Piero Comin-Chiaramonti & Celso de Barros Gomes

Editors

# Mesozoic to Cenozoic Alkaline Magmatism in the Brazilian Platform

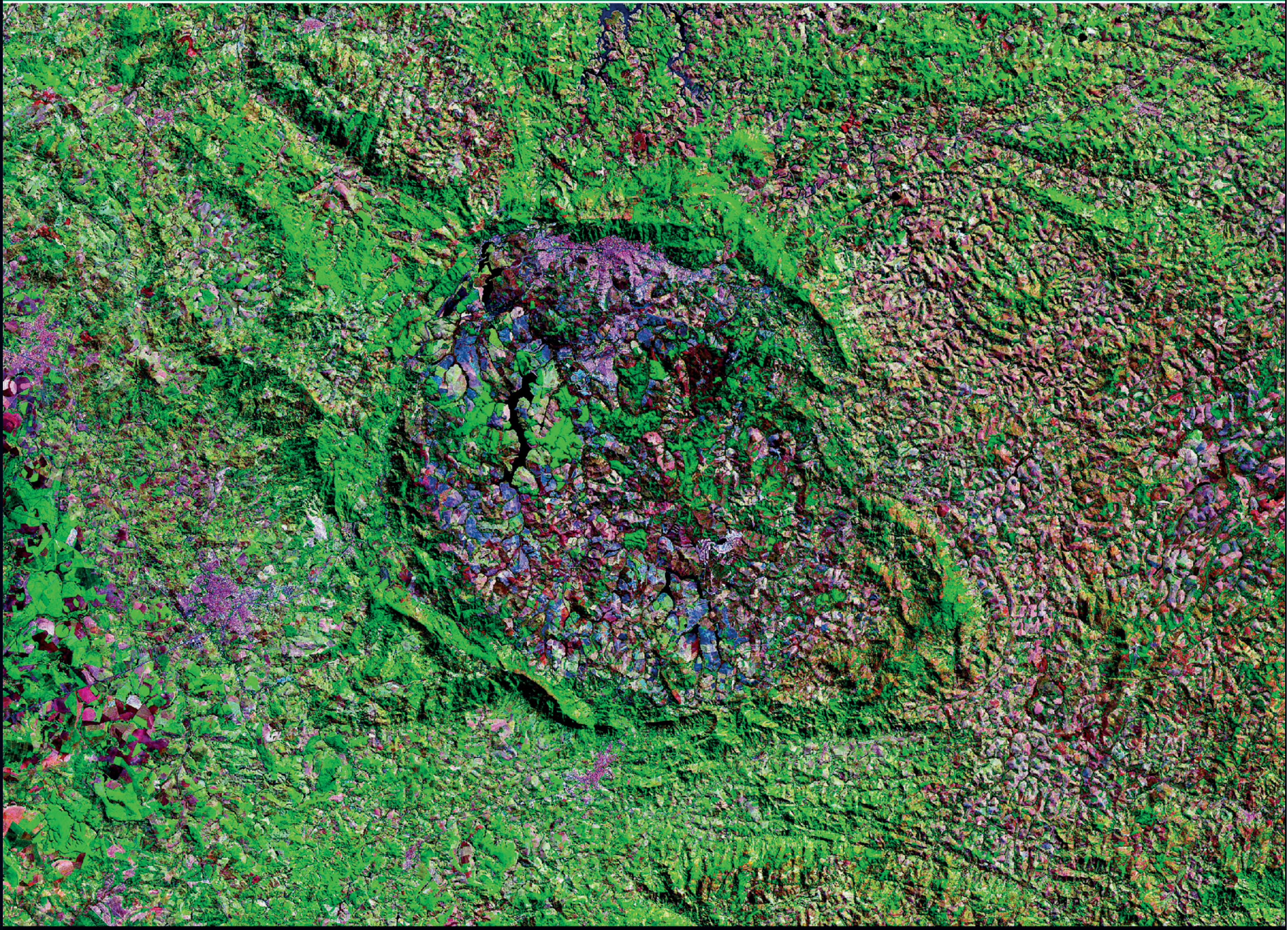

FAPESP

edusp

# MESOZOIC TO CENOZOIC ALKALINE MAGMATISM IN THE BRAZILIAL PLATFORM

P. COMIN-CHIARAMONTI and C.B.GOMES (Editors)

Dados Internacionais de Catalogação na Publicação (CIP)
(Câmara Brasileira do Livro, SP, Brasil)

P. Comin-Chiaramonti and C. B. Gomes
Mesozoic to Cenozoic Alkaline Magmatism in the Brazilian Platform / P. Comin-Chiaramonti and C. B. Gomes (editors). – São Paulo: Editora da Universidade de São Paulo, 2005

ISBN 85-314-0903-9

1. Geofísica – Paraguai 2. Geomorfologia – Paraguai 3. Magmatismo – Paraguai 4. Rochas ígneas alcalinas – Paraguai I. Comin-Chiaramonti, P. II Gomes, C.B.

96-3359 CDD-551.1309892

Índice para catálogo sistemático:
1. Paraguai: Magmatismo alcalino:
Geologia 551.1309892



Edusp – Editora da Universidade de São Paulo
Av. Prof. Luciano Gualberto, Travessa J, 374
6º andar – Ed. da Antiga Reitoria – Cidade Universitária
05508-900 – São Paulo – SP – Brasil Tel (11) 3091-4006
E-mail: edusp@edu.usp.br - SAC: (11) 3091-2911

Printed in Brazil, 2005

# CONTENTS

# LIST OF CONTRIBUTORS

| | |
|---|---|
| ANTONINI, P. | Dipartimento di Ingegneria Chimica, dell'Ambiente e delle Materie Prime, Università di Trieste<br>Piazzale Europa, 1<br>I-34127 Trieste, Italia<br>e-mail: paolo.antonini@dicamp.units.it |
| ARAÚJO, A.L.N | Centro de Estudos Gerais, Universidade Federal Fluminense<br>Avenida Litôranea, s/n<br>24210-340 Niterói, Brasil<br>email: alna@terra.com.br |
| AZZONE, R.G. | Instituto de Geociências, Universidade de São Paulo<br>Rua do Lago, 562<br>05508-900 São Paulo, Brasil<br>e-mail: rgazzone@yahoo.com.br |
| BARBOSA, E.S.R. | Instituto de Geociências, Universidade de Brasília<br>Campus Universitário “Darcy Ribeiro”<br>70910-900 Brasília, DF, Brasil<br>e-mail: elisabarbosa@unb.br |
| BIONDI, J.C. | Departamento de Geologia, Universidade Federal do Paraná<br>Caixa Postal 19.001<br>81531-990 Curitiba, Brasil<br>e-mail: jcbiondi@geologia.ufpr.br |
| BIZZI, L.A. | e-mail: luizbizzi@terra.com.br |
| BROD, J.A. | Instituto de Geociências, Universidade de Brasília<br>Campus Universitário “Darcy Ribeiro”<br>70910-900 Brasília, DF, Brasil<br>e-mail: brod@unb.br |

| | |
|---|---|
| BROTZU, P. | Dipartimento di Scienze della Terra, Università “Federico II”<br>Via Mezzocannone, 8<br>I-80134 Napoli, Italia<br>e-mail: pbrotzu@cds.unina.it |
| CARBONIN, S. | Dipartimento di Mineralogia e Petrologia, Università di Padova<br>Corso Garibaldi, 37<br>I-35137 Padova, Italia<br>e-mail: susanna.carbonin@unipd.it |
| CENSI, P. | Dipartimento di Scienze Geologiche, Università di Catania<br>Orso Italia, 55<br>I-95129 Catania, Italia<br>e-mail: pcensi@mbox.unict.it |
| COMIN-CHIARAMONTI, F. | Via Saval, 25<br>I-37124 Verona, Italia<br>e-mail: fchiaramonti@libero.it |
| COMIN-CHIARAMONTI, P. | Dipartimento di Ingegneria Chimica, dell'Ambiente e delle Materie Prime, Università di Trieste<br>Piazzale Europa, 1<br>I-34127 Trieste, Italia<br>e-mail: comin@univ.trieste.it |
| CRISTIANI, C. | Dipartimento di Scienze della Terra, Università di Pisa<br>Via S. Maria, 53<br>I-56126 Pisa, Italia<br>e-mail: cristiani@dst.unipi.it |
| D'AMELIO, F. | Dipartimento di Scienze della Terra, Università “Federico II”<br>Via Mezzocannone, 8<br>I-80134 Napoli, Italia |
| DEMAIFFE, D. | Départment des Sciences de la Terre et de l`Environnement, Université Libre de Bruxelles<br>Bruxelles, Bélgique |
| DINIZ-PINTO, H.S. | Instituto de Geociências, Universidade de Brasília<br>Campus Universitário “Darcy Ribeiro”<br>70910-900 Brasília, DF, Brasil<br>e-mail: hsenna@unb.br |
| ENRICH, G.E.R. | Instituto de Geociências, Universidade de São Paulo<br>Rua do Lago, 562<br>05508-900 São Paulo, Brasil<br>e-mail: gastonenrich@hotmail.com |
| ERNESTO, M. | Instituto de Astronomia, Geofísica e Ciências Atmosféricas, Universidade de São Paulo<br>Rua do Matão, 1226<br>05508-900 São Paulo, Brasil<br>e-mail: marcia@iag.usp.br |

FURTADO, S.M.A.
Departamento de Geociências, Universidade Federal de Santa Catarina
88040-90 Florianópolis, Brasil
e-mail: furtadosm@brturbo.com

FUSO, C.
Dipartimento di Mineralogia e Petrologia, Università di Padova
Corso Garibaldi, 37
I-35137 Padova, Italia
e-mail: lu.ni.cri@libero.it

GASPAR, J.C.
Instituto de Geociências, Universidade de Brasília
Campus Universitário “Darcy Ribeiro”
70910-900 Brasília, DF, Brasil
e-mail: gasp@unb.br

GASPARON, M.
Department of Earth Sciences, The University of Queensland Brisbane,
Queensland 4072, Australia
e-mail: massimo@earth.uq.edu.au

GOMES, C.B.
Instituto de Geociências, Universidade de São Paulo
Rua do Lago, 562
05508-900 São Paulo, Brasil
e-mail: cgomes@usp.br

JUNQUEIRA-BROD, T.C.
Companhia Vale do Rio Doce, Centro de Desenvolvimento Mineral
Rodovia BR-262, Km 296
Caixa Postal 09
33010-970 Santa Luzia, Brasil
e-mail: tcjbrod@uol.com.br

LIZIERO, F.
Dipartimento di Mineralogia e Petrologia, Università di Padova
Corso Garibaldi, 37
I-35137 Padova, Italia
e-mail: federica.liziero@unipd.it

LUSTRINO, M.
Dipartimento di Scienze della Terra, Università di Roma “La Sapienza”
Piazzale Aldo Moro, 5
I-00185 Roma, Italia
e-mail: michele.lustrino@uniroma1.it

MARQUES, L.S.
Instituto de Astronomia, Geofísica e Ciências Atmosféricas,
Universidade de São Paulo
Rua do Matão, 1226
05508-900 São Paulo, Brasil
e-mail:

MATTEINI, M.
Facultad de Ciencias Naturales, Universidad Nacional de Salta
Avenida Bolivia, 5150
4400 Salta, Argentina
e-mail: mmatteini@arnet.com.ar

MAZZUOLI, R.
Dipartimento di Scienze della Terra, Università di Pisa
Via S. Maria, 53
I-56126 Pisa, Italia
e-mail: mazzuoli@dst.unipi.it

| | |
|---|---|
| MELLUSO, L. | Dipartimento di Scienze della Terra, Università "Federico II"<br>Via Mezzocannone, 8<br>I-80134 Napoli, Italia<br>e-mail: melluso@cds.unina.it |
| OMARINI, R. | Facultad de Ciencias Naturales, Universidad Nacional de Salta<br>Avenida Bolivia, 5150<br>4400 Salta, Argentina<br>e-mail: rhomarini@arnet.com.ar |
| PETRINOVIC, I.A. | CONICET - Ministerio de Educación, Ciencia e Tecnología<br>Avenida Rivadavia, 1917<br>C1033AAJ Buenos Aires, Argentina<br>e-mail: petrino@unsa.edu.ar |
| PHILIPP, R.P. | Instituto de Geociências, Universidade Federal do Rio Grande do Sul<br>Avenida Bento Gonçalves, 9500<br>91501-970 Porto Alegre, Brasil<br>e-mail: philipp@terra.com.br |
| PUNTURO, R. | Dipartimento di Scienze Geologiche, Università di Catania<br>Orso Italia, 55<br>I-95129 Catania, Italia<br>e-mail: |
| RICCOMINI, C. | Instituto de Geociências, Universidade de São Paulo<br>Rua do Lago, 562<br>05508-900 São Paulo, Brasil<br>e-mail: riccomin@usp.br |
| RUBERTI, E. | Instituto de Geociências, Universidade de São Paulo<br>Rua do Lago, 562<br>05508-900 São Paulo, Brasil<br>e-mail: exrubert@usp.br |
| SCHEIBE, L.F | Departamento de Geociências, Universidade Federal de Santa Catarina<br>88040-90 Florianópolis, Brasil<br>e-mail: scheibe@cfh.ufsc.br |
| SGARBI, P.B.A. | Instituto de Geociências, Universidade Federal de Minas Gerais<br>Avenida Antônio Carlos, 6627-B<br>31270-910 Belo Horizonte, Brasil<br>e-mail: psgarbi@ciclope.lcc.ufmg.br |
| SOUSA, M.Z.A. | Universidade Federal de Mato Grosso, Cuiabá, Brasil<br>e-mail: mzaguiar@terra.com.br |
| SPEZIALE, S. | Department of Earth and Planetary Science, University of California<br>307 McCone Hall<br>94720-4767 Berkeley, U.S.A<br>e-mail: speziale@uclink.berkeley.edu |
| TASSINARI, C.C.G. | Instituto de Geociências, Universidade de São Paulo<br>Rua do Lago, 562<br>05508-900 São Paulo, Brasil<br>e-mail: ccgtassi@usp.br |

| | |
|---|---|
| ULBRICH, M.N.C. | Instituto de Geociências, Universidade de São Paulo<br>Rua do Lago, 562<br>05508-900 São Paulo, Brasil |
| ULBRICH, H.H.G.J | Instituto de Geociências, Universidade de São Paulo<br>Rua do Lago, 562<br>05508-900 São Paulo, Brasil<br>e-mail: hulbrich@usp.br |
| VELÁZQUEZ, V.F. | Instituto de Geociências, Universidade de São Paulo<br>Rua do Lago, 562<br>05508-900 São Paulo, Brasil<br>e-mail: vvf@usp.br |
| VIERO, A.P. | Instituto de Geociências, Universidade Federal do Rio Grande do Sul<br>Avenida Bento Gonçalves, 9500<br>91501-970 Porto Alegre, Brasil<br>e-mail: antonio.viero@ufrgs.br |
| VILLA, I.M. | Institut für Geologie, Universität<br>Earl strasse 9<br>Bern, Switzerland<br>e-mail: igor@geo.unibe.ch |
| VLACH, S.R.F. | Instituto de Geociências, Universidade de São Paulo<br>Rua do Lago, 562<br>05508-900 São Paulo, Brasil<br>e-mail: srfvlach@usp.br |

# PREFACE

The continental flood tholeiitic volcanism from the Paraná-Angola-Namibia was one of the most important events which has affected the Gondwanaland during the Mesozoic times. Associated with it in space, and sometimes in time, the alkaline magmatism is another relevant feature of pre-, syn- and post-Gondwana break-up in the region. Since the last century the alkaline magmatism from the Paraná-Angola-Namibia system has being the subject of many investigations which aim to enhance the knowledge of its different aspects, such as its genesis and evolution. However, most of these studies consist of isolated efforts restricted to relatively small portions of the area. The necessity of a better understanding of the relationships between the alkaline and alkaline-carbonatitic magmatism relative to the Gondwana evolution led Brazilian (C.B. Gomes and collaborators) and Italian (P. Comin-Chiaramonti and collaborators) researchers to elaborate the volume "Mesozoic to Cenozoic alkaline magmatism in the Brazilian Platform".

The main objective of this volume is to make available to the scientific community a survey of the published and unpublished data on the post-Paleozoic alkaline and alkaline-carbonatitic magmatism from the Brazilian Platform and neighbouring regions in South America, subdivided according to a regional distribution, although some papers also present a comparison with the African counterpart, i.e. Angola and Namibia. The several contributions are the results of a twenty years investigation program of various areas in and around the Paraná Basin and they were concluded in the period between 2002 and 2004. The studies, which have began in 1986 with the issue of Paraguay magmatism, were developed by means of multidisciplinary approaches involving geology, mineralogy, petrology, isotope geochemistry and paleomagnetism, in an effort to better define the geodynamic relationships between the alkaline (and tholeiitic) magmatism, in time and space, and the Gondwanaland break-up.

The program has been mainly carried out by researchers from Brazilian (São Paulo, Brasília, Curitiba, Florianópolis, Porto Alegre), Italian (Trieste, Catania, Naples, Rome, Pisa, Padova), Australian (Brisbane), American (Berkeley), Argentinian (Salta) and Swiss (Bern) Universities and CNR Italian centers (Consiglio Nazionale delle Ricerche: Padova, Pisa and Rome), besides several graduate students who prepared their theses mostly in São Paulo, Naples and Trieste.

A great many other people, particularly from Bolivia and Paraguay, both official and private citizens, gave freely of their time, knowledge and hospitality during the field work.

Finally, we would like to acknowledge our debts to our wives and sons (Paola, Caterina, Alessandro, Lorenzo, Francesco and Maria Beatrice, P.C.C.; and Maria Conceição, Anna Stella, Anna Lúcia and Anna Letícia, C.B.G.), who patiently took care of everything else while we were involved with this task.

Piero Comin-Chiaramonti
and
Celso de Barros Gomes

# ACKNOWLEDGEMENTS

The preparation and edition of this book was possible only by means of the continuous financial support provided by FAPESP (Fundação de Amparo à Pesquisa do Estado de São Paulo), CNPq (Conselho Nacional de Desenvolvimento Científico e Tecnológico), CNR (Consiglio Nazionale delle Ricerche), MIUR (Ministero della Pubblica Istruzione, della Università e della Ricerca), and by the Universities of São Paulo (USP), Trieste (UT) and Catania (UC).

The institutions below are acknowledged for their analytical support, laboratory facilities and collaboration:

1) Instituto de Geociências (USP)

2) Instituto de Astronomia, Geofísica e Ciências Atmosféricas (USP)

3) Dipartimento di Scienze della Terra (UT)

4) Istituto di Geocronologia e Geochimica Isotopica (CNR, Pisa)

5) Centro Studi Orogeno Alpi Orientali (CNR, Padova)

6) Centro di Studio per il Quaternario e l'Evoluzione Ambientale (CNR, Rome)

7) Dipartimento di Scienze della Terra (UC)

8) Dipartimento di Ingegneria Chimica, dell'Ambiente e delle Materie Prime (UT)

The following technicians participated in various stages of the work: M.S. Araújo, M.S. Mansueto, D.J. Oliveira, H.M. Sonoki and I.K. Sonoki (USP); L. Furlan, L. De Lorenzi and R. Zettin (UT); and R. Carampin (CNR, Padova).

The papers benefited of the following reviewers: K. Bell, S. Conticelli, A. Cundari, F. Innocenti, I. McReith, E.M. Piccirillo, F. Stoppa and A. Woolley.

Particular warm thanks go to both Clélia A. Monteiro, who patiently did all the typing work, and Anna Letícia Acquaviva, who was responsible for the formatting and layout of the volume.

# FOREWORD

In 1981 I was fortunate enough to receive funding to visit several countries in South America, with a view to gleaning as much information as possible on the alkaline rocks and carbonatites to be found there, which was to facilitate the writing of a book on the occurrences of these rocks in the Americas. My first couple of weeks were spent in São Paulo and Rio de Janeiro and aimed at compiling information on the alkaline rocks and carbonatites of Brazil, this being the country which is the most richly endowed with these rocks. The only generally available review at that time was that of Ulbrich & Gomes (1981) who listed and briefly described the occurrences of southern Brazil, with some information on the north, particularly those of the Amazon Basin. There was also a useful compilation of the 21 known carbonatites by Rodrigues & Lima (1984).

Although I had put a lot of effort into my Brazilian compilation in advance, it had generated a lot of frustration, principally because of the difficulty of obtaining copies of papers in relatively obscure Brazilian journals. My quest was transformed at the University of São Paulo where Professor Celso Gomes proved a wonderful host, as well as being an expert on the alkaline rocks of Brazil. Not only did he go through my lists and correct many errors but he added considerably to my number of localities. He also, incredibly generously, put at my disposal several boxes of papers and reprints which were just not generally available. These included many abstracts, short papers and maps presented at geological meetings in Brazil which could not be accessed outside the country. This information enriched considerably my own work and was the basis for my account published in 1987. The 'icing on the cake' of my São Paulo stay were field trips, organized by Celso Gomes, to Poços de Caldas and the Jacupiranga carbonatite.

Ulbrich & Gomes in their 1981 review pointed out that although there had been numerous papers in the last 20 years on the alkaline rocks of Brazil, which had added dozens of newly discovered occurrences, these were mostly "dispersed in Brazilian publications and these are usually unavailable to foreign readers.". The situation since then has been transformed and this transformation in no small part is owed to the efforts of Gomes and his many Brazilian colleagues, together with work by some of those "foreign readers" notably in Italy and particularly under the leadership of Professor Piero Comin-Chiaramonti. Apart from the 100s of widely published papers by these two petrologists and their colleagues their first major, single volume compilation was *Alkaline magmatism in central-eastern Paraguay* (Comin-Chiaramonti & Gomes, 1995) which included 15 papers and three extensive Appendices making available, for the first time, detailed information on the rich, but sadly neglected at that time, alkaline rocks and carbonatites of Paraguay. A glance at a map indicates why the alkaline rocks of eastern Paraguay are integral to any study of the same rock types in southern Brazil. A further perusal of that map might also indicate that any alkaline rocks occurring in northern Argentina, Uruguay and Bolivia might also be part of the same story.

The present volume probably represents the summit of the efforts that have been expended over the last 25 or so years on the alkaline rocks and carbonatites of Brazil, and again it comes under the driving editorships of Celso Gomes and Piero Comin-Chiaramonti. And not only does it cover Brazil, for there are substantial contributions on the alkaline rocks of Argentina, Uruguay, Bolivia and Paraguay, so that the whole province is now covered in a single, comprehensive volume. I myself was particularly looking forward to the contribution on the alkaline rocks of Uruguay, because I was totally unsuccessful in discovering anything significant whatsoever about these rocks in the 1980s.

This volume is remarkable in several ways. Firstly, it is probably the fullest comprehensive account of any of the world's major alkaline rock provinces. There are many partial accounts, descriptions of particular rock types, and descriptive lists but perhaps only Le Bas' (1977) book *Carbonatite-nephelinite volcanism* on western Kenya approaches it in comprehensiveness, although that is for a far smaller province. Secondly, it includes an enormous amount of primary chemical and mineralogical data. Most of the chapters are devoted to separate parts of the province but all of them contain many whole rock chemical analyses, including much isotope data, as well as a plethora of mineral analyses particularly of the rock-forming minerals. It is a bonus that most of the diagrams using these data are in colour. There are also chapters on tectonic controls, paleomagnetism and on the mineral deposits associated with the alkaline and alkaline-carbonatite complexes, from which Brazil is a major producer. Lastly, but certainly not least, are the numerous maps, all of them in colour. These range from maps of individual centres, to regional maps, to those that depict the whole province including adjacent countries. Needless to say, the perspective is also widened to take in the similar rocks found in the western part of southern Africa which, of course, are part of the general story.

As one would expect, much is written here on petrogenesis and in any book containing a lot of chemical, and particularly isotope, data this would be expected. It must be the ultimate aim of igneous petrology to arrive at a complete petrogenesis which will explain the full diversity of the igneous rocks we see, and the alkaline rocks and carbonatites present a particularly tough petrogenetic challenge. It seems to be part of the makeup of petrologists and geochemists that they must try to explain the origins of everything they see. We all do it, but I have always assumed that most of us will prove in time to be essentially wrong, and that it is those long sections at the end of very full papers in the Journal of Petrology and elsewhere which will date most rapidly and sometimes, perhaps, look foolish in the distant, if not near, future. We must, of course, keep hammering away producing 'petrogenetic models' for others to get their teeth into and worry to death. However, eventually, though I suspect long after my lifetime, somebody, or a combination of people, will arrive at a correct 'model for everything'.

In the meanwhile, here there is mention of mantle plumes, both for and against, sources in the lithosphere and asthenosphere, crystal fractionation and liquid immiscibility, metasomatism in the mantle and at higher levels, mixing of mantle components, and so on. Everyone will, I suspect, find opinions with which they agree and others with which they find fault, but I would suggest that in some ways this does not matter; what counts is that here a huge set of data are made available that you can pick over at your leisure and interpret as you please. On the whole I side with the Editors in being sceptical about plumes and support the idea that most alkaline rocks and carbonatites are generated in the lithosphere, but these are my prejudices. I have plenty of petrological friends who disagree with me completely on such issues. The point is that in this excellent book there are data for everyone, I am already picking over it for my own archives, and lots of ideas which are food for thought or disagreement.

I am grateful to all the authors for their efforts in researching for and writing this book. Needless to say, the Editors must be congratulated for persisting in their efforts over so many years and bringing to fruition this work so successfully.

Alan R. Woolley
Natural History Museum
London

REFERENCES

Comin-Chiaramonti, P. & Gomes, C.B. (1995). *Alkaline magmatism in central-eastern Paraguay: relationships with coeval magmatism in Brazil.* São Paulo: Edusp/Fapesp, 464p.

Le Bas, M.J. (1977). *Carbonatite-nephelinite volcanism*. London: John Wiley, 347p.

Rodrigues, C.S. & Lima, P.R.A.S. (1984). *Complexos carbonatíticos do Brasil: Geologia.* Companhia Brasileira de Metalurgia e Mineração, Araxá, 44p.

Ulbrich, H.H.G.J. & Gomes, C.B. (1981). Alkaline rocks from continental Brazil. *Earth-Science Reviews* **17**, 135-154.

# AN INTRODUCTION TO THE ALKALINE AND ALKALINE-CARBONATITIC MAGMATISM IN AND AROUND THE PARANÁ BASIN

*C.B. Gomes and P. Comin-Chiaramonti*

*The paper reviews general aspects of the alkaline and alkaline-carbonatitic complexes present in the South American Platform. This magmatic activity, which covers four different countries (Brazil, Paraguay, Bolivia and Uruguay, i.e. in and around the Paraná Basin), but particularly concentrated in the Brazilian and Paraguayan territories, started in Permo-Triassic times and lasted until the Oligocene period. Such rocks represent a large number of occurrences having dominantly Early Cretaceous age in Paraguay, Bolivia and Uruguay and Late Cretaceous age in Brazil. The emplacement of the alkaline rocks is clearly controlled by regional extensional tectonics and mainly on the basis of their geological setting they are grouped into various provinces showing distinct geographic distribution, rock associations and ages. On the whole, the alkaline magmatism is characterized by many occurrences essentially consisting of evolved rock-types and displaying wide variety of igneous forms, being prevalent the intrusive ones, and magma types. Carbonatites, usually occurring in association with several kinds of cumulate rocks, are very important economically in some Brazilian occurrences as a major source of phosphate, niobium, REE and vermiculite.*

## GENERAL OUTLINES

The emplacement of alkaline and alkaline-carbonatitic complexes in and around the Paraná-Angola-Etendeka igneous province (PAEP) occurred mainly along tectonic lineaments active at least since Early Mesozoic (Fig. 1; cf. Comin-Chiaramonti & Gomes, 1996, and therein references), being characterized by actual seismic activity (Berrocal & Fernandez, 1996).

Most of the Angola alkaline-carbonatitic bodies occur towards the apical part of the NE-trending Moçâmedes Arch, on an uplifted megastructure corresponding to the Ponta Grossa Arch of the southern Brazil at pre-drift times (Trompette, 1994; Alberti *et al.*, 1999). In the Etendeka region (NW Namibia), the Pan-African Damara fold belt was intruded by a large number of subvolcanic alkaline and alkaline-carbonatitic complexes (Trumbull *et al.*, 2004, and therein references). In the South American Platform, the alkaline complexes are distributed mainly along mobile belts (Brasiliano cycle) at the margins of the intracratonic Paraná Basin.

Several main pulses of alkaline magmatic activity are apparent in Brazil (Early and Late Cretaceous and Paleocene), Paraguay (Permo-Triassic to Eocene), Bolivia (Early and Late Cretaceous) and Uruguay (Early Cretaceous).

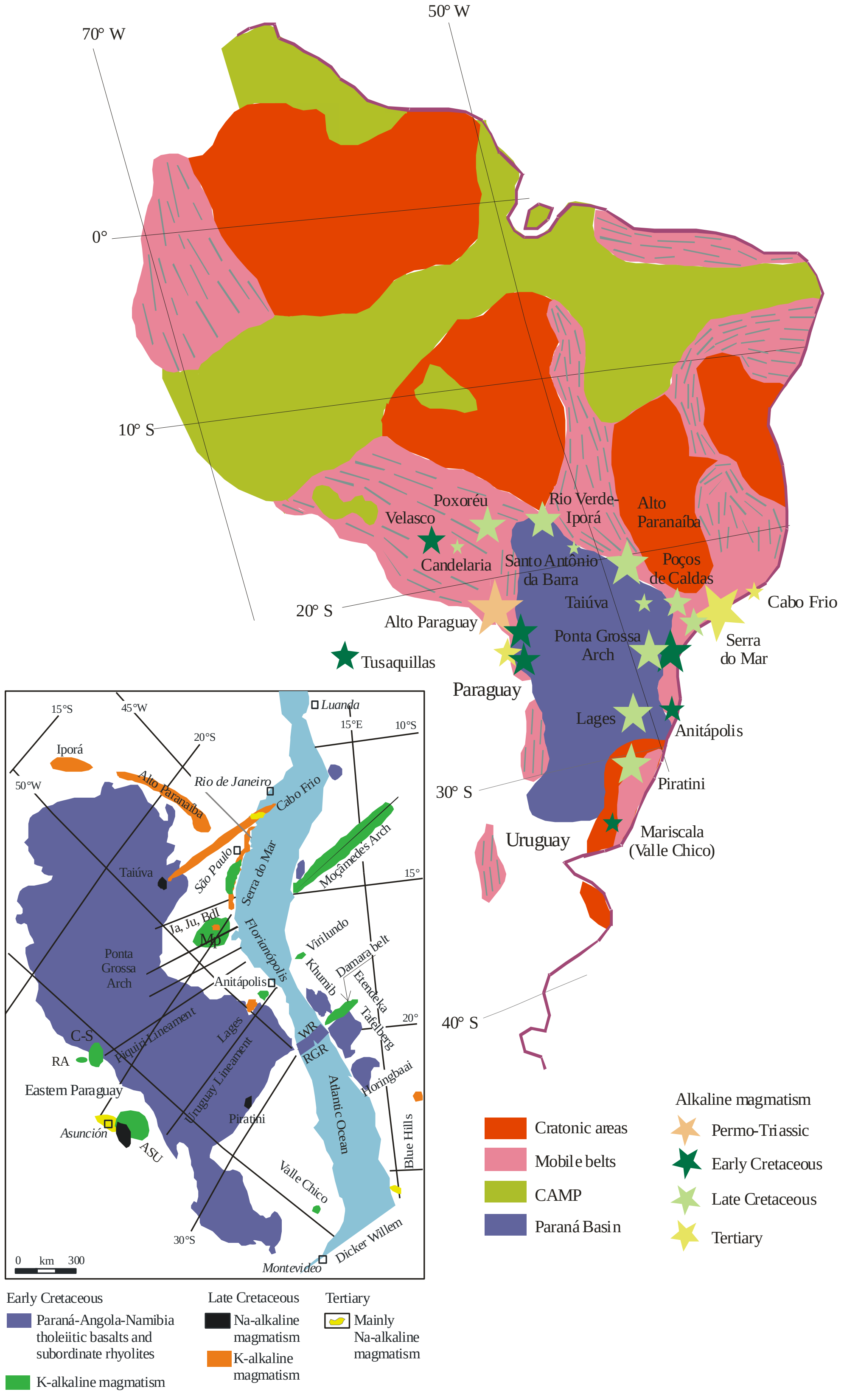


Fig. 1. Distribution of the post-Paleozoic alkaline magmatism (stars roughly proportional to the erupted volumes) in and around the Paraná Basin in the South American Platform. CAMP (Central Atlantic Magmatic Province), mobile belts and cratonic areas, as defined by De Min *et al.* (2003) and by Iacumin *et al.* (2003), and therein references. **Inset**: the main tectonic lineaments and simplified distribution of the alkaline rocks around the Paraná Basin, (cf. Fig. 1 of Comin-Chiaramonti *et al.*, in this volume, Carbonatites).

In the Brazilian territory, the alkaline occurrences are dominantly spread over its eastern flank, but they also form a large number of bodies arranged accordingly to two very distinctive belts extending for several hundred kilometers: the first (also referred to as Serra do Mar) is clearly NE-trending and parallels to the shoreline of the São Paulo and Rio de Janeiro states, and the second is approximately E-W-oriented and links more internal intrusions (e.g. Taiúva) with some found near the coast (e.g. Cabo Frio). Occurrences close to the Paraná Basin limits are abundant in the central and southern areas of the country, where they can be grouped following three prominent and mostly NW-trending alignments (Rio Verde-Iporá, Alto Paranaíba and Ponta Grossa). On the other hand, the alkaline bodies are scarcely represented in southern Brazil (Lages-Anitápolis and Rio Grande lineaments). A schematic structural map showing the main areas of alkaline outcrops (inset of Fig. 1) indicate that the Brazilian rocks are mainly concentrated north of the Rio Piqueri Lineament, in several groups related by emplacement ages and common tectonic features.

The southernmost alkaline rocks, also present in the eastern side of the Paraná Basin, correspond to the Uruguayan complex of Valle Chico, about 160 km SW of the Brazilian border.

In Paraguay, at the western side of the basin, the alkaline magmatism is widespread particularly in central-eastern region, where a considerable number of bodies is closely associated with a complex rifting structure, the Asunción-Sapucai-Villarrica graben (=Asunción Rift, cf. DeGraff, 1985), or even found in its northern part at the border with Brazil (Mato Grosso do Sul state), whose occurrences mainly lie along a NS-trending lineament at the both margins of the Paraguay river. The alkaline rocks are also abundant in the northeastern portion of the country (Amambay tectonic depression) and are less frequent in the southern one (Santa Rosa Lineament).

Additionally, alkaline bodies occur in southern Bolivia, whose different intrusions are mainly aligned in a northeasterly direction, that is considered an extension of the Tusaquillas rifting system in NW Argentina (Cristiani *et al.*, in this volume). This alkaline magmatism either covers a very extensive area at a great distance from the borders of the Paraná Basin, or its forms small bodies tectonically associated with the EW-ESE-trending Mercedes Rift, extending over 100 km.

As first suggested by Almeida (1971, 1972), the distribution of the alkaline rocks in the South American Platform is basically controlled by regional tectonics. In Eastern Paraguay, chiefly on the basis of Landsat imagery and geophysical evidence (aeromagnetic survey and Bouguer gravity map), Comin-Chiaramonti *et al.* (1997, 1999) argued that the tectonics in the area is clearly extensional and that major structures, NW-trending zones of tectonic subsidence, played an important role in the setting of the alkaline rocks. It is assumed for the whole magmatism that an old structural frame of the basement (NE-, NS- and NWW-trending lineaments and faulting zones), active since the Precambrian times and subject to intense reactivation in the Mesozoic (Wealdian reactivation of Almeida, 1966), in addition to positive, parallel, elongated deep fractures (arches), mainly NW-trending, transversal to the major axis of the Paraná Basin and generally surrounding it, has been important for the emplacement of such rocks. Besides dealing specifically with the arches, they have been also the sites of hundred of NW-trending basic dykes related to the Early Cretaceous (133-129 Ma; Renne *et al.*, 1997) basalt tholeiitic flows of the Serra Geral Formation (Piccirillo & Melfi, 1988), that occur associated with the alkaline rocks. In particular Fig. 1 draws the attention to the close relationships between the various alkaline centers and some important structural features such as arches (Rio Verde-Iporá, Alto Paranaíba, Ponta Grossa and Rio Grande in Brazil), rifts (Serra do Mar in Brazil; Asunción-Sapucai-Villarrica and Amambay in Paraguay; Mercedes in Bolivia) and lineaments (Lages-Anitápolis and Taiúva-Cabo Frio in Brazil; Alto Paraguay and Santa Rosa in Paraguay; Velasco in Bolivia; Valle Chico in Uruguay).

Taking into account both the tectonic setting and the geological-geophysical evidences, Riccomini *et al.* (in this volume) proposed a new assemblage for the various occurrences spread over the four countries (Brazil, Paraguay, Bolivia and Uruguay), which allows to distinguish 15 different alkaline provinces (cf. Fig. 1 of that paper): *Alto Paraguay, Ponta Grossa Arch*, *Valle Chico*, *Misiones*, *Central Paraguay*, *Amambay* and *Rio Apa*, all of them located at the borders of the Paraná Basin; *Rondonópolis Anteclise* and *Minas-Goiás*, lying along the borders of the Bauru Basin; *Serra do Mar* and *Piratini* adjoining to the borders of the Santos and Pelotas basins, respectively; *Asunción*, associated with the Cenozoic evolution of a rift system; the *Cabo Frio Magmatic Lineament*, encompassing asynchronic magmatic events along a major fracture zone; and the *Velasco* and *Candelaria*, in Bolivia, within the Amazon Craton. Data will be presented here and discussed mainly on the basis of the outlined classification, which in general terms does not differ significantly from that suggested by Almeida (1983).

The available literature on the alkaline magmatism lists a considerable number of occurrences, but their knowledge is far from being homogeneous. And for many of them only preliminary geological and petrographic data are available at present. This is partially due to the poor field geology which does not provide too much informations on such rocks as they are strongly influenced by weathering processes. In some places (e.g. the Brazilian Araxá carbonatite complex), the altered rocks may reach depths of more than 200 m, leading to the formation of a thick, residual mantle of lateritic soil. Furthermore progress in their knowledge has not been uniform in the last years, althought attention has being paid preferentially to occurrences that have economical interest and good facilities for field work (a typical example is the Jacupiranga carbonatite in Brazil).

The present monograph offers basically a synthesis of the information regarding the alkaline rocks from South America made available by a Brazilian-Italian research group and co-workers on the last years. However, it also contains non-published data and important review papers by others researchers focusing on their different aspects such as tectonic setting, regional distribution, formation ages, paleomagnetism, geochemistry of minerals and rocks, mineral resources etc. On the whole, the present released material will improve the knowledge on the alkaline magmatism that occurs in and around the Paraná Basin and will allow to throw some light on the genesis and evolution of the alkaline rocks.

## ALKALINE MAGMATISM IN THE SOUTH AMERICAN PLATFORM

The alkaline magmatism in the South American Platform started in Permo-Triassic times during the third of the four main stages of the geological evolution of the Paraná Basin, which is represented by general uplifts that promoted significant erosional processes and the final development of NW-trending arch structures (Almeida, 1971). The first two episodes (Devonian to Lower Carboniferous and Lower Carboniferous to Middle-Upper Permian, respectively) deal specifically with sediment deposition in a subsiding, synform basin, the fourth stage (end of Jurassic to Lower Cretaceous) being characterized by the outpouring of a huge volume of predominantly tholeiitic basalts and minor acid volcanics of the Serra Geral Formation in addition to important alkaline magmatic activity lasting up to Oligocene.

Individual occurrences are quite variable in size, the largest one corresponding to the Brazilian Poços de Caldas, which is basically composed of a nepheline syenite intrusion covering an area over 800 km$^2$. Others prominent massifs, also in Brazil and consisting dominantly of syenitic rocks, are Itatiaia (330 $km^2$) and Passa Quatro (165 $km^2$), the first one forming very impressive peaks up to 2787 m high. On the other hand, small bodies are represented by minor dykes or even veins either found penetrating the alkaline rock-types or the country-rocks. Excluded a few occurrences, such as Poços de Caldas, Lages and Pão de Açúcar, the more conspicuous alkaline centers in Brazil are found along the Serra do Mar. Over there they constitute massifs many kilometers away from the coastal line (e.g. Itatiaia, Passa Quatro, Tinguá) or form islands (e.g. São Sebastião, Búzios, Vitória). Although their more common rock associations consist of "syenites" of variable composition and texture (dominantly medium to coarse-grained), some of them are essentially made up of fine-grained, aphanitic rocks (e.g. Tinguá). In general, the alkaline rocks in the South American Platform are found intruding into the Precambrian crystalline basement or the Paraná Basin Paleozoic sediments; more rarely they occur associated with the flood tholeiites.

The mode of occurrence of the numerous bodies is also quite variable, being recognized intrusive, hypabyssal and extrusive types, sometimes all of them found together in the same complex. Intrusive formations are mainly represented by stocks of various dimensions, approaching to those of real batholiths in the case of the Brazilian Itatiaia and Passa Quatro massifs. Hypabyssal rocks occur as dykes (radial, concentric and more rarely as swarms), domes and plugs, whereas the extrusive ones comprise essentially lava flows. On the whole, the alkaline magmatism is characterized by a large number of occurrences displaying wide variety of igneous forms - but clearly prevailing the intrusive ones, except for a large number of occurrences associated with the Asunción-Sapucai-Villarrica graben in Paraguay-, and magma types.

Also, on the whole, the Brazilian alkaline rocks are characterized by a wide variation in composition, ranging chemically from ultrabasic to acidic types; in a few cases extreme differences are registered within the same complex, as indicated for instance by the presence of silica-undersaturated (syenitic) to silica-oversaturated (granitic) rock associations (Brazil: Itatiaia massif, Brotzu *et al.*, 1997; Alto Paraguay Province at the border with Paraguay, Gomes *et al.*, 1996; Bolivia: Velasco, Fletcher & Beddoe-Stephens, 1987). Potassic to ultrapotassic, mafic-ultramafic, strongly silica-undersaturated rock-types characterizing four distinct groups (kamafugitic, madupitic, kimberlitic and glimmeritic) are almost confined to two sets of occurrences, those found in the NW-trending belts related to the Alto Paranaíba Rift and Bom Jardim de Goiás Arch in Brazil and those (volcanics and dykes) associated with the Asunción-Sapucai-Villarrica graben in Paraguay. The more abundant silicate alkaline rocks are evolved nepheline syenites (and syenites), forming large isolated, simple or composite intrusions (e.g. Itatiaia and Passa Quatro in Brazil) or multiple plutons (a typical example is Velasco in Bolivia), and their equivalent fine-grained types. On the other hand, lithologies representative of the least evolved magmas are scarce and exclusively found as small dykes in a few complexes (e.g. Juquiá, Lages, Piratini in Brazil; Sapucai in Paraguay). Effusive suites are only significant in bodies cropping out in the area of Rio Verde-Iporá and Piratini in Brazil and, again, of Sapucai in Paraguay.

The alkaline rocks also vary considerably in mineralogy and have feldspars, feldspathoids and clinopyroxenes as the most important phases. Additional minerals include amphiboles, micas and a large number of accessories, some of them very common (opaques, titanite, apatite etc.) while others occur more rarely (mainly Zr and REE-rich phases). The mineralogy is typically agpaitic ($K_2O+Na_2O/Al_2O_3>1$, molar ratio, cf. Sørensen, 1974) in a very few complexes, such as Poços de Caldas and Lages in Brazil, where exotic minerals (lävenite, rosenbuschite, astrophyllite etc.) were described (e.g. Vlach *et al.*, 1996), and also in some

Cerro Bogianni and Cerro Siete Cabezas rocks (see Carbonin *et al.*, in this volume) in Alto Paraguay.

Carbonatites

Carbonatites are found in 22 occurrences in Brazil mainly associated with several kinds of cumulates, which vary from ultramafic (clinopyroxenites as the most frequent type) to basic-intermediate rocks and include all the members of the ijolite series; fenitic rocks are also particularly common. All the carbonatite types (cf. Woolley & Kempe, 1989) are recognized, although Ca-carbonatites (sövites and alvikites) represent the most widespread variety; Mg-carbonatites (berforsites) are important in the Juquiá and Araxá complexes. In Paraguay, such rocks are present in three different areas, the most relevant occurrences (Cerro Chiriguelo and Cerro Sarambí) being tectonically associated with the Amambay graben. They are calcitic in composition and also occur in contact with cumulate silicate rocks. In the Sapucai region, these rocks form a lava flow and have a beforsitic composition. Silicified carbonatites of the Cerro Manomó are found in the Bolivian territory in association with syenitic rocks of the Velasco Province. In general terms, the carbonatites occur as massive cores (plugs and stocks) and dykes/veins, the latter forming single bodies or complex systems (e.g. multiple stockwork in the Brazilian Barra do Itapirapuã body, cf. Ruberti *et al.*, 2002). Rarely they are found as lava flow (Brazil: Santo Antônio da Barra, Gaspar & Danni, 1981; Paraguay: Sapucai, Comin-Chiaramonti *et al.*, 1992).

Age

The alkaline magmatism in Brazil covers a large span of age (250-50 Ma), as confirmed by K/Ar, Ar/Ar and Rb/Sr determinations, and the periodicity of the numbers allows to place the rocks into different chronogroups. The oldest assemblage is Permo-Triassic (250-240 Ma) and comprises mostly syenitic rocks lying along both margins of the Paraguay river at the border of Brazil and Paraguay, and included in the Alto Paraguay Province (Gomes *et al.*, 1996; Comin-Chiaramonti *et al.*, in this volume). Only in Paraguay it is followed by rocks predating (c. 145 Ma) the Serra Geral Formation (tholeiitic) volcanics and present in two areas of the country, northern (Rio Apa Province) and northeastern (Amambay Province). The following group is Early Cretaceous (~130 Ma), consisting typically of alkaline-carbonatitic districts in Brazil, being the Jacupiranga complex the most representative occurrence. It is also represented by numerous alkaline bodies in association with the Asunción-Sapucai-Villarrica graben in Paraguay and by the syenitic rocks from Velasco and Valle Chico in Bolivia and in Uruguay, respectively. More recent events are suggested for the sodic rocks belonging to the Misiones Province in Paraguay (120-116 Ma, cf. Velázquez *et al.*, 2003) and for the Brazilian complexes of Banhadão and Itapirapuã (110-100 Ma). The most numerous assemblage, the Late Cretaceous-Eocene (90-50 Ma), consists of a large number of occurrences, with or without carbonatites, distributed over the central and southern parts of the Brazilian territory. Sodic rocks containing spinel-peridotite mantle xenoliths and cropping out in the Asunción neighborhood in Paraguay represent the most recent alkaline magmatic activity (61-39 Ma, Comin-Chiramonti *et al.*, 1991; 58-56 Ma, cf. Gomes *et al.*, 2003) in the South American Platform.

Economic geology

Alkaline-carbonatitic associations are very important as a major economical source of Nb, phosphate, REE and vermiculite (for a general review see Biondi, in this volume). Mineral deposits were formed in places by supergene processes that affected the alkaline rocks as well as by the residual concentration of minerals during the long period of weathering. Five carbonatitic bodies (Araxá, Catalão I and II, Jacupiranga and Tapira) are being mined nowadays, principally by open pit, for phosphate and niobium (only Araxá). Excepting Jacupiranga, where the fresh rock is mined as ore, mineral exploitation deals always with the weathered mantle. Concerning the Paraguayan, Bolivian and Uruguayan occurrences no application is presently registered.

Basic references

In terms of literature, the most accessible sources of data on the South American alkaline magmatism are the works by Ulbrich & Gomes (1981) and Morbidelli *et al.* (1995) regarding the Brazilian occurrences, and by Comin-Chiaramonti & Gomes (1996) on the Paraguayan rocks. On the whole, they contain data on the geology, petrography, mineral chemistry, geochemistry and geochronology of the numerous occurrences. In the latter paper a first attempt of comparison between the rocks from Brazil and Paraguay can also be found. An additional important source of information on such rocks is the book by Woolley (1987) that provides a general description of the alkaline bodies from different South American countries. Dealing specifically with the Brazilian carbonatites, it should be mentioned the review papers by Berbert (1984), Rodrigues & Lima (1984) and Gomes *et al.* (1990). The Bolivian literature is basically centered on the researches carried out by an English group in the 1970's, with much of the data made available in the papers by Fletcher & Litherland (1981) and Fletcher & Beddoe-Stephens (1987). Finally, the Uruguayan occurrence of Valle Chico has as major references the contributions presented by Kirstein *et al.* (2000), Muzio *et al.* (2002) and Lustrino *et al.* (2004).

## REFERENCES


Alberti, A., Castorina, F., Censi, P., Comin-Chiaramonti, P. & Gomes, C.B. (1999). Geochemical characteristics of Cretaceous carbonatites from Angola. *Journal of African Earth Sciences* **29**, 735-759.

Almeida, F.F.M. (1966). Origem e evolução da plataforma brasileira. *2ª Semana de Estudos Geológicos. Universidade Federal do Rio Grande do Sul, Porto Alegre, Anais*, pp. 45-128.

Almeida, F.F.M. (1971). Condicionamento tectônico do magmatismo alcalino mesozóico do Sul do Brasil e do Paraguai Oriental. *Anais da Academia Brasileira de Ciências* **43**, 835-836.

Almeida, F.F.M. (1972). Tectono-magmatic activation of the South American Platform and associated mineralization. *24th International Geological Congress, Montreal, Proceedings, Section* **3**, 339-346.

Almeida, F.F.M. (1983). Relações tectônicas das rochas alcalinas mesozóicas da região meridional da Plataforma Sul-Americana. *Revista Brasileira de Geociências* **13**, 139-158.

Berbert, C.O. (1984). Carbonatites and associated mineral deposits in Brazil. *Geological Survey of Japan Report* **263**, 269-290.

Berrocal, J. & Fernandes, C. (1996). Seismicity in Paraguay and neighbouring regions. In: Comin-Chiaramonti, P. & Gomes, C.B. (eds.) *Alkaline magmatism in central-eastern Paraguay. Relationships with coeval magmatism in Brazil.* São Paulo: Edusp-Fapesp, pp. 57-66.

Biondi, J.C. (in this volume). Brazilian mineral deposits associated with alkaline and alkaline-carbonatite complexes.

Brotzu, P., Gomes, C.B., Melluso, L., Morbidelli, L., Morra, E. & Ruberti, E. (1997). Petrogenesis of coexisting $SiO_2$-undersaturated felsic igneous rocks: the alkaline complex of Itatiaia, southeastern Brazil. *Lithos* **40**, 133-156.

Carbonin, S., Liziero, F. & Fuso, C. (in this volume). Mineral chemistry of accessory minerals in alkaline complexes from the Alto Paraguay Province.

Comin-Chiaramonti, P. & Gomes, C.B. (eds.) (1996). *Alkaline magmatism in central-eastern Paraguay. Relationships with coeval magmatism in Brazil.* São Paulo, Edusp-Fapesp, 464p.

Comin-Chiaramonti, P., Censi, P., Cundari, A. & Gomes, C.B. (1992). A silico-beforsitic lava flow from the Sapucai complex (Central-eastern Paraguay). *Geochimica Brasiliensis* **6**, 87-91.

Comin-Chiaramonti, P., Civetta, L., Petrini, R., Piccirillo, E.M., Bellieni, G., Censi, P., Bitschene, P., Demarchi, G., De Min, A., Gomes, C.B., Castillo, A.M.C. & Velázquez, J.C. (1991). Tertiary nephelinitic magmatism in Eastern Paraguay: petrology, Sr-Nd isotopes and genetic relationships with associated spinel-peridotite xenoliths. *European Journal of Mineralogy* **3**, 507-525.

Comin-Chiaramonti, P., Cundari, A., DeGraff, J.M., Gomes, C.B. & Piccirillo, E.M. (1999). Early Cretaceous-Tertiary magmatism in Eastern Paraguay (western Paraná basin): geological, geophysical and geochemical relationships. *Journal of Geodynamics* **28**, 375-391.

Comin-Chiaramonti, P., Cundari, A., Piccirillo, E.M., Gomes, C.B., Castorina, F., Censi, P., De Min, A., Marzoli, A., Speziale, S. & Velázquez, V.F. (1997). Potassic and sodic igneous rocks from Eastern Paraguay: their origin from the lithospheric mantle and genetic relationships with the associated Paraná flood tholeiites. *Journal of Petrology* **38**, 495-528.

Comin-Chiaramonti, P., Gomes, C.B., Censi, P.; Gasparon, M. & Velázquez, V.F. (in this volume). Alkaline complexes from the Alto Paraguay Province at the border of Brazil (Mato Grosso do Sul state) and Paraguay.

Comin-Chiaramonti, P., Gomes, C.B., Marques, L.S., Censi, P., Ruberti, E. & Antonini, P. (in this volume). Carbonatites from southeastern Brazil: geochemistry, O-C, Sr-Nd-Pb isotopes and relationships with the magmatism from the Paraná-Angola-Namibia Province.

Cristiani, C., Matteini, M., Mazzuoli, R., Omarini, R. & Villa, I. (in this volume). Petrology of Mesozoic Tusaquillas plutonic complex (Central Andes, 23º05'S-66º05'W): a comparison with rift related magmatism of NW Argentina and SE Bolivia.

DeGraff, J.M. (1985). Late Mesozoic crustal extension and rifting on the western edge of the Paraná Basin, Paraguay. *Geological Society of America, Abstracts with Programs* **17**, 560.

De Min, A., Piccirillo, E.M., Marzoli, A., Bellieni, G., Renne, P.R., Ernesto, M. & Marques, L.S. (2003). The Central Altlantic magmatic province (CAMP) in Brazil: petrology, geochemistry, $^{40}Ar/^{39}Ar$ ages, paleomagnetism and geodynamic implications. In: Hames, W.E., McHone, J.G., Renne, P.R. & Ruppel, C. (eds.) *The Central Atlantic magmatic province. AGU Geophysical Monograph* **136**, 91-128.

Fletcher, C.J.N. & Beddoe-Stephens, B. (1987) The petrology, chemistry and crystallization history of the Velasco alkaline province, eastern Bolivia. In: Fitton J.G. & Upton, B.G. (eds.) *Alkaline igneous rocks. Geological Society of London, Special Publication* **30**, 403-413.

Fletcher, C.J.N. & Litherland, M. (1981) The geology and tectonic setting of the Velasco Alkaline Province, eastern Bolivia. *Journal of the Geological Society of London* **138**, 541-548.

Gaspar, J.C. & Danni, J.C.M. (1981). Aspectos petrográficos e vulcanológicos da província alcalina-carbonatítica de Santo Antonio da Barra, sudoeste de Goiás. *Revista Brasileira de Geociências* **11**, 74-83.

Gomes, C.B., Laurenzi, M.A., Censi, P., De Min, A., Velázquez, V.F. & Comin-Chiaramonti, P. (1996). Alkaline magmatism from northern Paraguay (Alto Paraguay): a Permo-Triassic Province. In: Comin-Chiaramonti, P. & Gomes, C.B. (eds.) *Alkaline magmatism in central-eastern Paraguay. Relationships with coeval magmatism in Brazil.* São Paulo: Edusp-Fapesp, pp. 223-230.

Gomes, C.B., Milan, A., Velázquez, V.F., Riccomini, C., Comin-Chiaramonti, P., Vasconcelos, P.M. & Tassinari, C.C.G. (2003). Magmatismo alcalino na porção centro-oriental do Paraguai: novos dados geocronológicos para as rochas das Províncias Central e Assunção. *7º Congresso de Geoquímica dos Países de Língua Portuguesa, Maputo, Moçambique, Resumos,* p. 34.

Gomes, C.B., Ruberti, E. & Morbidelli, L, (1990). Carbonatites complexes from Brazil: a review. *Journal of South American Earth Sciences* **3**, 51-63.

Iacumin, M., De Min, A., Piccirillo, E.M. & Bellieni, G. (2003). Source mantle heterogeneity and its role in the genesis of Late Archean-Proterozoic (2.7-1.0 Ga) and Mesozoic (200 and 130 Ma) tholeiitic magmatism in the South American Platform. *Earth-Science Reviews* **62**, 365-391.

Kirstein, L.A., Peate, D.W., Hawkesworth, C.I., Turner, S.P., Harris, C. & Mantovani, M.S.M. (2000). Early Cretaceous basaltic and rhyolitic magmatism in Southern Uruguay associated with the opening of the South Atlantic. *Journal of Petrology* **41**, 1413-1438.

Lustrino, M., Melluso, L., Brotzu, P., Gomes, C.B., Morbidelli, L., Muzio, R., Ruberti, E. & Tassinari, C.C.G. (2005). Petrogenesis of the Early Cretaceous Valle Chico igneous complex (SE Uruguay): relationships with Paraná-Etendeka felsic rocks. *Lithos* (in press).

Morbidelli, L., Gomes, C.B., Beccaluva, L., Brotzu, P., Conte, A.M., Ruberti, E. & Traversa, G. (1995). Mineralogical, petrological and geochemical aspects of alkaline and alkaline-carbonatite associations from Brazil. *Earth-Science Reviews* **39**, 135-168.

Muzio S., R., Artur, A.C. & Wernick, E. (2002). Petrological and geochemical evolution of the alkaline Valle Chico massif, southeastern Uruguay. *International Geology Review* **44**, 352-369.

Piccirillo, E.M. & Melfi, A.J. (eds.) (1988). *The Mesozoic flood volcanism of the Paraná Basin: petrogenetic and geophysical aspects*. São Paulo: IAG-USP, 600p.

Renne, P.R., Ernesto, M. & Milner, S.C. (1997). Geochronology of the Paraná-Angola-Etendeka magmatic Province. *Eos, Transactions, American Geophysical Union* **78** (46), F742.

Riccomini, C., Velázquez, V.F. & Gomes, C.B. (in this volume). Tectonic controls of Mesozoic and Cenozoic alkaline magmatism in central-southeastern Brazilian Platform.

Rodrigues, C.S. & Lima, P.R.A.S. (1984). *Complexos carbonatíticos do Brasil: Geologia.* Companhia Brasileira de Metalurgia e Mineração, Araxá, 44p.

Ruberti, E., Castorina, F., Censi, P., Comin-Chiaramonti, P., Gomes, C.B., Antonini P. & Andrade, F.R.D. (2002). The geochemistry of the Barra do Itapirapuã carbonatite (Ponta Grossa Arch, Brazil): a multiple stockwork. *Journal of South American Earth Sciences* **15**, 215-228.

Sørensen, H. (ed.) (1974). *The alkaline rocks*. London: John Wiley & Sons, 622p.

Trompette, R. (1994). *Geology of Western Gondwana (2000-500 Ma). Panafrican-Brasiliano aggregation of South America and Africa*. Rotterdam: Balkema, 350p.

Trumbull, R.B., Harris, C., Frindt, S. & Wigand, M. (2004). Oxygen and Neodymium isotope evidence for source diversity in Cretaceous anorogenic granites from Namibia and implications for A-type granite genesis. *Lithos* **73**, 21-40.

Ulbrich, H.H.G.J. & Gomes, C.B. (1981) Alkaline rocks from continental Brazil. *Earth-Science Reviews* **17**, 135-154.

Velázquez, V.F.; Gomes, C.B.; Riccomini, C.; Comin-Chiaramonti, P.; Brumatti, M.; Vasconcelos, P.; Tassinari, C.C.G. (2003). Características isotópicas e idades $^{40}Ar/^{40}Ar$ para as rochas alcalinas da Província Misiones, Paraguai Meridional. *7° Congresso de Geoquímica dos Países de Língua Portuguesa, Maputo, Moçambique, Resumos*, p.39.

Vlach S.R.F., Ulbrich, M.N.C. Ulbrich, H.H.G.J. & Gualda, G.A.R. (1996). Rochas de afinidades alnoíticas e sílico-carbonatíticas periféricas ao maciço alcalino de Poços de Caldas (MG-SP). *XXXIX Congresso Brasileiro de Geologia, Salvador, Anais* **2,** 128-130.

Woolley, A.R. (1987). *Alkaline rocks and carbonatites of the World. Part I: North and South America*. London: British Museum (Natural History), 216p.

Woolley, A.R. & Kempe, D.R.C. (1989). Carbonatites: nomenclature, average chemical compositions, and element distribution. In: Bell, K. (ed.) *Carbonatites: genesis and evolution*. London: Unwin Hyman, pp. 1-14.

*Mesozoic to Cenozoic Alkaline Magmatism in the Brazilian Platform*
*Comin-Chiaramonti, P. & Gomes, C.B. (eds.)*
*Edusp/Fapesp, São Paulo, pp. 21-29, 2005*

# TECTONIC CONTROLS OF THE MESOZOIC AND CENOZOIC ALKALINE MAGMATISM IN CENTRAL-SOUTHEASTERN BRAZILIAN PLATFORM

*C. Riccomini, V.F. Velázquez and C.B. Gomes*

*An attempt is made in this paper in order to examine the tectonic relationships of the Mesozoic and Cenozoic alkaline magmatism in the central-southeastern part of the Brazilian Platform. This region is punctuated by more than one hundred occurrences of alkaline rocks, Permian-Triassic to Paleogene in age, including alkaline centers, associated dyke swarms and small bodies. These occurrences may be grouped into 15 provinces: Alto Paraguay, Ponta Grossa Arch, Valle Chico, Misiones, Central Paraguay, Amambay and Rio Apa, all of them located on the borders of Paraná Basin; Rondonópolis Anteclise and Minas-Goiás, lying along the borders of Bauru Basin; Serra do Mar and Piratini, adjoining to the borders of the Santos and Pelotas basins, respectively; Asunción, associated with the Cenozoic evolution of a rift system; the Cabo Frio Magmatic Lineament, encompassing asynchronic magmatic events along a major fracture zone; and the Velasco and Candelaria, in eastern Bolivia, within the Amazon Craton. The alkaline provinces are controlled by crustal discontinuities, mainly extensional or wrenching fault zones along the present-day borders of sedimentary basins. Their distribution along tectonic features does not show any age distribution pattern, and the isotopic data indicate a clear lithospheric mantle source to the alkaline magmatism. Taking into account the age span (ca. 210 Ma) and the large area of occurrence (ca. $2.10^6$ $km^2$), a long-lived process of mantle upwelling seems to explain the source of heating for the Permian-Triassic to Cenozoic alkaline magmatism in the region. Changes in the stress-fields and reactivations of regional structures (mainly inherited from Proterozoic crustal discontinuities), in different pulses from Permian-Triassic to the Paleogene, have generated a wide range of structural discontinuities along which alkaline magmas were emplaced or reached to the surface.*

## INTRODUCTION

The South American Plate is composed of four main geotectonic units: the Andean chain, to the west, the Brazilian Platform and the Patagonian block, in the central region, and the domain of oceanic crust which constitutes its eastern part. The Brazilian Platform (Almeida, 1967) is essentially composed of Archaean to Proterozoic cratonic areas surrounded by Neoproterozoic orogenic belts and covered by Phanerozoic sedimentary basins. From Late Neoproterozoic to Early Cretaceous the central-southeastern part of the Brazilian Platform has belonged to Gondwanaland. Tectonic reactivations along shear zones and other discontinuities in the basement rocks and cratonic boundaries have played a major role in the origin and in the stratigraphic and structural development of Phanerozoic sedimentary basins (Cordani *et al.*, 1984; Milani, 1997), as well as in the distribution of magmatic activity in space and time.

More than one hundred major alkaline centers and associated bodies, Permian-Triassic to Paleogene in age, are known in the central-southeastern region, particularly close to the borders of the Paraná Basin. These occurrences, in some cases known since the 19th century, were object of an extensive K-Ar dating program (Amaral *et al.*, 1967a) and of regional reviews dealing mainly with its petrographic and genetic aspects (e.g. Ulbrich & Gomes, 1981; Morbidelli *et al.*, 1995; Comin-Chiaramonti & Gomes, 1996). Only during the last 30 years, however, took place an increasing interest on the study of tectonic controls of the alkaline magmatism of the region. The main studies are those by Almeida (1971, 1972, 1983, 1986), Almeida & Carneiro (1989) and Almeida *et al.* (1996). Almeida (1983), in a comprehensive review of the subject, recognized that alkaline rocks south of 15° S parallel are concentrated in three main different geographical contexts: near the borders of the Paraná Basin; in a belt, 100 km wide, along the onshore Atlantic coastal region; and in the Bolivian territory, within the domain of the Amazon Craton, far from the borders of Paraná Basin and more than 1500 km away from the Atlantic Ocean. The author has introduced the concept of *alkaline province* in order to designate the regions of occurrence of clusters of alkaline bodies, with specific petrographic relationships and ages, and related to recognizable tectonic features. Based on this concept, Almeida (1983) defined the following provinces:

- *Poços de Caldas, Alto Paranaíba, Rio Verde-Iporá, Ponta do Morro, Eastern Paraguay, Mariscala, Piratini, Santa Catarina, Ponta Grossa Arch* and *Ipanema*, all along the borders of the Paraná Basin;
- *Serra do Mar*, on the onshore continental region along the western border of the Santos Basin;
- *Velasco* and *Candelaria*, in eastern Bolivia, within the Amazon Craton.

This paper examines the role of fracture zones as the main tectonic control of the alkaline magmatism in the region close to the geographic area of Paraná, Santos and Pelotas basins as well as in the eastern Bolivia. It follows the general approach given by Almeida (1983), but the interpretations herein presented are based on new geological, structural and geophysical data obtained during the last 20 years, including previously unpublished data, which have greatly improved the geological knowledge of the region. Special reference is given to the: 1) recognition of new structural lineaments hosting alkaline rocks; 2) identification of wrenching and associated structures as a control for alkaline bodies; 3) individualization of the Bauru Basin, a Late Cretaceous tectonic unit overlying Early Cretaceous tholeiites of the Serra Geral Formation (Paraná flood volcanism), within the geographical area of the Paraná Basin, and with bodies of alkaline rocks along its borders; 4) geochronological data indicating different ages for alkaline rocks previously included in a single province.

These new data have opened a new perspective to the analysis of the Mesozoic and Cenozoic magmatism in the region and, consequently, to a review of the model proposed by Almeida (1983).

## THE MAIN PULSES OF ALKALINE MAGMATIC ACTIVITY DURING THE MESOZOIC AND CENOZOIC IN THE CENTRAL-SOUTHEASTERN BRAZILIAN PLATFORM

Taking into account the available geochronological data at the beginning of the 80's (Amaral *et al.*, 1967a; Ulbrich & Gomes, 1981), Almeida (1983) verified that the Mesozoic and Cenozoic alkaline magmatism in the region has occurred in three main stages related to the opening of the South Atlantic: 1) Late Jurassic to Early Cretaceous, correlated with the rift stage in the Atlantic marginal basins; 2) Aptian to Maastrichtian, or even the beginning of the Paleogene, corresponding to the ocean stage (Asmus & Guazelli, 1981); and 3) Paleogene, coeval to the installation of the continental taphrogenic basins of southeastern Brazil (Almeida, 1976).

The more recently available geochronological data confirm the existence of such three stages. Moreover, they point to an older stage, Permian-Triassic in age (e.g. Velázquez *et al.*, 1996a, b; Gomes *et al.*, 1996a), and bring about the division of the Early Cretaceous stage in three main pulses of alkaline magmatic activity.

In the present paper, the alkaline magmatism of central-southeastern region of Brazilian Platform is grouped in 15 provinces (Fig. 1):

- the Permian-Triassic *Alto Paraguay* and the Early Cretaceous *Ponta Grossa Arch, Valle Chico, Misiones, Central Paraguay, Amambay* and *Rio Apa* provinces, distributed along the present-day borders of Paraná Basin;
- the Late Cretaceous *Rondonópolis Anteclise* and *Minas-Goiás* provinces, adjacent to the Bauru Basin;
- the Late Cretaceous *Serra do Mar* and *Piratini* provinces, developed on the onshore continental region at the western borders of Santos and Pelotas marginal basins, respectively;
- the *Asunción* province, related to the Cenozoic evolution of the Asunción Rift;
- the *Cabo Frio Magmatic Lineament* province, with at least two phases of alkaline magmatism, from Late Cretaceous to the Paleogene;
- the Early Cretaceous *Velasco* and *Candelaria* provinces of eastern Bolivia, within the Amazon Craton.

## ALKALINE PROVINCES AROUND THE PARANÁ BASIN

The boundaries of Paraná Basin, an interior cratonic sineclise, are delineated by syn- and post-tectonic activity of archs and structural lineaments, parallel or transverse to its borders. Their oldest sedimentary deposits, preserved in Eastern Paraguay, are Ordovician in age (Fúlfaro, 1996). Its sedimentary fill records the different Phanerozoic orogenic processes that occurred in the adjoining regions of the Western Gondwana at the end of the Ordovician and of the Devonian, and at the Permian-Triassic (Zalán *et al.*, 1990a, b; Tankard *et al.*, 1995; Milani, 1997). The present-day expression of the Paraná Basin summarizes a long, polycyclic evolution history, alternating periods of subsidence and uplift, largely influenced by archs and lineaments. The successive periods of erosion, including those actives nowadays, have restricted the original area of sedimentation.

The oldest alkaline rocks recognized around the Paraná Basin are of Permian-Triassic age (Amaral *et al.*, 1967a; Velázquez, 1996; Veláquez *et al.*, 1996a, b; Gomes *et al.*, 1996a). At this time occurred the convergence along the southern border of Western Gondwana (Ramos, 1988; Cobbold *et al.*, 1992; Dalziel & Grunow, 1992) and the consequent Cabo-La Ventana Orogeny (e.g. Tankard *et al.*, 1995; Milani, 1997). The propagation of stresses related to this event into the inner parts of the continent has caused syn-sedimentary tectonism and deformation (Riccomini, 1995a; Rostirolla *et al.*, 2000; Velázquez *et al.*, 2001) and generated N-S and NE-SW-trending zones of weakness in the central-western and the eastern part of the basin, respectively.

Early Cretaceous is marked by intense tectono-magmatic activity in the region of the Paraná Basin, with the extrusion of tholeiitic basaltic lavas (Amaral *et al.*, 1967b; Melfi *et al.*, 1988; Rocha-Campos *et al.*, 1988; Renne *et al.*, 1992; Turner *et al.*, 1994; Stewart *et al.*, 1996). The area covered by lava flows was larger than 1.6 x $10^6$ $km^2$ (Renne *et al.*, 1992), with a volume of about 7.9 x $10^5$ $km^3$ (Eyles & Eyles, 1993). High precision Ar-Ar age data (Turner *et al.*, 1994; Stewart *et al.*, 1996) show that the extrusion of lava flows started at 137 Ma along NE-trending geosutures, parallel to the present-day Paraná river, and has migrated to the southeast at 134-132 Ma along the NW-striking lineaments that constitute the Ponta Grossa Arch. Laterly, the magmatism occurred along the coastal regions of Santa Catarina, Paraná, São Paulo and Rio de Janeiro states, following older, NE to NNE-trending structures (nowadays represented by dykes, the feeders of lava flows), before reaching the Etendeka (Namibia) and the continental breakup occurred at 126 Ma.

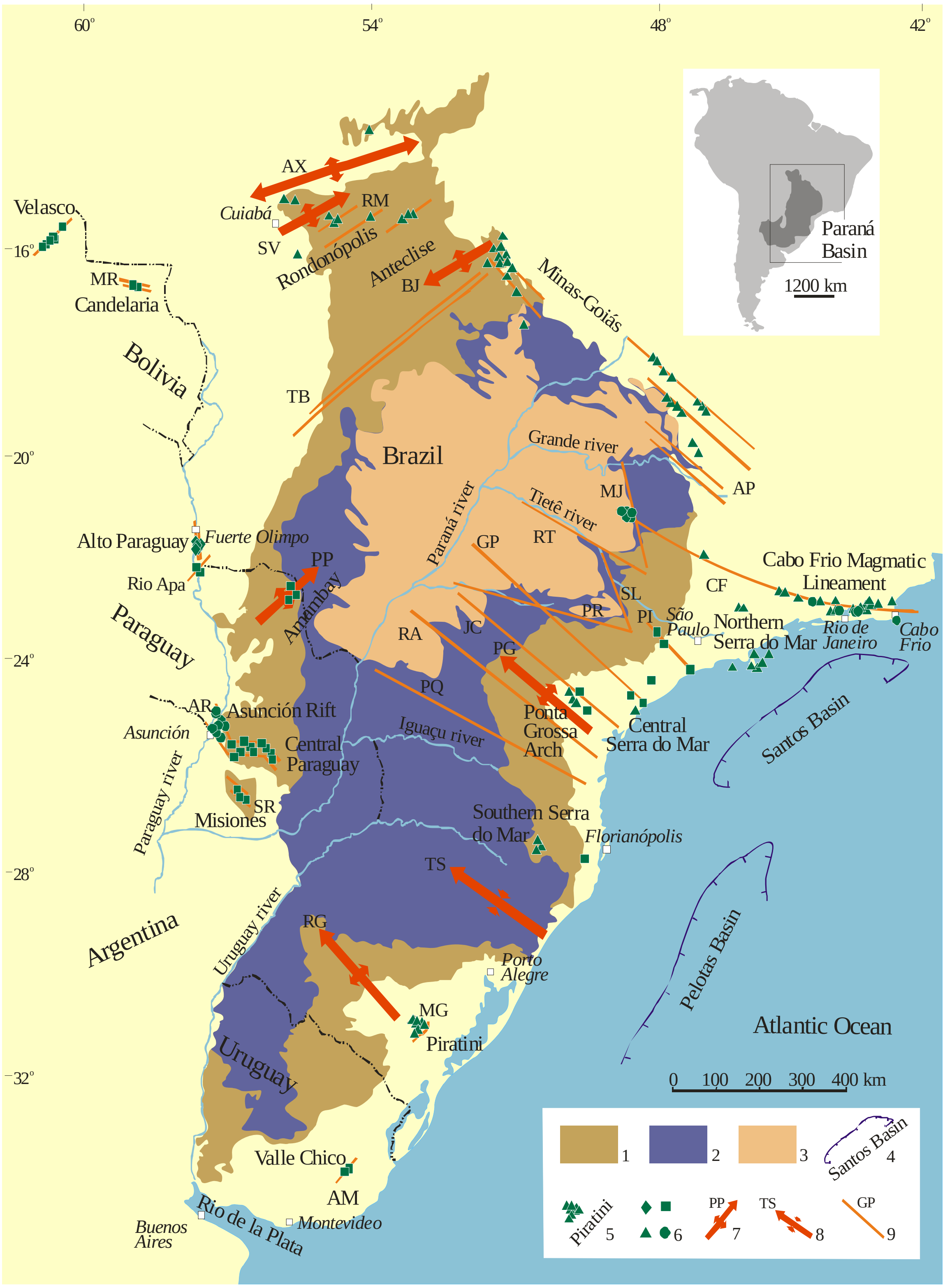


Fig. 1. Alkaline provinces of the central-southeastern region of the Brazilian Platform and their relationships with major structural features: 1) Late Ordovician to Early Cretaceous Paraná Basin; 2) Early Cretaceous tholeiitic lava flows; 3) Late Cretaceous Bauru Basin; 4) Offshore marginal basins; 5) alkaline provinces; 6) age of alkaline rocks (diamonds, Permian-Triassic; squares, Early Cretaceous; triangles, Late Cretaceous; circles, Paleogene); 7) Axes of main archs (AX, Alto Xingu; SV, São Vicente; BJ, Bom Jardim de Goiás; PG, Ponta Grossa; RG, Rio Grande; PP, Ponta Porã); 8) Torres Syncline; 9) Major fracture zones, in part deep lithospheric faults (Rifts: MR, Mercedes; RM, Rio das Mortes; MG, Moirão; SR, Santa Rosa; AR, Asunción; Lineaments: TB, Transbrasiliano; AP, Alto Paranaíba; MJ, Moji-Guaçu; CF, Cabo Frio; RT, Rio Tietê; SL, São Carlos-Leme; PR, Paranapanema; PI, Piedade; GP, Guapiara; JC, São Jerônimo-Curiúva; RA, Rio Alonzo; PQ, Rio Piquiri; AM, Santa Lucía-Aiguá-Merin).

The structure of the western border of Paraná Basin in Eastern Paraguay was first delineated in regional studies (DeGraff, 1985; Druecker & Gay Jr., 1987) and could be detailed thanks to the aeromagnetometric and gravimetric data obtained, respectively, by Aerial Geophysics Company (1991) and Photo Gravity Corporation (1991), during a survey under contract for the Anschutz Corporation. On the basis of the reinterpretation and integration of these data, Velázquez *et al.* (1998) identified the presence of NW-SE-striking structural lineaments in the regions of Asunción and San Juan Bautista (Fig. 1). Such structures correspond to deep-lithospheric faults filled with dykes of ultra-alkaline rocks, active either during the Early Cretaceous and the Paleogene (Riccomini *et al.*, 2001; Velázquez *et al.*, 2002). These lineaments are displayed similarly as those observed in the eastern border of the Paraná Basin, in Brazil (Velázquez *et al.*, 1998). New geochronological, structural and geophysical data obtained from the Paraguayan alkaline rocks allowed the individualization of six provinces in the region (Velázquez *et al.*, 1996b), which as a whole were so far considered as corresponding to the Eastern Paraguay Province and related solely to the Asunción Arch (Almeida, 1983).

Alto Paraguay

The Alto Paraguay Province encompasses the alkaline centers located north of Porto Murtinho, at the boundary zone between the Paraguay and the state of Mato Grosso do Sul, Brazil (Fig. 1). These rocks are related to the oldest recognized alkaline magmatic event around the Paraná Basin, of Permian-Triassic age (250-240 Ma) (Amaral *et al.*, 1967b; Velázquez, 1996; Velázquez *et al.*, 1996a, b; Gomes *et al.*, 1996a). They consist mainly of nepheline syenites and syenites occurring as ring-like complexes and stocks, with fine-grained equivalents, such as lavas and dykes.

Livieres & Quade (1987) related the magmatism of the Alto Paraguay Province to the Rio Apa Arch, whereas Velázquez *et al.* (1996a) to a cratonic margin. Because of the restricted area of occurrence, with bodies aligned in a narrow belt along the Paraguay river, and the presence of structural lineaments, Velázquez *et al.* (1998) pointed out the possibility of a control by N-S-trending faults. Taking into account that stresses related to the Cabo-La Ventana orogeny (Tankard *et al.*, 1995; Milani, 1997) have propagated to the inner parts of the Brazilian Platform in the general N-S-trending, it is here put forward the hypothesis of a genetical relationship between the convergence in southwestern Gondwana and the Permian-Triassic alkaline magmatism in the Alto Paraguay Province.

Ponta Grossa Arch

The Ponta Grossa Arch is composed of NW-SE-striking structural lineaments along which huge diabase dykes related to the tholeiite magmatism of the Serra Geral Formation were intruded (Ferreira, 1982; Ussami *et al.*, 1994). In this work the Ponta Grossa Arch Province includes only the Early Cretaceous alkaline rocks occurrences, with chronological links with the tholeiitic effusives and associated dykes and sills of the main magmatic phase of the arch. Some of the alkaline intrusions are situated on or close to the NW-SE-trending arch lineaments. Together with the bodies lying in the axial region of the arch, which originally integrated this province (Almeida, 1983), it is here believed to extend to northeast, in order to include the Ipanema (Araçoiaba da Serra), Salto de Pirapora, Piedade and Itanhaém alkaline bodies (São Paulo state), because of their distribution along a NW-SE-trending structure, parallel to the Guapiara Lineament, and to the south, to include the Anitápolis intrusion (Santa Catarina state). These new limits correspond to the extent of Early Cretaceous uplift along the arch.

Alkaline rocks with a mafic to ultramafic character predominate in this province, including carbonatites in Anitápolis, Itapirapuã, Jacupiranga, Juquiá and Ipanema (Gomes *et al.*, 1990), whereas in Tunas there are rocks with a felsic nature (Gomes *et al.*, 1987). The available geochronological determinations show that the Early Cretaceous alkaline magmatism occurred in two phases: the older, coeval to the tholeiitic event, as indicated by Ar-Ar age data of 132-131 Ma for Anitápolis (Renne *et al.*, 1993) and Jacupiranga (Renne *et al.*, 1993; Basu *et al.*, 1993), besides the K-Ar ages within the 130 to 122 Ma interval for Juquiá, Ipanema, Piedade and Itanhaém (Amaral *et al.*, 1967a; Sonoki & Garda, 1988); and the more recent event, with K-Ar age determinations of 101-105 Ma for Itapirapuã (Gomes & Cordani, 1965; Sonoki & Garda, 1988) and 110 Ma for Tunas (Gomes *et al.*, 1987; Sonoki & Garda, 1988). Ar-Ar data of alkaline massifs in northwestern Namibia, the African counterpart of the Ponta Grossa Arch Province, indicate similar ages, between 137 and 127 Ma (Milner *et al.*, 1995; Renne *et al.*, 1996).

With the exception of Anitápolis, without a clear structural control, the other Early Cretaceous occurrences of the Ponta Grossa Arch show a striking control along the NW-SE direction, as evidenced by the elongation of the Tunas and Itapirapuã massifs, the association of the Jacupiranga, Juquiá and Pariqüera-Açu massifs with the Guapiara Lineament, and the alignment of the Ipanema, Piedade and Itanhaém intrusions along this direction.

During the tholeiitic magmatism, the structural lineaments of the Ponta Grossa Arch acted as the conduit for lavas. In particular, the Guapiara Lineament (which integrates the Ponta Grossa Arch) was a 600 km long and 20-60 km wide fissure-zone along which a large volume of basaltic magma was intruded as dykes. This crustal section was thinned by 14%, with maximum mantle ascension of 5 km and minimum extension of 18% (Ferreira *et al.*, 1989), suggestive of a quite pure shearing regime, with the main extensive stress, $\sigma3$, horizontal, NE-SW-oriented (Riccomini, 1995a, b). Almost all of the older Early Cretaceous alkaline intrusions in this region probably were emplaced under this extensional stress-field. Mafic dykes constitute three swarms, with NW-SE-trending in the Ponta Grossa Arch, ENE-WSW-trending along the coast of São Paulo and Rio de Janeiro states, and a N-S-trending swarm along the coast of Paraná and Santa Catarina states, the branches of a triple-junction installed in the region (Herz, 1977; Riccomini, 1995a). The formation of the South Atlantic sea floor was older to the south and more recent to the north of São Paulo-Walvis Chain (Chang & Kowsmann, 1991). As a result, the stress-regime has changed to wrenching, related to a WNW-ESE-trending right-lateral binary. The principal extensive stress, $\sigma3$, remained in the NE-SW direction, but the principal compressive stress, $\sigma1$, has changed to NW-SE, horizontal (Riccomini, 1995a). The occurrence of diabase dykes showing syn-intrusive shortening along the NW-SE-direction in the region of the Guaratuba Bay, in the coast of the Paraná state (Soares, 1991) and of discontinuities developed during the cooling phase of the Jacupiranga intrusion (Hasui *et al.*, 1992) corroborate this change in the stress-field and allows to conclude that $\sigma1$ was positioned along the NW-SE-direction, thus indicating a clockwise block rotation in the region of the Ponta Grossa Arch at that time.

Valle Chico

The Valle Chico Province, in southern Uruguay, was formerly referred to as Mariscala Province by Almeida (1983). It is an igneous complex with about 250 km$^2$ (Muzio & Artur, 1998; Muzio, 2000) and includes syenites, trachytes and porphyry syenites of the Valle Chico Formation (Pirelli, 1999). Rb-Sr (Umpierre & Halpern, 1971), U-Pb and Sm-Nd data (Muzio *et al.*, 1999) have indicated an Early Cretaceous age for this province. A syenite from this region yielded an Ar-Ar age of 133 Ma (Stewart *et al.*, 1996). Dykes and veins within the complex are preferentially NW-SE-trending oriented (Pirelli, 1999). The province was first related to the Early Cretaceous evolution of the WNW-ESE-trending Santa Lucía Graben (Bossi, 1996) and more recently to the NE-SW-trending Santa Lucía-Aiguá-Merin Lineament, an extensional fault zone during the alkaline magmatism (Rosselo *et al.*, 2000).

Misiones

The Misiones Province includes the sodic alkaline rocks of the region of San Juan Bautista in the southern part of Eastern Paraguay (Comin-Chiaramonti *et al.*, 1992a). It is related to a late Early Cretaceous magmatic event, with Ar-Ar age-data of ca. 118 Ma (Velázquez *et al.*, 2003), and consists of small plugs and dykes of nephelinite, peralkaline phonolite (Comin-Chiaramonti *et al.*, 1992a) and tephrite (Velázquez *et al.*, 2003). Magnetometric and gravimetric data indicate a conspicuous set of NW-SE-striking structural lineaments, over 150 km long, about 100 km south of the Asunción Rift (Velázquez *et al.*, 1998). This feature was considered as a result of crustal fracturing, being named as Santa Rosa Graben (DeGraff & Orué, 1984). Recent investigations confirmed that the alkaline bodies of this province are distributed and oriented along NW-SE structures, and were emplaced under a NE-trending extension (Velázquez *et al.*, 2002).

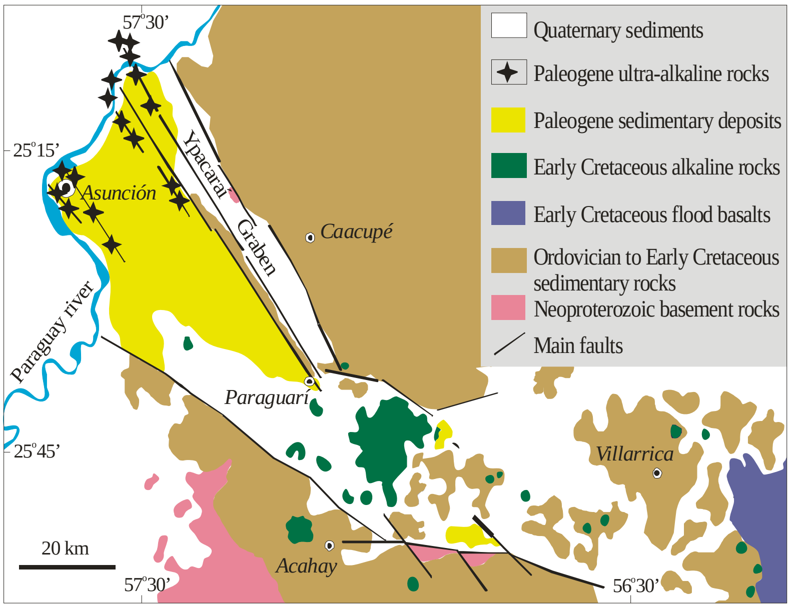


Fig. 2. Geologic map of the Asunción Rift with location of Early Cretaceous (Central Paraguay Province) and Paleogene (Asunción Province) alkaline rock occurrences (after Velázquez *et al.*, 1998, modified).

Central Paraguay

The Central Paraguay Province encompasses the occurrences of alkaline rocks related to the evolution of the central and eastern portions of the Asunción Rift (DeGraff, 1985), installed in the Early Cretaceous. This tectonic depression (Fig. 2), a striking feature either in magnetometric or gravimetric maps (Velázquez *et al.*, 1998; Comin-Chiaramonti *et al.*, 1999), is about 200 km long and has a variable width between 25 and 40 km. It is composed of three well-defined segments: the western segment, NW-SE oriented, between Benjamin Aceval (north of Asunción) and Paraguarí, with a length of about 90 km; the central segment, E-W oriented, from Paraguarí to Villarrica, with around 70 km in length; and the less well-defined eastern segment, NW-SE oriented, from Villarrica to the region of the Ybytyruzú mountains, with an approximate length of 40 km. The study of dyke swarms, faults and joints allowed Velázquez *et al.* (1998) to conclude that the rift was generated under a right-lateral wrenching tectonic regime, associated with an E-W-trending oriented binary. The Ar-Ar ages of alkaline rocks of the Central Paraguay Province range between 126 and 128 Ma (Gomes *et al.* 2003), characterizing an Early Cretaceous magmatic pulse, younger than the tholeiitic magmatism of Alto Paraná Formation (Serra Geral Formation in Brazil). The alkaline bodies occur as stocks, plugs, lavas and specially dykes and dyke swarms (Gomes *et al.*, 1989; Comin-Chiaramonti *et al.*, 1992b, 1995) and also includes the great, ring-like intrusion of Cerro Acahay (Comin-Chiaramonti *et al.*, 1990; Velázquez *et al.* 1992). The province consists of highly potassic rocks with a wide petrographic diversity (Velázquez, 1992; Comin-Chiaramonti *et al.,* 1997). These rocks are grouped in two distinct sets, one with basanites to phonolites and other with alkaline basalts to trachytes, both including its corresponding intrusive terms (Comin-Chiaramonti *et al.*, 1993, 1996; Gomes *et al.*, 1996b). In addition, a small occurrence of carbonatite rock has been identified in the surroundings of the locality of Sapucai (Comin-Chiaramonti *et al.*, 1992c).

Amambay

In the Amambay Province, located in northeastern Paraguay, along the boundary with Brazil, the alkaline magmatic activity is represented by the ring-like complexes of Cerro Chiriguelo and Cerro Sarambí (both with occurrence of carbonatite facies). Pyroxenites, shonkinites, fenites and dykes of trachytes and phonolites also occur in the region. The ages of this alkaline magmatism range between 140 and 135 Ma (Velázquez *et al.*, 1996b), indicating the presence of a prior event with respect to the tholeiitic basaltic magmatism. The Amambay Province is located within the domain of the NE-SW-trending Ponta Porã Arch (Thomas & Associates, 1976) and between two outstanding depressions, one to NW and the other to SE of Pedro Juan Caballero, as indicated by the Bouguer anomaly map (Velázquez *et al.*, 1998; Vidotti *et al.*, 1998; Comin-Chiaramonti *et al.*, 1999). These depressions are probably sedimentary basins and the uplifted block of the Ponta Porã Arch hosts the alkaline intrusions of Cerro Chiriguelo and Cerro Sarambí. The tectonic control of alkaline intrusions of Amambay Province by the Ponta Porã Arch was originally proposed by Livieres & Quade (1987). The presence of magnetic anomalies with higher intensity at the southwestern end of the arch seems to support this hypothesis (Velázquez *et al.*, 1998).

Rio Apa

The magmatism in the Rio Apa Province is not expressive and consists only of small occurrences of alkaline rocks near Puerto Valle-mí and San Lázaro, at the margins of the Paraguay river, northern part of Eastern Paraguay. It includes thin dykes of carbonatitic basanite afilliation (Comin-Chiaramonti *et al.*, 1997) along NE-SW-trending faults (Velázquez *et al.*, 1998). These faults were deep enough to allow the migration of primitive magmatic liquids from mantle to the surface across the entire block of Neoproterozoic carbonatic rocks (Velázquez *et al.*, 1998). As in the Amambay Province, the ages between 140 and 135 Ma (Velázquez *et al.* 1996b) show that this magmatic event preceded the tholeiitic magmatism of the Alto Paraná Formation, indicating an older Late Jurassic to Early Cretaceous magmatic pulse around the Paraná Basin.

## ALKALINE PROVINCES ADJOINING THE BAURU BASIN

The Late Cretaceous Bauru Basin (Fernandes & Coimbra, 1996) developed over the geographical area of the Paraná Basin. Its origin is related to subsidence above the Early Cretaceous tholeiite lava flows, with depocentre located over the thickest part of the volcanic pile (Riccomini, 1995a, 1997). The basin boundaries are essentially of tectonic nature (Riccomini, 1997) and delineated by the Rondonópolis Anteclise (Coimbra, 1991) to the northwest; by the Alto Paranaíba Uplift (Hasui *et al.*, 1975) to the northeast; by the Rio Moji-Guaçu (Coimbra *et al.*, 1981), São Carlos-Leme and Ibitinga-Botucatu lineaments (Riccomini, 1995a, 1997) to the east; by the Paranapanema Lineament (Fúlfaro, 1974) to the southwest, and by the Rio Piquiri Lineament (Ferreira, 1982) to the south (Fig. 1). Some of these archs and lineaments have also influenced the contours of the borders of the Paraná Basin.

Rondonópolis Anteclise

The Rondonópolis Anteclise (Coimbra, 1991) is a NE-SW-trending positive tectonic feature. It includes important structural elements such as the Alto Xingu Arch, its northern boundary, the São Vicente Arch at its central part, and the Transbrasiliano Lineament (Schobbenhaus *et al.*, 1981), its southern boundary. The main phase of tectonic activity of this structure occurred during the Late Cretaceous, with uplift along discontinuities of the Neoproterozoic Brasiliano Cycle. At that time the anteclise acted as a barrier between the Parecis and Bauru basins, both developed over a cratonic substrate (Coimbra, 1991). The transtensional reactivation of NE to ENE and NW-trending faults allowed the deposition of a thick continental sedimentary succession in rhomb-shaped, pull-apart basins, developed within the anteclise. A more recent reactivation is recorded during the Paleogene. Late Cretaceous alkaline manifestations occur within this feature. The alkaline intrusion of Ponta do Morro (Del'Arco *et al.*, 1982; Souza, 1997) mainly consists of syenites and granites. A Rb-Sr reference isochron obtained for the syenites has given an age of 97.1±1.1 Ma (Souza, 1997), in agreement with the age of the main tectonic event. The Poxoréu Igneous Province (Gibson *et al.*, 1997) is placed along the Rio das Mortes Rift, an extensional NE-SW-trending tectonic feature following the general structural trend of the anteclise. Ar-Ar determinations relative to one dyke (Gibson *et al.*, 1995) yielded an age of 83.4±2.4 Ma.

The magmatism in this area was related to intense lithospheric extension above the western margin of the supposed impact zone of the Trindade plume (Gibson *et al.*, 1997). Initial Sr- and Nd- isotopic ratios ($^{87}Sr/^{86}Sr = 0.704$ and $^{143}Nd/^{144}Nd = 0.51274$) of the Poxoréu basaltic lavas obtained by these authors indicate a clear lithospheric mantle source to the alkaline magmatism of this region, and do not point to a magma source from mantle plumes.

Minas-Goiás

Alkaline rocks from the Alto Paranaíba and the Rio Verde-Iporá provinces (as described by Almeida, 1983) were recently grouped in the Minas–Goiás Alkaline Province (Sgarbi & Gaspar, 2002).

In the northwestern portion of the province there are the occurrences of the previously named Rio Verde-Iporá Province (Almeida 1983). It includes more than 20 alkaline complexes, many dykes and local volcanic products occurring along a NW-SE oriented belt with about 250 km in lenght and 70 km in width, which parallels the faults that have served as conduits for the alkaline magma (Almeida, 1983). According to Danni (1974), the alkaline rocks are either intrusives (Morro do Engenho, Água Emendada, Santa Fé, Montes Claros de Goiás, Morro Preto, Areianópolis, Buriti, Córrego dos Bois and Morro do Macaco) or volcanics (Amorinópolis and Santo Antônio da Barra); among the intrusive types there are peridotites, pyroxenites, dunites, essexites, theralites, gabbros, tinguaites, nepheline syenites, nordmarkites, carbonatites and alaskite dykes, and lamprophyre dykes and sills, whereas among the volcanic rocks are found trachyandesites, alkali basalts and clinopyroxenites. Kamafugites occurring as lavas and pyroclastic rocks, with a subvolcanic facies, were described by Sgarbi & Gaspar (2002) in Santo Antônio da Barra, Goiás. The available geochronological data indicate a Late Cretaceous age (e.g. Cordani & Hasui, 1975), ranging from 90 to 79 Ma (Gibson *et al.*, 1995).

The southeastern portion of the Minas-Goiás Alkaline Province includes the occurrences of the previously named Alto Paranaíba Province (Almeida, 1983). Alkaline rocks occur along the Alto Paranaíba Uplift (Hasui *et al.*, 1975), a positive tectonic feature developed from Jurassic to Early Cretaceous as a barrier between the Paraná and São Francisco basins. During the Late Cretaceous, it corresponded to the northeast border of the Bauru Basin (Riccomini, 1997). With a general NW-SE-trending, the uplift develops upon the Brasília Fold Belt, near the southwestern border of the São Francisco Craton. This boundary region between the craton and the mobile belt also includes NW-SE-trending structural lineaments, as indicated in aeromagnetic surveys and taken as fracture zones, more than 400 km in length (Bosum, 1973). Seismic data suggest a present-day lithosphere thicker than 130 km in the northeastern region of the geographical area of the Paraná Basin and a crustal thickness of about 40 km southwest of the Alto Paranaíba Uplift (James *et al.*, 1993). This region comprises potassic to ultrapotassic mafic to ultramafic rocks (Gibson *et al.*, 1995), occurring as plutonic complexes, hypabissal intrusions, lavas and tuffs. The volcanic occurrences cover an area over 4500 km$^2$ (Leonardos *et al.*, 1991) and belong to the Mata da Corda Formation (Costa & Sad, 1968). It includes amigdaloidal lavas and pyroclastic rocks of kamafugitic affinity (volcanic ash, lapilli and blocks) bearing abundant dunite, melilitite and pyroxenite xenoliths, occasionally cut by thin olivinic dykes (Gibson *et al.*, 1995).

There are seven plutonic complexes ranging between 2 and 6 km in diameter (Tapira, Araxá, Salitre I and II, Serra Negra and Catalão I and II). All include carbonatites (Gomes *et al.*, 1990) and some of them glimmerites, pyroxenites, peridotites, dunites and peralkaline syenites (Barbosa *et al.*, 1970; Danni *et al.*, 1991; Mariano & Marchetto, 1991; Brod, 1993). Minor intrusive bodies occur as pipes and dykes with major axes no larger than some hundreds of meters (Svizero *et al.*, 1984). Generally, they have been altered and consist of agglomerates, tuffs and volcanic breccias with xenoliths of ultramafic rocks (glimmerites, hazburgites, dunites, spinel and garnet lherzolites). These bodies, in part previously considered as kimberlites (Svizero *et al.*, 1984), were recently studied in detail by Bizzi (1993) and Bizzi *et al.* (1994). Kamafugite (Serra do Bueno) and massive porphyritic hypabissal facies (Mata da Corda, Três Ranchos) are recognized in some bodies (Gibson *et al.*, 1995). Available K-Ar geochronological data (Amaral *et al.*, 1967a; Hasui & Cordani, 1968; Sonoki & Garda, 1988; Gomes *et al.*, 1990) indicated a Late Cretaceous age (97-79 Ma) for the plutonic carbonatite complexes of this province. K-Ar determinations in phlogopite furnished an age of 83.6±1.4 Ma for a lava flow of the Mata da Corda Formation (Gibson *et al.*, 1995), whereas Ar-Ar analysis of olivine phenocrysts of the Serra do Bueno kamafugite yielded 90±4 Ma (Gibson *et al.*, 1994), both within the age interval for the plutonic carbonatite complexes.

The source of heat in this province was related either to the Trindade (e.g. Herz, 1977; Gibson *et al.*, 1995) or Tristan da Cunha plumes (Bizzi, 1993; Van Decar *et al.*, 1995). In particular, Gibson *et al.* (1995) considered that the mafic alkaline magmatism of Alto Paranaíba and Iporá regions would represent the impact of installation of the Trindade plume within the subcontinental lithospheric mantle, whereas Van Decar *et al.* (1995) suggested the existence of a fossil mantle plume beneath this province. According to Gibson *et al.* (1995), the mafic potassic magmatic rocks from the Alto Paranaíba show initial Sr- and Nd-isotopic ratios varying between 0.7046-0.7058 and 0.5121-0.5123, respectively, suggesting that the magmas were derived from the remobilization of subcontinental lithospheric mantle.

The distribution of alkaline occurrences along NW-SE-trending crustal discontinuities extending over 800 km in length and the nature of the magmatism indicate that deep lithospheric faults played a major role in the tectonic control of this province.

## ALKALINE PROVINCES ADJOINING THE SANTOS AND PELOTAS BASINS

### Serra do Mar

Once defined the Cabo Frio Magmatic Lineament (Almeida, 1991), the alkaline occurrences of the Serra do Mar Province (*sensu* Almeida, 1983) were restricted to those of the islands close to the Atlantic coast and the Ponte Nova massif, all of them in the

São Paulo state. On account of the type of structural control by the basement discontinuities, ages and the relationship with the evolution of the Atlantic continental margin adjoining the Santos and Pelotas basins, in the present paper it has been grouped in the Serra do Mar Province the Late Cretaceous alkaline rocks of the region of the Ponta Grossa Arch, formerly included in the homonymous province, and of Lages, previously related to the Santa Catarina Province, by Almeida (1983). This province was divided into three sectors, north, central and south, corresponding to areas of major Cenozoic uplift along the onshore coastal region of southeastern Brazil.

In the northern sector, one can find the alkaline intrusions of the coastal islands of São Sebastião, the larger one, Montão de Trigo, Búzios and Vitória, besides the Ponte Nova plutonic body in the Serra da Mantiqueira highlands. The Ponte Nova massif is composed of nepheline melagabbros with leucogabbros and syenite veins, and associated minor melagabbro, phonolite and melanephelinite dykes (Thompson *et al.*, 1998). Three syenite and a probable alkaline gabbro stocks occur in São Sebastião Island (Freitas, 1947a); related mafic dykes are also present in the onshore coastal region (*e.g.* Garda *et al.*, 1995). Two generations of mafic and felsic alkaline dykes were recognized in the Búzios and Vitória islands, the older, radial, left-laterally dislocated by the younger NE-SW-trending dykes (Motoki, 1986; Alves, 1997). Available K-Ar and Rb-Sr geochronological data indicated ages of 90-80 Ma for the Vitória Island (Motoki, 1986), 86 Ma for the Ponte Nova (Sonoki & Garda, 1988), 81 Ma for the São Sebastião Island, 80 Ma for the Montão de Trigo Island (Amaral *et al.*, 1967b), and 81-79 Ma for the Búzios Island (Alves, 1997). An Ar-Ar determination for a mafic dyke of the Campos do Jordão region provided an age of 80 Ma (Regelous, 1993).

In the central sector, within the geographical area of the Ponta Grossa Arch, there are many Late Cretaceous alkaline bodies, such as Cananéia (Freitas, 1947b; Spinelli *et al.*, 2001), Barra do Teixeira and Mato Preto (Vasconcellos, 1995; Comin-Chiaramonti *et al.*, 2001a), consisting mainly of felsic alkaline rocks. Available K-Ar data indicated 82 Ma for Cananéia (Amaral *et al.*, 1967b), 73 Ma for Barra do Teixeira and 67 Ma for Mato Preto (Sonoki & Garda, 1988).

In the southern sector of the province, there is the Lages intrusion, a dome structure that uplifted the Paleozoic sedimentary rocks and the basalts of the Serra Geral Formation. In this occurrence nepheline syenite predominates, with minor dykes and veins of variable compositions, including carbonatites and kimberlitic rocks (Scheibe, 1979; Traversa *et al.*, 1994, 1996; Comin-Chiaramonti *et al.*, 2002). The intrusion was dated as of 78-63 Ma by K-Ar method (Scheibe, 1986). NE-SW-trending normal faults are the main structures in the massif (Scheibe, 1986).

The alkaline magmatism of the Serra do Mar Province has been frequently related to the evolution of the adjoining passive continental margin (e.g. Almeida, 1976, 1983, 1986; Ulbrich & Gomes, 1981; Morbidelli *et al.*, 1995). In this extensional context the reactivation of ancient zones of weakness are favoured, particularly the Proterozoic shear zones which parallels the present-day coast line. Indications in this sense are given by the alignment of the alkaline occurrences in the islands of the coastal region in northeastern São Paulo state, following a probable fault zone, as well as by the NE-SW-trending mafic dyke swarm. NE-SW-trending normal faults also occur in Lages.

The sedimentary record of the Santos Basin indicates that the uplift of the Serra do Mar started at 90 Ma. Relying on fission-track data, Vignol-Lelarge *et al.* (1994) obtained an age of 86 Ma for the uplift in the region of the Ponta Grossa Arch. More recent apatite fission-track data suggest that the region of the Serra da Mantiqueira and adjoining areas would have experienced an uplift of 2 to 6 km since the Early Cretaceous (Gallagher *et al.*, 1995), and the main phases of cooling, which indicate the accentuation of uplift rates, have occurred during the Cretaceous (120-100 and 85-70 Ma), the Paleocene (Tello Saenz *et al.*, 2003), and the Quaternary (Hackspacher *et al*., 1999). The erosional processes in the uplifting region and the load of the volcano-sedimentary pile in the Santos Basin lead to the installation of a self-supported stress-field, which gradually has accentuated the elevation of the emerged area and the subsidence in the basin, with an offset of about 15 km from the top of the Serra da Mantiqueira to the base of the Santos Basin (Almeida *et al.*, 2000).

Structural data (Riccomini, 1995b) as well as anisotropy of magnetic susceptibility data (C.J. Archanjo, personal communication) point out that during its emplacement the Cananéia alkaline body was under the action of a NW-SE-oriented compressive stress-field, 82 Ma ago, suggesting a new change in the regional stress-field from the Campanian.

### Piratini

Almeida (1983) included in the Piratini Province all known alkaline rocks in the so-called Sul-rio-grandense Shield. The occurrences, mainly phonolitic bodies, are generally hectometric and only in one case larger than 1 km in diameter. K-Ar age determinations in these rocks span between 99 and 76 Ma (Barbieri *et al.*, 1987). The occurrences are located in the inner part and along the borders of a NE-SW-trending tectonic depression, the Moirão Graben, which nestles the remains of Triassic continental sediments of the Caneleiras Formation. The distribution of the alkaline bodies is controlled by NE-SW-trending faults, parallel to the graben, as well as by NNW-SSE to NW-SE-trending fractures.

Due to its age, structural control and distribution with respect to the Pelotas Basin, we put forward an evolutive context to the alkaline magmatism of the Piratini Province analogue to the Serra do Mar Province, and related to the evolution of the Atlantic continental margin basins.

## ALKALINE PROVINCE RELATED TO THE CENOZOIC EVOLUTION OF THE ASUNCIÓN RIFT

### Asunción

The Asunción Province comprises the ultra-alkaline rocks of the western segment of the Asunción Rift in Eastern Paraguay. It marks an important tectono-magmatic activity during the Paleogene, with Ar-Ar ages ranging between 68 and 52 Ma, but with a clear predominance in the 58-56 Ma (Eocene) interval (Gomes *et al.*, 2003). Its rocks present a markedly sodic composition, mainly nephelinites and ankaratrites, bearing mantle nodules which range from dunites to lherzolites (Comin-Chiaramonti *et al.*, 1991, 2001b). Isotopic ratios ($^{87}Sr/^{86}Sr$=0.70362-0.70392 and $^{143}Nd/^{144}Nd$=0.51225-051242; Comin-Chiaramonti *et al.*, 1991, 1995, 1997) indicate a lithospheric mantle provenance for the ultra-alkaline magmatism of this region. The occurrences are related to NW-SE-striking magnetic lineaments and to a gravimetric low situated beneath the region of Asunción. This gravimetric low corresponds to a graben filled with fanglomeratic sediments containing nephelinite volcanic fragments and bombs (Riccomini *et al.*, 2002). Systematic studies of faults and fracture patterns of the Ñemby, Lambaré and Benjamin Aceval ultra-alkaline bodies and available petrological data allowed Riccomini *et al.* (2001) to conclude that these rocks were emplaced along NW-SE-striking deep lithospheric faults (more than 60 km deep), within an E-W-trending right-lateral wrenching tectonic regime, identical to those active during the rift installation, at the Early Cretaceous. Cooling and fracturing of the nephelinitic and ankaratritic bodies in relatively restricted areas indicate that the activity of deep faults caused great energy loss in the asthenosphere, leading to subsequent melting of the lithospheric mantle by decompression during a relatively short-time interval (Riccomini *et al.*, 2001).

## ALKALINE PROVINCE WITH A POLYPHASIC TECTONO-MAGMATIC EVOLUTION

### Cabo Frio Magmatic Lineament

The Cabo Frio Magmatic Lineament, as defined by Almeida (1991), is a WNW-ESE-trending structural feature developed from Jaboticabal (São Paulo state) eastwards, up to the border region between the continental and oceanic crusts (Almirante Saldanha Bank). It corresponds to a curved belt, 60 km wide by 1150 km in length, which follows a small circle centered on the 84-49 Ma plate rotation pole. This lineament includes 26 alkaline intrusive centers as stocks and larger massifs, plugs, effusive centers and an expressive number of alkaline dykes. Under this conception, Almeida (1991) has included in the Cabo Frio Magmatic Lineament the alkaline rocks of Poços de Caldas and Serra do Mar (the group of intrusions between the Passa Quatro and Cabo Frio alkaline massifs) provinces (Almeida, 1983).

The intrusive centers along the Cabo Frio Magmatic Lineament consist essentially of nepheline syenites and syenites and corresponding fine-grained rock-types (e.g. Ulbrich, 1983; Ulbrich, 1984; Shea, 1992; Brotzu *et al.*, 1989, 1992, 1997; Morbidelli *et al.*, 1995). Among these centers there is the Poços de Caldas massif, the largest alkaline complex of Brazil with about 800 $km^2$. Other important intrusions are, from west to the east, the Passa Quatro, Itatiaia, Morro Redondo, Tomazes, Tinguá, Mendanha, Tanguá, Soarinho, Rio Bonito, Morro de São João and Cabo Frio. The westernmost alkaline occurrences are located where the Cabo Frio Magmatic Lineament intercepts the Rio Moji-Guaçu Lineament, including the intrusions of Jaboticabal, a probable tinguaite sill (Gomes & Valarelli, 1970) emplaced in sedimentary rocks of the Bauru Basin, and the phonolite (tinguaite) of Guariba (Salles, 1999). The occurrences of Aparecida do Monte Alto, Taiúva and Piranji were found by drilling (Coutinho *et al.*, 1982), and probably are part of a large analcimite sill. A variety of mafic alkaline rocks also occur as dykes, sills and lava flows (Morbidelli *et al.*, 1995). There are references to kamafugite dykes in Poços de Caldas and to spinel lherzolite xenoliths in a dyke found in the Itatiaia massif (Gibson *et al.*, 1995). Ankaramite lava flows occur interbedded with the sediments of the Volta Redonda (Riccomini *et al.*, 1983) and Itaboraí (Klein & Valença, 1984) Cenozoic basins, which integrate the Serra do Mar Rift System (Almeida, 1976) or Continental Rift of Southeastern Brazil (Riccomini, 1989).

Marsh (1973) suggested that these alkaline rocks delineate a small cycle consistent with the South Atlantic rotation pole. He interpreted this lineament as an extension of an oceanic fracture or transform fault into the continent. In the same way, Herz (1977), taking into account that the available ages for the alkaline rocks of the coastal regions of São Paulo and Rio de Janeiro states point to an age decrease easthwards, has estimated the velocity of plate displacement above a fixed reference point. Sadowski & Dias Neto (1981) attributed a seismotectonic character to the lineament, taken as a deflexion of the oceanic crust along the northern border of the Santos Basin. Using tomographic models, Van Decar *et al.* (1995) interpreted a low velocity zone beneath the Paraná Basin as a remnant mantle plume tail and considered the Late Cretaceous and Tertiary alkaline magmatism of this region as an evidence of post-Early Cretaceous flood basalt heating. Based on Ar-Ar results for the alkaline bodies of Nova Iguaçu, Soarinho and Cabo Frio (all lying along the eastern segment of the lineament) and a selection of previous data, Thompson *et al.* (1998) revived the idea of an age decrease to the east, relating the alkaline magmatism of the Serra do Mar and Alto Paranaíba provinces (*sensu* Almeida 1983) to the trajectory of the Trindade plume. Thomaz Filho & Rodrigues (1999) followed this general conception for the Poços de Caldas-Cabo Frio segment of the lineament. Also on the basis of Ar-Ar determinations for some intrusions along a line extending 300 km inland from Cabo Frio, Smith *et al.* (1999) estimated that, between 69 and 61 Ma, the alkaline magmatism has migrated with a velocity of 3.4 cm/yr, in consonance with the plate tectonic model velocity of 3.6 cm/yr.

An evaluation of the available K-Ar and Ar-Ar data along the lineament, however, does not support these assumptions (Fig. 3). For instance, the Jaboticabal and Taiúva intrusions, to the west, were dated by the K-Ar method as of 54 Ma (Gomes & Valarelli, 1970) and 61 Ma (Coutinho *et al.*, 1982), respectively. From west to the east, Ar-Ar data shows 76 Ma for Poços de Caldas (Shea, 1992) and 84 Ma (Vlach *et al.*, 2003) for carbonatitic veins associated with this large massif, 82-54 Ma for dykes associated with the Mendanha massif (Deckart *et al.*, 1998; Smith *et al.*, 2001; Ferrari, 2001), 66 Ma for Itaúna, 57 Ma for Monjolos, 65 Ma for Country Club and 52 Ma for Cabo Frio (Ferrari, 2001). The ankaramite lavas of Volta Redonda and Itaboraí are more recent manifestations of Eocene age (Riccomini *et al.*, 1983, 1991; Riccomini & Rodrigues-Francisco, 1992). Therefore, an eastward age decrease does not seem to occur. Available age data indicate different phases of alkaline magmatism, from Late Cretaceous to the Paleogene. Sr- and Nd-isotopic ratios ($^{87}Sr/^{86}Sr$=0.705-0.707 and $^{143}Nd/^{144}Nd$=0.5123-0.5126) obtained for phonolites and nepheline syenites from the Poços de Caldas alkaline massif (Ulbrich *et al*., 2003) point to a lithospheric mantle source.

According to Almeida (1991), the Cabo Frio Magmatic Lineament would indicate the existence of subcrustal faults along which partial mantle melting and alkaline magma generation have occcurred. During its rising and emplacement, the magma probably was shaped accordingly with the Precambrian structural grain, resulting in various NE to NNE-elongated bodies. Ferrari (2001), after detailed structural studies in the Rio de Janeiro state, concluded that the emplacement of the Campanian and Paleocene alkaline massifs and the NE-SW-trending dyke swarms took place under a left-lateral transcurrent shear regime, with the principal compressive σ1 and extensive σ3 stresses oriented to the NE-SW and NW-SE directions, respectively. The Eocene extrusive magmatism occurred under a NW-SE-oriented extensional regime (Riccomini, 1989). These facts reinforce the idea that the lineament corresponds to a fracture zone under the action of a WNW-ESE-oriented left-lateral wrenching during Late Cretaceous and the Paleocene (Fig. 4), and NW-SE-oriented extension at the Eocene. The difference in age of the alkaline magmatic activity could be explained as a result of successive tectonic reactivations along the lineament.

## ALKALINE PROVINCES WITHIN THE AMAZON CRATON

### Candelaria

The Candelaria Alkaline Province is located in eastern Bolivia, about 70 km from the international boundary with Brazil. It includes nepheline syenites, quartz syenites, nordmarkites, phonolites, foyaites, pulaskites and trachyte dykes and lavas, with a K-Ar age of 116 Ma (Litherland *et al*., 1986). The province is controlled by E-W to WNW-ESE-trending faults of the Early Tertiary Mercedes Rift, with more than 100 km in length (Litherland *et al.*, 1986).

### Velasco

The Velasco Alkaline Province (Darbyshire & Fletcher, 1979) is also located in eastern Bolivia. It comprises a volcanic suite, a series of 14 interfering ring plutons, dykes and a silicified carbonatite complex (Cerro Manomó). Porphyritic trachyte is the main unit within the volcanic suite whereas the plutonic rocks include silica-undersaturated (pulaskite and foyaite) and oversaturated (quartz syenite and granite) rocks; dykes range in composition from microfoyaite to aplite (Fletcher & Beddoe-Stephens, 1987). Rb-Sr whole-rock isochron results of 143-140 Ma and K-Ar mineral determinations of 142-134 Ma indicate a Late Jurassic to Early Cretaceous age for these rocks (Darbyshire & Fletcher, 1979).

Alkaline bodies of this province are distributed over a NE-trending elongated narrow belt of about 80 km in length (Fletcher & Beddoe-Stephens, 1987). A major NE-SW structure was active during the em-placement of the plutons. Fletcher & Litherland (1981) suggested that the alkaline magmatism was generated along a deep crustal fracture, related to a possible triple-junction initiated during the Early Cretaceous rifting of the South America-Africa plate.

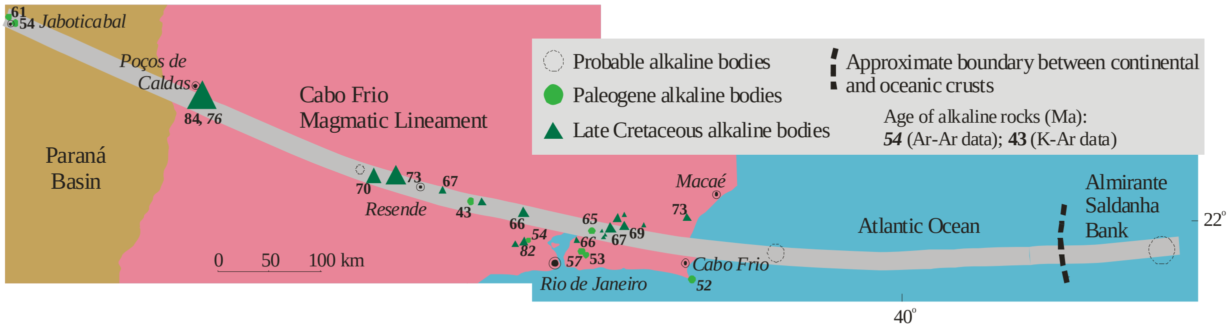


Fig. 3. The Cabo Frio Magmatic Lineament (after Almeida 1991, modified), with indications of available K-Ar and Ar-Ar data.

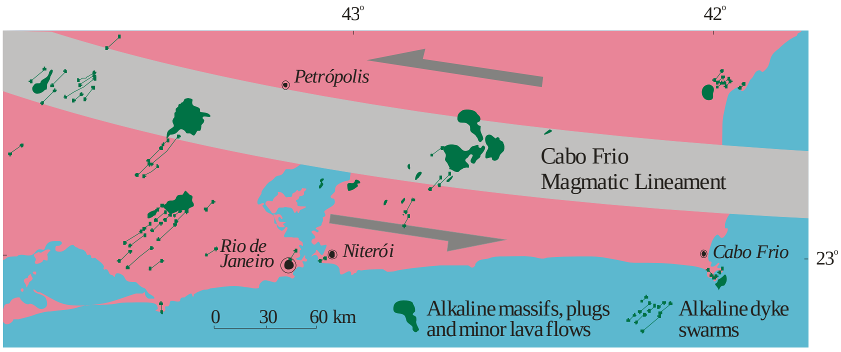


Fig. 4. Distribution of the Mesozoic-Cenozoic alkaline massifs, plugs, dyke swarms and minor lava flows along the Cabo Frio Magmatic Lineament in central-eastern Rio de Janeiro state (after Ferrari, 2001, modified). The emplacement of dykes and other alkaline bodies was controlled by a NE-SW compression related to a left-lateral WNW-ESE wrenching along the Cabo Frio Lineament.

## DISCUSSION

Many aspects concerning the genesis and tectonic controls of the continental alkaline magmatism remain poorly understood and controversial. Intraplate deformation and alkaline magmatism related to fracture zones have been first identified in continental regions (e.g. Bailey, 1979) and more recently in the oceanic crust (e.g. Fernandez *et al.*, 1997; Ferrari & Riccomini, 1999). However, the common assumption of genetic relationships of alkaline magmatism to mantle plumes, hot spot tracks or rifting of continents, frequently hinge on geochronology. Moreover, the continental lithosphere is thicker and structurally more complex than the oceanic lithosphere and, probably because of this fact, plume-related magmatism in continental intraplate regions usually does not exhibit age tendencies as clearly evidenced as in oceanic island chains (Fitton & Upton, 1987). In recent papers, some authors have argued against the model of mantle plume as a source of heat for large igneous provinces (e.g. Sheth, 1999) and alternative models have been proposed (e.g. Ernesto *et al.*, 2002).

Although the source of magmas of the alkaline provinces of the central-southeastern region of the Brazilian Platform has been frequently associated with mantle plumes, some characteristics of the magmatism, such as the provenance, extent and age distribution, do not support this hypothesis.

The available data on initial Sr- and Nd-isotopic ratios (Gibson *et al.*, 1995, 1997; Comin-Chiaramonti *et al.*, 1995, 1997, 1999; Thompson *et al.*, 1998; Ulbrich *et al.*, 2003) indicate a clear lithospheric mantle source for the alkaline magmatism of this region. All data are concentrated next or below the Bulk Earth line in the conventional Sr-Nd diagram of Hart (1998), showing no contribution of asthenospheric components in the alkaline magmas.

The alkaline magmatism in the region is distributed over an area with about 2000 km in the N-S and 1700 km in the E-W direction (more than

$2.10^6$ $km^2$). This extent is compatible with the large (ca. 2000 km diameter) mushroom-shaped head of the upwelling Tristan da Cunha mantle plume suggested by White & McKenzie (1995) to explain the lithospheric thinning prior to the breakup of Africa and South America. Nevertheless, considering the age span of the alkaline magmatism (Permian-Triassic to Cenozoic), the explanation for the long-term source of heating (ca. 210 Ma) still remains a matter of discussion.

From the Neoproterozoic to the Early Cretaceous the central-southeastern part of the Brazilian Platform was within a large plate (e.g. Ramos, 1988; Soares, 1988). Large plates prevent the mantle beneath them from being cooled by subduction (Condie, 2001) and the greater the plates the more effectively they act as insulators (e.g. Gillou & Jaupart, 1995). Consequently, large mantle upwellings develop beneath large plates (Condie, 2001). For layered-mantle convection, Lowman & Jarvis (1999) estimated a period of time of more than 600 Ma to generate stresses necessary to break supercontinents. This time-interval has been considered too large with respect to the duration of supercontinent cycles. Nd model ages, however, indicate that the incompatible elements enrichment in the source mantle of the Early Cretaceous sodic rocks of Misiones (Velázquez *et al.*, 2003), the Late Cretaceous alkaline rocks of the Cabo Frio Magmatic Lineament (Fetter *et al.*, 2003), the Late Cretaceous kamafugites of Alto Paranaíba and the Paleogene sodic rocks from Asunción (Comin-Chiaramonti *et al.*, 1997) are related to Neoproterozoic events of magma migration to the lithospheric mantle and hence in good agreement with a long-lived source of heat beneath the region. It would appear, therefore, that an alternative model of mantle upwelling would better explain the source of heating for the Permian-Triassic to Cenozoic alkaline magmatism in the region.

The data presented in this paper show that the Mesozoic and Cenozoic alkaline magmatism of the central-southeastern part of the Brazilian Platform has a clear tectonic control by crustal discontinuities and an evolutionary link with the main sedimentary basins. Regional structures were the main zones of weakness along which alkaline magmas were emplaced or reached to the surface. These extensional or wrench structures are mainly represented by fault zones situated along the borders of sedimentary basins. In some cases (e.g. Rondonópolis Anteclise, Alto Paranaíba Uplift, Rio Moji-Guaçu Lineament) they acted as barriers to the sedimentation, whereas in others (e.g. Ponta Grossa Arch, Santa Rosa Graben, Asunción Rift) as deformation zones in the basins. In the Asunción, Misiones and probably in the Alto Paranaíba provinces the magmatism was controlled by deep lithospheric faulting.

The available geochronological data indicate that alkaline magmatism in the region took place in four main stages, under different stress-fields. The first one, Permian-Triassic in age, possibly linked to the propagation of stress related to the Cape-La Ventana Orogeny (Tankard *et al.*, 1995; Milani, 1997) to the inner parts of the continent. The second, Early Cretaceous in age, with three pulses - older, coeval and younger than the tholeiitic magmatism of the Paraná basin (*Paraná flood basalts*) - is equivalent to the rift stage in marginal Atlantic basins. The third is Late Cretaceous and corresponds to the oceanic stage of the Atlantic Margin. The more recent, of Cenozoic (Paleogene) age, is associated with the evolution of continental rift systems in southeastern Brazil and Eastern Paraguay. Therefore, changes in the stress-fields and consequent fault reactivations at the Permian-Triassic, Early Cretaceous, Late Cretaceous and the Paleogene explain the regional distribution of alkaline magmatism in the central-southeastern region of the Brazilian Platform.

## CONCLUSIONS

The main conclusions of the present study can be summarized as follows:

1) The central-southeastern portion of the Brazilian Platform contains more than one hundred

occurrences of alkaline rocks. There are alkaline centers, associated dyke swarms and small bodies widespread in Brazilian, Bolivian, Paraguayan and Uruguayan territories, in different tectonic settings.

2) The alkaline magmatism in the region took place in four main stages: Permian-Triassic, possibly linked to the propagation of stress related to the Cape-La Ventana Orogeny; Early Cretaceous, equivalent to the rift stage in marginal Atlantic basins; Late Cretaceous, coeval to the oceanic stage of the Atlantic Margin; and Cenozoic (Paleogene), related to the evolution of continental rift systems in southeastern Brazil and eastern Paraguay.

3) The alkaline bodies may be grouped in 15 provinces. The first assemblage is located on the borders of Paraná (Alto Paraguay, Ponta Grossa Arch, Valle Chico, Misiones, Central Paraguay, Amambay and Rio Apa), Bauru (Rondonópolis Anteclise and Minas-Goiás), Santos (Serra do Mar) and Pelotas (Piratini) basins. The second assemblage is associated with the Cenozoic evolution of the Asunción Rift. The third, Cabo Frio Magmatic Lineament, with asynchronic magmatic alkaline pulses along a fracture zone. The later one includes the alkaline provinces of eastern Bolivia, within the Amazon Craton.

4) Available Ar-Ar geochronological data and the distribution of alkaline rocks along tectonic features do not make evident any age distribution pattern. Initial Sr- and Nd-isotopic ratios indicate a lithospheric mantle source to the alkaline magmatism of this region, and thus do not support the hypothesis of the action of mantle plumes. An alternative model comprising a long-lived process of mantle upwelling seems to explain the source of heating for the alkaline magmatism in the region.

5) The alkaline provinces show a clear tectonic control of magmatism by crustal discontinuities, mainly extensional or wrenching fault zones along the present-day borders of sedimentary basins. Inheritance of Proterozoic crustal discontinuities has played a major role on the alkaline magmatism. Changes in the stress-fields and reactivations of regional structures in different pulses from Permian-Triassic to the Paleogene produced a great range of structural weakness along which alkaline magmas were emplaced or reached to the surface. These tectonic controls explain the regional distribution of alkaline magmatism in the central-southeastern region of the Brazilian Platform.

## ACKNOWLEDGEMENTS

The manuscript benefited from comments by B.B. Brito Neves, U.G. Cordani and M. Assumpção (University of São Paulo), P. Comin-Chiaramonti (University of Trieste) and discussion with A.L. Ferrari (Flumi-nense Federal University, Rio de Janeiro). This work was supported by the Fundação de Amparo à Pesquisa do Estado de São Paulo - FAPESP (grants 97/01210-4, 97/12091-6 and 01/10714-3).

## REFERENCES

Aerial Geophysics Company (1991). *Composite Map of Aeromagnetic Survey Eastern Paraguay (Scale 1:1.000.000).* Asunción: Archivo DRM-MOPC.

Almeida, F.F.M. (1967). Origem e evolução da Plataforma Brasileira. *Boletim da Divisão de Geologia e Mineralogia,* Departamento Nacional de Produção Mineral **241**, 36p.

Almeida, F.F.M. (1971). Condicionamento tectônico do magmatismo alcalino mesozóico do Sul do Brasil e do Paraguai. *Anais da Academia Brasileira de Ciências* **43**, 835-836.

Almeida, F.F.M. (1972). Tectono-magmatic activation of the South American platform and associated mineralization. *24th International Geological Congress, Montreal, Proceedings, Section* **3**, pp. 339-346.

Almeida, F.F.M. (1976). The system of continental rifts bordering the Santos Basin, Brazil. *Anais da Academia Brasileira de Ciências* **48** (suplemento), 15-26.

Almeida, F.F.M. (1983). Relações tectônicas das rochas alcalinas mesozóicas da região meridional da Plataforma Sul-Americana. *Revista Brasileira de Geociências* **13**, 139-158.

Almeida, F.F.M. (1986). Distribuição regional e relações tectônicas do magmatismo pós-paleozóico do Brasil. *Revista Brasileira de Geociências* **16**, 325-349.

Almeida, F.F.M. (1991). O alinhamento magmático de Cabo Frio. *2º Simpósio de Geologia do Sudeste, São Paulo, Atas,* pp. 423-428.

Almeida, F.F.M. & Carneiro, C.D.R. (1989). Magmatic occurrences of post-Permian age of the South American Platform. *Boletim Instituto de Geociências da USP, Série Científica* **20**, 71-85.

Almeida, F.F.M., Brito Neves, B.B. & Carneiro, C.D.R. (2000). The origin and evolution of the South American Platform. *Earth-Science Reviews* **50**, 77-111.

Almeida, F.F.M., Carneiro, C.D.R. & Misuzaki, A.M.P. (1996). Correlação do magmatismo das bacias da margem continental brasileira com o das áreas emersas adjacentes. *Revista Brasileira de Geociências* **26**, 125-138.

Alves, F.R. (1997). *Contribuição ao conhecimento geológico e petrológico das rochas alcalinas da Ilha de Búzios, SP*. Ph.D. Thesis, University of São Paulo, 352p.

Amaral, G., Bushee, J., Cordani, U.G., Kawashita, K. & Reynolds, J.H. (1967a). Potassium-argon ages of alkaline rocks from southern Brazil. *Geochimica et Cosmochimica Acta* **31**, 117-142.

Amaral, G., Cordani, U.G., Kawashita, K. & Reynolds, J.H. (1967b). Potassium-argon dates of basaltic rocks from southern Brazil. *Geochimica et Cosmochimica Acta* **30**, 159-189.

Asmus, H.E. & Guazelli, W. (1981). Descrição sumária das estruturas da margem continental brasileira e das áreas oceânicas adjacentes, hipótese sobre o tectonismo causador e implicações para os prognósticos do potencial de recursos minerais. In: *Estruturas e tectonismo da margem continental sul brasileira e suas implicações nos processos sedimentares e na avaliação do potencial de recursos minerais. Petrobrás, Série Projeto REMAC* **9**, pp.187-269.

Barbieri, M., Beccaluva, L., Brotzu, P., Conte, A., Garbarino, C., Gomes, C.B., Loss, E.L., Macciotta, G., Morbidelli, L., Scheibe, L.F., Tamura, R.M. & Traversa, G. (1987). Petrological and geochemical studies of alkaline rocks from continental Brazil. 1. The phonolite suite from Piratini RS. *Geochimica Brasiliensis* **1**, 109-138.

Barbosa, O., Braun, O.P.G., Dyer, R.C. & Cunha, C.A.B.R. (1970). Geologia da região do Triângulo Mineiro. Departamento Nacional de Produção Mineral. *Boletim da Divisão de Geologia e Mineralogia,* **136**, 140p.

Basu, A.R., Renne, P.R., Mertz, D. & Poreda, R.J. (1993). Alkaline igneous complexes of the Deccan and Paraná: implications for the origin of continental flood basalts. *EOS Transactions, American Geophysical Union* **74**, p. 552.

Bailey, D.K. (1979). Continental rifting and alkaline magmatism. In: Sørensen, H. (ed.) *The alkaline rocks*. London: John Wiley, pp.148-159.

Bizzi, L.A. (1993). *Mesozoic alkaline volcanism and mantle evolution on the southwestern São Francisco craton, Brazil*. Ph.D. Thesis, University of Cape Town, 240p.

Bizzi, L.A., Smith, C.B., Meyer, H.O.A., Amstrong, R. & de Wit, M.J. (1994). Mesozoic kimberlites and related rocks in southwestern São Francisco craton, Brazil: a case for local mantle reservoirs and their interaction. *5th Internatio-nal Kimberlite Conference, Araxá, Proceedings,* pp.156–171.

Bossi, J. (1996). *Geología del Uruguay*. Montevideo, Universidad de la República, 464p.

Bosum, W. (1973). O levantamento aeromagnético de Minas Gerais e Espírito Santo e sua seqüência quanto à estrutura geológica. *Revista Brasileira de Geociências* **3**, 149-159.

Brod, J.A. (1993). Química mineral de calcitas e dolomitas dos carbonatitos de Tapira, MG. *4º Congresso Brasileiro de Geoquímica, Anais,* pp. 64-67.

Brotzu, P., Barbieri, M., Beccaluva, L., Gabarino, C., Gomes, C.B., Macciotta, G., Melluso, L., Morbidelli, L., Ruberti, E., Sigolo, J.B. & Traversa, G. (1992). Petrology and geochemistry of the Passa Quatro alkaline complex, southeastern Brazil. *Journal of South American Earth Sciences* **6**, 237-252.

Brotzu, P., Beccaluva, L., Conte, A., Fonseca, M., Garbarino, C., Gomes, C.B., Leong, R., Macciotta, G., Mansur, R.L., Melluso, L., Morbidelli, L., Ruberti, E., Sigolo, J.B., Traversa, G. & Valença, J.G. (1989). Petrological and geochemical studies of alkaline rocks from continental Brazil. The syenitic intrusion of Morro Redondo, RJ. *Geochimica Brasiliensis* **3,** 63-80.

Brotzu, P., Gomes, C.B., Melluso, L., Morbidelli, L., Morra, V. & Ruberti, E. (1997). Petrogenesis of coexisting $SiO_2$-undersaturated to $SiO_2$-saturated felsic igneous rocks: the alkaline complex of Itatiaia, southeastern Brazil. *Lithos* **40**, 133-156.

Chang, H.K. & Kowsmann, R.O. (1991). Significado dos diques do Arco de Ponta Grossa na abertura diferencial do Atlântico Sul. *3º Simpósio Nacional de Estudos Tectônicos, Rio Claro, Boletim,* pp. 77-78.

Cobbold, P.R., Gapais, D., Rosselo, E.R., Milani, E.J., & Szatmari, P. (1992). Permian-Triassic intracontinental deformation in SW Godwana. In: De Wit, M. & Ramsome, I.G.D. (eds.) *Inversion tectonics of the Cape fold belt, Karoo and Cretaceous basins of Southern Africa*. Rotterdam: Balkema, pp. 23-26.

Coimbra, A.M. (1991). *Sistematização crítica da obra*. Livre Docência Thesis, University of São Paulo, 54p.

Coimbra, A.M., Brandt Neto, M. & Coutinho, J.M.V. (1981). Silicificação dos arenitos da Formação Buru no Estado de São Paulo. In: *A Formação Bauru no Estado de São Paulo e regiões adjacentes.* São Paulo: *Sociedade Brasileira de Geologia, Coletânea de trabalhos e debates*, pp. 103-115.

Comin-Chiaramonti, P. & Gomes, C.B. (1996). *Alkaline magmatism in central-eastern Paraguay. Relationships with coeval magmatism in Brazil.* São Paulo: Edusp/Fapesp, 464p.

Comin-Chiaramonti, P., Castorina, F., Cundari, A., Petrini, R. & Gomes, C.B. (1995). Dykes and sills from eastern Paraguay: Sr and Nd systematics. In: Baer, G. & Heiman, A. (eds.) *Physics and chemistry of dykes*. Rotterdam: Balkema, pp. 267-278.

Comin-Chiaramonti, P., Censi, P., Cundari, A., De Min, A., Gomes, C.B., Marzoli, A. & Piccirillo, E.M. (1996). In: Comin-Chiaramonti, P. & Gomes, C.B. (eds.) *Alkaline magmatism in central-eastern Paraguay. Relationships with coeval magmatism in Brazil.* São Paulo: Edusp/Fapesp, pp. 123-150.

Comin-Chiaramonti, P., Censi, P., Cundari, A. & Gomes, C.B. (1992b). A silico-beforsitic flow from the Sapucai Complex (Central-Eastern Paraguai). *Geochimica Brasiliensis* **6**, 87-91.

Comin-Chiaramonti, P., Civetta, L., Petrini, P., Piccirillo, E.M., Bellieni, G., Censi, P., Bitschene, P.R., Demarchi, D., De Min, A., Gomes, C.B., Castillo, A.M.C. & Velázquez, J.C. (1991). Tertiary nephelinitic magmatism in eastern Paraguay: petrology, Sr-Nd isotopes and genetic relationships with associated spinel-peridotite xenoliths. *European Journal of Mineralogy* **3**, 507-525.

Comin-Chiaramonti, P., Cundari, A., DeGraff, J.M., Gomes, C.B. & Piccirillo, E.M. (1999). Early Cretaceous-Tertiary magmatism in eastern Paraguay (western Paraná Basin): geological, geophysical and geochemical relationships. *Journal of Geodynamics* **28**, 375-391.

Comin-Chiramonti, P., Cundari, A., Gomes, C.B., Piccirillo, E.M., Censi, P., De Min, A., Bellieni, G., Velázquez, V.F. & Orué, D. (1992c) Potassic dyke swarm in he Sapucai-graben Eastern Paraguay: petrographical, mineralogical and geochemical outlines. *Lithos* **28**, 283-301.

Comin-Chiaramonti, P., Cundari, A., Piccirillo, E.M., Gomes, C.B., Castorina, F., Censi, P., De Min, A., Marzoli, A., Speziale, S. & Velázquez, V.F. (1997). Potassic and sodic igneous rocks from eastern Paraguay: their origin from the lithospheric mantle and genetic relationships with the associated Paraná flood tholeiites. *Journal of Petrology* **38**, 495-528.

Comin-Chiramonti, P., Gomes, C.B., Castorina, F., Censi, P., Furtado, S., Ruberti, E. & Scheibe, L.F. (2002) Anitápolis and Lages alkaline-carbonatite complexes, Santa Catarina State, Brazil: geochemistry and geodynamic implications. *Revista Brasileira de Geociências* **32**, 629-653.

Comin-Chiaramonti, P., Gomes, C.B., Censi, P., De Min, A., Rotolo, S.G. & Velázquez, V.F. (1993). Geoquímica do magmatismo pós-paleozóico no Paraguai Centro-Oriental. *Geochimica Brasiliensis* **7**, 19-34.

Comin-Chiaramonti, P., Gomes, C.B., Petrini, R., De Min, A., Velázquez, V.F. & Orué, D. (1992a). A new area of alkaline rocks in Eastern Paraguay. *Revista Brasileira de Geociências* **22**, 500-506.

Comin-Chiaramonti, P., Gomes, C.B., Piccirillo, E.M., Bellieni, G., Castillo, A.M.C., Demarchi, G., Gallo, P. & Velázquez, J.C. (1990) Petrologia do maciço alcalino de Acahay, Paraguai Oriental. *Revista Brasileira de Geociências* **20**, 133-152.

Comin-Chiaramonti, P., Gomes, C.B., Ruberti, E., Antonini, P. & Censi, P. (2001a). Mato Preto alkaline-carbonatite complex: geochemistry and isotope (O-C, Sr-Nd) constraints. *Geochimica Brasiliensis* **15**, 23-34.

Comin-Chiaramonti, P., Princivalle, F., Girardi, V.A.V., Gomes, C., Laurora, A. & Zanetti, F. (2001b). Mantle xenoliths from Ñemby, Eastern Paraguay: O-Sr-Nd isotopes, trace elements and crystal chemistry of hosted clinopyroxenes. *Periodico di Mineralogia* **70**, 205-230.

Condie, K.C. (2001). *Mantle plumes and their record in Earth history*. Cambridge: Cambridge University Press, 306p.

Cordani, U.G. & Hasui, Y. (1975). Comentários sobre as idades geocronológicas disponíveis para a Folha de Goiânia. In: *Carta geológica do Brasil ao milionésimo; Folha Goiás (SD 22).* Brasília: Departamento Nacional de Produção Mineral, pp. 85-95.

Cordani, U.G., Brito Neves, B.B., Fuck, R.A., Thomaz Filho, A. & Cunha, F.M.B. (1984). Estudo preliminar de integração do Pré-Cambriano com os eventos tectônicos das bacias sedimentares brasileiras. *Petrobrás, Ciência Técnica Petróleo, Seção Exploração de Petróleo*, **15**, 70p.

Costa, M.T. & Sad, J.H.G. (1968). O Cretáceo em Minas Gerais. *22º Congresso Brasileiro de Geologia, Belo Horizonte, Anais,* pp. 23-36.

Coutinho, J.M.V., Coimbra, A.M., Brandt Neto, M. & Rocha, G.A. (1982). Lavas analcimíticas associadas ao Grupo Bauru (Kb) no Estado de São Paulo, Brasil. *5º Congreso Latinoamericano de Geologia, Buenos Aires, Actas* **2**, pp. 185-195.

Dalziel, I.W.D. & Grunow, A.M. (1992). Late Gondwanide tectonic rotations within Gondwanaland. *Tectonics* **11**, 603-606.

Danni, J.C.M. (1974). *Géologie des complexes ultrabasiques alcalins de la région d'Iporá, Goiás (Brésil)*. Ph.D. Thesis, University of Paris Sud, 104p.

Danni, J.C.M., Gaspar, J.C. & Gonzaga, G.M. (1991). The Fazenda Alagoinha intrusion, Três Ranchos, Goiás. *5th International Kimberlite Conference, Araxá, Field Guide Book*, pp. 31-35.

Darbyshire, D.P.F. & Fletcher, C.J.N. (1979). A Mesozoic alkaline province in eastern Bolivia. *Geology* **7**, 545-548.

Deckart, K., Féraud, G., Marques, L.S. & Bertrand, H. (1998). New time constraints on dyke swarms related to the Paraná-Etendeka magmatic province, and subsequent South Atlantic opening, southeastern Brazil. *Journal of Volcanology and Geothermal Research* **80**, 67-83.

DeGraff, J.M. (1985). Late Mesozoic crustal extension and rifting on the western edge of the Paraná Basin, Paraguay. *Geological Society of America, Abstracts with Programs* **17**, p. 560.

DeGraff, J.M & Orué, D. (1984). *Proyecto tectónico del Paraguay Suroriental: informe de progreso al termino del trabajo de campo (2da. etapa)*. Asunción: MDN-DIM, Relatório Interno, 12p.

Del'Arco, J.O., Silva, R.H., Tarapanoff, I., Freire, F.A., Pereira, L.G.M., Souza, S.L., Luz, D.S., Palmeira, R.C.B. & Tassinari, C.C.G. (1982). Geologia. In: *Folha SE-21 - Corumbá e parte da Folha SE-20 - Cuiabá*. Rio de Janeiro: *Projeto Radambrasil, Levantamento de Recursos Naturais* **27**, pp. 25-159.

Druecker, M.D. & Gay Jr., S.P. (1987). Mafic dyke swarms associated with Mesozoic rifting in Eastern Paraguay, South America. In: Halls, H.C. & Fahrig, W.F. (eds.) *Mafic dyke swarms. Geological Association of Canada, Special Publication* **34**, pp. 187-193.

Ernesto, M., Marques, L.S., Piccirillo, E.M., Molina, E.C., Ussami, N., Comin-Chiaramonti, P. & Bellieni, G. (2002). Paraná Magmatic Province - Tristan da Cunha plume system: fixed versus mobile plume, petrogenetic considerations and alternative heat sources. *Journal of Volcanology and Geothermal Research* **118**, 15-36.

Eyles, N. & Eyles, C.H. (1993). Glacial geologic confirmation of an intraplate boundary in the Paraná Basin of Brazil. *Geology* **21**, 459-462.

Fernandes, L.A. & Coimbra, A.M. (1996). A Bacia Bauru (Cretáceo Superior, Brasil). *Anais da Academia Brasileira de Ciências* **68**, 195-205.

Fernandez, C., Casillas, R., Ahijado, A., Perello, V. & Hernandez Pacheco, A. (1997). Shear zones as a result of intraplate tectonics in oceanic crust: The example of the Basal Complex of Fuerteventura (Canary Islands). *Journal of Structural Geology* **19**, 41-57.

Ferrari, A.L. (2001). *Evolução tectônica do Graben da Guanabara*. Ph.D. Thesis, University of São Paulo, 412p.

Ferrari, A.L. & Riccomini, C. (1999). Campo de esforços plio-pleistocênico na Ilha da Trindade (Oceano Atlântico Sul, Brasil) e sua relação com a tectônica regional. *Revista Brasileira de Geociências* **29**, 195-202.

Ferreira, F.J.F. (1982). Alinhamentos estruturais-magnéticos da região centro-oriental da Bacia do Paraná Basin e seu significado tectônico. In: *Geologia da Bacia do Paraná - reavaliação da potencialidade e prospectividade em hidrocarbonetos*. São Paulo: *Paulipetro, Consórcio CESP/IPT*, pp. 143-166.

Ferreira, F.J.F., Monma, R., Campanha, G.A.C. & Galli, V.L. (1989). An estimate of the degree of crustal extension and thinning associated with the Guapiara Lineament based on aeromagnetic modelling. *Boletim do Instituto de Geociências da USP, Série Científica* **20**, 69-70.

Fetter, A.H., Hackspacher, P.C., Dantas, E.L., Saad, A.R.L., Bistrichi, C.A. & Ávila, C.A. (2003). Nd provenance of local Cenozoic sedimentary deposits in continetal southeastern Brazil: evidence for limited mixing of sediment sources during erosion, transport and deposition. *4th South American Symposium on Isotope Geology, Salvador, Short Papers,* pp. 57-59.

Fitton, J.G. & Upton, G.G.J. (1987). Introduction. In: Fitton, J.G. & Upton, G.G.J. (eds.) *Alkaline igneous rocks. Geological Society of London, Special Publication* **30**, pp. ix-xiv.

Fletcher, C.J.N. & Beddoe-Stephens, B. (1987). The petrology and crystallization history of the Velasco alkaline province, eastern Bolivia. In: Fitton, J.G. & Upton, B.G.J. (eds.) *Alkaline igneous rocks. Geological Society of London, Special Publication* **30**, pp. 403-413.

Fletcher, C.J.N. & Litherland, M. (1981). The geology and tectonic setting of the Velasco alkaline Province, eastern Bolivia. *Journal of the Geological Society of London* **138**, 541-548.

Freitas, R.O. (1947a). Geologia e petrologia da Ilha de São Sebastião. *Boletim da Faculdade de Filosofia, Ciências e Letras da Universidade de São Paulo* **85,** 244p.

Freitas, R.O. (1947b). Eruptivas alcalinas de Cananéia, Estado de São Paulo. *Boletim da Faculdade de Filosofia, Ciências e Letras da Universidade de São Paulo, Geologia* **4**, 35p.

Fúlfaro, V.J. (1974). Tectônica do alinhamento estrutural do Paranapanema. *Boletim do Instituto de Geociências da USP* **5**, 129-138.

Fúlfaro, V.J. (1996). Geology of Eastern Paraguay. In: Comin-Chiaramonti, P. & Gomes, C.B. (eds.) *Alkaline magmatism in central-eastern*

*Paraguay. Relationships with coeval magmatism in Brazil.* São Paulo: Edusp/Fapesp, pp. 17-29.

Gallagher, K., Hawkesworth, C.J. & Mantovani, M.S.M. (1995). Denudation, fission track analysis and the long term evolution of passive margin topography: application to the Brazilian margin. *Journal of South American Earth Sciences* **8**, 65-77.

Garda, G.M., Schorscher, J.H.D., Esperança, S. & Carlson, R.W. (1995). The petrology and geochemistry of coastal dykes from São Paulo State Brazil: implications for variable lithospheric contributions to alkaline magmas from the western margin of the South Atlantic. *Anais da Academia Brasileira de Ciências* **67**, 191-216.

Gibson, S.A., Thompson, R.N., Leonardos, O.H., Dickin, A.P. & Mitchell, J.G. (1995). The Late Cretaceous impact of the Trindade mantle plume: evidence from large-volume, mafic, potassic magmatism in SE Brazil. *Journal of Petrology* **36**, 189-229.

Gibson, S.A., Thompson, R.N., Leonardos, O.H., Turner, S., Mitchell, J.G. & Dickin, A.P. (1994). The Serra do Bueno potassic diatreme: a possible hypabissal equivalent of the ultramafic potassic volcanics in the Cretaceous Alto Paranaíba Igneous Province, SE Brazil. *Mineralogical Magazine* **58**, 357-373.

Gibson, S.A., Thompson, R.N., Weska, R.K., Dickin, A.P. & Leonardos, O.H. (1997). Late Cretaceous rift-related upwelling and melting of the Trindade starting mantle plume head beneath western Brazil. *Contributions to Mineralogy and Petrology* **126**, 303-314.

Gomes, C.B. & Cordani, U.G. (1965). Estudos geocronológicos do maciço alcalino de Itapirapuã, SP, Brasil. *Anais da Academia Brasileira de Ciências* **37**, 497-501.

Gomes, C.B. & Valarelli, J.V. (1970). Nova ocorrência de rochas alcalinas no Estado de São Paulo. *24º Congresso Brasileiro de Geologia, Brasília, Resumo das Comunicações,* pp. 336-337.

Gomes, C.B., Barbieri, M., Beccaluva, L., Brotzu, P., Conte, A., Garbarino, C., Macciotta, G., Melluso, L., Morbidelli, L., Ruberti, E., Scheibe, L.F., Tamura, R.M. & Traversa, G. (1987). Petrological and geochemical studies alkaline rocks from continental Brazil. 2. The Tunas massif, State of Paraná. *Geochimica Brasiliensis* **1,** 201-234.

Gomes, C.B., Comin-Chiaramonti, P., De Min, A., Melfi, A.J., Bellieni, G., Ernesto, M., Castillo, A.M.C. & Velázquez, V.F. (1989) Atividade filoniana associada ao complexo alcalino de Sapukai, Paraguai Oriental. *Geochimica Brasiliensis* **3**, 93-114.

Gomes, C.B., Comin-Chiaramonti, P., Velázquez, V.F. & Orué, D. (1996b). Alkaline magmatism in Paraguay: a review. In: Comin-Chiaramonti, P. & Gomes, C.B. (eds.) *Alkaline magmatism in central-eastern Paraguay. Relationships with coeval magmatism in Brazil.* São Paulo: Edusp/Fapesp, pp. 31-56.

Gomes, C.B., Laurenzi, M.A., Censi, P., De Min, A., Velázquez, V.F., & Comin-Chiaramonti, P. (1996a). Alkaline magmatism from northern Paraguay (Alto Paraguay): a permo-triassic province. In: Comin-Chiaramonti, P. & Gomes, C.B. (eds.) *Alkaline magmatism in central-eastern Paraguay. Relationships with coeval magmatism in Brazil.* São Paulo: Edusp/Fapesp, pp. 223-230.

Gomes, C.B., Milan, A., Velázquez, V.F., Riccomini, C., Comin-Chiaramonti, P., Vasconcelos, P.M. & Tassinari, C.C.G. (2003). Magmatismo alcalino da porção centro-oriental do Paraguai: novos dados geocronológicos para as rochas das províncias Central e Assunção. *7º Congresso de Geoquímica dos Países de Língua Portuguesa, Maputo, Resumos,* p. 34.

Gomes, C.B., Ruberti, E. & Morbidelli, L. (1990). Carbonatite complexes from Brazil: a review. *Journal of South American Earth Sciences* **3**, 51-63.

Guillou, L. & Jaupart, C. (1995). On the effects of continents on mantle convection. *Journal of Geophysical Research* **100**, 24217-24238.

Hackspacher, P.C., Hadler, J.C., Iunes, P.J., Paulo, S.R., Ribeiro, L.F.B. & Tello Saez, C.A. (1999). Alguns dados sobre o Período Cretáceo na Serra da Mantiqueira através de traços de fissão em apatitas (ATFA). *5º Simpósio sobre o Cretáceo do Brasil/1º Simpósio sobre el Cretácico de América del Sur, Serra Negra, Boletim*, pp. 33-37.

Hart, S.R. (1988). Heterogeneous mantle domains: signatures, genesis and mixing chronologies. *Earth and Planetary Science Letters* **90**, 273-296.

Hasui, Y. & Cordani, U.G. (1968). Idades potássio-argônio de rochas eruptivas mesozóicas do leste mineiro e sul de Goiás. *22º Congresso Brasileiro de Geologia, Belo Horizonte, Anais*, pp. 139-143.

Hasui, Y., Magalhães, F.S., Coppedê Jr., A. & Margutti, R.L. (1992). Mina de carbonatito de Jacupiranga (SP): permeabilidade do maciço avaliada pelo método geoestrutural. In: Hasui, Y. & Mioto, J.A. (coords.) *Geologia Estrutural Aplicada*. São Paulo: Associação Brasileira de Geologia de Engenharia e Indústrias Votorantin, pp. 383-398.

Hasui, Y., Sadowski, G.R., Suguio, K. & Fuck, R.A. (1975). The Phanerozoic tectonic evolution of the western Minas Gerais State. *Anais da*

*Academia Brasileira de Ciências* **47**, 431-438.

Herz, N. (1977). Timing of spreading in the South Atlantic: information from Brazilian alkalic rocks. *Geological Society of America Bulletin* **88**, 101-112.

James, D.E., Assumpção, M., Snoke, J.A., Ribotta, L.C. & Kuehnel, R. (1993). Seismic studies of continental lithosphere beneath SE Brazil. *Anais da Academia Brasileira de Ciências* **65** (suplemento), 227-250.

Klein, V.C. & Valença, J.G. (1984). Estruturas almofadadas em derrame ankaramítico na Bacia de São José de Itaboraí, Rio de Janeiro. *33º Congresso Brasileiro de Geologia, Rio de Janeiro, Anais* **9**, 4335-4345.

Leonardos, O.H., Ulbrich, M.C.N. & Gaspar, J.C. (1991). The Mata da Corda volcanic rocks. *5th International Kimberlite Conference, Araxá, Field Guide Book,* pp. 17-24.

Litherland, M., Annells, R.N., Appleton, J.D., Berrange, J.P., Bloomfield, K., Burton, C.C.J., Darbyshire, D.P.F., Fletcher, C.J.N., Hawkins, M.P., Klinck, B.A., Llanos, A., Mitchell, W.I., O'Connor, E.A., Pitfield, P.E.J., Power, G. & Webb, B.C. (1986). The geology and mineral resources of the Bolivian Precambrian shield. *British Geological Survey Overseas Memoir* **9**, 153pp.

Livieres, R.A. & Quade, H. (1987). Distribución regional y asentamiento tectónico de los complejos alcalinos del Paraguay. *Zentralblat für Geologie und Paläontologie* **7/8**, 791-805.

Lowman, J.P. & Jarvis, G.T. (1999). Effects on mantle heat source distribution on supercontinent stability. *Journal of Geophysical Research* **104**, 12733-12746.

Mariano, A.N. & Marchetto, M. (1991). Serra Negra and Salitre carbonatite alkaline igneous complex. In: Leonardos, O.H., Meyer, H.O.A. & Gaspar, J.C. (eds.) *5th International Kimberlite Conference, Araxá, Field Guide Book,* pp. 75-79.

Marsh, J.S. (1973). Relationships between transform directions and alkaline igneous rock lineaments in Africa and South America. *Earth and Planetary Science Letters* **18**, 317-323.

Melfi, A.J., Piccirillo, E.M. & Nardy, A.J.R. (1988). Geological and magmatic aspects of the Paraná Basin - an introduction. In: Piccirillo, E.M. & Melfi, J.A. (eds.) *The Mesozoic flood volcanism of the Paraná Basin - petrogenetic and geophysical aspects*. São Paulo: IAG-USP, pp. 1-13.

Milani, E.J. (1997). *Evolução tectono-estratigráfica da Bacia do Paraná e seu relacionamento com a geodinâmica fanerozóica do Gondwana Sul-Ocidental.* Ph.D. Thesis, Federal University of Rio Grande do Sul, 255p.

Milner, S.C., Le Roex, A.P. & O'Connor, J.M. (1995). Age of Mesozoic rocks in northwestern Namibia, and their relationship to continental breakup. *Journal of the Geological Society of London* **152**, 97-104.

Morbidelli, L., Gomes, C.B., Becalluva, L., Brotzu, P., Conte, A.M., Ruberti, E. & Traversa, G. (1995). Mineralogical, petrological and geochemical aspects of alkaline-carbonatite associations in Brazil. *Earth-Science Reviews* **30**, 135-168.

Motoki, A. (1986). *Geologia e petrologia do maciço alcalino da Ilha da Vitória, SP*. Ph.D. Thesis, University of São Paulo, 245p.

Muzio, R.S. (2000). *Evolução petrológica e* geocronológica *do Maciço alcalino Valle Chico, Uruguai*. Ph.D. Thesis, Universidade Estadual Paulista, Rio Claro, 171p.

Muzio, R.S. & Artur, A.C. (1998). Petrografía y geoquímica del macizo alcalino Valle Chico, Depto. de Lavalleja, Uruguay: resultados preliminares. *2º* Congreso *Uruguayo de Geologia, Punta del Este, Actas,* pp. 145-150.

Muzio, R.S., Peel, E. & Artur, A.C. (1999). New geochronological data of the Valle Chico alkaline massif (Uruguay), using U-Pb and Sm-Nd systematics. *2º Simposio Sudamericano de Geología Isotópica, Córdoba, Extended Abstracts* (CD-ROM).

Photo Gravity Corporation (1991). *Regional Bouguer Gravity data and station lacation Map of the Paraguay (Scale 1:2.000.000).* Asunción: Archivo DRM-MOPC.

Pirelli, H. (1999). Contribución al conocimiento de la *Formación* Valle Chico, Uruguay. *5º Simpósio sobre o Cretáceo do Brasil/1º Simpósio sobre el Cretácico de América del Sur, Serra Negra, Anais,* pp. 433-437.

Ramos, V.A. (1988). Late Proterozoic-Early Cambrian of South America: a collisional history. *Episodes* **11**, 168-174.

Regelous, M. (1993). *Geochemistry of dolerites from the Paraná flood basalt province, southern Brazil*. Ph.D. Thesis, Open University, Milton Keynes, 256p.

Renne, P.R., Ernesto, M., Pacca, I.G., Coe, R.S., Glen, J.M., Prévot, M. & Perrin, M., (1992). The age of Paraná flood volcanism, rifting of Gondwanaland and the Jurassic-Cretaceous boundary. *Science* **258**, 975-979.

Renne, P.R., Glen, J.M., Milner, S.C. & Duncan, A.R. (1996). Age of Etendeka flood volcanism and associated intrusions in southwestern Africa. *Geology* **24**, 659-662.

Renne, P.R., Mertz, D.F., Ernesto, M., Marques, L.S., Teixeira, W., Ens, H.H. & Richards, M.A. (1993). Geochronologic constraints on magmatic and tectonic evolution of the Paraná Province. *EOS* **74**, 553p.

Riccomini, C. (1989). *O Rift continental do sudeste do Brasil*. Ph.D. Thesis, University of São Paulo, 256p.

Riccomini, C. (1995a). *Tectonismo gerador e deformador dos depósitos sedimentares pós-*gondvânicos *da porção centro-oriental do Estado de São Paulo e áreas vizinhas.* Livre-Docência Thesis, University of São Paulo, 100p.

Riccomini, C. (1995b). Padrão de fraturamentos do maciço alcalino de Cananéia, Estado de São Paulo: relações com a tectônica mesozóico-cenozóica do sudeste do Brasil. *Revista Brasileira de Geociências* **25**, 79-84.

Riccomini, C. (1997). Arcabouço estrutural e aspectos do tectonismo gerador e deformador da Bacia Bauru no Estado de São Paulo. *Revista* Brasileira *de Geociências* **27**, 153-162.

Riccomini, C. & Rodrigues-Francisco, B.H. (1992). Idade potássio-argônio do derrame de ankaramito da Bacia de Itaboraí, Rio de Janeiro: implicações tectônicas. *37º Congresso Brasileiro de Geologia, São Paulo, Boletim de Resumos Expandidos* **2**, 469-470.

Riccomini, C., Melo, M.S. & Coutinho, J.M.V. (1991). Late Cretaceous-Early Tertiary ultrabasic magmatism in the western part of the State of Rio de Janeiro, Brazil. *Boletim do Instituto de Geociências da USP, Publicação Especial* **10**, 77-84.

Riccomini, C., Melo, M.S., Carneiro, C.D.R., Almeida, F.F.M., Mioto, J.A. & Hasui, Y. (1983). Sobre a ocorrência de um derrame de ankaramito na Bacia de Volta Redonda, RJ, e sua importância na datação das bacias tafrogênicas continentais do sudeste brasileiro. *4º Simpósio Regional de Geologia, São Paulo, Resumos,* pp.23-24.

Riccomini, C., Velázquez, V.F. & Gomes, C.B. (2001). Cenozoic lithospheric faulting in the Asunción Rift, eastern Paraguay. *Journal of South American Earth Sciences* **14**, 625-630.

Riccomini, C., Velázquez, V.F., Gomes, C.B., Sallun, A.E.M. & Milan, A. (2002). Tectonic evolution of the Asunción Rift, Eastern Paraguay. *Anais da Academia Brasileira de Ciências* **74**, p. 555.

Rocha-Campos, A.C., Cordani, U.G., Kawashita, K., Sonoki, H.M. & Sonoki, I.K. (1988). Age of the Paraná flood volcanism. In: Piccirillo, E.M. & Melfi, J.A (eds.) *The Mesozoic flood volcanism of the Paraná Basin - petrogenetic and geophysical aspects*. São Paulo: IAG-USP, pp. 25-45.

Rosselo, E.A., Santa Ana, H. & Veroslavsky, G. (2000). El Lineamiento Santa Lucía - Aiguá - Merín (Uruguay): un corredor tectónico extensivo y transcurrente dextral precursor de la apertura Atlántica. *Revista Brasileira de Geociências* **30**, 749-756.

Rostirolla, S.P., Assine, M.L., Fernandes, L.A. & Artur, P.C. (2000). Reativação de paleolineamentos durante a evolução da Bacia do Paraná: o exemplo do Alto Estrutural de Quatiguá. *Revista Brasileira de Geociências* **30**, 639-648.

Sadowski, G.R. & Dias Neto, C.M. (1981). O lineamento sismo-tectônico de Cabo Frio. *Revista Brasileira de Geociências* **11**, 209-212.

Salles, A.M.F. (1999). *Análise morfotectônica do segmento meridional do Alinhamento do Rio Moji-Guaçu*. Bs.D. Dissertation, University of São Paulo, 106p.

Scheibe, L.F. (1979). *Estudo petrológico e* geoquímico *dos carbonatitos da Fazenda Varela, Lajes, Santa Catarina, Brasil.* M.Sc. Dissertation, Federal University of Rio Grande do Sul, 120p.

Scheibe, L.F. (1986). *Geologia e petrologia do distrito alcalino de Lages, SC*. Ph.D. Thesis, University of São Paulo, 224p.

Schobbenhaus, C., Campos, D.A., Derze, G.R. & Asmus, H.E. (1981). *Mapa geológico do Brasil e da área oceânica adjacente, incluindo depósitos minerais; escala 1:2.500.000*. Brasília: Departamento Nacional de Produção Mineral/Ministério das Minas e Energia, 4 folhas.

Sgarbi, P.B.D. & Gaspar, J.C. (2002). Geochemistry of Santo Antonio da Barra kamafugites, Goiás, Brazil. *Journal of South American Earth Sciences* **14**, 889-901.

Shea, M.E. (1992). Isotopic geochemical characterization of selected nepheline syenites and phonolites from Poços de Caldas alkaline complex, Minas Gerais, Brazil. *Journal of Geochemical Exploration* **45**,173-214.

Sheth, H.C. (1999). Flood basalts and large igneous provinces from deep mantle plumes: fact, fiction and fallacy. *Tectonophysics* **311**, 1-29.

Smith, P.E., Evensen, N.M., York, D., Szatmari, P., Conceição, J.C.J. & Destro, N. (1999). Getting it on track: Ar-Ar geochronology of alkali intrusions of the Serra do Mar Province, Brazil. *EOS* **80**, 1134-1135.

Soares, P.C. (1988). Tectônica colisional em torno do Bloco Paraná, Brasil. *7º Congresso Latinoamericano de Geologia, Belém, Anais* **1**, 63-79.

Soares, P.C. (1991). *Tectônica sinsedimentar cíclica na Bacia do Paraná - controles*. Full Professor Thesis, Federal University of Paraná, 131p.

Sonoki, I.K. & Garda, G.M. (1988). Idades K-Ar de rochas alcalinas do Brasil meridional e Paraguai oriental: compilação e adaptação às novas constantes de decaimento. *Boletim do Instituto de Geociências da USP, Série Científica* **19**, 63-85.

Souza, M.Z.A. (1997). *Petrologia e geoquímica do* *complexo ancalino Ponta do Morro, MT*. Ph.D. Thesis, University of São Paulo, 168p.

Spinelli, F.P., Gomes, C.B., Velázquez, V.F., Riccomini, C. & Comin-Chiaramonti, P. (2001). Considerações *petrográficas* e geoquímicas sobre a intrusão alcalina de Cananéia, litoral sul de São Paulo. *8° Congresso Brasileiro de Geoquímica/1º Simpósio de Geoquímica dos Países do Mercosul, Curitiba, Anais* (CD-ROM).

Stewart, K., Turner, S., Kelley, S., Hawkesworth, C., Kirstein, L. & Mantovani, M. (1996). 3-D, $^{40}$Ar-$^{39}$Ar *geochronology* in the Paraná continental flood basalt province. *Earth and Planetary Science Letters* **143**, 95-109.

Svizero, D.P., Meyer, H.O.A., Haralyi, N.L.E. & Hasui, Y. (1984). A note on the geology of some Brazilian kimberlites. *Journal of Geology* **92**, 331-338.

Tankard, A.J., Uliana, M.A., Welsink, H.J., Ramos, V.A., Turic, M., França, A.B., Milani, E.J., Brito Neves, B.B., Eyles, N., Skarmeta, J., Santa Ana, H., Wiens, F., Cirbián, M., Paulsen, O.L., Germs, G.J.B., De Wit, M.J., Machacha, T. & Miller, R. McG. (1995). Tectonic controls of basin evolution in southwestern Gondwana. In: Tankard, A.J., Suarez, R. & Welsink, H.J. (eds.) *Petroleum basins of South America. AAPG Memoir* **62**, 5-52.

Tello Saenz, C.A., Hackspacher, P.C., Hadler Neto, J.C., Iunes, P.J., Guedes, S., Ribeiro, L.F.B. & Paulo, S.R. (2003). Recognition of Cretaceous, Paleocene, and Neogene tectonic reactivation through apatite fission-track analysis in Precambrian areas of southeast Brazil: association with the opening of the south Atlantic Ocean. *Journal of South American Earth Sciences* **15**, 765-774.

Thomas & Associates (1976). *Preliminary ERTS interpretation southeastern Paraguay*. Asunción: DRM-MOPC, Relatório Interno, 20p.

Thomaz Filho, A. & Rodrigues, A.L. (1999). O alinhamento de rochas alcalinas Poços de Caldas - Cabo Frio (RJ) e sua continuidade na Cadeia Vitória Trindade. *Revista Brasileira de Geociências* **29**, 189-194.

Thompson, R.N., Gibson, S.A., Mitchell, J.G., Dickin, A.P., Leonardos, O.H., Brod, J.A. & Greenwood, J.C. (1998). Migrating Cretaceous-Eocene magmatism in the Serra do Mar alkaline province, SE Brazil: melts from the deflected Trindade mantle plume. *Journal of Petrology* **39**, 1493-1526.

Traversa, G., Barbieri, M., Beccaluva, L., Coltorti, M., Conte, A.M., Garbarino, C., Gomes, C.B., Macciotta, G., Morbidelli, L., Ronca, S. & Scheibe, L.F. (1996). Mantle sources and differentiation of alkaline magmatic suite of Lages, Santa Catarina, Brazil. *European Journal of Mineralogy* **8**, 193-208.

Traversa, G., Scheibe, L.F., Barbieri, M., Beccaluva, L., Coltorti, M., Conte, A.M., Garbarino, C., Gomes, C.B., Macciotta, G., Morbidelli, L. & Ronca, S. (1994). Petrology and mineral chemistry of the alkaline district of Lages, SC, Brazil. *Geochimica Brasiliensis* **8**, 179-214.

Turner, S., Regelous, M., Kelley, S., Hawkesworth, C. & Mantovani, M.S.M. (1994). Magmatism and continental break-up in the South Atlantic: high precision $^{40}$Ar-$^{39}$Ar geochronology. *Earth and Planetary Science Letters* **121**, 333-348.

Ulbrich, H.H.G.J. (1984). *A petrografia, a estrutura e o quimismo de nefelina sienitos do maciço alcalino de Poços de Caldas, MG-SP*. Livre-Docência Thesis, University of São Paulo, 477p.

Ulbrich, H.H.G.J. & Gomes, C.B. (1981). Alkaline *rocks* from continental Brazil: a review. *Earth-Science Review* **17**, 135-154.

Ulbrich, H.H.G.J., Demaiffe, D., Vlach, S.R.F. & Ulbrich, M.N.C. (2003). Geochemical and Sr, Nd and Pb isotope signatures of phonolites and nepheline syenites from Poços de Caldas alkaline massif, southeastern Brazil. *4th South American Symposium on Isotope Geology, Salvador, Short Papers,* pp. 698-701.

Ulbrich, M.N.C. (1983). *Aspectos mineralógicos e* petrológicos *de nefelina sienitos do maciço alcalino de Poços de Caldas, MG-SP*. Ph.D. Thesis, University of São Paulo, 369p.

Umpierre, M. & Halpern, H. (1971). Edades estroncio-rubidio en rocas cristalinas del sur de la República Oriental del Uruguay. *Revista de la Asociación Geológica Argentina*, **26**, 133-151.

Ussami, N., Kolisnyk, A., Raposo, M.I.B., Ferreira, F.J.F., Molina, E.C. & Ernesto, M. (1994). Detectabilidade magnética de diques do Arco de Ponta Grossa: um estudo integrado de magnetometria terrestre/aérea e magnetismo de rocha. *Revista Brasileira de Geociências* **21**, 317-327.

Van Decar, J.C., James, D.E. & Assumpção, M. (1995). Seismic evidence for a fossil mantle plume beneath South America and implications for plate driving forces. *Nature* **378**, 25-31.

Vasconcelos, E.M. (1995). *Petrologia e* geoquímica *de diques e "plugs" alcalinos da região do Vale do Ribeira, divisa dos estados do Paraná e São Paulo*. Ph.D. Thesis, University of São Paulo, 202p.

Velázquez, V.F. (1992). *Província Alcalina Central, Paraguai Centro-Oriental: aspectos tectônicos, petrográficos e geocronológicos*. M.Sc. Dissertation, University of São Paulo, 119p.

Velázquez, V.F. (1996). *Província Alcalina Alto Paraguai: características petrográficas, geoquímicas e geocronológicas*. Ph.D. Thesis, University of São Paulo, 101p.

Velázquez, V.F., Gomes, C.B., Capaldi, G., Comin-Chiaramonti, P., Ernesto, M., Kawashita, K., Petrini, R. & Piccirillo, E.M. (1992). Magmatismo alcalino mesozóico na porção centro-oriental do Paraguai: aspectos geocronológicos. *Geochimica Brasiliensis* **6**, 23-35.

Velázquez, V.F., Gomes, C.B., Orué, D. & Comin-Chiaramonti, P. (1996b). Magmatismo alcalino do Paraguai: uma revisão e atualização das *províncias*. *Boletim do Instituto de Geociências da USP, Série Científica* **27**, 61-79.

Velázquez, V.F., Gomes, C.B., Riccomini, C., Comin-Chiaramonti, P., Brumatti, M., Vasconcelos, P.M. & Tassinari, C.C.G. (2003). Características isotópicas e idades $^{40}Ar/^{39}Ar$ para as rochas alcalinas da Província Misiones, Paraguai meridional. *7º Congresso de Geoquímica dos Países de Língua Portuguesa, Maputo, Resumos,* p. 39.

Velázquez, V.F., Gomes, C.B., Teixeira, W. & Comin-Chiaramonti, P. (1996a). Contribution to the geochronology of the Permo-Triassic alkaline magmatism of the Alto Paraguay Province. *Revista Brasileira de Geociências* **26**, 103-108.

Velázquez, V.F., Riccomini, C. & Gomes, C.B. (2001). Tectônica rúptil da região da Cordillera de Ybytyruzú, segmento oriental do Rift de Asunción, Paraguay Oriental. *3º Congreso Uruguayo de Geología/11º Congreso Latinoamericano de Geología, Montevideo, Actas, Edición Eletrónica, paper n°*. 159, 3p.

Velázquez, V.F., Riccomini, C., Gomes, C.B. & Brumatti, M. (2002). Magmatismo alcalino da Província Misiones, Paraguai Oriental: aspectos geoquímicos e tectônicos. *41º Congresso Brasileiro de Geologia, João Pessoa, Anais,* pp.546.

Velázquez, V.F., Riccomini, C., Gomes, C.B., Figueredo, L.B. & Figueredo, C. (1998). Relações tectônicas do magmatismo alcalino do Paraguai Oriental. *Revista do Instituto Geológico* **19**, 43-49.

Vidotti, R.M., Ebinger, C.J. & Fairhead, J.D. (1998). Gravity signature of the western Paraná basin, Brazil. *Earth and Planetary Science Letters* **159**, 117-132.

Vignol-Lelarge, M.L.M., Soliani Jr., E. & Poupeau, G. (1994). Datação pelos traços de fissão do domínio meridional da Serra do Mar (Arco de Ponta Grossa). *38º Congresso Brasileiro de Geologia, Camboriú, Boletim de Resumos Expandidos* **2**, pp.379-380.

Vlach, S.R.F., Vilalva, F.C.J., Ulbrich, M.C.N., Ulbrich, H.H.G.J. & Vasconcelos, P.M. (2003). Phlogopite from carbonatitic veins associated with the Poços de Caldas alkaline massif, SE Brazil: mineralogy and $^{40}Ar/^{39}Ar$ dating by the laser step heating method. *4th South American Symposium on Isotope Geology, Salvador, Short Papers,* pp. 702-705.

White, R.S. & McKenzie, D.P. (1995). Mantle plumes and flood basalts. *Journal of Geophysical Research* **100**, 17543-17585

Zalán, P.V., Wolf, S., Astolfi, M.A.M., Vieira, I.S., Conceição, J.C.J., Appi, V.T., Santos Neto, E.V., Cerqueira, J.R. & Marques, A. (1990a). The Paraná Basin, Brazil. In: Leighton, M.W., Kolata, D.R., Oltz, D.F. & Eidel, J.J. (eds.) *Interior cratonic basins. AAPG Memoir* **51**, pp.681-708.

Zalán, P.V., Wolf, S., Conceição, J.C.J., Marques, A., Astolfi, M.A.M., Vieira, I.S., Appi, V.T. & Zanotto, O.A. (1990b). Bacia do Paraná. In: Raja Gabaglia, G.P. & Milani, E.J. (coords.) *Origem e evolução de bacias sedimentares*. Rio de Janeiro: *Petrobrás,* pp.135-168.

*Mesozoic to Cenozoic Alkaline Magmatism in the Brazilian Platform*
*Comin-Chiaramonti, P. & Gomes, C.B. (eds.)*
*Edusp/Fapesp, São Paulo, pp. 31-55, 2005*

# POST-PALEOZOIC MAGMATISM IN EASTERN PARAGUAY: Sr-Nd-Pb ISOTOPE COMPOSITIONS

*P. Antonini, M. Gasparon, P. Comin-Chiaramonti and C.B. Gomes*

*Eastern Paraguay is the westernmost part of the Paraná Basin and was the site of intense magmatic activity since Mesozoic. During the Early Cretaceous, potassic alkaline magmatism pre- and postdates the Paraná flood tholeiites of the Serra Geral Formation. Sodic magmatism occurred in Eastern Paraguay during late Early Cretaceous and Tertiary. Selected samples belonging to these distinct magmatic events have been investigated for incompatible elements and for Sr-Nd-Pb isotopes. The results suggest that two main mantle components have been involved in the genesis of the Cretaceous to Tertiary magmatism in Eastern Paraguay: an extreme and heterogeneous EMI and a HIMU component. The EMI component dominated the Early Cretaceous potassic alkaline magmatism, whereas the HIMU was important in the late Early Cretaceous and Tertiary sodic magmatism. Different contributions of EMI and HIMU components could also explain the Sr-Nd-Pb isotopic heterogeneity of the Early Cretaceous flood tholeiites in Eastern Paraguay.*

## INTRODUCTION

Eastern Paraguay represents the westernmost fringe of Early Cretaceous Paraná flood tholeiites (Serra Geral Formation, SGF). In addition it has been the site of alkaline magmatism since Early Cretaceous: Early Cretaceous potassic igneous rocks, late Early Cretaceous sodic lavas and Tertiary sodic lavas.

These magmatic rocks, closely related in time and space, offer the opportunity to investigate the petrogenetic significance of the potassic and sodic continental alkaline magmatism and their relationships with the SGF basalts. Due to the high Sr and Nd concentrations of the alkaline rocks, it is reasonable to assume that their $^{87}Sr/^{86}Sr$ and $^{143}Nd/^{144}Nd$ compositions have not been significantly affected by crustal contamination processes and, therefore, reflect the isotopic signature of the mantle source. This paper aims to discuss, through the review of the available data and new Pb isotopic data, the most important geochemical and isotopic features of the alkaline and tholeiitic magmatism of Eastern Paraguay in order to constrain the spatial and temporal evolution of the subcontinental mantle source(s).

## GEOLOGICAL SETTING

Eastern Paraguay lies in an intercratonic region which includes the westernmost side of the Paraná Basin of Brazil. It is bounded by an anticlinal structure established since Early Paleozoic, the Asunción Arch, separating the Paraná Basin (East) from the Gran Chaco Basin (West) (Fig. 1; Almeida, 1983; Comin-Chiaramonti *et al*., 1997).

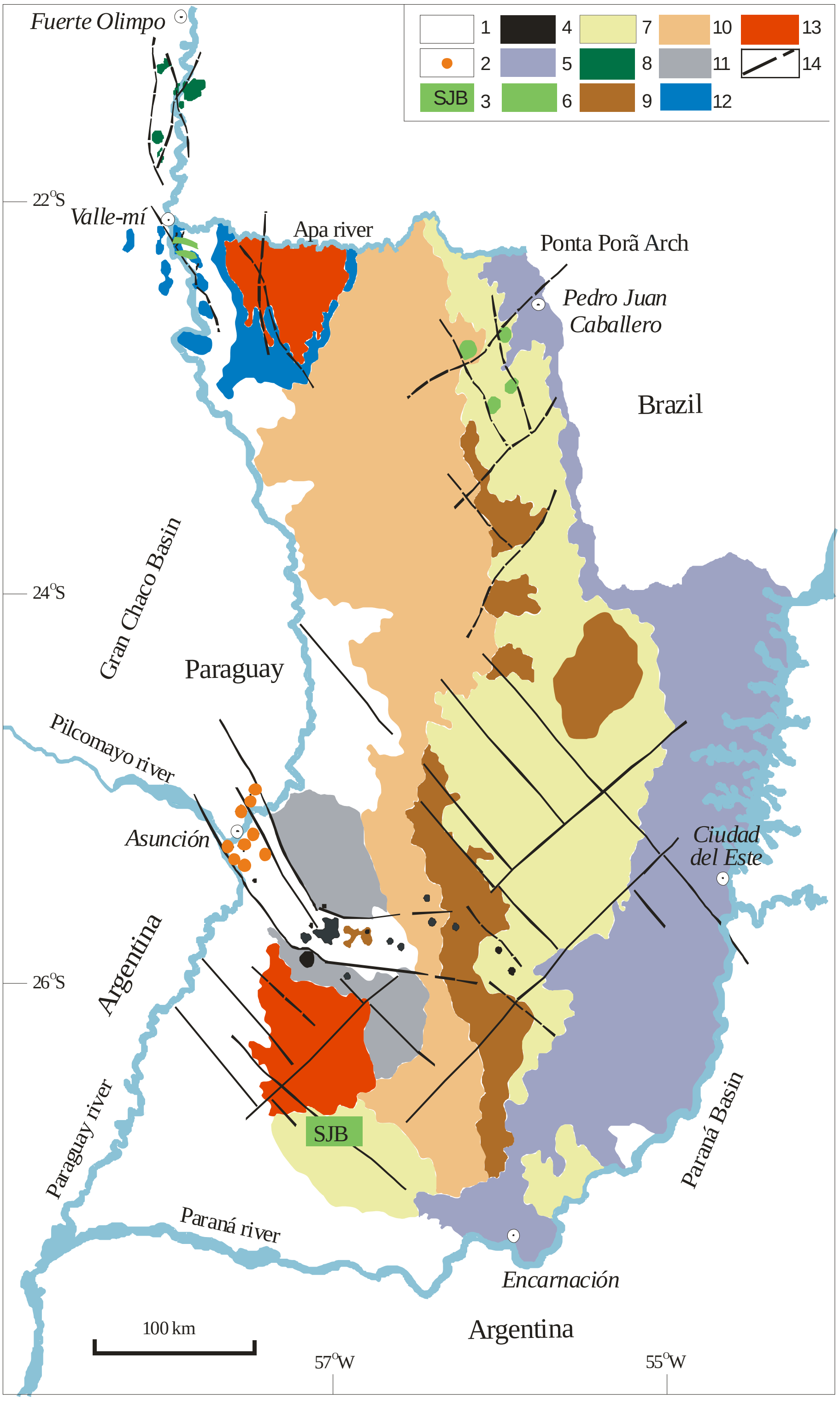


Fig. 1. Geological sketch-map showing the distribution of Post-Palaeozoic magmatism in Eastern Paraguay, modified after Fúlfaro (1996) and Velázquez *et al*. (1998). 1) Quaternary sedimentary cover; 2) Tertiary sodic alkaline rocks; 3) Late Early Cretaceous sodic alkaline rocks (San Juan Bautista, SJB); 4) Early Cretaceous potassic alkaline rocks (post-tholeiites); 5) Early Cretaceous tholeiites of the Paraná Basin; 6) Early Cretaceous potassic alkaline rocks (pre-tholeiites); 7) Cretaceous sedimentary rocks (Misiones Formation); 8) Permo-Triassic alkaline rocks (Alto Paraguay Province); 9) Permian sedimentary rocks (Independencia Group); 10) Permo-Carboniferous sedimentary rocks (Coronel Oviedo Group); 11) Ordovician-Silurian sedimentary rocks (Caacupé and Itacurubí Groups); 12) Cambro-Ordovician platform carbonates (Itacupumí Group); 13) Archean and Neoproterozoic crystalline basement: high- to low-grade metasedimentary rocks, metarhyolites and granitic intrusions; 14) faults.

The basement rocks are mainly Precambrian to Early Paleozoic granitic intrusions and high to low-grade metamorphic sediments, considered to be the northernmost occurrence of the Rio de la Plata craton and the southernmost tip of the Amazon craton (Fúlfaro, 1996), at the southern and northern region of Eastern Paraguay, respectively.

Eastern Paraguay was subjected to NE-SW-trending crustal extension during Late Mesozoic, probably related to the western Gondwana breakup. NW-SE fault trends, paralleling the dominant orientation of Mesozoic alkaline and tholeiitic dykes, reflect this type of structure (Comin-Chiaramonti *et al*., 1992; Riccomini *et al*., 2001). The resulting structural pattern controlled the development of the grabens or semigrabens as a response to NE-SW-directed extension and continued evolving into Upper Tertiary times (Comin-Chiaramonti & Gomes, 1996; Comin-Chiaramonti *et al*., 1999).

From the beginning of Mesozoic times, six main magmatic events have occurred in Eastern Paraguay (Fig. 1):

1) Early Triassic sodic magmatism of the Alto Paraguay Province (Gomes *et al*., 1996; Comin-Chiaramonti *et al.*, in this volume), widespread at the southernmost side of the Amazon craton (Fúlfaro, 1996).

2) Potassic alkaline-carbonatitic complexes and dykes from the Rio Apa (~145 Ma; Gibson *et al*., 1995) and Amambay area (avg. 137 Ma; Eby & Mariano, 1986), which predates the SGF basalts.

3) SGF flood tholeiites and dykes (133±1.1 Ma; Renne *et al*., 1992), both represented by high-Ti and low-Ti rock-types (cf. Piccirillo & Melfi, 1998).

4) Potassic alkaline complexes and dykes (128-126 Ma; Velázquez *et al*., 1996) with subordinate carbonatite flows and dykes, widespread mainly in the Asunción-Sapucai-Villarrica graben (Comin-Chiaramonti *et al*., 1999).

5) Sodic alkaline complexes, plugs and dykes (112-106 Ma; De Graff, personal communication), occurring mainly in the Misiones Province (Velázquez *et al*., 1996).

6) Sodic alkaline complexes, plugs and dykes (70-32 Ma; Comin-Chiaramonti *et al.*, 1991) cropping out at the western side of the Asunción-Sapucai-Villarrica graben.

## EARLY CRETACEOUS TO TERTIARY MAGMATISM

Early Cretaceous alkaline magmatism in Eastern Paraguay is moderately to strongly potassic, spanning from alkali basalt to trachyte (AB-suite) and from basanite to phonolite (BP-suite) and their intrusive analogues (Comin-Chiaramonti & Gomes, 1996; Comin-Chiaramonti *et al*., 1997).

Early Cretaceous SGF tholeiitic rocks are mainly basalts and andesibasalts, both of the high-Ti and the low-Ti suites (Piccirillo & Melfi, 1988; Comin-Chiaramonti & Gomes, 1996).

The Late Cretaceous-Tertiary sodic rocks include nephelinites, ankaratrites and phonolites.

### Incompatible elements

Incompatible elements (I.E.) patterns of the pre- and post-tholeiites potassic alkaline rocks are quite similar and are, in general, characterized by LILE enrichment and HFSE depletion (Fig. 2A). The latter geochemical features have been explained by enrichment processes (e.g. subduction: Hergt *et al*., 1991; Maury *et al*., 1992, or volatile-rich small-volume melts derived from the asthenosphere: McKenzie & O'Nions, 1995) occurred on a previously depleted mantle source. Comin-Chiaramonti *et al*. (1997) emphasize the lack of any geological evidence to support a subduction process in the Paraguayan region during Proterozoic, and suggest that the enrichment processes would be related to small-volume melts in the mantle.

In respect to the potassic alkaline magmatism, the Late Cretaceous to Tertiary sodic event differs, in general, by a marked K negative spike and Nb, P and Y positive spikes (Fig. 2A). As proposed by Comin-Chiaramonti *et al*. (1997), the relative K enrichment in Eastern Paraguay potassic rocks suggests that a K-bearing phase (e.g. phlogopite) did not represent a residual phase during the partial melting of the mantle. Phlogopite, instead, was probably a residual phase in the mantle source for the Tertiary sodic alkaline rocks, according to the lower melting degree inferred for the sodic magmatism in relation to the potassic one (e.g. 4-6% and 6-11%, of a garnet mantle melting, respectively).

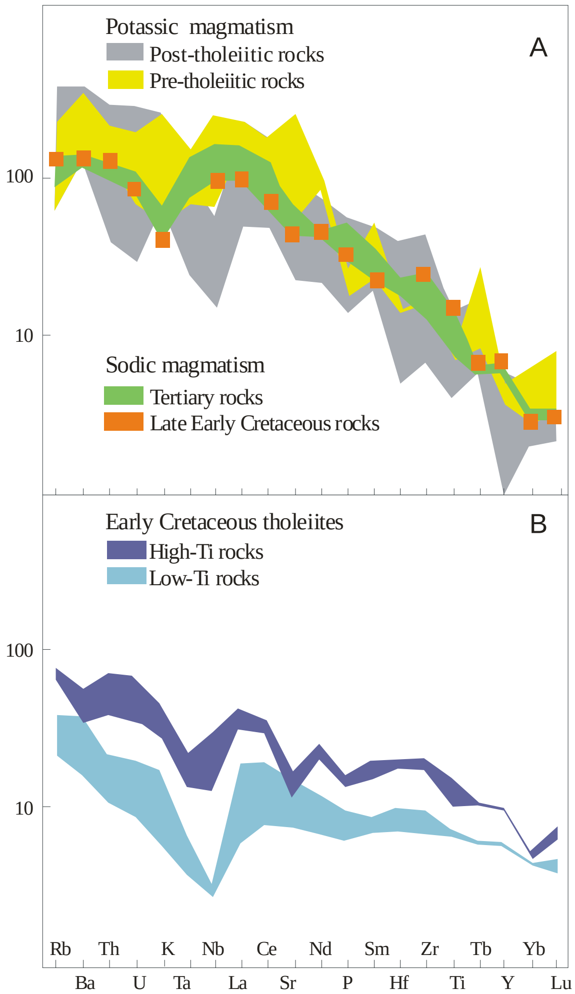


Fig. 2. Primordial mantle (Sun & McDonough, 1989) normalized I.E. of Early Cretaceous to Tertiary magmatic rocks of Eastern Paraguay. A: pre- and post-tholeiitic potassic rocks and Cretaceous and Tertiary sodic rocks; B: low- and high-Ti Early Cretaceous tholeiites of Serra Geral Formation. Data source: Comin-Chiaramonti *et al.* (1997, 1999).

I.E. from the Cretaceous tholeiites differ for their relatively low elemental abundances and low LILE/HFSE ratios (Fig. 2B). In general, low- and high-Ti tholeiites show I.E. characterized by slight LILE enrichment and by a marked Nb-negative spike. In particular, the high-Ti tholeiites have I.E. abundances higher than the low-Ti analogues and Sr-negative anomaly. These differences have been ascribed to different melting degree of a large-scale heterogeneous mantle source (i.e. 20% low-Ti and 5% high-Ti; Piccirillo *et al.*, 1988).

## Sr-Nd isotopes

The schematic petrography and the geographic coordinates of the samples are given in Table 1.

In Table 2 are reported selected Sr and Nd isotopic compositions representative of the Cretaceous to Tertiary magmatic rocks and also of the basement of Eastern Paraguay.

The investigated rocks cover a wide range of Sr-Nd isotopic compositions (Fig. 3) defining on the whole a trend similar to the low-Nd array of Hart *et al.* (1986) (Paraguay array of Comin-Chiaramonti *et al.*, 1995). Initial $^{87}Sr/^{86}Sr$ ($Sr_i$) and $^{143}Nd/^{144}Nd$ ($Nd_i$) ratios range from the depleted quadrant to the enriched one. The potassic alkaline rocks, both pre- and post-tholeiites, have the highest initial $Sr_i$ and the lowest $Nd_i$. Including the Cerro Chiriguelo carbonatite, which occurs associated with the pre-tholeiitic potassic rocks in northeast Paraguay, the $Sr_i$ and $Nd_i$ range from 0.70721 to 0.70636 and from 0.51165 to 0.51194, respectively. These values are quite distinct from those presented by the Early Cretaceous sodic rocks (ca. 110 Ma; $Sr_i$=0.70403, $Nd_i$=0.51243), which approach the Bulk Earth, and also by the Tertiary sodic rocks (ca. 45 Ma), which extends within the depleted quadrant ($Sr_i$=0.70351, $Nd_i$=0.51273) towards the HIMU and DMM compositional fields.

Due to the high Sr and Nd content of Eastern Paraguay alkaline rocks, it is reasonable to assume that crustal contamination processes played a secondary role. According to Comin-Chiaramonti *et al.* (1997), the $Sr_i$ and $Nd_i$ of such rocks can be considered crustally uncontaminated and, as a result, representative of the isotopic composition of the mantle source. The Sr-Nd isotopic variations (Fig. 3) may be explained by: 1) distinct portions of a large- and small-scale heterogeneous lithospheric mantle source, where the small-scale heterogeneity is required for the variations in the $Sr_i$ and $Nd_i$ ratios in each magmatic event; or 2) in terms of mixing by involving an enriched mantle component with extreme EMI signature and depleted mantle component(s) like DMM and/or HIMU. In any case, on the basis of that diagram, it is possible to infer that since Late Cretaceous up to Tertiary times depleted mantle domain(s) played progressively a major role in the genesis of alkaline magmatism in Eastern Paraguay (Comin-Chiaramonti *et al.*, 1999).

Notably, $Sr_i$ and $Nd_i$ of the "uncontaminated" tholeiites (both high- and low-Ti) are intermediate between the potassic and sodic rocks.

## Nd model ages

$T^{DM}$ ages calculated for the Cretaceous-Tertiary magmatic rocks of Eastern Paraguay (cf. Table 2) suggest that the trace elements enrichment in the Paraguayan rocks reflect metasomatic processes which took place in the mantle source at different times since Proterozoic (cf. Fig. 12 in Comin-Chiaramonti *et al.*, 1997).

The pre- and post-tholeiites potassic rocks yielded $T^{DM}$ ranging from 1800 to 1500 Ma, respectively, similar to those of the associated carbonatites (ca. 1600 Ma) and low-Ti tholeiites of central-eastern Paraguay (ca. 1700 Ma). The low-Ti tholeiites of northeast Paraguay yielded more recent $T^{DM}$ (1200-1400 Ma), whereas the oldest ages are given by the Paraguayan high-Ti tholeiites (1800-2000 Ma). The youngest $T^{DM}$ are shown by the late Early Cretaceous sodic alkaline rocks (ca. 800 Ma) and by the Tertiary sodic alkaline rocks (ca. 500 Ma). The model ages computed for the Eastern Paraguayan rocks suggest that two distinct major mantle metasomatic events occurred during Middle and Late Proterozoic as precursor to the genesis of tholeiitic and K-alkaline magmatism and Na-alkaline magmatism, respectively (cf. Comin-Chiaramonti et al., 1999).

## LEAD ISOTOPES

Pb isotopes are believed to discriminate between DMM and HIMU components (see chapter "Mantle components of Bell & Tilton", 2001, for a summary). For this purpose lead isotopic compositions have been carried out on selected Cretaceous to Tertiary rocks of Eastern Paraguay.

The measured and initial $^{206}Pb/^{204}Pb$, $^{207}Pb/^{204}Pb$ and $^{208}Pb/^{204}Pb$ ratios, the U, Th and Pb concentrations and the μ and κ values are reported in Table 3, and the results are shown in Fig. 4.

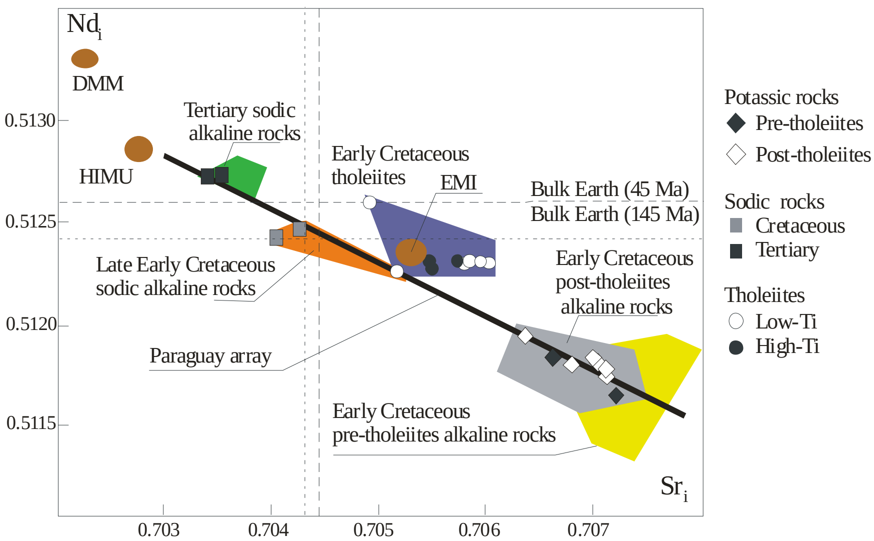


Fig. 3. Initial $^{87}Sr/^{86}Sr$ ($Sr_i$) vs. $^{143}Nd/^{144}Nd$ ($Nd_i$) diagram for the Early Cretaceous to Tertiary magmatic rocks of Eastern Paraguay. Data source: this work and Comin-Chiaramonti *et al.* (1991, 1997). DMM, HIMU and EMI fields after Hart & Zindler (1989). Paraguay array: $Nd_i = -0.23255Sr_i + 0.6763$; r = -0.84; Comin-Chiaramonti *et al.* (1995).

Table 1. Geographic location and schematic petrography of the investigated samples.

| Sample | Rock-type | Lat. | Long. | Texture | Mineral assemblage |
|---|---|---|---|---|---|
| **K-alkaline rocks (Pre-tholeiites)** | | | | | |
| VM | Basanite | 22.13 | 57.24 | Porphyritic | Olivine, clinopyroxene, carbonate (15%)±plagioclase |
| 3441 | Carbonatite | 22.37 | 55.57 | Granular | Carbonate±barite, quartz, phlogopite, sanidine, opaques, aegirine, zircon |
| **Low-Ti tholeiitic rocks** | | | | | |
| 3064 | Tholeiitic basalt | 27.44 | 56.73 | Subaphyric hypocrystalline | Plagioclase, clinopyroxene, opaques, olivine±pigeonite, glass |
| 3002 | Andesibasalt | 25.46 | 56.25 | Subophitic seriate | Clinopyroxene, plagioclase, opaques, pigeonite±glass, quartz, alkali feldspar |
| 3006 | Tholeiitic basalt | 25.43 | 55.12 | Subophitic seriate | Plagioclase, clinopyroxene, opaques±pigeonite, glass |
| PS-239 | Andesibasalt | 26.00 | 57.00 | Subophitic seriate | Clinopyroxene, plagioclase, opaques, pigeonite±glass, quartz, alkali feldspar |
| 987 | Tholeiitic basalt | 22.40 | 55.63 | Porphyritic seriate | Clinopyroxene, opaques, plagioclase, pigeonite, olivine±quartz, alkali feldspar |
| 983 | Tholeiitic basalt | 22.04 | 54.71 | Subaphyric holocrystalline | Clinopyroxene, plagioclase±opaques, pigeonite, olivine |
| 980 | Tholeiitic basalt | 21.59 | 54.42 | Subaphyric holocrystalline | Plagioclase, olivine, clinopyroxene, opaques±pigeonite |
| **High-Ti tholeiitic rocks** | | | | | |
| 3010 | Andesibasalt | 25.58 | 54.31 | Porphyritic holocrystalline | Plagioclase, clinopyroxene, opaques, olivine±glass, alkali feldspar |
| 3403 | Andesibasalt | 24.75 | 56.25 | Porphyritic holocrystalline | Plagioclase, clinopyroxene, opaques, olivine±glass, alkali feldspar |
| PS-306 | Andesibasalt | 25.55 | 56.56 | Ophitic | Plagioclase, clinopyroxene, opaques, biotite, apatite |
| **K-alkaline rocks (Post-tholeiites)** | | | | | |
| PS-204 | Phonolite | 25.35 | 56.21 | Porphyritic | Clinopyroxene, amphibole, biotite±opaques, apatite, alkali feldspar |
| PS-233 | Phonotephrite | 25.59 | 56.57 | Porphyritic | Olivine, clinopyroxene±plagioclase, opaques, alkali feldspar, calcite, apatite |
| PS-245 | Ijolite | 25.48 | 56.47 | Cumulitic | Clinopyroxene, olivine, biotite, opaques |
| PS-264 | Essexitic gabbro | 25.35 | 56.27 | Holocrystalline | Clinopyroxene, alkali feldspar, nepheline, olivine, opaques, biotite, apatite, zircon |
| PS-309 | Trachybasalt | 25.55 | 56.56 | Porphyritic | Clinopyroxene, olivine±plagioclase, amphibole, opaques, apatite |
| PS-519 | Tephrite | 25.53 | 56.17 | Porphyritic | Clinopyroxene, analcime, olivine, opaques±apatite, biotite |
| **Na-alkaline rocks** | | | | | |
| 3284 | Melanephelinite | 25.24 | 57.32 | Porphyritic | Olivine, clinopyroxene, opaques±nepheline, apatite, biotite, calcite |
| 3284-I | Harzburgite (Xen.) | 25.24 | 57.32 | Protogranular | Olivine, orthopyroxene, spinel exsolution in orthopyroxene, relict clinopyroxene |
| PS-558B | Dunite (Xen.) | 25.57 | 57.10 | Protogranular | Olivine±orthopyroxene, spinel |
| PS-577 | Melanephelinite | 26.57 | 57.10 | Porphyritic | Olivine, clinopyroxene, opaques±nepheline, apatite |
| **Basement rocks** | | | | | |
| RP-19B | Metarhyolite | 21.05 | 57.54 | Porphyroblastic | Alkali feldspar, plagioclase±quartz |
| AZ-2 | Granite | 21.80 | 57.60 | Heterogranular | Quartz, alkali feldspar, plagioclase, biotite |
| LIM | Metalimestone | 22.13 | 58.10 | Porphyroblastic | Carbonate |
| PS-608 | Metarhyolite | 25.90 | 56.90 | Porphyroblastic | Alkali feldspar, plagioclase±quartz |

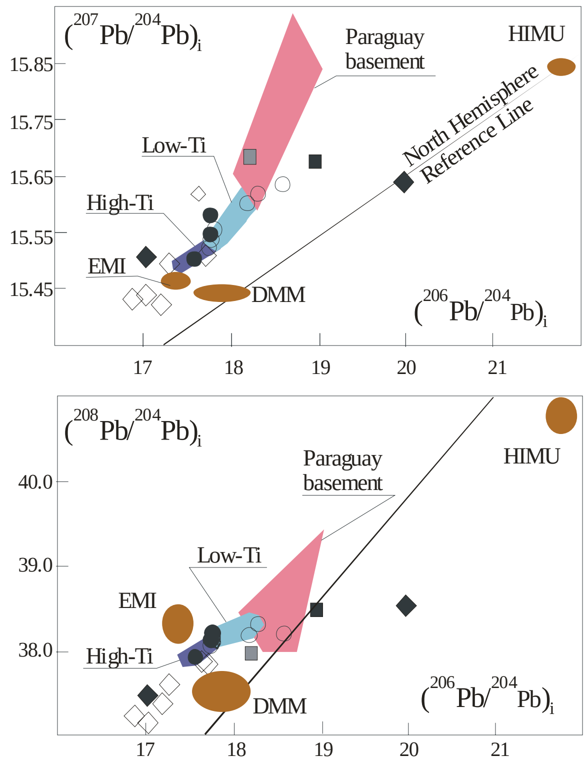


Fig. 4. Initial $^{206}Pb/^{204}Pb$ vs. $^{207}Pb/^{204}Pb$ and $^{208}Pb/^{204}Pb$ diagrams for the Early Cretaceous to Tertiary magmatic rocks of Eastern Paraguay. DMM, HIMU and EMI fields after Hart & Zindler (1989) and high-Ti and low-Ti tholeiites fields after Marques *et al*. (1999). North Hemisphere Reference Line after Hart (1984) and Paraguay basement field this work. Symbols as in Fig. 3.

Table 2. Sr and Nd isotopic compositions of selected Cretaceous to Tertiary magmatic rocks and of the basement of Eastern Paraguay (in brackets 2$\sigma$ error in the last digits). Initial isotopic composition and time integrated notation ($\varepsilon^t$) computed at the notional age reported in the table. * = 145 Ma, ** = 130 Ma. ($\varepsilon^t$) calculated using $^{87}Sr/^{86}Sr_{CHUR}=0.7045$, $^{87}Rb/^{86}Sr_{CHUR}=0.0816$, $^{143}Nd/^{144}Nd_{CHUR}=0.512638$ and $^{147}Sm/^{144}Nd_{CHUR}=0.1967$. Decay constants are those recommended by Faure (1986). $T^{DM}$: Nd depleted mantle model age (depleted mantle: $^{143}Nd/^{144}Nd=0.513151$, $^{147}Sm/^{144}Nd=0.2188$). Data source as follows: this work and Petrini *et al.* (1987), Castorina *et al.* (1996) and Comin-Chiaramonti *et al.* (1997). ASU, Asunción-Sapucai graben.

| | Sample | Rock-type | Notional age (Ma) | Rb (ppm) | Sr (ppm) | $^{87}Sr/^{86}Sr$ | $(^{87}Sr/^{86}Sr)_i$ | $\varepsilon(Sr)_T$ | Sm (ppm) | Nd (ppm) | $^{143}Nd/^{144}Nd$ | $(^{143}Nd/^{144}Nd)_i$ | $\varepsilon(Nd)_T$ | $T^{DM}$ (Ma) |
|---|---|---|---|---|---|---|---|---|---|---|---|---|---|---|
| **K-alkaline rocks (Pre-tholeiites)** | | | | | | | | | | | | | | |
| *North Paraguay* | | | | | | | | | | | | | | |
| Valle-mí | VM | Basanite | 145 | 41 | 1151 | 0.706822(4) | 0.70661 | 32.4 | 23.8 | 148.7 | 0.511956(6) | 0.51186 | -11.5 | 1609 |
| Cerro Chiriguelo | 3441 | Carbonatite | 137 | 27 | 17940 | 0.707218(10) | 0.70721 | 42.8 | 51.0 | 313.0 | 0.511740(10) | 0.51165 | -15.7 | 1783 |
| **Low-Ti tholeiitic rocks** | | | | | | | | | | | | | | |
| *South Paraguay* | | | | | | | | | | | | | | |
| 1. Yaciretá | 3064 | Tholeiitic basalt | 133 | 9 | 160 | 0.705210(10) | 0.70491 | 8.0 | 3.4 | 10.0 | 0.512780(10) | 0.51260 | 2.6 | |
| *Central Paraguay* | | | | | | | | | | | | | | |
| Coronel Oviedo | 3002 | Andesibasalt | 133 | 19 | 257 | 0.706191(7) | 0.70579 | 20.5 | 7.0 | 27.1 | 0.512434(7) | 0.51230 | -3.3 | 1740 |
| 1. Ciudad del Este | 3006 | Tholeiitic basalt | 133 | 14 | 163 | 0.705620(10) | 0.70516 | 11.5 | 3.1 | 12.2 | 0.512400(10) | 0.51226 | -4.0 | 1751 |
| La Rosada | PS-239 | Andesibasalt | 133 | 24 | 289 | 0.706477(5) | 0.70602 | 23.8 | 4.9 | 19.0 | 0.512433(6) | 0.51230 | -3.3 | 1735 |
| *Northeast Paraguay* | | | | | | | | | | | | | | |
| 1. Ponta Porã | 987 | Tholeiitic basalt | 133 | 17 | 273 | 0.706200(20) | 0.70593 | 22.5 | 4.4 | 19.0 | 0.512441(5) | 0.51232 | -2.9 | 1232 |
| 1. Ponta Porã | 983 | Tholeiitic basalt | 133 | 14 | 270 | 0.706120(20) | 0.70585 | 21.4 | 4.2 | 18.9 | 0.512427(7) | 0.51231 | -3.1 | 1305 |
| 1. Ponta Porã | 980 | Tholeiitic basalt | 133 | 13 | 273 | 0.706140(20) | 0.70585 | 21.4 | 4.1 | 19.3 | 0.512420(10) | 0.51231 | -3.1 | 1371 |
| **High-Ti tholeiitic rocks** | | | | | | | | | | | | | | |
| *Central Paraguay* | | | | | | | | | | | | | | |
| 1.Ciudad del Este | 3010 | Andesibasalt | 133 | 32 | 386 | 0.705944(4) | 0.70549 | 16.3 | 8.1 | 30.8 | 0.512416(6) | 0.51228 | -3.6 | 1867 |
| Carayo | 3403 | Andesibasalt | 133 | 23 | 244 | 0.706231(7) | 0.70572 | 19.4 | 7.6 | 27.7 | 0.512451(8) | 0.51231 | -3.1 | 2008 |
| Cerro Verá | PS-306 | Andesibasalt | 133 | 27 | 375 | 0.705868(6) | 0.70547 | 16.0 | 6.8 | 26.0 | 0.512448(8) | 0.51231 | -3.1 | 1761 |
| **K-alkaline rocks (Post-tholeiites)** | | | | | | | | | | | | | | |
| *Central Paraguay* | | | | | | | | | | | | | | |
| 2. Cerro Arrúa-í (ASU) | PS-204 | Phonolite | 126 | 103 | 1562 | 0.706721(6) | 0.70636 | 28.8 | 13.3 | 78.0 | 0.512027(9) | 0.51194 | -10.5 | 1478 |
| 3. Cerro San José (ASU) | PS-233 | Phonotephrite | 126 | 81 | 1555 | 0.707310(20) | 0.70704 | 38.1 | 10.6 | 62.7 | 0.511900(10) | 0.51181 | -13.0 | 1595 |
| 3. Cañada (ASU) | PS-245 | Ijolite | 126 | 114 | 1624 | 0.707370(20) | 0.70700 | 37.7 | 13.8 | 90.2 | 0.511920(10) | 0.51184 | -12.4 | 1710 |
| 3. Aguapety Portón (ASU) | PS-264 | Essexitic gabbro | 126 | 69 | 735 | 0.707610(10) | 0.70710 | 39.3 | 14.4 | 93.7 | 0.511820(10) | 0.51174 | -14.4 | 1712 |
| Cerro Verá (ASU) | PS-309 | Trachybasalt | 126 | 74 | 1364 | 0.707393(4) | 0.70711 | 39.2 | 8.3 | 54.0 | 0.511856(7) | 0.51178 | -13.6 | 1565 |
| Cerro Santa Helena (ASU) | PS-519 | Tephrite | 126 | 46 | 1594 | 0.706943(4) | 0.70679 | 34.6 | 10.7 | 60.0 | 0.511887(8) | 0.51180 | -13.2 | 1731 |
| **Na-alkaline rocks** | | | | | | | | | | | | | | |
| *Central Paraguay* | | | | | | | | | | | | | | |
| Ñemby (ASU) | 3284 | Melanephelinite | 45 | 56 | 1072 | 0.703609(6) | 0.70351 | -13.3 | 10.8 | 61.0 | 0.512758(6) | 0.51273 | 2.9 | 536 |
| Ñemby (ASU) | 3284-I | Harzburgite | | 7 | 63 | 0.703592(7) | n.d. | n.d. | 0.4 | 2.7 | 0.512749(7) | n.d. | n.d. | 473 |
| *South Paraguay* | | | | | | | | | | | | | | |
| San Juan Bautista | PS-558B | Dunite | | 8 | 262 | 0.704381(7) | n.d. | n.d. | 5.6 | 32.2 | 0.512533(7) | n.d. | n.d. | 823 |
| San Juan Bautista | PS-577 | Melanephelinite | 110 | 107 | 1136 | 0.704459(7) | 0.70403 | -4.8 | 9.9 | 58.5 | 0.512523(8) | 0.51243 | -1.3 | 822 |
| **Basement rocks** | | | | | | | | | | | | | | |
| *North Paraguay* | | | | | | | | | | | | | | |
| Fuerte Olimpo (1341 Ma) | RP-19B | Metarhyolite | * | 154 | 179 | 0.756843(8) | 0.75169 | 672.4 | 9.2 | 56 | 0.511475(7) | 0.51138 | -20.9 | 2129 |
| Porto Murtinho (1341 Ma) | AZ-2 | Granite | * | 207 | 120 | 0.776415(5) | 0.76606 | 876.4 | 5.5 | 28 | 0.511743(7) | 0.51163 | -16.0 | 2137 |
| Valle-mí (ca. 500 Ma) | LIM | Metalimestone | * | 7.3 | 2760 | 0.707521(7) | 0.70751 | 45.1 | 0.46 | 0.48 | 0.512010(15) | 0.51146 | -19.3 | n.d. |
| *Central Paraguay* | | | | | | | | | | | | | | |
| Acahay (500 Ma) | PS-608 | Mertarhyolite | ** | 154 | 180 | 0.715567(6) | 0.71096 | 91.1 | 8.0 | 50 | 0.511872(6) | 0.51179 | -13.3 | 1625 |

Table 3. Pb isotopic compositions of selected Cretaceous to Tertiary magmatic rocks and of the basement of Eastern Paraguay (in brackets 2σ error in the last digits). Initial isotopic composition computed at the notional age reported in Table 2. Data source: this work and Marques *et al*. (1999).

| Sample | U (ppm) | Th (ppm) | Pb (ppm) | $^{206}Pb/^{204}Pb$ | $^{207}Pb/^{204}Pb$ | $^{208}Pb/^{204}Pb$ | $(^{206}Pb/^{204}Pb)_i$ | $(^{207}Pb/^{204}Pb)_i$ | $(^{208}Pb/^{204}Pb)_i$ | μ | κ |
|---|---|---|---|---|---|---|---|---|---|---|---|
| **K-alkaline rocks (Pre-tholeiites)** | | | | | | | | | | | |
| VM | 5.40 | 18.30 | 23.58 | 20.3098(6) | 15.6578(6) | 38.9676(6) | 19.968 | 15.641 | 38.589 | 15.03 | 3.50 |
| 3441 | 2.25 | 3.28 | 10.52 | 17.3333(1) | 15.5211(1) | 37.6087(1) | 17.033 | 15.506 | 37.465 | 13.21 | 1.51 |
| **Low-Ti tholeiitic rocks** | | | | | | | | | | | |
| 3064 | 0.19 | 0.99 | 1.39 | 18.379 (6) | 15.613 (7) | 38.501 (24) | 18.199 | 15.604 | 38.193 | 8.66 | 5.38 |
| 3002 | 0.46 | 3.10 | 3.58 | 17.9573(1) | 15.5590(1) | 38.4667(1) | 17.788 | 15.551 | 38.094 | 8.10 | 6.96 |
| 3006 | 0.20 | 1.00 | 1.86 | 18.442 (6) | 15.625 (7) | 38.548 (24) | 18.300 | 15.618 | 38.315 | 6.83 | 5.17 |
| PS-239 | 0.63 | 3.24 | 5.06 | 18.7663(1) | 15.6415(1) | 38.4798(1) | 18.601 | 15.633 | 38.201 | 7.95 | 5.31 |
| 987 | 0.30 | 1.99 | 2.53 | 17.917 (6) | 15.533 (7) | 38.466 (24) | 17.761 | 15.525 | 38.128 | 7.47 | 6.85 |
| 983 | 0.29 | 1.88 | 2.43 | 17.915 (7) | 15.531 (8) | 38.407 (25) | 17.758 | 15.523 | 38.075 | 7.52 | 6.70 |
| 980 | 0.24 | 1.74 | 2.33 | 17.918 (6) | 15.547 (7) | 38.437 (24) | 17.782 | 15.540 | 38.115 | 6.50 | 7.49 |
| **High-Ti tholeiitic rocks** | | | | | | | | | | | |
| 3010 | 0.93 | 4.38 | 6.30 | 17.9460(1) | 15.5552(1) | 38.4443(1) | 17.752 | 15.546 | 38.145 | 9.31 | 4.87 |
| 3403 | 0.63 | 3.03 | 3.56 | 17.9959(3) | 15.5912(3) | 38.5723(3) | 17.762 | 15.580 | 38.205 | 11.20 | 4.97 |
| PS-306 | 0.58 | 2.82 | 3.30 | 17.8093(1) | 15.5132(1) | 38.2946(1) | 17.580 | 15.502 | 37.929 | 11.02 | 5.02 |
| **K-alkaline rocks (Post-tholeiites)** | | | | | | | | | | | |
| PS-204 | 1.90 | 2.40 | 15.10 | 17.8569(1) | 15.5181(1) | 37.9160(1) | 17.702 | 15.511 | 37.852 | 7.86 | 1.31 |
| PS-233 | 2.40 | 9.10 | 18.60 | 17.4529(9) | 15.5027(9) | 37.8206(9) | 17.295 | 15.495 | 37.624 | 8.00 | 3.92 |
| PS-245 | 1.70 | 6.60 | 8.73 | 17.8652(31) | 15.6322(31) | 38.2221(31) | 17.624 | 15.620 | 37.915 | 12.24 | 4.01 |
| PS-264 | 1.47 | 6.83 | 7.56 | 17.1239(4) | 15.4442(1) | 37.6031(1) | 16.888 | 15.433 | 37.244 | 11.96 | 4.80 |
| PS-309 | 1.10 | 7.20 | 5.70 | 17.2753(1) | 15.4505(1) | 37.6598(1) | 17.040 | 15.439 | 37.156 | 11.91 | 6.76 |
| PS-519 | 1.00 | 5.50 | 5.20 | 17.4353(7) | 15.4354(7) | 37.7963(7) | 17.200 | 15.424 | 37.373 | 11.91 | 5.68 |
| **Na-alkaline rocks** | | | | | | | | | | | |
| 3284 | 2.01 | 10.94 | 10.25 | 19.0526(1) | 15.6821(1) | 38.6424(1) | 18.964 | 15.678 | 38.484 | 12.60 | 5.62 |
| 3284-I | n.d. | n.d. | n.d. | 18.9639(17) | 15.6382(17) | 38.7041(17) | n.d. | n.d. | n.d. | n.d. | n.d. |
| PS-558B | n.d. | n.d. | n.d. | 19.0482(1) | 15.6602(1) | 38.5028(1) | n.d. | n.d. | n.d. | n.d. | n.d. |
| PS-577 | 1.83 | 9.85 | 9.13 | 18.4301(5) | 15.6930(5) | 38.3496(5) | 18.211 | 15.682 | 37.963 | 12.73 | 5.56 |
| **Basement rocks** | | | | | | | | | | | |
| RP-19B | n.d. | n.d. | n.d. | 19.0528(5) | 15.8429(5) | 39.4461(5) | | | | | |
| AZ-2 | n.d. | n.d. | n.d. | 18.723 (2) | 15.9432(2) | 38.0084(2) | | | | | |
| LIM | n.d. | n.d. | n.d. | 18.3447(5) | 15.5841(5) | 37.9951(5) | | | | | |
| PS-608 | n.d. | n.d. | n.d. | 18.0598(1) | 15.6521(1) | 38.4523(1) | | | | | |

Pre-tholeiitic potassic rocks

The initial Pb isotopic compositions of the Cerro Chiriguelo carbonatite and Valle-mí basanite are extremely different, in particular regarding the $^{206}Pb/^{204}Pb$ and $^{208}Pb/^{204}Pb$ ratios. The first rock-type has initial Pb compositions (17.033, 15.506, 37.465 for $^{206}Pb/^{204}Pb$, $^{207}Pb/^{204}Pb$ and $^{208}Pb/^{204}Pb$, respectively) similar to those of the post-tholeiites potassic alkaline rocks (i.e. 16.888-17.702, 15.433-15.620, 37.156-37.915, respectively), whereas the second one is characterized by very high initial $^{206}Pb/^{204}Pb$ ratio (19.968) and high $^{208}Pb/^{204}Pb$ and $^{207}Pb/^{204}Pb$ ratios (38.589 and 15.641, respectively). Notably, the Valle-mí basanite appears outside of a possible near-linear array formed by the investigated rocks in the initial Pb isotopic diagram (Fig. 4).

Tholeiites

The initial $^{206}Pb/^{204}Pb$, $^{207}Pb/^{204}Pb$ and $^{208}Pb/^{204}Pb$ compositions of the tholeiitic Paraguayan rocks generally agree with the Brazilian analogues reported by Marques *et al.* (1999), except for a low-Ti andesibasalt from central Paraguay (La Rosada).

Also it should be noted that some low-Ti tholeiites tend to plot in the field of the Paleozoic crustal rocks of Eastern Paraguay and that their lead isotopic compositions could be affected by interaction with crustal material.

Post-tholeiitic potassic rocks

In the initial Pb isotopic diagram (Fig. 4), the post-tholeiites potassic rocks form a general trend parallel to the NHRL of Hart (1984), but shifted towards higher $^{208}Pb/^{204}Pb$ ratios. They also extend towards $^{206}Pb/^{204}Pb$ and $^{208}Pb/^{204}Pb$ ratios lower than the EMI values.

Cretaceous and Tertiary sodic rocks

The sodic alkaline rocks-types have different Pb isotopic compositions and differ from the potassic analogues: the Cretaceous sodic rocks show initial

Pb compositions ($^{206}Pb/^{204}Pb = 18.211$, $^{207}Pb/^{204}Pb = 15.628$, $^{208}Pb/^{204}Pb = 37.963$) approaching those of the Cretaceous low-Ti tholeiites of southern Paraná (cf. Marques *et al*., 1999), whereas the Tertiary sodic rocks ($^{206}Pb/^{204}Pb = 18.964$, $^{207}Pb/^{204}Pb = 15.678$, $^{208}Pb/^{204}Pb = 38.484$) appear shifted towards the HIMU field (Fig. 4).

## THE ROLE OF DIFFERENT MANTLE COMPONENTS IN THE GENESIS OF THE CRETACEOUS TO TERTIARY PARAGUAYAN MAGMATISM

In order to constrain the role of possible distinct mantle components in the genesis of the Cretaceous to Tertiary magmatism, the correlation among Sr, Nd and Pb isotopes has been investigated. The initial $^{206}Pb/^{204}Pb$, $^{207}Pb/^{204}Pb$ and $^{208}Pb/^{204}Pb$ vs. $^{87}Sr/^{86}Sr$ and $^{143}Nd/^{144}Nd$ ratios are illustrated in Fig. 5.

In general, excluding the pre-tholeiites Valle-mí basanite, the potassic rocks are in the same trend common to the Early Cretaceous SGF tholeiites and to the sodic rocks (both Cretaceous and Tertiary). It is interesting to observe that the isotopic compositions trend towards the HIMU field rather than the DMM one, particularly in the $^{207}Pb/^{204}Pb$ vs. $^{87}Sr/^{86}Sr$ and $^{143}Nd/^{144}Nd$ diagrams (Fig. 5), suggesting that the HIMU component played an important role in the whole Cretaceous to Tertiary

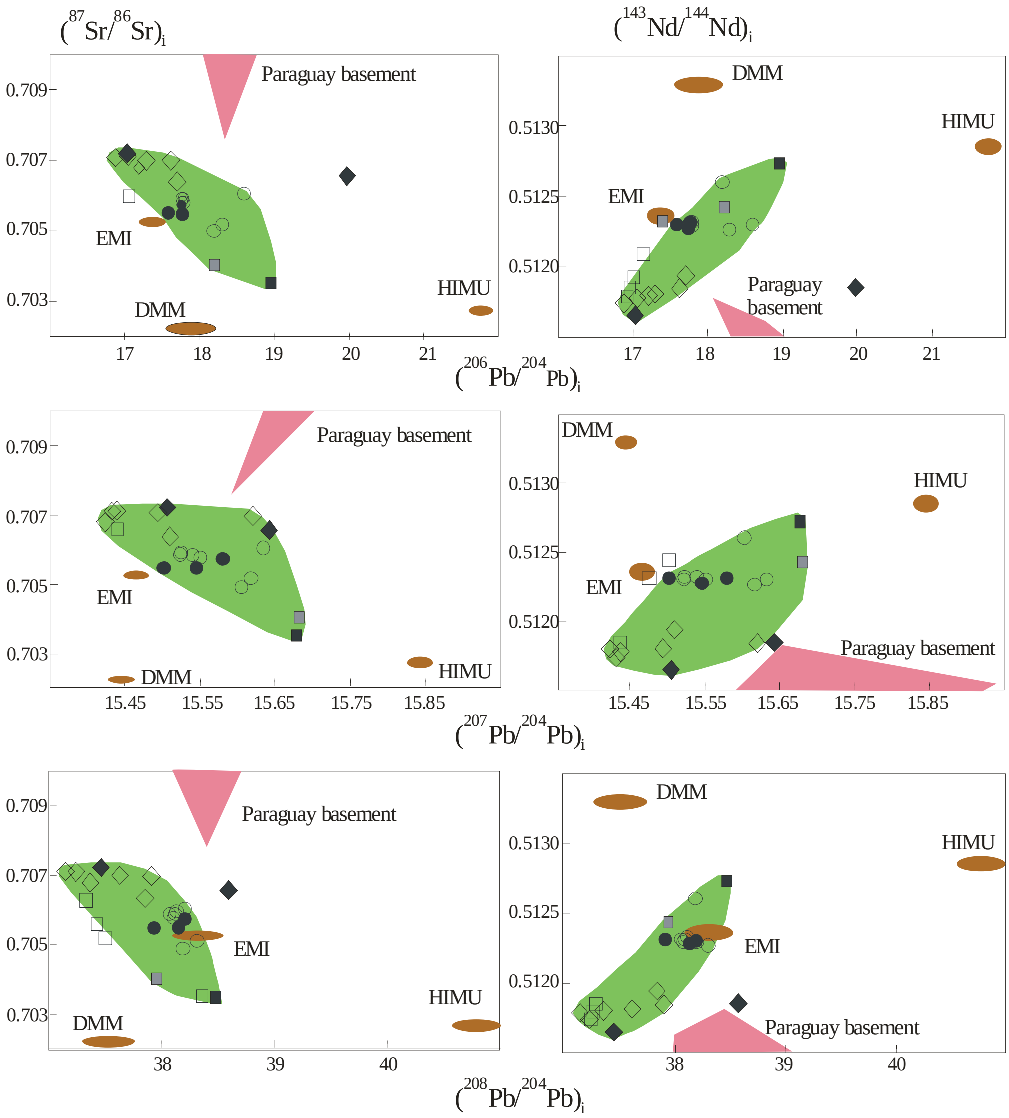


Fig. 5. Initial $^{206}Pb/^{204}Pb$, $^{207}Pb/^{204}Pb$ and $^{208}Pb/^{204}Pb$ vs. $Sr_i$ and $Nd_i$ diagrams for the Early Cretaceous to Tertiary alkaline rocks (green field) of Eastern Paraguay. DMM, HIMU and EMI fields after Hart & Zindler (1989). Symbols as in Fig. 3.

magmatism of Eastern Paraguay. However, the Pb isotopic compositions of some rocks (e.g. potassic rocks with highest $^{207}Pb/^{204}Pb$) tend towards the field of the basement rocks and, therefore, a partial contribution of crustal components can not be totally ruled out. The isotopic heterogeneity shown by the potassic magmatism, which represents extreme EMI compositions, could reflect old metasomatic events caused by small-volume melts with different U, Th and Pb ratios. Alternatively, the observed trends can be modelled by mixing process between the K-ASU magma (as defined by Comin-Chiaramonti *et al.*, 1997) with the lowest initial $^{206}Pb/^{204}Pb$ ratios and a HIMU magma. The calculated patterns (Fig. 6) show that 1) 10-30% of the HIMU end-member is consistent with the isotopic heterogeneity observed in the potassic magmatism; 2) the HIMU component appears dominant in the generation of the sodic magmatism. Notably, the proposed isotopic mixing model between K-ASU and HIMU-like magmas appear to be consistent also for reproducing some critical I.E. ratios of the sodic magmatism, e.g. Ba/Nb, La/Nb and Ti/Zr (Fig. 7).

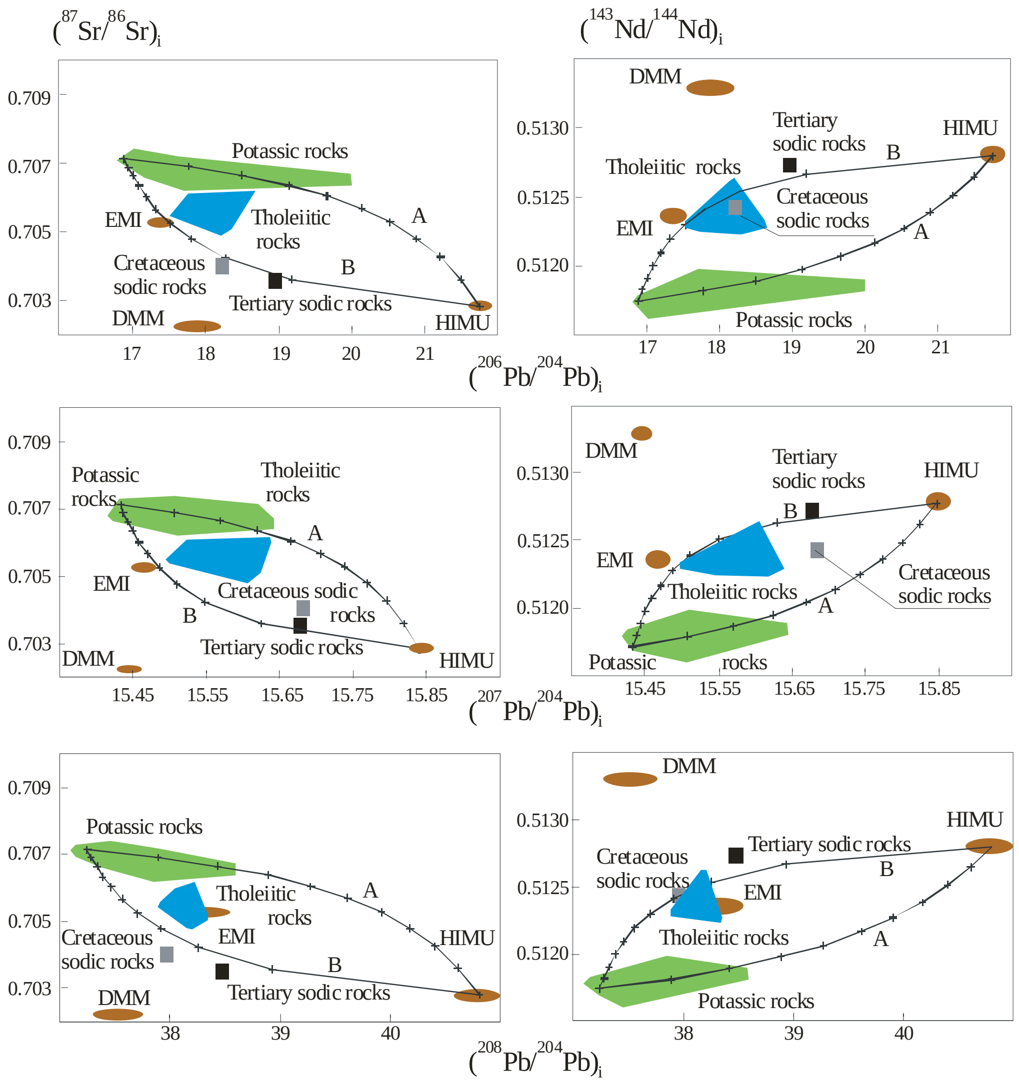


Fig. 6. Isotopic mixing curves between HIMU and potassic magma from the Asunción Sapucai graben (ASU), computed using the following isotopic composition: HIMU (St. Helena; Chaffey *et al.*, 1989); $^{87}Sr/^{86}Sr = 0.70282$, $^{143}Nd/^{144}Nd = 0.5130$, $^{206}Pb/^{204}Pb = 20.73$, $^{207}Pb/^{204}Pb = 15.77$ and $^{208}Pb/^{204}Pb = 40.80$; K-ASU; $^{87}Sr/^{86}Sr = 0.7071$, $^{143}Nd/^{144}Nd = 0.5117$, $^{206}Pb/^{204}Pb = 16.89$, $^{207}Pb/^{204}Pb = 15.43$, $^{208}Pb/^{204}Pb = 37.24$. The two curves differ for the Sr, Nd and Pb elemental concentrations (ppm) assumed in the end-members. A: HIMU; Sr = 650, Nd = 40, Pb = 4; K-ASU; Sr = 1300, Nd = 60, Pb = 2; B: HIMU; Sr = 678, Nd = 41, Pb = 2; K-ASU; Sr = 1317, Nd = 55, Pb = 15. Cross: 10% step of mixing. DMM, HIMU and EMI fields after Hart & Zindler (1989).

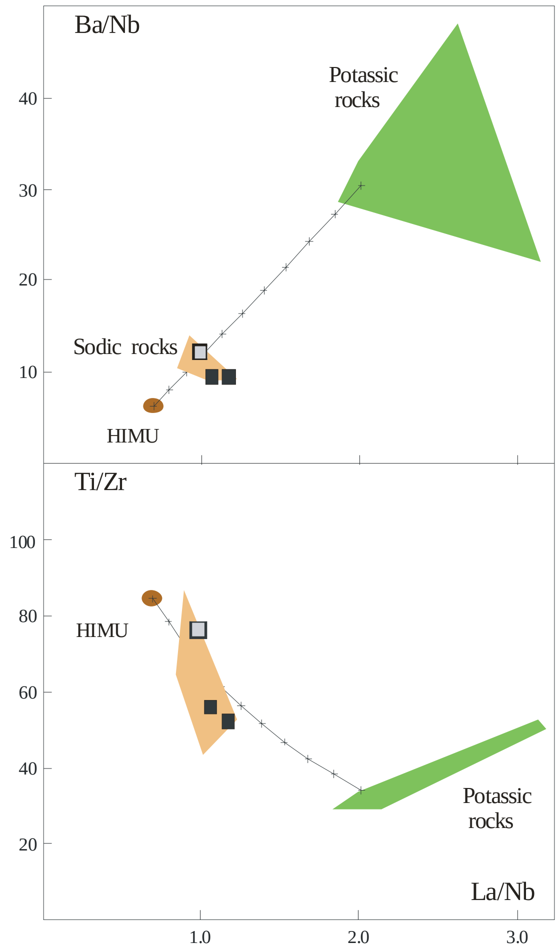


Fig. 7. La/Nb vs. Ba/Nb and Ti/Zr mixing curves between HIMU and potassic magma from the Asunción-Sapucai graben (ASU). Cross: 10% step of mixing. DMM, HIMU and EMI fields after Hart & Zindler (1989).

The Pb isotopes of the Early Cretaceous Brazilian tholeiites have been carefully studied by Marques *et al.* (1999). These authors interpreted the Sr-Nd-Pb isotopic relationships of the Brazilian tholeiites as owing to a prevalent EMI mantle component and to a possible EMII component, except for the low-Ti tholeiites from southern Brazil for which a major contribution of the EMII component is required. However, the Sr-Nd-Pb isotopic compositions of the investigated Paraguayan tholeiites suggest that HIMU could represent an important mantle component in the genesis of the Cretaceous tholeiites. The isotopic compositions of the studied Cretaceous tholeiites could be the result of mixing between K-ASU (extreme EMI type) and HIMU components. This indicates that a DMM component is not necessary to explain the isotopic compositions of the SGF Cretaceous tholeiites, even if a partial contribution of the DMM can not be rule out.

## CONCLUSIONS

Distinct magmatic events took place in Eastern Paraguay since Cretaceous time. During the Early Cretaceous, the potassic alkaline magmatism pre- and postdates the emissions of the Paraná Basin tholeiites. Since late Early Cretaceous to Tertiary, only sodic magmatism occurred in that area. The Sr-Nd-Pb isotopic data indicate that the two main mantle components could have been involved in the genesis of the Cretaceous to Tertiary magmatism in Eastern Paraguay: an extreme and heterogeneous EMI component, which was prevalent in the Cretaceous alkaline magmatism, and a HIMU component, which become more important in the Cretaceous and Tertiary sodic magmatism.

## ACKNOWLEDGEMENTS

This work has been financially supported by MURST 60%, COFIN 1998 and CNR (Contrib. n° 98.00243.CT05 and 98.00583.CT11) and by FAPESP (Proc. 01/10714-3).

## REFERENCES

Almeida, F.F.M. (1983). Relações tectônicas das rochas alcalinas mesozóicas de região meridional da Plataforma Sul-Americana. *Revista Brasileira de Geociências* **13**, 139-158.

Bell, K. & Tilton, G.R. (2001). Nd, Pb and Sr isotopic compositions of East African carbonatites: evidence for mantle mixing and plume inhomogeneity. *Journal of Petrology* **42**, 1927-1945.

Chaffey, D.J, Cliff, R.A. & Wilson, B.M. (1989). Characterization of the St Helena magma source. In: Sunders, D. & Norry, M.J. (eds.) *Magmatism in the ocean basins. Geological Society, Special Paper* **42**, 257-276.

Castorina, F., Petrini, R., Comin-Chiaramonti, P., Capaldi, G. & Pardini, G. (1996). Potassic magmatism from the Asunción-Sapucai Graben, Eastern Paraguay: inferences on mantle sources by Sr-Nd isotopic systematics. In: Comin-Chiaramonti, P. & Gomes, C.B. (eds.) *Alkaline* *magmatism in central-eastern Paraguay. Relationships with coeval magmatism in Brazil.* São Paulo: Edusp-Fapesp, pp. 195-206.

Comin-Chiaramonti, P. & Gomes, C.B. (eds.) (1996). *Alkaline magmatism in central-eastern Paraguay. Relationships with coeval magmatism in Brazil.* São Paulo: Edusp-Fapesp, 464p.

Comin-Chiaramonti P., Gomes, C.B., Censi, P., Gasparon, M. & Velázquez, J.C. (in this volume). Alkaline complexes from the Alto Paraguay Province at the border of Brazil (Mato Grosso do Sul State) and Paraguay.

Comin-Chiaramonti, P., Castorina, F., Cundari, A., Petrini, R. & Gomes, C.B. (1995). Dykes and sills from Eastern Paraguay: Sr and Nd isotope systematics. In: Baer, G. & Heimann, A. (eds.) *Physics and chemistry of dykes.* Rotterdam: Balkema, pp. 267-278.

Comin-Chiaramonti, P., Civetta, L., Petrini, R., Piccirillo, E.M., Bellini, G., Censi, P., Bitschene, P., Demarchi, G., De Min, A., Gomes, C.B., Castillo, A.M.C. & Velázquez, J.C. (1991). Tertiary nephelinitic magmatism in Eastern Paraguay: petrology, Sr-Nd isotopes and genetic relationships with associated spinel-peridotite xenoliths. *European Journal of Mineralogy* **3**, 507-525.

Comin-Chiaramonti, P., Cundari, A., De Graff, J.M., Gomes, C.B. & Piccirillo, E.M. (1999). Early Cretaceous-Tertiary magmatism in Eastern Paraguay (western Paraná basin): geological, geophysical and geochemical relationships. *Journal of Geodynamics* **28**, 375-391.

Comin-Chiaramonti P., Cundari, A., Gomes, C.B., Piccirillo, E.M., Censi, P., De Min, A., Bellieni, G., Velázquez, V.F. & Orué, D. (1992). Potassic dyke swarm in the Sapucai graben, Eastern Paraguay: petrographical, mineralogical and geochemical outlines. *Lithos* **28**, 283-310.

Comin-Chiaramonti, P., Cundari, A., Piccirillo, E.M., Gomes, C.B., Castorina, F., Censi, P., De Min, A., Marzoli, A., Speziale, S. & Velázquez, V.F. (1997). Potassic and sodic igneous rocks from Eastern Paraguay: their origin from the lithospheric mantle and genetic relationships with the associated Paraná flood tholeiites. *Journal of Petrology* **38**, 495-528.

Eby, N.G. & Mariano, A.N. (1986). Geology and geochronology of carbonatites peripheral to the Paraná Basin, Brazil-Paraguay. *Carbonatites Symposium*, *Ottawa*, 13p.

Faure, G. (1986). *Principles of isotope geology*. New York: J. Wiley & Sons, 589p.

Fúlfaro, V.J. (1996). Geology of Eastern Paraguay. In: Comin-Chiaramonti, P. & Gomes, C.B. (eds.) *Alkaline magmatism in central-eastern Paraguay. Relationships with coeval magmatism in Brazil.* São Paulo: Edusp-Fapesp, pp. 17-30.

Gibson, S.A., Thompson, R.N., Dickin, A.P. & Leonardos, O.H. (1995). High-Ti and low-Ti mafic potassic magmas: key to plume-lithosphere interactions and continental flood-basalt genesis. *Earth and Planetary Science Letters* **136**, 149-165.

Gomes, C.B., Laurenzi, M.A., Censi, P., De Min, A., Velázquez, V.F. & Comin-Chiaramonti, P. (1996). Alkaline magmatism from northern Paraguay (Alto Paraguay): a Permo-Triassic Province. In: Comin-Chiaramonti, P. & Gomes, C.B. (eds.) *Alkaline magmatism in central-eastern Paraguay. Relationships with coeval magmatism in Brazil.* São Paulo: Edusp-Fapesp, pp. 223-230.

Hart, S.R. (1984). A large scale isotopic anomaly in the Southern Hemisphere mantle. *Nature* **309**, 753-757.

Hart, S.R. & Zindler, A. (1989). Constraints on the nature and the development of chemical heterogeneities in the mantle. In: Peltier, W.R. (ed.) *Mantle convection plate tectonics and global dynamics.* New York: Gordon and Breach Sciences Publishers, pp. 261-388.

Hart, S.R., Gerlach, D.C. & White, W.M. (1986). A possible new Sr-Nd-Pb mantle array and consequences for mantle mixing. *Geochimica et Cosmochimica Acta* **50**, 1551-1557.

Hergt, J.M., Peate, D.W. & Hawkesworth, C.J. (1991). The petrogenesis of Mesozoic Gondwana low-Ti flood basalts. *Earth and Planetary Sciences Letters* **105**, 134-148.

Marques, L.S., Duprè, B. & Piccirillo E.M. (1999). Mantle source compositions of the Paraná Magmatic Province (southern Brazil): evidence from trace element and Sr-Nd-Pb isotope geochemistry. *Journal of Geodynamics* **28**, 439-458.

Maury, R., Defant, C. & Joron, M.J. (1992). Metasomatism of the sub-arc mantle inferred from trace elements in Philippine xenoliths. *Nature* **360**, 661.

McKenzie, D.P. & O'Nions, M.J. (1995). The source regions of ocean island basalts. *Journal of Petrology* **36**, 133-159.

Petrini, R., Civetta, L., Piccirillo, E.M., Bellieni, G., Comin-Chiaramonti, P., Marques, L.S. & Melfi, A.J. (1987). Mantle heterogeneity and crustal contamination in the genesis of low-Ti continental flood basalts from the Paraná plateau (Brazil): Sr-Nd isotope and geochemical evidence. *Journal of Petrology* **28**, 701-726.

Piccirillo, E.M. & Melfi, A.J. (eds.) (1988). *The Mesozoic flood volcanism of the Paraná Basin: petrogenetic and geophysical aspects.* São Paulo: IAG-USP, 600p.

Piccirillo, E.M., Comin-Chiaramonti, P., Bellieni, G., Civetta, L., Marques, L.S., Melfi, A.J., Petrini, R., Raposo, M.I.B. & Stolfa, D. (1988).

Petrogenetic aspects of continental flood basalt-rhyolite suites from the Paraná Basin (Brazil). In: Piccirillo, E.M. & Melfi, A.J. (eds.) *The Mesozoic flood volcanism of the Paraná Basin: petrogenetic and geophysical aspects.* São Paulo: IAG-SP, pp. 179-205.

Renne, P.R., Ernesto, M., Pacca, I.G., Coe, R.S., Glen, J.M., Prevot, M. & Perrin, M. (1992). The age of Paraná flood volcanism, rifting of Gondwananland, and Jurassic-Cretaceous boundary. *Science* **258**, 975-979.

Riccomini, V., Velázquez, V.F. & Gomes, C.B. (2001). Cenozoic lithospheric faulting in the Asunción Rift, Eastern Paraguay. *Journal of South American Earth Sciences* **14**, 625-630.

Sun, S.S. & McDonough, W.F. (1989). Chemical and isotopic systematics of oceanic basalts. In: Sunders, D. & Norry, M.J. (eds.) *Magmatism in the ocean basins*. *Geological Society of London, Special Publication* **42**, pp. 313-345.

Velázquez, V.F., Gomes, C.B., Orué, D. & Comin-Chiaramonti, P. (1996). Magmatismo alcalino do Paraguai: uma revisão e atualização das províncias. *Boletim do Instituto de Geociências da USP, Série Científica* **27**, 61-79.

Velázquez, V.F., Riccomini, C., Gomes, C.B., Figueredo, L. & Figueredo, C. (1998). Relações tectônicas do magmatismo alcalino do Paraguai Oriental. *Revista do Instituto Geológico de São Paulo* **19**, 43-49.

*Mesozoic to Cenozoic Alkaline Magmatism in the Brazilian Platform*
*Comin-Chiaramonti, P. & Gomes, C.B. (eds.)*
*Edusp/Fapesp, São Paulo, pp. 57-69, 2005*

# ALKALINE COMPLEXES FROM THE ALTO PARAGUAY PROVINCE AT THE BORDER OF BRAZIL (MATO GROSSO DO SUL STATE) AND PARAGUAY

*P. Comin-Chiaramonti, C.B. Gomes, P. Censi, M. Gasparon and V.F. Velázquez*

*The Alto Paraguay Province, at the northwesternmost side of the Paraná Basin l.s., consists of a series of almost seven circular and elliptical Na-alkaline intrusive-effusive complexes and scarce dykes. The alkaline rocks are res-tricted to a narrow N-S trending belt that has been traced for nearly 40 km along the Paraguay river. $^{40}Ar/^{39}Ar$ biotite ages (241±1Ma) have shown that the complexes were emplaced during Early Triassic times and repre-sent the oldest magmatic alkaline activity since Brasiliano cycle around the Paraná Basin. The rock-types are evoluted, prevailing silica-undersaturated agpaitic syenites, hypersolvus varieties, and phonolites. Subordinate silica-undersaturated and silica-oversaturated syenites, trachyphonolites and rhyolites are charac-terized by plagioclase and/or modal normative quartz. On the whole, the geochemical characteristics are quite similar: in particular, Eu negative anomalies point to a parent magma (basanite/theralite) subjected to plagio-clase fractionation. Sr-Nd isotope systematics highlight the possibility of contamination by almost 10% of upper crust for some silica-oversaturated rock-types. In contrast, the undersaturated rocks show no evidence of crustal influence, and isotope results cluster in a tendentiously depleted source with a model age 747±47 Ma old.*

## INTRODUCTION

The alkaline complexes from the Alto Paraguay Province (APP, cf. Gomes *et al*., 1996a; Velázquez *et al*., 1996a, b) form a narrow N-S belt along the Paraguay river between 21°00' and 23°35' lat S, and 57°10' and 58°00' long W, approximately. They are cropping out in the Pleistocenic Pantanal Formation (Oliveira & Leonardos, 1943) at the westernmost side of the Paraná Basin, and at the northwestern side of the Eastern Paraguay (Fig. 1; cf. Comin-Chiaramonti *et al*., 1997).

The belt may be traced for nearly 40 km between the Mato Grosso do Sul state (Brazil) and north-eastern Paraguayan Chaco in the Asunción Arch (cf. Piccirillo & Melfi, 1988; Comin-Chiaramonti *et al*., 1997, and therein references). It represents a structural lineament seismically active, as are the other structural lineaments along which the Brazilian alkaline complexes can be found (Berrocal & Fernandes, 1996). The APP alkaline rocks extend between the crystalline Amoguijá Group (Alumiador granite, Rb/Sr isochron: 1600±40 Ma; cf. Araújo *et al*., 1982) and the Rio Apa complex (granitic and gneissic rocks, Rb/Sr data: 1654±50 Ma; amphibolites, K/Ar data: 1302±62 Ma; cf. Araújo *et al*., 1982), at approximately 28 and 65 km west of Porto Murtinho, respectively, and the Meso-Proterozoic rhyolites of Fuerte Olimpo, about 60 km north of Porto Murtinho (Rb/Sr isochron: 1341±53

Ma, Velázquez *et al.*, 1996a; Gomes *et al.*, 2000). The southern regions are mainly formed by the Eocambrian sediments of Itapucumí Group (Wiens, 1986; inset B of Fig. 1). On the whole, the region corresponds to the southernmost tip of the Amazon Craton (Província Tapajós, Sub-Província Madeira of Amaral, 1984; Teixeira *et al.*, 1989; inset A of Fig. 1).

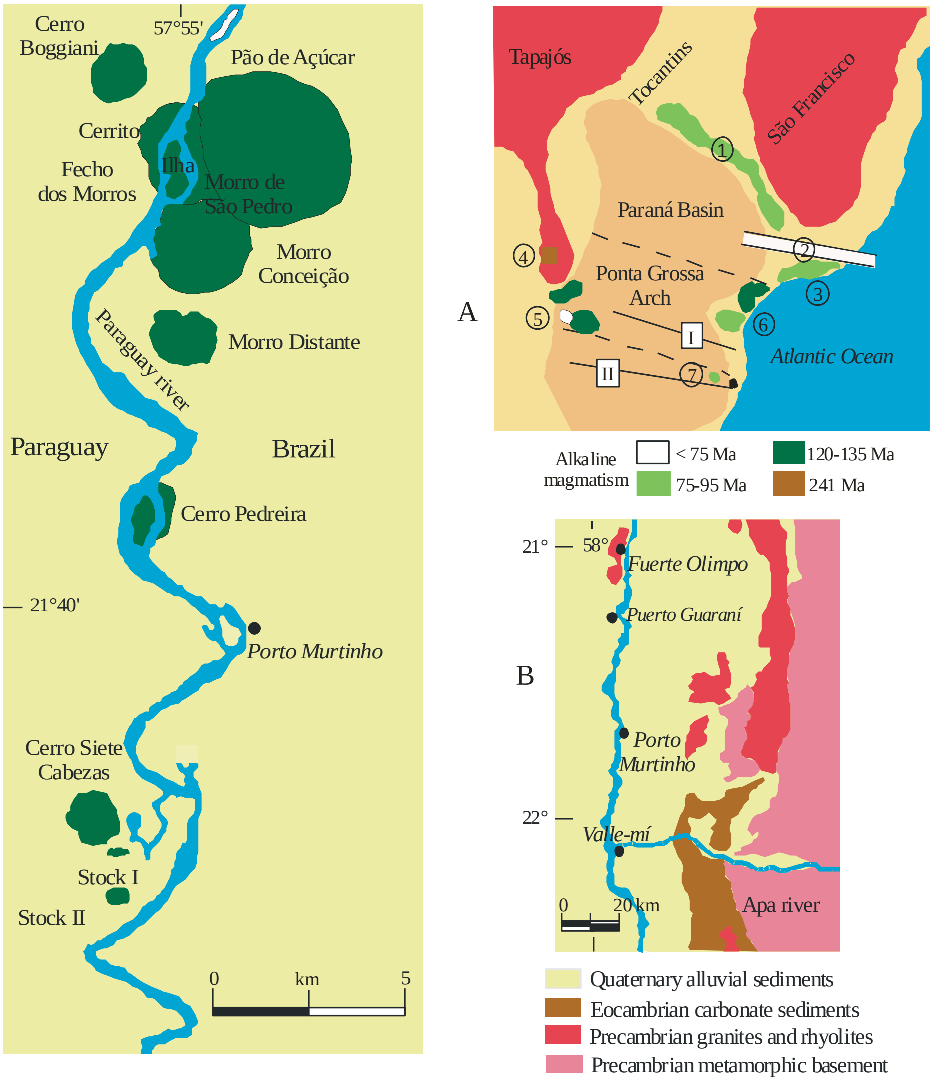


Fig. 1. Sketch map showing the main alkaline occurrences from the Alto Paraguay Province (after Velázquez *et al.*, 1996b, modified). Inset A: Schematic structural map representing the alkaline areas in and around the Paraná Basin (modified after Almeida, 1983; Trompette, 1994; Gomes *et al.*, 1996b); legend: 1) Alto Paranaíba; 2) Taiúva-Cabo Frio Lineament; 3) Ribeira Belt; 4) Alto Paraguay; 5) Paraguay; 6) Ponta Grossa Arch; 7) Santa Catarina State; I, II: Piquirí and Uruguay Lineaments, respectively. Inset B: Geological sketch map of the Alto Paraguay region; data source: Araújo *et al.* (1982) and Wiens (1986).

From a general point of view, the Alto Paraguay complexes, having an age of 241 Ma ($^{40}$Ar/$^{39}$Ar biotite preferred age; cf. Velázquez *et al.*, 1996a), represent the oldest alkaline occurrences linked to the Paraná Basin l.s.

They are mostly characterized by the presence of silica-oversaturated to silica-undersaturated, miaskitic and agpaitic rock-types, both within individual complexes as well as in the region as a whole. There has been considerable discussion in the literature dealing with the mechanism by which such silica-undersaturated and silica-oversaturated rocks may form from a common parental magma. This is constrained by the presence of the "alkali feldspar thermal divide" in the "Petrogeny's Residua System" (Bowen, 1937; Fudali, 1963). Velázquez *et al.*

(1998) cited the Alto Paraguay complexes as a possible example of magmas crossing that barrier by fractional crystallization processes. However, other processes, like crustal melting or assimilation of upper crustal material, and the effects of fluid activity during both the magmatic and sub-solidus stages, must also be considered. It is, of course, conceivable that silica-oversaturated and silica-undersaturated rocks are related by different mechanisms in different complexes.

Relevant petrogenetical constraints are the characteristics of the crystalline basement as a possible source of contamination of the magma(s) and the typology of the magmatic bodies.

The Alto Paraguay Province consists of at least seven major circular complexes, as inferred from field work and photointerpretation data (cf. Araújo *et al.*, 1982), i.e. Cerro Siete Cabezas, Cerro Pedreira, Morro Distante, Morro Conceição, Fecho dos Morros, Pão de Açúcar and Cerro Boggiani, some minor occurrences and a few dykes (Fig. 1). Intrusive rock-types are dominant, except for the Pão de Açúcar complex which is largely formed by a large volcanic field.

The major occurrences, as grouped below, will be discussed on the basis of mineralogical, petrological, geochemical and isotopical data:

1) Cerro Siete Cabezas and associated Stocks I and II;
2) Cerro Pedreira, Morro Distante and Morro Conceição;
3) Fecho dos Morros (Cerrito, Ilha Fecho dos Morros, Morro de São Pedro);
4) Pão de Açúcar volcanic field;
5) Cerro Boggiani.

## 1. CERRO SIETE CABEZAS

Cerro Siete Cabezas constitutes the southermost complex of the Alto Paraguay Province. It is circular in shape, with a central depression evidencing cauldron subsidence, and it is found associated with two minor bodies (Stock I and Stock II of Fig. 1). The circular intrusion covers an area of approximately 4 $km^2$ (Fig. 2), rising up to 248 m high above the sea level (158 m above the alluvial plain of the Paraguay river), and it is characterized by silica-undersaturated medium to coarse-grained syenitic rocks. Stock I forms an elongated body (1.0x0.2 km), 138 m high, with prevailing quartz-bearing rocks. Stock II is a circular body of about 0.4 $km^2$, 120 m high, and formed by coarse-grained syenitic quartz- or nepheline-bearing rock-types.


Fig. 2. Sketch map showing the Cerro Siete Cabezas circular complex and the Stock I.

## PETROGRAPHY

Representative modal analyses are given in Table 1. The common feature of mostly rocks is the abundance of alkali feldspar, mainly as simple-twinned mesoperthites. The exsolution texture varies from moderately fine vein perthites to coarsely exsolved patch perthites. Typically, nepheline occurs as euhedral or subhedral crystals, sometimes altered to cancrinite in rock-types from Cerro Siete Cabezas and in a few samples from Stock II. Stock I is characterized by prevailing quartz-bearing (modal quartz of 2% up to 20%), and scarce nepheline-bearing rock-types, respectively. Stock II is also characterized by prevailing quartz-bearing rocks, but in this case the mineral is present in constant amount (about 1-3%); subordinate nepheline-bearing rocks contain nepheline up to 20%. Plagioclase (An>5) is virtually absent. The main mafic mineral is amphibole, which is found associated with a green clinopyroxene and biotite in variable amounts and sometimes forming clusters and/or complex intergrowths. Opaques (magnetite and ilmenite) are ubiquitous. Many rock-types have as accessories apatite, titanite, zircon and fluorite. Eudialyte is a common phase in the Cerro Siete Cabezas complex. The rocks show variable degree of subsolidus (hydrothermal) alteration, as indicated by clouding of the K-feldspar component of the perthites, occurrence of coarse patch perthites, albite rims, interlocking crystal boundaries of feldspars, and recrystallization of clinopyroxene into brown-green amphibole. The latter often displays patchy blue-green regions at the crystal margins, or is related to tiny fractures within the grains.

On the whole, the petrography outlines an alkaline-peralkaline association with prevailing silica-undersaturated rocks and subordinate oversaturated variants.

Classification and nomenclature

The modal mineral content using the Streckeisen's QAPF diagram (in Le Maitre, 1989) allows to classify the whole population from Cerro Siete Cabezas and associated stocks as foid syenites (Cerro Siete Cabezas, 40%; Stock II, 2%), foid-bearing alkali feldspar syenites (Cerro Siete Cabezas, 15%; Stock II, 4%), alkali feldspar syenites to quartz-alkali feldspar syenites (Stock I, 19%; Stock II, 20%). Following the petrochemical nomenclature of De La Roche *et al.* (1980; cf. $R_1$-$R_2$ inset A of Fig. 3), the analyzed rocks (Table 2) range from nepheline syenites to syenites, quartz syenites and alkali granites, the two latter present only in Stock I.

Using the serial discriminant diagram (Le Maitre 1989; Comin-Chiaramonti & Gomes, 1996; cf. inset $Na_2O$ vs. $K_2O$ inset B of Fig. 3), it is apparent that most of the samples from the Cerro Siete Cabezas complex fall into the sodic field, whereas the Stock I rock-types are in the transitional field; the Stock II rocks straddle the field of Cerro Siete Cabezas and Stock I. Similarly, the Alkali Index [A.I. = molar $(Na_2O+K_2O)/Al_2O_3$] vs. Q-ne normative diagram (Fig. 3) defines a very well constrained under-saturated, tendentiously peralkaline, suite for Cerro Siete Cabezas: 85% of the samples have A.I. ranging from 1.0 to 1.2, normative nepheline between 2.5 and 18%; 15% of the samples show A.I. in the range 0.93-0.99, normative nepheline 2.6-8.5%, normative anorthite 0.5-3.3%, i.e. "miaskitic" tendency. The two stocks tend towards the silica-oversaturation: Stock I, A.I. 0.98-1.04, normative quartz 0-23.6%; Stock II, A.I. 1.01-1.10, normative quartz 1-4% in 75% of the samples, normative nepheline 2-20% in 25% of the samples (cf. Table 2).

Table 1. Representative modal analyses of selected rocks from Cerro Siete Cabezas, Stock I and Stock II. Abbreviations: Q, quartz; AF, alkali feldspar; Ne, nepheline; Cpx, clinopyroxene; Am, amphibole; Bi, biotite; Op, opaques (magnetite and ilmenite); Ap, apatite. Accessory phases: titanite, eudialyte, zircon and fluorite.

| | CERRO SIETE CABEZAS | | | | | STOCK I | | | STOCK II | | |
|---|---|---|---|---|---|---|---|---|---|---|---|
| Sample | RP-62 | RP-72 | RP-74 | RP-231 | RP-232 | RP-44 | RP-45 | RP-50 | RP-52 | RP-56 | RP-58 |
| vol% | | | | | | | | | | | |
| Q | | | | | | 2.0 | 16.5 | 1.0 | | 1.0 | 1.7 |
| AF | 72.6 | 69.0 | 71.0 | 65.6 | 60.0 | 87.2 | 76.3 | 88.6 | 86.1 | 91.3 | 90.2 |
| Ne | 6.5 | 10.1 | 9.2 | 9.0 | 17.7 | | | | | | |
| Cpx | 4.6 | 11.5 | 6.0 | 6.4 | 5.9 | 1.5 | 2.8 | 3.6 | 0.5 | 2.0 | 0.3 |
| Am | 10.6 | 1.7 | 3.0 | 8.2 | 8.7 | 5.8 | 1.1 | 1.8 | 9.5 | 7.1 | 5.0 |
| Bi | 3.1 | 3.8 | 8.0 | 4.5 | 3.4 | 1.1 | 0.9 | 1.6 | 1.2 | | 0.2 |
| Op | 1.0 | 1.9 | 1.0 | 3.1 | 0.9 | 0.8 | 0.4 | 1.0 | 0.5 | 1.2 | 1.0 |
| Ap | 0.5 | 1.0 | 0.5 | 1.5 | 1.9 | | | 0.5 | 0.1 | | |
| Accessories | 1.1 | 1.0 | 1.3 | 1.7 | 1.4 | 1.6 | 2.0 | 1.9 | 2.1 | 0.2 | 1.6 |

Table 2. Major element analyses, norms and classification (according to De La Roche *et al.*, 1980) of selected rocks from Cerro Siete Cabezas, Stock I and Stock II. A.I., agpaitic index: molar ratio $(Na_2O+K_2O)/Al_2O_3$; D.I.*, normative Q+or+ab+ne+ac; Q-ne-ks: recalculated to 100% values (wt%) relative to normative Q+or+ab+ne.

| | CERRO SIETE CABEZAS | | | | | | | | | | | | | |
|---|---|---|---|---|---|---|---|---|---|---|---|---|---|---|
| Sample | RP-61 | RP-62 | RP-63 | RP-64 | RP-65 | RP-66 | RP-67 | RP-68 | RP-69 | RP-70 | RP-71 | RP-72 | RP-74 | RP-75 |
| wt% | | | | | | | | | | | | | | |
| $SiO_2$ | 60.85 | 61.06 | 60.79 | 58.38 | 62.35 | 62.26 | 59.13 | 60.40 | 60.28 | 60.34 | 61.65 | 58.49 | 62.22 | 60.10 |
| $TiO_2$ | 0.80 | 0.84 | 0.78 | 1.18 | 0.75 | 0.69 | 1.14 | 0.75 | 0.82 | 0.85 | 0.62 | 1.11 | 0.58 | 0.93 |
| $Al_2O_3$ | 17.78 | 17.80 | 17.88 | 17.37 | 17.31 | 17.60 | 16.56 | 17.71 | 17.69 | 17.09 | 17.73 | 17.52 | 17.65 | 17.29 |
| $Fe_2O_3$ | 1.13 | 1.59 | 1.49 | 2.43 | 1.60 | 1.23 | 2.46 | 1.83 | 2.20 | 2.50 | 1.37 | 2.16 | 1.41 | 2.48 |
| FeO | 3.05 | 2.63 | 2.50 | 3.07 | 2.02 | 1.77 | 3.08 | 2.18 | 2.03 | 2.32 | 2.29 | 3.07 | 2.47 | 2.75 |
| MnO | 0.19 | 0.19 | 0.18 | 0.22 | 0.16 | 0.13 | 0.25 | 0.18 | 0.19 | 0.22 | 0.19 | 0.20 | 0.22 | 0.24 |
| MgO | 0.76 | 0.77 | 0.71 | 1.70 | 0.78 | 0.66 | 1.28 | 0.76 | 0.80 | 1.09 | 0.51 | 1.31 | 0.57 | 1.08 |
| CaO | 1.95 | 1.86 | 1.81 | 2.40 | 1.31 | 1.04 | 2.37 | 1.97 | 1.95 | 1.62 | 1.16 | 3.09 | 1.04 | 2.09 |
| $Na_2O$ | 8.02 | 7.91 | 8.16 | 7.16 | 7.08 | 7.22 | 6.81 | 8.20 | 7.96 | 7.83 | 8.25 | 7.37 | 8.30 | 7.78 |
| $K_2O$ | 4.76 | 4.86 | 4.80 | 4.99 | 5.49 | 5.31 | 4.57 | 5.04 | 4.89 | 4.97 | 5.08 | 3.85 | 5.28 | 4.18 |
| $P_2O_5$ | 0.33 | 0.35 | 0.34 | 0.62 | 0.24 | 0.20 | 0.55 | 0.35 | 0.37 | 0.33 | 0.23 | 0.66 | 0.25 | 0.47 |
| L.O.I. | 0.24 | 0.22 | 0.41 | 0.34 | 0.48 | 0.81 | 1.05 | 0.47 | 0.67 | 0.71 | 0.58 | 1.01 | 0.10 | 0.10 |
| Sum | 99.86 | 100.08 | 99.85 | 99.86 | 99.57 | 98.92 | 99.25 | 99.84 | 99.85 | 99.87 | 99.66 | 99.84 | 100.09 | 99.79 |
| or | 28.13 | 28.72 | 28.39 | 29.49 | 32.44 | 31.38 | 27.01 | 29.79 | 29.13 | 29.66 | 30.02 | 22.75 | 31.20 | 26.47 |
| ab | 48.90 | 50.26 | 46.60 | 45.95 | 53.40 | 56.42 | 52.83 | 44.02 | 47.42 | 46.60 | 51.07 | 52.59 | 49.89 | 51.80 |
| an | | | | 0.52 | | | 1.12 | | | | | 3.35 | | |
| ne | 8.70 | 7.71 | 11.96 | 7.92 | 2.75 | 2.46 | 2.60 | 10.30 | 9.17 | 7.70 | 3.98 | 5.30 | 6.23 | 6.60 |
| ac | 2.56 | 2.14 | 3.33 | | 1.27 | 0.11 | | 4.63 | 3.15 | 4.86 | 3.96 | | 4.97 | 1.62 |
| ns | | | | | | | | 0.08 | | 0.13 | 1.60 | | 0.97 | |
| di | 6.40 | 5.84 | 5.33 | 5.94 | 4.13 | 3.17 | 5.76 | 6.30 | 6.20 | 5.02 | 3.64 | 6.28 | 3.00 | 6.02 |
| ol | 2.30 | 1.54 | 1.80 | 2.49 | 1.96 | 1.06 | 1.88 | 1.36 | 1.90 | 3.63 | 2.22 | 1.58 | 2.90 | 1.54 |
| mt | 0.35 | 1.23 | 0.49 | 3.52 | 1.69 | 1.73 | 3.57 | | 0.55 | | | 3.13 | | 2.78 |
| il | 1.52 | 1.60 | 1.49 | 2.24 | 1.42 | 1.31 | 2.16 | 1.42 | 1.57 | 1.63 | 1.18 | 2.11 | 1.10 | 1.77 |
| ap | 0.78 | 0.83 | 0.95 | 1.47 | 0.55 | 0.46 | 1.27 | 0.81 | 0.87 | 0.78 | 0.53 | 1.53 | 0.59 | 1.11 |
| A.I. | 1.03 | 1.03 | 1.04 | 0.99 | 1.02 | 1.00 | 0.98 | 1.07 | 1.04 | 1.07 | 1.08 | 0.93 | 1.10 | 1.02 |
| D.I.* | 88.3 | 88.8 | 90.3 | 83.4 | 89.9 | 90.4 | 82.4 | 88.7 | 88.9 | 88.8 | 89.0 | 80.6 | 92.3 | 86.5 |
| $R_1$ | -42 | -12 | -98 | 3 | 240 | 244 | 275 | -193 | -87 | -72 | -125 | 211 | -157 | 30 |
| $R_2$ | 595 | 586 | 580 | 682 | 518 | 489 | 642 | 596 | 595 | 563 | 497 | 739 | 486 | 616 |
| Rock-type | Nephel-syenite | Nephel-syenite | Nephel-syenite | Nephel-syenite | Nephel-syenite | Nephel-syenite | Nephel-syenite | Nephel-syenite | Nephel-syenite | Nephel-syenite | Nephel-syenite | Nephel-syenite | Nephel-syenite | Nephel-syenite |
| Q | 40.3 | 40.9 | 37.4 | 40.5 | 43.4 | 43.4 | 43.5 | 39.3 | 40.0 | 40.7 | 42.7 | 42.1 | 41.6 | 41.4 |
| ne | 41.0 | 40.3 | 41.4 | 39.4 | 35.8 | 36.8 | 37.9 | 40.6 | 40.7 | 39.2 | 37.2 | 41.9 | 38.1 | 40.8 |
| ks | 18.7 | 18.8 | 21.2 | 20.1 | 20.8 | 19.8 | 18.6 | 20.1 | 19.3 | 20.1 | 20.1 | 16.0 | 20.3 | 17.8 |

| Sample | RP-230 | RP-231 | RP-232 | RP-235 | RP-236 | RP-237 | RP-238 | RP-240 | RP-241 | RP-242 | RP-244 | RP-246 |
|---|---|---|---|---|---|---|---|---|---|---|---|---|
| wt% | | | | | | | | | | | | |
| $SiO_2$ | 58.75 | 58.21 | 54.15 | 60.77 | 57.12 | 57.48 | 57.85 | 58.88 | 57.29 | 58.86 | 55.68 | 63.66 |
| $TiO_2$ | 0.80 | 0.85 | 1.62 | 0.75 | 1.05 | 0.88 | 0.70 | 0.91 | 1.06 | 1.02 | 1.28 | 0.39 |
| $Al_2O_3$ | 18.38 | 18.29 | 15.70 | 17.28 | 17.67 | 18.11 | 18.28 | 17.61 | 17.72 | 17.11 | 17.50 | 17.57 |
| $Fe_2O_3$ | 1.49 | 1.73 | 3.26 | 1.72 | 2.26 | 2.62 | 1.87 | 1.97 | 2.00 | 2.70 | 2.90 | 1.36 |
| FeO | 2.12 | 2.31 | 5.42 | 2.46 | 2.50 | 1.31 | 1.86 | 2.18 | 2.15 | 2.48 | 2.63 | 0.96 |
| MnO | 0.16 | 0.18 | 0.43 | 0.21 | 0.19 | 0.16 | 0.17 | 0.16 | 0.18 | 0.24 | 0.20 | 0.12 |
| MgO | 1.08 | 1.14 | 2.75 | 0.95 | 1.56 | 1.22 | 0.76 | 1.35 | 1.63 | 1.54 | 1.98 | 0.30 |
| CaO | 1.74 | 1.96 | 3.96 | 1.49 | 2.48 | 2.25 | 1.93 | 1.81 | 2.34 | 1.16 | 3.29 | 0.62 |
| $Na_2O$ | 9.85 | 9.78 | 6.42 | 7.92 | 8.78 | 10.01 | 10.37 | 8.74 | 9.55 | 7.28 | 8.25 | 8.23 |
| $K_2O$ | 4.36 | 4.22 | 4.35 | 5.30 | 4.48 | 4.20 | 4.54 | 4.68 | 4.10 | 5.87 | 4.13 | 5.48 |
| $P_2O_5$ | 0.34 | 0.37 | 1.13 | 0.26 | 0.54 | 0.44 | 0.30 | 0.37 | 0.50 | 0.29 | 0.68 | 0.08 |
| L.O.I. | 0.48 | 0.60 | 0.38 | 0.81 | 0.57 | 0.75 | 0.70 | 0.45 | 0.68 | 0.94 | 0.95 | 0.38 |
| Sum | 99.55 | 99.64 | 99.57 | 99.92 | 99.20 | 99.43 | 99.83 | 99.11 | 99.20 | 99.49 | 99.47 | 99.15 |
| or | 25.77 | 24.94 | 25.71 | 31.32 | 26.48 | 24.81 | 26.83 | 27.66 | 24.23 | 34.69 | 24.41 | 32.39 |
| ab | 41.99 | 40.58 | 38.57 | 45.11 | 36.26 | 36.83 | 36.68 | 41.69 | 38.75 | 38.92 | 38.39 | 54.45 |
| an | | | 1.17 | | | | | | | | | |
| ne | 15.32 | 16.26 | 8.54 | 7.73 | 16.08 | 17.85 | 17.37 | 12.37 | 16.02 | 8.89 | 15.51 | 2.93 |
| ac | 4.31 | 5.00 | | 4.98 | 6.54 | 7.58 | 5.41 | 5.70 | 5.79 | 5.53 | 2.46 | 3.93 |
| ns | 1.91 | 1.51 | | 0.46 | 0.22 | 1.47 | 2.99 | 0.69 | 1.38 | | | 1.24 |
| di | 5.32 | 6.07 | 9.11 | 4.78 | 7.22 | 6.68 | 6.37 | 5.49 | 6.80 | 3.16 | 9.49 | 2.15 |
| ol | 2.15 | 2.21 | 5.68 | 2.70 | 2.60 | 0.77 | 0.95 | 2.57 | 2.39 | 3.62 | 1.29 | 0.75 |
| mt | | | 4.73 | | | | | | | 1.15 | 2.97 | |
| il | 1.52 | 1.61 | 3.08 | 1.42 | 1.99 | 1.67 | 1.32 | 1.73 | 2.01 | 1.94 | 2.13 | 0.74 |
| ap | 0.79 | 0.86 | 2.62 | 0.60 | 1.25 | 1.02 | 0.69 | 0.86 | 1.16 | 0.67 | 1.57 | 0.19 |
| A.I. | 1.14 | 1.13 | 0.97 | 1.09 | 1.09 | 1.16 | 1.20 | 1.10 | 1.14 | 1.07 | 1.03 | 1.11 |
| D.I.* | 87.4 | 86.8 | 72.8 | 89.1 | 85.4 | 87.1 | 86.3 | 87.4 | 84.8 | 88.0 | 80.8 | 93.7 |
| $R_1$ | -721 | -711 | 36 | -134 | -513 | -832 | -1006 | -409 | -671 | -199 | -365 | -34 |
| $R_2$ | 600 | 625 | 868 | 546 | 689 | 657 | 603 | 606 | 679 | 536 | 794 | 426 |
| Rock-type | Nepheline syenite | Nepheline syenite | Nepheline syenite | Nephel-syenite | Nepheline syenite | Nepheline syenite | Nepheline syenite | Nepheline syenite | Nepheline syenite | Nephel-syenite | Nepheline syenite | Nephel-syenite |
| Q | 36.6 | 35.9 | 39.5 | 40.6 | 35.6 | 34.7 | 35.1 | 38.0 | 35.7 | 39.8 | 35.7 | 43.4 |
| ne | 45.8 | 46.8 | 40.4 | 38.2 | 45.3 | 47.6 | 39.9 | 42.8 | 46.8 | 36.3 | 46.1 | 36.1 |
| ks | 17.6 | 17.3 | 20.1 | 21.2 | 19.1 | 17.7 | 18.9 | 19.2 | 17.5 | 23.9 | 17.2 | 20.5 |

Table 2 (continued).

| | STOCK I | | | | | | | |
|---|---|---|---|---|---|---|---|---|
| Sample | RP-44 | RP-45 | RP-46 | RP-47 | RP-48 | RP-49 | RP-50 | RP-51 |
| wt% | | | | | | | | |
| $SiO_2$ | 64.75 | 66.53 | 64.66 | 72.33 | 63.53 | 66.83 | 62.89 | 64.35 |
| $TiO_2$ | 0.64 | 0.22 | 0.56 | 0.14 | 0.76 | 0.21 | 0.86 | 0.61 |
| $Al_2O_3$ | 17.23 | 14.04 | 17.49 | 13.26 | 16.75 | 17.24 | 17.01 | 16.51 |
| $Fe_2O_3$ | 1.05 | 4.60 | 1.14 | 1.88 | 2.17 | 0.82 | 1.43 | 1.60 |
| FeO | 2.10 | 2.69 | 1.94 | 1.57 | 1.53 | 1.34 | 2.82 | 2.78 |
| MnO | 0.11 | 0.24 | 0.12 | 0.08 | 0.13 | 0.06 | 0.18 | 0.21 |
| MgO | 0.42 | 0.03 | 0.38 | 0.02 | 0.65 | 0.05 | 1.03 | 0.41 |
| CaO | 0.63 | 0.39 | 0.59 | 0.03 | 0.90 | 0.07 | 1.23 | 0.88 |
| $Na_2O$ | 6.73 | 5.80 | 6.77 | 5.81 | 6.75 | 7.09 | 6.63 | 6.77 |
| $K_2O$ | 5.62 | 4.57 | 5.64 | 3.80 | 5.15 | 5.68 | 5.40 | 5.55 |
| $P_2O_5$ | 0.13 | 0.02 | 0.22 | 0.01 | 0.27 | 0.06 | 0.33 | 0.14 |
| L.O.I. | 0.51 | 0.40 | 0.40 | 0.88 | 0.52 | 0.63 | 0.35 | 0.24 |
| Sum | 99.92 | 99.53 | 99.91 | 99.81 | 99.11 | 100.08 | 100.16 | 100.05 |
| | | | | | | | | |
| or | 1.96 | 14.57 | 1.76 | 23.61 | 2.96 | 3.51 | | 1.30 |
| ab | 33.21 | 27.01 | 33.35 | 22.46 | 30.43 | 33.57 | 31.92 | 32.80 |
| an | 56.94 | 46.78 | 57.35 | 47.05 | 57.12 | 57.07 | 56.09 | 54.02 |
| ne | 0.21 | | 0.65 | | 0.19 | | 0.74 | |
| ac | | 2.03 | | 1.86 | | 2.36 | | 2.87 |
| ns | 1.75 | 1.60 | 0.69 | 0.07 | 1.95 | 0.06 | 2.65 | 2.98 |
| di | 2.29 | 1.03 | 2.49 | 1.79 | 0.71 | 2.35 | 3.43 | 3.47 |
| ol | | | | | | | 0.50 | |
| mt | 1.51 | 5.65 | 1.65 | 1.79 | 3.15 | | 2.08 | 0.88 |
| il | 1.22 | 0.42 | 1.06 | 0.27 | 1.44 | 0.39 | 1.63 | 1.16 |
| ap | 0.31 | 0.05 | 0.52 | 0.02 | 0.63 | 0.14 | 0.78 | 0.33 |
| | | | | | | | | |
| A.I. | 0.99 | 1.03 | 0.99 | 1.03 | 1.00 | 1.03 | 0.98 | 1.04 |
| D.I.* | 92.1 | 90.4 | 92.5 | 95.0 | 90.5 | 96.5 | 88.0 | 91.0 |
| $R_1$ | 508 | 1106 | 487 | 1770 | 506 | 542 | 436 | 451 |
| $R_2$ | 426 | 319 | 425 | 264 | 457 | 348 | 516 | 438 |
| Rock-type | Syenite | Quartz-syenite | Syenite | Alkali granite | Syenite | Syenite | Syenite | Syenite |
| Q | 46.0 | 58.9 | 45.9 | 58.9 | 46.7 | 46.9 | 44.9 | 44.4 |
| ne | 33.5 | 25.6 | 33.6 | 27.4 | 34.2 | 32.8 | 34.5 | 34.6 |
| ks | 20.5 | 15.5 | 20.5 | 13.7 | 19.1 | 20.3 | 20.6 | 21.0 |

| | STOCK II | | | | | | | | | | | |
|---|---|---|---|---|---|---|---|---|---|---|---|---|
| Sample | RP-52 | RP-53 | RP-54 | RP-55 | RP-56 | RP-57 | RP-58 | RP-59 | RP-60 | RP-211 | RP-212 | RP-214 |
| wt% | | | | | | | | | | | | |
| $SiO_2$ | 65.35 | 65.30 | 63.96 | 64.64 | 65.29 | 63.85 | 66.05 | 64.60 | 65.33 | 64.10 | 63.20 | 56.76 |
| $TiO_2$ | 0.44 | 0.43 | 0.45 | 0.63 | 0.33 | 0.33 | 0.30 | 0.50 | 0.51 | 0.24 | 0.36 | 0.94 |
| $Al_2O_3$ | 17.09 | 17.23 | 16.91 | 16.91 | 16.11 | 16.06 | 16.53 | 16.62 | 17.14 | 17.57 | 18.18 | 18.93 |
| $Fe_2O_3$ | 1.18 | 1.28 | 1.85 | 1.60 | 1.74 | 1.96 | 1.29 | 1.68 | 1.58 | 1.40 | 1.54 | 1.94 |
| FeO | 1.98 | 2.15 | 1.84 | 2.00 | 2.82 | 2.45 | 1.44 | 1.80 | 1.29 | 1.47 | 1.31 | 2.16 |
| MnO | 0.14 | 0.13 | 0.12 | 0.16 | 0.25 | 0.22 | 0.10 | 0.17 | 0.15 | 0.16 | 0.06 | 0.18 |
| MgO | 0.32 | 0.17 | 0.24 | 0.47 | 0.12 | 0.51 | 0.21 | 0.40 | 0.33 | 0.19 | 0.24 | 1.57 |
| CaO | 0.51 | 0.21 | 0.33 | 0.72 | 0.66 | 0.74 | 0.22 | 0.98 | 0.70 | 0.58 | 0.31 | 2.44 |
| $Na_2O$ | 6.91 | 6.84 | 6.70 | 6.89 | 7.49 | 7.20 | 6.99 | 6.82 | 6.74 | 8.40 | 8.85 | 9.45 |
| $K_2O$ | 5.71 | 5.77 | 5.64 | 5.43 | 4.83 | 4.85 | 5.73 | 5.38 | 5.83 | 4.55 | 4.97 | 4.15 |
| $P_2O_5$ | 0.08 | 0.14 | 0.13 | 0.16 | 0.02 | 0.04 | 0.05 | 0.10 | 0.08 | 0.03 | 0.09 | 0.56 |
| L.O.I. | 0.28 | 0.33 | 1.40 | 0.30 | 0.19 | 1.44 | 0.55 | 0.38 | 0.16 | 0.85 | 0.77 | 0.68 |
| Sum | 99.99 | 99.98 | 99.57 | 99.91 | 99.85 | 99.65 | 99.46 | 99.43 | 99.84 | 99.57 | 99.88 | 99.76 |
| | | | | | | | | | | | | |
| Q | 1.66 | 2.20 | 2.39 | 1.99 | 2.34 | 1.27 | 3.91 | 1.96 | 2.62 | | | |
| or | 33.78 | 34.11 | 33.33 | 32.08 | 28.54 | 28.66 | 33.86 | 31.79 | 34.45 | 26.89 | 29.37 | 24.52 |
| ab | 56.12 | 56.54 | 55.58 | 56.76 | 55.97 | 55.61 | 53.13 | 55.54 | 55.70 | 60.96 | 55.40 | 36.56 |
| ne | | | | | | | | | | 2.21 | 5.66 | 20.43 |
| ac | 2.08 | 1.18 | 0.98 | 1.35 | 5.03 | 4.69 | 3.73 | 2.66 | 1.16 | 4.05 | 4.46 | 5.02 |
| ns | | | | | 0.39 | | 0.42 | | | 0.33 | 0.93 | |
| di | 1.71 | 0.10 | 0.67 | 2.13 | 2.78 | 2.93 | 0.66 | 3.57 | 2.44 | 2.33 | 0.82 | 6.90 |
| hy | 2.70 | 3.12 | 1.86 | 2.09 | 3.93 | 3.85 | 2.51 | 1.35 | 0.45 | | | |
| ol | | | | | | | | | | 1.42 | 1.59 | 2.27 |
| mt | 0.66 | 1.26 | 2.19 | 1.64 | | 0.49 | | 1.11 | 1.71 | | | 0.30 |
| il | 0.83 | 0.81 | 0.85 | 1.20 | 0.63 | 0.63 | 0.57 | 0.95 | 0.97 | 0.46 | 0.68 | 1.79 |
| ap | 0.18 | 0.33 | 0.30 | 0.38 | 0.05 | 0.09 | 0.12 | 0.23 | 0.19 | 0.07 | 0.21 | 1.30 |
| | | | | | | | | | | | | |
| A.I. | 1.03 | 1.02 | 1.01 | 1.02 | 1.09 | 1.06 | 1.07 | 1.03 | 1.02 | 1.07 | 1.10 | 1.06 |
| D.I.* | 93.7 | 94.0 | 92.3 | 92.2 | 91.9 | 90.2 | 90.9 | 92.0 | 93.9 | 94.1 | 94.9 | 86.5 |
| $R_1$ | 468 | 468 | 453 | 477 | 429 | 436 | 497 | 511 | 506 | 142 | -180 | -678 |
| $R_2$ | 406 | 369 | 379 | 432 | 393 | 420 | 358 | 451 | 428 | 416 | 402 | 710 |
| Rock-type | Syenite | Syenite | Syenite | Syenite | Syenite | Syenite | Syenite | Syenite | Syenite | Nephel-syenite | Nephel-syenite | Nepheline syenite |
| Q | 45.8 | 46.1 | 46.3 | 46.1 | 46.4 | 45.7 | 47.2 | 46.1 | 46.4 | 43.9 | 42.1 | 33.5 |
| ne | 33.2 | 33.0 | 33.0 | 33.8 | 34.9 | 35.2 | 31.7 | 33.7 | 32.5 | 39.1 | 39.4 | 49.4 |
| ks | 21.0 | 20.9 | 20.7 | 20.1 | 18.7 | 19.1 | 21.1 | 20.2 | 21.1 | 17.0 | 18.5 | 17.1 |

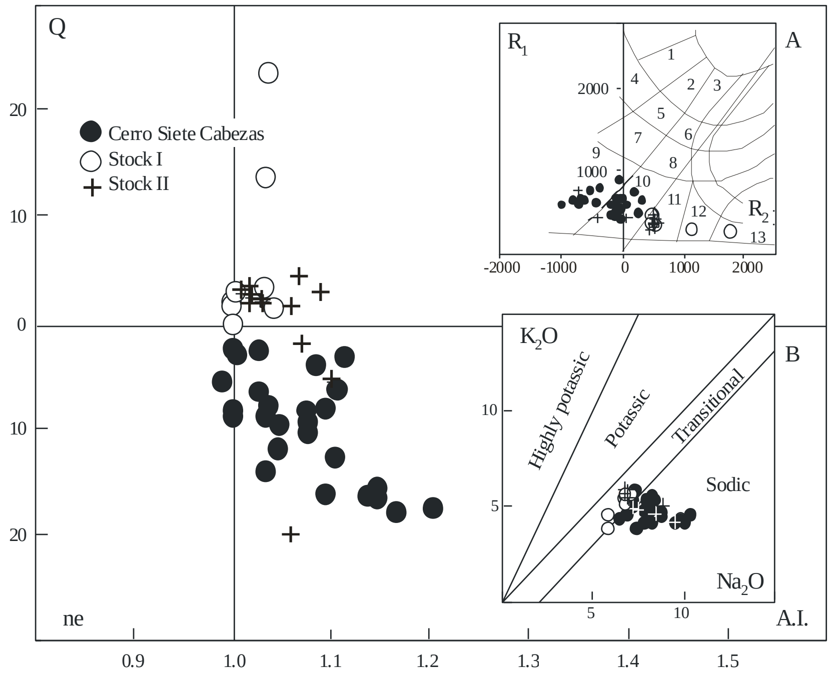


Fig. 3. A.I. [Alkali Index = ($Na_2O/K_2O$)/$Al_2O_3$ molar ratio] vs. Q-ne (normative quartz or nepheline) diagram for Cerro Siete Cabezas, Stock I and Stock II rocks. Inset A: $R_1$-$R_2$: classificative diagram of De La Roche *et al.* (1980) [$R_1$ = 4 Si-11(Na+K)-2(Fe+Ti), $R_2$ = 6 Ca+2Mg+Al; numbered fields: 9) nepheline syenite; 10) nephel-syenite; 11) syenite; 12) quartz syenite; 13) alkali granite]. Inset B: $Na_2O$-$K_2O$: serial (potassic and sodic series) discriminative diagram for alkaline rocks, after Le Maitre (1989), modified after Comin-Chiaramonti & Gomes (1996).

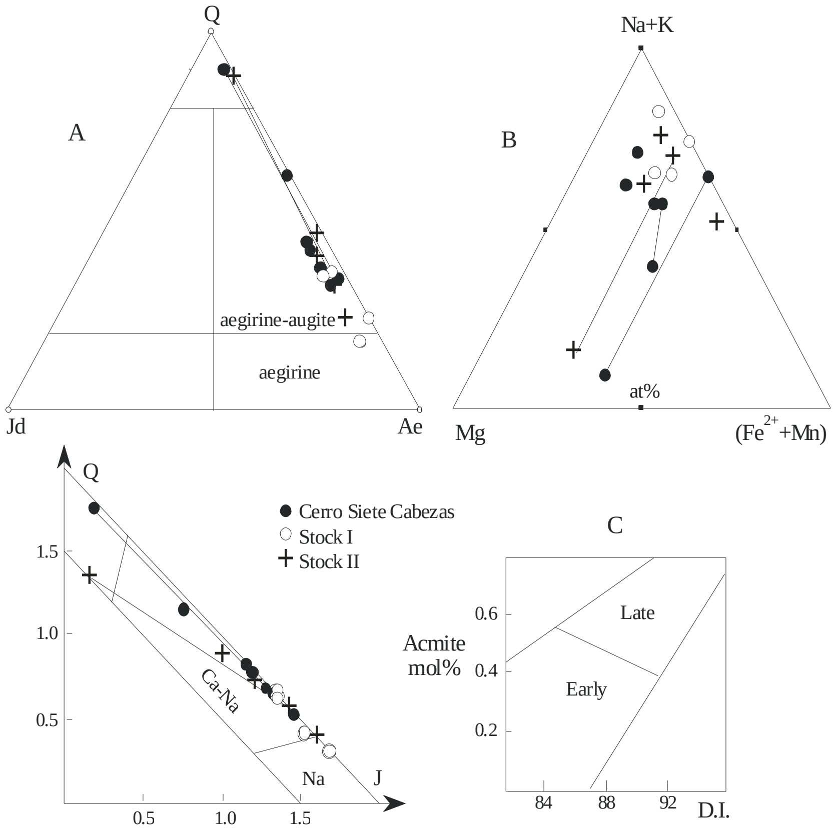


Fig. 4. A: Q-Jd-Ae and Q-J (inset A) nomenclature diagram for clinopyroxenes (Morimoto, 1988) from Cerro Siete Cabezas, Stock I and Stock II rocks. B: variation diagram in terms of Mg(Di)–$Fe^{2+}$+Mn(Hd)-Na+K(Ac). C: field representing the D.I. (Differentiation Index=normative Q+or+ab+ne+ac) vs. acmite content (mol%).

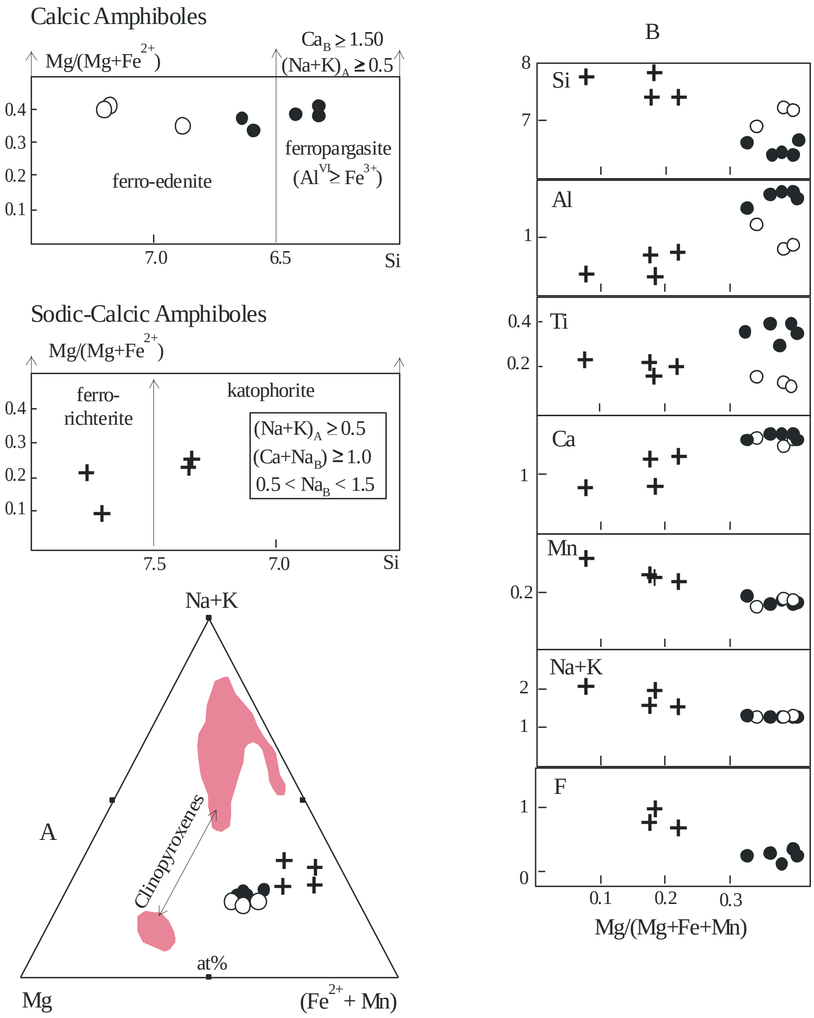


Fig. 5. Nomenclature diagram for amphiboles (Leake *et al.*, 1998) from Cerro Siete Cabezas, Stock I and Stock II rocks. A: elemental variations (atomic formula unity, a.f.u., values) in terms of Mg-($Fe^{2+}$+Mn)-(Na+K); also shown are the compositional fields for the clinopyroxenes. B: variation of Si, Al, Ti, Ca, Mn, Na+K and F in representative amphiboles vs. Mg/(Mg+Fe+Mn) atomic ratio. Symbols as in Fig. 4.

## MINERALOGY

### *Clinopyroxene*

Representative chemical analyses are given in Table 3 and the nomenclature and variation trends are presented in Fig. 4. The clinopyroxenes show a wide compositional range and plot mainly in the aegirine-augite field. Following to Morimoto (1988), the core of some crystals is calcic, but the bulk composition is sodic-calcic. Rarely some rims plot in the sodic field (inset A of Fig. 4) and in this case the mineral is mantled by amphibole. In the Mg(Di)–$Fe^{2+}$+Mn(Hd)–Na+K(Ac) diagram (inset B of Fig. 4), mostly magnesian and presumably least evolved compositions are found in the core of clinopyroxenes from the Cerro Siete Cabezas and Stock II specimens, whereas the more acmitic compositions are represented by bulk compositions of samples from the Stock I and Stock II. On the whole, the clinopyroxene composition overlaps the variation trends of many Cretaceous Brazilian alkaline complexes (Gomes *et al.*, 1987), and the acmite content tends to increase with the differentiation index of the rocks (inset C of Fig. 4).

### *Amphibole*

Selected representative analyses are given in Table 4 and the classificative diagrams are illustrated in Fig. 5. The overall chemical composition includes calcic to sodic-calcic varieties

Table 3. Representative clinopyroxene analyses from Cerro Siete Cabezas, Stock I and Stock II rocks. $Fe_2O_3$ and FeO recalculated on the basis of 4 cations. C, core; R, rim. Quad = Ca+Mg+$Fe^{2+}$, J=2Na (according to Morimoto, 1988).

| | CERRO SIETE CABEZAS | | | | | | | STOCK I | | | | STOCK II | | | | |
|---|---|---|---|---|---|---|---|---|---|---|---|---|---|---|---|---|
| Sample | RP-61 | RP-64 | RP-66 | RP-74C | RP-74R | RP-230C | RP-230R | RP-44 | RP-45 | RP-48 | RP-50 | RP-52C | RP-52R | RP-53 | RP-56 | RP-58 |
| wt% | | | | | | | | | | | | | | | | |
| $SiO_2$ | 52.54 | 52.77 | 51.48 | 50.32 | 50.68 | 51.71 | 51.90 | 53.13 | 51.05 | 51.67 | 51.28 | 50.85 | 51.66 | 51.77 | 49.82 | 52.26 |
| $TiO_2$ | 0.60 | 0.72 | 0.84 | 0.35 | 0.50 | 0.50 | 0.72 | 1.46 | 0.24 | 0.75 | 0.66 | 0.16 | 1.00 | 1.68 | 0.38 | 0.92 |
| $Al_2O_3$ | 1.04 | 1.04 | 1.00 | 1.31 | 1.09 | 1.32 | 1.03 | 1.06 | 0.24 | 0.93 | 1.07 | 0.52 | 1.07 | 0.98 | 0.50 | 0.99 |
| $Fe_2O_3$ | 22.60 | 19.62 | 16.82 | 12.53 | 16.88 | 2.48 | 20.10 | 24.96 | 25.69 | 19.55 | 19.48 | 17.03 | 20.25 | 22.22 | 16.71 | 19.54 |
| FeO | 3.93 | 6.03 | 6.42 | 7.92 | 7.47 | 9.83 | 5.08 | 3.11 | 6.59 | 7.16 | 4.95 | 3.42 | 7.07 | 5.42 | 12.90 | 5.01 |
| MnO | 1.28 | 1.48 | 1.55 | 1.43 | 1.05 | 1.06 | 1.43 | 0.96 | 1.74 | 1.15 | 1.40 | 1.68 | 1.17 | 0.98 | 1.65 | 1.52 |
| MgO | 2.28 | 2.76 | 3.13 | 4.58 | 2.53 | 9.68 | 2.72 | 1.02 | 0.24 | 2.06 | 2.51 | 6.74 | 1.00 | 1.02 | 0.45 | 3.23 |
| CaO | 6.43 | 8.42 | 9.33 | 15.00 | 10.26 | 21.88 | 8.06 | 3.77 | 4.47 | 7.61 | 7.62 | 20.33 | 6.46 | 3.85 | 10.49 | 9.30 |
| $Na_2O$ | 9.87 | 8.72 | 7.93 | 5.02 | 7.52 | 1.30 | 8.84 | 11.49 | 10.08 | 9.00 | 8.89 | 1.26 | 9.55 | 10.85 | 6.67 | 8.42 |
| $K_2O$ | 0.01 | 0.02 | 0.01 | 0.03 | 0.01 | 0.01 | 0.01 | 0.00 | 0.00 | 0.01 | 0.00 | 0.01 | 0.02 | 0.00 | 0.03 | 0.01 |
| Sum | 100.58 | 101.58 | 98.53 | 98.49 | 97.99 | 98.71 | 99.89 | 101.02 | 100.34 | 99.89 | 97.86 | 101.94 | 98.49 | 98.77 | 99.31 | 101.10 |
| | | | | | | | | | | | | | | | | |
| Si | 2.000 | 1.998 | 2.005 | 1.967 | 1.996 | 1.969 | 2.003 | 2.009 | 1.992 | 1.993 | 2.007 | 1.975 | 2.011 | 2.011 | 1.986 | 1.984 |
| $Al^{IV}$ | | 0.002 | | 0.033 | 0.004 | 0.031 | | | 0.008 | 0.007 | | 0.024 | 0.000 | 0.000 | 0.014 | 0.016 |
| Sum | 2.000 | 2.000 | 2.005 | 2.000 | 2.000 | 2.000 | 2.000 | 2.009 | 2.000 | 2.000 | 2.007 | 1.999 | 2.011 | 2.011 | 2.000 | 2.000 |
| $Al^{VI}$ | 0.047 | 0.044 | 0.046 | 0.010 | 0.047 | 0.028 | 0.030 | 0.047 | 0.003 | 0.035 | 0.049 | 0.000 | 0.029 | 0.045 | 0.009 | 0.028 |
| Ti | 0.017 | 0.020 | 0.025 | 0.010 | 0.015 | 0.014 | 0.021 | 0.042 | 0.007 | 0.022 | 0.019 | 0.005 | 0.029 | 0.050 | 0.011 | 0.026 |
| $Fe^{3+}$ | 0.648 | 0.559 | 0.493 | 0.369 | 0.501 | 0.071 | 0.584 | 0.710 | 0.754 | 0.568 | 0.574 | 0.111 | 0.593 | 0.650 | 0.534 | 0.556 |
| $Fe^{2+}$ | 0.125 | 0.191 | 0.209 | 0.259 | 0.246 | 0.313 | 0.164 | 0.098 | 0.215 | 0.231 | 0.162 | 0.498 | 0.230 | 0.176 | 0.405 | 0.159 |
| Mn | 0.041 | 0.047 | 0.051 | 0.057 | 0.035 | 0.034 | 0.047 | 0.031 | 0.057 | 0.038 | 0.046 | 0.055 | 0.039 | 0.032 | 0.056 | 0.049 |
| Mg | 0.129 | 0.156 | 0.182 | 0.267 | 0.149 | 0.550 | 0.156 | 0.057 | 0.014 | 0.118 | 0.147 | 0.390 | 0.058 | 0.059 | 0.027 | 0.183 |
| Ca | 0.262 | 0.342 | 0.389 | 0.628 | 0.433 | 0.893 | 0.333 | 0.153 | 0.187 | 0.315 | 0.320 | 0.846 | 0.269 | 0.160 | 0.448 | 0.379 |
| Na | 0.729 | 0.640 | 0.599 | 0.381 | 0.574 | 0.096 | 0.662 | 0.842 | 0.763 | 0.673 | 0.675 | 0.095 | 0.721 | 0.817 | 0.516 | 0.620 |
| K | 0.000 | 0.001 | 0.000 | 0.002 | 0.000 | 0.001 | 0.000 | 0.000 | 0.000 | 0.000 | 0.000 | 0.002 | 0.001 | 0.000 | 0.002 | 0.000 |
| Sum | 1.999 | 2.000 | 1.999 | 2.000 | 2.000 | 2.000 | 2.000 | 1.991 | 2.000 | 2.000 | 1.999 | 1.999 | 2.000 | 2.000 | 2.000 | 2.000 |
| | | | | | | | | | | | | | | | | |
| Mg/(Mg+Fe+Mn) | 0.136 | 0.164 | 0.195 | 0.280 | 0.160 | 0.568 | 0.164 | 0.064 | 0.015 | 0.124 | 0.158 | 0.370 | 0.063 | 0.064 | 0.026 | 0.193 |
| Quad | 0.52 | 0.69 | 0.78 | 1.15 | 0.83 | 1.76 | 0.65 | 0.31 | 0.42 | 0.66 | 0.63 | 1.35 | 0.56 | 0.40 | 0.88 | 0.72 |
| J | 1.46 | 1.28 | 1.20 | 0.76 | 1.15 | 0.19 | 1.32 | 1.68 | 1.53 | 1.35 | 1.35 | 0.19 | 1.44 | 1.63 | 1.03 | 1.24 |

Table 4. Representative amphibole analyses from Cerro Siete Cabezas, Stock I and Stock II rocks. $Fe_2O_3$ and FeO recalculated according to Schumacher (1997). Structural formulae calculated on the basis of 23 (O).

| | CERRO SIETE CABEZAS | | | | | STOCK I | | | STOCK II | | | |
|---|---|---|---|---|---|---|---|---|---|---|---|---|
| Sample | RP-61 | RP-64 | RP-66 | RP-74 | RP-230 | RP-44 | RP-48 | RP-50 | RP-52 | RP-53 | RP-56 | RP-58 |
| wt% | | | | | | | | | | | | |
| $SiO_2$ | 41.32 | 40.87 | 43.07 | 42.03 | 41.03 | 45.59 | 46.26 | 43.39 | 46.08 | 46.26 | 48.18 | 49.19 |
| $TiO_2$ | 3.33 | 3.35 | 2.95 | 3.01 | 2.51 | 0.98 | 1.14 | 1.31 | 1.73 | 1.54 | 1.76 | 1.25 |
| $Al_2O_3$ | 9.69 | 9.56 | 9.27 | 8.06 | 9.54 | 4.75 | 4.27 | 6.00 | 3.41 | 3.58 | 1.63 | 1.32 |
| $Fe_2O_3$ | 0.16 | | | 0.74 | 0.47 | 0.50 | 0.98 | 0.82 | 0.01 | 0.96 | 1.95 | 4.38 |
| FeO | 19.62 | 20.65 | 19.48 | 21.55 | 19.71 | 20.66 | 21.48 | 22.80 | 28.34 | 26.34 | 29.69 | 24.75 |
| MnO | 1.20 | 1.16 | 1.22 | 1.37 | 1.31 | 1.28 | 1.36 | 1.12 | 1.84 | 1.67 | 2.27 | 1.78 |
| MgO | 7.65 | 6.97 | 6.82 | 6.18 | 7.18 | 8.11 | 7.96 | 6.94 | 3.78 | 4.57 | 1.60 | 3.48 |
| CaO | 10.26 | 10.27 | 9.65 | 9.38 | 10.21 | 9.47 | 8.87 | 9.68 | 7.04 | 7.40 | 4.20 | 4.42 |
| $Na_2O$ | 3.36 | 3.28 | 3.46 | 3.53 | 3.23 | 3.61 | 3.46 | 3.39 | 4.11 | 4.04 | 5.67 | 5.45 |
| $K_2O$ | 1.44 | 1.44 | 1.29 | 1.34 | 1.43 | 1.09 | 1.16 | 1.22 | 1.27 | 1.21 | 1.27 | 1.25 |
| F | 1.01 | 0.88 | 0.80 | 0.82 | 0.59 | | | | 1.59 | 1.45 | | 1.94 |
| Cl | 0.04 | 0.03 | 0.10 | 0.08 | 0.02 | | | | 0.08 | 0.09 | | 0.06 |
| Sum | 98.65 | 98.00 | 97.75 | 97.65 | 96.98 | 96.04 | 96.84 | 96.67 | 98.59 | 98.49 | 98.23 | 98.41 |
| | | | | | | | | | | | | |
| Si | 6.380 | 6.379 | 6.650 | 6.604 | 6.441 | 7.162 | 7.215 | 6.879 | 7.358 | 7.331 | 7.693 | 7.761 |
| $Al^{IV}$ | 1.620 | 1.621 | 1.350 | 1.396 | 1.559 | 0.838 | 0.785 | 1.121 | 0.642 | 0.669 | 0.307 | 0.239 |
| Sum | 8.000 | 8.000 | 8.000 | 8.000 | 8.000 | 8.000 | 8.000 | 8.000 | 8.000 | 8.000 | 8.000 | 8.000 |
| $Al^{VI}$ | 0.144 | 0.136 | 0.337 | 0.096 | 0.206 | 0.041 | 0.000 | 0.000 | 0.000 | 0.000 | 0.000 | 0.007 |
| Ti | 0.387 | 0.393 | 0.343 | 0.356 | 0.296 | 0.116 | 0.134 | 0.156 | 0.208 | 0.184 | 0.211 | 0.148 |
| $Fe^{3+}$ | 0.018 | | | 0.087 | 0.056 | 0.059 | 0.114 | 0.098 | 0.001 | 0.115 | 0.235 | 0.520 |
| $Fe^{2+}$ | 2.534 | 2.695 | 2.515 | 2.831 | 2.587 | 2.715 | 2.802 | 3.023 | 3.785 | 3.491 | 3.965 | 3.268 |
| Mn | 0.157 | 0.153 | 0.160 | 0.182 | 0.174 | 0.170 | 0.180 | 0.150 | 0.249 | 0.224 | 0.307 | 0.238 |
| Mg | 1.761 | 1.622 | 1.570 | 1.448 | 1.681 | 1.899 | 1.851 | 1.640 | 0.900 | 1.080 | 0.381 | 0.819 |
| Sum | 5.000 | 5.000 | 4.925 | 5.000 | 5.000 | 5.000 | 5.081 | 5.067 | 5.143 | 5.094 | 5.099 | 5.000 |
| Ca | 1.697 | 1.717 | 1.596 | 1.579 | 1.717 | 1.594 | 1.483 | 1.644 | 1.204 | 1.257 | 0.719 | 0.748 |
| $Na_B$ | 0.303 | 0.283 | 0.404 | 0.421 | 0.283 | 0.406 | 0.438 | 0.289 | 0.653 | 0.650 | 1.182 | 1.252 |
| Sum | 2.000 | 2.000 | 2.000 | 2.000 | 2.000 | 2.000 | 1.921 | 1.933 | 1.857 | 1.907 | 1.901 | 2.000 |
| $Na_A$ | 0.703 | 0.710 | 0.632 | 0.654 | 0.700 | 0.693 | 0.609 | 0.753 | 0.619 | 0.592 | 0.573 | 0.416 |
| K | 0.284 | 0.287 | 0.254 | 0.269 | 0.286 | 0.218 | 0.231 | 0.247 | 0.259 | 0.245 | 0.259 | 0.252 |
| $Sum_A$ | 0.987 | 0.997 | 0.886 | 0.923 | 0.986 | 0.912 | 0.840 | 1.000 | 0.878 | 0.836 | 0.832 | 0.668 |
| F | 0.493 | 0.434 | 0.390 | 0.400 | 0.293 | | | | 0.794 | 0.722 | | 0.969 |
| Cl | 0.010 | 0.008 | 0.025 | 0.020 | 0.005 | | | | 0.021 | 0.024 | | 0.011 |
| | | | | | | | | | | | | |
| Mg/(Mg+$Fe^{2+}$) | 0.41 | 0.38 | 0.38 | 0.34 | 0.39 | 0.41 | 0.40 | 0.35 | 0.22 | 0.25 | 0.09 | 0.20 |

Table 5. Representative biotite analyses from Cerro Siete Cabezas, Stock I and Stock II rocks. Structural formulae calculated on the basis of 22 (O).

| | CERRO SIETE CABEZAS | | | | STOCK I | | | STOCK II | | |
|---|---|---|---|---|---|---|---|---|---|---|
| Sample | RP-61 | RP-64 | RP-74 | RP-230 | RP-44 | RP-48 | RP-50 | RP-52 | RP-53 | RP-56 |
| wt% | | | | | | | | | | |
| $SiO_2$ | 34.43 | 34.86 | 35.04 | 35.07 | 35.93 | 35.56 | 35.01 | 36.02 | 35.68 | 35.64 |
| $TiO_2$ | 3.43 | 3.37 | 3.42 | 2.92 | 4.31 | 4.53 | 4.47 | 4.13 | 4.60 | 4.37 |
| $Al_2O_3$ | 11.69 | 11.43 | 11.79 | 13.04 | 12.85 | 11.65 | 12.98 | 11.01 | 12.29 | 11.82 |
| $FeO_{tot}$ | 29.34 | 29.12 | 29.16 | 28.61 | 26.03 | 25.72 | 24.96 | 29.86 | 30.21 | 29.79 |
| MnO | 1.78 | 1.79 | 1.79 | 1.12 | 0.69 | 0.70 | 0.97 | 0.87 | 0.83 | 1.07 |
| MgO | 5.45 | 5.66 | 5.51 | 6.38 | 6.33 | 6.88 | 6.70 | 5.61 | 5.22 | 5.45 |
| CaO | 0.05 | 0.04 | 0.03 | 0.02 | 0.02 | 0.01 | 0.04 | 0.01 | 0.01 | 0.03 |
| $Na_2O$ | 0.29 | 0.28 | 0.22 | 0.30 | 0.20 | 0.31 | 0.23 | 0.36 | 0.50 | 0.38 |
| $K_2O$ | 8.91 | 8.85 | 8.84 | 9.27 | 9.04 | 8.79 | 9.18 | 8.96 | 8.93 | 8.73 |
| F | 1.07 | 1.00 | 1.04 | 1.01 | 1.01 | 1.02 | 0.96 | 2.05 | 1.83 | 1.80 |
| Cl | 0.02 | 0.01 | 0.00 | 0.01 | 0.19 | 0.15 | 0.10 | 0.12 | 0.10 | 0.10 |
| Less O=F,Cl | 0.46 | 0.42 | 0.44 | 0.43 | 0.47 | 0.46 | 0.43 | 0.89 | 0.79 | 0.78 |
| $H_2O^+_{calc}$ | 3.16 | 3.21 | 3.21 | 3.28 | 3.25 | 3.20 | 3.26 | 2.75 | 2.91 | 2.90 |
| Sum | 99.16 | 99.20 | 99.61 | 100.60 | 99.38 | 98.06 | 98.43 | 100.86 | 102.32 | 101.30 |
| Si | 5.616 | 5.670 | 5.665 | 5.583 | 5.694 | 5.718 | 5.602 | 5.478 | 5.609 | 5.655 |
| $Al^{IV}$ | 2.248 | 2.191 | 2.247 | 2.417 | 2.306 | 2.208 | 2.398 | 2.071 | 2.277 | 2.210 |
| $Ti^{IV}$ | 0.136 | 0.139 | 0.088 | 0.000 | 0.000 | 0.074 | 0.000 | 0.451 | 0.114 | 0.135 |
| Sum (Z) | 8.000 | 8.000 | 8.000 | 8.000 | 8.000 | 8.000 | 8.000 | 8.000 | 8.000 | 8.000 |
| $Al^{VI}$ | 0.000 | 0.000 | 0.000 | 0.030 | 0.094 | 0.000 | 0.050 | 0.000 | 0.000 | 0.000 |
| $Ti^{VI}$ | 0.283 | 0.273 | 0.328 | 0.349 | 0.514 | 0.474 | 0.538 | 0.045 | 0.430 | 0.386 |
| $Fe^{2+}$ | 4.002 | 3.961 | 3.943 | 3.809 | 3.449 | 3.459 | 3.340 | 3.985 | 3.972 | 3.953 |
| Mn | 0.246 | 0.246 | 0.245 | 0.151 | 0.093 | 0.095 | 0.131 | 0.118 | 0.111 | 0.144 |
| Mg | 1.325 | 1.372 | 1.328 | 1.514 | 1.495 | 1.649 | 1.598 | 1.334 | 1.223 | 1.289 |
| Sum (Y) | 5.856 | 5.852 | 5.844 | 5.853 | 5.645 | 5.677 | 5.657 | 5.482 | 5.736 | 5.772 |
| Ca | 0.009 | 0.007 | 0.005 | 0.003 | 0.003 | 0.002 | 0.007 | 0.002 | 0.002 | 0.005 |
| Na | 0.092 | 0.088 | 0.069 | 0.093 | 0.061 | 0.097 | 0.074 | 0.111 | 0.152 | 0.117 |
| K | 1.854 | 1.836 | 1.823 | 1.883 | 1.892 | 1.902 | 1.952 | 1.825 | 1.791 | 1.767 |
| Sum (X) | 1.955 | 1.932 | 1.897 | 1.979 | 1.892 | 1.902 | 1.952 | 1.938 | 1.945 | 1.889 |
| F | 0.552 | 0.514 | 0.532 | 0.509 | 0.506 | 0.519 | 0.486 | 1.035 | 0.910 | 0.903 |
| Cl | 0.006 | 0.003 | 0.000 | 0.003 | 0.051 | 0.041 | 0.027 | 0.032 | 0.027 | 0.027 |
| OH | 3.442 | 3.483 | 3.468 | 3.488 | 3.443 | 3.440 | 3.487 | 2.933 | 3.063 | 3.070 |
| Sum | 4.000 | 4.000 | 4.000 | 4.000 | 4.000 | 4.000 | 4.000 | 4.000 | 4.000 | 4.000 |
| Mg/(Mg+Fe+Mn) | 0.238 | 0.246 | 0.241 | 0.277 | 0.297 | 0.316 | 0.315 | 0.245 | 0.230 | 0.239 |

(nomenclature following Leake *et al.*, 1998) and plots in the gap between the core and rims, or bulks, of the clinopyroxene crystals (inset A of Fig. 5). Amphiboles from Cerro Siete Cabezas range from ferropargasite to ferro-edenite, whereas in the Stock I they lie in the last field. On the other hand, the Stock II analogues range from katophorite to ferro-richterite.

The Mg/(Mg+Fe+Mn) ratio varies from 0.24 to 0.40 in Cerro Siete Cabezas and Stock I and from 0.08 to 0.24 in Stock II. A trend of increasing Si, Mn, Na+K, and F, and a concomitant decrease of Al and Ca is apparent as the amphiboles become more Fe enriched (as shown in inset B of Fig. 5). This compositional variation is accompanied by the substitution of Mg for $Fe^{2+}$+Mn, while Ti tends to increase in Cerro Siete Cabezas amphiboles, and to be lower in Stock I equivalents.

### *Biotite*

Representative analyses are given in Table 5 and the biotite compositions are plotted in Fig. 6. In general, the data cluster close to the annite field and show iron enrichment in the Cerro Siete Cabezas and Stock II samples. Biotite has distinct Mg/(Mg+Fe+Mn) ratios: 0.23-0.28 for the main complex and Stock II, and 0.30-0.32 for the Stock I. Moreover, the biotite from Stock I and Stock II contains higher Ti and lower Mn than the Cerro Siete Cabezas equivalents. Notably, the biotite from Stock II presents the highest fluorine content.

### *Iron oxides*

The opaque minerals are almost entirely Fe-Ti oxides, confined to the magnetite-ulvöspinel and ilmenite-hematite solid solutions series, and coexist in all the analyzed samples (Table 6). In general, the grains display a high degree of exsolution, but discrete magnetite-ilmenite pairs are usually found.

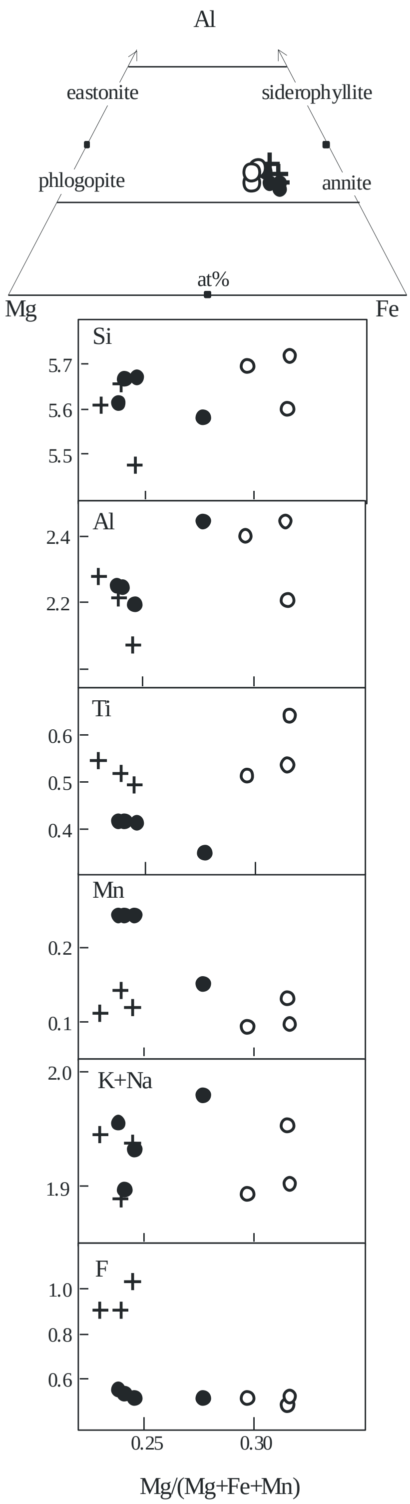


Fig. 6. Plot of biotites from Cerro Siete Cabezas, Stock I and Stock II rocks in the system Al-Mg-Fe, and variation of Si, Al, Ti, Mn, K+Na and F vs. Mg/(Mg+Fe+Mn) atomic ratio. Fe = total iron as $Fe^{2+}$. Symbols as in Fig. 4.

The high MnO content (9-14 wt%) of the ilmenite is noteworthy and similar to that of other ilmenites from peralkaline rocks (cf. e.g. Platt & Woolley, 1986). The cubic phases are represented by Ti-magnetite with ulvöspinel ranging from 14 to about 35 mol%, while the $R_2O_3$ (mol%) of the ilmenite ranges from 2 to 4%. The use of the Spencer & Lindsley (1981) geothermometry yielded very low equilibration temperatures (subsolidus) of equilibration, i.e. 515-665°C, and low oxygen activity (range of log $fO_2 = -20$ to $-26$) between the Magnetite-Wustite and Quartz-Fayalite-Magnetite buffers, contrasting with the peralkaline tendency of the suite (Fig. 7). As a matter of fact, the coexistence of magnetite and titanite and the lack of perovskite may indicate that $fO_2$ was originally above the QFM buffer and below the HM buffer throughout the crystallization history of the rock (cf. Flohr & Ross, 1990).

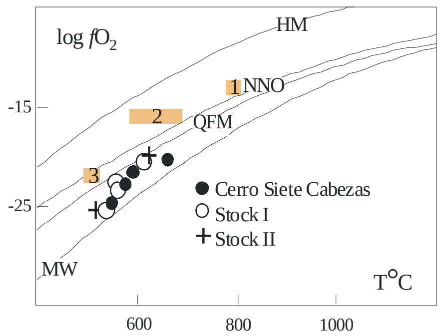


Fig. 7. Cerro Siete Cabezas complex: stability relationships in T°C-$fO_2$ diagram for the magnetite-ilmenite pairs (Spencer & Lindsley, 1981). MW, QFM, NNO, HM: Magnetite-Wustite, Quartz-Fayalite-Magnetite, Nickel-Nickel Oxide and Hematite-Magnetite buffers. 1) field of clinopyroxenes; 2) field of amphiboles; 3) field of micas (see later significance of the mineralogy).

### *Feldspars and nepheline*

Alkali feldspars are the only feldspathic phase (An content•10%) present in the rocks. The texture is variable, ranging from cryptoperthite to coarse braided and patch perthite. As far as possible, compositions were obtained from analyses of clear cryptoperthitic regions with a broad beam (10 µm) and on the coarse exsolved areas (Table 7). The bulk compositions approach those of anorthoclase, displaying Or content between 30 and 40 mol% (mesoperthites from original hypersolvus rock-types, subsolvus equilibration temperature below 500°C; cf. Brown & Parsons, 1989). In general, the An content of these feldspars is very low and tends to decrease with the increasing Or concentration. Notably, in the larger Na-exsolved patches, the An content is up to 7.3 mol% (Fig. 8).

Parsons (1978) pointed out that the coarseness of exsolution in felspars increases possibly in relation to the progressive enrichment in volatiles. Matos (2000) quoted plagioclase ($An_{19\text{-}12}$) as a coexisting phase with alkali feldspar in the Stock I rocks. If

Table 6. Representative magnetite and ilmenite analyses from Cerro Siete Cabezas, Stock I and Stock II rocks. $Fe_2O_3$ and FeO recalculated according to ulvöspinel basis and to ilmenite basis, magnetite and ilmenite, respectively. Structural formulae on the basis of 32 (O) and 3 (O), respectively. Equilibration temperatures (T°C) and $fO_2$ calculated according to the geothermometer of Spencer & Lindsley (1981).

| Magnetite | CERRO SIETE CABEZAS | | | | STOCK I | | | | STOCK II | |
|---|---|---|---|---|---|---|---|---|---|---|
| Sample | RP-61 | RP-64 | RP-74 | RP-230 | RP-44 | RP-45 | RP-48 | RP-50 | RP-52 | RP-56 |
| wt% | | | | | | | | | | |
| $SiO_2$ | 0.09 | 0.10 | 0.12 | 0.01 | 0.12 | 0.11 | 0.01 | 0.12 | 0.21 | 0.18 |
| $TiO_2$ | 7.45 | 7.55 | 8.47 | 7467 | 9.05 | 4.71 | 9.83 | 6.87 | 8.05 | 11.82 |
| $Al_2O_3$ | 0.14 | 0.21 | 0.17 | 0.35 | 0.27 | 0.01 | 0.12 | 0.34 | 0.12 | 0.04 |
| $Cr_2O_3$ | 0.01 | 0.03 | 0.02 | 0.02 | 0.05 | 0.01 | 0.03 | 0.01 | 0.01 | 0.04 |
| $Fe_2O_3$ | 53.75 | 53.50 | 51.30 | 53.23 | 49.78 | 58.99 | 49.75 | 55.11 | 52.15 | 45.44 |
| FeO | 36.38 | 35.88 | 36.91 | 35.37 | 37.87 | 32.63 | 38.18 | 35.13 | 36.42 | 40.09 |
| MnO | 1.26 | 1.90 | 1.63 | 2.11 | 1.21 | 2.59 | 1.94 | 2.30 | 1.98 | 1.89 |
| MgO | 0.13 | 0.12 | 0.07 | 0.06 | 0.04 | 0.01 | 0.02 | 0.06 | 0.02 | 0.02 |
| CaO | 0.01 | 0.02 | 0.04 | 0.03 | 0.01 | 0.04 | 0.000 | 0.01 | 0.05 | 0.11 |
| Sum | 99.22 | 99.31 | 98.73 | 98.64 | 98.40 | 99.10 | 99.88 | 99.90 | 99.01 | 99.63 |
| Si | 0.028 | 0.031 | 0.037 | 0.003 | 0.037 | 0.033 | 0.003 | 0.037 | 0.065 | 0.055 |
| Ti | 1.724 | 1.744 | 1.967 | 1.735 | 2.107 | 1.095 | 2.257 | 1.565 | 1.866 | 2.714 |
| Al | 0.051 | 0.076 | 0.062 | 0.128 | 0.099 | 0.004 | 0.043 | 0.122 | 0.044 | 0.014 |
| Cr | 0.002 | 0.007 | 0.005 | 0.003 | 0.012 | 0.002 | 0.007 | 0.000 | 0.002 | 0.009 |
| $Fe^{3+}$ | 12.444 | 12.368 | 11.923 | 12.391 | 11.600 | 13.730 | 11.431 | 12.673 | 12.094 | 10.439 |
| $Fe^{2+}$ | 9.360 | 9.218 | 9.535 | 9.150 | 9.807 | 8.440 | 9.478 | 8.978 | 9.387 | 10.235 |
| Mn | 0.328 | 0.494 | 0.426 | 0.553 | 0.317 | 0.678 | 0.502 | 0.595 | 0.517 | 0.489 |
| Mg | 0.060 | 0.055 | 0.032 | 0.028 | 0.018 | 0.005 | 0.009 | 0.027 | 0.009 | 0.009 |
| Ca | 0.003 | 0.007 | 0.013 | 0.009 | 0.003 | 0.013 | 0.000 | 0.000 | 0.016 | 0.036 |
| Sum | 24.000 | 24.000 | 24.000 | 24.000 | 24.000 | 24.000 | 24.000 | 24.000 | 24.000 | 24.000 |
| Ulvösp. mol% | 21.89 | 22.18 | 25.06 | 21.73 | 26.80 | 14.11 | 28.25 | 20.02 | 24.13 | 34.60 |
| Ilmenite | CERRO SIETE CABEZAS | | | | STOCK I | | | | STOCK II | |
| Sample | RP-61 | RP-64 | RP-74 | RP-230 | RP-44 | RP-45 | RP-48 | RP-50 | RP-52 | RP-56 |
| wt% | | | | | | | | | | |
| $SiO_2$ | 0.01 | 0.02 | 0.04 | 0.01 | 0.02 | 0.01 | 0.00 | 0.00 | 0.00 | 0.10 |
| $TiO_2$ | 50.02 | 50.30 | 50.21 | 49.98 | 49.32 | 50.10 | 50.06 | 50.92 | 51.34 | 50.12 |
| $Al_2O_3$ | 0.01 | 0.08 | 0.02 | 0.01 | 0.01 | 0.01 | 0.02 | 0.01 | 0.10 | 0.05 |
| $Cr_2O_3$ | 0.02 | 0.03 | 0.03 | 0.02 | 0.02 | 0.03 | 0.03 | 0.00 | 0.00 | 0.02 |
| $Fe_2O_3$ | 3.49 | 2.03 | 2.91 | 3.24 | 3.90 | 2.73 | 1.96 | 2.38 | 1.73 | 3.76 |
| FeO | 33.75 | 34.17 | 34.84 | 31.88 | 30.26 | 33.39 | 33.77 | 36.19 | 34.66 | 33.81 |
| MnO | 10.98 | 10.79 | 9.91 | 12.74 | 13.87 | 11.40 | 11.07 | 9.36 | 11.36 | 11.12 |
| MgO | 0.06 | 0.08 | 0.01 | 0.09 | 0.03 | 0.05 | 0.01 | 0.06 | 0.00 | 0.04 |
| CaO | 0.01 | 0.01 | 0.03 | 0.01 | 0.01 | 0.03 | 0.02 | 0.01 | 0.00 | 0.04 |
| Sum | 98.35 | 97.51 | 98.00 | 97.98 | 97.44 | 97.75 | 96.93 | 98.93 | 99.02 | 99.06 |
| Si | 0.000 | 0.001 | 0.001 | 0.000 | 0.001 | 0.000 | 0.000 | 0.000 | 0.000 | 0.002 |
| Ti | 0.966 | 0.978 | 0.972 | 0.968 | 0.961 | 0.973 | 0.980 | 0.977 | 0.982 | 0.960 |
| Al | 0.000 | 0.002 | 0.001 | 0.000 | 0.000 | 0.000 | 0.001 | 0.000 | 0.003 | 0.002 |
| Cr | 0.001 | 0.001 | 0.001 | 0.001 | 0.001 | 0.001 | 0.001 | 0.000 | 0.000 | 0.001 |
| $Fe^{3+}$ | 0.067 | 0.040 | 0.056 | 0.063 | 0.076 | 0.053 | 0.038 | 0.046 | 0.033 | 0.072 |
| $Fe^{2+}$ | 0.725 | 0.739 | 0.751 | 0.687 | 0.656 | 0.721 | 0.735 | 0.772 | 0.737 | 0.720 |
| Mn | 0.239 | 0.236 | 0.217 | 0.278 | 0.304 | 0.249 | 0.244 | 0.203 | 0.245 | 0.240 |
| Mg | 0.002 | 0.003 | 0.000 | 0.003 | 0.001 | 0.002 | 0.000 | 0.002 | 0.000 | 0.002 |
| Ca | 0.000 | 0.000 | 0.001 | 0.000 | 0.000 | 0.001 | 0.001 | 0.000 | 0.000 | 0.001 |
| Sum | 2.000 | 2.000 | 2.000 | 2.000 | 2.000 | 2.000 | 2.000 | 2.000 | 2.000 | 2.000 |
| $Fe^{2+}/(Mn+Fe^{2+})$ | 0.75 | 0.76 | 0.78 | 0.71 | 0.68 | 0.74 | 0.75 | 0.79 | 0.75 | 0.75 |
| $R_2O_3$ mol% | 3.74 | 2.14 | 2.72 | 3.25 | 3.80 | 2.70 | 1.98 | 2.43 | 1.81 | 3.88 |
| T°C | 665 | 536 | 566 | 587 | 614 | 558 | 525 | 551 | 515 | 628 |
| $\log_{10} fO^2$ | -20.2 | -24.8 | -23.0 | -21.7 | -20.5 | -23.3 | -25.4 | -22.7 | -26.0 | -20.1 |

Table 7. Representative alkali feldspar analyses from Cerro Siete Cabezas, Stock I and Stock II rocks. B, bulk compositions; ab and or, exsolved Na-rich and K-rich phases, respectively. Compositions are also expressed as end-member molecular proportions (Or, Ab and An).

| | CERRO SIETE CABEZAS | | | | | | | | | |
|---|---|---|---|---|---|---|---|---|---|---|
| Sample | RP-61B | RP-64B | RP-66B | RP-74B | RP-74ab | RP-74or | RP-230B | RP-230ab | RP-230or | |
| wt% | | | | | | | | | | |
| $SiO_2$ | 66.94 | 66.75 | 66.96 | 67.03 | 67.92 | 63.31 | 67.43 | 66.22 | 64.53 | |
| $Al_2O_3$ | 19.03 | 19.04 | 18.88 | 19.15 | 19.45 | 18.02 | 19.58 | 20.01 | 18.46 | |
| $Fe_2O_3$ | 0.10 | 0.08 | 0.44 | 0.21 | 0.23 | 0.24 | 0.10 | 0.10 | 0.17 | |
| BaO | 0.00 | 0.03 | 0.08 | 0.00 | 0.08 | 0.14 | 0.21 | 0.03 | 0.23 | |
| CaO | 0.19 | 0.13 | 0.16 | 0.15 | 0.05 | 0.01 | 0.18 | 0.50 | 0.03 | |
| $Na_2O$ | 7.24 | 7.12 | 7.51 | 8.00 | 11.74 | 0.50 | 7.59 | 10.19 | 1.91 | |
| $K_2O$ | 6.31 | 6.54 | 5.98 | 5.27 | 0.10 | 15.98 | 6.08 | 2.05 | 14.19 | |
| Sum | 99.81 | 99.70 | 100.01 | 100.52 | 99.57 | 98.20 | 101.13 | 99.03 | 99.52 | |
| Or | 35.8 | 37.2 | 33.8 | 29.8 | 0.5 | 95.4 | 34.2 | 11.4 | 82.8 | |
| Ab | 62.4 | 61.6 | 64.6 | 68.8 | 99.2 | 4.6 | 64.9 | 86.2 | 16.9 | |
| An | 1.8 | 1.2 | 1.6 | 1.4 | 0.3 | 0.0 | 0.9 | 2.3 | 0.3 | |
| | STOCK I | | | | | | | | | |
| Sample | RP-44B | RP-44ab | RP-44or | RP-45B | RP-48B | RP-48ab | RP-48or | RP-50B | RP-50ab | RP-50or |
| wt% | | | | | | | | | | |
| $SiO_2$ | 67.10 | 67.89 | 64.32 | 66.67 | 67.30 | 69.31 | 64.73 | 65.95 | 67.65 | 64.50 |
| $Al_2O_3$ | 187.75 | 20.04 | 18.58 | 18.37 | 19.09 | 19.07 | 17.41 | 18.73 | 19.55 | 18.37 |
| $Fe_2O_3$ | 0.29 | 0.10 | 0.16 | 1.21 | 0.22 | 0.06 | 0.73 | 0.19 | 0.10 | 0.11 |
| BaO | 0.10 | 0.04 | 0.14 | 0.03 | 0.05 | 0.01 | 0.00 | 0.11 | 0.06 | 0.13 |
| CaO | 0.06 | 0.80 | 0.01 | 0.01 | 0.04 | 0.01 | 0.01 | 0.10 | 0.59 | 0.01 |
| $Na_2O$ | 6.91 | 11.29 | 0.79 | 7.18 | 7.69 | 11.58 | 0.90 | 7.16 | 11.56 | 1.05 |
| $K_2O$ | 6.79 | 0.33 | 15.51 | 6.62 | 5.87 | 0.16 | 14.59 | 6.61 | 0.19 | 14.37 |
| Sum | 100.00 | 100.49 | 99.51 | 100.09 | 100.26 | 100.20 | 98.37 | 98.85 | 99.70 | 98.54 |
| Or | 39.0 | 1.8 | 92.9 | 37.7 | 33.3 | 0.9 | 91.4 | 37.4 | 1.0 | 89.9 |
| Ab | 60.4 | 94.5 | 7.1 | 62.2 | 66.3 | 99.1 | 8.6 | 61.6 | 93.7 | 10.0 |
| An | 0.6 | 3.7 | 0.0 | 0.0 | 0.4 | 0.0 | 0.0 | 1.0 | 7.3 | 0.1 |
| | STOCK II | | | | | | | | | |
| Sample | RP-52B | RP-52ab | RP-52or | RP-53B | RP-56B | RP-56ab | RP-56or | RP-58B | RP-58ab | RP-58or |
| wt% | | | | | | | | | | |
| $SiO_2$ | 66.38 | 70.10 | 67.27 | 67.40 | 66.57 | 70.44 | 64.81 | 68.38 | 67.96 | 65.31 |
| $Al_2O_3$ | 18.97 | 19.52 | 17.75 | 18.92 | 19.06 | 19.07 | 18.04 | 18.33 | 19.28 | 17.75 |
| $Fe_2O_3$ | 0.10 | 0.74 | 0.47 | 0.12 | 0.49 | 0.58 | 0.48 | 0.52 | 0.17 | 0.74 |
| BaO | 0.10 | 0.00 | 0.04 | 0.10 | 0.01 | 0.00 | 0.00 | 0.00 | 0.00 | 0.02 |
| CaO | 0.16 | 0.53 | 0.01 | 0.13 | 0.19 | 0.00 | 0.01 | 0.01 | 0.15 | 0.01 |
| $Na_2O$ | 6.68 | 10.19 | 1.17 | 7.47 | 7.56 | 11.36 | 1.08 | 7.09 | 11.24 | 1.70 |
| $K_2O$ | 7.10 | 0.42 | 15.27 | 6.20 | 5.79 | 0.74 | 15.37 | 6.89 | 0.31 | 14.47 |
| Sum | 99.49 | 101.50 | 101.98 | 100.34 | 99.67 | 102.19 | 99.79 | 101.20 | 99.11 | 100.00 |
| Or | 40.5 | 2.6 | 89.6 | 34.9 | 32.9 | 4.1 | 90.3 | 39.0 | 1.8 | 84.8 |
| Ab | 58.0 | 94.7 | 10.4 | 63.9 | 65.3 | 95.1 | 9.7 | 61.0 | 97.5 | 15.1 |
| An | 1.5 | 2.7 | 0.0 | 1.2 | 1.8 | 0.0 | 0.0 | 0.0 | 0.7 | 0.1 |

this is the case, it is suggested that these crystals represent an incomplete reabsorption of early-crystallized plagioclase as the magma moves towards crystallization of a single alkali feldspar (cf. Rahman & MacKenzie, 1961).

Representative analyses of nepheline are in Table 8. They are compositionally homogeneous. The silica excess ranges from 2.0 to 6.3 mol% and the kalsilite content is between 18.8 and 23.4 mol%. Compositions of nepheline partly lie near to and partly fall within the Morozewicz-Buerger convergence field of plutonic nephelines (Fig. 8; cf. Tilley, 1954), implying temperatures of about 600-500°C for re-equilibration (Hamilton, 1961; Hamilton & McKenzie, 1965).

### Accessory minerals

Representative analyses of eudialyte, titanite, apatite and zircon (Cerro Siete Cabezas) are given in Table 8, as well as that of an unknown phase present in Stock II samples.

In some cases the eudialyte amounts up to 1% modal content (e.g. RP-74, Cerro Siete Cabezas). This mineral is typical of high Zr peralkaline magmas, where the excess of alkalies over alumina increases the solubility of Zr and results in the formation of alkali-zircono-silicate complexes (Collins *et al*., 1982; Mitchell, 1996).

Table 8. Representative nepheline (RP-61 to RP-230, Cerro Siete Cabezas; RP-214, Stock I) and accessory mineral analyses (eudialyte, titanite, apatite, zircon from Cerro Siete Cabezas, and an unknown (?) mineral from Stock II). Nepheline compositions are also expressed in terms of molecular proportions of Q, Ne and Ks.

| Nepheline | | | | | | Accessories | | | | | | |
|---|---|---|---|---|---|---|---|---|---|---|---|---|
| | | | | | | | Eudialyte | Titanite | Apatite | | Zircon | (?) |
| Sample | RP-61 | RP-64 | RP-74 | RP-230 | RP-214 | | RP-74 | RP-67 | RP-244 | | RP-75 | RP-52 |
| wt% | | | | | | wt% | | | | | | |
| $SiO_2$ | 44.14 | 44.74 | 42.73 | 43.78 | 42.83 | $SiO_2$ | 51.80 | 30.35 | | $SiO_2$ | 32.22 | 20.90 |
| $Al_2O_3$ | 32.67 | 33.49 | 34.14 | 33.81 | 33.40 | $TiO_2$ | 0.26 | 37.65 | | $TiO_2$ | 0.14 | 36.09 |
| $Fe_2O_3$ | 0.74 | 0.73 | 0.14 | 0.38 | 0.56 | $ZrO_2$ | 13.35 | | | $ZrO_2$ | 66.21 | 1.11 |
| BaO | 0.00 | 0.05 | 0.04 | 0.01 | 0.02 | $Al_2O_3$ | | 0.46 | | $ThO_2$ | | 2.22 |
| CaO | 0.02 | 0.04 | 0.05 | 0.20 | 0.49 | $Ce_2O_3$ | 2.02 | 0.19 | | $Al_2O_3$ | 0.68 | 0.59 |
| $Na_2O$ | 16.58 | 16.07 | 16.33 | 16.11 | 16.11 | FeO | 4.90 | 0.88 | 0.24 | $Cr_2O_3$ | 0.59 | |
| $K_2O$ | 5.64 | 5.60 | 7.01 | 5.61 | 6.21 | MnO | 3.17 | 0.06 | | $La_2O_3$ | | 1.84 |
| Sum | 99.79 | 100.69 | 100.44 | 99.90 | 99.62 | MgO | 0.04 | 0.00 | | $Ce_2O_3$ | | 5.02 |
| | | | | | | CaO | 8.46 | 27.61 | 53.58 | FeO | 0.09 | 11.49 |
| Q | 4.8 | 6.3 | 2.0 | 5.1 | 2.7 | $Na_2O$ | 12.55 | 0.22 | | MnO | | 0.37 |
| Ne | 76.2 | 74.9 | 74.6 | 75.6 | 75.8 | $K_2O$ | 0.10 | 0.01 | | MgO | 0.02 | 0.01 |
| Ks | 19.0 | 18.8 | 23.4 | 19.3 | 21.5 | $Nb_2O_5$ | 0.56 | | | BaO | | 0.12 |
| | | | | | | $P_2O_5$ | | | 40.54 | CaO | 0.06 | 0.84 |
| | | | | | | F | 0.05 | 0.60 | 3.71 | $Na_2O$ | | 0.00 |
| | | | | | | Cl | 0.82 | 0.05 | 0.56 | $K_2O$ | | 0.18 |
| | | | | | | Sum | 97.72 | 97.82 | 96.93 | $Nb_2O_5$ | | 0.00 |
| | | | | | | | | | | $P_2O_5$ | | 8.88 |
| | | | | | | | | | | Sum | 100.02 | 89.66 |

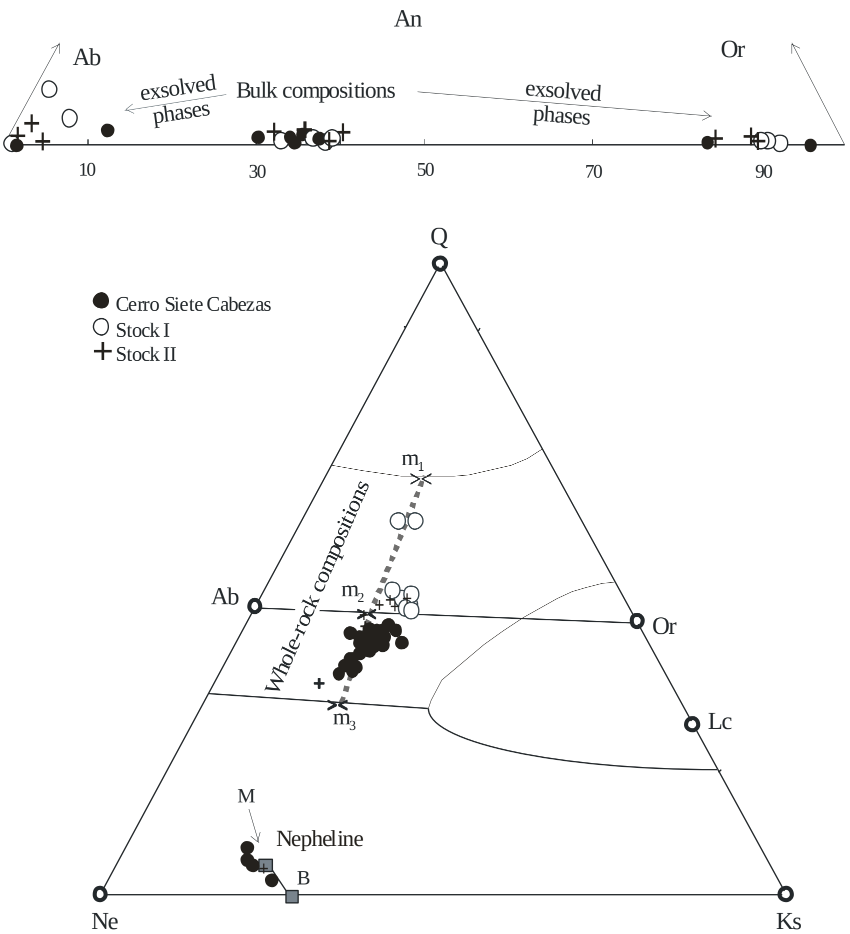


Fig. 8. Alkali feldspar from Cerro Siete Cabezas, Stock I and Stock II rocks plotted into the Or-Ab-An (mol%) diagram, and nepheline compositions plotted into the Ks-Ne-Q (wt%) space ($PH_2O = 1$ kb; Hamilton & McKenzie, 1965); M and B are Morozewicz's and Buerger's ideal nepheline composition, respectively. For comparison the whole-rock compositions are also plotted; it should be noted that the Cerro Siete Cabezas rocks trend towards the phonolitic minimum, whereas the Stock I and Stock II rocks tend to fit the trachytic minimum along the feldspar join.

Table 9. Trace element analyses of selected Cerro Siete Cabezas, Stock I and Stock II rocks.

| | CERRO SIETE CABEZAS | | | | | | | | | | | | | | | | | | | |
|---|---|---|---|---|---|---|---|---|---|---|---|---|---|---|---|---|---|---|---|---|
| | RP-61 | RP-62 | RP-63 | RP-64 | RP-65 | RP-66 | RP-67 | RP-68 | RP-69 | RP-70 | RP-71 | RP-72 | RP-74 | RP-75 | RP-232 | RP-235 | RP-236 | RP-241 | RP-244 | RP-246 |
| ppm | | | | | | | | | | | | | | | | | | | | |
| Cr | <1 | 2 | <1 | 1 | <1 | <1 | <1 | <1 | 1 | 1 | 1 | 1 | 1 | <1 | 5 | 2 | 5 | 2 | 9 | 10 |
| Ni | 8 | 9 | 6 | 6 | 8 | 5 | 8 | 6 | 9 | 7 | 6 | 8 | 7 | 7 | 12 | 2 | 2 | 3 | 5 | 4 |
| Rb | 100 | 110 | 105 | 92 | 86 | 75 | 86 | 117 | 104 | 83 | 110 | 69 | 137 | 74 | 93 | 89 | 78 | 90 | 56 | 111 |
| Ba | 831 | 877 | 894 | 1414 | 769 | 855 | 1379 | 911 | 876 | 1100 | 691 | 1656 | 679 | 867 | 859 | 1290 | 1522 | 2813 | 2285 | 182 |
| Th | 15.4 | 16.3 | 16.0 | | | 9.5 | | | | | 2.6 | 3.0 | 9.0 | | 8.6 | 6.2 | 8.9 | 11.5 | 10.9 | 5.6 |
| U | 5.6 | 7.3 | 6.4 | | | 2.1 | | | | | 0.9 | 1.1 | 4.3 | | 3.0 | 1.2 | 2.2 | 7.2 | 3.4 | 1.0 |
| Ta | 10.4 | 14.9 | 10.1 | | | 6.9 | 16.3 | | | | 12.8 | 7.0 | 12.3 | | 11.6 | 8.9 | 9.1 | 8.9 | 9.1 | 4.4 |
| Nb | 137 | 157 | 147 | 139 | 111 | 143 | 252 | 182 | 175 | 151 | 199 | 97 | 161 | 192 | 241 | 128 | 172 | 143 | 153 | 95 |
| Sr | 413 | 370 | 409 | 606 | 209 | 216 | 568 | 488 | 437 | 320 | 452 | 1062 | 266 | 393 | 384 | 280 | 647 | 909 | 1119 | 35 |
| Hf | 18.8 | 16.5 | 18.3 | | | | 15.4 | | | | 10.7 | 7.8 | 22.1 | | 13.9 | 6.8 | 11.4 | 8.8 | 14.7 | 15.3 |
| Zr | 684 | 621 | 701 | 433 | 366 | 572 | 573 | 725 | 688 | 508 | 348 | 315 | 905 | 1194 | 835 | 359 | 610 | 444 | 692 | 908 |
| Y | 46 | 44 | 46 | 46 | 30 | 28 | 72 | 49 | 48 | 47 | 36 | 36 | 49 | 65 | 71 | 36 | 37 | 49 | 52 | 29 |
| La | 101.00 | 96.91 | 90.01 | 81 | 44.51 | 54.70 | 141.00 | 91 | 94 | 86 | 94.01 | 75.99 | 82.31 | 114 | 136.00 | 90.31 | 107.11 | 124.13 | 155.73 | 83.11 |
| Ce | 193.00 | 199.49 | 194.98 | 160 | 111.10 | 126.01 | 291.00 | 177 | 182 | 169 | 201.98 | 151.03 | 154.79 | 218 | 273.01 | 181.19 | 172.18 | 229.36 | 233.04 | 167.20 |
| Pr | 22.91 | 23.32 | 21.70 | | 13.40 | 13.52 | 33.11 | | | | 22.20 | 17.80 | 17.72 | | 28.50 | 18.48 | 19.78 | 23.27 | 29.25 | 18.40 |
| Nd | 77.00 | 76.68 | 68.00 | 58 | 48.50 | 47.40 | 109.03 | 61 | 61 | 65 | 68.00 | 63.01 | 52.83 | 79 | 99.21 | 69.22 | 74.32 | 87.71 | 102.04 | 65.51 |
| Sm | 16.10 | 16.00 | 14.91 | | 10.30 | 8.09 | 22.20 | | | | 15.00 | 13.10 | 9.40 | 16 | 19.32 | 11.91 | 12.41 | 14.59 | 19.33 | 11.01 |
| Eu | 2.65 | 2.63 | 2.45 | | 1.68 | 2.40 | 3.93 | | | | 3.36 | 3.56 | 2.21 | | 2.40 | 2.56 | 2.99 | 2.79 | 3.62 | 2.19 |
| Gd | 13.50 | 13.40 | 12.41 | | 8.41 | 7.75 | 19.01 | | | | 13.91 | 12.21 | 9.70 | | 18.4 | 11.10 | 12.13 | 14.28 | 18.88 | 10.73 |
| Tb | 1.70 | 1.68 | 1.54 | | 1.04 | 0.99 | 2.96 | | | | 2.10 | 1.87 | 1.39 | | 2.71 | 1.69 | 1.82 | 2.39 | 3.12 | 1.75 |
| Dy | 9.89 | 10.21 | 9.39 | | 6.36 | 4.52 | 15.72 | | | | 12.12 | 11.00 | 7.35 | | 17.19 | 9.38 | 9.68 | 12.27 | 17.08 | 9.99 |
| Ho | 1.97 | 2.03 | 1.82 | | 1.23 | 0.94 | 3.28 | | | | 2.38 | 2.44 | 1.63 | | 2.12 | 1.55 | 1.93 | 2.08 | 2.78 | 1.53 |
| Er | 5.07 | 5.22 | 4.73 | | 3.07 | 2.53 | 8.14 | | | | 6.23 | 7.12 | 4.76 | | 6.42 | 5.10 | 5.41 | 6.80 | 9.22 | 4.98 |
| Tm | 0.79 | 0.82 | 0.70 | | 0.40 | 0.36 | 1.14 | | | | 0.78 | 0.94 | 0.75 | | 1.10 | 0.70 | 0.83 | 0.98 | 1.10 | 0.56 |
| Yb | 4.42 | 4.59 | 4.09 | | 2.24 | 2.00 | 6.43 | | | | 4.11 | 5.08 | 3.72 | | 5.80 | 3.57 | 4.50 | 5.57 | 6.48 | 2.85 |
| Lu | 0.50 | 0.51 | 0.48 | | 0.23 | 0.29 | 0.93 | | | | 0.44 | 0.71 | 0.57 | | 0.80 | 0.55 | 0.74 | 0.96 | 1.03 | 0.41 |

| | STOCK I | | | | | | | | STOCK II | | | | | | |
|---|---|---|---|---|---|---|---|---|---|---|---|---|---|---|---|
| | RP-44 | RP-45 | RP-46 | RP-47 | RP-48 | RP-49 | RP-50 | RP-51 | RP-52 | RP-53 | RP-54 | RP-57 | RP-211 | RP-212 | RP-214 |
| ppm | | | | | | | | | | | | | | | |
| Cr | 1 | 1 | 1 | 1 | 1 | 1 | 1 | 1 | 1 | 1 | 1 | 7 | 1 | 1 | 4 |
| Ni | 6 | 10 | 8 | 2 | 12 | 5 | 6 | 8 | 3 | 6 | 5 | 18 | 5 | 2 | 7 |
| Rb | 157 | 186 | 152 | 128 | 154 | 154 | 187 | 165 | 123 | 145 | 133 | 143 | 136 | 84 | 71 |
| Ba | 555 | 112 | 548 | 92 | 886 | 102 | 1229 | 381 | 195 | 223 | 249 | 119 | 207 | 246 | 256 |
| Th | 9.7 | | 3.1 | | 15.5 | 5.1 | 7.9 | 1.0 | 7.4 | 8.6 | 6.6 | 4.1 | 6.4 | 4.6 | 6.3 |
| U | 3.0 | | 4.9 | | 4.8 | 4.1 | 4.9 | 13.5 | 3.9 | 5.0 | | 2.2 | 3.5 | 1.4 | 1.5 |
| Ta | 15.1 | 38 | 15.4 | 61 | 13.8 | 14.9 | 18.5 | 36.2 | 13.7 | 17.1 | 11.7 | 13.1 | 12.0 | 4.5 | 5.5 |
| Nb | 157 | 424 | 141 | 684 | 144 | 128 | 167 | 188 | 120 | 159 | 114 | 127 | 105 | 89 | 95 |
| Sr | 92 | 22 | 87 | 36 | 177 | 47 | 258 | 62 | 36 | 49 | 42 | 27 | 32 | 33 | 711 |
| Hf | 12.4 | 27.9 | 10.1 | 37.2 | 16.8 | 12.4 | 14.4 | 37.8 | 18.4 | 27.2 | 19.3 | 15.0 | 24.3 | 12.0 | 13.7 |
| Zr | 681 | 1534 | 405 | 1820 | 782 | 676 | 487 | 1203 | 568 | 895 | 611 | 491 | 858 | 496 | 568 |
| Y | 30 | 77 | 52 | 66 | 50 | 36 | 53 | 59 | 29 | 52 | 28 | 45 | 42 | 22 | 33 |
| La | 27.20 | 114 | 47.41 | 51 | 80 | 51.79 | 66.30 | 179.33 | 62.21 | 89.11 | 47 | 220 | 76 | 55.54 | 50.65 |
| Ce | 65.60 | 281 | 112.19 | 169 | 182 | 123.04 | 171.50 | 398.94 | 105.12 | 171.21 | 116 | 383 | 137 | 87.64 | 93.53 |
| Pr | 7.40 | | 12.38 | | | 13.88 | 10.13 | 20.93 | 12.83 | 18.84 | | | | 10.93 | 10.42 |
| Nd | 26.90 | 75 | 45.82 | 44 | 76 | 53.13 | 67.62 | 118.52 | 46.40 | 62.11 | 38 | 107 | 55 | 42.30 | 38.71 |
| Sm | 5.60 | 16 | 9.81 | 8 | 15 | 10.59 | 14.10 | 24.70 | 9.70 | 13.90 | 7.2 | 23 | 11 | 8.80 | 8.10 |
| Eu | 1.44 | | 1.33 | | | 1.44 | 1.38 | 1.29 | 2.48 | 1.62 | | | | 1.66 | 1.46 |
| Gd | 5.10 | | 8.62 | | | 9.75 | 11.4 | 20.00 | 8.83 | 11.97 | | | | 7.79 | 7.07 |
| Tb | 0.71 | | 0.98 | | | 1.14 | 1.39 | 2.03 | 1.25 | 1.49 | | | | 1.26 | 1.15 |
| Dy | 4.41 | | 6.70 | | | 8.15 | 8.07 | 14.28 | 7.62 | 10.03 | | | | 8.37 | 6.10 |
| Ho | 0.90 | | 1.35 | | | 1.63 | 1.60 | 2.98 | 1.56 | 2.05 | | | | 1.65 | 1.20 |
| Er | 2.37 | | 3.53 | | | 4.24 | 4.10 | 8.14 | 4.16 | 5.62 | | | | 4.35 | 3.33 |
| Tm | 0.43 | | 0.43 | | | 0.53 | 0.63 | 1.05 | 0.69 | 0.91 | | | | 0.58 | 0.46 |
| Yb | 2.43 | | 1.96 | | | 1.90 | 2.69 | 4.81 | 4.04 | 4.82 | | | | 3.35 | 2.52 |
| Lu | 0.35 | | 0.41 | | | 0.40 | 0.43 | 0.79 | 0.45 | 0.47 | | | | 0.42 | 0.32 |

## Significance of the mineralogy

The clinopyroxenes, following an initial increase in hedenbergite molecule with a corresponding decrease in the Mg/$Fe^{2+}$ ratio, become progressively enriched in Na (and $Fe^{3+}$) as the Alkali Index (and D.I.*) increases. The trend towards the Na-$Fe^{3+}$ (i.e. aegirine) enrichment may be originated anywhere from the hedenbergite-rich compositions (Fig. 4), and the point of departure appears, at least, a function of the peralkalinity of the magma(s), rather than a merely control of oxygen fugacity. The Bailey's (1969) experimental data suggest temperatures around 780-800°C for the more acmitic compositions.

Using the free energy data of Nicholls & Carmichael (1969), $fO_2$ estimates are around $10^{-17}$ bar. From the Ti and $Al^{IV}$–$Al^{VI}$ content of amphiboles

(Helz, 1982), it can be inferred that the ferro-edenite-ferropargasite from Cerro Ciete Cabezas and Stock I have crystallization temperatures around 700-750°C, while the ferro-richterite-katophorite from Stock II points to equilibration temperatures around 600-700°C. The uniformly low $Al^{VI}$ content is consistent with the low pressure conditions of the intrusions.

Using the equation of Wones (1981) and the estimated activities of annite in biotite (0.65 as average), of $KAlSi_3O_8$ in alkali feldspar (0.35) and of $Fe_3O_4$ in magnetite (0.76), temperatures of 575°C and $fO_2=10^{-23}$ bar (average of the results for the magnetite-ilmenite pairs) give about 900 bar for both $fH_2O$ and water partial pressure (Burnham *et al.*, 1969). Finally, if the original magma is assumed to have been $H_2O$-saturated, a 3 km depth would be indicated for the intrusions.

The fluorine content of biotite, X=0.06–0.07 (Cerro Siete Cabezas and Stock I) and X=0.12–0.14 (Stock II), suggests log ($fH_2O/fHF$) ratios of about 4 and 3, respectively, for the hydrothermal fluids in equilibrium with biotite in subsolidus environment.

Major and trace elements distribution

From the Fig. 8 it is apparent that the investigated rocks tend to cluster between the trachytic and phonolitic minima (Cerro Siete Cabezas complex) and towards the trachytic minimum (Stock I and Stock II bodies), whereas some Q-normative-rich samples from Stock I approach to the rhyolitic minimum. Variation diagrams using D.I.* (normative Q+or+ab+ne+ac) values as parameter (Fig. 9) show a decrease of $TiO_2$, FeO (total iron), MgO, CaO and $P_2O_5$, corresponding to the continuous fractionation of mafic phases and of apatite. The FeO scattering in the two stocks probably reflects crystal sorting processes occurring either during or after the intrusion.

$Al_2O_3$ tends to increase up to D.I.*=86, and then to slightly decrease up to D.I.*=90, mainly because of the nepheline fractionation. K is an incompatible element as D.I.*=92 and then decreases together Na and Al. In conclusion, from the D.I.* diagrams the following main crystallization sequence is apparent: clinopyroxene+apatite+accessories→ nepheline→alkali feldspar, according to the petrographic observations.

D.I.* vs. incompatible trace elements (I.E.; Table 9) and some element-element variation diagrams are illustrated in Fig. 10. The I.E. show remarkable dispersion, in particular Th and U which are scattered between two, "high" and "low" trends. Rb displays a broad positive correlation in the main complex and appears negatively correlated to D.I.* in the stocks.

Ba, Sr, Y and REE are negatively correlated, although some high REE values are noticeable in the two minor intrusions. In particular, the Rb vs. Sr diagram points to two distinct groups, with negative and positive correlations for the main intrusion and for the two satellite bodies, respectively. On the other hand, Ba-Sr and Nd-Sm appear well correlated, with Ba/Sr and Sm/Nd ratios of 0.43 and 0.20, respectively. Ta, Nb, Hf and Zr show quite constant (and scattered) behaviour with a tendency towards higher contents at D.I.* between 90 and 95 in Stock I. The Rb enrichment in the Stocks I and II, along their modal and normative quartz contents, raises the question of a possible contamination from the crystalline basement for the origin of these rocks.

The spidergrams relative to the primitive mantle-normalized I.E. (Sun & McDonough, 1989) evidence overlapping fields for the main complex and associated stocks, with U, Nb-Ta, Zr-Hf and Yb positive spikes and K, Sr, P and Ti negative anomalies (Fig. 11). Notably, the spidergrams parallel to the upper continental crust (Taylor & McLennan, 1981) and the Precambrian rhyolites from Fuerte Olimpo (Gomes *et al.*, 2000), except for Nb and Ta which, in the latter, show negative anomalies.

The REE spidergrams (chondrite-normalized; Boynton, 1984) have similar behaviours in the Cerro Siete Cabezas and Stock II, with La/Sm and La/Yb averaging 4.4 and 15.7–13.0, respectively, and with similar Eu negative spikes (Eu/Eu*=0.64 and 0.57,

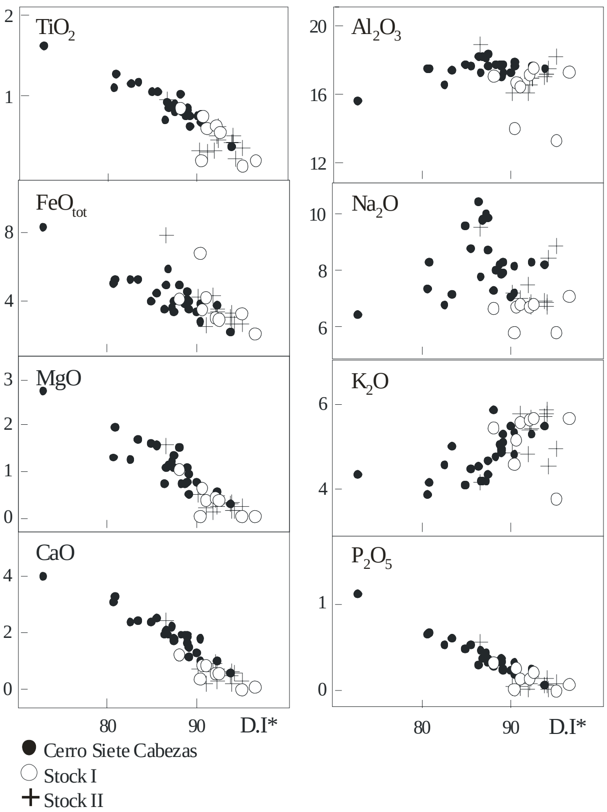


Fig. 9. D.I.* vs. major elements (wt%) for Cerro Siete Cabezas, Stock I and Stock II rocks.

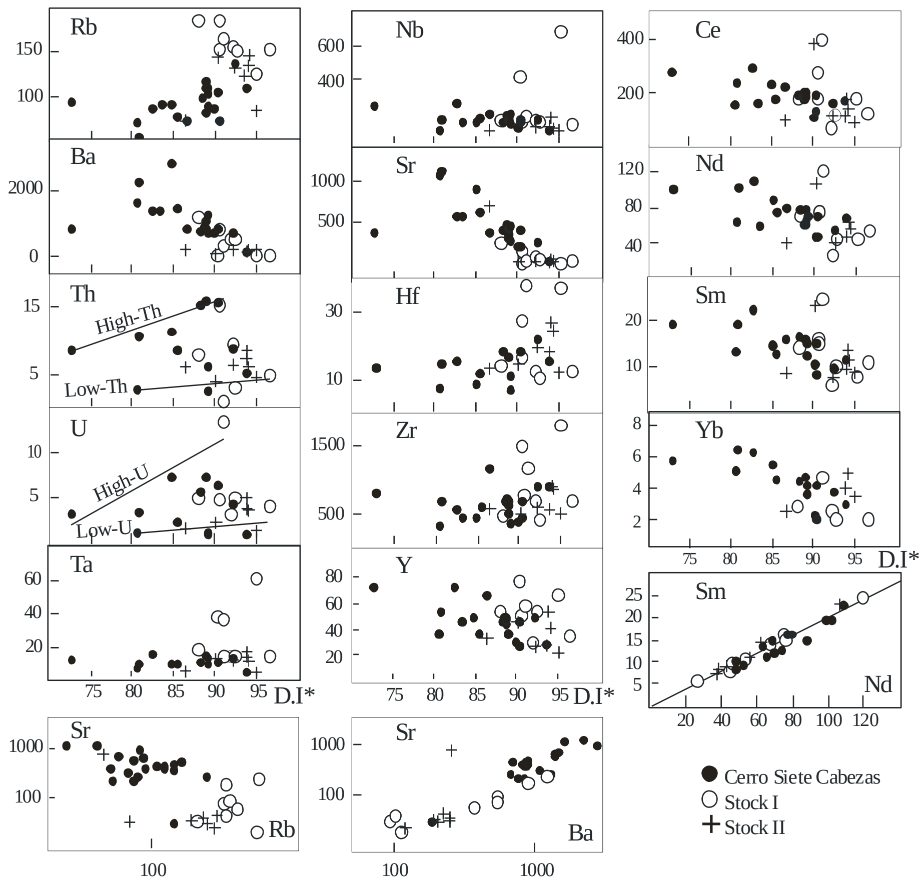


Fig. 10. D.I.* vs. trace elements (ppm) for Cerro Siete Cabezas, Stock I and Stock II rocks. Some element-element correlations (Sr-Rb, Sr-Ba and Sm-Nd) are also shown.

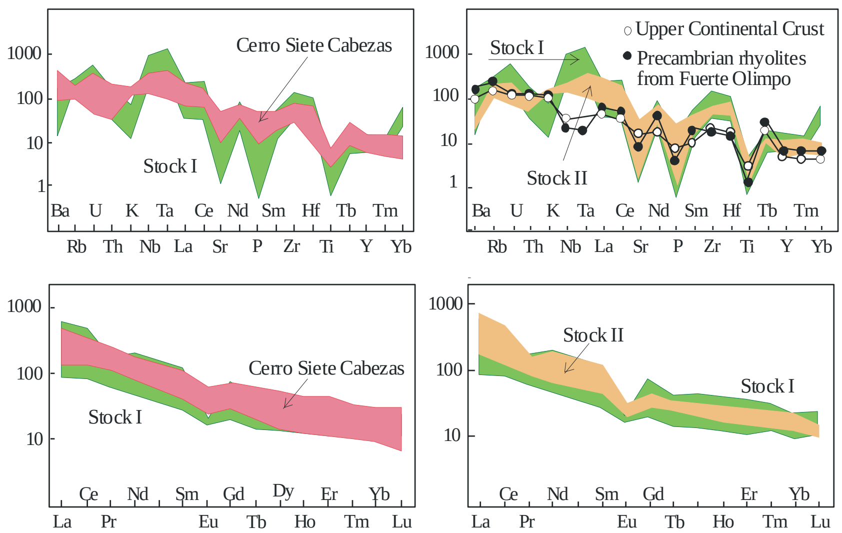


Fig. 11. Primitive mantle- (Sun & McDonough, 1989) and chondrite- (Boynton, 1984) normalized I.E. and REE distribution diagrams, respectively, for Cerro Siete Cabezas, Stock I and Stock II rocks. Upper Crust and Fuerte Olimpo values are from Taylor & McLennan (1981) and from Gomes *et al*. (2000), respectively.

respectively). Stock I is quite different having $(La/Sm)_C=3.6$, $(La/Yb)_C=17.8$ and the most negative Eu anomaly (Eu/Eu*=0.34). It should be noted that these pronounced Eu anomalies are probably due to an earlier crystallization of plagioclase in the parental (basanitic/theralitic) magma, and not only to the crystallization of phases such as titanite, eudialyte and so on.

## Sr-Nd isotopes

New results of selected isotopic analyses (whole rocks) are in Tables I and II of the Appendix. On the whole, the $^{87}Rb/^{86}Sr$ vs. $^{87}Sr/^{86}Sr$ ratios fit well a straigth line, $r^2=0.997$, initial $^{87}Sr/^{86}Sr$ $(R_0)=0.703788$, approaching the results of Velázquez *et al.* (1996a) that reported a $R_0=0.70361$. However, some important $R_0$ (241 Ma) differences are apparent for the rock-types from Cerro Siete Cabezas and two satellite bodies: all the samples from the main complex have quite constant $R_0$ (0.70380±0.00006), whereas the Q-normative rocks from the Stock I display the highest $R_0$ ratio (e.g. RP-47: $R_0=0.70988$, Q=23.61%; RP-45: $R_0=0.71602$, Q=14.57%). The samples from the Stock II show scattered $R_0$ values between 0.70374 and 0.70767. The data point to possible crustal contamination processes or to different magma types for the two minor intrusions. Mixing calculation between basement compositions (Araújo *et al*., 1982 and this work) and the "less evolved" magmas from the Cerro Siete Cabezas complex makes evident an unrealistic contamination by a rhyolitic source (e.g. sample RP-44) or that the basement contamination is outside of the mixing curves as shown in Figs. 12A, B. Probably there are complex relationships between a miaskitic magma and a peralkaline one (line 4 of Figs. 12A, B), the latter being subjected to fractional crystallization processes (cf. line FC of Fig. 12, and inset C).

Initial (241 Ma) $^{143}Nd/^{144}Nd$ ratios have a slightly depleted character, being between 0.51238 and 0.51239 in Cerro Siete Cabezas and Stock II, and between 0.51235 and 0.51236 in Stock I. Mixing between Sr-Nd isotopes of the less evolved rocks from the main complex (as RP-214) and basement rock-types (i.e. Fuerte Olimpo rhyolites and Porto Murtinho AZ-2 granite, cf. Table 1 of the Appendix), demonstrates that the contamination, in any case, is restricted to less than 10% of crustal components (inset D of Fig. 12).

Finally, it can be concluded that Nd-model ages, calculated with respect to a depleted reservoir (Table 1 of Appendix II; Faure, 1986), show, on the whole, an average value of 910±73 Ma (Cerro Siete Cabezas: 886±80; Stock I: 930±91; Stock II: 953±28).

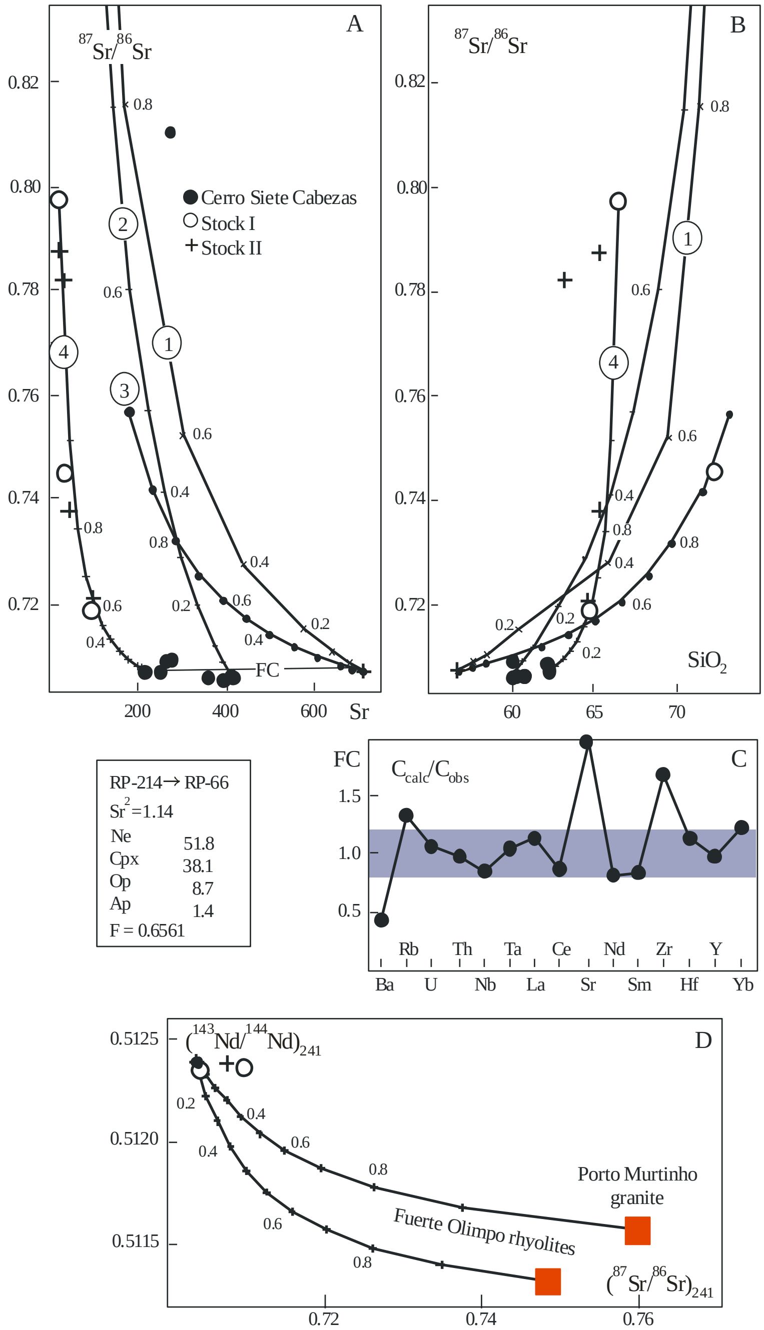


Fig. 12. Mixing curves between alkaline and basement rocks (Araújo *et al.*, 1982; Table 1). FC: fractional crystallization line between samples RP-214 to RP-66. A and B: fractional crystallization from RP-214 to RP-66 is consistent with fractionation of ~34% of nepheline+clinopyroxene+opaques+apatite. C: the calculated/observed ratios relative to the concentration of the trace elements are generally in the 20% gain or loss, Rb (calculated/observed ratio=1.3), Sr (2.0) and Zr (1.7) excepted (mineral/liquid partition coefficients after Marzoli, 1991, and Caroff *et al.*, 1993). D: Sr-Nd isotope mixing curves between the RP-214 sample and Fuerte Olimpo rhyolites and Porto Murtinho granite.

## 2. CERRO PEDREIRA, MORRO DISTANTE AND MORRO CONCEIÇÃO

Cerro Pedreira, Morro Distante and Morro Conceição (PDC) are three semi-circular stocks cropping out between Porto Murtinho town and the locality of Fecho dos Morros (Fig. 1). They cover areas of approximately 1, 2 and 4 $km^2$, respectively, and stand up to 20-30 m from the plain. Cerro Pedreira is also characterized by the presence of NE-SW-trending dykes, 1-2 m thick and porphyritic-aphanitic in texture.

### Petrography

The rocks are medium to coarse-grained, rarely pegmatoid, with equigranular to seriate texture. Representative modal analyses are given in Table 10. The main rock-types are syenites and subordinate nephel-syenites, whereas the dykes are quartz trachytes and alkali rhyolites. The intrusive rocks consist of perthitic alkali feldspar as the most abundant phase in addition to allotriomorphic quartz and plagioclase (oligoclase). The last mineral is subhedral in shape and zoned with An content ranging from 68 to 20. Nepheline-bearing varieties practically occur only at Morro Conceição. The main mafic minerals are amphibole, clinopyroxene and biotite. Opaques (magnetite and ilmenite) are ubiquitous, along with the accessory phases apatite, titanite and zircon. Eudialyte is typically absent. On the whole, the petrographic features outline an alkaline-miaskitic association where silica-saturated to slightly silica-oversaturated rock-types prevail on the silica-undersaturated variants.

The dykes exhibit phenocrysts and/or micro-phenocrysts of anorthoclase, amphibole and opaques set in a very fine groundmass consisting of alkali feldspar laths arranged in a trachytic texture and interstitial quartz. In the Cerro Pedreira stock, a xenolith consisting of cumulatic amphibole, plagioclase ($An_{70}$), opaques, biotite and apatite is noticeable (X RP-5B, Table 11).

### Classification and nomenclature

Following the petrochemical nomenclature ($R_1$-$R_2$ inset of Fig. 13; De la Roche *et al.*, 1980), the analyzed intrusives consist mainly of syenites and subordinate nephel-syenites, while the dykes plot into the quartz trachytes and alkali rhyolites, strictly corresponding to the petrographic (i.e. modal) classification.

Using the serial discrimination diagram (cf. inset $Na_2O$ vs. $K_2O$ of Fig. 13), it is apparent that the samples fall into the sodic-transitional and into the transitional fields.

The Alkali Index (A.I.) vs. Q-ne normative diagram (Fig. 13) defines two well-defined tendency: on one hand, the majority of the samples from Morro Conceição display an undersaturated character (A.I. ranging from 0.98 and 1.07), and, on the other one, the samples from Cerro Pedreira and Morro Distante have a silica-saturated to slightly oversaturated character with A.I.<1.0. All the dykes are oversaturated, varying from per-alkaline to metaluminous (Fig. 13).

Table 10. Representative modal analyses (vol%) of rocks from Cerro Pedreira, Morro Distante and Morro Conceição stocks. Accessory phases: titanite and zircon. For abbreviations see Table 1.

| | CERRO PEDREIRA | | | | | MORRO DISTANTE | | MORRO CONCEIÇÃO | |
|---|---|---|---|---|---|---|---|---|---|
| Sample | RP-1 | RP-5A | XRP-5B | RP-7 | RP-8 | RP-264 | RP-265 | RP-78 | RP-79 |
| vol% | | | | | | | | | |
| Q | 15.0 | | | | | 1.0 | 1.1 | 5.1 | 4.2 |
| AF | 78.5 | 75.0 | | 88.5 | 89.4 | 75.9 | 76.2 | 82.1 | 82.2 |
| Pl | | 8.9 | 36.9 | 1.4 | 1.1 | 0.5 | 0.8 | 0.9 | |
| Ne | | | | | | | | | |
| Cpx | 1.4 | 4.2 | | 0.1 | 2.3 | 1.4 | 1.0 | 1.0 | 2.1 |
| Am | 0.8 | 2.7 | 47.9 | 1.8 | | 9.8 | 9.5 | 7.4 | 6.8 |
| Bi | 1.2 | 3.7 | 4.0 | 6.2 | 3.4 | 7.7 | 8.0 | 0.5 | 0.9 |
| Op | 2.1 | 3.8 | 6.5 | 0.8 | 1.5 | 2.1 | 2.2 | 2.2 | 3.0 |
| Ap | 0.1 | 1.0 | 3.2 | 1.0 | 2.0 | 1.0 | 1.0 | 0.5 | 0.5 |
| Accessories | 0.9 | 0.7 | 1.5 | 0.2 | 0.3 | 0.9 | 0.2 | 0.3 | 0.3 |

Table 11. Major element analyses, norms and classification (according to De La Roche *et al.*, 1980) of selected Cerro Pedreira, Morro Distante and Morro Conceição rocks. D, dykes; X, xenolith. D.I. and A.I. differentiation and alkali indexes, respectively (cf. Table 2).

| | CERRO PEDREIRA | | | | | | | | | | |
|---|---|---|---|---|---|---|---|---|---|---|---|
| Sample | RP-1 D | RP-2 D | RP-3 | RP-4 | RP5A | RP-5B X | RP-6 D | RP-7 | RP-8 | RP-205 | RP-206 D |
| wt% | | | | | | | | | | | |
| $SiO_2$ | 68.41 | 69.93 | 66.24 | 59.57 | 59.17 | 41.70 | 68.94 | 60.21 | 60.31 | 65.26 | 68.93 |
| $TiO_2$ | 0.34 | 0.36 | 0.43 | 1.38 | 1.43 | 3.82 | 0.50 | 1.26 | 1.25 | 0.41 | 0.33 |
| $Al_2O_3$ | 14.82 | 14.23 | 16.91 | 16.29 | 16.42 | 16.81 | 14.71 | 16.46 | 16.5 | 17.63 | 15.39 |
| $Fe_2O_3$ | 3.40 | 2.90 | 1.29 | 3.59 | 1.79 | 3.07 | 2.55 | 3.34 | 3.39 | 1.39 | 2.44 |
| FeO | 1.01 | 1.03 | 0.70 | 1.54 | 3.01 | 8.92 | 1.07 | 1.39 | 1.47 | 0.61 | 1.06 |
| MnO | 0.31 | 0.09 | 0.13 | 0.15 | 0.14 | 0.20 | 0.20 | 0.17 | 0.16 | 0.15 | 0.12 |
| MgO | 0.12 | 0.35 | 0.32 | 2.87 | 2.88 | 7.34 | 0.14 | 2.19 | 2.00 | 0.14 | 0.03 |
| CaO | 0.03 | 0.49 | 0.44 | 3.18 | 3.25 | 11.02 | 0.95 | 2.96 | 2.71 | 0.11 | 0.16 |
| $Na_2O$ | 7.66 | 6.07 | 7.08 | 5.96 | 5.91 | 3.07 | 4.97 | 6.31 | 6.41 | 9.12 | 6.25 |
| $K_2O$ | 2.94 | 3.89 | 5.36 | 4.23 | 4.26 | 1.02 | 4.71 | 4.10 | 4.19 | 4.71 | 4.26 |
| $P_2O_5$ | 0.08 | 0.03 | 0.08 | 0.81 | 0.90 | 1.69 | 0.04 | 0.66 | 0.67 | 0.05 | 0.04 |
| L.O.I. | 0.40 | 0.38 | 0.35 | 0.30 | 0.66 | 1.05 | 1.00 | 0.81 | 0.73 | 0.33 | 0.50 |
| Sum | 99.52 | 99.75 | 99.33 | 99.87 | 99.82 | 99.71 | 99.78 | 99.86 | 99.79 | 99.91 | 99.51 |
| Q | 13.49 | 18.70 | 4.13 | 1.04 | | | 19.98 | 1.34 | 1.21 | | 15.99 |
| C | | | | | | | | | | | 0.30 |
| or | 17.37 | 22.98 | 31.67 | 24.99 | 25.17 | 6.02 | 27.83 | 24.23 | 24.76 | 27.83 | 25.17 |
| ab | 59.86 | 51.36 | 57.14 | 50.43 | 50.00 | 15.91 | 42.05 | 53.39 | 54.24 | 63.49 | 52.88 |
| an | | 0.09 | | 5.20 | 5.69 | 29.07 | 3.91 | 4.48 | 3.87 | | |
| ne | | | | | | 5.44 | | | | 0.52 | |
| ac | 4.36 | | 2.43 | | | | | | | 4.02 | |
| ns | | | | | | | | | | 1.89 | |
| di | | 1.66 | 1.33 | 4.10 | 3.62 | 11.74 | 0.41 | 4.58 | 4.03 | 0.18 | |
| hy | 0.32 | 0.09 | 0.58 | 5.23 | 6.90 | | 0.15 | 3.32 | 3.10 | | 0.07 |
| ol | | | | | 0.33 | 14.81 | | | | 0.27 | |
| mt | 2.74 | 2.56 | 0.64 | 1.45 | 2.59 | 4.45 | 2.65 | 1.38 | 1.63 | | 2.85 |
| hm | | 1.12 | | 2.58 | | | 0.72 | 2.38 | 2.26 | | 0.47 |
| il | 0.64 | 0.68 | 0.81 | 2.62 | 2.71 | 7.25 | 0.94 | 2.39 | 2.37 | 0.77 | 0.62 |
| ap | 0.18 | 0.07 | 0.18 | 1.91 | 2.13 | 4.00 | 0.09 | 1.56 | 1.58 | 0.11 | 0.09 |
| D.I.* | 95.1 | 93.1 | 95.4 | 76.5 | 75.2 | 27.4 | 93.8 | 79.0 | 80.2 | 95.9 | 94.0 |
| A.I. | 1.06 | 1.00 | 1.03 | 0.88 | 0.87 | 0.37 | 0.90 | 0.90 | 0.91 | 1.14 | 0.97 |
| $R_1$ | 1026 | 1481 | 582 | 694 | 681 | 1027 | 1618 | 656 | 603 | -56 | 1275 |
| $R_2$ | 300 | 348 | 395 | 802 | 813 | 1873 | 397 | 748 | 713 | 365 | 321 |
| Rock-type | Quartz trachyte | Quartz trachyte | Syenite | Syenite | Syenite | Basanite | Alkali rhyolite | Syenite | Syenite | Nephel-syenite | Quartz trachyte |
| Q | 53.4 | 56.1 | 47.3 | 45.7 | 45.0 | 36.1 | 57.1 | 45.9 | 45.8 | 44.8 | 54.3 |
| Ne | 35.7 | 29.9 | 33.3 | 35.7 | 36.0 | 51.4 | 25.3 | 36.6 | 36.6 | 38.0 | 30.5 |
| Ks | 10.9 | 14.0 | 19.4 | 18.6 | 19.0 | 12.5 | 17.6 | 17.5 | 17.6 | 17.2 | 15.2 |

| | MORRO DISTANTE | | | MORRO CONCEIÇÃO | | | | | | | | |
|---|---|---|---|---|---|---|---|---|---|---|---|---|
| Sample | RP-264 | RP-265 | RP-266 | RP-9 | RP-76 | RP-77 | RP-78 | RP-79 | RP-259 | RP-260 | RP-261 | RP-262 |
| wt% | | | | | | | | | | | | |
| $SiO_2$ | 64.35 | 65.15 | 64.32 | 62.16 | 61.83 | 58.65 | 64.33 | 65.39 | 61.52 | 61.49 | 61.21 | 61.45 |
| $TiO_2$ | 0.72 | 0.69 | 0.69 | 1.05 | 0.84 | 1.13 | 0.74 | 0.66 | 0.78 | 0.77 | 0.79 | 0.74 |
| $Al_2O_3$ | 16.60 | 16.30 | 16.58 | 17.43 | 17.55 | 17.78 | 16.69 | 16.85 | 17.48 | 17.54 | 17.34 | 17.54 |
| $Fe_2O_3$ | 2.00 | 1.91 | 1.93 | 1.28 | 1.93 | 1.96 | 2.12 | 1.71 | 2.40 | 2.34 | 2.43 | 2.33 |
| FeO | 0.99 | 0.95 | 0.97 | 2.04 | 0.98 | 2.73 | 1.09 | 0.84 | 1.30 | 1.27 | 1.30 | 1.26 |
| MnO | 0.11 | 0.10 | 0.10 | 0.16 | 0.13 | 0.20 | 0.12 | 0.09 | 0.17 | 0.16 | 0.16 | 0.15 |
| MgO | 1.29 | 1.26 | 1.09 | 1.12 | 0.99 | 1.44 | 0.95 | 0.44 | 1.05 | 1.06 | 1.05 | 0.98 |
| CaO | 1.80 | 1.64 | 1.85 | 1.22 | 1.04 | 2.74 | 1.44 | 0.66 | 1.86 | 1.73 | 1.98 | 1.90 |
| $Na_2O$ | 6.56 | 6.68 | 6.82 | 6.03 | 6.77 | 7.33 | 6.29 | 6.33 | 7.16 | 7.20 | 7.00 | 7.30 |
| $K_2O$ | 4.37 | 4.40 | 4.20 | 6.48 | 6.66 | 4.87 | 4.93 | 6.00 | 5.13 | 5.04 | 5.06 | 4.90 |
| $P_2O_5$ | 0.26 | 0.25 | 0.25 | 0.33 | 0.25 | 0.76 | 0.29 | 0.27 | 0.31 | 0.30 | 0.35 | 0.30 |
| L.O.I. | 0.65 | 0.50 | 0.65 | 0.40 | 0.55 | 0.23 | 0.62 | 0.62 | 0.65 | 0.81 | 0.93 | 0.77 |
| Sum | 99.70 | 99.83 | 99.45 | 99.70 | 99.52 | 99.82 | 99.61 | 99.86 | 99.81 | 99.71 | 99.60 | 99.62 |
| Q | 5.34 | 5.84 | 4.83 | | | | 5.72 | 4.69 | | | | |
| or | 25.82 | 26.00 | 24.82 | 38.29 | 39.35 | 28.78 | 29.13 | 35.45 | 30.31 | 29.78 | 29.90 | 28.95 |
| ab | 55.50 | 56.52 | 57.70 | 50.48 | 44.45 | 46.61 | 53.22 | 53.26 | 54.20 | 55.05 | 54.42 | 55.27 |
| an | 2.94 | 1.49 | 2.22 | 1.35 | | 1.23 | 2.74 | | 0.40 | 0.65 | 0.95 | 0.62 |
| ne | | | | 0.29 | 4.73 | 8.34 | | | 3.45 | 3.17 | 2.60 | 3.51 |
| ac | | | | | 3.60 | | | 0.25 | | | | |
| di | 4.33 | 3.17 | 4.14 | 2.04 | 2.74 | 5.99 | 1.94 | 1.17 | 5.28 | 4.64 | 5.12 | 5.29 |
| hy | 1.66 | 1.33 | 0.79 | | | | 1.46 | 0.55 | | | | |
| ol | | | | 2.19 | 0.88 | 1.85 | | | 0.11 | 0.34 | 0.16 | |
| mt | 1.46 | 1.38 | 1.45 | 1.85 | 0.99 | 2.84 | 1.75 | 1.08 | 2.48 | 2.38 | 2.42 | 2.40 |
| hm | 0.99 | 0.95 | 0.92 | | | | 0.90 | 0.86 | 0.68 | 0.69 | 0.75 | 0.67 |
| il | 1.36 | 1.31 | 1.31 | 1.99 | 1.59 | 2.14 | 1.40 | 1.25 | 1.48 | 1.46 | 1.50 | 1.40 |
| ap | 0.61 | 0.59 | 0.59 | 0.78 | 0.59 | 1.80 | 0.68 | 0.63 | 0.73 | 0.71 | 0.82 | 0.71 |
| D.I.* | 86.7 | 88.4 | 87.4 | 89.1 | 92.1 | 87.7 | 88.1 | 93.7 | 88.0 | 88.0 | 86.9 | 87.7 |
| A.I. | 0.94 | 0.97 | 0.95 | 0.97 | 1.05 | 0.97 | 0.94 | 1.00 | 0.99 | 0.99 | 0.98 | 0.99 |
| $R_1$ | 838 | 846 | 786 | 368 | 60 | 11 | 796 | 621 | 239 | 246 | 291 | 243 |
| $R_2$ | 582 | 558 | 577 | 528 | 505 | 713 | 529 | 423 | 594 | 582 | 604 | 596 |
| Rock-type | Syenite | Syenite | Syenite | Syenite | Nephel-syenite | Nephel-syenite | Syenite | Syenite | Nephel-syenite | Nephel-syenite | Nephel-syenite | Nephel-syenite |
| Q | 48.4 | 48.6 | 48.1 | 44.6 | 42.2 | 40.4 | 48.5 | 47.5 | 43.1 | 43.3 | 43.5 | 43.1 |
| Ne | 34.7 | 34.7 | 35.8 | 31.0 | 32.5 | 40.1 | 32.7 | 30.9 | 37.3 | 37.5 | 36.9 | 38.1 |
| Ks | 16.9 | 16.7 | 16.1 | 24.4 | 25.3 | 19.5 | 18.8 | 21.6 | 19.6 | 19.2 | 19.6 | 10.8 |

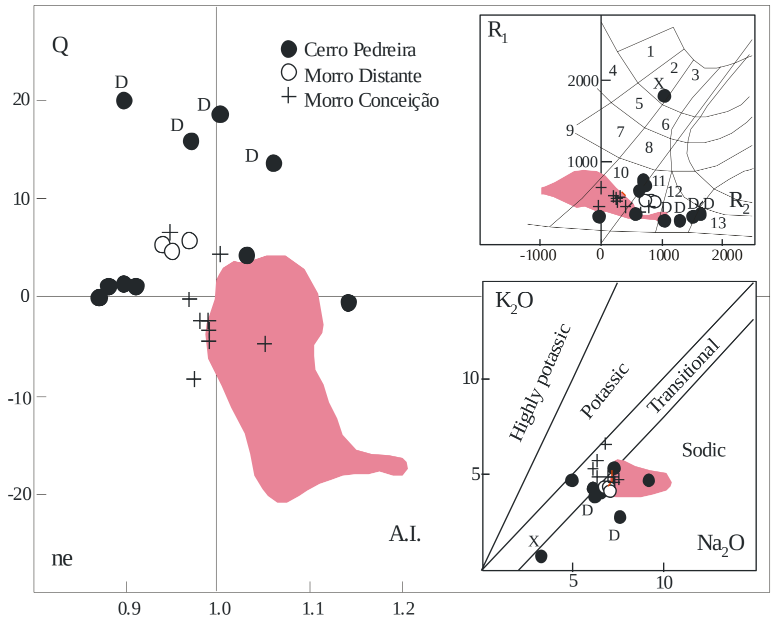


Fig. 13. A.I. vs. Q-ne diagram for Cerro Pedreira, Morro Distante and Morro Conceição rocks. For insets see Fig. 3; D, dykes; X, xenolith. In pink, the fields for the Cerro Siete Cabezas rocks.

Table 12. Representative clinopyroxene analyses from Cerro Pedreira, Morro Distante and Morro Conceição rocks. For additional information see Table 3.

| | CERRO PEDREIRA | | MORRO DISTANTE | | MORRO CONCEIÇÃO |
|---|---|---|---|---|---|
| Sample | RP-1 | RP-5A | RP-264C | RP-264R | RP-259 |
| wt% | | | | | |
| $SiO_2$ | 53.43 | 53.40 | 52.78 | 50.01 | 51.46 |
| $TiO_2$ | 0.48 | 0.54 | 0.34 | 1.01 | 0.77 |
| $Al_2O_3$ | 0.93 | 1.27 | 0.87 | 4.56 | 1.74 |
| $Cr_2O_3$ | 0.03 | 0.01 | | | |
| $Fe_2O_3$ | 2.30 | | 2.42 | 7.59 | 4.33 |
| FeO | 6.44 | 7.33 | 6.51 | 2.90 | 6.73 |
| MnO | 0.80 | 0.77 | 1.12 | 0.98 | 0.85 |
| MgO | 13.94 | 14.10 | 13.97 | 7.74 | 10.81 |
| CaO | 22.57 | 22.34 | 22.03 | 24.51 | 21.57 |
| $Na_2O$ | 0.74 | 0.63 | 0.58 | 2.09 | 1.65 |
| $K_2O$ | 0.00- | 0.02 | 0.01 | 0.64 | 0.01 |
| Sum | 101.76 | 100.40 | 100.63 | 98.16 | 99.92 |
| | | | | | |
| Si | 1.961 | 1.984 | 1.968 | 1.856 | 1.939 |
| $Al^{IV}$ | 0.039 | 0.016 | 0.032 | 0.144 | 0.061 |
| Sum | 2.000 | 2.000 | 2.000 | 2.000 | 2.000 |
| $Al^{VI}$ | 0.001 | 0.040 | 0.006 | 0.056 | 0.016 |
| Ti | 0.013 | 0.015 | 0.010 | 0.028 | 0.022 |
| Cr | 0.001 | 0.000 | | | |
| $Fe^{3+}$ | 0.063 | 0.000 | 0.068 | 0.212 | 0.123 |
| $Fe^{2+}$ | 0.197 | 0.228 | 0.203 | 0.091 | 0.212 |
| Mn | 0.025 | 0.024 | 0.035 | 0.031 | 0.027 |
| Mg | 0.761 | 0.781 | 0.776 | 0.428 | 0.607 |
| Ca | 0.885 | 0.888 | 0.880 | 0.975 | 0.871 |
| Na | 0.053 | 0.023 | 0.021 | 0.150 | 0.121 |
| K | | 0.001 | 0.01 | 0.030 | 0.001 |
| Sum | 2.000 | 2.000 | 2.000 | 2.000 | 2.000 |
| | | | | | |
| Mg/(Mg+Fe+Mn) | 0.728 | 0.756 | 0.717 | 0.561 | 0.626 |
| Quad | 1.84 | 1.90 | 1.86 | 1.49 | 1.69 |
| J | 0.11 | 0.05 | 0.04 | 0.30 | 0.24 |

Table 13. Representative amphibole analyses from Cerro Pedreira, Morro Distante and Morro Conceição rocks. C, core; R, rim. For additional information see Table 4.

| | CERRO PEDREIRA | | | | | | | MORRO DISTANTE | | MORRO CONCEIÇÃO | |
|---|---|---|---|---|---|---|---|---|---|---|---|
| Sample | RP-4 | RP-5AC | RP-5AR | RP-5B | RP-205C | RP-205R | RP-205R | RP-264C | RP-264R | RP-259C | RP-259R |
| wt% | | | | | | | | | | | |
| $SiO_2$ | 46.32 | 46.34 | 45.84 | 45.34 | 49.13 | 48.72 | 43.03 | 50.01 | 47.13 | 46.53 | 45.10 |
| $TiO_2$ | 0.98 | 1.08 | 1.91 | 4.54 | 3.04 | 2.00 | 5.05 | 1.01 | 1.00 | 1.08 | 1.73 |
| $Al_2O_3$ | 3.75 | 3.90 | 2.81 | 7.22 | 4.45 | 3.52 | 2.56 | 4.56 | 2.74 | 6.39 | 5.93 |
| $Fe_2O_3$ | 1.95 | 0.34 | 1.26 | | | 6.68 | 21.46 | 8.94 | 3.91 | 4.62 | 0.29 |
| FeO | 24.45 | 24.79 | 29.21 | 11.83 | 10.40 | 11.12 | 12.88 | 1.68 | 25.73 | 11.68 | 22.03 |
| MnO | 1.47 | 1.57 | 1.95 | 0.22 | 0.51 | 0.70 | 1.00 | 0.98 | 1.67 | 1.05 | 1.29 |
| MgO | 5.59 | 6.28 | 2.02 | 13.50 | 15.49 | 11.28 | 3.16 | 17.62 | 3.61 | 13.31 | 9.07 |
| CaO | 7.72 | 8.28 | 6.17 | 8.78 | 8.17 | 5.14 | 1.15 | 10.76 | 6.09 | 10.05 | 9.51 |
| $Na_2O$ | 4.01 | 4.02 | 4.18 | 4.15 | 4.90 | 5.87 | 7.16 | 2.09 | 4.45 | 2.44 | 2.37 |
| $K_2O$ | 1.18 | 1.04 | 0.97 | 1.96 | 1.31 | 1.83 | 1.65 | 0.64 | 0.95 | 0.93 | 0.97 |
| F | n.d. | n.d. | n.d. | n.d. | 1.73 | 1.23 | 0.18 | n.d. | n.d. | 1.60 | 1.37 |
| Cl | n.d. | n.d. | n.d. | n.d. | 0.01 | 0.01 | 0.01 | n.d. | n.d. | 0.06 | 0.11 |
| Sum | 97.42 | 97.64 | 96.32 | 97.64 | 98.41 | 97.57 | 99.21 | 98.29 | 97.28 | 99.06 | 99.17 |
| Si | 7.303 | 7.278 | 7.461 | 6.727 | 7.186 | 7.356 | 6.794 | 7.115 | 7.487 | 6.886 | 6.927 |
| $Al^{IV}$ | 0.697 | 0.722 | 0.539 | 1.260 | 0.767 | 0.626 | 0.476 | 0.764 | 0.513 | 1.114 | 1.073 |
| $Fe^{3+}$ | | | | | | 0.018 | 0.730 | 0.121 | | | |
| $Ti^{IV}$ | | | | 0.013 | 0.047 | | | | | | |
| Sum | 8.000 | 8.000 | 8.000 | 8.000 | 8.000 | 8.000 | 8.000 | 8.000 | 8.000 | 8.000 | 8.000 |
| $Al^{VI}$ | 0.000 | 0.000 | 0.000 | 0.000 | 0.000 | 0.000 | 0.000 | 0.000 | 0.000 | 0.000 | 0.000 |
| Ti | 0.116 | 0.128 | 0.234 | 0.492 | 0.287 | 0.227 | 0.600 | 0.108 | 0.119 | 0.120 | 0.200 |
| $Fe^{3+}$ | 0.231 | 0.040 | 0.154 | 0.000 | 0.000 | 0.456 | 1.092 | 0.696 | 0.468 | 0.515 | 0.034 |
| $Fe^{2+}$ | 3.224 | 3.256 | 3.976 | 1.465 | 1.272 | 1.688 | 2.430 | 0.341 | 3.418 | 1.445 | 2.829 |
| Mn | 0.196 | 0.209 | 0.269 | 0.028 | 0.063 | 0.090 | 0.134 | 0.118 | 0.225 | 0.132 | 0.168 |
| Mg | 1.314 | 1.470 | 0.490 | 2.979 | 3.378 | 2.539 | 0.744 | 3.737 | 0.855 | 2.969 | 2.077 |
| Sum | 5.081 | 5.104 | 5.123 | 4.964 | 5.000 | 5.000 | 5.000 | 5.000 | 5.085 | 5.148 | 5.307 |
| Ca | 1.304 | 1.393 | 1.076 | 1.393 | 0.993 | 0.831 | 0.195 | 1.640 | 1.037 | 1.593 | 1.565 |
| $Na_B$ | 0.615 | 0.503 | 0.802 | 0.607 | 1.007 | 1.169 | 1.805 | 0.360 | 0.878 | 0.258 | 0.128 |
| Sum | 1.919 | 1.896 | 1.878 | 2.000 | 2.000 | 2.000 | 2.000 | 2.000 | 1.915 | 1.851 | 1.693 |
| $Na_A$ | 0.611 | 0.721 | 0.518 | 0.584 | 0.383 | 0.550 | 0.387 | 0.217 | 0.492 | 0.442 | 0.578 |
| K | 0.237 | 0.208 | 0.201 | 0.370 | 0.244 | 0.352 | 0.332 | 0.116 | 0.193 | 0.176 | 0.190 |
| $Sum_A$ | 0.848 | 0.929 | 0.719 | 0.954 | 0.627 | 0.902 | 0.719 | 0.333 | 0.685 | 0.617 | 0.768 |
| F | | | | | 0.800 | 0.587 | 0.090 | | | 0.740 | 0.650 |
| Cl | | | | | 0.002 | | 0.003 | | | 0.015 | 0.028 |
| Mg/(Mg+Fe+Mn) | 0.265 | 0.295 | 0.100 | 0.666 | 0.716 | 0.532 | 0.169 | 0.764 | 0.172 | 0.587 | 0.407 |

## Mineralogy

Representative chemical compositions of minerals from selected samples are given in Tables 12 to 16.

### *Clinopyroxene and amphibole*

Mg/(Mg+Fe+Mn) ratio varies from 0.56 to 0.73 in clinopyroxene (Table 12). The classificative diagrams (Fig. 14) show that the clinopyroxenes have a narrow compositional range fitting the salite field, with Mg values higher than that of pyroxene cores from the Cerro Siete Cabezas analogues.

The amphiboles belong to the sodic-calcic series (Cerro Pedreira: katophorite and magnesio-katophorite) and to the calcic series (Morro Distante and Morro Conceição: edenite and hornblende); the Mg/(Mg+Fe+ Mn) ratio is quite variable, from 0.58 to 0.78, in the central parts of the grains, and up to 0.14 in the rims (cf. Table 13). The Fe (Na) enrichment follows two main trends: one similar to that of amphiboles from the Cerro Siete Cabezas complex, and the other towards more Na-rich compositions (Fig. 14). Notably, the amphibole from the xenolith falls in the same compositional range of the amphibole cores from Cerro Pedreira.

### *Biotite*

In general, the biotites cluster in a group of phlogopite-rich composition (Mg=3.5−3.7 a.f.u.; Table 14 and Fig. 15), except for the Cerro Pedreira mineral, which is Fe enriched (Mg=2.8 a.f.u.). The RP-5B xenolith shows the most Mg-rich and Ti-poor composition (Mg=4.8, Ti=0.047 a.f.u., respectively). The Mg-rich compositions correspond also to the Mn-poor compositions with respect to the

Cerro Siete Cabezas analogues.

*Iron oxides*

The opaque minerals are magnetite (Cerro Pedreira and Morro Distante: ulvöspinel 0.6-12.0 mol%), Ti-magnetite (Morro Conceição: ulvöspinel 32-54 mol%), and Mn-rich (MnO 4.4-7.5 wt%) ilmenite (Table 15) generally found as discrete pairs in the rocks.

The geothermometry of Spencer & Lindsley (1981) yielded temperatures between 612 and 797°C and log $fO_2$ from −13 to −16 between the Nickel-Nickel Oxide and Hematite-Magnetite buffers (Fig. 16), suggesting for these minerals more oxidizing conditions than those calculated for the Cerro Siete Cabezas analogues.

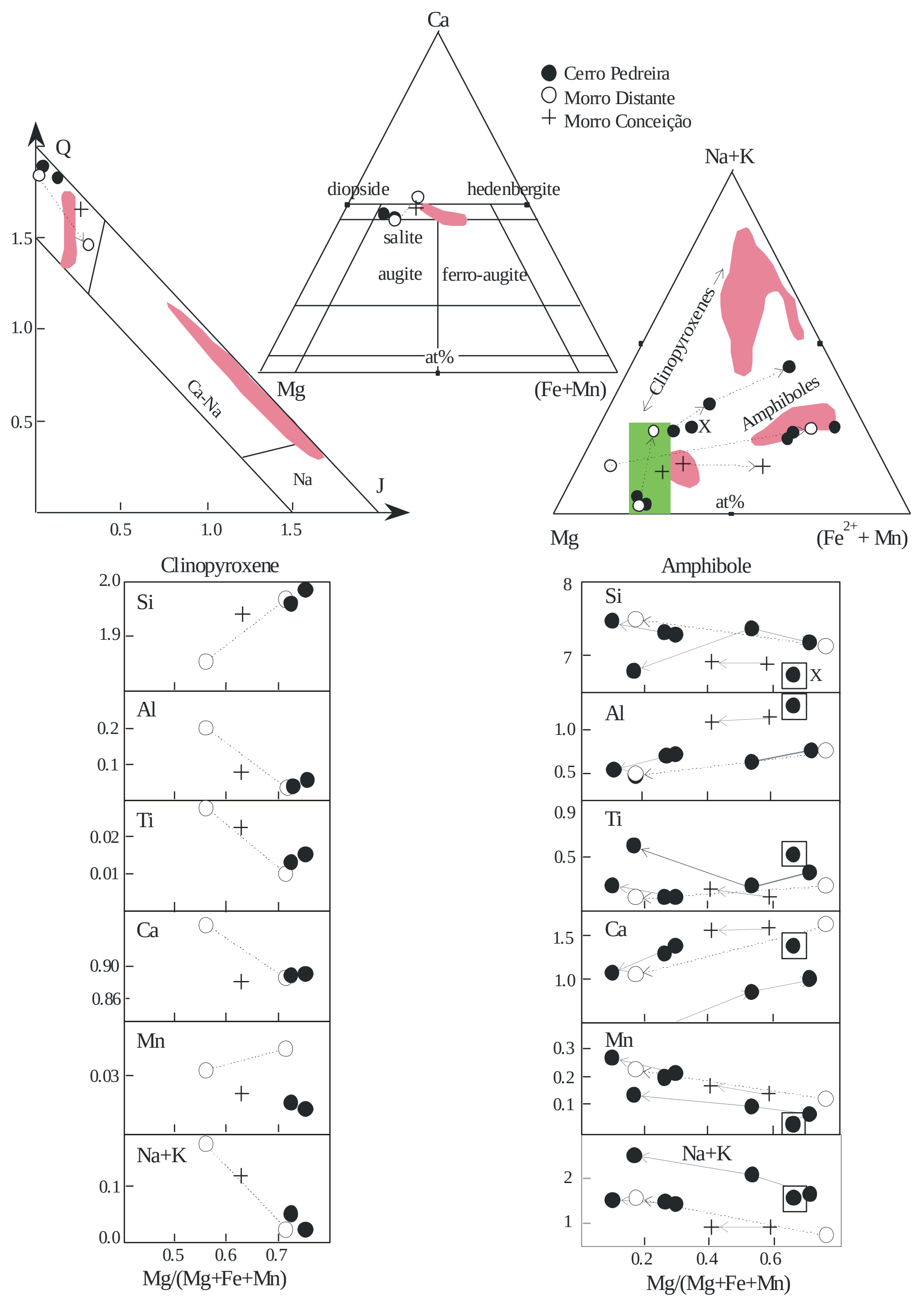


Fig. 14. Classificative and variation diagrams for clinopyroxenes and amphiboles from Cerro Pedreira, Morro Distante and Morro Conceição rocks; X: xenolith from Cerro Pedreira. For additional information see Fig. 4. In pink, the fields for the Cerro Siete Cabezas minerals.

Table 14. Representative biotite analyses from Cerro Pedreira, Morro Distante and Morro Conceição rocks. For additional information see Table 5.

| | CERRO PEDREIRA | | | | | MORRO DISTANTE | | MORRO CONCEIÇÃO |
|---|---|---|---|---|---|---|---|---|
| Sample | RP-4 | RP-5A | RP-5A | RP-5B | RP-205 | RP-264 | RP-264 | RP-259 |
| wt% | | | | | | | | |
| $SiO_2$ | 37.39 | 38.69 | 38.06 | 40.97 | 38.34 | 37.57 | 38.86 | 36.82 |
| $TiO_2$ | 5.35 | 4.98 | 5.51 | 0.43 | 1.88 | 4.02 | 4.01 | 5.03 |
| $Al_2O_3$ | 12.64 | 12.79 | 12.93 | 13.48 | 11.18 | 13.56 | 13.61 | 13.56 |
| $Cr_2O_3$ | 0.08 | n.d. | 0.04 | 0.01 | n.d. | 0.01 | 0.02 | n.d. |
| $FeO_{tot}$ | 12.64 | 12.73 | 12.19 | 7.91 | 21.87 | 13.23 | 11.99 | 13.45 |
| MnO | 0.28 | 0.35 | 0.31 | 0.14 | 0.52 | 0.42 | 0.39 | 0.53 |
| MgO | 16.54 | 17.01 | 16.23 | 22.20 | 12.22 | 16.93 | 17.07 | 16.25 |
| CaO | n.d. | 0.03 | n.d. | 0.03 | 0.01 | 0.02 | 0.02 | 0.01 |
| $Na_2O$ | 0.30 | 0.35 | 0.40 | 0.20 | 0.24 | 0.40 | 0.33 | 0.57 |
| $K_2O$ | 9.17 | 9.29 | 9.24 | 9.85 | 9.47 | 9.46 | 9.60 | 9.17 |
| F | n.d. | n.d. | n.d. | n.d. | 0.99 | 2.54 | 2.56 | 2.23 |
| Cl | n.d. | n.d. | n.d. | n.d. | 0.01 | 0.16 | 0.17 | 0.16 |
| Less O=F, Cl | | | | | 0.57 | 1.10 | 1.09 | 0.97 |
| $H_2O^+_{calc}$ | 3.99 | 4.09 | 4.04 | 4.16 | 3.45 | 2.91 | 2.95 | 3.02 |
| Sum | 98.38 | 100.31 | 98.95 | 99.38 | 99.61 | 100.13 | 100.49 | 99.83 |
| Si | 5.601 | 5.672 | 5.648 | 5.900 | 5.854 | 5.422 | 5.541 | 5.358 |
| $Al^{IV}$ | 2.232 | 2.210 | 2.262 | 2.100 | 2.012 | 2.307 | 2.287 | 2.326 |
| $Ti^{IV}$ | 0.167 | 0.118 | 0.090 | | 0.134 | 0.251 | 0.172 | 0.316 |
| Sum (Z) | 8.000 | 8.000 | 8.000 | 8.000 | 8.000 | 8.000 | 8.000 | 8.000 |
| $Al^{VI}$ | | | | 0.188 | | | | |
| $Ti^{VI}$ | 0.436 | 0.431 | 0.525 | 0.047 | 0.082 | 0.185 | 0.258 | 0.235 |
| Cr | 0.010 | | 0.005 | 0.001 | | 0.001 | 0.002 | |
| $Fe^{2+}$ | 1.584 | 1.561 | 1.513 | 0.953 | 2.793 | 1.597 | 1.430 | 1.637 |
| Mn | 0.036 | 0.043 | 0.039 | 0.017 | 0.067 | 0.051 | 0.047 | 0.065 |
| Mg | 3.693 | 3.717 | 3.590 | 4.766 | 2.782 | 3.643 | 3.628 | 3.525 |
| Sum (Y) | 5.759 | 5.752 | 5.672 | 5.972 | 5.724 | 5.477 | 5.365 | 5.462 |
| Ca | | 0.005 | | 0.005 | 0.002 | 0.003 | 0.003 | 0.002 |
| Na | 0.087 | 0.099 | 0.115 | 0.056 | 0.071 | 0.112 | 0.091 | 0.161 |
| K | 1.752 | 1.737 | 1.749 | 1.809 | 1.845 | 1.742 | 1.746 | 1.702 |
| Sum (X) | 1.839 | 1.841 | 1.864 | 1.870 | 1.918 | 1.857 | 1.840 | 1.865 |
| F | n.d. | n.d. | n.d. | n.d. | 0.478 | 1.159 | 1.154 | 1.026 |
| Cl | n.d. | n.d. | n.d. | n.d. | 0.003 | 0.039 | 0.041 | 0.039 |
| OH | 4.000 | 4.000 | 4.000 | 4.000 | 3.519 | 2.802 | 2.805 | 2.935 |
| Sum | 4.000 | 4.000 | 4.000 | 4.000 | 4.000 | 4.000 | 4.000 | 4.000 |
| Mg/(Mg+Fe+Mn) | 0.695 | 0.740 | 0.698 | 0.831 | 0.493 | 0.688 | 0.711 | 0.674 |

### *Feldspars, nepheline, accessory minerals and mineralogical inferences*

Plagioclase crystals ($An_{68-20}$) coexist with late crystallized perthitic anorthoclase ($Ab_{56-37}$) and/or oligoclase ($An_{20-13}$) phases. They typically follow K-Na enrichment and Ca-depletion trends from the core to the rim of the grains, and sometimes the grains are mantled by albite ($An_{8-7}$) (Fig. 17). Apparent closure temperatures of 1230-1100° were obtained at 1 kb $H_2O$ pressure (Kudo & Weill, 1970). Notably, the late phases (rims of plagioclase and alkali feldspars crystals) yielded temperatures below 700°C (Powell & Powell, 1977), indicating possible subsolidus exchanges.

In the scarce undersaturated rocks nepheline is usually altered into cancrinite. A representative analysis was taken from sample RP-259 (Table 16): the amount of silica excess is 11.3 mol% with kalsilite content of 16.9 mol%. The data plot close to the upper Q-Ks limit of nephelines from Cerro Siete Cabezas rocks (Fig. 17).

The accessory minerals are commonly apatite, zircon and titanite. No significant chemical differences between the titanites from the xenolith and Cerro Pedreira host rock (RP-5A and RP-5B, respectively) were detected (Table 16). The lack of "peralkaline accessories", such as eudialyte, is characteristic.

The mineralogy of the Cerro Pedreira, Morro Distante and Morro Conceição rock-types, showing, on the whole, both miaskitic (undersaturated) and oversaturated tendencies, is taken as indicative that they are formed from different source(s) with respect

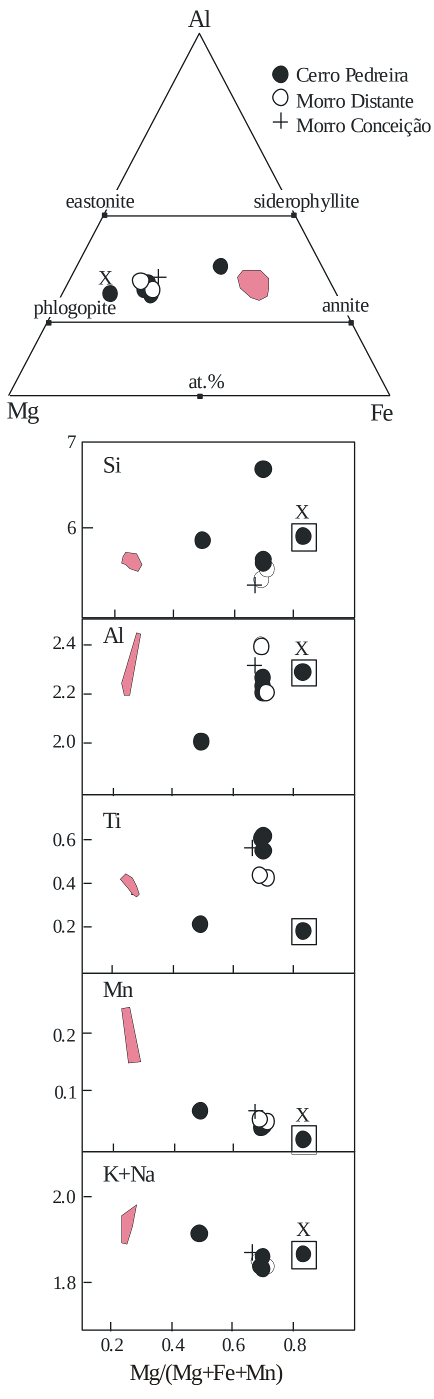


Fig. 15. Plot of biotites from Cerro Pedreira, Morro Distante and Morro Conceição rocks in the system Al-Mg-(Fe+Mn). Total iron as $Fe^{2+}$, and variation diagrams of Si, Al, Ti, Mn and K+Na vs. Mg/(Mg+Fe+Mn) atomic ratio. In pink, the fields for the Cerro Siete Cabezas micas. X: xenolith from Cerro Pedreira.

to the Cerro Siete Cabezas complex and also at comparatively higher equilibration temperatures. Moreover, the general occurrence of two feldspars gives a substantially subsolvus character for those rock-types. Using the same approach for the Cerro Siete Cabezas complex, the total pressure of the intrusions is believed to be in the range of 1-2 kb.

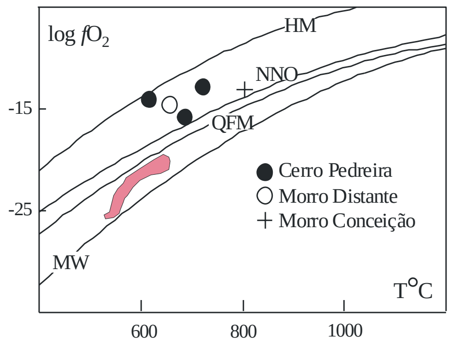


Fig. 16. Stability relationships in T°C- $fO_2$ diagram for the magnetite-ilmenite pairs from Cerro Pedreira, Morro Distante and Morro Conceição rocks (Spencer & Lindsley, 1981). The field of the Cierro Siete Cabezas minerals in pink is shown for comparison. For abbreviations see Fig. 7.

## Major and trace elements distribution

In the nepheline-kalsilite-silica diagram the intrusive specimens cluster in the trachytic minimum (Table 11 and Fig. 17), whereas the dykes trend towards the rhyolitic minimum. D.I.* vs. major element diagrams (Fig. 18) show, on the whole, similar characteristics to those of the Cerro Siete Cabezas complex. However, for the same D.I.* values, the Cerro Pedreira and Morro Distante rocks display higher silica and lower total iron and soda contents. Alumina is positively correlated with D.I.*, except for the dykes which have the lowest $Al_2O_3$ contents.

Moreover $Na_2O$ and $K_2O$ display an "incompatible" behaviour indicative of a continuous alkali enrichment, dykes excluded.

Modelling seems to suggest that quartz syenites and rhyolites were formed by simultaneous assimilation and fractional crystallization processes from a slightly silica-undersaturated magma (e.g. with assimilated/crystallized material ~0.2, and 10% of granitic composition). On the other hand, the nepheline syenites evolved from such a magma without accompanying contamination (paths of Fig. 17).

Representative trace element data are given in Table 17. Rb, Sr and REE vs. D.I.* plot with considerable scatter (Fig. 19; RP-5B xenolith, D.I.*=27.4, not shown), whereas the other I.E. have a quite constant tendency, excluded the strongly enriched (particularly in Th, U, Nb, Zr, Y and light REE) trachytic-rhyolitic dykes. The average Sm/Nd ratio is 0.16 (vs. 0.20 of Cerro Siete Cabezas complex) with a Nd-Sm correlation $r^2$>0.96.

Table 15. Representative magnetite and ilmenites analyses from Cerro Pedreira, Morro Distante and Morro Conceição rocks. C, core; R, rim. For additional information see Table 6.

| | CERRO PEDREIRA | | | | MORRO DISTANTE | MORRO CONCEIÇÃO | |
|---|---|---|---|---|---|---|---|
| Magnetite | | | | | | | |
| Sample | RP-4 | RP-5A | RP-5B | RP-205 | RP-264 | RP-259 C | RP-259 R |
| wt% | | | | | | | |
| $SiO_2$ | | | | 0.21 | 0.02 | 0.04 | 0.11 |
| $TiO_2$ | 0.22 | 2.04 | 0.52 | 4.82 | 0.72 | 18.67 | 11.05 |
| $Al_2O_3$ | 0.05 | 0.72 | 2.44 | 0.08 | 0.45 | 0.35 | 0.56 |
| $Cr_2O_3$ | 0.03 | | | 0.02 | 0.01 | | |
| $Fe_2O_3$ | 68.61 | 63.02 | 64.71 | 59.42 | 66.63 | 31.62 | 45.76 |
| FeO | 31.32 | 31.17 | 31.57 | 34.53 | 31.35 | 46.64 | 39.57 |
| MnO | | 1.35 | 0.02 | 1.10 | 0.06 | 1.78 | 1.18 |
| MgO | | | 0.10 | 0.15 | 0.08 | | 0.12 |
| CaO | | | | 0.05 | 0.06 | | 0.02 |
| Sum | 100.23 | 98.30 | 99.36 | 100.38 | 99.38 | 98.80 | 98.38 |
| Si | | | | 0.064 | 0.006 | 0.012 | 0.034 |
| Ti | 0.048 | 0.480 | 0.120 | 1.105 | 0.167 | 4.290 | 2.564 |
| Al | 0.016 | 0.264 | 0.880 | 0.029 | 0.164 | 0.126 | 0.203 |
| Cr | 0.008 | | | 0.005 | 0.002 | | |
| $Fe^{3+}$ | 15.872 | 14.776 | 14.880 | 13.628 | 15.489 | 7.270 | 10.620 |
| $Fe^{2+}$ | 8.056 | 8.120 | 8.072 | 8.801 | 8.099 | 11.841 | 10.205 |
| Mn | | 0.360 | 0.002 | 0.284 | 0.016 | 0.461 | 0.310 |
| Mg | | | 0.046 | 0.068 | 0.037 | | 0.056 |
| Ca | | | | 0.016 | 0.020 | | 0.008 |
| Sum | 24.000 | 24.000 | 24.000 | 24.000 | 24.000 | 24.000 | 24.000 |
| Ulvösp. mol% | 0.64 | 5.91 | 1.49 | 12.05 | 2.16 | 53.77 | 32.44 |

| | CERRO PEDREIRA | | | MORRO DISTANTE | MORRO CONCEIÇÃO |
|---|---|---|---|---|---|
| Ilmenite | | | | | |
| Sample | RP-4 | RP-5A | RP-205 | RP-264 | RP-259 |
| wt% | | | | | |
| $SiO_2$ | | | 0.15 | 0.05 | 0.05 |
| $TiO_2$ | 44.77 | 45.15 | 47.48 | 46.32 | 48.33 |
| $Al_2O_3$ | 0.18 | | 1.90 | 0.95 | 0.02 |
| $Cr_2O_3$ | | 0.03 | | 0.01 | |
| $Fe_2O_3$ | 14.81 | 13.56 | 6.20 | 8.69 | 5.33 |
| FeO | 34.83 | 35.60 | 34.97 | 35.34 | 39.03 |
| MnO | 5.17 | 4.77 | 7.47 | 6.12 | 4.40 |
| MgO | 0.07 | 0.10 | 0.07 | 0.09 | 0.01 |
| CaO | 0.06 | | 0.03 | 0.01 | 0.01 |
| Sum | 99.89 | 99.21 | 98.27 | 97.58 | 97.18 |
| Si | | | 0.004 | 0.001 | 0.001 |
| Ti | 0.856 | 0.869 | 0.909 | 0.901 | 0.946 |
| Al | 0.005 | | 0.057 | 0.029 | 0.001 |
| Cr | | 0.001 | | | |
| $Fe^{3+}$ | 0.283 | 0.261 | 0.119 | 0.169 | 0.104 |
| $Fe^{2+}$ | 0.740 | 0.762 | 0.746 | 0.763 | 0.850 |
| Mn | 0.111 | 0.103 | 0.161 | 0.134 | 0.097 |
| Mg | 0.003 | 0.004 | 0.003 | 0.003 | 0.001 |
| Ca | 0.002 | | 0.001 | | |
| Sum | 2.000 | 2.000 | 2.000 | 2.000 | |
| $Fe^{2+}/(Mn+Fe^{2+})$ | 0.87 | 0.88 | 0.82 | 0.85 | 0.90 |
| $R_2O_3$ mol% | 25.17 | 23.16 | 8.78 | 15.80 | 9.95 |
| T°C | 612 | 732 | 685 | 646 | 797 |
| $\log_{10} fO_2$ | -14.2 | -12.6 | -16.0 | -14.7 | -13.7 |

Table 16. Representative alkali feldspar, nepheline and titanite analyses from Cerro Pedreira, Morro Distante and Morro Conceição rocks. For additional information see Tables 7 and 8.

| Feldspar | CERRO PEDREIRA | | | | | | | | | |
|---|---|---|---|---|---|---|---|---|---|---|
| Sample | RP-4A | RP-4A | RP-5A | RP-5A | RP-5A | RP-5A | RP-5B | RP-205 | RP-205 | RP-205 |
| wt% | | | | | | | | | | |
| $SiO_2$ | 58.91 | 66.10 | 54.22 | 57.73 | 65.61 | 65.79 | 54.31 | 65.36 | 66.68 | 65.04 |
| $Al_2O_3$ | 24.67 | 18.56 | 27.95 | 24.89 | 20.87 | 18.60 | 28.33 | 18.37 | 19.33 | 18.33 |
| $Fe_2O_3$ | 0.39 | 0.49 | 0.34 | 0.40 | 0.34 | 0.33 | 0.43 | 0.30 | 0.06 | 0.30 |
| BaO | 0.15 | 0.10 | 0.05 | 0.08 | 0.01 | 0.21 | 0.05 | 0.16 | 0.30 | 0.16 |
| CaO | 6.76 | 0.11 | 10.57 | 7.25 | 2.08 | 0.09 | 10.91 | 0.01 | 0.31 | 0.05 |
| $Na_2O$ | 7.32 | 5.54 | 5.29 | 7.00 | 9.51 | 4.17 | 5.14 | 4.44 | 10.17 | 2.04 |
| $K_2O$ | 0.45 | 8.77 | 0.20 | 0.37 | 1.52 | 10.76 | 0.26 | 10.29 | 1.73 | 13.84 |
| Sum | 98.65 | 99.67 | 98.62 | 97.72 | 99.94 | 99.95 | 99.43 | 98.77 | 98.58 | 99.76 |
| | | | | | | | | | | |
| Or | 2.0 | 50.3 | 0.8 | 1.6 | 7.8 | 61.9 | 1.0 | 60.0 | 9.7 | 80.8 |
| Ab | 48.3 | 48.3 | 30.9 | 45.8 | 74.2 | 36.5 | 29.5 | 39.3 | 86.4 | 18.1 |
| An | 49.7 | 1.4 | 68.3 | 52.6 | 17.9 | 1.6 | 69.5 | 0.7 | 3.9 | 1.1 |

| Feldspar | MORRO DISTANTE | | | MORRO CONCEIÇÃO | | | |
|---|---|---|---|---|---|---|---|
| Sample | RP-264 | RP-264 | RP-264 | RP-259 | RP-259 | RP-259 | RP-259 |
| wt% | | | | | | | |
| $SiO_2$ | 58.67 | 66.37 | 66.65 | 62.73 | 66.18 | 65.68 | 67.17 |
| $Al_2O_3$ | 25.28 | 19.25 | 20.28 | 22.11 | 19.17 | 18.62 | 19.70 |
| $Fe_2O_3$ | 0.37 | 0.65 | 0.44 | 0.16 | 0.25 | 0.24 | 0.08 |
| BaO | 0.13 | 0.39 | 0.01 | 1.00 | 0.16 | 0.22 | 0.08 |
| CaO | 7.32 | 0.59 | 1.41 | 3.33 | 0.45 | 0.09 | 0.60 |
| $Na_2O$ | 7.04 | 8.08 | 10.41 | 8.23 | 6.63 | 4.22 | 10.78 |
| $K_2O$ | 0.51 | 4.65 | 0.80 | 1.81 | 6.92 | 10.33 | 0.81 |
| Sum | 99.32 | 99.98 | 100.00 | 99.37 | 99.76 | 99.40 | 99.22 |
| | | | | | | | |
| Or | 2.1 | 25.6 | 4.2 | 9.0 | 38.8 | 60.7 | 4.4 |
| Ab | 44.9 | 67.6 | 83.3 | 62.2 | 56.4 | 37.6 | 89.8 |
| An | 53.0 | 6.8 | 12.5 | 28.8 | 4.8 | 1.7 | 5.8 |

| Nepheline | MORRO CONCEIÇÃO | Titanite | CERRO PEDREIRA | |
|---|---|---|---|---|
| Sample | RP-259 | | RP-5A | X-RP-5B |
| wt% | | wt% | | |
| $SiO_2$ | 46.51 | $SiO_2$ | 30.42 | 30.47 |
| $Al_2O_3$ | 31.31 | $TiO_2$ | 33.65 | 35.91 |
| $Fe_2O_3$ | 0.42 | $Cr_2O_3$ | 0.03 | 0.13 |
| BaO | 0.02 | $Al_2O_3$ | 1.38 | 2.73 |
| CaO | 0.41 | $Ce_2O_3$ | 0.04 | |
| $Na_2O$ | 15.16 | FeO | 1.95 | 1.65 |
| $K_2O$ | 5.43 | MnO | 0.14 | |
| Sum | 99.26 | MgO | 0.08 | 0.19 |
| | | CaO | 27.91 | 28.81 |
| Q | 11.3 | $Na_2O$ | 0.16 | |
| Ne | 71.8 | $Nb_2O_5$ | 0.33 | |
| Ks | 16.9 | F | 0.82 | |
| | | Cl | 0.07 | |
| | | Sum | 96.78 | 99.99 |

The best results of mass balance calculations, relative to the RP-5B xenolith, demonstrate that this rock may be taken as an amphibole-plagioclase-biotite-magnetite-apatite cumulate derived from about 27% of crystallizing phases of syenitic magmas (RP-7 vs. RP-3: Table 18). The I.E. calculated/observed ratios are around the unity (1.0±0.1), both for the liquid fractions and for the crystallizing phases, except for the Sr of RP-5B sample where the calculated/observed ratio is 0.27. Probably this disagreement is due to the presence of some accessory cryptic phases not identified in the rock.

The I.E. (primitive mantle-normalized) spidergrams show overlapping fields for both Cerro Pedreira and Morro Conceição with the Cerro Siete Cabezas main body (Fig. 20). Cerro Pedreira rocks display strong positive U, Nb-Ta and Zr-Hf spikes, whereas Morro Distante and Morro Conceição have parallel patterns with a progressive decreasing of I.E. from La to Yb, and less pronounced positive Zr-Hf spikes.

Table 17. Trace element analyses of selected rocks from Cerro Pedreira, Morro Distante and Morro Conceição stocks. D, dykes.

| | CERRO PEDREIRA | | | | | | | | | | MORRO DISTANTE | | | MORRO CONCEIÇÃO | | | | | | | | |
|---|---|---|---|---|---|---|---|---|---|---|---|---|---|---|---|---|---|---|---|---|---|---|
| Sample | RP-1 D | RP-2 D | RP-3 | RP-4 | RP5A | RP-5B | RP-6 D | RP-7 | RP-8 | RP-206 D | RP-264 | RP-265 | RP-266 | RP-9 | RP-76 | RP-77 | RP-78 | RP-79 | RP-259 | RP-260 | RP-261 | RP-262 |
| ppm | | | | | | | | | | | | | | | | | | | | | | |
| Cr | 4 | 1 | 1 | 3 | 4 | 120 | 1 | 4 | 2 | 1 | 6 | 7 | 1 | 1 | 1 | 1 | 4 | 1 | 1 | 7 | 4 | 2 |
| Ni | 12 | 9 | 2 | 11 | 6 | 90 | 5 | 8 | 9 | 4 | 5 | 4 | 3 | 3 | 9 | 9 | 8 | 6 | 5 | 2 | 6 | 5 |
| Rb | 121 | 81 | 120 | 115 | 121 | 29 | 189 | 106 | 109 | 83 | 113 | 120 | 106 | 76 | 100 | 94 | 168 | 125 | 102 | 100 | 101 | 96 |
| Ba | 108 | 147 | 1348 | 1144 | 1149 | 600 | 85 | 1021 | 1036 | 790 | 672 | 677 | 650 | 225 | | 1187 | 777 | 453 | 302 | 355 | 515 | 350 |
| Th | | | 11.9 | | | 4.0 | 19.7 | 10.1 | 11.0 | 27.3 | 8.4 | 8.5 | 8.1 | | | 20.8 | 10.0 | 11.1 | | | | |
| U | | | 3.5 | | | 0.4 | 16.0 | 2.7 | 2.9 | 6.9 | 2.2 | 2.2 | 2.0 | | | 3.2 | 3.0 | 1.6 | | | | |
| Ta | | | 16.0 | | | 10.1 | 49.3 | 13.6 | 13.2 | | 4.1 | 5.4 | 4.5 | | | 13.1 | 12.7 | 8.1 | | | | |
| Nb | 329 | 325 | 105 | 95 | 103 | 72 | 480 | 112 | 112 | 263 | 60 | 68 | 61 | 92 | 116 | 150 | 137 | 88 | 74 | 82 | 76 | 72 |
| Sr | 49 | 88 | 600 | 704 | 725 | 2454 | 30 | 648 | 579 | 54 | 409 | 400 | 448 | 34.5 | 58 | 1048 | 396 | 217 | 407 | 414 | 442 | 399 |
| Hf | | | 9.4 | | | 2.8 | 33.7 | 7.1 | 7.5 | | 2.8 | 7.1 | 4.9 | | | 13.2 | 10.9 | 17.3 | | | | |
| Zr | 2374 | 1954 | 395 | 341 | 459 | 120 | 1337 | 300 | 319 | 2205 | 312 | 348 | 331 | 203 | 288 | 510 | 422 | 671 | 347 | 358 | 382 | 333 |
| Y | 88 | 80 | 28 | 34 | 39 | 18 | 84 | 26 | 22 | 80 | 26 | 27 | 28 | 29 | 30 | 38 | 27 | 27 | 32 | 32 | 35 | 33 |
| La | 147 | 264 | 69 | 81 | 74 | 20 | 159 | 63.1 | 69.0 | 128.4 | 36.82 | 40.09 | 37.05 | 67 | 101 | 89 | 66.0 | 51 | 90 | 106 | 88 | 89 |
| Ce | 325 | 460 | 147 | 166 | 141 | 47 | 325 | 134.0 | 194.0 | 198.0 | 71.31 | 78.64 | 72.22 | 136 | 205 | 168 | 139.8 | 99 | 183 | 225 | 181 | 180 |
| Pr | | | | | | | 31.8 | 14.4 | 19.9 | 20.24 | 8.11 | 8.37 | 7.95 | 14 | | 18 | 13.8 | 11 | | | | |
| Nd | 92 | 120 | 60 | 68 | 60 | 17 | 103.0 | 51.6 | 77.6 | 66.17 | 29.46 | 30.40 | 28.97 | 50 | 75 | 65 | 45.5 | 41 | 67 | 79 | 65 | 70 |
| Sm | | | 11 | | | 3.2 | 10.4 | 9.2 | 13.24 | 11.80 | 4.94 | 5.10 | 4.86 | 7.6 | 12 | 10.9 | 7.60 | 6.8 | 10 | 12 | 11 | 11 |
| Eu | | | | | | | 3.46 | 2.64 | 3.37 | 3.39 | 1.11 | 1.10 | 1.07 | 1.8 | | 2.6 | 1.79 | 1.6 | | | | |
| Gd | | | | | | | 11.66 | 8.90 | 13.00 | 11.42 | 4.78 | 5.01 | 4.74 | 7.4 | | 10.7 | 7.51 | 6.6 | | | | |
| Tb | | | | | | | 1.28 | 0.90 | 1.40 | | 0.49 | | | 0.8 | | | 0.84 | | | | | |
| Dy | | | | | | | 8.07 | 5.30 | 7.30 | 6.80 | 2.94 | 3.08 | 2.92 | 4.5 | | 6.50 | 4.60 | 4.1 | | | | |
| Ho | | | | | | | 1.37 | 0.83 | 1.27 | | 0.45 | | | 0.7 | | 0.76 | | | | | | |
| Er | | | | | | | 4.26 | 2.30 | 3.50 | 2.95 | 1.28 | 1.36 | 1.28 | 2.3 | | 3.40 | 2.40 | 2.1 | | | | |
| Tm | | | | | | | 0.57 | 0.31 | 0.54 | | 0.15 | | | 0.28 | | | 0.30 | | | | | |
| Yb | | | | | | | 3.40 | 1.92 | 2.31 | 2.46 | 1.20 | 1.31 | 1.22 | 2.12 | | 3.10 | 2.21 | 1.9 | | | | |
| Lu | | | | | | | 0.52 | 0.25 | 0.33 | 0.33 | 0.16 | 0.18 | 0.17 | 0.29 | | 0.40 | 0.30 | 0.26 | | | | |

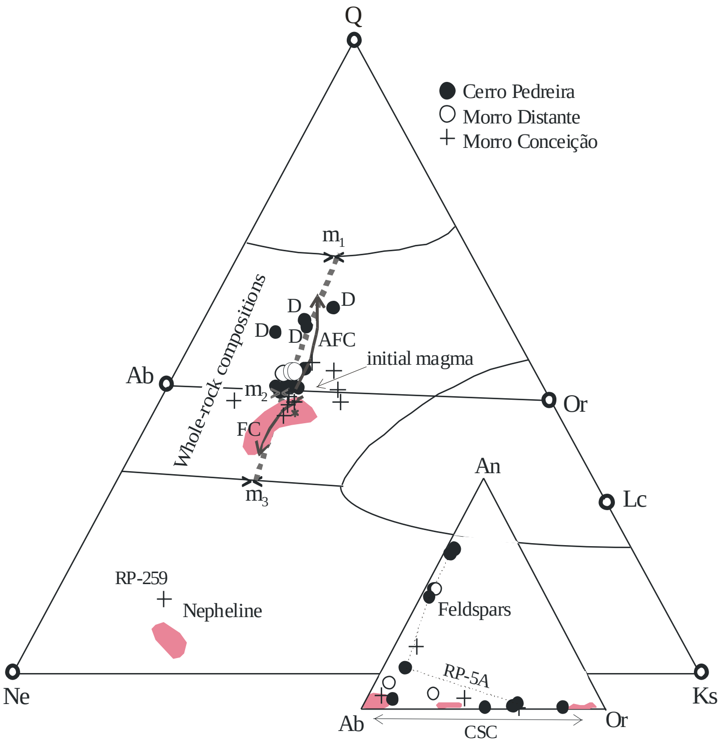


Fig. 17. Alkali feldspar from Cerro Pedreira, Morro Distante and Morro Conceição rocks plotted into the Or-Ab-An (mol%) diagram, and nepheline (RP-259) plotted into the Ks-Ne-Q (wt%) space (cf. Fig. 8). For comparison the whole-rock compositions are also plotted: it should be noted that the samples fit the trachytic minimum, whereas the dykes from Cerro Pedreira tend towards the rhyolitic minimum. The lines show liquid evolution paths for coupled assimilation and fractional crystallization (AFC) and fractional crystallization (FC) of an initial, crytically undersaturated, liquid. In pink, the fields for the Cerro Siete Cabezas minerals.

Table 18. Mass balance calculations (Stormer & Nicholls, 1978) showing the composition of the RP-5B mafic cumulate, and the observed and calculated concentrations and ratios of the trace elements relative to the liquid fraction (F) and to the RP-5B cumulate, using the compositons of RP-7 vs. RP-3 syenites and RP-5B phases (Rayleigh's fractionation model, mineral/liquid partition coefficients after Marzoli, 1991, and Caroff *et al.*, 1993).

| | Xenolith | | | Syenite → | Syenite | Cumulate | | | | |
|---|---|---|---|---|---|---|---|---|---|---|
| Sample | RP-5B modal | RP-5B mass balance | | RP-7 observed | RP-3 observed | RP-3 calculated | RP-3 calc/obs | RP-5B observed | RP-5B calculated | RP-5B calc/obs |
| | | | Ba | 1021 | 1348 | 1188 | 0.88 | 600 | 622 | 1.04 |
| | | | Rb | 106 | 120 | 137 | 1.14 | 29 | 20 | 0.97 |
| | | | U | 2.7 | 3.5 | 3.6 | 1.03 | 0.4 | 0.3 | 0.78 |
| | | | Th | 10.1 | 11.9 | 12.6 | 1.06 | 4 | 3.8 | 0.94 |
| Pl | 36.9 | 39.01 | Nb | 105 | 112 | 125.2 | 1.07 | 72 | 76 | 1.06 |
| Am | 47.9 | 48.94 | Ta | 13.6 | 16.0 | 15.4 | 0.96 | 10.1 | 9.5 | 0.94 |
| Bi | 4.0 | 2.80 | La | 63.1 | 69 | 80.8 | 1.17 | 20 | 18.1 | 0.90 |
| Op | 6.5 | 5.49 | Ce | 134 | 147 | 171 | 1.16 | 47 | 40 | 0.85 |
| Ap | 3.2 | 3.75 | Sr | 648 | 600 | 645 | 1.08 | 2454 | 655 | 0.27 |
| Accessory | 1.5 | | N.d. | 51.6 | 60 | 65.8 | 1.10 | 17 | 15.5 | 0.91 |
| | | | Sm | 9.2 | 10.7 | 11.4 | 1.06 | 3.2 | 3.7 | 1.17 |
| | | | Zr | 300 | 395 | 376 | 0.96 | 120 | 108 | 0.90 |
| | | | Hf | 7.1 | 9.0 | 8.9 | 0.99 | 2.8 | 2.6 | 0.91 |
| | | | Y | 26 | 28 | 28.6 | 0.93 | 18 | 20.1 | 0.90 |
| F | | | | | 0.7278 | | | | | |
| $\Sigma R^2$ | | 0.26 | | | | | | | | |

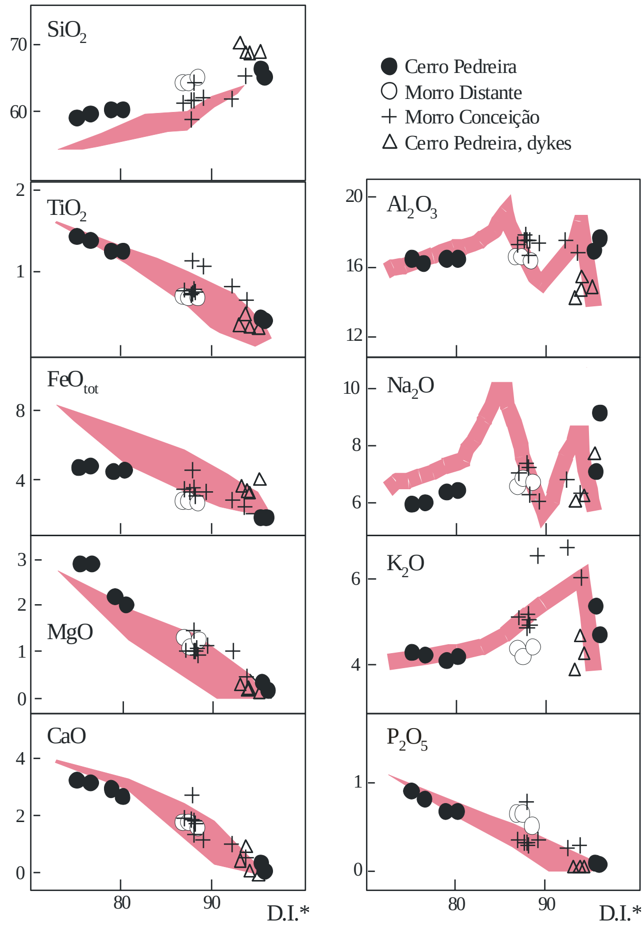


Fig. 18. D.I. vs. major elements (wt%) for Cerro Pedreira, Morro Distante and Morro Conceição rocks. The compositional fields for the Cerro Siete Cabezas rocks in pink are shown for comparison.

The REE (chondrite-normalized) spidergrams display similar strongly enriched patterns in the Cerro Pedreira and Morro Conceição rock-types and, also, more depleted compositions compared to the Morro Distante samples (Fig. 20).

Notably, the intrusive rocks and dykes from Cerro Pedreira give average $(La/Sm)_c$ and $(La/Yb)_c$ ratios of 5.0 and 8.2, and 28.3 and 34.7, respectively. Ratios of 4.8–5.2 and of 20.6–19.7 are here presented by samples from Morro Distante and Morro Conceição, respectively. These values are 1.1-2.5 times the calculated ratios for the rocks from the Cerro Siete Cabezas complex, indicating the more pronounced fractionation of LREE vs. MREE and of LREE vs. HREE. Eu/Eu* has mean values of 0.82 and 0.92 in Cerro Pedreira intrusives and in trachytic-rhyolitic dykes, respectively; in Morro Distante and Cerro Conceição rock-types the ratio is 0.67 and 0.72, respectively. The Eu/Eu* ratios obtained for Cerro Pedreira intrusives are considerably higher than those found for the Cerro Siete Cabezas equivalents (Eu/Eu*=0.64), and correspond to samples having discrete modal plagioclase.

## Sr-Nd isotopes

The rock-types from the three intrusions are poorly documented. Only one sample of each and one from a Cerro Pedreira dyke (RP-6) have been measured (Table I of the Appendix). The intrusive rocks point to $R_0$ (241 Ma) values between 0.70425 and 0.70480 and to initial $^{143}Nd/^{144}Nd$ ratios between 0.51230 and 0.51241. The dyke has quite different isotopic ratios, 0.70571 and 0.5126 for Sr and Nd, respectively, probably due to contamination by a crustal (granitic?) component. The Nd-model ages for Cerro Pedreira, Morro Distante, Morro Conceição and the dyke are 934, 834, 719 and 868

Ma, respectively, roughly in the same range of the Cerro Siete Cabezas complex.

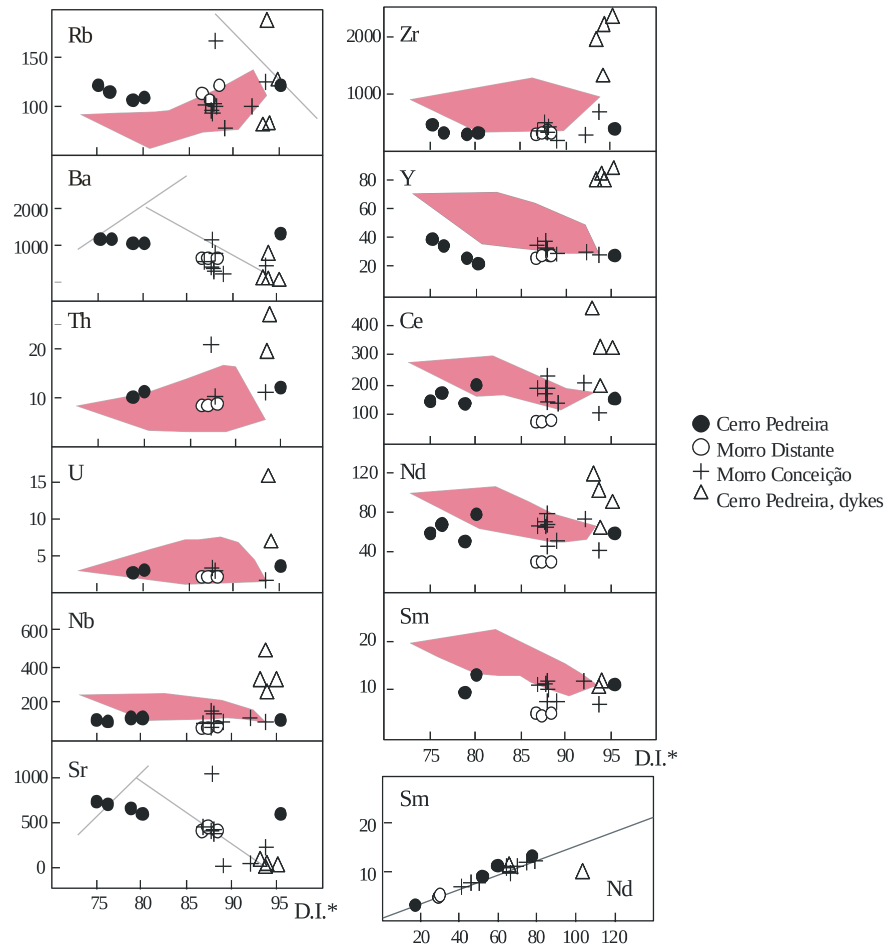


Fig. 19. D.I.* vs. trace elements (ppm) for Cerro Pedreira, Morro Distante and Morro Conceição rocks. The compositional fields for the Cerro Siete Cabezas rocks in pink are shown for comparison (cf. Fig. 10).

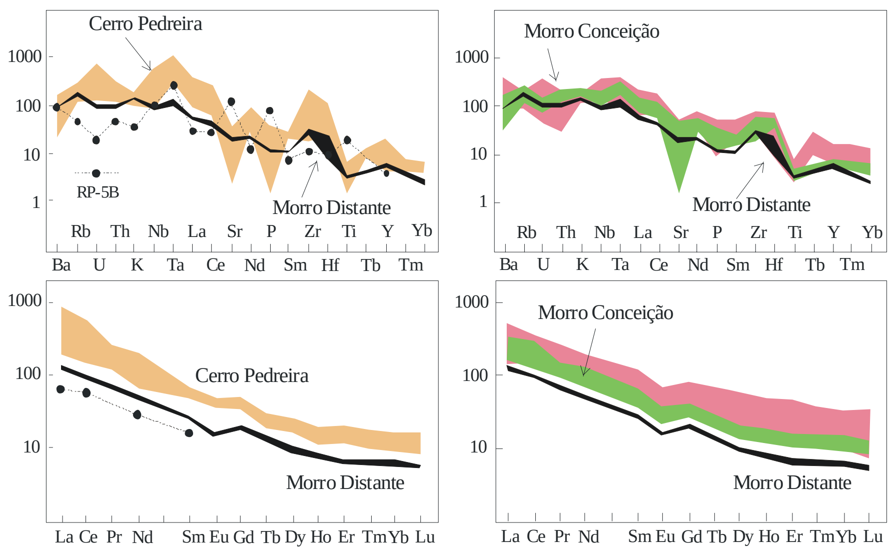


Fig. 20. Primitive mantle- (Sun & McDonough, 1984) and chondrite- (Boynton, 1984) normalized I.E. and REE distribution diagrams, respectively, for Cerro Pedreira, Morro Distante and Morro Conceição rocks. The Cerro Siete Cabezas field in pink is shown for comparison.

Table 19. Representative modal analyses relative to selected rocks from the Fecho dos Morros complex. So, sodalite; for other abbreviations see Table 1.

| | CERRITO | | | ILHA FECHO DOS MORROS | | | MORRO DE SÃO PEDRO | | |
|---|---|---|---|---|---|---|---|---|---|
| Sample | RP-83 | RP-85 | RP-88 | RP-91 | RP-95 | RP-201A | RP-202 | RP-256 | RP-257 |
| vol% | | | | | | | | | |
| AF | 95.0 | 64.6 | 71.5 | 59.3 | 62.8 | 50.5 | 61.8 | 69.4 | 79.6 |
| Ne | 0.3 | 16.9 | 13.1 | 20.5 | 19.4 | 27.2 | 17.2 | 15.9 | 11.5 |
| So | | 1.2 | 1.4 | 6.2 | 2.9 | 6.4 | 6.7 | 3.7 | |
| Cpx | 2.0 | 10.2 | 3.2 | 0.5 | 4.4 | 5.0 | 5.5 | 1.6 | 1.2 |
| Am | 0.3 | 1.1 | 7.7 | 9.0 | 3.8 | 4.3 | 6.8 | 7.8 | 5.9 |
| Bi | 0.5 | 4.0 | 1.5 | 2.0 | 3.4 | 2.8 | 0.7 | 0.2 | 0.5 |
| Op | 0.8 | 0.6 | 0.4 | 1.0 | 0.9 | 1.0 | 0.5 | 0.5 | 0.6 |
| Ap | 0.1 | 0.5 | 0.2 | 0.7 | 1.5 | 1.3 | 0.1 | | 0.2 |
| Accessories | 1.0 | 0.9 | 1.0 | 0.8 | 1.1 | 1.5 | 0.7 | 0.9 | 0.5 |

## 3. FECHO DOS MORROS

Cerrito, Ilha Fecho dos Morros and Morro de São Pedro are three intrusive bodies between the western and eastern sides of the Paraguay river. They have an overall circular structure and are partially covered in eastern areas by the lava flows and ignimbrites of the Pão de Açúcar volcano (Fig. 1). The rocks vary from medium- to coarse-grained syenites (normal facies) to a pegmatitic facies and are crossed by N-S phonolitic dykes (reaching up to 100 cm thick and with subvertical dip). In particular, the pegmatitic rocks present in the Cerrito body are prevailing in the Ilha Fecho dos Morros, at the core of the complex.

In a few places, mainly found in the Cerrito body, at the western side of this intrusive complex and also corresponding to the western flanks of the pegmatitic facies, igneous layering is exceptionally well developed (Matos, 2000). The individual layers can be traced for more than 100-200 m, with N-S attitude (the same of the Paraguay river) and vertical dips. The layering is decimeter-rhytmic and consists of concentrations of mafic minerals (pyroxene, magnetite, amphibole, zircon and apatite) alternated with alkali feldspar and nepheline-rich layers. The layers terminate by tapering into "normal" rock-type by a gradual decrease in the amount of mafic minerals. In some areas earlier layered rocks are intruded by mafic-rich syenites which in turn contain fragments of yet another layered syenite. All the above features suggest the existence of strong currents in the magmatic chamber.

On the whole, the intrusive rocks extend for about 14 km$^2$, with a top 156 m high (about 75 m over the river) in the island Ilha Fecho dos Morros.

### Petrography

Modal data (Table 19) indicate that the samples range from alkali feldspar syenites to foid-bearing and foid-syenites with a tendentiously peralkaline character. In particular, sodalite may be an important phase in this complex. The intrusive rocks are allotriomorphic, intergranular and sometimes porphyritic in texture. The phenocrysts are commonly clinopyroxene, nepheline and alkali feldspar, being the latter mineral represented by mesoperthitic Carlsbad twins. Clinopyroxene usually shows salitic cores and aegirinic rims. The pyroxene is sometimes replaced by amphibole which also occurs as euhedral prisms and forming patches with biotite, opaques, titanite and apatite. Biotite occurs as discrete crystals or substituting earlier generated amphibole and opaque phases. Interstitial sodalite is occasionally present in some samples from Cerrito and Morro de São Pedro, and it is particularly abundant, up to 10%, in the pegmatitic facies. Accessory minerals are opaques, apatite, titanite, zircon and fluorite. Secondary phases are mostly cancrinite and carbonates in sodalite-rich samples, replacing nepheline or at the contact between nepheline and sodalite. The pegmatitic facies (particularly in the Ilha Fecho dos Morros) consists mainly of mesoperthitic alkali feldspar, nepheline and sodalite up to 5 cm across. Locally zircon, up to 1 vol%, is a common phase.

The dykes exhibit porphyritic-microporphyritic fluidal texture, with pheno- and/or microphenocrysts of nepheline, alkali feldspar, sodalite, clinopyroxene, amphibole, biotite, opaques, apatite, titanite and zircon set in a groundmass made mainly of alkali feldspar and nepheline.

## Classification and nomenclature

The analyzed intrusives ($R_1$-$R_2$ diagram, De La Roche *et al.*, 1980; cf. Table 20 and inset of Fig. 21) range from nepheline syenites to syenites, while the dykes plot into the phonolite field. Applying the serial discriminant diagram (cf. inset $Na_2O$ vs. $K_2O$ of Fig. 21), it is apparent that the main population is represented by sodic rocks, with a few samples falling in the transitional field. The latter belong to the alkali feldspar-rich layers. The Alkali Index (A.I.) vs. Q-ne-normative diagram (Fig. 21) defines an undersaturated, prevailing miaskitic association for the Cerrito "normal" intrusive facies. On the other hand, an undersaturated peralkaline suite is indicated for the pegmatoid facies (both from Cerrito and Ilha Fecho dos Morros), for the "normal" facies from Morro de São Pedro and for the phonolitic dykes.

## Mineralogy

The chemical variations have been determined in a representative selection of samples and are given in Tables 21 to 25.

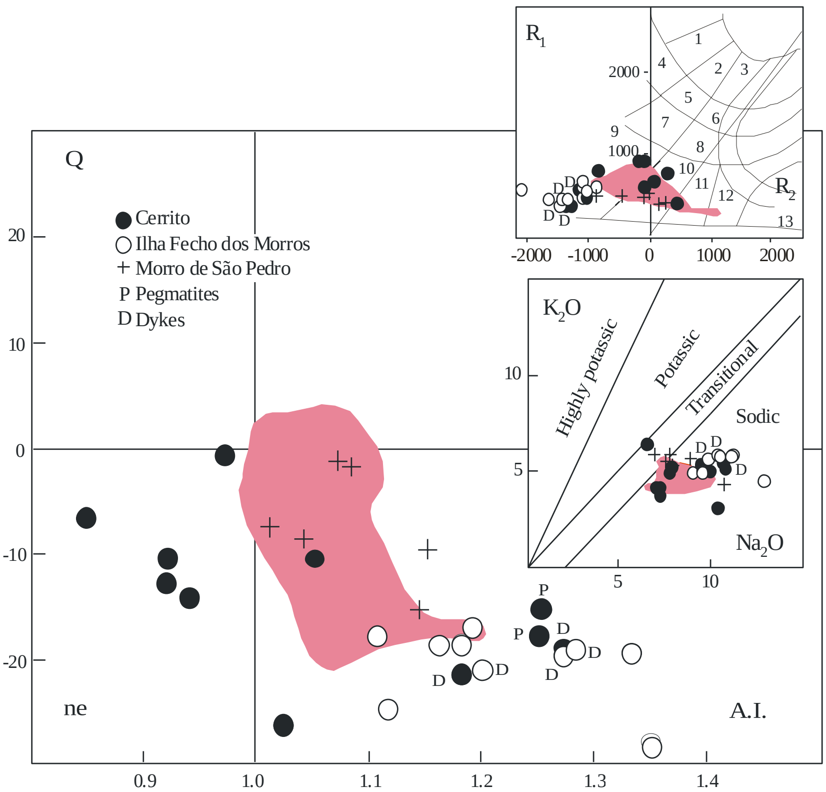


Fig. 21. A.I. vs. Q-ne diagram for rocks from the Fecho dos Morros complex (Cerrito, Ilha Fecho dos Morros and Morro de São Pedro). The fields of rock-types from the Siete Cabezas complex in pink are shown for comparison. For insets see Fig. 3.

Table 20. Major element analyses, norms and classification (according to De La Roche *et al.*, 1980) of selected rocks from the Fecho dos Morros complex (Cerrito, Ilha Fecho dos Morros and Morro de São Pedro bodies). D, dykes; P, pegmatitic facies. See Table 2 for abbreviations.

| | | | | | | CERRITO | | | | | |
|---|---|---|---|---|---|---|---|---|---|---|---|
| Sample | RP-80 | RP-81 D | RP-82A P | RP-82B | RP-83 | RP-84 | RP-85 D | RP-86 | RP-87 | RP-88 P | RP-202 |
| wt% | | | | | | | | | | | |
| $SiO_2$ | 53.83 | 57.33 | 58.19 | 57.78 | 64.21 | 60.49 | 54.34 | 53.68 | 59.72 | 57.10 | 55.42 |
| $TiO_2$ | 2.01 | 0.36 | 0.35 | 1.00 | 0.50 | 0.71 | 1.06 | 2.02 | 1.02 | 0.49 | 1.05 |
| $Al_2O_3$ | 17.72 | 18.73 | 18.85 | 19.10 | 18.24 | 19.96 | 18.18 | 17.51 | 17.75 | 17.40 | 20.26 |
| $Fe_2O_3$ | 2.75 | 2.62 | 2.60 | 2.44 | 0.77 | 0.47 | 2.43 | 2.46 | 1.13 | 2.19 | 1.35 |
| FeO | 3.65 | 0.80 | 0.86 | 0.82 | 0.80 | 1.37 | 2.46 | 4.06 | 2.51 | 3.22 | 1.98 |
| MnO | 0.18 | 0.28 | 0.28 | 0.08 | 0.04 | 0.05 | 0.22 | 0.18 | 0.15 | 0.35 | 0.09 |
| MgO | 2.64 | 0.11 | 0.09 | 1.01 | 0.22 | 0.41 | 1.16 | 2.54 | 0.99 | 0.72 | 1.26 |
| CaO | 4.43 | 0.57 | 0.57 | 3.58 | 1.36 | 2.77 | 1.88 | 4.54 | 2.16 | 1.25 | 3.29 |
| $Na_2O$ | 7.24 | 10.74 | 10.79 | 7.26 | 6.43 | 7.86 | 9.48 | 7.05 | 7.80 | 9.86 | 10.36 |
| $K_2O$ | 4.34 | 5.62 | 5.37 | 3.88 | 6.62 | 4.93 | 5.47 | 4.23 | 5.30 | 5.14 | 3.26 |
| $P_2O_5$ | 1.29 | 0.07 | 0.04 | 0.56 | 0.12 | 0.26 | 0.56 | 1.34 | 0.46 | 0.18 | 0.60 |
| L.O.I. | 0.19 | 2.42 | 1.60 | 2.01 | 0.50 | 0.43 | 2.48 | 0.14 | 0.81 | 1.68 | 0.80 |
| Sum | 100.27 | 99.65 | 99.59 | 99.52 | 99.81 | 99.71 | 99.72 | 99.75 | 99.80 | 99.58 | 99.72 |
| or | 25.64 | 33.21 | 31.73 | 22.92 | 39.12 | 29.13 | 32.32 | 24.99 | 31.32 | 30.37 | 19.26 |
| ab | 35.27 | 30.17 | 33.41 | 49.44 | 53.37 | 47.33 | 23.61 | 36.04 | 42.66 | 32.61 | 37.77 |
| an | 3.03 | | | 8.07 | 1.35 | 4.62 | | 3.64 | | | |
| ne | 14.08 | 18.89 | 18.22 | 6.49 | 0.56 | 10.38 | 21.37 | 12.78 | 10.36 | 15.31 | 26.15 |
| ac | | 7.58 | 7.52 | | | | 7.03 | | 3.26 | 6.33 | 1.40 |
| ns | | 4.00 | 3.65 | | | | 2.13 | | 0.11 | 3.57 | |
| di | 8.35 | 2.04 | 2.23 | 4.69 | 1.32 | 4.16 | 4.69 | 8.14 | 6.42 | 4.20 | 9.30 |
| wo | | | | | 1.21 | 0.99 | | | | | 0.35 |
| ol | 2.88 | 0.44 | 0.43 | 0.23 | | | 2.74 | 3.47 | 1.80 | 4.01 | |
| mt | 3.98 | | | | 1.11 | 0.68 | | 3.56 | | | 1.25 |
| hm | | | | 2.43 | | | | | | | |
| il | 3.81 | 0.68 | 0.66 | 1.89 | 0.94 | 1.34 | 2.01 | 3.83 | 1.93 | 0.93 | 1.25 |
| ap | 3.05 | 0.16 | 0.09 | 1.32 | 0.28 | 0.61 | 1.32 | 3.17 | 1.08 | 0.42 | 1.42 |
| D.I.* | 75.0 | 89.8 | 90.9 | 78.8 | 93.0 | 86.8 | 84.3 | 73.8 | 87.6 | 84.6 | 84.6 |
| A.I. | 0.94 | 1.27 | 1.25 | 0.85 | 0.97 | 0.92 | 1.18 | 0.92 | 1.05 | 1.25 | 1.02 |
| $R_1$ | -221 | -1406 | -1309 | 254 | 391 | 17 | -1182 | -142 | -155 | -1056 | -865 |
| $R_2$ | 953 | 434 | 435 | 808 | 514 | 708 | 615 | 955 | 628 | 511 | 812 |
| Rock-type | Nepheline syenite | Phonolite | Nepheline syenite | Syenite | Syenite | Nephel-syenite | Phonolite | Nepheline syenite | Nephel-syenite | Nepheline syenite | Nepheline syenite |
| Q | 36.3 | 34.2 | 34.8 | 41.3 | 44.4 | 39.5 | 32.0 | 37.0 | 39.2 | 35.8 | 30.8 |
| Ne | 44.3 | 42.8 | 43.6 | 42.2 | 31.7 | 41.5 | 44.2 | 43.8 | 39.7 | 42.1 | 56.0 |
| Ks | 19.4 | 23.0 | 21.6 | 16.5 | 23.9 | 19.0 | 23.8 | 19.2 | 21.1 | 22.1 | 13.2 |

| | | | | | | ILHA FECHO DOS MORROS | | | | |
|---|---|---|---|---|---|---|---|---|---|---|
| Sample | RP-89 | RP-90 | RP-91 | RP-92 D | RP-93 | RP-94 D | RP-95 | RP-96 D | RP-97 | RP-201A |
| wt% | | | | | | | | | | |
| $SiO_2$ | 57.68 | 56.27 | 55.40 | 58.73 | 55.93 | 58.70 | 56.02 | 58.02 | 54.16 | 53.60 |
| $TiO_2$ | 0.68 | 0.64 | 1.06 | 0.44 | 1.02 | 0.45 | 0.88 | 0.54 | 1.12 | 0.80 |
| $Al_2O_3$ | 18.91 | 18.49 | 18.40 | 19.28 | 18.41 | 19.12 | 18.45 | 19.50 | 18.81 | 19.26 |
| $Fe_2O_3$ | 0.88 | 1.13 | 0.84 | 2.50 | 2.02 | 2.69 | 1.27 | 2.59 | 2.61 | 1.93 |
| FeO | 2.49 | 2.82 | 4.08 | 0.70 | 2.70 | 0.51 | 2.94 | 0.92 | 3.02 | 2.25 |
| MnO | 0.17 | 0.19 | 0.29 | 0.23 | 0.23 | 0.24 | 0.21 | 0.22 | 0.25 | 0.22 |
| MgO | 0.74 | 0.98 | 1.24 | 0.09 | 1.29 | 0.11 | 1.43 | 0.43 | 1.68 | 1.42 |
| CaO | 1.24 | 0.94 | 1.74 | 0.53 | 1.76 | 0.61 | 1.72 | 0.87 | 2.23 | 1.60 |
| $Na_2O$ | 9.88 | 11.15 | 9.08 | 11.06 | 9.48 | 11.03 | 9.61 | 10.40 | 9.52 | 12.88 |
| $K_2O$ | 5.74 | 5.84 | 5.11 | 5.83 | 5.32 | 5.80 | 5.54 | 5.78 | 4.92 | 4.43 |
| $P_2O_5$ | 0.62 | 0.43 | 0.91 | 0.04 | 0.96 | 0.07 | 0.87 | 0.19 | 1.03 | 0.66 |
| L.O.I. | 0.72 | 0.81 | 1.48 | 0.34 | 0.62 | 0.44 | 0.83 | 0.32 | 0.31 | 0.55 |
| Sum | 99.75 | 99.69 | 99.63 | 99.77 | 99.74 | 99.77 | 99.77 | 99.78 | 99.66 | 99.60 |
| or | 33.92 | 34.51 | 30.19 | 34.45 | 31.43 | 34.27 | 32.74 | 34.15 | 29.07 | 26.18 |
| ab | 33.97 | 26.86 | 33.34 | 30.91 | 30.63 | 30.96 | 30.00 | 29.44 | 25.31 | 22.88 |
| ne | 16.98 | 19.35 | 17.79 | 19.39 | 18.66 | 19.00 | 18.45 | 20.95 | 23.86 | 27.91 |
| ac | 2.55 | 3.26 | 2.43 | 7.23 | 5.84 | 7.78 | 3.67 | 7.49 | 7.55 | 5.58 |
| ns | 3.59 | 6.52 | 1.83 | 4.34 | 1.97 | 4.29 | 3.04 | 2.64 | 0.6 | 6.57 |
| di | 1.78 | 1.55 | 2.27 | 2.03 | 2.03 | 1.78 | 2.37 | 2.54 | 3.58 | 2.98 |
| wo | | | | | | 0.19 | | | | |
| ol | 3.52 | 4.56 | 6.14 | 0.10 | 4.34 | | 4.96 | 0.74 | 4.82 | 3.87 |
| il | 1.29 | 1.21 | 2.01 | 0.83 | 1.93 | 0.85 | 1.67 | 1.02 | 2.12 | 1.51 |
| ap | 1.44 | 1.01 | 2.15 | 0.09 | 2.27 | 0.16 | 2.06 | 0.45 | 2.43 | 1.56 |
| D.I.* | 87.4 | 84.0 | 83.7 | 92.0 | 86.6 | 92.0 | 84.7 | 92.0 | 85.8 | 82.5 |
| A.I. | 1.19 | 1.33 | 1.11 | 1.27 | 1.16 | 1.28 | 1.18 | 1.20 | 1.12 | 1.35 |
| $R_1$ | -1117 | -1699 | -890 | -1471 | -1036 | -1456 | -1112 | -1284 | -1101 | -2170 |
| $R_2$ | 540 | 512 | 609 | 439 | 613 | 446 | 617 | 497 | 691 | 619 |
| Rock-type | Nepheline syenite | Nepheline syenite | Nepheline syenite | Phonolite | Nepheline syenite | Phonolite | Nepheline syenite | Phonolite | Nepheline syenite | Nepheline syenite |
| Q | 35.6 | 33.7 | 34.8 | 34.3 | 34.2 | 34.4 | 34.4 | 33.4 | 30.9 | 28.3 |
| Ne | 41.7 | 42.0 | 44.1 | 42.6 | 43.7 | 42.5 | 42.7 | 43.7 | 48.0 | 52.4 |
| Ks | 22.7 | 24.3 | 21.1 | 23.1 | 22.1 | 23.1 | 22.9 | 22.9 | 21.1 | 19.3 |

Table 20 (continued).

| | MORRO DE SÃO PEDRO | | | | | |
|---|---|---|---|---|---|---|
| Sample | RP-252 | RP-253 | RP-254 | RP-256 | RP-257 | RP-258 |
| wt% | | | | | | |
| $SiO_2$ | 59.86 | 64.20 | 64.32 | 61.69 | 61.70 | 60.48 |
| $TiO_2$ | 0.60 | 0.55 | 0.50 | 0.49 | 0.63 | 0.96 |
| $Al_2O_3$ | 18.18 | 17.27 | 17.44 | 18.19 | 18.47 | 17.94 |
| $Fe_2O_3$ | 1.77 | 1.56 | 1.57 | 1.68 | 1.67 | 2.30 |
| FeO | 1.17 | 0.78 | 0.63 | 0.84 | 0.84 | 1.17 |
| MnO | 0.14 | 0.12 | 0.11 | 0.12 | 0.11 | 0.15 |
| MgO | 0.63 | 0.50 | 0.50 | 0.38 | 0.68 | 1.18 |
| CaO | 1.61 | 0.75 | 0.74 | 1.16 | 1.27 | 1.66 |
| $Na_2O$ | 10.66 | 7.57 | 7.87 | 8.95 | 7.72 | 7.03 |
| $K_2O$ | 4.40 | 5.62 | 5.44 | 5.66 | 5.99 | 6.02 |
| $P_2O_5$ | 0.21 | 0.12 | 0.12 | 0.12 | 0.17 | 0.28 |
| L.O.I. | 0.30 | 0.51 | 0.47 | 0.49 | 0.50 | 0.38 |
| Sum | 99.53 | 99.55 | 99.71 | 99.77 | 99.75 | 99.55 |
| or | 26.00 | 33.21 | 32.14 | 33.44 | 35.39 | 35.57 |
| ab | 43.29 | 55.64 | 56.42 | 44.22 | 45.21 | 45.14 |
| ne | 13.93 | 1.02 | 1.62 | 9.65 | 8.9 | 7.37 |
| ac | 5.12 | 4.51 | 4.54 | 4.86 | 3.23 | 0.63 |
| ns | 3.57 | 0.32 | 0.46 | 1.89 | | |
| di | 5.44 | 2.37 | 2.31 | 3.82 | 4.08 | 4.98 |
| wo | | | | 0.13 | | |
| ol | 0.20 | 0.59 | 0.37 | | | |
| mt | | | | | 0.80 | 1.47 |
| hm | | | | | | 1.06 |
| il | 1.13 | 1.04 | 0.94 | 0.93 | 1.19 | 1.82 |
| ap | 0.49 | 0.28 | 0.28 | 0.28 | 0.40 | 0.66 |
| D.I.* | 88.3 | 94.4 | 94.7 | 92.2 | 92.7 | 88.7 |
| A.I. | 1.13 | 1.07 | 1.08 | 1.15 | 1.04 | 1.01 |
| $R_1$ | -919 | 199 | 148 | -470 | -113 | 10 |
| $R_2$ | 560 | 444 | 446 | 500 | 532 | 589 |
| Rock-type | Nepheline syenite | Nephel-syenite | Nephel-syenite | Nepheline syenite | Nephel-syenite | Nephel-syenite |
| Q | 37.3 | 44.3 | 44.1 | 39.7 | 40.2 | 40.9 |
| Ne | 44.9 | 34.7 | 35.7 | 38.5 | 37.3 | 36.1 |
| Ks | 17.8 | 21.0 | 20.2 | 21.8 | 22.5 | 23.0 |

Table 21. Representative clinopyroxene analyses from Fecho dos Morros rocks. C, core; R, rim. For additional information see Table 3.

| | CERRITO | ILHA FECHO DOS MORROS | | | | MORRO DE SÃO PEDRO | | | | |
|---|---|---|---|---|---|---|---|---|---|---|
| Sample | RP-202 | RP-91R | | RP-201C | RP-201R | RP-255C | | RP-256C | | RP-257C |
| wt% | | | | | | | | | | |
| $SiO_2$ | 51.56 | 51.04 | 50.07 | 52.42 | 50.98 | 51.08 | 50.99 | 52.43 | 50.89 | 51.68 |
| $TiO_2$ | 1.03 | 0.11 | 0.97 | 0.70 | 2.69 | 1.13 | 1.00 | 0.69 | 0.42 | 0.44 |
| $Al_2O_3$ | 2.62 | 0.26 | 0.19 | 1.21 | 0.91 | 2.50 | 2.34 | 1.10 | 1.57 | 1.33 |
| $Fe_2O_3$ | 2.98 | 21.96 | 25.52 | 3.68 | 25.96 | 3.29 | 4.50 | 3.16 | 6.39 | 4.37 |
| FeO | 5.12 | 5.24 | 5.43 | 5.38 | 1.79 | 6.51 | 6.76 | 5.66 | 8.65 | 8.36 |
| MnO | 0.47 | 1.17 | 0.75 | 0.54 | 0.57 | 0.64 | 0.75 | 0.74 | 1.27 | 1.13 |
| MgO | 13.26 | 2.89 | 0.78 | 13.35 | 1.05 | 11.37 | 10.74 | 12.68 | 8.41 | 9.65 |
| CaO | 22.29 | 7.16 | 2.87 | 21.23 | 1.28 | 22.09 | 22.08 | 21.77 | 20.10 | 20.81 |
| $Na_2O$ | 1.07 | 8.70 | 10.66 | 1.39 | 12.35 | 1.37 | 1.48 | 1.38 | 2.27 | 1.91 |
| $K_2O$ | 0.02 | 0.01 | 0.01 | 0.00 | 0.09 | 0.01 | 0.01 | 0.00 | 0.01 | 0.00 |
| Sum | 100.42 | 98.54 | 97.25 | 99.96 | 97.67 | 99.99 | 100.65 | 99.61 | 98.41 | 99.68 |
| Si | 1.908 | 1.998 | 1.996 | 1.952 | 1.988 | 1.916 | 1.911 | 1.962 | 1.945 | 1.965 |
| $Al^{IV}$ | 0.092 | 0.002 | 0.004 | 0.048 | 0.012 | 0.084 | 0.089 | 0.038 | 0.055 | 0.035 |
| Sum | 2.000 | 2.000 | 2.000 | 2.000 | 2.000 | 2.000 | 2.000 | 2.000 | 2.000 | 2.000 |
| $Al^{VI}$ | 0.022 | 0.010 | 0.005 | 0.005 | 0.030 | 0.027 | 0.014 | 0.011 | 0.016 | 0.025 |
| Ti | 0.029 | 0.003 | 0.029 | 0.020 | 0.079 | 0.032 | 0.028 | 0.019 | 0.012 | 0.013 |
| $Fe^{3+}$ | 0.083 | 0.647 | 0.766 | 0.103 | 0.762 | 0.093 | 0.127 | 0.089 | 0.184 | 0.125 |
| $Fe^{2+}$ | 0.158 | 0.171 | 0.181 | 0.168 | 0.058 | 0.204 | 0.212 | 0.178 | 0.277 | 0.266 |
| Mn | 0.015 | 0.039 | 0.025 | 0.017 | 0.019 | 0.020 | 0.024 | 0.023 | 0.041 | 0.036 |
| Mg | 0.731 | 0.169 | 0.046 | 0.740 | 0.061 | 0.636 | 0.600 | 0.707 | 0.478 | 0.546 |
| Ca | 0.884 | 0.300 | 0.123 | 0.847 | 0.053 | 0.888 | 0.887 | 0.873 | 0.823 | 0.848 |
| Na | 0.077 | 0.660 | 0.824 | 0.100 | 0.934 | 0.099 | 0.107 | 0.100 | 0.168 | 0.141 |
| K | 0.001 | 0.001 | 0.001 | 0.000 | 0.004 | 0.001 | 0.001 | 0.000 | 0.001 | 0.000 |
| Sum | 2.000 | 2.000 | 2.000 | 2.000 | 2.000 | 2.000 | 2.000 | 2.000 | 2.000 | 2.000 |
| Mg/(Mg+Fe+Mn) | 0.741 | 0.165 | 0.045 | 0.720 | 0.068 | 0.667 | 0.623 | 0.709 | 0.488 | 0.561 |
| Quad | 1.773 | 0.640 | 0.350 | 1.755 | 0.172 | 1.728 | 1.699 | 1.758 | 1.578 | 1.660 |
| J | 0.154 | 1.320 | 1.648 | 0.200 | 1.868 | 0.198 | 0.214 | 0.200 | 0.336 | 0.282 |

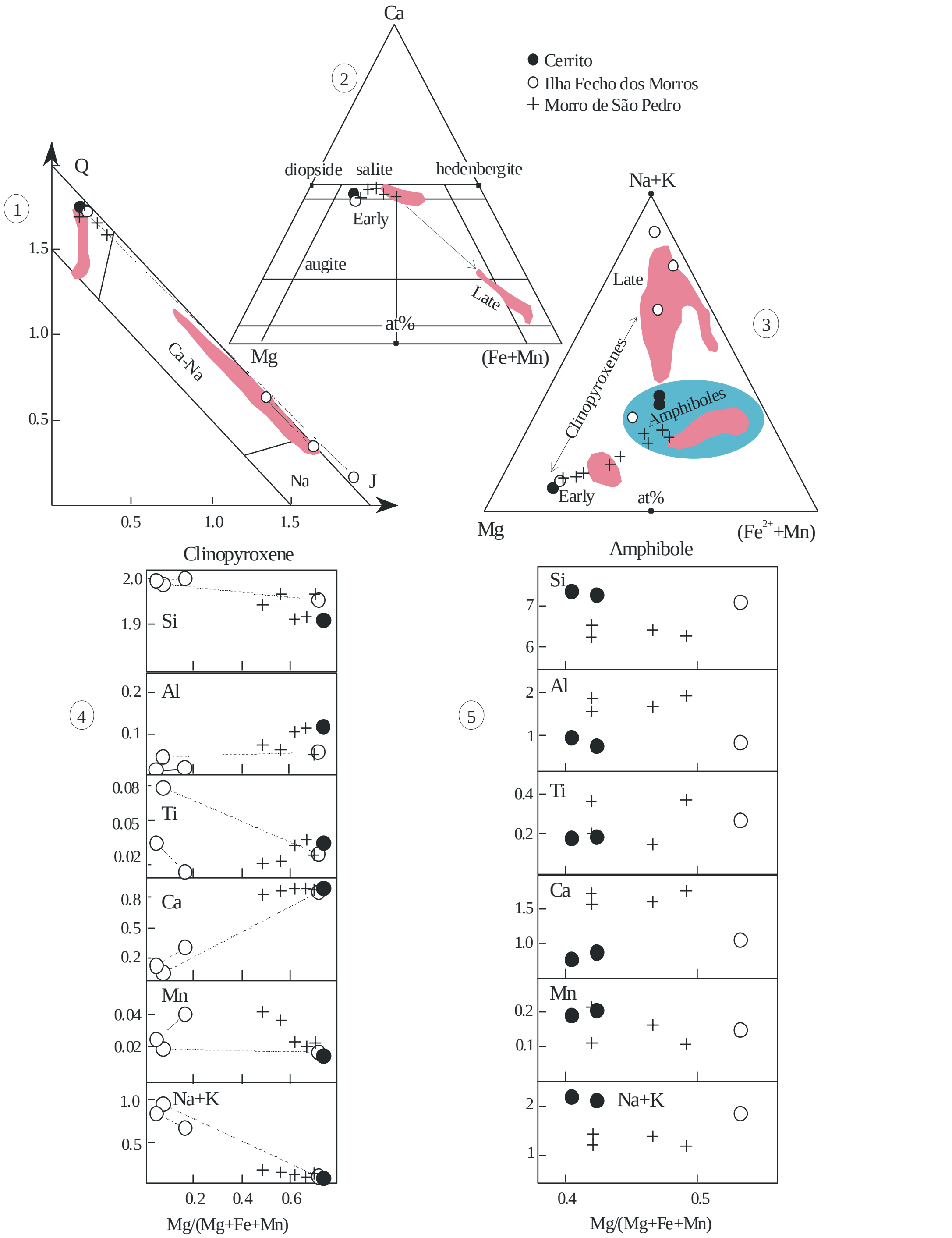


Fig. 22. Synoptical picture showing 1) Q-J and 2) Mg-(Fe+Mn)-Ca diagrams for clinopyroxenes (tie linens join core, early, and rim, late, compositions) from the Fecho dos Morros complex; for additional information see Fig. 4; 3) clinopyroxenes and amphiboles plotted into the Mg-($Fe^{2+}$+Mn)-(Na+K) diagrams; 4) and 5) elemental variations vs. Mg/(Mg+Fe+Mn) (Fe=total iron) atomic ratio for clinopyroxenes and amphiboles, respectively. Also shown in pink are the fields for the Cerro Siete Cabezas minerals.

Table 22. Representative amphibole analyses from Fecho dos Morros rocks. C, core; R, rim. For additional information see Table 4.

| | CERRITO | | ILHA FECHO DOS MORROS | MORRO DE SÃO PEDRO | | | |
|---|---|---|---|---|---|---|---|
| Sample | RP-88 | RP-102 | RP-201 | RP-255C | RP-255R | RP-256 | RP-257 |
| wt% | | | | | | | |
| $SiO_2$ | 47.75 | 47.76 | 47.56 | 41.12 | 40.81 | 42.05 | 41.82 |
| $TiO_2$ | 1.61 | 1.51 | 2.38 | 3.20 | 3.16 | 1.31 | 1.70 |
| $Al_2O_3$ | 4.30 | 5.26 | 4.74 | 10.60 | 10.22 | 9.24 | 8.36 |
| $Fe_2O_3$ | 3.81 | 2.19 | 3.30 | 0.82 | 1.47 | 4.59 | 3.17 |
| FeO | 16.36 | 17.39 | 13.81 | 16.19 | 18.21 | 14.28 | 16.28 |
| MnO | 1.60 | 1.45 | 1.17 | 0.84 | 9.84 | 1.26 | 1.64 |
| MgO | 8.88 | 7.97 | 11.44 | 9.66 | 8.30 | 9.66 | 8.49 |
| CaO | 5.35 | 4.65 | 6.68 | 10.86 | 10.61 | 9.89 | 9.46 |
| $Na_2O$ | 6.02 | 6.35 | 5.42 | 3.06 | 3.13 | 3.57 | 3.73 |
| $K_2O$ | 1.60 | 1.51 | 1.42 | 1.45 | 1.49 | 1.50 | 1.37 |
| F | 1.99 | 1.37 | 1.33 | 0.64 | 0.48 | 1.36 | 1.21 |
| Cl | 0.01 | 0.02 | 0.11 | 0.02 | 0.02 | 0.13 | 0.10 |
| Sum | 98.14 | 96.85 | 98.78 | 98.19 | 98.53 | 98.24 | 96.80 |
| | | | | | | | |
| Si | 7.288 | 7.357 | 7.116 | 6.268 | 6.267 | 6.447 | 6.550 |
| $Al^{IV}$ | 0.712 | 0.643 | 0.836 | 1.732 | 1.733 | 1.553 | 1.450 |
| $Fe^{3+}$ | | | 0.048 | | | | |
| Sum | 8.000 | 8.000 | 8.000 | 8.000 | 8.000 | 8.000 | 8.000 |
| $Al^{VI}$ | 0.062 | 0.312 | | 0.172 | 0.117 | 0.117 | 0.094 |
| Ti | 0.185 | 0.175 | 0.268 | 0.367 | 0.365 | 0.151 | 0.200 |
| $Fe^{3+}$ | 0.438 | 0.253 | 0.324 | 0.094 | 0.170 | 0.530 | 0.373 |
| $Fe^{2+}$ | 2.088 | 2.240 | 1.728 | 2.064 | 2.338 | 1.831 | 2.132 |
| Mn | 0.207 | 0.189 | 0.148 | 0.108 | 0.109 | 0.164 | 0.218 |
| Mg | 2.021 | 1.830 | 2.551 | 2.195 | 1.900 | 2.208 | 1.982 |
| Sum | 5.000 | 5.000 | 5.019 | 5.000 | 5.000 | 5.000 | 5.000 |
| § | | | | | | | |
| Ca | 0.875 | 0.767 | 1.071 | 1.773 | 1.746 | 1.625 | 1.588 |
| $Na_B$ | 1.125 | 1.233 | 0.910 | 0.227 | 0.254 | 0.375 | 0.412 |
| Sum | 2.000 | 2.000 | 1.981 | 2.000 | 2.000 | 2.000 | 2.000 |
| $Na_A$ | 0.656 | 0.664 | 0.663 | 0.678 | 0.678 | 0.686 | 0.720 |
| K | 0.312 | 0.297 | 0.271 | 0.282 | 0.292 | 0.293 | 0.274 |
| $Sum_A$ | 0.968 | 0.961 | 0.934 | 0.960 | 0.970 | 0.979 | 0.994 |
| F | 0.960 | 0.670 | 0.629 | 0.309 | 0.233 | 0.659 | 0.599 |
| Cl | 0.002 | 0.005 | 0.028 | 0.005 | 0.005 | 0.033 | 0.024 |
| | | | | | | | |
| Mg/(Mg+Fe+Mn) | 0.425 | 0.406 | 0.537 | 0.492 | 0.421 | 0.466 | 0.421 |

*Clinopyroxene and amphibole*

Clinopyroxenes (Table 21) display a very large compositional range, both in the whole population and in single specimens from calcic to sodic variants, i.e. salitic cores with Mg/(Mg+Fe+Mn) ratio (mg#) from 0.49 to 0.74 (similar to the mg# values of the clinopyroxenes from Cerro Pedreira, Morro Distante and Morro Conceição bodies (PDC), and higher than those from the Cerro Siete Cabezas complex), and rims with mg# ranging from 0.17 to 0.05. An important compositional gap between calcic and sodic pyroxenes is apparent (Fig. 22, insets 1-4). In the Mg–(Na+K)–($Fe^{2+}$+Mn) diagram, the calcic (early) clinopyroxenes demonstrate a well-defined trend of alkalies and iron enrichment. On the contrary, in terms of elemental correlation (a.f.u. values) vs. mg#, there are scattered variations, above all for Si and Al, confirming thus a general disequilibrium, that is, fast cooling, sub-solidus reactions and reactions with volatile-rich residua.

Amphiboles (Table 22) are sodic-calcic in the Cerrito and Ilha Fecho dos Morros bodies (katophorite and magnesiokatophorite, respectively; mg#=0.40–0.53), and tendentiously calcic in the Morro de São Pedro rock-types (ferropargasite to edenite; mg#=0.42–0.49). In the Mg–(Na+K)–($Fe^{2+}$+Mn) diagram (Fig. 22, inset 3), amphiboles appear in the same trend of the coexisting clinopyroxenes, and quite distinct from the amphiboles of the Cerro Siete Cabezas complex. However, as for the pyroxenes, the same elemental scatters are observed (Fig. 22, inset 5). Specially in the Cerrito body, where the pyroxenes show the highest and lowest Ca and Na+K values, respectively, the cognate amphiboles have the lowest and highest Ca and Na+K, respectively.

### *Biotite*

The biotites (Table 23; Fig. 23, where the results are compared with the compositions from the previous investigated occurrences), in terms of Mg/(Mg+Fe+Mn) ratio, span between the ranges of mineral analogues from Cerro Siete Cabezas and PDC. In the Mg-Al-Fe diagram, the samples show a trend of iron enrichment, where the highest iron contents are observed for biotites from the Ilha Fecho dos Morros (annite up to 62%). Specimens from Cerrito and Morro de São Pedro bodies have phlogopite-rich (annite about 31%) and intermediate compositions (annite about 49%), respectively. $Al^{IV}$ and Ti are correlated with increasing annite solid solution, whereas Mn tends to increase as FeO increases. K content is quite constant, between 1.8 and 1.9 a.f.u., but some biotites, having the highest F contents, display important depletions, up to 1.67 a.f.u., probably due to subsolidus reactions under the influence of F-rich magmatic fluids (cf. Finch *et al.*, 1995). Some Li-rich compositions are noticeable at the rims of the more F-rich compositions (taeniolite?).

Table 23. Representative biotite analyses from Fecho dos Morros rocks. For additional information see Table 5.

| | CERRITO | | ILHA FECHO DOS MORROS | MORRO DE SÃO PEDRO | | |
|---|---|---|---|---|---|---|
| Sample | RP-88 | RP-202 | RP-201 | RP-255 | RP-256 | RP-257 |
| wt% | | | | | | |
| $SiO_2$ | 37.40 | 37.20 | 36.94 | 38.86 | 37.94 | 36.56 |
| $TiO_2$ | 6.90 | 7.62 | 3.17 | 4.03 | 2.19 | 2.51 |
| $Al_2O_3$ | 13.68 | 14.09 | 10.56 | 13.21 | 12.71 | 12.49 |
| $Cr_2O_3$ | 0.03 | n.d. | n.d. | n.d. | n.d. | n.d. |
| $FeO_{tot}$ | 11.54 | 13.47 | 25.76 | 20.08 | 18.51 | 20.15 |
| MnO | 0.21 | 0.25 | 0.70 | 0.64 | 1.19 | 1.82 |
| MgO | 15.65 | 13.89 | 8.80 | 12.15 | 12.50 | 11.10 |
| CaO | 0.00 | 0.01 | 0.01 | 0.09 | 0.09 | 0.05 |
| $Na_2O$ | 0.33 | 0.44 | 0.17 | 0.57 | 0.44 | 0.31 |
| $K_2O$ | 9.71 | 9.56 | 9.42 | 9.05 | 9.47 | 8.40 |
| F | 0.82 | n.d. | 0.68 | 0.76 | 1.63 | 0.92 |
| Cl | 0.05 | n.d. | 0.15 | 0.00 | 0.02 | 0.12 |
| Less O=F,Cl | 0.36 | | 0.32 | 0.32 | 0.69 | 0.41 |
| $H_2O^+$calc | 3.66 | 4.07 | 3.45 | 3.62 | 3.20 | 3.38 |
| Sum | 99.63 | 100.60 | 99.49 | 100.74 | 99.20 | 97.39 |
| | | | | | | |
| Si | 5.520 | 5.475 | 5.807 | 5.546 | 5.720 | 5.696 |
| $Al^{IV}$ | 2.380 | 2.444 | 1.956 | 2.343 | 2.259 | 2.294 |
| $Ti^{IV}$ | 0.100 | 0.081 | 0.237 | 0.111 | 0.021 | 0.010 |
| Sum (Z) | 8.000 | 8.000 | 8.000 | 8.000 | 8.000 | 8.000 |
| $Al^{VI}$ | | | | | | |
| $Ti^{VI}$ | 0.666 | 0.762 | 0.138 | 0.345 | 0.227 | 0.284 |
| Cr | 0.003 | | | | | |
| $Fe^{2+}$ | 1.424 | 1.658 | 3.387 | 2.527 | 2.334 | 2.626 |
| Mn | 0.026 | 0.031 | 0.093 | 0.082 | 0.152 | 0.240 |
| Mg | 3.442 | 3.047 | 2.062 | 2.725 | 2.809 | 2.579 |
| Sum (Y) | 5.561 | 5.498 | 5.680 | 5.679 | 5.522 | 5.729 |
| Ca | | 0.002 | 0.002 | 0.015 | 0.015 | 0.008 |
| Na | 0.094 | 0.126 | 0.052 | 0.166 | 0.129 | 0.094 |
| K | 1.828 | 1.795 | 1.889 | 1.737 | 1.821 | 1.670 |
| Sum (X) | 1.922 | 1.923 | 1.943 | 1.918 | 1.965 | 1.772 |
| F | 0.382 | | 0.338 | 0.362 | 0.777 | 0.454 |
| Cl | 0.013 | | 0.040 | | 0.005 | 0.032 |
| OH | 3.605 | 4.000 | 3.622 | 3.638 | 3.218 | 3.514 |
| Sum | 4.000 | 4.000 | 4.000 | 4.000 | 4.000 | 4.000 |
| | | | | | | |
| Mg/(Mg+Fe+Mn) | 0.704 | 0.643 | 0.372 | 0.511 | 0.531 | 0.474 |

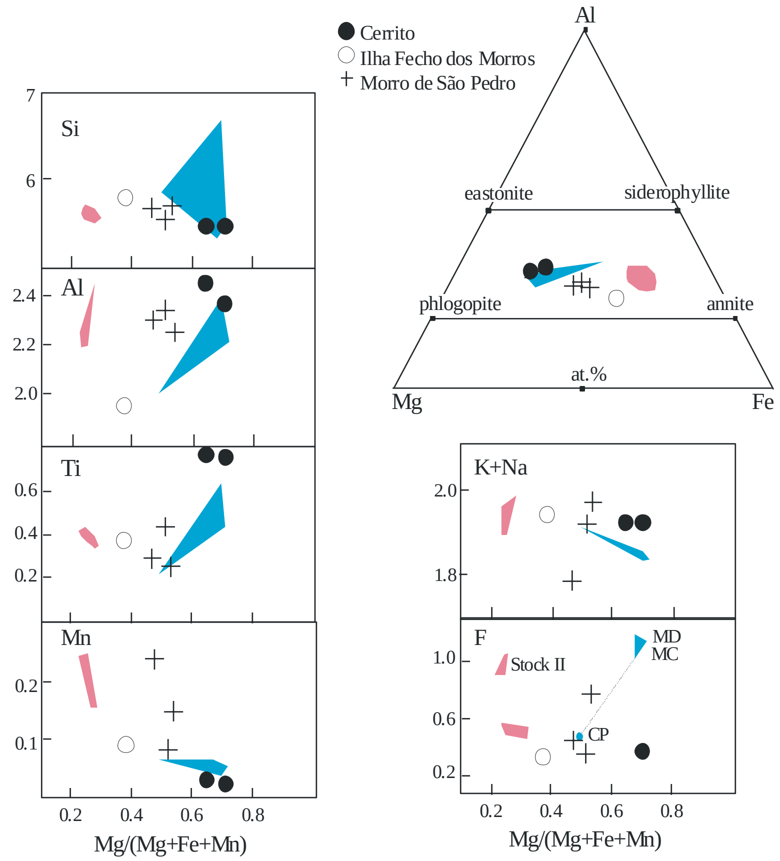


Fig. 23. Plot of biotites from the Fecho dos Morros complex in the system Al-Mg-(Fe+Mn), Fe=total iron as $Fe^{2+}$, and variations of Si, Al, Ti, Mn, K+Na and F vs. Mg/(Mg+Fe+Mn) atomic ratio. Fields for the Cerro Siete Cabezas and Cerro Pedreira (CP)+Morro Distante (MD)+Morro Conceição (MC) minerals are shown in pink and blue, respectively.

*Iron oxides*

The opaque minerals are often represented by oxydized phases (hematite). Magnetite-ilmenite pairs were identified in a few specimens (Table 24). The geothermometry of Spencer & Lindsley (1981) yielded subsolidus temperatures between 496°C and 690°C, and log $fO_2$ between −15 and −23 (spanning from above the Magnetite-Hematite and under the Quartz-Fayalite-Magnetite buffers, Fig. 24A). As previously observed, the ilmenites contain high Mn contents, generally in the range of the PDC compositions; however, the coexisting magnetites show higher Mn contents than those of the Cerro Siete Cabezas complex and PDC occurrences (Fig. 24B).

*Feldspars, nepheline and sodalite*

As noted for the Cerro Siete Cabezas occurrences, only alkali feldspar is present in the Fecho dos Morros complex (Table 25), with a variety of perthitic textures developed with cooling and subsequent subsolvus unmixing. Typically the bulk compositions have Or contents between 34 and 48 mol% (Fig. 25); some An-rich compositions are found in the groundmass or at the rims of alkali feldspar grains (i.e. $Or_{34-21}$, $Ab_{68-54}$, $An_{12-11}$).

Nepheline is in a few cases partially replaced by cancrinite a typical late-stage alteration phase. Representative analyses of nepheline are in Table 25 and plotted in the system Ks-Ne-Q (Fig. 25). The silica-excess, as quartz molecules, ranges from 7.4 to 8.8% (Cerrito and Ilha Fecho dos Morros) and is up to 12% in Morro de São Pedro, with kalsilite between 14.2 and 19.9%, and 15.2%, respectively (Table 25), from which crystallization temperatures between 740 and 980°C are obtained (cf. Hamilton & MacKenzie, 1965; Woolley & Platt, 1986).

Sodalite, that is found as a primary mineral phase together with nepheline and alkali felspar, especially in the pegmatitic facies, presents Cl contents between 4.5 and 7.6 wt% (Table 25). As a matter of fact, the necessary Cl activity required for the formation of sodalite in undersaturated liquids takes advantage of the Cl "ability" to concentrate in such liquids rather than partitioning into the vapour phase (Hards, 1976), according to the experimental studies performed by Barker (1976) which demonstrated the stabilility of liquidus sodalite-nepheline-alkali feldspar in undersaturated compositions.

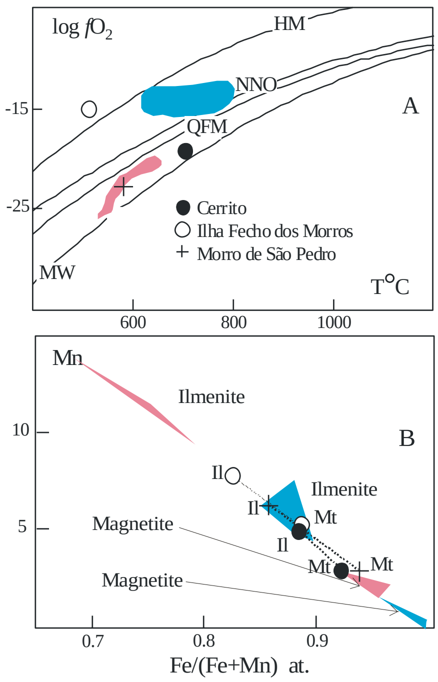


Fig. 24. Fecho dos Morros complex. A: stability relationships in T°C-$fO_2$ diagram for magnetite-ilmenite pairs (cf. Fig. 7). B: relationships between Mn content (wt%) and Fe/(Fe+Mn) (atomic ratio) for magnetite-ilmenite pairs (Mt, magnetite; Il, ilmenite). The fields representing the compositional variations of opaques from the Cerro Siete Cabezas complex and Cerro Pedreira+Morro Distante+Morro Conceição bodies are shown in pink and blue, respectively.

## Major and trace elements distribution

In the Ks-Ne-Q diagram (Fig. 25) all the samples fit the range between the trachytic and phonolitic minima, but the pegmatitic varieties from the Ilha Fecho dos Morros tend to place around the phonolitic minimum, whereas the Morro de São Pedro specimens are concentrated near to the trachytic minimum.

The normal facies of the Fecho dos Morros complex (Cerrito and Morro de São Pedro) displays a D.I.* range similar to that shown by the Cerro Siete Cabezas complex (CSC), that is, between 74 and 95.

However, important differences are apparent (Fig. 26): the normal facies from Cerrito and Morro de São Pedro, fitting the same CSC field, have the highest alumina content with a maximum at 84.5 D.I.* (petrographically corresponding to the beginning of the nepheline+sodalite fractionation), and comparatively higher and lower calcium and iron contents, respectively. The Ilha Fecho dos Morros facies clusters in a narrow D.I.* range (82-88), with lower silica, alumina and calcium concentrations. Some scattering values relative to the soda and phosphorous contents ($Na_2O$ up to 13% and $P_2O_5$ up to 1 wt%, at D.I.*=84) are noticeable. Pegmatitic facies and phonolitic dykes appear on the same trend of the Fecho dos Morros rocks.

Although not satisfactory because of the high $\Sigma R^2>3$, probably due to the presence of accessory (i.e. exotic) "cryptic" phases, and then only of qualitative significance, mass balance calculations demonstrate the possibility of fractional crystallization of prevailing mafic phases, e.g. about 19% (clinopyroxene 46%, biotite 36%, opaques 11%, apatite 6% and titanite 1%), from D.I.*=73.8 to D.I.*=84.6, and prevailing nepheline and sodalite from D.I.*=84.6 to D.I.*=93.1 (e.g. about 30% of a fractionated mineral assemblage containing 40% nepheline+60% sodalite).

As observed in the other occurrences, the trace elements appear strongly scattered vs. D.I.*, or follow broadly depletion-trends, in particular Y and REE (Table 26, Fig. 27), probably due to the fractionation of accessory minerals such as titanite or other cryptic phases. Syenitic rocks from Cerrito have high Sr contents in comparison with the other bodies, and some dykes and pegmatitic facies are strongly enriched in U (up to 111 ppm), Zr-Hf (up to 5939 and 161 ppm, respectively), Nb-Ta (up to 2236 and 246 ppm, respectively) and Y (up to 200 ppm; cf. Table 26). The Sm/Nd ratio is 0.17 (r>0.99), similar to that of the Cerro Pedreira occurrence (Sm/Nd=0.16), but lower in relation to the Cerro Siete Cabezas complex (Sm/Nd=0.20).

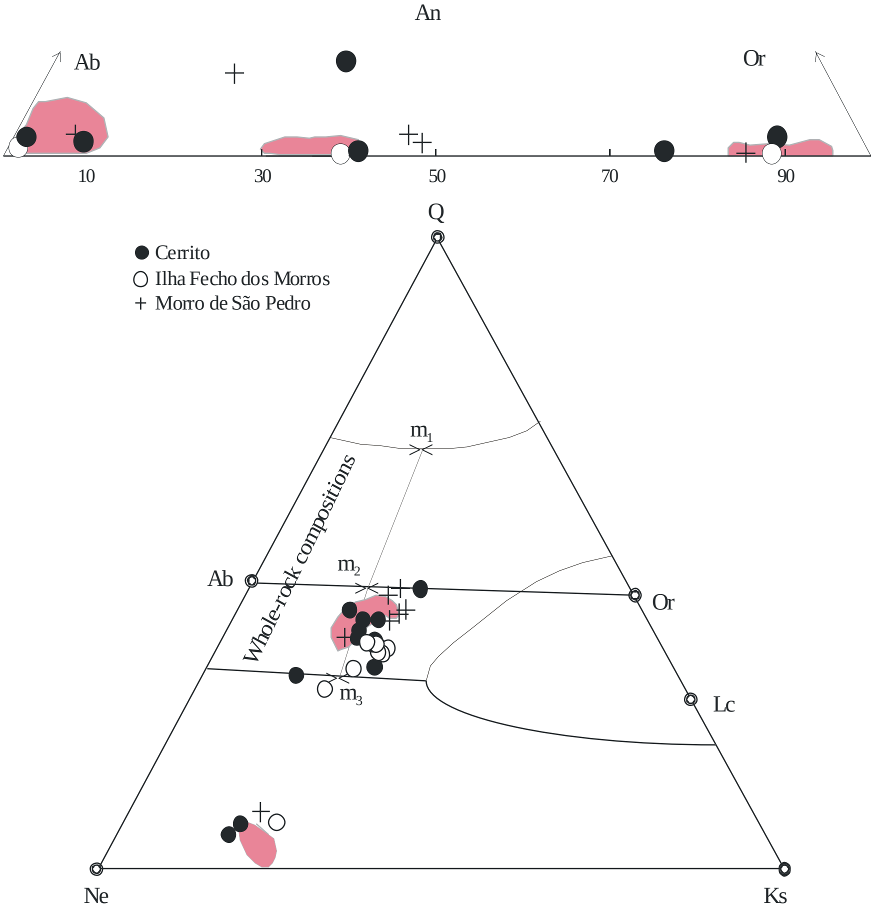


Fig. 25. Alkali feldspar and nepheline compositions from the Fecho dos Morros complex plotted into the Or-Ab-An (mol%) and Ks-Ne-Q (wt%) diagrams, respectively (see Fig. 8). For comparison the whole-rock compositions are also plotted. Compositional fields for the Cerro Siete Cabezas complex are shown in pink.

The I.E. (primitive mantle-normalized) spidergrams (Fig. 28) show in general similar behaviours, spikes and overlapping fields, with exception of Sr that in Cerrito exhibits a positive spike in comparison to a negative one for the other occurrences. The REE of the pegmatitic facies (RP-81 Cerrito dyke) tend to be strongly enriched. Notably, U from Morro de São Pedro is depleted with respect to Rb and Th, while in the other occurrences U seems to be strongly enriched in relation to Th.

Also the REE (chondrite-normalized) spidergrams display in general similar enriched behaviours, but the pegmatitic facies (and RP-81 dyke) is largely enriched. Some relatively depleted samples are noticeable in Morro de São Pedro (Fig. 28). The REE have similar fractionation patterns in the normal facies, that is, La/Sm=5.6-7.1, Sm/Yb=3.2-5.1, La/Yb=18.4-32.7 (cf. inset A of Fig. 28). In the RP-81 dyke, and also in the pegmatitic facies, the ratios are 4.8 to 5.9, 1.2 to 1.1 and 5.7 to 6.6, respectively and HREE are clearly enriched in comparison to the MREE (amphibole fractionation?). Eu/Eu* anomalies are pronounced in all the occurrences, with the more negative spikes corresponding to the RP-92 dyke, RP-82A pegmatitic facies and to the Morro de São Pedro samples (cf. inset B of Fig. 28).

Sr-Nd isotopes

The data relative to $^{87}Rb/^{86}Sr$ vs. $^{87}Sr/^{86}Sr$ isoto-pes of specimens from Ilha Fecho dos Morros and Morro de São Pedro occurrences (Table I of Appendix) fit a straigth line, r=0.99, initial $^{87}Sr/^{86}Sr$ ($R_0$)= 0.703864, defining an errorchron of 38 Ma younger than that obtained for CSC (i.e. 217 Ma; cf. Velázquez *et al.*, 1996a). The two samples from Cerrito show scattered values bridging the above correlation line. $^{143}Nd/^{143}Nd$ initial ratio ranges from 0.51222 to 0.51244. The differences are not easily modelled through AFC or RTF processes: probably, the isotopic systems are strongly perturbed by the action of convective movements in the magmatic chamber and also by the volatile pressure, as judged from petrographical and mineralogical evidence. The Nd model ages spread from 682 (Cerrito) up to 1038 Ma (Ilha Fecho dos Morros; cf. Table I of the Appendix) with an average of 834±165 Ma; Cerro Siete Cabezas and PDC present a mean value of 890±85 Ma.

Table 24. Representative magnetite and ilmenite analyses from Fecho dos Morros rocks. For additional information see Table 6.

| Magnetite | CERRITO | | ILHA FECHO DOS MORROS | | MORRO DE SÃO PEDRO | |
|---|---|---|---|---|---|---|
| Sample | RP-88 | RP-202 | RP-91 | RP-201 | RP-255 | RP-256 |
| wt% | | | | | | |
| $SiO_2$ | 0.06 | 0.02 | 0.02 | 0.05 | 0.03 | 0.05 |
| $TiO_2$ | 10.78 | 8.87 | 18.01 | 14.86 | 16.64 | 5.93 |
| $Al_2O_3$ | 0.23 | 0.15 | 0.16 | 0.48 | 0.64 | 0.58 |
| $Cr_2O_3$ | n.d. | n.d. | 0.02 | 0.01 | 0.05 | 0.04 |
| $Fe_2O_3$ | 45.92 | 50.90 | 32.55 | 39.29 | 35.36 | 55.57 |
| FeO | 37.06 | 35.78 | 44.13 | 39.62 | 43.48 | 33.36 |
| MnO | 3.37 | 2.83 | 2.99 | 5.13 | 2.81 | 2.58 |
| MgO | 0.02 | 0.10 | 0.06 | 0.26 | 0.02 | 0.04 |
| CaO | 0.00 | 0.01 | 0.05 | 0.01 | 0.04 | 0.13 |
| Sum | 97.44 | 98.66 | 97.99 | 99.71 | 99.07 | 98.28 |
| Si | 0.019 | 0.006 | 0.006 | 0.015 | 0.009 | 0.015 |
| Ti | 2.548 | 2.074 | 4.177 | 3.384 | 3.815 | 1.384 |
| Al | 0.085 | 0.055 | 0.058 | 0.170 | 0.230 | 0.212 |
| Cr | | | 0.004 | 0.002 | 0.012 | 0.010 |
| $Fe^{3+}$ | 10.780 | 11.771 | 7.554 | 8.960 | 8.111 | 12.979 |
| $Fe^{2+}$ | 9.669 | 9.305 | 11.382 | 10.040 | 11.084 | 8.660 |
| Mn | 0.890 | 0.745 | 0.781 | 1.309 | 0.725 | 0.679 |
| Mg | 0.009 | 0.046 | 0.028 | 0.117 | 0.009 | 0.018 |
| Ca | | 0.003 | 0.010 | 0.003 | 0.005 | 0.043 |
| Sum | 24.000 | 24.000 | 24.000 | 24.000 | 24.000 | 24.000 |
| Ulv. mol% | 31.93 | 26.03 | 52.35 | 42.63 | 48.52 | 17.49 |

| Ilmenite | CERRITO | ILHA FECHO DOS MORROS | MORRO DE SÃO PEDRO |
|---|---|---|---|
| Sample | RP-202 | RP-201 | RP-255 |
| wt% | | | |
| $SiO_2$ | 0.01 | 0.04 | |
| $TiO_2$ | 50.62 | 50.56 | 50.59 |
| $Al_2O_3$ | 0.02 | 0.02 | 0.10 |
| $Cr_2O_3$ | | 0.02 | |
| $Fe_2O_3$ | 6.44 | 1.71 | 2.68 |
| FeO | 37.54 | 37.59 | 38.83 |
| MnO | 4.82 | 7.75 | 6.30 |
| MgO | 0.11 | 0.02 | 0.16 |
| CaO | 0.01 | 0.03 | |
| Sum | 99.57 | 97.74 | 98.66 |
| Si | 0.001 | 0.001 | |
| Ti | 0.959 | 0.982 | 0.973 |
| Al | 0.001 | 0.000 | 0.003 |
| Cr | | 0.000 | |
| $Fe^{3+}$ | 0.122 | 0.033 | 0.052 |
| $Fe^{2+}$ | 0.791 | 0.812 | 0.830 |
| Mn | 0.103 | 0.170 | 0.136 |
| Mg | 0.004 | 0.001 | 0.006 |
| Ca | 0.001 | 0.001 | |
| Sum | | | |
| $Fe^{2+}/(Mn+Fe^{2+})$ | 0.885 | 0.826 | 0.859 |
| $R_2O_3$ mol% | 6.01 | 1.71 | 2.72 |
| T°C | 690 | 496 | 582 |
| $\log_{10} fO_2$ | -17.3 | -15.0 | -22.6 |

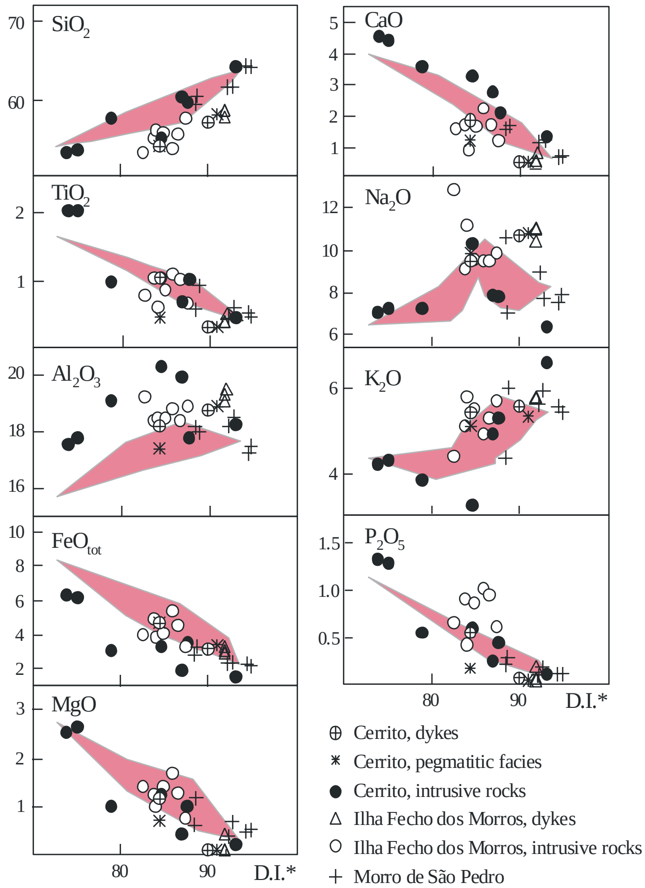


Fig. 26. D.I.* vs. major elements (wt%) for rocks from the Fecho dos Morros complex. The fields in pink represent the compositional variations of rock-types from the Cerro Siete Cabezas complex.

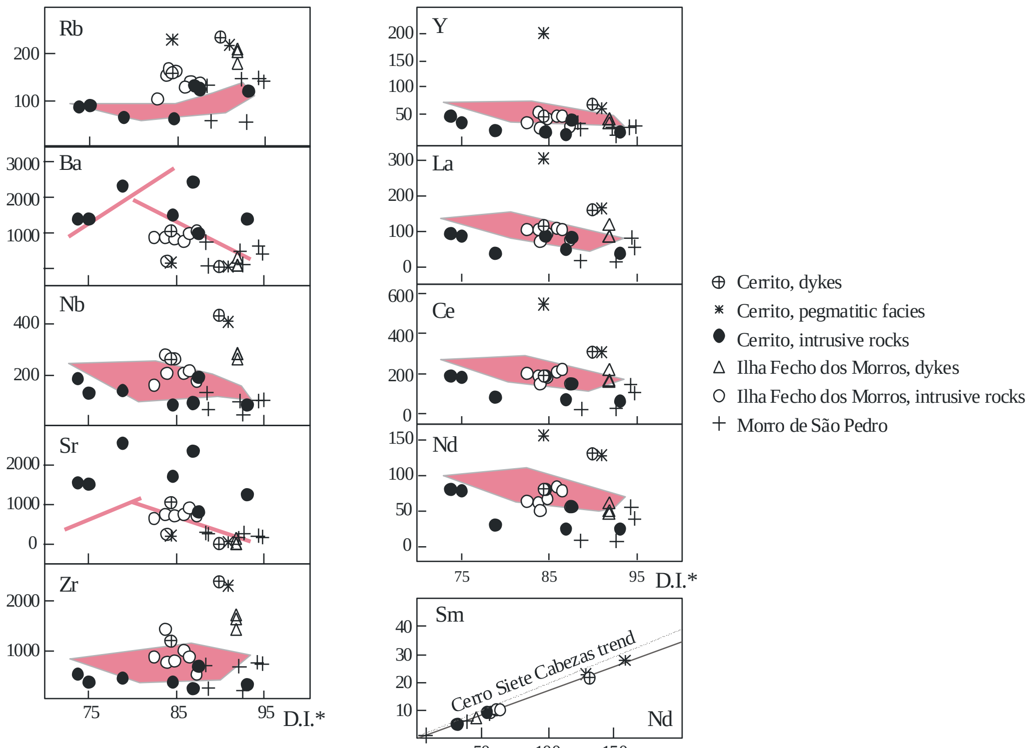


Fig. 27. D.I.* vs. trace elements (ppm) for rocks from the Fecho dos Morros complex and Nd-Sm correlation. The fields in pink represent the compositional variations of rock-types from the Cerro Siete Cabezas complex.

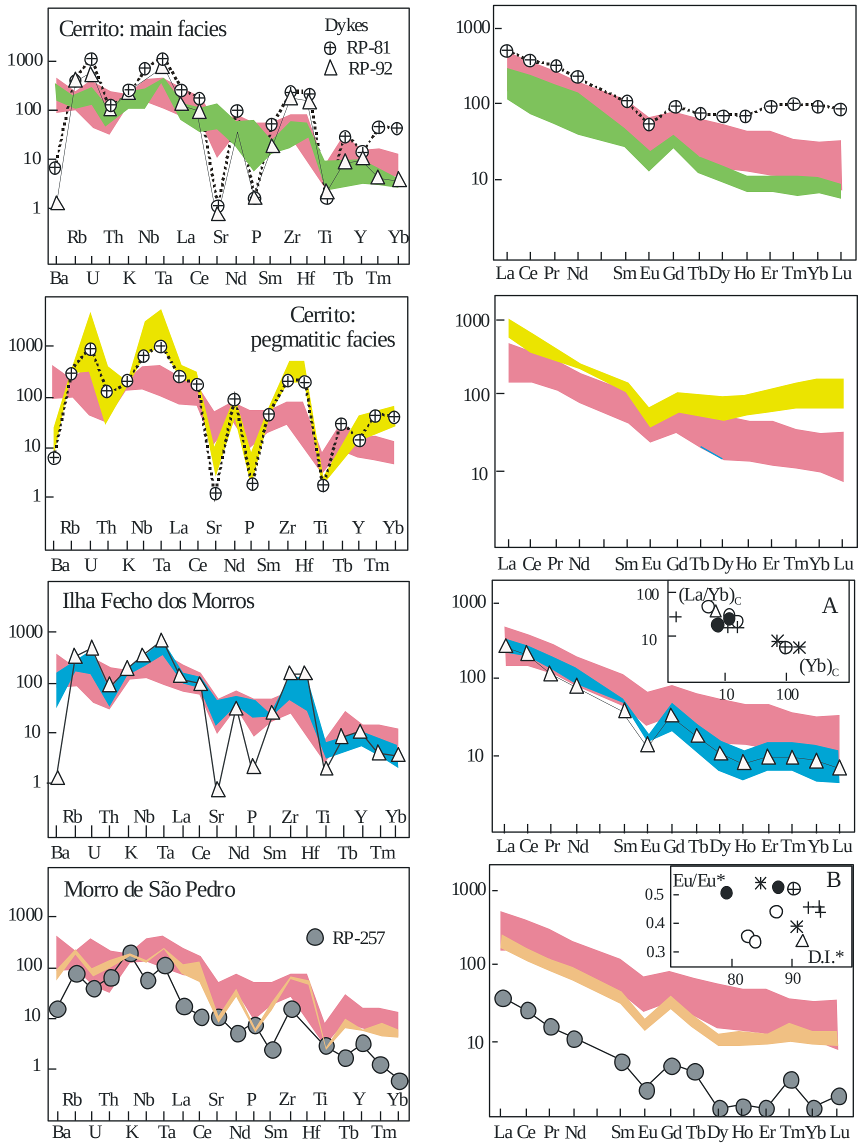


Fig. 28. Primitive mantle- (Sun & McDonough, 1989) and chondrite- (Boynton, 1984) normalized I.E. and REE distribution, respectively, for rocks from the Fecho dos Morros complex. The Cerro Siete Cabezas field in pink is shown for comparison. Inset A: $Yb_c$ vs. $(La/Yb)_c$; inset B: D.I. vs. Eu/Eu* (symbols as in Fig. 27).

Table 25. Representative alkali feldspar, nepheline and titanite analyses of rocks from the Fecho dos Morros complex, and representative analyses of sodalite (for the latter formulae on the basis of $3Al_2O_3$*$6SiO_2$ structural frame). For additional information see Tables 7 and 8.

| Feldspars | CERRITO | | | | | | ILHA FECHO DOS MORROS | | | MORRO DE SÃO PEDRO | | | | |
|---|---|---|---|---|---|---|---|---|---|---|---|---|---|---|
| Sample | RP-88B | RP-88or | RP-88ab | RP-202B | RP-202or | RP-202ab | RP-91B | RP-201or | RP-201ab | RP-255C | RP-255R | RP-256B | RP-256or | RP-256ab |
| wt% | | | | | | | | | | | | | | |
| $SiO_2$ | 66.52 | 65.38 | 67.29 | 66.07 | 65.59 | 68.04 | 67.51 | 65.56 | 68.58 | 65.83 | 65.91 | 66.43 | 65.18 | 67.87 |
| $Al_2O_3$ | 19.14 | 18.50 | 19.20 | 19.91 | 18.95 | 19.68 | 18.71 | 18.44 | 19.36 | 19.25 | 20.08 | 19.00 | 18.41 | 19.58 |
| $Fe_2O_3$ | 0.12 | 0.08 | 0.10 | 0.16 | 0.07 | 0.02 | 0.70 | 0.25 | 0.15 | 0.18 | 0.17 | 0.18 | 0.09 | 0.01 |
| BaO | 0.08 | 0.07 | 0.17 | 0.53 | 0.86 | 0.28 | 0.04 | 0.11 | 0.00 | 0.17 | 0.36 | 0.25 | 0.00 | 0.13 |
| CaO | 0.04 | 0.02 | 0.20 | 1.19 | 0.05 | 0.24 | 0.04 | 0.01 | 0.05 | 0.56 | 1.14 | 0.18 | 0.03 | 0.28 |
| $Na_2O$ | 6.62 | 2.65 | 10.48 | 6.65 | 1.14 | 10.71 | 7.23 | 1.37 | 11.62 | 5.79 | 8.33 | 5.76 | 1.70 | 10.52 |
| $K_2O$ | 7.29 | 13.03 | 1.53 | 6.38 | 15.20 | 0.12 | 6.62 | 15.02 | 0.23 | 8.06 | 3.86 | 8.45 | 14.43 | 1.56 |
| Sum | 99.81 | 99.73 | 98.97 | 100.89 | 101.86 | 99.09 | 101.11 | 100.76 | 99.99 | 99.84 | 99.85 | 100.25 | 99.84 | 99.95 |
| | | | | | | | | | | | | | | |
| Or | 41.7 | 76.0 | 8.5 | 33.9 | 86.6 | 0.7 | 37.4 | 87.4 | 1.3 | 45.0 | 20.7 | 47.8 | 84.6 | 8.6 |
| Ab | 57.6 | 23.5 | 89.0 | 53.7 | 9.9 | 95.9 | 62.1 | 12.1 | 98.2 | 49.1 | 67.9 | 49.6 | 15.1 | 88.3 |
| An | 0.7 | 0.5 | 2.5 | 12.4 | 3.5 | 3.4 | 0.5 | 0.5 | 0.5 | 5.9 | 11.4 | 2.6 | 0.3 | 3.1 |

Table 25 (continued).

| Nepheline | CERRITO | | ILHA FECHO DOS MORROS | MORRO DE SÃO PEDRO | Sodalite | CERRITO | ILHA FECHO DOS MORROS | MORRO DE SÃO PEDRO | |
|---|---|---|---|---|---|---|---|---|---|
| Sample | RP-88 | RP-202 | RP-201 | RP-255 | | RP-288 | RP-201 | RP-255 | RP-256 |
| wt% | | | | | | | | | |
| $SiO_2$ | 45.69 | 44.71 | 45.38 | 46.44 | $SiO_2$ | 37.03 | 36.79 | 38.12 | 37.99 |
| $Al_2O_3$ | 31.73 | 32.84 | 32.18 | 31.28 | $Al_2O_3$ | 29.50 | 28.40 | 32.71 | 30.23 |
| $Fe_2O_3$ | 0.30 | 0.37 | 0.21 | 0.41 | $Fe_2O_3$ | 0.70 | 0.66 | 0.18 | 0.32 |
| BaO | 0.01 | 0.01 | | 0.08 | CaO | 0.04 | 0.04 | 0.08 | 0.15 |
| CaO | 0.04 | 1.44 | | 0.80 | $Na_2O$ | 22.57 | 24.5 | 24.24 | 25.31 |
| $Na_2O$ | 16.69 | 15.68 | 15.36 | 15.12 | $K_2O$ | 0.01 | 0.09 | 0.02 | 0.05 |
| $K_2O$ | 4.69 | 4.31 | 6.51 | 4.81 | Cl | 6.91 | 7.04 | 4.53 | 7.58 |
| Sum | 99.15 | 99.06 | 99.64 | 98.94 | -O=Cl | 1.56 | 1.58 | 1.02 | 1.71 |
| | | | | | Sum | 95.20 | 95.94 | 98.86 | 99.92 |
| Q | 8.8 | 7.4 | 8.7 | 12.0 | | | | | |
| Ne | 77.0 | 78.4 | 71.4 | 72.7 | Si | 6.160 | 6.241 | 5.971 | 6.163 |
| Ks | 14.2 | 14.2 | 19.9 | 15.2 | Al | 5.786 | 5.679 | 6.725 | 5.781 |
| | | | | | $Fe^{3+}$ | 0.088 | 0.084 | 0.021 | 0.039 |
| | | | | | Sum | 12.034 | 12.004 | 12.267 | 11.983 |
| | | | | | Ca | 0.007 | 0.007 | 0;013 | 0.026 |
| | | | | | Na | 7.280 | 8.058 | 7.362 | 7.962 |
| | | | | | K | 0.002 | 0.020 | 0.004 | 0.010 |
| | | | | | Sum | 7.289 | 8.085 | 7.379 | 7.998 |
| | | | | | Cl | 1.818 | 1.889 | 1.219 | 2.085 |

Table 26. Trace element analyses of selected rocks from the Fecho dos Morros complex. D, dykes; P, pegmatitic facies.

| | CERRITO | | | | | | | | | | | ILHA FECHO DOS MORROS | | | | |
|---|---|---|---|---|---|---|---|---|---|---|---|---|---|---|---|---|
| Sample | RP-80 | RP-81 D | RP-82A P | RP-82B | RP-83 | RP-84 | RP-85 D | RP-86 | RP-87 | RP-88 P | RP-202 | RP-89 | RP-90 | RP-91 | RP-92 D | RP-93 |
| ppm | | | | | | | | | | | | | | | | |
| Cr | 2 | 1 | 1 | 1 | 1 | 1 | 1 | 5 | 1 | 1 | 6 | 1 | 1 | 4 | 1 | 1 |
| Ni | 11 | 8 | 4 | 7 | 3 | 5 | 9 | 8 | 6 | 13 | 8 | 10 | 7 | 8 | 4 | 1 |
| Rb | 89 | 235 | 216 | 67 | 120 | 133 | 160 | 87 | 123 | 232 | 60 | 138 | 165 | 156 | 207 | 142 |
| Ba | 1389 | 43 | 25 | 2329 | 1369 | 2467 | 1059 | 1378 | 1013 | 164 | 1525 | 1030 | 217 | 901 | 9 | 982 |
| Th | 3.4 | 9.5 | 2.2 | 6.2 | | | | | 8.0 | 36.8 | | 3.0 | | 5.3 | 7.0 | |
| U | 6.0 | 22 | 6.7 | 2.3 | | | | | 2.6 | 111 | | 3.4 | | 9.4 | 11.1 | |
| Ta | 13.2 | 46.0 | 45 | 13.1 | | | | | 17.5 | 246 | | 18.1 | | 29.6 | 28.9 | |
| Nb | 124 | 429 | 405 | 136 | 78 | 86 | 261 | 184 | 190 | 2230 | 78 | 172 | 205 | 276 | 285 | 210 |
| Sr | 1481 | 24 | 53 | 2514 | 1259 | 2360 | 1028 | 1565 | 816 | 213 | 1671 | 700 | 271 | 741 | 12 | 883 |
| Hf | 8.4 | 67 | 64 | 10.6 | | | | | 16.4 | 163 | | 8.7 | | 39.1 | 44.4 | |
| Zr | 320 | 2406 | 2322 | 409 | 281 | 188 | 1201 | 494 | 649 | 5939 | 320 | 505 | 722 | 1436 | 1712 | 851 |
| Y | 36 | 67 | 62 | 20 | 17 | 15 | 48 | 47 | 38 | 200 | 17 | 28 | 26 | 54 | 44 | 47 |
| La | 86 | 161 | 167 | 39.0 | 36 | 48 | 116 | 94 | 84 | 310.3 | 90 | 75 | 70 | 103.5 | 87 | 107 |
| Ce | 181 | 308 | 313 | 82.0 | 59 | 73 | 194 | 194 | 151 | 545.0 | 188 | 152 | 148 | 195.9 | 170 | 221 |
| Pr | | 38 | | 8.6 | | | | | 16 | 54.6 | | | | 19.4 | 15 | |
| Nd | 56 | 131 | 128 | 30.6 | 25 | 24 | 82 | 82 | 54 | 158.3 | 80 | 56 | 49 | 94.2 | 47 | 78 |
| Sm | 9.2 | 21.18 | 22.70 | 5.50 | | | | | 7.90 | 28.0 | | 9.20 | | 11.7 | 7.70 | |
| Eu | | 3.88 | 2.76 | 1.01 | | | | | 1.78 | 5.12 | | 1.10 | | 1.20 | 0.92 | |
| Gd | | 24.3 | 19.54 | 6.60 | | | | | 10.60 | 29.62 | | 5.59 | | 11.81 | 9.00 | |
| Tb | | 3.51 | 2.50 | 0.60 | | | | | 0.96 | 4.54 | | 0.57 | | 1.18 | 0.89 | |
| Dy | | 23.94 | 15.50 | 3.20 | | | | | 5.10 | 30.51 | | 2.05 | | 4.48 | 3.42 | |
| Ho | | 5.07 | 4.00 | 0.52 | | | | | 0.83 | 7.77 | | 0.33 | | 0.73 | 0.56 | |
| Er | | 19.06 | 12.78 | 1.50 | | | | | 2.39 | 24.96 | | 1.30 | | 2.70 | 2.06 | |
| Tm | | 3.35 | 2.25 | 0.20 | | | | | 0.38 | 4.69 | | 0.20 | | 0.39 | 0.30 | |
| Yb | | 19.00 | 14.35 | 1.40 | | | | | 2.23 | 34.8 | | 1.00 | | 2.35 | 1.80 | |
| Lu | | 2.81 | 2.18 | 0.19 | | | | | 0.30 | 5.13 | | 0.14 | | 0.30 | 0.23 | |

Table 26 (continued).

| | ILHA FECHO DOS MORROS | | | | | MORRO DE SÃO PEDRO | | | | | |
|---|---|---|---|---|---|---|---|---|---|---|---|
| Sample | RP-94 D | RP-95 | RP-96 D | RP-97 | RP-201A | RP-252 | RP-253 | RP-254 | RP-256 | RP-257 | RP-258 |
| ppm | | | | | | | | | | | |
| Cr | 1 | 1 | 2 | 1 | 2 | 1 | 2 | 8 | 8 | 3 | < 1 |
| Ni | 6 | 5 | 6 | 10 | 7 | 6 | 5 | 5 | 1 | 4 | 6 |
| Rb | 206 | 162 | 179 | 130 | 104 | 132 | 145 | 140 | 147 | 54 | 58 |
| Ba | 15 | 845 | 256 | 761 | 896 | 771 | 599 | 412 | 460 | 110 | 106 |
| Th | | | | | 3.9 | | 12.3 | 8.5 | | 5.4 | |
| U | | | | | 5.8 | | 2.1 | 1.5 | | 0.8 | |
| Ta | | | | | 15.2 | | 10.3 | 10.1 | | 4.5 | |
| Nb | 280 | 262 | 258 | 205 | 156 | 130 | 98 | 96 | 100 | 43 | 65 |
| Sr | 19 | 720 | 188 | 758 | 658 | 305 | 237 | 163 | 182 | 254 | 244 |
| Hf | | | | | 20.6 | | 17.6 | 17.9 | | | |
| Zr | 1630 | 768 | 1442 | 986 | 868 | 710 | 740 | 752 | 643 | 179 | 190 |
| Y | 44 | 43 | 37 | 45 | 35 | 31 | 27 | 27 | 26 | 15 | 24 |
| La | 119 | 95 | 90 | 111 | 105.2 | | 80.07 | 55.11 | | 12.00 | 12 |
| Ce | 219 | 186 | 158 | 214 | 200.1 | | 144.69 | 99.58 | | 20.05 | 19 |
| Pr | | | | | 19.5 | | 14.53 | 10.00 | | 1.97 | |
| Nd | 61 | 66 | 50 | 83 | 63.61 | | 54.60 | 37.58 | | 6.88 | 7 |
| Sm | | | | | 10.50 | | 8.90 | 6.09 | | 1.11 | |
| Eu | | | | | 1.35 | | 1.43 | 0.98 | | 0.18 | |
| Gd | | | | | 12.27 | | 10.34 | 7.11 | | 1.31 | |
| Tb | | | | | 1.28 | | 1.07 | 0.70 | | 0.20 | |
| Dy | | | | | 4.97 | | 4.19 | 2.88 | | 0.42 | |
| Ho | | | | | 0.81 | | 0.96 | 0.66 | | 0.09 | |
| Er | | | | | 3.15 | | 2.66 | 1.83 | | 0.27 | |
| Tm | | | | | 0.48 | | 0.57 | 0.33 | | 0.08 | |
| Yb | | | | | 2.94 | | 2.93 | 2.02 | | 0.30 | |
| Lu | | | | | 0.35 | | 0.47 | 0.32 | | 0.05 | |

## 4. PÃO DE AÇÚCAR

By far, the most voluminous surface manifestation of the alkaline magmatism in the Alto Paraguay Province are the lavas and tuffs of the Pão de Açúcar complex. Almost three well preserved cones, more than 300 m high, are present in the area (Fig. 29), but the field conditions (very closed vegetation) actually do not permit an accurate survey and sampling of the eastern outcrops. At any way, topographic maps and photointerpretation allow to the characterization of a volcanic field extending over 30 km$^2$, with almost three main emission centers, a central depression, a relevant cone at the west (Morro Pão the Açúcar, see later) and a crest at the eastern limits of the volcanic field (inset of Fig. 29). The latter may be interpreted as the caldera remnants, and on the whole the complex suggests a cauldron subsidence.

Morro Pão de Açúcar was the only outcrop extensively sampled. It is a cone 545 m high (460 m above the Paraguay river) spreading over a surface of approximately 7 km$^2$. The lower parts are formed by intrusive syenitic rocks covered by trachyphonolitic lavas which, at their turn, are topped by thicker beds of ignimbrites dipping outward at angles of 20-27°.

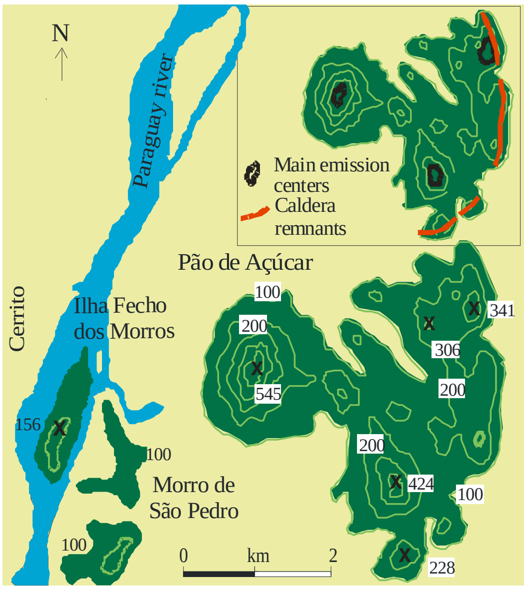


Fig. 29. Sketch map showing the Pão de Açúcar volcanic field. Inset: probable emission centers and caldera remnants, as inferred from the photointerpretation.

### Petrography

The basal intrusive rock-types are fine-grained syenites and nepheline syenites similar to those of the Fecho dos Morros complex. Trachyphonolites are porphyritic to glomeroporphyritic and contain pheno and microphenocrysts of alkali feldspar, nepheline, sodalite, clinopyroxene, biotite and amphibole set in a glassy to microcrystalline groundmass with apparent fluidal texture. Accessory are opaques, zircon, titanite and apatite. The ignimbrites consist of the same mineralogical assemblage of the associated lavas and have crystals and rock fragments set in matrix of glassy shares which are usually welded together. The nepheline content is more abundant than that in the associated lavas, i.e. the ignimbrites tend to have a phonolitic composition. Sometimes baddeleyte coexist with zircon among the accessory minerals.

## Classification and nomenclature

The intrusive rocks, as taken from modal results, are syenites (e.g. sample RP-114: alkali feldspar 82%, nepheline 5%, clinopyroxene 5%, bio-tite 3%, amphibole 2%, opaques and accessory mi-nerals 3%), and nepheline syenites (e.g. sample RP-207: alkali feldspar 70%, nepheline 15%, sodalite 4%, clinopyroxene 2%, biotite 1%, amphibole 4%, opaques and accessory minerals 3%).

A.I. vs. Q-ne normative diagram (Fig. 30) shows two main groups: the first containing A.I.<1.09 and the second one represented by prevailing ignimbritic rocks, with A.I.>1.14. In general, the majority of the samples (over 70%) has a peralkaline character.

In the $R_1$-$R_2$ inset of Fig. 30, the effusive rocks (Table 27) cluster the trachyphonolite (10) and phonolite (9) fields, respectively. Notably, the observed clusters correspond also to the sodic-transitional and sodic serial character of the analyzed samples (cf. $Na_2O$ vs. $K_2O$ inset of Fig. 30).

## Mineralogy

### *Clinopyroxene and amphibole*

Representative pheno-, micropheno and groundmass chemical analyses of clinopyroxenes are given in Table 28. They display the same compositional range shown by the intrusive analogues of the Fecho dos Morros complex, that is, cores with mg# up to 0.73 and rims with mg# up to 0.15. The variations appear to be continuous from calcic (salitic) vs. acmite-rich compositions in Q-J, Ca−Mg−(Fe+Mg)

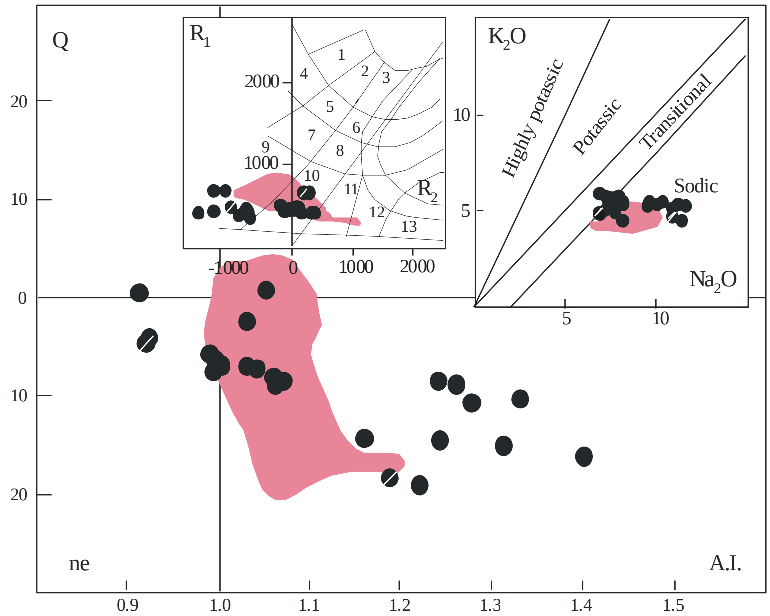


Fig. 30. A.I. vs. Q-ne for rocks from the Pão de Açúcar complex. The Cerro Siete Cabezas fields in pink are shown as reference. Full circles, lavas and ignimbrites; full circles with bar, intrusive rock-types. For insets see Fig. 3.

Table 27. Major element analyses, norms and classification (according to De La Roche *et al.*, 1980) from the Pão de Açúcar complex. See Table 2 for abbreviations.

| Sample | RP-98 | RP-99 | RP-100 | RP-101 | RP-102 | RP-103 | RP-104 | RP-105 | RP-106 | RP-107 | RP-108 | RP-109 | RP-110 |
|---|---|---|---|---|---|---|---|---|---|---|---|---|---|
| wt% | | | | | | | | | | | | | |
| $SiO_2$ | 60.80 | 61.70 | 60.89 | 60.66 | 62.32 | 61.34 | 60.74 | 60.87 | 58.77 | 58.46 | 58.60 | 61.25 | 59.78 |
| $TiO_2$ | 0.72 | 0.65 | 0.75 | 0.73 | 0.72 | 0.68 | 0.71 | 0.78 | 0.35 | 0.37 | 0.45 | 0.64 | 0.35 |
| $Al_2O_3$ | 18.33 | 18.07 | 17.84 | 18.06 | 18.87 | 18.13 | 18.20 | 18.19 | 17.88 | 17.59 | 17.77 | 18.03 | 18.39 |
| $Fe_2O_3$ | 0.71 | 1.64 | 2.18 | 1.71 | 2.21 | 1.88 | 1.84 | 2.22 | 2.77 | 3.68 | 3.01 | 0.75 | 2.78 |
| FeO | 2.81 | 1.65 | 1.68 | 1.93 | 1.85 | 1.74 | 1.74 | 1.48 | 1.85 | 1.09 | 1.88 | 2.54 | 1.66 |
| MnO | 0.21 | 0.19 | 0.22 | 0.21 | 0.14 | 0.23 | 0.20 | 0.19 | 0.36 | 0.38 | 0.36 | 0.21 | 0.33 |
| MgO | 0.57 | 0.52 | 0.64 | 0.66 | 0.56 | 0.63 | 0.60 | 0.65 | 0.16 | 0.19 | 0.31 | 0.44 | 0.62 |
| CaO | 1.40 | 1.07 | 1.36 | 1.36 | 0.16 | 1.51 | 1.32 | 1.42 | 0.68 | 0.68 | 0.89 | 1.35 | 0.77 |
| $Na_2O$ | 7.35 | 7.62 | 7.44 | 7.56 | 7.15 | 7.63 | 7.27 | 7.10 | 10.83 | 11.53 | 9.89 | 8.07 | 9.44 |
| $K_2O$ | 5.52 | 5.78 | 5.61 | 5.20 | 4.98 | 5.03 | 5.68 | 5.86 | 5.18 | 5.28 | 5.36 | 5.59 | 5.30 |
| $P_2O_5$ | 0.24 | 0.19 | 0.23 | 0.22 | 0.17 | 0.22 | 0.21 | 0.25 | 0.08 | 0.07 | 0.13 | 0.20 | 0.06 |
| L.O.I. | 1.18 | 0.65 | 1.03 | 1.50 | 0.61 | 0.83 | 1.36 | 0.81 | 0.88 | 0.46 | 1.14 | 0.77 | 0.33 |
| Sum | 99.84 | 99.73 | 99.87 | 99.80 | 99.74 | 99.85 | 99.87 | 99.82 | 99.79 | 99.78 | 99.79 | 99.84 | 99.81 |
| Q | | | | | 0.67 | | | | | | | | |
| C | | | | | 1.83 | | | | | | | | |
| or | 32.62 | 34.15 | 33.15 | 30.73 | 29.43 | 29.72 | 33.56 | 34.63 | 30.61 | 31.20 | 31.67 | 33.03 | 31.32 |
| ab | 48.69 | 47.60 | 48.04 | 51.45 | 60.50 | 53.69 | 49.21 | 48.96 | 35.45 | 31.32 | 34.67 | 46.12 | 38.12 |
| an | 0.72 | | | | | 0.36 | 0.25 | 0.45 | | | | | |
| ne | 7.31 | 7.13 | 6.76 | 6.76 | | 5.88 | 6.66 | 6.02 | 14.99 | 16.11 | 14.56 | 8.39 | 14.60 |
| ac | | 3.26 | 2.13 | 0.02 | | | | | 8.01 | 10.64 | 8.7 | 2.16 | 8.04 |
| ns | | | | | | | | | 4.51 | 5.67 | 2.84 | 0.97 | 1.31 |
| di | 3.96 | 3.39 | 4.27 | 4.34 | | 4.61 | 3.98 | 3.48 | 2.49 | 2.51 | 3.07 | 3.64 | 2.90 |
| wo | | | | | | | | 0.19 | | | | | |
| hy | | | | | 2.03 | | | | | | | | |
| ol | 2.37 | 1.08 | 0.40 | 0.59 | | 0.18 | 0.29 | | 1.96 | 0.95 | 1.93 | 2.03 | 2.35 |
| mt | 1.02 | 0.74 | 2.09 | 2.46 | 3.20 | 2.72 | 2.66 | 3.12 | | | | | |
| hm | | | | | | | | 0.06 | | | | | |
| il | 1.36 | 1.23 | 1.42 | 1.38 | 1.36 | 1.29 | 1.34 | 1.48 | 0.66 | 0.70 | 0.85 | 1.21 | 0.66 |
| ap | 0.56 | 0.45 | 0.54 | 0.52 | 0.40 | 0.52 | 0.49 | 0.59 | 0.18 | 0.16 | 0.30 | 0.47 | 0.14 |
| D.I.* | 88.6 | 92.1 | 90.1 | 89.0 | 90.6 | 89.3 | 89.4 | 89.6 | 89.1 | 89.3 | 89.6 | 89.7 | 92.1 |
| A.I. | 0.99 | 1.04 | 1.03 | 1.00 | 0.91 | 0.99 | 1.00 | 0.99 | 1.31 | 1.40 | 1.24 | 1.07 | 1.16 |
| $R_1$ | 35 | -48 | -18 | 25 | 322 | 87 | 24 | 46 | -1272 | -1567 | -1001 | -199 | -734 |
| $R_2$ | 538 | 495 | 527 | 533 | 415 | 538 | 528 | 541 | 431 | 427 | 459 | 520 | 474 |
| Rock-type | Trachy-phonolite | Trachy-phonolite | Trachy-phonolite | Trachy-phonolite | Trachy-phonolite | Trachy-phonolite | Trachy-phonolite | Trachy-phonolite | Phonolite | Phonolite | Trachy-phonolite | Trachy-phonolite | Phonolite |
| Q | 41.1 | 41.1 | 41.3 | 41.4 | 45.4 | 41.9 | 41.4 | 41.7 | 36.3 | 35.4 | 36.5 | 40.5 | 36.9 |
| ne | 38.0 | 37.1 | 37.3 | 39.0 | 36.2 | 39.2 | 37.3 | 36.3 | 42.2 | 42.1 | 41.2 | 38.1 | 41.9 |
| ks | 20.9 | 21.8 | 21.4 | 19.6 | 18.4 | 18.9 | 21.3 | 22.0 | 21.5 | 22.5 | 22.3 | 21.4 | 21.2 |

| Sample | RP-111 | RP-112A | RP-112B | RP-113A | RP-113B | RP-114 | RP-207 | RP-208 | RP-247 | RP-248 | RP-249 | RP-250 |
|---|---|---|---|---|---|---|---|---|---|---|---|---|
| wt% | | | | | | | | | | | | |
| $SiO_2$ | 59.37 | 61.56 | 64.01 | 61.30 | 62.82 | 59.32 | 59.05 | 58.65 | 61.18 | 60.07 | 61.32 | 60.26 |
| $TiO_2$ | 1.20 | 0.59 | 0.63 | 0.62 | 0.64 | 1.05 | 0.54 | 0.53 | 0.60 | 0.43 | 0.57 | 0.78 |
| $Al_2O_3$ | 18.07 | 18.12 | 16.61 | 18.11 | 17.55 | 18.16 | 19.36 | 19.34 | 18.18 | 17.59 | 17.59 | 17.16 |
| $Fe_2O_3$ | 2.72 | 1.65 | 2.09 | 2.30 | 2.31 | 2.68 | 1.70 | 1.68 | 1.84 | 1.64 | 2.04 | 2.33 |
| FeO | 1.51 | 1.77 | 1.48 | 1.15 | 1.28 | 1.49 | 1.14 | 1.11 | 0.93 | 0.91 | 1.37 | 1.38 |
| MnO | 0.17 | 0.20 | 0.20 | 0.21 | 0.21 | 0.16 | 0.17 | 0.17 | 0.13 | 0.12 | 0.17 | 0.19 |
| MgO | 1.30 | 0.45 | 0.41 | 0.41 | 0.44 | 1.20 | 0.45 | 0.43 | 0.29 | 0.30 | 0.42 | 0.50 |
| CaO | 2.46 | 0.99 | 0.85 | 1.12 | 0.90 | 2.54 | 1.02 | 1.06 | 0.55 | 0.44 | 0.52 | 0.82 |
| $Na_2O$ | 6.76 | 7.91 | 6.76 | 8.04 | 8.13 | 6.76 | 10.94 | 11.31 | 10.29 | 11.18 | 9.55 | 9.53 |
| $K_2O$ | 5.01 | 5.80 | 5.93 | 5.49 | 4.38 | 5.08 | 4.68 | 4.63 | 5.44 | 5.32 | 5.57 | 5.51 |
| $P_2O_5$ | 0.50 | 0.15 | 0.15 | 0.19 | 0.15 | 0.51 | 0.14 | 0.15 | 0.05 | 0.06 | 0.06 | 0.16 |
| L.O.I. | 0.71 | 0.58 | 0.76 | 0.80 | 1.01 | 0.94 | 0.41 | 0.53 | 1.10 | 0.61 | 0.61 | 1.25 |
| Sum | 99.78 | 99.77 | 99.88 | 99.74 | 99.82 | 99.89 | 99.60 | 99.59 | 99.75 | 99.79 | 99.79 | 99.87 |
| Q | | | 1.08 | | | | | | | | | |
| C | | | | | | | | | | | | |
| or | 29.60 | 34.27 | 35.04 | 32.44 | 25.88 | 30.02 | 27.65 | 27.36 | 32.14 | 31.43 | 32.91 | 32.56 |
| ab | 49.69 | 45.03 | 52.42 | 46.98 | 61.21 | 48.91 | 39.63 | 38.36 | 43.31 | 41.39 | 44.02 | 41.43 |
| an | 4.16 | | | | | 4.20 | | | | | | |
| ne | 4.06 | 8.60 | | 8.45 | 2.53 | 4.48 | 18.36 | 19.14 | 10.78 | 10.54 | 8.36 | 8.75 |
| ac | | 4.77 | 4.2 | 4.79 | 2.55 | | 4.91 | 4.86 | 5.32 | 4.74 | 5.90 | 6.74 |
| ns | | 0.13 | | | | | 3.13 | 3.83 | 4.14 | 6.59 | 3.40 | 3.58 |
| di | 3.71 | 3.33 | 2.70 | 3.55 | 2.81 | 3.93 | 3.45 | 3.57 | 2.00 | 1.49 | 1.84 | 2.51 |
| wo | | | | | | | | | | | | |
| hy | | | 1.17 | | | | | | | | | |
| ol | 1.06 | 1.53 | | 0.14 | 0.16 | 0.81 | 0.66 | 0.55 | 0.49 | 0.86 | 1.48 | 1.16 |
| mt | 1.94 | | 0.92 | 0.93 | 2.06 | 2.28 | | | | | | |
| hm | 1.37 | | | | | 1.10 | | | | | | |
| il | 2.27 | 1.12 | 1.19 | 1.17 | 1.21 | 1.99 | 1.02 | 1.00 | 1.13 | 0.81 | 1.08 | 1.48 |
| ap | 1.18 | 0.35 | 0.35 | 0.45 | 0.35 | 1.20 | 0.33 | 0.35 | 0.11 | 0.14 | 0.14 | 0.37 |
| D.I.* | 83.3 | 92.7 | 92.7 | 92.7 | 92.2 | 83.4 | 90.5 | 89.7 | 91.5 | 88.1 | 91.2 | 89.5 |
| A.I. | 0.92 | 1.06 | 1.06 | 1.06 | 1.03 | 0.92 | 1.19 | 1.22 | 1.28 | 1.33 | 1.24 | 1.26 |
| $R_1$ | 242 | -170 | 367 | -161 | 163 | 228 | -1134 | -1278 | -939 | -713 | -713 | -775 |
| $R_2$ | 682 | 484 | 437 | 495 | 462 | 688 | 511 | 514 | 419 | 422 | 422 | 449 |
| Rock-type | Trachy-phonolite | Trachy-phonolite | Trachy-phonolite | Trachy-phonolite | Trachy-phonolite | Syenite | Nepheline syenite | Phonolite | Phonolite | Phonolite | Phonolite | Phonolite |
| Q | 42.7 | 40.3 | 45.4 | 40.4 | 43.8 | 42.4 | 35.2 | 34.6 | 39.1 | 39.0 | 40.3 | 39.9 |
| ne | 37.1 | 37.5 | 32.1 | 38.6 | 39.8 | 37.1 | 46.5 | 47.0 | 39.7 | 39.5 | 37.8 | 37.7 |
| ks | 20.2 | 22.2 | 22.5 | 21.0 | 16.4 | 20.5 | 18.3 | 18.3 | 21.2 | 21.5 | 21.9 | 22.4 |

Table 28. Representative analyses of clinopyroxenes from Pão de Açúcar rocks. C, core; I, intermediate areas between core and rim; R, rim; gm, groundmass. For additional information see Table 3.

| Sample | RP-99C | RP-99R | RP-99gm | RP-100C | RP-100R | RP-107 | RP-108 | RP-109C | RP-109I | RP-109R | RP-207C | RP-207I | RP-207R |
|---|---|---|---|---|---|---|---|---|---|---|---|---|---|
| wt% | | | | | | | | | | | | | |
| $SiO_2$ | 51.80 | 51.05 | 51.58 | 52.12 | 51.91 | 51.26 | 52.62 | 52.68 | 51.46 | 51.76 | 52.22 | 52.21 | 52.05 |
| $TiO_2$ | 0.54 | 0.27 | 0.39 | 0.64 | 0.36 | 0.67 | 0.29 | 0.58 | 0.57 | 0.43 | 0.76 | 0.74 | 0.29 |
| $Al_2O_3$ | 0.97 | 0.98 | 0.33 | 1.42 | 0.70 | 1.28 | 0.79 | 1.28 | 1.10 | 0.82 | 1.89 | 0.95 | 0.54 |
| $Fe_2O_3$ | 4.55 | 18.67 | 23.89 | 2.93 | 18.67 | 7.80 | 9.95 | 2.53 | 4.33 | 13.86 | 1.94 | 19.15 | 23.35 |
| FeO | 9.86 | 4.22 | 3.28 | 7.76 | 5.57 | 8.82 | 7.45 | 7.11 | 9.48 | 6.90 | 6.67 | 6.13 | 4.35 |
| MnO | 0.48 | 0.99 | 0.85 | 1.20 | 1.01 | 1.49 | 0.44 | 1.13 | 1.74 | 1.23 | 0.84 | 0.57 | 0.72 |
| MgO | 9.00 | 5.17 | 2.64 | 12.00 | 3.72 | 7.48 | 7.41 | 13.10 | 8.97 | 5.47 | 13.89 | 2.90 | 1.96 |
| CaO | 21.40 | 12.10 | 7.01 | 21.21 | 9.00 | 18.38 | 16.46 | 21.84 | 20.11 | 12.80 | 21.37 | 8.76 | 5.18 |
| $Na_2O$ | 1.85 | 6.76 | 9.53 | 1.14 | 8.11 | 3.12 | 4.59 | 0.84 | 1.84 | 6.02 | 0.74 | 8.61 | 10.19 |
| $K_2O$ | 0.01 | 0.02 | 0.01 | 0.02 | 0.01 | 0.07 | 0.01 | 0.01 | 0.04 | 0.02 | 0.01 | 0.02 | 0.01 |
| Sum | 100.46 | 100.23 | 99.51 | 100.44 | 99.06 | 100.37 | 100.01 | 101.10 | 99.94 | 99.31 | 100.33 | 100.04 | 98.64 |
| Si | 1.966 | 1.952 | 1.991 | 1.951 | 2.006 | 1.957 | 1.996 | 1.951 | 1.966 | 1.993 | 1.937 | 2.001 | 2.021 |
| $Al^{IV}$ | 0.044 | 0.048 | 0.009 | 0.049 | | 0.043 | 0.004 | 0.049 | 0.034 | 0.007 | 0.063 | | |
| Sum | 2.000 | 2.000 | 2;000 | 2.000 | 2.006 | 2.000 | 2.000 | 2.000 | 2.000 | 2.000 | 2.000 | 2.001 | 2.021 |
| $Al^{VI}$ | 0.000 | 0.000 | 0.006 | 0.014 | 0.032 | 0.015 | 0.031 | 0.007 | 0.016 | 0.030 | 0.016 | 0.043 | 0.025 |
| Ti | 0.015 | 0.007 | 0.011 | 0.018 | 0.011 | 0.019 | 0.008 | 0.016 | 0.016 | 0.013 | 0.021 | 0.021 | 0.009 |
| $Fe^{3+}$ | 0.130 | 0.536 | 0.694 | 0.083 | 0.543 | 0.224 | 0.284 | 0.071 | 0.125 | 0.402 | 0.054 | 0.552 | 0.683 |
| $Fe^{2+}$ | 0.313 | 0.135 | 0.106 | 0.243 | 0.180 | 0.282 | 0.236 | 0.220 | 0.303 | 0.222 | 0.207 | 0.197 | 0.141 |
| Mn | 0.027 | 0.032 | 0.028 | 0.038 | 0.033 | 0.048 | 0.014 | 0.035 | 0.056 | 0.040 | 0.026 | 0.019 | 0.024 |
| Mg | 0.509 | 0.295 | 0.152 | 0.669 | 0.214 | 0.426 | 0.419 | 0.723 | 0.511 | 0.314 | 0.768 | 0.166 | 0.113 |
| Ca | 0.870 | 0.496 | 0.290 | 0.851 | 0.373 | 0.752 | 0.670 | 0.867 | 0.835 | 0.528 | 0.850 | 0.360 | 0.216 |
| Na | 0.136 | 0.500 | 0.713 | 0.083 | 0.608 | 0.231 | 0.338 | 0.060 | 0.136 | 0.450 | 0.053 | 0.640 | 0.768 |
| K | 0.000 | 0.002 | 0.000 | 0.001 | | 0.003 | 0.000 | 0.001 | 0.002 | 0.001 | | 0.001 | |
| Sum | 2.000 | 2.000 | 2.000 | 2.000 | 1.994 | 2.000 | 2.000 | 2.000 | 2.000 | 2.000 | 2.000 | 1.999 | 1.979 |
| Mg/(Mg+Fe+Mn) | 0.519 | 0.296 | 0.155 | 0.648 | 0.221 | 0.435 | 0.440 | 0.689 | 0.514 | 0.321 | 0.728 | 0.178 | 0.118 |
| Quad | 1.705 | 0.958 | 0.576 | 1.763 | 0.767 | 1.460 | 1.339 | 1.810 | 1.649 | 1.064 | 1.825 | 0.723 | 0.470 |
| J | 0.274 | 1.002 | 1.426 | 0.166 | 1.216 | 0.462 | 0.676 | 0.120 | 0.272 | 0.900 | 0.106 | 1.280 | 1.536 |

and in Mg−(Na+K)−($Fe^{2+}$+Mn) diagrams, without large differences between the high and low A.I. populations (>1.14 and <1.09, respectively). In particular the mg# vs. elemental variation graphs show continuous trends of Si and Na+K enrichment and corresponding depletion of Al (Ti) and Ca (Fig. 31, insets 1 to 4).

The amphiboles vary (nomenclature after Leake *et al.*, 1997) from calcic (ferro-edenite), sodic-calcic (katophorite and magnesiokatoforite) up to sodic (magnesioarfvedsonite) compositions (cf. Table 29). In the Mg−(Na+K)−($Fe^{2+}$+Mn) diagram (Fig. 31, inset 3), the amphiboles overlap the clinopyroxenes trend between their early and the late compositions and cluster the compositions of the analogues from the Fecho dos Morros complex. Similarly to the coexisting clinopyroxenes, the amphiboles from Pão de Açúcar display a large mg# range, between 0.70 and 0.39, differing from the Fecho dos Morros amphiboles that exhibit a narrow mg# range (0.54-0.41). In the mg# vs. elemental graphs, scatters are generally observed, except for Mn which tends to be enriched in the later phases (Fig. 31, inset 5). The F content, as an average, is about twice the F of Fecho dos Morros analogues (0.76±0.11 wt% vs. 0.45±0.05 wt%, respectively), testifying a higher F activity, similar to that of Stock II from the Cerro Siete Cabezas complex, where the F of amphiboles is 0.83±0.13 wt%.

### *Biotite*

The biotites (Table 30, Fig. 32) have Mg/(Mg+Fe+Mn) ratios between 0.51 and 0.35. The compositions cluster bout 52 and 63 annite mol%, the most iron-rich types being found at the rims of crystals from the high A.I. rocks. In the variation diagrams, there are very scattered values vs. Mg/(Mg+Fe+Mn) ratios, but the more iron-rich biotites display systematically higher Si, Mn and Na+K and correspondly lower Ti, Al and F contents than the Mg-rich variants. In general, the latter display higher Ti, Al and F and lower Si compared to the biotites from the Fecho dos Morros complex.

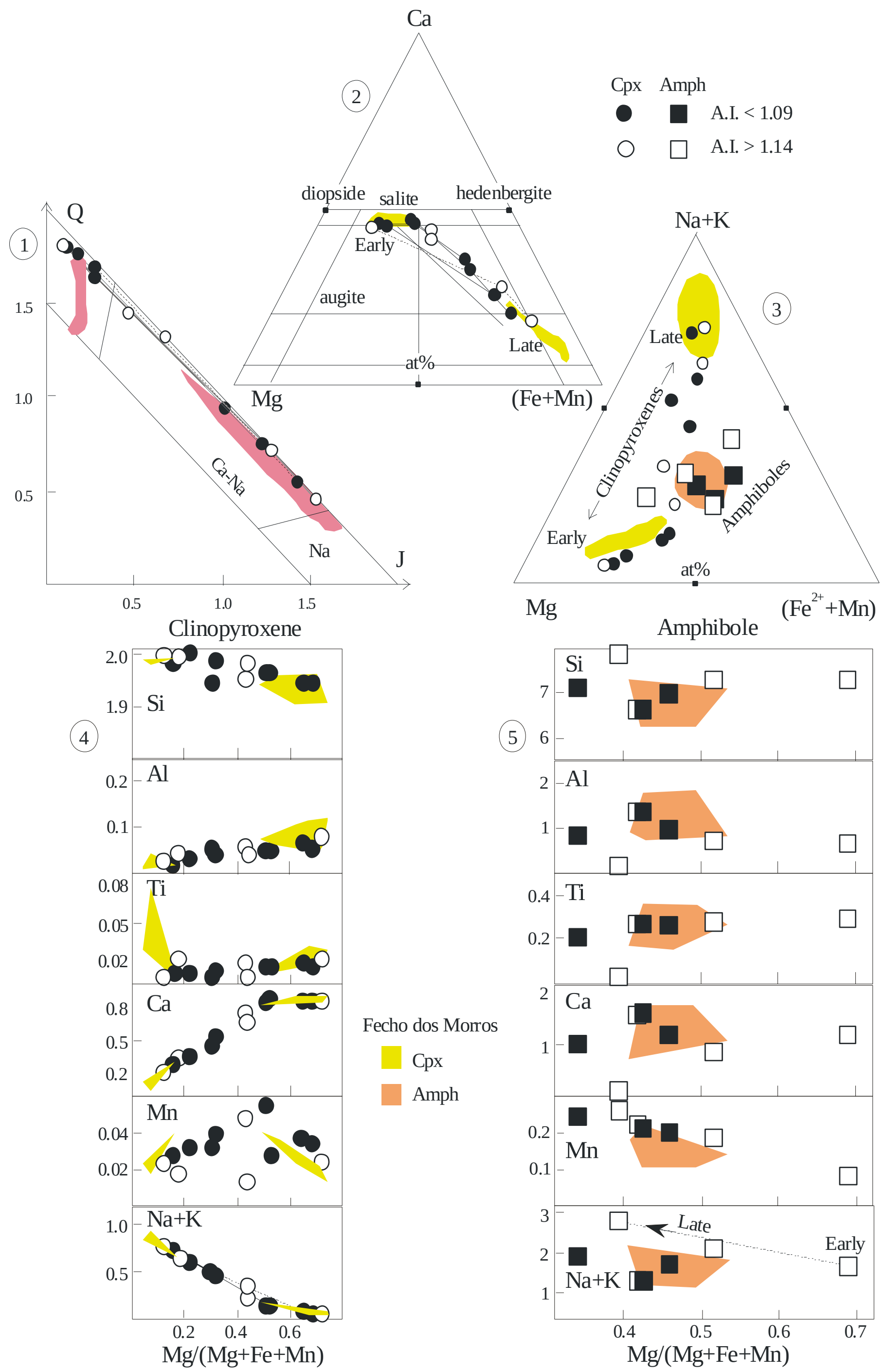


Fig. 31. Synoptical picture showing: 1) Q-J (in pink, the Cerro Siete Cabezas complex field) and 2) Mg-(Fe+Mn)-Ca diagrams for clinopyroxenes (tie lines join core, early, and rim, late, compositions) from the Pão de Açúcar complex; 3) clinopyroxenes and amphiboles plotted into the Mg-($Fe^{2+}$+Mn)-(Na+K) diagram with the fields of analogous phases from the Fecho dos Morros complex; elemental variations vs. Mg/(Mg+Fe+Mn) ratio (Fe=total iron) for clinopyroxenes 4) and amphiboles 5).

Table 29. Representative analyses of amphiboles from Pão de Açúcar rocks. C, core; R, rim. For additional information see Table 4.

| Sample | RP-100 | RP-109C | RP-109R | RP-207C-1 | RP-207R-A | RP-207R-B | RP-207C-2 |
|---|---|---|---|---|---|---|---|
| wt% | | | | | | | |
| $SiO_2$ | 45.91 | 43.57 | 45.87 | 49.77 | 52.31 | 48.82 | 43.17 |
| $TiO_2$ | 2.28 | 2.41 | 1.84 | 2.70 | 0.18 | 2.49 | 2.40 |
| $Al_2O_3$ | 5.50 | 7.67 | 4.77 | 4.05 | 1.14 | 4.12 | 7.69 |
| $Fe_2O_3$ | 2.85 | 1.70 | 3.22 | | 8.04 | 1.75 | 1.97 |
| FeO | 15.98 | 17.84 | 19.15 | 11.13 | 14.30 | 14.92 | 17.65 |
| MnO | 1.60 | 1.66 | 1.89 | 0.67 | 2.07 | 1.49 | 1.74 |
| MgO | 9.50 | 8.70 | 6.91 | 14.62 | 8.59 | 10.72 | 8.52 |
| CaO | 7.39 | 9.77 | 6.11 | 7.77 | 1.03 | 5.41 | 9.62 |
| $Na_2O$ | 4.89 | 3.55 | 5.38 | 4.94 | 8.68 | 6.32 | 3.58 |
| $K_2O$ | 1.40 | 1.46 | 1.53 | 1.40 | 1.20 | 1.41 | 1.48 |
| F | 1.55 | 1.76 | 1.69 | 1.58 | 1.70 | 1.14 | 1.72 |
| Cl | 0.01 | 0.02 | 0.02 | | | | 0.01 |
| Sum | 98.22 | 99.36 | 97.66 | 97.96 | 98.52 | 98.11 | 98.83 |
| | | | | | | | |
| Si | 7.010 | 6.664 | 7.166 | 7.332 | 7.875 | 7.330 | 6.644 |
| $Al^{IV}$ | 0.990 | 1.336 | 0.834 | 0.668 | 0.125 | 0.670 | 1.356 |
| Sum | 8.000 | 8.000 | 8.000 | 8.000 | 8.000 | 8.000 | 8.000 |
| $Al^{VI}$ | | 0.046 | 0.044 | 0.035 | 0.077 | 0.059 | 0.039 |
| Ti | 0.262 | 0.277 | 0.216 | 0.299 | 0.020 | 0.281 | 0.278 |
| $Fe^{3+}$ | 0.328 | 0.196 | 0.378 | | 0.911 | 0.198 | 0.229 |
| $Fe^{2+}$ | 2.041 | 2.282 | 2.502 | 1.371 | 1.800 | 1.873 | 2.272 |
| Mn | 0.207 | 0.215 | 0.250 | 0.084 | 0.264 | 0.189 | 0.227 |
| Mg | 2.162 | 1.984 | 1.609 | 3.211 | 1.928 | 2.399 | 1.955 |
| Sum | 5.000 | 5.000 | 5.000 | 5.000 | 5.000 | 5.000 | 5.000 |
| Ca | 1.209 | 1.601 | 1.023 | 1.226 | 0.166 | 0.870 | 1.586 |
| $Na_B$ | 0.791 | 0.399 | 0.977 | 0.774 | 1.834 | 1.130 | 0.414 |
| Sum | 2.000 | 2.000 | 2.000 | 2.000 | 2.000 | 2.000 | 2.000 |
| $Na_A$ | 0.657 | 0.654 | 0.652 | 0.638 | 0.700 | 0.710 | 0.655 |
| K | 0.273 | 0.285 | 0.305 | 0.263 | 0.230 | 0.270 | 0.291 |
| $Sum_A$ | 0.929 | 0.939 | 0.957 | 0.901 | 0.930 | 0.980 | 0.945 |
| F | 0.738 | 0.851 | 0.835 | 0.736 | 0.815 | 0.542 | 0.837 |
| Cl | 0.003 | 0.005 | 0.005 | | | | 0.003 |
| | | | | | | | |
| Mg/(Mg+Fe+Mn) | 0.456 | 0.424 | 0.339 | 0.688 | 0.393 | 0.515 | 0.417 |

Table 30. Representative analyses of biotites from Pão de Açúcar rocks. C, core; I, intermediate areas between core and rim; R, rim. For additional information see Table 5.

| Sample | RP-100C | RP-100R | RP-109C | RP-109R | RP-207C | RP-207I | RP-207R | RP-208R |
|---|---|---|---|---|---|---|---|---|
| wt% | | | | | | | | |
| $SiO_2$ | 36.67 | 36.60 | 35.82 | 38.23 | 36.38 | 36.24 | 37.56 | 37.32 |
| $TiO_2$ | 7.01 | 5.88 | 5.68 | 4.21 | 6.63 | 6.04 | 3.30 | 3.00 |
| $Al_2O_3$ | 13.11 | 13.22 | 13.47 | 11.99 | 13.36 | 13.43 | 10.51 | 10.58 |
| $Cr_2O_3$ | | | | | 0.04 | 0.01 | n.d. | 0.02 |
| $FeO_{tot}$ | 19.65 | 20.01 | 21.14 | 19.51 | 19.59 | 20.00 | 25.08 | 26.07 |
| MnO | 1.16 | 1.22 | 1.22 | 1.19 | 1.13 | 1.21 | 1.41 | 1.25 |
| MgO | 10.11 | 10.35 | 9.38 | 11.85 | 10.25 | 9.98 | 8.13 | 8.10 |
| CaO | 0.01 | 0.01 | 0.01 | 0.03 | 0.05 | 0.04 | 0.02 | 0.06 |
| $Na_2O$ | 0.73 | 0.73 | 0.70 | 0.54 | 0.70 | 0.68 | 0.29 | 0.22 |
| $K_2O$ | 8.97 | 8.99 | 8.61 | 9.34 | 8.92 | 8.69 | 9.55 | 9.34 |
| F | 1.66 | 1.81 | n.d. | n.d. | 1.79 | 2.28 | 0.99 | 0.82 |
| Cl | 0.01 | 0.04 | n.d. | n.d. | 0.02 | 0.01 | 0.03 | 0.03 |
| Less O=F, Cl | 0.70 | 0.76 | | | 0.76 | 0.96 | 0.42 | 0.35 |
| $H_2O^{+}_{calc}$ | 3.26 | 3.16 | 3.89 | 3.96 | 3.18 | 2.93 | 3.36 | 3.43 |
| Sum | 101.65 | 101.26 | 99.93 | 102.53 | 101.28 | 100.58 | 99.81 | 99.89 |
| | | | | | | | | |
| Si | 5.428 | 5.442 | 5.515 | 5.781 | 5.397 | 5.394 | 5.863 | 5.849 |
| $Al^{IV}$ | 2.287 | 2.317 | 2.445 | 2.137 | 2.336 | 2.356 | 1.934 | 1.954 |
| $Ti^{IV}$ | 0.285 | 0.241 | 0.040 | 0.082 | 0.267 | 0.250 | 0.203 | 0.197 |
| Sum (Z) | 8.000 | 8.000 | 8.000 | 8.000 | 8.000 | 8.000 | 8.000 | 8.000 |
| $Ti^{VI}$ | 0.495 | 0.417 | 0.619 | 0.397 | 0.473 | 0.426 | 0.184 | 0.157 |
| Cr | | | | | 0.005 | 0.001 | | 0.003 |
| $Fe^{2+}$ | 2.433 | 2.488 | 2.722 | 2.467 | 2.431 | 2.490 | 3.274 | 3.417 |
| Mn | 0.145 | 0.154 | 0.159 | 0.152 | 0.142 | 0.153 | 0.186 | 0.166 |
| Mg | 2.231 | 2.294 | 2.153 | 2.671 | 2.267 | 2.214 | 1.892 | 1.892 |
| Sum (Y) | 5.304 | 5.353 | 5.653 | 5.687 | 5.318 | 5.284 | 5.536 | 6.635 |
| Ca | 0.002 | 0.002 | 0.002 | 0.005 | 0.008 | 0.006 | 0.003 | 0.010 |
| Na | 0.210 | 0.211 | 0.209 | 0.158 | 0.201 | 0.196 | 0.088 | 0.067 |
| K | 1.694 | 1.705 | 1.691 | 1.802 | 1.688 | 1.650 | 1.902 | 1.867 |
| Sum (X) | 1.906 | 1.918 | 1.902 | 1.965 | 1.897 | 1.852 | 1.993 | 1.994 |
| F | 0.777 | 0.851 | | | 0.840 | 1.073 | 0.489 | 0.407 |
| Cl | 0.002 | 0.010 | | | 0.005 | 0.003 | 0.008 | 0.008 |
| OH | 3.221 | 3.139 | 4.000 | 4.000 | 3.155 | 2.924 | 3.503 | 3.585 |
| Sum | 4.000 | 4.000 | 4.000 | 4.000 | 4.000 | 4.000 | 4.000 | 4.000 |
| | | | | | | | | |
| Mg/(Mg+Fe+Mn) | 0.464 | 0.465 | 0.428 | 0.505 | 0.509 | 0.456 | 0.354 | 0.346 |

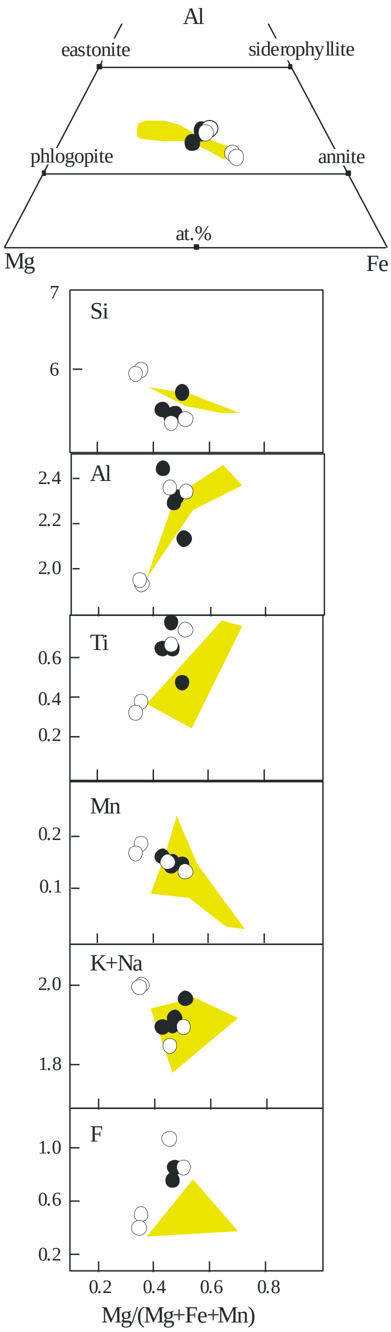


Fig. 32. Plot of biotites from the Pão de Açúcar complex in the Al-Mg-(Fe+Mn) diagram; Fe=total iron as $Fe^{2+}$. Variation of Si, Al, Ti, Mn, K+Na and F [atoms per 22(O)] with the Mg/(Mg+Fe+Mn) atomic ratio. In yellow, the field for the Fecho dos Morros complex.

*Opaques and other accessory minerals*

The accessory phases are not easily detectable by means of microprobe analyses, because they are present as microphenocrysts and/or in the groundmass, with size not exceeding a few dozens of microns. In Table 31 are reported some representative analyses. Opaques consist of Ti-magnetites, generally coexisting with ilmenite, and of alteration products (hematite). Magnetite from RP-100 sample has a Mn content similar to that shown by magnetites from the Fecho dos Morros complex, while ilmenite presents a very high Mn content (up to 16 wt%), that is, 2% higher than that of ilmenites from the Cerro Siete Cabezas complex. The Spencer & Lindsley's geothermometer yielded a temperature of 836°C and log $fO_2$=−13.5 on the Nickel-Nickel Oxide buffer.

Titanite and apatite have composition similar to those of the other occurrences. In particular, the phosphate is a fluorapatite (F=1.770 a.f.u.) showing a generally high F activity, just also indicated for the other complexes, and consistent with the relatively high F content of amphiboles and biotites, and with the presence of accessory fluorite in the intrusive facies. Finally, the coexistence of zircon and baddeleyte in the high A.I. samples, along with the presence of nepheline and Ab-rich feldspars, point to temperatures around 820°C, near to that determined for the magnetite-ilmenite pair, and to a silica activity (log $\alpha SiO_2$) of -0.66 (intersection of log silica activity in liquidus temperature versus temperature for the reactions zircon-baddeleyte and albite-nepheline; cf. Ghiorso & Carmichael, 1987). The calculated temperatures may be considered not far from liquidus temperatures for the lavas, also because powdered samples heated at 900°C for four hours turned to be completely melted.

*Feldspars, nepheline and sodalite*

Pheno and microphenocrysts are tendentiously anorthoclase or sodic sanidine (Or 30-43 mol%), whereas at the rims and also in the groundmass coexist albitic-rich compositions (Ab up to 85%) and sanidine ($Or_{80-75}$) falling below the 900°C solvus-solid isotherm (cf. Seck, 1971). The compositions fit those of the intrusive rocks from the Fecho dos Morros complex, as well as the composition of coexisting nepheline pheno and microphenocrysts (Table 32 and Fig. 33). The latter differ substantially from the corresponding Fecho dos Morros intrusives having higher $Fe_2O_3$, i.e., 1.00±0.12% wt% vs. 0.32±0.09 wt%, respectively. Silica excess is in the 11.8-4.8 wt% range. Isotherms, showing the limits of nepheline solid solutions (cf. Hamilton, 1961), indicate temperatures between 1068°C (RP-100 trachyphonolite) and 710°C (RP-107 phonolite).

Sodalite pheno and microphenocrysts, relatively abundant in phonolitic lavas with A.I.>1.14, also have compositions similar to those of the intrusive equivalents with high Cl contents (1.75±0.09 a.f.u.; cf. Table 32).

Significance of the mineralogy

A strictly compositional affinity between mineral assemblages from the Pão de Açúcar trachyphonolitic-phonolitic lavas/ignimbrites and intrusive rocks of the Fecho dos Morros complex is apparent, also in terms of temperatures and fluid activities. Probably, the Fecho dos Morros complex represents the highest structural levels of the magmatic chamber of the Pão de Açúcar volcanic field, actually exposed by the erosional activity done by the Paraguay river.

In this interpretation, the pegmatoid facies of the Ilha Fecho dos Morros should correspond to the western nucleous with fluid overpressures and the layering of Cerrito could represent the evidence of convective movements at the flanks of the magmatic chamber. The progressive empting of the magmatic chamber may justify the cauldron subsidence of the western area of the Pão de Açúcar volcanic field, and the general subvolcanic character of the complexes from the Alto Paraguay region.

*Major and trace elements distribution*

In the quartz-nepheline-kalsilite diagram (Fig. 33), the samples on the whole plot in the same field of the rocks from the Fecho dos Morros complex

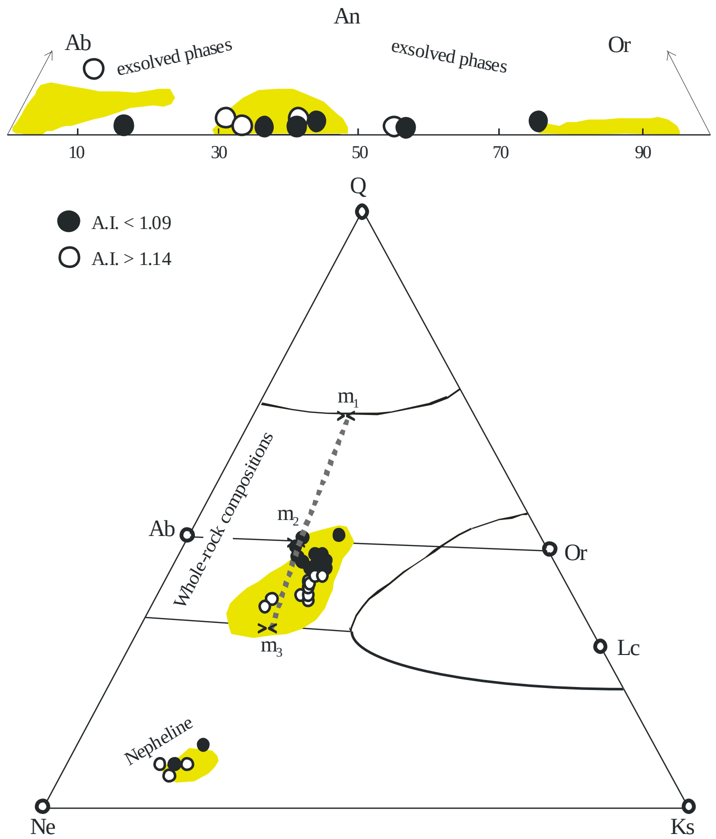


Fig. 33. Alkali feldspar from the Pão de Açúcar complex (rocks with A.I.<1.09 and >1.14, respectively) plotted into the Or-Ab-An (mol%) diagram, and nepheline compositions plotted into the Ks-Ne-Q (wt%) space (cf. Fig. 8). For comparison the compositional field of the Fecho dos Morros complex is also illustrated in yellow.

Table 31. Representative analyses of magnetite, ilmenite and accessory minerals from Pão de Açúcar rocks [titanite: 4 (Si) basis; apatite: 26 (O, F, Cl) basis; zircon: 16 (O) basis]. For additional information see Table 6.

| | Magnetite | Ilmenite | Titanite | | Apatite | | Zircon | |
|---|---|---|---|---|---|---|---|---|
| Sample | RP-100 | RP-100 | RP-113A | | RP-114 | | RP-114 | |
| wt% | | | | | | | | |
| $SiO_2$ | 0.07 | | $SiO_2$ | 30.03 | $SiO_2$ | 0.38 | $SiO_2$ | 32.52 |
| $TiO_2$ | 15.10 | 49.81 | $TiO_2$ | 38.20 | $La_2O_3$ | 0.23 | $TiO_2$ | 0.06 |
| $Al_2O_3$ | 0.30 | 0.02 | $Al_2O_3$ | 0.30 | $Ce_2O_3$ | 0.26 | $ZrO_2$ | 65.75 |
| $Cr_2O_3$ | 0.04 | | $Fe_2O_3$ | 1.25 | $Nd_2O_3$ | 0.14 | $Al_2O_3$ | 0.24 |
| $Fe_2O_3$ | 37.81 | 3.06 | FeO | 0.41 | FeO | 0.25 | $Cr_2O_3$ | 0.20 |
| FeO | 40.32 | 27.73 | MnO | 0.04 | CaO | 52.96 | $La_2O_3$ | 0.09 |
| MnO | 4.00 | 16.80 | MgO | 0.03 | SrO | 2.49 | CaO | 0.13 |
| MgO | 0.10 | 0.01 | CaO | 27.83 | $Na_2O$ | 0.12 | Sum | 98.96 |
| CaO | 0.01 | 0.02 | $Na_2O$ | 0.28 | $K_2O$ | 0.01 | | |
| Sum | 97.15 | 97.45 | $K_2O$ | 0.01 | $P_2O_5$ | 40.56 | Si | 4.000 |
| | | | F | 0.85 | F | 3.25 | Ti | 0.005 |
| Si | 0.022 | | Cl | 0.08 | Cl | 0.49 | Zr | 3.944 |
| Ti | 03.515 | 0.970 | Less O=F, Cl | 0.37 | Less O=F, Cl | 1.48 | Al | 0.052 |
| Al | 0.109 | 0.001 | Sum | 98.81 | Sum | 99.66 | Cr | 0.019 |
| Cr | 0.010 | | | | | | La | 0.004 |
| $Fe^{3+}$ | 8.808 | 0.060 | Si | 4.000 | Si | 0.065 | Ca | 0.017 |
| $Fe^{2+}$ | 10.438 | 0.600 | Al | 0.047 | La | 0.010 | Sum | 4.041 |
| Mn | 1.049 | 0.368 | Ti | 3.827 | Ce | 0.011 | | |
| Mg | 0.046 | | $Fe^{3+}$ | 0.125 | Nd | 0.006 | | |
| Ca | 0.003 | 0.001 | Sum | 3.999 | Fe | 0.036 | | |
| Sum | 24.000 | 2.000 | $Fe^{2+}$ | 0.046 | Ca | 9.775 | | |
| | | | Mn | 0.005 | Sr | 0.249 | | |
| | | | Mg | 0.006 | Na | 0.040 | | |
| Ulv. mol% | 44.21 | | Ca | 3.972 | K | 0.002 | | |
| $R_2O_3$ | | 8.52 | Na | 0.072 | Sum | 10.194 | | |
| | | | K | 0.001 | P | 5.917 | | |
| T°C | | 836 | Sum | 4.101 | F | 1.770 | | |
| $\log_{10} fO_2$ | | -13.50 | F | 0.358 | Cl | 0.143 | | |
| | | | Cl | 0.018 | Sum | 1.913 | | |
| $Fe^{2+}/(Fe^{2+}+Mn$ | 0.908 | 0.620 | Sum | 0.376 | | | | |

Table 32. Representative analyses of alkali feldspar (P and mP: pheno and microphenocrysts; gm: groundmass phases), nepheline and sodalite from Pão de Açúcar rocks. For additional information see Tables 7, 8 and 25.

| | Alkali feldspar | | | | | | | | | | |
|---|---|---|---|---|---|---|---|---|---|---|---|
| Sample | RP-100P | RP-107P | RP-108P | RP-109mP | RP-109mP | RP-109P | RP-109gm | RP-109gm | RP-207 | RP-207 | RP-207 |
| wt% | | | | | | | | | | | |
| $SiO_2$ | 66.45 | 67.17 | 66.24 | 65.80 | 66.71 | 66.78 | 66.26 | 67.91 | 66.49 | 66.26 | 66.31 |
| $Al_2O_3$ | 18.79 | 18.90 | 18.66 | 18.60 | 18.88 | 18.67 | 18.72 | 19.21 | 19.00 | 18.77 | 20.91 |
| $Fe_2O_3$ | 0.34 | 0.72 | 0.80 | 0.26 | 0.22 | 0.55 | 0.31 | 0.07 | 0.31 | 0.17 | 0.19 |
| BaO | 0.11 | 0.26 | 0.20 | 0.17 | 0.01 | 0.15 | 0.03 | 0.03 | 0.11 | 0.10 | 0.67 |
| CaO | 0.10 | 0.21 | 0.29 | 0.07 | 0.12 | 0.05 | 0.14 | 0.04 | 0.12 | 0.08 | 0.63 |
| $Na_2O$ | 6.39 | 7.71 | 7.80 | 4.85 | 6.79 | 7.54 | 2.67 | 9.68 | 6.38 | 5.18 | 9.40 |
| $K_2O$ | 7.57 | 5.66 | 5.25 | 9.74 | 7.04 | 5.92 | 13.17 | 3.00 | 7.59 | 9.37 | 1.99 |
| Sum | 99.75 | 100.63 | 99.24 | 99.49 | 99.77 | 99.66 | 101.30 | 99.93 | 99.99 | 99.93 | 99.91 |
| Mol% | | | | | | | | | | | |
| Or | 43.2 | 32.1 | 30.1 | 56.2 | 40.1 | 33.7 | 75.3 | 16.9 | 43.2 | 53.7 | 11.2 |
| Ab | 55.4 | 66.4 | 68.1 | 42.5 | 58.7 | 65.3 | 23.2 | 82.7 | 55.2 | 45.1 | 80.5 |
| An | 1.4 | 1.5 | 1.8 | 1.3 | 1.2 | 1.0 | 1.5 | 0.4 | 1.6 | 1.2 | 8.3 |

| | Nepheline | | | | | | Sodalite | | | |
|---|---|---|---|---|---|---|---|---|---|---|
| Sample | RP-100 | RP-107 | RP-108 | RP-109 | RP-207 | RP-207 | | RP-107 | RP-108 | RP-207 |
| wt% | | | | | | | | | | |
| $SiO_2$ | 47.69 | 44.15 | 45.29 | 46.11 | 45.32 | 44.87 | $SiO_2$ | 37.70 | 36.60 | 36.41 |
| $Al_2O_3$ | 30.44 | 31.70 | 31.63 | 32.09 | 31.49 | 32.55 | $Al_2O_3$ | 31.99 | 31.85 | 31.67 |
| $Fe_2O_3$ | 0.90 | 1.19 | 0.90 | 1.06 | 1.05 | 0.89 | $Fe_2O_3$ | 0.48 | 0.80 | 0.55 |
| BaO | | | | 0.05 | 0.10 | 0.07 | BaO | | | 0.01 |
| CaO | 0.05 | 0.13 | 0.06 | 0.02 | 0.05 | 0.10 | CaO | | 0.09 | 0.05 |
| $Na_2O$ | 15.09 | 16.45 | 16.80 | 16.70 | 15.91 | 16.80 | $Na_2O$ | 23.45 | 22.61 | 22.09 |
| $K_2O$ | 5.64 | 5.66 | 4.12 | 4.83 | 5.39 | 4.85 | $K_2O$ | 0.05 | 0.10 | 0.01 |
| Sum | 99.81 | 99.28 | 98.80 | 100.86 | 99.31 | 100.13 | Cl | 7.24 | 6.61 | 6.92 |
| | | | | | | | -O=Cl | 1.63 | 1.17 | 1.56 |
| Mol% | | | | | | | Sum | 99.28 | 97.49 | 95.75 |
| Q | 13.2 | 5.7 | 8.8 | 8.9 | 9.1 | 6.1 | | | | |
| Ne | 69.7 | 76.9 | 78.5 | 76.5 | 74.3 | 77.5 | Si | 5.999 | 5.935 | 5.936 |
| Ks | 17.1 | 17.4 | 12.7 | 14.6 | 16.6 | 16.4 | Al | 6.000 | 6.087 | 6.086 |
| | | | | | | | $Fe^{3+}$ | 0.057 | 0.098 | 0.087 |
| | | | | | | | Sum | 12.056 | 12.120 | 12.109 |
| | | | | | | | Ba | | | 0.001 |
| | | | | | | | Ca | | 0.016 | 0.009 |
| | | | | | | | Na | 7.236 | 7.109 | 6.982 |
| | | | | | | | K | 0.010 | 0.020 | 0.208 |
| | | | | | | | Sum | 7.247 | 7.145 | 7.200 |
| | | | | | | | Cl | 1.641 | 1.817 | 1.784 |

Table 33. Trace element analyses of selected rocks from the Pão de Açúcar complex.

| Sample | RP-98 | RP-99 | RP-100 | RP-101 | RP-102 | RP-103 | RP-104 | RP-105 | RP-106 | RP-107 | RP-108 | RP-109 | RP-110 |
|---|---|---|---|---|---|---|---|---|---|---|---|---|---|
| ppm | | | | | | | | | | | | | |
| Cr | < 1 | 3 | 1 | < 1 | 2 | 1 | < 1 | < 1 | 1 | < 1 | < 1 | 1 | 4 |
| Ni | 5 | 5 | 4 | 7 | 7 | 5 | 8 | 7 | 6 | 8 | 7 | 4 | 5 |
| Rb | 106 | 101 | 107 | 103 | 152 | 114 | 107 | 108 | 187 | 191 | 183 | 109 | 178 |
| Ba | 868 | 566 | 709 | 817 | 572 | 659 | 803 | 920 | 90 | 121 | 255 | 925 | 202 |
| Th | | | 13.7 | | | 8.2 | | | | 5,1 | | 7.0 | 4.8 |
| U | | | 2.9 | | | 4.3 | | | | 3,0 | | 3.4 | 2.7 |
| Ta | | | 14.3 | | | 15.0 | | | | 30,5 | | 18.3 | 28.8 |
| Nb | 166 | 144 | 145 | 159 | 151 | 157 | 169 | 132 | 330 | 343 | 325 | 176 | 314 |
| Sr | 358 | 255 | 303 | 352 | 308 | 308 | 355 | 439 | 37 | 51 | 112 | 399 | 87 |
| Hf | | | 15.3 | | | 20.0 | | | | 31,0 | | 16.9 | 29.1 |
| Zr | 669 | 491 | 573 | 613 | 620 | 730 | 553 | 555 | 1389 | 1432 | 1377 | 663 | 1364 |
| Y | 47 | 37 | 48 | 47 | 48 | 46 | 44 | 44 | 85 | 91 | 87 | 51 | 79 |
| La | 123 | 101 | 115.90 | 122 | 130 | 128.20 | 115 | 116 | 216 | 218 | 207 | 129.80 | 188 |
| Ce | 228 | 196 | 228.01 | 230 | 275 | 237.79 | 224 | 231 | 433 | 418 | 411 | 241.20 | 372 |
| Pr | | | 24.38 | | | 24.02 | | | | 44 | | 23.11 | 39 |
| Nd | 81 | 68 | 87.10 | 80 | 89 | 90.77 | 77 | 84 | 127 | 123 | 120 | 85.88 | 109 |
| Sm | | | 13.40 | | | 13.59 | | | | 20,9 | | 15.22 | 19,00 |
| Eu | | | 2.62 | | | 2.58 | | | | 3,13 | | 2.28 | 2,84 |
| Gd | | | 14.42 | | | 11.52 | | | | 19,4 | | 14.13 | 17,75 |
| Tb | | | 1.96 | | | 1.27 | | | | 2,49 | | 1.41 | 2,23 |
| Dy | | | 8.79 | | | 5.60 | | | | 9,67 | | 6.75 | 8,89 |
| Ho | | | 1.55 | | | 1.16 | | | | 2,20 | | 1.15 | 2,02 |
| Er | | | 5.25 | | | 3.66 | | | | 6,55 | | 4.57 | 6,01 |
| Tm | | | 0.80 | | | 0.55 | | | | 1,03 | | 0.76 | 0,89 |
| Yb | | | 4.06 | | | 3.11 | | | | 5,56 | | 3.81 | 5,21 |
| Lu | | | 0.65 | | | 0.43 | | | | 0,78 | | 0.50 | 0,72 |

| Sample | RP-111 | RP-112A | RP-112B | RP-113A | RP-113B | RP-114 | RP-207 | RP-208 | RP-247 | RP-248 | RP-249 | RP-250 |
|---|---|---|---|---|---|---|---|---|---|---|---|---|
| ppm | | | | | | | | | | | | |
| Cr | 4 | 3 | < 1 | < 1 | < 1 | < 1 | < 1 | 5 | 3 | 5 | 3 | 5 |
| Ni | 5 | 5 | 2 | 9 | 7 | 2 | 6 | 6 | 1 | 4 | 3 | 4 |
| Rb | 76 | 115 | 119 | 114 | 86 | 68 | 90 | 99 | 98 | 97 | 83 | 111 |
| Ba | 2023 | 752 | 156 | 800 | 508 | 2115 | 701 | 790 | 28 | 30 | 16 | 57 |
| Th | | | 5.2 | | | | 8.9 | 9.2 | | | 5.2 | 8.5 |
| U | | | 3.4 | | | | 2.2 | 2.3 | | | 1.5 | 2.2 |
| Ta | | | 17.3 | | | | 9.5 | 8.3 | | | 6.5 | 6.1 |
| Nb | 121 | 136 | 165 | 133 | 102 | 102 | 138 | 163 | 75 | 60 | 103 | 110 |
| Sr | 728 | 319 | 62 | 301 | 173 | 1307 | 283 | 320 | 7 | 7 | 12 | 15 |
| Hf | | | 16.6 | | | | 10.9 | 10.2 | | | 5.8 | 6.0 |
| Zr | 360 | 605 | 730 | 527 | 417 | 273 | 477 | 501 | 226 | 197 | 305 | 327 |
| Y | 39 | 50 | 56 | 43 | 34 | 35 | 30 | 35 | 23 | 19 | 23 | 42 |
| La | 105 | 118 | 118 | 119 | 113 | 85 | 94.04 | 105.98 | 58.95 | 114.72 | 50.52 | 70.51 |
| Ce | 204 | 237 | 226 | 230 | 221 | 167 | 169.28 | 184.62 | 122.88 | 208.17 | 115.90 | 151.76 |
| Pr | | | | | | | 16.28 | 17.83 | 12.48 | 19.53 | 11.89 | 14.67 |
| Nd | 86 | 78 | 78 | 84 | 77 | 68 | 60.34 | 65.88 | 46.84 | 73.81 | 45.22 | 57.50 |
| Sm | | | | | | | 9.67 | 9.47 | 7.84 | 10.5 | 7.42 | 8.85 |
| Eu | | | | | | | 1.70 | 1.90 | 0.85 | 2.37 | 0.72 | 1.40 |
| Gd | | | | | | | 9.10 | 8.91 | 7.38 | 9.84 | 6.98 | 8.29 |
| Tb | | | | | | | 0.54 | 0.89 | 0.58 | 0.98 | 0.70 | 0.79 |
| Dy | | | | | | | 5.44 | 6.39 | 4.27 | 6.87 | 4.17 | 5.03 |
| Ho | | | | | | | 0.97 | 1.15 | 0.76 | 1.13 | 0.71 | 0.78 |
| Er | | | | | | | 3.74 | 4.33 | 2.97 | 4.56 | 2.87 | 3.36 |
| Tm | | | | | | | 0.53 | 0.65 | 0.42 | 0.69 | 0.42 | 0.50 |
| Yb | | | | | | | 3.12 | 3.61 | 2.31 | 3.80 | 2.16 | 2.63 |
| Lu | | | | | | | 0.47 | 0.62 | 0.35 | 0.65 | 0.34 | 0.42 |

and cluster in two groups, rocks with A.I.<1.09 (trachyphonolites) and >1.14 (phonolites); the first group places near to the trachytic minimum and the latter trends towards the phonolitic minimum.

D.I.* displays "evolved" numbers clustering between 88 and 93 (at the highest values shown by rock-types from both Fecho dos Morros and Cerro Siete Cabezas complexes), with the exception of two saples which have D.I. around 83. In the elemental variation diagrams, the data fit the fields of the above quoted complexes; notably the high A.I. variants have higher $Na_2O$ and tend to present lower silica, titanium, magnesium, calcium and phosphorous than the low A.I. equivalents (Fig. 34).

In general, the concentrations of trace elements (Table 33), for the same D.I.*, fit the field of the Fecho dos Morros complex, but the phonolites tend to display lower Ba and Sr contents (Fig. 35). Moreover, the phonolites appear to be clustered in two main groups, distinct in having high and low

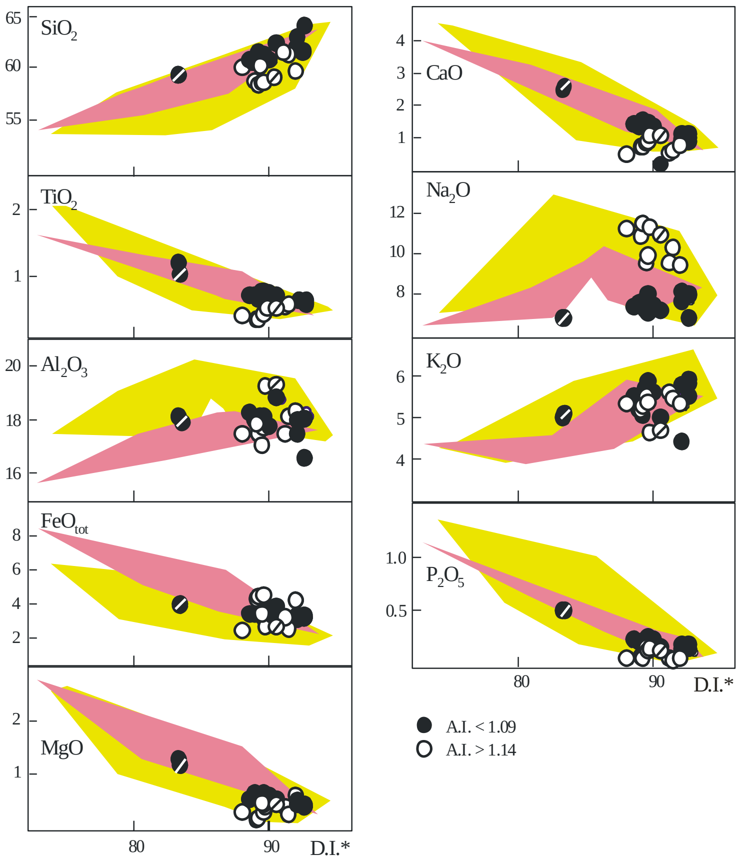


Fig. 34. D.I.* vs. major elements (wt%) for rocks from the Pão de Açúcar complex, compared with the variation fields of two Cerro Siete Cabezas and Fecho dos Morros complexes in pink and yellow, respectively. The samples are subdivided into two groups, A.I<1.09 and >1.14; circles with bar correspond to basal intrusive rocks.

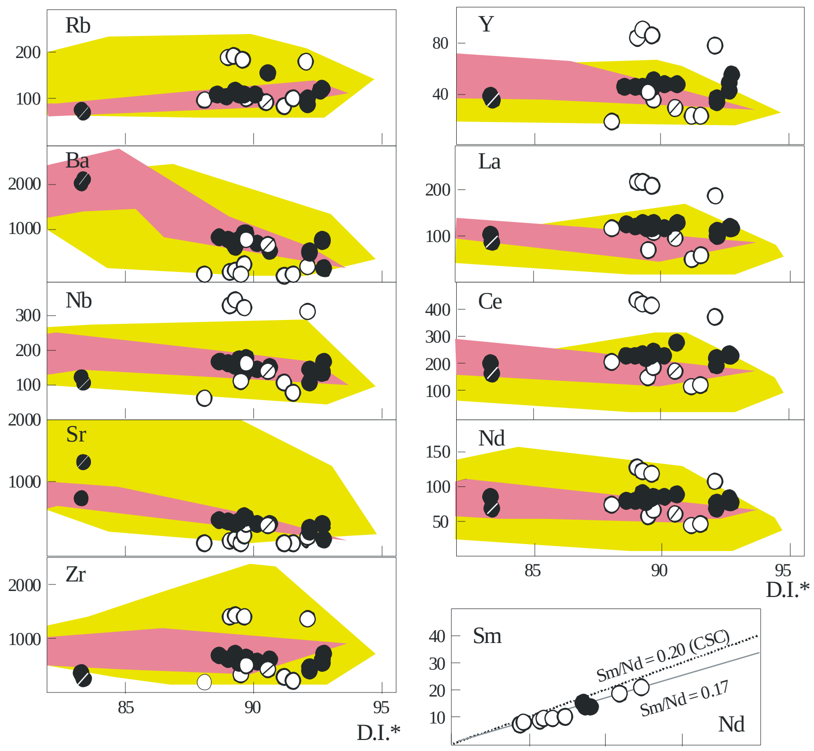


Fig. 35. D.I.* vs. trace elements (ppm) and Nd-Sm diagram for rocks from the Pão de Açúcar complex, compared with the variation fields of Cerro Siete Cabezas and Fecho dos Morros complexes in pink and yellow, respectively. Symbols as in Fig. 34.

contents of Rb, Nb, Zr, Y and REE, respectively (high-Zr and low-Zr variants). In spite of the observed differences, the Sm/Nd ratio of the analyzed samples is quite constant (0.17±0.01), that is the same value of rocks from the Fecho dos Morros complex.

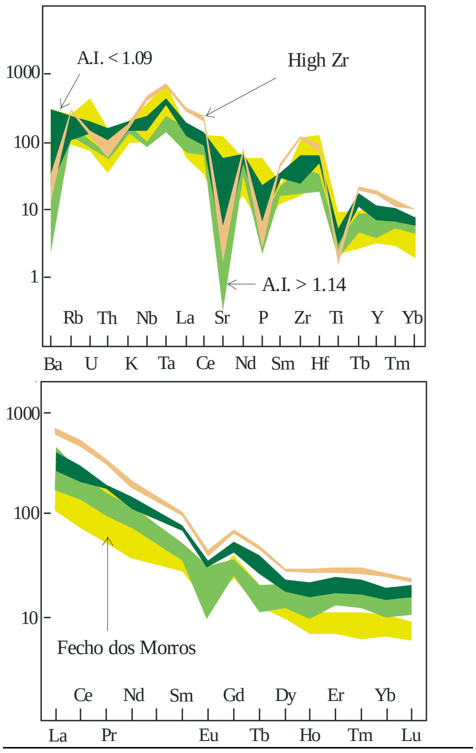


Fig. 36. Primitive mantle- (Sun & McDonough, 1989) and chondrite- (Boynton, 1984) normalized I.E. and REE diagrams, respectively, for rocks from the Pão de Açúcar complex. The field of the Fecho dos Morros complex is shown in yellow for comparison.

As illustrated in the I.E. spidergrams (primitive mantle-normalized, Fig. 36), the various rock-types, i.e. trachyphonolites, phonolites, lavas and ignimbrites, have subparallel trends, except for Sr showing a pronounced negative spike in trachyphonolites (A.I.<1.09). The REE diagram (chondrite-normalized) displays quite similar fractionation patterns, that is, La/Sm 4.3-7.0, Sm/Yb=2.8–4.7 and La/Yb=17.2–27.8. The Eu/Eu* negative anomaly spreads between 0.30 and 0.61, with the more negative values found in the low-Zr phonolites. In general, REE are more enriched with respect to the Fecho dos Morros rock-types, and are characterized by the following progressive enrichment: phonolites (A.I.>1.14)•trachyphonolites (A.I.<1.09)•high-Zr phonolites (A.I.>1.14).

Sr-Nd isotopes

There are only three isotopic Sr-Nd results for the Pão de Açúcar complex (Table I; Appendix), all of them taken from trachyphonolites with A.I.<1.09. They define an initial $^{87}Sr/^{86}Sr$ ratio of 0.70351 ($r^2$= 0.999). This $R_0$ value is not far from that relative to the Fecho dos Morros complex, excluding the two results given by the Cerrito rocks: in this case the best fitting of four results indicates a $R_0$=0.70363 ($r^2$=0.999). On the contrary, the Sm-Nd system is similar to that found for the Cerrito body, showing a depleted character with an initial (241 Ma) $^{143}Nd/^{144}Nd$ ratio of 0.51245±0.00001 (εNd 2.1-2.6).

Nd model ages give an average of 671±16 Ma, approaching those of the Cerrito body (695±18 Ma).

## 5. CERRO BOGGIANI AND COMPARISON WITH THE OTHER ALTO PARAGUAY COMPLEXES

Lying at 15 km NW of the Morro Pão de Açúcar, on the western side of the Paraguay river, Cerro Boggiani (or Cerros Boggiani, according to Putzer & Van den Boom, 1962) forms an expressive hill on the Chaco Boreal swamps. The complex is formed by three isolated monadnocks cropping out above the alluvial sediments of the Paraguay river.

The eastern and southeastern bodies extend for some hundreds of square meters, about 5 to 10 m above the plain, and are constituted by intrusive and extrusive rock-types. The western body covers about 1 $km^2$, is 65 m high and consists of intrusive rocks topped by lava flows; it is also cut by scarce dykes. On the whole, the three bodies define a circular structure extending over 4 $km^2$ (see Fig. 1). The intrusive varieties are usually coarse-grained in texture with alkali feldspar, nepheline and sodalite crystals sizing up to 1-2 cm in length. Sometimes the extrusive varieties contain scarce angular coarse to fine-grained xenoliths.

Petrography

The intrusive rocks are characterized by large euhedral-subhedral crystals of mesoperthite, nepheline and sodalite. Green clinopyroxenes represent the most abundant mafic phase. They form stubby prisms and are partially replaced by amphiboles at the rims. Notably, the textural relationships of the Cerro Boggiani amphiboles are consistent with subsolidus fluid-rock reactions. Biotite is a subordinate phase being found as xenomorphic aggregates associated with aenigmatite and opaques. The latter are ilmenite, pyrite and sphalerite. Typically magnetite is lacking. Common accessories include titanite and very rare apatite. Secondary minerals are cancrinite, carbonates, zeolites and a Li-rich mica.

The effusive rocks are porphyritic in texture and consist of pheno and microphenocrysts of sanidine-anorthoclase, sodalite, nepheline, clinopyroxene, amphibole, titanite and zircon set in a glassy to microcrystalline groundmass, sometimes exhibiting trachytic texture. In particular eudialyte, rosembuschite and låvenite microphenocrysts also occur.

The dykes have petrographic characteristics very similar to those of the effusive rock-types, being porphyritic in texture with the main phenocrysts of alkali feldspar, nepheline, sodalite and clinopyroxene set in a very fine trachytic matrix. The xenoliths are represented by angular inclusions of intrusive rocks in the lava flows (e.g. RP-31-B) or by volcanic breccias containing abundant lithic fragments of gneiss and granite set in a glassy to cryptocrystalline matrix (e.g. RP-32).

Classification and nomenclature

The intrusive rocks, as indicated by modal results, are foid syenites (modal nepheline+sodalite 28-42%; cf. Table 34), and nepheline syenites, following to De La Roche's classification (Table 35 and $R_1$-$R_2$ inset of Fig. 37). Extrusive rocks cluster the phonolite field, while the two xenoliths (sampled in the RP-31A phonolite) are made of nepheline syenite (RP-31B) and trachyphonolite (RP-32), respectively (cf. Table 35). A.I. vs. Q-ne normative diagram and insets (Fig. 37) make evident that the Cerro Boggiani intrusive and extrusive rocks have the same strong peralkaline, sodic-undersaturated character (A.I. up to 1.51 and normative nepheline up to about 25%). On the whole, they define a field well distinct from that related to the Cerro Siete Cabezas complex, and partly overlap the Ilha dos Fecho dos Morros and Pão de Açúcar agpaitic fields.

Table 34. Modal analyses of intrusive rock-types from Cerro Boggiani. Op, opaques (ilmenite, pyrite, sphalerite). Accessory phases: titanite, eudialyte, rosembuschite, lävenite and zircon; *: containing cancrinite about 0.5-1.0%. For other abbreviations see Table 3.

| Sample | RP-27 | RP-29 | RP-30 | RP-35 | RP-38B | RP-39 |
|---|---|---|---|---|---|---|
| vol% | | | | | | |
| AF | 52.2 | 61.3 | 56.6 | 56.0 | 51.7 | 60.0 |
| Ne | 28.2 | 20.5 | 15.5 | 17.8 | 21.0 | 17.9 |
| So | 13.9 | 8.1 | 17.1 | 15.2 | 8.0 | 13.5 |
| Cpx | 4.2 | 8.2 | 6.9 | 8.1 | 15.5 | 6.6 |
| Am | 0.2 | 0.4 | 0.9 | 0.6 | 0.4 | 0.2 |
| Bi | 0.5 | 0.3 | 0.3 | 0.2 | 0.2 | |
| Op | 0.3 | 0.2 | 0.2 | | | |
| Ap | | | | | | |
| Accessories | 0.5 | 1.0 | 2.5* | 2.0* | 2.1* | 3.2* |

Mineralogy

Representative chemical compositions of minerals from selected samples are given in Tables 36 to 39.

*Clinopyroxene and amphibole*

The Cerro Boggiani clinopyroxenes systematically have very low Mg/(Mg+$Fe_{tot}$+Mn) ratios, i.e. 0.18 to 0.14, at the core of the largest crystals and in phenocrysts from intrusive and effusive rock-types, respectively, and up to 0.03 at the rims and in groundmass (Table 36). The crystals from effusive lavas differ only for a few higher Ti content. In general, they represent the extreme side of the evolutionary trend expressed by the Pão de Açúcar and Fecho dos Morros minerals (Fig. 38).

The amphiboles vary between ferrorichteritic and arfvedsonitic compositions (Table 37 and Fig. 38) with Mg/(Mg+$Fe_{tot}$+Mn) ratios between 0.42 and 0.31, and overlap the compositions of late amphiboles from the Fecho dos Morros and Pão de Açúcar complexes (Fig. 38).

Table 35. Major element analyses, norms and classification of selected rocks from Cerro Boggiani (according to De La Roche, 1980). LF, lava flows; D, dykes; X, xenoliths. The other samples are intrusive rocks. See Table 2 for abbreviations.

| Sample | RP-27 | RP-28<br>D | RP-29 | RP-30 | RP-31A<br>LF | RP-31B<br>X | RP-32<br>X | RP-33<br>D | RP-34<br>LF |
|---|---|---|---|---|---|---|---|---|---|
| wt% | | | | | | | | | |
| $SiO_2$ | 56.60 | 57.83 | 57.65 | 58.52 | 57.46 | 58.25 | 62.88 | 57.34 | 58.44 |
| $TiO_2$ | 0.22 | 0.35 | 0.37 | 0.22 | 0.51 | 0.43 | 0.49 | 0.41 | 0.32 |
| $Al_2O_3$ | 19.97 | 19.42 | 19.40 | 19.57 | 18.86 | 19.34 | 16.35 | 19.07 | 19.08 |
| $Fe_2O_3$ | 1.34 | 1.74 | 1.08 | 0.83 | 2.40 | 1.17 | 3.76 | 1.23 | 2.15 |
| FeO | 0.78 | 0.76 | 1.99 | 1.51 | 0.98 | 2.17 | 0.67 | 2.27 | 0.47 |
| MnO | 0.13 | 0.14 | 0.24 | 0.16 | 0.22 | 0.23 | 0.14 | 0.22 | 0.18 |
| MgO | 0.04 | 0.10 | 0.26 | 0.06 | 0.26 | 0.21 | 0.09 | 0.17 | 0.13 |
| CaO | 0.29 | 0.96 | 1.29 | 0.66 | 1.33 | 1.01 | 0.61 | 1.20 | 0.65 |
| $Na_2O$ | 13.17 | 11.98 | 11.91 | 12.44 | 11.41 | 12.02 | 10.39 | 12.58 | 11.20 |
| $K_2O$ | 5.44 | 5.83 | 5.68 | 5.81 | 5.46 | 4.88 | 2.65 | 5.23 | 5.50 |
| $P_2O_5$ | 0.02 | 0.02 | 0.02 | 0.02 | 0.14 | 0.18 | 0.23 | 0.12 | 0.06 |
| L.O.I. | 1.22 | 0.75 | 0.31 | 0.36 | 0.72 | 0.28 | 1.12 | 0.54 | 1.10 |
| Sum | 99.22 | 0.75 | 100.21 | 100.16 | 99.75 | 100.17 | 99.15 | 100.38 | 99.28 |
| or | 32.15 | 34.45 | 33.57 | 34.33 | 32.26 | 28.88 | 15.66 | 30.90 | 32.50 |
| ab | 27.18 | 27.45 | 26.87 | 30.06 | 28.22 | 35.06 | 64.93 | 28.68 | 33.31 |
| ne | 24.51 | 21.66 | 22.37 | 20.72 | 20.80 | 20.17 | 2.39 | 21.82 | 18.53 |
| ac | 3.88 | 5.04 | 3.12 | 2.40 | 6.94 | 3.38 | 10.88 | 3.55 | 6.22 |
| ns | 8.05 | 6.57 | 6.77 | 7.96 | 5.13 | 5.94 | 1.45 | 7.78 | 4.70 |
| di | 1.15 | 2.56 | 5.45 | 2.77 | 3.96 | 3.34 | 1.31 | 4.52 | 1.96 |
| wo | | 0.70 | | | 0.42 | | | | 0.22 |
| ol | 0.62 | | 0.99 | 1.06 | | 1.88 | 0.18 | 1.48 | |
| il | 0.42 | 0.66 | 0.70 | 0.41 | 0.97 | 0.81 | 0.93 | 0.77 | 0.61 |
| ap | 0.05 | 0.05 | 0.05 | 0.05 | 0.33 | 0.42 | 0.53 | 0.28 | 0.14 |
| D.I.* | 87.7 | 88.6 | 85.9 | 87.5 | 88.2 | 87.5 | 93.9 | 84.5 | 90.6 |
| A.I. | 1.38 | 1.34 | 1.33 | 1.37 | 1.31 | 1.30 | 1.22 | 1.38 | 1.28 |
| $R_1$ | -2239 | -1838 | -1809 | -1946 | -1601 | -1630 | -247 | -1975 | -1445 |
| $R_2$ | 424 | 489 | 532 | 458 | 525 | 498 | 391 | 511 | 453 |
| Rock-type | Nepheline syenite | Phonolite | Nepheline syenite | Nepheline syenite | Phonolite | Nepheline syenite | Trachy-phonolite | Phonolite | Phonolite |
| Q | 32.5 | 32.9 | 32.4 | 33.6 | 33.0 | 33.9 | 45.3 | 32.5 | 34.7 |
| ne | 45.0 | 43.7 | 44.6 | 43.5 | 44.4 | 46.6 | 45.3 | 45.9 | 43.4 |
| ks | 22.5 | 23.4 | 23.0 | 22.9 | 22.6 | 19.5 | 9.4 | 21.6 | 21.9 |

| Sample | RP-35 | RP-36<br>LF | RP-37<br>LF | RP-38A<br>LF | RP-38B | RP-39 | RP-40<br>LF | RP-41<br>LF | RP-42<br>LF | RP-43<br>LF |
|---|---|---|---|---|---|---|---|---|---|---|
| wt% | | | | | | | | | | |
| $SiO_2$ | 59.07 | 59.35 | 58.06 | 59.70 | 57.57 | 58.80 | 55.72 | 57.01 | 57.55 | 59.11 |
| $TiO_2$ | 0.20 | 0.34 | 0.20 | 0.19 | 0.18 | 0.17 | 0.53 | 0.23 | 0.19 | 0.63 |
| $Al_2O_3$ | 19.96 | 19.43 | 18.68 | 20.73 | 19.07 | 19.89 | 17.10 | 18.90 | 18.93 | 17.71 |
| $Fe_2O_3$ | 0.70 | 0.98 | 3.57 | 0.92 | 2.33 | 1.00 | 3.81 | 2.93 | 3.55 | 2.64 |
| FeO | 1.26 | 1.78 | 1.39 | 1.67 | 2.51 | 0.97 | 1.70 | 2.04 | 1.06 | 1. 60 |
| MnO | 0.13 | 0.19 | 0.20 | 0.18 | 0.21 | 0.10 | 0.52 | 0.25 | 0.19 | 0.28 |
| MgO | 0.02 | 0.12 | 0.13 | 0.12 | 0.05 | <0.01 | 0.07 | 0.07 | 0.05 | 0.78 |
| CaO | 0.55 | 0.67 | 1.19 | 0.86 | 1.18 | 0.39 | 1.16 | 1.06 | 0.92 | 1.30 |
| $Na_2O$ | 11.56 | 11.20 | 10.24 | 9.65 | 10.15 | 12.00 | 12.81 | 10.82 | 10.93 | 10.44 |
| $K_2O$ | 6.38 | 5.72 | 5.54 | 5.80 | 5.59 | 5.47 | 4.36 | 5.55 | 5.50 | 4.33 |
| $P_2O_5$ | 0.01 | 0.07 | 0.01 | 0.01 | 0.01 | 0.01 | 0.01 | 0.01 | 0.01 | 0.20 |
| L.O.I.* | 0.30 | 0.55 | 0.55 | 0.49 | 0.75 | 1.05 | 1.65 | 1.14 | 0.90 | 0.75 |
| Sum | 100.17 | 100.40 | 99.76 | 100.32 | 99.60 | 99.85 | 99.44 | 100.01 | 99.78 | 99.77 |
| or | 37.70 | 33.80 | 32.73 | 34.27 | 33.03 | 32.39 | 25.76 | 32.80 | 32.50 | 25.59 |
| ab | 29.62 | 34.85 | 28.04 | 35.85 | 28.47 | 34.63 | 27.01 | 25.63 | 26.85 | 41.39 |
| ne | 20.32 | 18.00 | 20.15 | 20.84 | 20.86 | 20.17 | 19.88 | 22.04 | 21.61 | 13.86 |
| ac | 2.02 | 2.83 | 10.33 | 2.66 | 6.74 | 2.89 | 11.02 | 8.48 | 10.27 | 7.64 |
| ns | 6.60 | 5.45 | 2.25 | 0.99 | 2.62 | 6.15 | 7.49 | 3.63 | 3.28 | 2.95 |
| di | 2.35 | 2.50 | 5.11 | 3.68 | 5.14 | 1.66 | 5.03 | 4.65 | 3.98 | 4.29 |
| ol | 0.78 | 1.55 | 0.19 | 1.09 | 1.62 | 0.32 | 0.58 | 1.19 | | 1.64 |
| il | 0.37 | 0.64 | 0.38 | 0.36 | 0.34 | 0.32 | 0.99 | 0.44 | 0.36 | 1.19 |
| ap | 0.02 | 0.16 | 0.02 | 0.02 | 0.02 | 0.02 | 0.02 | 0.02 | 0.02 | 0.47 |
| D.I.* | 89.7 | 89.5 | 91.2 | 93.6 | 89.1 | 90.1 | 72.6 | 88.9 | 81.0 | 80.8 |
| A.I. | 1.30 | 1.27 | 1.22 | 1.07 | 1.19 | 1.29 | 1.51 | 1.26 | 1.26 | 1.23 |
| $R_1$ | -1719 | -1444 | -1197 | -881 | -1209 | -1680 | -2012 | -1478 | -1456 | -909 |
| $R_2$ | 451 | 459 | 500 | 505 | 503 | 432 | 463 | 488 | 472 | 525 |
| Rock-type | Nepheline syenite | Phonolite | Phonolite | Phonolite | Nepheline syenite | Nepheline syenite | Phonolite | Phonolite | Phonolite | Phonolite |
| Q | 34.1 | 33.3 | 33.3 | 34.3 | 33.2 | 34.2 | 32.4 | 32.2 | 32.5 | 37.1 |
| ne | 41.5 | 43.7 | 43.7 | 44.3 | 44.0 | 44.7 | 47.4 | 44.6 | 44.7 | 44.9 |
| ks | 24.4 | 23.0 | 23.0 | 21.4 | 22.8 | 21.1 | 20.2 | 23.2 | 22.8 | 18.0 |

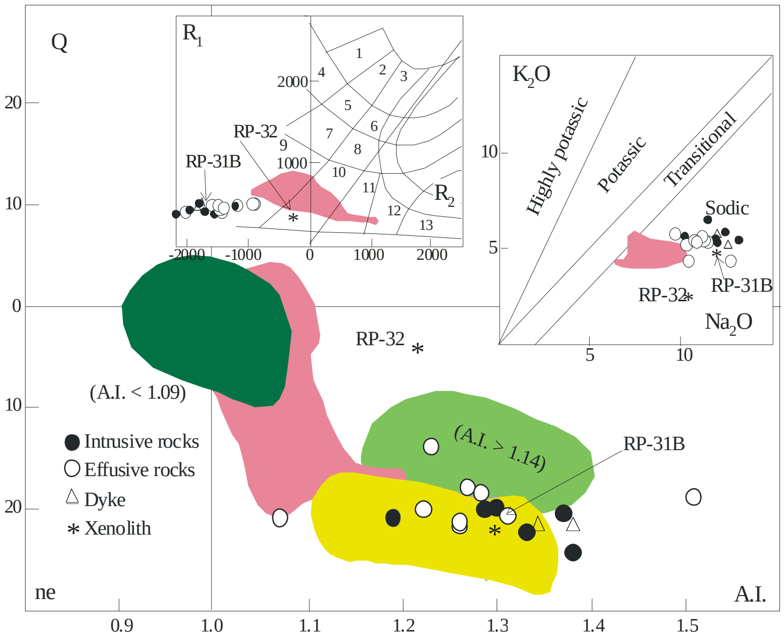


Fig. 37. A.I. vs. Q-ne for rocks from the Cerro Boggiani complex. For comparison the fields relative to the Pão de Açúcar (light and dark green) and Cerro Siete Cabezas (pink) complexes and to the Ilha Fecho dos Morros (yellow) body are shown. For insets see Fig. 3.

Table 36. Representative clinopyroxene analyses from Cerro Boggiani rocks. C, core; R, rim; Ph, mPh and gm, phenocryst, microphenocryst and groundmass phases, respectively. For additional information see Table 3.

| Sample | RP-29C | RP-30C | RP-30R | RP-31AC | RP-31AR | RP-33mPH | RP-37mPH | RP-40gm | RP-41gm | RP-42mPH | RP-43mPH |
|---|---|---|---|---|---|---|---|---|---|---|---|
| wt% | | | | | | | | | | | |
| $SiO_2$ | 51.62 | 52.25 | 52.95 | 51.42 | 51.90 | 52.40 | 51.47 | 52.02 | 51.38 | 51.74 | 51.14 |
| $TiO_2$ | 0.63 | 0.38 | 0.42 | 0.83 | 0.91 | 0.65 | 0.87 | 1.34 | 0.90 | 0.96 | 0.76 |
| $Al_2O_3$ | 1.02 | 0.98 | 1.06 | 0.97 | 0.99 | 1.13 | 0.99 | 1.33 | 0.89 | 1.05 | 1.35 |
| $Cr_2O_3$ | | | | 0.08 | 0.01 | 0.01 | 0.01 | 0.04 | | | 0.03 |
| $Fe_2O_3$ | 17.97 | 20.48 | 33.00 | 18.05 | 23.66 | 26.30 | 22.07 | 25.88 | 23.57 | 24.87 | 17.91 |
| FeO | 6.14 | 5.27 | 0.09 | 5.90 | 2.79 | 2.22 | 5.77 | 1.95 | 4.58 | 4.03 | 7.38 |
| MnO | 1.58 | 1.67 | 0.14 | 1.40 | 1.23 | 1.04 | 0.68 | 0.80 | 1.01 | 1.07 | 0.99 |
| MgO | 3.02 | 2.63 | 0.52 | 3.13 | 1.88 | 1.78 | 0.94 | 0.46 | 0.93 | 0.98 | 2.16 |
| CaO | 9.95 | 9.94 | 0.79 | 9.34 | 5.16 | 5.43 | 7.96 | 2.47 | 5.53 | 5.08 | 8.47 |
| $Na_2O$ | 7.82 | 8.28 | 12.84 | 8.05 | 10.52 | 10.74 | 9.48 | 11.91 | 10.33 | 10.61 | 8.33 |
| $K_2O$ | 0.01 | 0.01 | 0.01 | 0.01 | 0.03 | 0.01 | 0.01 | | | 0.05 | 0.03 |
| Sum | 99.66 | 101.89 | 101.82 | 99.18 | 99.08 | 101.71 | 100.25 | 98.20 | 99.12 | 100.05 | 98.55 |
| | | | | | | | | | | | |
| Si | 1.991 | 1.980 | 1.993 | 1.992 | 2.002 | 1.976 | 1.987 | 2.016 | 1.998 | 1.991 | 2.000 |
| $Al^{IV}$ | 0.009 | 0.020 | 0.007 | 0.008 | | 0.024 | 0.013 | | 0.002 | 0.009 | |
| Sum | 2.000 | 2.000 | 2.000 | 2.000 | 2.002 | 2.000 | 2.000 | 2.016 | 2.000 | 2.000 | 2.000 |
| $Al^{VI}$ | 0.037 | 0.024 | 0.040 | 0.036 | 0.045 | 0.026 | 0.032 | 0.061 | 0.039 | 0.039 | 0.062 |
| Ti | 0.018 | 0.011 | 0.019 | 0.024 | 0.026 | 0.018 | 0.025 | 0.039 | 0.026 | 0.028 | 0.022 |
| Cr | | | | 0.003 | | | | 0.001 | | | 0.001 |
| $Fe^{3+}$ | 0.522 | 0.584 | 0.935 | 0.526 | 0.687 | 0.747 | 0.641 | 0.755 | 0.690 | 0.709 | 0.528 |
| $Fe^{2+}$ | 0.198 | 0.167 | 0.003 | 0.191 | 0.090 | 0.070 | 0.186 | 0.063 | 0.149 | 0.130 | 0.241 |
| Mn | 0.052 | 0.053 | 0.004 | 0.046 | 0.040 | 0.033 | 0.022 | 0.026 | 0.033 | 0.035 | 0.033 |
| Mg | 0.174 | 0.149 | 0.029 | 0.181 | 0.108 | 0.100 | 0.054 | 0.027 | 0.054 | 0.056 | 0.126 |
| Ca | 0.412 | 0.407 | 0.032 | 0.388 | 0.213 | 0.219 | 0.329 | 0.103 | 0.230 | 0.210 | 0.355 |
| Na | 0.586 | 0.608 | 0.937 | 0.605 | 0.787 | 0.785 | 0.710 | 0.895 | 0.779 | 0.792 | 0.632 |
| K | 0.001 | 0.001 | 0.001 | 0.001 | 0.002 | 0.001 | 0.001 | | | 0.002 | 0.001 |
| Sum | 2.000 | 2.000 | 2.000 | 2.000 | 1.998 | 2.000 | 2.000 | 1.970 | 2.000 | 2.000 | 2.000 |
| | | | | | | | | | | | |
| Mg/(Mg+ΣFe+Mn) | 0.183 | 0.156 | 0.030 | 0.136 | 0.117 | 0.105 | 0.060 | 0.031 | 0.058 | 0.060 | 0.136 |
| Quad | 0.784 | 0.719 | 0.064 | 0.760 | 0.411 | 0.389 | 0.569 | 0.193 | 0.433 | 0.396 | 0.722 |
| J | 1.172 | 1.216 | 1.874 | 1.210 | 1.574 | 1.570 | 1.420 | 1.790 | 1.558 | 1.584 | 1.264 |

Table 37. Representative analyses of amphiboles mantling clinopyroxene crystals from Cerro Boggiani rocks. For additional information see Table 4.

| Sample | RP-30 | RP-31A | RP-32 | RP-37 | RP-40 | RP-43 |
|---|---|---|---|---|---|---|
| wt% | | | | | | |
| $SiO_2$ | 52.12 | 51.11 | 47.32 | 48.00 | 48.02 | 49.35 |
| $TiO_2$ | 1.08 | 1.04 | 1.49 | 1.66 | 1.74 | 1.07 |
| $Al_2O_3$ | 1.73 | 6.54 | 5.17 | 3.81 | 3.75 | 3.06 |
| $Cr_2O_3$ | | 0.02 | 0.03 | | 0.04 | 0.02 |
| $Fe_2O_3$ | 4.15 | 16.86 | 4.40 | 6.64 | 3.83 | 4.47 |
| FeO | 14.55 | 2.00 | 16.06 | 14.33 | 16.24 | 15.42 |
| MnO | 3.51 | 1.51 | 2.20 | 2.32 | 2.55 | 2.06 |
| MgO | 9.05 | 4.81 | 7.54 | 8.36 | 7.89 | 8.78 |
| CaO | 2.36 | 5.03 | 3.26 | 3.69 | 3.31 | 2.86 |
| $Na_2O$ | 8.05 | 7.30 | 7.44 | 6.86 | 7.45 | 7.76 |
| $K_2O$ | 1.40 | 2.15 | 1.44 | 1.41 | 1.33 | 1.42 |
| F | 1.45 | 1.11 | 1.12 | 1.36 | 1.21 | 1.26 |
| Cl | 0.01 | 0.10 | 0.01 | 0.01 | 0.08 | 0.08 |
| Sum | 98.80 | 99.09 | 97.01 | 97.87 | 96.91 | 97.06 |
| | | | | | | |
| Si | 7.809 | 7.603 | 7.289 | 7.329 | 7.417 | 7.560 |
| $Al^{IV}$ | 0.191 | 0.397 | 0.711 | 0.671 | 0.583 | 0.440 |
| Sum | 8.000 | 8.000 | 8.000 | 8.000 | 8.000 | 8.000 |
| $Al^{VI}$ | 0.115 | 0.673 | 0.226 | 0.014 | 0.099 | 0.112 |
| Ti | 0.122 | 0.108 | 0.173 | 0.191 | 0.202 | 0.123 |
| Cr | | 0.002 | 0.003 | | 0.005 | 0.002 |
| $Fe^{3+}$ | 0.468 | 1.761 | 0.555 | 0.763 | 0.486 | 0.559 |
| $Fe^{2+}$ | 1.829 | 0.232 | 2.024 | 1.829 | 2.058 | 1.932 |
| Mn | 0.445 | 0.177 | 0.287 | 0.300 | 0.334 | 0.267 |
| Mg | 2.021 | 0.995 | 1.731 | 1.903 | 1.817 | 2.005 |
| Sum | 5.000 | 3.948 | 5.000 | 5.000 | 5.000 | 5.000 |
| Ca | 0.379 | 0.748 | 0.538 | 0.604 | 0.548 | 0.469 |
| $Na_B$ | 1.621 | 1.252 | 1.462 | 1.396 | 1.452 | 1.531 |
| Sum | 2.000 | 2.000 | 2.000 | 2.000 | 2.000 | 2.000 |
| $Na_A$ | 0.718 | 0.713 | 0.760 | 0.634 | 0.779 | 0.774 |
| K | 0.268 | 0.381 | 0.283 | 0.275 | 0.262 | 0.278 |
| $Sum_A$ | 0.985 | 1.094 | 1.043 | 0.909 | 1.041 | 1.052 |
| F | 0.668 | 0.487 | 0.546 | 0.657 | 0.591 | 0.611 |
| Cl | 0.003 | 0.023 | 0.003 | 0.003 | 0.021 | 0.021 |
| | | | | | | |
| Mg/(Mg+ΣFe+Mn) | 0.425 | 0.314 | 0.377 | 0.397 | 0.383 | 0.421 |
| | | | | | | |
| Na+K | 37.8 | 62.6 | 35.3 | 32.5 | 34.7 | 38.1 |
| Mg | 29.3 | 26.5 | 24.4 | 26.8 | 25.3 | 29.5 |
| $Fe^{2+}$+Mn | 32.9 | 10.9 | 40.3 | 40.7 | 40.0 | 32.4 |

### *Biotite, ilmenite and accessory minerals*

The biotites (Table 38) have Mg/(Mg+Fe+Mn) ratios ranging from 0.44 to extreme iron-rich varieties, corresponding to annite 58 to 91 mol%, respectively, with F contents depleted and Mn enriched with the decreasing of the above ratio, respectively (Fig. 39). Probably, considering the close relationships among aenigmatite, ilmenite and annite-rich biotite, the latter are due to subsolidus reactions developing at the intersection of Ac-Ilm-Aen-Nds buffer, Na-amphibole and annite stability fields (cf. Nicholls & Carmichael, 1969), at temperatures around 500-570°C.

The compositional variations shown by biotite in the whole Alto Paraguay Province are fairly representative. Similar trends have been also noticed from silica-undersaturated nepheline syenites from the Cilwa Province (Woolley & Platt, 1986) and from peralkaline syenites and granites from Mulanje, Malawi (Platt & Woolley, 1986), suggesting no silica activity control on the compositional evolution of biotite in felsic alkaline rocks.

Ilmenite is extremely Mn enriched, up to 15wt% for a Fe/(Fe+Mn) ratio of 0.68 (Table 38), and plots at the end of the trend defined by the ilmenites from other Alto Paraguay complexes (cf. Fig. 24).

Titanite is relatively abundant. The low analytical totals of the microprobe analyses (cf. Table 38) suggest that significant amounts of other elements (e.g. Nb and REE) may be present. Zircono-silicates, like eudialyte, rosembuschite and låvenite (Table 38), are typical minerals in Cerro Boggiani rocks, along with aenigmatite (see also Carbonin *et al.*, in this volume). The Cerro Boggiani eudialyte differs from the Cerro Siete Cabezas ana-logues (cf. Table 8) above for the higher F, Nb and CaO contents vs. lower Si, Zr and Na. The presence of rosembuschite indicates high F activity (F up to 8.43 wt%). Aenigmatite appears as an exclusive phase of Cerro Boggiani and shows a composition similar to other Ti-bearing varieties from peralkaline rocks (cf. Woolley & Platt, 1986), stable to a $fO_2$ between NNO and QFM solid buffers (cf. Lindsley, 1971).

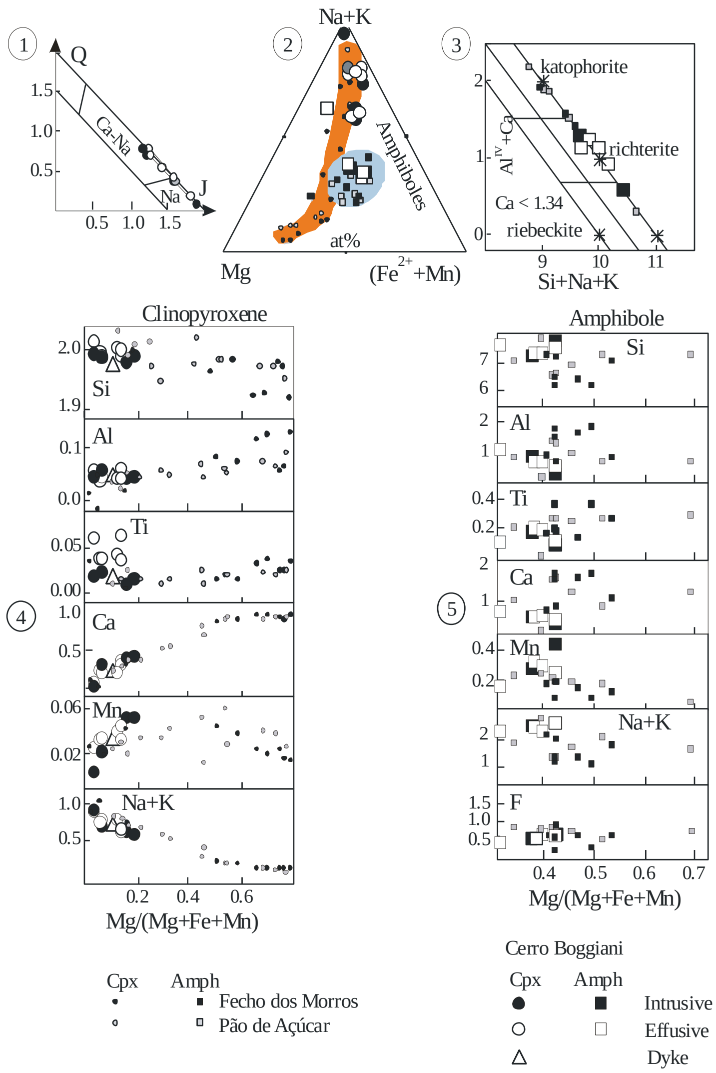


Fig. 38. Clinopyroxenes and amphiboles from Cerro Boggiani representative rock-types. 1) Q-J classification for clinopyroxenes (tie lines join core, early, and rim, late, compositions; 2) Mg-($Fe^{2+}$+Mn)-(Na+K) diagrams for clinopyroxenes and amphiboles (for comparison the compositions and fields from the Pão de Açúcar+Fecho dos Morros complexes in orange and light blue, respectively, are plotted); 3) classificative diagram for amphiboles (cf. Platt & Woolley, 1986); 4) and 5) elemental variations vs. Mg/(Mg+Fe+Mn) ratio (Fe=total iron).

Table 38. Representative biotite, ilmenite and accessory minerals analyses from Cerro Boggiani rocks; mPhC and mPhR, microphenocryst, core and rim, respectively.

| | Biotite | | |
|---|---|---|---|
| Sample | RP-41 | RP-42 mPhC | RP-42 mPhR |
| wt% | | | |
| $SiO_2$ | 34.98 | 38.32 | 35.24 |
| $TiO_2$ | 4.52 | 2.34 | 2.56 |
| $Al_2O_3$ | 9.80 | 10.81 | 8.55 |
| $Cr_2O_3$ | 0.06 | 0.01 | |
| $FeO_{tot}$ | 32.46 | 21.40 | 35.31 |
| MnO | 2.82 | 2.06 | 2.90 |
| MgO | 2.68 | 10.49 | 1.48 |
| CaO | | 0.01 | |
| $Na_2O$ | 0.19 | 0.29 | 0.15 |
| $K_2O$ | 8.55 | 9.24 | 8.84 |
| F | 0.28 | 1.59 | 0.33 |
| Cl | 0.03 | 0.04 | 0.02 |
| Less O=F, Cl | 0.12 | 0.69 | 0.15 |
| $H_2O^+_{calc}$ | 3.38 | 3.14 | 3.36 |
| Sum | 99.63 | 99.05 | 98.59 |
| Si | 5.772 | 5.885 | 6.001 |
| $Al^{IV}$ | 1.906 | 1.957 | 1.716 |
| $Ti^{IV}$ | 0.322 | 0.158 | 0.283 |
| Sum (Z) | 8.000 | 8.000 | 8.000 |
| $Ti^{VI}$ | 0.239 | 0.112 | 0.045 |
| Cr | 0.008 | 0.001 | |
| $Fe^{2+}$ | 4.480 | 2.749 | 5.029 |
| Mn | 0.394 | 0.268 | 0.418 |
| Mg | 0.659 | 2.401 | 0.334 |
| Sum (Y) | 5.780 | 5.531 | 5.826 |
| Ca | | 0.002 | |
| Na | 0.061 | 0.086 | 0.050 |
| K | 1.800 | 1.810 | 1.921 |
| Sum (X) | 1.861 | 1.898 | 1.971 |
| F | 0.151 | 0.772 | 0.177 |
| Cl | 0.008 | 0.010 | 0.006 |
| OH | 3.841 | 3.218 | 3.817 |
| Sum | 4.000 | 4.000 | 4.000 |
| Mg/(Mg+ΣFe+Mn) | 0.119 | 0.443 | 0.058 |

| | Ilmenite |
|---|---|
| | RP-32 |
| $SiO_2$ | |
| $TiO_2$ | 51.94 |
| $Al_2O_3$ | 0.01 |
| $Cr_2O_3$ | 0.08 |
| $Fe_2O_3$ | 0.12 |
| FeO | 31.74 |
| MnO | 15.02 |
| MgO | 0.02 |
| CaO | 0.02 |
| Sum | 98.95 |
| Si | |
| Ti | 0.995 |
| Al | |
| Cr | 0.001 |
| $Fe^{3+}$ | 0.002 |
| $Fe^{2+}$ | 0.677 |
| Mn | 0.323 |
| Mg | 0.001 |
| Ca | 0.001 |
| Sum | 2.000 |
| mol% | |
| $R_2O_3$ | 0.19 |

| | Eudialyte | Rosembuschite | |
|---|---|---|---|
| | RP-33 | RP-31A | RP-33 |
| $SiO_2$ | 48.81 | 31.56 | 31.46 |
| $TiO_2$ | 0.46 | 7.79 | 8.10 |
| $ZrO_2$ | 12.88 | 16.47 | 12.68 |
| $Al_2O_3$ | 0.16 | | |
| $Ce_2O_3$ | 0.40 | | |
| $FeO_{tot}$ | 4.90 | 0.78 | 0.70 |
| MnO | 3.36 | 3.48 | 2.32 |
| MgO | 0.07 | 0.12 | 0.07 |
| CaO | 10.54 | 22.46 | 26.39 |
| $Na_2O$ | 10.46 | 9.57 | 9.33 |
| $K_2O$ | 0.26 | | |
| $Nb_2O_5$ | 1.32 | 1.37 | 1.59 |
| F | 0.69 | 7.55 | 8.43 |
| Cl | 0.94 | | |
| Less O=F, Cl | 0.49 | 3.18 | 3.55 |
| | | 97.97 | 97.52 |
| Sum | 94.76 | | |

| | Lävenite | Aenigmatite | Titanite | |
|---|---|---|---|---|
| | RP-40 | RP-42 | RP-31A | RP-33 |
| $SiO_2$ | 32.58 | 41.50 | 30.26 | 30.02 |
| $TiO_2$ | 3.75 | 8.99 | 35.64 | 35.14 |
| $ZrO_2$ | 29.90 | | 1.05 | 0.93 |
| $Al_2O_3$ | | 0.35 | 1.05 | 0.93 |
| $Ce_2O_3$ | | | 0.03 | 0.02 |
| $FeO_{tot}$ | 2.97 | 39.80 | 1.62 | 1.78 |
| MnO | 5.99 | 1.94 | 0.07 | 0.15 |
| MgO | 0.10 | 0.01 | 0.01 | 0.01 |
| CaO | 12.43 | 0.19 | 28.02 | 27.05 |
| $Na_2O$ | 6.80 | 7.10 | 0.08 | 0.20 |
| $K_2O$ | | 0.01 | 0.03 | 0.01 |
| $Nb_2O_5$ | 1.40 | | | |
| F | 5.33 | | | |
| Cl | | | | |
| Less O=F, Cl | 2.25 | | | |
| Sum | 99.01 | 99.89 | 96.81 | 95.30 |

### *Feldspars, nepheline and sodalite*

Feldspars consist of mesoperthites in the nepheline syenites, while the phenocrysts in the phonolites are sodic sanidine. Exsolutions tend towards albite pure compositions and to Or 94 (Table 39 and Fig. 40). In general, the compositions plot in the fields of the other Alto Paraguay Province complexes. Sanidinic and albitic compositions may coexist in groundmass, and sometimes sanidine pheno- and microphenocrysts are mantled by albitic rims. Some X-ray precession determinations demonstrated that the sodic sanidine phenocrysts are cryptopertitic.

The nepheline has an average $Fe_2O_3$ content of 0.71±0.15 with silica excess between 10 and 5% (corresponding to temperatures between about 1000º and 700°C, according to Hamilton, 1961).

Sodalite, ranging from about 8 to 20 vol%, displays a quite constant composition with Cl= 1.82±0.09 a.f.u. (Table 39).

Concluding, the mineralogical assemblages on the whole seem to indicate temperatures of emplacement around or less than 1000°C and a very low total pressure for intrusive rock-types, as shown by the compositional overlapping of intrusive and effusive minerals (i.e.•1 kb), with high activity of F and Cl.

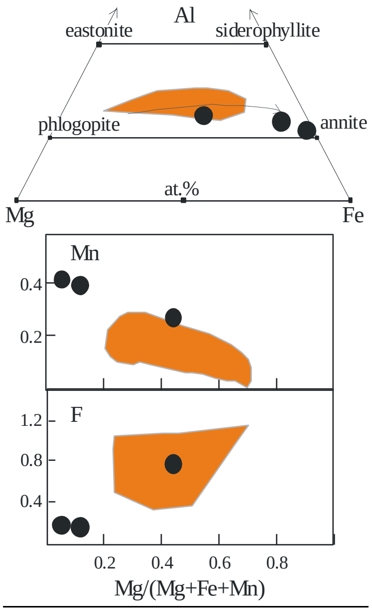


Fig. 39. Plot of biotites from Cerro Boggiani representative rocks in the Al-Mg-(Fe+Mn) diagram (Fe=total iron as $Fe^{2+}$), and variation of Mn and F [atoms per 22(O)] with Mg/(Mg+Fe+Mn) atomic ratio. The fields in orange represent the compositional variations of micas from the Pão de Açúcar+Fecho dos Morros complexes and the line with arrow corresponds to the trend of minerals from the Chilwa Province, Malawi (Wooley & Platt, 1986).

## Major and trace elements distribution

The analyzed intrusive and effusive rocks lie in the whole field of the Alto Paraguay complexes, clustering the phonolitic minimum, with the exception of the RP-32 xenolith that plots on the Ab side of the Ab-Or tie line (Fig. 40). The latter, as above evidenced, also chemically reflects the mixing with basement components.

D.I.* ranges between 72 and 94, that is the same interval given for the Fecho dos Morros and Pão de Açúcar rocks. However, in the elemental variation diagrams, the Cerro Boggiani complex can be distinguished by the very low and constant behaviour of Ti, Mg, Ca and P and for the high Na contents (Fig. 41).

The trace elements are also distinct with respect to the Fecho dos Morros and Pão de Açúcar rock-types for the very high Rb contents and low Ba and Sr concentrations, respectively (Table 40 and Fig. 42).

Nepheline syenites and phonolites have broadly similar I.E. and REE patterns (Fig. 43A), and are systematically enriched in Rb-U-Th, Nb-Ta and Zr-Hf with respect to the Pão de Açúcar rocks. The spidergrams parallel to some extent those relative to the Late Cretaceous-Tertiary melanephelinites (mg# 68-48) from central and southern Paraguay (Comin-Chiaramonti *et al.*, 1991, 1997, 1999).

The average Sm/Nd ratio is 0.156, compared to 0.17 given by both Fecho dos Morros and Pão the Açúcar rock-types. REE display slightly concave patterns with HREE enrichment ($Er/Lu_c$= 0.69±0.04). The LREE show steep slopes from La to Sm ($La/Sm_c$=14.0±3.5) and Eu negative anomalies (Eu/Eu*=0.68±0.05). In the $Yb_c$ vs. $La/Yb_c$ diagram, the Cerro Boggiani rocks plot between the main facies and pegmatitic facies of the Fecho dos Morros complex (the latter defining a field comprising the melanephelinites from central and southwestern Paraguay), and fit the field of the Cerro Siete Cabezas complex at the lower La/Yb (Fig. 43C).

Notably, the Eu negative anomaly is a peculiar feature in all the alkaline complexes from the Alto Paraguay Province (Fig. 43B). As a gabbroic-basaltic precursor has not been found yet in the Alto Paraguay petrographic associations, that anomaly may be attributed to a basanite-like parent magma subjected to plagioclase fractionation. For example, Beccaluva *et al.* (1992) and Morbidelli *et al.* (1995) demonstrated that in the Juquiá complex (Ponta Grossa Arch) the liquid line of descent is represented by the following sequence: basanitic magma•essexite•mafic nepheline syenite• nephelinesyenite•evolved nepheline syenite (D.I.* up to 90).

On the other hand, it is remarkable that melanephelinites from central Paraguay, which are believed to be primary magmas (e.g. sample 3399 of Table 1, mg#=0.68, in Comin-Chiaramonti *et al.*, 1997), have Eu/Eu*=0.80. Thus, there is also the possibility that a melanephelinitic magma may have been the precursor of Cerro Boggiani rock-types. As a matter of fact, mass balance calculations (e.g. nephelinitic parent magma n. 3, Table 3 of Comin-Chiaramonti *et al.*, 1997, vs. sample RP-43) give a F=8.62% ($r^2$=0.44) and a fractionated assemblage consisting of 18.87% olivine, 49.44% clinopyroxene, 8.31% Ti-magnetite, 20.29% nepheline and 3.08% apatite (mineral analyses from sample 3097 in Comin-Chiaramonti & Gomes, 1996). However, the modelling of trace elements is largely unsatisfactory (as also in the case of a basanitic parent magma), probably as a result of the fractionation of accessory phases (as eudialyte) and their $K_D$ values. Moreover, the preferential retention of F and Cl in agpaitic melts is crucial for a such approach, particularly for the concentrations of Nb, Th, U, Zr, REE.

Comparing the REE patterns of the Cerro Boggiani rocks with those of analogues from other Alto Paraguay complexes, apart for the systematic negative Eu anomalies, some different types of REE patterns can be distinguished among the various occurrences, independently from the alkali or differentiation indexes (Fig. 43B):

1) straight log-linear patterns with a steady decrease from La to Sm, and a reduced linear decrease from Gd to Lu (Cerro Siete Cabezas, Cerro Pedreira, Morro Distante and Morro Conceição), similar to REE patterns of ASU-SJB melanephelinites (cf. Comin-Chiaramonti *et al.*, 1997);

2) LREE patterns similar to the former type, but nearly constant HREE (Cerrito and Cerrito dykes);

3) patterns characterized by HREE plateau, strong increase in enrichment from Dy to Gd, followed by a steady increase from Sm to La (Ilha Fecho dos Morros, Morro de São Pedro and Pão de Açúcar rock-types);

4) concave patterns with HREE decreasing from Lu to Tb, and additionally LREE increasing from Gd to La (pegmatitic facies from the Ilha Fechos dos Morros body);

5) concave patterns with HREE decreasing from Lu to Tb, a reduced increase from Tb to Sm, and a steep increase from Sm to La, typical of the Cerro Boggiani rocks.

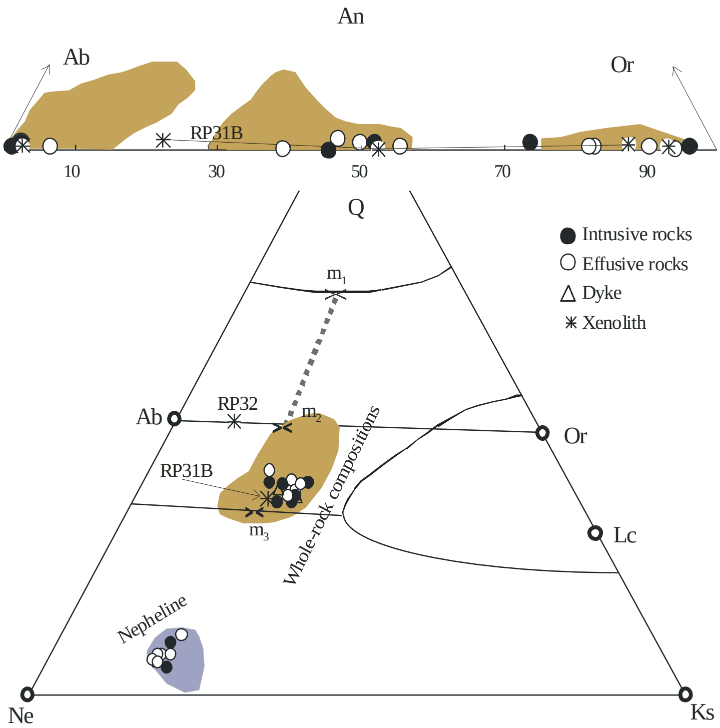


Fig. 40. Alkali feldspar from Cerro Boggiani representative rocks plotted into the Or-Ab-An (mol%) diagram, and nepheline compositions plotted into the Ks-Ne-Q (wt%) space (cf. Fig. 8). For comparison the representative fields of compositions of all the occurrences from Alto Paraguay Province are also shown in sand along the compositional variation of the whole-rocks.

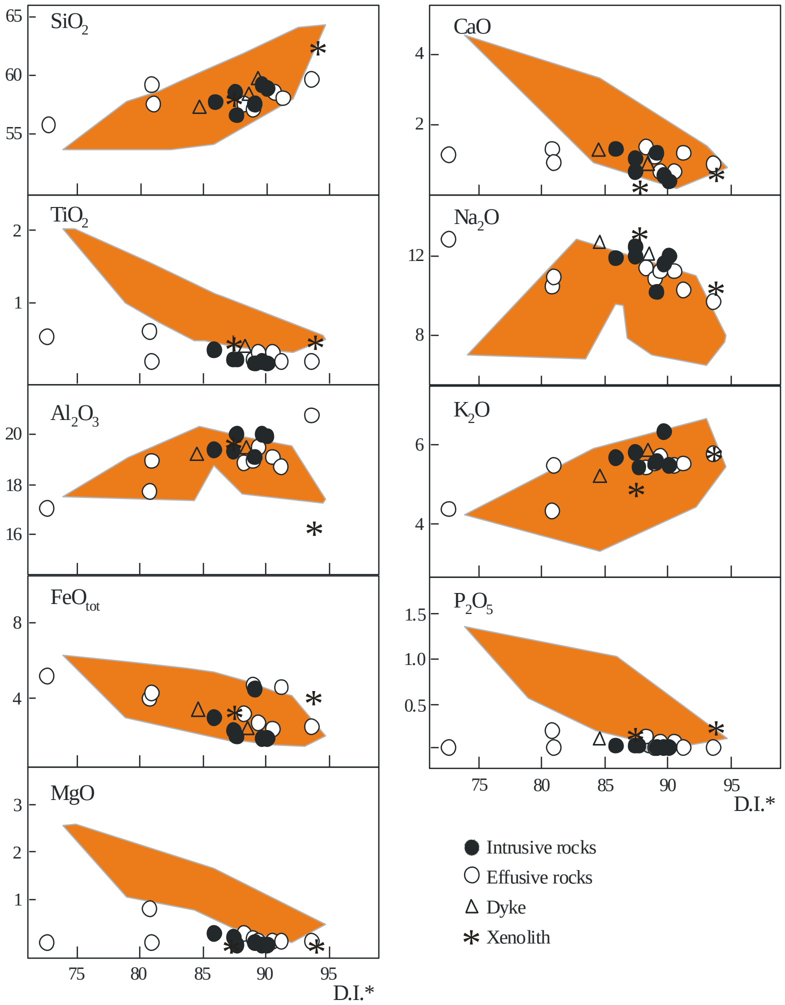


Fig. 41. D.I.* vs. major elements (wt%) for Cerro Boggiani rocks, compared with the variation field in orange for the Fecho dos Morros+Pão de Açúcar complexes.

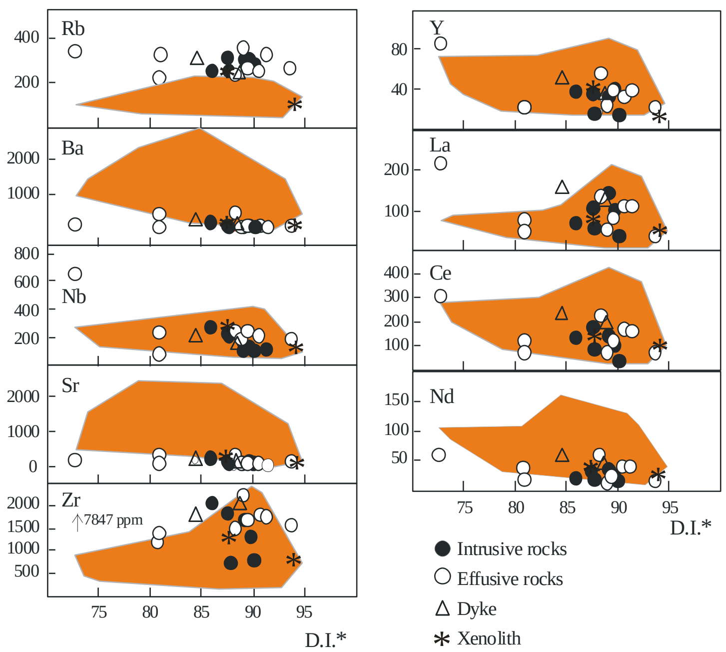


Fig. 42. D.I.* vs. trace elements (pppm) for Cerro Boggiani rocks, compared with the variation field in orange for the Fecho dos Morros+Pão de Açúcar complexes.

Table 39. Representative analyses of alkali feldspar, nepheline and sodalite (for the latter: crystal chemistry on the basis of the $3Al_2O_3$*$6SiO_2$ structural frame) from Cerro Boggiani rocks. For additional information see Tables 7, 8 and 25.

| | Alkali feldspar | | | | | | | | | | | |
|---|---|---|---|---|---|---|---|---|---|---|---|---|
| Sample | RP-29C | RP-29or | RP-29ab | RP-30C | RP-30gm | RP-30gm | RP-31APh | RP-31APhR | RP-31Agm | RP-31Agm | RP-32gm | RP-32gm |
| wt% | | | | | | | | | | | | |
| $SiO_2$ | 66.99 | 65.87 | 68.95 | 66.69 | 64.80 | 67.86 | 66.46 | 67.32 | 67.94 | 64.73 | 68.33 | 64.23 |
| $Al_2O_3$ | 18.88 | 18.50 | 19.34 | 18.81 | 18.27 | 19.05 | 18.73 | 19.19 | 19.03 | 18.18 | 18.90 | 18.39 |
| $Fe_2O_3$ | 0.20 | 0.25 | 0.29 | 0.13 | 0.10 | 0.31 | 0.20 | 0.29 | 0.36 | 0.37 | 0.72 | 0.30 |
| BaO | 0.15 | 0.08 | 0.02 | | | | 0.11 | 0.04 | 0.06 | 0.15 | 0.06 | 0.05 |
| CaO | | | 0.01 | 0.03 | | 0.04 | 0.02 | 0.26 | 0.02 | 0.04 | 0.01 | 0.02 |
| $Na_2O$ | 5.81 | 3.01 | 11.75 | 6.23 | 0.38 | 11.56 | 5.36 | 8.82 | 10.92 | 1.46 | 11.61 | 0.70 |
| $K_2O$ | 8.64 | 12.62 | 0.15 | 7.93 | 16.35 | 0.15 | 9.18 | 4.02 | 1.14 | 14.64 | 0.19 | 15.70 |
| Sum | 100.67 | 100.33 | 100.51 | 99.82 | 99.90 | 98.97 | 100.06 | 99.94 | 99.47 | 99.57 | 99.10 | 99.39 |
| Or | 49.3 | 73.3 | 0.8 | 45.5 | 96.6 | 0.8 | 52.8 | 22.8 | 86.4 | 6.4 | 93.5 | 1.1 |
| Ab | 50.4 | 26.6 | 97.5 | 54.3 | 3.4 | 99.0 | 46.9 | 75.9 | 13.0 | 93.4 | 6.3 | 98.8 |
| An | 0.3 | 0.1 | 1.7 | 0.2 | | 0.2 | 0.3 | 1.3 | 0.6 | 0.2 | 0.2 | 0.1 |

| | Alkali feldspar | | | | | | | | | | |
|---|---|---|---|---|---|---|---|---|---|---|---|
| Sample | RP-37Ph | RP-37gm | RP-37PhR | RP-40Ph | RP-41gm | RP-42mPh | RP-42gm | RP-42gm | RP-42Ph | RP-42PhR | RP-42gm |
| wt% | | | | | | | | | | | |
| $SiO_2$ | 65.97 | 65.15 | 68.48 | 66.54 | 63.86 | 66.87 | 63.92 | 68.37 | 66.36 | 66.05 | 67.50 |
| $Al_2O_3$ | 18.57 | 18.32 | 19.31 | 18.55 | 17.90 | 18.70 | 17.92 | 19.22 | 18.69 | 18.59 | 18.94 |
| $Fe_2O_3$ | 0.21 | 0.22 | 0.23 | 0.35 | 0.34 | 0.43 | 0.28 | 0.20 | 0.15 | 0.35 | 0.29 |
| BaO | 0.02 | 0.02 | 0.14 | | 0.08 | 0.12 | 0.06 | 0.02 | 0.01 | 0.19 | 0.03 |
| CaO | 0.03 | 0.02 | 0.02 | | 0.02 | 0.01 | | 0.01 | 0.02 | 0.04 | 0.02 |
| $Na_2O$ | 4.96 | 1.96 | 11.63 | 5.33 | 1.15 | 6.96 | 0.65 | 11.66 | 6.10 | 2.09 | 11.48 |
| $K_2O$ | 9.67 | 14.02 | 0.17 | 9.24 | 14.91 | 6.86 | 15.70 | 0.14 | 8.05 | 14.02 | 0.17 |
| Sum | 99.43 | 99.71 | 99.98 | 100.01 | 98.26 | 99.95 | 98.25 | 99.62 | 99.38 | 101.33 | 98.43 |
| Or | 56.1 | 82.4 | 1.0 | 53.3 | 89.3 | 39.2 | 94.0 | 0.8 | 46.4 | 81.1 | 1.0 |
| Ab | 43.7 | 17.5 | 98.7 | 46.7 | 10.5 | 60.5 | 5.9 | 99.1 | 53.5 | 18.4 | 98.9 |
| An | 0.2 | 0.1 | 0.3 | | 0.2 | 0.3 | 0.1 | 0.1 | 0.1 | 0.5 | 0.1 |

| | Nepheline | | | | | | | |
|---|---|---|---|---|---|---|---|---|
| Sample | RP-29 | RP-30 | RP-31A | RP-37 | RP-40 | RP-41 | RP-42 | RP-43 |
| wt% | | | | | | | | |
| $SiO_2$ | 45.53 | 43.83 | 45.89 | 44.87 | 45.00 | 45.26 | 44.75 | 45.05 |
| $Al_2O_3$ | 31.90 | 33.10 | 31.29 | 32.79 | 32.27 | 32.97 | 32.78 | 32.95 |
| $Fe_2O_3$ | 0.66 | 0.40 | 0.87 | 0.70 | 0.66 | 0.81 | 0.84 | 0.72 |
| BaO | | | 0.12 | | 0.03 | 0.07 | | 0.06 |
| CaO | | | | | | 0.03 | | 0.03 |
| $Na_2O$ | 15.87 | 16.42 | 15.41 | 16.60 | 16.08 | 16.53 | 16.58 | 16.53 |
| $K_2O$ | 5.74 | 5.86 | 5.92 | 5.48 | 5.75 | 5.73 | 5.58 | 5.67 |
| Sum | 99.70 | 99.61 | 99.49 | 100.44 | 99.79 | 101.40 | 100.53 | 101.00 |
| Mol% | | | | | | | | |
| Q | 8.9 | 5.4 | 10.1 | 6.8 | 7.7 | 6.8 | 6.6 | 6.7 |
| Ne | 73.6 | 76.6 | 71.8 | 76.6 | 74.7 | 75.9 | 76.5 | 76.1 |
| Ks | 17.5 | 18.0 | 18.1 | 16.6 | 17.6 | 17.3 | 16.9 | 17.2 |

| Sodalite | | | | |
|---|---|---|---|---|
| RP-31A | RP-31A | RP-41 | RP-42 | RP-43 |
| $SiO_2$ | 37.72 | 37.85 | 37.64 | 37.87 |
| $Al_2O_3$ | 31.53 | 31.82 | 33.14 | 33.69 |
| $Fe_2O_3$ | 0.48 | 0.40 | 0.58 | 0.39 |
| BaO | 0.06 | 0.01 | 0.06 | 0.01 |
| CaO | 0.03 | 0.05 | 0.06 | 0.02 |
| $Na_2O$ | 24.85 | 25.40 | 23.61 | 23.95 |
| $K_2O$ | 0.02 | 0.03 | 0.03 | 0.02 |
| Cl | 6.77 | 7.02 | 6.89 | 6.58 |
| -O=Cl | 1.16 | 1.47 | 1.45 | 1.38 |
| Sum | 100.03 | 101.11 | 100.56 | 101.15 |
| Si | 6.038 | 6.023 | 5.904 | 5.878 |
| Al | 5.949 | 5.969 | 6.127 | 6.163 |
| $Fe^{3+}$ | 0.058 | 0.048 | 0.068 | 0.046 |
| Sum | 12.045 | 12.040 | 12.099 | 12.087 |
| Ba | 0.004 | 0.001 | 0.004 | 0.001 |
| Ca | 0.005 | 0.009 | 0.101 | 0.003 |
| Na | 7.697 | 7.837 | 7.181 | 7.207 |
| K | 0.001 | 0.006 | 0.006 | 0.004 |
| Sum | 7.707 | 7.853 | 7.292 | 7.215 |
| Cl | 1.837 | 1.894 | 1.833 | 1.732 |

## Sr-Nd-Pb isotopes

The Cerro Boggiani rock-types show a tendentiously depleted character, having initial (241 Ma) $^{87}Sr/^{86}Sr$ ($R_0$) and $^{143}Nd/^{144}Nd$ ($Nd_0$) ratios of 0.70368-0.70463 and 0.51242-0.51235, respectively (cf. Table I of the Appendix). From a general point of view, the measured $^{87}Rb/^{86}Sr$ vs. $^{87}Sr/^{86}Sr$ ratios are on the same straight line of the other complexes, Stock I and Stock II excluded (see section relative to the Cerro Siete Cabezas complex). The correlation ($r^2$=0.998) defines a $R_0$ ratio of 0.70397 and a slope of 0.003483, corresponding to a whole rock age of 244.8 Ma. Notably, this value represents a younger age than that provided by Velázquez *et al.* (1996a), that is 251-255 Ma, but approaches the $^{40}Ar/^{39}Ar$ biotite ages obtained for the Alto Paraguay complexes, that is, 241-242 Ma (Velázquez *et al.*, 1996a and unpublished data). On the contrary, the isotopic results from Stock I and Stock II, that are also dealing with Q-normative (up to about 24%) samples, define a $R_0$ of 0.70439 and an artificial age of 259.6 Ma (mixing with the crystalline basement?), whereas the $^{40}Ar/^{39}Ar$ biotite age (sample RP-44) give 241 Ma.

In the silica vs. measured $^{87}Sr/^{86}Sr$ ratios diagram (Fig. 44A) two main trends are apparent: the first has relatively low isotopic ratio and points towards the Fuerte Olimpo rhyolites (Gomes *et al.*, 2000); the second one, represented mainly by Cerro Boggiani rocks and by some silica-rich varieties from Cerro Pedreira and Stock II, show high isotopic ratio and point towards the isotopic compositions of the Alumiador granites (cf. Table I of the Appendix). These behaviours draw the attention to the general question of a possible contamination of the Alto Paraguay alkaline complexes by basement rocks. The modelling relative to the initial isotopic Sr-Nd ratios, using as end-members the "less evolved" rocks and some basement compositions,

Table 40. Trace element analyses of selected rocks from Cerro Boggiani. Abbreviations as in Table 35.

| Sample | RP-27 | RP-28<br>D | RP-29 | RP-30 | RP-31A<br>LF | RP-31B<br>X | RP-32<br>X | RP-33<br>D | RP-34<br>LF | RP-35 |
|---|---|---|---|---|---|---|---|---|---|---|
| ppm | | | | | | | | | | |
| Cr | <1 | 1 | 2 | 1 | 4 | 1 | 2 | 1 | 2 | 1 |
| Ni | 4 | 9 | 9 | 6 | 8 | 4 | 2 | 11 | 3 | 8 |
| Rb | 258 | 247 | 258 | 310 | 243 | 254 | 121 | 307 | 256 | 305 |
| Ba | 36 | 100 | 175 | 76 | 437 | 189 | 150 | 246 | 74 | 66 |
| Th | | 3.9 | 10.7 | 10.1 | | 27.1 | | 4.9 | | 10.1 |
| U | | 12.1 | 4.8 | 18.9 | | 26.7 | | 17.4 | | 3.8 |
| Ta | | 19.4 | 16.9 | 14.6 | | 21.1 | | 28.4 | | 17.3 |
| Nb | 203 | 149 | 270 | 215 | 237 | 276 | 123 | 207 | 211 | 124 |
| Sr | 76 | 133 | 206 | 137 | 319 | 190 | 106 | 161 | 93 | 107 |
| Hf | | 33.1 | 44.6 | 33.9 | | 29.0 | | 33.9 | | 27.2 |
| Zr | 717 | 1696 | 2027 | 1829 | 1499 | 1288 | 848 | 1567 | 1775 | 1297 |
| Y | 15 | 34 | 38.0 | 35.5 | 55 | 39.5 | 9 | 51.5 | 33 | 40 |
| La | 60 | 130.4 | 71.9 | 108.1 | 137 | 80.5 | 56 | 160.8 | 113 | 48.4 |
| Ce | 83 | 204.3 | 132.5 | 175.8 | 225 | 161.0 | 99 | 240.5 | 171 | 102.1 |
| Pr | | 14.4 | 8.7 | 11.2 | | 11.6 | | 17.8 | | 7.3 |
| Nd | 17 | 45.8 | 20.1 | 31.0 | 59 | 35.6 | 25 | 59.5 | 39 | 21.9 |
| Sm | 2.5 | 5.81 | 3.0 | 4.0 | | 4.1 | | 7.6 | | 3.5 |
| Eu | | 1.43 | 0.80 | 1.07 | | 1.03 | | 1.88 | | 0.82 |
| Gd | | 6.43 | 3.80 | 5.20 | | 4.0 | | 8.55 | | 3.68 |
| Tb | | 0.97 | 0.50 | 0.62 | | 0.74 | | 1.29 | | 0.50 |
| Dy | | 5.72 | 3.59 | 4.52 | | 3.96 | | 7.60 | | 3.02 |
| Er | | 4.42 | 3.21 | 3.80 | | 2.93 | | 5.90 | | 2.37 |
| Tm | | 0.85 | 0.63 | 0.75 | | 0.70 | | 1.18 | | 0.43 |
| Yb | | 5.76 | 4.66 | 6.14 | | 5.30 | | 8.16 | | 2.87 |
| Lu | | 0.73 | 0.71 | 0.91 | | 0.58 | | 1.03 | | 0.37 |

| Sample | RP-36<br>LF | RP-37<br>LF | RP-38A<br>LF | RP-38B | RP-39 | RP-40<br>LF | RP-41<br>LF | RP-42<br>LF | RP-43<br>LF |
|---|---|---|---|---|---|---|---|---|---|
| ppm | | | | | | | | | |
| Cr | 1 | 1 | 1 | <1 | <1 | 1 | 1 | <1 | 2 |
| Ni | 6 | 9 | 8 | 8 | 4 | 10 | 5 | 5 | 5 |
| Rb | 271 | 328 | 273 | 305 | 285 | 340 | 354 | 331 | 223 |
| Ba | 66 | 12 | 73 | 17 | 44 | 135 | 13 | 19 | 428 |
| Th | 16.1 | 11.2 | 10.1 | | | 28.7 | 5.6 | 5.1 | |
| U | 14.3 | 9.9 | 3.8 | | | 78.8 | 1.8 | 1.6 | |
| Ta | 17.3 | 8.1 | 12.1 | | | 52.1 | 17.0 | 6.2 | |
| Nb | 240 | 116 | 179 | 98 | 98 | 653 | 186 | 71 | 230 |
| Sr | 93 | 48 | 135 | 74 | 74 | 180 | 72 | 59 | 298 |
| Hf | 35.8 | 34.8 | 32.8 | | | 149.4 | 70.3 | 39.8 | |
| Zr | 1679 | 1754 | 1577 | 1670 | 791 | 7847 | 2239 | 1394 | 1182 |
| Y | 39 | 39 | 22.7 | 33 | 14 | 85 | 23.3 | 23 | 22 |
| La | 82.1 | 110.3 | 36.6 | 96 | 28 | 216 | 54.0 | 52.0 | 81 |
| Ce | 116.9 | 164.2 | 70.8 | 143 | 38 | 309 | 71.9 | 68. 1 | 119 |
| Pr | | 11.0 | 4.3 | | | 23.7 | 4.6 | 4.2 | |
| Nd | 24.0 | 38.8 | 13.9 | 33 | 14 | 59.9 | 11.3 | 18.4 | 38 |
| Sm | 3.8 | 6.15 | 2.0 | | | 9.0 | 1.5 | 2.5 | |
| Eu | 0.87 | 1.39 | 0.46 | | | 2.19 | 0.36 | 0.58 | |
| Gd | 4.10 | 6.10 | 2.45 | | | 12.5 | 2.2 | 3.10 | |
| Tb | 0.46 | 0.67 | 0.33 | | | 1.62 | 0.3 | 0.39 | |
| Dy | 2.97 | 4.44 | 1.88 | | | 9.97 | 2.1 | 2.88 | |
| Er | 1.76 | 2.63 | 1.65 | | | 8.57 | 2.3 | 2.85 | |
| Tm | 0.37 | 0.51 | 0.33 | | | 1.57 | 0.5 | 0.58 | |
| Yb | 2.02 | 2.92 | 2.41 | | | 12.49 | 4.3 | 4.98 | |
| Lu | 0.34 | 0.49 | 0.41 | | | 1.78 | 0.75 | 0.82 | |

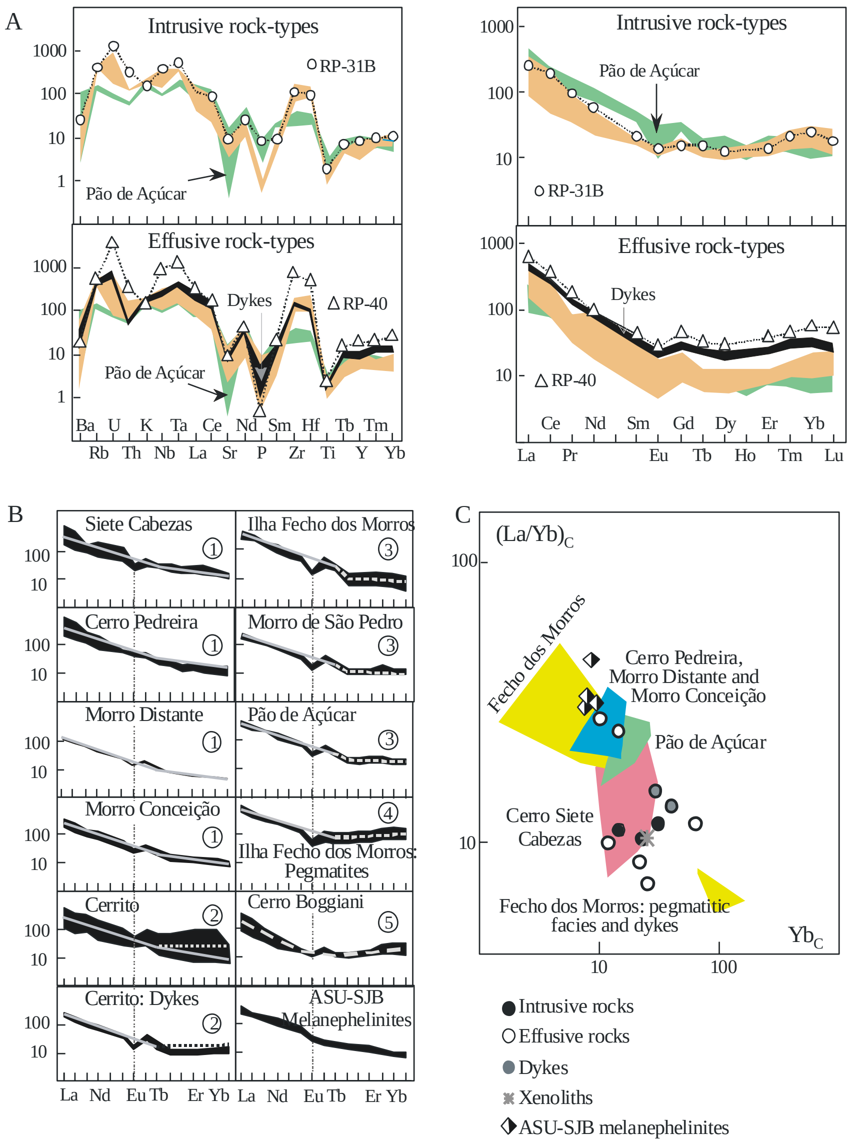


Fig. 43. A: Primitive mantle- (Sun & McDonough, 1989) and chondrite- (Boynton, 1984) normalized I.E. and REE distribution, respectively, for the Cerro Boggiani rocks. The variation fields of the Pão de Açúcar rock-types in light green are shown for comparison. B: Main type of REE spidergrams in the Alto Paraguay Province. For circled numbers see text. **C**: $Yb_c$ vs. $(La/Yb)_c$ of Cerro Boggiani rocks compared with the other occurrences from the Alto Paraguay Province and with sodic magmatic rock-types from central and soutwestern Paraguay (cf. Comin-Chiaramonti *et al*., 1997).

highlights the possibility of contamination by about 10% of upper crust for the most analyzed samples, and an eventual contribution of lower crust up to 20% (Fig. 44B).

In the time integrated $\varepsilon^t$Sr-$\varepsilon^t$Nd system (Fig 44C), the Cerro Boggiani samples plot together to the other rock-types of the Alto Paraguay complexes and fit the depleted field corresponding to the Na-alkaline rocks from southern and central Paraguay (Late Cretaceous and Tertiary melanephelinites from San Juan Bautista and Asunción regions, respectively; cf. Comin-Chiaramonti *et al*., 1997). Only two samples from Stock I and Stock II bodies (RP-47 and RP-212, respectively) and one dyke from Cerro Pedreira (RP-9) exhibit enriched features with high $\varepsilon^t$Sr, i.e. 77 and 18, respectively. Notably, the sodic, tholeiitic and potassic rocks from Paraguay delineate a well-defined array from depleted (Na-alkaline magmatism) to enriched rock-types (K-alkaline magmatism; Comin-Chiaramonti *et al.*, 1999).

The Nd-model ages indicate 747±42 Ma. The histogram regarding the distribution of the model ages (Fig. 44D) shows a bimodal behaviour driven

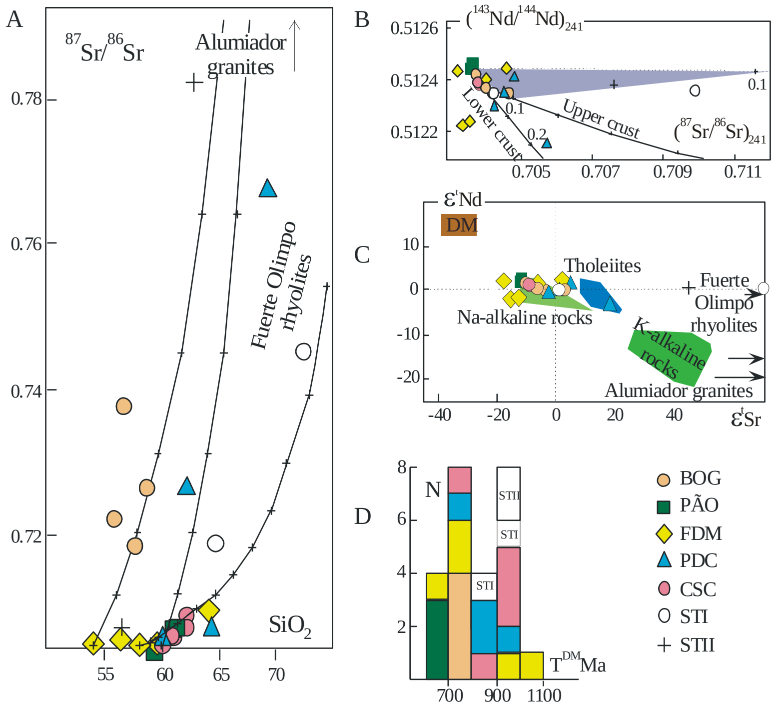


Fig. 44. A: Mixing between $SiO_2$ and Sr isotopic ratios (basement and magmatic from the Alto Paraguay Province, APP). B: Sr-Nd isotope correlation diagram (time-integrated) and mixing between basement and APP rocks. C: Time integrated, ε-notation, for magmatic rocks from Alto Paraguay (see text). D: Statistic distribution of model ages in the APP complexes (CSC, Cerro Siete Cabezas; STI and STII, Stocks I and II, respectively; PDC, Cerro Pedreira, Morro Distante and Morro Conceição; FDM, Fecho dos Morros; PÃO, Pão de Açúcar; BOG, Cerro Boggiani).

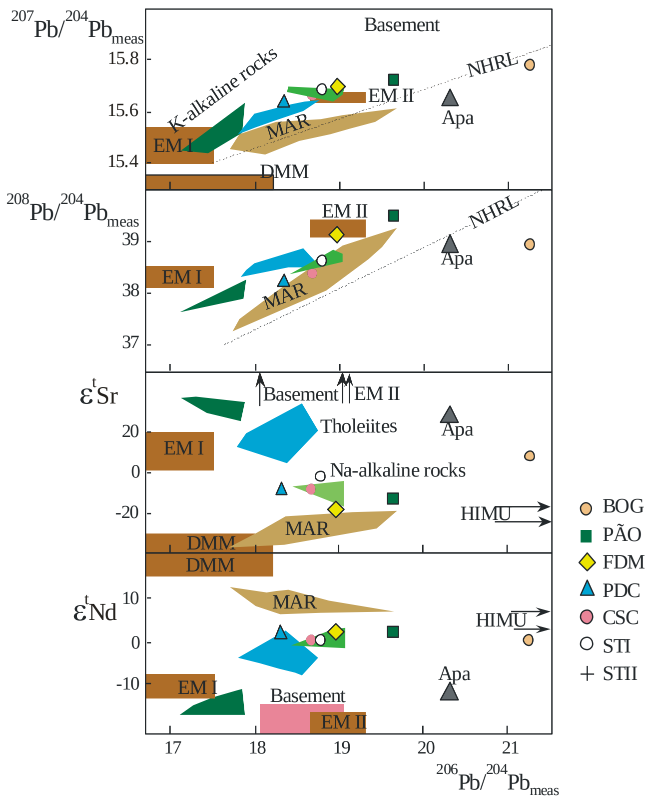


Fig. 45. Pb-Pb and Pb vs. Sr-Nd (ε notation) isotope correlation diagrams comparing the APP complexes with the fields of magmatic rocks and crystalline basement from Eastern Paraguay. MAR: Mid Atlantinc Ridge Basalts (Fontignie & Schilling, 1997); EMI, EMII, DMM and HIMU: hypothetical mantle end-member compositions (Zindler & Hart, 1986); NHRL, Northern Hemisphere Reference Line (Hart, 1984).

mainly by the Pão de Açúcar and Cerro Boggiani bodies, and by the Cerro Siete Cabezas complex, with model ages <800 Ma and around 950 Ma, respectively.

A few data on Pb isotopes relative to all the complexes (Table II of the Appendix) indicate that the $^{206}Pb/^{204}Pb$ and $^{208}Pb/^{204}Pb$ vs. $^{207}Pb/^{204}$ measured ratios are on the same array defined by the other rock-types from eastern Paraguay (Fig. 45). This array, a sample of Cerro Boggiani excluded, is between EMI and EMII components and parallels to the Northern Hemisphere Reference Line (cf. Hart, 1984). Moreover, the lead isotope ratios appear strongly negatively and positively correlated with Sr and Nd isotopic data, respectively (Fig. 45), with the Alto Paraguay rock-types representing an extension of the field defined by the younger sodic rocks from eastern Paraguay.

## PETROGENETIC CONSIDERATIONS

The formation of cogenetic saturated and undersaturated rocks within the constraints imposed by relationships in the Petrogeny's Residua System of Bowen (1937) (PRS) may be resumed into two categories (Foland *et al.*, 1993): 1) "special fractionation schemes or effects that otherwise obviate the thermal divide in the PRS, as effects of volatiles, mineral absorption, changing water pressures, incongruent melting of aegirine"; 2) "open-system processes that involve some type of magma interactions with silica-rich crustal materials via various mechanisms: hydrothermal modification, crustal contamination combined with fractional crystallization, or production of anatectic crustal melts that either directly produce oversaturated rocks or mix with undersaturated magmas to form oversaturated ones".

Foland *et al*. (1993) stated that a silica-undersaturated magma, lying close to the join of the alkali feldspars (at temperatures above the "$m_2$" minimum), can migrate to silica-oversaturated compositions with a ratio of assimilated/crystallizated materials •0.2 and less than 10% of "granitic" contamination. If the magma is significantly undersaturated, contamination may reduce the degree of undersaturation, but the crystallization may proceed on before crossing the alkali feldspar join.

Not excluding the first category above, all the PRS diagrams (cf. Figs. 8, 17, 25, 33 and 40) support the second category, evolving at very low total pressures and starting from temperatures above the feldspar minimum (~865°C). In particular the Stock I and Stock II rock-types (Fig. 8) and the Cerro Pedreira dykes (Fig. 17) constitute an excellent example regarding the Foland *et al.* (1993) hypothesis. In support to the above arguments, the isotopic data for Stock I and II indicate a possible contamination of less than 20% of crustal components (Figs. 12 and 44B). Thus, the quartz modal syenites, Q-normative phonolites and alkali rhyolitic dyke (e.g. RP-6) from the Alto Paraguay Province are thought to have been formed by simultaneous assimilation and fractional crystallization of a slightly undersaturated magma, whereas the undersaturated rock-types evolved from such a magma without appreciable contamination.

## CONCLUSIONS

The alkaline complexes from the Paraguay river, at the border of the Mato Grosso do Sul state (Brazil) and Chaco Boreal (Paraguay), represent the oldest magmatic occurrence around the Paraná Basin since the Brasiliano cycle. A common age, that is, Early Triassic (241 Ma), is inferred by radiometric $^{40}Ar/^{39}Ar$ data on biotite specimens.

The alkaline magmatism is assumed to extend for over 40 km within a relatively well-defined, rift-related continental structure along the Rio Paraguay Arch, a tectonic N-S lineament sysmically active up to present day.

The alkaline complexes have subvolcanic-volcanic characteristics, as shown by field relationships and by mineralogical associations. The outcrops display ring structures, sometimes cauldron subsidence and interfingering features. Such complexes contain evolved intrusive rocks, but not direct evidence for the presence of mafic rocks. Associated dykes and remnants of related volcanic sequences are also commonly observed.

The rocks consist predominantly of undersaturated agpaitic syenites (hypersolvus varieties) and phonolites.

Subordinate undersaturated and oversaturated syenites, trachyphonolites and rhyolites are characterized by plagioclase and/or modal or normative quartz.

The geochemistry shows, on the whole, quite similar behaviours. Although a nephelinitic magma may be considered as a source of the alkaline complexes from the Alto Paraguay Province, the strong Eu negative anomalies and the presence of An-rich plagioclase in some rocks from the central region (Cerro Pedreira, Morro Distante, Morro Conceição) seem to suggest a basanitic liquid as a possible parental magma.

The isotope results cluster in a tendentiously depleted source. However, some Q-normative rocks appear to have been subjected to crustal contamination.

All the available data confirm the unique character of this magmatic province in the southern Brazil.

## ACKNOWLEDGEMENTS

Special thanks are due to A. Alberti, S. Conticelli, A. Woolley and A. Cundari for their constructive critical review and helpful suggestions. This research was supported by grants from Italian (CNR, 05 and 11 Committes, and COFIN, 1998) and Brazilian (FAPESP, Proc. 01/10714-3) agencies.

## REFERENCES

Alaimo, R. & Censi, P. (1992). Quantitative determination of major, minor and trace elements on U.S.G.S. rock standards by inductively coupled plasma mass spectrometry. *Atomic Spectrometry* **13**, 113-119.

Alberti, A., Castorina, F., Censi, P., Comin-Chiaramonti, P. & Gomes, C.B. (1999). Geochemical characteristics of Cretaceous carbonatites from Angola. *Journal of African Earth Sciences* **29**, 735-759.

Almeida, F.F.M. (1983). Relações tectônicas das rochas alcalinas mesozóicas da região meridional da Plataforma Sul-Americana. *Revista Brasileira de Geociências* **13**, 139-158.

Amaral, G. (1984). Província Tapajós e Rio Branco. In: Almeida, F.F.A. & Hasui, Y. (eds.) *O Pré-Cambriano do Brasil*. São Paulo: Edgard Blücher Ltda., pp. 6-35.

Araújo, H.J.T., Santos Neto, A., Trindade, C.A.H., Pinto, J.C.A., Montalvão, R.M.G., Dourado, T.D.C., Palmeira, R.C.B. & Tassinari, C.C.G. (1982). Folha SF 21, Campo Grande: Geologia. In: *Projeto Radambrasil, MME/SG*, Rio de Janeiro **28**, pp. 83-84.

Bailey, D.K. (1969). The stability of acmite in the presence of $H_2O$. *American Journal of Sciences* **267A**, 1-16.

Barker, D.S. (1976). Phase relations in the system $NaAlSiO_4$-$SiO_2$-NaCl-$H_2O$ at 400-800°C and 1 kb and petrological implications. *Journal of Geology* **84**, 97-106.

Beccaluva, L., Barbieri, M., Born, H., Brotzu, P., Coltorti, M., Conte, A., Garbarino, C., Gomes, C.B., Macciotta, G., Morbidelli, L., Ruberti, E., Siena F. & Traversa, G. (1992). Fractional crystallization and liquid immiscibility processes in the alkaline-carbonatite complex of Juquiá (São Paulo, Brazil). *Journal of Petrology* **33**, 1371-1404.

Bellieni, G., Brotzu, P., Comin-Chiaramonti, P., Ernesto, M., Melfi, A.J., Pacca, I.G., Piccirillo E.M. & Stolfa, D. (1984). Flood basalt to rhyolite suites in the southern Paraná plateau (Brazil): paleomagnetism, petrogenesis and geodynamic implications. *Journal of Petrology* **25**, 579-618.

Berrocal, J. & Fernandes, C. (1996). Seismicity in Paraguay and neighbouring regions. In: Comin-Chiaramonti, P. & Gomes, C.B. (eds.) *Alkaline magmatism in central-eastern Paraguay. Relationships with coeval magmatism in Brazil*. São Paulo: Edusp/Fapesp, pp. 57-66.

Bowen, N.L. (1937). Recent high-temperature research on silicates and its significance in igneous geology. *American Journal of Sciences* **33**, 1-21.

Boynton, W.V. (1984). Cosmochemistry of the Rare Earth elements: meteorite studies. In: Henderson, P. (ed.) *Rare Earth Element geochemistry*. Amsterdam: Elsevier, pp. 63-114.

Brown, W.L. & Parsons, I. (1989). Alkali feldspars: ordering rates, phase transformation and behaviour diagrams for igneous rocks. *Mineralogical Magazine* **53**, 25-42.

Burnham, C.W., Holloway, J.R. & Davis, N.F. (1969). Thermodynamic properties of water to 1000°C and 10000 bar. *Geological Society of*

*America, Special Paper,* 132p.

Carbonin, S., Liziero, F. & Fuso, C. (in this volume). Mineral chemistry of acessory minerals in alkaline complexes from the Alto Paraguay Province.

Caroff, M., Maury, R.C., Leterrier, J., Joron, J.L., Cotten, J. & Guille, G. (1993). Trace element behaviour in the alkali basalt-comenditic trachyte series from Mururoa Atoll, French Polynesia. *Lithos* **30**, 1-22.

Collins, W.J., Beams, S.D., White, A.J.R. & Chappell, B.W. (1982). Nature and origin of A-type granites with particular reference to southeastern Australia. *Contributions to Mineralogy and Petrology* **80**, 189-200.

Comin-Chiaramonti, P. & Gomes, C.B. (eds.) (1996). *Alkaline magmatism in central-eastern Paraguay. Relationships with coeval magmatism in Brazil*. São Paulo: Edusp/Fapesp, 464p.

Comin-Chiaramonti, P., Civetta, L., Petrini, R., Piccirillo, E.M., Bellieni, G., Censi, P., Bitschene, P., Demarchi, G., De Min, A., Gomes, C.B., Castillo, A.M.C. & Velázquez, J.C. (1991). Tertiary nephelinitic magmatism in Eastern Paraguay: petrology, Sr-Nd isotopes and genetic relationships with associated spinel-peridotite xenoliths. *European Journal of Mineralogy* **3**, 507-525.

Comin-Chiaramonti, P., Cundari, A., DeGraff, J.M., Gomes, C.B. & Piccirillo, E.M (1999). Early Cretaceous-Tertiary magmatism in Eastern Paraguay (western Paraná basin): geological, geophysical and geochemical relationships. *Journal of Geodynamics* **28**, 375-391.

Comin-Chiaramonti, P., Cundari, A., Piccirillo, E.M., Gomes, C.B., Castorina, F., Censi , P., De Min A., Marzoli, A., Speziale, S. & Velázquez, V.F. (1997). Potassic and sodic igneous rocks from Eastern Paraguay: their origin from the lithospheric mantle and genetic relationships with the associated Paraná flood tholeiites. *Journal of Petrology* **38**, 495-528.

De La Roche, H., Leterrier, J., Grandclaude, P., Marchal, M. (1980). A classification of volcanic and plutonic rocks using R1-R2 diagram and major element analyses. Its relationships with current nomenclature. *Chemical Geology* **29**, 183-210.

Faure, G. (1986). *Principles of isotope geology*. New York: John Wiley & Sons, 589p.

Finch, A.A., Parsons, I. & Mingard, S.C. (1995). Biotites as indicators of fluorine fugacities in late-atage magmatic fluids: the Gardar Province of South Greenland. *Journal of Petrology* **36**, 1001-1028.

Flohr, M.J.K. & Ross, M. (1990). Alkaline igneous rocks of Magnet Cove, Arkansas: mineralogy and geochemistry of syenites. *Lithos* **26**, 67-98.

Foland, K.A., Landoll, J.D., Henderson, C.M.B. & Chen, J.F. (1993). Formation of cogenetic quartz and nepheline syenites. *Geochimica and Cosmochimica Acta* **29**, 1063-1075.

Fontignie, D. & Schilling, J.G. (1997). Mantle heterogeneities beneath the South Atlantic: a Nd-Sr-Pb isotope study along the Midatlantic Ridge (3ºS-46ºS). *Earth and Planetary Science Letters* **146**, 259-272.

Fudali, R.F. (1963). Experimental studies bearing on the origin of pseudoleucite and associated of alkaline rocks systen. *Geological Society of America Bulletin* **74**,1001-1026.

Ghiorso, M.S. & Carmichael, I.S.E. (1987). Modelling magmatic systems: petrologic applications. In: Carmichael, I.S.E. & Eugester, H.P. (eds.) *Thermodynamic modelling of geological materials. Reviews of Mineralogy* **17**, 467-499.

Gomes, C.B., Barbieri, M., Beccaluva, L., Brotzu, P., Conte, A., Garbarino, C., Macciotta, G., Melluso, L., Morbidelli, L., Ruberti, E., Scheibe, L.F., Tamura, R. & Traversa, G. (1987). Petrological and geochemical studies of alkaline rocks from continental Brazil. The Tunas massif, State of Paraná. *Geochimica Brasiliensis* **1**, 201-234.

Gomes, C.B., Laurenzi, M.A., Censi, P., De Min, A., Velázquez V.F. & Comin-Chiaramonti, P. (1996a). Alkaline magmatism from northern Paraguay (Alto Paraguay): a Permo-Triassic Province. In: Comin-Chiaramonti, P. & Gomes, C.B. (eds.) *Alkaline magmatism in central-eastern Paraguay. Relationships with coeval magmatism in Brazil*, São Paulo: Edusp/Fapesp, pp. 223-230.

Gomes, C.B., Morbidelli, L., Ruberti, R. & Comin-Chiaramonti, P. (1996b). A first attempt to compare Post-Palaeozoic alkaline rocks from western (Paraguay) and eastern (Brazil) margins of the Paraná Basin. In: Comin-Chiaramonti, P. & Gomes, C.B. (eds.) *Alkaline magmatism in central-eastern Paraguay. Relationships with coeval magmatism in Brazil*, São Paulo: Edusp/Fapesp, pp. 249-274.

Gomes, C.B., Velázquez V.F. & Comin-Chiaramonti, P. (2000). The Mesoproterozoic rhyolite occurrences of Fuerte Olimpo and Fuerte San Carlos, Northern Paraguay. *Revista Brasileira de Geociências* **30**, 785-788.

Hamilton, D.L. (1961). Nepheline as crystallization temperature indicators. *Journal of Geology* **69**, 321-329.

Hamilton, D.L. & McKenzie, W.S. (1965). Nepheline solid solutions in the system $NaAlSiO_4$-$KAlSiO_4$-$SiO_2$. *Journal of Petrology* **1**, 1-56.

Hards, N. (1976). Distribution of elements between the fluid phase and silicate melt phase of granites and nepheline syenites. Progress in Experimental

Petrology. *NERC Publication Series D*, pp. 88-90.

Hart, S.R. (1984). A large-scale isotope anomaly in the southern hemisphere. *Nature* **309**, 753-757.

Helz, R.T. (1982). Phase relations and compositions of amphiboles produced in studies on the melting behaviour of rocks. In: Veblen, D.R. & Ribbe, P.H. (eds.) *Amphiboles II. Petrology and experimental phase relations. Review in Mineralogy* **9B**, 279-353.

Kudo, A.M. & Weill, D.F. (1970). An igneous plagioclase thermometer. *Contributions to Mineralogy and Petrology* **26**, 52-65.

Leake, B.E. & 22 others (1998). Nomenclature of amphiboles. Report of the Subcommittee on Amphiboles of the International Mineralogical Commission on new minerals and mineral names. *European Journal of Mineralogy* **9**, 623-642.

Le Maitre, R.W. (1989). *A classification of igneous rocks and glossary of terms*. Oxford: Blackwell Science Publication, 193p.

Lindsley, D. (1971). Synthesis and preliminary results on the stability of aenigmatite ($Na_2Fe_5TiSi_6O_{20}$). Carnegie Institution of Washington, *Annual Report Geophysical Laboratory* 1969-1970, pp. 188-190.

Marzoli, A. (1991). *Studio petrologico e geochimico di complessi alcalini del rift di Sapucai (Paraguay)*. B.Sc. Thesis, University of Trieste, 201p.

Matos, J.B. (2000). *Petrografia e química mineral de ocorrências alcalinas da Província Alto Paraguai, Brasil-Paraguai*. Ph.D. Thesis, University of São Paulo, 261p.

Mitchell, R.H. (ed:) (1996). *Undersaturated alkaline rocks: mineralogy, petrogenesis, and economic potential*. Winnipeg: Manitoba, 312p.

Morbidelli, L., Gomes, C.B., Beccaluva, L., Brotzu, P., Conte, A., G., Ruberti, E. & Traversa, G. (1995). Mineralogical, petrological and geochemical aspects of alkaline and alkaline-carbonatite associations from Brazil. *Earth-Science Review* **39**, 135-168.

Morimoto, N. (1988). Nomenclature of pyroxenes. *Mineralogical Magazine* **52**, 535-550.

Nicholls, J. & Carmichael, I.S.E. (1969). Peralkaline acid liquids: a petrologic study. *Contributions to Mineralogy and Petrology* **20**, 268-294.

Oliveira, A.I. & Leonardos, O.H. (1943). *Geologia do Brasil*. 2a ed. Serviço de Informação Agrícola, Rio de Janeiro, 813p.

Parsons, I. (1978). Felspars and fluids in cooling plutons. *Mineralogical Magazine* **42**, 1-17.

Piccirillo, E.M. & Melfi, A.J. (1988). *The Mesozoic flood volcanism from the Paraná basin (Brazil). Petrogenetic and geophysical aspects*. São Paulo: IAG-USP, 600p.

Platt, R.G. & Woolley, A.R. (1986). The mafic mineralogy of the peralkaline syenites and granites of the Mulanje complex, Malawi. *Mineralogical Magazine* **50**, 85-99.

Powell, M. & Powell, R. (1977). Plagioclase-alkali feldspar geothermometer revisited. *Mineralogical Magazine*, **41**, 253-256.

Putzer, H. & Van den Bomm, G. (1962). Über einige Vorkommen von Alkaligesteinen in Paraguay. *Geologische Jahrbuch* **79**, 423-443.

Rahman, S. & MacKenzie, W.S. (1961). The crystallization of ternary feldspar: a study from natural rocks. *American Journal of Sciences* **267A**, 391-406.

Seck, H.A. (1971). Koexistierende alkalifeldspate und plagioclase im system $NaAlSi_3O_8$-$KAlSi_3O_8$-$CaAl_2Si_2O_8$-$H_2O$ bei temperaturen von 650°C bis 900°C. *Neues Mineralogische Abhanlungen* **115**, 315-395.

Spencer, K.J. & Lindsley, D.H. (1981). A solution model for coexisting iron-titanium oxides. *American Mineralogist* **66**, 1189-1201.

Stormer Jr., J.C. & Nicholls, J. (1978). A program for interactive testing of magmatic differentiation models. *Computer & Geocience* **4**, 143-159.

Sun, S.S. & McDonough, W. F. (1989). Chemical and isotopic systematics of oceanic basalts. In: Saunders, D. & Norry, M.J. (eds.) *Magmatism in the ocean basins. Geological Society of London, Special Publication* **42**, pp. 313-345.

Taylor, S.R. & McLennan, S.M (1981). The composition and evolution of continental crust: rare earth element evidence from sedimentary rocks. *Philosophical Transactions of the Royal Society* **A301**, 381-399.

Teixeira, W., Tassinari, C.C.G., Cordani, U.G. & Kawashita, K. (1989). A review of the geochronology of the Amazonian Craton: tectonic implications. *Precambrian Research* **42**, 213-227.

Tilley, C.E. (1954). Nepheline-alkali feldspar parageneses. *American Journal of Sciences* **252**, 65-75.

Trompette, R. (1994). *Geology of Western Gondwana (2000-500 Ma). Panafrican-Brasiliano aggregation of South America and Africa*. Rotterdam: Balkema, 350p.

Velázquez, V.F., Gomes, C.B., Censi, P., Comin-Chiaramonti, P. & De Min, A. (1998). Características geoquímicas e petrológicas do magmatismo alcalino da Província Alto Paraguai. *Anais da Academia Brasileira de Ciências* **70**, 69-89.

Velázquez, V.F., Gomes, C.B., Laurenzi, M., Teixeira, W. & Comin-Chiaramonti, P. (1996a). Contribution to the geochronology of the Permo-Triassic alkaline magmatism from the

Alto Paraguay Province. *Revista Brasileira de Geociências* **26**, 103-108.
Velázquez, V.F., Gomes, C.B., Orué, D. & Comin-Chiaramonti, P. (1996b). Magmatismo alcalino do Paraguai: uma revisão e atualização das províncias. *Boletim do Instituto de Geociências da USP, Série Científica* **27**, 61-79.
Wiens, F. (1986). *Zur lithostratigraphischen und strukturellen entwickelung des Rio Apa Hochlandes, Nordost Paraguay*. Ph.D. Thesis, Clausthal University, 280p.
Wones, D.R. (1981). Mafic minerals as indicators of intensive variables in granitic magmas. *Mining Geology* **31**, 191-212.
Woolley, A.R. & Platt, R.G. (1988). The peralkaline nepheline syenites of the Junguni intrusion, Chilwa Province, Malawi. *Mineralogical Magazine* **52**, 425-433.
Zindler, A. & Hart, S. (1986). Chemical geodynamics. *Annual Review of Earth and Planetary Science* **14**, 493-571.

## APPENDIX

### Analytical methods and Sr-Nd-Pb isotope ratios

Major and trace whole rock elements were determined by XRF fluorescence techniques using an automatic PW1400 spectrometer and pressed-powder pellets. FeO was determined chemically using the ammonium metavanadate. The analytical procedures are described in Bellieni *et al.* (1984).

Trace elements were also determined in selected samples by ICP mass procedures (cf. Alaimo & Censi, 1992). The mineral compositions have been determined in a representative selection of samples at Padova, Italy (CNR laboratory), and at São Paulo, Brazil (Laboratório de Microssonda Eletrônica do Instituto de Geociências) Universities. At Padova laboratory, an energy dispersive spectrometer EDS EG 1G connected to a SEM AUTOSCAN electron microprobe operating at 15 kV was employed; a MAGIC program in the ORTEC MAGIC IV M version was used to convert counting rates into wt% oxides.

At São Paulo laboratory, mineral compositions were obtained by means of an automated JEOL-JXA-8600S operating at 15 kV accelerating voltage and 20-30 nÅ specimen current.

The standards were oxides or simple silicate compositions and several samples were systematically analyzed in the two different microprobe equipaments, aiming at minimizing the interlaboratories bias. The reported analyses are averages of at least five point-determinations and the results are considered accurate to within 2-3% error for major elements and to about 10% for minor ones. Most amphibole analyses were rejected by usual crystallochemical computational programs, because of the insatisfactory stoichiometry, reflecting a systematic disequilibrium for this mineral, and in this paper only the best stoichiometric results are reported.

Sr, Nd and Pb isotope analyses were performed at Department of Earth Sciences, University of Queensland, Australia [NBS987: $^{87}Sr/^{86}Sr=0.710231$ ($2\sigma$:0.000008), $^{143}Nd/^{144}Nd=0.511971$ ($2\sigma$: 0.000015), n=21; NBS981: $^{206}Pb/^{204}Pb=19.9333$ (UQ isoprobe $\sigma$: 0.0033), $^{207}Pb/^{204}Pb=15.4869$ ($\sigma$:0.0025), $^{208}Pb/^{204}Pb=36.6919$ ($\sigma$:0.0073), $^{207}Pb/^{206}Pb=0.9146$ ($\sigma$:0.0001), $^{208}Pb/^{206}Pb=2.1669$ ($\sigma$:0.0002), n=16]. Additional data are from Velázquez *et al.* (1996a). Sr and Nd initial ratios calculated at 241 Ma; $T^{DM}$ values: calculation of model dates relative to a depleted reservoir, $^{143}Nd/^{144}Nd=0.513114$ and $^{147}Sm/^{144}Nd=0.222$, according to Faure, 1986). It should be noted that at 241 Ma the initial isotopic ratios for the Fuerte Olimpo rhyolites and for the AZ-2 Porto Murtinho granite are $Sr_i=0.74827$ and 0.76578, and $Nd_i=0.51132$ and 0.51157, respectively.

Table I. Rb, Sr, Sm and Nd contents (ppm) and Sr, Nd measured and initial isotopic ratios for Precambrian rock-types and for alkaline rocks from the Alto Paraguay complexes. (V): Velázquez *et al*. (1996a).

| | Rb | Sr | $^{87}Sr/^{86}Sr_m$ | $^{87}Sr/^{86}Sr_i$ | Sm | Nd | $^{143}Nd/^{144}Nd_m$ | $^{143}Nd/^{144}N_i$ | $\varepsilon_{Sr}$ | $\varepsilon_{Nd}$ | $T^{DM}$ |
|---|---|---|---|---|---|---|---|---|---|---|---|
| **BASEMENT** | | | | | | | | | | | |
| FUERTE OLIMPO | | | | | | | | | | | |
| RP-19B rhyolite (1341 Ma) | 154 | 179 | 0.756843 ( 8) | 0.70876 | 9.2 | 56.0 | 0.511475 ( 7) | 0.51060 | 80 | -6.0 | 2130 |
| PORTO MURTINHO; | | | | | | | | | | | |
| Alumiador AZ-2 granite (1600 Ma) | 197 | 185 | 0.776415 ( 5) | 0.70514 | 5.2 | 28.0 | 0.511743 ( 7) | 0.51056 | 33 | -0.1 | 2008 |
| **ALTO PARAGUAY COMPLEXES** | | | | | | | | | | | |
| CERRO SIETE CABEZAS | | | | | | | | | | | |
| RP-61 | 100 | 413 | 0.706146 ( 6) | 0.70374 | 16.10 | 77.0 | 0.512591 ( 8) | 0.51239 | -9.6 | 1.3 | 924 |
| RP-63 | 105 | 409 | 0.706299 ( 9) | 0.70375 | 14.91 | 68.0 | 0.512601 ( 9) | 0.51239 | -9.5 | 1.3 | 972 |
| RP-66 | 75 | 216 | 0.707247 ( 9) | 0.70380 | 8.09 | 47.7 | 0.512553 ( 9) | 0.51239 | -8.8 | 1.2 | 789 |
| RP-70 (V) | 83 | 335 | 0.70606 ( 6) | 0.70360 | | | | | | | |
| RP-70 (V, alkali feldspar) | 62 | 406 | 0.70542 ( 7) | 0.70390 | | | | | | | |
| RP-74 | 137 | 266 | 0.709005 (11) | 0.70390 | 9.40 | 52.8 | 0.512559 (12) | 0.51239 | -7.4 | 1.2 | 812 |
| RP-75 | 74 | 393 | 0.705653 ( 5) | 0.70379 | 16.41 | 79.0 | 0.512581 ( 7) | 0.51238 | -9.0 | 1.1 | 932 |
| **Stock I** | | | | | | | | | | | |
| RP-44 | 137 | 92 | 0.718966 ( 6) | 0.70418 | 5.6 | 26.9 | 0.512545 ( 7) | 0.51235 | -3.4 | 0.4 | 994 |
| RP-45 (V) | 187 | 23 | 0.79755 ( 7) | 0.71602 | | | | | | | |
| RP-47 | 128 | 36 | 0.745277 ( 9) | 0.70988 | 8.0 | 44.0 | 0.512533 ( 9) | 0.51236 | 77 | 0.6 | 865 |
| **Stock II** | | | | | | | | | | | |
| RP-54 (V) | 133 | 43 | 0.73800 (12) | 0.70730 | | | | | | | |
| RP-55 (V) | 154 | 97 | 0.72099 ( 6) | 0.70516 | | | | | | | |
| RP-56 (V) | 170 | 21 | 0.79646 ( 9) | 0.71385 | | | | | | | |
| RP-212 | 246 | 33 | 0.782149 (18) | 0.70767 | 8.8 | 42.4 | 0.512573 ( 9) | 0.51238 | 46 | 0.9 | 972 |
| RP-214 | 256 | 711 | 0.707305 ( 9) | 0.70374 | 8.1 | 38.7 | 0.512586 ( 6) | 0.51239 | -9.7 | 1.2 | 933 |
| CERRO PEDREIRA | | | | | | | | | | | |
| RP-6 Dyke | 189 | 30 | 0.768571 (11) | 0.70571 | 10.4 | 103.0 | 0.512253 (11) | 0.51216 | 18.4 | -3.3 | 868 |
| RP-7 | 106 | 648 | 0.705875 ( 9) | 0.70425 | 9.2 | 51.6 | 0.512471 (11) | 0.51230 | -2.4 | -0.5 | 934 |
| MORRO DISTANTE | | | | | | | | | | | |
| RP-264 | 113 | 409 | 0.707265 (15) | 0.70452 | 4.94 | 29.5 | 0.512509 (12) | 0.51235 | 1.5 | 0.4 | 834 |
| MORRO CONCEIÇÃO | | | | | | | | | | | |
| RP-9 | 76 | 35 | 0.726692 ( 6) | 0.70480 | 7.6 | 50.0 | 0.512553 ( 6) | 0.51241 | 5.4 | 1.6 | 719 |
| FECHO DOS MORROS | | | | | | | | | | | |
| **Cerrito** | | | | | | | | | | | |
| RP-80 | 89 | 1481 | 0.705192 ( 9) | 0.70460 | 9.2 | 56.0 | 0.512597 (10) | 0.51244 | 2.5 | 2.2 | 707 |
| RP-87 | 123 | 816 | 0.704678 ( 6) | 0.70318 | 7.9 | 53.8 | 0.512570 ( 9) | 0.51243 | -17.5 | 2.0 | 682 |
| **Ilha Fecho dos Morros** | | | | | | | | | | | |
| RP-89 | 98 | 1126 | 0.704862 (11) | 0.70400 | 9.2 | 56.0 | 0.512557 (10) | 0.51240 | -6.0 | 1.4 | 758 |
| RP-91 | 156 | 741 | 0.705620 (10) | 0.70353 | 11.7 | 64.2 | 0.512411 ( 9) | 0.51224 | -12.6 | -1.8 | 1038 |
| RP-95 | 155 | 642 | 0.705840 (10) | 0.70345 | | | | | -13.8 | | |
| **Morro de São Pedro** | | | | | | | | | | | |
| RP-253 | 145 | 237 | 0.709411 ( 8) | 0.70334 | 8.9 | 54.6 | 0.512375 (11) | 0.51222 | -15.3 | -2.1 | 983 |
| PÃO DE AÇÚCAR | | | | | | | | | | | |
| RP-100 | 107 | 303 | 0.707046 (12) | 0.70354 | 13.4 | 87 | 0.512588 (12) | 0.51244 | -12.4 | 2.2 | 683 |
| RP-103 | 114 | 308 | 0.707265 ( 8) | 0.70359 | 13.6 | 91 | 0.512601 (12) | 0.51246 | -11.7 | 2.6 | 653 |
| RP-114 | 68 | 1307 | 0.704066 (12) | 0.70355 | 10.1 | 68 | 0.512579 (12) | 0.51244 | -12.4 | 2.1 | 676 |
| CERRO BOGGIANI | | | | | | | | | | | |
| RP-27 | 258 | 76 | 0.737916 ( 8) | 0.70415 | 2.5 | 17.0 | 0.512487 ( 8) | 0.51235 | -3.9 | 0.4 | 780 |
| RP-29 | 278 | 195 | 0.718782 ( 5) | 0.70463 | 3.0 | 20.1 | 0.512489 ( 7) | 0.51235 | 2.9 | 0.4 | 785 |
| RP-30 | 310 | 137 | 0.726447 ( 8) | 0.70396 | 4.1 | 31.0 | 0.512496 ( 9) | 0.51237 | -6.5 | 0.8 | 720 |
| RP-40 | 340 | 180 | 0.722446 (10) | 0.70368 | 9.0 | 59.9 | 0.512561 ( 8) | 0.51242 | -10.4 | 1.8 | 703 |

Table II. U and Th contents (ppm) and measured Pb isotopic ratios for Precambrian rock-types and alkaline rocks from the Alto Paraguay Province.

| | U | Th | $^{206}Pb/^{204}Pb$ | $^{207}Pb/^{204}Pb$ | $^{208}Pb/^{204}Pb$ |
|---|---|---|---|---|---|
| **BASEMENT** | | | | | |
| FUERTE OLIMPO | | | | | |
| RP-19B rhyolite (1341 Ma) | | | 19.0528(5) | 15.8429(5) | 39.4461(5) |
| PORTO MURTINHO | | | | | |
| Alumiador AZ-2 granite (1600 Ma) | | | 18.7230(2) | 15.9432(2) | 38.0084(2) |
| **ALTO PARAGUAY COMPLEXES** | | | | | |
| CERRO SIETE CABEZAS | | | | | |
| RP-75 | 2.7 | 7.9 | 18.6761(3) | 15.6614(3) | 38.3646(3) |
| **Stock I** | | | | | |
| RP-44 | 3.0 | 9.7 | 18.7887(1) | 15.6866(2) | 38.6213(2) |
| MORRO CONCEIÇÃO | | | | | |
| RP-9 | | | 18.3339(1) | 15.6447(1) | 38.2633(1) |
| FECHO DOS MORROS | | | | | |
| **Cerrito** | | | | | |
| RP-87 | 3.4 | 3.0 | 18.9676(1) | 15.6973(1) | 39.1110(1) |
| PÃO DE AÇÚCAR | | | | | |
| RP-114 | 4.3 | 8.2 | 19.6350(2) | 15.7260(2) | 39.5113(2) |
| CERRO BOGGIANI | | | | | |
| RP-29 | 4.8 | 10.7 | 21.2584(5) | 15.7798(5) | 38.9307(6) |

*Mesozoic to Cenozoic Alkaline Magmatism in the Brazilian Platform*
*Comin-Chiaramonti, P. & Gomes, C.B. (eds.)*
*Edusp/Fapesp, São Paulo, pp. 71-148, 2005*

# MINERAL CHEMISTRY OF ACCESSORY MINERALS IN ALKALINE COMPLEXES FROM THE ALTO PARAGUAY PROVINCE

*S. Carbonin, F. Liziero and C. Fuso*

*Electron microprobe analyses were performed by wavelength dispersion method on some accessory silicate minerals of syenitic rocks from the Alto Paraguay Province. The identified rosenbuschite and låvenite mineral phases are quite rich in MnO. The structural formula of eudialyte was satisfactorily calculated on the basis of the number of cations, rather than of anions, and indicated intermediate characteristics between eudialytes s.s. and those REE-rich. The P-rich and REE-rich titanosilicate phases form small polycrystalline aggregates and are extremely heterogeneous in composition. Non-stoichiometry analyses are mainly interpreted as due to the partially amorphous state of these compounds.*

## INTRODUCTION

The study of alkaline rocks from the Alto Paraguay Province has revealed the presence in syenitic rocks of some accessory silicate minerals, generally rare, but commonly found in these rock-types. The main characteristic of these minerals is the abundance of strategic elements such as Ti, Nb, Zr, Th and Rare Earth Elements (REE). This paper presents the results of extensive microprobe analyses carried out in some of them.

## ROCK SAMPLES AND MINERAL CLASSIFICATION

The fundamental mineralogy, petrochemistry and geochemistry of the rocks in which the investigated minerals are present have already been the subject of comprehensive studies (Comin-Chiaramonti *et al.* and therein references, in this volume) to which readers are referred. Localities and rock-names are as follows:

1) Cerro Boggiani: RP-31A (peralkaline nephel-syenite), RP-33 and RP 40 (peralkaline phonolites);

2) Cerro Siete Cabezas: RP-52 (peralkaline syenite).

According to Gaines *et al.* (1997) classification, the accessory minerals are structurally sorosilicates, with additional O, OH, F and $H_2O$ (rosenbuschite, låvenite, chevkinite), and cyclosilicates (eudialyte). On the other hand, Deer *et al.* (1997) classify rosenbuschite and låvenite as disilicates of the seidozerite and cuspidine groups, respectively, and eudialyte as a ring silicate. However, all these minerals are still subject of extensive investigation by crystallographers all over the world (see references). The order of presentation here is on the basis of locality.

## CHEMICAL ANALYSES

Compositions were obtained on a Cameca/ Camebax electron microprobe at the Istituto di Geoscienze e Georisorse (IGG), CNR Padova. Analyses have been made by wavelength dispersion method at different accelerating voltages and beam currents, ranging between 15-20 kV and 10-20 nA, respectively, on the basis of the mineral phase. X-ray counts were converted into oxide mass percentage by a PAP correction program provided by Cameca. Minerals and synthetic oxides were used as standards. Particular care was taken in the analysis of Na (e.g. rosenbuschite, låvenite, eudialyte): where it was abundant, the element has been always analysed first with a defocalized electron beam; unfortunately, the loss of Na is still apparent in some analysed points. Particularly in rosenbuschite samples, quantitative analyses were difficult mainly as a result of the small size and needle-like shape of the mineral. Moreover, for REE-rich minerals, it was necessary to tackle the interference problems due to the extremely complex L spectra of these elements. A suitable strategy was adopted here to achieve satisfactory results: 1) interferences were minimized by employing L$\alpha$ peaks for La and Ce; 2) resolution was increased by using LIF as analysing crystal; 3) synthetic REE-phosphates were selected as appropriate standards.

### Disilicates

These minerals are all characterized by $(Si_2O_7)$ pairs of tetrahedra and by octahedral cations, varying from the small-radius high-charge $Ti^{4+}$, $Zr^{4+}$ and $Nb^{5+}$, to $Mn^{2+}$ and $Fe^{2+}$, and the larger-radius low-charge $Na^+$ and $Ca^{2+}$ (Bellezza *et al.*, 2003).

#### *Rosenbuschite*

Rosenbuschite grains from Cerro Boggiani samples RP-31A and RP-33 are needle-like to fibrous in shape and exhibit high relief and weak pleochroism (white to yellowish-white). The average analyses of samples RP-31A and RP-33 (Table 1) are quite comparable, having a MnO content (~3 wt%) significantly higher than that given by the mineral from Langesundfjord nepheline syenites (Norway) and similar to that found in Zaangar'ya rocks (Russia) (Deer *et al.*, 1997).

#### *Låvenite*

The låvenite crystals from Cerro Boggiani sample RP-40 are xenomorphic, showing medium to high relief and a pale yellow colour; pleochroism is weak (whitish to pinkish-yellow). Electron microprobe analyses (Table 2) contain quite variable $ZrO_2$ content (23-30 wt%); an inverse relationship between $ZrO_2$ and $TiO_2$ is also indicated in the analyses. Point analysis 30 in grain s6 yielded the following crystal chemical formula calculated on the basis of 9 (O, F):

$$(Na_{1.34}Ca_{0.66})_{2.00}(Mn_{0.38}Fe_{0.22}Mg_{0.01}Ti_{0.16}Ca_{0.18})_{0.95}$$
$$(Zr_{0.74}Ti_{0.16}Nb_{0.10})_{1.00}(Si_{1.97}O_{7.00})O_{0.88}F_{1.12}$$

which is particularly close to the comprehensive crystal chemical formula suggested by Mellini (1981): $W_2XY(Si_2O_7)O(O,OH,F)$, where, W=Na, Ca; X=Mn, Fe, Mg, Ti and some Ca; Y=Zr, Ti, Nb, Ta.

Also in låvenite, as in rosenbuschite, the high MnO concentration is noteworthy (~6 wt%) and similar to that shown by the same mineral crystallizing from the Junguni magmas and late fluids in Malawi (Woolley & Platt, 1988).

### Ring Silicates

The identified mineral phase is a Na-rich zirconosilicate characterized by both three- and nine-membered rings of $(SiO_4)$ tetrahedra.

#### *Eudialyte*

Eudialyte from Cerro Boggiani sample RP-33 is roundish oval in shape and has high relief and colour ranging from pale yellow to pale pink. This Na-rich zirconosilicate is particularly common in agpaitic syenitic rocks and associated pegmatites. According to more recent detailed crystal chemical studies

Table 1. Microprobe analyses of rosenbuschite from samples RP-31A and RP-33 (s1-8 are different grains in thin section; 1-41 are different point analyses). Numbers of ions on the basis of 9 (O, F); S1 = Ti+Zr+Nb+$Fe^{2+}$+Mn+Mg; S2 = Ca+Na

| RP-31A | s1 | s1 | s1 | s3 | s3 | s3 | s3 | s3 | s3 | s3 | s3 | s2 | s2 | s2 | s2 | s2 | s4 | s4 | s4 | s4 | Av. | St. |
|---|---|---|---|---|---|---|---|---|---|---|---|---|---|---|---|---|---|---|---|---|---|---|
| | 1 | 2 | 4 | 5 | 6 | 7 | 9 | 10 | 11 | 12 | 13 | 14 | 15 | 16 | 17 | 18 | 19 | 20 | 21 | 22 | | Dev. |
| $SiO_2$ | 31.56 | 31.32 | 31.38 | 31.29 | 31.12 | 31.65 | 31.32 | 31.34 | 31.03 | 31.61 | 31.55 | 31.35 | 30.84 | 31.09 | 30.69 | 31.18 | 30.61 | 30.96 | 31.19 | 31.27 | 31.22 | 0.29 |
| $TiO_2$ | 7.79 | 7.22 | 8.44 | 8.09 | 8.20 | 8.01 | 7.53 | 8.22 | 7.68 | 8.44 | 8.49 | 8.24 | 8.03 | 6.80 | 6.67 | 7.74 | 5.96 | 6.48 | 6.78 | 7.80 | 7.63 | 0.74 |
| $ZrO_2$ | 16.47 | 17.51 | 13.90 | 15.41 | 14.12 | 14.39 | 12.21 | 11.76 | 14.54 | 14.70 | 15.36 | 14.21 | 13.12 | 15.78 | 16.38 | 11.31 | 16.10 | 15.69 | 16.15 | 8.18 | 14.36 | 2.19 |
| $Nb_2O_5$ | 1.37 | 1.01 | 1.38 | 1.39 | 0.93 | 1.01 | 1.72 | 1.76 | 1.49 | 1.13 | 0.90 | 1.32 | 1.67 | 0.97 | 1.13 | 1.23 | 0.90 | 0.83 | 1.09 | 1.67 | 1.25 | 0.30 |
| FeO | 0.78 | 1.12 | 0.76 | 0.96 | 0.98 | 0.96 | 0.98 | 0.92 | 0.97 | 0.96 | 0.84 | 1.00 | 0.90 | 1.16 | 1.05 | 1.04 | 1.07 | 1.01 | 0.88 | 0.69 | 0.95 | 0.12 |
| MnO | 3.48 | 3.02 | 4.23 | 2.70 | 2.52 | 2.44 | 2.75 | 2.97 | 2.82 | 2.98 | 2.73 | 2.29 | 2.66 | 2.74 | 2.41 | 2.67 | 1.97 | 2.24 | 2.08 | 2.40 | 2.71 | 0.50 |
| MgO | 0.12 | 0.16 | 0.18 | 0.18 | 0.14 | 0.13 | 0.11 | 0.14 | 0.13 | 0.12 | 0.11 | 0.11 | 0.11 | 0.12 | 0.15 | 0.11 | 0.09 | 0.13 | 0.09 | 0.03 | 0.12 | 0.03 |
| CaO | 22.46 | 22.84 | 22.60 | 23.86 | 23.18 | 22.62 | 25.49 | 25.51 | 24.63 | 24.31 | 24.55 | 24.21 | 23.94 | 23.53 | 23.30 | 25.34 | 24.24 | 23.99 | 24.70 | 26.48 | 24.09 | 1.09 |
| $Na_2O$ | 9.57 | 9.79 | 9.28 | 9.54 | 9.38 | 9.40 | 9.19 | 9.28 | 9.53 | 9.44 | 9.61 | 9.27 | 9.28 | 9.48 | 9.46 | 9.04 | 9.47 | 9.52 | 9.48 | 8.80 | 9.39 | 0.22 |
| F | 7.55 | 7.73 | 7.81 | 8.05 | 7.67 | 7.55 | 8.61 | 8.05 | 8.01 | 7.54 | 7.49 | 8.57 | 8.21 | 8.19 | 8.15 | 8.88 | 8.02 | 8.69 | 8.80 | 9.57 | 8.16 | 0.55 |
| Total | 101.14 | 101.72 | 99.96 | 101.46 | 98.24 | 98.18 | 99.91 | 99.95 | 100.83 | 101.21 | 101.63 | 100.57 | 98.76 | 99.85 | 99.38 | 98.52 | 98.43 | 99.55 | 101.25 | 96.88 | 99.87 | 1.37 |
| O=F | 3.18 | 3.25 | 3.29 | 3.39 | 3.23 | 3.18 | 3.62 | 3.39 | 3.37 | 3.17 | 3.15 | 3.61 | 3.46 | 3.45 | 3.43 | 3.74 | 3.38 | 3.66 | 3.71 | 4.03 | 3.43 | 0.23 |
| Total | 97.96 | 98.46 | 96.67 | 98.07 | 95.01 | 95.00 | 96.29 | 96.56 | 97.46 | 98.04 | 98.47 | 96.96 | 95.31 | 96.40 | 95.95 | 94.78 | 95.05 | 95.89 | 97.55 | 92.86 | 96.44 | 1.48 |
| Si | 2.007 | 1.990 | 2.009 | 1.980 | 2.021 | 2.051 | 2.000 | 2.000 | 1.978 | 2.001 | 1.993 | 1.989 | 1.993 | 2.003 | 1.990 | 2.009 | 2.005 | 1.997 | 1.980 | 2.028 | 2.001 | 0.017 |
| Ti | 0.373 | 0.345 | 0.406 | 0.385 | 0.400 | 0.391 | 0.362 | 0.394 | 0.368 | 0.402 | 0.403 | 0.393 | 0.390 | 0.329 | 0.325 | 0.375 | 0.294 | 0.315 | 0.324 | 0.380 | 0.368 | 0.034 |
| Zr | 0.511 | 0.543 | 0.434 | 0.475 | 0.447 | 0.455 | 0.380 | 0.366 | 0.452 | 0.454 | 0.473 | 0.440 | 0.414 | 0.496 | 0.518 | 0.355 | 0.514 | 0.493 | 0.500 | 0.259 | 0.449 | 0.068 |
| Nb | 0.039 | 0.029 | 0.040 | 0.040 | 0.027 | 0.030 | 0.050 | 0.051 | 0.043 | 0.032 | 0.026 | 0.038 | 0.049 | 0.028 | 0.033 | 0.036 | 0.027 | 0.024 | 0.031 | 0.049 | 0.036 | 0.009 |
| $Fe^{2+}$ | 0.041 | 0.059 | 0.040 | 0.051 | 0.053 | 0.052 | 0.052 | 0.049 | 0.052 | 0.051 | 0.044 | 0.053 | 0.049 | 0.062 | 0.057 | 0.056 | 0.058 | 0.054 | 0.047 | 0.037 | 0.051 | 0.006 |
| Mn | 0.187 | 0.162 | 0.229 | 0.145 | 0.138 | 0.134 | 0.149 | 0.160 | 0.152 | 0.160 | 0.146 | 0.123 | 0.146 | 0.150 | 0.133 | 0.146 | 0.109 | 0.123 | 0.112 | 0.132 | 0.147 | 0.027 |
| Mg | 0.011 | 0.015 | 0.017 | 0.017 | 0.013 | 0.012 | 0.011 | 0.014 | 0.012 | 0.011 | 0.010 | 0.010 | 0.011 | 0.011 | 0.014 | 0.010 | 0.009 | 0.012 | 0.009 | 0.003 | 0.012 | 0.003 |
| Ca | 1.530 | 1.555 | 1.549 | 1.618 | 1.613 | 1.570 | 1.744 | 1.744 | 1.682 | 1.649 | 1.661 | 1.645 | 1.658 | 1.624 | 1.619 | 1.749 | 1.701 | 1.658 | 1.680 | 1.839 | 1.654 | 0.077 |
| Na | 1.180 | 1.207 | 1.152 | 1.171 | 1.181 | 1.181 | 1.137 | 1.148 | 1.178 | 1.159 | 1.177 | 1.140 | 1.164 | 1.185 | 1.190 | 1.129 | 1.203 | 1.190 | 1.167 | 1.106 | 1.167 | 0.026 |
| Sum | 5.881 | 5.905 | 5.877 | 5.880 | 5.894 | 5.876 | 5.884 | 5.926 | 5.918 | 5.919 | 5.934 | 5.831 | 5.872 | 5.887 | 5.878 | 5.866 | 5.919 | 5.867 | 5.849 | 5.832 | 5.885 | 0.029 |
| F | 1.519 | 1.553 | 1.581 | 1.610 | 1.575 | 1.547 | 1.738 | 1.624 | 1.616 | 1.510 | 1.496 | 1.720 | 1.678 | 1.669 | 1.670 | 1.809 | 1.660 | 1.773 | 1.767 | 1.961 | 1.654 | 0.117 |
| S1 | 1.163 | 1.154 | 1.167 | 1.112 | 1.080 | 1.074 | 1.003 | 1.034 | 1.079 | 1.110 | 1.102 | 1.057 | 1.057 | 1.076 | 1.079 | 0.978 | 1.011 | 1.022 | 1.022 | 0.860 | 1.062 | 0.071 |
| S2 | 2.711 | 2.761 | 2.702 | 2.789 | 2.794 | 2.751 | 2.881 | 2.892 | 2.860 | 2.808 | 2.839 | 2.786 | 2.821 | 2.808 | 2.808 | 2.879 | 2.904 | 2.848 | 2.847 | 2.945 | 2.822 | 0.063 |

Table 1 (continued).

| RP-33 | s4 31 | s4 32 | s4 33 | s4 34 | s4 35 | s5 36 | s5 37 | s5 38 | s6 40 | s8 41 | Av. | St. Dev. |
|---|---|---|---|---|---|---|---|---|---|---|---|---|
| $SiO_2$ | 31.46 | 31.09 | 30.92 | 32.61 | 31.33 | 32.30 | 31.63 | 31.43 | 30.44 | 30.46 | 31.37 | 0.70 |
| $TiO_2$ | 8.10 | 7.00 | 7.74 | 8.76 | 7.64 | 9.97 | 8.54 | 8.70 | 6.83 | 8.11 | 8.14 | 0.92 |
| $ZrO_2$ | 12.68 | 17.25 | 14.51 | 15.06 | 16.62 | 9.84 | 11.12 | 9.26 | 14.38 | 13.53 | 13.42 | 2.70 |
| $Nb_2O_5$ | 1.59 | 1.06 | 1.27 | 1.33 | 1.02 | 1.83 | 2.49 | 2.40 | 1.85 | 1.55 | 1.64 | 0.51 |
| FeO | 0.70 | 0.80 | 0.64 | 0.68 | 0.68 | 0.45 | 0.64 | 0.55 | 0.63 | 0.73 | 0.65 | 0.10 |
| MnO | 2.32 | 1.87 | 2.48 | 2.74 | 2.23 | 4.82 | 3.79 | 3.81 | 1.91 | 3.52 | 2.95 | 0.98 |
| MgO | 0.07 | 0.18 | 0.09 | 0.12 | 0.10 | 0.12 | 0.11 | 0.03 | 0.09 | 0.13 | 0.10 | 0.04 |
| CaO | 26.39 | 24.02 | 24.43 | 25.57 | 24.52 | 26.41 | 26.73 | 27.64 | 24.55 | 23.58 | 25.39 | 1.35 |
| $Na_2O$ | 9.33 | 9.66 | 9.22 | 8.38 | 9.59 | 8.27 | 8.89 | 8.63 | 9.50 | 9.93 | 9.14 | 0.57 |
| F | 8.43 | 8.32 | 8.08 | 8.39 | 8.05 | 8.73 | 8.60 | 8.64 | 8.84 | 8.84 | 8.49 | 0.29 |
| Total | 101.07 | 101.25 | 99.39 | 103.64 | 101.77 | 102.75 | 102.54 | 101.07 | 99.01 | 100.38 | 101.29 | 1.46 |
| O=F | 3.55 | 3.50 | 3.40 | 3.53 | 3.39 | 3.67 | 3.62 | 3.64 | 3.72 | 3.72 | 3.58 | 0.12 |
| Total | 97.52 | 97.75 | 95.99 | 100.11 | 98.38 | 99.07 | 98.92 | 97.44 | 95.29 | 96.65 | 97.71 | 1.47 |
| Si | 1.986 | 1.977 | 1.991 | 2.004 | 1.980 | 1.991 | 1.970 | 1.977 | 1.970 | 1.948 | 1.980 | 0.015 |
| Ti | 0.385 | 0.335 | 0.375 | 0.405 | 0.363 | 0.462 | 0.400 | 0.412 | 0.333 | 0.390 | 0.386 | 0.038 |
| Zr | 0.390 | 0.535 | 0.456 | 0.451 | 0.512 | 0.296 | 0.338 | 0.284 | 0.454 | 0.422 | 0.414 | 0.086 |
| Nb | 0.045 | 0.031 | 0.037 | 0.037 | 0.029 | 0.051 | 0.070 | 0.068 | 0.054 | 0.045 | 0.047 | 0.014 |
| $Fe^{2+}$ | 0.037 | 0.042 | 0.035 | 0.035 | 0.036 | 0.023 | 0.033 | 0.029 | 0.034 | 0.039 | 0.034 | 0.005 |
| Mn | 0.124 | 0.101 | 0.135 | 0.142 | 0.119 | 0.252 | 0.200 | 0.203 | 0.105 | 0.191 | 0.157 | 0.051 |
| Mg | 0.006 | 0.017 | 0.009 | 0.011 | 0.009 | 0.011 | 0.010 | 0.003 | 0.009 | 0.012 | 0.010 | 0.004 |
| Ca | 1.785 | 1.637 | 1.686 | 1.684 | 1.660 | 1.744 | 1.783 | 1.863 | 1.703 | 1.616 | 1.716 | 0.077 |
| Na | 1.142 | 1.191 | 1.152 | 0.998 | 1.175 | 0.988 | 1.074 | 1.053 | 1.193 | 1.232 | 1.120 | 0.086 |
| Sum | 5.901 | 5.866 | 5.876 | 5.767 | 5.884 | 5.818 | 5.878 | 5.892 | 5.854 | 5.895 | 5.863 | 0.041 |
| F | 1.682 | 1.674 | 1.645 | 1.632 | 1.608 | 1.701 | 1.694 | 1.720 | 1.809 | 1.788 | 1.695 | 0.064 |
| S1 | 0.988 | 1.060 | 1.046 | 1.081 | 1.069 | 1.095 | 1.051 | 0.999 | 0.988 | 1.099 | 1.048 | 0.042 |
| S2 | 2.927 | 2.828 | 2.838 | 2.682 | 2.835 | 2.732 | 2.857 | 2.916 | 2.895 | 2.848 | 2.836 | 0.077 |

(Johnsen & Grice, 1999), the "formula calculation is generally problematic because of the wide variety of chemical substitutions, site vacancies, variations in the total number of anions". Moreover, "an accurate formula for eudialyte can only be constructed from data based on structural information". However, according also to those authors, a reasonable formula can be derived from microprobe analyses on the basis of the number of cations, rather than anions: i.e. those accommodated in the silicate rings, in M(3) site, and the Zr octahedra ideally adding up to 29: (Si+Al+Zr+Ti+Hf+Nb+W+Ta). A general empirical formula may be written as follows: $Na_{15}[M(1)]_6[M(2)]_3Zr_3[M(3)](Si_{25}O_{73})(O,OH,H_2O)_3X_2$, where Na sites may also contain REE, Sr, Ca, K, Mn, $H_2O$; M(1)=Ca, Mn; M(2)=Fe, Mn; Zr sites may also contain Ti; M(3)=Nb, Ti, W, Mn, Si; X=Cl, F.

The calculated eudialyte analyses are listed in Table 3 and allow the mineral to be placed between eudialyte s.s. and an REE-rich type (Gula, 2002).

Point analysis 16 in grain s2 gave the following crystal chemical formula:

$$(Na_{10.85}Ca_{1.70}K_{0.19}Sr_{0.10}La_{0.13}Ce_{0.08})_{13.05}(Ca_{4.90}Mn_{1.10})_{6.00}(Fe_{2.02}Mn_{0.96}Mg_{0.02})_{3.00}Zr_{3.00}(Nb_{0.39}Ti_{0.20}Zr_{0.09}Si_{0.33})_{1.01}Si_{24.96}Al_{0.04}O_{74..23}Cl_{1.13}$$

which shows a cation deficiency in the Na sites, a phenomenon already reported in the literature. As mentioned above, structural analyses are in need to confirm the chemical characteristics of the mineral, but, from an analytical viewpoint, the data obtained may be considered as satisfactory.

Titanosilicates

In Cerro Siete Cabezas sample RP-52 at least two types of accessory minerals were identified, occurring often interstitially amongst the coarse-grained feldspar. They are all characterized by high relief, strong colours from brownish-yellow to reddish-orange, and rather small size, which ranges from ca. 200 to 50 μ from grain to grain. In general, the grains tend to form polycrystalline aggregates, indicating intergrowths among various mineral phases, even smaller in size, and quite heterogeneous compositions on electron microprobe analysis. Problems of non-stoichiometry were also found in the calculation of the formulas, the main reason being the partially metamictic state of the compounds (Liziero *et al.*, 2003), probably owing to the constant presence of $ThO_2$ (ca. 2 wt%) in the composition. On the basis of microprobe results alone, they were tentatively classified as P-rich and REE-rich titanosilicates.

Table 2. Microprobe analyses of låvenite from sample RP-40 (s3-6 are different grains in thin section; 25-30 are different point analyses). Numbers of ions on the basis of 9 (O, F).

| | s3 25 | s3 26 | s4 29 | s6 30 | Av. | St. Dev. |
|---|---|---|---|---|---|---|
| $SiO_2$ | 32.58 | 31.44 | 30.30 | 29.49 | 30.95 | 1.35 |
| $TiO_2$ | 3.75 | 3.03 | 4.30 | 6.40 | 4.37 | 1.45 |
| $ZrO_2$ | 29.90 | 29.99 | 28.47 | 22.68 | 27.76 | 3.46 |
| $Nb_2O_5$ | 1.40 | 1.86 | 1.77 | 3.36 | 2.10 | 0.86 |
| FeO | 2.97 | 2.39 | 1.93 | 3.99 | 2.82 | 0.89 |
| MnO | 5.99 | 5.33 | 6.25 | 6.80 | 6.09 | 0.61 |
| MgO | 0.10 | 0.09 | 0.15 | 0.12 | 0.11 | 0.02 |
| CaO | 12.43 | 13.53 | 13.01 | 11.83 | 12.70 | 0.73 |
| $Na_2O$ | 6.80 | 6.34 | 10.62 | 10.35 | 8.53 | 2.27 |
| F | 5.33 | 6.31 | 6.09 | 5.31 | 5.76 | 0.52 |
| Total | 101.25 | 100.32 | 102.90 | 100.32 | 101.20 | 1.22 |
| O=F | 2.24 | 2.66 | 2.57 | 2.24 | 2.43 | 0.22 |
| Total | 99.01 | 97.66 | 100.33 | 98.08 | 98.77 | 1.18 |
| | | | | | | |
| Si | 2.131 | 2.079 | 1.978 | 1.968 | 2.039 | 0.079 |
| Ti | 0.185 | 0.151 | 0.211 | 0.321 | 0.217 | 0.074 |
| Zr | 0.954 | 0.967 | 0.906 | 0.738 | 0.891 | 0.105 |
| Nb | 0.041 | 0.056 | 0.052 | 0.101 | 0.063 | 0.026 |
| $Fe^{2+}$ | 0.163 | 0.132 | 0.106 | 0.222 | 0.156 | 0.050 |
| Mn | 0.332 | 0.298 | 0.346 | 0.384 | 0.340 | 0.036 |
| Mg | 0.009 | 0.009 | 0.014 | 0.012 | 0.011 | 0.002 |
| Ca | 0.871 | 0.959 | 0.910 | 0.845 | 0.896 | 0.050 |
| Na | 0.862 | 0.814 | 1.345 | 1.338 | 1.090 | 0.291 |
| Sum | 5.548 | 5.465 | 5.868 | 5.929 | 5.703 | 0.230 |
| F | 1.103 | 1.321 | 1.259 | 1.120 | 1.201 | 0.106 |

### *P-rich titanosilicates*

Electron microprobe analyses are listed in Table 4. Considering the high $P_2O_5$ content, the paragenesis and also the preliminary transmission electron microscopy results (E. Belluso, pers. comm.), the mineral is believed to be structurally similar to bornemanite, with both $SiO_4$ and $PO_4$ groups and modular structure (Ferraris *et al.*, 2001). However, confirming its real structure will be only possible by means of structural analysis, presently in progress, although the extremely small size of the grains makes such study particularly difficult. Transmission electron microscopy data indicates that this P-titanosilicate is not homogeneous in composition, even on a submicrometric scale. Thus, it is admitted that the electron microprobe analyses are "contaminated" as a result of the presence of more than one mineral, smaller in size than the electron microprobe beam, and that the chemical data alone are not sufficient to provide a reliable structural formula.

### *REE-rich titanosilicates*

REE-rich titanosilicates are chemically heterogeneous in composition: on reflected light microscopy, the minerals exhibit complex zoning with patches of more and less metallic areas. Preliminary single-crystal CCD diffractometric results show that they are partially amorphous, with the crystalline portion allowing to determine the cell parameters of the chevkinite group minerals. They are Rare Earth titanosilicates with complex composition and general formula: $A_4BC_2D_2O_8$ $(Si_2O_7)_2$, where A=Ce Earth Elements, Ca, Th, Sr, Ba (coordination 8+3); B=Fe, Mn, Mg; C=Ti, Fe, Nb, Mg, Al; D=Ti, and rare Fe, Nb, Mg (B, C, D octahedral sites). However, the collapse of the interlayer *c* dimension in these samples points to a phenomenon already known among the Kola Peninsula titanosilicates as "decationization of interlayer population" (Ferraris, 1997): ions with greater radius (e.g. REE) lying between the layers tend to leave first the chevkinite framework.

Electron microprobe analyses (Tables 5a-d and Table 5e) draw the attention to the quite variable composition of these minerals and highlight the above phenomenon. Compositions relative to areas with low-, medium- and high-REE contents and those with particularly high Ti concentrations have been grouped in Tables 5a-c and Table 5d, respectively. From the data listed in Table 5c (high-REE) alone, a chevkinite-like formula was tentatively calculated on the basis of 22 atoms of oxygen. It resulted to be strongly non-stoichiometric, on average of the $A_2BC_2D_2Si_5O_{22}$ type, i.e. with both deficiency in interlayer population and overestimate of Si atoms with respect to the ideal chevkinite structure. Finally, the data are also indicating the more Fe enriched composition of sample 10 (Table 5e) in comparison to sample 6 (Tables 5a-d).

Table 3. Microprobe analyses of eudialyte from sample RP-33 (s1-3 are different grains in thin section; 1-23 are different point analyses). Numbers of ions on the basis of 29 (Si, Al, Zr, Ti, Nb).

| | s1 1 | s1 2 | s1 3 | s1 4 | s1 5 | s1 6 | s1 7 | s1 8 | s1 9 | s1 10 | s1 11 | s1 12 | s1 13 | Av. | St. Dev. | s2 15 | s2 16 | s2 17 | s2 18 | s2 19 | Av. | St. Dev. | s3 20 | s3 21 | s3 22 | s3 23 | Av. | St. Dev. |
|---|---|---|---|---|---|---|---|---|---|---|---|---|---|---|---|---|---|---|---|---|---|---|---|---|---|---|---|---|
| $SiO_2$ | 49.26 | 50.08 | 49.77 | 50.85 | 50.73 | 50.16 | 50.23 | 50.11 | 49.59 | 50.36 | 50.24 | 49.90 | 50.48 | 50.13 | 0.44 | 49.69 | 49.14 | 50.22 | 50.39 | 50.16 | 49.92 | 0.51 | 50.89 | 50.42 | 49.51 | 49.11 | 49.98 | 0.82 |
| $Al_2O_3$ | 0.25 | 0.22 | 0.11 | 0.13 | 0.09 | 0.27 | 0.07 | 0.25 | 0.07 | 0.12 | 0.27 | 0.15 | 0.06 | 0.16 | 0.08 | 0.23 | 0.06 | 0.22 | 0.23 | 0.08 | 0.16 | 0.09 | 0.09 | 0.12 | 0.13 | 0.06 | 0.10 | 0.03 |
| $TiO_2$ | 0.39 | 0.38 | 0.35 | 0.32 | 0.41 | 0.50 | 0.40 | 0.49 | 0.43 | 0.47 | 0.46 | 0.45 | 0.35 | 0.41 | 0.06 | 0.39 | 0.52 | 0.47 | 0.39 | 0.41 | 0.44 | 0.06 | 0.39 | 0.38 | 0.37 | 0.48 | 0.40 | 0.05 |
| $ZrO_2$ | 14.74 | 14.06 | 12.17 | 12.14 | 12.33 | 14.30 | 12.39 | 14.50 | 11.97 | 13.12 | 14.40 | 12.70 | 12.28 | 13.16 | 1.07 | 13.70 | 12.30 | 14.18 | 13.92 | 12.37 | 13.29 | 0.89 | 12.54 | 12.55 | 12.35 | 12.42 | 12.46 | 0.10 |
| $Nb_2O_5$ | 1.94 | 1.49 | 1.73 | 1.46 | 1.33 | 1.17 | 2.19 | 1.45 | 1.34 | 0.97 | 1.52 | 1.73 | 1.44 | 1.52 | 0.32 | 1.47 | 1.66 | 1.01 | 1.17 | 1.58 | 1.38 | 0.27 | 0.85 | 1.22 | 1.20 | 2.48 | 1.44 | 0.72 |
| FeO | 4.45 | 4.40 | 4.74 | 4.90 | 5.46 | 4.68 | 4.74 | 4.46 | 5.07 | 4.94 | 4.35 | 4.48 | 5.04 | 4.75 | 0.33 | 4.47 | 4.70 | 4.66 | 4.85 | 5.00 | 4.73 | 0.20 | 5.09 | 5.20 | 4.78 | 4.22 | 4.82 | 0.44 |
| MnO | 3.71 | 3.95 | 3.73 | 3.86 | 3.49 | 3.25 | 4.25 | 3.61 | 3.98 | 3.64 | 3.50 | 3.69 | 3.61 | 3.71 | 0.25 | 4.06 | 4.72 | 3.93 | 3.73 | 3.68 | 4.02 | 0.42 | 3.96 | 3.97 | 4.22 | 4.63 | 4.20 | 0.31 |
| MgO | 0.03 | 0.03 | 0.06 | 0.16 | 0.04 | 0.10 | 0.03 | 0.02 | 0.00 | 0.05 | 0.07 | 0.05 | 0.04 | 0.05 | 0.04 | 0.07 | 0.02 | 0.06 | 0.10 | 0.05 | 0.06 | 0.03 | 0.06 | 0.07 | 0.12 | 0.09 | 0.08 | 0.03 |
| CaO | 10.25 | 10.38 | 11.79 | 11.67 | 11.44 | 10.06 | 11.15 | 9.83 | 11.63 | 11.02 | 10.01 | 11.11 | 11.44 | 10.91 | 0.71 | 10.90 | 11.96 | 10.99 | 10.86 | 11.78 | 11.30 | 0.53 | 11.93 | 11.91 | 11.65 | 11.90 | 11.85 | 0.13 |
| $Na_2O$ | 10.49 | 11.48 | 10.35 | 10.04 | 11.64 | 11.28 | 10.92 | 10.75 | 10.87 | 10.64 | 11.16 | 11.36 | 10.03 | 10.85 | 0.53 | 10.39 | 10.87 | 11.22 | 11.02 | 11.56 | 11.01 | 0.43 | 11.60 | 11.10 | 11.17 | 10.77 | 11.16 | 0.34 |
| $K_2O$ | 0.28 | 0.33 | 0.22 | 0.24 | 0.29 | 0.30 | 0.29 | 0.38 | 0.16 | 0.17 | 0.23 | 0.29 | 0.22 | 0.26 | 0.06 | 0.22 | 0.28 | 0.26 | 0.26 | 0.23 | 0.25 | 0.02 | 0.26 | 0.23 | 0.29 | 0.27 | 0.26 | 0.02 |
| SrO | 0.00 | 0.28 | 0.06 | 0.56 | 0.28 | 0.09 | 0.62 | 0.41 | 0.17 | 0.00 | 0.21 | 0.02 | 0.24 | 0.23 | 0.20 | 0.21 | 0.34 | 0.21 | 0.26 | 0.50 | 0.31 | 0.12 | 0.15 | 0.00 | 0.17 | 0.13 | 0.11 | 0.08 |
| $La_2O_3$ | 0.25 | 0.35 | 0.53 | 0.24 | 0.62 | 0.35 | 0.53 | 0.62 | 0.16 | 0.42 | 0.24 | 0.53 | 0.25 | 0.39 | 0.16 | 0.45 | 0.67 | 0.38 | 0.31 | 0.49 | 0.46 | 0.14 | 0.24 | 0.51 | 0.27 | 0.60 | 0.40 | 0.18 |
| $Ce_2O_3$ | 0.32 | 0.19 | 0.31 | 0.43 | 0.39 | 0.53 | 0.68 | 0.66 | 0.36 | 0.36 | 0.36 | 0.39 | 0.17 | 0.40 | 0.15 | 0.61 | 0.44 | 0.32 | 0.34 | 0.31 | 0.41 | 0.13 | 0.27 | 0.31 | 0.31 | 0.77 | 0.41 | 0.24 |
| Cl | 1.29 | 1.27 | 1.18 | 1.15 | 1.32 | 1.23 | 1.37 | 1.25 | 1.28 | 1.21 | 1.23 | 1.23 | 1.22 | 1.25 | 0.06 | 1.45 | 1.29 | 1.31 | 1.40 | 1.33 | 1.36 | 0.07 | 1.13 | 1.25 | 1.07 | 1.21 | 1.16 | 0.08 |
| Total | 97.65 | 98.88 | 97.10 | 98.16 | 99.85 | 98.27 | 99.86 | 98.80 | 97.08 | 97.48 | 98.25 | 98.08 | 96.88 | 98.18 | 0.97 | 98.32 | 98.98 | 99.47 | 99.21 | 99.51 | 99.10 | 0.48 | 99.44 | 99.24 | 97.61 | 99.11 | 98.85 | 0.84 |
| O=Cl | 0.29 | 0.29 | 0.27 | 0.26 | 0.30 | 0.28 | 0.31 | 0.28 | 0.29 | 0.27 | 0.28 | 0.28 | 0.28 | 0.28 | 0.01 | 0.33 | 0.29 | 0.30 | 0.32 | 0.30 | 0.31 | 0.02 | 0.26 | 0.28 | 0.24 | 0.27 | 0.26 | 0.02 |
| Total | 97.36 | 98.59 | 96.83 | 97.90 | 99.56 | 97.99 | 99.55 | 98.52 | 96.79 | 97.20 | 97.97 | 97.80 | 96.61 | 97.90 | 0.96 | 97.99 | 98.69 | 99.18 | 98.90 | 99.21 | 98.79 | 0.49 | 99.19 | 98.96 | 97.37 | 98.84 | 98.59 | 0.82 |
| | | | | | | | | | | | | | | | | | | | | | | | | | | | | |
| Si | 24.667 | 24.973 | 25.374 | 25.502 | 25.473 | 24.923 | 25.270 | 24.840 | 25.481 | 25.319 | 24.855 | 25.214 | 25.476 | 25.182 | 0.293 | 25.017 | 25.290 | 25.018 | 25.079 | 25.387 | 25.158 | 0.170 | 25.541 | 25.419 | 25.408 | 25.110 | 25.369 | 0.183 |
| Al | 0.149 | 0.130 | 0.068 | 0.076 | 0.053 | 0.160 | 0.042 | 0.147 | 0.042 | 0.069 | 0.159 | 0.092 | 0.038 | 0.094 | 0.048 | 0.137 | 0.036 | 0.131 | 0.134 | 0.046 | 0.097 | 0.051 | 0.052 | 0.074 | 0.078 | 0.037 | 0.060 | 0.019 |
| Ti | 0.145 | 0.142 | 0.134 | 0.122 | 0.154 | 0.188 | 0.151 | 0.182 | 0.167 | 0.176 | 0.171 | 0.170 | 0.133 | 0.157 | 0.021 | 0.150 | 0.200 | 0.178 | 0.145 | 0.154 | 0.165 | 0.023 | 0.146 | 0.144 | 0.144 | 0.183 | 0.154 | 0.019 |
| Zr | 3.600 | 3.419 | 3.025 | 2.968 | 3.020 | 3.466 | 3.040 | 3.505 | 2.999 | 3.216 | 3.474 | 3.129 | 3.023 | 3.222 | 0.235 | 3.362 | 3.088 | 3.445 | 3.378 | 3.052 | 3.265 | 0.181 | 3.069 | 3.085 | 3.091 | 3.096 | 3.085 | 0.012 |
| Nb | 0.439 | 0.336 | 0.399 | 0.332 | 0.301 | 0.263 | 0.497 | 0.326 | 0.312 | 0.220 | 0.341 | 0.395 | 0.330 | 0.345 | 0.073 | 0.335 | 0.386 | 0.229 | 0.263 | 0.361 | 0.315 | 0.066 | 0.193 | 0.278 | 0.279 | 0.573 | 0.331 | 0.167 |
| $Fe^{2+}$ | 1.863 | 1.836 | 2.019 | 2.057 | 2.291 | 1.946 | 1.994 | 1.850 | 2.178 | 2.078 | 1.798 | 1.895 | 2.128 | 1.995 | 0.149 | 1.881 | 2.022 | 1.939 | 2.019 | 2.118 | 1.996 | 0.090 | 2.137 | 2.192 | 2.052 | 1.804 | 2.046 | 0.172 |
| Mn | 1.575 | 1.670 | 1.611 | 1.640 | 1.485 | 1.368 | 1.810 | 1.517 | 1.733 | 1.550 | 1.468 | 1.579 | 1.541 | 1.580 | 0.116 | 1.731 | 2.059 | 1.657 | 1.573 | 1.579 | 1.720 | 0.200 | 1.685 | 1.697 | 1.832 | 2.006 | 1.805 | 0.150 |
| Mg | 0.023 | 0.026 | 0.045 | 0.122 | 0.032 | 0.071 | 0.024 | 0.016 | 0.000 | 0.039 | 0.052 | 0.036 | 0.033 | 0.040 | 0.030 | 0.049 | 0.017 | 0.047 | 0.072 | 0.038 | 0.045 | 0.020 | 0.044 | 0.050 | 0.091 | 0.068 | 0.063 | 0.021 |
| Ca | 5.499 | 5.544 | 6.442 | 6.270 | 6.156 | 5.357 | 6.011 | 5.222 | 6.403 | 5.936 | 5.305 | 6.015 | 6.186 | 5.873 | 0.432 | 5.881 | 6.595 | 5.868 | 5.793 | 6.386 | 6.105 | 0.362 | 6.414 | 6.432 | 6.407 | 6.521 | 6.443 | 0.053 |
| Na | 10.189 | 11.100 | 10.229 | 9.762 | 11.328 | 10.870 | 10.652 | 10.334 | 10.826 | 10.376 | 10.708 | 11.128 | 9.815 | 10.563 | 0.494 | 10.140 | 10.845 | 10.841 | 10.638 | 11.343 | 10.762 | 0.434 | 11.289 | 10.849 | 11.115 | 10.673 | 10.981 | 0.274 |
| K | 0.178 | 0.209 | 0.144 | 0.154 | 0.188 | 0.190 | 0.184 | 0.238 | 0.104 | 0.106 | 0.143 | 0.187 | 0.139 | 0.166 | 0.039 | 0.143 | 0.185 | 0.168 | 0.163 | 0.149 | 0.161 | 0.017 | 0.164 | 0.146 | 0.187 | 0.173 | 0.168 | 0.017 |
| Sr | 0.000 | 0.081 | 0.019 | 0.162 | 0.082 | 0.025 | 0.182 | 0.117 | 0.051 | 0.000 | 0.061 | 0.006 | 0.069 | 0.066 | 0.059 | 0.063 | 0.103 | 0.062 | 0.074 | 0.145 | 0.089 | 0.035 | 0.044 | 0.000 | 0.051 | 0.038 | 0.033 | 0.023 |
| La | 0.047 | 0.064 | 0.099 | 0.044 | 0.115 | 0.063 | 0.098 | 0.113 | 0.031 | 0.078 | 0.043 | 0.098 | 0.047 | 0.072 | 0.029 | 0.084 | 0.128 | 0.070 | 0.057 | 0.092 | 0.086 | 0.027 | 0.044 | 0.095 | 0.052 | 0.113 | 0.076 | 0.033 |
| Ce | 0.059 | 0.034 | 0.057 | 0.078 | 0.072 | 0.096 | 0.125 | 0.120 | 0.067 | 0.066 | 0.065 | 0.073 | 0.032 | 0.073 | 0.028 | 0.113 | 0.083 | 0.059 | 0.062 | 0.057 | 0.075 | 0.024 | 0.050 | 0.057 | 0.058 | 0.143 | 0.077 | 0.044 |
| Sum | 48.432 | 49.563 | 49.666 | 49.288 | 50.748 | 48.986 | 50.080 | 48.527 | 50.393 | 49.228 | 48.642 | 50.017 | 48.990 | 49.428 | 0.730 | 49.085 | 51.037 | 49.712 | 49.451 | 50.906 | 50.038 | 0.882 | 50.871 | 50.517 | 50.844 | 50.539 | 50.693 | 0.191 |
| Cl | 1.092 | 1.072 | 1.018 | 0.977 | 1.119 | 1.036 | 1.165 | 1.049 | 1.112 | 1.033 | 1.029 | 1.057 | 1.044 | 1.062 | 0.050 | 1.238 | 1.125 | 1.107 | 1.178 | 1.141 | 1.158 | 0.052 | 0.963 | 1.065 | 0.933 | 1.046 | 1.002 | 0.064 |

Table 4. Microprobe analyses of P-rich titanosilicate from sample RP-52 (1-4 are different point analyses).

| | 1 | 2 | 3 | 4 | Av. |
|---|---|---|---|---|---|
| $SiO_2$ | 6.52 | 6.23 | 8.86 | 8.19 | 7.45 |
| $Al_2O_3$ | 7.72 | 7.82 | 7.99 | 8.42 | 7.99 |
| $TiO_2$ | 31.88 | 32.42 | 25.93 | 26.29 | 29.13 |
| $ZrO_2$ | 1.51 | 1.43 | 1.22 | 1.56 | 1.43 |
| $Nb_2O_5$ | 7.44 | 7.53 | 6.48 | 5.47 | 6.73 |
| FeO | 15.20 | 15.03 | 12.11 | 13.1 | 13.86 |
| MnO | 0.29 | 0.24 | 0.21 | 0.18 | 0.23 |
| MgO | 0.07 | 0.09 | 0.07 | 0.09 | 0.08 |
| CaO | 1.48 | 1.55 | 1.79 | 1.73 | 1.64 |
| $K_2O$ | 0.19 | 0.28 | 0.19 | 0.29 | 0.24 |
| BaO | 0.21 | 0.41 | 0.62 | 0.35 | 0.40 |
| $La_2O_3$ | 1.63 | 1.76 | 3.19 | 2.5 | 2.27 |
| $Ce_2O_3$ | 4.42 | 3.58 | 5.97 | 5.59 | 4.89 |
| $ThO_2$ | 2.98 | 2.96 | 2.46 | 2.53 | 2.73 |
| $P_2O_5$ | 12.65 | 12.49 | 12.61 | 13.41 | 12.79 |
| Total | 94.19 | 93.82 | 89.70 | 89.70 | 91.85 |

Table 5a. Microprobe analyses of low-REE area in titanosilicate 6 from sample RP-52 (36-80 are different point analyses).

| | 36 | 38 | 63 | 64 | 72 | 78 | 80 | Av. |
|---|---|---|---|---|---|---|---|---|
| $SiO_2$ | 28.05 | 27.60 | 24.56 | 27.00 | 26.87 | 28.65 | 28.42 | 27.31 |
| $Al_2O_3$ | 0.74 | 0.76 | 0.78 | 0.83 | 0.77 | 0.84 | 0.85 | 0.80 |
| $TiO_2$ | 25.65 | 28.76 | 27.43 | 24.81 | 24.97 | 24.55 | 26.19 | 26.05 |
| $ZrO_2$ | 1.12 | 1.26 | 1.21 | 1.51 | 1.30 | 1.21 | 1.24 | 1.27 |
| $Nb_2O_5$ | 7.25 | 7.30 | 7.63 | 7.43 | 7.46 | 7.40 | 7.70 | 7.45 |
| FeO | 8.19 | 8.78 | 9.22 | 8.70 | 7.82 | 8.20 | 8.37 | 8.47 |
| MnO | 0.22 | 0.28 | 0.31 | 0.27 | 0.29 | 0.32 | 0.25 | 0.28 |
| MgO | 0.06 | 0.03 | 0.05 | 0.04 | 0.04 | 0.05 | 0.04 | 0.04 |
| CaO | 1.43 | 1.49 | 1.42 | 1.43 | 1.60 | 1.39 | 1.30 | 1.44 |
| $K_2O$ | 0.17 | 0.20 | 0.19 | 0.17 | 0.16 | 0.12 | 0.20 | 0.17 |
| BaO | 0.42 | 0.11 | 0.08 | 0.23 | 0.00 | 0.07 | 0.00 | 0.13 |
| $La_2O_3$ | 3.45 | 3.19 | 3.68 | 3.42 | 3.97 | 3.64 | 2.91 | 3.46 |
| $Ce_2O_3$ | 8.82 | 7.44 | 7.79 | 8.12 | 8.40 | 8.61 | 7.41 | 8.08 |
| $ThO_2$ | 1.87 | 1.97 | 1.68 | 1.86 | 1.73 | 1.87 | 2.07 | 1.86 |
| Total | 87.45 | 89.16 | 86.03 | 85.82 | 85.37 | 86.89 | 86.96 | 86.81 |

Table 5b. Microprobe analyses of medium-REE area in titanosilicate 6 from sample RP-52 (37-71 are different point analyses).

| | 37 | 44 | 51 | 52 | 69 | 70 | 71 | Av. |
|---|---|---|---|---|---|---|---|---|
| $SiO_2$ | 27.72 | 27.50 | 29.64 | 27.91 | 26.78 | 27.23 | 26.32 | 27.59 |
| $Al_2O_3$ | 0.79 | 0.82 | 0.79 | 0.82 | 0.76 | 0.82 | 0.77 | 0.80 |
| $TiO_2$ | 25.32 | 26.96 | 21.33 | 21.24 | 24.38 | 24.77 | 26.42 | 24.35 |
| $ZrO_2$ | 1.14 | 1.28 | 1.20 | 1.11 | 1.25 | 1.30 | 1.38 | 1.24 |
| $Nb_2O_5$ | 6.76 | 7.01 | 6.48 | 6.76 | 7.22 | 7.05 | 7.26 | 6.93 |
| FeO | 8.01 | 8.05 | 7.35 | 7.32 | 7.70 | 8.29 | 8.30 | 7.86 |
| MnO | 0.17 | 0.30 | 0.34 | 0.23 | 0.23 | 0.29 | 0.24 | 0.26 |
| MgO | 0.03 | 0.06 | 0.06 | 0.04 | 0.09 | 0.08 | 0.05 | 0.06 |
| CaO | 1.54 | 1.61 | 1.65 | 1.75 | 1.68 | 1.61 | 1.56 | 1.63 |
| $K_2O$ | 0.18 | 0.15 | 0.20 | 0.13 | 0.13 | 0.15 | 0.11 | 0.15 |
| BaO | 0.00 | 0.26 | 0.00 | 0.08 | 0.18 | 0.22 | 0.53 | 0.18 |
| $La_2O_3$ | 4.46 | 4.48 | 4.83 | 4.89 | 5.39 | 4.18 | 4.06 | 4.61 |
| $Ce_2O_3$ | 9.29 | 9.44 | 11.11 | 11.04 | 9.08 | 9.41 | 9.33 | 9.82 |
| $ThO_2$ | 1.69 | 1.88 | 1.76 | 1.81 | 1.89 | 1.87 | 1.75 | 1.81 |
| Total | 87.08 | 89.81 | 86.74 | 85.13 | 86.77 | 87.27 | 88.08 | 87.27 |

## CONCLUDING REMARKS

Electron microprobe analyses of some accessory minerals in syenitic rocks from the Alto Paraguay Province confirmed the presence of Zr and Ti disilicates, such as rosenbuschite, in Cerro Boggiani samples RP-31A and RP-33 and also of låvenite in sample RP-40. Moreover, in sample RP-33, the Na, Zr-rich ring silicate eudialyte was determined. The mineral chemistry of these phases pointed to the significantly high concentration of MnO in both rosenbuschite and låvenite, and the intermediate nature of eudialyte, which displays characteristics between eudialyte s.s. and an REE-rich type.

In Cerro Siete Cabezas sample RP-52, microprobe analyses of REE-rich titanosilicates were not conclusive for mineral classification, mainly as a result of the non-stoichiometric structural formulae of the minerals. Probably, intergrowth textures among different REE-rich phases, both structurally complex and partially amorphous, and also smaller in size than the beam diameter, are thought to be responsible for the strong chemical variations shown by the different analysed points. Additional work from a structural viewpoint will be necessary for a better understanding of these complex phenomena.

## ACKNOWLEDGEMENTS

The Italian CNR financed the installation and maintenance of the microprobe laboratory at the University of Padova. The authors are grateful to P. Comin-Chiaramonti for suggesting this study and also for providing the samples. Elena Belluso, Giovanni Ferraris and Angela Gula are kindly acknowledged for advice on titanosilicates and eudialytes. Raul Carampin kindly assisted in the microanalyses. The authors are grateful to Gabriel Walton for revising the English text.

Table 5c. Microprobe analyses of high-REE area in titanosilicate 6 from sample RP-52 (41-77 are different point analyses). Numbers of ions on the basis of 22 (O).

| | 41 | 42 | 43 | 45 | 48 | 49 | 50 | 53 | 54 | 55 | 56 | 57 | 58 | 59 | 60 | 68 | 73 | 74 | 75 | 76 | 77 | Av. | St. Dev. |
|---|---|---|---|---|---|---|---|---|---|---|---|---|---|---|---|---|---|---|---|---|---|---|---|
| $SiO_2$ | 25.44 | 25.24 | 25.03 | 25.69 | 23.92 | 24.45 | 26.16 | 24.67 | 24.69 | 24.58 | 26.22 | 25.04 | 25.12 | 24.25 | 25.03 | 26.66 | 24.08 | 24.49 | 24.98 | 26.50 | 25.85 | 25.15 | 0.79 |
| $Al_2O_3$ | 0.67 | 0.61 | 0.61 | 0.71 | 0.58 | 0.61 | 0.73 | 0.58 | 0.61 | 0.60 | 0.72 | 0.72 | 0.63 | 0.59 | 0.66 | 0.67 | 0.52 | 0.53 | 0.63 | 0.83 | 0.73 | 0.64 | 0.07 |
| $TiO_2$ | 22.50 | 22.84 | 23.49 | 22.51 | 22.99 | 20.48 | 20.95 | 20.44 | 19.43 | 20.26 | 19.92 | 19.90 | 21.24 | 19.70 | 20.03 | 21.32 | 21.03 | 19.94 | 21.23 | 20.54 | 20.77 | 21.03 | 1.19 |
| $ZrO_2$ | 1.58 | 1.60 | 1.53 | 1.39 | 1.51 | 1.43 | 1.13 | 1.34 | 1.64 | 1.74 | 1.47 | 1.43 | 1.31 | 1.52 | 1.43 | 1.52 | 1.47 | 1.31 | 1.38 | 1.24 | 1.24 | 1.44 | 0.15 |
| $Nb_2O_5$ | 6.12 | 6.16 | 5.55 | 6.00 | 5.87 | 5.72 | 6.29 | 5.23 | 5.52 | 6.05 | 6.07 | 5.42 | 5.83 | 5.70 | 6.24 | 5.87 | 5.92 | 5.53 | 5.34 | 5.96 | 6.19 | 5.84 | 0.31 |
| FeO | 8.01 | 7.85 | 7.95 | 7.48 | 7.87 | 7.34 | 7.39 | 7.52 | 7.33 | 7.43 | 7.04 | 7.10 | 7.35 | 7.26 | 7.40 | 7.55 | 7.16 | 7.29 | 7.23 | 7.61 | 7.27 | 7.45 | 0.27 |
| MnO | 0.18 | 0.22 | 0.14 | 0.23 | 0.32 | 0.18 | 0.28 | 0.30 | 0.24 | 0.14 | 0.24 | 0.25 | 0.17 | 0.17 | 0.25 | 0.25 | 0.23 | 0.27 | 0.26 | 0.18 | 0.27 | 0.23 | 0.05 |
| MgO | 0.07 | 0.05 | 0.04 | 0.06 | 0.01 | 0.06 | 0.02 | 0.05 | 0.06 | 0.04 | 0.06 | 0.06 | 0.10 | 0.09 | 0.03 | 0.05 | 0.04 | 0.08 | 0.09 | 0.06 | 0.05 | 0.05 | 0.02 |
| CaO | 2.38 | 2.36 | 2.34 | 2.03 | 2.28 | 2.13 | 1.95 | 2.39 | 2.42 | 2.46 | 2.29 | 2.22 | 2.20 | 2.35 | 2.26 | 2.14 | 2.25 | 2.56 | 2.16 | 1.98 | 1.99 | 2.24 | 0.17 |
| $K_2O$ | 0.09 | 0.09 | 0.11 | 0.11 | 0.15 | 0.14 | 0.09 | 0.09 | 0.09 | 0.09 | 0.13 | 0.15 | 0.11 | 0.14 | 0.13 | 0.15 | 0.12 | 0.16 | 0.20 | 0.36 | 0.18 | 0.14 | 0.06 |
| BaO | 0.30 | 0.00 | 0.09 | 0.17 | 0.16 | 0.05 | 0.00 | 0.14 | 0.08 | 0.00 | 0.42 | 0.22 | 0.17 | 0.07 | 0.02 | 0.34 | 0.00 | 0.00 | 0.03 | 0.30 | 0.05 | 0.12 | 0.13 |
| $La_2O_3$ | 6.69 | 6.16 | 6.90 | 5.89 | 6.63 | 6.52 | 6.33 | 6.61 | 7.31 | 6.87 | 6.37 | 6.73 | 6.79 | 6.85 | 6.86 | 5.91 | 6.82 | 8.02 | 6.50 | 5.60 | 6.55 | 6.62 | 0.51 |
| $Ce_2O_3$ | 12.09 | 13.02 | 13.20 | 13.40 | 13.55 | 13.69 | 11.89 | 13.95 | 13.93 | 14.09 | 12.64 | 14.16 | 12.47 | 14.63 | 12.51 | 12.95 | 14.24 | 13.66 | 13.58 | 12.99 | 12.15 | 13.27 | 0.78 |
| $ThO_2$ | 1.65 | 1.50 | 1.49 | 1.41 | 1.23 | 1.20 | 1.54 | 1.26 | 1.04 | 1.11 | 1.41 | 1.49 | 1.45 | 1.18 | 1.27 | 1.41 | 1.28 | 1.16 | 1.43 | 1.56 | 1.45 | 1.36 | 0.16 |
| Total | 87.76 | 87.69 | 88.48 | 87.07 | 87.07 | 83.99 | 84.76 | 84.56 | 84.40 | 85.48 | 85.01 | 84.90 | 84.93 | 84.50 | 84.12 | 86.79 | 85.15 | 85.01 | 85.04 | 85.70 | 84.75 | 85.58 | 1.33 |
| | | | | | | | | | | | | | | | | | | | | | | | |
| Si | 4.861 | 4.825 | 4.771 | 4.926 | 4.670 | 4.931 | 5.108 | 4.955 | 4.992 | 4.899 | 5.151 | 5.018 | 4.962 | 4.920 | 5.005 | 5.108 | 4.827 | 4.935 | 4.952 | 5.145 | 5.075 | 4.954 | 0.124 |
| Al | 0.150 | 0.137 | 0.138 | 0.159 | 0.133 | 0.144 | 0.167 | 0.138 | 0.146 | 0.142 | 0.167 | 0.169 | 0.146 | 0.142 | 0.155 | 0.151 | 0.124 | 0.125 | 0.148 | 0.190 | 0.170 | 0.150 | 0.016 |
| Ti | 3.234 | 3.284 | 3.368 | 3.246 | 3.376 | 3.107 | 3.077 | 3.089 | 2.955 | 3.038 | 2.944 | 3.000 | 3.156 | 3.006 | 3.014 | 3.072 | 3.171 | 3.022 | 3.166 | 3.000 | 3.067 | 3.114 | 0.127 |
| Zr | 0.148 | 0.149 | 0.142 | 0.130 | 0.144 | 0.141 | 0.108 | 0.131 | 0.162 | 0.170 | 0.141 | 0.140 | 0.127 | 0.150 | 0.139 | 0.142 | 0.144 | 0.129 | 0.134 | 0.118 | 0.118 | 0.138 | 0.014 |
| Nb | 0.529 | 0.533 | 0.479 | 0.520 | 0.518 | 0.522 | 0.555 | 0.475 | 0.504 | 0.545 | 0.539 | 0.491 | 0.520 | 0.523 | 0.564 | 0.508 | 0.536 | 0.503 | 0.479 | 0.523 | 0.549 | 0.520 | 0.025 |
| $Fe^{2+}$ | 1.280 | 1.255 | 1.267 | 1.200 | 1.285 | 1.238 | 1.206 | 1.264 | 1.239 | 1.239 | 1.157 | 1.190 | 1.214 | 1.232 | 1.237 | 1.210 | 1.200 | 1.228 | 1.200 | 1.235 | 1.194 | 1.227 | 0.032 |
| Mn | 0.029 | 0.035 | 0.023 | 0.037 | 0.054 | 0.031 | 0.047 | 0.052 | 0.041 | 0.024 | 0.041 | 0.043 | 0.028 | 0.029 | 0.042 | 0.041 | 0.038 | 0.045 | 0.044 | 0.029 | 0.046 | 0.038 | 0.009 |
| Mg | 0.020 | 0.015 | 0.010 | 0.018 | 0.002 | 0.017 | 0.005 | 0.015 | 0.017 | 0.013 | 0.017 | 0.017 | 0.029 | 0.026 | 0.010 | 0.014 | 0.013 | 0.024 | 0.027 | 0.017 | 0.014 | 0.016 | 0.007 |
| Ca | 0.487 | 0.484 | 0.478 | 0.417 | 0.476 | 0.459 | 0.409 | 0.514 | 0.524 | 0.525 | 0.482 | 0.476 | 0.466 | 0.511 | 0.485 | 0.440 | 0.483 | 0.553 | 0.459 | 0.411 | 0.420 | 0.474 | 0.039 |
| K | 0.022 | 0.022 | 0.026 | 0.027 | 0.038 | 0.037 | 0.024 | 0.022 | 0.024 | 0.022 | 0.034 | 0.039 | 0.027 | 0.037 | 0.033 | 0.037 | 0.030 | 0.042 | 0.051 | 0.088 | 0.044 | 0.034 | 0.015 |
| Ba | 0.022 | 0.000 | 0.007 | 0.013 | 0.012 | 0.004 | 0.000 | 0.011 | 0.006 | 0.000 | 0.032 | 0.018 | 0.013 | 0.005 | 0.001 | 0.026 | 0.000 | 0.000 | 0.003 | 0.023 | 0.004 | 0.010 | 0.010 |
| La | 0.471 | 0.434 | 0.485 | 0.417 | 0.477 | 0.485 | 0.456 | 0.490 | 0.545 | 0.505 | 0.461 | 0.498 | 0.495 | 0.513 | 0.506 | 0.418 | 0.504 | 0.596 | 0.475 | 0.401 | 0.475 | 0.481 | 0.044 |
| Ce | 0.846 | 0.911 | 0.921 | 0.941 | 0.968 | 1.011 | 0.850 | 1.026 | 1.031 | 1.028 | 0.909 | 1.039 | 0.902 | 1.086 | 0.916 | 0.908 | 1.045 | 1.008 | 0.985 | 0.923 | 0.873 | 0.958 | 0.070 |
| Th | 0.072 | 0.065 | 0.065 | 0.061 | 0.055 | 0.055 | 0.068 | 0.057 | 0.048 | 0.050 | 0.063 | 0.068 | 0.065 | 0.055 | 0.058 | 0.061 | 0.058 | 0.053 | 0.064 | 0.069 | 0.065 | 0.061 | 0.007 |
| Sum | 12.170 | 12.148 | 12.178 | 12.111 | 12.208 | 12.182 | 12.081 | 12.239 | 12.237 | 12.199 | 12.139 | 12.204 | 12.151 | 12.234 | 12.166 | 12.135 | 12.174 | 12.263 | 12.187 | 12.171 | 12.114 | 12.176 | 0.046 |

Table 5d. Microprobe analyses of high-Ti area in titanosilicate 6 from sample RP-52 (33-67 are different point analyses).

| | 33 | 34 | 35 | 39 | 40 | 65 | 66 | 67 | Av. |
|---|---|---|---|---|---|---|---|---|---|
| $SiO_2$ | 21.16 | 20.90 | 21.18 | 25.59 | 20.50 | 21.01 | 23.56 | 21.68 | 21.95 |
| $Al_2O_3$ | 0.68 | 0.59 | 0.69 | 0.69 | 0.64 | 0.64 | 0.73 | 0.70 | 0.67 |
| $TiO_2$ | 35.55 | 36.09 | 35.78 | 32.25 | 36.42 | 32.46 | 30.91 | 33.19 | 34.08 |
| $ZrO_2$ | 1.22 | 1.11 | 1.03 | 1.03 | 1.16 | 1.23 | 1.21 | 1.14 | 1.14 |
| $Nb_2O_5$ | 8.18 | 8.88 | 8.71 | 8.51 | 8.51 | 7.99 | 8.32 | 9.13 | 8.53 |
| FeO | 11.69 | 11.49 | 11.37 | 10.01 | 11.73 | 11.09 | 10.36 | 11.03 | 11.10 |
| MnO | 0.31 | 0.37 | 0.36 | 0.28 | 0.34 | 0.37 | 0.26 | 0.33 | 0.33 |
| MgO | 0.03 | 0.01 | 0.01 | 0.05 | 0.02 | 0.06 | 0.05 | 0.04 | 0.03 |
| CaO | 1.00 | 0.84 | 0.91 | 1.18 | 0.82 | 0.99 | 1.00 | 0.86 | 0.95 |
| $K_2O$ | 0.17 | 0.18 | 0.19 | 0.16 | 0.14 | 0.19 | 0.11 | 0.19 | 0.17 |
| BaO | 0.35 | 0.12 | 0.50 | 0.07 | 0.13 | 0.16 | 0.16 | 0.18 | 0.21 |
| $La_2O_3$ | 1.69 | 1.84 | 2.16 | 2.52 | 2.45 | 2.64 | 2.53 | 2.08 | 2.24 |
| $Ce_2O_3$ | 5.67 | 5.02 | 5.77 | 7.38 | 5.05 | 5.31 | 6.02 | 4.88 | 5.64 |
| $ThO_2$ | 2.22 | 2.22 | 2.04 | 2.29 | 2.28 | 1.96 | 2.29 | 1.88 | 2.15 |
| Total | 89.92 | 89.66 | 90.70 | 92.01 | 90.19 | 86.10 | 87.51 | 87.31 | 89.18 |

Table 5e. Microprobe analyses of titanosilicate 10 from sample RP-52 (20-30 are different point analyses).

| | 20 | 21 | 22 | 23 | 24 | 25 | 26 | 27 | 28 | 29 | 30 | Av. |
|---|---|---|---|---|---|---|---|---|---|---|---|---|
| $SiO_2$ | 25.38 | 25.99 | 26.21 | 29.70 | 29.24 | 26.33 | 25.68 | 26.49 | 31.14 | 27.95 | 24.97 | 27.19 |
| $Al_2O_3$ | 0.87 | 0.88 | 0.92 | 1.02 | 0.95 | 0.92 | 1.00 | 0.93 | 1.13 | 1.03 | 0.79 | 0.95 |
| $TiO_2$ | 15.01 | 14.48 | 13.54 | 13.24 | 12.65 | 13.98 | 15.64 | 14.48 | 11.81 | 12.40 | 15.11 | 13.85 |
| $ZrO_2$ | 0.90 | 1.08 | 0.90 | 0.84 | 0.84 | 1.04 | 1.20 | 1.01 | 0.76 | 0.67 | 1.01 | 0.93 |
| $Nb_2O_5$ | 6.18 | 6.11 | 6.39 | 6.12 | 5.59 | 6.41 | 6.76 | 6.53 | 6.80 | 7.37 | 6.46 | 6.43 |
| FeO | 18.49 | 17.67 | 16.81 | 16.20 | 17.15 | 19.88 | 16.87 | 17.08 | 18.38 | 20.86 | 13.83 | 17.57 |
| MnO | 0.21 | 0.18 | 0.30 | 0.15 | 0.17 | 0.17 | 0.22 | 0.31 | 0.22 | 0.20 | 0.18 | 0.21 |
| MgO | 0.03 | 0.02 | 0.06 | 0.08 | 0.02 | 0.04 | 0.03 | 0.04 | 0.02 | 0.05 | 0.03 | 0.04 |
| CaO | 1.66 | 1.66 | 1.85 | 1.55 | 1.62 | 1.46 | 1.93 | 1.77 | 1.14 | 1.30 | 1.72 | 1.60 |
| $K_2O$ | 0.14 | 0.06 | 0.21 | 0.11 | 0.08 | 0.05 | 0.20 | 0.04 | 0.05 | 0.08 | 0.04 | 0.10 |
| BaO | 0.22 | 0.19 | 0.00 | 0.00 | 0.08 | 0.00 | 0.00 | 0.00 | 0.29 | 0.00 | 0.00 | 0.07 |
| $La_2O_3$ | 4.22 | 4.72 | 4.64 | 4.36 | 4.33 | 4.13 | 5.14 | 4.02 | 3.86 | 3.79 | 5.32 | 4.41 |
| $Ce_2O_3$ | 10.22 | 9.97 | 10.18 | 9.21 | 9.08 | 8.43 | 10.05 | 9.12 | 7.47 | 7.35 | 11.25 | 9.30 |
| $ThO_2$ | 1.39 | 1.48 | 1.48 | 2.23 | 2.46 | 1.36 | 1.38 | 1.45 | 1.28 | 1.22 | 1.25 | 1.54 |
| Total | 84.91 | 84.49 | 83.48 | 84.80 | 84.26 | 84.20 | 86.09 | 83.27 | 84.36 | 84.25 | 81.96 | 84.19 |

## REFERENCES


Bellezza, M., Merlino, S. & Perchiazzi, N. (2003). Chemical and structural study of the Zr, Ti-disilicates in the venanzite from Pian di Celle, Umbria, Italy. *GEOITALIA 2003 - 4° Forum Italiano di Scienze della Terra, Bellaria,* pp. 604-605.

Comin-Chiaramonti, P., Gomes, C.B., Censi, P., Gasparon, M. & Velázquez, V.F. (in this volume). Alkaline complexes from the Alto Paraguay Province at the border of Brazil (Mato Grosso do Sul state) and Paraguay.

Deer, W.A., Howie, R.A. & Zussman, J. (1997). *Rock-forming minerals, Vol. 1B, Disilicates and ring silicates*. The Geological Society, London.

Ferraris, G. (1997). Polysomatism as a tool for correlating properties and structure. In: Merlino, S. (ed.) *Modular aspects of minerals*. Budapest: European Mineralogical Union, pp. 275-295.

Ferraris, G., Belluso, E., Gula, A., Soboleva, S., Ageeva, O. & Borutskii, B. (2001) A structural model of the layer titanosilicate bornemanite based on seidozerite and lomonosovite modules. *Canadian Mineralogist* **39**, 1665-1673.

Gaines, R.V., Skinner, H.C.W., Foord, E.E., Mason, B. & Rosenzweig, A. (1997). *Dana's new mineralogy*. New York: John Wiley.

Gula, A. (2002). *Caratterizzazione e modellizzazione di silicati iperalcalini*. Ph.D. Thesis, University of Modena and Reggio Emilia, Italy.

Johnsen, O. & Grice, J.D. (1999) The crystal chemistry of the eudialyte group. *Canadian Mineralogist* **37**, 865-891.

Liziero, F., Carbonin, S., Belluso, E. (2003) Disomogeneità ed eterogeneità in titanosilicati di sieniti dell'Alto Paraguay. *GEOITALIA 2003 - 4° Forum Italiano di Scienze della Terra, Bellaria*, pp. 638-639.

Mellini, M. (1981) Refinement of the crystal structure of låvenite. *Tschermaks Mineralogische und Petrographische Mitteilungen* **28**, 99-112.

Woolley, A.R. & Platt, R.G. (1988) The peralkaline nepheline syenite of the Junguni intrusion, Chilwa province, Malawi. *Mineralogical Magazine* **52**, 425-433.

*Brazilian Platform*
*Comin-Chiaramonti, P. & Gomes, C.B. (eds.)*
*Edusp/Fapesp, São Paulo, pp. 149-158, 2005*

# ALKALINE COMPLEXES FROM SOUTHEASTERN BOLIVIA

*P. Comin-Chiaramonti, C.B. Gomes, V.F. Velázquez, P. Censi, P. Antonini, F. Comin-Chiaramonti and R. Punturo*

*Similarly to other peripheral areas of the Paraná Basin, southeastern Bolivia is characterized by the presence of Early Cretaceous potassic alkaline-carbonatitic rocks and Late Cretaceous potassic alkaline rocks in the regions of Velasco and Candelaria, respectively. These regions correspond to well-defined tectonic areas, i.e. Guaporé craton and Sunsas belt, respectively. The Velasco alkaline magmatism is represented by a group of interfingering plutons mainly lying along a narrow NE-trending belt, by an associated dyke swarm and by scarce volcanic remnants. Intrusive rocks consist of nepheline syenites, nephel-syenites, syenites, quartz syenites and granites; effusive types range from trachyphonolites to trachytes, whereas the dykes show both silica-oversaturated and silica-undersaturated varieties. Hypersolvus rocks seem to prevail, and agpaitic, metaluminous and peraluminous types occur even in a single pluton. Some carbonate-rich xenoliths or isolated blocks in the Velasco complex are indicative of an associated carbonatitic activity. Mineralogical results point up, in general, to a shallow depth and subvolcanic character for the intrusions and an apparent important activity of volatile phases such as F, Cl, $SO_2$ and $H_2O$. Petrochemical data are not indicative of simple genetic links among all the rock-types, e.g. derivation by crystal fractionation from a common source, and suggest several different trends or distinct rates of emplacement. In particular, quartz-normative magmas appear to have assimilated upper crust material, whereas nepheline-normative rocks usually seem to have been not appreciably affected by open-system crustal magma chamber processes. Sr isotope systematics display a common age of about 140 Ma for both undersaturated and oversaturated rocks, but with different initial isotopic ratios, i.e. $^{87}Sr/^{86}Sr = 0.70445$ (nepheline-bearing rock-types), 0.70619 (quartz syenites) and 0.70666-0.70745 (granites and aplogranites, respectively), indicating a possible role of progressive crustal contamination for the oversaturated types, probably due to the slow rate of emplacement. Sr-Nd data confirm the role played by crustal contamination processes due to mixing or mingling with the basement rocks. Nd model ages for the undersaturated types fit an age of 600±31 Ma, whereas the oversaturated ones span from 1031 to 1302 Ma (av. 1163±143 Ma), suggesting for the latter some mixing with the model ages of the basement rocks. Cerro Manomó, about 20 km NE of the northernmost fringe of the Velasco complex, forms a hill characterized by Fe- and Si-rich bands to which some authors have proposed a genesis linked to an important carbonatitic magmatism in the region. As a matter of fact, U-Th and REE concentrations along apatitite lens and sideritic-ankeritic blocks seem to support the above hypothesis. However, Cerro Manomó shows general characteristics which are very similar to those found in some worldwide banded iron formations. Candelaria rocks are represented by a few rock pavements and knolls, i.e. microsyenites, nephel-syenites and trachytes, roughly similar in composition to some Velasco rock-types and to Ponta do Morro alkaline rocks (Late Cretaceous: Mato Grosso state, Brazil, Poxoréu region). Rb/Sr errorchron provided an age around 80 Ma and initial $^{87}Sr/^{86}Sr = 0.70470$. Sr-Nd isotopes show values similar to those obtained for the Poxoréu igneous province, but with a Nd model age of 928±19 Ma. The coexistence of Early and Late Cretaceous alkaline magmatism in southeastern Bolivia, in analogy to other border areas of the Paraná Basin l.s., e.g. Eastern Paraguay and Namibia, puts severe constraints to any geodynamic interpretation based on mantle plume models.*

## INTRODUCTION

Southeastern Bolivia is part of the Rondônia block and of the Sunsas-Aguapeí belts, at the southwestern fringe of the Amazonian craton (Teixeira *et al*., 1989; Leite & Saes, 2000; Tohver *et al*., 2002), where about 30 km of crustal rocks overlap a thick continental lithospheric mantle (Jaillard *et al.*, 2002).

The Rondônia block (Paraguá craton or San Ignatio block, of Litherland *et al*., 1986, 1989) is characterized by high to medium grade metamorphic rocks and granitic complexes in the Paraguá region, mainly 2.0-1.3 Ga in age (Bolivian Chiquitania Gneissic Complex, Lomas Maneches Granulite Complex, San Ignatio Schist Supergroup and Pensamiento Granite Complex: cf. Litherland & Bloomfield, 1981; Litherland *et al*., 1989; Sousa, 1991).

The Rondônia block is bordered by the Rio Negro-Jurema Province (crystalline basement: 1.7-1.5 Ga) on the eastern side, through the Marechal Rondon Shear Zone (Teixeira & Tassinari, 1984).

The NW-SE-trending Sunsas belt (inset of Fig. 1), at the southern rim of the Paraguá (Rondônia) block, is bordered at the western side by the NNW-trending Aguapeí belt and represents the reactivated basement (1.3-0.9 Ga; cf. Litherland *et al.*, 1989; Sadowski & Bettencourt, 1996; Geraldes *et al*., 2000, 2001; Tohver *et al*., 2002).

The region was the site of two main alkaline magmatic episodes in Early and Late Cretaceous times (Almeida, 1983), i.e. Velasco and Candelaria igneous provinces (inset of Fig. 1), in the Rondônia block and in the Sunsas belt, respectively (Darbyshire & Fletcher, 1979; Litherland *et al*., 1986, 1989; Sadowski & Bettencourt, 1996).

*The Velasco Province* (Fletcher, 1979; Fletcher & Beddoe-Stephens, 1987), as shown in Fig. 1, consists of almost 14 overlapping ring and elliptical plutons (granite to nepheline syenite in composition), a western satellite body (Las Copas granite; Litherland *et al.*, 1986) and a northeastern complex (Cerro Manomó: "silicified ferrocarbonatitic complex", according to Fletcher *et al*., 1981), all emplaced in Precambrian gneisses, migmatites and granites of the San Ignatio-Rio Guaporé belt (1366 Ma; Darbyshire & Fletcher, 1979; Almeida *et al*., 2000). K/Ar determinations give an average value of 136±7 Ma, and Rb/Sr isochron ages are 141±5 Ma and 144±4 Ma for the Cabeza de Toro and Cerro Bamba plutons, respectively (Darbyshire & Fletcher, 1979; Litherland *et al.*, 1986).

*The Candelaria Province* (Pitfield, 1979) is poorly documented, with its alkaline magmatic rocks only represented by a few knolls, mostly buried under a thick alluvium of the Pantanal basin, which are overlying a Middle-Proterozoic sedimentary basin (Fortuna Formation of Alvarenga & Saes, 1992). According to Litherland *et al.* (1986), the main rock-types are micronordmarkites, quartz syenites and nordmarkites, displaying K/Ar ages of 76±2, 90±3 and 116±17 Ma, respectively.

The petrography, petrochemistry, mineral chemistry, geochemistry and Sr-Nd isotopic systematics of the alkaline rocks from southeastern Bolivia will be described mainly on the basis of a new extensive sampling chiefly performed (1999 and 2002) by the first three authors. Analytical procedures are discussed in Comin-Chiaramonti *et al*. (in this volume).

## VELASCO ALKALINE COMPLEXES

The alkaline plutons, with diameters of 1 to 8 km, crop out over an area of 500 km$^2$ and intrude the Precambrian metamorphic rocks, mainly along a NE-trending fault system. The main plutonic bodies are: Todos Santos, Taperas, Tirari, Retiro, San Miguelito, Cabeza de Toro, Bamba, San Francisco, Mercedes, Zuialito, Urucú, Tanomonia and Prado (Fig. 1). Volcanic rocks (agglomerates, tuffs and porphyritic trachytes) have been found only along the Paraguá river (cf. San Miguelito complexes of Fig. 1). Alkaline dykes (aphyric, porphyritic and fine-grained types, 1-3 m thick, with subvertical dip and mainly presenting NE and E-W attitudes) are widespread and penetrate both the plutons and the surrounding crystalline basement up to 30 km from the nearest complexes.

Petrography, classification and nomenclature

In the $R_1$-$R_2$ diagram (Fig. 2A; cf. De La Roche *et al.*, 1980) the intrusive samples that have been analysed are dominantly syenites, quartz syenites and granites (44, 8 and 20%, respectively), with subordinate nephel-syenites and nepheline syenites (18 and 10%, respectively; cf. Table 1). According to the IUGS classification (cf. Le Maitre, 1989), the rock-types are alkali feldspar granites and subordinate granites, quartz-alkali feldspar syenites and quartz syenites, alkali feldspar syenites, foid-bearing alkali feldspar syenites, foid-bearing syenites and foid syenites (Fig. 2B). The nepheline is the principal feldspathoid in the undersaturated rocks, and haüyne and/or sodalite megacrysts are present in the strongly undersaturated nepheline syenites (e.g. PV-22 and PV-27 samples).

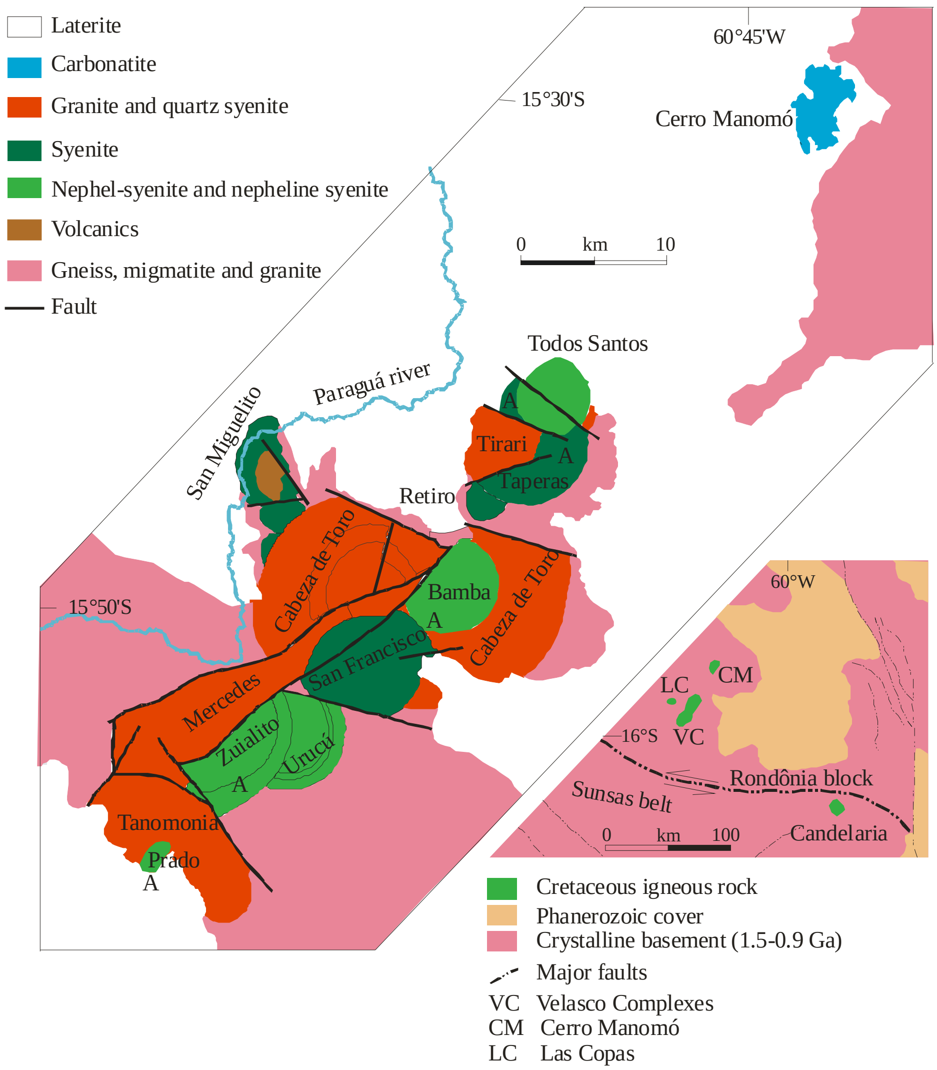


Fig. 1. Geological sketch-map of the Velasco alkaline province, modified after Litherland *et al.* (1986) and Fletcher & Beddoe-Stephens (1987). A, agpaitic rock-types (see Fig. 3). Inset: generalized geology of the Rondônia block and Sunsas belt, showing the location of the Candelaria alkaline province (modified after Litherland *et al.*, 1989; Sadowski & Bettencourt, 1996; Geraldes *et al.*, 2000, 2001).

Table 1. Major, trace element analyses and CIPW norms of representative rock-types from the Velasco complexes. A.I.=($Na_2O$+$K_2O$)/$Al_2O_3$ (molar ratio); R1-R2, as defined by De La Roche *et al.* (1980) (cf. Fig. 2). For analytical methods see Comin-Chiaramonti *et al.* (in this volume).

| | TODOS SANTOS | | | | TIRARI | | TAPERAS | | | RETIRO | | |
|---|---|---|---|---|---|---|---|---|---|---|---|---|
| Sample | 20 | 21 | 22 Dyke | 23 | 28 | 29 | 30 | 31 | 31A | 32 | 33 | 34 |
| wt% | | | | | | | | | | | | |
| $SiO_2$ | 58.57 | 58.60 | 56.42 | 55.34 | 73.06 | 71.84 | 62.42 | 66.71 | 63.58 | 63.25 | 43.45 | 63.88 |
| $TiO_2$ | 0.91 | 0.79 | 1.02 | 1.34 | 0.14 | 0.18 | 0.60 | 0.15 | 0.20 | 0.44 | 0.36 | 0.45 |
| $Al_2O_3$ | 17.14 | 19.05 | 18.07 | 18.10 | 13.20 | 13.13 | 16.51 | 16.96 | 16.53 | 16.99 | 10.64 | 17.16 |
| $Fe_2O_3$ | 2.42 | 2.40 | 2.99 | 3.17 | 1.00 | 1.39 | 2.47 | 0.99 | 3.47 | 1.13 | 0.51 | 1.14 |
| FeO | 2.37 | 2.24 | 3.10 | 3.64 | 1.02 | 1.41 | 1.96 | 0.72 | | 0.93 | 0.87 | 0.94 |
| MnO | 0.17 | 0.15 | 0.20 | 0.16 | 0.09 | 0.06 | 0.19 | 0.12 | 0.16 | 0.10 | 0.64 | 0.10 |
| MgO | 1.42 | 0.95 | 1.72 | 2.07 | 0.01 | 0.01 | 0.51 | 0.09 | 0.24 | 0.45 | 0.25 | 0.45 |
| CaO | 3.38 | 3.03 | 3.87 | 4.76 | 0.72 | 0.93 | 1.61 | 0.49 | 1.12 | 2.82 | 19.79 | 2.85 |
| $Na_2O$ | 5.56 | 6.10 | 5.73 | 5.29 | 4.24 | 4.41 | 6.47 | 6.57 | 7.12 | 6.01 | 3.72 | 6.07 |
| $K_2O$ | 5.23 | 5.12 | 4.66 | 4.22 | 5.30 | 5.25 | 6.03 | 6.53 | 5.47 | 6.15 | 4.48 | 6.21 |
| $P_2O_5$ | 0.49 | 0.36 | 0.55 | 0.64 | 0.05 | 0.05 | 0.18 | 0.09 | 0.05 | 0.20 | 2.46 | 0.20 |
| LOI | 1.39 | 1.43 | 1.45 | 1.15 | 0.82 | 0.95 | 0.82 | 0.40 | 1.91 | 1.41 | 12.82 | 0.50 |
| Sum | 99.05 | 100.22 | 99.78 | 99.88 | 99.64 | 99.60 | 99.77 | 99.81 | 99.85 | 99.88 | 99.99 | 99.95 |
| ppm | | | | | | | | | | | | |
| Cr | 21.22 | | | 5.21 | | | | 2.47 | | | 1.63 | |
| Ba | 681.71 | 1493.88 | 1517.20 | 1705.33 | 171.29 | 231.72 | 1219.80 | 428.52 | | 1433.84 | 514.60 | 1458 |
| Rb | 375.12 | 218.45 | 206.40 | 157.11 | 380.21 | 387.64 | 150.38 | 218.12 | | 200.81 | 147.93 | 204 |
| Sr | 1346.83 | 1086.45 | 1015.63 | 1417.74 | 79.34 | 99.69 | 339.62 | 737.58 | | 672.48 | 1484.02 | 680 |
| Pb | | 26.32 | 24.60 | 17.97 | 19.72 | 22.54 | 14.96 | | | 49.38 | | |
| Nb | 738.78 | 308.84 | 371.69 | 187.03 | 158.77 | 163.78 | 177.46 | 80.20 | | 130.29 | 65.57 | 133 |
| Ta | | 22.41 | 29.79 | 13.48 | 15.41 | 12.32 | 10.53 | | | 12.78 | | |
| Hf | | 17.86 | 20.57 | 38.85 | 13.04 | 15.02 | 13.54 | | | 4.35 | | |
| U | 26.34 | 23.71 | 41.09 | 11.99 | 12.38 | 10.88 | 6.61 | 6.38 | | 4.74 | 6.89 | 5 |
| Th | 86.34 | 51.70 | 46.83 | 23.44 | 56.92 | 47.17 | 64.12 | 28.19 | | 13.68 | 55.92 | 14 |
| Zr | 802.20 | 875.75 | 961.17 | 2084.89 | 375.53 | 504.92 | 655.71 | 175.17 | | 137.22 | 125.07 | 140 |
| Y | 85.85 | 38.46 | 55.34 | 41.59 | 90.90 | 93.74 | 57.93 | 218.46 | | 33.25 | 237.47 | |
| Ga | | 22.50 | 23.49 | 21.66 | 26.32 | 27.13 | 28.21 | | | 24.20 | | 26 |
| Ge | | 1.45 | 1.42 | 1.55 | 2.08 | 2.26 | 1.92 | | | 1.62 | | |
| La | 313.90 | 153.42 | 198.93 | 145.46 | 140.71 | 188.57 | 238.80 | 788.93 | | 90.26 | 469.97 | 105 |
| Ce | 592.68 | 271.66 | 371.87 | 265.72 | 277.30 | 255.24 | 487.77 | 869.80 | | 187.84 | 946.01 | 218 |
| Pr | 52.44 | 27.35 | 39.28 | 28.33 | 30.02 | 38.46 | 51.01 | 116.78 | | 21.29 | 95.32 | |
| Nd | 186.59 | 85.73 | 123.82 | 90.65 | 103.57 | 125.76 | 161.45 | 453.69 | | 73.07 | 523.42 | 85 |
| Sm | 25.85 | 11.62 | 17.51 | 12.79 | 19.25 | 21.52 | 23.05 | 57.05 | | 11.58 | 61.43 | |
| Eu | 6.10 | 3.74 | 3.94 | 3.92 | 0.64 | 0.93 | 4.07 | 8.39 | | 2.55 | 19.84 | |
| Gd | 19.02 | 7.76 | 11.52 | 8.86 | 14.95 | 16.74 | 15.49 | 38.59 | | 7.42 | 89.53 | |
| Tb | 3.17 | 1.34 | 1.93 | 1.41 | 2.57 | 2.71 | 2.30 | 5.37 | | 1.20 | 12.67 | |
| Dy | 14.39 | 7.23 | 10.06 | 7.41 | 15.13 | 15.93 | 12.05 | 33.89 | | 6.34 | 86.78 | |
| Ho | 3.17 | 1.37 | 1.96 | 1.39 | 3.07 | 3.14 | 2.06 | 5.37 | | 1.13 | 15.98 | |
| Er | 8.29 | 4.13 | 5.61 | 4.16 | 9.06 | 9.16 | 6.11 | 16.11 | | 3.33 | 24.52 | |
| Tm | 1.71 | 0.69 | 0.86 | 0.65 | 1.53 | 1.47 | 0.94 | 3.02 | | 0.51 | 5.23 | |
| Yb | 9.27 | 4.80 | 5.93 | 4.54 | 9.63 | 9.08 | 5.95 | 14.09 | | 3.22 | 25.34 | |
| Lu | 1.46 | 0.76 | 0.94 | 0.73 | 1.39 | 1.28 | 0.87 | 2.35 | | 0.47 | 3.58 | |
| Q | | | | | 26.54 | 24.34 | | | 0.03 | 0.97 | | 0.98 |
| or | 30.90 | 30.25 | 27.53 | 24.93 | 31.32 | 31.02 | 35.63 | 38.59 | 32.77 | 36.34 | | 36.70 |
| ab | 46.61 | 46.00 | 42.85 | 41.84 | 35.87 | 37.31 | 50.24 | 50.88 | 55.33 | 50.85 | | 51.36 |
| an | 6.36 | 9.47 | 9.82 | 13.18 | 1.33 | 0.52 | | | | 1.21 | | 1.22 |
| ne | 0.23 | 3.03 | 3.05 | 1.57 | | | 0.59 | | | | | |
| ac | | | | | | | 2.99 | 2.86 | 2.83 | | | |
| ns | | | | | | | | 0.33 | 0.59 | | | |
| di | 5.75 | 2.57 | 4.69 | 5.03 | 1.63 | 2.83 | 5.69 | 1.59 | 4.62 | 2.85 | | 2.88 |
| wo | | | | | | | | | | 3.28 | | 3.31 |
| hy | | | | | 0.06 | 0.28 | | 0.68 | 2.35 | | | |
| ol | 1.39 | 1.60 | 2.83 | 3.51 | | | 0.13 | | | | | |
| mt | 3.50 | 3.47 | 4.33 | 4.59 | 1.44 | 2.01 | 2.08 | | | 1.63 | | 1.65 |
| il | 1.72 | 1.50 | 1.93 | 2.54 | 0.26 | 0.34 | 1.13 | 0.28 | 0.38 | 0.83 | | 0.84 |
| ap | 1.16 | 0.85 | 1.30 | 1.51 | 0.11 | 0.11 | 0.42 | 0.21 | 0.12 | 0.47 | | 0.48 |
| Q | 44.6 | 43.1 | 42.9 | 43.8 | 60.3 | 59.2 | 44.4 | 47.0 | 45.0 | 45.3 | | 45.4 |
| Ne | 32.8 | 35.2 | 35.8 | 35.5 | 19.0 | 19.0 | 32.2 | 29.5 | 33.9 | 30.5 | | 31.2 |
| Ks | 22.6 | 21.7 | 21.3 | 20.7 | 20.7 | 21.8 | 23.4 | 23.5 | 21.1 | 24.2 | | 23.4 |
| A.I. | 0.86 | 0.82 | 0.80 | 0.73 | 0.96 | 0.99 | 1.04 | 1.05 | 1.07 | 0.97 | 1.03 | 0.97 |
| $K_2O/Na_2O$ | 0.94 | 0.84 | 0.81 | 0.80 | 1.25 | 1.19 | 0.93 | 0.99 | 0.77 | 1.02 | 1.20 | 1.02 |
| R1 | 554 | 397 | 446 | 606 | 2063 | 1912 | 318 | 535 | 335 | 575 | | 580 |
| R2 | 768 | 745 | 854 | 967 | 340 | 362 | 521 | 890 | 456 | 657 | | 664 |
| Rock-type | Syenite | Nephel-syenite | Trachy-phonolite | Nephel-syenite | Granite | Granite | Syenite | Syenite | Syenite | Syenite | Carbonate-rich xenolith | Syenite |

Table 1 (continued).

| | SAN MIGUELITO | | | | | | | | | | | | | |
|---|---|---|---|---|---|---|---|---|---|---|---|---|---|---|
| Sample | 17 | PV-57 | 2 | 3 | 4 | 5 | 10 | 11 | 12 | 13 | 14 | 15 | 16 | 18 |
| | | | | | | Dyke | | | | | | | | |
| wt% | | | | | | | | | | | | | | |
| $SiO_2$ | 66.26 | 60.40 | 63.08 | 63.87 | 64.04 | 65.84 | 59.11 | 64.01 | 62.13 | 65.01 | 66.57 | 63.93 | 64.93 | 60.67 |
| $TiO_2$ | 0.31 | 0.68 | 0.70 | 0.43 | 0.63 | 0.42 | 1.12 | 0.69 | 0.65 | 0.43 | 0.56 | 0.65 | 0.62 | 0.97 |
| $Al_2O_3$ | 16.90 | 16.07 | 17.86 | 17.45 | 17.10 | 17.22 | 18.58 | 17.14 | 18.17 | 17.65 | 16.73 | 16.63 | 16.30 | 16.57 |
| $Fe_2O_3$ | 1.37 | 2.29 | 1.66 | 1.60 | 1.72 | 1.55 | 2.45 | 1.79 | 1.95 | 1.52 | 1.10 | 2.17 | 1.98 | 2.86 |
| FeO | 1.09 | 2.28 | 1.27 | 1.18 | 1.43 | 1.30 | 2.35 | 1.51 | 1.60 | 1.19 | 0.97 | 2.13 | 1.85 | 3.10 |
| MnO | 0.11 | 0.15 | 0.13 | 0.19 | 0.12 | 0.11 | 0.18 | 0.17 | 0.20 | 0.09 | 0.09 | 0.14 | 0.15 | 0.17 |
| MgO | 0.20 | 1.23 | 0.51 | 0.80 | 0.59 | 0.25 | 1.38 | 0.74 | 0.70 | 0.25 | 0.28 | 0.74 | 0.68 | 1.73 |
| CaO | 0.63 | 2.42 | 0.92 | 0.40 | 1.32 | 0.96 | 2.94 | 1.56 | 1.29 | 0.72 | 1.37 | 1.92 | 1.75 | 3.28 |
| $Na_2O$ | 5.93 | 6.08 | 5.75 | 5.57 | 4.90 | 5.68 | 5.80 | 5.71 | 6.17 | 5.77 | 5.57 | 5.05 | 5.29 | 4.77 |
| $K_2O$ | 6.33 | 6.41 | 7.11 | 7.51 | 7.10 | 6.15 | 5.19 | 6.16 | 6.08 | 6.70 | 5.72 | 5.41 | 5.54 | 4.97 |
| $P_2O_5$ | 0.05 | 0.26 | 0.12 | 0.04 | 0.16 | 0.08 | 0.49 | 0.22 | 0.23 | 0.09 | 0.22 | 0.27 | 0.21 | 0.43 |
| LOI | 0.56 | 1.05 | 0.58 | 0.61 | 0.62 | 0.53 | 0.54 | 0.08 | 0.57 | 0.33 | 0.50 | 0.68 | 0.30 | 0.57 |
| Sum | 99.74 | 99.32 | 99.69 | 99.65 | 99.73 | 100.09 | 100.13 | 99.78 | 99.74 | 99.75 | 99.66 | 99.72 | 99.59 | 100.09 |
| ppm | | | | | | | | | | | | | | |
| Cr | | | | 5.75 | 4.53 | | | 3.12 | | | 3.83 | 5.87 | 5.23 | 17.16 |
| Ba | 203.63 | | 171.74 | 350.69 | 1379.75 | 231.52 | 2238.37 | 207.99 | 769.06 | 268.42 | 406.71 | 970.57 | 147.24 | 1129.88 |
| Rb | 253.76 | | 155.86 | 237.44 | 342.06 | 196.51 | 92.63 | 175.10 | 114.52 | 176.96 | 296.31 | 195.80 | 229.24 | 163.55 |
| Sr | 78.28 | | 71.02 | 731.05 | 1112.15 | 112.97 | 1804.14 | 750.76 | 527.07 | 159.93 | 771.48 | 357.15 | 557.67 | 524.22 |
| Pb | 15.23 | | 18.90 | | | 22.38 | 11.97 | | 11.80 | 16.68 | | 31.58 | | 15.49 |
| Nb | 146.81 | | 124.84 | 180.59 | 108.72 | 229.01 | 93.89 | 174.53 | 90.17 | 118.81 | 212.08 | 153.29 | 204.70 | 136.05 |
| Ta | 12.22 | | 11.35 | | | 18.59 | 6.90 | | 6.17 | 8.73 | | 12.06 | | 9.65 |
| Hf | 16.69 | | 8.54 | | | 20.24 | 9.72 | | 7.27 | 20.26 | | 15.00 | | 14.26 |
| U | 7.86 | | 3.21 | 3.65 | 6.85 | 8.49 | 1.92 | 3.61 | 1.94 | 5.58 | 7.38 | 5.17 | 6.75 | 4.08 |
| Th | 66.26 | | 14.72 | 38.58 | 61.99 | 64.45 | 15.70 | 35.93 | 21.29 | 53.32 | 51.01 | 40.82 | 46.42 | 28.14 |
| Zr | 634.07 | | 377.20 | 151.60 | 70.72 | 786.87 | 483.41 | 110.65 | 344.70 | 876.65 | 135.57 | 589.41 | 222.90 | 606.93 |
| Y | 42.60 | | 105.31 | 66.21 | 81.62 | 74.85 | 39.64 | 59.13 | 34.04 | 31.86 | 73.15 | 48.89 | 70.14 | 47.43 |
| Ga | 26.21 | | 22.75 | | | 25.13 | 20.51 | | 21.18 | 23.08 | | 23.84 | | 21.77 |
| Ge | 1.85 | | 1.69 | | | 1.86 | 1.62 | | 1.76 | 1.68 | | 2.01 | | 1.72 |
| La | 176.49 | | 197.16 | 248.40 | 367.91 | 260.52 | 199.00 | 223.38 | 251.04 | 157.42 | 183.56 | 160.32 | 154.81 | 153.03 |
| Ce | 324.47 | | 328.38 | 477.63 | 649.22 | 482.78 | 370.70 | 429.85 | 461.93 | 327.32 | 343.62 | 298.03 | 319.63 | 281.18 |
| Pr | 32.41 | | 38.66 | 44.29 | 61.99 | 49.07 | 39.14 | 38.40 | 44.21 | 31.25 | 33.22 | 31.86 | 32.52 | 30.19 |
| Nd | 97.40 | | 139.88 | 172.15 | 211.22 | 144.62 | 130.01 | 146.39 | 135.88 | 93.42 | 117.79 | 106.78 | 135.79 | 99.15 |
| Sm | 12.61 | | 20.41 | 20.78 | 26.79 | 20.08 | 17.04 | 17.87 | 16.04 | 11.55 | 18.12 | 15.05 | 19.43 | 14.60 |
| Eu | 1.04 | | 3.51 | 2.97 | 3.74 | 1.33 | 3.74 | 3.61 | 2.51 | 1.26 | 2.35 | 2.39 | 3.68 | 2.76 |
| Gd | 8.00 | | 16.83 | 14.84 | 13.71 | 12.77 | 11.72 | 11.22 | 9.77 | 7.41 | 15.10 | 10.56 | 21.68 | 10.45 |
| Tb | 1.35 | | 2.55 | 2.74 | 2.18 | 2.26 | 1.69 | 1.52 | 1.51 | 1.16 | 1.68 | 1.70 | 3.48 | 1.66 |
| Dy | 7.96 | | 14.68 | 12.79 | 12.77 | 13.04 | 8.53 | 9.32 | 7.26 | 6.04 | 12.08 | 9.27 | 13.91 | 9.51 |
| Ho | 1.56 | | 3.06 | 2.28 | 2.18 | 2.56 | 1.44 | 1.90 | 1.31 | 1.23 | 2.35 | 1.85 | 2.66 | 1.73 |
| Er | 4.99 | | 8.78 | 5.94 | 8.10 | 7.67 | 4.27 | 5.32 | 3.66 | 3.97 | 6.04 | 5.36 | 7.16 | 4.92 |
| Tm | 0.91 | | 1.33 | 1.14 | 1.56 | 1.21 | 0.61 | 1.14 | 0.56 | 0.74 | 1.34 | 0.90 | 1.43 | 0.79 |
| Yb | 6.56 | | 8.86 | 5.25 | 7.17 | 8.51 | 4.02 | 4.94 | 3.62 | 5.61 | 6.71 | 5.94 | 7.57 | 5.44 |
| Lu | 1.07 | | 1.46 | 0.91 | 1.25 | 1.34 | 0.64 | 0.76 | 0.61 | 0.99 | 1.01 | 1.00 | 1.23 | 0.86 |
| Q | 6.20 | | 0.40 | 0.84 | 5.31 | 6.97 | | 3.90 | | 4.07 | 9.83 | 9.02 | 8.95 | 5.51 |
| C | | | | | | | | | | | | | | |
| or | 37.40 | 37.88 | 42.01 | 44.38 | 41.95 | 36.34 | 30.67 | 36.40 | 35.93 | 39.59 | 33.80 | 31.97 | 32.74 | 29.37 |
| ab | 50.17 | 39.38 | 48.65 | 47.13 | 41.46 | 48.06 | 48.21 | 48.31 | 52.20 | 48.82 | 47.13 | 42.73 | 44.76 | 40.36 |
| an | 0.80 | | 1.92 | 0.43 | 3.69 | 3.32 | 9.33 | 2.94 | 3.92 | 2.47 | 3.75 | 6.73 | 4.37 | 9.12 |
| ne | | 4.11 | | | | | 0.46 | | | | | | | |
| ac | | 3.95 | | | | | | | | | | | | |
| ns | | | | | | | | | | | | | | |
| di | 1.64 | 8.35 | 1.44 | 1.01 | 1.43 | 0.74 | 1.62 | 2.66 | 0.76 | 0.40 | 1.26 | 0.84 | 2.32 | 3.50 |
| hy | 0.33 | | 0.63 | 1.98 | 1.16 | 0.86 | | 1.03 | 1.04 | 0.79 | 0.21 | 2.73 | 1.53 | 4.64 |
| ol | | 1.53 | | | | | 2.44 | | 0.67 | | | | | |
| mt | 1.98 | 1.34 | 2.4 | 2.31 | 2.49 | 2.24 | 3.55 | 2.59 | 2.82 | 2.20 | 1.59 | 3.14 | 2.87 | 4.14 |
| il | 0.58 | 1.29 | 1.32 | 0.81 | 1.19 | 0.79 | 2.12 | 1.31 | 1.23 | 0.81 | 1.06 | 1.23 | 1.17 | 1.84 |
| ap | 0.11 | 0.60 | 0.28 | 0.09 | 0.37 | 0.18 | 1.16 | 0.52 | 0.54 | 0.21 | 0.52 | 0.63 | 0.49 | 1.01 |
| Q | 48.3 | 42.3 | 44.9 | 45.0 | 48.1 | 48.9 | 44.9 | 47.1 | 44.7 | 47.1 | 50.7 | 50.6 | 50.4 | 48.8 |
| Ne | 29.0 | 31.3 | 28.9 | 27.7 | 25.0 | 28.5 | 33.1 | 29.6 | 32.1 | 28.6 | 28.1 | 27.7 | 28.1 | 29.0 |
| Ks | 22.7 | 26.4 | 26.2 | 27.3 | 26.9 | 22.6 | 22.0 | 23.3 | 23.2 | 24.3 | 21.2 | 21.7 | 21.5 | 22.2 |
| A.I. | 0.98 | 1.05 | 0.96 | 0.99 | 0.92 | 0.93 | 0.82 | 0.94 | 0.92 | 0.95 | 0.92 | 0.85 | 0.90 | 0.80 |
| $K_2O/Na_2O$ | 1.07 | 1.05 | 1.24 | 1.35 | 1.45 | 1.08 | 0.89 | 1.08 | 0.99 | 1.16 | 1.03 | 1.07 | 1.05 | 1.04 |
| R1 | 755 | 227 | 403 | 437 | 766 | 844 | 509 | 691 | 416 | 632 | 1049 | 1069 | 1034 | 1002 |
| R2 | 409 | 635 | 474 | 425 | 506 | 453 | 748 | 539 | 529 | 436 | 489 | 568 | 541 | 762 |
| Rock-type | Trachyte | Trachyte | Syenite | Syenite | Syenite | Syenite | Syenite | Syenite | Syenite | Syenite | Quartz syenite | Quartz syenite | Syenite | Syenite |

Table 1 (continued).

| | CABEZA DE TORO | | | | | | | | | | | | | |
|---|---|---|---|---|---|---|---|---|---|---|---|---|---|---|
| Sample | 1 | 6 | 7 | 7B | 8 | 9 | PV-1 | PV-2 | PV-5 | PV-6 | PV-7 | PV-8 | PV-9 | PV-10 |
| wt% | | | | | | | | | | | | | | |
| $SiO_2$ | 71.47 | 69.99 | 72.87 | 69.45 | 62.83 | 64.86 | 72.56 | 71.88 | 64.65 | 63.14 | 66.26 | 67.41 | 70.05 | 71.82 |
| $TiO_2$ | 0.26 | 0.17 | 0.19 | 0.40 | 0.47 | 0.67 | 0.28 | 0.32 | 0.56 | 0.58 | 0.40 | 0.33 | 0.20 | 0.20 |
| $Al_2O_3$ | 13.15 | 15.26 | 13.70 | 15.15 | 18.29 | 17.23 | 14.06 | 14.54 | 16.56 | 18.23 | 15.49 | 15.80 | 14.56 | 13.49 |
| $Fe_2O_3$ | 1.23 | 0.72 | 0.80 | 1.29 | 1.44 | 1.41 | 0.94 | 0.80 | 1.95 | 1.84 | 1.64 | 1.52 | 1.28 | 1.20 |
| FeO | 1.20 | 0.64 | 0.82 | 1.55 | 1.12 | 1.07 | 1.16 | 0.97 | 1.85 | 1.66 | 1.49 | 1.41 | 1.25 | 1.28 |
| MnO | 0.04 | 0.02 | 0.01 | 0.01 | 0.14 | 0.25 | 0.01 | 0.03 | 0.15 | 0.12 | 0.15 | 0.12 | 0.10 | 0.09 |
| MgO | 0.07 | 0.01 | 0.01 | 0.80 | 0.55 | 0.43 | 0.49 | 0.85 | 0.61 | 0.56 | 0.30 | 0.29 | 0.16 | 0.15 |
| CaO | 0.57 | 0.51 | 0.60 | 1.94 | 1.22 | 0.90 | 1.66 | 1.79 | 1.70 | 1.90 | 1.09 | 1.06 | 0.79 | 0.71 |
| $Na_2O$ | 4.57 | 5.10 | 4.23 | 3.13 | 6.05 | 6.14 | 2.98 | 3.39 | 5.04 | 5.82 | 5.15 | 4.88 | 4.38 | 4.05 |
| $K_2O$ | 5.52 | 5.88 | 5.30 | 5.13 | 6.60 | 6.67 | 4.83 | 4.66 | 5.70 | 5.47 | 5.85 | 5.92 | 5.82 | 5.23 |
| $P_2O_5$ | 0.01 | 0.01 | 0.05 | 0.10 | 0.16 | 0.08 | 0.10 | 0.04 | 0.20 | 0.18 | 0.08 | 0.11 | 0.06 | 0.07 |
| LOI | 1.22 | 1.12 | 1.16 | 0.77 | 0.83 | 0.05 | 0.64 | 0.60 | 0.83 | 0.38 | 1.10 | 0.90 | 1.05 | 0.78 |
| Sum | 99.31 | 99.43 | 99.72 | 99.71 | 99.70 | 99.76 | 99.70 | 99.87 | 99.80 | 99.88 | 99.00 | 99.75 | 99.70 | 99.07 |
| ppm | | | | | | | | | | | | | | |
| Cr | | 1.94 | | | | 2.95 | 6.30 | 2.57 | | | 5.84 | | | |
| Ba | | 252.57 | 378.13 | 972.69 | 482.01 | 180.05 | 579.82 | 247.05 | 1506.04 | 2086.40 | 389.42 | 709.69 | 174.19 | 236.17 |
| Rb | | 343.41 | 282.21 | 203.55 | 136.61 | 155.10 | 225.02 | 258.87 | 179.17 | 139.91 | 336.86 | 213.17 | 266.34 | 238.01 |
| Sr | | 480.87 | 33.11 | 193.35 | 165.62 | 564.03 | 140.33 | 55.32 | 297.41 | 409.41 | 1239.42 | 140.89 | 30.79 | 29.98 |
| Pb | | | 20.89 | 45.13 | 20.74 | | 37.58 | | 25.51 | 16.42 | | 38.34 | 36.33 | 27.30 |
| Nb | | 187.46 | 163.72 | 109.5 | 62.51 | 186.62 | 98.3 | 102.53 | 122.94 | 82.47 | 181.02 | 131.86 | 177.41 | 182.53 |
| Ta | | | 14.03 | 10.10 | 4.73 | | 6.01 | | 10.81 | 7.40 | | 12.40 | 14.03 | 13.76 |
| Hf | | | 14.57 | 7.80 | 3.09 | | | | 12.84 | 8.79 | | 13.26 | 13.58 | 13.23 |
| U | | 8.68 | 9.57 | 3.35 | 2.06 | 2.49 | 4.74 | 3.78 | 5.83 | 3.11 | 9.85 | 7.61 | 9.29 | 9.42 |
| Th | | 45.18 | 45.09 | 56.42 | 10.54 | 23.81 | 59.25 | 48.94 | 33.48 | 15.89 | 42.34 | 42.52 | 60.94 | 53.21 |
| Zr | | 89.71 | 487.94 | 239.79 | 114.23 | 87.76 | 190.25 | 71.87 | 548.71 | 384.52 | 104.02 | 521.70 | 444.92 | 428.81 |
| Y | | 743.41 | 130.96 | 20.90 | 16.08 | 53.97 | 20.76 | 17.26 | 52.13 | 34.84 | 122.99 | 61.56 | 75.81 | 138.36 |
| Ga | | | 31.41 | 19.08 | 19.96 | | 18.50 | | 24.37 | 22.60 | | 25.68 | 28.22 | 25.56 |
| Ge | | | 2.10 | 1.43 | 1.46 | | 1.44 | | 1.66 | 1.51 | | 1.74 | 1.99 | 1.81 |
| La | | 1442.77 | 182.07 | 75.96 | 92.61 | 213.15 | 84.05 | 51.54 | 153.66 | 96.22 | 170.07 | 165.27 | 210.83 | 140.06 |
| Ce | | 2026.52 | 283.63 | 157.88 | 148.99 | 395.69 | 172.37 | 115.60 | 287.32 | 174.42 | 308.03 | 299.28 | 392.80 | 267.65 |
| Pr | | 214.95 | 38.33 | 17.78 | 13.91 | 33.79 | 19.79 | 12.77 | 30.38 | 18.42 | 32.85 | 30.69 | 39.15 | 28.59 |
| Nd | | 760.77 | 129.61 | 64.01 | 40.51 | 143.08 | 69.25 | 49.41 | 98.97 | 64.40 | 135.04 | 96.86 | 120.77 | 93.23 |
| Sm | | 116.24 | 24.36 | 12.77 | 4.85 | 16.55 | 12.73 | 9.69 | 14.89 | 9.73 | 21.17 | 14.83 | 18.78 | 16.99 |
| Eu | | 4.18 | 1.18 | 1.45 | 2.38 | 2.04 | 1.33 | 0.95 | 2.70 | 3.71 | 2.19 | 1.62 | 0.56 | 0.55 |
| Gd | | 85.85 | 19.14 | 10.30 | 3.21 | 10.88 | 7.87 | 7.57 | 10.45 | 7.12 | 14.60 | 11.33 | 13.50 | 15.50 |
| Tb | | 12.54 | 3.32 | 1.34 | 0.53 | 2.49 | 0.99 | 0.71 | 1.72 | 1.08 | 2.56 | 1.79 | 2.39 | 2.65 |
| Dy | | 57.72 | 19.47 | 5.90 | 2.84 | 10.43 | 5.02 | 3.31 | 9.36 | 6.02 | 15.69 | 10.30 | 13.93 | 16.59 |
| Ho | | 9.81 | 3.80 | 0.72 | 0.54 | 2.04 | 0.76 | 0.71 | 1.78 | 1.12 | 2.56 | 2.08 | 2.72 | 3.81 |
| Er | | 29.10 | 10.76 | 1.43 | 1.74 | 5.22 | 1.65 | 1.89 | 5.39 | 3.59 | 9.12 | 5.98 | 8.43 | 11.00 |
| Tm | | 4.66 | 1.69 | 0.14 | 0.30 | 1.13 | 0.21 | 0.24 | 0.81 | 0.54 | 1.83 | 1.00 | 1.32 | 1.73 |
| Yb | | 23.79 | 10.99 | 0.79 | 1.99 | 4.99 | 1.35 | 1.18 | 6.17 | 3.94 | 9.49 | 7.18 | 9.23 | 11.75 |
| Lu | | 3.22 | 1.63 | 0.11 | 0.33 | 0.68 | 0.16 | 0.24 | 0.84 | 0.55 | 1.46 | 1.04 | 1.38 | 1.81 |
| Q | 22.88 | 16.82 | 26.43 | 26.00 | | 2.10 | 32.30 | 29.04 | 9.31 | 3.75 | 11.55 | 13.68 | 20.17 | 26.15 |
| C | | | 0.03 | 1.16 | | | 1.15 | 0.76 | | | | | | 0.04 |
| or | 32.62 | 34.74 | 31.32 | 30.31 | 39.00 | 39.41 | 28.54 | 27.53 | 33.68 | 32.32 | 34.57 | 34.98 | 34.39 | 30.90 |
| ab | 36.90 | 43.15 | 35.79 | 26.48 | 51.00 | 51.49 | 25.21 | 28.68 | 42.64 | 49.24 | 43.57 | 41.29 | 37.06 | 34.27 |
| an | | 1.38 | 2.65 | 8.97 | 3.25 | | 7.58 | 8.61 | 5.72 | 7.46 | 1.87 | 3.72 | 2.88 | 3.06 |
| ne | | | | | 0.10 | | | | | | | | | |
| ac | 1.55 | | | | | 0.40 | | | | | | | | |
| ns | | | | | | | | | | | | | | |
| di | 2.41 | 0.67 | | | 1.38 | 2.82 | | | 1.14 | 0.62 | 2.50 | 0.67 | 0.54 | |
| wo | | 0.12 | | | | 0.16 | | | | | | | | |
| hy | 0.18 | | 0.80 | 3.16 | | | | | 2.08 | 1.87 | 0.47 | 1.38 | 1.20 | 1.56 |
| ol | | | | | 0.74 | | | | | | | | | |
| mt | 1.00 | 1.04 | 1.15 | 1.87 | 2.08 | 1.84 | 1.36 | 1.15 | 2.82 | 2.66 | 2.37 | 2.20 | 1.85 | 1.73 |
| il | 0.49 | 0.32 | 0.36 | 0.75 | 0.89 | 1.27 | 0.53 | 0.60 | 1.06 | 1.10 | 0.75 | 0.62 | 0.37 | 0.37 |
| ap | 0.02 | 0.02 | 0.11 | 0.23 | 0.37 | 0.18 | 0.23 | 0.09 | 0.47 | 0.42 | 0.18 | 0.26 | 0.14 | 0.16 |
| Q | 58.3 | 54.5 | 60.2 | 61.9 | 44.6 | 45.9 | 65.3 | 63.4 | 50.7 | 47.2 | 51.8 | 53.0 | 56.8 | 60.5 |
| Ne | 21.6 | 24.7 | 20.7 | 17.3 | 30.8 | 30.0 | 15.9 | 18.2 | 27.0 | 31.3 | 26.3 | 24.9 | 21.9 | 20.3 |
| Ks | 20.1 | 20.8 | 19.1 | 20.8 | 24.6 | 24.1 | 18.8 | 18.4 | 22.3 | 21.5 | 21.9 | 22.1 | 21.3 | 19.2 |
| A.I. | 1.03 | 0.97 | 0.93 | 0.71 | 0.93 | 1.01 | 0.72 | 0.73 | 0.87 | 0.85 | 0.95 | 0.91 | 0.93 | 0.91 |
| $K_2O/Na_2O$ | 1.21 | 1.15 | 1.22 | 1.64 | 1.09 | 1.09 | 1.62 | 1.37 | 1.13 | 0.94 | 1.14 | 1.21 | 1.33 | 1.29 |
| R1 | 1775 | 1435 | 2063 | 2228 | 414 | 498 | 2580 | 2438 | 1068 | 752 | 1123 | 1286 | 1677 | 2051 |
| R2 | 322 | 354 | 334 | 544 | 516 | 456 | 478 | 519 | 537 | 589 | 435 | 438 | 378 | 348 |
| Rock-type | Granite | Quartz syenite | Granite | Granite | Syenite | Syenite | Granite | Granite | Quartz syenite | Syenite | Quartz syenite | Quartz syenite | Granite | Granite |

Table 1 (continued).

| | CABEZA DE TORO | | | | | | | | | BAMBA | | | |
|---|---|---|---|---|---|---|---|---|---|---|---|---|---|
| Sample | PV-11 | PV-12 | PV-13 | PV-3 | PV-4 | 24 | 25 | 26 | 27 | PV-39 | PV-40 | PV-41 | PV-42 |
| | | Dyke | Dyke | | | | | Dyke | Dyke | | | | |
| wt% | | | | | | | | | | | | | |
| $SiO_2$ | 71.23 | 67.05 | 55.61 | 70.16 | 68.92 | 64.46 | 69.87 | 53.76 | 75.71 | 63.97 | 64.98 | 63.57 | 59.83 |
| $TiO_2$ | 0.14 | 0.28 | 1.37 | 0.19 | 0.35 | 0.58 | 0.29 | 1.43 | 0.01 | 0.41 | 0.22 | 0.70 | 1.12 |
| $Al_2O_3$ | 14.86 | 14.88 | 16.11 | 14.79 | 13.55 | 16.04 | 14.48 | 15.61 | 12.79 | 16.74 | 16.81 | 17.19 | 17.12 |
| $Fe_2O_3$ | 0.92 | 2.50 | 3.96 | 1.19 | 1.67 | 2.00 | 1.41 | 3.87 | 0.13 | 2.00 | 1.42 | 1.40 | 2.59 |
| FeO | 0.88 | 2.30 | 5.19 | 1.13 | 1.64 | 1.80 | 1.31 | 5.29 | 0.14 | 1.55 | 1.11 | 1.10 | 2.24 |
| MnO | 0.04 | 0.27 | 0.23 | 0.06 | 0.13 | 0.17 | 0.10 | 0.21 | 0.01 | 0.22 | 0.22 | 0.13 | 0.27 |
| MgO | 0.01 | 0.18 | 1.99 | 0.13 | 0.21 | 0.48 | 0.18 | 2.03 | 0.01 | 0.34 | 0.53 | 0.54 | 1.20 |
| CaO | 0.58 | 0.60 | 4.16 | 0.61 | 1.06 | 1.40 | 0.80 | 4.41 | 0.79 | 1.16 | 1.56 | 2.00 | 2.33 |
| $Na_2O$ | 4.58 | 6.01 | 4.63 | 4.46 | 4.75 | 5.34 | 4.90 | 3.90 | 4.33 | 6.66 | 6.56 | 6.38 | 5.96 |
| $K_2O$ | 5.64 | 4.85 | 3.65 | 5.92 | 5.38 | 5.89 | 5.68 | 4.12 | 4.82 | 5.94 | 5.92 | 6.16 | 5.92 |
| $P_2O_5$ | 0.06 | 0.06 | 0.77 | 0.06 | 0.04 | 0.15 | 0.04 | 0.79 | 0.05 | 0.02 | 0.12 | 0.26 | 0.38 |
| LOI | 0.72 | 0.72 | 1.88 | 1.05 | 1.02 | 1.40 | 0.70 | 4.11 | 0.73 | 0.61 | 0.58 | 0.63 | 1.08 |
| Sum | 99.65 | 99.70 | 99.55 | 99.75 | 98.72 | 99.71 | 99.76 | 99.53 | 99.49 | 99.62 | 100.03 | 100.06 | 100.04 |
| ppm | | | | | | | | | | | | | |
| Cr | | | | | 5.27 | 3.88 | 3.18 | | | 4.33 | 4.88 | | |
| Ba | 437.89 | 67.19 | 2471.43 | 486.34 | 747.04 | 311.02 | 365.65 | 2300.78 | 121.49 | 319.33 | 292.48 | 3128.72 | 3682.46 |
| Rb | 226.88 | 286.68 | 93.00 | 253.64 | 359.11 | 246.12 | 418.12 | 111.98 | 358.73 | 201.33 | 175.49 | 176.95 | 212.96 |
| Sr | 77.81 | 19.01 | 643.10 | 76.23 | 465.27 | 1324.97 | 163.53 | 552.68 | 28.47 | 995.33 | 387.47 | 650.75 | 740.99 |
| Pb | 25.76 | 42.65 | 9.14 | 19.22 | | | | 7.16 | 51.16 | | | 11.94 | 24.75 |
| Nb | 108.53 | 339.59 | 95.54 | 147.53 | 214.04 | 140.82 | 224.00 | 88.43 | 169.14 | 138.00 | 139.28 | 208.59 | 255.53 |
| Ta | 12.25 | 24.06 | 6.52 | 13.19 | | | | 6.38 | 23.04 | | | 19.64 | 20.93 |
| Hf | 9.15 | 38.29 | 13.48 | 13.46 | | | | 12.06 | 7.32 | | | 8.74 | 9.32 |
| U | 7.65 | 28.34 | 3.51 | 6.49 | 8.87 | 4.49 | 7.77 | 3.33 | 11.02 | 4.33 | 1.95 | 2.47 | 1.04 |
| Th | 35.10 | 68.90 | 20.99 | 41.33 | 41.38 | 39.18 | 52.47 | 20.25 | 60.07 | 41.33 | 16.99 | 12.45 | 12.49 |
| Zr | 297.25 | 1582.80 | 554.31 | 461.77 | 164.78 | 129.80 | 138.82 | 523.53 | 110.27 | 147.33 | 137.05 | 274.70 | 351.09 |
| Y | 49.09 | 150.53 | 70.22 | 83.10 | 137.69 | 108.16 | 119.06 | 70.53 | 74.91 | 69.67 | 74.10 | 50.23 | 57.16 |
| Ga | 24.46 | 34.72 | 26.91 | 27.54 | | | | 25.97 | 29.02 | | | 20.59 | 21.04 |
| Ge | 1.81 | 2.74 | 2.05 | 1.71 | | | | 1.79 | 1.79 | | | 1.70 | 1.91 |
| La | 99.80 | 425.97 | 147.90 | 164.35 | 170.69 | 153.88 | 177.18 | 135.83 | 57.50 | 154.67 | 128.41 | 174.44 | 191.84 |
| Ce | 182.74 | 743.30 | 291.58 | 270.81 | 354.43 | 308.16 | 353.88 | 271.14 | 86.58 | 284.33 | 285.52 | 354.70 | 396.03 |
| Pr | 19.38 | 80.99 | 35.99 | 31.94 | 38.67 | 29.39 | 34.59 | 33.31 | 12.49 | 27.67 | 33.71 | 40.40 | 42.69 |
| Nd | 64.24 | 258.04 | 133.38 | 102.62 | 166.01 | 127.35 | 137.65 | 122.39 | 42.14 | 112.33 | 141.23 | 139.58 | 148.70 |
| Sm | 10.29 | 36.64 | 22.76 | 18.24 | 31.53 | 17.96 | 22.12 | 21.07 | 8.48 | 16.67 | 23.40 | 21.48 | 22.47 |
| Eu | 1.01 | 1.22 | 6.47 | 1.37 | 2.46 | 4.90 | 1.41 | 6.04 | 0.67 | 2.00 | 2.51 | 3.80 | 5.13 |
| Gd | 8.10 | 26.48 | 17.82 | 13.84 | 19.70 | 12.65 | 20.24 | 16.11 | 6.60 | 14.33 | 15.32 | 13.63 | 14.51 |
| Tb | 1.39 | 4.35 | 2.65 | 2.43 | 3.70 | 2.45 | 3.29 | 2.42 | 1.20 | 2.00 | 2.79 | 2.15 | 2.32 |
| Dy | 8.62 | 24.52 | 14.26 | 13.90 | 22.17 | 11.43 | 20.47 | 13.53 | 8.39 | 11.67 | 15.32 | 11.58 | 12.91 |
| Ho | 1.79 | 4.83 | 2.49 | 2.86 | 4.68 | 2.45 | 3.77 | 2.40 | 1.78 | 2.00 | 2.51 | 2.07 | 2.31 |
| Er | 5.27 | 14.05 | 6.54 | 8.26 | 11.82 | 6.94 | 9.65 | 6.40 | 6.12 | 5.67 | 7.52 | 5.12 | 6.01 |
| Tm | 0.85 | 2.31 | 0.96 | 1.31 | 2.71 | 1.63 | 2.12 | 0.95 | 1.21 | 1.33 | 1.39 | 0.79 | 0.81 |
| Yb | 6.26 | 14.60 | 6.02 | 8.83 | 12.81 | 7.76 | 9.88 | 5.61 | 8.90 | 6.33 | 6.96 | 4.96 | 5.02 |
| Lu | 0.89 | 2.06 | 0.84 | 1.18 | 2.22 | 1.22 | 1.65 | 0.81 | 1.43 | 1.00 | 1.11 | 0.78 | 0.69 |
| Q | 21.47 | 11.85 | 3.67 | 19.82 | 18.76 | 7.87 | 17.96 | 3.80 | 30.84 | 0.73 | 1.68 | 0.28 | |
| C | 0.31 | | | 0.08 | | | | | | | | | |
| or | 33.33 | 28.66 | 21.57 | 34.98 | 31.79 | 34.80 | 33.56 | 24.34 | 28.48 | 35.10 | 34.98 | 36.40 | 34.98 |
| ab | 38.75 | 49.43 | 39.17 | 37.73 | 39.74 | 45.18 | 41.46 | 33.00 | 36.63 | 53.03 | 53.50 | 53.98 | 46.63 |
| an | 2.48 | | 12.39 | 2.63 | | 2.40 | 0.74 | 12.92 | 1.22 | | | 0.07 | 2.47 |
| ne | | | | | | | | | | | | | 2.05 |
| ac | | | | | 0.39 | | | | | 2.92 | 1.76 | | |
| ns | | | | | | | | | | | | | |
| di | | 2.23 | 2.64 | | 3.76 | 2.92 | 2.50 | 3.12 | 0.70 | 4.75 | 5.49 | 2.89 | 5.33 |
| wo | | | | | 0.24 | | | | 0.61 | | 0.13 | 1.84 | |
| hy | 0.91 | 1.80 | 8.06 | 1.20 | | 0.75 | 1.11 | 8.05 | | 0.18 | | | |
| ol | | | | | | | | | | | | | 0.80 |
| mt | 1.33 | 3.04 | 5.74 | 1.72 | 2.22 | 2.89 | 2.04 | 5.61 | 0.18 | 1.43 | 1.17 | 1.94 | 3.75 |
| hm | | | | | | | | | | | | 0.06 | |
| il | 0.26 | 0.53 | 2.60 | 0.36 | 0.66 | 1.10 | 0.55 | 2.71 | 0.09 | 0.77 | 0.41 | 1.32 | 2.12 |
| ap | 0.14 | 0.14 | 1.82 | 0.14 | 0.09 | 0.35 | 0.09 | 1.87 | 0.11 | 0.04 | 0.28 | 0.61 | 0.90 |
| Q | 57.3 | 52.1 | 48.0 | 54.9 | 56.2 | 49.6 | 55.4 | 48.2 | 62.5 | 45.2 | 45.8 | 44.9 | 43.6 |
| Ne | 22.4 | 29.8 | 32.9 | 22.1 | 23.8 | 27.9 | 24.1 | 29.2 | 20.7 | 32.3 | 32.1 | 32.3 | 32.6 |
| Ks | 20.3 | 18.1 | 19.1 | 23.0 | 20.0 | 22.5 | 20.5 | 22.6 | 16.8 | 22.5 | 22.1 | 22.8 | 23.8 |
| A.I. | 0.92 | 1.02 | 0.72 | 0.93 | 1.01 | 0.95 | 0.98 | 0.70 | 0.96 | 1.04 | 1.02 | 1.00 | 0.95 |
| $K_2O/Na_2O$ | 1.23 | 0.81 | 0.79 | 1.33 | 1.13 | 1.10 | 1.16 | 1.06 | 1.11 | 0.89 | 0.90 | 0.97 | 0.99 |
| R1 | 1747 | 1063 | 928 | 1638 | 1549 | 904 | 1506 | 952 | 2368 | 403 | 542 | 445 | 329 |
| R2 | 358 | 365 | 860 | 362 | 390 | 488 | 379 | 879 | 339 | 469 | 523 | 578 | 645 |
| Rock-type | Granite | Quartz trachyte | Trachyte | Granite | Granite | Syenite | Granite | Trachyte | Aplo-granite | Syenite | Syenite | Syenite | Nephel-syenite |

Table 1 (continued).

| | BAMBA | | | SAN FRANCISCO | | | | | | | URUCÚ | | |
|---|---|---|---|---|---|---|---|---|---|---|---|---|---|
| Sample | PV-43 | PV-45 | PV-46 | PV-60 | PV-61 | PV-62 | PV-63 Dyke | PV-64 | PV-65 | PV-66 Dyke | PV-14 | PV-15 | PV-16 |
| wt% | | | | | | | | | | | | | |
| $SiO_2$ | 63.43 | 62.04 | 59.16 | 66.26 | 61.07 | 63.87 | 71.37 | 62.57 | 65.81 | 71.89 | 62.79 | 61.71 | 59.19 |
| $TiO_2$ | 0.59 | 0.79 | 0.87 | 0.71 | 0.99 | 0.42 | 0.17 | 0.71 | 0.22 | 0.16 | 0.62 | 0.70 | 0.76 |
| $Al_2O_3$ | 17.61 | 17.86 | 16.59 | 17.06 | 16.75 | 18.01 | 13.52 | 17.18 | 17.04 | 13.22 | 16.66 | 18.10 | 18.61 |
| $Fe_2O_3$ | 1.68 | 1.94 | 2.93 | 2.39 | 2.02 | 1.21 | 1.49 | 1.95 | 1.48 | 1.14 | 2.38 | 2.41 | 2.05 |
| FeO | 1.12 | 1.41 | 2.30 | 2.26 | 2.03 | 0.97 | 1.45 | 1.74 | 1.21 | 1.19 | 2.19 | 2.02 | 1.79 |
| MnO | 0.14 | 0.23 | 0.33 | 0.19 | 0.21 | 0.11 | 0.17 | 0.16 | 0.20 | 0.10 | 0.18 | 0.14 | 0.28 |
| MgO | 0.16 | 0.49 | 0.62 | 0.47 | 0.96 | 0.40 | 0.23 | 0.71 | 0.17 | 0.22 | 0.59 | 0.48 | 1.18 |
| CaO | 0.74 | 1.27 | 2.75 | 0.95 | 1.44 | 0.62 | 0.13 | 1.39 | 0.53 | 0.46 | 2.28 | 1.50 | 2.58 |
| $Na_2O$ | 8.00 | 7.28 | 7.89 | 5.75 | 5.77 | 5.77 | 4.60 | 5.78 | 6.73 | 4.52 | 5.20 | 5.62 | 5.77 |
| $K_2O$ | 6.00 | 6.05 | 4.91 | 6.15 | 5.64 | 6.55 | 5.46 | 5.64 | 5.36 | 4.80 | 5.90 | 6.42 | 6.01 |
| $P_2O_5$ | 0.01 | 0.16 | 0.06 | 0.13 | 0.27 | 0.12 | 0.01 | 0.23 | 0.01 | 0.01 | 0.20 | 0.20 | 0.33 |
| LOI | 0.27 | 0.54 | 1.23 | 1.42 | 2.02 | 1.17 | 1.21 | 0.93 | 1.26 | 1.48 | 0.76 | 0.48 | 1.49 |
| Sum | 99.76 | 100.06 | 99.64 | 99.74 | 99.17 | 99.22 | 99.81 | 98.99 | 100.01 | 99.19 | 99.75 | 99.78 | 100.04 |
| ppm | | | | | | | | | | | | | |
| Cr | 6.26 | | | | | | | | | | | | |
| Ba | 411.20 | 239.40 | 288.77 | 530 | 1762 | 1178 | 202 | 2013 | 103 | 84 | 983.11 | 894.33 | 2229.45 |
| Rb | 183.78 | 147.03 | 103.44 | 156.8 | 157.8 | 147.5 | 346.2 | 173.2 | 268.2 | 275.8 | 183.51 | 91.58 | 127.37 |
| Sr | 686.49 | 95.82 | 160.43 | 57.5 | 142.2 | 116.7 | 14.3 | 199.3 | 16.3 | 17.2 | 120.09 | 207.14 | 2041.16 |
| Pb | | 6.98 | 9.49 | 13.0 | 14.4 | 16.6 | 13.5 | 15.5 | 9.9 | 13.5 | 25.40 | 32.05 | 45.74 |
| Nb | 327.03 | 262.09 | 273.61 | 125.5 | 171.9 | 98.4 | 474.9 | 142.9 | 335.4 | 261.8 | 152.21 | 50.13 | 153.80 |
| Ta | | 16.41 | 16.99 | 7.67 | 10.61 | 7.34 | 25.60 | 10.69 | 16.50 | 26.28 | 10.31 | 4.28 | 9.66 |
| Hf | | 10.84 | 24.56 | 12.30 | 5.57 | 24.84 | 37.26 | 10.77 | 10.27 | 16.32 | 20.99 | 24.35 | 8.66 |
| U | 44.40 | 3.46 | 7.09 | 3.22 | 2.50 | 2.91 | 24.05 | 4.56 | 11.49 | 16.26 | 3.82 | 1.65 | 2.90 |
| Th | 9.65 | 35.42 | 23.69 | 29.65 | 16.01 | 15.71 | 109.1 | 23.46 | 49.42 | 66.06 | 29.10 | 10.17 | 19.71 |
| Zr | 361.39 | 485.30 | 819.16 | 622 | 249 | 1300 | 1591 | 458 | 370 | 507 | 855.36 | 1029.64 | 371.15 |
| Y | 23.94 | 48.93 | 83.93 | 71.15 | 49.84 | 63.01 | 172.8 | 55.29 | 122.7 | 70.82 | 127.05 | 70.94 | 47.24 |
| Ga | | 25.39 | 28.37 | 28.81 | 23.15 | 26.41 | 34.28 | 24.18 | 36.93 | 28.53 | 26.42 | 24.46 | 18.04 |
| Ge | | 2.07 | 2.60 | 2.17 | 1.78 | 1.67 | 2.40 | 1.84 | 2.28 | 2.11 | 2.33 | 1.71 | 1.29 |
| La | 30.12 | 260.44 | 144.96 | 250.2 | 118.6 | 110.6 | 343.5 | 137.2 | 178.3 | 137.3 | 415.50 | 204.20 | 261.91 |
| Ce | 72.59 | 509.48 | 362.29 | 435.8 | 228.7 | 168.6 | 373.6 | 240.5 | 292.7 | 258.5 | 547.52 | 354.77 | 448.93 |
| Pr | 8.11 | 48.48 | 41.75 | 47.8 | 24.8 | 21.7 | 65.7 | 26.2 | 35.6 | 26.0 | 80.49 | 39.65 | 44.84 |
| Nd | 31.66 | 154.85 | 143.36 | 154.3 | 85.9 | 73.6 | 200.0 | 86.6 | 114.1 | 78.7 | 277.48 | 131.89 | 137.39 |
| Sm | 5.41 | 21.16 | 22.66 | 22.81 | 13.92 | 11.87 | 33.70 | 13.65 | 22.05 | 13.84 | 40.85 | 17.04 | 17.54 |
| Eu | 1.16 | 3.89 | 4.30 | 3.10 | 3.77 | 3.81 | 3.28 | 3.87 | 1.91 | 0.44 | 4.26 | 3.54 | 5.92 |
| Gd | 3.86 | 14.39 | 15.99 | 16.41 | 10.16 | 9.71 | 25.14 | 10.19 | 18.33 | 10.42 | 30.18 | 11.11 | 10.59 |
| Tb | 0.67 | 2.22 | 2.79 | 2.45 | 1.57 | 1.57 | 4.80 | 1.60 | 3.37 | 1.96 | 4.41 | 1.70 | 1.64 |
| Dy | 4.63 | 11.17 | 15.45 | 13.48 | 8.95 | 9.58 | 30.80 | 9.43 | 21.30 | 12.63 | 23.00 | 8.51 | 9.23 |
| Ho | 0.77 | 2.04 | 3.01 | 2.44 | 1.69 | 1.92 | 6.39 | 1.85 | 4.22 | 2.55 | 4.38 | 1.71 | 1.60 |
| Er | 1.93 | 5.51 | 8.54 | 6.87 | 4.61 | 5.62 | 19.67 | 5.31 | 11.82 | 8.10 | 11.99 | 5.04 | 4.69 |
| Tm | 0.39 | 0.73 | 1.40 | 0.98 | 0.70 | 0.91 | 3.08 | 0.85 | 1.79 | 1.41 | 1.92 | 0.78 | 0.78 |
| Yb | 2.32 | 4.43 | 9.37 | 6.57 | 4.60 | 5.95 | 19.61 | 5.62 | 11.32 | 9.96 | 11.63 | 4.54 | 5.39 |
| Lu | 0.39 | 0.62 | 1.42 | 1.00 | 0.73 | 0.92 | 2.68 | 0.86 | 1.71 | 1.52 | 1.76 | 0.72 | 0.82 |
| Q | | | | 2.56 | 2.28 | 3.52 | 22.55 | 3.89 | 4.95 | 25.54 | 5.28 | 0.90 | |
| C | | | | | | 0.59 | | | | | | | |
| or | 35.45 | 35.75 | 29.01 | 36.35 | 33.33 | 38.71 | 32.27 | 33.33 | 31.68 | 28.37 | 34.86 | 37.94 | 35.51 |
| ab | 49.46 | 47.34 | 38.89 | 48.66 | 48.82 | 48.82 | 38.93 | 48.91 | 56.95 | 38.25 | 44.00 | 47.55 | 42.99 |
| an | | | | 2.58 | 3.15 | 2.29 | 0.12 | 4.28 | 0.46 | 1.61 | 4.69 | 5.20 | 7.13 |
| ne | 4.17 | 5.87 | 10.34 | | | | | | | | | | 3.15 |
| ac | 4.86 | 3.00 | 7.71 | | | | | | | | | | |
| ns | 1.16 | | | | | | | | | | | | |
| di | 3.09 | 4.30 | 9.31 | 1.07 | 1.79 | | | 0.90 | 1.80 | 0.52 | 4.37 | 0.761 | 2.79 |
| wo | | | 0.94 | | | | | | | | | | |
| hy | | | | 1.99 | 2.35 | 1.29 | 1.84 | 2.04 | 0.32 | 1.45 | 0.66 | 1.64 | |
| ol | 0.10 | 0.04 | | | | | | | | | | | 1.75 |
| mt | | 1.30 | 0.37 | 3.46 | 2.93 | 1.76 | 2.16 | 2.83 | 2.15 | 1.65 | 3.45 | 3.49 | 2.97 |
| il | 1.12 | 1.50 | 1.65 | 1.35 | 1.88 | 0.80 | 0.32 | 1.35 | 0.42 | 0.30 | 1.17 | 1.32 | 1.44 |
| ap | 0.02 | 0.37 | 0.14 | 0.30 | 0.63 | 0.28 | 0.02 | 0.53 | 0.02 | 0.02 | 0.47 | 0.47 | 0.78 |
| Q | 42.6 | 41.7 | 41.2 | 46.3 | 46.2 | 46.8 | 57.9 | 47.2 | 47.8 | 60.0 | 48.1 | 45.2 | 43.1 |
| Ne | 34.8 | 35.4 | 38.5 | 30.1 | 31.3 | 29.0 | 22.5 | 30.8 | 33.0 | 22.5 | 28.3 | 29.8 | 32.4 |
| Ks | 22.6 | 22.9 | 20.2 | 23.6 | 22.5 | 24.2 | 19.6 | 22.0 | 19.2 | 17.5 | 23.6 | 25.0 | 24.5 |
| A.I. | 1.05 | 1.04 | 1.10 | 0.95 | 0.93 | 0.92 | 0.99 | 0.91 | 0.99 | 0.96 | 0.90 | 0.90 | 0.86 |
| $K_2O/Na_2O$ | 0.75 | 0.83 | 0.62 | 1.07 | 0.98 | 1.14 | 1.19 | 0.98 | 0.80 | 1.06 | 1.13 | 1.14 | 1.04 |
| R1 | -107 | 25 | -169 | 526 | 568 | 606 | 1761 | 681 | 663 | 1994 | 820 | 479 | 368 |
| R2 | 433 | 511 | 650 | 460 | 530 | 440 | 291 | 521 | 399 | 319 | 600 | 539 | 700 |
| Rock-type | Nephel-syenite | Nephel-syenite | Nepheline syenite | Syenite | Syenite | Syenite | Micro-granite | Syenite | Syenite | Micro-granite | Syenite | Syenite | Nephel-syenite |

Table 1 (continued).

| | URUCÚ | | | | | | | | | | ZUIALITO | | |
|---|---|---|---|---|---|---|---|---|---|---|---|---|---|
| Sample | PV-47 | PV-48 | PV-49 | PV-50 | PV-51 | PV-52 | PV-53 | PV-54 | PV-55 | PV-56 | PV-17 | PV-18 | PV-19 |
| wt% | | | | | | | | | | | | | |
| $SiO_2$ | 61.73 | 59.22 | 60.03 | 58.11 | 60.07 | 59.52 | 61.73 | 62.62 | 59.18 | 54.78 | 59.51 | 59.69 | 54.73 |
| $TiO_2$ | 0.55 | 0.74 | 0.66 | 0.74 | 0.60 | 0.71 | 0.56 | 0.66 | 0.69 | 0.66 | 0.25 | 0.71 | 0.40 |
| $Al_2O_3$ | 18.73 | 18.43 | 18.72 | 18.84 | 19.40 | 19.11 | 18.20 | 18.00 | 18.66 | 20.82 | 21.23 | 17.41 | 22.98 |
| $Fe_2O_3$ | 1.37 | 2.24 | 1.79 | 2.24 | 1.67 | 1.89 | 1.85 | 1.73 | 2.13 | 2.79 | 1.36 | 2.45 | 1.99 |
| FeO | 1.13 | 1.90 | 1.52 | 1.73 | 1.37 | 1.58 | 1.31 | 1.34 | 1.66 | 2.16 | 0.79 | 1.71 | 1.15 |
| MnO | 0.13 | 0.16 | 0.12 | 0.25 | 0.11 | 0.14 | 0.23 | 0.17 | 0.18 | 0.48 | 0.09 | 0.36 | 0.28 |
| MgO | 0.62 | 1.28 | 1.11 | 1.17 | 0.94 | 1.17 | 0.57 | 0.59 | 0.97 | 0.86 | 0.01 | 0.97 | 0.57 |
| CaO | 2.00 | 2.32 | 2.05 | 2.03 | 2.16 | 1.98 | 1.26 | 1.44 | 2.01 | 1.77 | 0.22 | 0.79 | 0.83 |
| $Na_2O$ | 5.76 | 5.46 | 5.84 | 7.26 | 5.95 | 5.70 | 6.89 | 6.27 | 6.09 | 7.21 | 7.56 | 5.92 | 9.42 |
| $K_2O$ | 6.47 | 6.64 | 6.15 | 5.72 | 6.43 | 6.52 | 6.69 | 6.44 | 6.77 | 5.96 | 7.92 | 7.91 | 6.33 |
| $P_2O_5$ | 0.24 | 0.37 | 0.39 | 0.36 | 0.25 | 0.32 | 0.19 | 0.22 | 0.28 | 0.26 | 0.01 | 0.10 | 0.13 |
| LOI | 1.02 | 1.07 | 1.52 | 1.47 | 1.07 | 1.30 | 0.15 | 0.25 | 1.10 | 2.03 | 0.74 | 1.67 | 1.03 |
| Sum | 99.75 | 99.83 | 99.90 | 99.92 | 100.02 | 99.94 | 99.63 | 99.72 | 99.72 | 99.78 | 99.69 | 99.69 | 99.84 |
| ppm | | | | | | | | | | | | | |
| Cr | 2.37 | | | | | | 0.97 | 3.20 | | | | 10.69 | |
| Ba | 545.53 | 1546.73 | 1520.31 | 1834.56 | 2385.26 | 2308.02 | 539.55 | 1032.20 | 725.77 | 562.94 | 353.53 | 369.15 | 705.22 |
| Rb | 102.63 | 73.99 | 74.91 | 155.59 | 77.71 | 79.62 | 132.15 | 63.90 | 105.22 | 209.76 | 191.74 | 179.03 | 232.63 |
| Sr | 1358.95 | 1066.09 | 1182.55 | 1236.02 | 1618.54 | 1339.95 | 468.49 | 420.98 | 621.69 | 1118.37 | 779.76 | 1040.12 | 852.77 |
| Pb | | 10.10 | 17.41 | 45.39 | 14.70 | 11.13 | | | 14.13 | 32.55 | 15.45 | | 19.97 |
| Nb | 54.74 | 45.09 | 39.54 | 108.10 | 49.82 | 31.87 | 228.94 | 40.00 | 80.01 | 223.38 | 32.70 | 59.07 | 170.52 |
| Ta | | 3.16 | 2.82 | 5.28 | 3.66 | 2.62 | | | 7.05 | 13.90 | 3.11 | | 10.71 |
| Hf | | 2.72 | 1.95 | 9.24 | 3.10 | 1.67 | | | 4.22 | 12.83 | 0.96 | | 10.34 |
| U | 0.53 | 0.57 | 0.85 | 1.49 | 0.70 | 0.62 | 10.29 | 1.46 | 1.17 | 27.62 | 1.02 | 3.83 | 4.57 |
| Th | 5.00 | 3.48 | 4.03 | 19.17 | 3.94 | 3.35 | 45.66 | 5.85 | 8.10 | 400.53 | 2.77 | 13.51 | 22.63 |
| Zr | 85.26 | 110.50 | 98.78 | 317.62 | 141.49 | 75.85 | 237.62 | 93.17 | 185.98 | 485.33 | 50.97 | 75.40 | 444.38 |
| Y | 14.21 | 18.57 | 16.59 | 39.10 | 17.65 | 28.78 | 44.05 | 15.12 | 27.95 | 218.23 | 3.09 | 28.23 | 26.49 |
| Ga | | 14.60 | 14.45 | 17.64 | 15.08 | 14.38 | | | 16.20 | 34.92 | 25.59 | | 25.38 |
| Ge | | 1.22 | 1.06 | 1.31 | 1.05 | 1.08 | | | 1.30 | 3.09 | 0.97 | | 1.14 |
| La | 72.11 | 101.97 | 98.58 | 144.47 | 87.38 | 96.05 | 156.59 | 91.71 | 123.47 | 2153.88 | 14.17 | 99.19 | 149.56 |
| Ce | 142.90 | 188.12 | 184.04 | 242.00 | 152.13 | 167.54 | 268.81 | 158.54 | 233.40 | 3588.99 | 24.09 | 144.56 | 248.58 |
| Pr | 14.21 | 20.48 | 20.44 | 25.84 | 15.99 | 18.14 | 24.76 | 15.61 | 25.40 | 316.13 | 2.24 | 13.11 | 23.28 |
| Nd | 65.26 | 72.17 | 71.70 | 86.46 | 54.19 | 61.48 | 101.29 | 60.98 | 83.82 | 944.12 | 6.37 | 46.17 | 64.83 |
| Sm | 7.90 | 9.96 | 9.23 | 11.50 | 7.10 | 8.25 | 11.58 | 8.29 | 11.79 | 110.21 | 0.79 | 4.84 | 7.83 |
| Eu | 3.16 | 3.98 | 4.36 | 4.80 | 4.14 | 4.16 | 1.61 | 0.98 | 3.55 | 21.04 | 0.46 | 1.98 | 1.90 |
| Gd | 7.37 | 6.12 | 5.23 | 7.19 | 4.43 | 5.06 | 11.58 | 8.78 | 6.95 | 69.74 | 0.43 | 4.03 | 4.66 |
| Tb | 0.79 | 0.90 | 0.81 | 1.11 | 0.70 | 0.72 | 1.93 | 1.46 | 1.10 | 9.98 | 0.10 | 0.81 | 0.82 |
| Dy | 5.26 | 4.47 | 4.02 | 6.48 | 3.69 | 3.65 | 10.29 | 6.83 | 5.46 | 51.04 | 0.59 | 3.63 | 4.60 |
| Ho | 0.79 | 0.78 | 0.61 | 1.17 | 0.61 | 0.67 | 0.97 | 1.46 | 0.97 | 8.92 | 0.09 | 0.82 | 0.89 |
| Er | 2.37 | 1.91 | 1.76 | 3.54 | 1.57 | 1.80 | 4.82 | 2.44 | 2.72 | 25.08 | 0.28 | 2.02 | 2.61 |
| Tm | 0.26 | 0.27 | 0.20 | 0.55 | 0.22 | 0.27 | 0.97 | 0.49 | 0.37 | 3.41 | 0.06 | 0.40 | 0.45 |
| Yb | 1.58 | 1.60 | 1.47 | 4.33 | 1.60 | 1.63 | 5.15 | 1.95 | 2.58 | 23.16 | 0.35 | 2.02 | 3.58 |
| Lu | 0.26 | 0.24 | 0.19 | 0.62 | 0.23 | 0.22 | 0.64 | 0.98 | 0.36 | 3.26 | 0.06 | 0.40 | 0.52 |
| Q | | | | | | | | | | | | | |
| C | | | | | | | | | | | | | |
| or | 38.23 | 39.24 | 34.34 | 33.80 | 37.99 | 38.53 | 39.53 | 38.05 | 40.00 | 35.22 | 46.80 | 46.74 | 37.40 |
| ab | 47.79 | 40.34 | 45.92 | 40.21 | 42.37 | 42.00 | 43.81 | 50.74 | 38.40 | 30.50 | 30.85 | 32.08 | 22.89 |
| an | 6.14 | 6.17 | 6.70 | 1.92 | 7.23 | 7.30 | | 1.95 | 3.58 | 6.84 | 0.60 | | 1.72 |
| ne | 0.51 | 3.17 | 1.89 | 11.49 | 4.32 | 3.37 | 6.80 | 1.25 | 7.10 | 16.52 | 17.94 | 7.27 | 30.77 |
| ac | | | | | | | 1.70 | | | | | 4.03 | |
| ns | | | | | | | | | | | | | |
| di | 1.74 | 2.32 | 0.71 | 4.58 | 1.44 | 0.34 | 4.07 | 2.95 | 3.60 | 0.17 | 0.11 | 2.66 | 1.21 |
| wo | | | | | | | | | | | | | |
| hy | | | | | | | | | | | | | |
| ol | 0.69 | 1.99 | 2.02 | 0.92 | 1.44 | 2.25 | 0.20 | 0.22 | 0.84 | 2.56 | 0.17 | 2.09 | 0.82 |
| mt | 1.98 | 3.24 | 2.59 | 3.24 | 2.42 | 2.74 | 1.83 | 2.5 | 3.08 | 4.04 | 1.97 | 1.53 | 2.88 |
| il | 1.04 | 1.40 | 1.25 | 1.40 | 1.13 | 1.34 | 1.06 | 1.25 | 1.31 | 1.25 | 0.47 | 1.34 | 0.75 |
| ap | 0.56 | 0.87 | 0.92 | 0.85 | 0.59 | 0.75 | 0.45 | 0.52 | 0.66 | 0.61 | 0.11 | 0.23 | 0.30 |
| Q | 44.4 | 42.8 | 43.7 | 38.6 | 42.3 | 42.8 | 41.2 | 44.1 | 40.8 | 35.5 | 35.9 | 40.5 | 29.3 |
| Ne | 30.5 | 30.2 | 32.6 | 38.9 | 32.2 | 31.1 | 33.9 | 31.9 | 32.6 | 40.2 | 36.2 | 28.6 | 47.4 |
| Ks | 25.1 | 26.9 | 23.7 | 22.5 | 25.5 | 26.1 | 24.9 | 24.0 | 26.6 | 24.3 | 27.9 | 30.9 | 23.3 |
| A.I. | 0.88 | 0.88 | 0.87 | 0.96 | 0.86 | 0.86 | 1.02 | 0.90 | 0.93 | 0.88 | 0.99 | 1.05 | 0.97 |
| $K_2O/Na_2O$ | 1.12 | 1.22 | 1.05 | 0.79 | 1.08 | 1.14 | 0.97 | 1.03 | 1.11 | 0.83 | 1.05 | 1.34 | 0.67 |
| R1 | 474 | 325 | 383 | -168 | 290 | 307 | 4 | 341 | 79 | -452 | -634 | -102 | -1271 |
| R2 | 612 | 673 | 642 | 645 | 658 | 645 | 520 | 536 | 629 | 640 | 445 | 474 | 568 |
| Rock-type | Syenite | Syenite | Syenite | Nephel-syenite | Syenite | Syenite | Nephel-syenite | Syenite | Nephel-syenite | Nepheline syenite | Nephel-syenite | Nephel-syenite | Nepheline syenite |

Table 1 (continued).

| | ZUIALITO | | | | | | | | TANOMONIA | | | |
|---|---|---|---|---|---|---|---|---|---|---|---|---|
| Sample | PV-20 | PV-21 Dyke | PV-22 | PV-23 | PV-24 | PV-25 | PV-26 | PV-27 | PV-29 | PV-34 | PV-35 | PV-36 |
| wt% | | | | | | | | | | | | |
| $SiO_2$ | 53.70 | 56.56 | 58.15 | 49.28 | 61.67 | 59.97 | 65.43 | 59.05 | 65.53 | 66.97 | 74.82 | 64.77 |
| $TiO_2$ | 1.01 | 0.71 | 0.62 | 1.81 | 0.82 | 0.66 | 0.11 | 0.37 | 0.34 | 0.32 | 0.08 | 0.49 |
| $Al_2O_3$ | 19.94 | 21.97 | 19.71 | 20.43 | 16.10 | 18.00 | 18.37 | 20.03 | 16.72 | 16.64 | 12.88 | 17.26 |
| $Fe_2O_3$ | 2.64 | 1.83 | 1.84 | 3.51 | 2.72 | 2.62 | 0.87 | 1.50 | 1.84 | 1.59 | 0.67 | 1.64 |
| FeO | 1.79 | 1.97 | 1.22 | 2.33 | 2.23 | 2.23 | 0.63 | 0.78 | 1.56 | 1.41 | 0.68 | 1.52 |
| MnO | 0.26 | 0.33 | 0.21 | 0.36 | 0.30 | 0.21 | 0.05 | 0.25 | 0.15 | 0.12 | 0.04 | 0.08 |
| MgO | 0.90 | 0.41 | 0.52 | 1.09 | 1.01 | 1.29 | 0.16 | 0.16 | 0.24 | 0.18 | 0.01 | 0.64 |
| CaO | 2.60 | 3.33 | 1.38 | 3.19 | 1.27 | 1.84 | 0.46 | 0.57 | 0.62 | 0.83 | 0.33 | 1.69 |
| $Na_2O$ | 8.14 | 4.71 | 7.49 | 9.08 | 6.53 | 6.32 | 7.26 | 10.86 | 5.60 | 5.39 | 4.74 | 5.00 |
| $K_2O$ | 6.33 | 5.33 | 6.86 | 5.82 | 5.73 | 5.70 | 5.88 | 5.51 | 6.13 | 5.85 | 4.75 | 5.96 |
| $P_2O_5$ | 0.32 | 0.17 | 0.15 | 0.46 | 0.32 | 0.39 | 0.05 | 0.02 | 0.07 | 0.05 | 0.01 | 0.19 |
| LOI | 2.36 | 2.33 | 1.77 | 2.27 | 0.85 | 0.53 | 0.46 | 0.70 | 0.91 | 0.31 | 0.69 | 0.58 |
| Sum | 99.99 | 99.65 | 99.92 | 99.63 | 99.54 | 99.76 | 99.73 | 99.79 | 99.71 | 99.66 | 99.70 | 99.82 |
| ppm | | | | | | | | | | | | |
| Cr | | 19.40 | | | 3.63 | | | 11.35 | | | 0.85 | |
| Ba | 1510.21 | 424.13 | 1183.43 | 200.73 | 407.33 | 1661.64 | 153.85 | 107.09 | 236.27 | 101.76 | 244.02 | 1507.96 |
| Rb | 148.67 | 192.29 | 155.73 | 141.19 | 341.10 | 182.59 | 190.09 | 310.82 | 188.35 | 140.18 | 269.50 | 161.23 |
| Sr | 2355.13 | 719.40 | 1451.45 | 619.90 | 1514.40 | 691.66 | 95.13 | 1280.97 | 38.18 | 26.08 | 2079.92 | 440.07 |
| Pb | 15.83 | | 16.07 | 8.72 | | 16.33 | 12.11 | | 15.05 | 16.60 | | 19.77 |
| Nb | 198.48 | 198.51 | 160.90 | 347.38 | 421.47 | 131.80 | 72.36 | 599.25 | 147.33 | 115.90 | 118.15 | 106.63 |
| Ta | 14.94 | | 14.64 | 33.89 | | 7.25 | 7.60 | | 9.13 | 9.55 | | 8.66 |
| Hf | 6.89 | | 7.55 | 7.90 | | 3.98 | 5.13 | | 18.57 | 12.92 | | 10.90 |
| U | 2.34 | 6.22 | 2.87 | 2.37 | 31.94 | 2.17 | 6.06 | 33.58 | 4.87 | 3.21 | 14.67 | 3.86 |
| Th | 18.25 | 31.34 | 13.40 | 13.13 | 34.03 | 8.41 | 13.58 | 149.63 | 53.14 | 34.33 | 36.29 | 29.85 |
| Zr | 275.81 | 63.68 | 404.98 | 296.77 | 280.37 | 167.87 | 218.79 | 84.70 | 841.16 | 465.72 | 23.94 | 417.14 |
| Y | 51.75 | 61.19 | 33.24 | 81.65 | 92.15 | 31.66 | 22.08 | 62.69 | 61.91 | 41.14 | 151.35 | 50.20 |
| Ga | 19.75 | | 18.69 | 24.30 | | 18.78 | 26.04 | | 29.35 | 27.75 | | 22.49 |
| Ge | 1.40 | | 1.25 | 1.67 | | 1.37 | 1.50 | | 2.01 | 1.98 | | 1.48 |
| La | 318.26 | 302.49 | 243.01 | 484.02 | 245.81 | 151.50 | 51.91 | 314.18 | 385.18 | 248.40 | 63.71 | 134.71 |
| Ce | 572.93 | 542.79 | 431.34 | 956.75 | 470.68 | 282.49 | 92.76 | 565.30 | 725.66 | 431.51 | 84.94 | 253.89 |
| Pr | 56.55 | 48.76 | 43.83 | 99.72 | 46.34 | 29.70 | 9.46 | 44.40 | 71.52 | 45.23 | 11.97 | 26.77 |
| Nd | 171.44 | 197.26 | 128.85 | 322.49 | 170.68 | 96.57 | 31.70 | 136.57 | 231.03 | 146.02 | 42.47 | 90.99 |
| Sm | 22.25 | 20.90 | 15.63 | 41.07 | 24.35 | 13.07 | 4.79 | 16.79 | 29.99 | 17.64 | 11.58 | 15.10 |
| Eu | 5.95 | 5.47 | 3.73 | 9.90 | 3.40 | 3.40 | 0.87 | 2.61 | 1.39 | 0.87 | 1.16 | 2.81 |
| Gd | 12.72 | 15.92 | 8.65 | 22.11 | 15.97 | 7.80 | 2.77 | 10.08 | 17.82 | 10.01 | 8.88 | 10.50 |
| Tb | 2.09 | 2.49 | 1.42 | 3.54 | 2.36 | 1.18 | 0.55 | 2.61 | 2.67 | 1.68 | 1.93 | 1.73 |
| Dy | 10.87 | 14.43 | 7.27 | 18.40 | 13.35 | 6.36 | 2.89 | 12.31 | 13.80 | 8.36 | 11.20 | 9.53 |
| Ho | 1.91 | 1.99 | 1.26 | 3.25 | 2.88 | 1.14 | 0.62 | 3.36 | 2.47 | 1.50 | 2.32 | 1.95 |
| Er | 5.13 | 6.22 | 3.42 | 8.23 | 7.59 | 3.08 | 2.04 | 6.72 | 7.03 | 4.49 | 7.34 | 5.42 |
| Tm | 0.77 | 1.00 | 0.51 | 0.97 | 1.57 | 0.42 | 0.34 | 1.49 | 1.07 | 0.72 | 1.93 | 0.80 |
| Yb | 4.93 | 5.72 | 3.42 | 6.08 | 6.81 | 2.96 | 2.42 | 6.34 | 7.36 | 5.04 | 9.27 | 5.28 |
| Lu | 0.65 | 0.75 | 0.45 | 0.81 | 1.05 | 0.42 | 0.42 | 0.75 | 1.18 | 0.82 | 1.54 | 0.78 |
| Q | | 0.79 | | | | | | | 7.57 | 10.87 | 28.45 | 8.50 |
| C | | 2.80 | | | | | | | | 0.05 | | |
| or | 37.40 | 31.49 | 40.54 | 34.39 | 33.86 | 33.68 | 34.74 | 32.56 | 36.22 | 34.57 | 28.07 | 35.22 |
| ab | 20.76 | 39.85 | 33.22 | 8.74 | 50.91 | 48.22 | 61.09 | 35.27 | 47.38 | 45.60 | 39.80 | 42.30 |
| an | | 15.41 | | | | 3.91 | 0.17 | | 2.38 | 3.79 | | 7.05 |
| ne | 25.22 | | 16.23 | 34.63 | | 2.84 | 0.18 | 20.08 | | | | |
| ac | 1.36 | | 0.16 | 3.65 | 3.82 | | | 4.33 | | | 0.26 | |
| ns | | | | | | | | 3.40 | | | | |
| di | 5.41 | | 3.03 | 6.04 | 3.45 | 2.13 | 1.45 | 2.30 | 0.70 | | 1.38 | 0.06 |
| wo | 1.64 | | 0.83 | 2.12 | | | | | | | | |
| hy | | 2.56 | | | 0.53 | | | | 1.55 | 1.20 | | 2.32 |
| ol | | | | | 1.76 | 2.44 | | 0.37 | | | | |
| mt | 3.14 | 2.65 | 2.58 | 3.25 | 2.02 | 3.79 | 1.26 | | 2.66 | 2.30 | 0.83 | 2.37 |
| il | 1.91 | 1.34 | 1.17 | 3.43 | 1.55 | 1.25 | 0.20 | 0.70 | 0.64 | 0.60 | 0.15 | 0.93 |
| ap | 0.75 | 0.40 | 0.35 | 1.08 | 0.75 | 0.92 | 0.11 | 0.04 | 0.16 | 0.11 | 0.02 | 0.45 |
| Q | 30.8 | 45.3 | 36.4 | 24.2 | 44.8 | 43.2 | 44.8 | 34.4 | 49.3 | 51.3 | 61.0 | 50.1 |
| Ne | 43.7 | 29.9 | 38.0 | 50.6 | 32.5 | 34.2 | 34.6 | 44.6 | 28.1 | 27.1 | 22.4 | 26.6 |
| Ks | 25.5 | 24.8 | 25.6 | 25.2 | 22.7 | 22.6 | 20.6 | 21.0 | 22.6 | 21.6 | 16.6 | 23.3 |
| A.I. | 1.02 | 0.62 | 1.00 | 1.04 | 1.05 | 0.92 | 1.00 | 1.19 | 0.95 | 0.91 | 1.00 | 0.85 |
| $K_2O/Na_2O$ | 0.78 | 1.13 | 0.92 | 0.64 | 0.88 | 0.90 | 0.81 | 0.51 | 1.09 | 1.09 | 1.00 | 1.19 |
| R1 | -935 | 730 | -486 | -1500 | 298 | 273 | 363 | -1280 | 844 | 1091 | 2150 | 1048 |
| R2 | 714 | 808 | 560 | 796 | 502 | 614 | 418 | 462 | 406 | 424 | 289 | 551 |
| Rock-type | Nepheline syenite | Syenite | Nepheline syenite | Nepheline syenite | Syenite | Syenite | Syenite | Nepheline syenite | Quartz syenite | Quartz syenite | Granite | Quartz syenite |

Table 1 (continued).

| | PRADO | | | | MERCEDES | | | BASEMENT | |
|---|---|---|---|---|---|---|---|---|---|
| Sample | PV-30 | PV-31 | PV-32 Dyke | PV-33 | 35 | PV-58 | PV-59 | 19 Gneiss | PV-28 Migmatite |
| wt% | | | | | | | | | |
| $SiO_2$ | 56.58 | 58.08 | 45.14 | 58.73 | 70.31 | 71.51 | 73.79 | 70.59 | 74.00 |
| $TiO_2$ | 0.79 | 0.70 | 1.52 | 0.19 | 0.34 | 0.23 | 0.14 | 0.33 | 0.09 |
| $Al_2O_3$ | 18.46 | 18.12 | 26.82 | 22.16 | 13.86 | 13.90 | 13.18 | 14.67 | 13.90 |
| $Fe_2O_3$ | 2.80 | 2.60 | 4.34 | 0.97 | 1.62 | 0.69 | 0.52 | 1.09 | 0.74 |
| FeO | 2.42 | 1.95 | 3.67 | 0.50 | 1.62 | 1.82 | 1.38 | 1.13 | 0.79 |
| MnO | 0.21 | 0.27 | 0.69 | 0.18 | 0.13 | 0.09 | 0.06 | 0.03 | 0.04 |
| MgO | 1.55 | 0.87 | 1.73 | 0.20 | 0.19 | 0.09 | 0.11 | 0.39 | 0.36 |
| CaO | 2.88 | 2.03 | 0.87 | 0.33 | 0.94 | 0.62 | 0.50 | 1.02 | 0.61 |
| $Na_2O$ | 6.65 | 7.62 | 6.42 | 10.96 | 4.63 | 4.73 | 4.33 | 2.70 | 3.31 |
| $K_2O$ | 5.44 | 5.67 | 6.54 | 5.57 | 5.28 | 5.68 | 4.76 | 6.91 | 5.75 |
| $P_2O_5$ | 0.53 | 0.38 | 0.47 | 0.02 | 0.04 | 0.09 | 0.03 | 0.11 | 0.09 |
| LOI | 1.51 | 1.20 | 1.20 | 0.12 | 0.75 | 0.50 | 1.00 | 0.80 | 0.68 |
| Sum | 99.82 | 99.49 | 99.41 | 99.92 | 99.71 | 99.95 | 99.80 | 99.77 | 100.36 |
| ppm | | | | | | | | | |
| Cr | 5.45 | 18.82 | | 14.34 | 0.33 | | | 1.68 | |
| Ba | 1715.45 | 558.30 | 484.61 | 653.50 | 405.25 | | 544 | 347.57 | 954.46 |
| Rb | 103.17 | 131.73 | 275.40 | 329.72 | 265.02 | | 356 | 454.87 | 204.96 |
| Sr | 1107.85 | 2940.22 | 287.13 | 319.23 | 39.94 | | 49 | 657.05 | 94.41 |
| Pb | 26.36 | | 99.88 | | | | | | 34.97 |
| Nb | 174.60 | 267.16 | 376.04 | 104.55 | 279.59 | | 243 | 22.97 | 49.40 |
| Ta | 11.98 | | 52.86 | | | | | | 6.65 |
| Hf | 9.28 | | 6.44 | | | | | | 11.68 |
| U | 6.25 | 6.64 | 13.47 | 5.94 | 10.50 | | 10 | 3.51 | 4.17 |
| Th | 25.01 | 32.84 | 325.43 | 11.54 | 61.52 | | 58 | 15.62 | 22.97 |
| Zr | 481.96 | 319.56 | 264.55 | 40.21 | 125.07 | | 208 | 330.00 | 476.71 |
| Y | 40.05 | 54.98 | 147.98 | 22.73 | 136.74 | | 107 | 67.57 | 39.64 |
| Ga | 21.96 | | 54.99 | | | | | 15.03 | 17.51 |
| Ge | 1.55 | | 3.97 | | | | | 1.16 | 1.35 |
| La | 220.54 | 257.93 | 2856.99 | 87.76 | 194.75 | | 146 | 138.38 | 67.78 |
| Ce | 357.59 | 482.29 | 5773.68 | 163.64 | 374.34 | | 280 | 335.41 | 131.78 |
| Pr | 33.94 | 42.80 | 522.58 | 14.34 | 37.90 | | | 36.22 | 14.17 |
| Nd | 104.93 | 172.69 | 1676.01 | 59.44 | 139.65 | | 105 | 143.24 | 47.23 |
| Sm | 13.74 | 19.93 | 192.40 | 5.59 | 25.36 | | 19 | 28.11 | 8.41 |
| Eu | 3.47 | 5.90 | 22.69 | 1.40 | 1.46 | | 1.1 | 1.35 | 1.09 |
| Gd | 8.45 | 17.34 | 67.12 | 3.50 | 21.28 | | 16 | 16.22 | 6.61 |
| Tb | 1.40 | 2.58 | 12.63 | 0.70 | 3.50 | | 2.6 | 2.70 | 1.10 |
| Dy | 7.19 | 18.08 | 52.16 | 5.59 | 20.70 | | 15.5 | 14.87 | 6.63 |
| Ho | 1.41 | 2.21 | 6.40 | 0.70 | 4.67 | | | 2.43 | 1.51 |
| Er | 4.03 | 5.90 | 17.48 | 2.45 | 11.08 | | 8.3 | 5.95 | 3.90 |
| Tm | 0.59 | 1.11 | 1.73 | 0.35 | 2.62 | | | 1.08 | 0.64 |
| Yb | 3.98 | 5.54 | 9.73 | 2.10 | 11.37 | | 8.5 | 5.14 | 4.29 |
| Lu | 0.58 | 0.74 | 1.23 | 0.35 | 1.75 | | 1.3 | 0.81 | 0.65 |
| Q | | | | | 21.02 | 23.24 | 28.90 | 25.66 | 30.80 |
| C | | | 8.72 | | | | | 1.15 | 1.33 |
| or | 32.14 | 33.50 | 38.64 | 32.91 | 31.20 | 32.56 | 28.53 | 40.83 | 33.98 |
| ab | 38.06 | 38.19 | 11.76 | 33.45 | 39.17 | 37.88 | 37.15 | 22.84 | 28.00 |
| an | 4.45 | | 1.24 | | 1.44 | 2.18 | 2.29 | 4.34 | 2.43 |
| ne | 9.86 | 12.96 | 23.05 | 26.82 | | | | | |
| ac | | 2.50 | | 2.80 | | | | | |
| ns | | | | 1.53 | | | | | |
| di | 5.09 | 6.18 | | 1.26 | 2.52 | 0.69 | | | |
| wo | | | | | | | | | |
| hy | | | | | 0.49 | 1.98 | 1.96 | 1.65 | 1.65 |
| ol | 1.88 | 0.44 | 4.49 | 0.59 | | | | | |
| mt | 4.05 | 2.51 | 6.29 | | 2.34 | 1.00 | 0.76 | 1.58 | 1.07 |
| il | 1.50 | 1.32 | 2.88 | 0.36 | 0.64 | 0.44 | 0.27 | 0.62 | 0.17 |
| ap | 1.25 | 0.90 | 1.11 | 0.04 | 0.09 | 0.08 | 0.07 | 0.26 | 0.21 |
| Q | 39.1 | 37.8 | 30.0 | 31.7 | 57.4 | 58.3 | 61.6 | 60.2 | 62.8 |
| Ne | 38.1 | 39.8 | 40.0 | 48.2 | 23.2 | 21.9 | 21.3 | 13.8 | 16.4 |
| Ks | 22.8 | 22.4 | 30.0 | 20.1 | 19.4 | 19.8 | 17.1 | 26.0 | 20.8 |
| A.I. | 0.91 | 1.03 | 0.66 | 1.08 | 0.96 | 0.94 | 0.93 | 0.81 | 0.84 |
| $K_2O/Na_2O$ | 0.82 | 0.74 | 1.02 | 0.51 | 1.14 | 1.20 | 1.10 | 2.56 | 1.09 |
| R1 | -20 | -300 | -1051 | -1325 | 1709 | 1680 | 2207 | 2059 | 2365 |
| R2 | 747 | 616 | 705 | 480 | 382 | 344 | 318 | 416 | 356 |
| Rock-type | Nephel-syenite | Nepheline syenite | Nepheline syenite | Nepheline syenite | Granite | Granite | Granite | Granitic gneiss | Granitic migmatite |

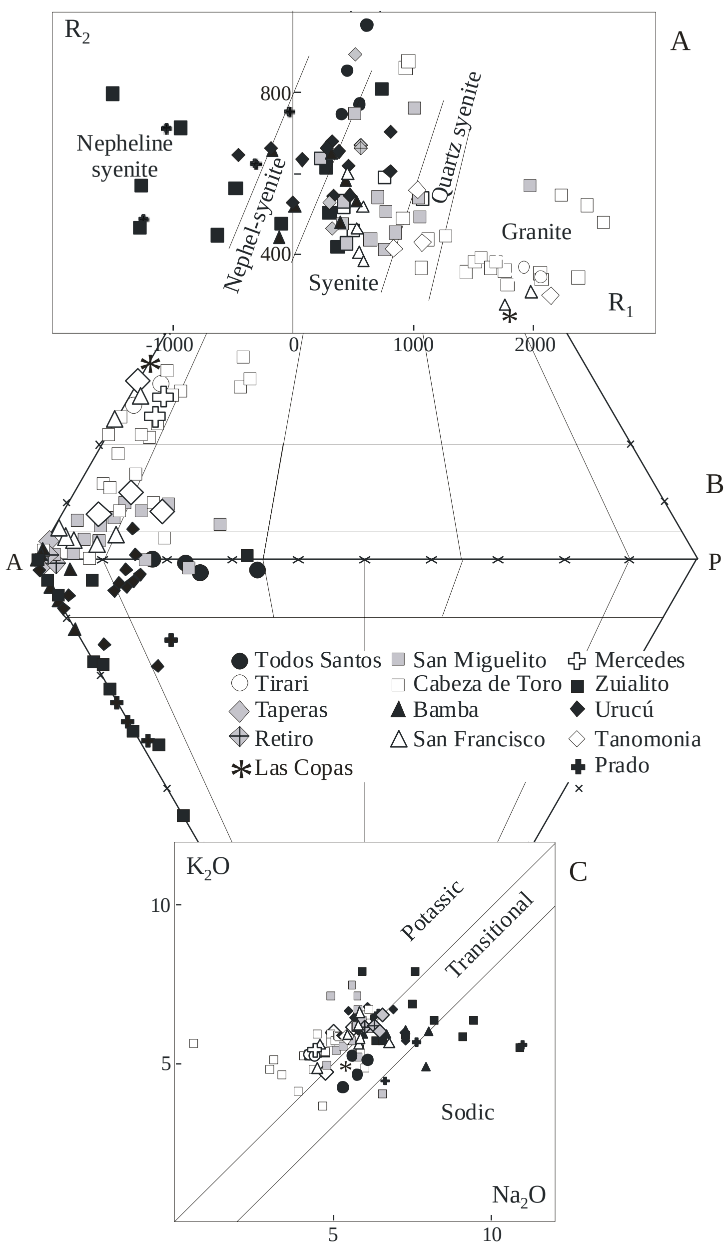


Fig. 2. A: part of the R1 [Si-11(Na+K)-2(Fe+Ti)]-R2 [6Ca+2Mg+Al] diagram (De La Roche *et al.*, 1980); B: Q-A-P-F Streckeisen's diagram (cf. Le Maitre, 1989); C: $Na_2O$ vs. $K_2O$ plot (after Comin-Chiaramonti & Gomes, 1996) for the Velasco rocks.

The rocks range from coarse to fine-grained in size, and include plagioclase-bearing (up to 30 vol%) and plagioclase-free varieties, the latter showing meso- and macroperthitic alkali feldspar laths (hypersolvus granites to hypersolvus foid syenites).

The textures are quite variable, from inequigranular allotriomorphic (very typical of granite types) through hypidiomorphic to trachytic and foyaitic, the latter due to the orientation of lath-shaped alkali feldspar crystals. Porphyritic textures are owing to macrocrystals of alkali feldspar randomly distributed along a fine-grained groundmass. Sometimes closely spaced elongated macrocrystals of alkali feldspar form adcumulate textures. The mafic minerals are chiefly represented by the assemblage biotite±amphibole±clinopyroxene and opaques. Common and ubiquitous accessories include zircon, titanite and apatite. Eudialyte, britholite and fluorite are frequent in the undersaturated, nepheline-rich rock-types.

More rarely carbonate-rich xenoliths, about 2x3 cm in size, are found in the syenites (e.g. Retiro complex, sample n. 33 of Table 1): they are formed by mesoperthitic alkali feldspar (~60 vol%) and quartz (~5 vol%) set in a groundmass of microcrystalline calcite (~30 vol%), apatite (~3%), biotite and opaques.

The scarce volcanic rocks (San Miguelito complexes; cf. Fig. 1) are porphyritic trachytes containing pheno- and microphenocrysts of micro to cryptoperthitic alkali feldspar, plagioclase, clinopyroxene (often replaced by amphibole and biotite) and opaques set in a groundmass consisting of the same minerals and occasional quartz (quartz trachyte varieties). A single fragment of carbonatite, 3 cm in length, containing calcite and minor amounts of quartz and fluorite, was described in a marginal breccia by Litherland *et al*. (1986).

The dykes usually range in composition from quartz trachytes to trachyphonolites (Table 1), showing mineralogical assemblages broadly similar to those of the corresponding plutonic facies. Microgranite dykes with aplitic texture are present in the San Francisco body, whereas melasyenite dykes are widespread in the whole region, according to Fletcher & Beddoe-Stephens (1987). The latter rocks contain augite-aegirine augite, hornblende, alkali feldspar and nepheline phenocrysts set in a groundmass made of the same minerals and opaques; zircon, titanite and britholite are the most common accessory phases.

A nepheline syenite dyke containing phenocrysts of corundum and hercynite is noticeable in the Prado body (sample PV-32 of Table 1) and an aplogranitic dyke was sampled in the Cabeza de Toro complex (sample 27 of Table 1; cf. also Fletcher & Beddoe-Stephens, 1987).

Finally, it should be stressed that in the $Na_2O$ vs. $K_2O$ diagram (Fig. 2C) the oversaturated-saturated samples from Velasco plot generally into the potassic fields (agpaitic types tendentially lying in the transitional field), whereas the undersaturated (and agpaitic) varieties belong to the sodic suites.

Petrochemistry

Most of the samples are metaluminous, but about 22% of the rock-types are peralkaline, i.e. molar ratio $(Na_2O+K_2O)/Al_2O_3$, A.I.>1: 60% of the nephel-syenites and nepheline syenites. The latter are concentrated in the Taperas, Bamba, Zuialito and Prado bodies, and have $K_2O/Na_2O$ ratios ranging from 0.4 to 1.4. Peraluminous, corundum-normative and corundum-bearing rock-types (9% of the samples) are present in the Cabeza de Toro, Prado, Zuialito and San Francisco intrusions.

Typically, the rocks having A.I.•0.95 are plagioclase-free (i.e. hypersolvus varieties, cf. Fig. 3A). The agpaitic, silica-oversaturated rocks, show a comenditic affinity (i.e. $Al_2O_3$ wt%>1.33 $FeO_{total}$ wt%+4.4), according to the Le Maitre classification (1989).

Mostly rock-types tend to fit the trachytic thermal minimum in the Petrogeny's Residua System (PRS, Fig. 3B), and two main trends are apparent in the potassic side of the diagram, towards the granitic and phonolitic residual melt compositítions, respectively. It should be also emphasized that the gneissic-migmatitic rocks from the crystalline basement plot near to the granitic compositions of some Velasco complexes.

Major elements vs. silica diagrams (Harker diagrams, Fig. 4A) illustrate the variations amongst the different rock-types and particularly draw the attention to the wide $SiO_2$ range which reflects the spread from undersaturated to oversaturated in silica magma types. In general, $TiO_2$, $FeO_{total}$, MgO, CaO, $Al_2O_3$, $Na_2O$ and $P_2O_5$ decrease as $SiO_2$ increases, while the $K_2O$ is widely scattered above all at $SiO_2$ about 60 wt%. However, it is apparent that the compositional ranges result from the presence of several main groups and trends, i.e. nepheline syenites, nephel-syenites+syenites, quartz syenites+granites and dykes+effusive rocks, even considering the agpaitic (cf. Fig. 4B) vs. metaluminous-peraluminous petrographic types. Notably, granites and quartz syenites tend to fit the fields of basement crystalline rocks, suggesting to some extent processes related to crustal contamination (see below).

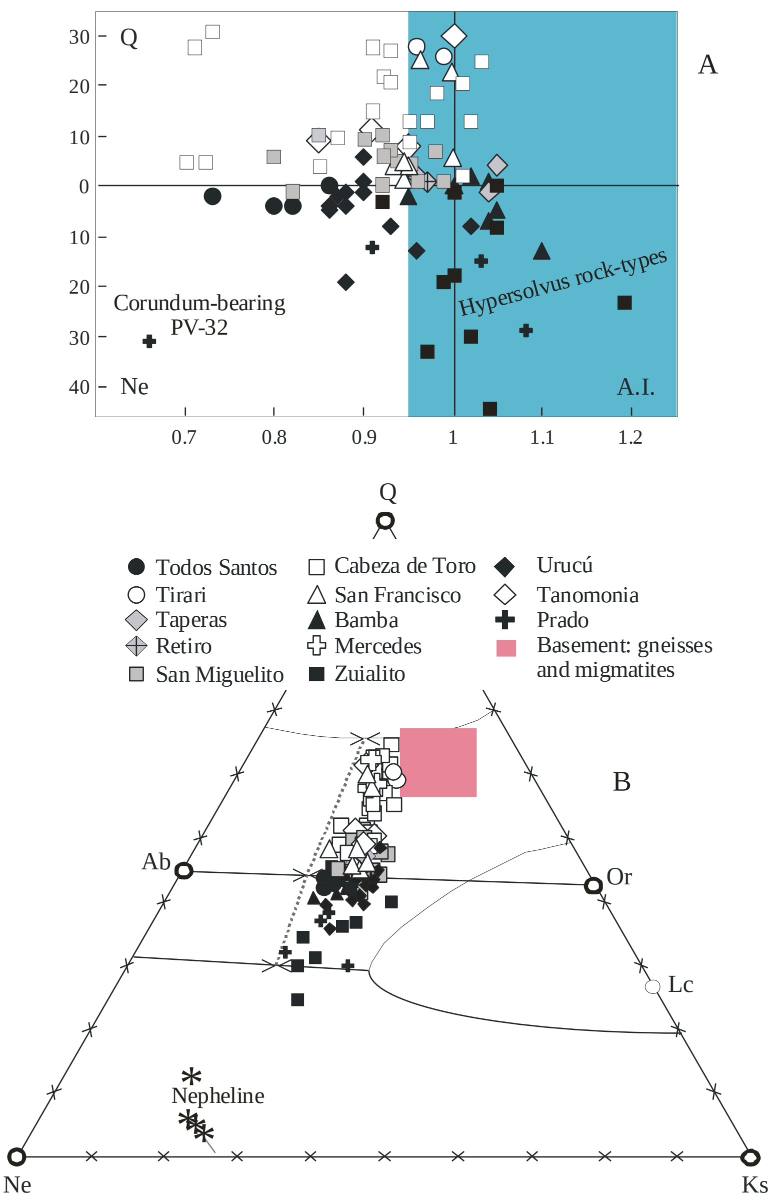


Fig. 3. A: normative Q-Ne vs. agpaitic index [A.I.=($Na_2O+K_2O$)/$Al_2O_3$ molar ratio] for the Velasco rocks (cf. Table 1). B: Velasco rock-types plotted into the Ne-Ks-$SiO_2$ system (Petrogeny's Residua System, after Hamilton & McKenzie, 1965, and Henderson, 1984). Phase boundaries are for $PH_2O$=1 kb and the thermal minima are linked by thermal valleys (broken lines) to the minimum on the Ab-Or join. Nepheline compositions are also plotted.

Defined trends are not apparent also for the trace elements that show very scattered variations, all about $SiO_2$~60 wt%, confirming the main groups observed for the major elements (Figs. 4C and D). It should be noted that Ga and Ge have a quite constant behaviour (23.6±4.6 ppm and 1.7±0.4 ppm, respectively), and that the PV-32 sample (corundum normative nepheline syenite dyke from Prado; cf. Table 1) displays very high Th (325 ppm), LREE (e.g. Ce=5774 ppm), Ga and Ge contents (55 and 4 ppm, respectively).

In particular, in terms of inter-elemental ratios and independently from the rock compositions, agpaitic or metaluminous, some general features should be stressed:

1) The quite constant behaviour of the Ba/Sr and Rb/Sr ratios up to $SiO_2$~60 wt% and the strong scattering of the quartz syenite to granite rock-types

(Fig. 5) (Ba/Sr: nepheline syenite 0.77±0.66; nephel-syenite 1.58±1.19; syenite 1.85±1.72; quartz syenite 3.08±2.21; granite 5.24±3.40. Rb/Sr: nepheline syenite 0.31±0.30; nephel-syenite 0.29±0.40; syenite 0.48±0.56; quartz syenite 1.63±2.03; granite 4.75±3.58). Notably, the latter rock-types display similar ratios to those shown by the basement rocks (cf. also Fletcher & Beddoe-Stephens, 1987, and Litherland *et al*., 1986).

2) The very different and scattered Nb/Ta ratios for the distinct rock-types, i.e. nepheline syenite 13.30±2.73, nephel-syenite 14.51±2.74, syenite 13.13±2.21, quartz syenite 12.55±1.90, granite and trachytic rocks 11.62±2.57. Moreover, in the Nb vs. Nb/Ta diagram (Fig. 5), the samples plot between the basement rocks and the mantle derived melts and associated worldwide alkaline rocks (cf. Green, 1995). The Hf/Zr ratio exhibits a quite uniform distribution for all the rock-types (0.024±0.004), with the exception of granites and aplogranite dykes (Hf/Zr=0.035±0.012 and 0.066, respectively).

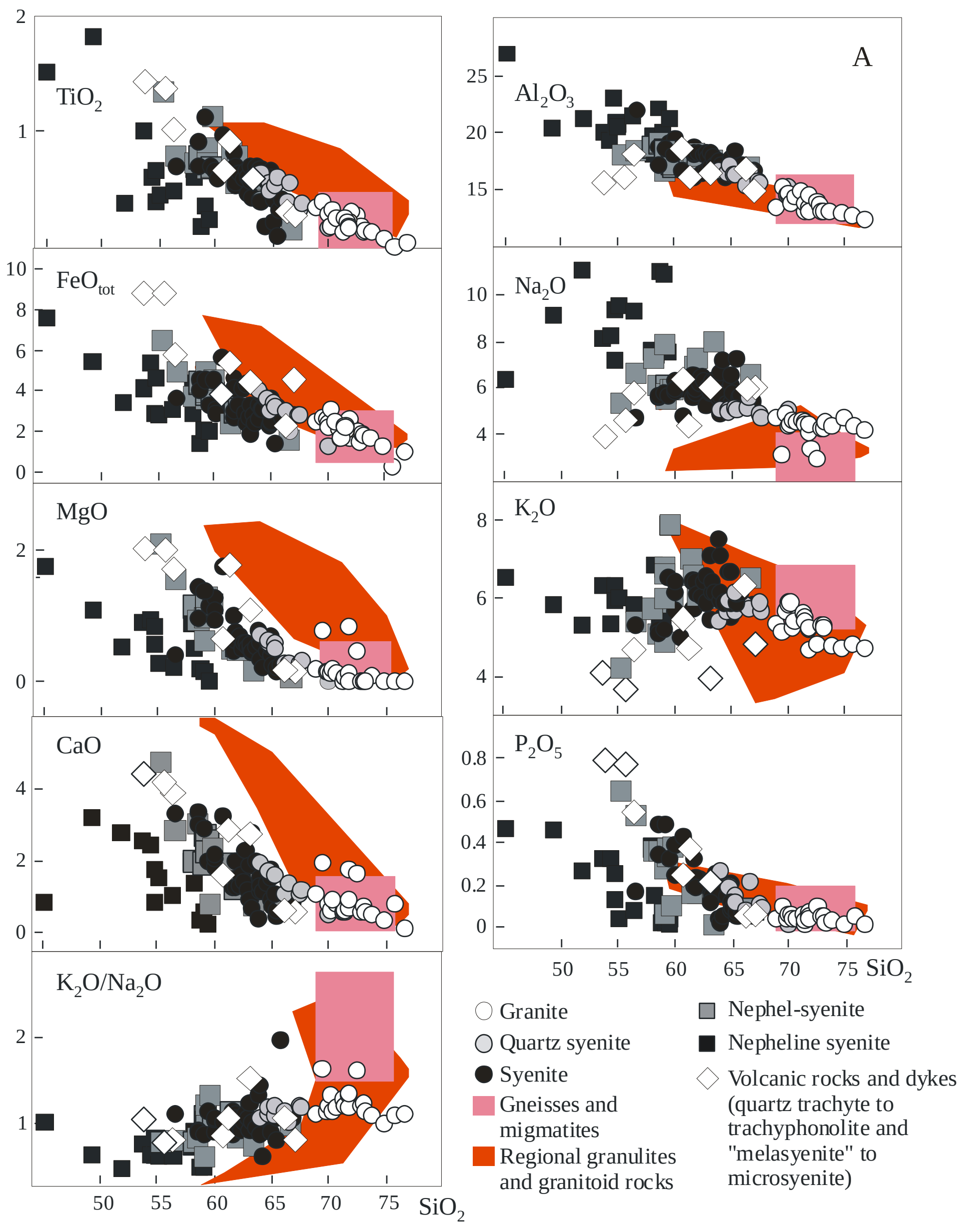


Fig. 4. A: Harker variation diagrams (major elements, wt%) for the whole population of Velasco rock-types.

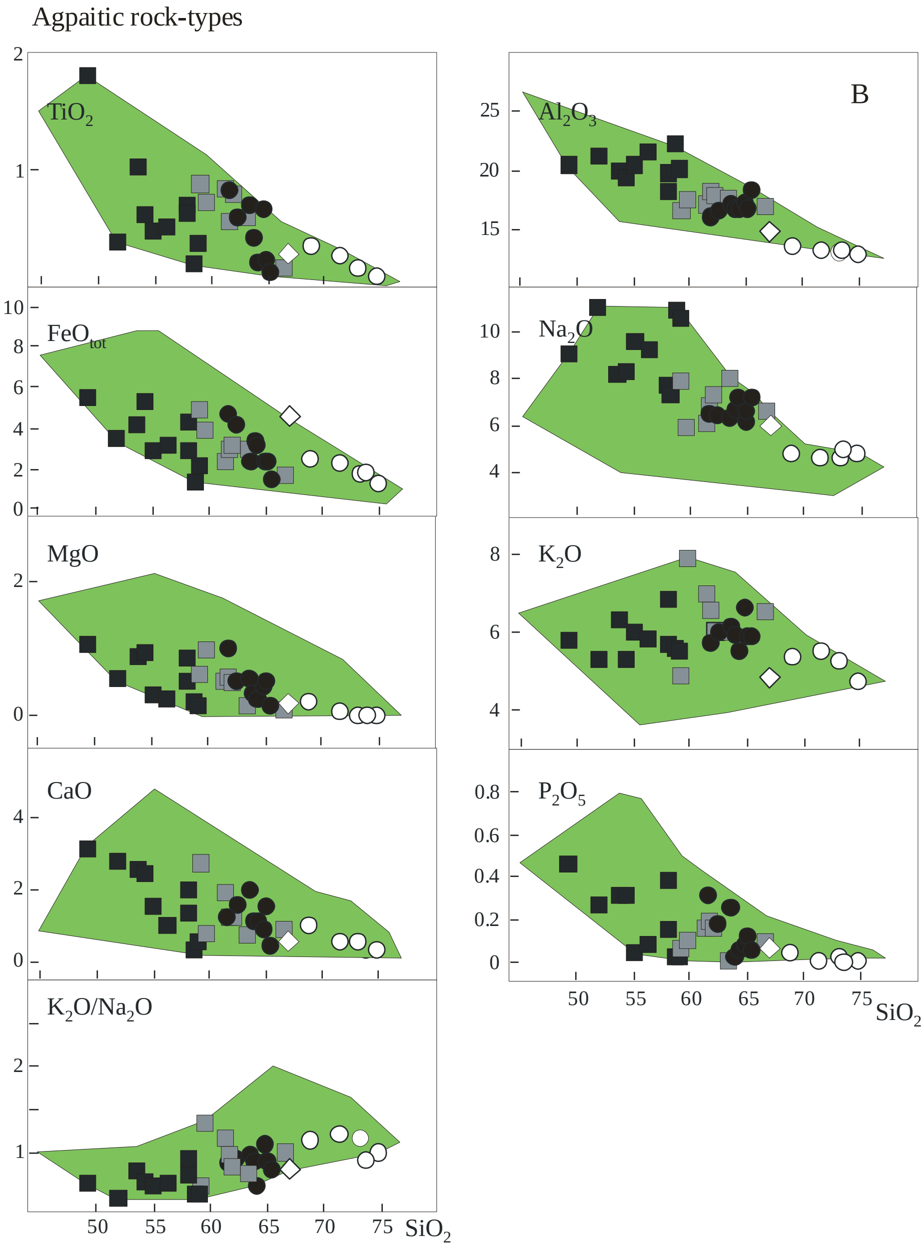


Fig. 4. B: Harker variation diagrams for only the agpaitic rock-types. In green, the whole population. Symbols as in Fig. 4A.

3) The apparent positive correlations (r=0.96 and 0.99, respectively) evidenced in the Y vs. Yb and Nd vs. Sm diagrams (Fig. 5). Granitic rocks tend to fit the Sm/Nd ratios of the metamorphic basement, following a linear correlation (Sm=0.170 Nd+1.222, r=0.97).

4) The scattered values shown by the La/Yb ratios (i.e. LREE/HREE): nepheline syenite 55.4±23.37, nephel-syenite 39.36±12.94, syenite 40.60±14.46, quartz syenite 34.22±15.43, granite 25.13±23.50. However, the chondrite-normalized La/Yb ratios [i.e. $(La/Yb)_c$, cf. Fig. 5] vs. $SiO_2$ display a tendency of decreasing fractionation of LREE/HREE from nepheline syenite to granite rock-types both in agpaitic and metaluminous-peraluminous varieties [i.e. $(La/Yb)_c$: nepheline syenite 35.77±25.66; nephel-syenite 26.93±7.82; syenite 20.65±12.30; quartz syenite 16.37±2.35; granite 10.83±2.64]. Some granites and quartz syenites have high $(La/Yb)_c$ values, i.e. 45.41±17.93 and 36.48±3.98, respectively.

5) On the whole, one can observe a strong enrichment in incompatible elements with respect to the primitive mantle (Sun & McDonough, 1989; cf.

Fig. 6), showing a very large spreading of elements such as Rb, U, Th, Nb, Ta and LREE, that vary from 100 to up to more than 1000 times the mantle values, and negative Sr, P and Ti spikes in all the rock-types. Notably, the spidergrams relative to the syenites (Fig. 6) parallel those from other worldwide occurences associated with continental rift areas (e.g. Kenia and Sudan; cf. Baker, 1987, and Harris *et al.*, 1983).

6) The distribution of REE in the chondrite-normalized diagrams (cf. Boynton, 1984; Figs. 7A, B) displays patterns characterized by different enrichments, steep fractionation of LREE, moderate fractionation of LREE with respect to MREE and a tendential flat behaviour of HREE for all the rock-types, and this even in a single complex [LREE/MREE, $(La/Sm)_c$: granite 4.47±1.22, quartz syenite 7.23±1.40, syenite 6.86±1.96, nephel-syenite 7.89±2.84, nepheline syenite 10.08±2.80, trachyphonolite to quartz trachyte dykes 6.44±2.41; MREE/HREE, $(Tb/Yb)_c$: granite 2.80±2.88, quartz syenite 1.48±0.55, syenite 1.73±0.54, nephel-syenite 1.55±0.40, nepheline syenite 1.68±0.64, trachyphonolite to quartz trachyte dykes 1.56±0.65].

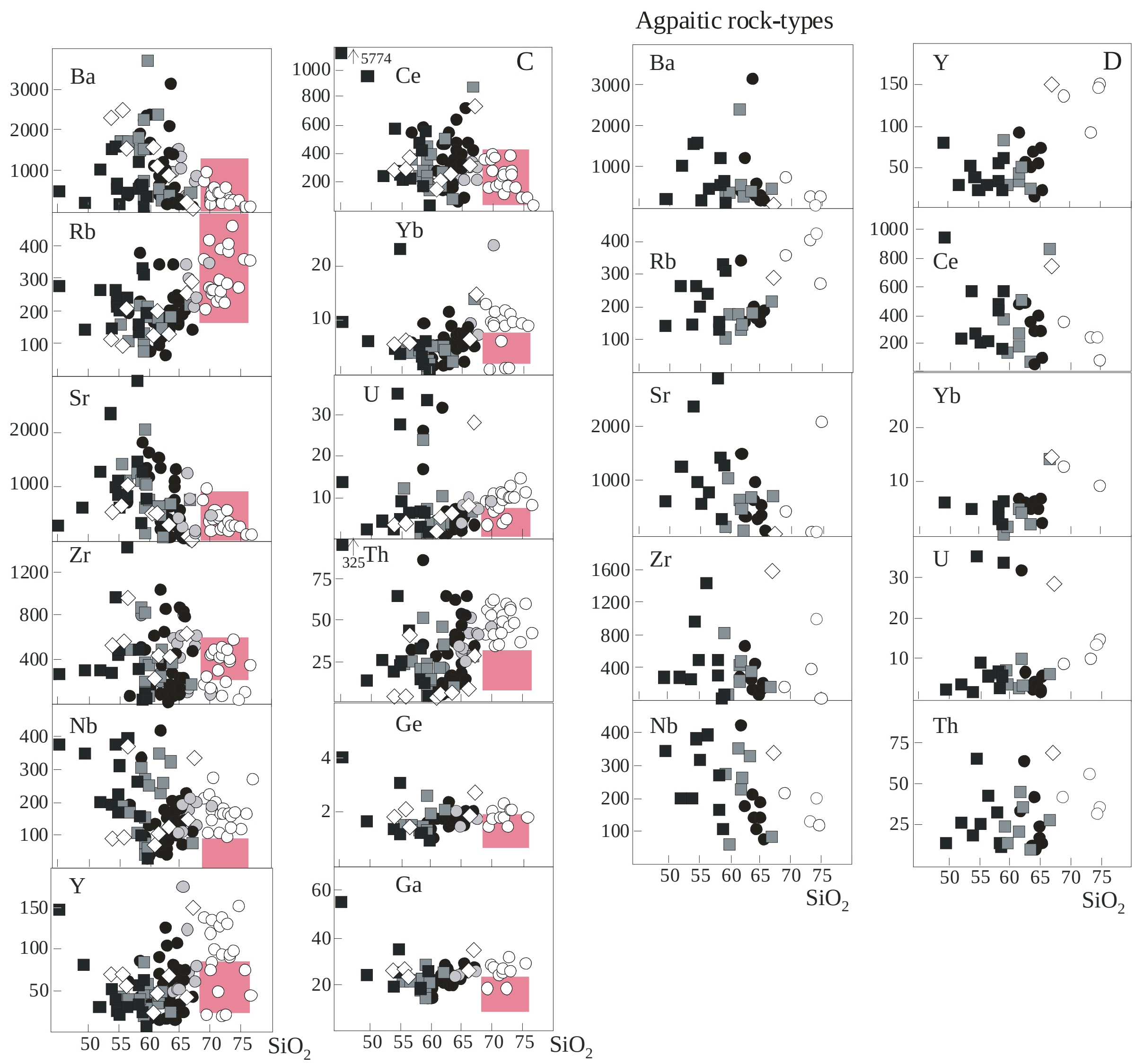


Fig. 4. C: Harker diagrams (trace elements, ppm) for the whole population. Symbols as in Fig. 4A. D: Harker diagrams for only the agpaitic rock-types. Data source for basement rocks: Litherland *et al.* (1986) and this work (cf. Table 1). Symbols as in Fig. 4A.

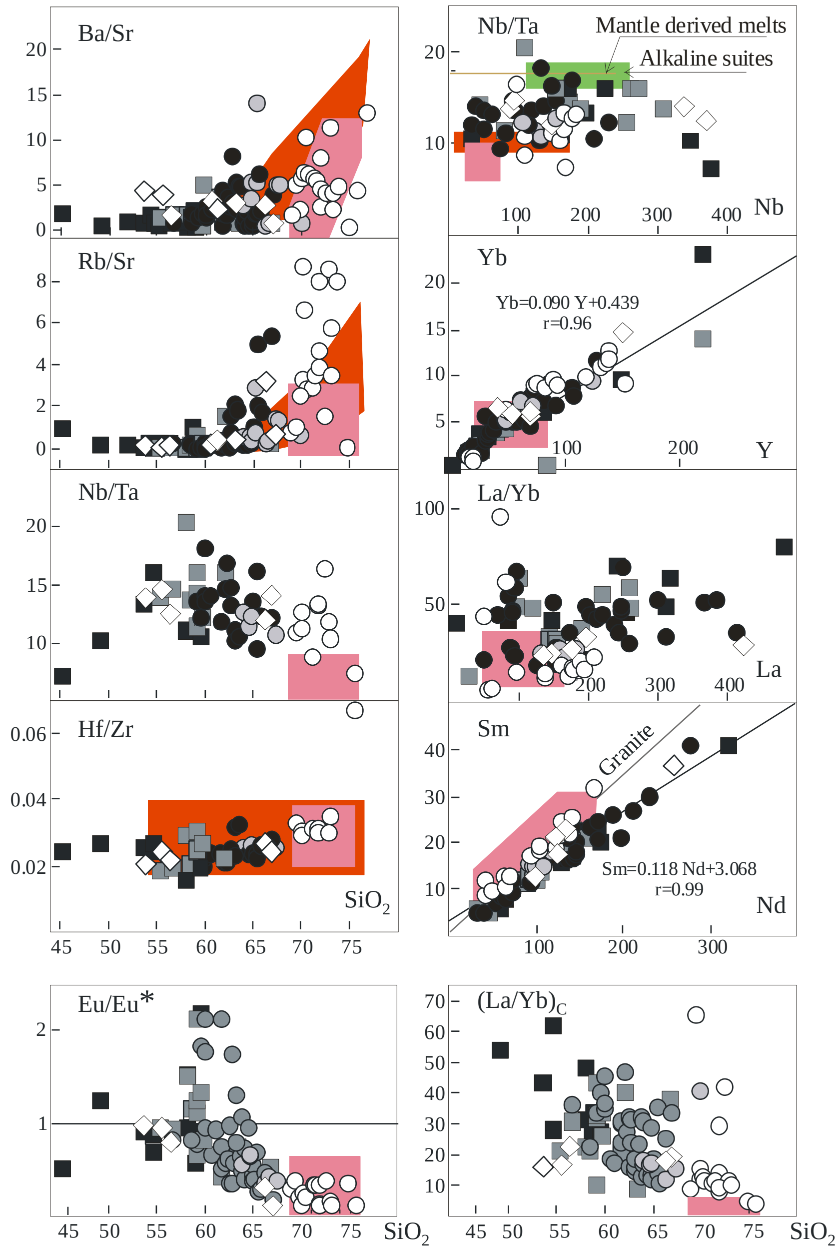


Fig. 5. Interelementar relationships for the Velasco complexes. Symbols and references as in Fig. 4A. In the Nb vs. Nb/Ta diagram, mantle derived melts and alkaline suites (worldwide alkaline rocks) are after Green (1995).

It should be also stressed that the granitic rock-types tend to fit the geochemical characteristics of gneisses and migmatites of the crystalline basement, and that the PV-32 dyke (corundum-hercynite-bearing nepheline syenite) exhibits a very different behaviour with $(La/Yb)_C$ 187.89, $(La/Sm)_C$ 9.34 and $(Tb/Yb)_C$ 5.72.

Eu anomalies (cf. Eu/Eu*, calculated according to Taylor & McLennan, 1985; Figs. 7A, B) are usually negative, but positive Eu/Eu* values are also found in some syenites (1.64±0.40), nephel-syenites (1.26±0.16) and nepheline syenites (1.65±0.49), both agpaitic and metaluminous. The origin of Eu anomalies has not yet been satisfactorily explained: feldspar fractionation, cumulus processes or mixtures of phenocryst (xenocryst)-loaded liquids from different stages of magmatic evolution are plausible means for producing Eu deficiency or excess.

7) The presence of a carbonate-rich xenolith (Retiro complex) with a strong enriched REE pattern (Fig. 7A), points up to some extent to the possibility of a not well-defined carbonatitic association.

In sum, the petrochemical data are consistent with different magma types, even in a single complex, probably derived from distinct parent sources and mixing in the magma chamber, or by crystallization in open system and/or affected by different crustal contamination (see below "Sr-Nd isotopes"), especially in the silica-oversaturated rock-types, i.e. quartz syenites (trachytes) and granites, in which an important role regarding the concentration of some trace elements may be also played by the fractional crystallization and cumulus of accessory phases such as titanite, eudialyte etc.

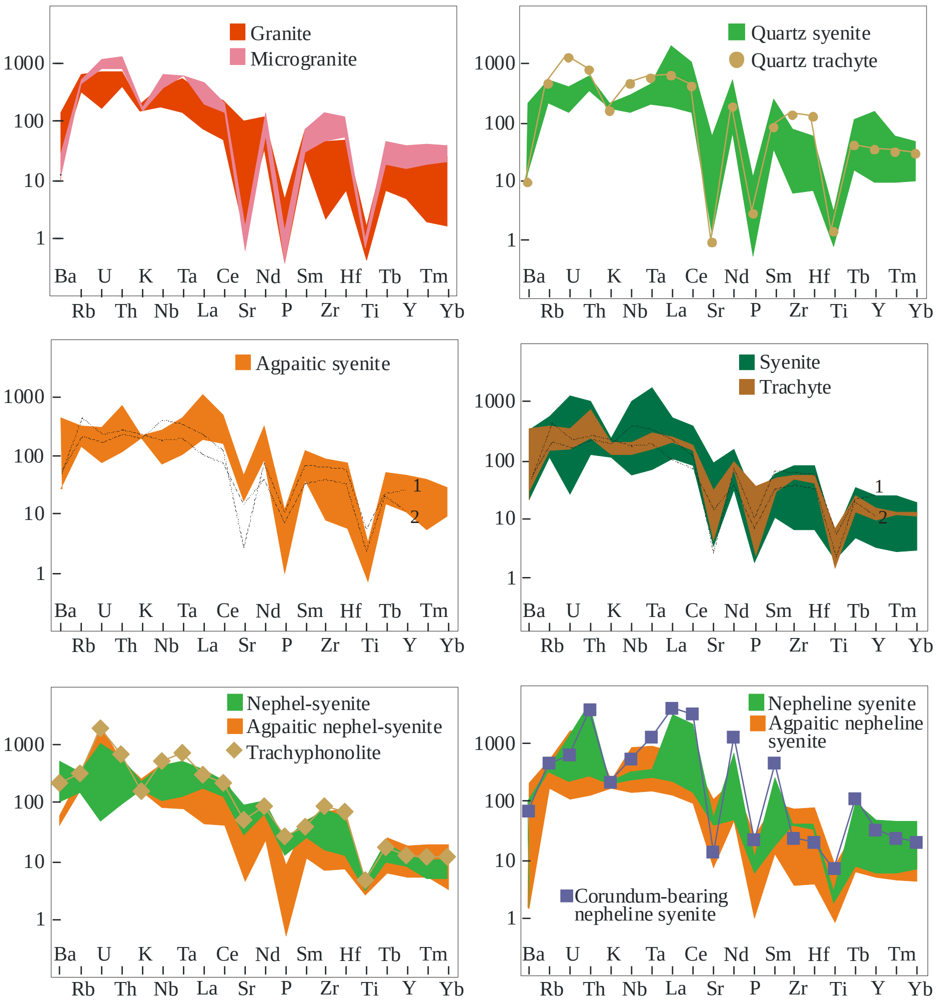


Fig. 6. Primitive mantle-normalized (Sun & McDonough, 1989) trace elements diagrams for the rock-types from Velasco complexes. 1) and 2): average data for trachytes and nepheline syenites from continental rift zones (Kenia and Sudan, respectively; data source: Baker, 1987, and Harris *et al.*, 1983).

## Mineralogy

Representative analyses of the main minerals from all the Velasco rock-types are given in Tables 2 to 6.

### *Feldspars*

Feldspars from Velasco rocks are alkali feldspar coexisting with plagioclase in subsolvus rock-types that have A.I.•0.95, or just mesoperthitic alkali feldspar in the hypersolvus varieties (Table 2; cf. Fig. 3).

Plagioclase is, in general, zoned ranging commonly from labradorite to oligoclase, but with prevailing andesine to oligoclase compositions in the syenites and trachytes, following Na-K-enrichment and Ca-depletion trends. The rims are often mantled by feldspars displaying Na-rich compositions (anorthoclase-albite).

The mesoperthitic alkali feldspar (principally characterized by patch- to hairperthites in coarse and fine-grained rock-types, respectively) shows for the whole composition an average value of $Ab_{55}Or_{45}$, whereas the exsolved phases are in the range of 60-98 Or and of 90-99 Ab, respectively.

Although the Velasco feldspars fall below the solvus-solidus intersection in the system $KalSi_3O_8$-$NaAlSi_3O_8$-$CaAl_2Si_2O_8$ at $P_{H_2O}$=0.5 kb and 900°C (Seck, 1971), some ternary compositions are noticeable as patches in syenites (Fig. 8).

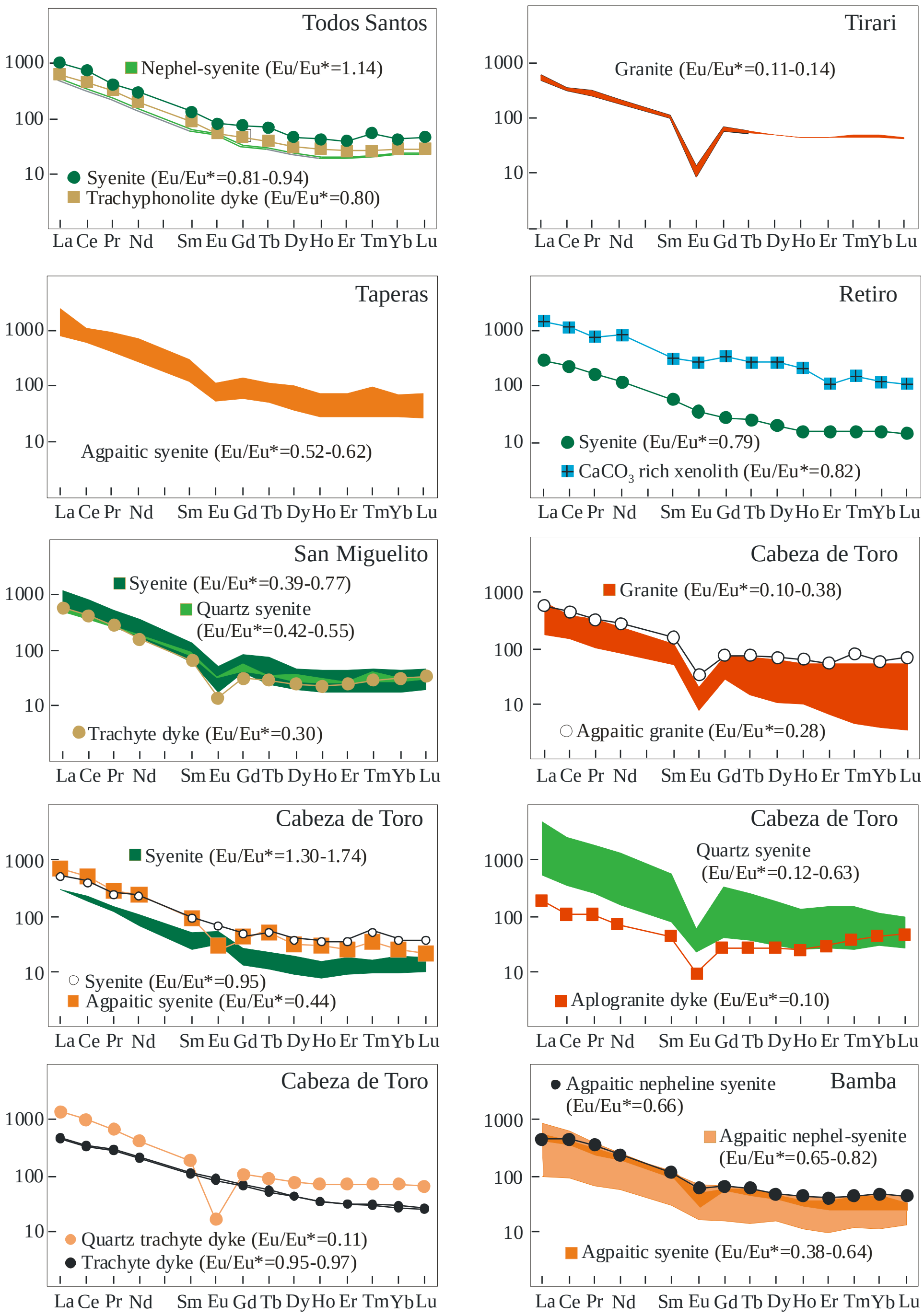


Fig. 7. A: Chondrite-normalized (Boynton, 1984) REE profiles for the rock-types from Velasco complexes. Eu/Eu* calculated according to Taylor & McLennan (1985).

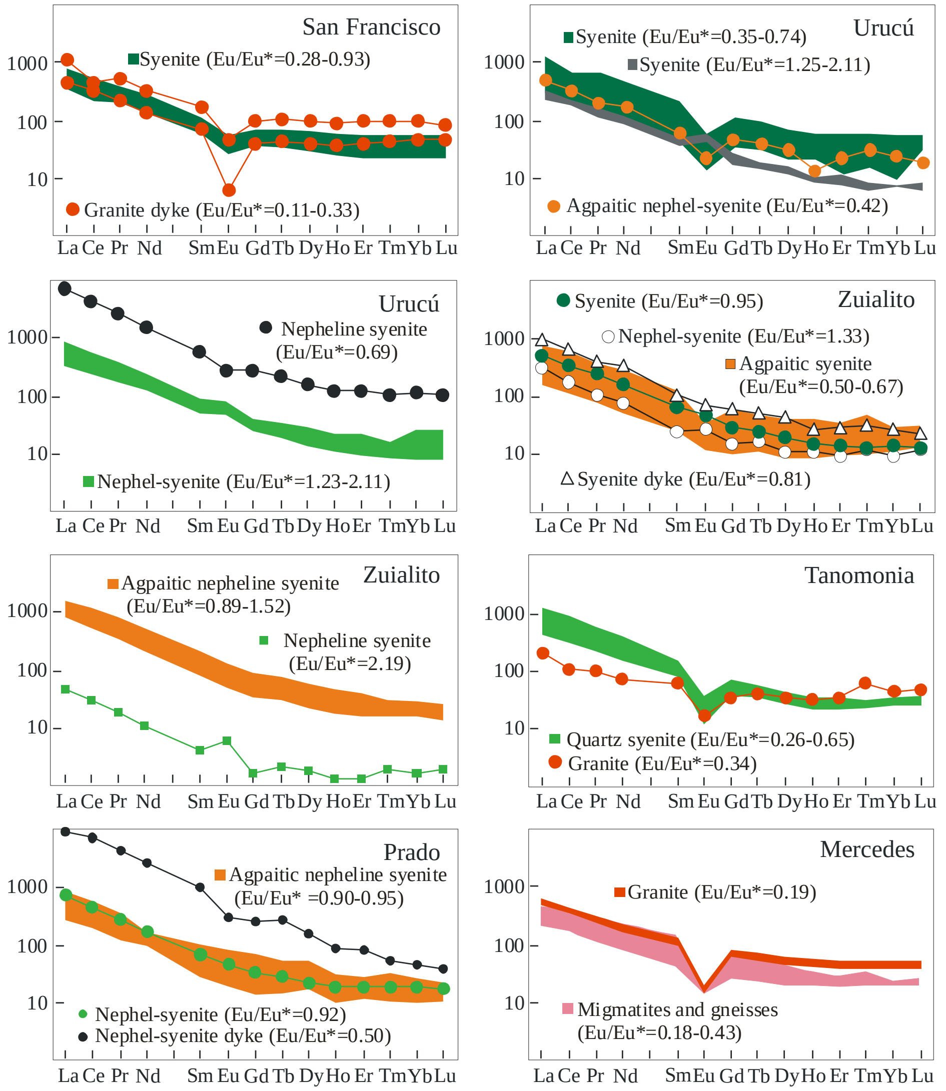


Fig. 7. B: Chondrite-normalized (Boynton, 1984) REE profiles for the rock-types from Velasco complexes.

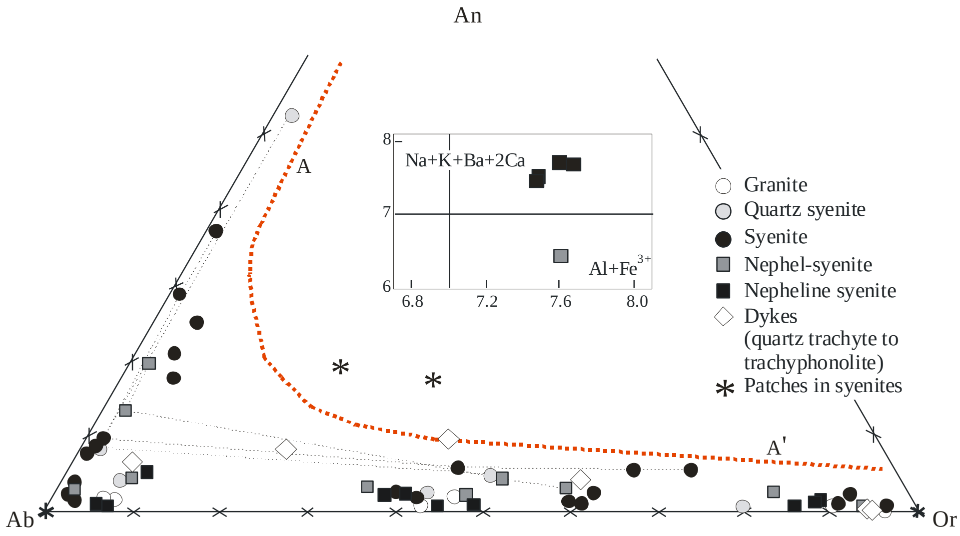


Fig. 8. Feldspar compositions plotted into the An-Ab-Or diagram (wt%). A-A' is the solvus-solidus intersection at 900°C (Seck, 1971). Inset: nepheline plotted in terms of $(Al+Fe^{3+})$ vs. (Na+K+Ba+2Ca), a.f.u.

Table 2. Representative probe analyses of feldspars and foids. Gr, granite; QS, quartz syenite; S, syenite; NS, nephel-syenite; NES, nepheline syenite; QTR, quartz trachyte; TRPH, trachyphonolite. AF, alkali feldspar, whole composition; K-ph and Na-ph, perthites and antiperthites, respectively; Pl, plagioclase; Neph, nepheline. C, core; R, rim; I, intermediate areas; ph, mph and gm, phenocrysts, microphenocrysts and groundmass phases, respectively. For analytical methods see Comin-Chiaramonti *et al*. (in this volume).

| Sample | | 7 | | | 28 | | | 15 | | | PV-8 | |
|---|---|---|---|---|---|---|---|---|---|---|---|---|
| | | Gr | | | Gr | | | QS | | | QS | |
| | AF | K-ph | Na-ph | AF | K-ph | Na-ph | AF | Pl-C | Pl-R | AF | K-ph | Na-ph |
| wt% | | | | | | | | | | | | |
| $SiO_2$ | 66.52 | 64.76 | 67.78 | 67.11 | 63.33 | 67.47 | 65.20 | 55.66 | 66.56 | 66.17 | 64.91 | 66.75 |
| $Al_2O_3$ | 18.88 | 18.18 | 19.52 | 19.14 | 17.93 | 19.37 | 19.38 | 27.79 | 20.64 | 19.18 | 18.38 | 19.76 |
| $Fe_2O_3$ | 0.14 | 0.25 | 0.11 | 0.06 | 0.14 | 0.20 | 0.11 | 0.47 | 0.19 | 0.14 | 0.13 | 0.14 |
| BaO | 0.06 | 0.04 | | 0.12 | 0.05 | 0.09 | 0.62 | 0.05 | 0.08 | 0.05 | 0.10 | |
| SrO | | 0.02 | | | | | 0.02 | 0.41 | | 0.02 | 0.02 | |
| CaO | 0.11 | | 0.35 | 0.14 | 0.07 | 0.31 | 0.61 | 10.18 | 1.57 | 0.43 | 0.04 | 0.8 |
| $Na_2O$ | 6.59 | 0.51 | 11.39 | 6.37 | 1.07 | 11.14 | 5.59 | 5.34 | 10.74 | 6.49 | 2.39 | 10.49 |
| $K_2O$ | 7.29 | 16.13 | 0.21 | 7.75 | 14.87 | 0.51 | 8.06 | 0.33 | 0.17 | 7.17 | 13.28 | 1.04 |
| Sum | 99.59 | 99.89 | 99.36 | 100.69 | 97.46 | 99.09 | 99.59 | 100.23 | 99.95 | 99.65 | 99.25 | 98.98 |
| | | | | | | | | | | | | |
| Si | 11.975 | 11.996 | 11.934 | 11.967 | 11.982 | 11.935 | 11.837 | 10.032 | 11.699 | 11.911 | 11.982 | 11.848 |
| Al | 4.006 | 3.969 | 4.051 | 4.023 | 3.999 | 4.038 | 4.147 | 5.904 | 4.276 | 4.070 | 4.000 | 4.134 |
| $Fe^{3+}$ | 0.019 | 0.035 | 0.015 | 0.008 | 0.019 | 0.027 | 0.015 | 0.064 | 0.025 | 0.019 | 0.018 | 0.018 |
| Ba | 0.004 | 0.003 | | 0.009 | 0.003 | 0.006 | 0.044 | 0.003 | 0.005 | 0.003 | 0.007 | |
| Sr | | 0.002 | | | | | 0.002 | 0.043 | | 0.002 | 0.002 | |
| Ca | 0.021 | | 0.066 | 0.027 | 0.014 | 0.058 | 0.119 | 1.966 | 0.296 | 0.083 | 0.008 | 0.152 |
| Na | 2.300 | 0.183 | 3.888 | 2.203 | 0.393 | 3.820 | 1.968 | 1.866 | 3.660 | 2.265 | 0.856 | 3.609 |
| K | 1.674 | 3.812 | 0.045 | 1.764 | 3.590 | 0.115 | 1.867 | 0.076 | 0.038 | 1.647 | 3.128 | 0.235 |
| (O=32) | | | | | | | | | | | | |
| Z | 16.000 | 16.000 | 16.000 | 15.998 | 16.000 | 16.000 | 15.999 | 16.000 | 16.000 | 16.000 | 16.000 | 16.000 |
| X | 3.999 | 4.000 | 3.999 | 4.003 | 4.000 | 4.000 | 4.000 | 3.954 | 4.000 | 4.000 | 4.001 | 3.996 |
| | | | | | | | | | | | | |
| wt% | | | | | | | | | | | | |
| Or | 43.3 | 95.7 | 1.2 | 45.5 | 90.2 | 3.0 | 48.2 | 2.0 | 1.0 | 42.5 | 79.1 | 6.2 |
| Ab | 56.0 | 4.3 | 97.0 | 53.5 | 9.3 | 95.2 | 47.1 | 45.6 | 90.9 | 55.1 | 20.4 | 89.8 |
| An | 0.7 | 0.0 | 1.8 | 1.0 | 0.5 | 1.8 | 4.7 | 52.4 | 8.1 | 2.4 | 0.5 | 4.0 |
| | | | | | | | | | | | | |
| A.I. | | 0.93 | | | 0.96 | | | 0.85 | | | 0.91 | |

| Sample | | | 10 | | | | | 18 | | | 30 | | | 32 | |
|---|---|---|---|---|---|---|---|---|---|---|---|---|---|---|---|
| | | | S | | | | | S | | | S | | | S | |
| | AF | K-ph | Na-ph | Pl-C | Pl-R | AF | Pl-C | Pl-I | Pl-R | AF | K-ph | Na-ph | AF | K-ph | Na-ph |
| wt% | | | | | | | | | | | | | | | |
| $SiO_2$ | 64.66 | 63.88 | 65.56 | 58.60 | 60.58 | 65.41 | 62.93 | 63.20 | 62.08 | 65.93 | 64.56 | 66.94 | 65.56 | 65.85 | 68.10 |
| $Al_2O_3$ | 19.49 | 19.04 | 20.67 | 25.34 | 23.80 | 18.85 | 22.86 | 21.96 | 21.98 | 18.89 | 18.26 | 19.68 | 18.66 | 18.58 | 19.38 |
| $Fe_2O_3$ | 0.19 | 0.19 | 0.15 | 0.16 | 0.38 | 0.12 | 0.11 | 0.24 | 0.16 | 0.15 | 0.16 | 0.24 | 0.38 | 0.34 | 0.24 |
| BaO | 0.33 | 0.90 | 0.23 | 0.22 | 0.06 | 0.33 | 0.01 | 0.09 | 1.37 | | 0.20 | 0.03 | 0.21 | 0.16 | 0.10 |
| SrO | 0.18 | 0.26 | 0.19 | 0.50 | 0.39 | 0.03 | 0.08 | 0.02 | 0.16 | | | | 0.11 | 0.09 | 0.10 |
| CaO | 0.88 | 0.44 | 1.65 | 6.97 | 5.47 | 0.22 | 4.18 | 3.46 | 3.13 | 0.28 | 0.01 | 0.73 | 0.16 | 0.04 | 0.13 |
| $Na_2O$ | 5.84 | 2.79 | 10.41 | 7.28 | 8.20 | 3.94 | 8.82 | 8.98 | 6.76 | 4.66 | 0.46 | 11.11 | 6.60 | 4.60 | 11.35 |
| $K_2O$ | 7.41 | 11.95 | 0.28 | 0.16 | 0.17 | 10.90 | 0.67 | 0.91 | 3.86 | 9.98 | 16.12 | 0.19 | 6.93 | 10.13 | 0.42 |
| Sum | 98.98 | 99.45 | 99.14 | 99.23 | 99.05 | 99.80 | 99.66 | 98.86 | 99.50 | 99.98 | 99.77 | 98.92 | 98.61 | 99.79 | 99.82 |
| | | | | | | | | | | | | | | | |
| Si | 11.786 | 11.777 | 11.650 | 10.583 | 10.901 | 11.931 | 11.193 | 11.328 | 11.274 | 11.946 | 11.983 | 11.859 | 11.942 | 11.972 | 11.958 |
| Al | 4.187 | 4.216 | 4.330 | 5.394 | 5.046 | 4.053 | 4.793 | 4.639 | 4.705 | 4.034 | 3.955 | 4.109 | 4.006 | 3.982 | 4.011 |
| $Fe^{3+}$ | 0.026 | 0.026 | 0.020 | 0.022 | 0.051 | 0.016 | 0.015 | 0.032 | 0.022 | 0.020 | 0.022 | 0.032 | 0.052 | 0.046 | 0.031 |
| Ba | 0.023 | 0.063 | 0.016 | 0.015 | 0.004 | 0.023 | 0.001 | 0.006 | 0.097 | | 0.014 | 0.002 | 0.015 | 0.011 | 0.006 |
| Sr | 0.019 | 0.028 | 0.019 | 0.052 | 0.041 | 0.003 | 0.008 | 0.002 | 0.017 | | | | 0.012 | 0.009 | 0.011 |
| Ca | 0.172 | 0.087 | 0.314 | 1.349 | 1.055 | 0.043 | 0.797 | 0.664 | 0.609 | 0.054 | 0.002 | 0.138 | 0.032 | 0.008 | 0.024 |
| Na | 2.064 | 0.997 | 3.587 | 2.549 | 2.861 | 1.394 | 3.042 | 3.121 | 2.381 | 1.638 | 0.165 | 3.817 | 2.331 | 1.622 | 3.864 |
| K | 1.723 | 2.811 | 0.063 | 0.037 | 0.039 | 2.536 | 0.152 | 0.208 | 0.894 | 2.306 | 3.817 | 0.043 | 1.611 | 2.350 | 0.095 |
| (O=32) | | | | | | | | | | | | | | | |
| Z | 15.999 | 16.019 | 16.000 | 15.999 | 15.998 | 16.000 | 16.001 | 15.999 | 16.001 | 16.000 | 16.000 | 16.000 | 16.000 | 16.000 | 16.000 |
| X | 4.001 | 3.986 | 3.999 | 4.002 | 4.000 | 3.999 | 4.000 | 4.001 | 3.998 | 4.000 | 4.000 | 4.000 | 4.001 | 4.000 | 4.000 |
| | | | | | | | | | | | | | | | |
| wt% | | | | | | | | | | | | | | | |
| Or | 44.3 | 71.0 | 1.7 | 1.0 | 1.0 | 64.6 | 4.0 | 5.4 | 23.0 | 59.1 | 95.6 | 1.1 | 41.6 | 60.1 | 2.5 |
| Ab | 49.9 | 23.7 | 88.9 | 62.1 | 70.2 | 33.4 | 74.9 | 77.0 | 57.5 | 39.5 | 3.9 | 95.1 | 56.7 | 39.0 | 96.3 |
| An | 5.8 | 5.3 | 9.4 | 36.9 | 28.8 | 2.0 | 21.1 | 17.6 | 19.5 | 1.4 | 0.5 | 3.8 | 1.7 | 0.9 | 1.2 |
| | | | | | | | | | | | | | | | |
| A.I. | | | 0.82 | | | | | 0.80 | | | 1.04 | | | 0.97 | |

Table 2 (continued).

| Sample | PV-6 | | | | | PV-14 | | PV-34 | | | 21 | | |
|---|---|---|---|---|---|---|---|---|---|---|---|---|---|
| | S | | | | | S | | S | | | NS | | |
| | AF | K-ph | Na-ph | Pl | Patch | K-patch | Na-patch | Na-ph | AF | AF-C | AF-R | Pl-C | Pl-R |
| wt% | | | | | | | | | | | | | |
| $SiO_2$ | 65.84 | 64.09 | 66.82 | 61.63 | 62.97 | 64.90 | 66.73 | 66.01 | 66.19 | 65.19 | 64.14 | 63.80 | 64.96 |
| $Al_2O_3$ | 19.11 | 18.42 | 20.68 | 22.94 | 21.74 | 18.40 | 19.34 | 20.62 | 19.00 | 19.38 | 18.93 | 22.82 | 21.65 |
| $Fe_2O_3$ | 0.05 | 0.25 | 0.10 | 0.30 | 0.13 | 0.20 | 0.14 | 0.11 | 0.36 | 0.03 | 0.09 | 0.14 | 0.05 |
| BaO | 0.23 | 0.98 | 0.10 | 0.52 | 1.49 | 0.31 | | 0.02 | 0.38 | 0.36 | 0.53 | 0.13 | 0.08 |
| SrO | 0.01 | | | 0.19 | 0.13 | 0.02 | | 0.02 | 0.20 | 0.23 | 0.19 | 0.16 | 0.17 |
| CaO | 0.34 | 0.01 | 1.48 | 4.42 | 2.70 | 0.02 | 0.46 | 1.66 | 0.19 | 0.52 | 0.41 | 3.87 | 2.61 |
| $Na_2O$ | 5.45 | 0.75 | 10.83 | 8.31 | 5.51 | 1.09 | 11.13 | 10.59 | 6.92 | 5.41 | 3.38 | 9.27 | 9.92 |
| $K_2O$ | 8.68 | 15.40 | 0.15 | 0.83 | 6.22 | 15.22 | 0.26 | 0.21 | 6.54 | 8.38 | 11.23 | 0.34 | 0.37 |
| Sum | 99.71 | 99.90 | 100.16 | 99.14 | 100.89 | 100.16 | 98.06 | 99.24 | 99.78 | 99.50 | 98.90 | 100.53 | 99.81 |
| | | | | | | | | | | | | | |
| Si | 11. 917 | 11.925 | 11.714 | 11.093 | 11.359 | 11.971 | 11.912 | 11.683 | 11.918 | 11.846 | 11.861 | 11.242 | 11.483 |
| Al | 4.077 | 4.040 | 4.273 | 4.867 | 4.623 | 4.001 | 4.069 | 4.302 | 4.032 | 4.151 | 4.126 | 4.740 | 4.511 |
| $Fe^{3+}$ | 0.006 | 0.035 | 0.013 | 0.040 | 0.018 | 0.028 | 0.019 | 0.015 | 0.049 | 0.004 | 0.013 | 0.018 | 0.006 |
| Ba | 0.016 | 0.072 | 0.006 | 0.037 | 0.105 | 0.022 | | 0.001 | 0.027 | 0.026 | 0.039 | 0.009 | 0.005 |
| Sr | 0.001 | | | 0.019 | 0.014 | 0.002 | | 0.002 | 0.020 | 0.024 | 0.020 | 0.016 | 0.017 |
| Ca | 0.066 | 0.002 | 0.278 | 0.852 | 0.522 | 0.004 | 0.088 | 0.315 | 0.037 | 0.101 | 0.081 | 0.731 | 0.494 |
| Na | 1.912 | 0.270 | 3.681 | 2.901 | 1.927 | 0.390 | 3.853 | 3.635 | 2.415 | 1.906 | 1.211 | 3.167 | 3.401 |
| K | 2.003 | 3.656 | 0.034 | 10.190 | 1.432 | 3.582 | 0.060 | 0.047 | 1.502 | 1.943 | 2.649 | 0.076 | 0.083 |
| (O=32) | | | | | | | | | | | | | |
| Z | 16.000 | 16.000 | 16.000 | 16.000 | 16.000 | 16.000 | 16.000 | 16.000 | 15.999 | 16.001 | 16.000 | 16.000 | 16.000 |
| X | 3.998 | 4.000 | 3.999 | 3.999 | 4.000 | 4.000 | 4.001 | 4.000 | 4.001 | 4.000 | 4.000 | 3.999 | 4.000 |
| | | | | | | | | | | | | | |
| wt% | | | | | | | | | | | | | |
| Or | 51.5 | 91.1 | 0.9 | 4.9 | 36.4 | 89.9 | 1.6 | 1.3 | 38.7 | 49.8 | 67.6 | 2.0 | 2.2 |
| Ab | 46.2 | 6.4 | 91.5 | 71.0 | 46.3 | 9.2 | 96.1 | 90.3 | 58.7 | 46.0 | 29.1 | 78.1 | 84.1 |
| An | 2.3 | 2.5 | 7.6 | 24.1 | 17.3 | 0.9 | 2.3 | 8.4 | 2.6 | 4.2 | 3.3 | 19.9 | 13.7 |
| | | | | | | | | | | | | | |
| A.I. | | | 0.85 | | | | 0.90 | | 0.91 | | | 0.82 | |

| Sample | PV-16 | | | PV-55 | | | | PV-22 | | | | PV-22 | |
|---|---|---|---|---|---|---|---|---|---|---|---|---|---|
| | NS | | | NS | | | | NES | | | | | |
| | AF | K-ph | Na-ph | AF | K-ph | Na-ph | Neph | AF | K-ph | Na-ph | Neph | Haüyne | |
| wt% | | | | | | | | | | | | | |
| $SiO_2$ | 67.31 | 64.83 | 66.28 | 66.15 | 63.83 | 67.67 | 46.00 | 66.55 | 64.45 | 67.80 | 44.13 | $SiO_2$ | 35.66 |
| $Al_2O_3$ | 19.67 | 18.83 | 19.66 | 19.06 | 18.11 | 19.61 | 33.81 | 18.91 | 18.38 | 19.19 | 32.47 | $Al_2O_3$ | 30.11 |
| $Fe_2O_3$ | 0.10 | 0.04 | 0.04 | 0.15 | 0.14 | 0.24 | 0.58 | 0.15 | 0.14 | 0.16 | 0.56 | $Fe_2O_3$ | 0.18 |
| BaO | 0.42 | 0.49 | 0.22 | 0.10 | 0.18 | 0.15 | | 0.14 | 0.25 | 0.03 | 0.04 | MnO | 0.02 |
| SrO | 0.30 | 0.10 | 0.58 | 0.20 | 0.08 | 0.25 | | 0.15 | .21 | 0.09 | | CaO | 4.90 |
| CaO | 0.30 | 0.10 | 0.58 | 0.24 | 0.02 | 0.33 | 0.71 | 0.02 | | 0.04 | 0.01 | $Na_2O$ | 19.36 |
| $Na_2O$ | 7.30 | 1.84 | 10.28 | 6.02 | 0.68 | 11.28 | 13.59 | 6.45 | 1.24 | 11.52 | 16.01 | $K_2O$ | 0.02 |
| $K_2O$ | 6.17 | 13.90 | 1.26 | 7.93 | 15.57 | 0.24 | 4.90 | 7.50 | 14.84 | 0.15 | 5.83 | $SO_3$ | 9.51 |
| Sum | 101.49 | 13.90 | 98.53 | 99.85 | 98.61 | 99.77 | 99.59 | 99.87 | 99.51 | 98.98 | 99.05 | Sum | 99.76 |
| | | | | | | | | | | | | | |
| Si | 11.891 | 11.915 | 11.851 | 11.927 | 11.975 | 11.903 | 8.685 | 11.970 | 11.961 | 11.981 | 8.529 | Si | 6.002 |
| Al | 4.096 | 4.079 | 4.144 | 4.051 | 4.004 | 4.066 | 7.524 | 4.009 | 4.020 | 3.997 | 7.397 | Al | 5.974 |
| $Fe^{3+}$ | 0.013 | 0.006 | 0.006 | 0.020 | 0.020 | 0.032 | 0.082 | 0.020 | 0.019 | 0.021 | 0.081 | $Fe^{3+}$ | 0.023 |
| Ba | 0.029 | 0.035 | 0.015 | 0.007 | 0.013 | 0.010 | | 0.010 | 0.018 | 0.002 | 0.003 | Sum | 11.999 |
| Sr | 0.022 | 0.030 | 0.021 | 0.020 | 0.009 | 0.026 | | 0.016 | 0.022 | 0.009 | | Mn | 0.003 |
| Ca | 0.056 | 0.019 | 0.111 | 0.047 | 0.004 | 0.063 | 0.144 | 0.004 | | 0.007 | 0.002 | Ca | 0.884 |
| Na | 2.501 | 0.656 | 3.565 | 2.104 | 0.248 | 3.847 | 4.975 | 2.250 | 0.446 | 3.948 | 6.000 | Na | 6.318 |
| K | 1.391 | 3.260 | 0.288 | 1.824 | 3.727 | 0.054 | 1.180 | 1.721 | 3.513 | 0.034 | 1.438 | K | 0.004 |
| (O=32) | | | | | | | | | | | | Sum | 7.209 |
| Z | 16.000 | 16.000 | 16.001 | 15.998 | 15.999 | 16.000 | 16.291 | 15.999 | 16.000 | 15.999 | 16.007 | $SO_3$ | 1.201 |
| X | 3.999 | 4.000 | 4.000 | 4.002 | 4.001 | 4.000 | 6.299 | 4.001 | 3.999 | 4.000 | 7.443 | | |
| | | | | | | | | | | | | (O=21) | |
| wt% | | | | | | | | | | | | Basis: | |
| Or | 36.0 | 81.8 | 7.6 | 46.9 | 93.3 | 1.4 | | 44.32 | 88.1 | 0.9 | | $3Al_2O_3{*}6SiO_2$ | |
| Ab | 60.8 | 15.5 | 88.2 | 51.0 | 5.9 | 95.7 | | 54.58 | 10.5 | 98.5 | | | |
| An | 3.2 | 2.7 | 4.2 | 2.1 | 0.8 | 2.9 | | 0.91 | 1.4 | 0.6 | | | |
| | | | | | | | | | | | | | |
| Q | | | | | | | 13.1 | | | | 5.7 | | |
| Ne | | | | | | | 68.7 | | | | 74.4 | | |
| Ks | | | | | | | 18.2 | | | | 19.9 | | |
| | | | | | | | | | | | | | |
| A.I. | | 0.86 | | | | 0.93 | | | | 1.00 | | | |

Table 2 (continued).

| Sample | PV-23 | | | | | PV-56 | | | PV-32 | | | |
|---|---|---|---|---|---|---|---|---|---|---|---|---|
| | NES | | | | | NES | | | Corundum-bearing NES | | | |
| | AF | K-ph | Na-ph | Neph | AF | K-ph | Na-ph | Neph | AF | Neph | Sodalite | |
| wt% | | | | | | | | | | | | |
| $SiO_2$ | 67.60 | 65.73 | 67.72 | 44.29 | 65.90 | 63.81 | 65.87 | 43.51 | 67.14 | 44.48 | $SiO_2$ | 37.23 |
| $Al_2O_3$ | 19.11 | 18.67 | 19.16 | 32.55 | 19.08 | 18.15 | 19.78 | 33.11 | 19.45 | 32.8 | $Al_2O_3$ | 31.49 |
| $Fe_2O_3$ | 0.13 | 0.07 | 0.22 | 0.78 | 0.15 | 0.15 | 0.10 | 0.46 | 0.03 | 0.43 | $Fe_2O_3$ | 0.14 |
| BaO | 0.06 | 0.10 | 0.03 | 0.03 | 0.14 | 0.13 | 0.06 | | 0.13 | 0.05 | BaO | 0.04 |
| SrO | 0.07 | 0.12 | 0.07 | | 0.08 | 0.05 | 0.08 | | 0.08 | | SrO | |
| CaO | | | 0.08 | 0.07 | 0.35 | 0.09 | 0.94 | | 0.31 | 0.89 | CaO | 0.08 |
| $Na_2O$ | 6.21 | 1.55 | 10.87 | 15.97 | 6.77 | 1.31 | 9.98 | 15.86 | 7.23 | 15.06 | $Na_2O$ | 25.51 |
| $K_2O$ | 8.19 | 14.76 | 1.10 | 6.12 | 6.68 | 14.59 | 1.48 | 6.76 | 6.33 | 6.14 | $K_2O$ | 0.06 |
| Sum | 101.37 | 101.00 | 99.25 | 99.81 | 99.15 | 98.28 | 98.29 | 99.70 | 100.70 | 99.85 | Cl | 7.06 |
| | | | | | | | | | | | F | 0.14 |
| Si | 11.988 | 11.980 | 11.977 | 8.513 | 11.914 | 11.967 | 11.807 | 8.399 | 11.924 | 8.327 | O=Cl, F | 1.65 |
| Al | 3.955 | 4.011 | 3.994 | 7.374 | 4.066 | 4.012 | 4.179 | 7.534 | 4.072 | 7.610 | Sum | 100.10 |
| $Fe^{3+}$ | 0.017 | 0.009 | 0.029 | 0.113 | 0.020 | 0.021 | 0.013 | 0.067 | 0.004 | 0.064 | | |
| Ba | 0.004 | 0.007 | 0.002 | 0.002 | 0.010 | 0.010 | 0.004 | | 0.009 | 0.001 | Si | 6.000 |
| Sr | 0.007 | 0.013 | 0.007 | | 0.008 | 0.005 | 0.008 | | 0.008 | | Al | 5.983 |
| Ca | | | 0.015 | 0.014 | 0.068 | 0.018 | 0.181 | | 0.059 | 0.188 | $Fe^{3+}$ | 0.017 |
| Na | 2.135 | 0.548 | 3.727 | 5.952 | 2.374 | 0.476 | 3.469 | 6.006 | 2.490 | 5.748 | Ba | 0.002 |
| K | 1.852 | 3.432 | 0.249 | 1.501 | 1.541 | 3.491 | 0.338 | 1.684 | 1.434 | 1.542 | Sr | |
| (O=32) | | | | | | | | | | | Ca | 0.014 |
| Z | 16.000 | 16.000 | 16.000 | 16.000 | 16.000 | 16.000 | 15.999 | 16.000 | 16.000 | 16.001 | Na | 7.972 |
| X | 3.998 | 4.000 | 4.000 | 7.469 | 4.001 | 4.000 | 4.000 | 7.690 | 4.000 | 7.479 | K | 0.012 |
| | | | | | | | | | | | Sum | 20.000 |
| | | | | | | | | | | | Cl | 1.929 |
| wt% | | | | | | | | | | | F | 0.071 |
| Or | 48.4 | 86.4 | 6.6 | | 39.8 | 87.7 | 8.9 | | 37.1 | | | |
| Ab | 51.2 | 13.0 | 92.7 | | 57.8 | 11.3 | 85.9 | | 60.8 | | | |
| An | 0.4 | 0.6 | 0.7 | | 2.4 | 1.0 | 5.2 | | 2.1 | | | |
| Q | | | | 5.4 | | | | 4.2 | | 5.8 | | |
| Ne | | | | 73.9 | | | | 73.0 | | 72.5 | | |
| Ks | | | | 20.7 | | | | 22.8 | | 27.7 | | |
| A.I. | 1.04 | | | | 0.88 | | | | 0.66 | | | |

| Sample | PV-12 | | | 22 | | |
|---|---|---|---|---|---|---|
| | QTR | | | TRPH | | |
| | Ph-AF | mPh | gm | Ph-AF | gm | gm |
| wt% | | | | | | |
| $SiO_2$ | 64.72 | 63.58 | 68.45 | 63.66 | 64.85 | 64.61 |
| $Al_2O_3$ | 18.09 | 17.42 | 19.12 | 19.98 | 20.21 | 19.17 |
| $Fe_2O_3$ | 0.46 | 0.92 | 0.53 | 0.10 | 0.06 | 0.05 |
| BaO | 0.03 | | 0.17 | 2.00 | 0.25 | 0.31 |
| SrO | | | | 0.17 | 0.13 | 0.19 |
| CaO | 0.05 | 0.02 | 0.02 | 0.86 | 1.41 | 0.55 |
| $Na_2O$ | 0.78 | 0.62 | 11.00 | 5.74 | 8.01 | 4.32 |
| $K_2O$ | 15.69 | 15.66 | 1.12 | 6.97 | 3.89 | 9.88 |
| Sum | 99.82 | 98.22 | 100.41 | 99.48 | 98.81 | 99.08 |
| Si | 11.987 | 11.996 | 11.984 | 11.669 | 11.696 | 11.850 |
| Al | 3.949 | 3.873 | 3.947 | 4.317 | 4.296 | 4.144 |
| $Fe^{3+}$ | 0.064 | 0.131 | 0.069 | 0.014 | 0.008 | 0.006 |
| Ba | 0.002 | | 0.011 | 0.144 | 0.017 | 0.022 |
| Sr | | | | 0.018 | 0.014 | 0.020 |
| Ca | 0.010 | 0.005 | 0.004 | 0.168 | 0.272 | 0.108 |
| Na | 0.280 | 0.227 | 3.735 | 2.040 | 2.801 | 1.536 |
| K | 3.708 | 3.768 | 0.250 | 1.630 | 0.895 | 2.312 |
| (O=32) | | | | | | |
| Z | 16.000 | 16.000 | 16.000 | 16.000 | 16.000 | 16.000 |
| X | 4.000 | 4.000 | 4.000 | 4.000 | 3.999 | 3.998 |
| wt% | | | | | | |
| Or | 93.1 | 94.5 | 6.6 | 41.4 | 23.3 | 59.0 |
| Ab | 6.6 | 5.4 | 92.9 | 48.8 | 68.6 | 36.9 |
| An | 0.3 | 0.1 | 0.5 | 9.8 | 8.1 | 4.1 |
| A.I. | | 1.02 | | | 0.80 | |

Table 3. Representative probe analyses of clinopyroxenes. Symbols as in Table 2. $Fe_2O_3$ and FeO recalculated on the cation basis. Formulae on 6 (O) basis. Mg#=Mg/(Mg+$Fe^{2+}$); Fe*=$Fe_{total}$+Mn-Na-K, Q=Ca+Mg+$Fe^{2+}$, J=2Na (cf. Morimoto, 1988).

| Sample | PV-8 | 10 | 30 | | 32 | | PV-55 | PV-22 | PV-23 | | PV-24 | PV-56 |
|---|---|---|---|---|---|---|---|---|---|---|---|---|
| | QS | S | S | | S | | NS | NES | NES | | NES | NES |
| | | | C | R | C | R | | | C | R | | |
| wt% | | | | | | | | | | | | |
| $SiO_2$ | 51.55 | 52.45 | 51.82 | 52.09 | 52.03 | 51.00 | 50.20 | 51.08 | 50.29 | 51.24 | 50.87 | 49.27 |
| $TiO_2$ | 0.50 | 0.17 | 0.40 | 0.52 | 0.27 | 0.23 | 0.73 | 0.37 | 0.75 | 0.28 | 0.24 | 0.97 |
| $Al_2O_3$ | 1.57 | 4.40 | 0.95 | 0.96 | 0.69 | 0.50 | 2.22 | 1.58 | 2.30 | 1.49 | 2.10 | 2.50 |
| $Fe_2O_3$ | 1.83 | | 12.48 | 21.32 | 3.13 | 2.50 | 6.36 | 15.44 | 6.68 | 12.04 | 21.13 | 4.79 |
| FeO | 10.34 | 14.77 | 4.92 | 3.68 | 8.99 | 14.08 | 6.77 | 7.44 | 7.91 | 7.30 | 4.84 | 7.37 |
| MnO | 0.94 | 0.99 | 1.38 | 1.12 | 0.98 | 0.97 | 1.24 | 1.53 | 1.55 | 1.67 | 1.22 | 2.82 |
| MgO | 12.22 | 14.07 | 4.00 | 3.26 | 10.64 | 7.69 | 9.46 | 3.77 | 8.25 | 5.58 | 3.02 | 9.38 |
| CaO | 20.28 | 11.91 | 9.71 | 7.65 | 22.91 | 21.96 | 19.96 | 11.57 | 18.72 | 14.89 | 7.52 | 19.67 |
| $Na_2O$ | 0.64 | 1.04 | 7.85 | 9.12 | 0.91 | 0.92 | 2.10 | 6.67 | 2.73 | 5.07 | 8.51 | 1.83 |
| $K_2O$ | 0.03 | | | | 0.01 | 0.02 | 0.01 | | | | 0.15 | 0.01 |
| Sum | 99.90 | 99.80 | 99.51 | 99.72 | 100.55 | 99.87 | 99.05 | 99.45 | 99.18 | 99.56 | 99.60 | 98.66 |
| | | | | | | | | | | | | |
| Si | 1.947 | 1.966 | 1.993 | 1.995 | 1.965 | 1.980 | 1.921 | 1.978 | 1.931 | 1.973 | 1.961 | 1.905 |
| $Al^{IV}$ | 0.053 | 0.034 | 0.007 | 0.005 | 0.031 | 0.020 | 0.079 | 0.022 | 0.069 | 0.027 | 0.039 | 0.095 |
| $Al^{VI}$ | 0.018 | 0.160 | 0.036 | 0.038 | | 0.003 | 0.021 | 0.050 | 0.035 | 0.041 | 0.056 | 0.019 |
| Ti | 0.014 | 0.005 | 0.011 | 0.015 | 0.008 | 0.007 | 0.021 | 0.011 | 0.022 | 0.008 | 0.007 | 0.028 |
| $Fe^{3+}$ | 0.053 | | 0.535 | 0.615 | 0.089 | 0.073 | 0.173 | 0.450 | 0.193 | 0.349 | 0.613 | 0.138 |
| $Fe^{2+}$ | 0.328 | 0.463 | 0.158 | 0.118 | 0.284 | 0.457 | 0.228 | 0.241 | 0.254 | 0.235 | 0.156 | 0.236 |
| Mn | 0.030 | 0.031 | 0.045 | 0.036 | 0.031 | 0.032 | 0.040 | 0.050 | 0.051 | 0.054 | 0.040 | 0.092 |
| Mg | 0.688 | 0.786 | 0.229 | 0.186 | 0.599 | 0.445 | 0.541 | 0.218 | 0.472 | 0.320 | 0.174 | 0.537 |
| Ca | 0.821 | 0.479 | 0.400 | 0.314 | 0.927 | 0.913 | 0.819 | 0.480 | 0.770 | 0.614 | 0.310 | 0.813 |
| Na | 0.047 | 0.076 | 0.586 | 0.678 | 0.066 | 0.069 | 0.156 | 0.500 | 0.203 | 0.379 | 0.636 | 0.137 |
| K | 0.001 | | | | | 0.001 | 0.001 | | | | 0.008 | 0.001 |
| | | | | | | | | | | | | |
| Sum | 4.000 | 4.000 | 4.000 | 4.000 | 4.000 | 4.000 | 4.000 | 4.000 | 4.000 | 4.000 | 4.000 | 4.000 |
| (O=6) | | | | | | | | | | | | |
| | | | | | | | | | | | | |
| Mg/(Mg+Mn+$Fe_{tot}$) | 0.63 | 0.61 | 0.24 | 0.19 | 0.60 | 0.44 | 0.55 | 0.23 | 0.49 | 0.33 | 0.18 | 0.54 |
| mg# | 0.68 | 0.63 | 0.59 | 0.61 | 0.68 | 0.49 | 0.70 | 0.47 | 0.65 | 0.58 | 0.53 | 0.69 |
| | | | | | | | | | | | | |
| Na+K | 4.4 | 5.9 | 60.6 | 71.0 | 6.6 | 6.9 | 15.9 | 52.1 | 20.9 | 39.6 | 64.7 | 13.7 |
| Mg | 62.6 | 61.4 | 23.7 | 19.5 | 59.7 | 44.2 | 55.1 | 22.7 | 48.6 | 33.4 | 17.7 | 53.5 |
| Fe* | 33.0 | 32.7 | 15.7 | 9.5 | 33.7 | 48.9 | 29.0 | 25.2 | 30.5 | 27.0 | 17.6 | 32.8 |
| | | | | | | | | | | | | |
| Q | 1.837 | 1.728 | 0.787 | 0.618 | 1.810 | 1.815 | 1.588 | 0.939 | 1.496 | 1.169 | 0.640 | 1.586 |
| J | 0.094 | 0.152 | 0.172 | 1.356 | 0.132 | 0.140 | 0.314 | 1.000 | 0.406 | 0.758 | 1.288 | 0.276 |
| | | | | | | | | | | | | |
| A.I. | 0.91 | 0.82 | 1.04 | | 0.97 | | 0.93 | 1.00 | | 1.04 | 1.05 | 0.88 |

The sum of cations in structural formulae ($X_4Z_{12}O_{32}$) and the X group (Ca+Sr+Ba+Na+K) are very close to the theoretical 20.00 and 4.00, respectively, even in the ternary feldspars, indicating that subsolidus processes have not substantially modified the chemistry of this mineral group.

Total iron, as expressed as $Fe^{3+}$, appears consistent with a tetrahedral coordination, varying from 0.012 to 0.049 a.f.u. in the alkali feldspar and plagioclase from all the rock-types. Ba and Sr show systema-tically low contents, i.e. less than 0.040 and 0.043 a.f.u., respectively; occasionally, Ba from ternary feldspars of some syenites corresponds to 0.101 a.f.u.

Apparent closure temperatures of 1100-890°C and 1150-810°C were obtained for the plagioclase at 1 kb $H_2O$ pressure (Kudo & Weill, 1970, and Mathez, 1973 geothermometers, respectively), whereas the calibration between plagioclase and coexisting alkali feldspar (whole compositions) yielded temperatures below 700°C, suggesting possible subsolidus exchange.

*Feldspathoids*

These are represented by nepheline, haüyne and sodalite in the silica-undersaturated rocks (cf. Table 2). Most nepheline compositions yielded (Si+Al+$Fe^{3+}$)=16.060±0.129 a.f.u., which falls well within the 1% of the expected theoretical values. However, some nepheline compositions from the nephel-syenites are cation deficient (inset of Fig. 8), probably reflecting vacancies in the potassium sites by omission of solid solution, and have $SiO_2$ excess around 13 wt% with kalsilite content about 18 wt%, from which a crystallization temperature of about 1070°C can be inferred (cf. Hamilton, 1961).

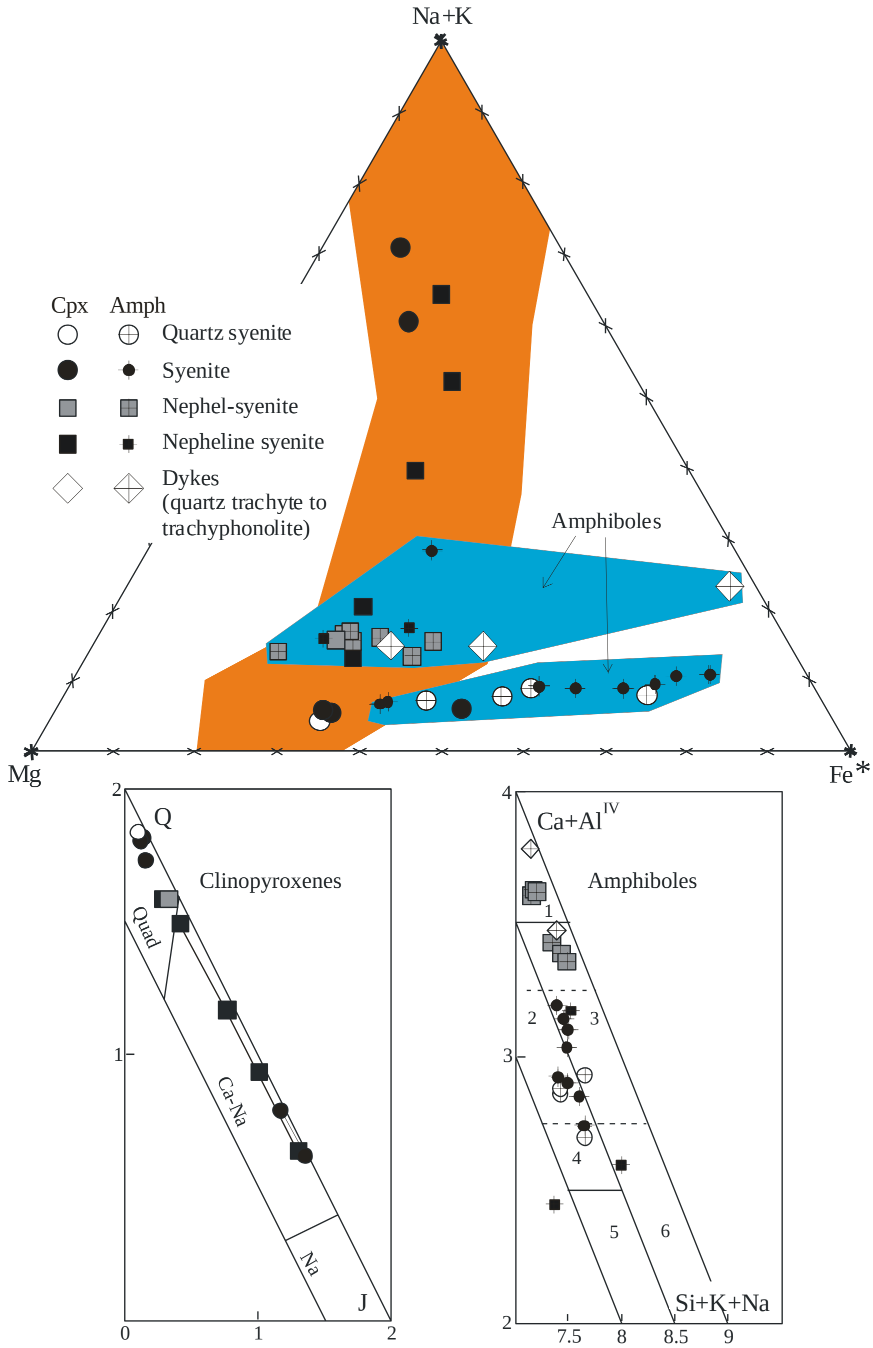


Fig. 9. Clinopyroxene and amphibole compositions plotted into the Na(+K)-Mg-Fe* diagram (Fe*=Fe+Mn-Na). The orange field indicates the pyroxene trend from other Brazilian provinces (cf. Brotzu *et al.*, 1997 and therein references, and Comin-Chiaramonti *et al.*, in this volume). Insets: clinopyroxenes [J (2Na) vs. Q (Ca+Mg+$Fe^{2+}$)] and amphiboles Si+K+Na vs. Ca+$Al^{IV}$ classificative diagrams (Morimoto, 1988, and Giret *et al.*, 1980, respectively). Clinopyroxenes: Quad, Ca-Mg-Fe pyroxenes; Ca-Na, calcic-sodic pyroxenes; Na, sodic pyroxenes. Amphiboles: 1, hastingsite; 2, hornblende; 3, 6, edenite; 4, actinolitic hornblende; 5, actinolite.

Table 4. Representative probe analyses of amphiboles. (*) uralitized cpx. $Fe_2O_3$/FeO partition made according to electrostatic minimization. Fe*=$FeO_{total}$+Mn-Na-K. Structural formulae calculated on the basis of 23(O, OH). $H_2O$ recalculated following the stoichiometry. Symbols as in Table 2.

| Sample | 15 | | PV-8 | | 18 | | 30 | PV-6 | | PV-14 | | PV-34 | |
|---|---|---|---|---|---|---|---|---|---|---|---|---|---|
| | QS | | QS | | S | | S | S | | S | | S | |
| | C | R | C | R | C | R | (*) | C | R | C | R | C | R |
| wt% | | | | | | | | | | | | | |
| $SiO_2$ | 45.36 | 43.33 | 41.87 | 42.79 | 44.63 | 44.97 | 49.94 | 43.42 | 43.62 | 41.49 | 41.76 | 41.58 | 41.05 |
| $TiO_2$ | 1.10 | 1.36 | 1.56 | 1.82 | 1.29 | 1.17 | 0.25 | 1.45 | 1.67 | 1.55 | 1.06 | 1.66 | 1.42 |
| $Al_2O_3$ | 6.41 | 6.93 | 7.36 | 7.03 | 6.88 | 6.82 | 0.71 | 7.23 | 6.46 | 8.24 | 7.57 | 7.44 | 7.92 |
| $Fe_2O_3$ | 5.14 | 9.75 | 6.40 | 5.40 | 5.97 | 5.73 | 4.59 | 7.24 | 7.02 | 7.08 | 6.73 | 7.61 | 7.37 |
| FeO | 15.94 | 15.02 | 22.06 | 18.63 | 13.56 | 13.08 | 11.49 | 17.77 | 19.46 | 21.86 | 20.87 | 22.22 | 22.69 |
| MnO | 1.09 | 1.39 | 1.50 | 1.22 | 0.80 | 0.80 | 0.94 | 1.14 | 1.27 | 1.35 | 1.17 | 1.62 | 1.78 |
| MgO | 10.07 | 7.16 | 3.84 | 6.59 | 10.58 | 10.71 | 7.28 | 6.14 | 5.40 | 3.44 | 4.19 | 3.13 | 2.18 |
| CaO | 9.85 | 9.69 | 9.74 | 10.24 | 10.54 | 10.65 | 17.04 | 9.56 | 9.32 | 10.23 | 10.45 | 9.72 | 9.81 |
| $Na_2O$ | 1.95 | 1.86 | 1.73 | 1.96 | 1.77 | 1.67 | 4.52 | 2.15 | 2.08 | 1.92 | 1.85 | 2.21 | 2.01 |
| $K_2O$ | 0.89 | 0.91 | 1.04 | 1.08 | 0.83 | 0.84 | | 1.00 | 0.98 | 1.26 | 1.16 | 1.13 | 1.29 |
| F | 1.56 | 1.16 | 0.45 | 0.98 | 0.73 | 0.73 | 2.14 | 0.87 | 0.56 | 0.68 | 0.57 | 0.77 | 0.53 |
| Cl | 0.06 | 0.10 | 0.38 | 0.30 | 0.19 | 0.17 | | 0.42 | 0.37 | 0.22 | 0.15 | 0.50 | 0.24 |
| $H_2O^+$ | 1.20 | 1.37 | 1.57 | 1.34 | 1.59 | 1.58 | 0.95 | 1.41 | 1.56 | 1.52 | 1.57 | 1.13 | 1.29 |
| Less O=F.Cl | 0.67 | 0.51 | 0.28 | 0.48 | 0.35 | 0.35 | 0.90 | 0.46 | 0.60 | 0.34 | 0.27 | 0.44 | 0.28 |
| Sum | 99.52 | 99.52 | 99.92 | 98.90 | 99.01 | 98.30 | 98.49 | 99.34 | 99.45 | 110.50 | 99.10 | 100.55 | 99.56 |
| mg# | 0.52 | 0.46 | 0.24 | 0.39 | 0.58 | 0.59 | 0.51 | 0.38 | 0.33 | 0.22 | 0.26 | 0.20 | 0.15 |
| Si+Na+K | 7.66 | 7.26 | 7.42 | 7.65 | 7.40 | 7.49 | 8.97 | 7.60 | 7.65 | 7.38 | 7.45 | 7.49 | 7.49 |
| $Ca+Al^{IV}$ | 2.70 | 2.86 | 2.99 | 2.93 | 2.92 | 2.90 | 2.92 | 2.84 | 2.74 | 3.08 | 3.14 | 3.04 | 3.10 |
| F | 0.767 | 0.566 | 0.227 | 0.494 | 0.347 | 0.351 | 0.966 | 0.428 | 0.277 | 0.339 | 0.287 | 0.385 | 0.270 |
| Cl | 0.016 | 0.026 | 0.103 | 0.083 | 0.050 | 0.043 | 0.000 | 0.111 | 0.098 | 0.059 | 0.049 | 0.134 | 0.066 |
| OH | 1.217 | 1.408 | 1.670 | 1.423 | 1.603 | 1.606 | 1.034 | 1.461 | 1.625 | 1.602 | 1.673 | 1.481 | 1.664 |
| Sum | 2.000 | 2.000 | 2.000 | 2.000 | 2.000 | 2.000 | 2.000 | 2.000 | 2.000 | 2.000 | 2.000 | 2.000 | 2.000 |
| Na+K | 7.7 | 8.5 | 8.4 | 9.1 | 7.5 | 7.2 | 19.0 | 9.8 | 9.4 | 9.8 | 9.3 | 10.4 | 10.5 |
| Mg | 48.1 | 38.0 | 20.5 | 34.5 | 52.5 | 53.7 | 47.2 | 33.0 | 28.7 | 18.8 | 22.9 | 16.3 | 12.3 |
| Fe* | 44.2 | 53.5 | 71.1 | 56.4 | 40.0 | 39.1 | 33.8 | 57.2 | 61.9 | 71.4 | 67.8 | 73.3 | 77.2 |
| A.I. | 0.90 | | 0.91 | | 0.80 | | 1.04 | 0.85 | | 0.90 | | 0.91 | |

| Sample | 21 | | PV-16 | | PV-55 | | | PV-22 | PV-56 | | PV-12 | 22 | |
|---|---|---|---|---|---|---|---|---|---|---|---|---|---|
| | NS | | NS | | NS | | | NES | NES | | QTR | TRPH | |
| | C | R | C | R | C | I | R | (*) | C | R | mPh | Ph-C | Ph-R |
| wt% | | | | | | | | | | | | | |
| $SiO_2$ | 41.74 | 40.43 | 1.13 | 0.84 | 41.05 | 39.65 | 40.80 | 43.99 | 41.73 | 41.31 | 45.85 | 39.27 | 41.43 |
| $TiO_2$ | 3.13 | 2.08 | 2.63 | 1.73 | 2.35 | 2.21 | 2.45 | 0.38 | 2.33 | 1.48 | 2.36 | 2.58 | 2.88 |
| $Al_2O_3$ | 9.79 | 10.65 | 10.40 | 10.26 | 10.86 | 12.03 | 10.76 | 2.65 | 8.96 | 9.58 | 4.86 | 11.58 | 9.80 |
| $Fe_2O_3$ | 5.37 | 5.68 | 6.52 | 7.85 | 7.34 | 7.69 | 7.51 | 21.26 | 9.08 | 9.27 | 14.98 | 9.93 | 10.18 |
| FeO | 9.03 | 13.61 | 11.83 | 12.85 | 10.29 | 10.63 | 10.31 | | 6.79 | 9.23 | 17.42 | 10.13 | 7.04 |
| MnO | 0.73 | 0.94 | 1.87 | 2.13 | 1.29 | 1.27 | 1.31 | 1.21 | 3.22 | 3.66 | 2.44 | 1.02 | 0.83 |
| MgO | 11.49 | 8.41 | 9.01 | 7.86 | 9.71 | 9.63 | 9.49 | 4.33 | 10.12 | 8.03 | 0.93 | 7.90 | 10.05 |
| CaO | 10.92 | 10.80 | 9.90 | 9.74 | 9.79 | 9.60 | 9.86 | 14.76 | 9.91 | 9.19 | 2.05 | 10.82 | 10.77 |
| $Na_2O$ | 2.90 | 2.59 | 3.51 | 3.32 | 3.54 | 3.27 | 3.45 | 6.56 | 3.36 | 3.57 | 4.53 | 2.69 | 2.89 |
| $K_2O$ | 1.57 | 1.75 | 1.67 | 1.65 | 1.62 | 1.64 | 1.67 | 1.21 | 1.61 | 1.66 | 1.95 | 1.77 | 1.57 |
| F | 1.74 | 1.43 | 1.01 | 1.18 | 1.21 | 1.03 | 1.28 | 6.36 | 1.86 | 1.62 | 0.57 | 1.26 | 1.71 |
| Cl | 0.04 | 0.02 | 0.01 | 0.01 | 0.02 | 0.02 | 0.03 | 0.01 | 0.02 | 0.01 | 0.01 | 0.03 | 0.05 |
| $H_2O^+$ | 1.12 | 1.24 | 1.43 | 1.35 | 1.35 | 1.42 | 1.31 | | 1.07 | 1.16 | 1.61 | 1.36 | 1.17 |
| Less O=F.Cl | 0.74 | 0.61 | 0.43 | 0.50 | 0.51 | 0.44 | 0.55 | 2.68 | 0.79 | 0.68 | 0.24 | 0.54 | 0.73 |
| Sum | 98.83 | 99.63 | 100.49 | 100.31 | 99.17 | 98.88 | 98.93 | 100.04 | 99.54 | 99.09 | 99.54 | 99.80 | 99.64 |
| mg# | 0.69 | 0.52 | 0.58 | 0.52 | 0.63 | 0.62 | 0.62 | | 0.73 | 0.61 | 0.09 | 0.58 | 0.72 |
| Si+Na+K | 7.19 | 7.14 | 7.43 | 7.47 | 7.36 | 7.15 | 7.33 | 8.03 | 7.35 | 7.49 | 8.96 | 7.14 | 7.38 |
| $Ca+Al^{IV}$ | 3.63 | 3.61 | 3.39 | 3.36 | 3.49 | 3.63 | 3.43 | 2.60 | 2.45 | 3.15 | 1.15 | 3.77 | 3.47 |
| F | 0.801 | 0.677 | 0.474 | 0.557 | 0.564 | 0.484 | 0.598 | 2.757 | 0.860 | 0.763 | 0.283 | 0.609 | 0.813 |
| Cl | 0.100 | 0.005 | 0.003 | 0.003 | 0.005 | 0.005 | 0.008 | 0.002 | 0.005 | 0.003 | 0.003 | 0.007 | 0.013 |
| OH | 1.189 | 1.318 | 1.523 | 1.440 | 1.431 | 1.511 | 1.394 | | 1.135 | 1.234 | 1.714 | 1.384 | 1.174 |
| Sum | 2.000 | 2.000 | 2.000 | 2.000 | 2.000 | 2.000 | 2.000 | 2.759 | 2.000 | 2.000 | 2.000 | 2.000 | 2.000 |
| Na+K | 14.0 | 13.5 | 16.3 | 15.7 | 16.6 | 15.5 | 16.5 | 46.1 | 15.9 | 17.2 | 23.8 | 15.0 | 15.0 |
| Mg | 62.7 | 46.7 | 49.1 | 43.0 | 53.7 | 52.7 | 53.0 | 41.7 | 56.1 | 45.5 | 5.9 | 47.4 | 59.0 |
| Fe* | 23.3 | 39.8 | 34.6 | 41.3 | 29.7 | 31.8 | 30.5 | 12.2 | 28.0 | 37.3 | 70.3 | 37.6 | 26.0 |
| A.I. | 0.82 | | 0.86 | | | 0.93 | | 1.01 | 0.88 | | 1.02 | 0.80 | |

Table 5. Representative probe analyses of biotites. Structural formulae calculated on the basis of 22 (O, OH). Symbols as in Table 2.

| Sample | 7 GR | 28 GR | 15 QS | PV-8 QS | | 18 S | 10 S | | 32 S | | PV-6 S | PV-14 S | | 21 NS | | PV-16 NS |
|---|---|---|---|---|---|---|---|---|---|---|---|---|---|---|---|---|
| | | | | C | R | | C | R | C | R | | C | R | C | R | C |
| wt% | | | | | | | | | | | | | | | | |
| $SiO_2$ | 35.35 | 33.62 | 35.45 | 34.97 | 34.45 | 36.09 | 36.09 | 34.99 | 37.22 | 37.29 | 35.31 | 35.65 | 35.40 | 38.44 | 35.46 | 37.73 |
| $TiO_2$ | 3.24 | 3.20 | 3.42 | 2.93 | 3.12 | 3.94 | 5.68 | 5.12 | 2.08 | 2.08 | 3.31 | 2.96 | 3.18 | 2.76 | 4.04 | 1.42 |
| $Al_2O_3$ | 11.15 | 10.40 | 12.85 | 12.04 | 11.81 | 13.56 | 13.64 | 13.63 | 11.27 | 9.19 | 11.75 | 11.59 | 11.68 | 11.83 | 13.14 | 12.59 |
| $FeO_{tot}$ | 34.55 | 34.41 | 23.52 | 29.67 | 29.55 | 21.76 | 16.39 | 20.66 | 23.26 | 31.34 | 29.13 | 29.50 | 30.61 | 16.18 | 25.01 | 19.65 |
| MnO | 0.95 | 1.14 | 0.32 | 0.66 | 0.47 | 0.36 | 0.47 | 0.80 | 0.52 | 0.86 | 0.53 | 0.79 | 0.61 | 0.66 | 0.51 | 1.77 |
| MgO | 1.11 | 1.73 | 9.16 | 4.39 | 5.01 | 10.03 | 12.46 | 9.94 | 11.09 | 5.38 | 5.41 | 4.84 | 3.98 | 13.81 | 7.16 | 12.47 |
| CaO | 0.04 | 0.01 | 0.03 | | 0.06 | 0.04 | | 0.02 | 0.04 | 0.04 | | 0.02 | | | 0.03 | |
| BaO | 0.02 | | | 0.09 | 0.41 | | 0.57 | 0.31 | 0.10 | 0.08 | 0.02 | 0.10 | 0.11 | 0.14 | 0.08 | 0.11 |
| $Na_2O$ | 0.05 | 0.09 | 0.06 | 0.03 | 0.06 | 0.06 | 0.15 | 0.14 | 0.14 | 0.03 | 0.08 | 0.06 | 0.04 | 0.23 | 0.19 | 0.22 |
| $K_2O$ | 8.82 | 8.87 | 9.73 | 9.02 | 8.97 | 9.28 | 9.56 | 9.28 | 9.35 | 9.10 | 9.20 | 8.98 | 9.26 | 9.57 | 9.17 | 9.91 |
| F | 0.53 | 0.98 | 2.12 | 1.04 | 1.08 | 1.21 | 0.83 | 0.80 | 2.41 | 0.67 | 0.90 | 0.32 | 0.49 | 3.39 | 0.92 | 1.51 |
| Cl | 0.22 | 0.29 | 0.16 | 0.45 | 0.40 | 0.24 | 0.05 | 0.06 | 0.11 | 0.79 | 0.47 | 0.33 | 0.31 | 0.04 | 0.10 | 0.01 |
| Less O=F.Cl | 0.27 | 0.48 | 0.93 | 0.54 | 0.55 | 0.56 | 0.36 | 0.35 | 1.04 | 0.46 | 0.49 | 0.21 | 0.28 | 1.44 | 0.41 | 0.64 |
| Sum | 95.76 | 94.26 | 95.89 | 94.75 | 94.96 | 96.01 | 95.53 | 95.40 | 96.55 | 96.39 | 95.63 | 94.33 | 95.39 | 95.61 | 95.40 | 96.75 |
| Mg | 3.7 | 5.8 | 28.6 | 14.20 | 16.0 | 30.3 | 38.1 | 30.3 | 35.2 | 17.5 | 17.3 | 15.6 | 12.9 | 42.3 | 22.5 | 37.4 |
| Fe+Mn | 66.8 | 66.7 | 39.6 | 55.0 | 54.1 | 37.4 | 28.1 | 36.8 | 36.5 | 58.8 | 53.1 | 54.8 | 57.1 | 29.0 | 44.9 | 32.7 |
| Al | 29.5 | 27.5 | 31.8 | 30.8 | 29.9 | 32.3 | 33.0 | 32.9 | 28.3 | 23.7 | 29.6 | 29.6 | 30.0 | 28.7 | 32.6 | 29.9 |
| Mg/(Mg+Fe+Mn) | 0.05 | 0.08 | 0.41 | 0.21 | 0.23 | 0.45 | 0.58 | 0.45 | 0.49 | 0.23 | 0.25 | 0.22 | 0.18 | 0.59 | 0.33 | 0.56 |
| A.I. | 0.93 | 0.96 | 0.90 | 0.91 | | 0.80 | 0.82 | | 0.97 | | 0.85 | 0.90 | | 0.82 | | 0.86 |

| Sample | PV-16 NS | PV-55 | | PV-22 NES | PV-23 NES | | PV-56 NES | | PV-32 Corundum-bearing NES | | PV-12 QTR | PV-12 QTR | 22 TRPH | 22 TRPH |
|---|---|---|---|---|---|---|---|---|---|---|---|---|---|---|
| | R | C | R | | C | R | | | | | Ph | mPh | Ph-C | Ph-R |
| wt% | | | | | | | | | | | | | | |
| $SiO_2$ | 35.92 | 37.11 | 37.69 | 34.71 | 37.69 | 35.69 | 36.17 | 36.25 | 32.44 | 32.03 | 34.99 | 36.53 | 38.16 | 39.07 |
| $TiO_2$ | 1.30 | 2.32 | 2.10 | 2.46 | 2.10 | 1.17 | 2.80 | 2.68 | 2.79 | 2.56 | 2.52 | 2.69 | 2.44 | 0.92 |
| $Al_2O_3$ | 14.34 | 13.56 | 13.63 | 12.74 | 13.63 | 11.92 | 14.05 | 13.95 | 18.10 | 19.18 | 8.74 | 8.33 | 12.46 | 12.43 |
| $FeO_{tot}$ | 21.06 | 15.77 | 16.64 | 24.87 | 16.64 | 24.98 | 18.00 | 18.07 | 21.50 | 22.68 | 35.13 | 33.63 | 15.73 | 14.82 |
| MnO | 2.27 | 1.02 | 1.25 | 2.46 | 1.25 | 2.32 | 3.33 | 3.28 | 1.59 | 1.76 | 1.29 | 1.63 | 0.53 | 0.52 |
| MgO | 10.64 | 14.30 | 13.18 | 8.00 | 13.18 | 8.33 | 9.99 | 10.10 | 7.32 | 6.45 | 1.59 | 2.28 | 14.73 | 16.29 |
| CaO | 0.01 | 0.04 | | 0.04 | | 0.06 | 0.02 | 0.01 | | | 0.05 | 0.01 | 0.02 | 0.05 |
| BaO | 0.05 | 0.04 | | | | 0.10 | | | | 0.06 | 0.12 | | 0.17 | 0.13 |
| $Na_2O$ | 0.13 | 0.19 | 0.20 | 0.17 | 0.20 | 0.15 | 0.17 | 0.15 | 0.19 | 0.22 | 0.04 | 0.03 | 0.30 | 0.24 |
| $K_2O$ | 9.78 | 9.94 | 10.06 | 9.44 | 10.06 | 9.57 | 9.40 | 9.34 | 9.65 | 9.50 | 9.06 | 9.05 | 9.63 | 9.42 |
| F | 0.99 | 2.37 | 2.30 | 1.27 | 2.30 | 0.63 | 2.31 | 2.43 | 2.12 | 2.08 | 0.45 | 1.27 | 3.13 | 3.66 |
| Cl | 0.03 | 0.10 | 0.02 | | 0.02 | 0.01 | 0.03 | | 0.01 | 0.01 | 0.04 | 0.04 | 0.03 | 0.03 |
| Less O=F.Cl | 0.42 | 1.02 | 0.97 | 0.53 | 0.97 | 0.27 | 0.98 | 1.02 | 0.90 | 0.88 | 0.20 | 0.54 | 1.35 | 1.55 |
| Sum | 96.10 | 95.74 | 96.10 | 95.63 | 96.10 | 94.66 | 95.29 | 95.24 | 94.82 | 95.65 | 93.82 | 95.41 | 96.01 | 96.03 |
| Mg | 30.8 | 43.7 | 39.9 | 24.6 | 39.9 | 25.5 | 30.2 | 30.5 | 21.8 | 18.3 | 5.5 | 8.0 | 46.5 | 52.1 |
| Fe+Mn | 36.3 | 23.5 | 27.4 | 44.5 | 27.4 | 45.6 | 36.2 | 36.2 | 35.7 | 38.8 | 70.6 | 69.0 | 22.4 | 16.5 |
| Al | 32.9 | 32.8 | 32.7 | 30.9 | 32.7 | 28.9 | 33.6 | 33.3 | 42.5 | 42.9 | 23.9 | 23.0 | 31.1 | 31.4 |
| Mg/(Mg+Fe+Mn) | 0.46 | 0.65 | 0.59 | 0.36 | 0.59 | 0.36 | 0.45 | 0.46 | 0.38 | 0.32 | 0.07 | 0.10 | 0.67 | 0.76 |
| A.I. | | 0.93 | | 1.00 | 1.04 | | 0.88 | 0.88 | | 0.66 | 1.02 | | 0.80 | |

Nepheline from nepheline syenites range in composition from $Ne_{73.0}Ks_{22.8}Q_{4.2}$ to $Ne_{72.5}Ks_{27.7}Q_{5.8}$, approaching the composition $Ne_{74.0}Ks_{22.1}Q_{3.9}$, commonly referred to as the ideal composition which lies on the experimental determined curve (700°C/1 kb) for nepheline solid solutions in the system nepheline-kalsilite-silica (cf. Fig. 3B; see Hamilton, 1961; Hamilton & McKenzie, 1965; Woolley & Platt, 1986).

Haüyne ($SO_3$=9.5 wt%) is found as a primary phase (euhedral phenochrysts) in some nephel-syenites, confirming the subvolcanic character of the host rock, whereas sodalite is particularly abundant in the corundum-normative PV-32 nepheline syenite dyke (Cl=7.1 wt%).

*Clinopyroxenes and amphiboles*

Clinopyroxenes (Table 3) are widespread in the syenitic rocks and range in composition from diopside-hedenbergite to sodic-calcic types (Quad to Ca-Na, following Morimoto, 1988; cf. Fig. 9) in the metaluminous and agpaitic rocks, respectively.

On the whole, they plot in the field defined by other alkaline suites from southern Brazil (Fig. 9; cf. Brotzu *et al.*, 1997 and therein references, and Comin-Chiaramonti *et al.*, in this volume).

In general, following an initial hedenbergite increase, with a corresponding decrease of the $Mg/Fe^{2+}$ ratio, the mineral becomes progressively enriched in Na and $Fe^{3+}$. As also indicated in Table 3, $Fe^{3+}$ appears as a function of the Na+K content, ranging in the metaluminous rocks between 0.00 to 0.19 [mg#=$Mg/(Mg+Fe^{2+}Mn)$]=0.70-0.49 vs. [$Mg/(Mg+Fe_{total}+Mn)$=0.63-0.42], and between 0.19 and 0.61 (mg#=0.65-0.47 vs. $Mg/(Mg+Fe_{total}+Mn$=0.49-0.18; cf. Table 3) in the agpaitic varieties.

The trend towards the $Na+Fe^{3+}$ (i.e. aegirine) enrichment can originate itself anywhere from diopside to hedenbergite-rich compositions (Fig. 9), and the point of departure seems to be in part a function of increasing soda activity rather than merely a control of oxygen fugacity, despite the obvious increase in the $Fe^{3+}/Fe^{2+}$ ratio (cf. Scott, 1976). Silica activity is believed to play no significant role in the pyroxene evolution, as similar trends have been noted in both silica-undersaturated and silica-oversaturated rocks from the Itatiaia complex in Brazil (e.g. Brotzu *et al.*, 1997 and therein references).

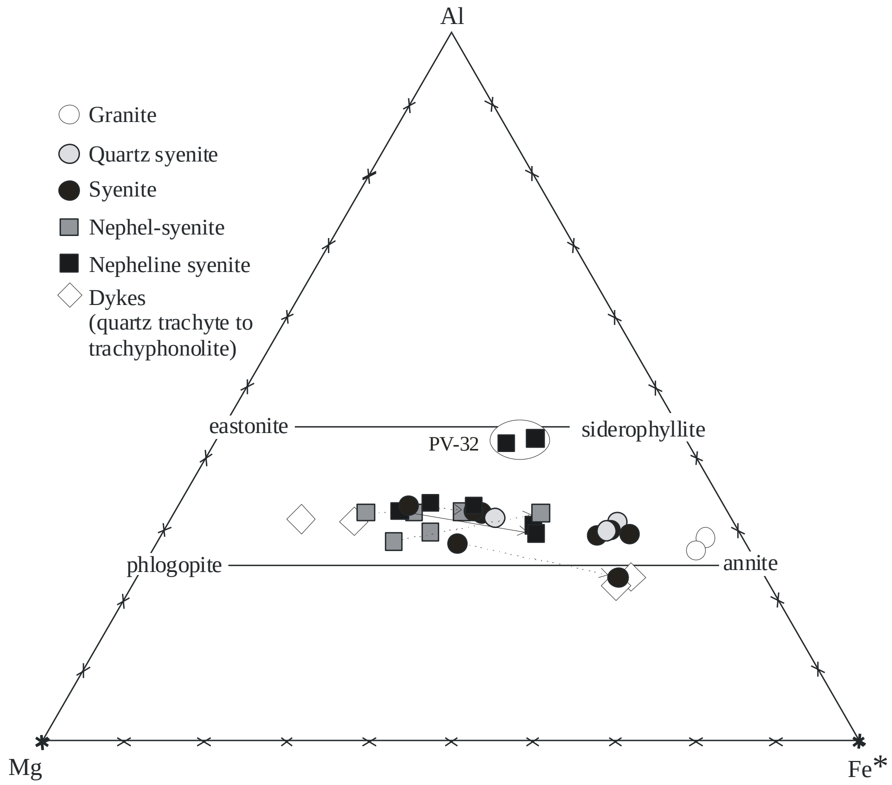


Fig. 10. Composition of micas from the Velasco rock-types in the Al-Mg-Fe* diagram (Fe*=Fe+Mn).

Table 6. Representative probe analyses of spinels and ilmenite. Mt, magnetite; Il, ilmenite; Hc, hercynite. Other symbols as in Table 2. $Fe_2O_3$ and FeO calculated on the ulvöspinel (magnetite: 32 O) and ilmenite (3 O) basis, respectively.

| Sample | 7 | 15 | | PV-8 | | | 18 | | 30 | | 32 | | | PV-6 |
|---|---|---|---|---|---|---|---|---|---|---|---|---|---|---|
| | Gr | QS | | QS | | | S | | S | | S | | | S |
| | Il | Mt | Il | Mt | Il-C | Il-R | Mt | Il | Mt | Il | Mt | Il-C | Il-R | Mt |
| wt% | | | | | | | | | | | | | | |
| $SiO_2$ | 0.08 | 0.21 | 0.05 | 0.08 | 0.03 | 0.12 | 0.07 | 0.04 | 0.05 | 0.12 | 0.03 | 0.04 | | 0.11 |
| $TiO_2$ | 50.11 | 1.30 | 50.33 | 4.38 | 48.41 | 47.90 | 11.18 | 46.49 | 4.51 | 49.09 | 2.90 | 48.10 | 48.84 | 2.36 |
| $Al_2O_3$ | 0.03 | 1.35 | | 0.18 | | 0.07 | 0.29 | 0.02 | 0.13 | 0.06 | 0.62 | | | 0.06 |
| $Fe_2O_3$ | 1.61 | 65.41 | 3.90 | 59.47 | 7.34 | 7.92 | 47.29 | 9.56 | 60.33 | 3.20 | 63.35 | 8.06 | 6.73 | 64.08 |
| FeO | 37.38 | 33.05 | 40.77 | 34.18 | 38.88 | 36.47 | 40.55 | 37.36 | 32.42 | 38.50 | 33.46 | 39.44 | 39.15 | 32.70 |
| MnO | 8.27 | 0.09 | 4.41 | 0.70 | 4.64 | 6.66 | 1.19 | 4.71 | 2.93 | 6.37 | 0.55 | 3.67 | 4.30 | 0.67 |
| MgO | 0.02 | 0.01 | 0.05 | 0.03 | 0.02 | 0.02 | 0.02 | 0.03 | 0.02 | 0.02 | 0.01 | 0.09 | 0.15 | |
| CaO | | 0.05 | 0.03 | 0.02 | 0.01 | | 0.02 | | 0.03 | 0.01 | 0.15 | 0.09 | 0.22 | |
| $Nb_2O_5$ | 2.31 | | 0.18 | 0.04 | 0.21 | 0.14 | 0.11 | 1.15 | | 2.62 | | 0.48 | 0.50 | |
| Sum | 99.81 | 101.47 | 99.70 | 99.20 | 99.54 | 99.30 | 100.72 | 99.33 | 100.42 | 99.99 | 101.07 | 99.97 | 99.89 | 99.98 |
| | | | | | | | | | | | | | | |
| Si | 0.002 | 0.063 | 0.001 | 0.025 | 0.001 | 0.003 | 0.021 | 0.001 | 0.015 | 0.003 | 0.009 | 0.001 | | 0.034 |
| Ti | 0.961 | 0.294 | 0.960 | 1.019 | 0.927 | 0.918 | 2.540 | 0.896 | 1.035 | 0.941 | 0.661 | 0.918 | 0.931 | 0.545 |
| Al | 0.001 | 0.479 | | 0.066 | | 0.002 | 0.103 | 0.001 | 0.047 | 0.002 | 0.221 | | | 0.022 |
| $Fe^{3+}$ | 0.031 | 14.806 | 0.074 | 13.839 | 0.141 | 0.152 | 10.753 | 0.185 | 13.853 | 0.061 | 14.439 | 0.154 | 0.129 | 14.820 |
| $Fe^{2+}$ | 0.797 | 8.314 | 0.865 | 8.840 | 0.828 | 0.778 | 10.247 | 0.800 | 8.274 | 0.821 | 8.476 | 0.837 | 0.830 | 8.405 |
| Mn | 0.179 | 0.023 | 0.095 | 0.184 | 0.100 | 0.144 | 0.304 | 0.102 | 0.757 | 0.138 | 0.141 | 0.079 | 0.092 | 0.174 |
| Mg | 0.001 | 0.005 | 0.002 | 0.014 | 0.001 | 0.001 | 0.009 | 0.001 | 0.009 | 0.001 | 0.004 | 0.003 | 0.006 | 0.005 |
| Ca | | 0.016 | 0.001 | 0.007 | | | 0.007 | | 0.010 | 0.001 | 0.049 | 0.002 | 0.006 | |
| Nb | 0.027 | | 0.002 | 0.006 | 0.002 | 0.002 | 0.015 | 0.014 | | 0.031 | | 0.006 | 0.006 | |
| Sum | 1.999 | 24.000 | 2.000 | 24.000 | 1.999 | 2.000 | 23.999 | 2.000 | 24.000 | 1.999 | 24.000 | 2.000 | 2.000 | 24.000 |
| | | | | | | | | | | | | | | |
| Mol% | | | | | | | | | | | | | | |
| ulvöspinel | | 4.46 | | 13.08 | | | 32.12 | | 13.13 | | 8.38 | | | 7.22 |
| $R_2O_3$ | 1.60 | | 3.72 | | 7.03 | 7.71 | | 9.28 | | 3.19 | | 7.71 | 6.43 | |
| | | | | | | | | | | | | | | |
| T (°C) | | | 556 | | 663 | 674 | | 783 | | 574 | | 652 | 626 | |
| $\log_{10} fO_2$ | | | -12.9 | | -17.2 | -16.7 | | -14.2 | | -22.2 | | -17.0 | -18.2 | |
| | | | | | | | | | | | | | | |
| A.I. | 0.93 | 0.90 | | | 0.91 | | 0.80 | | 1.04 | | | 0.97 | | 0.85 |

| Sample | PV-6 | PV-14 | | PV-34 | | 21 | | | PV-16 | PV-55 | | PV-56 |
|---|---|---|---|---|---|---|---|---|---|---|---|---|
| | S | S | | S | | NS | | | NS | NS | | NES |
| | Il | Mt | Il | Mt | Il | Mt-C | Mt-R | Il | Il | Mt | Il | Mt-C |
| wt% | | | | | | | | | | | | |
| $SiO_2$ | 0.04 | 0.06 | 0.04 | 0.10 | 0.08 | 0.06 | 0.09 | | | | | 0.07 |
| $TiO_2$ | 47.87 | 3.26 | 49.48 | 4.96 | 49.23 | 5.62 | 15.05 | 44.96 | 44.06 | 4.01 | 48.95 | 1.07 |
| $Al_2O_3$ | 0.02 | 0.27 | 0.05 | 0.28 | | 0.97 | 0.89 | 0.59 | 1.12 | 0.34 | 0.04 | 0.16 |
| $Fe_2O_3$ | 7.37 | 62.64 | 2.98 | 58.17 | 8.17 | 56.89 | 39.05 | 13.32 | 15.49 | 61.19 | 6.94 | 65.85 |
| FeO | 38.80 | 32.91 | 40.19 | 34.64 | 37.51 | 35.37 | 43.50 | 25.40 | 29.33 | 32.91 | 24.49 | 31.08 |
| MnO | 4.64 | 1.38 | 5.15 | 0.81 | 7.07 | 1.03 | 1.83 | 14.62 | 9.79 | 1.99 | 19.15 | 0.74 |
| MgO | 0.02 | | 0.03 | 0.05 | 0.03 | 0.04 | 0.03 | 0.15 | 0.21 | 0.01 | 0.09 | |
| CaO | | | 0.08 | | | 0.04 | 0.10 | | | 0.03 | 0.02 | |
| $Nb_2O_5$ | 1.62 | | 1.49 | | 1.30 | | 0.04 | 0.15 | | | 0.13 | |
| Sum | 100.38 | 100.25 | 99.49 | 99.01 | 100.17 | 100.02 | 100.58 | 99.19 | 100.00 | 100.48 | 99.81 | 98.97 |
| | | | | | | | | | | | | |
| Si | 0.001 | 0.018 | 0.001 | 0.031 | 0.002 | 0.018 | 0.027 | | | | | 0.022 |
| Ti | 0.914 | 0.749 | 0.949 | 1.153 | 0.911 | 1.287 | 3.398 | 0.862 | 0.837 | 0.921 | 0.932 | 0.251 |
| Al | 0.001 | 0.097 | 0.002 | 0.102 | | 0.348 | 0.315 | 0.018 | 0.033 | 0.081 | 0.001 | 0.059 |
| $Fe^{3+}$ | 0.141 | 14.381 | 0.058 | 13.531 | 0.152 | 13.040 | 8.822 | .0.255 | 0.294 | 14.065 | 0.133 | 15.397 |
| $Fe^{2+}$ | 0.824 | 8.397 | 0.857 | 8.955 | 0.772 | 9.010 | 10.922 | 0.541 | 0.619 | 8.496 | 0.518 | 8.076 |
| Mn | 0.099 | 0.357 | 0.112 | 0.212 | 0.147 | 0.266 | 0.465 | 0.316 | 0.209 | 0.514 | 0.410 | 0.195 |
| Mg | 0.001 | | 0.001 | 0.016 | 0.001 | 0.018 | 0.013 | 0.006 | 0.008 | 0.004 | 0.003 | |
| Ca | | | 0.002 | | | 0.013 | 0.032 | | | 0.009 | 0.001 | |
| Nb | 0.019 | | 0.018 | | 0.015 | | 0.005 | 0.002 | | | 0.002 | |
| Sum | 2.000 | 23.999 | 2.000 | 24.000 | 2.000 | 24.000 | 23.999 | 2.000 | 2.000 | 24.000 | 2.000 | 24.000 |
| | | | | | | | | | | | | |
| Mol% | | | | | | | | | | | | |
| ulvöspinel | | 9.47 | | 14.79 | | 16.31 | 42.81 | | | 11.51 | | 3.40 |
| $R_2O_3$ | 7.11 | | 3.00 | | 7.60 | | | 13.7 | | | 6.66 | |
| | | | | | | | | | | | | |
| T (°C) | 636 | | 560 | | 680 | | | 930 | | | 650 | |
| $\log_{10} fO_2$ | -17.1 | | -22.7 | | -16.6 | | | -10.9 | | | -16.4 | |
| | | | | | | | | | | | | |
| A.I. | | | 0.90 | 0.91 | | 0.82 | | | 0.86 | 0.93 | | 0.88 |

Table 6 (continued).

| Sample | PV-56 NES | | PV-32 Corundum-bearing NES | | | | | | | | 22 TRPH |
|---|---|---|---|---|---|---|---|---|---|---|---|
| | Il (at Mt rim) | Il | Hc-C | Hercynite-ilmenitic rim | Hc-C | Hercynite-ilmenitic rim | Ph Il-C | Il-Ph Mt R | mPh Mt-C | mPh Mt-R | gm Mt |
| wt% | | | | | | | | | | | |
| $SiO_2$ | 0.05 | 0.04 | 0.03 | 0.07 | 0.04 | | 0.03 | 0.05 | 0.05 | .06 | 0.04 |
| $TiO_2$ | 40.51 | 50.52 | 0.03 | 50.33 | 0.08 | 50.17 | 50.75 | 5.25 | 3.49 | 4.53 | 14.84 |
| $Al_2O_3$ | 1.78 | 2.76 | 56.73 | 0.03 | 56.88 | | 0.01 | 1.10 | 0.94 | 0.49 | 0.71 |
| $Fe_2O_3$ | 22.49 | 0.44 | 3.02 | 2.62 | 2.59 | 3.33 | 3.41 | 57.17 | 60.65 | 59.91 | 38.42 |
| FeO | 14.96 | 21.33 | 34.20 | 36.03 | 34.97 | 35.18 | 38.28 | 35.06 | 33.33 | 34.94 | 42.11 |
| MnO | 20.92 | 23.33 | 3.83 | 9.76 | 3.74 | 10.06 | 7.37 | 0.89 | 0.95 | 0.56 | 2.33 |
| MgO | 0.15 | 0.27 | 1.90 | 0.10 | 1.53 | 0.13 | 0.03 | 0.04 | 0.03 | 0.03 | 0.05 |
| CaO | 0.08 | 0.14 | | | | | 0.01 | 0.03 | | 0.02 | 0.06 |
| $Nb_2O_5$ | 0.13 | 0.22 | | 0.85 | | 0.72 | 0.14 | | | | 0.05 |
| Sum | 101.07 | 99.05 | 99.74 | 99.79 | 99.83 | 99.59 | 99.93 | 99.59 | 99.44 | 100.54 | 98.61 |
| Si | 0.001 | 0.001 | 0.007 | 0.002 | 0.009 | | 0.001 | 0.015 | 0.015 | 0.018 | 0.012 |
| Ti | 0.761 | 0.951 | 0.005 | 0.959 | 0.014 | 0.958 | 0.966 | 1.207 | 0.806 | 1.036 | 3.421 |
| Al | 0.052 | 0.081 | 15.450 | 0.001 | 15.503 | | | 0.396 | 0.340 | 0.176 | 0.256 |
| $Fe^{3+}$ | 0.422 | 0.008 | 0.525 | 0.050 | 0.451 | 0.064 | 0.64 | 13.156 | 14.016 | 13.715 | 8.862 |
| $Fe^{2+}$ | 0.313 | 0.447 | 6.609 | 0.764 | 6.763 | 0.748 | 0.810 | 8.967 | 8.561 | 8.900 | 10.794 |
| Mn | 0.442 | 0.495 | 0.750 | 0.210 | 0.733 | 0.217 | 0.158 | 0.231 | 0.247 | 0.144 | 0.605 |
| Mg | 0.006 | 0.010 | 0.654 | 0.004 | 0.527 | 0.005 | 0.001 | 0.018 | 0.014 | 0.014 | 0.023 |
| Ca | 0.002 | 0.004 | | | | | | 0.010 | | 0.007 | 0.020 |
| Nb | 0.001 | 0.002 | | 0.010 | | 0.008 | | | | | 0.007 |
| Sum | 2.000 | 1.999 | 24.000 | 2.000 | 24.000 | 2.000 | 2.000 | 24.000 | 23.999 | 24.000 | 24.000 |
| Mol% | | | | | | | | | | | |
| ulvöspinel | | | | | | | | 15.15 | 10.26 | 13.18 | 42.11 |
| $R_2O_3$ | 23.74 | 4.45 | | 2.55 | | 3.20 | 3.26 | | | | |
| T (°C) | 684 | | | | | | | 780 | | | 608 |
| $\log_{10} fO_2$ | -13.2 | | | | | | | -19.0 | | | -23.3 |
| Hercynite ($FeO{*}Al_2O_3$) | | | 78.95 | | 81.03 | | | | | | |
| A.I. | 0.88 | | | 0.66 | | | | | 0.80 | | |

Amphiboles are ubiquitous components in all the rock-types from Velasco, with the exception of granites (Table 4).

In the metaluminous petrographic varieties, these minerals may appear as primary phases, whereas in agpaitic rocks they systematically occur as uralitized products of clinopyroxene.

The amphiboles composition strongly reflects the nature of the host rocks and, as the alkalies activity increases, a trend from calcic to sodic-calcic varieties is observed, with two main populations represented by quartz syenite+syenite and by nephel-syenite+nepheline syenite+dyke (quartz trachyte to trachyphonolite), respectively (cf. Fig. 9).

In particular, a variation from hastingsitic to edenitic types is apparent (according to the classifications of Leake, 1978, and Giret *et al.*, 1980).

Notably, different F contents are also apparent: metaluminous quartz syenites and dykes (quartz trachytes to trachyphonolites) show quite variable concentrations, i.e. 0.51±0.22 and 1.18±0.57 wt%, whereas a systematic increase was noticed for the other metaluminous rock-types, i.e. syenites 0.34±0.06 wt%, nephel-syenites 0.59±0.11 wt% and nepheline syenites 1.74±0.16 wt%. Moreover, in some intrusive agpaitic rocks, the uralitic products have very high F content, i.e. in the range of 2.1-6.4 wt% (cf. Table 4), confirming thus a F activity increase as also shown by the occasional occurrence of fluorspar as an accessory phase.

Finally, it should be noted that in spite of the alkaline character of the host rocks, the amphiboles do not present alkaline compositions, even in the peralkaline varieties.

*Micas*

Biotite is an ubiquitous phase (cf. Table 5). The compositional variations tend to be dominated by the adjustaments in the Mg/Fe ratio along the phlogopite-annite join, the most evolved compositions from granite rock-types corresponding to annite (Fig. 10): $Mg/(Mg+Fe_{total}+Mn)$ ratio (Mg*) ranges from 0.05 to 0.10 in granites and quartz trachytes, being the averages 0.28 (±0.11), 0.36 (±0.15), 0.53 (±0.12), 0.45 (±0.09) and 0.72 (±0.06) in quartz syenites, syenites, nephel-syenites, nepheline syenites and trachyphonolites, respectively.

The wide Mg* range observed in syenites is coupled with $TiO_2$ increase (up to 5.7 wt%). MnO tends to have the highest concentration in the nepheline syenites, i.e. 2.53±0.85 wt% (granites 1.05±0.13, quartz syenites 0.48±0.17, syenites 0.62±0.18, nephel-syenites 1.25±0.67, quartz trachytes and trachyphonolites 0.99±0.56 wt%). Different compositions, trending to the siderophyllite corner, were observed in the corundum-hercynite-bearing PV-32 dyke (cf. Fig. 10).

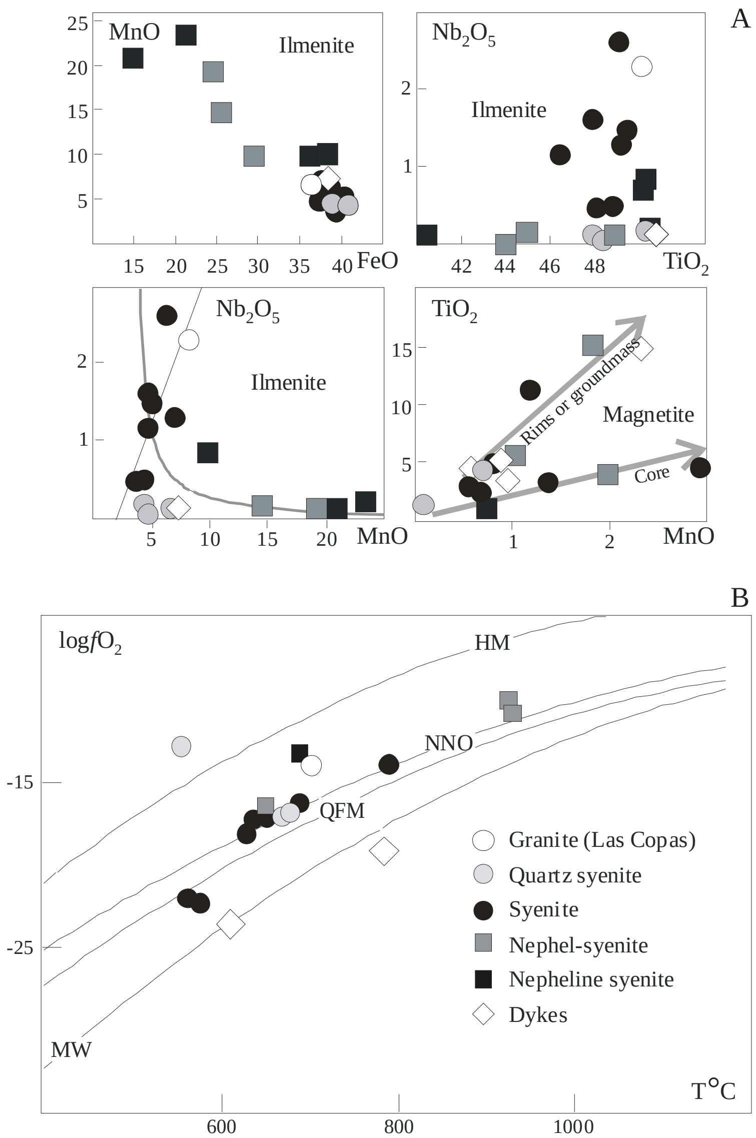


Fig. 11. A: Composition of opaques from the Velasco rock-types. Ilmenite: FeO vs. Mn, MnO and $TiO_2$ vs. $Nb_2O_5$ (wt%); Magnetite: MnO vs. $TiO_2$ (wt %). B: Temperature-oxygen fugacity diagram for the Velasco rocks.

Fluorine and chlorine contents are quite distinct and variable in the different rock-types: in the granites (F=0.76±0.32 wt%), quartz syenites (F=1.41±0.61 wt%) and syenites (F=0.95±0.65 wt%) the Cl content is relatively high, i.e. 0.26±0.05, 0.34±0.16, and 0.30±0.25 wt%, respectively; in the nephel-syenites, nepheline syenites and dykes the F content is 1.98±0.95, 1.88±0.67 and 2.13±1.52 wt%, respectively, and associated to Cl contents <0.05 wt%. In general, at increasing Mg* values, biotite tends to become progressively enriched in F (F=3.55 Mg*+0.165, r=0.75).

On the whole, the Velasco mica compositions are very similar to those of the Itatiaia rock-types at eastern Brazil (Brotzu *et al.*, 1997).

*Oxides*

Hematite is present in the granites and rarely occur associated with ilmenite. The latter is ubiquitous in all the Velasco rock-types and shows considerable, even variable, substitution of manganese for iron (FeO vs. MnO diagram; Fig. 11A). In syenites and granites, ilmenite displays a systematic Nb enrichment ($Nb_2O_5$ up to 2.62 wt%) correlated with MnO wt% content ($Nb_2O_5$=0.40 Mn+0.74, r=0.75), whereas in the nephel-syenites and nepheline syenites the mineral shows high Mn concentrations (pyrophanite-rich variants: MnO up to 23 wt%; cf. Table 6) coupled with very low $Nb_2O_5$ proportions. Probably, there are complex niobium substitutions for both manganese and titanium (cf. curves on the MnO vs. $Nb_2O_5$ diagram of Fig. 11A).

Magnetite shows a very large range in ulvöspinel content, i.e. from 4.5 to 42.1 mol%, and generally has low $Al_2O_3$ concentration (i.e.<1.4 wt%). Two main trends are apparent in the MnO vs. $TiO_2$ diagram of Fig. 11A: a behaviour represented by late magnetite (rims and/or groundmass phases, in the intrusive and effusive rock-types, respectively) and a trend related to the central parts of magnetite crystals.

Hercynite occurs as idiomorphic crystals only in the corundum-bearing dyke (nepheline syenite PV-32 of Table 1: $Al_2O_3$~57 wt%, hercynite ~79 mol%; cf. Table 6).

The presence of ilmenite-magnetite pairs allows very broad estimates of equilibration temperatures and oxygen fugacities (Fig. 11B), due to the presence of Nb and Ti substitutions. The results are scattered between the MW and HM buffers (Spencer & Lindsley, 1981; Andersen & Lindsley, 1988), but they trend mainly along the NNO buffer. The inferred temperatures are quite variable, from 930° to 556°C: even considering that peralkaline felsic magmas have a considerable temperature interval of crystallization (i.e. 990° to 580°C; cf. Piotrowski & Edgar, 1970, and Mitchell & Platt, 1978), the temperatures below 600°C reflect subsolidus non-equilibrium adjustment of composition.

*Intensive parameters, significance of the mineralogy and mass balance calculations*

It is hard to estimate the pressures that have prevailed at the time of the intrusions because the overlying volcanic sequences have not been well-preserved. The style of the intrusions and tectonic setting of the Velasco complexes are similar to that seen in other alkaline provinces (e.g. Chilwa Alkaline Province, Malawi, cf. Platt & Woolley, 1986, and therein references; Alto Paraguay Province, cf. Comin-Chiaramonti *et al.*, in this volume), suggesting a shallow depth of emplacement at pressure conditions probably not exceeding 1 kb, as also indicated by the presence of primary haüyne which is typically associated with volcanic-subvolcanic rock-types (cf. Burragato *et al.*, 1982). The validity of calculated crystallization temperatures is rendered dubious as a result of the extensive subsolidus and ion-exchange reactions described above. Thus, if plagioclase temperatures (1150°-810°C) in metaluminous rocks may represent liquid temperatures, the temperature of equilibration of plagioclase-alkali feldspar and alkali feldspar-nepheline pairs is •700°C, and the lowest temperature of equilibration of the magnetite-ilmenite pairs indicates less than 600°C (range 930° -556°C; cf. Table 6).

These wide temperature ranges are above the experimentally determined interval of syenites suites l.s. and clearly reflect subsolidus non-equilibrium adjustment in composition (cf. Mitchell & Platt, 1982 and therein references). Accordingly, it is here proposed a crystallization range between 1150° and 700°C for the Velasco complexes. The subsequent subsolidus reactions with hydrothermal fluids brought about ion-exchanges in feldspars, uralitization of clinopyroxenes and hematitization.

Oxygen fugacities calculated from coexisting magnetite and ilmenite (cf. Spencer & Lindsley, 1981) range from $10^{-11}$ (930°C) to $10^{-23}$ bars (608°C), but the best estimates of $fO_2$ prevailing during the course of crystallization are along the NNO buffer, located between $10^{-11}$ and $10^{-20}$ bars.

The best results relative to the mass balance calculations, performed in order to model the transition to the most differentiated rocks and to the peralkaline types, indicate that (Table 7): 1) a significant role for nepheline fractionation is required for the transition from the less to more evolved nepheline syenites; 2) the transition to nephel-syenites, syenites and quartz syenites requires, step by step, relatively high proportions of plagioclase (38, 23 and 20 wt%, respectively) plus alkali felspar (44, 55 and 61 wt%, respectively); 3) no reliable fractionation models allow the transition to the granites. However, these

Table 7. Selected mass balance results for Velasco rock-types. D: bulk partition coefficients calculated following mineral-liquid partition coefficients after Comin-Chiaramonti *et al.* (1997). F, residual liquid, $\Sigma R^2$, sum of the squares of major element residual.

| | NES PV-21 $SiO_2$ 50.62% to NES PV-46 $SiO_2$ 60.12% | NES PV-21 $SiO_2$ 50.62% to NS PV-43 $SiO_2$ 63.76% | NS PV-43 $SiO_2$ 63.76% to S 31 $SiO_2$ 67.10% | S 15 $SiO_2$ 64.55% to QS 6 $SiO_2$ 71.19% |
|---|---|---|---|---|
| Pl | 4.4 | 38.3 | 23.3 | 19.6 |
| Af | | 44.0 | 54.7 | 61.4 |
| Ne | 66.0 | | | |
| Cpx | 8.3 | | 4.7 | |
| Am | 5.0 | 5.0 | 9.2 | 11.6 |
| Bt | 10.1 | 6.6 | | |
| Mt | 0.4 | 4.4 | 4.0 | 4.7 |
| Il | 3.7 | 0.7 | 2.2 | 1.9 |
| Ap | 2.1 | 1.0 | 1.9 | 0.7 |
| F | 0.48 | 0.47 | 0.39 | 0.54 |
| $\Sigma R^2$ | 1.49 | 0.04 | 0.61 | 0.13 |
| D | | | | |
| Rb | 0.94 | 0.36 | 0.25 | 0.28 |
| Sr | 1.24 | 4.87 | 4.75 | 4.43 |
| Nb | 0.47 | 0.31 | 0.13 | 0.15 |
| Ba | 1.20 | 3.24 | 3.10 | 3.43 |
| Zr | 0.26 | 0.23 | 0.15 | 0.16 |
| Y | 2.70 | 1.28 | 2.33 | 1.16 |
| Nd | 2.05 | 1.10 | 1.84 | 0.91 |
| $C_{obs}/C_{calc}$ | | | | |
| Rb | 0.46 | 0.59 | 0.29 | 1.13 |
| Sr | 0.30 | 17.58 | 18.92 | 11.19 |
| Nb | 0.77 | 0.98 | 0.05 | 0.72 |
| Ba | 0.78 | 5.27 | 4.50 | 1.17 |
| Zr | 7.12 | 3.22 | 0.11 | 0.09 |
| Y | 7.63 | 1.41 | 8.72 | 16.09 |
| Nd | 2.55 | 0.36 | 5.34 | 6.73 |

Table 8. Chemical analysis of the Las Copas granite and microprobe analysis of the hosted amphibole (cf. Table 2 and Table 4).

| LAS COPAS | | | | | | Amphibole | | | |
|---|---|---|---|---|---|---|---|---|---|
| $SiO_2$ | 73.57 | Ba | 325 | Q | 28.92 | $SiO_2$ | 49.71 | Si | 7.761 |
| $TiO_2$ | 0.13 | Rb | 425 | or | 28.07 | $TiO_2$ | 0.12 | $Al^{IV}$ | 0.239 |
| $Al_2O_3$ | 11.10 | Sr | 39 | ab | 30.66 | $Al_2O_3$ | 1.64 | $Al^{VI}$ | 0.063 |
| $Fe_2O_3$ | 3.04 | Nb | 200 | ac | 8.80 | $Fe_2O_3$ | 16.34 | Ti | 0.014 |
| FeO | 0.42 | U | 13 | ns | 0.94 | FeO | 21.02 | $Fe^{3+}$ | 1.920 |
| MnO | 0.05 | Th | 32 | hy | 0.75 | MnO | 0.10 | $Fe^{2+}$ | 2.744 |
| MgO | 0.04 | Zr | 938 | il | 0.25 | MgO | 1.06 | Mn | 0.019 |
| CaO | 0.33 | Y | 144 | ap | 0.02 | CaO | 0.54 | Mg | 0.247 |
| $Na_2O$ | 5.28 | La | 130 | fr | 0.31 | $Na_2O$ | 6.40 | Ca | 0.090 |
| $K_2O$ | 4.75 | Ce | 241 | Q | 62.8 | $K_2O$ | 0.55 | Na | 1.937 |
| $P_2O_5$ | 0.01 | Nd | 92 | Ne | 18.2 | F | 1.10 | K | 0.109 |
| F | 0.15 | | | Ks | 19.0 | Cl | 0.10 | F | 0.543 |
| Cl | 0.01 | | | | | $H_2O$ | 1.37 | Cl | 0.027 |
| Sum | 99.69 | | | | | Less O=F,Cl | 0.48 | OH | 1.430 |
| | | | | | | Sum | 99.57 | $Mg/(Mg+Fe^{2+})$ | 0.083 |
| A.I. | 1.25 | | | | | | | $Fe^{3+}/(Fe^{3+}+Al^{VI})$ | 0.968 |
| $K_2O/Na_2O$ | 0.90 | | | | | | | | |
| R1 | 1819 | | | | | | | | |
| R2 | 253 | | | | | | | | |
| Rock-type | Granite | | | | | | | | |

algebric solutions are not consistent with the trace element contents because the calculated/observed concentrations (Rayleigh fractionation) are in the following ranges: Rb 0.46-1.13, Sr 0.17-18.9, Nb 0.05-1.03, Ba 0.78-5.27, Zr 0.09-7.45, Y 1.41-16.1, Nd 0.36-6.73 (cf. Table 7).

Whatever the origin of the felsic alkaline liquids (cf. Petrogeny's Residua System of Fig. 3B), phase relationships dominate in and between the silica-oversaturated, saturated and silica-undersaturated magmas. Foland *et al.* (1993) proposed that silica-oversaturated melts developed from felsic silica-undersaturated magmas in a coupled process of crustal assimilation (with a granitic minimum melt composition) and fractional crystallization, whereas nepheline-bearing syenites were formed without significant contamination. In these processes an important role may be played by the plagioclase, as e.g. fractionation of a mafic parental magma (such as alkali basalt or basanite) can potentially generate evolved liquids with a distinct peralkaline signature and Eu/Eu* negative anomalies. In addition, also the mixing with crustal derived melts, leaving plagioclase in the solid residue, gives Eu/Eu* negative anomalies. Notably, any interpretation of the origin of agpaitic magmas must account for the enhancement of alkalis with respect to the alumina, the impressive and variable enrichment of incompatible trace elements, a distinct order of crystallization in which felsic minerals tend to precipitate before the mafic phases, a typical high $Fe^{3+}/Fe^{2+}$ ratio, and an impressive enrichment in F and Cl (cf. Bailey, 1976), as shown by the amphibole and biotite compositions from the Velasco complexes.

## LAS COPAS BODY

Las Copas is a small body discovered by Hawkins (1982; in Litherland *et al.*, 1986) about 20 km to the west of the San Miguelito complex (cf. Fig. 1) and described as a satellite related to the Velasco Alkaline Province. However, there is also the possibility that the Las Copas rocks have an older age, because of their similarity with the La Junta granite (ca. 1300 Ma; Litherland *et al.*, 1986) that crops out not far from the Velasco complexes.

The Las Copas rocks are poorly exposed in a jungle-covered locality and only a sample is actually available. The analysed material is a hypersolvus granite characterized by a fine-grained granular texture and mineralogically made of quartz, mesoperthitic alkali feldspar, alkaline amphibole and, as accessory phases, zircon and fluorspar (the riebeckite-arfvedsonite granite of Fletcher & Beddoe-Stephens, 1987). Notably, the Las Copas sample differs from the Velasco specimens for the presence of an alkaline amphibole, and also from Velasco granites that are characteristically amphibole-free.

The chemical analysis (Table 8) indicates that the sample is agpaitic (A.I.=1.25) with normative acmite and sodium metasilicate (8.80 and 0.94 wt%, respectively) consistent with the occurrence of a riebeckitic amphibole (from crystallochemical data: $Na_B$>1.34, $(Na+K)_A$<0.5, $Mg/(Mg+Fe^{2+})$=0.083, $Fe^{3+}/(Fe^{3+}+Al^{VI})$=0.968; cf. Table 11 and Leake, 1978). On the whole, the rock appears to have a composition close to peralkaline silicic magmas (cf. BL 575 of Scaillet & MacDonald, 2001) for which experimental melting results give a mineralogical assemblage consisting of quartz-alkali feldspar-riebeckite/arfvedsonite-fluorite, at temperature and pressure about 700°C and 0.5 kb, respectively (log $fO_2$~-14; cf. Fig. 11B).

## CERRO MANOMÓ

Cerro Manomó lies about 22 km northeast of the Todos Santos alkaline body which represents the northeasternmost outcrop of the Velasco complexes (cf. Fig. 1). Cerro Manomó forms a mesa of 4x6 km, rising up to 300 m above the jungle-covered peneplain of laterized Precambrian basement. Fletcher (1979) and Fletcher *et al*. (1981) mapped the area and described the body as the largest silicified carbonatite complex so far listed in literature, strictly linked in time to the Velasco alkaline complexes. All the rock-types from Cerro Manomó are strongly altered, but the outcrop forms, macro- and micro-textures and alteration products allowed Burton (1982, in Litherland *et al*., 1986) to postulate that the complex consists of a central core of inten-sely brecciated and silicified gneisses surrounded by fenitized gneisses, cut by a network of steeply-dipping dykes and late-stage agglomerates. In particular, the dykes are composed by goethite-quartz-barite-bastnaesite assemblages, and were interpreted as altered ferrocarbonatites by Burton (1982). A lens of apatite-rich rock (cf. Fletcher *et al*., 1981) is noticeable on the north-eastern side of the complex associated with rare carbonate blocks. The latter rock-types are ferrocarbonatites (according to the nomenclature given by Gittings & Harmer, 1997; cf. Table 9), made of altered sideritic-ankeritic carbonate with subordinate calcite, goethite-limonite, quartz, apatite and REE-fluorcarbonates (mainly bastnaesite and synchysite).

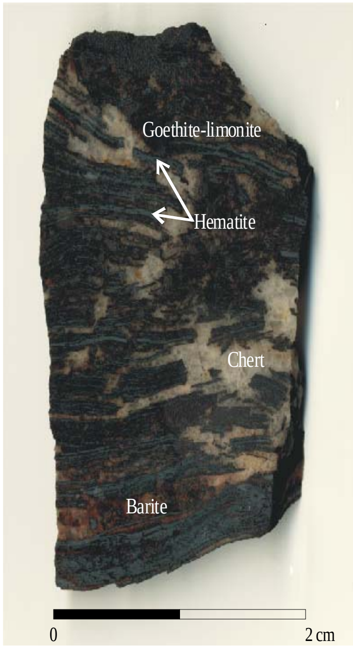


Fig. 12. Plate showing alternate succession of silica and iron-rich microbands in a sample from the Cerro Manomó.

Following Litherland *et al*. (1986), the stratigraphic relationships and the tectonic events suggest that Early Cretaceous faulting and intrusions in the area of the Velasco complexes predate the uplift, faulting and emplacement of the Cerro Manomó complex (Late Cretaceous?, cf. Fletcher *et al*., 1981). However, the Manomó hill is peculiar for his banding of Fe-rich and Si-rich layers: this banding can be observed on a wide range of scales, i.e. from coarse macrobands (meters in thickness) up to millimetric and sub-millimetric layers (microbands; cf. Fig. 12). If the macrobands correspond to the petrographical des-

Table 9. Chemical analyses of selected samples from the Cerro Manomó complex.; **, after Litherland *et al.* (1986).

| Sample | PV-67 Macro-band | PV-69 Macroband | | PV-67B Macroband | | PV-68 Macro-band | PV-69 Carbonate block | MW-3** Dyke | MR-16** Phosphate rock | PV-70 Basement gneiss |
|---|---|---|---|---|---|---|---|---|---|---|
| wt% | | | | | | | | | | |
| $SiO_2$ | 40.55 | 38.55 | | 22.02 | 92.88 | 87.66 | 3.02 | 46.92 | 5.67 | 74.18 |
| $TiO_2$ | 0.07 | 0.17 | 0.10 | 0.08 | 0.02 | 0.07 | 0.02 | 0.19 | 0.20 | 0.29 |
| $Al_2O_3$ | 0.27 | 0.12 | | 0.88 | 0.60 | 3.90 | 0.11 | 0.65 | 1.20 | 13.11 |
| $Fe_2O_3$ | 53.16 | 50.07 | | 74.13 | 0.86 | 5.64 | | 32.34 | 23.27 | 1.20 |
| FeO | | | | | | | 40.49 | | | |
| MnO | 0.36 | 0.42 | | 0.20 | 0.06 | 0.06 | 7.13 | 1.46 | 0.45 | 0.01 |
| MgO | 0.09 | 0.25 | | 0.08 | 0.01 | 0.11 | 0.34 | 0.24 | 0.40 | 0.02 |
| CaO | 0.16 | 0.50 | | 0.11 | 0.07 | 0.15 | 7.68 | 0.11 | 37.51 | 0.12 |
| BaO | 2.58 | 6.23 | 8.52 | | | | | 10.43 | 0.40 | |
| $Na_2O$ | 0.09 | 0.29 | | 0.09 | 0.01 | 0.01 | 0.08 | 0.34 | 0.57 | 2.89 |
| $K_2O$ | 0.02 | 0.07 | 0.08 | 0.01 | 0.12 | 0.40 | 0.02 | 0.04 | 0.03 | 4.40 |
| $P_2O_5$ | 0.12 | 0.32 | 0.29 | 0.05 | 0.01 | 0.18 | 0.10 | 0.15 | 25.19 | 0.07 |
| LOI | 1.41 | 2.11 | | 1.83 | 4.65 | 1.68 | 35.28 | 4.38 | 3.77 | 3.38 |
| F | | | | | | | 0.31 | | 1.69 | |
| Sum | 98.88 | 99.10 | | 99.48 | 99.28 | 99.86 | 94.58 | 97.25 | 99.66 | 99.67 |
| ppm | | | | | | | | | | |
| Cr | 46 | 9 | 12 | 74 | | | | 37 | 162 | 10 |
| Ni | 26 | 113 | 8 | 42 | | | | 14 | | |
| Ba | 25783 | 56728 | 76293 | 57 | 278 | 315 | 1560 | 93400 | 3600 | 137 |
| Rb | 19.2 | 10.3 | 0.2 | 10 | 0.72 | 13.5 | | | | 26 |
| Sr | 54.6 | 333.8 | 928.2 | 78 | 28 | 954 | 2342 | 214 | 7103 | 1058 |
| Pb | 57.3 | 64.4 | 58.8 | 82 | 7.3 | 29.8 | | 127 | 110 | 16.6 |
| Nb | 159 | 12.1 | 52.4 | 202 | 13.1 | 26.4 | 25 | 320 | 1025 | 43.4 |
| Ta | 9.5 | 0.25 | 0.6 | 19.6 | | 1.6 | | | | 0.9 |
| Hf | 0.9 | 0.38 | 0.2 | | | 0.3 | | | | 3.9 |
| U | 2.5 | 22.3 | 34.0 | 5.3 | 0.6 | 1.3 | 121 | 5 | 1010 | 0.9 |
| Th | 22.1 | 763.3 | 1739 | 46.9 | 5.2 | 11.3 | 481 | 714 | 1730 | 8.4 |
| Zr | 33.2 | 11.6 | 33.8 | 14.8 | 4.4 | 47.7 | 15 | 59 | 159 | 157 |
| Y | 18.0 | 714.9 | 965 | 38 | 1.5 | 9.0 | 49 | 70 | 755 | 18 |
| La | 40.3 | 101.3 | 469.2 | 11.3 | 2.12 | 18.1 | 2570 | 256 | 396 | 37.5 |
| Ce | 63.6 | 891.9 | 3519.0 | 12.8 | 4.37 | 28.6 | 5238 | 2170 | 1150 | 70.3 |
| Pr | 4.1 | 219.8 | 770.2 | 2.1 | 0.56 | 4.1 | 787 | | | 11.3 |
| Nd | 35.1 | 1237.9 | 3440.8 | 9.2 | 2.32 | 17.0 | 2142 | 880 | 655 | 44.2 |
| Sm | 8.54 | 272.6 | 532.8 | 2.02 | 0.58 | 4.69 | 369 | 145 | 330 | 7.66 |
| Eu | 2.10 | 76.3 | 128.4 | 0.47 | 0.32 | 1.37 | 79 | 26 | 95 | 1.60 |
| Gd | 5.98 | 233.1 | 513.4 | 1.51 | 0.49 | 3.43 | 221 | | | 4.55 |
| Tb | 0.82 | 52.5 | 73.0 | | | 0.41 | 13 | 4.3 | 23 | 0.60 |
| Dy | 3.74 | 289.6 | 357.6 | 1.42 | 0.47 | 1.97 | 60 | 15.0 | 137 | 3.10 |
| Ho | 0.60 | 51.0 | 61.8 | | | 0.31 | 10 | | | 0.58 |
| Er | 1.65 | 105.6 | 158.0 | 0.81 | 0.29 | 0.74 | 24 | | | 1.72 |
| Tm | 0.24 | 11.4 | 17.8 | | | 0.10 | 3 | | | 0.27 |
| Yb | 1.54 | 50.7 | 82.4 | 0.90 | 0.29 | 0.64 | 9 | 4.4 | 75 | 1.99 |
| Lu | 0.15 | 5.8 | 8.8 | | | 0.10 | 1 | 0.7 | 12 | 0.32 |

cription of Fletcher *et al.* (1981), being characterized by an association of hematite, goethite, limonite, barite, Ce-bastnaesite and Ce-synchysite with accessory monazite, the microbands show fine-scale banding of chert occasionally associated with some coarse-grained quartz, and hematite-goethite-limonite-rich levels.

Chemical analyses of selected samples (Table 9) outline the different compositions of alternating ferruginous-siliceous macro- and microbands.

Incompatible elements from the Fe-rich macrobands (values normalized to the primitive mantle, cf. Fig. 13) are strongly enriched for Ba (up to 6.23 wt%), Th (up to 1739 ppm) and REE (La excepted, i.e. La 40-469 ppm in comparison to Ce and Yb up to 3519 and 82 ppm, respectively), and show deep negative anomalies for Rb, K, Sr, P and Zr-Ti. The Th content of the macrobands accounts for the generalized high radioactivity of the area (Fletcher *et al*., 1981).

The carbonate blocks imitate to some extent the Fe-rich macrobands, excepting for the major La content (i.e. 2570 ppm). The apatitite displays high U and Th contents (1010 and 1730 ppm, respectively), but a flat Nb-P pattern (about 1000 times with respect to the primitive mantle; cf. Fig. 13).

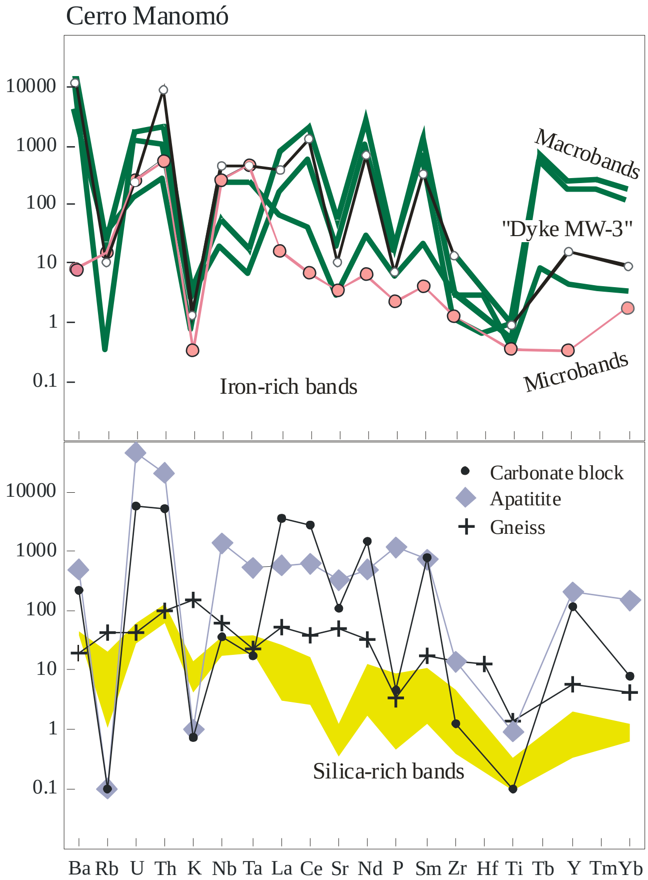


Fig. 13. Primitive mantle-normalized incompatible elements of rock-types from the Cerro Manomó complex.

REE spidergrams (chondritic normalization; Fig. 14) highlight the large variations relative to the iron-rich macrobands and a strong enrichment, in particular for Ce, Nd and Tb. But the striking similarity between the REE signature of the microbands and the banded iron formations (BIF; cf. Fig. 14), leads us to propose a genesis similar to the BIF for the Cerro Manomó complex and neighbouring areas (cf. mid-Archean BIF of Kato *et al*., 1998). Also the associated crystalline basement tends to have incompatible elements and REE patterns similar to those ones from the BIF, mostly in the MREE/HREE poor fractionation, and HREE flat behaviour, probably owing to a REE redistribution during later metamorphic events. The apatite-rich lens shows a strongly REE enriched pattern (10 times enriched with respect to the basement gneiss; cf. Fig. 14) and a poor LREE/HREE fractionation (chondritic La/Yb=3.5), contrasting with the strong REE fractionation of the associated carbonate blocks (chondritic La/Yb=192).

Considering that the region consists of a jungle-covered highland with development of a thick lateritic duricrust, and that Litherland *et al.* (1989) quoted "minor ferruginous quartzites and metaironstones" in the San Ignatio Schist Supergroup, on the whole the Cerro Manomó complex appears very similar to other BIF described, e.g. by Trendall & Blokey (1970), Trendall (2000) and Klein & Ladeira (2002) and also by Geraldes *et al.* (2000) and by Leite & Saes

(2000) in the states of Rondônia and Mato Grosso.

These characteristics, along with the appearance of apatite-rich lenses, carbonate blocks and the extensive enrichment in U, Th and REE probably point to a more complex history:

1) an old BIF-like formation deformed in Proterozoic and Fanerozoic times; 2) probable intrusion and fenitization by a carbonatitic magma in (Early, Late?) Cretaceous times; 3) lateritization processes and formation of a thick duricrust in Tertiary-Quaternary times.

Obviously, a more detailed field sampling and more systematic and extensive geological, mineralogical, petrographical and geochemical studies are in need for a more convincing regional picture.

## CANDELARIA ALKALINE MAGMATISM

The volcanic activity in the Candelaria region (Lat 16°50' S, Long 58°58' W) developed along an E-W-trending extensional zone (Mercedes rift) in the Sunsas block (cf. Litherland *et al.*, 1986, 1989; Geraldes *et al.*, 2001, and Fig. 1), 200 km west of the Late Cretaceous Poxoréu Igneous Province (PIP of Gibson *et al.*, 1997).

The latter consists of numerous outcrops of alkaline basaltic lavas and dykes (83.4±2.4 Ma; Gibson *et al.*, 1997), together with the Ponta do Morro intrusive complex (84±6 Ma, according to Del'Arco *et al.*, 1982; 100±1 Ma, according to Sousa & Ruberti, 1996).

The Candelaria region, which is characterized by reactivated basement formations of the Sunsas belt (mainly Mesoproterozoic gneisses), by Meso-Neoproterozoic sedimentary sequences and also by Neoproterozoic magmatic rocks (Litherland *et al.*, 1989; Alvarenga & Saes, 1992; Geraldes *et al.*,

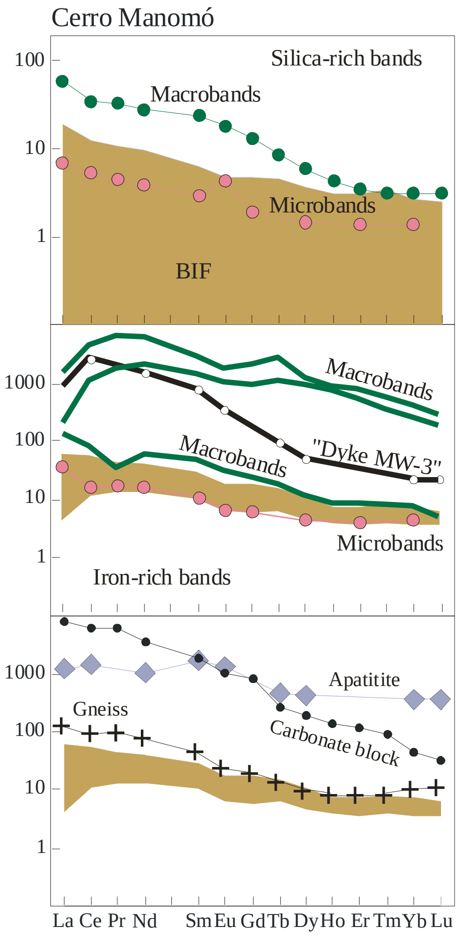


Fig. 14. Chondrite-normalized REE patterns of rock-types from the Cerro Manomó complex. The light brown fields represent Banded Iron Formations (BIF), after Kato *et al.* (1998).

Table 10. Chemical analyses of rock-types from the Candelaria region.

| | CANDELARIA | | | | | BASEMENT | | | |
|---|---|---|---|---|---|---|---|---|---|
| Sample | PV-75A | PV-76A | PV-76B | PV-77 | PV-77A | PV-72 | PV-73 | PV-75 | PV-78 |
| wt% | | | | | | | | | |
| $SiO_2$ | 53.68 | 59.32 | 61.17 | 61.78 | 63.70 | 73.38 | 71.61 | 76.83 | 78.18 |
| $TiO_2$ | 1.58 | 1.05 | 0.73 | 0.72 | 0.58 | 0.17 | 0.49 | 0.30 | 0.29 |
| $Al_2O_3$ | 15.08 | 15.02 | 16.39 | 15.44 | 14.20 | 13.62 | 13.64 | 9.60 | 9.55 |
| $Fe_2O_3$ | 4.02 | 2.30 | 3.21 | 3.19 | 3.35 | 0.71 | 1.30 | 2.81 | 2.80 |
| FeO | 5.79 | 3.70 | 3.05 | 2.85 | 2.95 | 0.87 | 1.60 | 3.43 | 3.42 |
| MnO | 0.20 | 0.14 | 0.17 | 0.22 | 0.15 | 0.06 | 0.06 | 0.01 | 0.01 |
| MgO | 2.44 | 1.22 | 0.42 | 0.57 | 0.91 | 0.24 | 1.05 | 0.01 | 0.01 |
| CaO | 4.60 | 3.30 | 1.00 | 1.20 | 0.55 | 0.86 | 2.48 | 0.13 | 0.26 |
| $Na_2O$ | 4.83 | 5.95 | 5.42 | 6.23 | 5.49 | 2.97 | 2.64 | 0.07 | 0.09 |
| $K_2O$ | 4.79 | 5.84 | 5.49 | 5.25 | 4.94 | 4.96 | 4.39 | 2.46 | 2.43 |
| $P_2O_5$ | 0.70 | 0.27 | 0.12 | 0.15 | 0.24 | 0.10 | 0.11 | 0.01 | 0.01 |
| LOI | 1.98 | 1.48 | 2.44 | 1.93 | 2.19 | 0.89 | 0.66 | 3.97 | 2.22 |
| Sum | 99.69 | 99.59 | 99.61 | 99.53 | 99.25 | 98.83 | 100.03 | 99.60 | 99.35 |
| ppm | | | | | | | | | |
| Cr | 10 | | | | | | 22 | | |
| Ni | 18 | | | | | | 11 | | |
| Ba | 653 | 583 | 514 | 441 | 410 | 378 | 972 | 32 | 32 |
| Rb | 140 | 125 | 149 | 118 | 162 | 71 | 119 | 240 | 241 |
| Sr | 1068 | 525 | 19.1 | 10.1 | 352 | 406 | 180 | 10 | 10.1 |
| Pb | | | 18.1 | 17.0 | 29.2 | 34 | 15 | 77 | 75.7 |
| Nb | 47 | 105 | 138 | 122 | 229 | 26.6 | 9 | 604 | 607 |
| Ta | 2.2 | | 6.9 | 6.3 | 11.4 | 4.9 | 3.0 | 31.2 | 30.7 |
| Hf | 3.8 | | 7.96 | 6.87 | 14.89 | 5.8 | 7.7 | 41.4 | 40.7 |
| U | 1.5 | | 4.0 | 3.88 | 7.33 | 4.3 | 0.4 | 14.4 | 14.1 |
| Th | 7.2 | 12 | 18.2 | 16.1 | 34.4 | 32.3 | 4.7 | 96.4 | 96.2 |
| Zr | 181 | 249 | 368 | 316 | 680 | 189 | 301 | 1882 | 1895 |
| Y | 68 | 40 | 46.5 | 60.1 | 95 | 70 | 36 | 204 | 205 |
| Ga | 22 | | 27.2 | 25.0 | 27.0 | 21.0 | 15.1 | 33.7 | 33.7 |
| Ge | | | | | 1.7 | 2.1 | 1.3 | 2.2 | 2.4 |
| La | 48.8 | 110 | 256.3 | 103.2 | 226 | 50.9 | 35.9 | 376 | 374 |
| Ce | 98.3 | 179 | 340.2 | 212.0 | 342 | 112.0 | 73.6 | 727 | 718 |
| Pr | 11.8 | | 55.5 | 23.0 | 43.4 | 12.9 | 8.9 | 85 | 84 |
| Nd | 39.4 | 89 | 179.5 | 79.7 | 145 | 45.8 | 34.4 | 281 | 281 |
| Sm | 12.7 | 14.3 | 26.45 | 12.71 | 25.2 | 9.80 | 7.2 | 49.3 | 48.9 |
| Eu | 3.3 | 3.0 | 3.86 | 2.71 | 3.17 | 0.81 | 1.49 | 2.88 | 2.80 |
| Gd | 8.7 | 10.2 | 16.23 | 9.62 | 17.24 | 8.34 | 6.10 | 37.89 | 38.90 |
| Tb | 2.0 | | 2.16 | 1.43 | 2.95 | 1.56 | 1.00 | 5.92 | 5.90 |
| Dy | 9.69 | | 10.47 | 8.56 | 15.64 | 10.45 | 6.12 | 34.20 | 33.83 |
| Ho | | | 1.70 | 1.64 | 2.91 | 2.16 | 1.23 | 6.69 | 6.58 |
| Er | 5.02 | | 4.85 | 4.85 | 8.63 | 6.67 | 3.54 | 19.94 | 19.79 |
| Tm | | | 0.67 | 0.68 | 1.26 | 1.12 | 0.53 | 3.05 | 2.91 |
| Yb | 5.50 | 3.7 | 4.90 | 4.58 | 8.74 | 8.11 | 3.52 | 21.00 | 20.77 |
| Lu | 0.81 | | 0.76 | 0.71 | 1.34 | 1.31 | 0.53 | 3.09 | 3.10 |
| Q | | | 5.26 | 2.98 | 10.46 | 34.54 | 32.35 | 65.15 | 66.58 |
| C | | | | | | 1.80 | 0.30 | 6.61 | 6.63 |
| or | 28.31 | 34.51 | 32.44 | 31.02 | 29.19 | 29.31 | 25.94 | 14.54 | 14.36 |
| ab | 36.05 | 37.88 | 45.87 | 50.19 | 45.54 | 25.13 | 22.34 | 0.59 | 0.76 |
| an | 5.32 | | 4.18 | | | 4.27 | 11.59 | 0.58 | 0.39 |
| ne | 2.61 | 3.72 | | | | | | | |
| ac | | 4.93 | | 2.23 | 0.81 | | | | |
| di | 10.53 | 12.22 | | 4.19 | 0.96 | | | | |
| hy | | | 3.11 | 1.76 | 3.99 | 1.44 | 3.78 | 3.53 | 3.51 |
| ol | | 1.36 | | | | | | | |
| mt | 5.83 | 0.86 | 4.65 | 3.51 | 4.45 | 1.03 | 1.88 | 4.07 | 4.06 |
| il | 3.00 | 1.99 | 1.39 | 1.37 | 1.10 | 0.32 | 0.93 | 0.57 | 0.55 |
| ap | 1.62 | 0.63 | 0.28 | 0.35 | 0.56 | 0.23 | 0.25 | 0.02 | 0.02 |
| Q | 42.9 | 42.4 | 48.2 | 42.8 | 51.6 | 66.0 | 66.7 | 89.3 | 89.5 |
| Ne | 33.1 | 31.8 | 29.7 | 32.3 | 28.9 | 15.3 | 15.0 | 0.4 | 0.5 |
| Ks | 24.0 | 25.8 | 22.1 | 24.9 | 19.5 | 18.7 | 18.3 | 10.3 | 10.0 |
| A.I. | 0.87 | 1.07 | 0.91 | 1.03 | 1.01 | 0.75 | 0.67 | 0.29 | 0.29 |
| $K_2O/Na_2O$ | 0.99 | 0.98 | 1.01 | 0.84 | 0.90 | 1.67 | 1.66 | 35.1 | 27.0 |
| R1 | 438 | 286 | 681 | 497 | 956 | 2625 | 2714 | 4341 | 4432 |
| R2 | 909 | 708 | 370 | 460 | 383 | 371 | 585 | 203 | 216 |
| Rock-type | Micro-syenite | Nephel syenite | Trachyte | Trachyte | Trachyte | Gneiss | Gneiss | Rhyolitic ignimbrite | Rhyolitic ignimbrite |

Table 11. Rb-Sr and Sm-Nd isotopic analyses of selected samples from the southeastern Bolivia alkaline outcrops. Initial isotopic ratios are calculated at 140 Ma and 84 Ma for the Velasco and Candelaria samples, respectively. The initial ratios for the basement are calculated at 140 Ma (Velasco) and 84 Ma (Candelaria). Model ages ($T^{DM}$) are calculated assuming the following values for the depleted mantle: $^{143}Nd/^{144}Nd = 0.513151$ and Sm/Nd=0.2188. Additional data (**) and sample numeration are from Litherland *et al.* (1986).

| | TODOS SANTOS | TIRARI | SAN MIGUELITO | CABEZA DE TORO | | | |
|---|---|---|---|---|---|---|---|
| Sample | 22<br>Dyke | 29 | 10 | 6 | 7B | PV-7 | PV-12<br>Dyke |
| Rb | 206.40 | 387.64 | 92.63 | 343.41 | 203.55 | 336.86 | 286.68 |
| Sr | 1015.63 | 99.69 | 1804.14 | 480.87 | 193.35 | 1239.42 | 19.01 |
| $(^{87}Sr/^{86}Sr)_{meas}$ | 0.705619 ( 9) | 0.729071 ( 9) | 0.704745 ( 8) | 0.710297 ( 9) | 0.712765 ( 9) | 0.707763 ( 8) | 0.793661 (10) |
| $R_0$ | 0.70445 | 0.70664 | 0.70445 | 0.70618 | 0.70670 | 0.70620 | 0.70611 |
| Sm | 17.51 | 21.52 | 17.04 | 116.24 | 12.77 | 21.17 | 36.64 |
| Nd | 123.82 | 125.76 | 130.01 | 760.77 | 64.01 | 166.01 | 258.04 |
| $(^{143}Nd/^{144}Nd)_{meas}$ | 0.512578 ( 7) | | 0.512629 ( 8) | | 0.512311 ( 9) | 0.512297 ( 7) | 0.512251 ( 9) |
| $(^{143}Nd/^{144}Nd)_{140}$ | 0.51250 | | 0.51256 | | 0.51220 | 0.51223 | 0.51217 |
| εSr | -1.25 | 29.79 | -1.25 | 23.37 | 30.70 | 23.57 | 22.25 |
| εNd | 0.82 | | 1.92 | | -5.02 | -4.52 | -5.57 |
| $T^{DM}$ | 656 | | 571 | | 1302 | 1049 | 1031 |
| $SiO_2$ | 56.42 | 71.84 | 59.11 | 69.99 | 69.45 | 66.26 | 67.05 |
| Q | | 24.34 | | 16.82 | 26.00 | 11.75 | 11.85 |
| ne | 3.05 | | 0.46 | | | | |
| Rock-type | Trachy-phonolite | Granite | Syenite | Quartz syenite | Granite | Quartz syenite | Quartz trachyte |

| | CABEZA DE TORO | | BAMBA | URUCÚ | | | |
|---|---|---|---|---|---|---|---|
| Sample | PV-3 | 27<br>Dyke | PV-46 | PV-16 | PV-48 | PV-55 | PV-56 |
| Rb | 253.64 | 358.73 | 103.44 | 127.37 | 73.99 | 105.22 | 209.76 |
| Sr | 76.23 | 28.47 | 160.43 | 2041.16 | 1066.09 | 621.69 | 1118.37 |
| $(^{87}Sr/^{86}Sr)_{meas}$ | 0.725843 ( 8) | 0.780107 (10) | 0.708159 ( 9) | 0.704809 ( 6) | 0.704849 ( 8) | 0.705423 (10) | 0.705429 ( 8) |
| $R_0$ | 0.70665 | 0.70705 | 0.70445 | 0.70445 | 0.70445 | 0.70444 | 0.70435 |
| Sm | 18.24 | 8.48 | 22.66 | 17.54 | 9.96 | 11.79 | 110.21 |
| Nd | 102.62 | 42.14 | 143.36 | 137.39 | 72.17 | 83.82 | 944.12 |
| $(^{143}Nd/^{144}Nd)_{meas}$ | 0.512223 ( 6) | | | | | | 0.512589 ( 9) |
| $(^{143}Nd/^{144}Nd)_{140}$ | 0.51242 | | | | | | 0.51252 |
| εSr | 30.01 | 35.62 | -0.03 | -1.29 | -1.25 | -1.27 | -2.67 |
| εNd | -6.50 | | | | | | 1.30 |
| $T^{DM}$ | 1269 | | | | | | 579 |
| $SiO_2$ | 70.16 | 75.71 | 59.16 | 59.19 | 59.22 | 59.18 | 54.78 |
| Q | 19.82 | 30.84 | | | | | |
| ne | | | 10.34 | 3.15 | 0.51 | 7.10 | 16.52 |
| Rock-type | Granite | Aplogranite | Nepheline syenite | Nephel-syenite | Syenite | Nephel-syenite | Nepheline syenite |

Table 11 (continued).

| | ZUIALITO | | | | | PRADO | | VELASCO BASEMENT |
|---|---|---|---|---|---|---|---|---|
| Sample | PV-19 | PV-20 | PV-22 | PV-23 | PV-25 | PV-30 | PV-31 | 19 |
| Rb | 232.63 | 148.67 | 155.73 | 141.19 | 182.59 | 103.17 | 131.73 | 454.86 |
| Sr | 852.77 | 2355.13 | 1451.45 | 619.9 | 691.66 | 1107.85 | 2940.22 | 657.05 |
| $(^{87}Sr/^{86}Sr)_{meas}$ | 0.706019 ( 5) | 0.704843 ( 7) | 0.705067 ( 7) | 0.705760 ( 7) | 0.705968 ( 8) | 0.704989 ( 8) | 0.704728 ( 7) | 0.771766 (15) |
| $R_0$ | 0.70445 | 0.70448 | 0.70445 | 0.70445 | 0.70445 | 0.70445 | 0.70447 | 0.76775 |
| Sm | 7.83 | 22.25 | 15.63 | 41.07 | 13.07 | 13.74 | 19.93 | 28.11 |
| Nd | 64.83 | 171.44 | 128.85 | 322.49 | 96.57 | 104.93 | 172.69 | 143.24 |
| $(^{143}Nd/^{144}Nd)_{meas}$ | | | | 0.512581 ( 7) | 0.512614 ( 5) | | 0.51279 ( 9) | 0.511558 ( 8) |
| $(^{143}Nd/^{144}Nd)_{140}$ | | | | 0.51251 | 0.51254 | | 0.51252 | 0.51145 |
| εSr | -1.26 | -0.82 | -1.25 | -1.26 | -1.27 | -1.20 | -0.96 | 897 |
| εNd | | | | 1.03 | 1.58 | | 1.12 | -19.7 |
| $T^{DM}$ | | | | 613 | 598 | | 586 | 2412 |
| $SiO_2$ | 54.73 | 53.70 | 58.15 | 49.28 | 59.97 | 56.58 | 58.08 | 70.59 |
| Q | | | | | | | | 25.66 |
| ne | 30.77 | 25.22 | 16.23 | 34.39 | 2.84 | 9.86 | 12.96 | |
| Rock-type | Nepheline syenite | Nepheline syenite | Nepheline syenite | Nepheline syenite | Syenite | Nephel-syenite | Nepheline syenite | Gneiss |

| | VELASCO BASEMENT | | MANOMÓ BASEMENT | CANDELARIA | | | CANDELARIA BASEMENT |
|---|---|---|---|---|---|---|---|
| Sample | 19A | PV-28 | PV-70 | PV-75A | PV-76B | PV-77A | PV-72 |
| Rb | 33 | 204.96 | 26 | 140 | 149 | 162 | 71 |
| Sr | 376 | 94.41 | 1058 | 1068 | 19.1 | 352 | 406 |
| $(^{87}Sr/^{86}Sr)_{meas}$ | 0.711561 (12) | 0.723191 (20) | 0.711081 ( 8) | 0.704921 ( 9) | 0.730211 (10) | 0.706492 ( 8) | 0.711865 (11) |
| $R_0$ | 0.71105 | 0.71061 | 0.71094 | 0.70449 | 0.70450 | 0.70498 | 0.71126 |
| Sm | | 8.41 | 7.66 | 12.7 | 26.45 | 25.2 | 9.80 |
| Nd | | 47.23 | 44.20 | 39.4 | 179.5 | 145 | 45.80 |
| $(^{143}Nd/^{144}Nd)_{meas}$ | | 0.511704 ( 7) | 0.511798 ( 7) | 0.513002 ( 8) | 0.512375 ( 7) | 0.512460 (11) | 0.512289 ( 7) |
| $(^{143}Nd/^{144}Nd)_{140}$ | | 0.51161 | 0.51170 | 0.51290 | 0.51233 | 0.51240 | 0.51222 |
| εSr | 92.5 | 86.3 | 90.9 | -1.66 | -1.52 | 5.27 | 94.5 |
| εNd | | -16.6 | -14.7 | 7.12 | -4.03 | -2.54 | -6.1 |
| $T^{DM}$ | | 1977 | 1803 | 948 | 911 | 926 | 1466 |
| $SiO_2$ | 73.5 | 74.0 | 74.18 | 53.68 | 61.17 | 63.70 | 73.38 |
| Q | 30.55 | 30.80 | 40.40 | | 5.26 | 10.46 | 34.54 |
| ne | | | | 2.61 | | | |
| Rock-type | Gneiss | Migmatite | Gneiss | Micro-syenite | Trachyte | Trachyte | Gneiss |

Table 11 (continued).

| Sample | Rock-type | Rb | Sr | $(^{87}Sr/^{86}Sr)_{meas}$ | $R_0$ | εSr | $SiO_2$ |
|---|---|---|---|---|---|---|---|
| | | | | Velasco complexes | | | |
| 25** | Granite | 221 | 89 | 0.72098 | 0.70667 | 30.19 | |
| 109** | Granite | 231 | 74 | 0.72420 | 0.70620 | 23.57 | |
| 118** | Granite | 374 | 53 | 0.74874 | 0.70795 | 48.41 | |
| 116** | Aplogranite | 285 | 10 | 0.87421 | 0.70745 | 41.32 | 76.75 |
| 26** | Quartz syenite | 182 | 256 | 0.71053 | 0.70643 | 26.94 | |
| 27** | Quartz syenite | 202 | 161 | 0.71350 | 0.70627 | 24.62 | |
| 44** | Quartz syenite | 93 | 765 | 0.70812 | 0.70742 | 40.91 | |
| 117** | Quartz syenite | 164 | 68 | 0.72074 | 0.70684 | 32.63 | |
| 22** | Syenite | 200 | 1197 | 0.70557 | 0.70461 | 1.00 | |
| 28** | Syenite | 125 | 78 | 0.71365 | 0.70442 | -1.70 | |
| 31** | Syenite | 143 | 300 | 0.70698 | 0.70424 | -4.28 | |
| 119** | Syenite | 123 | 344 | 0.70804 | 0.70598 | 20.49 | |
| 120** | Syenite | 169 | 584 | 0.70651 | 0.70484 | 4.35 | |
| 121** | Nephel-syenite | 193 | 749 | 0.70624 | 0.70476 | 3.11 | |
| 29-Dyke** | Nephel-syenite | 25 | 1043 | 0.70451 | 0.70437 | -2.35 | |
| 32-Dyke** | Nephel-syenite | 138 | 1457 | 0.70527 | 0.70472 | 2.66 | |
| 30** | Nepheline syenite | 149 | 640 | 0.70546 | 0.70412 | -5.93 | |
| | | | | Basement | | | |
| 23** | Gneiss | 33 | 376 | 0.71156 | 0.71105 | 92.50 | 73.50 |

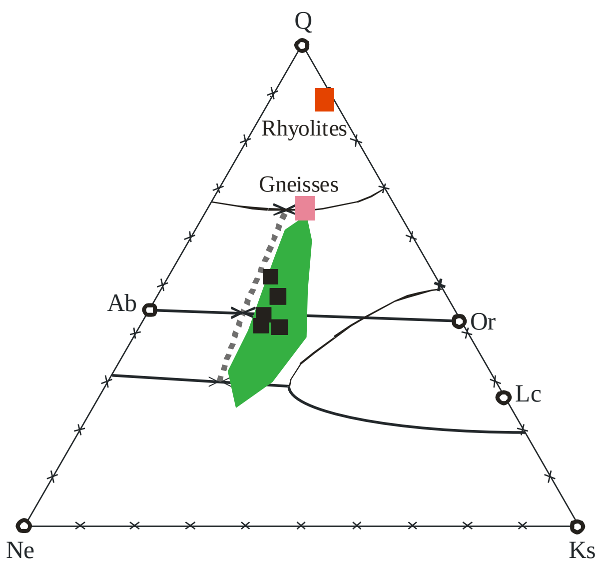


Fig. 15. Candelaria rock-types plotted into the Ne-Ks-$SiO_2$ system (Petrogeny's Residua System, after Hamilton & McKenzie, 1965, and Henderson, 1984). Phase boundaries are for $PH_2O$=1 kb and the thermal minima are linked by thermal valleys (broken lines) to the minimum on the Ab-Or join. Green field corresponds to the Velasco samples; full square represents Candelaria rocks.

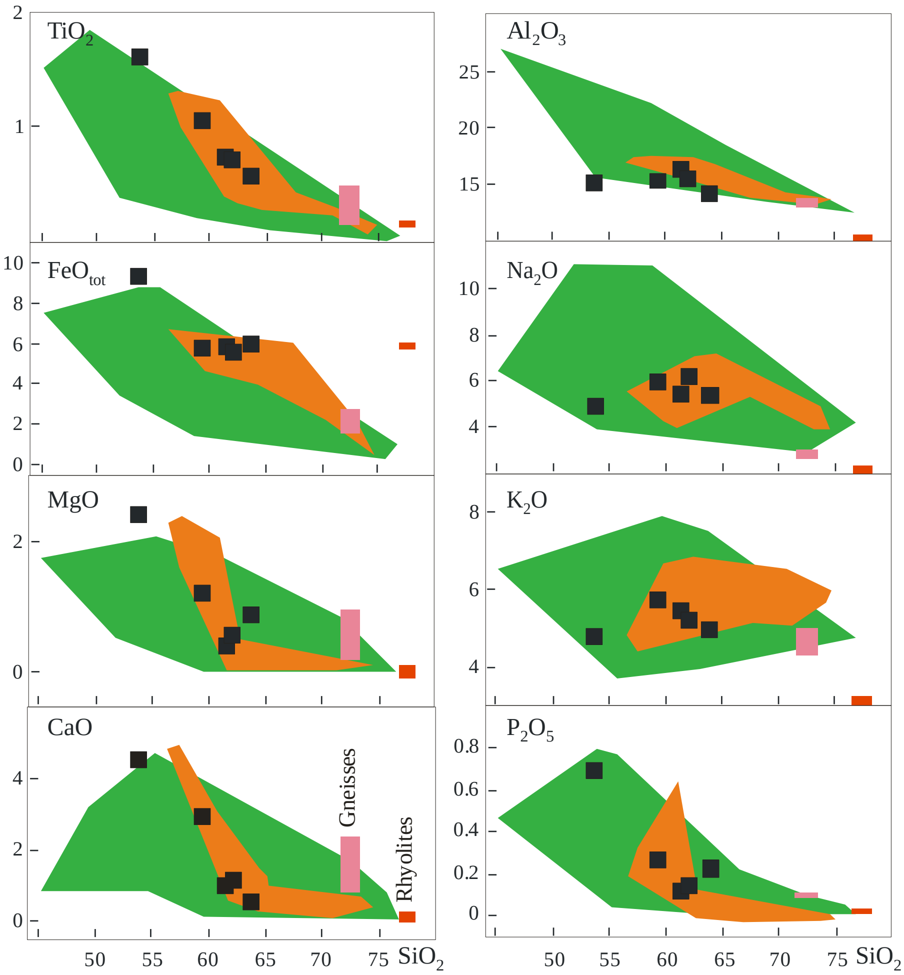


Fig. 16. Harker diagrams (major elements, wt%) for the Candelaria rock-types. For comparison the fields for the Velasco (green) and Ponta do Morro (orange) complexes are also shown as well as the fields for some basement rock-types (pink and red, respectively).

2000), is presently covered by the thick alluvium of the Pantanal Basin.

A few small hills are made of Neoproterozoic (?) ignimbrites, typical for their eutaxitic textures, and of quartz sandstones of the presumed Cretaceous Cerro Redondo Formation (Litherland *et al*., 1986) intruded by syenitic and trachytic dykes.

The sampled outcrops correspond to localities "Cerro Los Angeles" (PV-75A, PV-76A, B: Lat 16°45' 26"S, 59°03'31"W) and "Cerro Puntudo" (PV-77 and PV-77A: Lat 16°40'07" S, 59°02'38" W). The rock-types are microsyenites and trachytes: the former are hypersolvus varieties with mesoperthitic alkali feldspar±nepheline, and the trachytes show porphyritic texture with phenocrysts of sodic sanidine (mantled by anorthoclase)±clinopyroxene ±fluorite and microphenocrysts of alkali feldspar-opaques-biotite set in a hypohyaline to pilotaxitic groundmass made of glass and alkali feldspar, biotite, opaques, apatite and zircon microlites.

Metaluminous and peralkaline variants are present, i.e. A.I.=0.87-0.91 and 1.01-1.07, respectively (Table 10). The rock-types tend to plot near the trachytic thermal minimum in the Petrogeny's Residua System (Fig. 15), although some silica-oversaturated trachytes plot towards the rhyolitic minimum.

In the major and trace elements vs. silica Harker diagrams (Figs. 16 and 17), the Candelaria samples overlap the same fields of the Velasco complexes, and partially fit the fields of the samples from the Ponta do Morro Complex (cf. Sousa & Ruberti, 1996 and therein references).

Spidergrams relative to the incompatible elements (primitive mantle-normalized, according to Sun & McDonough, 1989) show that the nephel-syenites and trachytes have patterns similar to the corresponding rocks from the Velasco complexes and with the same strong Sr, P and Ti negative spikes common to the Precambrian country-rocks (Fig. 18A). On the contrary, the microsyenite displays Sr and P positive spikes and, on the whole, exhibits a behaviour quite similar to that of the "uncontaminated basalts" from the Poxoréu Igneous Province (cf. Fig. 5 of Gibson *et al.*, 1997).

Chondrite-normalized (Boynton, 1984) REE spidergrams highlight different LREE/HREE and MREE/HREE fractionation (Fig. 18B): $(La/Yb)_c$ and $(Sm/Yb)_c$ are 5.98 and 2.5, respectively, in microsyenite, and the ranges are of 15.2-35.3 and 3.0-5.9 in nephel-syenites and trachytes, respectively. Moreover, Eu/Eu* ratio is 0.91 in the microsyenite, while strong negative anomalies are apparent in the other rock-types (0.44-0.72), similar to the negative anomalies of the Precambrian gneisses (0.43; cf. Fig. 18B).

Sr-Nd isotopes

Twenty-one samples from the Velasco complexes have been analyzed for strontium and ten for strontium and neodymium isotopic compositions. The results were compared with the Sr isotopic data from Fletcher & Beddoe-Stephens (1987). In addition three samples from Candelaria, four basement rocks from the Guaporé craton and one gneiss from the Sunsas belt were also analysed (Table 11).

The geochronology of the Velasco complexes (cf. Litherland *et al.*, 1986) shows a high agreement between Rb/Sr and K/Ar ages, reaching uniformity around 140 Ma for all the outcrops. An attempt to recalculate the Rb/Sr ages, following the subdivision

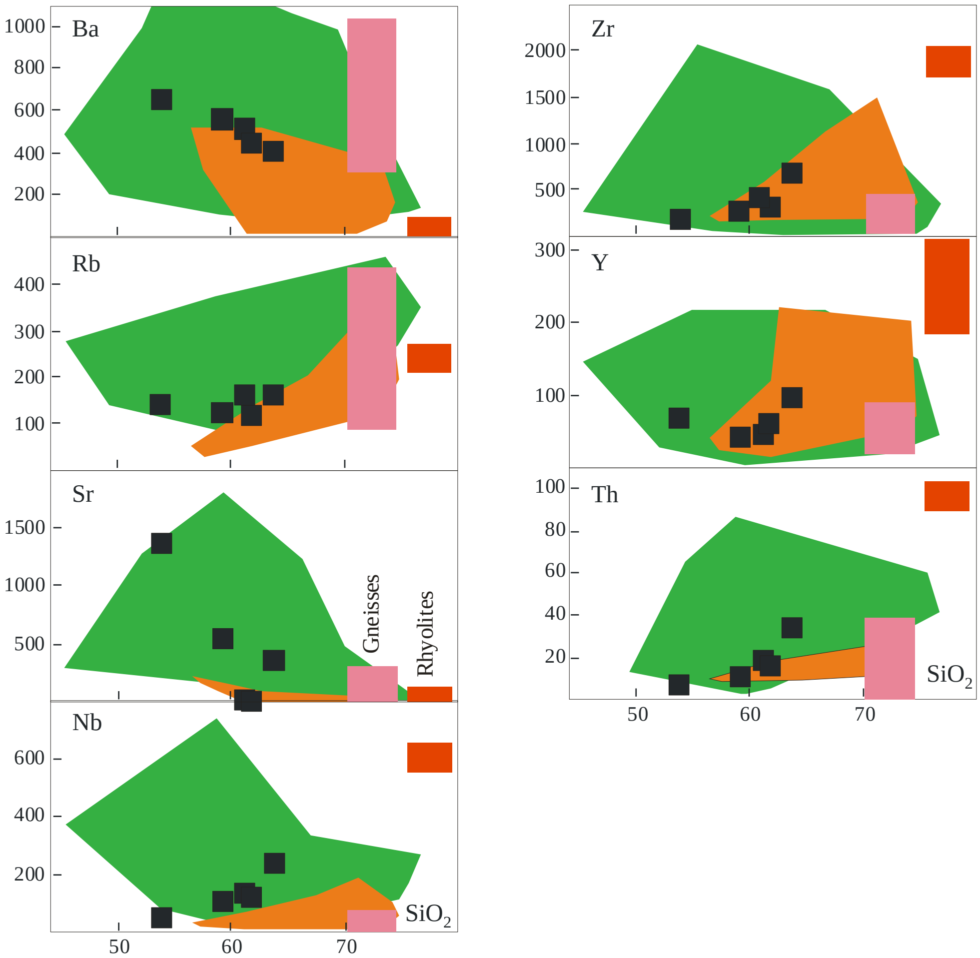


Fig. 17. Harker diagrams (trace elements, ppm) for the Candelaria rock-types. Fields as in Fig. 16.

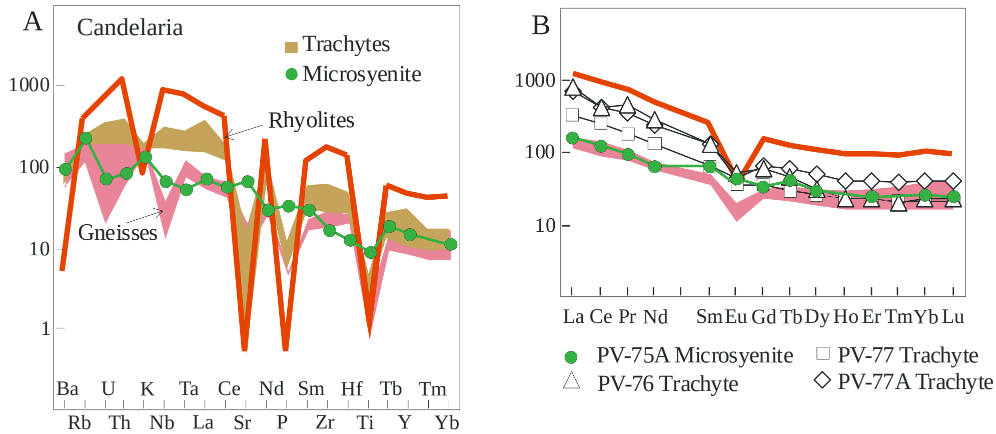


Fig. 18. A: Primitive mantle-normalized (Sun & McDonough (1989) trace element diagrams for the Candelaria rock-types. B. Chondrite-normalized (Boynton, 1984) REE profiles.

into silica-undersaturated and silica-overaturated rocks, gives errochrons of 139±3 and 140±1 Ma (Early Cretaceous), respectively (Figs. 19A, B), but with different initial $^{87}Sr/^{86}Sr$ ratios, i.e. 0.704452 and 0.706676, respectively.

The Candelaria samples seem to define an errorchron age of 79±8 Ma (Late Cretaceous) and an initial $^{87}Sr/^{86}Sr$ ratio=0.70474 (Fig. 19C), similar to the age determinations of uncontaminated lavas from the Poxoréu Igneous Province (83.4±2.4 Ma, initial $^{87}Sr/^{86}Sr$ ratio=0.70445±0.00004; cf. Gibson *et al.*, 1997). From a geochronological viewpoint, the Velasco complexes predate the tholeiitic flood basalts of the Paraná Basin (ca. 132 Ma), like those alkaline-carbonatitic occurrences from the Rio Apa and Amambay regions in Eastern Paraguay (ca. 140 Ma; cf. Comin-Chiaramonti *et al.*, 1997). On the other hand, the Candelaria magmatism displays an age that postdates the Paraná lavas, in conformity to numerous alkaline and alkaline-carbonatitic occurrences from southeastern Brazil (e.g. Poxoréu, Rio Verde-Iporá, Alto Paranaíba, Serra do Mar, Ponta Grossa Arch, Lages, Piratini; see other papers in this volume).

The isotopic data, as stressed by Fletcher & Beddoe-Stephens (1987), are strongly suggestive of silica-undersaturated suites that may be derived from a mantle not submitted to appreciable crustal contamination during the processes of fractionation and emplacement. On the contrary, the silica-oversaturated rocks-types appear to have suffered interactions with crustal materials (mixing and/or mingling), since the close spatial and temporal association precludes derivation from isotopically different mantle sources.

Attempts to calculate mixing of different magma types and the assimilation by magma bodies of the surrounding crystalline basement are represented in Fig. 20A: the plot of $SiO_2$ (wt%) vs. $^{87}Sr/^{86}Sr$ ($R_0$) ratios shows that almost 50-60% of the basement rocks are required to fit the quartz-bearing rock-types (mixing with migmatitic materials?). Alternatively, different parental liquids must be supposed, where, at any way, the high $R_0$ rocks may derived also from partial melting of crustal materials and mixing with more evolved liquids of appropriate isotopic composition.

The best fittings relative to assimilation-fractional crystallization processes (AFC, cf. DePaolo, 1985, 1988) are graphically illustrated in Fig. 20B: the different mixing lines reflect different bulk distribution for Sr between crystallizing minerals and the magma(s) at mass of assimilated basement/mass of the original magma=0.2.

In terms of ε time-integrated notations, the Velasco and Candelaria subsaturated rocks plot in the depleted quadrant (Fig. 21), and fit the most depleted alkaline and alkaline-carbonatite types from the southeastern Brazil, both Early and Late Cretaceous in age. In particular, the Candelaria microsyenite displays ε-values very close to those shown by the rock-types believed uncontaminated from the Poxoréu region (cf. Gibson *et al.*, 1997). Considering a depleted mantle source (cf. Comin-Chiaramonti *et al.*, 1997), both Velasco and Candelaria subsaturated petrographic types do not show any appreciable crustal contamination (i.e. << 1%; cf. curve 1 of Fig. 21), whereas the over-saturated rocks display up to 40% of mixing (or mingling) with the crystalline basement (curve 2 of Fig. 21, assuming a parent magma with εSr=-8 and εNd=+4).

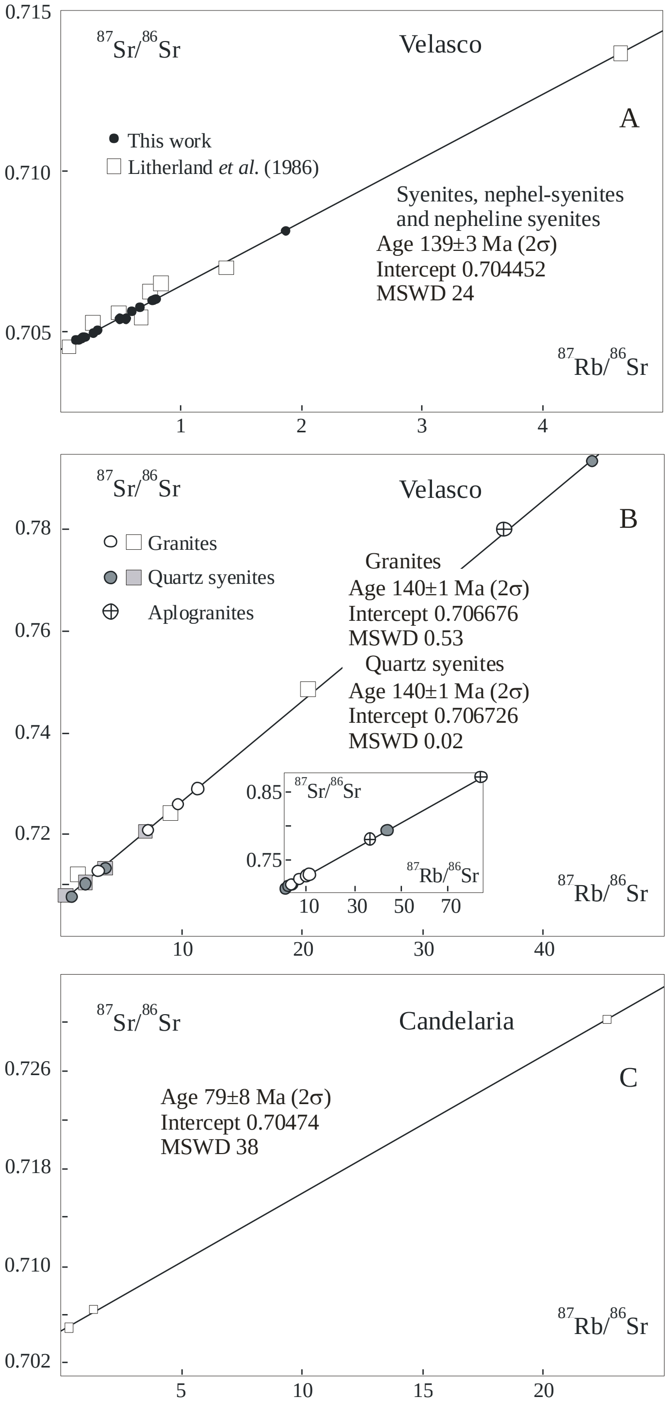


Fig. 19. $^{87}Rb/^{86}Sr$ vs. $^{87}Sr/^{86}Sr$ plot for the alkaline rocks from southeastern Bolivia. A: Velasco nepheline-normative syenitic rocks; B: Velasco quartz-normative rock-types (full circle, this work; square, Litherland *et al.*, 1986). **C**: Candelaria rock-types.

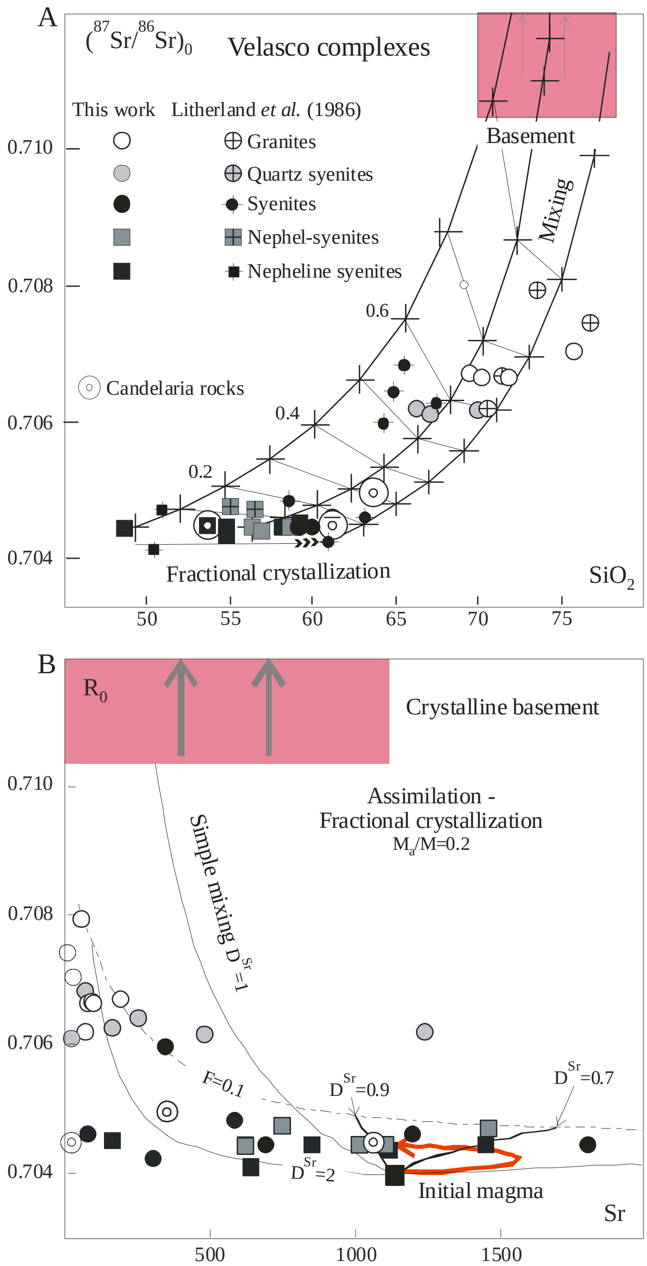


Fig. 20. A: $SiO_2$ vs. $^{87}Sr/^{86}Sr$ initial ratios for southeastern Bolivia alkaline rocks and mixing lines between supposed parental magmas ($SiO_2$=49 and 56 wt%) and crystalline basement ($SiO_2$=74 wt%); see text. B: Shifts in the $^{87}Sr/^{86}Sr$ initial ratios ($R_0$) and the Sr concentrations in a magma assimilating wall-rock (crystalline basement) and crystallizing (see text). $D^{Sr}$, Sr bulk distribution coefficient; F, ratio of the mass of the contaminated magma to that of the original magma; $M_a/M$, ratio of the mass of assimilated wall-rock and the mass of assimilated magma, respectively. The heavy red line represents plausible evolution for a magma moving through continental crust.

The apparent crustal contamination extends its effects to the model ages (depleted mantle, $T^{DM}$) which are 600±31 Ma and 1163±143 Ma for the Velasco undersaturated and oversaturated variants, respectively. On the contrary, the three values relative to the Candelaria samples are well constrained at 928±19 Ma, differing from the model ages inferred for the uncontaminated and contaminated varieties from the Poxoréu Igneous Province, i.e. 643±52 Ma and 1432±278 Ma, respectively. Notably, model ages of ca. 650 Ma were obtained for some alkaline complexes from Early Cretaceous Serra do Mar complexes, whereas model ages of ca. 750-1000 Ma were inferred for Late Cretaceous alkaline complexes from Alto Paranaíba, Iporá and Serra do Mar regions (cf. Comin-Chiaramonti *et al.*, 1999). This means that the supposed "impact zone of Trindade starting mantle plume head" (Gibson *et al.*,

1997) developed at about 250 km west of the Poxoréu Igneous Province (Late Cretaceous megaplume?) is very improbable.

## GEODYNAMIC CONSIDERATIONS

According to Litherland *et al.* (1986), the igneous and tectonical history of the Cretaceous is thought to be intimately related to the breakup of the South America-Africa plate and to the intrusions of the Velasco complexes predating this process. In contrast to this "Atlantic" model, Brown *et al.* (1984) interpreted the Velasco complexes as an evidence of a magmatism related to the back-arc zone of the Andean mobile belt, but a "subduction" signature is more less apparent with respect, e.g. to the coeval magmatism from Eastern Paraguay (inset of Fig. 21) for which intraplate rifting-related characteristics were inferred (Comin-Chiaramonti *et al.*, 1997, 1999).

The geochronological sequence (as also suggested by Litherland *et al.*, 1986) appears as follows: 1) ~140 Ma, uplift, faulting and intrusions of the Velasco complexes; 2) Albian-Aptian (?), deposition of (sediments) in intracontinental rift valleys; 3) Late Cretaceous, uplift, faulting and intrusion of the Cerro Manomó carbonatite; 4) ~80 Ma, Candelaria alkaline magmatism along the Mercedes rift.

Similar to other peripheral areas relative to the Paraná Basin l.s. (e.g. Namibia, Eastern Paraguay), southeastern Bolivia is characterized by intraplate Early- and Late Cretaceous K-alkaline magmatism associated with rifting processes.

The debate concerning the origin of these types of magmatism in and around the Paraná Basin with respect to the plate tectonics is still open and subject to controversy, and various models have been suggested invoking the presence of mantle plume/hot spots (Stefanick & Jurdy, 1984; Gibson *et al.*, 1997, 1999) or of shallow thermal anomalies (Holbrook & Kemelen, 1993). Smith & Lewis (1999) proposed an

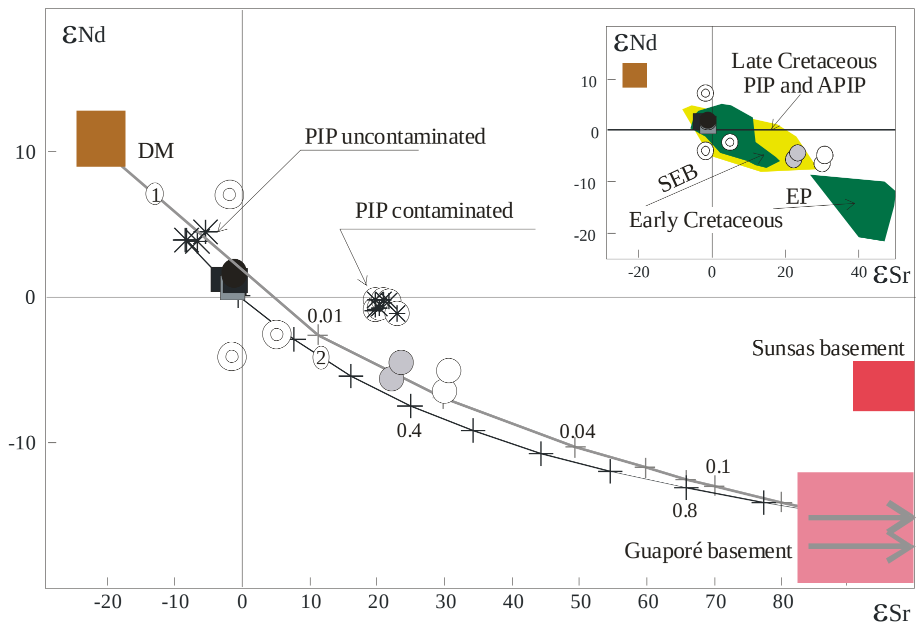


Fig. 21. Age integrated εSr vs. εNd diagram for the Velasco complexes (alkaline rocks and crystalline basement calculated at 140 Ma) and Candelaria samples (alkaline rocks and crystalline basement calculated at 84 Ma). For comparison the samples from the Poxoréu Igneous Province (PIP of Gibson *et al.*, 1997) are plotted. Symbols as in Fig. 20. DM, depleted mantle, as defined by Hart & Zindler (1987). Mixing curves are calculated with the following end-members: 1) Sr=12, $^{87}Sr/^{86}Sr$=0.70321, Nd=0.65, $^{143}Nd/^{144}Nd$=0.513151 vs. Sr=518, $^{87}Sr/^{86}Sr$=0.72509, Nd=70, $^{143}Nd/^{144}Nd$=0.51184; 2) Sr=628, $^{87}Sr/^{86}Sr$=0.704426, Nd=31.1, $^{143}Nd/^{144}Nd$=0.512815 vs. Sr=518, $^{87}Sr/^{86}Sr$=0.72509, Nd=70, $^{143}Nd/^{144}Nd$=0.51184. **Inset:** fields of the Early Cretaceous (EP: Eastern Paraguay; SEB, southeastern Brazil) and Late Cretaceous (PIP, Poxoréu Igneous Province; APIP, Alto Paranaíba Igneous Province; Gibson *et al.*, 1995, 1997).

alternative model: the forces acting on plates with different angular velocity and the presence of volatile-rich mantle sources (wet spots) would drive the rifting to occur parallel to the pre-existing N-S sutures in the South Atlantic areas. Intraplate alkaline and alkaline-carbonatite magmatism occurs where second order sutures (e.g. Alto Paranaíba, Rio Verde-Iporá, Poxoréu, Ponta Grossa-Moçâmedes Arch, Uruguay Lineament, Damara belt) intersect the axis of the major rifting, indicating erosion and cycling of continental mantle towards the ridge axis by local convenction taking the form of transverse rolls. Notably, in southern Brazil, the alkaline and alkaline-carbonatitic magmatism is concentrated in regions affected by positive geoid anomalies (Molina & Ussami, 1999; Ernesto *et al.*, 2002) that may refer to dense (and warm), very deep material. In this picture, the different westwards angular velocity of the lithospheric subplates, that are defined in South America by second order plate boundaries, may favour the decompression and melting of a variously metasomatized (wet spot) portion of the lithospheric mantle with different isotopic imprint and at different times. This scenario may explain the diffusion of the Late Cretaceous, and even of the Tertiary, magmatism in the whole Paraná-Angola-Namibia province, even up to the Eastern Paraguay where there is evidence of active rifting structures (cf. Comin-Chiaramonti *et al.*, 1999). In this case, the thermal perturbations may be channelled along the second order plate boundaries, as also pictured by the hypocenters of earthquakes in South America (cf. Berrocal & Fernandes, 1996).

## ACKNOWLEDGEMENTS

This research was supported by Brazilian (Fapesp, Proc. 01/10714-3) and Italian (CNR, 05 and 11 Committes, and COFIN 1998, MIUR 1998, 1999, 2000, 2001) agencies. The authors would like to thank the Department of Geological Sciences of the Catania University for the analytical facilities.

## REFERENCES

Almeida, F.F.M. (1983). Relações tectônicas das rochas alcalinas mesozóicas da região meridional da plataforma Sul-Americana. *Revista Brasileira de Geociências* **13**, 139-158.

Almeida, F.F.M., Brito Neves, B.B. & Carneiro, C.D.R. (2000). The origin and evolution of the South American Platform. *Earth-Science Reviews* **50,** 77-111.

Alvarenga, C.J.S. & Saes, G.S. (1992). Estratigrafia e sedimentologia do Proterozóico médio e superior da região sudoeste do cráton amazônico. *Revista Brasileira de Geociências* **22,** 493-499.

Andersen, D.J. & Lindsley, D.H. (1988). Internally consistent solution models for Fe-Mg-Mn-Ti oxides: Fe-Ti oxides. *American Mineralogist* **73,** 714-726.

Bailey, D.K. (1976). Applications of experiments to alkaline rocks. In: Bailey, D.K. & Macdonald, R. (eds.) *The evolution of crystalline rocks.* London: Academic Press, pp. 416-469.

Baker, B.H. (1987). Outline of the petrology of the Kenya rift alkaline province. In: Fitton, J.G. & Upton, B.G.J. (eds.) *Alkaline igneous rocks. Geological Society Special Publication* **30**, 293-311.

Berrocal, J. & Fernandes, C. (1996). Seismicity in Paraguay and neighbouring regions. In: Comin-Chiaramonti, P. & Gomes, C.B. (eds.) *Alkaline magmatism in central-eastern Paraguay. Relationships with coeval magmatism in Brazil.* São Paulo: Edusp/Fapesp, pp. 57-66.

Boynton, W.V. (1984). Cosmochemistry of the Rare Earth elements: meteorite studies. In: Henderson, P. (ed.) *Rare Earth Element geochemistry.* Amsterdam: Elsevier, pp. 63-114.

Brotzu, P., Gomes, C.B., Melluso, L., Morbidelli, L., Morra, V. & Ruberti, R. (1997). Petrogenesis of coexisting $SiO_2$-undersaturated to $SiO_2$-oversaturated felsic igneous rocks: the alkaline complex of Itatiaia, southeastern Brazil. *Lithos* **40**, 133-156.

Brown, G.C., Thorpe, R.S. & Webb, P.C. (1984). The geochemical characteristics of granitoids in contrasting arcs and comment on magma sources. *Journal of the Geological Society London* **141**, 4113-426.

Burragato, F., Maras, A. & Rossi, A. (1982). The sodalite group minerals in the volcanic areas of Latium. *Neues Jahrbuch Monatsheft,* pp. 433-445.

Burton, C.C.J. (1982). The geology and mineral resources of Cerro Manomó (with 6 maps 1:10000). In *Proyecto Precambrico. Fase II:*

*1980-1982.* Misión Geologica Británica/Servicio Geológico de Bolivia, Santa Cruz de la Sierra, Bolivia. Informe **19**, 29p.

Comin-Chiaramonti, P. & Gomes, C.B. (eds.) (1996). *Alkaline magmatism in central-eastern Paraguay. Relationships with coeval magmatism in Brazil.* São Paulo: Edusp-Fapesp, 464p.

Comin-Chiaramonti, P., Cundari, A., DeGraff, J., Gomes, C.B. & Piccirillo, E.M. (1999). Early Cretaceous magmatism from eastern Paraguay: geological, geophysical and geochemical constraints. *Journal of Geodynamics* **28**, 375-391.

Comin-Chiaramonti, P., Cundari, A., Piccirillo, E.M., Gomes, C.B., Castorina, F., Censi, P., De Min, A., Marzoli, A., Speziale, S. & Velázquez, V.F. (1997). Potassic and sodic igneous rocks from eastern Paraguay: their origin from the lithospheric mantle and genetic relationships with the associated Paraná flood tholeiites. *Journal of Petrology* **38,** 495-528.

Comin-Chiaramonti, P., Gomes, C.B., Censi, P., Gasparon, M., & Velázquez, V.F. (in this volume). Alkaline complexes from the Alto Paraguay Province at the border between Brazil (Mato Grosso do Sul state) and Paraguay.

Darbyshire, D.P.F. & Fletcher, C.J.N. (1979). A Mesozoic alkaline province in eastern Bolivia. *Geology* **7**, 545-548.

De La Roche, H., Leterrier, P., Grandclaude, P. & Marchal, E. (1980). A classification of volcanic and plutonic rocks using $R_1$-$R_2$ diagram and major element analyses. Its relationships with current nomenclature. *Chemical Geology* **29**, 183-210.

Del'Arco, J.O., Silva, R.H., Tarapanoff, I., Freire, F.A., Pereira, L.G.M., Souza, S.L., Luz, D.S., Palmeira, R.C.B. & Tassinari, C.C.G. (1982). *Geologia. Folha SE-21 – Corumbá e parte da Folha SE-20 – Cuiabá. Projeto Radambrasil, Levantamento de Recursos Naturais* **27**, 25-143.

DePaolo, D.J. (1985). Isotopic studies of processes in mafic magma chambers. 1. The Kiglapait intrusion, Labrador. *Journal of Petrology* **26,** 925-951.

DePaolo, D.J. (1988). Neodymium isotope geochemistry. An introduction. *Minerals and Rocks* **20**, 1-187.

Ernesto, M., Marques, L.S., Piccirillo, E.M., Molina, E.C., Ussami, N., Comin-Chiaramonti, P. & Bellieni, G. (2002). Paraná magmatic province - Tristan da Cunha plume system: fixed versus mobile plume, petrogenetic considerations and alternative heat sources. *Journal of Volcanology and Geothermal Research* **118**, 15-36.

Fletcher, C.J.N. (1979). La geología y potential de minerales de la Provincia Alcalina de Velasco y Cerro Manomó. Proyecto mineral de oriente Boliviano. In *Proyecto Precambrico. Fase I: 1976-1979.* Misión Geologica Británica/Servicio Geológico de Bolivia, Santa Cruz de la Sierra, Bolivia. Informe **8**, 129p.

Fletcher, C.J.N. & Beddoe-Stephens, B. (1987). The petrology, chemistry and crystallization history of the Velasco alkaline province, eastern Bolivia. In: Fitton, J.G. & Upton, B.G.J. (eds.) *Alkaline igneous rocks. Geological Society Special Publication* **30**, 403-413.

Fletcher, C.J.N., Appleton, J.D., Webb, B.C. & Basham, I.R. (1981). Mineralization in the Cerro Manomó carbonatite complex, eastern Bolivia. *Transaction Institution of Mining and Metallurgy, Section B, Applied Earth Sciences* **90**, B37-50.

Foland, K.A., Landoll, J.D., Henderson, C.M.B. & Chen, J-F. (1993). Formation of cogenetic quartz and nepheline syenites. *Geochimica et Cosmochimica Acta* **57**, 697-704.

Geraldes, M.C., Teixeira, W. & Van Schmus, W.R. (2000). Isotopic and chemical evidence for three accretionary magmatic arcs (1.79-1.42 Ga) in the SW Amazon craton, Mato Grosso State, Brazil. *Revista Brasileira de Geociências* **30,** 99-101.

Geraldes, M.C., Van Schmus, W.R., Condie, K.C., Bell, S., Teixeira, W. & Babinski, M. (2001). Proterozoic geologic evolution of the SW part of the Amazonian craton in Mato Grosso State, Brazil. *Precambrian Research* **111**, 91-128.

Gibson, S.A., Thompson, R.N., Leonardos, O.H., Dickin, A.P. & Mitchell, J.C. (1995). The Late Cretaceous impact of the Trindade mantle plume: evidence from large-volume, mafic potassic magmatism in SE Brazil. *Journal of Petrology* **36,** 189-229.

Gibson, S.A., Thompson, R.N., Leonardos, O.H., Dickin, A.P. & Mitchell, J.C. (1999). The limited extent of plume-lithosphere interactions during continental flood-basalt genesis: geochemical evidence frm Cretaceous magmatism in southern Brazil. *Contributions to Mineralogy and Petrology* **137**, 147-169.

Gibson, S.A., Thompson, R.N., Weska, R.K., Dickin, A.P. & Leonardos, O.H. (1997). Late Cretaceous rift-related upwelling and melting of the Trindade starting mantle plume head beneath western Brazil. *Contributions to Mineralogy and Petrology* **126,** 303-314.

Giret, A., Bonin, B. & Leger, J.M. (1980). Amphibole compositional trends in oversaturated and undersaturated alkaline plutonic ring-complexes. *Canadian Mineralogist* **18,** 481-495.

Gittings, J. & Harmer, R.E. (1997). What is ferrocarbonatite? A revised classification. *Journal of African Earth Sciences* **25,** 159-168.

Green, T.H. (1995). Significance of Nb/Ta as an indicator of geochemical processes in the crust-mantle system. *Chemical Geological* **120**, 347-359.

Hamilton, D.L. (1961). Nephelines as crystallization temperature indicators. *Journal of Geology* **69,** 321-329.

Hamilton, D.L. & McKenzie, W.S. (1965). Nepheline solid solutions in the system $NaAlSiO_4$–$KAlSiO_4$–$SiO_2$. *Journal of Petrology* **1**, 1-56.

Harris, N.B.W., Duyverman, H.J. & Almond, D.C. (1983). The trace element and isotope geochemistry of the Sabaloka Igneous Complex, Sudan. *Journal of Geological Society of London* **140,** 245-256.

Hart, S. & Zindler, A. (1989). Constraints on the nature and development of chemical heterogeneities in the mantle. In: Peltier W.R. (ed.) *Mantle convection. Plate tectonics and global geodynamics.* New York: Gordon & Breach Science Publishers, pp. 261-388.

Hawkins, M.P. (1982). The geology and mineral potential of the Manomó area. Map at 1:250000. In *Proyecto Precambrico. Fase II: 1980-1982.* Misión Geologica Británica/Servicio Geológico de Bolivia, Santa Cruz de la Sierra, Bolivia. Informe **13**, 15p.

Hendersdon, C.M.B. (1984). Feldspathoid stabilities and phase inversion - A review. In: Brown, W.L. (ed.) *Feldspars and feldspathoids; Structures, properties and occurrences.* London: Reidel, pp. 471-499.

Holbrook, W.S. & Kelemen, P.B. (1993). Large igneous province in the US Atlantic margin and implications for magmatism during continental breakup. *Nature* **364,** 433-436.

Jaillard, E., Hérail, G., Monfret, T. & Wörner, G. (2002). Andean geodynamics: main issues and contributions from the 4th ISAG, Göttingen. *Tectonophysics* **345**, 1-15.

Kato, Y., Ohta, I., Tsumenatsu, T., Watanabe, Y., Isozaki Y., Maruyama, S. & Imai, N. (1998). Rare earth element variations in mid-Archean banded iron formations: implications for the chemistry of ocean and continent and plate tectonics. *Geochimica et Cosmochimica Acta* **62,** 3475-3497.

Klein, C. & Ladeira, E.A. (2002). Petrography and geochemistry of the least altered banded iron-formation of archean Carajás Formation, northern Brazil. *Economic Geology* **97**, 643-651.

Kudo, A.M. & Weill, D.F. (1970). An igneous plagioclase geothermometer. *Contributions to Mineralogy and Petrology* **26**, 52-65.

Le Maitre, R.W. (1989). *A classification of igneous rocks and glossary of terms*. Oxford: Blackwell Scientific Publications, 193p.

Leake, B.E. (1978). Nomenclature of amphiboles. *Mineralogical Magazine* **42**, 533-565.

Leite, J.A.D. & Saes, G.S. (2000). Geology of the southern Amazon craton in southwestern Mato Grosso, Brazil: a review. *Revista Brasileira de Geociências* **30,** 91-94.

Litherland, M., & Bloomfield, K. (1981). The Proterozoic history of eastern Bolivia. *Precambrian Research* **15**, 157-179.

Litherland, M., Annels, R.N., Appleton, J.D., Berrange, J.P., Bloomfield, K., Burton, C.C., Darbyshire, D.P.F., Fletcher, C.J.N., Hawkins, M.P., Klink, B.A., Llanos, A., Mitchell, W.I., O'Connor, E.A., Pitfield, P.E., Power, G. & Webb, B.C. (1986). The geology and mineral resources of the Bolivian Precambrian Shield. *Keyworth Overseas Memoir* **9,** *British Geological Survey,* 153p.

Litherland, M., Annels, R.N., Darbyshire, D.P.F., Fletcher, C.J.N., Hawkins, M.P., Klink, B.A., Mitchell, W.I., O'Connor, E.A., Pitfield, P.E., Power, G. & Webb, B.C. (1989). The Proterozoic of eastern Bolivia and its relationship with the Andean Mobile Belt. *Precambrian Research* **43,** 157-174.

Mathez, E.A. (1973). Refinement of the Kudo-Weill plagioclase thermometer and its implication to basaltic rocks. *Contributions to Mineralogy and Petrology* **41**, 61-72.

Mitchell, R.H. & Platt, R.G. (1978). Mafic mineralogy of ferroaugite syenite from the Coldwell alkaline complex, Ontaro, Canada. *Journal of Petrology* **19**, 627-651.

Mitchell, R.H. & Platt, R.G. (1982). Mineralogy and petrology of nepheline syenites from the Coldwell alkaline complex, Ontaro, Canada. *Journal of Petrology* **23**, 186-214.

Molina, E.C. & Ussami, N. (1999). The geoid in southern Brazil and adjacent regions: new constraints on density distribution and thermal state of lithosphere. *Journal of Geodynamics* **28**, 321-340.

Morimoto, N. (1988). Nomenclature of pyroxenes. *Mineralogical Magazine* **52,** 535-550.

Piotrowski, J.M. & Edgar, A.D. (1970). Melting relations in undersaturated alkaline rocks from Greenland, Africa and Canada. *Meddelelser om Grönland* **181/9,** 61-89.

Pitfield, P.E.J. (1979). The geology and mineral potential of the Las Petas-San Matias area. In *Proyecto Precambrico. Fase I: 1976-1979.* Misión Geologica Británica/Servicio Geológico de Bolivia, Santa Cruz de la Sierra, Bolivia. Informe **4**, 26p.

Platt, R.G. & Woolley, A.R. (1986). The mafic mineralogy of the peralkaline syenites and granites of the Mulanje complex, Malawi.

*Mineralogical Magazine* **50**, 85-99.

Sadowski, G.R. & Bettencourt, J.S. (1996). Mesoproterozoic tectonic correlations between eastern Laurentia and the western border of the Amazon Craton. *Precambrian Research* **76**, 213-227.

Scaillet, B. & MacDonald, R. (2001). Phase relations of peralkaline silicic magmas and petrogenetic implications. *Journal of Petrology* **42**, 825-845.

Scott, P.W. (1976). Crystallization trends of pyroxenes from the alkaline volcanic rocks of Tenerife, Canary Islands. *Mineralogical Magazine* **40**, 805-816.

Seck, H.A. (1971). Koexistierende alkalifeldspate und plagioclase in the system $NaAlSi_3O_8$-$KalSi_3O_8$-$CaAl_3Si_2O_8$-$H_2O$ bei temperaturen von 650°C bis 900°C. *Neues Jahrbuch für Mineralogie Abhandlungen* **115**, 315-395.

Smith, A.D. & Lewis, C. (1999). The planet beyond the plume hypothesis. *Earth-Science Reviews* **48**, 135-182.

Sousa, F.J. (1991) Revisão da geologia da porção SW do estado de Mato Grosso, S do estado de Rondônia e do leste da Bolívia. *Revista Brasileira de Geociências* **21**, 74-81.

Sousa, M.Z.A. & Ruberti, E. (1996). Caracterização petrográfica e geocronológica do complexo intrusivo Ponta do Morro, MT. *XXXIX Congresso Brasileiro de Geologia, Salvador, Anais* **2**, 80-82.

Spencer, K.J. & Lindsley, D.H. (1981). A solution model for coexisting iron-titanium oxides. *American Mineralogist* **66,** 1189-1201.

Stefanick, M. & Jurdy, D.M. (1984). The distribution of hot spots. *Journal of Geophysical Research* **98**, 9919-9925.

Sun, S.S. & McDonough, W.F. (1989). Chemical and isotopic systematics of oceanic basalts. In: Saunders, D. & Norry, M.J. (eds.) *Magmatism in the ocean basins. Geological Society of London, SpecialPublication* **42**, 313-345.

Taylor, S.R. & McLennan, S.M. (1985). *The continental crust: its composition and evolution*. Oxford: Blackwell, 350p.

Teixeira, W. & Tassinari, C.C.G. (1984). Caracterização geocronológica da Província Rondoniana e suas implicações geotectônicas. *II Simpósio Amazônico, Manaus, Anais*, pp. 87-100.

Teixeira, W., Tassinari, C.C.G., Cordani, U.G. & Kawashita, K. (1989). A review of the geochronology of the Amazonian Craton: tectonic implications. *Precambrian Research* **42,** 213-227.

Tohver, E., Van der Pluijim, B.A., Van der Voo, R., Rizzotto, B. & Scandolara, J.E. (2002). Paleogeography of the Amazon craton at 1.2 Ga: early Grenvillian collision with the Llano segment of Laurentia. *Earth and Planetary Science Letters* **199**, 185-200.

Trendall, A. (2000). The significance of banded iron formations (BIF) in the Precambrian stratigraphic record. *Geoscientist* 1**0,** 4-7.

Trendall, A.F. & Blockley, J.G. (1970). The iron formations of the Precambrian Hamersley Group, Western Australia: with special reference to the associated crocidolite. *Western Australia Geological Survey Bulletin* **119**, 336-338.

Woolley, A.R. & Platt, R.G. (1986). The mineralogy of nepheline syenite complexes from the northern part of the Chilwa Province, Malawi. *Mineralogical Magazine* **50**, 597-610.

*Mesozoic to Cenozoic Alkaline Magmatism in the Brazilian Platform*
*Comin-Chiaramonti, P. & Gomes, C.B. (eds.)*
*Edusp/Fapesp, São Paulo, pp. 159-211, 2005*

# PETROLOGY OF LATE JURASSIC-EARLY CRETACEOUS TUSAQUILLAS AND ABRA LAITE-AGUILAR PLUTONIC COMPLEXES (CENTRAL ANDES, 23°05'S-66°05'W): A COMPARISON WITH RIFT-RELATED MAGMATISM OF NW ARGENTINA AND E BOLIVIA

*C. Cristiani, M. Matteini, R. Mazzuoli, R. Omarini and I.M. Villa*

*The Late Jurassic-Early Cretaceous Tusaquillas and the Abra Laite-Aguilar Plutonic Complexes represent the most extensive intrusive bodies belonging to the rift-related magmatism developed in NW Argentina from Upper Jurassic to Lower Eocene. Both complexes are characterized by rocks of a wide compositional spectrum, ranging from gabbro and diorite to syenogranite and monzogranite. Geochemical and isotopic data obtained on from samples of the two complexes allowed to distinguish rocks with: 1) basic composition ($SiO_2$=45-52 wt%), low HFSE and REE contents, low initial $^{87}Sr/^{86}Sr$ ratio ($R_0$=0.703198-0.705868) and high $\varepsilon^t Nd$ (3.82 to 1.51); 2) felsic compositions ($SiO_2$=70-77 wt%, low HFSE and REE, high $R_0$ (0.708677-0.722668) and low $\varepsilon^t Nd$ (-3.85 to -1.77); 3) intermediate features, i.e. $SiO_2$=53-69 wt%, $R_0$=0.703303-0.713121, $\varepsilon^t Nd$ 2.10 to -4.97. On the whole, the data suggest that the basic rocks could have been derived from a mantle source with OIB-like signature, whereas the granitic rocks could have been generated by partial melting of a radiogenic crust. Geochemical and isotopic characteristics of intermediate rocks suggest complex interactions (FC, AFC and mixing processes) between mantle derived magmas and crustal materials. In order to have a more complete scenario of the magmatic events which affected the south-central part of South America in the Jurassic-Cretaceous times, the Tusaquillas and the Abra Laite-Aguilar Plutonic Complexes have been compared with coeval NW Argentina (Rangel and Hornillos) and E Bolivia (Velasco) magmatic provinces. In view of the comparative data, we tentatively propose that the E Bolivia and NW Argentina magmatic provinces could be related to the same regional petrogenetic event, probably linked with the extensional tectonics that affected the western Gondwana at pre-drift times.*

## INTRODUCTION

The geodynamic evolution of the Andean margin since Early Mesozoic to present time was marked by a complex interaction of oceanic plates (Aluk-Phoenix, Farallon and Pacific) with the South American continental plate (Zonenshayn *et al.*, 1984; Jaillard *et al.*, 1990, 2000; Scheuber *et al.*, 1994). In the Jurassic times, the evolution of the western border of South America has been characterized by the presence of an extensive arc magmatism (Fig. 1A) related to the subduction of the paleo-pacific Aluk (Phoenix) plate, beneath the South American plate. At the same time, the southeastern sector of Bolivia and northwestern Argentina were affected by an extensive igneous

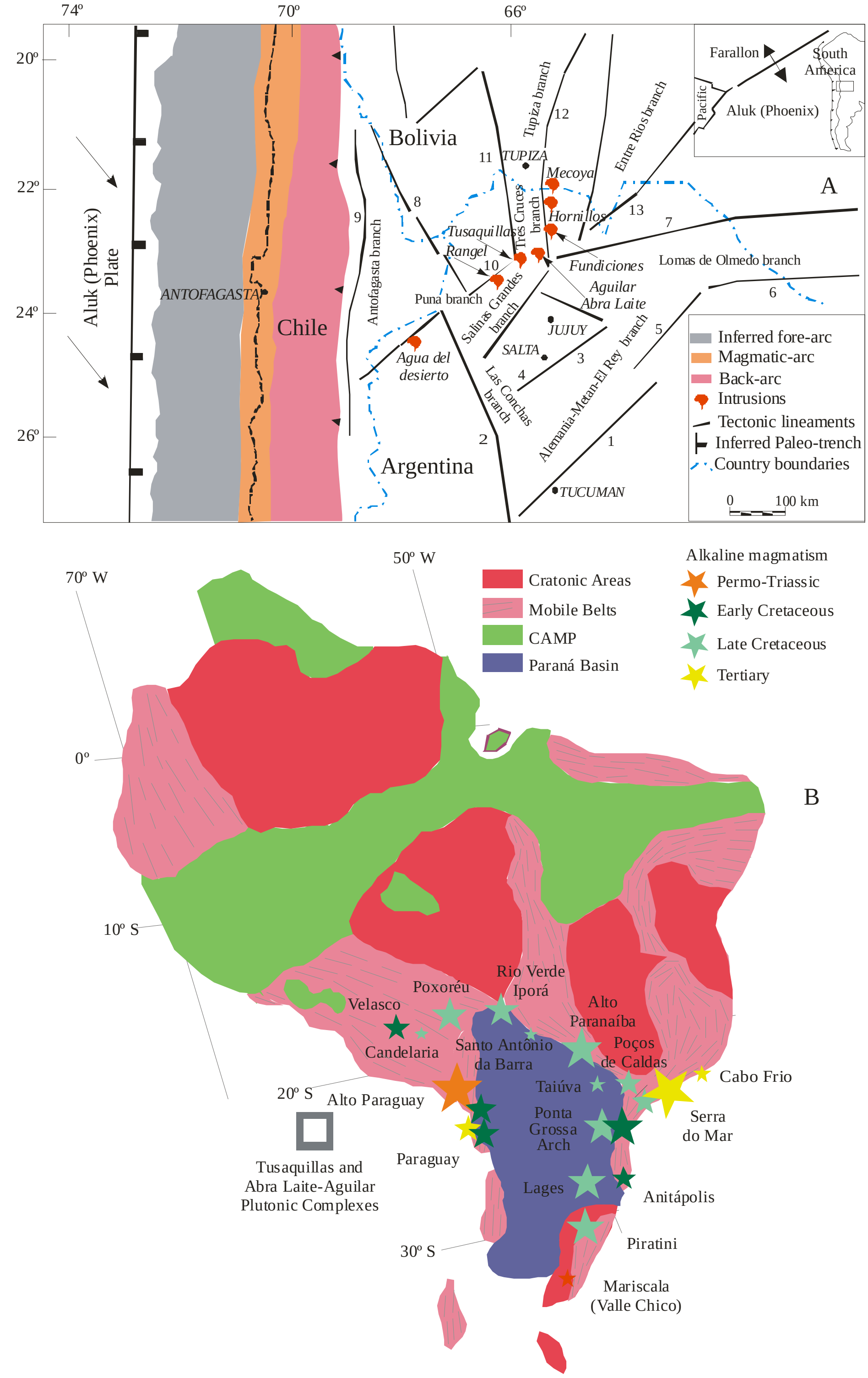


Fig. 1. A) Sketch-map showing the regional tectonic setting of the alkaline-subalkaline magmatism in the NW Argentina, Central Andes. The plate tectonic configuration for the Upper Jurassic time (c. 150 Ma) is from Zonenshayn *et al.* (1984) and Scheuber *et al.* (1994); the back-arc basin configuration is taken from Printz *et al.* (1994) and the paleo-tectonic patterns in the foreland region are modified after Marquillas & Salfity (1988). Reference numbers in figure, main faults: 1) Aconquija, 2) Transpampean, 3) Isonza, 4) El Toro, 5) Los Blancos, 6) Quirquincho, 7) Tomasito, 8) Calama, 9) Domeycko, 10) Cobres-Salinas Grandes, 11) San Pablo, 12) El Condor, 13) Michicola. B) Distribution of the post-Paleozoic alkaline magmatism (stars roughly proportional to the erupted volumes) in and around the Paraná Basin in the South American Platform (after Gomes & Comin-Chiaramonti, in this volume). CAMP (Central Atlantic Magmatic Province), mobile belts and cratonic areas, as defined by De Min *et al.* (2003) and by Iacumin *et al.* (2003) and therein references. The location of the Tusaquillas and Abra Laite-Aguilar Plutonic Complexes is also indicated.

activity, which produced abundant alkaline-subalkaline plutonic and volcanic rocks (e.g. Galliski & Viramonte, 1988; Rubiolo, 1992; Viramonte *et al*., 1999; Menegatti, 2001; Cristiani, 2004; Comin-Chiaramonti *et al*., in this volume). The magmatic events roughly span between 156 and 144 Ma, i.e. between the CAMP (Central Atlantic Magmatic Province, ~200 Ma) and the Paraná Basin magmatism (~130 Ma; De Min *et al*., 2003; Iacumin *et al*., 2003), at pre-drift times (cf. Fig. 1B). Notably, pre-drift magmatism affected also other extensional (rifting) areas of the South America plate, e.g. alkaline-carbonatitic complexes and dykes from northeastern Paraguay (138-140 Ma; Antonini *et al*., in this volume) and anatectic dacitic flows from Jaguarão, Rio Grande do Sul (143-144 Ma; Comin-Chiaramonti, 2000).

The northwestern Argentina and eastern Bolivia magmatism was linked to the formation and evolution of a continental rift system in a back-arc position with respect to the Jurassic-Cretaceous volcanic arc (Fig. 1A). The rifting, extending from southeastern Bolivia up to central Argentina with a roughly N-S trend, constitutes a geological structure of crucial importance in the evolution of the Andean Cordillera. There is no agreement on the rift origin and evolution among the workers who studied this Andean sector. Galliski & Viramonte (1988) interpreted the magmatism as being related to the back-arc zone of Jurassic subduction of the Aluk plate under the South America continent. Alternatively, Cristiani *et al*. (2000) associated the Upper Jurassic-Cretaceous magmatism in NW Argentina with the Gondwana break-up.

The intrusive rocks related to the rift system are mainly set in central and southeastern Bolivia (Velasco and Apopaya region) and NW Argentina (Puna Plateau and Eastern Cordillera). They show a considerable range in composition and geochemical affinity, being characterized by peralkaline, metaluminous and peraluminous signatures (e.g. Avila Salinas, 1986; Fletcher & Beddoe Stephens, 1987; Viramonte *et al*., 1999; Cristiani *et al*., 2000, 2002, 2003; Cristiani, 2004; Comin-Chiaramonti *et al*., in this volume and references therein). In this paper we present new petrological data on the Abra Laite-Aguilar (AL-APC) and Tusaquillas Plutonic Complexes (TPC), NW Argentina, attempting to define the potential magmatic sources responsible for the generation of magmas in the Jurassic-Cretaceous time in this sector of the eastern Central Andes. Our data are compared with the coeval intrusions outcropping in NW Argentina (Rangel and Hornillos) and in E Bolivia (Velasco), with the purpose of having a general view of the magmatism linked to the rift formation. The bulk of the data might give new insight on the petrogenesis and evolution of the rift-related magmatism in Late Jurassic-Early Cretaceous time.

## ANALYTICAL METHODS

Mineral compositions have been obtained by Scansion Electron Microprobe (SEM) at the Earth Sciences Department, Pisa University, following the methods listed in Marianelli & Sbrana (1998).

Major and trace elements ($SiO_2$, $TiO_2$, $Al_2O_3$, $Fe_2O_3$, MnO, CaO, $K_2O$, $P_2O_5$, La, Ce, Rb, Y, Zr, Nb, Ba, Sr, Ni, Cr, V, Co) analyses have been carried out by XRF techniques; MgO and $Na_2O$ were determinated by atomic absorption spectrometry whereas the $Fe^{2+}$ by titration methods. Measurement conditions and standards reproducibility are reported in Tamponi *et al*. (2003).

REE, Y, Th, U, Hf and Ta contents have been obtained by ICP-MS at the Geochemistry Laboratory of the Earth Science Department of the Monash University, Melbourne, Australia (measurement conditions and standards reproducibility are given in Frick *et al*., 2001).

Sr and Nd isotopic ratios for TPC samples have been measured by Finningan MAT 262V multicollector spectrometer. Reproducibility of $^{87}Sr/^{86}Sr$ ratio for NBS987 standard has been 0.710330±0.000016 ($2\sigma$, n=10); reproducibility of $^{143}Nd/^{144}Nd$ ratio for La Jolla standard has been 0.511860±0.000020. Rb and Sr concentrations for TPC samples have been determined by isotopic dilution using a VG-ISOMASS 54E monocollector spectrometer (IGGI-CNR, Pisa, Italy).

Sr and Nd isotopic ratios and Rb, Sr, Sm, Nd concentrations for AL-APC samples have been measured at the Institut für Geologie of Bern University, Switzerland. Sr isotopic compositions have been obtained by VG 354 monocollector spectrometer; Rb, Sm, Nd isotopic ratio have been measured by Nu multicollector ICP spectrometer. External reproducibility corresponds to ±37 ppm for

$^{143}Nd/^{144}Nd$ ratio and ±31 ppm for $^{145}Nd/^{144}Nd$ ratio (standard in-house Johnson-Matthey).

## GENERAL GEOLOGICAL REMARKS

During the Sinemurian-Pleinsbachian times, as a result of the subduction processes of the Aluk plate under the South American plate, an important orogenic magmatism began to be active on the western continental margin of South America. This magmatic activity was marked by the emplacement of subalkaline plutonic and volcanic rocks (Mpodozis & Ramos, 1990; Romeuf *et al*., 1995; Jaillard *et al*., 2000), presently outcropping in northern Chile (Fig. 1A). In close association with the magmatic arc, a fore-arc and a back-arc zone developed at the same time (Fig. 1A). The fore-arc realm is actually unknown because of the erosion due to the subduction processes from Jurassic to present time (Rutland, 1971; Ramos, 2000). The back-arc basin developed to the East of the magmatic arc as a consequence of extensional stress regime and was the place of intense deposition of continental-marine sediments outcropping nowadays in the Longitudinal Valley of Chile (Gröschke *et al*., 1988; Prinz *et al*., 1994; Jaillard *et al*., 2000; cf. Fig.1A).

To the East of the back-arc basin, from southern Bolivia to central Argentina, in the Early Jurassic-Cretaceous times, the structural framework was dominated by a general doming preceding the rift formation and by an intricate pattern of extensional faults. In this stage, anorogenic igneous complexes were emplaced along the most extensive tectonic structures with a rough NNE strike (i.e. Cobres Salinas Grandes fault, Fig. 1A). In the NW Argentina this magmatic activity includes Agua del Desierto, Rangel, Tusaquillas, Abra Laite, Aguilar, Fundiciones, Hornillos and Mecoya plutons, which are located in the Puna Plateau and in the Eastern Cordillera, ~450 km to the East of the volcanic arc. The plutonic complexes intruded the Late Precambrian-Lower Paleozoic metasedimentary sequences (Lanfranco, 1972; Rubiolo, 1992; Menegatti, 2001; Cristiani, 2004). During the subsequent thermal subsidence processes, alkaline volcanism and continental red-bed and marine carbonate sedimentation (Salta Group of Marquillas & Salfity, 1988) characterized the sin-rift (120-80 Ma) and post-rift (70-60 Ma) stages.

The evolution of the rift system was controlled by proto-lineaments (cf. Fig. 1A) reactivated during the Araucana (Late Jurassic) and Miriano (Lower Cretaceous) tectonic events. The reconstruction of tectonic lineaments delimiting the graben structures shows an asymmetrical geometry that permits to divide the proto-rift in four branches: Tres Cruces-Tupiza, Lomas de Olmedo, Alemania-Metan-El Rey and Puna. In the North, the Tres Cruces-Tupiza branch extends to southern Bolivia (Sempere *et al*., 2002), whereas in the South the Alemania-Metan-El Rey branch is connected with the Cordoba-San Luis proto-grabens, developed in the central sector of Argentina (Rossello & Mazetic, 1999). To the West, the Puna branch is linked to the NS Antofagasta branch and to the East with the Salinas-Grandes-Tres Cruces and the Las Conchas branches, respectively.

## THE TUSAQUILLAS COMPLEX

The Tusaquillas Plutonic Complex (TPC; 23°05'-23°25'S and 66°05'-65°55'W) is one of the most extensive intrusive body belonging to the Upper Jurassic-Lower Cretaceous magmatic activity in NW Argentina; it is located about 100 km northeast of San Antonio de Los Cobres village (Fig. 2A). The pluton forms a prominent and isolated structural block covering an area of about 200 $km^2$. It consists of a main central body of felsic composition (Tusaquillas batholith: Zappettini, 1998; Cristiani *et al*., 2002; Cristiani, 2004) and of three marginal stocks of mafic-intermediate composition (Castro Tolay stocks: Cristiani *et al*., 2000), outcropping at the southwestern and northwestern margins of the main body. Available Rb-Sr dates for the TPC give a range of ages between 140±1 and 144±2 Ma for the Tusaquillas Batholith and from 152±2 to 144±1 Ma for the marginal stocks (Cristiani, 2004). The host-rocks of the TPC are represented by a thick succession of marine sediments and minor volcanic rocks of the Ordovician Santa Victoria Group (Turner, 1960). The thermometamorphic contact aureole is generally very limited. The TPC is bordered at the western side by the Tusaquillas back-thrust and at the eastern side by the Salinas Grandes thrust (Fig. 2A). According to the geophysical data (Gangui & Götze, 1996), its western slope is steep and fault-controlled, whereas

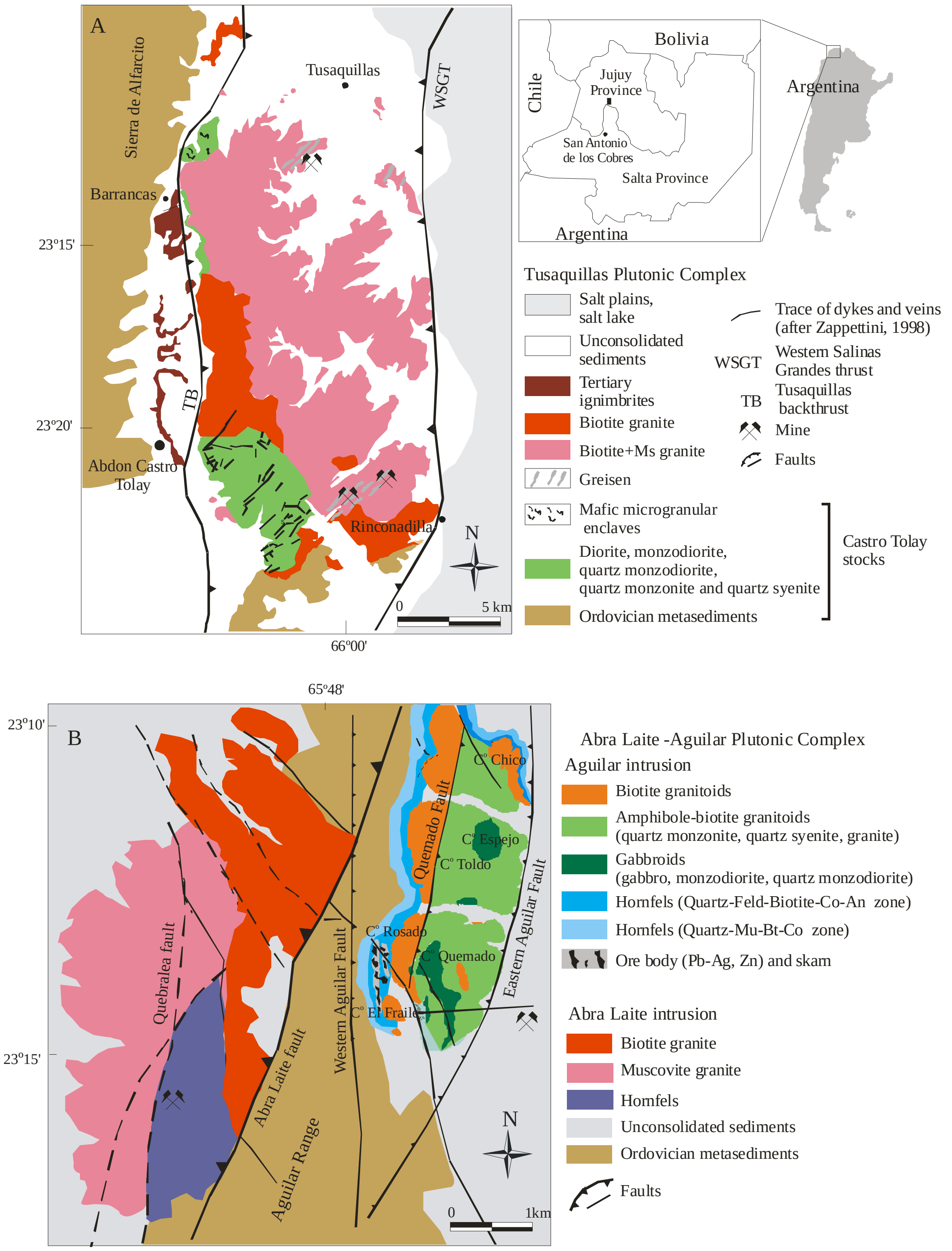


Fig. 2. Geological sketch-maps of the Tusaquillas Plutonic Complex (A) and of the Abra Laite-Aguilar Plutonic Complex (B).

its eastern side dips gradually under the Cenozoic sediment cover of the Guayatayoc salt lake. This structural pattern is probably linked to the Quechua tectonic event (~10 Ma), which is responsible for the strong shortening and uplift of the Puna plateau (Allmendinger *et al*., 1997).

The TPC rocks show a wide compositional range varying from gabbro (diorite), monzodiorite, quartz monzodiorite, quartz monzonite, quartz syenite to syenogranite and monzogranite (Fig. 3). Micro-granular enclaves with gabbroic composition are frequent in rocks from the marginal stocks. The main TPC body is constituted by biotite-muscovite granites with subordinate biotite granites. These rocks show an equigranular medium-grained texture with alkali feldspar (25-47 vol%), quartz (17-38 vol%), plagioclase (5-28 vol%), biotite (11-22 vol%) and occasional muscovite as the main phases, and zircon, apatite, tourmaline, Al-silicate and Fe,Ti oxides as accessory minerals.

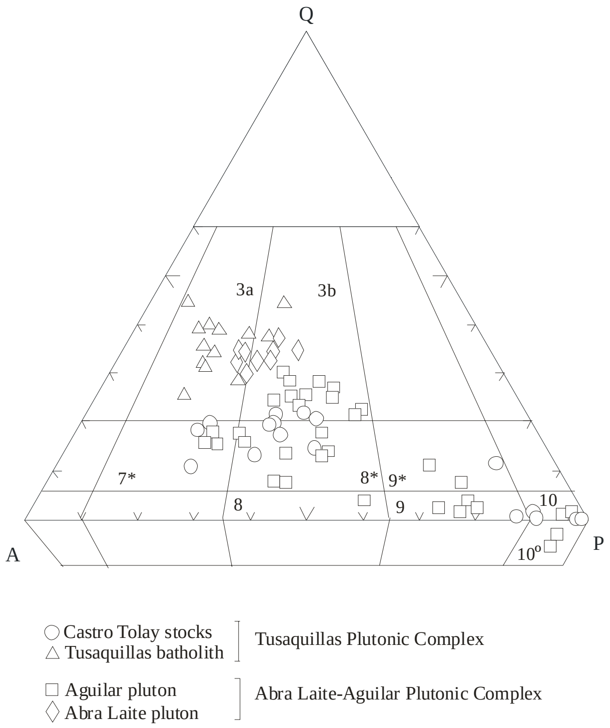


Fig. 3. QAPF modal diagram for rocks from Tusaquillas and Abra Laite-Aguilar Plutonic Complexes (Streckeisen, 1976). Fields: 3a) syenogranites, 3b) monzogranites, 7*) quartz syenites, 8*) quartz monzonites, 8) monzonites, 9*) quartz monzodiorites, 9) monzodiorites, 10) diorite (gabbros), 10°) foid diorites (foid gabbros).

From the mineral associations, two main felsic facies have been distinguished: biotite and biotite+muscovite granites (cf. Fig. 2A). Plagioclase ($An_{19-5}$) generally occurs as subeuhedral to euhedral crystals with weakly sericitized cores and unaltered rims and it exhibits normal continuous zoning. Alkali feldspar ($Or_{89-84}$) is the most abundant mineral, forming tabular microperthitic subhedral to euhedral crystals (up to 5 cm across) or granophyric intergrowths with quartz. Quartz is interstitial and appears as clusters of small grains, other than intergrowths with alkali feldspar. Biotite is the most common femic mineral in the granites, occurring both as pheno or microphenocrysts, and as a late interstitial phase in the granophyric groundmass. Microprobe analysis shows that the biotite is usually Fe and Al-rich, with Fe/(Fe+Mg) and $Al^{IV}$ ranging from 0.82 to 0.89 and from 2.5 to 2.6 a.f.u., respectively. In the muscovite-biotite granite facies, the muscovite forms large euhedral to subeuhedral lamellae (up to 5 mm across) of magmatic origin, as well as it appears as secondary phase being interstitial or replacing the alkali feldspar. The primary muscovite shows variable Al contents ranging between 4.06 and 5.25 a.f.u. Total Fe+Mg+Ti and Si range from 0.70 to 1.21 and from 6.20 to 7.04 a.f.u., respectively. This compositional range indicates magmatic crystallization at low temperature and high $H_2O$ fugacity, according to other peraluminous melt (Clarke, 1981; Miller *et al.* 1981). Tourmaline is generally scarce, but its abundance increases in the most differentiated rocks at the northern sector of the intrusive body (poikilitic inclusions in quartz and alkali feldspar, or concentrate in ovoids up to 30 cm across). According to Kasemann *et al.* (2000), isotope composition of TPC tourmalines ($\delta^{11}B$: -5.1 to -5.3) overlaps the compositional range of the tourmalines present in the Precambrian-Paleozoic basement of the Central Andes.

The mafic-intermediate marginal stocks (Castro Tolay stocks) of the TPC cover an area of about 30 $km^2$ (cf. Fig. 2A). The rock-types range from gabbros, diorites and monzodiorites to quartz monzodiorites, quartz monzonites and quartz syenites (Fig. 3). Small stocks of syenite-monzonite as well as of lamprophyre dykes and of carbonatite veins outcrop in the southern sector of the TPC (Santa Julia Alkaline Complex; Zappettini, 1998). Notably, diorites and monzodiorites contain abundant microgranular enclaves with gabbroic composition. Gabbros, diorites and monzodiorites show a fine-grained or porphyritic texture with plagioclase (30-50 vol%), amphibole (30-40 vol%), biotite (<15 vol%) and subordinate pyroxene and olivine. Fe-Ti oxides and apatite are accessory minerals. Anhedral to subeuhedral plagioclase appears usually zoned, i.e. $An_{71-64}$ core to $An_{22-16}$ rims. Euhedral to subhedral amphibole is a Mg-hornblende ($Mg/(Mg+Fe^{2+})$=0.81-0.56). Clinopyroxene, occurring in single crystals or at the central parts of amphibole, displays diopsidic-salitic compositions ($Wo_{47}En_{44-33}Fs_{9-20}$ mole%). Biotite from basic rocks has quite constant $Al^{IV}$, i.e. 2.49-2.40 a.f.u. and Fe/(Fe+Mg) ranging from 0.36 to 0.54

(more "primitive" to more evolved rock-types, respectively). Olivine ($Fo_{64-74}$, present only in the gabbros and representing the earliest phase) appears as rounded single grains up to 3 mm across, often partially to completely surrounded by hornblende-bearing coronas. These coronitic textures indicate that the olivine is not in equilibrium with the host liquid, thus representing a “remnant phase” of a more basic parental magma.

Quartz monzonites and quartz syenites are medium to coarse-grained (2-8 mm in size) with hypidiomorphic or xenomorphic textures. The rock-types are gray to dark gray in colours (C.I. 12.9-36.5), with modal compositions, vol%, 5-15 quartz, 30-40 plagioclase, 28-35 alkali feldspar, 7-22 biotite and 1-22 hornblende. Fe-Ti oxides, epidote, allanite and titanite are the main accessory minerals. Plagioclase is euhedral to subeuhedral and generally zoned ($An_{50-10}$ cores and $An_{29-7}$ rims). Two different generations of alkali feldspar are apparent, i.e. 1) subhedral perthitic feldspar ($Or_{97-84}$) in the most evolved rocks, and 2) rims ($Or_{89}$) mantling the plagioclase. This "rapakiwi" texture could be the result of crystallization during magma mixing processes (cf. Hibbard, 1981). Biotite is relatively homogeneous, $Al^{IV}$ 2.15-2.47 a.f.u. and Fe/(Fe+Mg) 0.80-0.65. Amphibole is Mg-hornblende tending to Fe-hornblende (Mg/(Mg+$Fe^{2+}$)=0.43-0.49). More occasionally, clinopyroxene ($Wo_{28-45}En_{36-39}Fs_{19-36}$) appears at the amphibo-le core, as a probable restitic phase of a mafic mag-ma, successively mixed with a more evolved one.

The gabbroic enclaves show an equigranular, fine-grained texture, whereas the most evolved ones (monzodiorites and quartz monzonites) display a porphyritic texture characterized by subhedral plagioclase and amphibole set in a dark groundmass composed by the same mineral plus alkali feldspar and biotite. The plagioclase phenocrysts have patchy zoning textures, with a compositional range from $An_{69}$ (cores) to $An_{23}$ (rims). On the other hand, the groundmass plagioclase is quite homogeneous ($An_{23-20}$).

## THE ABRA LAITE-AGUILAR COMPLEX

The Abra Laite-Aguilar Plutonic Complex (AL-APC; 24º58’-23º09’S and 65º51’-65º40’W) is constituted by two separate intrusions: the Aguilar pluton and the Abra Laite pluton (Fig. 2B).

The Abra Laite pluton is located in the western side of the Aguilar Range. It covers an area of approximately 108 $km^2$ and intrudes the Ordovician marine sedimentary sequences of the Santa Victoria Group (Turner, 1960). U/Pb dates (zircon, SHRIMP method) yielded an average age of 153±4 Ma (Cristiani, 2004). Seismic and gravimetric studies (Gangui & Götze, 1996) show an important west-dipping fault (Eastern Salinas Grandes fault) controlling the geologic and tectonic setting of the area. ALP consists of medium-grained biotite monzogranite and two micas syenogranite, having abundant alkali feldspar (32-40 vol %), plagioclase (17-21 vol %), quartz (~31 vol %) and minor biotite (~6 vol %), muscovite (~3 vol %), andalusite (~0.5 vol %), cordierite (~1.1 vol %) and garnet (~1.2 vol %). Alkali feldspar ($Or_{75-93}$) is subeuhedral to anhedral. Subeuhedral, zoned plagioclase ranges from $An_{48-43}$ (core) to $An_{17-7}$ (rim). Biotite (annite-siderophyllite) usually shows subeuhedral habitus, and FeO and $Al_2O_3$-rich compositions [(Fe/Fe+Mg): 0.59-0.86; $Al^{IV}$=2.71-2.47 a.f.u..)]. Muscovite is ubiquitous in the two-mica granite, with Si and $Al^{IV}$ ranging from 5.09 to 6.90 and 0.93 to 1.50 a.f.u., respectively. Pyralspitic garnet shows a range from $Alm_{76}Py_{15}Sp_{4.7}$ (cores) to $Alm_{74}Py_{18}Sp_{3.8}$ (rims).

The Aguilar pluton (23º00’-23º10’S and 65º44’-65º48’W) is located close to the eastern border of the Aguilar Range, about 35 km N-NE of the TPC (Fig. 2B). The body covers an area of about 40 $km^2$ and intrudes Ordovician marine sediments of the Santa Victoria Group (Turner, 1960). The latter is uncon-formably overlain by Cretaceous-Tertiary sediments deposited within fault-bounded sedimentary basins. The intrusion is fault-controlled (El Quemado, Eastern and Western Aguilar faults, cf. Fig. 2B). Its eastern side gently dips under the Pleistocene-Holocene cover and its western northern side is marked by a well-defined intrusive relationship with a metamorphic contact aureole, 500-1000 m wide (Lanfranco, 1972). A 149±1 Ma age (Rb-Sr isochron, whole-rock+biotite) is believed to be representative of the whole intrusion (cf. Cristiani, 2004).

According to the IUGS classification, the rock-types range from foid gabbro, gabbro, diorite, monzodiorite and quartz monzodiorite to monzonite, quartz monzonite, quartz syenite and monzogranite (cf. Fig. 3). Granitoid rocks (monzonite, quartz monzonite, quartz syenite, monzogranite) are medium to coarse-grained, with modal (vol %) alkali feldspar (30-47%; $Or_{68-94}$), plagioclase (20-26%; $An_{18-7}$), quartz (12-20%), biotite (13-11%) and occasional amphibole (up to 6.3%). Mineral assemblages and textural relationships allow to distinguish two groups of granitoid rock-types: 1) biotite granitoids, outcropping in the western sector of the pluton, and 2) biotite-amphibole granitoids, encompassing the central and eastern sector of the stock (cf. Fig. 2B). Biotite is characterized by $Al^{IV}$ from 2.33 to 2.55 a.f.u. and Fe/(Fe+Mg) ranging from 0.63 to 077. Amphibole is ferroedenite (according to Leake, 1977) with (Mg/(Mg+$Fe^{2+}$) from 0.25 to 0.46.

The gabbroid rocks (gabbros, monzodiorites, quartz monzodiorites) outcrop in the northern and southern sector of the Aguilar stock (cf. Fig. 2B). The contact between gabbroid and granitoid bodies is characterized by a high concentration of microgranular enclaves (30-35% by volume), displaying dioritic and monzodioritic composition (cf. Fig. 3). The enclaves (usually ellipsoidal or rounded) show crenulated borders and magmatic textures. The size ranges from a few centimeters up to 1 meter. Porphyritic textures with phenocrysts of plagioclase (up to 10 mm across) may be present. The gabbroid rocks are mainly characterized by plagioclase, clinopyroxene and amphiboles as primary phases and Fe-Ti oxides, apatite, allanite and zircons as accessories. Plagioclase is strongly zoned ($An_{55-46}$-$An_{20-26}$); clinopyroxene shows weak zoning, ranging from diopside to salite.

Brown-green amphibole, occurring both as large crystals and at the rims of the clinopyroxene grains tend to present ferropargasitic composition with Mg/(Mg+$Fe^{2+}$)=0.5-0.6.

## GEOCHEMISTRY

Major and trace element analyses of TPC and AL-APC rocks are displayed in Tables 1A, B. In the TAS diagram (Fig. 4; cf. Middlemost, 1994) the TPC and AL-APC rock-types range from gabbros to granites. The rocks display transitional features straddling over the line separating the alkaline and subalkaline fields (cf. Irvine & Baragar, 1971). In the NK/A vs. A/(CNK) diagram (Fig. 5), the granitic rocks of the TPC and AL-APC fall in the peraluminous field, whereas the intermediate rock-types from both complexes fall in the metaluminous and weakly peralkaline fields.

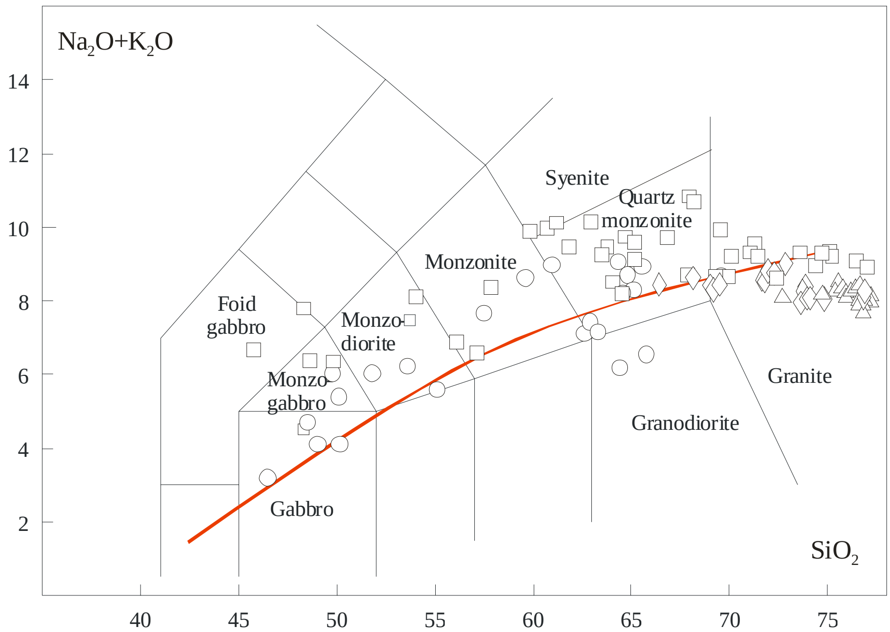


Fig. 4. TAS diagram modified by Middlemost (1994) for plutonic rocks. Symbols as in Fig. 3. Red-line separates alkaline and subalkaline fields (after Irvine & Baragar, 1971).

Table 1A. Major (wt%) and trace (ppm) elements (XRF) and CIPW norms for representative rocks from Tusaquillas (T) and Abra Laite (AB)-Aguilar (AG) plutonic complexes. MME: microgranular mafic enclaves.

| | Tusaquillas Plutonic Complex | | | | | | | | | | | | | | | | | | | | | | | | |
|---|---|---|---|---|---|---|---|---|---|---|---|---|---|---|---|---|---|---|---|---|---|---|---|---|---|
| Sample | T 6 | T103 | T2 | T73 | T91 | T31 | T55 | T98 | T 21 | T71 | T 30 | T34 | T81 | T104 | T5 | T 38 | T 11 | T79 | T83 | T94 | T 23 | T72 | T 9 | T100 | T 19 |
| Facies | MME | MME | MME | MME | | | MME | MME | | | | | | | | | | | | | | | | | |
| $SiO_2$ | 45.30 | 46.55 | 48.15 | 48.38 | 48.53 | 49.15 | 50.47 | 52.11 | 53.70 | 56.56 | 58.80 | 60.19 | 61.60 | 62.08 | 62.35 | 63.28 | 63.41 | 63.67 | 63.72 | 63.88 | 64.33 | 64.99 | 71.73 | 74.03 | 74.67 |
| $TiO_2$ | 2.19 | 3.30 | 2.50 | 2.96 | 2.04 | 1.66 | 2.16 | 1.85 | 1.59 | 1.79 | 1.32 | 1.15 | 1.22 | 1.33 | 1.36 | 1.02 | 0.90 | 0.99 | 0.97 | 0.93 | 0.90 | 0.92 | 0.36 | 0.25 | 0.17 |
| $Al_2O_3$ | 11.91 | 15.24 | 14.65 | 15.36 | 17.14 | 16.32 | 15.16 | 16.24 | 16.73 | 16.15 | 16.66 | 17.37 | 16.56 | 15.01 | 14.85 | 15.31 | 15.89 | 16.70 | 16.26 | 15.86 | 15.83 | 15.52 | 14.29 | 13.53 | 13.48 |
| $Fe_2O_3$ | 1.95 | 5.25 | 3.34 | 2.94 | 3.02 | 1.75 | 0.50 | 2.75 | 2.04 | 1.88 | 2.16 | 1.64 | 1.53 | 1.64 | 1.19 | 1.79 | 1.41 | 1.59 | 1.46 | 0.89 | 1.44 | 1.85 | 0.96 | 0.70 | 0.57 |
| FeO | 8.98 | 9.15 | 8.00 | 9.14 | 7.42 | 7.69 | 9.08 | 6.59 | 6.51 | 5.94 | 4.87 | 4.38 | 4.63 | 5.05 | 4.59 | 3.67 | 3.36 | 4.97 | 4.38 | 4.64 | 3.53 | 2.94 | 1.61 | 1.61 | 1.14 |
| MnO | 0.17 | 0.19 | 0.17 | 0.18 | 0.15 | 0.14 | 0.18 | 0.17 | 0.12 | 0.14 | 0.13 | 0.08 | 0.08 | 0.10 | 0.10 | 0.08 | 0.09 | 0.05 | 0.08 | 0.08 | 0.06 | 0.08 | 0.04 | 0.04 | 0.03 |
| MgO | 13.24 | 4.24 | 6.75 | 5.00 | 5.53 | 6.90 | 5.71 | 5.02 | 4.66 | 2.68 | 1.87 | 1.70 | 1.74 | 2.18 | 2.39 | 3.80 | 1.28 | 1.74 | 1.00 | 1.20 | 1.47 | 1.30 | 0.87 | 0.08 | 0.35 |
| CaO | 10.27 | 6.75 | 9.95 | 6.80 | 7.25 | 10.06 | 7.80 | 6.04 | 6.31 | 4.85 | 3.68 | 3.00 | 3.56 | 3.29 | 4.22 | 2.89 | 2.85 | 0.73 | 2.43 | 2.25 | 2.51 | 2.22 | 0.59 | 0.60 | 0.31 |
| $Na_2O$ | 2.21 | 2.76 | 3.03 | 3.59 | 3.44 | 2.82 | 3.76 | 4.07 | 2.92 | 4.39 | 3.77 | 3.51 | 3.27 | 3.24 | 4.03 | 3.22 | 4.63 | 2.87 | 3.39 | 3.65 | 3.15 | 4.15 | 3.21 | 2.90 | 3.18 |
| $K_2O$ | 0.89 | 1.80 | 1.02 | 2.29 | 1.78 | 1.18 | 2.11 | 2.00 | 2.52 | 3.14 | 4.71 | 5.33 | 3.74 | 3.85 | 3.32 | 2.85 | 4.28 | 3.44 | 4.71 | 4.94 | 5.04 | 4.72 | 4.78 | 5.18 | 5.03 |
| $P_2O_5$ | 0.46 | 0.76 | 0.53 | 0.70 | 0.61 | 0.33 | 0.43 | 0.47 | 0.42 | 0.79 | 0.69 | 0.39 | 0.45 | 0.48 | 0.47 | 0.29 | 0.40 | 0.20 | 0.31 | 0.35 | 0.38 | 0.35 | 0.24 | 0.14 | 0.06 |
| L.O.I. | 2.44 | 3.97 | 1.91 | 2.65 | 3.09 | 1.99 | 2.63 | 2.68 | 2.48 | 1.68 | 1.33 | 1.27 | 1.61 | 1.75 | 1.13 | 1.80 | 1.48 | 3.04 | 1.30 | 1.34 | 1.36 | 0.97 | 1.31 | 0.96 | 1.01 |
| Total | 100.01 | 99.96 | 100.00 | 99.99 | 100.00 | 99.99 | 99.99 | 99.99 | 100.00 | 99.99 | 99.99 | 100.01 | 99.99 | 100.00 | 100.00 | 100.00 | 99.98 | 99.99 | 100.01 | 100.01 | 100.00 | 100.01 | 99.99 | 100.02 | 100.00 |
| Y | 19 | 32 | 26 | 33 | 23 | 21 | 27 | 24 | 29 | 44 | 53 | 34 | 42 | 36 | 32 | 31 | 33 | 47 | 44 | 17 | 28 | 35 | 29 | 19 | 56 |
| La | 30 | 41 | 28 | 37 | 38 | 30 | 33 | 39 | 41 | 72 | 76 | 88 | 64 | 42 | 65 | 46 | 62 | 75 | 94 | 53 | 49 | 69 | 27 | 23 | 34 |
| Ce | 59 | 70 | 62 | 81 | 72 | 57 | 66 | 71 | 76 | 137 | 149 | 160 | 114 | 87 | 115 | 84 | 113 | 129 | 162 | 98 | 82 | 118 | 50 | 41 | 68 |
| Sr | 410 | 396 | 459 | 441 | 724 | 474 | 388 | 454 | 427 | 482 | 613 | 347 | 327 | 212 | 396 | 324 | 348 | 172 | 245 | 219 | 224 | 327 | 91 | 34 | 39 |
| Ba | 230 | 570 | 675 | 955 | 647 | 316 | 399 | 457 | 602 | 800 | 883 | 1509 | 983 | 505 | 416 | 453 | 474 | 621 | 1059 | 872 | 864 | 686 | 332 | 119 | 213 |
| Zr | 152 | 280 | 162 | 255 | 178 | 150 | 189 | 166 | 177 | 368 | 395 | 449 | 296 | 240 | 252 | 165 | 400 | 338 | 413 | 323 | 293 | 390 | 162 | 175 | 126 |
| Rb | 30 | 93 | 45 | 214 | 76 | 48 | 142 | 118 | 116 | 135 | 153 | 160 | 136 | 175 | 133 | 140 | 197 | 133 | 169 | 172 | 164 | 171 | 293 | 338 | 276 |
| Nb | 30 | 54 | 29 | 56 | 56 | 30 | 38 | 47 | 38 | 83 | 88 | 51 | 46 | 47 | 49 | 33 | 77 | 44 | 41 | 51 | 31 | 65 | 20 | 35 | 38 |
| Cr | 886 | 19 | 227 | 77 | 19 | 82 | 163 | 15 | 36 | 22 | 8 | 21 | 21 | 25 | 26 | 18 | 14 | 35 | 11 | 17 | 16 | 8 | 11 | 7 | 6 |
| Ni | 236 | 24 | 74 | 32 | 23 | 65 | 48 | 31 | 34 | 17 | 11 | 14 | 13 | 11 | 21 | 15 | 8 | 20 | 7 | 9 | 11 | 8 | 8 | 3 | 4 |
| Co | 64 | 48 | 47 | 37 | 39 | 46 | 41 | 34 | 37 | 23 | 19 | 17 | 19 | 19 | 21 | 20 | 13 | 14 | 14 | 12 | 15 | 13 | 5 | 3 | 2 |
| V | 267 | 275 | 294 | 280 | 152 | 220 | 252 | 156 | 180 | 114 | 58 | 83 | 94 | 126 | 114 | 94 | 45 | 87 | 58 | 61 | 73 | 46 | 29 | 9 | 11 |
| Q | | 2.62 | | | | | | | 4.96 | 4.64 | 7.75 | 9.27 | 16.87 | 16.87 | 13.61 | 20.91 | 11.88 | 27.36 | 17.70 | 18.12 | 18.44 | 15.95 | 32.14 | 35.40 | 35.27 |
| C | | | | | | | | | | | 0.32 | 1.31 | 1.74 | 0.68 | | 2.37 | | 7.41 | 1.91 | 1.26 | 1.54 | 0.39 | 3.34 | 2.40 | 2.38 |
| Or | 5.26 | 10.64 | 6.03 | 13.53 | 10.52 | 6.97 | 12.47 | 11.82 | 14.89 | 18.55 | 27.83 | 31.50 | 22.10 | 22.75 | 19.62 | 16.84 | 25.29 | 20.33 | 27.83 | 29.19 | 29.78 | 27.89 | 28.25 | 30.61 | 29.72 |
| Ab | 16.19 | 23.35 | 25.64 | 30.38 | 29.11 | 23.86 | 31.18 | 34.44 | 24.71 | 37.14 | 31.90 | 29.70 | 27.67 | 27.41 | 34.10 | 27.24 | 39.17 | 24.28 | 28.68 | 30.88 | 26.65 | 35.11 | 27.16 | 24.54 | 26.91 |
| Na | 19.95 | 23.88 | 23.36 | 19.03 | 26.07 | 28.39 | 18.26 | 20.14 | 25.10 | 15.09 | 13.75 | 12.34 | 14.72 | 13.19 | 12.62 | 12.44 | 9.93 | 2.32 | 10.03 | 8.88 | 9.97 | 8.73 | 1.36 | 2.06 | 1.15 |
| Ne | 1.36 | | | | | | 0.34 | | | | | | | | | | | | | | | | | | |
| Di | 22.46 | 3.80 | 18.23 | 8.32 | 4.81 | 15.76 | 14.55 | 5.49 | 2.83 | 3.16 | | | | | 4.32 | | 1.32 | | | | | | | | |
| Hy | | 16.07 | 8.53 | 4.77 | 9.47 | 8.20 | 0.00 | 16.62 | 18.09 | 11.77 | 9.88 | 9.17 | 9.71 | 11.34 | 9.20 | 13.19 | 6.21 | 10.60 | 7.87 | 2.99 | 7.58 | 5.74 | 3.81 | 2.24 | 2.27 |
| Ol | 24.30 | | 5.49 | 9.81 | 7.27 | 8.37 | 14.75 | 0.22 | | | | | | | | | | | | | | | | | |
| Mt | 2.83 | 7.61 | 4.84 | 4.26 | 4.38 | 2.54 | 0.72 | 3.99 | 2.96 | 2.73 | 3.13 | 2.38 | 2.22 | 2.38 | 1.73 | 2.60 | 2.04 | 2.31 | 2.12 | 3.83 | 2.09 | 2.68 | 1.39 | 1.01 | 0.83 |
| Il | 4.16 | 6.27 | 4.75 | 5.62 | 3.87 | 3.15 | 4.10 | 3.51 | 3.02 | 3.40 | 2.51 | 2.18 | 2.32 | 2.53 | 2.58 | 1.94 | 1.71 | 1.88 | 1.84 | 1.77 | 1.71 | 1.75 | 0.68 | 0.47 | 0.32 |
| Hm | | | | | | | | | | | | | | | | | | | | | | | | | |
| Ap | 1.09 | 1.80 | 1.26 | 1.66 | 1.44 | 0.78 | 1.02 | 1.11 | 0.99 | 1.87 | 1.63 | 0.92 | 1.07 | 1.14 | 1.11 | 0.69 | 0.95 | 0.47 | 0.73 | 0.83 | 0.90 | 0.83 | 0.57 | 0.33 | 0.14 |

Table 1A. (continued).

| | Tusaquillas Complex | | | | | | | | | | | | | | | | Abra Laite-Aguilar Complex: Aguilar Pluton | | | | | | | | | |
|---|---|---|---|---|---|---|---|---|---|---|---|---|---|---|---|---|---|---|---|---|---|---|---|---|---|---|
| Sample | T99 | T48 | T68 | T109 | T44 | T67 | T115 | T113 | T18 | T69 | T107 | T28 | T 25 | T 10 | T 40 | T63 | AG30 | AG31 | AG53 | AG8 | AG67 | AG42 | AG45s | AG16s | AG10s | AG26s |
| Facies | | | | | | | | | | | | | | | | | MME | | | | MME | | MME | MME | MME | MME |
| $SiO_2$ | 75.08 | 75.11 | 75.16 | 75.31 | 75.52 | 75.80 | 75.85 | 75.88 | 75.95 | 76.15 | 76.20 | 76.25 | 76.32 | 76.37 | 76.37 | 76.59 | 44.81 | 47.49 | 47.73 | 48.21 | 49.52 | 53.20 | 53.54 | 55.69 | 56.40 | 57.42 |
| $TiO_2$ | 0.13 | 0.18 | 0.14 | 0.26 | 0.11 | 0.11 | 0.12 | 0.13 | 0.10 | 0.14 | 0.05 | 0.11 | 0.12 | 0.08 | 0.05 | 0.06 | 2.72 | 2.77 | 2.84 | 2.45 | 2.65 | 2.05 | 1.68 | 1.51 | 1.70 | 1.45 |
| $Al_2O_3$ | 13.43 | 13.79 | 13.00 | 12.95 | 13.80 | 12.81 | 13.62 | 13.02 | 13.26 | 12.48 | 13.66 | 13.23 | 13.20 | 13.00 | 13.68 | 13.68 | 14.48 | 16.38 | 15.50 | 14.78 | 17.73 | 15.51 | 14.18 | 15.58 | 15.10 | 16.44 |
| $Fe_2O_3$ | 0.68 | 0.26 | 0.67 | 1.25 | 0.73 | 0.85 | 0.59 | 0.58 | 0.47 | 0.58 | 0.68 | 0.35 | 0.53 | 0.86 | 0.10 | 0.44 | 4.22 | 4.97 | 3.39 | 3.57 | 2.45 | 2.38 | 3.18 | 2.60 | 2.33 | 2.36 |
| FeO | 0.83 | 0.80 | 1.01 | 0.70 | 0.17 | 0.84 | 0.38 | 1.18 | 0.48 | 1.12 | 0.24 | 0.55 | 0.75 | 0.54 | 0.32 | 0.00 | 8.83 | 7.87 | 9.29 | 8.98 | 8.27 | 7.97 | 7.77 | 7.02 | 6.90 | 5.92 |
| MnO | 0.02 | 0.02 | 0.02 | 0.02 | 0.02 | 0.02 | 0.01 | 0.02 | 0.02 | 0.04 | 0.01 | 0.02 | 0.01 | 0.02 | 0.01 | 0.01 | 0.23 | 0.24 | 0.19 | 0.20 | 0.17 | 0.17 | 0.21 | 0.17 | 0.15 | 0.16 |
| MgO | 0.12 | 0.32 | 0.32 | 0.15 | 0.25 | 0.24 | 0.04 | 0.21 | 0.28 | 0.30 | 0.04 | 0.26 | 0.27 | 0.23 | 0.22 | 0.21 | 6.90 | 4.81 | 3.48 | 6.35 | 3.55 | 3.58 | 4.43 | 3.20 | 3.00 | 2.01 |
| CaO | 0.46 | 0.40 | 0.46 | 0.43 | 0.24 | 0.37 | 0.35 | 0.25 | 0.20 | 0.41 | 0.27 | 0.31 | 0.29 | 0.27 | 0.33 | 0.14 | 8.63 | 8.74 | 7.01 | 7.74 | 8.06 | 6.18 | 5.55 | 6.28 | 6.11 | 4.64 |
| $Na_2O$ | 3.38 | 3.02 | 2.96 | 2.98 | 3.01 | 2.93 | 3.12 | 2.82 | 3.19 | 2.87 | 3.31 | 2.94 | 2.66 | 3.21 | 3.24 | 3.43 | 4.18 | 2.75 | 5.16 | 3.34 | 4.54 | 4.53 | 5.26 | 4.61 | 3.98 | 4.61 |
| $K_2O$ | 5.11 | 5.21 | 5.14 | 5.07 | 5.19 | 4.96 | 5.18 | 4.97 | 5.14 | 4.98 | 4.77 | 4.99 | 4.97 | 4.60 | 4.62 | 4.63 | 2.34 | 1.69 | 2.66 | 2.97 | 1.78 | 2.89 | 2.78 | 2.20 | 2.50 | 3.69 |
| $P_2O_5$ | 0.18 | 0.08 | 0.09 | 0.09 | 0.13 | 0.09 | 0.06 | 0.11 | 0.03 | 0.10 | 0.10 | 0.14 | 0.21 | 0.07 | 0.09 | 0.03 | 0.49 | 0.66 | 0.89 | 0.54 | 0.65 | 0.56 | 0.39 | 0.37 | 0.44 | 0.54 |
| L.O.I. | 0.58 | 0.82 | 1.03 | 0.80 | 0.83 | 0.99 | 0.67 | 0.83 | 0.86 | 0.83 | 0.67 | 0.84 | 0.66 | 0.74 | 0.96 | 0.79 | 2.17 | 1.63 | 1.86 | 0.87 | 0.64 | 0.98 | 1.03 | 0.77 | 1.4 | 0.76 |
| Total | 100.00 | 100.01 | 100.00 | 100.01 | 100.00 | 100.01 | 99.99 | 100.00 | 99.98 | 100.00 | 100.00 | 99.99 | 99.99 | 99.99 | 99.99 | 100.01 | 100.00 | 100.00 | 100.00 | 100.00 | 100.01 | 100.00 | 100.00 | 100.00 | 100.01 | 100.00 |
| Y | 9 | 46 | 36 | 31 | 33 | 41 | 20 | 21 | 28 | 36 | 28 | 26 | 20 | 36 | 25 | 39 | 36 | 33 | 52 | 35 | 41 | 40 | 51 | 41 | 38 | 53 |
| La | 14 | 16 | 12 | 33 | 11 | 12 | 16 | 12 | 25 | 14 | 7 | 9 | 7 | 11 | 7 | 12 | 32 | 44 | 52 | 45 | 40 | 49 | 42 | 53 | 39 | 60 |
| Ce | 36 | 34 | 31 | 77 | 21 | 34 | 30 | 33 | 48 | 26 | 14 | 21 | 16 | 23 | 13 | 23 | 60 | 83 | 113 | 79 | 99 | 102 | 104 | 96 | 82 | 122 |
| Sr | 42 | 17 | 18 | 28 | 16 | 13 | 16 | 15 | 29 | 17 | 20 | 13 | 18 | 12 | 29 | 11 | 536 | 629 | 502 | 528 | 722 | 540 | 287 | 265 | 313 | 354 |
| Ba | 137 | 44 | 36 | 62 | 34 | 16 | 32 | 58 | 74 | 39 | 8 | 22 | 55 | 20 | 47 | 19 | 311 | 487 | 530 | 457 | 380 | 500 | 379 | 331 | 296 | 636 |
| Zr | 93 | 119 | 95 | 190 | 78 | 94 | 107 | 118 | 49 | 100 | 61 | 74 | 66 | 63 | 53 | 59 | 218 | 269 | 329 | 253 | 255 | 285 | 271 | 298 | 100 | 458 |
| Rb | 291 | 417 | 439 | 373 | 465 | 429 | 453 | 362 | 276 | 420 | 560 | 439 | 379 | 447 | 446 | 509 | 206 | 151 | 246 | 164 | 112 | 133 | 218 | 115 | 129 | 151 |
| Nb | 24 | 39 | 33 | 43 | 36 | 34 | 39 | 33 | 28 | 33 | 43 | 34 | 25 | 27 | 25 | 35 | 53 | 70 | 75 | 57 | 70 | 72 | 80 | 60 | 54 | 88 |
| Cr | 18 | 6 | 6 | 7 | 3 | 5 | 6 | 2 | 4 | 8 | 2 | 3 | 3 | 4 | 5 | 7 | 150 | 29 | 11 | 121 | 11 | 42 | 106 | 80 | 50 | 5 |
| Ni | 2 | 4 | 4 | 3 | 5 | 4 | 2 | 2 | 4 | 5 | 1 | 5 | 4 | 3 | 4 | 5 | 67 | 27 | 11 | 90 | 12 | 20 | 61 | 26 | 19 | 6 |
| Co | 2 | 1 | 2 | 2 | 0 | 2 | 1 | 2 | 1 | 2 | 1 | 1 | 0 | 1 | 0 | 0 | 35 | 38 | 25 | 44 | 26 | 28 | 29 | 26 | 26 | 15 |
| V | 10 | 6 | 6 | 11 | 5 | 4 | 4 | 5 | 5 | 5 | 2 | 3 | 5 | 3 | 3 | 2 | 264 | 261 | 132 | 198 | 144 | 162 | 127 | 133 | 138 | 58 |
| Q | 34.85 | 36.05 | 36.56 | 37.69 | 37.63 | 38.88 | 37.23 | 39.23 | 36.80 | 38.71 | 38.34 | 39.14 | 41.05 | 39.29 | 38.86 | 38.39 | | | | | | | | 2.27 | 6.10 | 3.31 |
| C | 1.93 | 2.65 | 1.95 | 1.99 | 3.11 | 2.16 | 2.39 | 2.81 | 2.16 | 1.86 | 2.80 | 2.76 | 3.42 | 2.42 | 2.96 | 2.84 | | | | | | | | | | |
| Or | 30.20 | 30.79 | 30.37 | 29.96 | 30.67 | 29.31 | 30.61 | 29.37 | 30.37 | 29.43 | 28.19 | 29.49 | 29.37 | 27.18 | 27.30 | 27.36 | 13.83 | 9.99 | 15.72 | 17.55 | 10.52 | 17.08 | 16.43 | 13.00 | 14.77 | 21.80 |
| Ab | 28.60 | 25.55 | 25.04 | 25.21 | 25.47 | 24.79 | 26.40 | 23.86 | 26.99 | 24.28 | 28.01 | 24.88 | 22.51 | 27.16 | 27.41 | 29.02 | 13.77 | 23.27 | 26.39 | 22.49 | 33.07 | 38.33 | 40.28 | 39.01 | 33.68 | 39.01 |
| Na | 1.11 | 1.46 | 1.69 | 1.55 | 0.34 | 1.25 | 1.34 | 0.52 | 0.80 | 1.38 | 0.69 | 0.62 | 0.07 | 0.88 | 1.05 | 0.50 | 13.84 | 27.36 | 11.28 | 16.56 | 22.74 | 13.45 | 6.87 | 15.32 | 15.95 | 13.27 |
| Ne | | | | | | | | | | | | | | | | | 11.70 | | 9.35 | 3.13 | 2.89 | | 2.29 | | | |
| Di | | | | | | | | | | | | | | | | | 20.88 | 9.48 | 14.70 | 14.92 | 10.77 | 11.24 | 14.90 | 11.13 | 9.53 | 5.21 |
| Hy | 1.08 | 1.79 | 1.90 | 0.37 | 0.62 | 0.60 | 0.13 | 2.03 | 1.06 | 2.17 | 0.10 | 1.22 | 1.43 | 0.76 | 0.99 | 0.52 | 0.00 | 13.60 | 0.00 | 0.00 | 0.00 | 2.83 | 0.00 | 11.01 | 10.95 | 9.22 |
| Ol | | | | | | | | | | | | | | | | | 11.40 | | 8.33 | 13.40 | 9.29 | 7.46 | 9.50 | | | |
| Mt | 0.99 | 0.38 | 0.97 | 1.57 | 0.29 | 1.59 | 0.86 | 0.84 | 0.68 | 0.84 | 0.66 | 0.51 | 0.77 | 1.25 | 0.14 | | 6.12 | 7.21 | 4.92 | 5.18 | 3.55 | 3.45 | 4.61 | 3.77 | 3.38 | 3.42 |
| Il | 0.25 | 0.34 | 0.27 | 0.49 | 0.21 | 0.21 | 0.23 | 0.25 | 0.19 | 0.27 | 0.09 | 0.21 | 0.23 | 0.15 | 0.09 | 0.02 | 5.17 | 5.26 | 5.39 | 4.65 | 5.03 | 3.89 | 3.19 | 2.87 | 3.23 | 2.75 |
| Hm | | | | 0.17 | 0.53 | 0.05 | | | | | 0.22 | | | | | 0.44 | | | | | | | | | | |
| Ap | 0.43 | 0.19 | 0.21 | 0.21 | 0.31 | 0.21 | 0.14 | 0.26 | 0.07 | 0.24 | 0.24 | 0.33 | 0.50 | 0.17 | 0.21 | 0.07 | 1.16 | 1.56 | 2.11 | 1.28 | 1.54 | 1.33 | 0.92 | 0.88 | 1.04 | 1.28 |

Table 1A. (continued).

| | Abra Laite-Aguilar Complex: Aguilar Pluton | | | | | | | | | | | | | | | | | | | | | | | | | |
|---|---|---|---|---|---|---|---|---|---|---|---|---|---|---|---|---|---|---|---|---|---|---|---|---|---|---|
| Sample | AG26gf | AG45ca | AG7 | AG44 | AG32 | AG26gg | AG45cb | AG40 | AG0 | AG47 | AG35 | AG1 | AG25 | AG23 | AG21 | AG29i | AG3 | AG13 | AG10c | AG2 | AG9 | AG57 | AG29 | AG62 | AG18 | AG68 |
| Facies | | | | | | | | | | | | | | | | | | | | | | | | | | |
| $SiO_2$ | 60.36 | 60.75 | 61.49 | 62.47 | 63.04 | 63.51 | 63.57 | 64.16 | 64.34 | 64.69 | 64.70 | 66.30 | 67.39 | 67.62 | 67.77 | 68.92 | 69.15 | 69.41 | 69.53 | 70.62 | 70.65 | 71.04 | 71.75 | 73.24 | 74.04 | 74.49 |
| $TiO_2$ | 0.83 | 0.98 | 0.94 | 0.78 | 0.81 | 0.77 | 0.79 | 0.77 | 0.68 | 0.67 | 0.63 | 0.64 | 0.60 | 0.29 | 0.26 | 0.60 | 0.28 | 0.48 | 0.40 | 0.25 | 0.35 | 0.39 | 0.33 | 0.22 | 0.21 | 0.11 |
| $Al_2O_3$ | 16.90 | 17.43 | 16.24 | 16.38 | 16.80 | 15.52 | 16.34 | 16.44 | 16.18 | 16.26 | 16.00 | 15.01 | 14.61 | 15.71 | 15.74 | 14.44 | 15.16 | 14.23 | 14.52 | 14.65 | 14.34 | 14.02 | 14.15 | 13.18 | 12.97 | 13.64 |
| $Fe_2O_3$ | 1.65 | 1.72 | 1.47 | 2.35 | 1.90 | 1.15 | 1.65 | 1.73 | 1.18 | 1.31 | 1.28 | 1.60 | 1.16 | 1.67 | 1.26 | 0.95 | 1.03 | 1 | 1.23 | 1.14 | 1.26 | 0.96 | 1.07 | 0.88 | 0.79 | 0.52 |
| FeO | 4.53 | 3.66 | 5.04 | 3.45 | 3.51 | 4.18 | 3.78 | 3.76 | 3.96 | 3.70 | 3.58 | 2.92 | 3.19 | 2.14 | 2.08 | 3.09 | 1.96 | 2.37 | 2.02 | 1.46 | 1.82 | 1.77 | 1.66 | 1.22 | 1.21 | 0.60 |
| MnO | 0.13 | 0.10 | 0.12 | 0.10 | 0.09 | 0.12 | 0.10 | 0.09 | 0.09 | 0.09 | 0.09 | 0.08 | 0.07 | 0.09 | 0.08 | 0.07 | 0.07 | 0.06 | 0.06 | 0.05 | 0.06 | 0.05 | 0.06 | 0.04 | 0.03 | 0.02 |
| MgO | 1.41 | 1.16 | 1.19 | 0.98 | 1.24 | 1.49 | 1.24 | 1.16 | 0.88 | 0.95 | 0.91 | 0.90 | 1.44 | 0.28 | 0.40 | 0.76 | 0.55 | 1.13 | 0.60 | 0.45 | 0.56 | 0.60 | 0.51 | 0.32 | 0.38 | 0.17 |
| CaO | 3.31 | 3.16 | 3.16 | 2.44 | 2.47 | 3.12 | 2.97 | 2.84 | 2.20 | 2.33 | 2.37 | 1.92 | 1.97 | 0.93 | 1.11 | 1.79 | 1.16 | 1.76 | 1.54 | 0.80 | 1.06 | 1.32 | 1.07 | 1.07 | 0.95 | 0.80 |
| $Na_2O$ | 5.51 | 5.65 | 5.32 | 5.34 | 4.21 | 4.56 | 4.06 | 4.44 | 5.23 | 4.15 | 5.15 | 4.91 | 4.42 | 5.59 | 5.47 | 4.69 | 4.72 | 4.35 | 4.65 | 4.42 | 4.42 | 3.96 | 3.79 | 4.23 | 3.94 | 4.11 |
| $K_2O$ | 4.41 | 4.41 | 4.10 | 4.72 | 4.95 | 4.85 | 4.39 | 3.69 | 4.45 | 4.90 | 4.37 | 4.74 | 4.23 | 5.21 | 5.14 | 3.96 | 5.15 | 4.27 | 4.48 | 5.06 | 4.86 | 5.20 | 4.71 | 5.04 | 4.96 | 5.17 |
| $P_2O_5$ | 0.41 | 0.27 | 0.34 | 0.23 | 0.24 | 0.32 | 0.29 | 0.28 | 0.20 | 0.21 | 0.18 | 0.20 | 0.19 | 0.04 | 0.05 | 0.20 | 0.18 | 0.17 | 0.14 | 0.16 | 0.11 | 0.14 | 0.15 | 0.06 | 0.05 | 0.06 |
| L.O.I. | 0.55 | 0.72 | 0.59 | 0.75 | 0.74 | 0.41 | 0.83 | 0.64 | 0.6 | 0.73 | 0.75 | 0.78 | 0.72 | 0.43 | 0.65 | 0.53 | 0.61 | 0.77 | 0.84 | 0.94 | 0.52 | 0.56 | 0.75 | 0.51 | 0.47 | 0.31 |
| Total | 100.00 | 100.01 | 100.00 | 99.99 | 100.00 | 100.00 | 100.01 | 100.00 | 99.99 | 99.99 | 100.01 | 100.00 | 99.99 | 100.00 | 100.01 | 100.00 | 100.02 | 100.00 | 100.01 | 100.00 | 100.01 | 100.01 | 100.00 | 100.01 | 100.00 | 100.00 |
| | | | | | | | | | | | | | | | | | | | | | | | | | | |
| Y | 51 | 43 | 44 | 44 | 47 | 53 | 52 | 45 | 47 | 44 | 46 | 45 | 31 | 63 | 56 | 47 | 36 | 35 | 38 | 36 | 42 | 44 | 43 | 43 | 33 | 38 |
| La | 49 | 49 | 52 | 62 | 63 | 65 | 67 | 52 | 66 | 67 | 58 | 57 | 39 | 77 | 80 | 48 | 50 | 43 | 55 | 39 | 43 | 56 | 40 | 66 | 56 | 39 |
| Ce | 118 | 91 | 108 | 119 | 118 | 129 | 124 | 101 | 123 | 124 | 120 | 114 | 78 | 146 | 150 | 89 | 82 | 77 | 99 | 73 | 91 | 111 | 80 | 121 | 92 | 65 |
| Sr | 281 | 356 | 282 | 267 | 237 | 285 | 277 | 274 | 204 | 222 | 205 | 175 | 213 | 67 | 74 | 140 | 116 | 139 | 147 | 101 | 113 | 111 | 102 | 69 | 75 | 109 |
| Ba | 724 | 792 | 660 | 750 | 678 | 746 | 558 | 480 | 653 | 630 | 680 | 508 | 475 | 649 | 371 | 333 | 411 | 310 | 400 | 394 | 351 | 432 | 303 | 173 | 185 | 225 |
| Zr | 622 | 636 | 474 | 570 | 671 | 396 | 556 | 492 | 556 | 586 | 562 | 426 | 310 | 598 | 542 | 325 | 406 | 270 | 345 | 312 | 306 | 241 | 226 | 196 | 206 | 176 |
| Rb | 175 | 139 | 147 | 162 | 193 | 140 | 122 | 148 | 180 | 164 | 172 | 205 | 176 | 311 | 288 | 229 | 252 | 218 | 179 | 251 | 229 | 283 | 242 | 300 | 220 | 355 |
| Nb | 80 | 93 | 76 | 82 | 80 | 88 | 81 | 80 | 76 | 86 | 74 | 65 | 53 | 90 | 81 | 43 | 67 | 56 | 59 | 49 | 66 | 35 | 44 | 37 | 35 | 47 |
| Cr | 6 | 9 | 4 | 3 | 2 | 11 | 9 | 3 | 14 | 2 | 2 | 7 | 18 | 2 | 4 | 12 | 2 | 13 | 10 | 4 | 13 | 8 | 4 | 10 | 3 | 19 |
| Ni | 3 | 5 | 4 | 3 | 5 | 3 | 4 | 5 | 3 | 2 | 3 | 4 | 6 | 5 | 1 | 3 | 10 | 16 | 3 | 4 | 4 | 3 | 3 | 3 | 2 | 3 |
| Co | 11 | 12 | 9 | 10 | 9 | 8 | 7 | 10 | 5 | 7 | 6 | 7 | 9 | 2 | 2 | 5 | 4 | 9 | 4 | 2 | 4 | 3 | 6 | 1 | 4 | 2 |
| V | 37 | 22 | 26 | 22 | 25 | 37 | 34 | 33 | 23 | 26 | 21 | 25 | 34 | 5 | 7 | 34 | 15 | 27 | 22 | 13 | 15 | 24 | 10 | 13 | 7 | 8 |
| | | | | | | | | | | | | | | | | | | | | | | | | | | |
| Q | 1.91 | 2.54 | 5.33 | 6.64 | 11.46 | 9.10 | 13.73 | 15.20 | 9.45 | 13.81 | 10.62 | 14.00 | 18.04 | 12.28 | 12.74 | 20.45 | 18.09 | 20.82 | 20.83 | 22.97 | 22.71 | 24.02 | 27.09 | 26.80 | 29.39 | 28.78 |
| C | | | | | 0.60 | | 0.20 | 0.65 | | 0.40 | | | | | | | 0.14 | | | 0.83 | 0.14 | | 0.48 | | | |
| Or | 26.06 | 26.06 | 24.23 | 27.89 | 29.25 | 28.66 | 25.94 | 21.80 | 26.30 | 28.95 | 25.82 | 28.01 | 25.00 | 30.79 | 30.37 | 23.40 | 30.43 | 26.53 | 26.47 | 29.90 | 28.72 | 30.73 | 29.31 | 29.78 | 29.31 | 30.55 |
| Ab | 46.62 | 47.81 | 45.01 | 45.18 | 35.62 | 38.58 | 34.35 | 37.57 | 44.25 | 35.11 | 43.57 | 41.54 | 37.40 | 47.30 | 46.28 | 39.68 | 39.94 | 36.81 | 39.34 | 37.40 | 37.40 | 33.51 | 32.07 | 35.79 | 33.34 | 34.78 |
| Na | 8.36 | 9.17 | 8.32 | 6.78 | 10.69 | 7.56 | 12.84 | 12.26 | 7.53 | 10.19 | 7.63 | 4.92 | 7.53 | 2.39 | 3.21 | 6.65 | 4.58 | 5.90 | 5.52 | 2.92 | 4.54 | 5.12 | 5.04 | 2.09 | 3.06 | 3.50 |
| Ne | | | | | | | | | | | | | | | | | | | | | | | | | | |
| Di | 4.53 | 3.96 | 4.36 | 3.19 | 0.00 | 4.90 | 0.00 | 0.00 | 1.77 | 0.00 | 2.50 | 2.76 | 0.83 | 1.69 | 1.68 | 0.78 | 0.00 | 2.17 | 1.01 | 0.00 | 0.00 | 0.43 | 0.00 | 2.37 | 1.11 | 0.06 |
| Hy | 7.05 | 4.77 | 7.45 | 4.13 | 6.79 | 6.93 | 7.55 | 7.26 | 6.63 | 7.14 | 5.64 | 3.99 | 7.21 | 2.07 | 2.64 | 5.52 | 3.79 | 4.58 | 3.13 | 2.54 | 3.23 | 3.19 | 3.00 | 0.83 | 1.67 | 0.92 |
| Ol | | | | | | | | | | | | | | | | | | | | | | | | | | |
| Mt | 2.39 | 2.49 | 2.13 | 3.41 | 2.75 | 1.67 | 2.39 | 2.51 | 1.71 | 1.90 | 1.86 | 2.32 | 1.68 | 2.42 | 1.83 | 1.38 | 1.49 | 1.48 | 1.78 | 1.65 | 1.83 | 1.39 | 1.61 | 1.28 | 1.15 | 0.75 |
| Il | 1.58 | 1.86 | 1.79 | 1.48 | 1.54 | 1.46 | 1.50 | 1.46 | 1.29 | 1.27 | 1.20 | 1.22 | 1.14 | 0.55 | 0.49 | 1.14 | 0.53 | 0.89 | 0.76 | 0.47 | 0.66 | 0.74 | 0.59 | 0.42 | 0.40 | 0.21 |
| Hm | | | | | | | | | | | | | | | | | | | | | | | | | | |
| Ap | 0.97 | 0.64 | 0.81 | 0.54 | 0.57 | 0.76 | 0.69 | 0.66 | 0.47 | 0.50 | 0.43 | 0.47 | 0.45 | 0.09 | 0.12 | 0.47 | 0.43 | 0.31 | 0.33 | 0.38 | 0.26 | 0.33 | 0.26 | 0.14 | 0.12 | 0.14 |

Table 1A. (continued).

| | Aguilar Pluton | | | | Abra Laite-Aguilar Plutonic Complex: Abra Laite Pluton | | | | | | | | | | | | | | | | | |
|---|---|---|---|---|---|---|---|---|---|---|---|---|---|---|---|---|---|---|---|---|---|---|
| Samples | AG27 | AG46 | AG24c | AG70 | AB21 | AB24 | AB30 | AB34 | AB26 | AB11 | AB27 | AB20 | AB9 | AB3 | AB23 | AB35 | AB13 | AB22 | AB1 | AB31 | AB18 | AB28 |
| Facies | | | | | | | | | | | | | | | | | | | | | | |
| $SiO_2$ | 74.63 | 74.73 | 76.14 | 76.65 | 65.84 | 67.60 | 68.42 | 68.60 | 68.64 | 70.84 | 71.00 | 71.48 | 71.80 | 72.06 | 72.85 | 73.07 | 73.34 | 73.35 | 73.52 | 74.24 | 76.33 | 76.41 |
| $TiO_2$ | 0.13 | 0.12 | 0.07 | 0.04 | 1.02 | 0.62 | 0.62 | 0.64 | 0.63 | 0.37 | 0.38 | 0.38 | 0.39 | 0.24 | 0.33 | 0.29 | 0.29 | 0.29 | 0.27 | 0.24 | 0.08 | 0.06 |
| $Al_2O_3$ | 12.50 | 13.08 | 12.87 | 12.22 | 14.41 | 16.00 | 15.28 | 14.55 | 14.75 | 13.76 | 14.43 | 14.09 | 13.46 | 13.54 | 13.54 | 13.79 | 13.71 | 13.57 | 13.38 | 13.10 | 12.87 | 13.46 |
| $Fe_2O_3$ | 0.55 | 0.83 | 0.61 | 0.39 | 1.75 | 1.22 | 0.88 | 0.83 | 1.09 | 0.77 | 0.89 | 1.03 | 1.13 | 0.06 | 0.83 | 1.29 | 0.92 | 0.73 | 0.88 | 0.34 | 0.69 | 0.38 |
| FeO | 1.11 | 0.73 | 0.18 | 0.79 | 5.15 | 2.57 | 3.05 | 3.14 | 3.24 | 2.45 | 2.21 | 1.91 | 2.15 | 2.59 | 1.96 | 1.36 | 1.68 | 1.77 | 1.74 | 1.92 | 0.74 | 0.25 |
| MnO | 0.04 | 0.03 | 0.02 | 0.02 | 0.09 | 0.04 | 0.04 | 0.05 | 0.06 | 0.07 | 0.05 | 0.04 | 0.07 | 0.04 | 0.04 | 0.04 | 0.04 | 0.04 | 0.05 | 0.05 | 0.02 | 0.01 |
| MgO | 0.23 | 0.17 | 0.18 | 0.08 | 1.28 | 0.81 | 0.73 | 0.86 | 0.80 | 0.48 | 0.58 | 0.51 | 0.38 | 0.91 | 0.46 | 0.35 | 0.46 | 0.41 | 0.43 | 0.38 | 0.13 | 0.12 |
| CaO | 0.86 | 0.48 | 0.47 | 0.44 | 1.09 | 1.66 | 1.63 | 1.54 | 1.64 | 1.43 | 0.86 | 1.01 | 1.17 | 0.49 | 0.91 | 0.61 | 0.62 | 0.70 | 0.74 | 0.83 | 0.40 | 0.35 |
| $Na_2O$ | 4.46 | 4.64 | 3.96 | 4.22 | 2.95 | 3.34 | 3.79 | 3.52 | 3.22 | 3.38 | 3.10 | 3.25 | 3.59 | 3.52 | 2.84 | 2.97 | 2.79 | 2.75 | 2.79 | 2.87 | 3.02 | 3.02 |
| $K_2O$ | 4.66 | 4.66 | 5.10 | 4.64 | 5.40 | 5.22 | 4.57 | 4.85 | 5.01 | 5.04 | 5.40 | 5.50 | 5.11 | 5.38 | 5.03 | 5.21 | 5.19 | 5.58 | 5.21 | 5.14 | 4.98 | 5.16 |
| $P_2O_5$ | 0.03 | 0.03 | 0.01 | 0.00 | 0.15 | 0.14 | 0.14 | 0.16 | 0.11 | 0.12 | 0.16 | 0.11 | 0.13 | 0.18 | 0.13 | 0.14 | 0.13 | 0.14 | 0.13 | 0.13 | 0.17 | 0.13 |
| L.O.I. | 0.8 | 0.51 | 0.4 | 0.51 | 0.87 | 0.78 | 0.85 | 1.26 | 0.80 | 1.30 | 0.95 | 0.68 | 0.62 | 1.10 | 1.07 | 0.87 | 0.83 | 0.68 | 0.86 | 0.76 | 0.57 | 0.64 |
| Total | 100.00 | 100.01 | 100.01 | 100.00 | 100.00 | 100.00 | 100.00 | 100.00 | 99.99 | 100.01 | 100.01 | 99.99 | 100.00 | 100.11 | 99.99 | 99.99 | 100.00 | 100.01 | 100.00 | 100.00 | 100.00 | 99.99 |
| | | | | | | | | | | | | | | | | | | | | | | |
| Y | 39 | 45 | 62 | 52 | 82 | 36 | 39 | 48 | 53 | 43 | 37 | 47 | 42 | 40 | 38 | 36 | 37 | 39 | 37 | 34 | 26 | 27 |
| La | 57 | 37 | 53 | 32 | 93 | 52 | 48 | 61 | 67 | 42 | 38 | 38 | 38 | 27 | 33 | 28 | 27 | 28 | 24 | 26 | 7 | 6 |
| Ce | 102 | 76 | 99 | 68 | 188 | 96 | 94 | 115 | 132 | 89 | 73 | 71 | 84 | 61 | 66 | 52 | 54 | 52 | 40 | 44 | 23 | 14 |
| Sr | 44 | 34 | 52 | 9 | 91 | 156 | 116 | 154 | 122 | 87 | 96 | 85 | 81 | 40 | 74 | 48 | 60 | 60 | 45 | 51 | 17 | 20 |
| Ba | 114 | 153 | 173 | 107 | 389 | 617 | 434 | 591 | 554 | 429 | 439 | 315 | 399 | 198 | 278 | 174 | 230 | 293 | 209 | 199 | 65 | 64 |
| Zr | 178 | 159 | 242 | 108 | 474 | 264 | 400 | 344 | 310 | 298 | 195 | 194 | 308 | 168 | 190 | 169 | 168 | 159 | 161 | 147 | 78 | 73 |
| Rb | 277 | 299 | 387 | 388 | 305 | 229 | 259 | 239 | 238 | 229 | 270 | 247 | 223 | 281 | 253 | 294 | 270 | 273 | 287 | 273 | 399 | 340 |
| Nb | 33 | 41 | 93 | 45 | 80 | 38 | 40 | 35 | 51 | 42 | 32 | 31 | 40 | 36 | 36 | 39 | 27 | 30 | 28 | 25 | 23 | 19 |
| Cr | 2 | 9 | 7 | 3 | 27 | 23 | 16 | 39 | 17 | 10 | 24 | 35 | 214 | 12 | 21 | 16 | 18 | 21 | 24 | 39 | 4 | 13 |
| Ni | 3 | 4 | 3 | 2 | 7 | 8 | 3 | 23 | 7 | 3 | 7 | 5 | 3 | 5 | 5 | 4 | 3 | 3 | 3 | 4 | 2 | 1 |
| Co | 2 | 2 | 3 | 1 | 10 | 5 | 6 | 5 | 5 | 5 | 2 | 5 | 6 | 5 | 6 | 5 | 5 | 3 | 5 | 3 | 2 | 3 |
| V | 10 | 8 | 8 | 6 | 69 | 49 | 34 | 52 | 45 | 18 | 33 | 31 | 11 | 24 | 22 | 18 | 24 | 24 | 23 | 21 | 12 | 8 |
| | | | | | | | | | | | | | | | | | | | | | | |
| Q | 28.91 | 28.71 | 32.34 | 33.11 | 21.24 | 22.57 | 22.92 | 23.56 | 24.47 | 26.91 | 28.78 | 27.96 | 27.52 | 28.22 | 33.70 | 33.96 | 34.73 | 33.27 | 34.53 | 34.56 | 38.82 | 38.51 |
| C | | | | | 2.09 | 2.17 | 1.47 | 1.09 | 1.31 | 0.43 | 2.30 | 1.22 | 0.21 | 1.47 | 2.08 | 2.49 | 2.69 | 2.07 | 2.12 | 1.62 | 2.19 | 2.58 |
| Or | 27.54 | 27.54 | 30.14 | 27.42 | 31.91 | 30.85 | 27.00 | 28.66 | 29.60 | 29.78 | 31.91 | 32.50 | 30.20 | 31.79 | 29.72 | 30.79 | 30.67 | 32.97 | 30.79 | 30.37 | 29.43 | 30.49 |
| Ab | 37.74 | 39.26 | 33.51 | 35.71 | 24.96 | 28.26 | 32.07 | 29.78 | 27.24 | 28.60 | 26.23 | 27.50 | 30.38 | 29.78 | 24.03 | 25.13 | 23.61 | 23.27 | 23.61 | 24.28 | 25.55 | 25.55 |
| Na | 0.33 | 1.10 | 2.27 | 0.70 | 4.43 | 7.32 | 7.17 | 6.60 | 7.42 | 6.31 | 3.22 | 4.29 | 4.96 | 1.26 | 3.67 | 2.11 | 2.23 | 2.56 | 2.82 | 3.27 | 0.87 | 0.89 |
| Ne | | | | | | | | | | | | | | | | | | | | | | |
| Di | 3.19 | 0.90 | | 1.29 | | | | | | | | | | | | | | | | | | |
| Hy | 0.39 | 0.49 | 0.45 | 0.63 | 9.68 | 4.78 | 5.74 | 6.26 | 6.11 | 4.58 | 4.23 | 3.37 | 3.45 | 6.70 | 3.59 | 1.90 | 3.07 | 3.26 | 3.19 | 3.89 | 1.02 | 0.36 |
| Ol | | | | | 0.00 | 0.00 | 0.00 | 0.00 | 0.00 | 0.00 | | | | | | | | | | | | |
| Mt | 0.80 | 1.20 | 0.44 | 0.57 | 2.54 | 1.77 | 1.28 | 1.20 | 1.58 | 1.12 | 1.29 | 1.49 | 1.64 | 0.00 | 1.20 | 1.87 | 1.33 | 1.06 | 1.28 | 0.49 | 1.00 | 0.55 |
| Il | 0.25 | 0.23 | 0.13 | 0.08 | 1.94 | 1.18 | 1.18 | 1.22 | 1.20 | 0.70 | 0.72 | 0.72 | 0.74 | 0.46 | 0.63 | 0.55 | 0.55 | 0.55 | 0.51 | 0.46 | 0.15 | 0.11 |
| Hm | | | 0.30 | | | | | | | | | | | | | | | | | | | |
| Ap | 0.07 | 0.07 | 0.02 | | 0.36 | 0.33 | 0.33 | 0.38 | 0.26 | 0.28 | 0.38 | 0.26 | 0.31 | 0.43 | 0.31 | 0.33 | 0.31 | 0.33 | 0.31 | 0.31 | 0.40 | 0.31 |

Table 1B. Trace elements (ppm), ICP-MS, of selected samples from the Tusaquillas and Abra Laite-Aguilar Plutonic Complexes. REE ratios are normalized to condrite compositions (Rollinson, 1993).

| Tusaquillas Plutonic Complex | | | | | | | | | | | | | | | |
|---|---|---|---|---|---|---|---|---|---|---|---|---|---|---|---|
| Sample | T 6 | T2 | T73 | T31 | T98 | T 30 | T34 | T5 | T 11 | T79 | T83 | T100 | T 19 | T48 | T69 |
| La | 25.79 | 29.30 | 45.93 | 28.80 | 42.28 | 79.80 | 103.00 | 62.65 | 77.50 | 91.34 | 99.75 | 31.15 | 41.80 | 28.05 | 21.70 |
| Ce | 55.27 | 59.00 | 96.23 | 55.30 | 82.21 | 172.05 | 194.00 | 120.69 | 146.00 | 169.87 | 193.62 | 64.61 | 81.10 | 61.78 | 46.40 |
| Pr | 7.01 | 7.41 | 12.12 | 6.60 | 9.71 | 20.90 | 20.40 | 13.27 | 16.30 | 21.61 | 21.59 | 7.27 | 9.40 | 7.29 | 5.30 |
| Nd | 28.68 | 30.40 | 47.14 | 25.40 | 36.15 | 77.73 | 71.00 | 45.39 | 53.30 | 75.50 | 75.84 | 23.91 | 30.70 | 24.44 | 17.20 |
| Sm | 5.94 | 6.40 | 9.67 | 5.70 | 7.03 | 14.90 | 12.40 | 8.24 | 9.80 | 14.49 | 13.84 | 5.41 | 6.80 | 6.01 | 4.50 |
| Eu | 1.83 | 2.19 | 2.66 | 1.80 | 1.99 | 3.01 | 2.88 | 1.93 | 2.14 | 1.88 | 2.72 | 0.40 | 0.40 | 0.22 | 0.15 |
| Gd | 5.24 | 7.09 | 8.33 | 4.90 | 6.36 | 12.19 | 10.30 | 7.01 | 7.90 | 11.04 | 11.21 | 5.41 | 6.50 | 5.52 | 3.90 |
| Tb | 0.76 | 1.02 | 1.22 | 0.80 | 0.96 | 1.86 | 1.50 | 1.04 | 1.40 | 1.54 | 1.58 | 0.96 | 1.40 | 1.13 | 1.00 |
| Dy | 4.10 | 5.79 | 6.38 | 4.70 | 5.15 | 9.91 | 7.70 | 5.56 | 6.70 | 7.50 | 8.11 | 5.45 | 9.40 | 7.01 | 6.70 |
| Ho | 0.79 | 1.04 | 1.24 | 0.90 | 1.04 | 1.93 | 1.44 | 1.10 | 1.39 | 1.32 | 1.54 | 1.03 | 1.94 | 1.47 | 1.37 |
| Er | 2.07 | 2.84 | 3.13 | 2.50 | 2.74 | 5.15 | 4.10 | 3.03 | 4.10 | 3.18 | 3.90 | 2.69 | 5.70 | 4.05 | 4.10 |
| Tm | 0.28 | 0.39 | 0.45 | 0.40 | 0.39 | 0.74 | 0.50 | 0.47 | 0.50 | 0.41 | 0.51 | 0.38 | 0.90 | 0.66 | 0.70 |
| Yb | 1.77 | 2.20 | 2.74 | 1.90 | 2.40 | 4.66 | 3.20 | 3.11 | 3.60 | 2.33 | 2.98 | 2.42 | 5.60 | 4.11 | 4.00 |
| Lu | 0.27 | 0.34 | 0.42 | 0.30 | 0.38 | 0.68 | 0.50 | 0.48 | 0.54 | 0.35 | 0.44 | 0.33 | 0.81 | 0.59 | 0.50 |
| Y | 22.52 | 24.90 | 35.15 | 22.00 | 29.96 | 56.65 | 34.00 | 32.96 | 33.00 | 35.10 | 44.76 | 32.45 | 50.00 | 45.05 | 37.00 |
| Th | 4.02 | 4.80 | 5.18 | 5.40 | 8.82 | 13.01 | 32.40 | 27.18 | 33.20 | 38.92 | 28.69 | 20.43 | 32.10 | 30.21 | 25.40 |
| U | 1.10 | 1.33 | 2.03 | 1.20 | 2.05 | 2.64 | 2.50 | 5.49 | 7.50 | 2.57 | 1.35 | 5.51 | 7.40 | 24.67 | 4.50 |
| Hf | 3.80 | 4.00 | 2.58 | n.d | 1.50 | 1.32 | n.d | 3.04 | n.d | 4.65 | 7.93 | 2.93 | n.d | 3.70 | n.d |
| Ta | 2.49 | 3.10 | 4.02 | n.d | 3.15 | 5.93 | n.d | 4.97 | n.d | 3.07 | 2.39 | 2.45 | n.d | 4.38 | n.d |
| $La/Sm_n$ | 2.80 | 2.96 | 3.07 | 3.26 | 3.88 | 3.46 | 5.36 | 4.91 | 5.11 | 4.07 | 4.65 | 3.72 | 3.97 | 3.01 | 3.11 |
| $Gd/Yb_n$ | 2.45 | 2.67 | 2.51 | 2.13 | 2.19 | 2.16 | 2.66 | 1.86 | 1.82 | 3.92 | 3.11 | 1.85 | 0.96 | 1.11 | 0.81 |
| $La/Yb_n$ | 10.45 | 9.55 | 12.02 | 10.87 | 12.64 | 12.28 | 23.09 | 14.45 | 15.44 | 28.12 | 24.01 | 9.23 | 5.35 | 4.90 | 3.89 |
| Eu/Eu* | 1.00 | 0.99 | 0.91 | 1.04 | 0.91 | 0.68 | 0.78 | 0.78 | 0.74 | 0.45 | 0.67 | 0.23 | 0.18 | 0.12 | 0.11 |

| Tusaquillas Plutonic Complex | | | | | Abra Laite-Aguilar Plutonic Complex | | | | | | | | | |
|---|---|---|---|---|---|---|---|---|---|---|---|---|---|---|
| Sample | T107 | T28 | T 25 | T 40 | AG 31 | AG 8 | AG 67 | AG 16s | AG 45ca | AG 13 | AG 18 | AB 21 | AB 34 | AB 18 |
| La | 8.86 | 14.00 | 9.50 | 7.00 | 47.80 | 46.40 | 49.80 | 52.00 | 52.20 | 54.40 | 72.80 | 129.00 | 75.40 | 11.80 |
| Ce | 20.43 | 30.00 | 20.20 | 15.80 | 93.20 | 84.60 | 105.00 | 98.20 | 103.00 | 95.80 | 127.00 | 250.00 | 147.00 | 24.50 |
| Pr | 2.57 | 3.50 | 2.40 | 1.90 | 10.70 | 9.62 | 12.70 | 10.70 | 11.70 | 9.58 | 12.50 | 27.80 | 16.30 | 2.77 |
| Nd | 8.21 | 11.40 | 8.80 | 6.90 | 42.40 | 36.90 | 51.60 | 39.70 | 43.10 | 32.20 | 39.40 | 100.00 | 58.70 | 9.70 |
| Sm | 2.66 | 3.00 | 2.60 | 2.40 | 8.40 | 7.20 | 10.30 | 8.10 | 8.50 | 5.90 | 7.00 | 18.60 | 10.80 | 2.40 |
| Eu | 0.10 | 0.10 | 0.13 | 0.12 | 2.47 | 2.15 | 3.24 | 1.99 | 2.28 | 0.98 | 0.78 | 1.06 | 1.57 | 0.16 |
| Gd | 2.62 | 3.00 | 3.10 | 2.60 | 8.62 | 7.05 | 10.80 | 8.13 | 8.35 | 5.77 | 6.16 | 17.70 | 10.10 | 2.68 |
| Tb | 0.65 | 0.70 | 0.60 | 0.60 | 1.23 | 1.03 | 1.50 | 1.21 | 1.33 | 0.96 | 0.97 | 2.61 | 1.53 | 0.55 |
| Dy | 4.14 | 5.00 | 4.00 | 4.30 | 7.02 | 5.90 | 8.32 | 6.99 | 7.72 | 5.67 | 5.80 | 14.60 | 8.74 | 3.68 |
| Ho | 0.86 | 1.04 | 0.62 | 0.79 | 1.28 | 1.08 | 1.49 | 1.34 | 1.49 | 1.14 | 1.11 | 2.77 | 1.66 | 0.62 |
| Er | 2.52 | 2.80 | 1.70 | 2.60 | 3.41 | 3.09 | 4.10 | 4.00 | 4.56 | 3.43 | 3.45 | 8.00 | 4.88 | 1.80 |
| Tm | 0.43 | 0.50 | 0.20 | 0.40 | 0.46 | 0.39 | 0.53 | 0.56 | 0.68 | 0.53 | 0.50 | 1.11 | 0.67 | 0.25 |
| Yb | 3.05 | 3.20 | 1.20 | 2.80 | 3.00 | 2.60 | 3.50 | 3.80 | 4.70 | 3.70 | 3.40 | 7.20 | 4.30 | 1.70 |
| Lu | 0.42 | 0.45 | 0.19 | 0.39 | 0.45 | 0.38 | 0.51 | 0.60 | 0.69 | 0.57 | 0.51 | 1.07 | 0.65 | 0.22 |
| Y | 27.92 | 30.00 | 19.00 | 23.00 | 30.80 | 27.10 | 37.00 | 34.10 | 38.60 | 29.30 | 28.80 | 70.30 | 41.20 | 17.80 |
| Th | 16.60 | 18.60 | 8.80 | 15.20 | 9.60 | 10.00 | 8.20 | 17.80 | 21.00 | 32.60 | 43.90 | 57.20 | 34.20 | 9.30 |
| U | 10.80 | 4.40 | 3.90 | 3.10 | 2.24 | 3.10 | 2.31 | 3.61 | 8.02 | 7.70 | 10.40 | 7.09 | 7.61 | 3.87 |
| Hf | 3.07 | n.d | n.d | n.d | 6.00 | 6.00 | 6.00 | 7.00 | 14.00 | 7.00 | 6.00 | 15.00 | 10.00 | 2.00 |
| Ta | 6.52 | n.d | n.d | n.d | 6.6 | 5.2 | 6.9 | 7 | 8.8 | 8.5 | 4.9 | 10.1 | 4.4 | 8.3 |
| $La/Sm_n$ | 2.15 | 3.01 | 2.36 | 1.88 | 3.67 | 4.16 | 3.12 | 4.14 | 3.96 | 5.95 | 6.71 | 4.48 | 4.51 | 3.17 |
| $Gd/Yb_n$ | 0.71 | 0.78 | 2.14 | 0.77 | 2.38 | 2.24 | 2.55 | 1.77 | 1.47 | 1.29 | 1.50 | 2.03 | 1.94 | 1.30 |
| $La/Yb_n$ | 2.08 | 3.14 | 5.68 | 1.79 | 11.43 | 12.80 | 10.21 | 9.82 | 7.97 | 10.55 | 15.36 | 12.85 | 12.58 | 4.98 |
| Eu/Eu* | 0.03 | 0.10 | 0.14 | 0.15 | 0.89 | 0.92 | 0.94 | 0.75 | 0.83 | 0.51 | 0.36 | 0.18 | 0.46 | 0.19 |

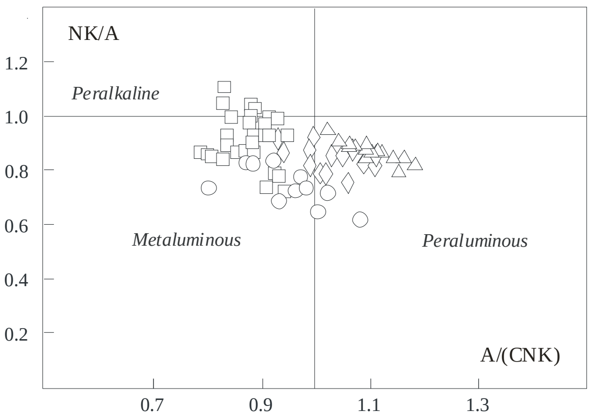


Fig. 5. A/CNK vs. NK/A diagram showing alumina saturation fields. Symbols as in Fig 3.

Major and trace elements

The Harker diagrams (Fig. 6A) show that MgO, CaO, $TiO_2$ and $FeO_t$ decrease with increasing $SiO_2$. $Al_2O_3$ exhibits a roughly positive correlation between 45 and 60 $SiO_2$ wt%; on the other hand, for intermediate to acid composition, alumina forms a negative trend. In the $K_2O$ and $P_2O_5$ vs. $SiO_2$ diagrams, the rocks define positive and negative trends, respectively. Scattered values appear for $Na_2O$.

The compatible elements, e.g. Ni, Cr, Co and V, show a negative correlation with $SiO_2$, depicting a steeper slope for basic to intermediate compositions (Fig. 6B).

Sr exhibits a "compatible" behaviour, being negatively correlated with the silica content, but showing a remarkable scattering for the rocks having $SiO_2$=60%.

The incompatible elements (I.E.) are characterized by contrasting behaviours: Rb displays a positive trend with $SiO_2$, whereas La, Ce, Ba and

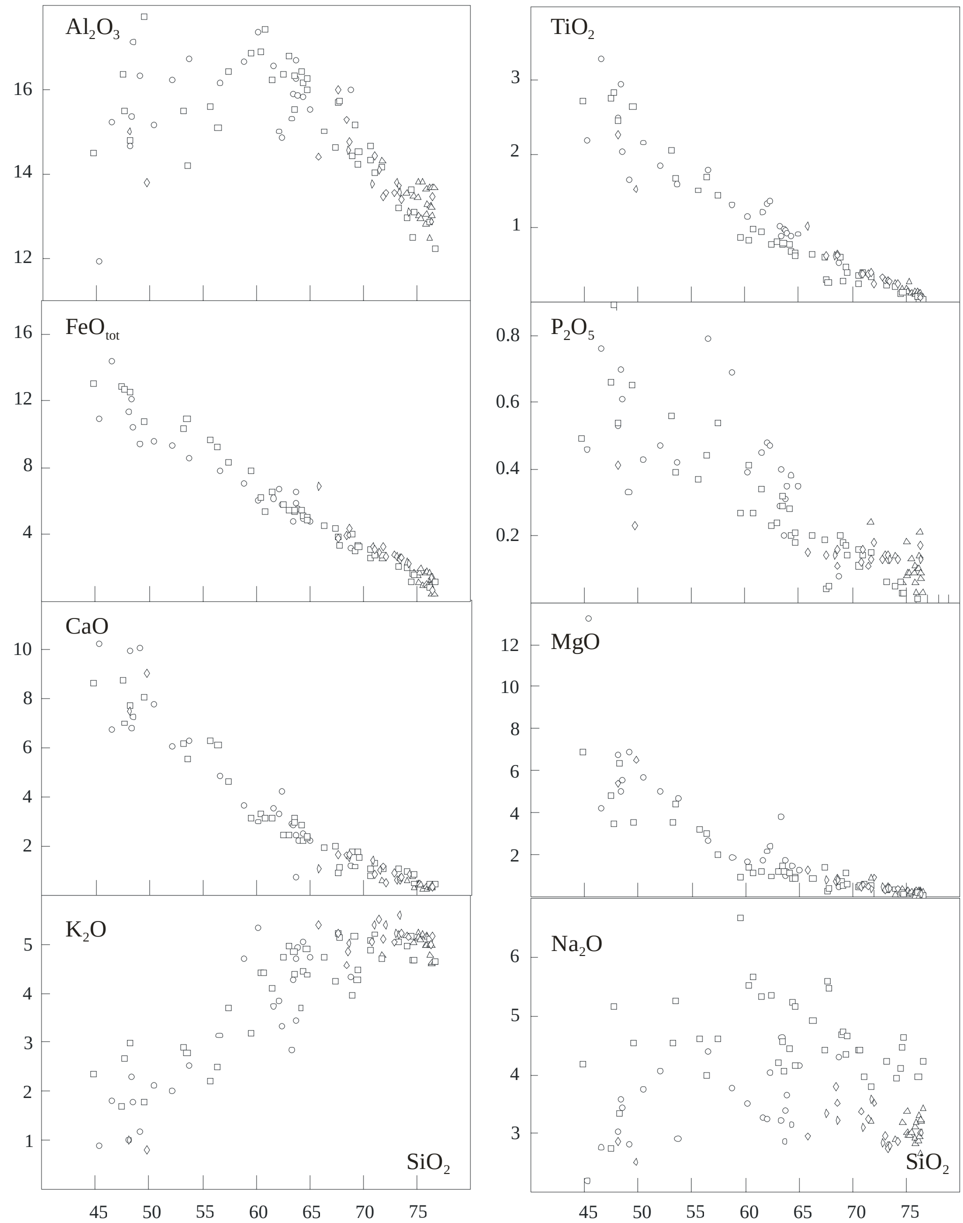


Fig. 6A. Harker diagrams, Tusaquillas Plutonic Complex (TPC) and Abra Laite-Aguilar Plutonic Complex (AL-APC). Symbols as in Fig. 3.

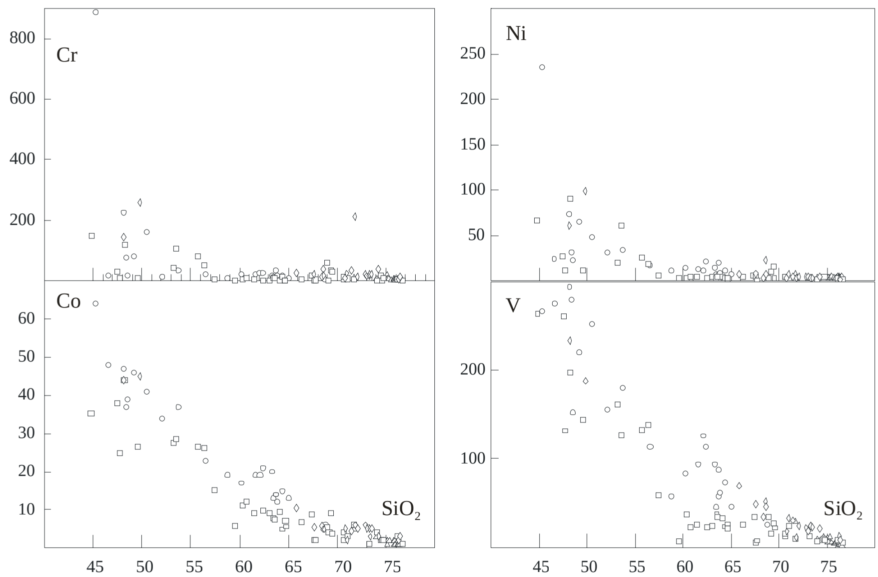


Fig. 6B. Compatible trace elements (ppm) vs. silica (wt%) for TPC and AL-APC rocks. Symbols as in Fig. 3.

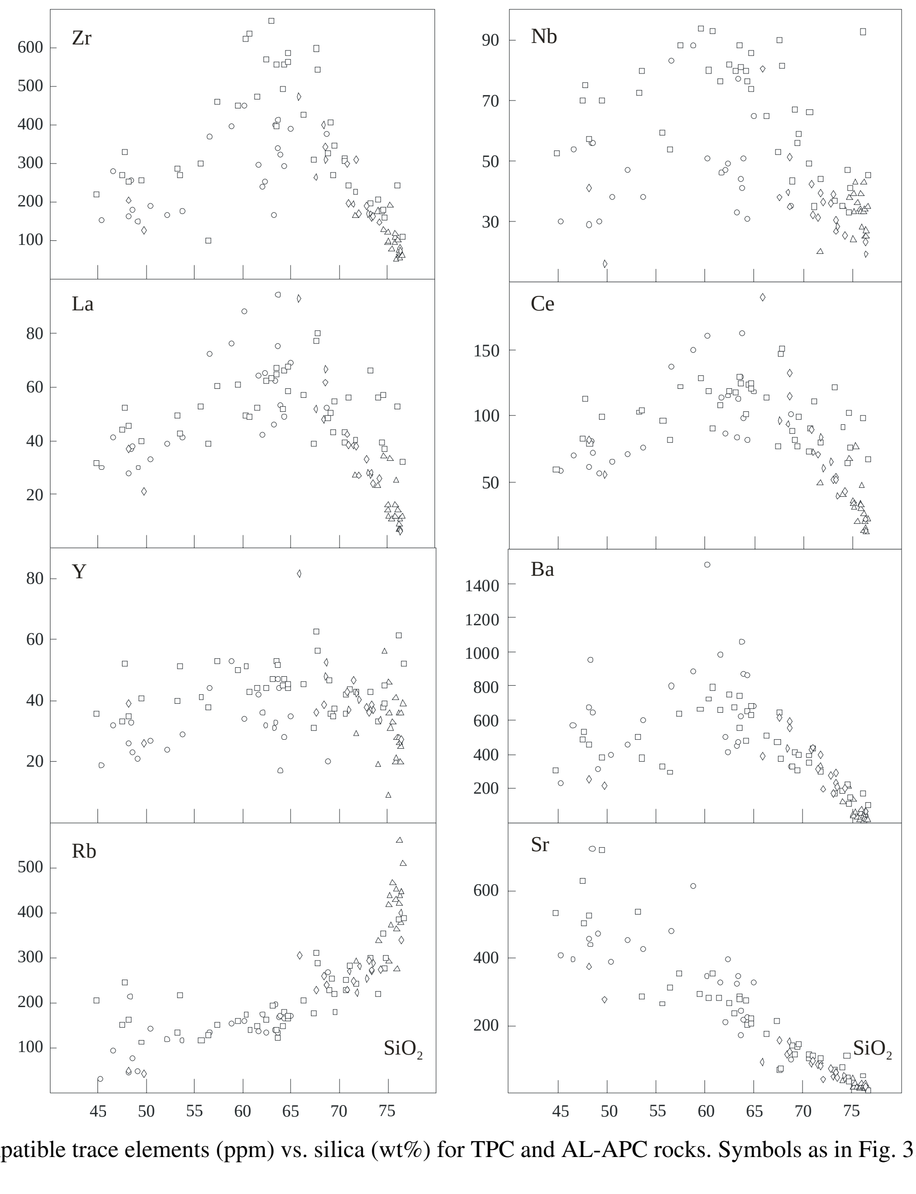


Fig. 6C. Incompatible trace elements (ppm) vs. silica (wt%) for TPC and AL-APC rocks. Symbols as in Fig. 3.

the HFSE present well-shaped trends, defining positive trends for the basic and intermediate compositions, and negative ones for higher $SiO_2$ contents. It is noteworthy that the most evolved rocks in both plutonic complexes, are characterized by the lowest contents of incompatible trace elements.

I.E. from basic to intermediate compositions of selected rock-types from AL-APC and TPC, normalized to the Primitive Mantle (Sun & McDonough, 1989; Fig. 7), display enriched patterns with negative anomalies in Sr and P.

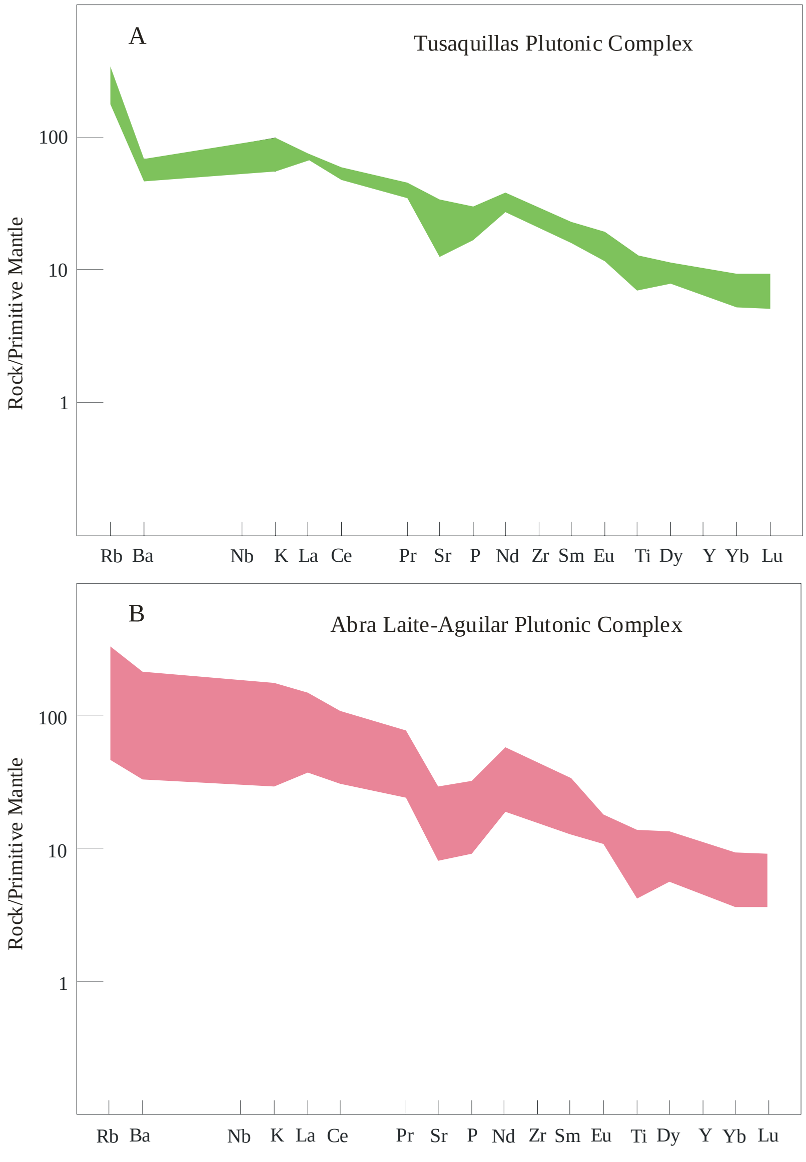


Fig. 7. Incompatible elements normalized to Primitive Mantle abundance (Sun & McDonough, 1989), basic to intermediate rocks from TPC (A) and AL-APC (B).

## Rare earth elements (REE)

Chondrite-normalized REE pattern for mafic and intermediate rocks from TPC (Fig. 8A) shows significant fractionation of LREE, $(La/Sm)_N$ ranging from 2.80 to 5.11, gabbro and quartz syenite, respectively. HREE appear poorly fractionated, $(Gd/Yb)_N$ ranging from 1.82 to 3.92, gabbroic and quartz syenitic compositions, respectively. Negative Eu anomalies (Eu/Eu*=0.68-0.75) are observed in samples with $SiO_2$>59 wt%, whereas the basic rocks show Eu/Eu* ranging from 1.00 to 0.91.

The TPC granites (Fig. 8B) have LREE contents lower than those of basic-intermediate rocks. All the samples display LREE fractionation decreasing with increasing $SiO_2$, i.e. $(La/Sm)_N$ 3.97-1.88 for $SiO_2$

74.7-76.37 wt%. HREE usually appear to be unfractionated, i.e. $(Gd/Yb)_N$ 0.71-1.11, T100 and T25 samples excepted [$(Gd/Yb)_N$~2)]. Significant negative Eu anomalies are observed in all the granites with a notable decrease of Eu/Eu* (0.23 to 0.03) with $SiO_2$ increase (74 to 76 wt%).

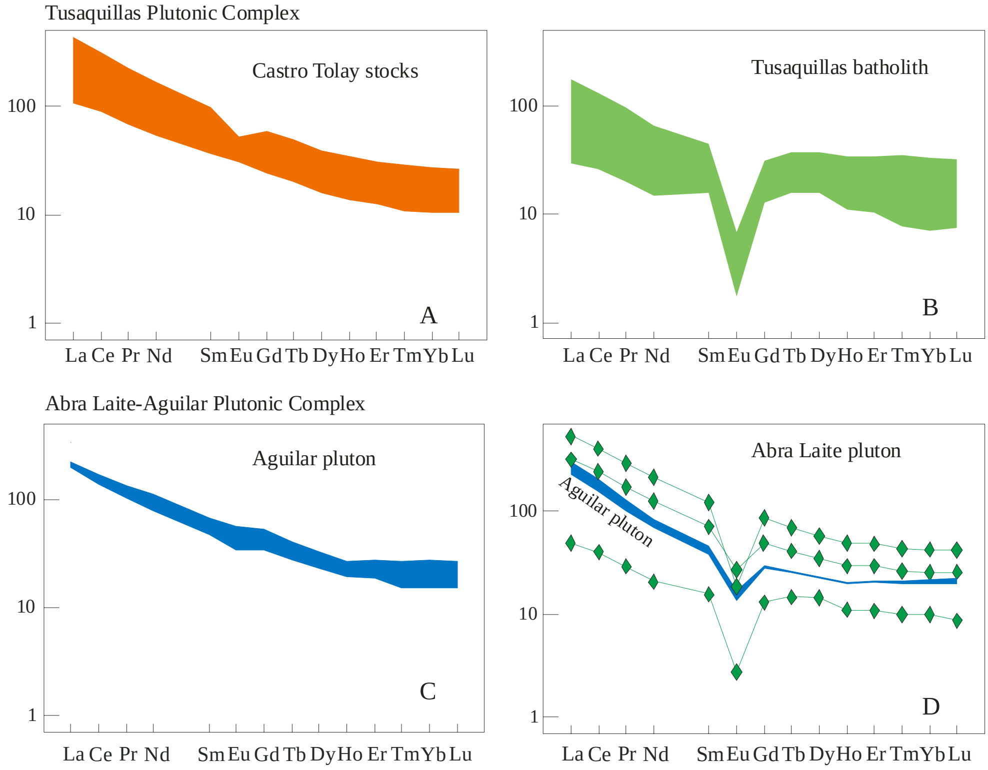


Fig. 8. Chondrite-normalized (Sun & McDonough, 1989) REE diagrams. A) basic to intermediate rocks from TPC; B) granitic rocks from TPC; C) basic to intermediate rocks from AL-APC; D) granitic rocks from AL-APC.

Mafic and intermediate rocks ($SiO_2$ 44.8-64.7 wt%) from AL-APC (Fig. 8C) show fractionated LREE, i.e. $(La/Sm)_N$ from 3.12 to 3.96 for gabbroic and monzonitic compositions, respectively, whereas HREE exhibit flattened patterns, $(Gd/Yb)_N$ ranging from 1.47 to 2.55. Eu/Eu* ranges from 0.75 to 0.94.

AL-APC granitic rocks (Fig. 8D) have REE contents similar to those of the TPC granites, showing LREE enrichment with $(La/Sm)_N$ varying from 3.17 to 4.51. Significant negative Eu anomalies are observed in all the granitic samples, Eu/Eu* ranging from 0.18 to 0.46.

## Isotopic (Sr, Nd) composition

Sr and Nd isotopic compositions of fifteen selected samples from TPC and eight from AL-APC were analyzed (Table 2).

Initial $^{87}Sr/^{86}Sr$ ($R_0$), $^{143}Nd/^{144}Nd$ ($Nd_i$) and $\varepsilon^tNd$ have been computed-back to 150 Ma for TPC marginal stocks and to 145 Ma for TPC granites. Initial isotopic ratios for AL-APC samples have been computed-back to 149 Ma (Table 2; cf. Cristiani *et al.*, 1999; Cristiani *et al.*, 2000).

TPC granites ($SiO_2$ 74-76 wt%) show $R_0$ ranging from 0.708677 to 0.722668, with relatively homogeneous $\varepsilon^tNd$ ranging from -1.77 to -2.65. The TPC marginal stocks have variable $R_0$: the most primitive rock-types ($SiO_2$~45 wt%) have low values (0.703545), whereas quartz syenite rock-types ($SiO_2$~64 wt%) exhibit relatively high values (0.713121). In the same rock-types, $\varepsilon^tNd$ ranges from 3.55 to -4.97.

AL-APC basic rocks ($SiO_2$<50 wt%) are characterized by low $R_0$ (0.703198-0.704605) and high $\varepsilon^tNd$ (3.82-3.65). More evolved monzodioritic and syenitic rocks have similar $R_0$ (0.703303-0.704008), and lower $\varepsilon^tNd$ (+2.01 to -1.06) in comparison with the more basic samples. Two granitic rocks are characterized by high $R_0$ (0.713735-0.710668) and low $\varepsilon^tNd$ values (-3.85 to -3.24).

Table 2. Rb-Sr and Sm-Nd isotopic analyses of selected samples from the Tusaquillas and Abra Laite-Aguilar Plutonic Complexes. (*), Rb/Sr isochron and (°), U/Pb SHRIMP (Cristiani, 2004).

| Tusaquillas Plutonic Complex (TPC) | | | | | | | | | | | | | |
|---|---|---|---|---|---|---|---|---|---|---|---|---|---|
| Sample | Rock-type | Rb | Sr | $^{87}Rb/^{86}Sr$ | $(^{87}Sr/^{86}Sr)_{meas}$ | $R_0$ | Sm | Nd | $^{147}Sm/^{144}Nd$ | $(^{143}Nd/^{144}Nd)_{meas}$ | $(^{143}Nd/^{144}Nd)_i$ | $\varepsilon^tNd$ | Age (Ma) |
| T 6 | Gabbro | 27.00 | 426.00 | 0.1833 | 0.703920±20 | 0.703545 | 5.42 | 25.84 | 0.1268 | 0.512754±09 | 0.512634 | 3.55 | |
| T 11 | Quartz monzonite | 202.00 | 354.00 | 16,510 | 0.707890±50 | 0.704511 | 9.80 | 53.30 | 0.1112 | 0.512617±10 | 0.512512 | 1.16 | 144±1(*) |
| T 30 | Quartz monzonite | 156.00 | 623.00 | 0.7244 | 0.707320±10 | 0.705755 | 12.67 | 67.21 | 0.1140 | 0.512505±01 | 0.512392 | -0.99 | |
| T 31 | Gabbro | 44.20 | 487.00 | 0.2625 | 0.704500±10 | 0.703933 | 5.70 | 24.40 | 0.1412 | 0.512675±09 | 0.512534 | 1.80 | 151±1(*) |
| T34 | Quartz syenite | 155.00 | 347.00 | 12,928 | 0.711420±20 | 0.708626 | 12.40 | 71.00 | 0.1056 | 0.512389±10 | 0.512284 | -3.09 | 152±2(*) |
| T 73 | Monzodiorite | 201.00 | 448.00 | 12,980 | 0.707060±10 | 0.704403 | 8.09 | 40.34 | 0.1212 | 0.512709±12 | 0.512595 | 2.77 | |
| T 79 | Quartz syenite | 132.00 | 170.00 | 22,488 | 0.717980±40 | 0.713121 | 12.42 | 66.90 | 0.1122 | 0.512299±09 | 0.512187 | -4.97 | |
| T 83 | Quartz syenite | 177.00 | 255.00 | 20,095 | 0.713780±20 | 0.709438 | 11.64 | 65.61 | 0.1072 | 0.512365±10 | 0.512257 | -3.61 | |
| T 5 | Quartz monzonite | 140.85 | 411.04 | 0.9912 | 0.705835±28 | 0.703806 | 7.49 | 40.92 | 0.1107 | 0.512657±11 | 0.512553 | 1.95 | |
| T 98 | Monzodiorite | 111.81 | 461.95 | 0.7003 | 0.707381±23 | 0.705868 | 6.38 | 32.16 | 0.1199 | 0.512649±12 | 0.512520 | 1.51 | |
| T 19 | Granite | 274.00 | 37.90 | 210,074 | 0.751920±40 | 0.708920 | 6.80 | 30.70 | 0.1339 | 0.512447±09 | 0.512321 | -2.57 | |
| T 69 | Granite | 430.00 | 15.20 | 832,205 | 0.879020±20 | 0.708677 | 4.50 | 17.20 | 0.1582 | 0.512445±12 | 0.512315 | -2.52 | 144±2(*) |
| T 100 | Granite | 329.00 | 34.00 | 281,659 | 0.769530±20 | 0.713480 | 4.55 | 21.33 | 0.1290 | 0.512440±11 | 0.512322 | -2.65 | 140±1(*) |
| T 48 | Granite | 464.98 | 20.69 | 659,521 | 0.853911±20 | 0.722668 | 5.37 | 23.85 | 0.1361 | 0.512492±12 | 0.512367 | -1.77 | |
| T 107 | Granite | 514.40 | 17.23 | 879,504 | 0.893790±40 | 0.718771 | 1.92 | 6.13 | 0.1893 | 0.512526±10 | 0.512352 | -2.05 | |
| Abra Laite-Aguilar Plutonic Complex (AL-APC) | | | | | | | | | | | | | |
| Sample | Rock-type | Rb | Sr | $^{87}Rb/^{86}Sr$ | $(^{87}Sr/^{86}Sr)_{meas}$ | $R_0$ | Sm | Nd | $^{147}Sm/^{144}Nd$ | $(^{143}Nd/^{144}Nd)_{meas}$ | $(^{143}Nd/^{144}Nd)_i$ | $\varepsilon^tNd$ | Age (Ma) |
| AGUILAR | | | | | | | | | | | | | |
| AG 31 | Gabbro | 149.28 | 602.65 | 0.717 | 0.706123±21 | 0.704605 | 8.69 | 43.76 | 0.120 | 0.512759±06 | 0.512642 | 3.82 | |
| AG 8 | Gabbro | 173.05 | 506.95 | 0.987 | 0.705289±30 | 0.703198 | 7.27 | 36.69 | 0.120 | 0.512755±06 | 0.512638 | 3.75 | |
| AG 67 | Diorite | 118.26 | 736.51 | 0.464 | 0.704343±10 | 0.703360 | 13.00 | 62.93 | 0.125 | 0.512755±06 | 0.512633 | 3.65 | |
| AG 16s | Monzodiorite | 119.66 | 264.71 | 1,308 | 0.706329±21 | 0.703559 | 8.28 | 43.64 | 0.115 | 0.512664±07 | 0.512552 | 2.07 | |
| AG 45c | Syenite Hbl+Bt | 143.38 | 299.82 | 1,383 | 0.706233±21 | 0.703303 | 7.40 | 38.27 | 0.117 | 0.512668±13 | 0.512554 | 2.10 | |
| AG 13 | Syenite Hbl+Bt | 218.51 | 131.82 | 4,799 | 0.714172±20 | 0.704008 | 4.61 | 21.85 | 0.128 | 0.512516±26 | 0.512392 | -1.06 | 149±1(*) |
| ABRA LAITE | | | | | | | | | | | | | |
| AB 21 | Granite Bt+Crd | 299.39 | 97.19 | 8,935 | 0.733296±10 | 0.713735 | 15.77 | 86.20 | 0.111 | 0.512385±11 | 0.512273 | -3.24 | 153±4(°) |
| AB 34 | Granite Bt+Grn | 235.63 | 151.84 | 4,495 | 0.720510±20 | 0.710668 | 10.30 | 55.87 | 0.111 | 0.512355±84 | 0.512243 | -3.85 | |

# DISCUSSION

## Magma source(s) and evolution

Trace elements and Sr and Nd isotopic compositions define two main groups, both for TPC and AL-APC complexes:

1) basic rock-types, $SiO_2$=45-52 wt%, low HFSE and REE contents, low $R_0$ (0.703198-0.705868) and high $\varepsilon^tNd$ (3.82 to 1.51);

2) felsic rock-types, $SiO_2$=70-77 wt%, low HFSE and REE, high $R_0$ (0.708677-0.722668) and low $Nd_i$ (-3.85 to -1.77).

Between the above two groups, a lot of rock-types with geochemical intermediate features (i.e. $SiO_2$=53-69 wt%, $R_0$=0.703303-0.713121; $\varepsilon^tNd$ 2.10 to -4.97) has been recognized.

The femic rocks from both the intrusive complexes show trace elements distribution and Sr-Nd isotopic ratios compatible with mantle derived magmas, and in particular with intraplate basalts. The geochemical characteristics of the felsic rocks ($SiO_2$ 70-76 wt%) are not in agreement with their derivation from basic-intermediate magmas through a simple fractional crystallization process (FC) or FC plus crustal assimilation (AFC). In fact, they show the highest $R_0$, and lowest $Nd_i$.

Also AFC process can be excluded because only a very high ratio of "r" (assimilation rate to fractionation rate; DePaolo, 1981) could explain a derivation of the felsic magmas from gabbroid liquids. These considerations and the high $R_0$ and low $\varepsilon^tNd$ from TPC granites suggest their derivation from partial melting of a crustal source. The scattered $R_0$ of the granites could be interpreted as due to a disequilibrated partial melting of crustal materials (cf. Knesel & Davidson, 1996; Tommasini & Davies, 1997).

Modelling of the trace elements indicates that magmas with intermediate composition ($SiO_2$ 60-65 wt%) could derive from magmas with low silica content (e.g. ~45 wt%) by fractional crystallization processes. In the diagrams La and Zr vs. $SiO_2$ (Fig. 9), the modelling suggests that a liquid with gabbroic composition (e.g.. T6 or AG 31 compositions of Table 1) could generate a quartz monzodioritic magma (e.g. T91 composition)

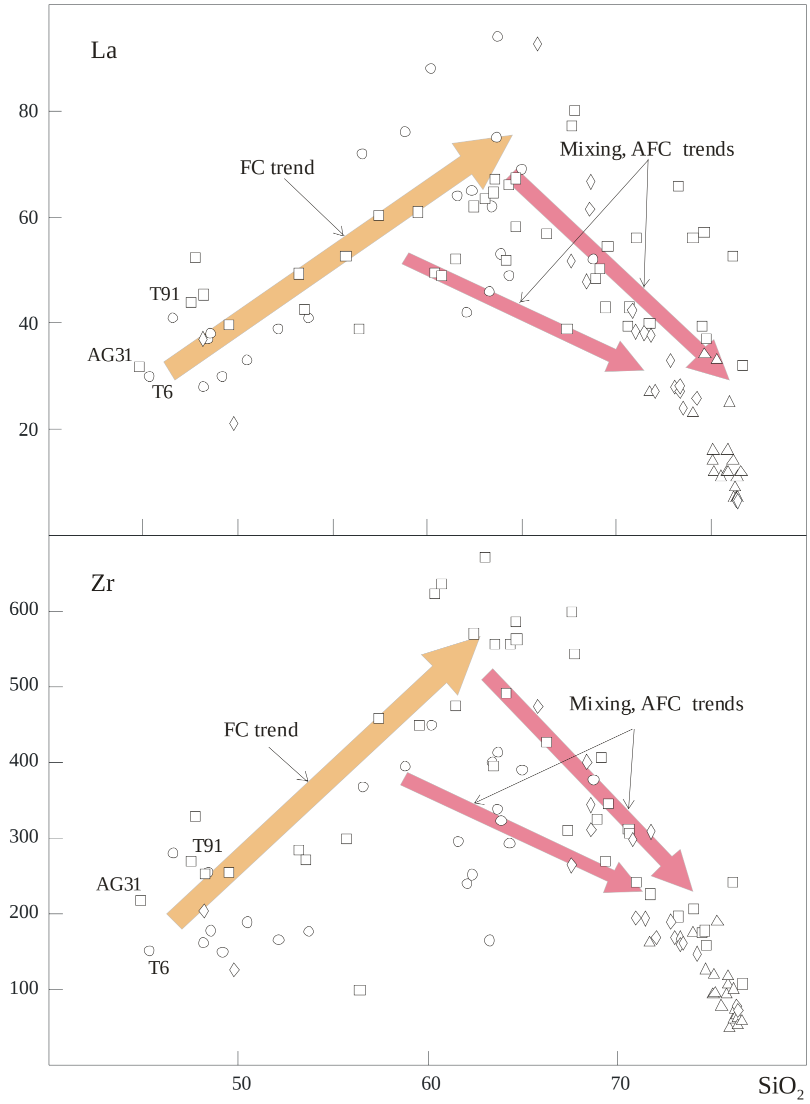


Fig. 9. $SiO_2$ vs. La and Zr showing the distribution of TPC and AL-APC rock-types. Symbols as in Fig. 3. The evolutionary trends (FC, fractional crystallization; mixing; AFC, assimilation plus fractional crystallization: cf. DePaolo, 1981) are also pictured (see text).

through crystallization (wt%) of olivine (30%), clinopyroxene (35%) and plagioclase (20%). If the FC process keeps going with separation of clinopyroxene (20%), plagioclase (50%) and hornblende (30%), it is possible to explain almost the whole compositional spectrum of intermediate TPC and AL-APC rocks up to $SiO_2$ 65 wt%. The homogeneity of the isotopic composition of the basic and intermediate rocks ($SiO_2$ 45-65 wt%) from AL-APC ($R_0$=0.703198-0.704605; $\varepsilon^t$Nd +3.65 to $\varepsilon^t$Nd +3.82) and TPC ($R_0$=0.703545-0.704403; $\varepsilon^t$Nd +3.55 to $\varepsilon^t$Nd +2.77) supports the hypothesis that FC processes have played an important role in the evolution of magmas (cf. trend 1 of Fig. 10).

These data suggest that at least two sources were involved in the production of the TPC and AL-APC magmas: one source characterized by mantle isotopic ratios, and other one with crustal geochemical signature. In this contex, the samples with $SiO_2$>60-65 wt%, plotting out of FC trend defined by basic rocks, possibly represent the result of contamination or mixing processes between mantle derived magmas and radiogenic crustal material (trend 2, Fig. 10). High concentrations of mafic microgranular enclaves in TPC and AL-APC support this hypothesis.

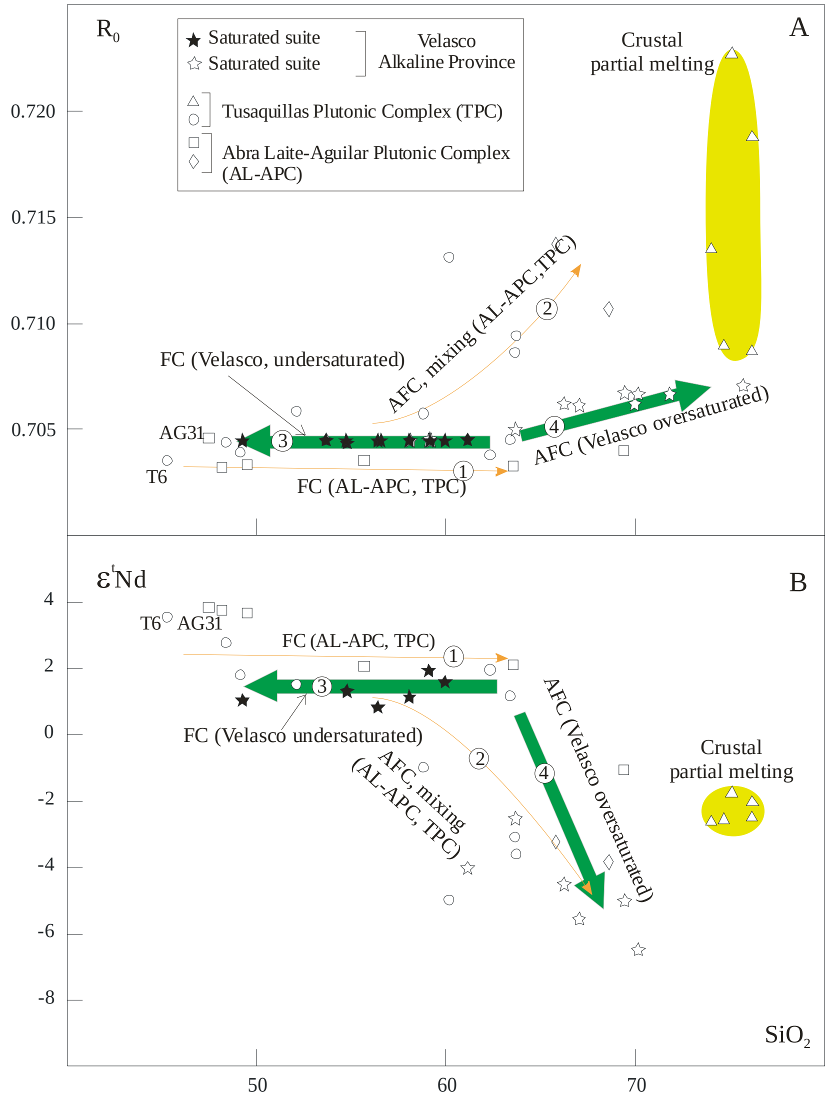


Fig. 10. $SiO_2$ vs. initial $^{87}Sr/^{86}Sr$ ($R_0$; A), and vs. time-integrated $^{143}Nd/^{144}Nd$ (ε-notation, $\varepsilon^tNd$; B) showing evolution of the different complexes from E Bolivia and NW Argentina. $R_0$ and $\varepsilon^tNd$ have been computed-back to 150 Ma for the TPC marginal stocks, to 145 Ma for the TPC granites, and to 149 Ma for AL-APC complex $\varepsilon^tNd$ (Cristiani *et al.*, 1999; Cristiani, 2004). Symbols as in Fig. 3. FC: fractional crystallization; AFC: assimilation plus fractional crystallization (DePaolo, 1981).

In conclusion, the intra-plate-type mantle melts could generate magmas with compositions up to $SiO_2$ 65 wt% by FC-AFC processes, whereas acid magmas could represent the product of partial melting of crustal material. Notably, anatectic melts are not unusual in the South American plate: e.g. at 143-144 Ma anatectic melts, with cordierite and orthopyroxene as liquidus phases, flowed at the Rio Grande do Sul (Jaguarão dacites-rhyodacites, $SiO_2$ 65 wt%, $R_0$ 0.72169, $\varepsilon^tNd$ -14.7; Comin-Chiaramonti, 2000). As a matter of fact, mixing-mingling processes between evolved and anatectic magmas would generate melts with intermediate geochemical and isotopic characteristics. In view of these considerations we propose a two-stage magmatic evolution for the TPC and AL-APC:

1) In a first stage, characterized by mantle upwelling, the asthenospheric upraising caused the emplacement of magmas with intraplate signatures at the base of continental crust, which were undergone by FC and AFC processes. This new geotectonic setting produced a general enhancement of the thermal gradient.

2) The storage of basaltic magmas in the crust and their ascent towards the shallower levels, accompanied by the consequent new physical

conditions, could have triggered partial melting processes in the continental crust, generating anatectic melts. At this point, gabbroic magmas and their differentiates mingled and blended with anatectic magmas.

NW Argentina Mesozoic magmatic Province: comparison with the Velasco Alkaline Province

Extensive outcrops of Mesozoic plutonic rocks represent prominent geologic features in E Bolivia (Velasco Alkaline Province) and NW Argentina (TPC, AL-APC, Rangel Alkaline Complex and Hornillos Alkaline Complex) (Fig. 11). Both magmatic provinces are commonly set along a lineament with a general NNE-SSW trend. The intrusions are interpreted as the product of magmatic episodes linked to the evolution of the Jurassic-Eocene continental rift systems, in western and central South America (Fletcher & Litherland, 1981; Avila Salinas, 1986; Cristiani *et al.*, 2000, 2003; Cristiani, 2004). A synoptical summary relative to the rock-types, associated minerals, geochemistry, isotopic data and ages of E Bolivia and NW Argentina Mesozoic suites is presented in Table 3.

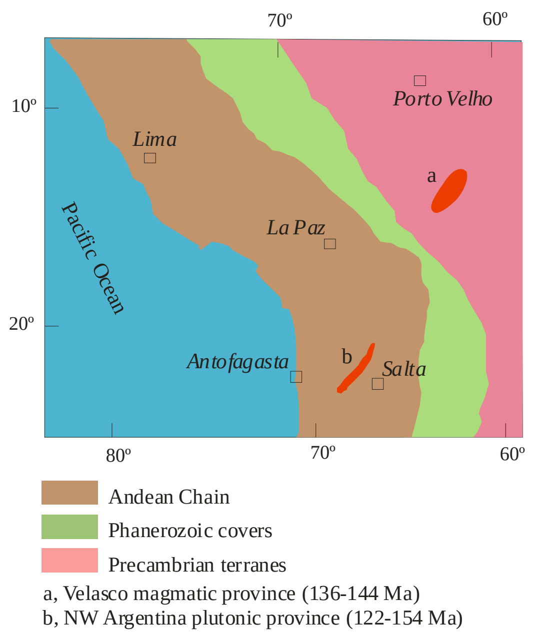


Fig. 11. Sketch-map of central-western South America showing the location of alkaline provinces from NW Argentina and E Bolivia.

In NW Argentina magmatic province, the Hornillos alkaline complex is represented by a small laccolith outcropping in the Eastern Cordillera, close to the Argentina-Bolivia boundary. Rocks of this complex, characterized by an undersaturated and a saturated series, range in compositions from monzodiorite, monzonite and syenite to pulaskite and nordmarkite. Geochemical and isotopic characteristics are comparable to alkaline intraplate basalts suggesting their derivation from an asthenospheric source enriched in incompatible elements. The Rangel Alkaline complex is constituted by a peralkaline syenitic intrusion outcropping in the Puna Plateau and covering an area of about 9 km$^2$. Geochemical and isotopic signatures suggest a derivation from an OIB-like mantle source, with scarce crustal contamination (Menegatti, 2001).

The Velasco Alkaline Province (Fletcher & Beddoe-Stephens, 1987) is situated near to the Bolivian-Brazilian border (Fig. 11). It consists of 14 inhomogeneous bodies with subcircular to sub-elliptical shapes covering an area of about 440 km$^2$. The plutons intrude the western Amazonian basement (1.8-1.0 Ga) and form part of the Sunsas-Aguapei mobile belt (1.3-0.95 Ga) in the Rondônia Block (Tassinari *et al.*, 2000). The ages determinated for the Cabeza de Toro and Cerro Bamba alkaline plutons from the Velasco Province range from 141±5 and 144±4 Ma (Rb/Sr isochron) to 134 and 136 Ma (K/Ar) (Fletcher & Beddoe Stephens, 1987). Syenites, quartz syenites and granites are the predominant rock-types. Subordinate nephel-syenites and nepheline syenites are present (Comin-Chiaramonti *et al.*, in this volume). Numerous alkaline dykes intrude the plutons of the Velasco complex and the metamorphic Precambrian basement. Dykes usually range in compositions from quartz trachyte to trachyphonolite and aplite showing mineralogical assemblages broadly similar to those of the host plutonic rocks (Fletcher & Litherland, 1981; Comin-Chiaramonti *et al.*, in this volume).

On the basis of petrologic, chemical and isotopic variations, some authors (Litherland *et al.*, 1986; Fletcher & Beddoe-Stephens, 1987; Comin-Chiaramonti *et al.*, in this volume) identified two main suites: a) an undersaturated suite (foyaite-pulaskite trend) and b) an oversaturated suite (quartz syenite-granite trend). Comin-Chiaramonti *et al.* (in this volume) suggest that the undersaturated rocks derived by mantle source without appreciable crustal contamination, whereas the oversaturated rocks appear to have suffered interactions with crustal materials.

Table 3. Synoptical comparison relative to the main rock-types, mineral assemblage ages and geochemical features of the Jurassic-Cretaceous plutons from NW Argentina and E Bolivia. Rangel Alkaline Complex after Menegatti (2001); Tusaquillas Plutonic Complex and Abra Laite-Aguilar Plutonic Complex after this paper; Hornillos Alkaline Complex after Rubiolo (1992); Velasco Plutonic Complex, after Comin-Chiaramonti *et al*. (in this volume) and therein references.

| Magmatic Province | NW Argentina | | | | | | E Bolivia |
|---|---|---|---|---|---|---|---|
| Plutonic Complex | Rangel Alkaline Complex | Tusaquillas Plutonic Complex | | AL-AG Plutonic Complex | | Hornillos Alkaline Complex | Velasco Plutonic Complex |
| | | Castro Tolay Stocks | Tusaquillas Granite | Aguilar Stock | Abra Laite Granite | | |
| Rock-types | Alkali granite<br>Alkali syenite<br>Foid alkali syenite<br>Dykes<br>Carbonatite dykes | Diorite-gabbro<br>Monzodiorite<br>Quartz monzodiorite<br>Quartz monzodiorite<br>Quartz syenite | Biotite granite<br>Bt+Ms granite | Monzodiorite<br>Quartz syenite<br>Quartz monzodiorite<br>Monzonite<br>Monzodiorite<br>Gabbro (diorite)<br>Foid gabbro | Bt-Ms granite<br>Biotite granite | Normarkite<br>Syenite<br>Monzonite<br>Monzodiorite<br>Pulaskite<br>Bostonite<br>Trachyte<br>Tinguaite | Syenite<br>Quartz syenite<br>Granite<br>Alkali granite<br>Trachyte<br>Quartz trachyte<br>Syenite<br>Nephel-syenodiorite<br>Nephel-syenite<br>Nepheline syenite<br>Trachyphonolite<br>Carbonatite |
| Paragenesis | Na-plagioclase<br>Alkali feldspar<br>Na-Feldspar<br>Hornblende | Plagioclase<br>Alkali feldspar<br>Olivine<br>Diopside-augite | Plagioclase<br>Alkali feldspar<br>Quartz<br>Biotite | Plagioclase<br>Alkali feldspar<br>Olivine<br>Diopside | Plagioclase<br>Alkali feldspar<br>Quartz<br>Biotite | K-feldspar<br>Plagioclase<br>Quartz<br>Clinopyroxene | Quartz<br>Alkali feldspar<br>Nepheline<br>Haüyne |
| Primary minerals | Diopside<br>Biotite<br>Arfvedsonite<br>Riebeckite<br>Aegirine<br>Nepheline | Hornblende<br>Biotite<br>Fe-Ti oxide<br>Allanite<br>Apatite | Muscovite<br>Al-silicate<br>Zircon<br>Apatite<br>Tourmaline<br>Fe-Ti oxide | Fe-edenite<br>Biotite<br>Fe-Ti oxide<br>Allanite<br>Apatite | Muscovite<br>Garnet<br>Cordierite<br>Al-silicate<br>Dumortierite<br>Tourmaline | Olivine<br>Nepheline<br>Sodalite<br>Biotite<br>Apatite | Sodalite<br>Diopside-hedenbergie<br>Hastingsite-edenite<br>Biotite<br>Magnetite<br>Hematite<br>Ilmenite |
| Microgranular mafic enclaves | Alkali syenite<br>Quartz alkali syenite | Diorite-gabbro | | Monzodiorite<br>Gabbro foid<br>Gabbro | | | |
| Geochemistry | | | | | | | |
| $SiO_2$ (wt%) | 59-76 | 45.30-64.99 | 71.73-76.59 | 44.81-76.65 | 62.42-78.83 | 44.0-69.8 | 54-72 |
| Alumina Index (A/CNK) | 0.6-1.1 | 0.88-1.02 | 1.02-1.16 | 0.80-1.07 | 0.81-0.97 | | 0.7-1.0 |
| Agpaitic Index (A.I.) | 0.8-1.5 | 1.22-1.63 | 1.06-1.23 | 0.89-1.33 | 1.07-1.32 | | 0.7-1.2 |
| $K_2O/Na_2O$ | 0.1-1.9 | 0.34-1.60 | 1.35-1.87 | 0.39-1.31 | 1.21-2.03 | 0.53-2.12 | 0.6-1.6 |
| $FeO_{tot}/(FeO_{tot}+MgO)$ | 0.04-0.9 | 0.45-0.88 | 0.66-0.96 | 0.65-0.94 | 0.74-0.92 | | 0.7-1.0 |
| Eu/Eu* | 0.18-1.10 | 0.45-1.04 | 0.030.23 | 0.36-0.94 | 0.18-0.46 | | 0.11-2.50 |
| $R_0$ | 0.704230-0.718438 | 0.703545-0.713121 | 0.708677-0.722668 | 0.703198-0.704605 | 0.710668-0.713735 | | 0.70412-0.70792 |
| $^{143}Nd/^{144}Nd_{initial}$ | 0.512517-0.512547 | 0.512299-0.512754 | 0.512315-0.512642 | 0.512392-0.512642 | 0.512243-0.512273 | | 0.51217-0.51256 |
| $\varepsilon^{t}Nd$ | 0.96-1.58 | 3.55 to -4.97 | - 1.77 to -2.65 | 3.82 to -1.06 | - 3.24 to -3.85 | | 1.92-6.50 |
| Age (Ma) | 122-134 | 144-152 | 140-144 | 149 | 154 | | 136 - 144 |
| $T^{DM}$ (Ma) | 527-757 | 529 | | 516-1507 | 977-1028 | | 600-1163 |

Petrogenetic considerations

For a better understanding of the relationships between the undersaturated and oversaturated magmas characterizing the Velasco and NW Argentina magmatic provinces, we have plotted the samples of the two provinces in the total alkalies-silica diagram (Fig. 12), with the thermal divide (Cox *et al.*, 1979). Most of the TPC and AL-APC basic and intermediate rocks exhibit a trend of alkali enrichment in the field of the oversaturated rocks, and define a continuous fractionation sequence from gabbros to syenites, as discussed in the previous sections. Fields representing the Hornillos rocks show evident coincidence with the over and undersaturated suites from the Velasco Province, whereas the Rangel compositional field straddles over the oversaturated trend of the same Velasco Province. The basic enclaves (i.e. T6 and AG31) and the basic rocks from Hornillos represent the most primitive oversaturated and slightly undersaturated terms from TPC and AL-APC intrusions (cf. Fig. 12). The different geochemical features of these two groups of rocks could be related to mantle source dishomogeneities or to different degrees of mantle partial melting. The parental end-members may generate, by fractionation of olivine, clinopyroxene and plagioclase in roughly cotectic proportions, residual over- or undersaturated liquids with syenitic composition (at about silica 62-65 wt%), depending of their position with respect to the thermal divide. For alkali feldspar fractionation, the over- or undersaturated syenite melts may evolve towards the rhyolites or phonolites, respectively. Thus, the compositional characteristics of Hornillos, Rangel and Velasco Alkaline Province may be explained.

The $SiO_2$ vs. $R_0$ and $\varepsilon^t Nd$ diagrams (cf. Fig. 10) illustrate the possible processes that led to the magma evolution of the NW Argentina and Velasco alkaline provinces. Undersaturated rocks from Velasco and most of the products from TPC-AL-APC with $SiO_2$ values ranging from 45 to 65 wt% show similar Sr isotopic ratios and εNd comparable with those from intra-plate basalts. This suggests that a basic magma with OIB signature similar to the TPC and AL-APC gabbroic rocks (i.e. AG31) could produce, by FC processes, liquids with undersaturated syenitic composition, which could represent the parent magmas of the Velasco suites. Magmas with these characteristics may evolve through FC processes towards the undersaturated suites (trend 3, Fig. 10). Finally, syenitic liquids, straddling over the thermal divide (Fig. 12), may generate oversaturated rocks by AFC processes (trend 4, Fig. 10).

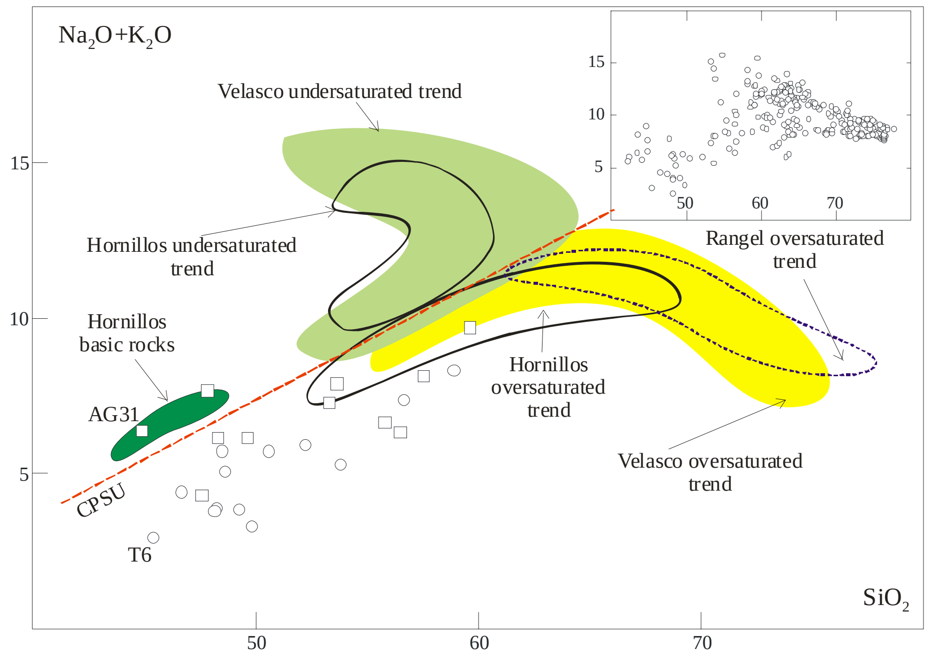


Fig. 12. $SiO_2$ vs. $Na_2O+K_2O$ (wt%) diagram showing the tendencies of the different alkaline complexes from E Bolivia and NW Argentina. Symbols as in Fig. 3; CPSU, red line: trace of the critical plane of silica saturation (Cox *et al.,* 1979). Inset: plot of the entire analyzed rocks from the NW Argentina and E Bolivia provinces. See text for explanation.

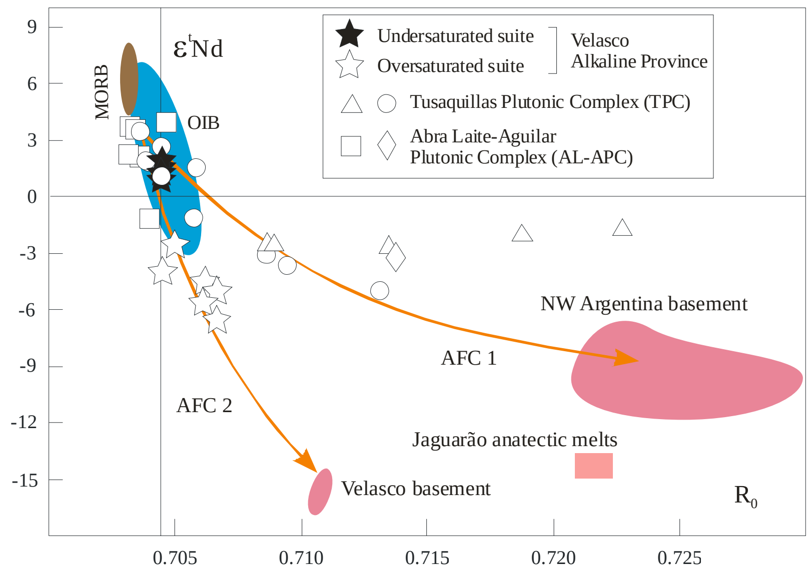


Fig. 13. $R_0$ vs. $\varepsilon^t$Nd diagram showing isotopic evolution for the different alkaline complexes from E Bolivia and NW Argentina. Symbols as in Fig. 3. Data sources: OIB and MORB, Rollinson (1993); Velasco complexes and basement, Comin-Chiaramonti *et al.* (in this volume); NW Argentina basement, Becchio *et al.* (1999). AFC: assimilation plus fractional crystallization (cf. DePaolo, 1981). For comparison the anatectic melts from Jaguarão, Rio Grande do Sul are shown (139 Ma, K/Ar; Comin-Chiaramonti, 2000).

The evolution frame of the intrusive products from NW Argentina and Velasco magmatic provinces can be summarized by $R_0$ vs. $\varepsilon^t$Nd (Fig. 13): a) the undersaturated terms of the Velasco magmatic province fall in the OIB field, as well as the TPC and AL-APC basic and some intermediate rock-types; b) the different trends, as depicted by oversaturated suite from Velasco and NW Argentina rocks, may be linked by FC processes plus assimilation of materials from the basement with distinct isotopic signatures; c) the rocks from TPC with similar $\varepsilon Nd_t$ and different $R_0$ could be related to a disequilibrated partial melting of crystalline basement as discussed above or by mixing processes between crustal materials with different isotopic characters and OIB-type magmas.

## CONCLUDING REMARKS

New petrological findings of Late Jurassic-Early Cretaceous plutonic rocks outcropping in NW Argentina, compared with the available geochemical data from the Velasco magmatic province (Comin-Chiaramonti *et al.*, in this volume), allow us to put forward some considerations on the magmatic history of the Mesozoic rifting in eastern Central Andes:

1) The Late Jurassic-Lower Cretaceous Tusaquillas and Abra Laite-Aguilar plutons in NW Argentina are a prominent example of an anorogenic suite, associated to Mesozoic rifting in the eastern Central Andes.

2) The TCP and AL-APC basic rocks show geochemical and isotopic features comparable with those of intra-plate (OIB) basaltic magmas.

3) The data suggest that the gabbroic TPC and AL-APC magmas (i.e. T6 and AG31) may represent the parent from mantle sources. These mafic magmas have originated intermediate products through FC and AFC processes. Taking into account the existence of coeval undersaturated and oversaturated alkaline suites in NW Argentina (Hornillos and Rangel complexes) the basic rocks from TPC and AL-APC may approach the composition of a regional parental magma.

4) Geochemical and isotopic signatures of the highly evolved Tusaquillas and Abra Laite granites suggest an anatectic origin.

5) The magmatic evolution of the NW Argentina Alkaline Province is comparable to that of Velasco alkaline province. We tentatively envisage that the Velasco rocks could derive from magma sources with geochemical features similar to those of basic enclaves from TPC and AL-APC and basic rocks from Hornillos. A simple FC process could have dominated the evolution of these magmas up to nepheline syenites, whereas the evolution up to the

oversaturated rocks could be mainly linked to AFC processes involving the Precambrian Velasco basement, as suggested by Comin-Chiaramonti *et al.* (in this volume).

6) The $T^{DM}$ ages (516-572 Ma, corresponding to the Brasiliano cycle; cf. Table 3) inferred for basic (AL-APC, TPC) and syenitic (Rangel alkaline complex) rocks from NW Argentina (Menegatti, 2001; Cristiani, 2004) are similar to those inferred for uncontaminated rocks from the Velasco Province (600 Ma; Comin-Chiaramonti *et al.*, in this volume), suggesting that a petrogenetic event at a regional scale may have generated both the magmatic provinces with similar signatures at pre-drift times of the South American plate.

7) The composition of the studied rock-types (alkaline OIB-like), and their location with respect to the Jurassic volcanic arc, reject the hypothesis that the rift formation is linked to a back-arc basin as suggested by some authors (e.g. Brown *et al.*, 1984; Viramonte *et al.*, 1999). It is plausible that the magmatic suites have been generated during extensional regimes preceeding the break-up of the South America-Africa plates (Litherland *et al.*, 1986; Cristiani *et al.*, 2000; Cristiani, 2004). Finally, we agree with Comin-Chiaramonti *et al.* (1997), that the role of the mantle plume as a possible cause in the generation of these magmatic provinces, in an extensional frame, remains highly controversial.

## ACKNOWLEDGEMENTS

This paper resulted from the "Jurassic-Cretaceous magmatism in the NW-Argentina" Scientific Project, part of an academic convention between the University of Pisa (Italy) and the University of Salta (Argentina). The research was supported by MIUR (Italy), CIUNSA (Consejo de Investigaciones de la Universidad Nacional de Salta) and CONICET (Consejo Nacional de Investigaciones Científicas y Tecnológicas de la República Argentina). We thank Piero Comin-Chiaramonti for providing the geochemical analyses of the Velasco alkaline complex and for reviewing this paper.

## REFERENCES

Allmendinger, R.W., Jordan, T.E., Kay, S.M. & Isacks, B.L. (1997). The evolution of the Altiplano-Puna Plateau of the Central Andes. *Earth and Planetary Science Letters* **25**, 139-174.

Antonini, P., Gasparon, M., Comin-Chiaramonti, P. & Gomes, C.B. (in this volume) Post-Paleozoic magmatism in Eastern Paraguay: Sr-Nd-Pb isotope compositions.

Avila Salinas, W.A. (1986). El magmatismo Cretácico en Bolivia: *Symposium IGCP Project 242, La Paz, Proceedings*, 52-66.

Becchio, R., Lucassen, F., Kasemann, S., Franz, G., & Viramonte, G.J. (1999). El basamento Paleozoico Inferior del Noroeste de Argentina (13°-27°S); metamorfismo y geocronologia. *XIV Congreso Geológico Argentino, Salta,* **14**, 58-72.

Brown, G.C., Thorpe, R.S. & Webb, P.C. (1984). The geochemical characteristic of granitoids in contrasting arcs and comment on magma sources. *Journal of the Geological Society of London* **141**, 4113-436

Clarke, D.B. (1981). The mineralogy of peraluminous granites: a review. *Canadian Mineralogist* **19**, 3-17.

Comin-Chiaramonti, P. (2000) Peraluminous lavas from Jaguarão (Rio Grande do Sul, Brazil). *DICAMP, Quaderni di Mineralogia, Petrografia e Geochimica Applicate* **17**, 1-15.

Comin-Chiaramonti, P., Cundari, A., Piccirillo, E.M., Gomes, C.B., Castorina, F., Censi, P., De Min, A., Marzoli, A., Speziale, S. & Velázquez, V.F. (1997). Potassic and sodic igneous rocks from Eastern Paraguay: their origin from the lithospheric mantle and genetic relationships with the associated Paraná flood tholeiites. *Journal of Petrology* **38**, 495-528.

Comin-Chiaramonti, P., Gomes, C.B., Velázquez, V.F., Censi, P., Antonini, P., Comin-Chiaramonti, F. & Punturo, R. (in this volume) Alkaline complexes from southeastern Bolivia.

Cox, K.G., Bell, J.D. & Pankhurst, R.J. (1979) *The interpretation of the igneous rocks*. London: Allen Unwin, 450p.

Cristiani, C. (2004). *Il plutonismo anorogenico Mesozoico nell'Altiplano della Puna (Argentina Nord Occidentale, Ande Centrali): implicazioni petrogenetiche e geodinamiche*. Ph.D. Thesis, University of Pisa, 229p.

Cristiani C., Del Moro, A., Matteini, M., Mazzuoli, R., Menegatti, N. & Omarini, R.H. (2000).The Jurassic-Cretaceous plutonism of NW Argentina (central Andes): age, geochemical characters and geological setting. *31st International Geological Congress, Rio de Janeiro, Symposium Volcanism and Associated Regime* (CD-ROM).

Cristiani, C., Del Moro, A., Matteini, M., Mazzuoli, R. & Omarini, R.H. (1999). The magmatism linked to the Jurassic-Cretaceous rift of NW Argentina: The Tusaquillas Plutonic Complex (Central Andes). *XIV Congreso Geologico Argentino, Salta, Actas II,* 190-193.

Cristiani, C., Matteini, M., Mazzuoli, R. & Omarini, R.H. (2002). Geochemical characters of the Aguilar and Tusaquillas plutonic complexes (NW Argentina): insights on the genesis and evolution of the magmas during the Jurassic. Cretaceous continental rift. *XV Congreso Geológico Argentino*, *Neuquén* **2**, 168-171.

Cristiani, C., Matteini, M., Mazzuoli, R. & Omarini, R. (2003). Petrological study of interaction processes between crustal and mantle magmas for reconstructing the geotectonic setting of a continental rift: the case of Jurassic-Cretaceous Tusaquillas Plutonic Complex in Central Andes (NW Argentina). *Geophysical Research Abstracts* **5**, 12577.

De Min, A., Piccirillo, E.M., Marzoli, A., Bellieni, G., Renne, P.R., Ernesto, M. & Marques, L.S. (2003). The Central Atlantic magmatic province (CAMP) in Brazil: petrology, geochemistry, $^{40}Ar/^{39}Ar$ ages, paleomagnetism and geodynamic implications. In: Hames, W.E., McHone, J.G., Renne, P.R. & Ruppel, C. (eds.) *The Central Atlantic magmatic province. AGU Geophysical Monograph* **136**, 91-128.

DePaolo, D. J. (1981). Trace element and isotopic effects of combined wall-rock assimilation and fractional crystallization. *Earth and Planetary Science Letters* **53**, 189-202.

Fletcher, C.J.N. & Beddoe Stephens, B (1987). The petrology, chemistry and crystallization history of the Velasco alkaline province, eastern Bolivia. In: Fitton, J.G. & Upton, B.G.J. (eds.) *Alkaline igneous rocks. Geological Society of London, Special Publication* **30***,* 403-413.

Fletcher, C.J.N. & Litherland, M. (1981). The geology and tectonic setting of the Velasco Alkaline Province, eastern Bolivia. *Journal of the Geological Society of London* **138**, 541-548.

Frick, L.R., Lambert, D.D. & Hoatson, D.M. (2001). Re-Os dating of the Radio Hill Ni-Cu deposit, West Pilbara Craton, Western Australia. *Australian Journal of Earth Sciences* **48**, 43-47.

Galliski, M.A. & Viramonte, J.G. (1988). The Cretaceous paleo-rift in northwestern Argentina: a petrologic approach. *Journal of South American Earth Sciences* **1**, 329-242.

Gangui, A. & Götze, H.J. (1996). The deep structure of the northern Puna, Argentina constraints from 2D seismic data and 3D gravity modeling. *XIII Congreso Geologico Argentino y III Congreso de Exploracion de Hidrocarburos, Buenos Aires* **2**, 545-565.

Gomes, C.B. & Comin-Chiaramonti, P. (in this volume) An introduction to the alkaline and alkaline-carbonatitic magmatism in and around the Paraná Basin.

Gröschke, M., Hillebrandt, A.v., Prinz, P., Quinzio, L.A. & Wilke, H.G. (1988). Marine Mesozoic Paleogeography in North Chile between 21º-26ºS. In: Bahlburg, H, Breitkreuz, C. & Giese, P. (eds.) *The Southern Central Andes. Lecture Notes in Earth Sciences* **17**, 105-119.

Hibbard, M.J. (1981). The magma mixing origin of mantled feldspar. *Contributions to Mineralogy and Petrology* **76**, 158-170

Iacumin, M., De Min, A., Piccirillo, E.M. & Bellieni, G. (2003). Source mantle heterogeneity and its role in the genesis of Late Archean-Proterozoic (2.7-1.0 Ga) and Mesozoic (200 and 130 Ma) tholeiitic magmatism in the South American Platform. *Earth-Science Reviews* **62**, 365-391.

Irvine, T.N. & Baragar, W.R.A., (1971). A guide to chemical classification of the common rocks. *Canadian Journal of Earth Sciences* **8**, 523-48.

Jaillard, E., Hérail, G., Monfret, T., Díaz-Martínez, E., Baby, P., Lavenu, A. & Mumont, J.F. (2000). Tectonic evolution of the Andes of Ecuador, Peru, Bolivia and Northernmost Chile. In: Cordani, U.G., Dilani, E.J., Thomaz Filho, A. & Campos, D.A. (eds.) *Tectonic evolution of South America. 31st International Geological Congress, Rio de Janeiro,* pp. 481-559.

Jaillard, E., Soler, P., Carlier, G. & Mourier, T. (1990). Geodynamic evolution of the northern and central Andes during early to middle Mesozoic time: a Tethyan model. *Journal of the Geological Society of London* **147**, 1009-1022.

Kasemann, S., Erzinger, J. & Franz, G. (2000). Boron recycling in the continental crust of the central Andes from the Paleozoic to Mesozoic, NW-Argentina. *Contributions to Mineralogy and Petrology* **140**, 328-343.

Knesel, K.M. & Davidson, J.P., 1996. Isotopic disequilibrium during melting of granite and implications for crustal contamination of magmas. *Geology Boulder* **24**, 243-246.

Lanfranco, J.J. (1972). *Estudio de la intrusion en la falda oriental de la Sierra de Aguilar y metamorfitas del area de contacto.* Ph.D. Thesis, University of Cordoba, 68p.

Leake, B.E. (1997). Nomenclature of amphiboles: report of the Subcommittee on Amphiboles of the International Mineralogical Association Commission on new minerals and mineral names. *Mineralogical Magazine* **61**, 295-321.

Litherland, M., Annels, R.N., Appleton, J.D., Berrange, J.P., Bloomfield, K., Burton, C.C., Derbyshire, D.P.F., Fletcher, C.J.N., Hawkins, M.P., Klink, B.A., Llanos, A., Mitchell, W.I., O'Connor, E.A., Pitfield, P.E., Power, G. & Webb, B.C. (1986). The geology and mineral resources of the Bolivian Precambrian Shield. *Keyworth Overseas Memoir* **9,** *British*

*Geological Survey,* 153p.

Marianelli, P. & Sbrana, A. (1998). Risultati di misure di standard di minerali e di vetri naturali in microanalisi a dispersione di energia. *Atti Società toscana di Scienze Naturali, Memorie, Serie A* **105**, 57-63.

Marquillas, R. & Salfity, J.A. (1988). Tectonic framework and correlations of the Cretaceous-Eocene Salta Group, Argentina. In: Bahlburg, H., Breitkreuz, C. & Giese, P. (eds.) *The Southern Central Andes. Lecture Notes in Earth Sciences.* **17**, 119-137.

Menegatti, N. (2001). *El complejo alcalino Sierra de Rangel, Provincia de Salta, Argentina.* Ph.D. Thesis, University of Salta, 157p.

Middlemost, E.A.K. (1994). Naming materials in the magma/igneous rock system. *Earth-Science Reviews* **37**, 215-224.

Miller, C.F., Stoddard, E.F. Bradfisch, J. & Dollase, W.A. (1981). Composition of plutonic muscovite: genetic implications. *Canadian Mineralogist* **19**, 25-34.

Mpodozis, C. & Ramos, V.A. (1990). The Andes of Chile and Argentina. In: Ericksen, G.E., Cañas, Pinochet, M.T. & Reinemuf, J.A. (eds.) *Geology of the Andes and its relation to Hydrocarbon and Mineral Resources. Circumpacific Council for Energy and Mineral Resources, Earth Sciences Series* **11**, 59-90.

Prinz, P., Wilke, H.G. & Hillebrand, A.V. (1994). Sediment accumulation and subsidence history in the Mesozoic marginal basin of Northern Chile. In: Reutter, K.J., Scheuber, E. & Wigger, P.J. (eds.) *Tectonic of the Southern Central Andes.* Berlin: Springer, pp. 219-233.

Ramos, V.A. (2000). The Southern Central Andes. In: Cordani, U.G., Milani, E.J., Thomaz Filho, A. & Campos, D.A. (eds.) *Tectonic Evolution of South America. 31st International Geological Congress,Rio de Janeiro*, pp. 561-604.

Rollinson, H.R. (1993). *Using geochemical data: evaluation, presentation, interpretation.* Burntmill: Longman, 353p.

Romeuf, N., Aguirre, L., Soler, P., Féraud, G., Jillard, E. & Ruffet, G. (1995). Middle Jurassic volcanism in the Northern and Central Andes. *Revista Geológica de Chile* **22**, 245-259.

Rossello, E. & Mazetic, M.E. (1999). Caracterización estructural y significado geotectónico de los depocentros cretácicos continentales del centro-oeste argentino. *5º Simpósio sobre Cretáceo do Brasil, Rio Claro, Boletim,* pp. 107-113.

Rubiolo, D.G. (1992). *Zur Geologie, Petrographie und Geochemie der Alcali Magmatite der Sierra de Santa Victoria (E-Kordillere, NW-Argentinien). Clausthaler Geowissenschaftliche Dissertationen* **41**, 145p.

Rutland**,** R.W.R. (1971). Andean orogeny and sea floor spreading. *Nature* **233**, 252-255.

Scheuber, E., Bogdanic, T., Jensen, A. & Reutter, K.J. (1994). Tectonic development of north Chilean Andes in relation to plate convergence and magmatism since the Jurassic. In: Reutter, K.J., Scheuber, E. & Wigger, P.J. (eds.) *Tectonic of the Southern Central Andes.* Berlin: Springer, pp. 121-139.

Sempere, T., Carlier, G., Soler, P., Fornari, Mm., Carlotto, V., Jacay, J., Arispe, O., Néraudeau, D., Cärdenas, J. & Rosas, N.J. (2002). Late Permian-Middle Jurassic lithospheric thinning in Peru and Bolivia, and its bearing on Andean-age tectonics. *Tectonophysics* **345**, 153-181.

Streickeisen, A. (1976). To each plutonic rocks its proper name. *Earth-Science Reviews* **12**, 1-32.

Sun, S.S. & McDonough, W.F. (1989). Chemical and isotopic systematics of oceanic basalt: implications for mantle composition and processes. In: Saunders, A.D. & Morry, M.J. (eds.) *Magmatism in ocean basins. Geological Society of London, Special Publication* **42***,* 313-345.

Tamponi, M., Bertoli, M., Innocenti, F. & Leoni, L. (2003). X-ray fluorescence analysis of major elements in silicate rocks using fused glass discs. *Atti Società toscana di Scienze Naturali, Memorie, Serie A (in press).*

Tassinari, C.G., Bettencourt, J.S., Geraldes, M.C., Macambira, M.J.B. & Lafon, J.M. (2000). The Amazonia Craton. In: Cordani, U.G., Dilani, E.J., Thomaz Filho, A. & Campos D.A. (eds.) *Tectonic evolution of South America. 31st International Geological Congress, Rio de Janeiro,* pp. 41-97.

Tommasini, S. & Davies, S. (1997). Isotope disequilibrium during anatexis: a case study of contact melting, Sierra Nevada, California. *Earth and Planetary Science Letters* **148**, 273-285.

Turner, J.C.M. (1960). Estratigrafia de la Sierra Santa Victoria y adyacencias. *Academia Nacional Ciencias*, *B. XLI* **2**, 163-196.

Viramonte, J.G., Kay, S.M., Becchio, R., Escayola, M. & Novitski, I. (1999). Cretaceous rift related magmatism in central-western South America. *Journal of South American Earth Sciences* **12**, 109-121.

Zappettini, E.O., (1989). *Geología y metalogénesis de la región comprendida entre las localidades de Santa Ana y Cobres, provincias de Jujuy y Salta. República Argentina.* Ph.D. Thesis, University of Buenos Aires, 215p.

Zappettini, E.O. (1998). El Complejo Alcalino Santa Julia, provincia de Jujuy, República Argentina. *X Congreso Latinoamericano de Geología y VI Congreso Nacional de Geología Econômica, Buenos Aires* **2,** 289-294.

Zonenshayn, L.P., Savotin, L.A. & Sedov, A.P. (1984). Global paleogeodynamic reconstructions for the last 160 million years. *Geotectonics* **18**, 181-195.

*Mesozoic to Cenozoic Alkaline Magmatism in the Brazilian Platform*
*Comin-Chiaramonti, P. & Gomes, C.B. (eds.)*
*Edusp/Fapesp, São Paulo, pp. 213-240, 2005*

# ALKALINE MAGMATISM FROM THE MATO GROSSO STATE, BRAZIL: THE PONTA DO MORRO COMPLEX

*M.Z.A. Sousa, E. Ruberti, P. Comin-Chiaramonti and C.B. Gomes*

*The Ponta do Morro complex (PMC) represents the only known occurrence of felsic rocks of Cretaceous age in the Mato Grosso state. The complex intrudes the Cuiabá metasediments at shallow level and consists mainly of granitic and syenitic rocks, both two feldspars and one feldspar variants, and scarce trachyte and rhyolite dykes. The one feldspar variants have a comenditic affinity. Variation diagrams, relative to the major elements, suggest fractionation trends mainly controlled by plagioclase and clinopyroxene. However, important scattering of the trace elements point also to different processes like subsolidus re-equilibration and crustal contamination, other than crystal fractionation. The few Sr isotope data for the PMC and for the alkaline dykes from the Poxoréu region indicate two main groups: one characterized by relatively low initial $^{87}Sr/^{86}Sr$, i.e. 0.7044, for rock-types ranging from trachybasalt to granite, and one characterized by initial $^{87}Sr/^{86}Sr>0.705$. For the latter, crustal contamination or AFC processes may be responsible for the high Sr isotope initial ratios.*

## INTRODUCTION

The emplacement of alkaline and alkaline-carbonatitic complexes in and around the Paraná-Angola-Etendeka igneous province (PAEP) occurred mainly along tectonic lineaments active at least since Early Mesozoic (Fig. 1 after Comin-Chiaramonti & Gomes, 1996 and therein references) and characterized by actual seismic activity (Berrocal & Fernandez, 1996).

The Cuiabá-Poxoréu-Paratininga magmatic province (CPP, Mato Grosso state, Brazil) is roughly aligned with the AZ 125 Lineament on the northwestern side (cf. Biondi, in this volume) that controls the main alkaline-mafic/ultramafic occurrences in Brazil, extending from almost Minas Gerais state to the Amazon region near the Bolivia border (Gonzaga & Tomkins, 1991). CPP was the site of repeated and different magmatic activities over an area of more than 60,000 km$^2$ during the Cretaceous times (Fig. 1). In particular, it consists of kimberlitic pipes (Greenwood *et al.*, 1999) with two distinct U-Pb ages, i.e. 91.6-94.6 and 122.6-127.2 Ma (Heaman *et al.*, 2003), of mafic dykes emplaced at about 84-97 Ma (this work and $^{40}$Ar-$^{39}$Ar determinations; cf. Gibson *et al.*, 1997), and of the Ponta do Morro syenite-granite complex dated at 100 Ma (Rb-Sr isochron; Sousa, 1997).

The kimberlitic pipes have been subdivided into two main groups, i.e. Paratininga and Batovi types (the latter containing perovskite; cf. Greenwood *et al.*, 1999).

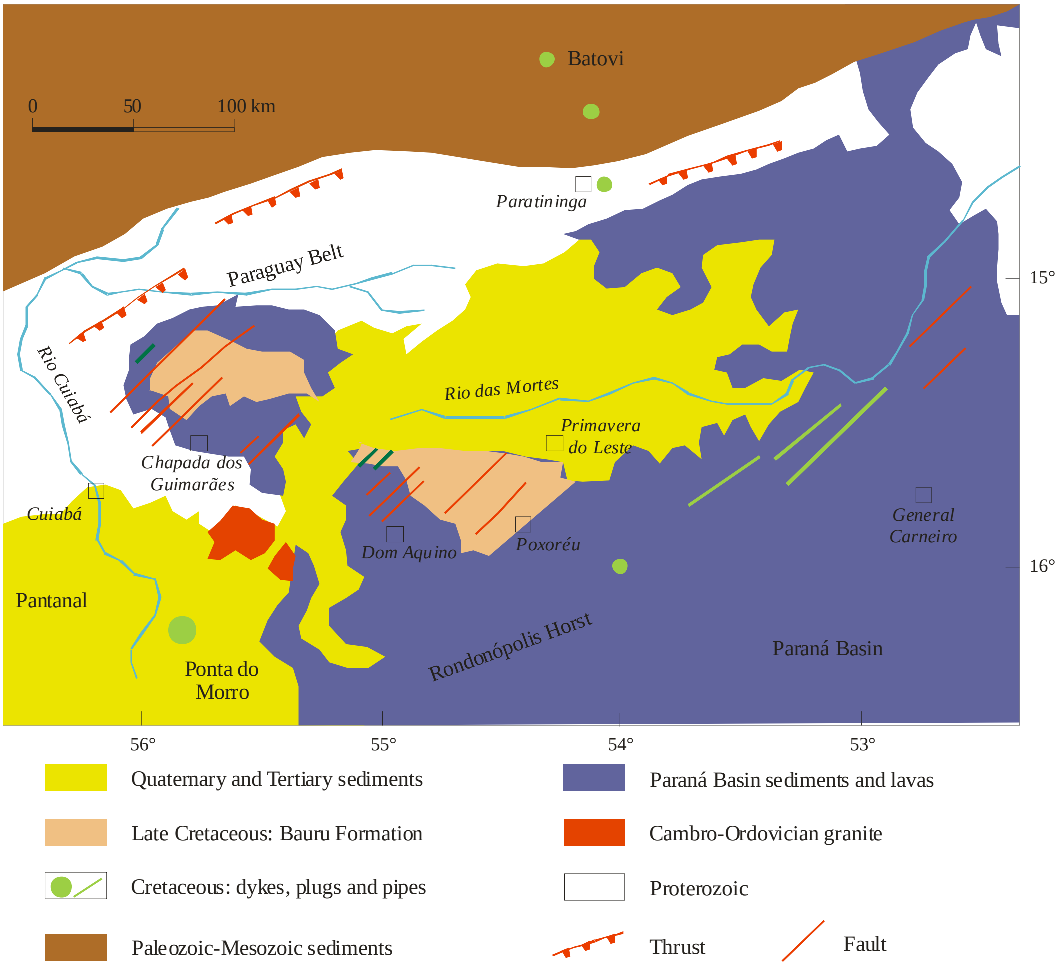


Fig. 1. Geological setting of the Cuiabá region, Mato Grosso state. After Gibson *et al.* (1997, modified).

The dykes are essentially alkali basalts, trachybasalts and trachyandesites widespread in a NE-SW-trending extensional zone (Rio das Mortes rift) that developed between the northernmost side of the Paraná Basin and a sedimentary basin on the southern side of the Amazonas craton, mainly within the Late Proterozoic Paraguay mobile belt (cf. Fig. 1). These dykes are characterized by 48-56 wt% $SiO_2$ and 5.1-7.4 wt% alkalis (this work and Gibson *et al.*, 1997).

The Ponta do Morro complex (PMC) is a crescent-shaped elevation, contrasting with the lowlands of the Pantanal Basin, and covers an area of about 7 $km^2$ (Fig. 2). The principal rock-types are granites and subordinate syenites intruded by scarce trachytic and rhyolitic dykes. The PMC represents the only felsic occurrence of Cretaceous age actually known in the Mato Grosso state.

Syenite-granite associations are unusual in southern Brazil where they are present only in a few complexes such as Ponta Grossa, Itatiaia and Cananéia (Brotzu *et al.*, 1997; Ruberti *et al.*, in this volume). On the other hand, syenite-granite associations, both two feldspars and one feldspar variants, are common in Uruguay and Bolivia (Valle Chico and Velasco complexes; Muzio *et al.*, 2002, and Comin-Chiaramonti *et al.*, in this volume).

In this study we adress the mineralogical and petrochemical aspects of the Ponta do Morro complex.

## PETROGRAPHICAL NOTES

The Ponta do Morro complex consists of alkali felspar-rich rock-types with variable amounts of quartz and plagioclase. According to the IUGS classification (cf. Le Maitre, 1989), the intrusive rocks are syenites, quartz syenites, alkali feldspar syenites, quartz-alkali feldspar syenites and alkali feldspar granites (Fig. 3). The subvolcanic activity is represented by trachytic and rhyolitic dykes. All the rock-types are silica-saturated to silica-over-saturated. Ubiquitous mafic constituents are clinopyroxene, amphibole and opaques. Biotite often occurs as a primary phase in granites, whereas in the syenitic variants the biotite usually replaces amphibole and clinopyroxene. Mafic enclaves, up to some decimeters in diameter, are widespread mainly at the western border of the complex.

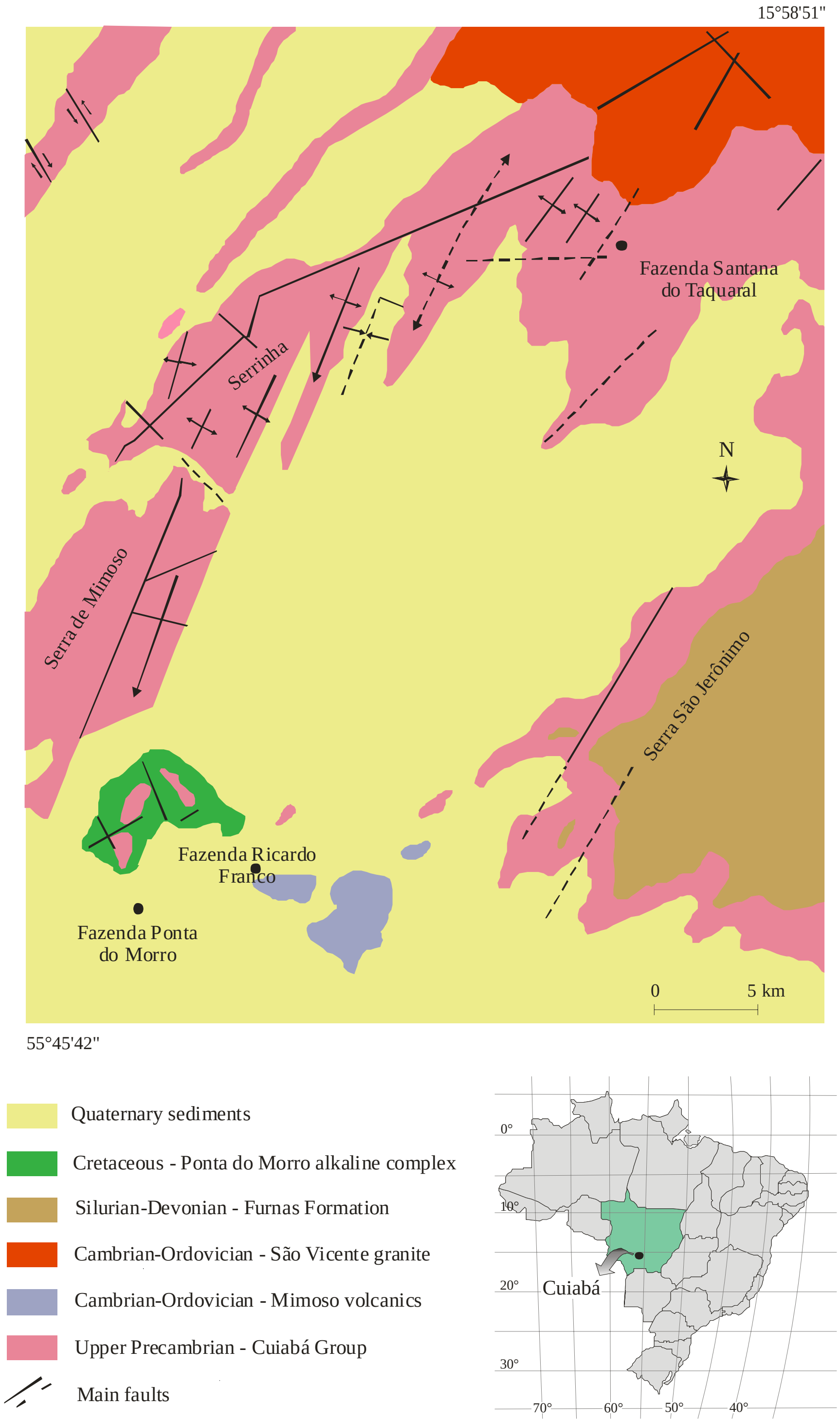


Fig. 2. Geological map of the Ponta do Morro area (after Sousa, 1997).

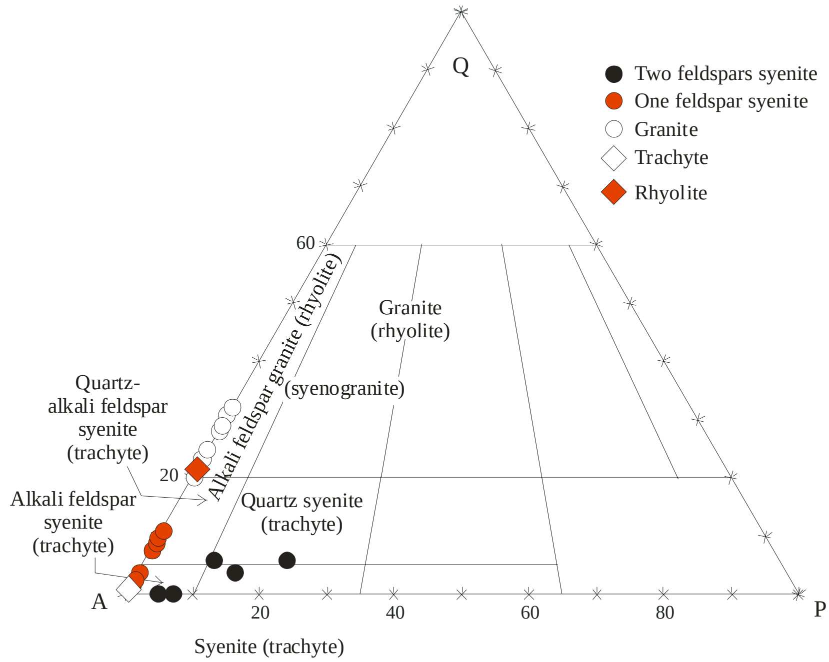


Fig. 3. Modal analyses of the Ponta do Morro rock-types plotted on the QAP diagram (cf. Le Maitre, 1989). Data source: Sousa (1997).

*Syenites*

Based on the feldspar assemblages two main subgroups may be recognized, i.e. two feldspars and one feldspar variants, respectively.

The two felspars syenites are fine to medium-grained with prevailing inequigranular hypidiomorphic and porphyritic textures. The porphyritic types are characterized by a fine to medium groundmass made of alkali feldspar, plagioclase, variable amounts of quartz (less than 5 vol%), clinopyroxene, amphibole, biotite, opaques and apatite. Phenocrysts of perthitic to mesoperthitic alkali felspar are dominant along with subordinate plagioclase and clinopyroxene. Groundmass plagioclase has an uniform composition (oligoclase), whereas the phenocrysts are strongly zoned (bytownite-labradorite core, andesine-albite rims). Quartz is generally interstitial or is present as graphic or micrographic intergrowths with the alkali feldspar.

Mafic minerals range from 14 to 32 vol%, i.e. up to mela-varieties. Clinopyroxene (augite, salite to ferrosalite) is the main mafic phase and usually displays uralitization rims made of light green actinolite/Fe-actinolite. Ferro-winchite and ferro-barroisite are also present in the medium-grained rock-types, the former as phenocrysts and the latter in the groundmass. Ferro-horthonolite and horthonolite are scarce and occur in the more mafic varieties. Common accessory minerals are apatite, titanite and zircon.

The one feldspar syenites, i.e. hypersolvus variants with mesoperthitic alkali feldspar, are also fine to medium-grained with inequigranular hipidiomorphic to xenomorphic textures. Porphyritic types with alkali felspar phenocrysts are occasionally present. Scarce quartz occurs as interstitial grains or micrographic intergrowths. Mafic minerals, ranging from 12 to 20 vol%, are mainly alkali amphibole, subordinate aegirinic pyroxene and rare biotite, fayalite and aenigmatite. Amphiboles are Na-rich varieties (arfvedsonite and riebeckite) and subordinate Ca-Na variants (ferro-winchite or ferro-barroisite). Sometimes they occur associated with, or replacing, clinopyroxene. The clinopyroxene usually ranges from aegirine-augite to aegirine, with sometimes hedenbergitic cores. Fayalite, aenigmatite and astrophyllite may occur as accessory phases along with opaques and apatite.

*Granites*

The granites are medium to coarse-grained and inequigranular to equigranular in texture. Porphyritic variants with quartz and alkali feldspar phenocrysts are also present. Mesoperthite is the most important felsic phase associated with interstitial or graphic quartz-alkali feldspar intergrowths. Notably, plagioclase is absent, i.e. hypersolvus granites. Mafic minerals (3-7 vol%) are mainly alkali amphibole and subordinate Na-bearing clinopyroxene and biotite. The last usually replaces both amphibole and clinopyroxene. Accessory minerals are apatite, zircon and opaques.

*Dykes*

Trachytic and rhyolitic dykes (30-40 cm thick) cut the syenites and granites, mainly along the eastern border of the complex. Trachytes are very fine-grained with porphyritic to glomeroporphyritic textures showing flow textures with aligned tabular alkali feldspar. Mafic phases are represented by riebeckite and opaques. Rhyolites are fine-grained with rare tabular alkali feldspar phenocrysts. The groundmass displays flow texture and contains subhedral alkali feldspar, quartz, riebeckite and opaques.

*Mafic enclaves*

Mafic enclaves exhibit porphyritic to glomeroporphyritic textures with plagioclase ($An_{85}$) phenocrysts and ocelli made mainly of edenitic hornblende partially replaced by biotite and subordinate clinopyroxene. The very fine-grained groundmass is made of amphibole, clinopyroxene, plagioclase ($An_{30}$), titanite and subordinate apatite.

## MINERALOGY

Mineral analyses were performed at the Instituto de Geociências of the University of São Paulo with a JEOL JXA-8600S electron microprobe, in wavelength-dispersion mode (WDS), employing the PROZA correction program (cf. Sousa, 1997). The used standards were oxides or simple silicate compositions.

The reported compositions represent averages of at least five point-analyses and the results are considered accurate to within 2-3% for major elements and to about 10% for minor ones. Representative analyses are given in Tables 1 to 6. A complete list of analyses may be found in Sousa (1997).

*Feldspars*

Plagioclase and alkali feldspar compositions are given in Table 1 and plotted in Fig. 4 in terms of Or, Ab, An.

Plagioclase occurs only in the two feldspars syenites and in the mafic enclaves. Plagioclase phenocrysts from syenites exhibit a compositional variation from $An_{85-59}$ (core) to $An_{46}$ (rims), and are usually mantled by anorthoclase ($Or_{43}Ab_{52}$) and/or by oligoclase ($An_{29}$). Mafic enclaves show homogeneous phenocrysts with bytownitic compositions ($An_{85}$). Notably, the more calcic cores from the two feldspars syenites have the same compositions of those from the mafic enclaves, suggesting a xenocrystic origin.

The groundmass plagioclase is mainly oligoclase ($An_{26-19}$) in the two feldspars syenites, whereas it ranges from andesine ($An_{37}$) to sodic oligoclase ($An_{12}$) in the enclaves.

The overall composition of the alkali feldspars, both phenocrysts and interstitial phases, averages 45 Or mol%. The exsolved phases may be up to $Ab_{95}$ and $Or_{94}$ in the syenites and up to $Ab_{98}$ and $Or_{96}$ mol% in the granites.

The Ponta do Morro feldspars fall below the solvus-solidus intersection in the system $KAlSi_3O_8$-$NaAlSi_3O_8$-$CaAl_2Si_2O_8$ at $PH_2O$=0.5 kb and 750°C (Seck, 1971). Apparent closure temperatures of 1250-1200°C were obtained from the plagioclase bytownitic compositions (1kb $PH_2O$ pressure; Kudo & Weill, 1970, and Mathez, 1973). Notably, groundmass plagioclase and alkali feldspar yielded temperatures below 700°C (Powell & Powell, 1977), according to the subsolidus exchange.

Table 1. Selected compositions of feldspars expressed in terms of Or, Ab and An mol%. Abbreviations: S, two feldspars syenite; AI-S, one feldspar syenite; TR, trachyte; GR, granite; E, mafic enclaves; Pl, plagioclase; AF, alkali feldspar; Ph, large crystals or phenocrysts; m, microlites; C, core; R, rim; GC, global composition.

| Sample | 2.1 | 2.1 | 2.4 | 3.4 | 3.4 | 3.4 | 34C | 34C | 34C | 2B | 2B | 2B |
|---|---|---|---|---|---|---|---|---|---|---|---|---|
| | S | S | S | S | S | S | S | S | S | S | S | S |
| | Pl | Pl | AF | Pl | Pl | AF | Pl | AF | AF | Pl | Pl | AF |
| | Ph-C | m | m | Ph-C | Ph-R | m-GC | Ph-C | Ph-R | Ph-GC | Ph-C | Ph-R | Ph-GC |
| Or | 0.2 | 2.4 | 34.0 | 0.6 | 1.6 | 77.8 | 1.8 | 30.5 | 47.3 | 0.2 | 2.2 | 39.9 |
| Ab | 22.7 | 74.3 | 61.6 | 33.0 | 61.3 | 21.8 | 48.6 | 68.0 | 52.3 | 13.2 | 80.7 | 57.7 |
| An | 77.1 | 23.3 | 4.4 | 66.4 | 37.1 | 0.4 | 49.6 | 1.5 | 0.4 | 86.6 | 17.2 | 5.4 |
| Sample | 50 | 28 | 18A | 20 | 20 | 10C | 30A | 4-2B | 3.1 | 4.3 | 4.3 | 4.3 |
| | AI-S | AI-S | AI-S | TR | TR | GR | GR | GR | GR | E | E | E |
| | AF | AF | AF | AF | AF | AF | AF | AF | AF | Pl | Pl | Pl |
| | Ph-GC | Ph-GC | m-GC | Ph-C | Ph-R | Ph-GC | Ph-GC | Ph-GC | Ph-GC | Ph-C | Ph-R | m |
| Or | 59.9 | 52.4 | 48.1 | 38.9 | 59.8 | 47.2 | 37.4 | 51.0 | 40.2 | 0.2 | 1.0 | 1.5 |
| Ab | 40.0 | 47.2 | 51.5 | 55.5 | 38.4 | 52.7 | 60.9 | 47.9 | 58.9 | 15.8 | 69.3 | 69.5 |
| An | 0.1 | 0.4 | 0.4 | 5.6 | 1.8 | 0.1 | 1.6 | 1.1 | 0.9 | 84.1 | 29.7 | 30.0 |

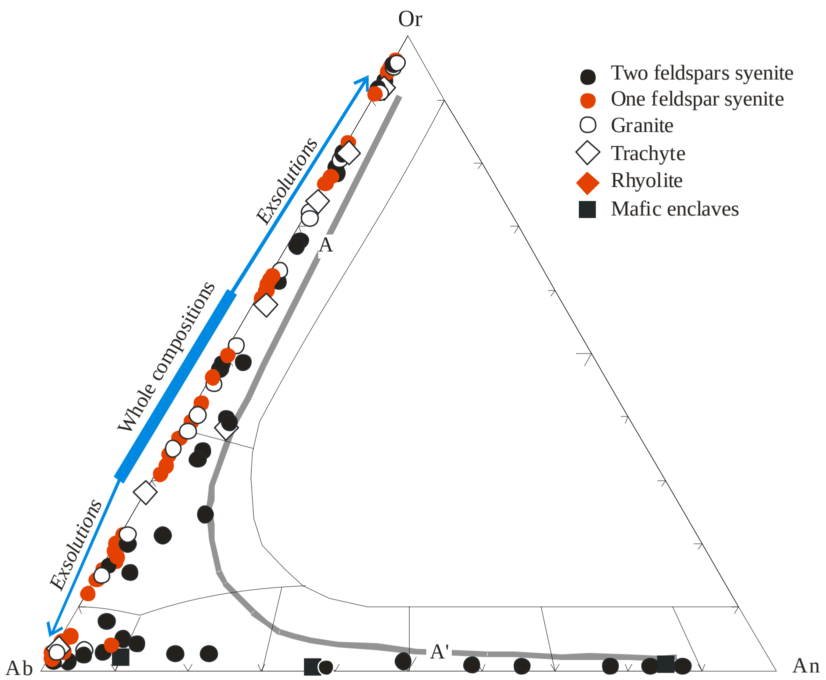


Fig. 4. Plot of the Ponta do Morro feldspars into the Or-Ab-An diagram space (cf. Deer *et al.*, 1992). A-A', solvus-solidus intersection at $PH_2O$ 0.5 kb and 750°C (Seck, 1971). Data source: this work (Table 1) and Sousa (1997).

The apparent P-T conditions along with the textural features, i.e. fine to very fine size of the interstitial phases, and the very low grade contact metamorphism with the roof rocks (Sousa, 1997), suggest a shallow level for the intrusion.

*Clinopyroxenes*

The compositions are plotted in Fig. 5 (cf. Table 2, and Sousa, 1997). Clinopyroxenes from the two feldspars syenites plot in the diopside-augite to hedenbergite fields (cores: mg#, $MgO/(MgO+Fe^{2+})$ molar ratio=0.79-0.63; rims: mg#=0.51-0.45). The clinopyroxenes from one feldspar syenites have mg# ranging from 0.45-0.22 (cores) to 0.10 (rims and/or interstitial phases). The clinopyroxenes from granites are restricted to the aegirine-augite field, mg# around 0.11 (cores) and 0.12 and 0.06 (rims and groundmass). On the other hand, the mafic enclaves show diopsidic-augitic cores (mg#=0.81) and hedenbergitic rims (mg#=0.37). All the clinopyroxenes contain low $Al^{IV}$ (i.e. 0.17•0.12 and •0.005 a.f.u. in the mafic enclaves, syenitic and granitic variants, respectively) and generally require Ti (occasionally $Fe^{3+}$) to fill the tetrahedral sites (cf. Table 3). It is noteworthy that the compositions with the highest mg# values appear in equilibrium with a hypothetical $Fo_{80}$ olivine (cf. Deer *et al.*, 1992), and that the clinopyroxene cores from the mafic enclaves overlap those from the two feldspar syenites (cf. Figs. 5A, B). Comparison with clinopyroxenes from other Brazilian occurrences (Fig. 5B) show a pattern similar to those of alkaline complexes from Piratini and Vitória island (cf. Barbieri *et al.* 1987).

*Amphiboles*

Amphiboles exhibit a wide compositional range from calcic to Na-rich varieties (Fig. 6). They usually require Ti-$Fe^{3+}$ in the tetrahedral sites (Table 3) and show appreciable K contents (up to 0.29 a.f.u.). The amphiboles mainly range (cf. Fig. 6A) from hornblende to winchite (two feldspars syenites), from barroisite to riebeckite-arfvedsonite

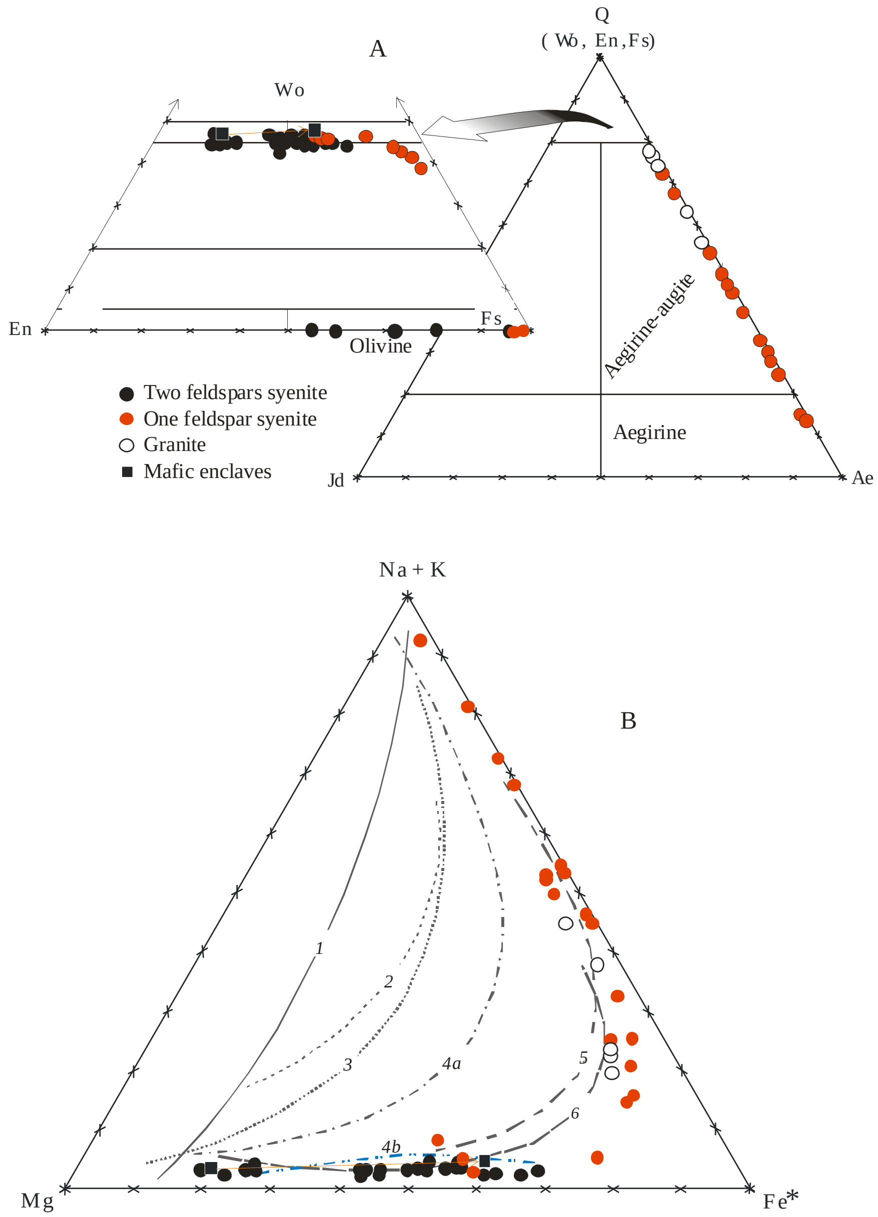


Fig. 5. Chemical analyses of clinopyroxenes from the Ponta do Morro complex (data source: Table 2 and Sousa, 1997), plotted on: A, classification diagram of Morimoto (1988); B, Na+K-Mg-Fe* space (Fe*=$Fe^{2+}$+$Fe^{3+}$+Mn-Na-K). For comparison, the main trends from other Brazilian alkaline complexe are shown: 1, Anitápolis; 2, Itapirapuã; 3, Banhadão; 4, Rio de Janeiro State (a, Tanguá-Rio Bonito-Itaúna-Morro de São João; b, Soarinho); 5, Piratini; 6, Vitória island (cf. Gomes *et al.*, 1987).

Table 2. Representative analyses of clinopyroxenes. $Fe^{3+}$ and $Fe^{2+}$ calculated according to the stoichiometry. Cations for 6 oxygens; mg#=Mg/(Mg+$Fe^{2+}$). C, core; R, rim; m, interstitial phases; P, phenocrysts. S, two feldspars syenite; AI-S, one feldspar syenite; GR, granite; E, mafic enclaves.

| Sample | 2.1 | 2.1 | 3.4 | 3.4 | 34 | 34 | 50 | 28 | 28 | 22-A | 22-A | 22 | 22 | 10-C | 10-C | 3.1 | 4.3 | 4.3 |
|---|---|---|---|---|---|---|---|---|---|---|---|---|---|---|---|---|---|---|
| | S | S | S | S | S | S | AI-S | AI-S | AI-S | AI-S | AI-S | AI-S | AI-S | GR | GR | GR | E | E |
| | C | R | C | R | C | R | m | C | m | C | m | C | R | C | R | m | P | m |
| $SiO_2$ | 51.08 | 52.16 | 51.11 | 50.50 | 51.67 | 51.18 | 50.58 | 50.05 | 49.12 | 49.35 | 48.87 | 48.83 | 49.12 | 50.26 | 50.28 | 49.50 | 49.80 | 50.53 |
| $TiO_2$ | 1.23 | 0.07 | 1.02 | 0.21 | 1.10 | 0.22 | 0.22 | 0.60 | 0.41 | 0.65 | 0.19 | 0.50 | 0.27 | 0.25 | 0.25 | 0.21 | 1.69 | 0.05 |
| $Al_2O_3$ | 2.88 | 0.25 | 3.03 | 0.75 | 3.22 | 0.60 | 0.19 | 0.88 | 0.31 | 1.22 | 0.21 | 0.68 | 0.25 | 0.28 | 0.23 | 0.22 | 5.24 | 0.62 |
| $Cr_2O_3$ | 0.03 | 0.03 | 0.10 | 0.01 | 0.01 | 0.02 | 0.01 | 0.00 | 0.05 | 0.02 | 0.01 | 0.02 | 0.02 | 0.01 | 0.03 | 0.00 | 0.13 | 0.08 |
| $FeO_{tot}$ | 9.78 | 17.48 | 8.88 | 17.41 | 8.13 | 16.81 | 28.37 | 18.72 | 26.73 | 18.17 | 28.41 | 23.86 | 27.20 | 27.70 | 28.57 | 27.19 | 7.29 | 18.75 |
| MnO | 0.34 | 0.67 | 0.27 | 0.78 | 0.17 | 0.84 | 1.08 | 0.76 | 1.00 | 0.78 | 0.89 | 0.93 | 0.95 | 1.29 | 1.35 | 1.13 | 0.08 | 0.75 |
| NiO | 0.04 | 0.00 | 0.02 | 0.03 | 0.00 | 0.04 | 0.03 | 0.01 | 0.06 | 0.03 | 0.01 | 0.05 | 0.04 | 0.03 | 0.05 | 0.03 | 0.02 | 0.10 |
| MgO | 13.12 | 7.91 | 14.08 | 8.47 | 14.99 | 8.94 | 0.73 | 7.05 | 1.14 | 7.35 | 1.16 | 3.37 | 1.34 | 1.12 | 0.52 | 1.65 | 14.04 | 6.05 |
| CaO | 21.49 | 21.96 | 21.90 | 20.47 | 21.91 | 21.66 | 10.29 | 21.42 | 16.02 | 21.29 | 16.84 | 18.79 | 18.02 | 13.45 | 11.78 | 16.12 | 22.01 | 21.68 |
| $Na_2O$ | 0.55 | 0.36 | 0.40 | 0.48 | 0.34 | 0.34 | 6.67 | 0.43 | 3.40 | 0.60 | 2.82 | 0.62 | 2.13 | 4.95 | 5.86 | 2.72 | 0.42 | 0.59 |
| $K_2O$ | 0.05 | 0.01 | 0.02 | 0.07 | 0.01 | 0.03 | 0.01 | 0.01 | 0.01 | 0.02 | 0.01 | 0.01 | 0.01 | 0.01 | 0.01 | 0.02 | 0.01 | 0.01 |
| Sum | 100.59 | 100.90 | 100.83 | 99.18 | 101.54 | 100.68 | 98.58 | 99.93 | 98.25 | 99.63 | 99.42 | 99.87 | 99.35 | 99.35 | 98.93 | 98.76 | 100.73 | 99.21 |
| Si | 1.898 | 2.001 | 1.885 | 1.973 | 1.884 | 1.967 | 2.000 | 1.960 | 1.994 | 1.936 | 1.974 | 1.962 | 1.991 | 1.995 | 1.999 | 2.000 | 1.830 | 1.998 |
| $Al^{IV}$ | 0.102 | | 0.115 | 0.027 | 0.116 | 0.027 | | 0.040 | 0.006 | 0.056 | 0.010 | 0.032 | 0.009 | 0.005 | 0.001 | | 0.170 | 0.002 |
| Ti | | | | | | 0.006 | | | | 0.008 | 0.006 | 0.006 | | | | | | |
| Sum | 2.000 | 2.001 | 2.000 | 2.000 | 2.000 | 2.000 | 2.000 | 2.000 | 2.000 | 2.000 | 2.000 | 2.000 | 2.000 | 2.000 | 2.000 | 2.000 | 2.000 | 2.000 |
| $Al^{IV}$ | 0.025 | 0.011 | 0.017 | 0.008 | 0.022 | | 0.009 | | 0.008 | | | | | | | | | |
| Ti | 0.034 | 0.002 | 0.028 | 0.006 | 0.030 | | 0.007 | 0.018 | 0.013 | | | | 0.003 | 0.008 | 0.010 | 0.011 | 0.057 | 0.027 |
| Cr | 0.001 | 0.001 | 0.003 | 0.000 | 0.000 | 0.001 | 0.000 | 0.000 | 0.002 | 0.011 | | 0.009 | 0.008 | 0.007 | 0.007 | 0.006 | 0.047 | 0.001 |
| $Fe^{3+}$ | 0.049 | | 0.068 | 0.047 | 0.057 | 0.053 | 0.474 | 0.037 | 0.239 | 0.001 | 0.000 | 0.001 | 0.001 | 0.000 | 0.001 | 0.000 | 0.004 | 0.002 |
| $Fe^{2+}$ | 0.255 | 0.564 | 0.206 | 0.523 | 0.191 | 0.487 | 0.468 | 0.576 | 0.668 | 0.080 | 0.225 | 0.062 | 0.156 | 0.363 | 0.428 | 0.178 | 0.045 | 0.015 |
| Mn | 0.011 | 0.022 | 0.008 | 0.026 | 0.005 | 0.027 | 0.036 | 0.025 | 0.034 | 0.515 | 0.709 | 0.740 | 0.767 | 0.558 | 0.523 | 0.743 | 0.179 | 0.605 |
| Mg | 0.727 | 0.455 | 0.774 | 0.493 | 0.815 | 0.513 | 0.043 | 0.412 | 0.069 | 0.026 | 0.030 | 0.032 | 0.033 | 0.043 | 0.045 | 0.039 | 0.002 | 0.025 |
| Ni | 0.001 | 0.000 | 0.001 | 0.001 | 0.000 | 0.001 | 0.001 | 0.000 | 0.002 | 0.429 | 0.070 | 0.203 | 0.081 | 0.066 | 0.031 | 0.100 | 0.769 | 0.357 |
| Ca | 0.856 | 0.907 | 0.865 | 0.857 | 0.856 | 0.892 | 0.438 | 0.899 | 0.697 | 0.001 | 0.000 | 0.002 | 0.001 | 0.001 | 0.002 | 0.001 | 0.001 | 0.003 |
| Na | 0.040 | 0.027 | 0.029 | 0.036 | 0.024 | 0.025 | 0.514 | 0.033 | 0.268 | 0.892 | 0.729 | 0.904 | 0.749 | 0.572 | 0.502 | 0.700 | 0.867 | 0.918 |
| K | 0.002 | 0.000 | 0.001 | 0.003 | 0.000 | 0.001 | 0.001 | 0.000 | 0.001 | 0.045 | 0.221 | 0.048 | 0.167 | 0.381 | 0.452 | 0.214 | 0.030 | 0.045 |
| Sum | 1.999 | 1.999 | 1.999 | 1.999 | 2.000 | 2.000 | 2.000 | 2.000 | 1.999 | 0.001 | 0.000 | 0.001 | 0.001 | 0.001 | 0.001 | 0.001 | 0.000 | 0.001 |
| | | | | | | | | | | 1.999 | 2.000 | 2.000 | 2.000 | 2.000 | 1.999 | 1.999 | 2.000 | 1.999 |
| mg # | 0.74 | 0.45 | 0.79 | 0.49 | 0.63 | 0.51 | 0.08 | 0.42 | 0.09 | 0.45 | 0.09 | 0.22 | 0.10 | 0.11 | 0.06 | 0.12 | 0.81 | 0.37 |

(one feldspar syenites and trachytes) and from barroisite to winchite (granites). The general trend overlaps to some extent that of the coexisting clinopyroxenes (Fig. 6B). The amphiboles from mafic enclaves plot in the hastingsite-edenite fields and display relatively high mg# values (i.e. 0.65-0.64; cf. Table 3).

*Biotites*

Biotites plot along the phlogopite-annite tie-line (Fig. 7) in the same field as the saturated to oversaturated complexes from Velasco (Bolivia). They have Mg/(Mg+Fe) ratios (Table 4) mainly between 0.52 to 0.17 (two feldspar syenites), 0.32 to 0.03 (one feldspar syenites and granites). The highest Mg/(Mg+Fe) ratios are shown by the biotite from the mafic enclaves and by some biotite cores from the two feldspars syenites. Some compositions from the one feldspar syenites present very low Al contents (Fig. 7). However, the Al is sufficient to fill the tetrahedral sites, i.e. with $Al^{VI}$ in octahedral sites ranging from 0-0.593 a.f.u.

*Oxides*

Oxides are ilmenite and Ti-magnetite. Ti-magnetite displays a wide compositional range with ulvöspinel contents from 3 to 78 mol% (Table 5 and Fig. 8A). A parallel increase of the Mn and Ti contents is observed (Table 5), i.e. from 0.044 to 0.741 and from 1.683 to 2.592 a.f.u., respectively.

Ilmenite plots close to the theoretical composition (Fig. 8A). $R_2O_3$ ranges between 1.5 and 11.4 mol%. MnO contents are usually high, 1.9 to 5.3, similar to the ilmenites from other alkaline oversaturated rocks, e.g. Velasco complexes, Valle Chico, Itatiaia.

The presence of ilmenite$_{ss}$-magnetite$_{ss}$ pairs allows calculation of equilibration temperatures and oxygen fugacities (Andersen & Lindsley, 1988). The results are scattered between 431 and 1015°C and -11 to -25 log$f$O$_2$, respectively (Fig. 8B), the lowest values representing the results of subsolidus reequilibration. The opaques tend to fit the QFM buffer, that is consistent with the occasional presence of quartz and fayalite both in the two feldspars and one feldspar syenites. The pattern appears close to the QFM buffer, being quite different with respect to other analogues from other oversaturated complexes, e.g. Valle Chico and Velasco, which straddle the MW and NNO buffers.

*Olivine and aenigmatite*

Olivines from the two feldspars syenites have average compositions (Table 6) between Fo$_{46}$ (cores) to Fo$_{18}$ (rims) mol%, whereas in the one feldspar

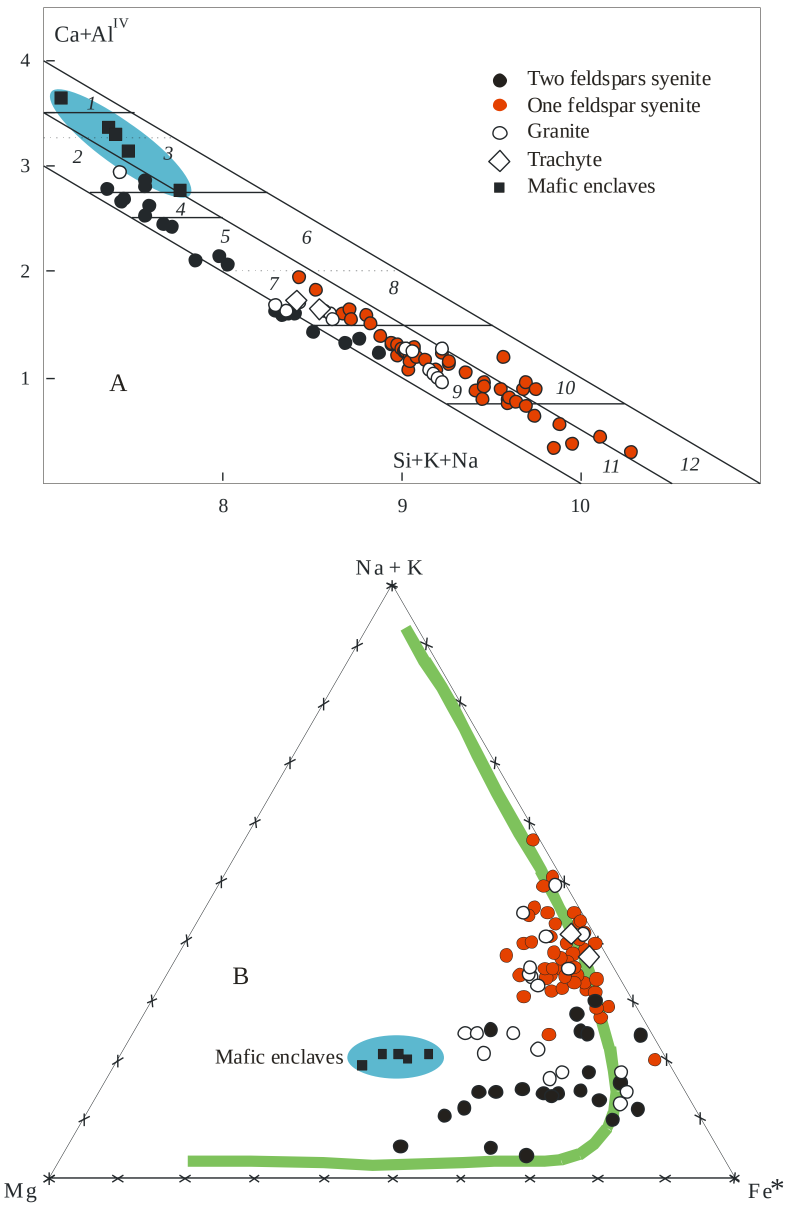


Fig. 6. Chemical analyses of amphiboles from the Ponta do Morro complex (data source: Table 3 and Sousa, 1997). A: classification diagram of Giret *et al.* (1980); 1, hastingsite; 2, hornblende; 3, edenite; 4 actinolitic hornblende; 5, actinolite; 6, edenite; 7, barroisite; 8, katophorite; 9, winchite; 10, richterite; 11, riebeckite; 12, arfvedsonite. B: Na+K-Mg-Fe* space (Fe*=Fe$^{2+}$+Fe$^{3+}$+Mn-Na-K). Green heavy line represents the trend of the associated clinopyroxenes.

Table 3. Representative analyses of amphiboles (cations per 23 oxygens). Symbols as in Table 2.

| Sample | 3.4 | 4.3 | 34 | 34C | 18A | 18A | 50 | 50 | 22 | 22R | 22A | 22A | 10C | 10C | 3.1 | 3.1 | 4-2B | 4-2B | 4.3 | 4.3 |
|---|---|---|---|---|---|---|---|---|---|---|---|---|---|---|---|---|---|---|---|---|
| | S | S | S | S | S | S | AI-S | AI-S | AI-S | AI-S | AI-S | AI-S | GR | GR | GR | GR | GR | GR | E | E |
| | C | R | C | m | m | m | C | m | C | R | C | R | C | R | C | m | C | m | C | m |
| $SiO_2$ | 50.12 | 46.34 | 45.69 | 48.08 | 47.47 | 48.79 | 49.54 | 50.02 | 46.16 | 47.26 | 47.40 | 47.57 | 50.57 | 48.61 | 48.78 | 47.49 | 42.20 | 42.16 | 46.13 | 42.50 |
| $TiO_2$ | 0.28 | 1.15 | 0.99 | 1.41 | 1.55 | 0.35 | 0.82 | 0.52 | 2.41 | 1.02 | 1.75 | 1.71 | 0.78 | 1.44 | 0.93 | 1.85 | 1.62 | 1.60 | 1.06 | 0.95 |
| $Al_2O_3$ | 2.65 | 4.53 | 4.18 | 1.48 | 1.66 | 1.15 | 0.93 | 0.54 | 2.76 | 1.77 | 1.82 | 1.98 | 1.57 | 1.66 | 2.15 | 1.45 | 6.70 | 6.85 | 5.87 | 8.59 |
| $Cr_2O_3$ | 0.04 | 0.03 | 0.02 | 0.02 | 0.05 | 0.03 | 0.03 | 0.00 | 0.40 | 0.00 | 0.02 | 0.02 | 0.01 | 0.05 | 0.05 | 0.00 | 0.02 | 0.02 | 0.00 | 0.03 |
| $FeO_{tot}$ | 21.18 | 23.53 | 30.00 | 34.69 | 34.87 | 34.65 | 31.55 | 30.62 | 31.19 | 34.46 | 32.81 | 32.63 | 25.21 | 30.82 | 26.82 | 31.80 | 28.68 | 28.83 | 19.46 | 21.11 |
| MnO | 0.73 | 0.61 | 0.89 | 1.00 | 0.79 | 0.96 | 1.55 | 1.31 | 0.78 | 0.98 | 0.89 | 0.88 | 1.16 | 1.45 | 1.04 | 0.89 | 0.75 | 0.71 | 0.52 | 0.55 |
| NiO | 0.06 | 0.06 | 0.03 | 0.01 | 0.00 | 0.05 | 0.06 | 0.00 | 0.06 | 0.00 | 0.03 | 0.03 | 0.00 | 0.01 | 0.04 | 0.00 | 0.00 | 0.00 | 0.00 | 0.00 |
| MgO | 10.14 | 7.82 | 4.50 | 1.67 | 1.10 | 1.86 | 2.25 | 1.26 | 2.25 | 0.90 | 1.64 | 1.57 | 7.15 | 2.89 | 5.76 | 1.69 | 3.76 | 3.47 | 9.17 | 7.52 |
| CaO | 10.31 | 10.50 | 9.40 | 5.15 | 5.58 | 8.18 | 3.59 | 6.74 | 6.70 | 5.28 | 5.58 | 5.37 | 6.18 | 4.70 | 7.54 | 8.36 | 9.93 | 9.97 | 10.81 | 11.11 |
| $Na_2O$ | 0.81 | 1.30 | 1.82 | 3.74 | 4.16 | 1.80 | 5.60 | 6.41 | 4.14 | 4.55 | 5.19 | 4.43 | 4.58 | 4.71 | 2.80 | 2.29 | 2.02 | 2.00 | 2.24 | 2.10 |
| $K_2O$ | 0.29 | 0.55 | 0.73 | 1.07 | 1.03 | 0.43 | 1.27 | 0.66 | 1.37 | 1.20 | 1.26 | 1.14 | 1.32 | 1.27 | 1.10 | 0.62 | 1.06 | 1.08 | 1.06 | 1.50 |
| Sum | 96.61 | 96.42 | 98.25 | 98.32 | 98.26 | 98.22 | 97.18 | 98.08 | 98.22 | 97.42 | 98.39 | 97.60 | 98.53 | 97.70 | 97.01 | 96.44 | 96.78 | 96.70 | 96.32 | 95.99 |
| Si | 7.552 | 7.079 | 7.028 | 7.511 | 7.406 | 7.687 | 7.658 | 7.556 | 7.150 | 7.417 | 7.288 | 7.439 | 7.493 | 7.498 | 7.508 | 7590 | 6.586 | 6.595 | 6.909 | 6.462 |
| $Al^{IV}$ | 0.488 | 0.815 | 0.757 | 0.027 | 0.305 | 0.213 | 0.169 | 0.096 | 0.503 | 0.327 | 0.330 | 0.365 | 0.274 | 0.302 | 0.390 | 0.273 | 1.231 | 1.262 | 1.035 | 1.538 |
| $Fe^{3+}$ | | 0.106 | 0.215 | 0.462 | 0.289 | 0.100 | 0.173 | 0.348 | 0.347 | 0.256 | 0.382 | 0.196 | 0.233 | 0.200 | 0.102 | 0.137 | 0.183 | 0.143 | 0.056 | |
| Sum | 8.000 | 8.000 | 8.000 | 8.000 | 8.000 | 8.000 | 8.000 | 8.000 | 8.000 | 8.000 | 8.000 | 8.000 | 8.000 | 8.000 | 8.000 | 8.000 | 8.000 | 8.000 | 8.000 | 8.000 |
| Ti | 0.032 | 0.132 | 0.115 | 0.166 | 0.182 | 0.041 | 0.094 | 0.059 | 0.281 | 0.120 | 0.202 | 0.201 | 0.087 | 0.167 | 0.108 | 0.222 | 0.190 | 0.188 | 0.119 | 0.109 |
| Cr | 0.005 | 0.004 | 0.002 | 0.002 | 0.006 | 0.004 | 0.004 | 0.000 | 0.049 | 0.000 | 0.002 | 0.002 | 0.001 | 0.006 | 0.006 | 0.000 | 0.004 | 0.002 | 0.000 | 0.004 |
| $Fe^{3+}$ | 0.538 | 0.931 | 1.141 | 1.075 | 1.278 | 0.690 | 1.576 | 2.076 | 1.213 | 1.487 | 1.605 | 1.218 | 1.399 | 1.320 | 0.890 | 0.548 | 1.430 | 1.417 | 1.300 | 1.646 |
| $Fe^{2+}$ | 2.131 | 1.970 | 2.503 | 2.996 | 2.983 | 3.776 | 2.331 | 1.445 | 2.481 | 2.780 | 2.232 | 2.853 | 1.492 | 2.455 | 2.460 | 3.565 | 2.130 | 2.221 | 1.082 | 1.038 |
| Mn | 0.093 | 0.079 | 0.116 | 0.132 | 0.104 | 0.128 | 0.203 | 0.168 | 0.102 | 0.130 | 0.116 | 0.117 | 0.147 | 0.201 | 0.136 | 0.120 | 0.099 | 0.094 | 0.066 | 0.071 |
| Mg | 2.278 | 1.781 | 1.032 | 0.634 | 0.256 | 0.430 | 0.519 | 0.284 | 0.520 | 0.211 | 0.376 | 0.366 | 1.579 | 0.665 | 1.322 | 0.403 | 0.875 | 0.809 | 2.047 | 1.810 |
| Ni | 0.009 | 0.009 | 0.004 | 0.001 | 0.000 | 0.010 | 0.009 | 0.000 | 0.009 | 0.000 | 0.002 | 0.002 | 0.000 | 0.001 | 0.006 | 0.000 | 0.000 | 0.000 | 0.000 | 0.000 |
| Sum | 5.086 | 4.906 | 4.913 | 5.006 | 4.809 | 5.079 | 4.736 | 4.032 | 4.655 | 4.728 | 4.535 | 4.759 | 4.705 | 4.815 | 4.928 | 4.858 | 4.728 | 4.731 | 4.614 | 4.678 |
| Ca | 1.664 | 1.719 | 1.549 | 0.862 | 0.933 | 1.381 | 0.594 | 1.091 | 1.112 | 0.887 | 0.920 | 0.900 | 0.981 | 0.777 | 1.243 | 1.431 | 1.661 | 1.671 | 1.734 | 1.810 |
| Na | 0.237 | 0.385 | 0.543 | 1.133 | 1.258 | 0.550 | 1.679 | 1.878 | 1.243 | 1.385 | 1.547 | 1.343 | 1.316 | 1.409 | 0.836 | 0.710 | 0.611 | 0.607 | 0.651 | 0.619 |
| K | 0.056 | 0.107 | 0.143 | 0.213 | 0.205 | 0.086 | 0.250 | 0.127 | 0.271 | 0.240 | 0.247 | 0.281 | 0.250 | 0.250 | 0.216 | 0.126 | 0.211 | 0.216 | 0.203 | 0.291 |
| Sum | 1.957 | 2.211 | 2.235 | 2.208 | 2.396 | 2.017 | 2.523 | 3.096 | 2.626 | 2.512 | 2.714 | 2.524 | 2.547 | 2.436 | 2.295 | 2.267 | 2.483 | 2.494 | 2.588 | 2.720 |
| mg# | 0.52 | 0.47 | 0.29 | 0.17 | 0.08 | 0.10 | 0.18 | 0.16 | 0.17 | 0.07 | 0.14 | 0.11 | 0.51 | 0.21 | 0.35 | 0.10 | 0.29 | 0.27 | 0.65 | 0.64 |

Table 4. Representative analyses of biotites (cations per 22 oxygens). Symbols as in Table 2.

| Sample | 3.4 | 2.1 | 2.1 | 32B | 34 | 22 | 10C | 3.1 | 30A | 4-2B | 4.3 | 4.3 |
|---|---|---|---|---|---|---|---|---|---|---|---|---|
| | S | S | S | S | S | AI-S | TR | GR | GR | GR | E | E |
| | m | C | m | m | m | m | m | C | m | C | C | m |
| $SiO_2$ | 35.23 | 37.48 | 36.31 | 36.10 | 35.10 | 36.08 | 37.34 | 39.93 | 33.66 | 35.27 | 38.33 | 38.59 |
| $TiO_2$ | 4.48 | 0.53 | 4.59 | 4.70 | 3.30 | 0.02 | 3.59 | 4.55 | 5.78 | 3.20 | 2.39 | 2.33 |
| $Al_2O_3$ | 12.07 | 13.23 | 12.08 | 12.66 | 11.16 | 6.13 | 9.60 | 8.53 | 10.92 | 11.45 | 11.63 | 11.84 |
| $Cr_2O_3$ | 0.02 | 0.03 | 0.04 | 0.04 | 0.00 | 0.00 | 0.01 | 0.01 | 0.00 | 0.02 | 0.00 | 0.04 |
| $FeO_{tot}$ | 26.67 | 21.00 | 25.47 | 24.08 | 33.66 | 43.12 | 31.06 | 24.38 | 31.49 | 31.26 | 20.33 | 20.14 |
| MnO | 0.20 | 0.17 | 0.26 | 0.15 | 0.37 | 0.84 | 0.48 | 0.47 | 0.29 | 0.49 | 0.31 | 0.28 |
| MgO | 6.93 | 12.93 | 7.14 | 8.51 | 3.77 | 0.71 | 5.59 | 6.39 | 3.50 | 4.34 | 11.52 | 11.78 |
| CaO | 0.00 | 0.00 | 0.00 | 0.00 | 0.00 | 0.00 | 0.00 | 0.00 | 0.00 | 0.00 | 0.00 | 0.00 |
| $Na_2O$ | 0.17 | 0.13 | 0.12 | 0.07 | 0.06 | 0.09 | 0.07 | 0.14 | 0.02 | 0.19 | 0.26 | 0.16 |
| $K_2O$ | 9.03 | 8.97 | 9.10 | 9.74 | 8.86 | 8.52 | 9.31 | 8.89 | 8.29 | 8.66 | 9.83 | 10.06 |
| Sum | 94.83 | 94.47 | 95.11 | 96.05 | 96.28 | 95.51 | 97.05 | 93.29 | 93.92 | 94.88 | 94.60 | 95.22 |
| Si | 5.901 | 6.070 | 6.007 | 5.891 | 5.994 | 6.566 | 6.233 | 6.659 | 5.847 | 6.038 | 6.218 | 6.212 |
| $Al^{IV}$ | 2.099 | 1.930 | 1.993 | 2.109 | 2.006 | 1.314 | 1.767 | 1.341 | 2.153 | 1.962 | 1.782 | 1.788 |
| $Al^{IV}$ | 0.282 | 0.593 | 0.361 | 0.324 | 0.238 | 0.000 | 0.120 | 0.334 | 0.081 | 0.346 | 0.440 | 0.457 |
| Ti | 0.564 | 0.065 | 0.571 | 0.577 | 0.424 | 0.003 | 0.451 | 0.571 | 0.755 | 0.412 | 0.292 | 0.282 |
| $Fe^{2+}$ | 3.740 | 3.844 | 3.524 | 3.286 | 4.807 | 6.563 | 4.336 | 3.400 | 4.575 | 4.475 | 2.758 | 2.711 |
| Cr | 0.003 | 0.004 | 0.005 | 0.005 | 0.000 | 0.000 | 0.001 | 0.001 | 0.000 | 0.003 | 0.000 | 0.005 |
| Mn | 0.028 | 0.023 | 0.036 | 0.002 | 0.054 | 0.129 | 0.068 | 0.066 | 0.038 | 0.071 | 0.043 | 0.038 |
| Mg | 1.730 | 3.122 | 1.761 | 2.070 | 0.960 | 0.193 | 1.391 | 1.589 | 0.906 | 1.108 | 2.786 | 2.827 |
| Ca | 0.000 | 0.000 | 0.000 | 0.000 | 0.000 | 0.000 | 0.000 | 0.000 | 0.000 | 0.000 | 0.000 | 0.000 |
| Na | 0.055 | 0.041 | 0.038 | 0.022 | 0.020 | 0.032 | 0.023 | 0.045 | 0.007 | 0.063 | 0.082 | 0.050 |
| K | 1.929 | 1.853 | 1.921 | 2.028 | 1.930 | 1.978 | 1.983 | 1.891 | 1.837 | 1.891 | 2.034 | 2.066 |
| mg# | 0.32 | 0.52 | 0.33 | 0.39 | 0.17 | 0.03 | 0.24 | 0.32 | 0.17 | 0.20 | 0.50 | 0.51 |

Table 5. Representative analyses of oxide minerals. Il, ilmenite (cation on basis of 3 oxygens); Mt, magnetite (cation on basis of 32 oxygens); other symbols as in Table 2.

| Sample | 1.1 | 2.1 | 3.4 | 3.4 | 34 | 34 | 15A | 15A | 50 | 50 | 28 |
|---|---|---|---|---|---|---|---|---|---|---|---|
| | S | S | S | S | S | S | S | AI-S | AI-S | AI-S | AI-S |
| | Il | Il | Il | Mt | Il | Mt | Il | Il | Il | Mt | Mt |
| $SiO_2$ | 0.09 | 0.13 | 0.21 | 0.17 | 0.06 | 0.24 | 0.04 | 0.02 | 0.07 | 0.19 | 0.21 |
| $TiO_2$ | 48.75 | 50.30 | 49.57 | 7.30 | 48.60 | 20.16 | 50.37 | 48.28 | 51.56 | 0.65 | 17.41 |
| $Al_2O_3$ | 0.16 | 0.09 | 0.05 | 2.72 | 0.02 | 1.17 | 0.03 | 0.03 | 0.04 | 0.16 | 0.10 |
| $Cr_2O_3$ | 0.09 | 0.03 | 0.09 | 0.80 | 0.03 | 0.11 | 0.00 | 0.01 | 0.00 | 0.06 | 0.10 |
| $Fe_2O_3$ | 7.88 | 3.33 | 6.50 | 49.22 | 9.11 | 27.96 | 5.29 | 8.27 | 1.96 | 66.73 | 34.55 |
| FeO | 39.16 | 42.28 | 40.75 | 37.29 | 40.02 | 48.29 | 40.32 | 40.42 | 41.54 | 31.30 | 45.68 |
| MnO | 4.46 | 1.87 | 3.55 | 0.17 | 3.62 | 1.97 | 4.91 | 2.91 | 4.77 | 0.31 | 1.69 |
| MgO | 0.15 | 0.11 | 0.13 | 0.29 | 0.05 | 0.00 | 0.03 | 0.04 | 0.04 | 0.09 | 0.05 |
| Sum | 100.74 | 99.14 | 100.85 | 97.96 | 101.51 | 99.90 | 100.99 | 99.98 | 99.98 | 99.49 | 99.79 |
| | | | | | | | | | | | |
| Si | 0.002 | 0.003 | 0.005 | 0.052 | 0.001 | 0.072 | 0.001 | 0.001 | 0.002 | 0.059 | 0.065 |
| Ti | 0.920 | 0.963 | 0.934 | 1.683 | 0.912 | 4.551 | 0.949 | 0.920 | 0.979 | 0.151 | 3.966 |
| Al | 0.005 | 0.003 | 0.001 | 0.983 | 0.001 | 0.414 | 0.001 | 0.001 | 0.001 | 0.058 | 0.037 |
| Cr | 0.002 | 0.001 | 0.002 | 0.194 | 0.001 | 0.026 | 0.001 | 0.001 | 0.001 | 0.058 | 0.037 |
| $Fe^{3+}$ | 0.149 | 0.064 | 0.123 | 11.353 | 0.171 | 6.315 | 0.100 | 0.158 | 0.037 | 15.510 | 7.876 |
| $Fe^{2+}$ | 0.822 | 0.900 | 0.854 | 9.559 | 0.835 | 12.121 | 0.845 | 0.857 | 0.877 | 8.085 | 11.574 |
| Mn | 0.095 | 0.062 | 0.075 | 0.044 | 0.077 | 0.501 | 0.104 | 0.062 | 0.102 | 0.081 | 0.434 |
| Mg | 0.005 | 0.004 | 0.005 | 0.132 | 0.002 | 0.000 | 0.001 | 0.002 | 0.001 | 0.041 | 0.023 |
| Sum | | | | | 2.000 | 24.000 | | | | | |
| | | | | | | | | | | | |
| Mol% | | | | | | | | | | | |
| Ulvöspinel | | | | 21.17 | | 59.41 | | | | 2.61 | 50.39 |
| $R_2O_3$ | 8.50 | 3.36 | 6.26 | | 9.11 | | 5.03 | 7.94 | 1.86 | | |
| | | | | | | | | | | | |
| T°C | | | | 675 | | 1015 | | | | 550 | |
| log$fO_2$ | | | | -18.0 | | -11.1 | | | | -23.5 | |

| Sample | AI-S | AI-S | TR | TR | TR | GR | GR | GR | GR | GR | GR |
|---|---|---|---|---|---|---|---|---|---|---|---|
| | 22A | 22A | 20 | 20 | 20 | 10C | 10C | 31 | 31 | 42-B | 42-B |
| | Il | Mt | Mt | Mt | Mt | Il | Mt | Il | Mt | Mt | Mt |
| $SiO_2$ | 0.06 | 1.09 | 0.16 | 0.48 | 0.90 | 0.08 | 0.29 | 0.13 | 0.22 | 0.24 | 0.24 |
| $TiO_2$ | 51.54 | 12.36 | 27.78 | 16.17 | 1.97 | 48.69 | 10.29 | 45.97 | 11.27 | 16.83 | 8.63 |
| $Al_2O_3$ | 0.02 | 0.44 | 0.69 | 0.24 | 0.41 | 0.00 | 0.16 | 0.02 | 0.16 | 0.41 | 0.25 |
| $Cr_2O_3$ | 0.00 | 0.04 | 0.02 | 0.00 | 0.00 | 0.02 | 0.03 | 0.05 | 0.02 | 0.00 | 0.05 |
| $Fe_2O_3$ | 1.50 | 41.81 | 13.97 | 34.88 | 62.13 | 9.51 | 48.41 | 11.81 | 46.15 | 33.89 | 51.18 |
| FeO | 44.09 | 42.46 | 54.69 | 44.32 | 33.68 | 38.43 | 39.48 | 36.78 | 38.57 | 43.75 | 38.01 |
| MnO | 2.67 | 1.32 | 2.35 | 1.62 | 0.22 | 5.29 | 1.47 | 4.57 | 2.86 | 2.28 | 1.07 |
| MgO | 0.03 | 0.10 | 0.04 | 0.07 | 0.02 | 0.05 | 0.08 | 0.05 | 0.12 | 0.18 | 0.13 |
| Sum | 100.25 | 99.62 | 99.70 | 97.78 | 99.33 | 102.07 | 100.21 | 99.38 | 99.37 | 97.58 | 99.56 |
| | | | | | | | | | | | |
| Si | 0.002 | 0.330 | 0.048 | 0.148 | 0.277 | 0.002 | 0.088 | 0.003 | 0.067 | 0.074 | 0.073 |
| Ti | 0.983 | 2.818 | 6.254 | 3.756 | 0.456 | 0.909 | 2.349 | 0.882 | 2.592 | 3.911 | 1.985 |
| Al | 0.001 | 0.157 | 0.243 | 0.087 | 0.149 | 0.000 | 0.057 | 0.001 | 0.058 | 0.149 | 0.090 |
| Cr | 0.000 | 0.010 | 0.004 | 0.000 | 0.000 | 0.000 | 0.007 | 0.001 | 0.005 | 0.000 | 0.012 |
| $Fe^{3+}$ | 0.028 | 9.537 | 3.147 | 8.106 | 14.385 | 0.178 | 11.060 | 0.227 | 10.620 | 7.880 | 11.780 |
| $Fe^{2+}$ | 0.928 | 10.763 | 13.691 | 11.447 | 8.667 | 0.798 | 10.024 | 0.785 | 9.863 | 11.306 | 9.723 |
| Mn | 0.057 | 0.339 | 0.596 | 0.424 | 0.057 | 0.111 | 0.378 | 0.099 | 0.741 | 0.597 | 0.277 |
| Mg | 0.001 | 0.045 | 0.018 | 0.032 | 0.009 | 0.002 | 0.036 | 0.002 | 0.055 | 0.083 | 0.059 |
| Sum | 2.000 | 23.999 | 24.001 | 24.000 | 24.000 | 2.000 | 23.999 | 2.000 | 24.001 | 24.000 | 23.999 |
| | | | | | | | | | | | |
| Mol% | | | | | | | | | | | |
| Ulvöspinel | | 39.35 | 78.73 | 48.80 | 9.16 | | 30.47 | | 33.23 | 49.82 | 25.73 |
| $R_2O_3$ | 1.45 | | | | | 8.88 | | 11.43 | | | |
| | | | | | | | | | | | |
| T°C | | 424 | | | | | 765 | | 831 | | |
| log$fO_2$ | | -28.2 | | | | | -15.5 | | -15.0 | | |

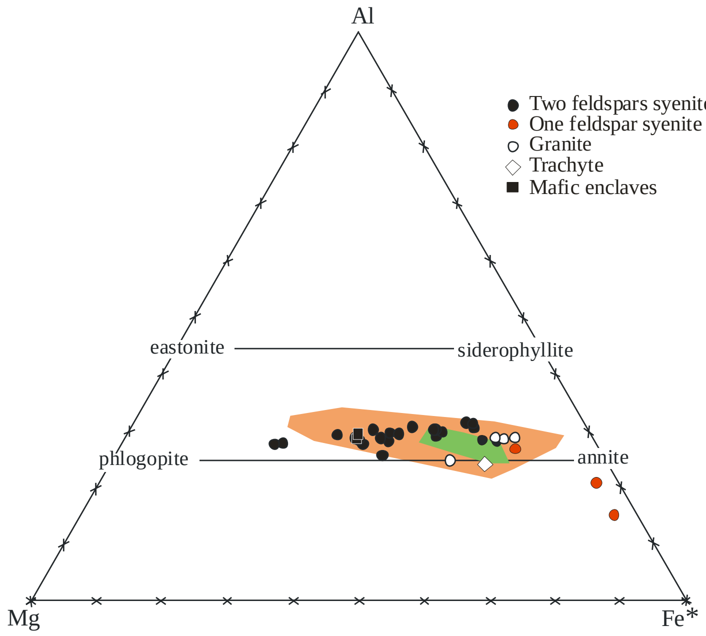


Fig. 7. Chemical analyses of biotites from the Ponta do Morro complex (data source: Table 4 and Sousa, 1997) plotted into the Al-Mg-Fe* diagram (cf. Bailey, 1984, and references therein). Green and light brown compositional fields represent the Valle Chico and Velasco complexes, respectively.

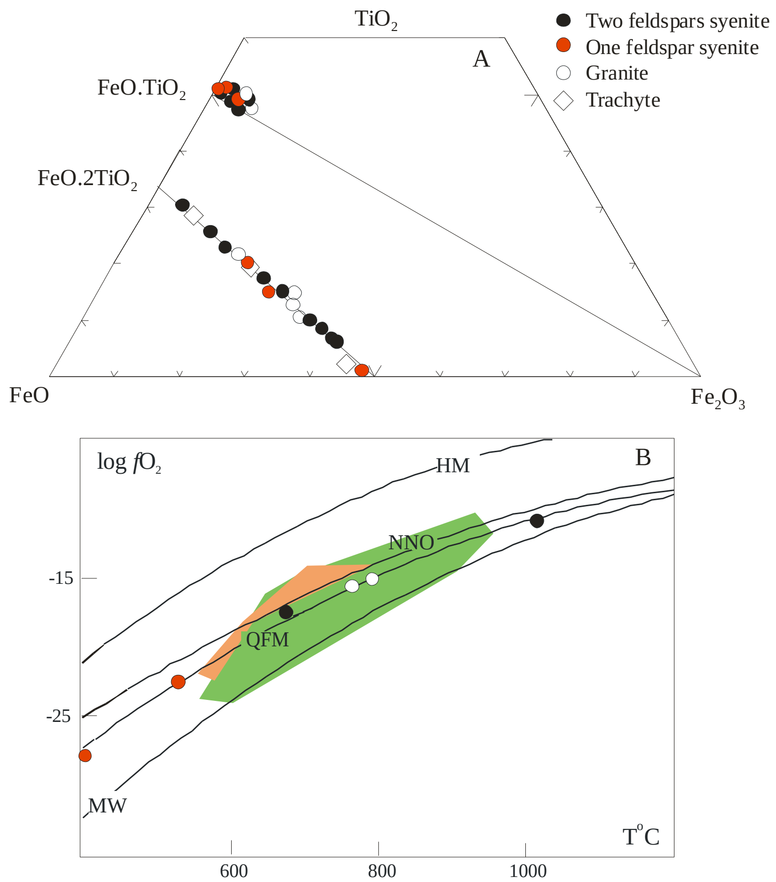


Fig. 8. A: Classification scheme of the Ponta do Morro opaque minerals (rhombohedral phases and spinel phases; Deer *et al.*, 1992). B: T(°C) vs. log $fO_2$ for Ti-magnetite and ilmenite pairs. The fields relative to magnetite-ilmenite pairs from Valle Chico and from Velasco alkaline complexes are shown for comparison.. Buffers: HM, haematite-magnetite; NNO, nickel-nickel oxide; QFM, quartz-magnetite-fayalite; MW, magnetite-wustite. Data source: Table 5 and Sousa, 1997. Green and light brown fields, as in Fig. 7.

Table 6. Representative analyses of olivines (cation on basis of 4 oxygens) and of aenigmatite (cation on basis of 20 oxygens).

| | Olivine | | | | Aenigmatite | | |
|---|---|---|---|---|---|---|---|
| Sample | 2.1 S mC | 2.1 S mR | 22A AI-S m | 2.2 AI-S m | | 22A AI-S m | 22-C AI-S m |
| $SiO_2$ | 34.23 | 31.22 | 32.35 | 29.58 | $SiO_2$ | 39.98 | 39.88 |
| $FeO_{tot}$ | 43.69 | 59.36 | 53.67 | 64.20 | $TiO_2$ | 8.26 | 7.08 |
| MnO | 1.23 | 2.58 | 1.88 | 3.39 | $Al_2O_3$ | 0.83 | 1.04 |
| MgO | 20.66 | 7.09 | 12.00 | 1.21 | $FeO_{tot}$ | 41.97 | 41.13 |
| CaO | 0.09 | 0.05 | 0.30 | 0.18 | MnO | 1.14 | 1.08 |
| Sum | 99.90 | 100.30 | 100.20 | 98.78 | MgO | 0.25 | 0.23 |
| | | | | | CaO | 0.80 | 0.82 |
| Si | 1.000 | 1.000 | 1.000 | 1.005 | $Na_2O$ | 6.88 | 6.21 |
| $Fe^{2+}$ | 1.067 | 1.590 | 1.388 | 1.824 | Sum | 100.11 | 97.47 |
| Mn | 0.030 | 0.070 | 0.049 | 0.098 | | | |
| Mg | 0.899 | 0.338 | 0.553 | 0.061 | Si | 5.802 | 5.917 |
| Ca | 0.003 | 0.002 | 0.010 | 0.007 | Al | 0.902 | 0.790 |
| Sum | 2.999 | 3.000 | 3.000 | 2.995 | Ti | 0.142 | 0.182 |
| | | | | | $Fe^{2+}$ | 5.094 | 5.103 |
| mg# | 0.46 | 0.18 | 0.28 | 0.03 | Mn | 0.140 | 0.136 |
| | | | | | Mg | 0.054 | 0.051 |
| | | | | | Ca | 0.124 | 0.130 |
| Equilibrium liquid, mg# | 0.22 | 0.07 | 0.11 | 0.01 | Na | 1.935 | 1.786 |
| | | | | | Sum | 14.113 | 14.095 |
| Observed mg# (host-rock) | 0.61 | 0.61 | 0.10 | 0.06 | | | |

syenites the range is between 0.28 and 0.03 Fo mol%. Notably, the more forsteritic cores could be in equilibrium with liquids with mg#=0.22, while the observed mg# of the host-rocks are around 0.61 (cf. Table 6). In general, the low mg# of the equilibrium liquids, with respect to the observed ones of the host-rocks, may be consistent with a late magmatic stage for the olivines from the two feldspars syenites.

In contrast, mg# of the olivines from one feldspar syenites appear consistent with those of the host-rocks (Table 6).

Aenigmatite (Table 6) is occasionally present in the one feldspar syenites, reflecting the increasing agpaitic index of the host-rocks, systematically •1. The presence of aenigmatite-olivine pairs suggests crystallization temperatures lower than 900° and $fO_2$ sightly below, or on the QFM buffer (cf. Marsh, 1975).

## PETROCHEMISTRY

Major and trace element analyses of representative Ponta do Morro (PMC) rock-types and some selected mafic to intermediate alkaline dykes from the Poxoréu area are reported in Table 7.

The PMC rocks show a large variation in $SiO_2$, i.e. 57-75 wt%, despite the restricted MgO content (2.4-0.3 wt%). In the TAS diagram (Fig. 9), these rocks fit the weakly alkaline fields (corresponding to the intrusive variants of trachyandesite, trachyte and rhyolite, respectively) with a transition to rocks of potassic affinity. The dykes from the Poxoréu area vary from trachybasalt to trachyandesite and the PMC dykes plot into the trachyte field. The modal PMC rhyolite (cf. Fig. 3) falls into the trachyte field. The two feldspar syenites straddle the trachyandesite and trachyte fields showing a saturated character (normative nepheline or quartz up to 3% and 5%, respectively), whereas the one feldspar syenites (A.I.•1; cf. Table 7) plot into the trachyte field and present both saturated and slightly oversaturated characteristics (normative nepheline up to 3.7% or normative quartz up to 10%). Notably, the latter rocks lie in the comendite field in the $Fe_2O_3$ vs. $Al_2O_3$ diagram (inset B of Fig. 9): on the whole the mineralogical (i.e. presence of fayalite and aenigmatite) and the petrochemical characteristics point to transitional series (cf. Barberi *et al.*, 1975).

Harker diagrams for the major elements (Fig. 10) show well distinct groups, i.e. mafic-intermediate dykes, syenites and granites, respectively, with overlapping of two feldspars and one feldspar syenites. The apparent trends may be referred to fractionation processes. In particular, the continuous decrease of $TiO_2$, FeO, MgO, CaO and $P_2O_5$ is consistent with magnetite, clinopyroxene and apatite fractionation. $Al_2O_3$, $Na_2O$ and $K_2O$ increase up to 58 $SiO_2$ wt%, and decrease for silica content •62 wt%, indicating feldspar fractionation.

Table 7. Chemical analyses of Ponta do Morro complex and Poxoréu rocks (*, Gibson *et al.*, 1997). A.I. = $(Na_2O+K_2O)/Al_2O_3$, molar ratio. Chemical methods in Sousa (1997). Abbreviations; BtrA, basaltic trachyandesite; TrA, tranchyandesite; TrB, trachybasalt.

| | Two feldspars syenite | | | | | | | | | | | | | | | One feldspar syenite | |
|---|---|---|---|---|---|---|---|---|---|---|---|---|---|---|---|---|---|
| Sample | 2.1 | 2-0 | 1.1 | 3.2 | 3.4 | 1D | 3.3 | 3.10 | 34A | 31C | 34C | 1.2 | 34 | 31B | 18 | 17 | 28 |
| wt% | | | | | | | | | | | | | | | | | |
| $SiO_2$ | 56.40 | 57.25 | 57.50 | 58.84 | 59.90 | 61.17 | 61.40 | 61.80 | 61.81 | 61.87 | 62.00 | 62.17 | 62.50 | 62.60 | 62.70 | 60.48 | 60.67 |
| $TiO_2$ | 1.30 | 1.32 | 1.00 | 0.92 | 0.86 | 0.88 | 0.78 | 0.80 | 0.73 | 0.74 | 0.74 | 0.76 | 0.71 | 0.70 | 0.71 | 0.64 | 0.65 |
| $Al_2O_3$ | 17.10 | 17.45 | 17.30 | 17.59 | 16.90 | 17.16 | 17.00 | 17.41 | 17.44 | 17.49 | 16.70 | 17.28 | 16.80 | 16.60 | 15.40 | 16.14 | 16.86 |
| $Fe_2O_3$ | 2.60 | 1.69 | 2.60 | 1.25 | 2.00 | 2.55 | 2.90 | 1.48 | 1.50 | 1.29 | 2.30 | 1.68 | 2.30 | 1.90 | 3.40 | 2.24 | 2.39 |
| FeO | 4.40 | 5.00 | 3.80 | 4.35 | 3.70 | 3.24 | 2.40 | 3.59 | 3.10 | 3.16 | 2.80 | 3.22 | 2.70 | 3.00 | 3.20 | 3.49 | 3.58 |
| MnO | 0.13 | 0.14 | 0.13 | 0.14 | 0.13 | 0.15 | 0.13 | 0.13 | 0.14 | 0.13 | 0.13 | 0.12 | 0.13 | 0.13 | 0.16 | 0.17 | 0.15 |
| MgO | 2.30 | 1.61 | 2.40 | 1.73 | 1.80 | 0.81 | 0.82 | 0.57 | 0.52 | 0.55 | 0.81 | 0.58 | 0.57 | 0.55 | 0.55 | 0.26 | 0.37 |
| CaO | 4.80 | 4.40 | 5.00 | 3.69 | 3.50 | 2.19 | 2.30 | 2.12 | 1.88 | 1.70 | 2.10 | 1.88 | 1.90 | 1.70 | 2.20 | 2.11 | 1.64 |
| $Na_2O$ | 5.60 | 5.59 | 5.30 | 5.85 | 5.10 | 5.69 | 5.30 | 5.46 | 5.69 | 5.80 | 5.10 | 5.72 | 5.00 | 5.50 | 5.40 | 6.09 | 6.34 |
| $K_2O$ | 4.10 | 4.47 | 3.60 | 4.78 | 5.00 | 5.90 | 6.20 | 6.01 | 6.41 | 6.51 | 6.20 | 6.19 | 6.50 | 6.50 | 5.00 | 6.14 | 6.18 |
| $P_2O_5$ | 0.32 | 0.35 | 0.19 | 0.23 | 0.18 | 0.21 | 0.19 | 0.19 | 0.17 | 0.16 | 0.17 | 0.17 | 0.15 | 0.15 | 0.14 | 0.12 | 0.13 |
| LOI | 0.38 | 0.38 | 0.64 | 0.20 | 0.37 | 0.10 | 0.19 | 0.14 | 0.29 | 0.05 | 0.47 | 0.10 | 0.33 | 0.21 | 0.73 | 1.44 | 0.81 |
| Sum | 99.43 | 99.65 | 99.46 | 99.57 | 99.41 | 100.05 | 99.61 | 99.70 | 99.68 | 99.45 | 99.52 | 99.87 | 99.59 | 99.33 | 99.59 | 99.32 | 99.77 |
| ppm | | | | | | | | | | | | | | | | | |
| Rb | 51 | 37 | 31 | 66 | 88 | 51 | 100 | 51 | 68 | 52 | 90 | 54 | 95 | 100 | 110 | 62 | 91 |
| Ba | 520 | | 320 | | 340 | 429 | 490 | 413 | 288 | | 370 | 450 | 300 | 260 | 520 | 131 | 187 |
| Sr | 220 | 162 | 160 | 97 | 140 | 74 | 77 | 70 | 33 | | 57 | 56 | 36 | 28 | 88 | 24 | 23 |
| Nb | 34 | 22 | 31 | 26 | 41 | 15 | 38 | 15 | 25 | 17 | 39 | 17 | 34 | 42 | 56 | 19 | 52 |
| Zr | 230 | 173 | 220 | 200 | 270 | 222 | 260 | 210 | 218 | 171 | 300 | 252 | 260 | 260 | 310 | 196 | 397 |
| Y | 41 | 22 | 52 | 36 | 62 | 31 | 61 | 45 | 34 | 15 | 49 | 54 | 49 | 48 | 62 | 33 | 57 |
| Th | 10 | | 10 | | 12 | | 16 | | | | 10 | | 14 | 12 | 10 | | |
| A.I. | 0.80 | 0.80 | 0.73 | 0.84 | 0.82 | 0.92 | 0.91 | 0.89 | 0.93 | 0.95 | 0.90 | 0.93 | 0.91 | 0.97 | 0.93 | 1.03 | 1.02 |
| $K_2O/Na_2O$ | 0.73 | 0.80 | 1.06 | 0.82 | 0.98 | 1.04 | 1.17 | 1.10 | 1.13 | 1.12 | 1.22 | 1.08 | 1.30 | 1.18 | 0.93 | 1.01 | 0.97 |

| | One feldspar syenite | | | | | | | | | | | | Trachyte Dykes | | Rhyolite Dyke |
|---|---|---|---|---|---|---|---|---|---|---|---|---|---|---|---|
| Sample | 29B | 26 | 22A | 22B | 27A | 50 | 11B | 2.2 | 6.3 | 11C | 15A | 16A | 1-D | 2-D | 3-D |
| wt% | | | | | | | | | | | | | | | |
| $SiO_2$ | 61.19 | 61.41 | 61.60 | 62.30 | 62.49 | 63.64 | 63.70 | 63.92 | 64.44 | 64.70 | 65.40 | 65.50 | 61.90 | 66.69 | 67.51 |
| $TiO_2$ | 0.41 | 0.46 | 0.64 | 0.64 | 0.35 | 0.47 | 0.44 | 0.50 | 0.35 | 0.28 | 0.40 | 0.41 | 0.47 | 0.33 | 0.44 |
| $Al_2O_3$ | 16.34 | 16.04 | 16.59 | 15.90 | 17.35 | 16.42 | 16.70 | 16.16 | 16.96 | 15.90 | 15.40 | 15.40 | 17.00 | 14.31 | 13.83 |
| $Fe_2O_3$ | 3.84 | 5.04 | 2.42 | 3.10 | 1.96 | 2.61 | 2.90 | 2.87 | 3.75 | 2.90 | 2.00 | 2.50 | 3.80 | 4.45 | 4.46 |
| FeO | 2.36 | 0.79 | 3.55 | 3.20 | 2.45 | 2.03 | 3.10 | 2.91 | 0.58 | 2.50 | 2.40 | 2.20 | 2.50 | 1.69 | 2.02 |
| MnO | 0.24 | 0.18 | 0.12 | 0.18 | 0.13 | 0.16 | 0.28 | 0.14 | 0.19 | 0.20 | 0.14 | 0.14 | 0.18 | 0.16 | 0.16 |
| MgO | 0.11 | 0.04 | 0.23 | 0.22 | 0.07 | 0.12 | 0.19 | 0.10 | 0.12 | 0.12 | 0.18 | 0.17 | 0.13 | 0.03 | 0.09 |
| CaO | 1.30 | 1.66 | 1.64 | 1.90 | 0.95 | 1.07 | 0.67 | 1.07 | 0.24 | 1.50 | 1.20 | 1.00 | 0.61 | 0.33 | 0.32 |
| $Na_2O$ | 6.35 | 5.82 | 6.62 | 6.00 | 7.10 | 6.45 | 6.60 | 6.40 | 7.21 | 6.40 | 6.00 | 6.00 | 6.00 | 6.51 | 5.34 |
| $K_2O$ | 5.60 | 6.29 | 5.58 | 5.60 | 5.76 | 6.26 | 5.30 | 5.59 | 5.30 | 5.30 | 5.60 | 5.70 | 5.90 | 4.53 | 4.46 |
| $P_2O_5$ | 0.06 | 0.06 | 0.06 | 0.09 | 0.03 | 0.10 | 0.07 | 0.06 | 0.02 | 0.05 | 0.05 | 0.05 | 0.06 | 0.01 | 0.08 |
| LOI | 1.35 | 1.81 | 0.56 | 0.45 | 0.65 | 0.19 | 0.05 | 0.21 | 0.75 | 0.05 | 0.76 | 0.51 | 1.13 | 0.56 | 1.01 |
| Sum | 99.15 | 99.60 | 99.43 | 99.58 | 99.30 | 99.52 | 100.00 | 99.93 | 99.91 | 99.90 | 99.53 | 99.58 | 99.68 | 99.60 | 99.75 |
| ppm | | | | | | | | | | | | | | | |
| Rb | 112 | 113 | 115 | 100 | 128 | 148 | 110 | 104 | 73 | 120 | 170 | 170 | 140 | 201 | 170 |
| Ba | 81 | 20 | 501 | 220 | 20 | 70 | 15 | 83 | 77 | 15 | 15 | 15 | 150 | 37 | 153 |
| Sr | 15 | 11 | 55 | 21 | 8 | 9 | 7 | 4 | 9 | 5 | 5 | 5 | 10 | 5 | 6 |
| Nb | 70 | 48 | 33 | 57 | 41 | 49 | 52 | 46 | 29 | 61 | 76 | 73 | 64 | 121 | 126 |
| Zr | 596 | 302 | 244 | 380 | 309 | 512 | 360 | 303 | 325 | 480 | 660 | 510 | 450 | 1121 | 512 |
| Y | 80 | 45 | 50 | 68 | 45 | 196 | 73 | 43 | 53 | 86 | 87 | 120 | 120 | 89 | 156 |
| Th | | | | 11 | | | 10 | | | 10 | 16 | 14 | 19 | | |
| A.I. | 1.01 | 1.02 | 1.02 | 1.00 | 1.03 | 1.06 | 0.99 | 1.03 | 1.04 | 1.02 | 1.03 | 1.04 | 0.96 | 1.09 | 0.98 |
| $K_2O/Na_2O$ | 0.88 | 1.08 | 0.84 | 0.93 | 0.81 | 0.97 | 0.80 | 0.87 | 0.74 | 0.83 | 0.93 | 0.95 | 0.98 | 0.70 | 0.84 |

Table 7 (continued).

| | Granite | | | | | | | | | | | Poxoréu dykes | Kimberlite pipes | | | | |
|---|---|---|---|---|---|---|---|---|---|---|---|---|---|---|---|---|---|
| | | | | | | | | | | | | TrB | TrB | BTrA | TrA | | |
| Sample | 19 | 30-A | 35-B | 10-A | 12-A | 4-2B | 5.5 | 10-D | 3-0 | 3.1 | 24-B | JM-8 | P-1 | B46b | B55b | JM-B | JM-P |
| wt% | | | | | | | | | | | | | | | | | |
| $SiO_2$ | 70.35 | 70.78 | 71.22 | 71.91 | 73.20 | 73.30 | 73.31 | 73.40 | 73.78 | 74.20 | 74.77 | 48.31 | 49.02 | 53.06 | 55.84 | 32.32 | 45.76 |
| $TiO_2$ | 0.27 | 0.24 | 0.32 | 0.21 | 0.18 | 0.20 | 0.21 | 0.22 | 0.10 | 0.08 | 0.16 | 2.97 | 2.70 | 2.35 | 1.96 | 2.71 | 2.44 |
| $Al_2O_3$ | 14.40 | 14.51 | 13.97 | 14.07 | 13.50 | 13.40 | 14.09 | 13.83 | 13.50 | 13.50 | 13.74 | 13.14 | 14.71 | 15.01 | 15.69 | 3.22 | 3.51 |
| $Fe_2O_3$ | 1.04 | 1.20 | 3.40 | 1.03 | 1.60 | 1.30 | 1.24 | 1.00 | 0.64 | 0.22 | 0.20 | | | | | | |
| FeO | 1.34 | 0.92 | 0.30 | 0.83 | 0.70 | 0.84 | 0.50 | 0.45 | 0.38 | 0.70 | 0.38 | *12.85 | *11.32 | *10.45 | *9.78 | *10.18 | *9.36 |
| MnO | 0.06 | 0.06 | 0.01 | 0.12 | 0.03 | 0.04 | 0.02 | 0.02 | 0.03 | 0.02 | 0.01 | 0.30 | 0.19 | 0.20 | 0.23 | 0.17 | 0.18 |
| MgO | 0.22 | 0.15 | 0.05 | 0.16 | 0.15 | 0.18 | 0.14 | 0.13 | 0.11 | 0.10 | 0.13 | 7.16 | 7.14 | 2.84 | 2.54 | 31.80 | 29.30 |
| CaO | 0.60 | 0.53 | 0.07 | 0.45 | 0.47 | 0.67 | 0.25 | 0.24 | 0.72 | 0.60 | 0.37 | 6.26 | 8.73 | 6.30 | 5.68 | 4.35 | 2.61 |
| $Na_2O$ | 4.73 | 4.50 | 4.98 | 4.73 | 4.00 | 4.10 | 4.58 | 4.57 | 4.92 | 4.70 | 4.00 | 1.66 | 3.68 | 4.34 | 4.48 | 0.72 | 0.13 |
| $K_2O$ | 5.93 | 6.10 | 4.41 | 5.71 | 5.30 | 5.20 | 5.23 | 5.55 | 5.26 | 5.10 | 5.49 | 3.79 | 1.96 | 2.60 | 2.89 | 0.35 | 0.40 |
| $P_2O_5$ | 0.03 | 0.06 | 0.01 | 0.01 | 0.05 | 0.05 | 0.01 | 0.02 | 0.01 | 0.05 | 0.02 | 0.58 | 0.55 | 0.50 | 0.44 | 0.63 | 0.15 |
| LOI | 0.57 | 0.48 | 0.96 | 0.32 | 0.57 | 0.45 | 0.31 | 0.37 | 0.31 | 0.56 | 0.75 | 1.30 | | 0.40 | 1.56 | 12.62 | 8.53 |
| Sum | 99.54 | 99.53 | 99.30 | 99.55 | 99.75 | 99.73 | 99.89 | 99.80 | 99.78 | 99.83 | 100.02 | 98.32 | 100.00 | 98.05 | 99.53 | 99.07 | 98.30 |
| ppm | | | | | | | | | | | | | | | | | |
| Rb | 191 | 198 | 320 | 149 | 260 | 260 | 123 | 161 | 164 | 310 | 198 | 99 | 95 | 76 | 95 | 23 | 48 |
| Ba | 191 | | 19 | 340 | 200 | 230 | 361 | 304 | 77 | 660 | | 685 | 652 | 602 | 674 | 1984 | 300 |
| Sr | 36 | 14 | 6 | 40 | 41 | 44 | 37 | 37 | 25 | 30 | 14 | 600 | 551 | 386 | 386 | 374 | 35 |
| Nb | 52 | 62 | 189 | 21 | 56 | 56 | 17 | 27 | 44 | 110 | 62 | 17 | 28 | 46 | 49 | 154 | 66 |
| Zr | 471 | 369 | 1513 | 319 | 380 | 370 | 359 | 341 | 196 | 290 | 369 | 185 | 190 | 458 | 504 | 103 | 57 |
| Y | 93 | 70 | 172 | 85 | 95 | 96 | 55 | 51 | 157 | 200 | 70 | 28 | 31 | 65 | 71 | 11 | 10 |
| Th | | | | | 12 | 28 | | | | 27 | | 3 | 5 | 8.5 | 7.4 | 14 | 3 |
| A.I. | 0.99 | 0.91 | 0.93 | 0.99 | 0.97 | 0.92 | 0.94 | 0.98 | 1.02 | 0.98 | 0.91 | 0.52 | 0.56 | 0.66 | 0.67 | 0.49 | 0.18 |
| $K_2O/Na_2O$ | 1.25 | 1.36 | 0.89 | 1.21 | 1.33 | 1.27 | 1.14 | 1.21 | 1.07 | 1.09 | 1.37 | 2.28 | 0.53 | 0.60 | 0.65 | 0.49 | 3.08 |

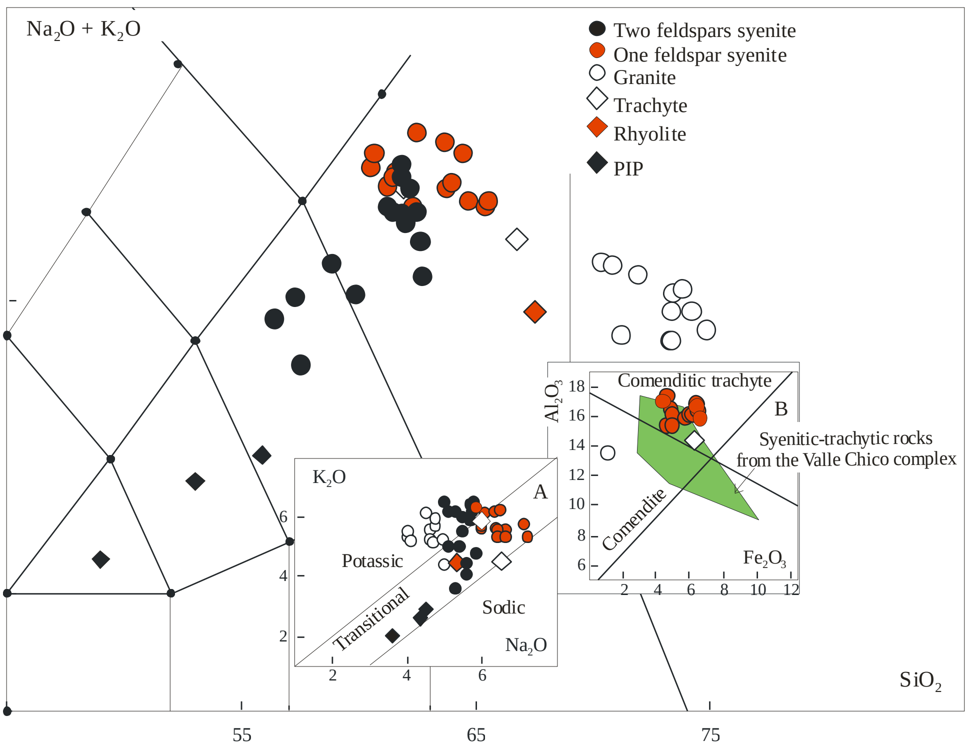


Fig. 9. TAS (total alkalies vs. silica, in wt%, cf. Le Maitre, 1989) diagram for the Ponta do Morro igneous rocks and Poxoréu dykes (PIP). Insets: A, $Na_2O$ vs. $K_2O$ showing the fields of the igneous variants. B, Classification grid for peralkaline rocks (Macdonald, 1974), total Fe (as $Fe_2O_3$) vs. $Al_2O_3$; the syenitic-trachytic rocks from the Valle Chico massif are shown for comparison (cf. Ruberti *et al.*, in this volume).

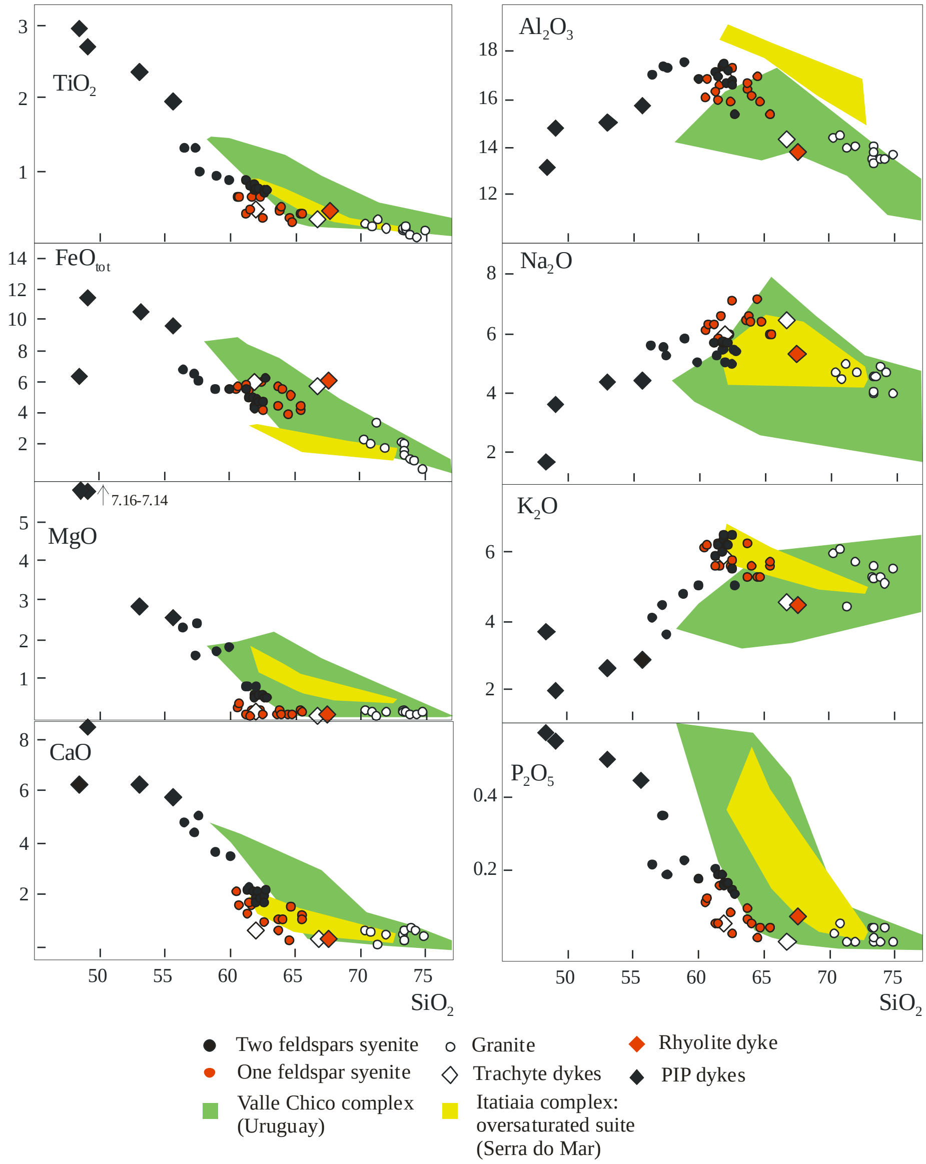


Fig. 10. $SiO_2$ vs. major elements of representative plutonic and hypabissal alkaline rock types from the Ponta do Morro complex and from the Poxoréu region (PIP). For comparison, the fields of the Valle Chico rocks and of the Itatiaia oversaturated suite are shown.

The trace elements (Fig. 11) display broad positive correlations against silica for Rb and Th, and negative ones for Sr, Zr, Ba, Nb and Y show very scattered variations, particularly around 62 (syenitic rocks) and 73 $SiO_2$ wt% (granites), probably due to complex reactions at subsolidus temperatures and hydrothermal conditions.

On the whole, the variations observed in the PMC rocks are different from those given by analogues from other complexes associated with the South American Platform, that display even larger scattering (cf. Figs. 10 and 11), e.g. Valle Chico (Muzio *et al.*, 2002) and Itatiaia (Brotzu *et al.*, 1997).

In order to quantitatively test the fractionation processes in the PMC suite, a series of mass balance calculations was performed based on the major element contents of the parent/daughter rock-types and their mineralogy (least squares fitting method of Stormer & Nichols, 1978), and on the trace elements contents of the melts derived by crystal fractionation (cf. Hanson, 1978). The results are consistent for a derivation of two feldspars and one feldspar syenites from a trachybasaltic parent (Table 8). Attempts to derive the one feldspar syenites and granites from the two feldspar syenites gave unrealistic results, due to high values of the square residuals (i.e. >> 1), or to inconsistent ratios between observed and calculated concentration of the trace elements. This is attributable either to subsolidus reactions, i.e. inadequate representativity of the utilized phases, or to wrong $K_D$ values used in the modelling, or both. Mixing processes between derivative liquids and the host-rocks of the Cuiabá Group may be also possible. Finally, it may be noted that Muzio *et al.* (2002) suggest different magmatic pulses for the various alkaline rocks from the Valle Chico complex (Uruguay), and that the granites may be attributable to a different parental magma.

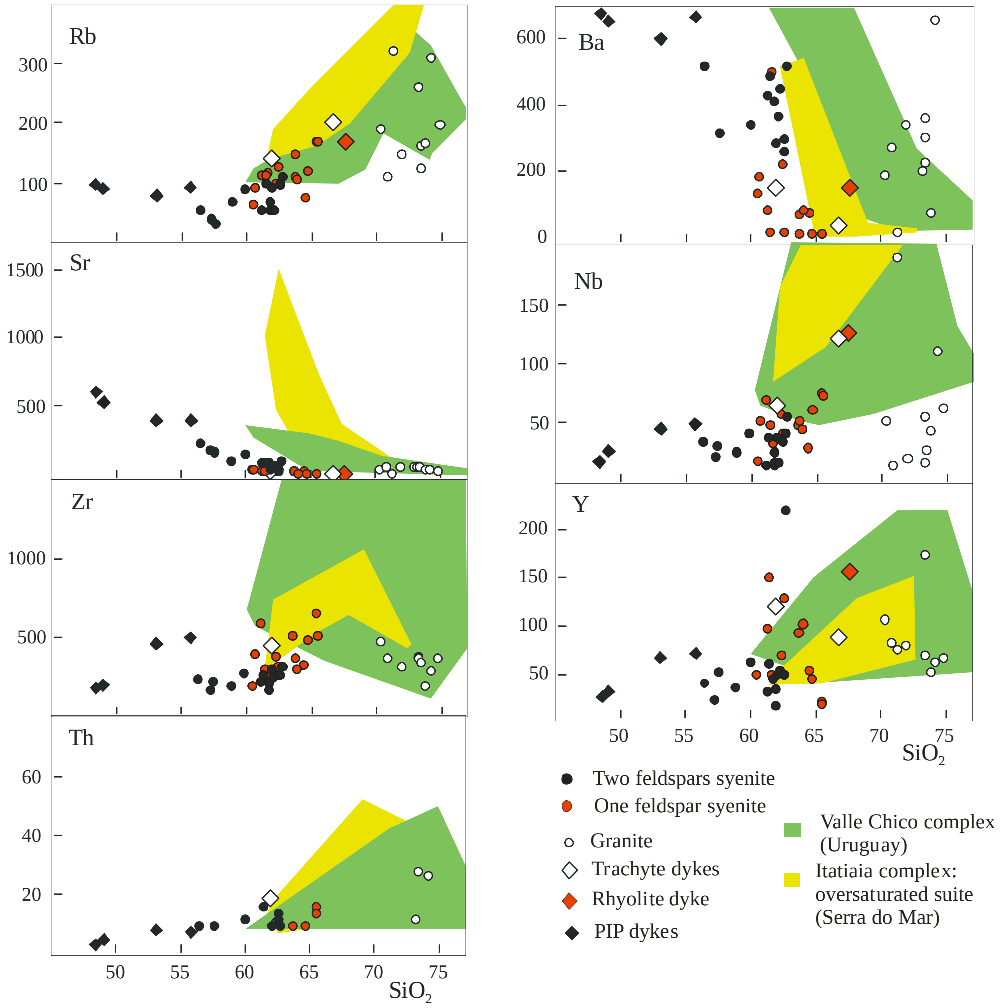


Fig. 11. $SiO_2$ vs. trace elements of representative plutonic and hypabissal alkaline rock-types from the Ponta do Morro complex and from the Poxoréu region (PIP). For comparison, the fields of the Valle Chico rocks and of the Itatiaia oversaturated suite are shown.

## Sr ISOTOPES

The isotope data for the different rock-types are given in Table 9. A positive correlation (r=0.999) between $^{87}Rb/^{86}Sr$ and $^{87}Sr/^{86}Sr$ (errorchron) allows the calculation of an age of 97.3±1.1 Ma with initial $^{87}Sr/^{86}Sr$ ($R_0$)=0.70435 for the Ponta do Morro complex, according to the isochron of Sousa (1997).

Important differences among the samples are apparent, in comparison with the dykes and kimberlitic pipes from the Poxoréu area: the PCC-1 trachybasalt dyke and the samples 3-4, 22-A, and 3-1 (two feldspars syenite, one feldspar syenite and granite), respectively. These rocks yielded an average $R_0$=0.70440±0.00001, indicating a substantial isotopically homogeneous parent magma.

On the other hand, the $R_0$ values, ranging from 0.70524 (two feldspars syenite) to 0.70770 (granite), are distinctly higher than those of the other Ponta do Morro rock-types, and do not support a simple fractionation origin from a common parent magma. The kimberlitic pipes that displays $R_0$ between 0.70364 and 0.70358 indicate substantially different (lithospheric) sources.

## CONCLUSIONS

The Ponta do Morro alkaline complex (97 Ma) intrudes the metasediments of the Cuiabá Group and consists of syenites, two feldspars and one feldspar variants, and of granitic rock-types. Scarce trachytic and rhyolitic dykes cut the complex. Mafic enclaves are widespread along the western borders.

Table 8. Modelling of fractional crystallization based on the least squares fit methods. Mineral-liquid partition coefficients after Caroff *et al.* (1993).

| Fractionation trends | | | | | |
|---|---|---|---|---|---|
| From trachybasalt (PCC-1) to two feldspars syenite (2-1) | | | From trachybasalt (PCC-1) to one feldspar syenite (28) | | |
| Subtracted solid 44.65% $R^2$=0.215 | | | Subtracted solid 57.98% $R^2$=0.841 | | |
| Ol | 8.82 | ($Fo_{80}$) | Ol | 9.92 | ($Fo_{80}$) |
| Cpx | 14.31 | ($En_{42}Fs_{13}Wo_{45}$) | Cpx | 19.07 | ($En_{42}Fs_{13}Wo_{45}$) |
| Mt | 7.12 | (Ulv60) | Mt | 7.94 | (Ulv60) |
| Pl | 13.44 | ($An_{85}$) | Pl | 20.25 | ($An_{85}$) |
| Ap | 0.96 | | Ap | 0.80 | |
| obs/calc | | | obs/calc | | |
| Rb | 0.99 | | Rb | 0.81 | |
| Ba | 0.87 | | Ba | 0.97 | |
| Sr | 0.86 | | Sr | 0.17 | |
| Nb | 1.00 | | Nb | 0.85 | |
| Zr | 0.83 | | Zr | 1.00 | |
| Y | 0.95 | | Y | 0.70 | |

Table 9. Isotopic Sr data for some selected rocks from the Ponta do Morro complex and from the Poxóreu area. Analytical methods in Sousa (1997) and (*) Gibson *et al.* (1997).

| | $SiO_2$ | Rb (ppm) | Sr (ppm) | $(^{87}Sr/^{86}Sr)_{meas}$ | $(^{87}Sr/^{86}Sr)_{97}$ (97 Ma) |
|---|---|---|---|---|---|
| Two feldspars syenite | | | | | |
| 2.1 | 56.40 | 50.5 | 212.4 | 0.70619 (9) | 0.70524 |
| 3.4 | 59.90 | 95.4 | 35.2 | 0.71554 (31) | 0.70438 |
| One felspar syenite | | | | | |
| 22-A | 61.60 | 114.9 | 42.4 | 0.71518 (9) | 0.70437 |
| Granite | | | | | |
| 4-2B | 73.31 | 241.7 | 38.9 | 0.73254 (5) | 0.70770 |
| 3.1 | 74.20 | 272.0 | 25.5 | 0.74725 (9) | 0.70455 |
| Dykes | | | | | |
| Trachybasalt | | | | | |
| JM-8 | 48.31 | 99 | 600 | 0.70506 (1) | 0.70440 |
| Trachybasalt | | | | | |
| PCC-1 | 49.02 | 95 | 551 | 0.70501 (1) | 0.70432 |
| Basaltic trachyandesite | | | | | |
| B46B* | 53.06 | 76 | 386 | 0.70667 (1) | 0.70588 |
| Trachyandesite | | | | | |
| B55b* | 55.84 | 95 | 386 | 0.70708 (1) | 0.70609 |
| Pipes (84 Ma*) | | | | | |
| JM-B | 32.32 | 23 | 374 | 0.70385 (2) | 0.70364 |
| JM-P | 45.76 | 48 | 35 | 0.70837 (1) | 0.70358 |

The textures and mineralogical assemblages suggest a shallow level intrusion at P-T around 1 kb and 1000°C. The subsolidus conditions developed along the QFM buffer. The mineralogical and petrochemical characteristics suggest a transitional affinity.

Harker diagrams for the major elements, as well as the mass balance calculations, are consistent with fractional crystallization, for both the two feldspar and one feldspar syenites, from a common trachybasalt magma.

A common source is also confirmed by constant $^{87}Sr/^{86}Sr$ initial ratios, i.e. 0.70440±0.00001, for trachybasalt to granite rocks. However, the important scattering relative to the contents of the trace elements and some high $^{87}Sr/^{86}Sr$ initial ratios (0.7052 to 0.7077) suggest the possibilty of crustal contamination or AFC processes for both the trachyandesite dykes of the region and the granitic rocks from the Ponta do Morro complex. Finally, the isotopic differences compared with the kimberlitic rocks of the region suggest distincts lithospheric sources.

## ACKNOWLEDGEMENTS

We are gratefull to Jayme A. Dexheimer Leite for the regional geological review and to Aldo Cundari and Alan Woolley for the constructive criticism of the manuscript.

## REFERENCES

Andersen, D.J. & Lindsley, D.H. (1988). Internally consistent solution models for Fe-Mg-Mn-Ti oxides: Fe-Ti oxides. *American Mineralogist* **73**, 714-726.

Bailey, S.W. (1984). Classification and structures of the micas. Crystal chemistry of the true micas. *Reviews in Mineralogy, Mineralogical Society of America* **13**, 1-60.

Barberi, F., Ferrara, G., Santacroce, R., Treuil, M. & Varet, J. (1975). A transitional basalt-pantellerite sequence of functional crystallization, the Boina Centre (Afar Rift, Ethiopia). *Journal of Petrology* **16**, 22-56.

Barbieri M., Beccaluva, L., Brotzu, P., Conte, A., Garbarino, C., Gomes, C.B., Loss, E.L., Macciotta, G., Morbidelli, L., Scheibe, L., Tamura, R.M. & Traversa, G. (1987). Petrological and geochemical studies of alkaline rocks from continental Brazil. 1. The phonolite suite from Piratini, RS. *Geochimica Brasiliensis* **1,** 109-138.

Berrocal, J. & Fernandes, C. (1996). Seismicity in Paraguay and neighbouring regions. In: Comin-Chiaramonti, P. & Gomes, C.B. (eds.) *Alkaline magmatism in the central-eastern Paraguay-Relationships with coeval magmatism in Brazil.* São Paulo: Edusp-Fapesp, pp. 57-66.

Biondi, J.C. (in this volume). Brazilian mineral deposits associated with alkaline and alkaline-carbonatite complexes.

Brotzu, P., Gomes, C.B., Melluso, L., Morbidelli, L., Morra, V. & Ruberti, E. (1997). Petrogenesis of coexisting $SiO_2$-undersaturated to $SiO_2$-oversaturated felsic igneous rocks: the alkaline complex of Itatiaia, southeastern Brazil. *Lithos* **40**, 133-156.

Caroff, M., Maury, R.C., Leterrier, J., Joron, J.L., Cotten, J. & Guille, G. (1993). Trace element behaviour in the alkali basalt-comenditic trachyte series from Mururoa Atoll, French Polynesia. *Lithos* ***30***, 1-22.

Comin-Chiaramonti, P. & Gomes, C.B. (1996) *Alkaline magmatism in the central-eastern Paraguay-Relationships with coeval magmatism in Brazil.* São Paulo: Edusp-Fapesp, 464p.

Comin-Chiaramonti, P., Gomes, C.B., Velázquez, V.F., Censi, P., Antonini, P., Comin-Chiaramonti, F. & Punturo, R. (in this volume). Alkaline complexes from southeastern Bolivia.

Deer, W.A., Howie, R.A. & Zussman, J. (1992). *An introduction to the rock-forming minerals.* London: Longman, 696p.

Gibson, S.A., Thompson, R.N., Weska, R.K., Dickin, A.P. & Leonardos, O.H. (1997). Late Cretaceous rift-related upwelling and melting of the Trindade starting mantle plume head beneath western Brazil. *Contributions to Mineralogy and Petrology* **126**, 303-314.

Giret, A., Bonin, B. & Leger, J.M. (1980). Amphibole compositional trends in oversaturated and undersaturated alkaline plutonic ring-complexes. *Canadian Mineralogist* **18**, 481-495.

Gomes, C.B., Barbieri, M., Beccaluva, L., Brotzu, P., Conte, A., Garbarino, C., Macciotta, G., Melluso, L., Morbidelli, L., Ruberti, E., Scheibe, L.F., Tamura, R.M. & Traversa, G. (1987). Petrological and geochemical studies of alkaline rocks from continental Brazil. 2. The Tunas massif, State of Paraná. *Geochimica Brasiliensis* **1**, 201-234.

Gonzaga, G.M. & Tomkins, L.A. (1991). Geologia do diamante. In: Schobbenhaus, C., Queiroz, E.T. & Coelho, C.E.S. (eds.) *Principais depósitos minerais do Brasil – Gemas e rochas ornamentais.* DNPM-CPRM, vol. VI, parte A, pp. 53-116.

Greenwod, J.C., Gibson, S.A., Thompson, R.N., Weska, R.K. & Dickin, A.P. (1999). Cretaceous kimberlites from the Paratininga-Batovi region, central Brazil: geochemical evidences for subcratonic mantle heterogeneity. *7th International Kimberlite Conference, Cape Town, Proceedings* **1**, 291-298.

Hanson, G.N. (1978). The application of trace elements to the petrogenesis of igneous rocks of granitic composition. *Earth and Planetary Science Letters* **38**, 26-43.

Heaman, L., Teixeira, N.A., Gobbo, L. & Gaspar, J.C. (2003). U-Pb mantle zircon ages for kimberlites from the Juina and Paratininga provinces, Brazil. *IV South American Symposium on Isotope Geology, Salvador,* CD-ROM, pp. 322-324.

Kudo, A.M. & Weill, D.F. (1970). An igneous plagioclase geothermometer. *Contributions to Mineralogy and Petrology* **26**, 52-65.

Le Maitre, R.W. (1989). *A classification of igneous rocks and glossary of terms*. Oxford: Blackwell, 193p.

Macdonald, R. (1974). Nomenclature and petrochemistry of the peralkaline oversaturated extrusive rocks. *Bullettin Volcanologique* **38**, 498-516.

Marsh, J.S. (1975). Aenigmatite stability in silica-undersaturated rocks. *Contributions to Mineralogy and Petrology* **50**, 135-144.

Mathez, E.A. (1973). Refinement of the Kudo-Weill plagioclase thermometer and its application to basaltic rocks. *Contributions to Mineralogy and Petrology* **41**, 61-72.

Morimoto, N. (1988). Nomenclature of pyroxenes. *Mineralogical Magazine* **52,** 535-550.

Muzio, R., Artur, A.C. & Wernick, E. (2002). Petrological and geochemical evolution of the alkaline Valle Chico massif, southeastern Uruguay. *International Geology Review* **44**, 352-369.

Powell, M. & Powell, R. (1977). Plagioclase-alkali feldspar geothermometer revisited. *Mineralogical Magazine* **41**, 253-256.

Ruberti, E., Gomes, C.B. & Comin-Chiaramonti, P. (in this volume). The alkaline magmatism from the Ponta Grossa Arch.

Ruberti, E., Gomes, C.B., Tassinari, C.C., Antonini, P. & Comin-Chiaramonti, P. (in this volume). The Early Cretaceous Valle Chico complex (Mariscala, SE Uruguay).

Seck, H.A. (1971). Koexistierende alkalifeldspate und plagioclase in the system $NaAlSi_3O_8$-$KAlSi_3O_8$-$CaAl_3Si_2O_8$-$H_2O$ bei temperaturen von 650°C bis 900°C. *Neues Jharbuch Mineralogische Abhandlungen* **115**, 315-395.

Sousa, M.Z.A. (1997). *Petrologia e geoquímica do complexo alcalino Ponta do Morro, MT*. Ph.D. Thesis, University of São Paulo, 171p.

Stormer, J.C. Jr. & Nicholls, J. (1978). XLFRAC, a programm for interactive testing of magmatic differentiation models. *Computational Geosciences* **4**, 143-159.

*Mesozoic to Cenozoic Alkaline Magmatism in the Brazilian Platform*
*Comin-Chiaramonti, P. & Gomes, C.B. (eds.)*
*Edusp/Fapesp, São Paulo, pp. 241-260, 2005*

# THE LATE CRETACEOUS GOIÁS ALKALINE PROVINCE (GAP), CENTRAL BRAZIL

*J.A. Brod, E.S.R. Barbosa, T.C. Junqueira-Brod, J.C. Gaspar, H.S. Diniz-Pinto, P.B.A. Sgarbi and I.A. Petrinovic*

*The Late Cretaceous Goiás Alkaline Province, located at the northern margin of the Paraná Basin, in central Brazil, is one of the largest areas of kamafugite exposure in the world. The northern portion of the province is dominated by alkaline plutonic ultramafic to mafic complexes, with subordinate dykes, plugs and sills. The central part is characterized by subvolcanic bodies (diatremes, plugs, and dykes) and the southern portion consists dominantly of volcanic rocks (lavas and pyroclastics). From north to south there is also a marked increase in the level of silica-undersaturation of the alkaline rocks, with a dominance of less silica-undersaturated (feldspar-bearing) rocks in northern GAP, and of strongly undersaturated, kamafugitic (katungite, mafurite, leucite mafurite and ugandite) rocks in the central and southern parts of the province. Textural, mineralogical and geochemical evidence indicate a complex evolution of the GAP. The mineralogical and chemical compositions of the less silica-undersaturated rocks that form the northern GAP plutonic complexes are indicative of a derivation from an alkaline picrite parent magma, through fractional crystallization. By their composition, katungites represent the most primitive rock-types, and ugandites correspond to the most evolved magmas within the kamafugite series, but the various kamafugitic rock-types cannot be easily connected through fractional crystallization. The trace element ranges of katungitic and mafuritic rock-types with MgO suggest that these groups represent independent sequences of rocks produced by various degrees of partial melting. Ugandites may also constitute an independent group or they may be the product of fractional crystallization of mafurites. Leucite mafurites are best explained as a result of mixing between picritic and mafuritic magma. The field relationships and the chemistry of phlogopite and olivine suggest that the kamafugite-carbonatite association is significant in the central and southern GAP.*

## INTRODUCTION

The Goiás Alkaline Province (GAP), located at the northern border of the Paraná Basin, is one of the largest kamafugite-dominated provinces of the world, comparable in volume of exposed kamafugitic rocks to the nearby Alto Paranaíba Igneous Province. Despite the wide variety of rock-types and the complete set of emplacement modes, from plutonic complexes through subvolcanic structures (plugs and diatremes) to lavas and pyroclastics, only a few of these alkaline rock occurrences have been studied in detail so far, and a substantial amount of mineral chemistry, geo-chemistry and isotope work is still required in order to fully understand their petrogenetic relationships.

The aim of this work is to provide a review of the existing knowledge on GAP rocks, and to suggest some alternatives for future research.

## GEOLOGICAL SETTING

During the Cretaceous, extensive alkaline magmatic activity took place around the margins of the Paraná Basin (Fig. 1). This was associated by Almeida (1967) with an extensional tectonic event, named Wealdenian reactivation, which led, in a first stage (Early Cretaceous), to the emplacement of alkaline rocks contemporaneous with the continental flood basalts of the Serra Geral Formation (Paraná Basalts). A second peak of alkaline magmatism occurred during the Late Cretaceous. Such tectonic event is thought to have reactivated ancient fault zones of the basement, through which the alkaline magmas ascended, and was considered to represent an inland expression of the opening of the South Atlantic Ocean (Almeida, 1983, 1986).

Gibson *et al.* (1997) suggested that the main cause for the Late Cretaceous magmatism in South Goiás is associated with the impact of Trindade Mantle Plume near the Iporá region. On the other hand, Van Decar *et al.* (1995), based on seismic data, linked the Late Cretaceous magmatism surrounding the Paraná Basin to the Early Cretaceous Tristan da Cunha Mantle Plume, considering the alkaline rocks as an extension of the earlier Paraná magmatism.

In the region extending from the towns of Araguaiana and Santa Fé, in the north, to Rio Verde, in the south, a series of alkaline rocks crop out mainly concentrated in a N30W-elongated area, approximately 250 km long and 70 km wide (Fig. 2), which coincides with a trend of basement faults. The major

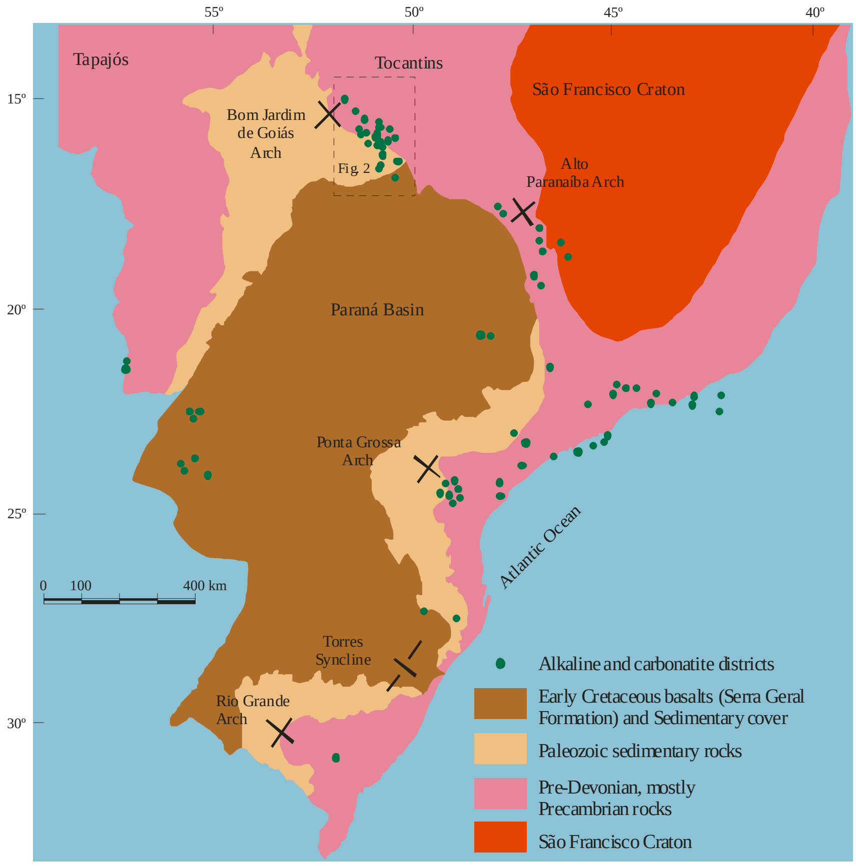


Fig. 1. Geological sketch-map of the distribution of Cretaceous alkaline provinces surrounding the Paraná Basin, showing the location of the Late Cretaceous Goiás Alkaline Province. Modified from Ulbrich & Gomes (1981).

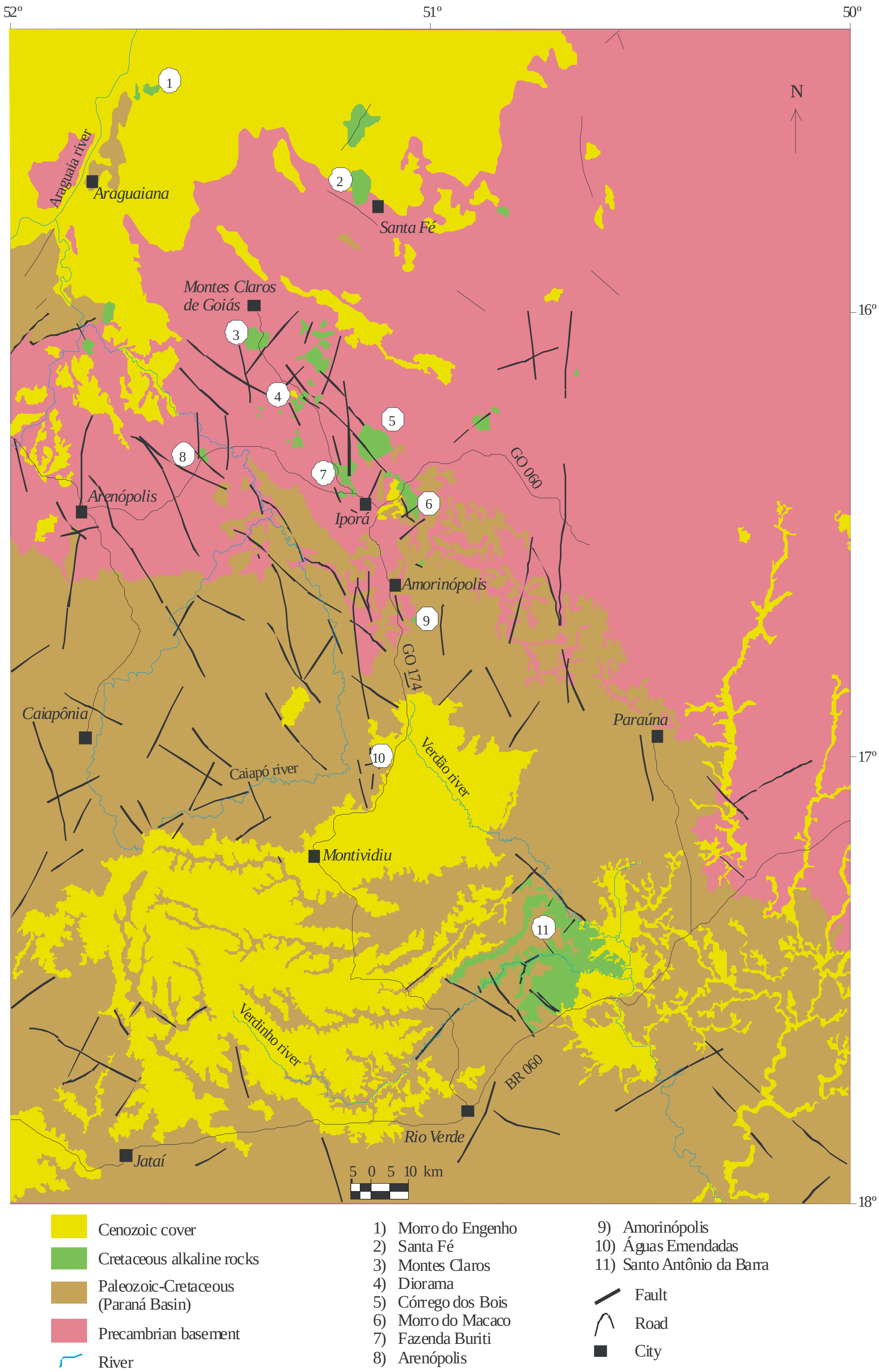


Fig. 2. Geological map of the Goiás Alkaline Province, showing the location of the main plutonic complexes in the north, subvolcanic rocks in the centre and lavas and pyroclastics in the south. Modified from Lacerda Filho *et al.* (2000).

Precambrian structures related with the ascent of the Cretaceous alkaline magmas are the Bom Jardim de Goiás Arch and the Transbrasiliano Lineament. The former is a regional anticline structure with a S80W-plunging axis (Pena, 1974), and the latter follows a general NE orientation (Schobbenhaus *et al.*, 1975).

Rift tectonics affected the central-north portion of the region during the Late Cretaceous (Almeida, 1983), forming the Caiapó Graben.

The Cretaceous alkaline igneous rocks that occur in the north of this region were first designated as Iporá Group by Guimarães *et al.* (1968). Later, Bez *et al.* (1971) added to that group the alkaline volcanic rocks of Santo Antônio da Barra, referring to the latter unit as Rio Verde Volcanic District. Almeida (1983) grouped the clusters of alkaline rocks around the margins of Paraná Basin into different provinces, designating all the alkaline rocks of southern Goiás as the Rio Verde-Iporá Igneous Province, a nomenclature later adopted by Danni *et al.* (1992) and Junqueira-Brod *et al.* (1999a, b, 2000). Lacerda Filho *et al.* (2000) suggested the name of Southern Goiás Alkaline Province for these occurrences. Sgarbi & Gaspar (2002) considered the Alto Paranaíba Igneous Province (Almeida, 1983; Gibson *et al.*, 1995a) and the Rio Verde-Iporá Igneous Province as a single unit, grouping them under the designation of Minas-Goiás Alkaline Province, subdivided into four subprovinces: Mata da Corda, Alto Paranaíba, Iporá and Santo Antônio da Barra. More recently, Gaspar *et al.* (2003), based on isotopic data, found that the rocks occurring in western Minas Gerais and near the city of Catalão, and those cropping out in the Iporá-Rio Verde region belong, in fact, to two different provinces; thus, the designation of Alto Paranaíba Igneous Province (APIP) was maintained for the former, whereas the latter was called Goiás Alkaline Province (GAP), which is the nomenclature adopted in this work. Sgarbi *et al.* (2004) characterized the kamafugites from Santo Antônio da Barra, in the GAP, as slightly older (88-90 Ma) than those of the Mata da Corda region, in the APIP (clustering at 80-81 Ma and 75-76 Ma), on the basis of U-Pb dating of perovskite, thus providing the first concrete evidence for an eastward age progression related to the Trindade Mantle Plume track in the northern border of the Paraná Basin.

A wide variety of petrographic types occur in the GAP, encompassing intrusive, subvolcanic and volcanic products. Volcanic and subvolcanic rocks dominate in the southern and central portions of the province, respectively, whereas plutonic alkaline complexes are more commonly found in the north (Bez *et al.*, 1971; Danni, 1978; Barbour *et al.*, 1979; Gaspar & Danni, 1981; Danni & Gaspar, 1992; Danni *et al.*, 1992; Junqueira-Brod *et al.*, 2002).

Plutonic complexes (northern GAP)

The extreme northwest limit of the GAP is distinguished by the **Morro do Engenho** complex (Fig. 2; 15º32'S, 51º40'W). This intrusion is made up of a central dunite body which is surrounded by clinopyroxenites and peridotites, and then by alkaline gabbros and nepheline syenites. The complex is approximately 5 km in diameter and intrudes the Furnas Formation of the Paraná Basin (Pena, 1974).

The mafic-ultramafic alkaline **Santa Fé** complex (Fig. 2; 15º45'S, 51º10'W) is an ellipsoidal body, measuring ca. 9.5 km along its N-S axis and 6.5 km across. It comprises dunites in the centre and clinopyroxenites, peridotites, alkaline gabbros and syenites at the borders. Lamprophyre and phonolite dykes also occur (Barbour *et al.*, 1979). K-Ar data on biotite from a missourite yielded an age of 86.7±1.8 Ma (Sonoki & Garda, 1988).

The **Montes Claros** complex (Fig. 2; 16º03'S, 51º23'W), located near the Montes Claros de Goiás city, is a 50 $km^2$ composite intrusion, comprising mainly dunites and subordinate pyroxenites, alkaline gabbros and nepheline syenites. The complex intrudes sedimentary rocks of the Furnas Formation, turning the country rocks into a pyroxene hornfels. The pyroxenites contain both ortho and clino-pyroxene and are concentrated in the southwestern portion of the complex. Dykes of monchiquite and other alkaline rocks are common both within and outside the complex (Bez, 1970; Woolley, 1987).

Near the town of Iporá, two Late Cretaceous concentrically zoned intrusions have been described by Danni (1978). The **Córrego dos Bois** complex

(Fig. 2; 16º17'S, 51º08'W) is composed of two domes, covering an area of approximately 33 $km^2$. The domes are formed mostly by central dunites, surrounded by wehrlites, olivine pyroxenites and websterites. To the north and to the south, rings of alkaline olivine gabbro, theralite and essexite are found. The whole structure is surrounded by a narrow and discontinuous intrusion of nepheline syenite. Dykes of syenite occur both in the complex and in the country-rocks. The other intrusion is the **Morro do Macaco** complex (Fig. 2; 16º25'S, 51º03'W), comprising four domes composed, from core to rim, of dunites, wehrlites, olivine pyroxenites and clinopyroxenites. Syenites are found to the west of the domes.

The **Fazenda Buriti** complex (Fig. 2; 16º22'S, 51º12'W) is located about 15 km NW of Iporá, occupying an approximate area of 35 $km^2$. The intrusive rocks are olivine clinopyroxenites, mela-gabbros, essexites, syenogabbros and syenites. Associated with the coarse-grained rocks, a trachyte sill and quartz microsyenites are also found (Cerqueira & Danni, 1994).

The **Arenópolis** complex is located to the west of the main cluster of plutonic complexes in northern GAP (Fig. 2; 16º22'S, 51º32'W) and comprises a N-S elongate elliptical intrusion covering an area of 12 $km^2$. The main rock-types are alkaline gabbros, with subordinate nepheline syenites and more rarely olivine clinopyroxenites and shonkinites. Danni *et al.* (1976) described the occurrence of ijolite series rocks (dominant melteigite, with subordinate ijolite and pyroxenite) in the southeast portion of the complex. Abundant syenitic fine-grained dykes occur within the complex and in the country-rocks, and often contain eudialyte, suggesting an agpaitic affiliation for these rocks.

In addition to the above-mentioned occurrences, a series of smaller intrusions are described in the north portion of GAP. For further information and location of these intrusions the reader is referred to Pena (1974), Woolley (1987) and Lacerda Filho *et al.* (2000).

Junqueira-Brod *et al.* (2005a) modelled the intensive variables of the GAP kamafugitic magmas, and their behaviour during ascent from the mantle source to the final emplacement in the crust. The physical and chemical characteristics of these magmas suggest that they did not rise directly to the surface, but stopped and differentiated in both deep and shallow magma chambers through a combination of fractional crystallization, liquid immiscibility and magma mixing. Junqueira-Brod *et al.* (2005a) concluded that the density barrier between the Precambrian basement and the Phanerozoic sedimentary rocks of the Paraná Basin is the most likely site for the establishment of the shallower magma chambers, which is in good keeping with most northern GAP plutonic complexes occurring exactly at this discordance.

Subvolcanic bodies and diatremes (central GAP)

Subvolcanic intrusions of *alkaline picrite* are commonly found in the GAP, especially in the Iporá region. They occur as dykes, plugs and sills. The dykes are often only a few meters wide and tens of meters long, filling fractures in the Precambrian basement, dominantly with N30W and N50E directions. The sills, normally emplaced into the Paraná Basin strata, are usually less than 5 m thick, but can extend laterally for more than 500 m. They have a homogeneous aspect, with no visible indication of differentiation. The plugs are cylindrical in shape and can be up to 200 m in diameter (Danni, 1994).

A subvolcanic association occurs near the Bebedouro farm, 10 km south of the city of **Amorinópolis** (Fig. 2; 16º41'S, 51º03'W), as the result of ultrabasic alkaline magmatism of per-potassic to sodic-potassic composition (Danni, 1985). The occurrence is about 1.2 km in diameter and consists of a central, cylindrical intrusion of basanitic to tephritic composition. Ring and radial dykes of olivine leucite melanephelinite, mela-analcimite and olivine nepheline melaleucitite preceded the main intrusion, and the last event in the complex was the degassing of the subvolcanic reservoir, forming breccia pipes (Danni, 1985). To the southwest of the main intrusion, a katungite pipe is the only known occurrence of this petrographic type in the province so far. It is composed of 18 vol % of olivine phenocrysts set in a groundmass of melilite (25 vol%), leucite (40 vol%), spinel (8 vol %) and perovskite (3 vol%), with interstitial diopside, nepheline, phlogopite and apatite (Danni, 1985; Danni & Gaspar, 1992, 1994). A striking feature pointed out by Danni & Gaspar (1994) is the high $TiO_2$ content in whole-rock analyses of this occurrence. Late Cretaceous, high-Ti alkaline rocks are geographically coincident with high-Ti continental flood basalts of the Paraná Basin, a feature that has been related to the source of the magmatism (Gibson *et al.*, 1995b).

Another important volcanic-subvolcanic association occurs in the **Águas Emendadas** region (Fig. 2; 17º02'S, 51º02'W), between the towns of Amorinópolis and Montividiu. It comprises dykes, plugs, volcanic vents and pyroclastic deposits, usually emplaced into the Aquidauana Formation and covered by the Bauru Group. Danni *et al.* (1990) described the petrographic types at Águas Emendadas as olivine melanephelinites, olivine-analcime melanephelinites, olivine analcimites, nephelinites, microijolites, basanites and tephrites. The same authors considered these rocks to be an extension of the alkaline-carbonatitic volcanic association of Santo Antônio da Barra, suggesting that the leucititic and nephelinitic rocks have originated from different magmas.

More recent studies redefined the highly silica-undersaturated (feldspar-free) rocks from Águas Emendadas as members of the kamafugite series, on the basis of the presence of kalsilite in the lavas (Junqueira-Brod *et al.*, 1999a, 2000) and of their geochemical characteristics (Junqueira-Brod, 1998, and this work).

Danni *et al.* (1990) suggested that the leucititic rocks of the Águas Emendadas region might be related to the sources of diamonds found in the alluvial deposits nearby. Based on aeromagnetic data and microprobe analyses of heavy mineral concentrates from stream sediments, Tompkins (1987) described the occurrence of a probable kimberlite to the south of Amorinópolis. However, she also considered that the lithosphere thickness is likely to be less than 150 km in the region, not deep enough for the kimberlite to be diamondiferous, and therefore interpreted the source of diamonds in the region as an older (Precambrian) one.

The volcanic structures in the Águas Emendadas area are diatremes (Junqueira-Brod, 1998, 2003; Junqueira-Brod *et al.*, 2004, 2005a, b) composed mostly of breccias and showing a range of distinct diatreme facies deposits with subordinate mafurite and leucite mafurite lavas and dykes.

Junqueira-Brod *et al.* (2004) presented a detailed study of the facies distribution within the central GAP diatremes, showing that these structures were formed under a highly heterogeneous environment, where variable degrees of confinement, fluidisation and magma fragmentation resulted in the formation of very distinctive pyroclastic deposits. Fig. 3 illustrates the effect of increasing magma fragmentation on the size of the finer-grained fraction (matrix) of the diatreme-filling breccias in the Águas Emendadas region.

Lavas and pyroclastics (southern GAP)

The volcanic rocks of the **Santo Antônio da Barra** region (Fig. 2; 17º30'S, 50º42'W) comprise alternate lavas and pyroclastic deposits. The lava flows occupy an area of 371 $km^2$, with a calculated volume of 23 $km^3$ (Junqueira-Brod *et al.*, 2002), which is consistent with the plutonic complexes occurring in northern GAP or in the adjacent Alto Paranaíba Province. The magmas ascended dominantly through the N40-50W Santo Antônio da Barra-Iporá tectonic-magmatic lineament. A volcaniclastic conglomerate (Rio Verdinho Formation; Gaspar & Danni, 1981) was deposited on the top of the volcanic rocks.

The Santo Antônio da Barra rocks were first described as analcimites, olivine analcimites, analcimitic breccias and carbonatitic pyroclastic rocks, with related late-stage dykes and plugs of fourchite, melamonchiquite, phonolite and trachyte. In view of these petrographic characteristics, their parental magma was originally interpreted as nephelinitic (Gaspar & Danni, 1981), but Sgarbi *et al.* (1998) argued that these rocks have a chemical affinity with kamafugites, as also suggested earlier by Moraes (1984, 1988) on the basis of whole-rock analyses, petrographic similarities with the Ugandan kamafugites and the presence of melilite in some flows. Sgarbi & Gaspar (2002) described kalsilite in the Santo Antônio da Barra lavas and pointed out that the originally recognized analcime is in fact the product of leucite alteration, thus redefining the previous petrographic types as mafurites and ugandites. Oxygen isotope data indicate a temperature range from 1050 to 1060ºC for the lavas during eruption (Sgarbi *et al.*, 1998). K-Ar whole-rock dating yielded an 85 Ma age for the volcanic rocks (Hasui *et al.*, 1971), whereas U-Pb dating of perovskite from the lava flows indicates ages between 88.3 and 89.6 Ma (Sgarbi *et al.*, 2000a, 2004).

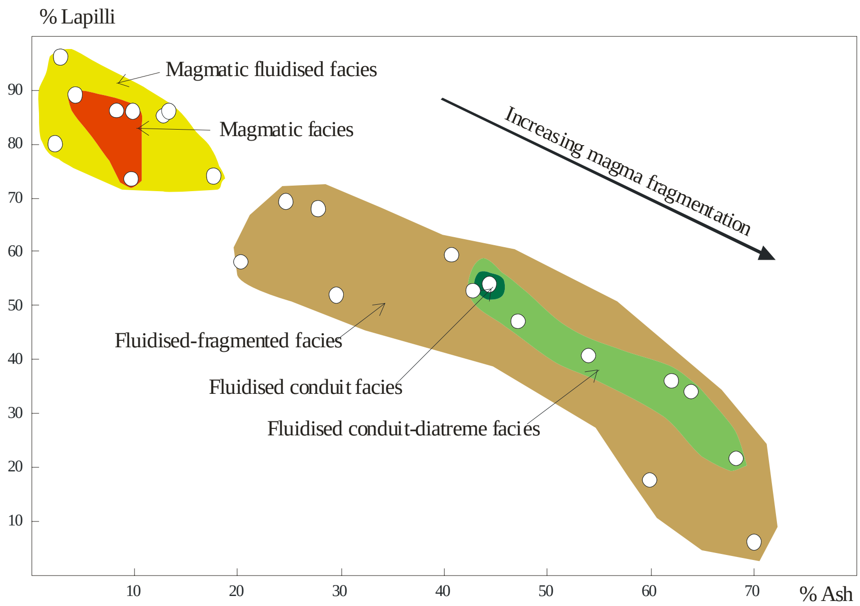


Fig. 3. Ash and lapilli distribution in the various facies of the Águas Emendadas diatreme. Magma fragmentation clearly increases from the magmatic facies and magmatic fluidised facies to the pyroclastic facies located at higher levels in the diatreme (fluidised conduit facies, fluidised conduit-diatreme facies and fluidised-fragmented facies). Data source: Junqueira-Brod *et al.* (2004).

Substantial evidence has now been put together to demonstrate the kamafugitic character of the GAP, in particular the works of Moraes (1984, 1988), Danni & Gaspar (1992, 1994), Sgarbi (1998), Sgarbi *et al.* (1998, 2000a), Junqueira-Brod (1998) and Junqueira-Brod *et al.* (2000). When petrographic descriptions are given in older published works, the corresponding samples were reclassified into one of the following petrographic terms: katungite, mafurite, leucite mafurite, kalsilite ugandite and ugandite, on the basis of their similarities with the more recently described specimens.

Similarly, in areas that were not studied in detail by the authors of the present work, such as the northern GAP plutonic complexes, we tried to keep rock nomenclature as simple as possible, by recasting the petrographic terms into three main groups: ultramafic, mafic and felsic rocks. In this sense, rock names which are fairly straightforward, such as dunite, wehrlite, pyroxenite, olivine basalt, basanite etc., were retained from older descriptions. On the other hand, a considerable profusion of rock names is used to designate varieties of alkaline mafic and felsic rocks in older literature, which is often misleading. In this work we opted to designate all the mafic petrographic varieties of feldspar-bearing alkaline rocks occurring in the northern GAP complexes as "gabbroic", whereas the felsic, feldspar-bearing alkaline rocks were all designated as "syenitic". Although this may result in some loss of petrographic accuracy, it would otherwise be an impossible task to achieve reasonable petrogenetic interpretations for such rocks, at least until more detailed studies are carried out in northern GAP.

Along with the Alto Paranaíba Igneous Province (northeast border of the Paraná Basin), the GAP is one of the largest kamafugite occurrence areas in the world. In this work, we will aim, as much as possible, to deal separately with the feldspar-free (kamafugitic) rocks which predominate in the southern and central GAP, and with the feldspar-bearing rocks which are dominant in the northern GAP plutonic complexes.

## MINERAL CHEMISTRY

The currently available set of data on the composition of minerals from the GAP rocks is relatively restricted, and much remains yet to be done regarding this subject. Most of the data discussed in the following sections comes from research works on the Santo Antônio da Barra lavas, the Águas Emendadas diatremes, the Amorinópolis subvolcanic association, and the Córrego dos Bois, Morro do Macaco and Fazenda Buriti plutonic complexes (Danni, 1978, 1994; Danni & Gaspar, 1992; Cerqueira, 1995; Junqueira-Brod, 1998; Sgarbi, 1998; Junqueira-Brod *et al.*, 1999a; Sgarbi *et al.*, 2000b). We will concentrate mostly on the mineral chemistry of spinel, olivine, clinopyroxene, mica, nepheline and kalsilite, which make up most of the available analytical set of data and are the most suitable phases to provide information on the origin and evolution of these rocks.

### *Spinel*

Spinel-group minerals are a frequent accessory in the GAP kamafugitic rocks. In katungites they occur as inclusions in olivine phenocrysts and as a groundmass phase. In the leucite mafurites they are present as inclusions in clinopyroxene, as phenocrysts and microphenocrysts, and in the groundmass. In the more fine-grained mafurites, ugandites and basanites, spinel-group minerals generally occur as small groundmass grains. Spinels are also present in most rock-types of the northern GAP plutonic complexes, often hosting ilmenite exsolution lamellae, which indicate re-equilibration at low temperature. Cerqueira (1995) described the common occurrence of reaction rims of biotite surrounding spinel-group minerals in rocks of the Fazenda Buriti complex.

Table 1 shows representative spinel compositions from the Águas Emendadas, Santo Antônio da Barra and Amorinópolis kamafugitic rocks, and from the Águas Emendadas basanites and Fazenda Buriti plutonic rocks. Typically, spinel from GAP rocks is rich in $TiO_2$ (up to 28.62 wt%), MgO (up to 10.23 wt%), FeO (26-54 wt%) and $Fe_2O_3$ (10-67 wt%). $Cr_2O_3$ (up to 17.61 wt%) and $Al_2O_3$ (up to 8.00 wt%) may be significant in some phenocrysts or in grains included in olivine.

Fig. 4 shows the composition of spinels from the GAP feldspar-free rocks plotted on the triangular face of both conventional spinel prisms. The Amorinópolis katungite spinels evolved initially along a trend of simultaneous Al and Cr decrease and Ti and $Fe^{3+}$ increase, defined by spinel inclusions in olivine, whereas groundmass spinel contains very little or no chromium, evolving towards Ti and $Fe^{3+}$-rich terms at the expense of aluminium only. Spinels from mafurites (Águas Emendadas) show an initial decrease of Cr at relatively constant Al, and then a decrease of Al at very low Cr, paralleling the trend of katungite groundmass spinels. Leucite mafurite spinels from Águas Emendadas display an evolution trend that is similar to that of mafurites, but which appears to initiate at significantly higher Cr and Al values. On the other hand, spinels from the SAB leucite mafurites follow an Al-depleted trend, evolving towards $Fe^{3+}$ and Ti-rich terms at the expense of Cr only. Spinels from ugandites (SAB) do not contain significant Cr and have very low Al contents, plotting near the Ti and $Fe^{3+}$ peaks (Fig. 4). Spinels from leucite ijolites (fergusites) of the Fazenda Buriti complex in northern GAP are similar to some of the Águas Emendadas leucite mafurites.

Spinel-group minerals from the feldspar-bearing rocks of Águas Emendadas (basanites) and Fazenda Buriti (gabbroic and syenitic rocks) all plot at the Al-$Fe^{3+}$ and Al-Ti lines of the diagrams in Fig. 5. These are Cr-poor spinels whose $Fe^{3+}$ contents increase, while those of Ti decrease, according to the degree of evolution of the host-rock (i.e. from basanite to gabbro to syenite).

The relationship between Ti and $Fe^{3+}$ in the kamafugitic spinels is better depicted in Fig. 6. The evolution trends for katungite and mafurite spinels show a marked inflection that results from initial enrichment in both Ti and $Fe^{3+}$ (different rate depending on the rock type), followed, in a second stage, by substitution of Ti for $Fe^{3+}$. Spinels from the Santo Antônio da Barra ugandites and leucite mafurites, and from the Fazenda Buriti leucite ijolites, on the other hand, display a single, continuous trend of Ti-$Fe^{3+}$ substitution. The approximate ratio of Ti:2$Fe^{3+}$ indicates substitution along the magnetite-ulvöspinel solid solution series. In leucite mafurites from both Águas Emendadas and Santo Antônio da Barra, however, spinels define two contrasting trends. One is a curved line similar to that observed in katungites and mafurites, and the other is a straight trend of $Fe^{3+}$-Ti substitution similar to that of ugandites and leucite ijolites. Spinels from feldspar-bearing rocks plot along a linear, $Fe^{3+}$-Ti exchange trend (not shown in Fig. 6), similar to that of ugandites and leucite ijolites.

Distribution of $Ti^{4+}$ and the main trivalent cations in spinels from the GAP feldspar-free and feldspar-bearing rocks are plotted against the $Fe^{2+}/(Fe^{2+}+Mg)$ ratio in Figs. 7 and 8.

Table 1. Representative electron microprobe analyses of spinels from GAP samples. Data source: 1) Danni & Gaspar (1994), 2) Junqueira-Brod (1998), 3) This work, 4) Sgarbi (1998) and 5) Cerqueira (1995). L-I = leucite ijolite.

| Locality | Amorinópolis | | Águas Emendadas | | | Santo Antônio da Barra | | | Fazenda Buriti | | | | |
|---|---|---|---|---|---|---|---|---|---|---|---|---|---|
| Rock | Katungite | | Mafurite | Leucite mafurite | | Leucite mafurite | | Ugandite | L-I | Gabbro | | Syenite | |
| Sample | Am04 | Am10 | 96ae46 | 96ae57 | 96ae01 | sabm01 | sabm03 | sabug01 | cfb020 | cfb002a | cfb047a | cfb033 | cfb112b |
| Remarks | incl ol | g | | | incl cpx | ph | | ph | | | | | |
| Reference | 1 | 1 | 2 | 2 | 3 | 4 | 4 | 4 | 5 | 5 | 5 | 5 | 5 |
| $SiO_2$ | 0.06 | 0.07 | 0.26 | 0.18 | 0.09 | 0.01 | 0.19 | 0.09 | 0.04 | 0.02 | 0.03 | 0.03 | 0.23 |
| $TiO_2$ | 14.84 | 19.92 | 14.45 | 11.09 | 14.88 | 16.73 | 17.77 | 20.84 | 16.10 | 6.94 | 21.00 | 13.98 | 3.09 |
| $Al_2O_3$ | 6.70 | 1.05 | 6.05 | 8.00 | 5.02 | 0.12 | 0.65 | 0.51 | 3.88 | 2.96 | 2.86 | 2.52 | 0.80 |
| FeO | 32.30 | 43.35 | 34.38 | 25.92 | 32.36 | 39.37 | 40.85 | 42.72 | 43.80 | 36.50 | 49.09 | 41.95 | 33.31 |
| $Fe_2O_3$ | 26.49 | 30.26 | 28.01 | 25.75 | 35.62 | 37.96 | 27.47 | 28.67 | 33.42 | 51.86 | 25.38 | 38.18 | 61.30 |
| $Cr_2O_3$ | 9.96 | 0.40 | 6.91 | 17.61 | 2.11 | 0.65 | 6.78 | 0.12 | 0.17 | 0.06 | 0.10 | 1.65 | 0.03 |
| MnO | 0.14 | 0.83 | 0.94 | 0.55 | 0.44 | 0.99 | 0.84 | 1.06 | 0.80 | 0.51 | 0.84 | 0.71 | 0.82 |
| MgO | 8.82 | 3.51 | 6.13 | 10.23 | 8.14 | 4.01 | 3.75 | 3.84 | 1.29 | 0.54 | 0.78 | 1.28 | 0.07 |
| CaO | 0.01 | 0.07 | 0.13 | 0.01 | 0.32 | 0.05 | 0.04 | 0.30 | | | | | |
| Total | 99.32 | 99.46 | 97.24 | 99.35 | 98.97 | 99.89 | 98.34 | 98.15 | 99.50 | 99.39 | 100.08 | 100.30 | 99.64 |
| Cations on the basis of 32 O | | | | | | | | | | | | | |
| Si | 0.017 | 0.021 | 0.073 | 0.049 | 0.024 | 0.003 | 0.056 | 0.027 | 0.012 | 0.006 | 0.009 | 0.009 | 0.071 |
| Al | 2.171 | 0.363 | 2.042 | 2.539 | 1.657 | 0.042 | 0.227 | 0.179 | 1.350 | 1.051 | 0.994 | 0.878 | 0.289 |
| Ti | 3.072 | 4.405 | 3.116 | 2.248 | 3.136 | 3.701 | 3.967 | 4.662 | 3.578 | 1.575 | 4.663 | 3.110 | 0.712 |
| $Fe^{2+}$ | 7.433 | 10.657 | 8.242 | 5.841 | 7.582 | 9.683 | 10.140 | 10.623 | 10.821 | 9.207 | 12.118 | 10.377 | 8.538 |
| $Fe^{3+}$ | 5.480 | 6.687 | 6.036 | 5.215 | 7.504 | 8.392 | 6.129 | 6.410 | 7.423 | 11.760 | 5.633 | 8.489 | 14.124 |
| Cr | 2.164 | 0.093 | 1.564 | 3.747 | 0.466 | 0.151 | 1.589 | 0.028 | 0.040 | 0.014 | 0.023 | 0.385 | 0.007 |
| Mn | 0.033 | 0.207 | 0.228 | 0.126 | 0.104 | 0.247 | 0.211 | 0.267 | 0.200 | 0.130 | 0.210 | 0.178 | 0.213 |
| Mg | 3.618 | 1.538 | 2.621 | 4.109 | 3.401 | 1.758 | 1.659 | 1.702 | 0.568 | 0.243 | 0.343 | 0.564 | 0.032 |
| Ca | 0.003 | 0.022 | 0.039 | 0.004 | 0.095 | 0.016 | 0.013 | 0.096 | | | | | |
| Total | 23.990 | 23.992 | 23.990 | 23.988 | 24.013 | 23.991 | 23.992 | 23.993 | 23.991 | 23.987 | 23.993 | 23.990 | 23.986 |

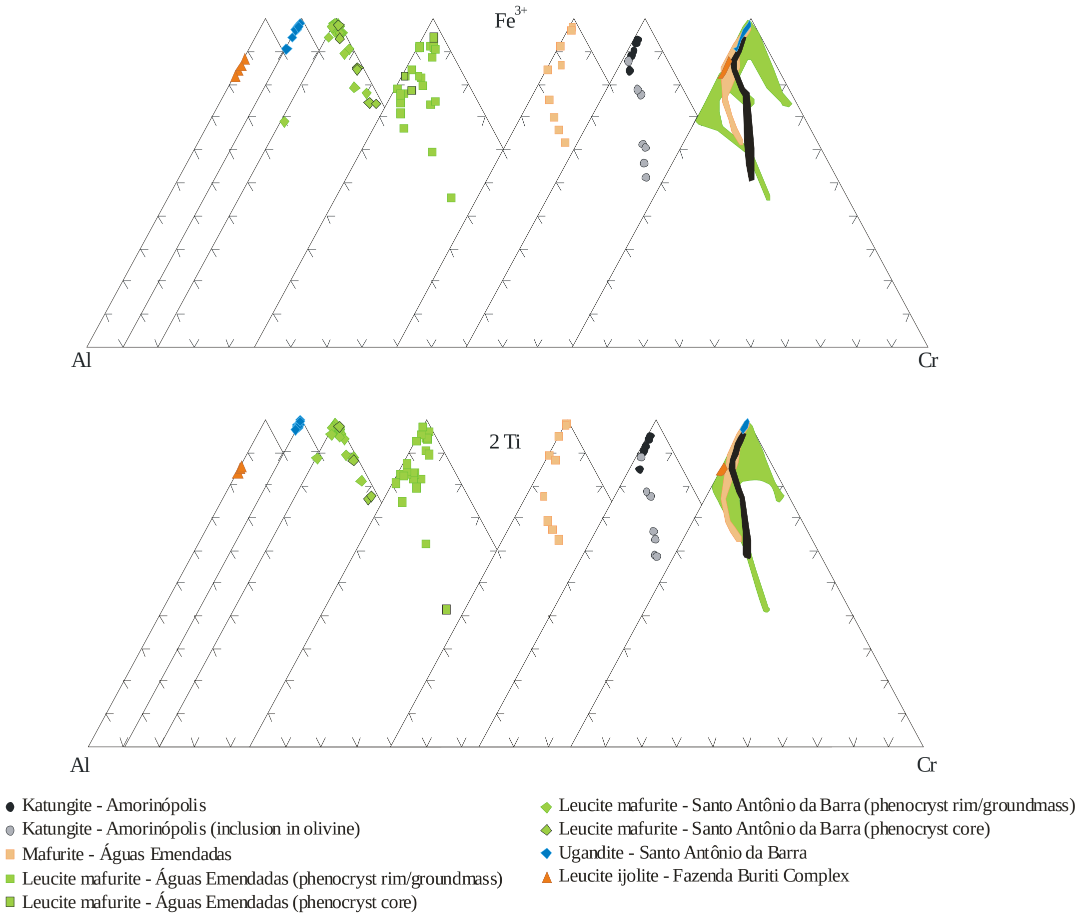


Fig. 4. Composition of GAP kamafugitic spinels plotted on the triangular faces of the two conventional spinel prisms. Data source: Danni & Gaspar (1994), Cerqueira (1995), Junqueira-Brod (1998), Sgarbi (1998) and this work.

Spinels from all feldspar-free rocks, except for the Fazenda Buriti leucite ijolites, show increasing Ti with increasing $Fe^{2+}/(Fe^{2+}+Mg)$. The compositional variations from phenocryst core to rim, from phenocrysts to groundmass, and from spinel inclusions in olivine to groundmass spinel, confirm this general evolution direction. In detail, however, spinels from the distinct rock-types differ (Fig. 7): 1) in katungites and ugandites they follow an almost continuous trend, with katungite spinels plotting at higher $Fe^{2+}/(Fe^{2+}+Mg)$; 2) mafurite spinels follow a trend of slightly lower Ti than those of katungites and ugandites; 3) in leucite mafurites, spinels have a much wider Ti range, with those from Santo Antônio da Barra concentrated at the higher $Fe^{2+}/(Fe^{2+}+Mg)$ end, but at lower Ti contents than those from Águas Emendadas.

Spinels from feldspar-bearing rocks of the Fazenda Buriti complex show an opposite Ti behaviour (Fig. 8). Although the analyses are concentrated in a much narrower $Fe^{2+}/(Fe^{2+}+Mg)$ range (>0.85), it is clear that Ti decreases and $Fe^{2+}/(Fe^{2+}+Mg)$ slightly increases in a spinel with increasing differentiation of the host-rock.

$Al^{3+}$ generally decreases with increasing $Fe^{2+}/(Fe^{2+}+Mg)$ in spinels from feldspar-free rocks (Fig. 7). As noted for Ti, it is possible to distinguish different groups of spinel within the GAP kamafugites on the basis of Al content. Spinels from katungites plot along a relatively Al-depleted trend. Those from Águas Emendadas leucite mafurites form a wider field, that nearly encloses the katungite trend but extends towards higher Al for a given $Fe^{2+}/(Fe^{2+}+Mg)$ ratio. In this respect, spinels from the Santo Antônio da Barra leucite mafurites are distinguished from the Águas Emendadas equivalents, as they plot in a restricted range of low Al and high $Fe^{2+}/(Fe^{2+}+Mg)$. Analyses from mafurites plot in a negative slope parallel to the previous types but at higher Al, and spinels from the Fazenda Buriti leucite ijolites have the highest Al content of all, although for a very restricted, $Fe^{2+}/(Fe^{2+}+Mg)$ range. Spinels from ugandites have very little Al, and cluster at the low-Al, high $Fe^{2+}/(Fe^{2+}+Mg)$ end of the katungite and mafurite trends (Fig. 7).

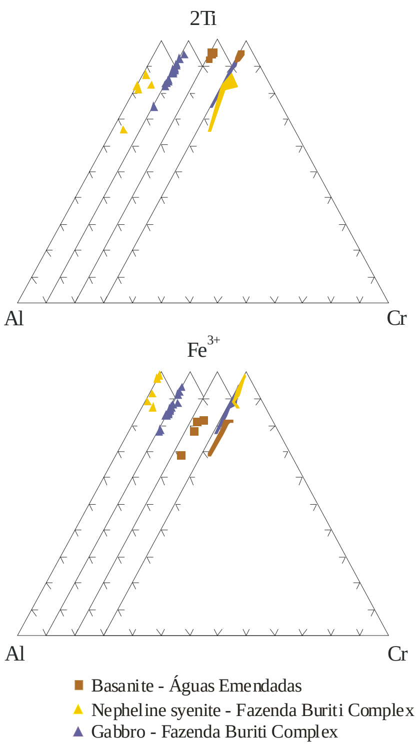


Fig. 5. Composition of spinels from the GAP feldspar-bearing rocks plotted on the triangular faces of the two conventional spinel prisms. Data source: Cerqueira (1995) and Junqueira-Brod (1998).

Spinels in the feldspar-bearing rocks from Águas Emendadas and Fazenda Buriti plot at the low-Al, high-$Fe^{2+}/(Fe^{2+}+Mg)$ end of the kamafugitic spinel trend (Fig. 8). Syenitic rocks contain less aluminous spinel than gabbros, whereas in the Águas Emendadas basanites spinel has Al intermediate between the former two types.

The Cr content of spinel is very low in the SAB ugandites and in the Fazenda Buriti leucite ijolites (Fig. 7). In katungites, mafurites and leucite mafurites, spinels may contain significant Cr, but its content rapidly decreases with increasing $Fe^{2+}/(Fe^{2+}+Mg)$. It is noteworthy from Fig. 7 that the high-Cr end of the spinel evolution trends in the kamafugitic rocks is located at highly variable $Fe^{2+}/(Fe^{2+}+Mg)$ values. High-Cr spinels in katungite have a $Fe^{2+}/(Fe^{2+}+Mg)$ ratio of ca. 0.67, whereas mafurite spinels are slightly more evolved, with trends starting at ca. 0.75 $Fe^{2+}/(Fe^{2+}+Mg)$. Spinels from leucite mafurites, on the other hand, cover a wide $Fe^{2+}/(Fe^{2+}+Mg)$ range, with evolution trends starting at 0.6, 0.88 and 0.96. The combination of spinel trends in Fig. 7 suggests that the leucite mafurites cannot be related to the other members by fractionation. Rather, leucite mafurite spinels and to a lesser extent, ugandite spinels appear to belong to multiple evolution trends.

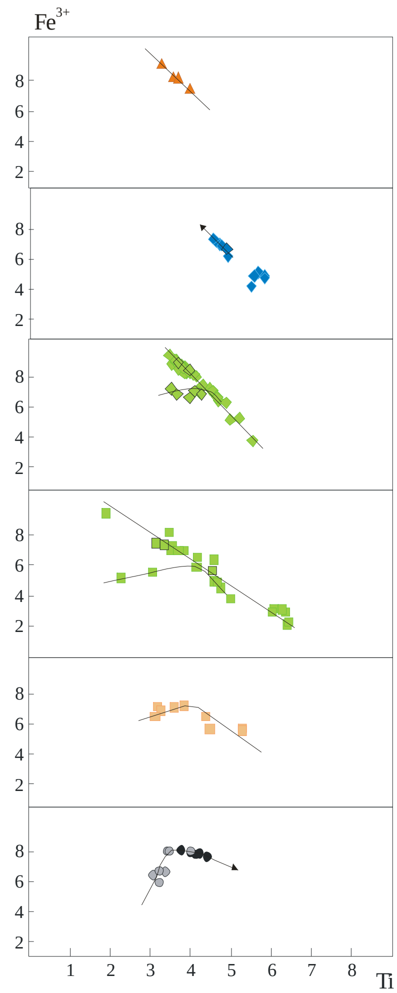


Fig. 6. Composition and evolution of GAP kamafugitic spinels in terms of $Fe^{3+}$ and Ti (a.f.u.). Data source and symbols as in Fig. 4.

Fig. 7. Ti, Al, Cr and $Fe^{3+}$ (a.f.u.) variation with $Fe^{2+}/(Fe^{2+}+Mg)$ for the GAP kamafugitic spinels. Dashed fields in Ti and $Fe^{3+}$ diagrams for the Águas Emendadas leucite mafurites represent spinel grains containing exsolved ilmenite lamellae, and are not considered in the overall trends. Data source and symbols as in Fig. 4.

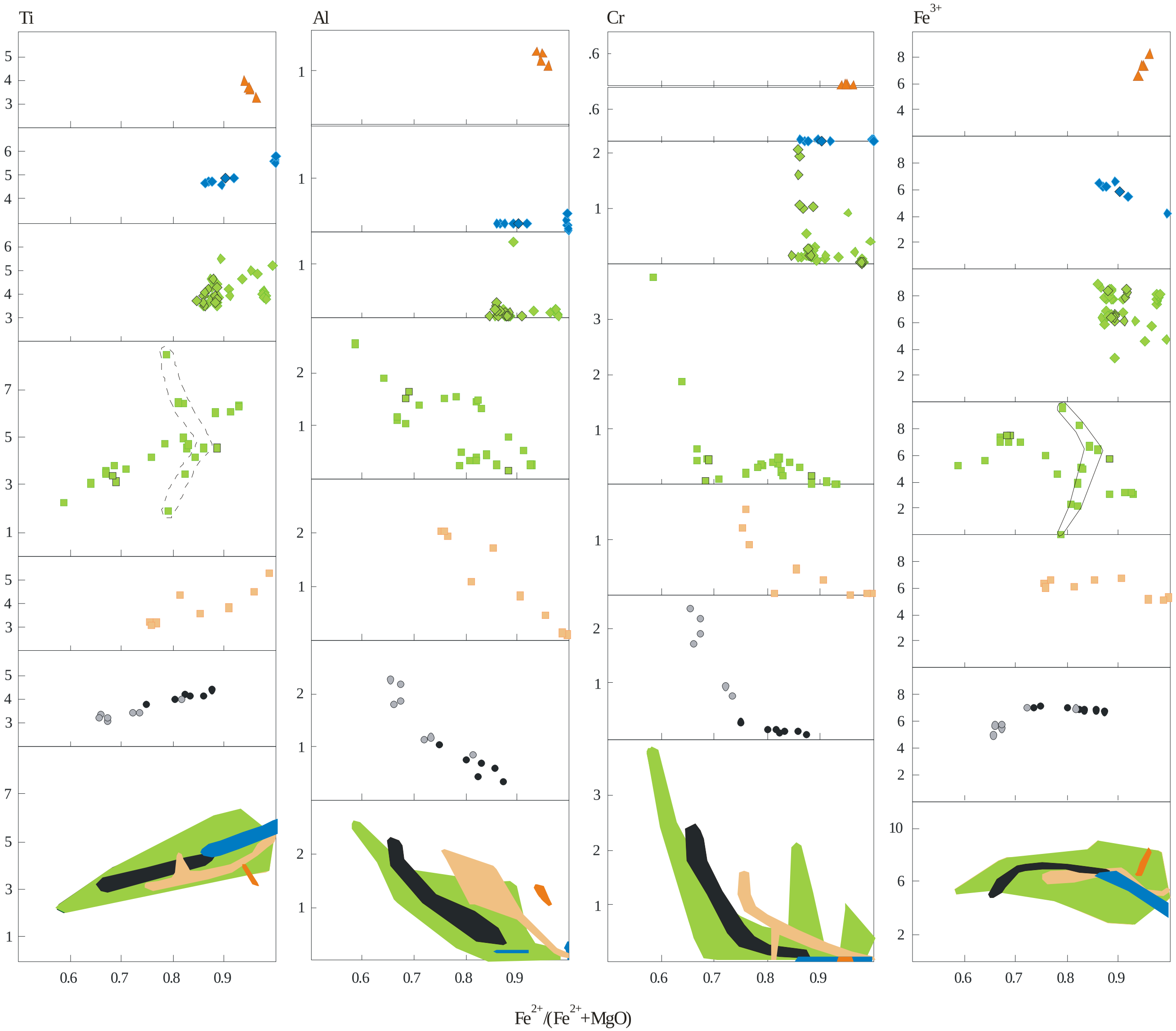

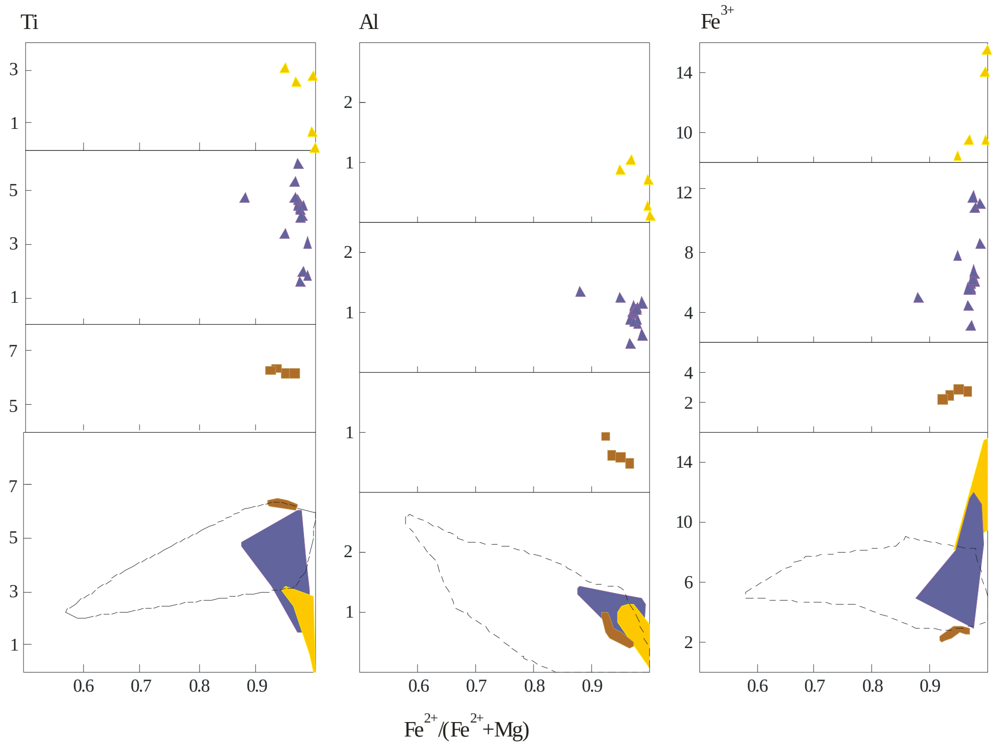


Fig. 8. Ti, Al and $Fe^{3+}$ (a.f.u.) variation with $Fe^{2+}/(Fe^{2+}+Mg)$ for spinels from the GAP feldspar-bearing rocks. Dashed lines depict the compositional range of kamafugitic spinels of Fig. 7. Data source and symbols as in Fig. 5.

The different proportions between Cr and $Fe^{2+}/(Fe^{2+}+Mg)$ for each spinel trend in Fig. 7 may be the result of distinct initial magma compositions, differ-rent $fO_2$ conditions during crystallization or variable degrees of olivine crystallization. Both low $fO_2$ and the concomitant crystallization of abundant olivine would result in increasing $Fe^{2+}/(Fe^{2+}+Mg)$ in spinel.

Spinels from feldspar-bearing rocks have very little Cr, clustering at the lower right corner of the Cr- $Fe^{2+}/(Fe^{2+}+Mg)$ diagram (not shown in Fig. 7), and do not define significant trends.

$Fe^{3+}$ is relatively insensitive to $Fe^{2+}/(Fe^{2+}+Mg)$ variations in spinels from katungites, mafurites and leucite mafurites (Fig. 7). Ugandite spinels tend to show decreasing $Fe^{3+}$ with increasing $Fe^{2+}/(Fe^{2+}+Mg)$, whereas the opposite behaviour is observed in spinels from the Fazenda Buriti leucite ijolites.

In feldspar-bearing rocks, $Fe^{3+}$ in spinel clearly increases with the evolution of the host-rock, from basanite to gabbro to syenite (Fig. 8).

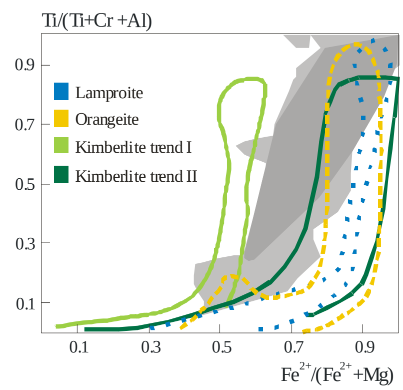


Fig. 9. $Fe^{2+}/(Fe^{2+}+Mg)$ vs. Ti/(Ti+Cr+Al) diagram for spinels of various types of ultrapotassic rocks. The dark shaded field represents the compositional range of GAP kamafugitic spinels and the light shaded field represents the compositional range of spinels from other kamafugite occurrences. Data source - GAP: Danni & Gaspar (1994), Cerqueira (1995), Junqueira-Brod (1998) and Sgarbi (1998); Other kamafugites: Lloyd *et al.* (1991), Cundari & Ferguson (1991), Sgarbi & Valença (1995) and Araújo (2000); Kimberlites (TI and TII), orangeites and lamproites: Mitchell & Bergman (1991).

Fig. 9 illustrates the comparison of spinels from the GAP kamafugites with that of spinels from other ultrapotassic rocks of the world. It should be noted that spinels from GAP and from other kamafugitic rocks follow a trend of increasing Ti/(Ti+Cr+Al) with increasing $Fe^{2+}/(Fe^{2+}+Mg)$, as also observed for other types of ultrapotassic rocks. Although there is a considerable overlap, especially at the highest Ti/(Ti+Cr+Al) values, most kamafugitic spinels occupy an intermediate region between "trend 1" kimberlitic spinels and the fields of spinels from lamproite, orangeite, and "trend 2" kimberlite.

In summary, the least evolved GAP spinels are from some leucite mafurites and katungites as indicated by their higher Cr and Al contents and lower $Fe^{2+}/(Fe^{2+}+Mg)$. During crystallization, Cr and Al were consumed and kamafugitic spinels evolved towards the ulvöspinel end-member. The multiple trends in leucite mafurite and ugandite spinels suggest a complex evolution for these magmas. Spinels from the feldspar-bearing rocks typically evolve from ulvöspinel towards magnetite, by decreasing Ti.

*Olivine*

Olivine occurs as phenocrysts and micropheno-crysts, and occasionally in the groundmass of volca-nic and subvolcanic rock-types of southern and cen-tral GAP. It may reach up to 16 modal % in leucite mafurites from Santo Antônio da Barra (Sgarbi, 1998), but it is much less abundant in ugandites. Junqueira-Brod (1998) distinguished two textural varieties of olivine phenocrysts in the Águas Emen-dadas mafurites and leucite mafurites, one euhedral to subhedral and the other anhedral, showing resorption features. In the Amorinópolis katungites, olivine occurs as phenocrysts and microphenocrysts that may reach up to 30% in volume. In the Águas Emendadas basanites, the mineral occurs as euhedral phenocrysts and as a groundmass phase. Olivine is also an important constituent of dunites, wehrlites, olivine clinopyroxenites and some gabbros from the northern GAP plutonic complexes.

Table 2 shows representative analyses of olivine from Águas Emendadas, Santo Antônio da Barra and Amorinópolis kamafugites, and from northern GAP plutonic rocks.

Olivine in kamafugitic rocks of southern and central GAP is a chrysolite ranging in composition from $Fo_{77}$ to $Fo_{88}$ (Fig. 10). A much wider range ($Fo_{45}$ to $Fo_{89}$) is observed in olivine from the northern GAP plutonic rocks, although the set of data is mainly restricted to the Fazenda Buriti complex, with only a few analyses of dunitic and peridotitic olivine from the Morro do Macaco and Córrego dos Bois complexes (Fig. 11). MnO reaches up to 1.1 wt% and is generally higher in olivine from the northern GAP complexes than in kamafugitic olivine. The latter, in turn, are substantially richer in CaO (up to 1.2 wt%) and NiO (up to 0.37 wt%).

The zoning pattern of katungite and mafurite olivines is one of decreasing forsterite content from core to rim. Furthermore, olivines in mafurites are slightly more evolved than those in katungites, suggesting that these two rock-types may be related through fractionation processes. On the other hand, olivine phenocrysts in leucite mafurites from both Santo Antônio da Barra and Águas Emendadas typically have rims enriched in Mg relatively to the respective cores, indicating that these are xeno-crystic olivines caught in a less-evolved magma, although a few crystals with normal zoning are reported from Águas Emendadas (Junqueira-Brod, 1998). This is consistent with the composition of groundmass olivine in leucite mafurites, which is only slightly more enriched in Fe than the phenocryst rims. Olivine in the leucite ijolites from the Fazenda Buriti is mainly hyalosiderite, showing both normal and reverse zoning patterns.

Olivines in the feldspar-bearing rocks of northern GAP follow the normal path of Fo decreasing with the degree of differentiation of the host-rock (Fig. 11), although reverse zoning patterns are observed in some crystals in gabbroic rocks from the Fazenda Buriti complex.

Table 2. Electron microprobe analyses of olivines from selected GAP samples. Data source: 1) Danni & Gaspar (1994), 2) Junqueira-Brod (1998), 3) Sgarbi (1998) and 4) Cerqueira (1995). SAB = Santo Antônio da Barra; MM = Morro do Macaco.

| Locality | Amorinópolis | | | Águas Emendadas | | | | | SAB | MM | Fazenda Buriti | | | | | | |
|---|---|---|---|---|---|---|---|---|---|---|---|---|---|---|---|---|---|
| Rock | Katungite | | | Mafurite | | | Leucite mafurite | | Leucite mafurite | Dunite | Leucite ijolite | | Pyro-xenite | Gabbro | | | Malig-nite |
| Sample | Am2 | Am3 | Am4 | 96ae08 | 96ae08 | 96ae08 | 96ae04 | 96ae11 | sabm8 | MM107 | cfb20 | cfb38 | cfb33a | cfb35 | cfb47 | cfb50 | cfb33 |
| Remarks | r | c | r | | | | | c | ph | | c | c | r | incl | r | r | r |
| Reference | 1 | 1 | 1 | 2 | 2 | 2 | 2 | 2 | 3 | 4 | 4 | 4 | 4 | 4 | 4 | 4 | 4 |
| $SiO_2$ | 39.71 | 39.81 | 39.65 | 38.44 | 38.08 | 39.04 | 38.67 | 40.11 | 39.69 | 41.10 | 37.56 | 36.22 | 38.08 | 37.56 | 34.57 | 35.85 | 37.06 |
| $Al_2O_3$ | | | | | | | 0.02 | | 0.03 | 0.02 | 0.03 | 0.10 | 0.03 | 0.02 | 0.04 | 0.02 | 0.01 |
| FeO | 16.12 | 14.75 | 15.90 | 19.24 | 20.69 | 16.13 | 18.45 | 11.35 | 15.18 | 10.24 | 25.97 | 33.00 | 23.38 | 28.62 | 43.28 | 37.25 | 28.79 |
| MnO | 0.32 | 0.23 | 0.37 | 0.54 | 0.73 | 0.22 | 0.53 | 0.21 | 0.46 | 0.11 | 0.59 | 0.87 | 0.49 | 0.59 | 1.11 | 0.87 | 0.79 |
| MgO | 43.51 | 44.20 | 42.53 | 40.79 | 38.68 | 44.21 | 41.01 | 47.70 | 43.32 | 46.79 | 34.76 | 29.63 | 37.79 | 33.20 | 20.67 | 26.32 | 32.47 |
| CaO | 0.62 | 0.39 | 0.94 | 0.54 | 0.97 | 0.27 | 1.21 | 0.30 | 0.69 | 0.42 | 0.43 | 0.19 | 0.14 | 0.24 | 0.29 | 0.38 | 0.18 |
| NiO | 0.13 | 0.11 | 0.07 | 0.06 | | 0.04 | 0.02 | 0.26 | 0.13 | 0.25 | 0.08 | 0.05 | 0.14 | 0.06 | 0.02 | 0.01 | 0.07 |
| $Cr_2O_3$ | | | | | 0.03 | 0.01 | 0.02 | 0.09 | 0.02 | 0.06 | | | | 0.01 | | | 0.01 |
| Total | 100.41 | 99.49 | 99.46 | 99.61 | 99.17 | 99.92 | 99.93 | 100.02 | 99.52 | 98.99 | 99.42 | 100.06 | 100.05 | 100.30 | 99.98 | 100.70 | 99.38 |
| Cations on the basis of 4 O | | | | | | | | | | | | | | | | | |
| Si | 1.000 | 1.004 | 1.008 | 0.993 | 0.997 | 0.988 | 0.993 | 0.993 | 1.005 | 1.019 | 1.003 | 0.996 | 0.997 | 1.005 | 1.005 | 1.000 | 1.005 |
| Al | | | | | | | 0.001 | | 0.001 | 0.001 | 0.001 | 0.003 | 0.001 | 0.001 | 0.001 | 0.001 | 0.000 |
| Ti | | | | | | | | | | 0.000 | 0.001 | 0.001 | 0.001 | 0.001 | 0.001 | 0.001 | 0.000 |
| $Fe^{2+}$ | 0.340 | 0.311 | 0.338 | 0.416 | 0.453 | 0.342 | 0.396 | 0.235 | 0.322 | 0.212 | 0.580 | 0.759 | 0.512 | 0.640 | 1.052 | 0.869 | 0.653 |
| Mn | 0.007 | 0.005 | 0.008 | 0.012 | 0.016 | 0.005 | 0.012 | 0.004 | 0.010 | 0.002 | 0.013 | 0.020 | 0.011 | 0.013 | 0.027 | 0.021 | 0.018 |
| Mg | 1.634 | 1.662 | 1.612 | 1.571 | 1.509 | 1.669 | 1.570 | 1.760 | 1.635 | 1.729 | 1.384 | 1.215 | 1.475 | 1.324 | 0.896 | 1.095 | 1.312 |
| Ca | 0.017 | 0.011 | 0.026 | 0.015 | 0.027 | 0.007 | 0.033 | 0.008 | 0.019 | 0.011 | 0.012 | 0.006 | 0.004 | 0.007 | 0.009 | 0.011 | 0.005 |
| Ni | 0.003 | 0.002 | 0.001 | 0.001 | | 0.001 | 0.000 | 0.005 | 0.003 | 0.005 | 0.002 | 0.001 | 0.003 | 0.001 | 0.001 | 0.000 | 0.002 |
| Cr | | | | | 0.001 | 0.000 | 0.000 | 0.002 | 0.000 | 0.001 | | | | 0.000 | | | 0.000 |
| Total | 3.000 | 2.996 | 2.992 | 3.007 | 3.002 | 3.011 | 3.006 | 3.005 | 2.994 | 2.979 | 2.996 | 3.001 | 3.002 | 2.993 | 2.993 | 2.998 | 2.995 |

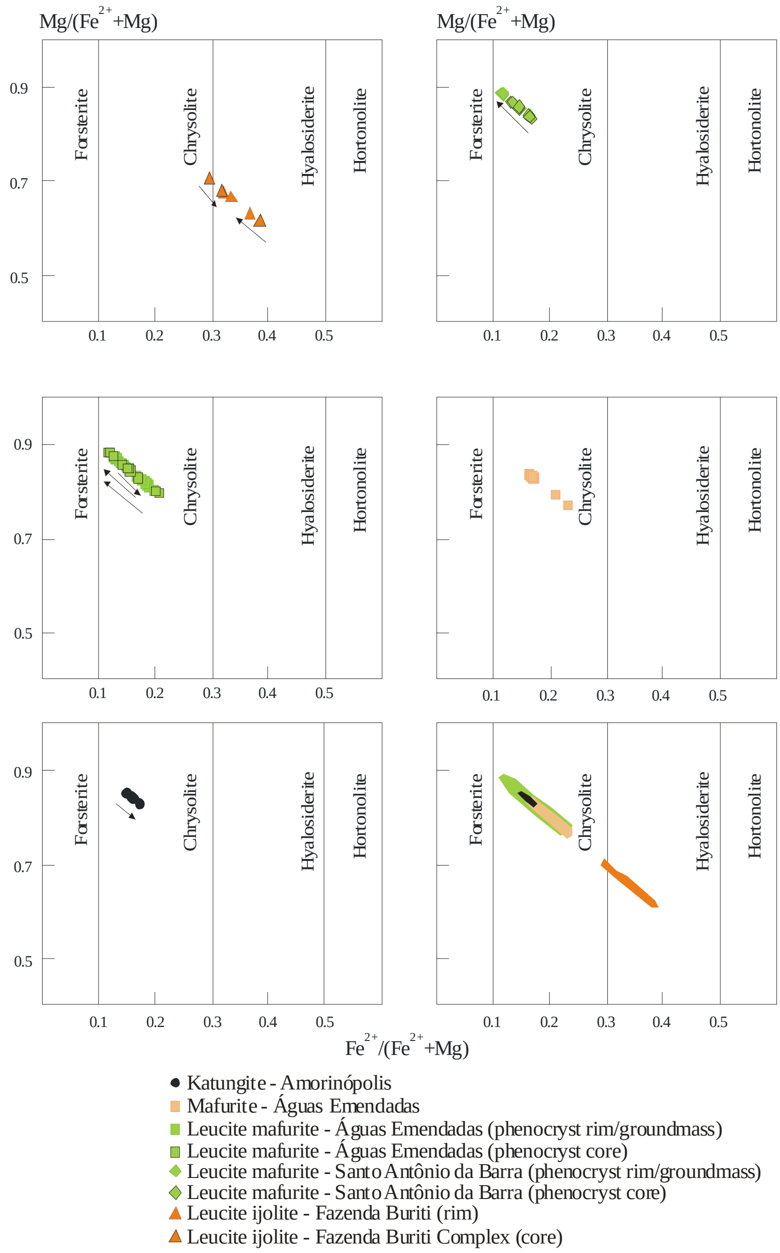


Fig. 10. Classification and zoning patterns of olivines from the GAP feldspar-free rocks. Data source: Danni & Gaspar (1994), Cerqueira (1995), Junqueira-Brod (1998) and Sgarbi (1998).

Ni behaviour in olivine is generally sympathetic, and Mn is generally antipathetic, with Fo content for all rock-types. On the other hand, Ca content in olivine clearly distinguishes the kamafugitic rocks of southern and central GAP from the feldspar-bearing plutonic rocks of northern GAP.

Fig. 12 shows the Ca variation with forsterite content for olivine in the GAP feldspar-free rocks. Olivines from katungites and mafurites show a fast increase in Ca for a small decrease in forsterite content from core to rim. In olivine phenocrysts from leucite mafurites the increase in forsterite content from core to rim is accompanied with a very little increase in Ca, defining a nearly horizontal trend in the diagram. From phenocryst to groundmass olivine, however, there is a small decrease in forsterite content and a significant increase in Ca. Olivine from the Fazenda Buriti leucite ijolites shows a sympathetic relationship between forsterite content and Ca with both normal and reverse zoning patterns.

Fig. 13 illustrates the Ca and Fo relationships for olivine in the feldspar-bearing rocks. Ca content is relatively insensitive to Fo variation. If all rock-types are considered, Ca slightly decreases at first, from dunite to pyroxenite olivine, and than increases with decreasing Fo content in the gabbros and malignite, although the zoning pattern is rather erratic in the former.

Fig. 12 shows the relationships between Ca and Mn in olivine from the feldspar-free rocks. If all analyses are considered, a positive correlation between these cations is observed (although with considerable dispersion), except for the Fazenda Buriti leucite ijolites. The Ca:Mn ratio is higher than 1 in katungite olivine and lower than 1 in mafurite olivine, whereas olivines from leucite mafurites define a wider field that overlaps the former two types. The cores of olivine phenocrysts from Águas Emendadas leucite mafurites define a negative slope in the diagram, in contrast with the phenocryst-to-groundmass sympathetic variation of Ca and Mn. In olivines from the SAB leucite mafurites, however, both phenocrystic and groundmass olivine trend along a positive slope in the diagram.

In olivine from the feldspar-bearing rocks (Fig. 13), Mn increases steadily with the degree of rock differentiation. Ca decreases at first, and then increases with increasing manganese in olivine from malignite and gabbroic rocks.

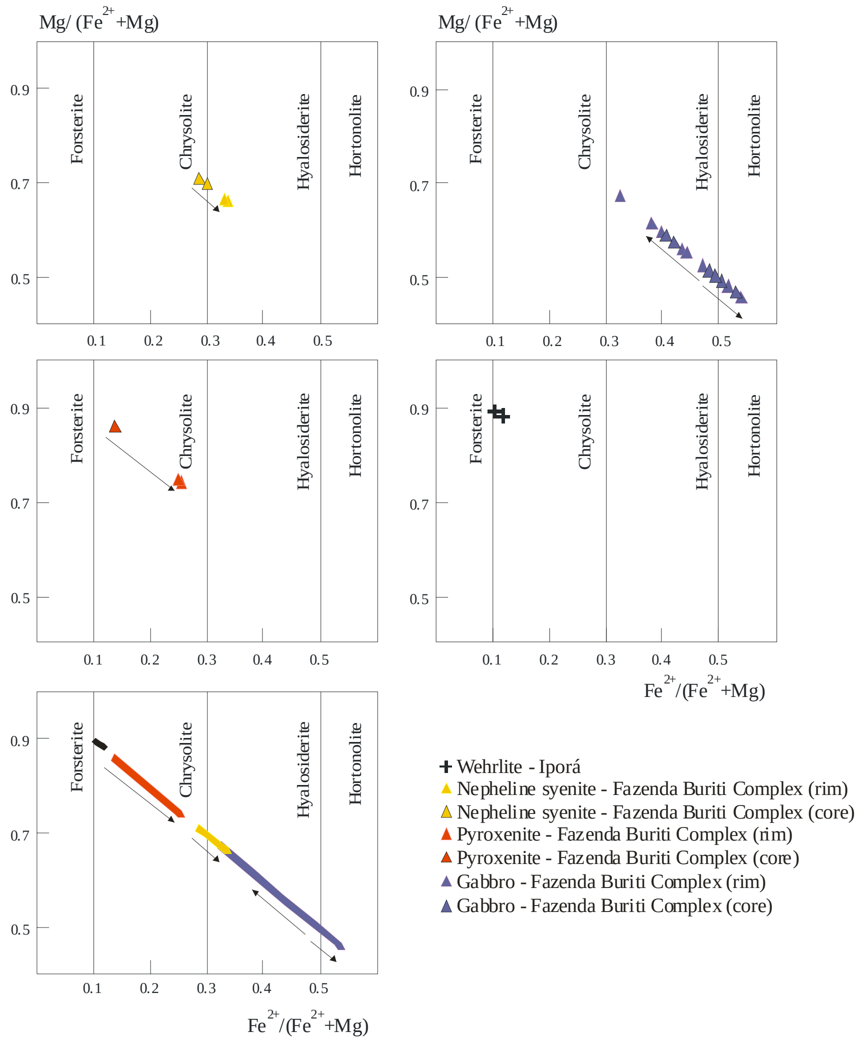


Fig. 11. Classification and zoning patterns of olivines from the GAP feldspar-bearing rocks. Data source: Cerqueira (1995).

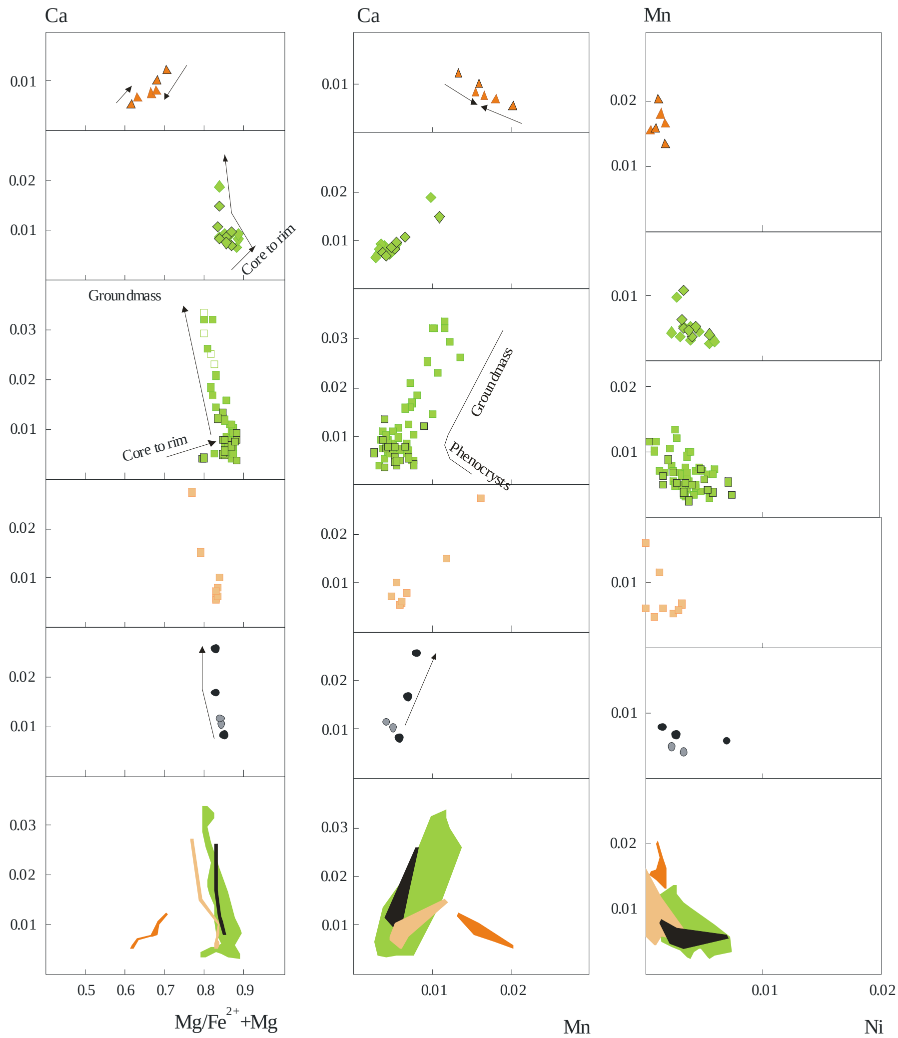


Fig. 12. Ca, Mn, Ni (a.f.u.) and Fo (mol %) relationships in olivines from feldspar-free rocks. Data source and symbols as in Fig. 10.

Olivine data show that Ca substitution is relevant in the GAP kamafugites, although the substitution mechanism is neither entirely clear nor it appears to be the same for all the rock-types. Ca substitution for Mn seems to be a feasible mechanism only in cores of leucite mafurite olivine from Águas Emendadas and in the least evolved olivine of the northern GAP plutonic complexes (dunite, pyroxenite, and the leucite ijolite from Fazenda Buriti) although some detailed core-to-rim variations in gabbroic olivine also define a negative Ca-Mn correlation. For the vast majority of kamafugitic olivine, and for evolved olivine in the plutonic complexes, Ca correlates negatively with Fo content, suggesting the Ca substitutes Mg in olivine. Considering that Ca content in olivine is a function of pressure (Simkin & Smith, 1970; Stormer, 1973), the Ca behaviour indicates that the discussed rock-types have had different crystallization histories.

Ni and Mn show a poorly defined negative correlation in olivines from feldspar-free rocks (Fig. 12) when the whole set of analyses is considered. When rock-types are considered independently, however, no significant correlation is observed between these two elements. In leucite mafurites from Águas Emendadas, groundmass olivine is slightly enriched in Mn for the same Ni content, but the opposite behaviour is noted in the SAB leucite mafurites. In all rock-types in Fig. 12, detailed Ni-Mn zoning patterns are erratic.

In the northern GAP plutonic complexes, Ni and Mn show a distinctive antipathetic behavior in olivine from pyroxenites and malignites (Fig. 13), but Ni varies irrespectively of Mn in olivine from dunites and peridotites, and Mn variation is insensitive to Ni content in olivine from the gabbros and syenites.

If the composition of olivine phenocrysts alone is taken into consideration it is not easy to relate the kamafugitic rock-types to one another through fractional crystallization and an alternative different-tiation process, such as magma mixing or liquid immiscibility, must have been in place during the evolution of these rocks. This is in consonance with the reverse zoning patterns observed in olivine, specially from leucite mafurites, and the reabsorption features present in olivine phenocrysts from mafurites and leucite mafurites, both from the Águas Emendadas and the Santo Antônio da Barra areas.

*Clinopyroxene*

Clinopyroxene occurs as phenocrysts and/or in the groundmass of central and southern GAP kamafugites. It is also an essential constituent of many rock-types of the northern GAP plutonic complexes. Table 3 shows representative clinopyroxene compo-sitions from kamafugitic rocks (katungite, mafurite, leucite mafurite and ugandite) of Águas Emendadas, Santo Antônio da Barra and Amorinópolis, along with data from feldspar-bearing rocks of Águas Emendadas (basanites) and of some northern GAP plutonic complexes (Morro do Macaco, Fazenda Buriti).

The compositions of GAP clinopyroxenes correspond to the diopside-hedenbergite solid solution ($Di_{1.00}$-$Di_{0.77}$) according to the classification of Morimoto *et al.* (1988). In addition to the consti-

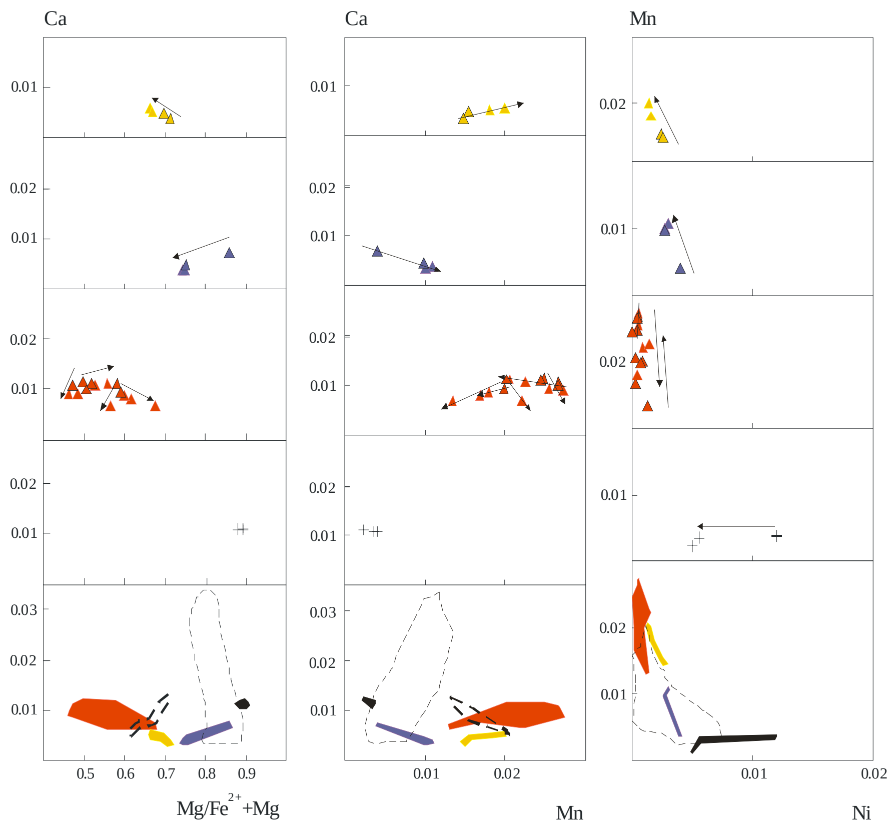


Fig. 13. Ca, Mn, Ni (a.f.u.) and Fo (mol. %) relationships in olivines from feldspar-bearing rocks. Dashed lines represent the compositional fields defined by feldspar-free rocks of Fig. 12. Data source and symbols as in Fig. 11.

Table 3. Representative electron microprobe analyses of clinopyroxenes from GAP samples. Data source: 1) Danni & Gaspar (1994), 2) In this work, 3) Junqueira-Brod (1998), 4) Sgarbi (1998), 5) Cerqueira (1995) and 6) Danni (1978). SAB=Santo Antônio da Barra; L-M=leucite mafurite; L-I=leucite ijolite; g=groundmass; mph=microphenocryst.

| Locality | Amori-nópolis | | Águas Emendadas | | | | | SAB | | Fazenda Buriti | | | | | | | Iporá | | |
|---|---|---|---|---|---|---|---|---|---|---|---|---|---|---|---|---|---|---|---|
| Rock | Katungite | | L-M | L-M | Basanite | L-M | Mafurite | Ugandite | | L-I | Pyroxenite | | Gabbro | | Syenite | | Wehrl. | Gabbro | Syenite |
| Sample | Am1 | Am3 | 96ae01 | 96ae04 | 96ae18 | 96ae22 | 96ae46 | sabug2 | sabug2 | cfb38 | cfb33a | cfb33a | cfb35 | cfb48 | cfb33 | cfb5 | D1 | D5 | D9 |
| Remarks | | | | c | r | | | g | mph | r | c | r | r | r | c | r | | | |
| Reference | 1 | 1 | 2 | 3 | 3 | 3 | 3 | 4 | 4 | 5 | 5 | 5 | 5 | 5 | 5 | 5 | 6 | 6 | 6 |
| $SiO_2$ | 49.62 | 46.58 | 47.63 | 50.98 | 47.82 | 50.31 | 47.04 | 50.26 | 50.52 | 49.05 | 52.85 | 47.80 | 46.13 | 52.41 | 51.81 | 47.61 | 50.07 | 49.64 | 47.46 |
| $TiO_2$ | 4.12 | 4.72 | 3.19 | 1.06 | 2.40 | 2.14 | 3.41 | 1.84 | 1.33 | 2.00 | 0.95 | 3.21 | 3.33 | 0.70 | 0.83 | 2.87 | 3.19 | 4.26 | 5.98 |
| $Al_2O_3$ | 1.81 | 3.32 | 5.20 | 3.36 | 5.47 | 1.88 | 4.94 | 2.76 | 3.51 | 5.97 | 2.69 | 6.78 | 6.62 | 1.91 | 2.54 | 6.13 | 1.39 | 1.77 | 2.74 |
| FeO | 7.87 | 7.90 | 6.00 | 4.48 | 7.30 | 6.46 | 5.94 | 5.50 | 4.93 | 7.80 | 4.16 | 6.64 | 8.02 | 10.49 | 4.13 | 7.06 | 4.40 | 7.46 | 11.51 |
| $Cr_2O_3$ | 0.07 | 0.01 | 0.09 | 1.25 | 0.08 | 0.09 | 0.13 | 0.28 | 0.06 | 0.01 | 0.34 | 0.06 | 0.02 | 0.02 | 0.59 | 0.02 | 0.44 | | |
| MnO | 0.13 | 0.18 | 0.01 | 0.13 | 0.24 | 0.11 | 0.03 | 0.08 | 0.16 | 0.16 | 0.04 | 0.11 | 0.13 | 0.35 | 0.08 | 0.14 | 0.03 | 0.07 | 0.44 |
| NiO | | | 0.03 | | 0.05 | | 0.05 | | | | | | | | | | | | |
| MgO | 12.28 | 11.96 | 13.55 | 15.97 | 13.61 | 13.83 | 14.00 | 15.45 | 15.34 | 12.15 | 16.03 | 12.21 | 11.86 | 11.83 | 15.85 | 12.17 | 16.86 | 13.18 | 10.60 |
| Cao | 22.48 | 22.39 | 23.89 | 21.82 | 22.40 | 24.38 | 24.53 | 23.72 | 23.07 | 22.53 | 23.11 | 21.91 | 22.48 | 21.84 | 24.37 | 22.69 | 22.26 | 19.54 | 22.39 |
| $Na_2O$ | 1.61 | 1.28 | 0.22 | 0.87 | 0.57 | 0.39 | 0.26 | 0.26 | 0.44 | 0.73 | 0.26 | 0.91 | 0.49 | 0.66 | 0.36 | 0.74 | 0.47 | 0.74 | 0.50 |
| $K_2O$ | | | | 0.03 | 0.01 | 0.04 | 0.02 | 0.03 | 0.01 | | | | | | | | 0.16 | 0.31 | |
| Total | 99.99 | 98.34 | 99.80 | 99.96 | 99.95 | 99.64 | 100.35 | 100.18 | 99.37 | 100.40 | 100.43 | 99.63 | 99.08 | 100.21 | 100.56 | 99.43 | 99.27 | 96.97 | 101.62 |
| Cations on the basis of 6 O | | | | | | | | | | | | | | | | | | | |
| TSi | 1.853 | 1.773 | 1.772 | 1.862 | 1.773 | 1.876 | 1.738 | 1.848 | 1.864 | 1.818 | 1.928 | 1.781 | 1.741 | 1.967 | 1.887 | 1.781 | 1.850 | 1.916 | 1.792 |
| TAl | 0.080 | 0.149 | 0.228 | 0.138 | 0.227 | 0.083 | 0.215 | 0.120 | 0.136 | 0.182 | 0.072 | 0.219 | 0.259 | 0.033 | 0.109 | 0.219 | 0.060 | 0.080 | 0.122 |
| $TFe^{3+}$ | 0.067 | 0.079 | | | | 0.041 | 0.046 | 0.032 | | | | | | | 0.005 | | 0.090 | | |
| M1Al | | | | 0.007 | 0.012 | | | | 0.017 | 0.079 | 0.043 | 0.079 | 0.035 | 0.051 | | 0.051 | | | |
| M1Ti | 0.116 | 0.135 | 0.089 | 0.029 | 0.067 | 0.060 | 0.095 | 0.051 | 0.037 | 0.056 | 0.026 | 0.090 | 0.095 | 0.020 | 0.023 | 0.081 | 0.089 | 0.124 | 0.170 |
| $M1Fe^{3+}$ | 0.030 | 0.051 | 0.061 | 0.099 | 0.120 | 0.031 | 0.087 | 0.061 | 0.075 | 0.043 | | 0.023 | 0.069 | | 0.076 | 0.058 | 0.001 | | |
| $M1Fe^{2+}$ | 0.149 | 0.122 | 0.094 | | 0.046 | 0.130 | 0.042 | 0.033 | 0.026 | 0.151 | 0.050 | 0.128 | 0.133 | 0.267 | 0.024 | 0.130 | | 0.118 | 0.234 |
| M1Cr | 0.002 | | 0.003 | 0.036 | 0.002 | 0.003 | 0.004 | 0.008 | 0.002 | | 0.010 | 0.002 | 0.001 | 0.001 | 0.017 | 0.001 | 0.013 | | |
| M1Mg | 0.684 | 0.679 | 0.752 | 0.829 | 0.752 | 0.769 | 0.771 | 0.847 | 0.844 | 0.671 | 0.872 | 0.678 | 0.667 | 0.662 | 0.860 | 0.679 | 0.898 | 0.758 | 0.597 |
| M1Ni | | | 0.001 | | 0.001 | | 0.002 | | | | | | | | | | | | |
| M2Mg | | | | 0.041 | | | | | | | | | | | | | 0.031 | | |
| $M2Fe^{2+}$ | | | 0.031 | 0.038 | 0.061 | | 0.008 | 0.043 | 0.051 | 0.048 | 0.077 | 0.056 | 0.051 | 0.063 | 0.021 | 0.032 | 0.046 | 0.123 | 0.130 |
| M2Mn | 0.004 | 0.006 | | 0.004 | 0.008 | 0.003 | 0.001 | 0.002 | 0.005 | 0.005 | 0.001 | 0.003 | 0.004 | 0.011 | 0.002 | 0.004 | 0.001 | 0.002 | 0.014 |
| M2Ca | 0.899 | 0.913 | 0.953 | 0.854 | 0.890 | 0.974 | 0.971 | 0.935 | 0.912 | 0.895 | 0.903 | 0.875 | 0.909 | 0.878 | 0.951 | 0.910 | 0.881 | 0.808 | 0.906 |
| M2Na | 0.117 | 0.094 | 0.016 | 0.062 | 0.041 | 0.028 | 0.018 | 0.019 | 0.031 | 0.052 | 0.018 | 0.066 | 0.036 | 0.048 | 0.025 | 0.054 | 0.034 | 0.055 | 0.037 |
| M2K | | | | 0.001 | | 0.002 | 0.001 | 0.001 | | | | | | | | | 0.008 | 0.015 | |
| Total | 4.000 | 4.000 | 4.000 | 3.999 | 4.000 | 3.998 | 3.999 | 3.999 | 4.000 | 4.000 | 4.000 | 4.000 | 4.000 | 4.000 | 4.000 | 4.000 | 3.992 | 3.985 | 4.000 |

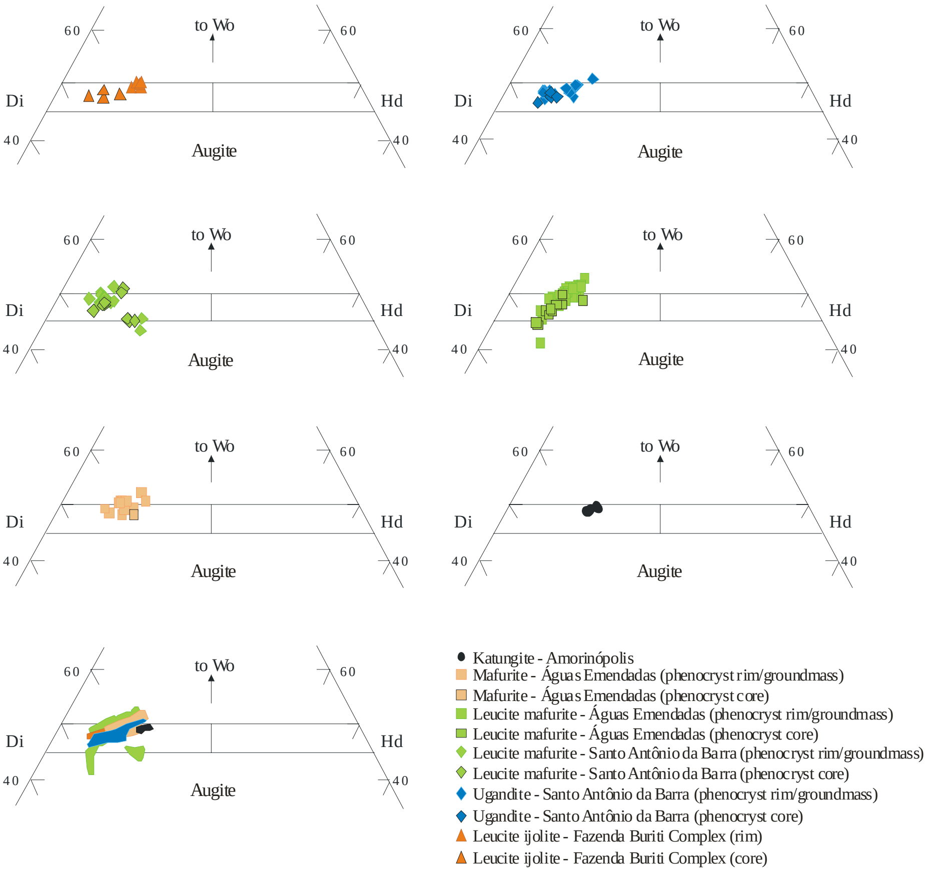


Fig. 14. Classification of clinopyroxenes from the GAP feldspar-free rocks in the Ca-Fe-Mg system (Morimoto *et al.*, 1988). Data source: Danni & Gaspar (1994), Cerqueira (1995), Junqueira-Brod (1998), Sgarbi (1998) and this work.

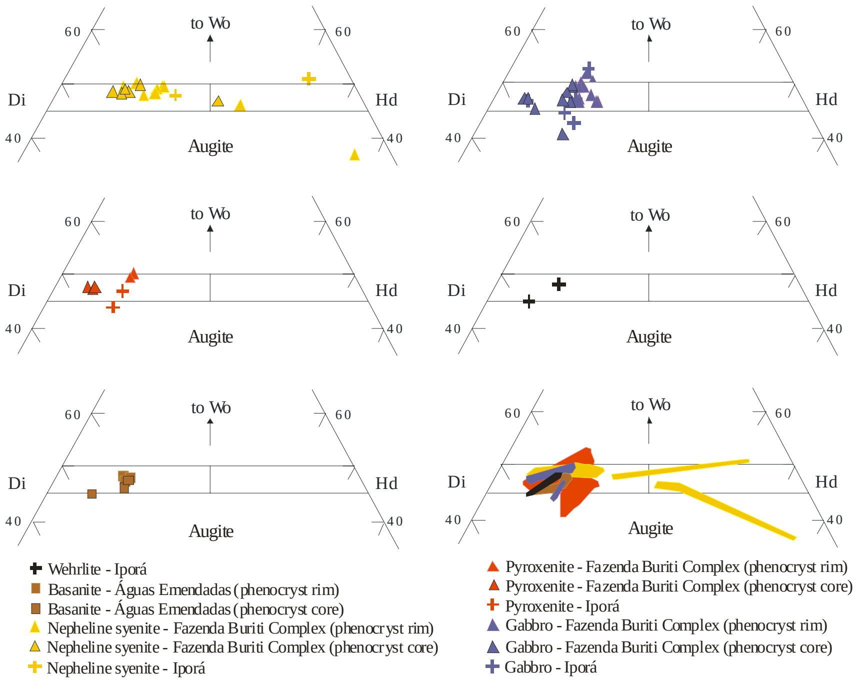


Fig. 15. Classification of clinopyroxenes from the GAP feldspar-bearing rocks in the Ca-Fe-Mg system (Morimoto *et al.*, 1988). Data source: Danni (1978) and Cerqueira (1995).

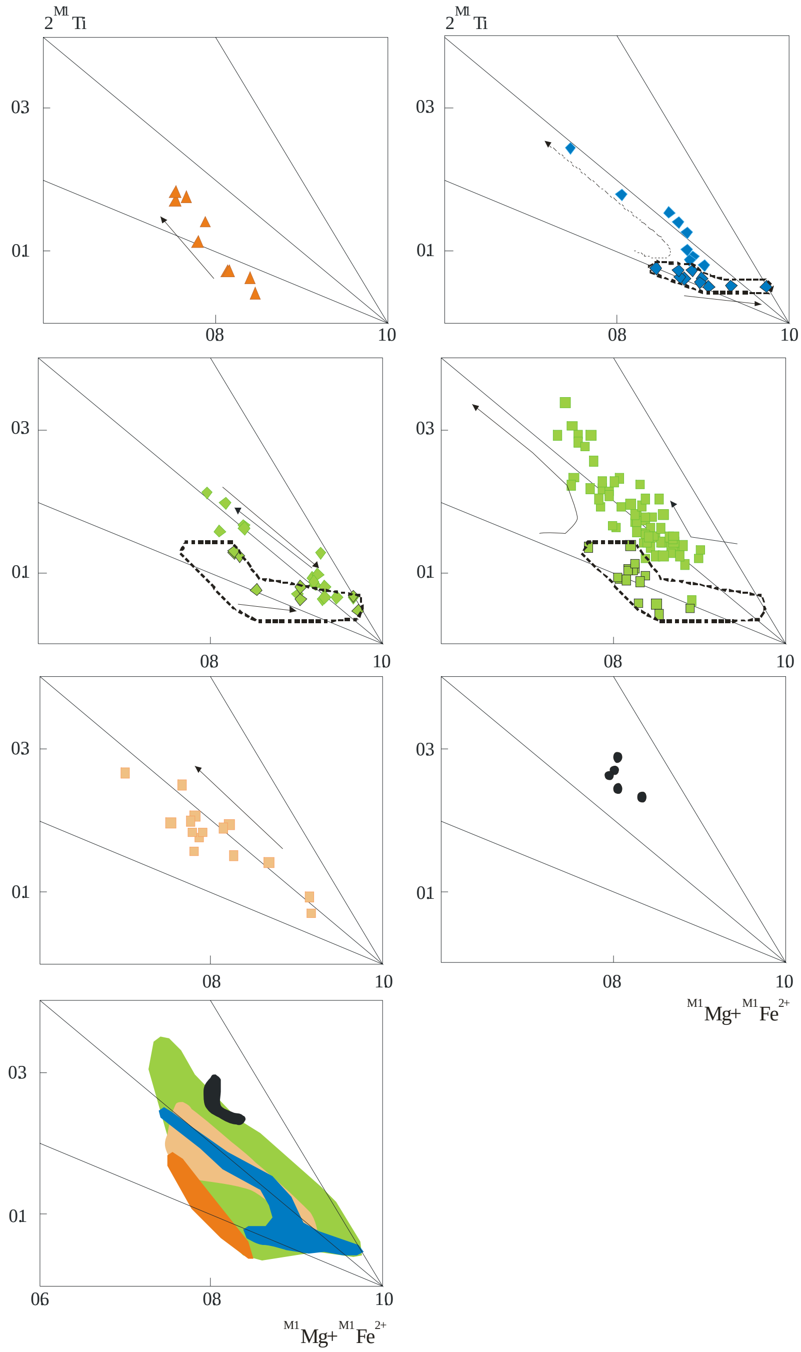


Fig. 16. Variations of octahedral (M1) Ti and Mg+Fe$^{2+}$ (a.f.u.) in clinopyroxenes from the GAP feldspar-free rocks. Dashed lines represent the field of phenocryst cores in leucite mafurite and ugandite clinopyroxenes. Data source and symbols as in Fig. 14.

tuents that make up these two end-members, other important oxides are $Al_2O_3$ (0.55-8.50 wt%), $Fe_2O_3$ (0.00-10.24 wt%), $TiO_2$ (0.61-5.98 wt%) and $Na_2O$ (0.19-4.34 wt%). Minor amounts of $Cr_2O_3$ (up to 1.25 wt%), MnO (up to 1.3 wt%) and NiO (up to 0.14 wt%) may also be present. Most GAP pyroxenes do not contain Al enough to fill the tetrahedral site in addition to Si, and therefore require the presence of $Fe^{3+}$ (Table 3).

The compositional ranges of diopside from kamafugitic rocks of most GAP locations largely overlap in the Ca-Mg-Fe pyroxene system (Fig. 14), except for the Amorinópolis katungites, whose pyroxenes are somewhat slightly more enriched in the hedenbergite molecule. Most kamafugitic pyroxenes have only small amounts of $Na_2O$ (lower than

1 wt%), but in the Amorinópolis katungites, pyroxene is distinctively more Na-rich, with $Na_2O$ varying from 1.28 to 1.66 wt%. The overall core-to-rim trends indicate a general evolution through hedenbergite enrichment in all the GAP kamafugitic rocks.

Diopside from ultramafic rocks of the northern GAP plutonic complexes largely overlap those of the kamafugites, but diopside from the gabbroic rocks extends slightly towards hedenbergite, whereas syenitic clinopyroxene may be highly enriched in the hedenbergite molecule (Fig. 15). The ranges for Fazenda Buriti and Morro do Macaco/Córrego dos Bois complexes are very similar, except for the most evolved (syenitic) pyroxene from Fazenda Buriti, which inflects toward augitic (aegirine-augite, not shown) composition. It is also noteworthy from Fig. 15 that in the Morro do Macaco/Córrego dos Bois complexes more differentiated rocks in the sequence wehrlite-pyroxenite-gabbro-syenite have progressively more hedenbergitic pyroxene, whereas in the Fazenda Buriti complex diopside compositions overlap the mafic rocks.

Despite the overall similarity of GAP clinopyroxenes in the diopside-hedenbergite system, some elemental substitutions may be used to discriminate between textural varieties of clinopyroxene, and between different rock-types and localities.

Fig. 16 shows that katungite clinopyroxenes are enriched in Ti, relatively to octahedral $Mg+Fe^{2+}$. Katungite and mafurite clinopyroxenes are characterized by negative correlation between these M1 cations, which indicates mutual substitution.

Diopside from leucite mafurites and ugandites, however, shows a distinct behaviour. The cores of pyroxene phenocrysts in these rocks are Ti-poor, and their Ti content is little or not affected at all by the amount of $Mg+Fe^{2+}$. On the other hand, phenocryst rims and groundmass diopside from leucite mafurites and ugandites behave in a similar way to that observed for the mafurites.

Diopside from the Fazenda Buriti leucite ijolites also shows a negative correlation between Ti and $Fe^{2+}+Mg$, though at a more pronounced slope perhaps akin to katungite diopside (but at lower Ti and $Fe^{2+}+Mg$).

The overall relationships in the diagram suggest that pyroxenes from the GAP kamafugitic rocks cannot be easily related to each other through simple fractionation processes. Particularly, the cores of diopside phenocrysts in leucite mafurites and in ugandites are likely to represent xenocryst pyroxene, whereas the respective phenocryst rims, microphenocrysts and groundmass pyroxene have an evolution pattern that is similar to that of mafurite diopside.

Fig. 17 represents the behaviour of the same cations in pyroxenes of feldspar-bearing rocks from the Fazenda Buriti and Morro do Macaco/Córrego dos Bois complexes (wehrlite, pyroxenite, gabbro and syenite) and from Águas Emendadas (basanite). The core-to-rim variation, as well as the changes in pyroxene composition with the differentiation degree of the host-rock, defines two very different trends. Unfortunately, the small number of analyses, and the lack of details regarding textural constraints on the pyroxenes of the Morro do Macaco/Córrego dos Bois complexes preclude a more detailed assessment of the pyroxene chemical variation within a single rock-type. However, when host-rocks at different differentiation degrees are considered, diopside from these complexes clearly evolves through strong Ti enrichment at relatively constant $Fe^{2+}+Mg$ values.

In rocks of the Fazenda Buriti complex clinopyroxene within a single rock-type evolves along a negative slope (increasing Ti with decreasing $Fe^{2+}+Mg$), which may change into a trend of $Fe^{2+}+Mg$ depletion at constant Ti. This latter pattern is dominant when distinct host-rocks are compared to each other.

Diopside from the Águas Emendadas basanites is similar in composition to that of the gabbroic rocks from the Fazenda Buriti complex.

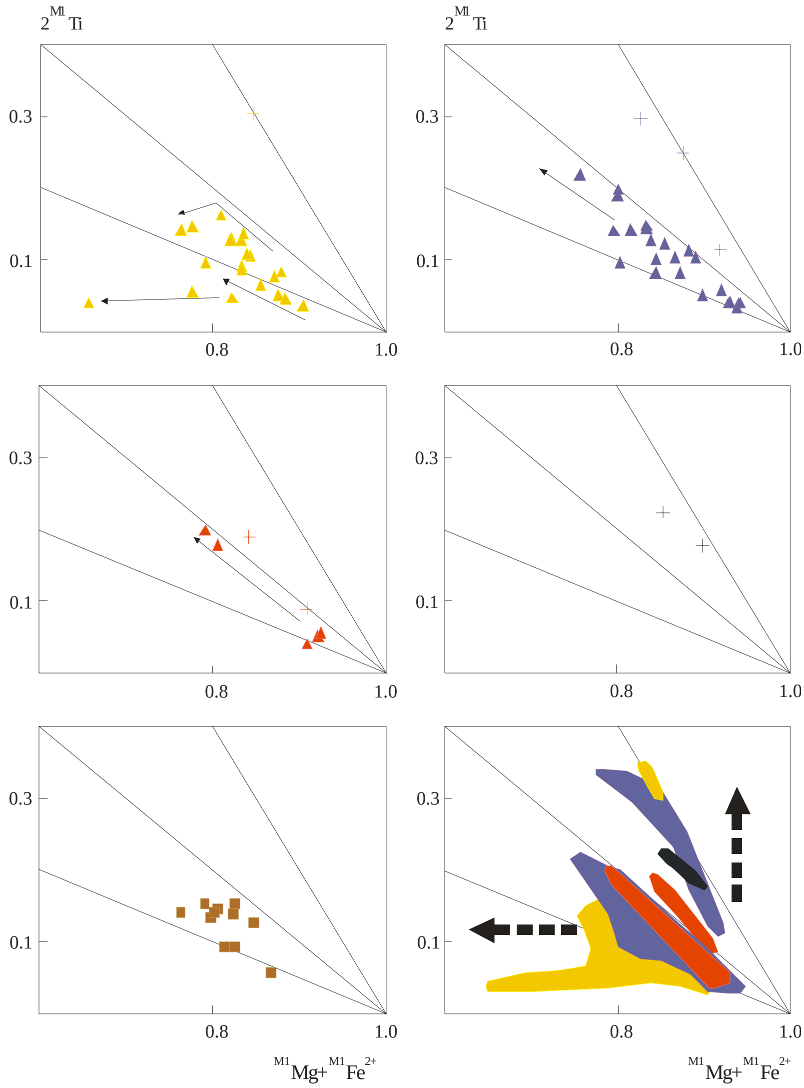


Fig. 17. Variations of octahedral (M1) Ti and Mg+Fe$^{2+}$ (a.f.u.) in clinopyroxenes from the GAP feldspar-bearing rocks. Dashed arrows represent the overall trend of pyroxenes with respect to the evolution stage of the host-rock. Data source and symbols as in Fig 15.

Fig. 18 shows the behaviour of Ti and Al in diopside from the various types of GAP feldspar-free rocks. Katungite diopside is clearly more enriched in Ti for a given Al content than all other kamafugitic rock-types. Mafurite diopside appears to evolve across different Al-Ti slopes, starting at an Al/Ti ratio similar to that of katungite diopside, but progressing towards Al/Ti ratios that are more similar to those of the leucite mafurite and ugandite pyroxene (see below). In leucite mafurite and ugandite samples from Águas Emendadas and SAB, there is a consistent discrepancy between Al and Ti contents in the cores of diopside phenocrysts, when compared to the respective rims and to the groundmass crystals. Although a generally sympathetic relationship between Al and Ti occurs in all cases, the cores of phenocrysts are typically aligned in a trend of higher Al/Ti ratio than that of the phenocryst rims and groundmass pyroxene, suggesting that the phenocryst cores represent xenocrysts that have been later overgrown by diopside with a different composition. This is consistent with the generally similar chemical character of phenocryst rims and groundmass crystals. Diopside from the Fazenda Buriti leucite ijolites is chemically similar to the cores of diopside phenocrysts in leucite mafurites and ugandites, in terms of the Al/Ti ratio.

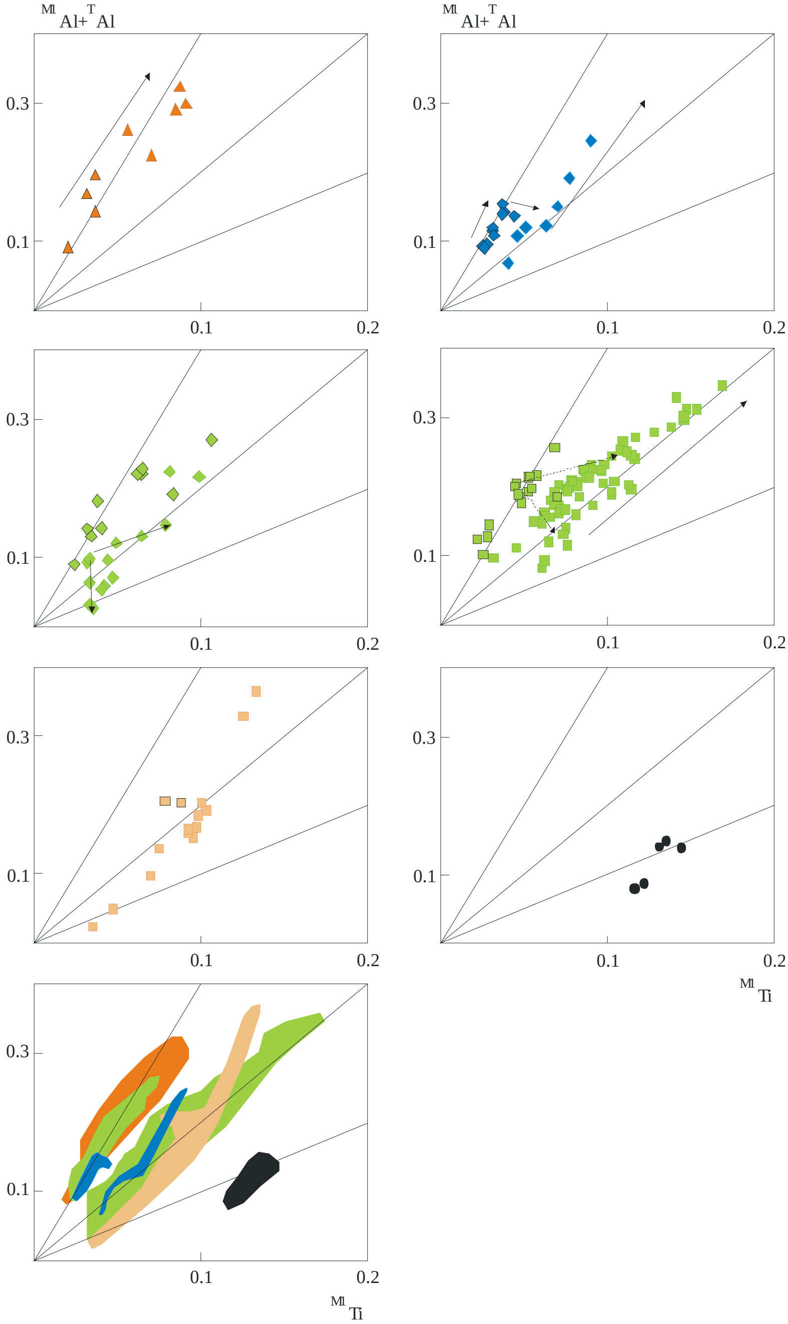


Fig. 18. Ti-Al relationships in clinopyroxenes from the GAP feldspar-free rocks. Data source as in Fig. 14.

Fig. 19 shows the compositional trends of diopside from feldspar-bearing rocks in the same diagram. The general evolution is one of sympathetically increasing Al and Ti, but it is clear from the diagram that diopside from the Morro do Macaco/Córrego dos Bois complexes is much enriched in Ti relatively to that occurring in the Fazenda Buriti rocks and in the Águas Emendadas basanites. When different degrees of evolution of the host-rock are considered, diopside from the Morro do Macaco/Córrego dos Bois complexes evolve in the sense of increasing Ti at constant Al, whereas no particular evolution pattern can be devised with fractionation degree in the Fazenda Buriti rocks.

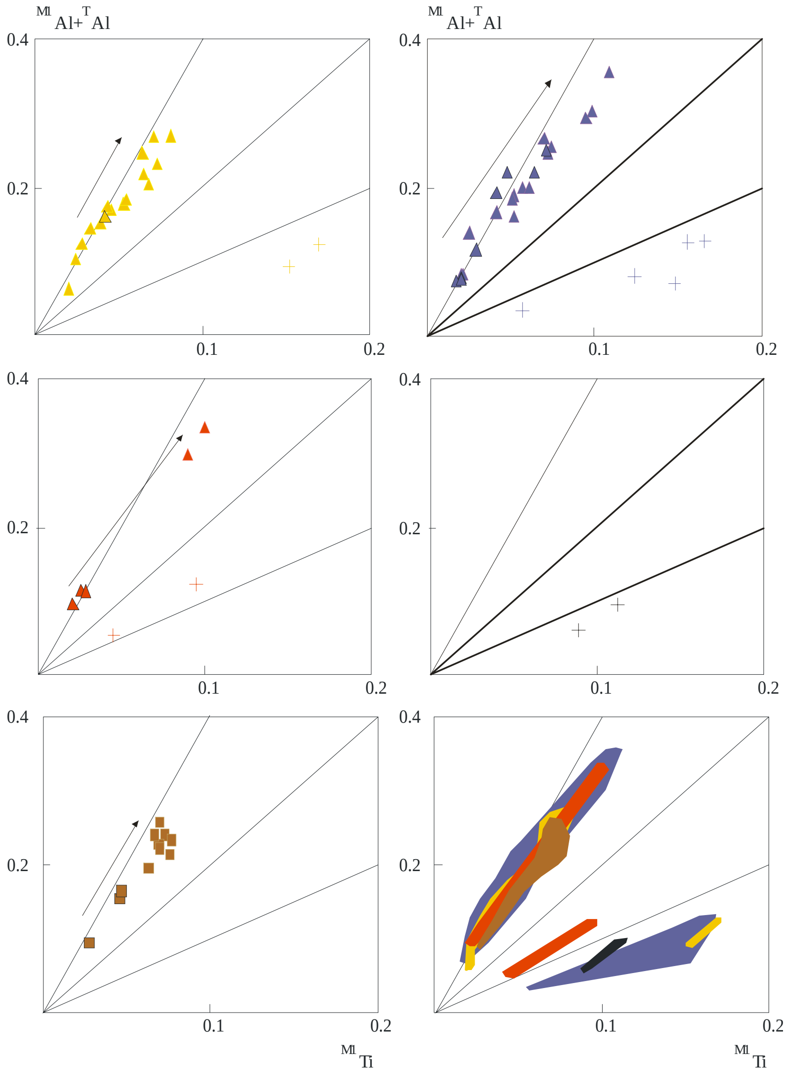


Fig. 19. Ti-Al relationships in clinopyroxenes from the GAP feldspar-bearing rocks. Data source as in Fig. 15.

Fig. 20 compares the pyroxenes from the GAP rocks with those of various kamafugites and other ultrapotassic rocks from the world. Within the GAP it is clear that the Al/Ti ratio varies widely, which is also the case in pyroxenes of other ultrapotassic rocks.

A group of analyses, including diopside in both feldspar-free and feldspar-bearing rocks of the Fazenda Buriti complex, the cores of diopside phenocrysts in the leucite mafurites from Águas Emendadas and Santo Antônio da Barra, and the cores of diopside in ugandites plot along a 4:1 (Al:Ti) ratio. A second group, comprising the phenocryst rims and groundmass pyroxene in leucite mafurites and ugandites, are more Ti-enriched, plotting along a 2:1 Al:Ti line. Both groups have the same range of Al:Ti ratios observed in pyroxenes from the Ugandan kamafugites, although in the GAP Al and Ti reach higher contents. A third group of GAP diopsides, including those in the Morro do Macaco/Córrego dos Bois complexes, and in the Amorinópolis katungites, show a much stronger Ti enrichment, plotting along a 1:1 Al:Ti line, which is more typical of the Italian (San Venanzo and Cupaello) kamafugites, and of orangeites.

Diopside from the Mata da Corda kamafugites (Alto Paranaíba Igneous Province) define a main field corresponding to Al:Ti=1:1 (Fig. 20), therefore similar to the Italian kamafugites, and to orangeites and lamproites. Two very distinct narrow trends derive from this main field, one evolving at higher Al/Ti and the other evolving at lower Al/Ti than all GAP pyroxenes. The low Al/Ti Mata da Corda offshoot comprises phenocryst rims and groundmass grains of late-stage (deuteric) aegirine in ugandite (Sgarbi *et al.*, 2000b), which appear to be lacking in the GAP rocks. The high Al/Ti Mata da Corda branch in Fig. 20 represents green diopside-to-hedenbergite cores in reversely zoned phenocrysts, which are interpreted (Sgarbi & Valença, 1995) as a result of comagmatic mixing.

This could possibly be also the case of the high Al/Ti phenocryst cores in GAP leucite mafurites and ugandites, although in this case the phenocryst cores are not particularly enriched in the hedenbergite component.

*Mica*

Phlogopite is a common mineral in most GAP rock-types. In the SAB kamafugites it occurs essentially in the groundmass, and also as pseudomorphs on olivine crystals. In the Águas Emendadas mafurites, phlogopite occurs as a late-stage poikilitic phase, while in leucite mafurites it is present both as phenocrysts and as a groundmass constituent (Junqueira-Brod, 1998). Águas Emendadas ugandites contain phlogopite both as phenocrysts and as a groundmass phase. In the Amorinópolis katungites, phlogopite forms an interstitial phase, resulting from the reaction of late-stage fluids with olivine crystals (Danni & Gaspar, 1994).

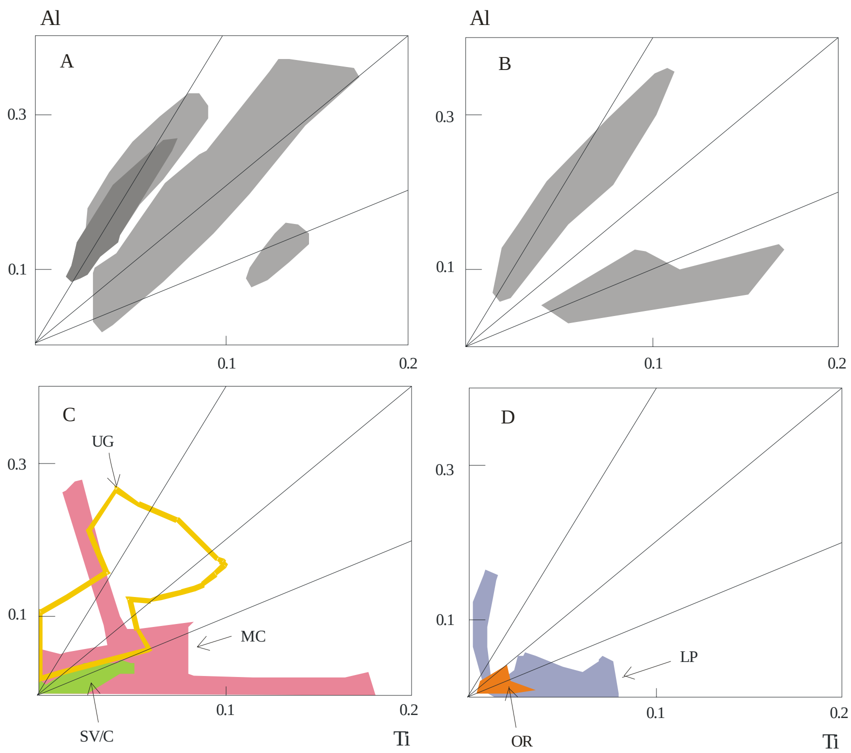


Fig. 20. Comparison between GAP clinopyroxenes and those of other ultrapotassic rocks, in terms of Ti-Al (a.f.u.) relationships. A) Fields of GAP clinopyroxenes from feldspar-free rocks (darker shaded area represents the fields of phenocryst cores in leucite mafurites and ugandites); B) Fields of GAP clinopyroxenes from feldspar-bearing rocks; C) Fields of clinopyroxenes from African kamafugites (UG), Mata da Corda kamafugites (MC), Italian kamafugites (SV/C); D) Fields of clinopyroxenes from orangeites (OR) and lamproites (LP). Data source - GAP: Danni & Gaspar (1994), Cerqueira (1995), Sgarbi (1998), Junqueira-Brod (1998), Sgarbi *et al.* (2000b), and this work; Other kamafugites: Lloyd *et al.* (1991), Cundari & Ferguson (1991), Sgarbi & Valença (1995) and Sgarbi *et al.* (2000c); Lamproites: Mitchell & Bergman (1991); Orangeites: Mitchell (1995).

Table 4. Electron microprobe analyses of micas from selected GAP samples. Data source: 1) Danni & Gaspar (1994), 2) This work, 3) Sgarbi (1998) and 4) Cerqueira (1995). L-M = leucite mafurite; L-I = leucite ijolite; g = groundmass.

| Locality | Amori-nópolis | Águas Emendadas | | | Santo Antônio da Barra | | | | Fazenda Buriti | | |
|---|---|---|---|---|---|---|---|---|---|---|---|
| Rock | Katungite | Breccia | Mafurite | L-M | L-M | L-M | Ugandite | Ugandite | L-I | Gabbro | Syenite |
| Sample | Amor4 | 96ae09 | 96ae46 | 96ae04 | sabmp08 | sabm01 | sabug02 | sabug03 | cfb020 | cfb048 | cfb047b |
| Remarks | | g | | | | | | | | r | |
| Reference | 1 | 2 | 2 | 2 | 3 | 3 | 3 | 3 | 4 | 4 | 4 |
| $SiO_2$ | 40.44 | 38.46 | 38.42 | 36.10 | 39.46 | 35.30 | 34.90 | 34.64 | 35.53 | 35.00 | 33.45 |
| $TiO_2$ | 3.22 | 7.23 | 5.54 | 7.50 | 3.86 | 5.52 | 7.91 | 6.47 | 9.31 | 6.33 | 9.15 |
| $Al_2O_3$ | 5.92 | 10.83 | 10.32 | 12.90 | 9.34 | 12.90 | 11.96 | 12.55 | 14.61 | 14.01 | 13.78 |
| $Cr_2O_3$ | 0.02 | 0.02 | | | | 0.01 | 0.01 | | | 0.01 | |
| $Fe_2O_3$ | 7.85 | 3.57 | 5.66 | 3.87 | 4.87 | 3.13 | 4.23 | 3.22 | 1.67 | 0.96 | 2.10 |
| FeO | 8.65 | 8.22 | 1.75 | 2.96 | 0.81 | 2.13 | 6.77 | 7.00 | 11.19 | 19.21 | 19.77 |
| MnO | 0.09 | 0.15 | 0.17 | 0.07 | 0.06 | 0.07 | 0.04 | 0.30 | 0.04 | 0.14 | 0.32 |
| MgO | 18.55 | 15.43 | 21.83 | 19.54 | 22.50 | 20.64 | 15.15 | 15.88 | 13.45 | 10.68 | 7.44 |
| CaO | 0.11 | 0.12 | 0.16 | 0.09 | | 0.11 | 0.24 | 0.11 | 0.01 | | |
| BaO | 0.49 | 2.54 | | | 2.35 | 6.51 | 6.27 | 7.33 | | | |
| $Na_2O$ | 0.48 | 1.01 | 0.81 | 0.37 | 0.62 | 0.11 | 0.30 | 0.51 | 0.51 | 0.24 | 0.36 |
| $K_2O$ | 9.23 | 8.08 | 9.28 | 9.92 | 9.96 | 7.39 | 7.18 | 7.05 | 9.03 | 9.23 | 8.36 |
| $H_2O$ | 3.99 | 2.02 | 4.10 | 4.06 | 4.06 | 2.59 | 3.23 | 2.86 | 4.05 | 3.83 | 3.84 |
| Total | 99.04 | 97.66 | 98.04 | 97.39 | 97.89 | 96.40 | 98.18 | 97.92 | 99.39 | 99.65 | 98.57 |
| Cations on the basis of 24 O (OH) | | | | | | | | | | | |
| Si | 6.065 | 5.708 | 5.603 | 5.326 | 5.831 | 5.343 | 5.351 | 5.344 | 5.264 | 5.361 | 5.220 |
| Ti | 0.363 | 0.807 | 0.608 | 0.832 | 0.429 | 0.628 | 0.912 | 0.751 | 1.038 | 0.729 | 1.074 |
| Al | 1.046 | 1.892 | 1.773 | 2.242 | 1.625 | 2.299 | 2.159 | 2.280 | 2.549 | 2.527 | 2.532 |
| $Fe^{2+}$ | 1.084 | 1.020 | 0.214 | 0.365 | 0.100 | 0.269 | 0.868 | 0.903 | 1.386 | 2.461 | 2.580 |
| $Fe^{3+}$ | 0.885 | 0.398 | 0.620 | 0.429 | 0.541 | 0.356 | 0.487 | 0.374 | 0.186 | 0.111 | 0.246 |
| Cr | 0.002 | 0.002 | | | | 0.001 | 0.001 | | | 0.001 | |
| Mn | 0.011 | 0.019 | 0.021 | 0.009 | 0.008 | 0.009 | 0.005 | 0.039 | 0.005 | 0.018 | 0.042 |
| Mg | 4.147 | 3.414 | 4.747 | 4.297 | 4.956 | 4.657 | 3.463 | 3.652 | 2.971 | 2.439 | 1.731 |
| Ca | 0.018 | 0.019 | 0.025 | 0.015 | | 0.018 | 0.039 | 0.018 | 0.002 | | |
| Ba | 0.029 | 0.148 | | | 0.136 | 0.386 | 0.377 | 0.443 | | | |
| Na | 0.140 | 0.291 | 0.229 | 0.105 | 0.178 | 0.032 | 0.089 | 0.153 | 0.147 | 0.071 | 0.109 |
| K | 1.766 | 1.530 | 1.727 | 1.868 | 1.878 | 1.427 | 1.404 | 1.388 | 1.707 | 1.804 | 1.664 |
| Cations | 15.556 | 15.246 | 15.566 | 15.488 | 15.681 | 15.426 | 15.156 | 15.344 | 15.254 | 15.523 | 15.199 |

Biotite is a common phase in the Fazenda Buriti complex, in northern GAP, where it occurs in gabbroic rocks either as an intercumulus phase or as a product of reaction of pyroxene or amphibole with the residual liquid, and also as reaction rims surrounding ilmenite and magnetite. In syenitic rocks biotite is present as a subordinate phase forming individual lamellae (Cerqueira, 1995).

Table 4 shows representative mica analyses for the main GAP petrographic types. In most GAP micas the sum of Si and Al is not enough to fill the tetrahedral site (i.e. Si+Al<8 a.f.u.), but in most cases this seems to be due to Si rather than to Al-deficiency with respect to the ideal phlogopite or biotite formula $K_2(Mg,Fe)_6(Si_6Al_2O_{20})(OH,F)_4$. Remarkable exceptions are the Amorinópolis katungite phlogopites, which have a strong Al deficiency (1 to 1.3 a.f.u.), along with some excess Si (6.04-6.19 a.f.u.). Some mafurite and leucite mafurite mica (particularly those forming olivine pseudomorphs) may be both Si and Al-deficient.

Tetrahedral deficiency requires the completion of this site with other cations such as $Fe^{3+}$ or $Ti^{4+}$. Some authors have proposed the presence of $^{(IV)}Ti^{4+}$, rather than $^{(IV)}Fe^{3+}$, to account for the tetrahedral deficiency (Farmer & Boetcher, 1981), suggesting that $Ti^{4+}$ comes before $Fe^{3+}$ in the order of preference to occupy tetrahedral positions, with $Fe^{3+}$ entering the tetrahedral site only if there is still any deficiency left. This seems to be an attractive hypothesis, considering the high Ti content (0.3 to 1.2 a.f.u) and the strong Si deficiency of the GAP micas. However, attempts to recalculate the structural formulae recasting Ti to the tetrahedral site have produced unsuitable charge balance results (up to 0.93 unbalanced negative charges) on the basis of 24 (O, OH ,F). On the other hand, when Fe is recast as $Fe^{3+}$ until completion of the tetrahedral site, all charge balances are less than 0.008 away from stoichiometry. Additionally, a strong anti-pathetic behaviour between Ti and Fe+Mg (Fig. 21), and the presence of significant octahedral vacancy (up to 2 a.f.u.) suggest that Ti is mainly an octahedral constituent. We therefore opted for recasting part of the iron as $Fe^{3+}$ and adjusting the $Fe_2O_3$ values in Table 4, according to the procedure proposed by Brod *et al.* (2001).

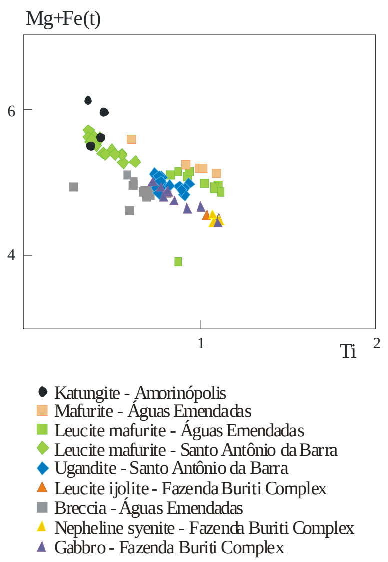


Fig. 21. Ti vs. $Mg+Fe_t$ diagram showing a strong negative correlation for these cations in mica from all GAP rock types. Data source: Danni & Gaspar (1994), Cerqueira (1995), Sgarbi (1998), and this work.

Most mica in the GAP feldspar-free rocks may be classified as phlogopite (Fig. 22) with compositions intermediate between the phlogopite-annite and the eastonite-siderophyllite series, sometimes with significant contribution from the tetra-ferri-phlogopite end-member (in katungite and in some mafurite and leucite mafurite mica). Micas from the Fazenda Buriti Complex are classified as biotite, with Al content intermediate between the phlogopite-annite series and the eastonite-siderophyllite series.

Phlogopites in GAP mafurites and leucite mafurites have the highest $Mg/(Fe^{2+}+Mg)$ content (respectively, 0.95-0.96 and 0.81-0.98) among the kamafugitic rocks. In ugandite micas this ratio varies from 0.76 to 0.84, suggesting that they are slightly more evolved, a relationship also noted between mafurite and ugandite micas from the Alto Paranaíba Igneous Province (Araújo, 2000). Analyses from katungite phlogopites have $Mg/(Fe^{2+}+Mg)$ values (0.75-0.85) that are mostly coincident with those of ugandites, but are clearly distinguished from the latter by the strong Al deficiency. Phlogopite in juvenile fragments from a breccia of the Águas Emendadas diatreme yielded $Mg/(Fe^{2+}+Mg)$ similar to ugandite mica, except for one analysis, which is compositionally a biotite ($Mg/(Fe^{2+}+Mg)=0.27$) and possibly represents a xenocryst.

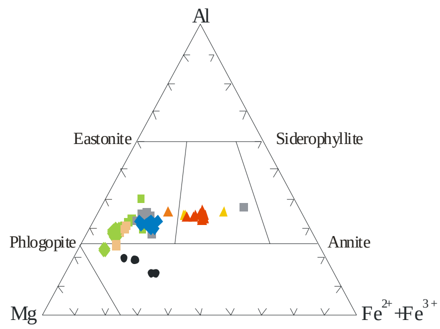


Fig. 22. Classification of micas from GAP feldspar-bearing and feldspar-free rocks in the system Mg-Fe-Al. Data source and symbols as in Fig. 21.

Although Ba data are not available for the whole set of GAP phlogopite analyses, at least micas from kamafugitic rocks have significant BaO contents. Phlogopite in leucite mafurites and ugandites has BaO ranging from 5.5 to 9 wt% (except pseudomorphs on olivine phenocrysts in leucite mafurites, where BaO varies from 1.88 to 2.35 wt%). Katungite phlogopites contain the least BaO (0.49-1.15 wt%) among the GAP kamafugites. A well-defined negative correlation between Ba and Si (Fig. 23) suggests that the K-Ba substitution is coupled with Si substitution by $Fe^{3+}$ or Al with phlogopite evolution.

$TiO_2$ is lower in micas from katungites (3.22-4.01 wt%) than in those from mafurites (5.53-9.52 wt%), from ugandites (6.19-7.95 wt%), and from the Águas Emendadas breccia (5.30-7.23 wt%). Phlogopite from leucite mafurites, however, covers the whole $TiO_2$ range observed for the other kamafugitic mica (3.23-9.87 wt%).

Al deficiency is most significant in the katungite micas (5.85-7.90 wt% $Al_2O_3$). Ugandite phlogopites contain 11.04-13.2 wt% $Al_2O_3$, while in mafurite mica $Al_2O_3$ ranges from 10.32 to 12.70 wt%. Leucite mafurite phlogopites contain 9.34 to 14.34 wt% $Al_2O_3$, therefore largely overlapping the range of other kamafugitic mica. Interestingly, phlogopites from the Águas Emendadas breccia are dominantly Al-saturated, even exceeding the amount necessary for completion of the tetrahedral site ($Al_2O_3$ up to 15.3 wt%).

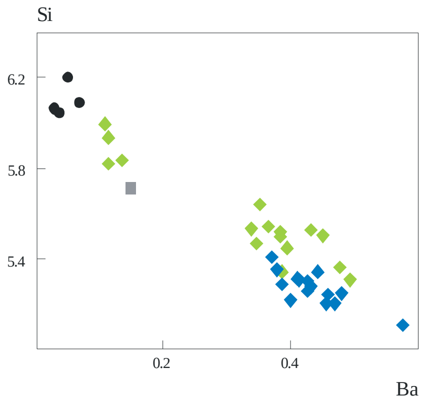


Fig. 23. Si-Ba negative correlation of GAP kamafugitic micas. Data source: Danni & Gaspar (1994), Sgarbi (1998), and this work. Symbols as in Fig. 21.

Mica in the feldspar-bearing rocks from the Fazenda Buriti complex has $Mg/(Fe^{2+}+Mg)$ varying from 0.4 to 0.6, and is therefore classified as biotite. It is enriched in $TiO_2$ (6.3-9.9 wt%) and $Al_2O_3$ (13.22-14.36 wt%) relatively to most kamafugitic phlogopites.

Fig. 24 shows the $Al_2O_3$-$TiO_2$ variation of GAP micas in comparison with other kamafugites and ultrapotassic rocks. GAP micas plot along a convex trend which may be divided into two sections: a trend of slow $Al_2O_3$ decrease over a wide range of decreasing $TiO_2$ values (10 to 4 wt%) and a trend of fast $Al_2O_3$ decrease over a limited $TiO_2$ range (4 to 3 wt%). The Al/Ti ratio of the former is similar to that of minettes and alnöites, whereas the latter resembles the behaviour of orangeite mica (Fig. 24a).

Similarly convex trends are observed in kamafugitic mica from the Mata da Corda volcanics and from kamafugite pipes from the Alto Paranaíba Igneous Province, which is the other main area of occurrence of kamafugitic rocks in Brazil (Fig. 24b). In this case, the field of GAP micas extends to a slightly higher $TiO_2$ maximum, and appears to follow a trend which is intermediate between those of the Alto Paranaíba/Mata da Corda mafurites and ugandites, although some overlap does exist.

Fig. 24c compares GAP micas with those in other kamafugitic provinces of the world. Again, convex Al-Ti trends are dominant. The GAP micas are more similar to those of Ugandan kamafugites, although the GAP trend extends to higher $TiO_2$ and lower $Al_2O_3$. The trend for micas in Italian kamafugites (San Venanzo and Cupaello) starts at significantly lower $TiO_2$, and reach significantly lower $Al_2O_3$ values than GAP.

Kamafugite mica is clearly different from other ultrapotassic rocks in terms of Al-Ti trends. The convex trends with rapid decrease in $Al_2O_3$ at low $TiO_2$ values appear to be the hallmark of kamafugite micas (Fig. 24d). Similar trends are observed in phlogopite from silicate rocks and carbonatites of some carbonatitic complexes (Fig. 24e), particularly those in the Alto Paranaíba Igneous Province. It is possible that the strong Al depletion at the low-Ti end of the trend of kamafugitic magmas is somehow related with the affinity between kamafugites and carbonatites. $CO_2$ is the dominant volatile phase in the kamafugitic magma, and the kamafugite-carbonatite association has been recognized both in Italy (Stoppa & Cundari, 1995, 1998) and in Brazil (Brod *et al.*, 2000). In Fig. 24e, the low-Al phlogopites (tetra-ferriphlogopite) at the low-Ti end of the trend representing Alto Paranaíba carbonatite complexes, which belong to the kamafugite-carbonatite association, clearly contrast with the Al enrichment trend in low-Ti phlogopite from the Jacupiranga complex (SE Brazil), where rocks of kamafugitic affinity are not known.

*Feldspathoids*

Feldspathoids are the felsic constituents of kamafugites and kalsilite is a key mineral in the recognition of alkaline volcanic rocks belonging to the kamafugitic series (Sahama, 1974; Le Maitre, 2002). In the GAP kamafugites, the primary feldspathoids comprise kalsilite, leucite, and nepheline. Analcime is a common subsolidus alteration product of leucite, and kalsilite may be affected by the late-stage substitution of $KAlSiO_4$ by the $NaFeSiO_4$ and $KFeSiO_4$ end-members (Sgarbi, 1998) or variably transformed to aggregates of alkali feldspar+nepheline during subsolidus alteration.

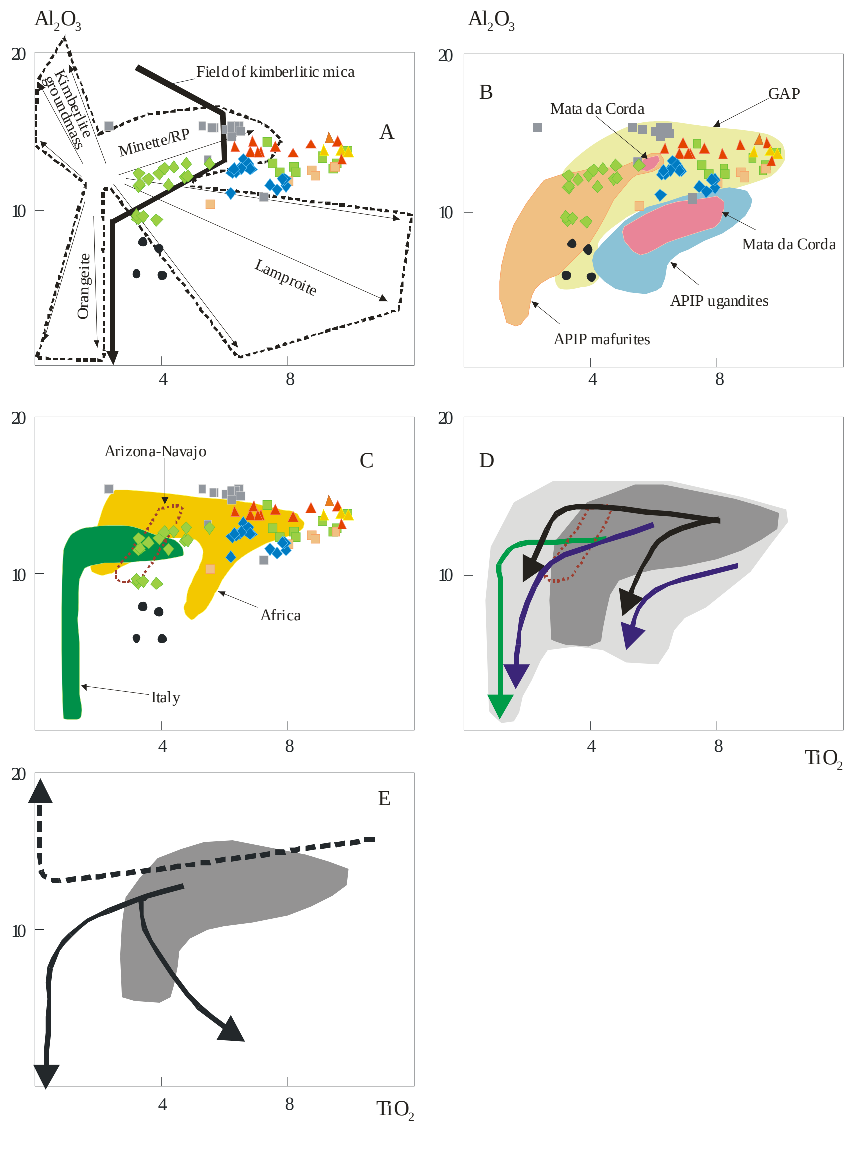


Fig. 24. $Al_2O_3$-$TiO_2$ trends, and comparison of GAP micas with those of other ultrapotassic rocks. A) GAP micas compared with trends observed in kimberlites, minettes and alnöites, lamproites and orangeites; B) GAP micas compared with kamafugitic micas from the Alto Paranaíba Igneous Province); C) GAP micas compared with micas from other kamafugitic provinces in the world; D) Field for all kamafugitic micas (light gray, GAP micas in darker shade) and the convex trends of micas from Ugandan kamafugites (black arrows), APIP kamafugites (blue arrows), Italian kamafugites (green arrow) and Arizona kamafugites (dashed field); E) Field of GAP kamafugitic micas compared with the trend of micas in APIP carbonatite complexes (solid arrow), and in the Jacupiranga carbonatite complex (dashed arrow). Symbols as in Fig. 21. Data source - GAP: Danni & Gaspar (1994), Cerqueira (1995), Sgarbi (1998), and this work. Fields for minette/RP (Roman Province) and kimberlite micas: Mitchell & Bergman (1991). Trends for kimberlites, lamproites, minettes and orangeites: Mitchell (1995). Kamafugites from the Alto Paranaíba Igneous Province (APIP): Sgarbi (1991, 1998) and Araújo (2000). Mata da Corda kamafugites: Sgarbi (1991, 1998), Leonardos *et al.* (1991) and Sgarbi & Valença (1994). African kamafugites: Lloyd *et al.* (1991). Italian kamafugites: Conticelli & Piccirillo (1992). Kamafugites from Arizona: Laughlin *et al.* (1989). Trends for the APIP kamafugite-carbonatite association: Brod *et al.* (2001). Trend for the Jacupiranga carbonatite complex: Gaspar & Wyllie (1987) and Gaspar (1989).

Table 5. Representative electron microprobe analyses of kalsilite from GAP samples. Data source: 1) Junqueira-Brod (1998) and 2) Sgarbi (1998).

| Locality | Águas | | Santo Antônio da Barra | | | | | | | |
|---|---|---|---|---|---|---|---|---|---|---|
| Rock | Mafurite | | Leucite mafurite | | | | | | | |
| Sample | 96ae08 | 96ae08 | sabM01 | sabM01 | sabM01 | sabM01 | sabM01 | sabM02 | sabM02 | sabM02 |
| Reference | 1 | 1 | 2 | 2 | 2 | 2 | 2 | 2 | 2 | 2 |
| $SiO_2$ | 37.77 | 37.77 | 37.95 | 38.00 | 38.86 | 38.34 | 38.05 | 39.60 | 38.05 | 38.53 |
| $TiO_2$ | 0.08 | 0.08 | 0.08 | 0.01 | 0.06 | | 0.11 | 0.11 | 0.05 | 0.14 |
| $Al_2O_3$ | 30.52 | 30.52 | 29.90 | 28.60 | 29.10 | 28.38 | 30.10 | 29.35 | 29.98 | 30.11 |
| $Fe_2O_3$ | 1.36 | 1.36 | 2.48 | 3.58 | 3.54 | 3.52 | 2.18 | 1.80 | 2.06 | 1.44 |
| MnO | 0.06 | 0.06 | 0.01 | 0.02 | 0.01 | | | | 0.01 | 0.05 |
| MgO | 0.22 | 0.22 | 0.18 | 0.52 | 0.35 | 0.38 | 0.26 | 0.88 | 0.19 | 0.19 |
| CaO | 0.02 | 0.02 | 0.04 | 0.24 | 0.02 | 0.04 | 0.01 | 0.92 | | 0.05 |
| $Na_2O$ | 1.35 | 1.35 | 1.94 | 1.63 | 2.18 | 1.54 | 1.47 | 1.24 | 1.35 | 1.10 |
| $K_2O$ | 28.83 | 28.83 | 27.20 | 27.16 | 26.54 | 28.19 | 27.63 | 26.30 | 26.36 | 26.42 |
| BaO | | | 0.13 | 0.17 | 0.17 | 0.32 | 0.10 | 0.28 | 0.20 | 0.22 |
| Total | 100.22 | 100.22 | 99.91 | 99.93 | 100.83 | 100.71 | 99.91 | 100.48 | 98.25 | 98.25 |
| Cations on the basis of 32 O | | | | | | | | | | |
| Si | 7.989 | 7.989 | 8.027 | 8.072 | 8.132 | 8.123 | 8.040 | 8.246 | 8.117 | 8.191 |
| Al | 7.604 | 7.604 | 7.448 | 7.154 | 7.171 | 7.081 | 7.490 | 7.197 | 7.532 | 7.538 |
| Ti | 0.013 | 0.013 | 0.013 | 0.002 | 0.009 | | 0.017 | 0.017 | 0.008 | 0.022 |
| $Fe^{3+}$ | 0.217 | 0.217 | 0.394 | 0.572 | 0.557 | 0.561 | 0.346 | 0.282 | 0.330 | 0.230 |
| Mg | 0.070 | 0.070 | 0.057 | 0.165 | 0.109 | 0.120 | 0.082 | 0.273 | 0.060 | 0.060 |
| Mn | 0.011 | 0.011 | 0.002 | 0.004 | 0.002 | | | | 0.002 | 0.009 |
| Na | 0.555 | 0.555 | 0.796 | 0.671 | 0.885 | 0.633 | 0.602 | 0.501 | 0.558 | 0.453 |
| Ca | 0.005 | 0.005 | 0.009 | 0.055 | 0.004 | 0.009 | 0.002 | 0.205 | | 0.011 |
| K | 7.780 | 7.780 | 7.340 | 7.360 | 7.085 | 7.619 | 7.448 | 6.986 | 7.174 | 7.165 |
| Ba | | | 0.011 | 0.014 | 0.014 | 0.027 | 0.008 | 0.023 | 0.017 | 0.018 |
| Total | 24.244 | 24.244 | 24.095 | 24.068 | 23.968 | 24.171 | 24.037 | 23.730 | 23.798 | 23.700 |

Kalsilite occurs as an interstitial phase in mafurites and leucite mafurites from Águas Emendadas and Santo Antônio da Barra (Table 5). Kalsilites from the Santo Antônio da Barra leucite mafurites usually contain excess Si (up to 3%) and are Al-depleted relatively to the ideal $KAlSiO_4$ formula. However, these features were not observed in kalsilite from the Águas Emendadas mafurites, which contains $SiO_2$ very close to stoichiometry. The $Fe_2O_3$ content in GAP kalsilite ranges from 1.36 to 3.58 wt%, and is higher in the Santo Antônio da Barra leucite mafurites. $Na_2O$ ranges from 1.1 to 2.18 wt%, corresponding to 5.8-11% of the nepheline molecule in solid solution.

GAP kalsilites are compositionally similar to those occurring in other kamafugites. In Fig. 25 they plot at the high-$Na_2O$ end of the fields for Ugandan and Alto Paranaíba kamafugite kalsilites and have slightly higher $Na_2O$ than those from Italian kamafugites. The $Fe_2O_3$ contents in GAP kalsilites partially overlap those of other kamafugites, though they seem restricted to the lower half of the overall $Fe_2O_3$ range, which may reach up to 6.4 wt% in kalsite from the Mata da Corda kamafugites (Sgarbi & Valença, 1993, not shown in Fig. 25).

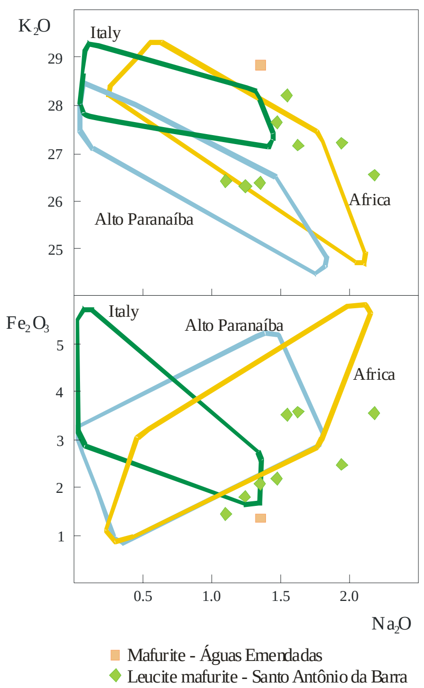


Fig. 25. GAP kalsilite compositions compared with other kamafugites, in terms of $Na_2O$, $K_2O$ and $Fe_2O_3$. Data source – GAP: Sgarbi (1998) and Junqueira-Brod (1998). Alto Paranaíba kamafugites: Araújo (2000). Mata da Corda kamafugites: Sgarbi & Valença (1993). African kamafugites: Lloyd *et al.* (1991). Italian kamafugites: Gallo *et al.* (1984).

The excess Si occurring in kalsilite from GAP leucite mafurites has also been observed in kalsilites from the Alto Paranaíba (up to 4 mol% Qz, cf. Araújo, 2000), Mata da Corda (average 2.66 mol% Qz, cf. Sgarbi & Valença, 1993), Uganda (0.8-2.0 mol% Qz, cf. Sahama, 1954; Edgar, 1979) and Cupaello (up to 2 mol% Qz, cf. Cundari & Ferguson, 1991), but kalsilites from San Venanzo are Si-deficient (Cundari & Ferguson, 1991).

Most kamafugite kalsilites contain an excess of alkalis (+Ca) relatively to Al+$Fe^{3+}$ (Fig. 26), which is a feature also noted in the GAP kamafugites.

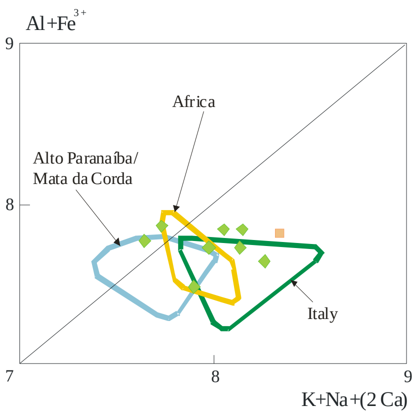


Fig. 26. GAP kalsilite compositions compared with other kamafugites, in terms of alkalis+Ca and Al+$Fe^{3+}$ (a.f.u.). Data source – GAP: Sgarbi (1998) and Junqueira-Brod (1998). Alto Paranaíba kamafugites: Araújo (2000). Mata da Corda kamafugites: Sgarbi & Valença (1993). Italian kamafugites: Cundari & Ferguson (1991). African kamafugites: Sahama (1954), Sahama *et al.* (1956), Hough (1972) and Edgar (1979). Symbols as in Fig. 25.

Nepheline occurs as an interstitial phase in the GAP kamafugites and is the dominant feldspathoid in the plutonic rocks of the Fazenda Buriti complex, where it is also present as an interstitial constituent. Representative analyses are given in Table 6.

GAP kamafugitic nephelines contain excess Si relative to the stoichiometric $NaAlSiO_4$. The Qz molecule in these nephelines ranges up to 0.84 % in the mafurites, up to 2.7 % in leucite mafurites and up to 3.34 % in the ugandites, but becomes more significant in the Amorinópolis katungites (2.75-5.71 %).

Nepheline in GAP kamafugites may contain up to 11.2 wt% of $K_2O$, corresponding to up to 35% of the kalsilite molecule in solid solution. The kalsilite content in nepheline is highest (27-35 mol%) in the leucite mafurites and lowest (19-27 mol%) in the ugandites, while katungites (28-31 mol%) and mafurites (29-31, exceptionally 25.5 mol%) contain nepheline with intermediate composition. GAP kamafugites show petrographic evidence for subsolidus re-equilibration (Sgarbi, 1998; Junqueira-Brod, 1998), which is reflected in the relatively wide ranges of solid solution in Fig. 27. This diagram suggests that the minimum crystallization temperature for the kalsilite-nepheline pair is ca. 750°C in the leucite mafurites and ca. 620°C in the mafurites. Kalsilite has not been reported from GAP katungites and ugandites, but the composition of nepheline in these rocks suggests minimum temperatures slightly above that of mafurite in the former, whereas ugandite nepheline records a much lower (ca. 500°C) temperature.

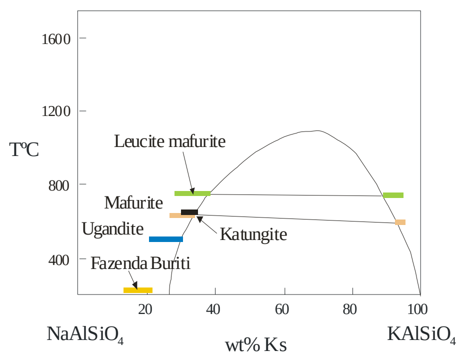


Fig. 27. Phase diagram in the $NaAlSiO_4$-$KalSiO_4$ system, showing the equilibration temperatures for various GAP nephelines and kalsilites. Data source: Danni & Gaspar (1994), Cerqueira (1995), Junqueira-Brod (1998), and Sgarbi (1998).

$Fe_2O_3$ in kamafugitic nepheline varies from 0.54 to 3.33 wt% in leucite mafurites, 1.07 to 3.06 wt% in mafurites, 1.84 to 2.62 wt% in katungites and 1.17 to 1.81 wt% in ugandites. CaO content is usually less than 1 wt%, although it can exceptionally reach 3.21 wt% in ugandititic nephelines.

Nepheline analyses are not reported for the Alto Paranaíba kamafugitic pipes (Araújo, 2000) and this mineral was not found in the Mata da Corda kamafugites (Sgarbi, 1998), suggesting that nepheline, if present, is not a prominent feldspathoid in kamafugites from the Alto Paranaíba Igneous Province.

Nephelines from the plutonic rocks of the Fazenda Buriti complex are compositionally distinct from those in the GAP kamafugites. They have a significantly higher excess of Si, containing 6.9 to 10.55 mol% of the quartz molecule, and are less enriched in K, with $K_2O$ contents ranging from 3.8 to 5 wt% (corresponding to 12-17.6 mol% of the kalsilite molecule in solid solution). Their $Fe_2O_3$ contents are the lowest (0.31-0.42 wt%) among the GAP nephelines discussed in this work.

Table 6. Electron microprobe analyses of nephelines from selected GAP samples. Data source: 1) Danni & Gaspar (1994), 2) Junqueira-Brod (1998), 3) Sgarbi (1998) and 4) Cerqueira (1995). L-M = leucite mafurite; L-I = leucite ijolite.

| Locality | Amorinópolis | Águas Emendadas | | | Santo Antônio da Barra | | | | | Fazenda Buriti | | |
|---|---|---|---|---|---|---|---|---|---|---|---|---|
| Rock | Katungite | Mafurite | | L-M | L-M | L-M | Ugandite | | | Syenite | Gabbro | L-I |
| Sample | Am | 96ae08 | 96ae08 | 96ae22 | sabM08 | sabM09 | sabug01 | sabug01 | sabug02 | cfb005 | cfb035 | cfb038 |
| Reference | 1 | 2 | 2 | 2 | 3 | 3 | 3 | 3 | 3 | 4 | 4 | 4 |
| $SiO_2$ | 43.33 | 39.61 | 40.88 | 40.65 | 39.68 | 41.66 | 41.30 | 42.71 | 41.66 | 45.42 | 44.64 | 44.66 |
| $TiO_2$ | | 0.48 | 0.04 | 0.08 | 0.05 | 0.09 | 0.12 | 0.09 | 0.10 | | | |
| $Al_2O_3$ | 31.32 | 32.45 | 32.84 | 33.02 | 32.54 | 32.64 | 32.89 | 34.22 | 34.41 | 32.92 | 32.92 | 33.44 |
| $Fe_2O_3$ | 1.84 | 3.06 | 1.22 | 1.01 | 3.10 | 1.08 | 1.59 | 1.81 | 1.18 | 0.34 | 0.32 | 0.40 |
| MnO | | 0.06 | 0.08 | | 0.01 | | 0.01 | | | | | |
| MgO | | 0.91 | 0.21 | 0.06 | 0.25 | 0.15 | 0.07 | 0.40 | 0.46 | | | |
| CaO | 0.16 | 0.22 | 0.08 | 0.05 | 0.13 | 0.25 | 0.19 | 0.41 | 3.21 | 1.38 | 1.18 | 1.72 |
| $Na_2O$ | 13.89 | 14.00 | 14.62 | 14.00 | 15.04 | 13.56 | 14.79 | 13.22 | 12.59 | 16.21 | 15.52 | 13.85 |
| $K_2O$ | 9.53 | 7.29 | 9.74 | 11.07 | 8.65 | 9.80 | 8.72 | 6.54 | 4.84 | 3.82 | 4.94 | 4.99 |
| BaO | 0.04 | | | | 0.03 | 0.10 | 0.00 | 0.01 | 0.01 | | | |
| Total | 100.11 | 98.08 | 99.71 | 99.95 | 99.48 | 99.35 | 99.68 | 99.41 | 98.46 | 100.09 | 99.52 | 99.06 |
| Cations on the basis of 24 O | | | | | | | | | | | | |
| Si | 8.462 | 7.890 | 8.068 | 8.043 | 7.882 | 8.212 | 8.110 | 8.226 | 8.076 | 8.597 | 8.538 | 8.539 |
| Al | 7.203 | 7.612 | 7.633 | 7.694 | 7.612 | 7.577 | 7.606 | 7.762 | 7.856 | 7.338 | 7.415 | 7.530 |
| Ti | | 0.071 | 0.006 | 0.012 | 0.007 | 0.013 | 0.018 | 0.013 | 0.015 | | | |
| $Fe^{3+}$ | 0.270 | 0.459 | 0.180 | 0.151 | 0.463 | 0.160 | 0.235 | 0.262 | 0.172 | 0.049 | 0.046 | 0.058 |
| Mg | | 0.271 | 0.063 | 0.019 | 0.074 | 0.044 | 0.020 | 0.115 | 0.133 | | | |
| Mn | | 0.010 | 0.014 | | 0.002 | | 0.002 | | | | | |
| Na | 5.260 | 5.406 | 5.597 | 5.369 | 5.793 | 5.183 | 5.632 | 4.937 | 4.732 | 5.949 | 5.755 | 5.135 |
| Ca | 0.033 | 0.047 | 0.018 | 0.011 | 0.028 | 0.053 | 0.040 | 0.085 | 0.667 | 0.280 | 0.242 | 0.352 |
| K | 2.374 | 1.853 | 2.453 | 2.795 | 2.192 | 2.465 | 2.185 | 1.607 | 1.197 | 0.922 | 1.205 | 1.217 |
| Ba | 0.003 | | | | 0.002 | 0.008 | | 0.001 | 0.001 | | | |
| Total | 23.607 | 23.620 | 24.032 | 24.094 | 24.054 | 23.718 | 23.848 | 23.008 | 22.848 | 23.135 | 23.201 | 22.832 |

Leucite is the main feldspathoid of GAP ugandites, where it occurs as phenocrysts and as a groundmass constituent. In leucite mafurites it occurs mainly as an interstitial groundmass phase and, more rarely, as microphenocrysts. It is also present as a major groundmass component of the Amorinópolis katungites. In the Fazenda Buriti complex, leucite and pseudoleucite occur as intercumulus material in malignites and as the major (intercumulus) felsic minerals in leucite ijolites (fergusites) and mela-essexites. Most leucite grains in the kamafugitic rocks are variably altered to analcime and other secondary phases. In the plutonic rocks of Fazenda Buriti the main alteration product is pseudoleucite. Table 7 presents representative analyses of GAP leucites.

The leucites from all rock-types have compositions close to stoichiometry (Fig. 28). The main traces present are $Fe_2O_3$ (0.6-0.73 wt% in katungites, 0.72-0.85 wt% in ugandites, 0.11-0.13 wt% in leucite ijolites), and $Na_2O$ (0.13-0.35 wt% in leucite from katungites, 0.04-0.49 wt% in leucite from ugandites, and 0.42-0.5 wt% in leucite from leucite ijolites).

Fig. 29 shows the composition of GAP leucites compared with other types of ultrapotassic rocks. The analyses of GAP kamafugite leucites plot in the overlapping region of kamafugites, leucitites and lamproites. Leucites from the Fazenda Buriti leucite ijolites are similar to those of leucitites.

*Melilite*

Melilite occurs scarcely in the GAP mafurites and leucite mafurites (Sgarbi *et al.*, 2004), but is an essential phase (up to 25 modal %) in the Amorinópolis katungites, where it occurs as a groundmass constituent, with an average composition of $Ak_{59}$-Fe-$Ak_{15}$-Na-$Mel_{26}$, and showing Na-enrichment and K-depletion from core to rim (Danni & Gaspar, 1994). Table 8 shows representative analyses.

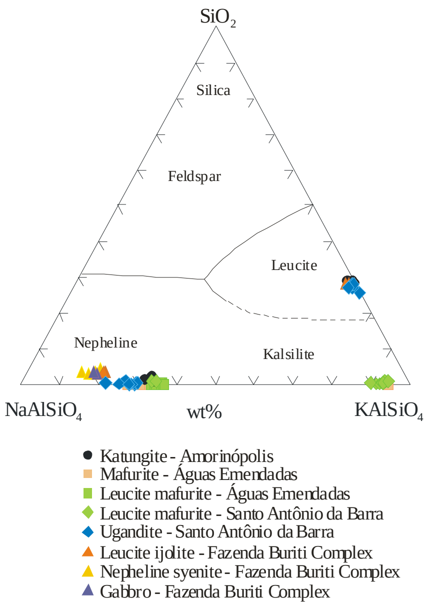


Fig. 28. Phase diagram in the quartz-nepheline-kalsilite system, showing the compositional range of GAP feldspathoids. Data source: Danni & Gaspar (1994), Cerqueira (1995), Junqueira-Brod (1998) and Sgarbi (1998).

*Perovskite*

Perovskite is a common mineral in kamafugites and a clear indication of strong silica-under-saturation. In the GAP kamafugites, perovskite occurs as an accessory mineral in the Amorinópolis katungites, in Águas Emendadas mafurites and leucite mafurites, and as a relatively rare accessory in the Santo Antônio da Barra leucite mafurites. Although the presently available database on the chemistry of GAP perovskites is restricted, they appear to be compositionally close to the $CaTiO_3$ end-member, irrespective of the host rock-type. Table 9 shows representative analyses of GAP perovskites.

In perovskite from the Águas Emendadas mafurites and leucite mafurites, Ca occupies 94-96 mol% of the A site and Ti exceeds 99 mol% of the B site in the $ABO_3$ general formula (Junqueira-Brod *et al.*, 1999a).

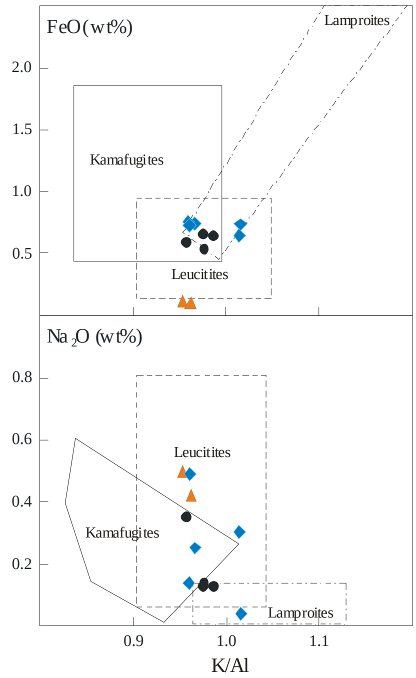


Fig. 29. Composition of GAP leucites compared with those occurring in various ultrapotassic rocks. Data source: Danni & Gaspar (1994), Cerqueira (1995) and Sgarbi (1998). Symbols as in Fig. 28.

In the Santo Antônio da Barra leucite mafurites (Sgarbi, 1998), Ca also fills 94-96 mol% of the A site, but Ti is slightly lower, filling 95 to 97 mol% of the B site. Phenocrysts are slightly enriched in $Fe_2O_3$, REE, $Na_2O$, and $Nb_2O_5$ relative to groundmass perovskite in these rocks. The sum of REE oxides ($REE_2O_3$) may reach up to 2.9 wt%, while $Nb_2O_5$ (0.49-0.59 wt%) and SrO (0.25-0.44 wt%) remain low.

Perovskite from other kamafugites worldwide are also very close to the $CaTiO_3$ end-member, usually with limited solid solution towards loparite [$(Na_{0.5}Ce_{0.5})TiO_3$] and very low Sr and Nb, therefore compositionally similar to perovskite in the GAP kamafugites.

Sgarbi *et al.* (2004) have recently dated kamafugitic rocks from the Goiás and Alto Paranaíba Provinces, using the U-Pb method on perovskite separates. They concluded that kamafugitic magmatism in the GAP kamafugites is slightly older (88.3-89.6 Ma.) than in the Alto Paranaíba Igneous Province (age clusters at 80-81 and 75-76 Ma).

Table 7. Representative electron microprobe analyses of leucites from GAP samples. Data source: 1) Danni & Gaspar (1994), 2) Cerqueira (1995) and 3) Sgarbi (1998).

| Locality | Amorinópolis | | | | Fazenda Buriti | | Santo Antônio da Barra | | | | |
|---|---|---|---|---|---|---|---|---|---|---|---|
| Rock | Katungite | | | | Leucite ijolite | | Ugandite | | | | |
| Sample | Am | Am | Am | Am | cfb038 | cfb038 | sabug1 | sabug1 | sabug1 | sabug1 | sabug1 |
| Reference | 1 | 1 | 1 | 1 | 2 | 2 | 3 | 3 | 3 | 3 | 3 |
| $SiO_2$ | 55.37 | 55.22 | 55.25 | 55.17 | 55.14 | 55.39 | 52.63 | 54.05 | 53.74 | 53.39 | 53.12 |
| $TiO_2$ | | | | | | | 0.25 | 0.39 | 0.35 | 0.29 | 0.31 |
| $Al_2O_3$ | 23.08 | 22.93 | 23.02 | 23.08 | 23.05 | 23.25 | 22.75 | 22.20 | 22.98 | 23.04 | 22.76 |
| $Fe_2O_3$ | 0.73 | 0.60 | 0.66 | 0.72 | 0.13 | 0.11 | 0.82 | 0.72 | 0.83 | 0.85 | 0.81 |
| MnO | | | | | | | 0.03 | 0.01 | | | |
| MgO | | | | | | | | | | | |
| CaO | | 0.03 | 0.06 | | | | | | 0.04 | | 0.03 |
| $Na_2O$ | 0.13 | 0.14 | 0.35 | 0.13 | 0.50 | 0.42 | 0.04 | 0.30 | 0.25 | 0.14 | 0.49 |
| $K_2O$ | 20.80 | 20.67 | 20.34 | 21.02 | 20.30 | 20.65 | 21.34 | 20.80 | 20.48 | 20.41 | 20.18 |
| BaO | | | 0.26 | 0.26 | | | 0.28 | 0.26 | 0.24 | 0.41 | 0.16 |
| Total | 100.11 | 99.59 | 99.94 | 100.38 | 99.12 | 99.82 | 98.14 | 98.73 | 98.91 | 98.53 | 97.86 |
| Cations on the basis of 6 O | | | | | | | | | | | |
| Si | 2.004 | 2.008 | 2.004 | 1.999 | 2.010 | 2.007 | 1.967 | 1.997 | 1.978 | 1.975 | 1.976 |
| Al | 0.984 | 0.982 | 0.983 | 0.985 | 0.989 | 0.992 | 1.001 | 0.966 | 0.996 | 1.004 | 0.997 |
| Ti | | | | | | | 0.007 | 0.011 | 0.010 | 0.008 | 0.009 |
| $Fe^{3+}$ | 0.020 | 0.016 | 0.018 | 0.020 | 0.004 | 0.003 | 0.023 | 0.020 | 0.023 | 0.024 | 0.023 |
| Mg | | | | | | | | | | | |
| Mn | | | | | | | 0.001 | | | | |
| Na | 0.009 | 0.010 | 0.025 | 0.009 | 0.035 | 0.030 | 0.003 | 0.021 | 0.018 | 0.010 | 0.035 |
| Ca | | | | | | | | | 0.002 | | 0.001 |
| K | 0.960 | 0.959 | 0.941 | 0.972 | 0.944 | 0.955 | 1.017 | 0.980 | 0.962 | 0.963 | 0.958 |
| Ba | | | | 0.004 | | | 0.004 | 0.004 | 0.003 | 0.006 | 0.002 |
| Total | 3.977 | 3.976 | 3.977 | 3.989 | 3.982 | 3.987 | 4.023 | 3.999 | 3.992 | 3.990 | 4.001 |

Table 8. Electron microprobe analyses of melilites from selected GAP samples. Data source: 1) Danni & Gaspar (1994).

| Locality | Amorinópolis | | | | | |
|---|---|---|---|---|---|---|
| Rock | Katungite | | | | | |
| Sample | Am | Am | Am | Am | Am | Am |
| Reference | 1 | 1 | 1 | 1 | 1 | 1 |
| $SiO_2$ | 43.28 | 42.26 | 43.12 | 43.34 | 42.73 | 42.96 |
| $TiO_2$ | 0.20 | 0.33 | 0.04 | 0.12 | 0.15 | 0.13 |
| $Al_2O_3$ | 4.60 | 5.08 | 4.52 | 4.50 | 4.60 | 4.50 |
| FeO | 3.69 | 4.02 | 3.82 | 3.88 | 3.85 | 3.67 |
| MnO | 0.02 | 0.08 | 0.10 | | 0.19 | 0.07 |
| MgO | 8.10 | 7.85 | 8.18 | 8.30 | 8.30 | 8.38 |
| CaO | 35.97 | 35.06 | 36.08 | 36.17 | 35.80 | 36.44 |
| $Na_2O$ | 2.96 | 2.73 | 2.75 | 2.45 | 2.78 | 2.69 |
| $K_2O$ | 0.18 | 0.75 | 0.12 | 0.18 | 0.18 | 0.21 |
| Total | 99.00 | 98.16 | 98.73 | 98.94 | 98.58 | 99.05 |
| Cations on the basis of 14 O | | | | | | |
| Si | 3.990 | 3.950 | 3.990 | 4.000 | 3.970 | 3.970 |
| Ti | 0.010 | 0.020 | | 0.010 | 0.010 | 0.010 |
| Al | 0.500 | 0.560 | 0.490 | 0.490 | 0.500 | 0.490 |
| Mg | 1.110 | 1.090 | 1.130 | 1.140 | 1.150 | 1.150 |
| Ca | 3.560 | 3.510 | 3.580 | 3.580 | 3.560 | 3.610 |
| Mn | | 0.010 | 0.010 | | 0.010 | 0.010 |
| Fe | 0.280 | 0.310 | 0.300 | 0.300 | 0.300 | 0.280 |
| Na | 0.530 | 0.490 | 0.490 | 0.440 | 0.500 | 0.480 |
| K | 0.020 | 0.090 | 0.010 | 0.020 | 0.020 | 0.020 |
| Total | 10.000 | 10.030 | 10.000 | 9.980 | 10.020 | 10.020 |

Table 9. Representative electron microprobe analyses of perovskites from GAP samples. Data source: 1) Sgarbi (1998) and 2) Junqueira-Brod (1998).

| Locality | Santo Antônio da Barra | | | | Águas Emendadas | | | | |
|---|---|---|---|---|---|---|---|---|---|
| Rock | Leucite mafurite | | | | Leucite mafurite | | Mafurite | | |
| Sample | M5(7) | M3(1) | M6(4) | M7(8) | 96ae22 | 96ae22 | 96ae46 | 96ae46 | 96ae46 |
| Reference | 1 | 1 | 1 | 1 | 2 | 2 | 2 | 2 | 2 |
| $SiO_2$ | 0.03 | 0.08 | 0.03 | 0.03 | 0.21 | 0.25 | 0.26 | 0.18 | 0.18 |
| $TiO_2$ | 54.72 | 55.83 | 54.66 | 54.92 | 58.89 | 59.29 | 58.54 | 58.15 | 58.43 |
| $Al_2O_3$ | 0.26 | 0.23 | 0.25 | 0.25 | 0.24 | 0.34 | 0.31 | 0.29 | 0.28 |
| FeO | 1.52 | 1.01 | 1.53 | 1.49 | 0.94 | 0.87 | 1.38 | 1.37 | 1.38 |
| CaO | 37.85 | 38.70 | 37.90 | 38.08 | 38.65 | 38.72 | 39.29 | 39.05 | 39.36 |
| $Na_2O$ | 1.74 | 1.20 | 1.74 | 1.66 | 0.63 | 0.30 | 0.40 | 0.21 | 0.22 |
| NiO | | | | | 0.07 | 0.03 | 0.07 | 0.08 | 0.16 |
| MgO | | | | | 0.06 | 0.10 | | 0.06 | |
| $K_2O$ | | | | | 0.04 | 0.04 | 0.03 | 0.03 | 0.06 |
| Cl | | | | | 0.01 | | 0.01 | | 0.03 |
| $Nb_2O_5$ | 0.54 | 0.49 | 0.59 | 0.54 | | | | | |
| $ZrO_2$ | 0.04 | 0.03 | 0.04 | 0.04 | | | | | |
| SrO | 0.40 | 0.25 | 0.44 | 0.40 | | | | | |
| $La_2O_3$ | 0.59 | 0.38 | 0.62 | 0.59 | | | | | |
| $Ce_2O_3$ | 1.47 | 0.90 | 1.49 | 1.46 | | | | | |
| $Pr_2O_3$ | 0.17 | 0.10 | 0.17 | 0.17 | | | | | |
| $Nd_2O_3$ | 0.58 | 0.34 | 0.56 | 0.58 | | | | | |
| $Sm_2O_3$ | 0.07 | 0.05 | 0.07 | 0.08 | | | | | |
| $Gd_2O_3$ | 0.04 | 0.03 | 0.04 | 0.04 | | | | | |
| $Y_2O_3$ | 0.03 | 0.04 | 0.04 | 0.03 | | | | | |
| Total | 100.06 | 99.66 | 100.18 | 100.37 | 99.73 | 99.92 | 100.29 | 99.41 | 100.10 |
| Cations on the basis of 6 O | | | | | | | | | |
| Si | 0.002 | 0.004 | 0.002 | 0.001 | 0.009 | 0.011 | 0.012 | 0.008 | 0.008 |
| Ti | 1.917 | 1.941 | 1.914 | 1.917 | 2.007 | 2.012 | 1.989 | 1.993 | 1.990 |
| Al | 0.014 | 0.012 | 0.014 | 0.014 | 0.013 | 0.018 | 0.017 | 0.015 | 0.015 |
| Fe | 0.059 | 0.039 | 0.060 | 0.058 | 0.035 | 0.033 | 0.052 | 0.052 | 0.052 |
| Ca | 1.888 | 1.917 | 1.890 | 1.894 | 1.876 | 1.872 | 1.901 | 1.906 | 1.910 |
| Na | 0.158 | 0.108 | 0.157 | 0.149 | 0.055 | 0.026 | 0.035 | 0.018 | 0.019 |
| Ni | | | | | 0.003 | 0.001 | 0.003 | 0.003 | 0.006 |
| Mg | | | | | 0.004 | 0.006 | | 0.004 | |
| K | | | | | 0.002 | 0.002 | 0.002 | 0.002 | 0.003 |
| Cl | | | | | 0.001 | | | | 0.002 |
| P | | | | | | | | | |
| Nb | 0.011 | 0.010 | 0.013 | 0.011 | | | | | |
| Zr | 0.001 | | 0.001 | 0.001 | | | | | |
| Sr | 0.011 | 0.007 | 0.012 | 0.011 | | | | | |
| La | 0.010 | 0.007 | 0.011 | 0.010 | | | | | |
| Ce | 0.025 | 0.015 | 0.026 | 0.025 | | | | | |
| Pr | 0.003 | | 0.003 | 0.003 | | | | | |
| Nd | 0.010 | 0.006 | 0.010 | 0.010 | | | | | |
| Sm | 0.001 | | 0.001 | 0.001 | | | | | |
| Gd | 0.001 | | 0.001 | 0.001 | | | | | |
| Y | 0.001 | | 0.001 | 0.001 | | | | | |
| Total | 4.112 | 4.071 | 4.116 | 4.107 | 4.006 | 3.982 | 4.010 | 4.002 | 4.005 |

## WHOLE-ROCK GEOCHEMISTRY

The Cretaceous alkaline rocks of Southern Goiás vary widely in texture and composition. Fine-grained, volcanic or hypabyssal rocks include members of the kamafugite series (rare katungite and abundant mafurite, leucite mafurite and ugandite), ultramafic lamprophyres, leucitite, nephelinite, alkali picrite, alkali olivine basalt, basanite, phonolite and trachyte. Coarse-grained plutonic rocks comprise, among other petrographic types, dunite, wehrlite, clinopyroxenite, and several varieties of alkaline gabbro and syenite. Although many authors have reported geochemical data from different parts of the province, most of the older analytical sets lack key trace elements, and some were carried out on coarse-grained, porphyritic and/or altered samples. A complete and integrated geochemical and isotopic study is, therefore, still to come. Some of the main features apparent from the published data and some unpublished analyses will be discussed below, with emphasis on fine-grained rocks. As in the mineral chemistry section of this work, samples are subdivided into the strongly undersaturated, feldspar-free rocks (kamafugites and related rocks) and the less undersaturated, feldspar-bearing rocks (basaltic or basanitic to trachytic, and the related coarse-grained rocks from the northern GAP plutonic complexes). For all analyses discussed in this work the major oxides were recast to 100% on a volatile-free basis.

Feldspar-free (kamafugitic) rocks

Despite the intense subsolidus alteration that may have substantially modified the contents of the more mobile elements, including a marked depletion in the $K_2O/Na_2O$ ratio, the majority of the strongly silica-undersaturated rocks occurring in the province are now interpreted as originally ultrapotassic, rather than sodic, and their affinity with the kamafugite series (Sahama, 1974) was established by Moraes (1984), Danni (1985), Danni & Gaspar (1994), Junqueira-Brod (1998), Junqueira-Brod *et al.* (2000) and Sgarbi *et al.* (2002). This is in consonance with petrographic evidence that indicates transformation of the original leucite into analcime and of the original kalsilite into nepheline (± K-feldspar). Therefore, these rocks will be treated in this work as members of the kamafugitic series, regardless of the original petrographic name given by the literature. Representative analyses of the GAP kamafugitic rocks are given in Table 10.

Kamafugitic rocks occur in several localities within the province. The main occurrences comprise, from South to North, the regions of Santo Antônio da Barra, Águas Emendadas, Amorinópolis and Iporá. They also become volumetrically less significant in this direction, while the amount of feldspar-bearing rocks increases.

The primitive character of the kamafugitic rocks is attested to by the high MgO contents, ranging up to 23.6 wt%. CaO contents are also high (up to 17.8 wt%) and $SiO_2$ and $Al_2O_3$ are as low as 34 wt% and 5 wt%, respectively, typical of rocks of the kamafugite series. Fig. 30 shows the GAP samples plotted in the classification diagrams of Foley *et al.* (1987) for ultrapotassic rocks. For these diagrams the data set was screened for MgO contents higher than 9 wt%, in order to assure that only primitive samples were plotted. For instance, most GAP ugandites were excluded by this criterion. Analyses containing over 3.5 wt% loss-on-ignition (L.O.I.) were also excluded, in order to avoid the effect of subsolidus alteration and/or metasomatism. The majority of the GAP primitive compositions plot within the field of kamafugites (Group II of Foley *et al.*, 1987). Their CaO, $Al_2O_3$, $SiO_2$ and MgO contents, and $K_2O/Al_2O_3$ are consistent with their kamafugitic character. For comparison, Fig. 30 also shows the field of kamafugites from the nearby Alto Paranaíba Igneous Province (APIP, Gibson *et al.*, 1995a), including the parental liquids (phlogopite picrites) of the APIP carbonatite-bearing complexes (Brod, 1999; Brod *et al.*, 2000). The major element composition of the GAP kamafugites agrees well with that of similar rocks from the APIP in most cases, but extends to higher $Al_2O_3$, $Na_2O$ and $SiO_2$ values in the GAP.

Fig. 31 compares the GAP kamafugites with rocks of other provinces and tectonic settings. GAP kamafugitic rocks agree well in composition with other kamafugites, particularly from Toro-Ankole and Alto Paranaíba (APIP), but differ strongly from the Italian kamafugites and alkaline rocks from Eastern Paraguay, which are both shifted towards lower Ta/Yb.

The ranges of major element oxides for the whole set of kamafugitic rocks containing less than 3.5 wt% L.O.I. are depicted in Fig. 32. The possible evolution trends in the diagram were interpreted on the basis of decreasing MgO and confirmed by Cr and Ni decrease (not shown).

The Amorinópolis katungites contain the lowest $SiO_2$ (37.3-33.9 wt%), and the highest $TiO_2$ (5.5-6.3 wt%), $Fe_2O_3$(T) (15.9-17.2 wt%) and $P_2O_5$ (0.71-1.36 wt%) of all the GAP kamafugitic rocks. $SiO_2$ decreases with magma evolution, at first coupled with decreasing MgO and later at relatively constant

Table 10. Representative whole-rock chemical analyses of GAP kamafugites. Data source: 1) Junqueira-Brod (1998), 2) Danni & Gaspar (1994), 3) This work, 4) Moraes (1984), and 5) Sgarbi & Gaspar (2002). SAB = Santo Antônio da Barra; AE = Águas Emendadas; MM = Morro do Macaco.

| Locality | Amorinópolis | | | Águas Emendadas | | | SAB | | Águas Emendadas | | | | AE | MM | | SAB |
|---|---|---|---|---|---|---|---|---|---|---|---|---|---|---|---|---|
| Rock | Katungite | | | Leucite mafurite | | | Leucite mafurite | | Mafurite | | | | | Ugandite | | |
| Sample | 96ae61 | 96ae63 | DG94-1 | 96ae06 | 96ae22 | ae09N16 | a178a | M12 | 96ae08 | ae09N01 | ae09N03 | ae09N08 | 96ae17 | 96ae68 | a267 | U2 |
| Reference | 1 | 1 | 2 | 1 | 1 | 3 | 4 | 5 | 1 | 3 | 3 | 3 | 1 | 1 | 4 | 5 |
| $SiO_2$ | 37.29 | 36.72 | 33.97 | 41.98 | 41.65 | 41.22 | 41.56 | 45.53 | 38.76 | 38.17 | 40.23 | 37.11 | 47.47 | 44.07 | 40.98 | 43.94 |
| $TiO_2$ | 5.57 | 5.93 | 6.36 | 4.35 | 3.49 | 4.53 | 4.31 | 2.99 | 4.68 | 5.30 | 4.56 | 5.29 | 4.03 | 4.40 | 3.47 | 3.83 |
| $Al_2O_3$ | 6.48 | 7.22 | 6.55 | 8.44 | 6.85 | 9.09 | 5.04 | 7.62 | 9.41 | 9.26 | 8.96 | 9.07 | 14.47 | 13.50 | 8.69 | 11.48 |
| $Fe_2O_{3\,total}$ | 15.95 | 16.02 | 16.65 | 14.37 | 13.39 | 15.11 | 13.95 | 12.64 | 16.09 | 15.38 | 15.94 | 15.91 | 11.45 | 12.66 | 13.62 | 13.29 |
| MnO | 0.21 | 0.22 | 0.20 | 0.22 | 0.20 | 0.20 | 0.21 | 0.21 | 0.25 | 0.21 | 0.22 | 0.20 | 0.46 | 0.20 | 0.21 | 0.23 |
| MgO | 17.29 | 15.01 | 15.26 | 11.90 | 18.46 | 10.52 | 23.58 | 14.11 | 10.43 | 12.02 | 10.50 | 10.79 | 4.25 | 5.33 | 11.96 | 7.75 |
| CaO | 11.28 | 13.19 | 13.16 | 15.43 | 13.39 | 13.55 | 10.13 | 14.01 | 13.91 | 13.63 | 13.88 | 14.05 | 9.54 | 12.03 | 15.02 | 12.92 |
| $Na_2O$ | 2.06 | 2.43 | 2.29 | 1.80 | 1.18 | 2.40 | 0.39 | 1.96 | 2.51 | 3.07 | 2.82 | 2.63 | 4.51 | 1.65 | 2.04 | 4.45 |
| $K_2O$ | 3.15 | 2.25 | 4.20 | 0.83 | 0.90 | 2.52 | 0.29 | 0.48 | 3.04 | 2.02 | 1.96 | 3.97 | 2.83 | 5.14 | 3.27 | 1.24 |
| $P_2O5$ | 0.71 | 1.01 | 1.36 | 0.69 | 0.49 | 0.85 | 0.55 | 0.46 | 0.91 | 0.94 | 0.92 | 0.96 | 0.98 | 1.01 | 0.73 | 0.87 |
| L.O.I. | 0.24 | 1.83 | 2.11 | 2.13 | 1.47 | 1.57 | 3.27 | 2.16 | 0.70 | 1.46 | 1.52 | 1.10 | 2.91 | 2.63 | 2.45 | 2.39 |
| Ba | 898 | 1257 | 1223 | 1209 | 872 | 1450 | 510 | 888 | 1308 | 1776 | 1233 | 1419 | 2346 | 1962 | 1600 | 1590 |
| Rb | 43.0 | 52.0 | 91.0 | 39.0 | 26.0 | 55.0 | 17.0 | 36.0 | 49.0 | | 30.0 | | 45.0 | 106.0 | 63.0 | 44.0 |
| Sr | 1221 | 1630 | 1597 | 1842 | 1110 | 1642 | 640 | 741 | 1605 | 1203 | 1141 | 1116 | 1366 | 1654 | 940 | 1346 |
| Ta | 8.99 | 10.38 | | 7.09 | 5.03 | | | | 11.12 | | | | 10.04 | 10.51 | | |
| Nb | 126 | 147 | | 95 | 69 | 155 | 89 | 84 | 148 | 165 | 135 | 162 | 132 | 118 | 150 | 130 |
| Hf | 9.68 | 12.45 | | 7.95 | 6.25 | | | | 11.22 | | | | 10.12 | 10.35 | | 10.00 |
| Zr | 390 | 518 | 580 | 331 | 241 | 408 | 320 | 256 | 426 | 531 | 422 | 386 | 383 | 445 | 480 | 418 |
| Y | 23.0 | 29.0 | 31.0 | 24.0 | 17.0 | 27.0 | 48.0 | 18.0 | 27.0 | 27.0 | 28.0 | 24.0 | 37.0 | 36.0 | 56.0 | 23.0 |
| Th | 12.3 | 14.3 | | 10.2 | 7.6 | 7.0 | | | 14.5 | | 5.0 | | 16.5 | 13.5 | | |
| U | 2.90 | 3.45 | | 2.39 | 1.79 | | 2.00 | | 3.37 | | | | 3.59 | 3.10 | 0.90 | |
| Cr | 846 | 511 | 506 | 585 | 1952 | 350 | 1500 | 889 | 86 | 290 | 124 | 128 | 28 | 60 | 900 | 219 |
| Ni | 504 | 356 | 287 | 262 | 470 | 137 | 510 | 322 | 93 | 133 | 86 | 98 | 17 | 58 | 280 | 63 |
| Sc | 26.7 | 28.2 | | 39.3 | 36.2 | | | | 37.5 | | | | 14.0 | 25.8 | | |
| V | 396 | 447 | 445 | 445 | 335 | 419 | 220 | | 415 | 438 | 331 | 412 | 373 | 364 | 380 | |
| La | 100.0 | 118.0 | 113.0 | 86.0 | 58.0 | 104.0 | 110.0 | 54.0 | 125.0 | 117.0 | 138.0 | 88.0 | 118.0 | 120.0 | 160.0 | 113.0 |
| Ce | 203.0 | 240.0 | 215.0 | 172.0 | 117.0 | 205.0 | | 130.0 | 242.0 | 227.0 | 279.0 | 185.0 | 231.0 | 239.0 | 300.0 | 253.0 |
| Nd | 95.0 | 111.0 | 105.0 | 80.0 | 55.0 | 91.0 | | 58.0 | 106.0 | 99.0 | 122.0 | 79.0 | 102.0 | 111.0 | | 102.0 |
| Sm | 15.31 | 17.95 | 18.60 | 12.90 | 9.00 | 12.75 | | 8.48 | 15.82 | 13.68 | 16.95 | 10.42 | 16.13 | 17.58 | | 13.44 |
| Eu | 4.13 | 4.89 | 4.90 | 3.57 | 2.52 | 3.62 | | 1.93 | 4.29 | 4.02 | 4.94 | 3.23 | 4.48 | 5.07 | | 3.07 |
| Gd | 10.63 | 12.31 | 13.70 | 9.08 | 6.71 | 9.03 | | 4.65 | 10.47 | 9.92 | 12.58 | 8.14 | 11.28 | 12.76 | | 7.18 |
| Dy | 5.62 | 6.76 | 7.60 | 5.33 | 4.03 | 4.99 | | 3.07 | 6.23 | 5.48 | 7.13 | 4.38 | 7.43 | 8.01 | | 4.46 |
| Ho | 0.849 | 1.021 | 1.300 | 0.856 | 0.644 | 0.888 | | 0.470 | 0.984 | 1.036 | 1.259 | 0.740 | 1.255 | 1.318 | | 0.798 |
| Er | 1.816 | 2.244 | 3.400 | 1.990 | 1.520 | 1.838 | | 1.100 | 2.388 | 1.942 | 2.252 | 1.632 | 3.177 | 3.113 | | 1.682 |
| Yb | 1.197 | 1.565 | 2.100 | 1.504 | 1.133 | 1.497 | 2.000 | 0.651 | 1.764 | 1.535 | 1.820 | 1.325 | 2.534 | 2.314 | 3.000 | 0.917 |
| Lu | 0.158 | 0.208 | 0.300 | 0.218 | 0.163 | 0.315 | | 0.100 | 0.247 | 0.315 | 0.273 | 0.273 | 0.362 | 0.313 | | 0.133 |

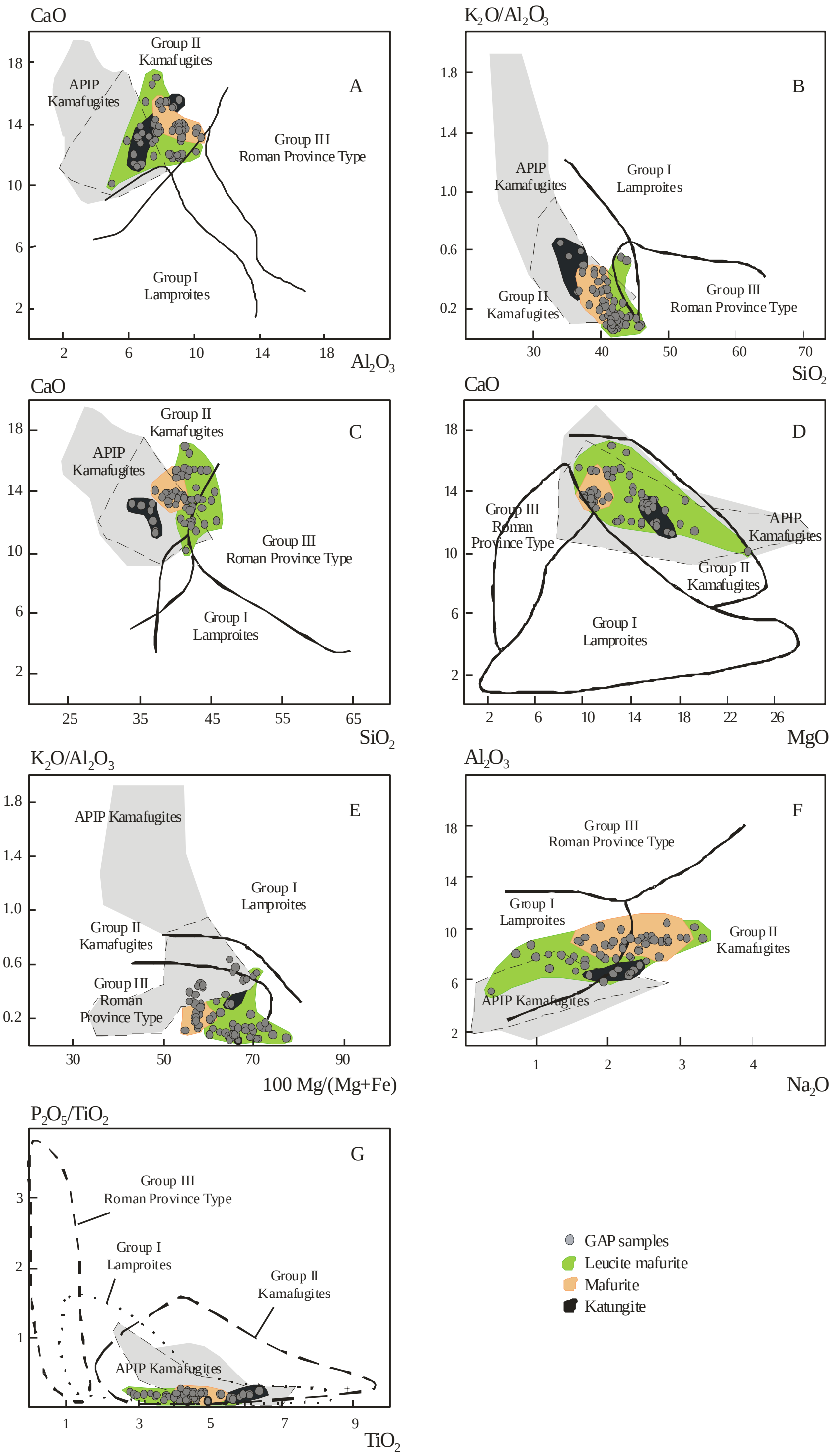


Fig. 30. Ultrapotassic rock classification diagrams of Foley *et al.* (1987), showing the composition of GAP kamafugitic rocks screened for MgO>9 wt% and loss-on-ignition <3.5 wt%. Also shown are fields of kamafugites from the Alto Paranaíba Igneous Province (dashed) and of the parental liquids (phlogopite picrites, shaded) of the kamafugite-carbonatite association occurring in that region. Data source: Moraes (1984), Danni (1985), Danni *et al.* (1990), Danni & Gaspar (1994), Junqueira-Brod (1998), Sgarbi & Gaspar (2002), and this work. Fields for the Alto Paranaíba rocks from Brod *et al.* (2000).

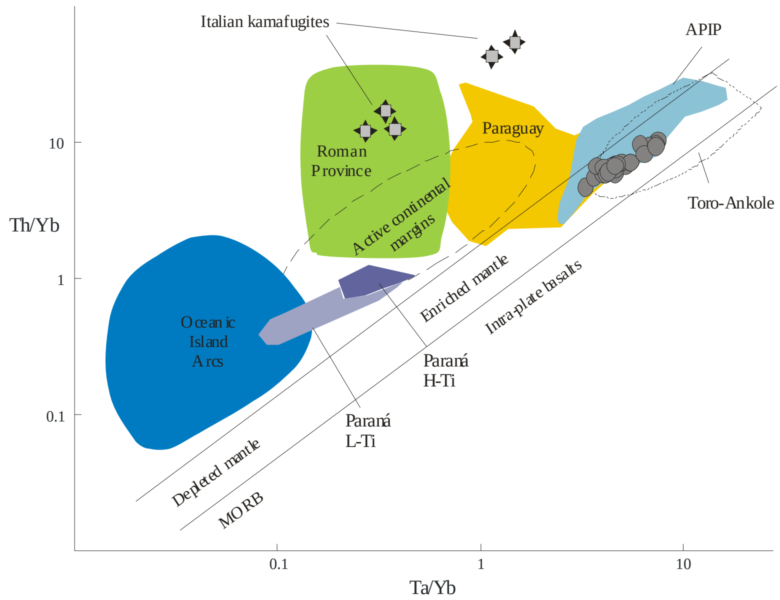


Fig. 31. Th/Yb vs. Ta/Yb diagram showing the composition of GAP kamafugitic rocks (circles), compared with other rock types. Data source - GAP: Junqueira-Brod (1998). Alkaline rocks from Eastern Paraguay: Comin-Chiaramonti *et al.* (1997). Italian kamafugites: Piccirillo *et al.* (1988) and Conticelli & Piccirillo (1992). Alto Paranaíba: Gibson *et al.* (1995a) and Brod *et al.* (2000). Other fields are from Wilson (1989) and references therein.

MgO. The generally positive $SiO_2$-MgO correlation may be explained by the removal of olivine, since the starting composition is less silica-rich (ca. 37 wt%) than olivine itself. The second part of the trend suggests an even faster $SiO_2$ depletion, which may be explained by the onset of clinopyroxene removal. $TiO_2$ shows a mirror trend, increasing firstly with decreasing MgO and later at constant MgO contents, which may correspond to increasing $TiO_2$ in the residual liquid as silicate phases are removed. $Al_2O_3$ shows a curved trend whereby the high-MgO samples have relatively constant $Al_2O_3$, inflecting towards $Al_2O_3$ enrichment at the low-MgO end. Total iron expressed as $Fe_2O_3$ initially increases and later decreases with MgO decrease. Manganese does not show significant variation with MgO, whereas CaO increases steadily with MgO decrease in katungites. $K_2O$ and $Na_2O$ show a somewhat erratic behaviour, which may result from subsolidus mobilization of theses elements. $P_2O_5$ behaves in a way similar to $TiO_2$.

Leucite mafurites and mafurites pose an intriguing question regarding magma evolution. Judging from their MgO (and Cr, Ni) contents leucite mafurites are less evolved than mafurites. However, the former have substantially higher $SiO_2$ contents than the latter, which is expressed both by the whole-rock analyses and by the appearance of leucite in addition to kalsilite as a major feldspathoid phase. This may be explained in two alternative ways: the increased $SiO_2$ contents may be related to a significantly higher content of olivine and clinopyroxene phenocrysts in the leucite mafurites, or it may result of leucite mafurites being involved in an episode of magma mixing with a less silica-undersaturated liquid. In several variation diagrams, the leucite mafurites appear to split into two or more trends, and their behaviour is not a straightforward one. For instance, $SiO_2$ contents are relatively constant for the higher MgO values, but at ca. 15 wt% a MgO part of the samples shows a $SiO_2$ decreasing trend, which is connected to mafurites after a sharp inflection, while other samples follow a $SiO_2$ increasing trend. $TiO_2$ apparently increases with MgO decrease for both leucite mafurites and mafurites, although the high degree of scatter suggests the existence of more than one trend in the former. As a general rule, there is a regional titanium variation in kamafugites, from higher Ti in the North (Amorinópolis) to progressively lower Ti towards the South (Águas Emendadas and then Santo Antônio da Barra). $Al_2O_3$ increases with MgO but, as observed for $TiO_2$, a wider scatter occurs in the leucite mafurites, compared with other rock-types, suggesting mixing of more than one trend. The total iron contents (expressed as $Fe_2O_3$ total) show two curved trends for the leucite mafurites, one of increasing iron with decreasing MgO, which seems to grade into the mafurites, and the other of decreasing iron with decreasing MgO. Manganese does not show significant correlation with MgO. CaO shows a curved trend of increasing and then decreasing values with decreasing MgO, typical of fractionation of olivine, at first, and then clino-pyroxene. Again, the leucite mafurites seem to follow two independent trends, one at higher CaO, which progresses into the mafurites, and the other at lower CaO, subparallel to the first. The interpretation of $K_2O$ and $Na_2O$ contents in leucite mafurites and mafurites is hampered by the wide scatter of the values, which probably derives from metasomatic alteration and/or weathering. As observed for other major elements, $P_2O_5$ contents suggest two or more independent trends for the

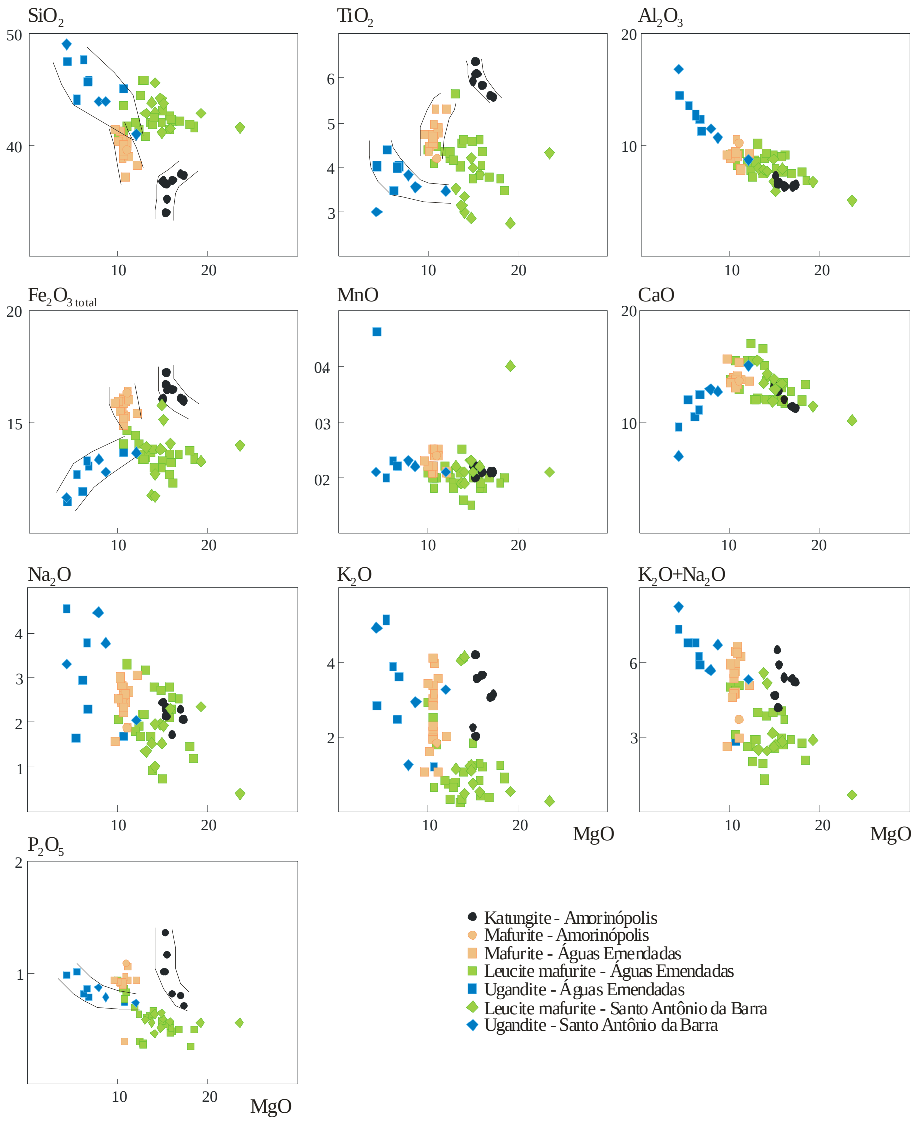


Fig. 32. Variation diagrams of major element oxides with MgO for the GAP feldspar-free rocks. Data source: Moraes (1984), Danni (1985), Danni *et al.* (1990), Danni & Gaspar (1994), Junqueira-Brod (1998) and Sgarbi & Gaspar (2002), and this work.

leucite mafurites, one of increasing $P_2O_5$ with decreasing MgO, progressing into the mafurites, and possibly one or two of decreasing $P_2O_5$ with increasing MgO.

Ugandites have the lowest MgO contents among the GAP kamafugites and are, therefore, interpreted as the most evolved terms in the kamafugitic series. Although there is some scatter in the distributions of various major elements with MgO, it can be seen from Fig. 32 that $SiO_2$, $Al_2O_3$, CaO, total alkalis and $P_2O_5$ behave in a way that is in consonance with normal crystal fractionation.

Fig. 33 shows the behaviour of selected trace elements of GAP kamafugitic rocks with MgO. Cr and Ni show a consistent positive correlation with MgO. A major discrepancy is observed between Cr and Ni contents of the Amorinópolis katungites: Ni values are consistent with the high-MgO content in these rocks but Cr is excessively low, suggesting that the katungites suffered previous fractionation of chromite (but not necessarily of olivine). Leucite mafurites contain considerably higher Cr and Ni than mafurites and ugandites, but this is difficult to interpret because the leucite mafurites are strongly porphyritic rocks with large amounts of xenocrysts in disequilibrium with the magma (see section on mineral chemistry above). Ugandites are clearly the most differentiated magma with respect to the compatible elements Cr, Ni and Mg. Sc shows an initial increase with decreasing MgO in katungites, mafurites and leucite mafurites, but the trend later inflects towards decreasing Sc in the ugandites, which probably reflects the onset of significant clinopyroxene removal from the magma.

The HFSE elements Nb, Zr, and Th also show marked behaviour differences among the various rock-types. Katungites have consistently higher contents of these elements relatively to the other kamafugite samples for the same MgO content. Mafurites, as well as katungites, have a much wider range of variation of incompatible elements than MgO, suggesting that these rocks are product of different degrees of partial melting, rather than of fractional crystallization. From the diagrams in Fig. 33 it seems difficult to relate the various petrographic types of the kamafugite series through simple fractional crystallization. In particular, Th behaviour seems to mark at least three distinct evolution trends, but these are not necessarily related to rock type. Light and heavy rare-earth elements do not appear to have suffered strong changes, apart from a slight increase with decreasing MgO contents, but the chondrite-normalized Ce/Yb ratio strongly increases from 25-50 to values up to 160 with decreasing Yb, suggesting the involvement of different degrees of partial melting, in the evolution of the GAP kamafugites, especially in the case of some of the Santo Antônio da Barra samples. The fact that the sudden Ce/Yb increase occurs at Yb values lower than 5 times the chondrite abundance seems to indicate that either garnet was a residual phase in the mantle source of the Santo Antônio da Barra magmas or a differentiation process capable of depleting the heavy rare-earths (e.g. liquid immiscibility, cf. Brod, 1999) was in place during the evolution of these magmas.

Fig. 34 shows the chondrite-normalized rare-earth patterns for the GAP kamafugitic rocks. The patterns for all rock-types are strongly enriched in LREE relatively to HREE and widely overlap each other. Katungites and mafurites are enriched in all REE relatively to average leucite mafurites and ugandites. The latter two rock-types, in turn, have a much wider range of absolute REE concentration. Rocks with high (>3.5 wt%) L.O.I. values (Fig. 34b) do not show significant changes in the slope of the REE in this diagram, but contain slightly higher REE than rocks with low values of L.O.I.

Fig. 35 shows multi-element diagrams for the GAP kamafugites. The general pattern for the GAP rocks is one of progressive enrichment in incompatible elements with a peak at Nb-La-Ce. Small negative anomalies occur at Rb, K, Sr and, less obviously, at P. This is similar to the general pattern of other kamafugitic provinces, such as the Alto Paranaíba (Gibson *et al.*, 1995a), Brod *et al.*

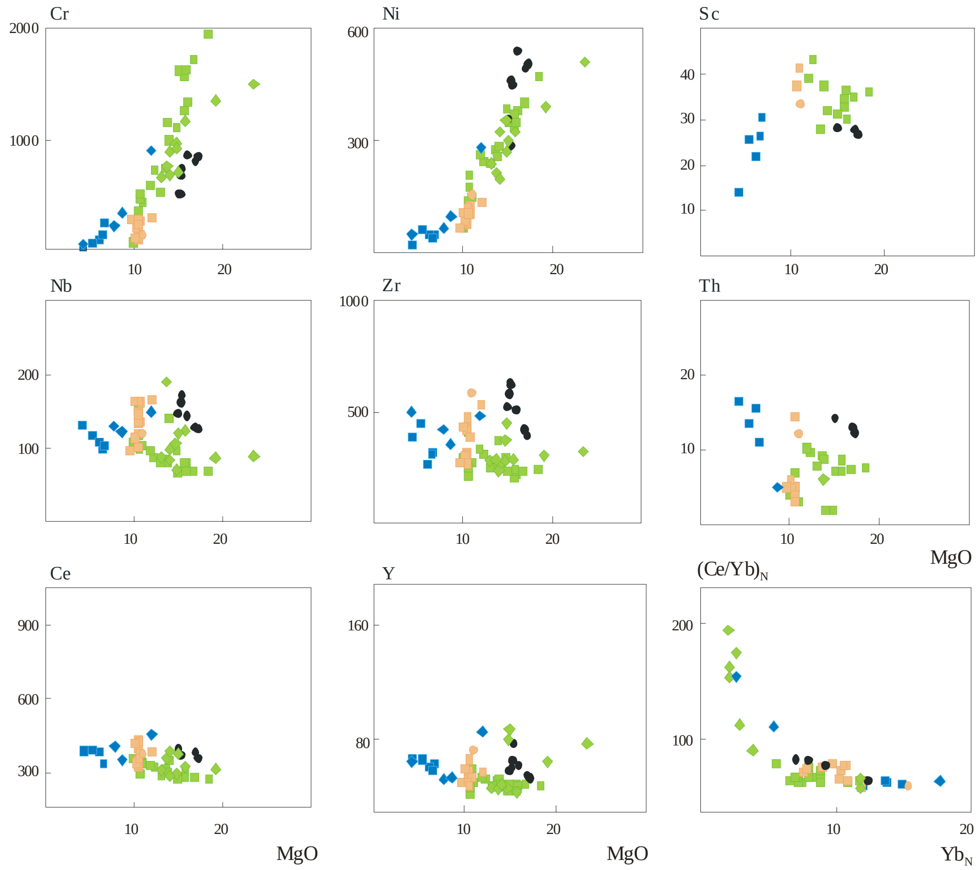


Fig. 33. Variation diagrams of selected trace elements with MgO for the GAP feldspar-free rocks. Data source and symbols as in Fig. 32.

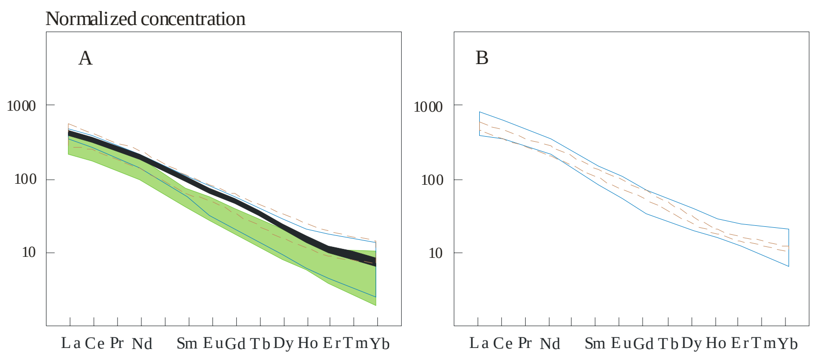


Fig. 34. Chondrite-normalized rare-earth element diagrams for GAP kamafugitic rocks with A) less and B) more than 3.5 wt% loss-on-ignition contents. Black: katungite; dashed line: mafurite; green: leucite mafurite; blue solid line: ugandite. Data source: Danni & Gaspar (1994), Junqueira-Brod (1998) and Sgarbi & Gaspar (2002), and this work.

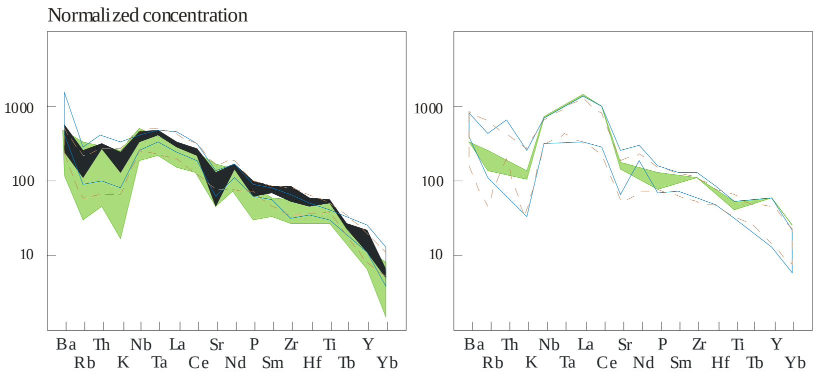


Fig. 35. Normalized trace element diagrams for GAP kamafugitic rocks with A) less and B) more than 3.5 wt% loss-on-ignition contents. Symbols as in Fig. 34. Data source: Moraes (1984), Danni (1985), Danni *et al.* (1990), Danni & Gaspar (1994), Junqueira-Brod (1998) and Sgarbi & Gaspar (2002), and this work.

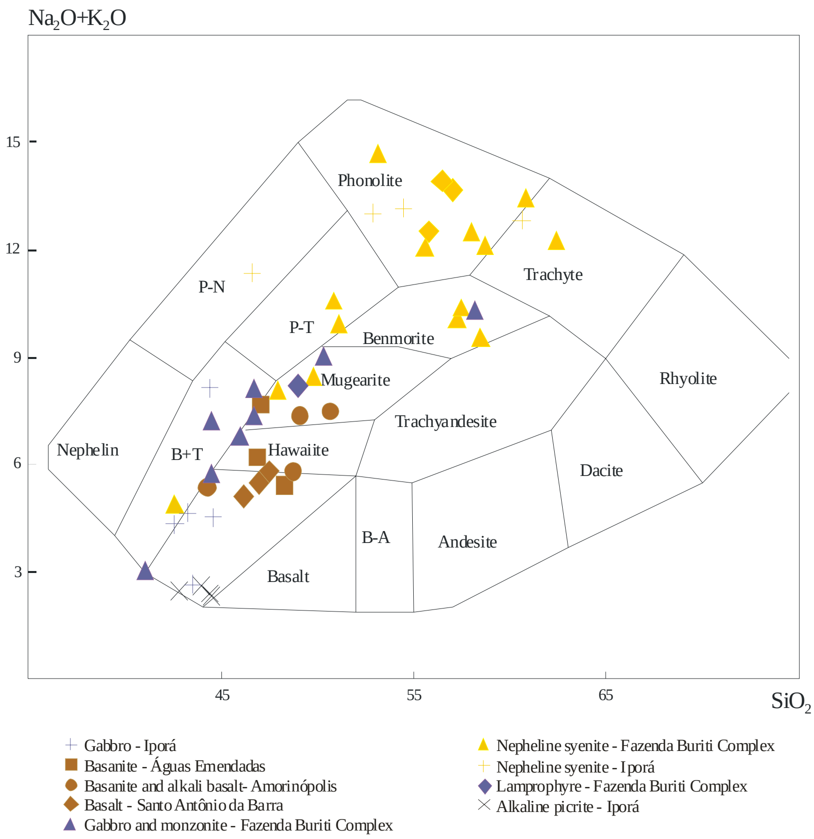


Fig. 36. Total alkalis-silica (TAS) classification diagrams for the feldspar-bearing rocks of the Goiás Alkaline Province. Data source: Danni (1978), Moraes (1984), Danni (1994), Cerqueira (1995) and Junqueira-Brod (1998).

2000), in the northeast border of the Paraná Basin. When rocks with L.O.I. contents higher than 3.5 wt% are considered, the Nb-La-Ce peak is distinctively enhanced (Fig. 35) relatively to adjacent incompatible trace elements. Despite the fact that many GAP kamafugites show evidence of subsolidus alteration, this consistent behaviour may suggest the involvement of a carbonatitic component in the high L.O.I. samples. Unfortunately, the lack of key element (Ta, Hf, and $CO_2$) determinations in the analyses reported in the literature does not allow to elaborate further on this hypothesis.

Feldspar-bearing rocks

Interpretation of the whole-rock geochemistry of the GAP feldspar-bearing rocks on a regional scale is difficulted by a number of reasons: 1) there are only a few geochemical studies regarding the plutonic complexes of northern GAP; 2) many of the available data refer to coarse-grained rocks in these complexes, which do not necessarily represent the composition of whole liquids; 3) many of the older sets of data do not include key trace elements. The available data for basanites (Águas Emendadas, Amorinópolis), alkali basalts (Amorinópolis, Santo Antônio da Barra), picrites (Iporá), trachytes (Fazenda Buriti), phonolites (Fazenda Buriti, Santo Antônio da Barra), as well as coarse-grained dunites, pyroxenites, gabbroic and syenitic rocks (Fazenda Buriti, Córrego dos Bois, Morro do Macaco) will be discussed below. Representative analyses of the GAP feldspar-bearing rocks are given in Table 11.

Fig. 36 shows the classification of GAP mafic to felsic feldspar-bearing rocks in the TAS diagram. The analyses plot along a silica-undersaturated trend ranging from basanite to phonolite. Fine-grained basanites and alkali basalts (Águas Emendadas, Santo Antônio da Barra) are slightly richer in $SiO_2$ than the plutonic rocks (Fazenda Buriti, Córrego dos Bois, Morro do Macaco), for the same alkali content.

Table 11. Representative whole-rock chemical analyses of GAP feldspar-bearing rocks. Data source: 1) Danni (1994), 2) Danni (1978), 3) Junqueira-Brod (1998), 4) Moraes (1984), and 5) Cerqueira (1995).

| Locality | Iporá | | | | | AE | SAB | Amorin. | Fazenda Buriti | | | | | | |
|---|---|---|---|---|---|---|---|---|---|---|---|---|---|---|---|
| Rock | Picrite | | | Dunite | Wehrlite | Basanite | Ol-basalt | Gabbro | Pyro-xenite | Gabbro | | | Syenite | | |
| Sample | D3-2 | D3-5 | D3-3 | D1-4 | D1-5 | 96ae52F | a215 | 96ae65 | cfb33a | cfb41 | cfb35 | cfb107 | cfb102 | cfb37b | cfb37a |
| Reference | 1 | 1 | 1 | 2 | 2 | 3 | 4 | 3 | 5 | 5 | 5 | 5 | 5 | 5 | 5 |
| $SiO_2$ | 44.40 | 42.78 | 44.47 | 39.06 | 43.04 | 46.88 | 46.90 | 49.10 | 43.49 | 50.34 | 40.98 | 49.69 | 52.54 | 55.56 | 60.80 |
| $TiO_2$ | 2.11 | 2.29 | 2.03 | 0.10 | 1.41 | 3.68 | 3.41 | 2.65 | 2.41 | 2.66 | 4.85 | 3.10 | 0.71 | 1.40 | 0.76 |
| $Al_2O_3$ | 9.15 | 9.00 | 6.18 | 0.46 | 2.34 | 13.13 | 14.05 | 14.25 | 6.33 | 16.06 | 8.32 | 14.84 | 19.90 | 18.21 | 18.46 |
| $Fe_2O_{3\ total}$ | 13.34 | 12.03 | 12.46 | 12.99 | 12.38 | 12.89 | 12.82 | 11.14 | 10.65 | 10.06 | 14.82 | 10.45 | 5.59 | 5.79 | 3.48 |
| MnO | 0.15 | 0.18 | 0.15 | 0.21 | 0.20 | 0.23 | 0.32 | 0.18 | 0.14 | 0.17 | 0.18 | 0.15 | 0.22 | 0.13 | 0.12 |
| MgO | 17.99 | 21.40 | 23.38 | 46.68 | 24.95 | 7.27 | 5.89 | 5.65 | 16.50 | 3.70 | 10.22 | 4.62 | 0.55 | 2.42 | 0.66 |
| CaO | 10.15 | 9.51 | 8.82 | 0.49 | 15.67 | 8.94 | 10.33 | 9.12 | 17.09 | 7.04 | 16.84 | 7.90 | 2.59 | 4.05 | 2.10 |
| $Na_2O$ | 1.42 | 1.04 | 1.36 | | | 2.23 | 3.20 | 2.43 | 1.49 | 4.30 | 1.61 | 3.75 | 7.85 | 6.18 | 5.73 |
| $K_2O$ | 0.99 | 1.44 | 0.96 | | | 4.00 | 2.27 | 4.94 | 1.50 | 4.76 | 1.43 | 4.70 | 9.96 | 5.90 | 7.75 |
| $P_2O_5$ | 0.29 | 0.32 | 0.19 | | | 0.74 | 0.81 | 0.55 | 0.40 | 0.91 | 0.76 | 0.82 | 0.09 | 0.37 | 0.14 |
| L.O.I. | 2.38 | 1.90 | 2.43 | 2.08 | 3.25 | 3.07 | 3.44 | 0.85 | 1.15 | 1.63 | 1.27 | 1.14 | 2.23 | 1.42 | 1.93 |
| Ba | 450 | 350 | 570 | | | 1617 | 1950 | 1251 | 275 | 1153 | 569 | 1243 | 2250 | 967 | 604 |
| Rb | | | 29.0 | | | 45.0 | 85.0 | 126.0 | | | | | | | |
| Sr | 350 | 600 | 410 | | | 1489 | 1040 | 802 | 453 | 1268 | 752 | 1137 | 2745 | 873 | 624 |
| Ta | | | | | | 5.90 | | | | | | | | | |
| Nb | | | 36 | | | 81 | 135 | 51 | | | | | | | |
| Hf | | | 23.00 | | | 8.22 | | | | | | | | | |
| Zr | 179 | 180 | 190 | | | 317 | 420 | 261 | 211 | 472 | 305 | 384 | 919 | 339 | 300 |
| Y | 15.0 | 17.0 | 18.0 | | | 30.0 | 64.0 | 29.0 | 19.0 | 29.0 | 29.0 | 30.0 | 42.0 | 23.0 | 16.0 |
| Th | | | 15.0 | | | 8.0 | | | | | | | | | |
| U | | | | | | 1.42 | 1.70 | | | | | | | | |
| Cr | 830 | 930 | 770 | | | 97 | 43 | 106 | 1389 | 25 | 173 | 39 | | 21 | |
| Ni | 780 | 750 | 800 | | | 32 | 50 | 36 | 301 | 29 | 134 | 54 | | 16 | |
| Sc | | | | | | 24.1 | | 24.7 | | | | | | | |
| V | 340 | 437 | | | | 304 | 390 | 287 | 262 | 176 | 497 | 255 | 213 | 101 | 43 |
| La | | | 39.0 | | | 78.0 | 250.0 | | | | | | | | |
| Ce | | | 93.0 | | | 157.0 | 300.0 | | | | | | | | |
| Nd | | | 43.7 | | | 74.9 | | | | | | | | | |
| Sm | | | 7.50 | | | 12.51 | | | | | | | | | |
| Eu | | | 1.67 | | | 3.72 | | | | | | | | | |
| Gd | | | 4.61 | | | 9.46 | | | | | | | | | |
| Dy | | | 3.60 | | | 6.24 | | | | | | | | | |
| Ho | | | 0.690 | | | 1.080 | | | | | | | | | |
| Er | | | 1.700 | | | 2.715 | | | | | | | | | |
| Yb | | | 1.260 | | | 2.249 | 4.000 | | | | | | | | |
| Lu | | | 0.160 | | | 0.342 | | | | | | | | | |

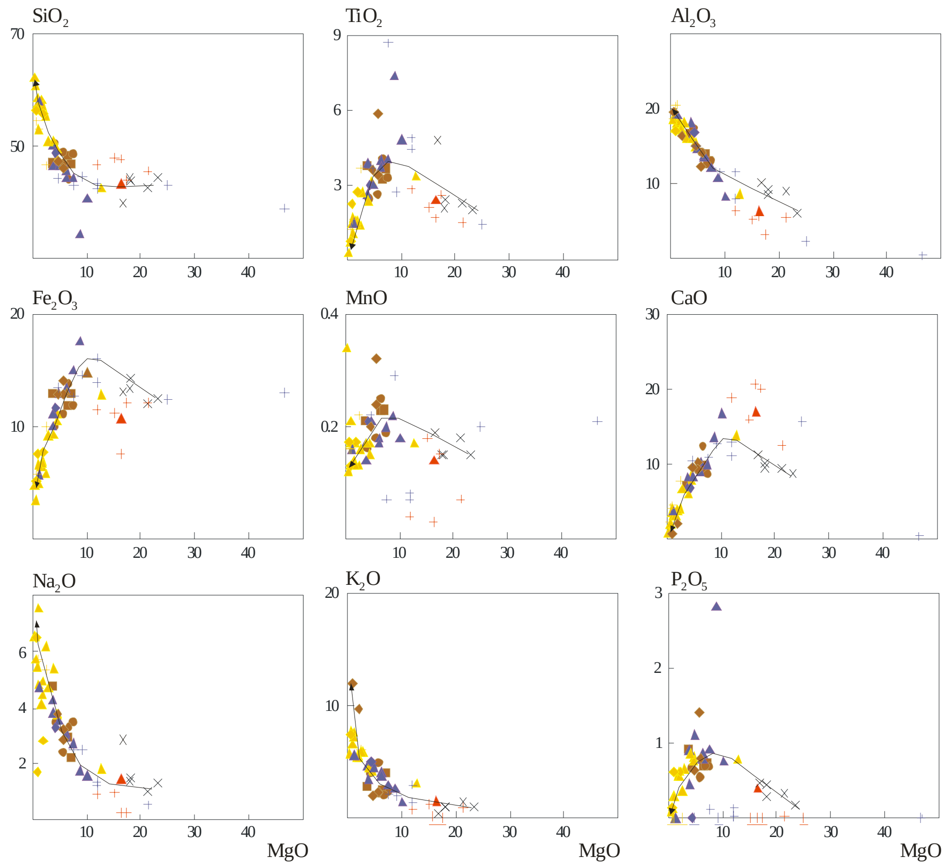


Fig. 37. Variation diagrams of major element oxides with MgO for the GAP feldspar-bearing rocks. Symbols and data source as in Fig. 36.

Fig. 37 shows the variation trends of major element oxides with MgO. Most of the evolution patterns are consistent with fractional crystallization from an alkali picrite magma, as suggested by Danni (1994), through the removal of olivine and, later, of clinopyroxene and/or plagioclase. Some mafic rocks from Iporá and Fazenda Buriti showing anomalously low $SiO_2$, and high $TiO_2$, $Fe_2O_3$(total) and $P_2O_5$, may represent crystal cumulates rather than whole liquids, and are disregarded for future interpretations.

The REE normalized contents of GAP basanites, alkali basalts and picrites are shown in Fig. 38. The patterns for these rock-types are essentially parallel, with the picrites showing lower abundances of all REE relatively to basanites and alkali basalts. The chondrite-normalized Ce/Yb ratios are 16 to 21 for the basanites and alkali basalts, and ca. 20 for the picrites, values that are only marginally lower than those obtained for the kamafugitic rocks with low L.O.I. contents. As observed for the kamafugites, the basanites and alkali basalts with high L.O.I. values (essentially samples from Santo Antônio da Barra) contain higher REE contents, although their chondrite-normalized Ce/Yb ratios (ca. 17) do not change substantially. High and low L.O.I. picrites appear to have essentially the same REE contents and patterns.

Fig. 39 presents multi-element normalized diagrams for basanites, alkali basalts and picrites. Rocks with L.O.I. values lower than 3.5 wt% display patterns which peak at Nb-La-Ce, with small negative anomalies at K, Rb, Sr, and P, and are essentially similar to those of the GAP kamafugites. As noted for the latter, alkali basalts with L.O.I.>3.5 wt% from Santo Antônio da Barra contain much higher Nb-La-Ce values. However, this feature is not present in the high L.O.I. picrites.

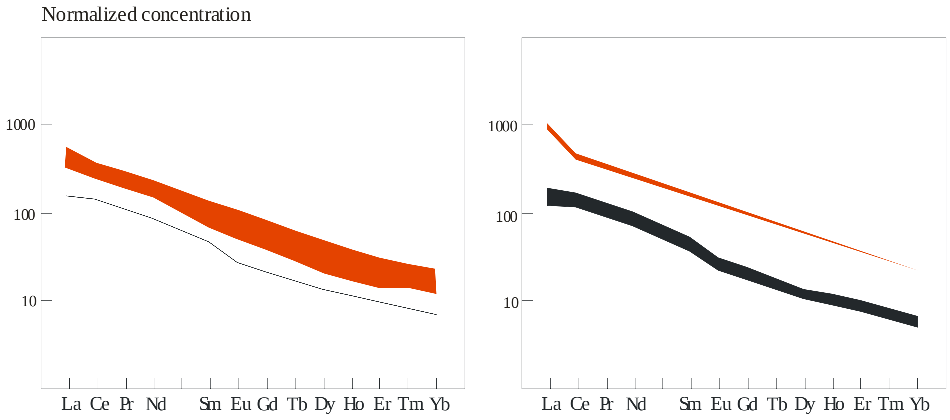


Fig. 38. Normalized rare-earth element diagrams for GAP feldspar-bearing rocks with A) less and B) more than 3.5 wt% loss-on-ignition contents. Black: alkaline picrite; red: other mafic rocks. Data source: Moraes (1984), Danni (1994) and Junqueira-Brod (1998).

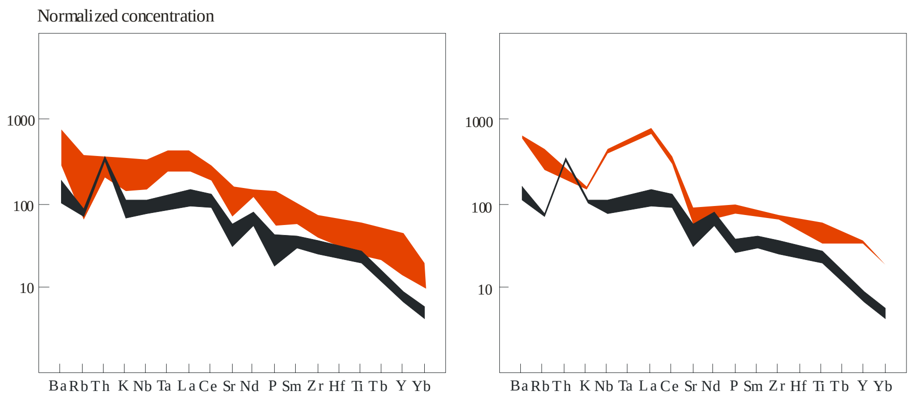


Fig. 39. Normalized trace element diagrams for GAP feldspar-bearing rocks with A) less and B) more than 3.5 wt% loss-on-ignition contents. Symbols and data source as in Fig. 38.

## Parental magmas, partial melt and fractional crystallization

The parental magma to the concentrically zoned plutonic complexes of northern GAP (e.g. Morro do Macaco, Córrego dos Bois) is believed to be alkaline picritic in composition, on the basis of the xenolithic content of these rocks (Danni *et al.*, 1992; Danni, 1994). This is in accordance with the petrographic ranges observed in the complexes and with the well-defined crystal fractionation trends indicated in whole-rock chemistry variation diagrams. The high MgO, Cr and Ni contents of the GAP picrites attest to the primitive character of the picritic magma. Fractional crystallization from an initial composition such as the GAP picrites must have been dominated initially by the fractionation of olivine and chromite and, later, of clinopyroxene. The local presence of both direct and reversal zoning in olivine from gabbroic rocks and leucite ijolites suggests occasional replenishment in the magma chamber (e.g. Fazenda Buriti complex).

The whole-rock chemistry, as well as the modal proportions of the essential phases (olivine, clinopyroxene, feldspathoids) suggest that, among the GAP kamafugitic rock-types, katungites are the most primitive and ugandites are the most evolved ones, with mafurites occupying a position intermediate between the former two.

However, some of the chemical and mineralogical aspects observed in the kamafugitic rocks are difficult to reconcile with the derivation of one rock type from another by means of fractional crystallization alone. For instance, if the katungite magma has fractionated olivine, it would evolve towards lower $SiO_2$ contents (therefore in the opposite direction from mafurites) due to the excessively low initial $SiO_2$. Furthermore, both katungites and mafurites show wider variation ranges in incompatible trace elements such as Rb, Nb, and Zr than in compatible constituents such as Mg, Cr and Ni, which suggests that the rocks within these two groups are related to each other through different degrees of partial melt, rather than fractional crystallization. This last crystallization process is only significant, perhaps, to produce ugandites from a mafuritic magma.

Compositionally, leucite mafurites do not fit in the sequence katungite-mafurite-ugandite as would be expected, and their evolution requires the intervention of some additional differentiation mechanisms.

Magma mixing

Several pieces of mineralogical evidence presented in this work suggest that magma mixing was involved in the evolution of GAP leucite mafurites and, possibly, of some GAP ugandites.

The multiple trends of spinel evolution in terms of Cr, Ti and Fe in the leucite mafurites suggest a complex evolution for these rocks. Spinel trends starting at high Cr for distinct values of $Fe^{2+}/(Fe^{2+}+Mg)$ effectively preclude evolution of leucite mafurites by fractional crystallization alone. This may also be true of ugandite spinel, although the Cr ranges in this case are too narrow to unequivocally establish the presence of more than one trend. On the other hand, the single trends of katungite and mafurite spinel suggest evolution through simpler differentiation processes (see partial melt and fractional crystallization above).

The reversal zoning of olivine phenocrysts in leucite mafurites suggests mixing with a more magnesian magma, such as the GAP alkaline picrites (MgO ranging from 17 to 23 wt%). There are no mineral chemistry data available on olivine from GAP picrites, but it is noteworthy that the highest Fo content observed in the magnesian rims of olivine phenocrysts from leucite mafurites (88.6 mol%) is only marginally lower than in dunitic olivine from the Morro do Macaco complex (89.0-89.3 mol% Fo) and slightly higher than peridotitic olivine from the Córrego dos Bois complex (87.99 mol% Fo). Olivine phenocryst cores in leucite mafurites, on the other hand, have Fo as low as 79.5 mol%, which is well within the range of olivine from GAP mafurites (76.9-83.5 mol% Fo). If the GAP picrites may be considered the parental magmas for the northern GAP plutonic complexes, then the mixing of picritic and mafuritic magma would provide a suitable alternative to explain the behaviour of leucite mafurite olivine.

The contrasting behaviour of clinopyroxene phenocryst cores and phenocryst rims+groundmass in some GAP rock-types is also indicative of magma mixing processes. The cores of pyroxene phenocrysts in the leucite mafurites and ugandites are clearly Ti-poor, relatively to both Al and $Fe^{2+}$+Mg, in comparison with the respective rims and with the groundmass crystals. These, in turn, show intermediate compositions between the clinopyroxene cores from leucite mafurites and ugandites and the clinopyroxene from the Morro do Macaco and Córrego dos Bois plutonic complexes in northern GAP. However, the interpretation of clinopyroxene data is not as straightforward as that of olivine, because:

1) there is no significant variation in the hedenbergite content among pyroxene grains from different mafic rock-types;

2) Ti contents in the pyroxene could possibly be affected by the concurrent crystallization of other phases (e.g. perovskite - in the kamafugitic rocks -, magnetite or ilmenite).

Fig. 40 shows the composition and evolution trends of both feldspar-free and feldspar-bearing GAP rocks. It is clear from the diagrams that the picrites are compositionally suitable to fractionate the whole sequence of feldspar-bearing rocks found in the northern GAP complexes, while producing ultramafic and mafic cumulates. Also plotted in Fig. 40 are the compositional fields for the rocks of the sequence katungite-mafurite-ugandite of south and central GAP. These rocks follow an independent trend (although not necessarily related to crystal fractionation, as seen above). The analyses of leucite mafurites plot systematically away from the compositional trend of other kamafugites, shifted toward the picritic compositions. This suggests that the leucite mafurites are the product of mixing of a highly magnesian, but less silica-undersaturated magma (picrite) with a mafuritic (and/or minor ugandite) magma, in accordance with the mineral chemistry evidence presented earlier.

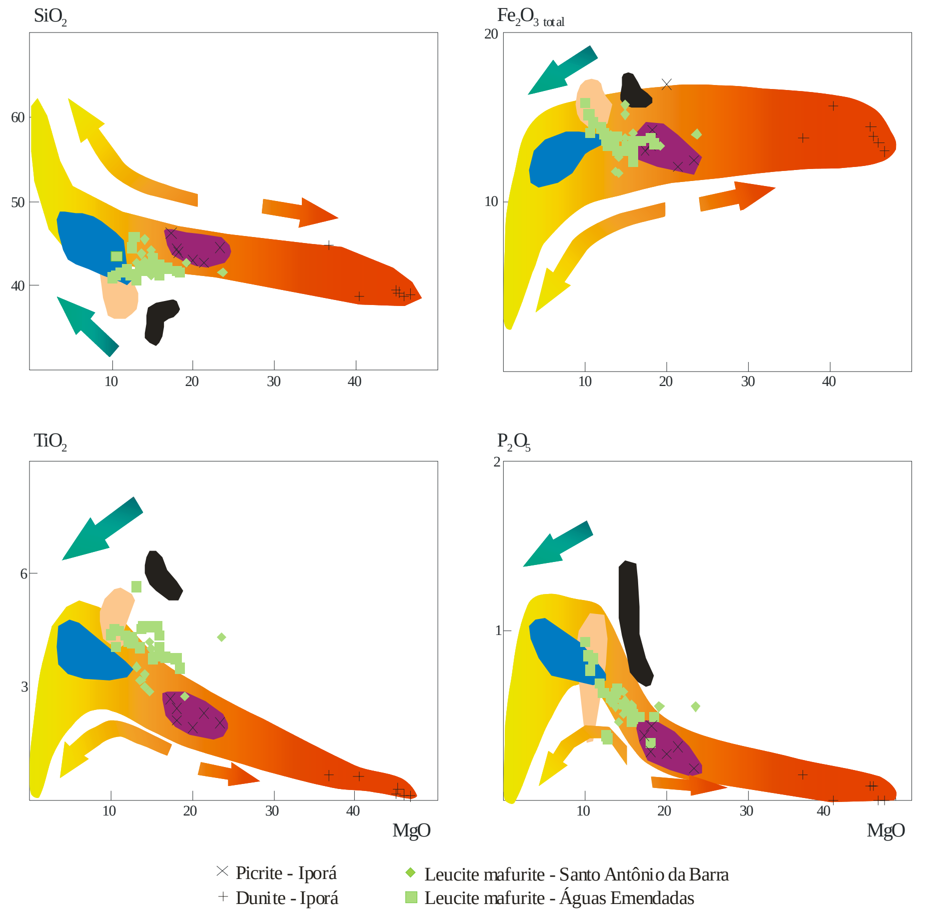


Fig. 40. Crystal fractionation and magma mixing relationships of GAP alkaline rocks. Black field=katungites; pink field=mafurites; blue field=ugandites, violet field=alkaline picrites; red to yellow field=all feldspar-bearing rocks and related ultramafic cumulates. Red arrow indicates the direction of olivine accumulation. Orange arrow indicates the direction of the crystal fractionation residual magma in northern GAP complexes. Green arrow indicates the general evolution trend of GAP kamafugites. It should be noted that leucite mafurites always plot between mafurites and picrites.

Temperature difference is a critical issue for the efficiency of the magma mixing process. Sgarbi *et al.*, (1998) determined a temperature of 1050 to 1060°C for the GAP mafuritic lavas on the basis of oxygen isotope data. Although this is an estimate of the closure temperature of the oxygen isotopic system, the small thickness of the GAP kamafugitic lava flows (Junqueira-Brod *et al.*, 2002, 2005a) suggests that these values should be fairly close to the actual eruption temperature. On the other hand, picritic magmas with the MgO content observed in the GAP picrites are expected to erupt at temperatures between 1350 and 1450°C (Nisbet, 1982; Green *et al.*, 2001; Van Thienen, 2004). Even if the actual eruption temperatures of the GAP picrites were lower than this estimate due to higher volatile contents, the temperature difference between the picritic and mafuritic magmas should be enough to allow mixing of the two liquids.

Several lines of evidence suggest that the leucite mafurite magma equilibrated at higher temperatures than the katungites, mafurites and ugandites: 1) reverse zoning in olivine; 2) the presence of various generations of Cr-rich spinel; 3) the higher equilibrium temperatures in the nepheline-kalsilite system.

Liquid immiscibility and the kamafugite-carbonatite association

The association of carbonatites with ultrapotassic rocks of the kamafugitic series has been recognized both in Italy (Stoppa & Cundari, 1995, 1998) and in Brazil (Brod, 1999; Brod *et al.*, 2000), and is now a firmly established fact. In the GAP, the association between the alkaline silicate rocks of Santo Antônio da Barra and carbonatites has been suggested as early as Gaspar & Danni (1981), but detailed chemical and mineralogical studies required to petrogenetically constrain the subject have not been carried out so far. Junqueira-Brod *et al.* (2005a) demonstrated that large amounts of carbonate globules (up to 70 vol%) occurring in kamafugitic lavas from the top flow unit at Santo Antônio da Barra could not be stable as gas bubbles in view of the extremely low viscosity of the kamafugitic host lava, and therefore these globules were taken as the result of silicate-carbonate liquid immiscibility.

The mineral chemistry of phlogopite presented earlier in this work is also strongly indicative of the presence of a kamafugite-carbonatite association similar to that recognized in the nearby Alto Paranaíba Igneous Province. The main characteristic of the phlogopite associated with carbonatites in the Alto Paranaíba region is its chemical evolution towards low-Ti tetra-ferriphlogopite (Brod *et al.*, 2001), a feature that is present in the GAP katungites and in some leucite mafurite samples.

The relatively high CaO content in GAP kamafugitic olivines (up to 1.2 wt%) is a feature shared with carbonatites and associated silicate rocks. CaO-rich olivines may result of the interaction with carbonatite or carbonate-rich residual liquid. Brenan & Watson (1991) demonstrated that olivines in equilibrium with carbonatite liquids show an increase in the percentage of the forsterite molecule and contain up to 0.5 wt% CaO. Dalton & Wood (1993) reported up to 0.81 wt% CaO in olivine crystallized at 15 kb and 1150°C, and established a positive correlation between the calcium content of olivine and that of the associated carbonatite liquid. Alternatively, high Ca content in olivine is dependent on pressure. Simkin & Smith (1970) suggested a strong relation between pressure and the Ca content of olivine, whereby extrusive and shallow intrusive igneous rocks contain olivine with distinc-tively higher Ca than deep-seated plutonic rocks.

Despite the indirect evidence reported here, a detailed petrogenetic work is still in need to investigate and constrain the relationships between kamafugites and carbonatites in the GAP.

## CONCLUSIONS

A striking feature of the Goiás Alkaline Province is the North-to-South zoning observed regarding the mode of emplacement and the degree of silica-undersaturation of the alkaline magmas.

Plutonic complexes are dominant in the northern part of the province, and consist mainly of feldspar-bearing rocks and related ultramafic cumulates. These complexes represent shallow magma chambers typically intruded at the discordance between the Precambrian basement and the Phanerozoic sedimentary rocks of the Paraná Basin (Junqueira-Brod *et al.*, 2005a). Dykes, plugs and sills of alkaline picrite are also present in northern GAP.

Most of the northern GAP plutonic complexes are concentrically zoned, with dunites in the centre, surrounded by rims of successively more differentiated, feldspar-bearing petrographic terms (noteworthy exceptions are the Montes Claros and Amorinópolis complexes, whose internal organization is less straightforward).

Subvolcanic bodies are dominant in the central portion of the province, consisting mainly of plugs, dykes and diatremes. They are basically composed of kamafugitic rocks (breccias, with subordinate lavas and dykes), but some feldspar-bearing rocks (e.g. basanites) may occur. Mafurites and leucite mafurites are very common in central GAP, whereas ugandites are subordinate and katungites were only recognized in the Amorinópolis region.

The southern portion of GAP is dominated by lavas and pyroclastic rocks which probably represent a kamafugite-carbonatite association similar to others described in the Alto Paranaíba region of Brazil, and in Italy. Leucite mafurites and ugandites are the main kamafugitic rock-types in this part of the province. Subordinate feldspar-bearing rocks (mainly alkali basalt to phonolite) also occur.

The whole-rock and mineral chemistry evidence suggest that the GAP feldspar-bearing rocks are mostly the product of fractional crystallization from an alkaline picritic parent, whilst the feldspar-free (kamafugitic) rocks underwent a more complex petrogenetic evolution.

The composition and chemical variation of spinel, olivine, clinopyroxene and feldspathoids, as well as the whole-rock geochemistry, indicate that katungites and mafurites derive from distinct degrees of partial melt and cannot be related to each other through simple fractional crystallization. However, a fractional crystallization link between mafurites and ugandites is a feasible alternative. Compositionally, katungites represent the most primitive and ugandites represent the most evolved magmas amongst the kamafugite series. Mafurites are compositionally intermediate between these two.

Leucite mafurites show a much more variable composition, which is difficult to reconcile with the sequence katungite-mafurite-ugandite. Textural, mineralogical and geochemical evidence indicate that leucite mafurites are best explained as a product of mixing between a picritic and a mafuritic (subordinately uganditic) magma.

The field relationships, the mineral chemistry of phlogopite and olivine, and some features of trace element whole-rock chemistry show that the kamafugite-carbonatite association is significant in southern and central GAP. Detailed geochemical, isotopic and mineralogical work is still required to petrogenetically constrain this association in the province.

## ACKNOWLEDGEMENTS

The authors are grateful to the Brazilian Council for Research and Development (CNPq), for research grants to JAB and JCG, a post-Doctoral grant to HSDP and post-graduate grants to TCJB and ESRB.

## REFERENCES

Almeida, F.F.M. (1967). Origem e evolução da Plataforma Brasileira. *Boletim da Divisão de Geologia e Mineralogia* **241**, 36p.

Almeida, F.F.M. (1983). Relações tectônicas das rochas alcalinas mesozóicas da região meridional da Plataforma Sul-Americana. *Revista Brasileira de Geociências* **13**, 139-158.

Almeida, F.F.M. (1986). Distribuição regional e relações tectônicas do magmatismo Pós-Paleozóico no Brasil. *Revista Brasileira de Geociências* **16**, 325-349.

Araújo, A.L.N. (2000). *Petrologia dos pipes kimberlíticos e kamafugíticos da Província Alcalina do Alto Paranaíba, Minas Gerais e Goiás.* Ph.D. Thesis, University of Brasilia, 297p.

Barbour, A.P., Girardi, V.A.V., Kawashita, K. & Souza, A.M.S. (1979). Geocronologia do complexo máfico-ultramáfico alcalino de Santa Fé, Goiás. *Boletim do Instituto de Geociências da USP* **10**, 11-18.

Bez, L. (1970). Petrografia do maciço alcalino de Montes Claros de Goiás, GO. *XXIV Congresso Brasileiro de Geologia, Brasília, Anais* **1**, 361-364.

Bez, L., Guimarães, J.E & Guimarães, D. (1971). Distrito vulcânico de Rio Verde. *XXV Congresso Brasileiro de Geologia, São Paulo, Anais* **2**, 121-128.

Brod, J.A. (1999). *Petrology and geochemistry of the Tapira alkaline complex, Minas Gerais State, Brazil.* Ph.D. Thesis, University of Durham, 486p.

Brod, J.A., Gaspar, J.C., Araújo, D.P., Gibson, S.A., Thompson, R.N. & Junqueira-Brod, T.C. (2001). Phlogopite and tetra-ferriphlogopite from Brazilian carbonatite complexes: petrogenetic constraints and implications for mineral-chemistry systematics. *Journal of Asian Earth Sciences* **19**, 265-296.

Brod, J.A., Gibson, S.A., Thompson, R.N., Junqueira-Brod, T.C., Seer, H.J., Moraes, L.C. & Boaventura, G.R. (2000). The kamafugite-carbonatite association in the Alto-Paranaíba Igneous Province, southeastern Brazil. *Revista Brasileira de Geociências* **30**, 408-412.

Cerqueira, M.R.S. (1995). *Geologia e evolução petrológica do complexo alcalino Fazenda Buriti, Iporá-Goiás.* M.Sc. Dissertation, University of Brasilia, 180p.

Cerqueira, M.R.S. & Danni, J.M.C. (1994). Aspectos petrográficos e químicos do complexo da Fazenda Buriti, Iporá, GO. *Boletim de Geociências do Centro-Oeste* **17**, 29-33.

Comin-Chiaramonti, P., Cundari, A., Piccirillo, E.M., Gomes, C.B., Castorina, F., Censi, P., De Min, A., Marzoli, A., Speziale, S. & Velázquez, V.F. (1997). Potassic and sodic igneous rocks from eastern Paraguay: their origin from the lithospheric mantle and genetic relationships with the associated Paraná flood tholeiites. *Journal of Petrology* **38**, 495-528.

Conticelli, S. & Peccerillo, A. (1992). Petrology and geochemistry of potassic and ultrapotassic volcanism in central Italy: petrogenesis and inferences on the evolution of the mantle sources. *Lithos* **28**, 221-240.

Cundari, A. & Ferguson, A.K. (1991). Petrogenetic relationships between melilitite and lamproite in the Roman Comagmatic Region: the lavas of S. Venanzo and Cupaello. *Contributions to Mineralogy and Petrology* **107**, 343-357.

Danni, J.C.M. (1978). Magmatic differentiation of the alkaline ultrabasic intrusions of the Iporá region, southwest Goiás, Brazil. *1st International Symposium Carbonatites, Poços de Caldas, Proceedings*, pp. 149-167.

Danni, J.C.M. (1985). Rochas da série kamafugítica na região de Amorinópolis, Goiás. Contribuições à Geologia e à Petrografia - Núcleo de Minas Gerais, Belo Horizonte, pp. 5-13.

Danni, J.C.M. (1994). Os picritos alcalinos da região de Iporá: implicações na gênese dos complexos do tipo central do Sul de Goiás. *Revista Brasileira de Geociências* **24**, 112-119.

Danni, J.C.M. & Gaspar, J.C. (1992). Mineralogia e química do katungito de Amorinópolis, Goiás. *XXXVII Congresso Brasileiro de Geologia, São Paulo, Anais*, pp. 85-86.

Danni, J.C.M. & Gaspar, J.C. (1994). Química do katungito de Amorinópolis - Goiás: contribuição ao estudo do magmatismo kamafugítico. *Geochimica Brasiliensis* **8**, 119-134.

Danni, J.C.M., Fuck, R.A. & Leonardos, O.H. (1976). Geologia e petrografia da intrusão ultramáfica alcalina de Arenópolis. *XXIX Congresso Brasileiro de Geologia*, *Ouro Preto, Resumos, pp.* 265-271.

Danni, J.C.M., Silva, A.J.G.C., Campos, J.E.G. & Cerqueira, M.R.S. (1992). Picritos alcalinos do sul de Goiás: características mineralógicas e geoquímicas. *XXXVII Congresso Brasileiro de Geologia, São Paulo, Anais*, p. 89.

Danni, J.C.M., Silva, A.J.G.C. & Cerqueira, M.R. (1990). Petrografia e petroquímica das rochas alcalinas cretácicas da Serra do Caipó, sudoeste de Goiás. *XXXVI Congresso Brasileiro Geologia, Natal, Anais*, pp. 1872-1882.

Dalton, J.A. & Wood, B.J. (1993). The compositions of primary carbonate melts and their evolution through wallrock reaction in the mantle. *Earth and Planetary Science Letters* **119**, 511-525.

Edgar, A.D. (1979). Mineral chemistry and petrogenesis of an ultrapotassic-ultramafic volcanic rock. *Contributions to Mineralogy and Petrology* **71**, 171-175.

Farmer, G.L. & Boetcher, A.L. (1981). Petrologic and crystal-chemical significance of some deep-seated phlogopites. *American Mineralogist* **66**, 1154-1163.

Foley, S.F., Venturelli, G., Green, D.H. & Toscani, L. (1987). The ultrapotassic rocks: characteristics, classification, and constraints of petrogenetic models. *Earth-Science Reviews* **24**, 81-134.

Gallo, F., Giammetti, F., Venturelli. G. & Vernia, L. (1984). The kamafugitic rocks of San Venanzo and Cupaello, Central Italy. *Neues Jahrbuch für Mineralogie Abhandlungen*, pp. 198-210.

Gaspar, J.C. (1989). *Géologie et mineralogie du complexe carbonatitique de Jacupiranga, Brésil.* Ph.D. Thesis, University of Orleans, France.

Gaspar, J.C. & Danni, J.C.M. (1981). Aspectos petrográficos e vulcanológicos da província alcalina-carbonatítica de Santo Antônio da Barra, sudoeste de Goiás. *Revista Brasileira de Geociências* **11**, 74-83.

Gaspar, J.C. & Wyllie, P.J. (1987). The phlogopites from the Jacupiranga carbonatite intrusions. *Mineralogy and Petrology* 36, 121-134.

Gaspar, J.C., Araújo, A.L.N., Carlson, R.W., Sichel, S.E., Brod, J.A., Sgarbi, P.B.A. & Danni, J.C.M. (2003). Mantle xenoliths and new constraints on the origin of alkaline ultrapotassic rocks from the Alto Paranaíba and Goiás Igneous Province, Brazil. *8th International Kimberlite Conference, Victoria, CD-ROM, FLA 0337*, pp. 1-5.

Gaspar, J.C., Brod, J.A., Sgarbi, P.B.A., Junqueira-Brod, T.C. & Araújo, A.L.N. (2000). A review of the Cretaceous alkaline magmatism in Western Minas Gerais and Southern Goiás. *31st International Geological Congress, Rio de*

*Janeiro, Abstracts,* CD-ROM.

Gibson, S.A., Thompson, R.N., Leonardos, O.H., Dickin, A.P. & Mitchell, J.G. (1995a). The Late Cretaceous impact of the Trindade mantle plume: evidence from large-volume, mafic, potassic magmatism in SE Brazil. *Journal of Petrology* **36**, 189-229.

Gibson, S.A., Thompson, R.N., Dickin, A.P. & Leonardos, O.H. (1995b). High-Ti and low-Ti mafic potassic magmas: key to plume-lithosphere interactions and continental flood-basalt genesis. *Earth and Planetary Science Letters* **136**, 149-165.

Gibson, S.A., Thompson, R.N., Weska, R.K., Dickin, A.P. & Leonardos, O.H. (1997). Late Cretaceous rift-related upwelling and melting of the Trindade starting mantle plume head beneath western Brazil. *Contributions to Mineralogy and Petrology*, **126**, 303-314.

Green, D.H., Falloon, T.J., Eggins, S.M. & Yaxley, G.M. (2001). Primary magmas and mantle temperatures. *European Journal of Mineralogy* 13, 437-451.

Guimarães, G., Glaser, I. & Marques, V.L. (1968). Sobre a ocorrência de rochas alcalinas na região de Iporá, Goiás. *Mineração Metalurgia* **48**, 11-15.

Hasui, Y., Cartner-Dyer, R.E. & Iwanuch, W. (1971). Geocronologia das rochas alcalinas de Santo Antônio da Barra, GO. *XXV Congresso Brasileiro de Geologia*, *São Paulo, Anais,* pp. 253-258.

Hough, F.E. (1972). *The petrogenesis of strongly alkaline mafic lavas and nodules from the West Eifel and southwest Uganda.* Ph.D. Thesis, University of Reading, 183p.

Junqueira-Brod, T.C. (1998). *Cretaceous alkaline igneous rocks from the Águas Emendadas region, Goiás, Central Brazil.* M.Sc. Dissertation, University of Durham, 161p.

Junqueira-Brod, T.C. (2003). *Vulcanologia das rochas kamafugíticas da Província Alcalina de Goiás.* Ph.D. Thesis, University of Brasilia, 168p.

Junqueira-Brod, T.C., Brod, J.A., Gaspar, J.C. & Jost, H. (2004). Kamafugitic diatremes: facies characterisation and genesis. Examples from the Goiás Alkaline Province, Brazil. *Lithos* **76**, 261-282.

Junqueira-Brod, T.C., Brod, J.A., Gibson, S.A. & Thompson, R.N. (2000). Mineral chemistry of kamafugites and related rocks from Águas Emendadas region, Goiás state. *Revista Brasileira de Geociências* **30**, 403-407.

Junqueira-Brod, T.C., Brod, J.A., Thompson, R.N. & Gibson, S.A. (1999b). Spinning droplets – A conspicuous lapilli-size structure of kamafugitic diatremes of southern Goiás, Brazil. *Revista Brasileira de Geociências* **29**, 557-560.

Junqueira-Brod, T.C., Gaspar, J.C., Brod, J.A., Jost, H., Barbosa, E.S.R. & Kafino, C.V. (2005a). Emplacement of kamafugite lavas from the Goiás Alkaline Province, Brazil: constraints from whole-rock simulations. *Journal of South America Earth Sciences* (in press).

Junqueira-Brod, T.C., Gaspar, J.C., Brod, J.A. & Kafino, C.V. (2005b). Kamafugitic diatremes: their textures and field relationships with examples from the Goiás Alkaline Province, Brazil. *Journal of South America Earth Sciences* (in press).

Junqueira-Brod, T.C., Gibson, S.A., Thompson, R.N. & Brod, J.A. (1999a). Mineral chemistry of Águas Emendadas kamafugitic rocks, Goiás. *VII Simpósio de Geologia do Centro-Oeste e X Simpósio de Geologia de Minas Gerais, Brasília, Boletim de Resumos*, p. 66.

Junqueira-Brod, T.C., Roig, H.L., Gaspar, J.C., Brod, J.A. & Meneses, P.R. (2002). A Província Alcalina de Goiás e a extensão do seu vulcanismo kamafugítico. *Revista Brasileira de Geociências* **32**, 559-566.

Lacerda Filho, J.V., Rezende, A. & Silva, A. (2000). Programa Levantamentos Geológicos Básicos do Brasil. Geologia e Recursos Minerais do Estado de Goiás e do Distrito Federal. Escala 1:500000 (mapa) 2ª Edição. CPRM/METAGO/UnB, 184p.

Laughlin, A.W., Charles, R.W. & Aldrich, M.J. (1989). Heteromorphism and crystallization paths of katungites, Navajo volcanic field, Arizona, USA. Kimberlites and related rocks. *Geological Society of Australia, Special Publication* **14**, 582-591.

Le Maitre, R.W. (2002). *Igneous rocks: a classification and glossary of terms. Recommendations of the International Union of Geological Sciences Subcommission on the Systematics of Igneous Rocks.* 2nd edition. Cambridge: Cambridge University Press, 252p.

Leonardos, O.H., Ulbrich, M.N. & Gaspar, J.C. (1991). The Mata da Corda volcanic rocks. In: Leonardos, O.H., Meyer, H.O.A. & Gaspar, J.C. (eds.). *5th International Kimberlite Conference, Araxá, Field Guide Book*, pp. 17-24.

Lloyd, F.E., Huntingdon, A.T., Davies, G.R. & Nixon, P.H. (1991). Phanerozoic volcanism of Southwest Uganda: a case for regional K and LIL enrichment of the lithosphere beneath a domed and rifted continental plate. In: *Magmatism in extensional structural settings*. Heidelberg: Springer-Verlag, pp. 23-72.

Mitchell, R.H. (1995). *Kimberlites, orangeites and related rocks.* New York: Plenum Press, 410p.

Mitchell, R.H. & Bergman, S.C. (1991). *Petrology of lamproites.* New York: Plenum Press, 447p.

Moraes, L.C. (1984). *Petrologia, estratigrafia e potencial diamantífero da suíte vulcânica alçalina da região de Santo Antônio da Barra, Goiás.* M.Sc. Dissertation, University of Brasilia, 133p.

Moraes, L.C. (1988). Aspectos petrológicos do magmatismo alcalino cretáceo de Santo Antônio da Barra, GO. *Revista Brasileira de Geociências* **18**, 33-42.

Morimoto, N., Fabries, J., Ferguson, A.K., Ginzburg, I.V., Ross, M., Seifert, F.A., Zussmann, J., Aoki, K. & Gotardi, G. (1988). Nomenclature of pyroxenes. *American Mineralogist* **73**, 1123-1133.

Nisbet, E.G. (1982). The tectonic setting and petrogenesis of komatiites. In: Arndt, N.T. & Nisbet, E.G. (eds.) *Komatiites*. London: George Allen & Unwin, pp. 501-520.

Peccerillo, A., Poli, G. & Serri, G. (1988). Petrogenesis of orenditic and kamafugitic rocks from central Italy. *Canadian Mineralogist* **26**, 45-65.

Pena, G.S. (1974). Geologia da Área do Projeto Goiânia II, Sudoeste de Goiás. *XXVIII Congresso Brasileiro de Geologia, Porto Alegre, Anais* **4**, 37-50.

Sahama, T.G. (1954). Mineralogy of mafurite. *Bulletin de la Comission Geologique de Finlande* **27**, 21-28.

Sahama, T.G. (1974). Potassium-rich alkaline rocks. In: Sørensen, H. (ed.) *The alkaline rocks*. New York: Wiley, pp. 2-5, 97-109.

Sahama, T.G., Neuvonen, K.J. & Hytonen, K. (1956). Determination of the composition of kalsilites by an X-ray method. *Mineralogical Magazine* **31**, 200.

Schobbenhaus, C., Ribeiro, C.L., Oliva, L.A., Takanohashi, J.T., Lindenmayer, Z.G., Vasconcelos, J.B. & Orlandi, V. (1975). Carta Geológica do Brasil ao milionésimo; Folha Goiás (SD.22). DNPM/MME, Brasília, 114p.

Sgarbi, P.B.A. (1991). *Petrografia e geoquímica da Formação Mata da Corda na região de Carmo do Paranaíba, MG,* M.Sc. Dissertation, Federal University of Rio de Janeiro, 214p.

Sgarbi, P.B.A. (1998). *Mineralogia e petrologia dos kamafugitos da região de Santo Antônio da Barra, sudoeste de Goiás*. Ph.D. Thesis, University of Brasilia, 226p.

Sgarbi, P.B.A. & Gaspar, J.C. (2002). Geochemistry of Santo Antônio da Barra kamafugites, Goiás, Brazil. *Journal of South America Earth Sciences* **14**, 889-901.

Sgarbi, P.B.A. & Valença, J.G. (1993). Kalsilite in Brazilian kamafugitic rocks. *Mineralogical Magazine* **57**, 165-171.

Sgarbi, P.B.A. & Valença, J.G. (1994). Mineral and rock chemistry of the Mata da Corda kamafugitic rocks (MG state, Brazil). *International Symposium on the Physics and Chemistry of the Upper Mantle, São Paulo, Extended Abstracts*, pp. 27-29.

Sgarbi, P.B.A. & Valença, J.G. (1995). Mineral and rock chemistry of Mata da Corda kamafugitic rocks (Minas Gerais, State, Brazil). *Anais da Academia Brasileira de Ciências* **27**, 257-269.

Sgarbi, P.B.A., Clayton, R.N., Toshiko, K.M. & Gaspar, J.C. (1998). Oxygen isotope thermometry of Brazilian potassic volcanic rocks of kamafugitic affinities. *Chemical Geology* **146**, 115-126.

Sgarbi, P.B.A., Gaspar, J.C. & Valença, J.G. (2000b). Clinopyroxene from Brazilian kamafugites. *Lithos* **53**, 101-116.

Sgarbi, P.B.A., Gaspar, J.C. & Valença, J.G. (2000c). Brazilian kamafugites. *Revista Brasileira de Geociências* **30**, 417-420.

Sgarbi, P.B.A., Heaman, L.M. & Gaspar, J.C. (2000a). U-Pb Perovskite ages for Brazilian kamafugites. *XXXI International Geological Congress, Rio de Janeiro, Abstracts,* CD-ROM.

Sgarbi, P.B.A., Heaman, L.M. & Gaspar, J.C. (2004). U-Pb perovskite ages for Brazilian kamafugitic rocks: further support for a temporal link to a mantle plume hotspot track. *Journal of South America Earth Sciences* **16**, 715-724.

Simkin, T. & Smith, J.V. (1970). Minor element distribution in olivine. *Journal of Geology* **78**, 304-325.

Sonoki, I.K. & Garda, G.M. (1988). Idades K-Ar de rochas alcalinas do Brasil Meridional e Paraguai Oriental: compilação e adaptação às novas constantes de decaimento. *Boletim IG-USP, Série Científica* **19**, 63-85.

Stoppa, F. & Cundari, A. (1995). A new Italian carbonatite occurrence at Cupaello (Rieti) and its genetic significance. *Contributions to Mineralogy and Petrology* **122**, 275-288.

Stoppa, F. & Cundari, A. (1998). Origin and multiple crystallisation of the kamafugite-carbonatite association: the San Venanzo-Pian di Celle occurrence (Umbria, Italy). *Mineralogical Magazine* **62**, 273-289.

Stormer Jr., J.C. (1973). Calcium zoning in olivine and its relationship to silica activity and pressure. *Geochimica Cosmochimica Acta* **37**, 1815-1821.

Tompkins, L.A. (1987). Exploration for kimberlites in southwest Goiás region, Brazil: mineral chemistry of stream sediment samples. *Journal of Geochemical Exploration* **27**, 1-28.

Ulbrich, H.H.G.J. & Gomes, C.B. (1981). Alkaline rocks from continental Brazil. *Earth-Science Reviews* **17**, 135-154.

Van Decar, J.C., James, D.E. & Assumpção, M. (1995). Seismic evidence for a fossil mantle plume beneath South America and implications for plate driving forces. *Nature* **378**, 25-31.

Van Thienen, P., Vlaar, N.J. & van den Berg, A.P. (2004). Plate tectonics on terrestrial planets. *Physics of Earth Planetary Interiors* **142**, 61-74.

Wilson, M. (1989). *Igneous petrogenesis - A global tectonic approach*. London: Harper Collins, 466p.

Woolley, A.R. (1987). Alkaline rocks and carbonatites of the world. Part 1: North and South America. London: British Museum (Natural History), 216p.

*Mesozoic to Cenozoic Alkaline Magmatism in the Brazilian Platform*
*Comin-Chiaramonti, P. & Gomes, C.B. (eds.)*
*Edusp/Fapesp, São Paulo, pp. 261-316, 2005*

# SOME NOTES ON THE ALTO PARANAÍBA IGNEOUS PROVINCE

*C.B. Gomes and P. Comin-Chiaramonti*

*An integrated synthesis of the available data, i.e. concentrations of major and trace elements and Sr-Nd-Pb isotope ratios, is herein presented in order to assess the mantle sources involved in the genesis of the Alto Paranaíba (APIP) magmatic occurrences (Late Cretaceous kamafugites, kimberlites, peridotites, basanites and associated carbonatites). The data cover a relatively large range of isotope compositions, which are accompanied by systematic changes in incompatible trace element ratios and Sr-Nd-Pb isotopes, indicating contributions from different mantle sources. The remarkable isotope differences between APIP rocks, N-MORB and a hypothetical Trindade plume indicate that asthenospheric sources did not play a significant role in the genesis of the APIP rocks. It is here put forward the hypothesis of melting of a veined lithospheric mantle.*

## INTRODUCTION

Attempts to sort out the Brazilian alkaline magmatic occurrences into different geographic provinces were made by e.g. Herz (1977) and by Ulbrich & Gomes (1981) on the basis of petrographic, geochronological and geological evidences. Almeida (1983), reviewing the Upper Jurassic to Eocene alkaline occurrences in Bolivia, Brazil, Paraguay and Uruguay, expanded the previous classifications by including some intrusions bordering the Paraná Basin in Bolivia (Velasco and Candelaria Provinces) and Uruguay (Mariscala Province). In Brazil, Almeida (1983) proposed the following provinces: Poços de Caldas, Alto Paranaíba, Rio Verde-Iporá, Piratini, Santa Catarina, Arco de Ponta Grossa, Ipanema and Serra do Mar.

In particular, the Alto Paranaíba province predominates in western Minas Gerais state (Gibson *et al.*, 1995a) and represents one of the most voluminous potassic provinces of the world (>$20x10^5$ $km^3$), probably extending from the Rio Verde-Iporá area (Goiás state) to roughly 1500 km southeast to the area of Bambuí and Poços de Caldas (?).

The aim of this report is to present a synthesis of the available petrochemical and Sr-Nd-Pb isotope data related to the various magmatic rock-types occurring in the Alto Paranaíba igneous province (APIP). In particular, the silicate rock-types will be taken into account. The associated carbonatites are discussed in the two detailed studies by Comin-Chiaramonti *et al*. included in this volume.

## THE ALTO PARANAÍBA ALKALINE PROVINCE

Alkaline rocks are widespread along the Alto Paranaíba uplift (cf. Hasui, 1975). A large number of intrusions and lava flows were emplaced during Late Cretaceous in/over Proterozoic metamorphosed and deformed supracrustal sequences referred to as the *Brasília mobile belt*. The latter is a suture that possibly welds the São Francisco craton in the East to a hypothetical ancient cratonic nucleus to the West (Leonardos & Fife, 1974). The Brasília mobile belt represents a strongly folded terrain for which the isotope data indicate peak metamorphism ages of 790 and 630-610 Ma (Pimentel *et al*., 1997). Pimentel *et al*. (1999) suggesting an early rift stage between 1.77 and 1.60 Ga and a collisional stage between 0.90 and 0.60 Ga on the basis of isotopic evidence from the granitic rocks associated with the mobile belt.

The Alto Paranaíba igneous province (APIP) consists of the volcanic rocks of the Mata da Corda Formation, major alkaline-carbonatite complexes and minor alkaline intrusions (Fig. 1). Its southeastern fringe is bounded by the large alkaline complex of Poços de Caldas, at the boundary with the Taiúva-Cabo Frio lineament (inset of Fig. 1).

The province corresponds to a strong Bouguer gradient anomaly, indicative of a probable suture zone between the São Francisco craton and the Paraná Basin (James *et al*., 1993; Van Decar *et al*., 1995 and therein references).

The different rock-types from the APIP, other than carbonatites, are represented by various suites of potassic/ultrapotassic, mafic/ultramafic, strongly silica-undersaturated lavas and by hypabissal intrusions with ages between 80-90 Ma (Bizzi *et al*., 1993, 1994, 1995; Meyer *et al*., 1994; Gibson *et al*., 1995a, b; Brod *et al*., 2000; Araújo *et al*., 2001). Spinel and garnet mantle xenoliths are also reported (Meyer *et al*., 1994; Danni & Gaspar, 1994).

Three major silicate rock types/group have been identified, i.e. kamafugites, kimberlites and peridotites. Phoscoritic, glimmeritic, melilitic and basanitic-ankaratritic rocks are occasionally present. The latter usually represent sodic varieties.

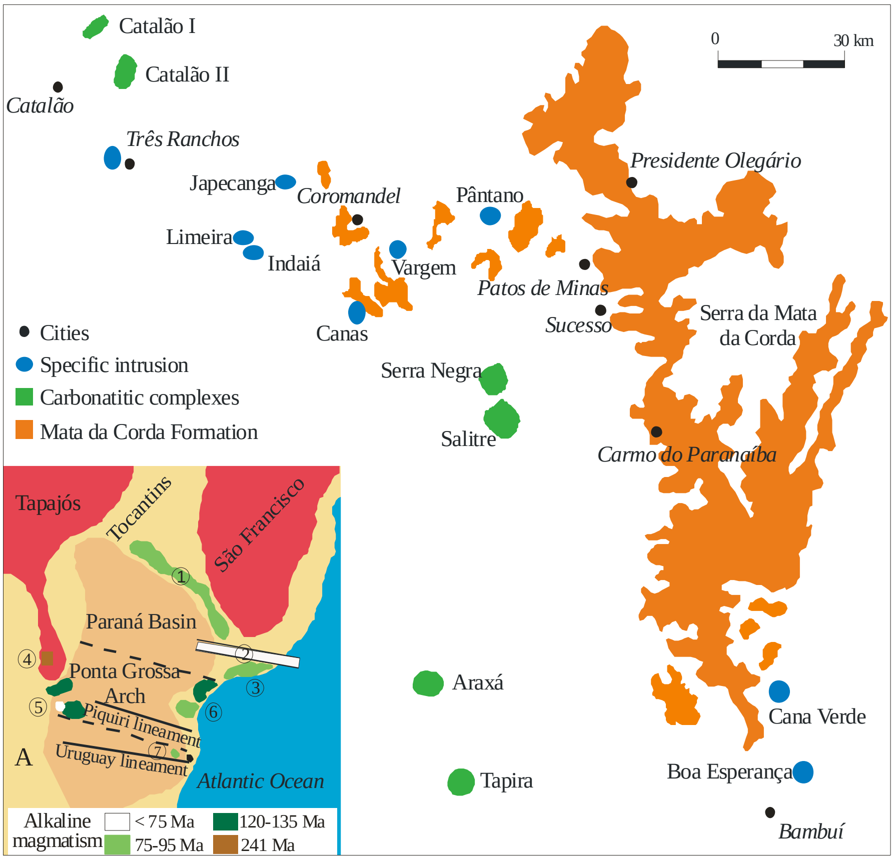


Fig. 1. Sketch-map showing the main alkaline outcrops in the Alto Paranaíba region (Meyer *et al.*, 1994, modified). **Inset**: schematic structural map representing the main areas of the alkaline outcrops in and around the Paraná Basin (modified after Almeida, 1983; Trompette, 1994; Gomes *et al.*, 1996).

*Kamafugites* (cf. Sgarbi & Valença, 1993; Bizzi *et al.*, 1994; Sgarbi *et al.*, 2000; Brod *et al.*, 2000) generally form lava flows characterized by high proportion of clinopyroxene, which is found not only as phenocrysts but also in the groundmass, associated with perovskite, magnetite±olivine±phlogopite±melilite±monticellite. Pseudomorphs of kalsilite, nepheline and leucite are ubiquitous along with accessory apatite and occasional wadeite. The more evolved rock-types contain aegirine-augite.

*Kamafugitic dykes* are also widespread and have abundant olivine and phlogopite both as phenocrysts and groundmass phases.

*Kimberlites* show high contents of modal olivine and minor amounts of diopside, Mg-ilmenite, phlogopite, chromite and occasional garnet set in a groundmass of carbonates, serpentine±perovskite±apatite±monticellite. (cf. Meyer *et al.*, 1994; Carlson *et al.*, 1996 and therein references).

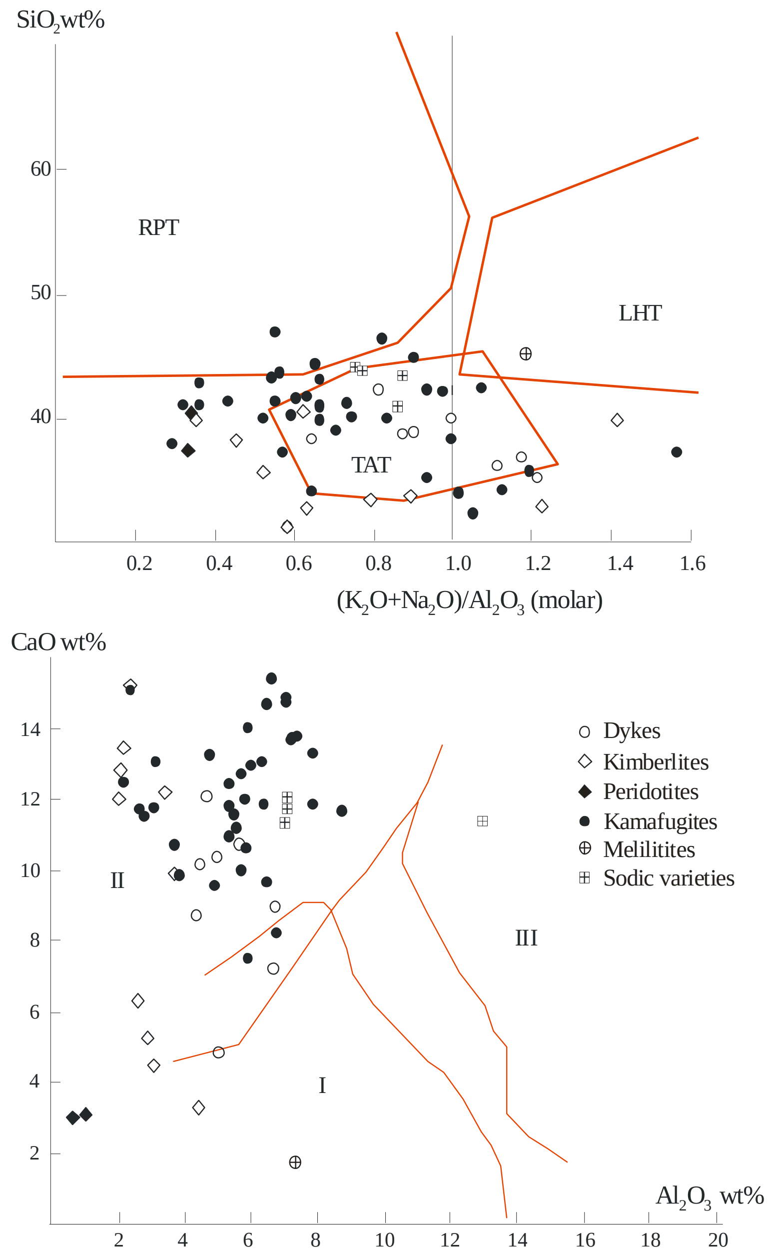


Fig. 2. Alto Paranaíba magmatic rocks: molar $(K_2O+Na_2O)/Al_2O_3$ vs. $SiO_2$ (wt% on a water-free basis) (LHT, Leucite Hills; TAT, Toro-Ankole; RPT, Roman Province type lavas; after Barton, 1979) and CaO vs. $Al_2O_3$ (Group I, LHT; Group II, TAT; and Group III, RPT; after Foley *et al.*, 1987). Data source: Bizzi *et al.* (1993, 1994, 1995); Danni & Gaspar (1994); Toyoda *et al.* (1994); Meyer *et al.* (1994); Gibson *et al.* (1995a, b); Araújo *et al.* (2001); Comin-Chiaramonti, unpublished data.

*Peridotites* are usually found as xenoliths in kimberlites and are represented by spinel lherzolites, harzburgites and dunites. Some melilite-rich xenoliths (melilitites) are noticeable.

*Glimmerites* and *phoscorites* form small dykes or veins that are usually associated with the carbonatite complexes. The former mainly consist of olivine surrounded by phlogopite laths. The latter substantially represent cumulates of magnetite, olivine, clinopyroxene and apatite

The rare *ankaratrite* and *basanite* dykes are melanocratic, biotite-bearing, olivine nephelinite, and rocks with dominant clinopyroxene, plagioclase, nepheline and olivine, respectively.

## PETROCHEMISTRY

The APIP rocks (Fig. 2; cf. Table 1, major oxides wt%, recalculated on a water-free basis) fit the TAT field of Barton (1979). Foley *et al.* (1987), using a CaO-$Al_2O_3$ diagram, recognized three end-member compositional groups that roughly correspond to those proposed by Barton, i.e. Group I (Leucite Hills type, LHT), Group II (Toro-Ankole type, TAT) and Group III (Roman Province type, RPT). Although this classification specifically refers to rock-types considered ultrapotassic (i.e., $K_2O/Na_2O>2$, $K_2O>3$ wt% and MgO>3 wt%) and only 13% of the APIP kamafugites conform with this definition, it is interesting to note that the RPT rocks fall in the Group II of Foley *et al.* (1987).

In particular, the kamafugites (lava flows and intrusive varieties) yielded (wt%) MgO= 17.60±5.46, $TiO_2$=5.25±1.61, $Al_2O_3$=5.36±1.83, CaO=12.44± 1.84 and $K_2O$=2.15±0.79 vs. MgO= 20.96±2.96, $TiO_2$=5.34±1.00, $Al_2O_3$=5.55±0.91, CaO=9.32±1.56 and $K_2O$=3.31±1.32 of the dykes. These values are well distinct from those of kimberlites that display higher MgO (34.35±2.35 wt%) and lower $TiO_2$, $Al_2O_3$ and CaO (2.08±0.64, 3.36±0.64 and 6.87±3.43 wt%, respectively), in the range of the associated peridotite xenoliths.

The variation diagrams (MgO vs. major oxides; Fig. 3) show a major olivine control for the kamafugitic types, the isolated field of the kimberlites+mantle xenoliths and the large variations of K, Na and P.

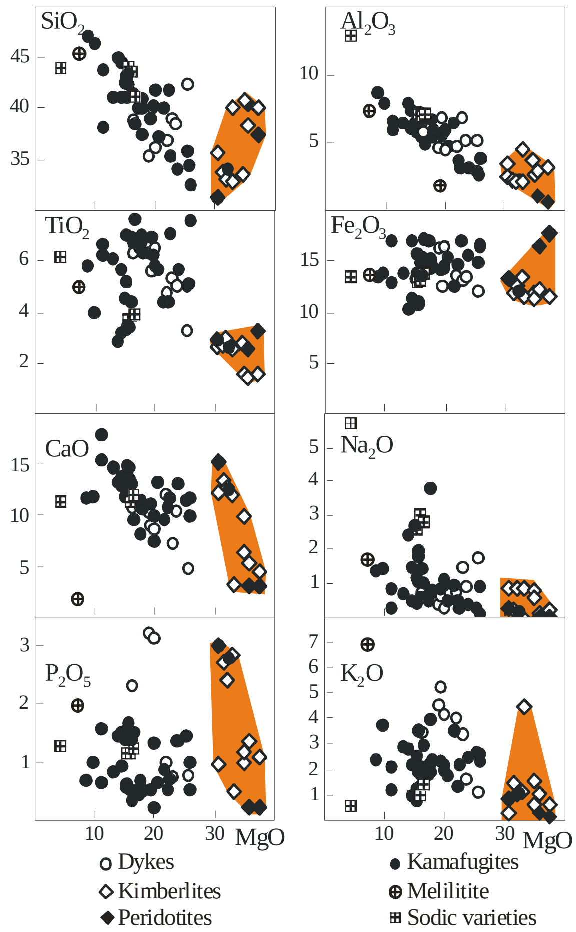


Fig. 3. Correlation of MgO vs. major oxides. Orange field: kimberlites+ultramafic xenoliths. Data source as in Fig. 2.

Trace elements exhibit wide ranges for both compatible and incompatible elements (Fig. 4): Ni contents are related to the amounts of olivine; similarly, the Cr reflects higher proportions of clinopyroxene in peridotites and in some kimberlites and kamafugites; kamafugites and kimberlites yielded a Th/U ratio around 5.7, quite distinct from that of the associated carbonatites (~2.3); Zr/Hf, Nb/Ta and La/Yb ratios show mainly ranges of 30-55, 12-21 and 70-200, respectively. On the whole, the comparison between compatible elements (e.g. Cr) and highly incompatible elements (e.g. Zr) indicates heterogeneous strongly enriched sources with initial Zr contents between 200 and 700 ppm (Fig. 4).

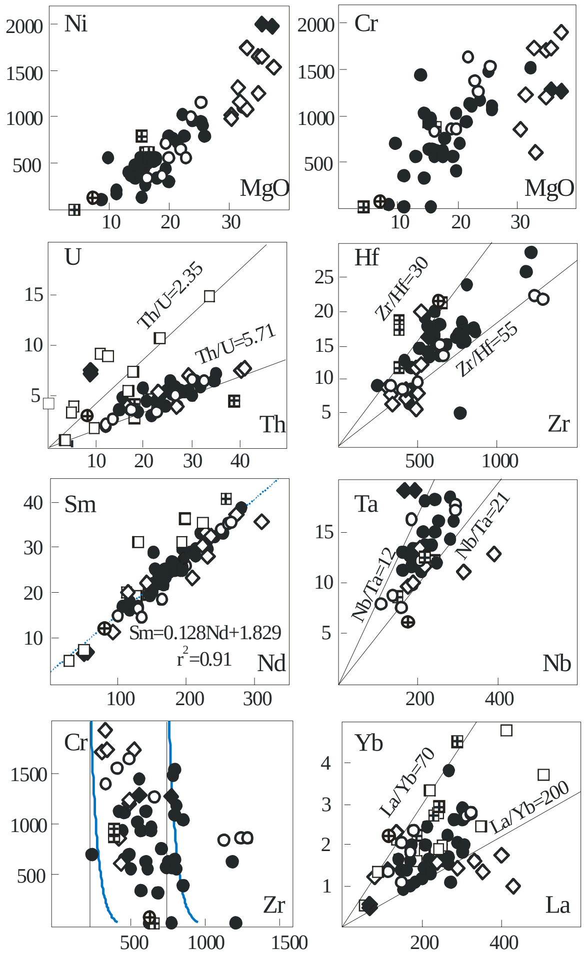


Fig. 4. Trace elements relationships. Open square: carbonatites; other symbols as in Fig. 3.

In spite of the observed large variations of the icompatible elements, the Sm/Nd ratio correlation is linear ($r^2$=0.91; cf. Fig. 4).

Incompatible elements, normalized to a primitive mantle composition (Fig. 5), for both different rock-types and single occurrences, show different behaviours. Melilitite displays negative spikes for Th, Sr-P, Sm and Tb, and positive spikes for Ba, K, Hf and Ti. Peridotites show negative spikes for Rb, K, Sr-P, Sm and Ti, and positive ones for U-Ta, La-Ce, Nd and Hf-Zr. Kimberlites and kamafugitic dykes have similar characteristics with common negative spikes, in particular for K, Sr-P and Hf, and positive spikes for La-Ce and Nd. The kamafugitic lavas, the intrusions and the sodic rock-types parallel to some extent the kamafugitic dykes, but exhibiting strong variation in the Ba contents.

Chondrite-normalized REE distribution (Fig. 5) displays similar behaviours with strong LREE/HREE fractionation, i.e. $(La/Yb)_C$: melilitite 35, peridotites 76-98, kimberlites 91-155, kamafugitic dykes 71-78, kamafugitic lava-flows 50-112, kamafugitic intrusions 61-136. Eu/Eu* (Sm-Tb normalization) presents negative anomalies in kimberlites, peridotites and kamafugitic dykes (0.77-0.92) and shows wide ranges in the kamafugitic intrusions and lava flows (0.70-1.56). Usually, positive Eu/Eu* anomalies are followed by strong Gd/Gd* anomalies (up to 2.22).

Considering the high MgO contents and Cr (Ni) vs. Zr relationships (Fig. 4), the REE distribution likely represents the products of partial melts of enriched (and veined) mantle sources rather than lherzolite or harzburgite mantle xenoliths.

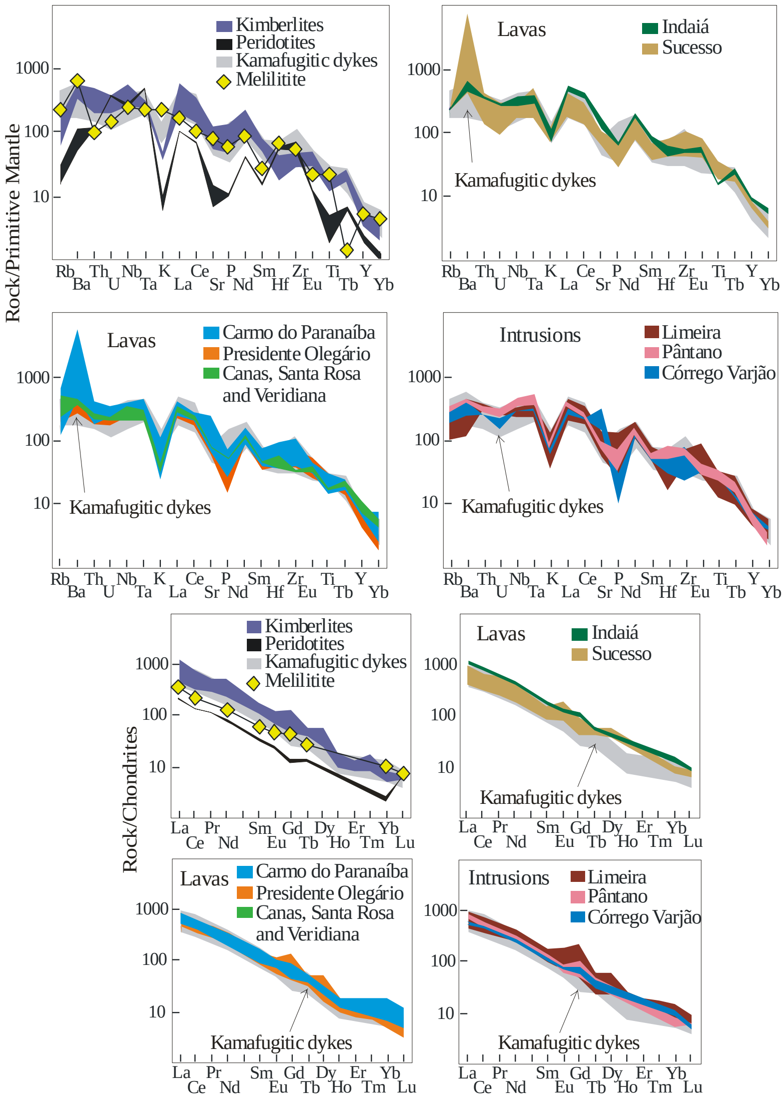


Fig. 5. Incompatible elements normalized to primitive mantle concentrations (Sun & McDonough, 1989) and chondrite-normalized (Boynton, 1984) REE distribution for the various rock-types and occurrences from the Alto Paranaíba region. Data source as in Fig. 2.

## MANTLE SOURCES

The strong LREE/HREE ratios of APIP magmas require melting of peridotite sources with an unrealistic high proportion of garnet in the solid residua. Notionally, for 3% of batch melting, the garnet proportion in APIP peridotite residua is higher than 14 wt% (Comin-Chiaramonti *et al.*, 1997). However, if portions of the mantle present suitable compositions (e.g. phlogopite-amphibole-rich veins), it is possible to obtain compositions similar to those of the APIP kamafugites through batch melting processes.

In the APIP lavas, some phlogopite-olivine-K-richterite-clinopyroxene xenoliths (Comin-Chiaramonti, unpublished data) may represent to some extent portions of a veined mantle. Mass balance calculations, starting from variously metasomatized mantle compositions (cf. Table 2), indicate that the APIP compositions of possible primary melts may be derived from relatively high melting degrees, i.e. 4-11%. The calculated trace elements (see Comin-Chiaramonti *et al.*, 1997 for discussion) are in consonance with the observed concentrations (Fig. 6).

Table 1. Representative whole-rock analyses for the different rock-types and localities of the Alto Paranaíba region. Data source: Bizzi *et al.* (1993, 1994, 1995); Danni & Gaspar (1994); Toyoda *et al.* (1994); Meyer *et al.* (1994); Gibson *et al.* (1995a); Araújo *et al.* (2001); Comin-Chiaramonti, unpublished data. Major oxides wt%, recalculated on a water-free basis. $T^{DM}$ values: calculation of model dates relative to a depleted reservoir, $^{143}Nd/^{144}Nd = 0.513114$ and $^{147}Sm/^{144}Nd = 0.222$, after Faure (1986).

| Locality | CATALÃO I | | | | | | | | CATALÃO II | |
|---|---|---|---|---|---|---|---|---|---|---|
| Age (Ma) | 87 | | | | | | | | 87 | |
| Rock-type | Kamafugite Dyke | Phoscorite Vein | Phoscorite Vein | Ca-carbonatite (søvite) | Mg-carbonatite (beforsite) | Mg-carbonatite (beforsite) carbonate fraction | Mg-carbonatite drill 56/07 N=11 | | Kamafugite Dyke | Kamafugite Dyke |
| wt% | | | | | | | | | | |
| $SiO_2$ | 38.77 | | | | | | | | 36.21 | 35.26 |
| $TiO_2$ | 6.28 | | | | 0.01 | | | | 6.51 | 6.34 |
| $Al_2O_3$ | 5.72 | | | | | | | | 4.42 | 4.53 |
| $Fe_2O_3$ | 15.45 | | | | | | | | 16.43 | 16.38 |
| FeO | | | | 0.24 | 1.58 | | | | | |
| MnO | 0.24 | | | 0.05 | 0.27 | | | | 0.28 | 0.24 |
| MgO | 16.27 | | | 1.17 | 19.90 | | | | 19.91 | 18.97 |
| CaO | 10.73 | | | 54.38 | 31.10 | | | | 8.72 | 10.16 |
| $Na_2O$ | 0.72 | | | 0.03 | 0.07 | | | | 0.25 | 0.35 |
| $K_2O$ | 3.48 | | | | 0.07 | | | | 4.16 | 4.55 |
| $P_2O_5$ | 2.33 | | | | 1.47 | | | | 3.11 | 3.21 |
| L.O.I. | 4.01 | | | 44.12 | 45.74 | | | | 2.63 | 1.59 |
| A.I. | 0.87 | | | | | | | | 1.11 | 1.21 |
| ppm | | | | | | | | | | |
| Cr | 836 | 1260 | | | | | | | 862 | 854 |
| Ni | 353 | 650 | | | | | | | 551 | 358 |
| Rb | 275 | 254 | 123.7 | <0.1 | <0.1 | 2.2 | | | 272 | 278 |
| Ba | 4051 | 1700 | 419 | 1730 | 1740 | 2063 | | | 3477 | 4119 |
| Th | | 34.1 | 10.0 | 4.17 | 78 | 17.8 | 18.46 | (13.40) | 32.8 | 30.3 |
| U | | 15.0 | 2.0 | 0.42 | | 0.69 | 3.00 | (0.93) | 6.45 | 6.71 |
| Nb | 302 | 26672 | | | | 15.80 | 96.71 | (60.79) | 296 | 294 |
| Ta | | 41.6 | 41 | 0.81 | 23.5 | 0.82 | 5.01 | (3.15) | 17.10 | 17.67 |
| Sr | 1619 | 3200 | 2218 | 15300 | 4000 | 9800 | | | 1246 | 1804 |
| Pb | | 5.1 | 5.08 | 1.79 | | | | | | |
| Zr | 1120 | 210 | 215 | | | 5.3 | 120.88 | (53.76) | 1285 | 1232 |
| Hf | | 8.2 | 8 | | 1.2 | | | | 21.81 | 22.27 |
| Y | 34 | 26 | | 20 | 23 | 23.5 | 85.93 | (23.03) | 37.1 | 36.3 |
| La | 311 | 243 | 247 | 193 | 204 | 216 | 5642 | -1547 | 325 | 325 |
| Ce | 633 | 557 | 542 | 375 | 449 | 447 | 9826 | -2335 | 688 | 636 |
| Pr | | | 63.2 | | | 55.8 | 1142 | -323 | | |
| Nd | 251 | 196 | 323.2 | 114 | 130 | 200.9 | 3831 | -1038 | 265 | 260 |
| Sm | 34 | 30.7 | 46.7 | 19.9 | 31.4 | 36.0 | 355 | -77 | 35.5 | 35.10 |
| Eu | 8.3 | 7.1 | 12.0 | 4.98 | 7.13 | 8.82 | 69.9 | (12.0) | 8.75 | 8.58 |
| Gd | | | 15.5 | | | 20.37 | 188.5 | (32.9) | 9.10 | 9.30 |
| Tb | 2.8 | 2.6 | 3.3 | 1.9 | 2.50 | 3.04 | 14.1 | (2.6) | 3.02 | 2.87 |
| Dy | | | | | | 15.26 | 29.8 | (6.5) | | |
| Ho | | | | | | | 3.23 | (0.71) | 1.16 | 1.42 |
| Er | | | | | | 6.35 | 6.78 | (1.19) | | |
| Tm | | | | | | 0.66 | 0.57 | (0.12) | 0.50 | 0.30 |
| Yb | 2.7 | 2.7 | 1.86 | 1.61 | 1.73 | 3.34 | 2.59 | (0.62) | 2.75 | 2.82 |
| Lu | | 0.32 | 0.16 | 0.14 | 0.19 | 0.39 | 0.24 | (0.07) | 0.29 | 0.27 |
| Measured ratios | | | | | | | | | | |
| $^{87}Sr/^{86}Sr$ | 0.705407 | 0.705542 | 0.70523 | 0.705248 | 0.705195 | 0.705231 | | | 0.705559 | 0.705372 |
| $^{143}Nd/^{144}Nd$ | 0.512249 | | 0.51232 | | | 0.512274 | | | 0.512242 | 0.512255 |
| $^{206}Pb/^{204}Pb$ | | 20.466 | 18.11 | 17.904 | 17.788 | | | | | |
| $^{207}Pb/^{204}Pb$ | | 15.640 | 15.43 | 15.496 | 15.503 | | | | | |
| $^{208}Pb/^{204}Pb$ | | 40.503 | 38.56 | 38.875 | 38.417 | | | | | |
| Initial ratios | | | | | | | | | | |
| $^{87}Sr/^{86}Sr$ | 0.70480 | 0.70526 | 0.70503 | 0.70525 | 0.70519 | 0.70523 | | | 0.70478 | 0.70482 |
| $^{143}Nd/^{144}Nd$ | 0.51220 | | 0.51227 | | | 0.51221 | | | 0.51220 | 0.51221 |
| $^{206}Pb/^{204}Pb$ | | 17.90 | | 17.71 | 17.52 | | | | | |
| $^{207}Pb/^{204}Pb$ | | 15.52 | | 15.49 | 15.49 | | | | | |
| $^{208}Pb/^{204}Pb$ | | 38.59 | | 38.25 | 38.37 | | | | | |
| εSr | 2.85 | 9.35 | 6.12 | 9.21 | 8.46 | 8.96 | | | 2.54 | 3.15 |
| εNd | -6.31 | | -4.99 | | | -6.12 | | | -6.44 | -6.19 |
| $T^{DM}$Ga | 1.00 | | 1.02 | | | 1.21 | | | 1.01 | 1.00 |

Table 1 (continued).

| Locality | CATALÃO II | | TRÊS RANCHOS | | | | | JAPECANGA | |
|---|---|---|---|---|---|---|---|---|---|
| Age (Ma) | 87 | | 85 | | | | | 85 | |
| Rock-type | Kamafugite Dyke | Ca-carbonatite (søvite) | Kimberlite Intrusion | Kimberlite Intrusion | Kimberlite Intrusion | Kimberlite Intrusion | Kamafugite Dyke | Peridotite Xenolith | Peridotite Xenolith |
| wt% | | | | | | | | | |
| $SiO_2$ | | | 39.95 | 40.66 | 38.83 | 33.48 | 40.12 | 40.46 | 37.47 |
| $TiO_2$ | | | 1.55 | 1.56 | 1.41 | 2.77 | 4.43 | 2.59 | 3.29 |
| $Al_2O_3$ | | | 3.11 | 2.63 | 2.89 | 3.72 | 6.46 | 1.05 | 0.67 |
| $Fe_2O_3$ | | | 11.46 | 11.30 | 12.29 | 11.84 | 12.55 | 16.50 | 17.72 |
| FeO | | | | | | | | | |
| MnO | | | 0.22 | 0.23 | 0.27 | 0.23 | 0.19 | 0.22 | 0.20 |
| MgO | | | 37.33 | 34.86 | 35.62 | 34.79 | 21.51 | 35.58 | 37.26 |
| Cao | | | 4.43 | 6.28 | 5.22 | 9.84 | 9.60 | 3.07 | 2.98 |
| $Na_2O$ | | | 0.22 | 0.56 | 0.10 | 0.78 | 0.95 | 0.02 | 0.02 |
| $K_2O$ | | | 0.67 | 0.66 | 1.05 | 1.55 | 3.51 | 0.29 | 0.17 |
| $P_2O_5$ | | | 1.07 | 1.17 | 1.36 | 1.00 | 0.87 | 0.22 | 0.21 |
| L.O.I. | | | | 13.60 | 11.22 | 10.84 | 4.05 | 14.24 | 12.56 |
| A.I. | | | 0.35 | 0.62 | 0.45 | 0.79 | 0.83 | 0.34 | 0.33 |
| ppm | | | | | | | | | |
| Cr | 512 | | 1913 | 1712 | 1725 | 1200 | 930 | 1280 | 1270 |
| Ni | | | 1530 | 1650 | 1647 | 1250 | 730 | 1999 | 1974 |
| Rb | 267 | 2.20 | 38 | 47.9 | 53.61 | 93.60 | 294 | 18.4 | 9.5 |
| Ba | 5400 | 2750 | 2659 | 3130 | 2730 | 3850 | 3400 | 760 | 335 |
| Th | 18 | 0.99 | 40.4 | 29.6 | 41.0 | | | 9.0 | 9.1 |
| U | 5.2 | | 7.5 | 7.08 | 7.70 | | | 7.6 | 7.2 |
| Nb | | | 216 | 392 | 317 | 254 | 174 | 166 | 193 |
| Ta | 10 | 0.84 | 11.5 | 12.8 | 11.0 | | | 19 | 19 |
| Sr | 2523 | 13346 | 1143 | 1811 | 1814 | 1770 | 1995 | 294 | 142 |
| Pb | | | | 19.5 | 12.6 | | | 3 | 5.8 |
| Zr | | | 332 | 307 | 342 | 490 | 452 | 561 | 770 |
| Hf | 16.4 | 0.13 | 7.54 | 8.76 | 6.5 | 5.6 | 6.4 | 16.1 | 16.4 |
| Y | | | 26.0 | 32.2 | 22 | 16.1 | 25.5 | 8.8 | 8.3 |
| La | 264 | 251 | 402 | 352 | 429 | 137 | 173 | 71.2 | 68.1 |
| Ce | 438 | 1010 | 601 | 582 | 614 | 259 | 374 | 116 | 117 |
| Pr | 54 | 101 | | 61.9 | 59.5 | | | 14.6 | 14.9 |
| Nd | 218 | 440 | 229 | 208.4 | 310.4 | 141.0 | 159.0 | 50.1 | 55.1 |
| Sm | 28.2 | 53 | 33.4 | 23.49 | 35.7 | 22.0 | 23.5 | 6.5 | 7.0 |
| Eu | 6.9 | 15.0 | 5.84 | 5.48 | 6.3 | 5.0 | 5.4 | 1.8 | 1.9 |
| Gd | 12.2 | 27.9 | 13.4 | 28.10 | 11.8 | 15.8 | 18.8 | 3.7 | 3.3 |
| Tb | 1.9 | 6.9 | 1.39 | 1.96 | 1.8 | | | 0.69 | 0.62 |
| Dy | | | | 12.80 | | 7.8 | 7.7 | | |
| Ho | | | 0.67 | 0.86 | | 1.31 | 1.52 | | |
| Er | | | | 1.78 | | 2.78 | 2.78 | | |
| Tm | 0.36 | 0.60 | | 0.22 | 0.26 | | | | |
| Yb | 1.35 | 1.98 | 1.75 | 1.34 | 1.01 | 1.33 | 1.61 | 0.55 | 0.47 |
| Lu | 0.23 | 0.23 | 0.17 | 0.19 | 0.19 | | | 0.16 | 0.17 |
| Measured ratios | | | | | | | | | |
| $^{87}Sr/^{86}Sr$ | 0.70592 | 0.70525 | 0.704774 | 0.705021 | 0.705175 | 0.705185 | 0.707339 | 0.70612 | 0.70598 |
| $^{143}Nd/^{144}Nd$ | 0.51227 | 0.51226 | 0.512349 | 0.512323 | 0.512305 | 0.512314 | 0.512127 | 0.51223 | 0.51230 |
| $^{206}Pb/^{204}Pb$ | 18.22 | | | 18.985 | 19.24 | 18.638 | 17.935 | 19.62 | 20.96 |
| $^{207}Pb/^{204}Pb$ | 15.50 | | | 15.544 | 15.57 | 15.538 | 15.521 | 15.59 | 15.68 |
| $^{208}Pb/^{204}Pb$ | 38.80 | | | 39.61 | 40.15 | 39.589 | 38.864 | 38.34 | 39.67 |
| Initial ratios | | | | | | | | | |
| $^{87}Sr/^{86}Sr$ | 0.70541 | 0.70525 | 0.70466 | 0.70493 | 0.70507 | 0.70511 | 0.70682 | 0.70590 | 0.70575 |
| $^{143}Nd/^{144}Nd$ | 0.51223 | 0.51222 | 0.51230 | 0.51229 | 0.51227 | 0.51226 | 0.51208 | 0.51219 | 0.51226 |
| $^{206}Pb/^{204}Pb$ | 17.53 | | | 18.63 | 18.68 | | | 18.30 | 18.73 |
| $^{207}Pb/^{204}Pb$ | 15.44 | | | 15.53 | 15.54 | | | 15.53 | 15.58 |
| $^{208}Pb/^{204}Pb$ | 38.20 | | | 39.13 | 39.08 | | | 37.79 | 38.80 |
| εSr | 13.38 | 9.23 | 0.80 | 4.64 | 6.67 | 7.22 | 31.54 | 18.45 | 16.25 |
| εNd | -5.86 | -6.00 | -4.46 | -4.75 | -5.12 | -5.21 | -8.80 | -6.68 | -5.29 |
| $T^{DM}$Ga | 0.96 | 0.93 | 0.94 | 0.84 | 0.86 | 1.02 | 1.20 | 1.04 | 0.91 |

Table 1 (continued).

| Locality | BOCAINA | | LIMEIRA | | | | | | | | |
|---|---|---|---|---|---|---|---|---|---|---|---|
| Age (Ma) | 85 | | 85 | | | | | | | | |
| Rock-type | Kama-fugite Dyke | Kama-fugite Dyke | Kama-fugite Intrusion | Kama-fugite Intrusion | Kama-fugite Intrusion | Kama-fugite Intrusion | Kama-fugite Intrusion | Kama-fugite Intrusion | Kimber-lite Intrusion | Kimber-lite Intrusion | Kimber-lite Intrusion |
| wt% | | | | | | | | | | | |
| $SiO_2$ | 38.94 | 36.87 | 43.31 | 34.11 | 43.22 | 45.01 | 32.38 | 37.34 | 33.75 | 32.77 | 32.97 |
| $TiO_2$ | 5.30 | 4.74 | 3.45 | 2.67 | 3.32 | 2.88 | 7.56 | 6.99 | 2.70 | 2.66 | 2.96 |
| $Al_2O_3$ | 6.77 | 4.75 | 7.06 | 2.18 | 7.06 | 7.88 | 3.84 | 6.75 | 2.20 | 2.04 | 2.11 |
| $Fe_2O_3$ | 13.18 | 13.70 | 10.98 | 12.10 | 10.85 | 10.31 | 16.56 | 14.37 | 11.87 | 13.44 | 12.67 |
| FeO | | | | | | | | | | | |
| MnO | 0.17 | 0.21 | 0.20 | 0.22 | 0.19 | 0.20 | 0.22 | 0.19 | 0.24 | 0.24 | 0.23 |
| MgO | 22.85 | 21.88 | 15.60 | 32.29 | 15.29 | 13.87 | 25.83 | 17.71 | 31.40 | 32.93 | 31.96 |
| CaO | 7.23 | 12.08 | 14.69 | 12.45 | 14.82 | 13.24 | 9.82 | 8.19 | 13.40 | 11.95 | 12.76 |
| $Na_2O$ | 1.47 | 0.75 | 1.07 | 0.16 | 1.14 | 2.44 | 0.92 | 3.79 | 0.22 | 0.02 | 0.86 |
| $K_2O$ | 3.37 | 4.02 | 1.90 | 1.04 | 2.56 | 2.85 | 2.32 | 3.98 | 1.46 | 1.16 | 1.08 |
| $P_2O_5$ | 0.73 | 1.00 | 1.67 | 2.77 | 1.54 | 1.44 | 0.54 | 0.68 | 2.71 | 2.83 | 2.41 |
| L.O.I. | 1.27 | 0.91 | 3.38 | 1.10 | 1.44 | 5.57 | 7.63 | 12.43 | 11.03 | 9.26 | 11.44 |
| A.I. | 0.90 | 1.17 | 0.54 | 0.64 | 0.66 | 0.90 | 1.05 | 1.56 | 0.89 | 0.63 | 1.22 |
| ppm | | | | | | | | | | | |
| Cr | 1390 | 1631 | 938 | 1521 | 923 | 1437 | 1111 | 571 | 1230 | 1725 | 2874 |
| Ni | 560 | 650 | 438 | 1110 | 393 | 372 | 790 | 550 | 1321 | 1747 | 1168 |
| Rb | 178 | 187 | 176 | 92 | 169 | 65 | 153 | 128 | 114 | 102 | 100 |
| Ba | 2502 | 2276 | 25200 | 2782 | 2937 | 3038 | 820 | 2800 | 2850 | 2351 | 2566 |
| Th | 22.6 | 26.5 | 26.1 | 27.0 | 30.9 | 29.0 | | | 16.7 | 23.0 | 32.0 |
| U | 3.41 | 5.08 | 5.25 | 5.40 | 6.46 | | | | 3.99 | 5.49 | |
| Nb | 136 | 206 | 190 | 162 | 179 | | 225 | 173 | 176 | 188 | |
| Ta | 8.85 | 12.16 | 9.76 | 13.01 | 12.67 | 15 | | | 9.70 | 9.99 | 16 |
| Sr | 1079 | 1673 | 2490 | 1818 | 2900 | 2987 | 1162 | 2268 | 2540 | 2278 | 2401 |
| Pb | | | 31.4 | | | | | | 8.6 | 8.0 | |
| Zr | 330 | 498 | 574 | 794 | 640 | 564 | 460 | 770 | 491 | 521 | 529 |
| Hf | 9.06 | 9.52 | 13.2 | 15.65 | 17.94 | 14 | 8.6 | 5.0 | 11.6 | 12.3 | 20 |
| Y | 11.4 | 23.2 | 39.0 | 37.3 | 39.5 | | 21.4 | 27.7 | 31.3 | 29.0 | |
| La | 149 | 180 | 309 | 302 | 303 | | 152 | 140 | 241 | 291 | |
| Ce | 304 | 418 | 536 | 598 | 583 | | 312 | 305 | 450 | 480 | |
| Pr | | | 70.5 | | | | | | 55.2 | 49.0 | |
| Nd | 134 | 163 | 226.1 | 254 | 240 | 213 | 148.3 | 151.9 | 224.6 | 229.8 | 236.7 |
| Sm | 14.5 | 18.7 | 30.70 | 33.30 | 32.60 | 29.51 | 20.28 | 28.84 | 30.25 | 27.90 | 32.41 |
| Eu | 3.83 | 4.65 | 14.60 | 8.85 | 8.79 | | 5.00 | 5.70 | 7.25 | 8.49 | |
| Gd | | | 57.5 | 24.8 | 22.4 | | 12.2 | 18.4 | 33.7 | 15.4 | |
| Tb | 1.34 | 1.65 | 3.03 | 2.18 | 2.71 | | | | 2.76 | 2.41 | |
| Dy | | | 19.6 | | | | 7.3 | 8.2 | 18.0 | | |
| Ho | | 0.91 | 1.41 | | | | 1.43 | 1.35 | 1.21 | | |
| Er | | | 2.82 | | | | 2.76 | 2.96 | 2.30 | | |
| Tm | | | 0.35 | 0.31 | 0.32 | | | | 0.26 | 0.53 | |
| Yb | 2.05 | 2.35 | 2.03 | 1.86 | 2.89 | | 1.39 | 1.66 | 1.58 | 1.44 | |
| Lu | 0.16 | 0.16 | 0.27 | 0.19 | 0.28 | | | | 0.21 | 0.22 | |
| Measured ratios | | | | | | | | | | | |
| $^{87}Sr/^{86}Sr$ | 0.705486 | 0.705341 | 0.705724 | 0.705436 | 0.705739 | 0.70631 | 0.705524 | 0.705711 | 0.705435 | 0.70543 | 0.70536 |
| $^{143}Nd/^{144}Nd$ | 0.512252 | 0.512340 | 0.512318 | 0.512235 | 0.512301 | 0.51228 | 0.512400 | 0.512188 | 0.512299 | 0.51228 | 0.51229 |
| $^{206}Pb/^{204}Pb$ | | | 17.753 | | | | 18.619 | 17.976 | 18.139 | 17.97 | 18.122 |
| $^{207}Pb/^{204}Pb$ | | | 15.386 | | | | 15.528 | 15.497 | 15.510 | 15.46 | 15.526 |
| $^{208}Pb/^{204}Pb$ | | | 38.33 | | | | 39.142 | 38.455 | 38.83 | 38.68 | 38.918 |
| Initial ratios | | | | | | | | | | | |
| $^{87}Sr/^{86}Sr$ | 0.70543 | 0.70495 | 0.70548 | 0.70526 | 0.70570 | 0.70623 | 0.70506 | 0.70551 | 0.70528 | 0.70527 | 0.70521 |
| $^{143}Nd/^{144}Nd$ | 0.51222 | 0.51230 | 0.51227 | 0.51228 | 0.51226 | 0.51223 | 0.51235 | 0.51212 | 0.51225 | 0.51224 | 0.51224 |
| $^{206}Pb/^{204}Pb$ | | | 17.39 | | | | | | 17.69 | 17.41 | |
| $^{207}Pb/^{204}Pb$ | | | 15.37 | | | | | | 15.49 | 15.43 | |
| $^{208}Pb/^{204}Pb$ | | | 37.76 | | | | | | 38.23 | 37.89 | |
| εSr | 11.73 | 4.95 | 12.43 | 9.34 | 13.26 | 23.17 | 6.56 | 12.95 | 9.60 | 9.55 | 8.70 |
| εNd | -6.11 | -4.43 | -5.00 | -4.83 | -5.33 | -5.76 | -3.40 | -7.89 | -5.36 | -5.65 | -5.55 |
| $T^{DM}$Ga | 0.93 | 0.83 | 0.93 | 0.90 | 0.95 | 0.98 | 0.84 | 1.41 | 0.95 | 0.91 | 0.96 |

Table 1 (continued).

| Locality | INDAIÁ | | | COROMANDEL | | | PÂNTANO | | | | | |
|---|---|---|---|---|---|---|---|---|---|---|---|---|
| Age (Ma) | 85 | | | 85 | | | 85 | | | | | |
| Rock-type | Kama-fugite Lava flow | Kama-fugite Lava flow | Kimber-lite Pipe | Kama-fugite Dyke | Kama-fugite Dyke | Kama-fugite Dyke | Kama-fugite Intrusion | Kama-fugite Intrusion | Kama-fugite Intrusion | Kama-fugite Intrusion | Kama-fugite Intrusion | Kama-fugite Intrusion |
| wt% | | | | | | | | | | | | |
| $SiO_2$ | 42.26 | 44.45 | 31.30 | 40.04 | 38.37 | 42.37 | 34.01 | 35.84 | | 35.24 | | 34.37 |
| $TiO_2$ | 3.38 | 3.20 | 2.91 | 5.62 | 5.06 | 3.27 | 5.69 | 5.03 | | 7.08 | | 5.09 |
| $Al_2O_3$ | 7.18 | 7.39 | 2.40 | 6.82 | 5.06 | 5.08 | 3.17 | 2.83 | | 3.08 | | 2.65 |
| $Fe_2O_3$ | 10.86 | 11.36 | 13.38 | 12.51 | 13.52 | 12.13 | 15.65 | 14.83 | | 16.97 | | 16.64 |
| FeO | | | | | | | | | | | | |
| MnO | 0.19 | 0.21 | 0.24 | 0.18 | 0.19 | 0.16 | 0.26 | 0.24 | | 0.20 | | 0.26 |
| MgO | 15.66 | 14.46 | 30.50 | 19.41 | 23.52 | 25.40 | 23.84 | 25.35 | | 22.52 | | 25.66 |
| CaO | 13.61 | 13.71 | 15.14 | 8.99 | 10.37 | 7.83 | 13.00 | 11.47 | | 11.71 | | 11.66 |
| $Na_2O$ | 1.94 | 1.50 | 0.29 | 0.65 | 0.90 | 1.75 | 0.35 | 0.29 | | 0.29 | | 0.11 |
| $K_2O$ | 3.50 | 2.19 | 0.85 | 5.24 | 1.63 | 1.15 | 2.45 | 2.66 | | 2.21 | | 2.58 |
| $P_2O_5$ | 1.41 | 1.52 | 2.99 | 0.54 | 1.37 | 0.76 | 1.36 | 1.45 | | 0.70 | | 0.99 |
| L.O.I. | 1.99 | 6.64 | 12.70 | 1.35 | 2.03 | 1.05 | 7.38 | 1.08 | | 10.31 | | 6.11 |
| A.I. | 0.97 | 0.65 | 0.58 | 0.99 | 0.64 | 0.81 | 1.01 | 1.19 | | 0.93 | | 1.12 |
| ppm | | | | | | | | | | | | |
| Cr | 970 | 1026 | 2600 | 2805 | 1260 | 1539 | 1173 | 1485 | | 1116 | | 1080 |
| Ni | 375 | 343 | 994 | 707 | 1005 | 1170 | 959 | 947 | | 788 | | 902 |
| Rb | 145 | 141 | 49 | 329 | 180 | 179 | 183 | 202 | 144.7 | 171.0 | 201.7 | 166 |
| Ba | 3184 | 4490 | 3451 | 2159 | 2244 | 1812 | 2980 | 2974 | | 2751 | | 2580 |
| Th | 29.5 | 32.0 | 27.0 | 17.4 | 13.5 | 12.3 | 25.4 | 22.7 | | 27.0 | | 26.0 |
| U | 5.61 | 5.99 | 4.00 | 3.70 | 2.84 | 2.24 | 6.39 | 4.55 | | | | 5.89 |
| Nb | 183 | 253 | 204 | 185 | 160 | 109 | 324 | 233 | | | | 288 |
| Ta | 11.58 | 16.01 | 13.41 | 16.13 | 7.57 | 7.93 | 21.20 | 13.73 | | | | 16.00 |
| Sr | 2433 | 3431 | 2687 | 1179 | 1493 | 1066 | 2029 | 1470 | 1766 | 1850 | 1784 | 1846 |
| Pb | | | | | | | 9.14 | | | | | 8.39 |
| Zr | 638 | 548 | 503 | 642 | 659 | 408 | 806 | 782 | | 608 | | 798 |
| Hf | 13.43 | 19.00 | 8.01 | 15.06 | 13.60 | 8.51 | 23.89 | 15.33 | | 20 | | 17.19 |
| Y | 38.2 | 43.0 | 40.0 | 22.9 | 23.2 | 19.5 | 30.7 | 20.4 | | | | 23.0 |
| La | 303 | 367 | 333 | 170 | 151 | 117 | 270 | 219 | | | | 274 |
| Ce | 599 | 726 | 670 | 289 | 311 | 238 | 468 | 380 | | | | 435 |
| Pr | | | | | | | 60 | | | | | 42 |
| Nd | 232 | 281 | 272 | 130 | 129 | 100 | 195 | 151 | 178.7 | 191.9 | 194.8 | 185 |
| Sm | 31.6 | 38.6 | 37.21 | 16.4 | 16.9 | 14.9 | 24.86 | 22.3 | 26.69 | 24.83 | 25.55 | 24.83 |
| Eu | 8.27 | 10.1 | 7.50 | 4.23 | 4.36 | 3.79 | 6.63 | 4.50 | | | | 6.50 |
| Gd | 24.2 | 29.6 | 23.5 | 12.8 | 9.3 | | 28.7 | | | | | 12.3 |
| Tb | 2.45 | 2.99 | | 1.34 | 1.25 | 1.16 | 2.31 | 1.52 | | | | 1.60 |
| Dy | | | | | | | 15.5 | | | | | |
| Ho | 1.16 | | | 0.57 | 0.58 | | 1.12 | | | | | |
| Er | | | | | | | 2.21 | | | | | |
| Tm | 0.40 | | | 0.30 | | | 0.25 | | | | | |
| Yb | 2.62 | 2.18 | 1.62 | 1.83 | 1.11 | 1.35 | 1.53 | 1.68 | | | | 1.09 |
| Lu | 0.25 | 0.30 | 0.16 | 0.15 | 0.13 | 0.17 | 0.20 | 0.17 | | | | 0.17 |
| Measured ratios | | | | | | | | | | | | |
| $^{87}Sr/^{86}Sr$ | 0.705712 | 0.70590 | 0.70528 | 0.705727 | 0.705399 | 0.706093 | 0.705637 | 0.705678 | 0.70548 | 0.70561 | 0.70570 | 0.705637 |
| $^{143}Nd/^{144}Nd$ | 0.512261 | 0.51221 | 0.512231 | 0.512288 | 0.512211 | 0.512175 | 0.512292 | 0.512379 | 0.51234 | 0.51233 | 0.51232 | 0.512292 |
| $^{206}Pb/^{204}Pb$ | | | | | | | 18.429 | | 18.474 | | 18.355 | 18.410 |
| $^{207}Pb/^{204}Pb$ | | | | | | | 15.496 | | 15.527 | | 15.504 | 15.507 |
| $^{208}Pb/^{204}Pb$ | | | | | | | 38.98 | | 39.181 | | 38.94 | 39.03 |
| Initial ratios | | | | | | | | | | | | |
| $^{87}Sr/^{86}Sr$ | 0.70550 | 0.70576 | 0.70522 | 0.70475 | 0.70498 | 0.70551 | 0.70532 | 0.70520 | 0.70519 | 0.70529 | 0.70531 | 0.70532 |
| $^{143}Nd/^{144}Nd$ | 0.51222 | 0.51216 | 0.51226 | 0.51224 | 0.51217 | 0.51218 | 0.51225 | 0.51233 | 0.51229 | 0.51229 | 0.51223 | 0.51225 |
| $^{206}Pb/^{204}Pb$ | | | | | | | 17.75 | | | | | 17.73 |
| $^{207}Pb/^{204}Pb$ | | | | | | | 15.46 | | | | | 15.28 |
| $^{208}Pb/^{204}Pb$ | | | | | | | 38.11 | | | | | 38.16 |
| εSr | 12.81 | 16.39 | 8.73 | 2.14 | 5.34 | 12.85 | 10.23 | 8.47 | 8.40 | 9.73 | 9.99 | 10.23 |
| εNd | -6.11 | -7.12 | -5.16 | -5.52 | -7.06 | -7.88 | -5.45 | -3.89 | -4.66 | -4.70 | -4.89 | -5.45 |
| $T^{DM}$Ga | 0.99 | 1.06 | 0.94 | 0.92 | 1.03 | 1.15 | 0.92 | 0.91 | 0.96 | 0.88 | 0.96 | 0.92 |

Table 1 (continued).

| Locality<br>Age (Ma) | CANAS<br><br>85 | | SANTA ROSA<br>85 | VERIDIANA<br><br>85 | SERRA NEGRA<br>85 | SALITRE<br><br>85 | | SUCESSO<br><br>85 | | |
|---|---|---|---|---|---|---|---|---|---|---|
| Rock-type | Basanite Lava flow | Basanite Lava flow | Basanite Lava flow | Basanite Lava flow | Kamafugite Dyke | Kimberlite Intrusion | Kimberlite Intrusion | Kamafugite Lava flow | Kamafugite Lava flow | Kamafugite Lava flow |
| wt% | | | | | | | | | | |
| $SiO_2$ | 43.49 | | 44.12 | 41.01 | 41.87 | 35.69 | 39.96 | 38.49 | 46.44 | 43.75 |
| $TiO_2$ | 3.72 | | 3.73 | 3.91 | 5.83 | 2.62 | 2.59 | 7.63 | 4.01 | 6.21 |
| $Al_2O_3$ | 7.01 | | 7.12 | 7.09 | 5.90 | 3.41 | 4.42 | 4.91 | 7.87 | 6.63 |
| $Fe_2O_3$ | 13.10 | | 12.95 | 13.74 | 14.52 | 13.28 | 11.60 | 17.25 | 13.77 | 13.03 |
| FeO | | | | | | | | | | |
| MnO | 0.21 | | 0.21 | 0.22 | 0.21 | 0.21 | 0.22 | 0.22 | 0.18 | 0.26 |
| MgO | 15.98 | | 15.43 | 16.55 | 19.91 | 30.48 | 33.01 | 16.51 | 9.76 | 11.15 |
| CaO | 11.27 | | 11.68 | 12.01 | 7.46 | 12.17 | 3.26 | 9.52 | 11.80 | 15.35 |
| $Na_2O$ | 3.03 | | 2.60 | 2.78 | 0.96 | 0.87 | 0.85 | 1.00 | 1.43 | 0.84 |
| $K_2O$ | 1.00 | | 0.99 | 1.38 | 2.00 | 0.30 | 4.45 | 2.96 | 3.75 | 2.13 |
| $P_2O_5$ | 1.13 | | 1.14 | 1.22 | 1.34 | 0.95 | 0.50 | 1.52 | 0.99 | 0.66 |
| L.O.I. | 4.09 | | 1.60 | 1.55 | 1.05 | 11.37 | 14.06 | 5.12 | 5.82 | 7.51 |
| A.I. | 0.87 | | 0.75 | 0.86 | 0.63 | 0.52 | 1.41 | 0.99 | 0.82 | 0.56 |
| ppm | | | | | | | | | | |
| Cr | 940 | | 918 | 884 | 408 | 860 | 608 | 624 | 697 | 347 |
| Ni | 626 | | 795 | 615 | 316 | 1020 | 1085 | 563 | 559 | 205 |
| Rb | 144 | 249.5 | 333 | 161 | 110 | 21.1 | 187 | 173 | 149.25 | 176 |
| Ba | 2510 | | 2640 | 3140 | 1203 | 1500 | 2150 | 3120 | 2979 | 49900 |
| Th | 22.9 | | 18.2 | 20.9 | 24.4 | | | 19 | 12 | 34.7 |
| U | 4.32 | | 4.25 | 4.76 | 4.02 | | | 3.4 | 2.0 | 6.40 |
| Nb | 219 | | 150 | 245 | 186 | 136 | 158 | 206 | 116 | 276 |
| Ta | 12.40 | | 8.56 | 12.20 | 9.80 | | | 12 | | 20.39 |
| Sr | 1632 | 1687 | 1668 | 1771 | 934 | 1450 | 733 | 2248 | 1374 | 1815 |
| Pb | 17.4 | | 23.2 | 16.4 | | | | 12.3 | 9.4 | 17.6 |
| Zr | 388 | | 387 | 387 | 859 | 425 | 433 | 1181 | 496 | 566 |
| Hf | 17.20 | | 11.70 | 18.70 | 16.97 | 7.2 | 8.5 | 25.8 | | 17.90 |
| Y | 53.5 | | 34.8 | 54.0 | 28.3 | 19.9 | 13.0 | 30 | 31 | 38.8 |
| La | 242 | | 188 | 229 | 263 | 116 | 84 | 197 | 122 | 292 |
| Ce | 440 | | 365 | 423 | 446 | 238 | 181 | 366 | 249 | 545 |
| Pr | 52.3 | | 41.4 | 49.8 | | | | 38.6 | | 70.2 |
| Nd | 164.4 | 156.1 | 144.0 | 162.3 | 193 | 116 | 92 | 150.6 | 107.1 | 230.8 |
| Sm | 22.21 | 21.5 | 19.70 | 22.00 | 29.5 | 20.0 | 11.37 | 20.40 | 17.00 | 29.76 |
| Eu | 6.58 | | 5.56 | 6.24 | 7.38 | 4.40 | 2.60 | 6.90 | | 13.89 |
| Gd | 28.0 | | 27.7 | 27.7 | 20.0 | 14.6 | 12.2 | 10.9 | | 23.7 |
| Tb | 2.56 | | 2.22 | 2.42 | 2.20 | | | 1.90 | | 2.75 |
| Dy | 16.3 | | 14.0 | 15.5 | | 6.8 | 4.4 | | | 18.3 |
| Ho | 1.68 | | 1.20 | 1.50 | 1.27 | 1.38 | 1.29 | | | 1.37 |
| Er | 3.77 | | 2.68 | 3.38 | | 2.92 | 2.59 | | | 2.79 |
| Tm | 0.48 | | 0.35 | 0.44 | 0.50 | | | | | 0.34 |
| Yb | 2.95 | | 2.23 | 2.73 | 2.22 | 1.39 | 1.22 | 1.51 | | 2.06 |
| Lu | 0.43 | | 0.32 | 0.41 | 0.25 | | | 0.21 | | 0.27 |
| Measured ratios | | | | | | | | | | |
| $^{87}Sr/^{86}Sr$ | 0.706256 | 0.70634 | 0.706334 | 0.706561 | 0.704764 | 0.705457 | 0.706901 | 0.70586 | 0.70678 | 0.706251 |
| $^{143}Nd/^{144}Nd$ | 0.512224 | 0.51221 | 0.512233 | 0.512227 | 0.512329 | | 0.512251 | 0.51210 | 0.51214 | 0.512270 |
| $^{206}Pb/^{204}Pb$ | 17.478 | 17.383 | 17.397 | 17.515 | | 19.225 | 18.472 | 17.70 | 17.07 | 18.144 |
| $^{207}Pb/^{204}Pb$ | 15.410 | 15.409 | 15.398 | 15.421 | | 15.615 | 15.603 | 15.45 | 15.31 | 15.473 |
| $^{208}Pb/^{204}Pb$ | 38.21 | 38.084 | 38.02 | 38.15 | | 39.787 | 39.046 | 38.25 | 38.16 | 38.52 |
| Initial ratios | | | | | | | | | | |
| $^{87}Sr/^{86}Sr$ | 0.70595 | 0.70582 | 0.70564 | 0.70624 | 0.70435 | 0.70541 | 0.70600 | 0.70556 | 0.70640 | 0.70591 |
| $^{143}Nd/^{144}Nd$ | 0.51218 | 0.51216 | 0.51219 | 0.51218 | 0.51228 | | 0.51221 | 0.51205 | 0.51209 | 0.51222 |
| $^{206}Pb/^{204}Pb$ | 17.24 | | 17.22 | 17.24 | | | | 17.57 | 17.07 | 17.79 |
| $^{207}Pb/^{204}Pb$ | 15.40 | | 15.39 | 15.41 | | | | 15.44 | 15.31 | 15.46 |
| $^{208}Pb/^{204}Pb$ | 37.81 | | 37.78 | 37.76 | | | | 38.00 | 37.84 | 37.91 |
| $\varepsilon Sr$ | 19.10 | 17.34 | 14.69 | 23.30 | -3.53 | 11.42 | 20.00 | 14.05 | 25.53 | 18.60 |
| $\varepsilon Nd$ | -6.83 | -7.12 | -6.67 | -6.77 | -4.90 | | -6.23 | -9.25 | -8.62 | -5.89 |
| $T^{DM}Ga$ | 1.03 | 1.06 | 1.03 | 1.03 | 0.99 | | 0.95 | 1.17 | 1.25 | 0.95 |

Table 1 (continued).

| Locality | PRESIDENTE OLEGÁRIO | | | | | | | | | |
|---|---|---|---|---|---|---|---|---|---|---|
| Age (Ma) | 85 | | | | | | | | | |
| Rock-type | Kama-fugite Lava flow | Kama-fugite Lava flow | Kama-fugite Lava flow | Kama-fugite Lava flow | Kama-fugite Lava flow | Kama-fugite Lava flow | Kama-fugite Lava flow | Kama-fugite Lava flow | Kama-fugite Lava flow | Kama-fugite Lava flow |
| wt% | | | | | | | | | | |
| $SiO_2$ | 41.10 | 41.39 | 39.99 | 40.31 | 41.16 | 41.75 | 40.03 | 40.99 | 39.06 | 41.47 |
| $TiO_2$ | 7.03 | 6.71 | 6.76 | 6.53 | 6.10 | 4.43 | 6.51 | 6.29 | 6.93 | 6.93 |
| $Al_2O_2$ | 5.72 | 5.82 | 5.36 | 5.50 | 6.47 | 3.71 | 5.32 | 5.87 | 5.56 | 5.33 |
| $Fe_2O_3$ | 15.71 | 15.21 | 15.00 | 15.18 | 13.86 | 14.64 | 16.98 | 14.45 | 14.12 | 14.80 |
| FeO | | | | | | | | | | |
| MnO | 0.21 | 0.22 | 0.20 | 0.21 | 0.24 | 0.23 | 0.22 | 0.20 | 0.19 | 0.18 |
| MgO | 15.31 | 16.33 | 17.70 | 17.57 | 13.06 | 22.20 | 17.34 | 17.92 | 19.32 | 15.99 |
| CaO | 12.66 | 11.98 | 11.79 | 11.52 | 14.63 | 10.69 | 10.91 | 10.59 | 11.13 | 12.37 |
| $Na_2O$ | 0.40 | 0.59 | 0.69 | 0.72 | 0.70 | 0.46 | 0.47 | 0.79 | 0.85 | 0.60 |
| $K_2O$ | 1.30 | 1.41 | 2.23 | 1.88 | 2.88 | 1.35 | 1.85 | 2.41 | 2.31 | 1.81 |
| $P_2O_5$ | 0.56 | 0.33 | 0.58 | 0.58 | 0.84 | 0.51 | 0.43 | 0.49 | 0.52 | 0.52 |
| L.O.I. | 1.70 | 1.26 | 2.00 | 2.32 | 7.90 | 9.17 | 5.72 | 3.65 | 4.03 | 5.12 |
| A.I. | 0.36 | 0.43 | 0.66 | 0.59 | 0.66 | 0.60 | 0.52 | 0.66 | 0.70 | 0.55 |
| ppm | | | | | | | | | | |
| Cr | 635 | 567 | 630 | 566 | 558 | 1129 | 582 | 752 | 570 | 650 |
| Ni | 534 | 509 | 556 | 557 | 412 | 1032 | 528 | 338 | 440 | 270 |
| Rb | 146 | 183 | 260 | 205 | 124 | 120 | 201 | 150 | 150 | 160 |
| Ba | 19400 | 11672 | 5977 | 14628 | 12700 | 1910 | 6540 | 10748 | 11644 | 11656 |
| Th | 30.2 | | 28.2 | 28.9 | 27.7 | 15.0 | 25.0 | | | |
| U | 5.0 | | 5.43 | 5.35 | 5.59 | 3.62 | 5.6 | | | |
| Nb | 243 | 238 | 220 | 217 | 245 | 165 | 214 | 200 | 192 | |
| Ta | 15.0 | | 13.67 | 17.89 | 18.2 | 11.2 | 15 | | | |
| Sr | 1926 | 1933 | 3659 | 2732 | 1823 | 1234 | 2278 | 1250 | 1310 | 1650 |
| Pb | | | | | 14.8 | 7.57 | 10.7 | | | |
| Zr | 757 | 805 | 608 | 615 | 508 | 422 | 744 | 710 | 790 | 800 |
| Hf | 16.77 | | 16.54 | 17.87 | 14.70 | 12.80 | 16.2 | | | |
| Y | 28.0 | 24.0 | 19.9 | 20.6 | 33.8 | 24.9 | 23 | 30 | 38 | |
| La | 223 | | 251 | 207 | 270 | 163 | 202 | 173 | 153 | 183 |
| Ce | 415 | | 446 | 421 | 481 | 307 | 364 | 348 | 294 | 340 |
| Pr | | | | | 61.7 | 35.4 | 46.8 | | | |
| Nd | 168 | 184 | 205 | 181 | 212.6 | 116.7 | 170.2 | 159 | 147 | 168 |
| Sm | 25.3 | 26.1 | 29.0 | 25.0 | 28.08 | 15.96 | 23.9 | 23.4 | 19.2 | 23.9 |
| Eu | 6.06 | | 7.02 | 6.97 | 8.59 | 4.44 | 6.6 | 5.5 | 4.2 | 5.1 |
| Gd | 19.8 | | 19.5 | 18.9 | 34.9 | 17.5 | 12.2 | 13.4 | 11.0 | 13.5 |
| Tb | 2.41 | | 1.92 | 2.36 | 2.52 | 1.53 | 1.7 | | | |
| Dy | | | | | 16.9 | 9.97 | | 6.2 | 4.8 | 6.1 |
| Ho | 0.76 | | 1.29 | | 1.29 | 0.90 | | 1.0 | 0.7 | 1.0 |
| Er | | | | | 2.52 | 1.84 | | 2.0 | 1.6 | 2.4 |
| Tm | 0.30 | | 0.40 | 0.40 | 0.30 | 0.23 | | | | |
| Yb | 1.59 | | 1.60 | 1.42 | 1.71 | 1.40 | 1.18 | 1.00 | 0.91 | 1.09 |
| Lu | 0.17 | | 0.18 | 0.14 | 0.23 | 0.19 | 0.18 | 0.13 | 0.10 | 0.18 |
| Measured ratios | | | | | | | | | | |
| $^{87}Sr/^{86}Sr$ | 0.705573 | 0.705674 | 0.705258 | 0.705483 | 0.705724 | 0.705579 | 0.705625 | | | |
| $^{143}Nd/^{144}Nd$ | 0.512330 | 0.512357 | 0.512352 | 0.512328 | 0.512318 | 0.512349 | 0.512265 | | | |
| $^{206}Pb/^{204}Pb$ | | | | | 17.753 | 17.849 | 17.95 | | | |
| $^{207}Pb/^{204}Pb$ | | | | | 15.386 | 15.417 | 15.47 | | | |
| $^{208}Pb/^{204}Pb$ | | | | | 38.33 | 38.43 | 38.68 | | | |
| Initial ratios | | | | | | | | | | |
| $^{87}Sr/^{86}Sr$ | 0.70531 | 0.70534 | 0.70501 | 0.70522 | 0.70549 | 0.70524 | 0.70532 | | | |
| $^{143}Nd/^{144}Nd$ | 0.51228 | 0.51223 | 0.51230 | 0.51228 | 0.51227 | 0.51230 | 0.51222 | | | |
| $^{206}Pb/^{204}Pb$ | | | | | 17.39 | 17.39 | 17.64 | | | |
| $^{207}Pb/^{204}Pb$ | | | | | 15.37 | 15.39 | 15.46 | | | |
| $^{208}Pb/^{204}Pb$ | | | | | 37.76 | 37.82 | 37.88 | | | |
| εSr | 10.03 | 10.52 | 5.80 | 8.79 | 12.56 | 9.05 | 12.56 | | | |
| εNd | -4.86 | -4.28 | -4.37 | -4.82 | -4.98 | -4.40 | -4.98 | | | |
| $T^{DM}$Ga | 0.98 | 0.91 | 0.91 | 0.93 | 0.91 | 0.90 | 0.91 | | | |

Table 1 (continued).

| Locality | CARMO DO PARANAÍBA | | | | | CÓRREGO VARJÃO | | | SERRA DO BUENO | |
|---|---|---|---|---|---|---|---|---|---|---|
| Age (Ma) | 85 | | | | | 85 | | | 85 | |
| Rock-type | Kama-fugite Lava flow | Kama-fugite Lava flow | Kama-fugite Lava flow | Kama-fugite Lava flow | Kama-fugite Lava flow | Kama-fugite Sill | Kama-fugite Block | Melilitite xenolith | Kama-fugite Sill | Kama-fugite Sill |
| wt% | | | | | | | | | | |
| $SiO_2$ | 42.94 | 42.37 | 47.04 | 38.07 | 41.15 | 40.16 | 37.29 | 45.33 | 41.30 | 42.48 |
| $TiO_2$ | 5.16 | 3.38 | 5.80 | 6.69 | 5.67 | 6.27 | 5.70 | 4.95 | 4.39 | 4.51 |
| $Al_2O_3$ | 5.89 | 7.24 | 8.74 | 5.94 | 6.02 | 5.71 | 4.76 | 7.32 | 6.33 | 6.40 |
| $Fe_2O_3$ | 13.85 | 10.87 | 13.51 | 16.97 | 17.04 | 14.35 | 15.43 | 13.64 | 13.71 | 13.23 |
| FeO | | | | | | | | | | |
| MnO | 0.34 | 0.19 | 0.19 | 0.21 | 0.37 | 0.20 | 0.20 | 0.18 | 0.19 | 0.20 |
| MgO | 15.30 | 15.56 | 8.69 | 11.20 | 14.41 | 19.83 | 20.53 | 7.28 | 16.12 | 15.04 |
| CaO | 13.98 | 13.66 | 11.60 | 17.90 | 12.93 | 9.95 | 13.19 | 11.72 | 13.01 | 11.82 |
| $Na_2O$ | 1.18 | 1.78 | 1.37 | 0.28 | 0.50 | 1.11 | 0.46 | 0.69 | 1.41 | 2.70 |
| $K_2O$ | 0.76 | 3.53 | 2.38 | 1.17 | 1.00 | 2.22 | 1.79 | 6.92 | 2.14 | 2.21 |
| $P_2O_5$ | 0.61 | 1.40 | 0.68 | 1.57 | 0.92 | 0.21 | 0.64 | 1.97 | 1.39 | 1.39 |
| L.O.I. | 2.10 | 2.50 | 3.38 | 5.72 | 8.41 | 1.44 | 1.69 | 1.80 | 1.32 | 5.46 |
| A.I. | 0.36 | 0.93 | 0.55 | 0.29 | 0.32 | 0.74 | 0.57 | 1.18 | 0.73 | 1.07 |
| ppm | | | | | | | | | | |
| Cr | 649 | 28 | 37 | 28 | 332 | 1028 | 706 | 78 | | |
| Ni | 564 | 125 | 115 | 171 | 484 | 788 | 776 | 137 | | |
| Rb | 190 | 389 | 418 | 239 | 76.7 | 177 | 115 | 151 | 69 | 106 |
| Ba | 16274 | 3023 | 38611 | 36684 | 17660 | 2746 | 1590 | 4551 | | |
| Th | 23.5 | 15.57 | 35.2 | 26.7 | 20 | 21.8 | 20.5 | 8.4 | | |
| U | 5.11 | 4.80 | 7.16 | 5.97 | 5.7 | 3.18 | 4.53 | 3.13 | | |
| Nb | 189 | 246 | 283 | 280 | 208 | 203 | 199 | 176 | | |
| Ta | 13.27 | 12.00 | 18.36 | 14.27 | 11 | 11.59 | 12.18 | 6.20 | | |
| Sr | 1407 | 5191 | 1978 | 3018 | 2355 | 6203 | 2899 | 1739 | 2866 | 1907 |
| Pb | | | | | 9 | | | | | |
| Zr | 461 | 623 | 775 | 1209 | 686 | 853 | 244 | 625 | | |
| Hf | 11.71 | 15.07 | 18.31 | 28.63 | 15.2 | 17.63 | 9.00 | 21.40 | | |
| Y | 34.5 | 33.9 | 35.5 | 35.6 | 30 | 33.4 | 24.6 | 24.2 | | |
| La | 214 | 170 | 270 | 280 | 224 | 176 | 208 | 116 | | |
| Ce | 395 | 362 | 494 | 519 | 366 | 364 | 399 | 194 | | |
| Pr | | | | | 44.1 | | | | | |
| Nd | 167 | 118 | 220 | 197 | 173.4 | 147 | 168 | 81 | 154 | 146.9 |
| Sm | 21.6 | 18.3 | 33.2 | 27.7 | 24.4 | 20 | 23.3 | 12.0 | 25.4 | 21.8 |
| Eu | 5.30 | 5.28 | 7.82 | 7.37 | 6.5 | 5.20 | 5.95 | 3.75 | | |
| Gd | | 17.2 | 23.3 | | 11.9 | 14.9 | 20.9 | 11.9 | | |
| Tb | 1.88 | 1.85 | 2.68 | 2.19 | 1.9 | 1.45 | 1.39 | 1.33 | | |
| Dy | | | | | | | | | | |
| Ho | 0.93 | 0.85 | 1.35 | 1.08 | | 0.91 | | | | |
| Er | | | | | | | | | | |
| Tm | | | | | | | 0.24 | | | |
| Yb | 2.47 | 1.82 | 3.81 | 2.63 | 1.29 | 2.00 | 2.00 | 2.25 | | |
| Lu | 0.15 | 0.20 | 0.38 | 0.33 | 0.21 | 0.23 | 0.15 | 0.25 | | |
| Measured ratios | | | | | | | | | | |
| $^{87}Sr/^{86}Sr$ | 0.705704 | 0.704934 | 0.706503 | 0.705247 | 0.70586 | 0.705933 | 0.704807 | 0.705808 | 0.705259 | 0.705346 |
| $^{143}Nd/^{144}Nd$ | 0.512323 | 0.512440 | 0.512303 | 0.512278 | 0.51223 | 0.512193 | 0.512356 | 0.512292 | 0.512367 | 0.512323 |
| $^{206}Pb/^{204}Pb$ | | | | | 17.78 | | | | | 18.205 |
| $^{207}Pb/^{204}Pb$ | | | | | 15.47 | | | | | 15.521 |
| $^{208}Pb/^{204}Pb$ | | | | | 38.21 | | | | | 38.74 |
| Initial ratios | | | | | | | | | | |
| $^{87}Sr/^{86}Sr$ | 0.70523 | 0.70467 | 0.70576 | 0.70497 | 0.70575 | 0.70583 | 0.70467 | 0.70550 | 0.70518 | 0.70515 |
| $^{143}Nd/^{144}Nd$ | 0.51280 | 0.51239 | 0.51225 | 0.51223 | 0.51218 | 0.51215 | 0.51231 | 0.51224 | 0.51231 | 0.51227 |
| $^{206}Pb/^{204}Pb$ | | | | | 17.59 | | | | | 17.86 |
| $^{207}Pb/^{204}Pb$ | | | | | 15.46 | | | | | 15.50 |
| $^{208}Pb/^{204}Pb$ | | | | | 37.99 | | | | | 38.25 |
| εSr | 8.95 | 1.00 | 16.51 | 5.23 | 16.25 | 17.48 | 0.95 | 12.82 | 8.14 | 7.81 |
| εNd | -4.86 | -2.75 | -5.39 | -5.81 | -6.75 | -7.44 | -4.28 | -5.59 | -4.24 | -4.99 |
| $T^{DM}$Ga | 0.90 | 0.87 | 1.01 | 0.99 | 1.05 | 1.06 | 0.90 | 1.01 | 1.00 | 0.98 |

Table 1 (continued).

| Locality<br>Age (Ma) | ARAXÁ<br>83 | | | | | | TAPIRA<br>81 | | | | |
|---|---|---|---|---|---|---|---|---|---|---|---|
| Rock-type | Mg-carbonatite (beforsite) | Mg-carbonatite (beforsite) | Mg-carbonatite (beforsite) carbonate fraction | Mg-carbonatite (beforsite) carbonate fraction | Mg-carbonatite (beforsite) silicate fraction | Mg-carbonatite (beforsite) silicate fraction | Ca-carbonatite (sövite) | Ca-carbonatite (sövite) | Ca-carbonatite (sövite) carbonate fraction | Ca-carbonatite (sövite) carbonate fraction | Ca-carbonatite (sövite) silicate |
| wt% | | | | | | | | | | | |
| $SiO_2$ | 9.74 | 9.93 | | | | | 0.70 | | | | |
| $TiO_2$ | 2.86 | 2.90 | | | | | 0.33 | | | | |
| $Al_2O_3$ | 2.76 | 2.81 | | | | | 0.20 | | | | |
| $Fe_2O_3$ | | | | | | | | | | | |
| FeO | 11.13 | 9.75 | | | | | 10.13 | 0.12 | | | |
| MnO | 0.19 | 0.16 | | | | | 0.17 | 0.06 | | | |
| MgO | 18.10 | 16.54 | | | | | 6.35 | 3.85 | | | |
| CaO | 13.70 | 14.61 | | | | | 38.48 | 51.35 | | | |
| $Na_2O$ | 0.21 | 0.11 | | | | | 0.04 | 0.02 | | | |
| $K_2O$ | 5.21 | 4.45 | | | | | 0.12 | | | | |
| $P_2O_5$ | 0.22 | 0.19 | | | | | 0.05 | | | | |
| L.O.I. | 35.07 | 39.85 | | | | | 45.14 | 44.59 | | | |
| A.I. | | | | | | | | | | | |
| ppm | | | | | | | | | | | |
| Cr | | | | | | | | | | | |
| Ni | | | | | | | | | | | |
| Rb | 149 | 138 | 1.1 | | | | 7.4 | 0.1 | 2.2 | | |
| Ba | | | 1648 | | | | 2360 | 11600 | 4590 | | |
| Th | 18.21 | 16.97 | 23.1 | 5.505 | 11.618 | 12.944 | 5.73 | 0.68 | 0.76 | 0.334 | 26.153 |
| U | 7.18 | 5.45 | 10.9 | 3.247 | 8.937 | 8.707 | 3.84 | 9.69 | 9.36 | 4.110 | 24.997 |
| Nb | 27750 | 25514 | 2.1 | | | | | | | | |
| Ta | 16.5 | 14.9 | 1.22 | | | | 1.40 | 0.53 | 0.72 | | |
| Sr | 1150 | 1230 | 5937 | | | | 12200 | 9570 | 9452 | | |
| Pb | 5.09 | 5.05 | | 5.885 | 6.001 | 4.893 | 10.96 | 30.84 | 2.81 | 1.251 | 8.335 |
| Zr | 170 | 100 | 7.8 | | | | 110 | 18.4 | 2.8 | | |
| Hf | | | 0.19 | | | | 2.7 | 0.5 | 0.31 | | |
| Y | 54 | 44 | 89.8 | | | | 17.0 | 11.0 | 80.5 | | |
| La | 506 | 351 | 413 | | | | 90.2 | 62.2 | 135 | | |
| Ce | 1083 | 657 | 751 | | | | 112 | 90 | 324 | | |
| Pr | | | 90.3 | | | | | | 38.9 | | |
| Nd | 320 | 225 | 324 | | | | 47.0 | 31.7 | 125.4 | | |
| Sm | 50.6 | 35.1 | 50.1 | | | | 7.11 | 4.68 | 19.0 | | |
| Eu | 12.5 | 7.74 | 15.50 | | | | 1.56 | 1.25 | 4.62 | | |
| Gd | | | 34.81 | | | | | | 13.20 | | |
| Tb | 4.6 | 2.8 | 4.53 | | | | 0.55 | 0.33 | 1.61 | | |
| Dy | | | 21.67 | | | | | | 7.96 | | |
| Ho | | | 3.34 | | | | | | | | |
| Er | | | 8.55 | | | | | | 3.09 | | |
| Tm | | | 1.01 | | | | | | | | |
| Yb | 3.72 | 2.46 | 4.78 | | | | 1.37 | 0.53 | 2.10 | | |
| Lu | 0.47 | 0.26 | 0.74 | | | | 0.15 | 0.06 | 0.26 | | |
| Measured ratios | | | | | | | | | | | |
| $^{87}Sr/^{86}Sr$ | 0.705067 | 0.705054 | 0.704999 | | | | 0.705316 | 0.705387 | 0.705356 | | |
| $^{143}Nd/^{144}Nd$ | | | 0.512292 | | | | | | 0.512239 | | |
| $^{206}Pb/^{204}Pb$ | 19.433 | 19.474 | | 18.525 | 19.698 | 20.237 | 18.189 | 18.043 | | 20.228 | 20.413 |
| $^{207}Pb/^{204}Pb$ | 15.612 | 15.579 | | 15.538 | 15.592 | 15.592 | 15.550 | 15.550 | | 15.641 | 15.642 |
| $^{208}Pb/^{204}Pb$ | 39.535 | 39.644 | | 39.029 | 39.644 | 39.840 | 38.483 | 38.483 | | 38.555 | 39.469 |
| Initial ratios | | | | | | | | | | | |
| $^{87}Sr/^{86}Sr$ | 0.70463 | 0.70467 | 0.70499 | | | | 0.70531 | 0.70539 | 0.70535 | | |
| $^{143}Nd/^{144}Nd$ | | | 0.51222 | | | | | | 0.51219 | | |
| $^{206}Pb/^{204}Pb$ | 18.18 | 18.52 | | 18.05 | 18.37 | 18.41 | 17.95 | 17.83 | | 17.89 | 18.25 |
| $^{207}Pb/^{204}Pb$ | 15.55 | 15.53 | | 15.52 | 15.53 | 14.72 | 15.54 | 15.54 | | 15.53 | 15.54 |
| $^{208}Pb/^{204}Pb$ | 38.49 | 38.67 | | 38.76 | 38.67 | 38.95 | 38.53 | 38.48 | | 38.49 | 38.73 |
| εSr | 0.30 | 0.96 | 5.60 | | | | 10.05 | 11.08 | 10.63 | | |
| εNd | | | -5.66 | | | | | | -6.70 | | |
| $T^{DM}$Ga | | | 1.04 | | | | | | 1.09 | | |

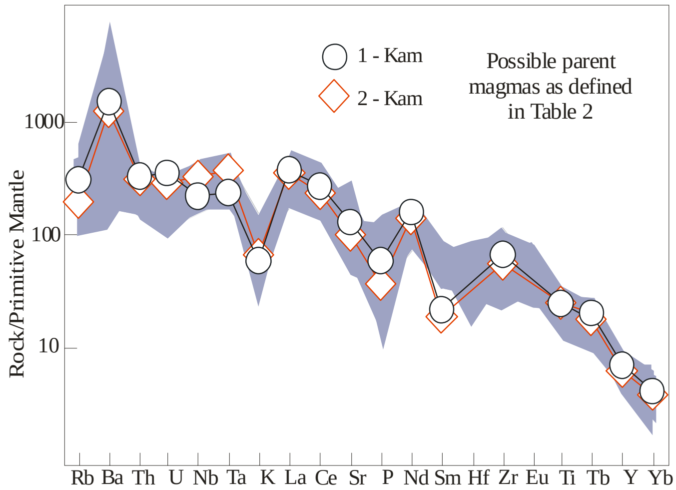


Fig. 6. Incompatible elements normalized to primitive mantle concentrations (Sun & McDonough, 1989) for supposed APIP parent melts (1 and 2 as defined in Table 2) compared with the whole field (light violet) of the APIP kamafugites.

Table 2. Possible compositions of parent magmas for APIP kamafugites; compositions of mantle rocks and xenoliths; chemical and mineralogical compositions. 1-Kam, APIP kamafugite [av. of 24 kamafugitic rock-types, after Gibson *et al.*, 1995a; +5% Ol ($Fo_{93}$)]; 2-Kam, kamafugite (av. of all kamafugitic rocks, in this work); mg#=Mg/(Mg+$Fe_{tot}$). PP, phlogopite peridotite (Erlank *et al.*, 1987, N=17); XEN, phlogopite-amphibole-bearing xenoliths (Comin-Chiaramonti, unpublished data, N=5). Ol, olivine, Opx, orthopyroxene (Nixon, 1987); Cpx, clinopyroxene, and Phl, phlogopite (Erlank *et al.*, 1987), K-richt, potassic richterite (Comin-Chiaramonti, unpublished data), Ap, apatite, stoichiometric composition. $\Sigma R^2$, sum of the squares of major element residuals; F%, melting degree.

| Possible parent magmas | | | Mantle compositions and mineral abundances (wt%) | | | | | | Mass balance Solid Residua | | |
|---|---|---|---|---|---|---|---|---|---|---|---|
| | 1-Kam | 2-Kam | | PP | XEN | | PP | XEN | | PP | XEN |
| $SiO_2$ | 40.24 | 41.22 | $SiO_2$ | 45.26 | 47.98 | | | | | | |
| $TiO_2$ | 5.40 | 5.45 | $TiO_2$ | 0.17 | 0.50 | Ol | 67.4 | 15.7 | Ol | 68.8 | 20.0 |
| $Al_2O_3$ | 5.64 | 6.11 | $Al_2O_3$ | 0.97 | 6.98 | Opx | 20.8 | | Opx | 26.5 | |
| FeOt | 12.93 | 14.33 | FeOt | 6.76 | 4.00 | Cpx | 4.6 | 10.4 | Cpx | 0.2 | 7.8 |
| MnO | 0.22 | 0.22 | MnO | 0.12 | 0.06 | Phl | 7.2 | 44.8 | Phl | 4.53 | 48.4 |
| MgO | 18.29 | 17.10 | MgO | 44.81 | 28.22 | K-richt | | 28.3 | K-richt | | 23.0 |
| CaO | 13.29 | 12.30 | CaO | 0.86 | 4.62 | Ap | | 0.8 | Ap | | 0.70 |
| $Na_2O$ | 0.86 | 0.61 | $Na_2O$ | 0.14 | 1.44 | | | | | | |
| $K_2O$ | 1.83 | 2.08 | $K_2O$ | 0.85 | 5.86 | $\Sigma R^2$ | 0.72 | 0.55 | $\Sigma R^2$ | 0.22 | 1.28 |
| $P_2O_5$ | 1.30 | 0.80 | $P_2O_5$ | 0.06 | 0.34 | | | | | | |
| mg# | 0.72 | 0.68 | mg# | 0.92 | 0.93 | | | | | | |

| Calculated trace elements | | |
|---|---|---|
| Cr | 918 | 1025 |
| Ni | 749 | 789 |
| Rb | 189 | 121 |
| Ba | 10298 | 8267 |
| Th | 27 | 25 |
| U | 7 | 6 |
| Ta | 9.4 | 15 |
| Nb | 151 | 230 |
| La | 260 | 232 |
| Ce | 479 | 415 |
| Sr | 2734 | 2039 |
| Nd | 209 | 184 |
| Sm | 28.70 | 28 |
| Zr | 772 | 633 |
| Tb | 2.22 | 2 |
| Y | 32.6 | 29 |
| Yb | 2.22 | 2 |

Mineral compositions

| | Ol | Opx | Cpx | Gt | Phl | K-richt | Ap |
|---|---|---|---|---|---|---|---|
| $SiO_2$ | 41.21 | 56.70 | 56.27 | 43.72 | 43.96 | 56.42 | |
| $TiO_2$ | 0.05 | 0.05 | 0.35 | 0.05 | 0.60 | 0.60 | |
| $Al_2O_3$ | 0.05 | 0.91 | 0.41 | 20.80 | 14.81 | 1.05 | |
| FeOt | 7.14 | 4.47 | 2.32 | 7.18 | 3.31 | 4.07 | |
| MnO | 0.10 | 0.14 | | 0.49 | | 0.15 | |
| MgO | 51.58 | 36.40 | 17.58 | 21.33 | 26.73 | 22.35 | |
| CaO | 0.05 | 0.34 | 20.64 | 6.43 | | 7.07 | 57.37 |
| $Na_2O$ | | 0.05 | 1.81 | 0.05 | 0.51 | 3.63 | |
| $K_2O$ | | | | | 10.08 | 4.76 | |
| $P_2O_5$ | | | | | | | 42.63 |
| mg# | 0.93 | 0.93 | 0.93 | 0.84 | 0.93 | 0.91 | |

The metasomatic processes responsible for mantle incompatible element enrichment are believed to be due mainly to fluids or melts related to subduction processes (cf. Maury *et al.*, 1992), or to volatile-rich small volume melts from the asthenosphere which would have veined the overlying lithospheric mantle at different depths and times (cf. Foley, 1992 a, b).

Lloyd *et al.* (1985) determined experimentally the composition of glasses produced from various degrees of partial melting at 20 and 30 kb, using a model phlogopite clinopyroxenite represented by the mantle-derived xenoliths sampled from the Uganda kamafugites. At about 25% partial melting at 30 kb (~100 km depth, stability field of the garnet peridotites), the glass composition is similar to that of the kamafugite lavas. On the other hand, at 20 kb the glass composition does not correspond to any of the kamafugitic rocks. This implies that these metasomatized xenoliths may be a potential source for kamafugitic magmas at high pressure and high melting degrees. If so, the source of the APIP kamafugites might be a veined mantle at a depth •30 km.

## Sr-Nd ISOTOPES

In general, the high concentration of most I.E. in all the APIP alkaline rocks suggests that the effects of crustal contamination on the Sr-Nd isotopic system were negligible and that the parental magma compositions are more likely linked to mantle-enriched sources related to variable degrees of metasomatism. The data (Table 1) are plotted in Fig. 7 (time-integrated ε-notations). The values are scattered mainly in the enriched quadrant, with εSr and εNd extending in the ranges from -4 to 31 and from -2.5 to -9, respectively. The field regarding the kamafugitic rocks contains all the other rock-types, i.e. kimberlites, peridotites, carbonatites, melilitite and basanites with sodic affinity. Notably, APIP Sr-Nd isotope data only partially overlap the fields relative to the alkaline rocks from the Serra do Mar and Poços de Caldas, and are quite distinct from those corresponding to the Abrolhos and Trindade islands (Fig. 7).

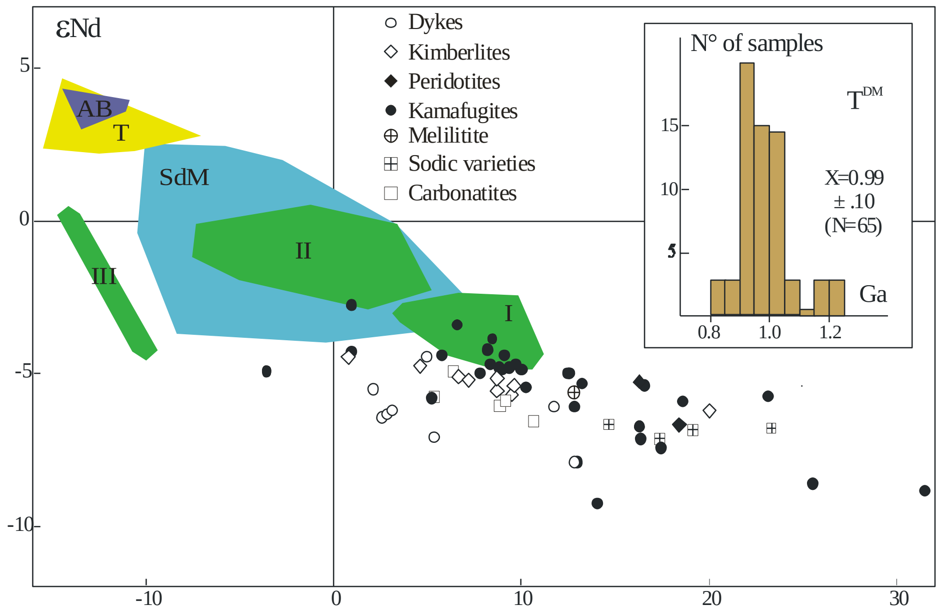


Fig. 7. Time integrated, ε notations, $^{87}Sr/^{86}Sr$ (εSr) vs. $^{144}Nd/^{143}Nd$ (εNd) correlation diagrams. SdM: Serra do Mar; AB, Abrolhos island; T, Trindade and Martin Vaz islands. I, II and III represent the fields from Poços de Caldas rock-types: phonolite-nepheline syenite clan (I), ankaratritic-tephritic blocks (II) and lamprophyric dykes (the latter calculated at 60 Ma). Data source: Bellieni *et al.* (1990), Bizzi *et al.* (1993, 1995), Toyoda *et al.* (1994), Meyer *et al.* (1994), Gibson *et al.* (1995a, b, 1997, 1999), Carlson *et al.* (1996); Serra do Mar: Thompson *et al.* (1998), Bennio *et al.* (2002); Poços de Caldas: Shea (1992), Vlach *et al.* (1998); Abrolhos: Fodor *et al.* (1989); Trindade and Martin Vaz islands: Marques *et al.* (1999b), Siebel *et al.* (2000). Inset: Nd model ages ($T^{DM}$) for Alto Paranaíba alkaline and carbonatitic rocks ($T^{DM}$ values: calculation of model dates relative to a depleted reservoir, $^{143}Nd/^{144}Nd = 0.513114$ and $^{147}Sm/^{144}Nd = 0.222$; Faure, 1986).

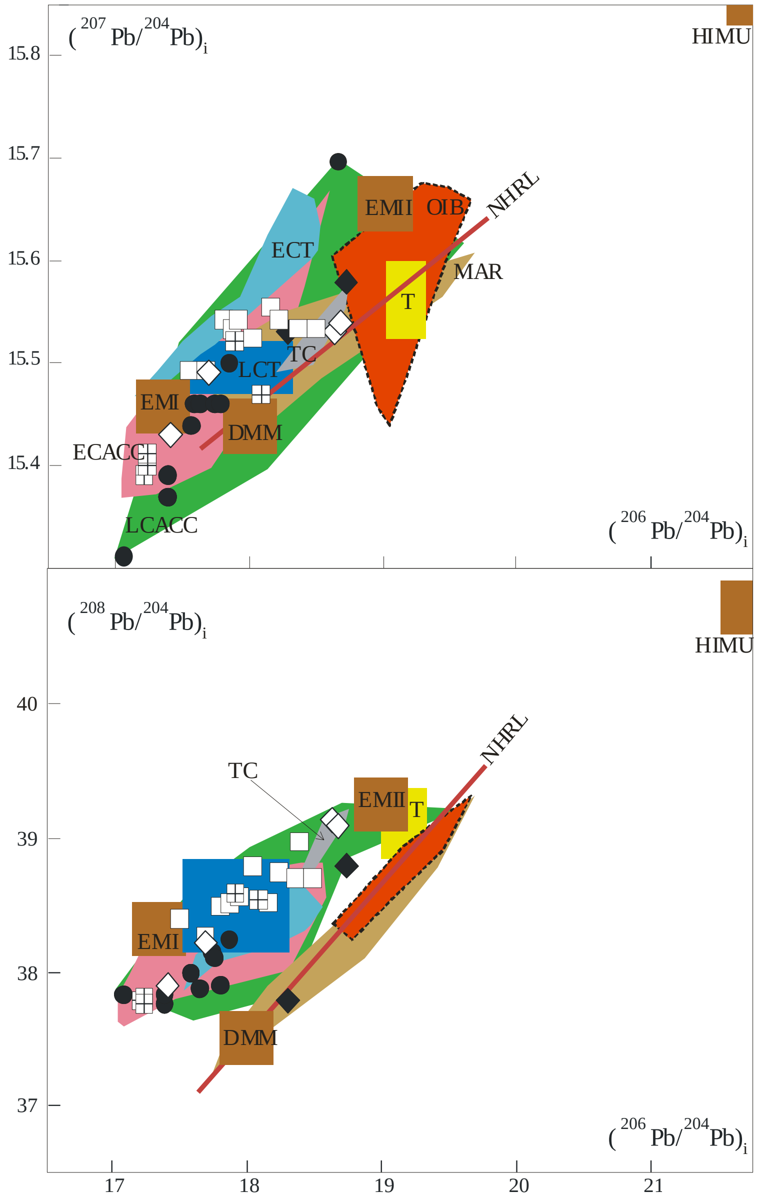


Fig. 8. $^{207}Pb/^{204}Pb$ and $^{208}Pb/^{204}Pb$ vs. $^{206}Pb/^{204}Pb$ (initial ratios) for rock-types from the Alto Paranaíba Province. Symbols as in Fig 7. ECT, Early Cretaceous Paraná tholeiites; ECACC, Early Cretaceous alkaline-carbonatite complexes in and around the Paraná Basin; LCACC, Late Cretaceous alkaline-carbonatite complexes in and around the Paraná Basin; LCT, Late Cretaceous tholeiites (Walvis Ridge); MAR, Middle Atlantic Ridge; OIB, Ocean island basalts; TC, Tristan da Cunha; T, Trindade and Martin Vaz. Data source: *Early Cretaceous* - Comin-Chiaramonti *et al.* (1991, 1995, 1997, 2002), Toyoda *et al.* (1995), Huang *et al.* (1995), Walter *et al.* (1995), Garda *et al.* (1995), Comin-Chiaramonti & Gomes (1996), Castorina *et al.* (1997), Marques *et al.* (1999a), Gibson *et al.* (1999), Andrade *et al.* (1999), Ruberti *et al.* (2002); Antonini *et al.* (in this volume); *Late Cretaceous* - Bellieni *et al.* (1990), Bizzi *et al.* (1994, 1995), Toyoda *et al.* (1994), Meyer *et al.* (1994), Gibson *et al.* (1995a, b, 1997, 1999), Carlson *et al.* (1996), Thompson *et al.* (1998); *Tertiary* - Serra do Mar, Thompson *et al.* (1998), Bennio *et al.* (2002); Abrolhos, Fodor *et al.* (1989); *Atlantic Ocean*: Walvis Ridge, Richardson *et al.* (1982), O'Connor & Duncan, 1990; Rio Grande Rise, Gamboa & Rabinowitz (1984); *Mid Atlantic Ridge* (MAR): Hamelin *et al.* (1984), Ito *et al.* (1987), Fontignie & Shilling (1996); OIB, Halliday *et al.* (1988, 1995); Trindade and Martin Vaz islands, Thompson *et al.* (1998), Marques *et al.* (1999b), Siebel *et al.* (2000); Tristan da Cunha, Le Roex, *et al.* (1990). DMM, HIMU, EMI and EMII are approximations of mantle end-members taken from Hart *et al.* (1992). It should be noted that the Rio Grande Rise basalts (not shown; cf. Gamboa & Rabinowitz, 1984) plot in the same field of the Walvis Ridge samples. NHRL, North Hemisphere Reference Line after Hart (1984).

The constant behaviour of the Sm/Nd ratio in APIP rocks ($^{147}Sm/^{144}Nd$ 0.085±0.009; cf. Fig. 4) allows to consider the Nd model ages as indicative of the main metasomatic events affecting the lithospheric sources beneath the Alto Paranaíba region. The model ages (calculated in relation to the depleted mantle, $T^{DM}$, cf. Table 1) for the whole APIP population (65 samples; cf. inset of Fig. 7) fit 0.99±0.10 Ga. Important differences with respect to other magmatic occurrences, as Poços de Caldas, Serra do Mar region and Abrolhos and Trindade islands are apparent: Poços de Caldas alkaline complex displays model ages ranging from 0.80±0.04 to 0.86±0.06 Ga ($^{147}Sm/^{144}Nd$ 0.074±0.008 to $^{147}Sm/^{144}Nd$ 0.100±0.009) vs. $T^{DM}$=0.75±0.12 Ga ($^{147}Sm/^{144}Nd$ 0.106±0.010) for the Serra do Mar occurrences (Thompson *et al.*, 1998). All these values are distinct from the model ages obtained for Abrolhos (0.69±0.06 Ga) and Trindade-Martin Vaz islands (0.47±0.06 Ga).

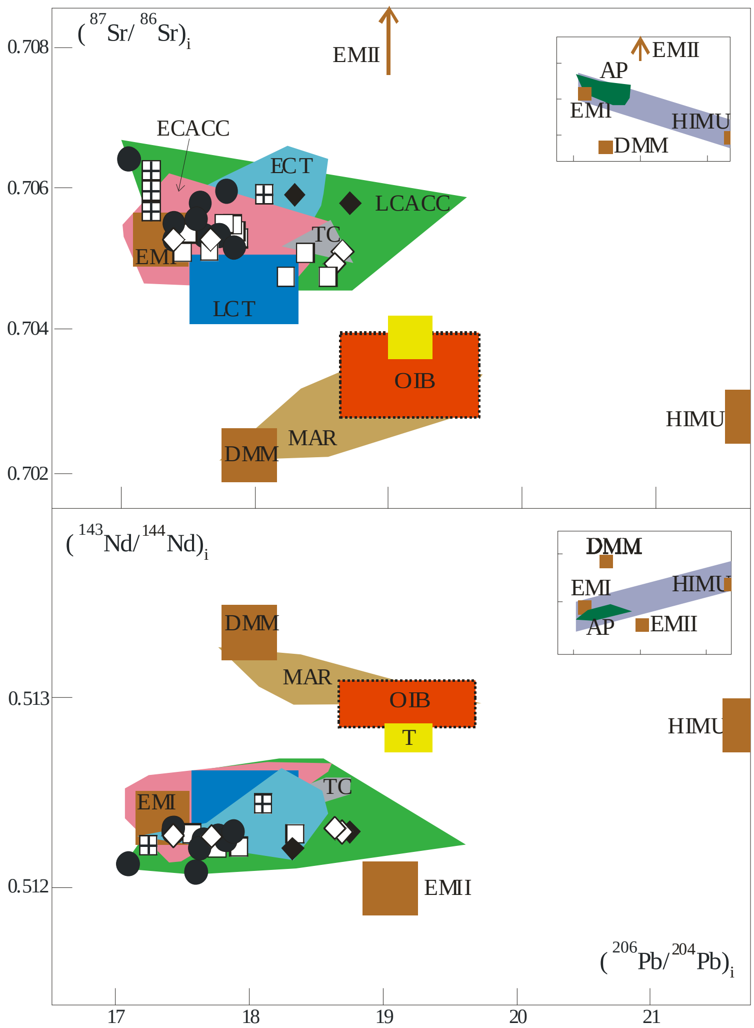


Fig. 9. $Sr_i$ and $Nd_i$ vs. $^{206}Pb/^{204}Pb$ (initial ratios). Symbols and data source as in Fig. 8. **Insets**: Alto Paranaíba rock-types (AP) compared with the mantle components: it should be noted the links between EMI and HIMU components (dark brown fields).

## Pb ISOTOPES

The initial isotopic compositions displayed on $^{206}Pb/^{204}Pb$ vs. $^{207}Pb/^{204}Pb$ and $^{208}Pb/^{204}Pb$ diagrams (Fig. 8; Table 1) define essential linear main arrays on the two diagrams, that are both subparallel to the Early Cretaceous tholeiites from the Paraná Basin (Marques *et al.*, 1999a) and to the Northern Hemisphere Reference Line (NHRL of Hart, 1984). A possible explanation for the Pb isotope behaviour is that the data represent a secondary isochron, establishing an apparent age of 2.5 Ga and suggesting an Archean-Proterozoic mantle source, as pointed out by Hawkesworth *et al.* (1986) for the tholeiites from the Paraná Basin. Alternatively, the observed trends are due to mixing of different mantle components.

On the whole, the APIP alkaline rock-types and associated carbonatites plot in the field of the Brazilian Late Cretaceous alkaline-carbonatite complexes. The latter contains the fields of all the magmatic rocks from the Paraná Basin (i.e. Early Cretaceous alkaline-carbonatite complexes and flood tholeiites). In particular, the APIP extends from EMI and DMM to EMII mantle components, overlapping the field of Tristan da Cunha volcanics (Fig. 8).

The lead isotope initial ratios (Figs. 9 and 10) are correlated with Sr and Nd isotopes (initial ratios). The overlapping fields are the same observed in Fig. 8, but the APIP rocks appear as a mixture of prevailing EMI and subordinate HIMU components (max. ~30%; cf. insets of Figs. 9 and 10).

In contrast to the crustal contamination effects that could be responsible for a whole increase in Pb contents and in radiogenic Pb, the APIP rock-types define a negative correlation between Pb and lead isotopes (Fig. 11). Th and U seem to delineate positive correlations with radiogenic Pb, but with different trends for the kamafugites and most of the carbonatites (Fig. 11). This likely reflects significant chemical differences in the mantle sources.

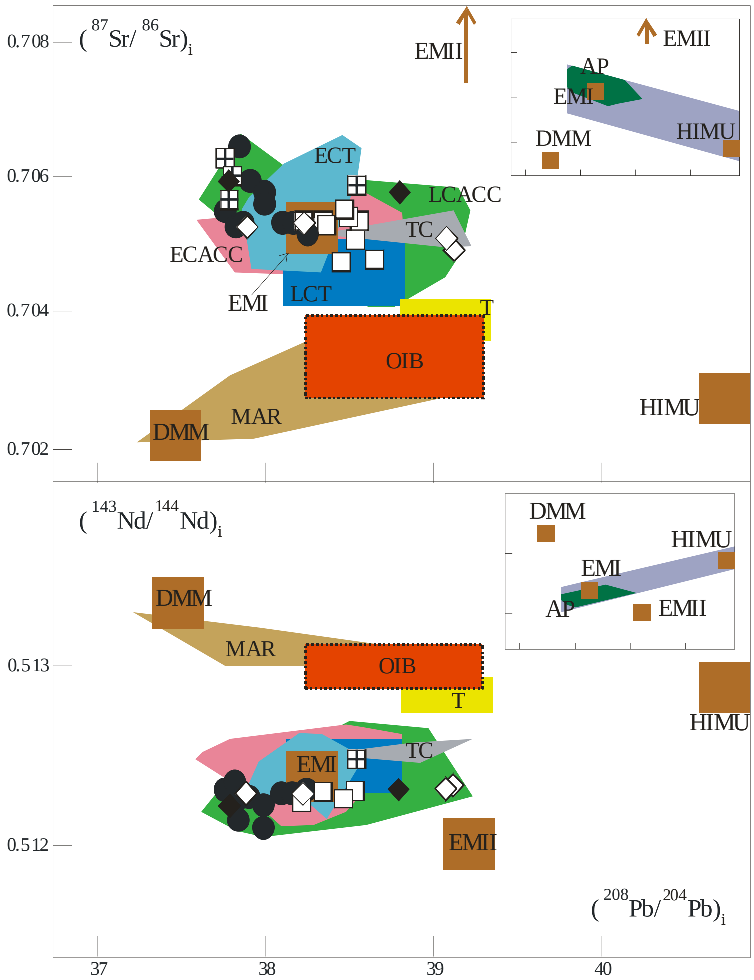


Fig.10. $Sr_i$ and $Nd_i$ vs. $^{208}Pb/^{204}Pb$ (initial ratios). Symbols and data source as in Fig. 8. **Insets**: Alto Paranaíba rock-types (AP) compared with the mantle components: it should be noted the links between EMI and HIMU components (dark brown fields).

The U/Pb and Th/Pb ratios, which may reflect the source compositions, are distinct when compared with $^{206}Pb/^{204}Pb$ and $^{208}Pb/^{204}Pb$ initial isotope ratios, respectively (Fig. 11). The low U/Pb ratios (kamafugites, kimberlites, sodic rock-types and carbonatites, partim) are associated with spread $^{206}Pb/^{204}Pb$ initial ratios; the data displayed on the Th/Pb vs. $^{208}Pb/^{204}Pb$ initial ratios are widely scattered, but appears to follow two main possible trends, one represented by the kamafugitic rocks, and another one involving most of the carbonatites.

A possible explanation for the distinct enrichment in these incompatible elements could be the presence of fluids and/or small volume melts at small scale (cf. Menzies & Hawkesworth, 1987), which probably occcurred simultaneously with melting in a relatively deep lithosphere.

## CONCLUDING REMARKS

The major, trace elements and isotope data here presented support the petrogenetic interpretation given in other studies (Comin-Chiaramonti *et al*. and Bizzi & Araújo, both in this volume), which consider the APIP alkaline rocks as generated from the melting of old lithospheric mantle reservoirs with heterogeneous chemical and isotope characteristics. In particular, the Trindade mantle source signature was not recognized, implying that the APIP alkaline rocks mainly reflect lithospheric source characteristics.

Therefore, the role of the Trindade mantle plume in the Paraná flood basalt generation would be that of providing enough heat to trigger the melting of the lithospheric mantle affected by decompression events due to a regional extensive tectonics in Late Cretaceous.

Arguments in favour of lithospheric sources for the APIP magma types are also suggested by Carlson *et al*. (1996) and by Araújo *et al.* (2001), who compared the rhenium-depletion ages of the kimberlites with Nd-depleted mantle model ages of all their analysed rock-types. The Os isotope data for the APIP rocks point to lithospheric mantle sources for the kimberlites ($^{187}Os/^{188}Os$ ratios 0.117 to 0.129) that were variously Re-depleted, probably at late Archean to mid-Proterozoic times. These lithospheric sources experienced LILE enrichment by fluid/melt metasomatism at ~1 Ga, possibly during the mobile belt formation along the western border of the São Francisco craton. Kamafugites yielded radiogenic $^{187}Os/^{188}Os$ (up to 0.147) indicative of a vein source that might have been stabilized in the lithospheric mantle in the mid to late Proterozoic.

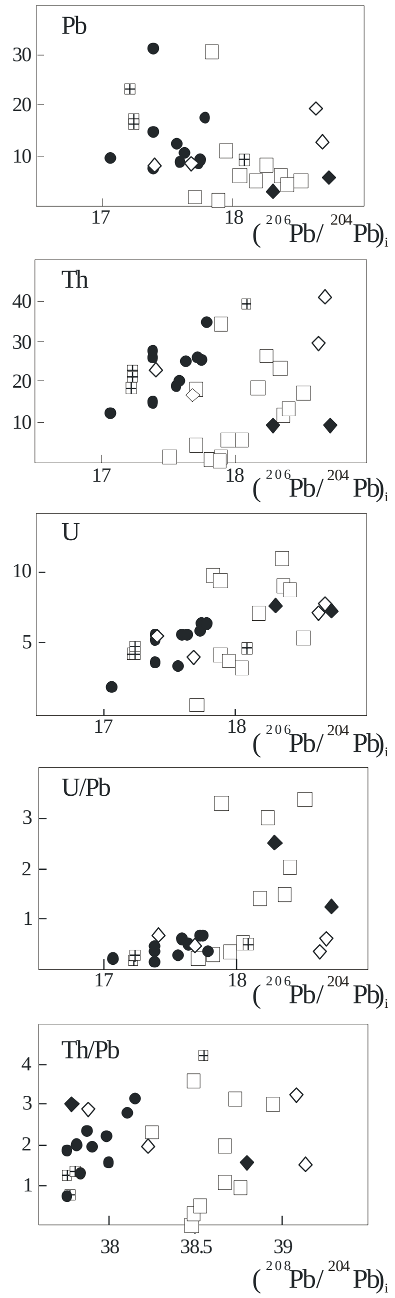


Fig. 11. Pb, Th, U concentrations and U/Pb ratios vs. initial $^{206}Pb/^{204}Pb$, and Th/Pb ratios vs. initial $^{208}Pb/^{204}Pb$ for the Alto Paranaíba rock-types. Symbols as in Fig 7. Data source as in Fig. 8.

Finally, it should be stressed that Carlson *et al.* (1996) suggest that the Os isotope evidences (coupled with Sr-Nd-Pb isotope systematics) most likely represent the influence of a delaminated Brazilian lithospheric mantle mixed into mantle circulation beneath the South Atlantic, being not related to the plume(s) commonly associated with the APIP magmatism (cf. Gibson *et al*., 1995a).

## ACKNOWLEDGEMENTS

This research was supported by Brazilian (Fapesp, Proc. 01/10714-3) and Italian (CNR, 05 and 11 Committes, and COFIN 1998, MIUR 1998, 1999, 2000, 2001) agencies.

## REFERENCES


Almeida, F.F.M. (1983). Relações tectônicas das rochas alcalinas mesozóicas da região meridional da plataforma Sul-Americana. *Revista Brasileira de Geociências* **13**, 139-158.

Andrade, F.R.D., Möller, P. & Höhndorf, A. (1999). The effect of hydrothermal alteration on the Sr and Nd isotopic signatures of the Barra do Itapirapuã carbonatite, southern Brazil. *Journal of Geology* **107**, 177-191.

Antonini, P., Gasparon, M., Comin-Chiaramonti, P. & Gomes, C.B. (in this volume). Post Paleozoic magmatism in the Eastern Paraguay: Sr-Nd-Pb isotope compositions.

Araújo A.L.N., Carlson, R.W., Gaspar, J.C. & Bizzi, L.A. (2001). Petrology of kamafugites and kimberlites from the Alto Paranaíba alkaline province, Minas Gerais, Brazil. *Contributions to Mineralogy and Petrology* **142**, 163-177.

Barton, M. (1979). A comparative study of some minerals occurring in K-alkaline rocks of the Leucite Hills, Wyoming, The Vico Volcano, Italy, and Toro-Ankole region, Uganda. *Neues Jahrbuch Mineralogische Abhandlungen* **137**, 113-134.

Bellieni, G., Montes-Lauar, C.R., De Min, A., Piccirillo, E.M., Cavazzini, G., Melfi A.J. & Pacca, I.G. (1990). Early and Late Cretaceous magmatism from São Sebastião island (SE-Brazil): geochemistry and petrology. *Geochimica Brasiliensis* **4**, 59-83.

Bennio, L., Brotzu, P., Gomes, C.B., D'Antonio, M., Lustrino, M., Melluso, L., Morbidelli, L. & Ruberti, E. (2002). Petrological, geochemical and Sr-Nd isotopic features of Eocene alkaline rocks of the Cabo Frio Peninsula (southern Brazil): evidence of several magma series. *Periodico di Mineralogia*, **71**, 137-158.

Bizzi, L.A., Smith, C.B., De Wit, M.J., Armstrong, R.A. & Meyer, H.O.A. (1993). Mesozoic kimberlites and related alkaline rocks in southwestern São Francisco craton: a case for local mantle reservoirs and their interaction. *5th International Kimberlite Conference, Araxá Proceedings,* pp. 156-171.

Bizzi, L.A., De Wit, M.J., Smith, C.B., McDonald, I. & Armstrong, R.A. (1995). Heterogeneous enriched mantle materials and Dupal-type magmatism along the southwestern margin of the São Francisco craton, Brazil. *Journal of Geodynamics* **20**, 469-491.

Bizzi, L.A., Smith, B.C., De Wit, M.J., Macdonald, I. & Armstrong, R.A. (1994). Isotope characteristics of the lithospheric mantle underlying the SW São Francisco craton margin, Brazil. *International Symposium on the Physics and Chemistry of the Upper Mantle, Invited Lectures*, São Paulo, pp. 227-256.

Boynton, W.V. (1984). Cosmochemistry of the Rare Earth elements: meteorite studies. In: Henderson, P. (ed.) *Rare Earth Element geochemistry*. Amsterdam: Elsevier, pp. 63-114.

Brod, J.A., Gibson, S.A., Thompson, R.N., Junqueira-Brod, T.C., Seer, H.J., Castanheira, L.M. & Boaventura, G.R. (2000). The kamafugite-carbonatite association in the Alto Paranaíba Igneous Province (APIP), southeastern Brazil. *Revista Brasileira de Geociências* **30**, 408-412.

Carlson, R.W., Esperança, S. & Svisero D.P. (1996). Chemical and Os isotopic study of Cretaceous potassic rocks from southern Brazil. *Contributions to Mineralogy and Petrology* **125**, 393-405.

Castorina, F., Censi, P., Comin-Chiaramonti, P.A., Gomes, C.B., Piccirillo, E.M., Alcover Neto, A., Almeida R.T., Speziale, S. & Toledo M.C. (1997). Geochemistry of carbonatites from Eastern Paraguay and genetic relationships with potassicc magmatism: C, O, Sr and Nd isotopes. *Mineralogy and Petrology* **61**, 237-260.

Comin-Chiaramonti, P. & Gomes, C.B. (1996). *Alkaline magmatism in central-eastern Paraguay. Relationships with coeval magmatism in Brazil.* São Paulo: Edusp/Fapesp, 464p.

Comin-Chiaramonti, P., Castorina, F., Cundari, A., Petrini, R. & Gomes C.B. (1995). Dykes and sills from Eastern Paraguay: Sr and Nd isotope systematics. In: Baer, G. & Heimann, A. (eds.) *Physics and chemistry of dykes*. Rotterdam: Balkema pp. 267-278.

Comin-Chiaramonti, P., Civetta, L., Petrini, R., Piccirillo, E.M., Bellieni, G., Censi, P., Bitschene, P., Demarchi, G., De Min, A., Gomes, C.B., Castillo, A.M.C. & Velázquez, J.C. (1991). Tertiary nephelinitic magmatism in Eastern Paraguay: petrology, Sr-Nd isotopes and genetic relationships with associated spinel-peridotite xenoliths. *European Journal of Mineralogy* **3**, 507-525.

Comin-Chiaramonti, P., Cundari, A., Piccirillo, E.M., Gomes, C.B., Castorina, F., Censi , P., De Min A., Marzoli, A., Speziale, S. & Velázquez, V.F. (1997). Potassic and sodic igneous rocks from Eastern Paraguay: their origin from the lithospheric mantle and genetic relationships with the associated Paraná flood tholeiites. *Journal of Petrology* **38**, 495-528.

Comin-Chiaramonti, P., Gomes, C.B., Castorina, F., Censi P., Antonini, P., Furtado, S., Ruberti , E. & Scheibe, L.F. (2002). Anitápolis and Lages alkaline-carbonatite complexes, Santa Catarina State, Brazil: geochemistry and geodynamic implications. *Revista Brasileira de Geociências* **32**, 639-653.

Comin-Chiaramonti, P., Gomes, C.B., Marques, L.S., P. Censi, P., Ruberti, E. & Antonini, P. (in this volume). Carbonatites from southeastern Brazil: geochemistry, O-C, Sr-Nd-Pb isotopes and relationships with the magmatism from the Paraná-Angola-Namibia Province.

Comin-Chiaramonti, P., Gomes, C.B., Ruberti, E., Antonini, P. & Censi, P. (2001). Mato Preto alkaline-carbonatite complex: geochemistry and isotope (O-C, Sr-Nd) constraints. *Geochimica Brasiliensis* **15**, 23-34.

Danni, J.C.M. & Gaspar, J.C. (1994). Chemistry of katungite from the Amorinópolis, Goiás: contribution to the study of kamafugitic magmatism. *Geochimica Brasiliensis* **8**, 119-134.

Erlank, A.J., Waters, F.G., Hawkesworth, C.J., Haggerty, S.E., Allsopp, H.L., Rickard, R.S. & Menzies, M.A., 1987. Evidence for mantle metasomatism in peridotite nodules from the kimberley pipes, South Africa. In: Menzies M.A. & Hawkesworth C.J. (eds.) *Mantle metasomatism*. London: Academic Press, pp. 221-311.

Faure, G. (1986). *Principles of isotope geology*. New York: John Wiley & Sons, 589p.

Fodor, R.V., Mukasa, S.B., Gomes, C.B. & Cordani, U.G. (1989). Ti-rich Eocene basaltic rocks, Abrolhos Platform, offshore Brazil, 18º S: petrology with respect to South Atlantic magmatism. *Journal of Petrology* **30**, 763-786.

Foley, S.F. (1992a). Petrological characterization of the source components of potassic magmas: geochemical and experimental constraints. *Lithos* **28**, 187-204.

Foley, S.F. (1992b). Vein plus wall-rock melting mechanism in the lithosphere and the origin of potassic alkaline magmas. *Lithos* **28**, 435-453.

Foley, S.F., Venturelli, G., Green, D.H. & Toscani, L. (1987). The ultrapotassic rocks: classification and constraints for petrogenetic models. *Earth-Science Reviews* **24**, 81-134.

Fontignie, D. & Schilling, J.G. (1996). Mantle heterogeneities beneath the South Atlantic: a Nd-Sr-Pb isotope study along the Mid-Atlantic Ridge (3°S-46°S). *Earth Planetary Science Letters* **146**, 259-272.

Gamboa, L.A.P. & Rabinowitz, P.D. (1984). The evolution of the Rio Grande Rise in Southwest Atlantic. *Marine Geology* **58**, 35-58.

Garda G.M., Schorscher, H.D., Esperança, S. & Carlson, R.W. (1995). The petrology and geochemistry of coastal dikes from São Paulo State, Brazil: implications for variable lithospheric contributions to alkaline magmas from the western margin of the South Atlantic. *Anais da Academia Brasileira de Ciências* **67**, 191-216.

Gibson, S.A., Thompson, R.N., Dickin, A.P. & Leonardos, O.H. (1995b). High-Ti and Low-Ti mafic potassic magmas: key to plume-lithosphere interactions and continental flood-basalt genesis. *Earth and Planetary Science Letters* **136**, 149-165.

Gibson, S.A., Thompson, R.N., Leonardos, O.H., Dickin, A.P. & Mitchell, J.G. (1995a). The late Cretaceous impact of the Trindade mantle plume: evidence form large-volume, mafic potassic magmatism in SE Brazil. *Journal of Petrology* **36**, 189-229.

Gibson, S.A., Thompson, R.N., Leonardos, O.H., Dickin, A.P. & Mitchell, J.G. (1999). The limited extent of plume-lithosphere interactions during continental flood-basalt genesis: geochemical evidence from Cretaceous magmatism in southern Brazil. *Contributions to Mineralogy and Petrology* **137**, 147-169.

Gibson, S.A., Thompson, R.N., Weska, R., Dickin, A.P. & Leonardos, O.H. (1997). Late Cretaceous rift-related upwelling and melting of the Trindade starting mantle plume head beneath western Brazil. *Contributions to Mineralogy and Petrology* **126**, 303-314.

Gomes, C.B., Morbidelli, L., Ruberti, R. & Comin-Chiaramonti, P. (1996). A first attempt to compare Post-Palaeozoic alkaline rocks from western (Paraguay) and eastern (Brazil) margins of the Paraná Basin. In: Comin-Chiaramonti, P. & Gomes, C.B. (eds.) *Alkaline magmatism in central-eastern Paraguay. Relationships with coeval magmatism in Brazil.* São Paulo: Edusp-Fapesp, pp. 249-274.

Halliday, A.N., Dickin, A.P., Fallick, A.E. & Fitton, J.G. (1988). Mantle dynamics: a Nd, Sr, Pb and O isotopic study of the Cameroon Line volcanic chain. *Journal of Petrology* **29**, 181-211.

Halliday, A.N., Lee, D.C., Tommasini, S., Davies, G.R., Paslick, C.R., Fitton, G.J. & James, D.E. (1995). Incompatible trace elements in OIB and MORB and source enrichment in the sub-oceanic mantle. *Earth and Planetary Science Letters* **133**, 379-395.

Hamelin, B., Dupré, B. & Allègre, C.J. (1984). Lead-strontium isotopic variations alongt the East Pacific Rise and Mid-Atlantic Ridge: a comparative study. *Earth and Planetary Science*

*Letters* **67**, 340-350.

Hart, S.R. (1984) A large-scale isotope anomaly in the southern hemisphere mantle. *Nature* **309**, 753-757.

Hart, S.R., Hauri, E.H., Oschmann, L.A. & Whithehead, J.A. (1992). Mantle plumes and entrainement: isotopic evidence. *Science* **256**, 517-520.

Hasui, Y. (1975). The phanerozoic tectonic evolution of the western Minas Gerais State. *Anais da Academia Brasileira de Ciências* **47**, 431-438.

Hawkesworth, C.J., Mantovani, M.S.M., Taylor, P.N. & Palacz, Z. (1986). Evidence from the Paraná of south Brazil for a continental contribution to Dupal basalts. *Nature* **322**, 356-359.

Herz, N. (1977). Timing and spreading in the South Atlantic: information from Brazilian alkaline rocks. *Geological Society of America Bulletin* **88**, 101-112.

Huang, H-M., Hawkesworth, C.J., Van Calsteren, P. & Mcdermott, F. (1995). Geochemical characteristics and origin of the Jacupiranga carbonatites, Brazil. *Chemical Geology* **119**, 79-99.

Ito, E., White, W.M. & Göpel, C. (1987). The O, Sr, Nd and Pb isotope geochemistry of MORB. *Chemical Geology* **62**, 157-176.

James, D.E., Assumpção, M., Snoke, J.A., Ribotta, L.C. & Kuehnel, R., 1993. Seismic studies of continental lithosphere beneth SE Brazil. *3rd Congress of the Brazilian Geophysical Society, Rio de Janeiro, Expanded Abstracts* **2**, 1110-1115.

Leonardos, O.H. & Fife, W.S. (1974). Ultrametamorphism and melting of a continental margin in the Rio de Janeiro region, Brazil. *Contributions to Mineralogy and Petrology* **46**, 201-214.

Le Roex, A.P., Cliff, R.A. & Adair, B.J.I. (1990). Tristan da Cunha, South Atlantic: geochemistry and petrogenesis of a basanite-phonolite lava series. *Journal of Petrology* **31**, 779-812.

Lloyd, F.E., Arima, M. & Edgar, A.D. (1985). Partial melting of phlogopite clinopyroxenite nodule from southwest Uganda. Experimental study bearing on the origin of highly potassic continental rift volcanics. *Contributions to Mineralogy and Petrology* **91**, 321-329.

Marques, L.S., Dupré, B. & Piccirillo, E.M. (1999a). Mantle source compositions of the Paraná magmatic province (southern Brazil): evidence from trace element and Sr-Nd-Pb isotope geochemistry. *Journal of Geodynamics* 28, 439-458.

Marques, L.S., Ulbrich, M.N.C., Ruberti, E. & Tassinari, C.G. (1999b). Petrology, geochemistry and Sr-Nd isotopes of the Trindade and Martin Vaz volcanic rocks (Southern Atlantic Ocean). *Journal of Volcanology and Geothermal Research* **93**, 191-216.

Maury, R., Defant, C. & Joron, M.J. (1992). Metasomatism of the sub-arc mantle inferred from trace elements in Philippine xenoliths. *Nature* **360**, 661.

Menzies, M.A. & Hawkesworth, C.J. (eds.) (1987). *Mantle metasomatism*. London: Academic Press, 472p.

Meyer, H.O.A., Blaine, L.G., Svisero, D.P. & Craig, B.S. (1994). Alkaline intrusions in western Minas Gerais, Brazil. *5th International Kimberlite Conference*, *Araxá, Proceedings,* pp. 140-155.

O'Connor, J.M. & Duncan, R.A. (1990). Evolution of the Walvis Ridge-Rio Grande Rise hot spot system: implications for African and South American plate motions over plumes. *Journal of Geophysical Researches* **95**, 17475-17502.

Nixon, P.H. (ed.) (1987). *Mantle xenoliths*. Chichester: Wiley Press, 844p.

Pimentel, M.M., Whitehouse M.J., Viana, M.G., Fuck R.A. & Machado, N. (1997). The Mara Rosa arc in the Tocantins Province: further evidence for Neoproterozoic crustal accretion in Central Brazil. *Precambrian Research* **81**, 299-310.

Pimentel, M.M., Fuck R.A. & Botelho, N.F. (1999). Granites and geodynamic history of the Neoproterozoic Brasilia belt, Central Brazil: a review. *Lithos* **46**, 463-483.

Richardson, S.H., Erlank, A.J., Duncan, A.R. & Reid, D.L., 1982. Correlated Sr, Nd and Pb isotope variations in Walvis Ridge basalts and implications for the evolution of their mantle source. *Earth and Planetary Science Letters* **59**, 327-342.

Ruberti, E., Castorina, F., Censi, P., Comin-Chiaramonti, P., Gomes, C.B., Antonini P. & Andrade, F.R.D. (2002). The geochemistry of the Barra do Itapirapuã carbonatite (Ponta Grossa Arch, Brazil): a multiple stockwork. *Journal of South America Earth Sciences* **15**, 215-228.

Sgarbi, P.B.A. & Valença, J.G. (1993). Mineral and rock chemistry of Mata da Corda kamafugitic rocks (MG State, Brazil). *Anais da Academia Brasileira de Ciências* **27**, 257-269.

Sgarbi, P.B.A., Gaspar, J.C. & Valença, J.G. (2000). Brazilian kamafugites. *Revista Brasileira de Geociências* **30**, 417-420.

Shea, M.E. (1992). Isotopic geochemical characterization of selected nepheline syenites and phonolites from the Poços de Caldas alkaline complex, Minas Gerais, Brazil. *Journal of Geochemical Exploration* **45**, 173-214.

Siebel, W., Becchio, R., Volker, F., Hansen, M.A.F., Viramonte, J., Trumbull, R.B., Haase, G. & Zimmer, M. (2000). Trindade and Martin Vaz islands, South Atlantic: isotopic (Sr, Nd, Pb) and trace element constraints on plume related magmatism. *Journal of South American Earth*

*Sciences* **13**, 79-103.

Sun, S.-S. & McDonough, W.F., 1989. Chemical and isotopic systematics of oceanic basalts: implications for mantle composition and processes. In: Saunders, A.D. & Norry, M.J. (eds.) *Magmatism in the ocean basins. Geological Society of London, Special Publication* **42**, pp. 313-345.

Thompson, R.N., Gibson, S.A., Mitchell, J.G., Dickin, A.P., Leonardos, O.H., Brod, J.A. & Greenwood J.C. (1998). Migrating Cretaceous-Eocene magmatism in the Serra do Mar Alkaline Province, SE Brazil: melts from the deflected Trindade mantle plume? *Journal of Petrology* **39**, 1493-1526.

Toyoda, K., Horiuchi, H. & Tokonami, M. (1994). Dupal anomaly of Brazilian carbonatites: geochemical correlations with hotspots in the South Atlantic and implications for the mantle source. *Earth and Planetary Science Letters* **126**, 315-331.

Trompette, R. (1994). *Geology of western Gondwana (2000-500 Ma). Pan-African-Brasiliano aggregation of South America and Africa*. Rotterdam: Bakelma, 350p.

Ulbrich, H.H.G.J. & Gomes, C.B. (1981). Alkaline rocks from continental Brazil. *Earth-Science Reviews* **17**,135-154.

Van Decar, J.C., James, D.E. & Assumpção, M. (1995). Seismic evidence for a fossil mantle plume beneath South America and implications for plate forces. *Nature* **378**, 25-31.

Vlach S.R.F., Ulbrich, H.H.G.J. & Ulbrich, M.N.C.. (1998). Isótopos radiogênicos (Sr, Nd) e estáveis (C,O) de rochas máfico-ultramáficas potássicas da região de Poços de Caldas, MG-SP: inferências sobre a natureza do manto litosférico Mesozóico. *XL Congresso Brasileiro de Geologia, Belo Horizonte, Anais,* p. 475.

Walter A.V., Flicoteaux, R., Parron, C., Loubet, M. & Nahon, D. (1995). Rare-earth elements and isotopes (Sr, Nd, O, C) in minerals from the Juquiá carbonatite (Brazil): tracers of a multistage evolution. *Chemical Geology* **120**, 27-44.

*Mesozoic to Cenozoic Alkaline Magmatism in the Brazilian Platform*
*Comin-Chiaramonti, P. & Gomes, C.B. (eds.)*
*Edusp/Fapesp, São Paulo, pp. 317-340, 2005*

# DYNAMICS OF MANTLE-DERIVED MAGMATISM IN THE SOUTHWESTERN SÃO FRANCISCO CRATON, BRAZIL

*L.A. Bizzi and A.L.N. Araújo*

*The nature and restricted range of Dupal-type Sr, Nd, Pb and Os isotopic compositions of Cretaceous kimberlites, tuffaceous diatremes of kamafugitic affinity and carbonatite complexes, which intrude the southwestern margin of the São Francisco craton in Brazil, indicate that these magmas either interacted extensively with, or were derived from, a LREE enriched homogeneous lithospheric mantle source isotopically similar to the "enriched mantle I" (EMI) component. The shallow-derived alkaline rocks contain a greater proportion of this component, whereas the lower time-averaged Rb/Sr, Nd/Sm, Re/Os and Pb/U ratios of the kimberlites compared to the other rock-types suggest mixing between the EMI mantle material and variable amounts of depleted mantle material (DMM) and high $^{238}U/^{234}Pb$ (HIMU) components. Systematic variations in rock-types and geochemistry on a regional scale are believed to be indicative of vertical geochemical heterogeneities that are translated into lateral heterogeneities by different depths of melting. Such components are concentrated in laterally extensive, but vertically distinctive portions of the mantle beneath the São Francisco craton. The EMI-type signatures are more prevalent in shallow-derived volcanism, whereas the HIMU-type signatures have originated from a DMM-dominated source that started melting deeper in the mantle. The Nd signatures of the EMI-type volcanics follow the evolutionary path defined by the Neoproterozoic crustal sequences that overlie and flank the craton margin. This suggests that the source of such mantle signatures was related to the tectono-thermal processes which led to the formation and evolution of such crustal sequences. The existence of such a mantle anomaly underlying the southwestern margin of the São Francisco craton since the Proterozoic severely constrains local mantle convection models. An upper-Mesozoic ternary mixing between up-welling HIMU-like melts, depleted mantle and volumetrically dominant EMI-type source materials resident in the lithospheric mantle is apparently capable of satisfying the constraints of the isotopic data. The HIMU-like component is thought to be representative of melts generated from a source at the base of the mechanical boundary layer (MBL) or deeper. This source could be the asthenosphere, brought up either by a mantle plume active at the time of the emplacement or, alternatively, by long-term entrapment of blobs and weak plumes accumulated in the lower subcontinental lithosphere. The time-integrated mobilization of Re, Pb and Rb in a ($CO_2$-charged?) metasomatic fluid and its subsequent removal from the mantle segment could be considered a plausible means by which to produce a residual, degassed, HIMU-like component and a complementary volatile-rich EMI-like component elsewhere in the mantle. The first batch of melt products, presumably has been generated at the base of the MBL or deeper, as a response to adiabatic decompression originated from rising diapirs or blobs of mantle material, and probably has underwent solid-state mixing during ascent. The final product, therefore, represents some average over-large mantle depths. The implied link means that the source of the Dupal-type signature in the studied volcanics could have been Tristan plume Dupal-type material that had once been trapped under the subcontinental lithosphere but was brought up under the thermal influence of the Trindade non-Dupal hot spot. The isotopic similarity of the sources of the studied rocks and of the high-Ti basalts of the northern Paraná Basin to those of some Ocean Island Basalts with Dupal signatures in the South Atlantic (e.g. in Walvis Ridge) is ascribed to processes by which overthickened continental lithosphere became* *firstly delaminated, and then contaminated a zone of South Atlantic asthenosphere from which hot spot islands have been erupting.*

## INTRODUCTION

The isotopic signatures of the Mesozoic alkaline magmas that intrude the southwestern São Francisco craton margin are used to characterize an isotopically discrete and physically continuous mantle domain that underlies the craton margin. A mixture of depleted mantle material (DMM) and at least three distinct enriched mantle end-member components (HIMU, EMI and EMII; acronyms that stand for High-, Enriched Mantle I and Enriched Mantle II) are necessary to accurately fingerprint the mantle signatures recorded in the area under investigation. Isotopic signatures and their relation to U, Pb, Rare Earth Elements (REE) and Platinum Group Elements (PGE) are used to constrain source characteristics and mixing of isotopic reservoirs. Modelling of mixing systematics and petrological data are employed to define the nature of the components and of the mixing process that took place beneath the southwestern São Francisco craton. The time-integrated Nd isotopic evolution of on and off craton supracrustal rocks are compared to the section of enriched subcontinental mantle lithosphere that was involved in the generation of the alkaline magmas. The isotopic characteristics of the alkaline volcanics are compared with those of the Paraná basalts, the Walvis Ridge basalts and other OIB-type enriched mantle components, and a conceptual geodynamic model capable of explaining the isotopic similarity observed among such distinctive rock types is presented.

## GEOLOGICAL SETTING

The São Francisco craton (Fig. 1; cf. also Fig. 1 of Gomes & Comin-Chiaramonti, in this volume) is a mid- to late-Archean granite-gneiss and granite-greenstone terrain. Its southern boundary is marked by a steep, seismically active, strike-slip fault system. Its western margin is overprinted by tectonism of Brasiliano age (Neoproterozoic; ~0.8-0.5 Ga) tectonism and is overlain by a thin-skinned fold and thrust belt of alloctonous to para-alloctonous units (the Brasília belt). This belt is coupled to an external Neoproterozoic orogenic zone (the Uruaçu belt) of metasediments, orthogneisses, metavolcanics and metaplutonic assemblages of various ages. Further to the West, the southern Uruaçu and Brasília fold belts are linked with the western Goiás area, which is characterized by a metamorphic basement composed largely of volcano-sedimentary arc assemblages and orthogneisses (Pimentel & Fuck, 1992). The entire orogenic zone to the west of the São Francisco craton, which includes a Neoproterozoic fold and thrust belt-foreland basin association formed along the craton margin, has been named as "Tocantins Province" by Almeida *et al.* (1981).

## MESOZOIC ALKALINE VOLCANICS

The southwestern São Francisco craton margin is intruded by Cretaceous kimberlites, olivine meli-litites, tuffaceous diatremes of kamafugitic affinity, and carbonatite complexes. The most important foci of alkaline magmatic activity occurred in the Alto Paranaíba area over a period of about 45 Ma (i.e. 120-75 Ma), concomitant with Early Cretaceous continental extension and the deposition of the Cretaceous volcanics comprising the Mata da Corda Formation. On a regional scale, the characteristics of the alkaline igneous activity are comparable to those along craton margins in southern Africa, western

Uganda and Montana, in U.S.A..

Some sixty of the freshest representatives of the alkaline magmatism had been investigated by Bizzi (1994) and Araújo (2000) in terms of age and mode of emplacement, petrography and whole-rock geochemistry. The sixty localities straddle across the western margin of the craton and were selected to represent a substantial range of different alkaline ultrabasic rock-types found in the area. The studied rocks have first been categorized by Bizzi (1994) into four groups: kimberlites, alkaline rocks of kimberlitic affinity, rift-related alkaline rocks (related either to the Paraná Basin volcanism or to the Mata da Corda Formation) and carbonatites. The latter group of rocks was also referred to as kamafugites by Araújo (2000), who further classified such rocks as either ugandites or mafurites on the basis of their petrography and mineral chemistry.

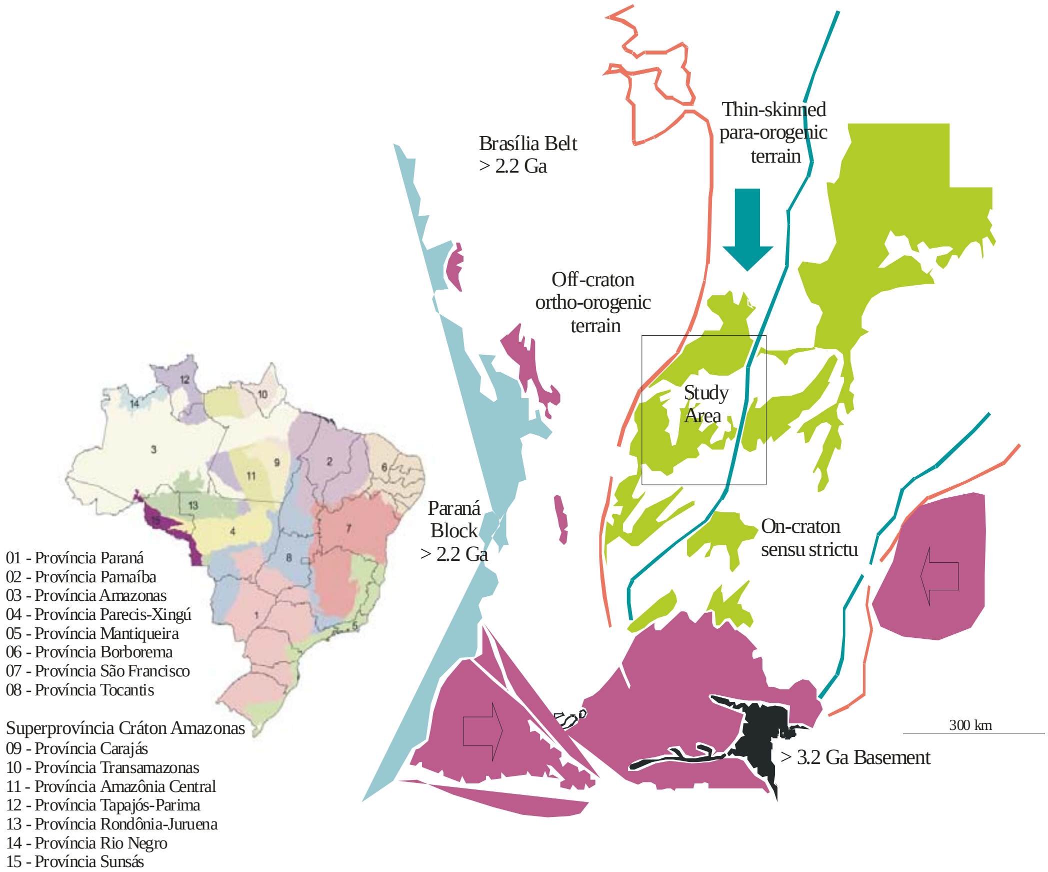


Fig. 1. Sketch-map showing the main structural outlines of the Alto Paranaíba region (after Bizzi, 1994).

On chemical, petrographical and mineralogical grounds, the studied kimberlites are similar to the South African Group I kimberlites (i.e. hypabyssal calcite-monticellite types with uniformly distributed groundmass minerals). Both ilmenite-rich and ilmenite-poor varieties occur. However, the peculiar composition of micas and other matrix minerals in these kimberlites, together with their distinct isotopic compositions, characterize the Brazilian group of kimberlites as being a distinctive "clan" compared to kimberlites elsewhere (Bizzi *et al.*, 1993). Xenoliths of spinel lherzolite, harzburgite and dunite are common and display evidence of spinel and phlogopite metasomatism similar to that observed in xenoliths found in South African kimberlites.

Some of the rocks were grouped as “alkaline rocks with kimberlitic affinity”. These are diatremes and plugs carrying high-Mg/low-Cr ilmenites and garnets of various compositions. Their hypabyssal phase have chemical, mineralogical and petrographic similarities with “true-kimberlites” (e.g. two generations of olivine and phlogopite and the mineralogy of the groundmass), suggesting a kimberlitic affinity for these rocks. Most of the studied samples from the latter group (e.g. those from the localities designated as Japecanga and Pântano) are texturally similar to hypabyssal aphanitic kimberlites, but differ in the shape of olivine phenocrysts and in the relative abundance of perovskite grains. On this respect, these occurrences have affinities with shallower derived melts (e.g. olivine melilitites and mildly alkaline ultrabasic rocks related to kamafugites). For the purpose of this study, these localities are referred to as “mica peridotites”. The term “alkaline rocks with kimberlitic affinity” is used here to denote a rock that in most aspects resembles a kimberlite, but in some aspects is anomalous, and as such is an “ambiguous” kimberlite.

Drill-core samples of phoscorite, sövite and lamprophyre representing late-stage magmatic and hydrothermal activity in the Catalão II carbonatite complex were also analyzed. Metasomatized magnetite and mica peridotites and pyroxenites of an early stage associated with five other late-stage magmatic carbonatites and late hydrothermal activity are represented herein by phoscorite, sövite, cryptocrystalline berforsite, glimmerite and lamprophyre samples. Metasomatic equilibration of magnetite pyroxenites and peridotites is accompanied by pervasive phlogopitization and exsolution of oxides. The subsequent magmatic carbonatitic phases, especially the phoscorite stage, introduced magnetite, phlogopite, apatite and pyroclore, resulting in an enrichment of incompatible elements.

The volcanic fields within the Mata da Corda Formation have a well-preserved record of volcanic breccias, pyroclastic flows and a variety of alkaline rocks containing silica-deficient minerals such as melitite, monticellite, nepheline, leucite and perovskite (Seer & Moraes, 1988; Leonardos *et al.*, 1991; Araújo, 2002). The volcanic and sedimentary stratigraphy of the Mata da Corda and Areado Formations was affected by large-scale synvolcanic listric normal faults, and there are evidences, both in the field and in satellite imagery, for tectonic control of the extrusives along major rift-related structures. Breccia-filled maars or diatremes of kamafugitic affinity (designated here as “rift-related alkaline rocks”) are widespread in the regions of Patos de Minas, Presidente Olegário and Carmo do Paranaíba. Samples from each of these areas were selected for this study, comprising ca. 85% of the investigated occurrences. Kamafugites (s.l.) of the Mata da Corda Formation consist of olivine, clinopyroxene and phlogopite set in a fine groudmass of clinopyroxene, olivine, phlogopite, kalsilite and/or leucite, spinels, perovskite, carbonate, apatite and serpentine. Among the Mata da Corda kamafugites, both ugandite (characterized by the presence of leucite as a dominant felsic phase) and mafurite (with kalsilite as a dominant felsic phase) end-members have been identified by Araújo (2002). Surge deposits of the Mata da Corda Formation contain coarse fragments of mela-syenite, wehrlites, dunites and pyroxenite or cognate cumulus peridotite nodules (with olivine and perovskite which alternate as cumulus and ad-cumulus phases, and minor magnetite and pyroxene as intercumulus). Such fragments and nodules indicate magma re-equilibration within temperature zoned reservoirs (see discussion below regarding mantle plumes).

Mineral chemistry, major elements and compatible trace elements

Mineral chemistry of samples used in the isotopic analyses was determined by microprobe and found to be efficient in distinguishing kimberlites s.l., mafurites and ugandites. Phlogopites in the kimberlites have low $TiO_2$ contents (ranging from 0.41 to 1.94 wt%) with $Al_2O_3$ ranging from 11.41 to 12.64 wt%. In mafurites, the $TiO_2$ of the phlogopites ranges from 0.46 to 4.97 wt%, and $Al_2O_3$ from 2.74 to 12.65 wt%. In ugandites, the phlogopites have high $TiO_2$ contents, i.e. 4.35 to 8.65 wt%, with $Al_2O_3$ from 5.14 to 11.38 wt%. Forsterite contents in the olivines from kimberlites range from $Fo_{82}$ to $Fo_{92}$. The olivines from the mafrites display a range from $Fo_{81}$ to $Fo_{82}$ and the olivines from the ugandites between $Fo_{79}$ and $Fo_{92}$. Pyroxenes (diopsides) have been identified only in the mafurites and ugandites. The nature of the spinel group minerals depends on the rock-type. Kimberlites have titano-magnetite phenocrysts and chromium-spinel xenocrysts; mafurites have titano-magnetite phenocrysts and chromite xenocrysts; ugandites have titano-magnetite phenocrysts, chromite and hercynite xenocrysts. Ilmenite (picroilmenite) was observed in kimberlites, with MgO contents ranging from 8.53 to 17.71 wt%, FeO from 18.54 to 29.81 wt%, and MnO varying from 0.34 to 0.86 wt%. Perovskites recognized in both kimberlites and kamafugites have a high $CaTiO_3$ component.

Bulk compositions of the samples used in the isotopic analysis have been determined by X-ray fluorescence (XRF) and Neutron Activation analysis (INAA) (Table 1). The studied rocks are ultrabasic ($SiO_2$ contents generally lower than 40 wt%) and plot in the highly alkaline field in the silica vs. total alkalies diagram. The kimberlites and rocks of kimberlitic affinity are ultrapotassic ($K_2O/Na_2O>3$), with mg# $[Mg/(Mg+ Fe^{2+})]*100$ ranging from 63 to 76, and the overall compositions are similar to those of primary liquids derived from the melting of mantle peridotites. On the basis of chemical compositions, the shallower-derived rock-types plot within the field of kamafugites (Foley *et al.*, 1987). Relative to the studied kimberlites, and to kimberlites in general, the "rift-related" alkaline rocks have more evolved bulk composition (mg# from 49 to 53), indicating olivine and possible chromite fractionation in the parent magmas.

On the whole, the analyzed samples exhibit trends of increasing $Al_2O_3$, $Fe_2O_3$, CaO and $Na_2O$ with increasing $SiO_2$. Variation diagrams show a tendency to display a continuum of major and trace element compositions. The apparent affinity of the different rock-types could be misleading, in that different proportions (and compositions) of macrocrystals of olivine, perovskite and phlogopite may, to a large extent, control the major element geochemistry. However, because of the common source character of the different rock-types (see below) and because of petrographic evidence for shallow-level differentiation, the linear relationships between various oxides and MgO (and other fractionation indexes) is tentatively ascribed to melt extraction trends and fractional crystallization dominated by Mg-rich olivine, pyroxene and chromite. Modal abundances, as well as increasing $SiO_2$ and CaO with decreasing MgO contents, point to a major role for clinopyroxene in controlling the whole-rock composition of the more evolved rock-types.

Table 1. Representative whole-rock analyses of different alkaline rocks (kimberlite, k; mica peridotite of kimberlitic affinity, p) from the Alto Paranaíba region (cf. Bizzi *et al.*, 1994, 1995). Notional age 85 Ma. REE and PGE were determined by induced neutron activation analysis (INAA) and mass spectrometry; major and other trace elements by XRF; total iron as FeO and LOI not adjusted for oxidation. For analytical methods see McDonald *et al*. (1995) and Bizzi *et al*. (1995).

| | Três Ranchos (k) | Limeira (k) | Japecanga (p) | Três Ranchos (k) | Limeira (k) | Japecanga (p) | Pântano (p) | Presidente Oligário (a) |
|---|---|---|---|---|---|---|---|---|
| wt % | | | | | | | | |
| $SiO_2$ | 34.47 | 29.74 | 34.71 | 32.27 | 37.74 | 37.69 | 36.52 | 43.74 |
| $TiO_2$ | 1.25 | 2.41 | 2.22 | 4.78 | 6.14 | 5.19 | 7.24 | 3.78 |
| $Al_2O_3$ | 2.57 | 1.85 | 0.89 | 2.49 | 5.02 | 5.51 | 4.66 | 7.41 |
| $FeO_{tot}$ | 9.82 | 10.98 | 12.74 | 14.06 | 14.41 | 14.05 | 14.73 | 10.50 |
| MnO | 0.24 | 0.22 | 0.19 | 0.24 | 0.21 | 0.34 | 0.21 | 0.17 |
| MgO | 31.62 | 29.88 | 30.51 | 24.09 | 16.35 | 13.20 | 15.66 | 9.19 |
| CaO | 4.63 | 10.84 | 2.63 | 10.95 | 10.29 | 11.84 | 9.03 | 11.11 |
| $Na_2O$ | 0.09 | 0.02 | 0.02 | 0.10 | 0.44 | 0.46 | 0.95 | 1.35 |
| $K_2O$ | 0.93 | 1.05 | 0.25 | 2.42 | 1.74 | 0.92 | 2.81 | 3.53 |
| $P_2O_5$ | 1.21 | 2.57 | 0.19 | 0.93 | 0.41 | 0.84 | 1.44 | 0.93 |
| L.O.I. | 12.71 | 9.73 | 15.38 | 6.63 | 5.57 | 6.43 | 6.03 | 6.53 |
| Sum | 99.73 | 99.25 | 99.70 | 98.96 | 98.32 | 96.47 | 99.27 | 98.24 |
| ppm | | | | | | | | |
| S | 554 | 701 | 982 | 3331 | 579 | 315 | 310 | |
| F | 3375 | 2141 | 1491 | 1754 | 2565 | 2829 | 1470 | |
| Sc | 19.7 | 23 | 11.6 | 24 | 25 | 28 | 23 | 20 |
| V | 72 | 141 | 136 | 53 | 250 | 261 | 247 | |
| Cr | 1725 | 1289 | 1280 | 1169 | 587 | 361 | 685 | 589 |
| Co | 99 | 89 | 121 | 98 | 79 | 70 | 84 | 53 |
| Ni | 1747 | 1295 | 2403 | 1094 | 544 | 459 | 603 | 524 |
| Cu | 37 | 53 | 11 | 124 | 122 | 129 | 92 | 55 |
| Zn | 75 | 79 | 68 | 88 | 103 | 106 | 128 | 103 |
| Cs | 7.7 | 8.6 | 0.7 | 9.1 | 9 | 9.6 | 10.8 | |
| Rb | 72 | 101 | 18.5 | 171 | 203 | 85 | 175 | 55 |
| Ba | 2730 | 2351 | 675 | 2560 | 6569 | 17620 | 3095 | 2980 |
| Th | 41.5 | 23.0 | 9.7 | 25.5 | 24.5 | 19.9 | 19.0 | 18.0 |
| U | 7.7 | 5.4 | 8.2 | 5.2 | 5.6 | 5.7 | 3.4 | 3.2 |
| Nb | 317 | 195 | 166 | 140 | 199 | 171 | 176 | 134 |
| Ta | 11 | 10 | 19 | 16 | 15 | 11 | 12 | 11 |
| Sr | 2290 | 2160 | 547 | 1828 | 1908 | 2158 | 2032 | 1260 |
| Pb | 12.6 | 8.2 | 5.8 | 8.4 | 10.9 | 8.9 | 12.3 | 9.0 |
| Zr | 378 | 632 | 632 | 820 | 774 | 669 | 1156 | 503 |
| Hf | 7.6 | 12.0 | 12.2 | 16.6 | 15.4 | 15.3 | 26.6 | 22.0 |
| Y | 22 | 34 | 8.8 | 23 | 23 | 30 | 30 | 31 |
| La | 429 | 291 | 68.1 | 274 | 202 | 224 | 197 | 192 |
| Ce | 614 | 480 | 117 | 435 | 364 | 366 | 366 | 360 |
| Pr | 59.5 | 49.1 | 14.9 | 42.1 | 46.8 | 44.1 | 38.6 | 39.1 |
| Nd | 191 | 194 | 45.2 | 160 | 156 | 156 | 150 | 154 |
| Sm | 28.7 | 35.6 | 7.9 | 26.9 | 26.0 | 25.7 | 23.8 | 23.6 |
| Eu | 6.3 | 8.5 | 1.9 | 6.5 | 6.6 | 6.5 | 6.9 | 6.7 |
| Gd | 11.8 | 15.4 | 3.3 | 12.3 | 12.2 | 11.9 | 10.9 | 10.8 |
| Tb | 1.8 | 2.4 | 0.62 | 1.6 | 1.7 | 1.9 | 1.9 | 1.9 |
| Tm | 0.26 | 0.53 | | | | | | |
| Yb | 1.01 | 1.44 | 0.47 | 1.09 | 1.18 | 1.29 | 1.51 | 1.44 |
| Lu | 0.19 | 0.22 | 0.16 | 0.17 | 0.18 | 0.21 | 0.21 | 0.22 |
| ppb | | | | | | | | |
| Os | 1.3 | 1.7 | 1.0 | 0.99 | 0.48 | 0.51 | 0.26 | 0.30 |
| Ir | 2.3 | 1.8 | 0.94 | 0.92 | 0.45 | 0.41 | 0.28 | 0.37 |
| Ru | 4.5 | 4.6 | 2.7 | 2.9 | 0.54 | 0.62 | 0.66 | 1.10 |
| Rh | 1.1 | 1.2 | 0.61 | | | | 0.30 | 0.35 |
| Pt | 14.1 | 11.7 | 4.3 | 9.9 | 8.6 | 8.5 | 7.4 | 7.1 |
| Pd | 9.9 | 8.8 | 2.4 | 6.2 | 5.7 | 6.9 | 5.3 | 5.2 |

### Incompatible trace elements

Mantle-normalized trace element compositions of the Três Ranchos Kimberlite display the greatest degree of enrichment in incompatible trace elements such as La, Ce, Th, Nb and Nd. This kimberlite is more enriched in these elements than the South African Group II kimberlites. The concentrations observed in the other kimberlites, however, are comparable to those of the South African kimberlites. Excepting for high Ba contents, the range of normalized trace element composition of the rift-related rocks is not dissimilar to that of the kimberlites and kimberlite-related rocks.

Chondrite-normalized rare earth elements (REE) compositions indicate that the studied occurrences are highly LREE enriched (La 70-430 ppm) and exhibit steep profiles (Ce/Yb = 130-425), which tend to flatten out in the heavy rare earth elements (HREE). All rock-types have similar parallel to subparallel trends and, with the exception of Japecanga, there are no significant variations in REE contents among the intrusions. The high LREE/HREE ratios, associated with the near constant low HREE contents, indicate that melting occurred in the presence of residual garnet, and that changes in depth of final melt segregation were not accompanied by significant variations in source mineralogy. The similarity in REE-normalized patterns suggests that all the investigated rocks have undergone similar processes. The lower LREE/HREE ratios of the rift-related alkaline rocks compared to those of the kimberlites indicate that higher degrees of partial melting were probably associated with their genesis. The samples from the Catalão II carbonatite have significant internal REE variability.

Uranium and thorium behave coherently and present positive correlations with LREE/HREE ratios. A negative correlation between U/Pb and K/U ratios indicates a process that fractionated both K and Pb relative to U, and suggests that the U/Pb fractionation was influenced by a potassic phase, probably phlogopite.

All the magma types recognized in this study have positive Nb anomalies on the mantle-normalized trace element diagrams. Niobium tends to correlate positively with LREE, and the high Nb/La ratios in these rocks are similar to those of OIB. Nb also correlates positively with Th and U, and negatively with Y and HREE. The lack of significant correlation between Zr and Nb indicates a rather erratic behavior of Nb. U/Nb, Th/Nb and Rb/Nb ratios are consistently lower than the ratios of the primitive mantle (Hofmann, 1988), probably indicating a phase that was enriched in Nb relative to these very incompatible elements. Ba/Nb ratios, with the exception of Japecanga, are higher than primitive mantle ratios.

### Platinum-group elements

Some of the inter PGE ratios and the chondrite-normalized PGE patterns are shown in Fig. 2. Noble metal concentrations (i.e. concentrations of Os, Ir and Ru in the range of 1-5 ppb) are compatible with the range of values from South African kimberlites (McDonald *et al.*, 1995), and are higher than those typically found in basalts (MORB, OIB and CFB; Hertogen *et al.*, 1980; Barnes *et al.*, 1985) and in many komatiites (Crocket & MacRae, 1986; Brugmann *et al.*, 1987), but lower than calculated PGE abundances in average spinel and garnet lherzolites (e.g. Mitchell & Keys, 1981).

Re contents determined by mass-spectrometry were found to be higher in kimberlites (average 0.5 ppb) than in kamafugites (Re contents of the order of 0.05 ppb). A weak negative correlation is noted between Re and $Al_2O_3$, thus suggesting that the variation in Re contents is not controlled by partial melting processes. Re and Al contents of kamafugites in general, and ugandites in particular, could possibly be related to mixing of a re-enriched peridotitic source and a magmatic fluid with low Re/Al ratio. Os contents have positive correlation with MgO and Ni contents. Different Re contents of kimberlite samples relative to kamafugite samples might thus be taken as indicative of the involvement of different sources.

Different PGE patterns were found. The samples from fractionated rock-types (e.g. Sucesso) display the strongest Os and Ir to Pd fractionation relative to chondrite. In contrast, the samples from primitive/ unfractionated rock-types (e.g. Japecanga) show the lowest Pd/Ir ratio and the least fractionated pattern, with only a slight depletion in Os and Ir, and almost chondritic proportions of Ru, Rh, Pt and Pd.

The other localities show a continuum of Pd/Ir ratios and pattern shapes intermediate between the fractionated and the unfractionated end-members.

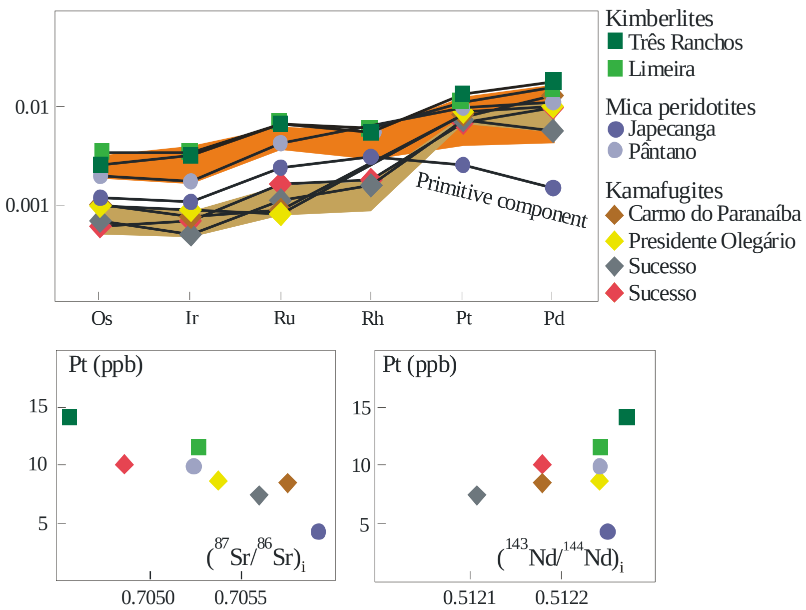


Fig. 2. Chondrite-normalized PGE concentrations (cf. Table 1). The kimberlite (orange) and kamafugite (light brown) fields are after Araújo *et al*. (2001). It should be noted the linear relationships of PGE with Sr and Nd isotopic ratios (cf. Table 2) which suggest that PGE and inter-element features are related to time-integrated source characteristics rather than to fractionation processes. This apparent affinity of PGE and isotopic signatures, however, does not necessarily imply that PGE is associated with ancient metasomatic events because such a relationship could have been inherited during a mixing process.

## Isotope geochemistry

Representative isotopic results are given in Tables 2 and 3.

The analyzed rocks have presently $^{143}Nd/^{144}Nd$ and $^{87}Sr/^{86}Sr$ ratios ranging from 0.51216 to 0.51234 and 0.7047 to 0708, respectively (initial ratios, calculated at 100 Ma, 0.51210-0.51228 and 0.7046-0.7066, respectively).

The kimberlites and carbonatites have slightly more radiogenic Nd (average for the present-day ratio $^{143}Nd/^{144}Nd=0.51230$) and less radiogenic Sr (average $^{87}Sr/^{86}Sr=0.705$) than the rift-related alkaline rocks. Nd model ages (depleted mantle) vary from 830-910 Ma for the kimberlites and from 1.00 to 1.12 Ga for the kamafugites. In general, present-day Pb isotopic signatures range as follows: $^{206}Pb/^{204}Pb=17.07$-$20.96$, $^{207}Pb/^{204}Pb=15.31$-$15.68$ and $^{208}Pb/^{204}Pb=30.16$-$40.15$. $^{238}U/^{204}Pb$ ratios vary from 10.18 to 144.73. Initial ratios (100 Ma) range from

17.44 to 19.41 and from 15.44 to 15.61 for $^{206}Pb/^{204}Pb$ and $^{207}Pb/^{204}Pb$, respectively. As shown in Fig. 3, the $^{206}Pb/^{204}Pb$ vs. $^{207}Pb/^{204}Pb$ data define a linear array with a small degree of scatter regarding a reference secondary isochron of 925 Ma.

In particular, the kimberlites have $^{206}Pb/^{204}Pb$ initial ratios>18, whereas the other alkaline rocks have $^{206}Pb/^{204}Pb$ initial ratios in the 17-18 range. Pb isotopic compositions of the carbonatites plot intermediate between the kimberlites and the rift-related rocks.

The Re-Os isotope systematics allowed a clear distinction among the different rock-types. Kimberlites have $^{187}Os/^{188}Os$ ratios ranging from 0.117 to 0.129 and γOs between 0 and -7. Mafurites and ugandites have $^{187}Os/^{188}Os$ ratios ranging from 0.127 to 0.145 and 0.142 to 0.147, respectively, and γOs between -1 and 15. The kimberlites have higher Re (0.2-1.3 ppb) and Os (1.2-1.9 ppb) contents relative to the more radiogenic kamafugites (Re 0.03-0.07 ppb, Os 0.2-1.9 ppb).

With one exception, TRD model ages range between 1.39 and 1.64 Ga, thus setting a minimum Re age of the source region protolith.

An important aspect of the studied alkaline rocks is that they show typical Dupal characteristics (in terms of $^{207}Pb/^{204}Pb$ and $^{208}Pb/^{204}Pb$ ratios, of deviation from a northern hemisphere reference line-NHR and of $^{87}Sr/^{86}Sr$ values; cf. Hart, 1984). The relevance of this observation is emphasized by the isotopic similarities between the Alto Paranaíba igneous rocks and some OIB with Dupal signatures in the South Atlantic (e.g. the Walvis Ridge basalts; Fig. 4) and by the hypothesis that the source region of the studied volcanics is likely to have been influenced by the Tristan da Cunha Dupal hot spot at ca. 130 Ma.

However, the relationships between the emplacement of these rocks and Dupal-type mantle plumes are yet not clear. The older "rift-related" volcanics (e.g. the Sucesso volcanics, dated at 119 Ma), and perhaps the kimberlites (emplace-ment ages ranging from 109 to 87 Ma), probably occurred

Table 2. Sr, Nd and Pb isotopic ratios relative to the samples of Table 1. Notional age 85 Ma. For analytical methods see Bizzi *et al*. (1994, 1995).

| | Três Ranchos (k) | Limeira (k) | Japecanga (p) | Pântano (p) | Presidente Olegário (a) | Carmo do Paranaíba (a) | Sucesso (a) | Sucesso (a) |
|---|---|---|---|---|---|---|---|---|
| Rb | 54.28 | 101.62 | 9.2 | 176.0 | 200.9 | 76.7 | 172.6 | 49.25 |
| Sr | 1215 | 2278 | 400 | 1899 | 2278 | 2355 | 2248 | 1374 |
| $(^{87}Sr/^{86}Sr)_m$ | 0.70473 | 0.70543 | 0.70599 | 0.70556 | 0.70568 | 0.70586 | 0.70586 | 0.70502 |
| Sm | 46 | 27.9 | 6.5 | 24.6 | 23.9 | 24.4 | 20.4 | 23.5 |
| Nd | 391.5 | 229.8 | 47.3 | 179.0 | 170.2 | 173.4 | 150.6 | 173.5 |
| $(^{143}Nd/^{144}Nd)_m$ | 0.51231 | 0.51228 | 0.51230 | 0.51229 | 0.51229 | 0.51223 | 0.51216 | 0.51223 |
| $(^{87}Sr/^{86}Sr)_i$ | 0.70457 | 0.70527 | 0.70591 | 0.70524 | 0.70537 | 0.70575 | 0.70559 | 0.70487 |
| $(^{143}Nd/^{144}Nd)_i$ | 0.51227 | 0.51224 | 0.51225 | 0.51224 | 0.51224 | 0.51218 | 0.51211 | 0.51218 |
| $\varepsilon^t Sr$ | -0.39 | 9.55 | 18.57 | 9.01 | 10.93 | 16.25 | 15.05 | 3.78 |
| $\varepsilon^t Nd$ | -5.03 | -5.65 | -5.36 | -5.55 | -5.58 | -6.75 | -8.08 | -6.71 |
| $T^{DM}$ (Ga) | 0.87 | 0.91 | 0.86 | 0.97 | 0.98 | 1.05 | 1.10 | 1.02 |
| $(^{206}Pb/^{204}Pb)_m$ | 19.21 | 17.97 | 20.96 | 18.44 | 17.95 | 17.78 | 17.70 | 17.07 |
| $(^{207}Pb/^{204}Pb)_m$ | 15.56 | 15.46 | 15.68 | 15.49 | 15.47 | 15.47 | 15.45 | 15.31 |
| $(^{208}Pb/^{204}Pb)_m$ | 40.01 | 38.68 | 39.67 | 38.96 | 38.68 | 38.21 | 38.25 | 38.16 |
| $^{238}Pb/^{204}Pb$ | 36.38 | 30.02 | 144.73 | 34.22 | 20.67 | 14.61 | 10.18 | 13.16 |

Table 3. Sr, Nd, Pb and Os-Re isotopic ratios relative to Alto Paranaíba samples (after Araújo *et al*. 2001).

| **Kimberlites** | D-04A | TR-72 | SR-16 | D-04B | D-01 | SR-04 |
|---|---|---|---|---|---|---|
| Rb | 93.63 | 37.83 | 21.05 | 123.51 | 131.64 | 186.82 |
| Sr | 2215.51 | 2926.76 | 4216.04 | 2267.04 | 1069.67 | 732.50 |
| ($^{87}$Sr/$^{86}$Sr)$_m$ | 0.70558 (3) | 0.70519 (2) | 0.70546 (8) | 0.70559 (3) | 0.70545 (5) | 0.70690 (3) |
| Sm | 41.84 | 42.89 | 20.02 | 25.64 | 42.90 | 11.37 |
| Nd | 311.85 | 347.87 | 116.52 | 185.96 | 324.77 | 91.99 |
| ($^{143}$Nd/$^{144}$Nd)$_m$ | 0.51227 (5) | 0.51231 (5) | 0.51236 (6) | 0.51225 (3) | 0.51227 (6) | 0.51225 (2) |
| | | | | | | |
| ($^{87}$Sr/$^{86}$Sr)$_i$ | 0.70544 | 0.70514 | 0.70540 | 0.70540 | 0.70505 | 0.70600 |
| ($^{143}$Nd/$^{144}$Nd)$_i$ | 0.51222 | 0.51227 | 0.51229 | 0.51220 | 0.51223 | 0.51221 |
| | | | | | | |
| $\varepsilon^t$Sr | 11.79 | 7.71 | 11.94 | 11.33 | 5.94 | 19.97 |
| $\varepsilon^t$Nd | -5.93 | -5.07 | -4.65 | -6.34 | -5.91 | -6.22 |
| T$^{DM}$(Ga) | 1.02 | 0.89 | 1.28 | 1.01 | 0.97 | 0.95 |
| | | | | | | |
| ($^{206}$Pb/$^{204}$Pb)$_m$ | 23.188 (5) | 18.638 (7) | 19.225 (4) | 23.506 (2) | 19.748 (1) | 18.472 (1) |
| ($^{207}$Pb/$^{204}$Pb)$_m$ | 15.742 (4) | 15.538 (1) | 15.615 (3) | 15.790 (1) | 15.606 (1) | 15.603 (1) |
| ($^{208}$Pb/$^{204}$Pb)$_m$ | 40.558 (9) | 39.589 (2) | 39.787 (8) | 40.669 (3) | 39.367 (2) | 39.046 (2) |
| | | | | | | |
| Os (ppb) | 12.213 | 12.624 | 19.271 | 11.646 | 14.295 | 16.918 |
| ($^{187}$Os/$^{188}$Os)$_m$ | 0.12987 (2) | 0.11984 (18) | 0.11985 (65) | 0.13050 (20) | 0.13174 (12) | 0.11940 (8) |
| ($^{187}$Os/$^{186}$Os) | 108.269 | 0.99609 | 0.99615 | 110.981 | 109.501 | 0.99247 |
| ($^{187}$Os/$^{188}$Os)$_i$ | 0.12813 | 0.11896 | 0.11721 | 0.12861 | 0.12546 | 0.11796 |
| $\gamma$Os | 0.02 | -7.14 | -8.50 | 0.40 | -2.06 | -7.92 |
| | | | | | | |
| Re (ppb) | 0.3148 | 0.2173 | 0.7192 | 0.3347 | 13.135 | 0.3363 |
| $^{187}$Re/$^{185}$Re | 1.2461 (89) | 1.1578 (28) | 1.4592 (42) | 1.2625 (11) | 1.4922 (25) | 1.2933 (33) |
| $^{187}$Re/$^{188}$Os | 12.313 | 0.6227 | 18.619 | 13.344 | 44.295 | 10.163 |
| T$^{RD}$(Ga) | | 1.39 | 1.65 | | 0.46 | 1.54 |

| **Mafurites** | L-06 | TR-83 | TR-84 | O-09 | O-22 | **Ugandites** | L-28 | O-24 | P-09 |
|---|---|---|---|---|---|---|---|---|---|
| Rb | 153.2 | 218.55 | 293.97 | 246.78 | 155.97 | | 127.57 | 355.13 | 339.89 |
| Sr | 1162.43 | 1570 | 2994.8 | 1337.96 | 846.34 | | 2267.57 | 1036.35 | 2267.57 |
| ($^{87}$Sr/$^{86}$Sr)$_m$ | 0.70552 (2) | 0.70555 (2) | 0.70734 (2) | 0.70614 (1) | 0.70563 (1) | | 0.70571 (3) | 0.70664 (2) | 0.70597 (3) |
| Sm | 20.28 | 23 | 33.5 | 19.69 | 12.6 | | 23.6 | 16.2 | 24.35 |
| Nd | 148.25 | 177.75 | 259 | 148.19 | 72.06 | | 151.88 | 98.04 | 169.34 |
| ($^{143}$Nd/$^{144}$Nd)$_m$ | 0.51240 (7) | 0.51229 (6) | 0.51213 (5) | 0.51213 (5) | 0.51228 (6) | | 0.51219 (5) | 0.51223 (5) | 0.51212 (5) |
| | | | | | | | | | |
| ($^{87}$Sr/$^{86}$Sr)$_i$ | 0.70506 | 0.70507 | 0.70686 | 0.70549 | 0.70498 | | 0.705474 | 0.705732 | 0.705437 |
| ($^{143}$Nd/$^{144}$Nd)$_i$ | 0.51235 | 0.51225 | 0.51209 | 0.5122 | 0.51222 | | 0.51213 | 0.51217 | 0.51207 |
| | | | | | | | | | |
| $\varepsilon^t$Sr | 6.5 | 6.63 | 34 | 12.69 | 5.46 | | 12.94 | 11.94 | 11.98 |
| $\varepsilon^t$Nd | -3.41 | -5.5 | -8.63 | -6.5 | -5.94 | | -7.63 | -6.9 | -8.92 |
| T$^{DM}$(Ga) | 0.84 | 0.93 | 1.11 | 1 | 1.08 | | 1.17 | 1.21 | 1.19 |
| | | | | | | | | | |
| ($^{206}$Pb/$^{204}$Pb)$_m$ | 18.619 (1) | 18.372 (8) | 17.935 (1) | 17.798 (8) | 18.303 (7) | | 17.976 (1) | 18.445 (1) | 17.943 (1) |
| ($^{207}$Pb/$^{204}$Pb)$_m$ | 15.528 (1) | 15.524 (1) | 17.935 (1) | 17.798 (1) | 18.303 (1) | | 15.497 (1) | 15.508 (1) | 15.464 (1) |
| ($^{208}$Pb/$^{204}$Pb)$_m$ | 39.142 (3) | 39.164 (2) | 38.684 (2) | 38.374 (2) | 38.858 (2) | | 38.455 (2) | 38.891 (3) | 38.398 (3) |
| | | | | | | | | | |
| Os (ppb) | 0.7001 | 0.1229 | 0.8434 | 10.172 | 17.823 | | 15.471 | 19.821 | 0.2657 |
| ($^{187}$Os/$^{188}$Os)$_m$ | (20) | (68) | 0.12794 (29) | 0.13913 (38) | 0.14547 (20) | | (32) | 0.14176 (16) | (103) |
| $^{187}$Os/$^{186}$Os | 108.502 | 112.686 | 115.646 | 115.646 | 12.091 | | 120.627 | 117.828 | 12.345 |
| ($^{187}$Os/$^{188}$Os)$_i$ | 0.12679 | 0.13313 | 0.12743 | 0.13887 | 0.14522 | | 0.14487 | 0.14161 | 0.14772 |
| $\gamma$Os | -1.02 | 3.93 | -0.52 | 8.4 | 13.37 | | 13.09 | 10.55 | 15.32 |
| | | | | | | | | | |
| Re (ppb) | 0.3845 | 0.0438 | 0.0645 | 0.0394 | 0.0649 | | 0.0706 | 0.0438 | 0.0337 |
| $^{187}$Re/$^{185}$Re | (54) | (46) | (100) | (141) | (245) | | (24) | (263) | 0.39971 (68) |
| $^{187}$Re/$^{188}$Os | 26.487 | 17.217 | 0.3569 | 0.1869 | 0.176 | | 0.18607 | 0.10517 | 0.56575 |
| T$^{RD}$(Ga) | 0.27 | | 0.18 | | | | | | |

under the thermal influence of the Tristan da Cunha hot spot. Conversely, the peak of activity within the Mata da Corda volcanic fields was coincident with the thermal influence of the Trindade non-Dupal hot spot at ca. 80 Ma (see discussion below on the influence of mantle plumes).

Despite their similarities in bulk composition, mineralogy and petrographic character, the Sr-Nd and U-Pb isotopic compositions of the kimberlites from Alto Paranaíba are unique when related to worldwide kimberlitic provinces (Figs. 3 and 4). Compared to Group I kimberlites (Smith, 1983), the Brazilian kimberlites have originated from mantle source rocks with higher time-averaged Rb/Sr, Nd/Sm and Pb/U ratios (indicative of ancient LILE enrichment in the source of the Brazilian kimberlites). Compared to the source of micaceous Group II kim-berlites (Smith, 1983) and isotopically transitional kimberli-tes (Clark *et al.*, 1991; Skinner *et al.*, 1991) from southern Africa, the Brazilian rocks have been for-med from sources with lower time-averaged Rb/Sr, Nd/Sm and Pb/U (Bizzi *et al.*, 1993). Therefore, the enrichment of the Brazilian kimberlite sources was either not as intense or not as old (or possibly both) as that of the source of the South African analogues. Alternatively, such lower time-averaged ratios could have been genera-ted shortly after the enrichment event, if the enriched source was depleted in some of its elements during tectonic process and left to evolve with time (see discussion below on the delamination processes).

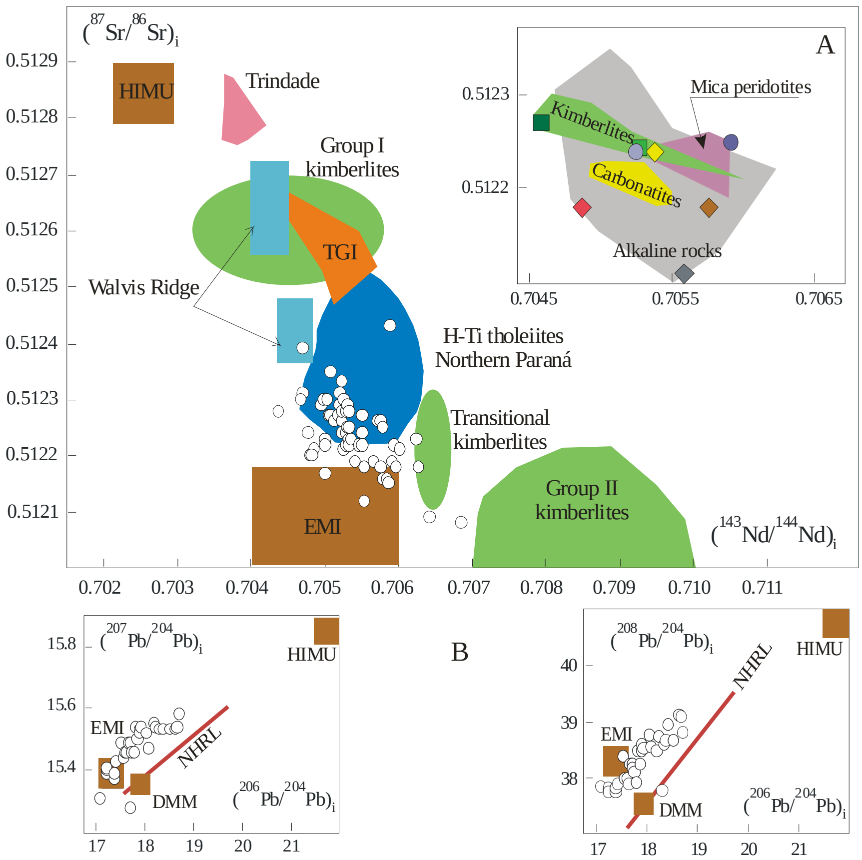


Fig. 3. Sr, Nd and Pb (inset B) isotopic signatures relative to the Alto Paranaíba whole population (open circles; cf. Table 2 of Gomes & Comin-Chiaramonti, in this volume). HIMU and EMI, as defined by Zindler & Hart (1986) and by Hart & Zindler (1989); Group I, Group II and transitional kimberlites after Smith (1983) and Clark *et al.* (1991); Walvis Ridge after Richardson *et al.* (1984); Paraná "uncontaminated" high-Ti tholeiites after Comin-Chiaramonti *et al.*, 1997 and therein references; Trindade after Siebel *et al.* (2000) and Marques *et al.* (2000); TGI, Tristan da Cunha-Gough-Inacessible Islands, after Le Roex *et al.* (1990). Inset A: Initial Sr-Nd isotopic ratios of the samples of Fig. 2 (same symbols) and the field of the various rock-types (cf. Gomes & Comin-Chiaramonti, in this volume).

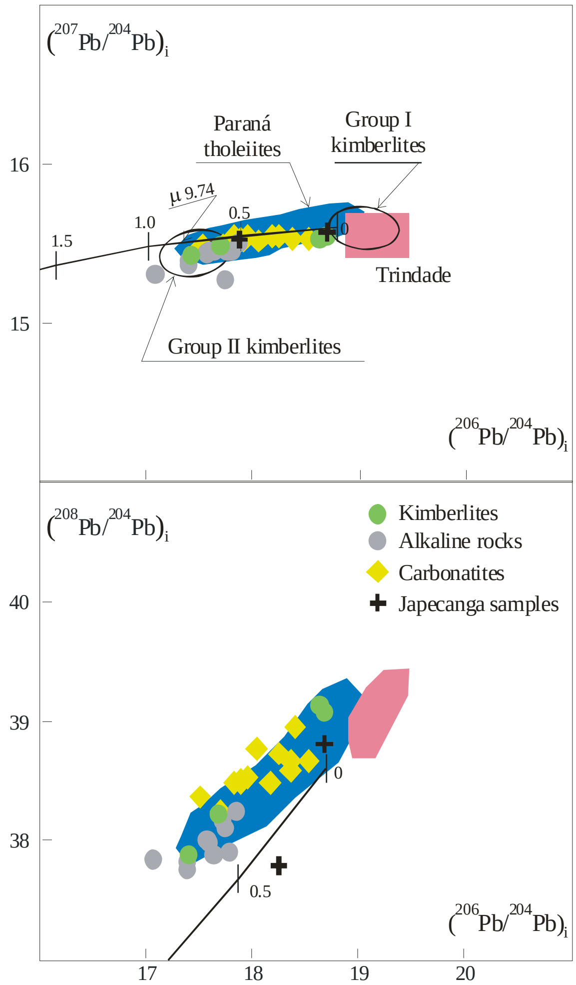


Fig. 4. Lead isotopic signature for selected samples from the Alto Paranaíba region. It should be noted that Pb isotopes define a linear array with a small degree of scatter regarding a reference secondary isochron at 925 Ma.

## SOURCE CHARACTERISTICS AND MIXING SYSTEMATICS

The tight clustering of Sr-Nd signatures (Fig. 3) is such that a common source component can be postulated to have been involved in the generation of the studied kimberlites, mica peridotites, carbonatites and other Mesozoic alkaline rocks. This source component was enriched in Rb (fRb>0) and depleted in Sm (fSm<0) relative to the Bulk Earth and remained isolated for a sufficient time span to acquire distinctive Sr and Nd isotopic compositions. Such compositions, typical of enriched lithosphere, together with the geochemical and petrographic characteristics of the rift-related rock-types and their xenoliths, indicate that the parent melts either interacted extensively with the local enriched lithosphere or were directly derived by various melting degrees of the enriched lithosphere. Os isotopes support such hypothesis, being $^{187}Os/^{188}Os$ ratios similar to those observed in mantle-derived xenoliths in kimberlites from the Kaapvaal, Wyoming and Siberian cratons.

On a larger scale, both the distinct source character and the relative homogeneity of the isotopic signatures suggest that a unique mantle lithosphere underlies the SW São Francisco craton margin. The isotopic similarities of the investigated rocks with the continental flood basalts from the northern Paraná Basin (Figs. 3 and 4) is indicative that their source(s) might be physically continuous. The magmatism which displays this isotopic similarity occur-red over an area of approximately 200x250 km for approximately 45 My. The magmatism does not show an obvious age progression on this scale, and its loci were apparently controlled mainly by intra-plate stresses focused along the preexisting Brasi-liano structural discontinuities (Bizzi, 1994). This implies prolonged tapping of a single mantle source between 130 and 85 Ma, a period during which the Coromandel area might have moved over a distance of 90 km during continuous Gondwana dispersion. The homogeneous mantle source, therefore, either moved with the South American plate or was available to be tapped over great distances.

Despite the clustering of Sr and Nd isotopic signatures of the province, it is evident that the internal variation within the groups of rocks (i.e. kimberlites, carbonatites etc.) is less than that among the different groups. Moreover, both Os and Pb isotopic signatures offer a clear discrimination between the groups, which mirrors the distinctive PGE characteristics of each group. Taken together, the range of the data provides evidence that more than one component was involved in the generation of the observed compositions, and that systematic change of end-member contributions exists among rock-types. It is proposed that the trends recognized for the Minas Gerais rocks depict mixing lines between two main end-members: 1) deep-derived melts represented by the kimberlites and related rocks; 2) a volumetrically prevailing lithospheric mantle peridotite which dominates the trace element characteristics of all the studied rocks, but it is clearly more significant in the shallower-derived alkaline rocks from the Mata da Corda Formation and in those related to the Paraná volcanics.

The first component has lower time-averaged Rb/Sr, Nd/Sm and Pb/U ratios and, therefore, it is isotopically more similar to the OIBS and Group I kimberlites (Smith, 1983) than the second component. Compared to the first component, the second one records higher time-averaged source enrichment in Nd, higher time-averaged enrichment in Rb and less radiogenic $^{206}Pb/^{204}Pb$ values, and is thus isotopically more similar to enriched subcontinental mantle lithosphere. Os signatures of the second component ($^{187}Os/^{188}Os$~0.135) plot within the range of ratios reported for pyroxenite veins in alpine-type peridotites and OIBs (Fig. 5).

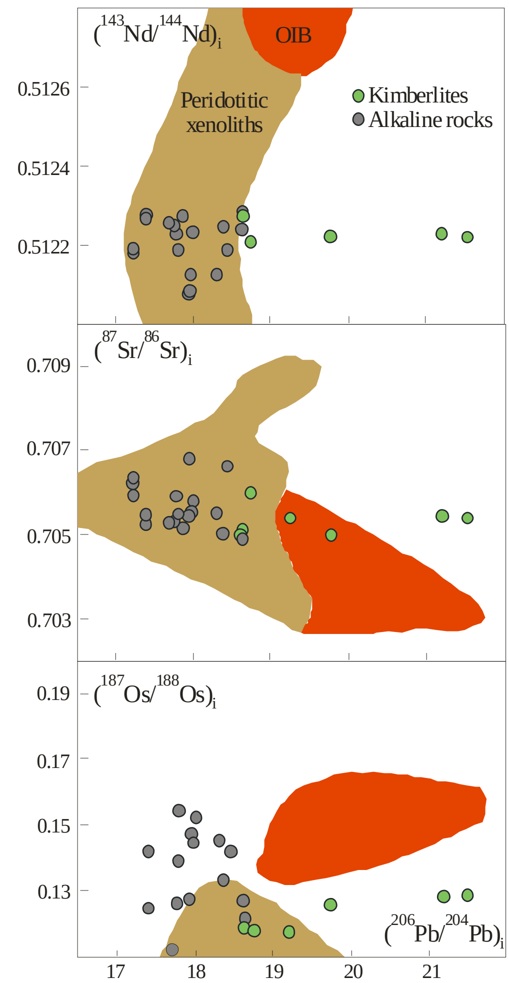


Fig. 5. $^{206}Pb/^{204}Pb$ isotopic ratios vs. $^{187}Os/^{188}Os$, $^{87}Sr/^{86}Sr$ and $^{143}Nd/^{144}Nd$ for selected samples from the Alto Paranaíba region. Data source: Carlson *et al.* (1996) and Araújo *et al.* (2001). OIB, Ocean Island Basalts, and peridotite xenoliths, after Smith (1983) and Smith *et al.* (1985).

Mixing processes are reflected by the relative positions of individual localities that, with respect to the end-member components, remain relatively constant from one isotopic space to the next (Fig. 6). Because of the restricted isotopic variation among the studied rocks, the definition of mixing lines is necessarily imprecise on this scale and highly dependent on chosen end-members and respective concentrations. Both analytical uncertainties and small-scale source heterogeneities are significant sources of scatter in the modelling, and preclude the possibility of delineating unique component contribution to the compositional varieties at the individual localities.

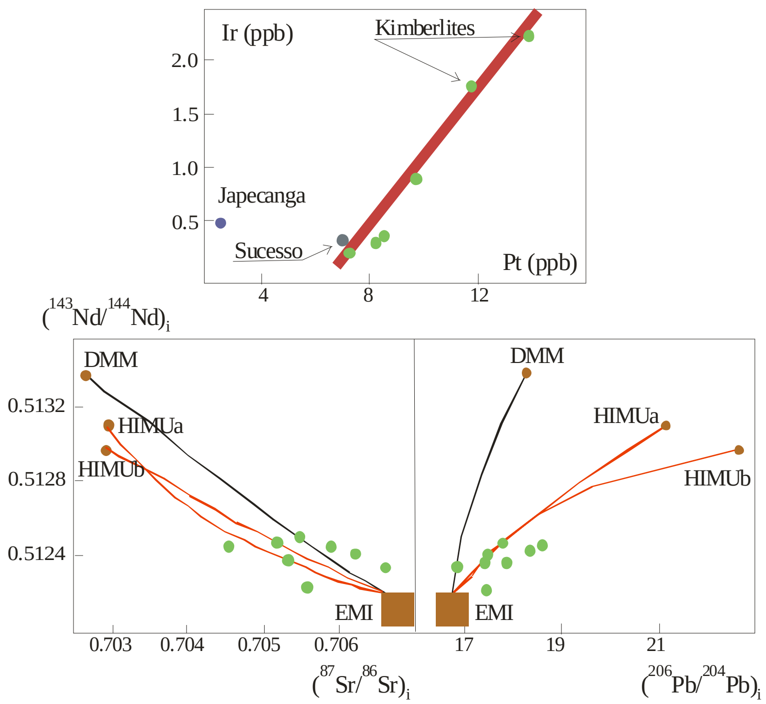


Fig. 6. Mixing systematics using both PGE and radiogenic isotopes. Isotope compositions of end-members after Hart & Zindler (1989). Though imprecise, the accuracy of the mixing lines betwen HIMU (DMM) and DMM is reflected by the fact that the relative positions of individual localities, with respect to the components, remain relatively constant from one isotopic space to the next. The plot of Pt vs. Ir shows a close correlation between the metal contents of the various rock-types. The slope of the line is very similar to the observed Pt/Ir ratio of Japecanga. The behaviour of these metals might be represented by a stright line (Ir=0.2775 Pt - 1.874) where the constant is the fractionated component "Sucesso" and the slope is the proportion of the "Japecanga" component. The mixing proportions calculated using the above equation are favorably comparable to the concentrations calculated using the radiogenic isotopes.

Assuming that Sucesso (fractioned) and Japecanga (unfractioned) PGE patterns represent two end-members which could be combined to produce the other patterns, both mixing and addition models were calculated (Fig. 6). It was concluded that none of the patterns can be generated by the mixing of an unfractionated Japecanga-like component with a fractionated Sucesso-like component, because deficiencies in Pt and Pd were found in all mixing combinations. However, if variable concentrations of PGE material with Japecanga's unfractionated characteristics are added to a fractionated reservoir, all other PGE patterns can be generated. The PGE compositions of the sampled rocks from Sucesso, Carmo do Paranaíba and Presidente Olegário can be satisfactorily duplicated by the addition of a small amount of Japecanga-like component to the Sucesso composition: the addition would cause only a negligible dilution of the fractionated reservoir, because of the relatively small volume of the contaminant. The patterns for Três Ranchos, Limeira and Pântano occurrences may also be closely modelled by the addition of the Japecanga component to the Sucesso component, but only if large amounts of the Japecanga end-member (up to two times PGE content) are added.

Employing such arguments, and comparing the data between the Brazilian and South African kimberlites, McDonald *et al.* (1995) suggested that the overall PGE characteristics of the studied Brazilian volcanics resulted from the assimilation and dilution of a PGE-enriched material by PGE-fractionated (Pt and Pd enriched) kimberlite-like melts. Notably, the PGE inter-element ratios ascribed to a theoretical PGE assimilated component are comparable to those reported to material from the 3.5 Ga Bon Acord Ni-Fe body, believed to be concentrated at depth in the Kaapval craton (cf. McDonald *et al.*, 1995). The lithosphere which forms the keel of the São Francisco craton may likewise be enriched in a similar component, entrained in the PGE-poor kimberlite-like magmas at the emplacement.

## THE INFLUENCE OF MANTLE PLUMES

The studied area has supposedly been under the influence of both the Trindade and the Tristan da Cunha mantle plumes. These plumes (cf. Fig. 3) have distinct Sr-Pb isotopic compositions, Trindade yielding non-Dupal-type volcanics, and Tristan da Cunha being associated with Dupal-type volcanism (cf. Duprè & Allégre, 1983).

In Tristan da Cunha island, the mantle plume manifested itself as a continuous series of ankaramitic basanites, tephriphonolites and phonolites that extend up to the ca. 89 Ma Rio Grande rise (Le Roex *et al.,* 1990). In the continent, the tholeiites from the northern Paraná Basin and the ca. 130 Ma alkaline complexes of Jacupiranga, Juquiá and Anitápolis, among others, have been generated from a garnet-bearing protolith under the "influence" of the Tristan plume (e.g. Mantovani *et al.*, 1985). The magnesium-rich end-members, also characterized by lower $Fe_2O_3$, $Al_2O_3$ and CaO, were derived from depths of the order of 60 to 100 km (Bizzi, 1994 and therein references).

Major and trace element variation trends suggest that the differentiation inside the prevailing high-Ti tholeiitic (HTi) and subordinate low-Ti tholeiitic suites from the northern Paraná Basin is compatible with crystal fractionation processes. The observed prevailing mineral assemblages are constituted by augite, pigeonite, plagioclase (labradorite), Ti-magnetite and rare olivine and orthopyroxene. These mineral assemblages are compatible with conditions of low pressure (e.g. 1 kb), low $fO_2$ (FMQ buffer), and near anhydrous conditions ($H_2O$~0.5 wt%). Conditions of higher pressure favour the crystallization of orthopyroxene rather than olivine, but would delay the crystallization of plagioclase (Bellieni *et al.*, 1984; Iacumin *et al.*, 2003). On the contrary, Mantovani *et al.* (1985) stated that modelling of incompatible elements are not consistent with crystal fractionation processes, even with varying partial melting degrees. Crustal contamination (e.g. ACF processes of De Paolo, 1981) is not apparent through the major and trace elements, and Sr-Nd istopes modelling (Peate *et al.*, 1992; Piccirillo *et al.*, 1990). Mantle heterogeneity due to ancient mixing processes that occurred in the source mantle is suggested by Iacumin *et al.* (2003) to explain the genesis of both L-Ti and H-Ti tholeiites.

The Trindade and Martin Vaz islands, as well as the 50 Ma Trindade-Vitória chain (Oversby, 1971;

Weaver, 1990; Halliday *et al.*, 1992; Siebel *et al.*, 2000) and the Abrolhos islands (Fodor *et al.* 1989), have been related to the Trindade plume. Most of the non-Dupal continental magmatism along the 125 AZ lineament (125° Azimut lineament: e.g. the kimberlitic provinces of Paranatinga-Batovi and Juína, Greenwood *et al.*, 1999, Araújo, 2002; the igneous provinces of Poxoréu, Gibson *et al.* 1997, and of Serra do Mar, Thompson *et al.* 1998, respectively) has also tentatively been related to the Trindade plume. Trace element compositions led the above mentioned authors to suggest different degrees of partial melting (5.5% for Poxoréu, 4.0% for Abrolhos, and 1.3% for Trindade) at different depths (generation would have taken place at 150 km for Trindade-Martin Vaz, whilst magma extraction for Poxoréu and Abrolhos would have taken place at shallower depths, of the order of 80 to 100 km). Such compositional differences would be due to the heterogeneous nature of the subcontinental lithosphere along the Trindade plume track. Compositional differences have also been observed along track across the South Atlantic oceanic lithosphere. As the South American plate drifted away, the plume entrained young oceanic lithosphere (some 30 Ma old) at first, and then impinged upon older (some 70 Ma old) and thicker oceanic lithosphere, the result of which being lower degrees of partial melting (1.3%) and the generation of subsaturated magmas to the East.

The influence of the Trindade plume has also been claimed for rocks generated at greater depths (Araújo, 2002 and therein references). Whereas basalts and basaltic trachyandesites from the Poxoréu igneous province were emplaced at ~84 Ma and the correspondig melts are believed to be generated at 80 to 100 km depth (Gibson *et al.* 1997), some of the Batovi-Paranatinga kimberlites, emplaced further to the northwest at 121-127 Ma (Heaman *et al.,* 1998), are diamonds-bearers, implying the generation of the corresponding melts at 140 km or deeper. In Juína, knorringitic garnets (with exsolved pyroxene), included in diamonds sampled by the 95 Ma old kimberlites, suggest that Trindade was a weak plume, originated at the thermoelastic discontinuity that separates the upper mantle from the lower one (400 to 670 km deep), which entrained both lower mantle and the subcontinental lithosphere (Hutchison, 1997). Araújo (2002) suggests that some rare magnesiowüstite and ferripericlase from the Juína diamonds are consistent with the silicate-perovskite paragenesis and the derivation from lower mantle (below the 670 km discontinuity). This implies the generation of the plume at the "D" thermal boundary layer, just above the core-mantle boundary. Significantly enough, the nature of the deep-seated diamond inclusions and the limited surface expression of the Juína magmatism would endorse the arguments posed by e.g. Bird *et al.* (1999) and Marquart & Schmeling (2000). The latter authors argue that deeply derived plumes would bear rare samples from the base of the mantle and would be efficient in incorporating materials from the lower mantle and the transition zone, reaching surface with about 30% of their initial temperature.

Gibson *et al.* (1995) inferred that the APIP (Alto Paranaíba Igneous Province) has been generated at 85 Ma under the influence of the Trindade hot spot on the basis of both plume track proposed by O'Connor & Duncan (1990) and geochemical similarities. Bizzi *et al.* (1995) and Van Decar *et al.* (1995) argued against Gibson's hypothesis for the Dupal-type signature of the rocks in the Paranaíba Province, and for the positioning of the volcanics relative to plume tracks and transform faults. It is possible, however, that both the Tristan and Trindade mantle plumes have had influence in the Alto Paranaíba region: the first would have had chemical influence, and the second would have been restricted to thermal influence.

Toyoda *et al.* (1994) investigating two groups of carbonatites, Catalão, Tapira and Araxá (ca. 80 Ma aged), and Jacupiranga and Anitápolis (ca. 130 Ma aged), respectively, suggested lower crust contamination for the first group of carbonatites, upper crust contamination for Anitápolis and no contamination at all for the Jacupiranga carbonatite.

It was inferred that the first generation of the Araxá and Tapira carbonatites was accompanied by widespread accumulation of carbonatitic materials at the base of the lithosphere, and that such materials were remobilized in the second carbonatitic event (80 to 70 Ma). Evidences from xenoliths (Bizzi *et al.*, 1993, 1995) support the accumulation model of Toyoda *et al.* (1994). Van Decar *et al.* (1995) positioned a fossil plume manifestation (Tristan da Cunha) beneath the Alto Paranaíba region and associated magmatism in that region and in the northern Paraná basin.

Geophysical data (Escalante, 2002) support Van Decar's assesment and identified another anomaly to the north which could be related to Trindade.

Alternatively, Comin-Chiaramonti *et al.* (1997), Comin-Chiaramonti *et al.* (in this volume) and Ernesto *et al*. (2002) suggest that on the whole the tholeiitic, alkaline and alkaline-carbonatitic magmatism in and around the Paraná Basin originated from a significant, but small scale, heterogeneous subcontinental mantle. In this scenario, the Tristan da Cunha, Walvis Ridge-Rio Grande Rise and Vitória-Trindade hot spot tracks might reflect the accomodation of stresses in the lithosphere during rifting, rather than continuous magmatic activity induced by mantle plumes beneath the moving lithosphere.

In geochemical terms, the reconciliation of the widespread distribution of Dupal-type signatures is possible if the chemical Tristan da Cunha signature (Dupal-type) was inherited by some of the volcanics generated under the thermal influence of the Trindade plume, as proposed by Toyoda *et al.* (1994) and Bizzi *et al.* (1995). Firstly, the process would involve the accumulation of metasomatic fluids brought up by a potent mantle plume active at the time of the emplacement or, alternatively, by long-term entrapment of blobs and weak plumes accumulated in the lower subcontinental lithosphere. Later, such materials would be preferentially remobilized by heat, given their lower solidus relative to the surrounding protolith. The Dupal signature would result of time-integrated mobilization of Pb and Rb in ($CO_2$-charged?) metasomatic fluids (cf. Comin-Chiaramonti *et al.*, 1997). The removal from the mantle segment could be considered a plausible means by which to produce a residual, degassed, HIMU-like component and a complementary volatile-rich EMI-like component.

## DISCUSSION

The nature, evolution and distribution of isotopically discrete mantle domains are the main constraints on models of mantle dynamics. Isotopic heterogeneities occur on both small and large scales in the mantle, and the case for a chemically heterogeneous mantle has been established for both suboceanic and subcontinental mantle (Allégre, 1982; Zindler & Hart, 1986; Hart, 1988; Hart & Zindler, 1989). Isotopic and trace element variations in mantle-derived potassic and ultrapotassic alkaline volcanics (Fitton & Upton, 1987; Menzies & Hawkesworth, 1987) and many mantle-derived xenoliths (Nixon, 1987) testify to the operation of mantle enrichment processes in continental settings. Evidence for similar enrichment processes has been recognized in the source regions of both Ocean Island Basalts (OIB) and Mid-Ocean Ridge Basalts (MORB) (Menzies & Hawkesworth, 1987).

The origin of the isotopic and trace element variations in the Alto Paranaíba rocks imply either involvement of different isotopic reservoirs in the source region (i.e. melting of distinct and variably enriched portions of the subcontinental lithosphere) or, alternatively, interaction of different source regions (i.e. "blending" of melts generated at both asthenospheric and lithospheric levels). The systematic changes in the nature of correlated rock-types, whole-rock isotopic composition and PGE signatures suggest that might be a progressive regional change in end-member proportions. A higher proportion of primitive magmas, with more "asthenospheric-like" εNd-values, occurs in western Alto Paranaíba region. On the contrary, a higher proportion of evolved magmas with "lithospheric-like" εNd values, is present in the eastern side.

Profiles relative to the depth of the source (Fig. 7) have been constructed on the basis of xenolith composition, geothermobarometry, and petrographic and compositional characteristics of the studied rocks as compared with experimental and theoretical studies (cf. Bizzi, 1994 and therein references). As the systematic changes in isotopes appear linked to the different rock-types, and as the latter are believed to have been derived from different depths, it is suggested that the different isotopic compositions in the area, as well as the variation in Pd/Ir ratios, may be related to different source depths. As kimberlite-type magmas tend to concentrate in western region and the Mata da Corda volcanics in the eastern side, systematic lateral variations of the source are ap-

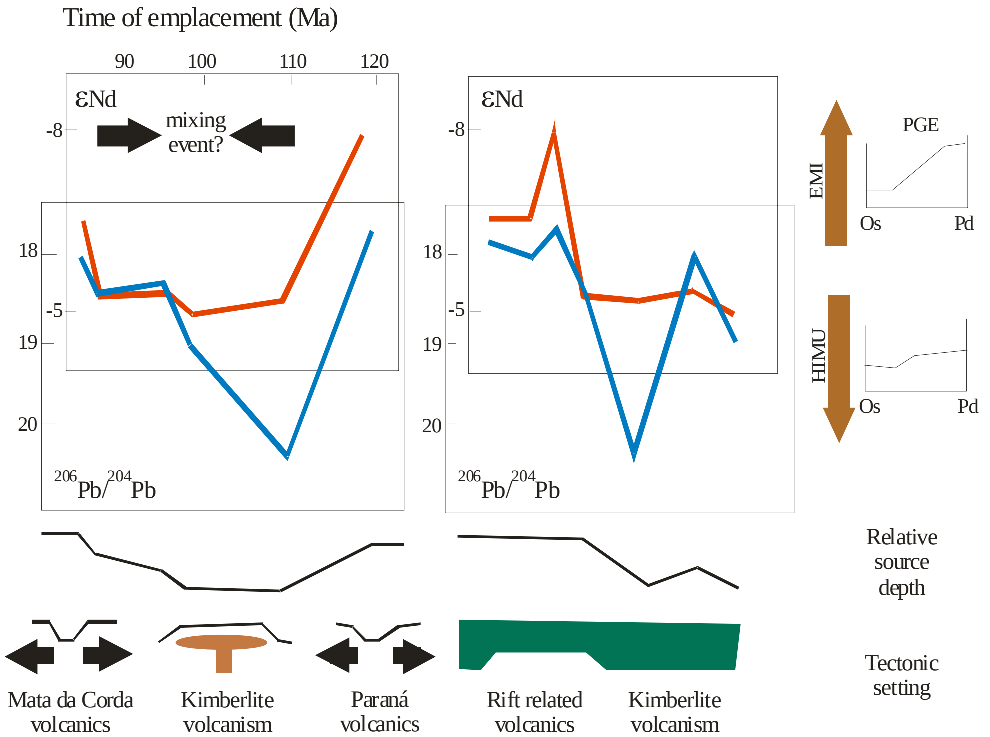


Fig. 7. Source depth profiles related to isotopes and PGE characteristics. The systematic changes with the nature of rock-types may be depth-related and represent differences in the tectonic setting of the intrusives. Possible implications for the nature and evolution of the local mantle lithosphere and for the ultimate origin of EMI- and HIMU-like signatures are discussed in the text.

parent on a regional scale. Such lateral variations appear to be the result of a progressive vertical shift in the zone of melting from West to East. Thus, vertical geochemical heterogeneities were translated into lateral geochemical heterogeneities by control of the source depth.

The negative covariation of $^{87}Sr/^{86}Sr$ with both $^{206}Pb/^{204}Pb$ and $^{143}Nd/^{144}Nd$, as well as the nature of Os isotopic signatures and their covariation with $Al_2O_3$ contents, provide evidence for the invol-vement of continental mantle lithosphere as a major component in the generation of all these rocks.

It is also demonstrated that the higher Rb/Sr ratios correlate with lower time-averaged U/Pb and Sm/Nd ratios. The negative correlation between Ba/Nb and $^{143}Nd/^{144}Nd$ indicates that the high Ba/Nb ratios were not generated during melting, but rather reflect lithospheric source composition related to some older enrichment event. These observations are relevant because the unique Sr, Nd, Os and Pb isotopic composition and the high Ba/Nb contents of the rift-related rocks correlate extremely well with the EMI component (Zindler & Hart, 1986; Hart, 1988; Hart & Zindler, 1989).

The kimberlitic rocks, generated at the greatest depths by smaller degrees of partial melting and representing small degrees of AFC, seem to show the least content of EMI component. The array linking the kimberlitic compositions to EMI subpa-rallels the mantle array with lower $^{143}Nd/^{144}Nd$ and lower $^{87}Sr/^{86}Sr$ and it is, therefore, distinctive from the trend observed in the Walvis Ridge basalts. Hart *et al.* (1986) described similar mixing for several oceanic localities, and suggested that such an array ("LoNd" array) may form a continuum between HIMU and EMI. This trend is presumed to be linked to some Dupal compositions in oceanic basalts (Zindler & Hart, 1986; Hart, 1988). The higher U/Pb and the lower Rb/Sr time-integrated compositions of the source of the kimberlites parallel the time-integrated source characteristics of the HIMU-OIBs: it is possible, therefore, that the kimberlites have a small HIMU component in the parental source.

## ORIGIN OF THE EMI- AND HIMU-LIKE COMPONENTS

The radiogenic isotopes are consistent with a sequence of events in which the local mantle lithosphere was enriched with incompatible elements during the formation of the Brasília fold and thrust belt. Plotted against crystallization age, the time-integrated εNd values of the studied volcanics fall on the evolution path defined by the Proterozoic crustal sequences of the Tocatins Province. Starting on the mantle evolution curve and linearly progressing to lower values with time, the data suggest that the enrichment event (reflected in the EMI-type Nd values) could be related to the tectonic processes which led to the formation and evolution of the crustal sequences within the Proterozoic Tocantins Province.

Compared to the source of micaceous Group II kimberlites, both the isotopically transitional kimberlites from Prieska in southern Africa and the Alto Paranaíba rocks, originated from sources with lower time-average Rb/Sr. It might not be a coincidence that the Prieska kimberlites, which in terms of isotopic composition and PGE signatures are the closest kimberlitic equivalents to the Brazilian kimberlites, also intrude a cratonic margin which has been affected by Proterozoic thin-skinned tectonism. The East-African carbonatites (Bell & Blenkinsop, 1987), which intrude the eastern margin of the Tanzanian craton (affected by Neoproterozoic thin-skinned tectonism during the pan-African orogeny), also have isotopic signatures very similar to the LoNd array. The high $^{143}Nd/^{144}Nd$-low $^{87}Sr/^{86}Sr$ North American lamproites also intrude overthickened craton margins which were tectonically reactivated in the Proterozoic (Mitchell & Bergman, 1991). It is possible, therefore, that the similar $^{87}Sr/^{86}Sr$ ratios observed in volcanics from all those areas might reflect first-order modifications of the ancient upper mantle lithosphere imposed by Proterozoic tectonic processes in thin-skinned pericratonic domains.

It has been speculated that the lower $^{87}Sr/^{86}Sr$ of Mesozoic volcanics relative to Group II kimberlites and other enriched mantle derived rocks may represent time-integrated Rb depletion attained *in situ* during gabbro-eclogite-granulite phase transformations (which could have been accompanied by $CO_2$ metasomatism) following tectonic overthickening at cratonic margins. The nature of the shallow-derived EMI-type materials could possibly be reconciled with the models of delamination of enriched continental lithosphere (McKenzie & O'Nions, 1983). This implies sufficient phase transformations along with density inversion and delamination, with a consequent removal of EMI-like material into the convecting asthenosphere. It would appear, however, that such a delamination process did not entirely remove the EMI-like material beneath the marginal São Francisco craton.

As an alternative to the *in situ* model of generation of the EMI-like source materials, it is conceivable that the source of the EMI-like component in these Dupal-type 119-87 Ma volcanics was the Tristan plume Dupal-type material which had once been trapped under the subcontinental lithosphere. Such a model, however, does not address the above mentioned similarities of the studied volcanics to the Prieska kimberlites and to the East-African carbonatites, nor the fact that the EMI-like signatures fit the Nd evolution path defined by the overlying crustal sequences.

The sources of the shallower alkaline rocks at Coromandel and the high-Ti basalts of the northern Paraná Basin, as well as some Ocean Island Basalts (OIB) with Dupal signatures in the South Atlantic (e.g. the Walvis Ridge basalts), all appear to be related to the EMI component. The similarity of such enriched sources is ascribed to processes by which Brazilian Neoproterozoic continental lithosphere was delaminated, and contaminated a zone of South Atlantic asthenosphere which is now erupting as hot spot islands and nearby sections of the Mid-Atlantic ridge (McKenzie & O'Nions, 1983; Hawkesworth *et al.,* 1986). The depth at which the recycled enriched material was stored until the sampling by the mantle plume is uncertain. According to this model, the Walvis Ridge basalts are mixtures of delaminated enriched subcontinental lithosphere and more typical "normal" oceanic compositions lying within the oceanic mantle array.

From this study it would appear that HIMU, and EMI in particular, may occur in laterally extensive but vertically distinctive portions of the continental lithosphere beneath the SW São Francisco craton. In general, EMI signatures seem to be restricted to more shallow-derived volcanism (e.g. carbonatites and rift related volcanics in Brazil and East Africa) compared to HIMU rocks (e.g. high-temperature megacrysts and diamond-bearing southern Africa kimberlites). The HIMU-type signatures are suggested to come from a DMM-dominated source that was hotter and which started melting deeper in the mantle. This source could be the asthenosphere, brought up either by a potent mantle plume active at the time of the emplacement or, alternatively, by long-term entrapment of blobs and weak plumes accumulated in the lower subcontinental lithosphere. Another possibility is that the time-integrated mobilization of Pb and Rb in a ($CO_2$-charged?) metasomatic fluid and subsequent removal from the mantle segment could be considered a plausible means by which to produce a residual, degassed, HIMU-like component and a complementary volatile-rich EMI-like component elsewhere in the mantle.

## CONCLUDING REMARKS

The data from Alto Paranaíba volcanics provide further evidence that large-scale geodynamical domains have existed in southern Gondwana at the time of breakup. The scale-length at which EMI-like source materials demonstrably exist beneath the southwestern margin of the São Francisco craton is comparable to mantle dimensions (i.e. 200 km). It is also clear from this work, however, that systematic small-scale isotopic variations accompany a progressive vertical shift in the zone of melting, and that isotopic characteristics are controlled by source depth. It is contemplated that the presence of the HIMU-like component might be restricted to melts generated at the base of the mechanical boundary layer (MBL), in a DMM-dominated environment, or deeper. However, inferring three-dimensional domain sizes of mantle heterogeneities, based on such heterogeneity projected at the surface, is problematic because of the poor control on the depth of segregation of the mantle-derived magmas. A major source of ambiguity resides in the fact that the first melt products, presumably generated as a response to the adiabatic decompression originated from rising diapirs or blobs of mantle material, probably underwent solid-state mixing during the ascent. The final product, therefore, represents some average over-large mantle depths.

The arguments herein presented suggest that the mantle anomalies underlying the southwestern margin of the São Francisco craton have existed at least since the Meso-Proterozoic, an observation that severely constrains local mantle convection models. An Upper-Mesozoic ternary mixing among up-welling HIMU-like melts, depleted mantle materials and volumetrically dominant EMI-type source materials (resident in the Mechanical Boundary Layer lithospheric mantle underneath the South American continent) is apparently capable of satisfying the constraints of the data obtained in this study. The implied link means that in some areas the Dupal anomaly represents a mixing of enriched subcontinental lithosphere and deep-level melts.

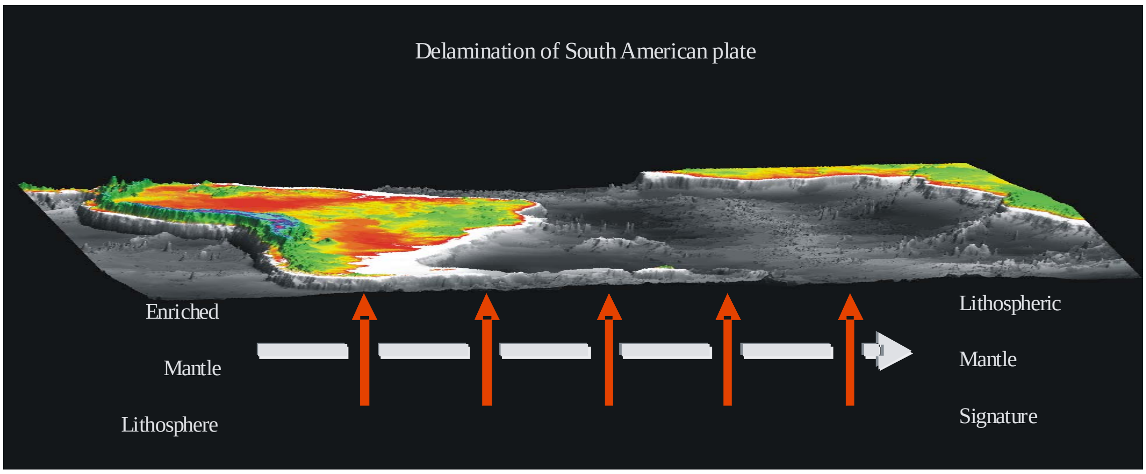


Asthenospheric Upwelling and South Atlantic IOBs

## ACKNOWLEDGEMENTS

De Beers is thanked for support to two Ph.D. research projects that were the basis for this contribution. Special thanks are due to P. Comin-Chiaramonti and C.B. Gomes for their constructive critical reviews and helpful suggestions.

## REFERENCES

Allègre, C.J. (1982). Chemical geodynamics. *Tectonophysics* **81**, 109-132.

Almeida, F.F.M. (1977). O cráton do São Francisco. *Revista Brasileira de Geociências* **7**, 364-394.

Almeida, F.F.M., Hasui, Y., Neves, B.B.B. & Fuck, R.A. (1981). Brazilian structural provinces: an introduction. *Earth-Science Reviews* **17**, 1-29.

Araújo, A.L.N. (2000). *Petrologia dos pipes kimberlíticos e kamafugíticos da Província Alcalina do Alto Paranaíba, Minas Gerais e Goiás.* Ph.D. Thesis, University of Brasília, 284p.

Araújo, A.L.N., Carlson, R.W., Gaspar, J.C. & Bizzi, L.A. (2001). Petrology of kamafugites and kimberlites from the Alto Paranaíba Alkaline Province, Minas Gerais, Brazil. *Contributions to Mineralogy and Petrology* **142**, 163-177.

Araújo, D.P. (2002). *Mineralogia dos diamantes da Província Kimberlítica de Juína, MT.* Ph.D. Thesis, University of Brasília, 325p.

Barnes, S. J., Naldret, A. J. & Gorten, M. P. (1985). The origin of the fractionation of platinum-group elements in terrestrial magmas. *Chemical Geology* **53**, 303-323.

Bellieni, G., Comin-Chiaramonti, P., Marques, L.S., Melfi, A.J., Nardy, A.J.R., Piccirillo, E.M. & Roisemberg, A. (1984). High- and low-$TiO_2$ flood basalts from the Paraná Plateau (Brazil): petrology and geochemical aspects bearing on their mantle origin. *Neues Jahrbuch Mineralogische Abhandlungen* **150**, 273-306.

Bell, K. & Blenkinsop, J. (1987). Archean depleted mantle evidence form Nd and Sr initial isotopic ratios of carbonatites. *Geochimica et Cosmochimica Acta* **51**, 291-298.

Bird, J.M., Meibom, A., Frei, R. & Nägler, Th.F. (1999). Osmium and lead isotopes of rare Os-Ir-Ru minerals: derivation from the core-mantle boundary region? *Earth Planetary Science Letters* **170**, 83-92.

Bizzi, L.A. (1994). *Mesozoic alkaline volcanism and mantle evolution of the souththwestern São Francisco craton, Brazil.* Ph.D. Thesis, University of Cape Town, 218p.

Bizzi, L.A., De Wit, M.J., Smith, C.B., McDonald, I. & Armstrong, R.A. (1995). Heterogeneous enriched mantle materials and Dupal-type magmatism along the southwestern margin of the São Francisco craton, Brazil. *Journal of Geodynamics* **20**, 469-491.

Bizzi, L.A., Smith, C.B., De Wit, M.J., Armstrong, R.A. & Meyer, H.O.A. (1993). Mesozoic kimberlites and related alkaline rocks in southwestern São Francisco craton: a case for local mantle reservoirs and their interaction. *5th International Kimberlite Conference*, *Araxá, Proceedings,* pp 156-171.

Brugmann, G.E., Arndt, N.T., Hofmann, A.W. & Tobschall, H.J.C (1987). Nobel metal abundances in komatiite suites from Alexo, Ontario and Gorgona Island, Colombia. *Geochimica et Cosmochimica Acta* **51**, 2159-2169.

Campos Neto, M.C. (1999). *Extensão sul do sistema orogênico Tocantins no contexto geodinâmico da aglutinação do Gondwana: exercício de tectônica.* M.Sc. Dissertation, University of São Paulo, 101p.

Carlson, R.W., Esperança, S. & Svisero, D.P. (1996). Chemical and Os isotopic study of cretaceous potassic rocks from southern Brazil. *Contributions to Mineralogy and Petrology* **125**, 393-405.

Clark, T.C., Smith, C.B., Bristow, J.W., Skinner, E.M. W. & Viljoen, K.S. (1991). Isotopic and geochemical variation in kimberlites from the southwestern craton margin, Prieska area, South Africa. *5th International Kimberlite Conference*, *Araxá, Proceedings,* pp. 46-48.

Comin-Chiaramonti, P., Cundari, A., Piccirillo, E.M., Gomes, C.B., Castorina, F., Censi, P., DeMin, A., Marzoli, A., Speziale, S. & Velázquez, V.F. (1997). Potassic and sodic igneous rocks from Eastern Paraguay: their origin from the lithospheric mantle and genetic relationships with the associated Paraná flood tholeiites. *Journal of Petrology* **38**, 495-528.

Comin-Chiaramonti, P., Gomes, C.B., Marques, L.S., Censi, P., Ruberti, E. & Antonini, P. (in this volume). Carbonatites from Southeastern Brazil: geochemistry, O-C, Sr-Nd-Pb isotopes and relationships with the magmatism from the Paraná-Angola-Namibia Province.

Crocket, J.H. & MacRrae, W.E. (1986). Platinum-group element distribution in komatiite and tholeiitic volcanic rocks from Munro Township, Otario. *Economic Geology* **81**, 1242-1251.

De Paolo, D.I. (1981). Trace element and isotopic effects of combined wallrock assimilation and fractional crystallization. *Earth and Planetary Science Letters* **43**, 201-211.

Duprè, B. & Allégre, C.J. (1983). Pb-Sr isotope variation in Indian Ocean basalts and mixing phenomena. *Nature* **303**, 142.

Ernesto, M., Marques, L.M., Piccirillo, E.M., Molina, E., Ussami, N., Comin-Chiaramonti, P. & Bellieni, G. (2002). Paraná Magmatic Province - Tristan da Cunha plume system: fixed versus mobile plume, petrogenetic considerations and alternative heat sources. *Journal of Volcanology and Geothermal Researches* **130**, 527-553.

Escalante, V.C. (2002). *Tomografia sísmica do manto superior abaixo do sudeste e centro-oeste do Brasil.* M.Sc. Dissertation, University of São Paulo, 74p.

Fitton, J.G. & Upton, B.G.J. (eds.) (1987). *Alkaline igneous rocks*. Oxford: Blackwell, 550p.

Fodor, R.V., Mukasa, S.B., Gomes, C.B. & Cordani, U.G. (1989). Ti-rich Eocene basaltic rocks, Abrolhos Platform, offshore Brazil, 18º S: petrology with respect to South Atlantic magmatism. *Journal of Petrology* **30**, 763-786.

Foley, S.F., Venturelli, G., Green, D.H. & Toscani, L. (1987). The ultrapotassic rocks: classification and constraints for petrogenetic models. *Earth-Science Reviews* **24**, 81-134.

Gibson, S.A., Thompson, R.N., Leonardos, O.H., Dickin, A.P. & Mitchell, J.G. (1995). The late Cretaceous impact of the Trindade mantle plume: evidence from large-volume, mafic potassic magmatism in SE Brazil. *Journal of Petrology* **36**, 189-229.

Gibson, S.A., Thompson, R.N., Weska, R., Dickin, A.P. & Leonardos, O.H. (1997). Late Cretaceous rift-related upwelling and melting of the Trindade starting mantle plume head beneath western Brazil. *Contributions to Mineralogy and Petrology* **126**, 303-314.

Gomes, C.B. & Comin-Chiaramonti, P. (in this volume). Some notes on the Alto Paranaíba Igneous Province.

Gomes, C.B., Morbidelli, L., Ruberti, E. & Comin-Chiaramonti, P. (1996). Comparative aspects between post-paleozoic alkaline rocks from the western and eastern margins of the Paraná basin. In: Comin-Chiaramonti, P. & Gomes, C.B. (eds.). *Alkaline magmatism in central-eastern Paraguay. Relationships with coeval magmatism in Brazil.* São Paulo: Edusp-Fapesp, pp. 249-274.

Greenwood, J.C., Gibson, S.A., Thmpson, R.N., Weska, R.K. & Dickin, A.P. (1999). Cretaceous kimberlites form the Paranatinga-Batovi region, central Brazil: geochemical evidence for subcratonic lithospheric mantle heterogeneity. *7st International Kimberlite Conference, Cape Town*, Vol. **1**, 291-298.

Halliday, A.N., Davies, G.R., Lee, D.C., Tommasini, S., Paslick, C.R., Fitton, J.G. & James, D.E. (1992). Lead isotope evidence for young trace element enrichment in the oceanic upper mantle. *Nature* **359**, 623-627.

Hawkesworth, C.J., Mantovani, M.S.M., Taylor, P.N. & Palacz, Z. (1986). Evidence from the Paraná of South Brazil for a continental distribution to Dupal basalts. *Nature* **322**, 356-359.

Hart, S.R. (1984). A large-scale isotope anomaly in the southern hemisphere mantle. *Nature* **309**, 753-757.

Hart, S.R. (1988). Heterogeneous mantle domains: signatures, genesis and mixing chronologies. *Earth and Planetary Science Letters* **90**, 273-296.

Hart, S.R. & Zindler, A. (1989). Constraints on the nature and development of chemical heterogeneities in the mantle. In: Peltier, W.R. (ed.) *Mantle convection*. Montreaux: Gordon and Breach, pp. 261-388.

Hart, S.R., Gerlach, O.C. & White, W.M. (1986). A possible new Sr-Nd-Pb mantle array and consequences for mantle mixing. *Geochimica et Cosmochimica Acta* **50**, 1551-1557.

Heaman, L., Teixeira, N.A., Gobbo, L. & Gaspar, J.C. (1998). U-Pb zircon ages for kimberlites from the Juína and Paranatinga provinces, Brazil. *7st International Kimberlite Conference, Cape Town*, Vol. **1**, 322-324.

Hertogen, J., Janssens, M.J. & Palme, H. (1980). Trace elements in ocean ridge basalt glasses: implications for fractionations during mantle evolution and petrogenesis. *Geochimica et Cosmochimica Acta* **44**, 2125-2143.

Hofmann, A.W. (1988). Chemical differentiation of the Earth: the relationship between mantle, continental crust and oceanic crust. *Chemical Geology* **90**, 297-314.

Hutchison, M.T. (1997). *Constitution of the deep transition zone and lower mantle shown by diamonds and their inclusions.* Ph.D. Thesis. University of Edinburgh, UK.

Iacumin, M., De Min, A., Piccirillo, E.M. & Bellieni, G. (2003). Source mantle heterogeneity and its role in the genesis of Late Archean – Proterozoic (2.7-1.0 Ga) and Mesozoic (200 and 130 Ma) tholeiitic magmatism in the South American Platform. *Earth-Science Reviews* **62**, 365-397.

Leonardos, O.H., Ulbrich, M.N. & Gaspar J.C. (1991). The Mata da Corda volcanic rocks. *5th International Kimberlite Conference*, *Araxá, Field Guide Book,* pp.5-74.

Le Roex, A.P., Cliff, R.A. & Adair, B.J.I. (1990). Tristan da Cunha, South Atlantic: geochemistry and petrogenesis of a basanite-phonolite lava series. *Journal of Petrology* **31**, 779-812.

Mantovani, M. S. M., Marques, L. S., Souza, M. A. D., Civetta, L., Atalla, M. & Innocenti, F. (1985). Trace element and strontium isotope constraints on the origin and evolution of Paraná Continental

Flood Basalts of Santa Catarina State (southern Brazil). *Journal of Petrology* **26**,187-209.

Marquart, G. & Schmeling, H. (2000). Interaction of small plumes with the spinel-perovskite phase boundary: implications for chemical mixing. *Earth and Planetary Science Letters* **177**, 241-254.

Marques, L.S., Ulbrich, M.N.C., Ruberti, E. & Tassinari, C.G. (2000). Petrology, geochemistry and Sr-Nd isotopes of the Trindade and Martin Vaz volcanic rocks (Southern Atlantic Ocean). *Journal of Volcanology and Geothermal Research* **93**, 191-216.

McDonald, I., Bizzi, L.A., Smith, C.B., De Wit, M.J. & Viljoen, K.S. (1995). The geochemistry of the platinum-group elements in Brazilian and southern African Kimberlites. *Geochimica et Comochimica Acta* **59**, 2883-2903.

McKenzie, D. & O'Nions, R.K. (1983). Mantle reservoirs and ocean island basalts. *Nature* **301**, 229-231.

Menzies, M.A. & Hawkesworth, C.J. (eds.) (1987). *Mantle metasomatism*. London: Academic Press, 472p.

Mitchell, R.H. & Bergman, S.C. (eds.) (1991). *The Petrology of lamproites*. New York: Plenum Press, 447p.

Mitchell, R.H. & Keys, R.R. (1981). Abundance and distribution of gold, palladium and iridium in some spinel and garnet lherzolites: implications for the nature and origin of precious metal-rich components in the upper mantle. *Geochimica et Cosmochimica Acta* **45**, 2425-2442.

Nixon, P.H. (ed.) (1987). *Mantle xenoliths*. New York, John Wiley, 844p.

O'Connor, J.M. & Duncan, R.A. (1990). Evolution of the Walvis Ridge-Rio Grande Rise hot spot system: implications for African and South American plate motions over plumes. *Journal of Geophysical Researches* **95**, 17475-17502.

Oversby, V.M. (1971). Lead in oceanic islands: Faial, Azores and Trindade. *Earth and Planetary Science Letters* **11**, 401-406.

Peate, D.W., Hawkesworth, C.J. & Mantovani, M.S.M. (1992). Chemical stratigraphy of the Paraná lavas (South America): classification of magma types and their spatial distribution. *Bulletin of Volcanology* **55**, 119-139.

Piccirillo, E.M., Bellieni, G., Cavazzini, G., Comin-Chiaramonti, P., Petrini, R., Melfi, A.J., Pinese, J.P.P., Zantedeschi, P. & De Min, A. (1990). Lower Cretaceous tholeiitic dyke systems from the Ponta Grossa Arch (southeast Brazil): petrology, Sr-Nd isotopes and genetic relationships with the Paraná flood volcanics. *Chemical Geology* **89**, 19-48.

Pimentel, M.M. & Fuck, R.A. (1992). Neoproterozoic crustal accretion in central Brazil. *Geology* **20**, 375-379.

Richardson, S.H., Gurney, J.J., Erlank, A.J. & Harris, J.W. (1984). Origin of diamonds in old enriched mantle. *Nature* **310**, 198-202.

Seer, H.J. & Moraes, L.C. (1988). Estudo petrográfico das rochas ígneas alcalinas da região de Lagoa Formosa, MG. *Revista Brasileira de Geociências* **18**, 134-140.

Siebel, W., Becchio, R., Volker, F., Hansen, M.A.F., Viramonte, J., Trumbull, R.B., Haase, G. & Zimmer, M. (2000). Trindade and Martin Vaz islands, South Atlantic: isotopic (Sr, Nd, Pb) and trace element constraints on plume related magmatism. *Journal of South American Earth Sciences* **13**, 79-103.

Skinner, E.M.W., Viljoen, K.S., Clark, T.C. & Smith, C.B. (1991). The petrography, tectonic setting and emplacement ages of kimberlites in the south western border region of the Kaapvaal craton, Prieska area, South Africa. *5th International Kimberlite Conference, Araxá, Proceedings*, pp. 80-97.

Smith, C.B. (1983). Pb, Sr and Nd isotopic evidence for sources of southern African Cretaceous kimberlites. *Nature* **304**, 51-54.

Smith, C.B., Gurney, J.J., Skinner, E.M.W., Clement, C.R. & Ebrahim, N. (1985). Geochemical character of southern African kimberlites. A new approach based on isotopic constraints. *Transaction of the Geological Society of South Africa* **88**, 267-280.

Thompson, R.N., Gibson, S.A., Mitchell, J.G., Dickin, A.P., Leonardos, O.H., Brod, J.A. & Greenwood J.C. (1998). Migrating Cretaceous-Eocene magmatism in the Serra do Mar Alkaline Province, SE Brazil: melts from the deflected Trindade mantle plume? *Journal of Petrology* **39**, 1493-1526.

Toyoda, K., Horiuchi, H. & Tokonami, M. (1994). Dupal anomaly of Brazilian carbonatites: geochemical correlations with hotspots in the South Atlantic and implications for the mantle source. *Earth and Planetary Science Letters* **126**, 315-331.

Van Decar, J.C., James, D.E. & Assumpção, M. (1995). Seismic evidence for a fossil mantle plume beneath South America and implications for plate forces. *Nature* **378**, 25-31.

Weaver, B.L. (1990). Geochemistry of highly-undersaturated ocean island basalt suites from the South Atlantic Ocean: Fernando de Noronha and Trindade Islands. *Contributions to Mineralogy and Petrology* **105**, 502-515.

Zindler, A. & Hart, S. (1986). Chemical geodynamics. *Annual Review Earth Planetary Sciences* **14**, 493-571.

*Mesozoic to Cenozoic Alkaline Magmatism in the Brazilian Platform*
*Comin-Chiaramonti, P. & Gomes, C.B. (eds.)*
*Edusp/Fapesp, São Paulo, pp. 341-365, 2005*

# STRUCTURE AND ORIGIN OF THE POÇOS DE CALDAS ALKALINE MASSIF, SE BRAZIL

*H.H. Ulbrich, S.R.F. Vlach, D. Demaiffe and M.N.C. Ulbrich*

*Poços de Caldas (PC), the largest Brazilian alkaline massif, is constituted mainly by phonolites and their subvolcanic and plutonic counterparts (tinguaites and nepheline syenites, NeS), forming a felsic undersaturated suite, associated with minor amounts of mafic-ultramafic rocks which are mostly concentrated along the volcanoclastic strip of the Vale do Quartel (VQ), appearing also as dykes in the Osamu Utsumi uranium mine (OU) and within basement mangerites, close to the massif´s border (Minas Pedras quarry, MP), showing a wide variety of ultrabasic to basic rock-types, in part also rare carbonatite dykes. The felsic rocks have K-feldspar, nepheline and sodic pyroxene as main minerals, with associated rare metal silicates, in part also rock-forming phases (eudialyte in lujavrites and khibinites). NeS, divided into agpaitic and intermediate-miaskitic varieties, are present as discrete bodies, each characterized by distinct facies; they are intrusive into tinguaites and phonolites. Tinguaites, in particular, were quickly quenched and invaded mostly as liquid magmas, at temperatures of over 1000°C, while NeS intruded as discrete magma batches and cooled within the still hot host-rock, registering re-equilibration temperatures of around 800°C (intermediate NeS) to less than 500°C (agpaitic types). Deuteric alteration is usually absent in tinguaites, but widespread in all NeS. Larger chemical variations in the felsic rocks are restricted to trace elements, unusually enriched in many of them. A critical appraisal of published K-Ar ages limits the age gap between 64 and 83 Ma, with a median value of 77 Ma. Recent Rb/Sr measurements yield an age of 78.6±6.6 Ma (internal isochron), i.r. 0.7053±0.0002, considered the best estimate for emplacement age of the felsic rocks (NeS and tinguaites). Hydrothermal alteration in the Utsumi mine, and the associated U-Zr-Mo mineralization, is dated at 75.6±2.2 Ma, i.r. 0.7053±0.0002, an age closely related to emplacement, as also attested by geologic arguments. Ar/Ar ages of phlogopites in the mica lamprophyres of OU and in a silico-carbonatitic dyke at MP yield around 76±0.6-1.6 Ma and 83.9±0.3 Ma, respectively. Thorites in a MP sample show a mean age of 79±3.2 Ma (U-Th-Pb measurement method with microprobe). All the felsic rocks present reverse magnetization, the agglomerates from VQ normal polarization, which should place the emplacement for the first rocks within the 33r Campanian interval (at around 80 Ma?), that of the agglomerates in the 33n, and possibly also in the 34n event, suggesting a wider time gap for the eruption of all ultramafic rocks. Rb-Sr, Sm-Nd and Pb-Pb isotopic data are presented for 10 NeS and 8 tinguaites, along with data for the ultramafic VQ (from literature) and MP (own data). NeS and tinguaites plot, in all three systems, as a continuous cluster, separated from the VQ and MP data. $^{87}Sr/^{86}Sr$ initial ratios for NeS and tinguaites are around 0.70515 (range 0.70475-0.70522). $(^{143}Nd/^{144}Nd)_{80}$ ratios vary from 0.51233 to 0.51239 ( Nd: -2.6 to -4.5). VQ and MP rocks are more primitive and clearly different from the PC samples, also presenting higher Sm/Nd ratios, reflecting a less fractionated REE pattern. In the Sr/Nd isotopic diagram, the felsic PC rocks plot to the right of BSE, in the quadrant of OIB and enriched crustal and mantle rocks with similar, but more primitive Nd isotopes, than the EMI reservoir. $T_{DM}$ ages for PC rocks (range: 650-750 Ma) show an almost normal distribution, with mean of 692±54 Ma (2 ), while VQ values range between 630 and 810 Ma (MP range: 580-640 Ma). The Pb isotopes for felsic PC rocks exhibit small ranges, and isotope ratios 206/204, 207/204 and 208/204 varying between 17.9-18.3, 15.43-15.48 and 38.10-38.55, respectively. In the 207/204 vs. 206/204* *diagram, they plot close to, but to the right of, the NHRL, also typical of OIB samples, roughly defining a 2.2 Ga reference line (possibly a mixing array). The felsic PC are intermediate and enriched rocks, NeS and tinguaites are very similar, but each one with heterogeneous trace element contents; they plot close to, or within, the undersaturated thermal valley in the residual diagram. MgO contents are low (below 1 or even 0.5%) and compatible elements Co, Ni, Cr, Cu are either not detected or lower than 1 to 2 ppm. Ultrabasic rocks are similar to nephelinites in chemistry, with larger variations in the MP samples. REE are enriched in all PC rocks, the ultrabasic samples showing an OIB pattern, and the felsic rocks a curved to concave one, with strong LREE over HREE enrichment. Variograms of the ultrabasic rocks are again similar to OIB, the felsic rocks characterized by negative Ba, Sr (in some), K (slight), Ti and P spikes, positive Nb, Pb and Zr spikes, and high LIL,Th and U. In trace element ratio diagrams, ultrabasic rocks plot usually close to OIB; felsic rocks are widely scattered. Geochemistry and isotopes thus indicate that the ultrabasic rocks have probably derived from an OIB asthenospheric source, whereas the felsic ones possibly have derived as single and discrete individual magma batches, from enriched mantle positioned at the base of the lithosphere, created by invasion of (ultrabasic alkaline?) magma veins and dykes, possibly during the Brasiliano tectonomagmatic event (~800-450 Ma). Melting of a source with garnet, a Ti-mineral and a K-bearing phase might explain the chemistry of the intermediate PC magmas (including the REE pattern, Nb positive anomaly and the negative K one), followed by direct emplacement (with little or no crystal fractionation, and little crustal contamination).*

## INTRODUCTION

The Poços de Caldas (PC) alkaline massif, positioned at the limit between the states of São Paulo and Minas Gerais, southeastern Brazil, is one of the largest alkaline igneous bodies in the world, covering over 800 $km^2$, behind only to the Khibina alkaline massif (1350 $km^2$) in the Kola Peninsula (Kramm *et al.*, 1993; Kramm & Kogarko, 1994).

The PC massif intrudes a thick part of the continental crust, the large and discontinuous Guaxupé-Socorro Nappe, structurally related to two other well-defined Precambrian tectonostratigraphic units, the Alto Rio Grande Belt, formed by folded supracrustal rocks, and the reworked Archean basement adjacent to, and being part of, the São Francisco Craton (Campos Neto & Caby, 1999, 2000; Figs.1 and 2).

PC is one among a large number of Mesozoic alkaline occurrences, although in a peculiar position, since it is found as an isolated massif, some distance away from the ones that constitute, to the NE, the Alto Paranaíba Igneous Province and, to the east, the Serra do Mar Province (e.g. Thompson *et al.*, 1998; Araújo *et al.*, 2001).

PC is distinctive in its petrographic composition, with a large predominance of nepheline syenites (NeS) and phonolites, with significant amounts of strongly agpaitic types (e.g. lujavrites and khibinites), thus sharing a similar geochemical signature with a few alkaline massifs worldwide: Khibina and Lovozero in the Kola Peninsula, Pilansberg in South Africa, Ilimaussaq in Greenland and the smaller Trans-Pecos agpaitic occurrences in Texas (Sorensen, 1970; Mathias, 1974; Larsen & Sorensen, 1987; Barker, 1987). The depressed area of the Vale do Quartel, a large curved structure outcropping close to the western border of the PC massif, is filled with pyroclastic rocks (agglomerates, lapilli, tuffs) and also with remnants of lava flows, constituted mostly by mafic-ultramafic rocks (Fig. 3). Ultramafic rocks are also found as phlogopite lamprophyre dykes in the Osamu Utsumi open pit uranium mine and within basement mangerite gneisses at the Minas Pedras quarry (Fig. 3). The former volcanic edifice is not preserved, but a few remnants of sediments attributed to the Poços de Caldas volcanic activity (lahars, reworked fluvial deposits, breccias; Oliveira *et al.*, 1975), extending 15-20 km from the actual limits of the massif, indicate that a widespread sheet of pyroclastic rocks may have once covered the entire area. Also observed as conspicuous enclaves and roof pendants, partly as mappable units, are sandstones of the eolian Jurassic-Lower Cretaceous Botucatu Formation, with their distinctive large-scale cross-stratification, and some siltstone and massive sandstone beds which have been attributed to the Lower Carboniferous Aquidauana Formation (Oliveira *et al.*, 1984), but may actually belong to the Jurassic-Lower Cretaceous Pirambóia Formation (Fig. 3). Significant areas in the inner parts of the massif are hydrothermally altered, and also brecciated to some extent as a result of late subvolcanic activity, resulting in numerous mineralized occurrences (mainly U, Th, Mo and Zr), the largest of which was developed as the Osamu Utsumi open pit uranium mine.

In the next pages, a general survey on PC will be presented, combining a historical overview with results based on mapping and petrographic, geo-chemical-isotopic and geophysical work, all of them combined to present an updated outlook on the origin of this large massif.

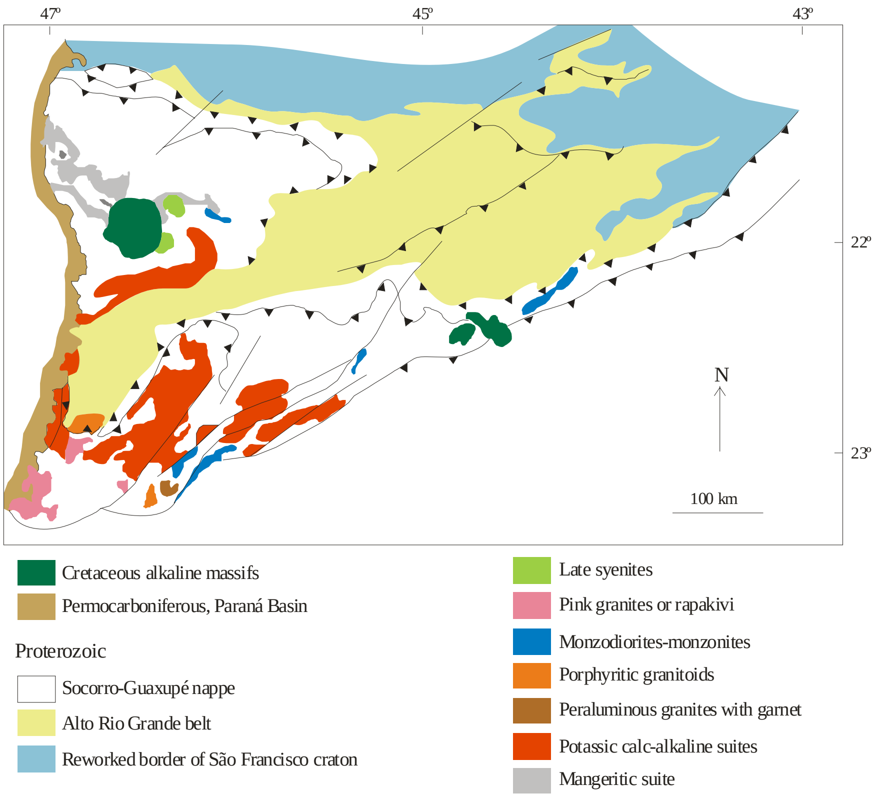


Fig. 1. Nappe structure in basement areas, states of São Paulo and Minas Gerais, SE Brazil. See text for comments. Source: Haddad (1995).

## PREVIOUS STUDIES

The bibliography on Poços de Caldas amounts, until 1984, to over 150 contributions (Ulbrich, 1984b), supplemented in the last 20 years with more than 50 further publications, mostly dealing with partial aspects (geology, petrography, ages, mineral deposits etc.).

The earliest references to the general geology of the district stretches back to the 19th century. Foremost among them is the contribution by Orville Derby (1887), who pointed out that intrusive "foyaites" (=NeS) coexist in the district with volcanic phonolites, while tinguaites (a term coined by Rosenbusch in 1887 to identify subvolcanic phonolites) might represent the gradation of the coarser rocks into finer-grained ones. The presence of pyroclastic rocks and sandstones was also mentioned. A post-Carboniferous age of the intrusion was proposed, in view of the incorporation of the eolian sandstones of the Botucatu Formation – then - considered to be Carboniferous - by the magmas. Barbosa (1948), on the other hand, interpreted the NeS as part of a batholithic mass of pre-Ordovician age, later covered by the Triassic (or post-Triassic) Botucatu sandstones, followed by the emplacement of late phonolites. However, later authors confirmed Derby's interpretation, mostly considering that NeS and phonolites grade into each other. But they disagreed as to the assignment of the age of the Botucatu sandstones (Jurassic for Leinz & Guimarães, and Lamego, cf. Freitas 1943, and, correctly, Cretaceous, as in Ellert, 1959, Björnberg, 1956, 1959, and Björnberg & Landim, 1966). Ellert, Björnberg and Coutinho presented in 1959 the first detailed map of the district, published as a separate sheet (cf. Ellert, 1959; Björnberg, 1959). Bushee (1971) produced a detailed map of the lujavrite-khibinite bodies found in the northern ring area.

The presence of several district-wide U and Th-REE occurrences as well as that of Zr minerals triggered new research and led to a second map of the district by geologists of the Brazilian Nuclear Energy Agency and the state company Nuclebrás,

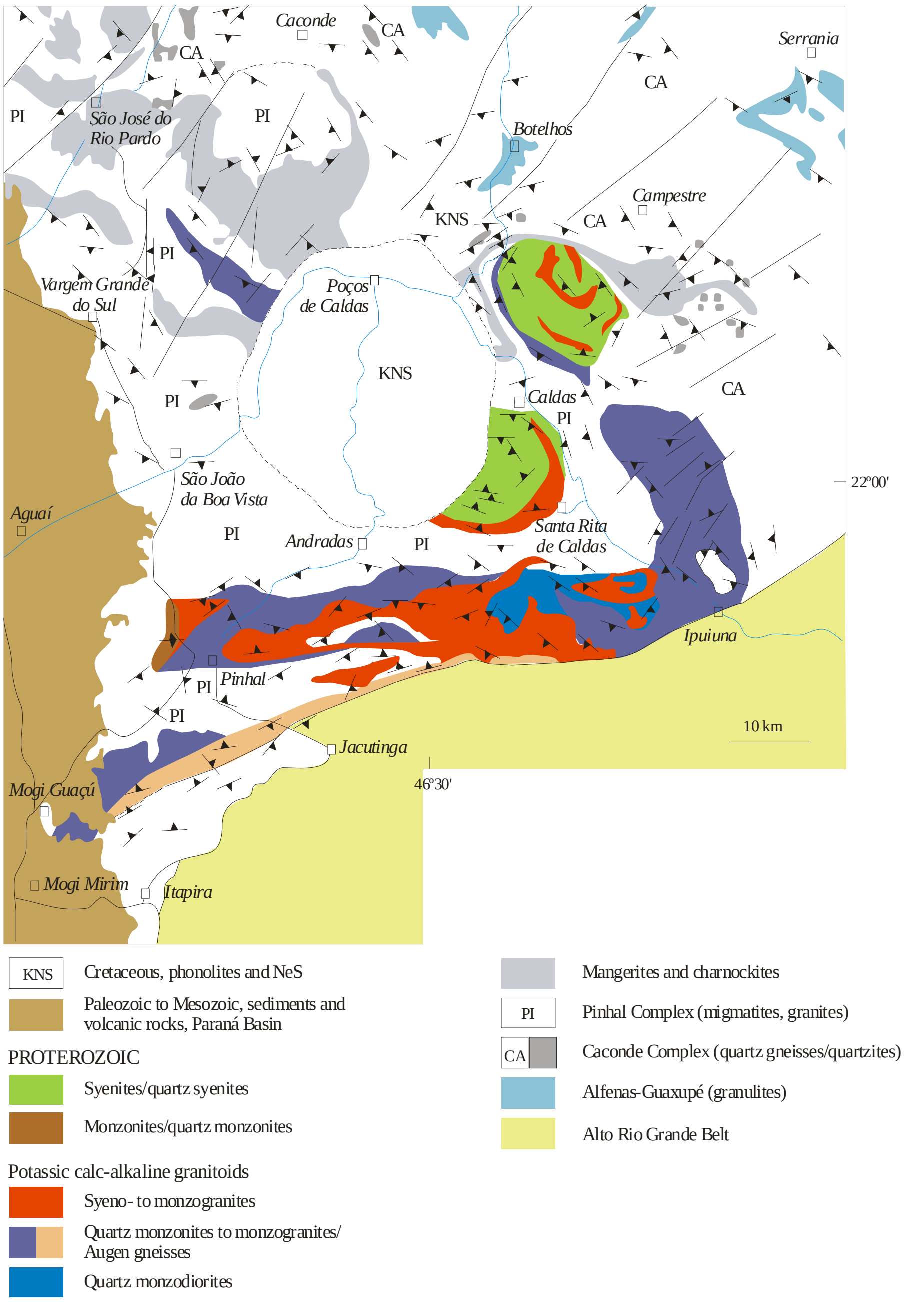


Fig. 2. The location of the Poços de Caldas massif within the Guaxupé block, with outlined basement units. See text for comments. Source: Haddad (1995).

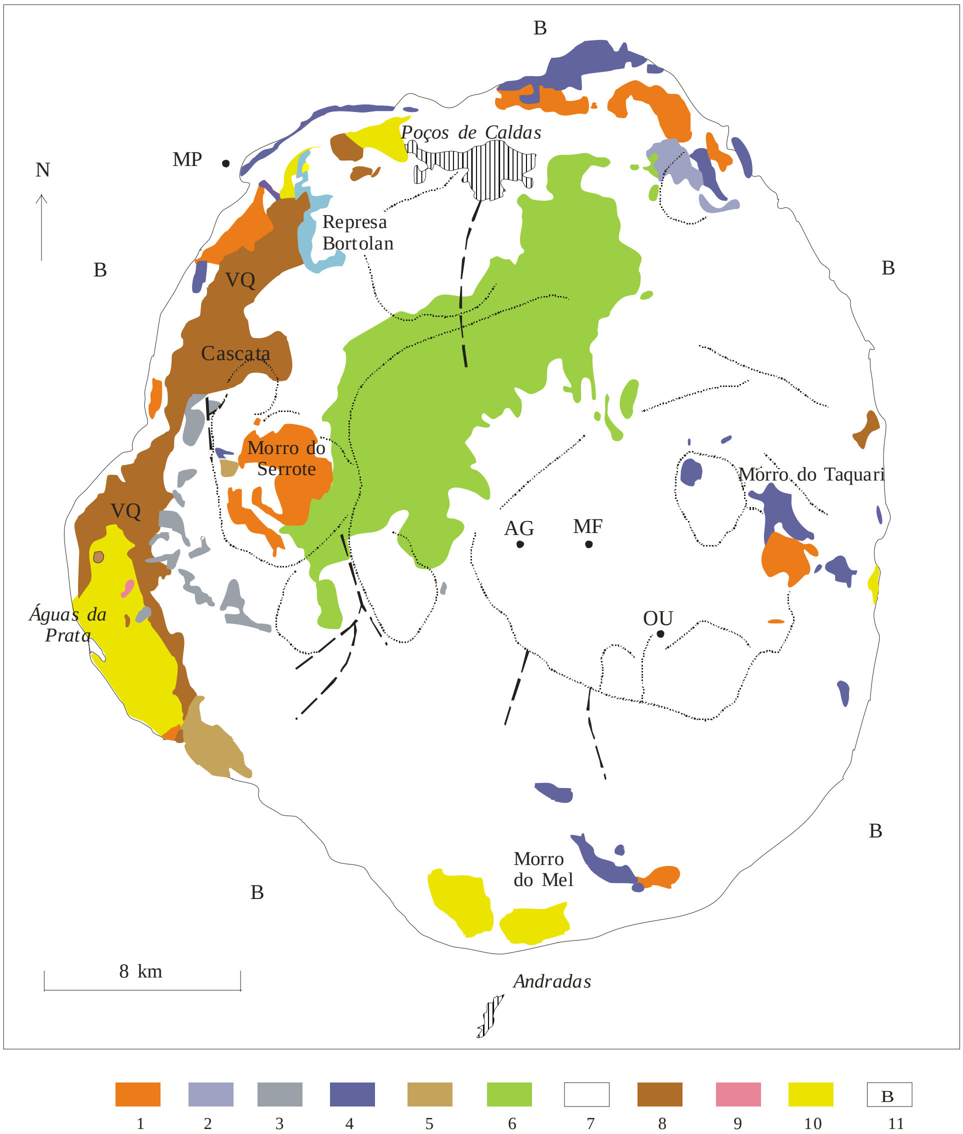


Fig. 3. Simplified map of the Poços de Caldas massif (Ulbrich, 1984a). 1) agpaitic NeS; 2) NeS with pseudoleucite; 3) porphyritic NeS; 4) grey NeS; 5) biotite-bearing NeS; 6) NeS, Pedreira type; 7) tinguaites and phonolites, undifferentiated; 8) volcanoclastic deposits (to the W, Vale do Quartel strip); 9) diabase, Serra Geral Formation; 10) sandstones and related sedimentary rocks, Paraná Basin; 11) B, undifferentiated basement (cf. Fig. 2). AG; Campo do Agostinho; MF; Morro do Ferro; MP; Minas Pedras; OU; Osamu Utsumi open pit (C-09 area); VQ; Vale do Quartel. Faults as heavy lines, "circular structures" as dotted lines. Reproduced in Garda (1990) and Ulbrich & Ulbrich (1992, 2000b, 2002).

now emphasizing the identification of hydrothermally altered areas (reproduced in Utsumi *et al.*, 1971; Gorsky & Gorsky, 1974; Oliveira, 1974; Ulbrich, 1984; Ulbrich & Ulbrich, 1992, 2000b). Several circular "structures" can be observed in satellite images and aerial photographs, in part controlling and confining the radioactive mineralization and hydrothermal alteration (Paradella & Almeida, 1976; Ulbrich & Ulbrich, 1992, 2000). A new faciological map by H. Ulbrich was presented in the 1980's, with emphasis on the NeS facies (Ulbrich, 1984a; Ulbrich & Ulbrich, 1992, 2000b). A detailed map of the Vale do Quartel pyroclastic rocks is found in Alves (2003).

Geomorphological insights are presented in Freitas (1943) and Christofoletti (1970, 1973), dealing with the topographic contrasts of the district, probably related to an ancient (Neocretaceous?) peneplaining event. Ellert (1959) proposed a caldera-like origin for the massif, initiated by a regional doming followed by the caldera collapse (cf. discussion in Garda, 1990), while Motoki and collaborators (Motoki & Oliveira, 1987; Motoki *et al.*, 1988; Vargas & Motoki, 1991) suggested that the massif represents a stock-like structure, limited by vertical or outward dipping contacts with the surrounding basement, the actual morphology displaying higher outer tinguaite rims and lowered interior as the result of differential erosion.

Several of the most recent studies were accompanied by geophysical field and laboratory work, mostly as unpublished reports (cf. references in Almeida Filho & Paradella, 1976, and Almeida *et al.*, 1980). Thermal studies show that thermal flow is as high as 50.6 $mW/m^2$ at sector C-09 (site of the Osamu Utsumi mine) and 96.5 $mW/m^2$ at Morro do Ferro (Th-REE anomaly), dropping to 31 $mW/m^2$ in the surrounding basement rocks, while the geothermal gradient is around 29°C/km (C-09 area) to over 33°C/km (Morro do Ferro) (cf. Araújo, 1980), or even over 39°C/km (Hamza, 1982). These data are mostly confirmed by Hamza (1982), who points out that the smaller thermal flow in the U-mineralized occurrences may be due to cooling effects brought about by more intense groundwater flow in these largely fractured areas. A mean district-wide value of 85.6 $mW/m^2$ is proposed, in comparison to values of 52.7 $mW/m^2$ found in basement areas; although heat production is unusually high in mineralized areas (up to 21.3 $\mu W/m^3$), a more conservative value of 7.0 $\mu W/m^3$ is proposed for the entire PC district, assuming a rather low mean Th+U content of 50 ppm for phonolites and NeS (Hamza, 1982; see more recent chemical data below). Unpublished gammaspectrometric surveys (Nuclebrás) clearly identified the radioactive anomalies and the Morro do Ferro site (Th and U channels). Unpublished magnetometric studies done on behalf of CPRM (Companhia de Pesquisas de Recursos Minerais), covered only a partial E-W trending strip of the central part of the district. The first comprehensive gravity survey was presented by Slavec (2002; also Slavec *et al.*, 2004), showing a flat regional residual Bouguer anomaly, dropping down to -45 mgal at the Poços de Caldas massif; preliminary model calculations, based on a geometric model with several blocks of different densities of alkaline rocks (2.47 to 2.66 $g/cm^3$, with a mean 2.66 $g/cm^3$ density for basement rocks), predict a downward tapering igneous body to a depth of around 7-8 km, with a total volume of alkaline rocks of about 7700 $km^3$. For comparison, seismological studies on the Khibina massif showed a cylindrical body (30x40 km) from the surface down to a depth of 7 km, then continuously decreasing in size to a depth of 15 km, where it still has a diameter of 15 km, with an estimated intrusive volume of over 12000 $km^3$ (Kramm *et al.*, 1993; Kramm & Kogarko, 1994).

The first petrographic and mineralogical descriptions were published by Derby (1887; cf. above), who also reported the existence of idiomorphic pseudoleucites (also Guimarães & Ilchenko, 1954). Machado (1888) indicated in his detailed report that NeS are a combination of "orthoclase", nepheline and pleochroic "augite", mentioning the presence of melanite and including new optical and chemical data on lavenite, $(Na,Ca)_2(Mn,Fe^{2+})(Zr,Ti,Nb)Si_2O_7(O,OH,F)$, a phase also cited by Graef (1887) in an alkaline rock from the Tinguá locality, Rio de Janeiro. Cm-sized idiomorphic zircons, abundant in some PC areas (e.g. Morro do Taquari), were mentioned by Sachsen-Coburg (1889). Also conspicuous is the occurrence, in restricted areas, of heavy pebbles of "caldasite" (a name given by Derby), an intergrowth of zircon and a fibrous mineral, first described erroneously as a new Nb-Ta oxide and named "brasilite" by Hussak (1892), and later identified as baddeleyite, $ZrO_2$, a mineral discovered by Fletcher (1894) in Ceylon (cf. also Hussak, 1899; Hussak & Reitinger, 1903; Franco, 1945; Franco & Loewenstein, 1948; Loewenstein, 1952). Guimarães & Moraes (1955) described lamprophyllite, $Na_3Sr_2Ti_3(Si_2O_7)_2(O,OH,F)_2$, in the Morro do Serrote NeS, also found in lujavrites by Baptista (1976). The complex silicate "giannetite" (Guimarães, 1948; also Winchell & Winchell, 1967), first described in PC, was recently identified as hainite, $Na_2Ca_5Ti(Si_2O_7)_2(OH)_2F_2$ (Atencio *et al.*, 1999). Chemical data on several rare minerals (lamprophyllite, eudialyte etc.) are given in Dirksen (1964) and Dutra (1965). Ashry (1962) described astrophyllite, $(K,Na)_3(Fe,Mn)_7(Ti,Zr)_2.Si_8(O,OH)_{31}$, sodalite, natrolite, $Na_2Al_2Si_3O_{10}.2H_2O$, pectolite, $Na(Ca,Mn)_2(Si_3O_8)(OH)$, titanite and fersmanite, $Na_4Ca_4Ti_4(O,OH,F)_3(SiO_4)_3$, in the northern rim khibinite. A discussion on the chemistry and optical properties of eudialyte-eucolite from the Pedra Balão lujavrites and khibinites is found in Gualda & Vlach (1996), who also reported the presence of lamprophyllite and normandite (titaniferous lavenite) in these rocks (Gualda & Vlach, 1998a). Pectolite, eudialyte-eucolite, lamprophyllite and lorenzenite, $Na_2(Ti, Zr)_2(Si_2O_9)$, were described in the agpaitic Taquari NeS (Gualda & Vlach, 1997, 1998b; Fig. 3). The presence of kalsilite was reported in PC altered rocks (Fujimori, 1982a), unconfirmed up to now, as well as that of leucite, with analcime, in some of the ultramafic rocks of the Vale do Quartel (e.g. Thompson *et al.*, 1998).

The monographs by Ellert (1959) and Björnberg (1959) accompanied the presentation of the first map of the district, with Ellert describing the igneous rocks of the massif and the second author the sedimentary ones. A detailed study of the lujavrites and khibinites of the northern rim was presented by Bushee (1971). A comprehensive set of chemical data on rock-forming minerals in NeS (feldspars, nephelines and pyroxenes), in part used to establish geothermometers, can be found in M. Ulbrich (1983, 1985, 1993). H. Ulbrich and collaborators presented partial aspects related to geochemistry, mineralogy and petrography in several abstracts (cf. summary in Ulbrich, 1984b). Descriptions of PC rocks (NeS, phonolites, pyroclastic rocks), along with selected chemical data are also reported in Schorscher & Shea (1992) and Alves (2003). Lamprophyre-like dykes observed in the Osamu Utsumi mine are described in Garda (1990), Schorscher *et al.* (1991), Shea (1992) and Alves (2003). A number of small dykes and plugs of silico-carbonatitic rocks (with carbonates, fluorite, phlogopite, and pyroxenes), within regional mangerites, were found in the Minas Pedras quarry (Fig. 1) and described in Vlach *et al.* (1996, 1998), and Ulbrich *et al.* (1998). Ulbrich *et al.* (2003), based on isotope and rock geochemistry, suggested that the PC rocks were derived from ultrabasic alkaline parental magmas (e.g. nephelinites), either directly by fractional crystallization or indirectly by melting of an enriched nephelinite protolith.

The interest in uranium mining, along with the creation of the state enterprise Nuclebrás, led to intensive research efforts to find nuclear materials, firstly focusing on the U-bearing caldasite deposits. As a result, several new occurrences of economic interest were discovered, such as areas with extensive hydrothermal alteration and main U-mineralization, which provided the stimulus for new studies and, in particular, the development of uranium mining in the open pit Osamu Utsumi mine by Nuclebrás in the 1970's and 1980's, along with yellow cake production in an adjacent industrial facility (cf. section on Mineralizations, below).

Early geochronologic work was presented by Dutra (1966), who analyzed zircons by means of the now abandoned alpha-lead method, obtaining ages for PC rocks that vary between 87 and 109 Ma. The first comprehensive K-Ar dating of a large number of alkaline occurrences in southeastern Brazil, including PC, was reported by Amaral *et al.* (1967), with later additions provided by Bushee (1971). Rb-Sr isochronic ages for PC are presented in Kawashita *et al.* (1984) and Shea (1992). Additional discussion about the age of the massif is found in Ulbrich *et al.* (2002), here summarized below in a section on Geochronology.

The first considerations about the geotectonic setting of the basaltic flows of the Lower Cretaceous Serra Geral Formation, along with the emplacement of the Cretaceous alkaline massifs, were made by

Freitas (1951), who favoured a control by tensional regimes. Herz (1977) proposed, on the base of geochronologic ages, that the string of alkaline massifs occurring along the São Paulo-Rio de Janeiro coastal belt have been caused by the passage of a diffuse hot-spot, moving from the initial southernmost "Jacupiranga node" (starting at around 130 Ma) along a northeastern direction, leaving the continent into the Atlantic ocean at around 53 Ma ago (the age of the Cabo Frio alkaline rocks). Almeida (1971, 1983) related the emplacement of the Mesozoic alkaline occurrences in southern Brazil to the evolution of the Paraná Basin. He noted that the alkaline occurrences positioned around the Paraná Basin occur within specific "provinces", each one with particular structural-tectonic features: the massifs within the Ponta Grossa Arch, others aligned at the northeastern and northern border of the Paraná Basin (related to the Bom Jardim de Goiás and Alto Paranaíba arches), the occurrences within the Rio Grande do Sul Arch, those in eastern Paraguay (in part controlled by tensional crustal structures), and a transversal rather wide E-W belt including massifs from Rio de Janeiro and São Paulo, leaving PC as a single isolated occurrence. Almeida *et al.* (1980) indicated that the Brasília and Uruaçú folded belts, at the NE border of the Paraná Basin, were invaded by alkaline occurrences during a reactivation phase of the Alto Paranaíba Arch, while the PC massif is located as the sole important alkaline occurrence within the Guaxupé block, at the crossing of the "coastal folded belt" with the Brasília-Uruaçú belts. Ulbrich & Gomes (1981) presented a summary overview of the alkaline occurrences in southern Brazil, divided into petrographic groups and alkaline provinces, probably emplaced as a result of tensional regimes. Sadowski & Dias Neto (1981) defined the seismic-tectonic east-west Cabo Frio alignment, along which many alkaline occurrences are found (Poços de Caldas, Itatiaia, Passa Quatro, Tinguá, Morro Redondo and Mendanha, among others). They observed that the Cabo Frio belt has a curved shape and may represent the continental continuation of the Rio de Janeiro oceanic fracture zone (at latitude 42°50´), which may have provided channels for the emplacement of alkaline magmas generated by hot-spot activity. Lapido-Loureiro & Valderano (1982) pointed out that pre-drift reconstructions show continuity between the belts of alkaline occurrences in Brazil and Angola, which they reunited in the large "Brazil-Angola alkaline-carbonatitic province", further divided into six subprovinces.

More recent work adopted entirely the concept of "igneous provinces" of alkaline rocks, mainly along the lines proposed by Almeida, each one identified by petrography, geochemistry and ages of emplacement (see also Riccomini *et al.*, in this volume). The provinces in Brazil are positioned mostly around the northern, northeastern and eastern margins of the Paraná Basin and are, from NW to SE and S, respectively, Iporá (Morro do Engenho, Santa Fé, Montes Claros de Goiás, Iporá, Córrego dos Bois, Amorinópolis, Água Emendada, Santo Antônio da Barra), Alto Paranaíba (Catalão, Pântano, Coromandel, Serra Negra, São Gotardo, Patos de Minas, Serra do Bueno, Salitre, Araxá, Tapira, Coromandel etc.), Serra do Mar (Passa Quatro, Itatiaia, Mendanha, Morro Redondo, Barra do Piraí, Tinguá, Canaã, Soarinho, Rio Bonito, Tanguá, Cabo Frio, Morro de São João, São Sebastião and Vitória islands, Búzios and Monte de Trigo), Ponta Grossa (Cananéia, Jacupiranga, Juquiá, Pariquera Açu, Tunas, Banhadão, Itapirapuã, Mato Preto) and Rio Grande do Sul (Piratini), leaving the occurrences at Lages and Anitápolis (the Ponta Grossa and Rio Grande do Sul "provinces") as well as PC, as isolated unattached alkaline occurrences (e.g. Thompson *et al.*, 1998; Araújo *et al.*, 2001). Lustrino *et al.* (2003) considered PC as the westernmost massif that may belong to the Serra do Mar Province, on account of similarities in rock and isotopic geochemistries. The topic of relationship between the basaltic magmatism in the Paraná Basin (erupted 130 Ma ago) and coeval alkaline occurrences is very pertinent and can shed light on assumptions about the structure, chemistry and dynamics of the mantle and, therefore, on the mechanisms that led to the generation of alkaline magmas; it is extensively discussed in Gibson *et al.* (1995, 1999), Comin-Chiaramonti & Gomes (1996), Comin-Chiaramonti *et al.* (1997) and Thompson *et al.* (1998). In contrast to the time-honoured assumption that correlated crustal extension and mantle uprising with the generation of basaltic and alkaline magmas (e.g. Almeida, 1971, 1983; Ulbrich & Gomes, 1981, Comin-Chiaramonti *et al.*, 2002), newer hypothesis rely on hot-spot and plume activity to provide explanations for the generation of a myriad of magmatic events, in Brazil and elsewhere, from minor alkaline occurrences to large igneous provinces (e.g. Herz, 1977; Sadowski & Dias Neto, 1981; Gibson *et al.*, 1995, Thompson *et al.*, 1998, 1999; Thomaz Filho & Rodrigues, 1999).

## REGIONAL GEOLOGIC AND STRUCTURAL OUTLINE

The Guaxupé-Socorro Nappe, with a complex intrusive and metamorphic history, may have been attached to the southernmost portion of the Brasília Folded Belt (general SE-NW direction), later transported during the Neoproterozoic over the São Francisco Craton in an easterly direction. Two possibly related segments are recognized in the Nappe, the northernmost triangular Guaxupé block, with its base covered by sediments of the Paraná Basin, and the southern Socorro structure (Campos Neto & Caby, 1999, 2000; Fig. 1).

Several Archean to Proterozoic units were recognized within the Guaxupé block: the complexes Caconde (supracrustal quartz gneisses), Alfenas-Guaxupé (assorted granulites of igneous origin), Varginha (high-grade gneisses and paragranulites) and Pinhal (migmatitic and deformed granite facies) (Fig. 1). The Nappe structure was invaded by many igneous bodies during the Brasiliano event (~800-450 Ma), presenting very different petrogenetic lineages, such as syenites (e.g. the Pedra Branca massif, 613±3 Ma), pink granites with rapakivi affinities (610-586±10 Ma), minor monzonites-monzodiorites (e.g. the Piracaia massif, 577±2 Ma), several porphyritic calc-alkaline granites, some peraluminous granitoids (624±2 Ma), mangeritic-charnockitic rocks (625±7 Ma) and calc-alkaline potassic granites (610-595±10-12 Ma) (Janasi, 1999; Figs. 1 and 2). To the southeast, PC is in direct contact with the syenitic Pedra Branca massif (Figs. 1 and 2). The study of paragneisses, which recrystallized at lower (?) crustal levels, and are exposed immediately to the N of the Guaxupé Nappe, yield thermobarometric results of around 900°C and pressures of 13.5-15 kbars (Heilbron *et al.*, 2004), therefore suggesting a minimum crustal thickness of around 40 km, if applied to the Guaxupé Nappe region.

The Alto Rio Grande Belt (Fig. 1) is formed mainly by highly deformed and recrystallized supra-crustal units, the complexes Andrelândia (schists and gneisses, sedimentation age less than 1.2 Ga) and Itapira (high-grade gneisses and quartzites), with some minor outcrops of rocks belonging to the São João del Rei Complex (low-grade phyllites and schists), while pieces of the Silvianópolis Complex, represented by migmatitic gneisses reworked during the Transamazonian cycle (ca. 1.8-2.2 Ga), crop out as basement rocks of the Andrelândia Complex. Reworked Precambrian basement (Fig. 1) is observed to the N and E of the Guaxupé block, comprising in part the Barbacena Group (granite-greenstone terranes, ages over 2 Ga), considered a part of the São Francisco Craton, and the Campos Gerais Complex (deformed granites and greenstones), grading into cratonic rocks and separating the Guaxupé Nappe from the adjacent Passos Nappe (not represented in Fig. 1).

The basement areas that constitute the Guaxupé block and the surrounding regions are cut by several linear features, clearly observed in aerial photo-graphs and Landsat images, interpreted mostly as older, in part reactivated faults. The predominant fault directions are NE and NW, parallel to the two most commonly observed structural trends in the basement of southern and SE Brazil. Observations on a regional scale show an increase in the amount of the NE and NW fractures in the region around PC, as well as an arching of structural trends in the basement rocks, to the east, thus creating, as interpreted by some authors, a probable zone of weakness that may have channeled the flow of the PC magmas (Paradella & Almeida, 1976; Fig. 4). More recent interpretations suggest that the emplacement of the PC massif, as well as that of other related bodies of the Serra do Mar alkaline province, are controlled by the passage of the Trindade plume, farther north, which may have been deflected to the south by the deep keel of old and cold cratonic areas, such as that of the São Francisco craton, generating magmas that rose to the surface along deep pre-existing structures (e.g. Thompson *et al.*, 1998; Thomaz Filho & Rodrigues, 1999). No geophysical studies of the crustal structure of the Guaxupé-Socorro Nappe are available, up to now, that can be used to identify whatever structures were actually responsible for magma flow and emplacement of such a large body as PC.

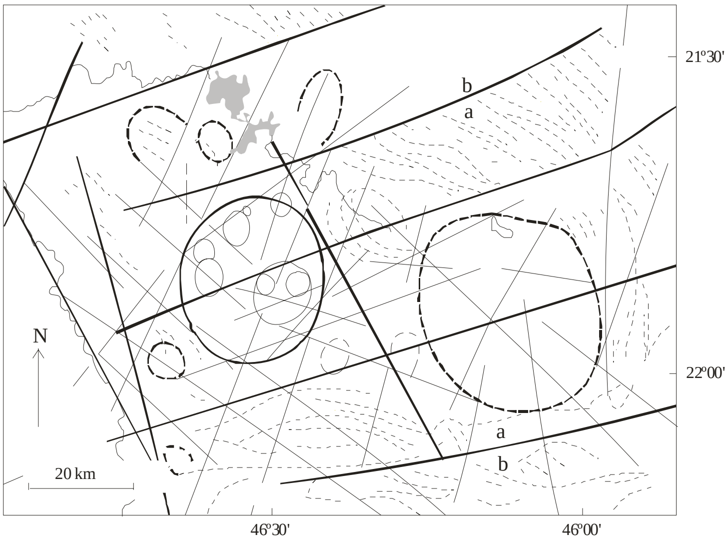


Fig. 4. Structural outline in basement rocks of the Guaxupé block and surrounding areas, as interpreted from Landsat images (Paradella & Almeida Filho, 1976). The PC massif is outlined, as well as the internal "circular structures". Other circular structures in the basement, indicated by dashed lines, are however devoid of Phanerozoic igneous activity. a: up; b: down.

## GEOMORPHOLOGIC FEATURES

The basement rocks around the PC massif crop out as a dissected plateau with irregular topographic ridges and peaks. Prevailing altitudes in the basement rocks are between 900 and 1300 m, with the highest elevations over 1400 m or even over 1600 m, found as conspicuous ridges constituted by specific geologic units (e.g. granitoid rocks, such as in the Ranges or Serras de Pau d'Alho and Mirante; Fig. 5). The Paraná Basin, to the west, is a depressed area, filled by subhorizontal sedimentary and volcanic units with a slight inward dip, presenting altitudes that are usually below 900 m. The PC massif stands out, in this landscape, as a remarkable topographic feature, with an outer rim composed by tinguaites (the so-called "ring dyke"), especially prominent in the northern and southern segments, with elevations over 1400 m (Fig. 5). A marked topographic crescent-shaped structure, in direct contact with PC to the SE, represents the outcrops of the syenitic Pedra Branca massif (Fig. 5). The areas around PC do not show a systematic outward sloping topography, at least within the region represented in Fig. 5. This topography suggests that the PC massif was intruded without any concomitant doming of the basement rocks, the present regional surface features of basement rocks being the result of differential erosion, in part enhanced by the presence of faults and joint systems. Equally, the topographic features observed in the inner part of the PC massif itself, although resembling a caldera topography, can alternatively be explained as result of differential erosion, as suggested by some authors (e.g. Motoki & Oliveira, 1987; Motoki *et al.*, 1988; Vargas & Motoki, 1991), in the sense that the fresh and massive ring tinguaites are more resistant rocks than the inner units, in part strongly affected by hydrothermal alteration.

Drainage patterns point out several "circular structures" within PC (Almeida Filho & Paradella, 1976), very visible in Landsat images and topographic maps, and which represent either the outline of intrusive tinguaite domes or NeS bodies

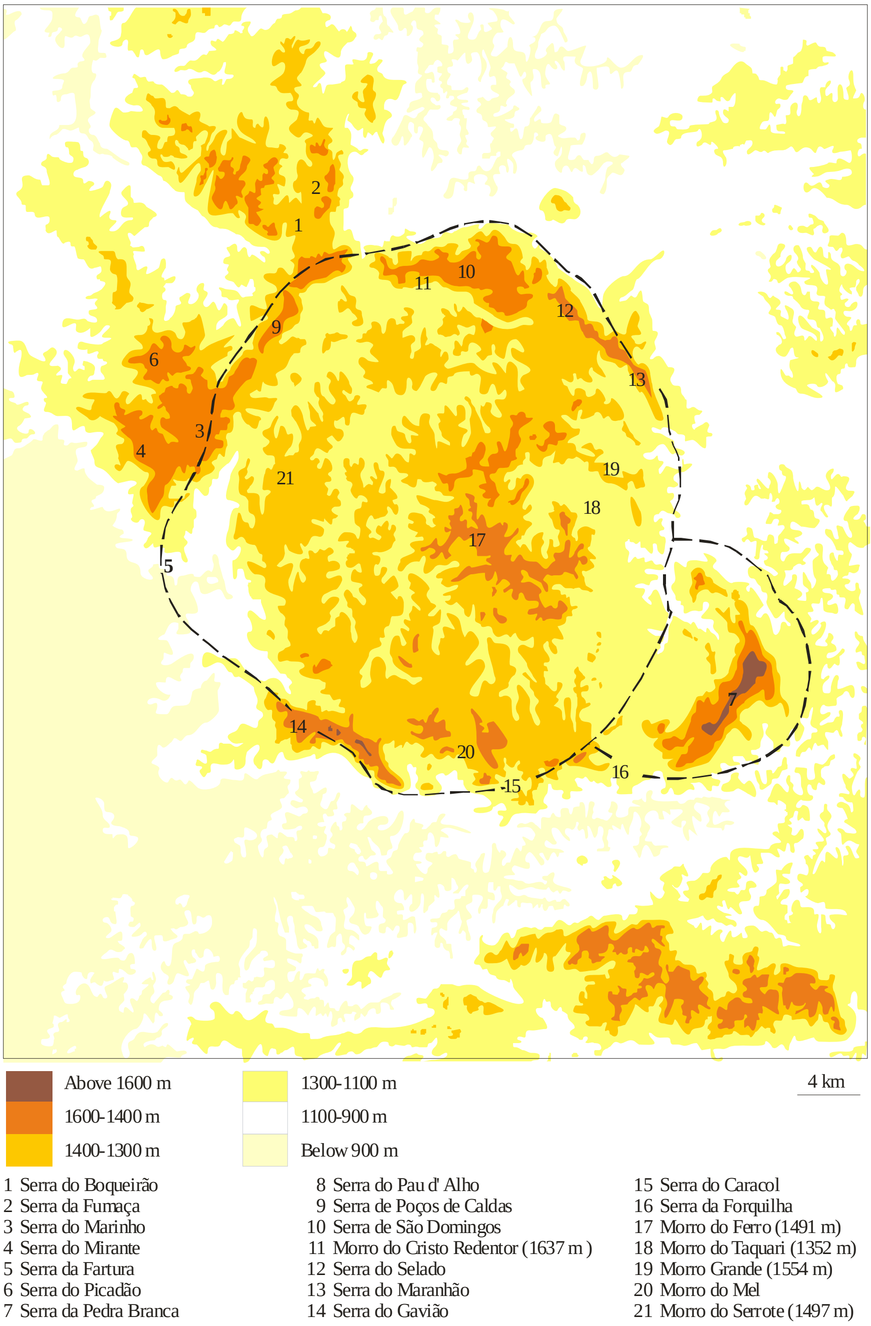


Fig. 5. Topographic features in the Poços de Caldas massif and surrounding basement areas (compare with Fig. 2). Dotted line: approximate outline of the PC massif. Source: Garda (1990).

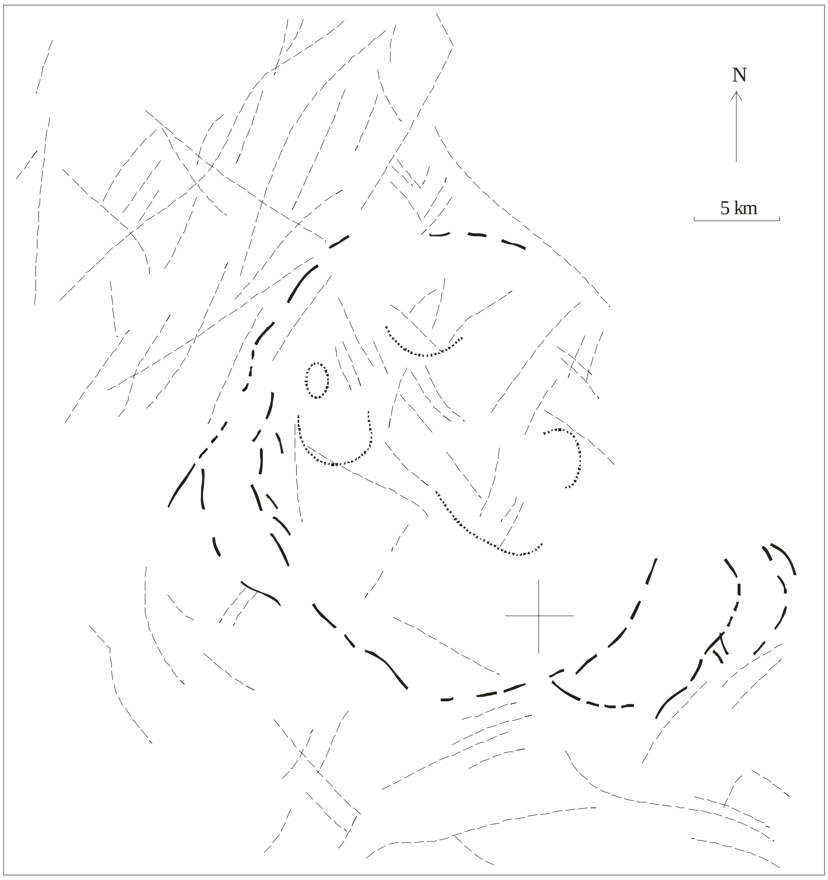


Fig. 6. Structural features in the Poços de Caldas massif (radar images). Finer dashed lines identify linear features (fracture systems and/or faults). Coarser lines are traced along the top of the topographic tinguaite rims in the massif and also identify the high rim limiting the Pedra Branca syenitic massif, to the SE. Source: Ulbrich (1984a).

(therefore controlled by differential erosion) or true structures caused by a combination of intrusive and explosive activities. The single most important "circular structure" is the one located off-center (Figs. 3 and 6), the "central-eastern structure", preferentially affected by hydrothermal alteration and concentrating, in its interior and neighboring outer areas, most of the U and Th occurrences in the district (among them, the Osamu Utsumi mine, the Campo do Agostinho prospect and the Morro do Ferro; cf. Mineralizations, below) (Fig. 7). Geometry, structure, concentration of mineralizations and hydrothermal alteration suggest that this structure represents the superficial manifestation of late subvolcanic intrusions accompanied by strong local brecciation. An even larger concentric structure is weakly outlined on the outside of the central-eastern structure, to the west within the massif, and may be interpreted in the same way (represented partially in Fig. 3).

The massif shows along its perimeter, to the SW, a bulge corresponding to a circle with a smaller diameter, occupied mainly by tinguaites and prominent sandstone outcrops, constituting the "Águas da Prata structure" (Fig. 3; Ulbrich, 1984a), suggesting a slight off-center displacement in the intrusive activity in that area. A slight but clearly visible bulge in the general geometry is also observed outside the northern ring, constituting the site of emplacement of tinguaites, gray NeS, lujavrites and khibinites (Fig. 3).

## PETROGRAPHY AND MINERALOGY

The PC rocks will be briefly described, separating them into two main lineages, broadly identified as the *felsic* and *mafic-ultramafic* suites. These terms, although loosely defined in the literature (e.g. Jackson, 1997), are here applied only to rocks and minerals, while chemical names will be used to characterize the equivalent magmas (e.g. *intermediate*, *basic-ultrabasic* etc.). The felsic rocks are NeS, tinguaites (subvolcanic pyroxene phonolites) and volcanic phonolites. Despite the large variety of rocks found in the Vale do Quartel, emphasis will be placed on those that represent the ultramafic lineage, leaving aside accidental rocks (e.g. some NeS blocks, phonolites, etc.) as well as the abundant blocks of metamorphic basement rocks concentrated in certain areas of the Vale do Quartel (cf. Alves, 2003).

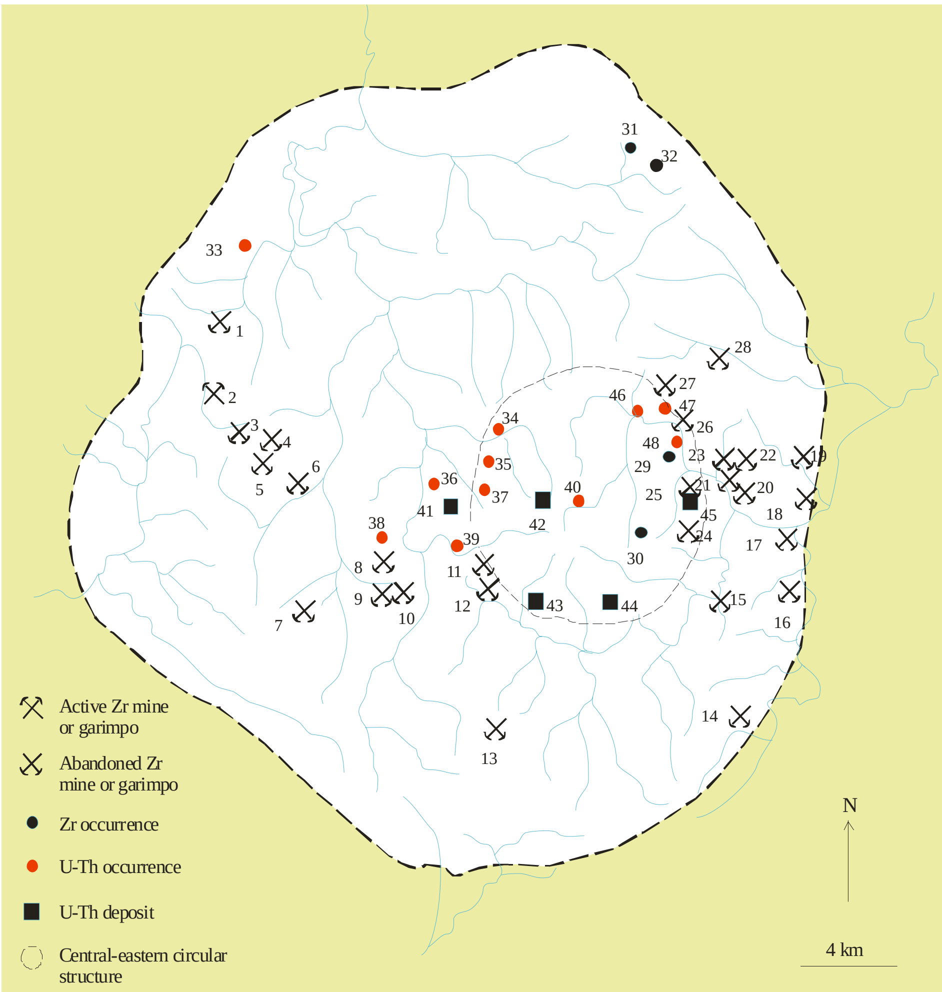


Fig. 7. Mineralized occurrences in the PC district, associated with hydrothermally altered rocks. The active exploration occurrences (in 1979) were all abandoned in the 1980's. Source: Almeida Filho & Paradella (1976) and Fraenkel *et al.* (1985); reproduced in Garda (1990).

*Nepheline syenites (=NeS)*

These rocks are subordinate among the felsic rocks (covering about 145 km$^2$ of the district, 17%), and can be separated into several clearly identifiable facies by differences in texture and structure, grain size, and amounts, type and distribution of mafic minerals, including rare metal silicates (RMS) such as eudialyte. Field observations and geometry indicate that NeS are mostly discrete bodies, intrusive into tinguaites. Most NeS bodies do not surpass a few km$^2$, with the exception of the Pedreira type with over 80 km$^2$ and a general NE-SW elongation. A significant amount of the smaller NeS bodies cluster in the rim areas, in part representing incomplete ring dykes (such as the fluorite NeS, at the NW contact with basement; Fig. 3).

NeS are mineralogically rather uniform, and constituted by cloudy to transparent K-feldspar (~55 to 66% modal), mostly slightly to strongly altered nepheline (35 to 20%) and greenish to slightly colored clinopyroxene (aegirine to sodic augite; 4 to 11%), along with some RMS usually in very subordinate amounts. Albite may be seen in some rocks, clearly as a late phase, probably the result of Na redistribution (unmixed in K-feldspars etc.); plagioclase is absent. Primary sodalite is a rare mineral in NeS, and primary kaersutite may be present in some of them (e.g. lujavrites). Eudialyte, $Na_{16}Ca_6Fe_3Zr_3(OH,Cl)_4(Si_3O_9)$ $(Si_9O_{22})_2$, is the most common RMS; it contains Nb, Ta, U, Th and REE as well. It is a rock-forming mineral in lujavrites and khibinites (9 to 12%, with other RMS) and can be present in minor amounts (up to 4%) in many other NeS, and so it is used as a field guide to separate the "agpaitic" NeS from the more intermediate-miaskitic varieties (Fig. 3; cf. discussion in Edgar, 1977), the latter ones being predominant over agpaitic facies (118.7 $km^2$ of outcrops vs. 24.8 $km^2$). The predominant mafic mineral in all NeS is clino-pyroxene, even in the more miaskitic facies, with the exception of the "biotite" NeS facies, with predominant primary biotite, which is also seen, in subordinate amounts, in some "gray" NeS; secondary biotite, on the other hand, is observed in many NeS. Opaques and titanite are accessory minerals. Fluorite is a late phase in NeS, especially noticeable in the "fluorite" NeS of the northern ring dyke (Fig. 3). Foyaitic textures (Sorensen, 1974b) are predominant in NeS, medium to coarse-grained, with tabular to bladed K-feldspars forming a framework that contains finer-grained tabular feldspars, short prisms of nepheline and prismatic to acicular Na-pyroxenes (cf. Ulbrich, 1983, 1993; Ulbrich, 1984a; Ulbrich & Ulbrich, 2000a). In the porphyritic NeS facies, K-feldspars are present as phenocrysts in a finer-grained groundmass. Nepheline may appear as subidiomorphic euhedral grains, in part also poikilitically enclosed in the coarser K-feldspars, as in rischorrites (Sorensen, 1974b). Khibinites and lujavrites in PC present eudialyte concentrated in cm- to dm-sized patches. The lujavrite is a mesocratic rock with prismatic to fibrous aegirines showing a fluidal disposition around nephelines and tabular larger K-feldspars, giving the rock a "gneissic" aspect (Shand, 1949; Sorensen, 1974a, b). In the Botelhos khibinite, outcropping to the east of the northern lujavrites and khibinites (Fig. 3), locally eudialyte and K-feldspar are segregated in bands, similar to the Ilimaussaq kakortokite (Sorensen, 1970, 1974a; Larsen & Sorensen, 1987). Primary fluidal structures are also observed in eudialyte-free hololeucocratic foliated NeS found within khibinites of the northern lujavrite body (Ulbrich & Ulbrich, 2000a).

NeS are always altered by high temperature deuteric alteration, partly or totally converting K-feldspar and nepheline into analcime, natrolite and cancrinite, and they often also show the imprint of incipient lower temperature hydrothermal alteration, characterized by the illitization-sericitization of nepheline and recrystallization of K-feldspar (Garda, 1990; Waber *et al.*, 1992).

*Tinguaites (subvolcanic pyroxene phonolites)*

These rocks are predominant in PC, making up about 75% of the entire massif. The rocks are massive greenish-gray types, usually aphyric or with low proportions of microphenocrysts, mostly fine-grained to aphanitic, indicating that they have intruded almost as liquid magmas. Fluidal structures, when present, show subvertical attitudes along the rim areas. Modal compositions are as in NeS, sometimes showing trace amounts of primary idiomorphic analcime and sodalite. Pseudoleucites (K-feldspar intergrown with nepheline) are present as irregular mm-sized aggregates (the xenomorphic variety) in many tinguaites, and are also present in the pseudoleucite tinguaites as large (up to 10 cm) idiomorphic phenocrysts (modally up to 30% or more), present as dykes and small intrusive bodies within tinguaites in the Morro do Serrote area and the Osamu Utsumi open pit (Fig. 3). The main mafic mineral in tinguaites is a sodic pyroxene (to aegirine). Eudialyte is less commonly observed than in NeS, but several RMS are conspicuously present in these rocks (among them hainite). The dominant textures are microgranular or tinguaitic (unoriented pyroxene needles among felsic minerals); oriented trachytoid textures are less common. Geologic and structural observations indicate that most tinguaites, whether aphanitic or fine- to medium-grained, invaded as subvolcanic plugs or domes.

*Phonolites*

Altered vesicular phonolites, covering about 5% of the district, are found in the central parts (cf. map by Ellert *et al.*, 1959) and close to Morro do Serrote (Fig. 3), and were interpreted as flows (Ellert, 1959): they show sometimes oriented vesicles and crop out in areas of flat relief. The rocks are almost always altered, presenting a typical violet alteration color. Contrary to tinguaites, phonolites are more frequently porphyritic, with irregular to subidiomorphic analcime and tabular sanidine phenocrysts; phenocrysts of nepheline, pyroxene and magnetite appear in smaller sizes and proportions. The groundmass is very fine-grained, microgranular or oriented, with altered K-feldspar and nepheline as main minerals, and smaller amounts of pyroxene. Alteration of pyroxene into green biotite and amphibole is frequent, both in the groundmass and as replacement in phenocrysts.

*Mafic-ultramafic rocks*

The Vale do Quartel presents a variety of fragmented rocks, most of them conspicuously volcanoclastic mafic-ultra-mafic appearing as agglomerates, lapilli and tuffs, accompanied by subordinate amounts of phonolitic rocks; brecciated basement rocks are also present in this area. The Vale do Quartel is flanked on both sides mainly by tinguaites. It has been subjected to significant subsidence, probably over 400 m (e.g. in the northern part); drilling on a mineral water property showed that mafic-ultramafic rocks continue at depth for at least some 150 m. Some mafic-ultramafic rocks, in particular, are later than most felsic PC types. The phonolite fragments (also remnants of lava flows) are aphanitic to fine-grained, often with vesicles and amygdules, with or without phenocrysts of K-feldspar, pyroxenes and analcimes, which also appear, along with alteration phases, in the aphanitic matrix. The larger mafic-ultramafic fragments present cm-sized phenocrysts of assorted minerals (pyroxene, analcime, altered olivine) with significant amounts of amygdules, in a finer-grained matrix with microphenocrysts of feldspathoids, as well as pyroxene and some nepheline, as main minerals; biotite may be present in the groundmass. Plagioclase is reported missing in these fragments by most authors (e.g. Ellert, 1959; Ulbrich, 1984a), but is cited in Alves (2003). The more mafic rocks have been rather loosely classified as ankaratrites (biotite-bearing melanephelinites), nephelinites, “leucitites”, “basanites” and “tephrites” (Ellert, 1959; Ulbrich & Ulbrich, 1992; Thompson *et al.*, 1998; Alves, 2003; Lustrino *et al.*, 2003). Alves (2003) also described pyroxenitic and some rare carbonatitic fragments (with pyrochlore, in part with a layered structure) in the Vale do Quartel breccias.

The ultramafic dykes showing idiomorphic phlogopite phenocrysts in the Osamu Utsumi open pit were described as lamprophyres (Ulbrich *et al.*, 2002) or lamproites (Shea, 1992; Waber *et al.*, 1992). Ultramafic rocks at the Minas Pedras quarry were reported as subvertical dykes and dykelets and a plug-like breccia (a few meters in height and width), associated with irregular subhorizontal sheets and dykes of tinguaites, occurring as border zone intrusions within the regional Neoproterozoic quartz mangerites (Figs. 1 and 3). The ultramafic rocks are here massive to laminated aphanitic silico-carbonatite (up to 40% carbonates), a pyroxene-rich variety, a fine-grained phlogopite rock with carbonate ocelli and megacrystic aggregates (pseudomorphs after olivine and/or pyroxene, with phlogopite+pyroxene+amphibole+ilmenite), and a laminated medium-grained rock with alternating phlogopite-rich and carbonate-rich layers. The breccia plug contains transformed metamorphic rocks and silico-carbonatitic and phlogopite-rich fragments, with abundant fluorite in veins and along fractures (Vlach *et al.*, 1996, 1998, 2003; Ulbrich *et al.*, 1998).

## STRUCTURE OF THE NEPHELINE SYENITE BODIES

Detailed mapping indicated that many of the smaller NeS bodies have vertical contacts. Several are concentrated at, or close to, the rim areas, which may have constituted a zone of weakness that opened preferential channels for the rise of late magmas; some represent incomplete ring dykes, such as the "fluorite NeS" in the northern rim (Fig. 3). Other NeS bodies, however, show outcrop patterns that are compatible with a central feeder zone followed by an upward and outward expansion along inclined to almost horizontal surfaces. The Pe-eia NeS, constituting the largest single NeS body, crops out as an elongated structure with an inferred mushoom-shaped cross-section (Fig. 8). The north-rnmost agpaitic lujavrites and khibinites are found as two small, unconnected bodies (Fig. 3) with a stra-ified structure of magmatic origin. The smaller of the two bodies is the Pedra Balão lujavrite-khibinite, to the west, intrusive both into tinguaites and the gray NeS facies, covering about 1.5 $km^2$ (Fig. 9).

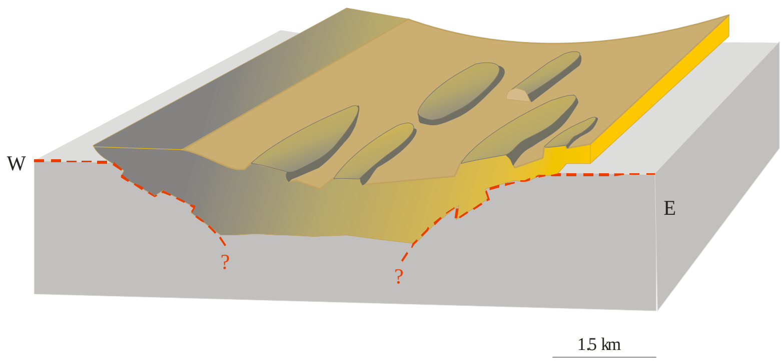


Fig. 8. Schematic block diagram depicting the inferred structure of the Pedreira NeS, at the center of the district. Source: Ulbrich (1984a).

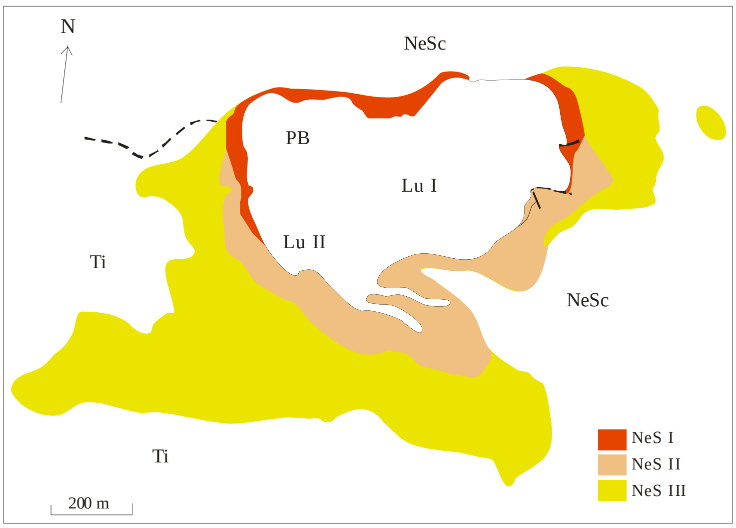


Fig. 9. Simplified map of the Pedra Balão lujavrite-khibinite body, at the northern rim area (Fig. 3). Lu I, Lu II, NeS I, NeS II, NeS III, as in text. NeSc: northern rim gray NeS. PB: Pedra Balão, a rounded meter-sized block made up of lujavrite, a local tourist attraction. Source: Ulbrich (1984a).

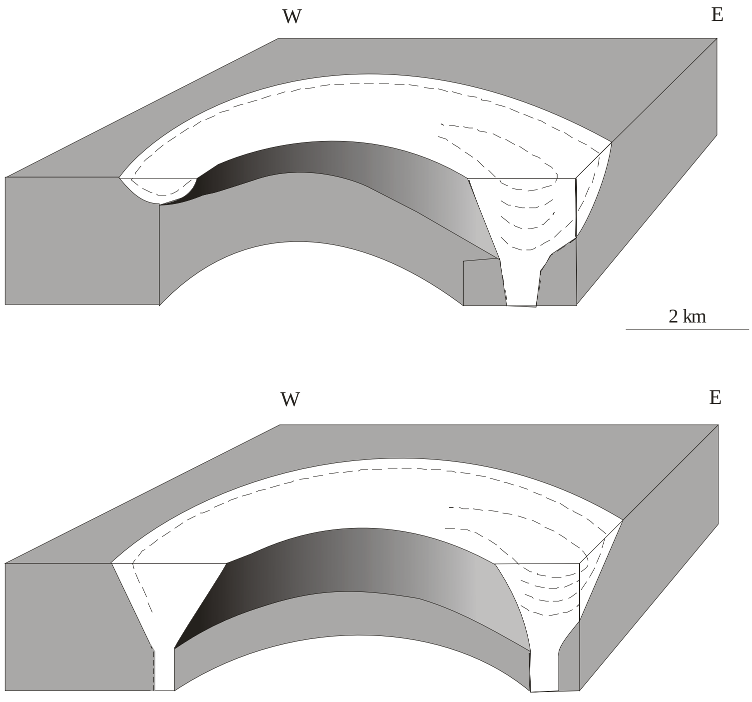


Fig. 10. Block diagrams showing the probable form of the northern rim Botelhos khibinite body. The upper diagram represents the body with a single feeder conduit, the lower one the case of a curved feeder dyke. Source: Ulbrich (1984a).

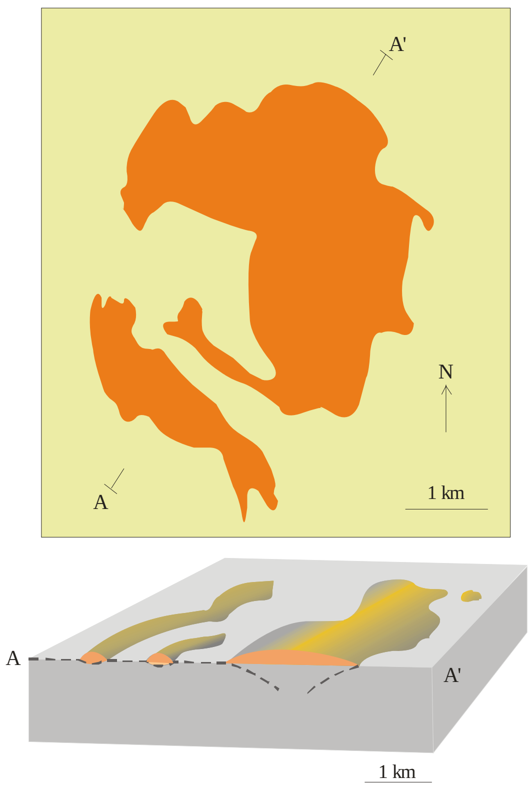


Fig. 11. The eudialyte-bearing Serrote NeS: outline (Fig. 3) and interpretative profile, assuming a single central feeder zone. Source: Ulbrich (1984a).

It shows at the center a coarse lujavrite (Lu I), surrounded by a rim of a finer-grained variety (Lu II) and two NeS with a trachytoid texture (NeS I and NeS II – the former is finer-grained and with some eudialyte, and the latter is more leucocratic and coarser-grained), followed by an outer subhorizontal to inclined apron of khibinites (NeS III; Fig. 9). The well-defined foliations are subhorizontal at the center (Lu I) and show steeper dips in the Lu II and NeS I and II, becoming less foliated and more massive in the outside khibinite. The eastern lujavrite-khibinite, poorly exposed, shows a similar petrographic and structural zonation. Strongly eroded lujavrites and khibinites are also observed at the Morro do Taquari (Fig. 3), where they probably have formed structures similar to those found at the northern rim. The origin of the strongly foliated structures in lujavrites was explained as the result of compaction processes in a crystallizing agpaitic magma (cf. discussion in Ulbrich & Ulbrich, 2000a). The Botelhos khibinite body, composed of several coarse NeS types with conspicuous eudialyte, shows an elongated curved form with inward sloping contacts (Fig. 10). Equally complex is the structure of the Serrote NeS, constituted by a whitish NeS with some eudialyte and other RMS, which probably represents the root zone of a subsidiary volcanic structure (Fig. 11).

## CRYSTALLIZATION TEMPERATURES AND SEQUENCE OF INTRUSIONS

Tinguaites, almost as entirely liquid magmas, have been emplaced as subvolcanic plugs and domes, and rapidly crystallized or quenched, as in the case of the aphanitic or very fine-grained rocks; some tinguaites appear as late dykes, cutting NeS and also pyroclastic rocks in the Vale do Quartel (cf. also Alves, 2003). Both textures and the lack of deuteric alteration indicate that fluids were not retained by these magmas; they were probably lost under a porous roof zone made up mainly by sandstones and, probably, also under a blanket of pyroclastic fall and flow deposits. Normative mineralogies for NeS, and for tinguaites as well, plot within, or close to, the experimentally determined "undersaturated thermal valley" at atmospheric pressure and 1 kb $H_2O$ pressure, which have practically coinciding minimum points M (e.g. Sood, 1981). $H_2O$ pressures, however, were probably much lower than load pressures, especially for the tinguaites, which represent early subvolcanic intrusions. The minimum temperatures M for atmospheric and 1 kb pressures are 1020 and 750°C, respectively, but liquidus temperatures for phonolites can reach as high as 1000°C (1 kb $H_2O$ pressures) or 1100°C (atmospheric pressure) (Sood, 1981), and these higher figures are probably representative of the true temperatures of emplacement for tinguaites.

NeS show sharp contacts and are mostly intrusive into tinguaites, partly incorporating them along contact zones, and sometimes present structures reminiscent of commingling features, characteristically interpreted as mixing between two (or more) incompletely crystallized magmas (e.g. Didier & Barbarin, 1991; cf. discussion in Ulbrich *et al.*, 2002). Each of the different NeS bodies is mineralogically rather homogeneous, a reminder that NeS invaded as discrete and rather uniform magma batches, slowly crystallizing within the still hot tinguaites. Agpaitic NeS are later than the miaskitic-intermediate varieties, as observed in the few cases in which the contrasted NeS facies are in contact (Ulbrich, 1984a; Ulbrich & Ulbrich, 2000a). The tinguaites acted as an impermeable cap, trapping late fluids in the crystallizing NeS batches until complete cooling was achieved, an explanation for the systematic presence of deuteric alteration in all NeS. The use of the Powell and Powell feldspar-nepheline and the Hamilton nepheline geothermometers gives support to this interpretation, showing that the intermediate-miaskitic Pedreira NeS type presented re-equilibration temperatures of around 800°C. The lowest re-equilibration temperatures of 540 to <500°C were obtained for the most agpaitic rocks (khibinites and lujavrites), other NeS yielding intermediate temperatures. Experimental data for miaskitic NeS magmas show liquidus temperatures, for $H_2O$ pressures of 1 kb, at around 1040°C, with an equivalent solidus at around 800°C, while the solidus of the agpaitic lujavrites is around 430-450°C, also presenting a much wider crystallization range (Sood, 1981).

Volcanic phonolites, extruded at the surface, were probably accompanied by large volumes of pyroclastic rocks, and may have marked the beginning of the felsic magmatism at PC. The mafic-ultramafic rocks at the Vale do Quartel and elsewhere are in part clearly later than the surrounding felsic tinguaites and NeS, but may have been formed during a more protracted time span, perhaps starting before the onset of the magmatism that emplaced the felsic rocks (cf. Ulbrich *et al.*, 2002; also Thompson *et al.*, 1998; Alves, 2003).

## HYDROTHERMAL ALTERATION AND MINERALIZATIONS

Large areas of the massif were affected by hydrothermal alteration, in part conditioned by clear structural controls, as in the cited "central-eastern circular structure" (Figs. 3 and 6). Altered rocks, especially tinguaites and phonolites, are usually strongly cracked by myriad of fractures, with the fragments preserving their orientation, thus showing a typical "craquelée" structure. The structural pattern controlling hydrothermal alteration is well-represented in the Osamu Utsumi open pit, where "cracked" rocks grade into "fragmentation" breccias by slight movement and rotation of the fragments and the creation of interfragmental voids, cut by the "intrusive" breccias with irregular to rounded, cm- to meter-sized blocks, that form the core of the structure (Fig. 12). Breccias of various types were also described at Campo de Agostinho (Fujimori, 1974, 1980). The general structural pattern indicates that the hydrothermal alteration, as elsewhere in deposits with a similar origin (e.g. in porphyry copper deposits), is intimately associated with a concomitant strong fracturing of the country-rocks, thus allowing the unhindered passage of $H_2O$-rich fluids through the rock fabric. This geologic model closely correlates the emplacement and cooling of the local magmas with the alteration and mineralization processes (e.g. Paradella & Almeida Filho, 1976; Garda, 1990; Ulbrich *et al.*, 2002); accordingly, radiometric ages of the fresh rocks and the hydrothermally altered ones must overlap each other (cf. Geochronology, below). Mineralized occurrences are especially concentrated in and around the "central-eastern circular structure", which probably represents the site of emplacement of late subvolcanic intrusions (Fig. 7).

The Osamu Utsumi mine (Fig. 12) was developed as an open pit in 1977, in a rolling landscape with hills (heights of 1475 to 1484 m) and ravines, and was closed down in 1988, with the pit floor standing at 1304 m; a lake now fills the pit. Predominant rocks in the mine are massive intrusive porphyritic phonolites, with tabular mm-sized K-feldspars (10-20 crystals per $dm^2$) and irregular or rounded aggregates of pseudoleucites (the xenomorphic variety); groundmass is aphanitic to very fine-grained, with illite and K-feldspar. Aphyric phonolites, turning rapidly into the porphyritic variety, are less frequent; they can also be seen as dykes. NeS are massive medium- to coarse-grained rocks, often with miaroles, forming small bodies, always showing reconstituted K-feldspars and altered nepheline. Pseudoleucite phonolites are seen as dykes and small irregular bodies, intrusive into the main phonolites and NeS; pseudoleucite is here of the idiomorphic variety (up to 5-7 cm in size), present in variable proportions (from 10-15% up to, locally, 50 to 60% of the rock), associated with tabular K-feldspar phenocrysts. The groundmass is fine-grained to aphanitic, showing K-feldspar and illite. Rare trachytes, as well as the already mentioned phonolites, appear as dykes with a steep to subvertical attitude. Mica lamprophyres are present as altered dykes (with one exception), usually showing intermediate dips and a predominant NE strike. A breccia pipe is at the center of the structure, with an irregular to lobate contour, accompanied on the outside by an irregular apron of fragmentation breccias, which grade farther out into heavily fractured rocks ("craquelée" structure). The mineralization is observed mainly in voids (breccia pipe and fragmentation breccias) and along fractures. Phonolites were the first rocks to be emplaced, followed by NeS and then by the dyke rocks. Brecciation, mineralization and hydrothermal alteration followed afterwards; the presence of altered and unaltered lamprophyres suggests that the ultramafic rocks have invaded during and after mineralization-alteration (Shea, 1992; Ulbrich *et al.*, 2002). The model suitable to explain this occurrence is that of a breccia pipe generated by a fragmentation that was triggered by intrusive events (Biondi, 1979; Garda, 1990; also the porphyry-Cu model, cf. literature in Sawkins,1990).

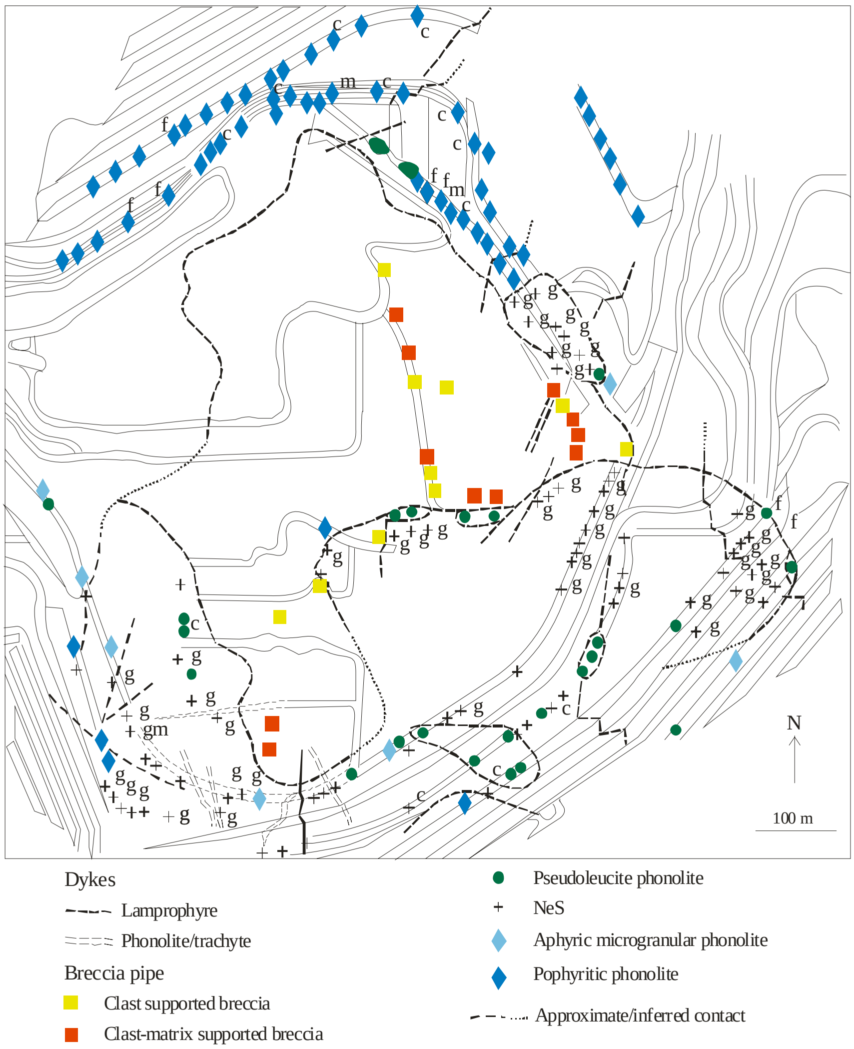


Fig. 12. Geologic sketch-map of the Osamu Utsumi open pit, with its central irregular breccia pipe. Based on a topographic map with the outline of the benches in 1982-1983, by Nuclebrás. All rocks are altered by hydrothermal alteration, as well as the phlogopite lamprophyres (with one exception). c: finely cracked rock ("craquelée"); f: fragmentation breccia; g: coarse to very coarse-grained texture; m: miarolitic structure. Geology by H.Ulbrich, 1982-1983. Reproduced in Garda (1990) and Ulbrich & Ulbrich (1992, 2000b).

Hydrothermal alteration preserves original magmatic textures and structures. The color of the altered rocks is a typical buff, grayish-beige to blue-gray in the *reduced* rock with the alteration assemblage in an unweathered state, but more yellowish-brown in the weathered (*oxidized*) types. With the progression of weathering, original textures tend to disappear, giving rise to structureless saprolites. The hydrothermal K-feldspar is chemically and structurally reconstituted, passing to almost pure $KAlSi_3O_8$, while very fine-grained illite completely replaces nepheline, and the pyroxenes and other mafic minerals are substituted by a combination of illite, carbonates and iron oxides and hydroxides (Moniz, 1969; Garda, 1990; Waber *et al.*, 1992). Pyrite is the main hydrothermal Fe-phase in the reduced rock, present especially in mineralized areas as pervasively distributed small cubes and also in veins and along fractures. Kaolinite is rare in the reduced rock, appearing only as minor aggregates or in veinlets. The altered rock turns gradationally into the completely weathered equivalent, with destruction of the primary textures and the appearance of kaolinite as main clay mineral, as well as gibbsite and amorphous and crystalline Fe-hydroxides (to a lesser extent, also Mn-hydroxides); sericite, illite and K-feldspar disappear. In the oxidized horizons, pyrite is replaced by goethite, other Fe-hydroxides and hematite. Geochemically, hydrothermal alteration leaches out mainly Ca, Na and Mg from the original rock, with concomitant introduction of $H_2O$, $CO_2$ and K, hence the local name "potassic rock" ("rocha potássica") that is applied to this alteration product. $K_2O$ contents in the "potassic rock" can be as high as 15-17%, which prompted several studies for its use as a potential fertilizer (e.g. Frayha, 1950, 1952; Castro & Souza, 1962; Almeida *et al.*, 1978; Garda, 1990; Waber *et al.*, 1992; Ulbrich & Ulbrich, 1992, 2000b).

Several ores are found in intimate association with hydrothermal alteration (Fig. 7). One ore-forming process is characterized by the generation of caldasite, which is found as subvertical veins always in hydrothermally altered areas. The veins are most often only a few centimeters thick, but in certain cases they can be meter-sized pockets. Caldasite is frequently found as gray pebbles on the ground. It also shows remarkable U contents, and was considered a possible source for uranium (Franco, 1945; Loewenstein, 1952; Dutra, 1954; Tolbert, 1958a, b, 1966; Wedow, 1961; Frayha, 1962a, b, c; Maciel *et al.*, 1973; Gorsky & Gorsky, 1974; Fujimori & Sardela, 1980; Sardela & Fujimori, 1980; Sardela, 1981). The ore was intensely mined by prospectors up to the 1980's. Large cm-sized zircon crystals are found locally on the surface (mainly in the Cerro Taquari area, Fig. 3), probably the weathering product of crystals concentrated in vugs and veins.

A second important hydrothermal ore is represented by the U-Zr-Mo mineralization, typically associated with brecciated pipes and linear structures. The two most important examples are the linear feature of Campo do Agostinho, within the "central-eastern circular structure", prospected but later abandoned as uneconomic, and the C-09 area at Campo de Cercado, developed as the Osamu Utsumi open pit mine (Fig. 3; Fujimori, 1974, 1980; Fujimori *et al.*, 1976). Uranium, REE, Mo and Zr minerals are found in the reduced breccias and in the oxidized potassic rock at the open pit; the mineralization was polyphasic, depositing minerals such as pitchblende (colloform to massive $UO_2$), uraninite (cubic $UO_2$), braunerite ($UTiO_6$) and monazite (Ce, REE)($PO_4$), as well as zircon and other species. Molibdenite probably represents the only primary Mo phase in the deposit. Several secondary minerals were also described, mainly phosphates and sulphates, among them the bluish Mo-coquimbite, $(Mo,Al,Fe)_2(SO_4)_3.9H_2O$, and other ill-defined Mo species. Significant mineral changes, such as the deposition of secondary pitchblende, occur at the mine along the irregular redox front, separating the reduced from the oxidized alteration assemblages (Garda, 1990; Waber *et al.*, 1992). Uranium ore was mined in the open pit, and transformed into yellow cake and Mo byproducts in an adjacent chemical plant (Forman & Angeiras, 1981).

Many additional smaller U-bearing occurrences were found in the district, including a linear radioactive anomaly along the N-S trending Assis Figueiredo street in the locality of Poços de Caldas (Fig. 7; Dutra, 1954; Frayha, 1957, 1962a, b, c;

Maciel *et al.*, 1973; Paradella & Almeida Filho, 1976).

Another unusual occurrence is the Th-REE supergene deposit at Morro do Ferro, covering a stockwork of magnetite dykes and dykelets, possibly representing the altered remnants of carbonatite-like bodies (Schorscher & Shea, 1992; Waber, 1992; Waber *et al.*, 1992). This deposit is found among tinguaites converted into "potassic rock", showing a discontinuous surficial patch with a remarkable Th-REE anomaly. Several primary minerals were recognized, such as bastnaesite (Ce,La,REE)($CO_3$)F, thorite $ThSiO_4$, monazite (REE)$PO_4$, pyrochlore $(Na,Ca)_2(Nb,Ti,Ta)_2(OH,F,O)$, and zircon, as well as many secondary phases, in part still unidentified, among them cerianite $(Ce,Th,U)O_2$, thorianite $(Th,U)O_2$, Nd lanthanide $(La,Nd)_2(CO_3)_3.8H_2O$, cheralite (Th,Ca,Ce,La)(PSi)$O_4$, and several others (Frondel & Marwin, 1959; Wedow, 1961a, b, 1967; Fujimori *et al.*, 1980; Fujimori, 1982b; Waber, 1992).

The single most important deposit of economic interest in PC is of course bauxite, always a product of weathering of fresh NeS and tinguaites; the already altered "potassic rocks" are not affected by bauxitization (Valeton *et al.*, 1997). Two varieties are recognized, the rim or ridge bauxites on the steeper hills developed on top of the rim tinguaites, richer in Al, and the plateau bauxites in the inner parts of the massif. The main laterite minerals are gibbsite (more abundant in the ridge bauxites) and goethite, while kaolinite and halloysite (in the plateau bauxites also with illite) are less abundant; also reported, usually as accessory minerals, were magnetite, lithiophorite, florencite, boehmite and anatase (Souza-Santos, 1937; Weber, 1959; Frayha, 1962a; Moniz, 1969; Moniz *et al.*, 1972; Almeida, 1977; Schulmann, 1993; Schulmann *et al.*, 1997; Valeton *et al.*, 1997).

A detailed general outline of ore deposits associated with alkaline occurrences, as well as complementary information on PC, is found in Biondi (in this volume).

## GEOCHRONOLOGY AND MAGNETIC REVERSALS

The oldest K-Ar age for PC rocks of around 89 Ma were obtained for an "ankaratritic" pyroclastic block in the Vale do Quartel, while most tinguaites and phonolites yielded ages around 72-78 Ma and most NeS around 60-64 Ma. The youngest date of 53 Ma was obtained for some inconspicuous phonolite dykes that cut NeS (Amaral *et al.*, 1967; Bushee, 1971; Sonoki & Garda, 1988). A mean K-Ar age for all 40 measurements is 73.7±8.6 Ma (2σ), with a median of 75.5 Ma, which can be corrected to a better mean and median of 75.6±6.8 (2σ) and 76.6 Ma, respectively, for a reduced set of 22 measurements, excluding some questionable values: all data based on K-feldspar analysis, those obtained from "amphiboles" (?) and a "pyroxene" with a low $K_2O$ value, and also measurements that show atmospheric $^{40}Ar$ significantly over 20% (Table 1, Fig. 13). Older and apparently "good" ages are reported for the JB-PC10 ankaratrite (89.3 Ma) and for two biotites from NeS (82.3 and 82.7 Ma, Table 1). A similar analysis by Thomaz Filho & Rodrigues (1999) with the same data set indicated 74.6 Ma as the "best mean" age for the massif, while Thompson *et al.* (1998), also incorporating their own data, propose an intrusion interval between 80 and 85 Ma.

A first try at Rb-Sr dating is reported in Kawashita *et al.* (1984), indicating isochron ages of around 83±21 (2σ), initial ratio 0.7052±0.0003 for lujavrites and khibinites of the northern lujavrite body, and 88.5±8.1 Ma (2σ), i.r. 0.7054±0.0002 for northern gray NeS (recalculation with the Isojob software, Ludwig, 1998; cf. also Shea, 1992; Ulbrich *et al.*, 2002; samples 1-14, Table 2). A recent Rb-Sr internal isochron from a fresh Pedreira NeS type yielded 77.9±6.2 (2σ), i.r. 0.70512±0.00002, MSWD=0.88 (Shea, 1992; samples 18-23, Table 2); calculations using the Isojob software with Shea's data yielded 78.6±6.6 (2σ) Ma, i.r. 0.70511±0.00001, MSWD=1.3 (Ulbrich *et al.*, 2002). The result of 78.6 Ma is considered the best age for the main NeS magmatism, also dating by extension the phonolite and tinguaite occurrences. Hydrothermally altered samples of NeS from a borehole in the Osamu Utsumi open pit give 75.8±2.4 (2σ) Ma, i.r. 0.70532±0.00011, MSWD= 1.08 (Shea, 1992; samples 24-35, Table 2), while our calculations with the Isojob software, excluding the poorly aligned samples 32 to 35, yield 76.8±2.6 Ma, i.r. 0.7053±0.0002, MSWD=0.49 (Ulbrich *et al.*, 2002), indicating a close age relationship between intrusion and alteration-mineralization ages, strongly supported by geologic evidence (Shea, 1992; Ulbrich *et al.*, 2002). Biotites from a fresh-looking lamprophyre dyke found in the same open pit yielded Ar-Ar plateau ages of 75.6±0.6 and 76.2±1.6 Ma (mica phenocryst and groundmass mica; Shea, 1992), again dates that closely correlate the intrusion and alteration of the felsic PC rocks in the Utsumi open pit with the intrusion of the subordinate ultramafic types, as also indicated by geological arguments (Shea, 1992; Ulbrich *et al.*, 2002).

The ultramafic pyroxenitic-carbonatitic dykelets occurring at the Minas Pedras quarry were dated with the Th-U-total Pb microprobe technique (Vlach & Gualda, 2000) on non-metamict cores of thorite crystals. The mineral, present in laminated carbonatitic veinlets with calcite+fluor-REE carbonate+fluorite+aegirine+anatase, yielded spot ages varying from 82 to 76±11 Ma (95% confidence interval), with a weighted mean age of 79±3.5 Ma (Ulbrich *et al.*, 2002; Table 3). Fresh phlogopites from a late Minas Pedras carbonatite vein with calcite+phlogopite+fluorite showed a best mean $^{40}Ar/^{39}Ar$ age of 83.9±0.3 Ma (Vlach *et al.*, 2003). The vein probably crystallized (or recrystallized) at temperatures of not more than 350-300°C, the closure temperature for the $^{40}Ar/^{39}Ar$ system. No newer age determinations were reported so far for the ultramafic rocks present in the Vale do Quartel pyroclastic strip.

Seventy-three paleomagnetic measurements were performed on PC rocks and some sandstone enclaves. All tinguaites, phonolites and NeS showed reverse polarity, while three successful measurements on ultramafic Vale do Quartel samples (out of five that were performed) showed normal polarity (Montes Lauar, 1988; Montes Lauar *et al.*, 1995). No paleomagnetic data are available for the dyke rocks in the Osamu Utsumi open pit and the Minas Pedras occurrences. These results, when compared with the known ages, indicate that the most probable interval of intrusion for the felsic PC rocks occurred during the Campanian 33r reverse

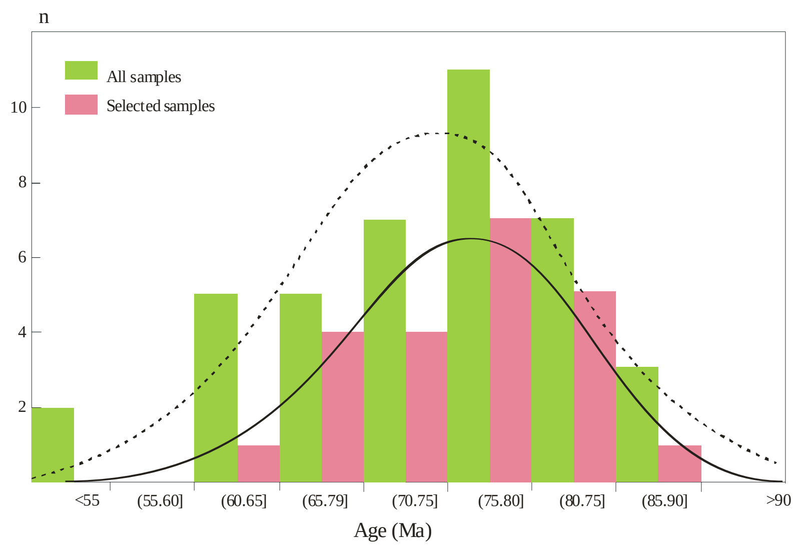


Fig. 13. Means and medians of the known K-Ar ages of the Poços de Caldas rocks. Source of data: Sonoki & Garda (1988).

Table 1. K-Ar ages of rocks from the Poços de Caldas massif.

| | Sample | Rock-type | Mineral/WR | $\%K_2O$ | $^{40}Ar$ atm (%) | Age (Ma) (error) | Ref. |
|---|---|---|---|---|---|---|---|
| 1 | JB PC 12 | W rim NeS | Biotite | 9.43 | 15.3 | 82.3 | 1 |
| 2 | KA 1832 | W rim NeS | Biotite | 9.37 | 20.3 | 82.7 | 2 |
| 3 | JB PC 38 | Tinguaite | WR | 8.69 | 37.5 | 76.9 | 1* |
| 4 | JB PC 38 | Tinguaite | WR | 8.69 | 34.5 | 75.0 | 1* |
| 5 | JB PC 24 | Tinguaite | WR | 7.93 | 13.1 | 78.2 | 1 |
| 6 | Berk6241 | Tinguaite | WR | 8.65 | 11.1 | 65.4(1.6) | 1 |
| 7 | UC6241 | Tinguaite | WR | 8.56 | 6.4 | 64.3 | 1 |
| 8 | UC6241a | Tinguaite | WR | 8.53 | 7.6 | 66.0 | 1 |
| 9 | JB PC 10 | Ankaratrite | WR | 5.14 | 15.1 | 89.3 | 2 |
| 10 | JB PC 17 | Ankaratrite | WR | 5.17 | 7.9 | 78.4 | 2 |
| 11 | JB PC 28 | Phonolite | WR | 7.75 | 19.70 | 77.1 | 2 |
| 12 | JB PC 29 | Phonolite | WR | 6.10 | 19.4 | 77.5 | 2 |
| 13 | JB PC 36 | N rim ting. | WR | 6.55 | 9.0 | 82.0 | 2 |
| 14 | JB PC 31 | S tinguaite | WR | 7.74 | 10.6 | 82.4 | 2 |
| 15 | KA 1821 | S tinguaite | WR | 8.35 | 24.3 | 82.9 | 2* |
| 16 | KA 1820 | Tinguaite | WR | 8.26 | 15.6 | 76.0 | 2 |
| 17 | JA 1820R | Tinguaite | WR | 8.26 | 7.3 | 75.7 | 2 |
| 18 | JB PC 5 | Tinguaite | WR | 8.42 | 20.0 | 74.9 | 2 |
| 19 | JB PC 53 | N rim ting. | WR | 8.46 | 7.0 | 71.1 | 2 |
| 20 | JB PC 44 | N rim ting. | WR | 8.47 | 5.0 | 74.5 | 2 |
| 21 | JB PC 48 | N rim ting. | WR | 8.28 | 5.4 | 74.2 | 2 |
| 22 | JB PC 51 | N rim ting. | WR | 8.78 | 6.2 | 65.4 | 2 |
| 23 | KA 1822 | Pedr. NeS | KF | 11.93 | 15.0 | 63.6 | 2* |
| 24 | KA 1833 | Grey NeS | KF | 16.39 | 11.0 | 61.2 | 2* |
| 25 | KA 1833R | Grey NeS | KF | 13.39 | 47.7 | 61.7 | 2* |
| 26 | KA 1829 | Lujavrite | KF | 15.84 | 7.8 | 62.3 | 2* |
| 27 | KA 1826 | N rim ting. | WR | 12.09 | 20.20 | 54.2 | 2* |
| 28 | VL3.1161 | NeS | Pyroxene | 0.13 | 71.50 | 85.5(15.1) | 3* |
| 29 | MZ | Phonolite | WR | 7.31 | 21.57 | 86.5(1.2) | 3* |
| 30 | RAA 414 | NeS | Amphibole? | 0.70 | 39.21 | 75.4(3.0) | 3* |
| 31 | RAA 420 | NeS | Amphibole? | 0.57 | 74.24 | 82.5(6.6) | 3* |
| 32 | RAA 416 | NeS | KF | 10.39 | 6.52 | 78.2(1.8) | 3* |
| 33 | RAA 419 | NeS | KF | 13.96 | 7.60 | 75.5(1.4) | 3* |
| 34 | RAA 419 | NeS | KF | 13.96 | 15.05 | 72.4(1.3) | 3* |
| 35 | RAA 418 | Tinguaite | WR | 11.20 | 5.73 | 78.0(1.3) | 3 |
| 36 | RAA 418 | Tinguaite | WR | 11.20 | 6.77 | 81.0(1.1) | 3 |
| 37 | RAA 417 | Tinguaite | WR | 7.59 | 5.73 | 66.3(4.0) | 3 |
| 38 | RAA 413 | NeS | Amphibole? | 1.05 | 41.38 | 66.2(2.0) | 3* |
| 39 | RAA 415 | NeS | Amphibole? | 0.65 | 44.07 | 54.3(1.7) | 3* |
| 40 | RAA 415 | NeS | KF | 11.09 | 31.13 | 71.7(2.5) | 3* |

NeS: nepheline syenite; WR: whole-rock; KF: K-feldspar. Errors refer to last figures. Asterisks mark the excluded data (cf. text). The K content of 0.508%, sample JB PC 29, as stated in Sonoki & Garda (1988), should read "K 5.08%". References: 1) Amaral *et al.* (1967); 2) Bushee (1974); 3) unpublished data, São Paulo Geochronology Center, Instituto de Geociências. All ages converted to Steiger & Jaeger's newer decay constants (cf. compilation in Sonoki & Garda, 1988). W & N rim, S, Pedr., Grey, refer to western and northern rim, southern, Pedreira NeS type, grey NeS (northern rim). Samples 28 to 40: no location registered.

polarity event, calibrated between 83 and 79.1 Ma, while the ultramafic rocks of the Vale do Quartel were erupted, at least in part, during the following 33n normal polarity event (79.1-73.6 Ma), some of them perhaps also being emplaced earlier, during the 34n event (>83 Ma; Cande & Kent, 1994). Most of the known ages ($\pm 2\sigma$) for the *felsic* PC rocks with reverse polarization plot within the time span of the 33n interval, thus suggesting that a slight correction should be made for the probable intrusion age of these rocks, to perhaps around 80 Ma, a slight error may be present in the adopted polarity calibration for the 33r episode (Fig. 14).

## ISOTOPE GEOCHEMISTRY

Isotopic data were obtained for 18 felsic PC rocks (10 NeS and 8 tinguaites; cf. location in Table 8). Data are found in Tables 4 to 7. Errors are quoted at the 95% confidence interval.

Also included in the present evaluation are published Sr and Nd data for the mafic-ultramafic Vale do Quartel rocks (Thompson *et al.*, 1998) and unpublished ones for the Minas Pedras varieties (Vlach *et al.*, 1998). To simplify matters, most initial ratios were calculated for an 80 Ma reference age (cf. Geochronology).

Table 2. Rb-Sr determinations in rocks from the Poços de Caldas massif.

| | Sample | Rock-type | Mineral/WR | Rb | Sr | $^{87}Rb/^{86}Sr$ (error) | $^{87}Sr/^{86}Sr$ (error) | $^{87}Sr/^{86}Sr$ (initial error) |
|---|---|---|---|---|---|---|---|---|
| 1 | P47 | Khibinite | KF | 413.3 | 627.9 | 1.905(54) | 0.70747(20) | 0.70533(21) |
| 2 | P11 | Khibinite$^{A}$ | WR | 316.7 | 965.9 | 0.949(27) | 0.70641(42) | 0.70535(42) |
| 3 | P224 | Khibinite | WR | 323.5 | 1139.8 | 0.821(23) | 0.70593(24) | 0.70500(34) |
| 4 | P215 | Khibinite | WR | 191.3 | 1112.8 | 0.494(14) | 0.70585(11) | 0.70530(11) |
| 5 | P223 | Lujavrite | WR | 216.9 | 2678.2 | 0.216(6) | 0.70538(18) | 0.70514(18) |
| 6 | P224 | NeS | KF | 400.7 | 557.1 | 2.084(59) | 0.70786(32) | 0.70552(33) |
| 7 | P220 | Grey NeS | WR | 576.8 | 1167.0 | 1.430(40) | 0.70680(9) | 0.70520(10) |
| 8 | P525 | NeS$^{B}$ | WR | 523.3 | 424.7 | 3.628 (103) | 0.70958(9) | 0.70551(15) |
| 9 | P432 | Grey NeS | WR | 289.5 | 722.8 | 1.159(33) | 0.70648(4) | 0.70518(6) |
| 10 | P176 | Grey NeS | WR | 617.8 | 691.0 | 2.588(73) | 0.70828(8) | 0.70538(12) |
| 11 | P205 | Grey NeS | WR | 593.6 | 1104.7 | 1.555(44) | 0.70708(6) | 0.70534(8) |
| 12 | P205 | Grey NeS | KF | 605.9 | 735.3 | 2.385(67) | 0.70813(6) | 0.70545(10) |
| 13 | P371 | Pedr. NeS | WR | 173.9 | 1814.2 | 0.277(8) | 0.70477(3) | 0.70446(3) |
| 14 | P384 | Pedr. NeS | WR | 152.0 | 2824.6 | 0.156(41) | 0.70518(13) | 0.70500(13) |
| 15 | NS 1 | Pedr. NeS | WR | 170.0 | 2130 | 0.2309 | 0.705335(7) | 0.705079(15)* |
| 16 | NS 4 | Pedr. NeS | WR | 162.0 | 2902 | 0.1614 | 0.705274(8) | 0.705095(12)* |
| 17 | NS 6 | Pedr. NeS | WR | 148.8 | 3263 | 0.1319 | 0.705250(7) | 0.705104(12)* |
| 18 | NS 7 | Pedr. NeS | WR | 159.5 | 2865 | 0.1610 | 0.705309(8) | 0.705131(12)* |
| 19 | NS 7 | Pedr. NeS | Titanite | 8.88 | 5038 | 0.00510 | 0.705121 | |
| 20 | NS 7 | Pedr. NeS | Titanite | 14.13 | 6242 | 0.00655 | 0.705133 | |
| 21 | NS 7 | Pedr. NeS | Aegirine | 0.648 | 291.2 | 0.00644 | 0.705105 | |
| 22 | NS 7 | Pedr. NeS | KF | 229.4 | 2605 | 0.2547 | 0.705398(8) | |
| 23 | NS 7 | Pedr. NeS | Nepheline | 12.89 | 186.5 | 0.2000 | 0.705326 | |
| 24 | 1A-A | Alt. NeS | WR | 418.3 | 174.9 | 6.924 | 0.712807(9) | |
| 25 | 1A-A | Alt. NeS | WR | 419.1 | 171.6 | 7.071 | 0.712898(8) | |
| 26 | 1A-C | Alt. NeS | WR | 419.6 | 172.7 | 7.034 | 0.712889(9) | |
| 27 | 1A-E | Alt. NeS | WR | 434.3 | 184.7 | 6.807 | 0.712635 | |
| 28 | 1A-H | Alt. NeS | WR | 420.0 | 168.4 | 7.222 | 0.713119 | |
| 29 | 1A-L | Alt. NeS | WR | 435.7 | 240.6 | 5.241 | 0.710941 | |
| 30 | 1A-N | Alt. NeS | WR | 439.6 | 194.5 | 6.543 | 0.712308(7) | |
| 31 | 1A-P | Alt. NeS | WR | 422.4 | 204.4 | 5.983 | 0.711740(9) | |
| 32 | 1AA | Alt. NeS | WR | 426.3 | 205.2 | 6.013 | 0.711768 | |
| 33 | 1AC | Alt. NeS | WR | 432.9 | 229.3 | 5.464 | 0.711229 | |
| 34 | 1AE | Alt. NeS | WR | 423.1 | 203.2 | 6.027 | 0.711900(8) | |
| 35 | 1AE | Alt. NeS | WR | 437.0 | 209.0 | 6.051 | 0.711878(7) | |

For newer Rb-Sr determinations, cf. Table 4. Abbreviations as in Table 1. Errors refer to last figures. Superscripts: A: pegmatoid facies; B: fluorite-bearing NeS. Initial ratios marked with (*) are calculated for an age of 78 Ma (Shea, 1992), the others with 80 Ma (cf. text). Samples 24 to 35 are from the F4-413 borehole cores, Osamu Utsumi Mine. Ref.: samples 1 to 14, unpublished data, obtained by K. Kawashita on a VG 54 single collector mass spectrometer at the University of Pará in Belém (cf. Kawashita *et al.*, 1984); samples 15 to 35: Shea (1992). Samples 1 to 5: Pedra Balão lujavrite-khibinite body, northern rim: 83±21 Ma, i.r. 0.7052±0.0003; northern rim gray NeS, samples 7 to 11: 88.5± 8.1 Ma, i.r. 0.7054±0.0002; samples 24 to 32: 75.6±2.23 Ma, i.r. 0.70953±0.0002; NS 7 whole rock and mineral isochron, samples 18 to 23: 78.6±6.6 Ma, i.r. 070511±0.00001. Ages and errors (2σ) calculated with the IsoPlot software.

Table 3. Th, U and Pb contents and ages for thorite, Minas Pedras quarry.

| | Spot | Th (error) | U (error) | Pb (error) | Spot age, Ma (error) |
|---|---|---|---|---|---|
| 1 | C11, cv | 65.16 (0.47) | 0.67(0.04) | 0.235(0.034) | 79 (11) |
| 2 | C11, c | 65.19 (0.48) | 0.57 (0.04) | 0.243 (0.034) | 82 (11) |
| 3 | C11, i | 64.38 (0.47) | 0.55 (0.03) | 0.229 (0.034) | 78 (11) |
| 4 | C11, i | 64.98 (0.47) | 0.51 (0.04) | 0.235 (0.034) | 79 (11) |
| 5 | C 11, r | 65.33 (0.48) | 0.48 (0.04) | 0.231 (0.033) | 78 (11) |
| 6 | C10, c | 67.22 (0.49) | 0.55 (0.04) | 0.237 (0.034) | 77 (11) |
| 7 | C 10, i | 65.27 (0.48) | 0.42 (0.04) | 0.230 (0.034) | 77 (11) |
| 8 | C 10, i | 64.76 (0.47) | 0.49 (0.04) | 0.238 (0.034) | 80 (12) |
| 9 | C 10, i | 64.97 (0.47) | 0.65 (0.04) | 0.233 (0.033) | 79 (11) |
| 10 | C 15, n | 66.19 (0.48) | 0.43 (0.04) | 0.244 (0.034) | 81 (11) |
| 11 | C 15, i | 65.85 (0.48) | 0.45 (0.04) | 0.243 (0.034) | 81 (11) |
| 12 | C 15, i | 64.71 (0.47) | 0.47 (0.04) | 0.223 (0.040) | 76 (12) |

Values are given in wt %. Analytical errors (95% confidence interval) refer to counting statistics. Weighted mean is 79.0±3.2 Ma.

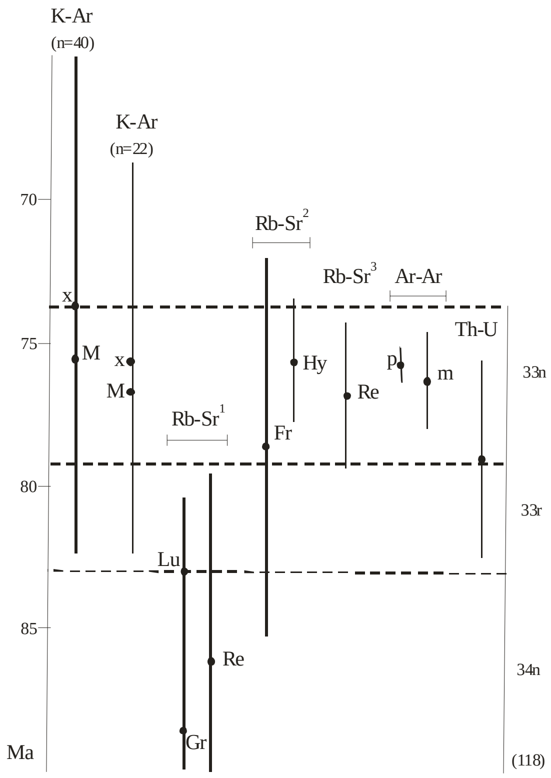


Fig. 14. Normal and reverse magnetic polarities during the Upper Cretaceous (Cande & Kent, 1994) and ages of Poços de Caldas rocks. 33n interval: 73.6-79.1 Ma; 33r interval: 79.1-83.0 Ma; 34n interval: 83.0-118 Ma. K-Ar ages, as quoted in text and Fig. 13 (for n=40 and n=22 data); x, M, mean and median values. Rb-Sr[1], Lu, Gr, Re: Rb-Sr ages for lujavrite-khibinite bodies and grey NeS; Re is reference age for all data. Rb-Sr[2]: Fr, Hy, fresh and hydrothermally altered NeS. Rb-Sr[3]: Re, reference isochron calculated from Shea's data for hydrothermally altered NeS (all data in Table 2). Ar-Ar: p, m, Ar-Ar ages for phenocrystic and groundmass micas, respectively. Th-U: thorite age with microprobe technique (Table 3). See text.

Table 4. Rb-Sr isotopic data for Poços de Caldas rocks.

| Sample | Rb | Sr | 1/Sr | $^{87}Rb/^{86}Sr)_m$ | $^{87}Sr/^{87}Sr)_m$ | $^{87}Sr/^{86}Sr)_{80}$ | $\varepsilon_{Sr(0)}$ | $\varepsilon_{Sr(80)}$ |
|---|---|---|---|---|---|---|---|---|
| NS1 | 136 | 2560 | 0.00039 | 0.1540(40) | 0.705318(10) | 0.705134(11) | 11.6 | 10.5 |
| NS2 | 135 | 1790 | 0.00056 | 0.2180(60) | 0.705675(09) | 0.705427(11) | 16.7 | 14.5 |
| NS3 | 292 | 840 | 0.00119 | 1.0060(280) | 0.706272(10) | 0.705129(33) | 25.2 | 10.3 |
| NS4 | 244 | 1770 | 0.00056 | 0.3990(110) | 0.705726(11) | 0.705272(17) | 17.4 | 12.3 |
| NS5 | 194 | 1530 | 0.00065 | 0.3670(100) | 0.705733(11) | 0.705316(16) | 17.5 | 12.9 |
| NS6 | 614 | 765 | 0.00131 | 2.3230(660) | 0.707389(11) | 0.704749(76) | 41.0 | 4.9 |
| NS7 | 197 | 3930 | 0.00025 | 0.1450(40) | 0.705195(10) | 0.705030(11) | 9.9 | 8.9 |
| NS8 | 112 | 894 | 0.00112 | 0.3630(100) | 0.705473(10) | 0.705060(15) | 13.8 | 9.3 |
| NS9 | 134 | 2750 | 0.00036 | 0.1410(40) | 0.705309(10) | 0.705149(11) | 11.5 | 10.5 |
| NS10 | 169 | 511 | 0.00196 | 0.9570(270) | 0.706169(07) | 0.705081(31) | 23.7 | 9.6 |
| T1 | 141 | 1090 | 0.00092 | 0.3740(110) | 0.705602(08) | 0.705177(15) | 15.6 | 10.9 |
| T2 | 171 | 1280 | 0.00078 | 0.3870(110) | 0.705541(10) | 0.705101(16) | 14.8 | 9.9 |
| T3 | 172 | 1310 | 0.00076 | 0.3800(110) | 0.705526(08) | 0.705094(15) | 14.6 | 9.8 |
| T4 | 172 | 1660 | 0.00060 | 0.3000(80) | 0.705504(10) | 0.705163(14) | 14.3 | 10.7 |
| T5 | 184 | 2400 | 0.00042 | 0.2220(60) | 0.705519(10) | 0.705267(12) | 14.5 | 12.2 |
| T6 | 243 | 207 | 0.00483 | 3.3980(960) | 0.709350(01) | 0.705488(110 | 68.8 | 15.4 |
| T7 | 142 | 2700 | 0.00037 | 0.1520(40) | 0.705450(10) | 0.705277(11) | 13.5 | 12.4 |
| T10 | 185 | 1640 | 0.00061 | 0.3260(90) | 0.705290(10) | 0.704919(14) | 11.2 | 7.3 |

Subscript m: measured data; subscript 809: data calculated for 80 Ma. Errors (2σ) in parenthesis as last significant figures (e.g. 0.1540±0.0040, 0.705318±0.000010, etc.).

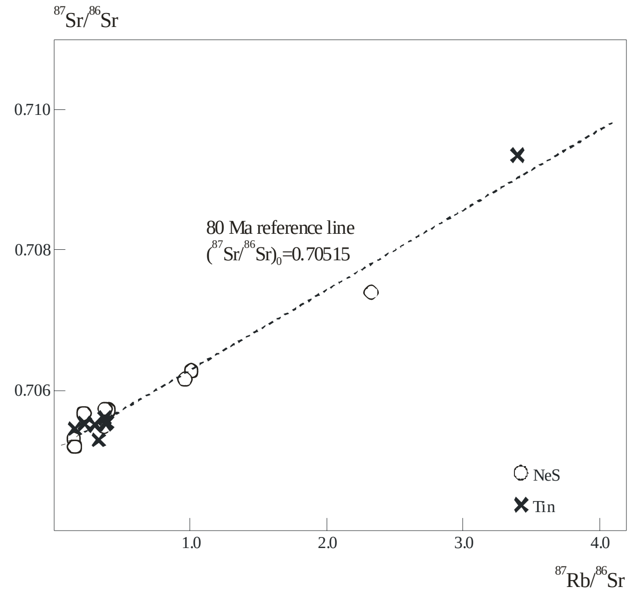


Fig. 15. $^{87}Sr/^{86}Sr$ vs. $^{87}Rb/^{86}Sr$ diagram for the PC NeS and tinguaites. Quoted initial ratio is calculated for a reference age of 80 Ma. NeS: nepheline syenite; Tin: tinguaite.

The complete set of measured $^{87}Rb/^{86}Sr$ and $^{87}Sr/^{86}Sr$ values (Table 4) plot close to an 80 Ma reference line with an initial ratio $(^{87}Sr/^{86}Sr)_{80}$ of 0.70515 (Fig. 15). The data do not fit a true isochron, on account of several possibilities (apart from laboratory errors): 1) the samples are not strictly contemporaneous; 2) various levels of crustal contamination; 3) disturbances in the Rb/Sr system by late- to post-magmatic deuteric-hydrothermal and/or supergene alteration. The second possibility can be ruled out, since the high Sr contents of these rocks, as well as the low calculated i.r. with a narrow range of variation (0.70475-0.70552), will probably not register any possible contamination that may have taken place. A similar argument can be used for the Sm-Nd isotopic data. There is no significant difference between the values obtained for NeS and tinguaites.

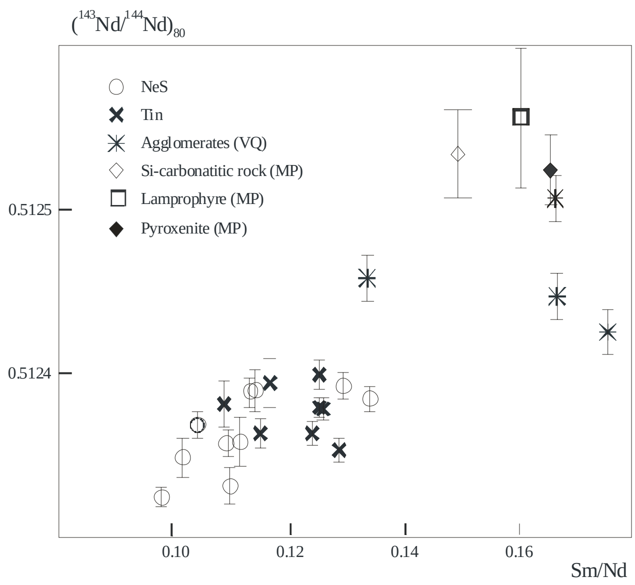


Fig. 16. $(^{143}Nd/^{144}Nd)_{80}$ vs. Sm/Nd plot for the PC felsic rocks and associated Vale do Quartel (VQ) and Minas Pedras (MP) occurrences. Error bars at 2σ. MP: Minas Pedras; VQ: Vale do Quartel.

Table 5. Sm-Nd isotopic data for Poços de Caldas rocks.

| Sample | Sm | Nd | 1/Nd | $^{147}Sm/^{143}Nd)_m$ | $^{143}Nd/^{144}Nd)_m$ | $^{143}Nd/^{144}Nd)_{80}$ | $\varepsilon_{Nd(0)}$ | $\varepsilon_{Nd(80)}$ | $f_{Sm/Nd}$ |
|---|---|---|---|---|---|---|---|---|---|
| NS1 | 22.60 | 175.00 | 0.00571 | 0.07810(30) | 0.512433(08) | 0.512392(08) | -4.0 | -2.8 | -0.60 |
| NS2 | 11.30 | 116.00 | 0.00862 | 0.05890(20) | 0.512355(06) | 0.512324(06) | -5.5 | -4.1 | -0.70 |
| NS3 | 3.67 | 35.40 | 0.028225 | 0.06270(30) | 0.512401(08) | 0.512368(08) | -4.6 | -3.3 | -0.68 |
| NS4 | 10.60 | 97.20 | 0.01029 | 0.06590(30) | 0.512392(08) | 0.512357(08) | -4.8 | -3.5 | -0.66 |
| NS5 | 2.79 | 25.50 | 0.03922 | 0.06620(30) | 0.512366(11) | 0.512331(11) | -5.3 | -4.0 | -0.66 |
| NS6 | 3.49 | 31.40 | 0.03185 | 0.06720(30) | 0.512393(15) | 0.512358(15) | -4.8 | -3.5 | -0.66 |
| NS7 | 6.96 | 61.70 | 0.01621 | 0.06820(30) | 0.512424(09) | 0.512388(09) | -4.2 | -2.9 | -0.65 |
| NS8 | 7.96 | 70.00 | 0.01429 | 0.06640(30) | 0.512424(13) | 0.512389(13) | -4.2 | -2.8 | -0.66 |
| NS9 | 19.40 | 145.00 | 0.00690 | 0.08090(30) | 0.512426(08) | 0.512384(08) | -4.1 | -3.0 | -0.59 |
| NS10 | 7.29 | 72.10 | 0.01387 | 0.06110(30) | 0.512380(12) | 0.512348(12) | -5.0 | -3.6 | -0.69 |
| T1 | 2.85 | 26.30 | 0.03802 | 0.06550(30) | 0.512415(14) | 0.512381(14) | -4.3 | -3.0 | -0.67 |
| T2 | 14.20 | 113.00 | 0.00885 | 0.07600(30) | 0.512418(07) | 0.512378(07) | -4.3 | -3.1 | -0.61 |
| T3 | 15.00 | 120.00 | 0.00833 | 0.07560(30) | 0.512419(06) | 0.512379(06) | -4.3 | -3.0 | -0.62 |
| T4 | 15.50 | 124.00 | 0.00806 | 0.07560(30) | 0.512439(09) | 0.512399(09) | -3.9 | -2.6 | -0.62 |
| T5 | 18.50 | 144.00 | 0.00694 | 0.07770(30) | 0.512394(07) | 0.512353(07) | -4.8 | -3.5 | -0.60 |
| T6 | 4.38 | 38.20 | 0.02618 | 0.06930(30) | 0.512399(09) | 0.512363(09) | -4.7 | -3.4 | -0.65 |
| T7 | 12.10 | 104.00 | 0.00962 | 0.07040(30) | 0.512431(15) | 0.512394(15) | -4.0 | -2.7 | -0.64 |
| T10 | 14.60 | 118.00 | 0.00847 | 0.97480(30) | 0.512402(07) | 0.512363(07) | -4.6 | -3.4 | -0.62 |

Subscript m: measured data; subscript 80: calculated for 80 Ma. Errors (2σ) in parenthesis as last significant figures (e.g. 0.07810±0.00030, 0.512433±0.000008, etc.)

The $(^{143}Nd/^{144}Nd)_{80}$ ratios show a moderate variation from 0.51233 to 0.51239 ($\varepsilon_{Nd}$: -2.6 to -4.5; Table 5). Three NeS stand out as the more evolved rocks (Fig. 16). The samples from the Vale do Quartel and Minas Pedras ultramafic rocks are clearly more primitive than the felsic PC rocks. With the exception of one Vale do Quartel sample, the ultramafic rocks present also higher Sm/Nd ratios, reflecting their less fractionated REE pattern (Fig. 16). There is little doubt that the felsic and ultramafic rocks from PC represent different isotopic populations. Depleted mantle model ages (De Paolo, 1981) of the felsic rocks vary within 650 and 750 Ma and present an almost normal distribution with a mean of 692±54 Ma (2σ), while the values for the Vale do Quartel and Minas Pedras samples range between 630-810 and 580-640 Ma, respectively (Fig. 17).

The correlation between $(^{87}Sr/^{86}Sr)_{80}$ and $(^{143}Nd/^{144}Nd)_{80}$ is depicted in Fig. 18. The felsic ro-cks plot to the right of, and below, the Bulk Silicate Earth (BSE) value at 80 Ma, in the lower right quadrant that corresponds to typical crustal material and to enriched mantle; they have similar Sr, but more primitive Nd isotopic characteristics than the EMI reference reservoir, and plot at the lower limit of the OIB field (cf. Zindler & Hart, 1986).

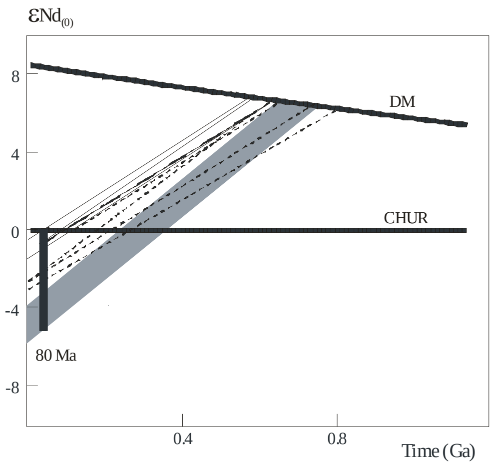


Fig. 17. Isotope evolution of εNd against time for NeS and tinguaites (shaded area). Vale do Quartel (VQ, dashed lines) and Minas Pedras (MP, full lines) data also plotted. Cf. text for references.

The Sr isotopic variations in the ultramafic rocks cover the same range as the felsic samples, with the exception of the silico-carbonatitic rocks from Minas Pedras and one of the agglomerates from Vale do Quartel. Sr and Nd data for the Lovozero and Khibina massifs, which share petrographic and geochemical characteristics with PC, emplaced about 370 Ma ago in the Kola Alkaline Province (Kramm *et al.*, 1993; Kramm & Kogarko, 1994), are also represented for comparative purposes, showing that the PC rocks have similar Nd, but more evolved Sr isotopic characteristics. The PC rocks plot to the right of the BSE reservoir, while the Khibina and Lovozero samples (at their crystallization ages) plot within the depleted mantle quadrant, as also do most carbonatites worldwide.

The PC data plot in the same quadrant as most of the Sr-Nd data of rocks belonging to the Alto Paranaíba and Serra do Mar alkaline provinces (Gibson *et al.*, 1995, 1999; Thompson *et al.*, 1998; Siebel *et al.*, 2000; Bennio *et al.*, 2002; Lustrino *et al.*, 2003; Enrich *et al.*, in this volume; Antonini *et al.*, in this volume; Comin-Chiaramonti *et al.*, in this volume), which led Lustrino *et al.* (2003) to include PC as the "westernmost massif of the Serra do Mar alkaline igneous province".

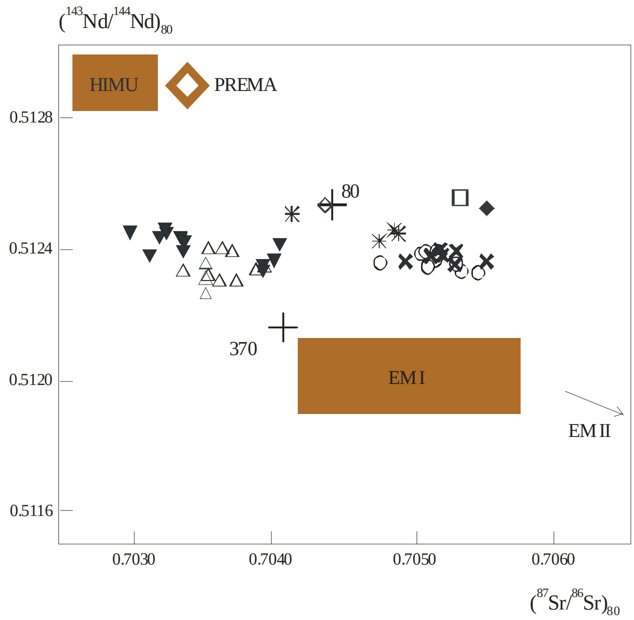


Fig. 18. Sr-Nd isotope correlation diagram for the PC felsic and ultramafic rocks, showing also the present-day composition of reference mantle reservoirs (Zindler & Hart, 1986; Hart *et al.*, 1986; cf. also Hoffmann, 1997). Inverted triangles: Khibina; upright triangles: Lovozero. Crosses are BSE compositions for indicated ages.

Table 6. Measured and calculated data for the Pb-Pb isotopes, Poços de Caldas rocks.

| Sample | U | Th | Pb | $^{206}Pb/^{204}Pb)_m$ | $^{207}Pb/^{204}Pb)_m$ | $^{208}Pb/^{204}Pb)_m$ | $^{204}Pb$ | $^{206}Pb$ | $^{207}Pb$ | $^{208}Pb$ |
|---|---|---|---|---|---|---|---|---|---|---|
| NS1 | 7.58 | 32.30 | 48 | 18.1801(55) | 15.4516(59) | 38.4829(66) | 0.0032 | 0.0576 | 0.0489 | 0.1219 |
| NS2 | 16.20 | 76.30 | 58 | 18.1951(30) | 15.4520(37) | 38.6594(46) | 0.0038 | 0.0695 | 0.0590 | 0.1476 |
| NS3 | 5.26 | 23.10 | 11 | 18.619(13) | 15.456(14) | 39.089(13) | 0.0007 | 0.0133 | 0.0111 | 0.0280 |
| NS4 | 26.10 | 99.00 | 124 | 18.1643(47) | 15.4450(59) | 38.5128(74) | 0.0082 | 0.1486 | 0.1264 | 0.3151 |
| NS5 | 7.34 | 24.00 | 48 | 18.0551(30) | 15.4416(37) | 38.3546(47) | 0.0047 | 0.0032 | 0.0491 | 0.1219 |
| NS6 | 11.50 | 27.90 | 77 | 18.0388(27) | 15.4372(27) | 38.2895(26) | 0.0051 | 0.0921 | 0.0788 | 0.1955 |
| NS7 | 8.73 | 38.50 | 40 | 18.3668(61) | 15.4772(66) | 38.6866(74) | 0.0026 | 0.0482 | 0.0406 | 0.1016 |
| NS8 | 8.04 | 36.40 | 15 | 18.3435(51) | 15.4768(44) | 38.7051(47) | 0.0010 | 0.0181 | 0.0152 | 0.0381 |
| NS9 | 7.74 | 32.70 | 24 | 18.1715(30) | 15.4463(30) | 38.4639(44) | 0.0016 | 0.0288 | 0.0245 | 0.0610 |
| NS10 | 5.72 | 30.90 | 26 | 18.3114(46) | 15.4677(50) | 38.7349(52) | 0.0017 | 0.0313 | 0.0264 | 0.0661 |
| T1 | 12.60 | 47.40 | 54 | 18.2021(45) | 15.4479(45) | 38.4814(44) | 0.0036 | 0.0649 | 0.0550 | 0.1371 |
| T2 | 6.22 | 28.60 | 28 | 18.2404(43) | 15.4541(43) | 38.5600(41) | 0.0018 | 0.0336 | 0.0285 | 0.0711 |
| T3 | 6.82 | 30.30 | 30 | 18.2777(28) | 15.4577(36) | 38.6142(44) | 0.0020 | 0.0361 | 0.0305 | 0.0762 |
| T4 | 2.87 | 31.30 | 33 | 18.0839(32) | 15.4451(37) | 38.5313(45) | 0.0022 | 0.0394 | 0.0337 | 0.0840 |
| T5 | 5.17 | 24.00 | 26 | 18.2129(80) | 15.4684(73) | 38.5648(81) | 0.0017 | 0.0312 | 0.0265 | 0.0661 |
| T6 | 13.60 | 59.90 | 67 | 18.2492(54) | 15.4619(54) | 38.5888(58) | 0.0044 | 0.0805 | 0.0682 | 0.1702 |
| T7 | 6.82 | 31.30 | 29 | 17.9773(23) | 15.4106(23) | 38.4784(24) | 0.0019 | 0.0345 | 0.0296 | 0.0739 |
| T10 | 2.78 | 30.80 | 43 | 18.1995(33) | 15.4579(37) | 38.5754(48) | 0.0028 | 0.0516 | 0.0438 | 0.1093 |

Subscript m: measured data. Errors (2σ) in parenthesis as last significant figures (e.g. 18.1801±0.0055, etc.).

Table 7. Calculated isotopic ratios for the Pb-Pb isotopes, Poços de Caldas rocks.

| Sample | $^{235}U/^{204}Pb$ | $^{238}U/^{204}P$ | $^{232}Th/^{204}P$ | $^{206}Pb/^{204}Pb)_{80}$ | $^{207}Pb/^{204}Pb)_{80}$ | $^{208}Pb/^{204}Pb)_{80}$ |
|---|---|---|---|---|---|---|
| NS1 | 0.072 | 9.979 | 43.941 | 18.0555(55) | 15.4457(59) | 38.3085(66) |
| NS2 | 0.128 | 17.696 | 86.128 | 17.9741(30) | 15.4415(37) | 38.3177(46) |
| NS3 | 0.222 | 30.651 | 139.096 | 18.2364(130) | 15.4380(137) | 38.5372(134) |
| NS4 | 0.097 | 13.302 | 52.140 | 17.99982(47) | 15.4371(59) | 38.3059(74) |
| NS5 | 0.070 | 9.628 | 32.532 | 17.9349(30) | 15.4359(37) | 38.2255(47) |
| NS6 | 0.068 | 9.393 | 23.547 | 17.9215(27) | 15.4316(27) | 38.1961(26) |
| NS7 | 0.101 | 13.870 | 63.208 | 18.1936(61) | 15.4689(66) | 38.4358(74) |
| NS8 | 0.247 | 34.061 | 159.349 | 17.9182(51) | 15.4565(44) | 38.0728(47) |
| NS9 | 0.148 | 20.370 | 88.930 | 17.9171(30) | 15.4342(30) | 38.1110(44) |
| NS10 | 0.101 | 13.978 | 79.030 | 18.1369(46) | 15.4594(50) | 38.4253(52) |
| T1 | 0.107 | 14.748 | 57.331 | 18.0179(45) | 15.4391(45) | 38.2539(44) |
| T2 | 0.102 | 14.064 | 66.826 | 18.0648(43) | 15.4458(43) | 38.2948(41) |
| T3 | 0.105 | 14.412 | 66.164 | 18.0977(28) | 15.4491(36) | 38.3517(44) |
| T4 | 0.040 | 5.492 | 61.890 | 18.0153(32) | 15.4418(37) | 38.2857(45) |
| T5 | 0.093 | 12.831 | 60.385 | 18.0527(80) | 15.4608(73) | 38.3252(81) |
| T6 | 0.093 | 12.859 | 58.527 | 18.0886(54) | 15.4543(54) | 38.3266(58) |
| T7 | 0.107 | 14.811 | 70.240 | 17.7924(23) | 15.4018(23) | 38.1997(24) |
| T10 | 0.030 | 4.092 | 46.848 | 18.1484(33) | 15.4555(37) | 38.3895(48) |

Subscripts: m: measured; 80: calculated for 80 Ma. Errors (2σ) in parenthesis as last significant figures (e.g. 18.0555±0.0055).

The $(^{206}Pb/^{204}Pb)_{80}$, $(^{207}Pb/^{204}Pb)_{80}$ and $(^{208}Pb/^{204}Pb)_{80}$ isotopic ratios for the NeS and tinguaites are similar and range between 17.9-18.3, 15.43-15.48 and 38.10-38.55, respectively (Tables 6 and 7). With the exception of two NeS and one tinguaite, which in part plot close to the Geochron, $(^{207}Pb/^{204}Pb)_{80}$ and $(^{208}Pb/^{204}Pb)_{80}$ show a good positive correlation with $(^{206}Pb/^{204}Pb)_{80}$. In the $(^{207}Pb/^{204}Pb)_{80}$ vs. $(^{206}Pb/^{204}Pb)_{80}$ diagram, the data plot to the right of the NHRL (Northern Hemisphere Reference Line; e.g. Zindler & Hart, 1986), as is also typical of OIB samples, and define a ca. 2.2 Ga reference line, which probably represents a mixing array (Fig. 19). In Fig. 20, a plot of $(^{87}Sr/^{86}Sr)_{80}$ vs $(^{206}Pb/^{204}Pb)_{80}$, the data cluster relatively close to the EMI reference reservoir.

Several general conclusions can be drawn from the analysis of these data: 1) the clustering of isotopic data in all diagrams indicates that NeS and tinguaites are cogenetic, confirming inferences from geological and petrographic observations, and clearly show that the Vale do Quartel and Minas Pedras mafic-ultramafic rocks belong to a different lineage (or lineages); 2) little post-magmatic change was brought about by late deuteric/hydrothermal alteration, which affected more the NeS than the finer-grained felsic rocks (cf. Petrography); 3) crustal contamination probably did not play a significant role in magma evolution, given the rather low initial ratios obtained for the Rb/Sr isotopes (but see comments below); 4) the $(Sr/Nd)_{80}$ data are represented in the quadrant that is characteristic of rocks that have derived from enriched mantle (whether lithospheric or sublithospheric).

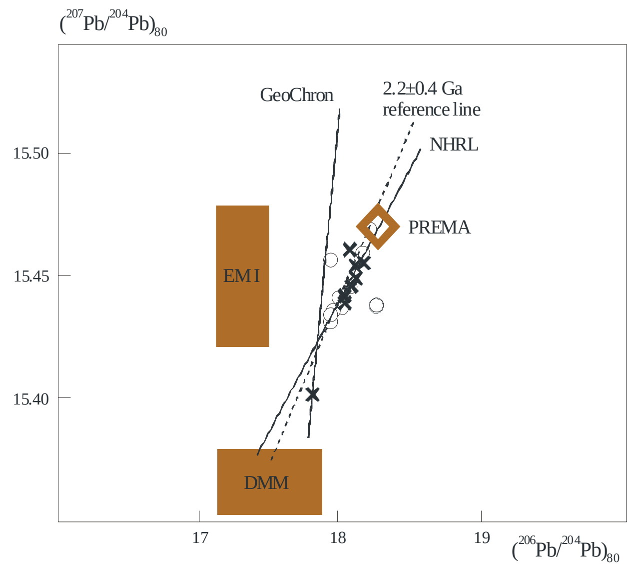


Fig. 19. $(^{207}Pb/^{204}Pb)_{80}$ vs. $(^{206}Pb/^{204}Pb)_{80}$ diagram showing the distribution for the felsic PC rocks and the present-day composition of some mantle reservoirs. Symbols as in Fig. 15. NHRL: northern hemisphere reference line. Mantle reservoirs as cited in Fig. 18.

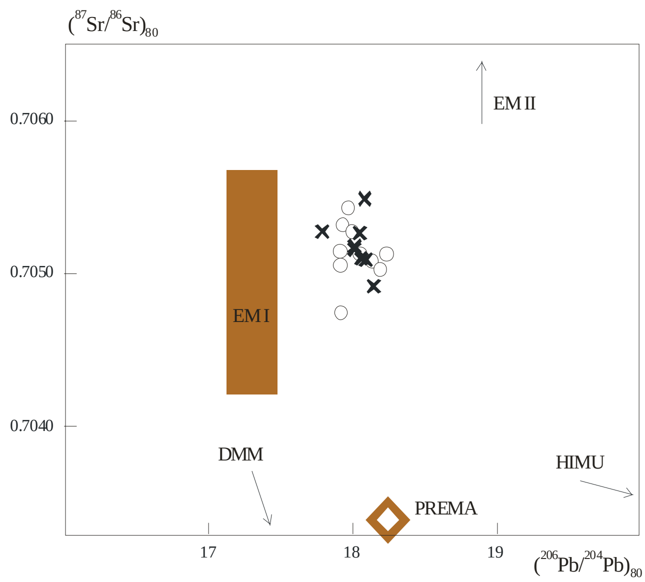


Fig. 20. $(^{87}Sr/^{86}Sr)_{80}$ vs. $(^{206}Pb/^{204}Pb)_{80}$ diagram indicating the distribution of the PC felsic rocks. Symbols and reservoirs as in previous figures.

Table 8. Representative chemical analysis of nepheline syenites (NeS) and tinguaites (T), Poços de Caldas.

| Nr | NeS1 Pedreira NeS, Pref. quarry | NeS2 Botelhos khibinite | NeS3 Fluorite gray NeS | NeS4 P.Balão khibinite | NeS5 P.Balão lujavrite | NeS6 Gray NeS | NeS7 Serrote eud. NeS | NeS8 Porph. NeS | NeS9 Pedreira NeS |
|---|---|---|---|---|---|---|---|---|---|
| $SiO_2$ | 52.34 | 51.00 | 53.20 | 52.82 | 51.44 | 55.85 | 52.83 | 53.92 | 52.96 |
| $TiO_2$ | 0.89 | 0.72 | 0.45 | 0.43 | 0.46 | 0.24 | 0.67 | 0.31 | 0.92 |
| $Al_2O_3$ | 19.49 | 16.38 | 20.94 | 19.52 | 15.23 | 20.80 | 20.76 | 20.65 | 19.07 |
| $Fe_2O_3$ | 4.59 | 8.27 | 3.97 | 4.44 | 11.22 | 2.38 | 3.72 | 3.31 | 4.69 |
| MnO | 0.27 | 0.53 | 0.17 | 0.40 | 0.46 | 0.11 | 0.28 | 0.25 | 0.28 |
| MgO | 0.47 | 0.30 | 0.18 | 0.13 | 0.56 | 0.04 | 0.29 | 0.15 | 0.50 |
| CaO | 2.08 | 2.92 | 0.89 | 1.57 | 2.53 | 0.66 | 1.70 | 1.16 | 2.15 |
| $Na_2O$ | 7.35 | 7.99 | 7.17 | 9.38 | 8.65 | 5.15 | 7.67 | 7.55 | 6.96 |
| $K_2O$ | 7.54 | 5.45 | 9.59 | 7.62 | 5.57 | 12.45 | 9.29 | 7.37 | 7.46 |
| $P_2O_5$ | 0.15 | 0.04 | 0.03 | 0.05 | n.d. | 0.02 | 0.08 | 0.03 | 0.13 |
| L.O.I. | 3.78 | 5.09 | 2.13 | 2.41 | 2.73 | 1.08 | 2.76 | 5.54 | 3.77 |
| Total | 98.94 | 98.69 | 98.71 | 98.77 | 98.86 | 98.76 | 100.04 | 100.24 | 98.88 |
| V | 81 | 165 | 72 | 66 | 286 | 35 | 88 | 58 | 88 |
| Zn | 203 | 347 | 139 | 177 | 347 | 173 | 192 | 133 | 144 |
| Ga | 36 | 43 | 40 | 60 | 51 | 42 | 35 | 37 | 35 |
| Rb | 138 | 135 | 292 | 244 | 194 | 614 | 197 | 112 | 134 |
| Sr | 2560 | 1790 | 840 | 1770 | 1530 | 765 | 3930 | 894 | 2750 |
| Y | 63.7 | 61.4 | 21.1 | 76.9 | 21.8 | 18.7 | 36.6 | 36.2 | 59.4 |
| Zr | 854 | 2320 | 728 | 4160 | 4450 | 1360 | 725 | 1110 | 875 |
| Nb | 235 | 532 | 127 | 614 | 368 | 184 | 242 | 217 | 251 |
| Cs | 2.0 | 3.2 | 4.3 | 5.6 | 7.3 | 2.6 | 1.8 | 1.2 | 1.8 |
| Ba | 535 | 144 | 75 | 286 | 132 | 236 | 1200 | 29 | 561 |
| La | 377 | 605 | 186 | 526 | 147 | 107 | 301 | 324 | 346 |
| Ce | 562 | 834 | 268 | 700 | 158 | 154 | 432 | 487 | 599 |
| Pr | 55.9 | 49.1 | 15.2 | 40.3 | 11.2 | 12.1 | 24.8 | 28.9 | 46.6 |
| Nd | 175 | 116 | 35.4 | 97.2 | 25.5 | 31.4 | 61.7 | 70.0 | 145 |
| Sm | 22.6 | 11.3 | 3.67 | 10.6 | 2.79 | 3.49 | 6.96 | 7.69 | 19.4 |
| Eu | 6.55 | 3.13 | 1.03 | 3.12 | 0.78 | 0.98 | 2.12 | 2.33 | 5.72 |
| Gd | 16.9 | 7.70 | 2.52 | 7.89 | 2.09 | 2.40 | 4.32 | 6.09 | 12.7 |
| Tb | 2.28 | 1.34 | 0.46 | 1.51 | 0.41 | 0.44 | 0.86 | 1.08 | 2.12 |
| Dy | 11.74 | 8.16 | 2.84 | 9.89 | 2.56 | 2.49 | 5.37 | 6.85 | 11.4 |
| Ho | 2.18 | 1.73 | 0.61 | 2.22 | 0.60 | 0.51 | 1.15 | 1.48 | 2.08 |
| Er | 6.24 | 5.70 | 2.21 | 8.17 | 2.30 | 1.73 | 3.87 | 4.74 | 5.97 |
| Tm | 0.826 | 0.930 | 0.383 | 1.42 | 0.421 | 0.303 | 0.647 | 0.735 | 0.831 |
| Yb | 4.96 | 5.93 | 2.52 | 9.63 | 3.02 | 2.01 | 4.13 | 4.73 | 5.14 |
| Lu | 0.582 | 0.799 | 0.371 | 1.47 | 0.510 | 0.280 | 0.591 | 0.644 | 0.564 |
| Hf | 16.2 | 35.7 | 14.7 | 71.5 | 82.4 | 22.9 | 13.4 | 21.2 | 19.2 |
| Ta | 15.0 | 8.91 | 4.09 | 12.4 | 8.33 | 4.75 | 6.77 | 7.13 | 15.5 |
| Tl | 0.42 | 0.65 | 0.60 | 0.66 | 0.70 | 0.48 | 0.50 | 0.28 | 0.25 |
| Pb | 48 | 58 | 11 | 124 | 48 | 77 | 40 | 15 | 24 |
| Th | 32.3 | 76.3 | 23.1 | 99.0 | 24.0 | 27.9 | 38.5 | 36.4 | 32.7 |
| U | 7.58 | 16.2 | 5.26 | 26.1 | 7.34 | 11.5 | 8.73 | 8.04 | 7.74 |
| K/Na1 | 1.025 | 0.68 | 1.34 | 0.81 | 0.64 | 2.42 | 1.21 | 0.98 | 1.07 |
| K/Na2 | 0.67 | 0.45 | 0.88 | 0.53 | 0.42 | 1.59 | 0.80 | 0.64 | 0.71 |
| A.I. | 1.04 | 1.16 | 1.06 | 1.21 | 1.33 | 1.06 | 1.09 | 0.99 | 1.02 |

Table 8 (continued).

| Nr | NeS10 Gray NeS | T1 Dike, Pref. quarry | T2 Northern rim | T3 N ring, outer part | T4 Cascata tinguaite | T5 Rio das Antas tinguaite | T6 Eastern ring tinguaite | T7 Minas Pedras tinguaite | T10 Southern ring tinguaite |
|---|---|---|---|---|---|---|---|---|---|
| $SiO_2$ | 53.51 | 54.98 | 54.90 | 54.94 | 56.92 | 53.58 | 53.98 | 53.61 | 56.00 |
| $TiO_2$ | 0.27 | 0.40 | 0.54 | 0.55 | 0.60 | 0.77 | 0.56 | 0.66 | 0.59 |
| $Al_2O_3$ | 21.38 | 20.81 | 20.55 | 20.45 | 21.14 | 19.89 | 19.82 | 19.83 | 21.09 |
| $Fe_2O_3$ | 3.15 | 3.26 | 3.75 | 3.80 | 3.81 | 4.11 | 4.14 | 4.66 | 3.80 |
| MnO | 0.23 | 0.21 | 0.25 | 0.26 | 0.24 | 0.24 | 0.25 | 0.27 | 0.24 |
| MgO | 0.13 | 0.19 | 0.24 | 0.23 | 0.26 | 0.37 | 0.28 | 0.29 | 0.25 |
| CaO | 0.95 | 1.04 | 1.51 | 1.56 | 1.37 | 2.05 | 0.90 | 1.86 | 1.37 |
| $Na_2O$ | 8.12 | 8.08 | 8.15 | 7.96 | 5.98 | 7.34 | 9.51 | 8.30 | 6.20 |
| $K_2O$ | 8.20 | 7.13 | 8.35 | 8.77 | 8.35 | 8.59 | 7.01 | 8.48 | 8.13 |
| $P_2O_5$ | 0.03 | 0.03 | 0.05 | 0.05 | 0.10 | 0.10 | 0.04 | 0.09 | 0.07 |
| L.O.I. | 3.63 | 3.21 | 0.89 | 1.16 | 1.42 | 1.65 | 2.68 | 1.35 | 1.12 |
| Total | 99.59 | 99.33 | 99.18 | 99.72 | 100.20 | 98.65 | 99.16 | 99.38 | 98.65 |
| V | 42 | 41 | 66 | 62 | 70 | 90 | 42 | 94 | 69 |
| Zn | 175 | 168 | 178 | 179 | 170 | 169 | 191 | 183 | 189 |
| Ga | 39 | 42 | 39 | 38 | 34 | 35 | 45 | 39 | 37 |
| Rb | 169 | 141 | 171 | 172 | 172 | 184 | 243 | 142 | 185 |
| Sr | 511 | 1090 | 1280 | 1310 | 1660 | 2400 | 207 | 2700 | 1640 |
| Y | 44.2 | 22.6 | 44.8 | 47.4 | 48.6 | 49.2 | 34.2 | 50.5 | 48.1 |
| Zr | 926 | 1460 | 952 | 975 | 679 | 782 | 1710 | 1050 | 673 |
| Nb | 198 | 217 | 224 | 210 | 227 | 244 | 323 | 245 | 246 |
| Cs | 1.4 | 1.8 | 2.1 | 2.2 | 2.3 | 2.6 | 4.8 | 1.4 | 2.5 |
| Ba | 16 | 26 | 32 | 34 | 74 | 186 | 3 | 548 | 81 |
| La | 347 | 200 | 282 | 305 | 321 | 297 | 260 | 309 | 307 |
| Ce | 531 | 229 | 500 | 528 | 564 | 563 | 319 | 495 | 529 |
| Pr | 31.4 | 11.7 | 38.2 | 39.1 | 40.9 | 45.3 | 16.8 | 36.5 | 39.0 |
| Nd | 72.1 | 26.3 | 113 | 120 | 124 | 144 | 38.2 | 104 | 118 |
| Sm | 7.29 | 2.85 | 14.2 | 15.0 | 15.5 | 18.5 | 4.38 | 12.1 | 14.6 |
| Eu | 2.03 | 0.851 | 4.08 | 4.20 | 4.38 | 5.39 | 1.26 | 3.66 | 4.15 |
| Gd | 5.39 | 1.86 | 10.0 | 9.84 | 9.86 | 13.3 | 3.40 | 9.00 | 10.3 |
| Tb | 1.06 | 0.41 | 1.60 | 1.71 | 1.74 | 1.95 | 0.69 | 1.50 | 1.74 |
| Dy | 6.93 | 2.80 | 8.38 | 8.93 | 9.43 | 9.91 | 4.55 | 8.19 | 8.97 |
| Ho | 1.53 | 0.66 | 1.59 | 1.67 | 1.74 | 1.80 | 1.08 | 1.64 | 1.70 |
| Er | 5.21 | 2.51 | 4.70 | 4.87 | 5.22 | 5.06 | 3.96 | 5.06 | 5.13 |
| Tm | 0.804 | 0.455 | 0.624 | 0.679 | 0.739 | 0.622 | 0.678 | 0.690 | 0.703 |
| Yb | 4.65 | 3.14 | 3.73 | 4.05 | 4.44 | 3.60 | 4.71 | 4.15 | 4.19 |
| Lu | 0.603 | 0.509 | 0.460 | 0.480 | 0.536 | 0.385 | 0.723 | 0.555 | 0.526 |
| Hf | 16.2 | 23.0 | 18.0 | 19.2 | 17.8 | 17.2 | 28.5 | 20.2 | 17.5 |
| Ta | 9.55 | 3.91 | 13.8 | 14.6 | 15.7 | 17.5 | 7.03 | 10.5 | 14.9 |
| Tl | 0.44 | 0.41 | 0.17 | 0.17 | 0.32 | 0.26 | 0.64 | 0.23 | 0.31 |
| Pb | 26 | 54 | 28 | 30 | 33 | 26 | 67 | 29 | 43 |
| Th | 30.9 | 47.4 | 28.6 | 30.3 | 31.3 | 24.0 | 59.9 | 31.3 | 30.8 |
| U | 5.72 | 12.6 | 6.22 | 6.82 | 2.87 | 5.27 | 13.6 | 6.82 | 2.78 |
| Na/K1 | 1.01 | 0.88 | 1.02 | 1.10 | 1.40 | 1.17 | 0.74 | 1.02 | 1.31 |
| Na/K2 | 0.66 | 0.58 | 0.67 | 0.72 | 0.92 | 0.77 | 0.48 | 0.67 | 0.86 |
| A.I. | 1.04 | 1.01 | 1.09 | 1.11 | 0.89 | 1.08 | 1.17 | 1.15 | 0.90 |

K/Na1, K/Na2: $K_2O/Na_2O$ (weight % ratios) and $K_2O/Na_2O$ (molar ratios), respectively. A.I., agpaitic index. Major and minor elements: weight %, others in ppm. Abbreviations: P, Pref, porph, NeS, respectively Pedra, Prefeitura, porphyritic and nepheline syenite. n.d.: not detected.

Table 9. Poços de Caldas felsic rocks: means and ranges of major and trace elements.

| | NeS (24) | Phon (15) | | NeS | Phon |
|---|---|---|---|---|---|
| $SiO_2$ | *53.55* | *54.82* | Ba (7) | 16-1200 | 3-548 |
| $TiO_2$ | *0.52* | *0.53* | Rb (0.6) | 92-614 | 91-243 |
| $Al_2O_3$ | *19.58* (15.23-21.87) | *20.28* (19.49-21.14) | Sr (21) | 410-6360 | 207-2700 |
| $Fe_2O_{3\ total}$ | 2.38-11.22 | 3.26-4.66 | Ta (0.04) | 1.98-17.5 | 2.70-17.50 |
| MnO | *0.30* (0.10-0.56) | *0.26* (0.21-0.34) | Nb (0.71) | 127-1000 | 198-323 |
| MgO | *0.22* (0.04-0.56) | *0.27* (0.15-0.43) | Hf (0.31) | 7.7-82.4 | 17.20-29.00 |
| CaO | *1.63* (0.45-3.42) | *1.41* (0.90-2.05) | Zr (11.2) | 383-4450 | 673-1710 |
| $Na_2O$ | *7.74* (5.15-10.15) | *7.76* (5.98-9.51) | Y (4.6) | ago/77 | 23-51 |
| $K_2O$ | *8.05* (5.45-12.45) | *7.80* (6.21-8.77) | Th (0.085) | 18.7-124 | 24.0-59.90 |
| $P_2O_5$ | *0.05* (0.01-0.15) | *0.06* (0.02-0.10) | U (0.021) | 2.78-30.60 | 2.78-13.60 |
| L.O.I. | *2.92* (1.08-5.54) | *2.41* (0.89-5.42) | Pb (0.07) | nov/77 | set/67 |
| Ni (2100) | n.d. | n.d. | La (0.7) | 75.6-1080 | 196-321 |
| Cr (3011) | n.d. | n.d. | Ce (1.8) | 81-1450 | 229-564 |
| Co (105) | n.d. | n.d. | Nd (1.354) | 11.30- | 26.30- |
| Cu (28.5) | n.d. | n.d. | Sm (0.444) | 1.57-23.90 | 2.85-18.50 |
| V (82) | 30-286 | 41-94 | Yb (0.49) | 0.93-13.40 | 3.14-5.60 |
| Zn (48.5) | 101-514 | 159-237 | Lu (0.07) | 0.12-2.00 | 0.35-0.75 |

Mean values in italics. NeS and Phon: respectively, nepheline syenites and subvolcanic phonolites (tinguaites); in parenthesis, number of selected samples for means and ranges. n.d.: not detected. In parenthesis, after symbol of trace elements: estimated values for primitive mantle (Sun & McDonough, 1989; V, Zn, Ni, Co, Cr, Cu, after Wänke *et al.*, 1984). Source: data in Table 1 and unpublished own data. For further chemical data on PC syenites and phonolites, cf. Shea & Schorscher (1992), Alves (2003) and Gomes *et al.* (unpublished data on PC rocks; work in progress, 2003).

Table 10. Poços de Caldas ultrabasic rocks: means and ranges of major and trace elements.

| | | | |
|---|---|---|---|
| $SiO_2$ | *39.47* | Ba (7) | 644-1433 |
| $TiO_2$ | *4.90* | Rb (0.6) | 51-81 |
| $Al_2O_3$ | *12.01* | Sr (21) | 674-2152 |
| $Fe_2O_{3\ total}$ | *13.69* | Ta (0.04) | 6.1-8.8 |
| MnO | *0.20* | Nb (0.71) | 97.0-128.0 |
| MgO | *6.12* | Hf (0.31) | 8.8-10.4 |
| CaO | *13.07* (9.94-19.16) | Zr (11.2) | 351-404 |
| $Na_2O$ | *3.66* | Y (4.5) | 31-38 |
| $K_2O$ | *1.74* | Th (0.085) | 9.9-15.0 |
| $P_2O_5$ | *0.95* | U (0.021) | 1.6-2.9 |
| L.O.I. | *4.96* (3.42-6.02) | Pb (0.07) | 0-8 |
| Ni (2100) | 35-79 | La (0.7) | 83.6-103 |
| Cr (3011) | 58-129 | Ce (1.8) | 167-218 |
| Co (105) | 35-48 | Yb (0.49) | 1.8-2.5 |
| Cu (28.5) | | Lu (0.07) | 0.23-0.32 |

Rocks from the Vale do Quartel (n=5; cf. also analytical data in Thompson *et al*., 1998). Means in italics. In parenthesis, after symbol of element, estimated values for primitive mantle (Sun & McDonough, 1985; Ni, Cr, Co and Cu, after Wänke *et al.*, 1984).

## PETROCHEMISTRY

The chemical data of the PC *felsic* rocks used for isotope studies are presented in Table 8; mean values for major elements and ranges for the trace elements are listed in Table 9. Element means and ranges of *ultrabasic* rocks from the Vale do Quartel are presented in Table 10. Variation diagrams of the set of data are depicted in Figs. 21 and 22, showing a bimodal distribution, as it is obvious in the case of modal compositions; no intermediate members between the felsic and ultramafic assemblages are found in PC at the present outcrop level. Fig. 23 depicts the Na-K relationships in these rocks, and Fig. 24 is a TAS diagram (Cox *et al.*, 1979). Fig. 25 shows the extreme range in trace elements (against La). Figs. 26 and 27 are REE diagrams and trace element variograms, which can be used, along with the previous figures, to define a frame of reference, together with isotopic information (cf. previous

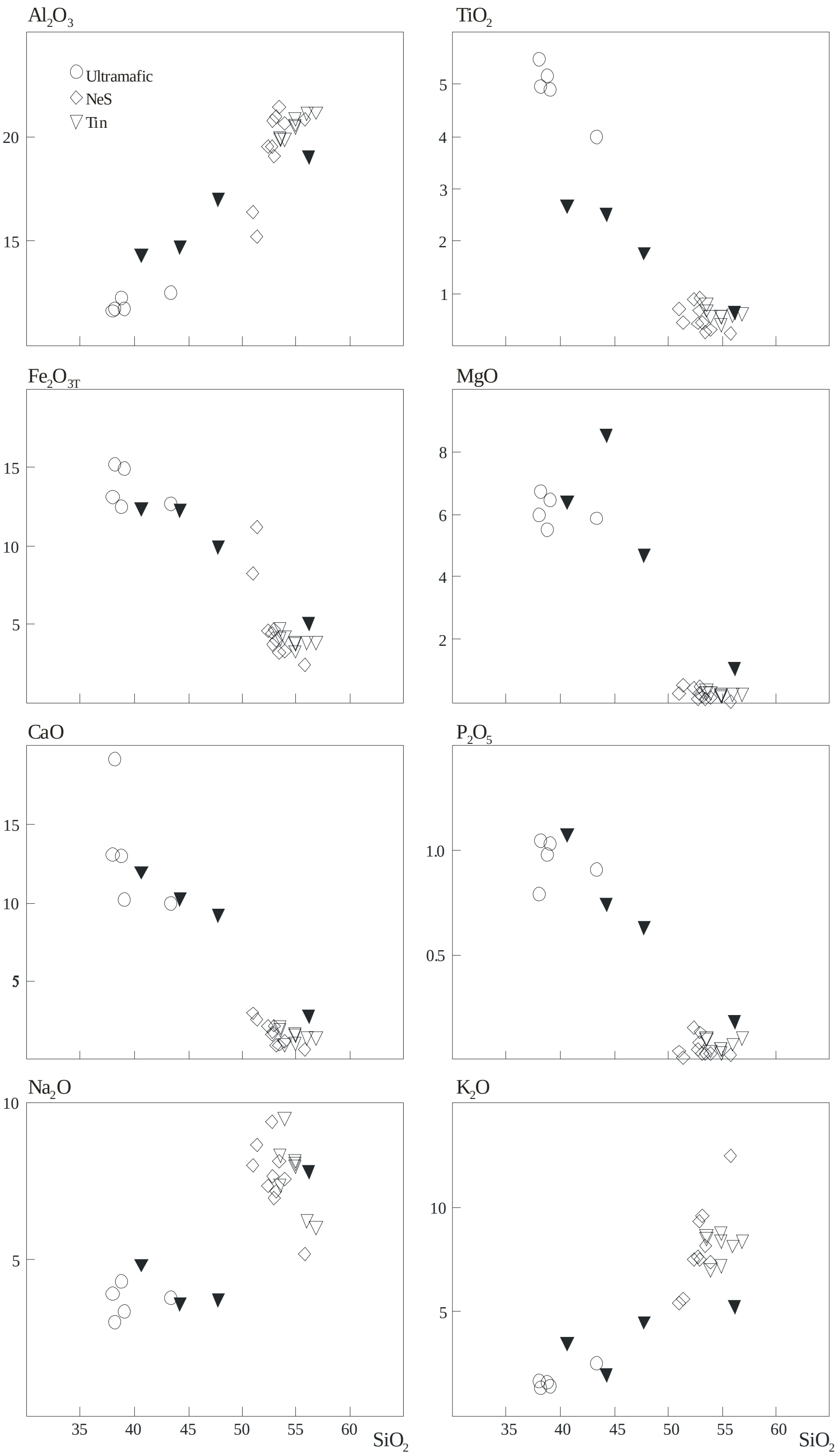


Fig. 21. Variation diagrams for PC rocks (major and minor oxides vs. $SiO_2$). Filled triangles represent the average nephelinite, basanite, tephrite and phonolite (Le Maitre, 1976), in order of increasing $SiO_2$ contents. Ultramafic: ultramafic rocks, Vale do Quartel; NeS: nepheline syenites; tin: tinguaites.

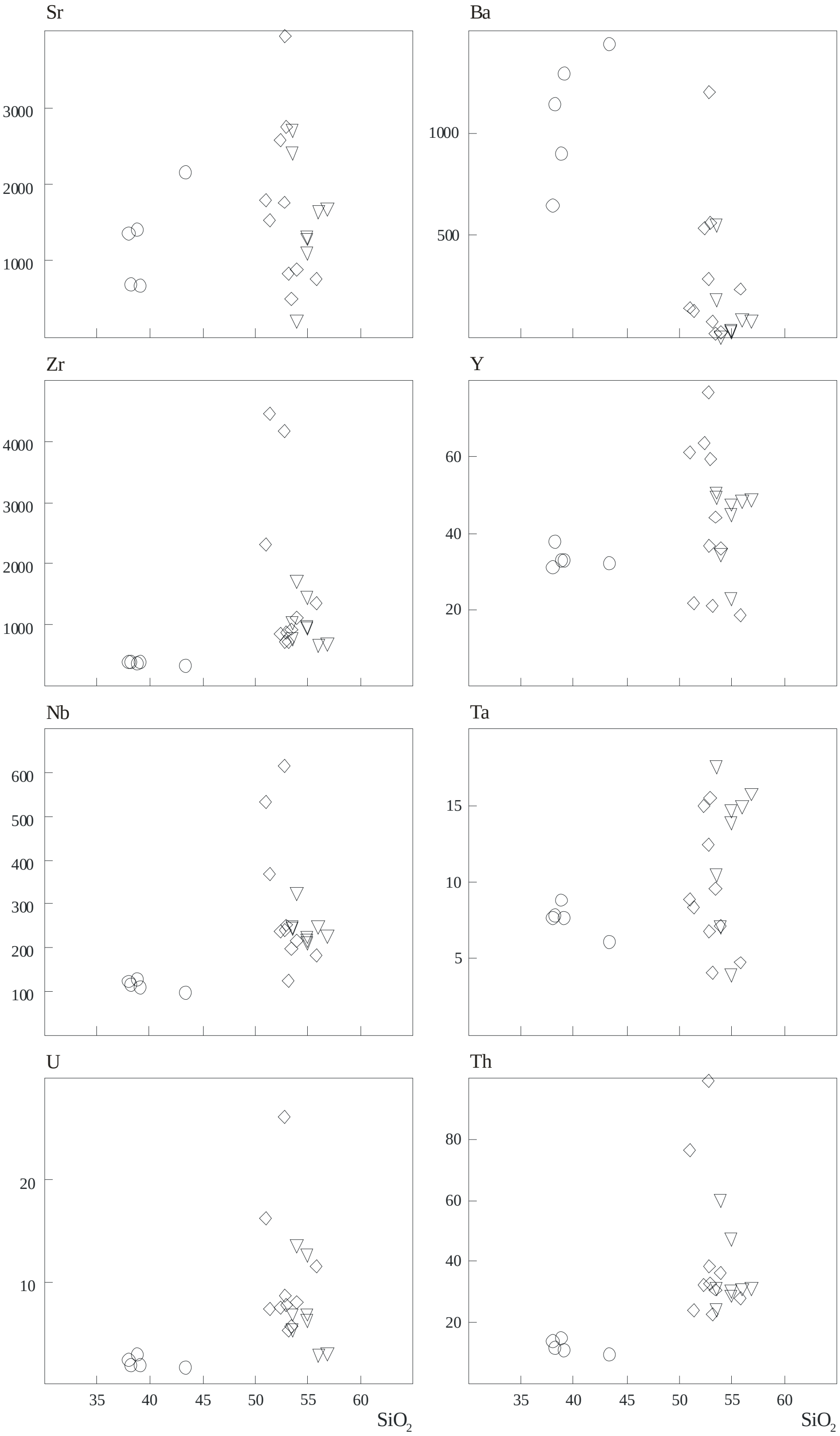


Fig. 22. Representative trace element contents in PC rocks (vs. $SiO_2$). Symbols as in Fig. 21.

item), for petrological statements. All figures were drawn using directly the data listed in the tables.

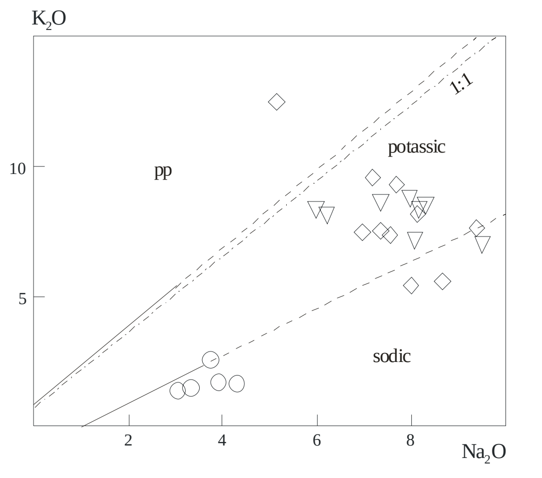


Fig. 23. $K_2O$ vs. $Na_2O$ plot of PC rocks. The lines limiting the sodic, potassic and perpotassic (pp) fields (weight proportions) are after Middlemost (1975). The "1:1" dashed line represents equal molar proportions. Symbols as in Fig. 21.

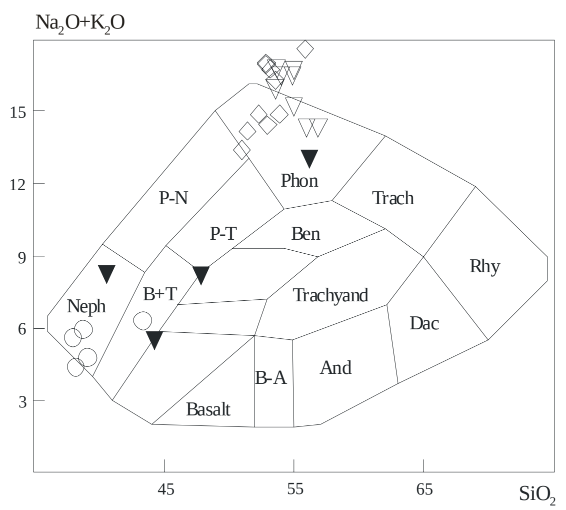


Fig. 24. TAS (total alkali-silica) diagram (after Cox *et al.*, 1979). Average nephelinite, tephrite, basanite and phonolite plotted as filled triangles (Le Maitre, 1978). Symbols as in Fig. 21.

Fig. 23 shows that the felsic PC rocks are mostly "sodic" to "potassic" (Middlemost, 1975; weight proportions). Actually, on a molar basis, most tinguaites and intermediate to agpaitic differentiated NeS present molar $Na_2O$ predominant over molar $K_2O$. Rocks with high molar $K_2O$ are less frequent, as shown by some of the less differentiated varieties of NeS (gray and fluorite NeS of the northern rim, southern biotite NeS, some typical Pedreira NeS; unpublished data, cf. Ulbrich, 1984a), on account of a large predominance of modal K-feldspar over nepheline; both these data and textures suggest the possibility of late K enrichment especially in NeS, as well as of some trace elements, during deuteric alteration (cf. also Fig. 25).

In the TAS diagram (Fig. 24) the ultrabasic rocks plot within, or close to, the nephelinite field, and the NeS and tinguaites spread across the phonolite field and into adjacent alkaline-rich areas. It should be noted that in the Le Bas and Le Maitre version of the TAS diagram (e.g. Le Bas *et al.*, 1986; Le Maitre *et al.*, 1989), the PC nephelinites (as well as the Fernando de Noronha melanephelinites, Ulbrich *et al.* 2004; also Trindade rocks, Marques *et al.*, 1999) plot within the basanite-tephrite field. These latter diagrams should not be used to represent basanites, tephrites and also nephelinites, since they can lead to a misguided "petrochemical" scheme of classification, so that, for instance, nephelinites may be erroneously classified as basanites or tephrites, although no modal plagioclase is present in the rocks.

Tinguaites, being usually rather fresh rocks, best represent the original magmas, while almost all NeS show clear signs of incipient and sometimes widespread deuteric alteration. Accordingly, chemical data for tinguaites clearly indicate that the *felsic* PC rocks have derived from magmas that were enriched in most "incompatible" (HFS and LILE) elements (Fig. 25), and extremely depleted in the "compatible" ones, such as Co, Cu, Ni and Cr (as well as in MgO; Table 8). Furthermore, data for tinguaites are less scattered than those for NeS, again suggesting that variations in the NeS may be related to late magmatic deuteric alteration (e.g. extreme enrichment in La, Ba, U, Th, Zr, also in $K_2O$, in some NeS; Fig. 25). Nb and Ta are also enriched in PC rocks, certainly an inheritance of the original magmas (or protoliths) that gave rise to NeS and tinguaites. Even so, Nb values are very high in a few NeS, as is La, suggesting mobility of La as well as Nb under high temperature alteration conditions (Fig. 25).

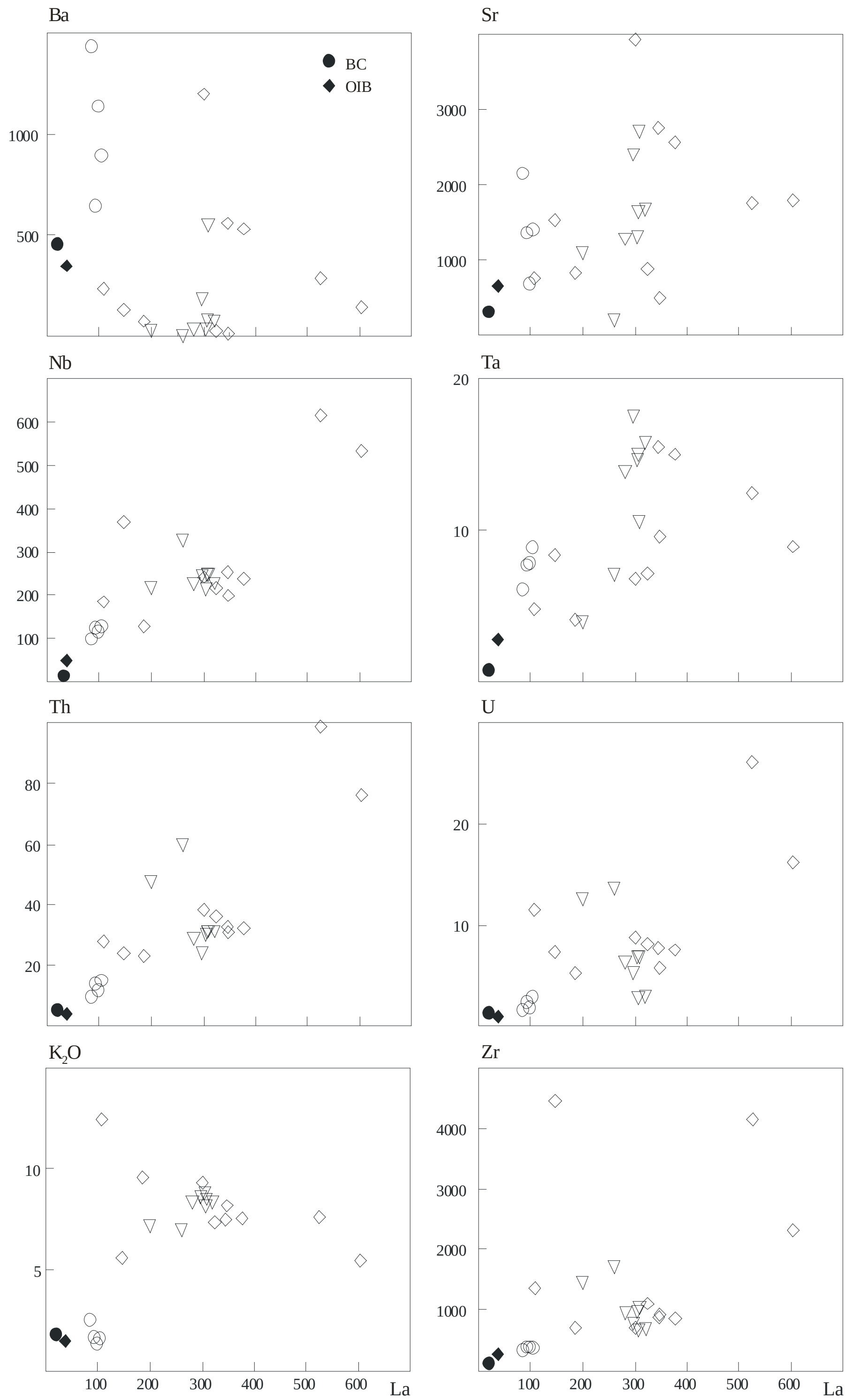


Fig. 25. Trace element and $K_2O$ contents (vs. La) for PC rocks. For comparative purposes, N-MORB and OIB (after Sun & McDonough, 1989) and average upper and bulk continental crusts (UC, BC, after Rudnick & Gao, 2004) are also indicated. BC: bulk continental crustal average (Rudnick & Gao, 2004; also); OIB after Sun & McDonough (1989).

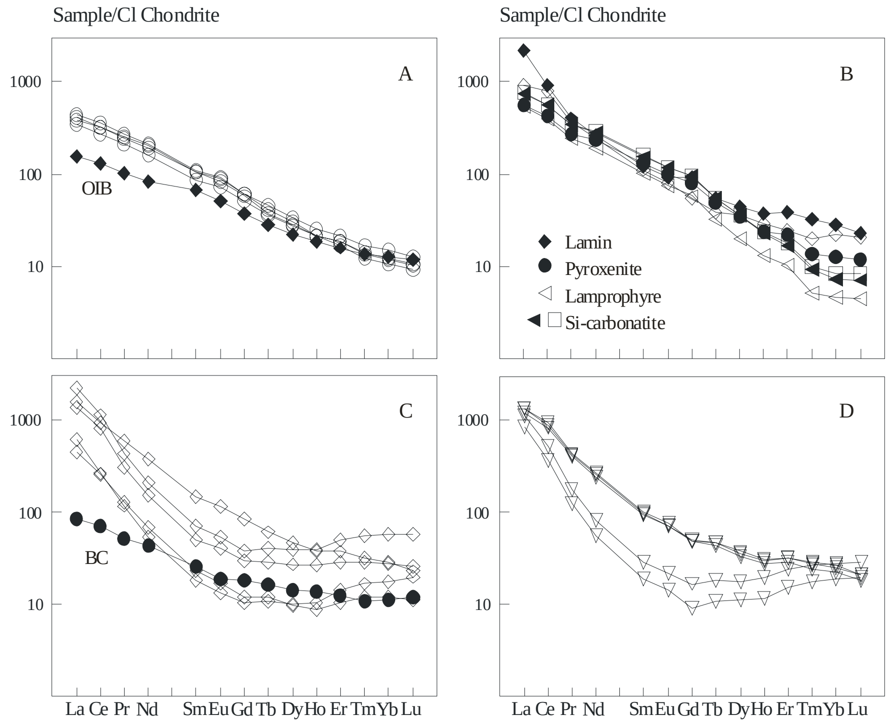


Fig. 26. C1-chondrite normalized REE patterns (after Sun & McDonough, 1989) for selected PC rocks. A) Vale do Quartel ultramafic rocks; OIB after Sun & McDonough (1989). B) Minas Pedras dyke rocks; lamin: laminated rock; Si-carbonatitic: silico-carbonatitic samples (cf. Petrography) C) Nepheline syenites (n=5) and BC, bulk continental crust (Rudnick & Gao, 2004); D) T, tinguaites (n=5). Other references in Fig. 21.

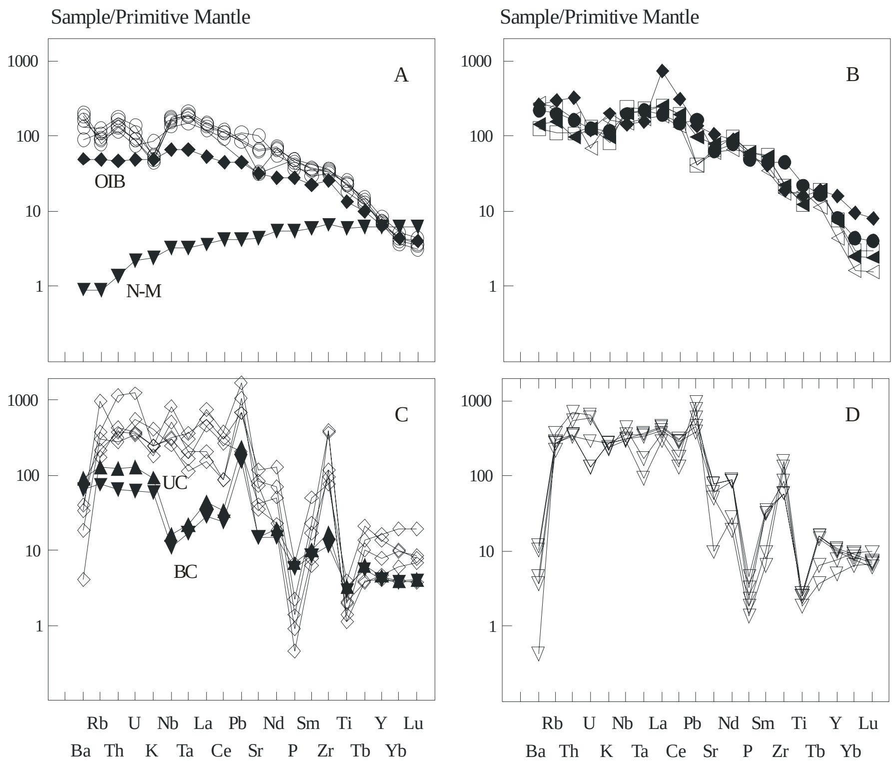


Fig. 27. Variograms for selected PC rocks. A) VQ, Vale do Quartel ultramafic rocks, N-MORB (N-M) and OIB after Sun & McDonough (1989); B) MP, Minas Pedras dykes; C) Nepheline syenites (n=5) and UC-BC, upper and bulk continental crusts (Rudnick & Gao, 2004); D) Tinguaites (n=5). For other references, see Figs. 21 and 26.

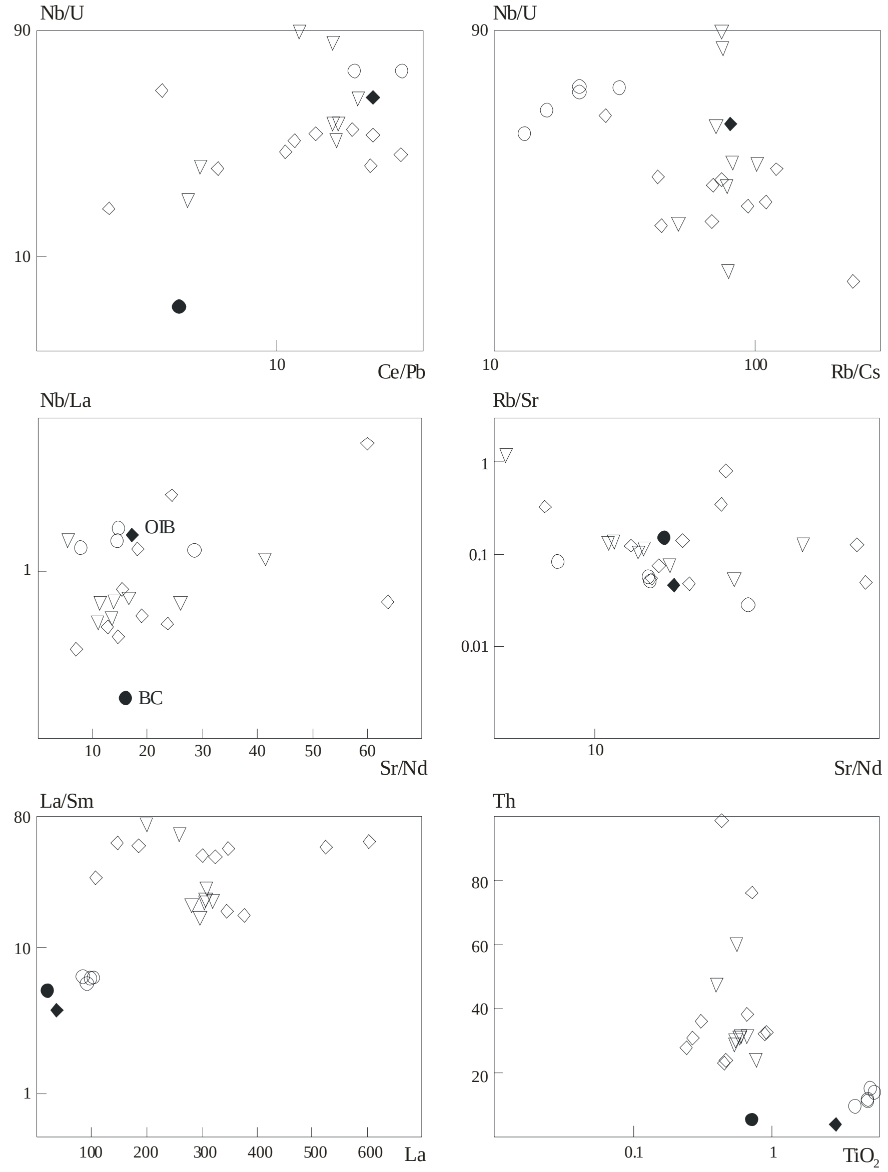


Fig. 28. Trace elements and trace element ratios for PC rocks. Also plotted are OIB (Sun & McDonough, 1989) and BC, bulk continental crust (Rudnick & Gao, 2004). Other references, see Fig. 21.

The C1 chondrite normalized diagrams in Fig. 26 for the Vale do Quartel *ultramafic* rocks present a flat continuous pattern, similar to the OIB signature, showing however a larger LREE enrichment ($La_N/Lu_N$ around 40-50, against $La_N/Lu_N$ around 20 in OIB; cf. also statements in Thompson *et al.*, 1998). The ultramafic Minas Pedras dykes were derived from liquids enriched in $H_2O$ and/or $CO_2$, which favored mobility of elements; probably due to this factor, they exhibit several anomalies (e.g. negative spikes for Sr, somewhat higher values for Nb and Ta) and are strongly enriched in LREE, with $La_N/Lu_N$ from ~60 to ~90. Even so, their pattern is similar to the general OIB trend. An exception is the laminated sample with phlogopite and carbonate bands at Minas Pedras ($La_N/Lu_N$ over 100), which shows LREE contents close to those expected in carbonatites. The *felsic* PC rocks present strong enrichment in LREE, more constant in tinguaites ($La_N/Lu_N$ around 50) and more variable in NeS ($La_N/Lu_N$ from ~50 to ~25), in the last case usually with correlated contents (the higher the LREE, the higher the HREE). The patterns in the NeS and tinguaites are effectively similar, showing a remarkable concave form, more pronounced in both rock-types when the MREE (Eu to Dy) appear with lower values than the corresponding HREE (Ho to Lu). The NeS again show a wider spread than tinguaites, presumably generated by element mobility during deuteric alteration. Considering that no garnet fractionation played a significant role in the evolution of the felsic rocks, the large $La_N/Yb_N$ (or $La_N/Yb_N$) ratio in all of them suggests petrogenetic processes that started with melting of a mantle protolith in the presence of garnet. Melanite, although reported in a few PC rocks as a rare accessory mineral (cf. previous studies), may not have played an important role in the crystallization of these rocks.

The variograms in Fig. 27 show that the *ultramafic* rocks in the Vale do Quartel and Minas Pedras present, again, a pattern similar to OIB, although enriched in "incompatible elements", including Nb and Ta; the small positive Nb-Ta anomaly observed in these rocks only enhances the one already present in OIB. The negative spike for K may be explained by K retention in a K-bearing phase in the protolith (assuming no spurious chemical deviations brought about by deuteric alteration in these rocks, which also present in most cases partially or totally filled vesicles). The patterns for Minas Pedras are more irregular, especially visible in the laminated rock with phlogopite and carbonatite bands, with a marked La and Ce enrichment, and the negative spike shown for Pb by a Minas Pedras lamprophyre and a silico-carbonatite sample. On the other hand, the *felsic* samples present variograms to be expected from rocks that crystallize from magmas within petrogenetic residual systems (whether over- or undersaturated), being enriched in incompatible elements and leaving behind the compatible ones. Thus, the general trends of NeS and tinguaites repeat the patterns shown by the average upper and bulk continental crusts (Fig. 27), although with a high plateau in LIL, U and Th, an irregular but always negative Ba anomaly, positive spikes for La, Pb and Zr, negative ones for P and Ti, and a visible Sr negative anomaly, particularly in the tinguaites. But, contrary to the upper and mean continental crusts, the felsic PC rocks show a remarkable positive Nb and Ta anomaly (Fig. 27).

The general conclusions to be drawn from these observations are that, as indicated especially by isotopic data, the *felsic* and *mafic-ultramafic* rocks have to be dealt with as separate lineages. There is a remarkable similarity between OIB and the *ultramafic* rocks in PC, strongly suggesting that at least these rocks have originated from magmas derived from asthenospheric sources (cf. Thompson *et al.*, 1998), in part with a carbonatite contribution, as observed in the rather inconspicuous Minas Pedras occurrence. Inversely, the *felsic* PC rocks repeat the pattern that is common to all differentiated crustal rocks (whether over- or undersaturated), namely, strong enrichment in all sorts of "incompatible" elements, brought to an extreme case in PC, with the important and significant difference that they show in variograms a weak, but visible Sr negative anomaly and, especially, a relative enrichment in Nb and Ta, in complete contradiction to what should be expected of typical differentiated crustal rocks. All these features, as well as the Sr and Ba negative spikes, are conspicuously present in all the differentiated felsic rocks occurring in the Serra do Mar belt of alkaline massifs (Itatiaia, Passa Quatro and São Sebastião; cf. Enrich *et al.*, in this volume; also Comin Chiaramonti *et al.*, in this volume; Antonini *et al.*, in this volume).

Ratios of trace elements may express some properties not immediately visible in the previous diagrams (Fig. 28). In most of them, the *ultramafic* Vale do Quartel rocks plot close to OIB (with the exception of the Nb/U vs. Rb/Cs diagram, on account of the dispersion in the Rb/Cs values, perhaps introduced by means of redistribution of elements during deuteric alteration).

No clear pattern of evolution can be observed in the plots for the *felsic* PC rocks (e.g. one that may involve the different tinguaites and, especially, the

NeS, in crystal fractionation processes). In a Nb/Ta-Zr/Sm diagram, the felsic PC rocks show either an unfractionated behaviour (relative to OIB) or fractionated trends (Nb vs. Ta and Zr vs. Sm). Foley *et al.* (2002) showed that these trends are to be expected during the melting process of eclogites with and without rutile (the first case controlling the increase in the Nb/Ta ratio); a decrease in the Nb/Ta ratio is to be expected during melting of amphibolites within a descending subduction slab (Foley *et al.*, 2002). This suggests that the felsic PC rocks inherited the relative Nb enrichment from the original magmas derived by melting of the PC protoliths; it also explains the presence of the positive Nb-Ta spike in the respective variograms (Fig. 27). A similar explanation is advanced for a Nb/Ta vs. Sr diagram, where most felsic PC rocks are either unfractionated (relative to OIB) or show fractionated trends (cf. Foley *et al.*, 2002). Possibly, lacking further information on geochemical behaviour of mantle minerals, the above explanation could be applied to include Ti-minerals, in general, found within dry mantle rocks (not necessarily only rutile in eclogites, but other Ti phases in any dry mantle rock; for the behaviour of Nb in amphibole and phlogopite, cf. Foley *et al.*, 2002; Farmer, 2004).

In the Nb/La and Rb/Sr (vs. Sr/Nd) diagrams, the felsic PC rocks cluster mainly around OIB (with some NeS as exceptions), separating them clearly from other rocks of different geotectonic environments (e.g. arc magmas).

In the Nb/U (vs. Ce/Pb and Rb/Cs) the felsic PC rocks have higher Nb/U ratios than crustal ones (cf. Farmer, 2004). The Nb/U ratio should be relatively constant during most petrogenetic processes such as melting and possibly also crystal fractionation (but not during deuteric and hydrothermal alteration), strongly suggesting that the protoliths of the felsic PC rocks were already enriched (kimberlites, for instance, plot close to OIB; Farmer, 2004).

It should be remembered that the several NeS have invaded as discrete bodies, each with its own chemical signature (especially in trace elements), thus representing discrete and different magma batches. The same conclusion may be extended to phonolites, although for obvious reasons it is impossible to map contacts between the different phonolite batches. It is however very difficult to create a single *parental* intermediate magma from which all the different magmas can be derived by crystal fractionation of feldspars and/or pyroxenes and/or nepheline, together with the help of several accessory minerals (titanite, RMS etc.). The individual intrusions possibly represent small volumes of magmas coming from the same protolith source but with little or no interaction among them (e.g. through crystal fractionation).

## PETROLOGICAL CONSIDERATIONS AND CONCLUSIONS

The data on rock chemistry and, especially, isotope geochemistry, discussed above, lead to the conclusion that at least *two contrasted lineages* of magmas were responsible for the generation of the PC rocks, one for the ultramafic Vale do Quartel and Minas Pedras rocks, the second for the predominant felsic lithotypes.

As suggested by isotopic data and decisively by rock chemistry, the *ultramafic rock lineage* shows a strong geochemical resemblance with OIB, indicating that the ultimate source is most likely an asthenospheric advecting mantle. The Minas Pedras occurrences clearly indicate that $CO_2$ as well as $H_2O$ were important components, probably also participating in the eruption of somewhat larger carbonatite bodies in other parts of the district, as suggested by the presence of the Th-REE supergene alteration patch at Morro do Ferro and the discovery of carbonatite clasts in the Vale do Quartel breccias (cf. Alves, 2003, and items on Petrography and Mineralizations).

The felsic PC rocks, on the other hand, show reasonably primitive isotopic values (initial ratios in the Rb/Sr and Sm/Nd systems), but must have been derived from enriched mantle rocks, after a rather efficient process controlling the loss of compatible elements and MgO. On a general basis, three possibilities must be considered:

1) Direct melting from peridotitic mantle protoliths, giving rise to a wide range of derived magmas (not only basalts) as shown in the recent literature (e.g. Draper & Green, 1997, and bibliography therein);

2) Melting of enriched mantle protoliths and generation of ultrabasic alkaline magmas (e.g. nephelinitic or melanephelinitic compositions), with derivation of intermediate alkaline magmas by crystal fractionation (extraction mainly of olivine and clinopyroxene in wehrlitic proportions; e.g. Ulbrich, 1984a);

3) Formation of an enriched mantle by invasion and crystallization of mantle magmas (e.g. with a "nephelinitic" composition) giving rise to "melt metasomatism" and percolation of lithospheric mantle rocks, later to be melted with the direct generation of intermediate alkaline magmas (e.g. Foley, 1992). The enriched mantle would be located at the base of the lithospheric mantle, perhaps in a zone that is transitional between the advecting asthenospheric mantle and the strictly rigid subcontinental mantle lithosphere (cf. Farmer, 2004, and bibliography therein). Nephelinites and melanephelinites may be produced in rather large volumes, as clearly shown in an oceanic environment by the Fernando de Noronha example (cf. Ulbrich *et al*., 2004), leading perhaps to a process that may be similar to basalt "underplating" at the base of the continental crust, or a concentration of differentiated rocks within the lithospheric mantle.

The absence of compatible elements and the low contents of MgO in the *PC felsic rocks* precludes the possibility that these rocks were generated by direct melting of ultramafic, olivine-rich, mantle protoliths: re-equilibration with a peridotitic mantle would certainly increase the contents of compatible elements (especially Cr, Co and Ni) and of MgO.

The second hypothesis can be tested with the help of gravity data. The gravity measurements were used to estimate the volume of the PC erupted rocks at certain depths (around 7700-8000 $km^3$, Slavec *et al.*, 2002). The passage to phonolitic magmas by crystal fractionation, starting from a parental magma with a nephelinite or melanephelinite composition, requires the withdrawal of around 70 to 80% (weight, somewhat less in volume) of wehrlitic material, with a mean density clearly over 3 $g/cm^3$ (e.g. Ulbrich, 1984a). This represents a volume of around 40000 $km^3$ of fractionated rock, so large that it should be detected in gravity surveys, provided this fractionation took place within the continental crust (N. Ussami, personal communication). The gravity survey conducted in PC shows a rather flat regional gravity anomaly, with very slight shoulders at the contact with the massif; no positive gravity anomalies in the deeper continental crust were, therefore, detected (Slavec *et al.*, 2002). It is a mute point to propose that the fractionation occurred in mantle regions, where it would go undetected.

This brief discussion shows that the third possibility has to be considered as the more realistic one, in part also bolstered by the absence of intermediate rock-types between the two ultramafic and felsic extremes (at least, at the present outcrop level; for a comparison with Khibina, cf. Arzamastsev *et al.*, 2002), possibly coupled with some fractionation of pyroxenes and accessory minerals. Melting of an extensively "veined" mantle, composed of "normal" mantle with interspersed "metasomatic" veins and dykes, would have generated more differentiated alkaline magmas, the more so the less the melting percentage (melt production less than 5%; e.g. Foley, 1992; Farmer, 2004), especially if the composition of the metasomatic component was already alkaline (e.g. a nephelinite or a melanephelinite). The point to be made is that the mantle is extremely heterogeneous (even the sublithospheric one; cf. discussion of mantle heterogeneities in Bodinier & Godard, 2004, and bibliography therein).

How did these magmas travel up to the surface? The rise may have occurred very rapidly along pre-existing fractures or other structures, possibly with no significant interaction with the continental crust; of course, the rocks (and the corresponding magmas) were so rich in REE and Sr that it would be difficult to prove that a significant contamination took place during the rise.

Rock geochemistry and geology indicate that each NeS intrusion (and hence also probably each phonolite) represent the emplacement of a discrete and individual magma batch, not related to the other magma batches (e.g. by crystal fractionation). If so, then each intrusion is a unique event, created by melting of a somewhat primitive lithospheric mantle (but not as primitive as the mantle that gave rise to the ultramafic rocks), differentially enriched with all sorts of incompatible elements. The $T_{DM}$ ages, although only tentatively, may indicate that the enrichment took place during the tectonomagmatic Brasiliano event (~800-450 Ma), thus leaving enough time to proceed to an isotopic homogeneization process of a petrographically and structurally heterogeneous subcontinental lower mantle lithosphere.

The heat source that started the whole process, in Brazil and elsewhere, may have been a more or less "passive" uprising of an "asthenospheric" advecting mantle (e.g. Comin-Chiaramonti *et al.*, 2002) or, as preferred by many authors, an "active" deep mantle plume, probably also responsible for the generation of other like alkaline occurrences along a path that is controlled by the relative mantle plume-plate motions (e.g. Thompson *et al.*, 1998; Gibson *et al.*, 1995, 1999; Thomaz Filho & Rodrigues, 1999). The first hypothesis has long been put forward, in various forms, as the explanation for magma generation in continental environments. The last one depends strongly on a rigid control on ages of the intrusions and the age interval of magmatism of the various basaltic and alkaline occurrences, as well as on still more refined reconstructions of the relative plume-lithosphere wandering paths. Plume action was hailed in the literature as a "saviour" hypothesis, explaining many difficult questions about magma generation, but it has come systematically under fire in more recent years (e.g. Smith & Lewis, 1999). Perhaps the study of Brazilian alkaline occurrences may help with important arguments in order to settle this question.

## ACKNOWLEDGMENTS

On several occasions field and laboratory work for PC projects were sponsored by grants from the Brazilian federal CNPq Science Council and the São Paulo State Science Foundation, mostly to H.U., who gratefully acknowledges them. The new Sr, Nd and Pb isotopic analysis were performed at the Laboratoire de Geochimie Isotopique of the Université Livre de Bruxelles by one of the coauthors (D.D.).

## REFERENCES

Almeida, E.B. (1977). *Geology of the bauxite deposits of the Poços de Caldas district, state of Minas Gerais, Brazil.* Ph.D. Thesis, Stanford University, 273p.

Almeida, E.B., Farjallat, J.E.S., Valarelli, J.V. & Yoshida, R. (1978). Fontes alternativas de potássio (Projeto do IPT). *XXX Congresso Brasileiro de Geologia, Recife, Anais* **4**, 1696-1705.

Almeida, F.F.M. (1971). Condicionamento tectônico do magmatismo alcalino mesozóico do Sul do Brasil e do Paraguai oriental. *Anais da Academia Brasileira de Ciências* **43**, 835-836.

Almeida, F.F.M. (1983). Relações tectônicas das rochas alcalinas mesozóicas da região meridional da plataforma sul-americana. *Revista Brasileira de Geociências* **13**, 139-158.

Almeida, F.F.M., Hasui, Y., Davino, A. & Haralyi, N.L.E. (1980). Informações geofísicas sobre o oeste mineiro e seu significado geotectônico. *Anais da Academia Brasileira de Ciências* **52**, 49-60.

Almeida Filho, R. & Paradella, W.R. (1976). *Estudo do maciço alcalino de Poços de Caldas através de imagens Landsat com ênfase em mineralizações radioativas.* M.Sc. Thesis, INPE-1112-TPT/065, 130p.

Alves, A.D. (2003). *Rochas vulcanoclásticas do complexo alcalino de Poços de Caldas-MG/SP.* M.Sc. Thesis, University of São Paulo, 106p.

Amaral, G., Bushee, J., Cordani, U.G., Kawashita, K. & Reynolds, J.H. (1967). Potassium-argon ages of alkaline rocks from southern Brazil.

*Geochimica et Cosmochimica Acta* **31**, 117-142.

Antonini, P., Gasparon, M., Comin-Chiaramonti, P. & Gomes, C.B. (in this volume). Post-Paleozoic magmatism in Eastern Paraguay: Sr-Nd-Pb isotopic compositions.

Araújo, A.L.N., Carlson, R.W., Gaspar, J.C. & Bizzi, L.A. (2001). Petrology of kamafugites and kimberlites from the Alto Paranaíba alkaline province, Minas Gerais, Brazil. *Contributions to Mineralogy and Petrology* **142**, 163-177.

Araújo, R.L.C. (1980). Pesquisa geotermal na chaminé alcalina de Poços de Caldas. *XXXI Congresso Brasileiro de Geologia, Camboriú. Anais* **2**, 1059-1074.

Arzamastsev, A.A., Bea, F., Arzamatseva, L.V. & Montero, P. (2002). Rare earth elements in rocks and minerals from alkaline plutons of the Kola Peninsula, NW Russia, as indicators of alkaline magma evolution. *Russian Journal of Earth Sciences* **4**, 187-209.

Ashry, M.M. (1962). Studies of three rock samples from Brazil. *Boletim da Sociedade Brasileira de Geologia* **11**, 89-107.

Atencio, D., Coutinho, J.M.V., Ulbrich, M.N.C. & Vlach, S.R.F. (1999). Hainite from Poços de Caldas, Minas Gerais, Brazil. *Canadian Mineralogist* **37**, 91-98.

Baptista, A. (1976). Lamprofilita no lujaurito de Pedra Balão, Poços de Caldas, Minas Gerais. *Anais da Academia Brasileira de Ciências* **48**, 475-492.

Barbosa, O. (1948). Sobre a idade das rochas alcalinas e a origem do Planalto de Poços de Caldas. *Mineralogia e Metalurgia* **13**, 235-236.

Barker, D.S. (1987). Tertiary alkaline magmatism in Trans-Pecos, Texas. In: Fitton, J.G. & Upton, B.G.J. (eds.) *Alkaline igneous rocks*. *Geological Society of London, Special Publication* **30**, 415-431.

Bennio, L., Brotzu, P., Gomes, C.B., D'Antonio, M., Lustrino, M., Melluso, L., Morbidelli, L. & Ruberti, E. (2002). Petrological, geochemical and Sr-Nd isotopic features of alkaline rocks from the Arraial do Cabo Frio (southeastern Brazil). *Periodico di Mineralogia* **71**, 137-158.

Biondi, J.C. (1979). "Pipes" e diques de brecha - um novo modelo de origem (implosão-fluidização). *Revista Brasileira de Geociências* **9**, 198-217.

Biondi, J.C. (in this volume). Brazilian mineral deposits associated with alkaline and alkaline-carbonatite complexes.

Björnberg, A.J.S. (1956). Arenitos do bordo do Planalto de Poços de Caldas. *Anais da Academia Brasileira de Ciências* **28**, 465-471.

Björnberg, A.J.S. (1959). Rochas clásticas do Planalto de Poços de Caldas. *Faculdade Filosofia Ciências e Letras Universidade de São Paulo*, *Boletim* 237, *Geologia* **18**, 65-123.

Björnberg, A.J.S. & Landim, P.M.B. (1966). Sobre os arenitos da Serra de Mantiqueira e os arenitos da Formação Botucatu (Eocretácico). *Boletim Paranaense de Geografia* **18-20**, 19-24.

Bodinier, J.L. & Godard, M. (2004). Orogenic, ophiolitic, and abyssal peridotites. In: Holland, H.D. & Turekian K.K. (eds.) *Treatise on geochemistry*, vol. 2, *The mantle and core*. Oxford: Elsevier, pp. 103-170.

Branco, J.J.R. (1956). Notas sobre a geologia e petrologia do Planalto de Poços de Caldas, MG. *Escola de Engenharia da Universidade de Minas Gerais*, *Instituto de Pesquisas Radioativas* no. **5**, 72p.

Bushee, J. (1971). Geochronological and petrographic studies of alkaline rocks from southern Brazil. I. Potassium-argon ages of some alkaline rocks from southern Brazil. II. A geochronological study of the alkaline massif of Poços de Caldas, Brazil. III. Geology and petrography of the lujaurite and nearby rocks, Poços de Caldas, Brazil. Ph.D. Thesis, University of California, 143p.

Campos Neto, M.C. & Caby, R. (1999). Tectonic constraints on Neoproterozoic high-pressure metamorphism and nappe systems south of the São Francisco craton, southeast Brazil. *Precambrian Research* **97**, 3-26.

Campos Neto, M.C. & Caby, R. (2000). Terrane accretion and upward extrusion of high-pressure granulites in the Neoproterozoic nappes of southeast Brazil: petrologic and structural constraints. *Tectonics* **19**, 669-687.

Cande, S.C. & Kent, D.V. (1994). Revised calibration of the geomagnetic polarity timescale for the Late Cretaceous and Cenozoic. *Journal of Geophysical Research* **100**, 6093-6095.

Castro L.O. & Souza, J.M. (1962). Ocorrência de molibdênio no depósito de urânio de Morro do Taquari, Planalto de Poços de Caldas, Minas Gerais. *Anais da Academia Brasileira de Ciências* **34**, 371-374.

Christofoletti, A. (1970). Análise morfogenética das bacias hidrográficas do Planalto de Poços de Caldas, MG. Habilitation Thesis, State University of São Paulo, 215p.

Christofoletti, A. (1973). A unidade morfoestrutural do Planalto de Poços de Caldas. *Notas Geomorfológicas* **13**, 77-85.

Comin-Chiaramonti, P. & Gomes, C.B. (1996). *Alkaline magmatism in central-eastern Paraguay. Relationship with coeval magmatism in Brazil*. São Paulo: Edusp-Fapesp, 464p.

Comin-Chiaramonti, P., Civetta, L., Petrini, R., Piccirillo, E.M., Bellieni, G., Censi, P., Bitschene, P., Demarchi, G., De Min, A., Gomes, C.B., Castillo, A.M.C. & Velázquez, J.C. (1991).

Tertiary nephelinitic magmatism in Eastern Paraguay: petrology, Sr-Nd isotopes and genetic relationships with associated spinel-peridotite xenoliths. *European Journal of Mineralogy* **3**, 507-525.

Comin-Chiaramonti, P., Cundari, A., Piccirillo, E.M., Gomes, C.B., Castorina, F., Censi, P., De Min, A., Marzoli, A., Speziale, S., & Velázquez, V.F. (1997). Potassic and sodic igneous rocks from Eastern Paraguay: their origin from the lithospheric mantle and genetic relationships with the associated Paraná flood tholeiites. *Journal of Petrology* **38**, 495-528.

Comin-Chiaramonti, P., Gomes, C.B., Castorina, F., Censi, P., Antonini, P., Furtado, S., Ruberti, E. & Scheibe, F. (2002). Geochemistry and geodynamic implications of the Anitápolis and Lages alkaline-carbonatitic complexes, Santa Catarina state, Brazil. *Revista Brasileira de Geociências* **32**, 27-42.

Comin-Chiaramonti, P., Marques, L.S., Gomes, C.B., Censi, P., Ruberti, E. & Antonini, P. (in this volume). Carbonatites from southeastern Brazil: geochemistry, O-C, Sr-Nd-Pb isotopes and relationships with magmatism from the Paraná-Angola-Namibia Province.

Cox, K.G., Bell, J.D. & Pankhurst, R.J. (1979). *The interpretation of igneous rocks*. London: Allen & Unwin, 450p.

De Paolo, D.J. (1981). Neodymium isotopes in the Colorado Front Range and crust-mantle evolution in the Proterozoic. *Nature* **291**, 193-196.

De Paolo, D.J. (1988). *Neodymium isotope geochemistry*. Berlin: Springer, 187p.

Derby, O.A. (1887). On nepheline rocks in Brazil, with special reference to the association of phonolite and foyaite. *Quarterly Journal of the Geological Society of London* **43**, 457-473.

Didier, J. & Barbarin, B. (eds.) (1991). *Enclaves and granite petrology*. Amsterdam: Elsevier, 625p.

Dirksen, M. 1964. Pesquisas em minerais zirconíferos de Poços de Caldas, Brasil. *Engenharia Mineralogia Metalurgia* **40**, 253-255.

Draper, D.S. & Green, T.H. (1997). P-T phase relations of silicic, alkaline, aluminous mantle-xenolith glasses under anhydrous and C-O-H fluid-saturated conditions. *Journal of Petrology* **38**, 1187-1224.

Dutra, E.B. (1954). Minas Gerais: importância das jazidas de minérios radioativos no Planalto de Poços de Caldas. *Departamento Nacional de Produção Mineral*, *Divisão de Fomento à Produção Mineral*, *Boletim* **102**, 29-56.

Dutra, C.V. (1965). Determinação espectroquímica de maiores e menores constituintes, em pequenas amostras de minerais. Análise completa de lamprofilita e eudialita. *Escola de Engenharia, Publicação* **4**, 8p.

Dutra, C.V. (1966). O método chumbo-alfa e idades de zircões do maciço alcalino de Poços de Caldas, MG. *Boletim do Instituto de Geologia* **1**, 125-135.

Edgar, A.D. (1977). A comment on "Agpaicity revisited: pattern recognization in the chemistry of nepheline syenite rocks" by Dagbert *et al. Geochimica et Cosmochimica Acta* **41**, 439-440.

Ellert, R. (1959). Contribuição à geologia do maciço alcalino de Poços de Caldas. *Boletim da Faculdade de Filosofia, Ciências e Letras*, *Universidade de São Paulo*, *Boletim* 237, no. **18**, 5-63.

Ellert, R., Björnberg, A.J.S. & Coutinho, J.M.V. (1959). Mapa geológico do maciço alcalino de Poços de Caldas.

Enrich, G.E.R., Azzone, R.B., Ruberti, E., Gomes, C.B. & Comin-Chiaramonti, P. (in this volume). Itatiaia, Passa Quatro and São Sebastião island, the major alkaline syenitic complexes from Serra do Mar region.

Farmer, G.L. (2004). Continental basaltic rocks. In: Holland, H.D. & Turekian, R.R. (eds.) *Treatise on geochemistry, vol. 3, The crust*. Oxford: Elsevier, pp. 85-121.

Faure, G. (1986). *Principles of isotope geology.*, New York: Wiley, 589p.

Fletcher, L. (1894). Hussak's brazilite. Appendix to "On baddeleyite (native zirconia) a new mineral from Rakwaha, Ceylon". *Mineralogical Magazine Journal* **10**, 148-159.

Foley, S. (1992). Vein-plus-wall-rock melting mechanisms in the lithosphere and the origin of potassic alkaline magmas. *Lithos* **28**, 435-453.

Foley, S., Tiepolo, M. & Vannucci, R. (2002). Growth of early continental crust controlled by melting of amphibolite in subduction zones. *Nature* **417**, 837-840.

Forman, J.M.A. & Angeiras, A.G. (1981). Poços de Caldas and Itatiaia: two case histories of uranium exploration in Brazil. In: *Uranium Exploration Case Histories*. *Proceedings International Atomic Energy Agency*, *IAEA-AG 250/14*, 99-139.

Fraenkel, M.O., Santos, R.C., Lapido-Loureiro, F.E.V. & Muniz, W.S. (1985). Jazida de urânio no Planalto de Poços de Caldas-Minas Gerais. In: Schobbenhaus, C. & Coelho, C.E.S. (coords.) *Principais depósitos minerais do Brasil*. DNPM **1**, 89-103.

Franco, R.R. (1945). Minerais de zircônio na região de Poços de Caldas, Minas Gerais. *Faculdade de Filosofia, Ciências e Letras*, *Universidade de São Paulo*, *Boletim* 49, *Mineralogia* **7**, 7-28.

Franco, R. & Loewenstein, W. (1948). Zirconium from the region of Poços de Caldas. *American Mineralogist* **33**, 142-151.

Frayha, R. (1950). Estudo preliminar e prospecção das jazidas de rochas potássicas de Poços de Caldas. *Departamento Nacional de Produção Mineral, Divisão de Fomento à Produção Mineral, Boletim* **87**, 109-111.

Frayha, R. (1952). Rochas potássicas (Planalto de Poços de Caldas) e estudo das jazidas zirconíferas. *Departamento Nacional de Produção Mineral, Divisão de Fomento à Produção Mineral, Boletim* **93**, 107-116.

Frayha, R. (1957). Ocorrências uraníferas no arenito de Águas da Prata, SP. *Engenharia Mineração Metalurgia* **26**, 201-208.

Frayha, R. (1962a). Bauxita e minerais radioativos, Poços de Caldas. *Departamento Nacional de Produção Mineral, Divisão de Fomento à Produção Mineral, Boletim* **113**, 49-61.

Frayha, R. (1962b). Urânio e tório no Planalto de Poços de Caldas. *Departamento Nacional de Produção Mineral, Divisão de Fomento à Produção Mineral, Boletim* **116**, 75p.

Frayha, R. (1962c). Poços de Caldas: estudo das jazidas de minérios radioativos. *Departamento Nacional de Produção Mineral, Divisão de Fomento à Produção Mineral, Boletim* **118**, 67-77.

Freitas, R.O. de (1943). As estruturas fósseis do sistema de Santa Catarina no Planalto de Poços de Caldas. *Boletim da Associação de Geógrafos Brasileiros* **III**, 25-37.

Freitas, R.O. de (1951). Ensaio sobre a tectônica moderna do Brasil. *Boletim da Faculdade de Filosofia, Ciências e Letras, Universidade de São Paulo, Boletim* 130, Geologia **6**, 120p.

Frondel, C. & Marwin, U.B. (1959). Cerianite, $CeO_2$, from Poços de Caldas, Brazil. *American Mineralogist* **44**, 882-884.

Fujimori, K. (1974). Minerais radioativos do Campo Agostinho, Poços de Caldas (MG). Habilitation Thesis, University of São Paulo, 161p.

Fujimori, K. (1980). Comportamento geoquímico uranífero no Campo de Agostinho, Poços de Caldas, MG. *XXXI Congresso Brasileiro de Geologia, Camboriú, Anais* **2**, 1125-1139.

Fujimori, K. (1982a). Kalsilita ($KAlSiO_4$) do complexo alcalino de Poços de Caldas, MG. *XXXII Congresso Brasileiro de Geologia, Salvador, Anais* **2**, 648-651.

Fujimori, K. (1982b). Silicato de terras raras $(Ce,La,Nd,Ca,Th)SiO_4$ e cheralita (Th,Ca,C,La) $(PSi)O_4$, minerais responsáveis pela anomalia no Morro do Ferro. *XXXII Congresso Brasileiro de Geologia, Salvador, Anais* **2**, 669-674.

Fujimori, K. & Sardela, I. (1980). Estudo mineralógico do "caldasito" dos Campos do Serrote, Brigida e Taquari, no Planalto de Poços de Caldas, MG. *XXXI Congresso Brasileiro de Geologia, Camboriú, Anais* **4**, 2023-2037.

Fujimori, K., Oliveira, A.G. & Utsumi, O. (1976). Minerais uraníferos do Campo do Cercado C-09, Poços de Caldas, MG. *XXIX Congresso Brasileiro de Geologia, Ouro Preto, Anais* **2**, 251-263.

Fujimori, K., Sardela, I.A. & Callari, R. 1980. Distribuição de anomalias radioativas no Morro do Ferro do complexo alcalino de Poços de Caldas, MG. *XXXI Congresso Brasileiro de Geologia, Camboriú, Anais* **2**, 1140-1148.

Garda, G.M. (1990). *A alteração hidrotermal no contexto da evolução geológica do maciço alcalino de Poços de Caldas, MG-SP*. M.Sc. Thesis, University of São Paulo, 161p.

Gibson, S.A., Thompson, R.N., Leonardos, O.H., Dickins, A.P. & Mitchell, J.G. (1995). The Late Cretaceous impact of the Trindade mantle plume: evidence from large-volume, mafic, potassic magmatism in SE Brazil. *Journal of Petrology* **36**, 189-229.

Gibson, S.A., Thompson, R.N., Leonardos, O.H., Dickin, A.P. & Mitchell, J.G. (1999). The limited extent of plume-lithosphere interactions during continental flood-basalt genesis: geochemical evidence from Cretaceous magmatism in southern Brazil. *Contributions to Mineralogy and Petrology* **137**, 147-169.

Gorsky, V.A. & Gorsky, E. (1974). Contribuição à mineralogia e petrografia do Planalto de Poços de Caldas. *Comissão Nacional de Energia Nuclear, Boletim* **13**, 93p.

Graef, F.F. (1887). Lavenit im brasilianischen Elaeolithsyenit. *Neues Jahrbuch für Mineralogie Geologie und Paläontologie* **I**, 201-203.

Gualda, G.A.R. & Vlach, S.R.F. (1996). Eudialita-eucolita do maciço alcalino de Poços de Caldas, MG-SP: quimismo e correlação com comportamento óptico. *XXXIX Congresso Brasileiro de Geologia, Salvador, Anais* **3**, 34-37.

Gualda, G.A.R. & Vlach, S.R.F. (1997). Lorenzenita em nefelina sienitos do maciço alcalino de Poços de Caldas (MG-SP). *V Simpósio Iniciação Científica da USP, Resumos* **2**, p. 420.

Gualda, G.A.R. & Vlach, S.R.F. (1998a). Lamprofilita e normandita (lavenita titanífera) em nefelina sienitos agpaíticos do maciço alcalino de Poços de Caldas (MG-SP): caracterização mineralógica e petrológica. *XL Congresso Brasileiro de Geologia, Belo Horizonte, Anais*, p. 284.

Gualda, G.A.R. & Vlach, S.R.F. (1998b). Controles na mineralogia acessória de rochas intermediárias a agpaíticas do Taquari – maciço alcalino de Poços de Caldas (MG-SP). *XL Congresso Brasileiro de Geologia,, Belo Horizonte, Anais*, p. 460.

Guimarães, D. (1948). The zirconium ore deposits of the Poços de Caldas Plateau, Brazil, and zirconium geochemistry. *Instituto Tecnológico Industrial do Estado de Minas Gerais, Boletim* **6**, 43-79.

Guimarães, D. & Ilchenko, W. (1954). Rochas com pseudoleucita ou epileucita de Poços de Caldas. *Boletim de Agricultura* **3**, 11-13.

Guimarães, D. & Moraes, L.J. (1955). Um mineral raro dos foiaitos de Serrote, Cascata, município de Águas da Prata, SP. *Instituto Tecnológico Industrial do Estado de Minas Gerais, Avulso* **19**, 10p.

Haddad, R.C. (1995). *O batólito granitóide Pinhal-Ipuiúna (SP-MG): um exemplo de magmatismo cálcio-alcalino potássico neoproterozóico no sudeste brasileiro*. Ph.D. Thesis, University of São Paulo, 270p.

Hamza, V.M. (1982). Terrestrial heat flow in the alkaline intrusive complex of Poços de Caldas, Brazil. *Tectonophysics* **83**, 45-62.

Hart, S.R., Gerlach, D.C. & White, W.M. (1986). A possible new Sr-Nd-Pb mantle array and consequences for mantle mixing. *Geochimica et Cosmochimica Acta* **50**, 1551-1557.

Heilbron, M., Pedrosa-Soares, A.C., Campos Neto, M.C., Silva, L.C., Trouw, R.A.J. & Janasi, V.A. (2004). Província Mantiqueira. In: Mantesso-Neto, V., Bartorelli, A., Carneiro, C.D.R. & Brito-Neves, B.B. (eds.). *Geologia do continente sul-americano: A evolução da obra de Fernando Flávio Marques de Almeida*. São Paulo: Beca, pp. 203-234.

Herz, N. (1977). Timing of spreading in the South Atlantic: information from Brazilian alkalic rocks. *Geological Society of America Bulletin* **88**, 101-112.

Hoffmann, A.W. (1997). Mantle geochemistry: the message from oceanic magmatism. *Nature* **385**, 219-229.

Hoffmann, A.W. (2004). Sampling mantle heterogeneity through oceanic basalts: isotopes and trace elements. In: Holland, H.D. & Turekian K.K. (eds.) *Treatise on geochemistry, vol. 2, The mantle and core*, Oxford: Elsevier, pp. 61-101.

Hussak, E. (1892). Ueber Brasilit, ein neues Tantal (Niob) Mineral von der Eisenmine Jacupiranga, Sued São Paulo. *Neues Jahrbuch für Mineralogie, Geologie und Paläontologie* **II**, 141-159.

Hussak, E. (1899). Ein Beitrag zur Kenntnis der sogenannten "Favas" der brasilianischen Diamantensande. *Tschermak's Mineralogische und Petrographische Mitteilungen* **18**, 335-359.

Hussak, E. & Reitinger, J. (1903). Ueber Monazit, Xenotim, Senait und natuerliches Zirkonoxyd aus Brasilien. *Zeitschrift für Kristallographie und Mineralogie* **37**, 550-574.

Jackson, J.A. (1997). *Glossary of geology. American Geological Institute,* Alexandria, 769 p.

Janasi, V.A. (1999). *Petrogênese de granitos crustais na Nappe de empurrão Socorro-Guaxupé (SP-MG): uma contribuição da geoquímica elemental e isotópica*. Habilitation Thesis, University of São Paulo, 302p.

Kawashita, K., Mahiques, M.M. & Ulbrich, H.H. (1984). Idades Rb-Sr de nefelina sienitos do anel Norte do maciço alcalino de Poços de Caldas, MG-SP. *XXXIII Congresso Brasileiro de Geologia, Rio de Janeiro, Resumos, pp.* 244-245.

Kramm, U. & Kogarko, L.N. (1994). Nd and Sr isotope signatures of the Khibina and Lovozero agpaitic centers, Kola Alkaline Province, Russia. *Lithos* **32**, 225-242.

Kramm, U., Kogarko, L.N., Kononova, V.A. & Vartiainen, H. (1993). The Kola Alkaline Province of the CIS and Finland: precise Rb-Sr ages define 380-360 Ma age range for all magmatism. *Lithos* **30**, 33-44.

Lapido-Loureiro, E.E. & Valderano, M.H.W. (1982). A província alcalina-carbonatítica Brasil-Angola e seus principais aspectos econômicos. *XXXII Congresso Brasileiro de Geologia, Salvador, Anais* **3**, 1049-1060.

Larsen, L.M. & Sorensen, H. (1987). The Ilimaussaq intrusion–progressive crystallization and formation of layering in an agpaitic magma. In: Fitton, J.G. & Upton, B.G.J. (eds.) *Alkaline igneous rocks. Geological Society of London, Special Publication* **30**, 473-488.

Le Bas, M.J., Le Maitre, R.W., Streckeisen, A. & Zanettin, B. (1986). A chemical classification of volcanic rocks based on the total alkali-silica diagram. *Journal of Petrology* **27**, 745-750.

Le Maitre, R.W., Bateman, P., Dudek, A., Keller, J., Lameyre, J., Le Bas, M.J., Sabine, P.A., Schmid, R., Sorensen, H., Streckeisen, A., Woolley, A.R. & Zanettin, B. (1989). *A classification of igneous rocks and glossary of terms*. Oxford: Blackwell, 193p.

Le Maitre, R.W. (1976). The chemical variability of some common igneous rocks. *Journal of Petrology* **17**, 589-597.

Loewenstein, W. (1952). Estudos sobre as propriedades químicas dos minerais de zircônio da região de Poços de Caldas, Minas Gerais. *Faculdade de Filosofia, Ciências e Letras, Universidade de São Paulo, Boletim 147, Mineralogia* **9**, 37-74.

Ludwig, K.R. (1998). Isoplet/Ex. A geo-chronological toolkit for Microsoft ExcelTM (version 1.00b). *Berkeley Geochronology Center, Special Publication* **1**, 44p.

Lustrino, M., Dallai, L., Giordano, R., Gomes, C.B., Melluso, L., Morbidelli, L., Ruberti, E. & Tassinari, C.C.G. (2003). Geochemical and Sr-

Nd-O isotopic features of the Poços de Caldas alkaline massif (SP-MG, SE Brazil): relationships with the Serra do Mar analogues. *IV South American Symposium on Isotope Geology, Salvador, Short Papers* **2**, 593-595.

Machado, J. (1888). Beitrag zur petrographie der suedwestlichen grenze zwischen Minas-Gerais und São Paulo. *Tschermak's Mineralogische und Petrographische Mitteilungen* **9**, 318-360.

Maciel, A.C., Azuaga, C.H.C. & Cruz, P.R. (1973). Reservas de urânio e tório no Brasil e no mundo. Capacidade de produção e perspectivas de demanda. *XXVII Congresso Brasileiro de Geologia, Aracaju, Anais* **2**, 353-368.

Marques, L.S., Ulbrich, M.N.C., Ruberti, E. & Tassinari, C.G. (1999). Petrology, geochemistry and Sr-Nd isotopes of the Trindade and Martin Vaz volcanic rocks (southern Atlantic Ocean). *Journal of Volcanology and Geothermal Research* **93**, 191-216.

Mathias, M. (1974). Alkaline rocks of southern Africa. In: Sorensen, H. (ed.) *The alkaline rocks*. New York: Wiley, pp.189-202.

Middlemost, E.A.K. (1975). The basalt clan. *Earth Sciences Review* **11**, 337-364.

Moniz, A.C. (1969). Estudo mineralógico de argilas do maciço alcalino de Poços de Caldas. *Faculdade de Filosofia, Ciências e Letras, Universidade de São Paulo, Boletim 304, Mineralogia* **19**, 134p.

Moniz, A.C., Williams, D.D., Souza-Santos, P. & Souza-Santos, H. (1972). Clay minerals in veins associated with bauxites of Poços de Caldas, Minas Gerais. *XXVI Congresso Brasileiro de Geologia, Belém, Anais* **1**, 221-230.

Montes Lauar, C.R. (1988). *Estudo paleomagnético dos maciços alcalinos de Poços de Caldas, Passa Quatro e Itatiaia*. M.Sc. Dissertation, University of São Paulo, 101p.

Montes Lauar, C.R., Pacca, I.G., Melfi, A.J. & Kawashita, K. (1995). Late Cretaceous alkaline complexes, southeastern Brazil: paleomagnetism and geochronology. *Earth and Planetary Sciences Letters* **134**, 425-440.

Motoki, A. & Oliveira, J.L.S. (1987). Reconsiderações vulcanológicas sobre a hipótese de caldeira vulcânica no complexo alcalino de Poços de Caldas, MG. *Simpósio de Geologia de Minas Gerais, Belo Horizonte, Anais* **4**, 420-433.

Motoki, A., Vargas, T., Chanello, E., Correa, F.J.G., Oliveira, J.L.S & Klotz, M. (1988). Nível de denudação atual do complexo alcalino de Poços de Caldas, MG-SP. *XXXV Congresso Brasileiro de Geologia, Belém, Anais* **6**, 2633-2648.

Oliveira, A.G. (1974). Mineralização de urânio e molibdênio no Planalto de Poços de Caldas, MG. *XXVIII Congresso Brasileiro de Geologia, Porto Alegre, Anais* **1**, 207-221.

Oliveira, M.A.F., Alves, F.R. & Coimbra, A.M. (1975). Sedimentação associada ao vulcanismo alcalino de Poços de Caldas (Divinolândia, SP). *Boletim do Instituto de Geociências da Universidade de São Paulo* **6**, 13-19.

Oliveira, M.A.F., Morales, N., Fúlfaro, V.J. (1984). Projeto Boa Vista. *Final Report of the SICCT, Rio Claro*, **1**, 109p.

Paradella, W.R. & Almeida Filho, R. (1976). Condicionamento das mineralizações radioativas no Planalto de Poços de Caldas baseado em imagens MSS do Landsat. *XXIX Congresso Brasileiro de Geologia, Ouro Preto, Anais* **3**, 181-190.

Riccomini, C, Velázquez, V.F. & Gomes, C.B. (in this volume) Tectonic controls of the Mesozoic and Cenozoic alkaline magmatism in the central-southeastern Brazilian Platform.

Rollinson, H. (1993). *Using geochemical data: Evaluation, presentation, interpretation*. London: Longmann, 352p.

Rudnick, R.L. & Gao, S. (2004). Composition of the continental crust. In: Holland, H.D. & Turekian K.K. (eds.) *Treatise on geochemistry, vol. 3, The crust*. Oxford: Elsevier, pp. 1-64.

Sachsen-Coburg, P.A. von (1889). Beitraege zur Mineralogie und Petrographie Brasiliens. *Tschermak's Mineralogische und Petrographische Mitteilungen* **10**, 451-463.

Sadowski, G.R. & Dias Neto, C.M. (1981). O lineamento sismo-tectônico de Cabo Frio. *Revista Brasileira de Geociências* **11**, 109-112.

Sardela, I.A. (1981). *Elementos radioativos nos minerais zirconíferos de Poços de Caldas, MG.* M.Sc. Dissertation, University of São Paulo, 120p.

Sardela, I. & Fujimori, K. (1980). Determinação do teor de Urânio lixiviável (método AIEA) e total no "caldasito" pela análise fluorimétrica. *XXXI Congresso Brasileiro de Geologia, Camboriú, Anais* **4**, 2263-2268.

Sawkins, F.J. (1990). *Metal deposits in relation to plate tectonics*. 2nd. edition. Berlin: Springer, 461p.

Schorscher, H.D. & Shea, M.E. (1992). The regional geology of the Poços de Caldas alkaline complex: mineralogy and geochemistry of selected nepheline syenites and phonolites. *Journal of Geochemical Exploration* **54**, 173-214.

Schorscher, H.D., Garda, G.M., Shea, M.E. & Waber, N. (1991). Lamprophyre dykes from the Utsumi uranium mine, Poços de Caldas (MG), Brazil. *International Symposium on Mafic Dykes, São Paulo, Extended Abstracts,* pp.166-124.

Schulmann, A. (1993). Changes in mineralogy and geochemistry of a nepheline syenite with increasing bauxitization, Poços de Caldas, Brazil. *Chemical Geology* **107**, 327-331.

Schulmann, A., Carvalho, A. & Valeton, I. (1997). Bauxites of Poços de Caldas. In: Carvalho, A., Boulangé, B. & Melfi, A.J. (eds.) *Brazilian bauxites*. São Paulo-Paris: USP-Fapesp-Orstom, pp. 231-254.

Shand, S.J. (1949). *Eruptive rocks*, 3rd. edition. London: Murby, 488p.

Shea, M.E. (1992). Isotopic geochemical characteristics of selected nepheline syenites and phonolites from the Poços de Caldas alkaline complex, Minas Gerais, Brazil. *Journal of Geochemical Exploration* **54**, 173-214.

Siebel, W., Becchio, R., Volker, F., Hansen, M.A.F., Viramonte, J., Trumbull, R.B., Haase, G. & Zimmer, M. (2000). Trindade and Martin Vaz Islands, South Atlantic: isotopic (Sr, Nd, Pb) and trace element constraints on plume related magmatism. *Journal of South American Earth Sciences* **13**, 79-103.

Slavec, G.B. (2002). *Estudo gravimétrico do maciço alcalino de Poços de Caldas, MG-SP*. M.Sc. Dissertation, University of São Paulo, 115p.

Slavec, G.B., Mantovani, M.S.M. & Shukowsky, W. (2004). Estudo gravimétrico do maciço alcalino de Poços de Caldas. *Revista Brasileira de Geociências* **34**, 275-280.

Smith, A.F. & Lewis, C. (1999). The planet beyond the plume hypothesis. *Earth Sciences Review* **48**, 135-182.

Sonoki, I.K. & Garda, G.M. (1988). Idades K-Ar de rochas alcalinas do Brasil meridional e Paraguai oriental: compilação e adaptação às novas constantes de decaimento. *Boletim do Instituto de Geociências da USP, Série Científica* **19**, 63-85.

Sood M.K. (1981). *Modern igneous petrology*. New York: Wiley, 244p.

Sorensen, H. (1970). Internal structures and geological setting of the three agpaitic intrusions - Khibina and Lovozero of the Kola peninsula and Ilimaussaq, south Greenland. *Canadian Mineralogist* **10**, 299-334.

Sorensen, H. (1974a). Alkali syenites, feldspathoidal syenites and related lavas. In: Sorensen, H. (ed.) *The alkaline rocks*. New York: Wiley, pp. 22-52.

Sorensen, H. (1974b). Glossary of alkaline and related rocks. In: Sorensen, H. (ed.) *The alkaline rocks*. New York: Wiley, pp. 577-588.

Souza-Santos, P. (1937). Contribuição para o estudo da bauxita do Planalto de Poços de Caldas. *Boletim do Instituto de Pesquisas Tecnológicas,* **17**, 109-134.

Sun, S.S. & McDonough, W.F. (1989). Chemical and isotopic systematics of oceanic basalts: implications for mantle composition and processses. In: Saunders A.D. & Norry M.J. (eds.) *Magmatism in the ocean basins. Geological Society of London, Special Publication* **42**, 313-345.

Taylor, S.R. & McLellan, S.M. (1985). *The continental crust: its composition and evolution*. Oxford: Blackwell, 312p.

Thomaz Filho, A. & Rodrigues, A.L. (1999). O alinhamento de rochas alcalinas Poços de Caldas-Cabo Frio (RJ) e sua continuidade na cadeia Vitória-Trindade. *Revista Brasileira de Geociências* **29**, 189-194.

Thompson, R.N., Gibson, S.A., Mitchell, J.G., Dickin, A.P., Leonardos, O.H., Brod, J.A. & Greenwood, J.C. (1998). Migrating Cretaceous-Eocene magmatism in the Serra do Mar alkaline province, SE Brazil: melts from the deflected Trindade mantle plume? *Journal of Petrology* **39**, 1493-1526.

Tolbert, G. (1958a). Preliminary report of the zirconium ore deposits of the Poços de Caldas Plateau. Part I. *Engenharia Mineração Metalurgia* **27**, 265-269.

Tolbert, G. (1958b). Preliminary report of the zirconium ore deposits of the Poços de Caldas Plateau. Part II. *Engenharia Mineração Metalurgia* **27**, 353-360.

Tolbert, G. (1966). The uraniferous zirconium deposits of the Poços de Caldas Plateau, Brazil. *U.S. Geological Survey Bulletin* **1185C**, 28p.

Ulbrich, H.H. (1984a). *A petrografia, a estrutura e o quimismo de nefelina sienitos do maciço alcalino de Poços de Caldas, MG-SP*. Habilitation Thesis, University of São Paulo, 480p.

Ulbrich, H.H. (1984b). Retrospecto histórico: os estudos anteriores sobre o distrito alcalino de Poços de Caldas. In: Ulbrich, H.H. *A petrografia, a estrutura e o quimismo de nefelina sienitos do maciço alcalino de Poços de Caldas, MG-SP*. Habilitation Thesis, University of São Paulo, *Apêndice A*, pp. A01-A62.

Ulbrich, H.H. & Gomes, C.B. (1981). Alkaline rocks from continental Brazil. *Earth Science Reviews* **17**, 135-154.

Ulbrich, H.H. & Ulbrich, M.N.C. (1992). O maciço alcalino de Poços de Caldas, MG-SP: características petrográficas e estruturais. *XXXVII Congresso Brasileiro de Geologia. São Paulo, Roteiro de Excursões*, 64p.

Ulbrich, H.H. & Ulbrich, M.N.C. (2000a). The lujavrite and khibinite bodies in the Poços de Caldas alkaline massif, southeastern Brazil: a structural and petrographic study. *Revista Brasileira de Geociências* **30**, 615-622.

Ulbrich, H.H. & Ulbrich, M.N.C. (2000b). The Poços de Caldas massif (Part II) – São Paulo and Minas Gerais states, eastern Brazil. In: Ruberti, E., Gomes, C.B., Melcher, G.C., Ulbrich, H.H. & Ulbrich, M.N.C. (eds.) *The Jacupiranga* *carbonatitic complex (Part I) and the Poços de Caldas massif (Part II). Field Trip Guide, Post-Congress Field Trip Aft 08, 31st International Geological Congress, Rio de Janeiro,* pp. 22-44.

Ulbrich, H.H., Demaiffe, D., Vlach, S.R.F. & Ulbrich, M.N.C. (2003). Geochemical and Sr, Nd and Pb isotope signatures of phonolites and nepheline syenites from the Poços de Caldas alkaline massif, southeastern Brazil. *IV South American Symposium on Isotope Geology, Salvador, Short Papers* **2**, 698-701.

Ulbrich, H.H., Vlach, S.R.F., Ulbrich, M.N.C. & Kawashita, K. (2002). Penecontemporaneous syenitic-phonolitic and basic-ultrabasic-carbonatitic rocks at the Poços de Caldas alkaline massif, SE Brazil: geologic and geochronologic evidence. *Revista Brasileira de Geociências* **32**, 15-26.

Ulbrich, M.N.C. (1983). *Aspectos mineralógicos e petrológicos de nefelina sienitos do maciço alcalino de Poços de Caldas, MG-SP*. Ph.D. Thesis, University of São Paulo, 369p.

Ulbrich, M.N.C. (1985). Geothermometry of the Poços de Caldas nepheline syenites, southern Brazil. *Anais da Academia Brasileira de Ciências* **57**, p.131.

Ulbrich, M.N.C. (1993). Mineralogy of nepheline syenites from the Poços de Caldas alkaline massif, SE Brazil: chemistry, X-ray data and microtextures of feldspars. *Revista Brasileira de Geociências* **23**, 388-399.

Ulbrich, M.N.C., Marques, L.S. & Lopes, R.P. (2004). As ilhas vulcânicas brasileiras: Fernando de Noronha e Trindade. In: Mantesso-Neto, V., Bartorelli, A., Carneiro, C.D.R. & Brito-Neves, B.B. (eds) *Geologia do continente sul-americano: a evolução da obra de Fernando Flávio Marques de Almeida*. São Paulo: Beca, pp. 555-573.

Ulbrich, M.N.C., Vlach, S.R.F. & Ulbrich, H.H. (1998). Geoquímica dos diques de rochas máfico-ultramáficas potássicas periféricas ao maciço de Poços de Caldas (MG-SP). *XL Congresso Brasileiro de Geologia, Belo Horizonte, Anais*, p. 469.

Utsumi, O. (1971). Mineralização urano-molibdenífera no Planalto de Poços de Caldas. *XXV Congresso Brasileiro de Geologia, São Paulo, Resumo das Comunicações, Boletim Especial* **1**, 40-41.

Utsumi, O., Oliveira, A.G., Parisi, C.A. & Williams, D.D. (1971). Roteiro de excursões: Poços de Caldas. *XXV Congresso Brasileiro de Geologia, São Paulo, Roteiro de Excursões, Boletim Especial* **2**, 7-13.

Valeton, I., Schulmann, A., Vinx, R. & Wieneke, M. (1997). Supergene alteration since the Upper Cretaceous on alkaline igneous and metasomatic rocks of the Poços de Caldas ring complex, Minas Gerais, Brazil. *Applied Geochemistry* **12**, 133-154.

Vargas, T. & Motoki, A. (1991). Inexistência dos diques anelares no ressalto topográfico da borda perimétrica (muralha) do complexo alcalino de Poços de Caldas, MG-SP. *II Simpósio Geologia do Sudeste, São Paulo, Boletim de Resumos*, p. 9.

Vlach, S.R.F. & Gualda, G.A.R. (2000). Microprobe Th-U-Pb systematics and dating of some granitic and metamorphic rocks from southeastern Brazil. *Revista Brasileira de Geociências* **30**, 214-218.

Vlach, S.R.F., Ulbrich, H.H. & Ulbrich, M.N.C. (1998). Isótopos radiogênicos (Sr, Nd) e estáveis (C, O) de rochas máfico-ultramáficas potássicas da região de Poços de Caldas, MG-SP: inferências sobre a natureza do manto litosférico mesozóico. *XL Congresso Brasileiro de Geologia, Belo Horizonte, Anais*, p. 475.

Vlach, S.R.F., Ulbrich, M.N.C., Ulbrich, H.H. & Gualda, G.A.R. (1996). Rochas de afinidades alnoíticas e sílico-carbonatíticas periféricas ao maciço alcalino de Poços de Caldas (MG-SP). *XXXIX Congresso Brasileiro de Geologia, Salvador, Anais* **2**, 128-130.

Vlach, S.R.F., Vilalva, F.C.J., Ulbrich, M.N.C., Ulbrich, H.H. & Vasconcelos, P.M. (2003). Phlogopite from carbonatitic veins associated with the Poços de Caldas alkaline massif, SE Brazil: mineralogy and $^{40}Ar/^{39}Ar$ dating by the laser step heating method. *IV South American Symposium on Isotope Geology, Salvador, Short Papers* **2**, 702-705.

Waber, N. (1992). The supergene thorium and rare-earth element deposit at Morro do Ferro, Poços de Caldas, Minas Gerais, Brazil. *Journal of Geochemical Exploration* **54**, 113-157.

Waber, N., Schorscher, H.D. & Peters, Tj. (1992). Hydrothermal and supergene uranium mineralization at the Osamu Utsumi mine, Poços de Caldas, Minas Gerais, Brazil. *Journal of Geochemical Exploration* **45**, 53-112.

Wänke, H., Dreibus, G. & Jagoutz, E. (1984). Mantle chemistry and accretion history of the Earth. In: Kröner, A. (ed.) *Archean geochemistry*. Berlin: Springer Verlag, pp. 1-24.

Weber, B.N. (1959). Bauxitization in the Poços de Caldas district, Brazil. *American Institute of Mining Metallurgy Engineering Transactions* **214**, 805-809.

Wedow Jr., H. (1961a). Thorium and rare earths in the Poços de Caldas zirconium district, Brazil. *U.S. Geological Survey Professional Paper* **424-D**, D214-D216.

Wedow Jr., H. (1961b). "Laterization" of allanite in the Morro do Ferro rare-earth and thorium deposit, Poços de Caldas Plateau, Brazil. *Geological*

*Society of America Special Paper* **68**, p. 293.
Wedow Jr., H. (1967). The Morro do Ferro thorium and rare-earth ore deposit, Poços de Caldas district, Brazil. *U.S. Geological Survey Bulletin* **1185-D**, 34p.
Winchell A.N. & Winchell H. (1967). *Elements of optical mineralogy, Part II. Descriptions of minerals,* 4th edition. New York: Wiley, 551p.
Zartman, R.E. & Doe, B.R. (1981). Plumbotectonics - the model. *Tectonophysics* **75**, 135-162.
Zindler, A. & Hart, S. (1986). Chemical geodynamics. *Annual Review of Earth Planetary Sciences* **14**, 493-571.

*Mesozoic to Cenozoic Alkaline Magmatism in the Brazilian Platform*
*Comin-Chiaramonti, P. & Gomes, C.B. (eds.)*
*Edusp/Fapesp, São Paulo, pp. 367-418, 2005*

# ITATIAIA, PASSA QUATRO AND SÃO SEBASTIÃO ISLAND, THE MAJOR ALKALINE SYENITIC COMPLEXES FROM THE SERRA DO MAR REGION

*G.E.R. Enrich, R.G. Azzone, E. Ruberti, C.B. Gomes and P. Comin-Chiaramonti*

*This paper reviews the main geological, petrographic and geochemical characteristics of the major Late Cretaceous alkaline syenitic complexes from the Serra do Mar Alkaline Province in SE Brazil: Itatiaia (220 km$^2$), Passa Quatro (165 km$^2$) and São Sebastião island (136 km$^2$). Itatiaia is characterized by a set of syenitic varieties ranging from early silica-undersaturated syenites to late quartz syenites and granites in the central parts of the massif. Passa Quatro dominant rock-types are nepheline syenites. São Sebastião island contains three zoned syenitic stocks with acid terms at the borders. Trachyte, phonolite and mafic dykes are found intruding the syenitic varieties and the country-rocks. Geochemical features indicate crystal fractionation of feldspars as the main evolution process for the formation of the syenitic varieties. Associated mafic dykes, basanites and tephrites (mg# 0.64 to 0.38) have quite similar geochemical features in comparison with those of the Trindade basanites; however, the overall characteristics indicate a main contribution of lithospheric mantle melts.*

## INTRODUCTION

Late Cretaceous to Paleocene alkaline complexes and dyke swarms intrude the basement of the Ribeira belt (750-450 Ma; Machado *et al.*, 1996) and constitute the Serra do Mar Alkaline Province (Ulbrich & Gomes, 1981; Almeida, 1983; Morbidelli *et al.*, 1995; Thompson *et al.*, 1998; Brotzu *et al.*, in this volume). These alkaline complexes (Fig. 1) are tectonically related to the Southeastern Brazilian Continental Rifting (Riccomini *et al.*, in this volume), which developed into the Ribeira belt (gneisses, migmatites, banded granulites and amphibolites) following ENE to E-W transcurrent systems reactivated during the Gondwana break-up.

This geological context appears to be well distinct from the Guaxupé block, the northern segment of the Socorro-Guaxupé nappe (Almeida, 1983; Iyer *et al.*, 1996; Janasi, 1999; Campos Neto & Caby, 1999; Almeida *et al.*, 2000), where Poços de Caldas, the largest Brazilian alkaline complex covering an area of 800 km$^2$ (Ulbrich *et al.*, in this volume), is found. As a matter of fact, the Guaxupé block structure separates the Brasília belt from the Ribeira belt (Fig. 1).

Complex arrangement in the Serra do Mar Province is conditioned by two alignments, following rifting structural systems - along the Cabo Frio alignment (Sadowski & Dias Neto, 1981; Almeida, 1991) and along the coastline, parallel to the Santos fault (Alves, 1996; Almeida & Carneiro, 1998; Alves & Gomes, 2001), where occur some of the largest Brazilian alkaline syenitic complexes: Itatiaia and Passa Quatro in the first alignment, and São Sebastião island in the second one.

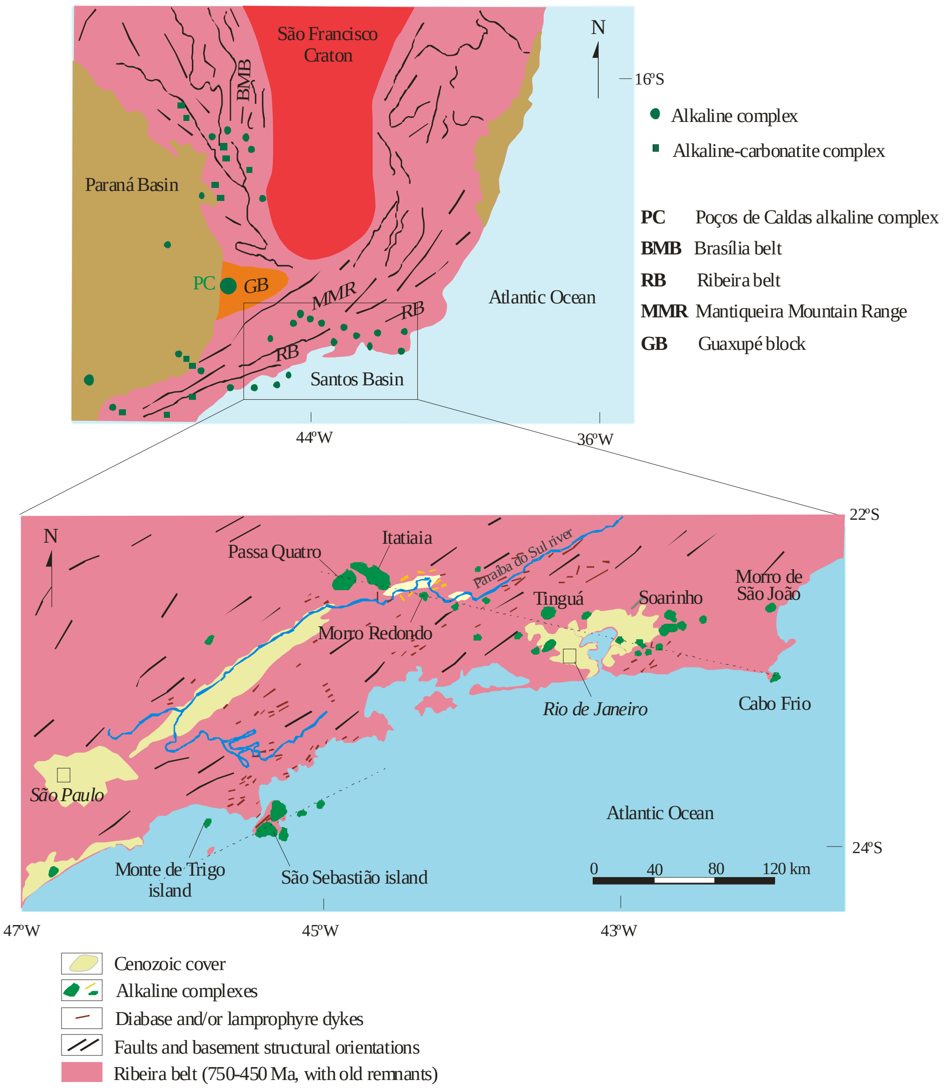


Fig. 1. Geological sketch-map of the Serra do Mar region, modified after Almeida (1983) and Schobbenhaus *et al.* (1984).

This paper focuses on the more important features of these occurrences mainly considering the previous literature (e.g. Bellieni *et al.*, 1990; Brotzu *et al.*, 1992, 1997; Sígolo *et al.*, 1992; Garda, 1995; Garda *et al.*, 1995; Thompson *et al.*, 1998).

## GEOLOGICAL SETTING

Derby (1887) provided the first geological descriptions of Brazilian nepheline syenitic rocks, including the Itatiaia and the São Sebastião island complexes. In the last century some works chiefly regarding the geological and petrographic characterization of these ocurrences were produced by, for instance, Freitas (1947), Ribeiro Filho (1967), Penalva (1967) and Hennies & Hasui (1977). On the late sixties, the first geochronological K-Ar data of these occurrences were made available by Ribeiro Filho & Cordani (1966), Amaral *et al.* (1967) and Hennies & Hasui (1968). Sonoki & Garda (1988) have recalculated these ages in accordance with new decay constants recommended by Steiger & Jäger (1977). From the late eighties up to now several papers were published contributing with a large amount of geochemical data (Brotzu *et al.*, 1989, 1992, 1997; Bellieni *et al.*, 1990; Garda *et al.*, 1995; Thompson *et al.*, 1998).

The *Itatiaia* complex (22°23'S, 44°40'W) forms a NW-SE ellipsoidal body spreading over an area of 220 $km^2$ and reaching a height of 2787 m (Agulhas Negras Peak, the highest point in SE Brazil). The complex consists of a set of syenitic rock-types ranging from early silica-undersaturated syenites and nepheline syenites to late quartz syenites and granites at the inner parts (Fig. 2). Syenitic breccias are associated with the late core. Scarce phonolitic, trachytic and mafic dykes intrude the complex (Ribeiro Filho, 1967; Brotzu *et al.*, 1997; Thompson *et al.*, 1998; Brotzu *et al.*, in this volume).

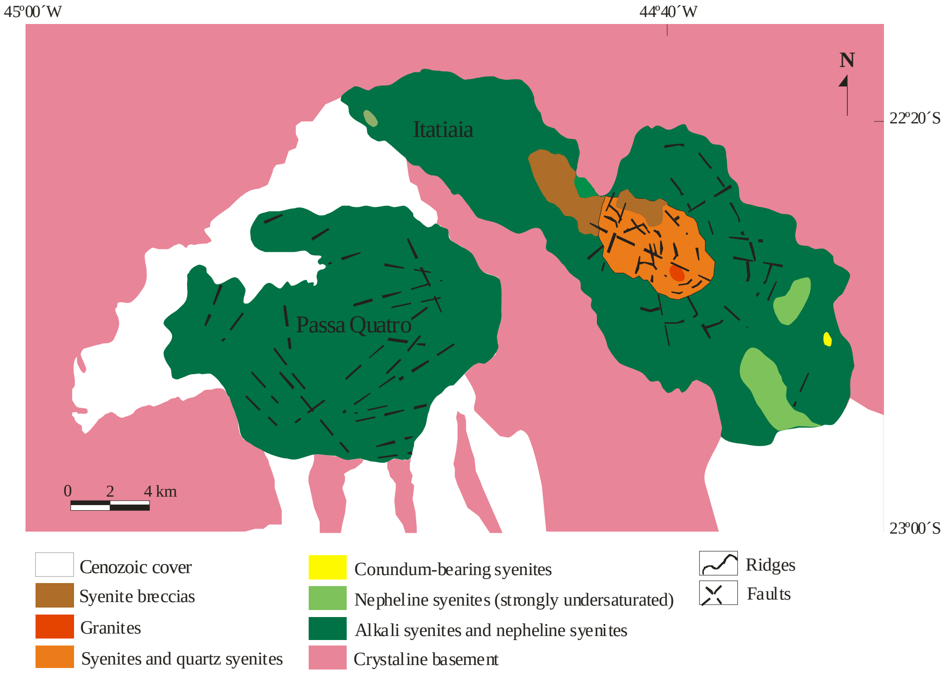


Fig. 2. Geological map of the Itatiaia and Passa Quatro complexes (after Ribeiro Filho, 1967; Penalva, 1967; Brotzu *et al.*, 1992, 1997).

Average K-Ar ages of 70.5±3.3 Ma (biotite) and 72±6 Ma are reported by Montes-Lauar *et al.* (1995) and Brotzu *et al.* (1997), respectively, from analyses compiled and recalculated by Sonoki & Garda (1988).

The *Passa Quatro* complex (22°25'S, 44°45'W) shows a subcircular shape, with 165 $km^2$ in area and reach up to 2780 m high. Dominant rock-types are nepheline syenites, intruded by alkaline polymictic breccias and phonolitic dykes with predominantly NE-SW direction (Fig. 2; Brotzu *et al.*, 1992; Sígolo *et al.*, 1992).

Ribeiro Filho & Cordani (1966) obtained only one K-Ar age of 67±3 Ma (amphibole; recalculated by Sonoki & Garda, 1988). Whole rock Rb-Sr ages of 77±3 Ma (MSWD=6) and 70.4±0.5 Ma (MSWD=3) were obtained by Brotzu *et al.* (1992) and Montes-Lauar *et al.* (1995), respectively. High MSWD values suggest a possible disturbance of the Rb-Sr system, as admitted by these authors.

The *São Sebastião island* (Fig. 3; 23°50'S, 45°20'W) represents a remnant of the granitic basement intruded by three syenitic stocks: Serraria (65 $km^2$), São Sebastião (55 $km^2$) and Mirante (16 $km^2$). They form a zoned structure with acid terms (quartz syenites) at the borders (Hennies & Hasui, 1977; Bellieni *et al.*, 1990). In the NNW region, layered gabbros occur at Ponta da Pacuíba and Canas showing transitional affinities (tholeiitic to alkaline), and alkaline affinity at the Armação beach. These occurrences extend to less than 1 $km^2$, along with their differentiation products (e.g. peridotites, pyroxenites, leucogabbros and anorthosites), near the Serraria stock (Lima & Schorscher, 1999; Lima, 2001). In the southern region, layered gabbros with transitional affinity also occur, dipping towards the

São Sebastião stock (Augusto, 2003).

Syenitic and gabbric bodies display an average K-Ar (biotite) age of 84±3 Ma, quoted by Bellieni *et al.* (1990) and Montes-Lauar *et al.* (1995) based on previous data compiled and recalculated by Sonoki & Garda (1988). A whole-rock Rb-Sr age of 81±3 Ma was determined by Montes-Lauar *et al.* (1995).

Early Cretaceous subalkaline dykes, both basic and acid rock-types in composition (not considered in this paper, and 129-136 Ma in age, cf. Bellieni *et al.*, 1990; Thompson *et al.*, 1998, and references therein), follow predominant NE direction with variable thickness (2-50 m) and extension (2-15 km). Late Cretaceous picritic lamprophyre (at the coastline, near the São Sebastião island), basanite, trachyte and phonolite dykes have a prevailing NW attitude, 0.5-3 m in thickness and an extension up to a few hundred meters (Bellieni *et al.*, 1990; Garda *et al.,* 1995). Notably, some alkaline dykes intrude the syenitic stocks, with K-Ar (whole-rock) ages from 78±8 to 83±6 Ma (Sonoki & Garda, 1988), thus representing the youngest magmatic activity in the São Sebastião island.

## PETROGRAPHIC OUTLINES

The descriptions below are based on the works done by Ribeiro Filho (1967), Penalva (1967), Brotzu *et al.* (1997) and Thompson *et al.* (1998) on the Itatitaia complex; Brotzu *et al.* (1992) and Sígolo *et al.* (1992) on the Passa Quatro complex; and Freitas (1947), Hennies & Hasui (1977), Bellieni *et al.* (1990), Garda *et al.* (1995), Thompson *et al.* (1998), Lima & Schorscher (1999), Lima (2001) and Augusto (2003) on the São Sebastião island complex.

### Itatiaia

*Nepheline syenites* and *nepheline-bearing syenites* present medium to coarse-grained inequigranular hypidiomorphic texture, with local variations to trachytic or banded texture. Felsic phases are euhedral to subhedral perthitic alkali feldspar, plagioclase (absent or up to 5 vol%), euhedral to interstitial nepheline (2 to 40 vol%) and rare sodalite. Mafic minerals include clinopyroxene (ranging from diopside to aegirine-augite and to aegirine), amphibole (mainly hastingsite, katophorite and richterite) and biotite. Accessory minerals are magnetite, ilmenite, titanite, apatite and less frequent zircon. Melanite and Ca-Zr-Nb silicates (e.g. wöhlerite) may occur in the nepheline syenites.

*Corundum-bearing syenites* rarely occur within the nepheline-bearing syenites. They are fine to medium-grained, with euhedral plagioclase and subhedral to interstitial alkali feldspar, biotite and

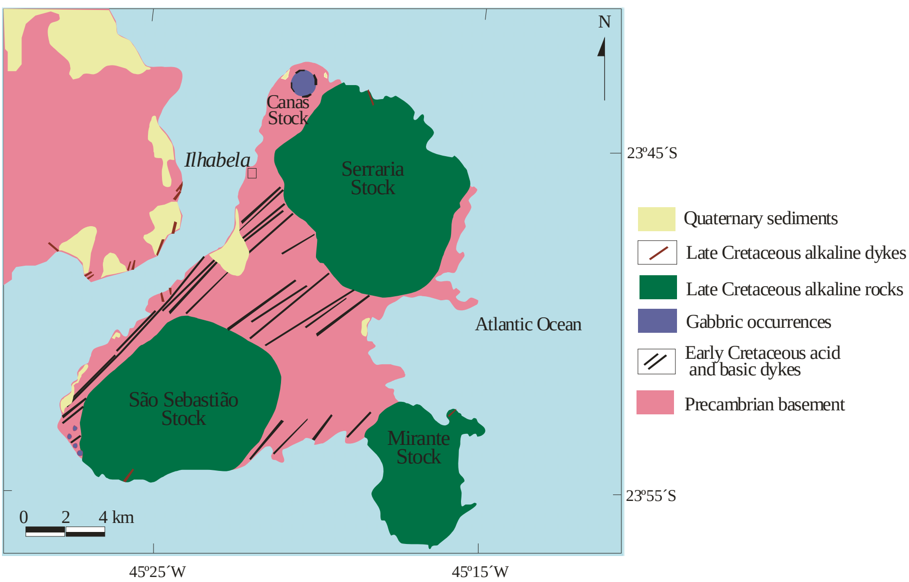


Fig. 3. Geological map of the São Sebastião island (after Hennies & Hasui, 1977; Bellieni *et al.*, 1990; Augusto, 2003).

cluster of small corundum grains with hercynite. Occasional nepheline is noticeable, whereas clino-pyroxene and amphibole are absent.

*Syenites* and *quartz syenites* are fine to medium-grained hypidiomorphic, varying from equigranular to porphyritic with alkali feldspar phenocrysts. Felsic phases are perthitic alkali feldspar, plagio-clase (oligoclase to andesine), sometimes mantled by anorthoclase and interstitial quartz (up to 12 vol%), some of them showing graphic texture with alkali feldspar. Mafic minerals are biotite, amphibole (mainly actinolite, richterite and arfvedsonite) and clinopyroxene (diopside and aegirine-augite). The accessory minerals consist of magnetite, ilmenite, titanite, apatite, zircon, with occasional fluorite, pseudobrookite, pyrite as well as an unidentified brown pleochroic REE-rich phase.

*Granites*, equigranular medium-grained, are characterized by hypidiomorphic alkali feldspar mantled by albitic rims, large amounts of interstitial quartz (up to 33 vol%) and graphic quartz-alkali feldspar intergrowths. The main mafic mineral is biotite, while accessory phases are represented by magnetite, titanite, apatite and fluorite.

*Phonolite* dykes contain dominant sanidine and nepheline, and subordinate nosean and mafic phenocrysts set in a groundmass of the same minerals. Occasional large euhedral pseudoleucite crystals (up to 10 cm in diameter) may be found in some hypocrystalline rock-types.

*Trachyte* dykes have sanidine phenocrysts set in a groundmass of sanidine, quartz, and subordinate opaques, biotite and amphibole.

*Mafic alkaline* dykes exhibit clinopyroxene, magnetite and occasional olivine, phlogopite pheno-crysts set in a groundmass of the same phases in addition to plagioclase, amphibole, alkali feldspar, apatite and interstitial glass.

*Magmatic breccias* are formed by angular to subangular clasts (1 to 50 cm in diameter), prevailling large feldspar crystals and volcanic and subvolcanic trachytic types over massive syenite and quartz syenites, set in fine-grained hypocrystalline feldspatic groundmass.

**Passa Quatro**

The main rock-types are hypersolvus *nepheline syenites*, characterized by large, abundant alkali feldspar crystals with variable amounts of interstitial to euhedral nepheline and rare sodalite or analcime. In rare subsolvus types, plagioclase appears mantled by large alkali feldspar rims. The rocks are medium to coarse-grained, with prevailing hypidiomorphic to slightly porphyritic textures. There are local texture variations to fine-grained or layered trachytic nepheline syenites. Mafic minerals (<10 vol%) are represented by clinopyroxene (augite to aegirine), amphibole (pargasitic to hastingsitic hornblende usually overgrowing on the clinopyroxene), and more occasionally biotite. Accessory minerals are Ti-magnetite, titanite, apatite and rare låvenite, eudyalite and pyrochlore.

*Phonolite* dykes have three main variants: 1) aphanitic varieties, containing sanidine, nepheline, clinopyroxene, amphibole, titanite and minor amounts of biotite, opaques and apatite; 2) porphy-ritic, showing phenocrysts of sanidine, biotite, opaques and occasional pseudoleucite set in a groundmass of nepheline, alkali feldspar and subordinate plagioclase with apatite and titanite as ubiquitous accessories (miaskitic type), and 3) phenocrysts of sanidine, nepheline and subordinate green clinopyroxene, amphibole and titanite set in a groundmass of the same minerals (agpaitic type).

*Magmatic breccias* are polymictic, with angular to subangular clasts of feldspar and clinopyroxene megacrystals and volcanic/subvolcanic felsic lithic types, set in a fine-grained to aphanitic phonolitic groundmass.

**São Sebastião island**

Syenitic stocks mainly consist of *quartz-bearing* and *nepheline-bearing syenites*, and subordinate *nepheline syenites*. Predominantly, they are medium to coarse-grained with large crystals of alkali feldspar, although locally fine-grained varieties (e.g. nepheline microsyenites) also occur locally. Main mafic minerals are clinopyroxene, biotite and amphibole. Typical accessory minerals include apatite, titanite and opaques; chevkinite-perrierite, pyrochlore and thorite rarely occur.

The *layered gabbros* are medium to coarse-grained with inequigranular to equigranular textures. Cumulatic textures are also common. Main mafic minerals are salitic clinopyroxene, olivine, opaques, kaersutite and Ti-rich biotite. Orthopyroxene occurs in small traces in transitional rocks. The main felsic phase is labradorite, whereas alkali feldspar locally occurs in the northern region. Alkaline varieties have modal nepheline up to 5%, while the transitional ones contain occasional traces of nepheline. Accessories are apatite and titanite.

*Phonolite* dykes are slightly porphyritic with phenocrysts of alkali feldspar, salitic clinopyroxene, biotite, rare opaques and apatite set in an aphanitic groundmass of sanidine, nepheline, sodalite and aegirine-augite.

*Quartz trachyte* dykes consist of pheno and microphenocrysts of alkali feldspar, opaques and quartz. The groundmass is composed of alkali feldspar and subordinate biotite, amphibole, quartz, opaques, glass and carbonates.

*Mafic alkaline* dykes have titanoaugite and olivine (occasional amphibole, biotite, plagioclase, opaques and apatite) phenocrysts set in a groundmass of clinopyroxene, olivine, opaques, alkali feldspar, apatite and interstitial carbonates.

*Ultramafic* dykes (picritic lamprophyre) exhibit cumulatic textures, with phenocrysts of olivine and clinopyroxene (in some cases) set in a fine-grained groundmass mainly of clinopyroxene and chromite.

## MINERAL CHEMISTRY

Source data from representative and average analyses of syenitic bodies and some alkaline dykes for the above occurrences are reported in Bellieni *et al.* (1990) and Brotzu *et al.* (1992, 1997). Mineral compositions are plotted in Figs. 4 to 9.

### Feldspars

Plagioclase in the Itatiaia syenitic rocks ranges from $An_{45}$ to $An_{16}$. Particularly, silica-undersaturated syenites (both normative corundum-bearing and corundum-free rock-types) contain plagioclase varying from $An_{45}$ to $An_{30}$. Some amphibole-bearing nepheline syenites may present plagioclase $An_{20\text{-}15}$. Quartz syenites and granites have plagioclase up to $An_{40}$ at the core, usually mantled by anorthoclase (average $Or_{11}An_{19}$). Plagioclase is rare in the Passa Quatro complex, being characterized by oligoclase

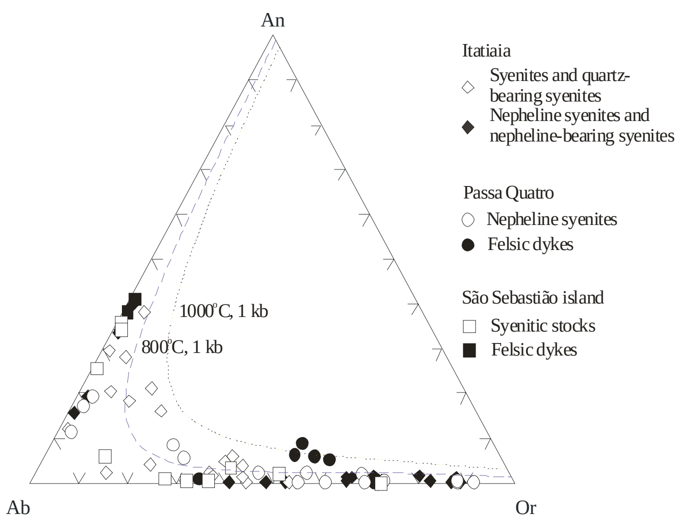


Fig. 4. Feldspars from the Itatiaia, Passa Quatro and São Sebastião island complexes in the An-Ab-Or (mol%) diagram. Solvus-solidus intersections, according to Elkins & Grove (1990) model, are plotted using SOLVCALC (Wen & Nekvasil, 1994). Data source: Bellieni *et al.* (1990) and Brotzu *et al.* (1992, 1997).

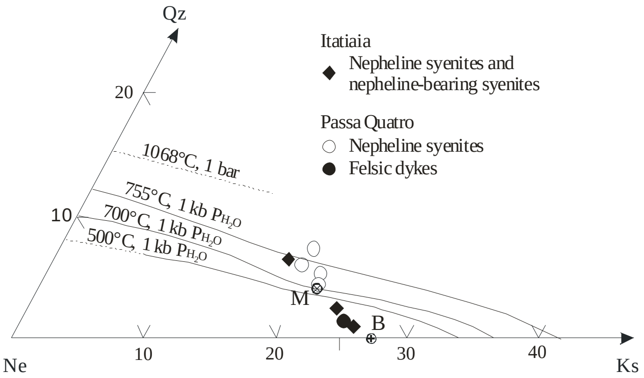


Fig. 5. Nephelines from the Itatiaia, Passa Quatro and São Sebastião island complexes in the Qz-Ne-Ks (wt %) diagram. Equilibrium temperatures according to Hamilton (1961). Data source as in Fig. 4.

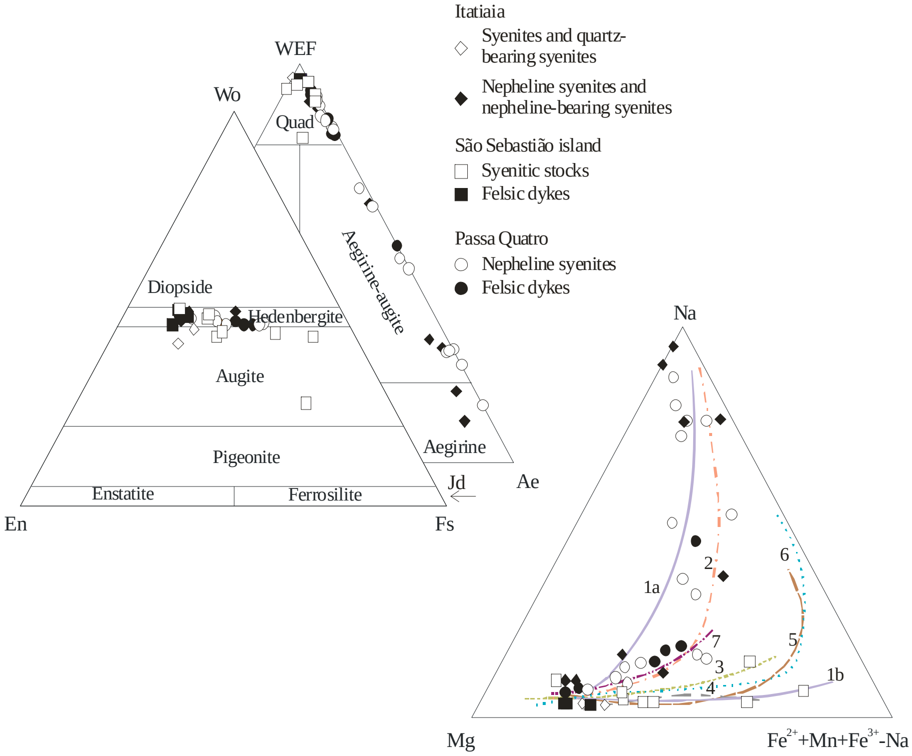


Fig. 6. Classification of clinopyroxenes from the Itatiaia, Passa Quatro and São Sebastião island complexes according to Morimoto (1988) and Na-Mg-($Fe^{2+}$+$Fe^{3+}$+Mn-Na) diagrams. Main trends of other syenitic complexes of Serra do Mar Alkaline Province are shown for comparison: 1) Búzios island (Alves, 1996; a, b-central and peripheric areas, respectively); 2) Itaúna (Valença, 1980); 3) Morro Redondo (Brotzu *et al.*, 1989); 4) Soarinho (Valença, 1980); 5) Vitória island (Motoki, 1986); 6) Monte de Trigo island (Enrich, 2000); 7) Tanguá-Rio Bonito-Morro de São João (Valença, 1980). Data source as in Fig. 4.

($An_{21-12}$) usually rimmed by anorthoclase ($Or_{30-26}$ $An_{9-5}$). Plagioclase in the São Sebastião island ranges from $An_{43}$ to $An_{26}$ both in the syenitic rock-types (as in Itatiaia) and in trachytic dykes (Fig. 4).

Alkali feldspar in Itatiaia displays a narrow compositional variation, i.e. from $Or_{72}Ab_{28}$ to $Or_{36}Ab_{62}$ in all the petrographic types, as a single crystal, even in graphic intergrowths, or mantling the plagioclase. Extreme compositions, i.e. $Or_{93-77}$ or Ab around 95 wt%, are found as exsolution phases or at the rims of some alkali feldspar crystals.

In Passa Quatro, alkali feldspar is zoned from $Or_{35}Ab_{64}$ (early crystallization) to $Or_{89}$ $Ab_{11}$ (late crystallization), with An up to 9 wt%.

In the São Sebastião island, alkali feldspar varies from $Or_{72}Ab_{28}$ (early crystallization) towards

$Or_{27}Ab_{72}$ (late crystallization). Therefore, chemical variations in alkali feldspar are the same for the three complexes, although Passa Quatro and São Sebastião island complexes have opposite evolution trends and Itatiaia displays both trends.

In the $KAlSi_3O_8$-$NaAlSi_3O_8$-$CaAl_2Si_2O_8$ system at $P_{H_2O}$=1.0 kb, most of feldspar compositions indicate temperatures below 800°C (Elkins & Groove, 1990), except for the Passa Quatro dykes and some Itatiaia quartz syenites with temperatures below 1000°C.

Nephelines

In the silica-undersaturated rock-types of the Itatiaia and Passa Quatro complexes, the nephelines (Fig. 5) range in composition from $Ne_{68}Q_{16}Ks_{16}$ to $Ne_{75}Q_2Ks_{23}$, close to the Morozewicz composition (Tilley, 1954). On the other hand, one Passa Quatro phonolitic dyke has a composition of $Ne_{75}Q_3Ks_{22}$, close to the Buerger composition (Tilley, 1954).

Average nepheline equilibrium temperatures, according to Hamilton (1961), are 500°C in Itatiaia syenitic rocks, 755°C in Passa Quatro nepheline syenites and below 500°C in Passa Quatro phonolitic dyke.

No analyses of nephelines are available for São Sebastião island syenitic rocks, although they are described in the petrographic literature.

Clinopyroxenes

Itatiaia clinopyroxenes (Fig. 6) from quartz-bearing syenites are classified as diopside. In silica-undersaturated syenitic varieties, the mineral ranges from diopside, with ferrian variants, and ferrian-sodian hedenbergite to aegirine-augite and aegirine.

Passa Quatro clinopyroxenes from nepheline syenites and dykes are similar to those from Itatiaia. Their compositions range from diopside, with ferrian and ferrian-sodian variants, and hedenbergite, with ferrian-sodian and sodian variants, to aegirine-augite and aegirine. Mg-richer clinopyroxenes are related to the core of zoned crystals, often mantled by amphiboles, the latter minerals suggesting late magmatic re-equilibration.

São Sebastião island clinopyroxenes have restricted compositions, ranging from diopside, with ferrian subsilicic variants, to augite, with ferrian-sodian variants. Differently from the Itatiaia and Passa Quatro clinopyroxenes, the strong Na enrichment is absent.

Such different trends are compatible with the main trends of other syenitic complexes of the Serra do Mar Alkaline Province (Fig. 6). Na-rich clinopyroxenes are typical in peralkaline magmas and could be crystallized at different stages of magmatic evolution (Morbidelli *et al.*, 1995).

Amphiboles

Amphiboles (classification after Leake, 1997) display two distinct compositional trends for the nepheline-bearing and quartz-bearing syenitic lithotypes, characterized by different contents of Si in T-sites and Na+K in A-sites (Fig. 7). According to Brotzu *et al.* (1997), the presence of both amphibole evolution trends in the same complex suggests two distinct liquid lines of descent.

Magnesiohastingsite and hastingsite are the dominant amphibole in the nepheline syenites and alkali syenites of the Passa Quatro and Itatiaia complexes, although hastingsite is also found substituting clinopyroxene in the Serraria syeno-diorite. Potassian and manganoan varieties are quite common, the first ones related to the potassic character of the host-rocks (Brotzu *et al.*, 1992, 1997). Early crystallized magnesiokatophorite and ferri-magnesiotaramite are also present in the Itatiaia and Passa Quatro nepheline syenites, respectively. Potassian kaersutites were found in one Passa Quatro dyke.

Amphiboles in the Itatiaia and São Sebastião quartz-bearing syenites range from magnesio-hornblende, edenite and actinolite to richterite, ferrorichterite, katophorite and arfvedsonite. Almost all the Itatiaia quartz-bearing syenite amphiboles are manganoan varieties. Main substitution pairs are $Ca+Al^{IV}=Na+Si$ and Mg=Fe+Mn.

## Biotites

In Itatiaia, biotite compositions are close to the phlogopite-annite join (mg# 0.79-0.24; Fig. 8) with some varieties trending towards siderophyllite-rich compositions. Ti and Mg-richer biotites ($TiO_2$ and MgO up to 7.6 and 19.5 wt%, respectively) are common in the silica-oversaturated rock-types.

Passa Quatro biotites also belong to the phlogopite-annite series, with compositional ranges similar to those of the Itatiaia complex.

No analyses of biotites for the São Sebastião rocks are presently available.

## Oxides

Itatiaia, Passa Quatro and São Sebastião island complexes have Ti-magnetite and ilmenite as main oxide phases (Fig. 9A). In Itatiaia, magnetite and ilmenite solid solutions occur with relatively high MnO contents, i.e. up to 7.2 and 34.4 wt%, respectively. Magnetite ranges from 34 to 1 ulvöspinel mol% in the silica-oversaturated syenites, whereas a more restricted range is shown by magnetite from nepheline syenites, i.e. 7.7 to 0.2 ulvöspinel mol%. Hercynite crystals ranging from 48 to 51 wt% $Al_2O_3$ are only found in corundum-bearing syenites.

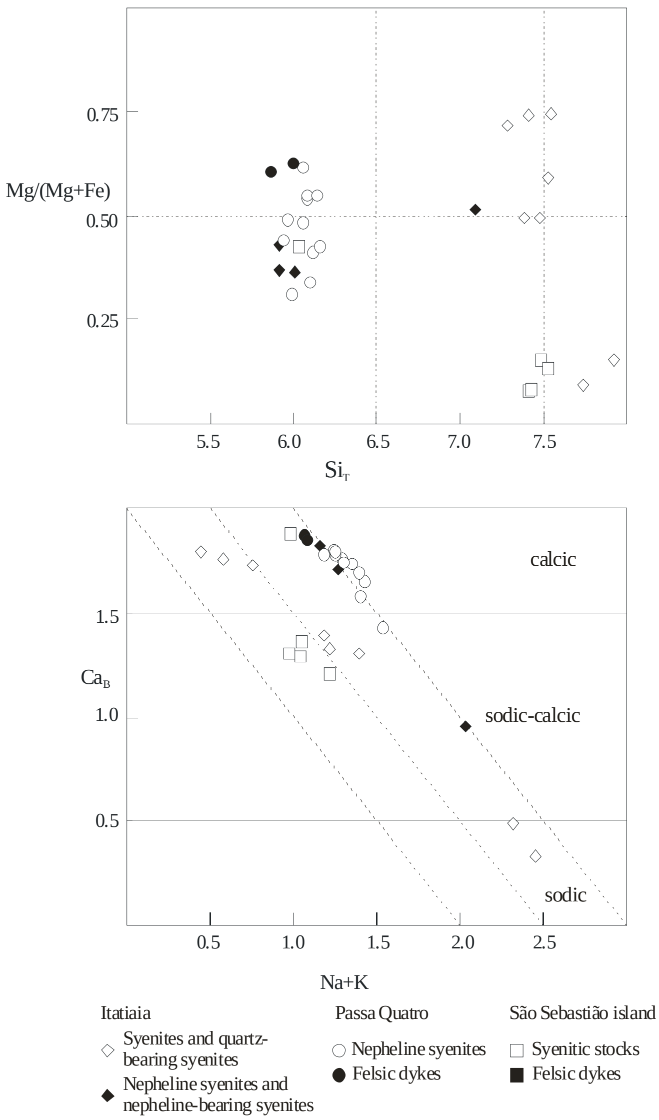


Fig. 7. Mg/Mg+Fe vs. $Si_T$ and $Ca_B$ vs. Na+K diagrams of amphiboles from the Itatiaia, Passa Quatro and São Sebastião island complexes. Data source as in Fig. 4.

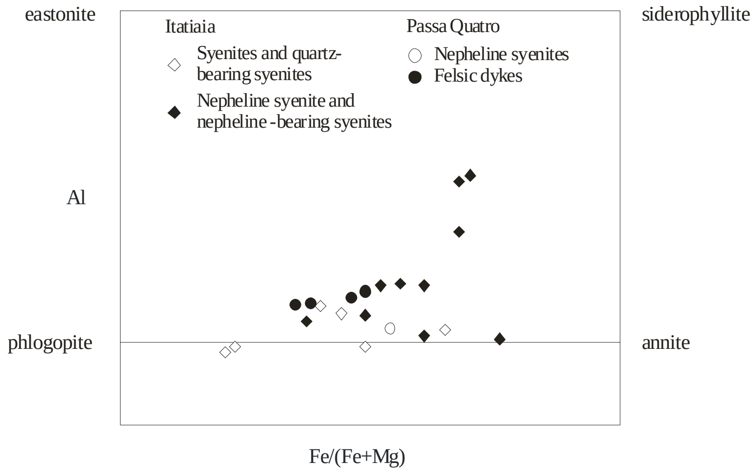


Fig. 8. Classification of biotites from the Itatiaia and Passa Quatro complexes in the Al vs. Fe/(Fe+Mg) diagram (Deer, 1992). Data source as in Fig. 4.

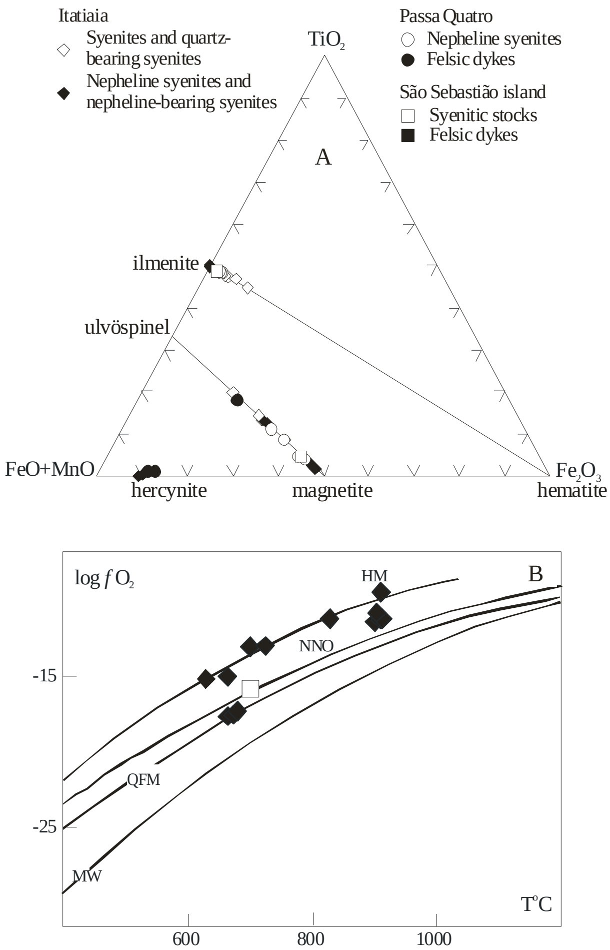


Fig. 9. A) $TiO_2$-(FeO+MnO)-$Fe_2O_3$ diagram (mol%) showing ilmenite and magnetite solid solutions (Deer *et al.*, 1992). B) T (°C) vs. log $fO_2$ for Ti-magnetite and ilmenite pairs (Andersen & Lindsley, 1988) from the Itatiaia and São Sebastião island complexes. Buffers: HM, haematite-magnetite; NNO, nickel-nickel oxide; QFM, quartz-magnetite-fayalite; MW, magnetite-wüstite. Data source as in Fig. 4.

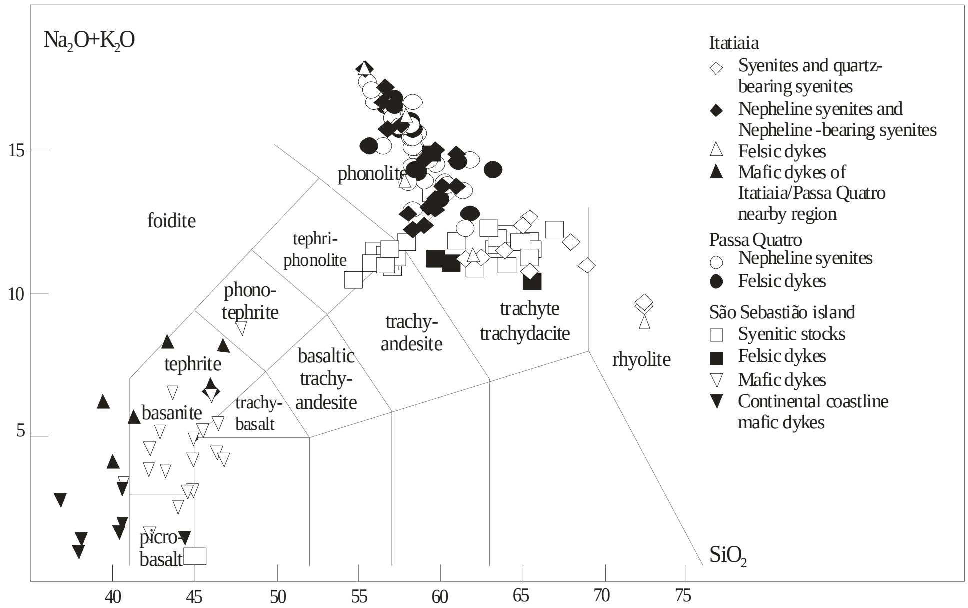


Fig. 10. TAS diagram (total alkalis vs. silica in wt%, cf. Le Maitre, 2002) for rock-types from the Itatiaia, Passa Quatro and São Sebastião island complexes. Data source: Bellieni *et al.* (1990), Brotzu *et al.* (1992, 1997), Garda *et al.* (1995) and Thompson *et al.* (1998).

In the Passa Quatro nepheline syenites, magnetite presents a range from 8 to 43 ulvöspinel mol% and up to 6.4 wt% MnO, and Mn-rich ilmenite exhibits a variation of 9.2-10.5 wt% MnO. Occurrences of hercynite are also found in some Passa Quatro felsic dykes.

In the São Sebastião island syenitic stocks, magnetite has aproximately 10 ulvöspinel mol%, coexisting with ilmenites showing about 6 mol% $Fe_2O_3$.

The high MnO concentrations in magnetites, in all of the above mentioned syenitic intrusions, follow the compositions of other alkaline plutonic rocks worldwide (Frost & Lindsley, 1991).

Coexisting magnetite-ilmenite pairs in the Itatiaia and Serraria stocks point to temperatures from 950 to 630°C, and conditions of $fO_2$ higher than the QFM buffer (Andersen & Lindsley, 1988; Fig. 9b). They indicate a relatively oxidized environment. The relatively high $fO_2$ is consistent with the absence of fayalite in all syenitic rocks (e.g. Brotzu *et al.*, 1997), except for the São Sebastião stock.

### Other phases

Mineral chemistry of some accessory and rare phases of the Itatiaia rocks have also been determined by Brotzu *et al.* (1997). Garnet has a melanite composition and is relatively Ti and Al-poor. A rare Zr-Nb-Ca-Na silicate was determined and classified as rosenbuschite by Brotzu *et al.* (1997). However, its compositions, with high Nb values (up to 12 wt%), indicate that it should correspond to wöhlerite, similar to other worldwide wöhlerites described by Mariano & Roeder (1989).

Augusto (2003) and Augusto & Vlach (2004) have recently reported the chemistry of fayalite ($Fa_{98-93}$), and other rare accessory minerals such as thorite, chevckinite and pyrochlore in the São Sebastião syenitic stock.

## PETROCHEMISTRY

Table 1 shows representative and average analyses (data source: Bellieni *et al.*, 1990; Brotzu *et al.*, 1992, 1997; Garda, 1995; Garda *et al.*, 1995; Thompson *et al.*, 1998).

The TAS diagram shows a bimodal distribution (Fig. 10): the alkaline mafic dykes from Itatiaia-Passa Quatro and São Sebastião island partially fit the tephrite-basanite field; the Itatiaia plutonic rocks and felsic dykes extend from the phonolite (nepheline syenite) to the rhyolite (granite) fields;

the other intrusive and felsic dykes from Passa Quatro and São Sebastião island straddle across the same alkaline fields, defining subgroups in the same Itatiaia trend.

Mafic dykes variation in the $Na_2O$ vs. $K_2O$ diagram (Fig. 11) is consistent with that of the associated felsic rocks. All these complexes have transitional to potassic affinities (Comin-Chiaramonti *et al.*, 1997).

In the Harker diagrams (Fig. 12) the mafic group (mg# 0.65-0.38) shows interelementary coherent variations, e.g. $TiO_2$, $FeO_{tot}$, MgO, CaO and $P_2O_5$ decrease and $Al_2O_3$, $Na_2O$ and $K_2O$ increase with increasing $SiO_2$ towards the sialic groups. Such inter-elementary variations are consistent with mafic mineral fractionation processes, suggesting that the

Table 1. Representative and average analyses for Itatiaia, Passa Quatro and São Sebastião island main rock-types, measured and time-integrated isotopic ratios ($Sr_i$, $Nd_i$, and ε notations, respectively), Eu/Eu*, $(La/Sm)_N$ and $(Gd/Yb)_N$ C1 chondritic normalization, and model ages (depleted mantle, $T^{DM}$). A.I.=$(Na_2O+K_2O)/Al_2O_3$, molar ratio. Data source: Bellieni *et al.* (1990), Brotzu *et al.* (1992, 1997), Garda (1995), Garda *et al.* (1995), Thompson *et al.* (1998 and therein references), and unpublished data by E.M. Piccirillo (written comunication).

| **Itatiaia** | Nepheline syenite | Syenite | Corundum-bearing syenite | Granite | Mafic dykes | **Passa Quatro** | Nepheline syenite | Phonolite dykes |
|---|---|---|---|---|---|---|---|---|
| wt% | | | | | | | | |
| $SiO_2$ | 56.41 (0.59) | 60.11 (0.98) | 58.08 | 70.47 (2.32) | 43.53 (2.40) | | 60.29 | 57.77 (3.06) |
| $TiO_2$ | 0.38 (0.05) | 0.52 (0.14) | 0.39 | 0.27 (0.07) | 3.81 (1.02) | | 0.73 | 0.82 (0.12) |
| $Al_2O_3$ | 23.09 (1.45) | 20.36 (0.29) | 23.7 | 16.37 (1.02) | 13.85 (0.88) | | 19.98 | 20.42 (1.02) |
| $FeO_{tot}$ | 1.75 (0.91) | 2.43 (0.75) | 2.11 | 1.58 (0.44) | 11.42 (2.07) | | 2.09 | 2.38 (0.37) |
| MnO | 0.24 (0.05) | 0.28 (0.08) | 0.27 | 0.23 (0.11) | 0.20 (0.03) | | 0.19 | 0.17 (0.01) |
| MgO | 0.20 (0.13) | 0.52 (0.39) | 0.46 | 0.16 (0.04) | 6.91 (0.86) | | 0.41 | 0.40 (0.31) |
| CaO | 1.09 (0.32) | 1.04 (0.43) | 1.90 | 0.43 (0.18) | 10.27 (0.93) | | 1.39 | 1.71 (0.11) |
| $Na_2O$ | 8.13 (1.58) | 6.77 (1.89) | 4.76 | 5.29 (1.10) | 4.16 (0.55) | | 6.82 | 6.21 (0.91) |
| $K_2O$ | 8.46 (1.18) | 7.50 (1.25) | 8.03 | 5.02 (0.23) | 2.67 (1.74) | | 7.03 | 7.96 (0.41) |
| $P_2O_5$ | 0.05 (0.02) | 0.24 (0.20) | 0.05 | 0.04 (0.02) | 1.14 (0.21) | | 0.08 | 0.12 (0.04) |
| L.O.I. | n.d. | n.d. | n.d. | n.d. | 2.07 (1.67) | | 0.75 | 1.74 (1.70) |
| Sum | 99.80 | 99.77 | 99.75 | 99.86 | 100.03 | | 99.76 | 99.70 |
| A.I. | 0.98 | 0.95 | 0.86 | 0.86 | 0.70 | | 0.94 | 0.92 |
| ppm | | | | | | | | |
| Cr | n.d. | n.d. | n.d. | n.d. | 207 (28) | | 4 | 5 (1) |
| Ni | n.d. | n.d. | n.d. | n.d. | 140 (30) | | 10 | 12 (2) |
| Rb | 180 (52) | 169 (59) | 116 | 321 (88) | 69 (29) | | 164 | 170 (15) |
| Sr | 862 (601) | 328 (319) | 374 | 19 (19) | 1611 (363) | | 228 | 516 (435) |
| Ba | 121 (57) | 36 (26) | 78 | 16 (6) | 1249 (194) | | 40 | 50 (13) |
| Nb | 227 (59) | 152 (23) | 135 | 272 (62) | 122 (27) | | 216 | 153 (75) |
| Zr | 588 (323) | 619 (170) | 470 | 658 (293) | 364 (84) | | 347 | 588 (33) |
| Y | 57 (41) | 42 (10) | 37 | 91 (27) | 38 (3) | | 38 | 40 (1) |
| La | 181 (32) | 182 (23) | 301 | 149 (56) | 110 (25) | | 144 | 183 (16) |
| Ce | 318 (110) | 388 (122) | 553 | 343 (134) | 198 (34) | | 265 | 331 (40) |
| Pr | 24 (4) | 36 (10) | 70 | 44 (21) | 26 (6) | | | |
| Nd | 60 (24) | 124 (48) | 187 | 102 (42) | 100 (22) | | 117 | 125 (7) |
| Sm | 6.3 (1.0) | 16.1 (5.9) | 29.9 | 21.1 (8.3) | 16.0 (2.9) | | 19.0 | 18.8 (0.4) |
| Eu | 1.74 (0.35) | 3.2 (2.0) | 6.0 | 0.80 (0.31) | 4.61 (0.71) | | 6.5 | 4.8 (0.1) |
| Gd | 6.11 (0.57) | 13.8 (3.2) | 24.5 | 19.1 (3.0) | 13.76 (0.93) | | 16.04 | 15.82 (0.31) |
| Dy | 4.80 (0.70) | 7.7 (3.4) | 11.7 | 12.8 (4.6) | 7.8 (0.8) | | 8.50 | 8.30 (0.20) |
| Yb | 3.04 (1.18) | 2.72 (0.41) | 4.55 | 1.89 (0.55) | 2.52 (0.09) | | 2.65 | 3.61 (0.04) |
| Lu | 0.36 (0.14) | 0.45 (0.21) | 1.04 | 0.86 (0.09) | 0.36 (0.03) | | 0.41 | 0.50 (0.02) |
| Eu/Eu* | 0.85 | 0.64 | 0.25 | 0.12 | 0.93 | | 1.10 | 0.83 |
| $(La/Sm)_N$ | 18.1 | 7.1 | 10.1 | 4.4 | 4.3 | | 4.8 | 6.1 |
| $(Gd/Yb)_N$ | 1.6 | 4.1 | 4.3 | 8.2 | 5.5 | | 4.9 | 3.5 |
| $^{87}Sr/^{86}Sr$ | 0.70547 (27) | 0.70656 (82) | 0.70642 (1) | 0.75557 (1) | 0.70503 (13) | | 0.70737 (15) | 0.70683 (18) |
| $^{143}Nd/^{144}Nd$ | 0.51228 (9) | 0.51238 (9) | 0.51247 (1) | 0.51258 (1) | 0.51247 (8) | | 0.51244 (11) | 0.51242 (17) |
| $Sr_i$ (72 Ma) | 0.70485 | 0.70504 | 0.70550 | 0.70533 | 0.7049 | (77 Ma) | 0.70509 | 0.70508 |
| $Nd_i$ (72 Ma) | 0.51225 | 0.51234 | 0.51243 | 0.51252 | 0.51242 | (77 Ma) | 0.51239 | 0.51237 |
| εSr | 3.34 | 5.94 | 12.57 | 10.19 | 4.10 | | 6.85 | 6.66 |
| εNd | -5.76 | -3.95 | -2.36 | -0.47 | -2.40 | | -2.89 | -3.21 |
| $T^{DM}$ | 855 | 838 | 900 | 928 | 851 | | 899 | 872 |

Table 1 (continued).

| **São Sebastião island** | Serraria syenite | São Sebastião syenite | Mirante syenite | Basanite dykes | Tephrite dykes | Phonolite dykes | Ultramafic dykes from coastline |
|---|---|---|---|---|---|---|---|
| wt% | | | | | | | |
| $SiO_2$ | 62.15 | 65.49 (0.10) | 62.86 | 43.31 (1.50) | 45.99 | 59.42 | 38.95 (3.16) |
| $TiO_2$ | 0.92 | 0.42 (0.13) | 0.66 | 2.22 (0.24) | 2.64 | 0.10 | 1.58 (0.62) |
| $Al_2O_3$ | 18.49 | 16.69 (1.04) | 19.47 | 12.59 (1.29) | 17.35 | 18.96 | 8.80 (2.18) |
| $FeO_{tot}$ | 4.08 | 4.24 (0.44) | 2.24 | 11.35 (0.67) | 12.84 | 5.05 | 10.52 (1.45) |
| MnO | 0.15 | 0.20 (0.01) | 0.08 | 0.21 (0.04) | 0.23 | 0.44 | 0.15 (0.02) |
| MgO | 0.85 | 0.29 (0.07) | 0.74 | 10.87 (3.03) | 5.94 | 0.10 | 15.09 (5.36) |
| CaO | 2.09 | 1.17 (0.06) | 1.52 | 14.91 (1.78) | 7.83 | 1.03 | 13.72 (3.54) |
| $Na_2O$ | 4.82 | 5.44 (0.17) | 4.85 | 1.52 (0.50) | 3.42 | 9.17 | 0.66 (0.40) |
| $K_2O$ | 6.03 | 5.97 (0.01) | 7.40 | 1.78 (0.46) | 3.02 | 5.69 | 0.90 (0.39) |
| $P_2O_5$ | 0.41 | 0.10 (0.01) | 0.20 | 0.82 (0.32) | 0.76 | 0.03 | 0.37 (0.32) |
| L.O.I. | 0.97 | 1.14 (0.10) | 0.97 | n.d. | n.d. | n.d. | 9.10 (4.21) |
| Sum | 100.96 | 101.15 | 100.99 | 99.58 | 100.41 | 99.8 | 99.85 |
| A.I. | 0.78 | 0.92 | 0.82 | 0.35 | 0.51 | 1.12 | 0.22 |
| ppm | | | | | | | |
| Cr | 1 | 2 (1) | 1 | 465 (303) | 12 | 1 | 1220 (883) |
| Ni | 5 | 3 (1) | 1 | 212 (124) | 34 | 3 | n.d. |
| Rb | 84 | 105 (3) | 120 | 58 (28) | 81 | 611 | 31 (16) |
| Sr | 220 | 32 (6) | 119 | 961 (265) | 1218 | 34 | 491 (326) |
| Ba | 1998 | 189 (46) | 259 | 754 (363) | 855 | 35 | 358 (211) |
| Nb | 73 | 55 (13) | 43 | 60 (11) | 110 | 459 | 33 (10) |
| Zr | 218 | 174 (87) | 192 | 233 (39) | 341 | 2411 | 151 (61) |
| Y | 32 | 31 (4) | 20 | 29 (6) | 36 | 125 | 25 (6) |
| La | 72 | 39 (2) | 54 | 55 (12) | 68 | 264 | 25 (16) |
| Ce | 132 | 80 (4) | 97 | 112 (25) | 122 | 424 | 55 (34) |
| Nd | 55 | 41 (3) | 41 | 53 (11) | 50 | 143 | 29 (16) |
| Sm | 10.2 | 8.5 (1.0) | 7.3 | 9.7 (1.7) | 9.0 | 24.3 | 6.0 (2.7) |
| Eu | 4.65 | 2.08 (0.30) | 2.41 | 2.94 (0.47) | 2.71 | 0.73 | 1.83 (0.82) |
| Gd | 9.10 | 7.96 (0.45) | 6.38 | 8.66 (0.81) | 10.03 | 23.50 | 6.63 (1.57) |
| Dy | 5.78 | 5.77 (0.73) | 3.81 | 5.51 (1.01) | 5.30 | 18.31 | 3.81 (1.47) |
| Yb | 2.06 | 2.17 (0.11) | 1.34 | 1.99 (0.44) | 1.75 | 9.82 | 1.35 (0.51) |
| Lu | 0.35 | 0.39 (0.02) | 0.27 | 0.30 (0.06) | 0.33 | 1.64 | 0.19 (0.08) |
| Eu/Eu* | 1.45 | 0.76 | 1.06 | 0.96 | 0.87 | 0.09 | 1.24 |
| $(La/Sm)_N$ | 4.4 | 2.9 | 7.1 | 3.6 | 4.8 | 6.8 | 2.47 |
| $(Gd/Yb)_N$ | 3.6 | 3.0 | 3.8 | 3.5 | 4.6 | 1.9 | 3.33 |
| $^{87}Sr/^{86}Sr$ | 0.70655 (2) | | 0.70855 (2) | 0.70508 (11) | 0.70458 (2) | | |
| $^{143}Nd/^{144}Nd$ | | | 0.51270 (2) | 0.512700 (2) | 0.51256 (1) | | |
| $Sr_i$ (81 Ma) | 0.70528 | | 0.70519 | 0.70488 | 0.70436 | | |
| $Nd_i$ (81 Ma) | | | 0.51264 | 0.51264 | 0.51250 | | |
| εSr | 9.54 | | 8.32 | 3.87 | -3.51 | | |
| εNd | | | 2.13 | 2.10 | -0.61 | | |
| $T^{DM}$ | | | 619 | 636 | 819 | | |

more evolved mafic rocks (Brotzu *et al.*, in this volume) have a tephrite-basanite parent magma.

In particular, some alkaline ultramafic dykes from the coastline, near the São Sebastião island (mainly picritic lamprophyres), have different patterns of $FeO_{tot}$, $TiO_2$ and $P_2O_5$ due to the presence of cumulatic olivine (Garda *et al.*, 1995). Olivine compositions ($Fo_{85-87}$, cf. Garda *et al.*, 1995) indicate liquids in equilibrium with mg# from 0.64 to 0.68 (Kushiro & Walter, 1998), while whole-rock analyses determined mg# range from 0.77 to 0.83, confirming their cumulatic character.

The intermediate-acid group ($SiO_2$•54 wt%) displays an overall trend to constant concentration of $TiO_2$, $FeO_{tot}$, MgO and CaO, and negative correlations with $Al_2O_3$, $Na_2O$ and $K_2O$, suggesting feldspar fractionation. However, some major differences are quite apparent: the São Sebastião island rocks are characterized by higher FeO for the same $SiO_2$ contents, and by $Na_2O$ increase, similar to the corundum-normative rocks from the Itatiaia syenites.

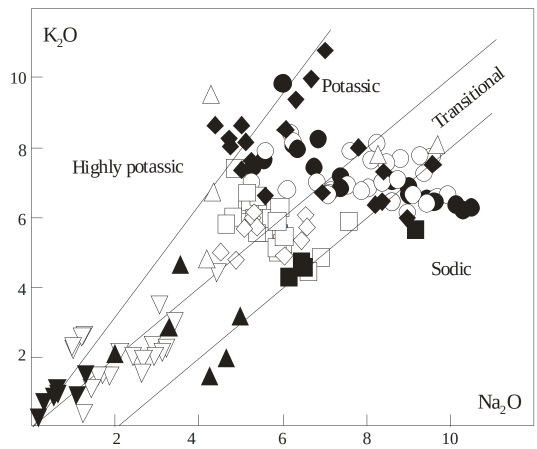


Fig. 11. $Na_2O$ vs. $K_2O$ diagram (wt%) (cf. Comin-Chiaramonti & Gomes, 1996) for rock-types from the Itatiaia, Passa Quatro and São Sebastião island complexes. Symbols and data source as in Fig. 10.

The above changes are also reflected on the large and random variations in $P_2O_5$, Rb, Ba, Sr, Zr, Nb and Y (Fig. 13), pointing to different degrees of alkali-feldspar accumulation and apatite, zircon and titanite fractionation.

It should be noted that the presence of amphibole rims or overgrowths on clinopyroxenes might be due to the control of microvariations in $P_{H_2O}$ (Parsons *et al.*, 1991). Moreover, cryptic variations in individual crystals may reflect crystallization from interstitial near-solidus liquids enriched in incompatible elements, thus suggesting that magmas have been evolved in independent microsystems, at least at later crystallization stages.

The agpaitic index increase may drive the evolution of clinopyroxenes and amphiboles which may contain Zr and Ti (Nb) in Na-richer compositions (Watson & Harrison, 1984), followed by a sudden fall to lower levels when these elements become compatible in other crystallizing phases (e.g. eudialyte, låvenite, wöhlerite). Moreover, different ratios of Zr/Nb (1.6-5.5; Fig. 13), even in the same complex and in the same rock-type, may indicate the presence of the above described typology.

In spite of the large variations of trace elements, incompatible elements (I.E.) from the felsic rock-types, normalized to the primitive mantle (McDonough & Sun, 1995), exhibit enriched subparallel patterns, but with negative spikes relative to Ba, Sr, P and Ti (Fig. 14A).

Mafic dykes (i.e. basanites and tephrites) associated with the three complexes present regular and similar patterns with decreasing enrichment from Rb to Lu. The main difference regards the relative enrichment in I.E.: dykes from the Itatiaia-Passa Quatro region, São Sebastião island and the coastline near the São Sebastião island have average enrichments of 130, 80 and 40 times, respectively, relative to the primitive mantle model (McDonough & Sun, 1995). Different enrichments between the first two occurrences could be attributed to heterogeneous mantle sources or different degrees of partial melting and, for the third group (picritic lamprophyres), they could be due to the presence of cumulatic olivine.

Itatiaia-Passa Quatro and São Sebastião island mafic dykes I.E. patterns are similar to those from Trindade basanites and other Serra do Mar mafic varieties of potassic affinity, and even to the Poços de Caldas ankaramites and tephrites of sodic filiation (Fig. 14A).

Chondrite-normalized REE patterns (C1 chondrite, Fig. 14B; McDonough & Sun, 1995) highlight some important differences among the three complexes and rocks. Higher LREE enrichments relative to MREE and HREE are present in silica-undersaturated rock-types. Average $La_N/Yb_N$ ratios of Itatiaia nepheline syenites, alkali syenites and phonolite dykes, Passa Quatro nepheline syenites and phonolite dykes, and mafic dykes from the Itatiaia-Passa Quatro region are 44.5, 32.8 and 28.5, respectively. Otherwise, average $La_N/Yb_N$ ratios of Itatiaia quartz syenites, Mirante syenites, Serraria syenites, São Sebastião syenites and mafic dykes from the São Sebastião island and coastline are 22.7, 26.8, 23.9, 12.2 and 11.9, respectively. Although most data show regular patterns in REE diagrams, some silica-undersaturated felsic varieties of Itatiaia and Passa Quatro have a slight enrichment of HREE relative to MREE.

Itatiaia felsic rocks exhibit increasing Eu negative anomalies with increasing silica contents. This anomaly is pratically absent in most silica-undersaturated varieties, whereas in other nepheline syenites and alkali syenites Eu/Eu* ranges from 1.55 to 0.35. In quartz-bearing syenites Eu/Eu* varies from 0.26 to 0.08. Passa Quatro nepheline syenites and phonolite dykes have variable Eu/Eu*, ranging from 1.21 to 0.43. Serraria, Mirante and São Sebastião syenitic stocks from the São Sebastião island have Eu/Eu* of 1.51, 0.80 and 1.11, respectively, whereas its associated phonolitic dyke has Eu/Eu* of 0.10, comparable to that of the Itatiaia quartz-bearing syenites. Eu/Eu* anomaly is absent in all the associated mafic dykes, ranging from 0.92 to 1.13. In summary, the Eu behavior seems to indicate feldspar fractionation (e.g. Itatiaia quartz-bearing syenites and phonolite dykes from the São Sebastião island) or accumulation (e.g. Serraria syenites) processes in the host rock-types.

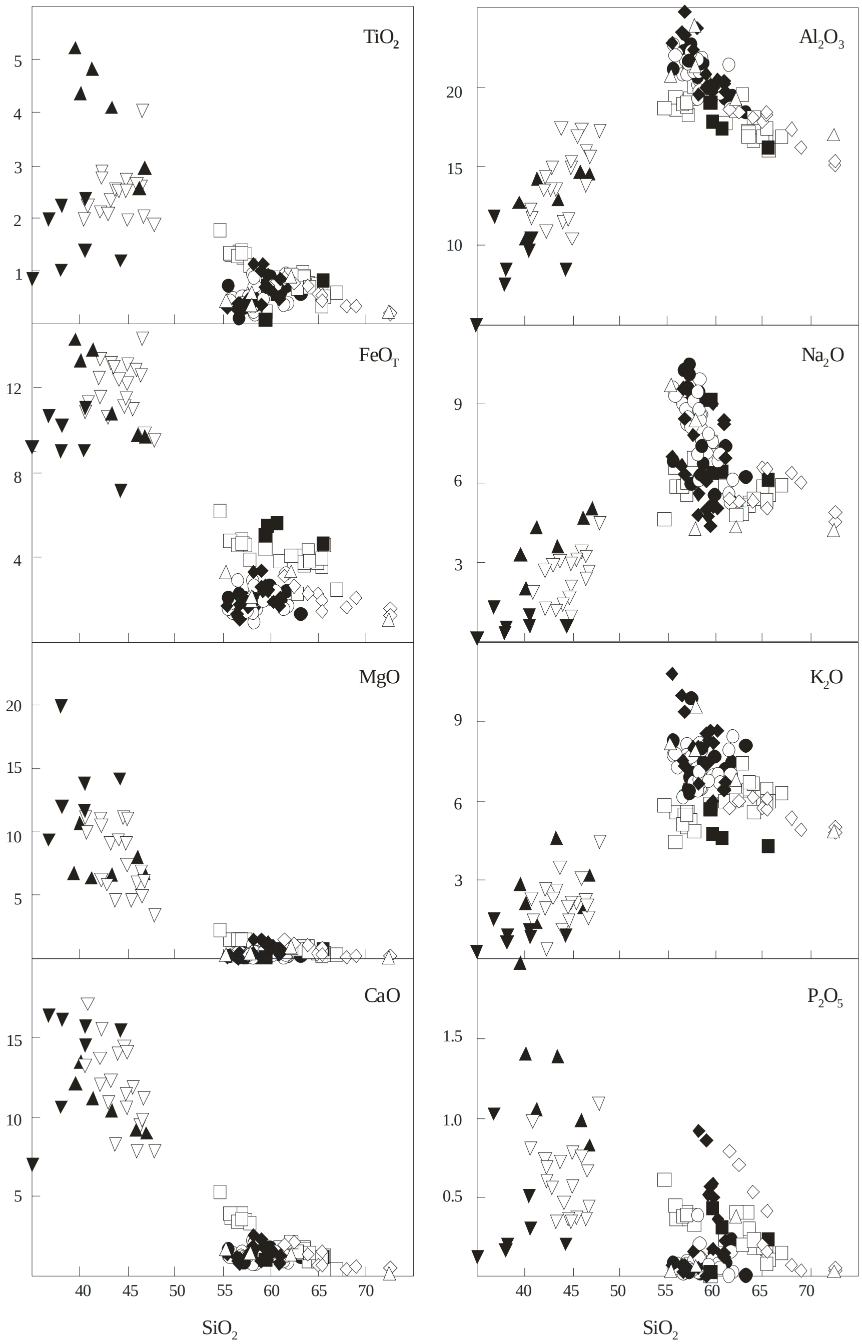


Fig. 12. Harker diagrams for major elements (wt%) of rock-types from the Itatiaia, Passa Quatro and São Sebastião island complexes. Symbols and data source as in Fig. 10.

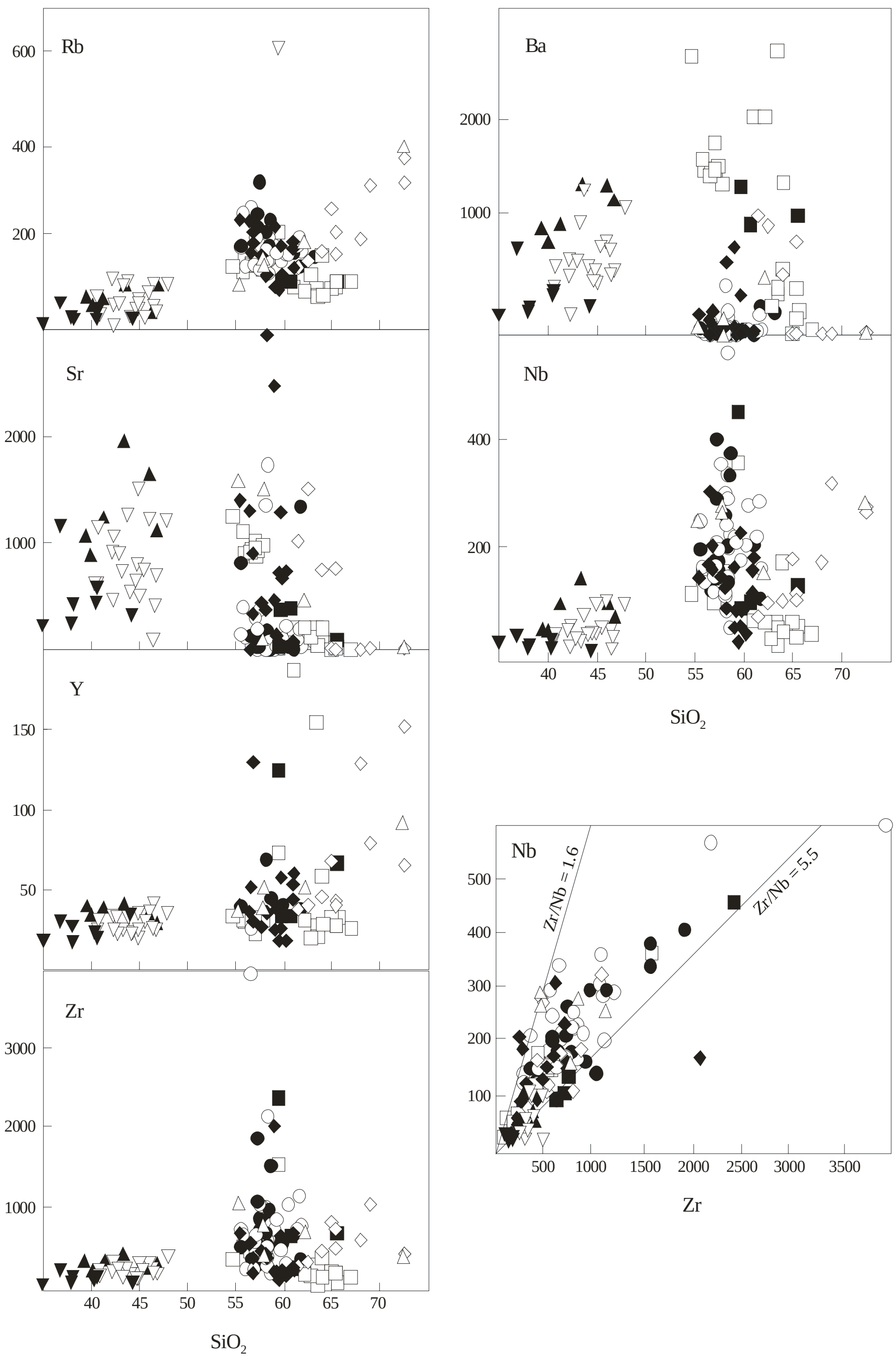


Fig. 13. Harker diagrams for trace elements (ppm) and Zr vs. Nb of rock-types from the Itatiaia, Passa Quatro and São Sebastião island complexes. Symbols and data source as in Fig. 10.

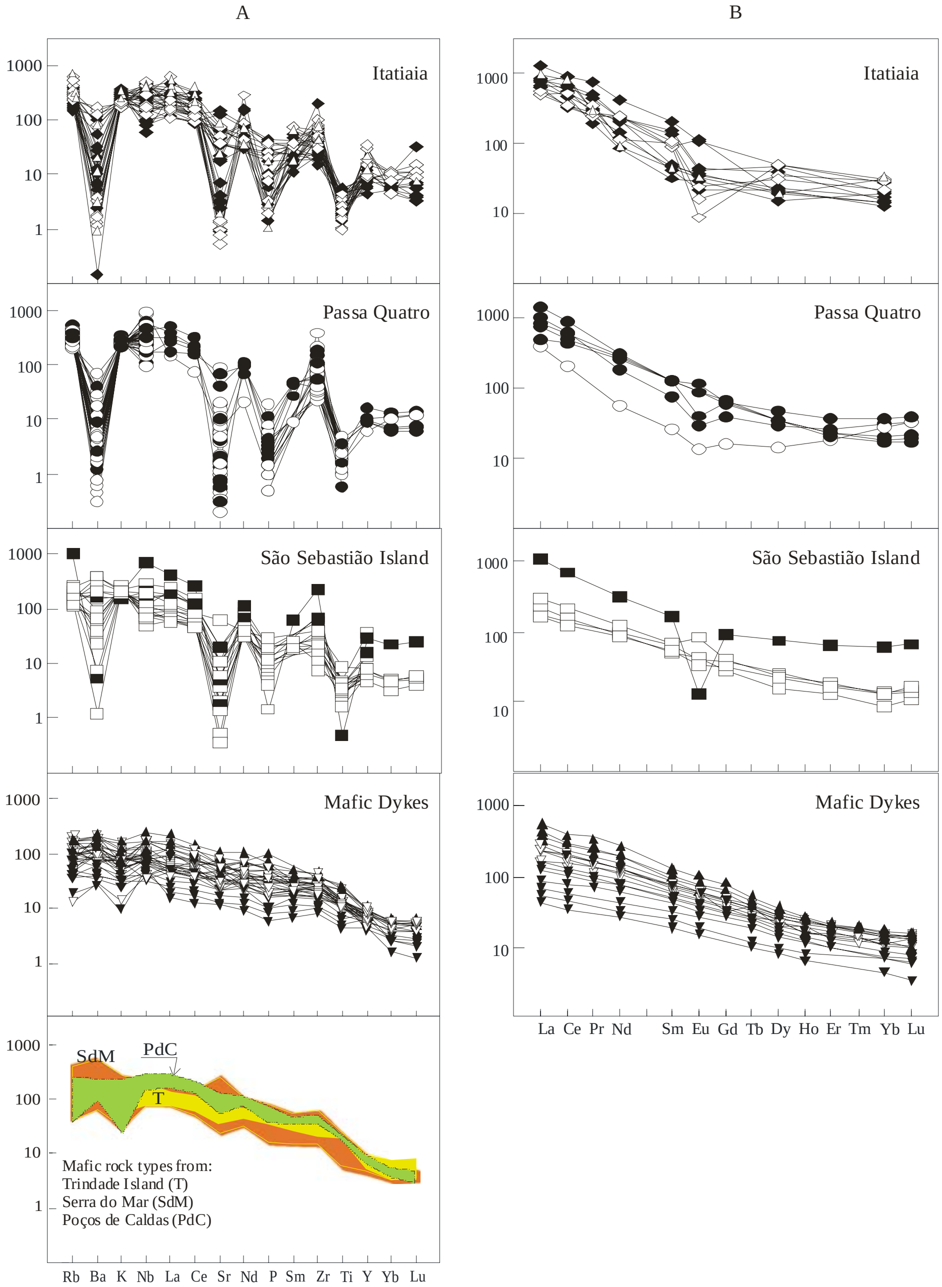


Fig. 14. A) Spidergrams of incompatible elements normalized to primordial mantle (McDonough & Sun, 1995); B) Chondrite-normalized (McDonough & Sun, 1995) REE distribution patterns of rock-types from Itatiaia, Passa Quatro and São Sebastião island complexes. Symbols and data source as in Fig. 10.

## Nd-Sr ISOTOPES

Average and representative analyses are presented in Table 1. The data are plotted on the εSr vs. εNd time-integrated diagram and compared with the tholeiitic and alkaline magmatism elsewhere in Brazil (Fig. 15). In general, εSr and εNd values range from -3.5 to 12.6 and from 2.1 to -5.8, respectively, being the highest εSr values given by the Itatiaia corundum-normative syenites and granites, thus suggesting that some radiogenic Sr-rich compositions could be due to a small participation of a crustal component.

The whole isotopic data follows the typical trend of uncontaminated Early Cretaceous tholeiitic and alkaline magmatism from the South American Platform. Most of the data have isotopic signature similar to that of the Serra do Mar Province

(Thompson *et al.*, 1998), except for some syenite and mafic dykes from the São Sebastião island, that fit the Ponta Grossa Arch field (Ruberti *et al.*, in this volume). The above exceptions suggest a mixed isotopic character for the alkaline magmatism and mantle radiogenic components in this region, probably due to large and small-scale metasomatism of the lithospheric mantle.

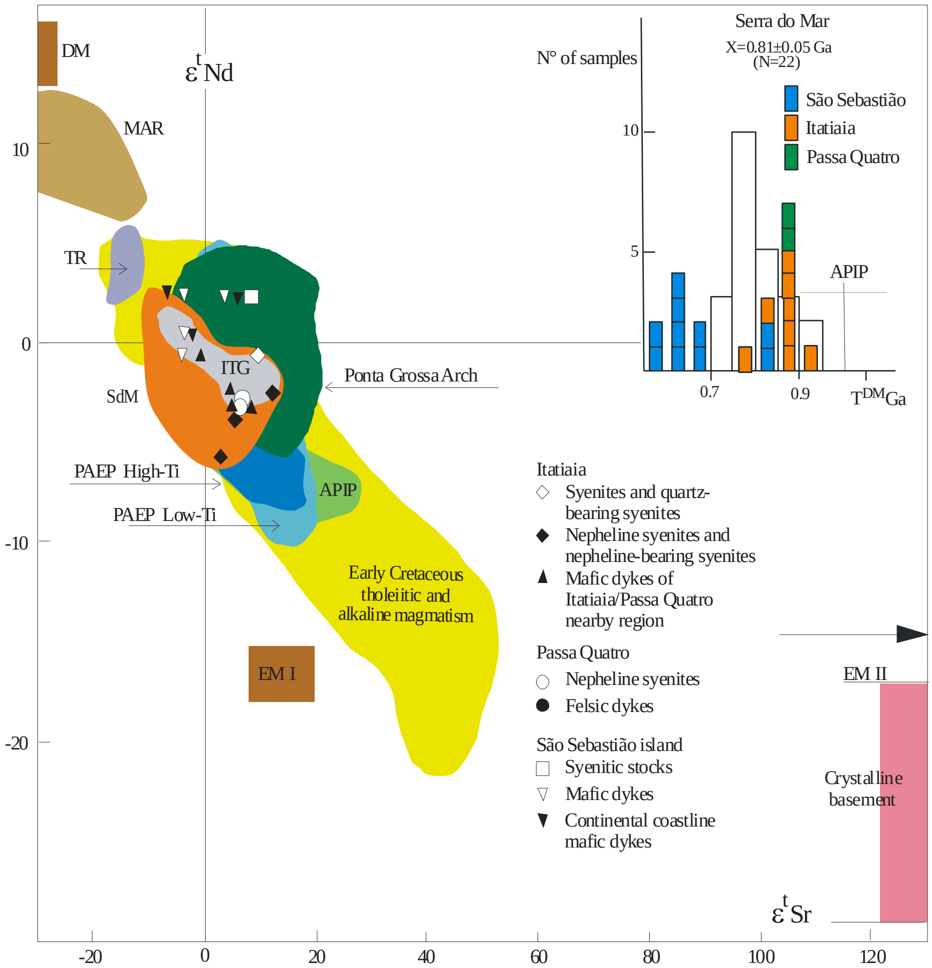


Fig. 15. Time-integrated, ε notations, $^{87}Sr/^{86}Sr$ (εSr) vs. $^{144}Nd/^{143}Nd$ (εNd) space. SdM: Serra do Mar; TR, Trindade and Martin Vaz islands; ITG, Inaccessible, Tristan and Gough islands; PAEP, Paraná-Etendeka Province; APIP, Alto Paranaíba Igneous Province; MAR, Median Atlantic Ridge; DM, EMI, EMII, depleted mantle and enriched mantle compositions, respectively. Data source: Hart (1984), Hart *et al.* (1992), Bizzi *et al.* (1993, 1995), Toyoda *et al.* (1994), Meyer *et al.* (1994), Garda *et al.* (1995), Gibson *et al.* (1995a, b, 1997, 1999), Carlson *et al.* (1996), Thompson *et al.* (1998), Marques *et al.* (1999), Siebel *et al.* (2000), Bennio *et al.* (2002) and unpublished data by M. Lustrino and E.M. Piccirillo. Inset: Nd model ages ($T^{DM}$) for the Serra do Mar rocks ($T^{DM}$ values: calculation of model dates relative to a depleted reservoir, $^{143}Nd/^{144}Nd$=0.513114 and $^{147}Sm/^{144}Nd$=0.222; Faure, 1986).

The latter peculiarity is also shown by model ages (calculated on the basis of depleted mantle; inset of Fig. 15), according to which a more recent age, i.e. around 625 Ma, is apparent for the São Sebastião island complex, similar to those calculated for phonolites and nepheline syenites from Poços the Caldas (692±54 Ma; Ulbrich *et al.*, 2003), but contrasting with some average model ages of Itatiaia, Passa Quatro and other Serra do Mar occurrences (800±50 Ma, Thompson *et al.*, 1998; Brotzu *et al.*, in this volume). Moreover, these model ages are quite different from the values obtained for the adjacent Alto Paranaíba Province (1.00±0.1 Ga; Gomes & Comin-Chiaramonti, in this volume), Poços de Caldas mafic rock-types (580-640 Ma; Vlach *et al.*, 1998) and Trindade island (470±60 Ma; Marques *et al.*, 1999).

According to the model of Gibson *et al.* (1995b) and Thompson *et al.* (1998), Trindade island, Alto Paranaíba Province and Serra do Mar Province magmatisms are related to the Trindade mantle plume. However, isotopic data of the Itatiaia, Passa Quatro and São Sebastião island complexes tend to fit the Inaccessible-Gough-Tristan da Cunha field (Fig. 15), well distinct from the Trindade island field.

## DISCUSSION AND FINAL REMARKS

Itatiaia, Passa Quatro and São Sebastião island alkaline complexes represent the largest syenitic intrusions in SE Brazil, after Poços de Caldas (Ulbrich *et al.*, in this volume). The distribution of these complexes, as already pointed out, is associated with two different alignments: Itatiaia and Passa Quatro in the first case, and São Sebastião, Serraria and Mirante, on São Sebastião island, in the second one. The geographical proximity of the Itatiaia and Passa Quatro syenitic massifs, in addition to geological/geomorphological, petrographic, geochemical and geochronological similarities, could support their comagmatic character (e.g. Ribeiro Filho, 1967). These similarities also suggest the comagmatic character among São Sebastião, Serraria and Mirante syenitic stocks.

Based upon oxides and feldspar geothermometries, supported also by experimental studies of Hamilton & Mackenzie (1965), it is possible to infer that syenitic crystallization temperatures might have been between 700°C and 900ºC. Some oxides, feldspar and nepheline lower temperature estimates could correspond to sub-solidus equilibrium. Low $Al^{VI}$, both in amphibole and pyroxene, along with the presence of magmatic breccias and aphanitic dykes, suggest a low-pressure crystallization environment for all these complexes (Brotzu *et al.*, 1992, 1997; Morbidelli *et al.*, 1995). Ilmenite-magnetite pairs, Na-rich late crystallized pyroxene lacking alkali amphibole and the absence of fayalite point out to a relatively oxidized environment for the Itatiaia, Passa Quatro, Serraria and Mirante syenitic bodies, with $fO_2$ higher than the QFM buffer. Fayalite ($Fa_{98-93}$), present in the São Sebastião stock (Augusto, 2003), indicates more reduced conditions, below the QFM buffer.

Geochemical features of the syenitic rocks are mainly characterized by feldspar fractionation or cumulus processes, with minor contributions of mafic phases. This fractionation trend evolves towards more peralkaline liquids, both in silica-undersaturated and oversaturated eutectics. Within each syenitic intrusion, scattered geochemical data, different mineral evolutions (mainly in amphiboles), and in least differentiated rocks the presence of both silica-oversaturated and silica-undersaturated types, suggest distinct liquid lines of descent, that might be formed due to different magma pulses (e.g. Brotzu *et al.*, 1997).

Petrogenesis of different syenitic rocks may be associated with a prolonged differentiation, originated from different silica-undersaturated mafic parental magmas (Brotzu *et al.*, in this volume), accompanied by variable crustal contamination in Itatiaia quartz syenites and granites (Brotzu *et al.*, 1997).

Such syenitic parental magma could be represented by associated mafic dykes, mainly basanites and tephrites from the Itatiaia-Passa Quatro region and the São Sebastião island. They show relative primitive features with mg# ranging from 0.64 to 0.38 and I.E. patterns fitting the Trindade island basanites.

The Itatiaia, Passa Quatro and São Sebastião island magmatisms have a potassic affinity, similar to that most of Brazilian alkaline complexes (Morbidelli *et al.*, 1995). Along with isotopic data, these magmatisms are interpreted as melts of enriched lithospheric mantle beneath southeastern Brazil (e.g. Brotzu *et al.,* 1997). However, as pointed out by Garda *et al.* (1995), geochemical evidences taken from mafic dykes of the São Sebastião island could also indicate a mantle source with larger proportion of asthenospheric derived melts.

The petrogenetic model proposed for the Serra do Mar Alkaline Province genesis by Thompson *et al.* (1998) sustains that, between 80 and 55 Ma, the hot upwelling Trindade plume-tail mantle was deflected by the deep lithosphere root beneath the São Francisco craton and flowed south until it finally became decompressed and partially melt beneath thinner lithosphere under a former adjacent mobile belt. Although ages and locations of the Itatiaia and Passa Quatro complexes are consistent with this model, there is no obvious explanation for the magmatism in São Sebastião island (Thompson *et al.*, 1998).

It should be stressed that Na-magmatism from the Poços de Caldas complex (~80 Ma) and also of nephelinites (ankaratrites) from Eastern Paraguay (60 Ma) have I.E. and Sr-Nd geochemical signatures overlapping those of the Trindade basanite magma. There-fore, overall geochemical characteristics common to Late Cretaceous-Tertiary magmatism from the Paraná system indicate a substantial contribution of a lithospheric mantle variously metasomatized in Middle to Early Proterozoic. Comin-Chiaramonti *et al.* (2002) and Scheibe *et al.* (in this volume) proposed that differential partial melting was driven by decompressive regimes due to different angular velocities of ancient sub-blocks from the region.

## ACKNOWLEDGEMENTS

This research was financially supported by the Brazilian agency FAPESP (Proc. 01/10714-3) and by the Institute of Geosciences of the University of São Paulo.

## REFERENCES


Almeida, F.F.M. (1983). Relações tectônicas das rochas alcalinas mesozóicas de região meridional da Plataforma Sul-Americana. *Revista Brasileira de Geociências* **13**, 139-158.

Almeida, F.F.M. (1991). O alinhamento magmático de Cabo Frio. *II Simpósio de Geologia do Sudeste, São Paulo*, *Atas*, pp. 423-428.

Almeida, F.F.M., & Carneiro, C.D.R. (1998). Origem e evolução da Serra do Mar. *Revista Brasileira de Geociências* **28**, 135-150.

Almeida, F.F.M. Brito Neves, B.B. & Carneiro, C.D.R. (2000). The origin and evolution of the South American Platform. *Earth-Science Reviews* **50**, 77-111.

Alves, F.R. (1996). *Contribuição ao conhecimento geológico e petrológico das rochas alcalinas da Ilha dos Búzios, SP*. Ph.D. Thesis, University of São Paulo, 274p.

Alves, F.R. & Gomes, C.B. (2001). Ilha dos Búzios, litoral norte do Estado de São Paulo: aspectos geológicos e petrográficos. *Geologia-USP Série Científica* **1**, 101-114.

Amaral, G., Bushee, J., Cordani, U.G., Kawashita, H. & Reynolds, J.H. (1967). Potassium-argon ages of alkalines rocks from southern Brazil. *Geochimica Cosmochimica Acta* **31**, 117-142.

Andersen, D.J. & Lindsley, D.H. (1988). Internally consistent solution models for Fe-Mg-Mn-Ti oxides: Fe-Ti oxides. *American Mineralogist* **73**, 714-726.

Augusto, T. (2003). *Petrografia e quimismo mineral de rochas gábricas e sieníticas do maciço de São Sebastião, Ilha de São Sebastião, SP*. Monografia de Trabalho de Formatura, University of São Paulo, 50p.

Augusto, T. & Vlach, S.R.F. (2004). Ocorrência e quimismo de minerais dos grupos da chevkinita e do pirocloro em rocha sienítica da Ilha de São Sebastião, litoral norte do Estado de São Paulo. *XLII Congresso Brasileiro de Geologia, Araxá*, *Anais (CD-ROM)*.

Bellieni, G., Montes-Lauar, C.R., De Min, A., Piccirillo, E.M., Cavazzini, G., Melfi A.J. & Pacca, I.G. (1990). Early and Late Cretaceous magmatism from São Sebastião island (SE-Brazil): geochemistry and petrology. *Geochimica Brasiliensis* **4**, 59-83.

Bennio, L., Brotzu, P., Gomes, C.B., D'Antonio, M., Lustrino, M., Melluso, L., Morbidelli, L. & Ruberti, E. (2002). Petrological, geochemical and Sr-Nd isotopic features of Eocene alkaline rocks of the Cabo Frio Peninsula (southern Brazil): evidence of several magma series. *Periodico di Mineralogia* **71**, 137-158.

Bizzi, L.A., De Wit, M.J., Smith, C.B., McDonald, I. & Armstrong, R.A. (1995). Heterogeneous enriched mantle materials and Dupal-type magmatism along the southwestern margin of the São Francisco craton, Brazil. *Journal of Geodynamics* **20**, 469-491.

Bizzi, L.A., Smith, C.B., De Wit, M.J., Armstrong, R.A. & Meyer, H.O.A. (1993). Mesozoic kimberlites and related alkaline rocks in southwestern São Francisco craton: a case for local mantle reservoirs and their interaction. *5th International Kimberlite Conference*, *Araxá, Proceedings*, pp.156-171.

Brotzu, P., Barbieri, M., Beccaluva, L., Garbarino, C., Gomes, C.B., Macciotta, G., Melluso, L., Morbidelli, L., Ruberti, E., Sígolo, J.B. & Traversa, G. (1992). Petrology and geochemistry of the Passa Quatro alkaline complex, southeastern Brazil. *Journal of South American*

*Earth Sciences* **6**, 273-252.

Brotzu, P., Beccaluva, L., Conte, A., Fonseca, M., Garbarino, C., Gomes, C.B., Leong, R., Macciotta, G., Mansur, R.L., Melluso, L., Morbidelli, L., Ruberti, E., Sígolo, J.B., Traversa, G. & Valença, J.G. (1989). Petrological and geochemical studies of alkaline rocks from continental Brazil. 8. The syenitic intrusion of Morro Redondo, RJ. *Geochimica Brasiliensis* **3**, 63-80.

Brotzu, P., Gomes, C.B., Melluso, L., Morbidelli, L., Morra, V. & Ruberti, E. (1997). Petrogenesis of coexisting $SiO_2$-undersaturated to $SiO_2$-oversaturated felsic igneous rocks: the alkaline complex of Itatiaia, southeastern Brazil. *Lithos* **40**, 133-156.

Brotzu, P., Melluso, L., D'Amelio, F. & Lustrino, M. (in this volume). Potassic dykes and intrusions of the Serra do Mar Igneous Province (SE Brazil).

Campos Neto, M.C. & Caby, R. (1999). Neoproterozoic high-pressure metamorphism and tectonic constraint from the nappe system south of the São Francisco Craton, southeast Brazil. *Precambrian Research* **97**, 3-26.

Carlson, R.W., Esperança, S. & Svisero D.P. (1996). Chemical and Os isotopic study of Cretaceous potassic rocks from southern Brazil. *Contributions to Mineralogy and Petrology* **125**, 393-405.

Comin-Chiaramonti, P. & Gomes, C.B. (1996). *Alkaline magmatism in central-eastern Paraguay. Relationships with coeval magmatism in Brazil.* São Paulo: Edusp/Fapesp, 464p.

Comin-Chiaramonti, P., Cundari, A., Piccirillo, E.M., Gomes, C.B., Castorina, F., Censi, P., De Min, A., Marzoli, A., Speziale, S., Velázquez, V.F. (1997). Potassic and sodic igneous rocks from Eastern Paraguay: their origin from the lithospheric mantle and genetic relationships with the associated Paraná flood tholeiites. *Journal of Petrology* **38**, 495-528.

Comin-Chiaramonti, P., Gomes, C.B., Castorina, F., Censi, P., Antonini, P., Furtado, S.M.A., Ruberti, E. & Scheibe, L.F. (2002). Anitápolis and Lages alkaline-carbonatite complexes, Santa Catarina State: geochemistry and geodynamic implications. *Revista Brasileira de Geociências* **32**, 639-653.

Deer, W.A., Howie, R.A. & Zussman, J. (1992). *An introduction to the rock-forming minerals*. London: Longman, 696p.

Derby, O.A. (1887). On nephelinic rocks in Brazil, with special reference to the association of phonolite and foyaite. *Quarterly Journal of the Geological Society of London* **43**, 457-473.

Elkins, L.T. & Grove, T.L. (1990). Ternary feldspar experiments and thermodynamic models. *American Mineralogist* **75**, 544-559.

Enrich, G.E.R. (2000). *Geologia e química mineral da Ilha Monte de Trigo, litoral norte do Estado de São Paulo*. M.Sc. Dissertation, University of São Paulo, 227p.

Faure, G. (1986). *Principles of isotope geology*. New York: John Wiley & Sons, 589p.

Freitas, R.O. (1947). Geologia e petrologia da Ilha de São Sebastião. *Boletim da Faculdade de Filosofia, Ciências e Letras, Geologia* **85**, 1-244.

Frost, B.R. & Lindsley, D.H. (1991). Occurrence of iron-titanium oxides in igneous rocks. *In*: Lindsley, D.H. (ed.) *Oxide minerals: petrologic and magnetic significance. Reviews in Mineralogy* **25**, 1-9.

Garda. G.M. (1995). *Os diques básicos e ultrabásicos da região costeira entre as cidades de São Sebastião e Ubatuba, Estado de São Paulo*. Ph.D. Thesis, University of São Paulo, 156p.

Garda, G.M., Schorscher, J.H.D., Esperança, S. & Carlson, R.W. (1995). The petrology and geochemistry of coastal dikes from São Paulo State, Brazil: implications for variable lithospheric contributions to alkaline magmas from the western margin of the South Atlantic. *Anais da Academia Brasileira de Ciências* **67**, 191-216.

Gibson, S.A., Thompson, R.N., Dickin, A.P., Leonardos, O.H. (1995a). High-Ti and low-Ti mafic potassic magmas: key to plume-lithosphere interactions and continental flood-basalt genesis. *Earth and Planetary Science Letters* **136**, 149-165.

Gibson, S.A., Thompson, R.N., Leonardos, O.H., Dickin, A.P. & Mitchell, J.G. (1995b). The late Cretaceous impact of the Trindade mantle plume: evidence form large-volume, mafic potassic magmatism in SE Brazil. *Journal of Petrology* **36**, 189-229.

Gibson, S.A., Thompson, R.N., Leonardos, O.H., Dickin, A.P. & Mitchell, J.G. (1999). The limited extent of plume-lithosphere interactions during continental flood-basalt genesis: geochemical evidence from Cretaceous magmatism in southern Brazil. *Contributions to Mineralogy and Petrology* **137**, 147-169.

Gibson, S.A., Thompson, R.N., Weska, R.K., Dickin, A.P. & Leonardos, O.H. (1997). Late Cretaceous rift-related upwelling and melting of the Trindade starting mantle plume head beneath western Brazil. *Contributions to Mineralogy and Petrology* **126**, 303-314.

Gomes, C.B. & Comin-Chiaramonti, P. (in this volume). Some notes on the Alto Paranaíba Igneous Province.

Hamilton, D.L. (1961). Nephelines as crystallization temperature indicators. *Journal of Geology* **69**, 321-329.

Hamilton, D.L. & Mackenzie, W.S. (1965). Phase equilibria studies in the system $NaAlSiO_4$ (nepheline)-$KAlSiO_4$ (kalsilite)-$SiO_2$-$H_2O$. *Mineralogical Magazine* **34**, 214-231.

Hart, S.R. (1984) A large-scale isotope anomaly in the southern hemisphere mantle. *Nature* **309**, 753-757.

Hart, S.R., Hauri, E.H., Oschmann, L.A. & Whithehead, J.A. (1992). Mantle plumes and entrainment: isotopic evidence. *Science* **256**, 517-520.

Hennies, W.T. & Hasui, Y. (1968). Geocronologia das rochas eruptivas alcalinas da Ilha de São Sebastião. *XXII Congresso Brasileiro de Geologia, Belo Horizonte, Anais,* pp. 145-148.

Hennies, W.T. & Hasui, Y. (1977). Contribuição ao reconhecimento da geologia da Ilha de São Sebastião. *I Simpósio de Geologia Regional, São Paulo*, *Atas*, pp.199-209.

Iyer, S.S., Chouduri, A. Pattison, D.R.M. & De Paoli, G.R. (1996). Petrology and geochemistry of the Neoproterozoic Guaxupé granulite facies terrain, southeastern Brazil. *Precambrian Research* **77**, 23-40.

Janasi, V.A. (1999). *Petrogênese de granitos crustais na nappe de empurrão Socorro-Guaxupé (SP-MG): uma contribuição da geoquímica elemental e isotópica*. Livre Docência Thesis, University of São Paulo, 304p.

Kushiro, I. & Walter, M.J. (1998). Mg-Fe partitioning between olivine and mafic-ultramafic melts. *Geophysical Research Letters* **25**, 2337–2340.

Le Maitre, R.W. (ed.) (2002). *Igneous rocks. A classification of igneous rocks and glossary of terms,* 2nd ed. Cambridge: Cambridge University Press, 236p.

Leake, B.E. (1997). Nomenclature of amphiboles, Report of the Subcommittee on Amphiboles of the International Mineralogical Association Commission on New Minerals and Minerals Names. *European Journal of Mineralogy* **9**, 623-651.

Lima, G.A. (2001). *Gabros estratiformes da região norte da Ilha de São Sebastião, SP*. M.Sc. Dissertation, University of São Paulo, 170p.

Lima, G.A. & Schorscher, J.H.D. (1999). Complexo gábrico estratiforme da Ponta da Pacuíba, Ilha de São Sebastião, São Paulo. *VI Simpósio de Geologia do Sudeste*, *São Pedro, Boletim de Resumos,* p. 65.

Machado, N., Valladares, C., Heilbron, M. & Valeriano, C. (1996). U-Pb geochronology of the central Ribeira belt (Brazil) and implications for the evolution of the Brazilian Orogeny. *Precambrian Research* **79**, 347-361.

Mariano, A.N. & Roeder, P.L. (1989). Wöhlerite: chemical composition, cathodoluminescence and environment of crystallization. *Canadian Mineralogist* **27**, 709-720.

Marques, L.S., Ulbrich, M.N.C., Ruberti, E. & Tassinari, C.C.G. (1999). Petrology, geochemistry and Sr-Nd isotopes of the Trindade and Martin Vaz volcanic rocks (Southern Atlantic Ocean). *Journal of Volcanology and Geothermal Research* **93**, 191-216.

McDonough, W.F. & Sun, S. (1995). The composition of the Earth. *Chemical Geology* **120**, 223-253.

Meyer, H.O.A., Blaine, L.G., Svisero, D.P. & Craig, B.S. (1994). Alkaline intrusions in western Minas Gerais, Brazil. *5th International Kimberlite Conference*, *Araxá, Proceedings,* pp.140-155.

Montes-Lauar, C.R., Pacca, I.G., Melfi, A.J. & Kawashita, K. (1995). Late Cretaceous alkaline complexes, southeastern Brazil: paleomagnetism and geochronology. *Earth and Planetary Science Letters* **134**, 425-440.

Morbidelli, L., Gomes, C.B., Beccaluva, L., Brotzu, P., Conte, A. M., Ruberti, E. & Traversa, G. (1995). Mineralogical, petrological and geochemical aspects of alkaline and alkaline-carbonatite associations from Brazil. *Earth-Science Reviews* **39**, 135-168.

Morimoto, N. (1988). Nomenclature of pyroxenes. *Mineralogical Magazine* **52**, 535-550.

Motoki, A. (1986). *Geologia e petrologia do maciço alcalino da Ilha de Vitória, SP*. Ph.D. Thesis, University of São Paulo, 245p.

Parsons, I., Mason, R.A., Becker, S.M., & Finch, A.A. (1991). Biotite equilibria and fluid circulation in the Klokken intrusion. *Journal of Petrology* **32**, 1299-1333.

Penalva, F. (1967). Geologia e tectônica da região do Itatiaia (Sudeste do Brasil). *Boletim da Faculdade de Filosofia, Ciências e Letras da Universidade de São Paulo* **302**, 95-196.

Ribeiro Filho, E. (1967). Geologia e petrologia dos maciços alcalinos do Itatiaia e Passa Quatro. *Boletim da Faculdade de Filosofia, Ciências e Letras da Universidade de São Paulo* **302**, 1-93.

Ribeiro Filho, E. & Cordani, U.G. (1966). Contemporaneidade das intrusões das rochas alcalinas do Itatiaia, Passa Quatro e Morro Redondo. *Publicação SBG, Núcleo Rio de Janeiro* **1**, 62-63.

Riccomini, C., Velázquez, V.F. & Gomes, C.B. (in this volume). Tectonic controls of the Mesozoic and Cenozoic alkaline magmatism in central-southeastern Brazilian Platform.

Ruberti, E., Gomes, C.B. & Comin-Chiaramonti, P. (in this volume). The alkaline magmatism from the Ponta Grossa Arch.

Sadowski, G.R. & Dias Neto, C.M. (1981). O lineamento sismotectônico de Cabo Frio. *Revista Brasileira de Geociências* **11**, 209-212.

Scheibe, L.F., Furtado, S.M.A., Gomes, C.B. & Comin-Chiaramonti, P. (in this volume). Cretaceous alkaline magmatism from Santa Catarina state, southern Brazil.

Schobbenhaus, F.C., Campos, P.A., Derze, G.R. & Asmus, H.E. (1984). Geologia do Brasil. Brasília: DNPM, 501p.

Siebel, W., Becchio, R., Volker, F., Hansen, M.A.F., Viramonte, J., Trumbull, R.B., Haase, G. & Zimmer, M. (2000). Trindade and Martin Vaz islands, South Atlantic: isotopic (Sr, Nd, Pb) and trace element constraints on plume related magmatism. *Journal of South American Earth Sciences* **13**, 79-103.

Sígolo, J.B., Ruberti, E. & Gomes, C.B. (1992). Complexo alcalino de Passa Quatro: dados geológicos preliminares. *Boletim do IG-USP, Publicação Especial* **12**, 109-111.

Sonoki, I.K. & Garda, G.M. (1988). Idades K-Ar de rochas alcalinas do Brasil Meridional e Paraguai Oriental: compilação e adaptação às novas constantes de decaimento. *Boletim do IG-USP, Série Científíca* **19**, 63-85.

Steiger, R.H. & Jäger, E. (1977). Subcommission on geochronology; convention on the use of decay constants in geo- and cosmochronology. *Earth and Planetary Science Letters* **36**, 359-362.

Thompson, R.N., Gibson, S.A., Mitchell, J.G., Dickin, A.P., Leonardos, O.H., Brod, J.A. & Greenwood, J.C. (1998). Migrating Cretaceous-Eocene magmatism in the Serra do Mar alkaline Province, SE Brazil: melts from the deflected Trindade mantle plume? *Journal of Petrology* **39**, 1493-1526.

Tilley, C.E. (1954). Nepheline-alkali feldspar parageneses. *American Journal of Science* **252**, 65-75.

Toyoda, K., Horiuchi, H. & Tokonami, M. (1994). Dupal anomaly of Brazilian carbonatites: geochemical correlations with hotspots in the South Atlantic and implications for the mantle source. *Earth and Planetary Science Letters* **126**, 315-331.

Ulbrich, H.H.G.J. & Gomes, C.B. (1981). Alkaline rocks from Brazil. *Earth-Science Reviews* **17**, 135-154.

Ulbrich, H.H.G.J., Demaiffe, D., Vlach, S.R.F. & Ulbrich, M.N.C. (2003). Geochemical and Sr, Nd and Pb isotope signatures of phonolites and nepheline syenites from the Poços de Caldas alkaline massif, southeastern Brazil. *IV South American Symposium on Isotope Geology, Salvador*, pp. 698-701.

Ulbrich, H.H.G.J., Demaiffe, D., Vlach, S.R.F. & Ulbrich, M.N.C. (in this volume). Structure and origin of the Poços de Caldas alkaline massif, SE Brazil.

Valença, J.G. (1980). *Geology, petrography and petrogenesis of some alkaline igneous complexes of Rio de Janeiro State, Brazil*. Ph.D. Thesis, University of Western Ontario, Canada, 248p.

Vlach, S.R.F., Ulbrich, M.N.C. & Ulbrich, H.H.G. (1998). Isótopos radiogênicos (Sr, Nd) e estáveis (C, O) de rochas máfico-ultramáficas potássicas da região de Poços de Caldas (MG-SP): inferências sobre a natureza do manto litosférico mesozóico. *XL Congresso Brasileiro de Geologia*, *Belo Horizonte, Anais*, p. 475.

Watson, E.B. & Harrison, T.M. (1984). Accessory minerals and the geochemical evolution of crustal magmatic systems: a summary and prospectus of experimental approaches. *Physics of the Earth and Planetary Interiors* **35**, 19-30.

Wen, S. & Nekvasil, H. (1994). SOLVCALC: an interactive graphics program package for calculating the ternary feldspar solvus and for two-feldspar geothermometry. *Computer & Geosciences* **20**, 1025-1040.

*Mesozoic to Cenozoic Alkaline Magmatism in the Brazilian Platform*
*Comin-Chiaramonti, P. & Gomes, C.B. (eds.)*
*Edusp/Fapesp, São Paulo, pp. 419-441, 2005*

# POTASSIC DYKES AND INTRUSIONS OF THE SERRA DO MAR IGNEOUS PROVINCE (SE BRAZIL)

*P. Brotzu, L. Melluso, F. d'Amelio and M. Lustrino*

*Mineralogy, petrography and geochemistry of the Late Cretaceous-Eocene (80-55 Ma) alkaline magmatism occurring from Poços de Caldas to Cabo Frio (SE Brazil) are reviewed and the most relevant petrogenetic processes are discussed. Dyke swarms and syenitic complexes are emplaced into the Proterozoic terrains of the Ribeira mobile belt and form the 500 km long "Serra do Mar Igneous Province". The age of this magmatism progressively decreases from NW to SE, towards the coastline, with the notable exception of the Morro de São João intrusion. The dykes have been divided into a prevailing strongly silica-undersaturated suite (SUS), ranging from foidites, basanites and tephrites to phonolites, and a minor weakly silica-undersaturated suite (WUS), ranging from alkali basalts to trachytes. Basanites/tephrites and phonolites are the most widespread rock-types and they have distinct potassic affinity. The near primary and/or poorly evolved dykes from the SUS suite are incompatible element-enriched, with Ba, Rb, Nb, La, Ce and Nd about 60-200 times and P, Zr and Ti about 10-20 times with respect to the primitive mantle. Alkali basalts of WUS are slightly less enriched in incompatible elements. Compositional variations of the main rock forming minerals, major and trace element trends, as well as Sr-Nd isotopic features, strongly indicate a magmatic evolution dominated by fractional crystallization and/or open system processes, starting from variably silica-undersaturated parental magmas. The occurrence of important syenitic (s.l.) intrusions, evolving towards nepheline syenite or granite residua, often with peralkaline affinity, is believed to be linked to the final evolution of mafic parents into low-pressure magmatic chambers. The most likely source(s) for the potassic to ultrapotassic melts of the Serra do Mar Igneous Province is an enriched, heterogeneous mantle, containing mica and small amounts of scattered LREE-Zr-Nb-P-Ti-rich phases.*

## INTRODUCTION

The Late Cretaceous to Eocene alkaline magmatism occurring along and near to the SE Brazilian coast (Serra do Mar Igneous Province of Thompson *et al.*, 1998) is formed by syenitic intrusions and by widespread dyke swarms (Fig. 1). Filtered K-Ar ages show that this magmatism is constrained between 80 and 55 Ma and has migrated progressively eastwards, from Poços de Caldas to Cabo Frio (Riccomini *et al.*, Fig. 3, in this volume and references therein).

The aim of this paper is to give a general picture of the petrography, mineral chemistry and geochemistry of the dykes and of the main felsic intrusions of the Serra do Mar Alkaline Province (SdM). The most relevant aspects that may prove helpful to petrogenetic modelling will be highlighted.

In order to compare the geochemical and isotopic data of the extensive literature on the SdM alkaline rocks, we have taken into account only the most recent papers (Brotzu *et al.*, 1992, 1997; Araújo *et al.*, 1995; Garda *et al.*, 1995; Gibson *et al.*, 1995, 1997; Morbidelli *et al.*, 1995; Valente, 1997; Thompson *et al.*, 1998; Bennio, 2001; Bennio *et al.*, 2002, 2003).

## GEOLOGICAL SETTING

The SdM alkaline rocks intrude a crystalline basement mainly formed by Proterozoic metamorphic terrains of the Ribeira mobile belt (cf. Almeida, 1983; Hackspacher & Godoy, 1999). Dykes and plutonic complexes are structurally related to an ENE to EW fault system developed at the end of the Brasiliano cycle. This system has been reactivated since the Cretaceous times by extensional movements linked to the opening of the South Atlantic (Morbidelli *et al.*, 1995; Brotzu *et al.*, 1997), and/or by the main regional uplift believed to be related to the track of the Trindade mantle plume (Thompson *et al.*, 1998) which occurred in Paleocene times (about 60 Ma; Tello Saenz *et al.*, 2003). The Early Cretaceous dykes are tholeiitic, and likely related to the Paraná-Etendeka igneous event (e.g., Comin-Chiaramonti *et al.* 1983), whereas Early Cenozoic tholeiitic dykes also crop out in the Cabo Frio area (Bennio *et al.* 2003).

The alkaline dykes trend predominantly NE-SW with minor subsets NW-SE oriented. They are tens of centimeters to a few meters wide and a few hundred meters long. Cross-cutting dykes with different compositions, as well as multiple intrusions are frequently observed. The dykes are often weathered; fresh samples may be found in quarries and along the coastline.

Several large alkaline intrusions (Itatiaia, Passa Quatro, São Sebastião island, Tinguá, Tanguá, Soarinho, Rio Bonito, Mendanha; for additional information on the three first complexes see Enrich *et al.*, in this volume) have been found in the Serra do Mar Province, from the large massif of Poços de Caldas to Cabo Frio and Morro de São João (Fig. 1; cf. Morbidelli *et al.* 1995). The plutonic complexes are represented by plugs or ring-type bodies, often formed by multiple intrusions at upper crustal levels.

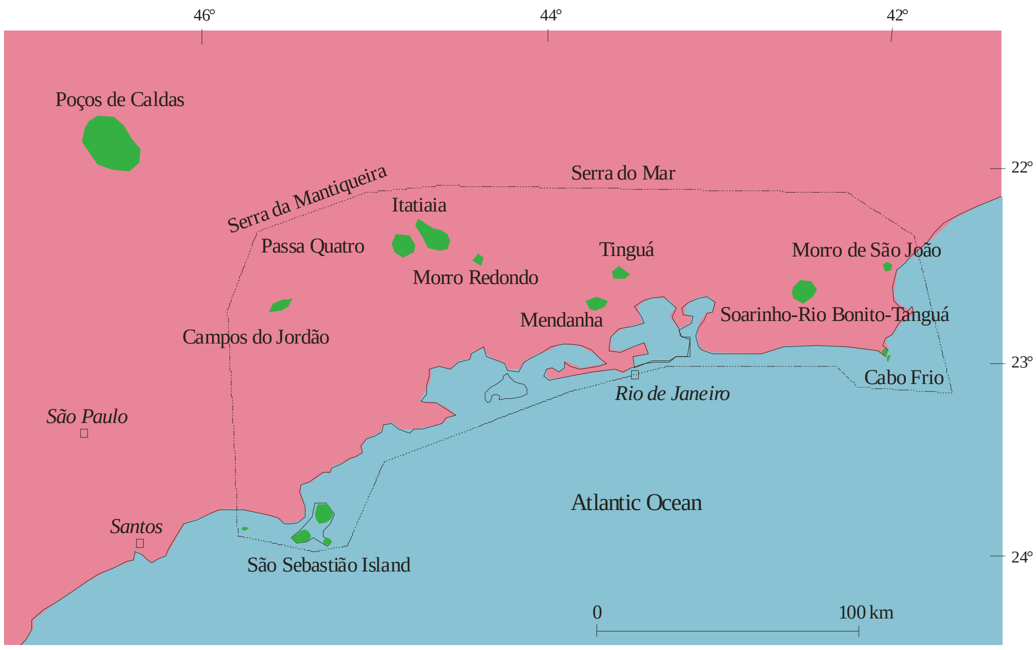


Fig. 1. Sketch-map of southwestern Brazil including location of the main igneous intrusions. The area covered by dyke swarms is indicated with a dashed line.

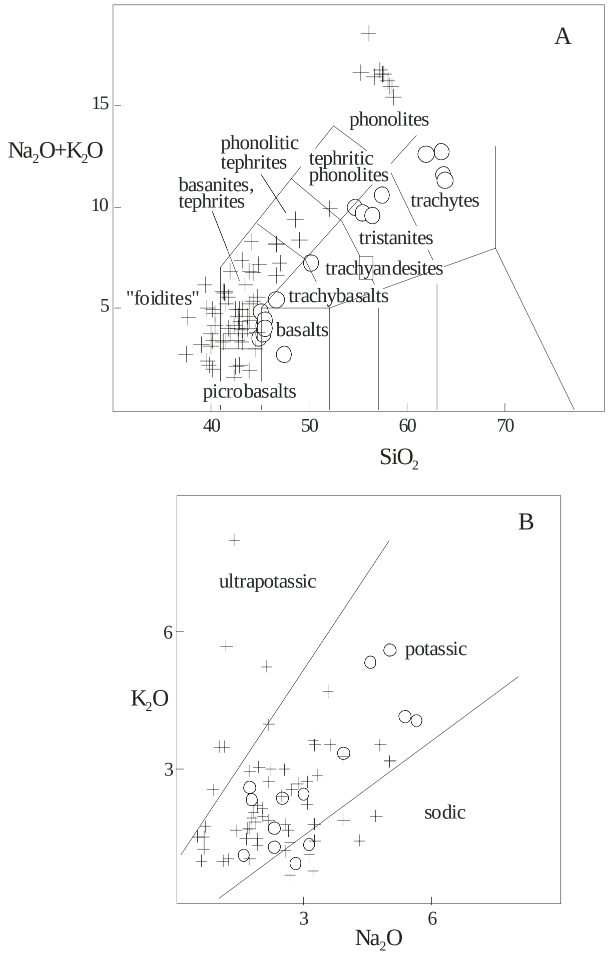


Fig. 2. A) Total alkali-silica classification diagram (Le Bas *et al.*, 1986) for the alkaline dykes of the Serra do Mar Province. Strongly undersaturated suite (SUS)=crosses and weakly undersaturated suite (WUS)=circles. Data source: Garda *et al.* (1995); Thompson *et al.* (1998); Bennio (2001), Bennio *et al.* (2002) and unpublished data by the authors. B) $K_2O$ vs. $Na_2O$ plot for the basic to ultrabasic dykes of the Serra do Mar Province. Lines according to Middlemost (1975).

## PETROGRAPHY

### Dykes

In the TAS (Le Bas *et al.*, 1986) diagram (Fig. 2A), the alkaline dykes form a spectrum ranging from ultrabasic/basic to felsic compositions. The ultrabasic rocks mainly plot in the foidite and basanite/tephrite fields; a few samples correspond to picrobasalts. The basalts straddle the alkaline/subalkaline boundary (Irvine & Baragar, 1971).

On the basis of the petrography, classification and whole-rock chemistry, two main suites have been distinguished: 1) a strongly $SiO_2$-undersaturated suite (SUS), ranging from foidites/basanites to phonolitic rocks, and 2) a weakly $SiO_2$-undersaturated suite (WUS) made up of alkali basalts, trachybasalts, rare hawaiites, trachyandesites and trachytes. A few basalts are hypersthene normative. Basanites/tephrites and phonolites are the most widespread rocks.

The mafic rocks have potassic affinity; a few samples are sodic or ultrapotassic (Fig. 2B, cf. Middlemost, 1975). The weakly $SiO_2$-undersaturated to rare weakly $SiO_2$-saturated basalts (WUS) straddle across the potassic/sodic boundary.

#### SUS suite

The ultrabasic rocks are variably phyric. Mineralogical and chemical compositions allow to distinguish two main groups, i.e. ultramafic lamprophyres and basanite/tephrites.

*Ultramafic lamprophyres* consist of a feldspar-poor/-free dyke group characterized by olivine and clinopyroxene phenocrysts set in a groundmass of clinopyroxene, olivine, amphibole, minor biotite, nepheline or analcime, opaques and sometimes glass. Subhedral Cr-spinel occasionally occurs within the olivine phenocrysts. A few samples are melilite-bearing, while others show clinopyroxene megacrysts. Patches and/or globular structures of exsolved carbonate are common. Finally, biotite phenocrysts may occur in the ultrapotassic foiditic rock-types (cf. Garda, 1995; Valente, 1997).

*Basanite* and *tephrite* dykes have olivine and clinopyroxene phenocrysts set in a groundmass made up of these phases, together with biotite, amphibole, minor plagioclase laths and sometimes glass. A few samples show chromite inclusions in the olivine phenocrysts. Apatite and Fe-Ti oxides are the main accessory phases. Several tephrites, olivine-poor/-free and containing biotite and amphibole phenocrysts, have been classified as minettes by Thompson *et al.* (1998). Spherical blebs, up to a few millimeters in size, of carbonates and/or made up of feldspar-feldspathoid intergrowths, are common. According to the nomenclature of the lamprophyres (Rock, 1991), these rocks have been classified as camptonites by Valente (1997) and Garda (1995). Some ultrabasic rocks have suffered late alteration processes responsible for the formation of secondary calcite on olivine grains, analcime and zeolites in the interstitial glass, and chlorite on biotite laths.

*Phonolitic tephrites* contain clinopyroxene, plagioclase, amphibole, biotite and olivine phenocrysts, in order of decreasing abundance. Feldspar-rich (sanidine and plagioclase) groundmass displays low content of mafic phases (clino-pyroxene, amphibole and biotite). The main accessory phases are magnetite and apatite.

*Tephritic phonolites* are porphyritic with sanidine, amphibole, clinopyroxene and scarce plagioclase phenocrysts set in a fine to coarse-grained groundmass made up of sanidine, nepheline and scarce amphibole, clinopyroxene and biotite microlites. Accessory phases are apatite, magnetite and titanite.

*Phonolites* show sub-aphyric to strongly porphyritic textures. Sanidine and nepheline are the main phenocryst phases, along with subordinate clinopyroxene, amphibole, biotite, apatite, magnetite and titanite. A few phonolites contain nosean and melanitic garnet. The fine to coarse-grained ground-mass is made up of the same phases.

WUS suite

The *alkali basalts* are plagioclase-phyric, along with olivine and clinopyroxene phenocrysts set in a fine-grained groundmass with olivine, clino-pyroxene, plagioclase and opaque minerals. In rare $SiO_2$-saturated basalts, orthopyroxene relics have been sometimes observed (Valente, 1997).

*Trachybasalts* are porphyritic with plagioclase, clinopyroxene and minor olivine phenocrysts set in a plagioclase-rich groundmass, together with clino-pyroxene, amphibole, opaques and apatite.

*Hawaiites* have a phenocryst assemblage similar to that of the trachybasalts, though richer in Ti-clinopyroxene.

*Trachyandesites* have plagioclase, sanidine, amphibole, biotite and opaque phenocrysts (in order of decreasing abundance) set in a sanidine-rich groundmass with minor amphibole and biotite.

*Trachytes* contain abundant sanidine phenocrysts, followed by biotite, amphibole and magnetite. The groundmass is dominated by sanidine and biotite.

**Alkaline intrusions**

Chemical (cf. Fig. 3, after De La Roche *et al.*, 1980) and modal analyses have been used for the classification of the intrusive SdM rock-types. Most of the alkaline intrusions are made up mainly of felsic rocks, whereas a few intrusions as those of Campos do Jordão and Morro de São João have also mafic and ultramafic lithologies (cf. Ulbrich & Gomes, 1981; Morbidelli *et al.*, 1995; Bennio, 2001). The common feature of the intrusive complexes is the presence of dominant alkali syenites and nepheline syenites. A few of these complexes (Itatiaia, Soarinho) contain also outcrops of quartz-bearing syenites and granites. Many of the most evolved rocks (both $SiO_2$-undersaturated and $SiO_2$-over-saturated) are weakly peralkaline.

*Pyroxene-biotite-amphibole-bearing ultramafics* (Morro de São João) have salitic clinopyroxene as the main cumulus phase, followed by apatite, titanite and Ti-magnetite. Reddish poikilitic biotite, strongly zoned kaersutitic amphibole, alkali feldspar, plagioclase and nepheline are intercumulus minerals.

*Melagabbros* (Morro de São João) are hypidiomorphic and seriate in texture with euhedral clinopyroxene, apatite, titanite, Ti-magnetite, euhedral to subhedral plagioclase, and poikilitic titaniferous minerals like biotite and amphibole. Alkali feldspar is interstitial.

*Shonkinites* and *malignites* (Morro de São João) have clinopyroxene, amphibole, titanite, magnetite and apatite as main cumulus phases. Subhedral alkali feldspar, interstitial nepheline and melanitic garnet represent the intercumulus phases.

*Nepheline syenites* and *alkali syenites* (pulaskites) (in most of the complexes) have dominant alkali feldspar and variable amounts of nepheline (rarely sodalite and nosean), usually interstitial, whereas in the most evolved syenites they become an idiomorphic phase. Plagioclase is not frequent, and it is commonly corroded and rimmed by alkali feldspar (antirapakivi textures).

The main mafic minerals are hastingsitic amphibole, salitic-ferrosalitic pyroxene and biotite. Ti-magnetite, titanite and apatite represent the liquidus phases and are present in accessory amounts; melanitic garnet is interstitial. Na-Ca-Zr silicates, such as lävenite and eudialyte, occasionally occur in a few evolved peralkaline syenites.

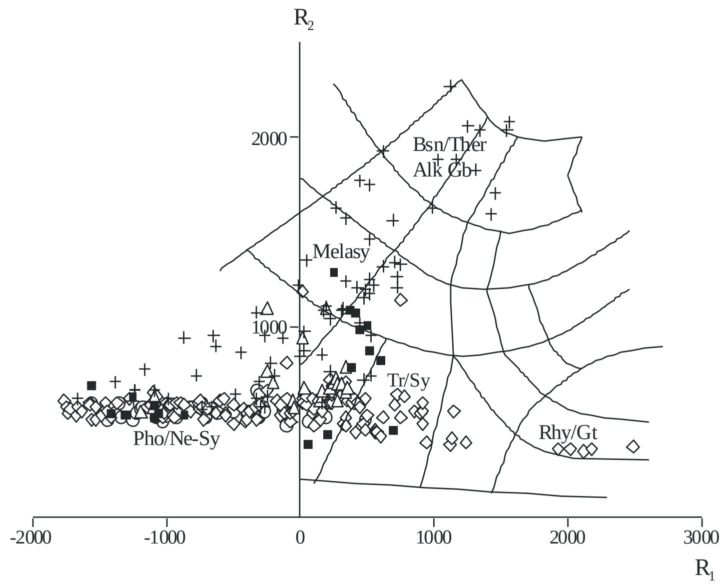


Fig. 3. R1[Si-11(Na+K)-2(Fe+Ti)]-R2 [6Ca+2Mg+Al] diagram (De La Roche *et al.*, 1980) for the rocks of the intrusive complexes from the Serra do Mar Province. Data source: Brotzu *et al.* (1989, 1992, 1997), Morbidelli *et al.* (1995), Bennio (2001) and Bennio *et al.* (2002). Abbreviations: Bsn/Ther (basanite/theralite), Alk Gb (alkali gabbro), Melasy (mela-syenite), Pho/Ne-Sy (phonolite/nepheline syenite), Tr/Sy (trachyte/syenite) and Rhy/Gt (rhyolite/granite). Symbols*:* crosses, Morro de São João; filled squares, Cabo Frio; triangles, Morro Redondo; open diamonds, Itatiaia; circles, Passa Quatro.

*Quartz syenites* (nordmarkites) (e.g. Itatiaia, Soarinho) are fine to medium-grained in size, sometimes with alkali feldspar phenocrysts. Quartz occurs in interstitial patches. The main mafic minerals are amphibole, clinopyroxene, biotite and oxides.

*Granites* (e.g. Itatiaia). These rocks are characterized by high amount of late-crystallized quartz, found in graphic intergrowths with alkali feldspar. Alkali feldspar has albite-rich rims; amphibole is altered, and the most important mafic phase is Fe-rich biotite, with minor amounts of oxides and fluorite.

**Volcanic-subvolcanic facies associated to the alkaline intrusions**

*Phonolitic tephrites* are strongly porphyritic with sanidine, nepheline, nosean, kaersutitic amphibole, salitic pyroxene and rare plagioclase and biotite phenocrysts set in a groundmass with the same phases or aphanitic. Titanite, apatite, magnetite and garnet are accessory phases.

*Phonolites* are more or less porphyritic, with sanidine and nepheline phenocrysts, along with lower amounts of nosean and mafic phases, set in a groundmass with the same phases. Some fine-grained nepheline syenites (grading to phonolites) also show pseudoleucite.

*Quartz trachytes* are found in the central part of the Itatiaia complex. They have sanidine phenocrysts set in a microcrystalline groundmass of sanidine, quartz and minor mafic phases (opaques, biotite and amphibole).

## MINERAL COMPOSITIONS

*Olivine* is a common constituent of ultrabasic-basic dykes and also occurs as an early phase in several intermediate rocks (e.g. tephrites, phonotephrites, trachybasalts and hawaiites). It is often partially or totally altered to serpentine, talc and carbonate minerals. The early-crystallized olivine of several ultrabasic rocks shows inclusions of Cr-spinel, zoning and biotite rims. Olivines from foidites and basanites are Mg-rich ($Fo_{89-86}$) CaO-poor (<0.30 wt%) and, using a $K_D$ $(Fe/Mg)_{Ol}/(Fe/Mg)_{Liq}=0.33$, are in broad equilibrium with their host-rocks, as well as with the olivines ($Fo_{78-67}$) from the basalts.

*Clinopyroxene* is by far the most important phenocryst phase in the dykes. It is often joined to biotite and amphibole crystals in the groundmass. The Ca content represents an important distinctive character between the strongly $SiO_2$-undersaturated rocks (SUS suite) and the $SiO_2$-undersaturated to weakly $SiO_2$-saturated ones (WUS suite). As shown in Fig. 4, the SUS clinopyroxenes have high Ca

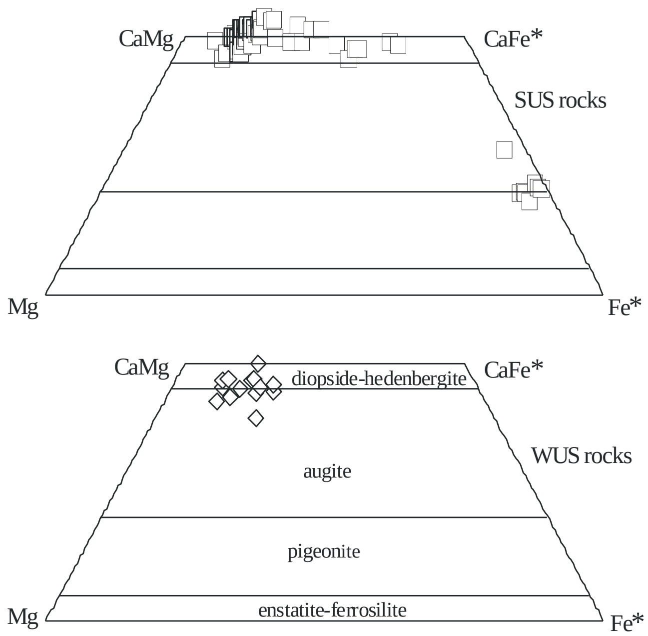


Fig. 4. Chemical variations of clinopyroxene in the dyke rocks. Fe*=$Fe_t$+Mn. Data source: Valente (1997), Bennio *et al.* (2002) and Bennio unpublished.

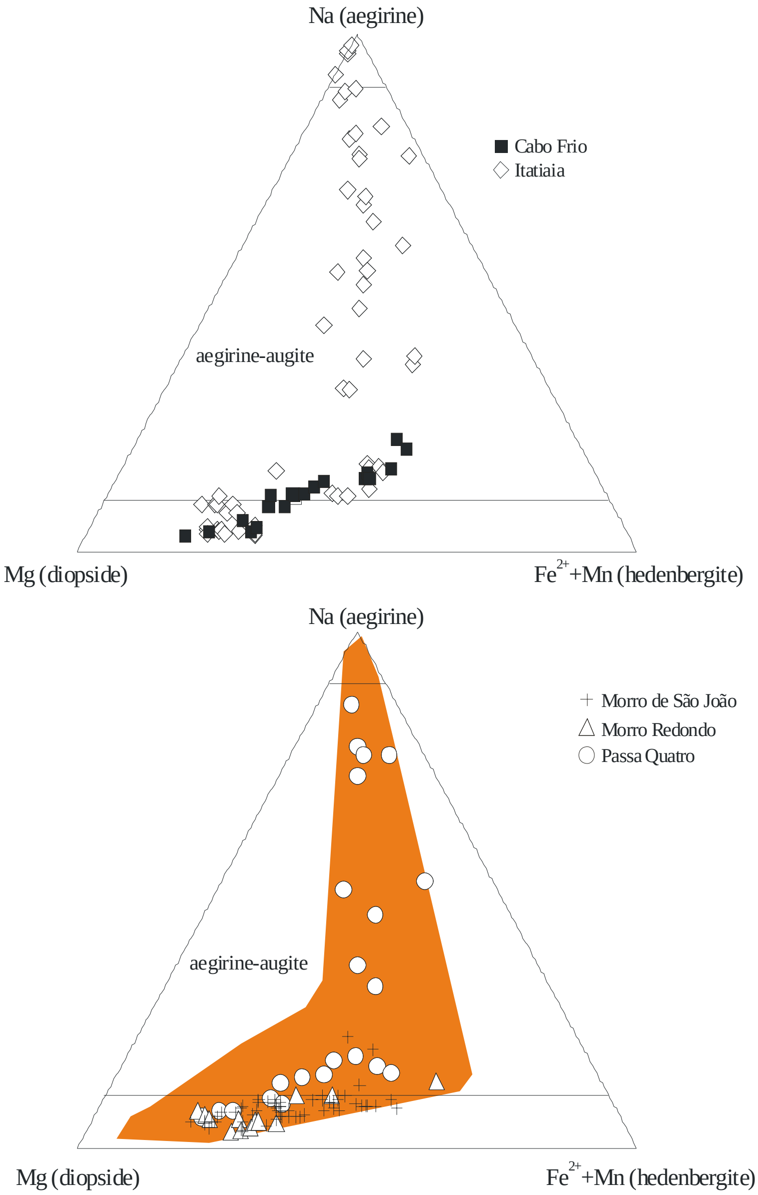


Fig. 5. Pyroxene compositions of the intrusive rocks from the Serra do Mar Province in the Na-Mg-($Fe^{2+}$+Mn) diagrams. The dotted orange field indicates the clinopyroxene composition of the dyke rocks. Data source: Brotzu *et al.* (1989, 1992, 1997), Morbidelli *et al.* (1995) and Bennio (2001).

content and mainly plot in the salite and ferrosalite fields, whereas the WUS ones plot in the augite and salite fields. The clinopyroxenes of the evolved phonolites reach aegirine compositions ($Na_2O$ content up to 12 wt%). Early clinopyroxenes of foidites and basanites have Mg# [atomic Mg/(Mg+Fe)] in the range of 0.89-0.73, and $Al_2O_3$ and $TiO_2$ contents up to 11 and 3 wt%, respectively.

Relatively low Mg# (0.80-0.66) and $Al_2O_3$ (2-6 wt%) characterize clinopyroxenes of the basaltic rocks. On average, Mg# values slightly decrease (0.78-0.74) in the clinopyroxenes of the phono-tephrites and then abruptly fall (0.10-0.02) in the most evolved fonolites. $Na_2O$ content tends to increase starting from phonotephrites.

Clinopyroxene compositions of the intrusive rocks range from diopside/salite (Mg# 0.84) to ferro-salite to aegirine in the most evolved and peralkaline compositions (Mg# 0.06; $Na_2O$ up to 13.4 wt%). Most trends, in the Na-Mg-($Fe^{2+}$+Mn) diagrams, show a kink which corresponds to the transition to peralkaline conditions of the whole-rocks (Fig. 5).

*Brown mica.* Green to brown phlogopites with Mg# values in the range 0.81-0.78 and low $TiO_2$ content (1.4-2.2 wt%) mainly occur in the foidites. Basanites and tephritic rocks typically show zoned phlogopites and biotites with yellow-brown cores and dark rims, characterized by Mg# values in the range 0.76 to 0.54 and high $TiO_2$ content (4.0-9.3 wt%). Ti-Fe-rich biotites ($TiO_2$=5.8-6.9 wt% and Mg# 0.43-0.10) occur in the phonotephrites and phonolites (Fig. 6). The latter biotites, when compared to those of basanites and foidites, have lower $Al_2O_3$ content (10.2-14.5 vs. 15.1-17.4 wt%). Biotites from trachybasalts and trachytes are moderately Ti-rich ($TiO_2$=3.1-4.8 wt%) and show a progressive Fe increase (Mg# 0.43-0.28) towards the most evolved rocks.

Biotite in the intrusive rocks (Fig. 6) has Mg# ranging from 0.77 to 0.21, and $TiO_2$ from 9.4 to 0.7 wt%. A few crystals are rich in $Al_2O_3$ (up to 21.7 wt% in a peraluminous syenite of Itatiaia).

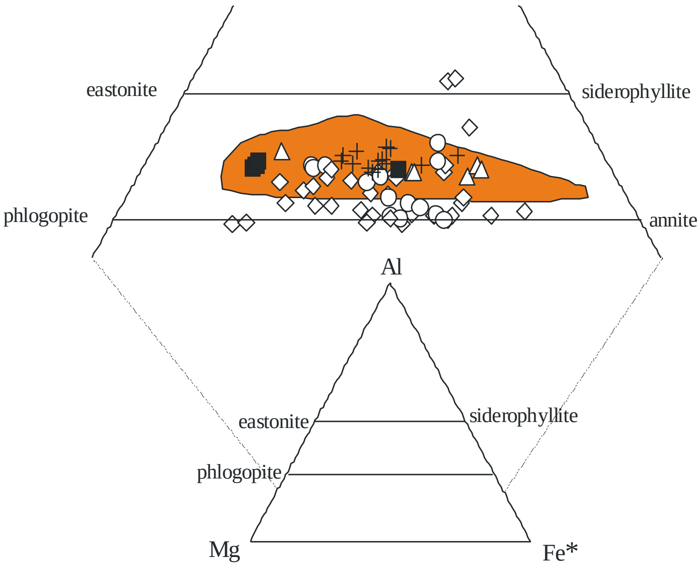


Fig. 6. Brown mica compositions of intrusive rocks of the Serra do Mar Province. Symbols as in Fig. 4. The orange field indicates the mica composition of dyke rocks (cf. Valente, 1997; Bennio *et al.*, 2002).

*Amphibole*. Kaersutite is a groundmass phase in most basanites, while it occurs as microphenocryst to phenocryst phase in tephritic and tephriphonolitic rocks. The compositional range is characterized by high $TiO_2$ (5.0-7.5 wt%). Slight zoning for Ti, Al, Mg and alkalies is often observable, with grain rims enriched in Na and K, and depleted in Mg, Al and Ti. Starting from tephriphonolites, amphiboles grade towards Mg-hastingsite up to Fe-hastingsite in phonolites (Mg# 0.62-0.57). Amphibole is a rare phase in the rocks of the WUS suite, and ranges from kaersutite (basalts) to Fe-hastingsite (trachy-andesites).

Amphiboles from the intrusive rocks range from kaersutite (in several complexes; Mg# up to 0.69, $TiO_2$ up to 6.7 wt%) through hastingsite and pargasitic hornblende to sodic amphiboles (arfvedsonite and richterite; Mg# 0.01, $Na_2O$=8.4 wt%). The latter Na-amphiboles are found in the Itatiaia quartz syenites and granites.

*Feldspars*. Rare groundmass plagioclase ($An_{55-40}$) is found in basanites and tephrites. Normally zoned plagioclase phenocrysts occur in the phonotephritic rocks and have $An_{61-45}$ composition. Plagioclase is labradoritic in the basalt groundmass ($An_{68-50}$), and it is mainly andesine in the intermediate rocks, i.e. trachybasalts and trachyandesites of the WUS suite ($An_{48-42}$). Lower An contents characterize the plagio-clase phenocrysts of trachytes ($An_{32-22}$). The Or content (2 to 12 mol%) of plagioclase progressively increases from basalts to trachytes. Sanidine ($Or_{52-95}$) is by far the most abundant feldspar of tephritic phonolites, phonolites and trachytes. Zoned crystals and phenocryst-groundmass relationships indicate Or increase in the late-crystallized phases. The most K-rich sanidine ($Or_{95}$) occurs in the groundmass of the most evolved phonolites. Some alkali feldspars ($Or_{91-80}$) from phonolites contain BaO up to 1.20 wt%.

Feldspars of the intrusive rocks are mostly represented by sodic plagioclase (up to $An_{41}$), rare anorthoclase and abundant K-rich alkali feldspar (Fig. 7). The widest feldspar variation ($Or_{1-92}$ $Ab_{8-97}$ $An_{0-40}$) is represented by the Itatiaia rocks. Plagioclase of the alkali gabbros from Morro de São João reaches highly calcic compositions ($An_{87-85}$), whereas some alkali feldspars of this complex have very high SrO (4.8 wt%) and BaO (6.8 wt%) contents.

*Feldspathoids*. Nepheline in the overall SUS rocks show narrow compositional variation ($Ne_{70-75}$ $Ks_{20-25}Qz_{5-7}$). No major differences have been found in the nepheline composition from ultrabasic, basic and phonolitic rocks, as well as in those found in the alkaline intrusions (see below Fig. 11).

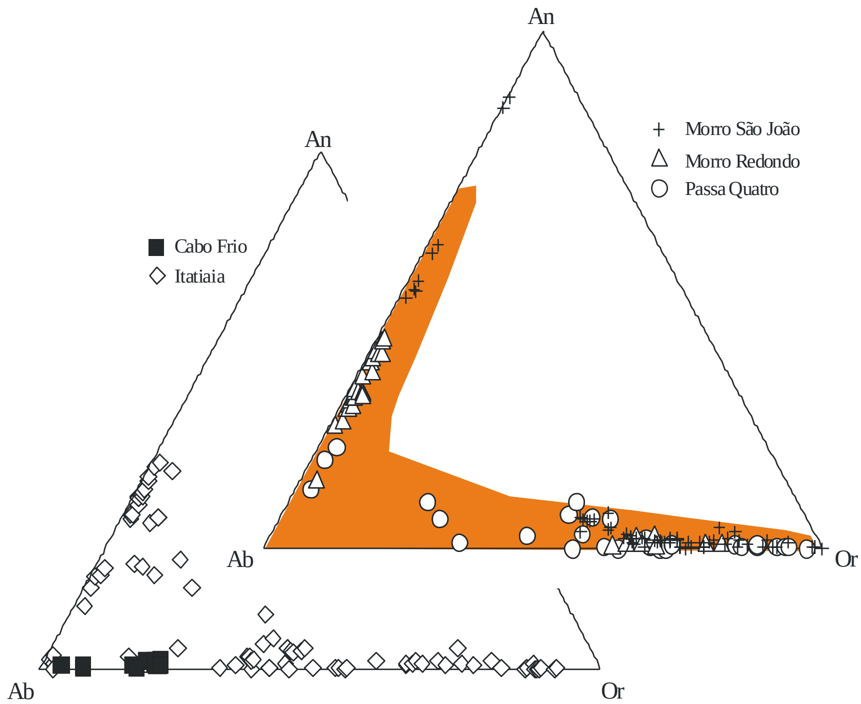


Fig. 7. Feldspar diagrams (mol%) of the intrusive rocks from the Serra do Mar Province (after Brotzu *et al.*, 1989, 1992, 1997; Bennio, 2001). The orange field indicates the feldspar compositions of the dyke rocks (cf. Valente, 1997; Bennio *et al.*, 2002, 2003).

## MAJOR AND TRACE ELEMENT GEOCHEMISTRY

### Dykes

Representative chemical compositions of the dyke rocks are given in Table 1.

The rocks of the dyke swarms greatly vary in MgO content (16–0.2 wt%). Several samples have high MgO (>10 wt%), Ni and Cr (>200 and 300 ppm, respectively) approaching to primary or poorly evolved magma compositions [Mg#=molar Mg/(Mg+$Fe^{2+}$) with $Fe_2O_3$/FeO=0.20, 0.78-0.62].

The WUS and SUS suites are distinguishable in several variation diagrams (e.g. $SiO_2$ and $Al_2O_3$ vs. MgO). $SiO_2$ and $Al_2O_3$ contents continuously increase with MgO decrease, while CaO and $Fe_2O_3$ total tend to remain constant and then abruptly decrease towards intermediate/felsic rocks (phonotephrites, phonolites and trachytes) (Fig. 8A). $TiO_2$ and $P_2O_5$ slightly increase up to 5 wt% MgO and then decrease. With decreasing MgO, the overall rock suites show Zr, Nb and Rb increase and a sharp Ni and Cr decrease. Sr and Ba slightly increase up to 5 wt% MgO and then decrease towards intermediate/felsic rocks, while Y tends to remain almost constant (Fig. 8B).

Ba, Rb, Nb, La, Ce and Nd concentrations in the Mg-rich ultrabasic rocks are 60-200 times mantle, while lower enrichments of Sr, K and Th occur. P, Zr and Ti are ca. 10-20 times mantle. The mantle normalized patterns of basanite and foidite are remarkably similar and characterized by Ba and Nb spikes, and more or less pronounced troughs at Sr and K (Fig. 9). No significant differences in the LILE concentrations have been observed between Ti-rich and Ti-poor rock-types. Mg-rich basalts (MgO>10 wt%) have mantle-normalized trace element patterns (Fig. 9) similar to those of the basanites and foidites at the lower mean LILE enrichment (20-60 times mantle). Trachytes and phonolites are enriched in Rb, Nb, Nd and Zr, and depleted in Sr, P, Ti, and Ba.

Table 1. Representative major, trace elements and isotopic data for the dyke swarms of the Serra do Mar Province. Data source: TH98, Thompson *et al.* (1998); GA, Garda *et al.* (1995); BEN, Bennio *et al.* (2002); *, in this paper.

| Data source | TH98 | * | TH98 | * | TH98 | TH98 | * | GA | TH98 | TH98 | GA | TH98 | TH98 |
|---|---|---|---|---|---|---|---|---|---|---|---|---|---|
| Suite | SUS | SUS | SUS | SUS | SUS | SUS | SUS | SUS | SUS | SUS | SUS | SUS | SUS |
| Sample | 94SOB13 | LN93 | 94SOB64 | BZ3F | 93SOB208 | 93SOB209 | LN07 | MV-2B | 94SOB31 | 94SOB92 | GPA-5 | 94SOB54 | 93SOB210 |
| $SiO_2$ | 42.86 | 39.72 | 44.65 | 43.73 | 40.16 | 40.39 | 42.63 | 42.91 | 44.45 | 40.35 | 39.86 | 41.18 | 39.55 |
| $TiO_2$ | 1.97 | 1.66 | 1.83 | 2.77 | 3.37 | 2.9 | 2.65 | 3.32 | 2.52 | 4.38 | 2.14 | 2.26 | 3.57 |
| $Al_2O_3$ | 11.57 | 9.26 | 12.86 | 8.93 | 9.83 | 11.48 | 9.74 | 12.67 | 11.56 | 10.46 | 12.82 | 11.88 | 12.63 |
| $Fe_2O_3$ total | 11.56 | 12.91 | 11.14 | 12.43 | 14.02 | 12.64 | 12.92 | 13.89 | 12.35 | 14.88 | 12.86 | 12.72 | 14.27 |
| MnO | 0.16 | 0.21 | 0.18 | 0.19 | 0.21 | 0.20 | 0.18 | 0.18 | 0.18 | 0.20 | 0.21 | 0.21 | 0.22 |
| MgO | 16.43 | 14.69 | 14.6 | 14.42 | 13.76 | 13.61 | 11.69 | 11.54 | 11.05 | 10.66 | 10.15 | 10.13 | 10.02 |
| CaO | 12.68 | 18.57 | 10.44 | 12.3 | 12.59 | 13.02 | 16.38 | 10.58 | 14.46 | 13.51 | 17.77 | 17.27 | 13.00 |
| $Na_2O$ | 0.65 | 1.21 | 1.8 | 1.13 | 3.19 | 3.27 | 1.70 | 2.64 | 1.62 | 2.02 | 1.42 | 1.89 | 3.25 |
| $K_2O$ | 1.51 | 1.03 | 2.03 | 3.5 | 1.78 | 1.41 | 1.70 | 1.65 | 1.45 | 2.13 | 1.66 | 1.47 | 1.77 |
| $P_2O_5$ | 0.61 | 0.75 | 0.47 | 0.6 | 1.1 | 1.08 | 0.41 | 0.63 | 0.36 | 1.41 | 1.12 | 0.99 | 1.71 |
| Sum | 100.00 | 100.00 | 100.00 | 100.00 | 100.00 | 100.00 | 100.00 | 100.00 | 100.00 | 100.00 | 100.00 | 100.00 | 100.00 |
| Mg# | 0.76 | 0.72 | 0.75 | 0.72 | 0.69 | 0.71 | 0.67 | 0.65 | 0.67 | 0.62 | 0.64 | 0.64 | 0.61 |
| V | 257 | 306 | 214 | 329 | 254 | 251 | 420 |  | 398 | 314 |  | 305 | 223 |
| Cr | 1066 | 591 | 752 | 598 | 369 | 370 | 372 | 379 | 483 | 332 | 280 | 334 | 127 |
| Ni | 460 | 299 | 310 | 258 | 364 | 257 | 173 | 221 | 191 | 141 | 169 | 177 | 113 |
| Zn | 83 | 84 | 82 | 126 | 100 | 96 | 82 |  | 94 | 84 |  | 67 | 112 |
| Rb | 62 | 24 | 138 | 114 | 39 | 71 | 37 | 51 | 46 | 54 | 58 | 32 | 71 |
| Sr | 656 | 682 | 639 | 220 | 1119 | 1268 | 655 | 1159 | 643 | 886 | 1164 | 1154 | 1767 |
| Y | 22 | 23 | 21 | 23 | 31 | 31 | 18 | 26.2 | 24 | 33 | 29.9 | 31 | 40 |
| Zr | 180 | 217 | 166 | 143 | 454 | 328 | 185 | 278 | 189 | 264 | 270 | 257 | 472 |
| Nb | 58 | 30 | 96 | 31 | 110 | 118 | 49 | 52 | 55 | 55 | 48.4 | 49 | 126 |
| Cs | 2.1 |  | 7.5 | 2.1 |  | 2.6 | 4.9 | 2.2 | 2.1 |  | 4.0 |  | 4.1 |
| Ba | 1477 | 485 | 1522 | 1174 | 1124 | 1353 | 667 | 925 | 501 | 849 | 795 | 624 | 1011 |
| La | 43 | 40.18 | 54 | 29.67 | 96 | 72 | 35.42 | 43.4 | 38 | 74 | 56.6 | 57 | 92 |
| Ce | 85 | 78.76 | 99 | 60.51 | 186 | 148 | 68.27 | 91 | 80 | 142 | 120 | 127 | 186 |
| Pr | 10.19 | 9.81 | 11.26 | 7.82 |  | 16.36 | 8.53 |  | 10.4 |  |  |  | 20.76 |
| Nd | 40 | 43.18 | 42 | 36.13 | 84 | 71 | 38.04 | 46.7 | 43 | 71 | 58.5 | 59 | 91 |
| Sm | 7.34 | 8.22 | 6.74 | 7.63 | 13.25 | 12.19 | 7.25 | 9.6 | 8.2 | 12.5 | 10.8 | 10.84 | 15.77 |
| Eu | 2.36 | 2.60 | 2.12 | 2.58 | 4.2 | 3.72 | 2.33 |  | 2.49 | 3.31 |  | 3.34 | 4.68 |
| Gd | 6.64 | 6.93 | 6.13 | 6.57 | 13.25 | 10.58 | 6.32 |  | 7.16 |  |  | 6.2 | 13.43 |
| Tb | 0.84 | 0.96 | 0.77 | 0.89 | 1.44 | 1.32 | 0.86 |  | 0.96 | 1.32 |  | 1.38 | 1.7 |
| Dy | 4.38 | 5.19 | 3.93 | 4.64 |  | 6.44 | 4.54 | 2.94 | 4.91 |  | 2.93 |  | 8.23 |
| Ho | 0.78 | 0.96 | 0.73 | 0.81 | 1.32 | 1.1 | 0.80 | 0.96 | 0.85 | 0.86 | 1.14 | 1.07 | 1.39 |
| Er | 1.69 | 2.64 | 1.84 | 2.14 |  | 2.6 | 2.14 | 2.23 | 2.08 |  | 2.9 |  | 3.32 |
| Tm |  | 0.32 |  | 0.24 |  |  | 0.24 |  |  |  |  |  |  |
| Yb | 1.65 | 1.94 | 1.56 | 1.48 | 2.64 | 1.97 | 1.55 | 1.56 | 1.65 | 1.98 | 2.24 | 2.27 | 2.56 |
| Lu | 0.25 | 0.28 | 0.24 | 0.19 | 0.35 | 0.29 | 0.21 | 0.21 | 0.24 | 0.24 | 0.32 | 0.32 | 0.38 |
| Hf | 4.12 | 4.70 | 3.83 | 3.96 | 8.69 | 6.84 | 5.28 |  | 5.14 | 7.1 |  | 5.89 | 10.06 |
| Ta | 3.74 | 2.20 | 5.5 | 2.09 | 7.1 | 6.86 | 3.38 |  | 3.29 | 3.55 |  | 3.36 | 8.21 |
| Pb | 3.02 | 0.00 | 4.61 | 15.9 |  | 4.95 |  |  | 5.44 |  |  |  | 6.02 |
| Th | 4.37 | 2.47 | 5.87 | 2.49 | 11.5 | 7.08 | 3.28 | 4.24 | 3.6 | 6.36 | 3.86 | 4.99 | 8.91 |
| U | 1.41 | 0.74 | 1.13 | 0.68 | 2.84 | 1.66 | 0.98 | 1.01 | 0.95 | 1.16 | 1.27 | 2.48 | 2.09 |
| $(^{87}Sr/^{86}Sr)_i$ | 0.70661 |  | 0.70474 |  | 0.70402 | 0.70433 |  |  | 0.70435 |  |  | 0.70434 | 0.70455 |
| εNd | -1.9 |  | -0.5 |  | -1.1 | -0.7 |  |  | 0.3 |  |  | 2.2 | -0.1 |

Table 1 (continued).

| Data source | TH98 | TH98 | TH98 | * | TH98 | TH98 | * | * | * | TH98 | TH98 | TH98 |
|---|---|---|---|---|---|---|---|---|---|---|---|---|
| Suite | SUS | SUS | SUS | SUS | SUS | SUS | SUS | SUS | SUS | SUS | SUS | SUS |
| Sample | 94SOB17 | 94SOB10 | 94SOB20 | RE006 | 94SOB50 | 93SOB212 | BZ312A | BZ312C | BZ29A | 94SOB95 | 94SOB12 | 93SOB197 |
| $SiO_2$ | 43.91 | 41.48 | 41.69 | 43.53 | 43.13 | 41.55 | 42.78 | 42.44 | 42.82 | 46.53 | 42.64 | 44.73 |
| $TiO_2$ | 2.54 | 2.48 | 3.07 | 4.92 | 3.70 | 4.09 | 5.63 | 5.65 | 5.52 | 2.62 | 1.99 | 3.33 |
| $Al_2O_3$ | 13.38 | 12.39 | 13.33 | 11.92 | 13.48 | 13.61 | 10.54 | 11.86 | 10.71 | 14.72 | 14.88 | 14.15 |
| $Fe_2O_3$ total | 12.46 | 12.78 | 15.39 | 13.53 | 11.57 | 14.47 | 13.10 | 13.56 | 12.92 | 10.93 | 12.69 | 12.91 |
| MnO | 0.20 | 0.21 | 0.24 | 0.22 | 0.22 | 0.19 | 0.18 | 0.18 | 0.21 | 0.18 | 0.20 | 0.17 |
| MgO | 10.01 | 9.17 | 8.71 | 8.55 | 8.46 | 8.41 | 8.38 | 8.07 | 8.02 | 7.99 | 7.61 | 7.26 |
| CaO | 12.18 | 17.11 | 12.13 | 9.89 | 14.07 | 11.39 | 13.09 | 11.58 | 13.13 | 9.37 | 14.68 | 10.55 |
| $Na_2O$ | 2.60 | 1.73 | 2.66 | 2.18 | 3.21 | 2.71 | 1.72 | 2.16 | 1.94 | 4.70 | 2.05 | 2.85 |
| $K_2O$ | 1.78 | 1.70 | 1.37 | 3.96 | 0.75 | 2.52 | 2.95 | 2.74 | 3.03 | 1.97 | 1.97 | 2.68 |
| $P_2O_5$ | 0.94 | 0.94 | 1.41 | 1.31 | 1.40 | 1.06 | 1.64 | 1.77 | 1.70 | 0.99 | 1.29 | 1.36 |
| Sum | 100.00 | 100.00 | 100.00 | 100.00 | 100.00 | 100.00 | 100.00 | 100.00 | 100.00 | 100.00 | 100.00 | 100.00 |
| Mg# | 0.64 | 0.62 | 0.56 | 0.59 | 0.62 | 0.57 | 0.59 | 0.57 | 0.58 | 0.62 | 0.57 | 0.56 |
| V | 246 | 322 | 265 | 385 | 310 | 316 | 485 | 467 | 464 | 198 | 260 | 233 |
| Cr | 309 | 333 | 170 | 49 | 304 | 201 | 112 | 79 | 106 | 187 | 28 | 134 |
| Ni | 174 | 143 | 138 | 25 | 159 | 106 | 65 | 53 | 54 | 118 | 122 | 71 |
| Zn | 100 | 99 | 131 | 118 | 96 | 97 | 102 | 103 | 95 | 89 | 97 | 109 |
| Rb | 54 | 46 | 26 | 84 | 31 | 68 | 68 | 56 | 75 | 41 | 47 | 31 |
| Sr | 1093 | 1250 | 1503 | 1368 | 2174 | 1253 | 1284 | 1113 | 1282 | 1638 | 1144 | 2213 |
| Y | 33 | 28 | 37 | 39 | 37 | 33 | 27 | 30 | 28 | 35 | 36 | 35 |
| Zr | 256 | 245 | 260 | 492 | 199 | 344 | 191 | 182 | 189 | 282 | 270 | 228 |
| Nb | 72 | 82 | 93 | 118 | 88 | 74 | 51 | 55 | 55 | 108 | 57 | 81 |
| Cs | 0.7 | 1.4 | 0.3 | | | | | | | 0.78 | 1.8 | |
| Ba | 615 | 732 | 664 | 1528 | 1713 | 1053 | 2299 | 2133 | 2336 | 1355 | 643 | 1802 |
| La | 61 | 68 | 75 | 35.42 | 83 | 75 | 57.70 | 56.11 | 59.59 | 104 | 67 | 111 |
| Ce | 125 | 136 | 152 | 68.27 | 161 | 146 | 117.38 | 114.50 | 120.58 | 180 | 134 | 222 |
| Pr | 15.42 | 14.83 | 16.72 | 8.53 | 21.96 | | 16.05 | 15.42 | 16.32 | 23.37 | 14.64 | |
| Nd | 62 | 64 | 72 | 38.04 | 88 | 69 | 74.94 | 72.32 | 76.42 | 88 | 64 | 113 |
| Sm | 11.17 | 11.24 | 12.94 | 7.25 | 14.41 | 11.64 | 14.11 | 13.37 | 14.33 | 13.55 | 11.28 | 17.29 |
| Eu | 3.39 | 3.34 | 3.99 | 2.33 | 4.62 | 3.17 | 4.56 | 4.43 | 4.67 | 4 | 3.39 | 5.49 |
| Gd | 9.63 | 9.52 | 11.87 | 6.32 | 12.04 | 56.25 | 11.42 | 10.63 | 11.28 | 11.36 | 10.16 | 14.03 |
| Tb | 1.29 | 1.21 | 1.54 | 0.86 | 1.48 | 1.34 | 1.36 | 1.32 | 1.37 | 1.39 | 1.33 | 1.69 |
| Dy | 6.61 | 5.97 | 7.74 | 4.54 | 7.45 | | 6.89 | 6.48 | 6.60 | 6.96 | 7.01 | |
| Ho | 1.16 | 1.01 | 1.34 | 0.80 | 1.28 | 1.18 | 1.41 | 1.08 | 1.11 | 1.24 | 1.25 | 1.45 |
| Er | 2.81 | 2.47 | 3.32 | 2.14 | 3.1 | | 2.71 | 2.55 | 2.75 | 3.13 | 3.19 | |
| Tm | | | | 0.24 | | | 0.27 | 0.24 | 0.26 | | | |
| Yb | 2.24 | 1.86 | 2.58 | 1.55 | 2.39 | 2.16 | 1.75 | 1.66 | 1.76 | 2.61 | 2.74 | 3.44 |
| Lu | 0.32 | 0.28 | 0.38 | 0.21 | 0.35 | 0.38 | 0.22 | 0.21 | 0.22 | 0.39 | 0.4 | 0.4 |
| Hf | 5.66 | 5.17 | 5.37 | 5.28 | 4.96 | 7.32 | 5.28 | 4.78 | 5.21 | 6.55 | 5.14 | 6.4 |
| Ta | 7.44 | 6.76 | 9.11 | 3.38 | 4.88 | 5.16 | 4.69 | 4.21 | 4.84 | 6.69 | 3.41 | 5.62 |
| Pb | 3.43 | 4.34 | 2.58 | 0.00 | 2.83 | | | | 0.00 | 5.99 | 3.82 | |
| Th | 4.64 | 7.01 | 2.71 | 3.28 | 4.56 | 8.4 | 4.30 | 3.75 | 4.33 | 7.92 | 6.9 | 6.68 |
| U | 4.53 | 5.15 | 2.95 | 0.98 | 0.91 | 1.86 | 1.09 | 0.92 | 1.09 | 1.98 | 2.54 | 1.28 |
| $(^{87}Sr/^{86}Sr)_i$ | 0.70389 | 0.70441 | 0.70399 | | 0.70455 | 0.7044 | | | | 0.70495 | 0.70419 | 0.7046 |
| $\varepsilon Nd$ | 2.4 | 1.8 | 1.5 | | -1.9 | -0.9 | | | | -3.4 | 2.4 | -3.0 |

Table 1 (continued).

| Data source | TH98 | TH98 | TH98 | TH98 | TH98 | TH98 | TH98 | TH98 | TH98 | TH98 | TH98 |
|---|---|---|---|---|---|---|---|---|---|---|---|
| Suite | SUS | SUS | SUS | SUS | SUS | SUS | SUS | SUS | SUS | SUS | SUS |
| Sample | 93SOB213 | 93SOB198 | 94SOB14 | 94SOB58 | 94SOB131 | 94SOB80 | 94SOB57 | 93SOB205 | 94SOB98 | 94SOB97 | 94SOB61 |
| $SiO_2$ | 41.48 | 41.62 | 41.27 | 47.07 | 37.58 | 46.68 | 44.18 | 44.27 | 44.10 | 41.31 | 43.95 |
| $TiO_2$ | 4.22 | 4.26 | 4.38 | 2.84 | 6.26 | 2.91 | 3.57 | 3.68 | 4.10 | 4.80 | 3.59 |
| $Al_2O_3$ | 13.97 | 14.21 | 14.03 | 15.29 | 11.72 | 14.49 | 14.37 | 13.22 | 12.98 | 14.18 | 14.71 |
| $Fe_2O_3$ total | 14.84 | 14.29 | 15.59 | 10.05 | 15.91 | 10.94 | 11.89 | 14.43 | 12.11 | 15.30 | 11.85 |
| MnO | 0.19 | 0.19 | 0.17 | 0.17 | 0.22 | 0.17 | 0.19 | 0.19 | 0.19 | 0.23 | 0.20 |
| MgO | 7.18 | 7.16 | 7.11 | 7.01 | 6.94 | 6.69 | 6.64 | 6.61 | 6.58 | 6.32 | 6.28 |
| CaO | 11.48 | 11.63 | 10.89 | 9.53 | 13.65 | 9.12 | 11.11 | 11.49 | 10.56 | 11.12 | 11.29 |
| $Na_2O$ | 3.08 | 2.53 | 3.91 | 3.95 | 1.02 | 4.99 | 3.24 | 3.09 | 3.59 | 4.28 | 3.20 |
| $K_2O$ | 2.73 | 2.98 | 1.88 | 3.25 | 3.49 | 3.18 | 3.53 | 2.21 | 4.70 | 1.41 | 3.63 |
| $P_2O_5$ | 1.13 | 1.13 | 0.77 | 0.86 | 2.34 | 0.86 | 1.26 | 0.80 | 1.39 | 1.05 | 1.29 |
| Sum | 100.00 | 100.00 | 100.00 | 100.00 | 100.00 | 100.00 | 100.00 | 100.00 | 100.00 | 100.00 | 100.00 |
| Mg# | 0.52 | 0.53 | 0.51 | 0.61 | 0.50 | 0.58 | 0.56 | 0.51 | 0.55 | 0.48 | 0.54 |
| V | 325 | 321 | 367 | 203 | 331 | 371 | 257 | 238 | 279 | 350 | 252 |
| Cr | 169 | 158 | 87 | 295 | 10 | 136 | 205 | 54 | 226 | 5 | 180 |
| Ni | 77 | 75 | 86 | 83 | 33 | 72 | 62 | 97 | 61 | 31 | 53 |
| Zn | 103 | 104 | 141 | 81 | 115 | 93 | 94 | 113 | 102 | 120 | 93 |
| Rb | 71 | 73 | 44 | 80 | 89 | 78 | 92 | 49 | 99 | 66 | 93 |
| Sr | 1280 | 1364 | 754 | 1562 | 5542 | 1286 | 1720 | 1009 | 1960 | 1236 | 1960 |
| Y | 31 | 33 | 32 | 31 | 43 | 30 | 36 | 33 | 40 | 38 | 35 |
| Zr | 340 | 332 | 223 | 259 | 253 | 186 | 246 | 287 | 450 | 361 | 241 |
| Nb | 85 | 104 | 48 | 99 | 71 | 58 | 99 | 74 | 154 | 105 | 98 |
| Cs | | 0.8 | 1.55 | 1.87 | 7.14 | 1.79 | 2.04 | 0.8 | 4.06 | 4.66 | 1.9 |
| Ba | 1038 | 1412 | 502 | 1540 | 3580 | 1634 | 1623 | 930 | 1367 | 1026 | 1515 |
| La | 84 | 79 | 45 | 68 | 84 | 58 | 76 | 55 | 137 | 88 | 75 |
| Ce | 167 | 156 | 97 | 139 | 178 | 124 | 161 | 111 | 237 | 176 | 149 |
| Pr | | 17.02 | 12.78 | 17.79 | 28.81 | 16.6 | 21.26 | 12.58 | 33.89 | 21.91 | 20.99 |
| Nd | 76 | 73 | 56 | 71 | 131 | 70 | 87 | 56 | 126 | 87 | 87 |
| Sm | 12.61 | 12.78 | 11.86 | 12.01 | 24.14 | 12.19 | 14.89 | 11.08 | 19.29 | 15.24 | 14.8 |
| Eu | 3.97 | 3.84 | 3.5 | 3.78 | 7.73 | 4.05 | 4.6 | 3.44 | 5.39 | 4.45 | 4.55 |
| Gd | 14.68 | 10.89 | 10.66 | 10.01 | 19.03 | 10.32 | 12.47 | 10.41 | 15.41 | 12.54 | 12.01 |
| Tb | 1.08 | 1.37 | 1.42 | 1.27 | 2.26 | 1.28 | 1.54 | 1.36 | 1.8 | 1.6 | 1.49 |
| Dy | | 6.74 | 7.03 | 6.45 | 10.55 | 6.25 | 7.57 | 6.87 | 8.62 | 7.87 | 7.36 |
| Ho | 1.07 | 1.15 | 1.16 | 1.09 | 1.7 | 1.08 | 1.27 | 1.17 | 1.41 | 1.33 | 1.26 |
| Er | | 2.77 | 2.64 | 2.68 | 3.75 | 2.57 | 3.06 | 2.79 | 3.4 | 3.12 | 3 |
| Tm | | | | | | | | | | | |
| Yb | 2.45 | 2.09 | 1.85 | 2.11 | 2.44 | 1.95 | 2.33 | 2.12 | 2.51 | 2.43 | 2.91 |
| Lu | 0.31 | 0.3 | 0.26 | 0.31 | 0.33 | 0.28 | 0.34 | 0.3 | 0.35 | 0.34 | 0.33 |
| Hf | 7.22 | 7.18 | 5.67 | 6.13 | 7.2 | 4.73 | 6.08 | 6.53 | 10.41 | 8.7 | 6.02 |
| Ta | 5.64 | 5.98 | 3.06 | 6.67 | 4.96 | 3.67 | 6.49 | 4.25 | 9.7 | 6.28 | 6.36 |
| Pb | | 5.44 | 9.78 | 6.82 | 3.97 | 3.65 | 5.7 | 4.96 | 8.82 | 6.19 | 5.86 |
| Th | 8.99 | 9.02 | 4.3 | 7.09 | 5.54 | 4.18 | 6.13 | 6.74 | 12.11 | 9.1 | 6.22 |
| U | 2.04 | 2.28 | 1.26 | 1.59 | 1.18 | 0.94 | 1.37 | 1.62 | 2.87 | 2.16 | 1.38 |
| $(^{87}Sr/^{86}Sr)_i$ | 0.70448 | 0.7045 | 0.70409 | 0.7047 | 0.70494 | | 0.70455 | 0.70415 | 0.70519 | 0.70453 | |
| εNd | -1.9 | - 2.3 | - 0.1 | - 0.9 | - 2.6 | | - 0.7 | - 0.1 | - 3.4 | 0.7 | |

Table 1 (continued).

| Data source | TH98 | TH98 | TH98 | TH98 | BEN | BEN | BEN | * | TH98 |
|---|---|---|---|---|---|---|---|---|---|
| Suite | SUS | SUS | SUS | SUS | SUS | SUS | SUS | WUS | WUS |
| Sample | 93SOB196 | 94SOB68 | 94SOB78 | 94SOB127 | F14 | F61 | F43 | LN11 | 94SOB67 |
| $SiO_2$ | 43.01 | 44.92 | 49.02 | 48.51 | 52.10 | 56.65 | 56.11 | 47.30 | 45.32 |
| $TiO_2$ | 2.87 | 2.91 | 2.53 | 3.07 | 2.29 | 0.45 | 0.27 | 1.47 | 2.38 |
| $Al_2O_3$ | 14.78 | 16.41 | 15.18 | 16.29 | 16.68 | 21.97 | 20.50 | 10.73 | 12.81 |
| $Fe_2O_3$ total | 12.50 | 11.41 | 10.36 | 10.06 | 7.88 | 2.25 | 3.09 | 10.85 | 10.50 |
| MnO | 0.22 | 0.19 | 0.18 | 0.17 | 0.22 | 0.13 | 0.26 | 0.18 | 0.17 |
| MgO | 6.09 | 5.74 | 5.33 | 3.21 | 2.47 | 0.34 | 0.15 | 13.69 | 12.30 |
| CaO | 12.15 | 10.38 | 8.16 | 7.47 | 7.78 | 1.69 | 1.09 | 12.83 | 12.20 |
| $Na_2O$ | 2.11 | 3.60 | 4.77 | 1.35 | 5.36 | 9.04 | 12.00 | 1.59 | 2.80 |
| $K_2O$ | 5.22 | 3.55 | 3.55 | 8.02 | 4.49 | 7.43 | 6.51 | 1.11 | 0.94 |
| $P_2O_5$ | 0.96 | 0.88 | 0.93 | 0.93 | 0.72 | 0.05 | 0.01 | 0.26 | 0.57 |
| Sum | 100.00 | 100.00 | 100.00 | 100.00 | 99.99 | 100.00 | 99.99 | 100.00 | 100.00 |
| Mg# | 0.52 | 0.53 | 0.54 | 0.42 | 0.41 | 0.25 | 0.10 | 0.74 | 0.72 |
| V | 283 | 243 | 181 | 93 | 159 | 34 | 15 | 233 | 234 |
| Cr | 30 | 73 | 216 | 119 | | | | 746 | 549 |
| Ni | 30 | 41 | 56 | 38 | | | | 330 | 252 |
| Zn | 88 | 88 | 105 | 92 | 126 | 59 | 139 | 68 | 78 |
| Rb | 113 | 96 | 93 | 164 | 92 | 173 | 274 | 27 | 34 |
| Sr | 1732 | 1234 | 1189 | 5166 | 1550 | 442 | 62 | 407 | 803 |
| Y | 33 | 28 | 28 | 41 | 40 | 25 | 46 | 20 | 25 |
| Zr | 336 | 219 | 286 | 366 | 391 | 392 | 1447 | 142 | 218 |
| Nb | 133 | 173 | 80 | 149 | 131 | 192 | 337 | 28 | 73 |
| Cs | | 4.7 | 2.64 | 10.74 | | | | | 12.59 |
| Ba | 1351 | 1338 | 1628 | 2696 | 1996 | 101.09 | 29 | 417 | 1132 |
| La | 122 | 81 | 73 | 142 | 130.88 | 150.54 | 178.43 | 22.57 | 41 |
| Ce | 230 | 148 | 146 | 247 | 220.00 | 11.96 | 198.72 | 43.19 | 80 |
| Pr | | 17.17 | 17.75 | 35.89 | 23.47 | 29.90 | 12.9 | 5.38 | 9.73 |
| Nd | 94 | 63 | 69 | 133 | 82.91 | 3.53 | 27.81 | 24.09 | 39 |
| Sm | 13.78 | 9.93 | 11.05 | 19.39 | 12.09 | 0.86 | 3.06 | 4.98 | 7.37 |
| Eu | 3.98 | 2.98 | 3.53 | 6.14 | 3.6 | 3.28 | 0.66 | 1.68 | 2.32 |
| Gd | 11.03 | 8.15 | 9.07 | 15.14 | 9.15 | 0.39 | 2.48 | 4.57 | 6.81 |
| Tb | 1.28 | 1.04 | 1.12 | 1.81 | 1.15 | 2.10 | 0.4 | 0.67 | 0.92 |
| Dy | | 5.39 | 5.63 | 8.87 | 5.87 | 0.41 | 2.66 | 3.81 | 4.88 |
| Ho | 1.21 | 0.97 | 0.98 | 1.48 | 1.06 | 1.42 | 0.61 | 0.73 | 0.87 |
| Er | | 2.51 | 2.43 | 3.51 | 2.95 | 1.42 | 2.27 | 1.96 | 2.2 |
| Tm | | | | | | | | 0.26 | |
| Yb | 2.8 | 2.16 | 1.99 | 2.59 | 2.62 | 1.55 | 3.72 | 1.54 | 1.86 |
| Lu | 0.31 | 0.33 | 0.29 | 0.36 | 0.38 | 0.24 | 0.62 | 0.23 | 0.28 |
| Hf | 8.4 | 5.22 | 6.53 | 8.55 | | | | 3.63 | 5.52 |
| Ta | 6.85 | 11.23 | 4.81 | 11.29 | | | | 1.84 | 4.58 |
| Pb | | 5.84 | 7.75 | 7.7 | | | | | 5.49 |
| Th | 15.17 | 8.41 | 7.1 | 9.55 | | | | 2.25 | 4.74 |
| U | 3.09 | 1.47 | 1.56 | 1.85 | | | | 0.56 | 1 |
| $(^{87}Sr/^{86}Sr)_i$ | 0.70404 | | | 0.70484 | 0.7044 | | 0.70439 | | 0.70484 |
| εNd | - 2.6 | | | - 1.5 | - 0.5 | | - 1.6 | | -1.7 |

Table 1 (continued).

| Data source | * | TH98 | * | * | * | TH98 | * | TH98 | BEN |
|---|---|---|---|---|---|---|---|---|---|
| Suite | WUS | WUS | WUS | WUS | WUS | WUS | WUS | WUS | WUS |
| Sample | LN215B | 94SOB66 | VR02 | BZ328B | BZ181A | 93SOB193 | BZ310 | 93SOB206 | F15 |
| $SiO_2$ | 44.79 | 45.35 | 45.34 | 45.28 | 45.37 | 46.54 | 45.09 | 50.12 | 61.83 |
| $TiO_2$ | 2.65 | 2.30 | 3.05 | 3.18 | 2.16 | 2.23 | 3.49 | 2.82 | 0.78 |
| $Al_2O_3$ | 10.65 | 13.35 | 12.16 | 11.79 | 14.39 | 14.25 | 14.84 | 15.66 | 18.20 |
| $Fe_2O_3$ total | 13.32 | 10.34 | 10.90 | 11.48 | 12.52 | 10.41 | 13.13 | 10.81 | 5.39 |
| MnO | 0.19 | 0.16 | 0.18 | 0.21 | 0.18 | 0.17 | 0.19 | 0.16 | 0.24 |
| MgO | 11.92 | 11.81 | 11.74 | 10.94 | 10.53 | 8.34 | 8.26 | 4.74 | 0.51 |
| CaO | 12.48 | 11.69 | 11.43 | 12.13 | 10.29 | 12.10 | 9.06 | 7.64 | 0.39 |
| $Na_2O$ | 2.29 | 3.10 | 1.72 | 1.78 | 2.33 | 2.98 | 2.51 | 3.94 | 6.50 |
| $K_2O$ | 1.27 | 1.31 | 2.57 | 2.31 | 1.67 | 2.46 | 2.34 | 3.35 | 6.08 |
| $P_2O_5$ | 0.42 | 0.60 | 0.90 | 0.90 | 0.55 | 0.51 | 1.09 | 0.77 | 0.09 |
| Sum | 100.00 | 100.00 | 100.00 | 100.00 | 100.00 | 100.00 | 100.00 | 100.00 | 100.00 |
| Mg# | 0.67 | 0.72 | 0.71 | 0.68 | 0.65 | 0.64 | 0.59 | 0.50 | 0.18 |
| V | 254 | 239 | 289 | 348 | 215 | 251 | 320 | 194 | 11 |
| Cr | 577 | 540 | 346 | 290 | 87 | 313 | 114 | 72 | |
| Ni | 244 | 234 | 159 | 154 | 68 | 105 | 55 | 52 | |
| Zn | 105 | 75 | 83 | 157 | 160 | 69 | 177 | 109 | 119 |
| Rb | 29 | 32 | 45 | 111 | 55 | 48 | 61 | 84 | 130 |
| Sr | 678 | 771 | 1468 | 795 | 989 | 1098 | 1305 | 1023 | 204 |
| Y | 22 | 25 | 31 | 23 | 19 | 25 | 30 | 35 | 48 |
| Zr | 182 | 219 | 272 | 176 | 134 | 201 | 209 | 381 | 621 |
| Nb | 34 | 77 | 80 | 37 | 24 | 63 | 46 | 75 | 182 |
| Cs | | 9.03 | | | | | | 0.87 | |
| Ba | 490 | 1136 | 1849 | 752 | 605 | 1047 | 1233 | 1159 | 1147 |
| La | 28.98 | 43 | 72.65 | 37.11 | 18.27 | 62 | 51.73 | 80 | 144.82 |
| Ce | 56.35 | 83 | 127.53 | 74.60 | 38.70 | 115 | 98.30 | 153 | 238.32 |
| Pr | 6.99 | 10.04 | 14.67 | 9.68 | 5.24 | | 12.41 | 18.23 | 26.86 |
| Nd | 31.68 | 40 | 60.32 | 44.76 | 23.10 | 51 | 54.83 | 72 | 81.52 |
| Sm | 6.69 | 7.44 | 10.05 | 8.99 | 5.02 | 7.85 | 10.24 | 12.81 | 12.13 |
| Eu | 2.28 | 2.33 | 3.12 | 2.75 | 2.13 | 2.18 | 3.29 | 3.71 | 2.75 |
| Gd | 6.00 | 6.74 | 7.81 | 7.59 | 4.52 | 38.74 | 8.35 | 10.98 | 8.36 |
| Tb | 0.87 | 0.92 | 1.07 | 1.02 | 0.74 | 0.98 | 1.14 | 1.43 | 1.22 |
| Dy | 4.73 | 4.91 | 5.61 | 5.32 | 3.84 | | 6.03 | 7.09 | 6.47 |
| Ho | 0.84 | 0.89 | 1.00 | 0.95 | 0.73 | 1.02 | 1.11 | 1.22 | 1.18 |
| Er | 2.14 | 2.2 | 2.65 | 2.41 | 1.69 | | 2.84 | 2.97 | 3.64 |
| Tm | 0.26 | | 0.33 | 0.27 | 0.22 | | 0.35 | | |
| Yb | 1.55 | 1.87 | 2.05 | 1.76 | 1.27 | 2.22 | 2.12 | 2.39 | 3.44 |
| Lu | 0.19 | 0.28 | 0.29 | 0.24 | 0.17 | 0.28 | 0.29 | 0.34 | 0.53 |
| Hf | 4.36 | 5.39 | 6.13 | 4.76 | 2.83 | 4.76 | .546 | 8.43 | |
| Ta | 2.67 | 4.45 | 5.36 | 2.93 | 1.62 | 4.15 | 3.11 | 4.2 | |
| Pb | | 5.62 | 8.30 | 6.54 | 10.56 | | 14.73 | 9.42 | |
| Th | 2.32 | 4.97 | 6.61 | 3.31 | 2.75 | 7.06 | 3.96 | 11.34 | |
| U | 1.08 | 1.03 | 2.02 | 0.90 | 0.80 | 1.38 | 1.19 | 2.15 | |
| $(^{87}Sr/^{86}Sr)_i$ | | 0.70485 | | | | | | | 0.70437 |
| εNd | | 0.1 | | | | | | | - 1.6 |

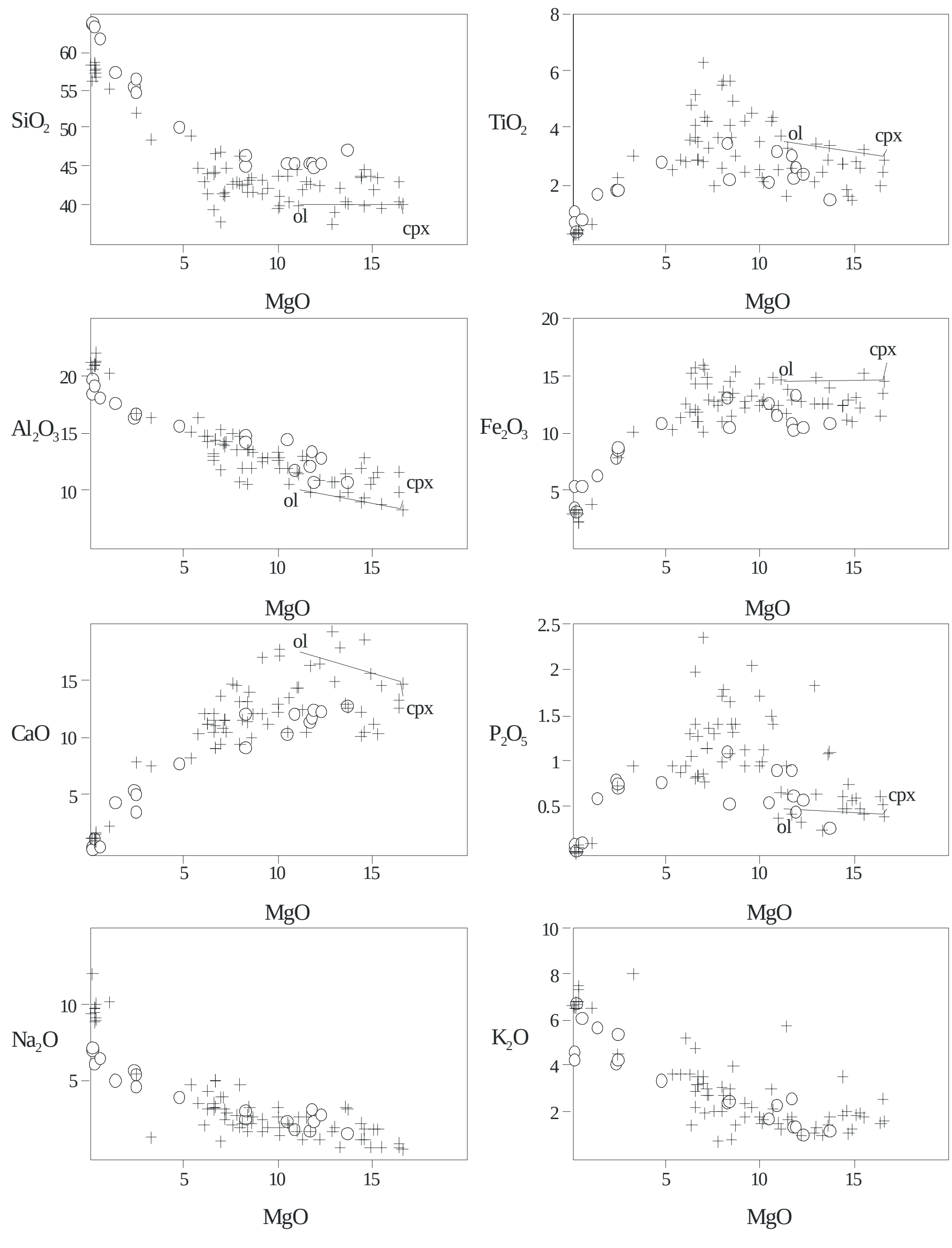


Fig. 8A. Representative major elements variation diagrams for the dyke rocks, using MgO as differentiation index. Symbols and data source as in Fig. 2. Trends after fractionation of 15% ol (olivine) or 15% cpx (clinopyroxene) starting from the most Mg-rich sample are shown in a few diagrams.

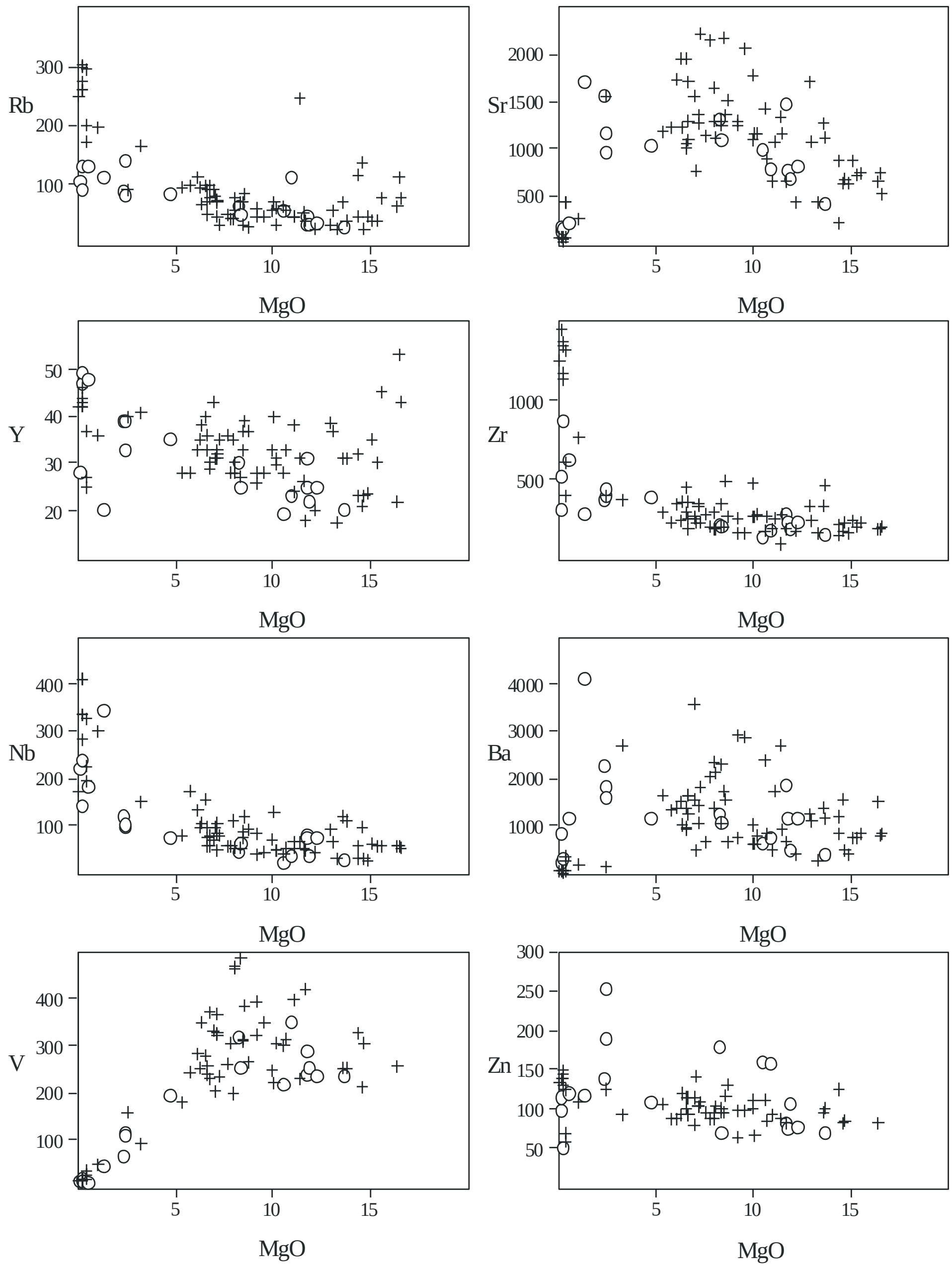


Fig. 8B. Representative trace elements variation diagrams for the dyke rocks, using MgO as differentiation index. Symbols and data source as in Fig. 2.

## Alkaline intrusions

Representative chemical compositions of the intrusive rocks are given in Table 2 and variation diagrams are plotted in Fig. 10.

Excluding Morro de São João, where ultramafic lithotypes are also found, most intrusions show rock-types trending to or closely approaching to the minima in the Nepheline-Kalsilite-Silica system (cf. Bailey, 1976; Luth, 1976), typical of silica-undersaturated and silica-oversaturated residual melts, i.e. nepheline syenites and quartz syenites to granites (Fig. 11). Most alkali syenites have feldspar accumulation responsible for their significant positive Eu anomaly (Eu/Eu* up to 2.7 in Morro Redondo alkali syenites; Brotzu *et al.* 1989) and displacement from typical liquid lines of descent (Brotzu *et al.*, 1992, 1997).

Table 2. Representative major and trace elements data for the intrusive complexes of the Serra do Mar Province. Abbreviations: ITA, Itatiaia; MR, Morro Redondo; MSJ, Morro de São João; PQ, Passa Quatro; m, massive; d, dyke. La/Yb ratio is chondrite normalized; Eu/Eu*=$Eu_n$/•$Sm_n$*$Gd_n$. Data source: Brotzu *et al.* (1989, 1992, 1997; Bennio, 2001).

| Complex | MSJ | MSJ | MSJ | MSJ | MSJ | MR | MR | MR | MR | MR | MR | MR | MR | MR | ITA | ITA | ITA |
|---|---|---|---|---|---|---|---|---|---|---|---|---|---|---|---|---|---|
| Facies | m | m | d | m | d | m | m | m | m | m | m | m | m | m | m | m | m |
| Group | | | | | | | | | | | | | | | A | A | A |
| Sample | MJ48 | MJ74 | MJ53 | MJ55 | MJ26 | MR22 | MR2 | MR15 | MR4 | MR3 | MR16 | MR11 | MR1 | MR26 | IT52 | IT54 | IT130 |
| $SiO_2$ | 44.39 | 52.83 | 56.65 | 60.08 | 58.34 | 52.26 | 51.36 | 54.24 | 58.70 | 59.14 | 58.80 | 60.31 | 56.03 | 57.31 | 60.95 | 60.92 | 59.04 |
| $TiO_2$ | 4.99 | 2.3 | 0.46 | 0.63 | 0.43 | 2.44 | 2.23 | 1.91 | 1.23 | 1.21 | 0.79 | 0.81 | 0.52 | 0.33 | 0.53 | 0.48 | 0.37 |
| $Al_2O_3$ | 10.55 | 19.44 | 21.47 | 19.13 | 20.46 | 17.93 | 17.90 | 17.45 | 18.41 | 18.45 | 19.89 | 18.84 | 21.92 | 21.80 | 20.36 | 20.19 | 20.77 |
| $Fe_2O_3$ | 13.25 | 6.41 | 2.49 | 2.48 | 2.60 | 7.51 | 7.08 | 6.86 | 4.42 | 3.71 | 2.90 | 3.14 | 2.23 | 2.02 | 1.95 | 2.13 | 3.75 |
| MnO | 0.36 | 0.18 | 0.17 | 0.13 | 0.20 | 0.22 | 0.19 | 0.32 | 0.19 | 0.16 | 0.15 | 0.16 | 0.14 | 0.11 | 0.24 | 0.28 | 0.39 |
| MgO | 5.81 | 1.65 | 0.15 | 0.36 | 0.22 | 2.22 | 2.40 | 1.54 | 0.90 | 0.69 | 0.40 | 0.46 | 0.22 | 0.08 | 0.49 | 0.25 | 0.12 |
| CaO | 12.89 | 5.95 | 1.76 | 1.79 | 1.44 | 5.90 | 5.81 | 4.84 | 2.76 | 2.92 | 2.77 | 2.04 | 1.85 | 1.41 | 0.75 | 0.79 | 0.96 |
| $Na_2O$ | 1.48 | 3.65 | 8.40 | 5.34 | 8.90 | 4.88 | 6.26 | 5.13 | 4.51 | 4.51 | 6.73 | 5.46 | 8.98 | 8.68 | 8.21 | 8.38 | 6.07 |
| $K_2O$ | 4.07 | 7.18 | 8.42 | 9.94 | 7.39 | 5.57 | 5.18 | 6.64 | 8.08 | 8.41 | 7.01 | 7.83 | 6.71 | 7.61 | 6.36 | 6.46 | 8.52 |
| $P_2O_5$ | 2.21 | 0.42 | 0.04 | 0.11 | 0.03 | 0.94 | 0.98 | 0.7 | 0.25 | 0.24 | 0.19 | 0.17 | 0.06 | 0.03 | 0.15 | 0.12 | 0.01 |
| Sc | 15 | 4 | | 2 | 1 | | | | | | | | | | | | |
| V | 386 | 179 | 44 | 37 | 22 | 100 | 160 | 93 | 26 | 32 | 29 | 17 | 16 | 9 | 22 | 22 | 26 |
| Cr | 9 | 3 | | | | | | | | | | | | | | | |
| Ni | 10 | 7 | 6 | 8 | 7 | | | | | | | | | | | | |
| Zn | 205 | 91 | 75 | 51 | 97 | | | | | | | | | | 66 | 104 | 216 |
| Rb | 53 | 94 | 82 | 217 | 199 | 110 | 125 | 158 | 116 | 112 | 145 | 129 | 131 | 160 | 177 | 190 | 223 |
| Sr | 2716 | 12733 | 1914 | 1782 | 109 | 3387 | 1784 | 1964 | 3141 | 3607 | 3141 | 2214 | 372 | 445 | 50 | 83 | 462 |
| Y | 61 | 35 | 18 | 30 | 30 | 38 | 32 | 68 | 23 | 29 | 40 | 21 | 23 | 14 | 44 | 53 | 42 |
| Zr | 616 | 134 | 485 | 263 | 782 | 463 | 573 | 684 | 372 | 329 | 773 | 612 | 475 | 568 | 299 | 717 | 2070 |
| Nb | 240 | 232 | 151 | 148 | 187 | 125 | 150 | 370 | 92 | 107 | 198 | 132 | 216 | 123 | 127 | 167 | 175 |
| Ba | 4091 | 10767 | 795 | 652 | 45 | 1908 | 1653 | 1219 | 2031 | 1951 | 1943 | 1100 | 79 | 95 | 16 | 16 | 70 |
| La | 218.5 | 158.0 | 113.7 | 94.6 | 131.5 | 148.7 | 114.5 | 306.7 | 74.4 | 82.4 | 169.0 | 93.8 | 110.0 | 87.0 | 155.9 | 186.9 | 210.1 |
| Ce | 374.1 | 299.6 | 142.6 | 167.2 | 189.6 | 290.1 | 212.0 | 567.2 | 157.2 | 165.3 | 287.4 | 199.1 | 171.0 | 135.0 | 376.5 | 403.8 | 237.2 |
| Pr | 44.5 | 31.5 | 10.2 | 16.9 | 15.0 | | | | | | | | | | 41.2 | 46.0 | 28.4 |
| Nd | 158.3 | 100.3 | 23.6 | 55.3 | 36.3 | 118.1 | 82.3 | 187.2 | 70.8 | 76.6 | 82.7 | 85.2 | 95.8 | 28.2 | 104.5 | 104.9 | 195.1 |
| Sm | 24.3 | 13.3 | 2.4 | 7.6 | 3.7 | 20.4 | 12.4 | 28.6 | 10.6 | 11.8 | 13.1 | 12.8 | 4.6 | 3.7 | 22.5 | 19.6 | 9.4 |
| Eu | 6.79 | 5.23 | 0.71 | 1.94 | 0.75 | 6.59 | 3.24 | 7.21 | 6.40 | 8.77 | 4.26 | 5.41 | 1.19 | 1.50 | 2.45 | 2.30 | 1.94 |
| Gd | 17.2 | 9.4 | 1.8 | 5.2 | 2.4 | 14.8 | 8.8 | 20.4 | 7.4 | 8.2 | 9.4 | 8.7 | 3.4 | 2.7 | 26.8 | 26.2 | 14.4 |
| Tb | 2.55 | 1.44 | 0.28 | 0.81 | 0.42 | | | | | | | | | | | | |
| Dy | 12.49 | 8.4 | 1.72 | 4.19 | 2.57 | 9.46 | 6.53 | 14.86 | 5.40 | 6.21 | 6.73 | 6.78 | 2.65 | 2.09 | 9.41 | 11.66 | 5.05 |
| Ho | 2.27 | 1.48 | 0.37 | 0.76 | 0.62 | | | | | | | | | | 3.85 | 1.51 | 1.01 |
| Er | 5.91 | 4.24 | 1.28 | 2.03 | 1.98 | 4.04 | 2.93 | 7.13 | 2.31 | 2.70 | 3.48 | 3.14 | 1.73 | 1.37 | | | |
| Tm | 0.79 | 0.59 | 0.26 | 0.29 | 0.40 | | | | | | | | | | | | |
| Yb | 4.44 | 3.55 | 1.78 | 1.70 | 2.57 | 3.21 | 2.55 | 6.35 | 1.75 | 2.06 | 3.38 | 2.68 | 2.99 | 1.57 | 2.47 | 3.26 | 2.82 |
| Lu | 0.65 | 0.47 | 0.28 | 0.26 | 0.44 | 0.41 | 0.31 | 0.73 | 0.21 | 0.24 | 0.46 | 0.32 | 0.28 | 0.22 | 0.45 | 0.73 | 0.38 |
| La/Yb | 33.2 | 30.0 | 43.0 | 37.5 | 34.5 | 31.2 | 30.3 | 32.6 | 28.7 | 27.0 | 33.7 | 23.6 | 24.8 | 37.4 | 42.5 | 38.6 | 50.2 |
| Eu/Eu* | 1.01 | 1.42 | 1.04 | 0.94 | 0.76 | 1.15 | 0.94 | 0.91 | 2.20 | 2.71 | 1.17 | 1.56 | 0.91 | 1.45 | 0.30 | 0.31 | 0.51 |

Table 2 (continued).

| Complex | ITA | ITA | ITA | ITA | ITA | ITA | ITA | ITA | ITA | ITA | ITA | ITA | PQ | PQ | PQ | PQ | PQ | PQ |
|---|---|---|---|---|---|---|---|---|---|---|---|---|---|---|---|---|---|---|
| Facies | m | m | m | dy | m | m | m | m | dy | m | m | m | d | d | d | m | d | d |
| Group | A | C | Q | Q | Q | Q | Q | SA | SA | SA | SA | SA | | | | | | |
| Sample | IT140 | IT42 | IT71 | IT97 | IT100 | IT102 | IT105 | IT20 | IT27 | IT60 | IT122 | IT128 | PQ55b | PQ7b | PQ42a | PQ40b | PQ22a | PQ22b |
| $SiO_2$ | 59.51 | 58.08 | 61.48 | 72.40 | 67.98 | 72.50 | 69.00 | 56.49 | 55.37 | 56.61 | 56.83 | 56.74 | 61.75 | 55.60 | 57.26 | 56.55 | 59.94 | 58.64 |
| $TiO_2$ | 0.70 | 0.39 | 0.86 | 0.21 | 0.33 | 0.21 | 0.32 | 0.29 | 0.43 | 0.40 | 0.40 | 0.37 | 0.72 | 0.73 | 0.30 | 0.32 | 0.90 | 0.38 |
| $Al_2O_3$ | 20.13 | 23.70 | 18.55 | 16.91 | 17.35 | 15.01 | 16.20 | 23.39 | 20.73 | 23.34 | 23.29 | 24.71 | 19.39 | 21.14 | 21.26 | 20.77 | 19.69 | 21.47 |
| $Fe_2O_3$ | 2.96 | 2.34 | 3.46 | 1.15 | 1.78 | 1.73 | 2.35 | 1.53 | 3.67 | 1.33 | 1.99 | 1.20 | 2.69 | 2.36 | 2.31 | 3.23 | 2.94 | 2.21 |
| MnO | 0.20 | 0.27 | 0.19 | 0.02 | 0.17 | 0.28 | 0.36 | 0.21 | 0.31 | 0.19 | 0.27 | 0.24 | 0.16 | 0.18 | 0.34 | 0.44 | 0.16 | 0.23 |
| MgO | 1.22 | 0.46 | 1.58 | 0.10 | 0.15 | 0.18 | 0.19 | 0.20 | 0.12 | 0.04 | 0.36 | 0.28 | 0.23 | 0.17 | 0.12 | 0.47 | 0.62 | 0.20 |
| CaO | 1.67 | 1.90 | 1.94 | 0.19 | 0.40 | 0.54 | 0.60 | 1.18 | 1.57 | 0.95 | 1.07 | 0.70 | 1.94 | 1.63 | 0.82 | 1.12 | 1.79 | 1.28 |
| $Na_2O$ | 4.40 | 4.76 | 5.41 | 4.19 | 6.42 | 4.51 | 6.03 | 6.67 | 9.68 | 9.58 | 8.42 | 6.31 | 5.29 | 6.85 | 10.48 | 8.99 | 5.56 | 6.74 |
| $K_2O$ | 8.64 | 8.03 | 5.74 | 4.81 | 5.34 | 5.00 | 49.1 | 9.99 | 8.09 | 7.54 | 7.30 | 9.39 | 7.45 | 8.25 | 6.28 | 6.14 | 7.67 | 7.44 |
| $P_2O_5$ | 0.57 | 0.05 | 0.79 | 0.02 | 0.07 | 0.04 | 0.04 | 0.07 | 0.03 | 0.03 | 0.07 | 0.06 | 0.23 | 0.09 | 0.03 | 0.02 | 0.15 | 0.04 |
| Sc | | | 7 | | 1 | | 2 | | | | | | | | | | | |
| V | 21 | 27 | 29 | 8 | 10 | 7 | 10 | 31 | 44 | 19 | 37 | 26 | 17 | 32 | 17 | 20 | 47 | 19 |
| Cr | | 4 | 2 | 10 | 1 | 21 | 11 | 1 | | | | | 7 | 4 | 10 | 7 | 6 | 7 |
| Ni | | | | | | | | | | | | | 12 | 11 | 11 | 12 | 13 | 15 |
| Zn | 80 | 116 | 86 | 45 | 113 | 145 | 134 | 85 | 167 | 70 | 120 | 41 | 81 | 102 | 242 | 231 | 87 | 130 |
| Rb | 86 | 116 | 136 | 397 | 199 | 373 | 314 | 235 | 99 | 167 | 188 | 211 | 139 | 180 | 250 | 265 | 159 | 170 |
| Sr | 717 | 374 | 1020 | 20 | 10 | 27 | 18 | 1301 | 1579 | 22 | 908 | 343 | 1347 | 823 | 30 | 136 | 108 | 39 |
| Y | 19 | 37 | 38 | 92 | 128 | 65 | 79 | 37 | 37 | 52 | 130 | 30 | | | | | | |
| Zr | 152 | 470 | 314 | 447 | 648 | 461 | 1075 | 583 | 1102 | 601 | 415 | 238 | 404 | 564 | 1911 | 3953 | 611 | 1566 |
| Nb | 38 | 135 | 84 | 293 | 183 | 284 | 326 | 178 | 260 | 312 | 171 | 214 | 116 | 206 | 409 | 600 | 100 | 382 |
| Ba | 43 | 78 | 1094 | 20 | 9 | 22 | 11 | 135 | 69 | 1 | 213 | 86 | 263 | 59 | 14 | 116 | 41 | 26 |
| La | 173.6 | 301.4 | 128.5 | 230.3 | 406 | 112.5 | 112.4 | 183.9 | 223.6 | 152.6 | 199.6 | 146.5 | 144.1 | 194.5 | 325 | 93.9 | 172.3 | 241.0 |
| Ce | 534.8 | 552.8 | 206.8 | 158.7 | 321.1 | 210.4 | 312.5 | 281.9 | 496.8 | 199.7 | 324.4 | 288.5 | 264.5 | 359.0 | 530.7 | 122.3 | 303.2 | 363.9 |
| Pr | 26.3 | 69.7 | 25.2 | 49.5 | 71.3 | 22.5 | 32.6 | 28.7 | 26.1 | 22.1 | 25.1 | 17.1 | | | | | | |
| Nd | 89.0 | 186.6 | 113.5 | 88.3 | 354.3 | 111.3 | 52.8 | 54.9 | 41.9 | 64.2 | 97.7 | 39.0 | 116.9 | 130.0 | 138.8 | 25.2 | 119.5 | 82.5 |
| Sm | 13.1 | 29.2 | 15.8 | 26.4 | 30.0 | 13.1 | 15.1 | 6.9 | 6.6 | 6.1 | 7.3 | 4.6 | 19.0 | 18.6 | 18.4 | 3.8 | 19.1 | 10.9 |
| Eu | 6.21 | 6.03 | 1.31 | 0.63 | 1.19 | 0.48 | 0.91 | 2.12 | 1.80 | 1.22 | 1.94 | 1.60 | 6.50 | 4.82 | 2.25 | 0.74 | 4.88 | 1.63 |
| Gd | 15.7 | 28.3 | 15.9 | 24.7 | 40.5 | 19.7 | 16.7 | 13.8 | 13.0 | 10.9 | 13.1 | 9.3 | 12.5 | 11.8 | 12.4 | 3.1 | 13.0 | 7.6 |
| Tb | | | | | | | | | | | | | | | | | | |
| Dy | 4.63 | 11.74 | 7.52 | 11.37 | 19.32 | 11.80 | 8.68 | 4.86 | 4.54 | 5.20 | 5.59 | 3.64 | 8.52 | 8.11 | 11.37 | 3.48 | 8.43 | 7.02 |
| Ho | 0.60 | 3.70 | 1.52 | 2.62 | 1.30 | 1.92 | 1.70 | 0.77 | 1.35 | 0.92 | 2.02 | 0.64 | | | | | | |
| Er | | | | | | | | | | | | | 3.25 | 3.64 | 5.73 | 2.87 | 3.58 | 3.95 |
| Tm | | | | | | | | | | | | | | | | | | |
| Yb | 2.34 | 4.55 | 3.34 | 4.76 | 2.02 | 4.95 | 4.64 | 2.36 | 5.02 | 2.01 | 2.64 | 3.13 | 2.65 | 2.97 | 5.88 | 4.41 | 3.15 | 4.85 |
| Lu | 0.22 | 2.21 | 0.62 | 0.98 | 0,98 | 0.76 | 0.73 | 0.28 | 0.51 | 0.23 | 0.50 | 0.26 | 0.41 | 0.48 | 0.93 | 0.79 | 0.51 | 0.80 |
| La/Yb | 50.0 | 44.7 | 25.9 | 32.6 | 135,3 | 15.3 | 16.3 | 52.5 | 30.0 | 51.2 | 50.4 | 31.6 | 36.7 | 44.1 | 37.3 | 14.3 | 36.9 | 33.5 |
| Eu/Eu* | 1.31 | 0.63 | 0.25 | 0.07 | 0,10 | 0.09 | 0.17 | 0.66 | 0.59 | 0.45 | 0.60 | 0.74 | 1.28 | 0.99 | 0.45 | 0.66 | 0.94 | 0.54 |

The *Itatiaia* rocks display a wide variation in terms of $SiO_2$, $Al_2O_3$ contents (55-75 and 14-25 wt%, respectively), and D.I.* values (normative Q+Or+Ab+Ne+Ac+Ns, from 55 to 97), despite the restricted MgO range (2-0 wt%) among the felsic intrusions of the Serra do Mar. The rocks have been subdivided into three main groups: 1) quartz-normative (and modal) samples (syenites and granites) (Q), 2) slightly Ne-normative syenites (A), and (3) associated C-normative syenites, and strongly Ne-normative (and modal) syenites (SA) (Brotzu *et al.*, 1997). Slightly peralkaline rocks (A.I., Agpaitic Index, molar $(Na_2O+K_2O)/Al_2O_3$, up to 1.2) are observable in the A and SA groups. With decreasing MgO, the coarse-grained rocks of the Q-group show $SiO_2$, Rb, Nb, and Th increase, along with $TiO_2$, CaO, $Fe_2O_3$ total, $P_2O_5$, Sr, and V decrease. $Al_2O_3$, alkalies and Zr firstly tend to remain constant and then decrease towards the alkali granites (MgO<0.5 wt%). The coarse-grained alkali syenites and nepheline syenites of the A-group have $SiO_2$ and $Al_2O_3$ contents almost constant, while $Na_2O$ increases with decreasing MgO. On the other hand, $TiO_2$, $P_2O_5$, CaO, $Fe_2O_3$ total, V, Sr, Ba (and $K_2O$) decrease throughout the A-group. The C-(corundum) normative syenites are remarkably different from the main A-group rocks, being displaced to higher $Al_2O_3$, CaO contents and $K_2O/Na_2O$ ratios, and to lower A.I., D.I.* and $Na_2O$, at a given MgO. On the other hand, these rock-types are similar to the SA-syenites, even though they are distinctly less $SiO_2$-undersaturated (Ne=0-14 wt%).

The SA-syenites have lower $K_2O/Na_2O$ ratio at a given $K_2O$, lower $SiO_2$ and higher $Al_2O_3$, CaO, Sr, and V, at a given MgO, with respect to the A-group syenites. Another distinctive feature of the SA rocks is the positive correlation between $K_2O$ and Rb, which is not observable in the other groups, except for the C-syenites. The SA group shows less clear trends, mostly caused by the very restricted MgO range. The compositions of SA rocks imply parental nepheline syenites different from those of the least differentiated A- and Q-syenites (e.g. higher alkalies, $Al_2O_3$, and lower $SiO_2$).

The *Passa Quatro* rocks have a narrow range of D.I.* (86 to 94) and A.I. (from 0.83 to 1.13), and are Ne-normative (14 to 27 wt%). The evolution towards the most modal nepheline-enriched rock-types (with subhedral nepheline and slightly peralkaline) is characterized by $Al_2O_3$ increase (18 to 23 wt%) and $Na_2O$ (from 5.6 to 9.9 wt%), while $SiO_2$, $K_2O$, CaO, Sr, Ba, $TiO_2$ and $P_2O_5$ tend to decrease. Rb and Nb tend to increase with differentiation. A strong scatter of the data is observable for Zr, Nb and Sr. The uneven distribution of apatite, titanite, eudialyte and lävenite is responsible for some unusually high contents of Zr and Nb.

The *Morro Redondo* rocks have D.I.* ranging from 64 to 93, and are characterized by increase of $Al_2O_3$, $Na_2O$, Rb and Nb, coupled with decreasing $TiO_2$ CaO, $Fe_2O_3$ total, Ba and Sr. $SiO_2$ content firstly increases towards the least evolved phonolites and nepheline syenites, and then tends to decrease towards the compositions plotting close to the phonolite minimum.

*Morro de São João*. The rocks of this complex have a large range of D.I.* (from 20 to 96). The clinopyroxene-amphibole-biotite-bearing ultramafic rocks have high CaO content (up to 16 wt%) and MgO ranging from 8.1 to 6.3 wt%, and low Ni (<19 ppm) and Cr (<38 ppm). Their chemical features (i.e. high $TiO_2$, $P_2O_5$, Zr and Ba contents, and the large $Na_2O/K_2O$ variations) reflect both the modal content of apatite and titanite, and the composition of the intercumulus material. Gabbroic rocks have a narrow range of MgO (6.5-4.9 wt%) and $SiO_2$ (42-46 wt%), and high $TiO_2$ (5.7-4.2 wt%), $P_2O_5$ (2.8-2.0 wt%) and CaO (13.4-9.5 wt%) contents. Decreasing

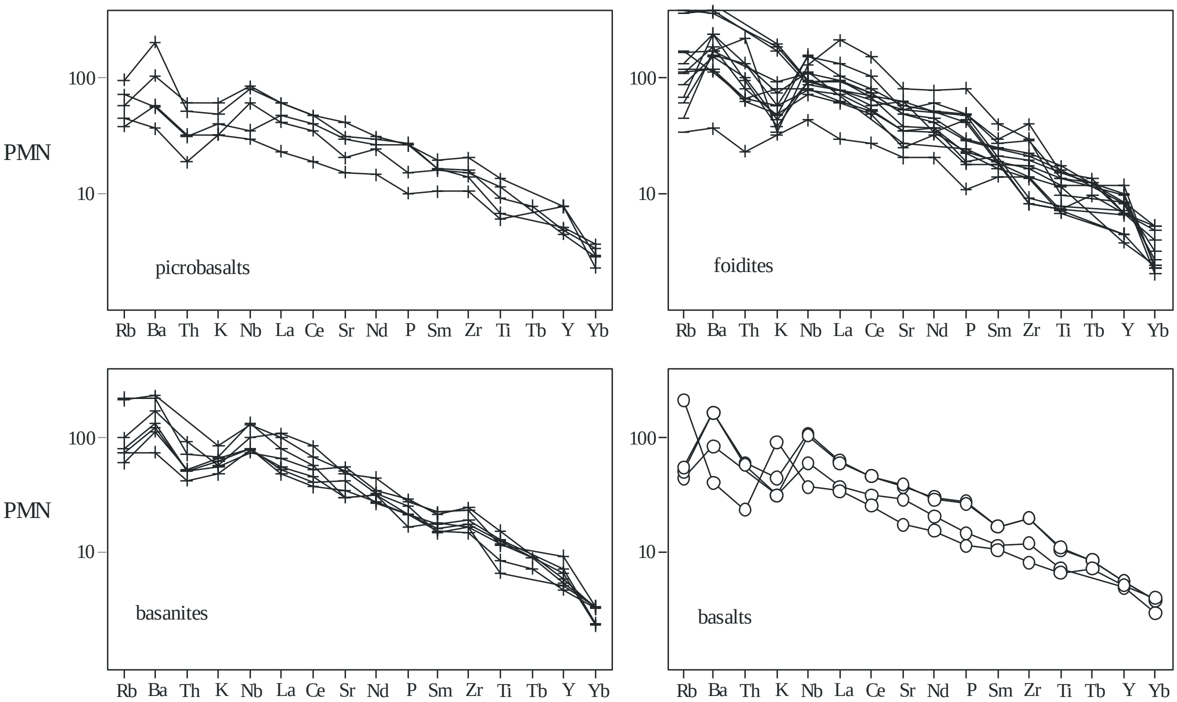


Fig. 9. Primitive mantle-normalized incompatible elements variation diagrams (PMN) for representative mafic dyke samples. Normalization values for primitive mantle are taken from Sun & McDonough (1989).

MgO, the high Sr and Ba concentrations decrease from 8000 to 2900 and from 10300 to 5700 ppm, respectively, as well as the already low Ni (17-5 ppm) and Cr (38-5 ppm) concentrations. Shonkinites and malignites reveal large compositional variations in $SiO_2$ (44.2-52.7 wt%), MgO (5.8-1.8 wt%), CaO (12.9-6.1 wt%) and $K_2O$ (3.4-9.8 wt%). Average malignite is richer in $SiO_2$ and $K_2O$ and poorer in MgO and CaO than average shonkinite. Ba and Sr contents may reach very high concentrations in malignites (up to 1.32 and 1.16 wt%, respectively). $SiO_2$, $Na_2O$, $K_2O$ and $Al_2O_3$ generally increase,

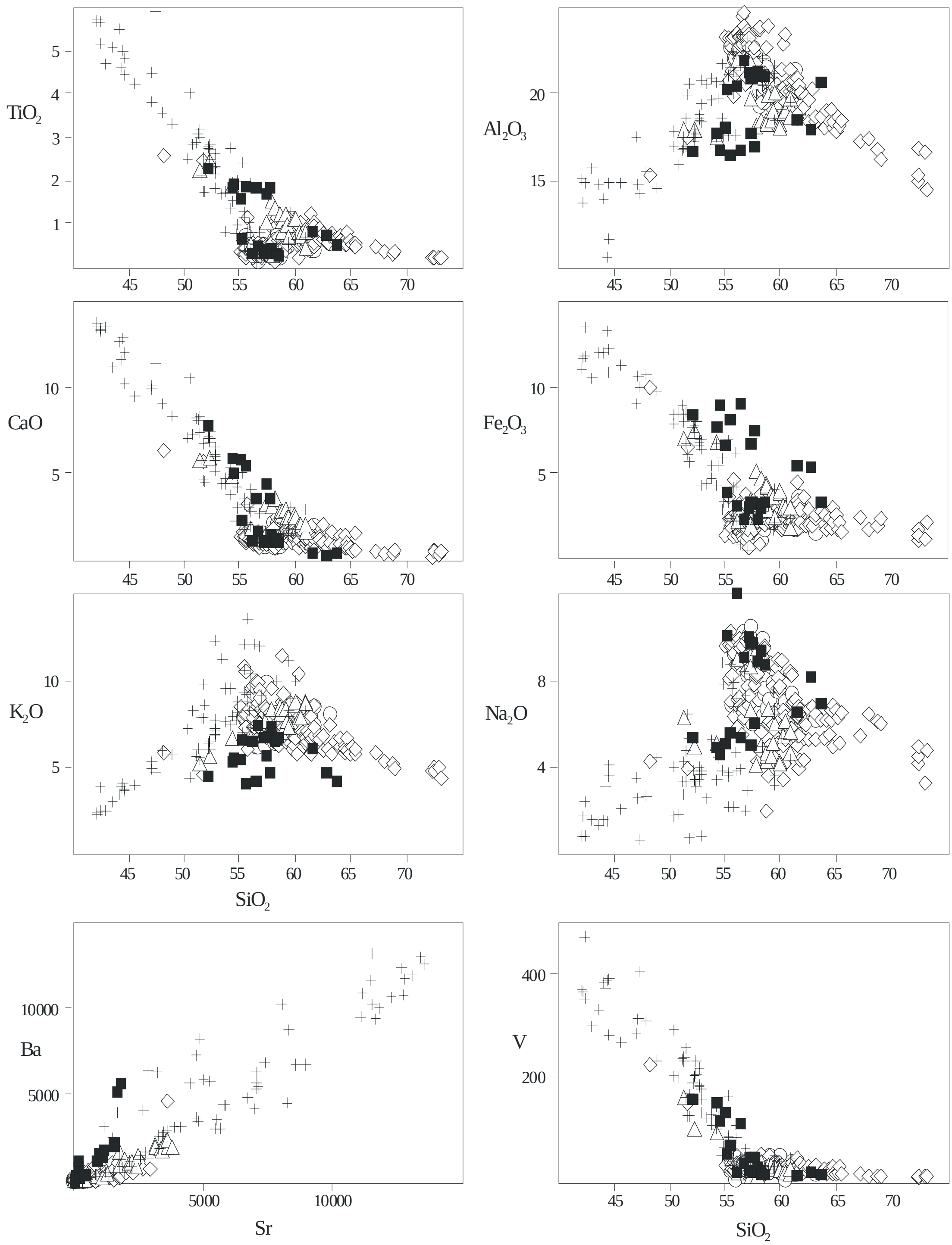


Fig. 10. Major oxides (wt%) and selected trace elements (ppm) variation diagrams for the intrusive rocks, using $SiO_2$ wt% as differentiation index. Symbols: crosses, Morro de São João; filled squares, Cabo Frio; triangles, Morro Redondo; open diamonds, Itatiaia; circles, Passa Quatro.

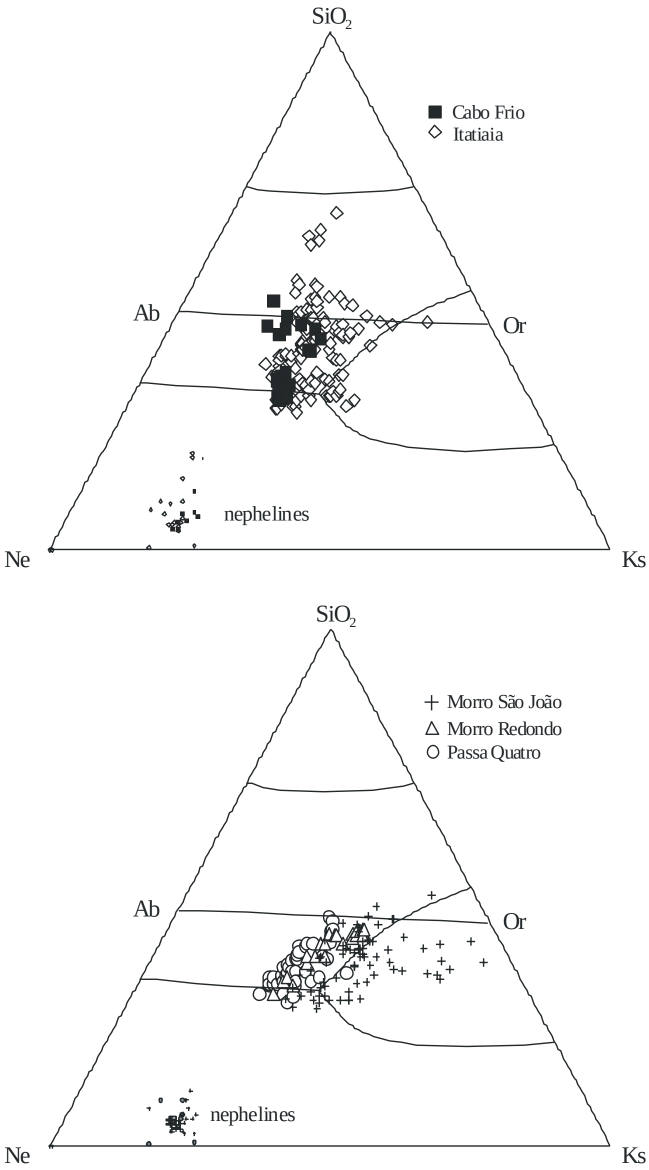


Fig. 11. The alkaline intrusive rocks of the Serra do Mar Province as plotted in the Ne-Ks-$SiO_2$ system (after Hamilton & MacKenzie, 1965). Symbols as in Fig. 10.

whereas MgO, $TiO_2$, CaO and $P_2O_5$ decrease. Rb and Zr increase as Ba, Sr, La, Ce and Y decrease in the evolved nepheline syenites and alkali syenites. Some coarse-grained alkali syenites and nepheline syenites have very high Ba, Sr, Nb, La and Ce contents.

## RARE EARTH ELEMENT GEOCHEMISTRY

### Dykes

The ultrabasic rocks (foidites, basanites and tephrites) have REE patterns characterized by La ranging from 100 to 300 times chondrite and $(La/Yb)_n$ from 17 to 30 (Fig. 12). Mg-rich alkali basalts (MgO>10 wt%) have linear REE patterns broadly similar to those of basanites and foidites but at slightly lower light REE (LREE) contents. Their $(La/Yb)_n$ varies between 9 and 17.

Trachytes and phonolites are variably enriched in LREE relative to middle REE with $(La/Sm)_n$ in the range 40-10. Several trachytes and phonolites show a variable negative Eu-anomaly (Eu/Eu* down to 0.09).

### Alkaline intrusions

The *Morro de São João* rocks are strongly LREE enriched: La and Ce abundances are about 300-800 times chondrite and $(La/Yb)_n$=29-34. Positive Eu anomalies are found in mela-gabbros, malignites and some coarse-grained syenites. Shonkinites do not show Eu anomalies. The most evolved fine-grained nepheline syenites and phonolites have MREE depletion (Fig. 13).

The REE patterns of the *Morro Redondo* syenites and nepheline syenites are strongly fractionated ($La/Yb_n$=25-37). Some alkali syenites also have marked positive Eu anomalies (Eu/Eu*=1.5-2.7), due to alkali feldspar accumulation.

The *Passa Quatro* nepheline syenites have strongly fractionated patterns ($La/Yb_n$=33-44). Positive or negative Eu anomalies (Fig. 13), which are not present in the less differentiated rocks, have been found in phenocryst-rich phonolites (Eu/Eu* =1.28) and in peralkaline phonolites (Eu/Eu*=0.65), respectively.

There is evidence of extensive fractionation (or,

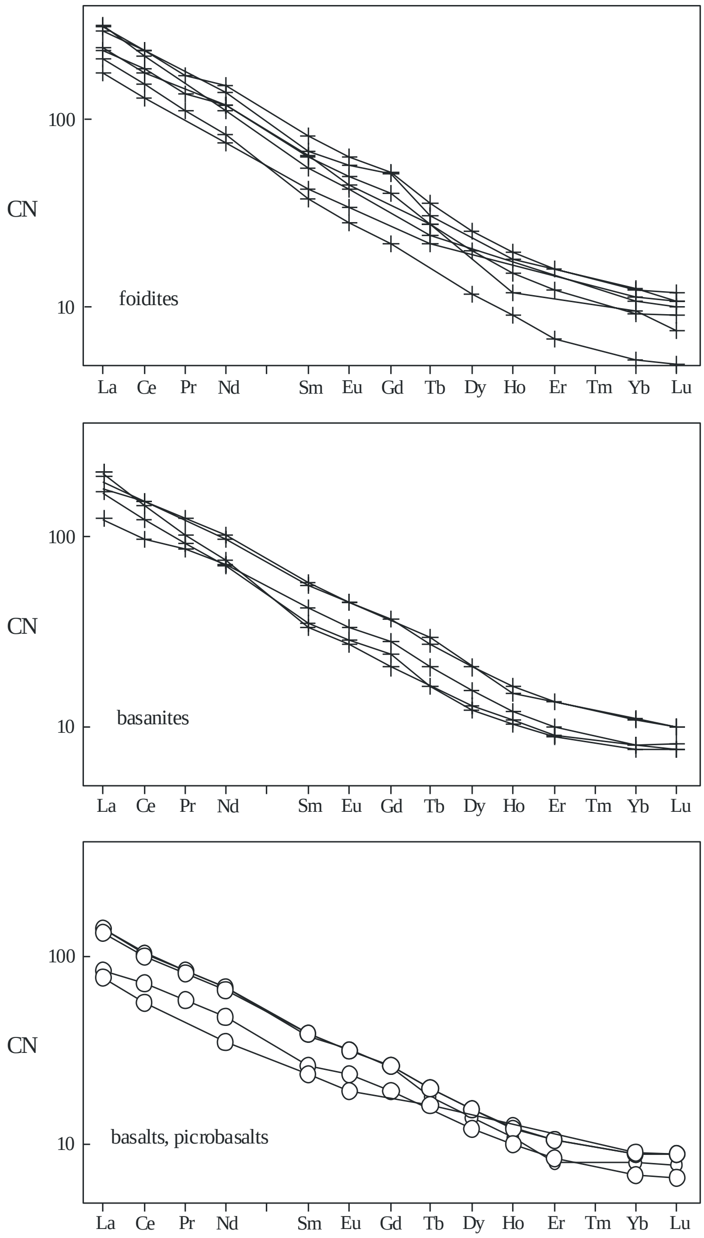


Fig. 12. Chondrite-normalized (CN, cf. Boynton, 1984) rare earth elements plots for representative foidites, basanites, basalts and picrobasalts of the Serra do Mar Province.

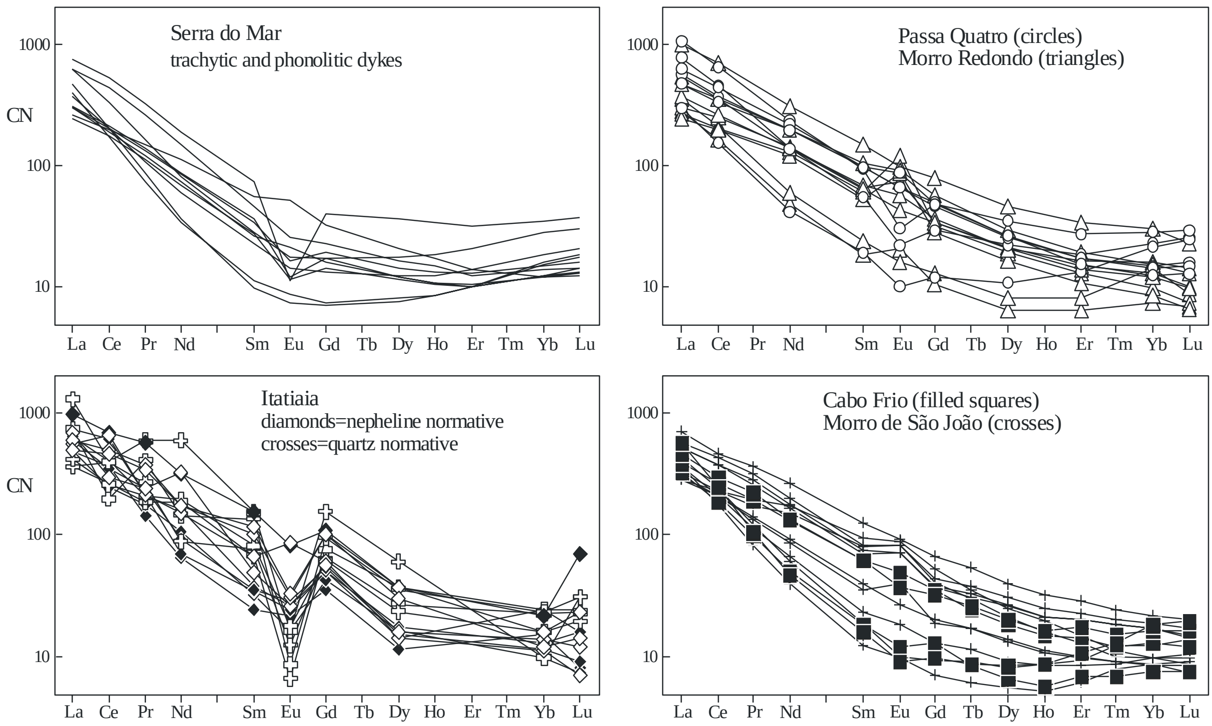


Fig. 13. Chondrite-normalized (CN) rare earth element plots for representative felsic rocks from the Serra do Mar Province.

in some cases, of local cumulus) of alkali feldspar at the transition to peralkaline conditions (Fig. 13). Chemically evolved nepheline syenites have upward concave patterns ($La/Sm_n$=15.6), the lowest REE and Y contents ($La/Yb_n$=14.3), and negative Eu anomalies (Eu/Eu*=0.66). Extensive fractionation of feldspar and titanite are the most likely explanation for these patterns.

The REE patterns of the *Itatiaia* syenitic rocks are distinctive for each rock group: the quartz syenites and granites (Q-group) have very pronounced negative Eu anomalies (Eu/Eu*=0.25-0.07), regardless the degree of differentiation of the lithologies, and moderate LREE fractionation ($La/Sm_n$=4.7-8.5). The alkali syenites, nepheline syenites, and C-syenites do not present strong negative Eu anomalies (Eu/Eu*=0.31-0.63 for the A group and 0.45-0.73 for the SA group). Moreover, for the same D.I.*, the patterns are steeper in the SA and C-syenites ($La/Sm_n$ is 4.4-14.1 for A-group and 17.1-21.3 for SA-group), suggesting that the different syenite groups cannot be related to simple fractional crystallization processes. The positive Eu anomaly values of some samples (Eu/Eu*=1.32) indicate accumulation of alkali feldspar (Fig. 13).

## Sr-Nd ISOTOPES

### Dykes

εNd and initial $^{87}Sr/^{86}Sr$ data of the SdM ultrabasic and basaltic rocks (Garda *et al.*, 1995; Valente, 1997; Thompson *et al.*, 1998) are plotted in Fig. 14, along with the fields from Trindade-Martin Vaz, Tristan da Cunha, Walvis Ridge, Rio Grande Rise and Alto Paranaíba magmatic rocks (Richardson *et al.*, 1982; Le Roex *et al.*, 1990; Gibson *et al.*, 1995; Marques *et al.*, 1999; Siebel *et al.*, 2000). The SdM rocks with MgO>10 wt% usually plot close to the Bulk Silicate Earth (BSE) and only a few samples have high $^{87}Sr/^{86}Sr_i$ values (0.70661 to 0.70820) with εNd -0.46, –1.86 and +1.96 (Valente, 1997; Thompson *et al.*, 1998). The authors mentioned above suggest that such isotopic features imply crustal contamination processes. On the other hand, some basanites from offshore islands (Monte de Trigo, São Sebastião; cf. Thompson *et al.*, 1998) plot in the depleted quadrant, having $^{87}Sr/^{86}Sr_i$ 0.70389-0.70435 and εNd +0.47 to +2.68.

The SdM intermediate and felsic rocks are scattered, with εNd ranging from +2 to -5 and $^{87}Sr/^{86}Sr_i$ ranging from 0.70389 to 0.70661; a few phonolitic and trachytic rocks have higher $^{87}Sr/^{86}Sr_i$ (up to 0.72375; cf. Valente, 1997; Thompson *et al*. 1998).

**Alkaline intrusions**

$^{87}Sr/^{86}Sr_i$ and εNd of the felsic intrusions comparatively display small variation ranges, with trachytes and syenites of the Arraial do Cabo (Bennio *et al.*, 2002) showing $^{87}Sr/^{86}Sr_i$ 0.7042-0.7045 and εNd -1.9 to -3.5. The alkaline rocks from the Passa Quatro, Itatiaia and Morro de São João complexes have similar and narrow ranges of both $^{87}Sr/^{86}Sr_i$ (0.7045-0.7058) and εNd (-2.7 to -4.3). It also should be noted that the Itatiaia quartz syenites present the highest $^{87}Sr/^{86}Sr_i$ (0.7068) and the lowest εNd (-6.36). Notably, the isotope data of the syenitic samples are very similar to those of the mafic dykes, and confirm the cogenetic nature of the evolved rocks.

## DISCUSSION

The Late Cretaceous-Eocene (80-55 Ma) alkaline magmas of the Serra do Mar Province belong both to a strongly and a weakly potassic alkaline suites. In regard to the rock-types, the basanites/tephrites and phonolites are by far much more widespread than the trachytes and alkali basalts. The following petrographical features are relevant for the petrogenetic modelling of the SUS suite: 1) the ultrabasic rocks (foidites and basanites) are dominated by early-crystallized olivine and clinopyroxene; 2) biotite becomes a phenocryst phase in the tephrites and intermediate rocks (phonotephrites and tephri-phonolites); 3) early-crystallized plagioclase, lacking in the ultramafic-mafic rocks, becomes a phenocryst phase in phonotephrites and tephriphonolites, along with clinopyroxene, biotite, amphibole and opaques; 4) sanidine phenocrysts are common in the tephriphonolites and phonolites, and 5) late stage alteration processes have variably affected the ultrabasic rocks, suggesting caution in the petrogenetic modelling, particularly when mobile elements are involved.

Source mantle

The least evolved rocks of the SUS suite, with Mg# in the 0.76-0.64 range, are enriched by up to 100-300 times in respect to the primitive mantle in Rb, Ba, Nb, and La (Fig. 9).

These plagioclase-free/-poor rocks, containing hydrous minerals in the groundmass and exsolved carbonate patches, are commonly considered to have been formed by small degrees of partial melting starting from an enriched, volatile-bearing mantle (Wilson *et al.*, 1995). Compared with the SUS suite, the least evolved (Mg# 0.70-0.68) rocks belonging to the WUS suite have strikingly similar patterns, displaced at slightly lower LILE contents.

In order to constrain source(s) mineralogy and melting processes, a subset of data showing MgO content in the range 10-17 wt% (mg# 0.70-0.64) and high Ni (>150 ppm) and Cr (>300 ppm) has been selected. This subset includes foidites, basanites, weakly silica-undersaturated basalts and ultra-potassic rock-types.

The potassic character of these rocks and the related strong incompatible element enrichment are a clear indication of a source completely different from that of the Mid Ocean Ridge basalts (MORB). Indeed, the most recent geochemical modelling of the mantle sources (Thompson *et al.*, 1998) started from a bulk silicate earth source (BSE), and obtained for the mafic volcanic rocks partial melting degrees variable from >1 to 0.1% of a mixed spinel-to-garnet source (30% sp to 70% gt). It is clear that melting of a bulk silicate earth cannot produce potassic or even ultrapotassic liquids with such a strong enrichment of incompatible elements, in view of realistic degrees of partial melting (e.g.>1%). We are more confident that mantle metasomatic processes took place in the source of the Serra do Mar Province prior to melting. This metasomatism was responsible for the formation of sources with small amounts of potassic phases like phlogopite, along with minor

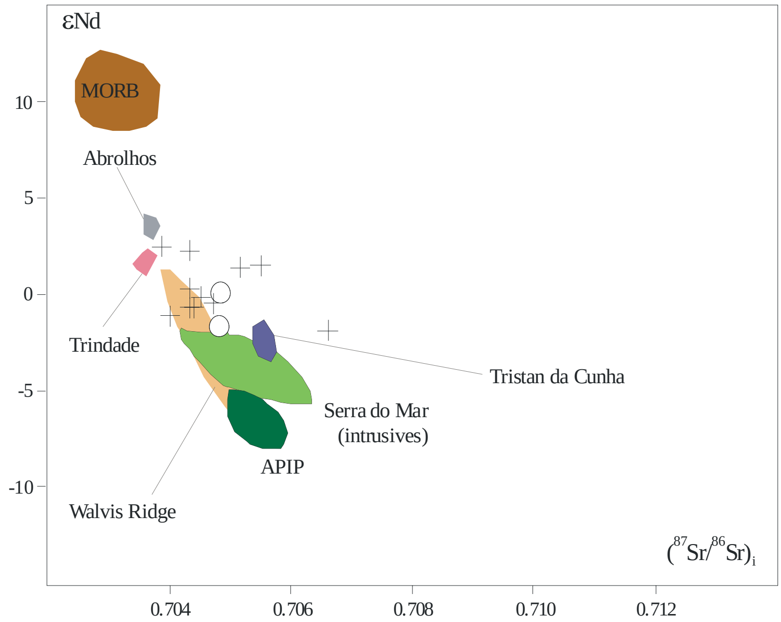


Fig. 14. Sr vs. Nd isotope diagram for the Serra do Mar mafic alkaline dykes. The fields of Trindade, Abrolhos, Tristan da Cunha, Walvis Ridge, and Alto Paranaíba Province are taken from Thompson *et al.* (1998) and references therein.

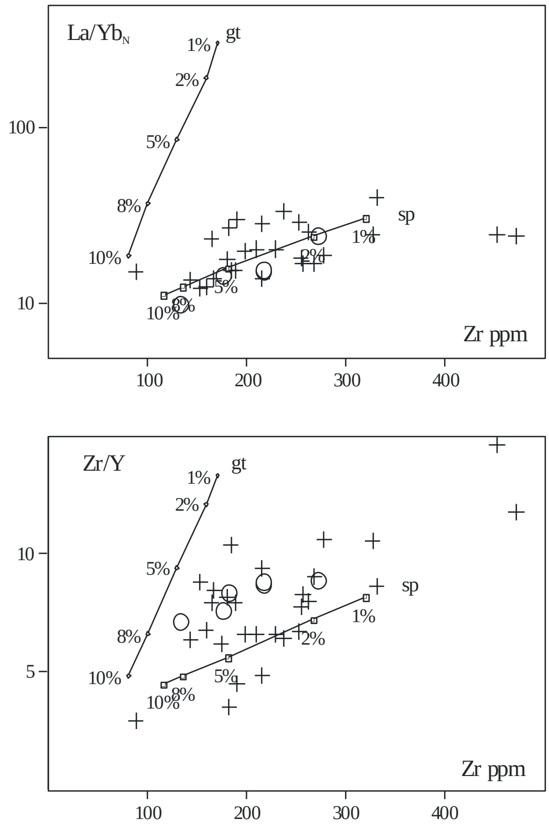


Fig. 15. Partial melting models of the Serra do Mar source. We hypothesized a 99% primitive mantle source contaminated for 1% of a kimberlitic melt with the composition of the Três Ranchos pipe (Gibson *et al.* 1995; unpublished data by the authors). Batch melting model was employed. Partition coefficients after Niu *et al.* (1996).

accessory phases, like titanium oxides and apatite. Moreover, the strong light rare earth elements fractionation of the mafic potassic rocks of the Serra do Mar could not *in se* been caused by melting in the presence of residual garnet, but it could have simply been a consequence of melting of an enriched source located in the shallow, garnet-free mantle. We hypothesized that a bulk silicate earth source was slightly metasomatized by kimberlitic melts (like the composition of the Três Ranchos kimberlite of the Alto Paranaíba Province; cf. Gibson *et al.*, 1995). In diagrams such as $La/Yb_N$ vs. Zr and Zr/Y vs. Zr (Fig. 15), the mafic potassic rocks plot in, or very close to the spinel-bearing (or simply garnet-free) melting trend at degrees of partial melting ranging from 1 to 8%.

These results also take for granted that phases like phlogopite cannot produce strong partitioning of these elements. Major element mass balance calculations to obtain the basanite BZ17A, starting from a phlogopite peridotite composition like that reported in Comin-Chiaramonti *et al.* (1997), obtained ca. 4.8% partial melting, leaving a phlogopite-bearing harzburgite residuum. We did not envisage major differences in the degree of partial melting between the SUS and WUS rocks. It is evident that the melting models can be source-dependent and not univocal, and thus any inference from them may be weakly based.

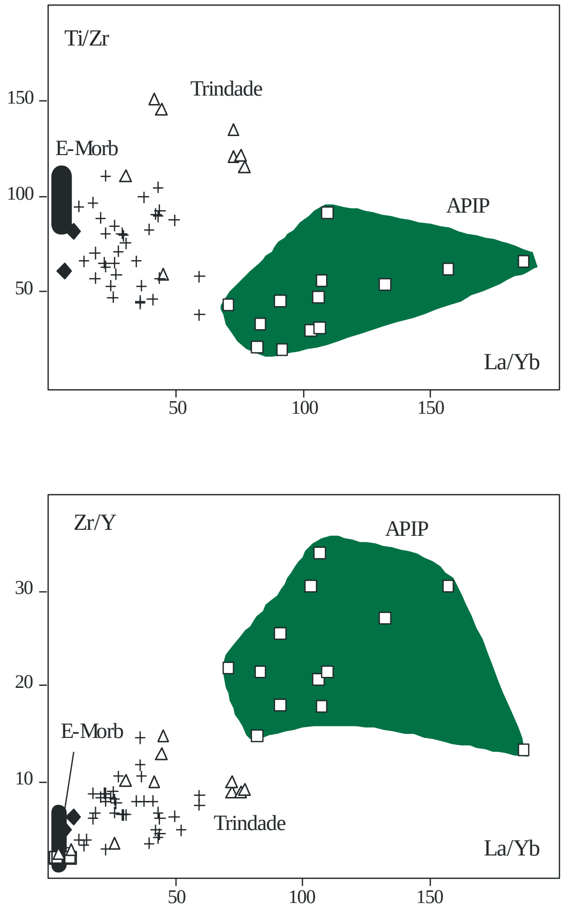


Fig. 16. Ti/Zr vs. La/Yb and Zr/Y vs. La/Yb diagrams for the most primitive WUS and SUS rocks. Alto Paranaíba kamafugites and kimberlites (unpublished data by the authors), Cabo Frio tholeiitic samples (Bennio *et al.*, 2003), and Trindade rocks (Marques *et al.*, 1999; Siebel *et al.*, 2000) are also shown.

The main petrogenetic models relative to the Serra do Mar Late Cretaceous mafic to ultramafic potassic magmas can be synthesized as follows: 1) interaction between a dominant, convecting OIB-like component and an EM1-like lithospheric mantle end-member (Thompson *et al.*, 1998); 2) melting of a heterogeneous subcontinental lithospheric mantle previously enriched by metasomatic processes (Valente, 1997; Brotzu *et al.*, 1997, Gibson *et al.*, 1999).

The first model is essentially based on the following geological and geochemical aspects: 1) Trindade plume-tail mantle was deflected southward beneath the São Francisco craton between 80 and 55 Ma; 2) close time-space relationships between migrating magmatism and predicted track of the Trindade plume tail; 3) the enriched geochemical patterns of the Serra do Mar potassic alkaline magmas. This model is inappropriate to explain the geochemical features of the Serra do Mar potassic magmas if some incompatible element ratios are considered. The near-primary Serra do Mar magmas and Trindade basanites and nephelinites plot in distinct fields so that significant and widespread interaction with lithospheric mantle is required to modify the Trindade melts, if they are required by the model (Fig. 16). The kamafugitic and kimberlitic rocks from the Alto Paranaíba Igneous Province, which have been related to low melting degrees of an EM1-like lithospheric mantle (Gibson *et al.*, 1995; Araújo *et al.*, 1995; Carlson *et al.*, 1996) plot in distinct fields and then may be considered the lithospheric (metasomatic) components able to modify the pristine mantle isotopic compositions.

## Magmatic evolution

### Dykes

The compositional variations of the main rock forming minerals (i.e. Na and Fe increase in clinopyroxenes, Fe increase in micas and amphiboles and, finally, Or increase from early to late-crystallized alkali feldspars) of the SUS suite are compatible with evolutive processes dominated by fractional crystallization. The genetic linkage between the rocks that form this strongly undersaturated suite is enhanced by relict and/or xenocryst phases (i.e. green clinopyroxene and corroded plagioclase) occurring in tephrites, phonotephrites and phonolites. Major and trace element trends are consistent with evolution processes dominated by olivine and clinopyroxene fractionation (cf. Figs. 8A, B). On the whole, the compositional variability of the olivine, clinopyroxene and Cr-spinel bearing cumulates well explains satisfactory that of the basanitic and foiditic rocks. The removal of clinopyroxene, titanomagnetite, apatite, and minor plagioclase, biotite and amphibole matches the compositional variations of phonotephrites and tephriphonolites. For example, the transition between the basanite BZ17A and phonolitic tephrite 94SOB78 was obtained by means of 54.8% fractionation of olivine (3%), clinopyroxene (20.9%), magnetite (2.1%), apatite (1.8%), phlogopite (16.9%) and kaersutite (10.1%), thus leaving ultramafic cumulates. The minor role of plagioclase in the fractionation process is also suggested by the $Al_2O_3$ increase with decreasing MgO (Fig. 8A). Finally, the feldspar fractionation could be the main phase responsible for the compositional variations of the felsic rocks and the "sodic" character of the evolved phonolites. Bennio (2002) modelled the transition from the tephritic phonolite F14 to the phonolite F21 of the Cabo Frio swarm by means of 75% fractionation of 32.1% sanidine, 29.9% sodic plagioclase, 3.4% amphibole, 23.1% clinopyroxene, 7.3% magnetite, 2.5% apatite and 1.8% titanite.

Regarding the WUS suite, petrography, mineralogy and geochemical trends suggest a magma evolution dominated by fractional crystallization processes. It should be noted that in this weakly undersaturated suite the plagioclase is an important fractionating phase (see $Al_2O_3$ trend, Fig. 8A) in the trachybasalts, as suggested by the crystallization sequence (plagioclase, clinopyroxene and minor olivine phenocrysts). As an example, the transition from the alkali basalt BZ181A to the trachyandesite 93SOB206 required ca. 63% fractionation of olivine (14.7%), clinopyroxene (18.4%), plagioclase (25.1%) and Fe-Ti oxides (5.0%).

The alkaline rock sequences of the Serra do Mar Province show Sr and Nd-isotopic trends which strongly suggest the involvement of crustal components during the magma evolution. The samples form a scattered trend starting from εNd ca. +2.7 and $^{87}Sr/^{86}Sr_i$ ca. 0.7039 to εNd ca. –5 and $^{87}Sr/^{86}Sr_i$ 0.7080. This trend is compatible with bulk assimilation involving ultrabasic magmas and local lower crust (Valente, 1997). Trachytic and phonolitic rocks show a greater scatter and suggest different contamination trends involving also local upper crust, even though a few samples have isotopic ratios comparable to those of the less evolved rocks.

In sum, there are several lines of evidence indicative that FC and/or AFC processes can explain the compositional variations of strongly and weakly silica-undersaturated dyke-rock sequence occurring in the Serra do Mar Province.

Geochemical modelling of these suites puts the question of why several elements, at a given MgO value, display relevant differences in their concentrations which cannot be related to space-time variations**.** From a geochemical point of view, the alkaline dykes emplaced into the western Serra do Mar Province are not distinguishable from those that outcrop along the eastern sector. Taking into consideration the CaO, $Fe_2O_3$ total, $TiO_2$, $P_2O_5$, Zr and Nb of the near-primary or poorly evolved rocks (MgO>10 wt%, high Ni and Cr, and relatively low LOI) high scatter is evident (Figs. 8A,B), and this points out to different parental magmas.

**Alkaline intrusions**

The magmatic evolution of the syenitic intrusions is closely related to the trends already noted in the differentiation of mafic and ultramafic dykes. From the observation of the diagrams shown in Fig. 12, and from the modelling of evolution trends of specific complexes (e.g. Brotzu *et al.*, 1989, 1992, 1997; Bennio, 2001) some features become clear: the rocks of the Morro de São João complex are formed by cumulus of calcic and titaniferous phases like clinopyroxene, amphibole, oxides and titanite, with low amounts of plagioclase and alkali feldspar, leaving more evolved liquids from which, in turn, the Al-rich nepheline syenites have been formed. The onset of major alkali feldspar fractionation is well displayed in the kinks of CaO, $Al_2O_3$, $Fe_2O_3$, $TiO_2$, and V at $SiO_2$ ca. 55 wt%. As exemplified by

Brotzu *et al.* (1997) for the Itatiaia rocks, extensive fractionation of K-rich alkali feldspar (in some cases up to 90% of the solid extracts), or coupled sodic plagioclase and alkali feldspar, drives the residual liquids either towards the more Al and Na-rich phonolites/nepheline syenites (Fig. 13; cf. also Brotzu *et al.*, 1989, 1992), or to the less Al, Na and K-rich rhyolite (granite) residual melts.

The oversaturated trend is well displayed at Itatiaia and likely at Soarinho. The Itatiaia, Passa Quatro and Morro Redondo nepheline-bearing rocks are very similar in their chemistry, whereas the Cabo Frio rocks tend to be less potassic and more iron-rich (Fig. 13). We argue that this slightly more sodic character of the evolved rocks is linked to the chemical composition of their mafic magmas, and thus ultimately linked to changes of the mantle source towards the sea.

We believe that there is no compelling doubt that the syenitic intrusions were filled by liquid residues of extensive crystallization starting from the mafic dykes of the Serra do Mar Province. Sporadic evidence of crustal contamination accompanying the transition towards the most evolved quartz normative samples has already been pointed out by Brotzu *et al.* (1997).

## CONCLUSIONS

The Serra do Mar Igneous Province is formed by plutonic complexes and by dyke swarms.

Regarding the latter, two main potassic suites have been distinguished: the most widespread suite is strongly silica-undersaturated and range from ultrabasic to phonolitic rocks; and minor weakly silica-undersaturated rocks range from basalts to trachytes. All the suites show major and trace element trends fully compatible with fractionation processes dominated by the already mentioned phenocrysts, locally accompanied by AFC processes. Distinct basanitic and foiditic parental magmas are required to explain the incompatible elements feature of the near primary/or poorly evolved magmas of the strongly undersaturated suite. Both suites have similarly enriched geochemical patterns even though the weakly silica-undersaturated suite display slightly lower incompatible element enrichment. The mantle sources were characterized by significant and heterogeneous incompatible element enrichment, which may have caused formation of small amounts of metasomatic phases like phlogopite, titanates and apatite. Degrees of partial melting variable from 1 to 8% of such metasomatized sources at shallow depths could be sufficient in order to generate the compositional variation in the mantle-derived rocks.

The syenitic intrusions have trends dominated by alkali feldspar fractionation towards phonolitic compositions, which often have weakly peralkaline chemistry. The evolution towards rhyolitic compositions is often accompanied by crustal contamination.

## ACKNOWLEDGEMENTS

The authors wish to gratefully thank E. Piccirillo, for the critical reading of an early draft of the manuscript, and L. Bennio, who provided data not yet published on the Morro de São João complex and on the mafic dyke swarm. This paper could not have been written without the scientific and logistic efforts of C.B. Gomes (Fapesp Proc. 01/10714-3) and E. Ruberti, throughout the more than twenty years of collaboration between Italian and São Paulo Universities.

## REFERENCES

Almeida, F.F.M. (1983). Relações tectônicas das rochas alcalinas mesozóicas de região meridional da Plataforma Sul-Americana. *Revista Brasileira de Geociências* **13**, 139-158.

Araújo, A.L.N., Sichel, S.E. & Valença, J.G. (1995). Geoquímica das rochas alcalinas de Arraial do Cabo (RJ): Ilha do Cabo Frio e áreas adjacentes. *V Congresso Brasileiro de Geoquímica, Niterói,* CD-ROM.

Bailey, D.K. (1976). Application of experiments to alkaline rocks. In: Bailey, D.K. & Macdonald, R. (eds.) *The evolution of the crystalline rocks*. London: Academic Press, pp. 419-473.

Bennio, L. (2001). *Petrogenesi del complesso alcalino tardo Cretacico di Morro São João*

*(Brasile sud-orientale)*. Ph.D. Thesis, University of Naples, 152p.

Bennio, L., Brotzu, P., D'Antonio, M., Feraud, G., Gomes, C.B., Marzoli, A., Melluso, L., Morbidelli, L., Morra, V., Rapaille, C. & Ruberti, E. (2003). The tholeiitic dyke swarm of the Arraial do Cabo peninsula (SE Brazil): $^{39}Ar/^{40}Ar$ ages, petrogenesis and regional significance. *Journal of South American Earth Sciences* **16**, 163-176.

Bennio, L., Brotzu, P., Gomes, C.B., D'Antonio, M., Lustrino, M., Melluso, L., Morbidelli, L. & Ruberti, E. (2002). Petrological, geochemical and Sr-Nd isotopic features of alkaline rocks from Arraial do Cabo peninsula (southeastern Brazil). *Periodico di Mineralogia* **71**, 137-158.

Boynton, W.B. (1984). Cosmochemistry of Rare Earth Elements: meteorite studies. In: Hendersen, P. (ed.) *Rare Earth Element geochemistry*. Amsterdam: Elsevier, pp. 63-114.

Brotzu, P., Barbieri, M., Beccaluva, L., Garbarino, G., Gomes, C.B., Macciotta, G., Melluso, L., Morbidelli, L., Ruberti, E., Sigolo, J.B. & Traversa, G. (1992). Petrology and geochemistry of the Passa Quatro complex, southeastern Brazil. *Journal of South American Earth Sciences* **6**, 237-252.

Brotzu, P., Beccaluva, L., Conte, A., Fonseca, M., Garbarino, C., Gomes, C.B., Leong, R., Macciotta, G., Mansur, R.L., Melluso, L., Morbidelli, L., Ruberti, E., Sigolo, J.B., Traversa, G. & Valença, J.G. (1989). Petrological and geochemical studies of alkaline rocks from continental Brazil. 8. The syenitic intrusion of Morro Redondo, RJ. *Geochimica Brasiliensis* **3**, 63-80.

Brotzu, P., Gomes, C.B., Melluso, L., Morbidelli, L., Morra, V. & Ruberti, E. (1997). Petrogenesis of coexisting $SiO_2$-undersaturated to $SiO_2$-saturated felsic igneous rocks: the alkaline complex of Itatiaia, southeastern Brazil. *Lithos* **40**, 133-156.

Carlson, R.W., Esperança, S. & Svisero, D.P. (1996). Chemical and Os isotopic study of Cretaceous potassic rocks from southern Brazil. *Contributions to Mineralogy and Petrology* **125**, 393-405.

Comin-Chiaramonti, P., Cundari, A., Piccirillo, E.M., Gomes, C.B., Castorina, F., Censi, P., De Min, A., Marzoli, A., Speziale, S. & Velázquez, V.F. (1997). Potassic and sodic igneous rocks from eastern Paraguay: their origin from the lithospheric mantle and genetic relationships with the associated Paraná flood tholeiites. *Journal of Petrology* **38**, 495-528.

Comin-Chiaramonti, P., Gomes, C.B., Piccirillo, E.M., Rivalenti, G. (1983). High-$TiO_2$ basaltic dykes in the coastline of São Paulo and Rio de Janeiro States (Brazil). *Neues Jahrbuch Mineralogische Abhandlungen* **146**, 133-150.

De La Roche, H., Leterrier, P., Grandclaude, P. & Marchal, E. (1980). A classification of volcanic and plutonic rocks using R1-R2 diagram and major element analyses. Its relationships with current nomenclature. *Chemical Geology* **29**, 183-210.

Enrich, G.E.R., Azzone, R.G., Ruberti, E., Gomes, C.B. & Comin-Chiaramonti, P. (in this volume). Itatiaia, Passa Quatro and São Sebastião island, the major alkaline syenitic complexes from the Serra do Mar region.

Garda, G.M. (1995). *Os diques básicos e ultra-básicos da região costeira entre as cidades de São Sebastião e Ubatuba, Estado de São Paulo*. Ph.D. Thesis, University of São Paulo, 360p.

Garda, G.M., Schorscher, J.H.D., Esperança, S. & Carlson, R.W. (1995). The petrology and geochemistry of coastal dykes from São Paulo State, Brazil: implication for variable lithospheric contributions to alkaline magmas from the western margin of the South Atlantic. *Anais da Academia Brasileira de Ciências* **67**, 191-216.

Gibson, S.A., Thompson, R.N., Leonardos, O.H., Dickin, A.P. & Mitchell, J.G. (1995). The Late Cretaceous impact of the Trindade mantle plume: evidence from large-volume mafic, potassic magmatism in SE Brazil. *Journal of Petrology* **36**, 189-229.

Gibson, S.A., Thompson, R.N., Leonardos, O.H., Dickin, A.P. & Mitchell, J.G. (1999). The limited extent of plume-lithosphere interactions during continental flood-basalt genesis: geochemical evidence from Cretaceous magmatism in southern Brazil. *Contributions to Mineralogy and Petrology* **137**, 147-169.

Gibson, S.A., Thompson, R.N., Weska, R., Dickin, A.P. & Leonardos, O.H. (1997). Late Cretaceous rift-related upwelling and melting of the Trindade starting mantle plume head beneath western Brazil. *Contributions to Mineralogy and Petrology* **126**, 303-314.

Hackspacher, P.C. & Godoy, A.M. (1999). Vertical displacement during late-collisional escape tectonics (Brasiliano orogeny) in the Ribeira belt, São Paulo State, Brazil. *Journal of African Earth Sciences* **29**, 25-32.

Hamilton, D.L. & MacKenzie, W.S. (1965). Phase equilibrium studies in the system $NaAlSiO_4$ (nepheline)-$KAlSiO_4$-(kalsilite)-$SiO_2$-$H_2O$. *Mineralogical Magazine* **34**, 214-231.

Irvine, T.N. & Baragar, W.R.A. (1971). A guide to chemical classification of the common rocks. *Canadian Journal of Earth Sciences* **62**, 365-391.

Le Bas, M.J., Le Maitre, R.W., Streckeisen, A. & Zanettin, B. (1986). A chemical classification of volcanic rocks based on the total alkali-silica diagram. *Journal of Petrology* **27**, 745-750.

Le Roex, A.P., Cliff, R.A. & Adair, B.J.I. (1990).

Tristan da Cunha, south Atlantic: geochemistry and petrogenesis of a basanite-phonolite lava series. *Journal of Petrology* **31**, 779-812.

Luth, W.C. (1976). Granitic rocks. In: Bailey, D.K. & Macdonald, R. (eds.) *The evolution of the crystalline rocks*. London: Academic Press, pp. 335-417.

Marques, L.S., Ulbrich, M.N.C., Ruberti, E. & Tassinari, C.G. (1999). Petrology, geochemistry, and Sr-Nd isotopes of the Trindade and Martin Vaz volcanic rocks (southern Atlantic Ocean). *Journal of Volcanology and Geothermal Research* **93**, 191-216.

Middlemost, E.A.K. (1975). The basalt clan. *Earth-Science Reviews* **11,** 337-364.

Morbidelli, L., Gomes, C.B., Beccaluva, L., Brotzu, P., Conte, A.M., Ruberti, E. & Traversa, G. (1995). Mineralogical, petrological and geochemical aspects of alkaline and alkaline-carbonatite associations from Brazil. *Earth-Science Reviews* **39**, 135-168.

Niu Y., Waggoner, D.G., Sinton, J.M., & Mahoney, J.J. (1996) Mantle source heterogeneity and melting processes beneath seafloor spreading centers: the East Pacific Rise, 18°-19°S. *Journal of Geophysical Research* **101**, 27711-27733.

Riccomini, C., Velázquez, V.F. & Gomes, C.B. (in this volume). Tectonic controls of the Mesozoic and Cenozoic alkaline magmatism in the central-southeastern Brazilian Platform.

Richardson, S.H., Erlank, A.J., Duncan, A.R. & Reid, D.L. (1982). Correlated Nd, Sr and Pb isotope variations in Walvis Ridge basalts and implications for the evolution of their mantle source. *Earth and Planetary Science Letters* **59**, 327-34

Rock, N.M.S. (1991) *Lamprophyres*. Glasgow: Blackie, 285p.

Ruberti, E., Gomes, C.B. & Comin-Chiaramonti, P. (in this volume). The alkaline magmatism from the Ponta Grossa Arch.

Siebel, W., Becchio, R., Volker, F., Hansen, M.A. F., Viramonte, J., Trumbull, R.B., Haase, G. & Zimmer, M. (2000). Trindade and Martin Vaz Islands, South Atlantic: isotopic (Sr, Nd, Pb) and trace element constraints on plume related magmatism. *Journal of South American Earth Sciences* **13**, 79-103.

Sun, S.-S. & McDonough, W.F. (1989). Chemical and isotopic systematics of oceanic basalts: implications for mantle composition and processes. In: Saunders, A.D. & Norry, M.J. (eds.) *Magmatism in the ocean basins*. *Geological Society of London, Special Publication* **42**, 313-345.

Tello Saenz, C.A., Hackspacher, P.C., Hadler Neto, J.C., Junes, P.J., Guedes, S., Ribeiro, L.F.B. & Paulo, S.R. (2003). Recognition of Cretaceous, Paleocene and Neogene tectonic reactivation trough apatite fission-track analysis in Precambrian areas of southeast Brazil: association with the opening of the south Atlantic Ocean. *Journal of South American Earth Sciences* **15**, 765-774.

Thompson, R.N., Gibson, S.A., Mitchell, J.G., Dickin, A.P., Leonardos, O.H., Brod, J.A. & Greenwood, J.C. (1998). Migrating Cretaceous-Eocene magmatism in the Serra do Mar alkaline Province, SE Brazil: melts from the deflected Trindade mantle plume? *Journal of Petrology* **39**, 1493-1526.

Ulbrich, H.H.G.J. & Gomes, C.B. (1981). Alkaline rocks from continental Brazil. *Earth-Science Reviews* **17**, 135-154.

Valente, S.C. (1997). *Geochemical and isotopic constraints on the petrogenesis of the Cretaceous dykes of the Rio de Janeiro, Brazil*. Ph.D. Thesis, University of Belfast, 297p.

Wilson, M., Downes, H. & Cebrià, J.M. (1995) Contrasting fractionation trends in coexisting continental alkaline magma series: Cantal, Massif Central, France. *Journal of Petrology*, **36**, 1729-1753.

*Mesozoic to Cenozoic Alkaline Magmatism in the Brazilian Platform*
*Comin-Chiaramonti, P. & Gomes, C.B. (eds.)*
*Edusp/Fapesp, São Paulo, pp. 443-472, 2005*

# THE ALKALINE MAGMATISM FROM THE PONTA GROSSA ARCH

*E. Ruberti, C.B. Gomes and P. Comin-Chiaramonti*

*The southeastern side of the Ponta Grossa Arch was the site of repeated alkaline and alkaline-carbonatitic activity in Early and Late Cretaceous times, respectively. Along two main NW-trending lineaments, i.e. Guapiara and São Jerônimo-Curiúva, a great number of complexes and dyke swarms intrude the country-rocks. A detailed description of the outcrops is presented. Some different parental mantle-derived magmas may be inferred from the geochemical characteristics, i.e. ankaratrite, basanite and theralite. Sr-Nd isotopes show that the primary magmas have signatures similar to the spatially associated Early Cretaceous tholeiites. The evolved rock-types may occasionally display isotopic ratios suggesting AFC processes, but the associated carbonatites usually have isotopic signatures similar to those of primary magmas. On the whole, the alkaline magmatism appears to be related to the litospheric mantle, where the contribution of asthenospheric components, derived from the hypothetical Tristan da Cunha and Trindade plumes, are not appreciable in terms of geochemical features.*

## INTRODUCTION

The Ponta Grossa Arch region (Fig. 1) was the site of alkaline and alkaline-carbonatitic intrusions in Cretaceous times ("Ponta Grossa Arch Alkaline Province” of Almeida, 1983).

The main complexes are represented by plutonic structures (e.g. Banhadão, Itapirapuã, Jacupiranga, Juquiá and Tunas), pipes and plugs (e.g. Barra do Ponta Grossa, Barra do Teixeira, Cerro Azul, Mato Preto, Morro do Chapéu and Sete Quedas). Alkaline dyke swarms are widespread mainly between the São Jerônimo-Curiúva and Rio Alonso lineaments.

The alkaline-carbonatitic complexes show nepheline syenite-syenite suites associated with mafic-ultramafic rocks (e.g. Jacupiranga and Juquiá), nepheline-bearing syenites (e.g. Ipanema), nepheline syenites (e.g. Itapirapuã), or prevailing phonolites (e.g. Mato Preto).

Systematic geological mapping and petrographical-geochemical studies were performed by Leinz (1940), Melcher (1966), Amaral *et al*. (1967), Gomes (1970), Born (1971), Fuck (1972), Lapido-Loureiro & Tavares (1983), Ruberti (1984, 1998), Ruberti & Gomes (1984), Morbidelli *et al*. (1986), Ruberti *et al*., (1987), Gomes *et al*. (1987), Germann *et al*. (1987), Morikiyo *et al*. (1987), Santos (1988), Gaspar (1989), Beccaluva *et al*. (1992), Vasconcellos (1995), Vasconcellos & Gomes (1998), Ruberti *et al*. (1997a, b, c), Andrade *et al*. (1999), Comin-Chiaramonti *et al*. (2001, 2002) and Ruberti *et al*. (2002).

The Ponta Grossa Arch (PGA), a NW structure extending for about 600 km and plunging towards the inner Paraná Basin, is characterized by the presence of hundreds NW-trending tholeiitic dykes (Piccirillo & Melfi, 1988; Piccirillo *et al.*, 1990) and by important NW-trending magnetic lineaments (Guapiara, São Jerônimo-Curiúva, Rio Alonso and Rio Piqueri; Fig. 1). In particular, its southeastern sector was the site of alkaline magmatism that has intruded Neoproterozoic basement (Gimenez Filho *et al.*, 2000) in the southern parts of the Guapiara and São Jerônimo-Curiúva lineaments, respectively.

Notably, at north of the Guapiara Lineament, the Ipanema complex and the nearby occurrences of Piedade and Tatuí intrude the same Neoproterozoic basement.

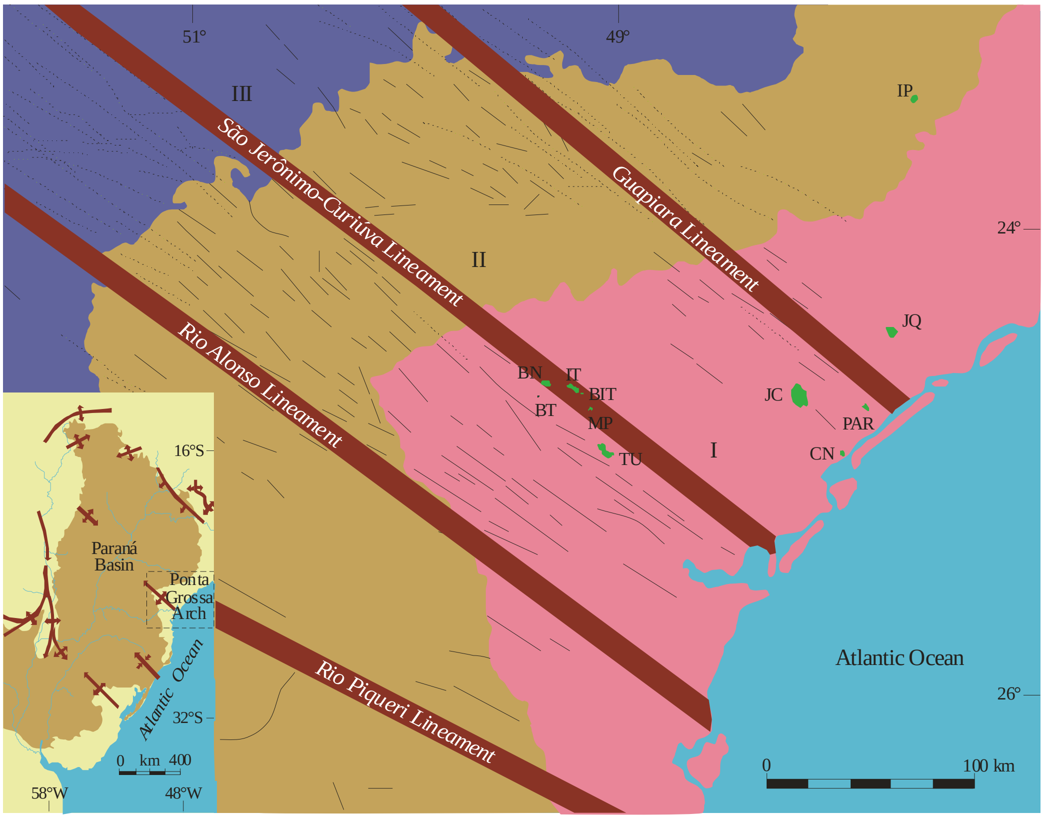


Fig. 1. Tectonic setting of Mesozoic alkaline magmatism in the Ponta Grossa Arch (after Almeida, 1986). The NW-SE swarms and the main intrusive complexes are indicated as follows: 1) and 2) dykes inferred by field geology and remote sensing and aeromagnetic survey, respectively; 3) alkaline complexes: BIT-Barra do Itapirapuã, BN-Banhadão, BT-Barra do Teixeira, CN-Cananéia, IP-Ipanema, IT-Itapirapuã, JC-Jacupiranga, JQ-Juquiá, MP-Mato Preto, PAR-Pariquera-Açu, TU-Tunas; I, Basement; II, Paraná Basin; III, Basalt flood. Inset shows the main structural features of southern Brazil.

## GENERAL OUTLINES

### Alkaline and alkaline-carbonatitic complexes from the Guapiara Lineament

The alkaline complexes from the Guapiara Lineament have Early Cretaceous (i.e. Jacupiranga, Juquiá and Pariquera-Açu) and Late Cretaceous (Cananéia) ages, respectively (Fig. 1).

Following Machado (2000), the first ones are linked to a tectonically active region, characterized by magnetic anomalies and by an intensive fault system. The Cananéia intrusives crop out in the southern area of the region out of the major faulting.

#### **Jacupiranga**

The Jacupiranga alkaline-carbonatite complex (24°42'S, 48°08'W) is a NNW-elongated body, 10.5x6.7 km, at 240 km SW of the city of São Paulo. It was discovered by Bauer (1877) and described for the first time by Derby (1891). Jacupiranga became world-famous after the Melcher's work (1966), who published a detailed map of the intrusive bodies and suggested a magmatic origin for the carbonatitic rocks intruded the magnetite-rich clinopyroxenites *(jacupirangites).*

The complex is emplaced into the Precambrian basement, that is locally represented by the Neo-proterozoic Açungui Group, and consists of two main intrusions, with dunites prevailing in the northern sector and clinopyroxenites in the southern one (Fig. 2). The nortwestern border of the clino-pyroxenites is rimmed by phlogopite and nepheline-bearing rocks. Two distinct bodies constituted by ijolites and carbonatites intrude the main clinopyroxenite outcrops. Dykes and small bodies, occurring at the margins of the dunites and clinopyroxenites, range from andesine-bearing phlogopite clinopyroxenites to melagabbros, essexites, theralites, quartz monzonites and quartz syenites. Veins of pegmatitic nepheline syenites are also widespread at the margins of the complex. Melcher (1966) described ijolitic, monchiquitic and tinguaitic dykes, and also a fenitized zone along the contact with the country-rocks. Syenites crop out at the transition zone between dunites and clino-pyroxenites.

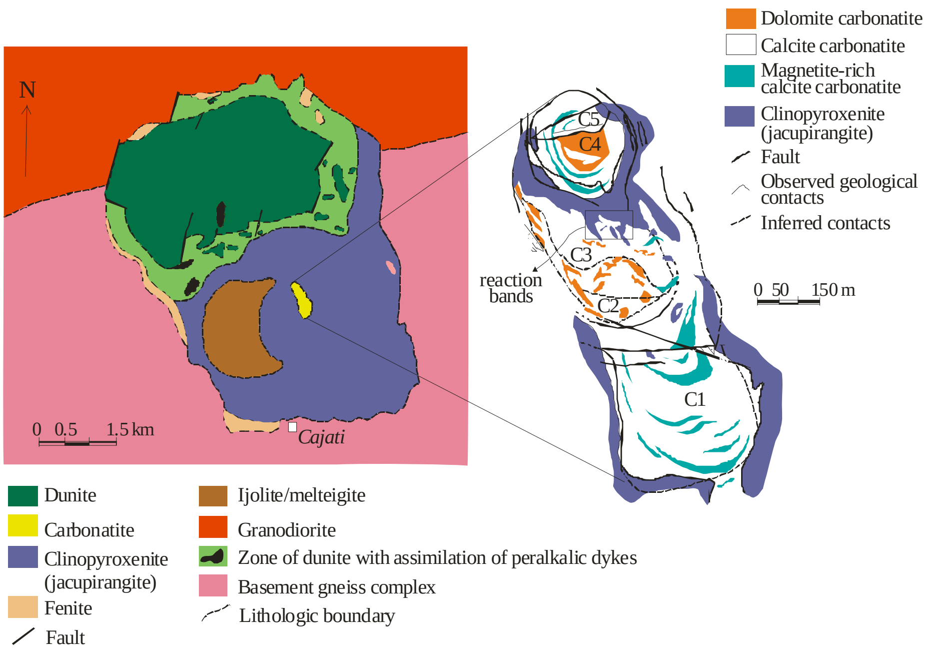


Fig. 2. Geological map of the Jacupiranga alkaline-carbonatite complex, São Paulo state (after Melcher, 1966; Germann *et al*., 1987). Inset shows the carbonatite geological map (Hirano *et al*., 1987) and outlines the C1 (sövite), C2 (calcitic rauhaugite), C3 (sövite), C4 (sövite) and C5 (rauhaugite) intrusions (after Gaspar & Wyllie, 1983a).

An age of 131 Ma on the basis of a Rb/Sr isochron for mica and carbonate (Roden *et al.*, 1985), and K/Ar data (Amaral, 1978) is indicated for the main Jacupiranga magmatic intrusive phase.

*1) Ultramafic-mafic and nepheline-bearing rock-types*

Ultramafic (cumulate) rocks, i.e. mainly dunites and clinopyroxenites, represent up to 70% of the outcrops.

*Dunites* are relatively homogeneous and fine-grained in texture, and mainly consist of forsterite ($Fo_{90}$), partially altered into serpentine. Scarce Al- and Ti-bearing ferrochromian spinels, iron hydroxides and carbonates also occur. Wehrlites are rare, occurring only as local blocks.

*Clinopyroxenites* (Fig. 2) show foliated fine to medium-grained equant texture and contain mainly diopside (sometimes augite) and magnetite, often with moderate amounts of perovskite, kaersutite and phlogopite. Dykes of nepheline-bearing clino-pyroxenites and melteigites intrude the phlogopite-rich clinopyroxene variants. Andesine-bearing phlogopite clinopyroxenites (magnetite, kaersutitic amphibole and apatite as accessories) are rare and regarding the structure concordant with the main clinopyroxenitic rock-type.

*Ijolites* are texturally fine to medium-grained and strongly oriented. They are made of clinopyroxene and nepheline, minor magnetite, perovskite, biotite, apatite and occasionally kalsilite. Locally *melteigites* and rare *melilite ijolites* may be found.

Additional lithologies include *phonolitic, lamprophyric, essexitic* and *theralitic* dykes in the northeastern area of the complex (cf. Germann *et al*., 1987).

*2) Plagioclase-bearing rock-types*

Gabbrodiorites, monzonites and syenites form veins, dyke swarms and minor intrusions. In particular gabbroic rocks comprise two principal occurrences, at the contact between dunites and clinopyroxenites, and at the southeastern side of the clinopyroxenite body.

*Monzonites* (*olivine-rich melamonzonites, porphyritic monzonites, monzonites and quartz monzonites variants*) are made of clinopyroxene, biotite, andesine, alkali feldspar, olivine ($Fo_{55-45}$), magnetite and accessory amphibole, apatite and zircon.

*Syenites, alkali syenites* and subordinate *quartz syenites* and *melasyenites* consist of perthitic alkali feldspar, oligoclase, clinopyroxene, biotite, amphibole, quartz, magnetite, titanite and apatite.

*3) Fenites*

Clinopyroxenitic and ijolitic rocks are differently fenitized in and around the complex. Particularly the clinopyroxenites show at the contact with the intrusive carbonatites a narrow zone of metasomatic reactions characterized by the presence of well-defined and mineralogically distinct bands (Morbidelli *et al*., 1986). Gaspar (1989) recognized incipient fenitization up to 2 km outwards the complex. A sodic character of the fenitization processes is suggested by the mineral assemblages, i.e. albite and sodic clinopyroxene and amphibole. Potassic fenitization is commonly related to ijolites and jacupirangites, i.e. local enrichments of phlogopite.

*4) Carbonatites*

The *carbonatites* form a small elongated body (1000-400 m) cropping out in a hill named “Morro da Mina”, standing over 225 m above the sea-level at the beginning of the mining operations in 1943. At the present time, fresh carbonatite exposures occur everywhere on the open-pit walls, at depths at least 80 m below the sea-level.

Melcher (1966) reported the occurrence of two independent plugs, the southern and the northern ones. Gaspar & Wyllie (1983a, b) described five distinct intrusions (inset of Fig. 2): C1 (sövite), C2 (dolomitic sövite) and C3 (sövite) correspond to the southern intrusions; C4 (sövite) and C5 (rauhaugite) represent the northern bodies. They evolved from the oldest C1 to the youngest C5 carbonatite. Swarms of beforsitic dykes are present in the complex. Metasomatic dolomitization processes are recognized by the presence of "patchy dolomite" in the C2, C3 and C4 sövites (Gaspar, 1989). Metasomatism of C4 occurred during the rauhaugite (C5) intrusion.

Hirano *et al*. (1987) assembled the carbonatitic rocks into four distinct categories (Table 1): calcite carbonatites (CC), magnetite-rich calcite carbonatites (CCmt), apatite-calcite carbonatites (CCap) and dolomite carbonatites (DC). The southern occurrences are mainly composed of CC, with CCmt bands, as well as of xenoliths and bands of CCap in the marginal portions, with the whole mass displaying a crescent-shaped structure. DC forms a swarm of small dykes in the northeastern portion of these bodies. Clinopyroxenite xenoliths showing reaction bands are frequently found close to the contacts with the silicate rocks. In the southern part, CC occurring as dyke swarms with nearly straight boundaries penetrate the magnetite clinopyroxenites, whereas plastic deformation is noticed in the host-rocks at the northern margin. CC and CCmt exhibit mineral banding given by the alignment of magnetite concentrations, probably due to flow structure (cf. Melcher, 1966). The northern body is a pipe-like composite plug, basically constituted by CC with a DC core. CCmt bands, within the CC, present a distinct concentric pattern with vertical dip. The mineralogy of the northern CC and CCmt is the same of the southern body, except for the absence of olivine-bearing CC and CCap.

Metasomatic reactions affecting the jacupirangite are believed to have occurred during the emplacement and crystallization of the carbonatitic magmas. Jacupirangite blocks (up to 50 m across) included in the carbonatites are enveloped by almost concentric shells whose width varies from a few centimeters up to 1 m. Some portions of the outermost part of the shells show plastic deformation due to the intrusion of carbonatitic veins. The normal sequence of the shells, from the magnetite clinopyroxenites towards the carbonatitic rocks, is the following (Morbidelli *et al*., 1986): amphibole-rich (A), phlogopite-rich (P) and olivine-rich (O) shells. Their relative thickness is variable, but in general the P shell-type is the most developed, whereas the O shell-type may be absent. The main mineralogical and petrographic features of the carbonatite intrusions are summarized in Table 2 (Gaspar & Wyllie, 1983a; Morbidelli *et al*., 1986).

Clinopyroxenite textural relationships are preserved only in A shell-type (Morbidelli *et al*., 1986). O shell-type (olivine, $Fo_{97\text{-}93}$) corresponds to a more evolved level as a consequence of the direct contact with the pervasive carbonatitic mass that sometimes seems to have disrupted and folded the preceeding silicate (especially phlogopitic in composition) aggregates.

The relationships between amphibole, olivine and phlogopite indicate that the carbonatitic fluids changed the clinopyroxenite diopside (or Ti-augite) into calcic, calcic-sodic and sodic amphibole. The formation of tetraferriphlogopite and richterite took place with the increase of the K-activity in an high $PH_2O$ and oxidizing environment.

Stable and radiogenic isotopic compositions (Huang *et al*., 1995, and references therein) reflect the isotopic signature of the mantle source(s). Initial $^{87}Sr/^{86}Sr$ isotopic ratios (Roden *et al*., 1985) for the southern carbonatites (C1, C2 and C3) are quite homogeneous (0.70494-0.70510) and are slightly less radiogenic than the northern analogues (0.70558-0.70535).

Table 1. Classification and main features of Jacupiranga carbonatites (after Hirano *et al*., 1987).

| **Rock-type** | **Main characteristics** | **Main carbonate mineral** | **Other major and accessory minerals (decreasing order of abundance)** |
|---|---|---|---|
| Calcite carbonatite (CC) | Major constituent of both southern and northern plugs. Some CC intrude into other CC as sheets and dykes. | calcite | Apatite, magnetite, dolomite; accessory phlogopite with more than 10% BaO (Gaspar & Wyllie, 1987), corroded olivine ($Fo_{93}$; Mitchell, 1978), anhedral pyrrhotite, chalcopyrite and valleriite (Boctor & Svisero, 1978). Clinohumite as olivine reaction borders. |
| Magnetite-rich calcite carbonatite (CCmt) | CCmt occurs as rhythmic bands in CC of the both plugs. | calcite | Magnetite (3 to 15 mm, frequently zoned), dolomite, phlogopite, apatite and minor olivine and sulphides. |
| Apatite-rich calcite carbonatite (CCap) | CCap occurs as xenoliths and bands in CC, especially in the marginal zones of the southern carbonatite plug. | calcite | Apatite (3 mm, euhedral to subhedral, more than 40% modal content), olivine (anhedral, includes apatite), magnetite, dolomite and minor phlogopite and sulphides. CCap may represent primitive carbonatitic magmas, mineralogically corresponding to phoscorites. |
| Fine to medium-grained dolomite carbonatite (DCfg) and coarse-grained dolomite carbonatite (DCcg) | DCfg intrude in the center of the both carbonatite plugs. DCcg occurs mainly in the center of the northern plug as rhythmic bands with DCfg. Some large crystals of dolomite develop from the walls of DCfg. | dolomite | Apatite (acicular and columnar, 10-30% modal content); minor amounts of magnetite (anhedral to subhedral), phlogopite and anhedral calcite (2-8%), sulphides and sometimes olivine with phlogopitic borders. |

Table 2. Main features of carbonatites, magnetite clinopyroxenites and reaction bands from Jacupiranga (after Gaspar & Wyllie, 1983a; Morbidelli *et al*., 1986).

| | Intrusion | Rock-type* | Main mineralogy** | Grain size | Other features |
|---|---|---|---|---|---|
| Southern Intrusions | C1 | Sövite | c, ap, mt, ol, phl, dl, sf | Coarse | Coarsely banded |
| | C2 | Dolomitic sövite | c, dl, ap, mt, phl, sf | Fine to medium | Finely banded |
| | C3 | Sövite | cc, ap, mt, phl, dl, ol, sf | Medium to coarse | Non-carbonate minerals less abundant than in other sövites. Banding less evident |
| Northern Intrusions | C4 | Sövite | cc, ap, mt, ol, phl, dl, sf | Medium | |
| | C5 | Rauhaugite | dl, ap, phl, mt, sf, cc | Medium to Coarse | Very few silicates, oxides and sulfides |
| Dykes*** | | Beforsite | dl, phl, mt, cc | Fine | Intruded in C4 sövite. Offshoot of the C5 |
| | | Beforsite | dl, cc, ap, mt, sf | Medium to fine | rauhaugite in C4 sövite |
| Rocks from the contact between carbonatite intrusions C2 and C3 | | Sövite | cc, dl, ap, phl, mt, sf | Medium to coarse | Diffuse banding |
| | | Beforsite | dl, cc, ap, mt, sf | Medium | Difuse banding |
| | Shell-type | | | | |
| Reaction zone between carbonatite intrusions and Mt cpx | A | Amphibolic shell | am psd after py, phl, mt, il | Fine | 1-5 cm thick, in contact with Mt cpx. Carbonate bands contain am, phl, ap cm-1 m thick. |
| | P | Phlogopitic shell | phl, am, il, mt | Fine | Carbonate horizon with apatite cm to dm wide. Carbonate bands |
| | O | Olivinic shell | ol, chm, phl, mt, il | | with apatite may be absent |
| Host-rock | Mt cpx | | py, Timt | Medium | |

* Other rock-types quoted in the text: alvikite (cc, ap, dl, phl) and ijolite (py, ne)
** Minerals arranged in decreasing order of abundance
*** Features common to these two type of dykes

Abbreviations: *Minerals* - am, amphibole; ap, apatite; cc, calcite; chm, clinohumite; dl, dolomite; ilm, ilmenite; mt, magnetite; ne, nepheline; ol, olivine; phl, phlogopite; psm, pseudomorfous; py, clinopyroxene; rch, richterite; sf, sulfide; Timt, titanomagnetite. *Rocks* – cpx, clinopyroxenite; Mt cpx, magnetite clinopyroxenite

Initial (130 Ma) $^{87}Sr/^{86}Sr$ (0.70467-0.70551), $^{143}Nd/^{144}Nd$ (0.51264-0.51251) and $^{206}Pb/^{204}Pb$ (17.0-18.2) isotopic ratios for carbonatites and clino-pyroxenites (Huang *et al*., 1995) are similar even to the isotopic ratios of high-Ti tholeiites from the Paraná Basin and also to the volcanic rocks from Walvis Ridge and Tristan da Cunha. The Jacupiranga carbonatites and clinopyroxenites may have been derived from similar mantle source regions and were not subjected to any significant contamination processes (cf. Comin-Chiaramonti *et al*., in this volume).

According to Morikiyo *et al*. (1987), Nelson *et al*. (1988) and Gaspar (1989), the Jacupiranga carbonatites show very uniform $\delta^{13}C$ (-5.6 to -6.9‰) and $\delta^{18}O$ (6.8 to 8.1‰) compositions lying in the primary carbonatites box (Taylor *et al*., 1967; Keller & Hoefs, 1995).

## Juquiá

The Juquiá alkaline-carbonatite complex (24°23’S, 47°49’W) is an irregularly shaped body covering about 14 km$^2$. The complex intrudes the Precambrian gneissic basement (Fig. 3).

More than 50% of the complex is made of olivine clinopyroxenites with subordinate lens of olivine alkali gabbros in the northernmost area. The southwestern area consists of a main occurrence of nepheline syenite. A satellite body of nepheline syenite crops out at the nortwestern side (Casa da Pedra hill, cf. Fig. 3). The central-western zone of the complex is represented by a subannular carbonatite surrounded by a ring of rocks that evolved from melteigites to ijolites and urtites.

Locally, essexite lens are present in the main nepheline syenite body. Syenodiorites are found as cumulates in the nepheline syenites at the southern border (Beccaluva *et al*., 1992). Basanite to phonotephrite dykes (some decimeters to 1-2 m thick) occur in many places, mainly within clinopyroxenites and nepheline syenites. Phonotephrite dykes are also present in the Casa de Pedra hill and contain xenoliths and xenocrysts of the enclosing nepheline syenites country-rocks. The estimated volumes are 48 km$^3$ and 5.5 km$^3$ for the clinopyroxenites (*l.s.*) and carbonatites, respectively (Slavec *et al*., 2001). An age of about 130 Ma is inferred from the K/Ar data (Amaral *et al*., 1967).

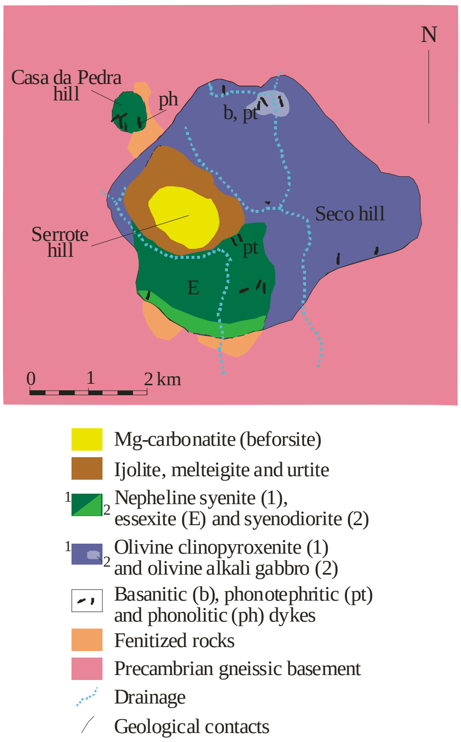


Fig. 3. Geological sketch-map of the Juquiá alkaline-carbonatite complex, São Paulo state (after Born, 1971; modified).

Fenitization with development of alkali feldspar, biotite and rare sodic amphibole affected the gneissic basement, chiefly around the southern and northwestern parts of the complex.

*Olivine clinopyroxenites* and *alkali gabbros* are cumulate that vary from olivine clinopyroxenites (olivine $Fo_{83-77}$) to plagioclase-bearing clinopyroxenites and alkali gabbros with the progressive increase of intercumulus feldspar. According to Beccaluva *et al*. (1992), the olivine clinopyroxenites change from adcumulate to mesocumulate types; in the latter ones, the intercumulus phases (10-30% in volume) are made of plagioclase, magnetite, ilmenite, phlogopite, brown-reddish amphibole, alkali feldspar in addition to little amounts of interstitial carbonate. The rare alkali gabbros are orthocumulates with euhedral olivine and clinopyroxene as main cumulate phases, and plagioclase, alkali feldspar, ilmenite, magnetite and phlogopite representing intercumulus materials (50-60 volume %).

*Nepheline syenites* are fine to medium-grained in texture and vary from mafic to felsic types. The mafic rocks contain abundant clinopyroxene and primary carbonates (large interstitial crystals or small "ocelli"). The more felsic rocks have a large amount of cumulitic alkali feldspar (3-7 mm) and intercumulus clinopyroxene, biotite and nepheline. Notably, coarse-grained, porphyritic nepheline syenites predominate in the eastern sector of the main body and at the Casa de Pedra hill.

*Ijolites*, *melteigites* and *urtites* are meso to orthocumulate rocks. In the ijolites and melteigites, the cumulus phases are represented by zoned clinopyroxene, magnetite and biotite, with nepheline as intercumulus; in the urtites, alkali feldspar may be an additional intercumulus phase.

*Carbonatites* are predominantly composed of dolomite and calcite and subordinate ankerite (beforsites). Magnesium-rich carbonatites form the core of the body with a rim of Ca-carbonatites (Born, 1971). Layering occurs in the inner carbonatites as a result of the enrichment of opaque minerals. The border rocks are characterized by abundant apatite forming policrystalline patches and by phlogopite, whereas barite is present in large amounts at the core. Accessory minerals are pyrochlore, monazite and Sr-Ba and REE-rich carbonates.

Initial $^{87}Sr/^{86}Sr$ and $^{143}Nd/^{144}Nd$ ratios range from 0.70492 to 0.70569 and from 0.51230 to 0.51251, respectively (Walter *et al*., 1995; Gibson *et al*., 1999), similar to the isotopic ratios of the Jacupiranga rocks.

**Pariquera-Açu**

The Pariquera-Açu complex (Fig. 4, inset A; 24°44'S, 47°49'W) is an elliptical northwestern aligned structure, 6 km$^2$ in area, intruding the Proterozoic metamorphic Turvo-Cajati Complex. It is partially covered by sediments of the Pariquera-Açu Formation (Silva & Algarte, 1981). The complex was discovered on the basis of geophysical evidence provided by a regional aeromagnetometric-scintillometric survey (Ferreira & Algarte, 1979).

The main rocks are theralites and essexites, and subordinate melatheralites, syenogabbros and syenodiorites. The estimated volume of the alkaline rocks is about 8.3 km$^3$ (Rugenski *et al*., 2001).

Geological evidence suggests that the complex could be coeval with the neighbouring alkaline-carbonatitic complexes of Jacupiranga and Juquiá (Morbidelli *et al*., 2000).

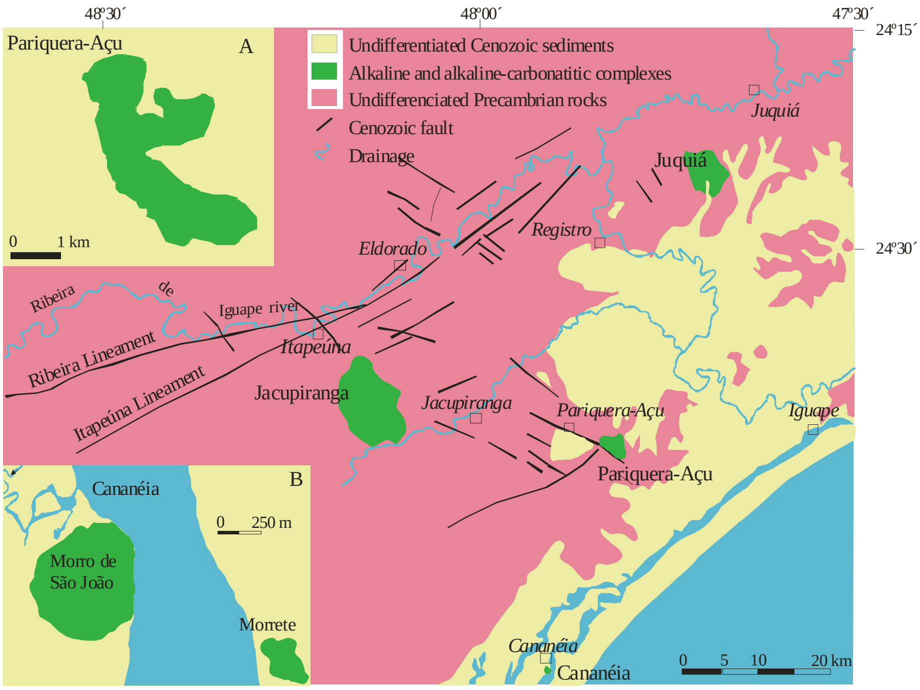


Fig. 4. Sketch-map showing the Jacupiranga, Juquiá, Pariquera-Açu and Cananéia alkaline complexes, São Paulo state, at the Guapiara Lineament. Insets: A, geological map of Pariquera-Açu (after Morbidelli *et al*., 2000); B, sketch map of Cananéia (after Spinelli, 2003).

*Theralites* are found in the central-northern part of the complex and are hypidiomorphic fine to coarse-grained in texture. They consist of clinopyroxene (diopsidic core and salitic rim), olivine ($Fo_{85-67}$) and minor alkali feldspar, nepheline, plagioclase and Ti-phlogopite. Accessory phases in-clude Ti-magnetite and apatite. Scarce alteration products are cancrinite after nepheline. Rare coarse-grained samples are clinopyroxene cumulophyric aggregates.

*Essexites* are fine-grained rocks, mainly seriate in texture with cotectic relationships between olivine and late crystallized salite. Mica mantling clinopyroxene crystals and late crystallized Ti-magnetite grains are believed to be reaction products. The interstitial feldspar-foid-bearing mesostasis is relatively abundant.

*Syenogabbros* and *syenodiorites* are hypidiomorphic and coarse to medium-grained in texture. Alkali feldspar, abundant plagioclase, clinopyroxene and olivine are the prevailing phases, occurring subordinately nepheline, amphibole and mica. Accessory minerals include Ti-magnetite and apatite. Textural relationships show that the mica laths represent a late phase more concentrated in the syenodiorites. Alkali feldspar is poikilitical and affected by subsolidus exsolution processes.

Morbidelli *et al*. (2000) suggest that the Pariquera-Açu complex is made of two distinct suites, theralite to essexite and syenogabbro to syenodiorite, evolved through fractional crystallization, i.e. from basanite and alkali basalt magmas, respectively. Both suites are characterized by similar $^{87}Sr/^{86}Sr$ initial ratios, i.e. 0.70605 and 0.70588, respectively.

**Cananéia**

The Cananéia intrusion (25°01'S, 47°54'W; Morro de São João) and the associated satellite body of Morrete crop out in the Cananéia and Comprida islands, respectively (Fig. 4, inset B). The bodies (0.6 and 0.2 km in diameter, respectively) are emplaced into Precambrian metamorphic rocks related to the Açungui Group, being partially covered by Pleistocenic sediments (Souza *et al*., 1996). Geophysical profiles suggest continuity between both the bodies (Suguio *et al*., 1987).

An age of 76.2±1.5 Ma was inferred by Rb/Sr isochron (Spinelli, 2000). Notably, this age (Late Cretaceous) is more recent compared to the other complexes from the Guapiara Lineament.

Both the outcrops are leucocratic, medium to coarse-grained *syenites* (alkali feldspar syenites and quartz alkali feldspar syenites), characterized by mesoperthitic alkali feldspar, quartz, clinopyroxene (ranging from diopsidic to hedenbergitic variants to sodic aegirine-augite), amphibole (ranging from hornblende to sodic amphibole), biotite and accessory opaques and zircon. Relics of plagioclase (oligoclase) may be present. Fine-grained syenite dykes are widespread mainly at the eastern border of the Morro de São João body and display trachytic and bostonitic textures (Spinelli, 2003).

Initial $^{87}Sr/^{86}Sr$ isotopic ratios range from 0.70615 to 0.70827 and are suggestive of the possibility of contamination by crustal materials.

Alkaline and alkaline-carbonatitic complexes at north of the Guapiara Lineament

**Ipanema**

The Ipanema complex (23°26'S, 47°36'W) is lo-

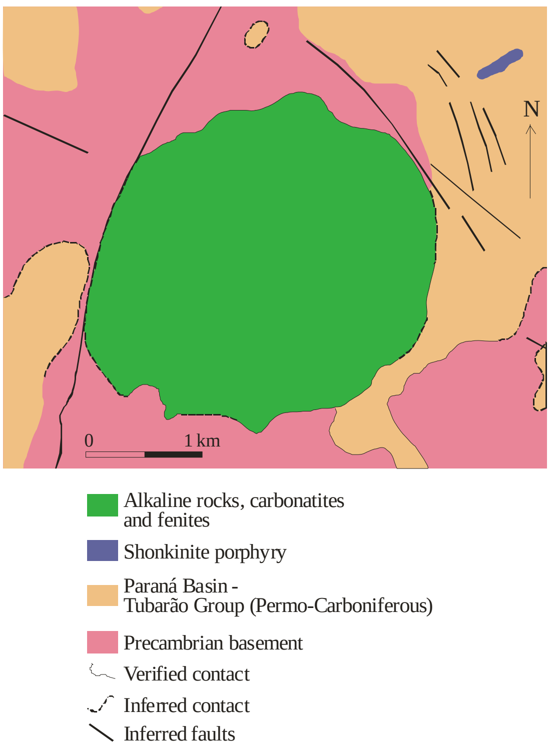


Fig. 5. Geological map of the alkaline-carbonatitic complex of Ipanema, São Paulo state (Davino, 1975; cf. Fig. 1).

cated 10 km NW of the city of Sorocaba (Fig. 5). The intrusion, subcircular form and 13 $km^2$ in area, is emplaced mostly into the crystalline basement but also into Permo-Carboniferous sediments belonging to the Tubarão Group at their eastern and southern sides (Davino, 1975). An age of 125 Ma was reported by Morbidelli *et al*. (1995).

A main glimmeritic core with subordinate clino-pyroxenitic rocks was intruded by clinopyroxene (aegirine), Na-amphibole and apatite-rich veins along with a network of carbonatitic veins and dykes. The latter rocks were found in boreholes up to 82 m deep. Notably, shonkinite dykes (melano-cratic foid syenites; cf. Fig. 5) penetrate the crystalline basement (Leinz, 1940).

Alkali metasomatism is believed to be responsi-ble for the formation of aegirine-augite, hastingsite, alkali feldspar and probably biotite and/or phlogopite. The metasomatic processes radially decrease from the central parts of the intrusion to the country-rocks. Syenitic rocks containing aegirine or egirine-augite, and sometimes hastingsite, show strong textural and modal variations, characterizing leucocratic to melanocratic petrographic types (following Leinz, 1940: orthoclase aegirinite, orthoclase lusitanite, umptekite and nordmarkite). The latter rock-types were considered to be fenitization products by Born (1975).

The Ipanema carbonatites (medium-grained, with granular hypidiomorphic texture) are sövites with modal calcite 95%, quartz 3%, barite 1%, opaques 1% and rare apatite. Yellowish-green, fine to me-dium-grained apatite concentrations display oriented granular hypidiomorphic texture, and mineral assemblage consisting of apatite (85 vol%), aegirine, hastingsite and occasional magnetite. Locally, piroxene-rich variants may grade to “aegirinites”.

**Piedade and Tatuí**

Knecht (1960) described shonkinite dykes intruding the crystalline basement along the Piedade-Juquiá road (23°42’S, 47°24’W), and near the city of Tatuí (23°22’S, 47°53’W).

The dykes are porphiritic with clinopyroxene, biotite, alkali feldspar and apatite phenocrysts set in an aphanitic, clinopyroxene-rich groundmass.

Alkaline and alkaline-carbonatitic complexes from the São Jerônimo-Curiúva Lineament

In the São Jerônimo-Curiúva Lineament (Fig. 1), large stocks as Tunas, Banhadão, Itapirapuã, Barra de Itapirapuã and Mato Preto, and minor bodies as Barra do Teixeira, Barra do Ponta Grossa, Morro do Chapéu, Cerro Azul and Sete Quedas, intrude the Neoproterozoic crystalline basement (Açungui Group), in association with dyke swarms (Fig. 6).

The alkaline structures, distributed over an area of 400 $km^2$, are arranged following two preferential lineaments, N45W and E-W, respectively, being both related to extensional tectonics (Algarte, 1972; Ferreira & Algarte, 1979).

On the whole, the available radiometric data for these rocks fit into two chronological groups: 100-110 Ma (Late Early Cretaceous) and 80-60 Ma (Late Cretaceous). Ages around 110-100 Ma include the Banhadão, Itapirapuã and Barra do Itapirapuã com-plexes, whereas the 80-60 Ma values characterize the Tunas, Barra do Teixeira and Mato Preto bodies (cf. Sonoki & Garda, 1988; Morbidelli *et al*., 1995).

**Banhadão**

The alkaline massif of Banhadão (24°39’S, 49°23’W) situated at 20 km NW of the city of Cerro Azul shows an oval shape and covers an area of about 8 $km^2$. It is composed of multiple intrusions emplaced into the Neoproterozoic Três Córregos Granite (Fig. 7). The better fitting of ages is around 106±5 Ma (Ruberti, 1984).

The complex mainly consists of gray or light-reddish nepheline syenites, basic to intermediate variants, respectively (Ruberti, 1984; Ruberti & Gomes, 1984). Its central areas are characterized by a phlogopite melteigite body (eastern area) and by a pipe-like late intrusion of a nepheline syenite body (western area) showing fingerprint textures, i.e. alkali feldspar-nepheline intergrowths. Fine to me-

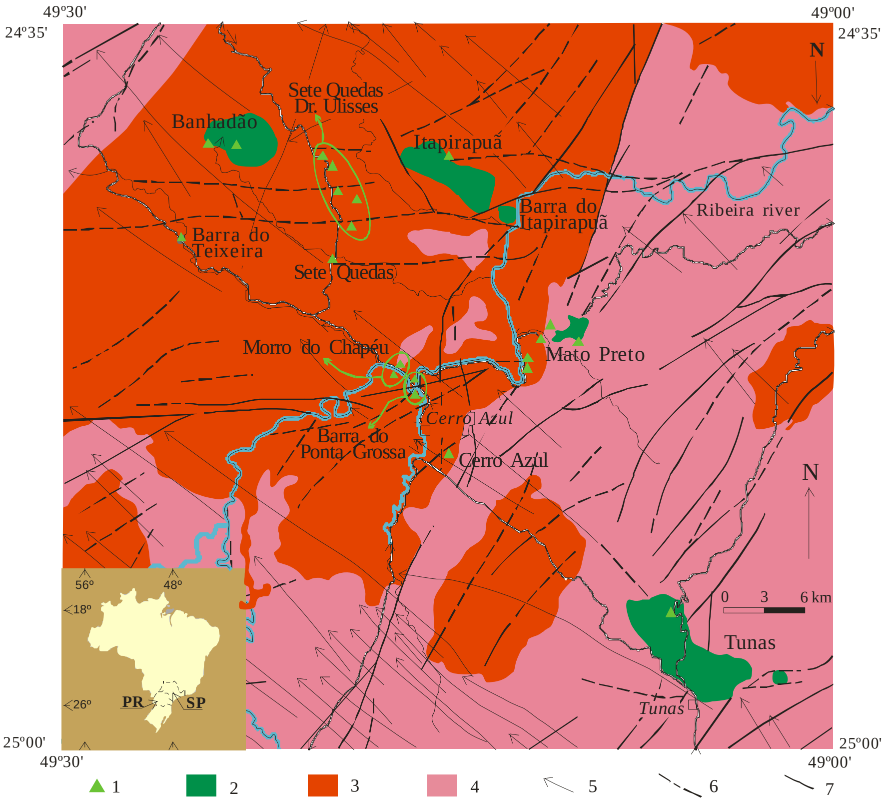


Fig. 6. Geological setting and location of alkaline complexes, plugs and dyke swarms in the Ribeira Valley, São Paulo and Paraná state, (São Jerônimo-Curiúva Lineament; cf. Vasconcellos & Gomes, 1998). 1) phonolitic dykes; 2) alkaline complexes and plugs; 3) Upper Precambrian-Cambrian Três Córregos granitic complex; 4) Middle to Upper Precambrian metasediments and meta-igneous rocks of the Açungui Group; 5) faults suggested by basic dykes; 6) inferred faults; 7) faults.

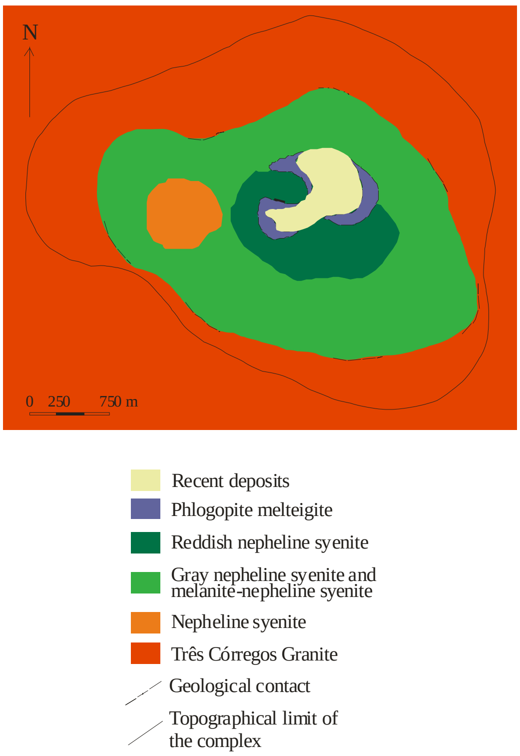


Fig. 7. Geological map of the Banhadão massif, Paraná state (after Ruberti & Gomes, 1984).

dium-grained malignites and alkali feldspar-melanite ijolites are believed to have formed by reactions between the phlogopite melteigites and the main nepheline syenites (Ruberti, 1984). Fine-grained to aphanitic phonolitic dykes intrude the nepheline syenites. A small carbonated sodalite-rich phonolitic lava flow is found in the surroundings of the western side of the complex. Fenitization processes are widespread along the contact with the wall-rocks.

*Nepheline syenites* contain alkali feldspar, nepheline, aegirine-augite ($Di_{70-13}Hd_{8-30}Ac_{22-57}$), aegirine and scarce brown biotite. Melanite is important in some rock-types (melanite-nepheline syenites). Accessory phases include titanite, apatite, opaques and sometimes wollastonite.

*Phlogopite melteigites* consist of large crystals of Na-augite ($Di_{87-70}Hd_{8-16}Ac_{5-14}$), phlogopite, nepheline, nosean-haüyne and accessories apatite, opaques and calcite.

*Malignites* contain nepheline, pyroxene (aegirine-augite, $Di_{42-55}Hd_{38-20}Ac_{20-25}$ with Na-augite cores, $Di_{83}Hd_{8}Ac_{9}$), poikilitic feldspar and occasional melanite.

*Alkali feldspar-melanite ijolites* are characterized by nepheline, Na-augite ($Di_{61-48}Hd_{29-32}Ac_{10-20}$) and melanite (up to 90% in volume).

*Phonolite dykes* consist of phenocrysts of alkali feldspar, aegirine-augite ($Di_{13-7}Hd_{27-25}Ac_{60-68}$) and nepheline set in a groundmass made of the same minerals besides sodalite, fluorite, carbonates and cancrinite.

**Itapirapuã**

The Itapirapuã alkaline complex (24°40'S, 49°15'W; Fig. 6), 130 km SSW from the city of Itapeva, intrudes the Neoproterozoic Três Córregos Granite (Gomes, 1970; Gimenez *et al.*, 2000). An average age of 109±5 Ma is given by Sonoki & Garda (1988).

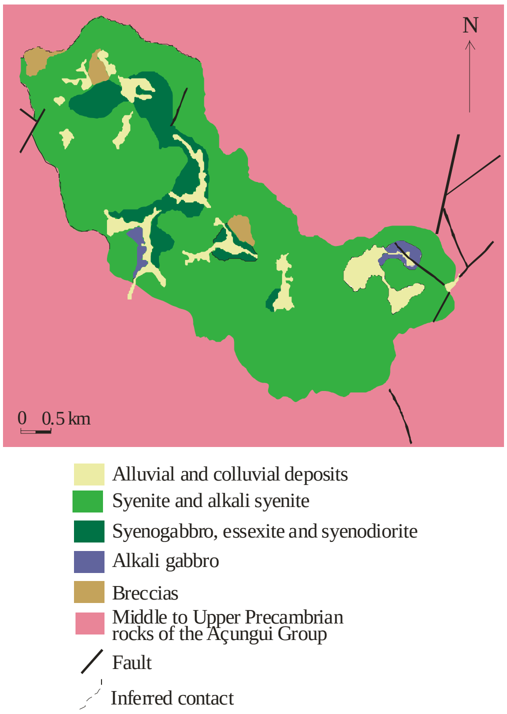


Fig. 8. Geological map of the Tunas alkaline complex, Paraná state (after Fuck, 1972).

The alkaline body, about 4 km$^2$, shows an irregular NW-trending shape and it is made of silica-undersaturated rocks, i.e. melanite-bearing or melanite-free nepheline syenites and subordinate biotite melteigites, melanite malignites and wollastonite-melanite-nepheline syenites (Gomes, 1970). Tinguaite decimetric dykes exhibiting NW attitude intrude both the massif and the granitic country-rocks. Carbonatite veins, few centimeters wide, penetrate the nepheline syenites at the core of the alkaline body. A magmatic breccia associated with fine to medium-grained nepheline syenites crops out in the southern area, covering a few tens of m$^2$; an iron ore, consisting of granular idiomorphic magnetite, is present in the southernmost area.

The *nepheline syenites* and their variants are composed of alkali feldspar, nepheline, pyroxene (with a wide compositional range including Na-augite, aegirine-augite and aegirine), melanite and subordinate magnetite, titanite and apatite, and secondary cancrinite.

**Tunas**

The Tunas alkaline complex (24°57'S, 49°6'W), outcropping 80 km from the city of Curitiba, covers an area of about 22 km$^2$ (Fig. 8). It intruded Precambrian meta-igneous rocks and metasediments of the Açungui Group about 80 Ma ago (K/Ar and Rb/Sr data; Gomes *et al.*, 1987). Five subcircular volcanic structures are recognized.

Syenites and alkali syenites are the main rock-types with subordinate alkali gabbros, syenogabbros, essexites and syenodiorites. Small late syenitic dykes are also found. Magmatic breccias containing clasts of all the rock-types are widespread (cf. Fig. 8).

The main minerals are feldspars (both alkali feldspar and plagioclase), Ca-clinopyroxene (Ti-salite grading towards ferrosalite and aegirine-augite), amphibole (mainly pargasite), Fe-biotite, olivine, quartz and/or feldspathoids (both nepheline and sodalite). Accessories include Ti-magnetite (with exsolved ilmenite) and apatite.

*Syenites* are hypidiomorphic equigranular to porphyritic with plagioclase phenocrysts. Perthitic alkali feldspar is the most important mineral. Sodalite, scarce nepheline and alteration products as cancrinite may be present (0.1 to 5.4 vol%; Fuck, 1972) in the undersaturated types, whereas quartz appears in the oversaturated ones. Femic phases as biotite, amphibole, occasional fayalitic olivine and Ca-clinopyroxene remnants represent about 2 vol% of the mineralogical assemblages (Fuck, 1972).

*Alkali gabbros* and *syenogabbros* show isotropic-orthocumulitic texture with abundant large size zoned plagioclase ($An_{88-39}$) and interstitial alkali feldspar. Magnetite, olivine ($Mg_{0.54-0.44}$) and Ca-rich clinopyroxene ($Mg_{0.75-0.59}$) are mostly corroded and often surrounded by poikilitic reddish amphibole and/or biotite. Apatite is the main accessory phase and alteration products comprise carbonates, sericite, chlorite and epidote.

*Essexites* show textures similar to the previous rocks with interstitial nepheline (high Qz molecule content).

*Syenodiorites* contain poikilitic amphibole and biotite (Ca-rich clinopyroxene inclusions). Plagioclase ($An_{41-20}$) and alkali feldspar are the principal felsic phases. Common accessories consist of apatite and titanite.

Dykes are mainly represented by *microsyenites* with trachytic to bostonitic texture. Sometimes they are porphyritic, with prevailing alkali feldspar phenocrysts and subordinate clinopyroxene, amphibole, plagioclase, biotite and rare fayalitic olivine. The groundmass is composed of the same minerals and minor opaques, titanite and apatite.

The strontium isotopic values mainly range from 0.705 to 0.707, being compatible with mantle derivation magmas. On the other hand, significant crustal contamination is indicated for some dykes ($^{87}Sr/^{86}Sr_i = 0.70777$ and 0.70806).

**Barra de Itapirapuã**

The Barra do Itapirapuã complex (24°41’S, 49°13’W), an ellipsoidal network of dykes and veins of Fe, Mg and Ca-carbonatites occupying area of approximately 2 km$^2$, intrudes the Neoproterozoic Três Córregos granitic rocks (Gimenez Filho *et al.*, 2000), which are emplaced into Mesoproterozoic to Neoproterozoic metasediments of the Açungui Group (Fig. 6). A crude errorchron of 128±19 Ma was inferred by Rb/Sr systematics (Ruberti *et al.*, 1997a).

A systematic bore-hole investigation confirms the stockwork-like structure of the carbonatite body (Lapido-Loureiro & Tavares, 1983) with prevailing millimeter to centimeter thick carbonatite veins at the surface and decimeter to meter thick dykes at depth (Ruberti, 1998). Fenitized rocks of syenitic affinity are found at various topographic levels up to 256 m deep; syenites seldom occur with magmatic texture (Ruberti *et al.*, 2002). Carbonatization processes led to the formation of feldspar-carbonatitic breccia and silico-carbonatitic rocks, the latter corresponding to the transition between fenites and carbonatites. Besides carbonatitic rocks, there are also carbonatitic lamprophyric breccias. Tardi-magmatic and/or hydrothermal veins bearing quartz, fluorite, REE-rich apatite, REE fluorcarbonates, barite and strontianite intrude the enclosing carbonatites and fenites.

The fine-grained varieties correspond to small dykes and centimetric veins that cut both the coarse carbonatites and the fenitized country-rocks. Ca-carbonatite variants occur as small veins associated with fenites *l.s.*

The magmatic evolution of the complex comprises four main phases of intrusive carbonatite: 1) medium to coarse-grained Mg and Fe-carbonatites; 2) medium to coarse-grained Mg and Fe-carbonatites overprinted by a first pervasive hydrothermal event; 3) medium to coarse-grained Mg and Fe-carbonatites overprinted by a second pervasive hydrothermal event; and 4) late, very fine to fine, mainly Mg-carbonatites (Andrade *et al.*, 1999; Ruberti *et al.*, 2002).

Texturally, the phase 1 carbonatites are inequigranular, xenomorphic to hypidiomorphic, and frequently seriate. The Mg-carbonatites are typically white to gray in colour, whereas the Fe-carbonatites are brownish to pinkish. The main minerals consist of Fe-dolomite to Mg-ankerite, sometimes with subordinate calcite and as accessories phlogopite, pyrochlore and scarce REE fluorcarbonates (1A subtype) or apatite (1B subtype).

The phase 2 carbonatites are very similar to the previous ones regarding the texture and also the mineralogical assemblage. However, they differ for the pervasive presence of microfractures and/or vesicles filled by quartz, REE fluorcarbonates as sinchysite, parisite, and bastnäsite (2A subtype) and/or apatite (2B subtype). The Fe-rich carbonates show reequilibration textures when in contact with "patches" of quartz and apatite.

The phase 3 is characterized by microveins of quartz and chalcedony (up to 20 vol%), barite, REE fluorcarbonates and fluorite, in addition to rare and disseminated sulphides, as galena and sphalerite (3A subtype).

All the rocks are cut by millimeter to centimeter thick veins of very fine to fine-grained carbonatites (phase 4) exhibiting flow texture at the chilled margins as a result of the alignement of phlogopite crystals. The predominant rock-types are Mg-carbonatites, but scarce Ca and Fe-carbonatites are also present.

The associate silicate rocks are syenites with magmatic texture, together with fenitized granitic rocks which constitute the wall-rocks of the complex. The syenites are inequigranular and fine-grained in texture and consist of alkali feldspar, edenitic amphibole, oligoclase, and as accessories apatite, zircon, titanite and opaques.

Field and petrographical evidences indicate that the complexity of the silicate rocks and the different carbonatite phases are driven by carbonate-fluid interactions. This is also apparent from the geochemistry that presents a wide compositional range from Mg to Fe and Ca-carbonatites. Thus, the Barra do Itapirapuã complex represents an example of probably full cycle of alkaline activity: from syenite to Mg-carbonatite, then Fe-carbonatite followed by late fine Mg, Fe and Ca-carbonatite with late stage mineralization concluding the sequence.

## Mato Preto

The Mato Preto alkaline complex (24°45'S, 49°12'W) includes several circular or irregular structures intruding Meso to Neoproterozoic metasediments of the Açungui Group and the Neoproterozoic Três Córregos Granite (Fig. 9). The structures are grouped into two main areas, Mato Preto I and Mato Preto II, respectively (Lapido-Loureiro & Tavares, 1983). K/Ar data suggest Late Cretaceous ages, i.e. 70-72±5 Ma, for the alkaline rocks (Sonoki & Garda, 1988).

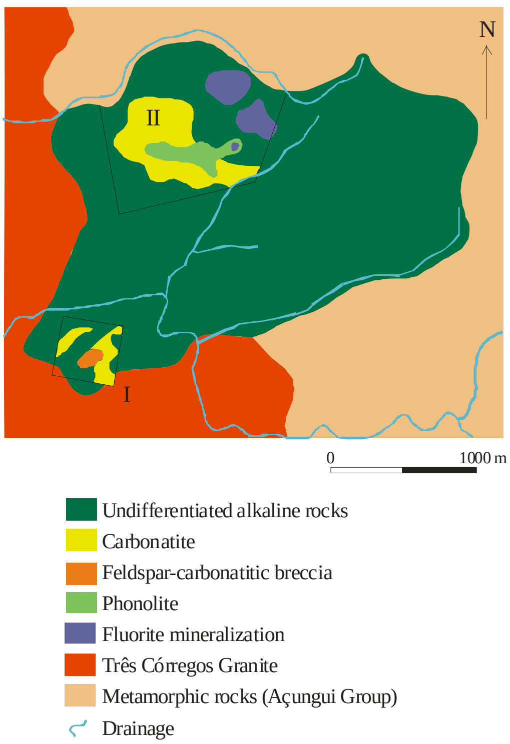


Fig. 9. Geological sketch-map of the Mato Preto alkaline-carbonatite complex, Paraná state (after Lapido-Loureiro & Tavares, 1983).

Mato Preto I (0.14 km$^2$) is mainly composed of porphyritic phonolites, breccia pipe (carbonate groundmass and phonolite clasts) and carbonatitic veins. In Mato Preto II (about 1.0 km$^2$), the dominant lithologies are Ca-carbonatites, breccia pipes (ankeritic groundmass and phonolites, fenitized granites or syenite fenites, nepheline microsyenites, "ijolites" and "melteigites" clasts), phonolites and phonolitic dykes (Jenkins, 1987). The structures are generated by a net of carbonatitic dykes and centimetric to millimetric veins (carbonatite stockwork) intruding an irregular body in contact with fenitized granites and syenitic fenites (Comin-Chiaramonti *et al*., 2001).

The *carbonatites* (fine to medium-grained Ca and Fe-carbonatites) have xenomorphic seriate texture with accessory opaques, apatite, pyrochlore and REE-fluorcarbonates. Alkali feldspar xenocrysts are widespread and locally abundant. The textural relationships show at least two different stages: prevailing early Ca-carbonatites and subordinate late Fe-carbonatites. Late millimetric veins of quartz, fluorite, barite and REE fluorcarbonates are found cutting the carbonatitic rocks.

The main silicate rocks are fine to medium-grained *nepheline syenites* (Lapido-Loureiro & Tavares, 1983; Comin-Chiaramonti *et al*., 2001), allotriomorphic in texture and with dominant alkali feldspar and nepheline, and subordinate aegirine-augite, opaques and biotite. Apatite, titanite and monazite are the chief accessories. *Alkali gabbros* and *ijolites* are also present. *Lamprophyre* (following Gibson *et al*., 1999; picritic alkali basalt?) and *trachybasalt* dykes cross cut the complex. The latter rocks are weakly porphyritic in texture and contain pheno and microphenocrysts of clinopyroxene, olivine, biotite, nepheline, amphibole, plagioclase and opaques set in a hypohyaline to hypocrystalline groundmass.

*Fenitized rocks*, widespread over the complex (Ruberti, 1998; Comin-Chiaramonti *et al*., 2001), generally show cataclastic texture with re-crystallizated alkali feldspar grains and micro-fractures filled by amphibole, aegirinic clino-pyroxene and carbonates.

Alkaline dykes and plugs from the Ribeira Valley at the border between the São Paulo and Paraná states

In the region of the so-called Ribeira Valley (between 49°00'-49°30'S and 24°30'-25°00'W; Fig. 6) tectonically related to the São Jerônimo-Curiúva and Rio Piquiri lineaments, alkaline dykes intrude alkaline complexes and regional country-rocks. Besides these dykes, small plugs, i.e. Barra do Ponta Grossa, Barra do Teixeira, Cerro Azul, Morro do Chapéu and Sete Quedas, are emplaced into crystalline basement (Neoproterozoic Açungui and Setuva Groups, and granitic rocks; cf. Vasconcellos & Gomes, 1998).

Notional ages between 70 and 78 Ma were inferred from the field relationships and a few radiometric data (Sonoki & Garda, 1988, and therein references).

The dykes and plugs are represented by widespread peralkaline phonolites and by local phonolites and trachyphonolites (Mato Preto), phonolitic nephelinites (Sete Quedas), micro-syenites (Itapirapuã) and trachytes (Tunas) (cf. Vasconcellos & Gomes, 1998).

The *phonolitic rocks l.s.* are subaphyric to porphyritic, with common alkaline feldspar, nepheline and clinopyroxene, and rare biotite and melanite phenocrysts, embedded in a groundmass formed by the same mineral phases and glass, and containing secondary zeolites and cancrinite. Peralkaline phonolites are Na-amphibole rich. Phonolitic nephelinites have very abundant micro-phenocrysts and groundmass melanite. Trachy-phonolites and trachytes show olivine, amphibole and opaques set in a hypocristalline groundmass.

The most important constituents are alkali feldspar (in generaly Or-rich), Ca-clinopyroxene (diopside, hedenbergite and augite) to Na-Ca and Na-clinopyroxene (aegirine-augite and aegirine) and nepheline. Subordinate minerals are Ti-biotite, mela-nite (phonolitic nephelinites and phonolites from Banhadão), amphibole (Mato Preto) and opaques.

Vasconcellos (1995) recognized two main dyke-types: 1) MgO-rich, i.e. phonolitic nephelinites, phonolites, microsyenites and peralkaline phonolites from Banhadão and Sete Quedas; 2) MgO-poor, i.e. the other rocks from Barra do Ponta Grossa, Barra do Teixeira, Cerro Azul, Mato Preto, Morro do Chapéu and Sete Quedas.

## GEOCHEMISTRY

A large data set of chemical compositions of alkaline rocks from both Guapiara and São Jerônimo-Curiúva lineaments in association with the Ponta Grossa Arch (PGA) is available, although for many occurrences trace elements and REE data are still scarce (Tables 3A, B, C and Table 4).

### Major elements

The PGA cumulate rocks are ultrabasic to basic ($SiO_2$, 35-46 wt%) and rarely intermediate. They show broad variation in MgO (<2-36 wt%), $Fe_2O_3$ (as total iron: 4-20 wt%), CaO (6-21 wt%), $Al_2O_3$ (<1-24 wt%) and alkalies (<1-17 wt %), defining ultramafic and mafic variants. Petrographically, they are mostly dunites, peridotites, clinopyroxenites, members of the ijolite series (melteigite, ijolite and urtite) and subordinate alkali gabbros, syenogabbros and syenodiorites. Ultramafic types may contain normative leucite and/or nefeline and sometimes modal perovskite.

$TiO_2$ contents are low in dunites and peridotites (<0.13 wt%) and high in clinopyroxenites (2-5 wt%), whereas the ijolite series shows intermediate values (1-2.9 wt%). $P_2O_5$ varies between <0.5 and 2.5 wt% and shows very different contents in the rock-types.

The PGA non-cumulate intrusive rocks have MgO ranging from 0.5 to 12 wt% (Figs. 10A, B).

The most "primitive" intrusives correspond to theralites (Pariquera-Açu), alkali gabbros (Jacupiranga, Juquiá, Pariquera-Açu and Tunas) and some essexites (Jacupiranga and Pariquera-Açu), while the more evolved rocks are represented by syenites and nepheline syenites. They are mainly silica-undersaturated, with large variation in $Al_2O_3$, $Na_2O$, $K_2O$ and CaO. On the other hand, the Tunas (São Jerônimo-Curiúva Lineament) and Cananéia (Guapiara Lineament) specimens are clearly silica-over-saturated.

In the TAS diagram, the Guapiara non-cumulate rocks mainly plot in the basanite, trachyandesite basalt to phonolite fields (Fig. 11A). A few Jacupiranga felsic rocks and the Cananéia complex plot in the trachyte to rhyolite fields. Most of the samples from the São Jerônimo-Curiúva Lineament fall in the foidite to phonolite fields, with rare tephriphonolites (Fig. 11B). On the other hand, the Tunas rock-types plot from the trachybasalt to trachyte fields showing a continuous evolutionary trend.

The most "primitive rock-types" (e.g. MgO>7 wt%) usually display a potassic affinity ($K_2O/Na_2O>$ 1.0). On the contrary, some alkali gabbros to syenodiorites from Tunas have $Na_2O$-2.0>$K_2O$ (i.e. sodic affinity). The evolved rock-types have $Na_2O$-2.0<$K_2O$ (i.e. potassic affinity). Notably, many evolved rocks such as nepheline syenites and phonolites (e.g. Banhadão and Itapirapuã) are peralkaline in composition.

The alkaline dykes and plugs intrude the alkaline complexes and the regional basement. In the TAS diagram (Fig. 11A partim, and Fig. 11C) such rocks display variations that extend from basanites to phonolites and trachytes. More than 75% of the PGA dykes consist of evolved strongly peralkaline rocks (A.I.>1.2).

Notably, the PGA "primitive dykes" are rare and only found in the Guapiara Lineament, close to the Early Cretaceous occurrrences (e.g. ankaratrite from Jacupiranga and basanite from Juquiá).

On the whole, the major oxides (for both intrusive and dykes variants from the two lineaments) follow similar trends, with CaO, MgO, $TiO_2$ and $FeO_{total}$ decreasing, and $Na_2O$, $K_2O$ and $Al_2O_3$ increasing with $SiO_2$ (cf. Figs. 10A, B). The Late Cretaceous rock-types from the Guapiara Lineament (Cananéia) represent the most evolved variants ($SiO_2$>59 wt%) as an extension of the main trends common to the Early Cretaceous complexes (cf. Fig. 10A). Alkaline rocks from the São Jerônimo-Curiúva Lineament, Early to Late Cretaceous in age, show two distinct tendencies, with the Tunas complex (Late Cretaceous) displaying for the same $SiO_2$ contents, lower $K_2O$ and higher CaO, $P_2O_5$, MgO, $FeO_{total}$ and $TiO_2$, respectively, compared to the other occurrences (cf. Fig. 10B).

Table 3A. Major (wt%) and trace elements (ppm) contents of selected Mesozoic alkaline rock-types from the Guapiara Lineament. Abbreviations: Ag, alkali gabbro; Ak, ankaratrite; Bsn, basanite; Cpx, clinopyroxenite; Ex, essexite; Ga, alkali granite; Ij, ijolite; Mdu, mica dunite; Me, melteigite; Mgb, melagabbro; mQSy, quartz microsyenite; mThe, melatheralite; neSy, nepheline syenite; olAg, olivine alkali gabbro; Olcpx, olivine clinopyroxenite; Ph, phonolite; pPh, peralkaline phonolite; PhTph, phonotephrite; Qm, quartz monzonite; qSy, quartz syenite; Ra, alkali microgranite; SD, syenodiorite; SG, syenogabbro; Sy, syenite; The, theralite; Tr, trachyte; Ur, urtite. mg#=MgO/(MgO+FeO) for molar ($Fe_2O_3/FeO=0.2$); A.I.=$(Na_2O+K_2O)/Al_2O_3$ molar ratio. References quoted in the text. In blank, not detected or not determined elements.

| Districts | Jacupiranga | | | | | | | | | | | | | | | | | |
|---|---|---|---|---|---|---|---|---|---|---|---|---|---|---|---|---|---|---|
| Sample | JC100 | JC98 | JC105 | JC106 | JC128 | JC129 | JC101 | JC127 | JC81 | JC114 | JC115 | JC116 | JC111-D | JC104 | JC126-D | JC122 | JC97 | JC85 |
| Rock-type | Cpx | Cpx | Cpx | Cpx | Cpx | Cpx | Cpx | Cpx | Cpx | Mdu | Mdu | Mdu | Ak | Ag | Mgb | SG | SD | Me |
| $SiO_2$ | 36.66 | 41.25 | 43.06 | 42.37 | 43.89 | 45.82 | 40.76 | 44.35 | 43.82 | 38.34 | 36.32 | 45.93 | 43.68 | 48.31 | 48.07 | 47.87 | 51.76 | 40.72 |
| $TiO_2$ | 4.56 | 4.55 | 4.62 | 4.84 | 3.14 | 2.51 | 3.83 | 2.61 | 3.06 | 0.13 | 0.08 | 0.11 | 2.78 | 3.5 | 3.91 | 3.52 | 2.21 | 2.94 |
| $Al_2O_3$ | 4.51 | 4.33 | 2.07 | 2.09 | 4.46 | 4.36 | 5.66 | 7.52 | 8.34 | 0.07 | 0.35 | 0.12 | 8.86 | 14.19 | 11.20 | 13.85 | 16.34 | 8.88 |
| $Fe_2O_{3\ total}$ | 19.80 | 20.06 | 16.54 | 17.50 | 12.03 | 9.48 | 14.27 | 12.27 | 10.89 | 14.69 | 10.89 | 15.47 | 11.99 | 11.84 | 13.46 | 11.81 | 9.58 | 13.39 |
| MnO | 0.17 | 0.18 | 0.19 | 0.21 | 0.12 | 0.11 | 0.13 | 0.16 | 0.14 | 0.17 | 0.09 | 0.20 | 0.17 | 0.18 | 0.19 | 0.17 | 0.14 | 0.15 |
| MgO | 13.07 | 13.18 | 16.00 | 15.29 | 15.52 | 16.05 | 14.73 | 12.41 | 11.79 | 30.99 | 39.4 | 23.86 | 12.31 | 7.59 | 7.47 | 6.82 | 4.47 | 10.87 |
| CaO | 19.01 | 17.07 | 17.43 | 17.25 | 19.89 | 20.30 | 19.48 | 16.99 | 18.13 | 0.02 | 0.01 | 0.04 | 11.63 | 9.43 | 8.02 | 8.89 | 6.47 | 19.18 |
| $Na_2O$ | | | | | | | | 1.25 | 1.78 | 0.02 | 0.05 | 0.05 | 3.13 | 2.55 | 2.46 | 2.70 | 4.23 | 2.56 |
| $K_2O$ | 0.01 | 0.02 | 0.02 | 0.02 | 0.02 | 0.07 | 0.09 | 1.47 | 1.33 | 0.02 | | 0.02 | 3.38 | 2.13 | 2.41 | 3.12 | 4.19 | 1.19 |
| $P_2O_5$ | 1.90 | 0.10 | 0.14 | 0.15 | 0.12 | 0.13 | 0.12 | 0.27 | 0.18 | 0.01 | | 0.01 | 0.50 | 0.31 | 0.45 | 0.99 | 0.65 | 0.11 |
| Sum | 99.69 | 100.74 | 100.07 | 99.72 | 99.19 | 98.83 | 99.07 | 99.30 | 99.46 | 84.46 | 87.19 | 85.81 | 98.43 | 100.03 | 97.64 | 99.74 | 100.04 | 99.99 |
| L.O.I | 2.27 | 1.25 | 1.56 | 2.00 | 2.00 | 2.11 | 2.33 | 1.91 | 1.62 | 18.01 | 13.89 | 15.72 | 2.75 | 1.14 | 3.69 | 1.44 | 0.91 | 1.35 |
| $K_2O/Na_2O$ | | | | | | | | 1.18 | 0.75 | 1.00 | | 0.40 | 1.08 | 0.84 | 0.98 | 1.16 | 0.99 | 0.46 |
| A.I. | | | | | | | | | | | | | 0.99 | 0.46 | 0.59 | 0.56 | 0.70 | 0.62 |
| mg# | 0.61 | 0.61 | 0.69 | 0.67 | 0.75 | 0.80 | 0.71 | 0.70 | 0.72 | 0.83 | 0.89 | 0.78 | 0.71 | 0.60 | 0.56 | 0.57 | 0.52 | 0.65 |
| V | 557 | 797 | 913 | 1000 | 291 | 174 | 322 | 450 | 447 | 26 | 16 | 29 | 319 | 436 | 371 | 322 | 207 | 499 |
| Cr | 78 | 314 | 591 | 490 | 437 | 1340 | 68 | 518 | 350 | 4210 | 1790 | 4790 | 733 | 213 | 217 | 142 | 93 | 164 |
| Co | 66 | 49 | 71 | 71 | 46 | 40 | 60 | 57 | 44 | 172 | 96 | 179 | 56 | 46 | 28 | 41 | 30 | 59 |
| Ni | 111 | 109 | 316 | 214 | 195 | 209 | 216 | 172 | 149 | 3460 | 3280 | 3790 | 221 | 85 | 86 | 71 | 51 | 125 |
| Rb | 2 | 2 | | 2 | | 2 | 3 | 45 | 37 | | | 5 | 100 | 53 | 48 | 65 | 95 | 17 |
| Sr | 427 | 160 | 226 | 199 | 277 | 334 | 321 | 472 | 522 | 15 | 12 | | 844 | 1540 | 549 | 1300 | 1040 | 1110 |
| Ba | 138 | 126 | 62 | 50 | 153 | 89 | 101 | 343 | 285 | 189 | 66 | 212 | 1820 | 1020 | 993 | 2350 | 1820 | 67 |
| Zr | 114 | 70 | 58 | 52 | 106 | 129 | 175 | 113 | 168 | | | | 252 | 145 | 419 | 222 | 228 | 61 |
| Nb | 1 | | 5 | 2 | | | 5 | 6 | 3 | | | 10 | 45 | 62 | 62 | 47 | 43 | |
| Y | 13 | 11 | 13 | 14 | 12 | 9 | 10 | 15 | 11 | 3 | 24 | | 17.9 | 22.5 | 27 | 20 | 27.6 | 6 |
| Districts | Jacupiranga (cont.) | | | | | | | | | | | | | | | | | |
| Sample | JC82 | JC78 | JC90 | JC80 | JC84 | JC76 | JC88 | JC73 | JC72 | JC83 | JC89 | JC70 | JC109 | JC71 | JC110 | JC86 | JC87 | JC79 |
| Rock-type | Me | Me | Me | Me | Ij | Ij | Ij | Ij | Ij | Ij | Ij | Ij | Ex | Ex | Ex | Ur | Ur | Ur |
| $SiO_2$ | 43.76 | 41.28 | 39.87 | 43.2 | 41.81 | 43.23 | 40.66 | 43.39 | 42.30 | 42.48 | 39.58 | 42.95 | 45.55 | 43.76 | 46.78 | 39.48 | 40.19 | 40.05 |
| $TiO_2$ | 2.08 | 2.45 | 2.56 | 1.85 | 2.65 | 1.73 | 2.67 | 1.63 | 2.81 | 1.44 | 2.32 | 2.40 | 3.90 | 2.97 | 3.05 | 1.19 | 1.06 | 1.15 |
| $Al_2O_3$ | 10.86 | 11.19 | 10.55 | 13.04 | 13.82 | 14.79 | 15.29 | 14.83 | 14.98 | 16.53 | 18.07 | 17.44 | 12.07 | 15.25 | 13.34 | 22.16 | 21.45 | 22.12 |
| $Fe_2O_{3\ total}$ | 8.95 | 11.56 | 13.13 | 8.06 | 10.28 | 8.89 | 9.97 | 8.70 | 10.89 | 7.19 | 9.40 | 9.52 | 11.97 | 10.61 | 10.05 | 6.11 | 4.88 | 6.08 |
| MnO | 0.12 | 0.14 | 0.16 | 0.11 | 0.12 | 0.12 | 0.13 | 0.12 | 0.15 | 0.10 | 0.12 | 0.15 | 0.20 | 0.15 | 0.20 | 0.09 | 0.08 | 0.09 |
| MgO | 10.48 | 9.90 | 9.32 | 9.29 | 9.28 | 7.63 | 7.87 | 7.56 | 6.11 | 7.17 | 6.52 | 4.27 | 8.77 | 5.28 | 7.04 | 4.24 | 4.54 | 4.25 |
| CaO | 17.48 | 16.99 | 17.81 | 16.24 | 14.16 | 13.68 | 13.19 | 13.82 | 11.82 | 13.77 | 11.24 | 9.72 | 8.24 | 11.06 | 8.10 | 10.02 | 10.19 | 9.45 |
| $Na_2O$ | 3.39 | 3.72 | 3.98 | 4.21 | 4.54 | 4.70 | 6.03 | 4.62 | 4.25 | 5.95 | 6.85 | 4.30 | 2.97 | 1.16 | 4.76 | 9.21 | 9.00 | 10.26 |
| $K_2O$ | 2.00 | 2.15 | 2.17 | 2.95 | 2.58 | 4.15 | 2.86 | 4.27 | 5.12 | 4.59 | 4.51 | 7.35 | 4.77 | 7.88 | 4.43 | 5.50 | 5.90 | 4.21 |
| $P_2O_5$ | 0.17 | 0.50 | 0.75 | 0.12 | 0.13 | 0.38 | 0.91 | 0.35 | 0.78 | 0.09 | 0.87 | 0.96 | 0.69 | 0.99 | 0.75 | 0.98 | 1.62 | 0.76 |
| Sum | 99.29 | 99.88 | 100.30 | 99.07 | 99.37 | 99.30 | 99.58 | 99.29 | 99.21 | 99.31 | 99.48 | 99.06 | 99.13 | 99.11 | 98.50 | 98.98 | 98.91 | 98.42 |
| L.O.I | 1.6 | 1.27 | 1.00 | 1.74 | 1.65 | 1.57 | 1.41 | 1.58 | 1.85 | 1.40 | 1.45 | 1.89 | 2.06 | 1.95 | 2.49 | 1.63 | 1.57 | 2.17 |
| $K_2O/Na_2O$ | 0.59 | 0.58 | 0.55 | 0.70 | 0.57 | 0.88 | 0.47 | 0.92 | 1.20 | 0.77 | 0.66 | 1.71 | 1.61 | 6.79 | 0.93 | 0.60 | 0.66 | 0.41 |
| A.I. | 0.71 | 0.75 | 0.84 | 0.78 | 0.74 | 0.73 | 0.75 | 0.82 | 0.84 | 0.89 | 0.89 | 0.86 | 0.83 | 0.68 | 0.95 | 0.95 | 0.99 | 0.97 |
| mg# | 0.73 | 0.67 | 0.62 | 0.73 | 0.68 | 0.67 | 0.65 | 0.67 | 0.57 | 0.70 | 0.62 | 0.51 | 0.63 | 0.54 | 0.62 | 0.62 | 0.68 | 0.62 |
| V | 308 | 350 | 407 | 269 | 407 | 290 | 467 | 264 | 4.68 | 237 | 417 | 431 | 407 | 479 | 335 | 216 | 167 | 209 |
| Cr | 414 | 195 | 108 | 323 | 169 | 209 | 58 | 208 | 72 | 162 | 24 | 26 | 370 | 34 | 276 | 16 | 18 | 15 |
| Co | 40 | 47 | 51 | 35 | 44 | 38 | 41 | 38 | 41 | 33 | 39 | 33 | 40 | 38 | 30 | 25 | 20 | 26 |
| Ni | 128 | 101 | 89 | 110 | 104 | 105 | 85 | 106 | 69 | 90 | 79 | 35 | 186 | 45 | 140 | 41 | 43 | 40 |
| Rb | 31 | 31 | 32 | 43 | 41 | 137 | 44 | 157 | 173 | 80 | 65 | 223 | 150 | 334 | 125 | 78 | 89 | 74 |
| Sr | 814 | 779 | 1170 | 840 | 413 | 1070 | 625 | 1000 | 771 | 859 | 533 | 772 | 1510 | 474 | 1840 | 817 | 671 | 784 |
| Ba | 181 | 79 | 196 | 222 | 177 | 254 | 226 | 314 | 655 | 239 | 249 | 675 | 2010 | 655 | 2190 | 210 | 269 | 182 |
| Zr | 86 | 52 | 39 | 74 | 92 | 41 | 86 | 53 | 45 | 39 | 60 | 65 | 350 | 167 | 465 | 24 | 44 | 12 |
| Nb | 2 | | 1 | | 3 | 2 | 10 | 2 | 5 | 6 | 7 | | 184 | 15 | 208 | 2 | | 11 |
| Y | 7.52 | 6.18 | 9 | 7 | 8.72 | 6 | 12.1 | 6 | 10 | 3 | 5 | 12 | 65.2 | 18 | 42 | 7.82 | 7 | |

Table 3A (continued).

| Districts | Jacupiranga (cont.) | | | | | | | | | | | | | | | | |
|---|---|---|---|---|---|---|---|---|---|---|---|---|---|---|---|---|---|
| Sample | JC91 | JC75 | JC74 | JC77 | JC108 | JC103 | JC107 | JC112 | JC96 | JC95 | JC102 | JC120 | JC94 | JC119 | JC93 | JC124-d | JC121-d | JC118-d |
| Rock-type | Ur | Ur | Ur | neSy | neSy | neSy | neSy | neSy | neSy | neSy | Sy | Sy | Sy | Sy | Sy | Ph | pPh | pPh |
| $SiO_2$ | 39.96 | 44.24 | 43.14 | 48.59 | 54.36 | 57.54 | 59.37 | 60.3 | 58.44 | 59.41 | 60.24 | 63.38 | 61.17 | 63.09 | 60.96 | 48.53 | 56.55 | 57.12 |
| $TiO_2$ | 1.15 | 1.39 | 2.36 | 2.41 | 1.79 | 1.37 | 0.96 | 0.71 | 1.37 | 1.21 | 1.14 | 0.89 | 1.05 | 0.94 | 0.22 | 1.91 | 0.73 | 0.70 |
| $Al_2O_3$ | 21.67 | 20.66 | 20.87 | 17.02 | 16.21 | 18.03 | 18.42 | 18.9 | 17.65 | 17.58 | 17.77 | 16.15 | 17.58 | 16.29 | 15.08 | 17.99 | 20.24 | 20.37 |
| $Fe_2O_{3\ total}$ | 6.07 | 6.03 | 6.64 | 7.23 | 5.85 | 4.08 | 3.16 | 2.85 | 4.56 | 4.01 | 3.77 | 3.73 | 3.64 | 3.93 | 6.53 | 7.85 | 3.16 | 2.74 |
| MnO | 0.09 | 0.09 | 0.10 | 0.15 | 0.12 | 0.09 | 0.09 | 0.08 | 0.12 | 0.12 | 0.12 | 0.09 | 0.12 | 0.1 | 0.13 | 0.16 | 0.13 | 0.13 |
| MgO | 4.39 | 4.03 | 2.79 | 2.05 | 3.80 | 1.39 | 0.83 | 0.55 | 1.60 | 1.15 | 1.34 | 1.24 | 1.51 | 1.03 | 0.55 | 2.08 | 0.32 | 0.21 |
| CaO | 10.00 | 8.06 | 7.58 | 6.71 | 4.56 | 3.15 | 2.31 | 2.00 | 3.05 | 2.95 | 2.54 | 2.36 | 2.25 | 1.96 | 2.32 | 6.55 | 1.88 | 1.58 |
| $Na_2O$ | 10.27 | 6.69 | 5.20 | 0.85 | 5.26 | 5.54 | 6.65 | 6.17 | 6.23 | 6.67 | 5.52 | 4.9 | 5.73 | 5.30 | 2.16 | 7.07 | 8.32 | 8.17 |
| $K_2O$ | 4.19 | 7.40 | 9.26 | 13.14 | 5.94 | 6.70 | 6.11 | 7.05 | 5.22 | 5.28 | 5.41 | 5.35 | 5.35 | 5.27 | 11.04 | 4.82 | 6.65 | 7.20 |
| $P_2O_5$ | 0.88 | 0.12 | 0.67 | 0.52 | 0.32 | 0.41 | 0.21 | 0.16 | 0.37 | 0.35 | 0.35 | 0.25 | 0.34 | 0.27 | 0.02 | 0.77 | 0.11 | 0.07 |
| Sum | 98.67 | 98.71 | 98.61 | 98.67 | 98.21 | 98.30 | 98.11 | 98.77 | 98.61 | 98.73 | 98.20 | 98.34 | 98.74 | 98.18 | 99.01 | 97.73 | 98.09 | 98.29 |
| L.O.I | 1.94 | 1.87 | 2.06 | 2.03 | 2.38 | 2.09 | 2.2 | 1.52 | 1.84 | 1.67 | 2.18 | 2.03 | 1.61 | 2.22 | 1.64 | 3.03 | 2.21 | 1.99 |
| $K_2O/Na_2O$ | 0.41 | 1.11 | 1.78 | 15.46 | 1.13 | 1.21 | 0.92 | 1.14 | 0.84 | 0.79 | 0.98 | 1.09 | 0.93 | 0.99 | 5.11 | 0.68 | 0.80 | 0.88 |
| A.I. | 0.99 | 0.92 | 0.89 | 0.92 | 0.93 | 0.91 | 0.95 | 0.94 | 0.90 | 0.95 | 0.84 | 0.86 | 0.87 | 0.89 | 1.03 | 0.94 | 1.03 | 1.04 |
| mg# | 0.63 | 0.61 | 0.50 | 0.40 | 0.60 | 0.44 | 0.38 | 0.31 | 0.45 | 0.40 | 0.45 | 0.44 | 0.49 | 0.38 | 0.16 | 0.38 | 0.19 | 0.15 |
| V | 217 | 207 | 215 | 201 | 181 | 126 | 85 | 80 | 56 | 30 | 50 | 55 | 49 | 53 | 373 | 201 | 39 | 32 |
| Cr | 15 | 21 | 10 | 24 | 169 | 13 | 6 | 5 | 5 | 2 | 5 | 10 | 2 | 10 | 23 | 24 | 5 | 4 |
| Co | 25 | 22 | 26 | 17 | 18 | 10 | 4 | 2 | 3 | 3 | 3 | 7 | 3 | 4 | 4 | 17 | 1 | 1 |
| Ni | 40 | 48 | 9 | 22 | 96 | 16 | 11 | 12 | 9 | 7 | 9 | 13 | 8 | 9 | 13 | 22 | 6 | 6 |
| Rb | 72 | 273 | 505 | 415 | 123 | 97 | 126 | 34 | 104 | 109 | 123 | 150 | 137 | 145 | 185 | 415 | 189 | 172 |
| Sr | 834 | 541 | 715 | 1650 | 3820 | 4450 | 2680 | 1520 | 955 | 860 | 842 | 540 | 789 | 426 | 524 | 1650 | 755 | 511 |
| Ba | 176 | 668 | 624 | 1700 | 2920 | 6770 | 2990 | 870 | 2440 | 2180 | 2480 | 1490 | 2140 | 1500 | 3720 | 1700 | 1200 | 792 |
| Zr | 17 | 68 | 43 | 61 | 277 | | 227 | | 276 | 363 | 370 | 347 | 114 | 359 | 137 | 61 | 367 | 236 |
| Nb | 12 | 1 | 131 | 41 | 123 | 45 | 93 | 16 | 43 | 60 | 67 | 46 | 53 | 51 | 1 | 41 | 107 | 107 |
| Y | | 7 | 19.5 | 14 | 24 | 17.1 | 31.3 | | 20 | 26 | 26 | 24 | 39 | 33.9 | 1.45 | 14 | 14 | 18.7 |

| Districts | Juquiá | | | | | | | | | | | | | | | | | | |
|---|---|---|---|---|---|---|---|---|---|---|---|---|---|---|---|---|---|---|---|
| Sample | S8 | S9 | S2 | S20 | S43 | S7-D | S5-D | S17 | S24 | S3 | S47bd | S10 | S11 | S38 | S27 | S37 | S32 | S30 | S22 |
| Rock-type | Olcpx | Olcpx | Olcpx | Me | Me | Bsn | Bsn | Ij | Ij | olAg | PhTph | Ur | Ur | SD | Ex | Ex | neSy | neSy | neSy |
| $SiO_2$ | 42.00 | 40.45 | 38.75 | 36.27 | 39.56 | 43.99 | 44.47 | 38.45 | 38.85 | 47.96 | 46.32 | 42.45 | 40.7 | 52.08 | 51.31 | 51.54 | 50.61 | 48.65 | 52.18 |
| $TiO_2$ | 3.06 | 3.64 | 1.80 | 4.30 | 4.76 | 3.74 | 3.69 | 3.78 | 3.26 | 3.21 | 2.84 | 2.17 | 1.37 | 2.95 | 3.08 | 1.86 | 2.51 | 1.92 | 2.46 |
| $Al_2O_3$ | 4.17 | 5.52 | 2.38 | 8.08 | 9.09 | 9.94 | 9.77 | 9.57 | 11.36 | 10.21 | 13.30 | 17.46 | 22.26 | 15.71 | 15.12 | 14.85 | 15.39 | 15.76 | 15.81 |
| $Fe_2O_{3\ total}$ | 15.39 | 17.00 | 17.55 | 18.15 | 14.30 | 13.85 | 13.55 | 16.14 | 12.31 | 12.45 | 11.52 | 9.58 | 4.95 | 9.55 | 9.81 | 9.27 | 10.23 | 9.28 | 9.16 |
| MnO | 0.21 | 0.22 | 0.25 | 0.24 | 0.21 | 0.19 | 0.19 | 0.24 | 0.23 | 0.18 | 0.19 | 0.13 | 0.11 | 0.15 | 0.16 | 0.17 | 0.18 | 0.17 | 0.18 |
| MgO | 20.15 | 18.73 | 31.96 | 9.88 | 8.42 | 11.74 | 12.88 | 8.63 | 5.45 | 11.66 | 5.39 | 4.65 | 2.03 | 4.03 | 4.19 | 6.19 | 3.14 | 2.98 | 2.55 |
| CaO | 13.59 | 13.42 | 5.42 | 15.56 | 16.33 | 10.65 | 9.54 | 14.17 | 17.06 | 9.43 | 9.83 | 9.36 | 8.83 | 5.99 | 6.00 | 5.76 | 5.90 | 5.74 | 5.29 |
| $Na_2O$ | 0.60 | 0.77 | 0.39 | 2.57 | 3.45 | 2.57 | 2.61 | 3.28 | 5.66 | 2.04 | 5.36 | 6.76 | 10.16 | 3.82 | 3.89 | 4.84 | 5.19 | 5.43 | 4.53 |
| $K_2O$ | 0.16 | 0.12 | 0.50 | 2.39 | 2.41 | 2.40 | 2.66 | 3.02 | 2.16 | 2.24 | 4.24 | 5.62 | 6.10 | 4.56 | 5.13 | 5.02 | 5.77 | 6.76 | 6.71 |
| $P_2O_5$ | 0.25 | 0.13 | 0.17 | 2.30 | 1.47 | 0.93 | 0.62 | 2.20 | 3.66 | 0.53 | 0.64 | 1.28 | 2.80 | 0.98 | 0.96 | 0.21 | 0.66 | 0.50 | 0.67 |
| Sum | 99.58 | 100.00 | 99.17 | 99.74 | 100.00 | 100.00 | 99.98 | 99.48 | 100.00 | 99.91 | 99.63 | 99.46 | 99.31 | 99.82 | 99.65 | 99.71 | 99.58 | 97.19 | 99.54 |
| L.O.I | 1.63 | 1.17 | 2.20 | 1.30 | 0.78 | 1.17 | 1.12 | 1.42 | 0.62 | 1.15 | 0.99 | 1.11 | 0.92 | 0.87 | 1.07 | 0.93 | 1.12 | 3.40 | 1.00 |
| $K_2O/Na_2O$ | 0.27 | 0.16 | 1.28 | 0.93 | 0.70 | 0.93 | 1.02 | 0.92 | 0.38 | 1.10 | 0.79 | 0.83 | 0.60 | 1.19 | 1.32 | 1.04 | 1.11 | 1.24 | 1.48 |
| A.I. | 0.28 | 0.25 | 0.50 | 0.84 | 0.91 | 0.69 | 0.73 | 0.91 | 1.03 | 0.57 | 1.01 | 0.99 | 1.05 | 0.72 | 0.79 | 0.90 | 0.96 | 1.03 | 0.93 |
| mg# | 0.75 | 0.72 | 0.81 | 0.56 | 0.58 | 0.66 | 0.69 | 0.56 | 0.51 | 0.69 | 0.52 | 0.53 | 0.49 | 0.50 | 0.50 | 0.61 | 0.42 | 0.43 | 0.39 |
| V | 331 | 330 | 177 | 501 | 404 | 329 | 326 | 411 | 397 | 293 | 299 | 367 | 142 | 221 | 231 | 167 | 183 | 211 | 205 |
| Cr | 1880 | 1600 | 2660 | 99 | 170 | 915 | 1000 | 41 | 28 | 942 | 129 | | | 11 | 37 | 516 | 8 | 30 | |
| Co | | | | | | | | | | | | | | | | | | | |
| Ni | 718 | 633 | 1570 | 91 | 76 | 420 | 478 | 56 | 31 | 356 | 61 | 39 | 14 | 24 | 30 | 214 | 18 | 25 | 4 |
| Rb | 10 | 9 | 18 | 61 | 67 | 57 | 64 | 81 | 42 | 57 | 132 | 150 | 94 | 94 | 98 | 159 | 142 | 190 | 142 |
| Sr | 407 | 613 | 206 | 1340 | 1580 | 1130 | 917 | 1350 | 1430 | 729 | 1530 | 757 | 716 | 2300 | 2060 | 1010 | 1980 | 1530 | 2510 |
| Ba | 133 | 202 | 276 | 1900 | 1670 | 952 | 1100 | 1910 | 420 | 850 | 2420 | 681 | 254 | 3280 | 3400 | 685 | 2260 | 1920 | 3050 |
| Zr | 95 | 117 | 70 | 277 | 225 | 334 | 310 | 505 | 432 | 271 | 264 | 92 | 101 | 161 | 167 | 242 | 320 | 497 | 191 |
| Nb | 12 | 10 | 10 | 85 | 187 | 61 | 62 | 111 | 258 | 48 | 131 | 15 | 163 | 65 | 61 | 81 | 132 | 162 | 134 |
| Y | 18 | 16 | 7 | 31 | 37 | 29 | 23 | 34 | 45 | 26 | 20 | 14 | 17 | 29 | 27 | 15 | 29 | 16 | 32 |

Table 3A (continued).

| Districts | **Juquiá (cont.)** | | | | | | | | **Pariquera-Açu** | | | |
|---|---|---|---|---|---|---|---|---|---|---|---|---|
| Sample | S48 | S40 | S28bd | S35 | S46-D | S36 | S47A | S4-D | Par 13 | Par 12 | Par 4 | Par 11 |
| Rock-type | neSy | neSy | neSy | neSy | neSy | neSy | neSy | pPh | mThe | The | The | The |
| $SiO_2$ | 49.03 | 53.76 | 53.88 | 52.53 | 57.80 | 57.30 | 54.11 | 56.97 | 43.92 | 43.2 | 43.43 | 43.13 |
| $TiO_2$ | 2.34 | 1.40 | 1.26 | 1.13 | 0.67 | 0.97 | 2.04 | 0.83 | 3.38 | 3.70 | 3.27 | 3.60 |
| $Al_2O_3$ | 17.24 | 17.74 | 19.01 | 19.13 | 20.17 | 18.67 | 16.65 | 20.47 | 8.64 | 8.88 | 9.35 | 8.70 |
| $Fe_2O_{3\ total}$ | 8.69 | 5.89 | 5.89 | 4.98 | 4.05 | 5.27 | 7.36 | 3.97 | 11.16 | 12.31 | 12.92 | 12.66 |
| MnO | 0.15 | 0.12 | 0.13 | 0.08 | 0.07 | 0.14 | 0.17 | 0.06 | 0.19 | 0.20 | 0.22 | 0.18 |
| MgO | 2.63 | 1.53 | 0.96 | 1.08 | 0.55 | 0.88 | 1.89 | 0.57 | 12.43 | 10.77 | 11.84 | 10.32 |
| CaO | 4.90 | 4.23 | 3.79 | 3.48 | 0.58 | 2.09 | 3.91 | 1.13 | 15.03 | 14.70 | 13.48 | 15.41 |
| $Na_2O$ | 6.65 | 6.67 | 7.14 | 6.57 | 7.24 | 6.86 | 6.52 | 9.14 | 2.00 | 1.64 | 1.63 | 2.23 |
| $K_2O$ | 6.65 | 6.95 | 6.92 | 8.52 | 8.36 | 7.30 | 6.12 | 6.25 | 1.62 | 2.30 | 2.14 | 1.99 |
| $P_2O_5$ | 0.52 | 0.42 | 0.25 | 0.24 | 0.02 | 0.23 | 0.37 | 0.16 | 0.36 | 0.63 | 0.78 | 0.39 |
| Sum | 98.80 | 98.71 | 99.23 | 97.74 | 99.51 | 99.71 | 99.14 | 99.55 | 98.73 | 98.33 | 99.06 | 98.61 |
| L.O.I | 1.66 | 1.57 | 1.09 | 2.52 | 0.72 | 0.60 | 1.24 | 0.59 | 2.19 | 2.65 | 2.01 | 2.23 |
| | | | | | | | | | | | | |
| $K_2O/Na_2O$ | 1.00 | 1.04 | 0.97 | 1.30 | 1.15 | 1.06 | 0.94 | 0.68 | 0.81 | 1.40 | 1.31 | 0.89 |
| A.I. | 1.05 | 1.04 | 1.01 | 1.05 | 1.04 | 1.03 | 1.04 | 1.07 | 0.58 | 0.58 | 0.53 | 0.67 |
| mg# | 0.41 | 0.38 | 0.28 | 0.34 | 0.24 | 0.28 | 0.37 | 0.25 | 0.72 | 0.67 | 0.68 | 0.66 |
| | | | | | | | | | | | | |
| V | 233 | 116 | 145 | 143 | 73 | 94 | 132 | 81 | 295 | 460 | 365 | 463 |
| Cr | | 9 | | | | 10 | | | 721 | 502 | 771 | 267 |
| Co | | | | | | | | | 56 | | | 54 |
| Ni | 12 | 13 | 7 | 8 | 6 | 12 | 10 | 10 | 224 | 765 | 235 | 140 |
| Rb | 152 | 181 | 163 | 148 | 244 | 241 | 166 | 123 | 34 | 63 | 55 | 63 |
| Sr | 1370 | 1670 | 1560 | 895 | 1030 | 1080 | 1800 | 2170 | 560 | 528 | 562 | 560 |
| Ba | 2080 | 1740 | 1980 | 2070 | 786 | 752 | 1750 | 1700 | 607 | 557 | 644 | 476 |
| Zr | 473 | 293 | 318 | 552 | 124 | 288 | 552 | 242 | 155 | 129 | 122 | 160 |
| Nb | 141 | 123 | 112 | 149 | 59 | 128 | 217 | 100 | 37 | 35 | 34 | 30 |
| Y | 26 | 19 | 16 | 13 | 4 | 10 | 40 | 17 | 12 | 10 | 13 | 15 |

| Districts | **Pariquera-Açu (cont.)** | | | | | | | | | | |
|---|---|---|---|---|---|---|---|---|---|---|---|
| Sample | Par 7 | Par 5 | Par 15 | Par 10 | Par 6 | Par 14 | Par 3 | Par 8 | Par 1 | Par 17 | Par 18 |
| Rock-type | The | The | The | The | The | The | Ex | Ex | SG | SD | SD |
| $SiO_2$ | 45.19 | 46.86 | 45.36 | 44.66 | 46.69 | 45.66 | 46.62 | 49.18 | 46.79 | 48.69 | 49.22 |
| $TiO_2$ | 3.57 | 2.59 | 3.02 | 3.79 | 2.94 | 2.97 | 2.76 | 2.07 | 3.60 | 3.49 | 3.53 |
| $Al_2O_3$ | 9.77 | 9.61 | 12.03 | 11.8 | 10.77 | 12.06 | 13.78 | 16.09 | 13.97 | 15.18 | 15.8 |
| $Fe_2O_{3\ total}$ | 12.16 | 10.45 | 11.68 | 11.61 | 10.93 | 11.15 | 10.54 | 7.90 | 12.18 | 11.38 | 11.32 |
| MnO | 0.17 | 0.17 | 0.20 | 0.19 | 0.18 | 0.19 | 0.17 | 0.14 | 0.19 | 0.18 | 0.18 |
| MgO | 10.29 | 11.35 | 8.15 | 10.41 | 9.84 | 8.14 | 7.18 | 5.58 | 6.19 | 4.85 | 4.11 |
| CaO | 13.14 | 13.31 | 12.47 | 10.55 | 11.51 | 12.13 | 9.76 | 8.35 | 8.53 | 7.47 | 6.67 |
| $Na_2O$ | 2.27 | 2.58 | 2.95 | 2.66 | 2.48 | 3.16 | 3.96 | 4.80 | 3.14 | 3.69 | 3.67 |
| $K_2O$ | 2.31 | 1.90 | 2.26 | 2.80 | 3.14 | 2.91 | 3.34 | 4.17 | 3.13 | 3.60 | 3.90 |
| $P_2O_5$ | 0.33 | 0.31 | 1.00 | 0.50 | 0.37 | 1.02 | 0.91 | 0.57 | 0.54 | 0.61 | 0.64 |
| Sum | 99.20 | 99.13 | 99.12 | 98.97 | 98.85 | 99.39 | 99.02 | 98.85 | 98.26 | 99.14 | 99.04 |
| L.O.I | 1.73 | 1.74 | 1.81 | 1.86 | 2.08 | 1.46 | 1.92 | 1.70 | 2.72 | 1.82 | 1.93 |
| | | | | | | | | | | | |
| $K_2O/Na_2O$ | 1.02 | 0.74 | 0.77 | 1.05 | 1.27 | 0.92 | 0.84 | 0.87 | 1.00 | 0.98 | 1.06 |
| A.I. | 0.64 | 0.66 | 0.61 | 0.63 | 0.69 | 0.69 | 0.74 | 0.77 | 0.61 | 0.66 | 0.65 |
| mg# | 0.66 | 0.72 | 0.62 | 0.68 | 0.68 | 0.63 | 0.61 | 0.62 | 0.54 | 0.50 | 0.46 |
| | | | | | | | | | | | |
| V | 525 | 303 | 326 | 368 | 306 | 345 | 291 | 212 | 337 | 332 | 303 |
| Cr | 463 | 811 | 314 | 674 | 574 | 313 | 223 | 236 | 140 | | 83 |
| Co | 58.9 | | 50.3 | | | 51 | | 35 | 59.3 | | 41 |
| Ni | 204 | 207 | 118 | 241 | 175 | 122 | 98 | 91 | 91.5 | 63 | 64 |
| Rb | 69.98 | 40 | 53.39 | 68 | 75 | 71 | 85 | 97 | 83 | 87 | 104 |
| Sr | 532 | 798 | 1090 | 991 | 587 | 776 | 920 | 1130 | 1250 | 1250 | 1330 |
| Ba | 547 | 957 | 1100 | 1090 | 680 | 903 | 1350 | 1800 | 1520 | 1570 | 1680 |
| Zr | 177 | 134 | 167 | 213 | 176 | 165 | 202 | 274 | 211 | 274 | 297 |
| Nb | 44.8 | 38 | 43 | 65 | 35 | 45 | 58 | 72 | 82 | 84 | 85 |
| Y | 15 | 11 | 16 | 16 | 16 | 15.3 | 16 | 17 | 21 | 22 | 21 |

Table 3A (continued).

| Districts | **Cananéia** | | | | | | | | | | | | | | | |
|---|---|---|---|---|---|---|---|---|---|---|---|---|---|---|---|---|
| Sample | 01B2 | 01C2 | 03-B2 | 03C2 | 04A2 | 04B2 | 04D1 | 04-D2 | 05A1 | 05-B1 | 06-B1 | 06-B2 | 07-A1 | 07B2 | 08-A2 | 08-B2 |
| Rock-type | Sy | Sy | Sy | Sy | Sy | Sy | Sy | Sy | Sy | Sy | Sy | Sy | Sy | Sy | Sy | Sy |
| $SiO_2$ | 63.21 | 64.5 | 64.75 | 66.65 | 66.46 | 64.9 | 66.02 | 65.00 | 65.23 | 64.42 | 60.25 | 60.55 | 62.77 | 63.46 | 60.71 | 60.54 |
| $TiO_2$ | 0.49 | 0.37 | 0.14 | 0.21 | 0.25 | 0.13 | 0.09 | 0.15 | 0.19 | 0.28 | 0.93 | 0.92 | 0.67 | 0.65 | 0.92 | 0.96 |
| $Al_2O_3$ | 16.26 | 17.16 | 17.47 | 17.8 | 17.74 | 17.55 | 18.24 | 17.93 | 17.55 | 16.91 | 16.41 | 16.5 | 16.42 | 16.6 | 16.41 | 16.39 |
| $Fe_2O_{3\ total}$ | 6.31 | 4.52 | 4.12 | 2.55 | 2.50 | 3.82 | 2.51 | 3.91 | 3.98 | 5.63 | 7.72 | 7.56 | 6.31 | 5.63 | 7.59 | 7.79 |
| MnO | 0.19 | 0.10 | 0.12 | 0.03 | 0.03 | 0.13 | 0.04 | 0.07 | 0.03 | 0.07 | 0.15 | 0.15 | 0.16 | 0.10 | 0.16 | 0.16 |
| MgO | 0.52 | 0.30 | 0.05 | 0.01 | 0.03 | 0.03 | | 0.04 | 0.04 | 0.06 | 1.55 | 1.47 | 0.90 | 0.90 | 1.54 | 1.56 |
| CaO | 1.53 | 1.20 | 0.19 | 0.26 | 0.28 | 0.33 | 0.05 | 0.13 | 0.38 | 0.50 | 3.54 | 3.26 | 2.10 | 1.94 | 3.11 | 3.33 |
| $Na_2O$ | 5.97 | 6.21 | 6.78 | 6.69 | 6.61 | 7.18 | 7.11 | 6.89 | 6.70 | 6.36 | 5.46 | 5.48 | 5.61 | 5.61 | 5.65 | 5.54 |
| $K_2O$ | 5.31 | 5.37 | 5.33 | 5.45 | 5.46 | 4.95 | 5.28 | 5.23 | 5.47 | 5.35 | 3.74 | 3.91 | 4.85 | 4.95 | 3.99 | 3.87 |
| $P_2O_5$ | 0.07 | 0.06 | 0.02 | 0.01 | 0.01 | 0.01 | 0.01 | 0.02 | 0.01 | 0.03 | 0.24 | 0.20 | 0.13 | 0.15 | 0.24 | 0.24 |
| Sum | 99.86 | 99.79 | 98.97 | 99.66 | 99.37 | 99.03 | 99.35 | 99.37 | 99.58 | 99.61 | 99.99 | 100.00 | 99.92 | 99.99 | 100.32 | 100.38 |
| L.O.I | 0.78 | 0.66 | 1.44 | 0.81 | 0.88 | 1.33 | 0.89 | 1.01 | 0.82 | 0.95 | 0.78 | 0.75 | 0.69 | 0.58 | 0.45 | 0.40 |
| | | | | | | | | | | | | | | | | |
| $K_2O/Na_2O$ | 0.89 | 0.86 | 0.79 | 0.81 | 0.83 | 0.69 | 0.74 | 0.76 | 0.82 | 0.84 | 0.68 | 0.71 | 0.86 | 0.88 | 0.71 | 0.70 |
| A.I. | 0.96 | 0.93 | 0.97 | 0.95 | 0.95 | 0.98 | 0.95 | 0.95 | 0.97 | 0.96 | 0.79 | 0.80 | 0.88 | 0.88 | 0.83 | 0.81 |
| mg# | 0.16 | 0.13 | 0.03 | 0.01 | 0.03 | 0.02 | | 0.02 | 0.02 | 0.02 | 0.32 | 0.31 | 0.25 | 0.27 | 0.32 | 0.32 |
| | | | | | | | | | | | | | | | | |
| V | | 17 | | | | 19 | | | | | 18 | | | | 50 | |
| Cr | 5 | 11 | 3 | 1 | 2 | 13 | | | 2 | | 6 | 8 | 4 | 7 | 16 | 8 |
| Co | | 2 | | | | 1 | | | | | 5 | | | | 7 | |
| Ni | 1 | 6 | 2 | 2 | 3 | 12 | 7 | 6 | 3 | 5 | 5 | 13 | 9 | 5 | 12 | 14 |
| Rb | 114 | 117 | 170 | 138 | 141 | 170 | 156 | 150 | 97 | 133 | 236 | 87 | 115 | 115 | 88 | 83 |
| Sr | 58 | 209 | 25 | 13 | 13 | 395 | 13 | 14 | 10 | 10 | 202 | 245 | 144 | 124 | 309 | 395 |
| Ba | 666 | 637 | 268 | 138 | 141 | 198 | 176 | 202 | 289 | 263 | 1434 | 1461 | 1310 | 1179 | 1334 | 1429 |
| Zr | 1165 | 1343 | 708 | 766 | 730 | 717 | 540 | 577 | 181 | 557 | 322 | 358 | 472 | 504 | 581 | 337 |
| Nb | 77 | 97 | 96 | 122 | 138 | 133 | 66 | 67 | 34 | 92 | 186 | 45 | 65 | 42 | 70 | 51 |
| Y | 79 | 193 | 69 | 66 | 73 | 77 | 47 | 59 | 34 | 62 | 46 | 147 | 53 | 39 | 73 | 53 |
| Districts | **Cananéia (cont.)** | | | | | | | | | | | | | | | |
| Sample | 09A2 | 09B2 | 10B2 | 10C2 | IC01C2 | IC01E2 | 03 | 05 | 07 | 10 | 11 | 18 | 20 | 24 | 41c | CR10 |
| Rock-type | Sy | Sy | Sy | Sy | qSy | qSy | mQSy | mQSy | QSy | Ga | qSy | Ra | Qm | mQSy | Tr | Tr |
| $SiO_2$ | 59.07 | 64.55 | 62.45 | 63.59 | 66.22 | 67.04 | 68.52 | 66.31 | 68.54 | 68.73 | 67.43 | 69.83 | 63.71 | 68.76 | 66.16 | 68.92 |
| $TiO_2$ | 0.32 | 0.26 | 0.69 | 0.43 | 0.33 | 0.29 | 0.17 | 0.23 | 0.30 | 0.28 | 0.18 | 0.15 | 0.71 | 0.11 | 0.23 | 0.09 |
| $Al_2O_3$ | 14.91 | 16.96 | 19.37 | 17.10 | 16.09 | 15.91 | 16.20 | 17.57 | 16.73 | 16.60 | 17.71 | 16.16 | 16.48 | 16.87 | 16.78 | 16.56 |
| $Fe_2O_{3\ total}$ | 14.01 | 4.60 | 6.99 | 5.67 | 5.31 | 4.60 | 3.96 | 4.37 | 3.83 | 4.05 | 3.17 | 3.60 | 6.43 | 3.08 | 5.55 | 3.51 |
| MnO | 0.47 | 0.22 | 0.22 | 0.18 | 0.08 | 0.08 | 0.05 | 0.12 | 0.08 | 0.09 | 0.10 | 0.08 | 0.14 | 0.1 | 0.18 | 0.15 |
| MgO | 0.23 | 0.11 | 0.50 | 0.36 | 0.21 | 0.15 | 0.00 | 0.06 | 0.15 | 0.17 | 0.10 | | 1.28 | | 0.06 | |
| CaO | 1.45 | 1.08 | 2.22 | 2.05 | 0.78 | 0.82 | 0.59 | 0.97 | 0.71 | 0.64 | 0.76 | 0.76 | 2.45 | 0.46 | 0.98 | 0.57 |
| $Na_2O$ | 5.77 | 6.4 | 5.73 | 6.05 | 5.92 | 6.00 | 6.05 | 6.34 | 5.76 | 5.51 | 5.61 | 5.68 | 5.31 | 6.86 | 6.02 | 5.81 |
| $K_2O$ | 4.96 | 5.50 | 4.66 | 4.55 | 4.74 | 4.88 | 3.53 | 3.90 | 3.86 | 3.65 | 4.47 | 3.48 | 3.27 | 3.51 | 3.80 | 3.95 |
| $P_2O_5$ | 0.09 | 0.03 | 0.17 | 0.12 | 0.07 | 0.05 | 0.00 | 0.03 | 0.04 | 0.04 | 0.01 | | 0.14 | | 0.02 | |
| Sum | 101.28 | 99.71 | 103.00 | 100.10 | 99.75 | 99.82 | 99.07 | 99.90 | 100.00 | 99.76 | 99.54 | 99.74 | 99.92 | 99.75 | 99.78 | 99.56 |
| L.O.I | 0.11 | 0.76 | 0.71 | 0.49 | 0.78 | 0.63 | 1.33 | 0.54 | 0.38 | 0.67 | 0.79 | 0.61 | 0.71 | 0.58 | 0.77 | 0.79 |
| | | | | | | | | | | | | | | | | |
| $K_2O/Na_2O$ | 0.86 | 0.86 | 0.81 | 0.75 | 0.80 | 0.81 | 0.58 | 0.62 | 0.67 | 0.66 | 0.80 | 0.61 | 0.62 | 0.51 | 0.63 | 0.68 |
| A.I. | 1.00 | 0.97 | 0.75 | 0.87 | 0.92 | 0.95 | 0.85 | 0.83 | 0.82 | 0.78 | 0.79 | 0.81 | 0.74 | 0.89 | 0.84 | 0.84 |
| mg# | 0.04 | 0.05 | 0.14 | 0.13 | 0.08 | 0.07 | | 0.03 | 0.08 | 0.09 | 0.07 | | 0.32 | | 0.02 | |
| | | | | | | | | | | | | | | | | |
| V | 21 | 18 | | 26 | | | | 24 | | | | 12 | | 57 | | |
| Cr | 9 | 8 | 10 | 13 | 8 | 5 | 1 | 16 | 2 | 2 | | 7 | 7 | 26 | 5 | 4 |
| Co | 1 | 2 | | 2 | | | | 5 | | | | 2 | | 9 | | |
| Ni | 27 | 7 | 9 | 17 | 3 | 4 | 5 | 12 | 1 | 1 | 2 | 8 | 5 | 14 | 4 | 4 |
| Rb | 112 | 101 | 75 | 79 | 140 | 149 | 117 | 113 | 124 | 124 | 109 | 127 | 100 | 75 | 101 | 146 |
| Sr | 174 | 388 | 156 | 209 | 89 | 83 | 14 | 257 | 73 | 73 | 29 | 704 | 165 | 359 | 16 | 9 |
| Ba | 64 | 59 | 1995 | 2242 | 980 | 897 | 77 | 306 | 825 | 825 | 315 | 89 | 1155 | 43 | 203 | 66 |
| Zr | 269 | 210 | 330 | 207 | 820 | 912 | 1037 | 851 | 756 | 756 | 726 | 1048 | 383 | 866 | 784 | 698 |
| Nb | 57 | 35 | 566 | 39 | 96 | 100 | 119 | 113 | 87 | 87 | 32 | 194 | 52 | 50 | 102 | 120 |
| Y | 39 | 28 | 42 | 26 | 83 | 76 | 110 | 52 | 56 | 56 | 29 | 89 | 38 | 89 | 65 | 71 |

Table 3B. Major (wt%) and trace elements (ppm) contents of selected Mesozoic alkaline rock-types from the São Jerônimo-Curiúva Lineament. Abbreviations: Ag, alkali gabbro; Asy, alkali syenite; Ex, essexite; flij, phlogopite-melanite ijolite; Ma, mariupolite; Mg, malignite; Me, melteigite; mlnSy, melanite nepheline syenite; neSy (c, r), nepheline syenites and varieties (c, gray; r, pink); Ph, phonolite; phMe, phlogopite melteigite; Pu, pulaskite; SD, syenodiorite; SG, syenogabbro; Sy, syenite; Ti, tinguaite; *, dykes. References quoted in the text. In blank, not detected or not determined elements.

| Districts | | | | | | | | **Tunas** | | | | | | | |
|---|---|---|---|---|---|---|---|---|---|---|---|---|---|---|---|
| Sample | 12 | 35 | 8 | 7 | 20 | 19 | 24 | 31 | 10 | 33 | 37* | 34* | 1 | 26 | 22 |
| Rock-type | Ag | SG | Ex | SD | SD | SD | SD* | SD* | SD | Sy | Sy | Sy | Sy | Sy | Sy |
| $SiO_2$ | 47.26 | 49.45 | 49.74 | 51.01 | 51.69 | 51.78 | 53.29 | 56.33 | 57.48 | 59.10 | 57.10 | 58.71 | 58.77 | 60.57 | 62.47 |
| $TiO_2$ | 1.95 | 1.41 | 1.66 | 1.74 | 1.59 | 2.35 | 1.28 | 0.82 | 1.29 | 0.86 | 1.08 | 0.79 | 0.84 | 0.81 | 0.55 |
| $Al_2O_3$ | 20.13 | 20.62 | 19.52 | 18.81 | 19.38 | 16.94 | 18.55 | 17.52 | 19.74 | 17.14 | 18.28 | 17.57 | 18.04 | 18.20 | 17.91 |
| $Fe_2O_{3\ total}$ | 9.63 | 8.23 | 9.66 | 9.37 | 7.87 | 9.57 | 7.90 | 7.46 | 6.02 | 6.78 | 7.06 | 6.15 | 6.22 | 5.66 | 4.48 |
| MnO | 0.14 | 0.14 | 0.20 | 0.17 | 0.13 | 0.18 | 0.12 | 0.13 | 0.16 | 0.10 | 0.14 | 0.12 | 0.18 | 0.14 | 0.14 |
| MgO | 4.15 | 3.28 | 2.63 | 2.26 | 2.37 | 2.86 | 3.45 | 2.17 | 0.69 | 1.46 | 1.54 | 1.66 | 1.26 | 1.02 | 0.61 |
| CaO | 10.74 | 9.26 | 7.74 | 6.77 | 6.88 | 6.18 | 6.10 | 5.39 | 4.89 | 3.64 | 3.70 | 3.87 | 2.71 | 2.44 | 2.65 |
| $Na_2O$ | 3.64 | 4.48 | 5.07 | 5.39 | 5.54 | 5.34 | 5.24 | 5.20 | 6.09 | 5.54 | 6.43 | 6.09 | 6.31 | 6.38 | 6.17 |
| $K_2O$ | 1.08 | 1.53 | 2.53 | 2.41 | 2.56 | 2.73 | 3.09 | 3.89 | 3.15 | 4.23 | 3.77 | 4.06 | 4.63 | 4.24 | 4.39 |
| $P_2O_5$ | 0.68 | 0.48 | 1.41 | 0.96 | 0.80 | 0.89 | 0.48 | 0.55 | 0.42 | 0.50 | 0.51 | 0.42 | 0.32 | 0.36 | 0.22 |
| Sum | 99.40 | 98.88 | 100.16 | 98.89 | 98.81 | 98.82 | 99.50 | 99.46 | 99.93 | 99.35 | 99.61 | 99.44 | 99.28 | 99.82 | 99.59 |
| L.O.I | 1.66 | 1.11 | 0.65 | 1.44 | 1.44 | 1.49 | 0.97 | 0.91 | 0.81 | 1.07 | 0.76 | 0.94 | 1.26 | 0.69 | 0.54 |
| | | | | | | | | | | | | | | | |
| $K_2O/Na_2O$ | 0.30 | 0.34 | 0.50 | 0.45 | 0.46 | 0.51 | 0.59 | 0.75 | 0.52 | 0.76 | 0.59 | 0.67 | 0.73 | 0.66 | 0.71 |
| A.I. | 0.36 | 0.44 | 0.57 | 0.61 | 0.61 | 0.69 | 0.65 | 0.73 | 0.68 | 0.80 | 0.80 | 0.82 | 0.85 | 0.83 | 0.83 |
| mg# | 0.50 | 0.48 | 0.39 | 0.36 | 0.41 | 0.41 | 0.51 | 0.40 | 0.21 | 0.33 | 0.34 | 0.39 | 0.32 | 0.30 | 0.24 |
| | | | | | | | | | | | | | | | |
| V | 224 | 143 | 130 | 115 | 81 | 97 | 111 | 60 | 42 | 48 | 36 | 63 | 34 | 25 | 16 |
| Cr | 23 | 35 | | 6 | 1 | | 50 | 32 | | | | | | | 3 |
| Co | 28 | 31 | 30 | 19 | | 22 | | | 21 | | | | | <10 | |
| Ni | 26 | 18 | 7 | 11 | 12 | 4 | 40 | 24 | 5 | 10 | 6 | 13 | 10 | 8 | 7 |
| Rb | 31 | 39 | 62 | 75 | 66 | 72 | 107 | 114 | 74 | 155 | 102 | 94 | 110 | 100 | 128 |
| Sr | 919 | 1282 | 997 | 940 | 1065 | 815 | 550 | 558 | 971 | 554 | 715 | 526 | 336 | 464 | 444 |
| Ba | 706 | 1338 | 1787 | 2070 | 2761 | 2024 | 1447 | 1444 | 1764 | 1539 | 2371 | 1651 | 2639 | 2514 | 1976 |
| Zr | 115 | 149 | 195 | 181 | 181 | 236 | 211 | 406 | 210 | 327 | 346 | 372 | 340 | 282 | 334 |
| Nb | 34 | 47 | 68 | 71 | 63 | 96 | 56 | 71 | 68 | 85 | 98 | 82 | 98 | 95 | 98 |
| Y | 10 | 8 | 20 | 25 | 19 | 30 | 22 | 17 | 16 | 27 | 17 | 18 | 27 | 16 | 36 |

| Districts | | | | | | | **Tunas (cont.)** | | | | | | | |
|---|---|---|---|---|---|---|---|---|---|---|---|---|---|---|
| Sample | 36 | 9 | 17 | 2 | 14 | 15 | 32 | 27 | 25 | 23 | 13 | 11 | 16 | 28 |
| Rock-type | Sy | Asy | Asy | Asy* | Asy* | Asy | Asy | Asy* | Asy | Asy | Asy | Asy | Asy | Asy* |
| $SiO_2$ | 61.63 | 61.49 | 61.93 | 61.74 | 62.29 | 63.22 | 63.79 | 67.33 | 65.95 | 65.9 | 64.28 | 63.99 | 64.55 | 63.03 |
| $TiO_2$ | 0.59 | 0.81 | 0.74 | 0.38 | 0.38 | 0.37 | 0.31 | 0.17 | 0.26 | 0.27 | 0.19 | 0.23 | 0.27 | 0.42 |
| $Al_2O_3$ | 18.71 | 17.21 | 17.76 | 18.66 | 17.88 | 17.12 | 17.92 | 15.6 | 16.57 | 16.48 | 17.49 | 17.53 | 17.85 | 17.94 |
| $Fe_2O_{3\ total}$ | 3.98 | 5.66 | 4.67 | 4.28 | 4.86 | 4.43 | 2.40 | 3.93 | 3.51 | 3.73 | 3.90 | 3.97 | 2.54 | 4.34 |
| MnO | 0.09 | 0.21 | 0.14 | 0.13 | 0.12 | 0.11 | 0.05 | 0.14 | 0.2 | 0.11 | 0.14 | 0.13 | 0.07 | 0.12 |
| MgO | 0.52 | 0.63 | 0.68 | 0.65 | 0.33 | 0.23 | 0.31 | 0.16 | 0.23 | 0.25 | 0.13 | 0.15 | 0.25 | 0.12 |
| CaO | 2.07 | 2.23 | 1.89 | 1.64 | 1.47 | 1.43 | 1.72 | 0.53 | 1.13 | 1.21 | 1.07 | 0.96 | 1.28 | 0.19 |
| $Na_2O$ | 6.33 | 5.75 | 6.23 | 7.49 | 7.08 | 6.78 | 6.13 | 6.85 | 6.38 | 6.31 | 7.24 | 7.08 | 6.82 | 7.16 |
| $K_2O$ | 4.72 | 5.18 | 5.29 | 4.62 | 5.04 | 5.38 | 5.94 | 4.84 | 5.83 | 5.65 | 5.33 | 5.3 | 5.74 | 5.09 |
| $P_2O_5$ | 0.2 | 0.25 | 0.22 | 0.11 | 0.1 | 0.06 | 0.13 | 0.01 | 0.06 | 0.05 | 0.04 | 0.03 | 0.05 | 0.11 |
| Sum | 98.84 | 99.42 | 99.55 | 99.70 | 99.55 | 99.13 | 98.70 | 99.56 | 100.12 | 99.96 | 99.81 | 99.37 | 99.42 | 98.52 |
| L.O.I | 0.87 | 0.78 | 0.71 | 0.56 | 0.7 | 1.21 | 1.24 | 0.78 | 0.66 | 0.65 | 0.59 | 0.92 | 0.71 | 1.51 |
| | | | | | | | | | | | | | | |
| $K_2O/Na_2O$ | 0.75 | 0.90 | 0.85 | 0.62 | 0.71 | 0.79 | 0.97 | 0.71 | 0.91 | 0.90 | 0.74 | 0.75 | 0.84 | 0.71 |
| A.I. | 0.83 | 0.88 | 0.90 | 0.93 | 0.96 | 0.99 | 0.92 | 1.06 | 1.01 | 1.00 | 1.01 | 0.99 | 0.98 | 0.96 |
| mg# | 0.23 | 0.21 | 0.25 | 0.26 | 0.14 | 0.11 | 0.23 | 0.09 | 0.13 | 0.14 | 0.07 | 0.08 | 0.19 | 0.06 |
| | | | | | | | | | | | | | | |
| V | 15 | 9 | 10 | 16 | 7 | 7 | 16 | 11 | 9 | 7 | | | 7 | 9 |
| Cr | | | | | 5 | | | | | | | | | |
| Co | <10 | <10 | | | | | | <10 | <10 | <10 | <10 | | | |
| Ni | 8 | 8 | 5 | 14 | 8 | 8 | 9 | 6 | 6 | 6 | 8 | 5 | 13 | 7 |
| Rb | 86 | 91 | 95 | 159 | 125 | 130 | 143 | 285 | 160 | 219 | 180 | 147 | 125 | 132 |
| Sr | 470 | 75 | 82 | 134 | 50 | 5 | 317 | 15 | 35 | 52 | 8 | 5 | 15 | 55 |
| Ba | 4897 | 4177 | 4134 | 713 | 2013 | 254 | 1516 | 75 | 367 | 613 | 211 | 114 | 282 | 698 |
| Zr | 200 | 171 | 128 | 724 | 273 | 311 | 267 | 1618 | 490 | 529 | 343 | 541 | 131 | 643 |
| Nb | 58 | 66 | 61 | 199 | 114 | 90 | 40 | 374 | 230 | 116 | 73 | 157 | 36 | 140 |
| Y | 16 | 17 | 17 | 49 | 27 | 29 | 10 | 74 | 97 | 46 | 17 | 56 | 5 | 26 |

Table 3B (continued).

| **Banhadão** | | | | | | | | | | | | | | |
|---|---|---|---|---|---|---|---|---|---|---|---|---|---|---|
| 1 | 2 | 3 | 4 | 5 | 6 | 7 | 8 | 9 | 10 | 11 | 12 | 13 | 14 | 15 |
| phMe | phMe | flij | flij | Mg | Mg | mlnSy | mlnSy | mlnSy | mlnSy | mlnSy | mlnSy | mlnSy | mlnSy | neSy |
| 43.9 | 41.00 | 42.10 | 46.10 | 48.70 | 48.20 | 41.40 | 41.00 | 51.30 | 49.00 | 48.50 | 49.5 | 45.00 | 51.1 | 50.30 |
| 1.70 | 2.10 | 1.30 | 0.76 | 0.64 | 0.67 | 2.00 | 2.30 | 0.41 | 1.10 | 0.82 | 0.51 | 0.65 | 0.13 | 0.52 |
| 11.2 | 11.60 | 14.10 | 23.4 | 18.5 | 19.2 | 17.10 | 13.20 | 20.90 | 20.8 | 20.6 | 20.7 | 23.50 | 23.8 | 23.10 |
| 9.07 | 10.66 | 13.51 | 5.71 | 4.89 | 8.18 | 10.52 | 14.40 | 4.15 | 6.90 | 7.11 | 6.55 | 4.73 | 2.18 | 4.15 |
| 0.20 | 0.14 | 0.35 | 0.17 | 0.18 | 0.23 | 0.22 | 0.32 | 0.09 | 0.21 | 0.22 | 0.19 | 0.15 | 0.06 | 0.12 |
| 12.6 | 11.10 | 2.00 | 0.80 | 2.40 | 1.20 | 1.60 | 1.60 | 0.51 | 0.80 | 0.75 | 0.80 | 0.80 | 0.28 | 0.36 |
| 9.70 | 12.9 | 14.50 | 8.10 | 8.00 | 6.80 | 13.5 | 15.70 | 4.20 | 4.70 | 6.60 | 6.00 | 7.50 | 4.10 | 4.00 |
| 4.84 | 4.00 | 6.52 | 7.35 | 7.27 | 6.90 | 7.69 | 5.39 | 6.13 | 7.21 | 7.00 | 6.09 | 9.70 | 9.44 | 7.15 |
| 4.82 | 4.57 | 4.00 | 7.18 | 5.71 | 8.18 | 5.16 | 4.99 | 10.67 | 8.70 | 8.14 | 8.72 | 7.18 | 7.66 | 10.14 |
| 0.99 | 1.80 | 0.34 | 0.30 | 0.59 | 0.26 | 0.54 | 0.36 | 0.36 | 0.17 | 0.20 | 0.19 | 0.46 | 0.19 | 0.20 |
| 99.02 | 99.87 | 98.72 | 99.87 | 96.88 | 99.82 | 99.73 | 99.26 | 98.72 | 99.59 | 99.94 | 99..25 | 99.67 | 98.94 | 100.04 |
| 0.46 | | 1.22 | | 1.79 | 0.10 | 0.62 | 0.88 | 1.02 | 0.40 | | 0.98 | 0.30 | 0.83 | |
| 1.00 | 1.14 | 0.61 | 0.98 | 0.79 | 1.19 | 0.67 | 0.93 | 1.74 | 1.21 | 1.16 | 1.43 | 0.74 | 0.81 | 1.42 |
| 1.18 | 0.99 | 1.07 | 0.85 | 0.98 | 1.05 | 1.07 | 1.08 | 1.04 | 1.02 | 0.99 | 0.94 | 1.01 | 1.00 | 0.98 |
| 0.76 | 0.71 | 0.26 | 0.25 | 0.53 | 0.26 | 0.26 | 0.21 | 0.22 | 0.21 | 0.20 | 0.22 | 0.28 | 0.23 | 0.17 |
| 130 | 280 | 450 | 146 | 94 | 260 | 400 | 550 | 110 | 128 | 136 | 158 | 120 | 19 | 110 |
| 525 | 560 | | | 112 | 5 | | | | | | | | 5 | |
| 32 | 45 | 22 | | 11 | 7 | 16 | 25 | | 7 | | | | | |
| 213 | 240 | 22 | 7 | 60 | 10 | 15 | 17 | | 7 | | 7 | 6 | | |
| 114 | 84 | 72 | 113 | 157 | 161 | 95 | 177 | 177 | 183 | 168 | 595 | 154 | | 457 |
| 1510 | 1960 | 500 | 260 | 2060 | 370 | 340 | | 560 | 1080 | 450 | 280 | 390 | 450 | 180 |
| 2520 | 4000 | 48 | 620 | 6600 | 1540 | 280 | 124 | 2620 | 2800 | 1840 | 840 | 840 | 1560 | 1030 |
| 190 | 360 | 460 | 236 | 162 | 240 | 590 | 620 | 152 | 440 | 200 | 162 | 240 | 20 | 300 |
| 70 | 110 | 86 | 44 | 66 | 108 | 98 | 118 | 46 | 560 | 84 | 23 | 58 | <20 | 180 |
| 14 | 44 | 200 | 30 | 16 | 12 | 70 | 56 | | 96 | 16 | | 26 | <20 | 12 |

| **Banhadão (cont.)** | | | | | | | | | | | | | | |
|---|---|---|---|---|---|---|---|---|---|---|---|---|---|---|
| 16 | 17 | 18 | 19 | 21 | 22 | 29 | 20 | 23 | 24 | 25 | 27 | 28 | 30 | 31 |
| neSy | neSy | neSyr | neSyr | neSyr | neSyr | neSyr | neSyc | neSyc | neSyc | neSyc | neSyc | neSyc | neSyc | Ph |
| 49.90 | 51.50 | 53.70 | 52.90 | 49.80 | 48.1 | 54.00 | 49.80 | 56.40 | 48.30 | 55.10 | 53.90 | 53.40 | 52.90 | 56.30 |
| 0.48 | 0.53 | 0.68 | 0.57 | 0.13 | 0.91 | 0.46 | 0.55 | 0.23 | 0.13 | 0.30 | 0.64 | 0.66 | 0.15 | 0.60 |
| 21.40 | 21.30 | 19.6 | 21.00 | 23.7 | 20.40 | 20.10 | 19.00 | 20.90 | 24.90 | 20.00 | 19.80 | 19.60 | 21.60 | 20.90 |
| 4.55 | 4.49 | 4.51 | 5.16 | 4.38 | 5.31 | 4.22 | 6.40 | 5.02 | 3.15 | 4.13 | 4.62 | 4.61 | 4.62 | 4.15 |
| 0.11 | 0.12 | 0.14 | 0.14 | 0.10 | 0.18 | 0.13 | 0.15 | 0.13 | 0.05 | 0.11 | 0.13 | 0.15 | 0.14 | 0.10 |
| 0.55 | 0.56 | 0.83 | 0.46 | 0.80 | 0.76 | 0.71 | 0.53 | 0.28 | 0.70 | 0.50 | 0.41 | 0.78 | 0.38 | 0.41 |
| 4.40 | 4.80 | 4.90 | 1.90 | 3.30 | 5.60 | 2.40 | 4.30 | 1.70 | 1.20 | 1.90 | 2.80 | 3.00 | 1.90 | 1.50 |
| 4.26 | 3.08 | 5.98 | 9.77 | 7.37 | 6.78 | 8.97 | 8.21 | 9.40 | 13.64 | 8.84 | 8.23 | 7.83 | 9.63 | 8.10 |
| 14.00 | 12.86 | 6.36 | 6.38 | 8.48 | 9.40 | 8.04 | 8.19 | 4.72 | 4.79 | 9.44 | 6.67 | 7.95 | 8.33 | 7.54 |
| 0.11 | 0.12 | 0.23 | | | 0.31 | 0.05 | 0.13 | | | | 0.08 | 0.19 | | 0.14 |
| 99.76 | 99.36 | 96.93 | 98.28 | 98.06 | 97.75 | 99.08 | 97.26 | 98.78 | 96.86 | 100.32 | 97.28 | 98.17 | 99.65 | 99.74 |
| 0.38 | 0.74 | 2.27 | 1.03 | 2.15 | 1.42 | 0.80 | 2.18 | 0.78 | 1.39 | 0.13 | 2.04 | 1.34 | 0.01 | 0.11 |
| 3.29 | 4.18 | 1.06 | 0.65 | 1.15 | 1.39 | 0.90 | 1.00 | 0.50 | 0.35 | 1.07 | 0.81 | 1.02 | 0.87 | 0.93 |
| 1.04 | 0.89 | 0.85 | 1.09 | 0.90 | 1.05 | 1.17 | 1.18 | 0.98 | 1.11 | 1.24 | 1.05 | 1.10 | 1.15 | 1.03 |
| 0.22 | 0.23 | 0.30 | 0.17 | 0.30 | 0.25 | 0.28 | 0.16 | 0.12 | 0.05 | 0.22 | 0.17 | 0.28 | 0.16 | 0.19 |
| 112 | 57 | 76 | 66 | 61 | 120 | 52 | 140 | 52 | 6 | 39 | 65 | 67 | 45 | 41 |
| | | 26 | | | | | | | | | | 21 | | |
| | | | | | | | | | | | | | | |
| | | 10 | | | | | | | | | | | | |
| 554 | 662 | 157 | 212 | 431 | 160 | 266 | 127 | 242 | 183 | 251 | 208 | 193 | 279 | 177 |
| 230 | 220 | 1820 | 94 | 246 | 1400 | <50 | 1160 | 470 | 140 | 700 | 1100 | 1880 | 425 | 490 |
| 380 | 520 | 2400 | 760 | 720 | 4000 | 900 | 3260 | 138 | 114 | 1120 | 690 | 1530 | 435 | 920 |
| 194 | 84 | 200 | 260 | 42 | 470 | 134 | 210 | 230 | 130 | 260 | 260 | 270 | 88 | 440 |
| 32 | | 82 | 96 | 23 | 80 | 32 | 54 | 54 | | 37 | 120 | 92 | 30 | 138 |
| 13 | | | | | 84 | | | | | | 21 | 10 | | |

Table 3B (continued).

| Districts | Itapirapuã | | | | | | | | | | | | | | | | | | | |
|---|---|---|---|---|---|---|---|---|---|---|---|---|---|---|---|---|---|---|---|---|
| Sample | IP1 | IP3 | IP4 | IP5 | IP6 | IP7 | IP8 | IP9 | IP10 | IP11 | IP12 | IP13 | IP14 | IP15 | IP16 | IP21 | IP2 | IP22 | IP18 | IP19 |
| Rock-type | Me | neSy | neSy | neSy | neSy | neSy | neSy | neSy | neSy | neSy | neSy | neSy | neSy | neSy | neSy | Pu | Ma | Ma | Ti | Ti |
| $SiO_2$ | 40.90 | 44.40 | 47.50 | 45.70 | 44.20 | 46.30 | 48.10 | 49.00 | 49.80 | 50.10 | 48.00 | 53.60 | 53.90 | 53.60 | 52.80 | 56.20 | 43.40 | 55.40 | 53.00 | 52.50 |
| $TiO_2$ | 2.75 | 1.28 | 1.00 | 1.07 | 1.50 | 1.00 | 1.00 | 0.93 | 0.55 | 0.44 | 0.37 | 0.50 | 0.12 | 0.24 | 0.60 | 0.52 | 2.15 | 0.35 | 0.58 | 0.35 |
| $Al_2O_3$ | 16.1 | 16.50 | 17.50 | 18.80 | 18.00 | 17.30 | 19.20 | 20.20 | 21.00 | 21.60 | 22.70 | 19.70 | 24.00 | 21.10 | 21.40 | 16.30 | 17.70 | 20.00 | 21.60 | 22.50 |
| $Fe_2O_{3\,total}$ | 10.11 | 9.84 | 8.04 | 6.09 | 9.12 | 9.92 | 6.02 | 6.24 | 7.01 | 4.33 | 2.69 | 6.08 | 4.11 | 4.84 | 5.40 | 6.80 | 8.91 | 6.52 | 3.75 | 4.30 |
| MnO | 0.23 | 0.29 | 0.21 | 0.24 | 0.28 | 0.22 | 0.13 | 0.14 | 0.21 | | 0.07 | 0.20 | | 0.10 | 0.19 | 0.15 | 0.27 | 0.17 | | |
| MgO | 3.82 | 1.69 | 0.24 | 1.76 | 1.65 | 1.50 | 1.28 | 0.89 | | 0.47 | 0.42 | 0.63 | 0.21 | | 0.10 | 0.89 | 3.24 | 0.10 | 0.12 | 0.18 |
| CaO | 13.5 | 11.40 | 9.31 | 9.22 | 8.64 | 7.20 | 6.55 | 6.05 | 4.00 | 3.87 | 3.59 | 2.51 | 2.20 | 2.55 | 1.90 | 3.03 | 12.4 | 1.52 | 1.69 | 1.24 |
| $Na_2O$ | 7.13 | 6.72 | 6.20 | 8.96 | 8.76 | 7.54 | 7.32 | 6.50 | 8.63 | 9.37 | 11.30 | 9.05 | 7.80 | 6.21 | 8.18 | 2.96 | 6.96 | 10.30 | 10.40 | 9.67 |
| $K_2O$ | 2.26 | 4.40 | 6.76 | 4.68 | 4.13 | 6.25 | 7.45 | 7.91 | 6.81 | 7.23 | 7.00 | 6.46 | 5.97 | 9.68 | 7.16 | 11.60 | 3.47 | 2.72 | 6.88 | 5.75 |
| $P_2O_5$ | 1.61 | 0.96 | 0.07 | 0.67 | 0.61 | 0.67 | 0.35 | 0.35 | 0.08 | 0.19 | 0.14 | 0.17 | 0.21 | 0.43 | 0.12 | 0.10 | 0.93 | 0.24 | 0.29 | 0.32 |
| Sum | 98.41 | 97.48 | 96.83 | 97.19 | 96.89 | 97.90 | 97.40 | 98.21 | 98.09 | 97.60 | 96.28 | 98.90 | 98.52 | 98.75 | 97.85 | 98.55 | 99.43 | 97.32 | 98.31 | 96.81 |
| L.O.I | 0.95 | 2.24 | 1.63 | 1.70 | 0.45 | 0.37 | 1.00 | 0.60 | 2.04 | 0.32 | 2.54 | 0.55 | 0.56 | 0.71 | 0.24 | 1.23 | 1.00 | 1.50 | 0.84 | 0.32 |
| | | | | | | | | | | | | | | | | | | | | |
| $K_2O/Na_2O$ | 0.32 | 0.5 | 1.08 | 0.52 | 0.47 | 0.83 | 1.02 | 1.22 | 0.79 | 0.77 | 0.62 | 0.71 | 0.77 | 1.56 | 0.88 | 3.92 | 0.50 | 0.26 | 0.66 | 0.59 |
| A.I. | 0.88 | 0.96 | 1.00 | 1.05 | 1.05 | 1.11 | 1.05 | 0.95 | 1.03 | 1.08 | 1.15 | 1.11 | 0.80 | 0.98 | 0.99 | 1.07 | 0.86 | 0.99 | 1.14 | 0.98 |
| mg# | 0.47 | 0.29 | 0.07 | 0.40 | 0.30 | 0.26 | 0.33 | 0.25 | | 0.20 | 0.27 | 0.20 | 0.11 | | 0.04 | 0.23 | 0.46 | 0.03 | 0.07 | 0.09 |
| | | | | | | | | | | | | | | | | | | | | |
| V | 168 | 270 | 400 | 180 | 172 | 156 | 200 | 200 | 164 | 76 | 70 | 80 | 70 | 108 | 84 | 140 | 230 | 18 | 44 | 54 |
| Cr | 96 | 15 | 10 | 12 | 6 | 13 | 9 | 7 | 2.8 | 1.3 | 9 | 3 | 3 | 1 | | | 5 | 1 | 1 | 1 |
| Co | 13 | 8 | 3 | 7 | 6 | 6 | 5 | 5 | 5 | 3.3 | 3.3 | 4 | 2 | 2 | 3 | | 13 | 1.5 | 3 | 2 |
| Ni | 60 | 11 | 18 | 8 | 8 | 9 | 3 | 3 | 7 | 3 | 2 | 5 | 3 | 3 | 3 | 5 | 11 | 2 | 3 | 5 |
| Rb | | | | | | | | | | | | | | | | | | | | |
| Sr | 920 | 760 | 570 | 840 | 740 | 640 | 590 | 490 | 820 | 780 | 1000 | 620 | 740 | 570 | 560 | 480 | 700 | 680 | 370 | 540 |
| Ba | 380 | 1200 | 3200 | 2800 | 5400 | 3000 | 4800 | 3200 | 3600 | 3200 | 3000 | 1080 | 320 | 3200 | 1200 | 3500 | 2000 | 3600 | 100 | 200 |
| Zr | 340 | 740 | 830 | 370 | 345 | 280 | 370 | 410 | 500 | 250 | 150 | 870 | 240 | 200 | 350 | 400 | 500 | 590 | 440 | 630 |
| Nb | 170 | 104 | 180 | 133 | 630 | 155 | 225 | 190 | 155 | 62 | 25 | 180 | 31 | 50 | 175 | 560 | 200 | 154 | 150 | 180 |
| Y | 62 | 124 | 280 | 54 | 90 | 48 | 49 | 58 | 43 | 13 | 35 | 63 | 5.5 | 11 | 24 | 230 | 115 | 13 | 20 | 35 |

Table 3C. Major (wt%) and trace elements (ppm) contents of selected Mesozoic alkaline dykes from the São Jerônimo-Curiúva Lineament. Abbreviations: mSy, microsyenite; Pnp, phonolitic nephelinite; pPh, peralkaline phonolite; Tph, trachyphonolite; Tr, trachyte. References quoted in the text. In blank, not detected or not determined elements.

| Districts | Barra do Ponta Grossa | | | | | Morro do Chapéu | | | | | | | | Barra do Teixeira | |
|---|---|---|---|---|---|---|---|---|---|---|---|---|---|---|---|
| Sample | 6A | 6B | 6C | 12A | 12B | 7A1 | 7A2 | 7B | 9A1 | 9A2 | 9A3 | 9B | 9C | 10A | 10B |
| Rock-type | pPh | pPh | pPh | pPh | pPh | pPh | pPh | pPh | pPh | pPh | pPh | pPh | pPh | pPh | pPh |
| $SiO_2$ | 53.17 | 52.55 | 53.08 | 54.35 | 51.88 | 54.16 | 54.56 | 53.95 | 54.72 | 53.76 | 54.43 | 53.69 | 54.57 | 53.44 | 53.71 |
| $TiO_2$ | 0.42 | 0.41 | 0.41 | 0.47 | 0.39 | 0.42 | 0.37 | 0.43 | 0.42 | 0.43 | 0.40 | 0.36 | 0.36 | 0.54 | 0.56 |
| $Al_2O_3$ | 18.28 | 18.24 | 18.55 | 18.81 | 17.61 | 19.76 | 18.37 | 18.61 | 18.39 | 18.93 | 18.46 | 18.65 | 19.15 | 18.96 | 18.61 |
| $Fe_2O_{3\,total}$ | 3.37 | 3.22 | 3.26 | 3.75 | 3.44 | 4.15 | 4.44 | 4.14 | 4.56 | 4.19 | 4.45 | 4.32 | 4.33 | 3.90 | 4.47 |
| MnO | 0.23 | 0.23 | 0.23 | 0.25 | 0.25 | 0.18 | 0.20 | 0.17 | 0.20 | 0.19 | 0.20 | 0.21 | 0.24 | 0.15 | 0.17 |
| MgO | 0.16 | 0.12 | 0.14 | 0.20 | 0.17 | 0.21 | 0.14 | 0.10 | 0.13 | 0.23 | 0.08 | 0.12 | 0.10 | 0.18 | 0.16 |
| CaO | 3.11 | 2.85 | 3.00 | 2.91 | 3.05 | 1.66 | 1.17 | 1.48 | 1.17 | 1.63 | 1.07 | 1.23 | 0.92 | 1.52 | 1.82 |
| $Na_2O$ | 10.01 | 11.81 | 10.19 | 12.42 | 12.72 | 8.50 | 9.43 | 10.39 | 9.34 | 9.57 | 9.57 | 10.51 | 8.37 | 9.81 | 9.60 |
| $K_2O$ | 5.18 | 5.35 | 4.81 | 5.97 | 5.86 | 6.35 | 6.30 | 6.45 | 6.09 | 5.73 | 6.01 | 5.28 | 6.53 | 7.10 | 7.92 |
| $P_2O_5$ | 0.18 | 0.16 | 0.13 | 0.21 | 0.20 | 0.06 | 0.05 | 0.07 | 0.04 | 0.06 | 0.06 | 0.07 | 0.06 | 0.10 | 0.13 |
| Total | 94.11 | 94.94 | 93.80 | 99.34 | 95.57 | 95.45 | 95.03 | 95.79 | 95.06 | 94.72 | 94.73 | 94.44 | 94.63 | 95.70 | 97.15 |
| L.O.I | 6.25 | 5.36 | 6.61 | 0.71 | 4.66 | 5.90 | 5.25 | 4.43 | 5.22 | 5.59 | 5.61 | 5.91 | 5.71 | 4.51 | 2.94 |
| | | | | | | | | | | | | | | | |
| $K_2O/Na_2O$ | 0.52 | 0.45 | 0.47 | 0.48 | 0.46 | 0.75 | 0.67 | 0.62 | 0.65 | 0.60 | 0.63 | 0.50 | 0.78 | 0.72 | 0.82 |
| A.I. | 1.21 | 1.38 | 1.18 | 1.43 | 1.55 | 1.11 | 1.22 | 1.29 | 1.19 | 1.16 | 1.21 | 1.23 | 1.09 | 1.26 | 1.31 |
| mg# | 0.10 | 0.08 | 0.09 | 0.11 | 0.10 | 0.10 | 0.07 | 0.05 | 0.06 | 0.11 | 0.04 | 0.06 | 0.05 | 0.10 | 0.08 |
| | | | | | | | | | | | | | | | |
| V | | | | | 14 | | | | | | | | 328 | | 22 |
| Cr | 1 | 1 | 2 | 1 | 1 | 1 | 2 | 2 | 4 | 3 | 1 | 2 | 4 | 2 | 3 |
| Co | | | | | 45 | | | | | | | | 23 | | 37 |
| Ni | 9 | 7 | 7 | 8 | 10 | 6 | 5 | 5 | 9 | 9 | 7 | 7 | 9 | 5 | 7 |
| Rb | 120 | 112 | 96 | 114 | 143 | 156 | 177 | 156 | 168 | 142 | 158 | 138 | 181 | 159 | 160 |
| Sr | 1600 | 1436 | 1432 | 1242 | 146 | 740 | 1072 | 1142 | 851 | 877 | 714 | 587 | 681 | 708 | 618 |
| Ba | 463 | 447 | 464 | 396 | 365 | 1161 | 369 | 860 | 585 | 770 | 559 | 354 | 442 | 502 | 450 |
| Zr | 1513 | 1531 | 1398 | 1545 | 1659 | 577 | 984 | 712 | 904 | 764 | 912 | 942 | 1184 | 1220 | 1619 |
| Nb | 522 | 529 | 446 | 509 | 534 | 165 | 206 | 170 | 183 | 166 | 180 | 188 | 273 | 337 | 380 |
| Y | 31 | 30 | 28 | 30 | 2 | 27 | 34 | 27 | 29 | 27 | 28 | 33 | 38 | 21 | 14 |

Table 3C (continued).

| Districts | Mato Preto | | | | | | | | | | | | | | | | | Sete Quedas | | | |
|---|---|---|---|---|---|---|---|---|---|---|---|---|---|---|---|---|---|---|---|---|---|
| Sample | 17A | 17B | 18A | 18B | 18C | 18C2 | 19A | 19B | 19C | 20A | 20B | 20C | 22A | 22B | 22C | 22D1 | 22D2 | 23A | 23B | 23C | 23D |
| Rock-type | pPh | pPh | pPh | pPh | pPh | pPh | Tph | Tph | Tph | pPh | pPh | pPh | pPh | pPh | pPh | pPh | pPh | pPh | Pnp | pPh | pPh |
| $SiO_2$ | 55.67 | 54.72 | 55.45 | 55.33 | 57.08 | 57.08 | 56.80 | 56.51 | 56.77 | 54.54 | 54.70 | 52.95 | 52.32 | 51.92 | 56.01 | 55.50 | 55.62 | 55.26 | 45.31 | 56.31 | 56.59 |
| $TiO_2$ | 0.37 | 0.21 | 0.22 | 0.44 | 0.22 | 0.22 | 0.25 | 0.26 | 0.26 | 0.18 | 0.18 | 0.18 | 0.76 | 0.77 | 0.27 | 0.26 | 0.26 | 0.35 | 0.96 | 0.33 | 0.34 |
| $Al_2O_3$ | 18.17 | 18.66 | 17.79 | 17.20 | 17.49 | 17.59 | 17.75 | 17.70 | 17.59 | 18.70 | 18.12 | 17.48 | 18.45 | 18.52 | 18.25 | 17.91 | 17.90 | 18.62 | 17.21 | 18.13 | 18.12 |
| $Fe_2O_{3\ total}$ | 4.69 | 5.16 | 5.11 | 6.39 | 5.28 | 5.21 | 4.61 | 4.70 | 4.69 | 5.52 | 5.38 | 5.47 | 5.42 | 5.50 | 4.77 | 4.93 | 4.89 | 4.38 | 8.83 | 3.93 | 4.35 |
| MnO | 0.26 | 0.35 | 0.41 | 0.36 | 0.41 | 0.40 | 0.23 | 0.24 | 0.23 | 0.39 | 0.39 | 0.42 | 0.18 | 0.19 | 0.31 | 0.27 | 0.28 | 0.23 | 0.31 | 0.25 | 0.25 |
| MgO | 0.12 | 0.11 | 0.08 | 0.41 | 0.11 | 0.11 | 0.64 | 0.75 | 0.89 | 0.27 | 0.30 | 0.36 | 1.53 | 1.68 | 0.05 | 0.09 | 0.09 | 0.10 | 1.30 | 0.09 | 0.22 |
| CaO | 0.90 | 1.09 | 0.77 | 2.59 | 1.07 | 1.04 | 1.03 | 1.12 | 1.22 | 0.85 | 0.87 | 0.94 | 3.97 | 4.08 | 0.78 | 0.68 | 0.68 | 0.91 | 8.09 | 0.66 | 0.85 |
| $Na_2O$ | 9.56 | 8.53 | 9.76 | 6.28 | 9.11 | 9.19 | 7.26 | 7.69 | 7.04 | 9.15 | 9.98 | 9.46 | 7.69 | 7.76 | 10.20 | 9.75 | 9.70 | 9.19 | 8.94 | 10.33 | 8.06 |
| $K_2O$ | 5.93 | 5.02 | 4.99 | 6.96 | 4.70 | 4.64 | 5.64 | 5.25 | 5.37 | 4.73 | 4.59 | 4.73 | 5.31 | 5.11 | 5.22 | 5.34 | 5.37 | 5.42 | 4.89 | 4.53 | 6.47 |
| $P_2O_5$ | 0.02 | 0.01 | | 0.12 | 0.01 | 0.01 | 0.05 | 0.03 | 0.03 | 0.01 | 0.01 | 0.01 | 0.52 | 0.49 | 0.03 | 0.01 | 0.01 | 0.06 | 0.37 | 0.02 | 0.04 |
| Total | 95.69 | 93.86 | 94.58 | 96.08 | 95.48 | 95.49 | 94.26 | 94.25 | 94.09 | 94.34 | 94.52 | 92.00 | 96.14 | 96.02 | 95.89 | 94.74 | 94.80 | 94.52 | 96.21 | 94.58 | 95.29 |
| L.O.I | 4.52 | 6.56 | 5.77 | 4.10 | 4.77 | 4.74 | 6.13 | 6.14 | 6.29 | 6.02 | 5.84 | 8.75 | 4.02 | 4.18 | 4.33 | 5.57 | 5.51 | 5.74 | 3.97 | 5.74 | 4.97 |
| $K_2O/Na_2O$ | 0.62 | 0.59 | 0.51 | 1.11 | 0.52 | 0.51 | 0.78 | 0.69 | 0.76 | 0.52 | 0.46 | 0.50 | 0.69 | 0.66 | 0.51 | 0.55 | 0.55 | 0.59 | 0.55 | 0.44 | 0.80 |
| A.I. | 1.22 | 1.04 | 1.21 | 1.04 | 1.15 | 1.15 | 1.02 | 1.04 | 0.99 | 1.08 | 1.18 | 1.18 | 1.00 | 0.99 | 1.23 | 1.22 | 1.22 | 1.13 | 1.16 | 1.21 | 1.12 |
| mg# | 0.06 | 0.05 | 0.03 | 0.13 | 0.05 | 0.05 | 0.24 | 0.27 | 0.31 | 0.10 | 0.12 | 0.13 | 0.40 | 0.42 | 0.02 | 0.04 | 0.04 | 0.08 | 0.26 | 0.05 | 0.10 |
| V | | | | | | | | | | | | | | | | | | | 343 | 91 | |
| Cr | 2 | 1 | 1 | 1 | 1 | 1 | 1 | 1 | 1 | 1 | 1 | 1 | 57 | 75 | 1 | 1 | 1 | 1 | 2 | 5 | 1 |
| Co | | | | | | | | | 19 | | | | | | | | | | 40 | 23 | |
| Ni | 8 | 11 | 8 | 7 | 14 | 11 | 11 | 11 | 10 | 11 | 10 | 14 | 26 | 33 | 10 | 9 | 10 | 11 | 8 | 9 | 9 |
| Rb | 327 | 457 | 420 | 252 | 423 | 431 | 294 | 301 | 295 | 347 | 312 | 372 | 147 | 142 | 329 | 351 | 346 | 191 | 127 | 263 | 229 |
| Sr | 312 | 175 | 130 | 1201 | 364 | 338 | 765 | 928 | 793 | 273 | 266 | 267 | 2004 | 2015 | 220 | 193 | 192 | 850 | 1172 | 134 | 752 |
| Ba | 54 | 169 | 97 | 2180 | 130 | 143 | 1172 | 940 | 781 | 282 | 139 | 222 | 2007 | 2112 | 103 | 91 | 59 | 69 | 708 | 18 | 142 |
| Zr | 1306 | 2623 | 2113 | 858 | 2385 | 2459 | 1224 | 1446 | 1658 | 2136 | 1955 | 2161 | 361 | 352 | 1490 | 1600 | 1703 | 1503 | 497 | 3192 | 1528 |
| Nb | 440 | 788 | 835 | 1111 | 1113 | 1148 | 378 | 461 | 671 | 671 | 608 | 696 | 216 | 209 | 539 | 637 | 697 | 409 | 361 | 711 | 454 |
| Y | 44 | 128 | 112 | 24 | 113 | 115 | 73 | 56 | 30 | 135 | 115 | 132 | 32 | 32 | 58 | 64 | 86 | 35 | 27 | 6 | 36 |

| Districts | Banhadão | | Itapirapuã | Sete Quedas-Dr. Ulisses | | | | | | | | | | Cerro Azul | | Tunas | |
|---|---|---|---|---|---|---|---|---|---|---|---|---|---|---|---|---|---|
| Sample | 24A | 24C | 34C | 36A | 36B | 37A | 37B | 39A | 39B | 40A | 40B | 41A | 41B | 42A | 42B | 44A | 44B |
| Rock-type | pPh | pPh | mSy | Pnp | Pnp | pPh | pPh | pPh | pPh | pPh | pPh | pPh | pPh | pPh | pPh | Tr | Tr |
| $SiO_2$ | 54.22 | 50.07 | 58.73 | 44.86 | 46.98 | 59.01 | 58.11 | 55.66 | 55.73 | 49.02 | 49.42 | 52.60 | 52.85 | 53.51 | 54.54 | 65.07 | 64.91 |
| $TiO_2$ | 0.48 | 0.82 | 0.77 | 1.53 | 1.32 | 0.42 | 0.44 | 0.41 | 0.40 | 1.23 | 1.23 | 0.56 | 0.56 | 0.54 | 0.51 | 0.22 | 0.18 |
| $Al_2O_3$ | 19.33 | 18.78 | 16.01 | 15.52 | 16.24 | 18.81 | 18.57 | 17.90 | 18.21 | 17.37 | 17.80 | 18.14 | 18.53 | 18.36 | 17.86 | 17.00 | 17.10 |
| $Fe_2O_{3\ total}$ | 5.19 | 6.42 | 5.05 | 8.74 | 8.38 | 3.86 | 3.95 | 4.62 | 4.46 | 6.28 | 6.38 | 5.01 | 4.90 | 4.11 | 3.96 | 3.98 | 4.19 |
| MnO | 0.19 | 0.20 | 0.20 | 0.25 | 0.25 | 0.20 | 0.24 | 0.22 | 0.22 | 0.23 | 0.23 | 0.20 | 0.17 | 0.11 | 0.11 | 0.18 | 0.17 |
| MgO | 0.19 | 0.86 | 0.85 | 2.50 | 3.26 | 0.11 | 0.10 | 0.07 | 0.05 | 0.93 | 0.90 | 0.21 | 0.34 | 0.24 | 0.28 | 0.05 | 0.04 |
| CaO | 2.49 | 6.72 | 4.29 | 10.90 | 8.37 | 0.64 | 0.65 | 1.01 | 0.99 | 4.29 | 4.19 | 2.83 | 3.52 | 2.15 | 2.72 | 0.57 | 0.41 |
| $Na_2O$ | 7.62 | 7.34 | 5.38 | 7.76 | 5.80 | 10.34 | 10.75 | 10.38 | 10.28 | 9.77 | 8.98 | 9.38 | 8.53 | 10.28 | 10.16 | 7.12 | 7.13 |
| $K_2O$ | 9.33 | 7.44 | 8.01 | 5.13 | 5.45 | 5.46 | 5.50 | 6.79 | 6.43 | 6.26 | 6.64 | 8.21 | 7.90 | 5.20 | 5.00 | 5.30 | 5.36 |
| $P_2O_5$ | 0.08 | 0.52 | 0.26 | 0.93 | 0.96 | 0.02 | 0.03 | 0.03 | 0.03 | 0.21 | 0.24 | 0.11 | 0.22 | 0.08 | 0.17 | 0.02 | 0.01 |
| Total | 99.12 | 99.17 | 99.55 | 98.12 | 97.01 | 98.87 | 98.34 | 97.09 | 96.80 | 95.59 | 96.01 | 97.25 | 97.52 | 94.58 | 95.31 | 99.51 | 99.50 |
| L.O.I | 0.89 | 0.86 | 0.45 | 1.93 | 3.10 | 1.16 | 1.70 | 3.01 | 3.33 | 4.64 | 4.19 | 2.84 | 2.54 | 5.77 | 5.10 | 0.50 | 0.50 |
| $K_2O/Na_2O$ | 1.22 | 1.01 | 1.49 | 0.66 | 0.94 | 0.53 | 0.51 | 0.65 | 0.63 | 0.64 | 0.74 | 0.88 | 0.93 | 0.51 | 0.49 | 0.75 | 0.75 |
| A.I. | 1.17 | 1.07 | 1.09 | 1.18 | 0.95 | 1.22 | 1.27 | 1.36 | 1.31 | 1.32 | 1.23 | 1.34 | 1.22 | 1.23 | 1.24 | 1.03 | 1.03 |
| mg# | 0.08 | 0.24 | 0.28 | 0.40 | 0.48 | 0.06 | 0.05 | 0.03 | 0.02 | 0.26 | 0.25 | 0.09 | 0.14 | 0.12 | 0.14 | 0.03 | 0.02 |
| V | 83 | | 38 | 359 | | 38 | | 166 | | 87 | | | | 176 | | 280 | |
| Cr | 7 | 4 | 27 | 14 | 6 | 10 | 1 | 2 | 4 | 2 | 3 | 4 | 4 | 7 | 2 | 9 | 1 |
| Co | 45 | | 57 | 55 | | 62 | | 33 | | 36 | | 18 | | 30 | | 48 | |
| Ni | 7 | 14 | 12 | 14 | 14 | 9 | 8 | 5 | 7 | 8 | 14 | 5 | 7 | 4 | 4 | 6 | 4 |
| Rb | 202 | 136 | 212 | 85 | 131 | 245 | 231 | 218 | 185 | 137 | 140 | 195 | 191 | 146 | 144 | 154 | 118 |
| Sr | 903 | 361 | 1349 | 848 | 1360 | 209 | 240 | 752 | 1064 | 1547 | 2189 | 693 | 992 | 752 | 893 | 41 | 18 |
| Ba | 786 | 432 | 1088 | 457 | 2945 | 114 | 128 | 260 | 245 | 1161 | 1422 | 1238 | 1441 | 1065 | 1181 | 344 | 225 |
| Zr | 931 | 603 | 517 | 482 | 438 | 1443 | 1655 | 770 | 720 | 753 | 741 | 640 | 527 | 1103 | 947 | 1269 | 1329 |
| Nb | 430 | 383 | 176 | 291 | 259 | 311 | 350 | 164 | 142 | 357 | 355 | 316 | 260 | 565 | 432 | 113 | 112 |
| Y | 11 | 42 | 11 | 6 | 47 | 24 | 44 | 16 | 38 | 20 | 47 | 21 | 28 | 15 | 16 | 17 | 25 |

Table 4. REE (ppm) of selected alkaline rock-types from the Guapiara and São Jerônimo-Curiúva lineaments. Abbreviations as in Tables 3A, B, C; additional abbreviations: BPG, Barra do Ponta Grossa; MCh, Morro do Chapéu; BT, Barra do Teixeira; MP, Mato Preto; SQ, Sete Quedas; BN, Banhadão; IT, Itapirapuã; SQ-DU, Sete Quedas-Dr. Ulisses; CA, Cerro Azul; TU, Tunas. References quoted in the text. In blank, not detected or not determined elements.

| Districts | **Jacupiranga** | | | | | | | | | | | | | | | | | |
|---|---|---|---|---|---|---|---|---|---|---|---|---|---|---|---|---|---|---|
| Sample | JC101 | JC127 | JC115 | JC111-D | JC104 | JC97 | JC82 | JC78 | JC84 | JC88 | JC109 | JC86 | JC75 | JC103 | JC107 | JC119 | JC93 | JC118-D |
| Rock-type | Cpx | Cpx | Mdu | Ak | Ag | SD | Me | Me | Ij | Ij | Ex | Ur | Ur | neSy | neSy | Sy | Sy | Pph |
| La | 13.00 | 19.70 | 12.73 | 65.00 | 49.30 | 73.40 | 10.70 | 10.70 | 10.70 | 26.40 | 291.00 | 22.00 | 254.00 | 109.00 | 149.00 | 70.80 | 5.23 | 80.10 |
| Ce | 42.00 | 49.70 | 29.43 | 128.00 | 103.00 | 149.00 | 32.60 | 34.80 | 38.10 | 58.40 | 583.00 | 45.70 | 638.00 | 189.00 | 304.00 | 139.00 | 8.20 | 126.00 |
| Pr | | | | | | | | | | | | | | | | | | |
| Nd | 23.50 | 24.80 | 17.20 | 53.90 | 43.70 | 59.00 | 17.20 | 17.20 | 15.80 | 28.70 | 199.00 | 21.50 | 239.00 | 65.20 | 112.00 | 50.10 | 2.22 | 35.20 |
| Sm | 4.80 | 5.31 | 3.92 | 9.09 | 8.44 | 10.70 | 3.61 | 3.57 | 3.88 | 5.55 | 31.90 | 4.16 | 31.70 | 9.67 | 17.90 | 9.37 | 0.28 | 5.46 |
| Eu | 1.45 | 1.56 | 0.69 | 2.37 | 2.72 | 2.91 | 0.95 | 0.88 | 1.11 | 1.52 | 7.80 | 1.13 | 7.49 | 4.44 | 4.49 | 2.30 | 0.10 | 1.32 |
| Gd | 1.45 | 2.33 | 0.94 | 4.41 | 4.18 | 3.87 | 0.40 | 0.43 | 0.77 | 2.46 | 45.10 | 1.51 | 24.50 | 4.33 | 13.60 | 4.48 | 0.08 | 4.83 |
| Tb | | | | | | | | | | | | | | | | | | |
| Dy | 2.44 | 3.03 | 1.64 | 3.10 | 3.73 | 4.69 | 1.73 | 1.69 | 1.91 | 3.51 | 11.10 | 1.65 | 6.95 | 3.20 | 6.29 | 5.32 | 0.31 | 2.82 |
| Ho | | | | | | | | | | | | | | | | | | |
| Er | 0.78 | 1.22 | 0.67 | 1.38 | 1.86 | 2.23 | 0.69 | 0.67 | 0.89 | 0.91 | 4.71 | 0.61 | 2.14 | 1.41 | 2.60 | 2.60 | 0.14 | 1.46 |
| Tm | | | | | | | | | | | | | | | | | | |
| Yb | 0.56 | 0.93 | 0.25 | 1.03 | 1.59 | 1.88 | 0.49 | 0.43 | 0.66 | 0.75 | 3.90 | 0.42 | 0.98 | 1.07 | 1.92 | 2.39 | 0.18 | 1.34 |
| Lu | 0.16 | 0.17 | 0.02 | 0.13 | 0.32 | 0.35 | 0.02 | 0.16 | 0.38 | 0.27 | 0.73 | 0.23 | 0.19 | 0.21 | 0.37 | 0.58 | 0.01 | 0.34 |
| Ga | | | | | | | | | | | | | | | | | | |
| | | | | | | | | | | | | | | | | | | |
| Eu/Eu* | 1.31 | 1.17 | 1.09 | 1.01 | 1.25 | 1.25 | 1.29 | 1.20 | 1.32 | 1.09 | 0.63 | 1.13 | 0.79 | 1.82 | 0.85 | 1.09 | 1.56 | 0.77 |
| $(La/Yb)_{CN}$ | 16.65 | 15.19 | 65.13 | 45.27 | 22.24 | 28.01 | 15.66 | 17.85 | 11.63 | 25.25 | 53.52 | 37.57 | 185.91 | 73.07 | 55.67 | 21.25 | 20.84 | 42.88 |
| La/Yb | 23.21 | 21.18 | 50.92 | 63.11 | 31.01 | 39.04 | 21.84 | 24.88 | 16.21 | 35.20 | 74.62 | 52.38 | 259.18 | 101.87 | 77.60 | 29.62 | 29.06 | 59.78 |
| $(La/Sm)_{CN}$ | 1.75 | 2.40 | 3.74 | 4.62 | 3.77 | 4.43 | 1.91 | 1.93 | 1.78 | 3.07 | 5.89 | 3.41 | 5.17 | 7.28 | 5.37 | 4.88 | 12.06 | 9.47 |

| Districts | **Juquiá** | | | | | | | | | | | | | | | | | | |
|---|---|---|---|---|---|---|---|---|---|---|---|---|---|---|---|---|---|---|---|
| Sample | S8 | S2 | S43 | S5-D | S17 | S24 | S10 | S11 | S38 | S37 | S32 | S30 | S22 | S40 | S28B-D | S46-D | S36 | S47A | S4-D |
| Rock-type | olcpx | olcpx | Me | Bsn | Ij | Ij | Ur | Ur | SD | Ex | neSy | neSy | neSy | neSy | neSy | neSy | neSy | neSy | pPh |
| La | 12.20 | 14.60 | 279.00 | 57.30 | 139.00 | 109.00 | 52.70 | 46.30 | 96.40 | 29.00 | 120.00 | 49.80 | 131.00 | 64.00 | 48.90 | 16.80 | 40.40 | 160.00 | 94.70 |
| Ce | 47.10 | 37.40 | 608.00 | 143.00 | 282.00 | 257.00 | 105.00 | 115.00 | 200.00 | 70.40 | 240.00 | 107.00 | 262.00 | 148.00 | 117.00 | 37.50 | 88.30 | 320.00 | 207.00 |
| Pr | | | | | | | | | | | | | | | | | | | |
| Nd | 30.20 | 17.50 | 328.00 | 64.30 | 116.00 | 125.00 | 42.40 | 56.90 | 84.40 | 32.60 | 88.20 | 40.80 | 96.80 | 57.10 | 48.00 | 12.40 | 30.50 | 112.00 | 73.30 |
| Sm | 7.50 | 3.88 | 32.40 | 11.60 | 17.90 | 21.60 | 7.03 | 10.40 | 14.40 | 6.13 | 13.30 | 6.55 | 14.80 | 9.07 | 7.86 | 2.06 | 4.71 | 16.40 | 11.00 |
| Eu | 2.12 | 1.08 | 7.61 | 2.86 | 4.44 | 5.78 | 1.87 | 3.17 | 4.22 | 1.59 | 3.18 | 1.68 | 3.70 | 2.39 | 2.01 | 0.44 | 1.19 | 3.83 | 2.78 |
| Gd | | | | | | | | | | | | | | | | | | | |
| Tb | | | | | | | | | | | | | | | | | | | |
| Dy | 4.47 | 1.60 | 10.10 | 5.95 | 7.05 | 10.20 | 2.98 | 4.13 | 6.26 | 3.34 | 6.25 | 3.26 | 6.65 | 4.24 | 3.70 | 0.99 | 2.27 | 7.80 | 4.49 |
| Ho | | | | | | | | | | | | | | | | | | | |
| Er | 1.83 | 0.69 | 3.86 | 2.37 | 3.04 | 3.93 | 1.30 | 1.60 | 2.55 | 1.40 | 2.87 | 1.55 | 2.97 | 1.91 | 1.69 | 0.55 | 1.08 | 3.64 | 1.73 |
| Tm | | | | | | | | | | | | | | | | | | | |
| Yb | 1.09 | 0.45 | 2.18 | 1.47 | 2.40 | 2.79 | 0.82 | 0.90 | 1.82 | 1.06 | 2.24 | 1.33 | 2.17 | 1.56 | 1.50 | 0.41 | 0.93 | 2.92 | 1.08 |
| Lu | 0.16 | 0.09 | 0.28 | 0.17 | 0.33 | 0.35 | 0.14 | 0.13 | 0.25 | 0.14 | 0.29 | 0.18 | 0.29 | 0.22 | 0.24 | 0.08 | 0.13 | 0.36 | 0.15 |
| Ga | | | | | | | | | | | | | | | | | | | |
| | | | | | | | | | | | | | | | | | | | |
| Eu/Eu* | 0.89 | 0.88 | 0.78 | 0.79 | 0.81 | 0.86 | 0.87 | 1.00 | 0.95 | 0.83 | 0.77 | 0.82 | 0.83 | 0.85 | 0.83 | 0.68 | 0.81 | 0.75 | 0.82 |
| $(La/Yb)_{CN}$ | 8.03 | 23.27 | 91.80 | 27.96 | 41.54 | 28.02 | 46.10 | 36.90 | 37.99 | 19.62 | 38.43 | 26.86 | 43.30 | 29.43 | 23.38 | 29.39 | 31.16 | 39.30 | 62.90 |
| La/Yb | 11.19 | 32.44 | 127.98 | 38.98 | 57.92 | 39.07 | 64.27 | 51.44 | 52.97 | 27.36 | 53.57 | 37.44 | 60.37 | 41.03 | 32.60 | 40.98 | 43.44 | 54.79 | 87.69 |
| $(La/Sm)_{CN}$ | 1.05 | 2.43 | 5.56 | 3.19 | 5.01 | 3.26 | 4.84 | 2.87 | 4.32 | 3.05 | 5.82 | 4.91 | 5.71 | 4.56 | 4.02 | 5.26 | 5.54 | 6.30 | 5.56 |

| Districts | **Pariquera-Açu** | | | | | | | | **Cananéia** | | | | | | | | | |
|---|---|---|---|---|---|---|---|---|---|---|---|---|---|---|---|---|---|---|
| Sample | Par 13 | Par 11 | Par 7 | Par 15 | Par 14 | Par 8 | Par 1 | Par 18 | 01/C2 | 04/B2 | 06/B1 | 08/A2 | 09/A2 | 09/B2 | 10/C2 | 5 | 18 | 24 |
| Rock-type | mThe | The | The | The | The | Ex | SG | SD | Sy | Sy | Sy | Sy | Sy | Sy | Sy | mQSy | Ra | mQSy |
| La | 33.10 | 31.97 | 49.77 | 48.32 | 44.10 | 73.15 | 95.12 | 97.90 | 162.93 | 133.17 | 95.37 | 47.35 | 44.83 | 31.27 | 21.50 | 84.30 | 118.65 | 43.36 |
| Ce | 69.41 | 68.09 | 100.50 | 99.47 | 93.17 | 138.20 | 185.60 | 189.20 | 254.63 | 237.70 | 170.69 | 82.84 | 90.94 | 60.22 | 44.73 | 167.21 | 224.37 | 82.00 |
| Pr | 8.03 | 8.25 | 11.45 | 11.31 | 10.80 | 14.59 | 20.38 | 19.79 | 27.01 | 23.71 | 21.39 | 10.34 | 11.38 | 7.50 | 5.78 | 18.38 | 22.51 | 9.82 |
| Nd | 33.28 | 33.93 | 43.43 | 44.72 | 41.61 | 51.48 | 73.19 | 72.78 | 114.78 | 91.94 | 88.40 | 43.63 | 51.80 | 34.34 | 27.76 | 79.88 | 91.08 | 44.75 |
| Sm | 5.74 | 6.52 | 7.06 | 7.45 | 7.08 | 7.62 | 10.18 | 10.39 | 21.79 | 16.22 | 16.77 | 8.95 | 9.47 | 6.66 | 5.81 | 14.55 | 18.26 | 9.01 |
| Eu | 1.61 | 1.77 | 1.98 | 2.19 | 1.98 | 2.42 | 3.10 | 2.94 | 2.73 | 1.00 | 2.41 | 2.87 | 1.86 | 1.03 | 0.72 | 1.64 | 2.03 | 2.79 |
| Gd | 4.28 | 4.79 | 4.96 | 5.65 | 4.98 | 5.09 | 7.59 | 7.50 | 26.15 | 14.78 | 16.64 | 10.77 | 9.71 | 8.30 | 7.25 | 15.09 | 19.95 | 10.10 |
| Tb | 0.50 | 0.61 | 0.66 | 0.65 | 0.65 | 0.73 | 0.95 | 0.91 | 4.16 | 2.33 | 2.83 | 1.74 | 1.51 | 1.12 | 1.10 | 2.18 | 3.18 | 1.50 |
| Dy | 2.72 | 3.18 | 3.12 | 3.63 | 3.14 | 3.59 | 4.65 | 4.57 | 21.87 | 10.18 | 14.52 | 8.94 | 4.43 | 4.49 | 4.52 | 11.93 | 18.97 | 6.71 |
| Ho | 0.47 | 0.58 | 0.63 | 0.64 | 0.60 | 0.68 | 0.84 | 0.77 | 5.30 | 2.36 | 2.84 | 1.56 | 1.37 | 0.68 | 1.28 | 2.27 | 3.42 | 1.69 |
| Er | 1.03 | 1.28 | 1.42 | 1.45 | 1.39 | 1.72 | 2.02 | 1.92 | 13.72 | 5.32 | 8.60 | 4.72 | 3.47 | 2.30 | 2.34 | 5.84 | 9.92 | 3.82 |
| Tm | 0.14 | 0.18 | 0.17 | 0.20 | 0.19 | 0.23 | 0.28 | 0.29 | 2.92 | 0.96 | 1.79 | 0.98 | 0.84 | 0.47 | 0.51 | 1.16 | 2.09 | 0.79 |
| Yb | 0.82 | 1.10 | 1.03 | 1.14 | 1.07 | 1.41 | 1.64 | 1.72 | 14.02 | 4.85 | 9.36 | 4.86 | 4.97 | 2.79 | 2.77 | 6.12 | 10.70 | 3.76 |
| Lu | 0.14 | 0.16 | 0.17 | 0.19 | 0.18 | 0.23 | 0.25 | 0.26 | 2.19 | 0.63 | 1.36 | 0.61 | 0.80 | 0.50 | 0.39 | 0.99 | 1.49 | 0.50 |
| Ga | | | | | | | | | | | | | | | | | | |
| | | | | | | | | | | | | | | | | | | |
| Eu/Eu* | 0.95 | 0.93 | 0.97 | 0.98 | 0.97 | 1.12 | 1.03 | 0.97 | 0.35 | 0.19 | 0.44 | 0.89 | 0.59 | 0.42 | 0.34 | 0.33 | 0.32 | 0.89 |
| $(La/Yb)_{CN}$ | 28.95 | 20.85 | 34.66 | 30.40 | 29.56 | 37.21 | 41.60 | 40.83 | 8.34 | 19.68 | 7.31 | 6.99 | 6.47 | 8.03 | 5.57 | 9.88 | 7.95 | 8.28 |
| La/Yb | 40.37 | 29.06 | 48.32 | 42.39 | 41.21 | 51.88 | 58.00 | 56.92 | 11.62 | 27.44 | 10.19 | 9.75 | 9.02 | 11.20 | 7.76 | 13.77 | 11.09 | 11.55 |
| $(La/Sm)_{CN}$ | 3.72 | 3.17 | 4.55 | 4.19 | 4.02 | 6.20 | 6.03 | 6.08 | 4.83 | 5.30 | 3.67 | 3.41 | 3.06 | 3.03 | 2.39 | 3.74 | 4.19 | 3.11 |

Table 4 (continued).

| Districts | **Tunas** | | | | | | | | **BPG*** | **MCh*** | **BT*** |
|---|---|---|---|---|---|---|---|---|---|---|---|
| Sample | 12 | 35 | 8 | 19 | 26 | 36 | 9 | 13 | 12B(*) | 9C(*) | 10B(*) |
| Rock-type | Ag | SG | Ex | SD | Sy | Sy | ASy | ASy | pPh | pPh | pPh |
| La | 26.61 | 41.37 | 77.95 | 86.76 | 88.93 | 63.43 | 67.09 | 52.6 | 118.35 | 118.24 | 66.98 |
| Ce | 52.96 | 72.95 | 126.94 | 153.45 | 139.46 | 90.75 | 98.43 | 100.35 | 199.61 | 197.53 | 120.73 |
| Pr | | | | | | | | | | | |
| Nd | 24.49 | 31.33 | 49.76 | 61.55 | 46.82 | 37.96 | 37.76 | 40.99 | 68.57 | 62.31 | 33.75 |
| Sm | 5.12 | 5.8 | 9.21 | 11.18 | 7.93 | 6.59 | 6.91 | 7.58 | 1.33 | 3.86 | 5.31 |
| Eu | 1.81 | 2.23 | 2.97 | 3.54 | 2.41 | 4.03 | 3.88 | 0.96 | 0.43 | 1.55 | 1.96 |
| Gd | 4.96 | 4.91 | 7.51 | 9.2 | 6.81 | 5.38 | 5.95 | 6.29 | | | |
| Tb | | | | | | | | | 0.41 | 0.96 | 1.08 |
| Dy | 3.91 | 3.7 | 5.77 | 6.96 | 5.12 | 4.46 | 4.72 | 5.3 | 0.77 | 4.39 | 4.14 |
| Ho | | | | | | | | | 0.37 | 0.83 | 0.69 |
| Er | 1.94 | 2.01 | 2.89 | 3.59 | 2.88 | 2.61 | 2.62 | 3.08 | 0.73 | 2.76 | 2.03 |
| Tm | | | | | | | | | 0.27 | 0.57 | 0.48 |
| Yb | 1.65 | 1.7 | 2.77 | 3.32 | 3.04 | 2.62 | 2.95 | 4.32 | 0.48 | 2.98 | 1.96 |
| Lu | 0.28 | 0.32 | 0.45 | 0.6 | 0.49 | 0.51 | 0.49 | 0.85 | 0.52 | 0.46 | 0.24 |
| Ga | | | | | | | | | 38.00 | 51.00 | 52.00 |
| Eu/Eu* | 1.10 | 1.25 | 1.06 | 1.04 | 0.98 | 2.01 | 1.81 | 0.41 | 0.79 | 1.06 | 0.97 |
| $(La/Yb)_{CN}$ | 11.57 | 17.46 | 20.19 | 18.74 | 20.98 | 17.37 | 16.31 | 8.73 | 176.86 | 28.46 | 24.51 |
| La/Yb | 16.13 | 24.34 | 28.14 | 26.13 | 29.25 | 24.21 | 22.74 | 12.18 | 246.56 | 39.68 | 34.17 |
| $(La/Sm)_{CN}$ | 3.36 | 4.60 | 5.46 | 5.01 | 7.24 | 6.21 | 6.27 | 4.48 | 57.45 | 19.78 | 8.14 |

| Districts | **MP*** | **SQ** | | **BN*** | **IT*** | **SQ-DU*** | | | | | **CA*** | **TU*** |
|---|---|---|---|---|---|---|---|---|---|---|---|---|
| Sample | 19C(*) | 23B(*) | 23C(*) | 24A(*) | 34C(*) | 36A(*) | 37A(*) | 39A(*) | 40A(*) | 41A(*) | 42A(*) | 44A(*) |
| Rock-type | TPh | Pnp | pPh | pPh | mSy | Pnp | pPh | pPh | pPh | pPh | pPh | Tr |
| La | 380.31 | 151.03 | 58.36 | 122.72 | 62.39 | 116.81 | 79.92 | 108.99 | 148.42 | 110.58 | 49.63 | 33.33 |
| Ce | 445.3 | 242.7 | 102.7 | 240.39 | 96.00 | 204.78 | 89.5 | 161.06 | 253.44 | 143.57 | 98.21 | 62.93 |
| Pr | | | | | | | | | | | | |
| Nd | 87.81 | 76.39 | 33.71 | 61.68 | 35.5 | 86.32 | 28.54 | 44.87 | 69.51 | 51.71 | 29.97 | 20.91 |
| Sm | 7.11 | 13.5 | 5.87 | 7.74 | 5.97 | 2.85 | 5.84 | 5.36 | 10.84 | 8.22 | 3.68 | 5.49 |
| Eu | 3.04 | 5.39 | 0.37 | 3.45 | 3.64 | 1.53 | 1.71 | 2.51 | 5.23 | 5.36 | 0.31 | 1.55 |
| Gd | | | | | | | | | | | | |
| Tb | 1.91 | 2.68 | 0.32 | 1.59 | 1.22 | 0.55 | 1.36 | 1.97 | 2.12 | 1.89 | 0.08 | 0.84 |
| Dy | 7.36 | 9.12 | 1.59 | 5.25 | 4.4 | 2.39 | 5.76 | 5.93 | 8.38 | 7.78 | 0.08 | 3.79 |
| Ho | 1.49 | 1.6 | 0.34 | 0.65 | 0.81 | 0.44 | 2.09 | 2.04 | 1.25 | 1.26 | 0.18 | 0.86 |
| Er | 4.94 | 4.63 | 1.23 | 2.14 | 2.27 | 0.8 | 3.25 | 3.93 | 3.99 | 4.25 | | 2.59 |
| Tm | 1.1 | 0.81 | 0.27 | 0.3 | 0.58 | | 0.76 | 1.4 | 0.57 | 0.71 | | 0.41 |
| Yb | 4.65 | 3.17 | 1.38 | 1.71 | 2.53 | 1.00 | 3.38 | 3.62 | 2.93 | 3.03 | 0.68 | 3.21 |
| Lu | 0.91 | 0.54 | | 0.24 | 0.6 | | 0.56 | 1.51 | 0.49 | 0.48 | 0.17 | 0.52 |
| Ga | 74.00 | 53.00 | 65.00 | 65.00 | 62.00 | 41.00 | 51.00 | 47.00 | 73.00 | 77.00 | 34.00 | 52.00 |
| Eu/Eu* | 1.10 | 1.17 | 0.22 | 1.28 | 1.71 | 1.53 | 0.79 | 1.06 | 1.37 | 1.76 | 0.32 | 0.96 |
| $(La/Yb)_{CN}$ | 58.67 | 34.17 | 30.33 | 51.48 | 17.69 | 83.79 | 16.96 | 21.60 | 36.34 | 26.18 | 52.35 | 7.45 |
| La/Yb | 81.79 | 47.64 | 42.29 | 71.77 | 24.66 | 116.81 | 23.64 | 30.11 | 50.66 | 36.50 | 72.99 | 10.38 |
| $(La/Sm)_{CN}$ | 34.53 | 7.22 | 6.42 | 10.24 | 6.75 | 26.46 | 8.83 | 13.13 | 8.84 | 8.68 | 8.71 | 5.98 |

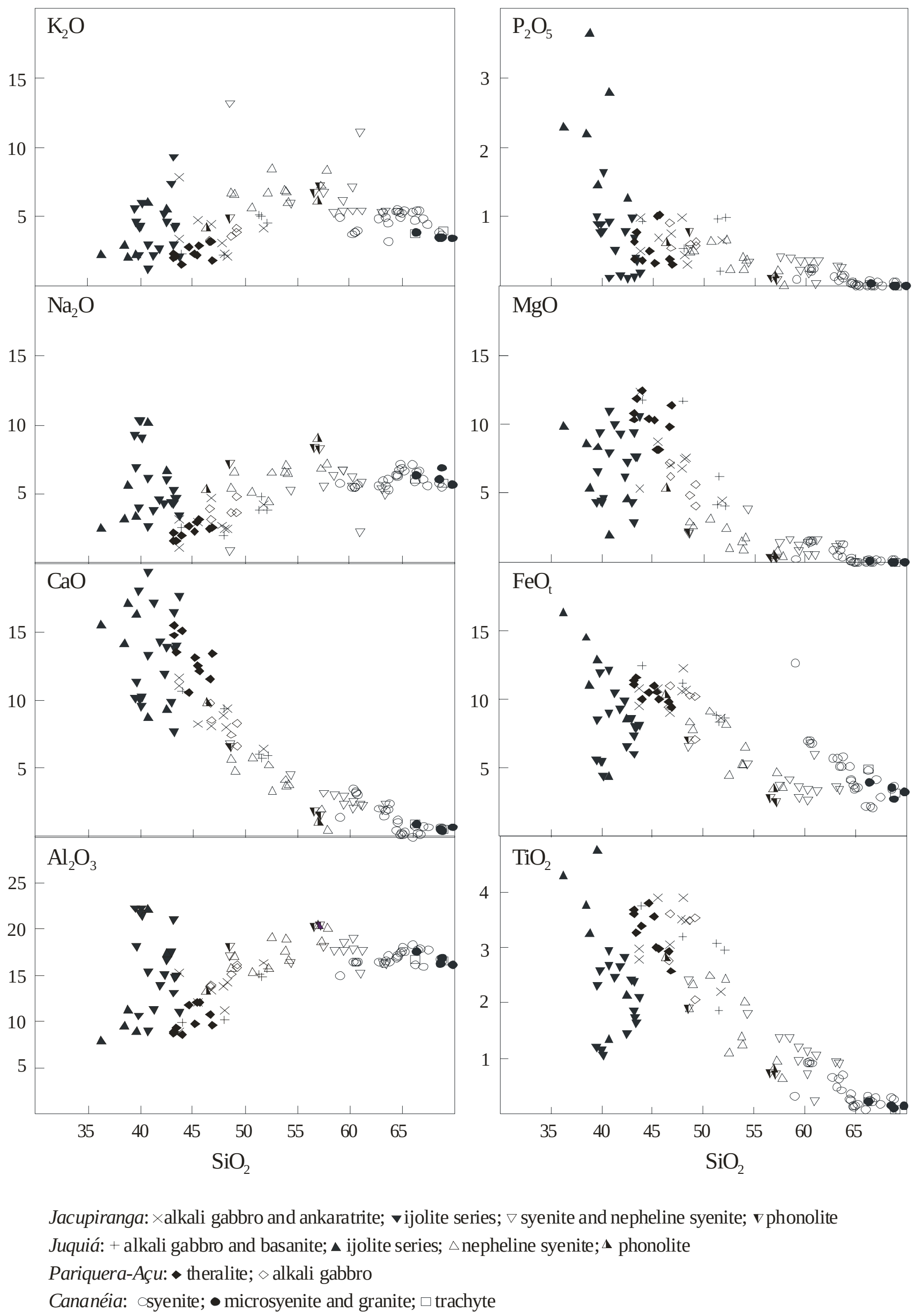


Fig. 10A. $SiO_2$ vs. major elements of representative plutonic and hypabissal alkaline rock-types from the Guapiara Lineament.

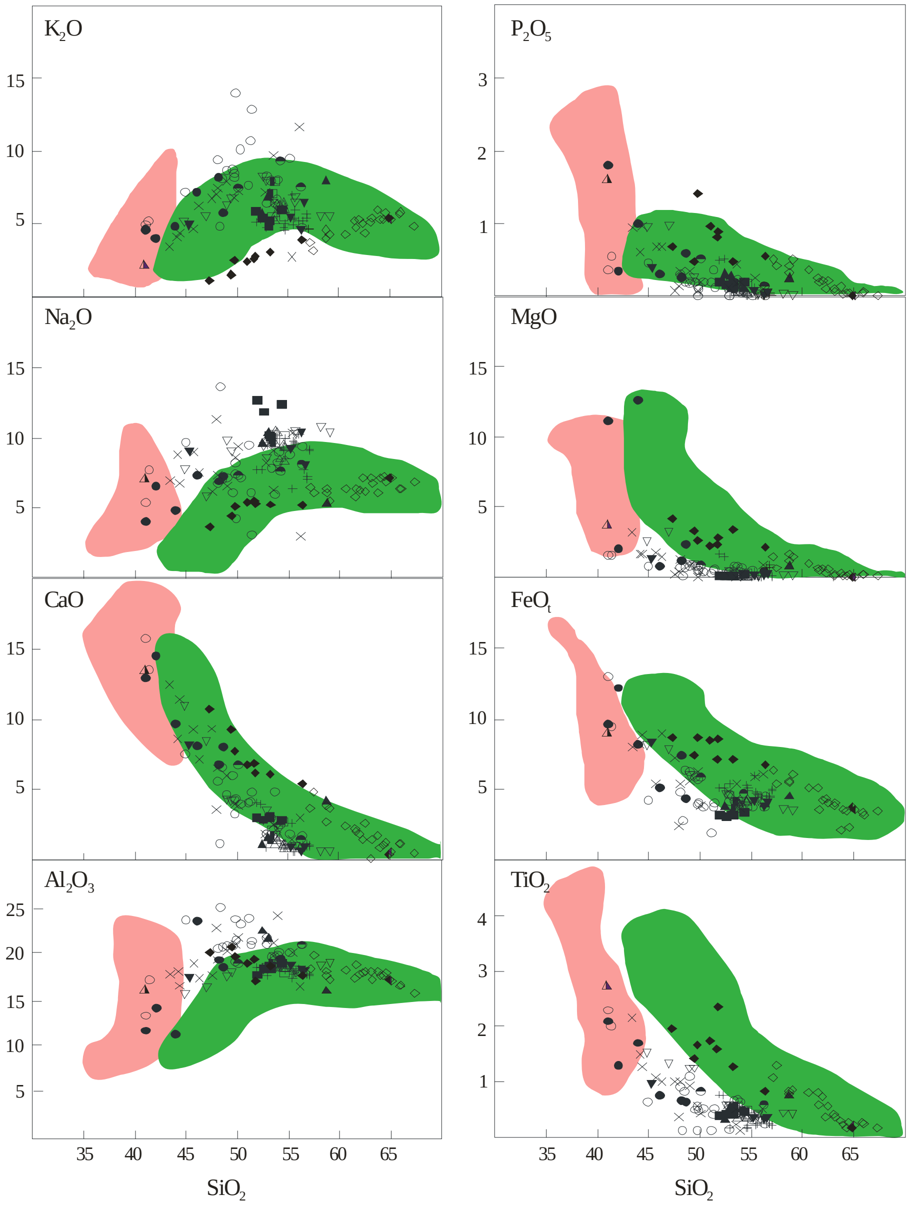


*Banhadão*: ● ijolite series; ○ nepheline syenite; ◓ phonolite. *Barra do Teixeira* : ◧ peralkaline phonolite
*Barra do Ponta Grossa*: ■ peralkaline phonolite. *Cerro Azul*: □ peralkaline phonolite
*Itapirapuã*: ▲ melteigite; × nepheline syenite; ▲ tinguaite and microsyenite. *Mato Preto*: + phonolitic and tephritic rocks
*Morro do Chapéu*: △ peralkaline phonolite; *Sete Quedas*: ▼ peralkaline phonolite and phonolitic nephelinite
*Sete Quedas-Dr. Ulisses*: ▽ peralkaline phonolite and phonolitic nephelinite
*Tunas*: ◆ alkali gabbroic rocks; ◇ syenitic rocks; ▷ trachyte

Fig. 10B. $SiO_2$ vs. major elements of representative plutonic and hypabissal alkaline rock-types from the São Jerônimo-Curiúva Lineament. Green and pink fields: non-cumulate and cumulate ijolite series, respectively, from the Guapiara Lineament.

Trace elements

Compatible elements (Ni and Cr) concentrate in the basic dykes and in the mafic to ultramafic intrusives, and more particularly in the cumulate rocks. The highest contents (Ni, 500-800 ppm; Cr, 1000-4800 ppm) found in some cumulates are controlled by the modal olivine, spinels and clinopyroxene. The most “primitive” rock-types (MgO>7 wt%), such as basanite and olivine gabbro from Juquiá, ankaratrite from Jacupiranga and theralite from Pariquera-Açu, have Ni 150-478 ppm, Cr 700-1000 ppm and mg#

0.67-0.72 [mg#=MgO/(MgO+FeO) molar ratio for $Fe_2O_3$/FeO=0.2)], compatible with 6-8% partial melting of a garnet peridotite mantle source (cf. Comin-Chiaramonti *et al.*, 1997).

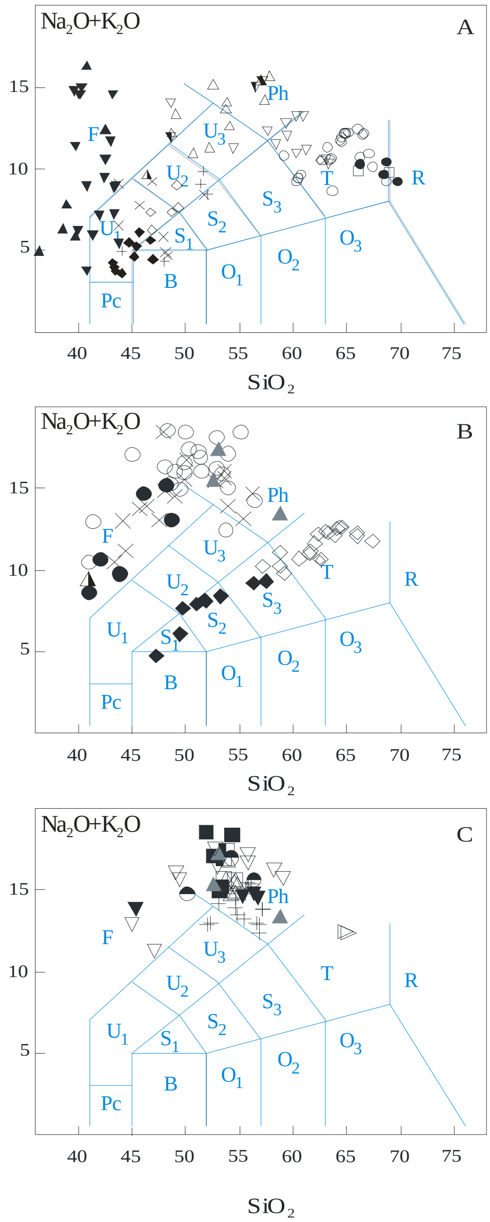


Fig. 11. TAS diagrams (Le Maitre *et al.*, 1989); cumulate rocks are not represented. A) Guapiara Lineament. B) São Jerônimo-Curiúva Lineament. C) dykes and plugs from the São Jerônimo-Curiúva Lineament. Symbols as in Figs. 10A, B.

Incompatible trace elements from the Guapiara Lineament usually show very large scattering. From Zr vs. the other elements (Fig. 12A), non-cumulate rock-types have $Zr_0$ (i.e. initial concentrations) between 150 and 300 ppm. Sr, Ba and Ce display broad positive correlations with $Zr_0$ only for the Pariquera-Açu complex. The Cananéia intrusion is characterized by two main suites, low and high Ba (200±84 and >500 ppm, respectively). Y appears positively correlated with $Zr_0$. $Zr_0$ vs. Nb shows on the whole an alkaline tendency for all the rock-types (cf. Leat *et al.*, 1986).

In the São Jerônimo-Curiúva area, "primitive" rock-types are virtually absent (i.e. Cr>500, Ni>150 ppm, mg#>0.60), but parents with $Zr_0$ between 125 and 200 ppm may be inferred. The incompatible trace elements roughly present the same scattering noted for the Guapiara Lineament. However, Sr, Ba and Y display the major scattering in the alkaline complexes, while the dykes tend to have broad negative and positive correlations between $Zr_0$ and Ba and between $Zr_0$ and Y, respectively (Fig. 12B).

High Y contents (i.e >100 ppm) are related to the presence of modal melanite in the nepheline syenites from Banhadão and Itapirapuã (cf. Ruberti, 1984). Notably, positive correlations are shown by the $Zr_0$ vs. Nb and Rb relationships, respectively. $Zr_0$ vs. Nb diagram suggests distinct $Zr_0$/Nb ratios for the various complexes and dyke swarms, probably associated with different melting degrees of (slightly different?) mantle sources.

On the whole, the comparative analysis among elements of different degree of incompatibility (cf. Treuil & Joron, 1976) indicates that the least evolved rock-types display patterns conforming to a partial melting curve, while the other types may fit crystal fractionation trends. This is shown, for example, by the best fitting in the $Zr_0$ vs. Y diagram of Fig. 12A. High field strenght elements (HFSE) exhibit a geochemical behaviour without apparent strong fractionation. Only the cumulate rocks of ijolite series show high, very scattered contents of Zr, Nb, Y, La and Ce.

In the Guapiara non-cumulate rocks and dykes, Y and Zr show positive correlations with $SiO_2$, whereas Nb, La and Ce are strongly scattered (Fig. 13A).

In the São Jerônimo-Curiúva rock-types, La, Ce and Y decrease with $SiO_2$ in the most occurrences,

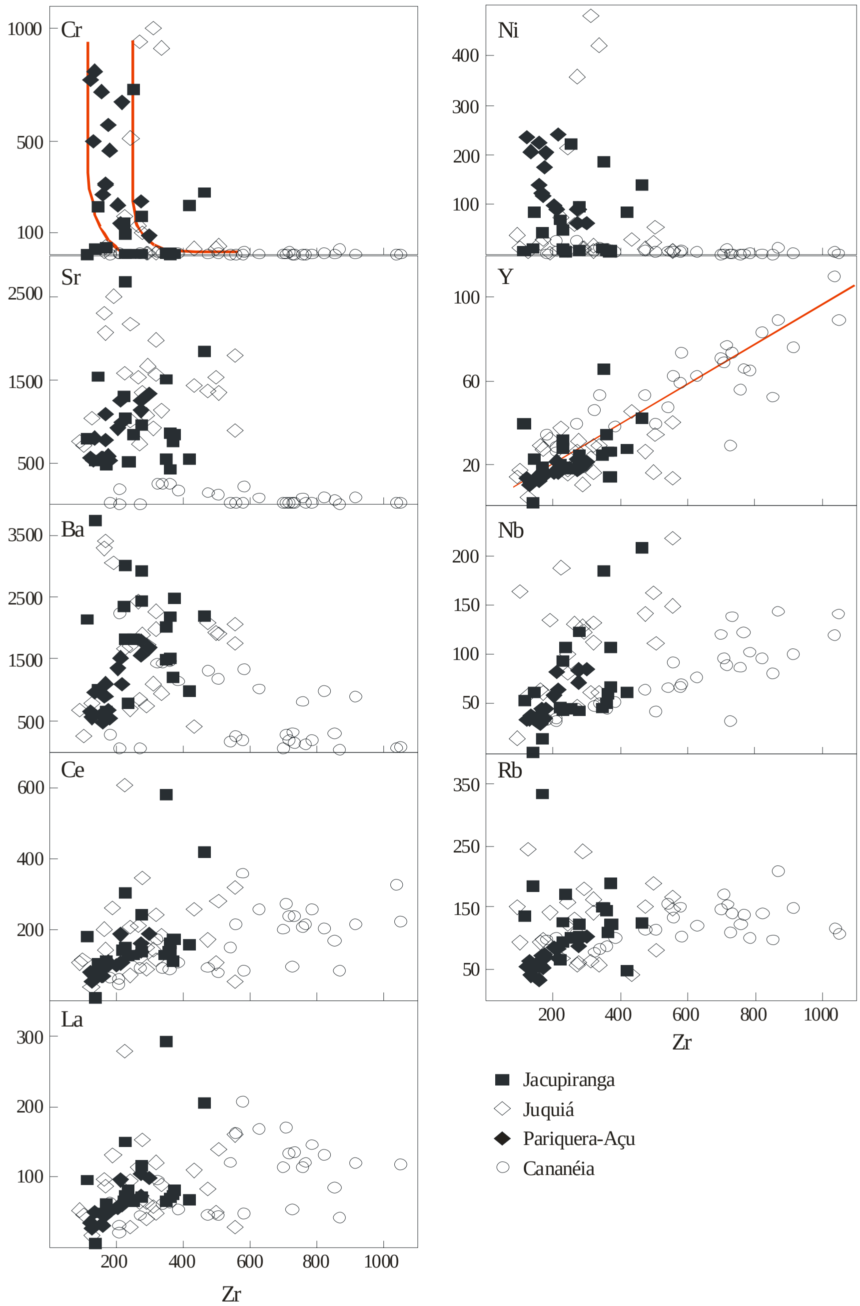


Fig. 12A. Zr (ppm) vs. trace elements (ppm) diagrams for representative plutonic and hypabyssal alkaline rock-types from the Guapiara Lineament. Ultramafic cumulate rocks are excluded. Possible $Zr_0$ initial concentrations are inferred from Cr and Ni concentrations.

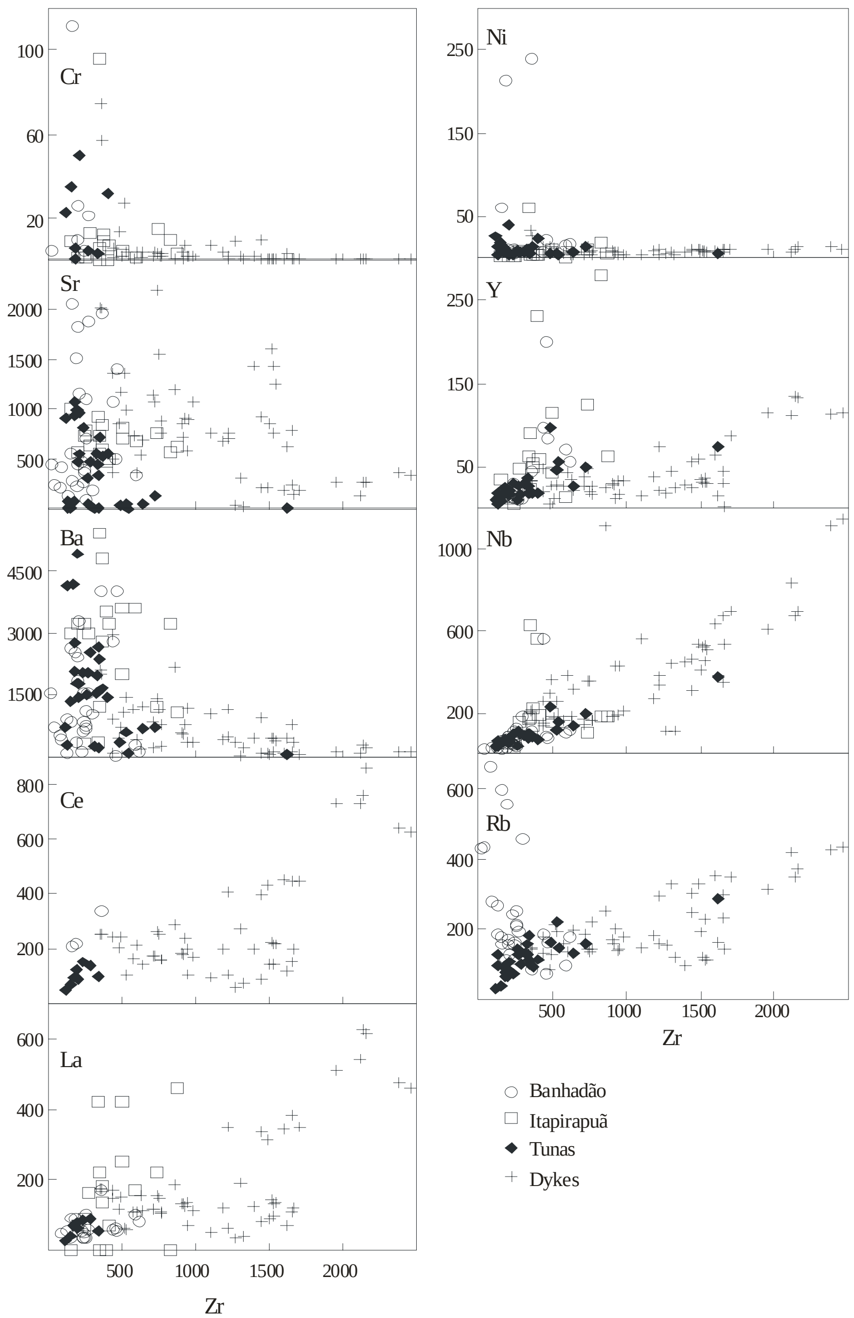


Fig. 12B. Zr (ppm) vs. trace elements (ppm) diagrams for representative plutonic and hypabyssal alkaline rock-types from the São Jerônimo-Curiúva Lineament.

while Zr and Nb are scattered (Fig. 13B). Notably, phonolites and tephrites from Tunas and Mato Preto display very scattered high contents of Rb, Nb, Zr, La, Ce and Y at $SiO_2$ around 55 wt%.

HFSE from the Guapiara suites have low Nb (<250 ppm) and high $TiO_2$ (up to 5 wt%) at similar $SiO_2$ contents, and in particular higher Zr/Nb (most between 1 and 9, some up to 24) than the São Jerônimo-Curiúva suites (Fig. 14).

Abundances of incompatible elements normalized to primitive mantle (Sun & McDonough, 1989) are shown in Figs. 15A, B (Guapiara Lineament and São Jerônimo-Curiúva Lineament, respectively).

In the Guapiara Lineament, cumulate rocks in general show similar patterns. However, the Jacupiranga melteigites are distinct for their Nb strong negative spike, and the Juquiá urtites are characterized by LREE contents lower than the

Jacupiranga analogues. Notably, the Jacupiranga ijolites display a pattern very similar to that shown by the clinopyroxenite variants, whereas the Juquiá ijolites appear almost ten times enriched with respect to the associated clinopyroxenites. Rock-types, which are believed to represent the most primitive magmas (e.g. ankaratrite from Jacupiranga, basanite and alkali gabbro from Juquiá and theralite from Pariquera-Açu, mg#=0.64-0.72, for $Fe_2O_3/FeO=0.2$), present very similar general patterns. The Pariquera-Açu theralite differs only for a more variable P and for Nb and Ti slightly negative and positive spike, respectively.

Ijolites, syenogabbros, syenodiorites and essexites show variable I.E. ranges, reflecting the modal mineralogy, but maintaining on the whole the steeps of the associate primitive rock-types. In particular, the Pariquera-Açu variants are about 1.5-

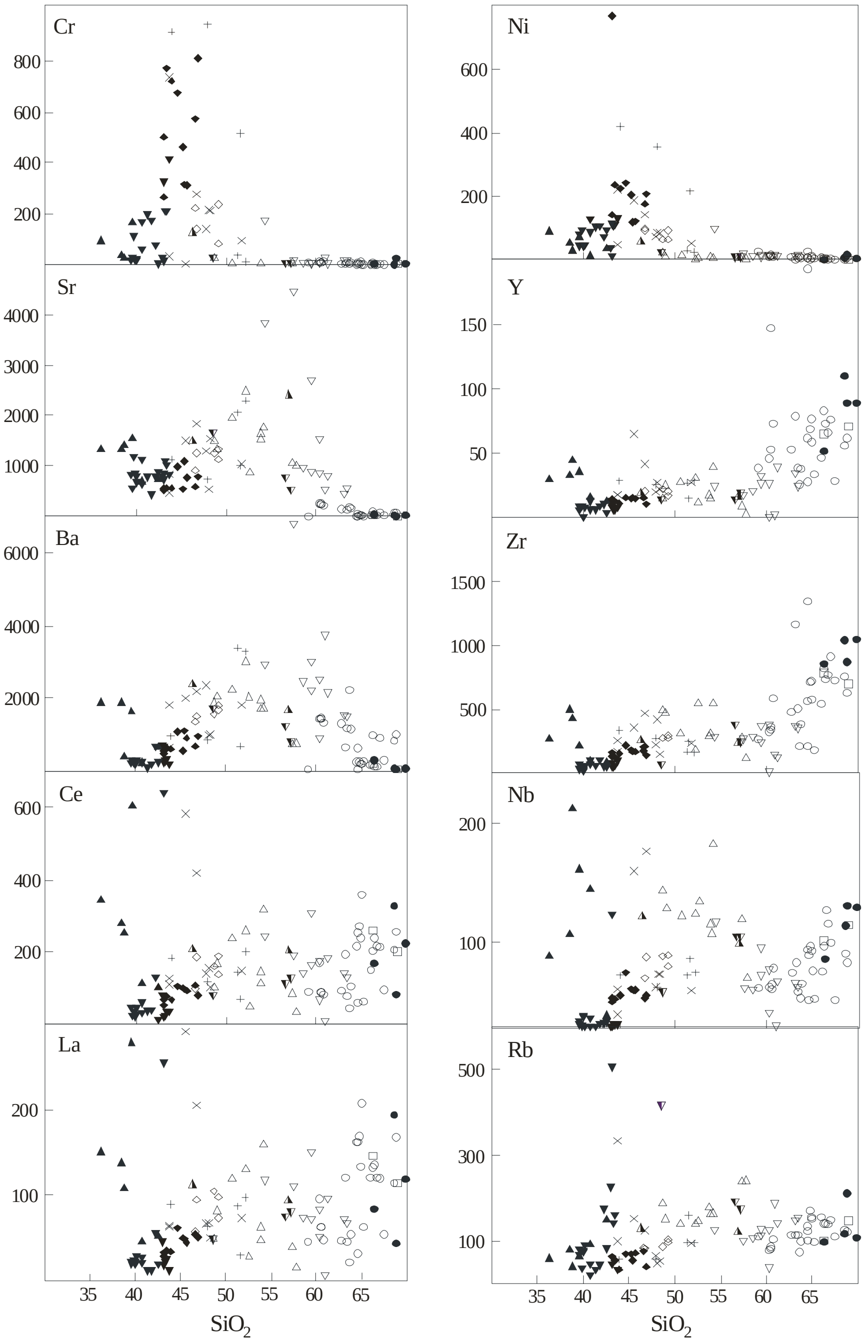


Fig. 13A. $SiO_2$ vs. trace elements for representative rock-types from the Guapiara Lineament. Symbols as in Fig. 10A.

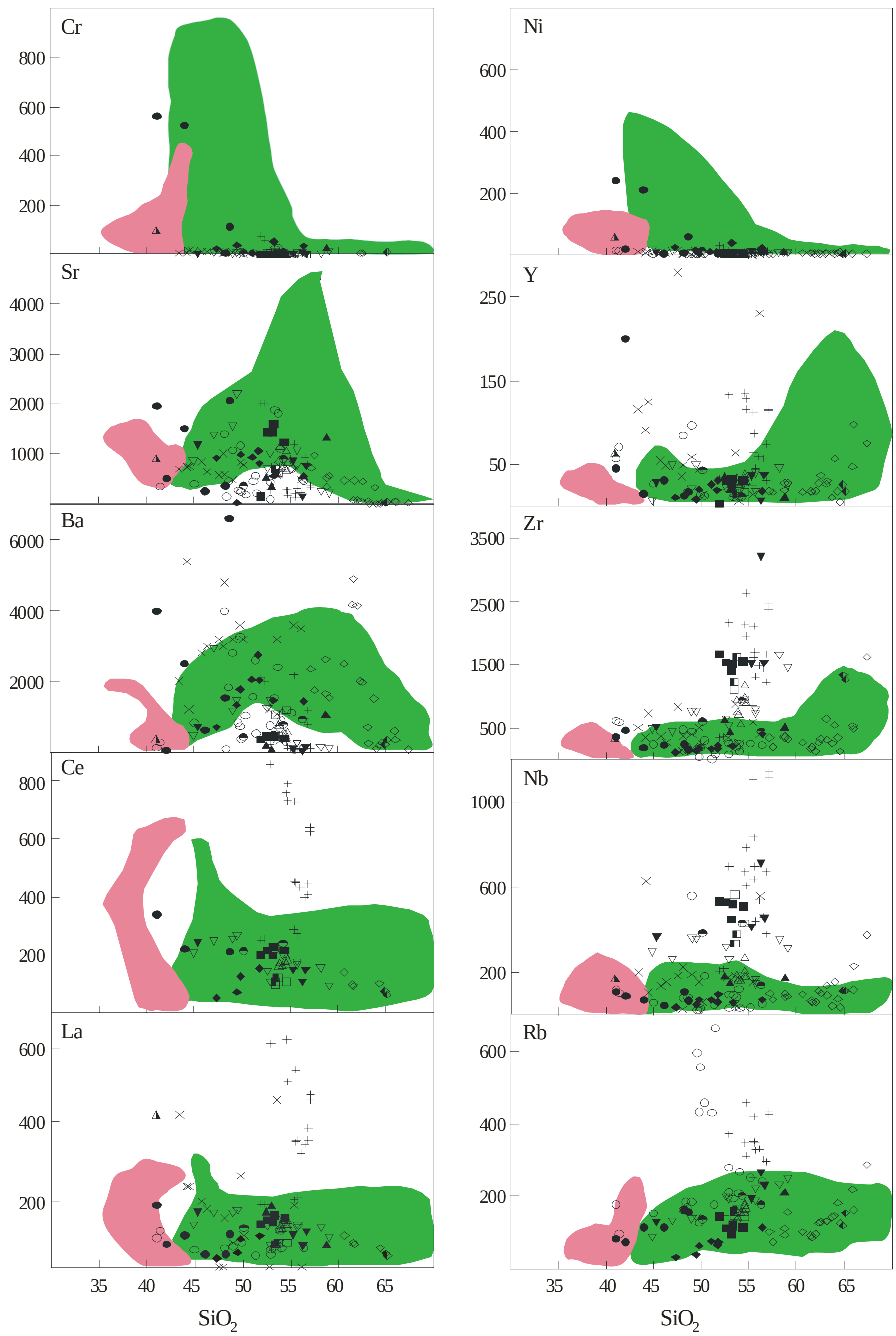


Fig. 13B. $SiO_2$ vs. trace elements for representative rock-types from the São Jerônimo-Curiúva Lineament. Symbols as in Fig. 10B. Green and pink fields: non-cumulate and cumulate ijolite series, respectively, from the Guapiara Lineament.

2 times enriched with respect to the associated theralites, P, Sm and Ti excepted.

The most evolved rocks, i.e. syenites and late peralkaline phonolites, display patterns with large I.E. ranges which cover the distribution relative to the other rock-types in the Jacupiranga and Juquiá complexes.

The Cananéia syenites (Late Cretaceous) are distinct for the presence of the enriched and depleted Ba suites, for the pronounced P and Ti negative anomalies and for the Zr and Y-Yb positive ones.

In the São Jerônimo-Curiúva Lineament, the gabbroic to essexitic rocks from the Tunas complex (Late Cretaceous) show spidergrams (Fig. 15B) paralleling those of the theralitic to essexitic rocks from Pariquera-Açu (Early Cretaceous; cf. Fig. 15A).

Notably, the evolved rocks (i.e. syenites and

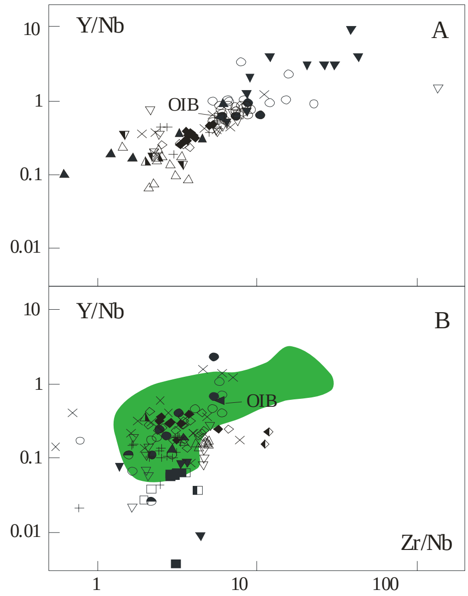


Fig. 14. Zr/Nb vs. Y/Nb ratios of silicate rocks for representative plutonic and hypabyssal alkaline rocks from the Guapiara (A) and São Jerônimo-Curiúva (B) lineaments, respectively. Symbols as in the Figs. 10A, B.

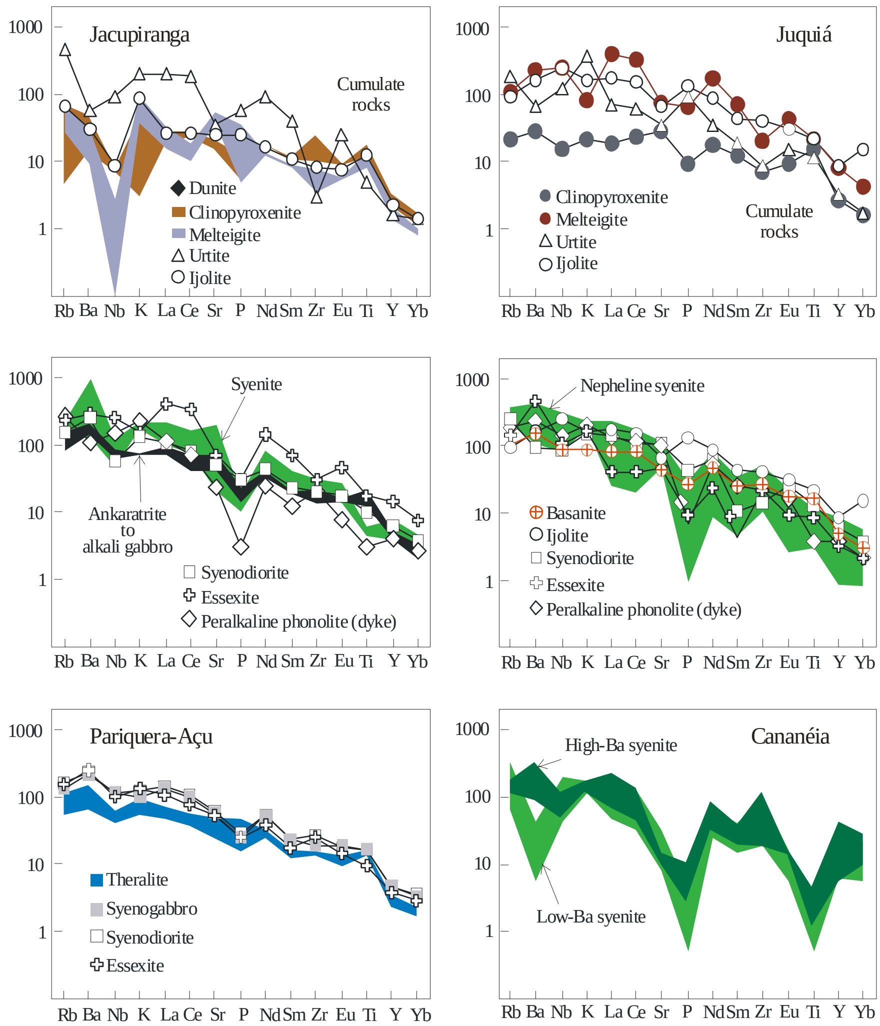


Fig. 15A. Primitive mantle-normalized (Sun & McDonough, 1989) incompatible elements of representative alkaline rocks from the Guapiara Lineament.

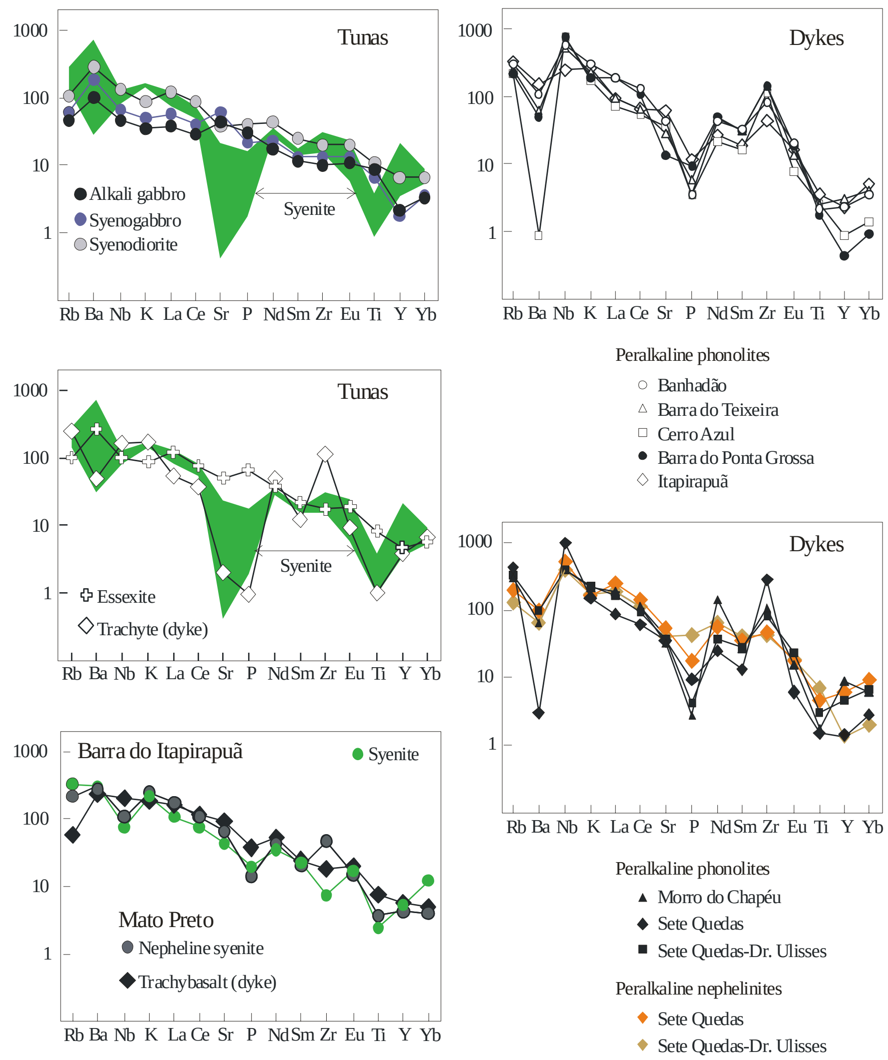


Fig. 15B. Primitive mantle-normalized (Sun & McDonough, 1989) incompatible elements of representative alkaline rocks from the São Jerônimo-Curiúva Lineament.

nepheline syenites) from Barra do Itapirapuã and Mato Preto (Late-Early Cretaceous and Late Cretaceous, respectively) display similar patterns. On the other hand, the syenites from Tunas are comparable with the Cananéia analogues, but the former display a strong Sr negative anomaly and the latter shows a pronounced P negative spike.

The dyke swarms (Late Cretaceous), i.e. per-alkaline phonolites and nephelinites, are mainly characterized by Nb and Zr strong positive anomalies and for Ba and P negative spikes.

REE behaviours

Available rare earth elements data are listed in Tables 4A, B, C. Chondrite-normalized REE patterns (according to Boynton, 1984) are shown in Figs. 16A, B.

The Jacupiranga (Guapiara Lineament) cumulate rocks display very different behaviours: dunites and melteigites have the lowest MREE and HREE concentrations with different Eu positive anomalies (Eu/Eu*=1.09 and 1.25, respectively). Urtite REE values are about ten times enriched with respect to the dunites, whereas ijolites and clinopyroxenites parallel the dunite patterns, but with Yb and Lu contents similar to the urtites. The cumulate rocks from Juquiá display more regular patterns, but with different REE concentrations and LREE/HREE fractionations, i.e. chondrite-normalized La/Yb ($La/Yb_C$), melteigites=91, urtites=41, ijolites=35 and clinopyroxenites=16.

Ankaratritic and “primitive” gabbroic rocks have very small to moderate Eu positive anomalies (Eu/Eu*=1.01-1.25). On the other hand, basanites, theralites, syenodiorites and essexites exhibit Eu negative anomalies (Eu/Eu*=0.63-0.95) both in Jacupiranga and Juquiá. On the contrary, the analogues from Pariquera-Açu and Tunas have Eu/Eu*=0.93-1.12. This fact suggests removal and accumulation of feldspar in the former and in the latter rocks, respectively. All these lithologies are enriched in LREE relative to MREE and HREE (La/Sm$_C$=3.2-6.2 and La/Yb$_C$=11-42).

The nepheline syenites and syenites from Guapiara and São Jerônimo-Curiúva lineaments present distinct characteristics. The Cananéia syenitic rocks have flattened HREE patterns with very strong negative Eu anomalies (Eu/Eu*=0.19-0.89), and show the lowest La/Sm$_C$ (2.4-5.3) and Gd/Yb$_C$ (about 1) ratios. Obviously, the behaviour indicates important feldspar removal. The Jacupiranga syenites have positive Eu anomalies (Eu/Eu*=1.09-1.56) and steep patterns (La/Sm$_C$= 4.8-12; La/Yb$_C$=20-21), whereas the Tunas syenites have a concave-shaped REE pattern (La/Sm$_C$=4.5-7.3; La/Yb$_C$=8.7-20.9) with both positive (Eu/Eu*=1.81 and 2.01) and negative (Eu/Eu*=0.41) Eu anomalies, respectively. These features may be indicative of a very complex environment, i.e. different cumulus and fractional plagioclase local processes. The Jacupiranga nepheline syenites have La/Sm$_C$=5.3-7.3 and La/Yb$_C$=73-55 and the Juquiá nepheline syenites have LaSm/=4-6.3 and La/Yb$_C$=23-43. The former show moderate positive

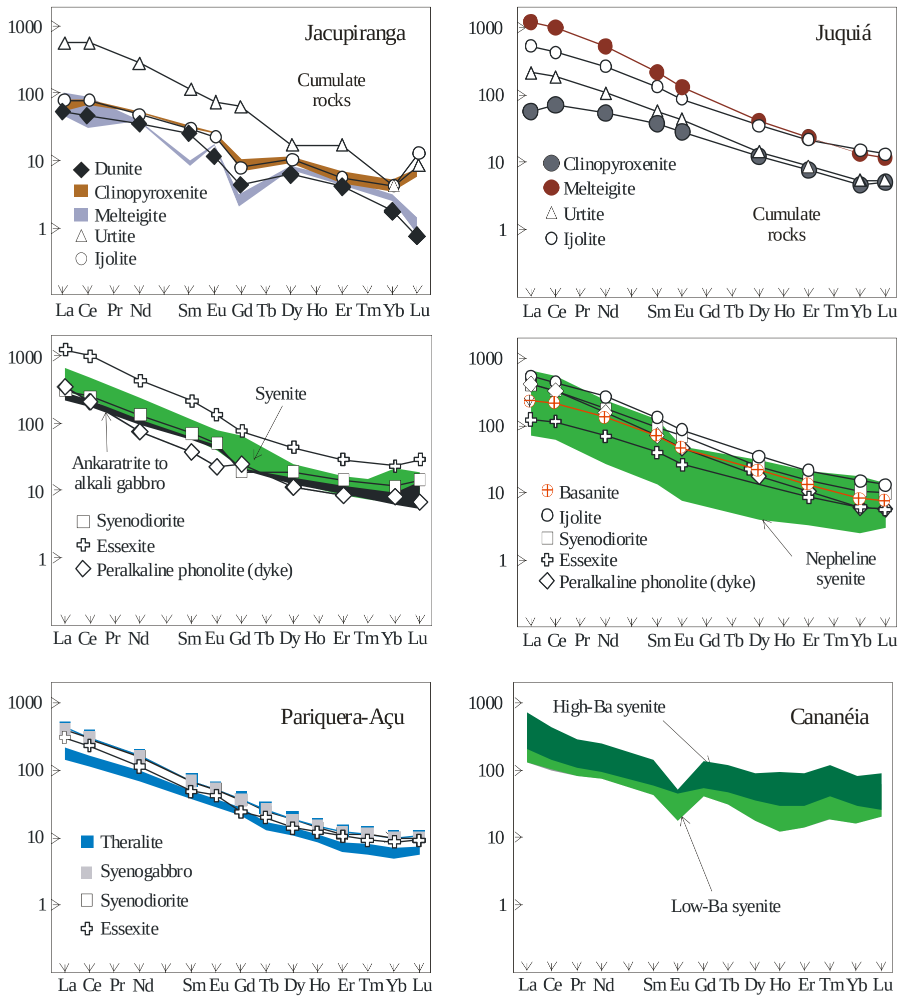


Fig. 16A. Chondrite-normalized (Boynton, 1984) REE patterns for silicate rocks of representative alkaline rocks from the Guapiara Lineament.

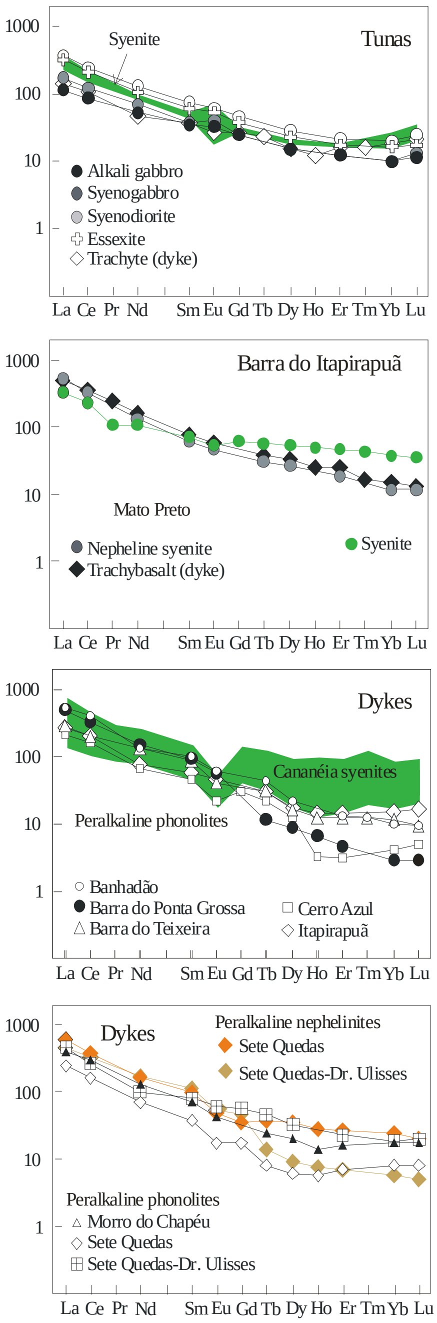


Fig. 16B. Chondrite-normalized (Boynton, 1984) REE patterns for silicate rocks of representative alkaline rocks from the São Jeronimo-Curiúva Lineament.

to poor negative Eu anomalies (Eu/Eu*=1.82-0.85), and the latter moderate negative anomalies (Eu/Eu*=0.68-0.85). The different patterns may indicate different parent magmas, not easily referred to fractional crystallization processes. For example, some concave-shaped REE patterns suggest titanite and apatite fractionation, whereas Eu positive and negative anomalies could be related to cumulus or removal of feldspar, respectively.

The peralkaline phonolitic and nephelinitic dykes display REE patterns comparable to syenites and nepheline syenites for the LREE, but with more apparent MREE and HREE fractionation. In comparison with the other evolved alkaline intrusives, all the phonolitic dykes are enriched in LREE relative to MREE and HREE, with $La/Sm_C$ ratios mainly in the range of 5.5-35 and $La/Yb_C$ ratios of 7.5-84. Significantly, the Barra do Ponta Grossa phonolites exhibit the most extreme enrichment in LREE relative to MREE and have the highest $La/Sm_C$ (57.4) and La/Yb (176) ratios. Mostly dykes present positive Eu anomalies (Eu/Eu*=1.04-1.76), but negative Eu anomalies (Eu/Eu*=0.96-0.22) are occasionally observed (i.e. Barra do Ponta Grossa, Barra do Teixeira, Cerro Azul, Sete Quedas and Sete Quedas-Dr. Ulisses). Notably, the Sete Quedas and Sete Quedas-Dr. Ulisses variants contain the highest MREE and HREE contents. The Jacupiranga and Juquiá phonolites show patterns similar to the Banhadão dykes, but with relatively low REE. The former present Eu anomalies (Eu/Eu*=0.8), whereas the Banhadão phonolites have Eu/Eu*=1.2. Phonolitic nephelinites (Sete Quedas and Sete Quedas-Dr. Ulisses) display significant LREE fractionation ($La/Sm_C$=7.2 and 27; $La/Yb_C$=34 and 83.8) with a nearly linear patterns associated with moderate or poor positive Eu anomalies (Eu/Eu*= 1.17 and 1.53). The Tunas trachytes, showing a concave-shaped behaviour, have Eu/Eu*=0.96, $La/Sm_C$=6 and $La/Yb_C$=7.45.

## Sr-Nd ISOTOPES

The available isotopic data for the silicate rocks from the Ponta Grossa Arch are reported in Tables 5A, B, C.

The initial $^{87}Sr/^{86}Sr$ ($R_0$) for the alkaline complexes from the Guapiara Lineament ranges from 0.70489 to 0.70572 (Early Cretaceous bodies, i.e. Jacupiranga, Juquiá and Pariquera-Açu), and 0.70709±0.00070 in syenites from the Late Cretaceous Cananéia intrusion.

In the alkaline complexes and dykes from the São Jerônimo-Curiúva Lineament, $R_0$ is 0.70454 in the Barra do Itapirapuã syenites (Late Early Cretaceous), and ranges from 0.70491 to 0.70588 in the Mato Preto and Tunas complexes (Late Cretaceous).

In general, the dyke swarms and plugs are well constrained at $R_0$ values of 0.70548±0.00079, but the syenitic dykes from Tunas are quite different, having $R_0$=0.70718±0.00087. Notably, a Tunas basanite dyke displays $R_0$=0.70499±0.00009.

On the whole, the $R_0$ variations are very consistent for both the two lineaments and for the Early and Late Cretaceous occurrences.

The associated carbonatites (i.e. Jacupiranga, Juquiá, Barra do Itapirapuã, Mato Preto) display substantially the same $R_0$ range (0.70425-0.70595) common to the related silicate rocks (cf. Comin-Chiaramonti *et al.*, in this volume).

Considering that a fundamental feature of the carbonatites is their buffering effect on the Sr-Nd isotopic contamination against crustal contamination (due to very high Sr and Nd abundances; cf. Bell & Tilton, 2001) the $R_0$ values of the alkaline-carbonatitic complexes may be considered as a primary characteristic. This is confirmed by the values of apatites (both from carbonate and silicate rocks) that are very similar to those of primitive mantle derived magmas, and by the $\delta^{13}C$ values of the carbonate phases that overlap those believed to be typical of upper mantle products (Nadeau *et al.*, 1999; Comin-Chiaramonti *et al.*, in this volume).

However, some high $R_0$ values (i.e. $R_0$>0.706) are common to complexes not associated with carbonatitic rocks, but sometimes they are also present in alkaline-carbonatitic complexes (e.g. Juquiá), probably due to crustal contamination or to AFC processes.

An attempt to model the $R_0$-$SiO_2$ relationships between the alkaline rocks and the basement (Fig. 17) shows that the $R_0$ lowest values (for both "primitive" and evolved rocks-types) may be mainly related to fractional crystallization processes (cf. also Beccaluva *et al.*, 1992). The $R_0$ values higher than 0.705 may be attributable or to AFC processes (cf. DePaolo, 1988) or to mixing with the crystalline basement starting from adequate compositions.

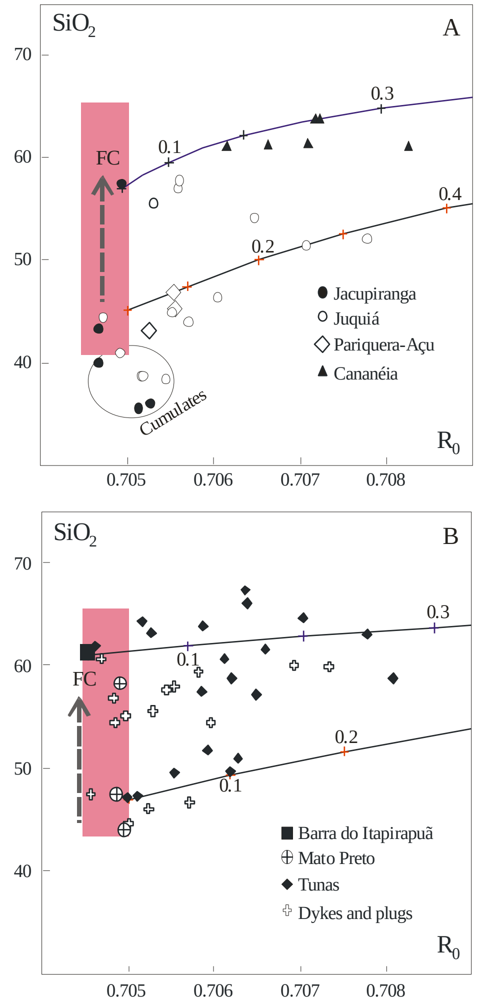


Fig. 17. Plot of initial Sr isotope ratios vs. $SiO_2$ (wt%) of representative silicate rock-types from the A) Guapiara and B) São Jerônimo-Curiúva lineaments, respectively. Mixing between the supposed primary magmas and crystalline basement are also shown (data source: Tables 5A, B, C). The vectors refer to the closed-system fractional crystallization (FC).

Taking into account simple mixing equations (Fig. 17; cf. Faure, 1986), the contribution of the crystalline basement up to 30% appears to be too high for a realistic process. AFC processes (not here quantified) are believed to be more appropriate to justify the important $R_0$ variations found in some Cananéia and Tunas rocks. Alternatively, for the latter complex may be considered the possibility of multiple intrusions starting from different sources (both mantle and lower crust?).

The $^{143}Nd/^{144}Nd$ initial ratios are in the range of

0.51228-0.51244 and of 0.51249-0.51268, Guapiara and São Jerônimo-Curiúva lineaments, respectively.

Considering the Sr-Nd time integrated notations (Fig. 18), the Ponta Grossa silicate rocks plot in the upper side of the array relative to the Early Cretaceous and Late Cretaceous magmatic rocks of the Paraná Basin (both tholeiitic and alkaline), as defined by the Paraná-Angola-Etendeka Province (PAEP, Comin-Chiaramonti *et al*., 1999).

Nd model ages (depleted mantle, $T^{DM}$) range from 0.9±0.1 to 0.7±0.1 Ga (Tables 5A, B), in the northeastern side and in the central area of the Ponta Grossa Arch, respectively, indicating a mantle reset mainly at the time of the Brasiliano cycle.

## MANTLE SOURCE CHARACTERISTICS

Thermobarometric data (cf. Klein & Langmuir, 1987; Albarede, 1992) relative to the most "primitive" rock-types (i.e. MgO 7-14 wt%) from the Ponta Grossa Arch (PGA) suggest PT melting in the ranges of 28-22 kbar and 1270-1400°C (garnet peridotite sources).

The origin of the PGA alkaline magmas appears to be related to and constrained by the geodynamic processes, which promoted the generation of the adjacent Early Cretaceous tholeiites.

The origin and emplacement of the latter rocks occurred before the opening of the South Atlantic,

Table 5A. Sr and Nd isotope compositions and concentrations of Rb, Sr, Sm and Nd for the alkaline rocks from the Guapiara Lineament. Abbreviations as in Table 3A. Data source: Beccaluva *et al*. (1992), Huang *et al*. (1995), Walter *et al.* (1995), Gibson *et al.* (1999), Morbidelli *et al.* (2000) and Gomes (unpublished data).

| Sample (Age, Ma) | Rock-type | Rb | Sr | $(^{87}Sr/^{86}Sr)_{meas}$ | $R_0$ | $SiO_2$ | Sm | Nd | $(^{143}Nd/^{144}Nd)_{meas}$ | $R_0$ | Sr | Nd | $T^{DM}$ |
|---|---|---|---|---|---|---|---|---|---|---|---|---|---|
| **Jacupiranga** | | | | | | | | | | | | | |
| 131 | | | | | | | | | | | | | |
| HB001 | Clinopyroxenite | 0.082 | 282 | 0.70467 | 0.70467 | 43.3 | 3.992 | 19.72 | 0.512638 | 0.51253 | 1.71 | 1.24 | 811 |
| HB008-1 | Clinopyroxenite | 1,000 | 332 | 0.70469 | 0.70467 | 40.0 | 5.13 | 26.49 | 0.512509 | 0.51241 | 1.78 | -1.19 | 962 |
| HB-004 | Melteigite | 100 | 2172 | 0.70538 | 0.70513 | 35.6 | 8.648 | 45.11 | 0.512649 | 0.51255 | 8.29 | 1.57 | 744 |
| HB008-2 | Melteigite | 75 | 2123 | 0.70546 | 0.70527 | 36.0 | 12.28 | 67.20 | 0.512620 | 0.51251 | 10.24 | 0.70 | 748 |
| JC103 | Nepheline syenite | 97 | 4450 | 0.70505 | 0.70493 | 57.5 | 9.7 | 65.2 | 0.512333 | 0.51225 | 5.46 | -4.22 | 967 |
| JC119 | Syenite | 145 | 426 | 0.70647 | 0.70464 | 63.9 | 9.4 | 50.1 | 0.512474 | 0.51238 | 1.26 | -1.81 | 979 |
| **Juquiá** | | | | | | | | | | | | | |
| 130 | | | | | | | | | | | | | |
| S2 | Clinopyroxenite | 18 | 206 | 0.70567 | 0.70518 | 38.8 | | | | | 8.91 | | |
| W13 | Clinopyroxenite | 155 | 1045 | 0.70571 | 0.70492 | 41.0 | 5.87 | 37.1 | 0.512342 | 0.51226 | 5.22 | -4.10 | 1001 |
| S17 | Ijolite | 81 | 1350 | 0.70576 | 0.70544 | 38.4 | | | | | 12.63 | | |
| S24 | Ijolite | 42 | 1430 | 0.70533 | 0.70517 | 38.8 | | | | | 8.85 | | |
| S38 | Syenodiorite | 94 | 2300 | 0.70800 | 0.70778 | 52.1 | | | | | 45.88 | | |
| S37 | Essexite | 159 | 1010 | 0.70791 | 0.70707 | 51.5 | | | | | 35.76 | | |
| S46-D | Nepheline syenite | 244 | 1030 | 0.70688 | 0.70561 | 57.8 | | | | | 15.11 | | |
| S-47A | Nepheline syenite | 166 | 1800 | 0.70696 | 0.70647 | 54.1 | | | | | 27.22 | | |
| W11 | Nepheline syenite | | | | | | 2.18 | 18.3 | 0.512295 | 0.51223 | 10.65 | -4.62 | 889 |
| W12 | Nepheline syenite | 86.7 | 970 | 0.705777 | 0.70530 | 55.5 | 13.2 | 90.8 | 0.512320 | 0.51225 | 10.65 | -4.40 | 967 |
| S7-D | Basanite | 57 | 1130 | 0.70598 | 0.70571 | 44.0 | | | | | 16.48 | | |
| S5-D | Basanite | 64 | 917 | 0.70510 | 0.70473 | 44.5 | | | | | 2.52 | | |
| S47B-D | Phonotephrite | 132 | 1530 | 0.70651 | 0.70605 | 46.3 | | | | | 21.28 | | |
| S4-D | Peralkaline phonolite | 123 | 2170 | 0.70589 | 0.70559 | 57.0 | | | | | 14.73 | | |
| B60B | Lamprophyre | 115 | 1556 | 0.70541 | 0.70501 | 44.9 | 19 | 112 | 0.51245 | 0.51236 | 6.61 | -2.11 | 919 |
| **Pariquera-Açu** | | | | | | | | | | | | | |
| (130?) | | | | | | | | | | | | | |
| Par 11 | Theralite | 62.94 | 560 | 0.705856 | 0.70526 | 43.1 | | | | | 10.02 | | |
| Par 7 | Theralite | 69.98 | 532 | 0.706254 | 0.70555 | 45.2 | | | | | 14.22 | | |
| Par 1 | Syenogabbro | 83.03 | 1250 | 0.705881 | 0.70553 | 46.8 | | | | | 13.86 | | |
| **Cananéia** | | | | | | | | | | | | | |
| 76 | | | | | | | | | | | | | |
| CN06 | Syenite | 119.29 | 74.97 | 0.71324 | 0.70825 | 61.1 | | | | | 51.86 | | |
| CN08 | Syenite | 183.89 | 74.67 | 0.71385 | 0.70615 | 61.1 | | | | | 21.85 | | |
| CN10 | Syenite | 146.0 | 95.65 | 0.71195 | 0.70718 | 63.8 | | | | | 36.43 | | |
| CN16 | Syenite | 129 | 178.06 | 0.70936 | 0.70709 | 61.5 | | | | | 35.26 | | |
| CN26 | Syenite | 98.52 | 246.52 | 0.70788 | 0.70663 | 61.2 | | | | | 28.66 | | |
| CN07 | Quartz syenite | 137.31 | 100.53 | 0.71150 | 0.70723 | 63.8 | | | | | 37.18 | | |

Table 5B. Sr and Nd isotope compositions and concentrations of Rb, Sr, Sm and Nd for the alkaline rocks from the São Jerônimo-Curiúva Lineament. Abbreviations as in Table 3B. Data source: Comin-Chiaramonti *et al.* (2001 and therein references), Gibson *et al.* (1999), Gomes *et al*. (1987) and Ruberti *et al*. (2002).

| Sample (Age, Ma) | Rock-type | Rb | Sr | $(^{87}Sr/^{86}Sr)_{meas}$ | $R_0$ | $SiO_2$ | Sm | Nd | $(^{143}Nd/^{144}Nd)_{meas}$ | $R_0$ | Sr | Nd | $T^{DM}$ |
|---|---|---|---|---|---|---|---|---|---|---|---|---|---|
| **Tunas** | | | | | | | | | | | | | |
| 80 | | | | | | | | | | | | | |
| 12 | Alkali gabbro | 31 | 919 | 0.70523 | 0.70512 | 47.3 | | | | | 7.26 | | |
| 35 | Syenogabbro | 39 | 1282 | 0.70563 | 0.70553 | 49.5 | | | | | 13.10 | | |
| 8 | Essexite | 62 | 997 | 0.70640 | 0.70619 | 49.7 | | | | | 22.54 | | |
| 19 | Syenodiorite | 70 | 815 | 0.70620 | 0.70592 | 51.8 | | | | | 18.60 | | |
| 10 | Syenodiorite | 74 | 970 | 0.70610 | 0.70585 | 57.5 | | | | | 17.63 | | |
| 7 | Syenodiorite | 75 | 940 | 0.70653 | 0.70627 | 51.0 | | | | | 23.56 | | |
| 1 | Syenite | 110 | 336 | 0.70728 | 0.70620 | 58.8 | | | | | 22.65 | | |
| 13 | Syenite | 180 | 10 | 0.76468 | 0.70516 | 64.3 | | | | | 7.78 | | |
| 15 | Syenite | 130 | 5 | 0.79147 | 0.70527 | 63.2 | | | | | 9.35 | | |
| 16 | Syenite | 125 | 15 | 0.73451 | 0.70703 | 64.6 | | | | | 34.43 | | |
| 17 | Syenite | 95 | 82 | 0.70843 | 0.70462 | 61.9 | | | | | 0.18 | | |
| 25 | Syenite | 160 | 35 | 0.72143 | 0.70638 | 66.0 | | | | | 25.11 | | |
| 26 | Syenite | 100 | 464 | 0.70683 | 0.70612 | 60.6 | | | | | 21.49 | | |
| 32 | Syenite | 143 | 317 | 0.70735 | 0.70587 | 63.8 | | | | | 17.87 | | |
| 36 | Syenite | 86 | 470 | 0.70720 | 0.70660 | 61.6 | | | | | 28.26 | | |
| 27 (Dyke) | Syenite | 285 | 15 | 0.76923 | 0.70637 | 67.3 | | | | | 25.03 | | |
| 28 (Dyke) | Syenite | 132 | 55 | 0.71568 | 0.70778 | 63.0 | | | | | 45.05 | | |
| 34 (Dyke) | Syenite | 94 | 526 | 0.70866 | 0.70807 | 58.7 | | | | | 49.18 | | |
| 37 (Dyke) | Syenite | 102 | 715 | 0.70695 | 0.70648 | 57.1 | | | | | 26.59 | | |
| 93SOB179 (Dyke) | Basanite | 13 | 900 | 0.70504 | 0.70499 | 47.1 | 4.7 | 23.4 | 0.51260 | 0.51254 | 5.47 | 0.03 | 863 |
| **Mato Preto** | | | | | | | | | | | | | |
| 70 | | | | | | | | | | | | | |
| 93S0B185 | Alkali basalt | 40 | 2324 | 0.70500 | 0.70495 | 44.0 | 12.2 | 79.3 | 0.51260 | 0.51258 | 4.71 | 0.19 | 668 |
| MP-C-1 | Trachybasalt | 36.8 | 2014 | 0.704925 | 0.70487 | 47.5 | 11.41 | 74.5 | 0.512543 | 0.51250 | 3.60 | -0.92 | 735 |
| MP-C-2 | Nepheline syenite | 140.7 | 1391 | 0.705191 | 0.70490 | 58.2 | 9.06 | 59.15 | 0.512585 | 0.51254 | 3.99 | -0.10 | 684 |
| **Barra do Itapirapuã** | | | | | | | | | | | | | |
| 128 | | | | | | | | | | | | | |
| 1-202.45 | Syenite | 206.3 | 924.4 | 0.705712 | 0.70454 | 61.2 | 10.62 | 50.44 | 0.512782 | 0.51268 | -0.20 | 3.94 | 615 |

Table 5C. Sr and Nd isotope compositions and concentrations of Rb, Sr, Sm and Nd for the alkaline dykes from the São Jerônimo-Curiúva Lineament and for the basement from the Ponta Grossa Arch. Abbreviations as in Table 3C. Data source: Gomes *et al*. (1987), Vasconcellos & Gomes (1998), Gibson *et al.* (1999), Comin-Chiaramonti *et al.* (2001 and therein references), Passarelli (2001) and Ruberti *et al*. (2002 and therein references)

| Sample (Notional age 74 Ma) | Rock-type | Rb | Sr | $(^{87}Sr/^{86}Sr)_{meas}$ | $R_0$ | $SiO_2$ | Sm | Nd | $(^{143}Nd/^{144}Nd)_{meas}$ | $R_0$ | Sr | Nd | $T^{DM}$ |
|---|---|---|---|---|---|---|---|---|---|---|---|---|---|
| **Dykes and Plugs** | | | | | | | | | | | | | |
| 9C Morro do Chapéu | Peralkaline phonolite | 181 | 681 | 0.70641 | 0.70554 | 57.9 | | | | | 13.18 | | |
| 10B Barra do Teixeira | Peralkaline phonolite | 156 | 704 | 0.70601 | 0.70528 | 55.5 | | | | | 9.57 | | |
| 12B Barra do Ponta Grossa | Peralkaline phonolite | 133 | 1471 | 0.70515 | 0.70485 | 54.5 | | | | | 3.48 | | |
| 19C Mato Preto | Phonotephrite | 319 | 1045 | 0.70569 | 0.70469 | 60.6 | | | | | 1.12 | | |
| 23B Sete Quedas | Phonolitic nephelinite | 125 | 1592 | 0.70483 | 0.70457 | 47.5 | | | | | -0.50 | | |
| 23C Sete Quedas | Peralkaline phonolite | 288 | 334 | 0.70944 | 0.70692 | 60.0 | | | | | 32.72 | | |
| 24A Banhadão | Peralkaline phonolite | 194 | 1086 | 0.70551 | 0.70497 | 55.0 | | | | | 5.00 | | |
| 93SOB175 Banhadão | Melteigite | 103 | 1733 | 0.70519 | 0.70501 | 44.6 | 13.61 | 92.2 | 0.51253 | 0.51249 | 5.61 | -1.09 | 731 |
| 34C Itapirapuã | Peralkaline phonolite | 190 | 1643 | 0.70617 | 0.70582 | 59.3 | | | | | 17.09 | | |
| 36A Sete Quedas-Dr. Ulisses | Phonolitic nephelinite | 92 | 1918 | 0.70538 | 0.70523 | 46.1 | | | | | 8.80 | | |
| 37A Sete Quedas-Dr. Ulisses | Peralkaline phonolite | 213 | 203 | 0.71051 | 0.70733 | 59.9 | | | | | 38.58 | | |
| 39A Sete Quedas-Dr. Ulisses | Peralkaline phonolite | 199 | 1079 | 0.70600 | 0.70544 | 57.6 | | | | | 11.71 | | |
| 41A Sete Quedas-Dr. Ulisses | Peralkaline phonolite | 207 | 1185 | 0.70649 | 0.70596 | 54.4 | | | | | 19.08 | | |
| 93SOB182 Cerro Azul | Basanite | 82 | 1530 | 0.70587 | 0.70571 | 46.6 | 7.5 | 50.9 | 0.51252 | 0.51248 | 15.51 | -1.29 | 742 |
| 42A Cerro Azul | Peralkaline phonolite | 146 | 752 | 0.70542 | 0.70483 | 56.8 | | | | | 3.06 | | |
| **Basement** | | | | | | | | | | | | | |
| Três Córregos | Granite | 168.4 | 868 | 0.716724 | 0.71613 | 68.5 | 4.56 | 29.82 | 0.511265 | 0.51122 | 163 | -25 | 2265 |
| "Bloco Registro" | Gneiss | 163 | 365 | 0.734826 | 0.73346 | 68.0 | 3.998 | 22.24 | 0.511119 | 0.51107 | 409 | -29 | 2795 |
| "Bloco Embu" | Granite | 211 | 244 | 0.748648 | 0.74600 | 70.4 | 7.852 | 50.816 | 0.511479 | 0.51143 | 587 | -22 | 2021 |
| "Bloco Mangaguá" | Gneiss | 175 | 510 | 0.719289 | 0.71824 | 70.0 | 6.99 | 60.939 | 0.511388 | 0.51135 | 193 | -23 | 1793 |

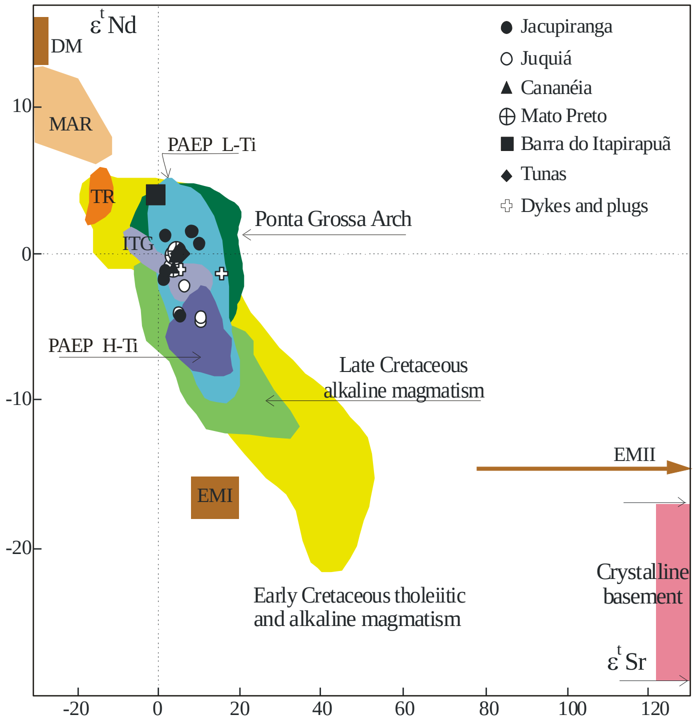


Fig. 18. εSr vs. εNd for representative alkaline rock-types from the Ponta Grossa Arch. Other data sources: Piccirillo & Melfi (1988); Gibson *et al.* (1995) and Comin-Chiaramonti *et al.* (in this volume and therein references). Abbreviations: DM, EMI and EMII, approximations of mantle end-members after Hart *et al.* (1992). Symbols as Fig. 17.

being associated with the early stages of lithosphere extension, and with variable melting degrees of garnet peridotite mantle sources, i.e. 5-8% and over 10-15% for high-$TiO_2$ and low-$TiO_2$ basalts, respectively (Piccirillo & Melfi, 1988; Piccirillo *et al.*, 1989; Peate & Hawkesworth, 1996; Ernesto *et al.*, 2002).

The major and trace element variations, as well the Sr-Nd isotope systematics of the PGA alkaline (and alkaline-carbonatitic complexes) support the view that the lithospheric mantle played an important role in their genesis (cf. Comin-Chiaramonti *et al.*, in this volume).

Mass balance calculations, starting from different garnet and garnet-phlogopite peridotites (Erlank *et al.*, 1987; whole-rock and mineral compositions in Table 6), indicate that the PGA "primary" melt compositions (i.e. Early Cretaceous Jacupiranga ankaratrite, Juquiá basanite and Pariquera-Açu theralite, $TiO_2$>2.5 wt%) can be derived by relatively high melting degrees, i.e. 4.7-5.3% or 5.0-5.9%, from an anhydrous garnet peridotite or phlogopite-bearing peridotite sources, respectively. On the other hand, the Late Cretaceous Tunas basanite can be derived from 6.5% or 9.4% of partial melting from an anhydrous garnet peridotite or phlogopite-bearing peridotite, respectively.

The presence of a relative K-enrichment in the PGA rocks (Fig. 15) suggests that a K-bearing phase (e.g. phlogopite) was not a residual phase during the partial melting processes (cf. Table 6). Phlogopite, instead, was probably a residual phase in the mantle sources of the Alto Paranaíba kamafugites (Late Cretaceous, 4-5% of partial melting of a garnet peridotite source; cf. Comin-Chiaramonti *et al.*, 1997).

The PGA primary melts, however, display relatively high abundances of I.E. and high LREE/HREE ratios (Fig. 19), which require mantle sources enriched in those elements before or sub-contemporaneously with the melting processes (Menzies & Wass, 1983). Nd model ages indicate that the I.E. enrichment in the source mantle probably occurred during the Late Proterozoic times:

ca. 0.9 Ga at the Guapiara Lineament and ca. 0.7 Ga at the São Jerônimo-Curiúva Lineament, Early Cretaceous and Late Cretaceous alkaline complexes, respectively. On the other hand, Nd model ages relative to the Alto Paranaíba kamafugites (Late Cretaceous) would be related to Middle Proterozoic events (cf. Gomes & Comin-Chiaramonti, in this volume).

Table 6. Compositions of depleted mantle rocks and mineral abundances (A). Mineral mantle compositions (B). Mass balances for batch melting (C) of the selected mantle rocks (cf. Comin-Chiaramonti *et al.*, 1997). Mineral-liquid partition coefficients from Caroff *et al.* (1993); mg#=Mg/(Mg+$Fe_{tot}$). Mantle compositions: GP, garnet peridotite (Erlank *et al.*, 1987); GPP, garnet phlogopite peridotite (Erlank *et al.*, 1987). Mantle mineral compositions: Ol, olivine, Opx, orthopyroxene, and Gt, garnet (Nixon, 1987); Cpx, clinopyroxene, and Phl, phlogopite (Erlank *et al.*, 1987). $R^2$, sum of the squares of major element residuals; F(%), melting degree (see text).

| Mantle compositions (wt%) | | | | | |
|---|---|---|---|---|---|
| | GP | GPP | | GP | GPP |
| $SiO_2$ | 46.24 | 45.64 | Ol | 62.80 | 65.38 |
| $TiO_2$ | 0.04 | 0.06 | Opx | 28.35 | 22.54 |
| $Al_2O_3$ | 1.26 | 1.40 | Cpx | 3.10 | 5.15 |
| $FeO_t$ | 6.80 | 6.81 | Gt | 5.75 | 6.97 |
| MnO | 0.12 | 0.13 | Phl | | 0.86 |
| MgO | 44.31 | 44.15 | | | |
| CaO | 1.01 | 1.42 | $R^2$ | 0.45 | 0.45 |
| $Na_2O$ | 0.09 | 0.17 | | | |
| $K_2O$ | 0.09 | 0.17 | | | |
| $P_2O_5$ | 0.04 | 0.05 | | | |
| mg# | 0.92 | 0.92 | | | |

| Mineral mantle compositions (wt%) | | | | | |
|---|---|---|---|---|---|
| | Ol | Opx | Cpx | Gt | Phl |
| $SiO_2$ | 41.21 | 56.70 | 56.27 | 43.72 | 43.96 |
| $TiO_2$ | 0.05 | 0.05 | 0.35 | 0.05 | 0.60 |
| $Al_2O_3$ | 0.05 | 0.91 | 0.41 | 20.80 | 14.81 |
| $FeO_t$ | 7.14 | 4.47 | 2.32 | 7.18 | 3.31 |
| MnO | 0.10 | 0.14 | | 0.49 | |
| MgO | 51.58 | 36.40 | 17.58 | 21.33 | 26.73 |
| CaO | 0.05 | 0.34 | 20.64 | 6.43 | |
| $Na_2O$ | 0.05 | 0.05 | 1.81 | 0.05 | 0.51 |
| $K_2O$ | | | | | 10.08 |
| mg# | 0.93 | 0.93 | 0.93 | 0.84 | 0.93 |

| Mass balances for batch melting of selected mantle rocks | | | | | | | | |
|---|---|---|---|---|---|---|---|---|
| | Ankaratrite Jacupiranga (JC111-D) | | Basanite Juquiá (S5-D) | | Theralite Pariquera-Açu (Par 11) | | Basanite Tunas (93SOB179) | |
| | GP | GPP | GP | GPP | GP | GPP | GP | GPP |
| Ol | 66.1 | 68.8 | 66.2 | 69.0 | 65.3 | 68.9 | 67.8 | 72.8 |
| Opx | 31.3 | 26.0 | 30.5 | 4.9 | 32.5 | 27.3 | 30.6 | 26.2 |
| Cpx | 0.2 | 1.5 | 1.0 | 2.7 | | 0.7 | | |
| Gt | 2.4 | 3.7 | 2.3 | 3.4 | 2.2 | 3.1 | 1.6 | 1.0 |
| Phl | | | | | | | | |
| F % | 5.34 | 5.11 | 5.05 | 5.03 | 4.68 | 5.89 | 6.49 | 9.38 |
| $R^2$ | 0.12 | 0.06 | 0.11 | 0.07 | 0.09 | 0.06 | 0.17 | 0.12 |

Trace element concentrations in the considered hypothetical mantle sources were calculated (batch melting) on the basis of the obtained melting degrees (Table 6) and using the partition coefficients of Caroff *et al.* (1993) and Comin-Chiaramonti *et al.* (1997).

It should be stressed that both the Pariquera-Açu (Early Cretaceous) theralite and the Tunas (Late Cretaceous) basanite present Nd to Ti contents for the calculated mantle source similar to those of the primitive mantle.

Notably, the patterns of the PGA primitive alkaline rocks are characterized by negative Nb (Jacupiranga and Pariquera-Açu), positive Ba (Jacupiranga, Juquiá and Tunas) and negative K (Tunas) spikes. On the other hand, the patterns for the mantle sources of the Alto Paranaíba kamafugites are distinct for their positive Nb and Zr and negative K and Sm spikes.

It seems, therefore, that the genesis of the PGA alkaline magmatism is dominated by a lithospheric mantle characterized by small-scale heterogeneity. The substantial differences between the mantle source patterns of the PGA alkaline complexes and the Alto Paranaíba kamafugites (as well as those inferred for the primitive rocks from e.g. Lages and Paraguay; cf. Comin-Chiaramonti *et al.*, 1997; Morbidelli *et al.*, 2000; Antonini *et al.*, in this volume) indicate also regional heterogeneity.

The metasomatic processes responsible for the I.E. enrichment in the mantle are believed to be due mainly to fluids or melts related to subduction processes (cf. Maury *et al.*, 1992) or to volatile rich small-volume melts from the asthenosphere which would have veined the overlying lithospheric mantle at different depths (cf. Foley, 1992a, b), or both. In general, the presence of carbonatites characterized by high I.E. concentrations (cf. Comin-Chiaramonti *et al.*, in this volume) suggest that the effect of crustal contamination on the Sr-Nd isotope systematics for the least evolved rocks was negligible and that the parental magma compositions were dominated by lithospheric mantle melts.

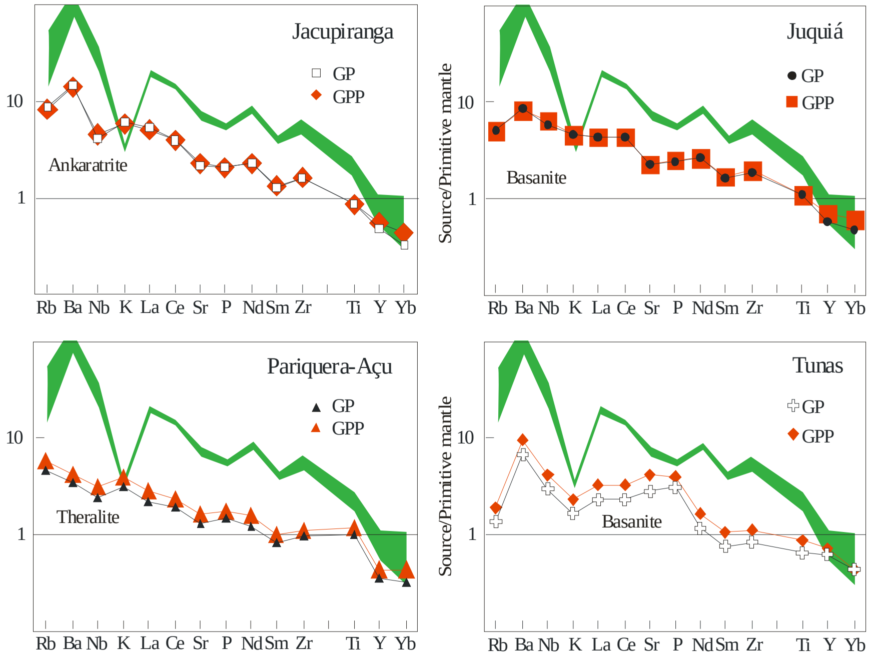


Fig. 19. I.E. distribution patterns for inferred mantle sources of the Early Cretaceous Jacupiranga, Juquiá and Pariquera-Açu alkaline-carbonatitic complexes and of the Late Cretaceous Tunas alkaline complex. Abreviations: GP, garnet peridotite; GPP, phlogopite-bearing garnet peridotite. The green field represents the APIP kamafugites (cf. Comin-Chiaramonti *et al.*, 1997).

Table 7. I.E., primitive mantle-normalized (Sun & McDonough, 1989), as inferred from mantle residual of Table 6. Calculated according to the Shaw equation (Hanson, 1978); $K_D$ values according to Caroff *et al.* (1993) and Comin-Chiaramonti *et al.* (1997).

| | Jacupiranga | | Juquiá | | Pariquera-Açu | | Tunas | |
|---|---|---|---|---|---|---|---|---|
| | GP | PP | GP | PP | GP | PP | GP | PP |
| Rb | 8.46 | 8.12 | 5.13 | 5.13 | 4.67 | 5.88 | 1.33 | 1.93 |
| Ba | 14.76 | 14.08 | 8.46 | 8.38 | 3.42 | 4.21 | 6.82 | 9.65 |
| Nb | 4.15 | 4.46 | 5.79 | 6.54 | 2.46 | 3.14 | 3.01 | 4.13 |
| K | 6.04 | 5.79 | 4.50 | 4.49 | 3.12 | 3.92 | 1.61 | 2.31 |
| La | 5.16 | 5.01 | 4.28 | 4.40 | 2.23 | 2.81 | 2.25 | 3.24 |
| Ce | 3.99 | 3.92 | 4.28 | 4.39 | 1.86 | 2.35 | 2.32 | 3.32 |
| Sr | 2.23 | 2.26 | 2.32 | 2.34 | 1.30 | 1.63 | 2.85 | 4.08 |
| P | 2.04 | 2.05 | 2.44 | 2.51 | 1.47 | 1.72 | 3.09 | 3.97 |
| Nd | 2.26 | 2.26 | 2.61 | 2.73 | 1.25 | 1.58 | 1.17 | 1.66 |
| Sm | 1.28 | 1.35 | 1.60 | 1.76 | 0.81 | 1.03 | 0.76 | 1.05 |
| Zr | 1.63 | 1.62 | 1.93 | 1.98 | 0.94 | 1.12 | 0.82 | 1.09 |
| Ti | 0.86 | 0.85 | 1.10 | 1.12 | 1.00 | 1.19 | 0.66 | 0.89 |
| Yb | 0.33 | 0.43 | 0.48 | 0.61 | 0.33 | 0.43 | 0.44 | 0.45 |

## CONCLUDING REMARKS

1) The southeastern side of the Ponta Grossa Arch, the major NW-SE structure of the Paraná Basin, is characterized by two main NW-SE lineaments, i.e. Guapiara and São Jerônimo-Curiúva, that were the site of alkaline and alkaline-carbonatitic magmatism in the Early Cretaceous and Late Cretaceous times, respectively.

2) At the Guapiara Lineament, Early Cretaceous complexes are prevailing (i.e. Jacupiranga, Juquiá and Pariquera-Açu), whereas at the São Jerônimo-Curiúva Lineament main Late Cretaceous complexes (e.g. Tunas, Mato Preto) and dykes swarms intrude the crystalline basement.

3) Four main parental magmas are inferred, i.e. ankaratrite, basanite and theralite, Jacupiranga, Juquiá and Pariquera-Açu, respectively (Guapiara Lineament), and the Tunas basanite (São Jerônimo-Curiúva Lineament).

4) The bodies display complex compositional variations ranging from cumulate rocks up to very evolved syenites/phonolites and associated carbonatites. In particular, in the Jacupiranga and Juquiá complexes, cumulate dunite and/or clino-pyroxenite may represent up to 70% in volume of the body. Ankaratrite and basanite to phonolite (nepheline syenite) represent continuous suites mainly related to fractional crystallization processes (cf. Beccaluva *et al.*, 1992).

Analogously, the Tunas complex shows a

continous variation from alkali gabbro (basanite) to syenite (trachyte). The Pariquera-Açu may represent a composite complex made of two distinct series, i.e. theralite to essexite, and syenogabbro to syeno-diorite.

Minor intrusions, i.e. Cananéia (Guapiara Lineament), Banhadão, Barra do Itapirapuã, Itapi-rapuã and Mato Preto (São Jerônimo-Curiúva Lineament) consist only of evolved rock-types, e.g. syenites and nepheline syenites (cf. Ruberti *et al*., 2002). The latter, probably may be related to different emplacement levels with respect to the more composite bodies, or to differential erosional processes (cf. Gomes *et al*., 1990).

Mostly of the plugs and dykes intruding the basement and the alkaline complexes of the São Jerônimo-Curiúva Lineament are basically made of peralkaline phonolites.

5) The least evolved rocks (i.e. supposed primary melts) have high I.E. abundances as well high LREE/HREE ratios, with very similar patterns, but least enriched in respect to the associated more evolved rocks.

The Cananéia syenites are distinct for the very negative Eu anomaly (Eu/Eu* up to 0.20), implying or a previous strong plagioclase fractionation or crustal (granitoid rock) assimilation or both.

6) Isotope systematics highlight that primary magmas have $^{87}Sr/^{86}Sr$ ratios (i.e. around 0.705) similar to those of the spatially associated “high”-$TiO_2$ not contaminated basalts (cf. Bellieni *et al*., 1986).

The evolved rock-types display $^{87}Sr/^{86}Sr$ ratios up to 0.708, pointing to an unrealistic mixing with the granitoid basement over 30%, or more likely AFC processes starting from different evolutive stages (cf. Fig. 17).

7) The Sr-Nd isotope values, relative to the PGA not contaminated rocks, in general overlap those of the associated carbonatites. The Sr-Nd integrated values plot on the array shown by the Early to Late Cretaceous tholeiites and alkaline magmatism from the Paraná-Angola-Etendeka Province (PAEP, cf. Fig. 18 and Comin-Chiaramonti *et al*., 1999). These put substantially two many questions, i.e. mantle source(s) and mantle metasomatism.

8) The close association of potassic rocks with different $K_2O/Na_2O$ ratios and tholeiitic basalts (both high and low-$TiO_2$) demands that their parental magmas have derived by different subcontinental masses, vertically and laterally heterogeneous in composition, and variously enriched in incompatible elements. Significant $H_2O$, $CO_2$ and F are also expected in the mantle sources for the occurrence of related carbonatites, sometimes strongly enriched in fluorocarbonates (Comin-Chiaramonti *et al.*, in this volume).

9) It is proposed that an isotopically enriched source, implied by the PGA alkaline magmas, originated from a depleted lithospheric mantle pervasively invaded by I.E.-C-H-rich fluids. These are expected to have promoted crystallization of K-rich phases (e.g. phlogopite) in a pristine peridotite, where they developed veined networks variously enriched in LILE and LREE under various redox conditions (cf. Foley 1988, 1992a, b). The newly formed veins (“enriched component”) underwent a different isotopic evolution with the time, depending on their parent/daughter ratio.

10) $T^{DM}$ systematics suggest that distinct magmas were generated following apparent two main enrichment events in the subcontinental mantle estimated at 0.9 Ga (Guapiara Lineament) and at 0.7 Ga (São Jerônimo-Curiúva Lineament).

Notably, $T^{DM}$ model ages of the flood tholeiites and tholeiitic dykes from the Paraná Basin and from Etendeka, as well as of the Early Cretaceous potassic rocks and carbonatites from Eastern Paraguay and Anitápolis (Santa Catarina state, southeastern Brazil) range from 1.1 to 1.6 Ga (Comin-Chiaramonti *et al*., 1999, 2002). By contrast, the other Early Cretaceous potassic rocks and carbonatites from eastern Paraná Basin, Angola and Namibia, as well as the younger sodic (Tertiary) and potassic (Late Cretaceous) rocks from Paraguay and Alto Paranaíba, respectively, yielded 0.6-1.0 Ga (Comin-Chiaramonti *et al*., 1999). It should be noted that the Tristan da Cunha and Trindade modern volcanics yielded 0.7 Ga and less than 0.5 Ga, respectively (cf. Le Roex, 1986; Le Roex *et al*., 1990; Marques *et al*., 1999; Siebel *et al*., 2000).

These model ages indicate that almost two distinct metasomatic events may have occurred during Middle and Late Proterozoic times, respectively, as precursor to the alkaline and tholeiitic magmas in the PAEP.

In summary, the alkaline and alkaline-carbonatitic magmatism from the Ponta Grossa Arch appears to be related to the lithospheric mantle, and the contribution of asthenospheric components derived from the hypothetical Tristan da Cunha and Trindade mantle plumes is not appreciable in terms of geochemistry and Sr-Nd isotopes. Moreover, the source(s) of the recurrent potassic, sodic and interposed tholeiitic magmatism may not easily accounted for the plume hypothesis (cf. Alberti *et al*., 1999; Ernesto *et al*., 2002).

## ACNOWLEDGEMENTS

Thanks are due to Brazilian (Fapesp, Proc. 01/10714-3) and Italian (MIUR 1998, 1999, 2000 and 2001) agencies for financial suport.

## REFERENCES

Albarede, F. (1992). How deep do common basaltic magmas form and differentiate? *Journal of Geophysical Research* **97**, 10997-11009.

Alberti, A., Castorina, F., Censi, P., Comin-Chiaramonti, P. & Gomes, C.B. (1999). Geochemical characteristics of Cretaceous carbonatites from Angola. *Journal of African Earth Sciences* **29**, 735-759.

Algarte, J.P. (1972). A influência dos arqueamentos cratônicos no condicionamento das alcalinas nos Estados de São Paulo e Paraná. *XXVI Congresso Brasileiro de Geologia, Belém, Anais* **1**, 65-69.

Almeida, F.F.M. (1983). Relações tectônicas das rochas alcalinas mesozóicas da região meridional da plataforma sul-americana. *Revista Brasileira de Geociências* **13**, 139-158.

Almeida, F.F.M. (1986). Distribuição regional e relações tectônicas do magmatismo Pós-Paleozóico no Brasil. *Revista Brasileira de Geociências* **16**, 325-349.

Amaral, G. (1978). Potassium-argon age studies on the Jacupiranga alkaline district, State of São Paulo, Brazil. *Proceedings 1st International Symposium on Carbonatites, Poços de Caldas*, pp. 297-302.

Amaral, G., Bushee, J., Cordani, U.G., Kawashita, K. & Reynolds, J.H. (1967). Potassium-argon ages of alkaline rocks from Southern Brazil. *Geochimica et Cosmochimica Acta* **31**, 117-142.

Andrade, F.R.D., Möller, P., Lüders, V., Dulski, P. & Gilg, H.A. (1999). Hydrothermal REE mineralization in the Barra do Itapirapuã carbonatite, southern Brazil: behavior of selected trace elements and stable isotopes (C,O). *Chemical Geology* **155**, 91-113.

Antonini, P., Gasparon, M., Comin-Chiaramonti, P. & Gomes, C.B. (in this volume). Post-Paleozoic magmatism in Eastern Paraguay: Sr-Nd-Pb isotope compositions.

Bauer, H.E. (1877). As minas de ferro de Jacupiranga. *Revista de Engenharia*, Rio de Janeiro, p. 213.

Beccaluva, L., Barbieri, M., Born, H., Brotzu, P., Coltorti, M., Conte, A., Garbarino, C., Gomes, C.B., Macciotta, G., Morbidelli, L., Ruberti, E., Siena, F. & Traversa, G. (1992). Fractional crystallization and liquid immiscibility processes in the alkaline-carbonatite complex of Juquiá (São Paulo, Brazil). *Journal of Petrology* **33**, 1371-1404.

Bell, K. & Tilton, G.R. (2001). Nd, Pb and Sr isotopic compositions of East African carbonatetes: evidence for mantle mixing and plume inhomogeneity. *Journal of Petrology* **42**, 1927-1945.

Bellieni, G., Comin-Chiaramonti, P., Marques, L.S., Melfi, A.J., Nardy, A.J.R., Papatrechas, C., Piccirillo, E.M., Roisenberg, A. & Stolfa, D. (1986). Petrogenetic aspects of acid and basaltic lavas from the Paraná Plateau (Brazil): geological, mineralogical and petrochemical relationships. *Journal of Petrology* **27**, 915-944.

Boctor, N.Z. & Svisero, D.P. (1978). Iron-titanium oxide and sulphide minerals in carbonatite from Jacupiranga, Brazil. *Annual Report of the Director of the Geophysical Laboratory* **77**, 876-880.

Born, H. (1971). *O complexo alcalino de Juquiá*. Ph.D. Thesis, University of São Paulo, 177p.

Born, H. (1975). Pesquisa do minério fosfático de Ipanema. *Geologia e Metalurgia, São Paulo* **37**, 24-34.

Boynton, W.V. (1984). Cosmochemistry of the Rare Earth elements: meteorite studies. In: Henderson, P. (ed.) *Rare Earth Element geochemistry*. Amsterdam: Elsevier, pp. 63-114.

Caroff, M., Maury, R.C., Leterrier, J., Joron, J.L., Cotten, J. & Guille, G. (1993). Trace element behaviour in the alkali basalt-comenditic trachyte series from Mururoa Atoll, French Polynesia. *Lithos 30*, 1-22.

Comin-Chiaramonti, P., Cundari, A., DeGraff, J.M., Gomes, C.B. & Piccirillo, E.M. (1999). Early Cretaceous-Tertiary magmatism in the Eastern Paraguay (western Paraná basin): geological, geophysical and geochemical relationships. *Journal of Geodynamics* **28**, 375-391.

Comin-Chiaramonti, P., Cundari, A., Piccirillo, E.M., Gomes, C.B., Castorina, F., Censi, P., De Min, A., Marzoli, A., Speziale, S. & Velázquez, V.F. (1997). Potassic and sodic igneous rocks from Eastern Paraguay: their origin from the lithospheric mantle and genetic relationships with the associated Paraná flood tholeiites. *Journal of Petrology* **38**, 495-528.

Comin-Chiaramonti, P., Gomes, C.B., Castorina, F., Censi, P., Antonini, P., Furtado, S., Ruberti, E. & Scheibe, F. (2002). Geochemistry and geodynamic implications of the Anitápolis and Lages alkaline-carbonatite complexes, Santa Catarina State Brazil. *Revista Brasileira de Geociências* **32**, 43-58.

Comin-Chiaramonti, P., Gomes, C.B., Marques, L.S., Censi, P., Ruberti, E. & Antonini, P. (in this volume). Carbonatites from southeastern Brazil: geochemistry, O-C, Sr-Nd-Pb isotopes and relationships with the magmatism from the Paraná-Angola-Namibia Province.

Comin-Chiaramonti, P., Gomes, C.B., Ruberti, E., Antonini, Castorina, F. & Censi, P. (2001). Mato Preto alkaline-carbonatite complex: geochemistry and isotope (O-C, Sr-Nd) constraints. *Geochimica Brasiliensis* **15**, 23-34.

Davino, A. (1975). Geologia da Serra de Araçoiaba, Estado de São Paulo. *Boletim do Instituto de Geociências da Universidade de São Paulo 6*, 129-144.

DePaolo, D.J. (1988). *Neodymium isotope geochemistry: an introduction*. New York: Springer Verlag, 187p.

Derby, O.A. (1891). On the magnetite ore districts of Jacupiranga and Ipanema, São Paulo, Brazil. *American Journal of Science* **41**, 311-321.

Erlank, A.J., Waters, F.G., Hawkesworth, C.J., Haggerty, S.E., Allsopp, H.L., Rickard, R.S. & Menzies, M.A. (1987). Evidence for mantle metasomatism in peridotite nodules from the Kimberley pipes, South Africa. In: Menzies M.A. & Hawkesworth, C.J. (eds.) *Mantle metasomatism*. London: Academic Press, pp. 221-311.

Ernesto, M., Marques, L.M., Piccirillo, E.M., Molina, E., Ussami, N., Comin-Chiaramonti, P. & Bellieni, G. (2002). Paraná Magmatic Province-Tristan da Cunha plume system: fixed versus mobile plume, petrogenetic considerations and alternative heat sources. *Journal of Volcanology and Geothermal Research* **130**, 527-553.

Faure, G. (1986). *Principles of isotope geology*. New York: John Wiley & Sons, 589p.

Ferreira, F.J.F. & Algarte, J.P. (1979). O comportamento aeromagnetométrico-cintilo-métrico das principais rochas alcalinas dos Estados de São Paulo e Paraná. *II Simpósio Regional de Geologia, Rio Claro, Atas,* pp. 195-208.

Foley, S.F. (1988). The genesis of continental basic alkaline magmas. An interpretation in terms of redox melting. *Journal of Petrology, Special Lithosphere Issue*, pp. 139-161.

Foley, S.F. (1992a). Petrological characterization of the source components of potassic magmas: geochemical and experimental constraints. *Lithos* **28**, 187-204.

Foley, S.F. (1992b). Vein plus wall-rock melting mechanism in the lithosphere and the origin of potassic alkaline magmas. *Lithos* **28**, 435-453.

Fuck, R.A. (1972). *Geologia do maciço alcalino de Tunas, Paraná, Brasil*. Ph.D. Thesis, University of São Paulo, 82p.

Gaspar, J.C. (1989). *Geologie et mineralogie du complexe carbonatique de Jacupiranga, Brésil.* Ph.D. Thesis, University of Orleans, 344p.

Gaspar, J.C. & Wyllie, P.J. (1983a). Magnetite in the carbonatites from the Jacupiranga complex, Brazil. *American Mineralogist* **68**, 195-213.

Gaspar, J.C. & Wyllie, P.J. (1983b). Ilmenite (high Mg, Mn, Nb) in the carbonatites from de Jacupiranga complex, Brazil. *American Mineralogist* **68**, 960-971.

Gaspar, J.C. & Wyllie, P.J. (1987). The phlogopites from the Jacupiranga carbonatite intrusions. *Contributions to Mineralogy and Petrology* **36**, 121-134.

Germann, A., Marker, A. & Friedrich, G. (1987). The alkaline complex of Jacupiranga, São Paulo, Brazil. Petrology and genetic considerations. *Zentralblatt für Geologie und Paläontologie* **1**, 807-818.

Gibson, S.A., Thompson, R.N., Leonardos, O.H., Dickin, A.P. & Mitchell, J.G. (1995). The late Cretaceous impact of the Trindade mantle plume: evidence from large-volume, mafic, potassic magmatism in SE Brazil. *Journal of Petrology* **36**, 189-229.

Gibson, S.A., Thompson, R.N., Leonardos, O.H., Dickin, A.P. & Mitchell, J.G. (1999). The limited extent of plume-lithosphere interactions during continental flood-basalt genesis: geochemical evidence from Cretaceous magmatism in southern Brazil. *Contributions to Mineralogy and Petrology* **137**, 147-169.

Gimenez Filho, A., Janasi, V.A., Campanha, G.A.C., Teixeira, W. & Trevizoli Júnior, L.E. (2000). U-

Pb dating and Rb-Sr isotope geochemistry of the eastern portion of the Três Córregos batholith, Ribeira fold belt, São Paulo. *Revista Brasileira de Geociências* **30**, 45-50.

Gomes, C.B. (1970). Petrologia do maciço alcalino de Itapirapuã, SP. *Boletim do Instituto de Geociências e Astronomia da Universidade de São Paulo* **1**, 77-197.

Gomes, C.B. & Comin-Chiaramonti, P. (in this volume). Some notes on the Alto Paranaíba Igneous Province.

Gomes, C.B., Barbieri, M., Beccaluva, L., Brotzu, P., Conte, A., Garbarino, C., Macciotta, G., Melluso, L., Morbidelli, L., Ruberti, E., Scheibe, L.F., Tamura, R.M. & Traversa, G. (1987). Petrological and geochemical studies of alkaline rocks from continental Brazil. 2. The Tunas massif, State of Paraná. *Geochimica Brasiliensis* **1**, 201-234.

Gomes, C.B., Ruberti, E. & Morbidelli, L. (1990). Carbonatite complexes from Brazil: a review. *Journal of South American Earth Sciences* **3**, 51-63.

Hanson, G.N. (1978). The application of trace elements to the petrogenesis of igneous rocks of granitic composition. *Earth and Panetary Science Letters* **38**, 26-43.

Hart, S.R., Hauri, E.H., Oschmann, L.A. & Whithehead, J.A. (1992). Mantle plumes and entrainement: isotopic evidence. *Science* **256**, 517-520.

Hirano, H., Kamitani, M. & Daitx, E.C. (1987). Jacupiranga carbonatites in the São Paulo State, Brazil: their mode of occurrence. *Report of International Research and Development Cooperation ITIT Projects*, Japan **8316**, 74-95.

Huang, J.-M., Hawkesworth, C.J., van Calsteren, P., & McDermott, F. (1995). Geochemical characteristics and origin of the Jacupiranga carbonatites, Brazil. *Chemical Geology* **119**, 79-99.

Jenkins, R.E. (1987). Geology of the Clugger-fluorite deposit, Mato Preto, Paraná, Brazil. *Revista Brasileira de Geociências* **17**, 288-294.

Keller, J. & Hoefs, J. (1995). Stable isotope characteristics of recent natrocarbonatites from Oldoinyo Lengai. In: Bell, K. & Keller, J. (eds.) *Carbonatite volcanism: Oldoynio Lengai and the petrogenesis of natrocarbonatites*. Berlin: Springer, pp. 113-123.

Klein, E.M. & Langmuir, C.H. (1987). Global correlation of ocean ridge basalt chemistry with axial depth and crustal thickness. *Journal of Geophysical Research* **92**, 8089-8115.

Knecht, T. (1960). Notas preliminares sobre novas ocorrências de rochas alcalinas no Estado de São Paulo. *Boletim da Sociedade Brasileira de Geologia* **9**, 71-76.

Lapido-Loureiro, F.E.V. & Tavares, J.R. (1983). Duas novas ocorrências de carbonatitos: Mato Preto e Barra do Rio Itapirapuã. *Revista Brasileira de Geociências* **13**, 7-11.

Le Maitre, R.W. (1989). *A classification of igneous rocks and glossary of terms*. Oxford: Blackwell, 193p.

Le Roex, A. P. (1986). Geochemical correlation between Southern African Kimberlites and South Atlantic hot spots. *Nature* **324**, 243-245.

Le Roex, A.P., Cliff, R.A. & Adair, B.J.I. (1990). Tristan da Cunha, south Atlantic: geochemistry and petrogenesis of a basanite-phonolite lava series. *Journal of Petrology* **31**, 779-812.

Leat, P.T., Jackson, S.E., Thorpe, R.S. & Stillman, C.G. (1986). Geochemistry of bimodal basalt subalkaline/peralkaline rhyolite provinces within the southern British Caledonides. *Journal of the Geological Society of London* **143**, 259-273.

Leinz, V. (1940). Petrologia das jazidas de apatita de Ipanema. *Boletim do Departamento Nacional da Produção Mineral, Divisão de Fomento da Produção Mineral* **40**, 1-52.

Machado Jr., D.L. (2000). *Condicionantes estruturais e contexto tectônico do "Alinhamento de Guapiara"*. Ph.D. Thesis, University of São Paulo, 143p.

Marques, L.S., Ulbrich, M.N.C., Ruberti, E. & Tassinari, C.G. (1999). Petrology, geochemistry and Sr-Nd isotopes of the Trindade and Martin Vaz volcanic rocks (Southern Atlantic Ocean). *Journal of Volcanology and Geothermal Research* **93**, 191-216.

Maury, R., Defant, C. & Joron, M.J. (1992). Metasomatism of the subarc mantle inferred from trace elements in Philippine xenoliths. *Nature* **360**, 661.

Melcher, G.C. (1966). The carbonatites of Jacupiranga, São Paulo, Brazil. In: Tuttle, O.F. & Gittins, J. (eds.) *Carbonatites*. Great Britain: Intersciences Publishers, pp. 169-181.

Menzies, M.A. & Wass, S.Y. (1983). $CO_2$ and LREE-rich mantle below eastern Australia; a REE and isotopic study of alkaline magmas and apatite-rich mantle xenoliths from the Southern Highlands Province, Australia. *Earth and Planetary Science Letters* **65**, 287-302.

Mitchell, R.H. (1978). Manganoan magnesian ilmenite and clinohumite from the Jacupiranga carbonatite, São Paulo, Brazil. *American Mineralogist* **63**, 544-547.

Morbidelli, L., Beccaluva, L., Brotzu, P., Conte, A., Garbarino, C., Gomes, C.B., Maciotta, G., Ruberti, E., Scheibe, L.F. & Traversa, G. (1986). Petrological and geochemical studies of alkaline rocks from continental Brazil. 3. Fenitization of jacupirangite by carbonatite magmas in the

Jacupiranga Complex, SP. *Periodico di Mineralogia* **55**, 261-295.

Morbidelli, L., Gomes, C.B., Beccaluva, L., Brotzu, P., Conte, A.M., Ruberti, E. & Traversa, G. (1995). Mineralogical, petrological and geochemical aspects of alkaline and alkaline-carbonatite associations from Brazil. *Earth-Science Reviews* **39**, 135-168.

Morbidelli, L., Gomes, C.B., L., Brotzu, P., D'Acquarica, S., Garbarino, C., Ruberti, E. & Traversa, G. (2000). The Pariquera Açu K-alkaline complex and southern Brazil lithospheric mantle source characteristics. *Journal of Asian Earth Sciences* **18**, 129-150.

Morikiyo, T., Hirano, H. & Matsuhisa, Y. (1987). Carbon and oxigen isotopic composition of the carbonates from the Jacupiranga and Catalão I carbonatite complexes, Brazil. *Report of International Research and Development Cooperation ITIT Projects, Japan* **8316**, 96-111.

Nadeau, S.L., Epstein, S. & Stolper, E. (1999). Hidrogen and carbon abundances and isotopic ratios in apatite from alkaline intrusive complexes, with a focus on carbonatites. *Geochimica et Cosmochimica Acta* **63**, 1837-1851.

Nelson, D.R., Chivas, A.R., Chapell, B.W. & McCulloch, M.T. (1988). Geochemical and isotopic systematics in carbonatites and implications for the evolution of ocean-island sources. *Geochimica et Cosmochimica Acta* **52**, 1-17.

Nixon, P.H. (1987). *Mantle xenoliths*. Chichester: John Wiley, 844p.

Passarelli, C.R. (2001). *Caracterização estrutural e geocronológica dos domínios tectônicos da porção sul-oriental do Estado de São Paulo*. Ph.D. Thesis, University of São Paulo, 254p.

Peate, D.W. & Hawkesworth, C.J. (1996). Lithospheric to asthenospheric transition in low-Ti flood basalts from Southern Paraná, Brazil. *Chemical Geology* **127**, 1-24.

Piccirillo, E.M. & Melfi, A.J. (eds.) (1988). *The Mesozoic flood volcanism from the Paraná Basin (Brazil). Petrogenetic and geophysical aspects*. São Paulo: IAG-USP, 600p.

Piccirillo, E.M., Bellieni, G., Cavazzini, G., Comin-Chiaramonti, P., Petrini, R., Melfi, A.J., Pinese, J.P.P., Zantedeschi, P. & De Min, A. (1990). Lower Cretaceous dyke swarms from the Ponta Grossa Arch. Petrology, Sm-Nd isotopes and genetic relationships with the Paraná flood volcanics. *Chemical Geology* **89**, 19-48.

Piccirillo, E.M., Civetta, L., Petrini, R., Longinelli, A., Bellieni, G., Comin-Chiaramonti, P., Marques, L.S. & Melfi, A.J. (1989). Regional variations within the Paraná flood basalts (Southern Brazil): evidence for subcontinental mantle heterogeneity and crustal contamination. *Chemical Geology* **75**, 103-122.

Roden, M.F., Murthy, V.R. & Gaspar, J.C. (1985). Sr and Nd isotopic composition of the Jacupiranga carbonatite. *Journal of Geology* **93**, 212-220.

Ruberti, E. (1984). *Petrologia do maciço alcalino do Banhadão, PR*. Ph.D. Thesis, University of São Paulo, 248p.

Ruberti, E. (1998). *Petrologia e geoquímica das suítes carbonatíticas de Mato Preto (PR) e da Barra de Itapirapuã (PR-SP), Brasil*. Livre-Docência Thesis, University of São Paulo, 211p.

Ruberti, E. & Gomes, C.B. (1984). O maciço alcalino do Banhadão, PR: geologia e petrografia. *XXXIII Congresso Brasileiro de Geologia, Rio de Janeiro, Anais* **9**, 4400-4412.

Ruberti, E., Castorina, F., Censi, P., Comin-Chiaramonti, P., Gomes, C.B., Antonini, P. & Andrade, F.R.D. (2002). The geochemistry of the Barra do Itapirapuã carbonatite (Ponta Grossa Arch, Brazil): a multiple stockwork. *Journal of South American Earth Sciences* **15**, 215-228.

Ruberti, E., Castorina, F., Censi, P., Gomes, C.B., Speziale, S. & Comin-Chiaramonti, P. (1997a). REE-C-O-Sr-Nd systematics in carbonatites from Barra do Itapirapuã and Mato Preto Southern Brazil). *1st South American Symposium on Isotope Geology, Campos de Jordão, Extended Abstracts*, pp. 271-275.

Ruberti, E., Gomes, C.B., Brotzu, P., Comin-Chiaramonti, P., Garbarino, C. & Morbidelli, L. (1997b). Aspectos geoquímicos dos carbonatitos de Mato Preto, PR. *VI Congresso Brasileiro de Geoquímica, Salvador, Anais*, pp. 676-679.

Ruberti, E., Gomes, C.B., Brotzu, P., Comin-Chiaramonti, P., Garbarino, C. & Morbidelli, L. (1997c). Estudo geoquímico dos carbonatitos da Barra do Itapirapuã, SP-PR. *VI Congresso Brasileiro de Geoquímica, Salvador, Anais*, pp. 730-733.

Ruberti, E., Gomes, C.B. & Dutra, C.V. (1987). Aspectos geoquímicos das rochas alcalinas do maciço do Banhadão, PR. *I Congresso Brasileiro de Geoquímica, Porto Alegre, Anais* **1**, 349-374.

Rugenski, A., Mantovani, M.S.M. & Shukowsky, W. (2001). Modelo gravimétrico do complexo alcalino de Pariquera-Açu (SP). *Revista Brasileira de Geociências* **31**, 365-374.

Santos, R.V. (1988). *Geologia e geoquímica do depósito de fluorita do complexo carbonatítico de Mato Preto, Paraná, Brasil*. M.Sc. Dissertation, University of Brasília, 144p.

Siebel, W., Becchio, R., Volker, F., Hansen, M.A.F., Viramonte, J., Trumbull, R.B., Haase, G. & Zimmer, M. (2000). Trindade and Martin Vaz islands, South Atlantic: isotopic (Sr, Nd, Pb) and trace element constraints on plume related magmatism. *Journal of South American Earth Sciences* **13**, 79-103.

Silva, A.T.S.F. & Algarte, J.P. (1981). Contribuição à geologia da Sequência Turvo-Cajati entre o Rio Pardo e Pariquera Açu, Estado de São Paulo. Litologia e petrologia. *Simpósio Regional de Geologia, Curitiba, Resumos* **1**, 109-120.

Slavec, G.B., Mantovani, M.S.M. & Shukowsky, W. (2001). Contribuição ao estudo do complexo de Juquiá. *Revista Brasileira de Geociências* **31**, 203-210.

Sonoki, I.K. & Garda, G.M. (1988). Idades K/Ar de rochas alcalinas do Brasil meridional e Paraguai oriental: compilação e adaptação às novas constantes de decaimento. *Boletim do Instituto de Geociências da USP, Série Científica* **19**, 63-85.

Souza, L.A.P., Tessler, M.G. & Galli, V.L. (1996). O gráben de Cananéia. *Revista Brasileira de Geociências* **26**, 139-150.

Spinelli, F.P. (2000). *A intrusão alcalina de Cananéia, SP: características petrográficas e geoquímicas.* Monografia de Trabalho de Formatura, University of São Paulo, 37p.

Spinelli, F.P. (2003). *As rochas alcalinas de Cananéia, Litoral Sul do Estado de São Paulo: características petrográficas, mineralógicas e geoquímicas*. M.Sc. Dissertation, University of São Paulo, 134p.

Suguio, K., Tessler, M.G., Furtado, V.V., Esteves, C.A. & Souza, L.A.P. (1987). Perfilagens geofísicas e sedimentação na área submersa entre Cananéia e Barra de Cananéia. *Simpósio sobre Ecossistemas da Costa Sul e Sudeste Brasileira, Cananéia*, Publicação ACIESP n 54-II **2**, 234-241.

Sun, S.S. & McDonough, W.F. (1989). Chemical and isotopic systematics of oceanic basalts: implications for mantle compositions and processes. In: Saunders, A.D. &, Norry, M.J. (Eds.) *Magmatism in the oceanic basins*. *Geological Society of London, Special Publication*, **42**, 313-345.

Taylor Jr., H.P., Frechen, J. & Degens, E.T. (1967). Oxygen and carbon isotope studies of carbonatites from Laacher See district, West Germany and Alnö district, Sweden. *Geochimica et Cosmochimica Acta* **31**, 407-430.

Treuil, M. & Joron, J.L. (1976). Etude géochimique des éléments en traces dans le magmatisme de l'Afar. Implications pétrogenétiques et comparison avec le magmatisme de l'Islande et de la dorsale medio-Atlantique. *Afar depression of Ethiopia, Stuttgart* **2**, 26-79.

Vasconcellos, E.M.G. (1995). *Petrologia e geoquímica de diques e plugs alcalinos da região do Vale do Ribeira, divisa dos Estados do Paraná e São Paulo.* Ph.D. Thesis, University of São Paulo, 202p.

Vasconcellos, E.M.G. & Gomes, C.B. (1998). Diques e plugs alcalinos da região do Vale do Ribeira, Divisa dos Estados do Paraná e São Paulo: características petrográficas e geoquímicas. *Geochimica Brasiliensis* **12**, 123-143.

Walter, A.V., Flicoteaux, R., Parron, C., Loubet, M. & Nahon, D. (1995). Rare-earth elements and isotopes (SR, Nd, O, C) in minerals from the Juquiá carbonatite (Brazil): tracers of a multi-stage evolution. *Chemical Geology* **120**, 27-44.

*Mesozoic to Cenozoic Alkaline Magmatism in the Brazilian Platform*
*Comin-Chiaramonti, P. & Gomes, C.B. (eds.)*
*Edusp/Fapesp, São Paulo, pp. 473-521, 2005*

# CRETACEOUS ALKALINE MAGMATISM FROM SANTA CATARINA STATE, SOUTHERN BRAZIL

*L.F. Scheibe, S.M.A. Furtado, P. Comin-Chiaramonti and C.B. Gomes*

*During the Cretaceous time, the Santa Catarina state, at the southern side of the Paraná Basin, experienced at least three main magmatic events. The first one, Early Cretaceous, included the emplacement of voluminous flood tholeiitic basalts of the Serra Geral Formation (133-130 Ma) and the small intrusion of the Anitápolis alkaline-carbonatite complex (132 Ma) in the Late Proterozoic crystalline basement. During late Early Cretaceous (120 Ma), a tholeiitic dyke swarm intruded the Late Proterozoic Pedras Grandes Suite in the Florianópolis region. The third event is represented by Late Cretaceous (76 Ma) alkaline-carbonatite outcrops in the Gondwana sedimentary sequences at the Lages district. The three magmatic events correspond to 1) the early stages of rifting before the Africa-South America separation; 2) the time of sea-floor spreading; 3) a more advanced stage of the continental separation. Mineralogical, geochemical and isotope data relative to the alkaline magmatism indicate subcontinental mantle sources which suffered processes of relatively low melting degrees of variously metasomatized layers and produced basanitic (or olivine nephelinitic) parent magmas. Leucocratic, evolved rock-types are consistent with fractional crystallization processes, sometimes with a contaminant component from the country-rocks. The coexistence in time and space of tholeiitic and alkaline magmatism in a region strongly affected by plate margin stresses, appear to be linked to the relative movement of plates and subplates and to the ancient geotectonic main lineaments. The forces acting on plates moving with different westwards angular velocity, and the presence of "second order plate boundaries", may have favoured the decompression and melting of variously metasomatized (wet spot) portions of the lithospheric mantle with distinct isotopic imprintings at different times.*

## INTRODUCTION

The Santa Catarina state, southern Brazil, is characterized by the occurrence of several alkaline and alkaline-carbonatitic bodies of Early to Late Cretaceous age (Fig. 1), as emphasized by Ulbrich & Gomes, (1981) and Almeida (1983), i.e. 1) Anitápolis alkaline-carbonatite complex (Furtado & Scheibe, 1987); 2) carbonatites, kimberlites and ultramafic rock-types from Lages, about 100 km W of Anitápolis (Traversa *et al.*, 1994); 3) an alkaline pipe and several alkaline dykes at the Quarenta locality, Botuverá municipality (D'Elboux *et al.*, 1982; Tavares, 1982). The alkaline magmatism is associated in time and/or in space with the Early Cretaceous flood tholeiites of the Serra Geral Formation (133-130 Ma, Renne *et al.*, 1997; Paraná Basin, Piccirillo & Melfi, 1988) and with the tholeiitic dyke swarm from Florianópolis (120 Ma; Raposo *et al.*, 1998) intruding the Late Proterozoic Pedras Grandes Suite (Babinski *et al.*, 1997). Tholeiitic and alkaline-carbonatitic magmatism occurring in and around the Paraná-Angola-Etendeka Province (PAEP) have been considered a marker of the subcontinental lithospheric mantle (Comin-Chiaramonti *et al.*, 1997a, b, 1999; Marques *et al.*, 1999a, Alberti *et al.*, 1999; Ernesto *et al.*, 2002). The emplacement of the alkaline rocks took place along tectonic lineaments which have been active at least since Early Mesozoic and probably up to the present day, as indicated by the distribution of earthquakes in southeastern Brazil (Berrocal & Fernandes, 1996). The Florianópolis dykes (also shown in Fig. 1) have approximately N-S attitude, the same holding true for some tectonic structures associated with the Anitápolis and Lages alkaline complexes which are roughly emplaced along the E-W Rio Uruguay Lineament.

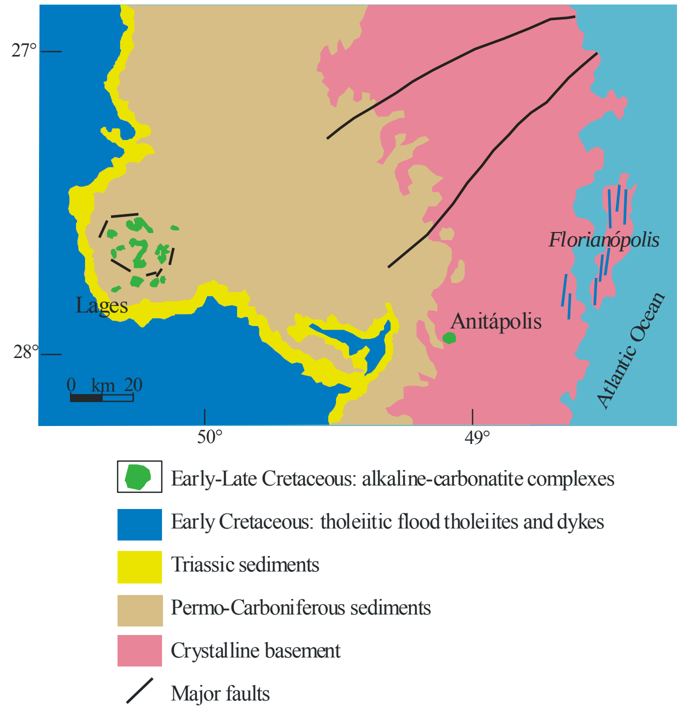


Fig. 1. Location of the Anitápolis alkaline complex and of the Lages district in the Santa Catarina state (Southern Brazil). Geological sketch map after Babinski *et al.* (1997) and Comin-Chiaramonti *et al.* (2002).

The aim of the present paper is to assess a synthesis relative to the alkaline-carbonatitic magmatism from the Santa Catarina state based on the main previous investigations on the Anitápolis complex and on the Lages district (cf. Scheibe, 1986; Furtado, 1989; Traversa *et al.*, 1994, 1996; Gibson *et al.*, 1999; Comin-Chiaramonti *et al.*, 2002, and therein references).

## THE ANITÁPOLIS ALKALINE COMPLEX

### Previous studies

Moraes Rego & Guimarães (1926) referred to magnetite ores occurring as veins cutting weathered materials. Leonardos (1956) included Anitápolis among the other Brazilian carbonatitic complexes, assuming for the outcrop at the Pinheiros river (formerly mentioned as a limestone) a carbonatitic affinity related to apatite, magnetite and pyrochlore deposits of economic interest. Mapping works (Carraro *et al.*, 1964; Scheibe & Teixeira, 1965; Melcher & Coutinho, 1966) described the thick weathering materials and the talus deposits overlaying the Anitápolis alkaline rocks. Drilling (CPRM and Indústria de Fosfatados Catarinenses) has shown that the Anitápolis igneous complex consists of a wide variety of rock-types including clinopyroxenites, nephelinites, ijolites, nepheline syenites, carbonatites and phonolites (Vergara, 1980; Rodrigues, 1985; Furtado, 1989).

Tavares (1982) described an alkaline pipe and some dykes associated with U-Th mineralization at

60 km N of Anitápolis (Quarenta locality) and without any apparent relationships with the Anitápolis alkaline rocks (Furtado & Scheibe, 1989). The Quarenta rock-types range from microsyenites to feldspathic breccias showing important metasomatic effects on the intruded country garnet schists. The microsyenites are mainly characterized by abundant alkali felspar set in an aphanitic groundmass. On the other hand, the breccias are made of pink to white feldspar fragments set in a reddish groundmass.

## Geological outlines

The Anitápolis complex, 90 km SW of the city of Florianópolis (Fig. 2), forms a circular concentric body of about 6 $km^2$ in area (Furtado & Scheibe, 1987). The alkaline rocks intrude Late Proterozoic leucogranites of the Dom Feliciano mobile belt (cf. Rodrigues, 1985). The latter are affected by deformational stresses (as evidenced by quartz and feldspar broken grains, biotite kink bands and bending of plagioclase twin planes) and by fenitization processes at the contact with the alkaline intrusion.

K/Ar data indicated ages of 131-132 Ma (Sonoki & Garda, 1988 and therein references; W. Teixeira, unpublished data), similar to those given by the Jacupiranga and Juquiá alkaline-carbonatite complexes (Ponta Grossa Arch; cf. Morbidelli *et al.*, 1995 and therein references). $^{40}Ar/^{39}Ar$ age determinations (Renne *et al.*, 1997) suggested that the emplacement of the Anitápolis complex was coeval to the eruption of the flood basalts from the Paraná Basin.

## Petrography

The rocks from the alkaline complex consist of magnetite-biotite pyroxenites and apatite-pyroxene biotitites at the central parts, surrounded by ijolites and nepheline syenites which are at their turn enveloped by melanocratic, mesocratic and leucocratic rocks, corresponding to high, medium and low fenitization degrees (Fig. 2). Apatite pyro-

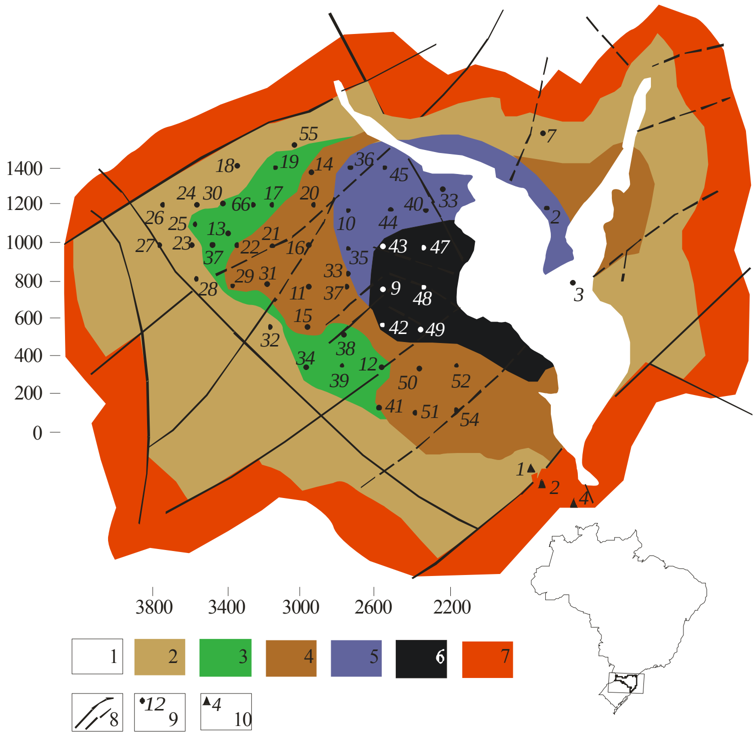


Fig. 2. Geological map of the Anitápolis alkaline complex (after Vergara, 1980; Rodrigues, 1985; Furtado, 1989). 1, Quaternary sediments; 2, border rocks; 3, nepheline syenite; 4, ijolite; 5, apatite-pyroxene biotitite; 6, magnetite-biotite pyroxenite; 7, granitoid country-rocks; 8, faults; 9, drill holes; 10, sampled dykes.

xenites occur as cumulates in the ijolites, nepheline syenites and fenites. Phoscorites and carbonatites are found penetrating into the silicate rocks as veins and dykes. Carbonatites, intruding the phoscorites, are made of sövitic, beforsitic and late-stage calcite-bearing variants. Melanephelinites were described only from boreholes. Phonolites and some lamprophyres intrude the granitoidic country-rocks up to 7 km from the main body. Furtado & Scheibe (1989) mentioned the occurrence of lamprophyre (referred to as nephelinites by Gibson *et al.*, 1999) at São Paulo dos Pinhais and Rio Branco localities, not far from the Anitápolis complex.

Notably, the silicate rocks may contain interstitial primary carbonates.

*Magnetite-biotite pyroxenites*

These rocks are deep green to black in colour and have fine to medium xenomorphic granular texture with apatite and titanite±nepheline as accessory minerals, and carbonates and amphiboles as occasional late phases.

Pyroxenes are poorly zoned with green rims and pale cores. Microprobe analyses (Furtado, 1989; Furtado & Gomes, 1994) show a compositional range from salite/Na-salite to diopside, respectively. Biotites (normal pleochroism), sometimes including clinoproxyene crystals, present a dominant brownish colour. Magnetite is xenomorphic and poikilitic, including clinopyroxenes, or occurs in fractures and patches; ilmenite occasionally appears as exsolution lamellae in magnetite or as minute grains at the magnetite rims.

*Apatite-pyroxene biotitites*

These rocks are found in the northern area of the massif, surrounding the magnetite-biotite pyroxenites through a gradational contact. The texture is granular xenomorphic with mica involving pyroxene and apatite grains. The clinopyroxenes have aegirine-augite optical characteristics, and biotite exhibits a brownish colour. Apatite, 5 to 23 vol.%, occurs as inclusions in the clinopyroxenes, but it is also present in the groundmass. The metasomatic effects over the clinopyroxenes produce Fe-richterite and Mg-arfvedsonite amphibole types, the latter at the contact with carbonates. Nepheline, pyrrhotite, pyrite, titanite, carbonates and rare alkali feldspar constitute the accessory phases. Carbonate "ocelli" are found where clinopyroxene, alkali feldspar and nepheline grains occur, sometimes mantled by biotite shells, indicating local increase of alkaline hydrous activity.

In general, the ultramafic rocks display typical cumulus texture with variable amounts of orthocumulus minerals, i.e. clinopyroxene, mica, apatite and magnetite; alkali feldspar, calcite and ankeritic dolomite appear as intercumulus phases.

*Ijolites, and urtite to melteigite types*

These rocks are prevailing mesocratic types, medium to coarse-grained and hypidiomorphic to heterogranular in texture, and consist of variable amounts of idiomorphic clinopyroxene (augite to Fe-augite cores and Na-rich aegirine-augite rims), biotite and opaques. Alkali feldspar and nepheline are the main felsic constituents. Titanite, opaques, amphibole, carbonates and albite occur as primary and secondary accessory phases, respectively. Notably, at the contact between ijolites and carbonatites, the clinopyroxene crystals show elongated and radial habit.

*Nepheline syenites*

These rocks have distinct granular texture with diferent mineral contents: alkali feldspar and nepheline represent the main constituents, but sometimes clinopyroxene and biotite are dominant, i.e. in malignite and shonkinite variants. Clinoyroxene, mainly poikilitic to skeletal aegirine-augite with apatite inclusions, is sandwiched between the alkali feldspar grains. The latter are also poikilitic, including an early alkali feldspar, nepheline and biotite. Similarly to the ijolitic rocks, the alkali feldspar, characterized by drop or/and film perthites, ranges from 83 to 95% Or.

*Apatite pyroxenites and pyroxene apatitites*

These rock-types are represented by veins up to 5 m thick intruding ijolites, nepheline syenites and fenitized granites near to the phoscorite or carbonatite outcrops. They are coarse-grained in size and composed by poikilitic aegirine-augite, about 6 cm long, with orientated, radial or comb texture, and by apatite occurring as inclusions in the groundmass.

*Fenites*

The border fenites range from melanocratic to leucocratic variants. The melanocratic types contain abundant aegirine-augite, sometimes with comb texture, and $Na_2O$ content varying from 3.5 to 6.6wt%. The mesocratic varieties are characterized by mortar texture, triple junctions and sometimes by the presence of clinopyroxene inclusions in the alkali feldspar. The leucocratic varieties maintain the original granitic texture with cloudy feldspar surrounded by clinopyroxene strings ($Na_2O$ up to 10.0 wt%).

*Phonolites*

Phonolite dykes, 0.3 to 3 m thick, present porphyritic texture with idiomorphic nepheline and clinopyroxene phenocrysts in addition to mica and melanite microphenocrysts set in a tinguaitic groundmass consisting of acicular aegirine, nepheline, alkali feldspar and zeolites. Clinopyroxenes, with apatite inclusions, vary from salitic cores to aegirine-augite rims, and may display aegirine fringes. Biotite occurs as phenocrysts with tetraferriphlogopite rims or as a groundmass phase.

*Lamprophyres*

These rocks, occurring as 5 to 40 cm thick dykes along the São Paulo dos Pinhais-Anitápolis road, 6 km SSE from the complex (Furtado & Scheibe, 1989), are fine-grained and show 0.4 cm thick chilled margins and porphyritic texture. They consist of mica, diopsidic pyroxene and pseudomorph olivine phenocrysts, and minor apatite, opaques, mica, clinopyroxene, titanite and carbonates set in a vitreous groundmass. Similar to the other rock-types, the mica displays tetraferriphlogopite rims and biotite core, whereas aegirine fringes appear at the contact clinopyroxene-carbonates. Globular structures, 2 mm wide, are composed by carbonates mantled by analcite, zeolites and opaques.

*Melanephelinites*

They are porphyritic in texture with phlogopite phenocrysts, and diopside, olivine and opaques microphenocrysts set in a hypohyaline groundmass.

*Nephelinites*

These rock-types (cf. Gibson *et al.*, 1999) are fine to medium-grained and contain olivine ($Fo_{80}$), clinopyroxene (diopside, ferrosilite 10-18) and biotite (phlogopite 80-53) phenocrysts set in a groundmass consisting of poikilitic nepheline enclosing aegirine and alkali feldspar needles.

*Phoscorites*

The phoscorites are coarse-grained, mainly with large poikilitic magnetite and mica crystals set in a groundmass made of altered olivine, saccharoid apatite and interstitial carbonates; accessory minerals include baddeleyite, pyrochlore, sulphides and carbonate-apatite. These rocks were affected by carbonatitic activity: olivine displays different alteration degrees with distinct mineralogical compositions and textures (Furtado *et al.*, 1986); mica exhibits different colours and pleochroic schemes, with prevailing late tetraferriphlogopite, typical for the inverse pleochroism (Furtado & Gomes, 1990).

*Sövites*

Ca-carbonatites, according to Woolley & Kempe (1989), constitute about 90 to 95% of the Anitápolis carbonatites and are medium to coarse-grained with euhedral calcite and subordinate Fe-dolomite, apatite, olivine, magnetite, pyrite, pyrrhotite and phlogopite layers or patches. Pyrochlore and baddeleyite represent occasional accessory phases. Notably, phlogopite crystals are light green in colour, sometimes orange or red, with reverse pleochroism.

### *Late carbonatites*

These rocks are represented by Mg-carbonatites occurring as veins in some drill holes at the inner part of the massif and display large textural variations. Quartz-free carbonatites show euhedral calcite and Mg-ankerite (including hydrous ferric oxides along the cleavage planes) associated with alstonite (Ca, Ba and Sr carbonate). Quartz-bearing carbonatites exhibit banded texture, with alternating white and yellowish layers, where the main minerals consist of calcite or Sr-rich Mg-ankerite and calcite associated with accessory alstonite, ancylite, bastnaesite, sphalerite, galena, pyrite, baddeleyite, fersmite and hematite.

Reactions at the carbonatite contacts may produce layers of newformed minerals (as also registered by Morbidelli *et al.*, 1986, in the Jacupiranga alkaline complex) with amphibole- or phlogopite- or olivine-rich bands. The glimmeritic types represent the most common layers which contain coarse-grained mica (ranging from biotite core to tetraferriphlogopite rims) associated with clinopyroxene and alkali feldspar. Notably, the glimmerite band thickness increases in the more silica-undersaturated rocks.

## Mineralogical aspects

### *Clinopyroxenes*

Clinopyroxenes from the Anitápolis complex are compositionally variable, ranging from diopside to salite in the magnetite-biotite pyroxenites to aegirine-augite (variable Na content) in the leucocratic rock-types (Table 1). In phonolites, the mineral composition varies from salite to soda-salite and aegirine-augite, with the late phases showing aegirine optical characteristics (cf. Table 1). Most of the analyses have Si+Al<2, suggesting the presence of Ti and $Fe^{3+}$ in tetrahedral sites. This peculiarity is believed to be typical of potassic rocks (e.g. Cundari & Salviulo, 1989).

The clinopyroxenes chemical trend displays Na increase and corresponding Mg depletion from the magnetite-biotite pyroxenites up to the border rocks, through the ijolites and nepheline syenites, with the phonolites showing the major compositional range (Furtado & Gomes, 1994). This evolutionary behaviour is distinct with respect to other Brazilian alkaline complexes (cf. Fig. 3), and exhibits some similarities (inset of Fig. 3) with clinopyroxenes, for instance, from the Cantal phonolites (Auvergne, France; cf. Varet, 1969) and from the Melteig area (Fen, Norway; cf. Kresten & Morogan, 1986). As well as in the latter two occurrences, the evolution of the Anitápolis clinopyroxenes is interpreted as due to high $fO_2$ conditions, which are responsible for the relatively low $Fe^{2+}$ content of the mineral even in the early stages of crystallization.

### *Micas*

Micas display a wide compositional range. Table 2 gives some representative analyses from different rock-types, the pleochroic scheme, the cationic distribution, and a classification according to Forster (1960). Following this author, phlogopites have more than 70% Mg in the octahedral sites.

Similarly to the clinopyroxenes, the Anitápolis micas have the Si+Al sum insufficient to fill the tetrahedral site, whereas a cationic excess is detectable in the octahedral layer. This is a common characteristic of micas from many alkaline rocks, but the deficient Si+Al occupancy in the tetrahedral sites is particularly evident in phoscorites, carbonatites and glimmerites.

Colour variations are clearly related to the $TiO_2$, MgO and FeO contents (cf. Furtado, 1989; Furtado & Gomes, 1990): dark brown types are characterized by the highest $TiO_2$ and FeO amounts (and corresponding low MgO), while the clear varieties show low $TiO_2$ and FeO contents, corresponding to relatively high MgO. Also in the carbonatites, phoscorites and glimmerites, the mica brownish colour is driven by the $TiO_2$+FeO content higher than that of the green varieties. In the orange-red micas, the more intense red colour at the X optical index is correlated with the low $TiO_2$ concentration and the high FeO/MgO ratio. Micas having low Si+Al amounts exhibit inverse pleochroism (more pronounced red colour at the $FeO_{total}$ increasing) indicating partial iron partitioning as $Fe^{3+}$ in the tetrahedral sites (tetraferriphlogopite).

On the whole, the Anitápolis bulk mineralogy suggests that $fO_2$ was sufficiently high during the crystallization processes, as also confirmed by the pyroxene chemical trend, the low annite amount in the micas and the almost ubiquitous magnetitetitanite. Notably, the late crystallized mineralogical assemblages point to $fO_2$ increase with tetraferriphlogopite, Mg-arfvedsonite and richterite characterizing glimmerites, phoscorites and carbonatites. More precise data for $fO_2$ could be obtained from the magnetite-ilmenite pairs. However, the MnO content of the ilmenite ranges from 5 to 11 wt% making unrealistic the geobarometry, as already stressed by Furtado (1989).

Petrochemistry

Representative analyses of alkaline and carbonatitic rocks are given in Table 3. The non-cumulate silicate rocks display distinct characteristics in terms of $K_2O/Na_2O$ ratios and a bimodal distribution (Fig. 4A). In particular the sodic affinity of lamprophyres, nephelinites and phonolites is apparent, clearly contrasting with the potassic affinity of the melanephelinites, ijolites and nepheline syenites.

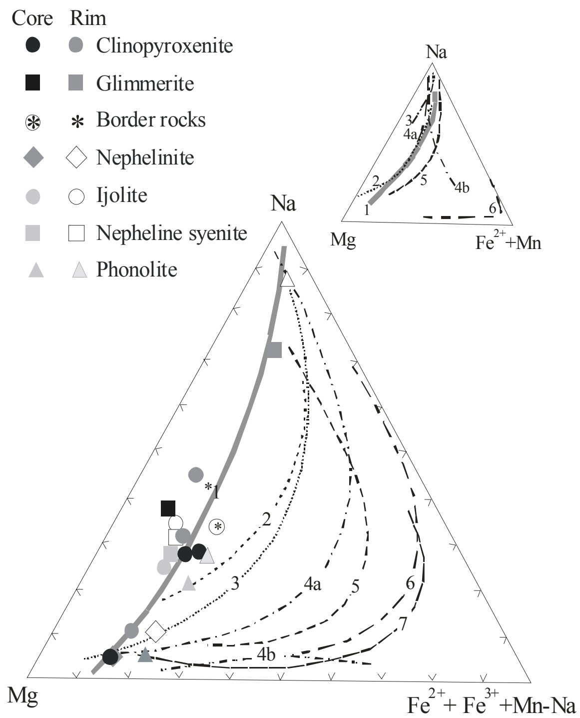


Fig. 3. Anitápolis clinopyroxenes plotted into the Na-Mg-($Fe^{2+}$+$Fe^{3+}$+Mn-Na) diagram. Whole chemical trends for Anitápolis clinopyroxenes and for clinopyroxenes from other alkaline and alkaline-carbonatite Brazilian complexes (Furtado, 1989) are as follows: 1, Anitápolis; 2, Itapirapuã (Gomes *et al.*, 1970); 3, Banhadão (Ruberti, 1984); 4, Rio de Janeiro State (Valença, 1980): a) Tanguá-Rio Bonito-Itaúna-Morro de São João, b) Soarinho; 5, Piratini (Barbieri *et al.*, 1987); 6, Vitória Island (Motoki, 1986); 7, Tunas (Gomes *et al.*, 1987). Inset: Na-Mg-($Fe^{2+}$+Mn) diagram showing the Anitápolis clinopyroxene trend (1) (Furtado, 1989), compared with clinopyroxenes from some worldwide alkaline complexes; 2, Cantal (Varet, 1969); 3, Sokli (Vartiainen & Woolley, 1976); 4, Fen (Kresten & Morogan, 1986): a) Melteig area, b) Holla area; 5, Itapirapuã (Gomes *et al.*, 1970); 6, Ilimaussaq (Larsen, 1976).

Table 1. Microprobe analyses of representative clinopyroxenes from the Anitápolis rock-types. Data source: Furtado (1989) and Gibson *et al.* (1999). Atomic formula units, a.f.u., on the basis of 6 (O). C, core; R, rim; gm, groundmass. Analyses are also expressed in terms of Na, Mg and ($Fe^{2+}$+$Fe^{3+}$+Mn-Na) components.

| | Magnetite-biotite pyroxenite | | Pyroxene biotitite | | Apatite pyroxenite | | Ijolite | | Nepheline syenite | | Border rock | | Glimmerite | | Phonolite | | | Nephelinite | |
|---|---|---|---|---|---|---|---|---|---|---|---|---|---|---|---|---|---|---|---|
| | 42-54 C | 42-54 R | 2-98.6 C | 2-98.6 R | 27-33.2 C | 27-33.2 R | 23-71.3 C | 23-71.3 R | 13-91.5 C | 13-91.5 R | 4-61.0 C | 4-61.0 R | 4-27.2 C | 4-27.2 R | 4-1 C | 4-1 R | 4-1 gm | 4-2 C | 4-2 R |
| $TiO_2$ | 1.33 | 0.92 | 0.38 | 0.39 | 0.29 | 0.55 | 0.46 | 0.68 | 0.36 | 0.37 | 0.56 | 0.51 | 0.60 | 0.70 | 0.72 | 0.88 | 0.84 | 1.36 | 1.46 |
| $Al_2O_3$ | 2.59 | 1.76 | 1.15 | 1.05 | 0.64 | 0.31 | 1.30 | 0.82 | 0.68 | 0.74 | 0.79 | 0.66 | 0.61 | 0.51 | 2.60 | 2.46 | 0.95 | 3.23 | 4.05 |
| $Fe_2O_3$ | 1.75 | 6.63 | 10.91 | 11.66 | 11.68 | 17.39 | 10.50 | 13.58 | 10.29 | 11.98 | 13.37 | 15.35 | 15.01 | 24.40 | 7.00 | 8.10 | 26.07 | 5.60 | 6.32 |
| FeO | 3.68 | 2.56 | 4.21 | 4.50 | 4.50 | 1.74 | 4.05 | 1.36 | 3.97 | 2.69 | 15.16 | 3.45 | 1.50 | 3.87 | 6.30 | 7.29 | 2.61 | 1.34 | 3.56 |
| MnO | 0.09 | 0.15 | 0.29 | 0.28 | 0.27 | 0.43 | 0.53 | 0.54 | 0.26 | 0.25 | 0.43 | 0.33 | 0.20 | 0.09 | 0.34 | 0.31 | 0.75 | 0.09 | 0.20 |
| MgO | 14.23 | 13.13 | 9.70 | 8.94 | 8.81 | 7.19 | 11.45 | 9.30 | 9.89 | 9.72 | 7.30 | 7.40 | 8.71 | 2.74 | 10.02 | 8.61 | 0.63 | 14.09 | 11.85 |
| CaO | 24.23 | 22.69 | 18.43 | 16.96 | 18.40 | 15.30 | 16.91 | 18.59 | 17.95 | 17.78 | 16.40 | 14.63 | 17.27 | 6.44 | 19.71 | 18.24 | 7.01 | 24.10 | 22.40 |
| $Na_2O$ | 0.56 | 1.49 | 3.77 | 4.36 | 3.78 | 5.90 | 3.70 | 4.39 | 3.79 | 4.25 | 4.73 | 5.78 | 4.87 | 9.58 | 2.71 | 3.48 | 10.53 | 0.71 | 1.33 |
| Sum | 100.60 | 100.33 | 101.07 | 100.20 | 99.91 | 100.34 | 101.44 | 101.34 | 99.15 | 99.97 | 99.05 | 99.81 | 99.49 | 99.35 | 100.58 | 100.61 | 100.82 | 100.25 | 100.03 |
| $FeO^t$ | 5.25 | 8.52 | 14.20 | 14.99 | 15.01 | 17.39 | 13.50 | 13.58 | 13.25 | 13.47 | 17.19 | 17.27 | 15.01 | 25.83 | 12.60 | 14.57 | 26.06 | 6.38 | 9.25 |
| Si | 1.911 | 1.894 | 1.947 | 1.959 | 1.953 | 1.948 | 1.940 | 1.934 | 1.967 | 1.956 | 1.939 | 1.961 | 1.926 | 1.973 | 1.917 | 1.929 | 1.969 | 1.839 | 1.829 |
| $Al^{IV}$ | 0.089 | 0.077 | 0.051 | 0.041 | 0.029 | 0.014 | 0.057 | 0.036 | 0.030 | 0.033 | 0.036 | 0.030 | 0.027 | 0.023 | 0.083 | 0.071 | 0.031 | 0.141 | 0.171 |
| Ti | | 0.026 | 0.002 | | 0.008 | 0.016 | 0.003 | 0.019 | 0.003 | 0.011 | 0.016 | 0.009 | 0.017 | 0.004 | | | | 0.020 | |
| $Fe^{3+}$ | | 0.003 | | | 0.010 | 0.022 | | 0.011 | | | 0.009 | | 0.030 | | | | | | |
| Sum | 2.000 | 2.000 | 2.000 | 2.000 | 2.000 | 2.000 | 2.000 | 2.000 | 2.000 | 2.000 | 2.000 | 2.000 | 2.000 | 2.000 | 2.000 | 2.000 | 2.000 | 2.000 | 2.000 |
| $Al^{VI}$ | 0.023 | | | 0.005 | | | | | | | | | | | 0.032 | 0.028 | 0.012 | | 0;008 |
| Ti | 0.037 | 0.026 | 0.009 | 0.011 | | 0.016 | 0.010 | | 0.007 | | | 0.006 | | 0.016 | 0.020 | 0.025 | 0.024 | 0.018 | 0.041 |
| $Fe^{3+}$ | 0.048 | 0.185 | 0.306 | 0.330 | 0.321 | 0.473 | 0.292 | 0.368 | 0.293 | 0.339 | 0.377 | 0.438 | 0.399 | 0.710 | 0.197 | 0.229 | 0.751 | 0.156 | 0.178 |
| $Fe^{2+}$ | 0.113 | 0.079 | 0.131 | 0.142 | 0.143 | 0.055 | 0.125 | 0.042 | 0.126 | 0.085 | 0.166 | 0.110 | 0.048 | 0.125 | 0.197 | 0.229 | 0.083 | 0.041 | 0.111 |
| Mn | 0.003 | 0.005 | 0.009 | 0.007 | 0.009 | 0.014 | 0.017 | 0.017 | 0.008 | 0.008 | 0.014 | 0.011 | 0.006 | 0.003 | 0.010 | 0.010 | 0.024 | 0.003 | 0.006 |
| Ca | 0.952 | 0.903 | 0.736 | 0.684 | 0.747 | 0.620 | 0.669 | 0.739 | 0.728 | 0.717 | 0.677 | 0.595 | 0.703 | 0.267 | 0.791 | 0.736 | 0.288 | 0.995 | 0.898 |
| Sum | 1.993 | 2.006 | 2.002 | 1.998 | 1.996 | 2.016 | 2.008 | 1.999 | 2.008 | 2.004 | 2.007 | 2.003 | 2.008 | 1.998 | 2.004 | 1.994 | 2.000 | 2.000 | 2.000 |
| Na | 4.2 | 10.7 | 27.6 | 32.4 | 28.6 | 45.7 | 24.9 | 33.6 | 28.2 | 31.1 | 36.3 | 43.5 | 37.9 | 72.2 | 20.5 | 26.7 | 87.5 | 5.2 | 10.0 |
| Mg | 8.6 | 73.0 | 54.7 | 51.1 | 51.3 | 42.8 | 59.2 | 54.6 | 56.6 | 54.7 | 42.9 | 42.8 | 52.1 | 15.9 | 58.2 | 50.8 | 4.0 | 79.5 | 69.2 |
| $Fe^{2+}$+$Fe^{3+}$+Mn-Na | 13.2 | 16.3 | 17.7 | 16.5 | 20.1 | 11.5 | 15.9 | 11.8 | 15.2 | 14.2 | 20.8 | 13.7 | 10.0 | 11.9 | 21.3 | 22.5 | 8.5 | 15.3 | 20.9 |

Table 2. Microprobe compositions of representative phlogopites and biotites from the Anitápolis rock-types (Furtado, 1989). Structural formulae on the basis of 22 (O); b, biotite and ph, phlogopite (according to Forster, 1960).

| | Magnetite-biotite pyroxenite | | | | Ijolite | | Nepheline syenite | Phoscorite | | | | Carbonatite | | Glimmerite |
|---|---|---|---|---|---|---|---|---|---|---|---|---|---|---|
| | 42-54 C | 42-54 I | 42-54 R | 43-29 C | 16A-108 | 57-58.5 | 19-73 | 33-113 C | 33-113 R | 2-40 C | 2-40 R | 16A-50 C | 50-54 R | 1-23.3 C |
| $SiO_2$ | 36.13 | 36.01 | 37.48 | 37.01 | 37.74 | 36.21 | 38.33 | 40.71 | 41.26 | 42.04 | 41.69 | 43.34 | 41.05 | 41.50 |
| $TiO_2$ | 4.04 | 3.32 | 3.83 | 3.37 | 1.91 | 2.38 | 3.35 | 0.13 | 0.81 | 0.19 | 0.16 | 0.09 | 2.90 | 0.39 |
| FeO | 16.17 | 14.26 | 15.83 | 12.24 | 14.64 | 16.82 | 18.19 | 19.50 | 6.95 | 13.81 | 15.97 | 4.35 | 7.56 | 9.95 |
| MnO | 0.19 | 0.20 | 0.19 | 0.22 | 0.31 | 0.47 | 0.45 | 0.17 | 0.13 | 0.15 | 0.15 | 0.05 | 0.21 | 0.05 |
| MgO | 16.24 | 17.59 | 16.53 | 19.71 | 18.74 | 16.65 | 16.33 | 22.82 | 24.20 | 26.04 | 25.23 | 27.77 | 24.91 | 25.73 |
| CaO | 0.31 | 0.33 | 0.16 | 0.27 | 0.22 | 0.12 | 0.12 | 0.89 | 0.11 | 0.43 | 0.56 | 0.28 | 0.60 | 0.01 |
| $Na_2O$ | 0.27 | 0.28 | 0.42 | 0.56 | 0.34 | 0.24 | 0.23 | 0.19 | 0.36 | 0.08 | 0.11 | 0.28 | 0.43 | 0.22 |
| $K_2O$ | 9.38 | 9.46 | 9.57 | 9.24 | 0.57 | 9.81 | 9.74 | 9.20 | 10.07 | 10.12 | 9.47 | 10.22 | 9.46 | 10.40 |
| BaO | 0.47 | 0.61 | 0.22 | 0.43 | 0.09 | 0.01 | 0.02 | 0.00 | 0.10 | 0.00 | 0.00 | 0.02 | 0.00 | 0.08 |
| F | 0.21 | 0.26 | 0.55 | 0.46 | 0.03 | 0.50 | 0.21 | 0.28 | 0.25 | 0.46 | 0.23 | 0.43 | 0.33 | 0.25 |
| Cl | 0.00 | 0.01 | 0.00 | 0.00 | 0.00 | 0.00 | 0.00 | 0.08 | 0.01 | 0.10 | 0.05 | 0.01 | 0.01 | 0.00 |
| Sum | 98.02 | 97.03 | 98.18 | 97.27 | 97.47 | 96.08 | 97.70 | 95.93 | 96.05 | 97.07 | 97.71 | 96.65 | 99.07 | 97.16 |
| O=F, Cl | 0.09 | 0.11 | 0.23 | 0.19 | 0.01 | 0.21 | 0.09 | 0.12 | 0.11 | 0.19 | 0.10 | 0.18 | 0.14 | 0.11 |
| | 97.93 | 96.92 | 97.95 | 97.08 | 97.46 | 95.87 | 97.61 | 95.81 | 95.94 | 96.88 | 97.61 | 96.47 | 98.93 | 97.05 |
| Si | 5.342 | 5.345 | 5.526 | 5.421 | 5.534 | 5.507 | 5.729 | 6.283 | 5.913 | 6.237 | 6.251 | 6.099 | 5.726 | 5.992 |
| Al | 2.545 | 2.573 | 2.329 | 2.392 | 2.397 | 2.305 | 1.892 | 0.356 | 1.993 | 0.657 | 0.503 | 1.626 | 1.908 | 1.461 |
| Ti | 0.449 | 0.370 | 0.425 | 0.371 | 0.211 | 0.273 | 0.377 | 0.015 | 0.088 | 0.022 | 0.018 | 0.010 | 0.304 | 0.042 |
| Fe | 1.999 | 1.770 | 1.952 | 1.498 | 1.796 | 2.140 | 2.273 | 2.516 | 0.833 | 1.714 | 2.006 | 0.512 | 0.882 | 1.202 |
| Mn | 0.024 | 0.025 | 0.024 | 0.016 | 0.039 | 0.061 | 0.057 | 0.022 | 0.016 | 0.019 | 0.019 | 0.006 | 0.025 | 0.006 |
| Mg | 3.578 | 3.891 | 3.632 | 4.304 | 4.097 | 3.775 | 3.638 | 5.249 | 5.169 | 5.758 | 5.648 | 5.825 | 5.180 | 5.537 |
| Ca | 0.049 | 0.052 | 0.023 | 0.042 | 0.034 | 0.019 | 0.019 | 0.147 | 0.017 | 0.068 | 0.090 | 0.043 | 0.090 | 0.002 |
| Na | 0.077 | 0.082 | 0.119 | 0.159 | 0.097 | 0.070 | 0.067 | 0.057 | 0.099 | 0.023 | 0.033 | 0.077 | 0.115 | 0.061 |
| K | 1.768 | 1.790 | 1.801 | 1.727 | 1.789 | 1.903 | 1.857 | 1.615 | 1.840 | 1.914 | 1.815 | 1.836 | 1.683 | 1.916 |
| Y | 6.050 | 6.056 | 5.694 | 6.190 | 6.143 | 6.249 | 6.345 | 7.802 | 6.106 | 7.513 | 7.691 | 6.353 | 6.391 | 6.749 |
| X | 1.921 | 1.960 | 1.956 | 1.953 | 1.925 | 2.003 | 1.954 | 2.015 | 1.962 | 2.005 | 1.938 | 1.957 | 1.888 | 1.984 |
| Classif. | b<br>Z=Y<br>dark brown<br>X<br>yellow | ph<br>Z=Y<br>greenish brown<br>X<br>yellow | b<br>Z=Y<br>pale brown<br>X<br>yellow | ph<br>Z=Y<br>reddish brown<br>X<br>yellow | ph<br>Z=Y<br>olive green<br>X<br>yellow | b<br>Z=Y<br>brown<br>X<br>reddish orange | b<br>Z=Y<br>brown<br>X<br>yellow orange | ph<br>Z=Y<br>dark green<br>X<br>reddish orange | ph<br>Z=Y<br>green<br>X<br>yellow orange | ph<br>Z=Y<br>yellow orange<br>X<br>orange | ph<br>Z=Y<br>yellow orange<br>X<br>reddish orange | ph<br>Z=Y<br>pale green<br>X<br>yellow orange | ph<br>Z=Y<br>brown<br>X<br>yellow | ph<br>Z=Y<br>pale yellow<br>X<br>reddish orange |

Table 3. Selected chemical analyses from Anitápolis rock-types (data source: Furtado, 1989; Comin-Chiaramonti *et al.*, 2002). (*) total iron as FeO. Biot-Cpx, biotite clinopyroxenite; Ap-Cpx, apatite clinopyroxenite; Lamp, lamprophyre; Carb, carbonatite.

| | Biot-Cpx | | Ap-Cpx | | Ijolite | | Mela nephelinite | Nepheline syenite | | Border rock | Phonolite |
|---|---|---|---|---|---|---|---|---|---|---|---|
| | SAN.2N | 43-29 | SAN.8 | 27-33.2 | SAN.24 | 36-69.3 | SAN.6A | SAN.25 | 13-91.5 | 4-51.65 | 04.2 |
| wt% | | | | | | | | | | | |
| $SiO_2$ | 38.19 | 42.30 | 33.57 | 44.90 | 40.61 | 40.90 | 38.54 | 44.88 | 43.40 | 50.10 | 47.80 |
| $Al_2O_3$ | 6.12 | 4.00 | 7.60 | 1.30 | 14.56 | 14.40 | 10.97 | 18.91 | 8.30 | 3.10 | 14.90 |
| $Fe_2O_3$ | | 12.00 | | 9.10 | | 5.70 | | | 3.50 | 10.10 | 5.50 |
| FeO | *13.59 | 8.93 | *11.80 | 4.84 | *9.99 | 3.61 | *10.61 | *8.14 | 7.00 | 4.11 | 2.62 |
| MnO | 0.22 | 0.19 | 0.17 | 0.36 | 0.19 | 0.11 | 0.19 | 0.18 | 0.17 | 0.29 | 0.16 |
| MgO | 14.15 | 10.40 | 13.78 | 5.80 | 6.64 | 4.70 | 10.00 | 2.15 | 5.70 | 6.10 | 2.40 |
| CaO | 12.73 | 15.30 | 15.47 | 20.90 | 11.34 | 14.30 | 10.93 | 8.44 | 14.40 | 15.70 | 7.60 |
| $Na_2O$ | 1.66 | 0.87 | 0.71 | 3.80 | 2.71 | 5.60 | 2.94 | 4.08 | 3.50 | 4.40 | 8.90 |
| $K_2O$ | 3.30 | 2.10 | 4.55 | 0.99 | 4.95 | 2.60 | 4.14 | 5.48 | 4.80 | 2.10 | 5.00 |
| $P_2O_5$ | 1.45 | 0.11 | 6.34 | 5.50 | 1.46 | 3.80 | 0.96 | 0.63 | 5.10 | 1.50 | 1.20 |
| L.O.I. | 4.98 | 1.08 | 2.18 | 1.71 | 2.81 | 3.34 | 6.93 | 2.66 | 1.68 | 1.58 | 2.96 |
| Sum | 98.32 | 99.88 | 99.57 | 99.74 | 98.75 | 99.34 | 98.82 | 98.06 | 98.47 | 99.73 | 99.65 |
| BaO | | 0.12 | | 0.02 | | 0.27 | | | 0.14 | 0.05 | 0.13 |
| F | | 0.06 | | 0.26 | | 0.15 | | | 0.26 | 0.08 | 0.10 |
| S | | 0.04 | | 0.03 | | 0.24 | | | 0.50 | 0.95 | 0.16 |
| ppm | | | | | | | | | | | |
| Rb | 104.6 | | 213.7 | | 124.5 | | 107.9 | 103.0 | | | |
| Ba | 1758.3 | | 3800.0 | | 2357.5 | | 2509.0 | 1300.0 | | | |
| Th | 6.9 | | 1.2 | | 5.1 | | 3.3 | 8.2 | | | |
| Nb | 26.2 | | 22.8 | | 54.3 | | 28.6 | 67.1 | | | |
| Ta | 1.9 | | 1.8 | | 2.7 | | 1.3 | 3.1 | | | |
| Hf | 6.9 | | 3.6 | | 5.4 | | 3.5 | 7.1 | | | |
| Y | 16.4 | | 56.1 | | 33.4 | | 29.1 | 15.2 | | | |
| La | 42.15 | 12.11 | 116.08 | 37.98 | 47.66 | 35.72 | 59.76 | 29.71 | 35.98 | 12.09 | 23.43 |
| Ce | 90.52 | 38.53 | 243.64 | 103.98 | 103.77 | 93.15 | 98.65 | 67.37 | 80.58 | 26.83 | 54.16 |
| Pr | 11.16 | | 26.77 | | 13.46 | | 14.89 | 10.15 | | | |
| Nd | 46.70 | 15.00 | 104.32 | 60.29 | 54.73 | 48.18 | 73.22 | 42.31 | 57.84 | 17.71 | 26.77 |
| Sm | 9.07 | 3.26 | 19.71 | 12.67 | 10.59 | 10.26 | 16.80 | 8.31 | 10.7 | 3.20 | 5.92 |
| Eu | 2.78 | 1.38 | 5.41 | 2.98 | 2.89 | 3.04 | 3.04 | 2.22 | 2.69 | 0.81 | 1.74 |
| Gd | 8.05 | 2.5 | 15.74 | 9.71 | 8.38 | 7.67 | 13.90 | 6.42 | 8.25 | 2.73 | 4.58 |
| Tb | 1.37 | | 2.22 | | 1.29 | | 2.30 | 1.03 | | | |
| Dy | 7.67 | 1.58 | 10.59 | 7.31 | 5.97 | 4.52 | 13.19 | 4.45 | 5.1 | 2.00 | 3.80 |
| Ho | 1.39 | | 1.92 | | 1.13 | | 2.25 | 0.87 | 1.0 | 0.34 | |
| Er | 3.67 | 0.77 | 5.00 | 3.16 | 2.83 | 1.78 | 5.46 | 2.11 | 2.36 | 0.91 | 1.85 |
| Tm | 0.54 | | 0.74 | | 0.41 | | 0.73 | 0.30 | | | |
| Yb | 3.31 | 0.71 | 4.37 | 3.69 | 2.38 | 1.44 | 2.79 | 1.70 | 1.53 | 1.97 | 1.86 |
| Lu | 0.47 | 0.15 | 0.61 | 0.6 | 0.34 | 0.3 | 0.38 | 0.25 | 0.23 | 0.40 | 0.27 |

| | Phoscorite | Glimmerite | Lamp 11C | | Ca-carb | | | | | Late Carb | |
|---|---|---|---|---|---|---|---|---|---|---|---|
| | 2-40.2 | 4-27.2 | clear | dark | SAN 1.0 | 14-49 | 12-78 | 11-101 | 16A-50.5 | 39-83.5 | 49-82 |
| wt% | | | | | | | | | | | |
| $SiO_2$ | 4.50 | 38.00 | 37.00 | 40.50 | 0.31 | 0.20 | 2.45 | 1.20 | 0.47 | 20.40 | 3.00 |
| $TiO_2$ | 1.10 | 3.00 | 1.90 | 2.10 | 0.01 | 0.01 | 0.06 | 0.05 | 0.07 | 0.05 | 0.08 |
| $Al_2O_3$ | 0.10 | 9.20 | 8.40 | 9.90 | 0.21 | 0.02 | 0.01 | 0.09 | 0.10 | 1.80 | 0.52 |
| $Fe_2O_3$ | 32.10 | 5.40 | 5.00 | 5.10 | | | | | 3.10 | 3.30 | 3.00 |
| FeO | 14.13 | 12.90 | 5.20 | 5.60 | *0.08 | *2.59 | *2.03 | *2.95 | 1.70 | 2.83 | 3.26 |
| MnO | 0.36 | 0.28 | 0.21 | 0.23 | 0.07 | 0.08 | 0.23 | 0.22 | 0.23 | 0.60 | 1.80 |
| MgO | 5.00 | 9.60 | 8.20 | 7.60 | 1.55 | 2.30 | 4.13 | 1.83 | 1.70 | 6.80 | 12.80 |
| CaO | 23.20 | 6.00 | 13.00 | 12.30 | 53.59 | 51.25 | 49.36 | 52.15 | 51.80 | 31.31 | 31.43 |
| $Na_2O$ | 0.51 | 1.20 | 4.20 | 4.10 | 0.05 | 0.16 | 0.34 | 0.01 | 0.07 | 0.29 | 0.51 |
| $K_2O$ | 0.11 | 8.30 | 1.70 | 2.60 | 0.49 | 0.78 | 0.07 | 0.02 | 0.06 | 0.03 | 0.01 |
| $P_2O_5$ | 12.10 | 2.80 | 0.43 | 1.10 | 0.48 | 1.31 | 2.37 | 2.89 | 1.80 | 3.00 | 0.12 |
| L.O.I. | 6.45 | 2.92 | 15.25 | 8.59 | 42.06 | 40.13 | 38.72 | 38.25 | 38.37 | 28.10 | 38.50 |
| Sum | 99.66 | 99.60 | 100.49 | 99.72 | 98.90 | 98.83 | 99.77 | 99.66 | 100.37 | 97.91 | 95.03 |
| BaO | 0.01 | 0.08 | 0.13 | 0.28 | | | | | 0.04 | 2.30 | 8.00 |
| F | 0.43 | 0.33 | 0.10 | 0.05 | | | | | 0.07 | 0.33 | 0.05 |
| S | 1.60 | 0.09 | 0.24 | 0.21 | | | | | 0.30 | 0.47 | 0.16 |
| ppm | | | | | | | | | | | |
| Rb | | | | | 3.2 | 6.1 | 6.5 | 6.9 | | | |
| Ba | | | | | 1051.8 | 950.6 | 1579.4 | 1120.6 | | | |
| Th | | | | | 5.6 | 3.5 | 10.2 | 4.2 | | | |
| Nb | | | | | 5.2 | 8.9 | 7.8 | 10.4 | | | |
| Ta | | | | | 1.4 | 0.5 | 1.5 | 1.8 | | | |
| Sr | | | | | 2462.3 | 2982.9 | 6848.5 | 4462.3 | | | |
| Hf | | | | | 0.4 | 0.4 | 1.8 | 0.8 | | | |
| Zr | | | | | 15.8 | 7.7 | 46.2 | 15.5 | | | |
| Y | | | | | 43.7 | 18.8 | 45.9 | 42.9 | | | |
| La | 136.25 | 26.27 | 27.10 | 24.40 | 67.13 | 41.20 | 125.38 | 48.57 | 158.02 | 1046.00 | 978.56 |
| Ce | 346.76 | 63.92 | 53.80 | 27.10 | 142.32 | 90.30 | 286.66 | 106.45 | 372.06 | 1377.00 | 2657.33 |
| Pr | | | | | 16.80 | 12.24 | 29.17 | 14.44 | | | |
| Nd | 201.82 | 34.35 | 30.30 | 27.40 | 69.62 | 47.54 | 115.73 | 53.49 | 170.37 | 398.50 | 1153.69 |
| Sm | 35.83 | 7.33 | 6.00 | 5.50 | 13.78 | 9.43 | 21.33 | 9.44 | 29.22 | 39.80 | 326.28 |
| Eu | 10.06 | 1.85 | 1.70 | 1.60 | 3.99 | 2.53 | 6.51 | 3.91 | 8.55 | 8.79 | 129.43 |
| Gd | 24.95 | 5.50 | 4.70 | 4.40 | 12.57 | 7.91 | 19.83 | 8.90 | 20.61 | 22.91 | 475.50 |
| Tb | | | | | 1.87 | 1.35 | 2.37 | 1.59 | | | |
| Dy | 13.11 | 3.96 | 3.50 | 2.90 | 9.62 | 7.67 | 11.63 | 9.04 | 12.17 | 7.69 | 728.30 |
| Ho | | | 0.62 | 0.55 | 1.74 | 1.39 | 2.44 | 1.64 | | 1.48 | |
| Er | 3.99 | 1.58 | 1.90 | 1.20 | 4.81 | 3.17 | 5.80 | 3.74 | 4.43 | 2.29 | 155.65 |
| Tm | | | | | 0.63 | 0.56 | 0.81 | 0.67 | | | |
| Yb | 1.97 | 1.19 | 1.50 | 1.00 | 3.74 | 3.09 | 4.83 | 3.48 | 3.02 | 0.94 | 25.00 |
| Lu | 0.20 | 0.16 | 0.20 | 0.14 | 0.59 | 0.44 | 0.65 | 0.51 | 0.36 | 0.15 | 2.21 |

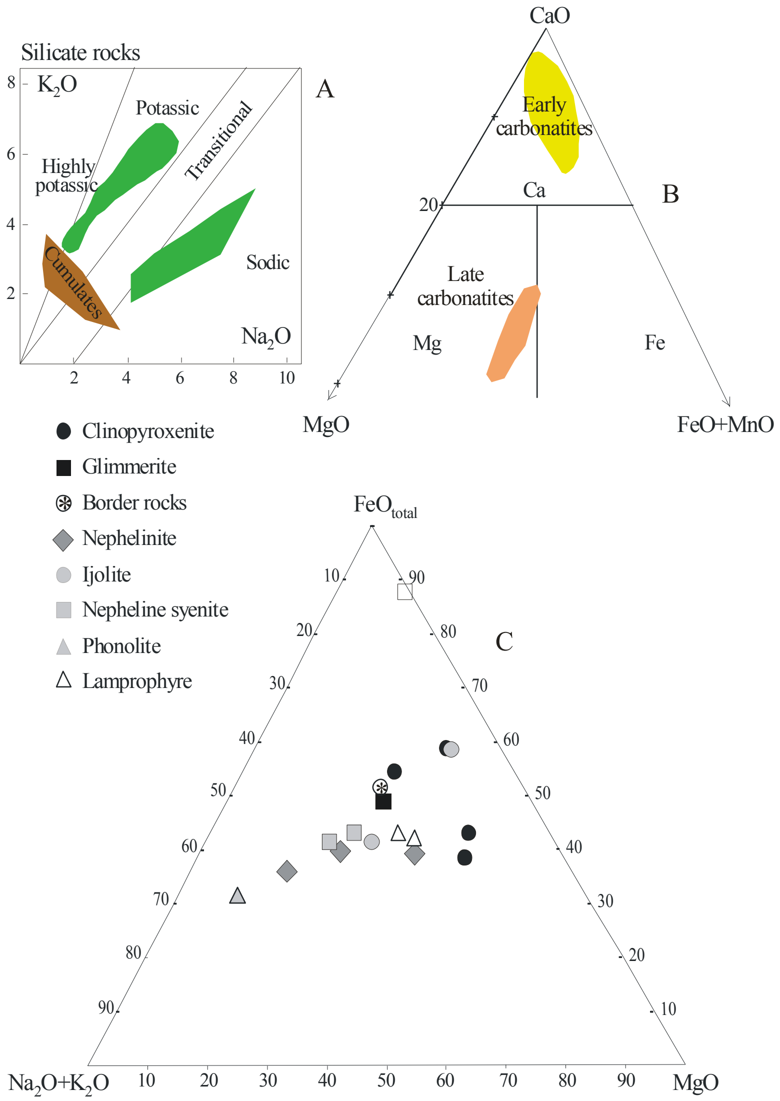


Fig. 4. A. Silicate rocks: $Na_2O$ vs. $K_2O$ diagram (cf. Comin-Chiaramonti & Gomes, 1996). B. Carbonatites: CaO-MgO-(FeO+Mn) diagram (cf. Woolley & Kempe, 1989). C. Silicate rocks ($Na_2O+K_2O$)-($FeO+Fe_2O_3$)-MgO diagram.

The relationships between alkalies, total iron and magnesium are illustrated in the AFM diagram (Fig. 4C). Notably, the samples show relatively low MgO proportions, even in cumulate rocks, coupled with high iron contents, mainly in the magnetite-biotite pyroxenites and ijolites, and with iron depletion and alkali enrichment in the felsic rock-types. Also the carbonatites present a bimodal distribution, the early-carbonatites fitting the Ca-carbonatite field, whereas the late carbonatites trend from the Mg-carbonatite to the Fe-carbonatite fields (Fig. 4B).

The patterns relative to the contents of incompatible elements and rare earths (REE), normalized to the primitive mantle (Sun & McDonough, 1989) and to the chondrites (Boynton, 1984), respectively, are given in Fig. 5. The potassic alkaline rock-types, notwithstanding some scattered values (e.g., La, Ce, P, Nd and Sm), display patterns compatible to those of the sodic varieties.

The lamprophyres (i.e. 11C, "clear" and 11C, "dark" types; cf. Table 3) exhibit the same behaviour of other Anitápolis silicate rocks, but the 11C "clear" sample (also bearing abundant globular structures) shows REE enrichment (particularly in LREE) in comparison with the 11C "dark" sample. The magnetite-biotite pyroxenites are REE depleted regarding the lamprophyres, in agreement with the cumulate texture. The other silicate rocks (ijolites, nepheline syenites and phonolites) have patterns similar to that indicated for the 11C "dark" sample.

The border rocks (e.g. 4-51.65 sample) have the lowest LREE contents, but relatively high Yb and Lu, showing a distinct pattern similar to that of the apatite pyroxenites (27-33.2 sample), probably due to metasomatic effects. The phoscorites pattern, characterized by negative Sm anomaly, parallels the glimmerites spidergram. The Ca-carbonatites are quite distinct for their high La-Ce-Sr "band" and strong negative anomalies for K, Zr and Ti, in comparison with the other silicate rocks. The late carbonatites contain the higher REE contents. In particular, the 49-82 sample (an alstonite-bearing dolomite carbonatite) is strongly enriched in MREE and HREE, giving a singular pattern. The 39-83.5 sample (an ancyllite- and quartz-bearing carbonatite) displays a very high $(La/Yb)_N$ ratio (1112.8) indicating a late genesis, as proposed by Kapustin (1980) for similar rock-types.

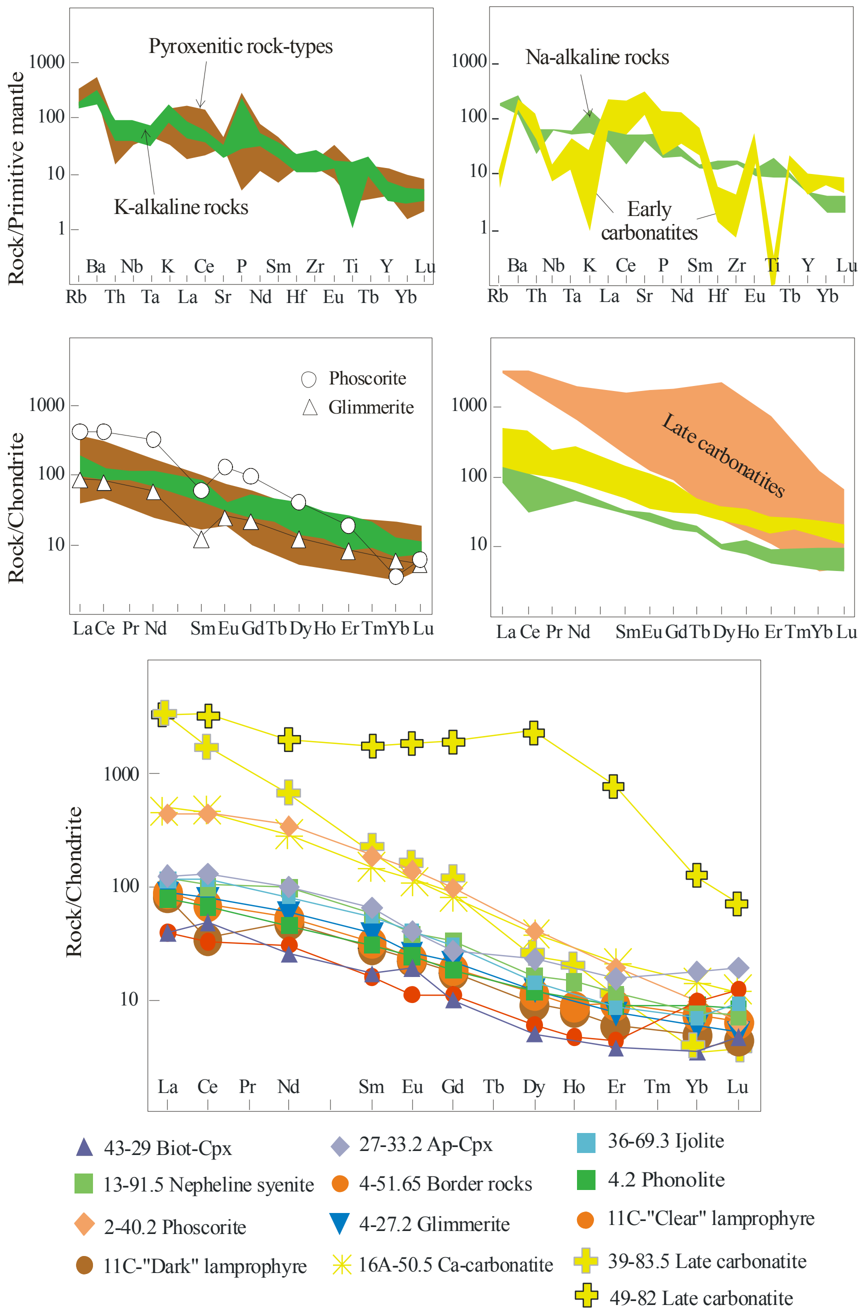


Fig. 5. Incompatible elements normalized to the primitive mantle (Sun & McDonough, 1984) and chondrite-normalized (Boynton, 1984) REE patterns for the Anitápolis rocks and for selected samples. Data source: Furtado (1989), Gibson *et al.* (1999) and Comin-Chiaramonti *et al.* (2002).

In summary, mantle-normalized Anitápolis early Ca-carbonatites have positive Sr-P, Sm, Eu and Tb spikes, and negative Nb, K, Hf-Zr and Ti. The late carbonatites (cf. Furtado *et al.*, 1986) are ten, or more times, enriched in Ba-Th-U-Nb, La-Ce, Nd and Y-Yb compared with the early analogues, and show negative Sr and P spikes. The associated alkaline rocks (ijolites, nepheline syenites and nephelinite dykes) exhibit a more "flattened" behaviour, characterized by a positive K spike. The cumulate rocks (mainly phlogopite and apatite-biotite clinopyroxenites) overlap to some extent the field of the alkaline rocks, showing positive anomalies of P, Eu and Tb.

In the $(REE)_N$ diagrams, the cumulate rocks fall roughly in the same range of the early carbonatites, but contain lower LREE, $(La/Yb)_N=13.3\pm6.6$ (clinopyroxenites) vs. 13.5±4.3 (early carbonatites), whereas the ijolites to nepheline syenites and nephelinites show the lowest LREE, with $(La/Yb)_N=$ 13.2±1.3 and negative Eu anomaly ($Eu/Eu^*=$ 0.65±0.24). The late carbonatites have $(La/Yb)_N=$ 3.0 and are strongly REE enriched.

On the whole, the Anitápolis complex (mass balance and trace element modellization data not shown) is consistent with a basanitic parental magma from which approximately 70% of cumulate rocks, 29% of ijolite+nepheline syenite and 1% of carbonatite are derived, showing an overall potassic affinity, in contrast to the "sodic" imprinting of the more evolved rocks.

## THE LAGES ALKALINE DISTRICT

### Geological background

The Lages alkaline-carbonatitic rocks were emplaced close to the present limit of the flood basalts of the Serra Geral Formation (Fig. 1) and mainly intruded the sedimentary Gondwanic sequences (Permian to Triassic, Itararé to Botucatu Formations, respectively). The latter are bordered at the western and southern sides by the Paraná flood basalts, and mark the uplift of a large crustal block underlined by a concentric structural arrangement (the so-called Lages Dome, about 2100 $km^2$; Scheibe, 1986) bounded by the Corupá, Rio Engano, Rio Canoas and Ponte Alta lineaments (Fig. 6; cf. Scheibe & Furtado, 1989).

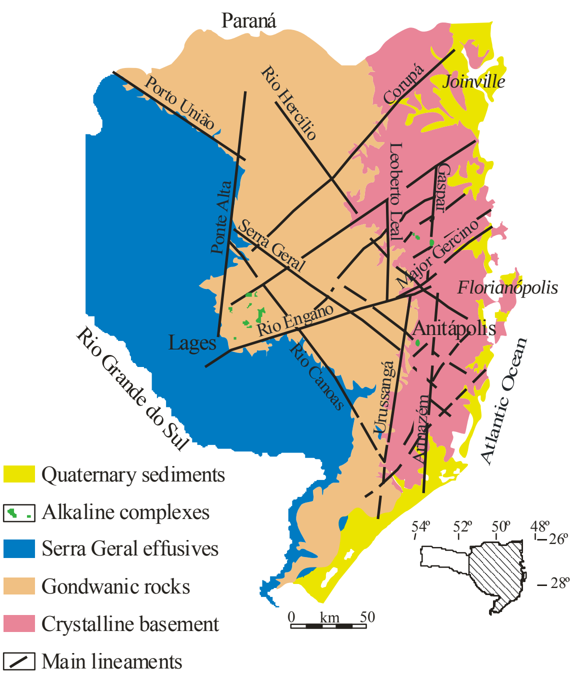


Fig. 6. Main lineaments characterizing the block tectonics in eastern Santa Catarina (after Scheibe & Furtado, 1989).

The Lages magmatic bodies mainly consist of shallow level intrusions, with dominant hypabissal and subvolcanic rock-types following a roughly ring arrangement. The outcrops range from several square kilometers discontinuous clusters to less than 1 m thick dykes, mostly concentrated along a 10 km wide, N60°E-trending belt, in the eastern area (Fig. 6).

Scheibe *et al.* (1984) clustered the Lages alkaline rocks into four main groups: carbonatites and associated rocks; kimberlites and pipe breccias; leucocratic rocks; and ultrabasic rocks.

The Fazenda Varela carbonatites (Fig. 7) intrude the sediments of the Itararé Sub-Group in the central part of the Lages Dome (Scheibe, 1978, 1979). According to Scheibe & Formoso (1982), the carbonatite occurrences are evidenced by higher radioactivity levels over an area of about 600 m in diameter, bordered by N-S and NE-SW fault lines.

The major outcrop occurs at the top of a Permian sandstone hill and forms a tabular 20 m wide body which is represented by a white ankeritic carbonatite and by dykelets and veins (ranging from centimeters to decimeters thick) of dark brownish carbonatite. The latter intrude fenitic feldspathic breccias, characterized by oriented orthoclase neogrowths over the original rounded grains of goethitic sandstone (Scheibe, 1986).

Diatremes, pipe breccias, kimberlites and kimberlitic dykes were described by Oliveira (1927), Paiva (1933), Loczy (1968) and Scheibe (1986). In particular, the "Janjão" kimberlite (Guarujá area in the city of Lages) is a completely weathered rock consisting of angular fragments of different sedimentary rocks and of minerals, being recognized by Scheibe (1978): pyrope-rich garnet, subvitreous rounded ilmenite, centimetric corroded and fracturated dark pyroxene, Cr-diopside, partially altered phlogopite, zircon, spinels and perovskite. Svisero *et al.* (1985) interpreted the geophysical data as indicative of an irregular diatreme with reverse polarity and at least 190x50 m wide. This diatreme and the sedimentary country-rocks (Rio do Rastro Formation) were penetrated by a kimberlitic dyke, about 10 m thick, showing normal polarity (Scheibe & Svisero, 1988; Traversa *et al.*, 1994).

Leucocratic rocks cover about 50 km$^2$ and are represented by four main types i.e. nepheline syenites, trachyphonolites, porphyritic peralkaline phonolites and peralkaline phonolites (Scheibe *et al.*, 1984).

Basic and ultramafic rocks include olivine melilitites, olivine nephelinites, basanites and phonotephrites. The most striking occurrence consists of a semi-ring dyke of olivine melilitite, about 50m wide, found in a quarry at east of Cerro Alto de Cima. Other occurrences are represented by matrix and/or fragments in pipe breccias or small dykes. Some of the latter cut the flood basalts of the Serra Geral Formation at the southernmost and at the northeastern part of the Lages district (Furtado & Scheibe, 1989).

K/Ar data indicate a Late Cretaceous age, with a range from 68 Ma (Amaral *et al.*, 1967; Teixeira, 1969; Sonoki & Garda, 1988) to 76 Ma (Gibson *et al.*, 1999). A Rb/Sr whole-rock errorchrone (Scheibe *et al.*, 1985) yielded an age of 82±6 Ma. On the whole, the results suggest for the nepheline syenites an age older than the phonolites, pipe breccias, olivine melilitites and Janjão kimberlite, as also apparent from the field relationships.

## Petrography

The main rock-types have been classified following Le Maitre (1989; TAS) and De La Roche *et al.* (1980; $R_1$-$R_2$) as olivine melilitites, olivine nephelinites, basanites, tephrites and phonotephrites, nepheline syenites, trachyphonolites, carbonatites and peralkaline phonolites. The latter include porphyritic and aphyric (microporphyritic) types.

### *Olivine melilitites*

Olivine melilitites are hypabissal rocks with fine-grained equigranular texture, sometimes containing olivine and phlogopite macrocrystals (Traversa *et al.*, 1994). The main mineral assemblages are Ti-magnetite (included in the other minerals), euhedral Mg-olivine, zoned and corroded millimeter in size melilite (sometimes showing peg-like structure), anhedral nepheline and poikilitic phlogopite. Accessory minerals are apatite and perovskite. Reabsorbed diopside macrocrystals and monticellite (associated with Mg-olivine) are rarely found. In particular, the Rancho de Tábuas dyke contains corroded and fractured olivine phenocrysts, spinel and perovskite microphenocrysts set in a groundmass composed of phlogopite, nepheline, monticellite and a greenish glass tending to melilitic composition.

*Olivine nephelinites*

Almost all the analyzed samples plot in the melanephelinites field of Le Bas (1989; Traversa *et al.*, 1994). The texture varies from granular and inequigranular to porphyritic (being the latter typical of dykes).

The olivine nephelinites are characterized by euhedral olivine and light green zoned diopside, frequently included in poikilitic nepheline, and leucite, kalsilite, interstitial phlogopite and Ti-magnetite. Apatite and perovskite are found as accessory phases.

The porphyritic varieties have abundant olivine and subordinate diopside phenocrysts, and nepheline, Ti-magnetite, apatite, perovskite, melilite and leucite microphenocrysts. The groundmass is made of clinopyroxene, nepheline, phlogopite and glass. The latter may be partially replaced by zeolites and/or carbonates.

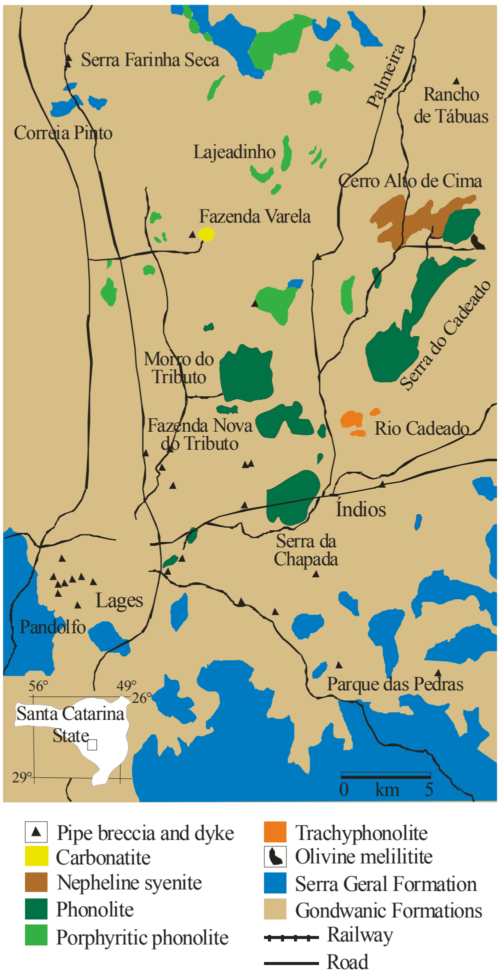


Fig. 7. Geologic sketch map of the Lages district (after Scheibe, 1986; Traversa *et al.*, 1994).

*Basanites*

A basanite dyke (Furtado & Scheibe, 1989; Traversa *et al.*, 1994) intrudes the tholeiitic flood basalts. The texture is porphyritic with euhedral olivine, phlogopite and clinopyroxene phenocrysts. Rare unstable orthopyroxene xenocrysts may be found. Notably, the phlogopite shows reaction rims, and the clinopyroxene is characterized by the presence of two generations of zoned crystals. The groundmass is composed by olivine, clinopyroxene, phlogopite, Ti-magnetite, anorthite-rich plagioclase, alkali feldspar, nepheline and interstitial carbonates. Olivine-clinopyroxene intergrowths (with intergranular euhedral phlogopite) are interpreted as crystal-liquid reaction products of unstable orthopyroxene relicts (Traversa *et al.*, 1994).

*Tephrites and phonotephrites*

These rock-types occur as small porphyritic dykes near the localities of Palmeira and Guarujá (Traversa *et al.*, 1994; Gibson *et al.*, 1999; Comin-Chiaramonti *et al.*, 2002). Greenish to yellow-green diopside, brown amphibole, biotite and nepheline phenocrysts are present. Ocelli-like shaped nepheline appears altered into zeolite and calcite aggregates. Ti-magnetite microphenocrysts are also present. Clinopyroxene shows opaque and apatite inclusions, while nepheline, clinopyroxene, Ti-magnetite and apatite are found inside the poikilitic brown amphibole. The groundmass is made of clinopyroxene rods, zoned dark reddish to brownish-yellow biotite, brown amphibole, calcic plagioclase and Ti-magnetite microlites set in a weakly zeolitized nepheline-alkali feldspar aggregate.

*Nepheline syenites*

Nepheline syenites occur forming discontinuous outcrops mostly at Cerro Alto de Cima (cf. Fig. 7). The rocks are coarse to fine-grained and strongly porphyritic (Scheibe *et al.*, 1984; Traversa *et al.*, 1994). The main minerals are alkali feldspar, ranging from zoned megacrysts (up to 20 mm) to submillimetric laths, nepheline and diopsidic-hedenbergitic to aegirine-augitic clinopyroxene (oscillatory zoning). Euhedral titanite, Ti-magnetite and apatite are systematically present. Sodalite, noseane, biotite and brown amphibole (karsutite-pargasite) may be found, the latter two phases showing corroded and oxidated rims. The fine-grained phaneritic groundmass of the porphyritic rock-types may contain analcite and aegirinic clinopyroxene microlites or rims around the mafic phenocrysts. Natrolite and carbonates may be present as alteration products.

*Trachyphonolites*

Small subaphyric, vesicular dykes cropping out near to Rio Cadeado (Fig. 7) show scarce clinopyroxene, titanite, Ti-magnetite and sodalite microphenocrysts set in a trachytic groundmass made of alkali feldspar, nepheline and interstitial secondary analcite. Vesicles are sometimes filled by carbonates, catapleiite and occasionally by hydrocarbons or "dead oil", probably related to the intruded Irati shale (Scheibe, 1986).

*Porphyritic peralkaline phonolites*

Porphyritic peralkaline phonolites are strongly bauxitized (Serra da Farinha Seca; cf. Fig. 7). Fresh samples from prospection wells under the bau-xitic and kaolinitic cover (more than 20 m deep; Lindstaedt, 1972; Szubert & Vergara, 1975; Dani, 1998) display porphyritic to strongly porphyritic texture characterized by the presence of zoned clinopyroxene (diopside-hedenbergite-aegirine), alkali feldspar, sodalite and nepheline phenocrysts, and also by Ti-magnetite, apatite and titanite microphenocrysts. In some samples, kaersutitic amphibole, included in clinopyroxene grains, titanite and Ti-magnetite macrocrystals are present. Biotite and melanite, showing aegirinic rims, rarely occur. The groundmass consists of alkali feldspar, nepheline, aegirine, poikilitic pectolite and interstitial analcite.

Natrolite and gibbsite are occasionally found as secondary products.

*Peralkaline phonolites*

Peralkaline phonolites crop out as large bodies at the Morro do Tributo, Fazenda Nova do Tributo, Serra da Chapada and Serra do Cadeado areas (Fig. 7). Drill holes (cf. Aumond & Scheibe, 1996) point out to roughly tabular bodies (rarely more than 30 m thick and intercalated in the Gondwanic sediments) forming relatively thin and shallow intrusions with aphyric to fluidal texture due to the isorientation of alkali feldspar and clinopyroxene needles.

Late poikilitical and skeletal aegirine aggregates, submillimetric to centimetric in size, give to the rock a mottled aspect, particularly at Morro do Tributo (Scheibe *et al.*, 1984; Traversa *et al.,* 1994). Rare alkali feldspar, nepheline, sodalite and green clinopyroxene phenocrysts are found in the weakly porphyritic types. Ti-magnetite, titanite and apatite occur as microphenocrysts.

The rocks from Fazenda Nova do Tributo show nodules consisting of diopside and biotite; rare biotite xenocrysts with coronitic texture made of aegirine needles are noticeable. The groundmass is constituted by K- to Na-feldspar, nepheline, aegirine, skeletal or poikilitical manganoan pectolite and calcic serandite. Ti-Zr minerals, typical of agpaitic rocks, include eudialyte-eucolite, neptunite, murmanite, lävenite and astrophyllite, in addition to fluorite and cryolite, testifying high F activity.

*Carbonatites*

Scheibe (1978, 1979), Scheibe & Formoso (1982) and Comin-Chiaramonti *et al.* (2002) described early and late carbonatites, and related fenitized feldspathic breccias (Fazenda Varela, Fig. 7).

Early carbonatites are medium-grained, hypidiomorphic, white to brownish in colour, consisting of prevailing Mg-ankerite and subordinate calcite with alkali feldspar xenocrysts and local concentrations of tetraferriphlogopite; accessory phases include apatite, quartz, pyrochlore and pyrite.

Late carbonatites are characterized by fibrous and radial aggregates of synchysite and also by barite veins and patches.

The carbonate minerals follow a crystallization order, which is represented by cloudy rhombohedral core and progressively clear rims, and by neocrystals containing barite and alkali feldspar. The later mineral is usually zoned or corroded and coloured by neoformed goethite or hematite.

Scheibe & Formoso (1982) reported the occurrence of associated metric in size blocks of coarse-grained magnetite.

*Pipe breccias*

Widespread pipes are characterized by tuffisitic breccias containing angular fragments of carbonatite, dunite, nepheline syenite, leucitite and tholeiitic basalt (Scheibe, 1986; Comin-Chiaramonti *et al.*, 2002). Fragments of red sandstone, shale and other sedimentary rocks are also present (cf. Oliveira, 1927).

Phlogopite, diopside, garnet (red pyrope), ilmenite, magnetite and zircon are set in a strongly altered groundmass.

In particular, the enclosed fragments of tholeiitic basalts consist of hypohyaline to microporphyritic texture and contain plagioclase, augite, pigeonite and opaques microphenocrysts. Leucititic fragments are made of pheno and microphenocrysts of leucite, phlogopite, diopsidic clinopyroxene set in a glassy-carbonatitic (Mg-ankerite) groundmass.

Mineral chemistry

Summarizing the petrographical evidences, the Lages alkaline rock-types are mainly characterized by the presence of: 1) monticellite in some olivine melilitites; 2) large alkali feldspar megacrysts (up to 20 mm) in the nepheline syenites; 3) xenocrysts, i.e. orthopyroxene in basanites, kaersutite or pargasite in nepheline syenites, melanite, kaersutite and phogopite in porphyritic peralkaline phonolites; 4) composition of the phogopite xenocrysts in the phonolitic rocks very similar to those of the phlogopite phenocrysts from the basanites; 5) strongly zoning of diopside-aegirine-augite phenocrysts in the phonolitic rocks, which may be interpreted as xenocrysts from less differentiated cogenetic melts (as proposed, e.g. for the Laacher See rocks, by Duda & Schminke, 1978); 6) pectolite-serandite, Ti-Zr phases such as eudialyte-eucolite, neptunite, murmanite, lävenite and astrophyllite, fluorite and cryolite in the peralkaline rock-types.

Average compositions of the main phases are given in Tables 4 to 12 and represent a selection of more than 850 microprobe analyses (data source: Scheibe, 1986, and Traversa et al., 1994).

*Melilite*

Melilite, present in variable amounts in the olivine melilitites, shows composition typical of both volcanic and plutonic occurrences (cf. El Goresy & Yoder, 1974). A slight FeO and $Na_2O$ enrichment, and concomitant depletion of CaO from the core to the rims of the crystals is apparent. In particular, the melilites from the Cerro Alto de Cima (LM6 and LM16 samples; cf. Table 4) contain Na>Al, suggesting the presence of a ferrisodamelilite end-member component (cf. Nielsen, 1980). According to the synthetic system of Velde & Yoder (1977), the composition of the Lages melilites is in agreement with the nearly constant amount of normative nepheline (i.e. 15.9-13.6 wt%).

*Olivine and monticellite*

Olivine is an ubiquitous phase in olivine melilitites, olivine nephelinites and basanites; monticellite may be an important mineral in olivine melilitites. As a rule, the Lages olivines (Table 5) show narrow compositional ranges (cf. Traversa *et al.*, 1994). Olivines from the melilitites are quite homogeneous, having Fo content between 91 and 87 and CaO enrichment from core to the rims (Δ•=0.57 wt%); olivine from the nephelinites displays a normal zoning from Fo 90 to 80 with FeO enrichment paralleling a small increase in CaO concentration; olivine from basanites is very homogeneous, having Fo content in the 86.3 to 85.5 range.

Table 4. Microprobe compositions of representative melilites from the Lages melilitic rocks. C, core; R, rim. Cationic numbers on the basis of 14 (O).

| | 1<br>LM98<br>C | 2<br>LM98<br>R | 3<br>LM6<br>C | 4<br>LM6<br>R | 5<br>LM16<br>C | 6<br>LM16<br>R |
|---|---|---|---|---|---|---|
| $SiO_2$ | 42.34 | 42.85 | 43.58 | 44.10 | 44.27 | 44.45 |
| $Al_2O_3$ | 6.53 | 5.83 | 5.70 | 6.44 | 5.78 | 5.68 |
| FeO | 2.00 | 2.37 | 2.20 | 2.61 | 1.95 | 2.20 |
| MnO | 0.06 | 0.05 | 0.00 | 0.09 | 0.07 | 0.00 |
| MgO | 9.39 | 9.20 | 9.70 | 8.60 | 9.63 | 9.13 |
| CaO | 36.69 | 35.78 | 35.25 | 33.70 | 34.81 | 34.30 |
| $Na_2O$ | 2.70 | 3.56 | 3.79 | 4.78 | 3.80 | 4.26 |
| $K_2O$ | 0.16 | 0.11 | 0.05 | 0.18 | 0.13 | 0.16 |
| Sum | 99.92 | 99.80 | 100.29 | 100.50 | 100.60 | 100.18 |
| | | | | | | |
| Si | 3.848 | 3.904 | 3.935 | 3.970 | 3.970 | 4.005 |
| Ti | 0.003 | 0.003 | 0.001 | 0.000 | 0.011 | 0.000 |
| Al | 0.699 | 0.626 | 0.607 | 0.683 | 0.611 | 0.603 |
| $Fe^{2+}$ | 0.152 | 0.181 | 0.166 | 0.197 | 0.146 | 0.166 |
| Mn | 0.005 | 0.004 | 0.000 | 0.007 | 0.005 | 0.000 |
| Mg | 1.272 | 1.249 | 1.306 | 1.154 | 1.287 | 1.226 |
| Sum | 5.979 | 5.967 | 6.018 | 6.011 | 6.030 | 6.000 |
| | | | | | | |
| Ca | 3.572 | 3.492 | 3.410 | 3.250 | 3.345 | 3.311 |
| Na | 0.476 | 0.629 | 0.664 | 0.834 | 0.661 | 0.744 |
| K | 0.019 | 0.013 | 0.006 | 0.021 | 0.015 | 0.018 |
| Sum | 4.067 | 4.134 | 4.080 | 4.105 | 4.021 | 4.073 |

Table 5. Microprobe compositions of representative olivines (1-17) and monticellites (18-20) from the Lages rocks; 1-7 and 18-20, OM: olivine melilitite; 8-15, ON, olivine nephelinite; 16-17, BA: basanite. C, core; R, rim; mg#=Mg/(Mg+$Fe^{2+}$). Structural formulae calculated on the basis of 4 (O).

| | 1 | 2 | 3 | 4 | 5 | 6 | 7 | 8 | 9 | 10 |
|---|---|---|---|---|---|---|---|---|---|---|
| | OM | OM | OM | OM | 0M | OM | OM | ON | ON | ON |
| | PA1 | PA1 | LM98 | LM6 | LM6 | LM16 | LM16 | LM70 | LM70 | LA29 |
| | C | R | C | C | R | C | R | C | R | C |
| $TiO_2$ | | | | | | | | | 0.05 | |
| $Al_2O_3$ | | 0.06 | | | | | | 0.06 | 0.18 | |
| FeO | 10.50 | 10.80 | 12.66 | 9.60 | 10.90 | 10.57 | 9.68 | 11.62 | 16.7 | 12.77 |
| MnO | 0.10 | 0.13 | 0.18 | 0.05 | 0.40 | 0.25 | 0.48 | 0.12 | 0.56 | 0.21 |
| MgO | 47.91 | 47.71 | 47.41 | 48.35 | 46.79 | 48.14 | 47.5 | 46.82 | 42.42 | 46.73 |
| CaO | 0.12 | 0.22 | 0.11 | 0.41 | 1.28 | 0.12 | 1.31 | 0.27 | 0.95 | 0.25 |
| NiO | 0.20 | 0.21 | | | | | | 0.12 | | 0.17 |
| $Cr_2O_3$ | | | 0.02 | 0.16 | | | | | | |
| Sum | 99.49 | 99.38 | 100.59 | 99.59 | 99.80 | 99.9 | 99.11 | 99.15 | 100.42 | 100.10 |
| Si | 1.005 | 0.998 | 0.993 | 1.008 | 1.002 | 1.004 | 0.997 | 1.001 | 1.000 | 0.994 |
| Ti | 0.000 | 0.000 | 0.000 | 0.000 | 0.000 | 0.000 | 0.000 | 0.000 | 0.001 | 0.000 |
| Al | 0.000 | 0.002 | 0.000 | 0.000 | 0.000 | 0.000 | 0.000 | 0.002 | 0.005 | 0.000 |
| $Fe^{2+}$ | 0.227 | 0.224 | 0.261 | 0.197 | 0.226 | 0.218 | 0.201 | 0.242 | 0.353 | 0.266 |
| Mn | 0.002 | 0.003 | 0.004 | 0.001 | 0.008 | 0.005 | 0.010 | 0.003 | 0.012 | 0.004 |
| Mg | 1.764 | 1.764 | 1.745 | 1.771 | 1.728 | 1.765 | 1.759 | 1.741 | 1.599 | 1.732 |
| Ca | 0.003 | 0.006 | 0.003 | 0.011 | 0.034 | 0.003 | 0.035 | 0.007 | 0.026 | 0.007 |
| Ni | 0.004 | 0.004 | 0.000 | 0.000 | 0.000 | 0.000 | 0.000 | 0.002 | 0.000 | 0.003 |
| Cr | 0.000 | 0.000 | 0.001 | 0.003 | 0.000 | 0.000 | 0.000 | 0.000 | 0.000 | 0.000 |
| Sum | 2.995 | 3.001 | 3.008 | 2.991 | 2.998 | 2.995 | 3.002 | 2.998 | 2.996 | 3.006 |
| mg# | 0.891 | 0.887 | 0.870 | 0.900 | 0.884 | 0.890 | 0.897 | 0.878 | 0.819 | 0.867 |
| | 11 | 12 | 13 | 14 | 15 | 16 | 17 | 18 | 19 | 20 |
| | ON | ON | ON | ON | ON | BA | BA | OM | OM | OM |
| | PA3 | LM115 | LM115 | LM116 | LM116 | PA4 | PA4 | LM6 | LM16 | LM16 |
| | C | C | R | C | R | C | R | C | C | C |
| $SiO_2$ | 40.10 | 41.06 | 39.55 | 40.79 | 40.63 | 39.51 | 39.89 | 37.18 | 36.11 | 35.89 |
| $TiO_2$ | | | | | | | 0.04 | | | |
| $Al_2O_3$ | 0.04 | | | | | | 0.03 | | | |
| FeO | 11.78 | 11.06 | 18.06 | 10.46 | 12.51 | 13.70 | 13.88 | 10.2 | 10.92 | 10.74 |
| MnO | 0.17 | | | 0.01 | 0.19 | 0.22 | 0.18 | 0.61 | 0.333 | 0.58 |
| MgO | 48.01 | 47.88 | 41.54 | 47.92 | 45.88 | 45.45 | 46.13 | 19.68 | 19.11 | 18.69 |
| CaO | 0.18 | 0.30 | 0.93 | 0.22 | 0.98 | 0.15 | 0.13 | 33.12 | 33.34 | 33.59 |
| NiO | 0.17 | | | | | 0.17 | 0.20 | | | |
| $Cr_2O_3$ | | 0.01 | 0.04 | | | | | 0.04 | | |
| Sum | 100.45 | 100.31 | 100.12 | 99.40 | 100.19 | 99.2 | 100.48 | 100.83 | 99.81 | 99.49 |
| Si | 0.989 | 1.007 | 1.007 | 1.007 | 1.008 | 0.996 | 0.993 | 1.003 | 0.991 | 0.989 |
| Ti | 0.000 | 0.000 | 0.000 | 0.000 | 0.000 | 0.000 | 0.001 | 0.000 | 0.000 | 0.000 |
| Al | 0.001 | 0.000 | 0.000 | 0.000 | 0.000 | 0.000 | 0.001 | 0.000 | 0.000 | 0.000 |
| $Fe^{2+}$ | 0.243 | 0.227 | 0.384 | 0.216 | 0.259 | 0.289 | 0.289 | 0.230 | 0.251 | 0.248 |
| Mn | 0.004 | 0.000 | 0.000 | 0.000 | 0.001 | 0.005 | 0.004 | 0.014 | 0.008 | 0.014 |
| Mg | 1.765 | 1.751 | 1.576 | 1.764 | 1.696 | 1.707 | 1.711 | 0.791 | 0.781 | 0.768 |
| Ca | 0.005 | 0.008 | 0.025 | 0.006 | 0.026 | 0.004 | 0.004 | 0.957 | 0.980 | 0.992 |
| Ni | 0.003 | 0.000 | 0.000 | 0.000 | 0.000 | 0.003 | 0.004 | 0.000 | 0.000 | 0.000 |
| Cr | 0.000 | 0.000 | 0.001 | 0.000 | 0.000 | 0.000 | 0.000 | 0.001 | 0.000 | 0.000 |
| Sum | 3.010 | 2.993 | 2.993 | 2.993 | 2.993 | 3.004 | 3.006 | 2.996 | 3.011 | 3.011 |
| mg# | 0.879 | 0.885 | 0.804 | 0.891 | 0.867 | 0.855 | 0.856 | 0.775 | 0.7572 | 0.756 |

Table 6. Compositions of representative clinopyroxenes from the Lages rocks. 1-2=OM; 3-6=ON; 7-8=BA; 9-10=PhTe; 11-15=NeSy; 16-22=PPPh; 23-30=PPh. Additional rock name abbreviations: PhTe, phonotefrite; NeSy, nepheline syenite; PPPh, porphiritic peralkaline phonolite; PPh, peralkaline phonolite. C, core; R, rim; gm, groundmass. Atomic proportions on the basis of 6 (O). $Fe^{2+}$ and $Fe^{3+}$ calculated according to Papike *et al.* (1974).

| | 1 | 2 | 3 | 4 | 5 | 6 | 7 | 8 | 9 | 10 | 11 | 12 | 13 | 14 | 15 |
|---|---|---|---|---|---|---|---|---|---|---|---|---|---|---|---|
| | OM | OM | ON | ON | ON | ON | BA | BA | PhTe | PhTe | NeSy | NeSy | NeSy | NeSy | NeSy |
| | LM6 | LM6 | LA70 | LA70 | LM115 | LM115 | PA4 | PA4 | LA3 | LA3 | LM53 | LM53 | LM2 | LM2 | LM2 |
| | C | R | C | R | C | R | C | gm | C | R | C | R | C | R | gm |
| $TiO_2$ | 1.63 | 0.46 | 1.58 | 1.18 | 2.69 | 1.33 | 0.48 | 0.71 | 1.99 | 1.75 | 1.43 | 0.67 | 2.26 | 1.80 | 1.08 |
| $Al_2O_3$ | 0.13 | | 1.95 | 4.70 | 4.72 | 0.19 | 2.31 | 2.19 | 5.69 | 6.25 | 5.69 | 1.93 | 6.29 | 4.94 | 3.95 |
| FeO | 4.72 | 3.45 | 5.75 | 6.77 | 5.30 | 5.08 | 10.78 | 6.69 | 13.00 | 10.05 | 14.90 | 20.09 | 9.69 | 10.71 | 14.83 |
| MnO | 0.19 | 0.09 | 0.20 | 0.16 | | 0.14 | 0.17 | 0.12 | 0.64 | 0.30 | 0.80 | 2.38 | 0.30 | 0.52 | 1.34 |
| MgO | 15.60 | 16.56 | 14.23 | 12.56 | 13.80 | 15.21 | 12.73 | 15.63 | 8.50 | 10.72 | 7.30 | 4.41 | 10.79 | 9.89 | 7.32 |
| CaO | 21.64 | 23.70 | 24.73 | 22.71 | 24.07 | 23.12 | 22.3 | 22.09 | 21.68 | 22.31 | 20.39 | 14.75 | 20.72 | 21.28 | 18.11 |
| $Na_2O$ | 1.61 | 0.98 | 0.39 | 1.44 | 0.59 | 0.91 | 0.68 | 0.52 | 1.44 | 1.15 | 2.00 | 4.76 | 1.17 | 1.20 | 2.24 |
| $Cr_2O_3$ | | | | | | | | | | | 0.06 | 0.09 | 0.15 | 0.13 | 0.12 |
| Sum | 99.50 | 99.69 | 100.37 | 99.29 | 99.28 | 99.61 | 99.66 | 98.82 | 98.39 | 99.7 | 97.86 | 97.08 | 99.34 | 99.58 | 99.85 |
| Si | 1.985 | 1.990 | 1.905 | 1.846 | 1.790 | 1.983 | 1.888 | 1.895 | 1.752 | 1.770 | 1.761 | 1.900 | 1.808 | 1.859 | 1.945 |
| $Al^{IV}$ | 0.006 | | 0.085 | 0.154 | 0.207 | 0.008 | 0.102 | 0.096 | 0.248 | 0.230 | 0.239 | 0.090 | 0.192 | 0.141 | 0.055 |
| Ti | 0.009 | 0.010 | 0.001 | | 0.003 | 0.037 | 0.010 | 0.009 | | | | 0.010 | | | |
| Sum | 2.000 | 2.000 | 2.000 | 2.000 | 2.000 | 2.000 | 2.000 | 2.000 | 2.000 | 2.000 | 2.000 | 2.000 | 2.000 | 2.000 | 2.000 |
| $Al^{VI}$ | | | | 0.052 | 0.052 | | | | 0.010 | 0.046 | 0.022 | | 0.087 | 0.079 | 0.124 |
| Ti | 0.036 | 0.003 | 0.043 | 0.033 | 0.072 | 0.028 | 0.004 | 0.011 | 0.058 | 0.049 | 0.042 | 0.010 | 0.064 | 0.051 | 0.031 |
| $Fe^{3+}$ | 0.030 | 0.044 | 0.025 | 0.140 | 0.099 | | 0.125 | 0.094 | 0.229 | 0.169 | 0.282 | 0.413 | 0.057 | 0.043 | 0.033 |
| $Fe^{2+}$ | 0.115 | 0.061 | 0.153 | 0.070 | 0.066 | 0.157 | 0.214 | 0.115 | 0.190 | 0.146 | 0.203 | 0.253 | 0.249 | 0.297 | 0.441 |
| Mn | 0.006 | 0.003 | 0.006 | 0.005 | | 0.004 | 0.005 | 0.004 | 0.021 | 0.010 | 0.026 | 0.080 | 0.010 | 0.017 | 0.044 |
| Mg | 0.855 | 0.902 | 0.784 | 0.694 | 0.765 | 0.838 | 0.713 | 0.868 | 0.488 | 0.599 | 0.423 | 0.260 | 0.606 | 0.558 | 0.417 |
| Ca | 0.853 | 0.928 | 0.979 | 0.902 | 0.959 | 0.916 | 0.898 | 0.881 | 0.896 | 0.897 | 0.849 | 0.826 | 0.837 | 0.863 | 0.742 |
| Cr | | | | | | | | | | | 0.002 | 0.003 | 0.004 | 0.004 | 0.004 |

| | 16 | 17 | 18 | 19 | 20 | 21 | 22 | 23 | 24 | 25 | 26 | 27 | 28 | 29 | 30 |
|---|---|---|---|---|---|---|---|---|---|---|---|---|---|---|---|
| | PPPh | PPPh | PPPh | PPPh | PPPh | PPPh | PPPh | PPH | PPh | PPh | PPh | PPh | PPh | PPh | PPh |
| | LM99 | LM99 | LM99 | LM99 | LM106 | LM106 | LM106 | LM97 | LM97 | LM97 | LM97 | LM112 | LM112 | LM88 | LM25 |
| | C | R | gmA | gmB | R | R | gm | C | R | gmA | gmB | C | R | gm | gm |
| $SiO_2$ | 46.56 | 44.71 | 48.26 | 48.52 | 45.02 | 50.08 | 50.86 | 48.90 | 50.45 | 50.64 | 50.46 | 46.04 | 48.94 | 50.35 | 50.5 |
| $TiO_2$ | 1.86 | 1.03 | 1.18 | 2.57 | 1.55 | 0.68 | 1.72 | 1.66 | 1.14 | 1.67 | 1.27 | 1.55 | 0.76 | 0.72 | 0.91 |
| $Al_2O_3$ | 5.57 | 4.24 | 1.96 | 1.16 | 5.58 | 0.88 | 1.39 | 5.49 | 1.67 | 0.88 | 0.83 | 4.06 | 1.63 | 1.01 | 1.07 |
| FeO | 9.69 | 20.09 | 20.3 | 26.39 | 14.73 | 27.35 | 26.83 | 4.86 | 12.81 | 17.67 | 26.65 | 15.66 | 22.77 | 27.41 | 27.05 |
| MnO | 0.22 | 2.42 | 2.23 | 2.22 | 0.61 | 0.98 | 0.76 | 0.09 | 0.59 | 0.76 | 0.04 | 2.62 | 3.43 | 1.00 | 1.06 |
| MgO | 11.05 | 3.91 | 4.43 | 0.11 | 8.19 | 0.29 | | 13.42 | 10.20 | 7.33 | 1.29 | 6.83 | 1.53 | 0.6 | 0.33 |
| CaO | 21.85 | 18.83 | 12.97 | 3.55 | 20.16 | 4.89 | 2.61 | 23.80 | 17.15 | 11.54 | 3.51 | 18.89 | 10.31 | 2.29 | 4.39 |
| $Na_2O$ | 1.52 | 2.41 | 5.69 | 10.69 | 2.02 | 10.44 | 11.71 | 0.80 | 3.83 | 6.40 | 11.26 | 2.42 | 7.27 | 11.72 | 10.61 |
| $Cr_2O_3$ | 0.03 | 0.04 | | | | | | 0.12 | 0.13 | 0.07 | | | | | |
| Sum | 98.35 | 97.68 | 97.02 | 95.21 | 97.86 | 95.59 | 95.88 | 99.14 | 97.97 | 96.96 | 95.31 | 98.07 | 96.64 | 95.1 | 95.92 |
| Si | 1.763 | 1.792 | 1.900 | 1.936 | 1.744 | 1.979 | 1.987 | 1.813 | 1.916 | 1.950 | 1.975 | 1.803 | 1.942 | 1.976 | 1.986 |
| $Al^{IV}$ | 0.237 | 0.200 | 0.091 | 0.055 | 0.255 | 0.021 | 0.013 | 0.187 | 0.075 | 0.040 | 0.025 | 0.187 | 0.058 | 0.024 | 0.014 |
| Ti | | 0.008 | 0.009 | 0.009 | 0.001 | 0.020 | | | 0.009 | 0.010 | | 0.010 | | | |
| Sum | 2.000 | 2.000 | 2.000 | 2.000 | 2.000 | 2.000 | 2.000 | 2.000 | 2.000 | 2.000 | 2.000 | 2.000 | 2.000 | 2.000 | 2.000 |
| $Al^{VI}$ | 0.012 | | | | | 0.020 | 0.051 | 0.053 | | | 0.013 | | 0.018 | 0.022 | 0.036 |
| Ti | 0.053 | 0.023 | 0.026 | 0.068 | 0.044 | 0.020 | 0.050 | 0.046 | 0.024 | 0.038 | 0.037 | 0.036 | 0.023 | 0.021 | 0.027 |
| $Fe^{3+}$ | 0.231 | 0.324 | 0.455 | 0.727 | 0.316 | 0.761 | 0.747 | 0.096 | 0.288 | 0.419 | 0.792 | 0.280 | 0.553 | 0.851 | 0.734 |
| $Fe^{2+}$ | 0.076 | 0.349 | 0.213 | 0.153 | 0.161 | 0.143 | 0.129 | 0.055 | 0.119 | 0.150 | 0.080 | 0.233 | 0.202 | 0.049 | 0.155 |
| Mn | 0.007 | 0.082 | 0.074 | 0.075 | 0.020 | 0.033 | 0.025 | 0.003 | 0.019 | 0.025 | 0.001 | 0.087 | 0.115 | 0.033 | 0.035 |
| Mg | 0.623 | 0.233 | 0.260 | 0.006 | 0.473 | 0.017 | | 0.741 | 0.577 | 0.421 | 0.075 | 0.399 | 0.091 | 0.035 | 0.019 |
| Ca | 0.886 | 0.808 | 0.547 | 0.152 | 0.836 | 0.208 | 0.109 | 0.945 | 0.698 | 0.476 | 0.147 | 0.792 | 0.438 | 0.096 | 0.185 |
| Na | 0.112 | 0.187 | 0.434 | 0.827 | 0.152 | 0.800 | 0.887 | 0.058 | 0.282 | 0.478 | 0.854 | 0.184 | 0.559 | 0.892 | 0.809 |
| Cr | 0.001 | 0.001 | | | | | | 0.004 | 0.004 | 0.002 | | | | | |
| Sum | 2.001 | 2.007 | 2.009 | 2.008 | 2.002 | 2.002 | 1.998 | 2.001 | 2.011 | 2.009 | 1.999 | 2.011 | 1.999 | 1.999 | 2.000 |

Monticellite, a typical phase of the Cerro Alto de Cima body, shows a quite uniform composition, with Ca ranging from 0.957 to 0.990, and with Mn=0.012±0.03 (vs. Mn=0.004±0.003 of the coexisting olivine).

*Clinopyroxenes*

Clinopyroxene is an ubiquitous mineral in the Lages rocks. Table 6 reports selected compositions plotted in the classificative diagrams of Morimoto (1988) (Fig. 8).

Clinopyroxenes cover a very large compositional range, varying from diopside-hedenbergite to aegirine, even in the same sample (cf. Traversa *et al.*, 1994).

Minerals from olivine melilitites, olivine nephelinites, basanites and phonotephrites are plotted in the Quad subfield (Fig. 8A), displaying iron enrichment (hedenbergitic component) from olivine melilitites to phonotephrites (Fig. 8B). Notably, the tetrahedral site is saturated by Si+Al±Ti. The diopside from the olivine melilitites is in general represented by Al- and Fe-rich types with Ti-bearing rims. Clinopyroxenes from nepheline syenites exhibit compositional variations from diopside to hedenbergite and from augite to aegirine-augite. In particular, the minerals from the LM2 (and LM1) nepheline syenite (cf. Table 6) have aluminian and ferroan cores evolving to Na-rich rims. As a rule, core vs. rim compositions show trends of Na, Fe and Si enrichment, corresponding to Ca, Mg and Al decrease. In some cases an oscillatory zoning is present in the phenocrysts (Fig. 9; cf. Scheibe, 1986) that should be interpreted as rhythmical $PH_2O$ variations in the magmatic system before the eruption (cf. Vieten, 1980).

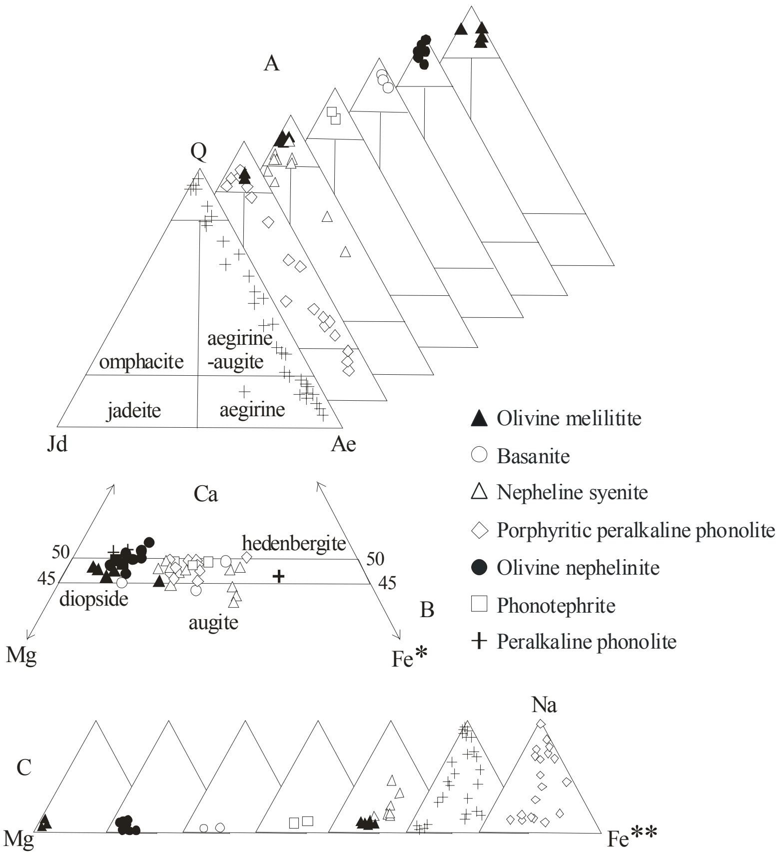


Fig. 8. Lages clinopyroxenes plotted into classificative diagrams: A. Q(Wo, En, Fs)-Jd-Ae (Morimoto, 1988); B. Ca-Mg-Fe* (Fe*=$Fe^{2+}$+$Fe^{3+}$+Mn) (Cpx from Q field of A); C. Na-Mg-Fe** (Fe**=$Fe^{2+}$+$Fe^{3+}$+Mn-Na).

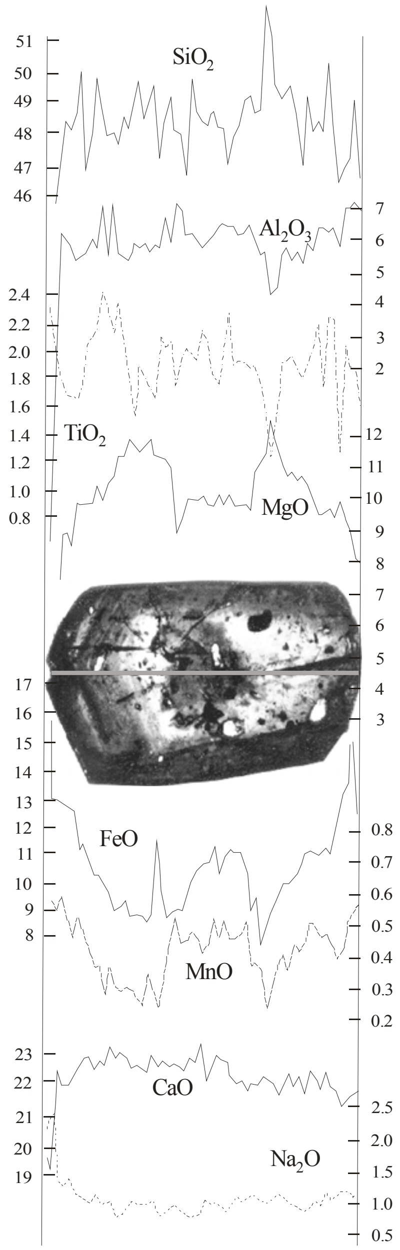


Fig. 9. Compositional variations in clinopyroxene grain from a Lages nepheline syenite (after Scheibe, 1986).

Finally, it should be stressed that clinopyroxenes from nepheline syenites and phonotephrites are systematically characterized by the presence of octahedral aluminium.

Clinopyroxenes from porphyritic and subaphyric peralkaline phonolites tend to present the major compositional ranges, i.e. from diopside to aegirine, even in a single crystal ($Na_2O$ up to 12.43 wt%; Figs. 8A and C). According to Traversa *et al.* (1994), different $PH_2O$ and $fO_2$ values could also explain the Na–$Fe^{3+}$ enrichment trends (cf. Fig. 8C) in the porphyritic peralkaline phonolites and in peralkaline phonolites.

*Micas*

Phlogopite and Mg-biotite are important constituents in mafic and ultramafic rocks and occur as minor phases in leucocratic types, sometimes displaying xenocrystal character. Representative analyses are given in Table 7.

Micas from the olivine melilitites are represented by a titaniferous phlogopite (Rock's nomenclature, 1982), homogeneous in composition and clustering the phlogopite-annite join (Fig. 10A). Micas from the olivine nephelinites plot along the phlogopite-Mg-biotite boundary, and Al and Ti values suggest the presence of $Fe^{3+}$ in tetrahedral sites (tetraferriphlogopite). Following Traversa *et al.* (1994), the phlogopites from the Fazenda Nova do Tributo peralkaline phonolites (e.g. LM97 sample) are believed to represent xenocryst phases: as matter of fact they are very different with respect to the groundmass phases from the other peralkaline phonolites (e.g. Rio do Cadeado peralkaline phonolites; cf. LM76 sample), and show a crystallochemistry similar to the cores of the micas from the basanitic rocks (cf. Fig. 10B).

In general, the micas from the mafic rocks vary from titanphlogopites to titanbiotites, and those from peralkaline phonolites from titaniferous phlogopites to titaniferous biotites (Rock's classification, 1982).

*Amphiboles*

Primary amphiboles occur in phonotephrites as phenocrysts and groundmass phases, but are also occasionally present in some nepheline syenites and phonolites as rare xenocrysts mantled by aegirine-augite rims (Table 8).

According to Giret *et al.* (1980), the amphiboles fit the hastingsite field. In conformity to Leake (1978), the amphiboles from nepheline syenites range from potassian kaersutite to K-Ti ferroan pargasite (LM1 and LM2 nepheline syenites of Table 8). The latter type is similar to the amphiboles

Table 7. Microprobe compositions of representative phlogopites and biotites from the Lages rocks. 1-6=OM; 7-10=ON; 11-13=BA; 14-15=PhTe; 16-17=NeSy; 18-20=PPh. Abbreviations as in Table 6. C, core; R, rim; gm, groundmass; structural formulae calculated on the basis of 23 (O); mg# =Mg/Mg+$Fe^{2+}$. Data source: Traversa *et al.* (1994).

| | 1 | 2 | 3 | 4 | 5 | 6 | 7 | 8 | 9 | 10 |
|---|---|---|---|---|---|---|---|---|---|---|
| | OM | OM | OM | OM | OM | OM | ON | ON | ON | ON |
| | PA1 | LM98 | LM98 | LM6 | LM16 | LM16 | LA29 | LM115 | LM116 | LM116 |
| $SiO_2$ | 36.24 | 37.80 | 39.06 | 39.96 | 39.73 | 40.66 | 37.42 | 44.11 | 40.6 | 40.36 |
| $TiO_2$ | 6.68 | 2.15 | 2.34 | 3.45 | 2.13 | 1.96 | 4.57 | 4.7 | 3.78 | 5.72 |
| $Al_2O_3$ | 8.39 | 11.91 | 11.02 | 13.12 | 12.42 | 11.81 | 16.22 | 5.98 | 8.6 | 7.25 |
| FeO | 6.72 | 6.84 | 7.37 | 6.31 | 4.94 | 5.76 | 6.13 | 10.08 | 10.45 | 12.42 |
| MnO | 0.12 | 0.11 | 0.10 | | 0.04 | | | 0.05 | | 0.07 |
| MgO | 21.85 | 23.29 | 22.97 | 23.24 | 24.17 | 23.96 | 20.02 | 19.86 | 19.91 | 15.55 |
| CaO | 3.83 | 0.04 | 0.02 | | | 1.09 | 0.04 | 0.01 | | |
| $Na_2O$ | 0.44 | 0.09 | 0.12 | 0.35 | 0.18 | 0.35 | 0.37 | 1.68 | 0.55 | 3.16 |
| $K_2O$ | 8.96 | 9.72 | 10.14 | 9.93 | 9.81 | 9.84 | 9.91 | 9.64 | 9.27 | 9.12 |
| $Cr_2O_3$ | | | | | | | 0.27 | 0.05 | | |
| BaO | | | | 0.93 | 1.99 | 0.99 | | 1.63 | 1.63 | 0.31 |
| Sum | 93.43 | 91.95 | 93.14 | 97.29 | 95.41 | 96.42 | 94.95 | 97.79 | 94.79 | 93.96 |
| Si | 5.702 | 5.925 | 6.062 | 5.920 | 6.011 | 6.079 | 5.648 | 6.656 | 6.327 | 6.412 |
| Ti | 0.814 | 0.253 | 0.273 | 0.384 | 0.242 | 0.220 | 0.519 | 0.533 | 0.443 | 0.683 |
| Al | 1.556 | 2.200 | 2.015 | 2.291 | 1.214 | 2.081 | 2.885 | 1.063 | 1.579 | 1.357 |
| $Fe^{2+}$ | 0.884 | 0.897 | 0.956 | 0.782 | 0.625 | 0.720 | 0.774 | 1.272 | 1.362 | 1.650 |
| Mn | 0.016 | 0.015 | 0.013 | | 0.005 | | | 0.006 | | 0.009 |
| Mg | 5.124 | 5.441 | 5.313 | 5.131 | 5.450 | 5.339 | 4.504 | 4.467 | 4.625 | 3.682 |
| Ca | 0.646 | 0.007 | 0.003 | | | 0.175 | 0.006 | 0.002 | | |
| Na | 0.134 | 0.027 | 0.036 | 0.101 | 0.05' | 0.1014 | 0.108 | 0.491 | 0.166 | 0.973 |
| K | 1.798 | 1.943 | 2.007 | 1.876 | 1.893 | 1.877 | 1.908 | 1.856 | 1.843 | 1.848 |
| Cr | | | | | | | | | | |
| Sum | 16.673 | 16.707 | 16.679 | 16.539 | 16.612 | 16.649 | 16.383 | 16.449 | 16.445 | 16.636 |
| mg# | 0.853 | 0.858 | 0.848 | 0.868 | 0.897 | 0.881 | 0.853 | 0.778 | 0.772 | 0.891 |

| | 11 | 12 | 13 | 14 | 15 | 16 | 17 | 18 | 19 | 20 |
|---|---|---|---|---|---|---|---|---|---|---|
| | BA | BA | BA | PhTe | PhTe | NeSy | NeSy | PPh | PPh | PPh |
| | PA4 | PA4 | PA4 | LA3 | LA3 | LAG3 | LAG7 | LM97 | LM97 | LM76 |
| | C | R | gm | C | gm | C | R | C | R | gm |
| $SiO_2$ | 36.99 | 36.88 | 35.69 | 34.92 | 35.38 | 36.54 | 33.72 | 37.58 | 37.17 | 35.60 |
| $TiO_2$ | 4.67 | 4.19 | 7.79 | 5.77 | 5.72 | 5.05 | 6.96 | 4.20 | 3.88 | 2.85 |
| $Al_2O_3$ | 14.78 | 15.06 | 13.03 | 14.34 | 15.44 | 15.30 | 14.42 | 16.43 | 15.72 | 13.71 |
| FeO | 8.09 | 6.53 | 14.29 | 16.89 | 10.67 | 10.86 | 21.62 | 6.49 | 6.76 | 19.99 |
| MnO | 0.07 | 0.09 | 0.08 | 0.27 | 0.10 | 0.10 | 0.96 | 0.02 | 0.1 | 1.42 |
| MgO | 19.63 | 19.79 | 14.30 | 13.36 | 16.70 | 19.86 | 11.11 | 20.7 | 19.89 | 12.01 |
| CaO | 0.08 | 0.06 | 0.13 | | 0.06 | | | | | |
| $Na_2O$ | 0.70 | 0.54 | 0.64 | 0.68 | 0.75 | | | 0.87 | 0.8 | 0.38 |
| $K_2O$ | 7.31 | 9.49 | 8.73 | 8.53 | 8.79 | 9.04 | 8.51 | 9.38 | 9.39 | 9.64 |
| NiO | 0.11 | 0.13 | | | | | | 0.02 | | |
| $Cr_2O_3$ | 0.15 | 0.12 | | | | | | 0.25 | 0.07 | |
| BaO | | | | | | 0.60 | 2.75 | 0.04 | | |
| Sum | 92.58 | 92.88 | 94.68 | 94.76 | 93.61 | 97.35 | 100.05 | 95.98 | 93.78 | 95.60 |
| Si | 5.713 | 5.708 | 5.631 | 5.569 | 5.538 | 5.111 | 5.336 | 5.614 | 5.692 | 5.764 |
| Ti | 0.542 | 0.488 | 0.924 | 0.692 | 0.673 | 0.573 | 0.828 | 0.472 | 0.447 | 0.347 |
| Al | 2.690 | 2.747 | 2.423 | 2.695 | 2.848 | 2.720 | 2.689 | 2.892 | 2.837 | 2.616 |
| $Fe^{2+}$ | 1.045 | 0.845 | 1.885 | 2.252 | 1.396 | 1.370 | 2.861 | 0.811 | 0.866 | 2.706 |
| Mn | 0.009 | 0.012 | 0.011 | 0.037 | 0.013 | 0.013 | 0.129 | 0.002 | 0.013 | 0.195 |
| Mg | 4.519 | 4.565 | 3.362 | 3.175 | 3.896 | 4.465 | 2.620 | 4.609 | 4.540 | 2.898 |
| Ca | 0.013 | 0.010 | 0.022 | | 0.010 | | | | | |
| Na | 0.210 | 0.162 | 0.196 | 0.210 | 0.228 | | | 0.252 | 0.237 | 0.119 |
| K | 1.440 | 1.874 | 1.757 | 1.735 | 1.755 | 1.739 | 1.718 | 1.787 | 1.834 | 1.991 |
| Ni | 0.014 | 0.016 | | | | | | 0.002 | | |
| Cr | 0.018 | 0.015 | | | | | | 0.029 | 0.008 | |
| Ba | | | | | | 0.035 | 0.170 | 0.002 | | |
| Sum | 16.215 | 16.441 | 16.210 | 16.365 | 16.357 | 16.426 | 16.350 | 16.473 | 16.474 | 16.636 |
| mg# | 0.812 | 0.844 | 0.641 | 0.585 | 0.7361 | 0.765 | 0.478 | 0.850 | 0.840 | 0.517 |

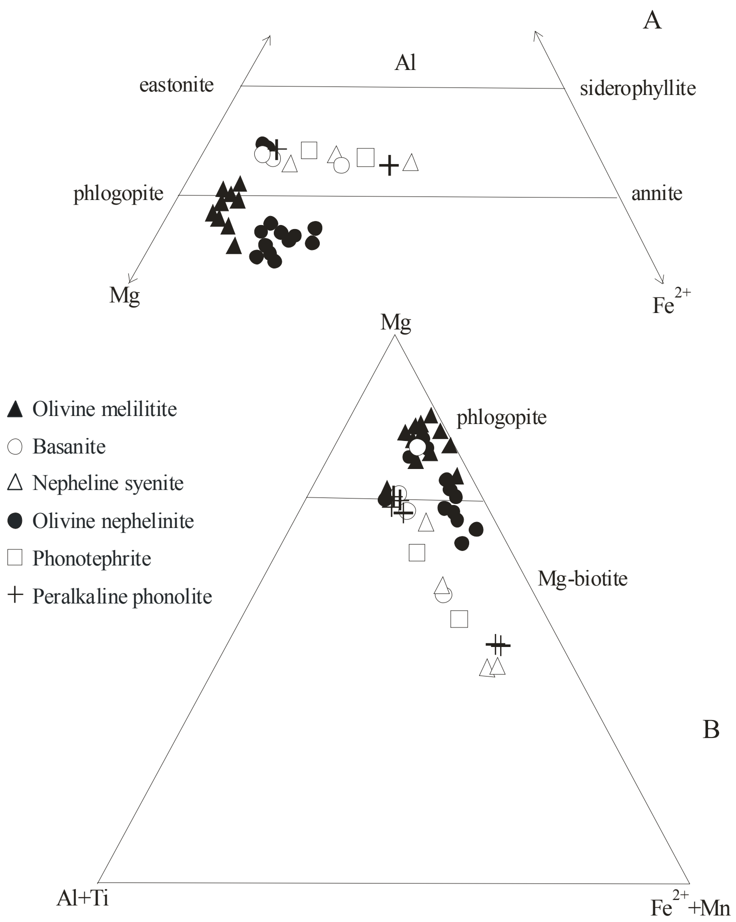


Fig. 10. Phlogopite and biotite compositions from Lages alkaline rocks: A. Al-Mg-$Fe^{2+}$; B. Mg-(Al+Ti)-($Fe^{2+}$+Mn) diagrams (after Rock, 1982).

from phonotephrites (cf. LA3 sample). Notably, the phonotephrite amphiboles show mg# (0.57) in apparent equilibrium with the host rock composition.

On the contrary, mg# values relative to the amphiboles from nepheline syenites are in the range 0.43-0.56 vs. host rock mg# varying from 0.22 to 0.25. This disagreement may indicate a xenocrystic origin for the amphiboles from the nepheline syenites, probably due to mixing with cogenetic less evolved magmas.

*Oxides*

Olivine melilitites and olivine nephelinites contain brown Cr-Al spinels mantled by Ti-magnetite. The first ones display MgO and $Cr_2O_3$ contents ranging from 10.0 to 17.6 and from 20.0 to 30.0 wt%, respectively, and furthermore $Al_2O_3$, negatively correlated with $Cr_2O_3$, varying from 43.8 to 32.5 wt% (Table 9, Fig. 11A). The spinels from olivine melilitites and olivine nephelinites contain spinel s.s. end-member about 37 and 65 mol%, respectively, vs. magnesiochromite about 34 and 4 mol%, respectively (average values). Notably, the spinel compositions plot in the lamproitic field of the spinel prism (cf. Mitchel & Bergman, 1991).

Ti-magnetite is ubiquitous and shows a wide compositional variation, with the ulvöspinel end-member ranging from 20 to 70 mol% (Table 9 and Fig. 11B).

*Alkali feldspar, nepheline, leucite and kalsilite*

According to Traversa *et al.*, (1994), large HS potassian sanidine (51 to 75 Or wt%; cf. Smith & Brown, 1988) characterizes basanites, phonotephrites and nepheline syenites (cf. Table 10). In the latter, an almost pure K-sanidine (96 Or wt%) is frequently present in the groundmass. Relatively high An contents (around 7 wt%) may be found at the cores of zoned macrophenocrysts from porphyritic nepheline syenites.

Table 8. Representative compositions of amphiboles from the Lages rocks (data source: Traversa *et al.*, 1994). 1-3, PhTe; 4-6, NeSy. Abbreviations as in Table 6. C, core; R, rim; gm, groundmass. Structural formulae calculated on the basis of 23 (O) basis; mg# = Mg/(Mg+$Fe^{2+}$).

| | 1<br>PhTe<br>LA3<br>C | 2<br>PhTe<br>LA3<br>R | 3<br>PhTe<br>LA3<br>gm | 4<br>NeSy<br>LM1<br>C | 5<br>NeSy<br>LM2<br>C | 6<br>NeSy<br>LM2<br>R |
|---|---|---|---|---|---|---|
| $TiO_2$ | 3.56 | 3.69 | 3.58 | 4.53 | 3.40 | 4.26 |
| $Al_2O_3$ | 13.89 | 13.55 | 12.95 | 13.40 | 13.38 | 12.49 |
| FeO | 14.87 | 14.59 | 14.91 | 13.98 | 18.68 | 16.21 |
| MnO | 0.22 | 0.27 | 0.29 | 0.34 | 0.92 | 0.47 |
| MgO | 10.86 | 10.71 | 11.10 | 10.17 | 7.95 | 8.85 |
| CaO | 11.96 | 11.65 | 11.96 | 11.38 | 11.32 | 11.38 |
| $Na_2O$ | 2.28 | 2.28 | 2.36 | 2.74 | 2.91 | 2.72 |
| $K_2O$ | 1.90 | 1.87 | 1.94 | 2.20 | 2.29 | 2.16 |
| Sum | 98.26 | 96.54 | 97.38 | 98.01 | 99.18 | 97.47 |
| | | | | | | |
| Si | 5.844 | 5.830 | 5.853 | 5.926 | 5.874 | 5.981 |
| $Al^{IV}$ | 2.156 | 2.170 | 2.147 | 2.074 | 2.126 | 2.016 |
| Sum | 8.000 | 8.000 | 8.000 | 8.000 | 8.000 | 8.000 |
| | | | | | | |
| $Al^{VI}$ | 0.315 | 0.285 | 0.186 | 0.315 | 0.291 | 0.246 |
| Ti | 0.404 | 0.427 | 0.411 | 0.514 | 0.392 | 0.492 |
| $Fe^{2+}$ | 1.877 | 1.875 | 1.906 | 1.764 | 2.394 | 2.083 |
| Mn | 0.028 | 0.035 | 0.038 | 0.043 | 0.119 | 0.061 |
| Mg | 2.443 | 2.454 | 2.529 | 2.287 | 1.816 | 2.027 |
| Ca | 1.934 | 1.918 | 1.959 | 1.840 | 1.858 | 1.873 |
| Na | 0.667 | 0.679 | 0.699 | 0.801 | 0.865 | 0.810 |
| K | 0.366 | 0.367 | 0.378 | 0.423 | 0.448 | 0.423 |
| | | | | | | |
| Ca+$Al^{IV}$ | 4.090 | 4.088 | 4.106 | 3.914 | 3.984 | 3.889 |
| | | | | | | |
| mg# | 0.566 | 0.567 | 0.570 | 0.565 | 0.431 | 0.493 |

Sanidine phenocrysts (70-77 Or wt%) characterize also many porphyritic peralkaline phonolites, coexisting with both sanidine (Or around 100%) and albite (Ab 99 wt%) of the groundmass.

Nepheline is an ubiquitous phase, while leucite and kalsilite are occasionally present in the olivine nephelinites (kamafugitic affinity). The nepheline ranges from Ks 30 wt% in the olivine melilitites to Ks 11-13 wt% in nepheline syenites and peralkaline phonolites.

In general, the groundmass varieties have higher silica than the corresponding phenocryst cores (i.e. Q 8 vs. 2 wt%, as mean values, respectively). Leucite and kalsilite, which are occasionally found in some olivine nephelinites, display compositions close to the stoichiometry (cf. Table 10).

*Perovskite and pectolite-serandite*

Small dark brown perovskite typically occurs in olivine melilitites and olivine nephelinites. Quantitative partial analyses are given in Table 11, but Nb and Ce contents (as from qualitative microprobes) suggest the presence of knopite and dysanalite components and a lamproitic affinity (cf. Mitchell & Bergman, 1991).

Late crystallized pectolite-serandite phases are common in peralkaline phonolites (Table 11). In particular, pectolites from Lageadinho and Chapada plot between pectolite and schizolite (manganoan pectolite), while the Tributo outcrop contains a variety between schizolite and serandite (Fig. 12).

Diatremes and related minerals

The systematic presence in the heavy mineral concentrates from diatremes of deep red, pyrope-rich garnet, vitreous ilmenite, dark pyroxene and grass green Cr-diopside, phlogopite, zircon, spinels and perovskite, is indicative of a kimberlitic or lamproitic affinity.

In particular, in the Janjão diatreme (50x200 m, and found intruding the Gondwanic sedimentary formations of the Lages dome), microprobe analyses on heavy mineral concentrates (i.e. garnet, ilmenite, clinopyroxene, spinel and zircon) show some typical "mantle" compositions (Scheibe & Svisero, 1988). Red garnets contain about MgO 21 wt%, and $Cr_2O_3$ ranging from 0.2 to 2.0 wt%, similar to kimberlite garnets. Ilmenites have MgO 3.5 wt% as average content, in analogy to that from kimberlitic and basaltic analogues, and low MnO proportions (i.e.<3.0 wt%), well distinct with respect to the high MnO of carbonatitic ilmenites. Clinopyroxenes include Cr-diopsides with Ca, Fe and Mg atomic contents close to clinopyroxenes from kimberlite ultramafic xenoliths. Red-brown translucent spinels have magnesiochromite-rich compositions fitting those from spinel harzburgites.

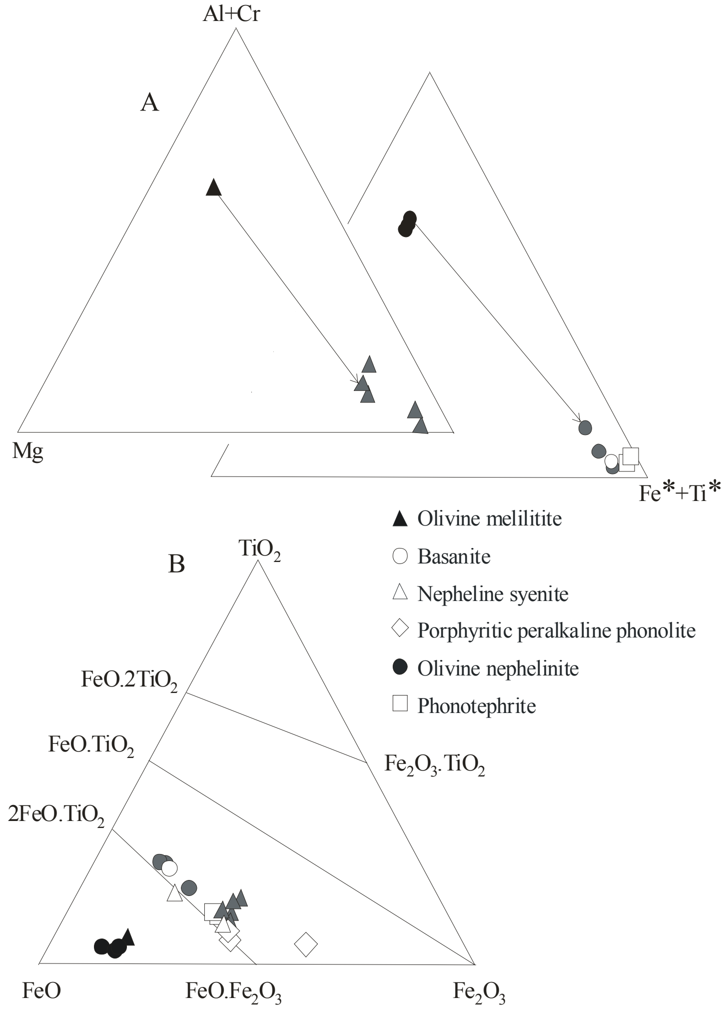


Fig. 11. Oxides in A. Al+Cr-Mg-Fe*+Ti* ($Fe^* = Fe^{2+}+Fe^{3+}+Mn+Ni$, $Ti^* = Ti+Si$) and B. $TiO_2$-FeO-$Fe_2O_3$ diagrams.

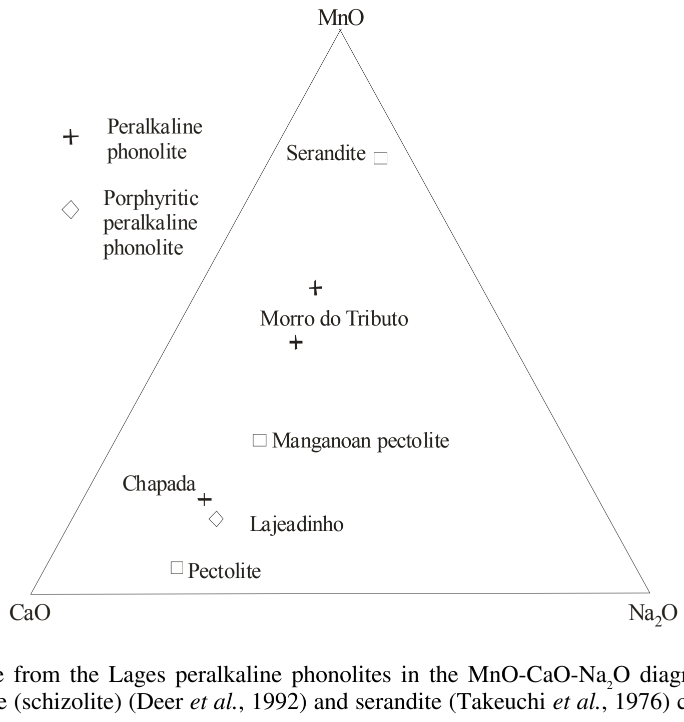


Fig. 12. Pectolite-serandite from the Lages peralkaline phonolites in the MnO-CaO-$Na_2O$ diagram. Pectolite (Deer *et al.*, 1992), manganoan pectolite (schizolite) (Deer *et al.*, 1992) and serandite (Takeuchi *et al.*, 1976) compositions are plotted for comparison.

Table 9. Representative compositions of oxides [$Fe_2O_3$ and FeO calculated on the ulvöspinel basis and structural formule on the basis of 32 (O)]. Abbreviations as in Table 6. Data source: Traversa *et al.* (1994).

| | 1 | 2 | 3 | 4 | 5 | 6 | 7 | 8 | 9 | 10 |
|---|---|---|---|---|---|---|---|---|---|---|
| | OM | OM | OM | OM | OM | OM | ON | ON | ON | ON |
| | PA1 | PA1 | PA1 | LM98 | LM98 | LM16 | LA70 | LA70 | LA29 | LA29 |
| | C | R | gm | | | | C | R | C | R |
| $TiO_2$ | 1.10 | 8.51 | 6.67 | 8.41 | 8.61 | 6.77 | 0.84 | 12.96 | 0.70 | 0.74 |
| $Al_2O_3$ | 32.49 | 2.56 | 6.66 | 0.49 | 8.93 | 0.09 | 35.93 | 3.36 | 43.84 | 43.46 |
| $Cr_2O_3$ | 30.43 | 5.35 | 12.04 | 0.10 | 0.13 | 3.68 | 28.00 | 6.57 | 20.04 | 19.98 |
| $Fe_2O_3$ | 6.58 | 46.50 | 40.68 | 54.54 | 46.41 | 53.90 | 4.49 | 33.76 | 5.93 | 6.34 |
| FeO | 12.14 | 25.28 | 26.41 | 31.90 | 26.86 | 31.11 | 12.52 | 34.93 | 13.05 | 12.85 |
| MnO | 0.28 | 0.43 | 0.52 | 1.06 | 1.02 | 0.65 | 0.19 | 0.78 | 0.26 | 0.20 |
| NiO | 0.16 | 0.13 | | | | | 0.17 | 0.10 | 0.17 | 0.23 |
| MgO | 16.85 | 8.47 | 7.87 | 3.96 | 8.20 | 3.84 | 16.50 | 4.58 | 17.59 | 17.61 |
| Sum | 100.19 | 97.38 | 100.97 | 100.46 | 100.16 | 100.20 | 98.75 | 97.04 | 101.80 | 101.58 |
| Si | 0.037 | 0.046 | 0.033 | | | 0.047 | 0.025 | | 0.048 | 0.037 |
| Ti | 0.191 | 1.851 | 1.378 | 1.862 | 1.782 | 1.506 | 0.146 | 2.885 | 0.115 | 0.121 |
| Al | 8.844 | 0.873 | 2.156 | 0.170 | 2.779 | 0.031 | 9.776 | 1.172 | 11.252 | 11.191 |
| Cr | 5.556 | 1.223 | 2.614 | 0.023 | 0.028 | 0.861 | 5.111 | 1.537 | 3.450 | 3.450 |
| $Fe^{3+}$ | 1.144 | 10.122 | 8.409 | 12.086 | 9.610 | 12.001 | 0.780 | 7.520 | 0.972 | 1.043 |
| $Fe^{2+}$ | 2.345 | 6.124 | 6.067 | 7.856 | 6.181 | 7.697 | 2.417 | 8.647 | 2.377 | 2.348 |
| Mn | 0.055 | 0.105 | 0.121 | 0.264 | 0.238 | 0.1630 | 0.037 | 0.195 | 0.048 | 0.037 |
| Ni | 0.030 | 0.030 | | | | | 0.032 | 0.024 | 0.030 | 0.040 |
| Mg | 5.799 | 3.626 | 3.222 | 1.739 | 3.362 | 1.694 | 5.676 | 2.020 | 5.708 | 5.734 |
| Sum | 24.001 | 24.000 | 24.000 | 24.000 | 24.000 | 24.000 | 23.999 | 24.000 | 24.000 | 24.000 |
| Mol% | | | | | | | | | | |
| Magnesiochromite | 34.25 | 6.73 | 15.02 | 0.11 | 0.17 | 4.91 | 9.88 | 8.14 | 1.01 | 1.71 |
| Ferrochromite | | | | | | | 21.28 | | | |
| Spinel | 37.26 | 4.81 | 12.38 | 9.03 | 16.41 | 0.18 | 61.29 | 6.21 | 69.26 | 69.25 |
| Hercynite | 17.27 | | | | | | | | | |
| Magnesioferrite | | 30.08 | 9.61 | 17.42 | 21.41 | 14.06 | | 7.05 | | |
| Magnetite | 7.00 | 27.04 | 38.67 | 42.81 | 30.68 | 54.25 | 4.33 | 32.78 | 6.51 | 6.45 |

| | 11 | 12 | 13 | 14 | 15 | 16 | 17 | 18 | 19 | 20 |
|---|---|---|---|---|---|---|---|---|---|---|
| | ON | ON | BA | PhTe | PhTe | NeSy | NeSy | PPPh | PPPh | PPPh |
| | LA29 | LM115 | PA4 | LA3 | LA3 | LM2 | LM2 | LM99 | LM106 | LM106 |
| | gm | | | C | R | C | R | | C | R |
| $SiO_2$ | 0.14 | 0.11 | 0.15 | 0.26 | 0.11 | 0.79 | | 0.27 | 0.03 | 0.11 |
| $TiO_2$ | 20.40 | 22.04 | 21.46 | 8.32 | 8.52 | 12.00 | 6.99 | 4.60 | 6.25 | 5.67 |
| $Al_2O_3$ | 1.30 | 0.87 | 1.37 | 1.69 | 2.09 | 0.57 | 0.71 | 0.24 | 1.28 | 1.21 |
| $Cr_2O_3$ | 0.85 | 0.03 | | | | | | 0.05 | 0.02 | 0.03 |
| $Fe_2O_3$ | 28.53 | 26.79 | 29.65 | 52.29 | 51.49 | 31.20 | 52.97 | 59.45 | 54.99 | 55.88 |
| FeO | 43.95 | 45.56 | 46.55 | 35.41 | 36.58 | 38.19 | 34.38 | 34.09 | 34.42 | 33.71 |
| MnO | 0.89 | 0.70 | | 1.10 | 1.17 | 4.17 | 1.75 | 1.74 | 1.79 | 1.90 |
| NiO | | 0.08 | 0.06 | 0.09 | | | | | | |
| MgO | 3.55 | 3.50 | 3.73 | 2.07 | 1.38 | | 0.42 | | 0.41 | 0.47 |
| Sum | 99.61 | 99.68 | 102.97 | 101.23 | 101.34 | 96.92 | 97.22 | 100.44 | 99.19 | 98.98 |
| Si | 0.041 | 0.032 | 0.042 | 0.076 | 0.032 | 0.246 | | 0.082 | 0.009 | 0.034 |
| Ti | 4.493 | 4.859 | 4.570 | 1.841 | 1.890 | 2.814 | 1.642 | 1.054 | 1.436 | 1.306 |
| Al | 0.449 | 0.301 | 0.457 | 0.586 | 0.726 | 0.209 | 0.262 | 0.086 | 0.461 | 0.436 |
| Cr | 0.197 | 0.007 | | | | | | 0.012 | 0.005 | 0.007 |
| $Fe^{3+}$ | 6.287 | 5.910 | 6.318 | 11.579 | 11.429 | 9.669 | 12.454 | 13.630 | 12.644 | 12.877 |
| $Fe^{2+}$ | 10.763 | 11.169 | 11.025 | 8.714 | 9.023 | 9.960 | 8.983 | 8.686 | 8.795 | 8.633 |
| Mn | 0.221 | 0.074 | | 0.274 | 0.294 | 1.102 | 0.463 | 0.449 | 0.463 | 0.493 |
| Ni | | 0.019 | 0.014 | 0.021 | | | | | | |
| Mg | 1.549 | 1.529 | 1.574 | 0.908 | 0.606 | | 0.196 | | 0.187 | 0.214 |
| Sum | 24.000 | 24.000 | 24.000 | 23.999 | 24.000 | 24.000 | 24.000 | 23.999 | 24.000 | 24.000 |
| Mol% | | | | | | | | | | |
| Ulvöspinel | 66.23 | 70.23 | 67.14 | 32.10 | 32.18 | 48.17 | 28.68 | 19.88 | 24.85 | 23.18 |
| Magnesiochromite | 0.96 | 0.03 | | | | | | | | |
| Chromite | | | | | | | | 0.07 | 0.03 | 0.02 |
| Spinel | 2.19 | 1.44 | 2.22 | 3.28 | 4.05 | | 1.52 | | 2.14 | 2.47 |
| Hercynite | | | | | | 1.10 | | 0.50 | 0.50 | 0.04 |
| Magnesioferrite | 11.95 | 13.17 | 13.06 | 6.86 | 2.72 | | 0.76 | | | |
| Magnetite | 18.67 | 15.13 | 17.58 | 57.76 | 61.05 | 50.73 | 69.04 | 79.55 | 72.48 | 74.29 |

Table 10. Representative compositions of alkali feldspar, nepheline, leucite and kalsilite from the Lages rock-types. Abbreviations as in Table 6. Data source: Traversa *et al.* (1994) and Gibson *et al.* (1999).

| | Alkali feldspar | | | | | | | | | | |
|---|---|---|---|---|---|---|---|---|---|---|---|
| | 1 | 2 | 3 | 4 | 5 | 6 | 7 | 8 | 9 | 10 | 11 |
| | BA | PhTe | NeSy | NeSy | NeSy | NeSy | NeSy | NeSy | NeSy | PPPh | PPPh |
| | PA4 | 93SOB165 | LA3 | LM1 | LM1 | LM1 | LM1 | LM2 | LM2 | LM106 | LM106 |
| $SiO_2$ | 61.40 | 65.70 | 62.50 | 62.86 | 65.50 | 65.13 | 64.34 | 65.39 | 64.53 | 65.48 | 65.04 |
| $Al_2O_3$ | 20.11 | 18.52 | 21.28 | 20.33 | 19.02 | 18.46 | 18.47 | 18.76 | 18.59 | 18.85 | 18.72 |
| FeO | 1.90 | 0.12 | 0.40 | 0.27 | 0.26 | 0.08 | | 0.15 | | 0.14 | 0.17 |
| CaO | 0.18 | 0.02 | 0.18 | 1.26 | 0.33 | 0.00 | 0.16 | 0.15 | | | |
| $Na_2O$ | 2.78 | 4.84 | 4.38 | 4.71 | 4.45 | 3.54 | 0.31 | 3.75 | 0.42 | 3.53 | 2.69 |
| $K_2O$ | 12.61 | 9.79 | 10.41 | 8.12 | 10.16 | 11.76 | 16.27 | 11.31 | 16.21 | 11.81 | 12.99 |
| BaO | | | | 2.30 | 0.21 | 0.09 | 0.11 | 0.13 | 0.16 | 0.01 | |
| Sum wt% | 98.98 | 98.99 | 99.15 | 99.85 | 99.93 | 99.06 | 99.66 | 99.64 | 99.91 | 99.82 | 99.61 |
| Or | 75.32 | 58.48 | 61.84 | 51.00 | 60.44 | 69.88 | 96.57 | 67.30 | 96.42 | 70.03 | 77.13 |
| Ab | 23.78 | 41.41 | 37.26 | 42.36 | 37.91 | 30.12 | 2.63 | 31.95 | 3.58 | 29.97 | 22.87 |
| An | 0.90 | 0.11 | 0.90 | 6.64 | 1.65 | 0.00 | 0.80 | 0.75 | 0.00 | 0.00 | 0.00 |

| | Alkali feldspar | | | | | | | | | |
|---|---|---|---|---|---|---|---|---|---|---|
| | 12 | 13 | 14 | 15 | 16 | 17 | 18 | 19 | 20 | 21 |
| | PPPh | PPPh | PPPh | PPh | PPh | PPh | PPh | PPh | PPh | PPh |
| | LM106 | LM106 | LM106 | LM112 | LM112 | LM112 | LM88 | LM88 | LM25 | LM25 |
| | gm | gm | gm | gm | gm | gm | gm | gm | gm | gm |
| $SiO_2$ | 64.62 | 65.61 | 68.18 | 64.65 | 66.66 | 68.29 | 64.95 | 68.17 | 64.43 | 68.32 |
| $Al_2O_3$ | 18.62 | 18.84 | 19.51 | 18.41 | 18.86 | 19.50 | 18.38 | 19.61 | 18.43 | 19.35 |
| CaO | | | 0.09 | | | | | | 0.02 | |
| $K_2O$ | 15.64 | 11.14 | 0.16 | 16.35 | 8.67 | 0.22 | 15.45 | 0.13 | 16.17 | 0.14 |
| BaO | | | | | | | | 0.13 | | |
| Sum wt% | 99.96 | 99.96 | 99.70 | 99.93 | 99.87 | 99.82 | 99.93 | 99.97 | 99.62 | 99.72 |
| Or | 92.54 | 65.93 | 0.95 | 97.11 | 51.59 | 1.30 | 91.52 | 0.77 | 95.99 | 0.83 |
| Ab | 7.46 | 34.07 | 98.61 | 2.89 | 48.31 | 98.70 | 8.48 | 99.23 | 3.91 | 99.17 |
| An | | | 0.45 | | | | | | 0.10 | |

| | Nepheline | | | | | | | | | | |
|---|---|---|---|---|---|---|---|---|---|---|---|
| | 1 | 2 | 3 | 4 | 5 | 6 | 7 | 8 | 9 | 10 | 11 |
| | OM | OM | OM | ON | ON | ON | PhTe | NeSy | NeSy | NeSy | NeSy |
| | LM6 | LM6 | SOB162 | LM115 | LM115 | SOB168 | LA3 | LM1 | LM1 | LM1 | LM2 |
| | C | R | | C | R | | | C | R | gm | C |
| $SiO_2$ | 40.55 | 40.54 | 40.81 | 40.64 | 41.30 | 41.45 | 45.32 | 42.08 | 45.10 | 45.71 | 45.30 |
| $Al_2O_3$ | 33.74 | 33.76 | 33.40 | 34.12 | 32.93 | 34.69 | 31.87 | 35.48 | 32.44 | 32.00 | 31.78 |
| FeO | 1.05 | 1.16 | 1.08 | 0.45 | 1.24 | 0.66 | 0.34 | 0.35 | 0.35 | 0.80 | 0.42 |
| CaO | | | | | | 1.02 | 0.16 | 0.44 | 0.08 | 0.03 | 0.13 |
| $Na_2O$ | 15.63 | 16.34 | 15.47 | 15.54 | 14.34 | 11.58 | 15.78 | 17.63 | 16.59 | 16.44 | 15.89 |
| $K_2O$ | 8.59 | 7.82 | 9.31 | 7.85 | 9.46 | 7.06 | 5.02 | 3.12 | 5.38 | 4.75 | 5.18 |
| Sum wt% | 99.67 | 99.62 | 100.07 | 98.60 | 99.27 | 96.46 | 98.49 | 99.10 | 99.94 | 99.73 | 98.70 |
| Q | | | | 1 | 2 | 2 | 9 | 4 | 6 | 8 | 8 |
| Ne | 71 | 75 | 69 | 72 | 66 | 68 | 74 | 85 | 76 | 76 | 74 |
| Ks | 29 | 25 | 31 | 27 | 32 | 30 | 17 | 11 | 18 | 16 | 18 |

| | Nepheline | | | | | | | | | Leucite | Kalsilite |
|---|---|---|---|---|---|---|---|---|---|---|---|
| | 12 | 13 | 14 | 15 | 16 | 17 | 18 | 19 | 20 | 21 | 22 |
| | NeSy | PPPh | PPPh | PPPh | PPPh | PPh | PPh | PPh | PPh | ON | ON |
| | LM2 | LM73 | LM99 | LM106 | LM106 | LM97 | LM19 | LM88 | LM25 | LM116 | LM116 |
| | R | gm | gm | C | R | gm | gm | gm | gm | | |
| $SiO_2$ | 44.82 | 47.91 | 41.95 | 43.64 | 45.28 | 48.78 | 46.13 | 44.51 | 44.87 | 55.44 | 37.93 |
| $Al_2O_3$ | 31.73 | 30.44 | 34.82 | 32.93 | 31.55 | 28.96 | 30.96 | 31.67 | 32.38 | 22.31 | 31.39 |
| FeO | 0.41 | 0.77 | 0.09 | 0.91 | 0.32 | 1.06 | 0.10 | 0.63 | 0.89 | 0.40 | 1.20 |
| CaO | 0.11 | 0.04 | | | | | | | 0.07 | | 0.56 |
| $Na_2O$ | 16.64 | 17.00 | 16.09 | 17.04 | 14.68 | 16.95 | 14.24 | 16.42 | 15.43 | 0.28 | 0.72 |
| $K_2O$ | 4.85 | 4.11 | 7.38 | 5.48 | 7.27 | 4.01 | 7.73 | 5.22 | 6.19 | 21.69 | 27.99 |
| Sum wt% | 98.56 | 100.27 | 100.33 | 100.00 | 99.10 | 99.77 | 99.16 | 98.45 | 99.83 | 100.12 | 100.34 |
| Q | 6 | 10 | 1 | 4 | 8 | 11 | 9 | 6 | 7 | 27 | 1 |
| Ne | 77 | 77 | 74 | 78 | 68 | 76 | 65 | 76 | 72 | 1 | 3 |
| Ks | 17 | 13 | 25 | 18 | 24 | 13 | 26 | 18 | 21 | 72 | 96 |

Table 11. Representative compositions of perovskites and pectolite-serandites. Abbreviations as in Table 6. Data source: Traversa *et al.* (1994) and Gibson *et al.* (1999).

| | Perovskite | | | | Pectolite-serandite | | | |
|---|---|---|---|---|---|---|---|---|
| | 1 | 2 | 3 | 4 | 1 | 2 | 3 | 4 |
| | OM | OM | OM | ON | PPh | PPPh | PPPh | PPPh |
| | LM16 | LM115 | B162 | B168 | LM106 | LM19 | LM88 | LM88 |
| $SiO_2$ | | | 0.21 | 0.23 | 53.82 | 52.00 | 51.69 | 50.99 |
| $TiO_2$ | 54.82 | 55.54 | 57.91 | 55.81 | | 0.18 | 0.19 | |
| $Al_2O_3$ | 0.30 | | | | 1.37 | | 0.09 | |
| FeO | 1.28 | 0.93 | | 1.09 | 0.17 | 0.95 | 0.66 | 0.97 |
| MnO | | | | | 5.87 | 7.15 | 19.63 | 24.39 |
| MgO | | | | | | 0.07 | 0.01 | |
| CaO | 37.89 | 36.34 | 38.94 | 35.66 | 26.48 | 26.73 | 15.71 | 11.95 |
| $Na_2O$ | 0.55 | 0.77 | 1.11 | 0.74 | 9.77 | 8.92 | 9.40 | 9.22 |
| $K_2O$ | | | | | 0.74 | | 0.10 | |
| SrO | | 0.55 | | | | | | |
| Sum | 94.84 | 94.13 | 98.17 | 93.53 | 98.22 | 96.00 | 97.48 | 97.52 |

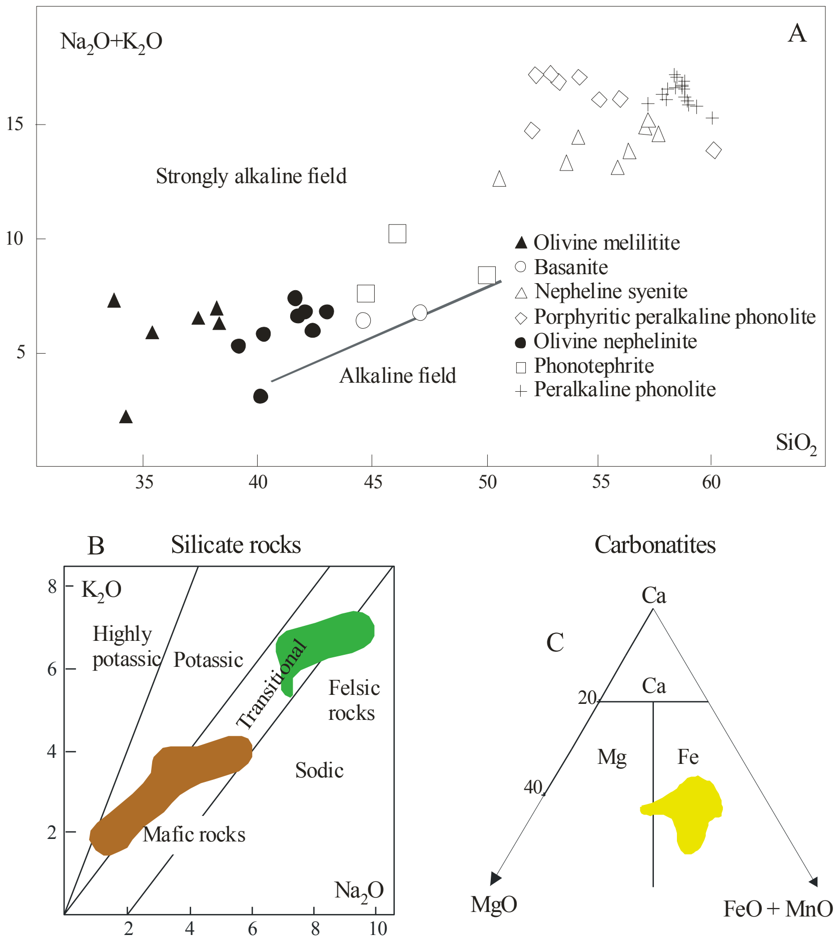


Fig. 13. A. Alkali-silica diagram for Lages alkaline rocks. Field boundary according to Saggerson & Williams (1964). B. Silicate rocks: $Na_2O$ vs. $K_2O$ diagram (cf. Le Maitre, 1989, and Comin-Chiaramonti & Gomes, 1996). C. Carbonatites: CaO-MgO-(FeO+Mn) space (cf. Woolley & Kempe, 1989). Data source: Traversa *et al.* (1996), Gibson *et al.* (1999) and Comin-Chiaramonti *et al.* (2002).

Table 12. Selected chemical analyses of Lages rock-types (data source: Traversa *et al.*, 1996; Comin-Chiaramonti *et al.*, 2002).

| | 1 | 2 | 3 | 4 | 5 | 6 | 7 | 8 | 9 | 10 | 11 | 12 |
|---|---|---|---|---|---|---|---|---|---|---|---|---|
| | PAI | LM98 | LM6 | LM16 | LA70 | LA29 | PA3 | LM115 | LM116 | PA4 | LA3 | SB.08 |
| | OM | OM | OM | OM | ON | ON | ON | ON | ON | BA | PhTe | Te |
| $SiO_2$ | 34.23 | 35.34 | 38.28 | 37.45 | 40.15 | 39.18 | 40.25 | 41.75 | 41.75 | 44.62 | 46.10 | 44.71 |
| $Al_2O_3$ | 8.29 | 9.71 | 9.29 | 8.98 | 11.30 | 11.64 | 10.85 | 11.50 | 11.45 | 12.08 | 17.55 | 16.46 |
| $Fe_2O_3$ | 4.10 | 3.14 | 2.58 | 2.76 | 5.37 | 4.63 | 4.91 | 4.36 | 4.62 | 4.44 | 4.00 | 2.84 |
| FeO | 5.42 | 5.74 | 6.10 | 6.42 | 4.69 | 5.84 | 5.34 | 6.10 | 5.92 | 5.35 | 3.48 | 3.80 |
| MnO | 0.17 | 0.21 | 0.18 | 0.20 | 0.16 | 0.16 | 0.15 | 0.17 | 0.17 | 0.14 | 0.14 | 0.16 |
| MgO | 18.42 | 14.18 | 17.47 | 17.04 | 14.53 | 13.88 | 13.17 | 10.74 | 10.38 | 12.56 | 3.95 | 5.02 |
| CaO | 16.65 | 18.32 | 14.59 | 15.17 | 13.25 | 12.86 | 12.29 | 12.88 | 12.59 | 8.06 | 7.24 | 9.40 |
| $Na_2O$ | 0.87 | 2.96 | 3.16 | 3.48 | 2.00 | 3.55 | 4.90 | 3.73 | 4.00 | 3.19 | 6.06 | 3.78 |
| $K_2O$ | 1.54 | 2.84 | 3.17 | 3.02 | 1.07 | 1.73 | 0.88 | 2.82 | 3.36 | 3.16 | 4.07 | 3.99 |
| $P_2O_5$ | 1.10 | 2.33 | 1.37 | 1.52 | 1.15 | 1.08 | 1.60 | 1.15 | 1.04 | 0.60 | 0.60 | 0.65 |
| L.O.I | 6.95 | 3.41 | 2.24 | 2.51 | 3.86 | 2.36 | 3.21 | 1.93 | 1.97 | 3.04 | 4.90 | 7.27 |
| Sum | 99.28 | 99.99 | 99.94 | 99.99 | 99.51 | 99.36 | 99.53 | 100.01 | 100.00 | 99.45 | 99.62 | 99.58 |
| ppm | | | | | | | | | | | | |
| V | 165 | 220 | 232 | 302 | 224 | 266 | 196 | 217 | 217 | 284 | 175 | |
| Cr | 676 | 402 | 642 | 723 | 498 | 538 | 426 | 320 | 325 | 474 | 22 | 165 |
| Co | 54 | 40 | 54 | 56 | 50 | 53 | 49 | 44 | 45 | 50 | 24 | |
| Ni | 32 | 171 | 417 | 404 | 305 | 342 | 327 | 233 | 243 | 288 | 18 | 95 |
| Zn | 87 | 83 | 83 | 83 | 95 | 99 | 99 | 108 | 108 | 96 | 84 | |
| Rb | 64 | 100 | 92 | 89 | 39 | 70 | 45 | 85 | 92 | 43 | 79 | 105.5 |
| Sr | 1910 | 1950 | 1470 | 1460 | 1370 | 1230 | 1360 | 1650 | 1640 | 1010 | 1270 | 1650.0 |
| Ba | 1720 | 3210 | 2290 | 2110 | 1620 | 1630 | 1970 | 1920 | 1940 | 1220 | 1660 | 2202.0 |
| Th | 27 | | | | 14 | 11 | 13 | | | 11 | 15 | 27.8 |
| Pb | 10 | 22 | 19 | 12 | 10 | 8 | 10 | 19 | 8 | 11 | 17 | |
| Y | 31 | 45.72 | 30.04 | 28.13 | 25 | 25 | 26 | 25.49 | 25.85 | 22 | 22 | 23.6 |
| La | 123.6 | 167.06 | 140.95 | 122.5 | 88.3 | 87 | 89.6 | 91.48 | 94.74 | 65.5 | 94 | 104.68 |
| Ce | 213.8 | 314.63 | 266.25 | 209.85 | 148.3 | 173 | 150.3 | 175.22 | 178.14 | 121.4 | 176 | 173.74 |
| Nd | 88.2 | 115.32 | 85.43 | 74 | 63.1 | | 65.8 | 69.08 | 71.47 | 55 | | 57.51 |
| Sm | 14.9 | 19.03 | 14.55 | 13.24 | 10.9 | | 11.8 | 12.08 | 12.2 | 9.4 | | 8.22 |
| Eu | 4.1 | 5.52 | 4.4 | 3.93 | 3 | | 3.1 | 3.4 | 3.45 | 2.5 | | 2.20 |
| Gd | 10.9 | 13.44 | 9.59 | 8.88 | 7.8 | | 8.6 | 8.29 | 8.47 | 6.5 | | 6.45 |
| Dy | 6.1 | 8.43 | 5.32 | 5.14 | 4.5 | | 5.1 | 5.01 | 5.04 | 4 | | 4.09 |
| Er | 2.5 | 3.3 | 2.22 | 2.08 | 1.9 | | 2.1 | 1.96 | 1.91 | 1.7 | | 1.28 |
| Yb | 1.5 | 2.58 | 1.72 | 1.55 | 1 | | 1.3 | 1.33 | 1.35 | 1. 1 | | 1.49 |
| Lu | 0.2 | 0.36 | 0.25 | 0.25 | 0.14 | | 0.19 | 0.18 | 0.21 | 0.15 | | 0.15 |
| or | | | | | 6.32 | | 5.20 | | | 18.67 | 24.05 | 23.58 |
| ab | | | | | 0.43 | | 0.08 | | | 8.00 | 9.48 | 5.08 |
| an | 14.17 | 4.82 | 1.80 | 0.00 | 18.70 | 10.72 | 5.01 | 6.31 | 3.36 | 9.31 | 8.67 | 16.16 |
| lc | 7.14 | 13.16 | 14.69 | 13.99 | | 8.02 | | 13.07 | 15.57 | | | |
| ne | 3.99 | 13.57 | 14.48 | 15.91 | 8.93 | 16.27 | 22.42 | 17.10 | 18.33 | 10.29 | 22.64 | 14.58 |
| di | 4.25 | 3.07 | 7.47 | 5.57 | 30.87 | 26.29 | 35.73 | 38.19 | 35.79 | 21.02 | 18.32 | 20.81 |
| wo | | | | | | | | | | | | |
| ol | 34.09 | 27.85 | 33.32 | 33.67 | 16.18 | 17.95 | 13.30 | 8.47 | 8.20 | 17.10 | 1.47 | 3.63 |
| cs | 17.28 | 20.72 | 16.15 | 18.05 | | 3.89 | | 0.49 | 2.10 | | | |
| mt | 5.94 | 4.55 | 3.74 | 3.97 | 7.79 | 6.71 | 7.12 | 6.32 | 6.70 | 6.44 | 5.80 | 4.11 |
| il | 2.92 | 3.44 | 2.87 | 2.73 | 3.76 | 4.65 | 3.76 | 5.47 | 5.56 | 4.20 | 2.91 | 2.85 |
| ap | 2.61 | 5.52 | 3.25 | 3.60 | 2.72 | 2.56 | 3.79 | 2.72 | 2.46 | 1.42 | 1.42 | 1.51 |
| A.I. | 0.37 | 0.82 | 0.93 | 1.00 | 0.39 | 0.66 | 0.83 | 0.80 | 0.89 | 0.72 | 0.82 | 0.64 |
| D.I. | 11.12 | 26.73 | 29.17 | 29.97 | 15.69 | 24.29 | 27.70 | 30.16 | 33.90 | 36.96 | 56.17 | 43.24 |

Table 12 (continued).

| | 13 | 14 | 15 | 16 | 17 | 18 | 19 | 20 | 21 | 22 | 23 | 24 | 25 |
|---|---|---|---|---|---|---|---|---|---|---|---|---|---|
| | LM61 | LM54 | LM53 | LMI | LM60 | LM2 | LM80 | LM99 | LM67 | LM106 | LA97 | LM76 | LM19 |
| | NeSy | NeSy | NeSy | NeSy | NeSy | NeSy | TrPh | PPPh | PPPh | PPPh | PPh | PPh | PPh |
| $SiO_2$ | 50.45 | 53.48 | 55.81 | 56.23 | 57.57 | 58.02 | 60.06 | 54.94 | 54.01 | 55.88 | 57.09 | 59.91 | 57.93 |
| $Al_2O_3$ | 17.87 | 19.31 | 20.18 | 19.98 | 20.42 | 20.43 | 19.75 | 21.03 | 19.59 | 21.04 | 19.97 | 20.11 | 20.95 |
| $Fe_2O_3$ | 3.01 | 2.13 | 1.15 | 1.49 | 1.00 | 1.89 | 1.01 | 1.21 | 3.41 | 2.25 | 2.29 | 1.01 | 1.34 |
| FeO | 3.20 | 2.28 | 3.02 | 1.52 | 1.26 | 1.04 | 1.07 | 1.22 | 0.92 | 0.76 | 0.70 | 0.82 | 0.64 |
| MnO | 0.18 | 0.18 | 0.15 | 0.14 | 0.12 | 0.12 | 0.19 | 0.12 | 0.25 | 0.23 | 0.11 | 0.22 | 0.17 |
| MgO | 1.62 | 1.00 | 1.51 | 0.48 | 0.21 | 0.38 | 0.13 | 0.16 | 0.17 | 0.09 | 0.37 | 0.06 | 0.05 |
| CaO | 6.32 | 4.21 | 3.67 | 2.39 | 1.98 | 2.40 | 1.49 | 1.87 | 1.27 | 1.03 | 0.78 | 0.96 | 0.76 |
| $Na_2O$ | 7.29 | 7.38 | 7.02 | 6.90 | 7.48 | 8.24 | 7.74 | 9.22 | 9.92 | 9.78 | 10.67 | 9.68 | 10.87 |
| $K_2O$ | 5.26 | 5.79 | 5.97 | 6.77 | 6.96 | 6.82 | 5.99 | 6.71 | 7.02 | 6.05 | 5.01 | 5.51 | 5.58 |
| $P_2O_5$ | 0.59 | 0.43 | 0.40 | 0.17 | 0.09 | 0.17 | 0.06 | 0.06 | 0.03 | 0.01 | 0.09 | 0.03 | 0.01 |
| L.O.I. | 2.87 | 2.97 | 0.34 | 3.28 | 2.48 | | 2.22 | 3.08 | 2.97 | 2.67 | 2.55 | 1.48 | 1.57 |
| Sum | 100.00 | 100.00 | 100.01 | 100.00 | 100.01 | 100.16 | 99.99 | 100.00 | 100.01 | 99.99 | 99.99 | 100.01 | 100.00 |
| ppm | | | | | | | | | | | | | |
| V | 143 | 82 | 74 | 52 | 34 | 49 | 15 | 43 | 63 | 24 | 51 | 12 | 12 |
| Cr | 1 | 3 | 1 | | | | | | | | 14 | | |
| Co | 12 | 10 | 7 | 4 | 2 | 5 | | 3 | 2 | 2 | 5 | 2 | 2 |
| Ni | 14 | 18 | 14 | 15 | 14 | 14 | 14 | 12 | 14 | 16 | 18 | 13 | 11 |
| Zn | 96 | 84 | 91 | 2990 | 69 | 73 | 113 | 77 | 119 | 184 | 94 | 142 | 133 |
| Rb | 95 | 110 | 122 | 115 | 124 | 117 | 174 | 125 | 126 | 186 | 122 | 208 | 203 |
| Sr | 2820 | 3630 | 3730 | 4320 | 3720 | 4370 | 259 | 2200 | 1480 | 498 | 310 | 71 | 30 |
| Ba | 2660 | 2860 | 2650 | 2990 | 2360 | 3247 | 148 | 1260 | 966 | 38 | 293 | 55 | 29 |
| Zr | 14 | 259 | 394 | 203 | 237 | 216 | 730 | 310 | 730 | 869 | 1840 | 1080 | 685 |
| Nb | 121 | 108 | 120 | 109 | 100 | 109 | 154 | 98 | 227 | 169 | 626 | 175 | 90 |
| La | 153 | 156 | 151.7 | 147.57 | 106.79 | | 187.71 | 130.58 | 110.01 | 183.66 | 21.28 | 143.80 | 146.69 |
| Cc | 252 | 234 | 246.49 | 231.57 | 167.5 | | 284.44 | 186.75 | 202.39 | 247.55 | 41.84 | 223.32 | 169.25 |
| Nd | | | 75.05 | 67.12 | 44.78 | | 65.18 | 39.98 | 54.79 | 42.39 | 13.01 | 48.03 | 25.62 |
| Sm | | | 11.09 | 10.46 | 6.35 | | 8.56 | 5.75 | 7.87 | 5.54 | 2.23 | 6.50 | 3.48 |
| Eu | | | 2.77 | 3.41 | 1.8 | | 1.83 | 1.6 | 1.83 | 1.52 | 0.63 | 1.37 | 0.90 |
| Gd | | | 7.21 | 6.73 | 4.01 | | 5.44 | 3.93 | 5.02 | 3.95 | 1.60 | 4.32 | 2.45 |
| Dy | | | 4.65 | 4.23 | 2.83 | | 3.82 | 2.82 | 3.4 | 2.65 | 1.21 | 3.32 | 1.54 |
| Er | | | 2.34 | 2.2 | 1.52 | | 2.36 | 1.69 | 1.79 | 1.83 | 0.70 | 2.26 | 1.24 |
| Yb | | | 2.3 | 2.21 | 1.6 | | 2.89 | 1.81 | 1.98 | 2.48 | 0.79 | 3.03 | 1.96 |
| Lu | | | 0.29 | 0.35 | 0.21 | | 0.45 | 0.26 | 0.27 | 0.38 | 0.12 | 0.47 | 0.35 |
| Or | 31.08 | 34.21 | 35.28 | 40.00 | 41.13 | 40.31 | 35.40 | 39.65 | 41.48 | 35.75 | 29.60 | 32.56 | 32.97 |
| Ab | 15.36 | 22.83 | 25.59 | 27.94 | 29.10 | 25.65 | 42.87 | 17.13 | 9.60 | 22.40 | 32.46 | 39.68 | 31.17 |
| An | 0.50 | 2.46 | 5.92 | 3.55 | 1.59 | | 1.46 | 0.00 | 0.00 | 0.00 | | | |
| Ne | 25.09 | 21.46 | 18.32 | 16.49 | 18.52 | 23.88 | 12.25 | 29.09 | 28.21 | 28.24 | 22.95 | 17.92 | 24.66 |
| Ac | | | | | | 2.30 | | 3.50 | 9.87 | 6.51 | 6.63 | 2.92 | 3.88 |
| Ns | | | | | | | | 0.75 | 2.57 | 0.19 | 1.85 | 1.36 | 2.53 |
| Di | 11.54 | 7.96 | 7.99 | 3.98 | 2.98 | 2.03 | 2.62 | 4.31 | 3.57 | 3.29 | 2.71 | 3.24 | 2.67 |
| Wo | 5.27 | 2.43 | | 0.96 | 1.72 | 2.80 | 1.04 | 1.63 | 0.82 | 0.53 | | 0.37 | 0.28 |
| Ol | | | 2.49 | | | | | | | | 0.35 | | |
| Mt | 4.36 | 3.09 | 1.67 | 2.16 | 1.45 | 1.57 | 1.46 | 0.00 | 0.00 | 0.00 | | | |
| 11 | 2.54 | 1.60 | 1.50 | 1.23 | 0.84 | 1.19 | 0.53 | 0.72 | 0.85 | 0.38 | 0.68 | 0.42 | 0.25 |
| Ap | 1.40 | 1.02 | 0.95 | 0.40 | 0.21 | 0.39 | 0.14 | 0.14 | 0.07 | 0.02 | 0.21 | 0.07 | 0.02 |
| A.I. | 0.99 | 0.95 | 0.89 | 0.93 | 0.97 | 1.02 | 0.97 | 1.07 | 1.22 | 1.08 | 1.15 | 1.09 | 1.14 |
| D.I. | 71.54 | 78.51 | 79.18 | 84.44 | 88.75 | 92.14 | 90.52 | 90.12 | 91.74 | 93.10 | 93.49 | 94.44 | 95.21 |

Table 12 (continued).

| | 26 | 27 | 28 | 29 | 30 | 31 | 32 | 33 | 34 | 35 | 36 | 37 |
|---|---|---|---|---|---|---|---|---|---|---|---|---|
| | LM112 | LM3 | LM46 | LM88 | LM25 | LM83 | LM37 | SB.09 | SB.05 | SB.02 | SB.10.-61. | SB.11.-24.4 |
| | PPh | PPh | PPh | PPh | PPh | PPh | PPh | Leucititic xenolith | Fe-carbonatite | Fe-carbonatite | Si-carbonatite | Phlogopite carbonatite |
| $TiO_2$ | 0.20 | 0.26 | 0.12 | 0.19 | 0.10 | 0.20 | 0.11 | 0.59 | 0.05 | 0.04 | 0.44 | 0.37 |
| $Al_2O_3$ | 20.80 | 20.93 | 20.99 | 21.02 | 21.17 | 20.88 | 20.85 | 20.73 | 0.87 | 0.83 | 12.11 | 8.18 |
| $Fe_2O_3$ | 1.32 | 1.51 | 1.31 | 1.36 | 1.40 | 1.30 | 1.71 | | | | | |
| FcO | 0.62 | 0.55 | 0.67 | 0.50 | 0.53 | 0.58 | 0.36 | 3.69 | 10.28 | 17.74 | 10.06 | 11.61 |
| MnO | 0.21 | 0.25 | 0.17 | 0.30 | 0.17 | 0.30 | 0.18 | 0.16 | 1.06 | 2.39 | 0.54 | 0.66 |
| MgO | 0.05 | 0.06 | 0.01 | 0.04 | 0.03 | 0.04 | 0.04 | 2.15 | 14.16 | 12.72 | 0.35 | 6.12 |
| CaO | 0.89 | 0.39 | 0.70 | 0.45 | 0.65 | 0.46 | 0.71 | 11.36 | 34.27 | 29.41 | 19.77 | 17.37 |
| $Na_2O$ | 9.89 | 11.19 | 11.18 | 11.70 | 10.84 | 11.91 | 11.16 | 0.59 | 0.02 | 0.02 | 0.07 | 0.19 |
| $K_2O$ | 5.79 | 4.80 | 5.46 | 5.02 | 5.32 | 5.01 | 5.33 | 17.89 | 0.26 | 0.20 | 3.69 | 5.76 |
| $P_2O_5$ | 0.03 | 0.05 | 0.01 | 0.02 | 0.01 | 0.03 | 0.01 | 0.41 | 0.03 | 0.04 | 0.54 | 0.05 |
| L.O.I. | 0.97 | 2.12 | 0.84 | 1.19 | 0.93 | 0.92 | 0.88 | 10.52 | 35.33 | 33.16 | 18.83 | 22.39 |
| Sum | 100.00 | 99.99 | 100.00 | 100.00 | 100.02 | 100.00 | 100.00 | 99.88 | 98.86 | 98.01 | 98.90 | 98.71 |
| ppm | | | | | | | | | | | | |
| V | 14 | 14 | 13 | 11 | 9 | 10 | 11 | | | | | |
| Cr | 5 | | | | | | | | | | | |
| Co | 2 | 2 | 4 | | 3 | | 3 | | | | | |
| Ni | 15 | 13 | 15 | 11 | 19 | 12 | 16 | | | | | |
| Zn | 147 | 196 | 130 | 185 | 139 | 195 | 147 | | | | | |
| Rb | 168 | 196 | 219 | 289 | 222 | 296 | 222 | 1078.0 | 6.1 | 3.5 | 78.3 | 394.0 |
| Sr | 108 | 65 | 27 | 19 | 32 | 19 | 21 | 4243.0 | 2983.0 | 8057.0 | 616.2 | 5237.0 |
| Ba | 48 | 54 | 2860 | 30 | 45 | 27 | 20 | 6940.0 | 951.0 | 13528.0 | 1756.0 | 581.5 |
| Zr | 840 | 1160 | 787 | 1330 | 741 | | 911 | 203.0 | 7.7 | 14.3 | 188.9 | 59.1 |
| Nb | 165 | 298 | 111 | 254 | 108 | 255 | 123 | 25.2 | 8.9 | 8.4 | 26.2 | 4.8 |
| Y | 26.47 | 34.54 | 13.62 | 46.98 | 14.48 | 45.27 | 14.40 | 24.2 | 18.8 | 45.5 | 16.4 | 59.3 |
| La | 183.03 | 116.14 | 120.09 | 177.90 | 136.77 | 174.63 | 130.97 | 1109.00 | 41.20 | 2569.00 | 42.15 | 106.44 |
| Cc | 264.55 | 187.52 | 148.90 | 295.02 | 162.40 | 287.46 | 158.22 | 2260.00 | 90.31 | 5236.00 | 90.52 | 223.75 |
| Nd | 50.76 | 43.27 | 23.56 | 64.36 | 24.23 | 61.43 | 24.24 | 354.33 | 47.54 | 2184.00 | 46.70 | 103.19 |
| Sm | 6.50 | 7.17 | 2.99 | 8.97 | 3.19 | 8.50 | 3.15 | 73.23 | 9.43 | 375.60 | 9.07 | 17.74 |
| Eu | 1.35 | 1.97 | 0.48 | 1.33 | 0.83 | 1.30 | 0.85 | 20.58 | 2.53 | 80.11 | 2.78 | 6.81 |
| Gd | 4.32 | 4.83 | 2.05 | 5.93 | 2.27 | 5.72 | 2.09 | 48.17 | 7.91 | 225.32 | 8.05 | 17.78 |
| Dy | 3.17 | 4.07 | 1.35 | 5.26 | 1.32 | 5.07 | 1.39 | 23.17 | 7.67 | 56.91 | 7.67 | 13.47 |
| Er | 2.13 | 2.73 | 1.08 | 3.61 | 1.11 | 3.50 | 1.09 | 7.39 | 3.17 | 22.45 | 3.67 | 6.04 |
| Yb | 2.75 | 3.87 | 1.66 | 5.14 | 1.73 | 4.95 | 1.74 | 4.17 | 3.09 | 8.72 | 3.31 | 4.89 |
| Lu | 0.38 | 0.58 | 0.26 | 0.74 | 0.31 | 0.74 | 0.26 | 0.42 | 0.44 | 0.86 | 0.61 | 0.57 |
| Or | 34.21 | 28.36 | 32.26 | 29.66 | 31.44 | 29.60 | 31.50 | | | | | |
| Ab | 34.70 | 36.85 | 32.91 | 34.84 | 35.14 | 35.08 | 33.72 | | | | | |
| Ne | 21.7 | 23.88 | 24.19 | 24.56 | 23.91 | 24.06 | 23.75 | | | | | |
| Ac | 3.82 | 4.37 | 3.79 | 3.93 | 4.05 | 3.76 | 4.95 | | | | | |
| Ns | 1.07 | 2.05 | 2.96 | 3.34 | 1.83 | 3.96 | 2.62 | | | | | |
| Di | 2.52 | 1.41 | 2.59 | 1.85 | 2.28 | 1.84 | 1.75 | | | | | |
| Wo | 0.56 | | 0.21 | | | | 0.61 | | | | | |
| Ol | | 0.35 | | 0.22 | | 0.33 | | | | | | |
| Il | 0.38 | 0.49 | 0.23 | 0.36 | 0.19 | 0.38 | 0.21 | | | | | |
| Ap | 0.07 | 0.12 | 0.02 | 0.05 | 0.02 | 0.07 | 0.02 | | | | | |
| A.I. | 1.08 | 1.13 | 1.16 | 1.17 | 1.11 | 1.20 | 1.16 | | | | | |
| D.I. | 95.50 | 95.51 | 96.12 | 96.33 | 96.36 | 96.47 | 96.53 | | | | | |

Petrochemistry

Selected whole-rock compositions (Table 12) are representative of the main rock-types. The silicate rocks are strongly alkaline (Fig. 13A) and are represented by three main clans: 1) ultramafic (olivine melilitites and olivine nephelinites), 2) mafic (basanites, tephrites and phonotephrites) and 3) leucocratic rock-types (nepheline syenites and peralkaline phonolites). All the rock-types are ne-normative (Table 12); in particular, the olivine melilites are lc- and cs-normative, the olivine nephelinites range from lc-cs- to strongly ne-di-normative and the phonolitic rocks are ac-ns-normative (A.I. = 1.01-1.22).

A bimodal distribution is apparent in the $Na_2O$ vs. $K_2O$ diagram (Fig. 13B), where the mafic and ultramafic rock-types fit the potassic and transitional fields, whereas the felsic rocks straddle the sodic field, the latter being mainly characterized by peralkaline phonolites having $Na_2O$-2$\geq K_2O$ (cf. Fig. 13B).

The associated carbonatites are Fe-carbonatite types (Fig. 13C).

Variation diagrams (Figs. 14 and 15) indicate that the leucocratic rocks may derive from basanitic or olivine nephelinitic liquids through fractional crystallization processes. In general, D.I.* values are positively correlated with $SiO_2$, $Al_2O_3$ and $Na_2O$, and negatively correlated with $FeO_{tot}$, MgO, CaO and $P_2O_5$, according to early olivine, clinopyroxene and apatite removal, followed by nepheline and alkali feldspar fractionation in the more differentiated peralkaline phonolites. In particular, the alkali feldspar fractionation is suggested by $K_2O$, Ba and Sr decrease after D.I.* = 90 (Figs. 14 and 15).

Mass balance results for major elements, starting from a basanite parent magma (e.g. sample n. 25, BA PA4 of Table 12), show that the derived melts, which are represented, e.g. by phonotephrite (sample n. 11, PhTe LA3), nepheline syenite (sample n. 18, NeSy LM2), and peralkaline phonolite (sample n. 26, PPh Lm112), correspond to 51, 24 and 11% of the parent liquid ($\sum Res^2$=0.38, 0.18 and 0.19, respectively; cf. Table 4 of Traversa *et al.*, 1996). The major element calculations are also consistent with trace element modelling (Rayleigh's law), where the calculated/observed ratios mostly range from 0.95 to 1.20 (Table 13). Some low ratios relative to Nb, Sr and Zr of the phonotephrite, nepheline syenite and peralkaline phonolite, respectively, are probably related to the presence of exotic phases, or to crustal contamination, or to an unadequate $K_D$ value for titanite.

The fact that peralkaline phonolites (sodic affinity in the $Na_2O$ vs. $K_2O$ diagrams of Fig. 13B) may be originated from a K-basanitic magma points to a pristine potassic affinity even for the leucocratic rock-types plotting in the sodic field. Moreover, mass balances also show that the 11 LA3 phonotephrite may derive from an olivine nephelinite magma (e.g. sample n. 8 LM115; cf. Table 6 of Traversa *et al.*, 1996).

Notably, the relationships between the olivine melilitites and the other rock-types do not give plausible physical solutions.

$(I.E.)_N$ diagrams for the early Fe-carbonatites display positive spikes for Ba, La, Nd-Sm and Tb, and negative ones for Th, P, Hf-Zr, Ti and Y (Fig. 16). The large range shown by U-Nb-Ta-K reflects the local concentrations of uranpyrochlore, alkali feldspar and tetraferriphlogopite. On the other hand, the late carbonatites are systematically enriched in Ba, Th, La-Ce, Nd-Sm and Tb in comparison with the early analogues.

Leucititic xenoliths, found in the Lages pipes and containing large carbonatitic fragments, show the same enrichment (plus K) of the late carbonatites, probably reflecting the presence of carbonatitic material. However, these leucititic xenoliths considerably differ from the cognate tholeiitic xenoliths (L-Ti tholeiitic basalts), which display a flattened trend and I.E. and REE contents similar to those of the low-$TiO_2$ Early Cretaceous Paraná basalts (Fig. 16; cf. also Marques *et al.*, 1989).

The alkaline rocks from the region display $(I.E.)_N$ and $(REE)_N$ values roughly in the same range of the early carbonatites, excepting for some leucocratic rock-types (peralkaline phonolites) that have strongly Nb and Zr positive spikes and the lowest $(La/Yb)_N$. The latter ratios are: 13.6±4.0 (early carbonatites); 289±238 (late carbonatites); 179 (leucitites); 3.0 (L-Ti tholeiitic basalts); 36.1±12.5 (olivine melilitites+melanephelinites+basanites); 47.7±4.4 (tephrites+nepheline syenites); 35.3±16.7 (peralkaline phonolites).

Traversa *et al.* (1996) suggested that I.E. trends and REE patterns of the "primitive" rock-types (i.e. olivine melilitites, melanephelinites, basanites) are consistent with a metasomatized mantle source, enriched in HFSE, LILE and LREE with respect to the primitive mantle, which suffered relatively low degrees of partial melting of wet layers (e.g. 4-10%; cf. also Comin-Chiaramonti *et al.*, 1997a, b), and gradually melting increase from olivine melilitites to basanites.

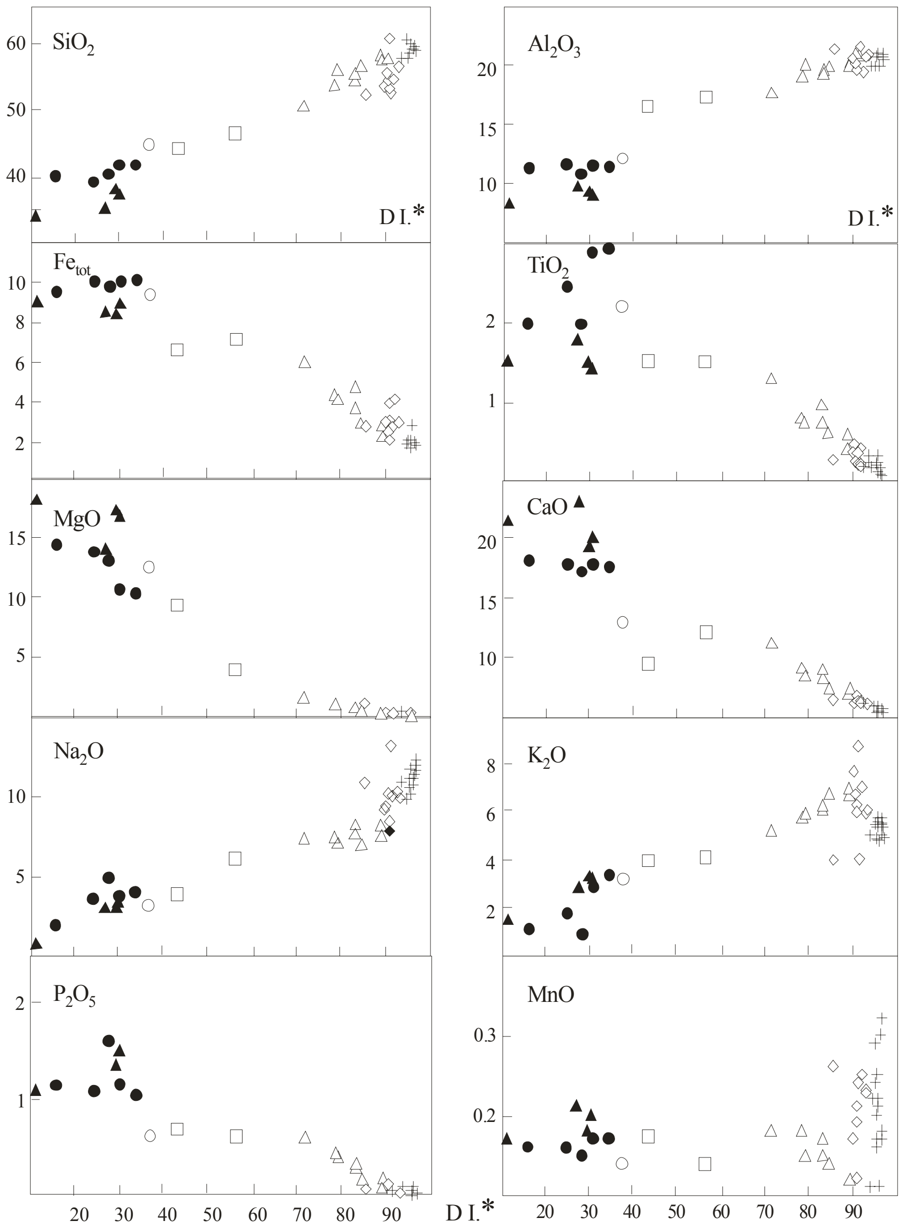


Fig. 14. Major elements (wt%) vs. D.I.* diagrams for Lages alkaline rocks (D.I.*=or+ab+ne+lc+ac+ns). Symbols as in Fig. 13.

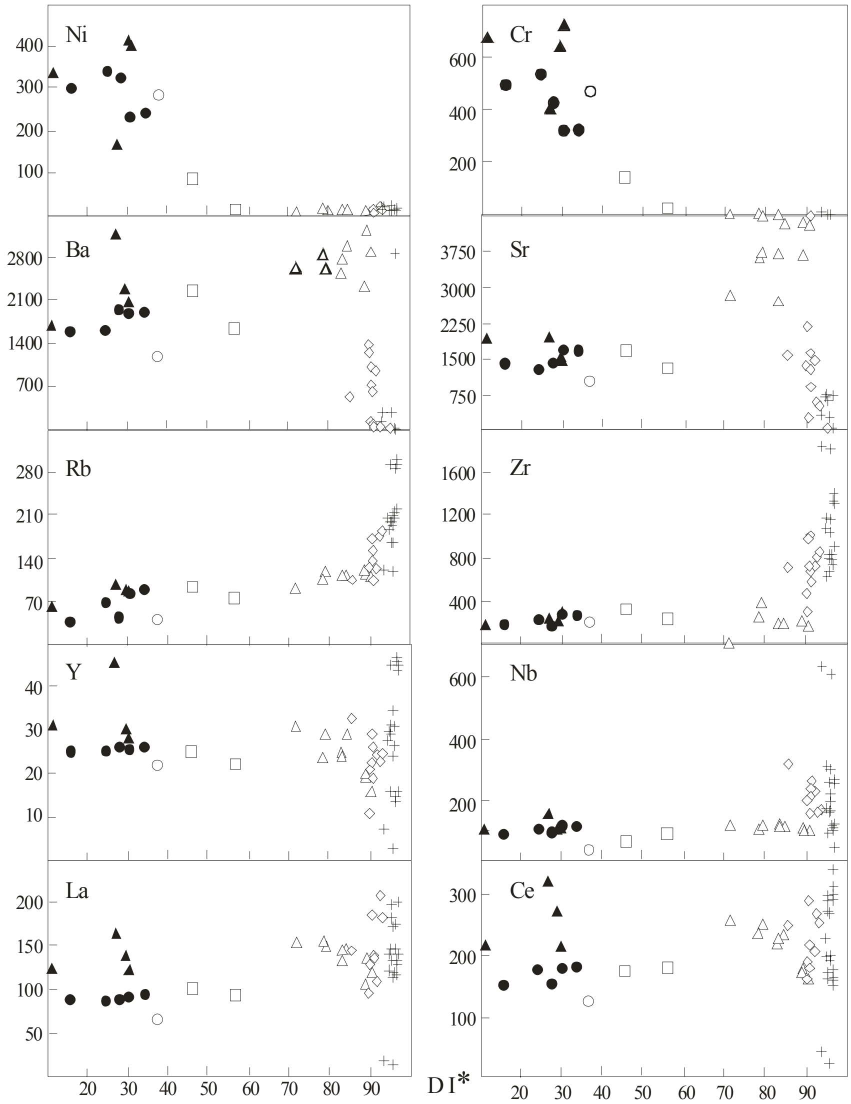


Fig. 15. Trace elements (ppm) vs. D.I.* diagrams for Lages alkaline rocks. Symbols as in Fig. 13.

Table 13. Calculated/observed ratios from the modelling of trace elements, Rayleigh's law, for selected samples from Lages rock-types. F, weight fraction of residual liquid, $Res^2$, sum of the residual squares for the major element compositions (cf. Tables 4 and 6 of Traversa *et al.*, 1996).

| | 10<br>BA<br>Observed | 11<br>PhTe<br>Calculated/<br>observed | 18<br>NeSy<br>Calculated/<br>observed | 26<br>PPh<br>Calculated/<br>observed | 8<br>ON<br>Observed | 11<br>PhTe<br>Calculated/<br>observed |
|---|---|---|---|---|---|---|
| Cr | 474 | 1.00 | | | 320 | 0.95 |
| Co | 50 | 0.96 | 1.20 | 1.00 | 44 | 1.08 |
| Ni | 288 | 1.00 | 1.00 | 1.00 | 233 | 1.00 |
| Zn | 96 | 1.01 | 1.00 | 0.97 | 108 | 0.99 |
| Rb | 43 | 0.96 | 1.07 | 1.01 | 85 | 2.19 |
| Sr | 1010 | 1.08 | 0.62 | 1.00 | 1657 | 1.01 |
| Ba | 1220 | 1.01 | 1.01 | 1.17 | 1924 | 1.15 |
| Zr | 207 | 0.99 | 0.99 | 0.56 | 276 | 1.03 |
| Nb | 36 | 0.72 | 1.00 | 0.98 | 113 | 0.97 |
| Y | 22 | 0.95 | 1.00 | 1.00 | 25 | 1.00 |
| La | 65 | 0.97 | 0.99 | 1.09 | 91 | 0.98 |
| Ce | 121 | 1.04 | 1.01 | 0.99 | 175 | 0.97 |
| F | | 0.51 | 0.24 | 0.11 | | 0.36 |
| $\sum Res^2$ | 0.38 | 0.18 | 0.19 | | 0.49 | |

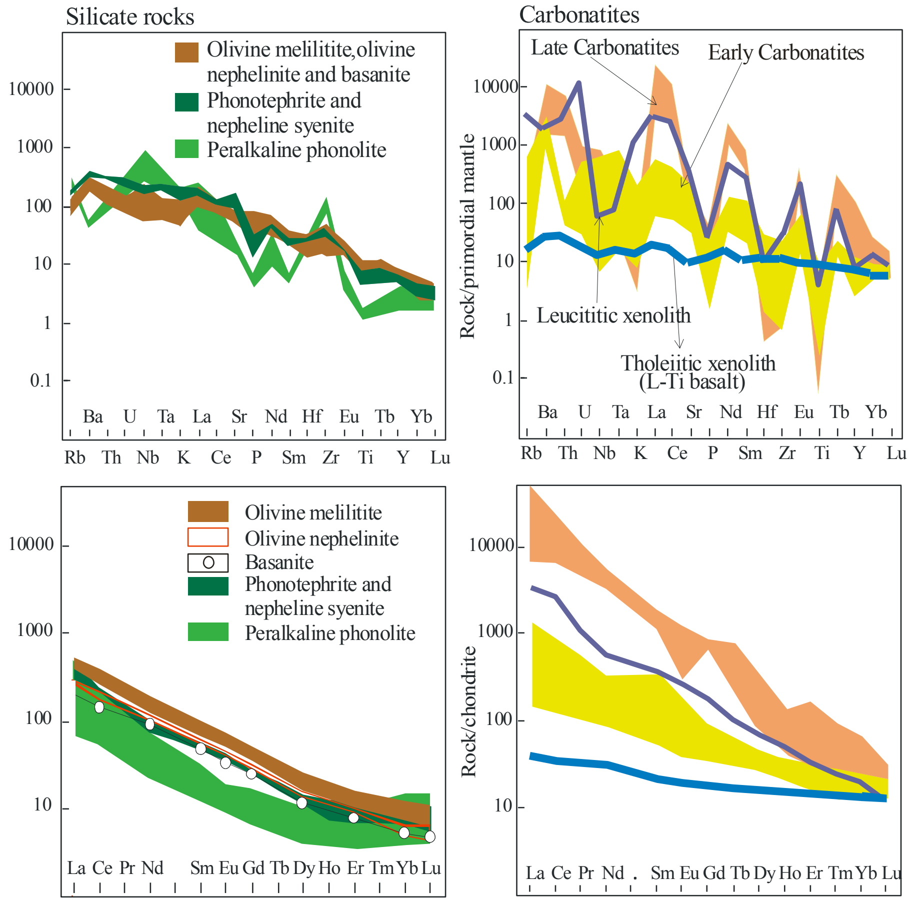


Fig. 16. Spidergrams representing the I.E. and REE fields of the main Lages rock-types normalized to the primitive mantle and to the chondrites (Sun & McDonough, 1989, and Boynton, 1984, respectively). Data source: Table 13 and Comin-Chiaramonti *et al.* (2002).

## LOCAL STRUCTURES AND TECTONICS

Many differences between Anitápolis and Lages outcrops may be explained by the different erosion stages reached by both complexes: while Anitápolis was already submitted to high erosion taxes, exposing the roots of the alkaline complex and attaining the crystalline basement level, the Lages rocks are representative of hypabissal and subvolcanic levels.

Using air photographs, Melcher & Coutinho (1966) detected different structural patterns in the regional granitoids related to the Anitápolis alkaline complex: radial and concentric fractures and a whole regional N-S trend (N10°E to N10°W) appear cut by a great number of N55°E joints, and the alkaline massif was placed in an important (10 km broad and NE-trending) fault zone. Scheibe & Furtado (1988) noted that alkaline dykes occurring around the Anitápolis massif have a widespread direction mainly at the NW quadrant, while the tholeiitic dykes have a predominant N-S and N10°W direction.

Any interpretation relative to the Santa Catarina structural emplacement, by radar and satellite images, is linked to a "block tectonics" system affecting the whole eastern part of the Santa Catarina state and resulting in the relative uplift of many trapezoidal blocks, among which the Lages Dome would be one of the more important geostructures, according to Scheibe & Furtado (1989). The latter authors also stressed the presence of two important NS-NNE sets of lineaments (i.e. Urussanga-Leoberto Leal and Armazém-Gaspar Lineaments) observed in the litoranean sediments extending from southern to the northern areas (Blumenau city). As it has been noted by Furtado

(1989), the Anitápolis alkaline massif crops out between these two lineaments and at the intersection with an important NW fault, parallel to the Serra Geral Lineament, characterizing another uplifted block (cf. Fig. 6).

Loczy (1968) described the domic character of the Lages area, quoting faultings with displacement of more than 360 m, and emphasizing the rectilinear character of many important rivers in the region. Scheibe (1986) drawed the attention that the Lages Dome caused an important retreat of the basaltic scarps, that the North and South limits of the dome correspond to important NE lineaments (Corupá and Rio Engano Lineaments), and that the whole geotectonics is similar to that of “crustal warpings” (e.g. Bailey, 1964, 1974) and of “crustal upwellings” (cf. Le Bas, 1977).

Scheibe & Furtado (1989) also defined the N-S "Ponte Alta Lineament" as the western border of the Lages Dome. The importance of these structural features (active since the Archean, according to Haralyi *et al.*, 1982) are apparent by the uplift of the sedimentary rocks along the Serra Geral Lineament, up to the upper level of the western flood basalts, reversing the drainage of this area to the Rio da Prata Basin.

NS-trending lineaments related to the opening of the South Atlantic Ocean are extensively filled by the tholeiitic dykes that are so frequent at Florianópolis, in the Santa Catarina Island, and have already been mapped by Petrobrás geologists at the continental platform, where they are responsible for the origin of the submarine petroleum deposits (Scheibe & Furtado, 1989).

Scheibe (1979) mentioned the Florianópolis fracture zone (Asmus, 1978) as a possible structural control for these two alkaline districts.

Fúlfaro *et al.* (1982) suggested that the alkaline rocks from Lages and Anitápolis, as well as those from the Eastern Paraguay, would be related to the E-W Rio Uruguay Lineament, a continental continuity of the same Florianópolis fracture zone.

## STABLE ISOTOPES: OXYGEN AND CARBON

In the Early Cretaceous Anitápolis Ca-carbonatites, where Fe-dolomite or Mg-ankerite are coupled with prevailing calcite, $\delta^{18}O$ and $\delta^{13}C$ isotopes vary in a restricted range, close to the "primary" magmatic carbonatite box (Table 14), and tend to fit a straight line along with the Juquiá carbonatites (Fig. 17; cf. Walter *et al.*, 1995). The isotopic data are in the same range as those for carbonates in some of the associated silicate rocks (e.g. phlogopite clinopyroxenites and ijolites; Table 15).

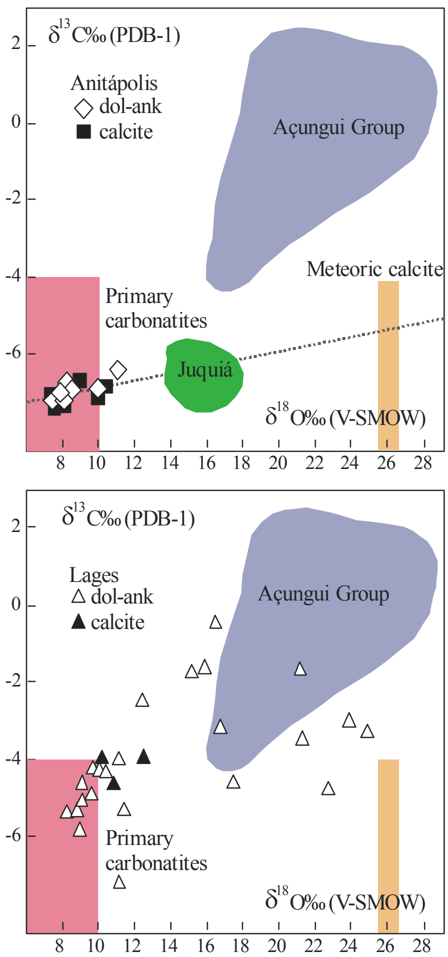


Fig. 17. Stable O-C isotope compositions (  notations) from selected samples from Anitápolis and Lages rock-types. Data source: Fassbinder (1996) and Comin-Chiaramonti *et al.* (2002). PCB, primary carbonatite box after Taylor *et al.* (1967) and Keller & Hoefs (1995). For comparison the fields relative to the alkaline-carbonatitic complex of Juquiá (P. Comin-Chiaramonti unpublished data), Açungui Group (Fassbinder, 1996) and meteoric calcite (Alcover Neto *et al.*, 1995).

Table 14. Oxygen and carbon isotope data for carbonates from selected samples of carbonatites and associated silicate rocks from the Anitápolis complex and Lages district (+, early carbonatites; *, late carbonatites). Main mineral assemblages are also reported. Data source: Scheibe, 1986; Toyoda *et al.*, 1995; Comin-Chiaramonti *et al.*, 2002. Abbreviations: af=alkali felspar; ank=ankerite; ap=apatite; ba=barite; biot=biotite; cc=calcite; ccpx=Ca-clinopyroxene; dol=dolomite; fcc=fluorocarbonates; lc=leucite; ne=nepheline; ol=olivine; op=opaques; phl=phlogopite; px=pyroxene; qz=quartz.

| ANITÁPOLIS | CaO | MgO | FeO | MgO/FeO | $\delta^{18}O$‰ | $\delta^{13}C$‰ | $\delta^{18}O$‰ | $\delta^{13}C$‰ | Main mineralogy |
|---|---|---|---|---|---|---|---|---|---|
| | | wt% | | mol | dol-ank | dol-ank | calcite | calcite | |
| CARBONATITE | | | | | | | | | |
| ***Borehole*** | | | | | | | | | |
| SAN 14-49 | 90.9 | 4.2 | 4.9 | 1.53 | 8.21 | | | | cc, ap, phl, (af) |
| SAN 12-78 | 87.9 | 4.8 | 7.3 | 3.25 | 8.19 | -6.78 | 7.47 | -7.15 | cc, dol, ap, phl |
| S-83.6 (F) | | | | | | | | | cc, Mg-ank, phl, fcc, ap, op |
| SAN 11-101 | 90.6 | 3.4 | 6.0 | 1.03 | 8.04 | -7.21 | 7.55 | -7.38 | cc, dol, ap, (qz) |
| ***Surface samples*** | | | | | | | | | |
| AP 891** | 84.5 | 6.0 | 9.5 | 1.13 | | | 9.0 | -6.7 | cc, ap, op |
| SAN-1 | 96.9 | 2.8 | 0.3 | 1.85 | 8.24 | -7.07 | 7.65 | -7.24 | cc, dol, ap |
| SAN 2 | 68.9 | 13.8 | 17.3 | 1.42 | 8.51 | -6.93 | 7.94 | -7.34 | cc, ap, dol, op, af, phl |
| SAN 13 | 91.7 | 5.6 | 2.7 | 3.78 | 7.65 | -7.25 | 7.52 | -7.37 | cc, dol, op, phl |
| SILICATE ROCKS | | | | | | | | | |
| SAN 2N Phlogopite clinopyroxenite | | | | | 8.01 | -7.00 | 7.89 | -7.26 | px, phl, op, ap, cc |
| SAN 6A Melanephelinite (dyke) | | | | | 10.12 | -6.89 | 10.02 | -7.15 | phl, px, ol, op, glass, dol, ap |
| SAN 8 Apatite-biotite clinopyroxenite | | | | | 11.05 | -6.43 | 10.38 | -6.82 | ap, biot, px, op, cc |
| Nephelinite (G) (dyke) | | | | | | | | | biot, px, ol, af, ne, op |
| Nephelinite (G) (dyke) | | | | | | | | | biot, cpx, ol, af, ne, op |
| SAN 24 Ijolite | | | | | 7.99 | -6.65 | 7.51 | -7.17 | px, phl, af, ne, op, ap, cc |
| SAN 25 Nepheline syenite | | | | | | | 8.98 | -7.10 | af, ne, px, biot, op |
| LAGES | CaO | MgO | FeO | MgO/FeO | $\delta^{18}O$‰ | $\delta^{13}C$‰ | $\delta^{18}O$‰ | $\delta^{13}C$‰ | Main mineralogy |
| | | wt% | | mol | dol-ank | dol-ank | calcite | calcite | |
| CARBONATITE | | | | | | | | | |
| ***Borehole*** | | | | | | | | | |
| (S)FV-14* | 60.3 | 10.9 | 2.8 | 0.67 | 16.67 | -3.09 | | | dol, cc, ba, fcc |
| (S)FV-24* | 61.8 | 9.7 | 28.5 | 0.62 | 23.91 | -3.02 | | | ank, cc, ba, fcc |
| (S)FV-26+ | | | | | 11.24 | -7.15 | | | |
| (S)FV-32* | 64.2 | 10.4 | 25.4 | 0.73 | 12.43 | -2.44 | | | ank, cc, fcc, ap |
| (S)FV-33* | | | | | 11.44 | -5.27 | | | |
| (S)LG-1/2-64.5* | 60.9 | 7.9 | 31.2 | 0.45 | 10.63 | -4.26 | | | ank, ba, fcc |
| (S)LG-1/4* | 63.4 | 8.9 | 27.7 | 0.54 | 21.19 | -1.66 | | | ank, ba, fcc |
| (S)LG-1/6+ | 57.2 | 10.7 | 32.1 | 0.59 | 8.95 | -4.38 | | | ank, ba, fcc |
| (S)LG-1/8-101.4+ | 62.3 | 8.0 | 29.7 | 0.47 | 9.74 | -4.07 | 9.02 | -4.48 | ank, cc, ba, fcc |
| (S)LG-1/10-109.8* | 59.5 | 10.7 | 29.8 | 0.63 | 9.26 | -4.89 | 8.64 | -5.27 | ank, cc, ba, ap |
| (S)LG-1/12-123.8+ | 55.1 | 11.8 | 33.1 | | 9.11 | -4.89 | 8.38 | -5.30 | ank, cc, phl, ap |
| (S)LG-3/5-34.3* | 88.1 | 1.9 | 10.0 | 0.33 | | | | | cc, ank, fcc, ba |
| (S)LG-3/8-27.9* | 58.7 | 10.0 | 31.3 | 0.57 | | | | | ank, cc, ba, phl |
| SB10 -61+ | | | | | 17.45 | -4.56 | | | ank, qz, phl, ap |
| SB 11-24.4+ | 48.6 | 17.1 | 34.3 | 0.89 | 11.12 | -3.94 | 12.54 | -3.90 | ank, cc, phl |
| SB 14-60+ | 95.0 | 2.0 | 3.0 | 1.20 | | | 10.92 | -4.54 | cc |
| SB 15-20+ | 58.5 | 10.3 | 31.2 | 0.58 | 9.59 | -4.67 | | | ank |
| SB 16-28.34+ | 60.7 | 16.0 | 23.3 | 1.22 | 10.17 | -4.2 | 10.19 | -3.86 | ank, cc, phl |
| SB 17-34.38+ | 55.2 | 19.2 | 25.6 | 1.35 | 10.37 | -4.29 | | | ank |
| SB 18-50* | 61.9 | 9.3 | 28.8 | 0.54 | 10.55 | -4.33 | | | ank, phl, ap |
| SB 19-80* | 54.7 | 16.6 | 28.7 | 1.03 | 24.84 | -3.24 | 22.73 | -4.76 | ank, cc, ap |
| SB 20-85* | 55.2 | 17.0 | 27.8 | 1.05 | 8.99 | -5.76 | | | ank |
| ***Surface samples*** | | | | | | | | | |
| SB-02* | 47.2 | 20.4 | 32.4 | 1.12 | 15.18 | -1.66 | | | ank, ba, fcc |
| SB-03+ | 57.6 | 22.5 | 19.9 | 2.00 | 15.82 | -1.55 | | | ank |
| SB-05+ | 57.3 | 23.7 | 19.0 | 2.22 | 16.45 | -0.46 | | | ank |
| XENOLITHS | | | | | | | | | |
| SB-09- Leucitite | | | | | 21.30 | -3.42 | | | glass, cc, lc, px, phl, op |

Table 15. Sr-Nd isotope data (ppm) for carbonatites and alkaline rock-types from selected samples of the Anitápolis complex and Lages district. Data source: Scheibe et al. (1986) (S), Toyoda et al. (1995), Carlson et al. (1996) (C), Gibson et al. (1996) (G), Traversa et al. (1996) (T) and Comin-Chiaramonti et al. (2002).

| ANITÁPOLIS | Rb | Sr | Measured $^{87}Sr/^{86}Sr$ | $R_0$ 132 Ma | Sm | Nd | Measured $^{143}Nd/^{144}Nd$ | $R_0$ 132 Ma | εSr | εNd | $T^{DM}$ Ma |
|---|---|---|---|---|---|---|---|---|---|---|---|
| CARBONATITE | | | | | | | | | | | |
| ***Borehole*** | | | | | | | | | | | |
| SAN 14-49 | 6.10 | 2983 | 0.705952 ( 8) | 0.70594 | 9.43 | 47.54 | 0.512281 ( 8) | 0.51218 | 19.8 | -5.7 | 1339 |
| SAN 12-78 | 6.48 | 6849 | 0.705953 ( 6) | 0.70595 | 21.33 | 115.73 | 0.512279 ( 7) | 0.51222 | 19.9 | -5.6 | 1237 |
| S-83.6 (F) | | | | | 180.18 | 672.60 | | | | | |
| SAN 11-101 | 6.87 | 4462.3 | 0.705952 ( 6) | 0.70594 | 9.44 | 53.49 | 0.512259 ( 7) | 0.51213 | 19.8 | -6.7 | 1266 |
| ***Surface samples*** | | | | | | | | | | | |
| AP 891** | 0 | 4000 | 0.706151 ( 6) | 0.70615 | 36.10 | 150.00 | | | 22.7 | | |
| SAN-1 | 3.22 | 2462.3 | 0.705947 (10) | 0.70594 | 13.78 | 69.62 | 0.512262 ( 8) | 0.51222 | 19.8 | -6.0 | 1365 |
| SAN 2 | 271.90 | 1738.7 | 0.706779 ( 8) | 0.70593 | 14.75 | 72.33 | 0.512278 ( 8) | 0.51217 | 19.6 | -5.8 | 1391 |
| SAN 13 | 113.94 | 7194 | 0.706029 ( 8) | 0.70594 | 22.12 | 103.19 | 0.512332 (10) | 0.51222 | 19.8 | -4.8 | 1397 |
| SILICATE ROCKS | | | | | | | | | | | |
| SAN 2N Phlogopite clinopyroxenite | 104.5 | 616 | 0.706850 (10) | 0.70593 | 9.07 | 46.70 | 0.512278 (11) | 0.51215 | 19.6 | -6.2 | 1350 |
| SAN 6A Melanephelinite (dyke) | 825.9 | 798 | 0.711471 ( 5) | 0.70585 | 18.86 | 101.35 | 0.512333 (10) | 0.51224 | 18.5 | -4.5 | 1172 |
| SAN 8 Apatite-biotite clinopyroxenite | 213.7 | 955 | 0.707139 (11) | 0.70592 | 19.71 | 104.32 | 0.512290 ( 6) | 0.51219 | 19.5 | -5.4 | 1254 |
| Nephelinite (G) (dyke) | 111.0 | 1082 | 0.70678 ( ?) | 0.70622 | 6.04 | 33.40 | 0.51220 ( ?) | 0.51211 | 23.8 | -7.1 | 1322 |
| Nephelinite (G) (dyke) | 120.0 | 834 | 0.70736 ( ?) | 0.70658 | 6.61 | 38.80 | 0.51225 ( ?) | 0.51216 | 28.8 | -6.0 | 1185 |
| SAN 24 Ijolite | 124.5 | 724.5 | 0.706836 ( 9) | 0.70590 | 10.59 | 54.73 | 0.512286 (11) | 0.51218 | 19.3 | -5.5 | 1295 |
| SAN 25 Nepheline syenite | 103.1 | 677 | 0.706751 (10) | 0.70593 | 8.31 | 42.31 | 0.512285 (10) | 0.51218 | 19.6 | -5.6 | 1317 |
| LAGES | Rb | Sr | Measured $^{87}Sr/^{86}Sr$ | $R_0$ 132 Ma | Sm | Nd | Measured $^{143}Nd/^{144}Nd$ | $R_0$ 132 Ma | εSr | εNd | $T^{DM}$ Ma |
| CARBONATITE | | | | | | | | | | | |
| ***Borehole*** | | | | | | | | | | | |
| (S)FV-14* | 78.3 | 616.2 | 0.706240 ( 5) | 0.70584 | 9.07 | 46.70 | 0.512100 ( 4) | 0.51214 | 17.48 | -9.72 | 1576 |
| (S)FV-24* | 394 | 5237 | 0.705887 ( 9) | 0.70565 | 17.74 | 103.19 | 0.512229 ( 9) | 0.51218 | 14.76 | -7.08 | 1222 |
| (S)FV-26+ | 10.39 | 3738 | 0.706101 ( 6) | 0.70609 | 10.95 | 60.16 | 0.512112 ( 6) | 0.51204 | 21.01 | -9.42 | 1454 |
| (S)FV-32* | 3.8 | 4879 | 0.706946 ( 7) | 0.70694 | 18.86 | 86.96 | 0.511969 ( 5) | 0.51190 | 33.09 | -12.95 | 1718 |
| (S)FV-33* | 155.64 | 954 | | | 19.71 | 104.32 | | | | | |
| (S)LG-1/2-64.5* | 6.48 | 6849 | | | 21.33 | 115.73 | | | | | |
| (S)LG-1/4* | 236.3 | 3937 | 0.706263 (9) | 0.70618 | 358.70 | 2086 | 0.512232 ( 6) | 0.51218 | 20.77 | -7.02 | 1218 |
| (S)LG-1/6+ | 120.85 | 1094 | | | 38.43 | 158.24 | | | | | |
| (S)LG-1/8-101.4+ | 1.90 | 1544 | 0.706126 ( 5) | 0.70612 | 42.84 | 185.92 | 0.512151 (13) | 0.51208 | 21.43 | -8.94 | 1910 |
| (S)LG-1/10-109.8* | | | | | | | | | | | |
| (S)LG-1/12-123.8+ | 3.52 | 8057 | 0.705967 (13) | 0.70596 | 375.60 | 2184 | 0.512156 ( 5) | 0.51210 | 19.21 | -8.50 | 1319 |
| (S)LG-3/5-34.3* | 6.87 | 4462 | | | 16.44 | 53.49 | | | | | |
| (S)LG-3/8-27.9* | 6.10 | 2983 | 0.706263 (10) | 0.70626 | 9.43 | 47.54 | 0.512138 (11) | 0.51208 | 23.34 | -9.01 | 1558 |
| SB 11-24.4+ | 9.40 | 183 | 0.705596 (11) | 0.70532 | 4.28 | 19.75 | 0.512353 (10) | 0.51224 | 10.96 | -4.47 | 1383 |
| SB 14-60+ | 1078 | 4243 | 0.705916 ( 7) | 0.70512 | 73.23 | 354.30 | 0.512132 (17) | 0.51207 | 7.24 | -9.18 | 1651 |
| SB 15-20+ | 3.80 | 4879 | 0.706946 ( 7) | 0.70694 | 18.86 | 86.96 | 0.511969 ( 5) | 0.51190 | 33.09 | -12.95 | 1718 |
| SB 16-28.34+ | 155.64 | 954 | | | 19.71 | 104.32 | | | | | |
| SB 17-34.38+ | 6.48 | 6849 | | | 21.33 | 115.73 | | | | | |
| SB 18-50* | 236.3 | 3937 | 0.706263 (9) | 0.70618 | 358.70 | 2086 | 0.512232 ( 6) | 0.51218 | 20.77 | -7.02 | 1218 |
| SB 19-80* | 120.85 | 1094 | | | 38.43 | 158.24 | | | | | |
| SB 20-85* | 1.90 | 1544 | 0.706126 ( 5) | 0.70612 | 42.84 | 185.92 | 0.512151 (13) | 0.51208 | 21.43 | -8.94 | 1910 |
| ***Surface samples*** | | | | | | | | | | | |
| SB-02* | 3.52 | 8057 | 0.705967 (13) | 0.70596 | 375.60 | 2184 | 0.512156 ( 5) | 0.51210 | 19.21 | -8.50 | 1319 |
| SB-03+ | 6.87 | 4462 | | | 16.44 | 53.49 | | | | | |
| SB-05+ | 6.10 | 2983 | 0.706263 (10) | 0.70626 | 9.43 | 47.54 | 0.512138 (11) | 0.51208 | 23.34 | -9.01 | 1558 |
| SILICATE ROCKS | | | | | | | | | | | |
| SB-08 -Tephrite | 105.47 | 1650 | 0.705111 ( 9) | 0.70491 | 8.22 | 57.51 | 0.512434 ( 8) | 0.51236 | 4.28 | -2.91 | 826 |
| (C)-Chapada-Tephrite | 76.70 | 1881 | 0.705285 ( 9) | 0.70516 | 9.74 | 63.04 | 0.512405 ( 9) | 0.51236 | 7.82 | -3.54 | 907 |
| (G) B162-Ol melilitite | 58 | 1639 | 0.70462 ( 1) | 0.70451 | 11.82 | 76.20 | 0.51244 ( 1) | 0.51239 | -1.45 | -2.86 | 867 |
| (G) B161-Ol melilitite | 96 | 1810 | 0.70472 ( 1) | 0.70455 | 18.87 | 105 | 0.51243 ( 1) | 0.51238 | -0.82 | -3.2 | 997 |
| (T) LM6-Ol melilitite | 92 | 1470 | 0.70445 ( 2) | 0.70425 | 14.55 | 85.43 | 0.51244 ( 2) | 0.51239 | -5.07 | -2.95 | 936 |
| (T) PA1-Ol melilitite | 64 | 1910 | 0.70443 ( 3) | 0.70433 | 14.90 | 88.20 | 0.51250 ( 2) | 0.51245 | -4.07 | -2.95 | 851 |
| (G) B169-Melanephelinite | 78 | 1941 | 0.70439 ( 1) | 0.70426 | 11.70 | 66.30 | 0.51252 ( 1) | 0.51247 | -4.93 | -1.43 | 858 |
| (G) B168-Melanephelinite | 87 | 1648 | 0.70443 ( 1) | 0.70427 | 11.42 | 65.90 | 0.51250 ( 1) | 0.51245 | -4.92 | -1.8 | 870 |
| (T) PA3-Ol nephelinte | 45 | 1360 | 0.70466 ( 2) | 0.70456 | 11.8 | 65.80 | 0.51232 ( 2) | 0.51227 | -0.78 | -5.34 | 1147 |
| (T) LM115-Ol nephelinite | 85 | 1650 | 0.70477 ( 3) | 0.70461 | 12.08 | 69.08 | 0.51235 ( 3) | 0.51230 | -0.03 | -4.73 | 1079 |
| (G) B166-Ol nephelinite | 80 | 1353 | 0.70547 ( 1) | 0.70529 | 10.20 | 61.20 | 0.51220 ( 1) | 0.51215 | 9.55 | -7.61 | 1227 |
| (T) PA4-Basanite | 43 | 1010 | 0.70445 ( 2) | 0.70431 | 9.40 | 55 | 0.51250 ( 3) | 0.51245 | -4.18 | -1.79 | 859 |
| (T) LM-1-Nepheline syenite | 115 | 4320 | 0.70550 ( 2) | 0.70542 | 10.46 | 67.12 | 0.51199 ( 3) | 0.51194 | 11.42 | -11.65 | 1418 |
| (T) LM-53-Nepheline syenite | 122 | 3730 | 0.70540 ( 3) | 0.7053 | 11.09 | 75.05 | 0.51201 ( 2) | 0.51197 | 9.74 | -11.21 | 1342 |
| (T) LM97-Peralkaline phonolite | 122 | 310 | 0.70589 ( 1) | 0.70466 | 2.23 | 13.01 | 0.51242 ( 3) | 0.51237 | 0.69 | -3.35 | 967 |
| (T) LM-99-Peralkaline phonolite | 125 | 2200 | 0.70535 ( 2) | 0.70517 | 5.75 | 39.98 | 0.51204 ( 3) | 0.512 | 7.96 | -10.6 | 1283 |

The data suggest crystallization temperatures starting close to magmatic conditions (Comin-Chiaramonti *et al.*, 2002). Mass balance equations for oxygen and carbon of early carbonatites are consistent with a carbonatitic liquid under nearly closed conditions, in a temperature range from about 700ºC to 400ºC (cf. Speziale *et al.*, 1997). If this is the case, the Anitápolis early carbonatites may represent a type of unfractionated parental carbonatite magma from which the composition of the Juquiá Mg-carbonatites could be obtained by fractionating of about 70-80% calcite (cf. Beccaluva *et al.*, 1992).

The Late Cretaceous Lages Fe-carbonatites are characterized by a large spreading of $\delta^{18}O$ values (av. 13.55±5.15‰) coupled with a relatively narrow $\delta^{13}C$ variation (av.-3.98±1.40‰). Notably, all the late carbonatites tend to shift towards the meteoric calcite and sedimentary carbonate fields (Fig. 17). This behaviour may be indicative, other than hydrothermal processes, also of groundwater weathering and/or of biogenic contamination (cf. Castorina *et al.*, 1997).

## STRONTIUM AND NEODIMIUM ISOTOPES

The Ca-carbonatites from Anitápolis have $Sr_i$ and $Nd_i$ (initial $^{87}Sr/^{86}Sr$ and $^{143}Nd/^{144}Nd$ isotope ratios, respectively) in the same range as those of the associated silicate rocks (Table 15; cf. Fig. 18A), i.e. $Sr_i$=0.70597±0.00008, $Nd_i$=0.51219±0.00004 (carbonatite) vs. $Sr_i$=0.70605±0.00026, $Nd_i$=0.51217±0.00004 (alkaline rocks and cumulates), supporting the hypothesis for a common parent magma for both carbonatites and associated silicate rocks. Correlationships between stable and radiogenic isotopes are not apparent (Comin-Chiaramonti *et al.*, 2002). Only a sample (Toyoda *et al.*, 1995; cf. Table 15) shows relatively high $Sr_i$ and low $\delta^{18}O$‰ values (0.70615 and 9.0, respectively), but in this case possible crustal contamination effects are not valuable.

The alkaline rock-types from Lages show isotope compositions (Table 15 and Fig. 18) spreading from $Sr_i$=0.70425 and $Nd_i$=0.51247 (olivine nephelinites) to $Sr_i$=0.70542 and $Nd_i$=0.51192 (nepheline syenites). On the other hand, the associated Fe-carbonatites have $Sr_i$=0.70622±0.00032 and $Nd_i$=0.51209±0.00009, similar to the values found for the Anitápolis Ca-carbonatites, but with a major $Nd_i$ spread. Regarding these considerable different isotope compositions it is not possible to assume a direct genetic link between the carbonatites and the silicate rocks. Notably, no positive correlations between oxygen isotopes and $Sr_i$ are apparent (cf. Comin-Chiaramonti *et al.*, 2002), probably owing to the weathering evidences and the “late” emplacement for the Lages Fe-carbonatites. Some peralkaline phonolites display a "crustal" signature ($Sr_i$ up to 0.73106 and $Nd_i$=0.51188; not shown in this paper; cf. Traversa *et al.*, 1996, Table 3, sample LM83), whereas the isotopic ratios of other analogues (e.g. LM112 peralkaline phonolite, Table 3 of Traversa *et al.*, 1996) approach those for the carbonatites. Therefore, these latter rocks may have originated by immiscibility from a carbonate-rich liquid. Following Traversa *et al.* (1996), since even leucocratic rock-types appear to have been formed through crystal fractionation processes starting from mafic rock-types, the extent of crustal assimilation is assumed to be relatively small. This is also supported by ACF models, showing that the leucocratic rocks were affected by less than 8% crustal contamination (Traversa *et al.*, 1996). Finally, it is noticeable that the analysed xenoliths from a Lages pipe, i.e. a leucitite and a tholeiitic basalt, are in the same isotopic range as that for the alkaline rocks and low-Ti tholeiites of the region, respectively (cf. Table 15, and Piccirillo & Melfi, 1988).

## SIGNIFICANCE OF THE RADIOGENIC ISOTOPES

In spite of the large variations in the petrographic features, incompatible elements distribution and O-C isotopes, the radiogenic isotopes are in the same ranges as those of the associated alkaline rocks, specifically nepheline syenites and phonolites. It should also be noted that in general the carbonatites from the whole Paraná-Angola-Etendeka Province (PAEP) have $Sr_i$ and $Nd_i$ values similar to those of the associated alkaline rocks, even in the samples affected by hydrothermal processes, spanning from time integrated depleted (Angola and Namibia) to enriched types (Paraguay and Uruguay; cf. Alberti *et al.*, 1999; Kirkstein *et al.*, 2000). This magmatism overlaps the subcoeval PAEP flood tholeiites and, on the whole, the data strongly suggest that the PAEP magmatism is related to large- and small-scale heterogeneous subcontinental mantle variously "contaminated" by ancient metasomatic processes (Comin-Chiaramonti *et al.*, 1997a, b; 1999). Notably, the time-integrated depleted signature of the Trindade Island is similar to that of Angola and Namibia alkaline-carbonatitic magmatism presenting Early Cretaceous (and Late Cretaceous) age, but different from that (EMI to B.E. signature) of the Late Cretaceous analogues in Brazil (Alto Paranaíba, Ponta Grossa Arch and Lages). The alkaline magmatism of Tristan da Cunha, Gough and Inaccessible Islands, and Walvis Ridge have B.E.-EMI Sr-Nd isotopic characteristics which are distinct or partly overlap those of the Early Cretaceous alkaline-carbonatitic (and tholeiitic) magmatism. Therefore, the contribution of the asthenospheric components derived from the Tristan da Cunha plume are not appreciable (cf. Comin-Chiaramonti *et al.*, 1997a, b; 1999; Ernesto *et al.*, 2002).

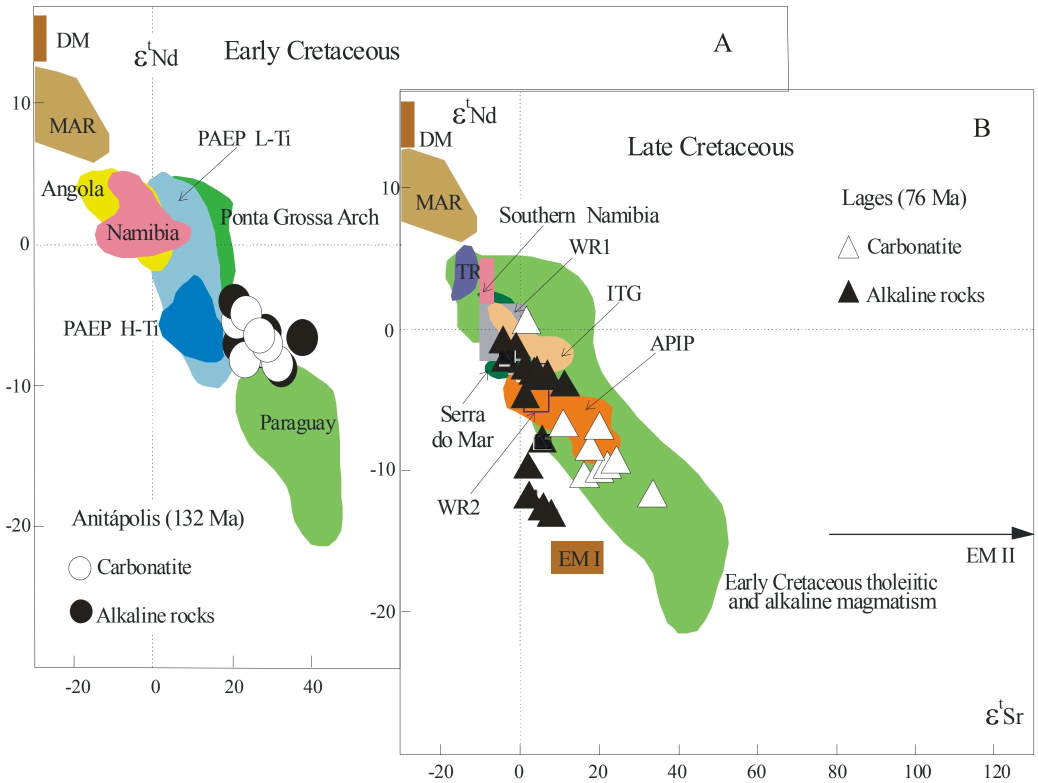


Fig. 18. Early Cretaceous: Synoptical $\varepsilon^t$Sr-$\varepsilon^t$Nd time-integrated diagrams for the Early Cretaceous Anitápolis alkaline-carbonatite complex compared with alkaline-carbonatite complexes from Angola, Namibia, Ponta Grossa Arch (Brazil) and Paraguay and with the Paraná-Etendeka-Angola Province tholeiites (PAEP: Early Cretaceous "uncontaminated low-Ti and H-Ti tholeiites" (i.e. measured $^{87}Sr/^{86}Sr<0.706$). Late Cretaceous: Lages alkaline-carbonatite complex compared with subcoeval K-alkaline-carbonatitic rocks from Alto Paranaíba (APIP), Taiúva-Cabo Frio Lineament-Serra do Mar (Serra do Mar) and Blue Hills, Southern Namibia (Kurszlaukis *et al.*, 1999). Post Mesozoic magmatism (ITG, Inaccessible, Tristan da Cunha and Gough Islands; WR1 and WR2, Walvis Ridge; MAR, Mid-Atlantic Ridge; TR, Trindade) is also shown. Data source: Bizzi *et al.* (1994), Gibson *et al.* (1995), Huang *et al.* (1995), Toyoda *et al.* (1995), Fontignie & Schilling (1996 and therein references), Milner & Le Roex (1996 and therein references), Traversa *et al.* (1996), Castorina *et al.* (1997 and therein references), Le Roex & Lanyon (1998 and therein references), Smithies & Marsh (1998), Thompson *et al.* (1998), Marques *et al.* (1999b) and Comin-Chiaramonti *et al.* (1999 and therein references). DMM, EMI and EMII components taken from Zindler & Hart (1986).

Hawkesworth *et al.* (1986) interpreted the EMI signature of the Etendeka basalts as resulting from melting of ancient lithospheric mantle, which in the case of Walvis Ridge (WR2 basalts), occurred as remnant within the shallow oceanic asthenosphere following the opening of the South Atlantic. Alternatively, this signature may result from contamination of the oceanic mantle by ancient continental lithospheric mantle that was eroded from the base of the lithosphere at the time of continental break-up (cf. Milner & Le Roex, 1996).

Nd-model ages provide a broad estimate of the time when a "metasomatic" event may have occurred, assuming that the Sm/Nd ratios were not substantially modified by melting and magma differentiation. Early Cretaceous and also Late Cretaceous carbonatites from the Ponta Grossa Arch display the same average model ages (0.64±0.08 and 0.65±0.07 Ga, respectively), similar to those of the Early Cretaceous (and Late Cretaceous) alkaline-carbonatitic complexes from Angola and Namibia (cf. Alberti *et al.*, 1999 and therein references). Early Cretaceous Anitápolis alkaline-carbonatite complex (Santa Catarina state, along the Rio Uruguay Lineament, cf. Fúlfaro *et al.*, 1982), has an average model age of 1.3±0.1 Ga, intermediate between H-Ti and L-Ti tholeiites from the PAEP. Finally, the Late Cretaceous Lages alkaline-carbonatitic rocks (Santa Catarina state, along the same Rio Uruguay Lineament) show a broad variation with an average model age of 1.2±0.2 Ga, but the bimodal distribution (mafic rocks: 0.9±0.1 Ga; peralkaline phonolites+carbonatites: 1.4±0.1 Ga) suggests at least two different mantle metasomatized sources, as already proposed by Traversa *et al.* (1996). In this scenario, the model ages of Lages carbonatites trend towards the ancient model ages of alkaline complexes from Paraguay and Uruguay (i.e.~1.5 and 1.7 Ga, respectively).

## CONCLUDING REMARKS

During the Cretaceous time, the Santa Catarina state, at the southern side of the Paraná Basin, experienced at least three main magmatic events. The first one, Early Cretaceous, included the emplacement of the voluminous flood tholeiitic basalts of the Serra Geral Formation (133-130 Ma) and the small intrusion of the Anitápolis alkaline-carbonatite complex (132 Ma) in the Late Proterozoic Dom Feliciano mobile belt. During the “late” Early Cretaceous (120 Ma), a tholeiitic dyke swarm intruded the Late Proterozoic Pedras Grandes Suite in the Florianópolis region. The third event is represented by Late Cretaceous (76 Ma) alkaline-carbonatite outcrops penetrating into the Gondwana sedimentary sequences at the Lages district.

The link with the geodynamic processes which led to the opening of the South Atlantic Ocean is crucial to the magma genesis in the Paraná-Angola-Etendeka Province. According to Nürberg & Müller (1991), the sea-floor spreading in the South Atlantic, at the Paraná Basin latitude, was initiated at ~125-127 Ma (Chron M4). To the North of the Walvis-Rio Grande ridges (latitude>28°), the onset of the oceanic crust should be more recent (~113 Ma; Chang *et al.*, 1988). The Early Cretaceous Anitápolis alkaline-carbonatite complex (and in general the coeval analogues from Angola, NW Namibia, Ponta Grossa Arch, Paraguay and Uruguay) is subcoeval with the main flood tholeiites of the Paraná Basin, and therefore occurred during the early rifting stages, before the continental separation. The Florianópolis tholeiitic dyke swarm approaches the time of sea-floor spreading (~120 Ma, cf. Raposo *et al.*, 1998). The Late Cretaceous alkaline-carbonatite complexes from Lages (and the subcoeval analogues from Ponta Grossa Arch, Serra do Mar, Taiúva-Cabo Frio Lineament, Alto Paranaíba, Iporá and Namibia) correspond to an advanced stage of the Africa-South America continental separation.

Despite the geochemical and geophysical studies concerning the genesis of the continental magmatic provinces with respect to the plate tectonics, there is still no clear consensus on the origin of the magmas. Thus, e.g. Stefanik & Jurdy (1984) invoked the presence of 16 hot spots, and Holbrook & Kelemen (1993) postulated shallow thermal anomalies. However, even considering the large flexibility permitted in the plume semantic concept (such as composition, temperature, size and depth of origin, and adoption of any hot spot numbers), this model cannot account for all the types of magmatic occurrences (see Smith & Lewis for a general discussion). Gibson *et al.* ( 1999) suggested that the Late Cretaceous magmatism of Lages, lying more than 1000 km to the South of the postulated center of the Trindade plume, was induced by high temperature melts channelled away southwards from the thick keels of the São Francisco craton (other occurrences of Late Cretaceous alkaline rocks, e.g. Piratini complexes from Rio Grande do Sul, and the mechanical barriers formed by the second order plate boundaries, e.g. Ponta Grossa Arch, Rio Piquiri and Rio Uruguay Lineaments were not discussed by those workers).

A more convincing model has been suggested by Smith & Lewis (1999): the forces acting on plates with different angular velocities and the presence of volatile-rich mantle sources (wet spots) would drive the rifting to parallel the pre-existing N-S sutures in the South Atlantic areas. Intraplate alkaline and alkaline-carbonatite magmatism is candidate to occur where second order sutures (e.g. Alto Paranaíba, Ponta Grossa-Moçâmedes Arch, Rio Uruguay Lineament, Damara Belt and so on) intersect the axis of major rifting, indicating an erosion and cycling of continental mantle towards the ridge axis by local convection taking the form of transverse rolls.

## APPENDIX

### Analytical techniques

Microprobe analyses were obtained at the Cagliari, Padova and São Paulo Universities (Instituto de Geociências) using various microprobe systems. At Cagliari laboratory, the mineral analyses were obtained by an ARL-SEMQ instrument, operating at 15 kV and 20 nÅ. At Padova laboratory, an energy dispersive spectrometer EDS EG 1G connected to a SEM AUTOSCAN electron microprobe operating at 15 kV was employed. At São Paulo, mineral compositions were obtained by means of an automated JEOL JXA-8600S electron microprobe, operating at 15 kV accelerating voltage and 20-30 nÅ specimen current. The standards were oxides or simple silicate compositions, and several samples were systematically analysed in the different instruments. The reported analyses are averages of at least three point-determinations and the results are considered accurate within 2-3% for major elements and to about 10% for the minor ones.

Whole-rock, major and trace elements were determined on pressed powder discs by a PW 1400 XRF spectrometer system (Rh as target tube) incorporating a sample automatic changer. REE plus Th, U, Hf and Ta were analysed by ICP-MS (Perkin Elmer Elan 5000) in solutions obtained from mixed HF-$HClO_4$ digestion under pressure in a sealed teflon vessel. Samples were spiked with Rh to monitor internal drift and calibration was achieved using international and in-house rock standards. The overall precision and accuracy for the major and trace elements, including REE, are better than 2% and 15%, respectively.

The carbonate composition was determined by X-ray diffraction methods, in order to establish the amounts of dolomite/ankerite and calcite. Oxygen and carbon isotopic compositions on carbonates were obtained by reacting the samples with 100% $H_3PO_4$ at 5°C. The released $CO_2$ was subsequently analysed on a Finnigan Mat Delta S mass spectrometer and its oxygen isotopic composition was corrected to calcite and dolomite (or ankerite) by applying the fractionation factors 1.01025 and 1.0111, respectively, according to Santos & Clayton (1995). Since most of the samples contain both simple and double carbonate phases, they were analysed by using double extraction techniques (Epstein & Taylor, 1967): the $CO_2$ corresponding to calcite and dolomite/ankerite was extracted after 1 hour and between 24 and 38 hours after reaction, respectively. The isotopic results are given in terms of δ‰ notations, the reference standards being PDB-1 for carbon and V-SMOW for oxygen. The resulting precision is better than 1‰.

$^{87}Sr/^{86}Sr$ and $^{143}Nd/^{144}Nd$ isotopic ratios were measured on a MAT 262 multicollector mass spectrometer. The average value of NBS 987 standard during data acquisition was 0.710220± 0.000012 (2σ), $^{86}Sr/^{88}Sr$ normalized to 0.1194. La Jolla standard gave 0.511856±0.000015 (2σ), and Nd isotopic ratios were normalized for within-run fractionation to $^{146}Nd/^{144}Nd$=0.7219. Standard deviations of the isotopic ratios are expressed at 95% confidence level as 2σ of the mean value. The $\varepsilon^t$Sr-Nd notations were calculated using the following values for the Bulk Earth: $^{87}Sr/^{86}Sr$=0.7045, $^{87}Rb/^{86}Sr$=0.827, $^{143}Nd/^{144}Nd$ =0.512638 and $^{147}Sm/^{144}Nd$=0.1967. TDM, Nd depleted mantle model ages, were calculated assuming $^{143}Nd/^{144}Nd$=0.513151 and $^{147}Sm/^{144}Nd$=0.2188.

## ACKNOWLEDGEMENTS

This research was supported by Brazilian (Fapesp, Proc. 01/10714-3) and Italian (CNR, 05 and 11 Committes, and COFIN 1998, MIUR 1998, 1999, 2000, 2001) agencies.

## REFERENCES

Alberti, A., Castorina, F., Censi, P., Comin-Chiaramonti, P. & Gomes, C.B. (1999). Geochemical characteristics of Cretaceous carbonatites from Angola. *Journal of African Earth Sciences* **29**, 735-759.

Alcover Neto, A., Almeida, T.I.R., Karmann, I., Toledo, M.C.M. (1995). Estudo da composição isotópica de C e O em carbonatitos primários e secundários de Juquiá e da caverna Santana, Vale do Ribeira (SP). *III Congresso de Geoquímica dos Países de Língua Portuguesa*, *Niterói*, CD-ROM.

Almeida, F.F.M. (1983). Relações tectônicas das rochas alcalinas mesozóicas da região meridional da Plataforma Sul-Americana. *Revista Brasileira de Geociências* **13**, 139-158.

Amaral, G., Bushee, J., Cordani, U.G. & Kawashita, K. (1967). Potassium-argon ages of alkaline rocks from southern Brazil. *Geochimica Cosmochimica Acta* **31**, 117-142.

Asmus, H.E. (1978). Hipótese sobre a origem dos sistemas de zonas de fraturas oceânicas/alinhamentos continentais que ocorrem nas regiões sudeste e sul do Brasil. In: *Aspectos estruturais da Margem Continental Leste e Sudeste do Brasil, Petrobrás, Série Projeto REMAC* **4**, 39-73.

Aumond, J.J. & Scheibe, L.F. (1996). O fonolito de Lages-SC, um novo fundente cerâmico brasileiro. *Cerâmica Industrial* **1**, 17-21.

Babinski, M., Chemale Jr., F., Van Schmus, W.R., Hartmann, L.A. & Silva, L.C. (1997). U-Pb and Sm-Nd geochronology of the Neoproterozoic Granitic-Gneissic Dom Feliciano Belt, Southern Brazil. *Journal of South American Earth Sciences* **10**, 263-274.

Bailey, D.K. (1964). Crustal warping - a possible tectonic control of alkaline magmatism. *Geophysical Research* **69**, 1103-1111.

Bailey, D.K. (1974). Continental rifting and alkaline magmatism. In: Sörensen, H. (ed.) *The alkaline rocks.* New York: Wiley, pp.148-159.

Barbieri, M., Beccaluva, L., Brotzu, P., Conte, A., Garbarino, C., Gomes, C.B., Loss, E.L., Macciotta, G., Morbidelli, L., Scheibe, L., Tamura, R.M. & Traversa, G. (1987). Petrological and geochemical studies of alkaline rocks from continental Brazil. 1. The phonolite suite from Piratini, RS. *Geochimica Brasiliensis* **1**, 109-138.

Beccaluva, L., Barbieri, M., Born, H., Brotzu, P., Coltorti, M., Conte, A., Garbarino, C., Gomes, C.B., Macciotta, G., Morbidelli, L., Ruberti, E., Siena, F. & Traversa, G. (1992). Fractional crystallization and liquid immiscibility processes in the alkaline-carbonatite complex of Juquiá. *Journal of Petrology* **33**, 1371-1404.

Berrocal, J. & Fernandes, C. (1996). Seismicity in Paraguay and neighbouring regions. In: Comin-Chiaramonti, P. & Gomes, C.B. (eds.) *Alkaline magmatism in central-eastern Paraguay. Relationships with coeval magmatism in Brazil.* São Paulo: Edusp/Fapesp, pp. 57-66.

Bizzi, L.A., Witt, M.J., Smith, C.B., McDonald, I. & Armstrong, R.A. (1994). Isotope characteristics of the lithospheric mantle underlying the SW São Francisco craton, Brazil. *International Symposium on the Physics and Chemistry of the Upper Mantle, São Paulo, Invited Lectures,* pp. 227-256.

Boynton, W.V. (1984). Cosmochemistry of the Rare Earth elements: meteorite studies. In: Henderson, P. (ed.) *Rare Earth Element geochemistry.* Amsterdam: Elsevier, pp. 63-114.

Carmichael, I.E.S. (1967). The iron-titanium oxides of salic volcanic rocks and their associated ferro-magnesian silicates. *Contributions to Mineralogy and Petrology* **14**, 36-64.

Carraro, C.C., Issler, R.S. & Formoso, M.L.L. (1964). Mapeamento do Distrito Alcalino de Alto Rio Pinheiros, Santa Catarina. Convênio UFRGS/ILM, Relatório Interno, Porto Alegre, 40p.

Castorina, F., Censi, P., Comin-Chiaramonti, P., Gomes, C.B., Piccirillo, E.M., Alcover Neto, A., Almeida, R.T. Speziale, S. & Toledo, M.C. (1997). Geochemistry of carbonatites from Eastern Paraguay and genetic relationships with potassic magmatism: C, O, Sr and Nd isotopes. *Mineralogy and Petrology* **61**, 237-260.

Chang, H.K., Kowsmann, R.O. & Figuereido, A.M.F. (1988). New concept on the development of east Brazilian margin basins. *Episodes* **11**, 194-202.

Comin-Chiaramonti, P. & Gomes, C.B. (eds.) (1996). *Alkaline magmatism in central-eastern Paraguay-Relationships with coeval magmatism in Brazil.* São Paulo: Edusp/Fapesp, 464p.

Comin-Chiaramonti, P., Cundari, A., DeGraff, J.M., Gomes, C.B & Piccirillo, E.M. (1999). Early Cretaceous-Tertiary magmatism in Eastern Paraguay (western Paraná Basin): geological, geophysical and geochemical relationships. *Journal of Geodynamics* **28**, 375-391.

Comin-Chiaramonti, P., Cundari, A., Piccirillo, E.M., Gomes, C.B., Castorina, F., Censi, P., De Min, A., Marzoli, A., Speziale, S. & Velázquez, V.F. (1997a). Potassic and sodic igneous rocks from Eastern Paraguay: their origin from the lithospheric mantle and genetic relationships with the associated Paraná flood tholeiites. *Journal of Petrology* **38**, 495-528.

Comin-Chiaramonti, P., Cundari, A., Piccirillo, E.M., Gomes, C.B. & De Min, A. (1997b). Carbonatitic magmatism in the Paraná-Angola mantle plume (?) system: petrological and isotope-geochemical bearing on the mantle source. *EOS, Transaction, AGU* **78** (46), F741.

Comin-Chiaramonti, P., Gomes, C.B., Castorina, F., Censi, P., Antonini, P., Furtado, S.M.A., Ruberti, E. & Scheibe, L.F. (2002). Geochemistry and geodynamic implications of the Anitápolis and Lages alkaline-carbonatite complexes, Santa Catarina State, Brazil. *Revista Brasileira de Geociências* **32**, 43-58.

Cundari, A. & Salviulo, G. (1989). Ti solubility in diopsidic clinopyroxenes from a suite of New South Wales leucitites (Australia). *Lithos* **22**, 191-198.

Dani, N. (1998). *Alteração supergênica de rochas alcalinas na região de Lages, Santa Catarina-formação de bauxita.* M.Sc. Dissertation, Federal University of Rio Grande do Sul, 240p.

Deer, W.A., Howie, R.A. & Zussman, J. (1992). *An introduction to the rock-forming minerals.* London: Longman, 696p.

De La Roche, H., Leterrier, J., Grandclaude, P. & Marchal, M. (1980). A classification of volcanic and plutonic rocks using R1-R2 diagram and major-element analyses: its relationships with current nomenclature. *Chemical Geology* **29**, 183-210.

D'Elboux, C.V., Tavares, J.R.P. & Paiva, I.B. (1982). Proposição de modelo mineralizador básico-alcalino para pesquisa mineral na região meridional do Escudo Pré-Cambriano. *XXXII Congresso Brasileiro de Geologia, Salvador, Anais* **3**, 1061-1072.

Duda, A. & Schminke, H.U. (1978). Quaternary basanites, melilitites, nephelinites and tephrites from the Laacher See area (Germany). *Neues Jahrbuch für Mineralogie Abdhalungen* **132**, 1-33.

El Goresy, A. & Yoder, H.S. Jr. (1974). Natural and synthetic melilite compositions. *Carnegie Institution Washington Yearbook* **73**, 359-371.

Epstein, S. & Taylor, H.P.Jr. (1967). Variation of $^{18}O/^{16}O$ in minerals and rocks. In: Abelson, P.H. (ed.) *Researches in geochemistry.* New York: J. Wiley, pp. 29-62.

Ernesto, M., Marques, L.S., Piccirillo, E.M., Molina, E.C., Ussami, N., Comin-Chiaramonti, P. & Bellieni, G. (2002). Paraná magmatic province-Tristan da Cunha plume system: fixed versus mobile plume, petrogenetic considerations and alternative heat sources. *Journal of Volcanology and Geothermal Research* **118**, 15-36.

Fassbinder, E. (1996). *A Unidade Água Clara no contexto do Grupo Açungui: um modelo transpressivo de colisão oblíqua no Neoproterozóico paranaense.* Ph.D. Thesis, University of São Paulo, 212p.

Fontignie, D. & Schilling, J.G. (1996). Mantle heterogeneities beneath the South Atlantic: a Nd-Sr-Pb isotope study along the Mid-Atlantic Ridge (3°S-46°S). *Earth Planetary Science Letters* **146**, 259-272.

Foster, M.D. (1960). Interpretation of the composition of trioctaedral micas. *Geological Survey Professional Paper* **354-B**, 49p.

Fúlfaro, V.F., Saad, A.R., Santos, M.V. & Vianna, R.B. (1982). Compartimentação e evolução tectônica da Bacia do Paraná. *Revista Brasileira de Geociências* **12**, 590-610.

Furtado, S.M. (1989). *Petrologia do maciço alcalino de Anitápolis, SC.* Ph.D. Thesis, University of São Paulo, 245p.

Furtado, S.M.A. & Gomes, C.B. (1990). Quimismo das micas do maciço alcalino de Anitápolis. *Geochimica Brasiliensis* **4**, 33-47.

Furtado, S.M.A. & Gomes, C.B. (1994). Caracterização química dos clinopiroxênios do maciço alcalino de Anitápolis. *Geochimica Brasiliensis* **8**, 65-78.

Furtado, S.M.A. & Scheibe, L.F. (1987). Geologia dos complexos alcalinos Mesozóicos de Santa

Catarina. In: *Textos básicos de geologia e recursos minerais.* Departamento Nacional de Produção Mineral/ Secretaria de Minas e Energia do Estado de Santa Catarina, pp.170-192.

Furtado, S.M.A. & Scheibe, L.F. (1989). Ocorrências de lamprófiros associados aos distritos alcalinos de Lages e de Anitápolis, SC. *Geochimica Brasiliensis* **3**, 149-160.

Furtado, S.M.A., Gomes, C.B., Scheibe, L.F. (1986). Ocorrência de foscoritos no maciço alcalino de Anitápolis. *XXXIV Congresso Brasileiro de Geologia, Goiânia, Anais* **4**, 1604-1614.

Gibson, S.A., Thompson, R.N., Leonardos, O.H., Dickin, A.P. & Mitchell, J.G. (1995). The Late Cretaceous impact of the Trindade mantle plume: evidence from large-volume, mafic potassic magmatism in SE Brazil. *Journal of Petrology* **36**, 189-229.

Gibson, S.A., Thompson, R.N., Leonardos, O.H., Dickin, A.P. & Mitchell, J.G. (1999). The limited extent of plume-lithosphere interactions during continental flood-basalt genesis: geochemical evidence from Cretaceous magmatism in southern Brazil. *Contributions to Mineralogy and Petrology* **137**, 147-169.

Giret, A., Bonin, B. & Leger, J.M. (1980). Amphibole compositional trends in oversaturated and undersaturated alkaline plutonic ring-complexes. *Canadian Mineralogist* **18**, 481-495.

Gomes, C.B., Barbieri, M., Beccaluva, L., Brotzu, P., Conte, A., Garbarino, C., Macciotta, G., Melluso, L., Morbidelli, L., Ruberti, E., Scheibe, L.F., Tamura, R.M. & Traversa, G. (1987). Petrological and geochemical studies of alkaline rocks from continental Brazil - The Tunas massif, State of Paraná. *Geochimica Brasiliensis* **1**, 201-234.

Gomes, C.B., Moro, S.L. & Dutra, C.V. (1970). Pyroxenes from the alkaline rocks of Itapirapuã, São Paulo, Brazil. *American Mineralogist* **55**, 224-240.

Haralyi, N.L.E., Hasui, Y. & Kaul, P.F.T. (1982). Dados gravimétricos da região costeira do Paraná e Santa Catarina e sua interpretação estrutural. *XXXII Congresso Brasileiro de Geologia, Salvador, Anais* **1**, 64-67.

Hawkesworth, C.J., Mantovani, M.S.M., Taylor, P.N. & Palacz, Z. (1986). Evidence from the Paraná of South Brazil for a continental contribution to Dupal basalts. *Nature* **322**, 356-359.

Holbrook, W.S. & Kelemen, P.B. (1993). Large igneous province on the US Atlantic margin and implications for magmatism during continental breakup. *Nature* **364**, 433-436.

Huang, Y-M, Hawkesworth, C.J., Van Calsteren, P. & McDermott, F. (1995). Geochemical characteristics of the Jacupiranga carbonatite, Brazil. *Chemical Geology* **119**, 79-99.

Kasputin, Y.L. (1980). *Mineralogy of carbonatites*. New Delhi: Amerind Publishing Co. Put. Ltd., 256p.

Keller, J. & Hoefs, J. (1995). Stable isotope characteristics of recent natrocarbonatites from Oldoinyo Lengai. In: Bell, K. & Keller, J. (eds.) *Carbonatite volcanism: Oldoinyo Lengai and the petrogenesis of natrocarbonatites.* Berlin: Springer, pp. 113-123.

Kirkstein, L.A., Peate, D.W., Hawkesweorth, C.J., Turner, S.P., Harris, C. & Mantovani, M.S.M. (2000). Early Cretaceous basaltic and rhyolitic magmatism in Southern Uruguay associated with the opening of the South Atlantic. *Journal of Petrology* **41**, 1413-1438.

Kresten, P. & Morogan, V. (1986). Fenitization at the Fen Complex, Southern Norway. *Lithos* **19**, 27-42.

Kurszlaukis, S., Franz, L. & Brey, G.P. (1999). The Blue Hills intrusive complex in southern Namibia: relationships between carbonatites and monticellite picrites. *Chemical Geology* **160**, 1-18.

Larsen, L.M. (1976). Clinopyroxenes and coexisting mafic minerals from the alkaline Ilimaussak intrusion, South Greenland. *Journal of Petrology* **17**, 258-290.

Le Bas, M.J. (1977). *Carbonatite-nephelinite volcanism.* London: Wiley, 347p.

Le Bas, M.J. (1989). Nephelinitic and basanitic rocks. *Journal of Petrology* **30**, 1299-1322.

Le Maitre, R.W. (1989). *A classification of igneous rocks and glossary of terms.* Oxford: Blackwell Scientific Publications, 193p.

Le Roex, A.P. & Lanyon, R. (1998). Isotope and trace element geochemistry of Cretaceous Damaraland lamprophyres and carbonatites, northwestern Namibia: evidence for plume-lithosphere interaction. *Journal of Petrology* **39**, 1117-1146.

Leake, B.E. (1978). Nomenclature of amphiboles. *American Mineralogist* **63**, 1023-1052.

Leonardos, O.H. (1956). Carbonatitos com apatita e pirocloro. *Departamento Nacional da Produção Mineral/Divisão de Fomento da Produção Mineral, Avulso* **80,** 30p.

Lindstaedt, H.P. (1972). *A alteração das rochas alcalinas, Lages, Santa Catarina*. M.Sc. Dissertation, Federal University of Rio Grande do Sul, 54p.

Loczy, L. (1968). Basic and alkalic volcanics of the State of Santa Catarina, Brazil. *Anais da Academia Brasileira de Ciências* **40**, 187-193.

Marques, L.S., Dupré, B. & Piccirillo, E.M. (1999a). Mantle source compositions of the Paraná magmatic province (southern Brazil): evidence from trace element and Sr-Nd-Pb isotope geochemistry. *Journal of Geodynamics* **28**, 439-458.

Marques, L.S., Piccirillo, E.M., Melfi, A.J. & Comin-Chiaramonti, P. (1989). Distribuição de terras raras e outros elementos traços em basaltos da Bacia do Paraná (Brasil meridional). *Geochimica Brasiliensis* **3**, 33-50.

Marques, L.S., Ulbrich, M.N.C., Ruberti, E. & Tassinari, C.G. (1999b). Petrology, geochemistry and Sr-Nd isotopes of the Trindade and Martin Vaz volcanic rocks (Southern Atlantic Ocean). *Journal of Volcanology and Geothermal Research* **93**, 191-216.

Melcher, G.C. & Coutinho, J.M.V. (1966). Rochas alcalinas e carbonatito de Anitápolis, Estado de Santa Catarina. *Boletim da Sociedade Brasileira de Geologia* **15**, 59-93.

Milner, S.C. & Le Roex, A.P. (1996). Isotope characteristics of the Okenyenia igneous complex, northjweestern Namibia: constraints on the composition of the early Tristan plume and the origin of the EM1 mantle component. *Earth Planetary Science Letters* **141**, 277-291.

Mitchel, R.H. & Bergman, S.C. (1991). *Petrology of lamproites.* New York: Plenum Press, 447p.

Moraes Rego, L.F. & Guimarães, D. (1926). Estudos geológicos e petrográficos da jazida de magnetita de Anitápolis, Estado de Santa Catarina, Brasil. *Departamento Nacional da Produção Mineral/Serviço Geológico Mineralógico,* **21**, 3-27.

Morbidelli, L, Beccaluva, L., Brotzu, P., Conte, A., Garbarino, G., Gomes, C.B., Macciotta, G., Ruberti, E., Scheibe, L.F. & Traversa, G., (1986). Petrological and geochemical studies of alkaline rocks from continental Brazil. 3. Fenitization of jacupirangite by carbonatite magmas in the Jacupiranga complex. *Periodico di Mineralogia* **55**, 261-295.

Morbidelli, L., Gomes, C.B., Beccaluva, L., Brotzu, P., Conte, A., Ruberti, E. & Traversa, G., (1995). Mineralogical, petrological and geochemical aspects of alkaline-carbonatite associations from Brazil. *Earth Science Review* **39**, 135-168.

Morimoto, N. (1988). Nomenclature of pyroxenes. *Mineralogical Magazine* **52**, 535-550.

Motoki, A. (1986). *Geologia e petrologia do maciço alcalino da Ilha de Vitória, São Paulo.* Ph.D. Thesis, University of São Paulo, 254p.

Nielsen, T.F.D. (1980). The petrology of a melilitolite, melteigite, carbonatite and syenite ring dyke system in the Gardiner Complex, East Greenland. *Lithos* **13**,181-197.

Nürberg, D. & Müller, R.D. (1991). The tectonic evolution of South Atlantic from Late Jurassic to present. *Tectonophysics* **191**, 27-43.

Oliveira, E.P. (1927). Geologia e recursos minerais do Estado do Paraná. *Serviço Geológico e Mineralógico Brasileiro, Monographia* **6**, 172p.

Paiva, G. (1933). Geologia do município de Lages, Santa Catarina. *Serviço Geológico e Mineralógico Brasileiro, Boletim* **69**, 23p.

Papike, J.J., Cameron, K. & Baldwin, K. (1974). Amphiboles and pyroxenes: characterization of other than quadrilateral components and estimates of ferric iron from microprobe data. *Bulletin Geological Society of America* **6**, 1053-1054.

Piccirillo, E.M. & Melfi, A.J. (1988). *The Mesozoic flood volcanism from the Paraná Basin (Brazil–Petrogenetic and geophysical aspects.* São Paulo: IAG-USP, 600p.

Raposo, M.I.B., Ernesto, M., Renne, P.R. (1998). Paleomagnetism and $^{40}Ar/^{39}Ar$ dating of Early Cretaceous Florianópolis dike swarm (Santa Catarina Island), southern Brazil. *Physic Earth Planetary Interior* **108**, 275-290.

Renne, P.R., Ernesto, M. & Milner, S.C. (1997). Geochronology of the Paraná-Etendeka magmatic province. *EOS American Gephysical Union* **78**, F742.

Rock, N.M.S. (1982). Chemical mineralogy of the Monchique alkaline complex, southern Portugal. *Contributions to Mineralogy and Petrology* **81**, 64-78.

Rodrigues, E.P. (1985). *O complexo alcalino de Anitápolis. Um estudo petrológico.* Ph.D. Thesis, University of São Paulo, 174p.

Ruberti, E. (1984). *Petrologia do maciço alcalino do Banhadão, PR.* Ph.D. Thesis, University of São Paulo, 249p.

Saggerson, E.P. & Williams, L.A.V. (1964). Ngurumanite from southern Kenia and its bearing on the origin of rocks in the northern Tanganika alkaline district. *Journal of Petrology* **5**, 40-81.

Santos, R.V. & Clayton, R.N. (1995). Variations of oxygen and carbon isotopes in carbonatites: a study of Brazilian alkaline complexes. *Geochimica et Cosmochimica Acta* **59**, 1339-1352.

Scheibe, L.F. (1978). Fazenda Varela carbonatite, Lajes, Santa Catarina, Brazil. *International Symposium on Carbonatites, Poços de Caldas, Brazil. Departamento Nacional da Produção Mineral, Anais* **19**, 137-146.

Scheibe, L.F. (1979). *Estudo petrológico e geoquímico dos carbonatitos da Fazenda Varela, Lages, SC, Brasil.* M.Sc. Dissertation, Federal University of Rio Grande do Sul, 120p.

Scheibe, L.F. (1986). *Geologia e petrologia do distrito alcalino de Lages, SC, Brasil.* Ph.D. Thesis, University of São Paulo, 224p.

Scheibe, L.F. & Formoso, M.L.L. (1982). Contribuição da geoquímica das terras raras à caracterização dos carbonatitos da Fazenda Varela, Lages, SC. *Revista Brasileira de Geociências* **12**, 553-561.

Scheibe, L.F. & Furtado, S.M.A. (1988). Geologia e petrografia de novas ocorrências de rochas alcalinas para caracterização da província alcalina de Santa Catarina. CNPq, Florianópolis, Relatório Interno, 24p.

Scheibe, L.F. & Furtado, S. M. A. (1989). Proposta de alinhamentos estruturais para um esboço geotectônico de Santa Catarina. *Geosul* **8**, 78-91.

Scheibe, L.F. & Svisero, D.P. (1988). Minerais de origem mantélica em concentrados do diatrema Janjão, Lages, SC. *XXXV Congresso Brasileiro de Geologia, Belém, Anais* **3**, 1326-1338.

Scheibe, L.F. & Teixeira, V.H. (1965). Distrito alcalino de Alto Pinheiros. Laboratório de

Química Agrícola da Secretaria da Agricultura de Florianópolis, Relatório Interno, 49p.

Scheibe, L.F., Gomes, C.B. & Coutinho, J.M.V. (1984). Caracterização petrográfica das rochas alcalinas de Lages. SC. *XXXIV Congresso Brasileiro de Geologia, Rio de Janeiro, Anais* **9**, 4377-4391.

Scheibe, L.F., Kawashita, K. & Gomes, C.B. (1985). Contribuição à geocronologia do complexo alcalino de Lages, SC. *2º Simpósio Sul-Brasileiro de Geologia, Florianópolis, Anais,* pp. 299-307.

Smith, J.V. & Brown, W.L. (1988). *Feldspar minerals 1. Crystal structures, physical chemical and microtextural proprties,* Berlin: Springer Verlag, 828p.

Smith, A.D. & Lewis, C. (1999). The planet beyond the plume hypothesis. *Earth-Science Reviews* **48**, 135-182.

Smithies, R.H. & Marsh, J.S. (1998). The Marinkas Quellen carbonatite complex, southern Namibia: carbonatite magmatism with an uncontaminated depleted mantle signature in continental setting. *Chemical Geology* **148**, 201-212.

Sonoki, I.K. & Garda, G.M. (1988). Idades K/Ar de rochas alcalinas do Brasil Meridional e Paraguai Oriental : compilação e adaptação às novas constantes de decaimento. *Boletim do Instituto de Geociências da USP, Série Científica* **19**, 63-87.

Speziale, S., Censi, P., Comin-Chiaramonti, P., Ruberti, E. & Gomes, C.B. (1997). Oxygen and Carbon isotopes in the Barra do Itapirapuã and Mato Preto carbonatites (southern Brazil). *Mineralogica et Petrographica Acta* **40**, 1-21.

Stefanick, M. & Jurdy, D.M. (1984). The distribution of hot spots. *Journal of Geophysical Researches* **98**, 9919-9925.

Sun, S.S. & McDonough, W.F. (1989). Chemical and isotopic systematics of oceanic basalts. In: Saunders, D. & Norry, M.J. (eds.). *Magmatism in the ocean basins*. *Geological Society of London, Special Publication* **42**, pp. 313-345.

Svisero, D.P., Haralyi, N.L.E. & Scheibe, L.F. (1985). Magnetometria, radiometria e gamaespectrometria na diatrema Janjão, Lages, SC. *2º Simpósio Sul-Brasileiro de Geologia, Florianópolis, Anais,* pp. 261-272.

Szubert, E.C. & Vergara, V. (1975). Avaliação das reservas e da qualidade dos depósitos de bauxita do município de Lages, SC. SUDESUL - CPRM, Relatório Interno, 68p.

Takeuchi, Y., Kudoh, Y. & Yamanaka, T. (1976). Crystal chemistry of the serandite-pectolite series and related minerals. *American Mineralogist* **61**, 229-237.

Tavares, J.R.P. (1982). Projeto Brusque - Sondagem e Perfilagem. Nuclebrás, Rio de Janeiro, Relatório Interno, 43p.

Taylor, H.P. Jr., Frechen, J. & Degens, E.T. (1967). Oxygen and carbon studies of carbonatites from Laacher See district, West Germany and Alnø district, Sweden. *Geochimica et Cosmochimica Acta* **31**, 407-430.

Teixeira, C.A.S. (1969). Relatório de estágio. Centro de Pesquisas Geocronológicas da Universidade de São Paulo, 48p.

Thompson, R.N., Gibson, S.A., Mitchell, J.G., Dickin, A.P., Leonardos, O.H., Brod, J.A. & Greenwood, J.C. (1998). Migrating Cretaceous-Eocene magmatism in the Serra do Mar alkaline province, SE Brazil: melts from the deflected Trindade mantle plume ? *Journal of Petrology* **39**, 1493-1526.

Toyoda, K., Horiuchi, H. & Tokonami, M. (1995). Dupal anomaly of the Brazilian carbonatites: geochemical correlations with hotspots in the South Atlantiuc and implicatiomns for the mantle source. *Earth Planetary Science Letters* **126**, 315-331.

Traversa, G., Barbieri, M., Beccaluva L., Coltorti, M. Conte, A.M., Garbarino, C., Gomes, C.B., Macciotta, G., Morbidelli, L., Ronca, S. & Scheibe, L.F. (1996). Mantle sources and differentiation of alkaline magmatic suite of Lages, Santa Catarina, Brazil. *European Journal of Mineralogy* **8**, 193-208.

Traversa, G., Scheibe, L.F., Barbieri, M., Beccaluva L., Coltorti, M., Conte, A.M., Garbarino, C., Gomes, C.B., Macciotta, G., Morbidelli, L. & Ronca, S. (1994). Petrology and mineral chemistry of the alcaline district of Lages, SC, Brazil. *Geochimica Brasiliensis* **8**, 179-214.

Ulbrich, H.H.G.J. & Gomes, C.B. (1981). Alkaline rocks from continental Brazil. *Earth-Science Reviews* **17**, 135-154.

Valença, J.C. (1980). *Geology, petrography and petrogenesis of some alkaline igneous complexes of Rio de Janeiro State, Brazil.* Ph.D. Thesis, Western Ontario University, 248p.

Varet, J. (1969). Les pyroxenes des phonolites du Cantal (Auvergne, France). *Neues Jahrbuch für Mineralogie Monathseft* **4**, 174-184.

Vartiainen, H. & Wooley, A. R. (1976). The petrography, mineralogy and chemistry of the fenites of the Sokli Carbonatite Intrusion, Finland. *Geological Survey Finland Bulletin* **280**, 1-87.

Velde, S. & Yoder, H.S. Jr. (1977). Melilite and melilite-bearing igneous rocks. *Carnegie Institution Washington Year Book* **76**, 478-485.

Vergara, V.D. (1980). Pesquisa geológica no complexo alcalino de Anitápolis. *XXXI Congresso Brasileiro de Geologia, Camboriú, Anais* **4**, 2504-2517.

Vieten, K. (1980). The minerals of the volcanic rock association of the Siebengebirge. I. Clinopyroxenes. 2. Variation of chemical composition of Ca-rich clinopyroxenes (salites) in the course of crystallization. *Neues Jahrbuch für Mineralogishe Abhanlungen* **135**, 270-286.

Walter, A.V., Flicoteaux, R., Parron, C., Loubet, M. & Nahon, D. (1995). Rare-earth and isotopes (Sr, Nd, O, C) in minerals from the Juquiá carbonatite (Brazil): tracers of a multistage

evolution. *Chemical Geology* **120**, 27-44.
Woolley, P.J. & Kempe, D.R.C. (1989). Carbonatites: nomenclature, average chemical compositions and element distribution. In: Bell, K. (ed.) *Carbonatites, genesis and evolution.* London: Unwin Hyman, pp. 500-545.
Zindler, A. & Hart, S.R. (1986). Chemical geodynamics. *Annual Review of Earth and Planetary Sciences* **14**, 493-571.

*Mesozoic to Cenozoic Alkaline Magmatism in the Brazilian Platform.*
*Comin-Chiaramonti, P. & Gomes, C.B. (eds.)*
*Edusp/Fapesp, São Paulo, pp. 523-571, 2005*

# MESOZOIC ALKALINE ROCKS OF RIO GRANDE DO SUL

*R.P. Philipp, A.P. Viero, P. Comin-Chiaramonti and C.B. Gomes*

*Late Cretaceous alkaline magmatic rocks are intruding the Phanerozoic cover and the crystalline basement at the central-eastern area of the Sul-rio-grandense Shield. A main phonolitic suite (Piratini suite) occurs as plugs, dykes and pipes. An average age of 84.6± Ma is suggested for that suite on the basis of K/Ar data. The rock-types are mainly tephritic phonolites and subordinate phonolites, both metaluminous and peralkaline varieties. Mineral assemblages include alkali feldspar, feldspathoids and clinopyroxene, and as accessory phases garnet, apatite, Ti-magnetite and titanite. Scarce and strongly altered diatremes and small dykes, probably having kimberlitic and lamproitic affinity, are also found in the shield area. Geochemical characteristics of the Piratini suite point to a parental basanite magma and are indicative that the phonolitic rocks were submitted to fractional crystallization processes without appreciable crustal contamination. Sr-Nd isotopes plot in the same typical fields of the subcoeval Alto Paranaíba igneous province and of the Lages alkaline rocks. However, Nd model ages suggest different lithospheric mantle sources that suffered low degrees of partial melting of variously metasomatized segments. The Cretaceous alkaline magmatism from the Rio Grande do Sul state appears strictly related to continental E-W lineaments representing the extension of oceanic lineaments. The oceanic expansion processes led to the reactivation of old Precambrian discontinuities in the continent, and may have favoured the melting of metasomatized sectors of the lithospheric mantle by decompression processes.*

## *INTRODUCTION*

In the Rio Grande do Sul state, southern Brazil, Mesozoic alkaline rocks are mainly concentrated in the central-eastern area of the Sul-rio-grandense Shield and intrude both the Phanerozoic cover and the Precambrian basement. The latter is part of the Mantiqueira Province and consists of Archean to Early Paleozoic crystalline terrains of three main cycles (Shobbenhaus *et al.*, 1984), i.e. Jequié (Archean), Transamazonian (Paleoproterozoic) and Brasiliano (Neoproterozoic to Early Paleozoic). The major structural feature of the Sul-rio-grandense Shield is the Rio Grande Arch, a positive structure NW-trending (Fig. 1; Almeida, 1983). According to Ribeiro (1978), the intersection of nearly orthogonal system of deep geosutures (i.e. N50°E and N50°W-trending, respectively) was the site of magmatic activity since Precambrian times.

In general, the Mantiqueira Province was strongly affected by the Brasiliano tectonic activity, as evidenced by the main NE-SW structures, by the granitic intrusions and by the "reworking" of Jequié to Transamazonian formations. In particular, its southern side (Fig. 1) is represented by the Dom Feliciano belt, a granitic gneissic-migmatitic complex extending from Uruguay to the Santa Catarina state (Almeida & Hasui, 1984). This belt is covered by Phanerozoic units at the eastern side, while the western areas are defined by tectonic contacts with the NE-SW Tijucas belt (Porongos Metamorphic Complex; cf. Chemale Jr. *et al.*, 1995).

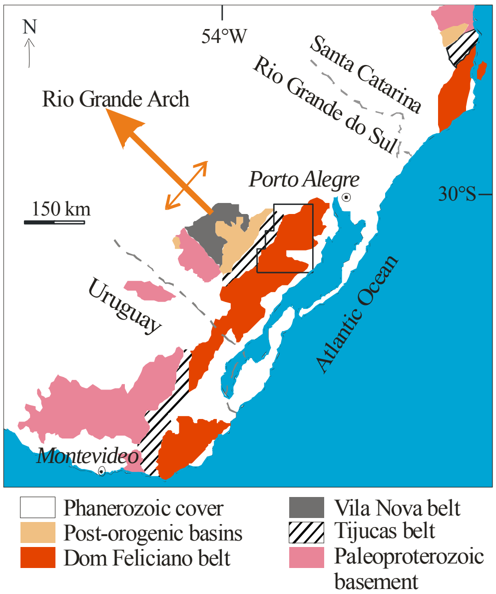


Fig. 1. Geological sketch-map of southern part of the Mantiqueira Province in the Rio Grande do Sul state.

The Dom Feliciano belt consists mainly of syn-thrust granites and several xenoliths of gneissic rocks, strike-slip related granites and late to post tectonic granites (650-500 Ma; cf. Babinski *et al.*, 1997; Philipp, 1998; Chemale Jr., 2000; Philipp *et al.*, 2002). The following main lithostratigraphic units have been described by several authors (Fig. 2): 1) Várzea do Capivarita and Arroio dos Ratos Gneissic Complex; 2) Capivarita Anorthosite; 3) Pinheiro Machado and Camboriú complexes (gneisses, migmatites and high-K calc-alkaline granites); 4) syn-trascurrent granites related to the development of a megashear zone (Dorsal de Canguçú Shear Zone of Fernandes *et al.*, 1990); 5) Piquiri Syenite and Dom Feliciano; 6) Encruzilhada do Sul Suite.

Presently, the Sul-rio-grandense Shield is affected by NNW drift in contrast to the W-E and NE motions of the Nazca plate and the Andean belt, respectively (Fig. 3). These motions have probably not significatively changed in the last 80 Ma (cf. Ernesto *et al.*, 2002). Notably, from a mechanical viewpoint, the resulting vectors produce ENE-WSW and NE-SW rotational components, and the induced rotation of deep faulted blocks would represent favorable sites for the emplacement of magmatic rocks.

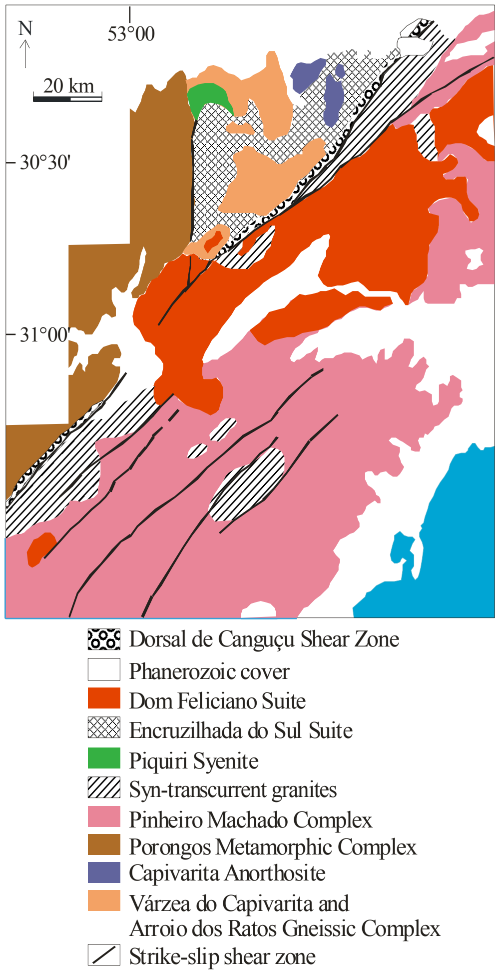


Fig. 2. Geological map of the Dom Feliciano belt in the Rio Grande do Sul state (after Chemale Jr. *et al.*, 1995 and Philipp *et al.* 2002).

As a matter of fact, Ribeiro (1978) outlines that the alkaline magmatism occurs mainly in the Canguçu-Caçapava NW-trending belt (Santana de Boa Vista, Piratini and Canguçu areas: Fig. 4), where the rising and distribution of the main alkaline bodies (plugs, dykes and pipes) are strongly controlled by fracturing zones reactivated or active since Mesozoic times and by E-W-trending lineaments (Camaquã River Lineament, and the offshore transform faults from the "Alto de Porto Alegre" of Viero *et al.*, 1995).

The alkaline rocks are mainly phonolites (Piratini suite: encircled area of Fig. 4) and subordinate kimberlites/lamproites (Tedesco & Robaina, 1991; Svisero & Chieregati, 1991; Caldasso & Sander, 1994). The latter are strongly altered and their characteristics were inferred from the crystallochemistry of the preserved heavy minerals. Viero (1998) also referred to the presence of some alkali basalts at the localities of Rondina, Palmas and Jaguari.

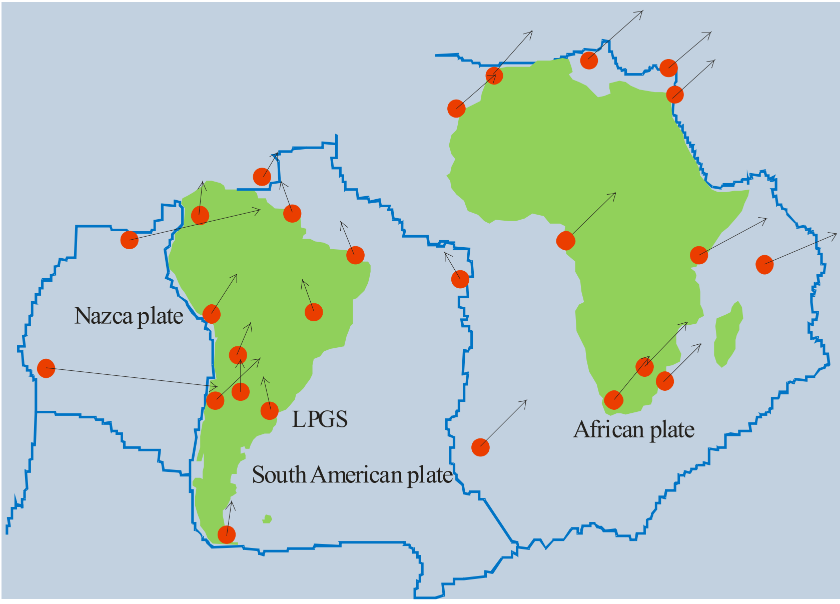


Fig. 3. Present-day plate motion vectors inferred from space geodesy, with reference to an hypothetical fixed Earth center (ITRF, International Terrestrial Reference Frame). LPGS: Rio Grande do Sul-Uruguay Latitude. Database after Heflin *et al.* (2001).

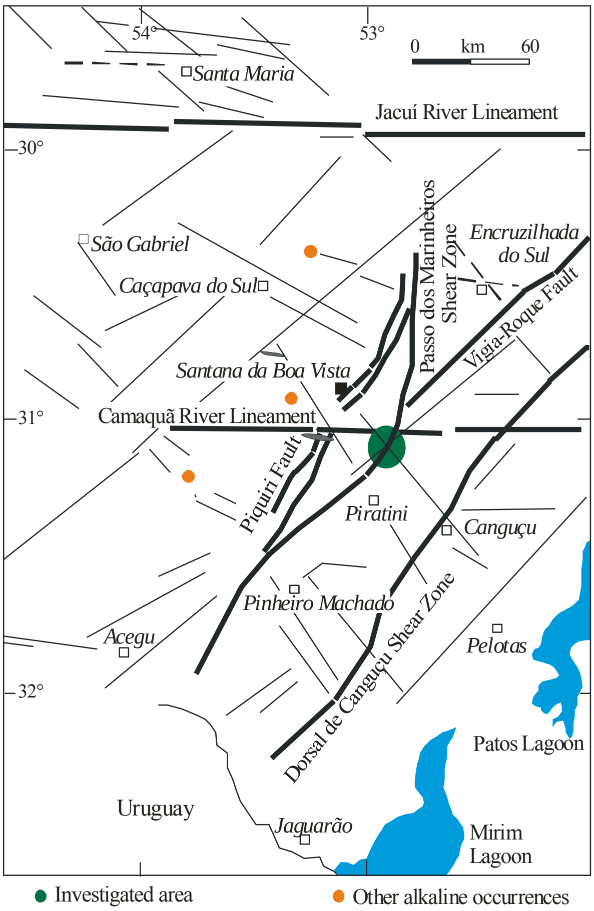


Fig. 4. Map showing the main tectonic structures associated with the Sul-rio-grandense Shield (after Viero, 1998).

This paper, other than being a trivial report on the kimberlite/lamproite occurrences, will be addressed to the Piratini phonolitic suite, chiefly relying upon the previous works by Barbieri *et al.* (1987) and Viero (1998).

## KIMBERLITES AND LAMPROITES

Deeply weathered rocks with kimberlitic/lamproitic affinity outcrop at Santiago, Jaguari, São Vicente, Rosário do Sul, Cachoeira do Sul and Canguçu localities. They form small diatremes (less than 25 m in diameter) and dykes (3 to 10 m thick and less than 100 m long) intruding the contacts between Neoproterozoic granites (Pelotas Batolith) and the Paleozoic to Mesozoic sedimentary and volcanic sequences of the Paraná Basin (Tedesco & Robaina, 1991; Almeida & Svisero, 1991; Svisero & Chieregati, 1991; Caldasso & Sander, 1994).

Partially preserved primary structures and textures are found only in the Canguçu diatreme (subcircular in shape and 24 m in diameter; cf. Caldasso & Sander, 1994). The geological structure is conditioned by the crossing between a ductile shearing zone and a fault, N40°E and N35-50°W, respectively, along the contact between the Arroio Moinho granite and the granitic rocks of the Pinheiro Machado complex. The intrusion is cut by a zoned dyke, about 5 m thick, and mainly characterized by breccias at the borders in addition to a massive core. The breccias are 10 to 30 cm wide and contain subangular to subrounded fragments of kimberlite set in an aphanitic matrix altered into an oxidated clay association. The fragments show massive structure and porphyritic texture with diopside, phlogopite, pyrope and ilmenite phenocrysts, 1 to 4 mm in size, and olivine pseudomorphs. The same mineral assemblage (about 30 to 40 vol% of the rock) occurs in the central portion of the diatreme. The core displays subaphyric texture and a few clinopyroxene phenocrysts, 2 to 12 cm long, set in a semi-aphanitic yellow-brown groundmass. It should be noted that other similar dykes were also recognized in the proximity of the Canguçu diatreme (R.P. Philipp, pers. com.).

Some lamproitic bodies at the Jaguari, Santiago, Rosário do Sul and Cachoeira do Sul regions are not exposed in surface. These occurrences were described by Tedesco & Robaina (1991) only on the basis of the presence of diopside, garnet and picroilmenite in heavy mineral concentrates: e.g. clinopyroxene, orthopyroxene and garnet from the São Vicente lamproitic rocks display characteristics similar to those analogous from other lamproitic occurrences (cf. Nixon *et al.*, 1987), i.e. Cr-diopside clinopyroxene (Ca 47, Mg 48, Fe+Mn 5 a.f.u.; $Cr_2O_3$ 1 wt%); enstatitic orthopyroxene [Mg/(Mg+Fe) ratio between 0.904 and 0.922; $Al_2O_3$, $Cr_2O_3$ and $TiO_2$=3.53%, 0.39% and 0.09%, respectively]; Cr-rich pyrope [Mg/(Mg+Fe)=0.80-0.86, $Cr_2O_3$=1.2-2.8 wt%].

## PIRATINI SUITE

The alkaline rocks form 34 subcircular phonolitic bodies (50 to 100 m in diameter), mainly intruding the Triassic sediments of the Rosário do Sul Formation, along a NW-trending strip subordinated NE-trending (Fig. 5).

All the rock-types contain nepheline as phenocrysts and/or microphenocrysts and groundmass phases. Two main petrographic types are apparent, i.e. tephritic phonolites and phonolites, on the basis of the modal mineral contents (Streckeisen, 1978).

Tephritic phonolites show porphyritic texture with phenocrysts of clinopyroxene, alkali feldspar, plagioclase, feldspathoids (nepheline and nosean), melanite, magnetite and titanite set in a trachytic microcrystalline groundmass made of the same minerals. Rare biotite and interstitial analcime may occur. Cumulatic nodules, in general less than 2 cm in diameter, are occasionally present. They consist of cumulate clinopyroxene or clinopyroxene+ plagioclase and by intercumulus magnetite and apatite with mineralogical characteristics similar to those of the host rock (i.e. salitic clinopyroxene and andesinic plagioclase).

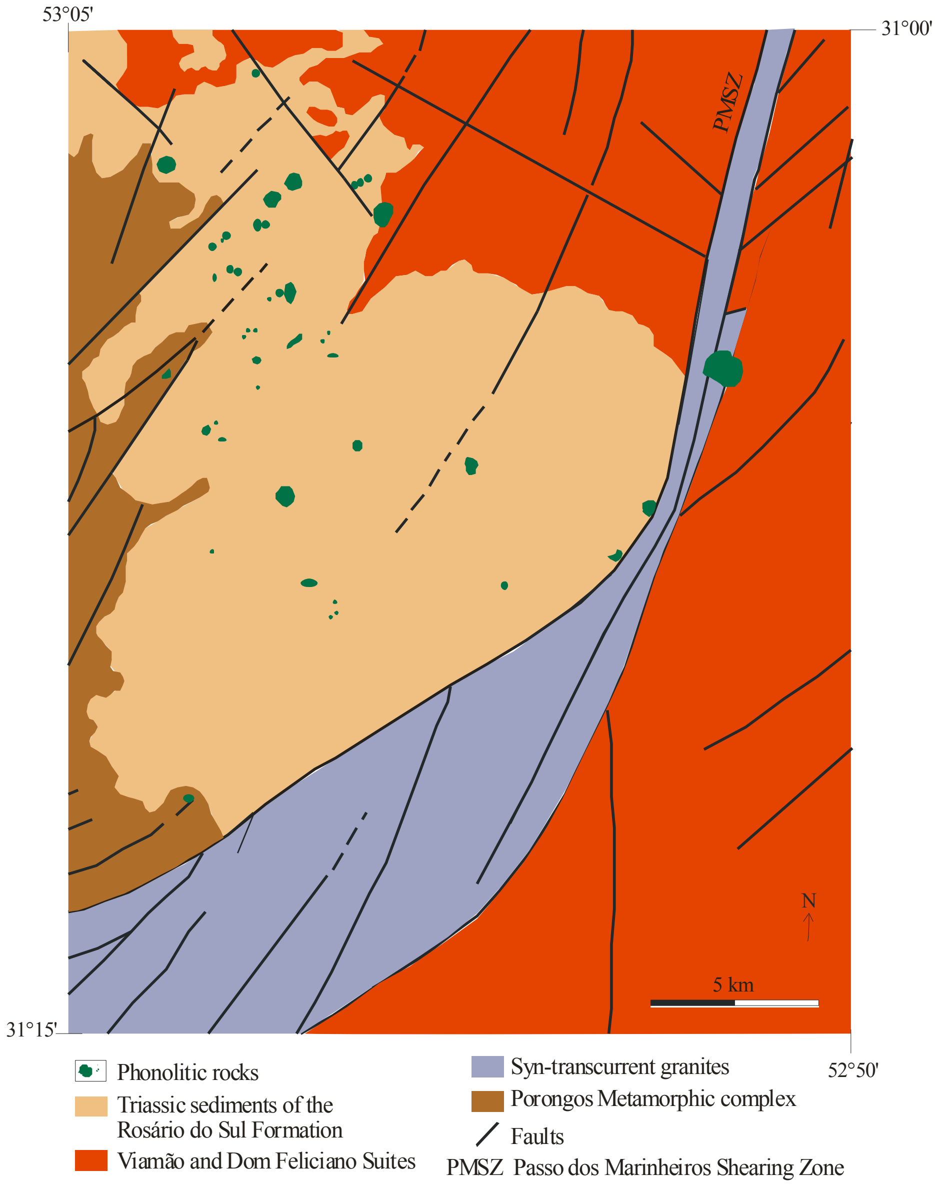


Fig. 5. Geologic aspects of the investigated area (after Barbieri *et al.*, 1987; UFRGS, 1995).

Phonolites are one of the feldspar rocks and have porphyritic or subaphyric/aphyric texture. The porphyritic types display alkali feldspar, clinopyroxene, nepheline, nosean and melanite phenocrysts, and magnetite, apatite and titanite microphenocrysts set in a hypocrystalline-hypohyaline groundmass. The aphyric varieties may contain scarce pheno- and microphenocrysts (less than 5 vol%) of sanidine, nepheline, nosean, acmitic clinopyroxene, garnet and titanite.

K-Ar data, whole-rock and feldspar, cluster at 84.6±6.7 Ma (Barbieri *et al.*, 1987). Fission track data indicated ages of 97.7 to 133 Ma (Baitelli, 1992).

Petrochemistry

Representative whole-rock analyses are given in Table 1. According to the TAS classification (Le Maitre, 1989), the samples fit the tephriphonolite and phonolite fields (Fig. 6), with transitional to sodic affinity ($Na_2O$ vs. $K_2O$ inset of Fig. 6). In turn, the phonolites may be subdivided in metaluminous and peralkaline variants on the basis of the alkali index (A.I.=$Na_2O$+$K_2O$/$Al_2O_3$ molar ratio), being higher and lower than 1, respectively (tephriphonolites, 0.74-0.92; phonolites, 0.88-1.00; peralkaline phonolites, 1.01-1.07). Notably, the peralkaline phonolites correspond to subaphyric-aphyric petrographic types. In the R1-R2 diagram (De La Roche *et al.*, 1980) all the samples plot in the phonolite field (R1-R2 inset of Fig. 6).

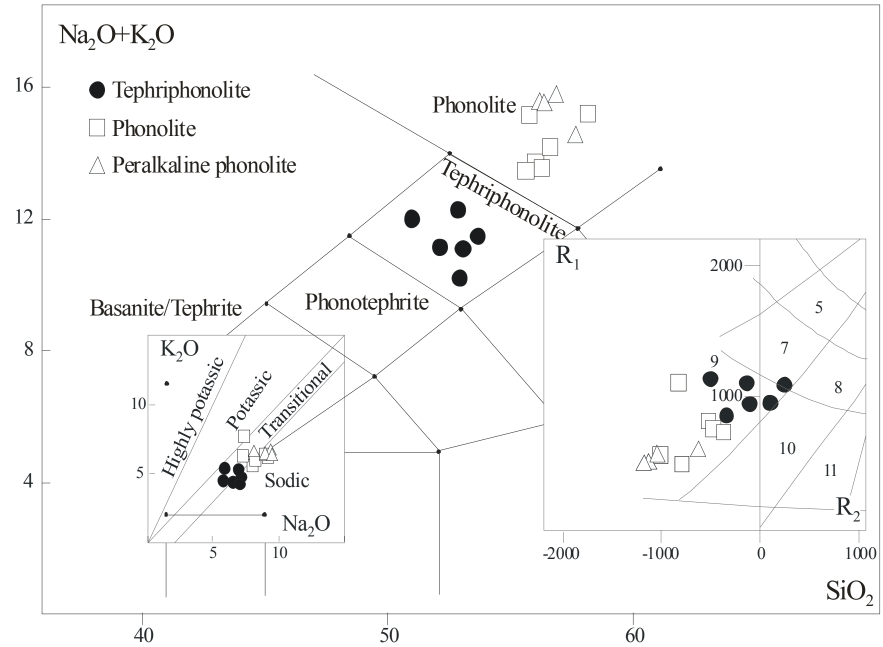


Fig. 6. TAS diagram (cf. Le Maitre, 1989) for the Piratini rock-types. Insets: $Na_2O$ vs. $K_2O$ plot (cf. Comin-Chiaramonti & Gomes, 1996) and part of the R1 [Si-11(Na+K) -2(Fe+Ti)]-$R_2$ [6Ca+2Mg+Al] diagram (De La Roche *et al.*, 1980).

Thereafter, tephriphonolites, phonolites and peralkaline phonolites will be indicated as TP, P and PP, respectively.

In the Q-Ne-Ks Petrogeny's Residual System (Fig. 7), all the Piratini rocks tend to cluster the phonolitic minimum, starting from the potassic field. The normative compositions (cf. Table 2) display a progressive or+ne increase from TP to PP, corresponding to a concomitant variation of the differentiation index (D.I.=or+ab+ne normative) values (TP=66-77; P=82-93; PP=87-93). In the D.I. vs. major elements plot (Fig. 8), the three rock-types are characterized by a decrease of $TiO_2$, $FeO_{total}$, MgO, CaO and $P_2O_5$ and by an increase of $SiO_2$, $Na_2O$ and $K_2O$, defining trends well distinct from those shown by the subcoeval analogues from the Lages district (cf. Scheibe *et al.*, in this volume). Considering the trace elements, a positive correlation between D.I. and Rb is apparent, whereas Nb decreases up to D.I. 90, followed by a steep increase in the more differentiated rocks. Ba, Zr and Sr display wide compositional ranges, with relatively narrow clusters at the lowest (Ba and Sr) and highest (Zr) contents for some phonolitic rocks having D.I.>90 (Fig. 8).

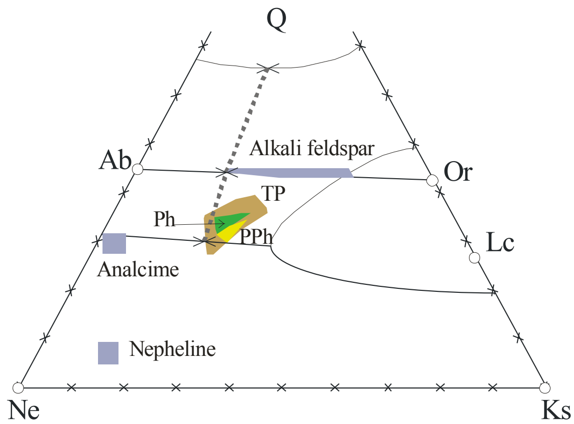


Fig. 7. Piratini rock-types plotted into the Ne-Ks-$SiO_2$ diagram (Petrogeny's Residua System, after Hamilton & McKenzie, 1965, and Henderson, 1984). Phase boundaries are for $PH_2O$=1 kb and the thermal minima are linked by thermal valleys (broken lines) to the minimum on the Ab-Or join. Alkali feldspar, analcime and nepheline compositions are also plotted. Data source: Barbieri *et al.* (1987) and Viero *et al.* (1995).

Multi-elemental diagrams, normalized to the primitive mantle of Sun & McDonough (1989), show that the phonolitic rocks are characterized by pronounced negative P-Ti and positive Zr spikes and by Ba and Lu spread. On the other hand, the tephriphonolites are enriched in Ce to Lu with respect to the phonolitic varieties and exhibit a weak Nb negative anomaly (Fig. 9). The latter is similar to the Early Cretaceous tholeiites from southern Brazil (both low- and high-Ti types), but contrasts with the strong Nb positive anomaly shown by coeval Alto Paranaíba alkaline rocks (cf. Gibson *et al.*, 1995).

REE (chondrite normalized; Boynton, 1984) distribution points to patterns with steep LREE fractionation, where the tephriphonolites display the most enriched values and a slight HREE fractionation. In turn, the phonolitic rocks have a remarkable range on the M- and HREE with an overall U-shaped distribution (Fig. 9).

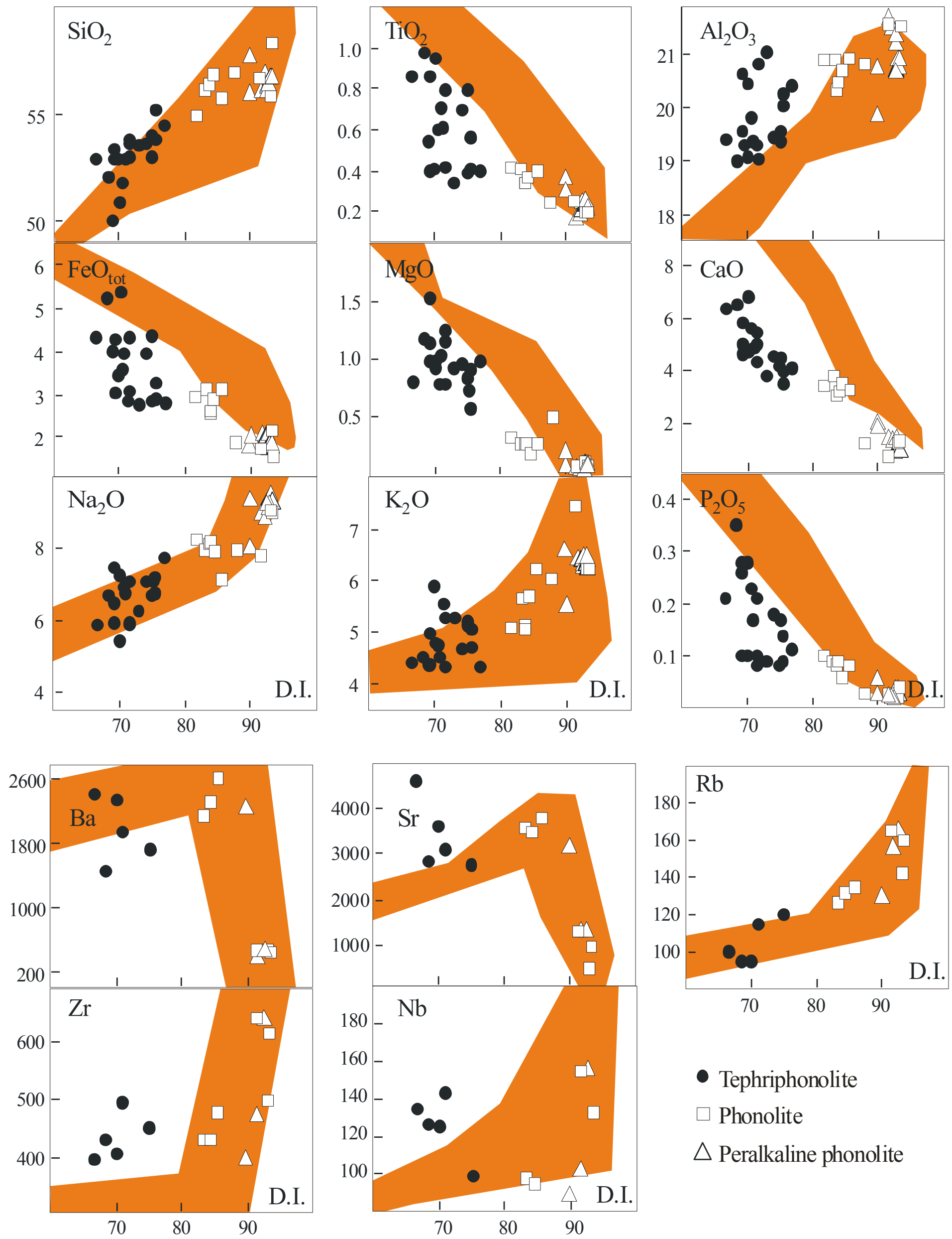


Fig. 8. D.I. (Differentiation Index=or+ab+ne normative) vs. major (wt%) and trace (ppm) elements for the Piratini suite. Orange fields: silicate rocks from the Lages alkaline-carbonatitic district (Scheibe *et al.*, in this volume).

Table 1. Representative analyses, (major and trace elements), CIPW norms and Sr-Nd isotope data for selected samples from the Piratini suite. Abbreviations: TP, tephriphonolite; P, phonolite; PP, peralkaline phonolite. R1=4Si-11(Na+K)-2(Fe+Ti), R2=6Ca+2Mg+Al (De La Roche *et al.*, 1980); A.I.=($Na_2O$=$K_2O$)/$Al_2O_3$ molar ratio, i.e. agpaitic index; D.I.=or+ab+an, i.e. differentiation index. Initial isotopic ratios and $\varepsilon^t$ notations, calculated at 86.4 Ma. Data source: Barbieri *et al.* (1987) and Viero (1998).

| | TP | TP | TP | TP | TP | TP | P | P | P | P | P | P | PP | PP | PP | PP |
|---|---|---|---|---|---|---|---|---|---|---|---|---|---|---|---|---|
| $SiO_2$ | 52.92 | 52.01 | 50.87 | 53.60 | 52.94 | 52.95 | 56.18 | 56.8 | 55.81 | 56.6 | 55.84 | 58.3 | 57.8 | 56.14 | 56.11 | 56.75 |
| $TiO_2$ | 0.86 | 0.98 | 0.95 | 0.61 | 0.79 | 0.79 | 0.41 | 0.37 | 0.40 | 0.25 | 0.19 | 0.19 | 0.37 | 0.21 | 0.17 | 0.24 |
| $Al_2O_3$ | 19.41 | 18.98 | 19.05 | 19.30 | 19.04 | 19.55 | 20.88 | 20.7 | 20.93 | 21.5 | 22.61 | 51.5 | 19.8 | 21.39 | 21.71 | 20.94 |
| $Fe_2O_3$ | 2.40 | 2.76 | 3.14 | 0.88 | 2.28 | 2.33 | 1.77 | 1.64 | 1.96 | 1.19 | 1.45 | 1.05 | 0.67 | 1.11 | 1.44 | 1.33 |
| FeO | 2.16 | 2.73 | 2.55 | 2.07 | 2.26 | 2.24 | 1.54 | 1.41 | 1.35 | 0.67 | 0.86 | 0.65 | 1.23 | 0.79 | 0.80 | 0.63 |
| MnO | 0.24 | 0.21 | 0.24 | 0.23 | 0.19 | 0.17 | 0.17 | 0.17 | 0.17 | 0.21 | 0.16 | 0.19 | 0.17 | 0.20 | 0.15 | 0.19 |
| MgO | 0.81 | 1.18 | 0.93 | 0.15 | 1.24 | 0.74 | 0.27 | 0.19 | 0.28 | 0.08 | 0.12 | 0.08 | 0.10 | 0.09 | 0.08 | 0.12 |
| CaO | 6.33 | 6.51 | 6.83 | 5.44 | 4.97 | 4.47 | 3.78 | 3.48 | 3.28 | 0.74 | 1.23 | 1.35 | 2.07 | 1.01 | 1.45 | 1.10 |
| $Na_2O$ | 5.89 | 6.69 | 7.26 | 5.87 | 7.08 | 7.10 | 7.95 | 7.90 | 7.15 | 7.80 | 9.06 | 8.98 | 8.08 | 9.26 | 9.00 | 9.53 |
| $K_2O$ | 4.40 | 4.53 | 4.77 | 5.54 | 4.34 | 5.21 | 5.66 | 5.70 | 6.22 | 7.45 | 6.21 | 6.22 | 6.59 | 6.48 | 6.45 | 6.26 |
| $P_2O_5$ | 0.21 | 0.35 | 0.28 | 0.08 | 0.21 | 0.17 | 0.09 | 0.06 | 0.08 | 0.03 | 0.02 | 0.04 | 0.03 | 0.04 | 0.03 | 0.04 |
| L.O.I | 4.83 | 2.81 | 2.47 | 5.67 | 4.46 | 3.75 | 0.83 | 0.93 | 1.53 | 3.43 | 2.43 | 1.85 | 2.77 | 3.07 | 2.30 | 2.85 |
| Sum | 100.46 | 99.74 | 99.34 | 99.-45 | 99.80 | 99.47 | 99.53 | 99.4 | 99.16 | 100. | 100.0 | 100. | 99.7 | 99.78 | 99.69 | 99.98 |
| | | | | | | | | | | | | | | | | |
| V | 27 | 30 | 30 | 28 | | 22 | 14 | 14 | | | | 23 | 13 | 23 | 25 | |
| Cr | | 12 | | | | 13 | | | | | | | | | | |
| Rb | 100 | 95 | 95 | 115 | | 120 | 126 | 132 | 135 | 165 | 142 | 160 | 131 | 166 | 157 | |
| Sr | 4601 | 2850 | 3633 | 3095 | | 2753 | 3586 | 3470 | 3793 | 1293 | 1344 | 947 | 3194 | 1322 | 1323 | |
| Ba | 2406 | 1449 | 2329 | 1948 | | 1723 | 2143 | 2304 | 2612 | 462 | 460 | 449 | 2262 | 481 | 388 | |
| Zr | 395 | 428 | 404 | 493 | | 449 | 430 | 429 | 477 | 640 | 497 | 612 | 400 | 640 | 473 | |
| Nb | 135 | 126 | 125 | 143 | | 99 | 98 | 95 | | 154 | | 133 | 90 | 157 | 104 | |
| Y | | 36.1 | 44.2 | | | 28 | 20.6 | 18.9 | 19 | 23.7 | 7 | 24 | | 25.0 | 5.6 | |
| La | | 130.1 | 173.5 | | | 140.2 | 154.4 | 153. | 140.7 | 104. | 116.0 | 116. | | 108.6 | 152.6 | |
| Ce | | 223.8 | 278.4 | | | 209.6 | 203.3 | 201. | 212.1 | 142. | 178.2 | 157. | | 148.7 | 183.4 | |
| Nd | | 88.2 | 103.5 | | | 67.1 | 58.9 | 55.6 | 49.9 | 36.2 | 31.5 | 38.1 | | 39.4 | 37.1 | |
| Sm | | 13.6 | 16.3 | | | 10.0 | 8.1 | 7.2 | 4.5 | 5.1 | 2.1 | 5.2 | | 5.5 | 3.7 | |
| Eu | | 3.8 | 4.5 | | | 2.6 | 2.1 | 1.8 | 1.0 | 1.3 | 0.4 | 1.3 | | 1.4 | 0.8 | |
| Gd | | 10.6 | 12.2 | | | 8.0 | 5.8 | 5.3 | 2.3 | 4.4 | 1.0 | 4.1 | | 4.4 | 2.9 | |
| Dy | | 6.5 | 7.5 | | | 4.8 | 3.3 | 3.0 | 1.2 | 3.3 | 0.4 | 3.2 | | 3.5 | 0.9 | |
| Er | | 3.2 | 3.7 | | | 2.5 | 1.8 | 1.6 | 0.3 | 2.1 | 0.1 | 2.1 | | 2.3 | 0.6 | |
| Yb | | 2.6 | 3.3 | | | 2.3 | 1.6 | 1.5 | 0.2 | 2.6 | 0.1 | 2.6 | | 2.7 | 0.5 | |
| Lu | | 0.4 | 0.6 | | | 0.4 | 0.2 | 0.3 | 0.03 | 0.4 | 0.01 | 0.5 | | 0.4 | 0.1 | |
| | | | | | | | | | | | | | | | | |
| or | 26.0 | 26.8 | 28.2 | 32.7 | 25.6 | 30.8 | 33.5 | 33.7 | 37.7 | 44.0 | 37.6 | 36.8 | 38.9 | 38.3 | 38.1 | 37.0 |
| ab | 29.7 | 23.9 | 18.9 | 25.7 | 29.6 | 25.6 | 29.1 | 31.6 | 31.3 | 25.5 | 28.4 | 33.7 | 29.0 | 23.6 | 26.4 | 26.0 |
| an | 13.6 | 8.4 | 5.3 | 10.0 | 7.3 | 6.1 | 4.6 | 4.2 | 6.8 | 1.8 | 2.7 | 0.1 | | | | |
| ne | 10.9 | 17.7 | 23.1 | 13.0 | 16.4 | 18.7 | 20.7 | 19.1 | 16.6 | 21.9 | 27.1 | 22.9 | 19.8 | 27.3 | 26.8 | 25.4 |
| ac | | | | | | | | | | | | | 1.9 | 3.2 | 0.4 | 3.9 |
| ns | | | | | | | | | | | | | 0.1 | 0.2 | 0.2 | 0.8 |
| di | 6.3 | 9.2 | 6.8 | 5.5 | 9.1 | 7.3 | 3.3 | 2.8 | 2.6 | 0.9 | 1.4 | 1,1 | 4.2 | 3.3 | 1.2 | 2.7 |
| wo | 3.7 | 4.3 | 7.6 | 4.3 | 1.9 | 3.1 | 4.0 | 3.9 | 1.3 | 0.3 | 0.7 | 2.1 | 2.2 | 0.4 | 2.4 | 0.8 |
| mt | 3.5 | 4.0 | 4.6 | 1.3 | 3.3 | 3.4 | 2.6 | 2.4 | 2.9 | 1.7 | 2.2 | 1.5 | | | 1.9 | |
| il | 1.6 | 1.9 | 1.8 | 1.2 | 1.5 | 1.5 | 0.8 | 0.7 | 0.8 | 0.5 | 0.4 | 0.4 | 0.7 | 0.4 | 0.3 | 0.5 |
| ap | 0.5 | 0.8 | 0.7 | 0.2 | 0.5 | 0.4 | 0.2 | 0.1 | 0.2 | 0.1 | | 0.1 | 0.1 | 0.1 | 0.1 | 0.1 |
| | | | | | | | | | | | | | | | | |
| R1 | 262 | -141 | -472 | 95 | -143 | -353 | -502 | -441 | -372 | -791 | -1015 | -805 | -618 | -1119 | -1028 | -1160 |
| R2 | 1098 | 1127 | 1151 | 968 | 967 | 898 | 827 | 788 | 775 | 506 | 581 | 1159 | 616 | 532 | 586 | 534 |
| A.I. | 0.74 | 0.84 | 0.90 | 0.81 | 0.86 | 0.88 | 0.92 | 0.93 | 0.88 | 0.97 | 0.96 | 1.00 | 1.03 | 1.04 | 1.01 | 1.07 |
| D.I. | 66.59 | 68.40 | 70.11 | 71.44 | 71.64 | 75.07 | 83.22 | 84.3 | 85.60 | 91.4 | 93.10 | 93.3 | 86.9 | 89.16 | 91.24 | 88.36 |
| | | | | | | | | | | | | | | | | |
| $(^{87}Sr/^{86}Sr)_m$ | | 16 | 52 | | | 59 | 81 | 553 | 61 | 567 | 59 | 626 | 569 | 00 | 76 | |
| $(^{143}Nd/^{144}Nd)_m$ | | | | | | | | | 28 | | 32 | | | | | |
| $(^{87}Sr/^{86}Sr)_i$ | | 04 | 43 | | | 43 | 69 | 539 | 48 | 522 | 15 | 566 | 554 | 56 | 34 | |
| $(^{143}Nd/^{144}Nd)_i$ | | | | | | | | | 25 | | 30 | | | | | |
| | | | | | | | | | | | | | | | | |
| εSr | | 6.3 | 11.7 | | | 11.9 | 15.4 | 11.3 | 12.5 | 8.8 | 7.9 | 15.1 | 13.4 | -0.6 | 10.5 | |
| εNd | | | | | | | | | -5.4 | | -4.5 | | | | | |

Table 2. Representative chemical analyses of feldspars from the Piratini suite. Data source: Barbieri *et al.* (1987). Atomic formulae units (a.f.u.) on the basis of 32 (O). Additional abbreviations: Ph, phenocryst; mPh, microphenocryst; gm, groundmass; C, core; R, rim. Other abbreviations as in Table 1.

| | TP | TP | TP | TP | TP | TP | TP | TP | TP | TP | P | P | P | P | P | P | P | P | P | PP | PP | PP | PP | PP |
|---|---|---|---|---|---|---|---|---|---|---|---|---|---|---|---|---|---|---|---|---|---|---|---|---|
| | Ph | mPh | PhC | PhR | gm | PhC | PhR | PhC | PhR | gm | PhC | PhR | PhR | mPh | gm | gm | PhC | PhR | gm | Ph | gm | gm | gm | gm |
| $SiO_2$ | 58.18 | 59.49 | 60.00 | 62.38 | 63.74 | 57.56 | 65.41 | 58.59 | 62.00 | 65.15 | 59.21 | 65.51 | 65.51 | 62.72 | 67.00 | 66.16 | 64.39 | 64.49 | 65.21 | 64.62 | 67.11 | 65.02 | 65.87 | 65.74 |
| $Al_2O_3$ | 25.87 | 25.03 | 22.00 | 20.23 | 20.36 | 21.59 | 18.73 | 21.64 | 20.54 | 19.30 | 21.08 | 19.57 | 19.57 | 20.44 | 19.00 | 18.90 | 19.47 | 19.67 | 19.19 | 19.85 | 19.69 | 18.46 | 19.40 | 18.94 |
| $Fe_2O_3$ | 0.36 | 0.41 | 0.13 | 0.43 | 0.21 | 0.28 | 0.40 | 0.28 | 0.22 | 0.36 | 0.33 | 0.24 | 0.24 | 0.32 | 0.51 | 0.38 | 0.01 | 0.17 | 0.20 | 0.23 | 0.17 | 0.42 | 0.40 | 0.99 |
| CaO | 7.21 | 6.04 | 1.97 | 0.43 | 0.81 | 0.71 | 0.12 | 1.33 | 0.79 | 0.36 | 0.61 | 0.73 | 0.73 | 0.70 | | | | | | 0.55 | | | 0.20 | |
| $Na_2O$ | 6.61 | 7.16 | 5.43 | 4.55 | 4.56 | 3.47 | 3.47 | 4.33 | 4.53 | 4.67 | 4.62 | 5.77 | 5.77 | 5.73 | 8.43 | 5.72 | 4.87 | 5.76 | 5.16 | 5.55 | 9.32 | 2.01 | 7.15 | 6.29 |
| $K_2O$ | 0.83 | 1.3 | 5.17 | 8.71 | 9.06 | 7.57 | 11.78 | 6.41 | 8.15 | 9.70 | 6.39 | 7.75 | 7.75 | 6.57 | 4.70 | 8.61 | 9.03 | 7.78 | 8.99 | 7.99 | 3.49 | 13.95 | 6.22 | 7.80 |
| BaO | 0.17 | 0.12 | 3.06 | 2.70 | 0.42 | 7.30 | | 6.22 | 2.67 | 0.05 | 6.31 | | | 2.98 | 0.27 | 0.16 | 2.11 | 2.13 | 1.27 | 1.04 | | 0.05 | 0.19 | |
| SrO | 0.82 | 0.48 | 2.00 | 0.30 | 0.86 | 1.46 | 0.14 | 1.10 | 0.92 | 0.36 | 1.49 | 0.55 | 0.55 | 0.63 | | 0.12 | 0.12 | 0.05 | 0.02 | 0.18 | 0.19 | 0.12 | 0.31 | 0.20 |
| Sum | 100.05 | 100.03 | 99.76 | 99.73 | 100.02 | 99.40 | 10.05 | 99.90 | 99.82 | 99.95 | 100.04 | 100.12 | 100.12 | 100.09 | 99.88 | 100.05 | 100.00 | 100.05 | 100.04 | 100.01 | 99.97 | 100.03 | 99.74 | 99.96 |
| | | | | | | | | | | | | | | | | | | | | | | | | |
| Si | 10.477 | 10.679 | 11.158 | 11.561 | 11.626 | 11.079 | 11.929 | 11.125 | 11.496 | 11.836 | 11.238 | 11.809 | 11.809 | 11.537 | 11.950 | 11.939 | 11.802 | 11.769 | 11.869 | 11.738 | 11.892 | 11.952 | 11.852 | 11.837 |
| Al | 5.490 | 5.295 | 4.822 | 4.418 | 4.376 | 4.897 | 4.025 | 4.842 | 4.488 | 4.132 | 4.715 | 4.157 | 4.157 | 44.311 | 3.994 | 4.019 | 4.206 | 4.230 | 4.116 | 4.249 | 4.112 | 3.999 | 4.114 | 4.019 |
| $Fe^{3+}$ | 0.048 | 0.056 | 0.019 | 0.060 | 0.029 | 0.040 | 0.055 | 0.040 | 0.031 | 0.049 | 0.048 | 0.033 | 0.033 | 0.044 | 0.068 | 0.0551 | 0.001 | 0.023 | 0.027 | 0.031 | 0.023 | 0.058 | 0.054 | 0.134 |
| Ca | 1.391 | 1.612 | 0.392 | 0.085 | 0.158 | 0.146 | 0.023 | 0.270 | 0.157 | 0.070 | 0.124 | 0.141 | 0.141 | 0.138 | | | | | | 0.107 | | | 0.039 | |
| Na | 2.308 | 2.492 | 1.958 | 1.635 | 1.613 | 1.295 | 12.267 | 1.594 | 1.628 | 1.645 | 1.700 | 2.016 | 2.016 | 2.043 | 2.905 | 2.001 | 1.730 | 2.038 | 1.821 | 1.954 | 3.202 | 0.716 | 2.494 | 2.196 |
| K | 0.191 | 0.298 | 1.226 | 2.059 | 2.108 | 1.858 | 2.740 | 1.552 | 1.928 | 2.248 | 1.547 | 1.782 | 1.782 | 1.542 | 1.069 | 1.982 | 2.111 | 1.811 | 2.087 | 1.851 | 0.789 | 3.271 | 1.427 | 1.792 |
| Ba | 0.012 | 0.008 | 0.223 | 0.196 | 0.030 | 0.550 | | 0.463 | 0.194 | 0.004 | 0.469 | | | 0.215 | 0.019 | 0.011 | 0.152 | 0.152 | 0.091 | 0.074 | | 0.004 | 0.013 | |
| Sr | 0.086 | 0.050 | 0.216 | 0.032 | 0.091 | 0.163 | 0.015 | 0.121 | 0.099 | 0.038 | 0.164 | 0.058 | 0.058 | 0.067 | | 0.013 | 0.013 | 0.005 | 0.002 | 0.019 | 0.019 | 0.013 | 0.032 | 0.021 |
| Sum | 20.003 | 20.039 | 20.014 | 20.047 | 20.031 | 20.029 | 20.015 | 20.007 | 20.022 | 20.020 | 20.005 | 19.996 | 19.996 | 20.018 | 20.006 | 20.021 | 20.015 | 20.029 | 20.013 | 20.025 | 20.036 | 20.013 | 20.025 | 19.999 |
| | | | | | | | | | | | | | | | | | | | | | | | | |
| wt% | | | | | | | | | | | | | | | | | | | | | | | | |
| Ab | 57.89 | 61.68 | 53.26 | 41.80 | 40.13 | 37.83 | 29.49 | 45.17 | 42.40 | 40.07 | 48.94 | 49.70 | 49.70 | 53.41 | 71.90 | 48.75 | 43.57 | 51.46 | 45.11 | 48.46 | 79.27 | 17.10 | 61.58 | 53.59 |
| An | 37.03 | 30.50 | 11.33 | 2.32 | 4.18 | 4.54 | 0.60 | 8.13 | 4.33 | 1.81 | 3.79 | 3.69 | 3.69 | 3.83 | | | | | | 2.82 | | | 1.01 | |
| Or | 5.08 | 7.82 | 35.41 | 55.88 | 55.69 | 57.63 | 69.91 | 46.70 | 53.27 | 58.12 | 47.27 | 46.62 | 46.62 | 42.77 | 28.10 | 51.25 | 56.43 | 48.54 | 54.89 | 48.72 | 20.73 | 82.90 | 37.41 | 46.41 |

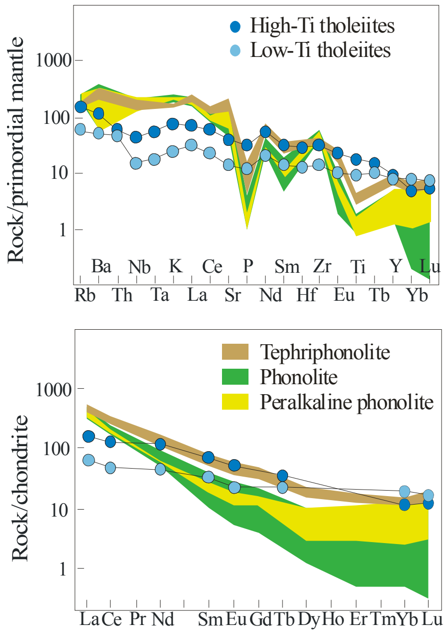


Fig. 9. Spidergrams representing the I.E. and REE fields of the main rock-types from Piratini normalized to the primitive mantle and to the chondrites (Sun & McDonough, 1989, and Boynton, 1984, respectively). Low- and high-Ti representative basalt tholeiites from southern Brazil are also shown (Piccirillo & Melfi, 1988).

## Mineral chemistry

### *Feldspars*

Representative analyses are listed in Table 2. Plagioclase is present only in TP, varying from sodic andesine to oligoclase. Alkali feldspar is ubiquitous, being a barium-rich sanidine in TP and P, and a low-barium anorthoclase to sodic sanidine in PP. The sum of cations in the structural formulae ($X_8Z_{12}O_{32}$) falls within the range 19.9-20.1, i.e.±0.5% of the theoretical 20.0. The X group (Ca+Sr+Ba+Na+K) is very close to the theoretical 4.00±0.1 (±2.5%). This indicates that subsolidus processes have not signify-cantly modified the chemistry of this mineral group.

Significant Sr (up to 0.21 atoms per formula unit) and Ba (up to 0.55) occur in the alkali feldspar from TP and P, whereas in the TP plagioclase Sr and Ba are lower than 0.11 and 0.04, respectively. Usually the feldspars fall below the solvus-solidus intersection in the system (Ca+Sr)-Na-(K+Ba) at $PH_2O$=0.5 kb and 900°C (Fig. 10; Seck, 1971).

Apparent closure temperatures of 950-920°C were obtained from plagioclase pheno- to microphenocrysts at 1 kb $H_2O$ pressure (Kudo & Weill, 1970; Mathez, 1973). Geothermobarometric calculations using the equilibrium system of two feldspars (Brown & Parson, 1981; Ghiorso, 1984) indicate for the tephritic phonolites crystallization temperature around 925°C at 1.0 kb pressure. This temperature value is about 100°C higher than that of the thermal trough (at $PH_2O$=1 kb; Hamilton & Mackenzie, 1965) in the Q-Ne-Ks system (cf. Fig. 7), suggesting comparatively lower water pressure for the crystallization conditions.

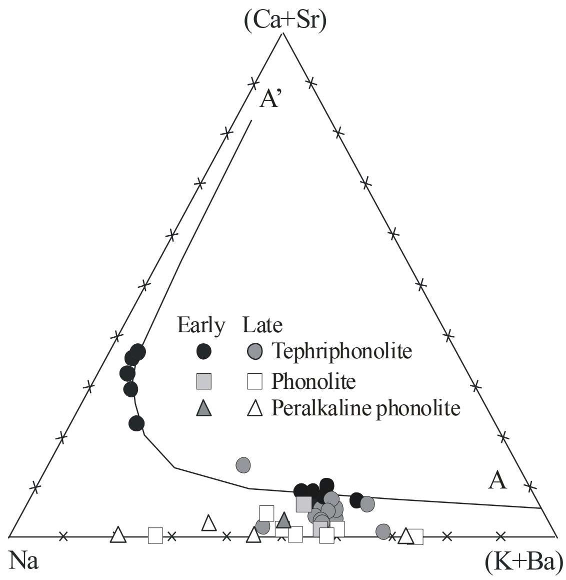


Fig. 10. Feldspar compositions in terms of (Ca+Sr)-Na-(K+Ba) diagram (at%). A-A' is the solvus-solidus intersection at 900°C (Seck, 1971).

### *Feldspathoids*

Several feldspathoids usually coexist in the phonolitic rocks: nepheline, nosean and analcime are ubiquitous, whereas sodalite characterizes the PP (cf. Table 3). The feldspathoids are generally modified: it is well-known that nepheline may be altered to analcime and cancrinite during subsolidus interaction with deuteric and/or hydrothermal fluids (Deer *et al.*, 1992). Cancrinite presumably is formed by the reactions of $SO_4$- or $CO_2$-bearing fluids with nepheline in subsolidus, whereas subsolidus sodalite has been associated with the chloritization of nepheline by metasomatic brines (Barker, 1976; Sharp *et al.*, 1989).

Nepheline is a widespread phase as pheno- and microphenocrysts, usually and strongly altered to zeolite, cancrinite and carbonates. It also occurs as microlites in the groundmass and as euhedral to subeuhedral microphenocrysts. The low Q content and homogeneous composition, i.e. within the range of nepheline solid solutions (cf. Fig. 7 and Table 3), suggest subsolidus temperatures between 500 and 650°C (cf. Hamilton, 1961).

Nosean occurs either in the groundmass or as hexagonal to rounded microphenocrysts strongly altered to an isotropic clay mass. Chemical data indicate high $K_2O$ and $SO_3$ contents (Table 3). Analcime, usually as a groundmass phase, has a constant, near stoichiometric composition in all the samples (Table 3; cf. Fig. 7).

Table 3. Representative chemical analyses of foids. Data source: Barbieri *et al.* (1987) and unpublished data. A.f.u. (Deer *et al.*, 1992) on the basis of: nepheline, 32 (O), analcime, 98 (O); cancrinite, (Si+Al)=12; sodalite group, $3Al_2O_3$+$6SiO_2$=21 (O). Abbreviations as in Table 2.

| | Nepheline TP Ph | Nepheline P gm | Analcime TP gm | Analcime P gm | Analcime PP gm | Cancrinite P gm | Nosean TP Ph | Nosean TP gm | Sodalite PP | Sodalite PP |
|---|---|---|---|---|---|---|---|---|---|---|
| $SiO_2$ | 44.06 | 45.65 | 53.00 | 53.20 | 54.65 | 34.50 | 36.54 | 36.81 | 38.04 | 38.36 |
| $Al_2O_3$ | 31.89 | 30.64 | 24.00 | 24.07 | 23.00 | 30.00 | 28.28 | 29.55 | 29.04 | 31.42 |
| $Fe_2O_3$ | 0.86 | 1.26 | | 0.11 | 0.11 | 1.47 | 0.03 | 0.64 | 0.04 | 0.92 |
| CaO | 0.49 | | 0.72 | 0.03 | 0.08 | 3.20 | 0.50 | 0.72 | 1.26 | 0.02 |
| $Na_2O$ | 16.79 | 17.02 | 13.08 | 13.50 | 13.00 | 17.52 | 21.53 | 21.46 | 22.37 | 21.95 |
| $K_2O$ | 4.76 | 3.79 | 1.05 | 0.42 | 1.22 | 0.60 | 0.31 | 0.97 | 0.06 | 0.10 |
| Cl | | | | | | 0.40 | | | 6.30 | 6.40 |
| $SO_3$ | | | | | | 3.70 | 10.82 | 7.63 | 1.75 | 0.93 |
| Sum | 98.85 | 98.36 | 91.85 | 91.33 | 92.06 | 91.30 | 98.01 | 97.78 | 97.74 | 98.66 |
| | | | | | | | | | | |
| Si | 8.529 | 8.810 | 31.300 | 30.619 | 32.077 | 5.926 | 6.193 | 6.142 | 6.269 | 6.090 |
| Al | 7.276 | 6.970 | 16.706 | 17.989 | 15.912 | 6.074 | 5.743 | 5.811 | 5.641 | 5.880 |
| $Fe^{3+}$ | 0.125 | 0.183 | | 0.048 | 0.049 | 0.190 | 0.004 | 0.080 | 0.005 | 0.110 |
| Ca | 0.102 | | 0.456 | 0.018 | 0.050 | 0.5835 | 0.092 | 0.129 | 0.223 | 0.003 |
| Na | 6.302 | 6.369 | 14.978 | 15.065 | 14.795 | 5.835 | 7.193 | 6.943 | 7.148 | 6.757 |
| K | 1.176 | 0.930 | 0.791 | 0.308 | 0.913 | 0.131 | 0.068 | 0.207 | 0.013 | 0.020 |
| Cl | | | | | | 0.116 | | | 1.760 | 1.722 |
| S | | | | | | 0.477 | 1.399 | 0.955 | 0.216 | 0.111 |
| Sum | 23.510 | 23.262 | 64.231 | 64.047 | 63.976 | 19.338 | 20.692 | 20.267 | 21.275 | 20.693 |
| | | | | | | | | | | |
| Ne | 78.23 | 80.18 | 67.95 | 68.98 | 65.19 | | | | | |
| Ks | 16.24 | 12.90 | 3.99 | 1.57 | 4.49 | | | | | |
| Q | 5.44 | 7.82 | 28.06 | 29.45 | 30.32 | | | | | |

Cancrinite is usually found associated with carbonates as late altered products of nepheline (Barbieri *et al.*, 1987). A high $CO_2$ activity is assumed to be present in the late fluids, and a stoichiometric a.f.u. $CO_2$ value (not determined in the analysis of Table 3) up to 1.407 can be inferred for the cancrinite.

Sodalite, a typical constituent in the peralkaline phonolites, occurs both as phenocryst and as a groundmass phase. The constant compositions is characterized by Cl up to 6.4%. The phenocrysts, i.e. early phases, are in agreement with the stability of liquidus sodalite in undersaturated compositions, and with its ability to coexist with nepheline (Binsted, 1981).

*Clinopyroxenes*

A large majority of clinopyroxene compositions (Table 4) falls within the salite field of the conventional pyroxene quadrilateral (Fig. 11A), independently from the rock-type, i.e. TP, P or PP. Those compositions are also well distinct from kimberlite clinopyroxenes (e.g. São Vicente kimberlite; Tedesco & Robaina, 1991). Late phases from P and PP samples plot in the Ca-Na field of Morimoto (1988) (Fig. 11B). In sum, the chemical variations straddle over all the clinopyroxene trends from other Brazilian alkaline complexes (Fig. 11C).

Table 4. Representative chemical analyses of clinopyroxenes from the Piratini suite (data source: Barbieri *et al.*, 1987). Abbreviations as in Table 2. A.f.u. on the basis of 6 (O). $Fe^{2+}$ and $Fe^{3+}$ calculated by stoichiometry; Fe*=$Fe^{3+}$+$Fe^{2+}$+Mn; Fe**=$Fe^{3+}$+$Fe^{2+}$+Mn-Na.

| | TP | TP | TP | TP | TP | TP | TP | P | P | P | P | P | P | PP | PP | PP | PP | PP |
|---|---|---|---|---|---|---|---|---|---|---|---|---|---|---|---|---|---|---|
| | PhC | PhR | PhC | PhR | Ph | mPh | gm | Ph | mPh | gm | Ph | gm | gm | mPh | gm | gm | Ph | gm |
| $SiO_2$ | 46.89 | 44.73 | 43.66 | 44.62 | 44.65 | 45.11 | 41.59 | 43.69 | 47.17 | 46.66 | 43.01 | 46.00 | 50.56 | 47.05 | 49.58 | 49.19 | 43.75 | 49.41 |
| $TiO_2$ | 0.80 | 0.12 | 2.23 | 1.15 | 2.18 | 1.44 | 1.61 | 1.74 | 0.73 | 0.87 | 1.50 | 0.76 | 0.59 | 1.77 | 1.08 | 1.37 | 1.70 | 0.88 |
| $Al_2O_3$ | 6.34 | 7.29 | 8.78 | 6.62 | 7.89 | 6.75 | 9.16 | 7.99 | 3.29 | 3.28 | 7.86 | 3.99 | 1.51 | 4.45 | 2.34 | 2.19 | 6.21 | 2.35 |
| $Cr_2O_3$ | 0.14 | 0.02 | | | 0.03 | 0.05 | | | | | | | | | | 0.12 | | |
| $Fe_2O_3$ | 6.42 | 9.53 | 9.67 | 9.59 | 6.80 | 7.82 | 10.58 | 13.19 | 8.49 | 9.47 | 10.28 | 9.86 | 18.24 | 10.65 | 16.28 | 22.84 | 10.85 | 14.18 |
| FeO | 5.52 | 8.45 | 3.46 | 9.66 | 5.56 | 8.33 | 9.08 | 0.76 | 11.14 | 11.05 | 9.01 | 11.25 | 5.07 | 9.27 | 5.59 | 4.72 | 8.61 | 11.71 |
| MnO | 0.32 | 0.88 | 0.56 | 1.08 | 0.39 | 0.80 | 0.81 | 0.43 | 2.05 | 2.01 | 0.72 | 1.93 | 2.32 | 2.84 | 2.35 | 2.25 | 1.53 | 2.58 |
| MgO | 9.88 | 5.94 | 8.47 | 5.27 | 9.38 | 6.88 | 4.66 | 9.48 | 5.23 | 4.79 | 5.25 | 4.26 | 3.24 | 3.35 | 4.10 | 1.38 | 4.77 | 1.40 |
| CaO | 22.98 | 21.76 | 21.93 | 20.72 | 22.22 | 21.56 | 21.54 | 21.98 | 19.75 | 20.33 | 21.41 | 20.00 | 11.75 | 16.75 | 12.89 | 7.32 | 20.52 | 11.47 |
| $Na_2O$ | 0.84 | 1.25 | 1.51 | 1.66 | 0.91 | 1.34 | 1.16 | 1.63 | 1.99 | 1.94 | 1.35 | 2.00 | 7.06 | 3.94 | 6.13 | 8.89 | 1.92 | 6.12 |
| Sum | 100.13 | 99.97 | 100.27 | 100.37 | 100.00 | 100.08 | 100.19 | 100.88 | 99.84 | 100.3 | 100.39 | 100.05 | 100.34 | 100.07 | 100.34 | 100.27 | 99.86 | 100.11 |
| | | | | | | | | | | | | | | | | | | |
| Si | 1.773 | 1.737 | 1.657 | 1.737 | 1.697 | 1.741 | 1.629 | 1.646 | 1.853 | 1.833 | 1.676 | 1.815 | 1.948 | 1.838 | 19.091 | 1.909 | 1.719 | 1.943 |
| $Al^{IV}$ | 0.227 | 0.263 | 0.343 | 0.263 | 0.303 | 0.259 | 0.371 | 0.354 | 0.147 | 0.152 | 0.324 | 0.185 | 0.052 | 0.162 | 0.0909 | 0.091 | 0.281 | 0.057 |
| Ti | | | | | | | | | | 0.015 | | | | | | | | |
| Sum | 2.000 | 2.000 | 2.000 | 2.000 | 2.000 | 2.000 | 2.000 | 2.000 | 2.000 | 2.000 | 2.000 | 2.000 | 2.000 | 2.000 | 2.000 | 2.000 | 2.000 | 2.000 |
| | | | | | | | | | | | | | | | | | | |
| $Al^{VI}$ | 0.056 | 0.071 | 0.050 | 0.040 | 0.050 | 0.048 | 0.052 | 0.001 | 0.005 | 0.010 | 0.037 | 0.001 | 0.017 | 0;043 | 0.015 | 0.0092 | 0.006 | 0.052 |
| Ti | 0.023 | 0.003 | 0.064 | 0.034 | 0.062 | 0.042 | 0.047 | 0.049 | 0.022 | 0.643 | 0.044 | 0.002 | 0.017 | 0.052 | 0.031 | 0.040 | 0.050 | 0.027 |
| Cr | 0.004 | 0.001 | | | 0.001 | 0.001 | | | | | | | | | | 0.004 | | |
| $Fe^{3+}$ | 0.183 | 0.278 | 0.276 | 0.281 | 0.194 | 0.227 | 0.312 | 0.374 | 0.251 | 0.280 | 0.301 | 0.293 | 0.529 | 0.313 | 0.472 | 0.667 | 0.321 | 0.420 |
| $Fe^{2+}$ | 0.175 | 0.274 | 0.110 | 0.315 | 0.177 | 0.269 | 0.298 | 0.024 | 0.366 | 0.363 | 0.293 | 0.371 | 0.163 | 0.303 | 0.180 | 0.153 | 0.283 | 0.385 |
| Mn | 0.010 | 0.029 | 0.018 | 0.036 | 0.013 | 0.026 | 0.027 | 0.014 | 0.068 | 0.067 | 0.024 | 0.065 | 0.076 | 0.094 | 0.077 | 0.074 | 0.051 | 0.085 |
| Mg | 0.557 | 0.343 | 0.479 | 0.306 | 0.531 | 0.396 | 0.271 | 0.532 | 0.306 | 0.280 | 0.305 | 0.250 | 0.186 | 0.195 | 0.235 | 0.080 | 0.279 | 0.082 |
| Ca | 0.931 | 0.905 | 0.892 | 0.864 | 0.905 | 0.891 | 0.904 | 0.887 | 0.831 | 0.852 | 0.894 | 0.845 | 0.485 | 0.701 | 0.532 | 0.304 | 0.864 | 0.483 |
| Na | 0.062 | 0.094 | 0.111 | 0.125 | 0.067 | 0.100 | 0.088 | 0.119 | 0.152 | 0.148 | 0.102 | 0.153 | 0.527 | 0.299 | 0.458 | 0.669 | 0.146 | 0.466 |
| Sum | 2.000 | 2.000 | 2.000 | 2.000 | 2.000 | 2.000 | 2.000 | 2.000 | 2.000 | 2.000 | 2.000 | 2.000 | 2.000 | 2.000 | 2.000 | 2.000 | 2.000 | 2.000 |
| | | | | | | | | | | | | | | | | | | |
| Ca | 50.2 | 49.4 | 50.2 | 48.0 | 49.7 | 49.2 | 49.9 | 48.4 | 45.6 | 46.2 | 49.2 | 46.3 | 33.7 | 43.7 | 35.6 | 23.8 | 48.1 | 33.2 |
| Mg | 30.0 | 18.8 | 27.0 | 17.0 | 29.2 | 21.9 | 15.0 | 29.1 | 16.8 | 15.2 | 16.8 | 13.7 | 12.9 | 12.1 | 15.7 | 6.2 | 15.5 | 5.6 |
| Fe* | 19.8 | 31.8 | 22.8 | 35.0 | 21.1 | 28.9 | 35.1 | 22.5 | 37.6 | 38.5 | 34.0 | 39.9 | 53.4 | 44.2 | 48.7 | 69.9 | 36.4 | 61.2 |
| | | | | | | | | | | | | | | | | | | |
| Na | 6.7 | 10.2 | 12.6 | 13.4 | 7.3 | 10.9 | 9.7 | 12.6 | 15.3 | 14.9 | 11.0 | 15.6 | 55.3 | 33.0 | 47.5 | 68.7 | 15.7 | 48.0 |
| Mg | 60.2 | 37.2 | 54.3 | 32.6 | 58.1 | 43.1 | 30.0 | 56.4 | 30.9 | 28.3 | 33.0 | 25.6 | 19.5 | 21.6 | 24.4 | 8.2 | 29.9 | 8.4 |
| Fe** | 33.1 | 52.7 | 33.2 | 54.0 | 34.6 | 46.0 | 60.3 | 31.0 | 53.8 | 56.8 | 55.9 | 58.8 | 25.2 | 45.5 | 28.1 | 23.1 | 54.4 | 43.6 |

In TP and P types, pheno- and microphenocryst cores usually display the major Ti and Al contents, whereas the rims of the grains and microlites from P and PP show a gradual increase of hedenbergitic and/or acmitic molecules (Fig. 11).

Major element substitutions regard (Si, $Al^{IV}$)$_T$ and (Ti, $Fe^{3+}$, $Fe^{2+}$, Mg) M1, whereas M2 is essentially occupied by Ca+Na (0.99±0.01). Although Si+Al is usually higher than 2, some groundmass P microlites tend to show a small deficiency in the tetrahedral site, suggesting that some $Ti^{4+}$ may fill the tetrahedral site (up to 0.015; cf. P2/4 gm sample of Table 4).

### *Garnet*

Garnet, occurring both as phenocrysts and in the groundmass, contains $TiO_2$ 3.4-8.1 wt% (Table 5), andradite and grossularia about 69-84 and 8-21 mole%, respectively, and a minor pyralspitic component. $Fe^{3+}$/Ti ratio in octahedral site ranges from 2.4 to 6.2 (av. 4.08±1.09, according to the melanite variety). $Al^{IV}$/$Al^{VI}$ ratio shows a very wide variation, i.e. from 0.12 to 3.72, with the lowest values found in the peralkaline phonolites.

### *Opaques*

Magnetite is ubiquitous as phenocrysts and as a groundmass phase. Hematite is a common groundmass constituent of PP, but also mantles and/or replaces magnetite in the other rock-types.

Magnetite compositions vary in a narrow range, characterized by ulvöspinel content between 9 and

17.5 mol% and by low amounts of $Al_2O_3$ (<2.0%), MgO (<0.4%), NiO (<0.05%) and $Cr_2O_3$ (<0.4%) (Table 6). It should be noted that the MnO content increases from TP to PP.

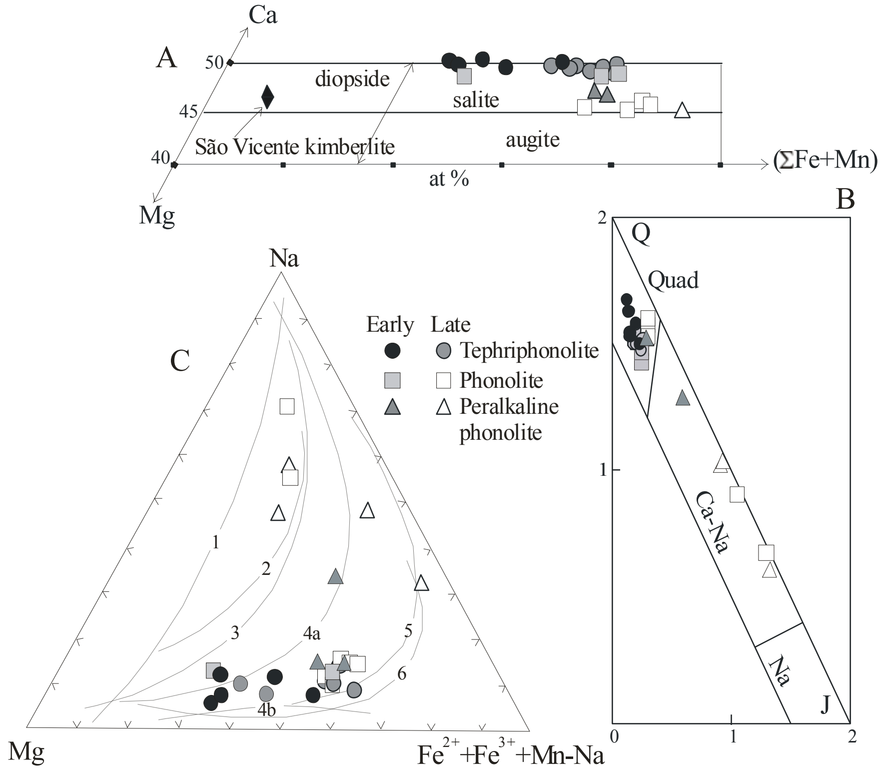


Fig. 11. Piratini clinopyroxenes plotted into classificatory diagrams. A: Ca-Mg-(∑Fe+Mn); B: Q(Wo, En, Fs)-Jd (Morimoto, 1988); C: Na-Mg-Fe** (Fe**=$Fe^{2+}$+$Fe^{3+}$+Mn-Na); compositional trends for clinopyroxenes from various Brazilian alkaline occurrences are shown. Data source: 1, Anitápolis (Furtado & Gomes, 1994); 2, Itapirapuã (Gomes *et al.*, 1970); 3, Banhadão (Ruberti, 1984); 4, Eastern Rio de Janeiro state: a, Tanguá-Rio Bonito-Itaúna-Morro de São João; b, Soarinho (Valença, 1980); 5, Ilha de Vitória (Motoki, 1986); 6, Tunas (Gomes *et al.*, 1987).

On the basis of ulvöspinel molecules of Ti-magnetite phenocrysts, a $fO_2$~$10^{-10}$ at 900-950°C may be inferred for the tephriphonolites (i.e. above the Ni-NiO buffer; cf. Buddington & Lindsley, 1964). These $fO_2$ and temperature values are substantially in consonance with the experimental results of Russel (1981).

On the whole, these data, along with the replacement of nepheline by cancrinite, suggest a significant $CO_2$ activity in the magmatic fluids and a moderate oxidizing environment.

Radiogenic isotopes

The average $^{87}Sr/^{86}Sr$ initial ratio for the whole Piratini suite is 0.70533±0.00031 (Barbieri *et al.*, 1987; Viero, 1998); $^{143}Nd/^{144}Nd$ initial ratios for two phonolites (Viero, 1998) are 0.51225 and 0.51230, respectively (samples 91 and 105 of Table 1). These values are in the same range of other Brazilian alkaline complexes (e.g. Lages district, Santa Catarina state; Scheibe *et al.*, in this volume), and even of the spatially associated high-Ti tholeiitic basalts from the southern Paraná Basin (Early Cretaceous; cf. Piccirillo & Melfi, 1988).

A significant crustal contamination for the Piratini magmas can be dismissed because of: 1) the lack of silica saturated to oversaturated rocks; 2) the high Sr contents of the phonolitic suite; 3) the high $^{87}Sr/^{86}Sr$ ratios of the crustal derived magmas from the Rio Grande do Sul state (e.g. Jaguarão Late Jurassic peraluminous dacites, $^{87}Sr/^{86}Sr$= 0.72234±0.00084, recalculated at 86.4 Ma; Vieira Jr., 1985), that precluded any possibility of modelling in terms of crustal contamination (Fig. 12A). Notably, "open system processes involve some type of magma interactions with silica-rich crustal materials via hydrothermal modification, crustal contamination combined with crystal fractionation (ACF) or anatectic crustal melts that either directly produce oversaturated rocks or mix with under-saturated magmas to form oversaturated ones".

Table 5. Representative analyses of garnets from the Piratini suite (data source: Barbieri *et al.*, 1987). Abbreviations as in Table 2. $Fe^{3+}$ and $Fe^{2+}$ calculated according to stoichiometry.

| | TP | TP | TP | TP | P | P | PP | PP |
|---|---|---|---|---|---|---|---|---|
| | Ph | gm | Ph | gm | Ph | gm | PhC | PhR |
| $SiO_2$ | 33.32 | 33.21 | 34.51 | 32.74 | 34.94 | 32.08 | 35.81 | 35.49 |
| $TiO_2$ | 5.09 | 5.66 | 3.40 | 5.79 | 3.92 | 8.10 | 3.98 | 4.67 |
| $Al_2O_3$ | 4.58 | 3.31 | 5.91 | 4.56 | 6.69 | 4.15 | 6.62 | 6.64 |
| $Fe_2O_3$ | 22.04 | 22.17 | 21.08 | 21.16 | 18.25 | 19.40 | 16.28 | 15.89 |
| FeO | 1.90 | 1.95 | 0.82 | 3.15 | 2.74 | 2.64 | 3.65 | 3.57 |
| MnO | 1.17 | 1.26 | 1.51 | 1.05 | 1.37 | 1.03 | 1.41 | 1.96 |
| MgO | 0.33 | 0.19 | 0.25 | 0.24 | 0.25 | 0.19 | 0.39 | 0.45 |
| CaO | 31.81 | 32.19 | 32.42 | 31.00 | 31.80 | 32.49 | 31.71 | 31.44 |
| Sum | 100.24 | 99.94 | 99.90 | 99.69 | 99.96 | 100.08 | 99.85 | 100.11 |
| | | | | | | | | |
| Si | 5.537 | 5.563 | 5.695 | 5.486 | 5.740 | 5.356 | 5.867 | 5.807 |
| $Al^{IV}$ | 0.463 | 0.437 | 0.305 | 0.514 | 0.260 | 0.644 | 0.133 | 0.193 |
| Sum | 6.000 | 6.000 | 6.000 | 6.000 | 6.000 | 6.000 | 6.000 | 6.000 |
| | | | | | | | | |
| $Al^{VI}$ | 0.434 | 0.216 | 0.844 | 0.387 | 1.035 | 0.173 | 1.145 | 1.087 |
| Ti | 0.636 | 0.713 | 0.422 | 0.730 | 0.484 | 1.017 | 0.490 | 0.575 |
| $Fe^{3+}$ | 2.756 | 2.795 | 2.617 | 2.668 | 2.256 | 2.437 | 2.007 | 1.956 |
| $Fe^{2+}$ | 0.264 | 0.273 | 0.113 | 0.441 | 0.376 | 0.369 | 0.500 | 0.489 |
| Mn | 0.165 | 0.179 | 0.211 | 0.149 | 0.191 | 0.146 | 0.196 | 0.272 |
| Mg | 0.082 | 0.047 | 0.062 | 0.060 | 0.061 | 0.047 | 0.095 | 0.110 |
| Ca | 5.663 | 5.777 | 5.731 | 5.565 | 5.597 | 5.811 | 5.566 | 5.511 |
| Sum | 10.000 | 10.000 | 10.000 | 10.000 | 10.000 | 10.000 | 10.000 | 10.000 |

Table 6. Representative chemical analyses of Ti-magnetites fom the Piratini suite (data source: Barbieri *et al.*, 1987 and unpublished data). $Fe^{3+}$ and $Fe^{2+}$ calculated on the ulvöspinel basis; a.f.u. on the basis of 32 (O).

| | TP | TP | TP | TP | P | P | PP |
|---|---|---|---|---|---|---|---|
| | Ph | Ph | Ph | gm | gm | gm | gm |
| $TiO_2$ | 4.31 | 4.57 | 6.05 | 5.08 | 3.08 | 5.16 | 5.22 |
| $Al_2O_3$ | 1.50 | 1.71 | 2.19 | 1.00 | 0.68 | 0.77 | 0.86 |
| $Fe_2O_3$ | 58.92 | 58.09 | 54.58 | 58.20 | 62.38 | 58.17 | 57.99 |
| FeO | 32.86 | 33.45 | 34.71 | 33.32 | 30.45 | 31.17 | 30.66 |
| MnO | 2.01 | 1.71 | 1.70 | 2.31 | 3.08 | 4.25 | 4.57 |
| MgO | 0.22 | 0.23 | 0.39 | 0.20 | 0.17 | 0.25 | 0.41 |
| CaO | 0.02 | 0.07 | 0.02 | 0.02 | 0.17 | 0.06 | 0.06 |
| NiO | | | 0.01 | | 0.05 | | |
| $Cr_2O_3$ | | 0.25 | 0.36 | | 0.01 | | 0.03 |
| Sum | 99.84 | 100.08 | 100.01 | 100.17 | 100.07 | 99.83 | 99.80 |
| | | | | | | | |
| Ti | 0.986 | 1.042 | 1.372 | 1.161 | 0.707 | 1.184 | 1.196 |
| Al | 0.538 | 0.610 | 0.778 | 0.358 | 0.245 | 0.277 | 0.309 |
| $Fe^{3+}$ | 13.490 | 13.247 | 12.390 | 13.311 | 14.332 | 13.356 | 13.292 |
| $Fe^{2+}$ | 8.362 | 8.476 | 8.756 | 8.469 | 7.773 | 7.952 | 7.811 |
| Mn | 0.518 | 0.439 | 0.434 | 0.594 | 0.797 | 1.098 | 1.179 |
| Mg | 0.100 | 0.022 | 0.175 | 0.091 | 0.077 | 0.114 | 0.186 |
| Ca | 0.006 | | 0.006 | 0.006 | 0.056 | 0.020 | 0.020 |
| Ni | | | 0.002 | | 0.012 | | |
| Cr | | 0.060 | 0.086 | 0.010 | 0.002 | | 0.007 |
| Sum | 24.000 | 24.000 | 23.999 | 24.000 | 24.000 | 24.001 | 24.000 |
| | | | | | | | |
| Mol% | | | | | | | |
| Ulv | 12.5 | 13.2 | 17.5 | 14.6 | 8.9 | 14.9 | 15.0 |

Regarding the εNd/εSr correlation, it should be noted that the Piratini phonolites fit the same fields of Late Cretaceous alkaline rocks from Lages and APIP (Alto Paranaíba Igneous Province of Gibson *et al.*, 1995), extending to the south of the South American plate the occurrence of Late Cretaceous alkaline rocks with the same isotopic imprint (Fig. 12B).

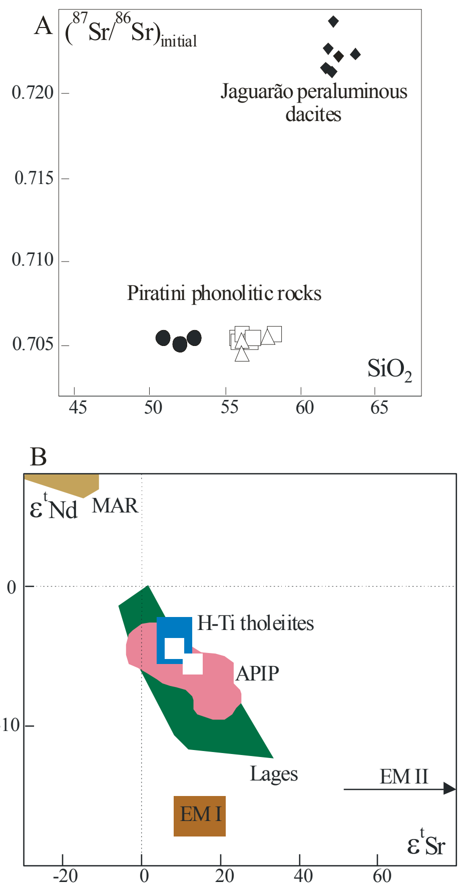


Fig. 12. A: $SiO_2$ vs. $^{87}Sr/^{86}Sr$ initial ratios of the phonolitic suite from Piratini. Symbols as in Fig. 11. B: Piratini rocks compared with subcoeval K-alkaline-carbonatitic material from Alto Paranaíba (APIP) and Lages district. Data source: Barbieri *et al.* (1987); Bizzi *et al.* (1994); Gibson *et al.* (1995); Traversa *et al.* (1996); Viero (1998); Scheibe *et al.* (in this volume). MAR, EMI and EMII components, as from Zindler & Hart (1986).

Finally, Nd model ages are 710 and 809 Ma, respectively, similar to the values obtained for APIP and Early Cretaceous Jacupiranga alkaline-carbonatitic complex, but different from those calculated for the Lages silicate rocks (c. 900 Ma) and for the Early Cretaceous Anitápolis alkaline-carbonatitic complex (c. 1300 Ma) (cf. Comin-Chiaramonti *et al.*, 1997, 2002). This suggests that different segments of the lithospheric mantle were variously metasomatized with the superimposed effects of the Archean, Transamazonian and Brasiliano cycles, and that mantle source heterogeneities were well established at least since Late Archean times (cf. Iacumin *et al.*, 2003).

## CONCLUDING REMARKS

Considering the geochemical trends, the mineral compositions and the presence of clinopyroxenite/gabbro enclaves in the tephriphonolites, Barbieri *et al.* (1987) inferred for the Piratini phonolitic suite a parental basanite magma which led tephriphonolites to evolve through crystal fractionation processes without appreciable crustal contamination. Moreover, mass balance calculations, relative to the less differentiated tephriphonolites (e.g. P11/3 sample of Table 1), are consistent with 31% fractionation of solid phases (9.1 clinopyroxene, 8.3 plagioclase, 8.2 alkali feldspar, 2.6 magnetite, 1.7 apatite and 1.1 garnet) to obtain the phonolites (e.g. P1/5 sample). The most evolved peralkaline phonolites (e.g. P7/1 sample) may be derived from the phonolites through 53% removal (equivalent to 36% of the initial tephriphonolite liquid) of solids involving prevailing alkali feldspar and clinopyroxene. Accordingly, Ba and Sr show a steep decrease in the most fractionated phonolites (cf. Fig. 8), owing to their high alkali feldspar/liquid partition coefficients.

However, the crystal fractionation processes are not in simple agreement with the REE distribution patterns that are characterized by the higher concentration of the tephriphonolites with respect to the phonolites, the latter showing a U-shaped MREE-HREE distribution and a slight negative Eu anomaly (cf. Fig. 9). To constrain the above patterns, it would be necessary to assume the fractionation of REE-rich phases (e.g. apatite and titanite that are ubiquitous microphenocrysts in the sampled rocks).

Rayleigh fractionation model (cf. Shaw, 1970; REE partition coefficients after Worner *et al.*, 1983, and Henderson, 1984) shows that the removal of titanite and apatite (1.1% and 1.4%, respectively, in addition to the prevailing sanidine removal) from the tephriphonolites is required to reach the observed variations in the REE patterns. The very low HREE abundance in some samples is believed to be consistent with an additional fractionation of 3% garnet.

On the other hand, the presence of $CO_2$-rich fluids is in consonance with the derivation of Piratini rocks from $CO_2$ enriched alkaline basic magmas (carbonatitic affinity?) generated by low melting degree in the subcontinental lithosphere (cf. Comin-Chiaramonti *et al.*, in this volume).

Finally, it should be noted that the Piratini suite straddle over the E-W Camaquã River Lineament, which represents an extension of the Porto Alegre Oceanic fracture system. As in the Santa Catarina state (cf. Scheibe *et al.*, in this volume), those tectonic lineaments lead to associate the Rio Grande do Sul alkaline magmatism with the dynamic expansion of the South Atlantic Ocean, as already suggested by Marsh (1973). The expansion process, as stressed by Piccirillo & Melfi (1988), manifests itself in the continent, probably through the transmission of tangent efforts, which are responsible for the development of transforming faults, as a result of thermal stress (Turcotte, 1974) and/or of the shift of the rotation poles of subplates (Franchetau & Pichon, 1972), leading to the reactivation of old fractures of intersialic dimensions, later converted into magmatic conducts (Viero *et al.*, 1995). If this is the case, the melting of variously metasomatized lithospheric mantle was primed by decompression processes.

## REFERENCES

Almeida, F.F.M. (1983). Relações tectônicas das rochas alcalinas mesozóicas da região meridional da plataforma Sul-Americana. *Revista Brasileira de Geociências* **13**, 139-158.

Almeida, F.F.M. & Hasui, Y. (1984). *O Pré-Cambriano do Brasil.* São Paulo: Edgard

Blücher Ltda., 378p.

Almeida, F.F.M. & Svisero, D.P. (1991). Structural setting and tectonic control of kimberlite and associated rocks of Brazil. *5th International Kimberlite Conference, Araxá, Annals,* pp.3-5.

Babinski, M., Chemale Jr., F., Van Schmus, W.R., Hartmann, L.A. & Silva, L.C. (1997). U-Pb and Sm-Nd geochronology of the Neoproterozoic Granitic-Gneissic Dom Feliciano Belt, Southern Brazil. *Journal of South American Earth Sciences* **10**, 263-274.

Baitelli, R. (1992). *Geocronologia por traços de fissão de maciços alcalinos do Brasil meridional.* M.Sc. Thesis, University of São Paulo, 204p.

Barbieri, M., Beccaluva, L., Brotzu, P., Conte, A., Garbarino, C., Gomes, C.B., Loss, E., Macciota, G., Morbidelli, L., Scheibe, L.F., Tamura, R.M. & Traversa, G. (1987). Petrological and geochemical studies of alkaline rocks from continental Brazil. 1. The phonolite suite from Piratini, RS. *Geochimica Brasiliensis* **1**, 109-138.

Barker, D.S. (1976). Phase relations in the system $NaAlSiO_4$-$SiO_2$-NaCl-$H_2O$ at 400-800°C and 1 kbar and petrological implications. *Journal of Geology* **84**, 97-106.

Binsted, N. (1981). The system Ab-Ne-NaCl-$H_2O$. *Progress in experimental petrology. NERC Publication Series* **D**, 34-35.

Bizzi, L.A. Witt, M.J., Smith, C.B., McDonald, I. & Armstrong, R.A. (1994). Isotope characteristics of the lithospheric mantle underlying the SW São Francisco craton, Brazil. *International Symposium on the Physics and Chemistry of the Upper Mantle, São Paulo, Invited Lectures*, pp. 227-256.

Boynton, W.V. (1984). Cosmochemistry of the Rare Earth Elements: meteorite studies. In: Henderson, P. (ed.) *Rare Earth Element geochemistry*. Amsterdam: Elsevier, pp. 63-114.

Brown, W.L. & Parson, I. (1981). Towards a more pratical two-feldspar geothermometer. *Contributions to Mineralogy and Petrology* **76**, 369-377.

Buddington, A.F. & Lindsley, D.H. (1964). Iron-titanium oxide minerals of syntetic equivalents. *Journal of Petrology* **5**, 310-357.

Caldasso, A.L.S. & Sander, A. (1994). O diatrema de Canguçú e rochas alcalinas associadas. *XXXVIII Congresso Brasileiro de Geologia, Camboriú,* Anais **3**, 59-60.

Chemale Jr., F. (2000). Evolução geológica do Escudo Sul-rio-grandense. In: Holz, M. & De Ros, L.F. (eds.) *Geologia do Rio Grande do Sul*. Porto Alegre, pp.13-52.

Chemale Jr., F., Hartmann, L.A. & Silva, L.C. (1995). Stratigraphy and tectonism of the Precambrian to Early Paleozoic units of Southern Brazil and Uruguay. *Acta Geológica Leopoldensia* **42**, 4-115.

Comin-Chiaramonti, P. & Gomes, C.B. (eds.) (1996). *Alkaline magmatism in central-eastern Paraguay. Relationships with coeval magmatism in Brazil.* São Paulo: Edusp/Fapesp, 464p.

Comin-Chiaramonti P., Cundari, A., Piccirillo, E.M., Gomes, C.B., Castorina,. F., Censi, P., De Min, A., Marzoli, A., Speziale, S. & Velázquez, V.F. (1997). Potassic and sodic igneous rocks from Eastern Paraguay: their origin from the lithospheric mantle and genetic relationships with the associated Paraná flood tholeiites. *Journal of Petrology* **38**, 495-528.

Comin-Chiaramonti, P., Gomes, C.B., Castorina, F., Censi, P., Antonini, P., Furtado S.M.A., Ruberti, E. & Scheibe, L.F. (2002). Geochemistry and geodynamic implications of the Anitápolis and Lages alkaline-carbonatite complexes, Santa Catarina State, Brazil. *Revista Brasileira de Geociências* **32**, 43-58.

Comin-Chiaramonti, P., Gomes, C.B., Marques, L.S., Censi, P., Ruberti, E. & Antonini, P. (in this volume). Carbonatites from southeastern Brazil: geochemistry, O-C, Sr-Nd-Pb isotopes and relationships with the magmatism from the Paraná-Angola-Namibia Province.

Deer, W.A., Howie, R.A. & Zussman, J. (1992). *An introduction to the rock-forming minerals*. Longman, 696p.

De La Roche, H., Leterrier, J., Grandclaude, P. & Marchal, M. (1980). A classification of volcanic and plutonic rocks using R1-R2 diagram and major-element analyses: its relationships with current nomenclature. *Chemical Geology* **29**, 183-210.

Ernesto, M., Marques, L.S., Piccirillo, E.M., Molina, E.C., Ussami, N., Comin-Chiaramonti, P. & Bellieni, G. (2002). Paraná magmatic province-Tristan da Cunha plume system: fixed versus mobile plume, petrogenetic considerations and alternative heat sources. *Journal of Volcanology and Geothermal Research* **118**, 15-36.

Fernandes, L.A.D., Tommasi, A., Porcher, C.C. (1990). Esboço estrutural de parte do Batólito Pelotas, região de Quitéria-Capivarita. *Acta Geológica Leopoldensia* **30**, 117-138.

Francheteau, J. & Le Pichon, X. (1972). Marginal fracture zones as structural framework of continental margins of the South Atlantic ocean. *Bulletin of American Association of Petroleum Geology* **56**, 991-1010.

Furtado, S.M..A. & Gomes, C.B. (1994). Caracterização química dos clinopiroxênios do maciço alcalino de Anitápolis, SC. *Geochimica Brasiliensis* **8**, 65-78.

Ghiorso, M.S. (1984). Activity composition relations in the ternary feldspars. *Contributions to Mineralogy and Petrology* **87**, 282-296.

Gibson, S.A., Thompson, R.N., Leonardos, O.H., Dickin, A.P. & Mitchell, J.G. (1995). The Late Cretaceous impact of the Trindade mantle plume: evidence from large-volume, mafic potassic magmatism in SE Brazil. *Journal of Petrology* **36**, 189-229.

Gomes, C.B., Barbieri, M., Beccaluva, L., Brotzu, P., Conte, A., Garbarino, C., Macciotta, G., Melluso, L., Morbidelli, L., Ruberti, E., Scheibe, L. F., Tamura, R.M. & Traversa, G. (1987). Petrological and geochemical studies of alkaline rocks from continental Brazil: the Tunas massif, state of Paraná. *Geochimica Brasiliensis* **1**, 201-234.

Gomes, C.B., Moro, S.L. & Dutra, C.V. (1970). Pyroxenes from the alkaline rocks of Itapirapuã, São Paulo, Brazil. *American Mineralogist* **55**, 224-240.

Hamilton, D.L. (1961). Nephelines as crystallization temperature indicators. *Journal of Geology* **69**, 321-329.

Hamilton, D.L. & Mackenzie, W.S. (1965). Phase-equilibrium studies in the system $NaAlSiO_4$ (nepheline)-$KAlSiO_4$ (kalsilite)-$SiO_2$-$H_2O$. *Mineralogical Magazine* **34**, 214-231.

Heflin, M. *et al.* (2001). http://sideshow.jpl.nasa.gov/mbh/series.html

Henderson, P. (1984). *Rare Earth Element geochemistry. Development in geochemistry*, Amsterdam: Elsevier, **2**, 510p.

Iacumin, M., De Min, A., Piccirillo, E.M. & Bellieni, G. (2003). Source mantle heterogeneity and its role in the genesis of Late Archean-Proterozoic (2.7-1.0 Ga) and Mesozoic (200 and 130 Ma) tholeiitic magmatism in the South American Platform. *Earth-Science Reviews*, **62**, 365-397.

Kudo, A.M. & Weill, D.F. (1970). An igneous plagioclase thermometer. *Contributions to Mineralogy and Petrology* **26**, 52-65.

Le Maitre, R.W. (1989). *A classification of igneous rocks and glossary of terms*. Oxford: Blackwell Scientific Publications, 193p.

Marsh, J.S. (1973). Relationships between transform directions and alkaline igneous rock lineaments in Africa and South America. *Earth and Planetary Science Letters* **18**, 317-323.

Mathez, E.A. (1973). Refinement of the Kudo-Weill plagioclase thermometer and its application to basaltic rocks. *Contributions to Mineralogy and Petrology* **41**, 61-72.

Morimoto, N. (1988). Nomenclature of pyroxenes. *Mineralogical Magazine* **52**, 535-550.

Motoki, A. (1986). *Geologia e petrologia do maciço alcalino da Ilha de Vitória, São Paulo*. Ph.D. Thesis, University of São Paulo, 254p.

Nixon, P.H., Boyd, F.R. & Lee, D.C. (1987). Western Australia xenoliths from kimberlites and lamproites. In: Nixon, P.H. (ed.) *Mantle xenoliths.* J. Wiley & Sons, pp. 281-286.

Philipp, R.P. (1998). *Evolução geológica e tectônica do Batólito Pelotas no Rio Grande do Sul.* Ph.D. Thesis, University of São Paulo, 379p.

Philipp, R.P., Machado, R., Nardi, L.V.S. & Lafon, J.M. (2002). O magmatismo granítico Neoproterozóico do Batólito Pelotas no sul do Brasil: novos dados e revisão da geocronologia regional. *Revista Brasileira de Geociências,* **32**, 277-290.

Piccirillo, E.M. & Melfi, A.J. (1988). *The Mesozoic flood volcanism from the Paraná basin (Brazil). Petrogenetic and geophysical aspects.* São Paulo: IAG-USP, 600p.

Ribeiro, M. (1970). Geologia da Folha Bom Jardim, Rio Grande do Sul. *Boletim da Divisão de Geologia e Mineralogia* **247**, 1-142.

Ribeiro, M. (1978). Structural setting of some alkaline pipes in the Rio Grande do Sul Shield. *International Symposium on Carbonatites, Poços de Caldas* **1**, 171-175.

Ruberti, E. (1984). *Petrologia do maciço alcalino de Banhadão, PR.* Ph.D. Thesis, University of São Paulo, 249p.

Russel, D.G. (1981). Estimation of FeO and $Fe^{2+}$ nor $Fe^{3+}$ in glasses from experimental charges. *Progress in Experimental Petrology, Edimburgh* **4**, 91-94.

Seck, H.A. (1971). Koexistierende alkalifeldspate und plagioclase im system $NaAlSi_3O_8$-$KAlSi_3O_8$-$CaAl_2Si_2O_8$-$H_2O$ bei temperaturen von 650°C bis 900°C. *Neues Jahrbuch für Mineralogie Abhandlungen* **115**, 315-395.

Sharp, Z.D., Helfrich, G.R., Bohlen, S.R. & Essene, E.J. (1989). The stability of sodalite in the system $NaAlSiO_4$-NaCl. *Geochimica et Cosmochimica Acta* **53**, 1943-1954.

Shaw, D.M. (1970). Trace elements during anatexis. *Geochimica et Cosmochimica Acta* **34**, 237-241.

Scheibe, L.F., Furtado S.M.A., Comin-Chiaramonti, P. & Gomes, C.B. (in this volume). Cretaceous alkaline magmatism from Santa Catarina state, Southern Brazil.

Shobbenhaus, C., Campos, D.A., Derze, G.R. & Asmus, H.A. (eds.) (1984). *Geologia do Brasil. Texto explicativo do mapa geológico do Brasil e da área oceânica adjacente incluindo depósitos minerais. Escala 1:2.500.000.* Departamento Nacional de Produção Mineral, 501p.

Streckeisen, A. (1978). IUGS Subcommission on the syestematics of igneous rocks. Classification and nomenclature of volcanic rocks, lamprophyres, carbonatites and melilite rocks. Reccomendations and suggestions. *Neues Jahrbuch für Mineralogie Abhandlungen* **143**, 1-14.

Sun, S.S. & McDonough, W.F. (1989). Chemical and isotopic systematics of oceanic basalts. In: Saunders, D. & Norry, M.J. (eds.) *Magmatism in the ocean basins*. *Geological Society of London, Special Publication* **42**, pp. 313-345.

Svisero, D.P. & Chieregati, L.A. (1991). Contexto geológico de kimberlitos, lamproítos e ocorrências diamantíferas do Brasil. *Boletim do Instituto de Geociências da USP, Publicação Especial* **9**, 75-81.

Tedesco, M.A. & Robaina, L.E.S. (1991). Caracterização geoquímica de piroxênios e granadas da brecha kimberlítica de São Vicente, RS. *3° Congresso Brasileiro de Geoquímica/1° Congresso de Geoquímica dos Países de Língua Portuguesa, São Paulo, Anais* **1**, 707-710.

Traversa, G., Barbieri, M. Beccaluva, L., Coltorti, M., Conte, A.M., Garbarino, C., Gomes, C.B., Macciota, G., Morbidelli, L., Ronca, S. & Scheibe, L.F. (1996). Mantle sources and differentiation of alkaline magmatic suite of Lages, Santa Catarina, Brazil. *European Journal of Mineralogy* **8**, 193-208.

Turcotte, D.L. (1974). Are transform faults thermal contraction cracks? *Journal of Geophysical Research* **79**, 2573-2577.

UFRGS (1995). Projeto Arroio da Bica, mapa geológico 1:50.000. Trabalho de Conclusão do Curso de Geologia do Instituto de Geociências–UFRGS, Porto Alegre.

Valença, J.G. (1980). *Geology, petrography and petrogenesis of some alkaline igneous complexes of Rio de Janeiro State, Brazil.* Ph.D. Thesis, University of Western Ontario, 248p.

Vieira Jr., N. (1985). *Petrologia e geoquímica do vulcanismo mesozóico de Jaguarão, RS.* M.Sc. Thesis, Federal University of Rio Grande do Sul, 136p.

Viero, A.P. (1998). *O magmatismo máfico alcalino Mesozóico do Rio Grande do Sul.* Ph.D. Thesis, Federal University of Rio Grande do Sul, 249p.

Viero, A.P., Tedesco, M.A. & Roisenberg, A. (1995). O papel das falhas transformantes no controle do magmatismo alcalino Mesozóico do RS. *5º Simpósio Nacional de Estudos Tectônicos, Gramado, Anais,* pp. 219-221.

Worner, G., Beusen, J.M., Duchateau, N., Gijbells, R., Schminke, H.U. (1983). Trace element abundances and mineral/melt distribution coefficients in phonolites from the Laacher see Volcano (Germany). *Contributions to Mineralogy and Petrology* **84**, 152-173.

Zindler, A. & Hart, S.R. (1986). Chemical geodynamics. *Annual Review of Earth and Planetary Sciences* **14**, 493-571.

*Mesozoic to Cenozoic Alkaline Magmatism in the Brazilian Platform*
*Comin-Chiaramonti, P. & Gomes, C.B. (eds.)*
*Edusp/Fapesp, São Paulo, pp. 573-590, 2005*

# THE EARLY CRETACEOUS VALLE CHICO COMPLEX (MARISCALA, SE URUGUAY)

*E. Ruberti, C.B. Gomes, C.C.G. Tassinari, P. Antonini and P. Comin-Chiaramonti*

*The Early Cretaceous (128 Ma) igneous complex of Valle Chico (VC), Mariscala, southeastern Uruguay, intrudes Precambrian to Mesozoic terrains and it is made of felsic intrusive rocks and subordinate volcanic rocks and dykes that crop out over an area of about 250 km$^2$. The intrusive rocks range from monzonite to granite. The volcanic rocks and the dykes range from latite to rhyolite. The rocks are both metaluminous (two feldspars variants) and peralkaline (one feldspar variants) and usually fit the A-type granite field. The one feldspar variants plot mainly on the comenditic trachyte and pantellerite fields, respectively. The mineralogical assemblages strongly suggest an (mild) alkaline affinity, also for the metaluminous variants. Primitive mantle-normalized multi-elemental plots show fractionated concentration of incompatible trace elements: in general, the rock-types display strong negative peaks at Sr and Ti, along with frequent positive peaks at Nb and Nd. The Eu/Eu* negative anomalies range from 0.78 (syenites and trachytes) to 0.09 (granites and rhyolites), suggesting increasing contribution of feldspars in the fractionating assemblages. The Arequita peralkaline rhyolites (pantellerites) are very similar, in terms of petrographical and geochemical characteristics, to the Valle Chico one feldspar rhyolites and may be related to the same emission center(s), but at the present time the relationships between the two suites are still unclear. Comparisons with other A-type suites and other felsic variants in and around the Paraná-Etendeka Igneous Province indicate that the VC rocks are quite different in their geochemistry and isotope systematics with respect to the Lavalleja, Aiguá, Palmas and Jaguarão suites (eastern Uruguay and Rio Grande do Sul, Brazil) and with respect to the Damaraland (Namibia), Choiyoi (Argentina), Velasco (Bolivia), Itatiaia and São Sebastião (Serra do Mar Province, southeastern Brazil) complexes. Only the Ponta do Morro intrusion (Mato Grosso) fits the geochemical trends of the VC complex, but it is different since it evolves along the QFM buffer. The trace element modelling and Sr-Nd systematics suggest that the VC peralkaline rocks cannot have been derived from the metaluminous variants through simple fractional crystallization, but both the two suites may be the result of partial melting of distinct crustal melts at different levels. Alternatively, partial melting of underplated basaltic compositions plus differential AFC processes may have produced the observed VC rocks. The Nd-model ages seem to support the latter interpretation, with overprinting of different Proterozoic events that concern the investigated area. In this context, the Valle Chico alkaline magmatism appears linked to decompressive events along extensional lineaments rather than related to mantle plume head (e.g. Tristan da Cunha plume).*

## INTRODUCTION

The Paraná-Etendeka Igneous Province (PEIP) forms one of the largest continental flood basalt provinces (Piccirillo & Melfi, 1988; Hawkesworth *et al.*, 1999; Comin-Chiaramonti *et al.*, 1999). Over 800.000 km$^3$ of prevailing basaltic tholeiites and subordinate rhyodacitic to rhyolitic sequences were erupted predominantly in the 135-130 Ma span (Piccirillo *et al.*, 1987, 1988; Renne *et al.*, 1992, 1997; Turner *et al*., 1994; Stewart *et al*., 1996) in response to precursor and initial stages of the South Atlantic Ocean opening. In addition, small volume Early and Late Cretaceous alkaline districts are widely scattered in and around the PEIP in Brazil, Bolivia, Paraguay, Uruguay, Angola and Namibia (Almeida, 1983; Alberti *et al*., 1999; Comin-Chiaramonti *et al*., 1999; Almeida *et al*., 2000).

In Uruguay, Early Cretaceous magmatic rocks occur mainly in two regions, i.e. in the northwestern part of the country where the PEIP flood basalts cover an area of about 20.000 $km^2$, and in the eastern one where Mesozoic magmatism extends from the Santa Lucia to the Laguna Merín basins (Bossi *et al*., 2001). In the latter region, outcrops of bimodal basaltic and acid sequences, intruded by the Valle Chico (Mariscala) syenites and felsic dykes, spread over an area of about 10.000 $km^2$ (Turner *et al*., 1999; Kirstein *et al*., 2000). Ar-Ar ages, 132-133 Ma for the basaltic sequences and 128-132 Ma for the overlying felsic rocks (Stewart *et al*., 1996; Féraud *et al*., 1999; Turner *et al*., 1999; Muzio & Artur, 1999), overlap those of the PEIP.

Notably, dacitic stratoid flows up to 50 m thick (143-144 Ma, K-Ar whole-rock; cf. Vieira, 1986) are exposed over about 160 $km^2$ near to the Jaguarão town (Fig. 1), at the Brazil-Uruguay eastern border. This magmatism, which predates the opening of the Atlantic Ocean at the Uruguayan latitudes (cf. Piccirillo & Melfi, 1988) and shows cordierite+orthopyroxene as liquidus phases, indicating P-T conditions of 920°C and •2 kb, respectively, was interpreted as the partial melting product of a S-granitic upper crust (Vieira, 1986; Comin-Chiaramonti, 2000).

The Valle Chico (VC, also referred in the literature as Mariscala) syenitic-granitic complex and associated felsic rock-types, lying between the localities of Mariscala and Colón (Lavalleja department), will be reviewed in detail from a mineralogical, petrographical and geochemical point of view (cf. Balestra, 1985; Kirstein *et al*., 2000; Muzio, 2000; Muzio *et al*., 2002; Lustrino *et al*., 2002, 2005, Comin-Chiaramonti, unpublished data) in order to better characterize the felsic magmatism in the southernmost part of the PEIP. In particular, a comparison with the Lavalleja and Aiguá series (Kirstein *et al*., 2000) will allow to verify if the VC may be also considered as the emission center for the former rock-types.

A comparison with similar felsic alkaline rocks in and around the PEIP will be also presented, i.e. Velasco complexes (Bolivia), Ponta do Morro (Mato Grosso, Brazil), Itatiaia and São Sebastião (Serra do Mar, Brazil), Damaraland complexes (Namibia) and Choiyoi Group (Argentina). In fact, the spatial association between subcoeval tholeiitic and acid and felsic alkaline bodies is not unusual in the Paraná Basin, e.g. Guayaquil tholeiitic sill and Aguapety Portón alkaline intrusion in Paraguay (Bellieni *et al*., 1986a; Comin-Chiaramonti & Gomes, 1996) and layered tholeiitic gabbro and alkaline stocks in the São Sebastião island in Brazil (Enrich *et al*., in this volume).

## GENERAL BACKGROUND

Uruguay represents part of the southern and northeastern end of the Brazilian and Rio de La Plata shields, respectively (Almeida *et al*., 2000).

The Uruguayan portions of these shields have ages spanning from the Paleoarchean to Neoproterozoic times and are represented by three main geotectonic units (Hartmann *et al*., 2002; Mallmann *et al*., 2003, and therein references), i.e. Piedra Alta (PAT) and Nico Pérez (NPT) terrains and Dom Feliciano Belt (DFB; Fig. 1). Large areas of granitic intrusions (0.5 up to >2.2 Ga) are found in all the geotectonic units (cf. Preciozzi & Bourne, 1993; Muzio & Artur, 1999, and therein references). PAT and NPT make up together the Rio de La Plata Craton in Uruguay, whereas DFB corresponds to the southernmost extension of the Brasiliano cycle of Brazil (cf. Mallmann *et al*., 2003). Paleo-proterozoic (1.86 Ga; Florida region) and Neo-proterozoic (~0.7 Ga; Nico Pérez and Treinta y Tres regions) dyke swarms intrude the Piedra Alta and Nico Pérez

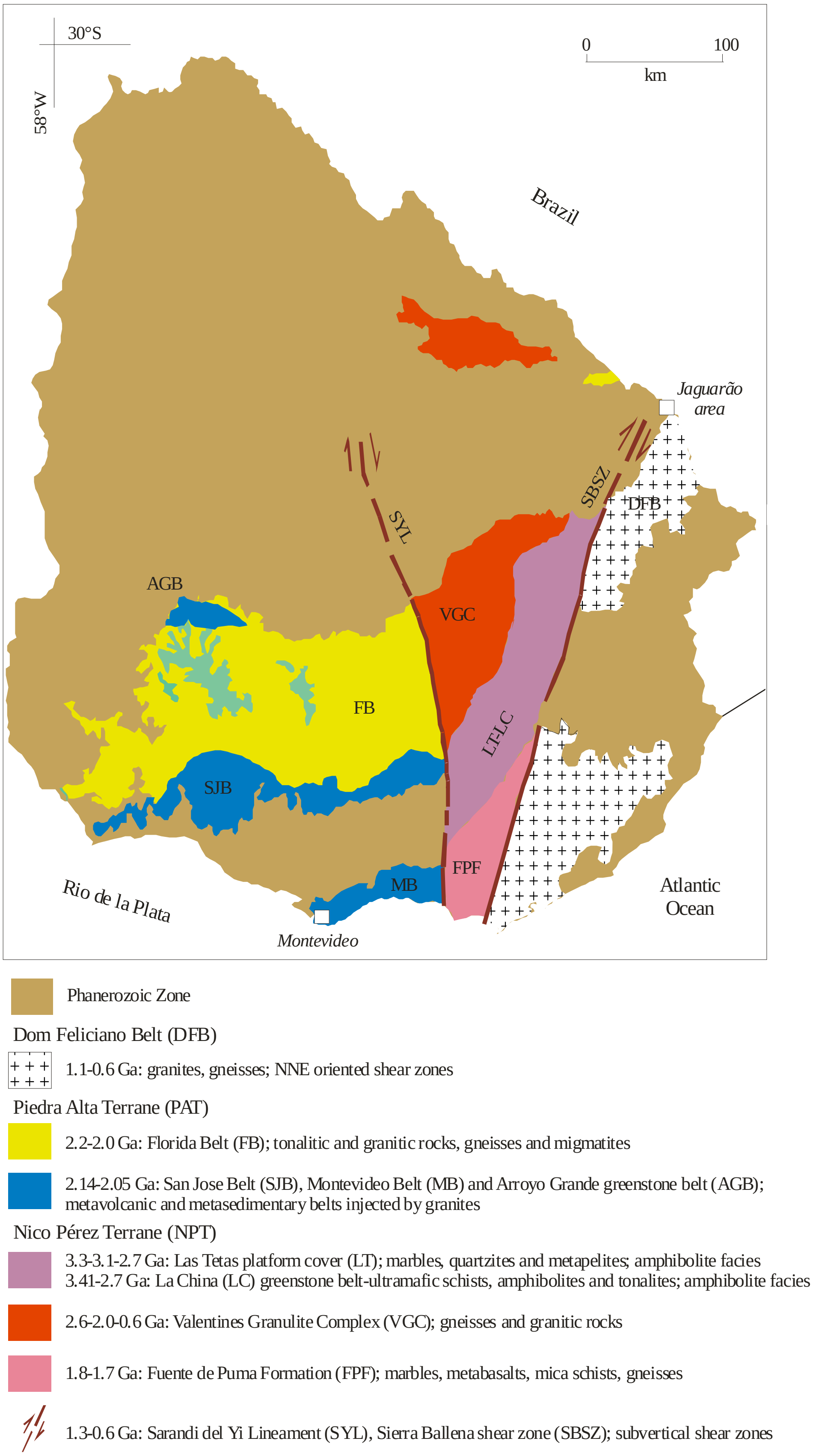


Fig. 1. Major geotectonic units of Uruguay (after Bossi *et al*., 2001; Hartmann *et al*., 2002; Mallmann *et al*., 2003, modified).

terrains, respectively (Preciozzi & Bourne, 1993; Mazzucchelli *et al.*, 1995; Girardi *et al.*, 1996). The Florida and Nico Pérez dykes are basalts, basaltic andesites and andesites of tholeiitic affinity, whereas the Treinta y Tres dykes consist of transitional to alkaline basalts. According to Mazzucchelli *et al.* (1995), the geochemical and isotopic characteristics are on the whole similar to those of the Mesozoic basalts related to the Gondwana break-up, supporting the view that the latter rocks have derived from a heterogeneous lithospheric source which recorded Proterozoic enrichment processes.

The Mesozoic magmatism from eastern Uruguay, extending from Santa Lucía to Laguna Merín basins (Figs. 2A, B), rests along a N60°E-trending system of faulted basement rocks (Riccardi, 1988; Bossi *et al.*, 2001), and crops out in a region characterized by an important positive gravity anomaly (about +30 to +90 mgal). The latter, following Turner *et al.* (1999), reflects an associated large mid-crustal intrusive mafic body. The Mesozoic magmatic rocks from this region are bimodal in composition, i.e. tholeiitic basalts and andesites, and trachytes, dacites and rhyolites.

The mafic lavas have general characteristics similar to the low-Ti tholeiites from the southern PEIP (Treinta y Tres magma types of Kirstein *et al.*, 2000; e.g. strong Nb-Ta negative anomalies), but

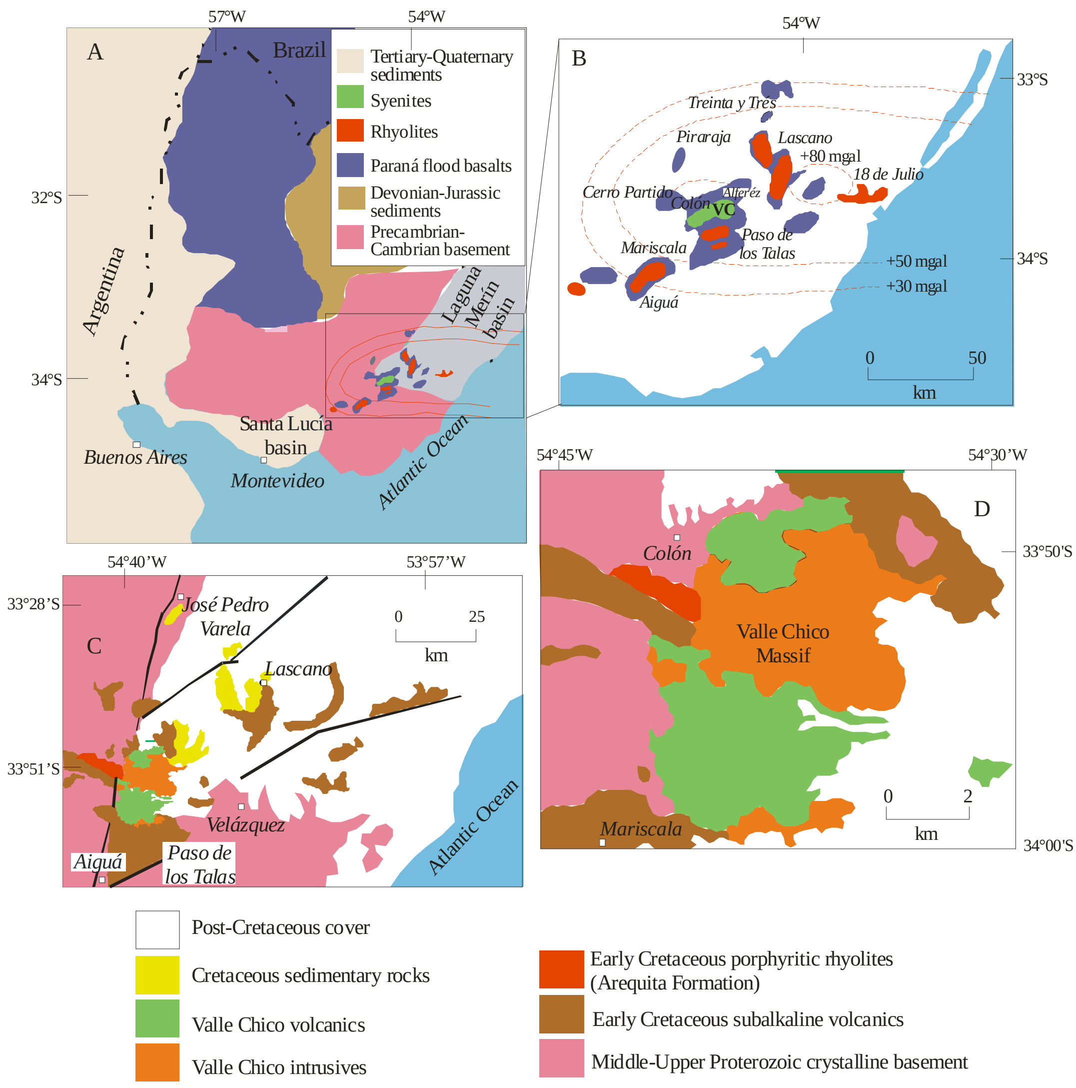


Fig. 2. Simplified geological map of Uruguay (A, after Bossi *et al.,* 2001); location of the Valle Chico igneous complex, eastern Uruguay, in relation with other igneous outcrops and gravity positive anomalies (B, after Turner *et al.*, 1999; Rossello *et al.*, 2000); geological sketch map of northeastern Uruguay (C, after Rossello *et al.*, 2000, modified) and geological sketch-map of the Valle Chico massif (D, after Muzio, 2000).

some types (Santa Lucía magma type) display transitional traits. In particular, the 92-U12 sample of Turner *et al.* (1999; Aiguá locality of Fig. 2B) is a ne-normative trachybasalt without the Nb-Ta negative anomaly which is common to all the tholeiitic products of the Paraná Basin (cf. Comin-Chiaramonti *et al*., 1999, and therein references).

Two chemically distinct felsic series, overlying the mafic lavas, were described by Kirstein *et al*. (2000), i.e. Lavalleja and Aiguá Series (not better defined field relationships) characterized by high (ca. 3-20) and low Ti/Zr (ca. 1-7) ratios, respectively.

An intrusive syenitic body associated with trachytic volcanics and ring trachyte-rhyolite dykes ("Valle Chico suite"; Bossi & Navarro, 1991) is exposed in the region comprising Cerro Partido, Alferéz, Paso de los Talas and Mariscala villages, and it is surrounded by ~132 Ma old basaltic flows (Figs. 2B, C, D). Geochronological data for the VC rocks span from 131 Ma (Stewart *et al.*, 1996; $^{40}Ar/^{39}Ar$) to 128 Ma (Muzio *et al.*, 1999; U/Pb on zircon fractions). Porphyritic rhyolites (Arequita Formation; cf. Fig. 2D) partially overlap the VC massif. Therefore, the VC igneous rocks can be considered roughly coeval, but of more recent age in comparison with the PEIP continental flood basalts at the Uruguayan latitudes.

## CLASSIFICATION OF THE VALLE CHICO ROCKS

The VC igneous rocks (Muzio, 2000) are both plutonic (~44% of the outcrops; average grain size generally >10 mm) and volcanic (~54% of the outcrops, average groundmass grain size <1 mm). The dyke swarms (~2% of the outcrops) have intermediate grain size and thereafter are grouped into the volcanic rocks. A striking feature is a bi-modal distribution of one feldspar and two feldspars rocks, i.e. hypersolvus and subsolvus variants, respectively.

Taking the classification according to modal composition (Fig. 3; QAPF diagram of Streckeisen, 1978, in Le Maitre, 2000), the plutonic rocks range

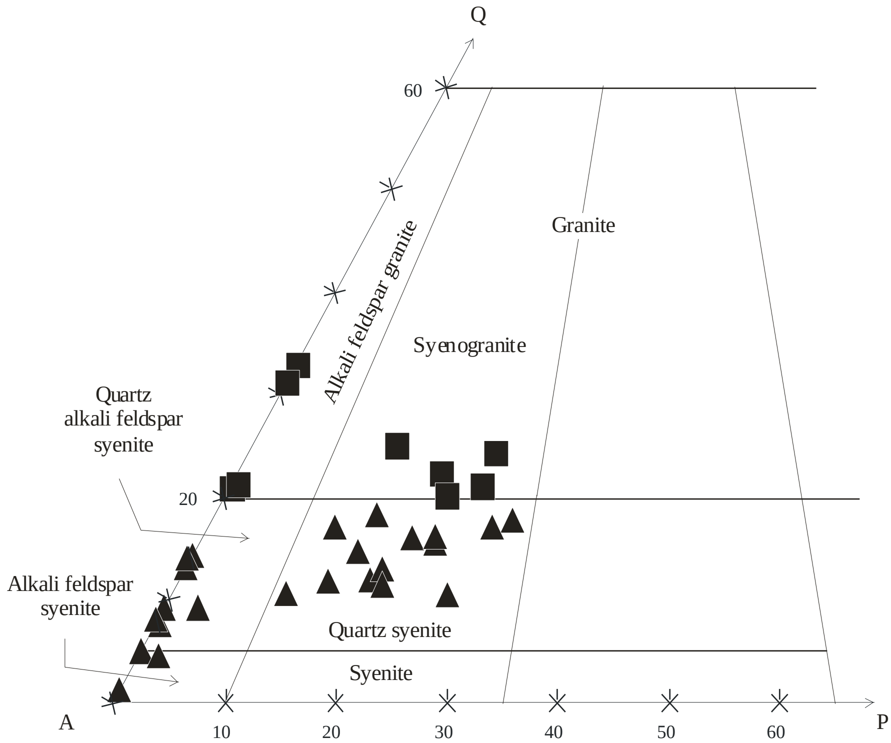


Fig. 3. Classification of the Valle Chico plutonic rocks on the Q-A-P Streckeisen's diagram (Le Maitre, 2000). Data source: Balestra (1985), Muzio (2000) and Comin-Chiaramonti (unpublished analyses).

from alkali feldspar syenites to alkali feldspar granites (one feldspar variants), and from quartz syenites to granites (two feldspars variants).

The volcanic rocks are classified as latites, trachytes and rhyolites according to the total alkalies-silica diagram (TAS, Le Maitre, 2000; Fig. 4; cf. also Table 1). Both two feldspars and one feldspar variants are well distinct if compared with the Palmas rock-types and with the Jaguarão lavas.

Notably, some two feldspars syenites plot in the latite (monzonite) field, partially fitting the Lavalleja series (Fig. 4). The hypersolvus variants lie over the Aiguá series, being peralkaline, i.e. with agpaitic index (A.I.) higher than the unity (inset A of Fig. 4),

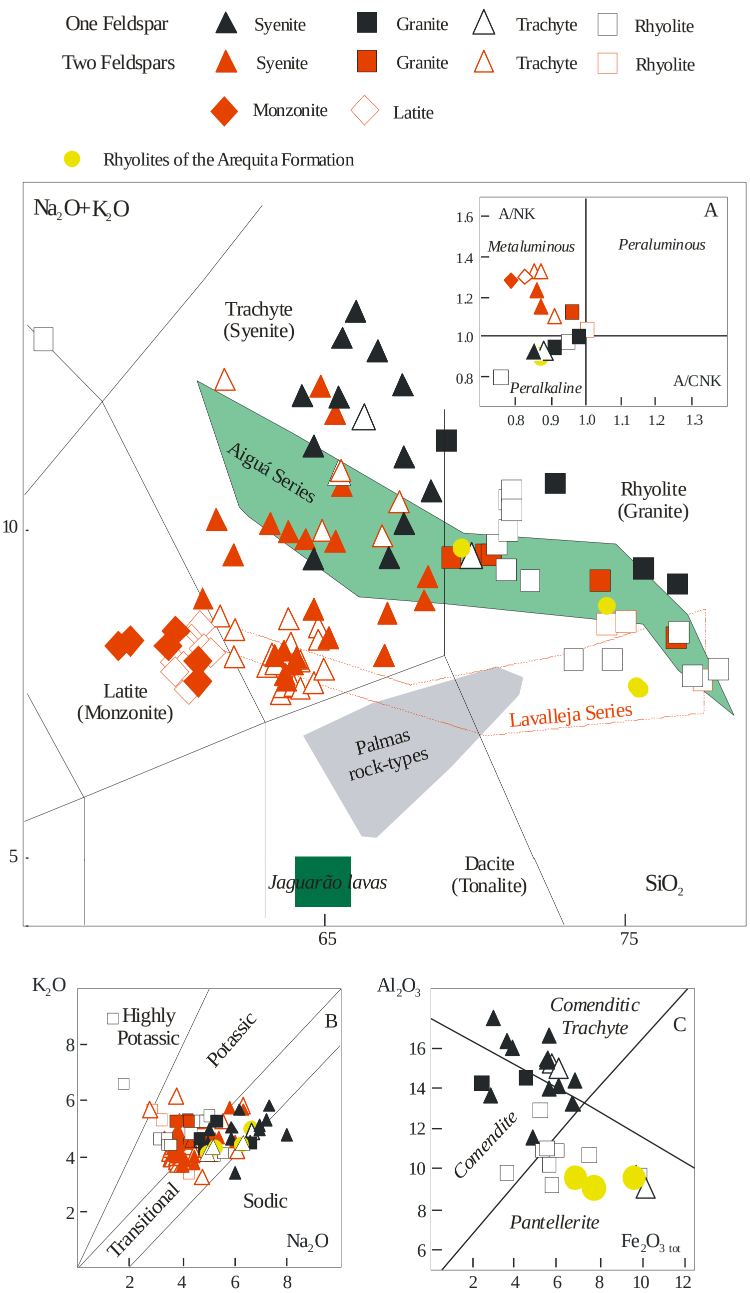


Fig. 4. TAS (total alkalies vs. silica, in wt%, cf. Le Maitre, 2000) for the Valle Chico volcanics and related plutonic rocks (data source: Balestra, 1985; Muzio, 2000; Muzio *et al.*, 2002; Lustrino *et al.*, 2005; Comin-Chiaramonti, unpublished analyses). The compositional fields for the coeval felsic rocks from eastern Uruguay and for the Palmas rock-types are plotted for comparison (data source: Balestra, 1985; Vieira, 1986; Bellieni *et al.*, 1986b, 1988; Piccirillo & Melfi, 1988; Garland *et al.*, 1995; Kirstein *et al.*, 2000). Insets: A) A/CNK, $Al_2O_3/(CaO+Na_2O+K_2O)$ vs. A/NK, $Al_2O_3/(Na_2O+K_2O)$ molar ratios; B) $Na_2O$ vs. $K_2O$ (cf. Comin-Chiaramonti & Gomes, 1996); C, classification grid for peralkaline rocks (Macdonald, 1974), total Fe (as $Fe_2O_3$) vs. $Al_2O_3$.

Table 1. Major (wt%) and trace elements content (ppm) and CIPW norms of Valle Chico igneous rocks, average and selected compositions. N, number of samples; in brackets, standard deviations. 1-9, two feldspars variants; 10-16, one feldspar variants. Data source: Kirstein *et al.* (2000), Muzio (2000), Muzio *et al.* (2002), Lustrino *et al.* (2005) and Comin-Chiaramonti (unpublished data). A.I., agpaitic index = molar ($Na_2O$+$K_2O$)/$Al_2O_3$; mg# = MgO/(MgO+FeO). Additional analyses, i.e. Aiguá 92-U12 trachybasalt, Arequita rhyolites and Jaguarão rhyodacites are from Kirstein *et al.* (2000), Muzio *et al.* (2002) and Comin-Chiaramonti (2000), respectively.

| Two feldspar variants | 1 Monzonite (N=6) | 2 Latite (N=10) | 3 Syenite (N=10) | 4 Syenite (N=10) | 5 Trachyte (N=9) | 6 Trachyte (N=9) | 7 Trachyte (N=4) | 8 Granite (N=6) | 9 Rhyolite (N=3) | 10 Syenite (N=6) |
|---|---|---|---|---|---|---|---|---|---|---|
| wt% | | | | | | | | | | |
| $SiO_2$ | 60.04 (1.09) | 60.56 (0.37) | 62.33 (0.89) | 65.89 (1.19) | 62.03 (0.30) | 63.49 (0.36) | 65.34 (1.01) | 71.85 (1.90) | 74.47 (1.67) | 64.67 (0.68) |
| $TiO_2$ | 1.41 (0.07) | 1.32 (0.07) | 1.11 (0.16) | 0.82 (0.11) | 1.19 (0.05) | 1.12 (0.08) | 0.61 (0.15) | 0.43 (0.19) | 0.27 (0.09) | 0.51 (0.19) |
| $Al_2O_3$ | 14.66 (0.51) | 14.19 (0.21) | 14.56 (0.70) | 14.95 (0.97) | 13.85 (0.21) | 13.89 (0.12) | 15.60 (0.78) | 13.77 (1.16) | 11.06 (0.12) | 15.39 (1.38) |
| $Fe_2O_{3tot}$ | 8.96 (0.65) | 9.17 (0.33) | 7.77 (0.59) | 5.39 (0.84) | 7.95 (0.37) | 7.45 (0.27) | 4.70 (0.76) | 3.14 (0.76) | 4.81 (1.10) | 5.88 (1.96) |
| MnO | 0.18 (0.01) | 0.19 (0.01) | 0.16 (0.02) | 0.12 (0.01) | 0.15 (0.01) | 0.14 (0.01) | 0.11 (0.05) | 0.06 (0.04) | 0.08 (0.04) | 0.15 (0.06) |
| MgO | 1.63 (0.22) | 1.44 (0.24) | 1.38 (0.61) | 0.95 (0.41) | 1.85 (0.16) | 1.72 (0.25) | 0.63 (0.17) | 0.36 (0.19) | 0.06 (0.03) | 0.18 (0.17) |
| CaO | 3.88 (0.28) | 3.47 (0.38) | 2.84 (0.56) | 2.24 (0.65) | 3.19 (0.18) | 3.03 (0.22) | 1.59 (0.35) | 1.12 (0.47) | 0.13 (0.07) | 0.99 (0.49) |
| $Na_2O$ | 4.27 (0.32) | 3.81 (0.15) | 4.22 (0.72) | 4.78 (0.98) | 3.82 (0.44) | 3.56 (0.40) | 5.67 (0.49) | 4.33 (0.55) | 3.36 (0.74) | 6.59 (1.03) |
| $K_2O$ | 4.04 (0.29) | 4.26 (0.24) | 4.44 (0.47) | 4.77 (0.57) | 3.85 (0.30) | 4.22 (0.64) | 4.53 (0.44) | 4.80 (0.53) | 4.72 (1.20) | 4.99 (0.58) |
| $P_2O_5$ | 0.51 (0.05) | 0.57 (0.07) | 0.43 (0.13) | 0.29 (0.19) | 0.51 (0.04) | 0.53 (0.07) | 0.18 (0.06) | 0.11 (0.05) | 0.01 (0.01) | 0.08 (0.06) |
| LOI | 0.33 (0.15) | 1.45 (0.92) | 0.76 (0.59) | 0.72 (0.29) | 1.61 (0.64) | 0.85 (0.28) | 1.04 (0.39) | 1.57 (0.06) | 1.04 (0.10) | 0.57 (0.29) |
| Sum | 99.91 | 100.43 | 100.00 | 100.92 | 100.00 | 100.00 | 100.00 | 100.54 | 100.01 | 100.00 |
| | | | | | | | | | | |
| $Fe_2O_3$/FeO | 0.35 | 0.35 | 0.5 | 0.5 | 0.8 | 0.5 | 0.9 | 0.5 | 0.9 | 0.3 |
| mg# | 0.30 | 0.30 | 0.34 | 0.34 | 0.44 | 0.40 | 0.32 | 0.25 | 0.04 | 0.07 |
| | | | | | | | | | | |
| ppm | | | | | | | | | | |
| Rb | 121(19) | 123(14) | 132(19) | 140(18) | 123(17) | 137(26) | 132(13) | 170(34) | 261(72) | 130(12) |
| Ba | 1286(46) | 1457(67) | 1432(136) | 1195(182) | 1412(88) | 1371(92) | 1207(323) | 820(305) | 47(13) | 516(366) |
| U | 2.4(0.3) | 2.7(0.1) | 2.8(0.6) | 3.2(0.6) | 2.8(0.6) | 3.1(0.8) | 4.7(0.9) | 10.8(3.2) | 9.8(3.4) | 7.5(2.1) |
| Th | 9.5(1.3) | 10.8(0.6) | 11.2(2.4) | 12.9(2.7) | 10.7(1.3) | 11.8(1.5) | 18.0(2.1) | 14.1(5.6) | 41.3(12.0) | 14.2(1.8) |
| Nb | 75(8) | 62(8) | 81(31) | 86(37) | 60(3) | 55(2) | 109(22) | 79(28) | 356(119) | 149(51) |
| Ta | 5.1(0.1) | 4.2(0.4) | 5.5(1.1) | 5.8(2.5) | 4.4(0.5) | 4.0(0.1) | 7.9(1.6) | 5.7(2.0) | 25.8(9.1) | 12.6(6.1) |
| Sr | 288(40) | 298(27) | 229(50) | 163(81) | 262(36) | 253(21) | 143(34) | 226(121) | 10(4) | 43(35) |
| Zr | 594(89) | 447(36) | 548(102) | 508(104) | 451(21) | 477(16) | 687(159) | 581(91) | 2198(600) | 887(417) |
| Hf | 14(2) | 12(4) | 13(2) | 12(2) | 11(1) | 13(0) | 20(4) | 16(2) | 53(17) | 24.5(13.9) |
| Y | 67(4) | 59(4) | 65(12) | 60(13) | 57(4) | 57(3) | 69(8) | 62(8) | 196(42) | 77(38) |
| Ga | 21(2) | 22(1) | 25(1) | 29(1) | 22(4) | 26(4) | 33(2) | 30(1) | 25(1) | 31(7) |
| | | | | | | | | | | |
| La | 79.6(2.7) | 79.6(2.7) | 78.7(16.5) | 78.6(7.5) | 75.0(2.7) | 68.2(2.1) | 91.6(7.2) | 68.8(19.6) | 33.5(14.8) | 138.0(45.7) |
| Ce | 152.4(5.6) | 152.4(5.6) | 150.2(27.9) | 145.6(12.6) | 143.0(6.3) | 128.6(3.3) | 163.0(6.1) | 129.8(37.7) | 106.0(26.9) | 230.2(70.5) |
| Pr | | 13.9(0.7) | | 14.0(1.2) | 13.9(0.5) | 13.1(0.6) | 16.5(1.5) | | | 21.4(6.5) |
| Nd | 64.8(4.5) | 59.3(3.1) | 63.0(6.4) | 55.1(4.5) | 59.6(6.6) | 59.8(4.0) | 73.3(11.3) | 54.8(17.2) | 44.8(23.6) | 101.0(38.0) |
| Sm | 12.16(0.74) | 11.50(0.80) | 11.89(1.34) | 10.43(0.96) | 11.42(1.43) | 12.54(0.84) | 15.74(2.42) | 9.6(1.3) | 14.1(7.1) | 22.2(8.9) |
| Eu | 3.38(0.44) | 2.90(0.24) | 3.08(0.25) | 1.82(0.46) | 3.00(0.27) | 2.87(0.27) | 2.68(0.41) | 1.00(0.40) | 0.70(0.55) | 2.31(0.98) |
| Gd | | 11.10(0.80) | | 9.91(0.87) | 11.00(0.84) | 12.10(0.81) | 15.59(2.67) | | 17.5(7.3) | 21.9(8.8) |
| Tb | 1.89(0.09) | 1.62(0.23) | 1.95(0.31) | 1.56(0.15) | 2.42(0.63) | 1.80(0.12) | 2.48(0.22) | 1.09(0.36) | 4.05(1.48) | 3.10(1.34) |
| Dy | | 10.40(0.40) | 10.40(0.40) | 9.67(0.15) | 10.08(0.15) | 10.95(0.73) | 14.70(2.61) | | 29.6(9.3) | 22.4(4.7) |
| Ho | | | | | | | | | 6.40(6.9) | |
| Er | | 6.60(0.29) | | 6.03(0.66) | 6.32(0.39) | 6.41(0.45) | 8.97(0.52) | | 22.0(2.61) | 14.8(3.1) |
| Tm | | | | | | | | | 3.56(1.20) | |
| Yb | 6.85(0.32) | 6.18(0.25) | 8.65(1.55) | 6.07(0.78) | 6.18(0.24) | 6.00(0.42) | 8.58(0.26) | 9.10(2.35) | 22.15(7.84) | 12.4(5.9) |
| Lu | 1.00(0.09) | 0.94(0.06) | 1.28(0.22) | 0.90(0.19) | 0.92(0.03) | 0.91(0.06) | 1.26(0.06) | 0.89(0.12) | 3.17(1.17) | 1.73(0.76) |
| | | | | | | | | | | |
| $(La/Yb)_C$ | 7.83 | 8.11 | 16.13 | 8.73 | 8.18 | 7.66 | 7.20 | 5.09 | 1.02 | 7.50 |
| $(Sm/Yb)_C$ | 1.90 | 1.99 | 1.47 | 1.84 | 1.98 | 2.24 | 1.97 | 1.13 | 0.68 | 1.92 |
| Eu/Eu* | 0.84 | 0.77 | 0.77 | 0.54 | 0.81 | 0.70 | 0.52 | 0.34 | 0.14 | 0.32 |
| | | | | | | | | | | |
| Q | 8.03 | 12.23 | 12.21 | 13.63 | 16.16 | 17.25 | 11.10 | 24.86 | 35.46 | 3.89 |
| C | | | | | | | | | 0.21 | 29.49 |
| or | 23.88 | 25.17 | 26.24 | 28.19 | 22.75 | 24.94 | 26.77 | 28.37 | 27.90 | 51.38 |
| ab | 36.13 | 32.32 | 35.71 | 40.45 | 32.32 | 30.13 | 47.98 | 36.64 | 28.43 | |
| an | 8.90 | 9.04 | 7.67 | 5.25 | 9.28 | 9.46 | 3.74 | 3.96 | 0.58 | 3.62 |
| di | 5.95 | 3.76 | 3.03 | 3.33 | 2.63 | 1.76 | 2.46 | 0.75 | | 0.06 |
| hy | 9.63 | 7.96 | 7.24 | 4.33 | 6.52 | 8.39 | 1.94 | 2.70 | 2.47 | 3.87 |
| mt | 3.44 | 4.13 | 3.49 | 2.42 | 4.83 | 3.35 | 3.33 | 1.41 | 3.12 | 5.50 |
| il | 2.68 | 2.51 | 2.11 | 1.56 | 2.26 | 2.13 | 1.16 | 0.82 | 0.51 | |
| ap | 1.18 | 1.32 | 1.00 | 1.67 | 1.18 | 1.23 | 0.42 | 0.25 | 0.02 | 0.97 |
| | | | | | | | | | | |
| A.I. | 0.78 | 0.77 | 0.81 | 0.87 | 0.75 | 0.75 | 0.91 | 0.90 | 0.96 | 1.06 |
| $K_2O/Na_2O$ | 0.95 | 1.12 | 1.05 | 1.00 | 1.01 | 1.19 | 0.80 | 1.11 | 1.40 | 0.76 |

Table 1 (continued).

| One feldspar variants | 11 Syenite (N=6) | 12 Trachyte (N=1) | 13 Granite (N=2) | 14 Granite (N=3) | 15 Rhyolite (N=10) | 16 Rhyolite (N=1) | 17 92-U12 Trachy-basalt | 18 Arequita rhyolite (N=1) | 19 Arequita rhyolite (N=3) | 20 Jaguarão rhyodacites (N=22) |
|---|---|---|---|---|---|---|---|---|---|---|
| wt% | | | | | | | | | | |
| $SiO_2$ | 66.79(0.59) | 65.12 | 70.27(1.89) | 76.72(0.69) | 71.09(0.99) | 77.20 | 47.89 | 69.41 | 74.97(0.61) | 63.07(0.96) |
| $TiO_2$ | 0.50(0.21) | 0.70 | 0.26(0.07) | 0.12(0.01) | 0.36(0.14) | 0.13 | 1.87 | 0.45 | 0.31(0.07) | 1.03(0.05) |
| $Al_2O_3$ | 14.06(1.79) | 14.76 | 14.28(0.13) | 11.27(2.08) | 10.71(1.15) | 9.77 | 16.88 | 9.59 | 9.79(0.96) | 15.43(0.43) |
| $Fe_2O_{3tot}$ | 6.08(2.66) | 5.90 | 3.45(1.03) | 2.56(1.54) | 7.11(2.05) | 3.65 | 12.23 | 9.55 | 6.39(1.03) | 6.56(0.66) |
| MnO | 0.14(0.07) | 0.13 | 0.09(0.05) | 0.03(0.02) | 0.16(0.05) | 0.04 | 0.18 | 0.23 | 0.13(0.04) | 0.15(0.01) |
| MgO | 0.12(0.05) | 0.28 | 0.04(0.00) | 0.05(0.02) | 0.07(0.04) | 0.05 | 6.40 | 0.14 | 0.03(0.02) | 1.97(0.24) |
| CaO | 0.81(0.21) | 0.54 | 0.43(0.33) | 0.10(0.09) | 0.33(0.12) | 0.10 | 8.52 | 0.62 | 0.17(0.13) | 4.29(0.57) |
| $Na_2O$ | 6.07(0.80) | 6.48 | 5.90(0.67) | 3.98(1.15) | 4.83(0.62) | 3.13 | 3.76 | 5.03 | 3.86(0.49) | 2.23(0.19) |
| $K_2O$ | 4.70(0.69) | 4.81 | 4.84(0.39) | 4.40(0.24) | 5.08(1.45) | 4.57 | 1.13 | 4.34 | 4.21(0.35) | 2.27(0.25) |
| $P_2O_5$ | 0.05(0.03) | 0.12 | 0.02(0.01) | 0.03(0.02) | 0.03(0.01) | 0.04 | 0.52 | 0.04 | 0.02(0.01) | 0.18(0.02) |
| LOI | 0.68(0.21) | 1.16 | 0.43(0.17) | 0.81(0.10) | 0.71(0.20) | 1.32 | 0.86 | 0.64 | 0.51(0.21) | 2.81(0.35) |
| Sum | 100.00 | 100.00 | 100.00 | 100.00 | 100.00 | 100.00 | 100.24 | 100.00 | 100.00 | 100.00 |
| $Fe_2O_3/FeO$ | 0.5 | 1.17 | 1.4 | 1;0 | 0.6 | 0.6 | 0.2 | 0.5 | 0.6 | 0.175 |
| mg# | 0.05 | 0.16 | 0.05 | 0.19 | 0.03 | 0.04 | 0.55 | 0.04 | 0.01 | 0.38 |
| ppm | | | | | | | | | | |
| Rb | 143(37) | 123 | 189(11) | 288(123) | 307(47) | 375 | 22 | 262 | 290(57) | 95(13) |
| Ba | 481(331) | 610 | 134(160) | 71(50) | 51(14) | 122 | 551 | 59 | 39(19) | 891(67) |
| U | 7.9(1.0) | | 4.4(1.5) | 7.5(2.9) | 10.6(0.6) | | 0.6 | | | |
| Th | 15.0(1.0) | | 19.7(1.0) | 17.3(2.3) | 45.0(4.6) | 66 | 2.29 | 49 | 32(5) | |
| Nb | 164(59) | 100 | 106(7) | 189(110) | 429(100) | 267 | 28 | 510 | 297(61) | |
| Ta | 13.9(1.2) | | 9.1(1.8) | 17.5(10.2) | 28.5(3.7) | | 1.56 | | | |
| Sr | 43(44) | 46 | 15(16) | 5.7(3.2) | 11.2(6.3) | 8 | 597 | 14 | 8(4) | 318(34) |
| Zr | 917(367) | 610 | 545(129) | 495(57) | 2569(715) | 1535 | 154 | 2555 | 1545(218) | 303(15) |
| Hf | 20.4(6.1) | | 18.4(2.5) | 18.0(2.1) | 62(6) | 46 | 3.44 | 59 | 37(6) | |
| Y | 85(21) | 75 | 60(18) | 77(42) | 196(63) | 207 | 30 | 214 | 152(40) | 26(8) |
| Ga | 29(2) | 30 | 29(1) | 32(1) | 30(3) | 23 | | 28 | 31(3) | |
| La | 150(53) | 110 | 63.5(31.8) | 59.7(26.4) | 222(32) | 78.3 | 27.3 | 253 | 73(9) | 52(4) |
| Ce | 265(104) | 182 | 133.0(68.0) | 116.0(43.8) | 420(50) | 147.0 | 57.7 | 487 | 139(13) | 101(13) |
| Pr | | 103 | 11.3(3.9) | 10.1(2.2) | 38(8) | | | | | |
| Nd | 117(36) | | 43.4(15.4) | 53.3(22.3) | 158(23) | 74.0 | 27.2 | 179 | 70(22) | 46.5(2.1) |
| Sm | 20.6(3.6) | | 9.75(1.91) | 13.9(5.8) | 27.6(6.5) | 19.4 | 6.20 | 32.3 | 23.8(5.3) | 9.5(1.0) |
| Eu | 3.6(0.6) | | 0.53(0.39) | 0.50(0.35) | 2.05(0.98) | 1.0 | 2.07 | 3.5 | 1.63(0.12) | |
| Gd | | | 9.3(2.2) | 10.2(3.6) | 30.1(4.6) | | | | | |
| Tb | 3.2(0.6) | | 1.75(0.21) | 2.54(1.21) | 5.37(1.05) | 3.9 | 0.93 | 6.5 | 3.47(1.36) | |
| Dy | | | 11.6(1.7) | 13.5(4.3) | 36.7(2.4) | | | | | |
| Ho | | | 2.35(0.35) | | | | | | | |
| Er | | | 8.1(1.1) | 8.38(1.54) | 25.3(2.8) | | | | | |
| Tm | | | 1.36(0.16) | | | | | | | |
| Yb | 15.3(2.7) | | 8.75(1.06) | 8.60(0.84) | 27.6(4.0) | 27.3 | 2.50 | 29.3 | 21.5(3.4) | |
| Lu | 2.28(0.40) | | 1.26(0.20) | 1.15(0.06) | 4.07(0.56) | 3.89 | 0.37 | 4.28 | 2.86(0.63) | |
| $(La/Yb)_C$ | 6.61 | | 4.89 | 4.68 | 5.42 | 1.93 | 7.36 | 5.82 | 2.29 | |
| $(Sm/Yb)_C$ | 1.44 | | 1.19 | 1.73 | 1.07 | 0.76 | 2.66 | 1.18 | 1.19 | |
| Eu/Eu* | 0.53 | | 0.17 | 0.12 | 0.22 | 0.15 | 1.02 | 0.30 | 0.21 | |
| Q | 10.70 | 8.23 | 17.37 | 36.33 | 25.05 | 40.33 | | 24.53 | 34.30 | 26.98 |
| C | | | | | | | | | | 2.00 |
| or | 27.77 | 28.43 | 28.60 | 26.00 | 29.99 | 27.01 | 6.67 | 25.65 | 24.88 | 13.83 |
| ab | 46.15 | 49.14 | 46.51 | 33.32 | 26.84 | 24.81 | 28.80 | 25.17 | 26.92 | 19.46 |
| an | | | | | | | 25.85 | | | 20.69 |
| ne | | | | | | | 1.63 | | | |
| ac | 3.27 | 5.01 | 3.01 | 0.02 | 7.20 | 1.47 | | 8.56 | 5.06 | |
| ns | 0.23 | | | | 1.36 | | | 1.79 | | |
| di | 3.27 | 1.64 | 1.77 | 0.26 | 1.28 | 0.21 | 10.67 | 2.50 | 0.71 | |
| ol | | | | | | | 17.26 | | | |
| hy | 5.50 | 2.63 | 0.34 | 1.07 | 6.82 | 3.15 | | 9.60 | 6.32 | 13.15 |
| mt | | | 1.27 | 1.75 | | 1.12 | 2.70 | | 0.71 | 1.44 |
| il | 0.95 | 1.33 | 0.49 | 0.23 | 0.68 | 0.25 | 3.55 | 0.85 | 0.59 | 2.01 |
| ap | 0.12 | 0.28 | 0.05 | 0.07 | 0.04 | 0.09 | 1.20 | 0.09 | 0.05 | 0.44 |
| A.I. | 1.06 | 1.08 | 1.05 | 1.01 | 1.26 | 1.03 | 0.44 | 1.35 | 1.11 | 0.40 |
| $K_2O/Na_2O$ | 0.77 | 0.74 | 0.82 | 1.11 | 1.05 | 1.46 | 0.30 | 0.86 | 1.09 | 1.02 |

in composition, and tend to straddle over the sodic field (inset B of Fig. 4). These rocks are classified as comenditic trachyte, comendite and pantellerite, according to the $Al_2O_3$ vs. $Fe_2O_3$ grid (Macdonald, 1974; inset C of Fig. 4).

The dykes are mainly peralkaline rhyolites and metaluminous trachytes (cf. Muzio *et al*., 2002). It should be noted that some of the rhyolites (and one feldspar granite) fall in the comendite field, and one trachyte plots in the pantellerite field, whereas the syenites straddle over the comenditic trachyte-comendite fields.

Alteration processes (cf. Lustrino *et al*., 2005), i.e. argillification, affect above all the alkali feldspars, resulting in occasional corundum in the norms (up to 2 wt%). It corresponds to a maximum of 5 wt% of kaolinite for the whole-rock, not substantially changing the classification grid.

## PETROGRAPHY

### Plutonic rocks

#### *One feldspar syenites and quartz syenites*

One feldspar syenitic variants show prevailing hypidiomorphic and subordinate allotriomorphic textures, with large crystals (up to 3 cm across) of perthitic, sometimes poikilitic, alkali feldspar. Occasional graphic alkali feldspar-quartz intergrowths are present. Quartz, amphibole, Ca-clinopyroxene to acmite-rich varieties, chloritized biotite, apatite, zircon and opaque minerals are common interstitial phases.

#### *Two feldspars monzonites and quartz syenites*

Monzonites and quartz syenites are inequigranular, with subhedral to anhedral plagioclase ($An_{50-22}$, often poikilitic and mantled by anorthoclase), alkali feldspar and interstitial to acicular quartz. Ca-clinopyroxene, anhedral amphibole, chloritized biotite, opaque minerals, zircon and apatite are interstitial and accessory constituents. Rims or overgrowths of amphibole on pyroxene and glomeroporphyritic textures (plagioclase, amphibole, opaque minerals and apatite glomerules) are usually present.

#### *Granites*

Granitic rocks range from hypidiomorphic to allotriomorphic inequigranular, sometimes porphyritic (porphyritic index, P.I., ~30%) with isotropic texture and medium grain size (~0.5 cm). Large, often poikilitic, anhedral to subhedral, commonly perthitic-mesoperthitic alkali feldspar (microcline, up to 1 cm long) prevails over anhedral plagioclase, quartz, partially chloritized biotite, amphibole, opaque minerals and zircon. Alkali feldspar-quartz intergrowths are common in the mesostasis.

### Volcanic rocks and dykes

#### *One feldspar quartz trachytes*

These variants are holocrystalline with porphyritic seriate (P.I. up to 20%), isotropic, texture. The paragenesis consists of euhedral alkali feldspar phenocrysts and amphibole microphenocrysts set in a groundmass made of subhedral alkali feldspar, opaque minerals, interstitial or granophiric quartz, apatite, chloritized biotite, clinopyroxene (partially enclosed in poikilitic alkali feldspar), zircon and titanite.

#### *Two feldspar latites and quartz trachytes*

Two feldspars latites and quartz trachytes are holocrystalline, rarely hypocrystalline, with porphyritic to glomeroporphyritic (P.I. between 10 and 40%) and occasional trachytic texture. Plagioclase occurs both as euhedral to subhedral phenocrysts (average size 1 cm, sometimes poikilitic and/or with sieved aspect; $An_{48-29}$) and as groundmass phase ($An_{42-26}$). The glomerules are constituted only of plagioclase or of plagioclase+clinopyroxene+apatite+opaque minerals. In some cases melanocratic patches of opaque minerals, apatite, clinopyroxene and amphibole have been found.

Alkali feldspar may occur as pheno and/or micro-phenocrysts. Groundmass is fine-grained to crypto-crystalline and consists of poikilitic plagioclase, euhedral altered (kaolinitized) alkali feldspar, acicular to interstitial quartz, opaque minerals, anhedral pyroxene, apatite, amphibole, zircon and rare glassy patches. Sometimes amygdales filled by zeolite, calcite and quartz are present.

*Rhyolites*

Rhyolites range from hypocrystalline to holocrystalline and from aphanitic to porphyritic (P.I. 5-30%), with isotropic to weakly trachytic texture. Embayed quartz and alkali feldspar are common. The very fine to fine-grained groundmass is made of alkali feldspar, quartz, rare plagioclase (~$An_{20-12}$, two feldspars variants), spherulites of opaque minerals, anhedral amphibole and accessory zircon and fluorite with occasional associated fluorcarbonates (one feldspar variants).

## MINERAL CHEMISTRY

Average and selected analyses of feldspars, clinopyroxene, amphibole, biotite and magnetite-ilmenite pairs from plutonic and volcanic rocks are presented in Tables 2 to 6.

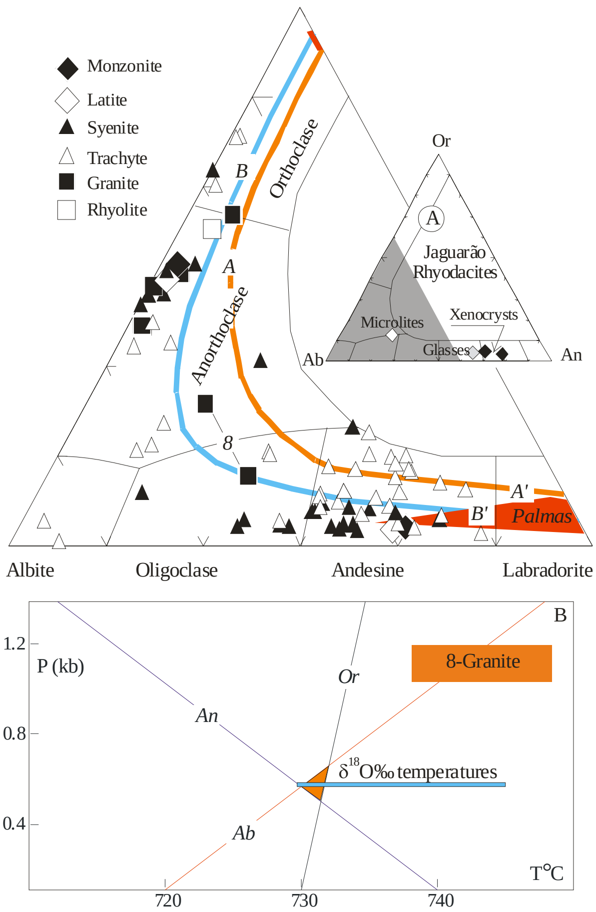


Fig. 5. Plot of the Valle Chico feldspars and plagioclase field from the Palmas rock-types (Bellieni *et al.*, 1988; Garland *et al.*, 1995) into the Or-Ab-An space (cf. Deer *et al.*, 1992). A-A', B-B' solvus-solidus intersection at $P_{H2O}$=0.5 kb and 900°C, and at $P_{H2O}$=1.0 kb and 750°C, respectively (Seck, 1971). Insets: A) Field of the Fig. 5 (gray) and compositions of feldspars and glasses of anatectic melts from the Jaguarão rhyodacites (Balestra, 1985; Vieira, 1986; Comin-Chiaramonti, unpublished data) shown for comparison; B) P-T diagram showing the calculated ternary-feldspar equilibria of the two feldspars granite (cf. Table 2), according to the geothermometer of Fuhrman & Lindsley (1988) and Green & Usdansky (1986) and the stable isotope equilibration temperatures (see text).

Table 2. Average compositions of feldspars from the Valle Chico complex expressed as An-Ab-Or wt%. TFV and OFV, two feldspars and one feldspar variants, respectively; order numbers and data source as in Table 1. Details of selected compositions are in Lustrino *et al.* (2005).

| | 1 | | 2 | | 3 | | 4 | | 5-6 | |
|---|---|---|---|---|---|---|---|---|---|---|
| TFV | Monzonite | | Latite | | Syenite | | Syenite | | Trachyte | |
| An | 49.2-22.9 | 1.2 | 47.8-26.4 | 1.2 | 36.3-29.0 | 0.5-3.4 | 23.7 | 1.7 | 34.6 | 2.3-1.2 |
| Ab | 49.2-73.8 | 66.9 | 50.7-70.7 | 68.5 | 60.5-65.1 | 72.5-55.2 | 66.4 | 50.3 | 58.9 | 61.9-58.8 |
| Or | 1.6-3.3 | 31.9 | 1.5-2.9 | 30.3 | 3.2-5.9 | 27.0-41.4 | 3.9 | 32.0 | 6.5 | 35.8-40.0 |

| | 7 | | 8 | | | 10 | 11 | 12 | 13 | 15 |
|---|---|---|---|---|---|---|---|---|---|---|
| TFV | Trachyte | | Granite | | OFV | Syenite | Syenite | Trachyte | Granite | Rhyolite |
| An | 30.0 | 0.4 | 16.5 | 8.0 | | 0.5-2.2 | 0.1 | 0.0 | 4.6-1.5 | 2.2 |
| Ab | 65.9 | 57.0 | 71.5 | 71.0 | | 58.8-94.9 | 62.4 | 63.3 | 58.4-74.1 | 52.0 |
| Or | 4.1 | 32.6 | 12.0 | 21.0 | | 40.7-2.9 | 37.5 | 36.7 | 37.0-24.4 | 45.8 |

Table 3. Selected microprobe analyses of clinopyroxenes from the Valle Chico igneous rocks. TFV and OFV, two feldspars and one feldspar variants, respectively; order numbers and data source as in Table 1. C, core of the crystals; R, rims or groundmass phases. $Fe^{2+}$-$Fe^{3+}$ repartition as from stoichiometry; mg#=Mg/(Mg+$Fe^{2+}$).

| | 1 | 4 | | 8 | | 10 | 11 | | 13 | 15 |
|---|---|---|---|---|---|---|---|---|---|---|
| TFV | Monzonite | Syenite | | Trachyte | OFV | Syenite | Syenite | | Granite | Rhyolite |
| | C | C | R | R | | R | C | R | R | R |
| $SiO_2$ | 49.88 | 49.92 | 49.96 | 49.91 | | 50.63 | 48.16 | 49.06 | 50.01 | 51.00 |
| $TiO_2$ | 0.45 | 0.25 | 0.06 | 0.37 | | 0.09 | 0.40 | 0.50 | 0.01 | 0.08 |
| $Al_2O_3$ | 0.87 | 0.55 | 0.30 | 0.47 | | 0.20 | 0.18 | 0.19 | 0.21 | 0.32 |
| $Fe_2O_3$ | 4.88 | 5.18 | 7.59 | 4.13 | | 25.10 | 6.03 | 7.33 | 12.20 | 28.36 |
| FeO | 15.31 | 12.71 | 13.83 | 16.85 | | 6.90 | 23.75 | 22.00 | 13.02 | 4.18 |
| MnO | 1.00 | 1.23 | 1.15 | 1.58 | | 0.85 | 0.97 | 0.98 | 3.12 | 0.51 |
| MgO | 9.75 | 8.66 | 5.89 | 7.50 | | 0.44 | 1.64 | 1.70 | 2.28 | 0.82 |
| CaO | 17.65 | 19.94 | 18.22 | 19.75 | | 6.32 | 17.21 | 17.08 | 14.86 | 3.46 |
| $Na_2O$ | 0.67 | 1.07 | 2.37 | 0.62 | | 9.48 | 1.77 | 2.41 | 4.44 | 10.85 |
| $K_2O$ | 0.02 | 0.00 | 0.00 | 0.00 | | 0.01 | 0.01 | 0.02 | 0.00 | 0.03 |
| Sum | 100.48 | 99.50 | 99.35 | 101.18 | | 100.00 | 100.12 | 101.26 | 100.17 | 99.61 |
| Si | 1.926 | 1.945 | 1.969 | 1.942 | | 1.983 | 1.961 | 1.964 | 1.982 | 1.985 |
| $Al^{IV}$ | 0.040 | 0.025 | 0.014 | 0.022 | | 0.009 | 0.009 | 0.009 | 0.010 | 0.015 |
| Ti | 0.013 | 0.007 | 0.002 | 0.010 | | 0.003 | 0.012 | 0.015 | | |
| $Fe^{3+}$ | 0.021 | 0.023 | 0.015 | 0.026 | | 0.005 | 0.018 | 0.012 | 0.008 | |
| Sum | 2.000 | 2.000 | 2.000 | 2.000 | | 2.000 | 2.000 | 2.000 | 2.000 | 2.000 |
| $Al^{VI}$ | | | | | | | | | | |
| Ti | | | | | | | | | | 0.002 |
| $Fe^{3+}$ | 0.121 | 0.129 | 0.210 | 0.095 | | 0.735 | 0.167 | 0.209 | 0.359 | 0.831 |
| $Fe^{2+}$ | 0.492 | 0.414 | 0.456 | 0.548 | | 0.231 | 0.809 | 0.736 | 0.432 | 0.136 |
| Mn | 0.033 | 0.041 | 0.038 | 0.052 | | 0.028 | 0.033 | 0.033 | 0.105 | 0.017 |
| Mg | 0.561 | 0.503 | 0.346 | 0.435 | | 0.026 | 0.100 | 0.101 | 0.135 | 0.048 |
| Ca | 0.730 | 0.832 | 0.769 | 0.823 | | 0.265 | 0.751 | 0.732 | 0.631 | 0.145 |
| Na | 0.050 | 0.081 | 0.181 | 0.047 | | 0.720 | 0.139 | 0.187 | 0.341 | 0.819 |
| K | 0.010 | | | | | 0.001 | 0.001 | 0.001 | | 0.001 |
| Sum | 2.000 | 2.000 | 2.000 | 2.000 | | 2.001 | 2.000 | 1.999 | 2.000 | 1.999 |
| mg# | 0.53 | 0.55 | 0.43 | 0.44 | | 0.10 | 0.11 | 0.12 | 0.24 | 0.26 |

### *Feldspars*

The VC compositional variations are shown in Fig. 5, where the differences with the Palmas and Jaguarão feldspars become apparent.

Following Lustrino *et al.* (2005), the sum of cations in the structural formula ($X_4Z_{16}O_{32}$) falls within the range 19.8-20.1, i.e.±1% of the theoretical 20.0. The X group (Ca+Sr+Ba+Na+K) averages 3.82 (±0.09) and 3.88 (±0.14) a.f.u. in plagioclase and alkali feldspar, respectively, vs. the theoretical 4.00: a fact that indicates that subsolidus processes may have modified the chemistry of this mineral group. Systematically, low Ba occurs both in the plagioclase and alkali feldspar (less than 0.015 a.f.u.). Notably, about 13% and 54% of the feldspars, respectively, plot above and below the solvus-solidus intersections at $P_{H_2O}$=0.5 kb and

900°C and at $P_{H_2O}$=1 kb and 750°C, respectively (Fig. 5), in the system $KAlSi_3O_8$-$NaAlSi_3O_8$-$CaAl_2Si_2O_8$ (Seck, 1971).

Plagioclase from the two feldspars variants is slightly zoned and range from andesine core ($An_{49}Ab_{49}Or_2$) to oligoclase rim ($An_{23}Ab_{74}Or_3$). The associated alkali feldspar is usually anorthoclase ($Or_{27-35}$) with K-rich rims ($Or_{40-45}$).

Alkali feldspar from the hypersolvus variants has whole compositions ranging from 24 to 46% Or, but exsolved phases display compositions up to Ab 95%.

Calculated closure temperatures of plagioclase at dry conditions (Mathez, 1973) yielded mean values of 989±36°C and 843±90°C (early and late phases, respectively) for the monzonitic and syenitic rocks, and 1061±58°C (phenocrysts and microphenocrysts) and 943±83°C (groundmass phases) for the latitic and trachytic variants.

The crystallization temperatures obtained for the phenocrysts and microphenocrysts of the VC trachytes approach those (1032±36°C) calculated for the Palmas rhyodacitic-rhyolitic sequences from the southern Paraná Basin (Bellieni *et al.*, 1986b, 1988). On the other hand, the temperatures estimated for the groundmass plagioclase are similar to the eruption ones inferred by Kirstein *et al.* (2000) for the Uruguayan rhyolites (i.e. 850-950°C). Some two feldspars granites display ternary feldspars, i.e. $An_{16.5}Ab_{71.5}Or_{12.0}$ and $An_8Ab_{71}Or_{21}$, respectively. P-T diagram (inset B of Fig. 5) relative to the calculated equilibria shows that the centroid of An, Ab and Or univariant curve intersections (cf. Green & Usdansky, 1986; Fuhrman & Lindsley, 1988) indicates temperature and pressure of about 730°C and 0.6 kb, respectively (subvolcanic conditions).

Stable isotope equilibration temperatures for two feldspars syenitic rocks (alkali feldspar, plagioclase and quartz: $^{18}O$‰ SMOW=9.9, 9.4 and 11.3, respectively; Censi, unpublished data) indicate values of 747 and 727°C for the alkali feldspar-plagioclase and quartz-plagioclase pairs, respectively (cf. Friedman & O'Neal, 1977; Matsuhisa *et al.*, 1979). The latter temperatures are about 100-200°C lower than those calculated by means of the Mathez geothermometry.

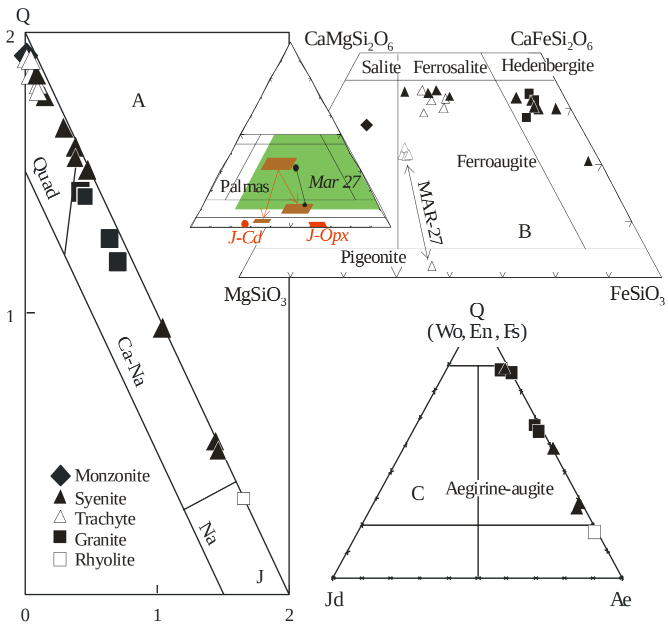


Fig. 6. A) Clinopyroxenes from VC selected samples plotted into the Q-J space of Morimoto (1988). B) VC clinopyroxenes from "Q" field plotted into the Di-Hd-Fs-En quadrilateral. Inset: fields of the VC clinopyroxenes (green field), of the Palmas clinopyroxenes (dark brow fields) and of cordierite and orthopyroxene from Jaguarão rhyodacites (red). C: VC clinopyroxenes from "Ca-Na" and "Na" fields plotted into the Q (wollastonite, enstatite, ferrosilite)-Jd (jadeite)-Ae (aegirine) diagram. Symbols as in Fig. 5. Data source: Bellieni *et al.* (1986b), Comin-Chiaramonti (2000 and unpublished data) and Lustrino *et al.* (2005).

*Clinopyroxenes*

On the whole, compositional variations display low $Al^{IV}$ (a.f.u.), requiring Ti ($Fe^{3+}$) to fill the tetrahedral sites. Two fold behaviours (Table 4; Fig. 6) are apparent: the clinopyroxenes from the two feldspars variants mostly plot in the Quad (Wo, En, Fs; Ca-rich clinopyroxenes), and have mg# ranging from 0.53 to 0.43, and Na (a.f.u.) from 0.047 to 0.181; clinopyroxenes from one feldspar variants plot on the Ca-Na and Na fields (Morimoto, 1988), and have mg#=0.10-0.26 and Na=0.139-0.819.

The relatively Na-rich compositions of some clinopyroxenes of Valle Chico and the systematic Al deficiency in the tetrahedral sites are typical features of other alkaline and alkaline-carbonatitic complexes in and around the Paraná Basin (Comin-Chiaramonti & Gomes, 1996).

In the intrusive rocks, the compositional range extends from Quad (Ca-rich clinopyroxenes) to Ca-Na fields of Morimoto (1988) in monzonitic to granitic variants. In the conventional pyroxene quadrilateral (Fig. 6B), Ca-clinopyroxenes from such rocks are in the ferroaugite field and vary from ferrosalitic to hedenbergitic rich compositions, paralleling the modal quartz increase. The Na-Ca clinopyroxenes plot in the aegirine-augite field (Fig. 6C).

As a rule, Ca-clinopyroxenes show important Al deficiency in the tetrahedral site, suggesting $Ti^{4+}$ and $Fe^{3+}$ in T sites. Si-Ti ($Fe^{3+}$) tetrahedral substitution has been documented for Ca-rich clinopyroxenes of potassic rocks (e.g., leucitites: Cundari & Salviulo, 1989; syenites, Ponta do Morro complex, Sousa *et al.*, in this volume).

In the volcanic rocks and dykes, Ca-rich clinopyroxenes from the latites and some trachytic rocks plot in the Quad field and correspond to ferroaugites, which cluster at $Wo_{41}$ to $Wo_{32}$ (Fig. 6B). As for the intrusive variants, such clino-pyroxenes require $Ti^{4+}$ and $Fe^{3+}$ in T site.

It is notable that pigeonite ($Wo_{12}En_{37}Fs_{51}$), enclosed in plagioclase of the trachyte MAR-27 of Lustrino *et al.* (2005), is associated with augite ($Wo_{32}En_{31}Fs_{37}$; cf. Fig. 6B). These clinopyroxenes are compositionally similar to those of the silicic Palmas flows (cf. inset of Fig. 6B). According to Ishii (1975), the crystallization temperature of the MAR-27 pigeonite is 1005°C as the Palmas pigeoni-tes, (1030-995±21°C; cf. Bellieni *et al.*, 1986b).

The presence of pigeonite and Na-rich clinopyroxene (aegirine component up to 73 mol%) in VC silicic rocks, with albite never in the same specimen, is a very interesting and uncommon feature among the Early Cretaceous alkaline complexes from South America (cf. Morbidelli *et al.*, 1995).

On the other hand, the felsic rocks from the Neoproterozoic Damara belt (Namibia) are dominated by silicic units ($SiO_2$>67 wt%) with a large compositional range, with peraluminous, metaluminous and peralkaline types, e.g. pigeonite-bearing quartz latites to aegirine-arvfedsonite granites (Schmitt *et al.*, 2000; Trumbull *et al.*, 2004).

The presence of low-Ca clinopyroxenes, coupled with Ca-rich ones enriched in hedenbergite component, is relatively common in the Paraná felsic rocks (quartz latites, rhyodacites and rhyolites, Chapecó and Palmas variants; cf. Bellieni *et al.*, 1986b), which are associated with the tholeiitic basalts (Piccirillo & Melfi, 1988).

In this case, the low $fO_2$ conditions would not promote $Fe^{2+}$ oxidation to $Fe^{3+}$; on the other hand, low $fO_2$ conditions may be responsible for Fe enrichment in weakly alkaline magmas (cf. Carbonin *et al.*, 1984, and therein references).

*Amphiboles*

Representative amphibole compositions (Table 4) were recalculated as atom numbers on the basis of 24 (O, OH, F, Cl), assuming the theoretical formula $A_{0-1}B_2C_5T_8O_{22}$ (OH,F,Cl)$_2$ and using the software of Yavuz (1999), and was also classified according to the IMA rules (cf. Leake, 1978; Giret *et al.*, 1980). Representative analyses of amphiboles of plutonic (quartz syenites and trachytes) and volcanic rocks (trachytes) are plotted in Fig. 7A and compared with the analogues from the Brazilian Ponta do Morro complex (Sousa *et al.*, in this volume). The amphiboles mainly belong to the edenite-katophorite (two feldspars variants) and richterite-arfvedsonite fields (one feldspar variants). The amphiboles from the two feldspars variants have mg# ranging from 0.69 to 0.39, whereas the one feldspar variants contain amphiboles with very low mg# (0.02-0.09).

Some syenitic to granitic compositions show amphiboles with Al deficiency in the tetrahedral sites and, according to Leake's suggestion, is expected that $Fe^{3+}$ completes the T site to the theoretical 2.00 a.f.u. Notably, strong Al deficiency has been reported in amphiboles from some alkaline rocks such as lamproites (Mitchell & Bergmann, 1991) and leucitites (Cundari, 1975). F is quite variable, ranging from 0.28 to 1.58 a.f.u., attesting a relatively high fluorine activity both in the meta-luminous and in the peralkaline variants (i.e. two feldspars and one feldspar variants, respectively): comparable values were obtained in amphiboles from felsic variants (both peralkaline and meta-luminous) of eastern Paraguay and southeastern Bolivia alkaline complexes (Comin-Chiaramonti & Gomes, 1996; Comin-Chiaramonti *et al.,* in this volume, respectively).

Table 4. Selected analyses of amphiboles from the Valle Chico igneous rocks. Abbreviations, order numbers and data source as in Table 1. $Fe^{2+}$-$Fe^{3+}$ repartition according to Yavuz (1999). Nomenclature according to Leake (1978).

| | 3 | 4 | | | 7 | 11 | | | 13 |
|---|---|---|---|---|---|---|---|---|---|
| TFV | Syenite | Syenite | | | OFV Trachyte | Syenite | | | Granite |
| | C | C | | R | R | C | | R | C |
| $SiO_2$ | 42.67 | 43.47 | 46.67 | 50.43 | 45.39 | 47.52 | 47.92 | 48.73 | 47.59 |
| $TiO_2$ | 1.35 | 1.57 | 0.96 | 0.28 | 1.09 | 2.12 | 1.55 | 0.91 | 1.16 |
| $Al_2O_3$ | 6.68 | 7.11 | 4.79 | 2.02 | 5.21 | 1.73 | 0.97 | 0.75 | 1.14 |
| $Fe_2O_3$ | | 0.19 | 4.34 | 7.44 | 0.52 | 0.81 | 2.29 | 8.96 | 8.56 |
| FeO | 20.14 | 22.91 | 13.31 | 10.47 | 23.77 | 31.47 | 31.50 | 24.41 | 26.43 |
| MnO | 0.22 | 0.52 | 0.85 | 0.93 | 1.10 | 0.85 | 1.48 | 1.18 | 1.08 |
| MgO | 9.59 | 8.66 | 11.88 | 13.21 | 8.56 | 1.66 | 0.44 | 0.53 | 0.62 |
| CaO | 10.02 | 10.05 | 9.59 | 8.19 | 9.96 | 5.75 | 4.15 | 3.16 | 4.20 |
| $Na_2O$ | 2.21 | 1.91 | 3.29 | 3.74 | 2.45 | 4.93 | 5.96 | 5.23 | 5.82 |
| $K_2O$ | 1.26 | 1.06 | 1.12 | 1.00 | 0.97 | 1.26 | 1.49 | 1.10 | 1.26 |
| F | 2.86 | 1.94 | 2.53 | 3.38 | 2.61 | 1.98 | 2.34 | 0.54 | 1.44 |
| Cl | 0.35 | 0.17 | 0.11 | 0.02 | 0.17 | 0.09 | 0.08 | 0.08 | 0.15 |
| O=F, Cl | 1.28 | 0.86 | 1.09 | 1.42 | 1.13 | 0.85 | 1.13 | 0.28 | 0.70 |
| $H_2O_{calc}$ | 0.87 | 1.93 | 1.46 | 0.84 | 1.33 | 1.81 | 1.42 | 3.16 | 2.30 |
| Sum | 96.94 | 100.63 | 99.81 | 100.53 | 100.89 | 101.90 | 100.46 | 99.46 | 101.05 |
| | | | | | | | | | |
| Si | 6.867 | 6.763 | 7.144 | 7.458 | 6.994 | 7.635 | 7.815 | 7.860 | 7.260 |
| $Al^{IV}$ | 1.193 | 1.237 | 0.856 | 0.354 | 0.946 | 0.327 | 0.185 | 0.140 | 0.215 |
| $Fe^{3+}$ | | | | 0.188 | 0.060 | 0.038 | | | 0.525 |
| Sum | 8.000 | 8.000 | 8.000 | 8.000 | 8.000 | 8.000 | 8.000 | 8.000 | 8.000 |
| $Al^{VI}$ | 0.063 | 0.067 | 0.008 | | | | 0.004 | 0.004 | |
| Ti | 0.162 | 0.184 | 0.111 | 0.031 | 0.126 | 0.256 | 0.253 | 0.110 | 0.140 |
| $Fe^{3+}$ | | 0.022 | 0.500 | 0.640 | | 0.060 | 0.281 | 1,088 | 0.508 |
| $Fe^{2+}$ | 2.689 | 2.984 | 1.704 | 1.295 | 3.064 | 4.228 | 4.296 | 3.293 | 3.543 |
| Mn | 0.030 | 0.069 | 0.111 | 0.117 | 0.143 | 0.116 | 0.204 | 0.161 | 0.146 |
| Mg | 2.280 | 2.008 | 2.710 | 2.912 | 1.966 | 0.397 | 0.107 | 0.127 | 0.148 |
| Ca | 1.713 | 1.675 | 1.573 | 1.298 | 1.644 | 0.990 | 0.725 | 0.546 | 0.721 |
| Na | 0.063 | | 0.284 | 0.707 | 0.057 | 0.953 | 1.130 | 1.671 | 1.794 |
| Sum | 7.000 | 7.000 | 7.000 | 7.000 | 7.000 | 7.000 | 7.000 | 7.000 | 7.000 |
| $Na_A$ | 0.621 | 0.576 | 0.692 | 0.365 | 0.675 | 0.583 | 0.705 | 0.277 | 0.015 |
| $K_A$ | 0.257 | 0.210 | 0.219 | 0.189 | 0.191 | 0.258 | 0.300 | 0.226 | 0.258 |
| Sum | 0.878 | 0.786 | 0.911 | 0.554 | 0.866 | 0.841 | 1,005 | 0.503 | 0.273 |
| F | 1.443 | 0.954 | 1,225 | 1.581 | 1.272 | 1.06 | 1.207 | 0.275 | 0.730 |
| Cl | 0.095 | 0.044 | 0.029 | 0.005 | 0.044 | 0.024 | 0.022 | 0.022 | 0.041 |
| OH | 0.462 | 1,002 | 0.746 | 0.414 | 0.684 | 0.970 | 0.771 | 1,703 | 1,229 |
| Sum | 2.000 | 2.000 | 2.000 | 2.000 | 2.000 | 2.000 | 2.000 | 2.000 | 2.000 |
| | | | | | | | | | |
| mg# | 0.46 | 0.40 | 0.61 | 0.69 | 0.39 | 0.09 | 0.02 | 0.04 | 0.04 |
| | Ferro-edenite | Ferro-edenite | Edenite | Magnesio-katophorite | Ferro-edenite | Ferro-richterite | Ferro-richterite | Arfved-sonite | Arfved-sonite |

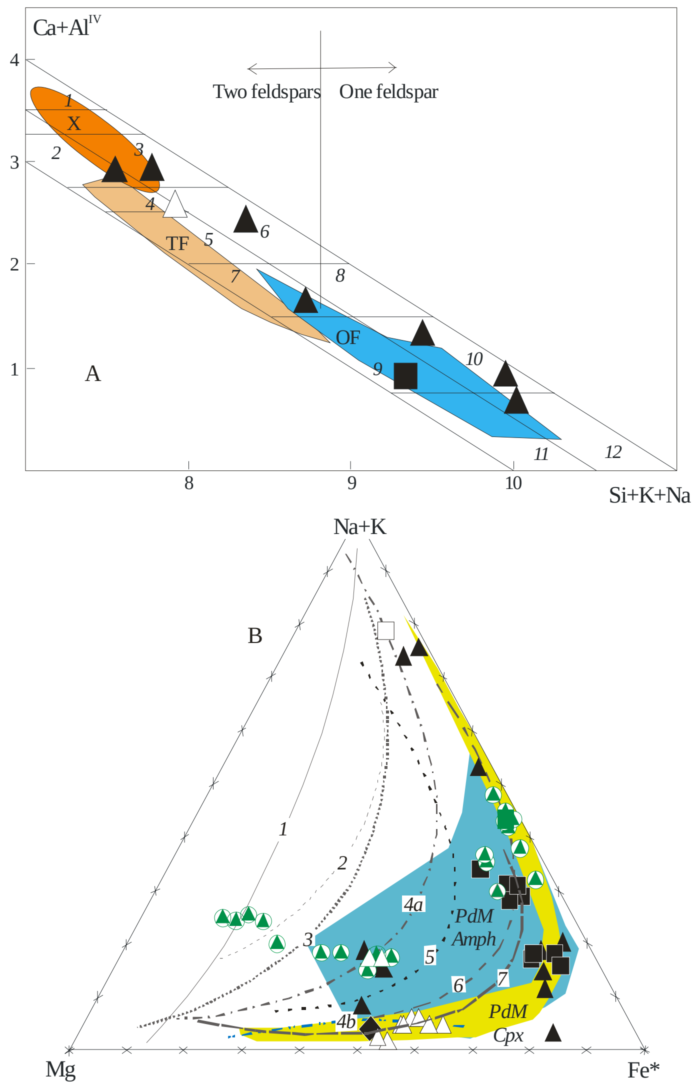


Fig. 7. A) Classificative diagrams of Giret *et al.* (1980) for the VC amphiboles (data source: Lustrino *et al.*, 2005; Comin-Chiaramonti, unpublished data); 1, hastingsite; 2, hornblende; 3, edenite; 4, actinolitic hornblende; 5, actinolite; 6, edenite; 7, barroisite; 8, katophorite; 9, winchite; 10, richterite; 11, riebeckite; 12, arfvedsonite (symbols as in Fig. 5). Fields for the Ponta do Morro amphiboles are illustrated for comparison (cf. Sousa *et al.*, in this volume). Mafic xenoliths (orange), two feldspars variants (sand) and one feldspar variants (blue). B) Compositional variations of VC clinopyroxenes and amphiboles (green symbols) into the Na+K-Mg-Fe* ($Fe^{2+}$+$Fe^{3+}$+Mn-Na-K) diagram. The trends of the clinopyroxene compositions from the main alkaline complexes are shown for comparison (Gomes *et al.*, 1987). 1, Anitápolis; 2, Itapirapuã; 3, Banhadão; 4, Rio de Janeiro state: a) Tanguá-Rio Bonito-Itaúna-Morro de São João, b) Soarinho; 5, Piratini; 6, Vitória island; 7, Tunas. Fields for the Ponta do Morro amphiboles and clinopyroxenes are shown in light blue and yellow, respectively.

Finally, it should be noted that the composition of the VC clinopyroxenes and amphiboles (Fig. 7B) straddles over the trends observed for the alkaline complexes from southern Brazil, with a tendency to fit the trend characterizing the Ponta do Morro complex (cf. Sousa *et al.*, in this volume).

*Biotite*

Biotites plot along the phlogopite-annite tie-line (Fig. 8), partially overlapping the analogues from the Ponta do Morro complex (cf. Sousa *et al.*, in this volume). They have mg# (Table 5) mainly between 0.56 and 0.21; the highest mg# is shown by the biotite from monzonitic rocks (mg#=0.56). Some compositions from the two feldspars and one feldspar syenites show relatively low Al contents, and the T site requires 0.092 to 0.191 $Fe^{3+}$ a.f.u. (cf. Table 5). However, in monzonites and in some two feldspars syenites the Al is enough to fill the tetrahedral sites, i.e. $Al^{VI}$ in octahedral sites ranges from 0.423 to 0.044 a.f.u.

*Fe-Ti oxides*

They are mostly magnetite and ilmenite (Table 6 and Fig. 9A).

Magnetite compositions for both intrusive and volcanic variants cluster near to the $Fe_2TiO_4$-$Fe_3O_4$ of the spinel prism (Deer *et al*., 1992), ranging from almost pure magnetite (ulvöspinel=7 mol%) to ulvöspinel 86 mol%. Notably, magnetite from one feldspar variants is occasionally present in some syenitic rocks, but it is characteristically absent in the granitic/rhyolitic rocks where the opaque phases are represented by ilmenite and hematite.

Ilmenite shows quite constant compositions: $R_2O_3$=1-12 mol%, low Al (0.000-0.003 a.f.u.) and Mg (0.001-0.011 a.f.u.) and relatively high Mn (0.060-0.134 a.f.u.). MnO contents (mean 4.2±1.2 wt%), similar to those of ilmenites from other PEIP alkaline complexes, are significantly higher (mean 1.05±0.33 wt%) than those of ilmenites from the Palmas rock-types (Bellieni *et al.*, 1988).

Coexisting magnetite-ilmenite pairs yielded closure temperatures in the range 560 to 922°C and $fO_2$ values (Spencer & Lindsley, 1981) spanning from MW and slightly higher NNO buffers (Fig. 9B). The latter $fO_2$ conditions are similar to those estimated for the eastern Paraguay and Bolivia alkaline complexes (cf. Comin-Chiaramonti & Gomes, 1996, and Comin-Chiaramonti *et al.*, in this volume, respectively), but quite different with respect to the alkaline rocks from the Ponta do Morro complex (cf. Sousa *et al.*, in this volume) which develop mainly along the quartz-fayalite-magnetite buffer (Fig. 9B).

It should be noted that magnetite-ilmenite pairs are extremely rare in the Palmas rock-types (cf. Bellieni *et al.*, 1988).

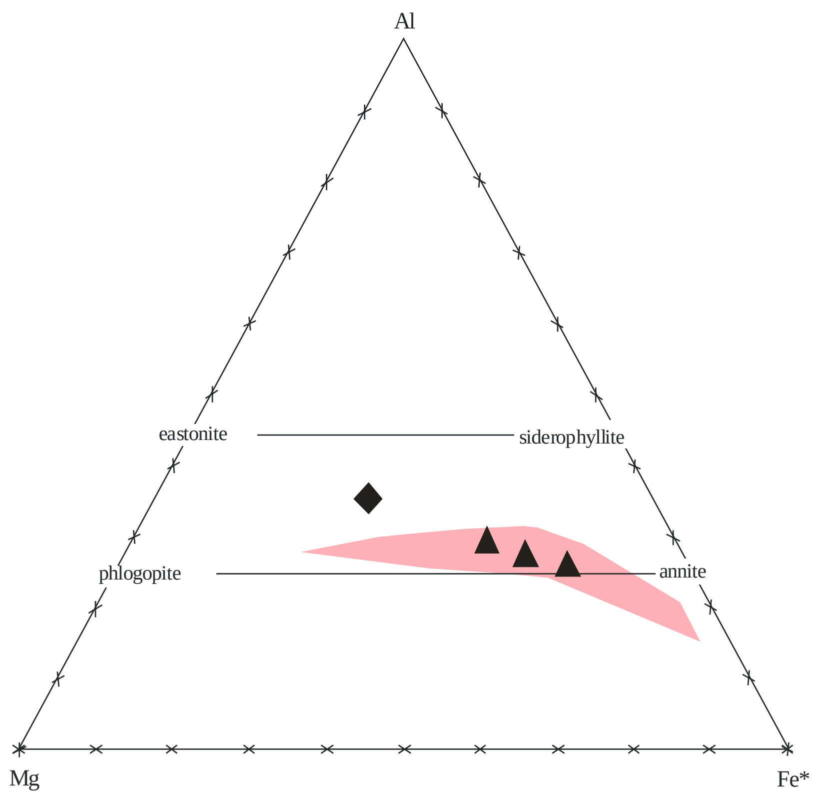


Fig. 8. Representative chemical analyses of biotites (data source: Comin-Chiaramonti, unpublished data) plotted into the Al-Mg-Fe* space (cf. Bailey, 1984, and therein references). Symbols as in Fig. 5. The Ponta do Morro field (cf. Sousa *et al.*, in this volume) is shown in pink.

Table 5. Selected analyses of biotites from the Valle Chico igneous rocks. Abbreviations and order numbers as in Table 1.

| TFV | 1 Monzonite C | 4 Syenite R | | OFV 11 Syenite R |
|---|---|---|---|---|
| $SiO_2$ | 38.44 | 36.23 | 36.59 | 36.22 |
| $TiO_2$ | 2.89 | 3.03 | 3.09 | 3.45 |
| $Al_2O_3$ | 15.27 | 10.99 | 12.09 | 10.38 |
| $FeO_{tot}$ | 16.98 | 29.29 | 26.21 | 32.36 |
| MnO | 0.22 | 0.35 | 0.33 | 0.43 |
| MgO | 12.22 | 6.51 | 7.73 | 4.68 |
| CaO | 0.34 | | 0.10 | |
| $Na_2O$ | 0.20 | 0.10 | 0.12 | 0.07 |
| $K_2O$ | 9.44 | 9.08 | 9.25 | 9.52 |
| Sum | 96.00 | 95.58 | 95.51 | 97.11 |
| | | | | |
| Si | 5.737 | 5.825 | 5.789 | 5.837 |
| $Al^{IV}$ | 2.263 | 2.083 | 2.211 | 1.972 |
| $Fe^{3+}$ | | 0.092 | | 0.191 |
| Sum | 8.000 | 8.000 | 8.000 | 8.000 |
| $Al^{VI}$ | 0.423 | | 0.044 | |
| Ti | 0.324 | 0.366 | 0.367 | 0.418 |
| $Fe^{2+}$ | 2.119 | 3.846 | 3.468 | 4.170 |
| Mn | 0.028 | 0.048 | 0.044 | 0.058 |
| Mg | 2.718 | 1.560 | 1.823 | 1.124 |
| Ca | 0.054 | | 0.017 | |
| Na | 0.058 | 0.031 | 0.037 | 0.022 |
| K | 1.797 | 1.862 | 1.867 | 1.957 |
| Sum | 7.575 | 7.713 | 7.667 | 7.749 |
| | | | | |
| mg# | 0.560 | 0.290 | 0.350 | 0.210 |

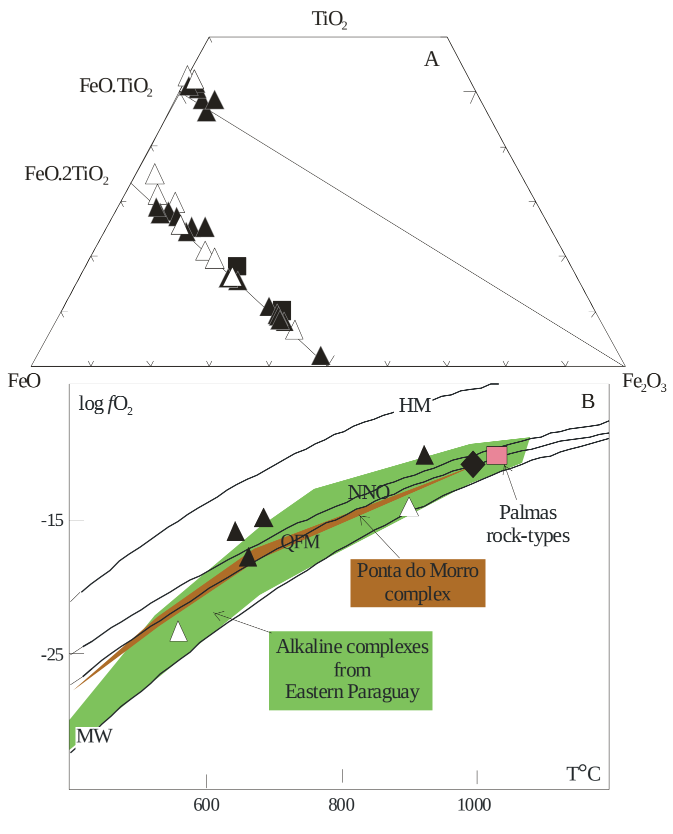


Fig. 9. A) Classification scheme of Valle Chico opaque minerals (rhombohedral phases and spinel phases; Deer *et al.*, 1992). B) T°C vs. log $fO_2$ for Ti-magnetite and ilmenite pairs for rock-types from Valle Chico (symbols as in Fig. 5). The fields relative to the magnetite-ilmenite pairs from the Eastern Paraguay alkaline complexes, from the Palmas rock-types and from the Ponta do Morro complex are also shown (data source: Piccirillo & Melfi, 1988; Comin-Chiaramonti & Gomes, 1996; Lustrino *et al.*, 2005; Sousa *et al.*, in this volume). Buffers: HM, hematite-magnetite; NNO, nickel-nickel oxide; QFM, quartz-fayalite-magnetite; MW, magnetite-wustite.

Table 6. Selected microprobe analyses of opaque minerals (Mt, magnetite; Il, ilmenite) from the Valle Chico igneous rocks. Abbreviations as in Table 2. $Fe^{2+}$-$Fe^{3+}$ repartition as from stoichiometry. T°C and log $fO_2$ calculated according to Spencer & Lindsley (1981).

| | 1 | | 3 | | 4 | | | | 7 | | 11 | | | 13 |
|---|---|---|---|---|---|---|---|---|---|---|---|---|---|---|
| TFV | Monzonite Il | Monzonite Mt | Syenite Il | Syenite Mt | Syenite Il | Syenite Mt | Syenite Il | Syenite Mt | Trachyte Il | Trachyte Mt | OFV | Syenite Il | Syenite Mt | Granite Il |
| $SiO_2$ | 0.06 | 0.24 | 0.35 | 0.70 | 0.01 | 0.10 | | | | | | 0.04 | 0.43 | 0.08 |
| $TiO_2$ | 48.60 | 20.16 | 46.11 | 15.43 | 49.75 | 6.59 | 48.87 | 5.01 | 51.02 | 36.60 | | 51.89 | 0.66 | 47.41 |
| $Al_2O_3$ | 0.02 | 1.17 | 0.11 | 0.94 | 0.01 | 0.15 | 0.02 | 0.73 | 0.01 | 0.19 | | | 0.01 | |
| $FeO_{tot}$ | 9.11 | 27.96 | 11.79 | 36.35 | 5.33 | 55.56 | 5.14 | 55.84 | 3.03 | 10.08 | | 0.71 | 65.87 | 9.26 |
| FeO | 40.02 | 48.29 | 37.55 | 45.36 | 40.98 | 35.99 | 40.98 | 35.84 | 39.41 | 56.27 | | 42.22 | 31.63 | 37.42 |
| MnO | 3.62 | 1.97 | 4.24 | 0.93 | 3.21 | 1.15 | 2.75 | 0.55 | 6.26 | 3.13 | | 4.38 | 0.25 | 5.15 |
| MgO | 0.05 | 0.00 | 0.02 | 0.08 | 0.29 | 0.03 | 0.010 | 0.02 | 0.07 | 0.13 | | 0.06 | 0.02 | 0.05 |
| Sum | 101.51 | 99.90 | 100.17 | 99.79 | 99.58 | 99.57 | 97.86 | 98.99 | 99.80 | 100.40 | | 99.30 | 98.87 | 99.37 |
| Si | 0.001 | 0.072 | 0.009 | 0.211 | | 0.031 | | | | | | 0.001 | 0.133 | 0.002 |
| Ti | 0.912 | 4.551 | 0.877 | 3,498 | 0.949 | 1.521 | 0.950 | 1,393 | 0.971 | 6,841 | | 0.992 | 0.154 | 0.909 |
| Al | 0.001 | 0.414 | 0.003 | 0.334 | | 0.054 | 0.001 | 0.265 | | 0.067 | | | 0.003 | |
| $Fe^{3+}$ | 0.171 | 6.315 | 0.225 | 8,247 | 0.102 | 12.839 | 0.100 | 12.950 | 0.058 | 2.255 | | 0.014 | 15.412 | 0.178 |
| $Fe^{2+}$ | 0.835 | 12.121 | 0.794 | 11.437 | 0.869 | 9.242 | 0.886 | 9.238 | 0.834 | 13.990 | | 0.897 | 8.224 | 0.798 |
| Mn | 0.077 | 0.501 | 0.091 | 0.237 | 0.069 | 0.299 | 0.060 | 0.144 | 0.134 | 0.788 | | 0.094 | 0.065 | 0.111 |
| Mg | 0.002 | 0.000 | 0.001 | 0.036 | 0.011 | 0.014 | 0.004 | 0.010 | 0.003 | 0.058 | | 0.002 | 0.009 | 0.002 |
| Sum | 2.000 | 24.000 | 2.000 | 24.000 | 2.000 | 24.000 | 2.001 | 24.000 | 2.000 | 23.999 | | 2.000 | 24.000 | 2.000 |
| Mol | | | | | | | | | | | | | | |
| Ulvöspinel | | 0.59 | | 0.46 | | 0.19 | | 0.17 | | 0.86 | | | 0.07 | |
| Ilmenite | 0.91 | | 0.89 | | 0.95 | | 0.95 | | 0.97 | | | 0.99 | | 0.91 |
| T°C | | 1000 | | 922 | | 667 | | 646 | | 914 | | | 689 | |
| log $fO_2$ | | -11.5 | | -11.5 | | -18.5 | | -16.0 | | -14.5 | | | -15.0 | |

*Apatite*

Apatite contains high F contents, i.e. 4.72±1.25 wt%, both in the one feldspar and in the two feldspars variants (Lustrino *et al*., 2005).

Occasionally (rhyolite 633 of Balestra, 1985), some flakes (bastnaesite?) are associated with the accessory fluorite: a semiquantitative analysis shows $La_2O_3$=22, $Ce_2O_3$=41, $Nd_2O_3$=10 and F=7 wt%. The high F concentrations of the apatites, coupled with high F contents of amphiboles and the presence of fluorite and fluorcarbonates in the more evolved rock-types, point to a high F activity in the Valle Chico complex, similar to other alkaline and alkaline-carbonatitic complexes from the PEIP, e.g. Mato Preto, Ponta Grossa Arch, Brazil (cf. Comin-Chiaramonti *et al.*, 2002b, and therein references) and Brandberg, Namibia (Schmitt *et al*., 2002).

## PETROCHEMISTRY

### *Major elements*

From Fig. 4 it is apparent that the one feldspar (i.e. peralkaline) and the two feldspars variants (i.e. metaluminous) tend to fit the fields of the Aiguá and the Lavalleja series of Kirstein *et al*. (2000), respectively, and are well distinct from the Palmas felsic volcanics.

The Harker diagrams for the VC rocks (average compositions; Fig. 10A) together with the 92-U12 trachybasalt (Turner *et al.*, 1999), the behaviours of the low-Ti tholeiitic suites from southern regions of the Paraná Basin and the fields of the coeval felsic igneous rocks from eastern Uruguay and Palmas flows (Kirstein *et al*., 2000, and Bellieni *et al*., 1986b, respectively) show important differences:

1) both one and two feldspars variants display spreadings quite different from the low-Ti suites from southern Brazil and appear to some extent correlated with the 92-U12 trachybasalt;

2) the field of the Palmas rocks partially overlaps that of the Lavalleja suite;

3) the one feldspar group is well distinct, for the same silica contents, from the two feldspars variants, above all for the lower $TiO_2$, MgO, CaO and $P_2O_5$ and for the higher $Na_2O$ contents;

4) regarding the other coeval felsic lithologies from eastern Uruguay, the one feldspar rocks show

major $Na_2O$ and minor $K_2O$ contents; the two feldspars varieties display higher MgO and CaO contents and a quite constant attitude for $K_2O$ (av. ~4.5 wt%), lower than the analogous contents of the Aiguá suite (av. ~5.5 wt%);

5) the Arequita rhyolites are in the same trend of the VC rhyolites;

6) the rhyolites systematically have high Fe contents (i.e. pantelleritic trend).

If the comparison is made with other felsic suites from the PEIP and Argentina (Fig. 10B), it becomes apparent that:

1) the fields representing Early Cretaceous felsic oversaturated rocks from the Damaraland complexes

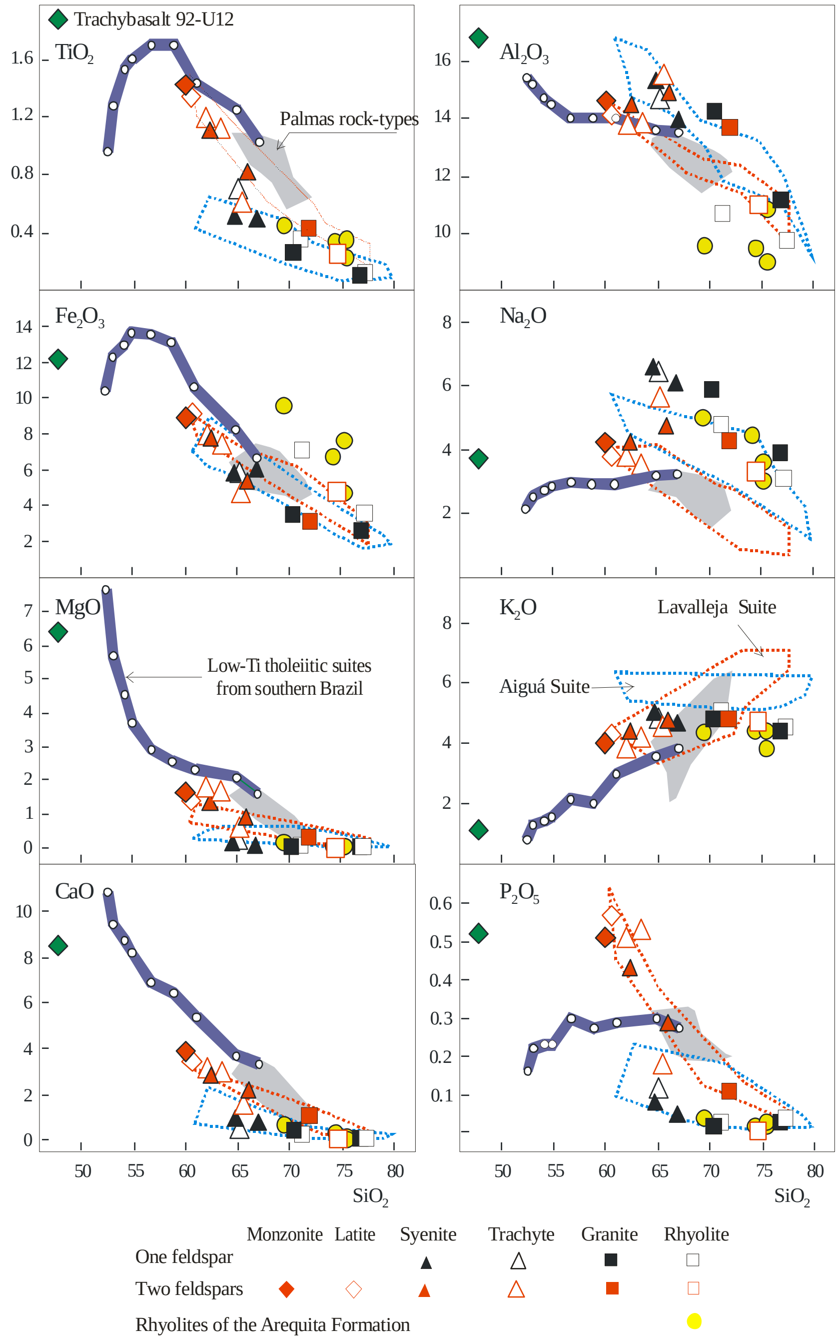


Fig. 10A. Major elements, Harker diagrams, for the Valle Chico rock-types (Table 1), 92-U12 Aiguá trachybasalt (Turner *et al.*, 1999; Kirstein *et al.*, 2000), and evolution line of low-Ti rock-types from southern Brazil (violet heavy line; cf. Bellieni *et al.*, 1986). The fields of coeval-subcoeval felsic rocks from eastern Uruguay (Lavalleja, dotted red line; Aiguá, dotted blue line) and from Palmas (gray) are shown for comparison (data source: Bellieni *et al.*, 1986b; Piccirillo & Melfi, 1988; Garland *et al.*, 1995; Kirstein *et al.*, 2000).

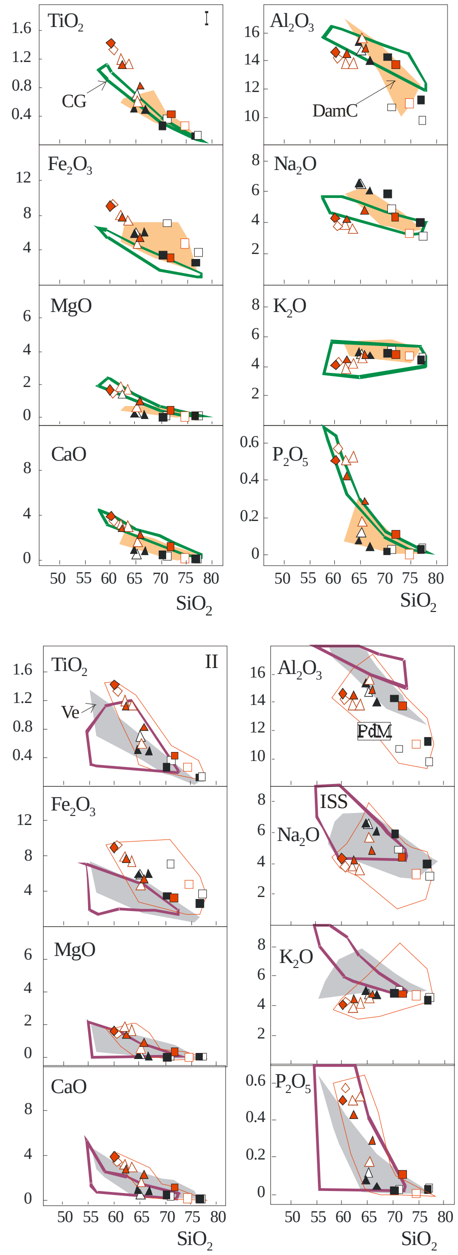


Fig. 10B. Major elements, Harker diagrams, for the Valle Chico rock-types (symbols as in Fig. 10A), compared with I: fields of alkaline felsic rock-types from the Choiyoi Group (CG, heavy green line; Permo-Triassic "trachytic shoshonites" from central Argentina; Llambías *et al.*, 2003) and from Damaraland complexes (DamC, sand field; Early Cretaceous complexes from Namibia; Trumbull *et al.*, 2004); II: fields of alkaline felsic rock-types from the Velasco complexes (Ve, light blue field; Early Cretaceous complexes from southeastern Bolivia; Comin-Chiaramonti *et al.*, in this volume), from Ponta do Morro complex (PdM, brown line; Late Early Cretaceous, Mato Grosso; Sousa *et al.*, in this volume) and from Itatiaia and São Sebastião complexes (ISS, heavy red lines; Late Cretaceous, southeastern Brazil; Enrich *et al.*, in this volume).

(Namibia; Trumbull *et al.*, 2004) and analogous alkaline rocks from the Choiyoi Group (Permo-Triassic "trachytic shoshonites" from central Argentina; Llambías *et al.*, 2003) do not show consistent whole elementary correlation with the VC rock-types (Fig. 10B, I);

2) the field representing the Ponta do Morro felsic complex (Late Early Cretaceous, Mato Grosso; Sousa *et al.*, in this volume) appears well covering the Valle Chico trend (Fig. 10B II). On the other hand, Lustrino *et al.* (2005) proposed a genetic similarity between the Messum complex (Damaraland,

Namibia) and the Valle Chico complex, because the first one is believed to be, on the whole, the feeding system for all the silica-oversaturated igneous rock-types.

In order to test the evolutionary processes for the Valle Chico and Arequita felsic variants based on major elements, a series of fractional crystallization processes, starting from the 92-U12 trachybasalt (mg#=0.55), was computed (cf. Stormer & Nicholls, 1978). The inferred liquid of descent for the major elements from slightly ne-normative trachybasalt through metaluminous hy-normative monzonite and the more evolved variants may be mainly related to the extent of plagioclase fractionation (Table 7).

Any attempt to derive the one feldspar variants from the trachybasalt or from the other more evolved two feldspars variants gives unrealistic solutions.

The evolution of one feldspar variants, starting from the less evolved syenite (10) of Table 1, implies a fractionation process essentially of alkali feldspar+amphibole for syenitic and trachytic rocks, whereas the best solutions for the rhyolites require fractionation of alkali feldspar+clinopyroxene.

Table 7. Modelling of fractional crystallization through mass balance calculations (Stormer & Nicholls, 1978) for major elements. Only the best results are presented. Abbreviations: Ol, olivine; Cpx, Ca-clinopyroxene; Pl, plagioclase; AK, alkali feldspar; Bi, biotite; Am, amphibole; Mt, magnetite; Il, ilmenite; Ap, apatite. Rock numbers as in Table 1.

| Fractional trends<br>Two feldspar variants | | | | | | | |
|---|---|---|---|---|---|---|---|
| (I)<br>From trachybasalt 92-U12 to monzonite 1<br>Subtracted solid 80.6 ($r^2$=0.08) | | (II)<br>From trachybasalt 92-U12 to latite 2<br>Subtracted solid 81.9 ($r^2$=0.11) | | (III)<br>From trachybasalt 92-U12 to syenite 3<br>Subtracted solid 82.7 ($r^2$=0.09) | | (IV)<br>From trachybasalt 92-U12 to syenite 4<br>Subtracted solid 83.5 ($r^2$=0.17) | |
| Ol | 13.1 ($Fo_{80}$) | Ol | 13.1 ($Fo_{80}$) | Ol | 12.8 ($Fo_{80}$) | Ol | 12.8 ($Fo_{80}$) |
| Cpx | 13.4 ($En_{38}$-$Fs_{14}$-$Wo_{48}$) | Cpx | 13.1 ($En_{38}$-$Fs_{14}$-$Wo_{48}$) | Cpx | 13.6 ($En_{38}$-$Fs_{14}$-$Wo_{48}$) | Cpx | 12.8 ($En_{38}$-$Fs_{14}$-$Wo_{48}$) |
| Pl | 60.9 ($An_{65}$) | Pl | 61.3 ($An_{65}$) | Pl | 60.7 ($An_{65}$) | Pl | 61.3 ($An_{65}$) |
| Mt | 11.1 | Mt | 11.0 | Mt | 11.0 | Mt | 11.5 |
| Ap | 1.5 | Ap | 1.5 | Ap | 1.6 | Ap | 1.6 |
| (V)<br>From monzonite 1 to syenite 3<br>Subtracted solid 12.3 $r^2$=0.04 | | (VI)<br>From syenite 3 to trachyte 7<br>Subtracted solid 10.3 ($r^2$=1.19) | | (VII)<br>From syenite 3 to rhyolite 9<br>Subtracted solid 63.1% ($r^2$=0.17) | | | |
| Cpx | 24.3 ($En_{38}$-$Fs_{14}$-Wo $_{48}$) | Cpx | 63.2 ($En_{28}$-$Fs_{34}$-$Wo_{37}$) | Cpx | 2.7 ($En_{28}$-$Fs_{34}$-Wo $_{37}$) | | |
| Pl | 51.2 ($An_{65}$) | Pl | 8.5 ($An_{49}$) | Amp | 11.9 | | |
| Bi | 7.0 | Mt | 24.4 | Pl | 18.0 ($An_{49}$) | | |
| Mt | 10.2 | Ap | 3.9 | AK | 58.1 | | |
| Il | 3.7 | | | Mt | 7.8 | | |
| Ap | 3.6 | | | Ap | 1.6 | | |
| Fractional trends<br>One feldspar variants | | | | | | | |
| (VIII)<br>From syenite 10 to syenite 11<br>Subtracted solid 57.5% $r^2$=0.04 | | (IX)<br>From syenite 10 to granite 13<br>Subtracted solid 69.6% ($r^2$=0.06) | | (X)<br>From syenite 10 to rhyolite 15<br>Subtracted solid 86.5% ($r^2$=0.91) | | (XI)<br>From monzonite 1 to Arequita rhyolites 15<br>Subtracted solid 90.4% ($r^2$=0.93) | |
| Cpx | 2.9 ($En_2$-$Fs_{78}$-$Wo_{21}$) | Cpx | 3.4 ($En_2$-$Fs_{78}$-$Wo_{21}$) | Cpx | 16.3 ($En_2$-$Fs_{78}$-$Wo_{21}$) | Cpx | 16.8 ($En_2$-$Fs_{78}$-$Wo_{21}$) |
| Amp | 10.2 | Amp | 11.9 | AF | 83.4 ($Or_{38}$) | AF | 82.9 ($Or_{38}$) |
| AF | 85.2 ($Or_{38}$) | AF | 82.6 ($Or_{38}$) | Ap | 0.3 | Ap | 0.3 |
| Mt | 0.7 | Mt | 1.1 | | | | |
| II | 0.5 | Il | 0.6 | | | | |
| Ap | 0.4 | Ap | 0.4 | | | | |

### *Trace elements*

The importance of plagioclase fractionation in the Valle Chico complex is demonstrated by the strong positive correlation between the Sr concentration and the Eu/Eu* ratios (Fig. 11A), overlapping the fields relative to the oversaturated felsic rocks from Damaraland and Choiyoi. It is important to note that the latters, regardless of their differentiation degree, have trace element contents corresponding to the

"A-type" granites as defined by Whalen *et al.* (1987), e.g. the high Ga/Al ratios and elevated contents of high field strength trace elements similar to the VC analogues (Fig. 11B).

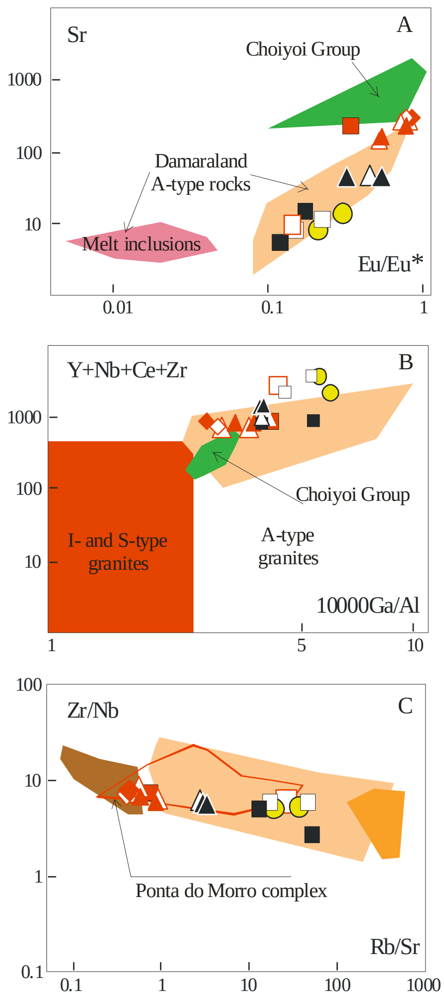


Fig. 11. Selected trace elements characteristics of the Valle Chico rock-types (symbols as in Fig. 10A) showing: A) The strong positive correlation between Sr and Eu/Eu*, suggesting a control of magma composition by feldspar fractionation. B) The discrimination plot of Whalen *et al.* (1987) and the fields of the Damaraland and Choiyoi A-type felsic rocks. C) The Rb/Sr vs. Zr/Nb ratios that mainly fit the peralkaline trend outlined by the Paresis and Brandberg complexes (Damaraland) and the Ponta do Morro intrusion (Mato Grosso). Data source: Llambías *et al.* (2003), Trumbull *et al.* (2004) and Sousa *et al.* (in this volume).

It should to be stressed that the variation of Rb/Sr vs. Zr/Nb (Fig. 11C) for the Valle Chico rocks shows Rb/Sr increase and a quite constant attitude for the Zr/Nb ratio, similar to the behaviour of the Ponta do Morro complex.

The diagrams relative to the trace elements vs. $SiO_2$ wt% (Fig. 12A) show that:

1) Rb and Sr (Ba) display positive and negative correlations, respectively, with the silica content, while La, Zr, Nb and Y show variable but large scattering (Fig. 12A). In particular the one feldspar variants are characterized by higher Nb, Zr, and La, and by lower Sr and Ba contents, respectively, than the corresponding two feldspars variants.

2) In spite of the scattering, the differences between the VC complex and the felsic volcanic series from SE Uruguay are also apparent in the trace element diagrams, particularly for the VC rhyolitic variants. The latter are systematically characterized by very high Zr, Nb and Y contents. It is remarkable that the Palmas flows contain very low Zr and Nb concentrations (average 283±52 ppm and 20±10 ppm, respectively). On the other hand, the Chapecó rock-types ($SiO_2$ 63-68 wt%; Bellieni *et al.*, 1986b; Garland *et al.*, 1995) have average Zr=604±54 ppm and Nb=50±3 ppm, but they are characterized by higher Sr (369±42 ppm) than the corresponding VC two feldspars analogues (210±54).

3) In general the one feldspar and two feldspars variants tend to fit the fields defined by the Aiguá and Lavalleja suites, respectively.

4) In the Zr vs. Nb diagram (cf. Leat *et al.*, 1986; Fig. 12A), the VC (and Arequita) rocks significantly differ from the Palmas, Aiguá and Lavelleja series: the VC rocks tend to plot in the peralkaline field, the Palmas and the Lavalleja suites fit the subalkaline field, and the Aiguá series straddle over subalkaline, transitional and peralkaline fields.

5) Sm/Nd mean ratios increase from the Aiguá and Lavalleja series (0.185±0.026 and 0.194±0.011, respectively) to the VC syenites+trachytes (0.206± 0.010) and to the VC granites+rhyolites (0.264± 0.053). The Palmas and Chapecó felsic rocks have mean Sm/Nd=0.211±0.018 and 0.196±0.004, respectively.

6) If the comparison is made with the other felsic A-type complexes related to the PEIP, the best

correspondence with the Valle Chico complex seems to be that defined by the rock-types from the Ponta do Morro complex (Fig. 12B).

*Modelling of fractional crystallization*

In order to test the mass balances of Table 7, the Rayleigh equation (Neumann *et al.*, 1954) was used in the modelling of the trace elements. The results are listed in Table 8 and illustrated in Fig. 13. The compositional ranges of the observed/calculated ratios are consistent with crystal fractionation from trachybasalt and monzonite for all the two feldspars variants, rhyolite excepted, so that in the latter strong positive and negative variations for Nb-Zr and Sr, respectively, are noted.

The one feldspar variants display a broad accordance in fractionation from the less to more evolved syenites, La-Ce and Sr excepted. On the other hand, the trace modelling is not consistent with the derivation of granitic and rhyolitic rocks from a

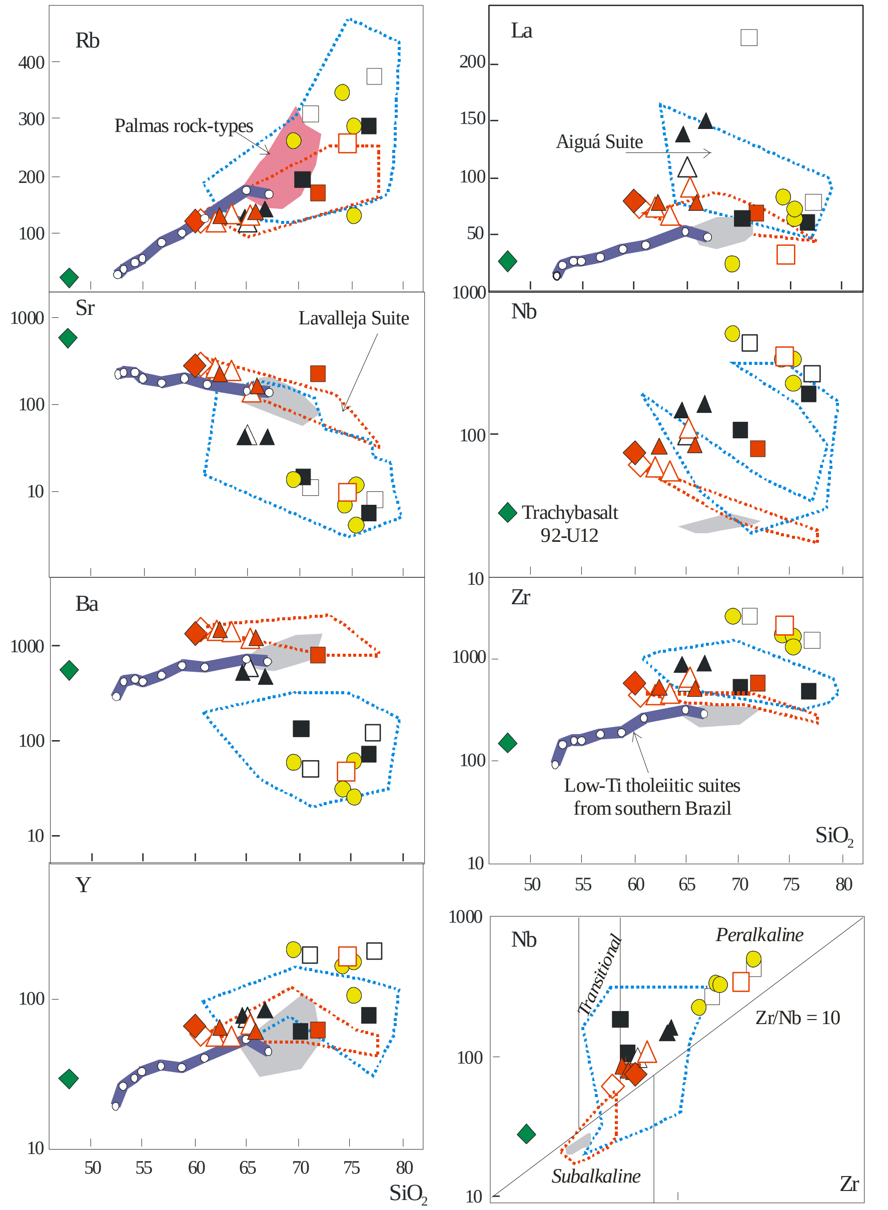


Fig. 12A. Trace elements (ppm) vs. silica diagrams for the Valle Chico rock-types compared with the analogous fields of Fig. 10A (symbols as in Fig. 10A) and Zr vs. Nb diagram with subalkaline, transitional and peralkaline fields according to the divisions of Leat *et al.* (1986). Data source as in Fig. 10 B.

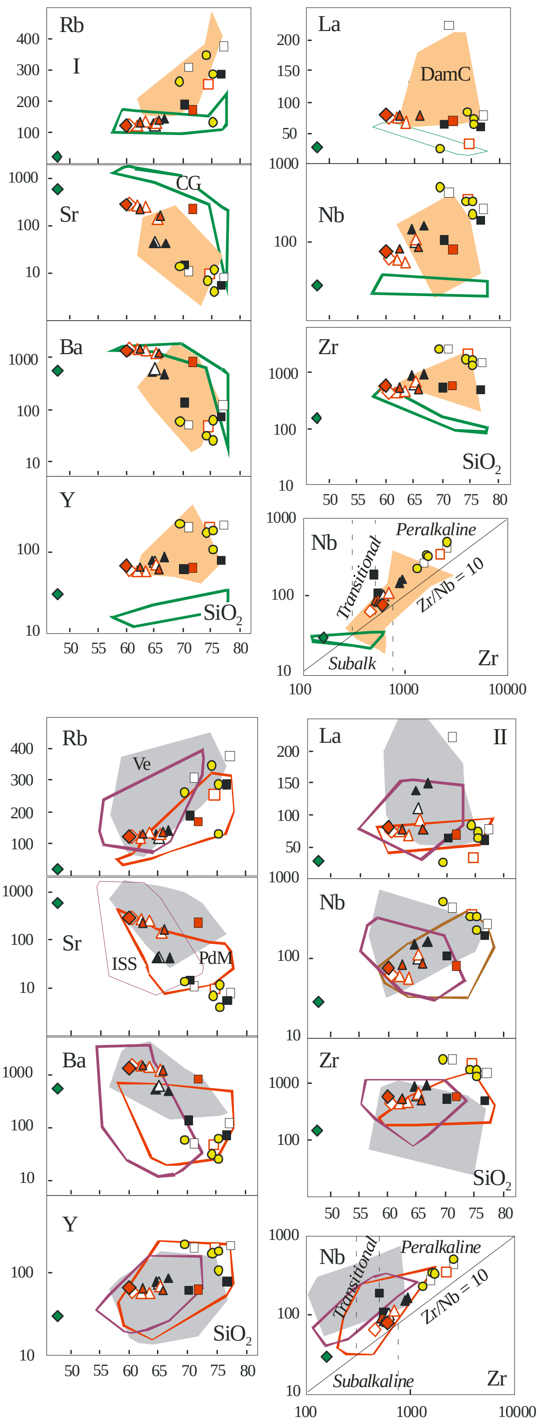


Fig. 12B. Trace elements (ppm) vs. silica diagrams for the Valle Chico rock-types compared with the analogous fields of Fig. 10B, I and II, respectively (cf. also Fig. 11A).

Table 8. Fractional crystallization model for trace elements from the Valle Chico variants (cf. Table 7): $C_{obs}/C_{calc}$ (observed/calculated) ratios with relative ranges (rock numbers and concentrations as in Table 1). The equation $C_L=C_0F^{(D-1)}$ is used where $C_L$ is the concentration of an element in the residual liquid, $C_0$ is the concentration of an element in the initial liquid, F is the fraction of melt left, and D is the bulk distribution coefficient for the minerals settling out of the melt (Neumann *et al.*, 1954). Mineral/melt partition coefficients are from Rollinson (1993) and therein references.

Fractional trends

Two feldspar variants

| (I) From trachybasalt 92-U12 to monzonite 1 | $C_{obs}/C_{calc}$ | (II) From trachybasalt 92-U12 to latite 2 | $C_{obs}/C_{calc}$ | (III) From trachybasalt 92-U12 to syenite 3 | $C_{obs}/C_{calc}$ | (IV) From trachybasalt 92-U12 to syenite 4 | $C_{obs}/C_{calc}$ |
|---|---|---|---|---|---|---|---|
| Rb | 1.12 (0.94-1.30) | Rb | 1.07 (0.95-1.19) | Rb | 1.10 (0.94-1.26) | Rb | 1.05 (0.94-1.15) |
| Ba | 0.80 (0.77-0.82) | Ba | 0.86 (0.82-0.90) | Ba | 0.90 (0.81-0.98) | Ba | 0.88 (0.65-1.19) |
| Nb | 0.82 (0.74-0.82) | Nb | 0.70 (0.68-0.73) | Nb | 0.76 (0.47-1.05) | Nb | 0.99 (0.79-1.19) |
| La | 0.99 (0.90-1.02) | La | 0.87 (0.84-0.91) | La | 0.92 (0.72-1.11) | La | 1.04 (0.96-1.13) |
| Ce | 1.03 (0.99-1.07) | Ce | 0.91 (0.86-0.97) | Ce | 0.99 (0.80-1.17) | Ce | 1.05 (1.00-1.09) |
| Sr | 0.99 (0.86-1.13) | Sr | 1.14 (1.03-1.24) | Sr | 1.17 (0.91-1.42) | Sr | 0.62 (0.47-0.76) |
| Nd | 1.24 (1.16-1.33) | Nd | 1.10 (1.04-1.16) | Nd | 1.21 (1.09-1.33) | Nd | 1.16 (0.98-1.34) |
| Sm | 1.20 (1.14-1.19) | Sm | 1.28 (1.19-1.37) | Sm | 1.19 (1.05-1.32) | Sm | 1.57 (1.33-1.82) |
| Zr | 1.06 (0.90-1.22) | Zr | 0.90 (0.82-0.97) | Zr | 0.9 (0.73-1.07) | Zr | 0.91 (0.70-1.12) |
| Y | 0.84 (0.89-1.00) | Y | 0.95 (0.89-1.02) | Y | 0.89 (0.83-1.05) | Y | 0.92 (0.81-1.03) |

| (V) From monzonite 1 to syenite 3 | $C_{obs}/C_{calc}$ | (VI) From syenite 3 to trachyte 7 | $C_{obs}/C_{calc}$ | (VII) From syenite 3 to rhyolite 9 | $C_{obs}/C_{calc}$ |
|---|---|---|---|---|---|
| Rb | 1.1 (0.94-1.26) | Rb | 0.90 (0.88-0.99) | Rb | 1.26 (0.91-1.61) |
| Ba | 1.08 (0.98-1.18) | Ba | 0.77 (0.57-0.98) | Ba | 0.73 (0.53-0.94) |
| Nb | 1.05 (0.65-1.45) | Nb | 1.27 (1.01-1.52) | Nb | 1.81 (1.20-2.41) |
| La | 1.02 (0.78-1.19) | La | 1.11 (1.03-1.20) | La | 0.69 (0.38-0.99) |
| Ce | 1.01 (0.82-1.20) | Ce | 1.08 (1.04-1.12) | Ce | 1.20 (0.90-1.51) |
| Sr | 0.89 (0.70-1.09) | Sr | 0.76 (0.58-0.94) | Sr | 0.43 (0.26-0.61) |
| Nd | 1.05 (0.94-1.16) | Nd | 1.20 (1.01-1.39) | Nd | 0.98 (0.46-1.49) |
| Sm | 1.08 (0.96-1.20) | Sm | 1.43 (1.21-1.65) | Sm | 1.13 (0.54-1.63) |
| Zr | 0.85 (0.69-1.01) | Zr | 1.19 (0.92-1.47) | Zr | 1.64 (1.19-2.09) |
| Y | 1.00 (0.82-1.18) | Y | 1.01 (0.90-1.13) | Y | 1.24 (0.97-1.51) |

Fractional trends

One feldspar variants

| (VIII) From syenite 10 to syenite 11 | $C_{obs}/C_{calc}$ | (IX) From syenite 10 to granite 13 | $C_{obs}/C_{calc}$ | (X) From syenite 10 to rhyolite 15 | $C_{obs}/C_{calc}$ | (XI) From syenite 10 Arequita rhyolites 16 | $C_{obs}/C_{calc}$ |
|---|---|---|---|---|---|---|---|
| Rb | 0.97 (0.72-1.22) | Rb | 0.89 (0.84-0.94) | Rb | 0.63 (0.53-0.72) | Rb | 0.59 (0.47-0.70) |
| Ba | 1.02 (0.32-1.72) | Ba | 0.92 (0.00-2.03) | Ba | 3.4 (2.47-4.33) | Ba | 2.16 (1.11-3.22) |
| Nb | 0.81 (0.52-1.00) | Nb | 0.62 (0.58-0.66) | Nb | 0.67 (0.51-0.82) | Nb | 0.33 (0.27-0.40) |
| La | 0.55 (0.36-0.75) | La | 0.18 (0.09-0.27) | La | 0.40 (0.34-0.46) | La | 0.10 (0.08-0.12) |
| Ce | 0.61 (0.37-0.85) | Ce | 0.25 (0.12-0.37) | Ce | 0.43 (0.38-0.48) | Ce | 0.10 (0.09-0.11) |
| Sr | 1.87 (0.00-3.35) | Sr | 15.00 (0.00-16.00) | Sr | 1.12 (0.49-1.75) | Sr | 0.80 (0.40-1.20) |
| Nd | 0.74 (0.51-0.96) | Nd | 0.29 (0.19-0.40) | Nd | 0.44 (0.38-0.51) | Nd | 0.14 (0.10-0.19) |
| Sm | 0.95 (0.77-1.10) | Sm | 0.32 (0.26-0.39) | Sm | 0.41 (0.31-0.51) | Sm | 0.26 (0.21-0.32) |
| Zr | 0.93 (0.56-1.30) | Zr | 0.35 (0.27-0.44) | Zr | 0.96 (0.69-1.23) | Zr | 0.43 (0.37-0.49) |
| Y | 0.83 (0.63-1.04) | Y | 0.59 (0.42-0.77) | Y | 0.8 (0.54-1.05) | Y | 0.45 (0.33-0.57) |

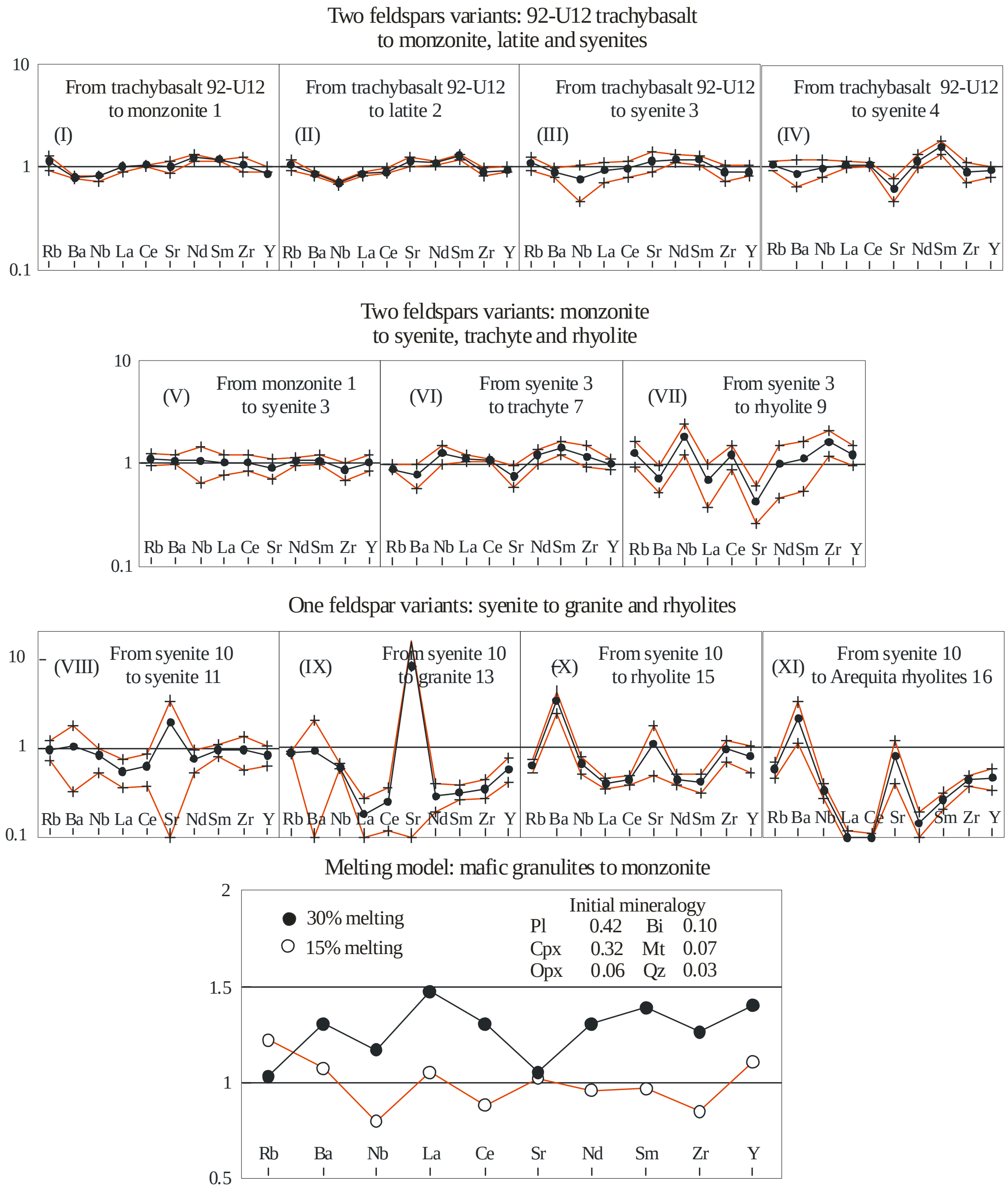


Fig. 13. $C_{observed}/C_{calculated}$ ratios for selected trace elements (cf. Table 8). The full circles and crosses correspond to the average values and to the maximum and minimum concentrations (as from Table 1); I - XI: various steps of Table 8. Melting model (batch equilibrium melting; Shaw, 1970) represents the $C_{observed}/C_{calculated}$ ratios of trace elements (monzonite 1 of Table 1, 15-30% batches) melts from a mafic granulite source.

precursor syenitic material. The granites show very strong HFSE and REE negative, and Sr positive spikes, respectively, whereas the rhyolites are above all characterized by positive Ba, and REE negative spikes, respectively. In particular, it can be seen that the Valle Chico and Arequita rhyolites present similar patterns.

These behaviours cannot simply be attributed to the accessory phases or to adequate mineral/liquid partition coefficients, but may be related to different sources or to mixing and/or assimilation processes.

Alternatively, the monzonite 1 may be modelled through batch melting of 15% of mafic granulites (Fig. 13), while the one feldspars syenites may be the products of about 20 to 50% of intermediate to acid granulites (charnockitic compositions).

*Normalized trace elements*

Primitive mantle-normalized multi-elemental plots (Sun & McDonough, 1989) show a tendency to positive Nb-Ta and Zr-Hf spikes, especially in one feldspar syenites and rhyolites, strongly contrasting with the Nb-Ta negative anomaly of the Lavalleja series (Fig. 14A) and with all the tholeiitic flood basalts of the Paraná Basin as well as with the felsic associated rocks, i.e. Palmas and Chapecó types (cf. Bellieni *et al.*, 1988; Piccirillo & Melfi, 1988; Comin-Chiaramonti *et al.*, 1997, 1999, and therein

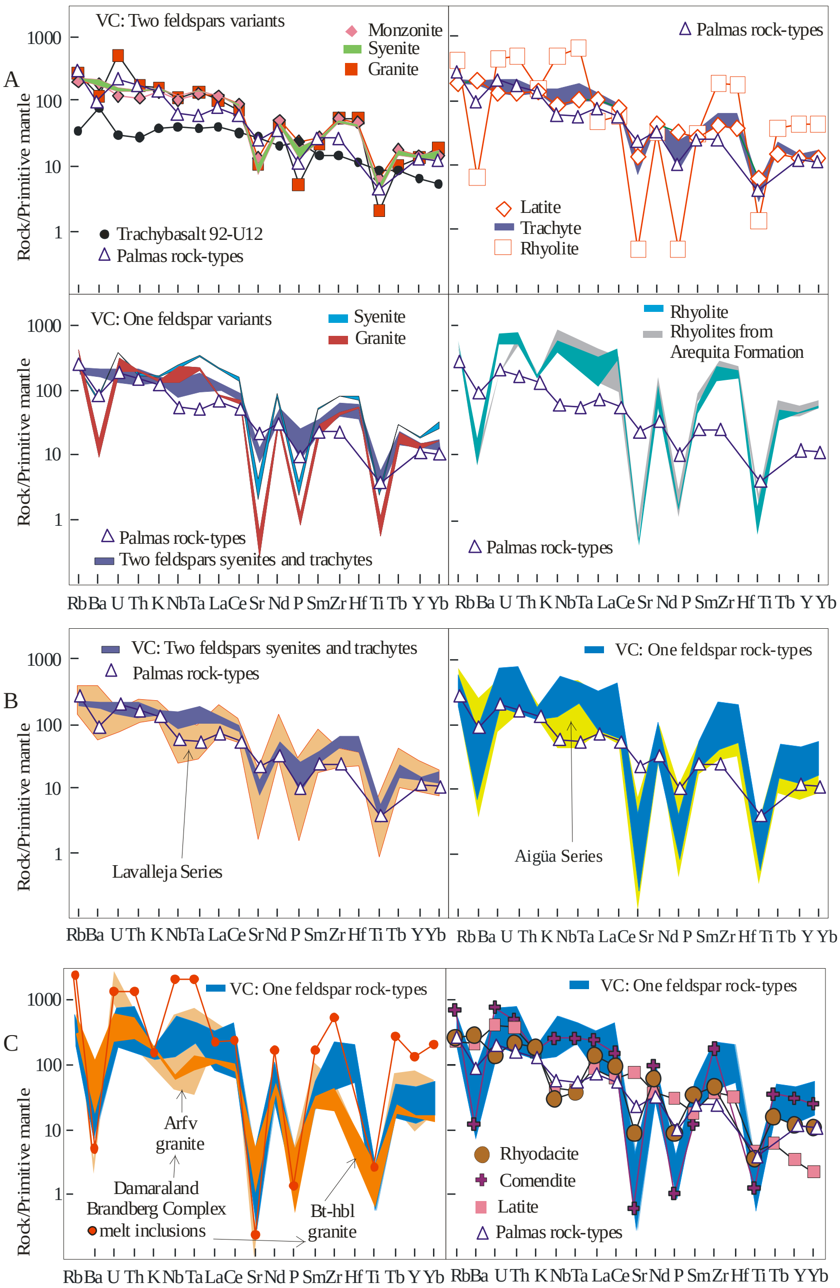


Fig. 14. A) Primitive mantle-normalized (Sun & McDonough, 1989) for average compositions of Valle Chico igneous rocks and Arequita Formation compared with averaged composition of the Palmas rock-types and with the trachybasalt 92-U12 from SE Uruguay (data source:Table 1; Garland *et al.*, 1995; Kirstein *et al.*, 2000; Muzio *et al.*, 2002). B) Comparison between the Valle Chico two feldspars and one feldspar variants with the Lavalleja and Aiguá suites of Kirstein *et al.* (2000), respectively. C) Valle Chico one feldspar variants compared with some other felsic rocks: Brandberg biotite-hornblende and arfvedsonite granites and related melt inclusions (Damaraland, Namibia; Trumbull *et al.*, 2004; Schmitt *et al.*, 2002); Paresis rhyodacite and comendite (Damaraland, Trumbull *et al.*, 2004), Palmas rock-types (Garland *et al.*, 1995) and with latites from the Choiyoi Group, central Argentina (Llambías *et al.*, 2003).

references).

All the VC rocks have marked negative spikes at Sr and Ti, and rhyolites and granites also at Ba and P. One feldspar syenites and trachytes tend to parallel the upper and lower boundaries, respectively, of the Aiguá series, but the latter display marked P negative spike (Fig. 14A). On the contrary, the VC granites and rhyolites overlap the field of the Aiguá felsic series. The Palmas rhyodacites-rhyolites (N=107, Bellieni *et al.*, 1986b; Piccirillo & Melfi, 1988; Garland *et al.*, 1995) partially overlap the one feldspar trachyte pattern, but are distinct for the Nb-Ta negative anomaly (Fig. 14B).

In comparison to the alkaline complexes from Damaraland (Fig. 14C), it is apparent a tendency for Nb-Ta negative anomaly for the granitic rocks of the Brandberg complex, but the melt inclusions strictly parallels the one feldspar behaviour of the Valle Chico complex, as well as the peralkaline variants from the Paresis complex (Damaraland, cf. Trumbull *et al.*, 2004). On the other hand, the Damaraland rhyodacites (Paresis complex; Trumbull *et al.*, 2004) and the Choiyoi shoshonitic latites (extensive and orogenic environments, respectively) clearly show strong negative Nb-Ta anomalies (Fig. 14C).

According to Trumbull *et al.* (2004), it should be remembered that the unifying features of the different felsic rocks in the Damaraland is likely to be related to the high temperature involved, which allows partial melting of dehydrated, and possibly melt-depleted, lower crustal lithologies.

The REE patterns, chondrite-normalized as given in Fig. 15A, show that the trachybasalt 92-U12 has

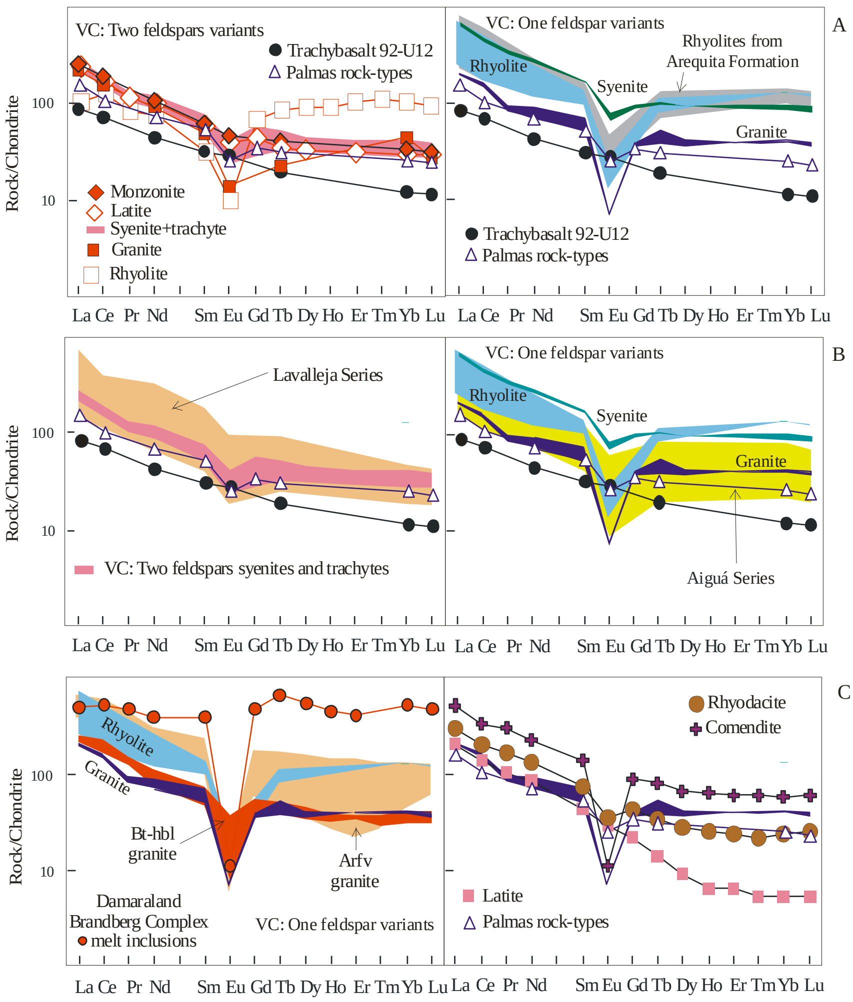


Fig. 15. Chondrite normalized (Boynton, 1984) for REE contents from the Valle Chico igneous rocks and Arequita Formation compared with the same rock-types as in Fig. 14 (A, B and C).

$La_N/Sm_N$=2.70, $Tb_N/Yb_N$=1.64 and Eu/Eu*=1.02. The trachyte/syenite group displays LREE enrich-ment over MREE ($La_N/Sm_N$=3.9-4.3), with quite flat HREE pattern ($Tb_N/Yb_N$=1.1-1.3); Eu/Eu* ratio is systematically <1 (0.70-0.36), attesting the feldspar fractionation.

The rhyolite/granite group has $La_N/Sm_N$ ranging from 1.5 to 4.1, $Tb_N/Yb_N$ from 0.8 to 1.0, and a very marked Eu negative anomaly, i.e. Eu/Eu*=0.14-0.19.

Two feldspar rhyolites, as well as the one feldspar and Arequita rhyolites, present a remarkable HREE enrichment with respect to the other variants.

On the whole, the REE patterns of the Valle Chico felsic rocks are quite similar to those shown by the Lavalleja and Aiguá felsic suites (cf. Fig. 15B and Kirstein *et al*., 2000; Lavalleja: $La_N/Sm_N$=3.5-4.1, $Tb_N/Yb_N$=1.3-2.1; Eu/Eu*=0.52-0.63; Aiguá: $La_N/Sm_N$=3.5-5.0, $Tb_N/Yb_N$=0.9-1.0; Eu/Eu*=0.26-0.55), and the Palmas rock-types overlap the two feldspars syenites and trachytes.

The Damaraland granites and comendites parallel the VC rhyolitic-granitic variants, but are quite different from the Choiyoi latites ($La_N/Sm_N$=4.8, $Tb_N/Yb_N$=2.6; Eu/Eu*=0.89; Fig. 15C).

In sum, the Valle Chico alkaline complex shows both some compositional similarities and differences regarding the other felsic Early Cretaceous sequences from eastern Uruguay in terms of incompatible elements and REE patterns. However, important differences are apparent from the variation diagrams (vs. silica) and from the elemental ratios.

## Sr-Nd ISOTOPES

Sr-Nd isotope analyses have been carried out on a

Table 9. $^{87}Sr/^{86}Sr$ and $^{143}Nd/^{144}Nd$ isotopic ratios for some selected Valle Chico igneous rocks. Model ages ($T^{DM}$) are calculated assuming the following values for the depleted mantle: $^{143}Nd/^{144}Nd$ = 0.513151 and Sm/Nd = 0.2188.

| Two feldspars rock-types | 92-U12 Trachybasalt | 1 Monzonite | 2 Latite | 3 Syenite | 5 Trachyte | 6 Trachyte | 7 Trachyte | 8 Granite | 9 Rhyolite |
|---|---|---|---|---|---|---|---|---|---|
| Rb (ppm) | 22 | 121 | 123 | 132 | 125.8 | 132.4 | 155.3 | 201 | 256.98 |
| Sr (ppm) | 597 | 288 | 298 | 229 | 256.5 | 270.8 | 157.9 | 154 | 6.88 |
| $(^{87}Sr/^{86}Sr)_{meas}$ | 0.70480 | 0.70861 | 0.70801 | 0.70878 | 0.71102 | 0.71101 | 0.71016 | 0.71151 | 0.92401 |
| $(^{87}Sr/^{86}Sr)_{128}$ | 0.70461 | 0.70640 | 0.70584 | 0.70688 | 0.70844 | 0.70844 | 0.70498 | 0.70464 | 0.72325 |
| Sm (ppm) | 6.20 | 12.16 | 11.5 | 11.89 | 12.8 | 12.5 | 14.2 | 10.8 | 20.1 |
| Nd (ppm) | 27.2 | 64.8 | 59.3 | 63.0 | 65.1 | 63.5 | 72.4 | 42.6 | 70.7 |
| $(^{143}Nd/^{144}Nd)_{meas}$ | 0.51247 | 0.51187 | 0.51201 | 0.51188 | 0.51199 | 0.51209 | 0.51212 | 0.51244 | 0.51204 |
| $(^{143}Nd/^{144}Nd)_{128}$ | 0.51235 | 0.51178 | 0.51191 | 0.51178 | 0.51189 | 0.51192 | 0.51202 | 0.51231 | 0.51190 |
| εSr | 0.77 | 26.21 | 18.25 | 33.06 | 55.16 | 55.13 | 6.11 | 1.22 | 265 |
| εNd | -2.32 | -13.62 | -10.96 | -13.45 | -11.31 | -10.81 | -8.79 | -3.19 | -11.18 |
| $T^{DM}$ | 1.3 | 1.8 | 1.7 | 1.8 | 1.8 | 1.7 | 1.6 | 1.7 | 3.5 |
| $SiO_2$ (wt%) | 47.89 | 60.04 | 60.56 | 62.33 | 62.03 | 63.49 | 65.34 | 71.85 | 74.47 |
| Q (wt%) | | 8.93 | 12.23 | 12.21 | 16.16 | 17.25 | 11.10 | 24.86 | 35.46 |

| One feldspar rock-types | 10 Syenite | 11 Syenite | 13 Granite | 15 Rhyolite | Jaguarão Rhyodacite |
|---|---|---|---|---|---|
| Rb (ppm) | 122.2 | 115 | 200.88 | 261 | 94.4 |
| Sr (ppm) | 34.0 | 48 | 3.13 | 6 | 318.3 |
| $(^{87}Sr/^{86}Sr)_{meas}$ | 0.72530 | 0.71811 | 111.028 | 0.94055 | 0.72331 |
| $(^{87}Sr/^{86}Sr)_{128}$ | 0.70635 | 0.70549 | 0.75917 | 0.70637 | 0.72169 |
| Sm. (ppm) | 22.65 | 18.8 | 9.0 | 27.3 | 9.5 |
| Nd (ppm) | 116.2 | 97.4 | 37.4 | 136.0 | 46.5 |
| $(^{143}Nd/^{144}Nd)_{meas}$ | 0.51195 | 0.51210 | 0.51183 | 0.51193 | 0.51182 |
| $(^{143}Nd/^{144}Nd)_{128}$ | 0.51185 | 0.51201 | 0.51171 | 0.51183 | 0.51171 |
| εSr | 25.5 | 13.27 | 775 | 25.85 | 243 |
| εNd | -12.2 | -9.13 | -14.92 | -12.6 | -14.7 |
| $T^{DM}$ | 1.8 | 1.7 | 2.7 | 1.9 | 2.1 |
| $SiO_2$ (wt%) | 64.67 | 66.79 | 70.27 | 71.09 | 64.96 |
| Q (wt%) | 3.89 | 10.70 | 17.37 | 25.05 | 26.98 |

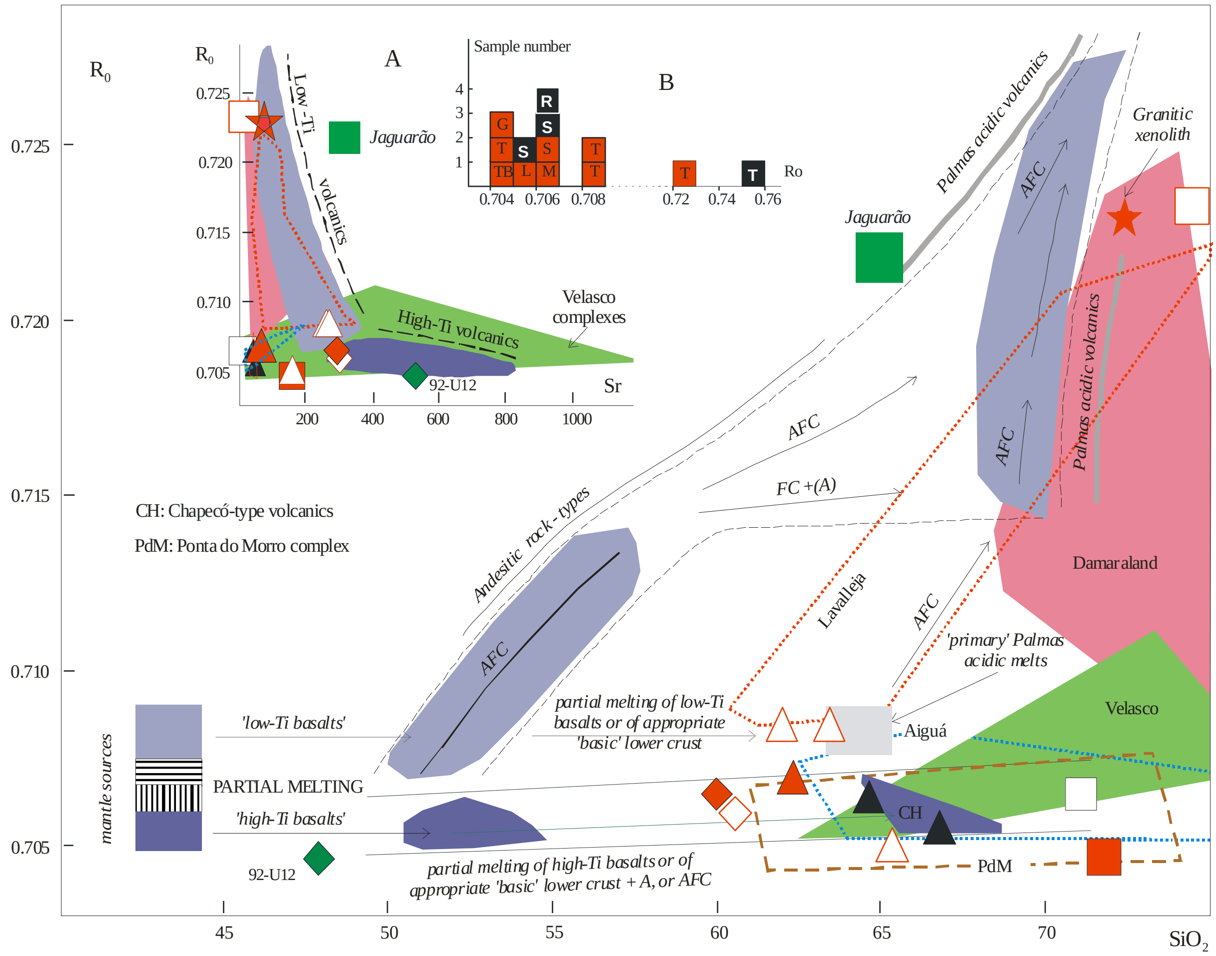

Fig. 16. Silica vs. $R_0$ ($^{87}Sr/^{86}Sr$ initial (128 Ma) ratios for 92-U12 trachybasalt and selected rocks from the Valle Chico complex (symbols as in Fig.10A). The fields of Aiguá and Lavalleja series (Kirstein *et al.*, 2000), Jaguarão rhyodacites (Comin-Chiaramonti, 2000), high- and low-Ti volcanics (also included the Chapecó and Palmas felsic variants) from the Paraná Basin (Bellieni *et al.*, 1986b; Garland *et al.*, 1995; Kirstein *et al.*, 2000), Ponta do Morro complex (Sousa *et al.*, in this volume), alkaline felsic complexes from Velasco, Bolivia (Comin-Chiaramonti *et al.*, in this volume) and felsic rocks from the Damaraland complexes (Trumbull *et al.*, 2004) are shown. AFC=crustal assimilation (A) associated with fractional crystallization (FC). Insets: A) relationships between Sr and $R_0$ for the considered rock-types; B) VC $R_0$ histogram (red and black squares, two feldspars and one feldspar variants, respectively; TB trachybasalt, M monzonite, L latite, S syenite, T trachyte, G granite, R rhyolite).

representative subset of samples and initial values were calculated at 128 Ma (Table 9).

At a large scale (Fig. 16), the VC rocks plot in a wide $SiO_2$ range, but the initial $^{87}Sr/^{86}Sr$ ratios ($R_0$, 128 Ma) of the most variants are in the same restricted $R_0$ range of the Chapecó acid rock-types, i.e. 0.705-0.706, distinctly related to the Palmas analogues (i.e. 0.714-0.728; Bellieni *et al.*, 1986b). In particular, the $R_0$ of the trachybasalt 92-U12 (0.70461; cf. Kirstein *et al.*, 2000, and Table 9) is quite comparable to the $R_0$ values of the feldspar trachyte 7 and granite 8; some two feldspars variants, i.e. monzonite 1 to syenite 3, have the $R_0$ range (0.706-0.707) similar to that of one feldspar variants, i.e. syenites 10-11 and rhyolite 15. On the other hand, the rhyolite 9 displays $R_0$=0.723, as the Jaguarão rhyodacites ($R_0$=0.722), and the granite 13 shows very high $R_0$, i.e. 0.759 (see also inset of Fig. 16).

On the whole, the VC initial $^{87}Sr/^{86}Sr$ ratios are well distinct from the fields defined by the Lavalleja, Damaraland and Palmas suites, and tend to fit the Aiguá, Ponta do Morro and Chapecó fields. Notably, the Chapecó rock-types are well distinct for their Sr contents (Sr>300 ppm; inset Sr-$R_0$ of Fig. 16) and the rhyolite 9 plots near to the granitic mantle xenolith as defined by Bellieni *et al.* (1986b). It is important to observe that the basic granulites from the crystalline basement of the southern Paraná Basin have (128 Ma) av. $R_0$=0.705 (Kaul & Teixeira, 1982), roughly corresponding to the value of the 92-U12 trachybasalt (0.70461). Thus, a picture similar to that illustrated by Bellieni *et al.* (1986b) and by Piccirillo *et al.* (1988) for the Palmas and Chapecó rock-types may be also considered for the VC genesis:

1) melting models indicate that the Paraná acidic melts may have been generated through melting (e.g. 10-15%) of basic materials corresponding to mafic granulites or, alternatively, to basalts of specific composition (e.g. Proterozoic dyke swarms of Uruguay; Mazzucchelli *et al.*, 1995);

2) the melting of lower crust mafic granulites or underplated basaltic rocks requires acid melts $R_0$ similar to those of the parents, and being in general relatively low (•0.705);

3) radiogenic crustal components have been introduced during the ascent of the primary acid melts to the surface, possibly during the low-pressure fractional crystallization process;

4) the application of assimilation-fractional crystallization processes (AFC; DePaolo, 1981, 1988) to the VC calculated "primary" melts ($R_0$~0.705; Sr~200 ppm; cf. Table 9), which evolved to the actual VC rock-types (liquid fraction=0.85; D(Sr)=1.4, assimilation/crystallization ratio=0.4 of granitic material, $R_0$=0.740; Sr=300 ppm), yielded $R_0$=0.708 and Sr=240 ppm. These values are similar

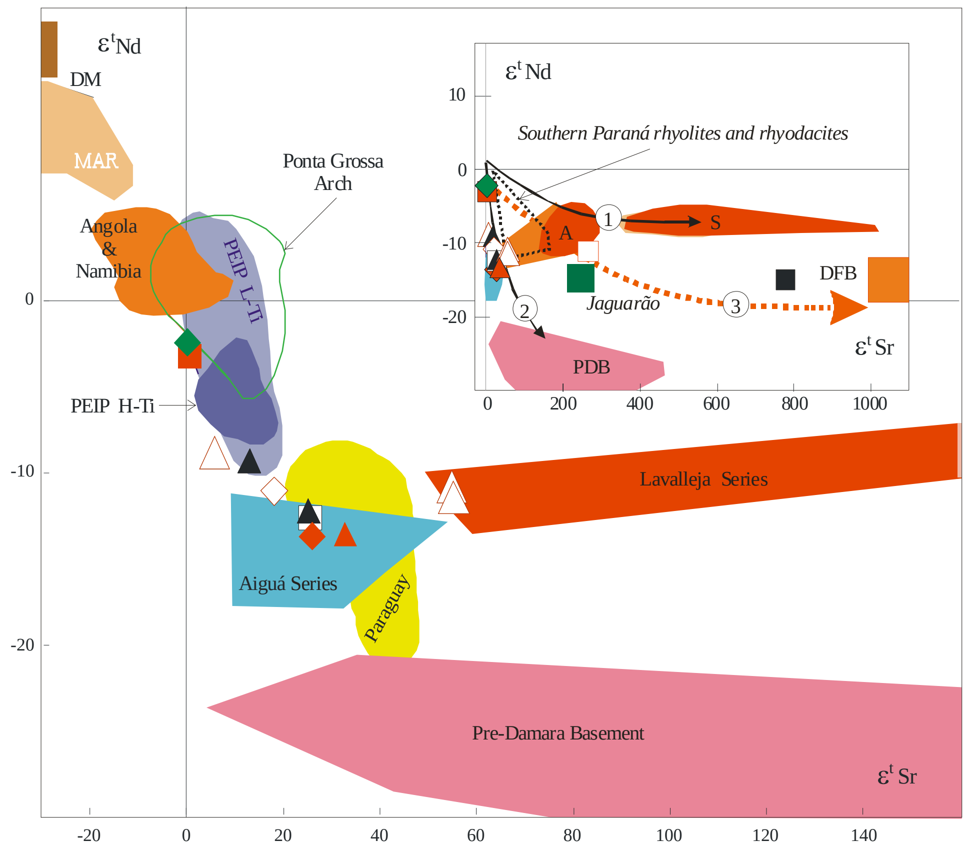


Fig. 17. $^t$Sr vs. $^t$Nd time-integrated notations (128 Ma) showing the Valle Chico rock-types (symbols as in Fig. 10A) and the fields of the main Early Cretaceous alkaline complexes and tholeiites (uncontaminated low and high-Ti tholeiites, PEIP L-Ti and PEIP H-Ti, respectively) from the Paraná-Etendeka Igneous Province. Data source as in Fig. 10A, and Piccirillo & Melfi (1988), Comin-Chiaramonti *et al.* (1997, 1999), Alberti *et al.* (1999) and Comin-Chiaramonti (2000). DM (depleted mantle) and MAR (Mid Atlantic Ridge) shown for comparison (data source: Hart *et al.*, 1992; Fontignie & Shilling, 1997; Le Roex *et al.*, 1990, respectively). Inset: enlarged range for $^t$Sr axis; PDB, A, S: Pre-Damara basement, A- and S-type Damara granite, respectively; (1) main trend and (2) Paresis trend of the Damaraland silicic complexes (Trumbul *et al.*, 2004, and therein references). DFB: Dom Feliciano belt (1.9 Ga) leucogranites (Babinski *et al.*, 1997; Jung *et al.*, 2001).

to those shown by the trachytes 5 and 6 of Table 9.

The variations of the $^{87}Sr/^{86}Sr$ vs. $^{143}Nd/^{144}Nd$ ratio (ε• notation; Fig. 17) indicate that most of the VC rock-types cluster the PEIP array (uncontaminated variants; cf. Comin-Chiaramonti *et al*., 1997, 1999; Alberti *et al*., 1999) between the field of the Angola-Namibia and eastern Paraguay alkaline occurrences, well distinct in comparison with the values shown by the Lavalleja suite and by the two feldspars rhyolite 9 and granite 13. The latters define a broad trend between the Palmas rocks and the Jaguarão rhyodacites, up to 1.9 Ga leucogranites (Preciozzi & Bourne, 1993; Babinski *et al*., 1997). This trend parallels the main Damaraland acid trend which extends towards the compositional field defined by metasediment and S-granites of the Damara belt (Trumbull *et al.*, 2004). On the other hand, the PEIP array overlaps the metaluminous "Paresis trend" (inset of Fig. 17), extending towards the composition of the pre-Damara gneisses defined by exposures at north of the Damara belt and from coastal Brazil (Seth *et al*., 1998; Teixeira *et al*., 1996).

Trumbull *et al.* (2004) suggest that the two Damaraland trends represent mixing or assimilation between mantle-derived magmas and two different crustal components.

*Model ages*

Although the model ages have little real meaning as they do not reflect the ages of the sources (cf. Arndt & Goldstein, 1987), the VC rock-types may be monitored to some extent by the Sm-Nd, depleted mantle ($T^{DM}$), model ages (DePaolo, 1988). The syenites and trachytes, both two feldspars and one feldspar variants, display $T^{DM}$ ranging from 1.6 to 1.8 Ga (mean 1.74±0.07) that overlaps those of the Palmas (av. 1.71±0.17 Ga) and Lavalleja (av. 1.64±0.11 Ga) volcanics. The Aiguá suite and the Early Cretaceous low-Ti tholeiites display more scattered values, around 1.91±0.33 Ga and 1.8±0.3, respectively. On the other hand, some more acid rocks (Table 9) show very variable model ages, i.e. 3.5 Ga (rhyolite 9) and 2.7 (granite 13).

According to Mallmann *et al*. (2003), Mazzucchelli *et al*. (1995) and Girardi *et al*. (1996), the Proterozoic mafic magmatism in Uruguay ($T^{DM}$ 1.81-1.86 Ga) yielded model ages quite similar to those common to the Dom Feliciano crystalline basement ($T^{DM}$ 1.9 Ga), and older than the Treinta y Tres Eoproterozoic mafic dyke swarms ($T^{DM}$ 1.5 Ga).

The gneisses and granitoids from the basement are interpreted as a direct melting product of Palaeoproterozoic terrains (Babinski *et al*., 1997), as a consequence of the interaction between the Rio de La Plata and Kalahari cratons during the Brasiliano/Pan-African collage (Mallmann *et al*., 2003).

Mantle melting responsible for the ancient mafic magmatism, which intruded ensialic terrains, occurred in Paleo and Neoproterozoic times. On the whole, the geochemical and isotopic characteristics of the Uruguayan Proterozoic dyke swarms are quite similar to those of the Mesozoic basalts related to the Gondwana break-up, supporting the possibility that the latter tholeiitic melts derived from similar heterogeneous subcontinental lithospheric mantle which recorded Proterozoic enrichment processes (cf. Mazzucchelli *et al.*, 1995; Iacumin *et al.*, 2003).

In this context (cf. Fig. 18), the alkaline VC magmatism may represent the evolved products of partial melting of an underplated mafic magmatism related to Proterozoic (or older) protoliths, and variously affected by crustal contamination during the ensialic emplacement.

## CONCLUDING REMARKS

The mineralogical, petrochemical and geochemical results indicate that the Valle Chico complex represents a felsic magmatism quite different with respect to the other acid rocks from the south-southeastern Paraná Basin in general, and eastern Uruguay in particular, i.e. Palmas, Jaguarão, Lavalleja and Aiguá suites. Only the rhyolites of the Arequita Formation are able to present geochemical characteristics overlapping those of the agpaitic VC rhyolites, and thus may be considered to some extent as the products from the same emission center, but geological information are still in need in order to clarify the relationships between the two suites.

Regarding the other PEIP felsic occurrences, the major affinities with the VC complex are presented by the Ponta do Morro complex (Mato Grosso), probably due to similar petrogenetic mechanisms. Anyway, a common feature is that the alkaline complexes in and around the PEIP were emplaced in areas characterized by tectonic lineaments indicating extensional environments and lithospheric thinning, generally after the emission of huge volumes of the PEIP stratoid volcanics (see Trumbull *et al.*, 2004, for a discussion). This suggests the possibility of subsequent partial melting of adequate compositions of lithospheric mantle portion and/or of lower to upper crustal levels, driven above all by the lithosphere thinning and decompressive environments.

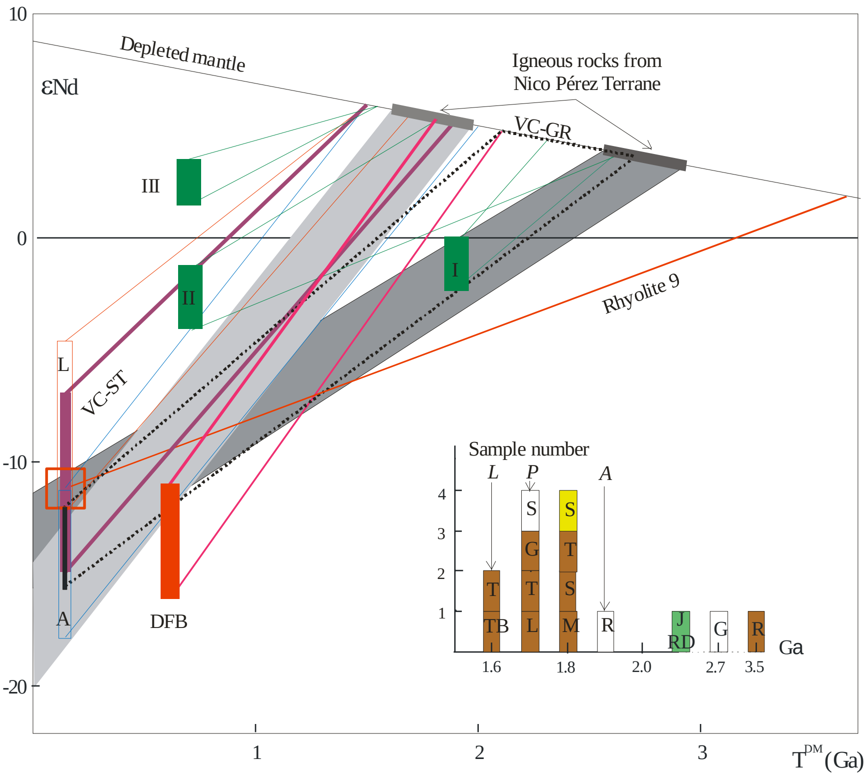


Fig. 18. $T^{DM}$ vs. 'Nd diagram (CF De Paolo, 1988) for rock-types from Uruguay. I, II, III: Florida, Nico Pérez and Treinta y Tres dyke swarms (Mazzucchelli *et al.*, 1995); DFB: Dom Feliciano belt (Babinski *et al.*, 1997); A and L: Aiguá and Lavalleja series, respectively (Kirstein *et al.*, 2000); VC-ST, Valle Chico syenites and trachytes; VC-GR, Valle Chico granites and rhyolites. It should be noted that the Palmas felsic rocks (not shown, Garland *et al.*, 1995) exactly overlap the VC-ST rocks. Inset: histogram representing the model ages for the VC rocks. Dark brown and yellow fields, two feldspars and one feldspar variants, respectively; symbols as in Fig. 16; green field: Jaguarão rhyodacites (JRD).

Finally, in order to explain the widespread distribution of the South American Early Cretaceous tholeiitic and alkaline magmatism, it is not necessary to imply an active role of hypothetical mantle plume head (cf. Ernesto *et al.*, 2002, and Ernesto, in this volume): we support an "edge drive convection" model (cf. King & Ritsema, 2000), by which the rifting processes were triggered by different lithospheric thickness beneath the edge of cratonic shields, and where a small-scale convection cell might be operative.

## ACKNOWLEDGEMENTS

P. Censi kindly performed O isotope and some ICPM trace analyses, and F. Castorina is gratefully acknowledged for some Sr-Nd isotope analyses. An early version of the manuscript benefited from constructive reviews by E.M. Piccirillo.

## REFERENCES


Alberti, A., Castorina, F., Censi, P., Comin-Chiaramonti, P. & Gomes, C.B. (1999). Geochemical characteristics of Cretaceous carbonatites from Angola. *Journal of African Earth Sciences* **29**, 735-759.

Almeida, F.F.M. (1983). Relações tectônicas das rochas alcalinas mesozóicas da região meridional da plataforma Sul-Americana. *Revista Brasileira de Geociências* **13**, 139-158.

Almeida, F.F.M., Neves, B.B. & Carneiro, C.D.R. (2000). The origin and evolution of the South American platform. *Earth-Science Reviews* **50**, 77-111.

Arndt, N.T. & Goldstein, L.S. (1987). Use and abuse of crust-formation ages. *Geology* **15**, 893-895.

Babinski, M., Chemale Jr., F., Van Schmus, W.R., Hartmann, L.A. & Silva, L.C. (1997). U-Pb and Sm-Nd geochronology of the Neoproterozoic Granitic-Gneissic Dom Feliciano Belt, Southern Brazil. *Journal of South American Earth Sciences* **10**, 263-274.

Bailey, S.W. (1984). Classification and structures of the micas. Crystal chemistry of the true micas. *Reviews in Mineralogy, Mineralogical Society of America* **13**, 1-60.

Balestra, R. (1985). *Studio vulcanologico e petrochimico di sequenze vulcaniche stratoidi dell'Uruguay (Bacino del Paraná).* M.Sc. Dissertation, University of Trieste, 127p.

Bellieni, G., Comin-Chiaramonti, P., Marques, L.S., Martinez, A.J., Melfi, A.J., Nardi, J.R., Piccirillo, E.M. & Stolfa, D. (1986a). Continental flood basalts from the central-western regions of the Paraná plateau (Paraguay and Argentina): petrology and petrogenetic aspects. *Neues Jahrbuch für Mineralogie Abhandlungen* **150**, 111-139.

Bellieni, G., Comin-Chiaramonti, P., Marques, L.S., Melfi, A.J., Nardi, J.R., Papatrechas, C., Piccirillo, E.M., Roisemberg, A. & Stolfa, D. (1986b). Petrogenetic aspects of acid and basaltic lavas from the Paraná Plateau (Brazil): geological, mineralogical and petrochemical relationships. *Journal of Petrology* **27**, 915-944.

Bellieni, G., Piccirillo, E.M., Comin-Chiaramonti, P., Melfi, A.J. & Da Roit, P. (1988). Mineral chemistry of continental stratoid volcanics and related intrusives from the Paraná basin (Brazil). In: Piccirillo, E.M., & Melfi, A.J. (eds.). *The Mesozoic flood volcanism of the Paraná basin: petrogenetic and geophysical aspects.* São Paulo: IAG-USP, pp. 73-92.

Bossi, J. & Navarro, R. (1991). Geologia del Uruguay. *Departemento de Publicaciones, Universidad de la República, Montevideo* Vol. **I**, 580p.

Bossi, J., Ferrando, L., Schipilov, A. (2001). Carta geológica 1/500.000 del Uruguay: versión 2001. Geoeditores, Montevideo.

Boynton, W.V. (1984). Cosmochemistry of the Rare Earth elements: meteorite studies. In: Henderson, P. (ed.) *Rare Earth Element Geochemistry*. Elsevier, Amsterdam, 63-114.

Carbonin, S., Dal Negro, A, Molin, G.M., Munno, R., Rossi, G., Lirer, L. & Piccirillo, E.M. (1984). Crystal-chemical of Ca-rich pyroxenes from undersaturated to oversaturated trachytic rocks, and their relationships with pyroxenes from basalts. *Lithos* **17**, 191-202.

Comin-Chiaramonti, P. (2000) Peraluminous lavas from Jaguarão (Rio Grande do Sul, Brazil). *DICAMP, Quaderni di Mineralogia, Petrografia e Geochimica Applicate* **17**, 1-15.

Comin-Chiaramonti, P. & Gomes, C.B. (eds.) (1996). *Alkaline magmatism in central-eastern Paraguay. Relationships with coeval magmatism in Brazil.* São Paulo: Edusp/Fapesp, 464p.

Comin-Chiaramonti, P., Cundari, A., DeGraff, J.M., Gomes, C.B. & Piccirillo, E.M. (1999). Early Cretaceous-Tertiary magmatism in eastern Paraguay (western Paraná basin): geological, geophysical and geochemical relationships. *Journal of Geodynamics* **28**, 375-391.

Comin-Chiaramonti, P., Cundari, A., Piccirillo, E.M., Gomes, C.B., Castorina, F., Censi, P., De Min, A., Marzoli, A., Speziale, S. & Velázquez, V.F. (1997). Potassic and sodic igneous rocks from eastern Paraguay: their origin from the lithospheric mantle and genetic relationships with the associated Paraná flood tholeiites. *Journal of Petrology* **38**, 495-528

Comin-Chiaramonti, P., Gomes, C.B., F., Castorina, Censi, P., Antonini, P., Furtado, S.M., Ruberti, E. & Scheibe, L.F. (2002a). Geochemistry and geodynamic implications of the Anitápolis and Lages alkaline carbonatite complexes, Santa Catarina State, Brazil. *Revista Brasileira de Geociências* **32**, 43-58.

Comin-Chiaramonti, P., Gomes, C.B., Ruberti, E., Antonini, P. & Censi, P. (2002b). Mato Preto alkaline-carbonatite complex: geochemistry and isotope (O-C, Sr-Nd) constraints. *Geochimica Brasiliensis* **15**, 23-24.

Comin-Chiaramonti, P., Gomes, C.B., Velázquez, V.F., Censi, P., Antonini, P., Comin-Chiaramonti, F. & Punturo, R. (in this volume) Alkaline complexes from southeastern Bolivia.

Cundari, A. (1975). Mineral chemistry and petrogenetic aspects of the Vico lavas, Roman Volcanic Region, Italy. *Contributions to Mineralogy and Petrology* **70**, 9-21.

Cundari, A. & Salviulo, G. (1989). Ti solubility in diopsidic clinopyroxenes from a suite of New South Wales leucitites (Australia). *Lithos* **22**, 191-198.

Deer, W.A., Howie, R.A. & Zussman, J. (1992). *An introduction to the rock-forming minerals*. London: Longman, 696p.

DePaolo, D.J. (1981). Trace element and isotopic effects of combinated wall rock assimilation and fractional crystallization. *Earth Planetary Science Letters* **53**, 59-68.

DePaolo, D.J. (1988). Neodymium isotope geochemistry. An introduction. *Mineral and Rocks* **20**, 1-187.

Enrich, G.E.R., Azzone, R.G., Ruberti, E., Gomes, C.B. & Comin-Chiaramonti, P. (in this volume). Itatiaia, Passa Quatro and São Sebastião Island, the major alkaline syenitic complexes from the Serra do Mar region.

Ernesto, M., Marques, L.M., Piccirillo, E.M., Molina, E., Ussami, N., Comin-Chiaramonti, P. & Bellieni, G. (2002). Paraná Magmatic Province-Tristan da Cunha plume system: fixed versus mobile plume, petrogenetic considerations and alternative heat sources. *Journal of Volcanology and Geothermal Researches*, **130**, 527-553.

Féraud, G., Bertrand, H., Martinez, M., Ures, C., Shilipov, A. & Bossi, J. (1999). $^{40}Ar/^{39}Ar$ age and geochemistry of the southern extension of Paraná traps in Uruguay. *II South American Symposium on Isotope Geology, Actas*, pp. 57-59.

Fontignie, D. & Schilling, J.G. (1997). Mantle heterogeneities beneath the South Atlantic: a Nd-Sr-Pb isotope study along the Mid-Atlantic Ridge (3°S-46°S). *Earth Planetary Science Letters* **146**, 259-272.

Friedman, I. & O'Neal, J.R. (1977). Compilation of stable isotope fractionation factors of geochemical interest. In: Fleischer, M. (ed) Data of geochemistry, 6th ed. *U.S. Geological Survey Professional Papers*, 440p.

Fuhrman, M.L. & Lindsley, D.H. (1988). Ternary-feldspar modelling and thermometry. *American Mineralogist* **73**, 201-215.

Garland, F., Hawkesworth, C.J. & Mantovani, M.S.M. (1995). Description and petrogenesis of the Paraná rhyolites, southern Brazil. *Journal of Petrology* **36**, 1193-1227.

Girardi, V.A.V., Mazzucchelli, M., Molesini, M., Civetta, L., Petrini, R., Bossi, J., Campal, N., Teixeira, W. & Correia, C.T. (1996). Petrology and geochemistry of the mafic dyke swarm of the Treinta y Tres region, northeast Uruguay. *Journal of South American Earth Sciences* **9**, 243-249.

Giret, A., Bonin, B. & Leger, J.M. (1980). Amphibole compositional trends in oversaturated and undersaturated alkaline plutonic ring complexes. *Canadian Mineralogist* **18**, 481-495.

Gomes, C.B., Barbieri, M., Beccaluva, L., Brotzu, P., Conte, A., Garbarino, C., Macciotta, G., Melluso, L., Morbidelli, L., Ruberti, E., Scheibe, L.F., Tamura, R.M. & Traversa, G. (1987). Petrological and geochemical studies of alkaline rocks from continental Brazil.: The Tunas massif, State of Paraná. *Geochimica Brasiliensis* **1**, 201-234.

Green, N.L. & Usdansky, S.I. (1986). Ternary-feldspar mixing relations and thermobarometry. *American Mineralogist* **71**, 1100-1108.

Hart, S.R., Hauri, E.H., Oschmann, L.A. & Whithehead, J.A. (1992). Mantle plumes and entrainment: isotopic evidence. *Science* **256**, 517-520.

Hartmann, L.A., Santos, J.O.S., Bossi, J., Campal, N., Schipilov, A. & McNaughton, N.J. (2002). Zircon and titanite U-Pb SHRIMP geochronology of Neoproterozoic felsic magmatism on the eastern border of the Rio de la Plata Craton, Uruguay. *Journal of South American Earth Sciences* **15**, 229-236.

Hawkesworth, C., Kelley, S., Turner, S., Le Roex, A. & Storey, B. (1999). Mantle processes during Gondwana break-up and dispersal. *Journal of African Earth Sciences* **28**, 239-261.

Iacumin, M., De Min, A., Piccirillo, E.M. & Bellieni, G. (2003). Source mantle heterogeneity and its role in the genesis of Late Archaean–Proterozoic (2.7-1.0 Ga) and Mesozoic (200 and 130 Ma) tholeiitic magmatism in the South American Platform. *Earth-Science Reviews* **62**, 265-391.

Ishii, T. (1975). The relations between temperature and composition of pigeonite in some lavas and their application to geothermometry. *Mineralogical Journal* **8**, 48-57.

Jung, S., Mezger K. & Hoernes, S. (2001). Trace element and isotopic (Sr, Nd, Pb, O) arguments for a mid-crustal origin of Pan-African garnet-bearing S-type granites from the Damara orogen (Namibia). *Precambrian Research* **110**, 325-355.

Kaul, P.F.T. & Teixeira, W. (1982). Archean and Early Proterozoic complexes of Santa Catarina, Paraná and São Paulo States, south-southeastern Brazil: an outline of their geological evolution. *Revista Brasileira de Geociências* **12**, 171-182.

King, S.D. & Ritsema, J. (2000). African hot spot volcanism: small scale convection in the upper mantle beneath cratons. *Science* **290**, 1137-1140.

Kirstein, L.A., Peate, D.W., Hawkesworth, C.J., Turner, S.P., Harris, C. & Mantovani, M.S.M. (2000). Early Cretaceous basaltic and rhyolitic magmatism in southern Uruguay associated with the opening of the South Atlantic. *Journal of Petrology* **41**, 1413-1438.

Llambías, E.J., Quenardelle, S. & Montenegro, T. (2003). The Choiyoi Group from Central Argentina: a subalkaline transitional to alkaline association in the craton adjacent to the active margin of the Gondwana continent. *Journal of South American Earth Sciences* **16**, 243-257.

Le Maitre, R.W. (2000). *Igneous rocks - a classification and glossary of terms*. Oxford: Blackwell Scientific Publications, 236p.

Le Roex, A.P., Cliff, R.A. & Adair, B.J.I. (1990). Tristan da Cunha, south Atlantic: geochemistry and petrogenesis of a basanite-phonolite lava series. *Journal of Petrology* **31**, 779-812.

Leake, B.E. (1978). Nomenclature of amphiboles. *American Mineralogist* **63**, 1023-1052.

Leat, P.Y., Jackson, S.E., Thorpe, R.S. & Stillman, C.J. (1986). Geochemistry of bimodal basal - subalkaline/peralkaline rhyolite provinces within the Southern British Caledonides. *Journal of the Geological Society of London* **143**, 259-273.

Lustrino, M., Melluso, L., Brotzu, P., Gomes, C.B., Morbidelli, L., Muzio, R., Ruberti, E. & Tassinari, C.C.G. (2005). Petrogenesis of the Early Cretaceous Valle Chico igneous complex (SE Uruguay): relationships with Paraná-Etendeka felsic rocks. *Lithos* (in press).

Lustrino, M., Morbidelli, L., Gomes, C.B., Melluso, L., Ruberti, E. & Tassinari, C.C.G. (2002) Geochemistry and petrology of Cretaceous silicic rocks from Uruguay. *XLI Congresso Brasileiro de Geologia, João Pessoa,* pp. 540-541.

Macdonald, R. (1974). Nomenclature and petrochemistry of the peralkaline oversaturated extrusive rocks. *Bullettin Volcanologique* **38**, 498-516.

Mallmann, G., Chemale Jr., F., Armstrong, R. & Kawashita, K. (2003). Sm-Nd and U-Pb SHRIMP zircon studies on the Nico Pérez terrane, reworked Rio de La Plata Craton, Uruguay. *IV South American Symposium on Isotope Geology*, *Salvador*.

Mathez, E.A. (1973). Refinement of the Kudo-Weill plagioclase thermometer and its application to basaltic rocks. *Contributions to Mineralogy and Petrology* **41**, 61-72.

Matsuhisa, Y., Goldsmith, J.R. & Clayton, R.N. (1979). Oxygen isotopic fractionation in the system quartz-albite-anorthite-water. *Geochimica et Cosmochimica Acta* **43**, 1131-1140.

Mazzucchelli, M., Rivalenti, G., Piccirillo, E.M., Girardi, V.A.V., Civetta, L. & Petrini, R. (1995). Petrology of the Proterozoic mafic dyke swarms of Uruguay and constraints on their mantle source composition. *Precambrian Research* **74**, 177-194.

Mitchell, R.H. & Bergmann, S.C. (1991). *Petrology of lamproites*. New York: Plenum Press, 447p.

Morbidelli, L., Gomes, C.B., Beccaluva, L., Brotzu, P., Conte, A.M., Ruberti, E. & Traversa, G. (1995). Mineralogical, petrological and geochemical aspects of alkaline and alkaline-carbonatite associations from Brazil. *Earth-Science Reviews* **39**, 135-168.

Morimoto, N. (1988). Nomenclature of pyroxenes. *Mineralogical Magazine* **52,** 535-550.

Muzio, R.S. (2000). *Evolução petrológica e geocronologia do maciço alcalino Valle Chico, Uruguai.* Ph.D. Thesis, Universidade Estadual Paulista, Rio Claro, 171p.

Muzio, R.S. & Artur, A.C. (1999). Petrological features of the Santa Teresa granitic complex, southeastern Uruguay. *Journal of South American Earth Sciences* **12**, 501-510.

Muzio, R.S., Artur, A.C. & Wernick, E. (2002). Petrological and geochemical evolution of the alkaline Valle Chico massif, southeastern Uruguay. *International Geology Review* **44**, 352-369.

Muzio, R.S., Peel, E. & Artur, A.C. (1999). New geochronological data of the Valle Chico alkaline massif using Sm/Nd and U/Pb systematics. *II Simposio Sudamericano de Geologia Isotopica*, *Cordoba, Actas*, p. 25.

Neumann, H., Mead, J. & Vitaliano, C.J. (1954). Trace element variations during fractional crystallization as calculated from the distribution law. *Geochimica and Cosmochimica Acta* **6**, 90-99.

Pearce, J.A., Harris, N.B.W. & Tindle, A.G. (1984). Trace element discrimination diagrams for the tectonic interpretation of granitic rocks. *Journal of Petrology* **25**, 956-983.

Piccirillo, E.M., & Melfi, A.J. (eds.) (1988). *The Mesozoic flood volcanism of the Paraná basin: petrogenetic and geophysical aspects.* São Paulo: IAG-USP, 600p.

Piccirillo, E.M., Comin-Chiaramonti, P., Bellieni, G., Civetta, L., Marques L.S., Melfi, A.J., Petrini, R., Raposo, M.I.B. & Stolfa, D. (1988). Petrogenetic aspects of continental flood basalt-rhyolite suites from the Paraná basin (Brazil). In: Piccirillo, E.M., & Melfi, A.J. (eds.) *The Mesozoic flood volcanism of the Paraná basin: petrogenetic and geophysical aspects.* São Paulo: IAG-USP, pp. 179-205.

Piccirillo, E.M., Raposo, M.I.B., Melfi, A.J., Comin-Chiaramonti, P., Bellieni, G., Cordani, U. & Kawashita, K. (1987). Bimodal fissural volcanic suites from the Paraná Basin (Brazil): K-Ar age, Sr isotopes and geochemistry. *Geochimica Brasiliensis* **1**, 53-69.

Preciozzi, F. & Bourne, J.H. (1993). Geochemistry and geochronology of three plutons from Central Uruguay: tectonic implications for the Transamazonian orogeny. *Revista Brasileira de Geociências* **23,** 52-60.

Renne, P.R., Ernesto, M., Pacca, I.G., Coe, R.S., Glen, J.M., Prévot, M. & Perrin, M. (1992). Rapid eruption of the Paraná flood volcanics, rifting of Gondwanaland and the Cretaceous boundary. *Science* **258**, 975-979.

Renne, P.R., Ernesto, M. & Milner, S.C. (1997). Geochronology of the Paraná- Angola - Etendeka magmatic Province. *Eos, Transaction, AGU* **78** (46), F742.

Riccardi, A.C. (1988). The Cretaceous system of southern South America. *Geological Society of America, Memoir* **168**, 1-161.

Rollinson, H. R. (1993). Using geochemical data: evaluation, presentation, interpretation. *Longman Geochemistry*, 353p.

Rossello, E.A., Santa Ana, H., & Veroslavsky, G. (2000). El lineamento Santa Lucía-Aiguá-Merín (Uruguay): un corredor tectónico extensivo y transcurrente dextral precursor de la apertura atlántica. *Revista Brasileira de Geociências* **30**, 749-756.

Schmitt, A.K., Emmermann, R., Trumbull, R.B., Buhn B. & Henjes-Kunst, F. (2000). Petrogenesis and $^{40}Ar/^{40}Ar$ geochronology of the Brandberg complex, Namibia: evidence for a major mantle contribution in metaluminous and peralkaline granites. *Journal of Petrology* **41**, 1207-1239.

Schmitt, A.K., Trumbull, R.B., Dulski, P. & Emmermann, R. (2002). Zr-Nb-REE mineralization in peralkaline granites from the Amis complex, Brandberg (Namibia): evidence for magmatic pre-enrichment from melt inclusions. *Economic Geology* **97**, 399-413.

Seck, H.A. (1971). Koexistierende Alkalifeldspäte und Plagioklase im System $NaAlSi_3O_8$-$KAlSi_3O_8$-$CaAl_3Si_2O_8$-$H_2O$ bei Temperaturen von 650°C bis 900°C. *Neues Jahrbuch für Mineralogie Abhandlungen* **115**, 315-345.

Seth, B., Kröner, A., Mezger, K., Nemchin, A., Pidgeon, R.T. & Okrusch, M. (1998). Archean to Neoproterozoic magmatic events in the Kaoko Belt of NW Namibia and their geodynamic significance. *Precambrian Research* **92**, 341-363.

Shaw, D.M. (1970). Trace element fractionation during anatexis. *Geochimica et Cosmochimica Acta* **34**, 237-243.

Sousa, M.Z.A., Ruberti, E., Comin-Chiaramonti, P. & Gomes, C.B. (in this volume). Alkaline magmatism from Mato Grosso state, Brazil: the Ponta do Morro alkaline complex.

Spencer, K.J. & Lindsley, D.H. (1981). A solution model for coexisting iron-titanium oxides. *American Mineralogist* **66,** 1189-1201.

Stewart, K., Turner, S., Kelley, S., Hawkesworth, C., Kirstein, L. & Mantovani, M. (1996). 3-D, $^{40}Ar$-$^{39}Ar$ geochronology in the Paraná continental flood basalt province. *Earth and Planetary Science Letters* **143**, 95-109.

Stormer, J.C. & Nicholls, J. (1978). XLFRAC: a program for interactive testing of magmatic differentiation model. *Computational Geosciences* **4**, 143-159.

Sun, S.S. & McDonough, W.F. (1989). Chemical and isotopic systematics of oceanic basalts. In: Saunders, D. & Norry, M.J. (eds.) *Magmatism in the ocean basins*. *Geological Society of London, Special Publication* **42**, 313-345.

Teixeira, W., Carneiro, A., Noce, C.M., Machado, N., Sato, K. & Taylor P.M. (1996). Pb, Sr and Pb isotope constraints on the Archean evolution of gneissic-granitoid complexes in the southern São Francisco craton, Brazil. *Precambrian Research* **78**, 151-164.

Trumbull, R.B., Harris, C., Frindt, S. & Wigand, M. (2004). Oxygen and Neodymium isotope evidence for source diversity in Cretaceous anorogenic granites from Namibia and implications for A-type granite genesis. *Lithos* **73**, 21-40.

Turner, S.P., Kirstein, L.A., Hawkesworth, C.J., Peate, D.W., Hallinan, S. & Mantovani, M.S.M. (1999). Petrogenesis of an 800 m lava sequence in eastern Uruguay: insights into magma chamber processes beneath the Paraná flood basalt province. *Journal of Geodynamics* **28**, 471-487.

Turner, S., Regelous, M., Kelley, S., Hawkesworth, C.J. & Mantovani, M. (1994). Magmatism and continental break-up in the South Atlantic: high precision $^{40}Ar$-$^{39}Ar$ geochronology. *Earth and Planetary Science Letters* **121**, 333-348.

Vieira, J.N. (1986). *Petrologia e geoquímica do vulcanismo mesozóico de Jaguarão, RS*. M.Sc. Dissertation, Federal University of Rio Grande do Sul, 136p.

Whalen, J.B., Currie, K.L. & Chappell, B.W. (1987). A-type granites: geochemical characteristics, discrimination and petrogenesis. *Contributions to Mineralogy and Petrology* **95**, 407-419.

Yavuz, F. (1999). A revised program for microprobe-derived amphibole analyses using the IMA rules. *Computational Geosciences* **25**, 909-927.

Zindler, A. & Hart, S. (1986). Chemical geodynamics. *Annual Earth and Planetary Science* **14**, 493-571.

*Mesozoic to Cenozoic Alkaline Magmatism in the Brazilian Platform*
*Comin-Chiaramonti, P. & Gomes, C.B. (eds.)*
*Edusp/Fapesp, São Paulo, pp. 591-627, 2005*

# CARBONATITES FROM SOUTHEASTERN BRAZIL: A MODEL FOR THE CARBON AND OXYGEN ISOTOPE VARIATIONS

*P. Comin-Chiaramonti, C.B. Gomes, P. Censi and S. Speziale*

*Carbonatitic complexes show large compositional ranges relative to oxygen and carbon isotopes. The variations are mostly attributed to 1) magmatic processes, 2) hydrothermal processes, 3) crustal contamination and 4) deuteric processes. Determining to what extent the oxygen and carbon isotope variations are "primary" or related to crustal processes has important implications for evaluating the isotopic characteristics of the source regions. In order to address some of these questions, a model of isotopic O-C fractionation regarding the carbonatites from the Paraná Basin (Southern Brazil) has been developed. The oxygen and carbon isotope data are taken from borehole and surface specimens. The model of isotopic fractionation of $\delta^{18}O$ and $\delta^{13}C$ is consistent with isotope exchange during fractional crystallization of the carbonatite liquid (magmatic processes) and by isotope exchange between carbonatitic rocks and $H_2O$-$CO_2$ fluids at different temperatures and with different $H_2O/CO_2$ ratios in hydrothermal conditions.*

## INTRODUCTION

Comprehensive studies on the geology and petrology of Brazilian alkaline and alkaline-carbonatitic complexes, in and around the Paraná Basin, were carried out by Morbidelli *et al.* (1995), Gomes *et al.* (1996) and Comin-Chiaramonti *et al.* (in this volume). Stable carbon and oxygen isotope studies on the carbonatites were systematically presented in several papers (Censi *et al*., 1989; Castorina *et al*., 1994, 1996, 1997; Santos & Clayton, 1995; Speziale *et al*., 1997; Comin-Chiaramonti *et al*., 1997, 2001, 2002; Alberti *et al.*, 1999; Andrade *et al.*, 1999; Ruberti *et al*., 2002).

Variations in $^{13}C$ and $^{18}O$ values in carbonatites may be attributed to differences in parameters such as 1) age, 2) tectonic setting, 3) magma source, 4) country-rocks, 5) mineralogy and 6) post-magmatic alteration.

This study presents a synthesis of all the O and C isotope analyses from carbonatite complexes of different ages and levels of exposure throughout the Paraná Basin, and addresses the evolution of the stable isotope patterns, especially in the light of magmatic-metasomatic processes and hydrothermal and/or meteoric water alteration (cf. also Comin-Chiaramonti *et al.*, in this volume), for the following carbonatites from the Paraná Basin (Fig. 1).

**Early Cretaceous***:* Eastern Paraguay (Cerro Chiriguelo, Cerro Sarambí, Rio Apa and Sapucai), Jacupiranga, Juquiá, Barra do Itapirapuã and Anitápolis;

**Late Cretaceous**: Mato Preto, Lages and Alto Paranaíba (Catalão I, Limeira, Araxá and Tapira).

In general, the alkaline-carbonatite complexes are characterized by subcircular or oval forms, but some carbonatites display complex relationships as the Barra do Itapirapuã stockwork carbonatite, where almost four generations of carbonatite dykes are emplaced in the Três Córregos granite (Ruberti *et al.*, 2002).

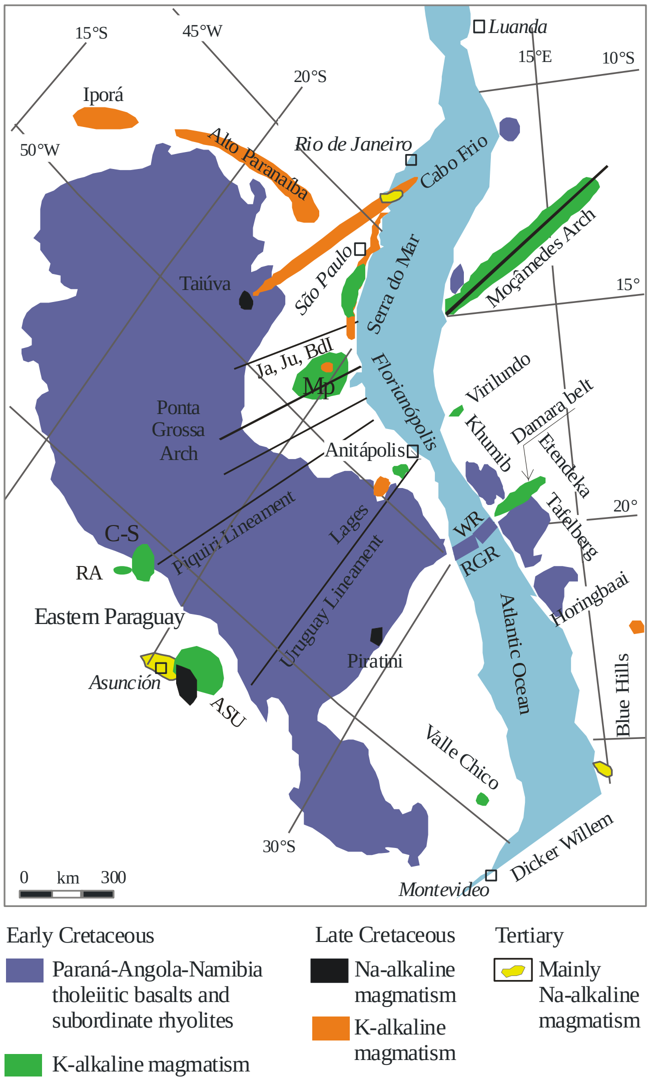


Fig. 1. Distribution of the magmatism in the Paraná-Angola-Namibia Province (South American and African plates, Western Gondwana, arranged at about 110 Ma; modified after Comin-Chiaramonti *et al.*, 1997, 1999), and location of the main alkaline-carbonatitic occurrences. Ja, Jacupiranga; Ju, Juquiá; BdI, Barra do Itapirapuã; MP, Mato Preto; RA, Rio Apa; C-S, Cerros Chiriguelo and Sarambí; ASU, Asunción-Sapucai Province; RGR, Rio Grande Rise; WR, Walvis Ridge.

According to the nomenclature of Gittings & Harmer (1997), the studied carbonatites are calcio-, magnesio- and ferruginous carbonatites (Fig. 2), but rarely the three rock-types are found in the same complex (e.g. Barra do Itapirapuã and Mato Preto).

The Jacupiranga body is considered to be a primary carbonatite (Huang *et al.*, 1995; Nadeau *et al.*, 1999), and the Juquiá magnesiocarbonatite was modeled as the result of fractionation from an exsolved calcio- carbonatite magma (Beccaluva *et al.*, 1992).

In general, the silicate rock-types at the contact with the carbonatite bodies are syenitic-trachytic to phonolitic (*l.s.*) in composition. Experimental data (e.g. Kjarsgaard & Hamilton, 1988; Kjasgaard *et al.*, 1995) show that carbonatitic liquids in equilibrium with trachytic/phonolitic magmas should have high alkali contents, whereas all the investigated carbonatites display very low alkali concentrations. This points to an exsolving carbonatite melt from

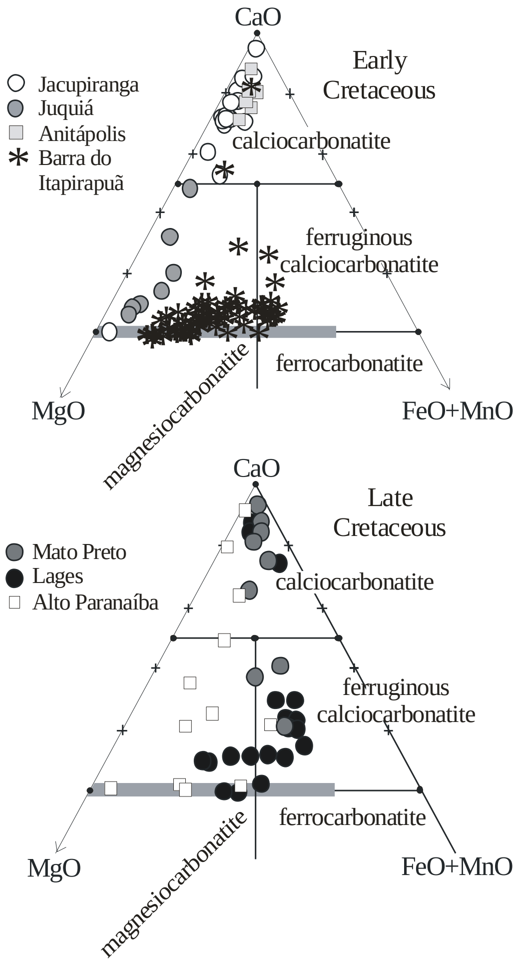


Fig. 2. Classificatory diagrams for Brazilian carbonatites (molar proportions) after Gittings & Harmer (1997).

parental basic magmas or to a more complex evolution involving alkali-rich carbonated melts exsolved from evolved magmas with loss of alkalis during depressurization, hydrothermal stages and volatile transfer (cf. Castorina *et al.*, 1996; Speziale *et al.*, 1997). The Juquiá model of Beccaluva *et al.* (1992) may represent a suitable picture for the examined carbonatites, where the various stages are: 1) fractionation from a parental basanite melt to an essexitic magma by crystallization of olivine clinopyroxenite and minor cumulus of olivine alkali gabbro, 2) derivation of the least differentiated maphic nepheline syenite from the essexitic magma through subtraction of syenodioritic assemblages and 3) exsolution of a carbonate liquid from a $CO_2$-enriched magma (cf. Fig. 3).

In this picture, the oxygen and carbon isotopes provided important information about the evolution of a $CO_2$ rich magma, both in terms of "magmatic processes" (including partial melting, fractional crystallization and liquid immiscibility) and of "fluid processes" (interaction between rocks and fluids at different temperatures, including low-temperature weathering).

The so-called "carbonatite box" of $\delta^{18}O$ and $\delta^{13}C$ compositions for primary carbonatites, which is believed to represent the primary isotope composition for the source of typical carbonatites (Taylor *et al.*, 1967; Deines & Gold, 1973; Andersen, 1987; Keller & Hoefs, 1995), ranges between 6 and 10‰ for $\delta^{18}O$ and between −4 and −8 for $\delta^{13}C$. However, a considerable number of carbonatite samples have significantly higher O and C isotope ratios. Pineau *et al.* (1973) explained the isotope variations regarding the carbonatite box as due to late magmatic and deuteric processes. Nelson *et al.* (1988) considered the isotope heterogeneity in the mantle to be one of the causes for the $\delta^{18}O$ and $\delta^{13}C$ variability in carbonatites. Clarke *et al.* (1991) and Shürmann *et al.* (1997) suggested hydrothermal alteration during equilibration with groundwaters at low temperatures (ca. 100-200°C) accompanying fluorite mineralizations to explain high $\delta^{18}O$ values. Following Santos & Clayton (1995), any isotopic variation is likely to be the result of interaction between the intruding carbonatites and surrounding carbonate country-rocks as well as of post-crystallization alteration processes.

## O-C ANALYSES

A compilation of the O-C isotopic data for calcite and dolomite-ankerite is given in Table 1 (Eastern Paraguay, Early Cretaceous; data source: Censi *et al.* 1989; Castorina *et al.*, 1997), Table 2 (Jacupiranga, Juquiá and Anitápolis, Early Cretaceous; data source: Nelson *et al.*, 1988; Castorina *et al.*, 1994, 1996; Huang *et al.*, 1995; Santos & Clayton, 1995; Toyoda *et al.*, 1995; Walter *et al.*, 1995; Comin-Chiaramonti *et al.*, 2002 and unpublished data), Table 3 (Barra do Itapirapuã, Early Cretaceous; data source: Andrade *et al*., 1999; Ruberti *et al*., 2002 and unpublished data), Table 4 (Alto Paranaíba: Catalão I, Limeira, Araxá and Tapira complexes, Late Cretaceous; data source: Morikiyo *et al*., 1990; Meyer *et al*., 1994; Bizzi *et al*., 1994; Toyoda *et al*., 1995; Santos & Clayton, 1995 and unpublished data) and Table 5 (Mato Preto and Lages, Late Cretaceous; data source: Scheibe & Formoso, 1982; Santos & Clayton, 1995; Andrade *et al*., 1999; Comin-Chiaramonti et al., 2001, 2002 and unpublished data). Analytical methods are described in the papers referred to above.

The whole distribution of $\delta^{18}O$ and $\delta^{13}C$ values in the carbonatite samples, subdivided into Early and Late Cretaceous times, is displayed in Fig. 4. A large spread in $\delta^{18}O$ and $\delta^{13}C$ values from 6 to 26‰ and from −8 to 2‰, respectively, is apparent for both suites and for both calcite and dolomite-ankerite assemblages. The Early Cretaceous carbonatites show a well-defined unimodal distribution within the primary carbonatite box and contain $\delta^{18}O$ between 8 and 10‰, and $\delta^{13}C$ between −7 and −5‰ with a maximum between −7 and −6% for calcite and between −6 and −5‰ for dolomite-ankerite. The Late Cretaceous carbonatites display two modes, the first one having a broad variation of $\delta^{18}O$ between 8

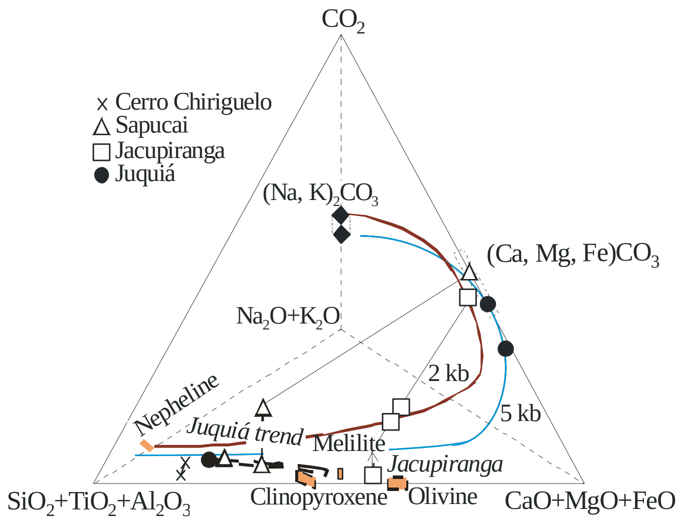


Fig. 3. Quaternary diagram showing residual liquid trends (after Kjarsgaard & Hamilton, 1989). For data source: Castorina *et al*. (1996). The curves labelled 2 kb and 5 kb are theoretical isobaric-polythermal solvi.

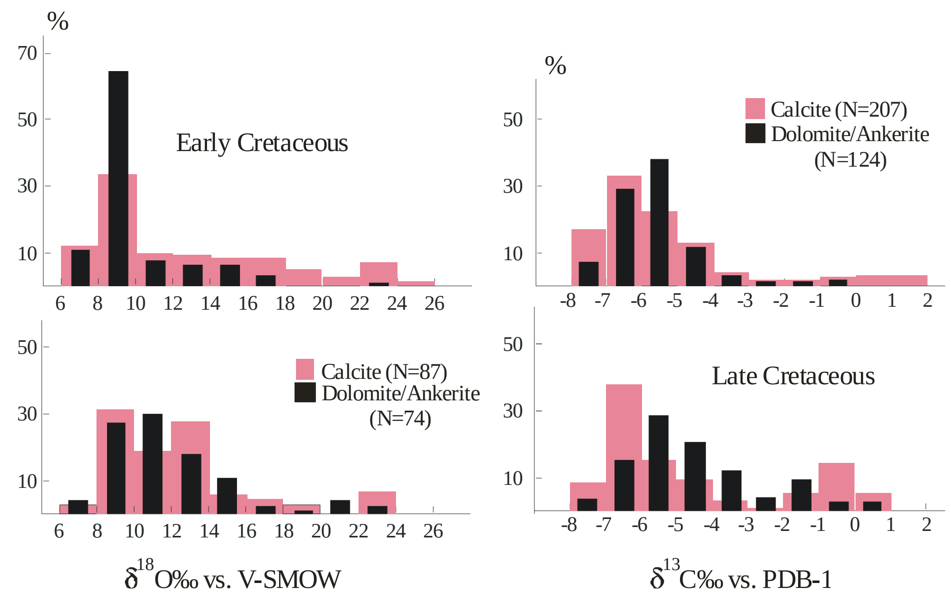


Fig. 4. Oxygen and carbon isotope distribution of carbonatites from the Paraná Basin.

and 14‰ and between 20 and 24 for both calcite and calcite-ankerite, respectively. $\delta^{13}C$ shows a more distinct bimodal variation, between −7 and −6‰ and between −1 and 0‰, respectively (calcite), and dolomite-ankerite shifted in the ranges −5 to −6‰ and −2 to −1, respectively. However, important differences in the isotopic composition are apparent in each carbonatitic complex (see later and Figs. 5 to 9).

## EARLY CRETACEOUS CARBONATITES

### Eastern Paraguay

The oxygen and carbon isotopic data are plotted in Fig. 5. $\delta^{18}O$ and $\delta^{13}C$ values from magmatic carbonates mainly vary between 6.5 and 24‰, and between −8 and 1‰, respectively. $\delta^{18}O$ and $\delta^{13}C$ from weathering and meteoric calcites are in the range of 13 to 18‰ and of 23 to 30‰, and of −11 to −5‰ and of −8 to −4‰, respectively (Table 1). It should be noted that the sedimentary carbonates from Valle-mí contain $\delta^{18}O$ and $\delta^{13}C$ ranging from 20.6 to 23.9‰, and from −1.7 to 0.6‰, respectively (Castorina *et al*., 1997).

Two main linear trends may be defined for these carbonatitic rocks. The first one corresponds to carbonates of silicate rocks taken from Cerro Chiriguelo wells (linear correlation coefficient r=0.84), while the second trend includes the magmatic carbonates of calciocarbonatites (alvikites and søvites of Censi *et al*., 1989) sampled near to, or at the topographic surface (r=0.86). The two trends intercept at $\delta^{18}O$=7.45‰ and $\delta^{13}C$=−8.52‰, close to the primary carbonates ($\delta^{18}O$=6.9‰ and $\delta^{13}C$=−8.5‰) of the Cañada K-ijolite (sample PS-245; cf. Table 1 and Comin-Chiaramonti & Gomes, 1996). These carbonates coexist with olivine ($\delta^{18}O$=4.63‰), clinopyroxene ($\delta^{18}O$=5.20‰) and biotite ($\delta^{18}O$= 5.54‰). In that last rock, the silicate minerals show isotopic equilibration temperature of about 1200°C as given by the clinopyroxene-biotite and clinopyroxene-olivine pairs (1208°C and 1201°C, respectively; cf. Bottinga & Javoy, 1975), whereas the clinopyroxene and calcite pairs yielded an equilibration temperature of 690°C (Matthews *et al*., 1983).

### Jacupiranga

The investigated Jacupiranga samples (medium-grained calciocarbonatites showing subhedral-granular texture with dominant calcite and subordinate dolomite) fit the primary carbonatite field (Fig. 6) and have $\delta^{18}O$=7.94±0.94‰ (calcite, n=23) and 8.02±0.83‰ (dolomite, n=19), and $\delta^{13}C$= −5.82±0.72‰ (calcite) and −5.41±0.82‰ (dolomite).

### Juquiá

Two main types of carbonatites can be distinguished (Beccaluva *et al*., 1992): an equigranular and coarse-grained outer ring magnesiocarbonatite and a fine-grained, “aplitic”, inner magnesiocarbonatite body. In the former (beforsite, dolomite 56 wt%, calcite 16 wt%) the apatite is around 30%, whereas in the latter, which has a more magnesian composition (beforsite, dolomite 80 wt%, calcite 10 wt%), the apatite is up to 12%. Occasional calciocarbonatites (søvite, calcite 87−78 wt%, dolomite 13 −22 wt%) may be found in the outer ring. The analyzed samples are representative of coarse-grained and fine-grained beforsites and søvites, respectively.

In the søvites, the $\delta^{18}O$ fall near to or into the carbonatite box ($\delta^{18}O$=9.89−10.29‰, and $\delta^{13}C$=−6.82−6.44‰), whereas the beforsites appear strongly enriched in heavy oxygen for both calcite and dolomite components (cf. Fig. 6: calcite, $\delta^{18}O$=14.14±1.11‰, and $\delta^{13}C$=−6.94±0.91‰; dolomite $\delta^{18}O$=15.09±1.25‰, and $\delta^{13}C$= −6.46±0.90‰). These values are very close to those of the coexisting apatite, i.e. $\delta^{18}O$=15.35±1.87‰, and $\delta^{13}C$=−6.6±0.39‰ (Walter *et al*., 1995).

### Anitápolis

The complex is basically formed by phlogopite clinopyroxenites and apatite-biotite-magnetite clinopyroxenites surrounded by ijolites and nepheline syenites that intrude Late Proterozoic granitic-gneissic rocks. A dyke like carbonatitic core of about ten square meters crops out at the center of the complex in contact with phlogopite clinopyroxenites. Carbonatite dykes and veins are widespread, dominantly in the clinopyroxenites. Field volume estimates for the main lithologies are 60% of cumulate rock-types, 39% of ijolite+nepheline syenite and about 1% of carbonatite.

Early carbonatites are coarse- to medium-grained, whitish in colour and allotriomorphic in texture. The main minerals are calcite, apatite and subordinate Fe-dolomite. Late carbonatite veins appear only from drill cores, fine- to coarse-grained, pink-greish coloured and showing allotriomorphic to hypidiomorphic texture. They are made of calcite and subordinate Mg-ankerite, quartz, apatite and phlogopite with accessory RE fluorcarbonates (ancylite, bastnaesite), alstonite, fersmite, magnetite, pyrite and galena.

$\delta^{18}O$ and $\delta^{13}C$ values vary in a restricted range, not so far from the "primary" magmatic carbonatite box (Fig. 6). The data suggest crystallization temperature starting close to magmatic conditions. Mass balance equations for oxygen and carbon of early carbonatites are consistent with a carbonatitic liquid under nearly closed condititions, in a temperature interval from about 700ºC to 400ºC (cf. Comin-Chiaramonti *et al.*, 2002).

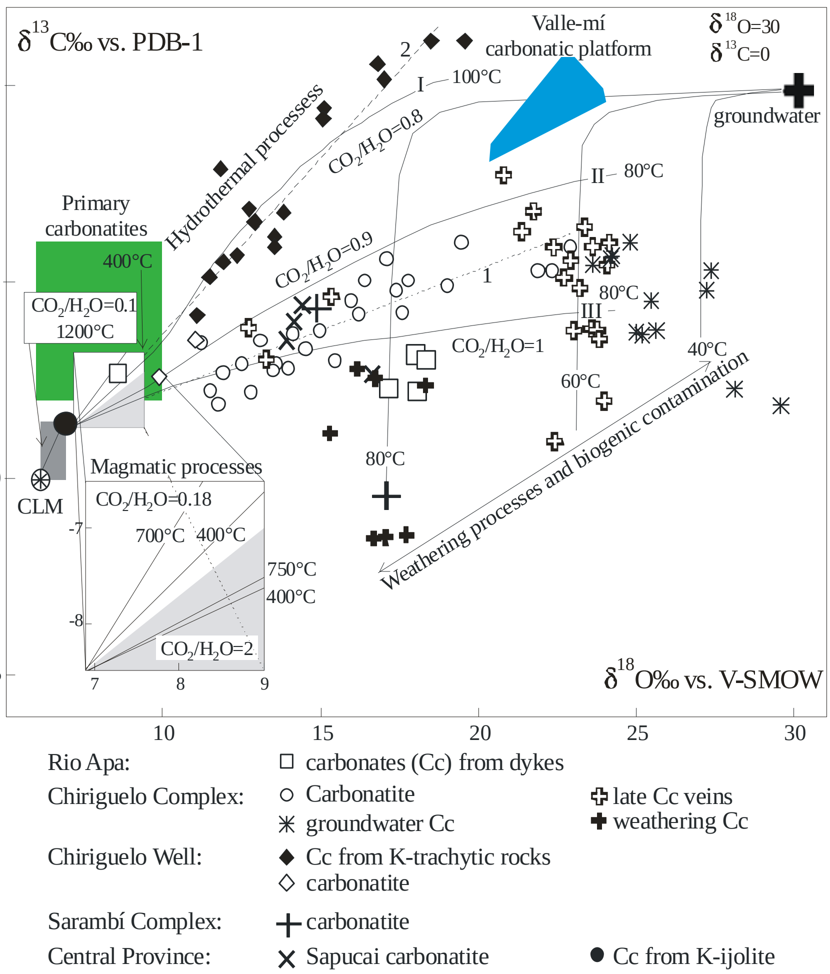


Fig. 5. Plot of $\delta^{18}O$ vs. $\delta^{13}C$ for the primary carbonates and carbonatites from Eastern Paraguay (Early Cretaceous, cf. Table 1) and evolution of the O-C isotope composition of carbonates (magmatic conditions, i.e. 1200-400°C; hydrothermal environment: I up to 100°C, II and III up to 80°C, cf. Appendix; low temperature conditions: biogenic component with pH~5 and temperature=40-80°C. Arbitrary starting compositions: $\delta^{13}O$=30‰, $\delta^{18}O$=0; cf. Taylor, 1978, and Usdowski, 1982). CLM: continental lithospheric mantle (Kyser, 1990). Cc, carbonates; I and 2: regression lines from field and borehole samples, respectively. Primary carbonatites field after Taylor *et al.* (1967) and Keller & Hoefs (1995). Data source for Valle-mí carbonate platform: Castorina *et al.* (1996).

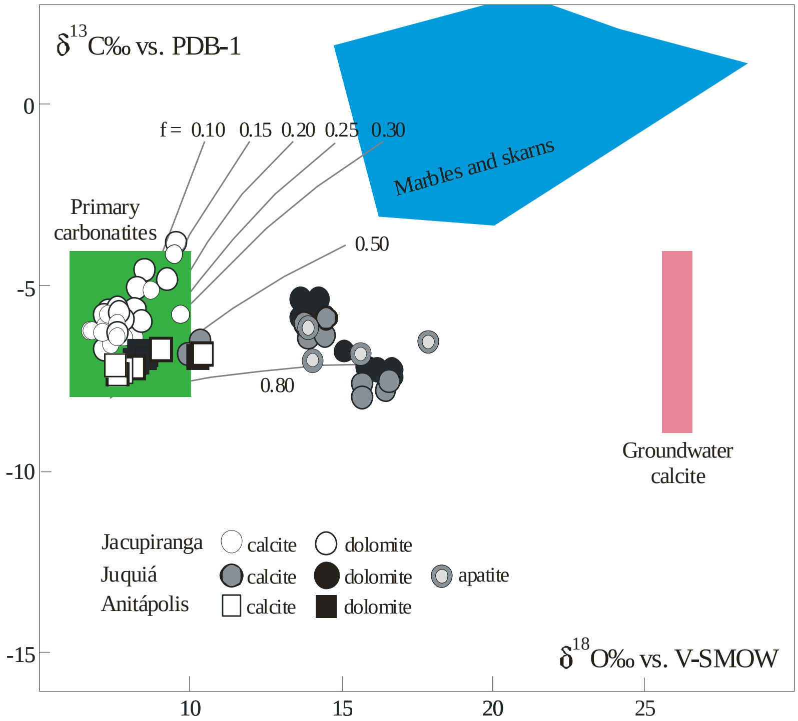


Fig. 6. Plot of $\delta^{18}O$ vs. $\delta^{13}C$ for Jacupiranga, Juquiá and Anitápolis carbonatite samples (Early Cretaceous, cf. Table 2) compared with the results from the elaborated model {*f*=[(A-b)/A], see text and Table II of the Appendix}. Data for Meso and Neoproterozoic marbles and skarns after Mello & Bettencourt (1998); groundwater calcite after Alcover *et al.* (1995); for primary carbonatites field see Fig. 5.

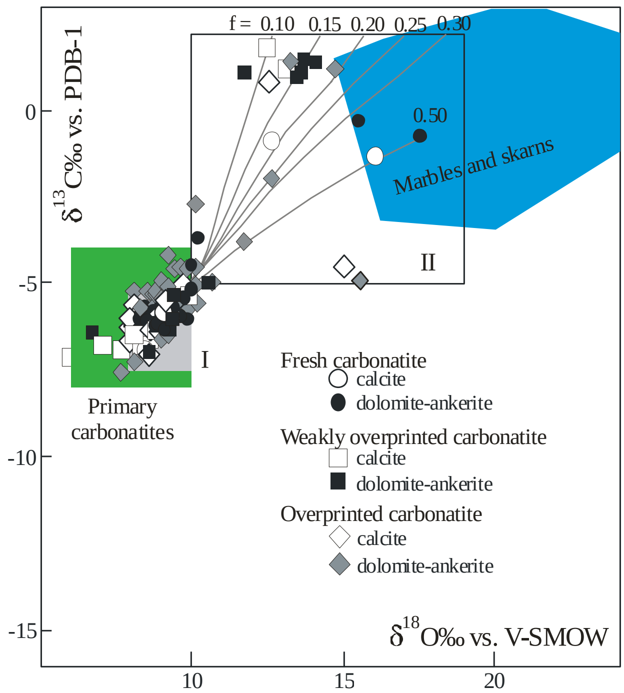


Fig. 7. Plot of $\delta^{18}O$ vs. $\delta^{13}C$ for the carbonatite samples from the Barra do Itapirapuã complex (Early Cretaceous, cf. Table 3) compared with the results from the elaborated model {I: magmatic evolution; II: fluid-related hydrothermal recrystallization; *f*=[(A-b)/A], see text and Tables I and II of the Appendix}. Data for Mesozoic and Neoproterozoic marbles and skarns after Mello & Bettencourt (1998); for primary carbonatites field see Fig. 5.

Table 1. Isotope O-C values for carbonate and silicate phases of different rock-types from Eastern Paraguay. Data source: Castorina *et al*. (1997). Abbreviations: Cc, calcite; Dol, dolomite; Cpx, clinopyroxene (wollastonite 0.5, enstatite 0.4, ferrosilite, 0.1); Ol, olivine (Fo 86); Bt, biotite [$Mg/(Mg+Fe^{2+})=0.70$]. The numbers in brackets represent the deep parts of borehole samples. K-1* to K-8*: data after Livieres (1987). The standard deviation for the whole analytical procedure is about 0.05‰ (1σ) for both carbon and oxygen isotopes.

| Sample | $\delta^{18}O$‰ (V-SMOW) | $\delta^{13}C$‰ (PDB-1) | Sample | $\delta^{18}O$‰ (V-SOW) | $\delta^{13}C$‰ (PDB-1) |
|---|---|---|---|---|---|
| RIO APA | | | ***Cerro Chiriguelo, Cc,*** | | |
| STE-A, Phonotephrite, Cc | 17.12 | | ***late hydrothermal veins*** | | |
| STE-B, Phonotephrite, Cc | 17.96 | -7.68 | CAU-08 | 23.62 | -6.19 |
| STE-C, Basanite, Cc | 8.53 | -6.82 | CHI-01 | 24.22 | -3.98 |
| STE-D, Phonotephrite, Cc | 18.30 | -7.30 | CHI-02 | 23.21 | -4.11 |
| STE-E, Phonotephrite, Cc | 18.03 | -6.96 | CHI-03 | 24.08 | -4.55 |
| PS-279, Dolostone, Cc | 23.88 | -7.75 | CHI-05 | 22.40 | -4.12 |
| Dol | 20.55 | -0.27 | CHI-07 | 23.87 | -6.45 |
| PS-280, Limestone, Cc | 22.85 | -1.68 | CHI-12 | 22.77 | -4.92 |
| | | 0.57 | CHI-15 | 21.42 | -3.71 |
| CERRO CHIRIGUELO | | | | | |
| 3407, Søvite, Cc | 17.87 | -7.01 | CHI-16 | 24.04 | -8.07 |
| 3408, Søvite, Cc | 18.14 | -5.97 | CHI-17 | 22.97 | -4.47 |
| 3409, Søvite, Cc | 14.14 | -6.30 | CHI-19 | 23.77 | -6.19 |
| 3410, Søvite, Cc | 22.33 | -4.71 | CHI-20 | 23.07 | -6.24 |
| 3411, Alvikite, Cc | 15.93 | -5.48 | CHI-21 | 22.29 | -4.70 |
| 3412, Søvite, Cc | 17.76 | -4.98 | CHI-22 | 20.85 | -2.31 |
| 3413, Søvite, Cc | 16.21 | -5.80 | CHI-23 | 21.79 | -3.21 |
| 3414, Alvikite, Cc | 17.56 | -5.75 | CHI-25 | 23.28 | -5.26 |
| 3416, Søvite, Cc | 16.53 | -6.40 | CHI-27 | 23.40 | -3.61 |
| 3417, Søvite, Cc | 16.38 | -4.98 | CHI-28 | 22.41 | -9.10 |
| 3418, Søvite, Cc | 15.56 | -6.74 | ***Weathering calcite*** | | |
| 3419, Søvite, Cc | 19.44 | -3.97 | CAU-9 | 16.21 | -7.22 |
| 3420, Alvikite, Cc | 15.45 | -6.98 | Chi-04 | 15.36 | -5.38 |
| 3422, Alvikite, Cc | 13.48 | -7.26 | Chi-06 | 16.79 | -7.47 |
| 3423, D-trachyte, Cc | 18.04 | -6.89 | Chi-11 | 12.70 | -6.06 |
| 3433, Trachyte, Cc | 18.71 | -5.34 | Chi-18 | 17.80 | -11.42 |
| 3434, Søvite, Cc | 11.22 | -6.52 | Chi-24 | 15.29 | -8.86 |
| 3435A, Søvite, Cc | 11.53 | -7.77 | Chi-26 | 13.29 | -6.95 |
| 3435B, Søvite, Cc | 14.94 | -6.25 | CAU-7f | 17.10 | -11.50 |
| 3436, Søvite, Cc | 12.51 | -7.07 | CAU-7g | 16.69 | -11.54 |
| 3440, Ferruginous carbonatite, Ank | 22.91 | -4.10 | CAU-7h | 18.39 | -7.63 |
| 3442, Søvite, Cc | 11.76 | -8.08 | ***Groundwater calcite*** | | |
| 3443, Alvikite, Cc | 13.07 | -6.49 | Chi-13 | 27.21 | -5.21 |
| K-1* | 19.0 | -5.1 | Chi-14 | 29.58 | -8.13 |
| K-2* | 12.8 | -7.8 | CCh-20a | 23.61 | -4.58 |
| K-3* | 13.6 | -7.1 | CCh-20b | 25.49 | -5.55 |
| K-4* | 17.4 | -5.2 | CCh-20c | 24.13 | -4.37 |
| K-5* | 11.9 | -7.3 | CCh-20d | 24.25 | -4.31 |
| K-6* | 21.9 | -4.7 | CCh-05 | 28.09 | -7.72 |
| K-7* | 14.5 | -6.7 | CCh-20e | 24.80 | -3.98 |
| K-8* | 14.0 | -7.2 | C-602 | 27.38 | -4.70 |
| ***Cerro Chiriguelo, Well-24*** | | | C-700 | 24.98 | -6.28 |
| 49 (-93.5), Trachyte, Cc | 12.36 | -4.33 | CCh-20f | 25.20 | -6.36 |
| 50 (-97.5), Phonotephrite, Cc | 13.55 | -3.86 | CCh-03 | 25.61 | -6.24 |
| 51 (-101.2), Trachyphnolite, Cc | 15.12 | -0.62 | | | |
| 52 (-108.0), Trachyte, Cc | 11.45 | -4.86 | CERRO SARAMBÍ | | |
| 53 (-121.7), Trachyphonolite, Cc | 11.04 | -4.51 | SA-90, Søvite, Cc | 21.68 | -5.68 |
| 54 (-136.8), Trachyte, Cc | 11.04 | -5.84 | SA-91, Silicocarbonatite, Cc | 17.11 | -10.37 |
| 55 (-142.0), Phonotephrite, Cc | 13.25 | -3.25 | SA-95, Silicocarbonatite, Cc | 14.96 | -5.68 |
| 56 (-155.2), Silicocarbonatite, Cc | 10.99 | -6.50 | | | |
| 57 (-175.0), Silicocarbonatite, Cc | 14.96 | 0.14 | SAPUCAI | | |
| 58 (-176.3), Phonotephrite, Cc | 16.77 | 0.53 | PS-72, Silicobeforsite, Dol | 14.47 | -5.63 |
| 59 (-183.6), Trachyte, Cc | 18.47 | 1.12 | PS-72, Silicobeforsite, Dol | 14.00 | -6.54 |
| 60 (-187.0), Silicocarbonatite, Cc | 16.98 | 0.14 | PS-94, Phonolite, Cc | 16.70 | -7.37 |
| 61 (-197.0), Phonotephrite, Cc | 18.53 | 1.12 | | | |
| 63 (-203.5), Trachyphonolite, Cc | 15.06 | -0.84 | CAÑADA | | |
| 64 (-233.0), Søvite, Cc | 9.90 | -7.40 | PS-245, Ijolite, whole-rock | 5.91 | |
| 65 (-235.0), Trachyphonolite, Cc | 12.87 | -3.47 | PS-245, Cpx | 5.20 | |
| 68 (-294.0), Trachyphonolite, Cc | 19.54 | 1.12 | PS-245, Bt | 5.54 | |
| 69 (-333.0), Phonolite, Cc | 11.79 | -2.13 | PS-245, Cc | 6.90 | -8.5 |
| 70 (-361.0), Phonotephrite, Cc | 13.55 | -4.11 | PS-245, Ol | 4.63 | |
| 71 (-387.0), Trachyte, Cc | 12.67 | -3.13 | | | |

Table 2. CaO-MgO-(FeO+MnO) mol%, isotope O-C values and calcite-dolomite/ankerite wt% for carbonates from Jacupiranga, Juquiá and Anitápolis carbonatites and carbonates from different rock-types and apatite. Data source: (N) Nelson *et al.* (1988); (SC), Santos & Clayton (1995); (H), Huang *et al*. (1995); (A), Alcover *et al*. (1995); (W) Walter *et al.* (1995); (T), Toyoda *et al*. (1995) and unpublished data. Abbreviations: Cc, calcite; Dol, dolomite-ankerite. The numbers in brackets represent the deep parts of borehole samples.

| Sample | CaO | MgO mol% | FeO+MnO | $\delta^{18}O$ Cc | $\delta^{13}C$ Cc | $\delta^{18}O$ Dol | $\delta^{13}C$ Dol | Cc% wt% | Dol-Ank% wt% | Notes |
|---|---|---|---|---|---|---|---|---|---|---|
| JACUPIRANGA | | | | | | | | | | |
| JM-1 | 90.3 | 8.9 | 0.8 | 8.0 | -6.3 | | | 96 | 4 | |
| JM-2 | 89.0 | 10.2 | 0.8 | 7.48 | -6.07 | 8.12 | -5.03 | 84 | 16 | |
| JM-6A | 87.2 | 12.3 | 0.5 | 8.12 | -5.03 | 8.41 | -4.59 | 79 | 21 | |
| JM-12B | 85.7 | 12.7 | 1.6 | 9.38 | -4.12 | 9.51 | -3.8 | 81 | 19 | |
| JM-15 | 93.0 | 6.2 | 0.8 | 8.62 | -5.15 | 9.2 | -4.8 | 84 | 16 | |
| JC-11 | 98.0 | 1.5 | 0.5 | 7.5 | -6.4 | | | 100 | 0 | |
| JC-18 | 98.0 | 1.5 | 0.5 | 8.1 | -6.4 | | | 100 | 0 | |
| JC-26 | 86.5 | 12.0 | 1.5 | 7.3 | -6.2 | 7.1 | -5.8 | 74 | 26 | |
| JC-27 | 50.0 | 48.0 | 2.0 | | | 7.7 | -5.9 | | 100 | |
| JC-44 | 87.0 | 11.8 | 1.2 | 9.6 | -5.8 | 7.3 | -6.1 | 80 | 20 | |
| JC-46 | 86.5 | 12.3 | 1.2 | 7.7 | -6.4 | 8.1 | -5.6 | 78 | 22 | |
| JC-99 | | | | 10.05 | -6.39 | | | 100 | 0 | |
| JC-100 | | | | 7.48 | -6.07 | 7.6 | -5.71 | 40 | 60 | |
| JC-101 | | | | 8.12 | -5.03 | 8.41 | -4.59 | 35 | 75 | |
| JC-102 | | | | 9.38 | -4.12 | 9.51 | -3.8 | 80 | 20 | |
| JC-103 | | | | 8.62 | -5.15 | 9.2 | -4.8 | 70 | 30 | |
| JP881 | 85.9 | 8.6 | 5.5 | 7.4 | -5.8 | 7.2 | -5.7 | 71 | 29 | |
| JP882 | 76.7 | 17.3 | 6.0 | 7.7 | -6.5 | 7.5 | -6.3 | 54 | 46 | |
| C1-A-5 (SC) | | | | 6.6 | -6.2 | 7.2 | -5.8 | | | |
| C1-C-3 (SC) | | | | 7.0 | -6.3 | 8.3 | -6.0 | | | |
| C3-4 (SC) | | | | 6.7 | -6.2 | 7.1 | -6.7 | | | |
| C4-5 (SC) | | | | 7.3 | -6.6 | 7.4 | -6.2 | | | |
| P1C-21 (SC) | | | | | | 7.5 | -5.6 | | | |
| HB 009-2 (H) | 86.5 | 10.6 | 2.9 | | | | | | | |
| HB 011 (H) | 80.4 | 17.2 | 2.4 | | | | | | | |
| 5961 (N) | 93.5 | 4.9 | 1.6 | 7.1 | -6.1 | | | 87 | 13 | |
| 5963 (N) | 88.6 | 10.7 | 0.7 | 7.3 | -5.6 | | | 78 | 22 | |
| JUQUIÁ | | | | | | | | | | |
| JQ 1 | | | | 10.29 | -6.44 | | | 80 | 20 | |
| JQ 2 | | | | 9.89 | -6.82 | | | 85 | 15 | |
| | | | | | | 15.05 | -6.75 | | | |
| S16C | 66.7 | 30.9 | 2.4 | 16.58 | -7.57 | 15.83 | -7.20 | 35 | 65 | |
| S25 | 54.8 | 42.2 | 3.0 | 15.68 | -7.60 | 16.13 | -7.27 | 10 | 90 | |
| S26A | 54.6 | 42.8 | 2.6 | 16.42 | -7.84 | 16.64 | -7.27 | 8 | 92 | |
| S26B | 54.0 | 43.4 | 2.6 | 15.68 | -8.02 | 16.64 | -7.45 | 7 | 93 | |
| 1 (A) | 74.0 | 23.5 | 2.5 | 14.39 | -6.31 | 14.19 | -5.78 | 49 | 51 | |
| 2 (A) | 60.0 | 29.6 | 10.4 | 14.50 | -5.82 | 14.19 | -5.32 | 16 | 84 | |
| 3 (A) | 60.0 | 29.1 | 10.9 | 13.90 | -6.39 | 13.59 | -5.78 | 16 | 84 | |
| 4 (A) | 57.1 | 36.8 | 6.2 | 13.79 | -5.95 | 13.59 | -5.32 | 15 | 85 | $\delta^{18}O$‰ $\delta^{13}C$‰ |
| Apatite (W) | | | | | | | | | | 13.9 -6.1 |
| Apatite (W) | | | | | | | | | | 14.0 -7.0 |
| Apatite (W) | | | | | | | | | | 17.9 -6.5 |
| Apatite (W) | | | | | | | | | | 15.6 -6.8 |
| ANITÁPOLIS | | | | | | | | | | |
| AP891 (T) | 87.4 | 8.7 | 3.9 | 9.0 | -6.7 | | | 75 | 25 | |
| SAN-1 | 95.0 | 3.9 | 1.1 | 7.55 | -7.24 | 8.24 | -7.07 | 91 | 9 | |
| SAN-2A | | | | 7.94 | -7.34 | 8.51 | -6.93 | 95 | 5 | Phlogopite pyroxenite |
| SAN-2B | | | | 7.89 | -7.29 | | | 100 | 0 | Cpx cumulate |
| SAN-3 | | | | 7.53 | -7.26 | 8.17 | -7.02 | | | |
| SAN-4 | | | | 7.63 | -7.27 | 8.11 | -7.00 | | | |
| SAN-5 | | | | 8.08 | -7.16 | 8.39 | -6.80 | | | |
| SAN-6A | | | | | | 10.12 | -6.89 | 0 | 100 | Lamprophyre |
| SAN-8 | | | | 10.38 | -6.82 | | | 100 | 0 | Ap-Cpx-Bi cumulate |
| SAN-11 (-101.0) | 90.6 | 4.8 | 4.6 | 7.55 | -7.38 | 8.04 | -7.21 | 81 | 19 | |
| SAN-12 (-78.0) | 86.0 | 10.7 | 3.3 | 7.47 | -7.15 | 8.19 | -6.78 | 73 | 27 | |
| SAN-13 (-27.0) | 88.5 | 8.5 | 3.0 | 7.52 | -7.37 | 7.45 | -7.25 | 82 | 18 | |
| SAN-14 (-49.3) | 90.5 | 5.8 | 3.7 | 7.50 | -7.15 | 8.22 | -6.78 | 81 | 19 | |

Table 3. CaO-MgO-(FeO+MnO) mol%, isotope O-C values and calcite-dolomite/ankerite wt% for carbonates from the Barra do Itapirapuã carbonatite (Early Cretaceous). The first sample-number indicates the borehole-number and the second the depth. Data source: Andrade *et al*. (1999), Ruberti *et al*. (2002) and unpublished data. Fresh, weakly and overprinted carbonatites are after Andrade *et al*. (1999); see text. Abbreviations: Cc, calcite; Dol, dolomite-ankerite.

| BARRA DO ITAPIRAPUÃ | CaO | MgO | FeO+MnO | $\delta^{18}O$ | $\delta^{13}C$ | $\delta^{18}O$ | $\delta^{13}C$ | Xχ% | Dol-Ank% | Notes |
|---|---|---|---|---|---|---|---|---|---|---|
| | mol% | | | Cc | Cc | Dol | Dol | wt% | wt% | |
| Sample | | | | | | | | | | |
| 1 -34.9 | 50.9 | 32.7 | 16.4 | | | 8.5 | -6.1 | 0 | 100 | **Fresh carbonatites** |
| 1 -66.5 | 50.3 | 39.9 | 9.8 | | | 8.87 | -6.13 | 0 | 100 | |
| 1 -87.4 | 50.6 | 35.6 | 13.8 | | | 9.37 | -5.69 | 0 | 100 | |
| 1 -100.7 | 49.5 | 42.2 | 8.3 | | | 8.85 | -6.2 | 0 | 100 | |
| 2 -16.2 | 50.5 | 34.8 | 14.7 | | | 8.2 | -6.0 | 0 | 100 | |
| 2 -31.0 | 50.3 | 38.4 | 11.3 | | | 8.7 | -5.8 | 0 | 100 | |
| 2 -110.5 | 50.3 | 37.1 | 12.6 | | | 9.97 | -4.43 | 0 | 100 | |
| 3 -35.7 | 91.5 | 6.5 | 2.0 | 12.64 | -0.89 | 15.55 | -0.3 | 84 | 16 | |
| 3 -44.7 | 78.5 | 16.3 | 5.2 | 16.08 | -1.3 | 17.53 | -0.73 | 58 | 42 | Silicocarbonatite |
| 4 -10.3 | 51.0 | 23.0 | 26.0 | | | 8.3 | -5.9 | 0 | 100 | |
| 5 -13.0 | 50.4 | 38.9 | 10.7 | | | 8.4 | -5.7 | 0 | 100 | |
| 5 -79.0 | 51.7 | 29.4 | 18.9 | 9.06 | -5.82 | 10.0 | -5.19 | 3 | 97 | |
| 5 -98.0 | 52.3 | 32.5 | 15.2 | 8.42 | -6.92 | 9.08 | -6.35 | 5 | 95 | |
| 5 -256.0 | 51.6 | 34.1 | 14.3 | 9.09 | -6.43 | 9.6 | -5.94 | 3 | 97 | |
| 6 -20.0 | 50.0 | 41.1 | 8.9 | | | 9.13 | -5.76 | 0 | 100 | |
| 6 -30.0 | 50.0 | 40.0 | 10.0 | | | 8.76 | -6.22 | 0 | 100 | |
| 6 -66.0 | 50.0 | 37.4 | 12.6 | | | 9.23 | -5.71 | 0 | 100 | |
| 6 -78.8 | 50.0 | 39.6 | 10.4 | | | 10.19 | -3.69 | 0 | 100 | |
| 6 -95.0 | 50.0 | 40.2 | 9.8 | | | 8.63 | -6.44 | 0 | 100 | |
| 6 -99.7 | 50.0 | 39.5 | 10.5 | | | 8.73 | -6.52 | 0 | 100 | |
| 6 -110.0 | 50.0 | 38.7 | 11.3 | | | 9.81 | -6.04 | 0 | 100 | |
| 6 -170.7 | 50.0 | 34.9 | 15.1 | | | 9.72 | -5.42 | 0 | 100 | |
| 1 -18.8 | 50.6 | 34.7 | 14.7 | | | 9.0 | -5.8 | 0 | 100 | **Weakly overprinted carbonatites** |
| 1 -30.5 A | 51.1 | 36.9 | 12.0 | 12.5 | 1.8 | 13.5 | 1.1 | 2 | 98 | |
| 1 -32.5 | 51.0 | 33.4 | 15.6 | 7.67 | -6.91 | 8.64 | -6.19 | 1 | 99 | |
| 1 -33.45 | 50.9 | 33.8 | 15.3 | | | 9.4 | -5.4 | 0 | 100 | |
| 1 -37.4 | 51.2 | 29.8 | 19.0 | 6.0 | -7.1 | 6.7 | -6.4 | 2 | 98 | |
| 1 -39.3 | 51.8 | 29.8 | 18.4 | 8.08 | -6.48 | 9.0 | -5.78 | 4 | 96 | |
| 1 -57.6 | 51.0 | 33.5 | 15.5 | 7.0 | -6.8 | 7.9 | -6.1 | 2 | 98 | |
| 1 -128.7 | 48.7 | 42.7 | 8.6 | | | 9.28 | -6.31 | 0 | 100 | |
| 2 -72.4 | 50.0 | 40.9 | 9.1 | | | 8.84 | -6.13 | 0 | 100 | |
| 3 -37.9 | 52.5 | 37.9 | 9.6 | | | 13.6 | 1.1 | 5 | 95 | |
| 3 -54.0 B | 51.2 | 37.0 | 11.8 | | | 11.7 | 1.1 | 2 | 98 | |
| 3 -67.4B | 52.0 | 38.1 | 9.9 | 13.1 | 1.2 | 13.7 | 1.5 | 4 | 96 | |
| 3 -72.2 | 50.0 | 40.9 | 9.1 | | | 8.54 | -6.98 | 0 | 100 | |
| 3 -183.4 | 51.5 | 32.5 | 16.0 | 8.27 | -6.77 | 9.26 | -6.0 | 3 | 97 | |
| 5 -90.4 | 50.3 | 41.7 | 8.0 | | | 14.13 | 1.38 | 0 | 100 | Silicocarbonatite |
| 5 -160.5 | 52.8 | 26.8 | 20.4 | 8.8 | -6.36 | 9.36 | -5.99 | 6 | 94 | |
| 5 -172.3 | 52.0 | 27.9 | 20.1 | 8.33 | -6.6 | 9.09 | -6.03 | 4 | 96 | |
| 5 -190.0 | 54.7 | 26.3 | 19.0 | 8.6 | -6.61 | 9.14 | -6.12 | 9 | 91 | |
| 5 -230 | 56.7 | 25.8 | 17.5 | 9.88 | -5.38 | 10.55 | -4.99 | 13 | 87 | |
| 1 -12.9 | 6.5 | 29.6 | 13.9 | 7.9 | -6.3 | 8.8 | -5.6 | 13 | 87 | **Overprinted carbonatites** |
| 1 -54.7 | 51.8 | 30.5 | 17.7 | 8.3 | -5.8 | 9.2 | -5.1 | 4 | 96 | |
| 1 -188.6 | 50.8 | 38.6 | 10.6 | | | 8.97 | -6.58 | 0 | 100 | |
| 2 -40.3 | 52.2 | 22.2 | 25.6 | 8.1 | -5.6 | 8.5 | -5.2 | 4 | 96 | |
| 2 -40.9 A | 53.1 | 28.7 | 18.2 | 7.9 | -6.0 | 8.3 | -5.7 | 6 | 94 | |
| 2 -40.9 B | 52.9 | 20.4 | 26.6 | 15.0 | -4.5 | 15.6 | -4.9 | 6 | 94 | |
| 2 -43.3 | 53.4 | 24.9 | 21.7 | 7.91 | -6.65 | 9.17 | -6.04 | 7 | 93 | |
| 2 -75.6 | 58.9 | 17.9 | 23.2 | 9.71 | -5.05 | 10.69 | -4.99 | 18 | 82 | |
| 2 -115.0 | 64.4 | 20.8 | 14.8 | 8.8 | -6.12 | 9.24 | -5.75 | 29 | 71 | |
| 3 -35 Si | 53.5 | 23.2 | 23.3 | | | 9.4 | -4.6 | 7 | 93 | |
| 3 -39.3 | 51.6 | 29.2 | 19.2 | | | 8.1 | -5.2 | 3 | 97 | |
| 3 -51.1 | 52.4 | 29.7 | 17.9 | | | 9.6 | -4.5 | 5 | 95 | Silicocarbonatite |
| 3 -54.0 A | 52.9 | 33.7 | 13.4 | | | 9.2 | -4.2 | 6 | 94 | |
| 3 -55.3 | 51.5 | 34.7 | 13.8 | | | 8.8 | -5.2 | 3 | 97 | |
| 3 -59.1 | 52.3 | 30.9 | 16.8 | | | 8.8 | -5.3 | 5 | 95 | |
| 3 -64.9 | 52.6 | 22.0 | 25.4 | 8.1 | -6.1 | 9.0 | -5.4 | 5 | 95 | |
| 3 -67.4 A | 51.7 | 34.4 | 13.9 | | | 9.0 | -4.9 | 3 | 97 | |
| 3 -69.5 | 50.0 | 24.8 | 25.2 | | | 10.1 | -4.5 | 0 | 100 | |
| 3 -93.6 | 50.0 | 36.6 | 13.4 | | | 12.63 | -1.95 | 0 | 100 | |
| 3 -142.0 | 53.6 | 28.2 | 18.2 | 8.95 | -6.39 | 9.9 | -5.72 | 7 | 93 | |
| 5 -11.0 | 50.0 | 30.0 | 20.0 | | | 9.8 | -4.6 | 0 | 100 | |
| 5 -32.5 | 52.5 | 21.0 | 26.5 | | | 11.7 | -3.8 | 5 | 95 | |
| 5 -40.0 A | 53.6 | 23.3 | 23.1 | | | 10.1 | -2.7 | 7 | 93 | |
| 5 -40.0 B | 53.6 | 33.2 | 13.2 | 8.43 | -6.0 | 9.41 | -5.65 | 8 | 92 | |
| 5 -43.0 | 51.4 | 27.5 | 21.1 | | | 8.7 | -5.6 | 3 | 97 | |
| 5 -50.7 | 50.0 | 23.5 | 26.5 | | | 9.32 | -6.03 | 0 | 100 | |
| 5 -55.7 | 52.2 | 22.1 | 25.7 | | | 8.7 | -5.3 | 4 | 96 | |
| 5 -61.2 | 59.3 | 28.8 | 11.9 | 9.05 | -6.03 | 10.18 | -5.57 | 19 | 81 | Silicocarbonatite |
| 5 -87.3 | 52.1 | 39.0 | 8.9 | 12.55 | 0.81 | 13.26 | 1.42 | 4 | 96 | |
| 5 -130.0 | 63.3 | 16.7 | 20.0 | 9.13 | -5.5 | 10.12 | -5.04 | 27 | 73 | |
| 5 -150.0 | 52.6 | 34.3 | 13.1 | 8.54 | -7.04 | 9.2 | -6.47 | 5 | 95 | |
| 5 -210.0 | 55.1 | 21.9 | 23.0 | 8.95 | -5.9 | 9.64 | -5.78 | 10 | 90 | |
| 6 -6.8 | 55.9 | 20.9 | 23.2 | 8.65 | -6.35 | 9.36 | -5.85 | 11 | 89 | |
| 6 -141.0 | 50.6 | 38.3 | 11.1 | | | 14.74 | 1.18 | 0 | 100 | |

### Barra do Itapirapuã

The Barra do Itapirapuã occurrence differs from the other alkaline-carbonatite complexes being represented by an ellipsoidal network of dykes and veins of calcio-, magnesio and ferruginous carbonatites. This network is intruding the Neoproterozoic Três Córregos granite, which in its turn penetrates Mesoproterozoic to Neoproterozoic metasediments of the Açungui Group (Mello & Bettencourt, 1998; Ruberti *et al.*, 2002 and therein references). The samples were mostly obtained from drill cores at various depths (up to 210 m; cf. Table 3). On the basis of textural and mineralogical relationships and following Andrade *et al.* (1999), the rock-types are grouped here into:

1) fresh carbonatites consisting of prevailing magnesio- and ferruginous carbonatites (mineral composition: Fe-dolomite with or without calcite) or scarce calciocarbonatites;

2) hydrothermal weakly overprinted carbonatites, i.e. magnesio- and ferruginous carbonatites with calcite content less than 13 wt% and characterized by small amounts of secondary quartz, apatite, fluorite and REE-fluorcarbonates;

3) hydrothermal overprinted carbonatites consisting of magnesio- and ferruginous carbonatites with Fe-dolomite, subordinate calcite (0-29 wt%) and accessory pyrochlore, quartz, apatite, REE-fluorcarbonates, fluorite, barite, galena and sphalerite.

In spite of the hydrothermal overprinting, the mean $\delta^{18}O$ values for dolomite-ankerite are 11.06±3.26 (fresh carbonatites), 10.07±2.17 (weakly overprinted carbonatites) and 9.92±1.73‰, and $\delta^{13}C$ −5.28±1.68, −4.11±3.31 and −4.83±1.73‰, respectively (Table 3). Notably, many carbonates from the overprinted carbonatites (about 7%) tend to have $\delta^{18}O$ between 11 and 15‰ and $\delta^{13}C$ between 0 and 2‰ (cf. Fig. 7).

Anyway, the carbonatite isotopic values are well distinct in comparison to those presented by the marbles and skarns of the region (Mello & Bettencourt, 1998 and therein references; cf. Fig. 7).

## LATE CRETACEOUS CARBONATITES

### Alto Paranaíba

The Alto Paranaíba carbonatites (Catalão I, Limeira, Araxá and Tapira bodies) are mostly characterized by magnesiocarbonatites and subordinate calcio- and ferruginous carbonatites and furthermore by large $\delta^{18}O$ and relatively narrow $\delta^{13}C$ variations, i.e. between 7 and 23‰, and between −8 and −3‰, respectively, for both calcite and dolomite-ankerite (Table 4 and Fig. 8). However, more than 93% of the samples fit a $\delta^{18}O$ range between 7 and 16‰, with the other samples trending towards the groundwater calcite field (Meyer *et al.*, 1994).

### Mato Preto

Mato Preto samples vary from calciocarbonatites to ferruginous carbonatites, the latter containing accessory fluorcarbonates and fluorite, and displaying patterns very similar to those shown by the Barra do Itapirapuã rocks (Table 5 and Fig. 9).

### Lages

The Lages samples are represented by magnesio- and ferruginous carbonatites made of prevailing Fe-dolomite or Mg-ankerite and subordinate calcite. They show very large spreads of $\delta^{18}O$ and $\delta^{13}C$ values for the two carbonatic phases, i.e. $\delta^{18}O$ 9−24‰ and $\delta^{13}C$ −7.2 to −0.5‰. (cf. Fig. 9).

## MODEL OF ISOTOPIC FRACTIONATION

The O-C isotopic variations falling out of the primary carbonatite box, the differences in isotopic composition between coexisting calcite and dolomite/ankerite, the petrographical and geochemical characteristics of the investigated carbonatites as well as the relationships to be expected if coexisting carbonates were formed in isotopic equilibrium (Sheppard & Schwarz, 1970: metamorphic equilibrium; Deines, 1989: fractionation processes at about 700°C) indi-

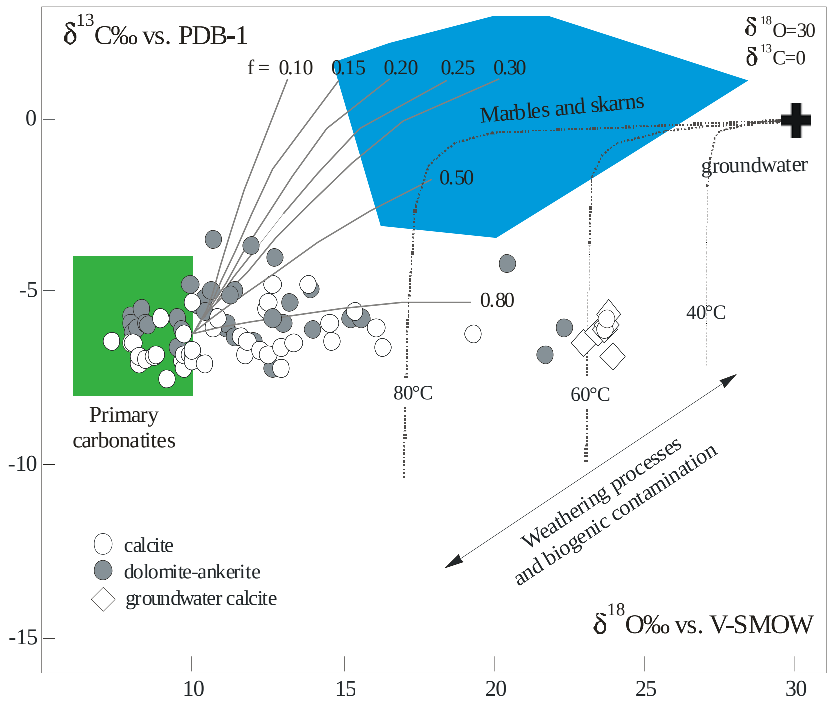


Fig. 8. Plot of $\delta^{18}O$ vs. $\delta^{13}C$ for carbonatite samples from the Alto Paranaíba complexes (Catalão I, Limeira, Araxá and Tapira; Early Cretaceous, cf. Table 4) compared with the results from the elaborated model (cf. Figs. 5 and 6); for primary carbonatites field see Fig. 5.

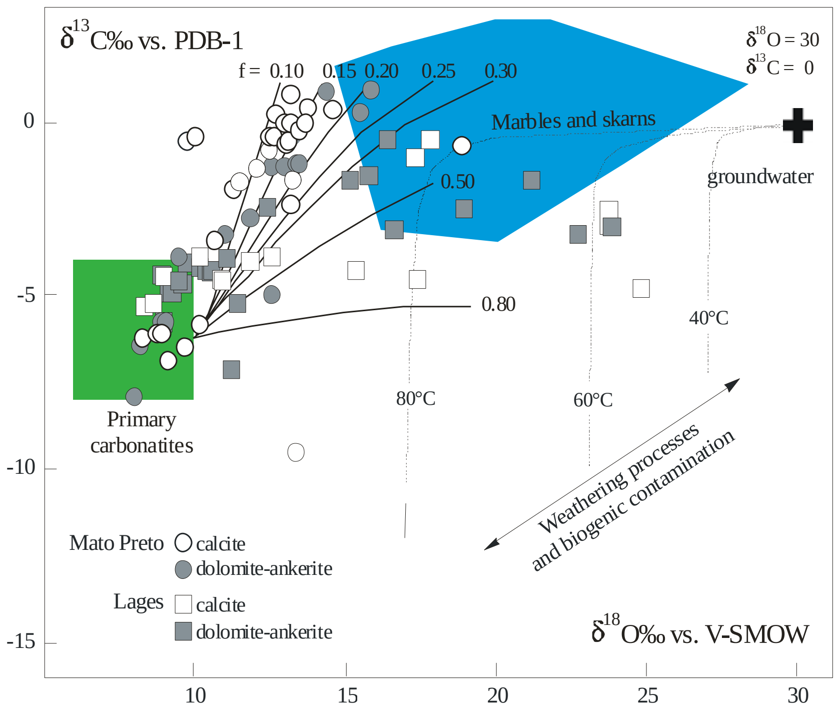


Fig. 9. Plot of $\delta^{18}O$ vs. $\delta^{13}C$ for carbonatite samples from the Mato Preto and Lages complexes compared with the results from the elaborated model (cf. Figs. 5 and 6); for primary carbonatites field see Fig. 5.

Table 4. CaO-MgO-(FeO+MnO) mol%, isotope O-C values and calcite-dolomite/ankerite wt% for carbonates from Alto Paranaíba (Catalão I, Limeira, Araxá and Tapira, Late Cretaceous) carbonatites and carbonates of various rock-types. Data source: (MO) Morikiyo *et al*. (1990), (B) Bizzi *et al*. (1994), (M) Meyer *et al*. (1994), (T) Toyoda *et al*. (1995), (SC) Santos & Clayton (1995) and unpublished data. Abbreviations: Cc, calcite; Dol, dolomite-ankerite.

| Sample | CaO | MgO | FeO+MnO | $\delta^{18}O$ | $\delta^{13}C$ | $\delta^{18}O$ | $\delta^{13}C$ | Xχ% | Dol-Ank% | Notes |
|---|---|---|---|---|---|---|---|---|---|---|
| | | mol% | | Cc | Cc | Dol | Dol | wt% | wt% | |
| CATALÃO I | | | | | | | | | | |
| CT-36 (MO) | | | | | | 13.2 | -5.3 | | | |
| CT-38 (MO) | | | | 10.7 | -6.0 | 8.4 | -5.9 | | | |
| CT-39A (MO) | | | | | | 10.4 | -5.2 | | | |
| CT-40 (MO) | | | | | | 22.3 | -6.0 | | | |
| CT-41(MO) | | | | | | 21.7 | -6.8 | | | |
| CT-351(MO) | | | | | | 12.6 | -5.8 | | | |
| CT-352(MO) | | | | | | 10.4 | -5.6 | | | |
| CTSC-1 (T) | 50.5 | 48.0 | 1.5 | | | 9.5 | -6.6 | | | |
| CTITB (T) | 50.0 | 27.2 | 22.8 | | | 9.6 | -6.1 | | | |
| CTITW(T) | 96.9 | 2.9 | 0.2 | 9.6 | -7.0 | | | | | |
| 13E-21N-1A (SC) | | | | 13.3 | -6.5 | 11.4 | -5.0 | | | |
| 13E-21N-2A(SC) | | | | 14.6 | -6.4 | 10.2 | -5.4 | | | |
| 13E-21N-3A(SC) | | | | 19.3 | -6.2 | 20.4 | -4.2 | | | |
| 13E-21N-4B(SC) | | | | | | 15.2 | -5.8 | | | Interstitial carbonates in phlogopite-magnetite-apatite cumulate |
| C3-B1-1B (SC) | | | | 7.3 | -6.4 | | | | | |
| C3-B1-2B (SC) | | | | 12.5 | -5.3 | 9.9 | -4.8 | | | |
| C3-B1-3C (SC) | | | | 8.9 | -5.8 | 11.2 | -5.1 | | | Interstitial carbonates in phlogopite-magnetite-apatite cumulate |
| SC-1-Y-1B (SC) | | | | 7.9 | -6.5 | | | | | |
| SC-2AB-12B(SC) | | | | 12.2 | -6.7 | 8.3 | -5.5 | | | |
| SC-2AB-17B(SC) | | | | | | 7.9 | -5.7 | | | |
| SC-2-CD-12B(SC) | | | | 16.1 | -6.0 | 12.0 | -6.4 | | | |
| SC-2-2-16B(SC) | | | | 8.2 | -7.1 | 7.9 | -5.9 | | | |
| 1 (B) | 96.9 | 2.9 | 0.2 | 8.8 | -6.8 | | | | | |
| 2(B) | | | | 10.8 | -5.8 | | | | | |
| CAT-I-1 | 60.0 | 17.0 | 23.0 | 8.45 | -6.97 | 8.03 | -6.17 | 20 | 80 | |
| CAT-I-2 | 67.7 | 26.1 | 6.2 | 8.03 | -6.47 | 8.51 | -5.97 | 37 | 63 | |
| CAT-I-3 | 51.1 | 26.8 | 21.1 | 8.23 | -6.85 | 8.15 | -6.01 | 3 | 97 | |
| LIMEIRA | | | | | | | | | | |
| 1A(M) | | | | 23.69 | -5.97 | | | | | Groundwater calcite |
| 1B(M) | | | | 23.62 | -6.07 | | | | | Groundwater calcite |
| 1C(M) | | | | 23.8 | -5.61 | | | | | Groundwater calcite |
| 2(M) | | | | 23.42 | -6.13 | | | | | Groundwater calcite |
| 3(M) | | | | 22.94 | -6.50 | | | | | Groundwater calcite |
| 4(M) | | | | 23.91 | -6.89 | | | | | Groundwater calcite |
| ARAXÁ | | | | | | | | | | |
| AR-891 (T) | 50.0 | 36.1 | 13.9 | | | 14.0 | -6.1 | 0 | 100 | |
| AR-892 (T) | 50.0 | 36.6 | 13.4 | | | 12.6 | -7.2 | 0 | 100 | |
| 750W-1150S-A (SC) | | | | | | 9.5 | -5.8 | | | Carbonate veins in ultramafite |
| 850W-1150S-B (SC) | | | | 11.6 | -6.3 | | | | | Carbonate veins in mafic silicate rock |
| 900W-1400S-A (SC) | | | | 8.7 | -6.9 | | | | | |
| 900W-1450A-S (SC) | | | | 9.1 | -7.5 | | | | | Carbonatized mafic/ultramafic rock |
| 900W-1450E-S (SC) | | | | 16.3 | -6.6 | | | | | Interstitial carbonate in phlogopite cumulate |
| 1250W-900S-A (SC) | | | | 11.8 | -6.4 | | | | | Veins of carbonate in phlogopite cumulate |
| ARX-1B-A(SC) | | | | 14.5 | -5.9 | | | | | Grounwater calcite |
| ARX-90-1A(SC) | | | | 9.7 | -7.2 | | | | | Carbonatized pyroxenite |
| ARX-90-2B(SC) | | | | 10.0 | -6.9 | 11.1 | -6.0 | | | |
| ARX-90-3B(SC) | | | | 10.4 | -7.1 | 11.4 | -6.3 | | | |
| ARX-90-4B(SC) | | | | 13.8 | -4.8 | 10.7 | -3.5 | | | |
| ARX-90-5B(SC) | | | | 10.0 | -7.0 | | | | | |
| AR | | | | 12.5 | -6.8 | | | | | |
| TAPIRA | | | | | | | | | | |
| TP891(T) | 75.0 | 17.2 | 7.8 | 12.9 | -7.2 | | | 51 | 49 | |
| TP892(T) | 90.5 | 9.4 | 0.1 | 11.7 | -6.8 | | | 82 | 18 | |
| S22-11-C (SC) | | | | 9.9 | -6.8 | 11.1 | -5.9 | | | |
| S22-4-B (SC) | | | | 10.0 | -6.7 | 13.9 | -4.9 | | | Interstitial carbonates in glimmerite |
| S22-5-B (SC) | | | | 15.4 | -5.6 | 15.6 | -5.8 | | | |
| S22-8-F (SC) | | | | 9.7 | -6.8 | | | | | |
| TP-90-1-C(SC) | | | | 10.0 | -5.3 | 11.9 | -3.7 | | | Carbonate veins in phlogopite-rich rock |
| TP-90-1-D(SC) | | | | 9.7 | -6.2 | 10.6 | -5.0 | | | Carbonate veins in phlogopite-rich rock |
| TP-90-12B(SC) | | | | 12.6 | -4.8 | 12.7 | -4.0 | | | |
| TP-90-5(SC) | | | | 12.4 | -5.5 | | | | | |
| TAP-1 | 81.5 | 13.8 | 4.7 | 12.89 | -6.61 | 12.95 | -5.92 | 64 | 36 | |

Table 5. CaO-MgO-(FeO+MnO) mol%, isotope O-C values and calcite-dolomite/ankerite wt% for carbonates from Mato Preto and Lages carbonatites (Late Cretaceous) and carbonates of various rock-types. The first sample-number indicates the borehole-number and the second the depth. Data source: (SH) Scheibe & Formoso (1982), (A) Andrade *et al.* (1999), Comin-Chiaramonti *et al*. (2001, 2002) and unpublished data. Abbreviations: Cc, calcite; Dol, dolomite-ankerite.

| Sample | CaO | MgO | FeO+MnO | $\delta^{18}O$ | $\delta^{13}C$ | $\delta^{18}O$ | $\delta^{13}C$ | Xχ% | Dol-Ank% | Notes |
|---|---|---|---|---|---|---|---|---|---|---|
| | | mol% | | Cc | Cc | Dol | Dol | wt% | wt% | |
| MATO PRETO | | | | | | | | | | |
| 1(A) | | | | | | 8.0 | -7.9 | | | |
| 2(A) | | | | | | 13.4 | -1.2 | | | |
| 3(A) | | | | | | 13.5 | -1.2 | | | |
| 4(A) | | | | | | 8.2 | -6.4 | | | |
| 7-DB46-A(SC) | | | | 12.7 | 0.2 | | | | | |
| 8-DB46-B(SC) | | | | 12.5 | -0.4 | | | | | |
| 8745-B(SC) | | | | 13.5 | -0.2 | | | | | |
| DB45-8733-A-B(SC) | | | | 13.0 | 0.0 | | | | | |
| DB47-8747-B(SC) | | | | 13.2 | 0.8 | 14.4 | 0.9 | | | |
| DB47-8748(SC) | | | | 13.7 | 0.0 | | | | | |
| DB47-8751-B(SC) | | | | 13.8 | 0.4 | 15.5 | 0.3 | | | |
| DB47-8764-B(SC) | | | | 13.2 | 0.0 | | | | | |
| SR-301-A(SC) | | | | | | 11.0 | -3.2 | | | Syenite with disseminated carbonate |
| SR-501-8778B(SC) | | | | | | 9.5 | -3.9 | | | |
| SR-502-8780-B(SC) | | | | 9.7 | -6.5 | | | | | Carbonatized alkaline silicate rock |
| SR-502-8781-B(SC) | | | | 11.5 | -1.7 | 12.6 | -1.3 | | | |
| SR-503-8723-C(SC) | | | | 9.1 | -6.9 | | | | | Alkaline silicate rock with carbonate |
| 44 (-62.2) | 69.9 | 15.2 | 14.9 | 10.68 | -3.45 | 11.88 | -2.74 | 40 | 60 | |
| 45 (-70.0) | 96.1 | 1.2 | 2.7 | 18.9 | -0.7 | | | 100 | 0 | |
| 46 (-77.0) | 92.6 | 3.3 | 4.1 | 11.32 | -1.91 | 13.0 | -1.3 | 85 | 15 | |
| 47 (-84.0) | 92.7 | 0.8 | 1.5 | 12.64 | -0.41 | | | 100 | 0 | |
| 48 (-93.1) | 97.3 | 0.9 | 1.8 | 13.06 | -0.63 | | | 100 | 0 | |
| 49 (-119.3) | 94.8 | 2.5 | 2.7 | 12.49 | -0.81 | 13.31 | -0.45 | 90 | 10 | |
| 50 | 97.3 | 0.2 | 2.5 | 13.26 | -1.66 | | | 100 | 0 | |
| 51 | 83.5 | 9.1 | 7.4 | 14.61 | 0.38 | 15.91 | 0.95 | 67 | 33 | |
| 52 | 99.3 | 0.1 | 0.5 | 8.26 | -6.25 | | | 100 | 0 | |
| 53 | 97.2 | 1.7 | 1.1 | 10.07 | -0.45 | | | 100 | 0 | |
| 54 | 96.1 | 1.2 | 2.7 | 12.06 | -1.36 | | | 92 | 8 | |
| 55 | 98.6 | 0.2 | 1.2 | 13.19 | -2.41 | | | 100 | 0 | |
| 56 | 88.9 | 3.9 | 7.2 | 10.19 | -5.84 | 12.6 | -4.98 | 77 | 23 | |
| 57 | 99.1 | 0.2 | 0.7 | 13.11 | -0.56 | | | 100 | 0 | |
| 58 | 98.0 | 0.4 | 1.6 | 9.77 | -0.57 | | | 100 | 0 | |
| 59 | 60.9 | 14.9 | 24.2 | 8.91 | -6.09 | 9.05 | -5.75 | 21 | 79 | |
| 60 | 70.2 | 11.2 | 18.6 | 8.76 | -6.12 | 8.94 | -5.78 | 40 | 60 | |
| LAGES | | | | | | | | | | |
| FV-1 (SH) | 60.6 | 13.5 | 25.9 | | | 19.0 | -2.49 | 21 | 79 | |
| FV-14 (SH) | 61.5 | 15.5 | 23.0 | | | 16.67 | -3.09 | 23 | 77 | |
| FV-24 (SH) | | | | | | 23.91 | -3.02 | | | |
| FV-26 (SH) | | | | | | 11.24 | -7.15 | | | |
| FV-32 (SH) | 65.5 | 14.6 | 19.9 | | | 12.43 | -2.44 | 31 | 69 | |
| FV-33 (SH) | | | | | | 11.44 | -5.27 | | | |
| LG-1-3 (SH) | | | | | | 10.63 | -4.26 | | | |
| LG-1-4 (SH) | | | | | | 21.19 | -1.66 | | | |
| LG-1-6 (SH) | | | | | | 8.95 | -4.38 | | | |
| LG-1-8 (SH) | | | | 9.02 | -4.48 | 9.74 | -4.07 | | | |
| LG-1-10 (SH) | 60.7 | 15.2 | 24.1 | 8.64 | -5.27 | 9.26 | -4.89 | 21 | 79 | Silicocarbonatite |
| LG-1-12 (SH) | 56.6 | 16.9 | 26.5 | 8.38 | -5.3 | 9.11 | -4.89 | 13 | 87 | |
| LG-1-14 (SH) | 89.5 | 2.6 | 7.9 | 15.41 | -4.27 | | | 78 | 23 | |
| LG-3-8 (SH) | 60.5 | 14.3 | 25.2 | | | | | | | |
| LG-3-13 (SH) | 57.6 | 14.5 | 27.9 | | | | | | | |
| SB-02 | 50.0 | 28.1 | 21.9 | | | 15.18 | -1.66 | 0 | 100 | |
| SB-03 | 55.3 | 29.8 | 14.9 | 17.35 | -1.0 | 15.82 | -1.55 | 11 | 89 | |
| SB-05 | 55.2 | 31.7 | 13.1 | 17.87 | -0.51 | 16.45 | -0.46 | 11 | 89 | |
| SB-10 | | | | 17.45 | -4.56 | | | | | Silicocarbonatite |
| SB-11 | 55.0 | 22.0 | 23.0 | 12.54 | -3.9 | 11.12 | -3.94 | 10 | 90 | |
| SB-14 | 94.8 | 2.8 | 2.4 | 10.92 | -4.52 | 9.5 | -4.58 | 90 | 10 | |
| SB-15 | 60.2 | 14.7 | 25.1 | 10.96 | -4.6 | 9.59 | -4.67 | 20 | 80 | |
| SB-16 | 60.0 | 22.0 | 18.0 | 10.19 | -3.86 | 10.17 | -4.2 | 20 | 80 | |
| SB-17 | 50.2 | 30.2 | 19.6 | | | 10.37 | -4.29 | 0 | 100 | |
| SB-18 | 63.6 | 13.3 | 23.1 | 11.9 | -4.0 | 10.55 | -4.33 | 27 | 73 | |
| SB-19 | 54.6 | 23.0 | 22.4 | 11.84 | -4.76 | 10.73 | -4.24 | 9 | 81 | |
| SB-20 | 50.9 | 25.5 | 23.6 | | | 8.99 | -5.76 | 0 | 100 | |

cate that, in general, the data are not consistent with the existence of isotopic equilibrium at magmatic temperatures between coexisting Fe-dolomite/Mg-ankerite and calcite. This fact points to metasomatic changes at low temperatures, not far from hydrothermal conditions (i.e. •375°C at P=1 atm). Subsolidus groundwater interaction might be an explanation for $\delta^{18}O$ values of carbonates higher than 12‰. The known carbonate-$H_2O$ oxygen fractionation values (Deines, 1989) and the typically negative $\delta^{18}O$ values for meteoric groundwaters (Hoefs, 1987) require that any interaction with groundwater must have occurred at low temperatures (<250°C; Deines, 1989; Speziale *et al.*, 1997). Alteration of Fe-dolomite/Mg-ankerite by groundwater may be related to the low temperature hydrothermal cycle (112-150°C; Roedder, 1973) responsible for the formation of the fluorite deposits, such as at Mato Preto and Barra do Itapirapuã, where the carbonatite emplacement and the fluorite deposition are closely related (cf. Santos *et al.*, 1996). On the whole, the data support the hypothesis that isotopic re-equilibrations have occurred during both the magmatic stage and the subsequent low-temperature hydrothermal stage, and with interaction with groundwaters. A model regarding the whole evolution of the isotopic O-C compositions, starting from magmatic processes, is developed in the next sections and graphically illustrated in Figs. 5 to 9.

## MAGMATIC PROCESSES

Assuming the K-ijolite PS-245 [mg#=Mg/ (Mg+ $Fe^{2+}$)=0.68; Comin-Chiaramonti & Gomes, 1996] as representative of an O-C near primary, mantle-derived melt (Table 1: intercumulus calcite: $\delta^{18}O$=6.9‰ and $\delta^{13}C$=−8.5‰, $\Delta O$=0.7, $\Delta C$=1.5, cf. Kyser, 1990), and that fractional crystallization + liquid immiscibility were responsible for variations not higher than 2‰ for both $\delta^{18}O$ and $\delta^{13}C$ (cf. Santos & Clayton, 1995), the expected values for $\delta^{18}O$ and $\delta^{13}C$ should not exceed 9‰ and −6.5‰, respectively.

The magmatic paths may be related to two evolutionary steps, i.e: 1) partial melting of subcontinental mantle ($\delta^{18}O$=6.9‰ and $\delta^{13}C$=−10‰) and differentiation of the primary magmas to the values given by the Cañada K-ijolite (PS-245), with $CO_2/H_2O$ ratio=0.1, and 2) evolution with a $CO_2/H_2O$~0.2 (shallow intrusions), and with a $CO_2/H_2O$~2.0 ("surface" conditions), respectively (cf. Fig. 5).

### Magmatic evolution

Hypothesis:

A) crystallization of the carbonatitic liquid under nearly closed conditions in temperature interval from 700°C to about 400°C (cf. Kuellmer *et al.*, 1966; Wyllie, 1989, and therein references), according to the reaction:

$$CO_2+H_2O \rightarrow CO_3^{2-}+2H^+;$$

The initial isotopic composition is assumed to have been $\delta^{18}O$‰=8.0 and $\delta^{13}C$=−7.5‰;

B) only $CO_2$ and $H_2O$ are oxygen carriers, and $CO_2$ is carbon carrier too;

C) mass balance equations for oxygen and carbon are:

$$[1]\ 2A\delta^{18}O(CO_2)i+B\delta^{18}O(H_2O)i=2a\delta^{18}O(CO_2)+3b\delta^{18}O(cc)+c\delta^{18}O(H_2O) \text{ and:}$$

$$[2]\ A\delta^{13}C(CO_2)i=a\delta^{13}C(CO_2)+b\delta^{13}C(cc)$$

where a, b, c are $CO_2$, $CO_3^{2-}$ and $H_2O$ molar concentrations in the fluid-mineral system at time "t". A and B are the initial $CO_2$ and $H_2O$ molar concentrations, respectively, in the magmatic fluid at "i" before crystallization of the carbonate (cc) (i.e., fixed A, from $CO_2/H_2O$ initial molar ratio, B is defined). From the equations the concentration values of the various components can be defined at each time "t" as b=A-a and c=B-b. It follows that the $\delta^{18}O$‰ and $\delta^{13}C$‰ compositions of the carbonate can be written in terms of a, b and c, as well as of fractionation factors $\Delta^{18}O(CO_2\text{-cc})$, $\Delta^{18}O(\text{cc-}H_2O)$ and $\Delta^{13}C(CO_2\text{-cc})$ (O'Neil *et al.*, 1969), according to the equations:

$$[3]\ \delta^{18}O_{(cc)}=[2A\delta^{18}O(CO_2)i+B\delta^{18}O(H_2O)i-2a\,\Delta^{18}O(CO_2-cc)+c\,\Delta^{18}O(cc\text{-}H_2O)]/[3b+2a+c]$$

$$[4]\ \delta^{13}C(cc)=[A\delta^{13}C(CO_2)i-(A-b)\,\Delta^{13}C(CO_2-cc)]/A$$

## Fluid-related hydrothermal recrystallization

After the crystallization of primary carbonates, recrystallization occurs by interactions with hydrothermal fluids at T<400°C. According to Zheng & Hoefs (1993), isotopic effects may be described by the equation:

[5] $\delta^{18}O(cc)=(\delta^{18}O(H_2O)i+\Delta^{18}O(cc\text{-}H_2O)-[\Delta^{18}O(H_2O)i+\Delta^{18}O(cc\text{-}H_2O)-\delta^{18}O(cc)i)\exp(-W/R(O)]$

[6] $\delta^{13}C(cc)=(\delta^{13}C(HCO_3)i+\Delta^{13}C(cc\text{-}HCO_3))-[(\delta^{13}C(HCO_3)i+\Delta^{13}C(cc\text{-}HCO_3)-\delta^{13}C(cc)i)\exp(-W/R(C)\,\chi(HCO_3))]$

with $\delta^{18}O$ and $\delta^{13}C$: initial isotopic composition of the carbonate; $\delta^{13}C(HCO_3)i$: initial carbon isotopic composition of $HCO_3^-$ in the fluid; $\chi(HCO_3)$: $HCO_3^-$ molar fraction in the fluid; W/R(O) and W/R(C): rock/water ratios in atom percentages of oxygen and carbon in the fluid and in the rock, and related to the calcite solubility product (Kps) that depends on temperature according to the equation (Jacobson & Langmuir, 1974):

[7] $\log Kps=-13.870-3059/T°K-0.04035*T°K$

Similarly to the W/R ratios, also the $HCO_3^-$ molar fraction in the fluid is a function of the temperature, due to the equilibria $CO_2+H_2O \rightleftarrows H_2CO_3$ ($K_0$), $H_2CO_3 \rightleftarrows H^++HCO_3^-$ ($K_1$), $HCO_3^- \rightleftarrows H^++CO_3^{2-}$ ($K_2$) and related equilibrium constants:

[8] $\log K_0=-14.0184+2385.73/T°K+0.0152642*T°K$ (Harned & Davis, 1943)

[9] $\log K_1=14.8435+3404.71/T°K-0.032786*T°K$ (Harned & Davis, 1943)

[10] $\log K_2=6.498-2902.39/T°K-0.02379*T°K$ (Harned & Sholes, 1941)

where the carbon speciation depends on the temperature and the pH. The initial $\delta^{13}C(HCO_3^-)i$ can be calculated from the isotopic fractionation factors relative to $\Delta^{13}C(CO_2\text{-}HCO_3^-)$ (Ohmoto & Rye, 1979), for various $\delta^{13}C$ values for $CO_2$ in the fluid. Numerical calculations are shown in Table II of the Appendix, and the model is graphicallly represented in Figs. 5 to 9, where a continuous variation of intensive parameters (i.e. $f=[(A\text{-}b)/A]$) is apparent.

Concluding, the magmatic paths may be related to two main evolutionary steps, i.e.: 1) partial melting of subcontinental mantle ($\delta^{18}O=6.9‰$ and $\delta^{13}C=-10‰$) and differentiation of the primary magmas to the values $\delta^{18}O=7.5‰$ and $\delta^{13}C=-8.5‰$, with $CO_2/H_2O$ ratio=0.1, and 2) evolution with a $CO_2/H_2O$~0.2 (shallow intrusions), and with $CO_2/H_2O$~0.2 ("surface" conditions), respectively (Fig. 5). After the crystallization of primary carbonates, the residual fluids may migrate and fenitize the country-rocks as well as the crystallized carbonates. The variations of O-C isotopes of the neo-carbonates, due to the interaction between fluid and primary carbonates, will follow paths which will depend on the temperature and the rock/water ratio (Zheng & Hoefs, 1993). In Fig. 5, the variation paths relative to the O-C isotopic compositions during hydrothermal water-rock interaction are shown for a temperature range of 400-100°C (curve I), and of 400-80°C (curves II and III). It should be noted that the low temperature carbonates plot between curves II and III, or below III. The lowest values of $\delta^{13}C$ (enrichment in $^{12}C$) may be related to hydrolisis of biogenic $CO_2$. In this case, if the pH of the solutions is determined by humic acids, the ratio $[HCO_3^-]/[Ca^{++}]$ is a temperature function (Taylor, 1978; Usdowski, 1982). The major contribution of biogenic components, at temperatures between 40 and 80°C and for pH • 5, is displayed in Fig. 5.

Examples of numerical calculations are given in Tables I and II of the Appendix and illustrated in Fig. 5.

## Trace elements

In hydrothermal environments, the rock/water (R/W) interaction modifies also the trace element content.

Following Nabelek (1987):

$$[R/W(O)]^{-1}=1/D\,\{\ln[Cwi-C(cc)i\,D)/(Cwi-C(cc)fD)]\},$$

where Cwi, C(cc)i and C(cc)f are the concentrations of a trace element in the fluid (w) and in the carbonate (cc), at the beginning (i) and at the end (f) of the interaction, respectively; D [Cwf/C(cc)f] is the ratio between a trace element in the fluid (wf) and in the carbonate (ccf) at the end of the interaction. From calculated rock/fluid ratios (Castorina *et al.*, 1997; Speziale *et al.*, 1997), and for fixed Cwi, C (cc)i and C (cc)f values, the variation of a trace element and $\delta^{18}O$ is calculated by the above equation. According to the Nabelek's (1987) model, the highest concentration of trace elements like Sr and REE are associated with temperatures higher than 200°C.

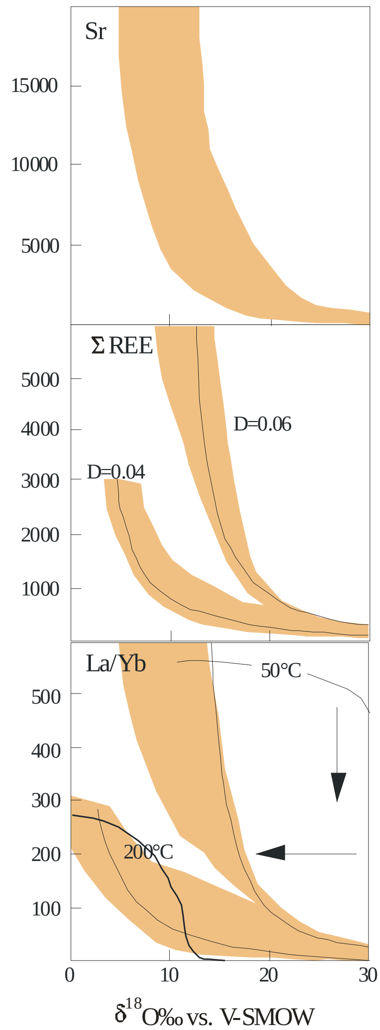


Fig. 10. Calculated paths of $\delta^{18}O$ vs. Sr, REE (ppm) and La/Yb ratio in neo-carbonates (following fluid-rock interaction in a hydrothermal environment, after Castorina *et al.*, 1997) compared with the analytical results (light brown fields). D=Cwf/C$^{(cc)}$ (see text). The temperature range is 200-50°C and the arrows show the trend of positive ΔT.

The variation paths of $\delta^{18}O$ vs. Sr, ΣREE contents (ppm) and La/Yb ratio are represented in Fig. 10. In the model Cwi is >C(cc)i, i.e. "fenitizing" fluid enriched in incompatible elements with respect to the primary carbonates, according to the enrichment of halogens in the fluid and Sr, REE, and other elements as halogen-complexes (Wood, 1990; Bau, 1991; Rubin *et al.*, 1993; Bühn *et al.*, 2002). In hydrothermal environments, the speciation of halogen-, hydroxide- and carbonate- complexes is a pH function in the fluid (Haas *et al.*, 1995). According to the interaction model of fluid-carbonatite, the pH range compatible with the system will depend on the $CO_2/H_2O$ ratio of the fluid, varying from 8.4-6.5 at 350°C to 5.3-3.4 at 50°C, respectively. It seems conceivable that a variable speciation in the hydrothermal fluid will start with REE strongly linked to hydroxides, and will stop with F-Cl-REE complexes at the end of the hydrothermal process (cf. Haas *et al.*, 1995).

## CONCLUSIONS

The O-C isotope compositions of the Paraná Basin carbonatites appear in general to be in agreement essentially with a magmatic origin from hypercrytical fluids with $CO_2/H_2O$~0.2-0.6 molar ratios and temperatures ranging from 700 to 499°C (i.e. "orthomagmatic vs. pegmatitic" environment; cf. Wyllie, 1989). However, significant variations in O-C isotope compositions are noticed in primary carbonates of alkaline rock-types and associated carbonatites and are mainly due to isotope exchange between carbonates and $H_2O$-$CO_2$ rich fluids; magmatic processes, i.e. fractional crystallization or liquid immiscibility, probably affect the $\delta^{18}O$ and $\delta^{13}C$ values by not more than 2‰. The isotope exchange model implies that the main isotopic changes occurred at low temperatures, in a hydrothermal environment, e.g. in the range 400-80°C, involving fluids with a $CO_2/H_2O$ ratio ranging from 0.8 to 1.

Two main paths of $\delta^{18}O$ and $\delta^{13}C$ fractionation seem to be generated by the emplacement levels (cf. Fig. 5).

Weathering and groundwater fluids are locally important, as well as meteoric water, which yielded samples strongly enriched in light carbon due to the contamination by a biogenic component.

The behavior of trace elements (e.g. Sr and REE) is consistent with the above conclusions.

The addition of carbonates from the country-rocks to "fresh" and even to "overprinted" carbonatites, as suggested by Santos & Clayton (1995) (e.g. Açunguí Group: $\delta^{18}O$=25.0 to 24.4‰ and $\delta^{13}C$=3.5 to −8.6‰), appears to be unnecessary to explain the considerably enrichment in both heavy oxygen and carbon of some samples. This interpretation is also supported by the initial $^{87}Sr/^{86}Sr$ and $^{143}Nd/^{144}Nd$ isotope ratios of the carbonatites that maintain the same values of the associated alkaline rocks (cf. Comin-Chiaramonti *et al.*, this volume).

## ACKNOWLEDGEMENTS

This research was supported by grants from Italian (CNR, 05 and 11 Committes, and COFIN, 1998, MURST 1998, 1999, 2000, 2001) and Brazilian (FAPESP, Proc. 01/10714-3) agencies.

## REFERENCES

Alcover, A.N., Almeida, T.I.R., Karmann, I. & Toledo, M.C.M. (1995). Estudo da composição isotópica de C e O em carbonatos primários e secundários de Juquiá e da caverna Santana, Vale do Ribeira (SP). *V Congresso Brasileiro de Geoquímica e III Congresso de Geoquímica dos Países de Língua Portuguesa, Niterói, CD-ROM*.

Alberti, A., Castorina, F., Censi, P., Comin-Chiaramonti, P. & Gomes, C.B. (1999). Geochemical characteristics of Cretaceous carbonatites from Angola. *Journal of African Earth Sciences* **29**, 735-759.

Andersen, T. (1987). Mantle and crustal components in a carbonatite complex, and the evolution of carbonatite magma: REE and isotopic evidence from the Fen complex, southeast Norway. *Isotope Geoscience* **65**, 147-166.

Andrade, F.R.D., Möller, P., Lüders, V., Dulski, P. & Gilg, H.A. (1999). Hydrothermal rare earth elements mineralization in the Barra do Itapirapuã carbonatite, southern Brazil: behavior of selected trace elements and stable isotopes (C, O). *Chemical Geology* **155**, 91-113.

Bau, M. (1991). Rare earth elements mobility during hydrothermal and metamorphic fluid-rock interactions and the significance of the oxydation state of europium. *Chemical Geology* **93**, 219-230.

Beccaluva, L., Barbieri, M., Born, H., Brotzu, P., Coltorti, M., Conte, A., Garbarino, C., Gomes, C.B., Macciotta, G., Morbidelli, L., Ruberti, E., Siena, F. & Traversa, G. (1992). Fractional crystallization and liquid immiscibility processes in the alkaline-carbonatite complex of Juquiá (São Paulo, Brazil). *Journal of Petrology* **33**, 1371-1404.

Bizzi, L.A., Smith, B.C., De Wit, M.J., Macdonald, I. & Armstrong, R.A. (1994). Isotope characteristics of the lithospheric mantle underlying the SW São Francisco craton margin, Brazil. *International Symposium on the Physics and Chemistry of the Upper Mantle*, *São Paulo, Invited Lectures*, pp. 227-256.

Bottinga, Y. & Javois, M. (1975). Oxygen isotope partitioning among the minerals in igneous and metamorphic rocks. *Review Geophysical Space Physics* **13**, 401-418.

Bühn, B., Rankin, A.H., Schneider, J. & Dulski, P. (2002). The nature of orthomagmatic, carbonatitic fluids precipitating REE, Sr-rich fluorite: fluid-inclusions evidence from the Okurusu fluorite deposit, Namibia. *Chemical Geology* **186**, 75-98.

Carlson, R.W., Esperança, S. & Svisero D.P. (1996). Chemical and Os isotopic study of Cretaceous potassic rocks from southern Brazil. *Contributions to Mineralogy and Petrology* **125**, 393-405.

Castorina, F., Censi, P., Barbieri, M., Comin-Chiaramonti, P., Cundari, A. & Gomes, C.B. (1994). Carbonatites from the Paraná basin: a 130 Ma transect. *International Symposium on the Physics and Chemistry of the Upper Mantle, São Paulo, Extended Abstracts,* pp. 52-55.

Castorina, F., Censi, P., Barbieri, M., Comin-Chiaramonti, P., Cundari, A., Gomes, C.B. & Pardini, G. (1996). Carbonatites from Eastern Paraguay: a comparison with coeval carbonatites from Brazil and Angola. In: Comin-Chiaramonti, P. & Gomes, C.B. (eds.) *Alkaline magmatism in central-eastern Paraguay. Relationships with coeval magmatism in Brazil.* São Paulo: Edusp-Fapesp, pp. 231-248.

Castorina, F., Censi, P., Comin-Chiaramonti, P., Gomes, C.B., Piccirillo, E.M., Alcover Neto, A., Almeida R.T., Speziale, S. & Toledo M.C. (1997). Geochemistry of carbonatites from Eastern Paraguay and genetic relationships with potassic magmatism: C, O, Sr and Nd isotopes. *Mineralogy and Petrology* **61**, 237-260.

Censi, P., Comin-Chiaramonti, P., Demarchi, G., Longinelli, A. & Orué, D. (1989). Geochemistry and C-O isotopes of the Chiriguelo carbonatite, northeastern Paraguay. *Journal of South American Earth Sciences* **3**, 295-303.

Clarke, L.B., Le Bas, M.J. & Spiro, B. (1991). Rare earth, trace element and stable isotope fractionation of carbonatites at Kruidfontein, Transvaal, South Africa. *Proceedings 5th International Kimberlite Conference, Araxá,* pp. 236-251.

Comin-Chiaramonti, P. & Gomes, C.B. (1996). *Alkaline magmatism in central-eastern Paraguay. Relationships with coeval magmatism in Brazil.* São Paulo: Edusp-Fapesp, 464p.

Comin-Chiaramonti, P., Cundari, A., Piccirillo, E.M., Gomes, C.B. & De Min, A. (1997). Carbonatitic magmatism in the Paraná-Angola mantle plume (?) system: petrological and isotope-geochemical bearing on the source mantle. *Eos, Transaction, AGU* **78** (46), F741.

Comin-Chiaramonti, P., Gomes, C.B., Castorina, F., Censi, P., Antonini, P., Furtado, S., Ruberti, E. & Scheibe, L.F. (2002). Anitápolis and Lages alkaline-carbonatite complexes, Santa Catarina State, Brazil: geochemistry and geodynamic implications. *Revista Brasileira de Geociências* **32**, 639-653.

Comin-Chiaramonti, P., Gomes, C.B., Marques, L.S., Censi, P., Ruberti, E. & Antonini, P. (in this volume). Carbonatites from Southeastern Brazil: geochemistry, O-C, Sr-Nd-Pb isotopes and relationships with the magmatism from the Paraná-Angola-Namibia Province.

Comin-Chiaramonti, P., Gomes, C.B., Ruberti, E., Antonini, P. & Censi, P. (2001). Mato Preto alkaline-carbonatite complex: geochemistry and isotope (O-C, Sr-Nd) constraints. *Geochimica Brasiliensis* **15**, 23-34.

Deines, P. (1989). Stable isotope variations in carbonatite. In: Bell, K. (ed.) *Carbonatites, genesis and evolution*. London: Unwin Hyman, pp. 301-359.

Deines, P. & Gold D.P. (1973). The isotopic composition of carbonatites and kimberlite carbonates and their bearing on the isotopic composition of deep-seated carbon. *Geochimica et Cosmochimica Acta* **51**, 1227-1243.

Gittings, J. & Harmer, R.E. (1997). What is ferrocarbonatite? A revised classification. *Journal of African Earth Sciences* **25**, 159-168.

Gomes, C.B., Morbidelli, L., Ruberti, E. & Comin-Chiaramonti, P. (1996). A first attempt to compare Post-Palaeozoic alkaline rocks from western (Paraguay) and eastern (Brazil) margins of the Paraná Basin. In: Comin-Chiaramonti, P. & Gomes, C.B. (eds.) *Alkaline magmatism in central-eastern Paraguay. Relationships with coeval magmatism in Brazil.* São Paulo: Edusp-Fapesp, pp. 249-274.

Haas, J.R., Shock, E.L. & Sassani, D.C. (1995). Rare earth elements in hydrothermal systems: estimates of standard partial molar thermodynamic properties of aqueous complexes of rare earth elements at high pressures and temperatures. *Geochimica et Cosmochimica Acta* **59**, 4329-4350.

Harned, H.S. & Davis, R. (1943). The ionization constant of carbonic acid in water and the solubility of carbon dioxide in water and acqueous salt solution from 0° to 50°C. *Journal of American Chemical Society* **65**, 2030-2039.

Harned, H.S. & Scholes, S.R. (1941). The ionization constant of $HCO_3^-$ from 0° to 50°C. *Journal of American Chemical Society* **65**, 1706-1711.

Hoefs, J. (1987). *Stable isotope geochemistry*. Berlin: Springer, 241p.

Huang, H-M., Hawkesworth, C.J., Van Calsteren, P. & Mcdermott, F. (1995). Geochemical characteristics and origin of the Jacupiranga carbonatites, Brazil. *Chemical Geology* **119**, 79-99.

Jacobson, R.L. & Lungmair, D. (1974). Dissociation constants of calcite and $CaHCO_3^+$ from 0° to 50°C. *Geochimica et Cosmochimica Acta* **38**, 301-312.

Keller, J. & Hoefs, J. (1995). Stable isotope characteristics of recent natrocarbonatites from Oldoinyo Lengai. In: Bell, K. & Keller, J. (eds.) *Carbonatite volcanism: Oldoynio Lengai and the petrogenesis of natrocarbonatites*. Berlin: Springer, pp. 113-123.

Kjarsgaard, B.A. & Hamilton, D.L. (1988). Liquid immiscibility and the origin of alkali-poor carbonatites. *Mineralogical Magazine* **52**, 43-55.

Kjarsgaard, B.A., Hamilton, D.L. & Peterson, T.D. (1995). Peralkaline nephelinite/carbonatite liquid immiscibility: comparison of phase composition in experiments and natural lavas from Oldoinyo Lengai. In: Bell, K. & Keller, J. (eds.) *Carbonatite volcanism: Oldoinyo Lengai and the petrogenesis of natrocarbonatites*. Berlin: Springer, pp. 163-190.

Kuellmer, F.J., Visocky, A.P. & Tuttle, O.F. (1966). Preliminary survey of the system barite-calcite-fluorite at 500 bars. In: Tuttle, O.F. & Gittings, J. (eds.) *Carbonatites*. New York: John Wiley & Sons, pp. 353-364.

Kyser, T.K. (1990). Stable isotopes in the continental lithospheric mantle. In: Menzies, M.A. (ed.) *Continental mantle*. Oxford: Clarendon Press, pp. 127-156.

Matthews, A., Goldsmith, J.R. & Clayton, R.N. (1983). Oxygen isotope fractionations involving pyroxenes: the calibration of mineral-pair geothermometers. *Geochimica Cosmochimica Acta* **47**, 631-644.

Mello, I.S.C. & Bettencourt, J.S. (1998). Geologia e gênese das mineralizações do maciço Itaoca, Vale do Ribeira, SP e PR. *Revista Brasileira de Geociências* **28**, 269-284.

Meyer, H.O.A., Blaine, L.G., Svisero, D. P. & Craig, B.S. (1994). Alkaline intrusions in western Minas Gerais, Brazil. *5th International Kimberlite Conference*, *Araxá, Proceedings,* pp. 140-155.

Morbidelli, L., Gomes, C.B., Brotzu, P., D'Acquarica, S., Garbarino, C., G., Ruberti, E. & Traversa, G. (1995). Mineralogical, petrological and geochemical aspects of alkaline and alkaline-carbonatite associations from Brazil. *Earth-Science Reviews* **39**, 135-168.

Morikiyo, T., Hirano, H. & Matsushita, Y. (1990). Carbon and oxygen isotopic composition of the carbonatites from Jacupiranga and Catalão I carbonatite complexes, Brazil. *Bulletin of Geological Survey of Japan* **41**, 619-626.

Nabelek, P.I. (1987). General equation for modelling fluid/rock interaction using trace elements and isotopes. *Geochimica et Cosmochimica Acta* **51**, 1765-1769.

Nadeau, S.L., Epstein, S.E. & Stolper, E. (1999). Hydrogen and carbon abundances and isotopic ratios in apatite from alkaline intrusive complexes, with a focus on carbonatites. *Geochimica et Cosmochimica Acta* **63**, 1837-1851.

Nelson, D.H., Chivas, A.R., Chappell, B.W. & McCulloch, M.T. (1988). Geochemical and isotopic systematics in carbonatites and implications for the evolution of ocean-island sources. *Geochimica et Cosmochimica Acta* **52**, 1-17.

Ohmoto, H. & Rye, R.O. (1979). Isotopes of sulfur and carbon. In: Barnes, H.L. (ed.). *Geochemistry of hydrothermal ore deposits.* New York: John Wiley & Sons, pp. 509-567.

O'Neil, J.R., Clayton, R.N. & Mayeda, T.K. (1969). Oxygen isotope fractionation in divalent metal carbonates. *Journal of Chemistry and Physics* **51**, 5547-5558.

Pineau, F., Javoy, M. & Allègre, C.J. (1973). Etude systématique des isotopes de l'oxygène, du carbone et du strontium dans les carbonatites. *Geochimica et Cosmochimica Acta* **37**, 2363-2377.

Robaina, L.S.S., Formoso, M.L.L. & Spadini, A.R. (1991). Carbonatos reservatório da Formação Macaé, Bacia de Campos, RJ, Brasil. *Geochimica Brasiliensis* **5**, 69-78.

Roedder, E. (1973). Fluid inclusions from the fluorite deposits associated with the carbonatite of Amba Dongar, India and Okurusu, south west Africa. *Transactions of the Institute of Mineralogy and Metallurgy* **82B**, 35-39.

Ruberti, E., Castorina, F., Censi, P., Comin-Chiaramonti, P., Gomes, C.B., Antonini P. & Andrade, F.R.D. (2002). The geochemistry of the Barra do Itapirapuã carbonatite (Ponta Grossa Arch, Brazil): a multiple stockwork. *Journal of South American Earth Sciences* **15**, 215-228.

Rubin, J.N., Christopher, D.H. & Price, J.G. (1993). The mobility of zirconium and other "immobile" elements during hydrothermal alteration. *Chemical Geology* **110**, 29-47.

Rudnik, R.L., McDonough, W.F. & Chappell, B.W. (1993). Carbonatite metasomatism and the Northern Tanzania mantle: petrographic and geochemical characteristics. *Earth and Planetary Science Letters* **114**, 463-474.

Santos, R.V. & Clayton, R.N. (1995). Variations of oxygen and carbon isotopes in carbonatites: a study of Brazilian alkaline complexes. *Geochimica et Cosmochimica Acta* **59**, 1339-1352.

Santos, R.V., Dardenne, M.A. & Oliveira, C.G. (1996). Rare earth elements geochemistry of fluorite from the Mato Preto carbonatite complex, southern Brazil. *Revista Brasileira de Geociências* **26**, 81-86.

Scheibe, L.F. & Formoso, M.L.L. (1982). Contribuição da geoquímica de terras raras à caracterização dos carbonatitos da Fazenda Varela, Lages, SC. *Revista Brasileira de Geociências* **12**, 553-561.

Sheppard, S.M.F. & Schwartz, H.P. (1970). Fractionation of carbon and oxygen isotopes and magnesium between coexisting metamorphic calcite and dolomite. *Contributions to Mineralogy and Petrology* **26**, 161-198.

Shurmann, L.W., Horstmann, U.E. & Cloete, H.C.C. (1997). Geochemical and stable isotope patterns in altered volcaniclastic and intrusive rocks of the Kruidfontein Carbonatite complex, South Africa. *Journal of African Earth Sciences* **25**, 77-101.

Speziale, S., Censi, P., Comin-Chiaramonti, P., Ruberti, E. & Gomes, C.B. (1997). Oxygen and Carbon isotopes in the Barra do Itapirapuã and Mato Preto carbonatites (southern Brazil). *Mineralogica et Petrographica Acta* **40**, 1-21.

Taylor, H.O. Jr. (1978). Water/rock interactions and origin of $H_2O$ in granitic batholiths. *Journal of the Geological Society of London* **133**, 509-558.

Taylor, H.P.Jr., Frechen, J. & Degens, E.T. (1967). Oxygen and carbon isotope studies of carbonatites from Laacher See district, West Germany and Alnø district, Sweden. *Geochimica et Cosmochimica Acta* **31**, 407-430.

Toyoda, K., Horiuchi, H. & Tokonami, M. (1995). Dupal anomaly of the Brazilian carbonatites: geochemical correlations with hotspots in the South Atlantic and implications for the mantle source. *Earth and Planetary Science Letters* **126,** 315-331.

Usdowski, E. (1982). Reaction and equilibria in the system $CO_2$-$H_2O$ and $CaCO_3$-$CO_2$-$H_2O$ (0°-50°). A review. *Neues Jahrbuch für Mineralogie Abhandlungen* **144**, 148-171.

Walter, A.V., Flicoteaux, R., Parron, C., Loubet, M. & Nahon, D. (1995). Rare-earth elements and isotopes (Sr, Nd, O, C) in minerals from the Juquiá carbonatite (Brazil): tracers of a multistage evolution. *Chemical Geology* **120**, 27-44.

Wood, S.A. (1990). The aqueous geochemistry of the rare earth elements and yttrium, 2. Theoretical prediction of speciation in hydrothermal solutions to 350°C at saturated water pressure. *Chemical Geology* **88**, 99-125.

Wyllie, P.J. (1989). Origin of carbonatites: evidence from phase equilibrium studies. In: Bell, K. (ed.), *Carbonatites, genesis and evolution*. London: Unwin Hyman, pp. 500-545.

Zheng, Y.F. & Hoefs, J. (1993). Carbon and oxygen isotopic covariations in hydrothermal calcites. Theoretical modelling on mixing processes and application to Pb-Zn deposits in the Harz Mountains, Germany. *Mineralium Deposita* **28**, 79-89.

*Mesozoic to Cenozoic Alkaline Magmatism in the Brazilian Platform*
*Comin-Chiaramonti, P. & Gomes, C.B. (eds.)*
*Edusp/Fapesp, São Paulo, pp. 629-656, 2005*

## APPENDIX

Oxygen-carbon modelling (Tables I and II) for magmatic and hydrothermal evolution of carbonatites, respectively (retyped after Speziale *et al.*, 1997).

Table I. O-C model for magmatic evolution of a carbonatitic liquid. $f$ is the residual fraction of fluid defined by $f$ =[(A-b)/A] (see text). The model previews that during "high temperature" stage the carbonate crystallization takes place between 700 and 400°C.

| $\delta^{18}O_i$ 8 a | $\delta^{13}C_i$ -7.5 c | $(XO_2/H_2O)_i$ 0.6 b | | | | | | |
|---|---|---|---|---|---|---|---|---|
| $(CO_2)_f$ | $(H_2O)_f$ | $(CaCO_3)$ | $\delta^{18}O(cc)_f$ | $\delta^{13}C(cc)_f$ | $\delta^{18}O(H_2O)_f$ | $\delta^{18}O(CO_2)_f$ | $\delta^{13}C(CO_2)_f$ | T°C |
| 100.00 | 166.67 | 0.00 | 8.00 | -7.50 | 7.55 | 13.72 | -5.24 | 700 |
| 95.00 | 161.67 | 5.00 | 8.05 | -7.41 | 7.69 | 13.88 | -5.12 | 685 |
| 90.00 | 156.67 | 10.00 | 8.11 | -7.32 | 7.84 | 14.05 | -5.01 | 670 |
| 85.00 | 151.67 | 15.00 | 8.17 | -7.22 | 8.01 | 14.23 | -4.89 | 655 |
| 80.00 | 146.67 | 20.00 | 8.24 | -7.12 | 8.19 | 14.42 | -4.77 | 640 |
| 75.00 | 141.67 | 25.00 | 8.31 | -7.02 | 8.37 | 14.61 | -4.65 | 625 |
| 70.00 | 136.67 | 30.00 | 8.40 | -6.91 | 8.57 | 14.82 | -4.52 | 610 |
| 65.00 | 131.67 | 35.00 | 8.48 | -6.80 | 8.78 | 15.04 | -4.40 | 595 |
| 60.00 | 126.67 | 40.00 | 8.58 | -6.69 | 9.01 | 15.26 | -4.27 | 580 |
| 55.00 | 121.67 | 45.00 | 8.68 | -6.58 | 9.25 | 15.50 | -4.14 | 565 |
| 50.00 | 116.67 | 50.00 | 8.79 | -6.46 | 9.51 | 15.74 | -4.02 | 550 |
| 45.00 | 111.67 | 55.00 | 8.91 | -6.34 | 9.78 | 16.00 | -3.89 | 535 |
| 40.00 | 106.67 | 60.00 | 9.04 | -6.22 | 10.07 | 16.27 | -3.77 | 520 |
| 35.00 | 101.67 | 65.00 | 9.17 | -6.10 | 10.37 | 16.55 | -3.64 | 505 |
| 30.00 | 96.67 | 70.00 | 9.32 | -5.97 | 10.70 | 16.85 | -3.52 | 490 |
| 25.00 | 91.67 | 75.00 | 9.47 | -5.85 | 11.05 | 17.15 | -3.40 | 475 |
| 20.00 | 86.67 | 80.00 | 9.64 | -5.73 | 11.42 | 17.48 | -3.29 | 460 |
| 15.00 | 81.67 | 85.00 | 9.81 | -5.60 | 11.82 | 17.81 | -3.18 | 445 |
| 10.00 | 76.67 | 90.00 | 10.00 | -5.48 | 12.24 | 18.17 | -3.08 | 430 |
| 5.00 | 71.67 | 95.00 | 10.20 | -5.36 | 12.68 | 18.53 | -2.99 | 415 |
| 0.00 | 66.67 | 100.00 | 10.41 | -5.24 | 13.16 | 18.92 | -2.91 | 400 |

Table II. Oxygen and carbon model for hydrothermal evolution of a carbonatitic rock. $f$ is the residual fraction of fluid defined by $f = [(A-b)/A]$ (see text). The model previews that the residual fluid fraction, remained after the "high-temperature" stage, is involved in the hydrothermal stage at temperature •375°C. In this residual fluid fraction the amount of dissolved $CO_2$, as $CO_2$, is related to the variation of $CO_2$ fraction in the late magmatic fluid, that is $f$ .

| $f$ 0.10 $K_0$ | $\delta^{13}C_i$ ($HCO_3$) 12.57 $K_1$ | [$CO_2$] 0.04 $K_2$ | $K_{ps}$ | [$H_2CO_3$] | pH | [$HCO_3$] | Solubility of calcite | R/W (C) | X[$HCO_3$] | R/W (O) | T°C | $\delta^{18}O_{cc}$ | $\delta^{13}C_{cc}$ |
|---|---|---|---|---|---|---|---|---|---|---|---|---|---|
| 3.58E-01 | 2.21E-12 | 4.01E-14 | 1.01E-17 | 7.20E-01 | 5.90 | 1.26E-06 | 2.51E-04 | 3.48E-04 | 1.75E-06 | 1.36E-05 | 375 | 9.76 | -5.46 |
| 3.07E-01 | 3.28E-12 | 5.26E-14 | 1.71E-17 | 6.18E-01 | 5.85 | 1.42E-06 | 3.26E-04 | 5.27E-04 | 2.30E-06 | 1.76E-05 | 368 | 9.76 | -5.46 |
| 2.64E-01 | 4.86E-12 | 6.87E-14 | 2.91E-17 | 5.31E-01 | 5.79 | 1.61E-06 | 4.23E-04 | 7.96E-04 | 3.03E-06 | 2.28E-05 | 361 | 9.76 | -5.46 |
| 2.28E-01 | 7.19E-12 | 8.97E-14 | 4.92E-17 | 4.57E-01 | 5.74 | 1.81E-06 | 5.48E-04 | 1.20E-03 | 3.96E-06 | 2.96E-05 | 354 | 9.76 | -5.46 |
| 1.96E-01 | 1.06E-11 | 1.17E-13 | 8.30E-17 | 3.95E-01 | 5.69 | 2.04E-06 | 7.12E-04 | 1.80E-03 | 5.18E-06 | 3.85E-05 | 347 | 9.76 | -5.46 |
| 1.70E-01 | 1.55E-11 | 1.51E-13 | 1.40E-16 | 3.42E-01 | 5.64 | 2.30E-06 | 9.23E-04 | 2.70E-03 | 6.75E-06 | 4.99E-05 | 340 | 9.76 | -5.46 |
| 1.47E-01 | 2.27E-11 | 1.96E-13 | 2.34E-16 | 2.96E-01 | 5.59 | 2.60E-06 | 1.20E-03 | 4.04E-03 | 8.76E-06 | 6.47E-05 | 333 | 9.76 | -5.46 |
| 1.28E-01 | 3.32E-11 | 2.53E-13 | 3.92E-16 | 2.57E-01 | 5.53 | 2.92E-06 | 1.55E-03 | 6.03E-03 | 1.14E-05 | 8.39E-05 | 326 | 9.76 | -5.46 |
| 1.12E-01 | 4.82E-11 | 3.25E-13 | 6.54E-16 | 2.24E-01 | 5.48 | 3.29E-06 | 2.01E-03 | 8.97E-03 | 1.47E-05 | 1.09E-04 | 319 | 9.76 | -5.46 |
| 9.76E-02 | 6.98E-11 | 4.16E-13 | 1.09E-15 | 1.96E-01 | 5.43 | 3.70E-06 | 2.61E-03 | 1.33E-02 | 1.89E-05 | 1.41E-04 | 312 | 9.76 | -5.46 |
| 8.55E-02 | 1.01E-10 | 5.32E-13 | 1.80E-15 | 1.72E-01 | 5.38 | 4.16E-06 | 3.38E-03 | 1.97E-02 | 2.42E-05 | 1.83E-04 | 305 | 9.76 | -5.46 |
| 7.51E-02 | 1.45E-10 | 6.78E-13 | 2.97E-15 | 1.51E-01 | 5.33 | 4.67E-06 | 4.38E-03 | 2.91E-02 | 3.10E-05 | 2.37E-04 | 298 | 9.76 | -5.46 |
| 6.62E-02 | 2.07E-10 | 8.60E-13 | 4.88E-15 | 1.33E-01 | 5.28 | 5.24E-06 | 5.68E-03 | 4.27E-02 | 3.94E-05 | 3.07E-04 | 291 | 9.76 | -5.46 |
| 5.85E-02 | 2.95E-10 | 1.09E-12 | 8.00E-15 | 1.17E-01 | 5.23 | 5.88E-06 | 7.36E-03 | 6.27E-02 | 5.01E-05 | 3.98E-04 | 284 | 9.76 | -5.46 |
| 5.18E-02 | 4.18E-10 | 1.37E-12 | 1.31E-14 | 1.04E-01 | 5.18 | 6.59E-06 | 9.53E-03 | 9.16E-02 | 6.33E-05 | 5.15E-04 | 277 | 9.76 | -5.46 |
| 4.61E-02 | 5.90E-10 | 1.72E-12 | 2.12E-14 | 9.26E-02 | 5.13 | 7.39E-06 | 1.23E-02 | 1.33E-01 | 7.98E-05 | 6.67E-04 | 270 | 9.76 | -5.46 |
| 4.11E-02 | 8.28E-10 | 2.15E-12 | 3.43E-14 | 8.26E-02 | 5.08 | 8.27E-06 | 1.60E-02 | 1.93E-01 | 1.00E-04 | 8.64E-04 | 263 | 9.77 | -5.46 |
| 3.68E-02 | 1.16E-09 | 2.67E-12 | 5.52E-14 | 7.40E-02 | 5.03 | 9.26E-06 | 2.07E-02 | 2.80E-01 | 1.25E-04 | 1.12E-03 | 256 | 9.77 | -5.46 |
| 3.31E-02 | 1.61E-09 | 3.31E-12 | 8.85E-14 | 6.65E-02 | 4.99 | 1.03E-05 | 2.68E-02 | 4.03E-01 | 1.56E-04 | 1.45E-03 | 249 | 9.77 | -5.46 |
| 2.99E-02 | 2.23E-09 | 4.08E-12 | 1.41E-13 | 6.00E-02 | 4.94 | 1.16E-05 | 3.46E-02 | 5.77E-01 | 1.93E-04 | 1.87E-03 | 242 | 9.78 | -5.46 |
| 2.70E-02 | 3.06E-09 | 5.00E-12 | 2.24E-13 | 5.43E-02 | 4.89 | 1.29E-05 | 4.48E-02 | 8.24E-01 | 2.37E-04 | 2.42E-03 | 235 | 9.78 | -5.46 |
| 2.46E-02 | 4.19E-09 | 6.11E-12 | 3.54E-13 | 4.94E-02 | 4.84 | 1.44E-05 | 5.79E-02 | 1.17E+00 | 2.91E-04 | 3.13E-03 | 228 | 9.79 | -5.46 |
| 2.25E-02 | 5.69E-09 | 7.42E-12 | 5.56E-13 | 4.51E-02 | 4.80 | 1.60E-05 | 7.49E-02 | 1.66E+00 | 3.55E-04 | 4.05E-03 | 221 | 9.80 | -5.45 |
| 2.06E-02 | 7.68E-09 | 8.96E-12 | 8.67E-13 | 4.14E-02 | 4.75 | 1.78E-05 | 9.68E-02 | 2.34E+00 | 4.31E-04 | 5.23E-03 | 214 | 9.82 | -5.44 |
| 1.90E-02 | 1.03E-08 | 1.08E-11 | 1.35E-12 | 3.82E-02 | 4.70 | 1.98E-05 | 1.25E-01 | 3.27E+00 | 5.19E-04 | 6.76E-03 | 207 | 9.84 | -5.43 |
| 1.76E-02 | 1.37E-08 | 1.29E-11 | 2.08E-12 | 3.53E-02 | 4.66 | 2.20E-05 | 1.61E-01 | 4.56E+00 | 6.23E-04 | 8.73E-03 | 200 | 9.87 | -5.40 |
| 1.64E-02 | 1.82E-08 | 1.53E-11 | 3.18E-12 | 3.29E-02 | 4.61 | 2.44E-05 | 2.08E-01 | 6.33E+00 | 7.42E-04 | 1.13E-02 | 193 | 9.90 | -5.36 |
| 1.53E-02 | 2.38E-08 | 1.80E-11 | 4.84E-12 | 3.08E-02 | 4.57 | 2.71E-05 | 2.69E-01 | 8.73E+00 | 8.79E-04 | 1.45E-02 | 186 | 9.95 | -5.30 |
| 1.44E-02 | 3.10E-08 | 2.11E-11 | 7.31E-12 | 2.90E-02 | 4.52 | 3.00E-05 | 3.47E-01 | 1.20E+01 | 1.03E-03 | 1.88E-02 | 179 | 10.01 | -5.20 |
| 1.37E-02 | 4.01E-08 | 2.45E-11 | 1.10E-11 | 2.74E-02 | 4.48 | 3.32E-05 | 4.48E-01 | 1.63E+01 | 1.21E-03 | 2.42E-02 | 172 | 10.09 | -5.05 |
| 1.30E-02 | 5.13E-08 | 2.83E-11 | 1.63E-11 | 2.61E-02 | 4.44 | 3.66E-05 | 5.77E-01 | 2.21E+01 | 1.40E-03 | 3.12E-02 | 165 | 10.20 | -4.82 |
| 1.25E-02 | 6.50E-08 | 3.24E-11 | 2.41E-11 | 2.50E-02 | 4.39 | 4.04E-05 | 7.43E-01 | 2.96E+01 | 1.61E-03 | 4.02E-02 | 158 | 10.34 | -4.47 |
| 1.20E-02 | 8.17E-08 | 3.68E-11 | 3.52E-11 | 2.42E-02 | 4.35 | 4.44E-05 | 9.58E-01 | 3.95E+01 | 1.84E-03 | 5.18E-02 | 151 | 10.53 | -3.98 |
| 1.17E-02 | 1.02E-07 | 4.14E-11 | 5.11E-11 | 2.35E-02 | 4.31 | 4.89E-05 | 1.23E+00 | 5.24E+01 | 2.08E-03 | 6.66E-02 | 144 | 10.78 | -3.28 |
| 1.14E-02 | 1.25E-07 | 4.62E-11 | 7.34E-11 | 2.30E-02 | 4.27 | 5.36E-05 | 1.59E+00 | 6.88E+01 | 2.33E-03 | 8.58E-02 | 137 | 11.10 | -2.33 |
| 1.13E-02 | 1.52E-07 | 5.11E-11 | 1.04E-10 | 2.27E-02 | 4.23 | 5.88E-05 | 2.04E+00 | 8.97E+01 | 2.58E-03 | 1.10E-01 | 130 | 11.53 | -1.10 |
| 1.12E-02 | 1.83E-07 | 5.60E-11 | 1.47E-10 | 2.26E-02 | 4.19 | 6.43E-05 | 2.62E+00 | 1.16E+02 | 2.84E-03 | 1.42E-01 | 123 | 12.08 | 0.44 |
| 1.13E-02 | 2.17E-07 | 6.06E-11 | 2.04E-10 | 2.27E-02 | 4.15 | 7.02E-05 | 3.37E+00 | 1.48E+02 | 3.09E-03 | 1.82E-01 | 116 | 12.79 | 2.26 |

Table II (continued).

| $f$ | $\delta^{13}C_i$ ($HCO_3$) | [$CO_2$] | | | | | | | | | | | |
|---|---|---|---|---|---|---|---|---|---|---|---|---|---|
| 0.15 | 12.68 | 0.05 | | | | | | | | | | | |
| $K_0$ | $K_1$ | $K_2$ | $K_{ps}$ | [$H_2CO_3$] | pH | [$HCO_3$] | Solubility of calcite | R/W (C) | X[$HCO_3$] | R/W (O) | T°C | $\delta^{18}O_{cc}$ | $\delta^{13}C_{cc}$ |
| 3.58E-01 | 2.21E-12 | 4.01E-14 | 1.01E-17 | 1.01E+00 | 5.82 | 1.50E-06 | 2.51E-04 | 2.47E-04 | 1.48E-06 | 1.36E-05 | 375 | 9.47 | -5.58 |
| 3.07E-01 | 3.28E-12 | 5.26E-14 | 1.71E-17 | 8.70E-01 | 5.77 | 1.69E-06 | 3.26E-04 | 3.74E-04 | 1.94E-06 | 1.76E-05 | 368 | 9.47 | -5.58 |
| 2.64E-01 | 4.86E-12 | 6.87E-14 | 2.91E-17 | 7.48E-01 | 5.72 | 1.91E-06 | 4.23E-04 | 5.65E-04 | 2.55E-06 | 2.28E-05 | 361 | 9.47 | -5.58 |
| 2.28E-01 | 7.19E-12 | 8.97E-14 | 4.92E-17 | 6.44E-01 | 5.67 | 2.15E-06 | 5.48E-04 | 8.52E-04 | 3.34E-06 | 2.96E-05 | 354 | 9.47 | -5.58 |
| 1.96E-01 | 1.06E-11 | 1.17E-13 | 8.30E-17 | 5.56E-01 | 5.62 | 2.43E-06 | 7.12E-04 | 1.28E-03 | 4.36E-06 | 3.85E-05 | 347 | 9.47 | -5.58 |
| 1.70E-01 | 1.55E-11 | 1.51E-13 | 1.40E-16 | 4.81E-01 | 5.56 | 2.73E-06 | 9.23E-04 | 1.92E-03 | 5.68E-06 | 4.99E-05 | 340 | 9.48 | -5.58 |
| 1.47E-01 | 2.27E-11 | 1.96E-13 | 2.34E-16 | 4.17E-01 | 5.51 | 3.08E-06 | 1.20E-03 | 2.87E-03 | 7.38E-06 | 6.47E-05 | 333 | 9.48 | -5.58 |
| 1.28E-01 | 3.32E-11 | 2.53E-13 | 3.92E-16 | 3.63E-01 | 5.46 | 3.47E-06 | 1.55E-03 | 4.28E-03 | 9.57E-06 | 8.39E-05 | 326 | 9.48 | -5.58 |
| 1.12E-01 | 4.82E-11 | 3.25E-13 | 6.54E-16 | 3.16E-01 | 5.41 | 3.90E-06 | 2.01E-03 | 6.37E-03 | 1.24E-05 | 1.09E-04 | 319 | 9.48 | -5.58 |
| 9.76E-02 | 6.98E-11 | 4.16E-13 | 1.09E-15 | 2.76E-01 | 5.36 | 4.39E-06 | 2.61E-03 | 9.46E-03 | 1.59E-05 | 1.41E-04 | 312 | 9.48 | -5.58 |
| 8.55E-02 | 1.01E-10 | 5.32E-13 | 1.80E-15 | 2.42E-01 | 5.31 | 4.93E-06 | 3.38E-03 | 1.40E-02 | 2.04E-05 | 1.83E-04 | 305 | 9.48 | -5.58 |
| 7.51E-02 | 1.45E-10 | 6.78E-13 | 2.97E-15 | 2.12E-01 | 5.26 | 5.54E-06 | 4.38E-03 | 2.06E-02 | 2.61E-05 | 2.37E-04 | 298 | 9.48 | -5.58 |
| 6.62E-02 | 2.07E-10 | 8.60E-13 | 4.88E-15 | 1.87E-01 | 5.21 | 6.22E-06 | 5.68E-03 | 3.04E-02 | 3.32E-05 | 3.07E-04 | 291 | 9.48 | -5.58 |
| 5.85E-02 | 2.95E-10 | 1.09E-12 | 8.00E-15 | 1.65E-01 | 5.16 | 6.98E-06 | 7.36E-03 | 4.45E-02 | 4.22E-05 | 3.98E-04 | 284 | 9.48 | -5.58 |
| 5.18E-02 | 4.18E-10 | 1.37E-12 | 1.31E-14 | 1.47E-01 | 5.11 | 7.83E-06 | 9.53E-03 | 6.50E-02 | 5.34E-05 | 5.15E-04 | 277 | 9.48 | -5.58 |
| 4.61E-02 | 5.90E-10 | 1.72E-12 | 2.12E-14 | 1.30E-01 | 5.06 | 8.77E-06 | 1.23E-02 | 9.47E-02 | 6.72E-05 | 6.67E-04 | 270 | 9.48 | -5.58 |
| 4.11E-02 | 8.28E-10 | 2.15E-12 | 3.43E-14 | 1.16E-01 | 5.01 | 9.82E-06 | 1.60E-02 | 1.37E-01 | 8.44E-05 | 8.64E-04 | 263 | 9.48 | -5.58 |
| 3.68E-02 | 1.16E-09 | 2.67E-12 | 5.52E-14 | 1.04E-01 | 4.96 | 1.10E-05 | 2.07E-02 | 1.99E-01 | 1.05E-04 | 1.12E-03 | 256 | 9.49 | -5.58 |
| 3.31E-02 | 1.61E-09 | 3.31E-12 | 8.85E-14 | 9.36E-02 | 4.91 | 1.23E-05 | 2.68E-02 | 2.86E-01 | 1.31E-04 | 1.45E-03 | 249 | 9.49 | -5.58 |
| 2.99E-02 | 2.23E-09 | 4.08E-12 | 1.41E-13 | 8.45E-02 | 4.86 | 1.37E-05 | 3.46E-02 | 4.10E-01 | 1.62E-04 | 1.87E-03 | 242 | 9.49 | -5.57 |
| 2.70E-02 | 3.06E-09 | 5.00E-12 | 2.24E-13 | 7.65E-02 | 4.82 | 1.53E-05 | 4.48E-02 | 5.85E-01 | 2.00E-04 | 2.42E-03 | 235 | 9.50 | -5.57 |
| 2.46E-02 | 4.19E-09 | 6.11E-12 | 3.54E-13 | 6.96E-02 | 4.77 | 1.71E-05 | 5.79E-02 | 8.32E-01 | 2.45E-04 | 3.13E-03 | 228 | 9.51 | -5.57 |
| 2.25E-02 | 5.69E-09 | 7.42E-12 | 5.56E-13 | 6.36E-02 | 4.72 | 1.90E-05 | 7.49E-02 | 1.18E+00 | 2.99E-04 | 4.05E-03 | 221 | 9.52 | -5.57 |
| 2.06E-02 | 7.68E-09 | 8.96E-12 | 8.67E-13 | 5.83E-02 | 4.67 | 2.12E-05 | 9.68E-02 | 1.66E+00 | 3.63E-04 | 5.23E-03 | 214 | 9.53 | -5.56 |
| 1.90E-02 | 1.03E-08 | 1.08E-11 | 1.35E-12 | 5.37E-02 | 4.63 | 2.35E-05 | 1.25E-01 | 2.33E+00 | 4.38E-04 | 6.76E-03 | 207 | 9.55 | -5.55 |
| 1.76E-02 | 1.37E-08 | 1.29E-11 | 2.08E-12 | 4.98E-02 | 4.58 | 2.61E-05 | 1.61E-01 | 3.24E+00 | 5.25E-04 | 8.73E-03 | 200 | 9.58 | -5.54 |
| 1.64E-02 | 1.82E-08 | 1.53E-11 | 3.18E-12 | 4.63E-02 | 4.54 | 2.90E-05 | 2.08E-01 | 4.50E+00 | 6.26E-04 | 1.13E-02 | 193 | 9.62 | -5.52 |
| 1.53E-02 | 2.38E-08 | 1.80E-11 | 4.84E-12 | 4.34E-02 | 4.49 | 3.21E-05 | 2.69E-01 | 6.20E+00 | 7.41E-04 | 1.45E-02 | 186 | 9.66 | -5.48 |
| 1.44E-02 | 3.10E-08 | 2.11E-11 | 7.31E-12 | 4.08E-02 | 4.45 | 3.56E-05 | 3.47E-01 | 8.50E+00 | 8.71E-04 | 1.88E-02 | 179 | 9.72 | -5.42 |
| 1.37E-02 | 4.01E-08 | 2.45E-11 | 1.10E-11 | 3.86E-02 | 4.41 | 3.93E-05 | 4.48E-01 | 1.16E+01 | 1.02E-03 | 2.42E-02 | 172 | 9.81 | -5.32 |
| 1.30E-02 | 5.13E-08 | 2.83E-11 | 1.63E-11 | 3.68E-02 | 4.36 | 4.34E-05 | 5.77E-01 | 1.57E+01 | 1.18E-03 | 3.12E-02 | 165 | 9.91 | -5.18 |
| 1.25E-02 | 6.50E-08 | 3.24E-11 | 2.41E-11 | 3.53E-02 | 4.32 | 4.79E-05 | 7.43E-01 | 2.11E+01 | 1.36E-03 | 4.02E-02 | 158 | 10.06 | -4.97 |
| 1.20E-02 | 8.17E-08 | 3.68E-11 | 3.52E-11 | 3.40E-02 | 4.28 | 5.27E-05 | 9.58E-01 | 2.81E+01 | 1.55E-03 | 5.18E-02 | 151 | 10.25 | -4.66 |
| 1.17E-02 | 1.02E-07 | 4.14E-11 | 5.11E-11 | 3.31E-02 | 4.24 | 5.80E-05 | 1.23E+00 | 3.72E+01 | 1.75E-03 | 6.66E-02 | 144 | 10.50 | -4.23 |
| 1.14E-02 | 1.25E-07 | 4.62E-11 | 7.34E-11 | 3.24E-02 | 4.20 | 6.36E-05 | 1.59E+00 | 4.89E+01 | 1.96E-03 | 8.58E-02 | 137 | 10.82 | -3.62 |
| 1.13E-02 | 1.52E-07 | 5.11E-11 | 1.04E-10 | 3.20E-02 | 4.16 | 6.97E-05 | 2.04E+00 | 6.37E+01 | 2.18E-03 | 1.10E-01 | 130 | 11.25 | -2.81 |
| 1.12E-02 | 1.83E-07 | 5.60E-11 | 1.47E-10 | 3.18E-02 | 4.12 | 7.63E-05 | 2.62E+00 | 8.23E+01 | 2.39E-03 | 1.42E-01 | 123 | 11.80 | -1.77 |
| 1.13E-02 | 2.17E-07 | 6.06E-11 | 2.04E-10 | 3.19E-02 | 4.08 | 8.33E-05 | 3.37E+00 | 1.05E+02 | 2.60E-03 | 1.82E-01 | 116 | 12.51 | -0.48 |

Table II (continued).

| *f*<br>0.20<br>$K_0$ | $\delta^{13}C_i$<br>($HCO_3$)<br>12.79<br>$K_1$ | [$CO_2$]<br>0.06<br>$K_2$ | $K_{ps}$ | [$H_2CO_3$] | pH | [$HCO_3$] | Solubility of calcite | R/W (C) | X[$HCO_3$] | R/W (O) | T°C | $\delta^{18}O_{cc}$ | $\delta^{13}C_{cc}$ |
|---|---|---|---|---|---|---|---|---|---|---|---|---|---|
| 3.58E-01 | 2.21E-12 | 4.01E-14 | 1.01E-17 | 1.27E+00 | 5.78 | 1.68E-06 | 2.51E-04 | 1.97E-04 | 1.32E-06 | 1.36E-05 | 375 | 9.19 | -5.69 |
| 3.07E-01 | 3.28E-12 | 5.26E-14 | 1.71E-17 | 1.09E+00 | 5.72 | 1.89E-06 | 3.26E-04 | 2.98E-04 | 1.73E-06 | 1.76E-05 | 368 | 9.19 | -5.69 |
| 2.64E-01 | 4.86E-12 | 6.87E-14 | 2.91E-17 | 9.39E-01 | 5.67 | 2.14E-06 | 4.23E-04 | 4.50E-04 | 2.28E-06 | 2.28E-05 | 361 | 9.19 | -5.69 |
| 2.28E-01 | 7.19E-12 | 8.97E-14 | 4.92E-17 | 8.09E-01 | 5.62 | 2.41E-06 | 5.48E-04 | 6.78E-04 | 2.98E-06 | 2.96E-05 | 354 | 9.19 | -5.69 |
| 1.96E-01 | 1.06E-11 | 1.17E-13 | 8.30E-17 | 6.98E-01 | 5.57 | 2.72E-06 | 7.12E-04 | 1.02E-03 | 3.89E-06 | 3.85E-05 | 347 | 9.19 | -5.69 |
| 1.70E-01 | 1.55E-11 | 1.51E-13 | 1.40E-16 | 6.04E-01 | 5.51 | 3.06E-06 | 9.23E-04 | 1.53E-03 | 5.07E-06 | 4.99E-05 | 340 | 9.19 | -5.69 |
| 1.47E-01 | 2.27E-11 | 1.96E-13 | 2.34E-16 | 5.24E-01 | 5.46 | 3.45E-06 | 1.20E-03 | 2.29E-03 | 6.59E-06 | 6.47E-05 | 333 | 9.19 | -5.69 |
| 1.28E-01 | 3.32E-11 | 2.53E-13 | 3.92E-16 | 4.55E-01 | 5.41 | 3.89E-06 | 1.55E-03 | 3.41E-03 | 8.53E-06 | 8.39E-05 | 326 | 9.19 | -5.69 |
| 1.12E-01 | 4.82E-11 | 3.25E-13 | 6.54E-16 | 3.97E-01 | 5.36 | 4.37E-06 | 2.01E-03 | 5.07E-03 | 1.10E-05 | 1.09E-04 | 319 | 9.19 | -5.69 |
| 9.76E-02 | 6.98E-11 | 4.16E-13 | 1.09E-15 | 3.47E-01 | 5.31 | 4.92E-06 | 2.61E-03 | 7.53E-03 | 1.42E-05 | 1.41E-04 | 312 | 9.19 | -5.69 |
| 8.55E-02 | 1.01E-10 | 5.32E-13 | 1.80E-15 | 3.04E-01 | 5.26 | 5.53E-06 | 3.38E-03 | 1.11E-02 | 1.82E-05 | 1.83E-04 | 305 | 9.19 | -5.69 |
| 7.51E-02 | 1.45E-10 | 6.78E-13 | 2.97E-15 | 2.67E-01 | 5.21 | 6.21E-06 | 4.38E-03 | 1.64E-02 | 2.33E-05 | 2.37E-04 | 298 | 9.19 | -5.69 |
| 6.62E-02 | 2.07E-10 | 8.60E-13 | 4.88E-15 | 2.35E-01 | 5.16 | 6.97E-06 | 5.68E-03 | 2.42E-02 | 2.97E-05 | 3.07E-04 | 291 | 9.19 | -5.69 |
| 5.85E-02 | 2.95E-10 | 1.09E-12 | 8.00E-15 | 2.08E-01 | 5.11 | 7.82E-06 | 7.36E-03 | 3.54E-02 | 3.76E-05 | 3.98E-04 | 284 | 9.19 | -5.69 |
| 5.18E-02 | 4.18E-10 | 1.37E-12 | 1.31E-14 | 1.84E-01 | 5.06 | 8.77E-06 | 9.53E-03 | 5.17E-02 | 4.76E-05 | 5.15E-04 | 277 | 9.20 | -5.69 |
| 4.61E-02 | 5.90E-10 | 1.72E-12 | 2.12E-14 | 1.64E-01 | 5.01 | 9.83E-06 | 1.23E-02 | 7.53E-02 | 6.00E-05 | 6.67E-04 | 270 | 9.20 | -5.69 |
| 4.11E-02 | 8.28E-10 | 2.15E-12 | 3.43E-14 | 1.46E-01 | 4.96 | 1.10E-05 | 1.60E-02 | 1.09E-01 | 7.53E-05 | 8.64E-04 | 263 | 9.20 | -5.69 |
| 3.68E-02 | 1.16E-09 | 2.67E-12 | 5.52E-14 | 1.31E-01 | 4.91 | 1.23E-05 | 2.07E-02 | 1.58E-01 | 9.40E-05 | 1.12E-03 | 256 | 9.20 | -5.69 |
| 3.31E-02 | 1.61E-09 | 3.31E-12 | 8.85E-14 | 1.18E-01 | 4.86 | 1.38E-05 | 2.68E-02 | 2.28E-01 | 1.17E-04 | 1.45E-03 | 249 | 9.21 | -5.69 |
| 2.99E-02 | 2.23E-09 | 4.08E-12 | 1.41E-13 | 1.06E-01 | 4.81 | 1.54E-05 | 3.46E-02 | 3.26E-01 | 1.45E-04 | 1.87E-03 | 242 | 9.21 | -5.69 |
| 2.70E-02 | 3.06E-09 | 5.00E-12 | 2.24E-13 | 9.61E-02 | 4.77 | 1.72E-05 | 4.48E-02 | 4.66E-01 | 1.78E-04 | 2.42E-03 | 235 | 9.22 | -5.69 |
| 2.46E-02 | 4.19E-09 | 6.11E-12 | 3.54E-13 | 8.74E-02 | 4.72 | 1.91E-05 | 5.79E-02 | 6.62E-01 | 2.19E-04 | 3.13E-03 | 228 | 9.22 | -5.69 |
| 2.25E-02 | 5.69E-09 | 7.42E-12 | 5.56E-13 | 7.98E-02 | 4.67 | 2.13E-05 | 7.49E-02 | 9.37E-01 | 2.67E-04 | 4.05E-03 | 221 | 9.24 | -5.68 |
| 2.06E-02 | 7.68E-09 | 8.96E-12 | 8.67E-13 | 7.33E-02 | 4.62 | 2.37E-05 | 9.68E-02 | 1.32E+00 | 3.24E-04 | 5.23E-03 | 214 | 9.25 | -5.68 |
| 1.90E-02 | 1.03E-08 | 1.08E-11 | 1.35E-12 | 6.75E-02 | 4.58 | 2.64E-05 | 1.25E-01 | 1.85E+00 | 3.91E-04 | 6.76E-03 | 207 | 9.27 | -5.67 |
| 1.76E-02 | 1.37E-08 | 1.29E-11 | 2.08E-12 | 6.25E-02 | 4.53 | 2.93E-05 | 1.61E-01 | 2.58E+00 | 4.68E-04 | 8.73E-03 | 200 | 9.30 | -5.66 |
| 1.64E-02 | 1.82E-08 | 1.53E-11 | 3.18E-12 | 5.82E-02 | 4.49 | 3.25E-05 | 2.08E-01 | 3.58E+00 | 5.58E-04 | 1.13E-02 | 193 | 9.33 | -5.65 |
| 1.53E-02 | 2.38E-08 | 1.80E-11 | 4.84E-12 | 5.45E-02 | 4.44 | 3.60E-05 | 2.69E-01 | 4.93E+00 | 6.61E-04 | 1.45E-02 | 186 | 9.38 | -5.62 |
| 1.44E-02 | 3.10E-08 | 2.11E-11 | 7.31E-12 | 5.13E-02 | 4.40 | 3.99E-05 | 3.47E-01 | 6.76E+00 | 7.77E-04 | 1.88E-02 | 179 | 9.44 | -5.57 |
| 1.37E-02 | 4.01E-08 | 2.45E-11 | 1.10E-11 | 4.85E-02 | 4.36 | 4.41E-05 | 4.48E-01 | 9.21E+00 | 9.08E-04 | 2.42E-02 | 172 | 9.52 | -5.51 |
| 1.30E-02 | 5.13E-08 | 2.83E-11 | 1.63E-11 | 4.62E-02 | 4.31 | 4.87E-05 | 5.77E-01 | 1.25E+01 | 1.05E-03 | 3.12E-02 | 165 | 9.63 | -5.41 |
| 1.25E-02 | 6.50E-08 | 3.24E-11 | 2.41E-11 | 4.43E-02 | 4.27 | 5.37E-05 | 7.43E-01 | 1.68E+01 | 1.21E-03 | 4.02E-02 | 158 | 9.77 | -5.25 |
| 1.20E-02 | 8.17E-08 | 3.68E-11 | 3.52E-11 | 4.28E-02 | 4.23 | 5.91E-05 | 9.58E-01 | 2.24E+01 | 1.38E-03 | 5.18E-02 | 151 | 9.96 | -5.03 |
| 1.17E-02 | 1.02E-07 | 4.14E-11 | 5.11E-11 | 4.16E-02 | 4.19 | 6.50E-05 | 1.23E+00 | 2.96E+01 | 1.56E-03 | 6.66E-02 | 144 | 10.21 | -4.71 |
| 1.14E-02 | 1.25E-07 | 4.62E-11 | 7.34E-11 | 4.07E-02 | 4.15 | 7.13E-05 | 1.59E+00 | 3.89E+01 | 1.75E-03 | 8.58E-02 | 137 | 10.54 | -4.27 |
| 1.13E-02 | 1.52E-07 | 5.11E-11 | 1.04E-10 | 4.02E-02 | 4.11 | 7.82E-05 | 2.04E+00 | 5.07E+01 | 1.94E-03 | 1.10E-01 | 130 | 10.96 | -3.66 |
| 1.12E-02 | 1.83E-07 | 5.60E-11 | 1.47E-10 | 4.00E-02 | 4.07 | 8.55E-05 | 2.62E+00 | 6.55E+01 | 2.14E-03 | 1.42E-01 | 123 | 11.51 | -2.88 |
| 1.13E-02 | 2.17E-07 | 6.06E-11 | 2.04E-10 | 4.01E-02 | 4.03 | 9.34E-05 | 3.37E+00 | 8.38E+01 | 2.32E-03 | 1.82E-01 | 116 | 12.22 | -1.89 |

Table II (continued).

| *f* 0.25 $K_0$ | $\delta^{13}C_i$ ($HCO_3$) 12.91 $K_1$ | [$CO_2$] 0.08 $K_2$ | $K_{ps}$ | [$H_2CO_3$] | pH | [$HCO_3$] | Solubility of calcite | R/W (C) | X[$HCO_3$] | R/W (O) | T°C | $\delta^{18}O_{cc}$ | $\delta^{13}C_{cc}$ |
|---|---|---|---|---|---|---|---|---|---|---|---|---|---|
| 3.58E-01 | 2.21E-12 | 4.01E-14 | 1.01E-17 | 1.51E+00 | 5.74 | 1.82E-06 | 2.51E-04 | 1.67E-04 | 1.21E-06 | 1.36E-05 | 375 | 8.91 | -5.80 |
| 3.07E-01 | 3.28E-12 | 5.26E-14 | 1.71E-17 | 1.29E+00 | 5.69 | 2.06E-06 | 3.26E-04 | 2.52E-04 | 1.59E-06 | 1.76E-05 | 368 | 8.91 | -5.80 |
| 2.64E-01 | 4.86E-12 | 6.87E-14 | 2.91E-17 | 1.11E+00 | 5.63 | 2.32E-06 | 4.23E-04 | 3.81E-04 | 2.09E-06 | 2.28E-05 | 361 | 8.91 | -5.80 |
| 2.28E-01 | 7.19E-12 | 8.97E-14 | 4.92E-17 | 9.56E-01 | 5.58 | 2.62E-06 | 5.48E-04 | 5.74E-04 | 2.74E-06 | 2.96E-05 | 354 | 8.91 | -5.80 |
| 1.96E-01 | 1.06E-11 | 1.17E-13 | 8.30E-17 | 8.25E-01 | 5.53 | 2.96E-06 | 7.12E-04 | 8.62E-04 | 3.58E-06 | 3.85E-05 | 347 | 8.91 | -5.80 |
| 1.70E-01 | 1.55E-11 | 1.51E-13 | 1.40E-16 | 7.14E-01 | 5.48 | 3.33E-06 | 9.23E-04 | 1.29E-03 | 4.67E-06 | 4.99E-05 | 340 | 8.91 | -5.80 |
| 1.47E-01 | 2.27E-11 | 1.96E-13 | 2.34E-16 | 6.19E-01 | 5.43 | 3.75E-06 | 1.20E-03 | 1.93E-03 | 6.06E-06 | 6.47E-05 | 333 | 8.91 | -5.80 |
| 1.28E-01 | 3.32E-11 | 2.53E-13 | 3.92E-16 | 5.38E-01 | 5.37 | 4.23E-06 | 1.55E-03 | 2.88E-03 | 7.85E-06 | 8.39E-05 | 326 | 8.91 | -5.80 |
| 1.12E-01 | 4.82E-11 | 3.25E-13 | 6.54E-16 | 4.69E-01 | 5.32 | 4.75E-06 | 2.01E-03 | 4.29E-03 | 1.01E-05 | 1.09E-04 | 319 | 8.91 | -5.80 |
| 9.76E-02 | 6.98E-11 | 4.16E-13 | 1.09E-15 | 4.10E-01 | 5.27 | 5.35E-06 | 2.61E-03 | 6.37E-03 | 1.30E-05 | 1.41E-04 | 312 | 8.91 | -5.80 |
| 8.55E-02 | 1.01E-10 | 5.32E-13 | 1.80E-15 | 3.59E-01 | 5.22 | 6.01E-06 | 3.38E-03 | 9.42E-03 | 1.67E-05 | 1.83E-04 | 305 | 8.91 | -5.80 |
| 7.51E-02 | 1.45E-10 | 6.78E-13 | 2.97E-15 | 3.15E-01 | 5.17 | 6.75E-06 | 4.38E-03 | 1.39E-02 | 2.14E-05 | 2.37E-04 | 298 | 8.91 | -5.80 |
| 6.62E-02 | 2.07E-10 | 8.60E-13 | 4.88E-15 | 2.78E-01 | 5.12 | 7.58E-06 | 5.68E-03 | 2.04E-02 | 2.73E-05 | 3.07E-04 | 291 | 8.91 | -5.80 |
| 5.85E-02 | 2.95E-10 | 1.09E-12 | 8.00E-15 | 2.46E-01 | 5.07 | 8.50E-06 | 7.36E-03 | 3.00E-02 | 3.46E-05 | 3.98E-04 | 284 | 8.91 | -5.80 |
| 5.18E-02 | 4.18E-10 | 1.37E-12 | 1.31E-14 | 2.18E-01 | 5.02 | 9.54E-06 | 9.53E-03 | 4.38E-02 | 4.38E-05 | 5.15E-04 | 277 | 8.91 | -5.80 |
| 4.61E-02 | 5.90E-10 | 1.72E-12 | 2.12E-14 | 1.94E-01 | 4.97 | 1.07E-05 | 1.23E-02 | 6.38E-02 | 5.52E-05 | 6.67E-04 | 270 | 8.91 | -5.80 |
| 4.11E-02 | 8.28E-10 | 2.15E-12 | 3.43E-14 | 1.73E-01 | 4.92 | 1.20E-05 | 1.60E-02 | 9.25E-02 | 6.92E-05 | 8.64E-04 | 263 | 8.91 | -5.80 |
| 3.68E-02 | 1.16E-09 | 2.67E-12 | 5.52E-14 | 1.55E-01 | 4.87 | 1.34E-05 | 2.07E-02 | 1.34E-01 | 8.65E-05 | 1.12E-03 | 256 | 8.92 | -5.80 |
| 3.31E-02 | 1.61E-09 | 3.31E-12 | 8.85E-14 | 1.39E-01 | 4.83 | 1.50E-05 | 2.68E-02 | 1.93E-01 | 1.08E-04 | 1.45E-03 | 249 | 8.92 | -5.80 |
| 2.99E-02 | 2.23E-09 | 4.08E-12 | 1.41E-13 | 1.25E-01 | 4.78 | 1.67E-05 | 3.46E-02 | 2.76E-01 | 1.33E-04 | 1.87E-03 | 242 | 8.93 | -5.80 |
| 2.70E-02 | 3.06E-09 | 5.00E-12 | 2.24E-13 | 1.14E-01 | 4.73 | 1.87E-05 | 4.48E-02 | 3.94E-01 | 1.64E-04 | 2.42E-03 | 235 | 8.93 | -5.80 |
| 2.46E-02 | 4.19E-09 | 6.11E-12 | 3.54E-13 | 1.03E-01 | 4.68 | 2.08E-05 | 5.79E-02 | 5.60E-01 | 2.01E-04 | 3.13E-03 | 228 | 8.94 | -5.80 |
| 2.25E-02 | 5.69E-09 | 7.42E-12 | 5.56E-13 | 9.44E-02 | 4.64 | 2.32E-05 | 7.49E-02 | 7.93E-01 | 2.45E-04 | 4.05E-03 | 221 | 8.95 | -5.80 |
| 2.06E-02 | 7.68E-09 | 8.96E-12 | 8.67E-13 | 8.66E-02 | 4.59 | 2.58E-05 | 9.68E-02 | 1.12E+00 | 2.98E-04 | 5.23E-03 | 214 | 8.97 | -5.79 |
| 1.90E-02 | 1.03E-08 | 1.08E-11 | 1.35E-12 | 7.98E-02 | 4.54 | 2.87E-05 | 1.25E-01 | 1.57E+00 | 3.59E-04 | 6.76E-03 | 207 | 8.99 | -5.79 |
| 1.76E-02 | 1.37E-08 | 1.29E-11 | 2.08E-12 | 7.39E-02 | 4.50 | 3.19E-05 | 1.61E-01 | 2.18E+00 | 4.31E-04 | 8.73E-03 | 200 | 9.01 | -5.78 |
| 1.64E-02 | 1.82E-08 | 1.53E-11 | 3.18E-12 | 6.88E-02 | 4.45 | 3.53E-05 | 2.08E-01 | 3.03E+00 | 5.13E-04 | 1.13E-02 | 193 | 9.05 | -5.77 |
| 1.53E-02 | 2.38E-08 | 1.80E-11 | 4.84E-12 | 6.44E-02 | 4.41 | 3.92E-05 | 2.69E-01 | 4.18E+00 | 6.08E-04 | 1.45E-02 | 186 | 9.09 | -5.75 |
| 1.44E-02 | 3.10E-08 | 2.11E-11 | 7.31E-12 | 6.06E-02 | 4.36 | 4.34E-05 | 3.47E-01 | 5.72E+00 | 7.15E-04 | 1.88E-02 | 179 | 9.16 | -5.71 |
| 1.37E-02 | 4.01E-08 | 2.45E-11 | 1.10E-11 | 5.74E-02 | 4.32 | 4.79E-05 | 4.48E-01 | 7.80E+00 | 8.35E-04 | 2.42E-02 | 172 | 9.24 | -5.66 |
| 1.30E-02 | 5.13E-08 | 2.83E-11 | 1.63E-11 | 5.46E-02 | 4.28 | 5.29E-05 | 5.77E-01 | 1.06E+01 | 9.68E-04 | 3.12E-02 | 165 | 9.35 | -5.58 |
| 1.25E-02 | 6.50E-08 | 3.24E-11 | 2.41E-11 | 5.24E-02 | 4.23 | 5.84E-05 | 7.43E-01 | 1.42E+01 | 1.11E-03 | 4.02E-02 | 158 | 9.49 | -5.46 |
| 1.20E-02 | 8.17E-08 | 3.68E-11 | 3.52E-11 | 5.05E-02 | 4.19 | 6.43E-05 | 9.58E-01 | 1.89E+01 | 1.27E-03 | 5.18E-02 | 151 | 9.68 | -5.28 |
| 1.17E-02 | 1.02E-07 | 4.14E-11 | 5.11E-11 | 4.91E-02 | 4.15 | 7.06E-05 | 1.23E+00 | 2.51E+01 | 1.44E-03 | 6.66E-02 | 144 | 9.93 | -5.03 |
| 1.14E-02 | 1.25E-07 | 4.62E-11 | 7.34E-11 | 4.81E-02 | 4.11 | 7.75E-05 | 1.59E+00 | 3.29E+01 | 1.61E-03 | 8.58E-02 | 137 | 10.25 | -4.67 |
| 1.13E-02 | 1.52E-07 | 5.11E-11 | 1.04E-10 | 4.75E-02 | 4.07 | 8.50E-05 | 2.04E+00 | 4.29E+01 | 1.79E-03 | 1.10E-01 | 130 | 10.68 | -4.19 |
| 1.12E-02 | 1.83E-07 | 5.60E-11 | 1.47E-10 | 4.72E-02 | 4.03 | 9.30E-05 | 2.62E+00 | 5.54E+01 | 1.96E-03 | 1.42E-01 | 123 | 11.23 | -3.56 |
| 1.13E-02 | 2.17E-07 | 6.06E-11 | 2.04E-10 | 4.74E-02 | 3.99 | 1.01E-04 | 3.37E+00 | 7.10E+01 | 2.14E-03 | 1.82E-01 | 116 | 11.94 | -2.75 |
| 1.14E-02 | 2.55E-07 | 6.49E-11 | 2.81E-10 | 4.80E-02 | 3.96 | 1.11E-04 | 4.33E+00 | 8.99E+01 | 2.30E-03 | 2.34E-01 | 109 | 12.85 | -1.76 |
| 1.17E-02 | 2.95E-07 | 6.87E-11 | 3.81E-10 | 4.91E-02 | 3.92 | 1.20E-04 | 5.55E+00 | 1.13E+02 | 2.44E-03 | 3.00E-01 | 102 | 13.99 | -0.59 |
| 1.21E-02 | 3.36E-07 | 7.18E-11 | 5.11E-10 | 5.07E-02 | 3.88 | 1.31E-04 | 7.12E+00 | 1.40E+02 | 2.57E-03 | 3.85E-01 | 95 | 15.41 | 0.70 |
| 1.26E-02 | 3.77E-07 | 7.41E-11 | 6.76E-10 | 5.30E-02 | 3.85 | 1.41E-04 | 9.12E+00 | 1.72E+02 | 2.66E-03 | 4.93E-01 | 88 | 17.15 | 2.08 |

Table II (continued).

| $f$ | $\delta^{13}C_i$ ($HCO_3$) | [$CO_2$] | | | | | | | | | | | |
|---|---|---|---|---|---|---|---|---|---|---|---|---|---|
| 0.30 | 13.02 | 0.09 | | | | | | | | | | | |
| $K_0$ | $K_1$ | $K_2$ | $K_{ps}$ | [$H_2CO_3$] | pH | [$HCO_3$] | Solubility of calcite | R/W (C) | X[$HCO_3$] | R/W (O) | T°C | $\delta^{18}O_{cc}$ | $\delta^{13}C_{cc}$ |
| 3.58E-01 | 2.21E-12 | 4.01E-14 | 1.01E-17 | 1.71E+00 | 5.71 | 1.95E-06 | 2.51E-04 | 1.46E-04 | 1.14E-06 | 1.36E-05 | 375 | 8.62 | -5.91 |
| 3.07E-01 | 3.28E-12 | 5.26E-14 | 1.71E-17 | 1.47E+00 | 5.66 | 2.20E-06 | 3.26E-04 | 2.22E-04 | 1.49E-06 | 1.76E-05 | 368 | 8.62 | -5.91 |
| 2.64E-01 | 4.86E-12 | 6.87E-14 | 2.91E-17 | 1.26E+00 | 5.61 | 2.48E-06 | 4.23E-04 | 3.35E-04 | 1.96E-06 | 2.28E-05 | 361 | 8.62 | -5.91 |
| 2.28E-01 | 7.19E-12 | 8.97E-14 | 4.92E-17 | 1.09E+00 | 5.55 | 2.80E-06 | 5.48E-04 | 5.04E-04 | 2.57E-06 | 2.96E-05 | 354 | 8.62 | -5.91 |
| 1.96E-01 | 1.06E-11 | 1.17E-13 | 8.30E-17 | 9.39E-01 | 5.50 | 3.15E-06 | 7.12E-04 | 7.58E-04 | 3.36E-06 | 3.85E-05 | 347 | 8.62 | -5.91 |
| 1.70E-01 | 1.55E-11 | 1.51E-13 | 1.40E-16 | 8.13E-01 | 5.45 | 3.55E-06 | 9.23E-04 | 1.14E-03 | 4.37E-06 | 4.99E-05 | 340 | 8.62 | -5.91 |
| 1.47E-01 | 2.27E-11 | 1.96E-13 | 2.34E-16 | 7.05E-01 | 5.40 | 4.00E-06 | 1.20E-03 | 1.70E-03 | 5.68E-06 | 6.47E-05 | 333 | 8.62 | -5.91 |
| 1.28E-01 | 3.32E-11 | 2.53E-13 | 3.92E-16 | 6.13E-01 | 5.35 | 4.51E-06 | 1.55E-03 | 2.54E-03 | 7.36E-06 | 8.39E-05 | 326 | 8.62 | -5.91 |
| 1.12E-01 | 4.82E-11 | 3.25E-13 | 6.54E-16 | 5.34E-01 | 5.29 | 5.07E-06 | 2.01E-03 | 3.77E-03 | 9.50E-06 | 1.09E-04 | 319 | 8.62 | -5.91 |
| 9.76E-02 | 6.98E-11 | 4.16E-13 | 1.09E-15 | 4.66E-01 | 5.24 | 5.70E-06 | 2.61E-03 | 5.60E-03 | 1.22E-05 | 1.41E-04 | 312 | 8.62 | -5.91 |
| 8.55E-02 | 1.01E-10 | 5.32E-13 | 1.80E-15 | 4.09E-01 | 5.19 | 6.41E-06 | 3.38E-03 | 8.28E-03 | 1.57E-05 | 1.83E-04 | 305 | 8.62 | -5.91 |
| 7.51E-02 | 1.45E-10 | 6.78E-13 | 2.97E-15 | 3.59E-01 | 5.14 | 7.20E-06 | 4.38E-03 | 1.22E-02 | 2.01E-05 | 2.37E-04 | 298 | 8.62 | -5.91 |
| 6.62E-02 | 2.07E-10 | 8.60E-13 | 4.88E-15 | 3.16E-01 | 5.09 | 8.09E-06 | 5.68E-03 | 1.80E-02 | 2.56E-05 | 3.07E-04 | 291 | 8.63 | -5.91 |
| 5.85E-02 | 2.95E-10 | 1.09E-12 | 8.00E-15 | 2.79E-01 | 5.04 | 9.07E-06 | 7.36E-03 | 2.63E-02 | 3.25E-05 | 3.98E-04 | 284 | 8.63 | -5.91 |
| 5.18E-02 | 4.18E-10 | 1.37E-12 | 1.31E-14 | 2.48E-01 | 4.99 | 1.02E-05 | 9.53E-03 | 3.85E-02 | 4.11E-05 | 5.15E-04 | 277 | 8.63 | -5.91 |
| 4.61E-02 | 5.90E-10 | 1.72E-12 | 2.12E-14 | 2.20E-01 | 4.94 | 1.14E-05 | 1.23E-02 | 5.60E-02 | 5.17E-05 | 6.67E-04 | 270 | 8.63 | -5.91 |
| 4.11E-02 | 8.28E-10 | 2.15E-12 | 3.43E-14 | 1.97E-01 | 4.89 | 1.28E-05 | 1.60E-02 | 8.13E-02 | 6.49E-05 | 8.64E-04 | 263 | 8.63 | -5.91 |
| 3.68E-02 | 1.16E-09 | 2.67E-12 | 5.52E-14 | 1.76E-01 | 4.85 | 1.43E-05 | 2.07E-02 | 1.17E-01 | 8.11E-05 | 1.12E-03 | 256 | 8.63 | -5.91 |
| 3.31E-02 | 1.61E-09 | 3.31E-12 | 8.85E-14 | 1.58E-01 | 4.80 | 1.60E-05 | 2.68E-02 | 1.69E-01 | 1.01E-04 | 1.45E-03 | 249 | 8.64 | -5.91 |
| 2.99E-02 | 2.23E-09 | 4.08E-12 | 1.41E-13 | 1.43E-01 | 4.75 | 1.78E-05 | 3.46E-02 | 2.43E-01 | 1.25E-04 | 1.87E-03 | 242 | 8.64 | -5.91 |
| 2.70E-02 | 3.06E-09 | 5.00E-12 | 2.24E-13 | 1.29E-01 | 4.70 | 1.99E-05 | 4.48E-02 | 3.46E-01 | 1.54E-04 | 2.42E-03 | 235 | 8.65 | -5.91 |
| 2.46E-02 | 4.19E-09 | 6.11E-12 | 3.54E-13 | 1.18E-01 | 4.65 | 2.22E-05 | 5.79E-02 | 4.93E-01 | 1.89E-04 | 3.13E-03 | 228 | 8.66 | -5.91 |
| 2.25E-02 | 5.69E-09 | 7.42E-12 | 5.56E-13 | 1.07E-01 | 4.61 | 2.47E-05 | 7.49E-02 | 6.97E-01 | 2.30E-04 | 4.05E-03 | 221 | 8.67 | -5.91 |
| 2.06E-02 | 7.68E-09 | 8.96E-12 | 8.67E-13 | 9.85E-02 | 4.56 | 2.75E-05 | 9.68E-02 | 9.82E-01 | 2.79E-04 | 5.23E-03 | 214 | 8.68 | -5.91 |
| 1.90E-02 | 1.03E-08 | 1.08E-11 | 1.35E-12 | 9.08E-02 | 4.51 | 3.06E-05 | 1.25E-01 | 1.38E+00 | 3.37E-04 | 6.76E-03 | 207 | 8.70 | -5.90 |
| 1.76E-02 | 1.37E-08 | 1.29E-11 | 2.08E-12 | 8.41E-02 | 4.47 | 3.40E-05 | 1.61E-01 | 1.92E+00 | 4.04E-04 | 8.73E-03 | 200 | 8.73 | -5.90 |
| 1.64E-02 | 1.82E-08 | 1.53E-11 | 3.18E-12 | 7.83E-02 | 4.42 | 3.77E-05 | 2.08E-01 | 2.66E+00 | 4.81E-04 | 1.13E-02 | 193 | 8.76 | -5.89 |
| 1.53E-02 | 2.38E-08 | 1.80E-11 | 4.84E-12 | 7.33E-02 | 4.38 | 4.18E-05 | 2.69E-01 | 3.67E+00 | 5.70E-04 | 1.45E-02 | 186 | 8.81 | -5.87 |
| 1.44E-02 | 3.10E-08 | 2.11E-11 | 7.31E-12 | 6.90E-02 | 4.33 | 4.63E-05 | 3.47E-01 | 5.03E+00 | 6.70E-04 | 1.88E-02 | 179 | 8.87 | -5.84 |
| 1.37E-02 | 4.01E-08 | 2.45E-11 | 1.10E-11 | 6.53E-02 | 4.29 | 5.11E-05 | 4.48E-01 | 6.85E+00 | 7.83E-04 | 2.42E-02 | 172 | 8.95 | -5.80 |
| 1.30E-02 | 5.13E-08 | 2.83E-11 | 1.63E-11 | 6.22E-02 | 4.25 | 5.65E-05 | 5.77E-01 | 9.27E+00 | 9.07E-04 | 3.12E-02 | 165 | 9.06 | -5.73 |
| 1.25E-02 | 6.50E-08 | 3.24E-11 | 2.41E-11 | 5.96E-02 | 4.21 | 6.23E-05 | 7.43E-01 | 1.25E+01 | 1.04E-03 | 4.02E-02 | 158 | 9.21 | -5.63 |
| 1.20E-02 | 8.17E-08 | 3.68E-11 | 3.52E-11 | 5.75E-02 | 4.16 | 6.85E-05 | 9.58E-01 | 1.66E+01 | 1.19E-03 | 5.18E-02 | 151 | 9.39 | -5.48 |
| 1.17E-02 | 1.02E-07 | 4.14E-11 | 5.11E-11 | 5.59E-02 | 4.12 | 7.54E-05 | 1.23E+00 | 2.20E+01 | 1.35E-03 | 6.66E-02 | 144 | 9.64 | -5.27 |
| 1.14E-02 | 1.25E-07 | 4.62E-11 | 7.34E-11 | 5.47E-02 | 4.08 | 8.27E-05 | 1.59E+00 | 2.89E+01 | 1.51E-03 | 8.58E-02 | 137 | 9.97 | -4.97 |
| 1.13E-02 | 1.52E-07 | 5.11E-11 | 1.04E-10 | 5.40E-02 | 4.04 | 9.06E-05 | 2.04E+00 | 3.77E+01 | 1.68E-03 | 1.10E-01 | 130 | 10.39 | -4.57 |
| 1.12E-02 | 1.83E-07 | 5.60E-11 | 1.47E-10 | 5.37E-02 | 4.00 | 9.92E-05 | 2.62E+00 | 4.87E+01 | 1.84E-03 | 1.42E-01 | 123 | 10.94 | -4.03 |
| 1.13E-02 | 2.17E-07 | 6.06E-11 | 2.04E-10 | 5.39E-02 | 3.97 | 1.08E-04 | 3.37E+00 | 6.24E+01 | 2.00E-03 | 1.82E-01 | 116 | 11.66 | -3.34 |
| 1.14E-02 | 2.55E-07 | 6.49E-11 | 2.81E-10 | 5.46E-02 | 3.93 | 1.18E-04 | 4.33E+00 | 7.90E+01 | 2.16E-03 | 2.34E-01 | 109 | 12.56 | -2.49 |
| 1.17E-02 | 2.95E-07 | 6.87E-11 | 3.81E-10 | 5.58E-02 | 3.89 | 1.28E-04 | 5.55E+00 | 9.92E+01 | 2.29E-03 | 3.00E-01 | 102 | 13.71 | -1.48 |
| 1.21E-02 | 3.36E-07 | 7.18E-11 | 5.11E-10 | 5.77E-02 | 3.86 | 1.39E-04 | 7.12E+00 | 1.23E+02 | 2.41E-03 | 3.85E-01 | 95 | 15.13 | -0.33 |
| 1.26E-02 | 3.77E-07 | 7.41E-11 | 6.76E-10 | 6.03E-02 | 3.82 | 1.51E-04 | 9.12E+00 | 1.51E+02 | 2.50E-03 | 4.93E-01 | 88 | 16.86 | 0.90 |
| 1.33E-02 | 4.16E-07 | 7.54E-11 | 8.81E-10 | 6.37E-02 | 3.79 | 1.63E-04 | 1.17E+01 | 1.83E+02 | 2.55E-03 | 6.31E-01 | 81 | 18.93 | 2.15 |

Table II (continued).

| *f* 0.50 $K_0$ | $\delta^{13}C_i$ ($HCO_3$) 13.47 $K_1$ | [$CO_2$] 0.12 $K_2$ | $K_{ps}$ | [$H_2CO_3$] | pH | [$HCO_3$] | Solubility of calcite | R/W (C) | X[$HCO_3$] | R/W (O) | T°C | $\delta^{18}O_{cc}$ | $\delta^{13}C_{cc}$ |
|---|---|---|---|---|---|---|---|---|---|---|---|---|---|
| 3.58E-01 | 2.21E-12 | 4.01E-14 | 1.01E-17 | 2.37E+00 | 5.64 | 2.29E-06 | 2.51E-04 | 1.06E-04 | 9.66E-07 | 1.36E-05 | 375 | 7.49 | -6.37 |
| 3.07E-01 | 3.28E-12 | 5.26E-14 | 1.71E-17 | 2.03E+00 | 5.59 | 2.58E-06 | 3.26E-04 | 1.60E-04 | 1.27E-06 | 1.76E-05 | 368 | 7.49 | -6.37 |
| 2.64E-01 | 4.86E-12 | 6.87E-14 | 2.91E-17 | 1.74E+00 | 5.54 | 2.91E-06 | 4.23E-04 | 2.42E-04 | 1.67E-06 | 2.28E-05 | 361 | 7.49 | -6.37 |
| 2.28E-01 | 7.19E-12 | 8.97E-14 | 4.92E-17 | 1.50E+00 | 5.48 | 3.29E-06 | 5.48E-04 | 3.65E-04 | 2.19E-06 | 2.96E-05 | 354 | 7.49 | -6.37 |
| 1.96E-01 | 1.06E-11 | 1.17E-13 | 8.30E-17 | 1.30E+00 | 5.43 | 3.71E-06 | 7.12E-04 | 5.49E-04 | 2.86E-06 | 3.85E-05 | 347 | 7.49 | -6.37 |
| 1.70E-01 | 1.55E-11 | 1.51E-13 | 1.40E-16 | 1.12E+00 | 5.38 | 4.18E-06 | 9.23E-04 | 8.23E-04 | 3.72E-06 | 4.99E-05 | 340 | 7.49 | -6.37 |
| 1.47E-01 | 2.27E-11 | 1.96E-13 | 2.34E-16 | 9.73E-01 | 5.33 | 4.70E-06 | 1.20E-03 | 1.23E-03 | 4.83E-06 | 6.47E-05 | 333 | 7.49 | -6.37 |
| 1.28E-01 | 3.32E-11 | 2.53E-13 | 3.92E-16 | 8.46E-01 | 5.28 | 5.30E-06 | 1.55E-03 | 1.84E-03 | 6.26E-06 | 8.39E-05 | 326 | 7.49 | -6.37 |
| 1.12E-01 | 4.82E-11 | 3.25E-13 | 6.54E-16 | 7.37E-01 | 5.22 | 5.96E-06 | 2.01E-03 | 2.73E-03 | 8.09E-06 | 1.09E-04 | 319 | 7.49 | -6.37 |
| 9.76E-02 | 6.98E-11 | 4.16E-13 | 1.09E-15 | 6.44E-01 | 5.17 | 6.70E-06 | 2.61E-03 | 4.05E-03 | 1.04E-05 | 1.41E-04 | 312 | 7.49 | -6.37 |
| 8.55E-02 | 1.01E-10 | 5.32E-13 | 1.80E-15 | 5.64E-01 | 5.12 | 7.53E-06 | 3.38E-03 | 6.00E-03 | 1.34E-05 | 1.83E-04 | 305 | 7.49 | -6.37 |
| 7.51E-02 | 1.45E-10 | 6.78E-13 | 2.97E-15 | 4.96E-01 | 5.07 | 8.46E-06 | 4.38E-03 | 8.85E-03 | 1.71E-05 | 2.37E-04 | 298 | 7.49 | -6.37 |
| 6.62E-02 | 2.07E-10 | 8.60E-13 | 4.88E-15 | 4.37E-01 | 5.02 | 9.50E-06 | 5.68E-03 | 1.30E-02 | 2.18E-05 | 3.07E-04 | 291 | 7.49 | -6.37 |
| 5.85E-02 | 2.95E-10 | 1.09E-12 | 8.00E-15 | 3.86E-01 | 4.97 | 1.07E-05 | 7.36E-03 | 1.91E-02 | 2.76E-05 | 3.98E-04 | 284 | 7.49 | -6.37 |
| 5.18E-02 | 4.18E-10 | 1.37E-12 | 1.31E-14 | 3.42E-01 | 4.92 | 1.20E-05 | 9.53E-03 | 2.79E-02 | 3.49E-05 | 5.15E-04 | 277 | 7.49 | -6.37 |
| 4.61E-02 | 5.90E-10 | 1.72E-12 | 2.12E-14 | 3.04E-01 | 4.87 | 1.34E-05 | 1.23E-02 | 4.06E-02 | 4.40E-05 | 6.67E-04 | 270 | 7.49 | -6.37 |
| 4.11E-02 | 8.28E-10 | 2.15E-12 | 3.43E-14 | 2.72E-01 | 4.82 | 1.50E-05 | 1.60E-02 | 5.89E-02 | 5.52E-05 | 8.64E-04 | 263 | 7.49 | -6.37 |
| 3.68E-02 | 1.16E-09 | 2.67E-12 | 5.52E-14 | 2.43E-01 | 4.78 | 1.68E-05 | 2.07E-02 | 8.51E-02 | 6.90E-05 | 1.12E-03 | 256 | 7.50 | -6.36 |
| 3.31E-02 | 1.61E-09 | 3.31E-12 | 8.85E-14 | 2.19E-01 | 4.73 | 1.88E-05 | 2.68E-02 | 1.23E-01 | 8.58E-05 | 1.45E-03 | 249 | 7.50 | -6.36 |
| 2.99E-02 | 2.23E-09 | 4.08E-12 | 1.41E-13 | 1.97E-01 | 4.68 | 2.09E-05 | 3.46E-02 | 1.76E-01 | 1.06E-04 | 1.87E-03 | 242 | 7.51 | -6.36 |
| 2.70E-02 | 3.06E-09 | 5.00E-12 | 2.24E-13 | 1.79E-01 | 4.63 | 2.34E-05 | 4.48E-02 | 2.51E-01 | 1.31E-04 | 2.42E-03 | 235 | 7.51 | -6.36 |
| 2.46E-02 | 4.19E-09 | 6.11E-12 | 3.54E-13 | 1.62E-01 | 4.58 | 2.61E-05 | 5.79E-02 | 3.57E-01 | 1.61E-04 | 3.13E-03 | 228 | 7.52 | -6.36 |
| 2.25E-02 | 5.69E-09 | 7.42E-12 | 5.56E-13 | 1.48E-01 | 4.54 | 2.90E-05 | 7.49E-02 | 5.05E-01 | 1.96E-04 | 4.05E-03 | 221 | 7.53 | -6.36 |
| 2.06E-02 | 7.68E-09 | 8.96E-12 | 8.67E-13 | 1.36E-01 | 4.49 | 3.23E-05 | 9.68E-02 | 7.11E-01 | 2.38E-04 | 5.23E-03 | 214 | 7.55 | -6.36 |
| 1.90E-02 | 1.03E-08 | 1.08E-11 | 1.35E-12 | 1.25E-01 | 4.44 | 3.59E-05 | 1.25E-01 | 9.97E-01 | 2.87E-04 | 6.76E-03 | 207 | 7.57 | -6.36 |
| 1.76E-02 | 1.37E-08 | 1.29E-11 | 2.08E-12 | 1.16E-01 | 4.40 | 3.99E-05 | 1.61E-01 | 1.39E+00 | 3.44E-04 | 8.73E-03 | 200 | 7.59 | -6.35 |
| 1.64E-02 | 1.82E-08 | 1.53E-11 | 3.18E-12 | 1.08E-01 | 4.35 | 4.43E-05 | 2.08E-01 | 1.93E+00 | 4.10E-04 | 1.13E-02 | 193 | 7.63 | -6.35 |
| 1.53E-02 | 2.38E-08 | 1.80E-11 | 4.84E-12 | 1.01E-01 | 4.31 | 4.91E-05 | 2.69E-01 | 2.66E+00 | 4.85E-04 | 1.45E-02 | 186 | 7.67 | -6.34 |
| 1.44E-02 | 3.10E-08 | 2.11E-11 | 7.31E-12 | 9.52E-02 | 4.26 | 5.44E-05 | 3.47E-01 | 3.64E+00 | 5.70E-04 | 1.88E-02 | 179 | 7.74 | -6.32 |
| 1.37E-02 | 4.01E-08 | 2.45E-11 | 1.10E-11 | 9.01E-02 | 4.22 | 6.01E-05 | 4.48E-01 | 4.96E+00 | 6.66E-04 | 2.42E-02 | 172 | 7.82 | -6.29 |
| 1.30E-02 | 5.13E-08 | 2.83E-11 | 1.63E-11 | 8.59E-02 | 4.18 | 6.64E-05 | 5.77E-01 | 6.72E+00 | 7.72E-04 | 3.12E-02 | 165 | 7.93 | -6.25 |
| 1.25E-02 | 6.50E-08 | 3.24E-11 | 2.41E-11 | 8.23E-02 | 4.14 | 7.32E-05 | 7.43E-01 | 9.03E+00 | 8.88E-04 | 4.02E-02 | 158 | 8.07 | -6.18 |
| 1.20E-02 | 8.17E-08 | 3.68E-11 | 3.52E-11 | 7.94E-02 | 4.09 | 8.06E-05 | 9.58E-01 | 1.20E+01 | 1.01E-03 | 5.18E-02 | 151 | 8.26 | -6.09 |
| 1.17E-02 | 1.02E-07 | 4.14E-11 | 5.11E-11 | 7.72E-02 | 4.05 | 8.86E-05 | 1.23E+00 | 1.60E+01 | 1.15E-03 | 6.66E-02 | 144 | 8.51 | -5.95 |
| 1.14E-02 | 1.25E-07 | 4.62E-11 | 7.34E-11 | 7.56E-02 | 4.01 | 9.72E-05 | 1.59E+00 | 2.10E+01 | 1.28E-03 | 8.58E-02 | 137 | 8.83 | -5.75 |
| 1.13E-02 | 1.52E-07 | 5.11E-11 | 1.04E-10 | 7.46E-02 | 3.97 | 1.07E-04 | 2.04E+00 | 2.73E+01 | 1.43E-03 | 1.10E-01 | 130 | 9.26 | -5.49 |
| 1.12E-02 | 1.83E-07 | 5.60E-11 | 1.47E-10 | 7.42E-02 | 3.93 | 1.17E-04 | 2.62E+00 | 3.53E+01 | 1.57E-03 | 1.42E-01 | 123 | 9.81 | -5.13 |
| 1.13E-02 | 2.17E-07 | 6.06E-11 | 2.04E-10 | 7.45E-02 | 3.90 | 1.27E-04 | 3.37E+00 | 4.52E+01 | 1.71E-03 | 1.82E-01 | 116 | 10.52 | -4.67 |
| 1.14E-02 | 2.55E-07 | 6.49E-11 | 2.81E-10 | 7.54E-02 | 3.86 | 1.39E-04 | 4.33E+00 | 5.73E+01 | 1.84E-03 | 2.34E-01 | 109 | 11.43 | -4.09 |
| 1.17E-02 | 2.95E-07 | 6.87E-11 | 3.81E-10 | 7.71E-02 | 3.82 | 1.51E-04 | 5.55E+00 | 7.18E+01 | 1.95E-03 | 3.00E-01 | 102 | 12.57 | -3.39 |
| 1.21E-02 | 3.36E-07 | 7.18E-11 | 5.11E-10 | 7.97E-02 | 3.79 | 1.64E-04 | 7.12E+00 | 8.91E+01 | 2.05E-03 | 3.85E-01 | 95 | 13.99 | -2.58 |
| 1.26E-02 | 3.77E-07 | 7.41E-11 | 6.76E-10 | 8.32E-02 | 3.75 | 1.77E-04 | 9.12E+00 | 1.09E+02 | 2.12E-03 | 4.93E-01 | 88 | 15.73 | -1.68 |
| 1.33E-02 | 4.16E-07 | 7.54E-11 | 8.81E-10 | 8.79E-02 | 3.72 | 1.91E-04 | 1.17E+01 | 1.33E+02 | 2.17E-03 | 6.31E-01 | 81 | 17.80 | -0.73 |

*Mesozoic to Cenozoic Alkaline Magmatism in the Brazilian Platform*
*Comin-Chiaramonti, P. & Gomes, C.B. (eds.)*
*Edusp/Fapesp, São Paulo, pp. 629-656, 2005*

# CARBONATITES FROM SOUTHEASTERN BRAZIL: GEOCHEMISTRY, O-C, Sr-Nd-Pb ISOTOPES AND RELATIONSHIPS WITH THE MAGMATISM FROM THE PARANÁ-ANGOLA-NAMIBIA PROVINCE

*P. Comin-Chiaramonti, C.B. Gomes, L.S. Marques, P. Censi, E. Ruberti and P. Antonini*

*Early and Late Cretaceous carbonatitic complexes from southern Brazil occur along the main tectonic Lineaments of the South America platform. A similar situation is recognized for the Angolan and Namibian occurrences in Africa. Processes of liquid immiscibility are believed to have generated carbonatitic liquids, as evidenced by the field relationships and by the geochemical characteristics. Ca-, Mg- and Fe-carbonatites are widespread even in the same complex. The remarkable scatters of the incompatible elements is mainly due to 1) the control of accessory phases, e.g. apatite, pyrochlore, fluorcarbonates and fluorite, and 2) the repeated overprinting of hydrothermal over magmatic processes. The O-C isotope results show trends ranging from magmatic to hydrothermal temperatures, at variable $CO_2/H_2O$ ratios. The Fe-carbonatites appear to be systematically related to low-temperature hydrothermal stages. Sr-Nd-Pb systematics highlight hetero-geneous mixtures between HIMU and EMI mantle components, likewise to the associated alkaline rocks and the flood tholeiites of the Paraná-Angola-Namibia Province. The areal distribution shows that the time-integrated isotopic enrichment of the carbonatites and alkaline rocks decreases from West (Eastern Paraguay) to East (Angola and Namibia), and it is associated with the age decrease of the alkaline magmatism, i.e. from Early Cretaceous to Tertiary. As a whole, the data indicate that the alkaline-carbonatitic magmatism originated from a significant but small scale heterogeneous subcontinental mantle. In this scenario, the Walvis Ridge-Rio Grande Rise and Vitória-Trindade hot spot tracks might reflect the accomodation of stresses in the lithosphere during rifting, rather than continuous magmatic activity induced by mantle plumes beneath the moving lithosphere.*

## INTRODUCTION

The Paraná Basin is part of the Paraná-Angola-Namibia (Etendeka) Province (PAEP of Comin-Chiaramonti *et al*., 1999), characterized by Early Cretaceous flood tholeiites and dyke swarms (129-133 Ma; Piccirillo & Melfi, 1988; Renne *et al*., 1997; Ernesto *et al*., 1999, 2002 and therein references) associated with alkaline and alkaline-carbonatite complexes of Early Cretaceous to Tertiary age (Gomes *et al*., 1990; Reid *et al*., 1990; Morbidelli *et al*., 1995; Le Roex & Lanyon, 1998; Alberti *et al*., 1999). The emplacement of the alkaline and alkaline-carbonatitic complexes, in and around the PAEP, occurred mainly along tectonic Lineaments active at least since Early Mesozoic (Fig. 1), and up to present day, as indicated by the distribution of the earthquakes in southern Brazil (Berrocal & Fernandes, 1996). Recently, Molina & Ussami (1999) and Ernesto *et al*. (2000, 2002) stressed to a clear correlation between geoid anomalies and magmatic/tectonic provinces along southeastern Brazil and Uruguay.

**Early Cretaceous** alkaline and alkaline-carbonatite complexes from southern Brazil and Paraguay are found mainly along 1) Uruguay Lineament (Anitápolis and Sapucai, at the eastermost and westernmost side of the Paraná Basin, respectively); 2) Piquiri Lineament (Eastern Paraguay: Cerros Chiriguelo and Sarambí); 3) Ponta Grossa Arch (e.g. Jacupiranga, Juquiá and Barra do Itapirapuã) and 4) Serra do Mar, at the northern fringe of the Ponta Grossa Arch (e.g. Itanhaém). Relative to flood basalts, these occurrences are pre-tholeiitic (e.g. Cerros Chiriguelo and Sarambí; 136-143 Ma), syn-tholeiitic (e.g. Anitápolis, Jacupiranga, Juquiá; 130-133 Ma), and post-tholeiitic (e.g. Sapucai, 128 Ma; Ipanema, 124 Ma; Barra do Itapirapuã, 115 Ma; cf. Comin-Chiaramonti *et al.*, 1997a, b, 1999; Ruberti *et al.*, 2002).

In Angola, the alkaline-carbonatitic complexes, dated at 138-130 Ma (Issa Filho *et al*., 1991; Coltorti *et al.*, 1993), occur mainly at the Moçâmedes Arch (e.g. Sulima, Bailundo, Longonjo, Coola and Tchivira-Bonga) and at the Khumib region (e.g. Virilundo).

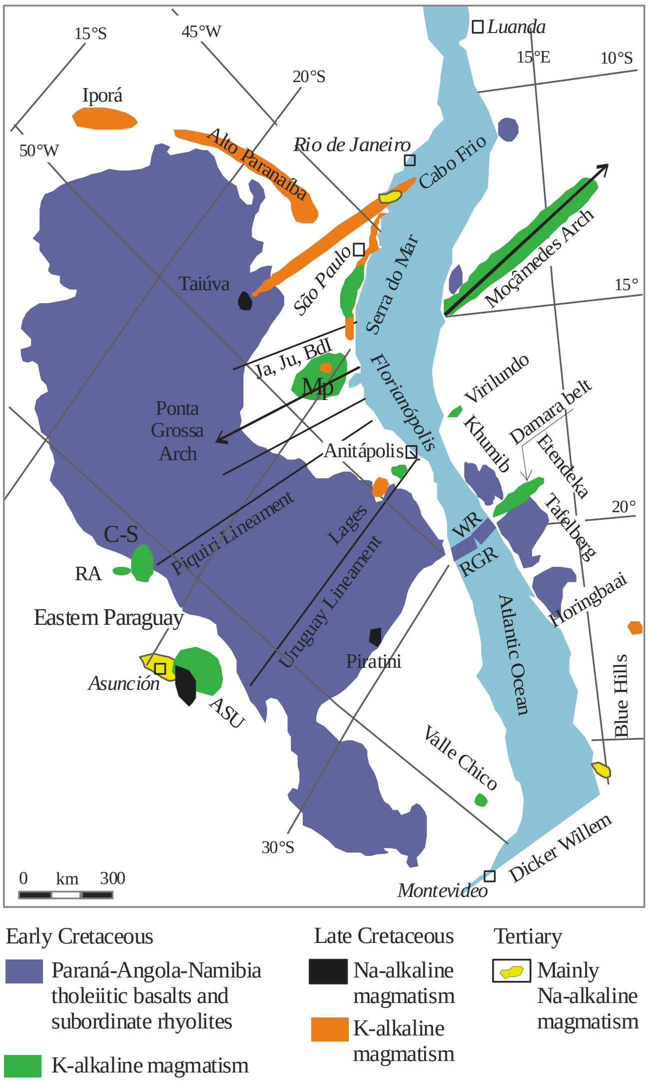


Fig. 1. Distribution of the magmatism in the Paraná-Angola-Namibia Province (South American and African plates, Western Gondwana, arranged at about 110 Ma; modified after Comin-Chiaramonti *et al.*, 1997a, 1999) and location of the main alkaline-carbonatitic occurrences. Abbreviations: Ja, Jacupiranga; Ju, Juquiá; BdI, Barra do Itapirapuã; MP, Mato Preto; RA, Rio Apa; C-S, Cerros Chiriguelo and Sarambí; ASU, Asunción-Sapucai Province; RGR, Rio Grande Rise; WR, Walvis Ridge.

In nortwestern Namibia, the alkaline-carbonatitic complexes, dated at 137-124 Ma, are widespread mainly along the inland of the Damara belt (Milner *et al.*, 1995; Le Roex & Lanyon, 1998: Osongombo, Kalkfeld, Ondurakorume, Okorusu).

**Late Cretaceous** alkaline-carbonatite complexes from southern Brazil are all concentrated along the 1) Iporá-Alto Paranaíba Lineament (e.g. Iporá: Morro do Engenho, Caiapó, Santo Antonio da Barra; Alto Paranaíba: Catalão I-II, Salitre, Serra Negra, Araxá, Tapira and São Gotardo), 2) Ponta Grossa Arch (e.g. Mato Preto), 3) Taiúva-Cabo Frio Lineament and 4) Uruguay Lineament (Lages).

In Namibia, a Late Cretaceous carbonatite complex (Blue Hills, 79 Ma) was described by Kurszlaukis *et al.* (1999).

**Tertiary** alkaline complexes (mainly 64-45 Ma) are distributed along the Taiúva-Cabo Frio Lineament (Serra do Mar igneous province; cf. Thompson *et al.*, 1998), but a Tertiary alkaline-carbonatite complex has been only found in southwestern Namibia (Dicker Willem carbonatite: 49 Ma; Cooper & Reid, 1998). Notably, the latter is not far from a Cambrian-Ordovician carbonatite complex (Marinkas Quellen; Smithies & Marsh, 1998).

The carbonatites from South America are rarely effusive (e.g. Sapucai and Santo Antonio da Barra), as well as the associated extrusive rocks are rarely exposed. The scarcity of volcanic rocks is probably due to the intense erosion which was responsible for their removal. Hegarty *et al.* (1996) suggested a kilometre-scale uplift and erosion which started at 80-90 Ma.

Often the pediplane is characterized by extensive soil and laterites, where the drainage led to the development of thick soils (up to 200-300 m) originated from weathering of cumulate (ultramafic) rocks and dissolution of carbonates from carbonatites (cf. Fig. 2, Catalão I, and Danni *et al.*, 1991). As a result, large supergenic and residual deposits of apatite, pyrochlore, vermiculite, anatase, and REE carbonates and phosphates were formed.

The general features of the alkaline-carbonatitic complexes in and around the Paraná Basin are summarized in Table 1.

Intrusive-subintrusive rock-types show different configurations, as network-like intrusion (e.g. Barra do Itapirapuã; Ruberti *et al.*, 2002), dykes cutting the alkaline complex (e.g. Anitápolis), plugs (e.g. Lages; Comin-Chiaramonti *et al.*, 2002), or have a well-defined circular or oval shaped form roughly at the core of the intrusions (e.g. Cerro Chiriguelo, Jacupiranga, Juquiá, Anitápolis, Araxá, Catalão; cf. Fig. 2 ).

The ring styles are particularly characteristic, also in Angola and Namibia (Reid & Cooper, 1992; Alberti *et al.*, 1999; Le Roex & Lanyon, 1998; Kurszlaukis *et al.*, 1999). The configuration has been frequently utilized for the identification of the complexes by aerophotogrammetry (cf. Censi *et al.*, 1989). Sometimes the carbonatites display a remarkable complexity, and multiple different carbonatitic events may be recognized (e.g. Barra do Itapirapuã; Ruberti *et al.*, 2002).

The Brazilian carbonatites vary from Ca-carbonatites to Mg-carbonatites and Fe-carbonatites (Fig. 3; Woolley & Kempe, 1989), but these three rock-types are rarely associated in the same complex (e.g. Barra do Itapirapuã, Mato Preto, Araxá; Ruberti *et al.* 2002, Comin-Chiaramonti *et al.*, 2001a, Traversa *et al.*, 2001, respectively). The Angolan carbonatites show a compositional range wider than that of the Brazilian analogues in each complex, roughly corresponding to the distribution of the whole population (Fig. 3).

The Namibian carbonatites are represented by Fe-carbonatites and scarce Ca-carbonatites (Early Cretaceous) and by Mg-carbonatites (Late Cretaceous). The data point to multistage carbonatite processes in the assemblages with changes of the rock-forming minerals (Table 2; cf. Sokolov, 2002).

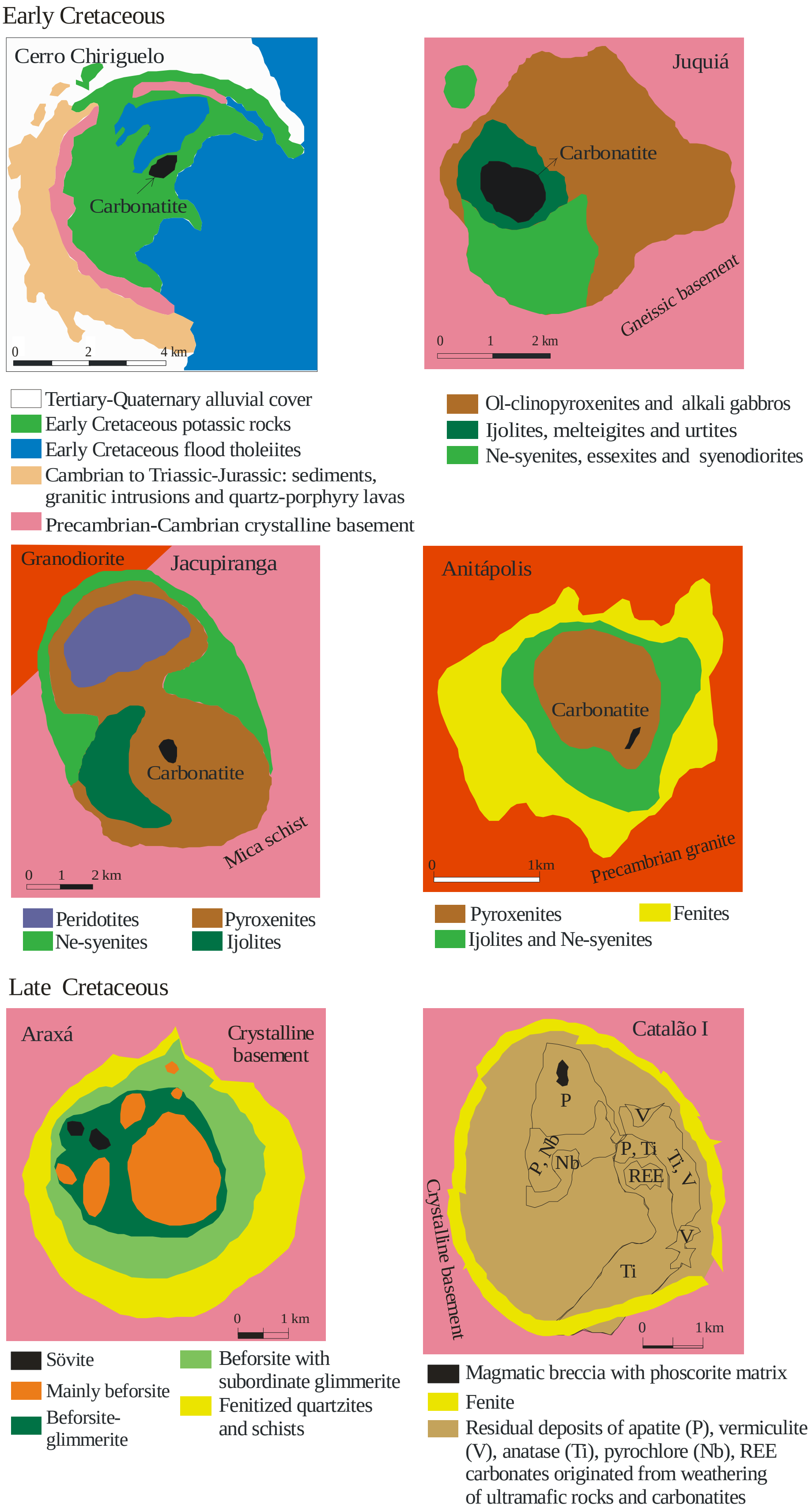


Fig. 2. Examples of ring style characteristic of the many alkaline-carbonatitic complexes from the Paraná Basin (after Issa Filho *et al.*, 1984; Censi *et al.*, 1989; Danni *et al.*, 1991; Beccaluva *et al.*, 1992; Huang *et al.*, 1995; Comin-Chiaramonti *et al.*, 2002).

Table 1. General features relative to the alkaline-carbonatitic complexes from Eastern Paraguay and southern Brazil. Abbreviations: ASU, Asunción region; RPL, Rio Piquiri Lineament; SdM, Serra do Mar; PGA, Ponta Grossa Arch; UL, Uruguay Lineament; AP, Alto Paranaíba; IP, Iporá. Data source: Grossi Sad (1972), Rodrigues & Lima (1984), Gomes *et al.* (1990) and Morbidelli *et al.* (1995). The ages are averages (2σ of standard deviation) of radiometric data.

| EARLY CRETACEOUS | Age (Ma) | Region | Main rock-associations | Form | References |
|---|---|---|---|---|---|
| **Pre-tholeiitic** | | | | | |
| Rio Apa | 145 (9) | North Paraguay<br>RPL | Basanite, phonotephrite, phonolite, carbonatitic K-basanite dykes | Globular Ca-carbonate patches in dykes<br>Circular | Castorina *et al*. (1997) |
| Cerro Chiriguelo | 143 (9) | Amambay, Paraguay<br>RPL | Tephrite, trachyte, phonolite, Si-carbonatite, Ca-carbonatite | | Comin-Chiaramonti & Gomes (1996);<br>Comin-Chiaramonti *et al.* (1999) |
| Cerro Sarambí | 136 (2) | Amambay, Paraguay<br>RPL | Pyroxenite, glimmerite, trachyte, Si-carbonatite, carbonatite | Subcircular | Castorina *et al.* (1997);<br>Comin-Chiaramonti *et al.* (1999) |
| **Syn-tholeiitic** | | | | | |
| Anitápolis | 131 (1) | Santa Catarina, Brazil<br>UL | Pyroxenite, glimmerite, ijolite, nepheline syenite, dunite pyroxenite, ijolite, syenite, tinguaite, Ca-carbonatite | Subcircular | Comin-Chiaramonti *et al.* (2002) |
| Jacupiranga | 130 (1) | São Paulo, Brazil<br>PGA | Dunite, pyroxenite, ijolite, alkali gabbro, syenogabbro, syenodiorite, syenite, nepheline syenite, carbonatite, basanite, phonolite | Oval | Morbidelli *et al.* (1995) |
| Juquiá | 132 (2) | São Paulo, Brazil<br>PGA | Pyroxenite, alkali gabbro, ijolite, essexite, nepheline, syenite, melteigite, ankaratrite, phonotephrite, phonolite, Mg-, Ca-carbonatite | Suboval | Beccaluva *et al*. (1992) |
| Itanhaém | 133 (5) | São Paulo, Brazil<br>PGA | Tinguaite, carbonatite | Dyke | Gomes *et al*. (1990) |
| **Post-tholeiitic** | | | | | |
| ASU | 128 (1) | Central Paraguay,<br>UL | K-tephrite to phonolite, K-alkaline basalt to trachyte, K-theralite, alkali gabbro, syenogabbro, essexite, (Mg-carbonatite, Ca-carbonatite) | Lava flow interbedded in the volcanic sequence. Ijolite with primary carbonate | Comin-Chiaramonti & Gomes (1996) |
| Barra do Itapirapuã | 115 (10) | São Paulo, Brazil<br>PGA | Syenite, Ca-Mg-Fe-carbonatite | Stockwork | Ruberti *et al.* (2002) |
| Itapirapuã | 109 (7) | São Paulo, Brazil<br>PGA | Melteigite, tinguaite, nepheline syenite, melteigite, carbonatite | Irregular, elongated intrusion | Gomes *et al.* (1990); Morbidelli *et al.* (1995) |
| Ipanema | 125 (10) | São Paulo, Brazil<br>PGA | Pyroxenite, glimmerite, syenite, shonkinite, Ca-carbonatite | Circular | Gomes *et al.* (1990) |
| LATE CRETACEOUS | Age (Ma) | Region | Main rock-associations | Form | References |
| Morro do Engenho | 86 (6) | Goiás, Brazil<br>IP | Dunite, pyroxenite, alkali gabbro, nepheline syenite, carbonatite | Circular | Gomes *et al*. (1990); Morbidelli *et al.* (1995) |
| Caiapó | 86 (6) | Goiás, Brazil<br>IP | Ijolite, monchiquite, carbonatite | Oval | Gomes *et al.* (1990); Morbidelli *et al.* (1995) |
| Santo Antonio da Barra | 86 (6) | Goiás, Brazil<br>IP | Basanite, fourchite, monchiquite, analcimite, phonolite, carbonatite | Volcanic field comprising lava flows, pyroclastites, vents, plugs and dykes | Gomes *et al.* (1990); Morbidelli *et al.* (1995) |
| Catalão I | 85 (6) | Goiás, Brazil<br>AP | Peridotite, pyroxenite, glimmerite, phoscorite, nepheline syenite, Ca-Mg-Fe-carbonatite | Circular | Gomes *et al.* (1990); Morbidelli *et al.* (1995) |
| Catalão II | 85 (6) | Goiás, Brazil<br>AP | Glimmerite, phoscorite, carbonatite | Circular | Gomes *et al.* (1990); Morbidelli *et al.* (1995) |
| Salitre | 84 (7) | Minas Gerais, Brazil<br>AP | Pyroxenite, nepheline syenite, syenite, trachyte, carbonatite | Oval | Gomes *et al.* (1990); Meyer *et al.* (1994);<br>Morbidelli *et al*. (1995) |
| Serra Negra | 83 (5) | Minas Gerais, Brazil<br>AP | Dunite, pyroxenite, shonkinite, tinguaite, carbonatite | Oval | Gomes *et al.* (1990); Meyer *et al.* (1994);<br>Morbidelli *et al*. (1995) |
| Araxá | 88 (10) | Minas Gerais, Brazil<br>AP | Pyroxenite, glimmerite, phoscorite, Ca-Mg-Fe-carbonatite | Circular | Gomes *et al*. (1990); Morbidelli *et al*. (1995);<br>Traversa *et al.* (2002) |
| Tapira | 79 (9) | Minas Gerais, Brazil<br>AP | Dunite, pyroxenite, phoscorite, uncompahgrite, syenite, trachyte, Ca-Mg-Fe-carbonatite | Oval | Gomes *et al.* (1990); Meyer *et al.* (1994);<br>Morbidelli *et al*. (1995) |
| Lages | 76 (4) | Santa Catarina, Brazil<br>UL | Olivine melilitite, nephelinite, melteigite, nepheline syenite, trachyte, phonolite, Ca-Fe-carbonatite | Magmatic field comprising sheet-like intrusions, dykes, sills, stocks and plugs | Gomes *et al*. (1990); Traversa *et al*. (1996);<br>Comin-Chiaramonti *et al.* (2002) |
| Mato Preto | 71 (5) | Paraná, Brazil<br>PGA | Nepheline syenite, phonolite, Ca-Mg-Fe-carbonatite | Subcircular complex | Gomes *et al.* (1990);<br>Comin-Chiaramonti et al. (2001a) |

Table 2. Mineral assemblages in the various evolutionary stages in carbonatites from PAEP. Data source: Rodrigues & Lima (1984), Censi *et al.* (1989), Walter *et al.* (1995), Andrade (1998), Speziale *et al.* (1997), Comin-Chiaramonti *et al.* (2001a, 2002) and Ruberti *et al*. (2002).

| | Main major minerals | Main accessory minerals |
|---|---|---|
| I STAGE | Calcite, diopside, forsterite, melilite, monticellite, nepheline, phogopite-biotite, apatite I, Ti-magnetite | Nb-perovskite (Nb), calzirtite (Zr, Nb), monazite (Ce, REE) |
| II STAGE | Mg-calcite ± dolomite, diopside, tetraferriphlogopite, apatite II, Mg-magnetite | Baddeleyte (Zr), pyrochlore-I (Nb), hatchettoloite (Nb, Ta, U, Th), zirkelite (Zr, Nb) |
| III STAGE | Calcite, dolomite (Fe-dolomite), tetrapherriplogopite, apatite III, magnetite, titanite | Pyrochlore (Nb, Th, U), burbankite (Sr, Ba, REE) |
| IV STAGE | Dolomite (Fe-dolomite), ankerite, siderite, magnesite, fluorite, rodochrosite, K-feldspar, quartz | Pyrochlore (U, Th, Nb), bastnäsite (REE), parisite (REE), ancylite (Sr, REE), synkisite (REE), strontianite (Sr), celestine (Sr) |

The Early Cretaceous carbonatites from Brazil and Angola are in general strictly associated with a potassic magmatism which shows, following Foley's classification (1992), "plagioleucitic" affinity (Gomes *et al.*, 1996; Alberti *et al.*, 1999). It is mainly represented by evolved rock-types (syenite-phonolite). In Namibia, they are related to lamprophyric rocks, both of potassic and sodic affinities (Le Roex & Lanyon, 1998). On the other hand, the Late Cretaceous carbonatites are usually caracterized by kamafugitic associations (Gibson *et al.*, 1995; Traversa *et al.*, 1994, 1996). "Less evolved" (gabbro-basalt clans) and cumulatic assemblages (e.g. dunite, clinopyroxenite, phoscorite) are common to both Early and Late Cretaceous complexes. The Tertiary Dicker Willem carbonatite (Southwestern Nabibia) is associated with alkaline sodic rock-types (melanite ijolite; Cooper & Reid, 1998).

The carbonatite occurrences are believed to have originated by processes of liquid immiscibility (Beccaluva *et al.*, 1992; Castorina *et al.*, 1996). In particular, at Juquiá, a parental basanitic magma fractionated under virtually closed system conditions, with the development of an inner zone side-wall cumulates of olivine clinopyroxenite to nepheline syenite, progressively enriched in trapped liquid. At an advanced fractionation stage, an immiscible carbonatitic liquid was exsolved from a $CO_2$-rich mafic nepheline syenite magma, resulting in the formation of carbonatite liquid which crystallized as Mg-carbonatite at the core of the intrusion. Continuous crystal fractionation of the silicatic magma gave rise to ijolite-melteigite-urtite cumulates. Primary carbonates occurs either as large interstitial crystals, or forming "ocelli" in some nepheline syenites. The "ocelli", where clinopyroxene and alkali feldspar may be present, are frequent in the more evolved rock-types and are commonly surrounded by biotite shells, indicating local increasing of fluid activity (Beccaluva *et al.*, 1992).

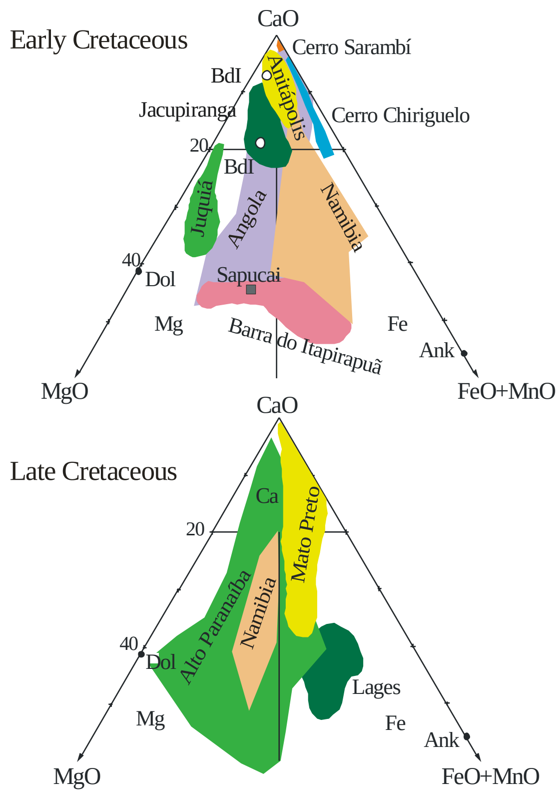


Fig. 3. Classification of the carbonatitic associations (after Woolley & Kempe, 1989) in the various complexes and fields from southern Brazil, Angola and Namibia. Data source, Brazil: Morbidelli *et al.* (1986), Censi *et al.* (1989), Beccaluva *et al.* (1992), Meyer *et al.* (1994), Huang *et al.* (1995), Toyoda *et al.* (1995), Ruberti *et al.* (2002), Comin-Chiaramonti *et al.* (2001a, 2002) and unpublished data; Angola: Alberti *et al.* (1999) and therein references; Namibia: Milner & Le Roex (1996), Le Roex & Lanyon (1998) and Kurszlaukis *et al.* (1999).

A similar picture is also apparent for the carbonatites from Eastern Paraguay (Castorina *et al*., 1996). The Jacupiranga carbonatites tend to present a more complex scenario, with the evolution line (alkali gabbro → syenogabbro → nepheline syenite) linked to the removal of large amounts of cumulatic material, mainly olivine and clinopyroxene, as indicated by the abundance of pyroxenitic and dunitic rocks in the field. Pyroxene and olivine fractionation is required for the transition from olivine nephelinite/ankaratrite to phonolite/peralkaline phonolite. The exsolution of carbonatite liquids appears to be associated with the evolution of phonolite to peralkaline phonolite melts (Morbidelli *et al*., 1986).

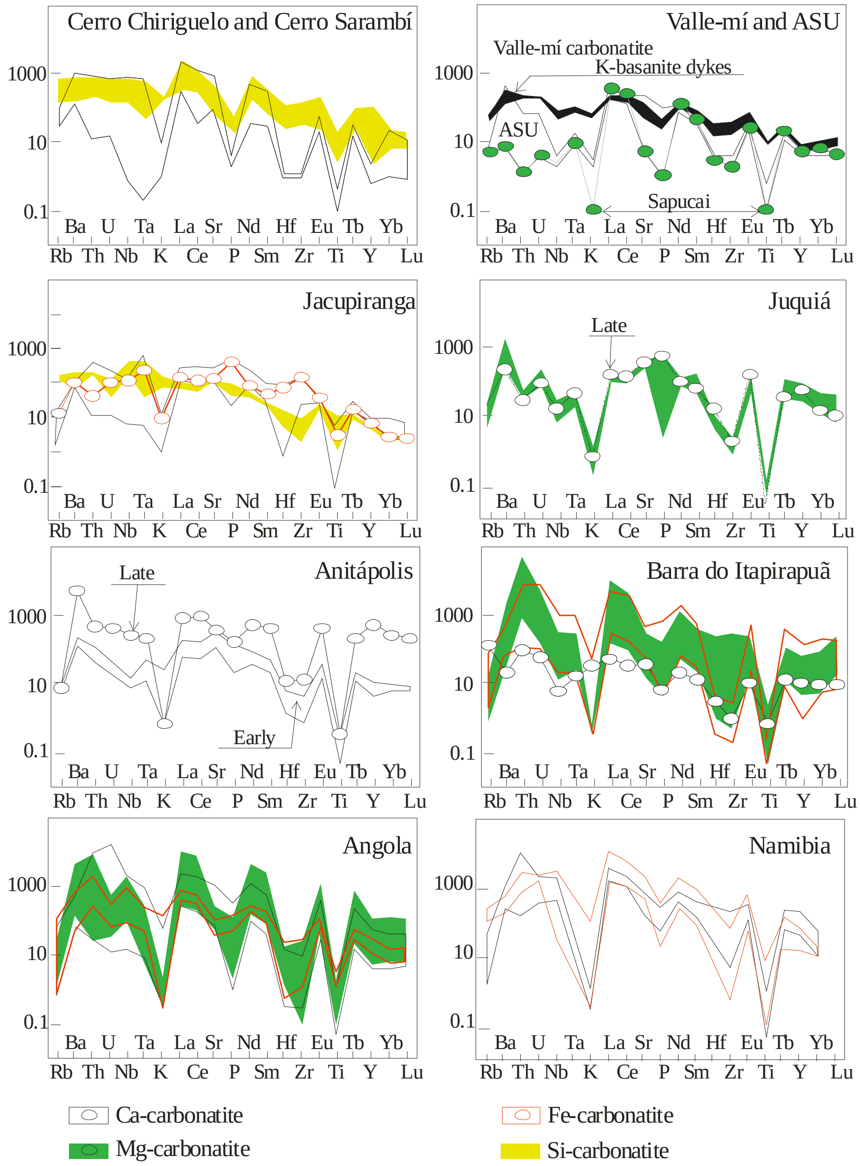


Fig. 4A. Early Cretaceous carbonatites from the PAEP: incompatible elements normalized to the primitive mantle concentrations (Sun & McDonough, 1989). See Fig. 4B, for data source.

However, sometimes the criteria by which a carbonate-rich rock can be proved to be a true carbonatite are difficult to apply with confidence, particularly if the geological and petrological relationships are not clear. The following evidences, although not conclusive, are the strongest clues, especially when their occur together (Barker, 1996): association with melilite- or nepheline-bearing rocks, calcite with >1 wt% SrO, presence of perovskite, pyrochlore, REE-carbonates and apatite with high silica content (e.g. >2 wt%), enrichment in Sr, Ba, Nb, U, Th and rare-earth elements (with high LREE vs. HREE fractionation) and depletion in other elements (e.g. K, Rb, Zr and Ti) relative to mantle and continental crust (Woolley & Kempe, 1989), $^{87}Sr/^{86}Sr$ initial ratios similar to those of the related alkaline rocks (cf. Castorina *et al.*, 1997), and stable isotopes (O-C) in the "primary carbonatitic box" (Taylor *et al.*, 1967; Keller & Hoefs, 1995) or following well distinct isotopic fractionation trends (Speziale *et al.*, 1997).

Based on the above cryteria this study will be used in a synthesis of the geochemical characteristics in terms of incompatible elements (I.E.), rare earth elements (REE), O-C and Sr-Nd-Pb isotopical data of the well-known alkaline-carbonatitic complexes and occurrences in southern Brazil, in particular, and of PAEP, in general.

## GEOCHEMISTRY

Molar [D.I.=CaO/(CaO+MgO+$FeO_t$+MnO)] of Ca-, Mg- and Fe- carbonatites is negatively correlated with (MgO+$FeO_t$+MnO) wt%, due to the Ca-Mg-Fe substitutions. Some other correlations are significant: $SiO_2$ versus $Al_2O_3$ (r=+0.90) and $Na_2O$+$K_2O$ (r=+0.96), whereas in the rocks with $SiO_2$<9 wt%, $P_2O_5$ is negatively correlated with LOI (assumed to represent $CO_2$; r=−0.98), in good agreement with the modal content of alkali feldspar and apatite, respectively (Gomes *et al.*, 1996; Castorina *et al.*, 1996, 1997; Alberti *et al.*, 1999). In general terms, there are very large variations in the normalized values (Figs. 4A, B) from one carbonatite complex to another for any given incompatible element. The incompatible elements (I.E.) scatter for the different carbonatites reflects to some extent the variable distribution and concentration of mineral phases such as phosphates (e.g. apatite and monazite: REE), oxides (e.g. pyrochlore: Nb, REE, Th, U; calzirtite: Ti, Zr; zirconolite: Ti, Zr, Nb; loparite: REE, Ti, Nb), REE-carbonates and fluorcarbonates (e.g. burbankite, ancylite, bastnäsite, parisite).

Model experiments with natural and artificial mixtures show that carbonatite melts might be enri-

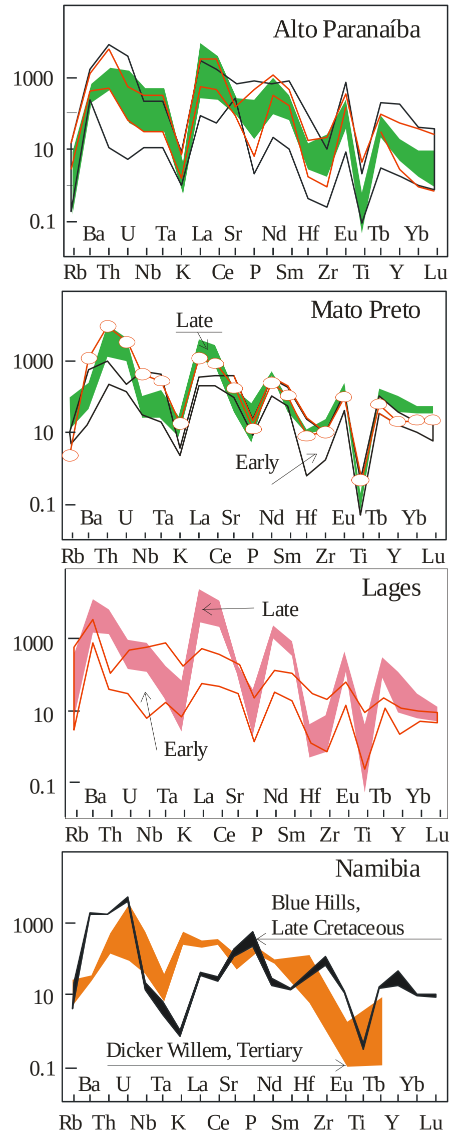


Fig. 4B. Late Cretaceous carbonatites from the PAEP: incompatible elements normalized to the primitive mantle concentrations (Sun & McDonough, 1989). Data source, Eastern Paraguay (Cerro Chiriguelo, Cerro Sarambí, Valle-mí and ASU): Comin-Chiaramonti *et al.* (1995) and unpublished data; Comin-Chiaramonti & Gomes (1996) and Castorina *et al.* (1996, 1997); Brazil, Jacupiranga: Morbidelli *et al.* (1986), Nelson *et al.* (1988), Toyoda *et al.* (1994), Huang *et al.* (1995) and Castorina *et al.* (1996); Juquiá: Beccaluva *et al.* (1992) and Castorina *et al.* (1996); Anitápolis: Comin-Chiaramonti *et al.* (2002); Barra do Itapirapuã: Ruberti *et al.* (2002); Alto Paranaíba: Toyoda *et al.* (1994), Meyer *et al.* (1994), Traversa *et al.* (2001), Comin-Chiaramonti & Censi and unpublished data; Mato Preto: Comin-Chiaramonti *et al.* (2001a); Lages: Traversa *et al.* (1996) and Comin-Chiaramonti *et al.* (2002); Angola, Alberti *et al.* (1999); Namibia, Damaraland: Le Roex & Lanyon (1998); Blue Hills: Kurszlaukis (1999); Dicker Willem: Cooper & Reid (1998).

ched in K, P, Sr, Ba, U, Th, REE, and also in F and

Cl (Kjarsgaard *et al.*, 1995, and therein references). F in silicate-carbonate systems positively influences the entry of Nb (Ta, U, Th, REE) into the carbonate fraction. Transfer of I.E. and REE are supported by experimental results on Nb and LREE solubility in synthetic carbonate liquids (cf. Jones *et al.*, 1995). According to Jago & Gittings (1993), Ca-carbonatite liquids are able to dissolve 5-7.5 wt% of $Nb_2O_5$ at 950-600°C. Crystallization of these liquids at first promotes the precipitation of a perovskite-type phase and then of pyrochlore togheter with calcite. Phase relationships in the section calcite-REE hydroxide (Jones & Wyllie, 1983) show that with the temperature variation from 610 to 700°C and increasing $CO_2/H_2O$ ratio, the solubility of the LREE hydroxides in simplified carbonatite systems changes from 20 to 40%: bastnäsite may crystallize togheter with calcite from magmatic carbonate liquids with temperature falling from liquidus (650-625°C) to eutectic (about 540°C) and under definite relations of carbon dioxide, water and fluorine.

On the other hand, REE-carbonates, fluor-carbonates and oxydes, which are the products of "low temperature" (mainly hydrothermal) environment, represent to some extent the fenitizing fluids enriched in I.E. with respect to the primary carbonates (cf. Castorina *et al.*, 1997). For example, four distinct generations of carbonatite dykes are present in the Barra do Itapirapuã complex, two of which clearly displaying overprint of hydrothermal alteration (Andrade *et al.*, 1999a; Ruberti *et al.*, 2002).

On the whole, the PAEP carbonatites cover the wide variation field of Andersen (1987), in terms of La vs. La/Yb relationships. The carbonate fractions of carbonatites display La/Yb ratios and La content 2-3 times higher than those of the corresponding rocks. On the contrary, the carbonate fractions from the associated silicate rocks show both higher La and La/Yb than those of the corresponding silicate fractions (Castorina *et al.*, 1997; Alberti *et al.*, 1999).

As an example, Fig. 5 illustrates the La/Yb relationships for basanite-tephrite and phonolite-trachyte suites and associated primary carbonates from Eastern Paraguay. If the differentiation of the $CO_2$-bearing parental magma is relatively restricted (i.e. basanite to phonotephrite), the exsolved carbonatitic melt is relatively small and crystallizes forming groundmass patches or "ocelli". On the other hand, if the evolution from basic melts leads to phonolite or trachyte, the latter magmas may exsolve carbonatite melts having high La and La/Yb relative to the parental fluid-rich basic magmas.

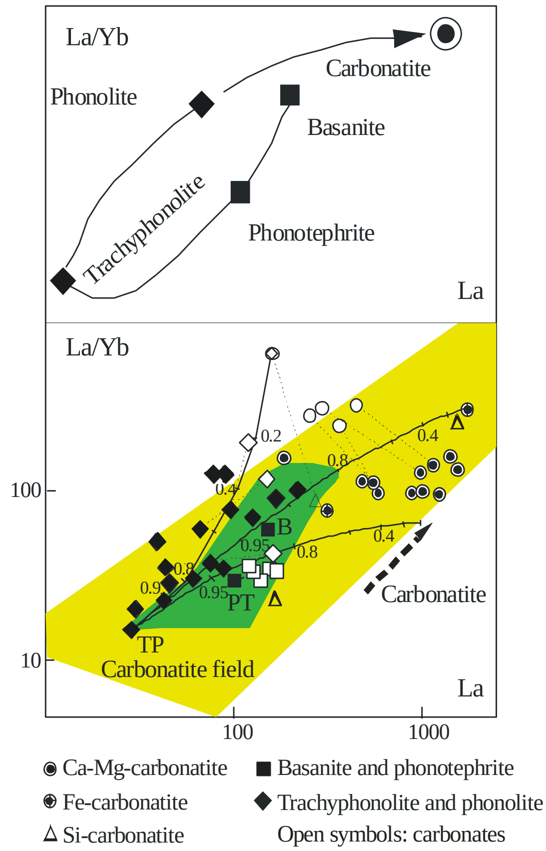


Fig. 5. La (ppm) vs. La/Yb ratios for silicate rocks, carbonatites and carbonates from Eastern Paraguay (after Castorina *et al.*, 1997, modified). B, basanite; PT, phonotephrite; TP, trachyphonolite. Carbonatite field after Andersen (1987).

The mixing curves between parental magma(s) and carbonatites (Fig. 5) provide an estimation of the $CO_2$-rich melt fraction(s). Considering that the primary carbonates (up to 15-20 wt%) of the silicate rocks represent late crystallized phases, and that the carbonatites may represent the carbonatitic liquid exsolved from the trachytic/phonolitic magma, the total carbonatitic magma appears to be higher than 30-35 wt% of the carbonate content in the parental silicate melt.

Thus, if the basanite of Fig. 5 is assumed as the parental magma of a carbonatite, the evolution consists of two main steps: 1) the first one (basanite →trachyphonolite) leads to differentiated rock-types by crystal fractionation and allows the concentration of $CO_2$-rich fluids, and 2) the second one promotes the exsolution of about 20 wt% carbonatitic liquids from the differentiated phonolitic magma.

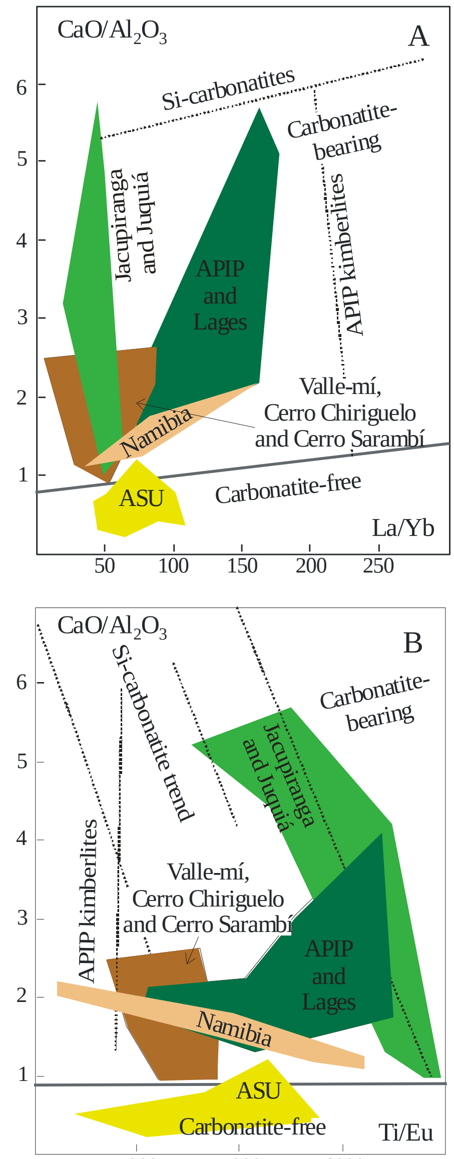


Fig. 6. A: $CaO/Al_2O_3$ vs. La/Yb B: and $CaO/Al_2O_3$ vs. Ti/Eu diagrams for carbonatite-free and carbonatite-bearing alkaline complexes from PAEP (see text). Data source as in Fig. 4B.

The fact that both the parental magmas and the associated carbonatites plot within the "carbonatite field" (Andersen, 1987) suggests that the parental magmas are characterized by high $CaO/Al_2O_3$, La/Yb and Ti/Eu (cf. Dalton & Wood, 1993; Rudnik *et al.*, 1993). $CaO/Al_2O_3$ vs. La/Yb and Ti/Eu diagrams, respectively (Fig. 6), show that primitive rocks belonging to carbonatite-free and carbonatite-bearing complexes plot into distinct fields (cf. Castorina *et al.*, 1997; Morbidelli *et al.*, 2000). It is remarkable that the K-basanites from the Valle-mí and Cerro Chiriguelo occurrences have higher $CaO/Al_2O_3$ ratios than those from ASU and, therefore, may reflect mantle regions which underwent significant carbonatitic metasomatism. The initial stages of differentiation of the $CO_2$-rich K-basanites are characterized by a silicate fraction that prevails on the carbonatitic component (cf. kamafugitic rock-types from Alto Paranaíba, APIP of Gibson *et al.*, 1995), which, instead, is prominent on the last stages of differentiation.

The REE display remarkable scatters even in any single complex, particularly for samples belonging to different stages of crystallization, i.e. from magmatic, to late-magmatic and to hydrothermal conditions. Scatters may be due, at least in part, to main accessory minerals such as apatite, REE fuorcarbonates, fluorite and barite. REE fuorcarbonates are relatively abundant in Fe-carbonatites.

Apart from well distinct anomalies, e.g. Eu (Cerro Chiriguelo) and Sm (ASU) negative spikes, some different types of REE distributions may be distinguished (Figs. 7A, B):

1) Patterns with a strong increase from Lu to La, as indicated for the Cerro Chiriguelo, Jacupiranga (Mg-carbonatites), Alto Paranaíba (Mg-carbonatites), Mato Preto and Lages (early and late carbonatites), and Angolan and Namibian complexes. It should be noted that the Cerro Chiriguelo patterns, for both Ca- and Si-carbonatites, parallel that of the coexisting apatite (note also Eu negative spike). The Mato Preto and Lages behaviours appear to be controlled by the coexisting fluorite and by late carbonatite veins, barite and fluorcarbonate-rich.

The Namibian carbonatites display patterns driven by their bulk fluids (cf. Bühn et al., 2002).

2) Flat LREE, or patterns with a weakly decrease from La to Lu, as shown in the Jacupiranga (Ca-carbonatites), Juquiá (Mg- and Ca-carbonatites), Anitápolis, Barra do Itapirapuã (late Ca-carbonatites) and Blue Hills complexes. In these occurrences the distribution seems to be related to the apatite composition (early-crystallized: apatite I, and late-crystallized: apatite II).

3) Concave patterns with HREE plateau and a steady increase from Dy to LREE, found in the Valle-mí and Barra do Itapirapuã occurrences. In the latter, showing four distinct generations of carbonatitic dykes, the most "hydrothermally altered" dykes (field III of Fig. 7A; cf. Andrade *et al.*, 1999a, b) contain the highest LREE concentrations as a result of the presence of REE fluorcarbonates (Andrade, 1998).

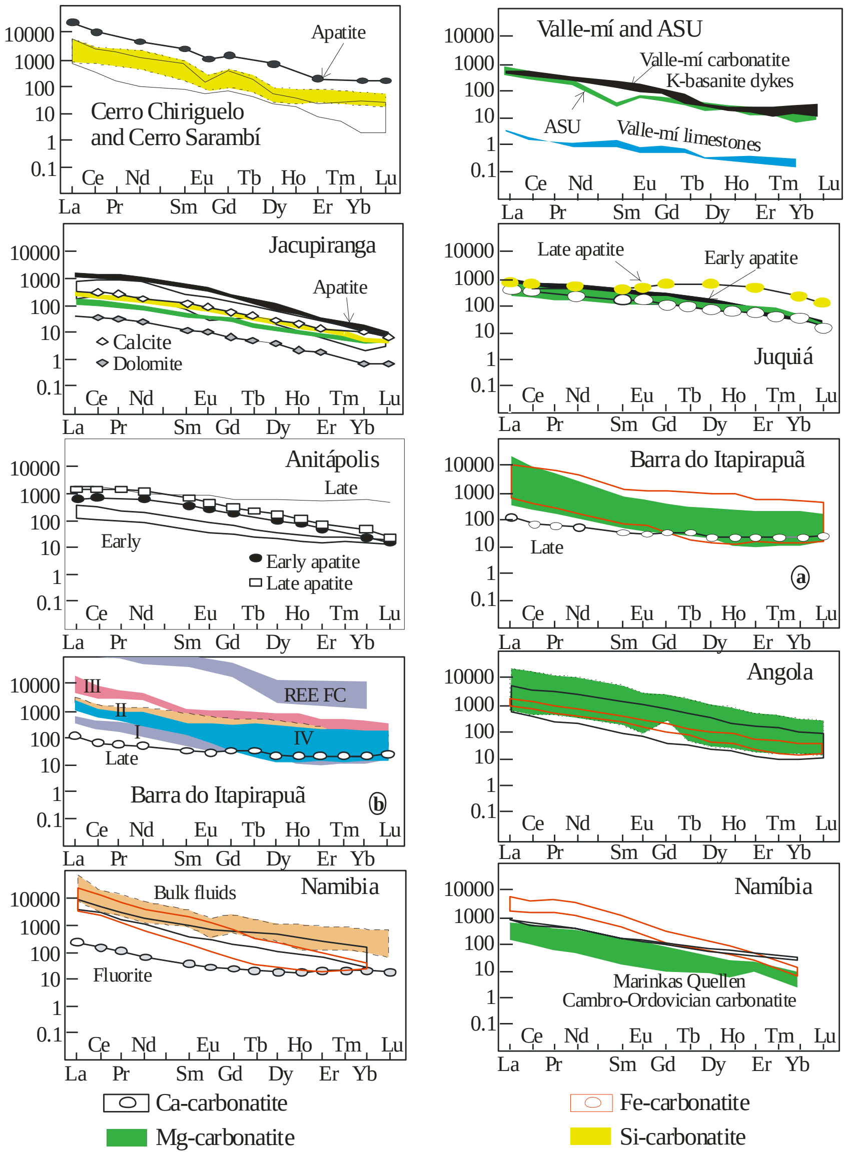


Fig. 7A. Early Cretaceous: Chondrite-normalized (Boynton, 1984) REE distribution for the various complexes from the PAEP and for some associated minerals. Data source as in Fig. 4B; additionally: Walter *et al.* (1995), Andrade (1998), Hornig-Kjarsgaard (1998), Smithies & Marsh (1998) and Bühn *et al.* (2002). Barra do Itapirapuã complex was subdivided into two diagrams: a, representing the whole population of the three carbonatite-types, i.e. Ca-, Mg- and Fe-carbonatites; b, showing the different types of carbonatite dykes (oldest I, youngest IV) and the field of the REE fluorcarbonates. For comparison the patterns of the Cambro-Ordovician carbonatitic complex of Marinkas Quellen (Namibia) are also reported.

Notably, the Valle-mí dykes that cut a Cambrian carbonatic platform are REE enriched by a factor 1000 relative to the sedimentary carbonates.

Concluding, the different behaviours of the early-crystallized carbonatites, believed to be "primary" carbonatitic liquids (Figs. 7A, B), would reflect the chemical signatures of their parental melts (cf. primary Ca-carbonatites and Mg-carbonatites of the Jacupiranga and Juquiá complexes). The presence of late-crystallized Fe-carbonatites, variably enriched in fluorcarbonates, points to hydrothermal processes.

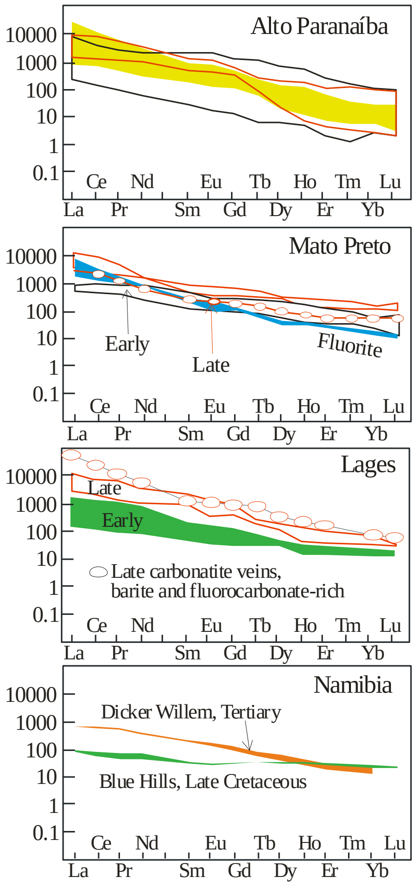


Fig. 7B. Late Cretaceous: Chondrite-normalized (Boynton, 1984) REE distribution for the various complexes from the PAEP and for some associated minerals. Data source as in Fig. 4B and as shown in Fig. 7A.

## VARIATIONS OF OXYGEN AND CARBON ISOTOPES

Carbonatite complexes display in general large compositional ranges in terms of oxygen and carbon isotopes (Taylor *et al.*, 1967; Pineau *et al.*, 1973; Nelson *et al.*, 1988; Deines, 1989; Censi *et al.*, 1989; Santos & Clayton, 1995). The $\delta^{18}O$ values cover a wide range from about 5 to 25‰ vs. V-SMOW (Deines, 1989), but about 50% of the analyses fall into a narrow interval between 6 and 10‰. The variation of $\delta^{13}C$ is more restricted, i.e. 91% of $\delta^{13}C$ values fall in the range between −2‰ and −8‰ vs. PDB-1 (Deines, 1989). Ranges of $\delta^{18}O$ and $\delta^{13}C$ between 6 and 10‰ and between −4 and −8‰, respectively, may reflect "primary carbonatites" (cf. Taylor *et al.*, 1967; Keller & Hoefs, 1995).

Different emplacement levels (i.e. deep-seated, up to near surface, or near-surface environments; Deines & Gold, 1973), and superimposed "primary" and "secondary" processes are believed to play a role in the isotopic variations. These variations may be attributed to 1) isotopic compositional differences in the source, 2) frac-tionation processes during the magmatic evolution, 3) loss of fluids during pressure reduction at the time of emplacement, 4) crustal contamination, 5) post-magmatic and deuteric-groundwater processes. Most of the largest variations in heavy oxygen from car-bonatites may be explained by the interaction with hydrothermal fluids, whereas the changes in heavy carbon are related to both primary (i.e. isotopic composition of parental magma) and secondary (i.e. hydrothermal re-equilibration) processes (Taylor *et al.*, 1967; Pineau *et al.*, 1973; Deines, 1989). Determining to what extent the oxygen and carbon isotopic variations in carbonatites are prima-ry or secondary has important implications for eva-luating the geochemical characteristics of the source regions. For example, the carbonatite complexes may be useful for deciphering the nature of the sub-continental mantle (cf. Castorina *et al.*, 1994, 1997).

In order to address some of these problems, this chapter developes a model of isotopic O-C fractionation relative to the PAEP carbonatites substantially starting from three main considerations: 1) the carbonatitic complexes from the PAEP are some of the best known in the worldwide literature from geological, petrological and geochemical view point (Scheibe & Formoso, 1982; Nelson *et al.*, 1988; Morikiyo *et al.*, 1990; Castorina *et al.*, 1994, 1997; Bizzi *et al.*, 1994; Meyer *et al.*, 1994; Toyoda *et al.*, 1995; Huang *et al.*, 1995; Walter *et al.*, 1995; Santos & Clayton, 1995; Le Roex & Lanyon, 1998; Alberti *et al.*, 1999; Comin-Chiaramonti *et al.*, 2001a, 2002; Ruberti *et al.*, 2002); 2) over 500 O-C isotopic data and a large number of radiogenic isotope data are available for the known occurrences (quoted references and unpublished data); 3) the interpretation of the isotopic data is controversial as to the role of primary processes versus crustal contamination.

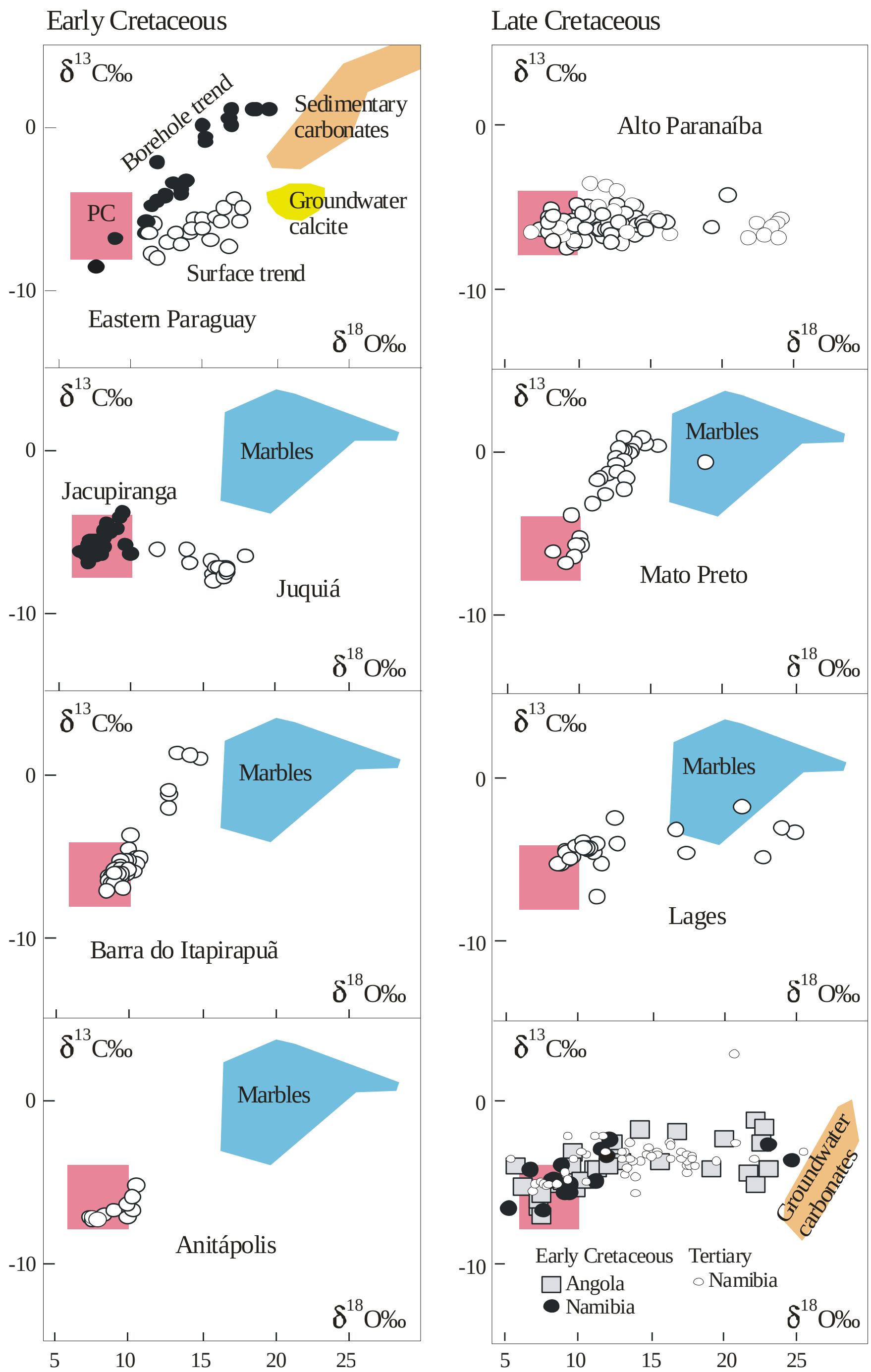


Fig. 8. Plot of $\delta^{18}O$‰ (V-SMOW) vs. $\delta^{13}C$‰ (PDB-1) for the carbonatites from the PAEP. For comparison the fields relative to the "primary carbonatites", PC (Taylor *et al.*, 1967; Hoefs, 1987), sedimentary carbonates, groundwater calcite and marbles are also shown. Data source: Scheibe & Formoso (1982), Censi *et al.* (1989), Robaina *et al.* (1991), Reid & Cooper (1992), Castorina *et al.* (1994, 1997), Huang *et al.* (1995), Walter *et al.* (1995), Santos & Clayton (1995), Speziale *et al.* (1997), Mello & Bettencourt (1998), Le Roex & Lanyon (1998), Alberti *et al.* (1999), Comin-Chiaramonti *et al.* (2001a, 2002 and unpublished data) and Ruberti *et al.* (2002).

Notably, Santos & Clayton (1995) suggested that the large isotopic variations, like those observed in the Mato Preto and Barra do Itapirapuã carbonatites, may be produced when these rocks intruded the limestone country-rocks (e.g. Mato Preto carbonatite) and/or have been subjected to post-crystallization alteration processes (e.g. Barra do Itapirapuã).

The oxygen and carbon isotopic results (Fig. 8) allow comparison with the isotopic composition of sedimentary carbonates, groundwater calcite and marbles of the regions (Castorina *et al.*, 1994, 1997 and unpublished data; Mello & Bettencourt, 1998).

$\delta^{18}O$ (V-SMOW) and $\delta^{13}C$ (PDB-1) data for the PAEP carbonatites mainly range between 5.5 and 24‰, and between −8.5 and 1.5‰, respectively, with values typical of "primary carbonatites", along with a number of samples with higher $\delta^{18}O$ and $\delta^{13}C$ values. Enrichments in heavy isotopes are interpreted in terms of heterogeneity in the mantle source (Nelson *et al.*, 1988), or contamination by host rocks (Santos & Clayton, 1995), or magmatic vs. hydrothermal evolution of the carbonatite at shallow level (Censi *et al.*, 1989; Castorina *et al.*, 1997; Speziale *et al.*, 1997).

$\delta^{18}O$ and $\delta^{13}C$ for sedimentary carbonates and groundwater calcite are in the range 20 to 30‰ and 20 to 24‰, and −4 to 5‰ and −6 to −4‰, respectively. It should be noted that the marbles from southern Brazil have $\delta^{18}O$ and $\delta^{13}C$ ranging from 16 to 23‰ and from −4 to 3‰, respectively (cf. Fig. 8).

The Fig. 8 also delineates two main isotopic C-O variations for the Brazilian carbonatites: 1) a trend characterized by a shifting towards positive values for $\delta^{13}C$, and $\delta^{18}O$ increase (Jacupiranga, Barra do Itapirapuã, Anitápolis, Mato Preto and Lages), and 2) a trend of heavy oxygen increase at about constant $\delta^{13}C$ (Juquiá, Alto Paranaíba). The Angola and Namibia carbonatites display characteristics similar to the first trend up to $\delta^{18}O=15‰$ and $\delta^{13}C=2‰$. The trend (1) appears to be an extension of the Jacupiranga carbonatite, which is believed to have a primary signature (cf. Huang *et al.*, 1995).

Also in Eastern Paraguay two main linear trends are apparent (Fig. 8), in this case the first being defined by carbonatitic samples and primary carbonate of silicate rocks from boreholes (Castorina *et al.*, 1997), while the other represents carbonatitic specimens sampled near to or at the topographic surface, or carbonatitic lava flows. The two trends intercept at $\delta^{18}O=7.5‰$ and $\delta^{13}C=-8.5‰$, similar to the values obtained for primary carbonate phases of an ijolite from Cañada (Central Paraguay Province), i.e. $\delta^{18}O=6.9‰$ and $\delta^{13}C=-8.5$ ‰, respectively, which coexist with olivine ($\delta^{18}O=4.63‰$), clinopyroxene ($\delta^{18}O=5.20‰$) and biotite ($\delta^{18}O=5.54‰$). In the ijolite, the silicate minerals provide isotopic equilibration temperature of about 1200°C (Cpx-Biot =1208°C; Cpx-Ol=1201°C), according to the equations of Bottinga & Javoy (1975), whereas the Cpx and Cc pair gives 690°C (Matthews *et al.*, 1983).

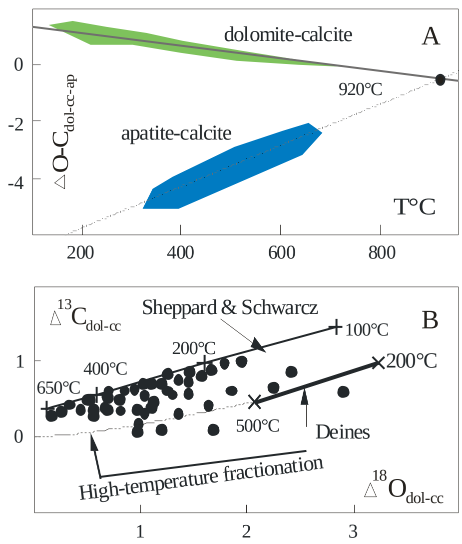


Fig. 9. A: Plots $\Delta O_{apatite\text{-}calcite}$ and $\Delta O\text{-}C_{dolomite\text{-}calcite}$ vs. temperature (°C), according to Alberti *et al.* (1999). B: $\Delta^{18}O_{dolomite\text{-}calcite}$ vs. $\Delta^{13}C_{dolomite\text{-}calcite}$, respectively, for coexisting calcite-Fe-dolomite pairs. Equilibration lines, metamorphic and magmatic-hydrothermal, are after Sheppard & Schwartz (1970), Deines (1989) and Jenkin *et al.* (1991), respectively. Data source as in Fig. 8.

Oxygen isotopes of the dolomite-calcite and apatite-calcite pairs are positively correlated and define two distinct temperature trends intercepting at about 920°C (Fig. 9A). It should be noted that this temperature is consistent with the range (i.e. 850-950°C) estimated for the exsolution of carbonatitic liquids from trachyphonolitic magmas by Comin-Chiaramonti e*t al*. (1992, 1995) and Castorina *et al*. (1994, 1996).

Castorina *et al*. (1997) and Speziale *et al*. (1997) developed a model in terms of C-O isotopic fractionation of carbonates for "magmatic differentiation processes" (i.e. liquid immiscibility and fractional crystallization), and "fluid processes" (i.e. interaction between rocks and fluids at different hydrothermal temperatures and $CO_2/H_2O$ ratios; see later). On the basis of this model, which will be discussed in this volume, about 30% of the analyzed samples plot in the box of "magmatic processes" (i.e. temperatures in the range 900-400°C, $\delta^{18}O$ 5.5-9‰), while the other samples follow trends related to "fluid processes" (i.e. temperatures in the range 400-100°C) at $CO_2/H_2O$ ratios roughly between 0.8 and 2.

In general, ferrodolomite displays higher $\delta^{18}O$ and $\delta^{13}C$ values than those for the coexisting calcite (cf. Speziale *et al*., 1997). The differences in isotopic composition between the two coexisting carbonates, as well as the relationship which would be expected if coexisting carbonates were formed in isotopic equilibrium (Sheppard & Schwartz, 1970: metamorphic equilibrium; Gittings, 1979; Deines, 1989: fractionation processes at about 700°C), are shown in Fig. 9B. The data are not consistent with an isotopic equilibrium at magmatic temperatures between Fe-dolomite and calcite, although a roughly equilibrium between the variables is apparent. This points to metasomatic changes at low temperatures, trending to hydrothermal conditions. Groundwater interaction might be an explanation for the $\delta^{18}O$ carbonate values higher than 12‰. The known carbonate-$H_2O$ oxygen fractionation values (e.g. Deines, 1989, and therein references) and the typically negative $\delta^{18}O$-values for meteoric groundwaters (e.g. Hoefs, 1987) require that any interaction with groundwater must have occurred at low temperatures (e.g.<250°C; Deines, 1989). Alteration of Fe-dolomite by grounwater may be related to the low-temperature hydrothermal cycle (e.g. 112-150°C: cf. Roedder, 1973) which is also responsible for the formation of the massive fluorite deposits (e.g. Mato Preto and Barra do Itapirapuã; cf. Santos *et al*., 1996; Andrade, 1998).

On the whole, the data support the hypothesis that isotopic re-equilibrations may have occurred both during the magmatic stage and the subsequent hydrothermal stage, as supported also by the fluid inclusions (Andrade, 1998; Bühn *et al*., 2002).

## Sr, Nd, Pb ISOTOPIC COMPOSITIONS

Previously published data on the PAEP magmatic rocks (tholeiitic, alkaline and carbonatitic samples) are diagrammatically summarized in the Figs. 10 to 13. Isotopic ratios included for comparison are those for the carbonatites from the East African Rift (Bell & Tilton, 2001) and from the Atlantic Ocean (Hoerne *et al*., 2002), as well as the basalts from the Median Atlantic Ridge and oceanic islands (MAR and OIB, respectively: Hamelin *et al*., 1984; Ito *et al*., 1987; Fontignie & Schilling, 1997; Halliday *et al*., 1995), rock-types from the Brazilian offshore islands (Abrolhos: Fodor *et al*., 1989; Fernando de Noronha: Gerlach *et al*., 1987), rock-types of Tertiary alkaline complexes from northeastern Brazil (Fodor *et al*., 1998), and the data relative to the rock-types from Tristan da Cunha (Le Roex, 1985; Le Roex *et al*., 1990) and Trindade islands (Marques *et al*., 1999b; Siebel *et al*., 2000). DMM, HIMU, EM I and EM II are approximations of mantle end-members as in Bell & Tilton (2001), taken from Hart *et al*. (1986, 1992).

In particular, Tristan da Cunha and Trindade islands are believed to be mantle plumes related to the genesis of the Early Cretaceous tholeiitic and Late Cretaceous tholeiitic and Late Cretaceous alkaline magmatism from the PAEP, respectively (e.g. Milner & Le Roex, 1996; Müller *et al*., 1993; O'Connor & Duncan, 1990; VanDeccar *et al.*, 1995; Gibson *et al*., 1995, 1999; Thompson *et al*., 1998). It should be noted that Ernesto *et al*. (2002) provided petrological, geochemical and geophysical data that do not support a genesis of the Early Cretaceous

Paraná magmatism closely related to Tristan da Cunha plume (see discussion).

Sr-Nd isotopes

The carbonatites from the PAEP usually show the same isotopic $^{87}Sr/^{86}Sr$ ($Sr_i$) and $^{143}Nd/^{144}Nd$ ($Nd_i$) initial ratios of the associated alkaline rocks, even in the late stages of fluid-rock re-equilibration (i.e. hydrothermal environment), as shown by Casto-rina *et al.* (1997) and Speziale *et al.* (1997).

In Eastern Paraguay, at the westermost fringe of the PAEP, typical specimens from the Early Cretaceous K-alkaline rocks (both pre- and post-Early Cretaceous tholeiitic magmatism) and associated carbonatites yielded $Sr_i$ and $Nd_i$ within the ranges 0.70612-0.70754 and 0.51154-0.51184 (Fig. 10A). These are distinct from the values obtained for the Late Cretaceous to Tertiary

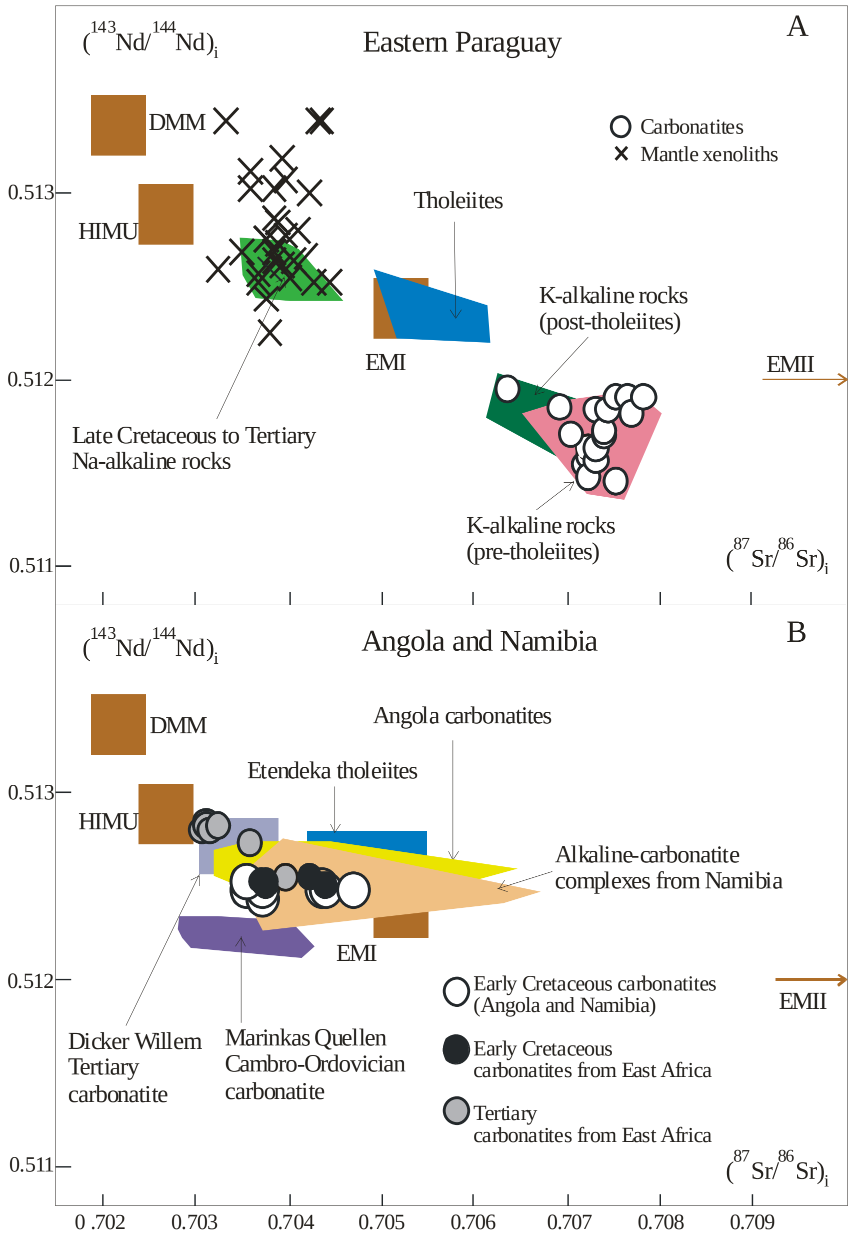


Figs. 10A, B. Initial $^{87}Sr/^{86}Sr$ ($Sr_i$) vs. initial $^{144}Nd/^{143}Nd$ ($Nd_i$) correlation diagrams. Data source, A, Eastern Paraguay: Comin-Chiaramonti *et al.* (1991, 1995, 1996, 1997a, 2001b), Comin-Chiaramonti & Gomes (1996), Castorina *et al.* (1997), Marques *et al.* (1999a) and Antonini *et al.* (in this volume). B, Angola and Namibia: Milner & Le Roex (1996), Le Roex & Lanyon (1998), Ewart *et al.* (1998), Cooper & Reid (1998), Smithies & Marsh (1998), Alberti *et al.* (1999), Kurzslaukis *et al.* (1999), Gibson *et al.* (1999) and Harris *et al.* (1999); East Africa: Bell & Tilton (2001), DMM, HIMU, EMI and EMII are approximations of mantle end-members taken from Hart *et al.* (1992). It should be noted that in all the diagrams (Figs. 10 to 13) the Rio Grande Rise basalts (not shown) plot in the same field of the Walvis Ridge samples.

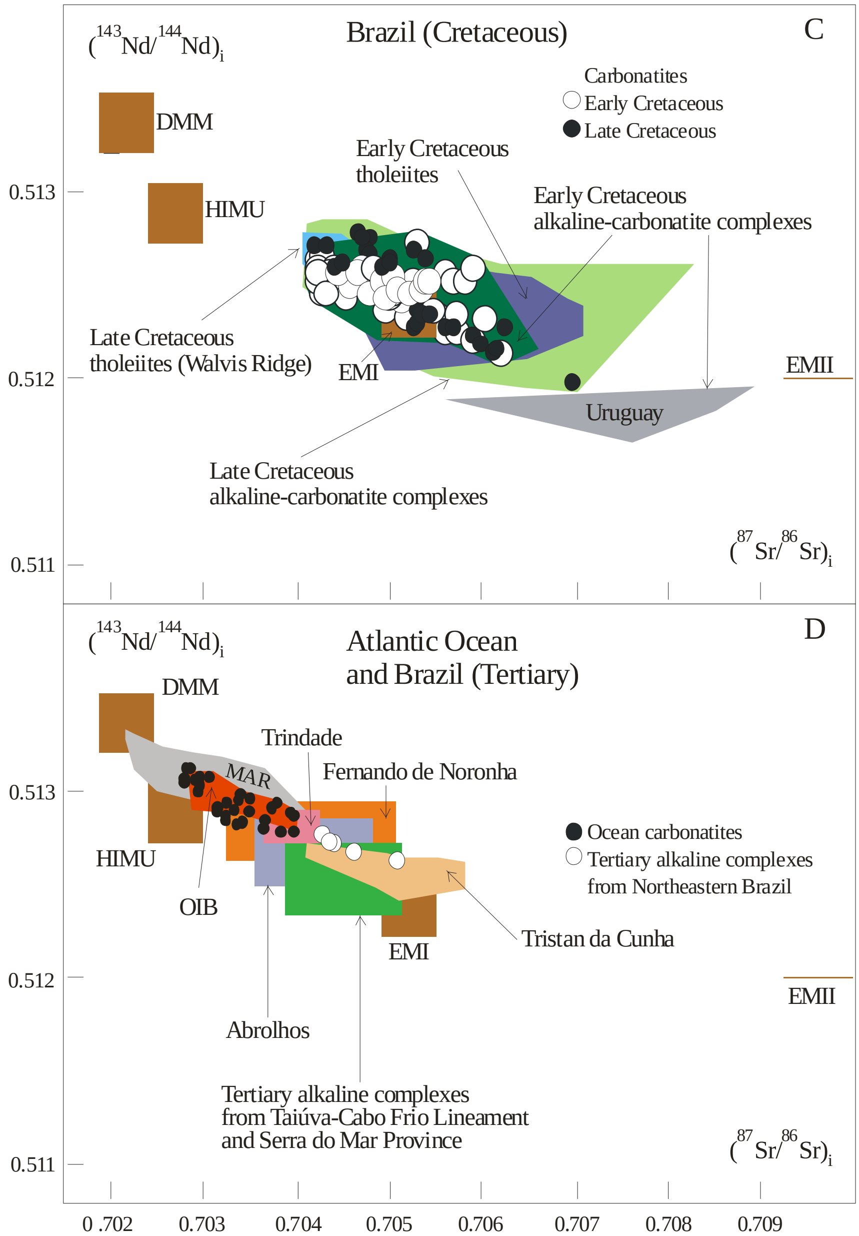


Figs. 10C, D. Initial $^{87}Sr/^{86}Sr$ ($Sr_i$) vs. initial $^{144}Nd/^{143}Nd$ ($Nd_i$) correlation diagrams. Data source, C, Brazil, *Early Cretaceous*: Toyoda *et al.* (1995), Huang *et al.* (1995), Walter *et al.* (1995), Garda *et al.* (1995), Marques *et al.* (1999a), Gibson *et al.* (1999), Andrade *et al.* (1999a), Comin-Chiaramonti *et al.* (2001a, 2002) and Ruberti *et al.* (2002); Uruguay, *Early Cretaceous*: Kirkstein *et al.* (2000); Brazil, *Late Cretaceous*: Bellieni *et al.* (1990), Bizzi *et al.* (1994, 1995), Toyoda *et al.* (1994), Meyer *et al.* (1994), Gibson *et al.* (1995, 1997, 1999), Carlson *et al.* (1996) and Thompson *et al.* (1998); D, Atlantic Ocean: *Walvis Ridge*, Richardson *et al.* (1982); *Rio Grande Rise*, Gamboa & Rabinowitz (1984); *Mid Atlantic Ridge* (MAR), Hamelin *et al.* (1984), Ito *et al.* (1987) and Fontignie & Shilling (1997); *OIB*, Halliday *et al.* (1988, 1995); *Atlantic carbonatites*, Hoernle *et al.* (2002); *Tristan da Cunha*, Le Roex (1985) and Le Roex *et al.* (1990); *Trindade*, Marques *et al.* (1999b) and Siebel *et al.* (2000); Brazil, *Tertiary*: *Serra do Mar*, Thompson *et al.* (1998), Bennio *et al.* (2002); *Abrolhos*, Fodor *et al.* (1989); *Northeastern Brazil*, Fodor *et al.* (1998); *Fernando de Noronha*, Gerlach *et al.* (1987).

Na-alkaline rocks, i.e: $Sr_i$=0.70362−70524 and $Nd_i$=0.51225−0.51277. As shown in Fig. 10A, the carbonatites and associated K-alkaline rocks have higher $Sr_i$ and lower $Nd_i$ values compared to the Low Nd array of Hart *et al.* (1986; cf. Comin-Chiaramonti et al., 1997a), whereas the Na-alkaline rocks and associated mantle xenoliths (Comin-Chiaramonti *et al.*, 2001b) approach to the Bulk Earth (BE) values, varying from the depleted quadrant to the enriched one. The Paraguayan flood tholeiites are intermediate between the K- and the Na-alkaline rocks. On the whole, a trend between

HIMU and the potassic rocks is apparent ("Paraguay array" of Comin-Chiaramonti *et al*., 1995).

In Angola and Namibia, at the easternmost fringe of the PAEP, $Sr_i$ and $Nd_i$ values for most Early Cretaceous Angolan carbonatites (Fig. 10B) vary between 0.70321 and 0.70466, and between 0.51273 and 0.51237, respectively, showing on the whole depleted characteristics relative to BE (Alberti *et al*., 1999).

On the other hand, the Early Cretaceous carbonatites from Namibia have a similar $Sr_i$ range (0.70351-0.70466), but almost constant $Nd_i$ (0.51250 to 0.51244; Milner & Le Roex, 1996; Le Roex & Lanyon, 1998). Mixing models (not shown) between the parental magmas and crustal compo-nents imply unrealistic (up to 50%) contaminant fractions (Alberti *et al*., 1999). According to Bell & Blenkinsop (1989), $Sr_i$ and $Nd_i$ values from the Angola-Namibia carbonatites may result from either mixing between a depleted and enriched mantle components, or from ancient mantle reservoirs.

Angola-Namibia, as well as the East Africa Early Cretaceous carbonatites show similar $Sr_i$ and $Nd_i$ values, whereas the Tertiary East Africa and Namibia analogues generally have lower $Sr_i$ and higher $Nd_i$ values (0.70307-0.70367 and 0.51268-0.51283, respectively; East Africa: Bell & Tilton, 2001; Namibia: Cooper & Reid, 1998). Also the Cambro-Ordovician carbonatitic samples from Namibia (Marinkas Quellen: Smithies & Marsh, 1998) show $Sr_i$ values similar to those of the Tertiary carbonatites of the country (0.70285-0.70415), but their $Nd_i$ ratios are significatively lower than the other carbonatitic specimens (0.51218-0.51228). Notably, the Early Cretaceous Namibia flood tholeiites (Ewart *et al*., 1998 and therein references) have $Sr_i$ and $Nd_i$ values between 0.70419 and 0.7055 and 0.51237 and 0.51277, respectively.

In Brazil (Fig. 10C), the Early Cretaceous carbonatites have $Sr_i$ between 0.70425 and 70595 and $Nd_i$ between 0.51213 and 0.51280 (mean $Sr_i$=0.70527± 0.00034 and mean $Nd_i$=0.51224±0.00011; Comin-Chiaramonti *et al*., 1999).

The $Sr_i$ and $Nd_i$ values of the Early Cretaceous Brazilian rocks are higher and lower, respectively, than those of the coeval, both sodic and potassic, rocks from Namibia (mean $Sr_i$=0.70398±0.00046 and $Nd_i$=0.51248±0.00002). The alkaline complexes from Uruguay, interpreted as crustally contaminated (Kirkstein *et al*., 2000), are distinct in having $Sr_i$ 0.70560-0.70893 and $Nd_i$ 0.51166-0.51195 (Fig. 10C).

Brazilian Late Cretaceous alkaline-carbonatitic complexes have the following $Sr_i$ and $Nd_i$ mean values, respectively: Alto Paranaíba (APIP), $Sr_i$=0.70527±0.00036 and $Nd_i$=0.51224±0.00006 (Bizzi *et al*., 1994; Gibson *et al*., 1995, and therein references); Taiúva-Cabo Frio and Serra do Mar, $Sr_i$=0.70447±0.00034 and $Nd_i$= 0.51252±0.00008 (Thompson *et al.,* 1998); Lages, $Sr_i$= 0.70485±0.00053 and $Nd_i$=0.51218±0.00022 (Traversa *et al*., 1996; Comin-Chiaramonti *et al*. 2002). It should be noted that the alkaline-carbonatite magmatism trends to the $Sr_i$ and $Nd_i$ field delineated by the Late Cretaceous tholeiites from Walvis Ridge and Rio Grande Rise (Richarson *et al*., 1982; Gamboa & Rabinowitz, 1984).

Alkaline rocks, carbonatites and tholeiites from the Atlantic Ocean Islands, Mid Atlantic Ridge (MAR) and Northeastern Brazil define a linear array between DMM and EMI mantle components (Fig. 10D).

The alkaline and alkaline-carbonatite complexes from the PAEP appear to follow a well-defined array involving depleted and enriched mantle components. Both the Early and Late Cretaceous Brazilian alkaline-carbonatite complexes vary from close to the BE to the enriched quadrant, fitting the fields of the "uncontaminated" low-Ti and high-Ti tholeiites from Paraná-Angola-Etendeka Province (Castorina *et al*., 1997; Speziale *et al*., 1997; Comin-Chiaramonti *et al*., 1997a, b; Comin-Chiaramonti *et al*., 1999). The isotopically Sr-enriched rocks (e.g. Eastern Paraguay alkaline-carbonatite complexes) are not easily explained by crustal contamination, since this requires high percentages of crustal components in a mixing process (up to 90%; cf. Comin-Chiaramonti *et al*., 1997a). On the contrary, we stress that oxygen isotope data suggest a primary, mantle-derived origin for silicate phases (cf. Comin-Chiaramonti *et al*., 1997a): whole-rock $\delta^{18}O$ data for the potassic rocks yielded +5.45 to +5.91‰ (V-SMOW), which are consistent with the values for its mineral constituents, clinopyroxene (+5.09 to +5.20‰) and biotite (+4.85 to +5.54‰) and the expected mantle values (Comin-Chiaramonti *et al*., 1997a).

On the whole, the Na-rocks, close to the BE, and the K-rocks, typically high in radiogenic Sr worldwide, represent the range of virtually uncontaminated source magmas from the PAEP. In summary, the data support the view that the carbonatites from Angola, mainly ranging in composition from a depleted component to the BE, and the carbonatites and alkaline rocks from Eastern Paraguay, represent the end-members of virtually uncontaminated source magmas from subcontinental mantle segments variously affected by "metasomatic l.s. processes" (Comin-Chiaramonti *et al*., 1997a, 1999; Alberti *et al*., 1999).

Studies of the initial $^{143}Nd/^{144}Nd$ ratios from Precambrian terrains suggest that the mantle which supplied continental crust (as in the PAEP; cf. Comin-Chiaramonti *et al.,* 1999) has evolved since earliest time with Sm/Nd ratios higher than that of CHUR (chondritic uniform reservoir; cf. Faure, 1986). For this reason, model ages ($T^{DM}$) for the continental crust are usually calculated with reference to the depleted mantle (DM: $^{143}Nd/^{144}Nd=0.513151$, $^{147}Sm/^{144}Nd=0.2188$) reser-voir rather than CHUR.

Nd-model ages for the K-alkaline rocks and carbonatites (depleted mantle: $T^{DM}$) range from 1.4 to 2.0 Ga (mean=1.5±0.2 Ga), whereas the Na-rocks yielded 0.5 to 0.9 Ga. In general, high-Ti and low-Ti tholeiites from the Paraná Basin (H-Ti and L-Ti, respectively) give $T^{DM}$ mean values of 1.1±0.1 and 1.5±0.2 Ga, respectively. These calculations require that the Sm/Nd fractionation was not significant during mantle melting.

The Angolan carbonatites have $T^{DM}$ ranging from 0.9 to 0.4 Ga (mean 0.64±0.17). This value fits the model ages of the Early Cretaceous alkaline outcrops from NW Namibia (i.e. 0.7±0.2; Milner & Le Roex, 1996, Le Roex & Lanyon, 1998) and of the Cambro-Ordovician Marinkas Quellen complex (southern Namibia, 0.68±0.02; Smithies & Marsh, 1998). High-Ti and low-Ti tholeiites and associated K-alkaline rocks from the Paraná Basin have mean $T^{DM}$ 1.1±0.1 and 1.5±0.2 Ga, respectively. Thus, the range of model ages in the PAEP (cf. Fig. 9 of Alberti *et al.*, 1999) implies that the corresponding Paleozoic, Cretaceous and Tertiary magmas were derived from subcontinental lithospheric mantle modified by "metasomatic l.s processes" (asthenospheric components ?) since Middle to Late Proterozoic times (Comin-Chiaramonti *et al.*, 1997a, b; 1999).

Pb isotopes

The available data for the alkaline-carbonatite complexes and tholeiites from the PAEP are illustrated in Figs. 11 to 13. These show patterns compatible with mixing processes mainly involving HIMU and EMI end-members, and subordinaterly DMM and EMI, as well crustal l.s. components (e.g. EMII).

MAR, OIB and oceanic carbonatites delineate trends between the DMM and HIMU mantle components. In comparison, the PAEP carbonatites plot close to the EMI-HIMU mixing lines for both Pb-Sr and Pb-Nd in Figs. 12 and 13. This observation seems to confirm the advantages in using carbonatite over silicate rocks, as indicators of mantle sources, because of their rapid ascent to the surface conditions, and buffering against crustal assimilation due to their high Sr, Nd and Pb concentrations in the liquids.

The results indicate that any model proposed for the evolution of the HIMU and EMI end-members must be consistent with the following constraints: 1) HIMU and EMI are not restricted to the oceanic environment; 2) end-members are variously associated in space as a function of the various protoliths; 3) mantle regions with HIMU and EMI isotope characteristics are capable of generating melts that can lead to the formation of a wide variety of silicate rocks, including melts enriched in $CO_2$ (cf. Bell, 1998).

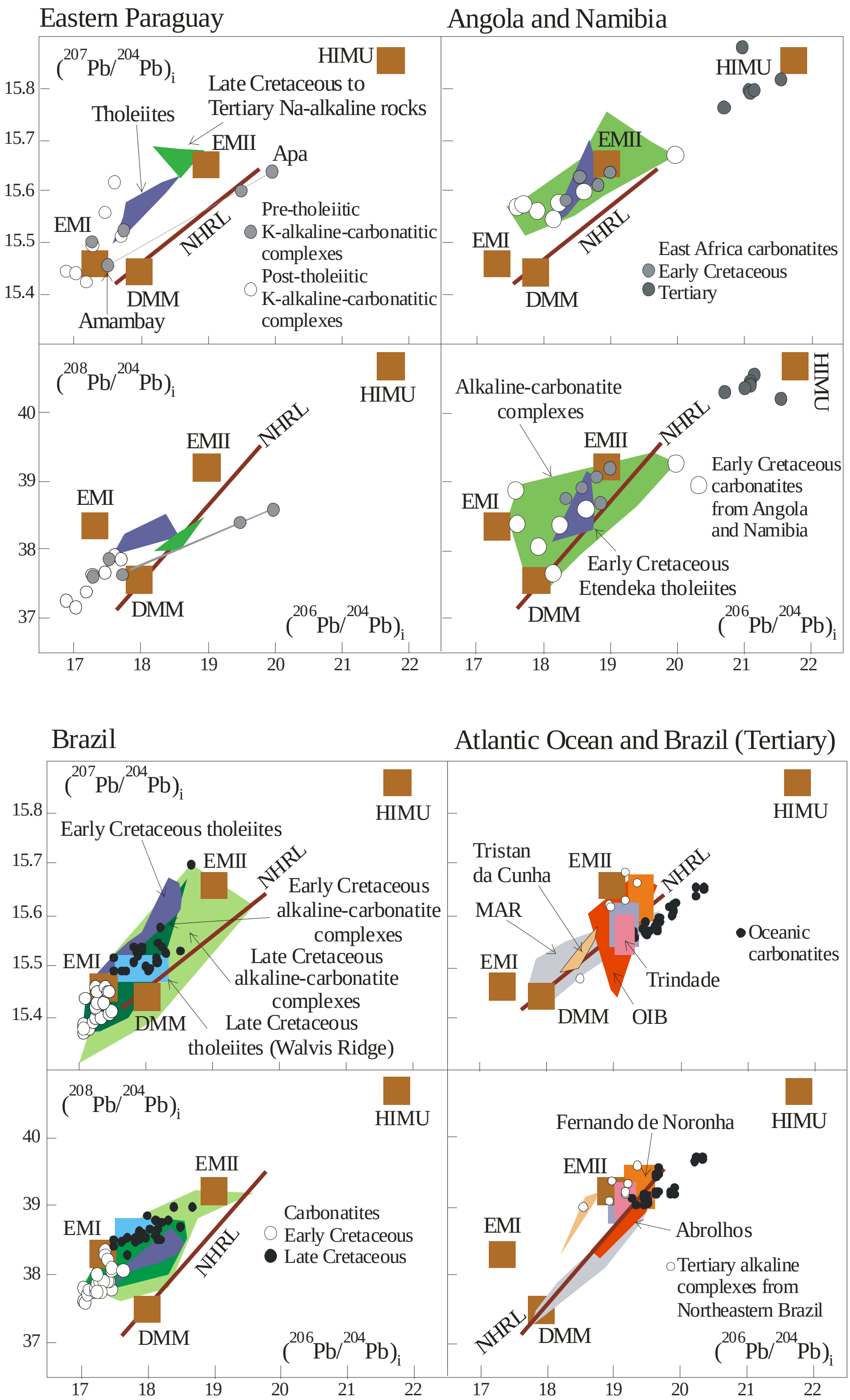


Fig. 11. $^{207}Pb/^{204}Pb$ and $^{208}Pb/^{204}Pb$ vs. $^{206}Pb/^{204}Pb$ (initial ratios) for rock-types from the PAEP. Data source as in Fig. 10. NHRL (North Hemisphere Reference Line) after Hart (1984).

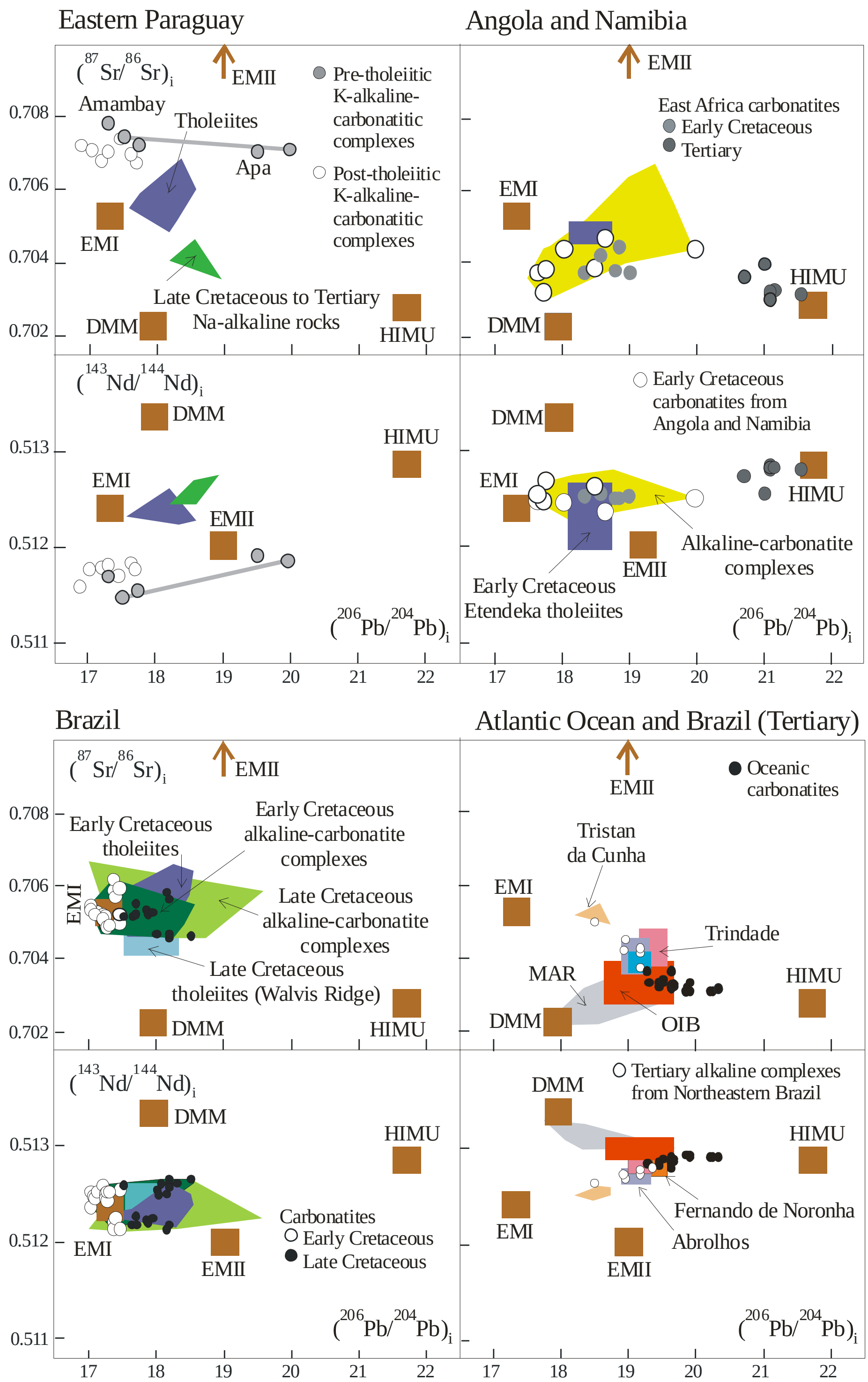


Fig. 12. $Sr_i$ and $Nd_i$ vs. $^{206}Pb/^{204}Pb$ (initial ratios). Data source as in Fig. 10.

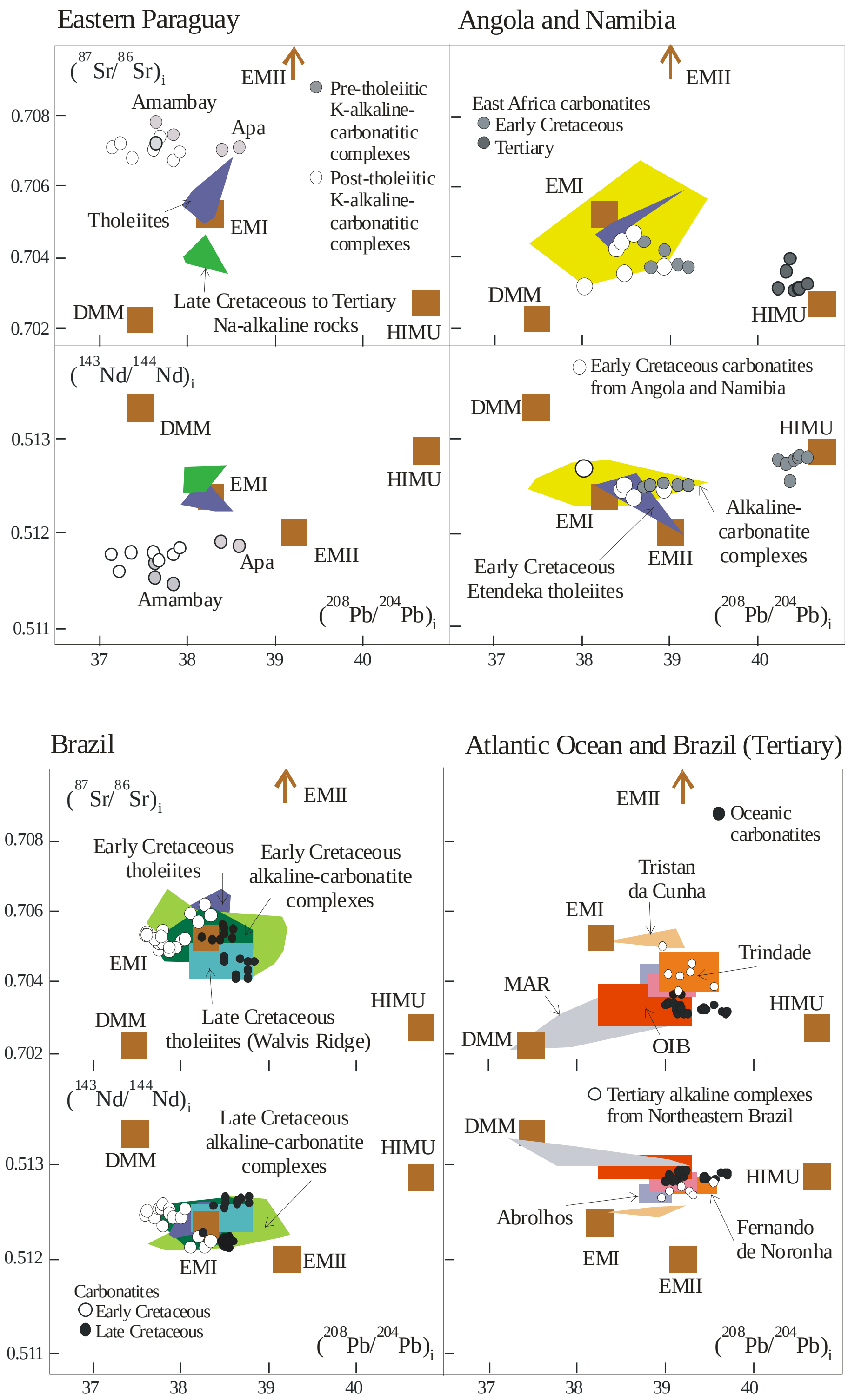


Fig. 13. $Sr_i$ and $Nd_i$ vs. $^{208}Pb/^{204}Pb$ (initial ratios). Data source as in Fig. 10.

## DISCUSSION AND GEODYNAMIC HYPOTHESES

Le Roex & Lanyon (1998) and Thompson *et al.* (1998) postulated that the Early Cretaceous alkaline-carbonatitic and tholeiitic magmatism from northwestern Namibia and the Late Cretaceous alkaline and alkaline-carbonatitic magmatism from Alto Paranaíba-Serra do Mar (southern Brazil) would reflect the variable contributions of the asthenospheric mantle components related to the Tristan da Cunha and Trindade plumes, respectively. On the contrary, Comin-Chiaramonti *et al.* (1997a, 1999), Castorina *et al.* (1997), Alberti *et al.* (1999) suggested that the alkaline and alkaline-carbonatitic magmatism in the PAEP originated from lithospheric mantle sources without appreciable participation of plume-derived materials. On the basis of geochemical and geophysical data, Ernesto *et al.* (2002) proposed that the genesis of the PAEP tholeiites mainly reflects melting of heterogeneous subcontinental mantle reservoirs, and that the geochemical and isotopic signatures of the Walvis Ridge and Rio Grande Rise basalt compositional variations may be explained by contamination through detached continental lithospheric mantle left behind during the continental breakup processes.

In the isotopic diagrams (Figs. 10 to 13), the Early Cretaceous alkaline magmatism from the PAEP appears to be related to heterogeneous mantle sources spanning from time-integrated HIMU and enriched mantle components. This alkaline magmatism mimics, in terms of isotopic compositions, the coeval flood tholeiites. We stress that, in general, the enriched isotopic signatures of the Early Cretaceous alkaline magmatism decreases from West (Paraguay) to East (Brazil, SE-continental margin, and Namibia). A similar decreasing isotopic shift is also observed for the age of the magmatism, in Paraguay and Brazil, i.e. Early-Late Cretaceous to Tertiary. These results suggest that the PAEP magmatism is related both to large- and small-scale heterogeneous source mantle. Also it should be noted that the the isotopic signature of the Trindade and Abrolhos islands (Figs. 10 to 13) is consistent with that of the alkaline-carbonatitic magmatism of Early Cretaceous from Angola and Namibia, but quite different from that (EMI signature) of the Late Cretaceous-Tertiary analogues from the Alto Paranaíba (APIP), Ponta Grossa Arch, and Cabo Frio-Taiúva-Serra do Mar areas. According to Thompson *et al.* (1998), the APIP would be the inland surface expression of the "dogleg" track left by the Trindade plume, but, in terms of Sr-Nd-Pb isotopes, the contribution, if any, of the asthenospheric components related to the that plume is difficult to account for.

The Tristan da Cunha (Gough and Inaccessible islands) alkaline magmatism and the Walvis Ridge-Rio Grande Rise basalts have isotopic characteristics which are distinct or partly overlap those of the PAEP Early Cretaceous alkaline-carbonatititic and tholeiitic magmatism, respectively. Therefore, also in this case, the contribution of mantle components derived from the Tristan da Cunha Plume is not appreciable.

Hawkesworth *et al.* (1986) interpreted the Etendeka (Namibia) high-$TiO_2$ (HTZ) basalts as resulting from melting of a Proterozoic lithospheric mantle, which, in the case of the Walvis Ridge (WR2 basalts, cf. Richardson *et al.*, 1982), was floating inside the oceanic asthenosphere during the opening of the South Atlantic. Alternatively, the elemental and isotopic signature of the HTZ basalts could be related to contamination of oceanic mantle by ancient subcontinental lithospheric mantle. In summary, the isotopic signature of the Early and Late Cretaceous carbonatites from the PAEP reflects ancient heterogeneities preserved in the subcontinental lithospheric mantle.

Therefore, we believe, as documented by Ernesto *et al.* (2000, 2002), that the hypothesis of asthenospheric plumes for the PAEP magmatism is not compelling, except that it may represent a thermal perturbation.

Also crucial to the PAEP magma genesis is the link with the geodynamic processes which promoted the opening of the South Atlantic. According to Nürberg & Müller (1991), the sea-floor spreading in the South Atlantic at PAEP latitude started at ~125-127 Ma (Chron M4). North of the Walvis-Rio Grande ridges (latitude >28°), the onset of the oceanic crust would be younger (~113 Ma; Chang *et al*., 1988).

The Early Cretaceous alkaline-carbonatitic complexes are subcoeval with the main flood tholeiites of the Paraná Basin and, therefore, occurred during the early stages of rifting, before the continental separation. On the other hand, the Late Cretaceous analogues emplaced during advanced stages of Africa-South America continental separation.

The origin of alkaline-carbonatitic magmatism in terms of plate tectonics is currently debated. Various models have been proposed involving deep mantle plume/hot spots (up to 16; Stefanick & Jurdy, 1984), or shallow thermal anomalies (Holbrook & Kelemen, 1993), which, whatever the temperature, size, depth of origin and number of hot spots, the plume model cannot explain to account for the worldwide occurrence of the alkaline-carbonatitic magmatism (see Smith & Lewis, 1999 for a discussion). Gibson *et al.* (1999) suggested that the Late Cretaceous alkaline-carbonatitic magmatism of Lages, located more than 1000 km south of the postulated head of the Trindade plume, was induced by "impressive" southward channelling of high temperature melts away from the thick keels of the São Francisco craton. This suggestion does not account for the occurrences of Late Cretaceous alkaline rocks from the Rio Grande Arch (e.g. Piratini) and also for the mechanical barriers formed by, e.g., Ponta Grossa Arch, Piquiri and Uruguay Lineaments ("second order plate boundaries"; cf. Comin-Chiaramonti & Gomes, 1996).

A more convincing model for South Atlantic is that proposed by Smith & Lewis (1999). The forces acting on plates which move at differential angular velocity and the presence of volatile-rich mantle sources (wet spot) would drive the rifting to occur parallel to the pre-existing (e.g. N-S) sutures, i.e. "Adamastor Ocean" (Fig. 14). Intraplate alkaline and alkaline-carbonatitic magmatism occurred where second order "plate boundaries" (e.g. Alto Paranaíba, Ponta Grossa-Moçâmedes Arch, Uruguay Lineament, Damara belt) intersect the axis of major rifting, possibly related to the erosion and cycling of continental mantle towards the ridge axis.

In southern Brazil, the alkaline and alkaline-carbonatitic magmatism is concentrated in regions showing positive geoid anomalies (Molina & Ussami, 1999) that may be related to dense (and warm) very deep materials. Moreover, the different westwords angular velocity of the lithospheric fragments in the South American plate, as defined by the "second order plate boundaries", may favour the decompression and melting at different times of variously metasomatized (wet spot) portion of the lithospheric mantle with variable isotopic imprint (cf. also Comin-Chiaramonti *et al.*, 1999).

This scenario could explain the presence of Late Cretaceous to Tertiary sodic magmatism in the PAEP (cf. Fig. 1), even at the Eastern Paraguay longitude, where there is evidence of active rifting structures (Comin-Chiaramonti *et al*., 1992, 1999). In this case, the thermal perturbations may be channeled along the "second order plate boundaries", as envisioned also by the hypocenters of earthquakes in South America (cf. Berrocal & Fernandes, 1996).

## CONCLUDING REMARKS

The alkaline-carbonatitic magmatism from the PAEP is distributed along tectonic lineaments, both in American and African continents. The carbonatites mainly occur in the inner parts of circular/oval shaped alkaline-carbonatitic complexes, being rock bodies usually associated with evolved silicate rocks. Liquid immiscibility processes are believed to have originated the carbonatites in the PAEP.

The large variations of the I.E. and REE appear to be mainly related to hydrothermal processes. This is supported by the O-C isotope systematics and by the calcite-dolomite isotopic equilibrium temperatures indicating complex trends from magmatic to hydrothermal environments at variable $CO_2/H_2O$ ratios.

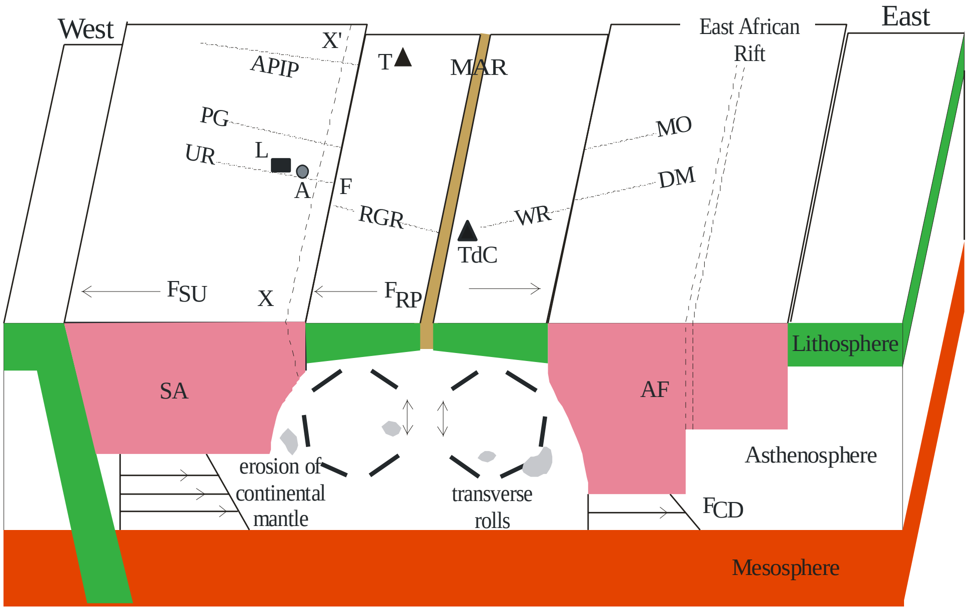


Fig. 14. Forces acting on plates in rotational model illustrated for the South Atlantic Ocean (after Smith & Lewis, 1999, modified). Major rifting occurs parallel to X-X' pre-existing suture. Intraplate volcanism follows the second order sutures (e.g. PG-MO: Ponta Grossa-Moçâmedes Arch; UR: Uruguay Lineament; DM: Damara belt). SA: South America plate; AF, African plate; RGR: Rio Grande Rise; WR: Walvis Ridge; TdC: Tristan da Cunha; T: Trindade. $F_{CD}$: continental drag; $F_{RP}$: ridge push; $F_{SU}$: trench suction. F, Florianópolis; A, Anitápolis; L, Lages.

On the whole, the geochemical data show that the genesis of PAEP magmatism requires heterogeneous mantle sources, also in terms of radiogenic isotopes. Such heterogeneity is probably related to "metasomatic l.s. processes" which would have occurred at about 0.6-0.7 Ga (Angola, Namibia and Brazil) and 1.6 Ga (Eastern Paraguay).

The areal distribution indicates that the time-integrated isotopic enrichment of the carbonatites and associated alkaline rocks decreases from West (Eastern Paraguay) to East (Angola and Namibia), concomitantly with the decreasing age of the magmatism (Early to Late Cretaceous). This also indicates that the PAEP alkaline-carbonatitic magmatism originated from large- to small-scale heterogeneous subcontinental mantle. Sr-Nd-Pb isotope data yield clear evidence of that HIMU and EMI mantle components were important in the genesis of PAEP magmatism.

All the results are consistent in indicating that the contribution of asthenospheric components, derived from mantle plumes (i.e. Tristan da Cunha and Trindade), to the genesis of the alkaline-carbonatitic magmatism of the PAEP, was not significant. This is consistent with the conclusions reached for the Paraná flood tholeiites (Comin-Chiaramonti *et al.*, 1997a; Marques *et al.*, 1999a; Ernesto *et al.*, 2002). Regional thermal anomalies in the deep mantle, mapped by geoid and seismic tomography data, offer an alternative for a non-plume-related heat source (Ernesto *et al.*, 2002). In this scenario, the "hot spot tracks" of Walvis Ridge and Rio Grande Rise, as well as the Vitória-Trindade chain, might reflect the accomodation of stresses in the lithosphere during rifting rather than continuous magmatic activity induced by mantle plumes beneath the moving lithospheric plates.

## ACKNOWLEDGEMENTS

Special thanks are due to A. Alberti, K. Bell, A. Cundari, F. Innocenti, F. Stoppa, E.M. Piccirillo and A. Woolley for their constructive critical review and hepful suggestions. This research was supported by grants from Italian (CNR, 05 and 11 Committes, and COFIN, 1998, MIUR 1998, 1999, 2000, 2001) and Brazilian (FAPESP, Proc. 01/10714-3) agencies.

## REFERENCES

Alberti, A., Castorina, F., Censi, P., Comin-Chiaramonti, P. & Gomes, C.B. (1999). Geochemical characteristics of Cretaceous carbonatites from Angola. *Journal of African Earth Sciences* **29**, 735-759.

Andersen, T. (1987). Mantle and crustal components in a carbonatite complex, and the evolution of carbonatite magma: REE and isotopic evidence from the Fen complex, southeast Norway. *Isotope Geoscience* **65**, 147-166.

Andrade, F.R.D. (1998). *Geoquímica do sistema de alteração do carbonatito de Barra do Itapirapuã (PR/SP).* Ph.D. Thesis, Universidade Estadual Paulista, Rio Claro, 136p.

Andrade, F.R.D., Möller, P. & Höhndorf, A. (1999a). The effect of hydrothermal alteration on the Sr and Nd isotopic signatures of the Barra do Itapirapuã carbonatite, southern Brazil. *Journal of Geology* **107**, 177-191.

Andrade, F.R.D., Möller, P., Lüders, V., Dulski, P. & Gilg, H.A. (1999b). Hydrothermal rare earth elements mineralization in the Barra do Itapirapuã carbonatite, southern Brazil: behaviour of selected trace elements and stable isotopes (C, O). *Chemical Geology* **155**, 91-113.

Antonini, P., Gasparon, M., Comin-Chiaramonti, P. & Gomes, C.B. (in this volume). Post-Paleozoic magmatism in the Eastern Paraguay: Sr-Nd-Pb isotope compositions.

Barker, D.S. (1996). Carbonatite volcanism. In: Mitchell, R.H. (ed.) *Undersaturated alkaline rocks: mineralogy, petrogenesis, and economic potential.* Mineralogical Association of Canada, Nepean, Ontario, pp. 45-62.

Beccaluva, L., Barbieri, M., Born, H., Brotzu, P., Coltorti, M., Conte, A., Garbarino, C., Gomes, C.B., Macciotta, G., Morbidelli, L., Ruberti, E., Siena, F. & Traversa, G. (1992). Fractional crystallization and liquid immiscibility processes in the alkaline-carbonatite complex of Juquiá (São Paulo, Brazil). *Journal of Petrology* **33**, 1371-1404.

Bell, K. (1998). Radiogenic isotope constraints on relationships between carbonatites and associated silicate rocks - A brief review. *Journal of Petrology* **39**, 99-102.

Bell, K. & Blenkinsop, J. (1989). Neodymium and strontium isotope geochemistry of carbonatites. In: Bell, K. (ed.) *Carbonatites, genesis and evolution.* London: Unwin Hyman, pp. 278-300.

Bell, K. & Tilton, G.R. (2001). Nd, Pb and Sr isotopic compositions of East African carbonatites: evidence for mantle mixing and plume inhomogeneity. *Journal of Petrology* **42**, 1927-1945.

Bellieni, G., Montes-Lauar, C.R., De Min, A., Piccirillo, E.M., Cavazzini, G., Melfi, A.J. & Pacca, I.G. (1990). Early and Late Cretaceous magmatism from São Sebastião island (SE-Brazil): geochemistry and petrology. *Geochimica Brasiliensis* **4**, 59-83.

Bennio, L., Brotzu, P., Gomes, C.B., D'Antonio, M., Lustrino, M., Melluso, L., Morbidelli, L. & Ruberti, E. (2002). Petrological, geochemical and Sr-Nd isotopic features of alkaline rocks from the Arraial do Cabo peninsula (southeastern Brazil). *Periodico di Mineralogia* **71**, 137-158.

Berrocal, J. & Fernandes, C. (1996). Seismicity in Paraguay and neighbouring regions. In: Comin-Chiaramonti, P. & Gomes, C.B. (eds.) *Alkaline magmatism in central-eastern Paraguay. Relationships with coeval magmatism in Brazil.* São Paulo: Edusp-Fapesp, pp. 57-66.

Bizzi, L.A., De Witt, M.J., Smith, C.B., McDonald, I. & Armstrong, R.A. (1995). Heterogeneous enriched mantle materials and Dupal-type magmatism along SW margin of the São Francisco craton, Brazil. *Journal of Geodynamics* **20**, 469-491.

Bizzi, L.A., Smith, B.C., De Witt, M.J., Macdonald, I. & Armstrong, R.A. (1994). Isotope characteristics of the lithospheric mantle underlying the SW São Francisco craton margin, Brazil. *International Symposium on the Physics and Chemistry of the Upper Mantle, São Paulo, Invited Lectures*, pp. 227-256.

Bottinga, Y. & Javois, M. (1975). Oxygen isotope partitioning among the minerals in igneous and metamorphic rocks. *Reviews of Geophysics and Space Physics* **13**, 401-418.

Boynton, W.V. (1984). Cosmochemistry of the Rare Earth elements: meteorite studies. In: Henderson, P. (ed.) *Rare Earth Element geochemistry.* Amsterdam: Elsevier, pp. 63-114.

Bühn, B., Rankin, A.H., Schneider, J. & Dulski, P. (2002). The nature of orthomagmatic, carbonatitic fluids precipitating REE, Sr-rich fluorite: fluid-inclusions evidence from the Okurusu fluorite deposit, Namibia. *Chemical Geology* **186**, 75-98.

Carlson, R.W., Esperança, S. & Svisero, D.P. (1996). Chemical and Os isotopic study of Cretaceous potassic rocks from southern Brazil. *Contributions to Mineralogy and Petrology* **125**, 393-405.

Castorina, F., Censi, P., Barbieri, M., Comin-

Chiaramonti, P., Cundari, A. & Gomes, C.B. (1994). Carbonatites from the Paraná basin: A 130 Ma transect. *International Symposium on the Physics and Chemistry of the Upper Mantle, São Paulo, Extended Abstracts,* pp. 52-55.

Castorina, F., Censi, P., Barbieri, M., Comin-Chiaramonti, P., Cundari, A., Gomes, C.B. & Pardini, G. (1996). Carbonatites from Eastern Paraguay: a comparison with coeval carbonatites from Brazil and Angola. In: Comin-Chiaramonti, P. & Gomes, C.B. (eds.) *Alkaline magmatism in central-eastern Paraguay. Relationships with coeval magmatism in Brazil.* São Paulo: Edusp-Fapesp, pp. 231-248.

Castorina, F., Censi, P., Comin-Chiaramonti, P., Gomes, C.B., Piccirillo, E.M., Alcover Neto, A., Almeida, R.T., Speziale, S. & Toledo, M.C. (1997). Geochemistry of carbonatites from Eastern Paraguay and genetic relationships with potassicc magmatism: C, O, Sr and Nd isotopes. *Mineralogy and Petrology* **61**, 237-260.

Censi, P., Comin-Chiaramonti, P., Demarchi, G., Longinelli, A. & Orué, D. (1989). Geochemistry and C-O isotopes of the Chiriguelo carbonatite, northeastern Paraguay. *Journal of South American Earth Sciences* **3**, 295-303.

Chang, H.K., Kowsmann, R.O. & Figuereido, A.M.F. (1988). New concept on the development of east Brazilian margin basins. *Episodes* **11**, 194-202.

Coltorti, M., Alberti, A., Beccaluva, L., Santos, A.B., Mazzucchelli, M., Morais, E., Rivalenti, G. & Siena, F. (1993). The Tchivira-Bonga alkaline-carbonatite complex (Angola): petrological study and comparison with some Brazilian analogues. *European Journal of Mineralogy* **5**, 1001-1024.

Comin-Chiaramonti, P. & Gomes, C.B. (1996). *Alkaline magmatism in central-eastern Paraguay. Relationships with coeval magmatism in Brazil.* São Paulo: Edusp/Fapesp, 464p.

Comin-Chiaramonti, P., Castorina, F., Cundari, A., Petrini, R. & Gomes, C.B. (1995). Dykes and sills from Eastern Paraguay: Sr and Nd isotope systematics. In: Baer, G. & Heimann, A. (eds.) *Physics and chemistry of dykes*. Rotterdam: Balkema, pp. 267-278.

Comin-Chiaramonti, P., Civetta, L., Petrini, R., Piccirillo, E.M., Bellieni, G., Censi, P., Bitschene, P., Demarchi, G., De Min, A., Gomes, C.B., Castillo, A.M.C. & Velázquez, J.C. (1991). Tertiary nephelinitic magmatism in Eastern Paraguay: petrology, Sr-Nd isotopes and genetic relationships with associated spinel-peridotite xenoliths. *European Journal of Mineralogy* **3**, 507-525.

Comin-Chiaramonti, P., Cundari, A., DeGraff, J.M., Gomes, C.B. & Piccirillo, E.M. (1999). Early Cretaceous-Tertiary magmatism in Eastern Paraguay (western Paraná basin): geological, geophysical and geochemical relationships. *Journal of Geodynamics* **28**, 375-391.

Comin-Chiaramonti, P., Cundari, A., Gomes, C.B., Piccirillo, E.M., Censi, P., De Min, A., Bellieni, G. & Velázquez, V.F. (1992). Potassic dyke swarm in the Sapucai graben, Eastern Paraguay: petrographical, mineralogical and geochemical outlines. *Lithos* **28**, 283-301.

Comin-Chiaramonti, P., Cundari, A., Piccirillo, E.M., Gomes, C.B., Castorina, F., Censi, P., De Min, A., Marzoli, A., Speziale, S. & Velázquez, V.F. (1997a). Potassic and sodic igneous rocks from Eastern Paraguay: their origin from the lithospheric mantle and genetic relationships with the associated Paraná flood tholeiites. *Journal of Petrology* **38**, 495-528.

Comin-Chiaramonti, P., Cundari, A., Piccirillo, E.M., Gomes, C.B. & De Min, A. (1997b). Carbonatitic magmatism in the Paraná-Angola mantle plume (?) system: petrological and isotope-geochemical bearing on the source mantle. *Eos, Transaction, AGU* **78** (46), F741.

Comin-Chiaramonti, P., Gomes, C.B., Castorina, F., Censi P., Antonini, P., Furtado, S., Ruberti , E. & Scheibe, L.F. (2002). Anitápolis and Lages alkaline-carbonatite complexes, Santa Catarina State, Brazil: geochemistry and geodynamic implications. *Revista Brasileira de Geociências* **32**, 639-653.

Comin-Chiaramonti, P., Gomes, C.B., Ruberti, E., Antonini, P. & Censi, P. (2001a). Mato Preto alkaline-carbonatite complex: geochemistry and isotope (O-C, Sr-Nd) constraints. *Geochimica Brasiliensis* **15**, 23-34.

Comin-Chiaramonti, P., Princivalle, F., Girardi, V.A.A., Gomes, C.B., Laurora, A. & Zanetti F. (2001b). Mantle xenoliths from Ñemby, Eastern Paraguay: O-Sr-Nd isotopes, trace elements and crystal chemistry of hosted clinopyroxenes. *Periodico di Mineralogia* **70**, 205-230.

Cooper, A.F. & Reid, D.L. (1998). Nepheline sövites as parental magmas in carbonatite complexes: evidence from Dicker Willem, soutwest Namibia. *Journal of Petrology* **39**, 2123-2136.

Dalton, J.A. & Wood, B.J. (1993). The composition of primary carbonate melts and their evolution through wallrock reaction in the mantle. *Earth and Planetary Science Letters* **119**, 511-525.

Danni, J.C.M., Baecker, M.L. & Ribeiro, C.C. (1991). The geology of the Catalão I carbonatite complex. *5th International Kimberlite Conference*, *Araxá*, *Field Guide Book*, pp. 25-30.

Deines, P. (1989). Stable isotope variations in carbonatite. In: Bell, K. (ed.) *Carbonatites, genesis and evolution*. London: Unwin Hyman, pp. 301-359.

Deines, P. & Gold D.P. (1973). The isotopic composition of carbonatites and kimberlite carbonates and their bearing on the isotopic composition of deep-seated carbon. *Geochimica et Cosmochimica Acta* **51**, 1227-1243.

Ernesto, M., Marques, L.M., Piccirillo, E.M., Comin-Chiaramonti, P. & Bellieni, G. (2000). Paraná-Tristan da Cunha system: plume mobility and petrogenetic implications. *31 International Geological Congress, Rio de Janeiro*, *Extended Abstracts*.

Ernesto, M., Marques, L.M., Piccirillo, E.M., Molina, E., Ussami, N., Comin-Chiaramonti, P. & Bellieni, G. (2002). Paraná Magmatic Province-Tristan da Cunha plume system: fixed versus mobile plume, petrogenetic considerations and alternative heat sources. *Journal of Volcanology and Geothermal Researches* **130**, 527-553.

Ernesto, M., Raposo, M.I.B., Marques, L.S., Renne, P.R., Diogo, L.A. & De Min, A. (1999). Paleomagnetism, geochemistry and $^{40}$Ar/$^{39}$ Ar dating of the Northeastern Paraná Magmatic province: tectonic implications. *Journal of Geodynamics* **28**, 321-340.

Ewart, A. Milner, S.C., Armstrong, R.A. & Duncan, A.R. (1998). Etendeka volcanism of the Goboboseb Mountains and Messum igneous complex, Namibia. Part I: geochemical evidence of Early Cretaceous Tristan plume melts and the role of crustal contamination in the Paraná-Etendeka CFB. *Journal of Petrology* **39**, 191-225.

Faure, G. (1986). *Principles of isotope geology*. New York: John Wiley & Sons, 589p.

Foley, S. (1992). Potassic and ultrapotassic magmatism and their origin. Lithos **28**, 181-186.

Fodor, R.V., Mukasa, S.B., Gomes, C.B. & Cordani, U.G. (1989). Ti-rich Eocene basaltic rock, Abrolhos plattform, offshore Brazil, 18°S: petrology with respect to South Atlantic magmatism. *Journal of Petrology* **30**, 763-786.

Fodor, R.V., Mukasa, S.B. & Sial, A.N. (1998). Isotopic and trace-element indications of lithospheric and asthenospheric components in Tertiary alkalic basalts, northeastern Brazil. *Lithos* **43**, 197-217.

Fontignie, D. & Schilling, J.G. (1996). Mantle heterogeneities beneath the South Atlantic: a Nd-Sr-Pb isotope study along the Mid-Atlantic Ridge (3°S-46°S). *Earth Planetary Science Letters* **146**, 259-272.

Gamboa, L.A.P. & Rabinowitz, P.D. (1984). The evolution of the Rio Grande Rise in Southwest Atlantic. *Marine Geology* **58**, 35-58.

Garda, G.M., Schorscher, H.D., Esperança, S. & Carlson, R.W. (1995). The petrology and geochemistry of coastal dikes from São Paulo State, Brazil: implications for variable lithospheric contributions to alkaline magmas from the western margin of the South Atlantic. *Anais da Academia Brasileira de Ciências* **67**, 191-216.

Gerlach, D.C., Stormer, J.C. & Mueller, P.A. (1987). Isotope geochemistry of Fernando de Noronha. *Earth and Planetary Science Letters* **85**, 129-144.

Gibson, S.A., Thompson, R.N., Leonardos, O.H., Dickin, A.P. & Mitchell, J.G. (1995). The Late Cretaceous impact of the Trindade mantle plume: evidence from large-volume, mafic, potassic magmatism in SE Brazil. *Journal of Petrology* **36**, 189-229.

Gibson, S.A., Thompson, R.N., Leonardos, O.H., Dickin, A.P. & Mitchell, J.G. (1999). The limited extent of plume-lithosphere interactions during continental flood-basalt genesis: geochemical evidence from Cretaceous magmatism in southern Brazil. *Contributions to Mineralogy and Petrology* **137**, 147-169.

Gibson, S.A., Thompson, R.N., Weska, R.K., Dickin, A.P. & Leonardos, O.H. (1997). Late-Cretaceous rift-related upwelling and melting of the Trindade starting mantle plume head beneath western Brazil. *Contributions to Mineralogy and Petrolog*y **126**, 303-314.

Gittings, J. (1979). Problems inherent in the application of calcite-dolomite geothermometry to carbonatites. *Contributions to Mineralogy and Petrology* **69**, 1-4.

Gomes, C.B., Morbidelli, L., Ruberti, R. & Comin-Chiaramonti, P. (1996). A first attempt to compare Post-Palaeozoic alkaline rocks from western (Paraguay) and eastern (Brazil) margins of the Paraná Basin. In: Comin-Chiaramonti, P. & Gomes, C.B. (eds.) *Alkaline magmatism in central-eastern Paraguay. Relationships with coeval magmatism in Brazil.* São Paulo: Edusp-Fapesp, pp. 249-274.

Gomes, C.B., Ruberti, E. & Morbidelli, L. (1990). Carbonatite complexes from Brazil: a review. *Journal of South American Earth Sciences* **3**, 51-63.

Grossi Sad, J.H. (1972). Complexos ultramáficos alcalinos com carbonatitos do Brasil Meridional. Departamento Nacional da Produção Mineral, 58p.

Halliday, A.N., Dickin, A.P., Fallick, A.E. & Fitton, J.G. (1988). Mantle dynamics: a Nd, Sr, Pb and O isotopic study of the Cameroon Line volcanic chain. *Journal of Petrology* **29**, 181-211.

Halliday, A.N., Lee, D.C., Tommasini, S., Davies, G.R., Paslick, C.R., Fitton, G.J. & James, D.E. (1995). Incompatible trace elements in OIB and MORB and source enrichment in the sub-oceanic mantle. *Earth and Planetary Science Letters* **133**, 379-395.

Hamelin, B., Dupré, B. & Allègre, C.J. (1984). Lead-strontium isotopic variations alongt the East Pacific Rise and Mid-Atlantic Ridge: a comparative study. *Earth and Planetary Science Letters* **67**, 340-350.

Harris, C., Marsh, J.S. & Milner, S.C. (1999). Petrology of the alkaline core of the Messum igneous complex, Namibia: evidence for the progressively decreasing effect of crustal contamination. *Journal of Petrology* **40,** 1377-1397.

Hart, S.R. (1984). A large-scale isotope anomaly in the southern hemisphere. *Nature* **309**, 753-757.

Hart, S.R., Gerlach, D.C. & White, W.M. (1986). A possible new Sr-Nd-Pb mantle array and consequences for mantle mixing. *Geochimica et Cosmochimica Acta* **50**, 1551-1557.

Hart, S.R., Hauri, E.H., Oschmann, L.A. & Whithehead, J.A. (1992). Mantle plumes and entrainement: isotopic evidence. *Science* **256**, 517-520.

Hawkesworth, C.J., Mantovani, M.S.M., Taylor, P.N. & Palacz, Z. (1986). Evidence from the Paraná of south Brazil for a continental contribution to Dupal basalts. *Nature* **322**, 356-359.

Hegarty, K.A., Duddy, I.R. & Green, P.F. (1996). The thermal history in around the Paraná Basin using apatite fission track analysis. Implications for hydrocarbon occurrences and basin formation. In: Comin-Chiaramonti, P. & Gomes, C.B. (eds.) *Alkaline magmatism in Central-Eastern Paraguay. Relationships with coeval magmatism in Brazil.* São Paulo: Edusp-Fapesp, pp. 223-230.

Hoefs, J. (1987). *Stable isotope geochemistry*. Berlin: Springer, 241p.

Hoernle, K., Tilton, G., Le Bas, M.J., Duggen, S. & Garbe-Schömberg, D. (2002). Geochemistry of oceanic carbonatites compared with continental carbonatites: mantle recycling of oceanic crustal carbonate. *Contributions to Mineralogy and Petrology* **142**, 520-542.

Holbrook, W.S. & Kelemen, P.B. (1993). Large igneous province on the US Atlantic margin and implications for magmatism during continental breakup. *Nature* **364**, 433-436.

Hornig-Kjarsgaard, I. (1998). Rare Earth Elements in sövitic carbonatites and their mineral phases. *Journal of Petrology* **39**, 2105-2121.

Huang, H-M., Hawkesworth, C.J., Van Calsteren, P. & Mcdermott, F. (1995). Geochemical characteristics and origin of the Jacupiranga carbonatites, Brazil. *Chemical Geology* **119**, 79-99.

Issa Filho, A., Santos, A.B.R.M.D., Riffel B.F., Lapido Loureiro, F.E.V. & McReath, I. (1991). Aspects of the geology, petrology and chemistry of some Angolan carbonatites. *Journal of Geochemical Explorations* **40**, 205-226.

Issa Filho, A., Santos P.R.A.S. & Souza, O.M. (1984). Aspects of the geology of the Barreiro Carbonatitic Complex, Araxá, MG, Brazil. In: Rodrigues, C.S. & Lima, P.R.A.S. (eds.). *Complexos Carbonatíticos do Brasil: Geologia.* Companhia Brasileira de Metalurgia e Mineração, pp. 21-44.

Ito, E., White, W.M. & Göpel, C. (1987). The O, Sr, Nd and Pb isotope geochemistry of MORB. *Chemical Geology* **62**, 157-176.

Jago, B.C. & Gittings, J. (1993). Pyrochlore crystallization in carbonatites: the role of fluorine. *South African Journal of Geology* **96**, 149-159.

Jenkin, G.R.T., Fallik, A.E., Farrow, C.M. & Bowes, G.E. (1991). COOL: a FORTRAN-77 computer program for modelling stable isotopes in cooling closed systems. *Computational Geoscience* **17**, 391-412.

Jones, A.P., Walker, D., Pickett, D.A., Murrell, M.T. & Beattie, P. (1995). Experimental investigations of the partitioning of Nb, Mo, Ba, Ce, Pb, Ra, Th and U between immiscible carbonate and silicate liquids. *Geochimica et Cosmochimica Acta* **59**, 1307-1320.

Jones, A.P. & Wyllie, P.J. (1983). Low-temperature glass quenched from a synthetic, rare earth carbonatite: implication for the origin of the Mountain Pass deposit, California. *Economic Geology* **78**, 1721-1723.

Keller, J. & Hoefs, J. (1995). Stable isotope characteristics of recent natrocarbonatites from Oldoinyo Lengai. In: Bell, K. & Keller, J. (eds.) *Carbonatite volcanism: Oldoynio Lengai and the petrogenesis of natrocarbonatites*. Berlin: Springer, pp. 113-123.

Kirkstein, L.A., Peate, D.W., Hawkesworth, C.J., Turner, S.P., Harris, C. & Mantovani, M.S.M. (2000). Early Cretaceous basaltic and rhyolitic magmatism in southern Uruguay associated with the opening of the South Atlantic. *Journal of Petrology* **41**, 1413-1438.

Kjarsgaard, B.A., Hamilton, D.L. & Peterson, T.D. (1995). Peralkaline nephelinite/carbonatite liquid immiscibility: comparison of phase composition in experiments and natural lavas from Oldoinyo Lengai. In: Bell, K. & Keller, J. (eds.) *Carbonatite volcanism: Oldoinyo Lengai and the petrogenesis of natrocarbonatites*. Berlin: Springer, pp. 163-190.

Kurszlaukis, S., Franz, L. & Brey, G.P. (1999). The Blue Hill intrusive complex in southern Namibia.

Relationships between carbonatites and monticellite picrites. *Chemical Geology* **160**, 1-18.

Kyser, T.K. (1990). Stable isotopes in the continental lithospheric mantle. In: Menzies, M.A. (ed.) *Continental mantle*. Oxford: Clarendon Press, pp. 127-156.

Le Roex, A.P. (1985). Geochemistry, mineralogy and magmatic evolution of the basaltic and trachytic lavas from Gough Island, South Atlantic. *Journal of Petrology* **26**, 149-186.

Le Roex, A.P. & Lanyon, R. (1998). Isotope and trace element geochemistry of Cretaceous Damaraland lamprophyres and carbonatites, northwestern Namibia: evidence for plume-lithosphere interaction. *Journal of Petrology* **39**, 1117-1146.

Le Roex, A.P., Cliff, R.A. & Adair, B.J.I. (1990). Tristan da Cunha, south Atlantic: geochemistry and petrogenesis of a basanite-phonolite lava series. *Journal of Petrology* **31**, 779-812.

Marques, L.S., Dupré, B. & Piccirillo, E.M. (1999a). Mantle source compositions of the Paraná magmatic province (southern Brazil): evidence from trace element and Sr-Nd-Pb isotope geochemistry. *Journal of Geodynamics* **28**, 439-458**.**

Marques, L.S., Ulbrich, M.N.C., Ruberti, E. & Tassinari, C.G. (1999b). Petrology, geochemistry and Sr-Nd isotopes of the Trindade and Martin Vaz volcanic rocks (Southern Atlantic Ocean). *Journal of Volcanology and Geothermal Research* **93**, 191-216.

Matthews, A., Goldsmith, J.R. & Clayton, R.N. (1983). Oxygen isotope fractionations involving pyroxenes: the calibration of mineral-pair geothermometers. *Geochimica Cosmochimica Acta* **47**, 631-644.

Mello, I.S.C. & Bettencourt, J.S. (1998). Geologia e gênese das mineralizações do maciço Itaoca, Vale do Ribeira, SP e PR. *Revista Brasileira de Geociências* **28**, 269-284.

Meyer, H.O.A., Blaine, L.G., Svisero, D. P. & Craig, B.S. (1994). Alkaline intrusions in western Minas Gerais, Brazil. *5th International Kimberlite Conference*, *Araxá, Proceedings,* pp. 140-155.

Milner, S.C. & Le Roex, A.P. (1996). Isotope characteristics of the Okenyenya igneous complex, nortwestern Namibia: constraints on the composition of the early Tristan plume and the origin of the EMI mantle component. *Earth Planetary Science Letters* **141**, 277-291.

Milner, S.C., Le Roex, A.P. & O'Connor, G.M. (1995). Ages of Mesozoic igneous rocks in northwestern Namibia, and their relationship to continental breakup. *Journal of the Geological Society of London* **152**, 97-104.

Molina, E.C. & Ussami, N. (1999). The geoid in southern Brazil and adjacent regions: new constraints on density distribution and thermal state of lithosphere. *Journal of Geodynamics* **28**, 321-340.

Morbidelli, L., Beccaluva, L., Brotzu, P., Conte, A., G., Garbarino, C., Gomes, C.B., Macciotta, G., Ruberti, E., Scheibe, L.F. & Traversa, G. (1986). Petrological and geochemical studies of alkaline rocks from continental Brazil. 3. Fenitization of jacupirangite by carbonatite magmas from Jacupiranga. *Periodico di Mineralogia* **55**, 261-295.

Morbidelli, L., Gomes, C.B., Beccaluva, L., Brotzu, P., Conte, A., Ruberti, E. & Traversa, G. (2000). The Pariquera Açú K-alkaline complex and southern Brazil lithospheric mantle source characteristics. *Journal of Asian Earth Sciences* **18**, 129-150.

Morbidelli, L., Gomes, C.B., Brotzu, P., D'Acquarica, S., Garbarino, C., G., Ruberti, E. & Traversa, G. (1995). Mineralogical, petrological and geochemical aspects of alkaline and alkaline-carbonatite associations from Brazil. *Earth Science Reviews* **39**, 135-168.

Morikiyo, T., Hirano, H. & Matsushita, Y. (1990). Carbon and oxygen isotopic composition of the carbonatites from Jacupiranga and Catalão I carbonatite complexes, Brazil. *Bullettin of Geological Survey of Japan* **41**, 619-626.

Müller, R.D., Royer, J.-Y & Lawver, L.A. (1993). Revised plate motions relative to the hotspots from combined Atlantic an Indian Ocean hotspots tracks. *Geology* **21**, 275-278.

Nelson, D.H., Chivas, A.R., Chappell, B.W. & McCulloch, M.T. (1988). Geochemical and isotopic systematics in carbonatites and implications for the evolution of ocean-island sources. *Geochimica et Cosmochimica Acta* **52**, 1-17.

Nürberg, D. & Müller, R.D. (1991). The tectonic evolution of South Atlantic from Late Jurassic to present. *Tectonophysics* **191**, 27-43.

O'Connor, J.M. & Duncan, R.A. (1990). Evolution of the Walvis Ridge-Rio Grande Rise hot spot system: implications for African and South American plate motions over plumes. *Journal of Geophysical Researches* **95**, 17475-17502.

Piccirillo, E.M. & Melfi, A.J. (eds.) (1988). *The Mesozoic flood volcanism from the Paraná basin (Brazil). Petrogenetic and geophysical aspects*. São Paulo: IAG-USP, 600p.

Pineau, F., Javoy, M. & Allègre, C.J. (1973). Etude systématique des isotopes de l'oxygène, du carbone et du strontium dans les carbonatites. *Geochimica et Cosmochimica Acta* **37**, 2363-2377.

Reid, D.L. & Cooper, A.F. (1992). Oxygen and carbon isotope patterns in the Dicker Willem carbonatite complex, southern Namibia. *Chemical Geology* **94**, 293-305.

Reid, D.L., Cooper, A.F., Rex, D.C. & Harmer, R.E.

(1990). Timing of post-Karroo alkaline magmatism in southern Namibia. *Geological Magazine* **127**, 427-433.

Renne, P.R., Ernesto, M. & Milner, S.C. (1997). Geochronology of the Paraná-Angola-Etendeka magmatic Province. *Eos, Transaction, AGU* **78** (46), F742.

Richardson, S.H., Erlank, A.J., Duncan, A.R. & Reid, D.L. (1982). Correlated Nd, Sr and Pb isotope variations in Walvis Ridge basalts and implications for the evolution of their mantle source. *Earth and Planetary Science Letters* **59**, 327-342.

Robaina, L.S.S., Formoso, M.L.L. & Spadini, A.R. (1991). Carbonatos reservatório da Formação Macaé, Bacia de Campos, RJ, Brazil. *Geochimica Brasiliensis* **5**, 69-78.

Rodrigues, C.S. & Lima, P.R.A.S. (1984). *Complexos Carbonatíticos do Brasil: Geologia.* Companhia Brasileira de Metalurgia e Mineração, Araxá, 44pp.

Roedder, E. (1973). Fluid inclusions from the fluorite deposits associated with the carbonatite of Amba Dongar, India and Okurusu, south west Africa. *Transactions of the Institution of Mining and Metallurgy* **82B**, 35-39.

Ruberti, E., Castorina, F., Censi, P., Comin-Chiaramonti, P., Gomes, C.B., Antonini P. & Andrade, F.R.D. (2002). The geochemistry of the Barra do Itapirapuã carbonatite (Ponta Grossa Arch, Brazil): a multiple stockwork. *Journal of South America Earth Sciences* **15**, 215-228.

Rudnik, R.L., McDonough, W.F. & Chappell, B.W. (1993). Carbonatite metasomatism in the Northern Tanzania mantle: petrographic and geochemical characteristics. *Earth and Planetary Science Letters* **114**, 463-474.

Santos, R.V. & Clayton, R.N. (1995). Variations of oxygen and carbon isotopes in carbonatites: a study of Brazilian alkaline complexes. *Geochimica et Cosmochimica Acta* **59**, 1339-1352.

Santos, R.V., Dardenne, M.A. & Oliveira, C.G. (1996). Rare earth elements geochemistry of fluorite from the Mato Preto carbonatite complex, southern Brazil. *Revista Brasileira de Geociências* **26**, 81-86.

Scheibe, L.F. & Formoso, M.L.L. (1982). Contribuição da geoquímica de terras raras à caracterização dos carbonatitos da Fazenda Varela, Lages, SC. *Revista Brasileira de Geociências* **12**, 553-561.

Sheppard, S.M.F. & Schwartz, H.P. (1970). Fractionation of carbon and oxygen isotopes and magnesium between coexisting metamorphic calcite and dolomite. *Contributions to Mineralogy and Petrology* **26**, 161-198.

Siebel, W., Becchio, R., Volker, F., Hansen, M.A.F., Viramonte, J., Trumbull, R.B., Haase, G. & Zimmer, M. (2000). Trindade and Martin Vaz islands, South Atlantic: isotopic (Sr, Nd, Pb) and trace element constraints on plume related magmatism. *Journal of South American Earth Sciences* **13**, 79-103.

Smith, A.D. & Lewis, C. (1999). The planet beyond the plume hypotesis. *Earth-Science Reviews* **48**, 135-182.

Smithies, R.H. & Marsh, J.S. (1998). The Marinkas Quellen carbonatite complex, southern Namibia: carbonatite magmatism with an uncontaminated depleted mantle signature in a continental setting. *Chemical Geology* **148**, 201-212.

Sokolov, S. (2002). Melt inclusions as indicator of the magmatic origin of carbonatite rare metal and rare earth minerals. *Chemical Geology* **183,** 373-378.

Speziale, S., Censi, P., Comin-Chiaramonti, P., Ruberti, E. & Gomes, C.B. (1997). Oxygen and Carbon isotopes in the Barra do Itapirapuã and Mato Preto carbonatites (southern Brazil). *Mineralogica et Petrographica Acta* **40**, 1-21.

Stefanick, M. & Jurdy, D.M. (1984). The distribution of hot spots. *Journal of Geophysical Researches* **98**, 9919-9925.

Sun, S.S. & McDonough, W.F. (1989). Chemical and isotopic systematics of oceanic basalts. In: Saunders, D. & Norry, M.J. (eds.) *Magmatism in the ocean basins*. *Geological Society of London, Special Publication* **42**, pp. 313-345.

Taylor, H.P.Jr., Frechen, J. & Degens, E.T. (1967). Oxygen and carbon isotope studies of carbonatites from Laacher See district, West Germany and Alnø district, Sweden. *Geochimica et Cosmochimica Acta* **31**, 407-430.

Thompson, R.N., Gibson, S.A., Mitchell, J.G., Dickin, A.P., Leonardos, O.H., Brod, J.A. & Greenwood, J.C. (1998). Migrating Cretaceous-Eocene magmatism in the Serra do Mar alkaline Province, SE Brazil: melts from the deflected Trindade mantle plume? *Journal of Petrology* **39**, 1493-1526.

Toyoda, K., Horiuchi, H. & Tokonami, M. (1995). Dupal anomaly of the Brazilian carbonatites: geochemical correlations with hotspots in the South Atlantic and implications for the mantle source. *Earth and Planetary Science Letters* **126**, 315-331.

Traversa, G., Barbieri, M., Beccaluva, L., Coltorti, M., Conte, A.M., Garbarino, C., Gomes, C.B., Macciotta, G., Morbidelli, L., Ronca, S. & Scheibe, L.F. (1996). Mantle sources and differentiation of alkaline magmatic suite of Lages, Santa Catarina, Brazil. *European Journal of Mineralogy* **8**, 193-208.

Traversa G., Gomes, C.B., Brotzu, P., Buraglini, N., Morbidelli, L., Principato, M.S., Ronca, S. & Ruberti, E. (2001). Petrography and mineral chemistry of carbonatites and mica-rich rocks from the Araxá complex (Alto Paranaíba Province, Brazil). *Anais da Academia Brasileira de Ciências* **73**, 71-98.

Traversa, G., Scheibe, L.F., Barbieri, M., Beccaluva, L., Coltorti, M., Conte, A.M., Garbarino, C., Gomes, C.B., Macciotta, G., Morbidelli, L. & Ronca, S. (1994). Petrology and mineral chemistry of the alkaline district of Lages, S.C., Brazil *Geochimica Brasiliensis* **8**, 179-214.

Walter A.V., Flicoteaux, R., Parron, C., Loubet, M. & Nahon, D. (1995). Rare-earth elements and isotopes (Sr, Nd, O, C) in minerals from the Juquiá carbonatite (Brazil): tracers of a multistage evolution. *Chemical Geology* **120**, 27-44.

Van Decar, J.C., James, D. & Assumpção, M. (1995). Seismic evidence for a fossil mantle plume beneath South America and implications for driving forces. *Nature* **378**, 25-31.

Woolley, A.R. & Kempe, D.R.C. (1989). Carbonatites: nomenclature, average chemical compositions, and element distribution. In: Bell, K. (ed.) *Carbonatites, genesis and evolution.* London: Unwin Hyman, pp. 1-1.

*Mesozoic to Cenozoic Alkaline Magmatism in the Brazilian Platform*
*Comin-Chiaramonti, P. & Gomes, C.B. (eds.)*
*Edusp/Fapesp, São Paulo, pp. 657-688, 2005*

# PALEOMAGNETISM OF THE POST-PALEOZOIC ALKALINE MAGMATISM IN THE BRAZILIAN PLATFORM: QUESTIONING THE MANTLE PLUME MODEL

*M. Ernesto*

*A review of the available paleomagnetic data on the post-Paleozoic alkaline rocks in the Brazilian Platform and other South America poles of the same age allows the proposition of a new apparent polar wander path, revealing rotations of the plate associated with the emplacement of the alkaline provinces. By means of an analysis of the magnetization polarity of the rocks, some inferences of the relative ages of the igneous complexes are possible, as the investigated time span comprises the long normal polarity interval of the Cretaceous (Cretaceous Normal Superchron). Absolute reconstructions of the drift movement of South America was achieved by means of paleomagnetic rotations and longitude control through the sea-floor magnetic anomalies. By assuming a fixed hotspot reference frame, the relative position of the alleged causative hotspots, in relation to the respective igneous province, is discussed. None of these hotspots was in favorable position when the corresponding magmatic activity occurred. A model based on long-lived deep mantle thermal anomalies, as revealed by geoid heights, is presented as an alternative for the heat source necessary for the magma generation.*

## INTRODUCTION

The concept of mantle plumes (Morgan, 1971, 1972) gained such strength in geodynamic literature since it has been proposed that all igneous provinces and continental magmatism are tentatively associated with a hotspot, the ultimate expression of the plume activity. However, the identification of the corresponding hotspot in most of the cases has no geological or geophysical basis. It is merely chosen by its proximity to the considered province, and frequently shows a striking feature that may be considered a hotspot track. Consequently, paleo-geographic reconstructions simply force the igneous province into the present hotspot position, even if the paleomagnetism may offer a different interpretation of the plate movement.

In recent years, much has been written (e.g. Sheth, 1999; Smith & Lewis, 1999; King & Ritsema, 2000) against plume model, providing geophysical, geochemical, isotopic and/or numerical modelling evidences that weaken the plume theory. On the other hand, supporters of the theory have presented several alternatives in order to explain the mismatch of the magmatic province and the associated hotspot: 1) when chemical signatures of the rocks are not compatible with plume signature, then the plume contributed with heat, but not with material; 2) if plumes appear displaced from the large igneous provinces, then plumes are not tightly anchored in deep mantle but they move in relation to each other at velocities that may exceed 100 mm/yr. (e.g. Molnar & Stock, 1987; Vandamme & Courtillot, 1990; Duncan, 1990); they are supposed to have generated ~500 mm/yr. fast (Larsen *et al.*, 1999) laterally spreading plumes; plumes would be channeled for a few thousands kilometers to the appropriate position (Thompson *et al.*, 1998); paleomagnetic data may be affected by true polar wander, thus giving wrong plate reconstructions and mislocating the magmatic provinces in relation to the corresponding plumes when the main magmatic phase was occurring (Courtillot *et al.*, 1999).

One of the best examples of a fallacious plume-generated magmatism is the Paraná Magmatic Province (PMP, ~133-132 Ma), one of the largest igneous province in the world, and associated with the Tristan da Cunha (TC) hotspot (e.g. Richards *et al.*, 1989; White & McKenzie, 1989; Milner & Le Roex, 1996; Gibson *et al.*, 1995; Courtillot *et al.*, 1999). The association of the PMP with the TC plume is widely accepted in literature because Walvis Ridge (Fig. 1) has a strong appeal to be taken as a trace left by the Tristan da Cunha hotspot, despite the difficulty of interpreting the expected western symmetrical magmatic chain (i.e. Rio Grande Rise) in terms of a simple mantle plume-hotspot model. As a matter of fact, the Rio Grande Rise (RGR) is composed of two distinct arms (Gamboa & Rabinowitz, 1984): an elevated western portion of elliptical shape (WRGR) and an eastern arm, about 600 km long, trending north-south (ERGR) and parallel to the trend of the present Mid-Atlantic Ridge (MAR).

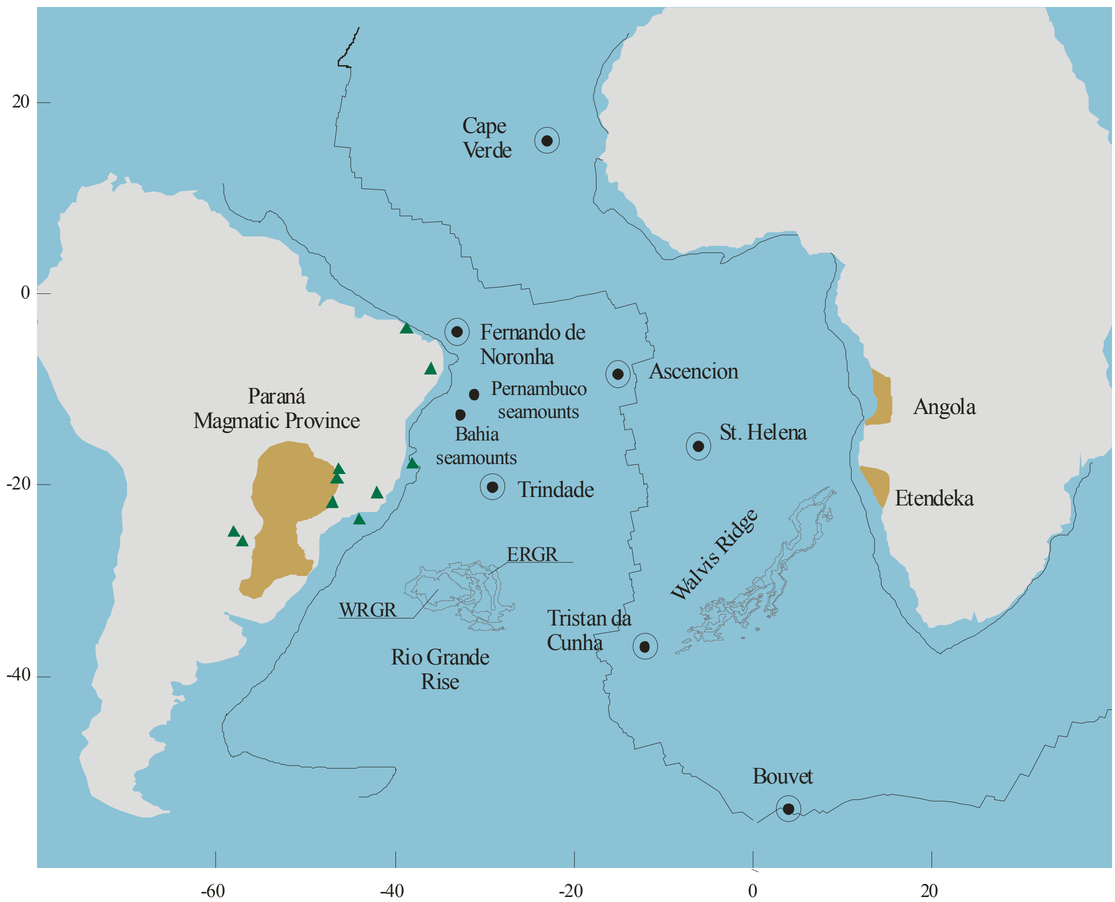


Fig. 1. Distribution of hotspots in Central and South Atlantic in relation to the Paraná Magmatic Province (and its extension into Africa) and the location of some alkaline provinces (triangles) in northeastern and southeastern Brazil.

The quoted authors claim that ERGR, and its conjugate portion of Walvis Ridge, has been formed at the same time by the same processes, and could represent an abandoned spreading center. However, ERGR and WRGR are morphologically different and may have had distinct origins. Le Pichon & Hayes (1971) suggested that WRGR represents a transverse ridge formed along a fracture zone trend, and that the North-South ERGR is due to a modification in the stress field during the opening of the South Atlantic.

Recently, Ernesto *et al.* (2002) demonstrated that PMP could not be generated by TC plume, because TC has never been under the region affected by the Paraná magmatism, and also because does not exist a geochemical plume signature in the Paraná tholeiites, or because the complexity of chemical types and ages distribution in the province does not allow the application of a simple plume model.

The PMP tholeiites are surrounded by alkaline rocks of variable ages. Early Cretaceous (145 Ma) K-alkaline and alkaline-carbonatitic magmatisms (Comin-Chiaramonti *et al.*, 1997, 1999) are found in northwestern PMP (northeastern Paraguay); in the southeastern margins of PMP (Jacupiranga, Juquiá, Anitápolis, and Uruguay) the alkaline rocks are coeval with the tholeiitic magmatism (130-132 Ma); in central Eastern Paraguay more recent activities (i.e. 128-126, 118, 60 Ma) took place (Comin-Chiaramonti & Gomes, 1996).

The alkaline magmatism follows tectonic lineaments (e.g. Ponta Grossa Arch, Rio Uruguay and Rio Pilcomayo), which were also sites of Late Cretaceous (and Tertiary) alkaline magmatism. The latter is also found along other important tectonic lineaments, as the Taiúva-Cabo Frio and Alto Paranaíba-Iporá, and is often attributed to the activity of the Trindade plume (Gibson *et al*, 1995).

In northeastern Brazil, the Tertiary alkaline basalts (Almeida, 1986) have been attributed both to Santa Helena and/or to Ascencion hotspot-mantle plume systems, which include Bahia and Pernambuco seamounts (O'Connor & Le Roex, 1992), or to Fernando de Noronha (Fodor *et al.*, 1998). On the other hand, Courtillot *et al.* (2003) suggested that Fernando de Noronha could be linked to the Early Jurassic Central Atlantic Magmatic Province (cf. Hames *et al.*, 2002).

The distribution of alkaline rocks around PMP and the recurrent magmatic activity in some areas (e.g. western PMP margins, Serra do Mar Province, northeastern Brazil) are also difficult to explain by only one plume model. Furthermore, paleomagnetic data indicate that the plate movement was different from those described by the hypothetical hotspot traces.

In this paper it will be discussed the relationship between mantle plumes and Mesozoic-Cenozoic alkaline magmatism in the Brazilian Platform, by means of plate reconstructions based on paleomagnetic data and sea-floor anomalies.

## PALEOMAGNETIC POLES AND AGE RELATIONSHIP

There are few paleomagnetic poles of post-Paleozoic alkaline rocks in the Brazilian Platform (Table 1; Fig. 2). Most of them refer to the alkaline provinces surrounding the Paraná (Brazil) and the Chaco-Paraná (Paraguay) basins (Ernesto *et al.*, 1996), where magmatic activity took place since the Triassic, and they are most concentrated from Campanian to Eocene (87-42 Ma; Almeida *et al.*, 2000). The alkaline magmatism in these areas is quite variable, including ultrabasic rocks, carbonatites and kimberlites. Literature on these rocks is quite abundant (e.g. Almeida, 1983; Gomes *et al.*, 1990; Comin-Chiaramonti *et al.*, 1997, 1999; Thompson *et al.*, 1998); updated papers are presented in this volume. The available paleomagnetic data from southeastern Brazil belongs to the Alto Paranaíba (Tapira and Salitre complexes; Montes-Lauar, 1993) and Serra do Mar (Poços de Caldas, Itatiaia and Passa Quatro complexes, Santos-Rio de Janeiro dyke swarm, and the São Sebastião necks; Montes-Lauar *et al.*, 1995; unpublished data).

In northeastern Brazil, the Borborema Province (Ulbrich & Gomes, 1981; Almeida *et al.*, 2000) was also affected by an alkaline magmatic activity, ranging from Early Cretaceous to Tertiary times (Fodor *et al.*, 1998; Almeida *et al.*, 2000). The older rocks are best represented by the Cabo Magmatic Province (CMP) in Pernambuco state (Nascimento, 2003), whereas the more abundant Tertiary activity occurs inside (Macau Formation; cf. Mizusaki, 1989) or southwards the Potiguar Basin (Cabugi Magmatism), as well as around Fortaleza city (Macciotta *et al.*, 1990). Paleomagnetic data are only available from CMP (Schult & Guerreiro, 1980), and from the Fortaleza Province (Schult *et al.*, 1986).

In the compilation shown in Table 1, all the existent poles were included, although some of them do not satisfy the commonly accepted reliability criteria. Some other reference poles for the stable South America plate, and some ages of interest for this paper, were included. Poles from the alkaline provinces in Paraguay are considered along with the Brazilian alkaline magmatism, due to the intrinsic geodynamic relationship of these provinces.

The restricted number of poles that are useful to trace the apparent polar wander path (APWP) for South America does not allow a rigorous selection, but poles based on less than five sites were discarded. An exception was made for the Fortaleza Province (only four sites), originally with seven sites (Schult *et al.*, 1986), but recalculated here to lessen scattering.

The Mesozoic-Cenozoic APWP for South America is displayed in Fig. 3, based on the paleomagnetic and radiometric data given in Table 1. It is noticeable the divergence between the APWP proposed by Randall (1998), which combine paleomagnetic poles from South America and Africa, and the path proposed here. As a matter of fact, Randall's curve does not fit the most reliable poles, mainly for the Paleocene-Eocene epochs.

Although much uncertainties still persist regarding the displacement of the South America plate from ~120 Ma to the present, due to scarcity of reference poles (those satisfying the acceptable reliability criteria; e.g. Beck, 1988), and lack of precise radiometric dating in some cases, the available data is sufficient to calculate the amount of drift and rotations that the South America plate underwent during that time interval. It is also possible to draw some inferences about the Brazilian alkaline magmatism ages by means of a comparative analysis.

The APWP Early Cretaceous segment is best defined by high quality paleomagnetic poles satisfying rigorous reliability criteria. Of particular interest are the PMP poles (Fig. 3), including the tholeiitic extrusive rocks of the Serra Geral Formation (SG: 133-132 Ma; Ernesto *et al.*, 1990, 1999) and the Ponta Grossa dolerites (PG: 129-131 Ma; Renne *et al.*, 1996).

The paleomagnetic pole of the Central Alkaline Province (CAP) in Paraguay is in consonance with the Ponta Grossa pole. K-Ar ages (127-130 Ma; Velázquez *et al.*, 1992) also indicate that the alkaline activity on the western side of the PMP have occurred at the same time as the tholeiitic activity (Ponta Grossa dykes) on the eastern side. The record of the most recent activity in PMP is given by the Florianópolis dykes (FL pole), with $^{40}Ar$-$^{39}Ar$ ages ranging from ~119 to 128 Ma (preferred age <127 Ma; Raposo *et al.*, 1998), although Deckart *et al.* (1998) assigned an age of 129±0.3 Ma. However, the FL pole significantly differs from the CAP and PG poles, leading to the conclusion that CAP rocks really concentrate on the older, ~130 Ma, ages. To the North, the Cabo Magmatic Province, represented by trachytes, rhyolites, ignimbrites, basalts/trachyandesites, monzonites and alkali feldspar granites with radiometric age of 102±1 Ma (Nascimento, 2003), was emplaced during the Cretaceous Normal Superchron (CNS of ~121-84 Ma; Gradstein *et al.*, 1994) of normal geomagnetic polarity, as also indicated by the normal polarity magnetizations of those rocks.

The paleomagnetic poles with ages assigned to Late Cretaceous come from the southeastern region

Table 1. Selected paleomagnetic poles for stable South America.

| Formation | Code | Age (Ma) | Paleomagnetic Pole Pol | N | Long (°E) | Lat (°S) | $\alpha_{95}$ (°) | References |
|---|---|---|---|---|---|---|---|---|
| *Alkaline rocks in the Brazilian Platform* | | | | | | | | |
| Fortaleza Province | FO | 28.7±2.5* | M | 4 | 269.5 | 80.8 | 19.3 | Schult *et al.* (1986), recalculated |
| Asunción alkaline plug | PP | 61-39* | M | 13 | 325.4 | 79.4 | 13.6 | Ernesto *et al.* (1996) |
| Serra do Mar Province | SM1 | 70† | R | 7 | 320.3 | 75.3 | 6.9 | Ernesto *et al.* (2004); †Deckart *et al.* (1998) |
| Itatiaia and Passa Quatro combined | IP | 70.5±3.3* | M | 18 | 360.0 | 79.5 | 5.7 | Montes-Lauar *et al.* (1995) |
| Serra do Mar Province | SM2 | 80† | N | 26 | 331.3 | 79.0 | 4.5 | Ernesto *et al.* (2004); †Deckart *et al.* (1998) |
| Poços de Caldas alkaline complex | PC | 84† | N | 36 | 325.7 | 82.2 | 3.2 | Montes-Lauar *et al.* (1995), recalculated |
| Salitre complex | SC | 82.0±2.5# | M | 8 | | (47.2) | | Montes-Lauar (1993) |
| Tapira complex | TP | 82.9±1.5# | R | 10 | 289.8 | 70.6 | 11.2 | Montes-Lauar (1993) |
| Cabo de Santo Agostinho | SA | 102±1† | N | 9 | 315.1 | 87.6 | 4.5 | Schult and Guerreiro (1980); †Nascimento (2003) |
| Central Alkaline Province, Paraguay | CAP | 127-130* | M | 75 | 62.3 | 85.4 | 3.1 | Ernesto *et al.* (1996) |
| *Related poles for the stable South America Platform* | | | | | | | | |
| Abrolhos | AB | 46* | M | 18 | 321.8 | 80.4 | 3.3 | Montes-Lauar (1993), corrected for bedding |
| Patagonian basalts | PB1 | 42-56* | M | 15 | 336.5 | 78.0 | 6.7 | Butler *et al.* (1991) |
| Patagonian basalts | PB2 | 64-79* | M | 18 | 358.4 | 78.7 | 6.3 | Butler *et al.* (1991) |
| Florianópolis dykes, SE Brazil | FL | ~121† | M | 65 | 3.3 | 89.1 | 2.6 | Raposo *et al.* (1998) |
| Serra do Mar Province | SM3 | ~130† | M | 53 | 43.9 | 87.2 | 4.6 | Ernesto *et al.* (2004); †Deckart *et al.* (1998) |
| Ponta Grossa dykes, SE Brazil | PG | 129-131† | M | 115 | 58.5 | 84.5 | 2.0 | Ernesto *et al.* (1999) and references therein |
| Serra Geral Formation | SG | 133-132† | M | 339 | 90.1 | 84.3 | 1.2 | Ernesto *et al.* (1999) |

N=number of sites; *K-Ar ages; † $^{40}Ar/^{39}Ar$ ages; #Rb-Sr ages; (47.2)=mean inclination

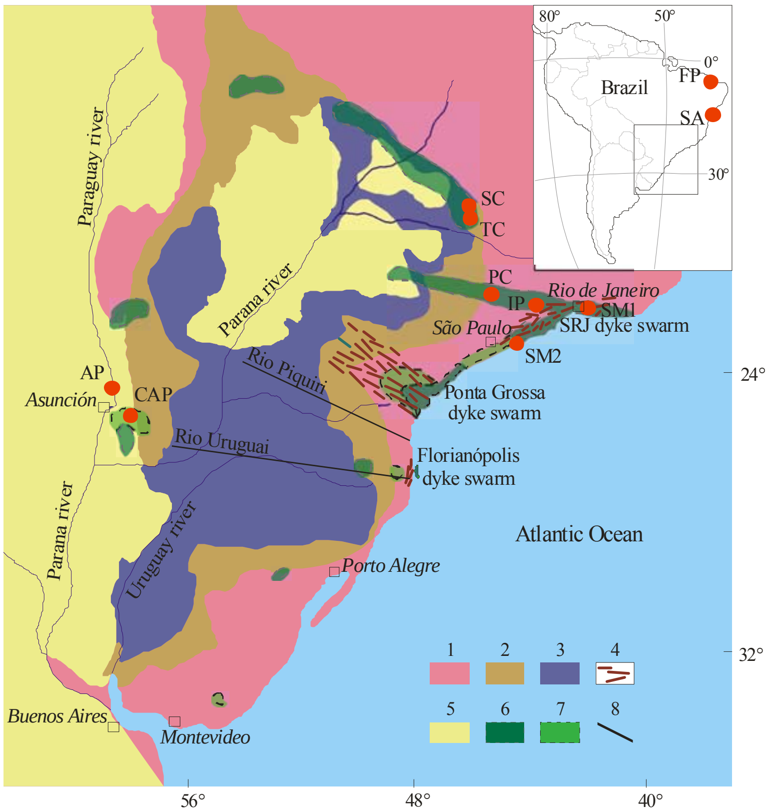


Fig. 2. General map of the Paraná Basin showing the location of the alkaline provinces from which paleomagnetic data are available. Symbols as in Table 1. Other legends: 1) pre-Devonian crystalline basement; 2) pre-volcanic sediments; 3) flood volcanics of the Paraná Magmatic Province; 4) dyke swarms; 5) post-volcanic sediments; 6) main areas of Early Cretaceous alkaline and alkaline-carbonatitic rocks; 7) main areas of Late Cretaceous alkaline and alkaline-carbonatitic rocks; 8) tectonic and/or magnetic lineaments.

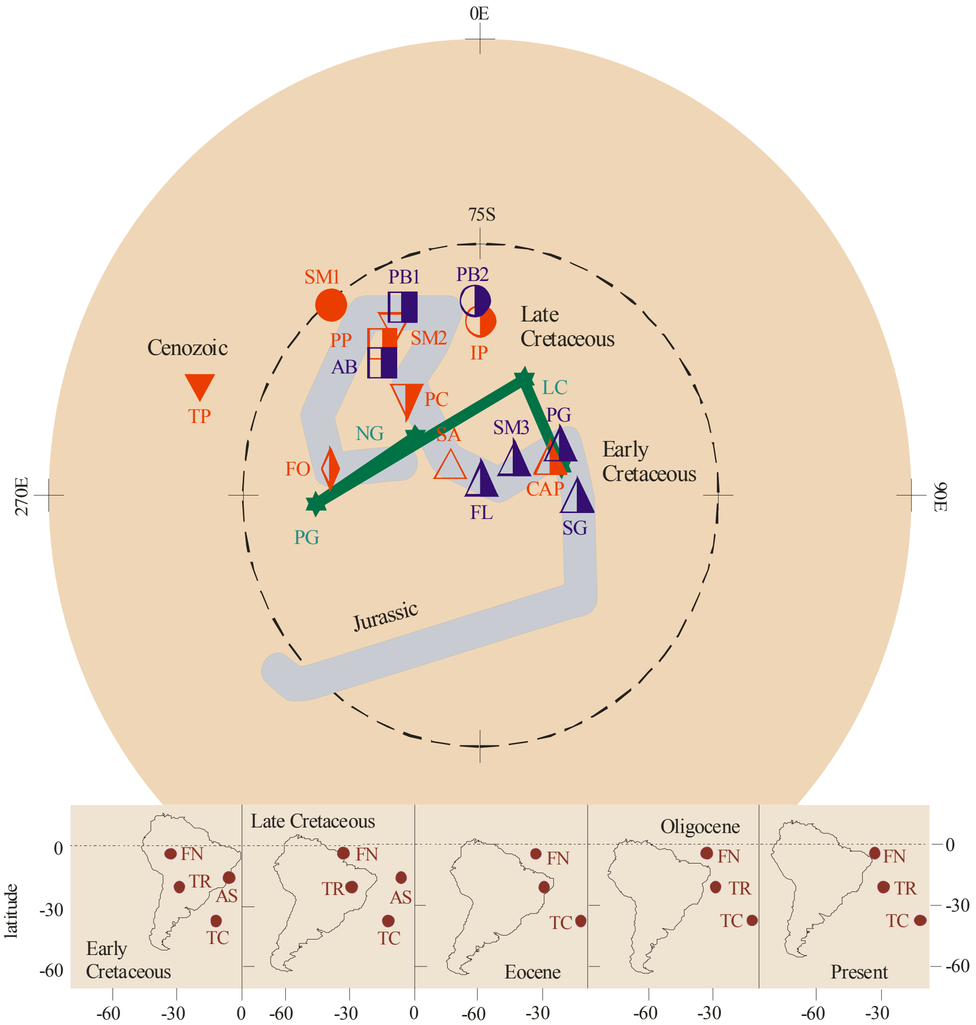


Fig. 3. Paleomagnetic data from post-Paleozoic Brazilian alkaline rocks along with other coeval poles from South America. Triangles: Early Cretaceous; Inverted triangles: Late Cretaceous (~80 Ma); circles: Late Cretaceous (~70 Ma); squares: Eocene (~50 Ma); diamond: Oligocene (~28 Ma). Open, full and half-full symbols represent normal, mixed and reversed polarity, respectively. Green line is the apparent polar wander path (APWP) proposed in this paper. Gray line represents Randall's (1998) APWP combining South American and African poles for Late Cretaceous (LC), Paleogene (PG) and Neogene (NG). Figures bottom: paleomagnetic reconstructions and the relative position of hotspots: Fernando de Noronha (FN), Trindade (TR), Ascension (AS) and Tristan da Cunha (TC).

(Fig. 1): 1) Serra do Mar Province (SM2; Marques *et al.*, 1992; Montes-Lauar *et al.*, 1995; and unpublished data), including the stocks and dykes in the São Sebastião island, and 2) the dykes along the coast between Santos and Rio de Janeiro cities, Poços de Caldas (Montes-Lauar *et al.*, 1995) and Tapira (Montes-Lauar, 1993) complexes, about 80 Ma in age. The Salitre complex (Montes-Lauar, 1993), from the same region and ~80 Ma in age, did not give a paleomagnetic pole because the data were obtained from unoriented cores, but the mean magnetic inclination of 47° is well in accordance with those obtained from other rocks of same age. Except for SM2, which shows only a normal polarity, all other poles of this group include reversed polarities. Although very short chrons of reversed polarity are found inside the CNS (Poornachandra Rao & Mallikharjuna Rao, 1996), they often show ages >95 Ma. Therefore, the ages of the reversed polarity rocks may fall between 84 and 81 Ma (Campanian), approximately the limits of the first reversed chron after CNS, according to Gradstein *et al.* (1994), if we consider that the majority of the analyzed rocks displayed reversed polarities. The Tapira pole, however, is far away from the other two poles, and will not be considered for further interpretations. In fact, as mentioned by Montes-Lauar (1993), this complex is composed by only one plug of 6 km in diameter and shows deep weathering.

In the city of Rio de Janeiro it is frequent to see the dykes of the Serra do Mar Province (normal polarity) being cut by a younger generation of alkaline dykes of reversed polarity. The latter are represented by more evolved lithotypes (Marques *et al.*, 1992), and $^{40}Ar$-$^{39}Ar$ ages fit 70 Ma (Deckart *et al.*, 1998). The same magnetic and chemical characteristics are displayed by other widespread dykes along the coast between Santos and Rio de Janeiro (SRJ dyke swarm in Fig. 2). These evidences are strong enough to allow the calculation of two distinct paleomagnetic poles for the Serra do Mar Province: SM1 and SM2 for the reversed and normal polarity rocks, respectively. However, these two poles do not differ significantly on statistical basis, in part due to the low number of sites (only 7) included in SM1. The younger SM1 pole should be closer to the combined Itatiaia-Passa Quatro pole (IP; Montes-Lauar *et al.*, 1995) as the ages are also around 70 Ma, as well as to the pole based on the basaltic rocks from Patagonia (PB1; Butler *et al.*, 1991), although in this case the available K-Ar ages are more scattered (64-79 Ma). The SM1 pole seems to best fit into the pole group formed by the Asunción plugs (AP; Ernesto *et al.*, 1996), the Patagonian basalts of younger ages (PB1; Butler *et al.*, 1991), and the transitional basalts from Abrolhos islands (AB; Montes-Lauar, 1993), all of them showing K-Ar data ranging from 39 to 56 Ma. Despite this observation, SM1 pole will be considered along with IP and PB2 for the purpose of calculating a mean pole, as the three poles agree in radiometric ages (~70 Ma). To the other pole group (AP, AB and PB1) a mean age of ~50 Ma will be considered. The only available Oligocene pole for the Brazilian Platform is the one from the Fortaleza plugs in Ceará state (pole FP; Schult *et al.*, 1986) with an age of about 28 Ma.

Mean paleomagnetic poles for each age group are given in Table 2. Excepting those from Early Cretaceous, the mean poles show large uncertainties, for they are based on few independent results. However, they give good indications of the successive paleolatitudes and rotations of South America since about 130 Ma. The rotation poles derived from the paleomagnetic poles are also given in Table 2. The paleomagnetic reconstructions of South America, considered as a rigid plate, are shown in Fig. 3. As reference, the Atlantic islands Fernando de Noronha (FN), Trindade (TR), and Tristan da Cunha (TC) are plotted in the same picture. From Early Cretaceous to Eocene, the South America plate was rotating clockwise and latitudes varied slightly up and down in relation to the present latitudes. From Oligocene to present times, the plate described a counterclockwise rotation, and moved northwards to recover the present position.

Table 2. Paleomagnetic mean poles, rotation poles on the equator used in the reconstructions, and corresponding sea-floor anomalies (Nürnberg & Müller, 1991).

| Mean Paleomagnetic Poles | | | | | Rotation Poles | | |
|---|---|---|---|---|---|---|---|
| Age | N | Long. (°E) | Lat. (°S) | $\alpha_{95}$ (°) | Long. (°E) | Angle (°) | Longitude adjustments |
| Early Cretaceous (~130 Ma) | 5 | 76.6 | 85.3 | 1.5 | 180.1 | 5.7 | pre-drift (Ernesto *et al.*, 2002) |
| Late Cretaceous (~80 Ma) | 2 | 328.9 | 80.6 | 7.3 | 73.9 | 9.7 | Anomaly 33R (80.17 Ma) |
| Late Cretaceous (~70 Ma) | 3 | 343.7 | 78.5 | 8.1 | 53.7 | 11.5 | Anomaly 32 (71.37 Ma) |
| Paleocene (~50 Ma) | 3 | 320.8 | 79.1 | 5.7 | 50.8 | 10.9 | Anomaly AN22 (51.95 Ma) |
| Oligocene (~28 Ma) | 1 | 269.5 | 80.8 | | 359.5 | 9.2 | Anomaly AN9 (28.15 Ma) |

## PALEOMAGNETIC RECONSTRUCTIONS AND THE MANTLE PLUME MODEL

Although paleomagnetism is insensitive to longitude variations, absolute paleogeographic reconstructions of the South America plate back to Early Cretaceous are possible if longitude information from sea-floor magnetic anomalies is taken into account. In Table 2 the magnetic anomalies corresponding in age to the mean paleomagnetic poles are indicated, as given by Nürnberg & Müller (1991). These authors give Euler poles for each anomaly that may be used to bring South America plate to its former longitudes for each considered age. For Early Cretaceous, when South America and Africa were still in pre-drift configuration, the spreading center of the ocean floor (Mid Atlantic Ridge, MAR) constitutes a very good longitude indicator. At about 130 Ma rifting between the two plates was already taking place at southern latitudes reaching 38°S (Nürnberg & Müller, 1991), and therefore it is reasonable to admit that the eastern border of the South America platform was close to the site where MAR would later develop.

Following the same procedures presented by Ernesto *et al.* (2002) to investigating alternative heat sources for the generation of the Paraná Magmatic Province, the reconstructed South America plate (SA) at 130, 80 and 50 Ma is plotted on a map of geoid anomalies, as well as the hotspots of interest in their present coordinates (Fig. 4). Large circles around the hotspots mark the ~1000 km radius, correspondent to the area of the plume head spreading (White & McKenzie, 1989). For each considered age, SA plate is rotated by the Euler pole derived from the sea-floor anomalies after being rotated by the corresponding paleomagnetic rotation poles.

Considering the hotspots anchored in the deep mantle, i.e. they are all fixed in relation to each other, it can be inferred that there is no possible relation between Fernando de Noronha and the

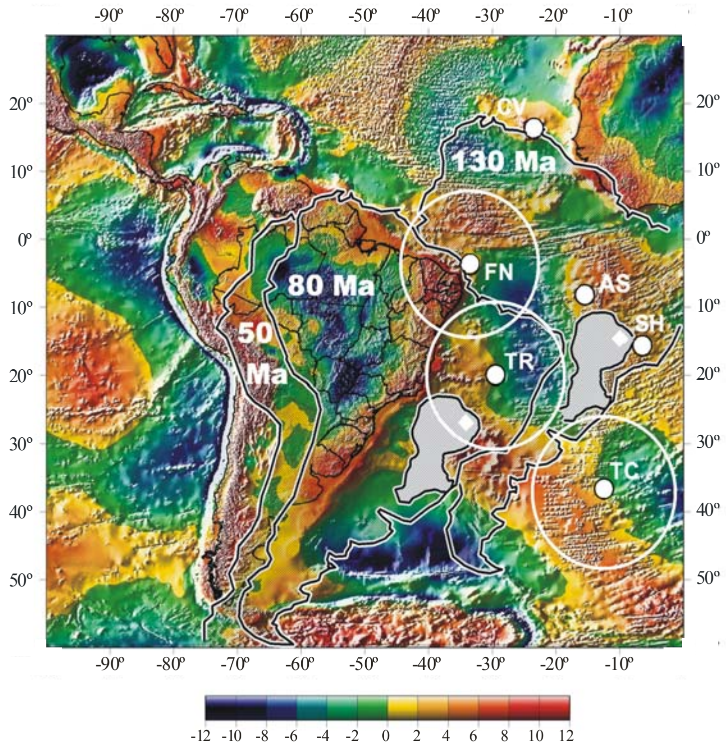


Fig. 4. Geoid anomalies for South Atlantic and South American continental lithosphere (Ernesto et al., 2002). Anomalies in meters. South American plate at 130, 80 and 50 Ma are placed on top of the picture, along with the location of present hotspots and the fossil plume of Van Decar *et al.* (1995).

Tertiary alkaline provinces in Northeastern Brazil as proposed by Fodor *et al.* (1998). Even less chance has Ascencion of having any participation in the northeastern magmatism generation, unless the hypothesis of a hot plume being deflected hundreds of kilometers from the impacted area (Thompson *et al.*, 1998) is taken into consideration. The same may be said of the Late Cretaceous Iporá, Alto Paranaíba and Serra do Mar Provinces and the island of Trindade (Thompson *et al.*, 1998; Gibson *et al.*, 1995).

The hypothesis of mobile plumes is often raised when the hotspot is found away from the magmatic province which it has supposedly generated. This has been so for the case of the Paraná Magmatic Province and Tristan da Cunha hotspot, in order to justify the ~1,000 km offset encountered when paleomagnetic sea-floor spreading reconstruction is used (Ernesto *et al.*, 2002), instead of unconstrained reconstructions (e.g. O'Connor & Duncan, 1990; Turner *et al.*, 1996). However, even in the case of the Paraná-Tristan da Cunha system, for ages from about 80 Ma to the present, the supposed trace of the hotspot (Walvis Ridge) marks the real Africa plate movement. This dichotomy in the hotspot trace-APWP relationship is usually explained as an effect of a true polar wander (TPW) on the paleomagnetic data. TPW corresponds to the differential movement of the mantle reference frame relative to the Earth's spin axes (Andrews, 1985; Gordon & Livermore, 1987). If considerable amounts of TPW are admitted, then paleomagnetic poles are mis-calculated as they are referred to the present rotation axis. Thus, depending on the considered time interval, paleomagnetic data would fall into correctly located large igneous provinces in relation to its correspondent plume head. But calculations of the TPW amount presuppose the concept that the volcanic chains (interpreted as hotspot traces) exactly indicate the movement of the lithospheric plates, and that paleomagnetic APWP deviations reflect TPW. Therefore, these results are not based on an independent source of information, neither from the paleomagnetic data nor from hotspot traces. Furthermore, most of the analyses are restricted to the last 100 Ma, when hotspots are more easily traceable. Although large amounts of TPW have been proposed during Mesozoic, Prévot *et al.* (2000) concluded that no TPW occurred after 80 Ma, and that a single period of shifting existed between 150 and 80 Ma culminating at 110 Ma with an abrupt tilting of 20°.

If TPW cannot be invoked to justify the misfit indicated by paleomagnetic reconstructions between the igneous province and the associated hotspot, then hotspots tracks must be seen as tectonic features reflecting accommodation of stresses in the lithosphere (e.g. LePichon & Hayes, 1971; Ferrari & Riccomini, 1999) rather than continuous magmatic activity induced by mantle plumes beneath the moving lithospheric plates. According to some authors (e.g. Popoff, 1988; Unternehr *et al.*, 1988), the western arm of the Rio Grande Rise represents the accommodation of stresses during the initial opening of the South Atlantic, and its prolongation within South America plate, between the Campos and Pelotas basins, is a dextral deformation. The eastern sector of the Rio Grande Rise is also in accordance with the change of South America movement at about 80 Ma when a north-south drifting component is clear, as already pointed out by LePichon & Hayes (1971). Similar interpretation was given by Ferrari & Riccomini (1999) for the Vitória-Trindade chain, believed to be the Trindade hotspot trace.

From the above discussion it comes out that if plumes have been anchored in the mantle for the last 80 Ma, then TC, TR and FN hotspots have been fixed relatively to the mantle, and therefore could not be under the expected areas in South America plate in order to generate the respective magmatic provinces: PMP and the alkaline provinces on its western and eastern margins (TC; Richards *et al.*, 1989; Courtillot *et al.*, 1999); Iporá, Alto Paranaíba and Serra do Mar provinces (TR; Gibson *et al.*, 1995; Thompson *et al.*, 1998); and the northeastern alkaline provinces (FN; Fodor *et al.* 1998). The Tertiary magmatism in northeastern Brazil has also been associated with the Santa Helena or Ascencion hotspots (O'Connor & Le Roex, 1992), which are even weaker candidates if the above considerations are taken for granted.

## MANTLE PLUMES VERSUS MANTLE THERMAL ANOMALIES

Van Decar *et al.* (1995) mapped a low-velocity zone in the mantle in northeastern PMP, which they interpreted as a thermal anomaly corresponding to the "fossil" TC plume that moved with the lithospheric plate. Considering that the lithosphere has a typical time constant of about 60 Ma (McKenzie, 1978; Gallagher & Brown, 1997) for dissipating heat and consequently attenuating topography, it is quite improbable that the heat of a plume that reached the base of the lithosphere more than 130 m.yr. ago could still persist. It would be more acceptable an association of the low-velocity zone with a plume related to the alkaline magmatic provinces nearby, where magmatism younger than 50 m.yr. can be found. However, no geoid anomaly, nor a surface expression of the TC thermal anomaly, is recognized in this region (Molina & Ussami, 1999), except for the Iporá and Alto Paranaíba Late Cretaceous alkaline provinces (Comin-Chiaramonti *et al.*, 1997, and references therein) further to the north.

Geoid anomalies constitute a source of information about the thermal condition of the Earth's interior. They are defined as the difference in geoid height between the measured geoid and some reference model (cf. Anderson, 1989). Positive geoid anomalies (>4 m) extend along the eastern Brazilian coast (Ussami *et al.*, 1999), except onshore the Bahia coast, where they are smaller than 4 m, and between the São Paulo and Curitiba towns in the southeastern area. In the northeastern area (Borborema Province), anomalies as high as 10 m have been calculated. Apatite fission tracks (AFT; Hegarty *et al.*, 1996; Harman *et al.*, 1998) suggest a re-heating of the area (along the Pernambuco lineament) in the Early Tertiary (~60 Ma). Northward the Potiguar basin, at least two rising episodes were identified in the stratigraphy (Campanian and Oligocene; Cremonini, 1993). The later one possibly occurred at about 25 Ma based on the geoid height in the area (Ussami *et al.*, 1999).

In the southeastern side of the São Francisco craton, where a part of the Alto Paranaíba Province and the Serra do Mar Province are located, the geoid anomaly is also expressive and extends towards de Abrolhos islands and Trindade. AFT data (Gallagher *et al.*, 1994; Ribeiro Filho *et al.*, 1995) indicate a Late Cretaceous age for the last thermal event in the area, which coincides with the age of the alkaline rocks (80-50 Ma). When these thermal events were taking place, none of the presumed plumes were under the corresponding lithospheric areas where they are supposed to have impinged, as indicated by the paleomagnetic reconstructions (Fig. 3). For example, during Late Cretaceous (~80 Ma) the Trindade plume was about 1,000 km to the north of the Serra do Mar Province and APIP. Even considering a 1,000 km plume head radius, it is difficult to explain why the main igneous activity would manifest only at the border of the plume. Moreover (cf. Fig. 3), the displacement of South America plate in relation to the fixed hotspot framework would not result in a hotspot track trending ~E-W, as suggested by the oceanic features. Curiously, the same situation has already been observed for the hypothetical system PMP-TC plume (Ernesto *et al.*, 2002), and for TC, located 1,000 km to the south of PMP during the emplacement of the main volcanic event. On its turn, the FN plume had kept away from the Borborema Province in northeastern Brazil until the Oligocene, whereas Trindade was closer to that area since Late Cretaceous.

In view of this scenario, the hypothesis of a mantle plume/hotspot origin for the alkaline provinces must be reviewed, at least regarding the plumes that have had more chances of being active at the right place and time when a specific province is considered. Moreover, geochemical signatures of the magmatic rocks are distinct from those presented by the commonly related plumes. For example, this is the case for TC and PMP (Peate, 1997; Marques *et al.*, 1999), but even for TC and Walvis Ridge-Rio Grande Rise, the alleged hotspot traces. Coring at the basement of WRGR provided tholeiitic basalts of about 85 Ma, but rocks dredged from the escarpments of the guyots, towering over the platform of the rise, indicated the presence of Eocene alkaline basalts (K-Ar date: 47 Ma; Bryan & Duncan, 1983; cf. Fodor *et al.*, 1997). In addition, the geochemical and Sr-Nd-Pb isotope data are different from those of Walvis Ridge basalts. All the geochemical data (Piccirillo & Melfi, 1988; Marques *et al.*, 1999) indicate that the genesis of the PMP tholeiites mainly reflects melting of heterogeneous lithospheric mantle reservoirs (cf. Comin-Chiaramonti *et al.*, 1997, 1999). Furthermore, the geochemical and isotope signatures of Walvis Ridge and RGR basalts may be explained by the detached continental lithospheric mantle left behind during the continental break-up processes (e.g. Hawkesworth *et al.*, 1986; Peate *et al.*, 1999).

It is also important to stress that the mantle heterogeneity, involved in the Paraná magmatism, is not confined to the tholeiites, but also to the PMP Early (and Late) Cretaceous alkaline magmatism. Even the carbonatites have on the whole a Sr-Nd-Pb isotope imprinting close to that of the related alkaline rocks and the spatially associated tholeiites (Comin-Chiaramonti *et al.*, 1997, 1999, and in this volume; Alberti *et al.*, 1999; Peate *et al.*, 1999; Marques *et al.*, 1999), indicating similar mantle components in their genesis.

In conclusion, the simplistic model of mantle plumes is not satisfactory for explaining most of the continental flood basalts and the recurrent intraplate magmatism; therefore, following Ernesto *et al.* (2002), alternative thermal sources can be found in the mantle with no implication of material transfer from the lower mantle to the lithosphere. Besides the indications from geoid anomalies, the existence of long-living thermal anomalies in the mantle have already been demonstrated by velocity distribution models based on seismic tomography techniques, using both P- and S-waves (e.g. Zhang & Tanimoto, 1992; Zhou, 1996; Li & Romanowicz, 1996; Van der Hilst *et al.*, 1997).

In Fig. 4, the residual geoid anomalies for the South Atlantic, including the continental lithosphere of the South America map, are overlaid by a shaded relief map of the 5'x5' digital topography/bathymetry (cf. Ernesto *et al.*, 2002). The most important residual geoid anomalies clearly correlate with major lithospheric scale features, such as a belt of subtle positive anomalies along the mid-ocean ridges, negative anomalies along deep oceanic basins, thick cratons and, above all, along the Paraná Province.

Two conspicuous intermediate wavelength positive anomalies are observed along the South Atlantic. The first one starts in the equatorial fault system which separates the Central and South Atlantic, then obliquely cross-cuts the ridge axis, and continues along the Ascencion and Santa Helena hotspots, as well as along the Walvis Ridge. The second one extends from southern Brazil, continues along the Rio Grande Rise and get linked to the Antarctic Ridge System. The extent of these anomalies indicates that their source must lie within the mantle. In fact, these two large positive anomalies correlate with a low-velocity zone mapped within the mantle, extending from 165-210 km to 660-710 km (Zhou, 1996). Below this depth, the low-velocity zones almost disappear. For the first 150 km upper mantle interval, Tanimoto & Zhang (1992) proposed a S-wave seismic tomographic model, which shows that the mid-ocean ridges are characterized by a focussed and shallow (~100 km) depth interval of low-velocity distribution. This may explain why geoid anomalies are also not very strong over these features, except in those places where an extra deep seated mantle thermal anomaly is present, as it is the case of those two plate scale positive geoid anomalies. Anderson *et al.* (1992) also observed that the upper mantle is characterized by vast domains of high temperatures rather than by small regions surrounding hotspots, and that low-velocity anomalies record previous positions of migrating ridges, or, in Tanimoto & Zhang's (1992) view, it marks the place where the Western Gondwana break-up occurred. Whatever the interpretation, this is a clear indication that this anomaly persisted for over 100 Ma, and the existence of long-living deep mantle thermal anomalies is very likely.

When the South America plate is represented (Fig. 4) in the geoid anomaly map, in its paleopositions at approximately 130 Ma (pink contour), as calculated in the previous section and displayed in Fig. 3, it comes out that the Paraná Province and the surrounding alkaline provinces plot over the NW-SE geoid/mantle thermal anomaly that contains also Ascencion and Santa Helena hotspots. Most of the alkaline activity concentrates in the 90-50 Ma interval. At 80 Ma (blue contour) the plate moves slightly southwards placing the area correspondent to the Alto Paranaíba and Serra do Mar provinces under the strong geoid anomaly that is now located over the Rio Grande Rise, and continues along the mid-ocean ridge. The same anomaly continues toward the South America eastern continental margin describing a path that nearly coincides with the plate drift path itself. Therefore, the alkaline magmatism that developed in the time interval of 90-70 Ma bordering the Paraná Province does not necessarily need an associated plume to be explained, because, as in the case of PMP, all the affected region was (and part of it still is) over a mantle thermal anomaly.

Paleomagnetic data indicate that drifting velocity was relatively high, and varied from about 23 mm/yr. in the 130-80 Ma interval, to about 7 mm/yr. in the 80-50 Ma interval. However, the path described by the South America plate as seen in Figs. 3 and 4, was such that the areas where the alkaline igneous provinces developed were kept under important mantle thermal anomalies for a time interval long enough for the lithosphere to incorporate the necessary heat. For example, as stressed by Ernesto *et al.* (2002) the area occupied by the PMP was kept under the thermal anomaly for at least ~50 Ma since the Jurassic. If sufficient heat is incorporated to the lithosphere, then magmatism will occur when adequate tectonic conditions take place, and this could mean stress accommodations (Ferrari & Riccomini, 1999) to the plate successive rotations.

The same can be said in relation to the Borborema Province, which moved from a mild anomaly close to the Trindade island to an area of stronger geoid/thermal anomaly near Fernando de Noronha, from 50 Ma to the present.

## CONCLUDING REMARKS

The paleomagnetic data for the post-Paleozoic alkaline rocks in the Brazilian Platform is still poor, and very few paleomagnetic poles satisfy most of the usually accepted reliability criteria, regarding number of independent sampled sites, field tests and precise radiometric dating. The same can be said for the whole paleomagnetic database for the same age interval. Besides this fact, the available data suggest that APWP describes the South America plate movements with very reasonable fidelity, although some refinement is still needed. In particular, the definition of mean poles corresponding to 80, 70 and 50 Ma, based on both paleomagnetic and radiometric information so far is not unique. The group of poles, mixing up rocks of ages in the range from ~80 to ~50 Ma, could also indicate that in this time span the plate displacement was exclusively E-W, and consequently without latitude variation for the paleomagnetic method to detect plate movements.

Changes in the APWP, which account for this alternative drifting scenario, will not change the relative position of the magmatic provinces and the presumed causative hotspot shown in Figs. 3 and 4. This remark reinforces the observed inconsistency between igneous provinces and plate reconstructions

(Heller *et al.*, 1996). In fact, plate reconstructions, usually used to check out the correspondence between igneous provinces and hotspots, are 1) all based on the hotspot frame itself (e.g. O'Connor & Duncan, 1990), and 2) considered to be indicator of absolute plate motions. Therefore, these attempts of reconstruction constitute a vicious proposition.

Paleomagnetic data represent an independent source of information which suggests a very different relationship. If some of the oceanic islands do represent hotspots or the final stage of a mantle plume, then Santa Helena rather than Tristan da Cunha should be associated with the Paraná Igneous Province, as well as Trindade, and not Fernando de Noronha, would be responsible for the Tertiary magmatism in northeastern Brazil.

Courtillot *et al.* (2003) recognized that not all hotspots have deep mantle origin as to characterize mantle plumes, as envisaged by Morgan (1972). Among the hotspots of interest in this paper, only Tristan da Cunha meets the necessary conditions to be classified as deep or primary plume in those authors' view. All the others, i.e. TR, FN, AS and SH, were considered to be a passive response to the lithosphere break-up, with origin in the asthenosphere, as already pointed out by Anderson (2000).

## ACKNOWLEDGMENTS

This work was supported by the Brazilian funding agencies FAPESP and CNPq. Thanks are due to P. Comin-Chiaramonti, L.S. Marques, N. Ussami, E.C. Molina and E.M. Piccirillo, who collaborated to this paper in many different ways.

## ACRONIMOUS LIST QUOTED IN THE TEXT

| | |
|---|---|
| AS | Ascension island |
| AB | Abrolhos islands |
| AFT | Apatite fission tracks |
| AP | Asunción plugs |
| APWP | Apparent polar wander path |
| CAP | Central Alkaline Province, Paraguay |
| CMP | Cabo Magmatic Province |
| CNS | Cretaceous Normal Superchron |
| ERGR | Eastern Rio Grande Rise |
| FL | Florianópolis |
| FN | Fernando de Noronha islands |
| FP | Fortaleza plug |
| IP | Itatiaia-Passa Quatro |
| MAR | Mid Atlantic Ridge |
| PB | Patagonia basalts |
| PG | Ponta Grossa Arch |
| PMP | Paraná Magmatic Province |
| RGR | Rio Grande Rise |
| SA | South America plate |
| SG | Serra Geral Formation |
| SM | Serra do Mar Province |
| SRJ | Santos-Rio de Janeiro |
| TPW | True polar wander |
| TC | Tristan da Cunha island |
| TR | Trindade island |
| WRGR | Western Rio Grande Rise |

## REFERENCES

Alberti, A., Castorina, F., Censi, P., Comin-Chiaramonti, P. & Gomes, C.B. (1999). Geochemical characteristics of Cretaceous carbonatites from Angola. *Journal of African Earth Sciences* **29**, 735-759.

Almeida, F.F.M. (1983). Relações tectônicas das rochas alcalinas mesozóicas da região meridional da plataforma Sul-Americana. *Revista Brasileira de Geociências* **13**, 139-158.

Almeida, F.F.M. (1986). Distribuição regional e relações tectônicas do magmatismo pós-paleozóico do Brasil. *Revista Brasileira de Geociências* **16**, 325-349.

Almeida, F.F.M., Brito Neves, B.B. & Carneiro, C.D.R. (2000). The origin and evolution of the South American Platform. *Earth-Science Reviews* **50**, 77-111.

Anderson, D.L. (1989). *Theory of the Earth*. Oxford: Blackwell Science Publication, 366p.

Anderson, D.L. (2000). The thermal state of the upper mantle: no role for mantle plumes. *Geophysics Research Letters* **27**, 3623-3626.

Anderson, D.L., Tanimoto, T. & Zhang, Y.S. (1992). Plate tectonics and hotspots - The 3rd dimension. *Science* **256**, 1645-1651.

Andrews, J.A. (1985). True polar wander: an analysis of Cenozoic and Mesozoic paleomagnetic poles. *Journal of Geophysical Research* **90**, 7737-7750.

Beck, M.E. Jr. (1988). Analysis of late Jurassic-Recent paleomagnetic data from active plate margins of South America. *Journal of South American Earth Sciences* **1**, 39-52.

Bryan, W.B. & Duncan, R.A. (1983). Age and provenance of clastic horizons from Hole 516F. In: Baker, P.F. *et al.* (eds.) *Initial Reports of the Deep Sea Drilling Project. U.S. Government Printing Office, Washington D.C.* **72**, 475-477.

Butler, R.F., Hervé, F., Munizaga, F., Beck M.E. Jr., Burmester, R.F. & Oviedo, E.S. (1991). Paleomagnetism of the Patagonian plateau basalts, southern Chile and Argentina. *Journal of Geophysical Research* **96**, 6023-6034.

Comin-Chiaramonti, P. & Gomes, C.B. (1996). *Alkaline magmatism in central-eastern Paraguay. Relationships with coeval magmatism in Brazil*. São Paulo: Edusp/Fapesp, 464p.

Comin-Chiaramonti, P., Cundari, A., DeGraff, J.M., Gomes, C.B. & Piccirillo, E.M. (1999). Early Cretaceous-Tertiary magmatism in Eastern Paraguay (western Paraná basin): geological, geophysical and geochemical relationships. *Journal of Geodynamics* **28**, 375-391.

Comin-Chiaramonti, P., Cundari, A., Piccirillo, E.M., Gomes, C.B., Castorina, F., Censi, P., Demin, A., Marzoli, A., Speziale, S. & Velázquez, V.F. (1997). Potassic and sodic igneous rocks from Eastern Paraguay: their origin from the lithospheric mantle and genetic relationships with the associated Paraná flood tholeiites. *Journal of Petrology* **38**, 495-528.

Courtillot, V., Davaille, A., Besse, J. & Stock, J. (2003). Three distinct types of hotspot in the Earth's mantle. *Earth and Planetary Science Letters* **205**, 295-308.

Courtillot, V., Jaupart, C., Manighetti, P., Taponier, P. & Besse, J. (1999). On causal links between flood basalts and continental breakup. *Earth and Planetary Science Letters* **166**, 177-195.

Cremonini, O.A. (1993). *Caracterização estrutural e evolução tectônica da área de Ubarana, porção submersa da Bacia Potiguar, Brasil*. Ph.D. Thesis, Federal University of Ouro Preto, 213p.

Deckart, K., Féraud, G., Marques, L.S. & Bertrand, H. (1998). New time constraints on dyke swarms related to the Paraná-Etendeka magmatic province, and subsequent South Atlantic opening, southeastern Brazil. *Journal of Volcanology and Geothermal Research* **80**, 67-83.

Duncan, R.A. (1990). The volcanic record of the Réunion hotspot. *Proceedings of the ODP Scientific Research* **115**, 3-10.

Ernesto, M. Comin-Chiaramonti, P., Gomes, C.B., Piccirillo, E.M., Castillo, A.M.C. & Velázquez, J.C. (1996). Paleomagnetic data from the Central Alkaline Province, Eastern Paraguay; In: Comin-Chiaramonti, P. & Gomes, C.B. (eds.) *Alkaline magmatism in central-eastern Paraguay. Relationships with coeval magmatism in Brazil*. São Paulo: Edusp/Fapesp, pp. 85-102.

Ernesto, M., Marques, L.M., Piccirillo, E.M., Molina, E., Ussami, N., Comin-Chiaramonti, P. & Bellieni, G. (2002). Paraná Magmatic Province-Tristan da Cunha plume system: fixed versus mobile plume, petrogenetic considerations and alternative heat sources. *Journal of Volcanology and Geothermal Researches*, **130**, 527-553.

Ernesto, M., Pacca, I.G., Hiodo, F.Y. & Nardy, A.J.R. (1990). Paleomagnetism of the Mesozoic Serra Geral Formation, southern Brazil. *Physics of Earth Planetary Interiors* **64**, 153-175.

Ernesto, M., Raposo, M.I.B., Marques, L.S., Renne, P.R., Diogo, L.A. & De Min, A. (1999). Paleomagnetism, geochemistry and $^{40}Ar/^{39}Ar$ dating of the Northeastern Paraná Magmatic province: tectonic implications. *Journal of Geodynamics* **28**, 321-340.

Ferrari, A.L. & Riccomini, C. (1999). Campo de esforços plio-pleistocênico na Ilha de Trindade (Oceano Atlântico Sul, Brasil) e sua relação com a tectônica regional. *Revista Brasileira de Geociências* **29**, 195-102.

Fodor, R.V., Husler, J.W. & Kumar, N. (1997). Petrology of volcanic rocks from an aseismic rise: implications for the origin of the Rio Grande Rise, South Atlantic Ocean. *Earth and Planetary Science Letters* **35**, 225-233.

Fodor, R.V., Mukasa, S.B. & Sial, A.N. (1998). Isotopic and trace-element indications of lithospheric and asthenospheric components in Tertiary alkalic basalts, northeastern Brazil. *Lithos* **43**, 197-217.

Gallagher, K. & Brown, R. (1997). The onshore record of passive margin evolution. *Journal of Geological Society of London* **154**, 451-457.

Gallagher, K., Hawkesworth, C.J. & Mantovani, M. (1994). The denudation history of the onshore continental margin of SE Brazil inferred from apatite fission track data. *Journal of Geophysical Research* **99**, 18117-18146.

Gamboa, L.A.P. & Rabinowitz, P.D. (1984). The evolution of the Rio Grande Rise in Southwest Atlantic. *Marine Geology* **58**, 35-58.

Gibson, S.A., Thompson, R.N., Leonardos, O.H., Dickin, A.P. & Mitchell, J.G. (1995). The Late Cretaceous impact of the Trindade mantle plume: evidence from large-volume, mafic, potassic magmatism in SE Brazil. *Journal of Petrology* **36**, 189-229.

Gomes, C.B., Ruberti, E. & Morbidelli, L. (1990). Carbonatite complexes from Brazil: a review. *Journal of South American Earth Sciences* **3**, 51-63.

Gordon, R.G. & Livermore, R.A. (1987). Apparent polar wander of the mean-lithosphere reference frame. *Geophysical Journal of the Royal Astronomical Society* **91**, 1049-1057.

Gradstein, F.M., Fritis, P.A., Ogg, J.G., Hardenbol, J., van Veen, P., Thierry, J. & Huang, Z. (1994). A Mesozoic time scale. *Journal of Geophysical Research* **99**, 24051-24074.

Hames, W.E., McHone, J.G., Renne, P.R. & Ruppel, C. (2002). The Central Atlantic Magmatic Province: insights from fragments of Pangea. *Geophysical Monograph, AGU* **136**, 128-151.

Harman, R., Gallagher, K., Brown, R., Raza, A. & Bizzi, L. (1998). Accelerated denudation and tectonic/geomorphic reactivation of the cratons of northeastern Brazil during the Late Cretaceous. *Journal of Geophysical Research* **103,** 27091-27105.

Hawkesworth, C.J., Mantovani, M.S.M., Taylor, P.N. & Palacz, Z. (1986). Evidence from the Paraná of South Brazil for a continental contribution to Dupal basalts. *Nature* **322**, 356-359.

Hegarty, K.A., Duddy, I.R. & Green, P.F., (1996). The thermal history in and around the Paraná Basin using apatite track analysis: implications for hydrocarbon occurrences and basin formation. In: Comin-Chiaramonti, P. & Gomes, C.B. (eds.) *Alkaline magmatism in central-eastern Paraguay. relationships with coeval magmatism in Brazil*. São Paulo: Edusp/Fapesp, pp. 41-50.

Heller, P.L., Anderson, D.L. & Angevine, C.L. (1996). Is the middle Cretaceous pulse of rapid sea-floor spreading real or necessary? *Geology* **24**, 491-494.

King, S.D. & Ritsema, J. (2000). African hot spot volcanism: small-scale convection in the upper mantle beneath cratons. *Science* **290**, 1137-1140.

Larsen, T.B., Yuen, D.A. & Storey, M. (1999). Ultrafast mantle plumes and implications for flood basalt volcanism in the Northern Atlantic Region. *Tectonophysics* **311**, 31-43.

Li, X-D. & Romanowicz, B. (1996). Global mantle shear-velocity model developed using nonlinear asymptotic coupling theory. *Journal of Geophysical Research* **101**, 22245-22272.

LePichon, X. & Hayes, D.E. (1971). Marginal offsets, fracture zones, and the early opening of the South Atlantic. *Journal of Geophysical Research* **76**, 6283-6293.

Macciotta, G., Almeida, A., Barbieri, M., Beccaluva, L., Brotzu, P., Coltorti, M., Conte, A., Garbarino, C., Gomes, C.B., Morbidelli, L., Ruberti, E., Siena, F. & Traversa, G. (1990). Petrology of the tephrite-phonolite suite and cognate xenoliths of the Fortaleza district (Ceará, Brazil). *European Journal of Mineralogy* **2**, 687-709.

Marques, L.S., Duprè, B. & Piccirillo, E.M. (1999). Mantle source compositions of the Paraná Magmatic Province (southern Brazil): evidence from trace element and Sr-Nd-Pb isotope geochemistry. *Journal of Geodynamics* **28**, 439-458.

Marques, L.S., Ernesto, M., Piccirillo, E.M., De Min, A. & Figueiredo, A.M.G. (1992). O magmatismo intrusivo cretáceo do Município do Rio de Janeiro: resultados geoquímicos e paleomagnéticos preliminares. *XXXVII Congresso Brasileiro de Geologia, São Paulo, Extended Abstracts* **1**, 511-512.

McKenzie D. (1978). Some remarks on development of sedimentary basins. *Earth Planetary Science Letters* **40**, 25-32.

Milner, S.C. & Le Roex, A.P. (1996). Isotope characteristics of the Okenyenya igneous complex, northwestern Namibia: constraints on the composition of the early Tristan plume and the origin of the EM 1 mantle component. *Earth and Planetary Science Letters* **141**, 277-291.

Mizusaki, A.M.P. (1989). A Formação Macau na porção submersa da Bacia Potiguar. *Boletim Geológico, Petrobrás* **3**, 191-200.

Molina, E.C. & Ussami, N. 1999. The geoid in southern Brazil and adjacent regions: new constraints on density distribution and thermal state of lithosphere. *Journal of Geodynamics* **28**, 321-340.

Molnar, P. & Stock, J.M. (1987). Relative motions of hotspots in the Pacific, Atlantic and Indian Oceans since Late Cretaceous time. *Nature* **327**, 587-591.

Montes-Lauar, C.R. (1993). *Paleomagnetismo de rochas magmáticas mesozóico-cenozóicas da Plataforma Sul-Americana*. Ph.D. Thesis, University of São Paulo, 250p.

Montes-Lauar, C.R., Pacca, I.G., Melfi, A.J. & Kawashita, K. (1995). Late Cretaceous alkaline complexes, southeastern Brazil: paleomagnetism and geochronology. *Earth and Planetary Science Letters* **134**, 425-440.

Morgan, W.J. (1971). Convection plumes in the lower mantle. *Nature* **230**, 42-43.

Morgan, W.J. (1972). Plate motion and deep convections. *Geological Society of America Memoirs* **132**, 7-22.

Nascimento, M.A.L. (2003). *Geologia, geocronologia, geoquímica e petrogênese das rochas ígneas cretácicas da Província Magmática do Cabo e sua relações com as* *unidades sedimentares da Bacia de Pernambuco (NE Brasil).* Ph.D. Thesis, Federal University of Rio Grande do Norte, 233p.

Nürnberg, D. & Müller, R.D. 1991. The tectonic evolution of South Atlantic from Late Jurassic to present. *Tectonophysics* **191**, 27-43.

O'Connor, J.M. & Duncan, R.A. (1990). Evolution of the Walvis Ridge-Rio Grande Rise Hot Spot System: implications for African and South American plate motions over plumes. *Journal of Geophysical Research* **95 B11**, 17475-17502.

O'Connor, J.M. & Le Roex, A.P. (1992). South Atlantic hot spot-plume system: 1. Distribution of volcanism in time and space. *Earth and Planetary Science Letters* **113**, 343-364.

Peate, D.W. (1997). The Paraná-Etendeka Province. In: Mahoney, J.J. & Coffin, M.F. (eds.) *Large igneous provinces: continental, oceanic and planetary flood volcanism. Geophysical Monograph, AGU* **100**, 217-246.

Peate, D.W., Hawkesworth, C.J., Mantovani, M.S.M., Rogers, N.W. & Turner, S.P. (1999). Petrogenesis and stratigraphy of the high-Ti/Y Urubici magma type in the Paraná flood basalt province and implications for the nature of "Dupal-type" mantle in the South Atlantic Region. *Journal of Petrology* **40**, 451-473.

Piccirillo, E.M. & Melfi, A.J. (eds.) (1988). *The Mesozoic flood volcanism from the Paraná basin (Brazil). Petrogenetic and geophysical aspects.* São Paulo: IAG-USP, 600p.

Poornachandra Rao, G.V.S. & Mallikharjuna Rao, J. (1996). Paleomagnetism of the Rajmahal Traps of India: implications to the reversal in the Cretaceous Normal Superchron. *Journal of Geomagnetism and Geoelectrics* **48**, 993-1000.

Popoff, M. (1988). Du Gondwana à l'Atlantique sud: les connexions du fossé de la Bénoué avec les bassins du Nord-Est brésilien jusqu'à l'ouverture de Guineé au Cretacé inférieur. *Journal of African Earth Sciences* **7**, 409-431.

Prévot, M., Mattern, E., Camps, P. & Daignières, M. (2000). Evidence for a 20° tilting of the Earth's rotation axis 110 million years ago. *Earth and Planetary Science Letters* **179**, 517-528.

Randall, D.E. (1998). A new Jurassic-Recent apparent polar wander path for South America and a review of central Andean tectonic models. *Tectonophysics* **299**, 49-74.

Raposo, M.I.B., Ernesto, M. & Renne, P.R. (1998). Paleomagnetic and $^{40}Ar/^{39}Ar$ data on the Early Cretaceous dyke swarm from the Santa Catarina island, Southern Brazil. *Earth and Planetary Science Letters* **144**, 199-211.

Renne, P.R., Deckart, K., Ernesto, M., Féraud, G. & Piccirillo, E.M. (1996). Age of the Ponta Grossa dyke swarm (Brazil) and implications to Paraná flood volcanism. *Earth and Planetary Science Letters* **144**, 199-211.

Ribeiro, L.F.B., Hackspacher, P.C., Hasui, Y., Hadler, J.C., Iunes, P.J. & Tello, C.A. (1995). Datação pelo método de traços de fissão de apatitas presentes em falhas da região de Bragança Paulista (SP). *5º Simpósio Nacional de Estudos Tectônicos, Gramado, Atas* **1**, 191-393.

Richards, M.A., Duncan, R.A. & Courtillot, V.E. (1989). Flood basalts and hot spot tracks: plume heads and tails. *Science* **246**, 103-107.

Schult, A. & Guerreiro, S.D.C. (1980). Paleo-magnetism of Upper Cretaceous volcanic rocks from Cabo de Sto. Agostinho, Brazil. *Earth and Planetary Science Letters* **144**, 199-211.

Schult, A., Calvo Rathert, M., Guerreiro, S.D.C. & Bloch, W. (1986). Paleomagnetism and rock magnetism of Fernando de Noronha, Brazil. *Earth and Planetary Science Letters* **79**, 208-216.

Sheth, H.C. (1999). Flood basalts and large igneous provinces from deep mantle plumes: fact, fiction and fallacy. *Tectonophysics* **311**, 1-29.

Smith, A.D. & Lewis, C. (1999). The planet beyond the plume hypothesis. *Earth-Science Reviews* **48**, 135-182.

Tanimoto, T. & Zhang, Y.S. (1992). Cause of low velocity anomaly along the South Atlantic hotspots. *Geophysical Research Letters* **19**, 1567-1570.

Thompson, R.N., Gibson, S.A., Mitchell, J.G., Dickin, A.P., Leonardos, O.H., Brod, J.A. & Greenwood, J.C. (1998). Migrating Cretaceous-Eocene magmatism in the Serra do Mar alkaline Province, SE Brazil: melts from the deflected Trindade mantle plume? *Journal of Petrology* **39**, 1493-1526.

Turner, S., Hawkesworth, C.J., Gallagher, K., Stewart, K., Peate, D. & Mantovani, M. (1996). Mantle plumes, flood basalts, and thermal models for melt generation beneath continents: assessment of conductive heating model and application to the Paraná. *Journal of Geophysical Research* **101**, 11503-11518.

Ulbrich, H.H.G.J. & Gomes, C.B. (1981). Alkaline rocks from continental Brazil. *Earth-Science Reviews* **17**, 135-182.

Unternehr, P., Curie, D., Olivet, J.L., Goslin, J. & Beuzart, P. (1988). South Atlantic fits and intraplate boundaries in Africa and South America. *Tectonophysics* **155**, 169-179.

Ussami, N., Molina, E.C. & Medeiros, W.E. (1999). Novos vínculos sobre a evolução térmica da margem continental leste do Brasil. *V Simpósio de Estudos Tectônicos, Lençóis-BA, Extended Abstracts*, pp. 20-23.

Van Decar, J.C., James, D. & Assumpção, M.

(1995). Seismic evidence for a fossil mantle plume beneath South America and implications for driving forces. *Nature* **378**, 25-31.

Van der Hilst, R.D., Widyantoro, S. & Engdahl, E.R. (1997). Evidence for deep mantle circulation from global tomography. *Nature* **386**, 578-584.

Vandamme, D. & Courtillot, V. (1990). Paleomagnetism of Leg 115 basement rocks and latitudinal evolution of the Réunion hotspot. *Proceedings of the ODP Scientific Results* **115**, 111-117.

Velázquez, V.F., Gomes, C.B., Capaldi, G., Comin-Chiaramonti, P. Ernesto, M., Kawashita, K., Petrini, R. & Piccirillo, E.M. (1992). Magmatismo alcalino mesozóico na porção centro-oriental do Paraguai: aspectos geocronológicos. *Geochimica Brasiliensis* **6**, 23-35.

White, R. & McKenzie, D.J. (1989). Magmatism at rift zones: the generation of volcanic continental margins and flood basalts. *Journal of Geophysical Research* **94**, 7685-7729.

Zhang, Y-S & Tanimoto, T. (1992). Ridges, hotspots and their interaction as observed in seismic velocity maps. *Nature* **355**, 45-49.

Zhou, H.W. (1996). A high resolution P wave model for the top 1200 km of the mantle. *Journal of Geophysical Research* **101**, 27791-27810.

*Mesozoic to Cenozoic Alkaline Magmatism in the Brazilian Platform*
*Comin-Chiaramonti, P. & Gomes, C.B. (eds.)*
*Edusp/Fapesp, São Paulo, pp. 689-705, 2005*

# BRAZILIAN MINERAL DEPOSITS ASSOCIATED WITH ALKALINE AND ALKALINE-CARBONATITE COMPLEXES

*J.C. Biondi*

*Alkaline and alkaline-carbonatitic complexes in Brazil are not only petrologically interesting, but are also economically important. Metals and industrial minerals are produced from alkaline rocks or are known to occur in potentially economic amounts. Many of the largest alkaline provinces of the world are located in Brazil. Some of them, such as the Amazonian one, are still almost unknown and new alkaline complexes and mineral deposits may be discovered in this region. The present paper aims to synthetize the available data and discuss the Brazilian economic geology related to alkaline rocks. The main alkaline rock associations containing mineral deposits are: 1) miaskitic alkaline complexes (syenites+pyroxenites+ijolites+carbonatites, and/or their effusive equivalents); 2) agpaitic alkaline complexes (nepheline syenites and/or their effusive equivalents, without carbonatites); 3) kimberlites l.s.; 4) lamproites, lamprophyres and ultrapotassic complexes; 5) Alaska-type mafic-ultramafic complexes (peridotites, pyroxenites, gabbros and diorites); 6) peralkaline associations of granites+syenites+ gabbros; 7) metasomatic "episyenites" and albitites formed in shearing zones. In Brazil, the most important mineral ores are found close to the association 1. Nickel ores (garnierite) related to the association 5 have a minor economic interest. Important concentrations of U, Zr, Mo, REE and fluorspar are present in complexes of type 2. Brazilian kimberlitic and lamproitic rocks, representing associations 3 and 4, respectively, are seldom mineralized. The "episyenites" of association 7 show important uranium deposits.*

## INTRODUCTION

Dyke swarms, necks, mono- or polyphasic effusions and intrusions of alkaline rocks are widespread in Brazil (Fig. 1). Except for the diamond deposits in kimberlites and lamproites, which are found associated with sub circular intrusions having diameters of a few tens of meters, all the important mineral deposits occur in alkaline complexes covering areas of some square kilometers (Table 1).

At least three major structural controls are apparent in the distribution of the alkaline magmatism: 1) complexes trending to the anteclises side of flexure regions, between positive (*anteclises*) and negative (*syneclises*) structures (Milashev, 1965; Frantsesson, 1970; Bardet, 1973, 1974; Biondi, 1974); 2) intrusions paralleling deep and rigid structures (*"crustal faults"* of Lumbers, 1978, or "*fractures of continental disjunction*" of Bardet, 1973) in the flexure regions and generally found near to second (or third) order fractures; 3) intrusions cropping out mainly in cratonic regions. The kimberlites and lamproites seem chiefly to have been mineralized only when occurring in areas that remained tectonically stable for long periods of time, e.g. at least 1500 Ma (Gonzaga & Tompkins, 1991).

In particular, the alkaline-carbonatitic complexes and the kimberlitic provinces occur associated with flexure and fractured zones at the borders of the Paraná, Parnaíba and Amazonas basins (cf. Almeida, 1986), where at least three main structural lineaments are observable (Fig. 1):

1) *125ºAZ Lineament* (125° azimuth of Bardet, 1977, corresponding to the "Alto Paranaíba Lineament", at the border between São Paulo and Minas Gerais states), extending from the Rio de Janeiro coast up to the eastern Rondônia state. The most economically important alkaline complexes are widespread in Minas Gerais ("*Triângulo Mineiro*") in association with the largest kimberlitic-lamproitic province known in the country. Alkaline-

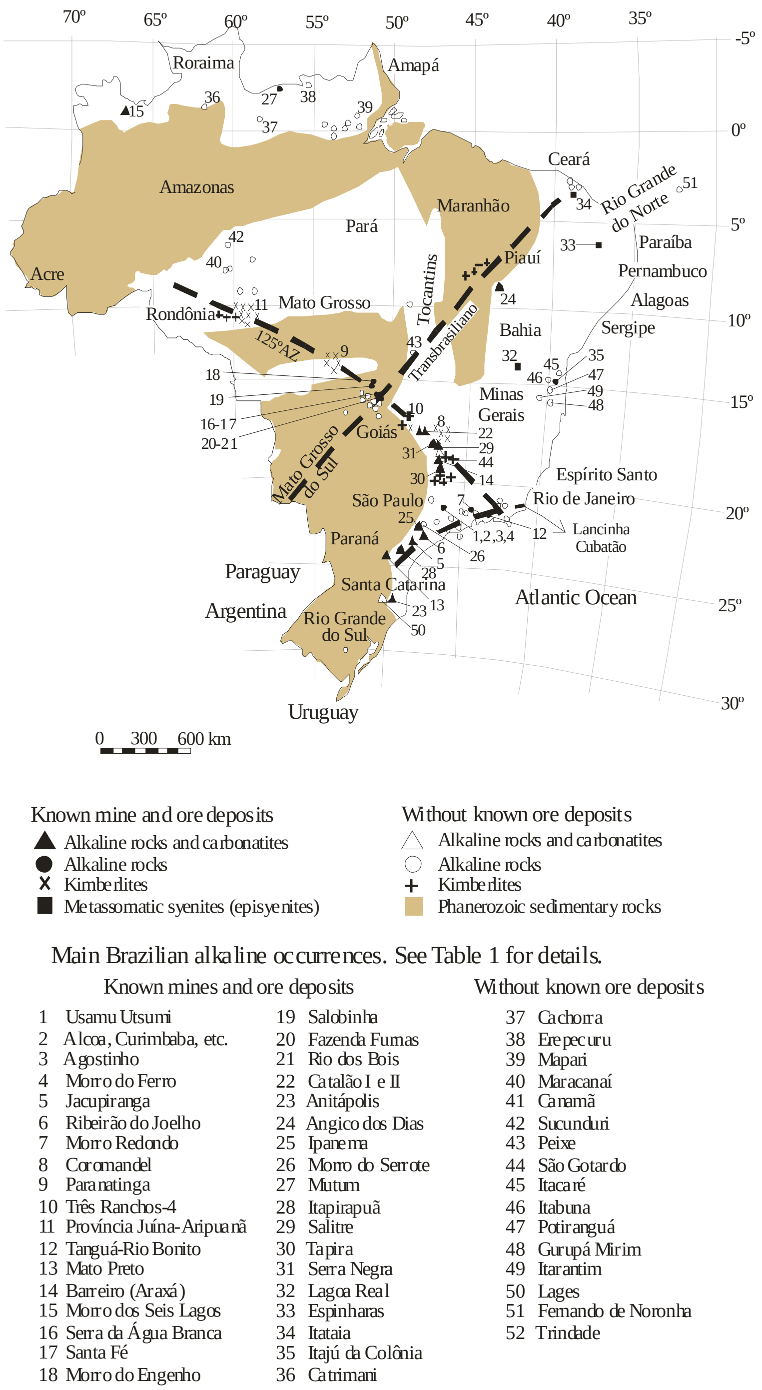


Fig. 1. Distribution of the main alkaline rocks in Brazil (numbers as in Table 1). The 125º AZ, Transbrasiliano and Lancinha-Cubatão lineaments are after Bardet (1973, 1977) and Biondi (1974).

Table 1. Main mineral deposits related to the Brazilian alkaline rocks (ornamental stones and limestones not included). Numbers as in Fig. 1.

| Nº | Mine or deposit | Locality (State) | Ore | Approximate contents | Genetic model | Host rock Age (Ma) | Mineralization Age (Ma) | References |
|---|---|---|---|---|---|---|---|---|
| 1 | **Osamu Utsumi (Cercado)** | Poços de Caldas (Minas Gerais) | U, Mo, Zr, REE | (a) 26,800 ton $U_3O_8$, ?g/ton<br>(b) 25,000 ton $MoO_3$, ?g/ton<br>(c)172,400 ton, 55-60% $ZrO_2$ | 1. Primary ore: veins (fluidization) and disseminated hydrothermal ore<br>2. Secondary ore: supergenic, nodular petchblende. Enrichment related to am oxidation front (only petchblende) | 64-83 (K/Ar) Average=77 Rb/Sr=79±7 | Primary U-Zr-Mo ore: » 60 Ma Secondary, supergenic, nodular, uranium ore: related to erosional Surface | Andrade Ramos & Fraenkel (1974), Fraenkel *et al.* (1985), Biondi (1976), Ulbrich *et al.* (2002) |
| 2 | **Alcoa, Curimbaba and many others** | Poços de Caldas (Minas Gerais) | Al | 50 Mt, 46 wt% $Al_2O_3$, 4.5 wt% $SiO_2$ | Bauxites over fonolites and tinguaites | 64-83 Average=77 Rb/Sr=79±7 | 25-40 | Parisi (1988a), Ulbrich *et al.* (2002) |
| 3 | **Agostinho** | Poços de Caldas (Minas Gerais) | U, Mo | (a) 5,000 ton $U_3O_8$<br>(b) Mo? | U and Mo in the fluidification matrix of brecciated alkaline dykes | 64-83 Average=77 Rb/Sr=79±7 | Primary U-Zr-Mo ore: » 60 My | Biondi (1976), Ulbrich *et al.* (2002) |
| 4 | **Morro do Ferro** | Poços de Caldas (Minas Gerais) | Th, REE | 1.2 Mt, 3.9 wt% $REE_2O_3$ (Ce, La, Nd e Pr) and 1.14 wt% ThO2. | Hydrothermal magnetite dyke with monazite, coffinite and pyrochlore | 64-83 Average=77 Rb/Sr=79±7 | Primary Th, REE, Nb ore: » 60 My | Wedow (1967), Lapido-Loureiro (1994), Ulbrich *et al.* (2002), |
| 5 | **Jacupiranga** | Jacupiranga (São Paulo) | P, lime, (Fe) | 80 Mt, 5.3 wt% $P_2O_5$ (probable reserves: 220 Mt). Carbonatite with less than 4 wt%. MgO (42Mt) is used for Portland cement | Primary ore: carbonatites with 5.5 wt% $P_2O_5$ and less than 4 wt% MgO. Residual ore (run out in 1969): enrichment of apatite over carbonatites | 130 | 130 | Melcher (1966), German et al. (1987), Ruberti *et al.* (1991), Reis (1997) |
| 6 | **Ribeirão do Joelho** | Jacupiranga (São Paulo) | Ni | 2.2 Mt, 1.39 wt% Ni (probable reserves: 1.0 Mt) | Residual, garnieritic ore over ultrabasic alkaline rocks | | | Schobbenhaus (1986) |
| 7 | **Morro Redondo** | Rezende (Rio de Janeiro) | Al | 1.1 Mt, 58 wt% $Al_2O_3$, 3.0 wt% $SiO_2$, 6.33 wt%, $Fe_2O_3$, 1.35 wt% $TiO_2$ | Residual bauxites over alkaline syenites | 64.6-90.5 | Less than 50 My | Parisi (1988b) |
| 8 | **Coromandel** | Coromandel (Minas Gerais) 125ºAZ Lineament, "CK" section | Diamond | ? | Kimberlites, alluvial placers | Neoproterozoic | 53-87 | Souza (1991), Kaminsky *et al.* (2002) |
| 9 | **Paranatinga** | Paranatinga (Mato Grosso) 125ºAZ Lineament, "PA" section | Diamond | ? | Kimberlites | Mesoproterozoic | 121.1 | Berbert (1984), Gonzaga & Tompkins (1991), Weska & Svisero (2002) |
| 10 | **Três Ranchos-4** | Catalão (Goiás) 125ºAZ Lineament, "CK" section | Diamond | ? | Kimberlites | | 80-87 | Gonzaga & Tompkins (1991) |

Table 1 (continued).

| Nº | Mine or deposit | Locality (State) | Ore | Approximate contents | Genetic model | Host rock Age (Ma) | Mineralization Age (Ma) | References |
|---|---|---|---|---|---|---|---|---|
| 11 | **Província Juína-Aripuanã** | Aripuanã (Mato Grosso and Rondônia) 125ºAZ Lineament, "PA" section | Diamond | ? | Kimberlites | | Cretaceous | Gonzaga & Tompkins (1991), Haraly (1991)<br>Araújo *et al.* (2002) |
| 12 | **Tanguá-Rio Bonito** | Itaboraí (Rio de Janeiro) | F (fluorite) | 0.18Mt, 45 wt% $CaF_2$ (probable: 0.4Mt, 45 wt% $CaF_2$) | Shear zone: hydrothermalized veins related to alkaline intrusions | Paleo- to Mesoproterozoic | 100-120 (?) | Coelho *et al.* (1986), Becker *et al.* (1997) |
| 13 | **Mato Preto** | Mato Preto (Paraná) | F, REE | 2.6 Mt, 60 wt% $CaF_2$, 160,000 ton, 41-55 wt% $CaF_2$, ? ton, 7.7 wt% REE,, 41-55 wt% $CaF_2$, ? ton, 7.7 wt% REE, ? ton, 12.82 wt% REE in sideritic carbonatites | Hydrothermal massive and disseminated fluorite in carbonatites. (Hydrothermal ore). | 70.2±4.8<br>71.7±4.7<br>63.2±1.3 | 70.2±4.8<br>71.7±4.7<br>63.2±1.3 | Jenkins II (1987), Gomes *et al.* (1990), Ruberti *et al.* (1997), Jenkins II (1997) |
| 14 | **Barreiro** | Araxá (Minas Gerais) | Nb, P, REE, (Ba, Ti) | Supergenic ore:<br>414 Mt, 3.3 wt% $P_2O_5$,<br>462 Mt, 2.5 wt% $Nb_2O_5$, 546,000 ton, 4.4 wt% $REE_2O_3$<br>Primary ore (unweathered carbonatites):<br>940 Mt, 1.6 wt% $Nb_2O_5$ | 1. Primary ore: carbonatite with barium-pyrochlore (pandaite), apatite and REE<br>2. Secondary ore: Residual enrichment of apatite and bario-pyrochlore over carbonatites | 77.4±1.0 to 97.6±6.1 | Primary ore: 77.4±1.0 to 97.6±6.1 | Issa Filho *et al.* (1984), Silva *et al.* (1986), Gomes *et al.* (1990) |
| 15 | **Morro dos Seis Lagos** | São Gabriel das Cachoeiras (Amazonas) | Nb, REE, Th, Ti | 38.4 Mt,<br>Total ore: 2898 Mt, 2.81 wt% $Nb_2O_5$ and 50 wt% $Fe_2O_3$ ? ton, 3.68 wt% REE | Lateritic ferruginous breccia ore: residual enrichment over carbonatites, with Nb-rich ilmenite-rutile-brookite, monazite and gorceixite | | Lateritic ore: 25-55<br>carbonatite:? | Issler & Silva (1980), Bonow & Issler (1980), Justo & Souza (1986), Lapido Loureiro (1994) |
| 16 | **Serra da Água Branca** | Jussara (Goiás) | Ni vermiculite | 78.7 Mt, 1.30% Ni (?) | Residual, garnieritic ore over ultrabasic alkaline rocks | Cretaceous | 55(?)-0 | Castro Filho & Mattos (1986), Schobbenhaus (1986), |
| 17 | **Santa Fé (Tira Pressa)** | Jussara (Goiás) | Ni | 60.2 Mt, 1.55 wt% Ni | Residual, garnieritic ore over ultrabasic alkaline rocks | Cretaceous | | Schobbenhaus (1986) |
| 18 | **Morro do Engenho** | Montes Claros de Goiás (Goiás) | Ni | Cut off 1.1 wt% Ni: 12.0 Mt, 1.34 wt% Ni<br>Cut off 0.8 wt% Ni: 26.8 Mt, 1.2 wt% Ni<br>Probable total reserves:<br>Cut off 0.8% Ni = 38.6 Mt, 1,10 wt% Ni | Residual, garnieritic ore over ultrabasic alkaline rocks | Cretaceous | | Chaban (1973), Berbert (1986), Schobbenhaus (1986) |

Table 1 (continued).

| Nº | Mine or deposit | Locality (State) | Ore | Approximate contents | Genetic model | Host rock Age (Ma) | Mineralization Age (Ma) | References |
|---|---|---|---|---|---|---|---|---|
| 19 | **Salobinha** | Montes Claros de Goiás (Goiás) | Ni | 52.5 Mt, 1.27 wt% Ni | Residual, garnieritic ore over ultrabasic alkaline rocks | Cretaceous | | Schobbenhaus (1986) |
| 20 | **Fazenda Furnas** | Jaupaci (Goiás) | Ni | 11.1 Mt, 1.34 wt% Ni | Residual, garnieritic ore over ultrabasic alkaline rocks | Cretaceous | | Schobbenhaus (1986) |
| 21 | **Rio dos Bois** | Iporá (Goiás) | Ni | 17.0 Mt, 1.43 wt% Ni (?) | Residual, garnieritic ore over ultrabasic alkaline rocks | Cretaceous | | Schobbenhaus (1986) |
| 22 | **Catalão I e II** | Catalão (Goiás) | P, Nb, Ti, REE, vermiculite | 250.0 Mt, 10.48 wt% $P_2O_5$ plus 121.5 Mt > 7.0 $P_2O_5$ 339.4 Mt > 10 wt% $TiO_2$ 19.2 Mt, 1.3 wt% $Nb_2O_5$ 15.1 Mt >4.0 wt% $CeO_2$+$La_2O_3$, 35.9 Mt, 17.0 wt% vermiculite > 0,5 mm | Residual and supergenic enrichment of monazite-florencite, apatite, anatase, vermiculite and pyrochlore over carbonatites and ultrabasic rocks | 85.0±6.9 to 84.0±4 | | Hasui & Cordani (1962), Carvalho (1974), Schobbenhaus & Campos (1984), Gierth & Baecker (1986), Gomes *et al.* (1990), Carvalho & Bressan (1997) |
| 23 | **Anitápolis** | Anitápolis (Santa Catarina) | P | Secondary, residual ore: 53.5 Mt, 8.2 wt% $P_2O_5$ Primary ore (unweathered rocks): 206.5 Mt, 5.9 wt% $P_2O_5$ | Primary ore: patite- rich ultramafic, nepheline syenites, urtites and carbonatites. Secondary ore: residual enrichment of apatite over ultramafic, nepheline syenites, urtites and carbonatites. | 130.6±3.0 to 136.4±1.6 | Primary ore: 130.6±3.0 to 136.4±1.6 Residual enrichment: 55(?)-0 | Schobbenhaus & Campos (1984), Gomes *et al.* (1990), Vergara (1997) |
| 24 | **Angico dos Dias** | Monte Alegre de Lourdes (Bahia) | P | Primary carbonatitic ore: ? ton, » 9.6 wt% $P_2O_5$ Residual ore: 15.0 Mt, 15.4 wt% $P_2O_5$ | Primary ore: apatite- rich carbonatites. Residual enrichment of apatite over carbonatites | 2011±6 | Primary ore (carbonatites): 2011±6 Residual ore: ~55(?)-0 | Silva *et al.* (1987), Silva *et al.* (1997) |
| 25 | **Ipanema** | Ipanema (São Paulo) | P, vermiculite, (Fe, Ti) | 117 Mt, 6.7 wt% $P_2O_5$ 5.0 Mt, 20 wt% vermiculite | Residual enrichment of apatite over carbonatites and carbonatites and alkaline rocks | 124.9±9.5 to 126.1±5.4 | | Leinz (1940), Gomes *et al.* (1990) |
| 26 | **Morro do Serrote** | Juquiá (São Paulo) | P | 18 Mt, 10.0 wt% $P_2O_5$ | Residual enrichment of apatite over carbonatites | 131.7±1.6 to 134.0±1.6 | | Born (1972), Gomes *et al.* (1990) |
| 27 | **Mutum** | Mutum (Amazonas) | P | (?) | Presence of phosphate- rich rocks (?) | 1026±28 | | Gomes *et al.* (1990) |

Table 1 (continued).

| Nº | Mine or deposit | Locality (State) | Ore | Approximate contents | Genetic model | Host rock Age (Ma) | Mineralization Age (Ma) | References |
|---|---|---|---|---|---|---|---|---|
| 28 | **Barra do Itapirapuã** | (São Paulo-Paraná) | REE, P | Paraná State: 1.4 Mt, 0.94 wt% $REE_2O_3$<br>2.1 Mt, 3.0 wt% $P_2O_5$<br>São Paulo State:<br>44.8 Mt, 0.7 wt% $REE_2O_3$<br>1.1 Mt, 2.5 wt% $P_2O_5$ | Primary ore: bastnaesite-synchisite and apatite in carbonatites | 96.9±1.9 to 114.7±9.7 | 96.9±1.9 to 114.7±9.7 | Gomes *et al.* (1990) |
| 29 | **Salitre** | Patrocínio (Minas Gerais) | P, Ti, Nb | Total reserves:<br>852.0 Mt, 10.7 wt% $P_2O_5$<br>694.3 Mt, 17.5 wt% $TiO_2$<br>196.0 Mt, 0.48 wt% $Nb_2O_5$ | Residual enrichment of apatite, anatase and pyrochlore over carbonatites and alkaline rocks | 79.0±1.2 to 86.3±5.7 | | Gomes *et al.* (1990), Melo *et al.* (1997) |
| 30 | **Tapira** | Tapira (Minas Gerais) | P, Ti, Nb, REE | Total reserves:<br>1381 Mt, 8.19 wt% $P_2O_5$<br>166 Mt, 0.73 wt% $Nb_2O_5$<br>414 Mt, 17.82 wt% $TiO_2$,<br>? ton, 1 to 10% $REE_2O_3$<br>( $Eu_2O_3$: 0.36 wt% ; Y2O3: 1.9 wt%) | Residual enrichment of apatite, anatase and pyrochlore and REE over carbonatites and alkaline rocks | 71.2±5.1 to 87.2±1.2 | | Hasui & Cordani (1962), Gomes *et al.* (1990), Ruberti *et al.* (1991), Lapido Loureiro (1994), Melo (1997) |
| 31 | **Serra Negra** | Serra Negra (Minas Gerais) | (Zr, Ti) | | Occurrences on outcrops and alluvial placers | 83±3 | | Gomes *et al.* (1990) |
| 32 | **Lagoa Real** | Lagoa Real (Bahia) | U | Proven reserves:<br>61.8 tons $U_3O_8$<br>Total reserves:<br>93,190 tons $U_3O_8$, ? g/ton | U in metasomatic episyenites | Paleo proterozoic | Regional metamorphism at 1500 Ma<br>Uranium remobilization at 820 Ma | Oliveira *et al.* (1985), Lobato & Fyfe (1990) |
| 33 | **Espinharas** | Patos (Paraiba) | U | Total probable reserves:<br>10,000 tons $U_3O_8$<br>Ore grades:<br>500 to 1000 ppm $U_3O_8$ | U in metasomatic episyenites | Neo proterozoic | 395-450 | Santos & Anacleto (1985) |
| 34 | **Itataia** | Itataia (Goiás) | U, P | (a) 142,500 tons $U_3O_8$,<br>0.19 wt% $U_3O_8$<br>(b) 18.0 Mt,<br>26.35 wt% $P_2O_5$ | 1. Primary ore: uranium in metasomatic episyenites<br>2. Secondary ore: supergenic enrichment of U in collophanites<br>3. Secondary, supergenic ore: collophanite | Paleo to Neo proterozoic | 1. Apatitic marbles: 2000-2500 Ma(?)<br>2. Episyenites- 550-600 Ma(?)<br>3. Supergenic enrichment- collophanites <550 Ma(?) | Mendonça *et al.* (1985) |
| 35 | **Fazenda Hiassu** | Itajú da Colônia (Bahia) | Sodalite | » 80,000 tons of sodalite | Magmatic differentiation? | 411 to | 411 to | Cassedane & Cassedane (1976), Cassedane (1991) |

carbonatitic complexes are found in the states of Minas Gerais (Catalão, Araxá, Tapira), and kimberlites (Iporá) and ultrabasic-alkaline complexes occur in Goiás. In Mato Grosso and Rondônia states are located the kimberlitic provinces of Paranatinga and Juína-Aripuanã, respectively, the former containing kimberlites with large chances of being economically mined (Gonzaga & Tompkins, 1991).

2) *Lancinha-Cubatão Lineament*, following the Brazilian southeastern coast line between the Paraná and Rio de Janeiro states. Main occurrences are Mato Preto, Tunas and Banhadão in Paraná State; Itapirapuã, Barra do Itapirapuã, Jacupiranga, Morro do Serrote and Ipanema in São Paulo and the intrusions nearby Rezende in Rio de Janeiro (e.g. Morro Redondo, Tanguá, Rio Bonito). The alkaline complexes of Lages and Anitápolis in Santa Catarina (Fig. 1) may be associated with this lineament. Almeida (1986) relates the latter alkaline complexes to the "Blumenau Lineament" (cf. Hartmann *et al.*, 1980), which is located at the inflexion zone between the Ponta Grossa Arch (Paraná) and the Torres Synclinal (Rio Grande do Sul). According to Janse (1984), this lineament extends into Africa, from Angola (alkaline and kimberlitic complexes of Nova Lisboa and kimberlitic province of Luanda) to Zaire (kimberlites of Mbuji Mayi). Gomes *et al.* (1990) suggest that the alkaline intrusions from Paraná and south of São Paulo are controlled by the semi parallel NW-SE-trending lineaments of Guapiara, São Jerônimo-Curiúva, Rio do Alonzo and Rio Piquiri, all of them associated with the Ponta Grossa Arch of Jurassic age.

3) *Transbrasiliano Lineament*, having a general direction given by the azimuth 45° and extending from the northeastern Paraguay up to Fortaleza in the Ceará state. This structural feature crosses the 125°AZ lineament in southwestern Goiás, showing in the intersection zone many mineralized ultrabasic-alkaline complexes such as Água Branca, Santa Fé, Morro do Engenho, Salobinha, Fazenda Furnas and Rio dos Bois. Kimberlitic rocks also occur in the area of Picos in the Piauí state and alkaline rocks are described in the vicinities of Fortaleza.

Alkaline and alkaline-carbonatitic occurrences and many diamond placers (suggesting the presence of kimberlites and/or lamproites) are found in the Amazonian Basin (Fig. 1) without apparent structural control. Also a group of alkaline intrusions in southeastern Bahia is apparently not related to structural lineaments.

The available data indicate that most of the Amazonian complexes are Early- to Middle Proterozoic in age, whereas the Bahia bodies are from the Late Proterozoic to Cambrian. On the other hand, the remaining Brazilian occurrences are concentrated in the Mesozoic and subordinately in the Cenozoic.

Even assuming that the majority of the mineralized alkaline centers are located along the 125°AZ structure, it cannot be inferred that this lineament is markedly fertile. It is noticeable, however, that four regions with mineralized kimberlitic pipes (Coromandel, Paranatinga, Três Ranchos-4 and Juína-Aripuanã, cf. Table 1 and Fig. 1) are associated with that structural feature. According to Gonzaga & Tompkins (1991), the pipes with more significant mineralization are found in tectonically stable regions since the Parguazense times (1600-1500 Ma).

## MAIN MINERAL DEPOSITS

Table 1 lists the 35 main Brazilian mineral deposits genetically related to alkaline rocks. Some of these deposits, such as those of niobium from the Barreiro mine (Araxá complex), and titanium from the Tapira and Salitre complexes, in Minas Gerais state, have international economic importance. Other ones, such as the rare-earths deposit of Catalão I, in Goiás, and the uranium deposit of Itataia, in Ceará, depend on technological and management solutions in order to become productive, but they are distinguished by the importance of their reserves and contents. The phosphate deposits of Tapira, Catalão, Araxá and Anitápolis, this last one in Santa Catarina, which produce large amounts of phosphate fertilizers, are also of national relevance.

The following detailed description of the occurrences according to genetic criteria may provide guidelines for the prospection of similar new mineral deposits.

## U, Zr, Mo, Th and REE deposits from the Poços de Caldas complex

The largest Brazilian Poços de Caldas alkaline complex, lying at the border of Minas Gerais and São Paulo states, forms a circular multiple structure of 1100 m high, with about 28 km of diameter (Fig. 2), emplaced between 83 and 64 Ma (average K/Ar value of 77 Ma). More recent Rb/Sr data from various nepheline syenites resulted in an isochron age of 79±7 Ma (Ulbrich *et al.*, 2002). The border is almost completely marked by a large tinguaitic ring-dyke (Andrade Ramos & Fraenkel, 1974; Fraenkel *et al.*, 1985). Notably, at least twelve secondary circular structures, with diameters ranging from 1 to 5 km, and believed to be remnants of ancient volcanoes, form the largest structure. The main rocks are phonolites, tuffs and tinguaitic breccias, occupying nearly two-thirds of the complex; subordinate rock-types are nepheline syenites (foyaites). Lujavrites (eudialyte-lamprophyllite-sodalite hypersolvus mela-nepheline syenites with pronounced lamination) and khibinites (eudialyte-lamprophillite-clinopyroxene hypersolvus nepheline syenites) crop out in the northeastern border of the intrusion (Ulbrich & Ulbrich, 2000). On the whole, the petrochemistry indicates miaskitic and agpaitic suites with agpaitic index ranging from 0.77 (tinguaites) to 1.14 (nepheline syenites, foyaites, phonolites and lujavrites). Although carbonatite occurrences are not known inside the complex, 79±3 Ma carbonatite veins (Th-U-total Pb age of thorite) associated with lamprophyric-pyroxenitic dykes and fenites occur in basement gneisses at the southeastern border (Ulbrich *et al.*, 2002). Fenites are also found at the southeastern border. Alkaline rocks strongly altered by hydrothermal and weathering processes occur in the central areas of the complex, where the following main mineral deposits were mined:

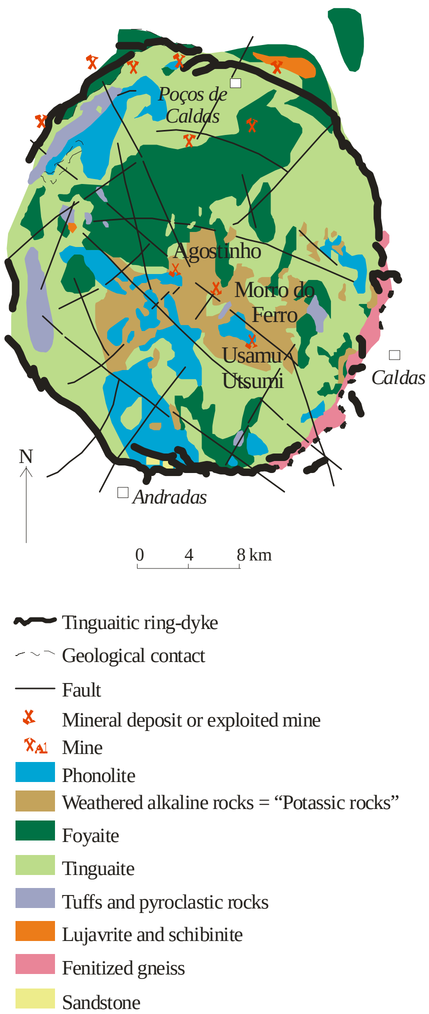


Fig. 2. Simplified geological map of the Poços de Caldas alkaline complex.

1) the exhausted Usamu Utsumi or Cercado mine, with U-Mo-Zr-REE ore (Table 1, n. 1);

2) the Agostinho Mo-U-Zr deposit (Table 1, n. 3);

3) the Morro do Ferro Th-REE-Nb deposit (Table 1, n. 3).

Bauxite mines (Table 1, n. 3) are associated with the tinguaite ring-dyke and are found in the interior of the plateau, mainly in the region around the city of Poços de Caldas.

### *U-Mo-Zr-REE Usamu Utsumi (Cercado) mine*

Mining activities in Usamu Utsumi ended in 1995. 26,800 tons of 0.15 wt% $U_3O_8$, plus 25,000 tons of $MoO_3$ and 172,400 tons of 55-60% wt% $ZrO_2$ concentrate, have been so far mined. The mineralized bodies of the Usamu Utsumi mine were formed in the inner part of a brecciate conical chimney, measuring about 1200x600 m in the surface. The chimney is almost completely filled by tinguaitic breccias intersected by dykes and necks of tinguaite and phonolite. It is limited at the south by a fracture system leaving the breccias in contact with the tinguaitic and phonolitic lavas (Fig. 3). All the rocks found inside and at the borders of the breccia chimney are strongly hydrothermally altered by a pervasive formation of clay minerals and pyrite. Fluorspar and calcite are less frequent alterated products, occurring mainly in fractures.

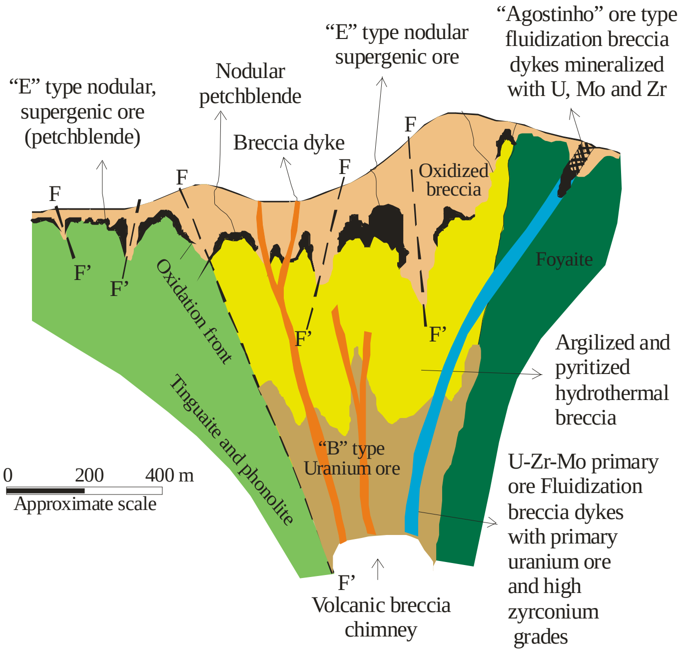


Fig. 3. Simplified sketch showing the ore types in the Usamu Utsumi and Agostinho U-Mo-Zr mines (Biondi, 1976).

Three main kinds of ore were extracted from the Usamu Utsumi mine:

1) "B" type ore (Fig. 3), disseminated in the inner parts of the breccias cone and formed by hydrothermal alteration of breccias and tinguaitic and phonolitic lavas. Such ore represents the largest part of the reserves (nearly 60%) and contains as main minerals uraninite, zircon and molibdenite, the latter generally altered into jordisite and ilsemannite. The gangue is made of clay minerals (mainly kaolinite), pyrite and residual phases of the hydrothermalized rocks.

2) "Fluidization" breccia-type ore (Reynolds, 1954; Lorenz *et al.*, 1970; Biondi, 1974; Woolsey, 1975; Burnham, 1985; Lorenz, 1985; McCallum, 1985), found in places where the mine is crossed by dykes and breccia pipes. The latter ones were emplaced mainly in the inner parts of the breccia chimney and subordinately in the country-rocks. The breccias, formed by a sequence of phreatic implosions followed by the percolation of fluids under high pressure (water steam+volcanic gas), are composed of fragments of all the rock-types cut by pipes and dykes, and cemented by a matrix material consisting of pulverized rocks and phonolitic lava. They constitute mineralized bodies (Fig. 3) having as main minerals uraninite, uranium-rich zircon, baddeleyite, molibdenite (jordsite), pyrite, sphalerite, galena and fluorspar. This ore type corresponds to nearly 10% of the reserves.

3) "E" type nodular ore associated with oxidation fronts, formed by meteoric and oxidizing water. The hydrothermalized-mineralized breccias are permeable rocks, easily percolated by water flowing from the surface. These waters, after the oxidation of pyrite, generated sulfates and iron hydroxides. Moreover, the resulting acid water, by lixiviation processes of the breccias and lavas, tend to

concentrate the uranium in the reduced side of the oxidation fronts. Mineralized bodies originated from this process are greatly irregular on shape and discontinuous (Fig. 3), occurring usually as pods strongly enriched uranium, in which the resulting spotted black mark is characterized by the concentration of microcrystalline pitchblende and by centimetric nodules of massive pitchblende and pyrite. In these ores, the mean content exceed 2 wt% $U_3O_8$. The supergenic nodular ore represents about 30% of the mining reserves.

*Mo-U-Zr Agostinho deposit*

The Agostinho deposit contains nearly 5,000 tons of $U_3O_8$, with about 0.1 wt% $MoO_3$ and 1.0 wt% $ZrO_2$ grades, respectively. Breccia dykes submitted to fluidization form the deposit, which is very similar to the same type present in the Usamu Utsumi mine. The Agostinho ore is characterized by high Mo content (molibdenite, jordisite and ilsemannite) having U as sub product. In addition to uraninite and zircon, the ore has minerals as fluorspar and pyrite disseminated in the breccia matrix.

*Morro do Ferro Th-REE-(Nb) deposit*

The Morro do Ferro deposit contains about 1.2 Mt with 3.9 wt% $REE_2O_3$ (Ce, La, Nd and also P), 1.14 wt% $ThO_2$ and non-determined Nb content; Wedow, 1967; Lapido Loureiro, 1994). It consists of hydrothermal veins of massive magnetite, 1 to 5 m thick, set in a magnetite stockwork. The whole structure is hosted by strongly lateritized rocks (tinguaites, phonolites and foyaites; Fig. 4) with supergenic concentration of resistant minerals and insoluble substances.

Primary ore minerals are allanite, bastnaesite, thorbastnaesite, monazite, coffinite, thorogumite, cerianite and fersunite (Lapido-Loureiro, 1994) set in a gangue consisting of magnetite, sericite, clay minerals, pyrite, zircon, rutile and anatase, with fissural fluorspar and molibdenite. The lateritic ore is composed of iron and manganese hydroxides forming a crust enriched of resistant minerals, mainly uranium and REE oxides, covering a clayey regolith also containing supergenic concentration of thorium, titanium and REE oxides and hydroxides.

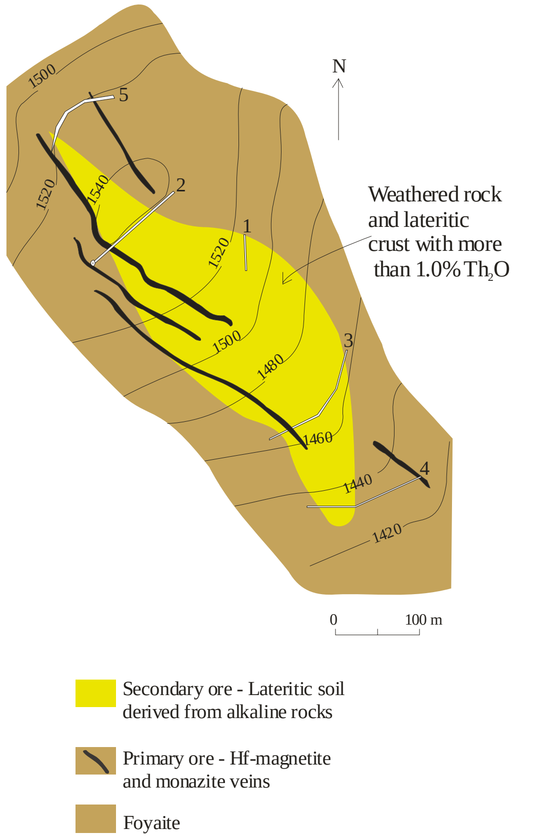


Fig. 4. Map of the Morro do Ferro REE and Th deposit (Wedow, 1967).

Phosphate and limestone, Morro da Mina mine, Jacupiranga

The Jacupiranga alkaline-carbonatite complex (an oval intrusion of 6.6 km long and 4.8 km wide; Fig. 5A) intrudes the Turvo-Cajati Group (Paleoproterozoic) and the Graciosa granite (513±13 Ma; cf. Germann *et al.*, 1987). A Rb/Sr isochron provided an age of 131±3 Ma (Gomes *et al.*, 1990; Ruberti *et al.*, 1991).

The northern and southern areas of the complex are formed by prevailing dunites and jacupirangites, respectively. Ijolites crop out in the southwestern part of the intrusion and carbonatites are found intruding the jacupirangites (Fig. 5A). Alkaline gabbros, melagabbros, quartz monzonites and quartz syenites are present in the western side of the complex, and in its southern area a dyke swarm of essexites, theralites and syenites is noticeable (Germann *et al.*, 1987). Fenites occur in the inner and border zones of the complex. At the contact between carbonatites and jacupirangites, metasomatic reactions led to the formation of silicate-rich (amphibole, phlogopite and olivine) and carbonatite bands or shells (Morbidelli *et al.*, 1986).

The mined area is the carbonatite body (Fig. 5B),

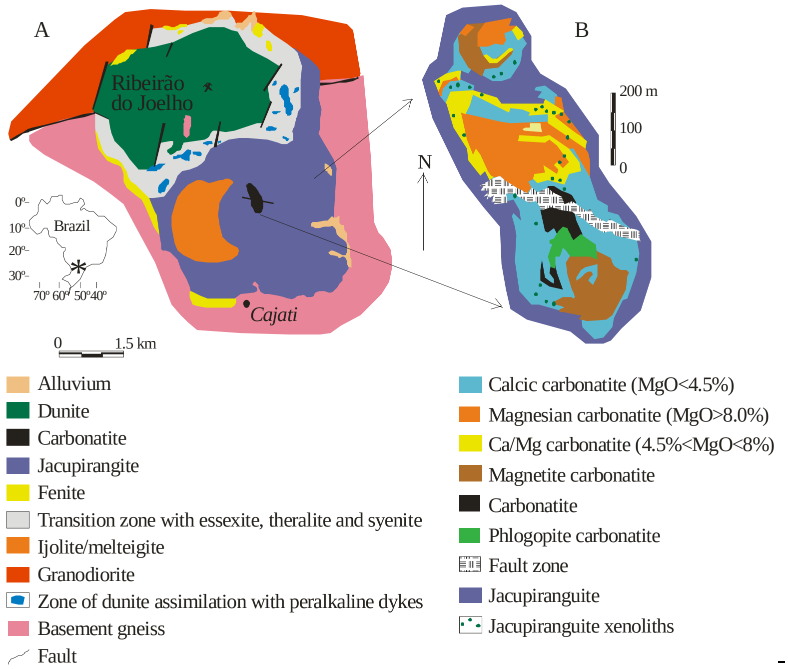


Fig. 5. A: Jacupiranga alkaline-carbonatitic complex, after Germann *et al.* (1987, modified). B: Carbonatitic body, after Ruberti *et al.* (1991).

1000 m long and 350 m wide, in which five intrusion phases were identified: C1 sövites; C2 dolomitic sövites; C3 sövites; C4 sövites; C5 rauhaugite (Gaspar & Wyllie, 1983). All these rocks are mined as phosphate ore and the flotation residue with less than 4 wt% MgO is used for the production of Portland cement.

The supergenic terrains covering the carbonatites, formed by the residual concentration of apatite, were mined between 1943 and 1969. The Morro da Mina mine has an 80 Mt ore with 5.3 wt% $P_2O_5$ and 42 Mt of carbonatitic rocks with less than 4 wt% MgO (Reis, 1997). Drillings up to 400 m depth have indicated the existence of more than 300 Mt of ore.

Notwithstanding the fact that all the carbonatite types are mined, the rocks have $P_2O_5$ grades ranging from less than 0.5 wt% to more than 11 wt%. Fig. 6 6A and B show that the $P_2O_5$ grade of the carbonatites is inversely proportional to the MgO content: the concentration of apatite in the sövites

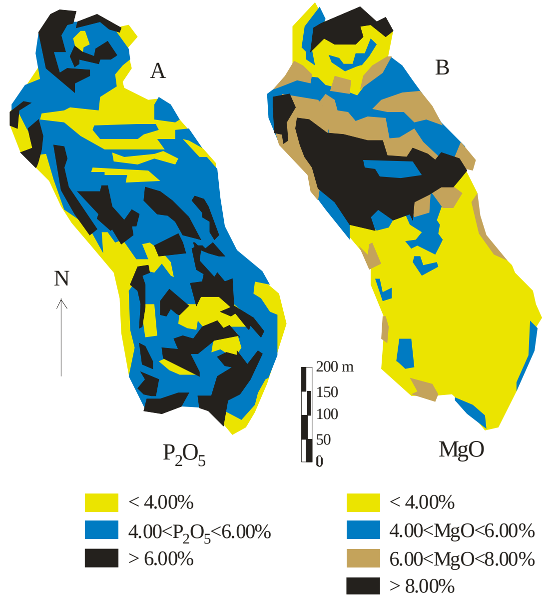


Fig. 6. $P_2O_5$ (A) and MgO (B) distribution (wt%) in the Morro da Mina mine.

decrease at the transition from sövites to the magnesian carbonatites (C2 type; see also Fig. 5B), emplaced in the central part of the mineralized body (Ruberti *et al.*, 1991). The lowest $P_2O_5$ contents are found in the phlogopite carbonatites, a virtually apatite-free rock.

## Fluorspar

### *Tanguá fluorspar mine*

In the Tanguá-Rio Bonito region, a group of alkaline complexes, 100-120 Ma, intrudes K-feldspar sillimanite-biotite gneisses and migmatites (Fig. 7; cf. Table 1, n. 12). The calculated reserves are of the order of 0.18-0.40 Mt, with an ore of 45 wt% $CaF_2$.

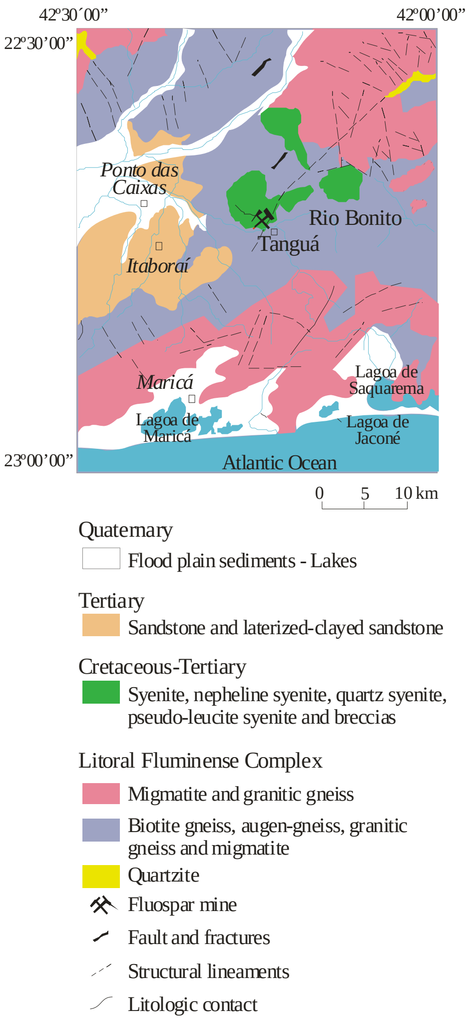


Fig. 7. Alkaline intrusions of the Tanguá-Rio Bonito complex near the city of Itaboraí, Rio de Janeiro state (Coelho *et al.*, 1986; Becker *et al.*, 1997).

The alkaline rocks are subvolcanic syenites showing a concentric zonation, from the border to the core of the intrusions, of saturated to silica-under-saturated rock-types, respectively. Moreover, in the border regions (Fig. 8), trachytic dykes, porphyritic phonolites and alkaline breccias are associated with fluorspar veins, forming the Tanguá mine ore.

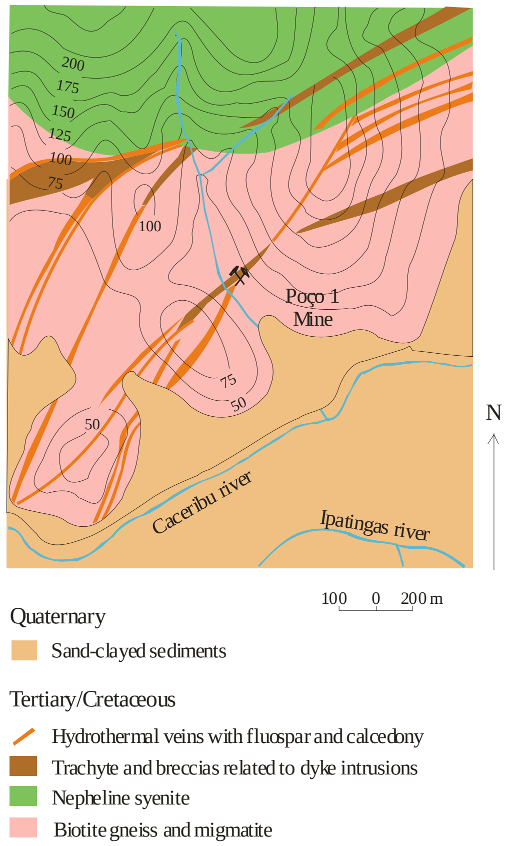


Fig. 8. The Tanguá alkaline massif. The main intrusions are predominantly pseudoleucite syenites. At the borders of the intrusions, a net of trachytic dykes, phonolites and breccias is emplaced in zones of shearing, where fluorspar and different minerals of hydrothermal alteration are crystallized (Becker *et al.*, 1997).

The fluorspar veins, 0.5 to 6.0 m thick, contain quartz, chalcedony, limonite, pyrite and clay minerals and are found in the interior of trachytes and porphyritic biotitic trachytes, close to alkaline breccias. Fluorspar-free veins made of quartz and clay minerals and of chalcedony, quartz, limonite, pyrite and clay minerals are also common (Fig. 9). According to Becker *et al.* (1997), the mineralizing fluids were composed of meteoric water that infiltrated the alkaline rocks and provocated the dissolution of silica, fluorine and calcium. Rising towards the surface and percolating the shearing zones, the fluids precipitated fluorspar, quartz and chalcedony.

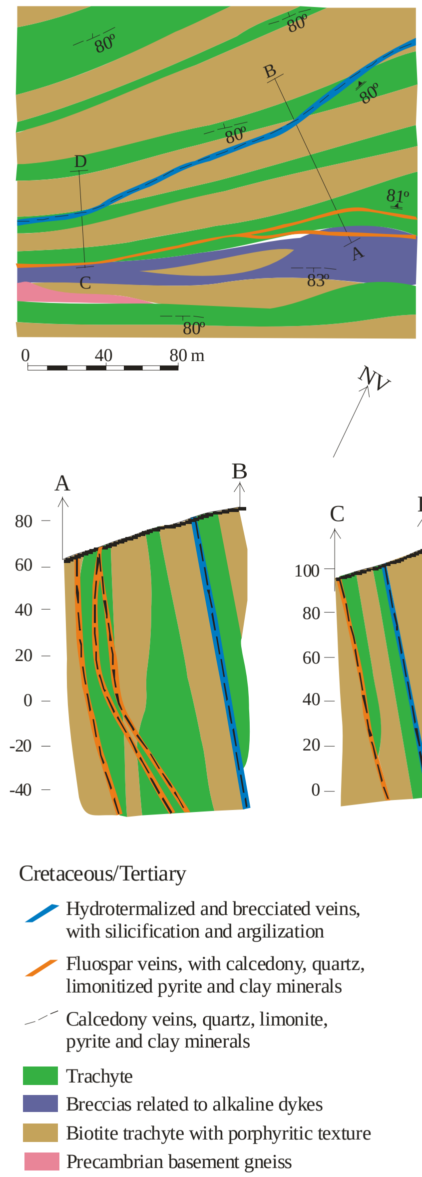


Fig. 9. Detail of the fluorspar mineralization of the Poço 9 Mine in the Tanguá intrusion. Fluorspar veins are closely associated with the trachytic dykes. The gangue is made of quartz, chalcedony, limonite, pyrite and clay minerals. Fluorspar-free veins having quartz and clay minerals or with quartz, chalcedony, limonite, pyrite and clay minerals are also present (Becker *et al*., 1997).

## Mato Preto fluorspar mine

Mato Preto (Table 1, n. 13) is a small carbonatitic complex and part of a group of alkaline intrusions (Tunas, Banhadão, Itapirapuã and Barra do Itapirapuã, Fig. 10A) tectonically associated with the Lancinha-Cubatão Lineament (Fig. 1). K/Ar ages are between 60.0±3.4 Ma and 71.7±4.7 Ma (Gomes *et al*., 1990; Ruberti *et al*., 1997). The Clugger mine, presently closed, is situated in the northern portion of the intrusion (Fig. 10B). In the same complex, other non-mined (FS-P, FS and Pinheirinho, Fig. 10B) deposits are known. The calculated fluorspar reserves are 2.6 Mt of 60 wt% $CaF_2$ and 160,000 tons of 41-55 wt% $CaF_2$. Lapido-Loureiro (1994) calculated a mean grade of 7.7 wt% $REE_2O_3$ in the Mato Preto carbonatites, assuming a 12.82 wt% $REE_2O_3$ concentration in the ferrocarbonatites.

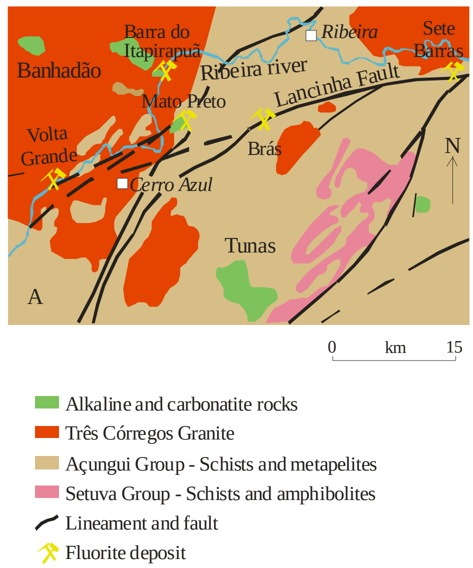


Fig. 10. A: Mato Preto alkaline-carbonatitic complex (Paraná state) and the associated alkaline intrusions of Tunas, Banhadão Itapirapuã and Barra do Itapirapuã. Other fluorspar mines and deposits related to the Lancinha-Cubatão Lineament, but without clear relation with alkaline rocks, are noticeable in the Vale do Ribeira region (Paraná and São Paulo states).

Mato Preto is an alkaline complex with nepheline syenites, phonolites and tinguaites containing calcio-carbonatites and ferruginous carbonatites (Comin-Chiaramonti *et al*., 2001). Subordinate outcrops of tuffs, agglomerates and other silicate rocks (ijolites and melteigites) are present (Fig. 10B). A shear zone belonging to the Lancinha-Cubatão system (Fig. 1) cuts the complex. The late hydrothermal fluorspar (Fig. 11) is related to the intrusion of phonolitic and tinguaitic dykes (60.0±3.4 Ma and 65.2±3.3 Ma). The fluorspar replaces carbonatites, nepheline syenites, breccias and undifferentiated alkaline rocks strongly affected by the hydrothermal alteration. The mineralizations form irregular, lenticular, dyke-like or podiform bodies. The mineralogy of the ore is very complex. More than 60 different minerals have been described in the mineralized areas (Jenkins II, 1987). The main hydrothermal processes may be thus summarized: 1) replacement of the sövites by quartz+fluorspar; 2) epidotization; 3) hydrothermal carbonatization; 4) pyritization; 5) baritization; 6) feldspatization; and 7) alteration into a clay mineral association. It is possible to identify at least three mineralization phases corresponding to: 1) purple fluorspar, with a great amount of pyrite; 2) yellow-brown fluorspar and 3) uncolored fluorspar. The second phase was the most important one, representing about 80%-85% of the known reserves.

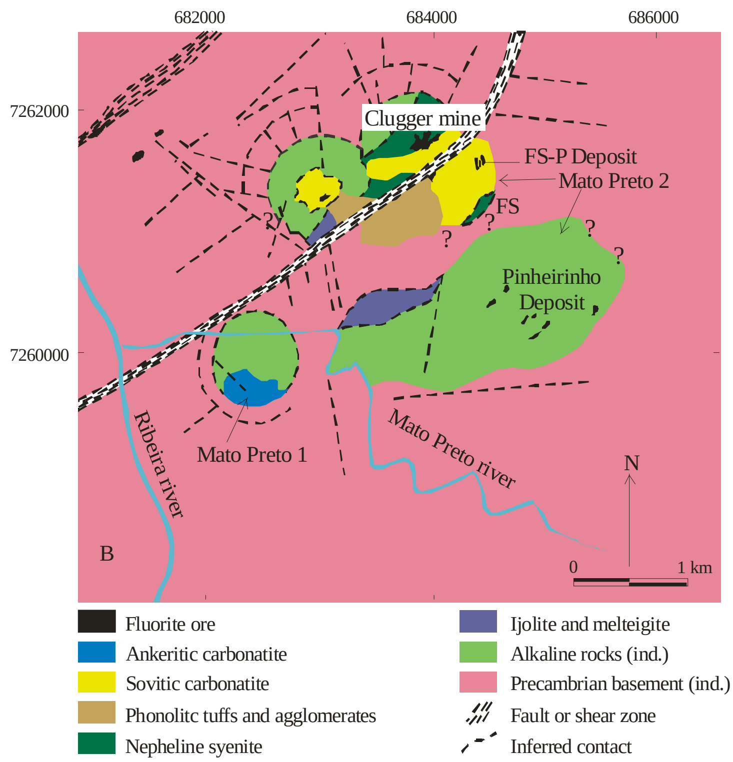


Fig. 10. B: Map of the Mato Preto alkaline-carbonatitic complex showing the fluorspar mineralized bodies (Clugger mine and the not-mined FS-P, FS and Pinheirinho deposits; cf. Jenkins II, 1987, 1997).

## Barra do Itapirapuã REE and phosphate deposit

Barra do Itapirapuã (Table 1, n. 28) is an alkaline-carbonatitic complex with 5 km long and 1.5 km wide. The largest part of the outcropping surface is located in the São Paulo state and the remaining area in Paraná, the border zone corresponding to the Ribeira river (Figs. 10A and 12). In the Paraná fringe, 1.4 Mt of ore with 0.94 wt% average $REE_2O_3$ grade and 2.1 Mt of phosphate ore with nearly 3.0 wt% $P_2O_5$ have been calculated. In the São Paulo side, the estimated reserves are of 44.8 Mt of rare-earths ore with 0.7 wt% $REE_2O_3$ and 1.1 Mt of phosphate ore with 2.5 wt% $P_2O_5$. Until 1980 the Maringá mining exploited magnetite in veins hosted inside phonolites and syenites at the northwestern side of the complex. K/Ar determinations indicate ages ranging from 96.9±1.9 Ma to 114.7±9.7 Ma (Gomes *et al.*, 1990).

The complex is a stockwork carbonatite intruding syenites and the Proterozoic Três Córregos granite (Ruberti *et al.*, 2002). The stockwork, made of prevailing magnesio to ferrocarbonatites, crops out only in the southeastern sector, sectioned by the Ribeira River (Fig. 12). The latest magmatic event is represented by the intrusion of lamprophyres, at their turn crossed by carbonatitic hydrothermal veins (cf. Ruberti *et al.*, 2002).

Bastanaesite-synchisite bearing carbonatites constitute the main ore in the Barra do Itapirapuã complex, an occurrence among other Brazilian REE mineralized carbonatites. REE minerals occur disseminated in the primary ankeritic carbonatites and also in veins and breccias cemented by late hydrothermal ferrocarbonatites (Biondi, 1987). The

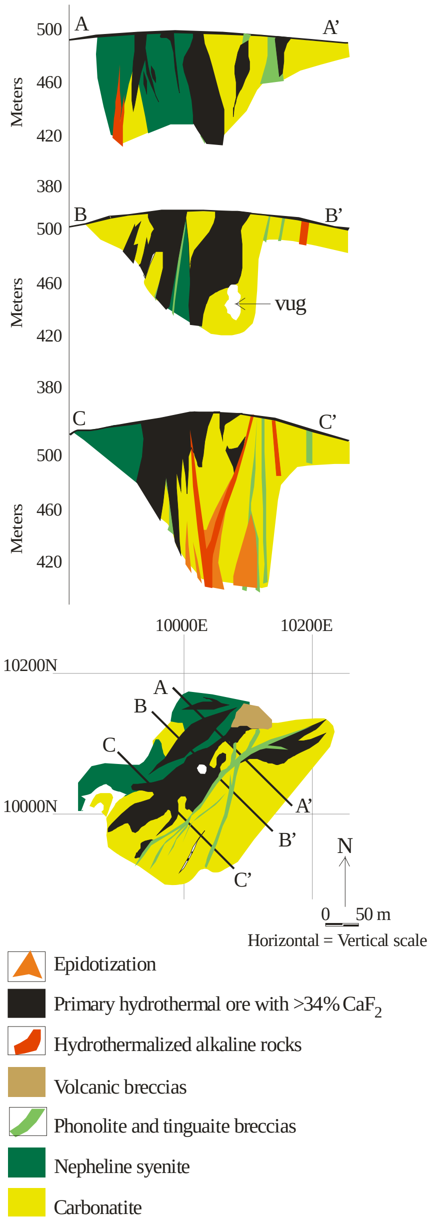


Fig. 11. Map and three sections (A-A', B-B' e C-C') of the mineralized body of fluorspar from the Clugger mine in the Mato Preto complex (Jenkins II, 1987).

REE contents of non-altered ankeritic carbonatites range from 0.05 to 6.30 wt% $REE_2O_3$, whereas the soil covering the mineralized areas contains more than 11% $REE_2O_3$. The $P_2O_5$ contents are low and the phosphate could be mined only as an eventual byproduct of the REE. Moreover, minerals as pyrochlore, galena, fluorspar, barite, molibdenite, sphalerite and Nb-rutile disseminated in the carbonatites are also present.

Diamond deposits in kimberlites from the 125ºAZ Lineament

Kimberlitic and lamproitic rocks may be diamond-carriers and usually crop out at the borders of the major sedimentary basins, in the flexure regions, along *crustal faults* (Lumbers, 1978) or along *continental disjunction faults* (Bardet, 1973). Many factors contribute to the economic interest of the kimberlites/lamproites diamond deposits: the diamond contents (carats/ton), the quality of the gems (expressed by their dimensions and by the proportion between graphitized, black, and non-graphitized diamonds), the amount of inclusions and the degree of microfracturing, and other factors common to the evaluation of other ores (dimension, geographic location, energy availability etc.). In general, rocks with contents ranging from 0.1 carats/ton (large and good gems) to 3-4 carats/ton (small gems or high proportion of black diamonds) are mined.

In the last 30 years hundreds of kimberlitic pipes and dykes and a few lamproites (Leonardos & Ulbrich, 1987) have been discovered in Brazil (cf. Fig. 1). Along the 125ºAZ Lineament, mineralized pipes were recognized in four regions: Coromandel, Três Ranchos-4, Paranatinga (Weska & Svisero, 2002) and Juína-Aripuanã (Araújo *et al.*, 2002) (Fig. 13), but the estimated diamond contents are considered to be very low and therefore without economic interest (Gonzaga & Tompkins, 1991).

Supergenic and residual deposits: phosphate, niobium, titanium, REE and vermiculite

The lixiviation of the carbonate constituents of the carbonatites leads to the formation of thick altered soils with residual concentrations of niobium, titanium, phosphorus and REE. Many Brazilian carbonatites, in particular the occurrences of Catalão and Araxá, show residual concentrations of niobium, phosphate, REE and vermiculite. The Barreiro deposit, near the city of Araxá, represents the richest niobium deposit of the world, and Catalão I has a very significant REE reserve. Common primary phosphate ores from the alkaline-carbonatitic complexes are fluorapatite-rich carbonatites. The primary, "Anitápolis type" phosphate ore deposit, contains 7.41 wt% $P_2O_5$ in ultramafic rocks, 6.27 wt% in nepheline syenites, 5.15 wt% in urtites and 4.33 wt% in carbonatites. Secondary ores have $P_2O_5$ proportions ranging from 7.0% to 9.0 wt%, in the same range of other complexes, but they are very low if compared to the 30 wt% $P_2O_5$ contents of the sedimentary ore phosphorites. In spite of the low concentrations, all the phosphate produced in Brazil derives from carbonatites. Deposits with many tens of millions tons reserves are common.

The main niobium ore mineral of these deposits is a barium-pyrochlore, with subordinate Nb-Fe-Ti minerals such as perovskite and anatase. The latter are usually found associated with superficial ferruginous crusts, rich in magnetite, and with underlying regoliths bearing goethite, barite, carbonates, limonite, ilmenite and quartz.

There are no published reports about the existence in Brazil of economic REE concentrations in lateritic and/or supergenic deposits outside the areas of occurrence of carbonatites. The main minerals are monazite, rabdophanite (hydrated monazite), parisite, florencite, apatite and gorceixite. Titanium – mainly related to anatase, ilmenite, perovskite, titanite, leucoxene and rutile – forms deposits with hundreds of millions tons of ore with 10 wt% to 30 wt% $TiO_2$. Magnetite, barite and pyrochlore occur associated with anatase in soils and regoliths, containing carbonated minerals and ferromagnesian silicates as groundmass phases.

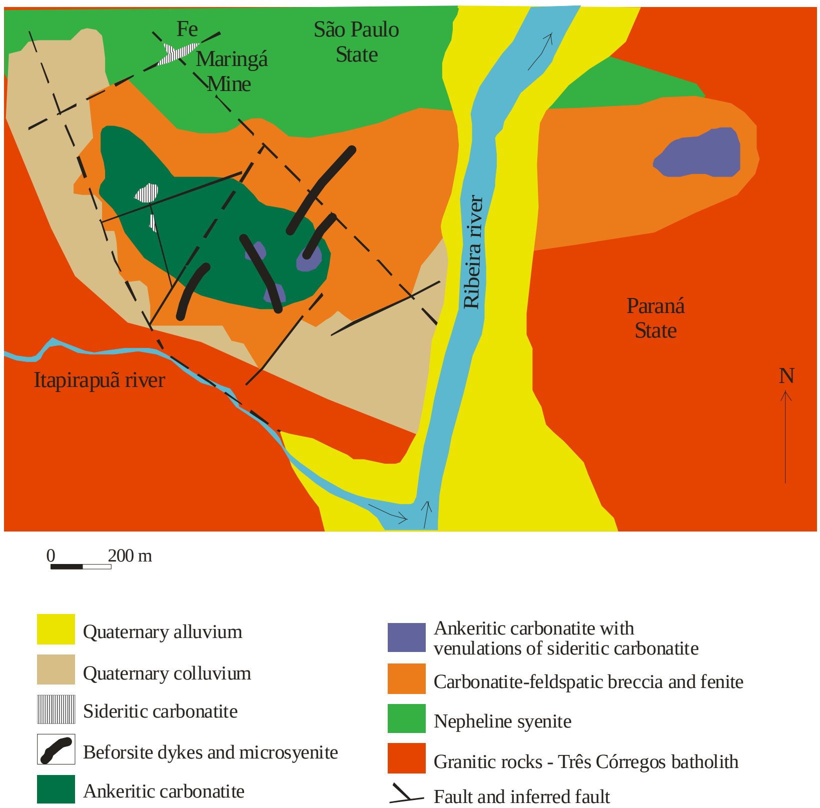


Fig. 12. Barra do Itapirapuã carbonatites. REE are disseminated in the ankeritic carbonatites and also in dykes and breccias cemented by sideritic carbonatites (Biondi, 1987).

*The Barreiro mine: niobium, phosphate and REE (Araxá carbonatite complex)*

The Araxá (Table 1, n. 14), Tapira, Salitre and Serra Negra alkaline-carbonatite complexes (Fig. 14) are associated with kimberlitic rock-types in the "CK" section of the 125°AZ Lineament (Fig. 13A).

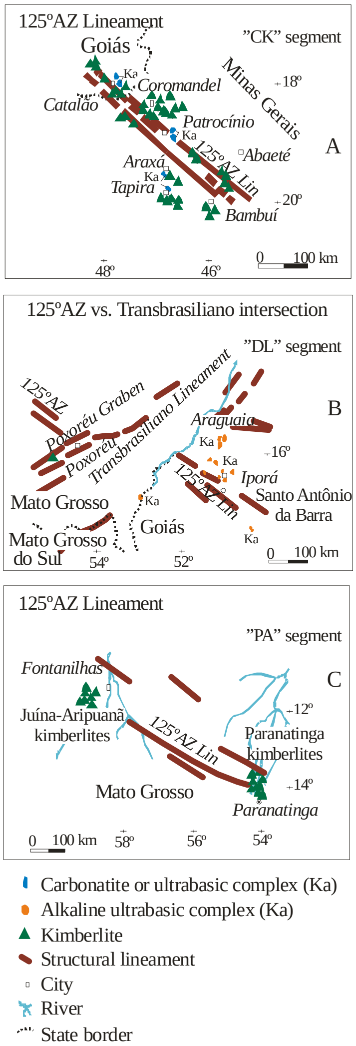


Fig. 13. Details of segments of the 125°AZ Lineament, where the majority of the pipes and dykes of kimberlites (80-87 Ma; cf. Gonzaga & Tompkins, 1991) known in Brazil are found. A) "CK" segment between Bambuí and Catalão, containing the major number of pipes. The Três Ranchos-4 pipe, with marginal mineralization, crops out near the Catalão town. In the Coromandel region, the largest Brazilian diamonds were found in alluvium deposits, but the pipes have sub economic interest. B) "DL" segment at the crossing between 125°AZ and Transbrasiliano lineaments. In the area, ultrabasic-alkaline complexes containing secondary nickel (garnierite) deposits outcrop. C) "PA" segment with the kimberlitic provinces of Paranatinga and Aripuanã. In the Aripuanã province, at least 10 mineralized pipes are known, all of them of sub economic interest. In Paranatinga, there are at least 40 identified pipes, many of them with mineralization without economic importance (Gonzaga & Tompkins, 1991).

The circular Araxá complex, about 5 km in diameter, intrudes Proterozoic quartzites and schists of the Araxá Group and consists of a central core of dolomitic carbonatite (beforsite) surrounded by a zone of prevailing dolomite carbonatite and subordinate glimmerite that are encircled by a glimmeritic zone with subordinate dolomitic carbonatite (Fig. 15, cf. Silva, 1986). Some coarse- to medium-grained calcite carbonatite (sövite) is also present in the northwestern part of the complex. Fenitization extends up to about 2 km from the contact, and it is characterized by the formation of alkali feldspar, eckermanite, arfvedsonite, aegirine-augite, apatite and dolomite in the host quartzites. K/Ar data resulted in ages ranging from 77.4±1.0 to 97.6±6.1 Ma (Gomes *et al.*, 1990).

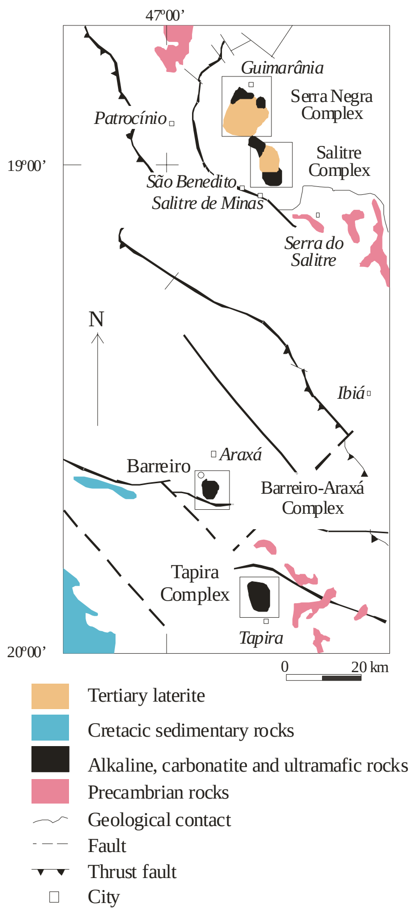


Fig. 14. Araxá (Barreiro), Salitre and Serra Negra complexes in the "CK" section of the 125°AZ Lineament.

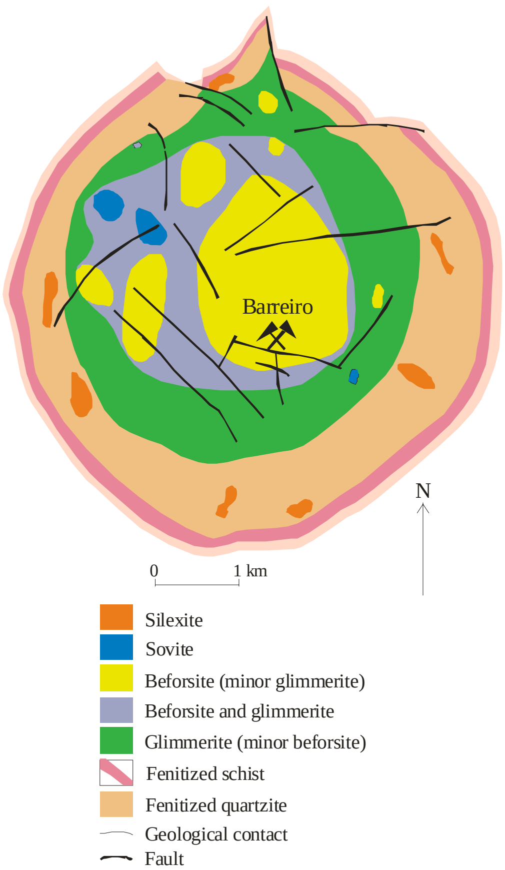


Fig. 15. Geological map of the alkaline-carbonatitic complex of Araxá (after Silva, 1986).

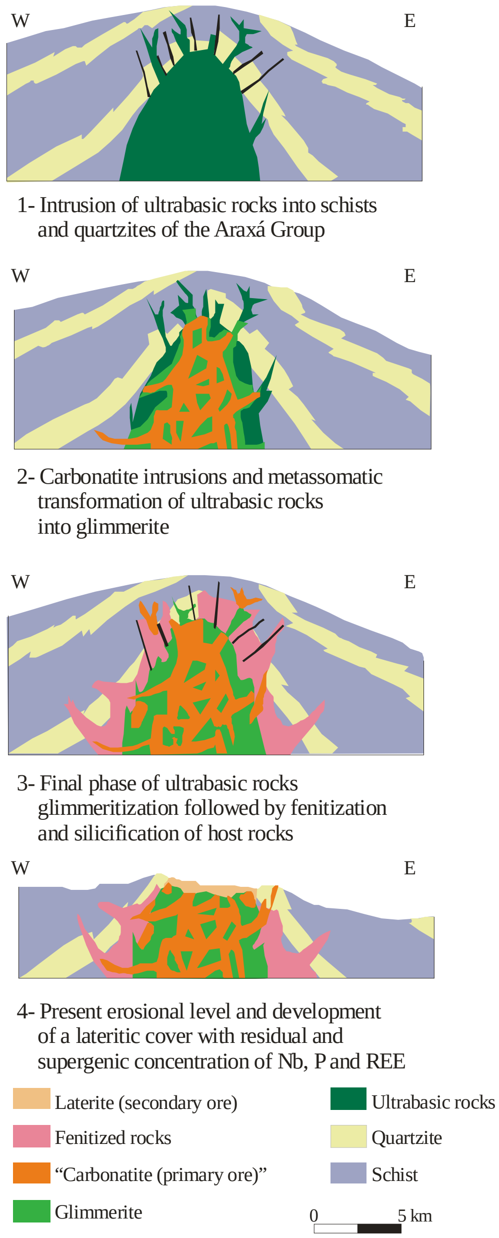


Fig. 16. Evolutionary sketch of the Araxá complex: 1) intrusion of ultrabasic rocks; 2) intrusion of carbonatites and metasomatic transformation of ultrabasic rocks into glimmerites; 3) fenitization of the host rocks, generating lenses and pods of silexite inside the quartzites; 4) erosion and intemperism forming residual and supergenic concentration of resistant minerals. The main ore in the Barreiro Mine is made of soil and regolith, with niobium and apatite concentrates (Issa Filho *et al.*, 1984).

The Araxá complex represents an eroded structure (Issa Filho *et al.*, 1984; cf. Fig. 16) showing the following evolution: 1) intrusion of dunites and periodites in the supracrustal rocks of the Araxá Group (Fig. 16.1); 2) intrusion of the carbonatitic magma and metasomatism of the ultrabasic rocks, generating glimmerites and fenitizing the host rocks (Fig. 16.2); 3) formation of lenses and pods of silexites in quartzites as a result of fenitization processes (Fig. 16.3); 4) erosion and formation of the intemperism mantle of the alkaline rocks in which residual resistant minerals are enriched (Fig. 16.4). Weathering has produced a friable lateritic residuum, more than 100 m thick, in which the supergenic and residual ores contain 414 Mt with 3.3 wt% $P_2O_5$, 462 Mt with 2.5 wt% $Nb_2O_5$ and 546,000 tons with 4.4 wt% $REE_2O_3$. Carbonatite drilling reveals about 940 Mt of primary unaltered carbonatitic rocks with 1.6 wt% $Nb_2O_5$ grade.

The Barreiro mine is an open pit since 1961 average mineralogical and chemical compositions are given in Table 2), with pyrochlore recovered by flotation. The mined ore is essentially the surface lateritic ferruginous crust, which is made of limonite/goethite and magnetite concentrating pyrochlore. Below the lateritic crust, the main mineralized body is a regolith formed by the alteration and lixiviation of carbonatites and it concentrate barium-pyrochlore, apatite and monazite (Fig. 17).

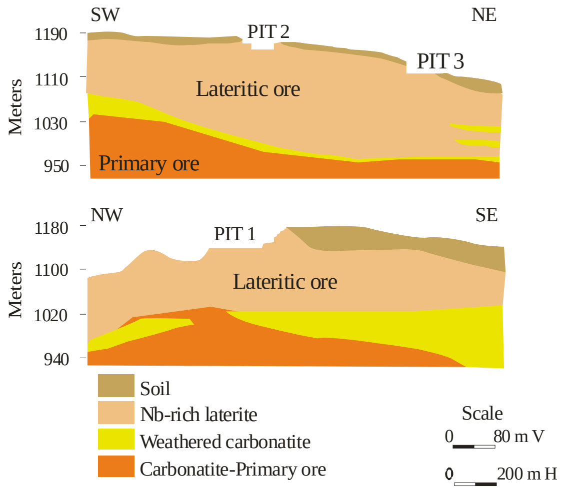


Fig. 17. Sections from the Barreiro mine. The main mineralized body is a regolith covered by a lateritic, Nb-rich limonite duricrust (Silva, 1986).

The primary ore is a fresh plutonic cumulate rock forming the core of the complex. It consists of carbonate and apatite cumulates, magnetite with exsolved ilmenite, phlogopite, pyrochlore and ilmenite. The ore is crossed by thin veins of dolomite+magnetite and dolomite+(Fe-Cu) sulphides+barium carbonate (norsethite). Primary ore occurs at least up to 844 m depth, as shown by drill cores (Issa Filho *et al.*, 2001).

Until 1976, phosphorus was separated from the niobium concentrate; after that year, the introduction of a new type of processing and metallurgy allowed the elimination of phosphorus, sulfur and lead at the same time. Presently, the CBMM produces only niobium.

*Tapira mine: phosphate, niobium and titanium*

The Tapira ultramafic-carbonatitic alkaline complex, southeast of Araxá (Figs. 13 and 14), has an elliptical shape, 6.5 km in diameter and covers an area of 36 km$^2$. The central portion of the complex consists of silica-carbonatites and carbonatites associated with carbonate phlogopite peridotites (olivine, pyroxene, carbonate, apatite, perovskite, magnetite and ilmenite), carbonate phlogopite pyroxenites (pyroxene, calcite, perovskite and apatite) and calcite glimmerites. Such rocks are intruded by trachyte and lamprophyre dykes and veins, containing pods of apatites and fenites. Alkaline rocks, with prevailing malignites, melteigites and syenites, tend to surround the core (Fig. 18; cf. Melo, 1997). Quartzites and fenitized phyllites encircle the entire complex. K/Ar determinations indicate ages ranging from 71.0±4.0 Ma to 87.2±1.2 Ma (Hasui & Cordani, 1962; Gomes *et al.*, 1990).

Table 2. Average mineralogical and chemical composition (wt%) of the ore from the main Barreiro mine. 1) Residual ore; 2) Barium-pyrochlore; 3) Barium-pyrochlore; 4) Barium-pyrochlore - composition adjusted from analysis of high purity concentrate containing micro inclusions of gorceixite. 1, Total iron reported in the most appropriate oxidation state; 2, $Fe_2O_3$ determined by difference between total Fe and FeO; 3, Total of analyzed rare-earth elements (REE); 4, $La_2O_3$+$Ce_2O_3$; n.d., not determined (after Silva, 1986; Issa Filho *et al.*, 2001).

| Sample | 1 | 2 | 3 | 4 | Minerals (%) | |
|---|---|---|---|---|---|---|
| wt% | | | | | Barium-pyrochlore | 4.6 |
| $Fe_2O_3$ [1] | 45.0 | 1.19 | n.d. | 0.92 [2] | Limonite and goethite | 35.0 |
| FeO [1] | | n.d. | 2.37 | 0.28 | Barite | 20.0 |
| BaO | 16.0 | 14.21 | 16.51 | 10.9 | Magnetite | 16.0 |
| $SO_3$ | 7.0 | n.d. | n.d. | n.d. | Gorceixite | 5.0 |
| $TiO_2$ | 4.0 | 4.74 | 2.3 | 4.3 | Monazite | 5.0 |
| $SiO_2$ | 5.3 | n.d. | n.d. | n.d. | Ilmenite | 4.0 |
| $P_2O_5$ | 3.7 | n.d. | n.d. | n.d. | Quartz | 5.0 |
| $(RE)_2O_3$ [3] | 3.2 | 1.62 [3] | 3.29 | 4.0 | Others | 5.4 |
| $Nb_2O_5$ | 2.5 | 65.97 | 63.42 | 66.0 | | |
| $Al_2O_3$ | 2.0 | n.d. | n.d. | n.d. | | |
| MnO | 0.9 | 0.01 | 0.16 | 0.01 | | |
| MgO | 0.3 | 0.01 | n.d. | 0.2 | | |
| CaO | 0.4 | 0.06 | 0.44 | 0.02 | | |
| PbO | tr. | 0.90 | 0.42 | 0.63 | | |
| $K_2O$ | tr. | n.d. | n.d. | 0.04 | | |
| $Ta_2O_5$ | tr. | 0.07 | 0.15 | 0.14 | | |
| SrO | n.d. | n.d. | n.d. | 0.07 | | |
| $ThO_2$ | tr. | 1.65 | 2.34 | 2.7 | | |
| $SnO_2$ | tr. | 0.08 | 0.10 | 0.06 | | |
| $ZrO_2$ | n.d. | 0.41 | n.d. | 0.18 | | |
| $UO_2$ | n.d. | 0.08 | n.d. | 0.05 | | |
| LOI | 6.5 | n.d. | n.d. | n.d. | | |
| $H_2O$ | n.d. | 8.26 | 8.50 | 7.83 | | |
| Total | 96.8 | 99.26 | 100 | 98.33 | | |

Presently, the mining joint venture CVRD-FOSFÉRTIL detains the rights for exploring all Tapira mineral reserves (previously belonging to CVRD-PETROBRÁS, FOSFÉRTIL and to CMM.

The total reserves (pondered average grades) are 1381 Mt of ore with 8.19 wt% $P_2O_5$, 166 Mt with 0.73% $Nb_2O_5$ and 414 Mt with 17.82 wt% $TiO_2$, (anatase). Lapido-Loureiro (1994) found in Tapira

$REE_2O_3$ grades ranging from 1.0 to 10.0 wt% ($Eu_2O_3$=0.36 wt% and $Y_2O_3$=1.9 wt%). Nowadays, the mined ore is used by FOSFÉRTIL to separate apatite for the production of phosphate fertilizer, and the CVRD concentrates anatase in order to produce a concentrate with 96 wt% $TiO_2$.

The Tapira ore was originated by intemperism and lixiviation of carbonatites and carbonated ultra-basic rocks. The supergenic processes led to the formation of differentiated concentrations with bands and lenses showing distinct compositions. The mineralized body is formed mainly by a regolith, with less than 5 wt% $P_2O_5$ (Fig. 19, section A-B). Inside the regolith, an upper stratiform zone having more than 15 wt% $TiO_2$ ($Nb_2O_5$>0.5 wt%) lies over a phosphatic horizon with more than 7.5 wt% $P_2O_5$.

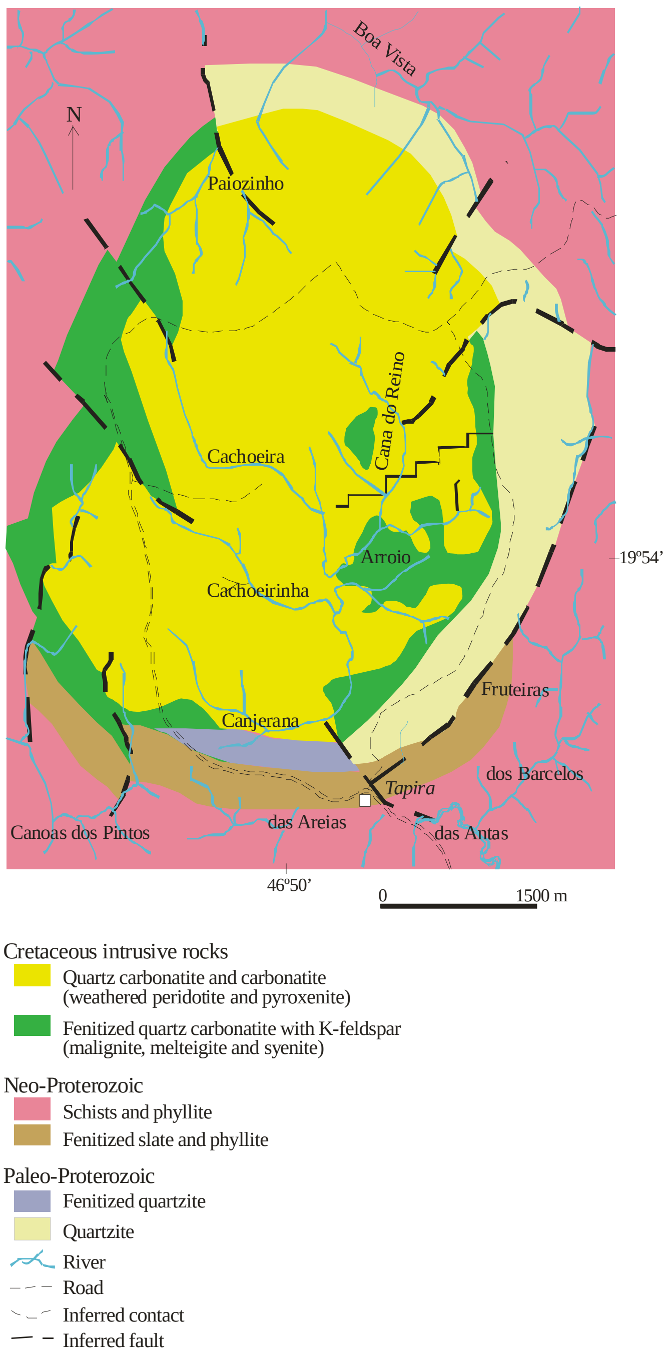


Fig. 18. Geological map of the Tapira ultrabasic-carbonatitic alkaline complex (after Melo, 1997).

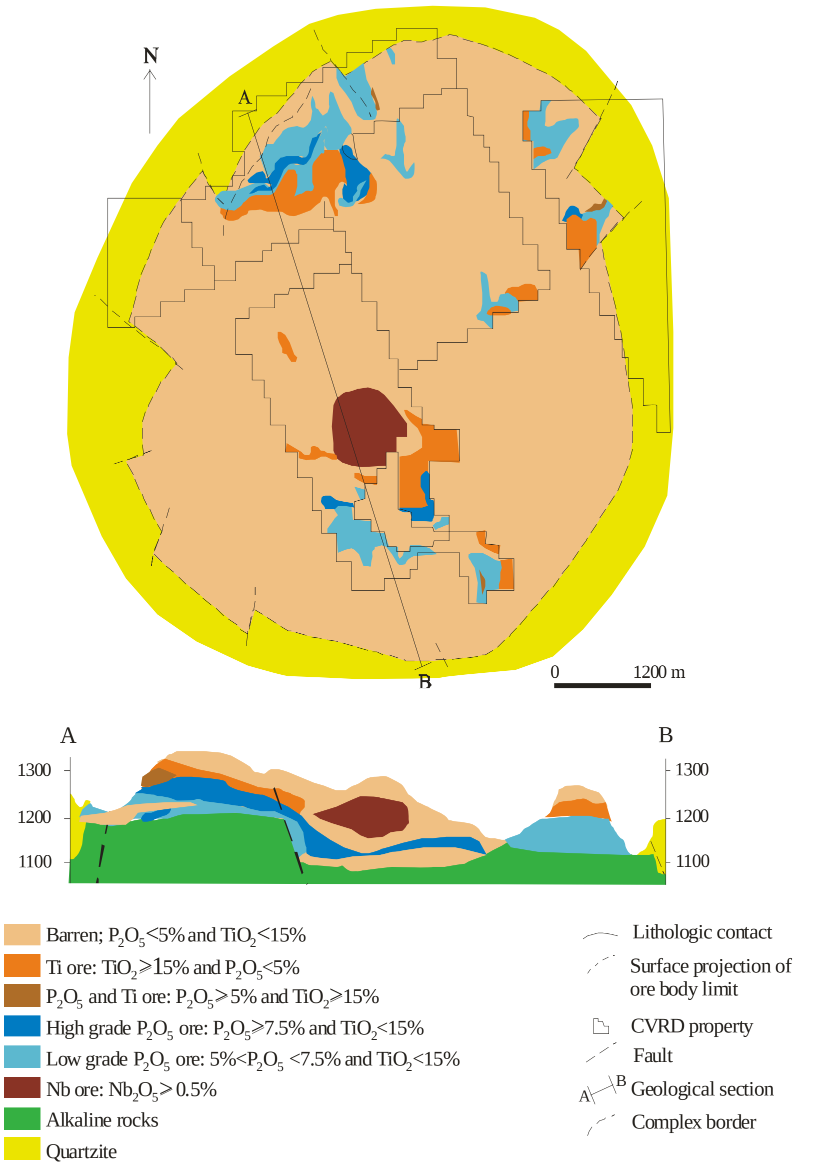


Fig. 19. Distribution of various types of residual and supergenic ores in Tapira. The stratified ores inside the regolith are the result of the alteration of carbonated rocks. The titanium (and niobium) concentrates in a horizon above the phosphate ore (after Melo, 1997).

*Salitre and Serra Negra mines: phosphate, niobium and titanium*

Salitre and Serra Negra are twinned complexes, separated by NE faults (Fig. 14). Together they show almost an eight-shape, with nearly 21 km of extension and width ranging from 5 to 10 km (Fig. 20). Mineral deposits are only found in the Salitre complex. In Serra Negra, mineral assemblages are compatible to those of Salitre and suggest similar ores, but the potential grades were poorly defined because of the touristy interest of the region and the poor geological conditions (i.e. scarce outcrops of alkaline rocks, and thick and extensive lateritic cover).

Salitre is a carbonatitic alkaline ultramafic complex. The existence of few outcrops and the lack of detailed drillings limit the geological knowledge of the area. According to Melo *et al.* (1997), the prevailing rocks are mica-bearing peridotites and subordinate clinopyroxenites cut by carbonatites. The latter rocks occur as small veins and also forming an elongated plug, approximately 500 m$^2$ in area (Morbidelli *et al.,* 1997). The peridotites are fenitized at the rims of the complex. Some drills suggest that in the Campestre Lake area (Fig. 20) carbonatites intrude the clinopyroxenites. Trachyte, foyaite, shonkinite and dunite dykes are present in the region. K/Ar data (Salitre and Serra Negra whole rocks) show ages ranging from 79.0±1.2 Ma to 86.3±5.7 Ma and from 83.0±3.0 to 83.7±4.5 Ma, respectively (Gomes *et al.*, 1990).

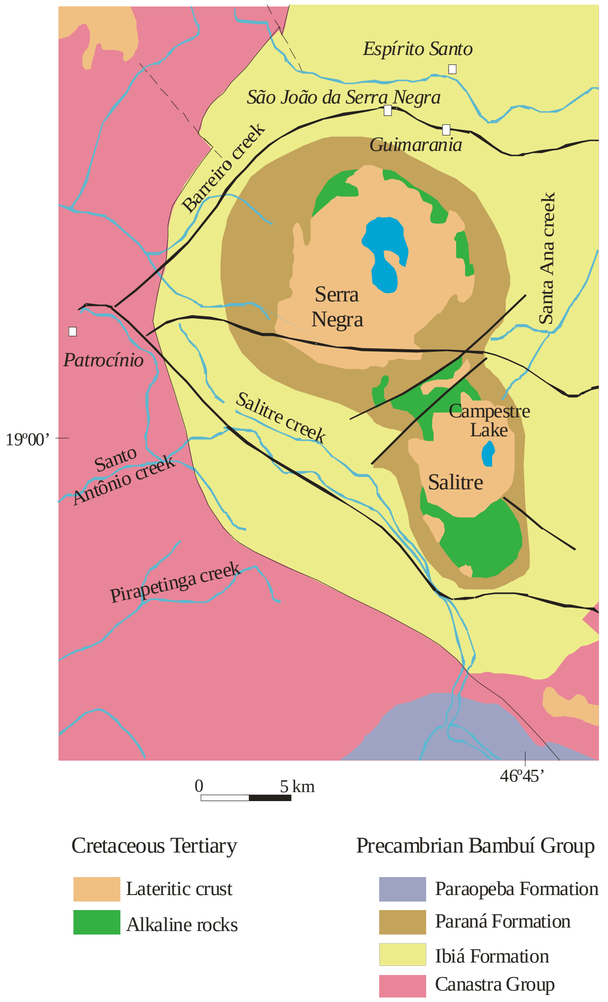


Fig. 20. Geological sketch of the Salitre and Serra Negra carbonatitic-ultrabasic alkaline complexes (after Melo *et al.*, 1997).

Mineral prospection was performed mainly by three companies in the residual and supergenic deposits: CVRD (Cia. Vale do Rio Doce), CMM (Cia. Meridional de Mineração) and CBMM (Cia. Brasileira de Metalurgia e Mineração). The total reserves (pondered average grades) are 852.0 Mt of apatite-rich ore with 10.7 wt% $P_2O_5$, 694.3 Mt of titanium ore (anatase) with 17.5 wt% $TiO_2$ and 196.0 Mt of niobium ore (pandaite) with 0.48 wt% $Nb_2O_5$ (Melo *et al.*, 1997). Occurrences of vermiculite (non-dimensioned) suggest the presence of deposits that could be mined as by products.

*Catalão I mine: phosphate, niobium, titanium, REE and vermiculite*

Catalão I and II are ultramafic-alkaline-carbonatitic complexes lying on the "CK" segment of the 125°AZ Lineament (Figs. 1 and 13A). Economic mineralizations are only found in Catalão I, a circular structure, about 5 km in diameter, intruding granitic-gneissic rocks and schists of the Proterozoic Araxá Group.

The deposit occurs inside the lateritic residuum, up to 80 m thick, overlying carbonatitic lenses in pyroxenites. Nodular laterites, limonitic conglomerates, vermiculite-rich or magnetite-rich soils and a magnetite-rich lateritic crust have been identified. The main Nb ore (secondary Ba-Ce pyrochlore) is found in association with the magnetite-rich lateritic soil (Fig. 21). Drillings have showed mainly the presence of pyroxenites and peridotites cut by carbonatitic (sövites and beforsites) veins and dykes responsible for the phlogopitization, serpentinization and carbonatization of the host rocks. Fenitized quartzites and silexites surround the whole complex. K/Ar determinations indicate ages of 82.9±4.2-85.0±6.9 Ma (Hasui & Cordani, 1962; Gomes *et al.*, 1990).


Fig. 21. Geological map of the carbonatitic-ultramafic alkaline complex of Catalão. On the surface, only literate and lateritic soils are found. Drillings show prevailing serenities and glimmerites intruded by dykes and apophyges of silica-carbonatites, sövites and beforsites (Carvel & Pressman, 1997).

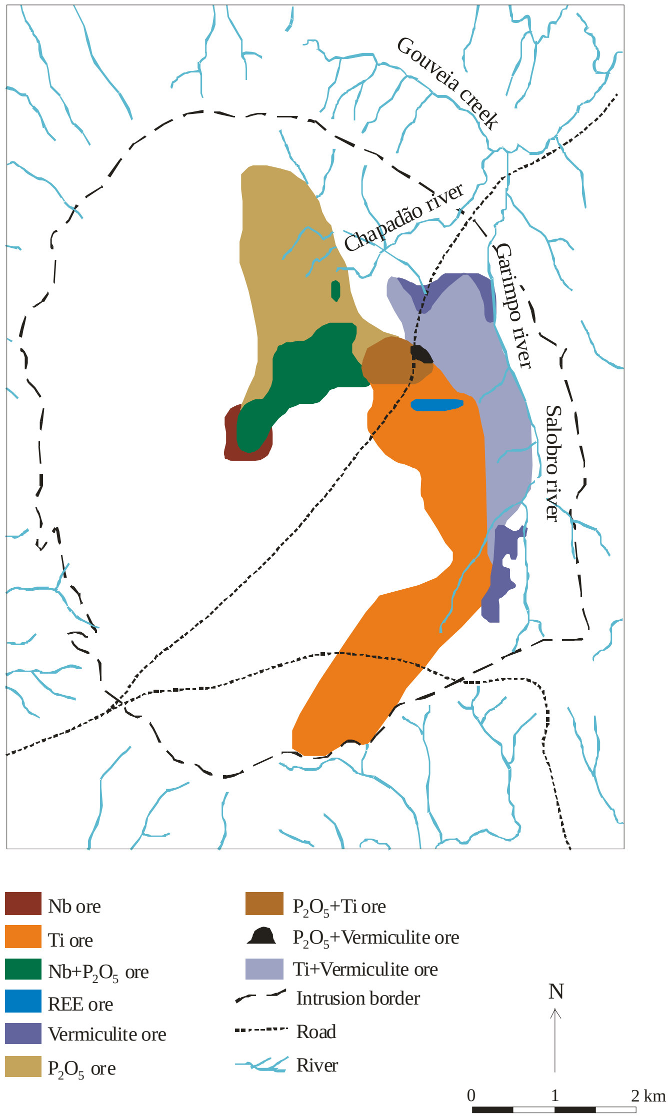


Fig. 22. Catalão I main mineral deposit containing ores formed through residual and/or supergenic concentration of resistant minerals of the underlying alkaline rocks (Carvel & Pressman, 1997).

A thick megalithic mantle, variously enriched in resistant minerals, underlies the lateritic horizon. Although ore minerals as apatite, vermiculite, titanium-rich phases (anatase, perovskite, ilmenite), barium-pyrochlore (niobium) and REE carriers (monazite, rabdofanite, parisite and florencite) are widespread in the central parts of the complex, the economic concentrations are found mainly in the eastern area (Fig. 22; cf. Carvalho & Bressan, 1997).

Presently, Catalão I is mined only for phosphate, niobium and vermiculite. According to Carvalho & Bressan (1997), the total reserves of phosphate ore (pondered average grades) are of the order of 250.0 Mt with 10.48 wt% $P_2O_5$. The known reserves of niobium are 19.2 Mt (1.3 wt% $Nb_2O_5$), of vermiculite 35.9 Mt (>0,5 mm, 17.0 wt% vermiculite), of titanium 339.4 Mt (10 wt% $TiO_2$) and of REE 15.1 Mt (4.0 wt% $Ce_2O_3$+$La_2O_3$).

## Anitápolis phosphate deposit

The Anitápolis alkaline-carbonatite complex (Table 1, n. 23; Fig. 23) intrudes granitoid rocks of the Santa Catarina crystalline basement. It lies at the southern side of the Lancinha-Cubatão Lineament (cf. Fig. 1) and shows a concentric zonation with a central portion made of pyroxenites, biotite pyroxenites, glimmerites and dunitic pods (Comin-Chiaramonti *et al.*, 2002 and therein references). The central-northern area contains a net of carbonatite veins (prevailing sövites and subordinate beforsites) mixed with glimmerites and pyroxenites. Nepheline-bearing rocks, i.e. ijolites, melteigites and urtites surround the ultramafic rocks and carbonatites. The outermost sector is constituted by nepheline and quartz syenites, which are believed to be fenitization products of the granitoid hosting rocks (Vergara, 1997). K/Ar ages range from 130.6±3.0 to 136.4±1.6 Ma (Gomes *et al.*, 1990).

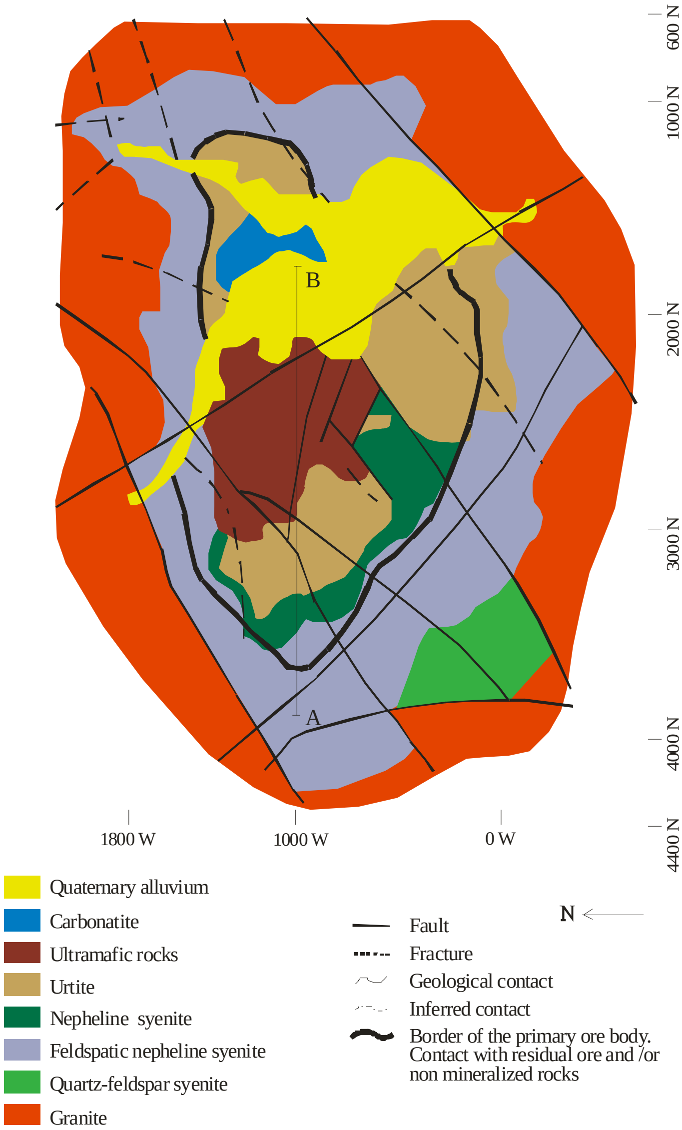


Fig. 23. Geological map of the Anitápolis alkaline-carbonatitic complex. The syenitic rocks are interpreted as being fenitization products of the host granitoids (Vergara, 1997).

Apatite is the only mineral worth exploiting economically. Non-mineralized talus deposits (Fig. 24) cover the residual and/or supergenic ore (regolith up to 50 m thick; Fig. 25A), where the reserves reach about 53.5 Mt with 8.2 wt% to 12 wt% $P_2O_5$ (Fig. 25B).

Primary apatite (concentrated in all the rock-types in which apatite veins and pods are usually present) corresponds to reserves of 206.5 Mt, according to fresh rocks distribution from the boreholes: ultramafic rocks, nepheline syenites, urtites and carbonatites show $P_2O_5$ of 7.41, 6.27, 5.15 and 4.33 wt%, respectively.

## Angico dos Dias phosphate deposit

Angico dos Dias (Campo Alegre de Lourdes;

Table 1, n. 24) is the only Brazilian ultramafic-alkaline carbonatitic complex of Paleoproterozoic age (2011 Ma, U-Pb method in baddeleyite and zircon; Mariano, 1987). The alkaline rocks intrude Archean gneisses and migmatites are deformed, folded and metamorphosed (Fig. 26; cf. Silva *et al.*, 1997; see also Antonini *et al.,* 2003). The most part of the complex is composed of syenites, alkali diorites, albitites, pyroxenites, olivine-apatite sövites, biotite-apatite sövites and magnetite-olivine-apatite sövites, being the rock-types covered by soils and by apatite-rich regoliths.

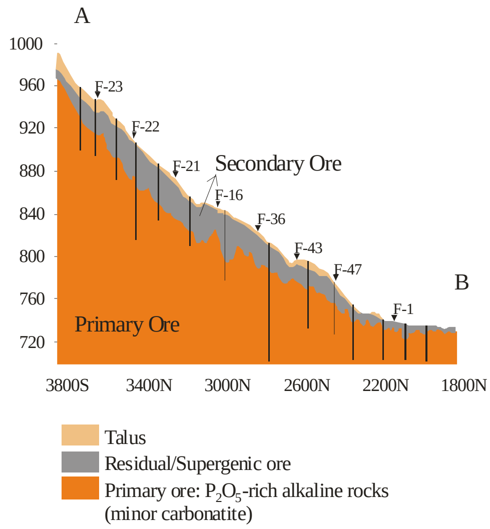


Fig. 24. Section A-B (West to East) showing the thickness variation of the residual, regolithic ore and the talus cover in the Anitápolis complex (Vergara, 1997).

Calculated reserves of the residual-supergenic ore are of 15.0 Mt, with 15.4 wt% $P_2O_5$ average grade. Reserves of non-intemperized rocks were not calculated, but the average $P_2O_5$ grade of some carbonatite samples is 9.6 wt% (0.3 wt% $REE_2O_3$; cf. Silva *et al*., 1997).

### *Morro dos Seis Lagos niobium deposit*

Morro dos Seis Lagos (Table 1, n. 15) is an almost circular structure, about 4 km in diameter, intruding Meson to Paleoproterozoic migmatites and gneisses of the Guyana craton. A lateritic mantle, more than 250 m thick, covers the entire structure (Justo & Souza, 1986). Drilling cores show lenses of carbon-clayey sediments within the laterites, probably corresponding to remnants of ancient lakes. The drillings did not reach the fresh rocks under the lateritic crust, but mineralogical and chemical compositions suggest the existence of a carbonatitic horizon.

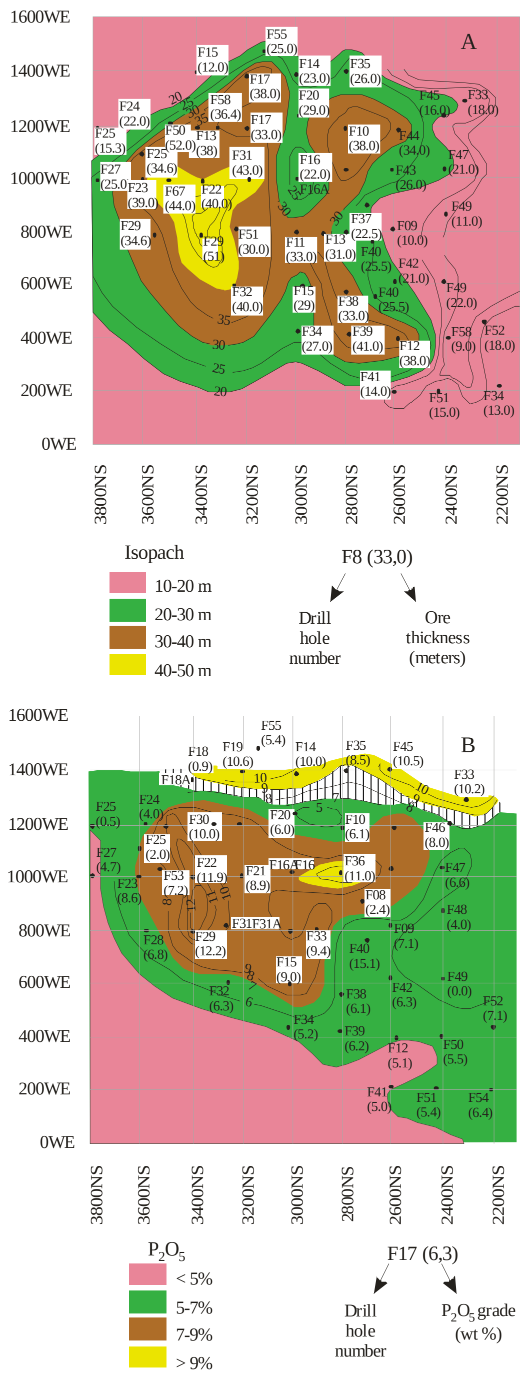


Fig. 25. A: Isopaches relative to the Anitápolis apatitic residual ore (cf. Fig. 23). B: $P_2O_5$ isogrades of the regolith ore. It should be noted that the area having the highest grade (up to 12 wt % $P_2O_5$) shows the largest regolith thickness (Vergara, 1997).

The laterites have average grade of 50 wt% $Fe_2O_3$. The main ore minerals are rutile and niobium-rich brookite. The ore has 38.4 Mt of ferruginous niobium-rich laterite, with 2.85 wt% $Nb_2O_5$. Estimated total reserves are of 2,898 Mt with 2.81 wt% $Nb_2O_5$ grade (Justo & Souza, 1986). It must be emphasized that some laterite samples have 3.68 wt% $REE_2O_3$ as average content (Lapido-Loureiro, 1994). Manganese crusts were also identified in many places over the ferruginous crust (Fig. 27).

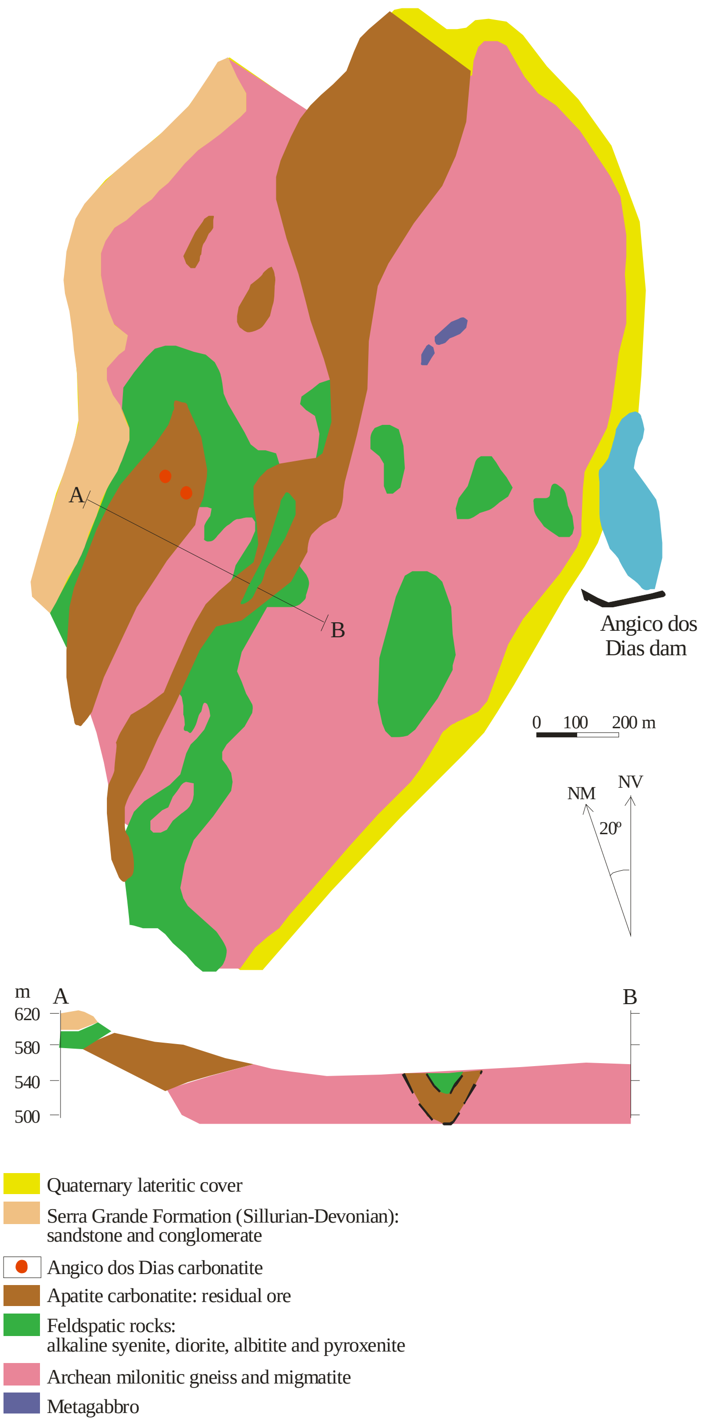


Fig. 26. Geological map of the Angico dos Dias alkaline-carbonatitic complex, Bahia state (after Silva *et al*., 1987, 1997).

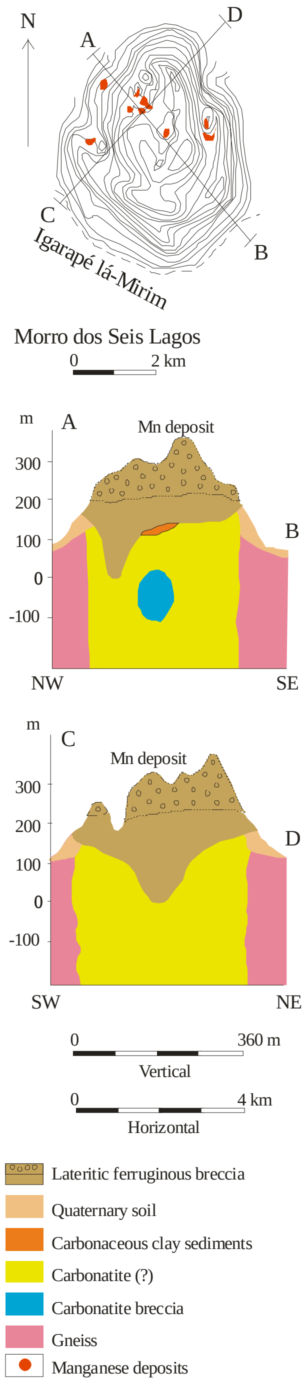


Fig. 27. Topographic map and geological sections (A-B and C-D) of the Morro dos Seis Lagos complex. A poliphasic lateritic ferruginous crust covers the entire structure (cf. Justo & Souza, 1986).

Ipanema complex: phosphate and vermiculite deposits

The Ipanema complex (Table 1, n. 25) is an ultramafic-alkaline carbonatitic complex showing circular shape and covering an area of about 13 $km^2$. The prevailing rocks are glimmerites, syenites, pyroxenites (aegirinites), shonkinites, umptekites and carbonatites. The carbonatites are composed of sövite veins and dykes intruding the glimmerites (Leinz, 1940). Fenitized granites crop out at the border of the complex. K/Ar ages ranges from 124.9±9.5 to 141.6±5.4 Ma (Gomes *et al.*, 1990). The Ipanema complex has 117.0 Mt of residual phosphate ore with 6.7 wt% $P_2O_5$ and 5.0 Mt of ore with 29 wt% vermiculite (Rodrigues & Lima, 1984).

*Morro do Serrote (Juquiá): phosphate deposit*

Morro do Serrote (Table 1, n. 26) is an alkaline carbonatitic complex with about 14 $km^2$ of outcropping rocks (Fig. 28; Born, 1971). The intrusion consists chiefly of pyroxenites and nepheline syenites and subordinate cumulus peridotites, alkaline gabbros and ijolites (Beccaluva *et al.*, 1992). Sövites surrounded by beforsites are present at the western side of the complex. Late carbonatites, phonolites and ankaratrites occur mainly as dykes. K/Ar ages range from 131.7±1.6 to 148±5 Ma (Gomes *et al.*, 1990). The phosphate deposit is residual and/or supergenic and contains 18.0 Mt of ore with 10.0 wt% $P_2O_5$.

Mutum alkaline complex: phosphate deposits

Gomes *et al* (1990) described the Mutum complex (Table 1, n. 27) as a circular intrusion covering an area of 16 $km^2$. The main rock-types are nepheline syenites, carbonatites, ijolites, urtites and fenites (albitites). The intrusion contains phosphate-rich rock-types, but the reserve estimates or grades are not available. K/Ar determinations show an age of 1026±28 Ma.

Aluminum (bauxites) and nickel (garnierites) supergenic and residual lateritic deposits

The development of *laterites* in general, and bauxites and garnierites in particular, is facilitated by the formation of erosion surfaces or peneplains. The Cretaceous-Tertiary laterization, related to the South American peneplains (King, 1956; Almeida, 1966), formed lateritic crusts in regions 600 to 850 m high, most of them closely associated with alkaline complexes. In Tertiary times, the elevation of the South American Platform, modifying the base level of the rivers and reactivating the erosive processes, promoted the destruction of the old surfaces and generated areas cut by valleys and hills, where generally the tops of the hills keep the level of the ancient surface, ranging from 600 to 850 m high. In some places the more recent erosive cycle originated a new peneplain ("Velhas Surface" of King, 1956), 400 to 600 m high, also linked to extensive lateritic deposits.

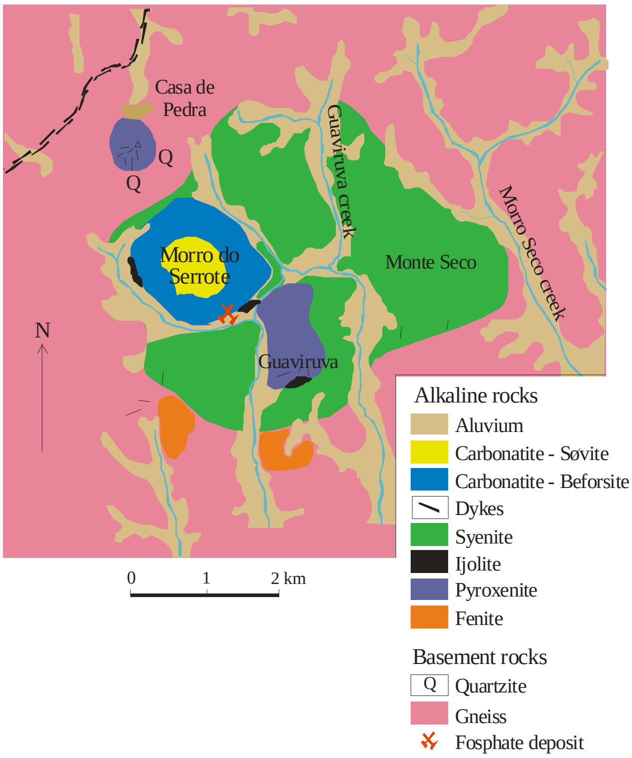


Fig. 28. Geological map of the Morro do Serrote (or Juquiá) carbonatitic-ultrabasic alkaline complex (Born, 1971).

The term bauxite is herein used to designate laterites with 80 to 90 wt% $Al_2O_3$ (anhydrous basis). From an economic viewpoint, bauxites are referred to as ore according to the presence of free-$Al_2O_3$ content, in consonance with the relation: $Al_2O_{3(free)} = Al_2O_{3(total)}$-0.85 $SiO_2$.

Bauxite ores occur as oxides and hydroxides, representing two series denominated $\alpha$ and $\gamma$ (Table 3). Minerals of the $\alpha$ series are less common as ore minerals. Despite the fact that jasper is a common mineral, gibbsite and boehmite are the major components in bauxites. The more ancient and evolved bauxites have more boehmite and less evolved gibbsite. The bohemitic bauxite duricrusts are hematitic, whereas the gibbsitic bauxites are goethitic.

The *lateritic bauxites*, derived from the silica-alumina-rich rock-types ("*lateritic type bauxite*") are essentially gibbsitic. This type of bauxite is characteristic of the alkaline complexes, usually developing from syenitic and phonolitic rocks. When bauxites are formed from iron-poor rocks (nepheline syenites, phonolites etc.), the duricrust is aluminous or pisolitic. On the other hand, when they are originated from iron-rich rocks, a ferruginous duricrust is formed at the surface, superimposed to an aluminous duricrust. In both cases, the deposits are stratiform with very irregular and gradational lower contacts, and the thickness ranges from 3 to 10 m.

The description of 122 deposits indicated that the lateritic bauxites represent reserves of 25.0 Mt of ore with mean contents of 45.0 wt% $Al_2O_3$. Deposits with reserves ranging from 100,000 tons to more than

6.3 Mt are generally mined. Rarely the mined deposits have mean contents of less than 35 wt% $Al_2O_3$, the best ones containing more than 55 wt% $Al_2O_3$. The gallium may be a byproduct of the aluminum, when the mean content is at least 20 g/ton.

Table 3. Most common minerals from bauxite deposits (Perkins *et al.*, 1979).

| | Composition | Molar volume |
|---|---|---|
| **α series** | | |
| Bayerite | $Al(OH)_3$ | 31.15 |
| Diaspore | AlOOH | 17.76 |
| Corundum | $Al_2O_3$ | 25.37 |
| **γ series** | | |
| Gibbsite | $Al(OH)_3$ | 32.00 |
| Boehmite | AlOOH | 19.35 |
| Synthetic boehmite | $Al_2O_3$ | 27.80 |
| **Others** | | |
| Norstrandite | $Al(OH)_3$ | 32.38 |

The term *garnierite* is commonly used to designate lateritic Ni oxi-silicate ore formed by the intemperism of ultrabasic rocks. The most common minerals are goethite, serpentine, talc, chlorite and smectites, in which Ni replaces Fe and/or Mg (Table 4).

Table 4. Mg-Fe-Ni silicates of the garnierite group (Brindley, 1978). Minerals having <0.05 Ni mol% are classified as Ni-chrisotile, Ni-talc etc.

| Ni-free | Nickel > 0.5 mol% |
|---|---|
| Chrisotile | Pecoraite |
| Lizardite | Nepouite |
| Montmorillonite or kerolite | Pimelite |
| Talc | Willemsite |
| Chlorite | Nimite |
| Sepiolite | Falcondoite |

In the lateritic profiles, the duricrust is essentially represented by goethite. Hematite and sometimes maghemite occur near the surface. The goethite displays $Al(OH)_3$ decreasing proportions as depth and silicate content increase. Ni occur either in contact with goethite, forming *oxidized ore*, or as criptocrystalline masses associated with Mn and Co oxides (asbolite or "asbolan"). The latter may form economic concentrations up to 2 wt% Co below the duricrust. Under the oxidized zone, Ni-free smectite and opale-rich soils are present, covering a silicate, garnierite-rich zone.

The *silicate ore* constitutes the largest mineralized part of the garnieritic deposits, where nickeliferous serpentines (lizardite/nepouite and chrisotile/pecoraite) and talc predominate. The Ni content decreases as the depth increases.

The nickel-cobaltiferous laterites are superficial deposits with mineralized stratiform bodies, more than 50 m thick. The major deposits have thickness ranging from 10 to 20 m. The area extension of the nickeliferous laterites depends on the underlying (altered) bodies. In general, the major Ni-rich zone is placed between 0.5 and 6.0 m (rarely up to 15 m) below the surface. The bottom of the ore body is very irregular due to the fracturing system of the original rocks and the topographic conditions.

Garnieritic deposits are very common: 71 deposits give 44 Mt ore reserves, with average grade of 1.4 wt% Ni (Co=0.066 wt%). Rarely the grades exceed 2.0 wt% Ni, but values with more than 10 wt% Ni are noticeable.

It should be stressed that all the Brazilian lateritic deposits genetically linked to ultramafic-alkaline complexes are situated in the area of intersection of the 125ºAZ with the Transbrasiliano lineaments (Fig. 1). According to Haggerty (1986), the ultrabasic-alkaline complexes are associated with weakly mineralized kimberlites at the marginal regions of cratonic areas, as confirmed by the Brazilian complexes located close to the kimberlites of the Iporá-Poxoréu region (Fig. 13B).

*Poços de Caldas alkaline complex: bauxite mines and deposits*

There are nearly 30 bauxite mines and deposits in the Poços de Caldas alkaline complex (Table 1, n. 2). In general, they have about 50.0 Mt ore with average grade of 46 wt% $Al_2O_3$ and 4.5 wt% of reactive $SiO_2$ (Parisi, 1988a). The main deposits ("jazidas da serra") (cf. Fig. 2) are lateritic concentrations formed by the alteration of the tinguaite ring-dyke surrounding the complex and they are represented by thick and continuous bauxites with low reactive silica contents. The highlands are characterized by the presence of the "*jazidas do campo*" (deposits in peneplained regions) constituting thin and discontinuous bauxite levels with high reactive silica contents.

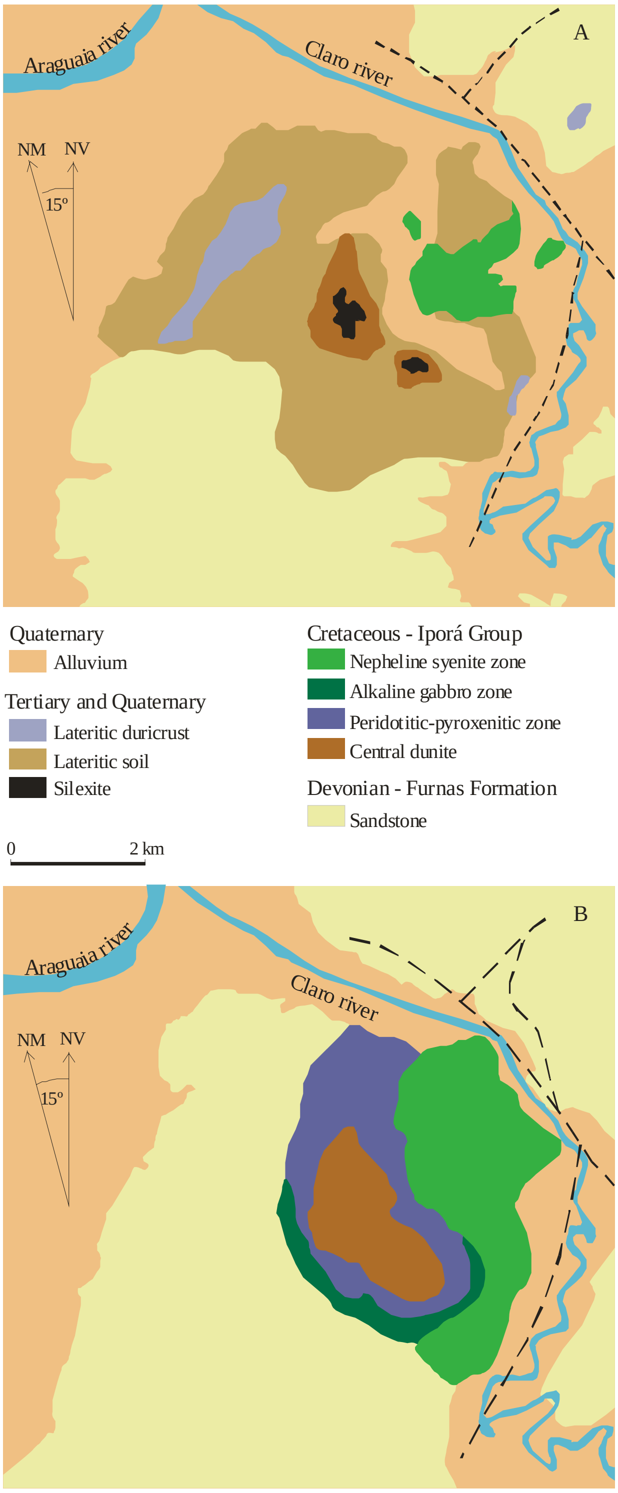


Fig. 29. A: Geological map of the Morro do Engenho ultrabasic-alkaline complex. B: Subsurface geological map. Note that the complex has concentric differentiation with a dunitic core involved progressively by peridote-pyroxenitic and gabbroic rocks and by nepheline syenites (Chaban, 1973).

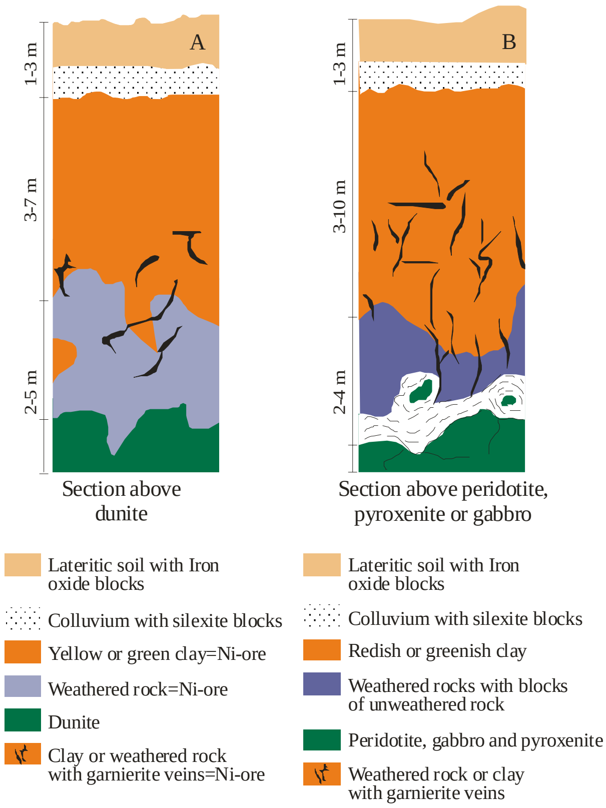


Fig. 30. Schematic profiles of the Morro do Engenho complex. In dunites (A), the mineralization reaches high contents in the clayey regoliths and in the altered rock. In the cover from the other rock-types (B), only regoliths are mineralized (Chaban, 1973).

The bauxites change, according to depth, to clayey-kaolinitic soils, and the latter into foyaites. In most of the places the clayey soils are abundant in zirconium, and have been mined as refractory ceramic ore.

*Morro Redondo bauxite mines*

Morro Redondo (Table 1, n. 7) is a circular intrusion, 5 km in diameter and 840 m high, belonging to a group of alkaline complexes that include Itatiaia and Passa Quatro. The main rock-types are syenites, alkali syenites and nepheline syenites cut by subordinate dykes ranging in composition from phonotephrite to peralkaline phonolite (Brotzu *et al.*, 1989). K/Ar ages for whole rock and mineral concentrates range from 68.0 to 79.8 Ma, being 73.6 Ma the preferred value following these authors.

The thickness of the bauxite deposits varies from 0.1 to 6.8 m, with a mean value of about 1.6 m. The bauxites change gradually into kaolinitic clays and into fresh alkaline rocks according to depth. Reserves of 1.1 Mt were calculated, with an ore averaging 58 wt% $Al_2O_3$, 3.0 wt% $SiO_2$, 6.33 wt% $Fe_2O_3$ and 1.35 wt% $TiO_2$ (Parisi, 1988b).

*Morro do Engenho nickel deposit*

The Morro do Engenho ultrabasic-alkaline complex (Table 1, n. 18) displays an oval shape (5.3x4.7 km), with a partially serpentinized dunitic core surrounded by peridotitic-pyroxenitic and gabbroic rocks, and bordered by nepheline syenites (Figs. 29A and B, cf. Chaban, 1973). A thick lateritic mantle with ferruginous duricrust and soils with garnieritic compositions showing high Ni grades covers the rocks of the complex.

In the laterite derived from the dunite alteration, two types of ore are present: 1) a clayey yellowish or greenish regolith with 0.8 to 1.6 wt% Ni; 2) a covering altered rock with 1.0 to 3.0 wt% Ni (Fig. 30A). The mineralized cover of the peridotites, pyroxenites and gabbros is restricted to the red or greenish clayey regoliths in which the nickel content ranges from 0.8 wt% to 1.6 wt% (Fig. 30B, cf. Chaban, 1973). The already known reserves, calculated at 1.1 wt% Ni cut-off, have 12.0 Mt of ore with average grade of 1.34 wt% Ni. The confirmed reserves, at 0.8 wt% Ni cut-off, amount to 26.8 Mt with average grade of 1.2 wt% Ni. Considering the same cut-off, the total estimated reserve has 38.6 Mt of ore with 1.1 wt% Ni average grade (Berbert, 1986).

*Ribeirão do Joelho (Jacupiranga complex), Serra da Água Branca, Santa Fé, Salobinha, Fazenda Furnas and Rio dos Bois lateritic nickel deposits (Table 1, n. 6, 16, 17, 19, 20 and 21)*

In the northern area of the Jacupiranga complex (Fig. 5), the intense weathering of peridotites and serpentinized dunites formed a 13 Mt deposit reaching 1.4 wt% Ni. The irregular Ni distribution and the thick cover are negative factors for the deposit exploitability.

There are not detailed information concerning the Goiás occurrences. Schobbenhaus (1986), in the "Anuário Mineral Brasileiro DNPM" and "Brazilian National Bureau of Mines DNPM-DFPM" files, suggests that they are garnieritic deposits similar to those from the Morro do Engenho complex. The reserves and contents are listed in Table 1.

Uranium deposits in metasomatic syenites or episyenites

The uranium deposits in episyenites are formed in shearing zones at medium to high metamorphic environment. Such deposits are usually uraninite albitites, i.e. episyenites from metasomatized orthogneisses.

Lobato & Fyfe (1990) suggest that mineralizing fluids from metasediments (500º-550ºC T and ~ 4 kb P) are responsible for metasomatic reactions percolating the sheared rocks. The fluid salinity ranges from 0 to 20% NaCl wt equivalent. $\delta^{18}O$‰ (SMOW) varies from −0.8 to +7.3 and from −3.7 to +2.6 in non-mineralized and mineralized albitites, respectively, in which the light oxygen enrichment seems to be the result of local processes. In this environment, the amphibole and biotite breakup releases hypercritical fluids enriched in $Na_2O$, $Fe_2O_3$, Sr, Pb, V and U (Lobato & Fyfe, 1990). At their turn, the fluids leaching $SiO_2$, $K_2O$, Rb and Ba from the gneisses and milonites produce a further $Na_2O$, $Fe_2O_3$, Sr, Pb, V and U enrichment. Finally, the steam generates metasomatic albitites lixiviating quartz, destroying amphiboles and crystallizing albite, aegirine-augite, andradite and hematite-magnetite. The uraninite precipitates in places where there is interaction between the oxidizing fluid and the meteoric water, which occasionates the decrease of the oxy-reduction potential of the metasomatic fluids and desestabilizes the uranium complexes (cf. Lobato & Fyfe, 1990).

*Lagoa Real uranium mine*

In the Lagoa Real deposit (Table 1, n. 32), coarse-grained and porphyritic granites host the mineralized bodies. As a result of the Espinhaço metamorphism (~1500 Ma; Pb-Pb 820 Ma on uraninite, considered to be remobilization ages by Oliveira *et al.*, 1985) these granitic rocks have been transformed into ophitic gneisses containing K-feldspar porphyroclasts, plagioclase and quartz set in a fine groundmass made of K-feldspar, plagioclase, hornblende, biotite and minor chlorite and calcite. Accessory phases are ilmenite, magnetite, apatite, zircon, fluorspar and rare allanite. Probably the metasomatic rocks of the shearing zones are associated with the main metamorphic events. The resulting episyenites (tabular bodies about 1000 m long and 100 m wide; cf. Fig. 31) are mainly made of albite+aegirine-augite+andradite+hematite, and, when mineralized, the deposit forms an uraninite-rich ore.

The estimated reserves amount to $U_3O_8$ 93,190 tons (Oliveira *et al.*, 1985).

*Espinharas episyenite uranium deposit*

The Espinharas (Table 1, n. 33) is an uranium episyenite deposit similar to Lagoa Real. The morphology of the mineralized bodies is mainly controlled by N60E/45° NW shear zones hundreds meters long. They consist of very irregular pods and lenses. In the sheared zones, biotite-amphibole gneisses were metasomatized into albite gneisses, granites into banded albitites, aplogranites into massive albitites and amphibolites into mineralized amphibolites.

After the metasomatic event, hydrothermal processes precipitated uraniferous collophane, thus generating the ore. The mineralization is assumed to have occurred at the end of the Brasiliano cycle (450-395 Ma; Santos & Anacleto, 1985). The estimated reserves are of 10,000 ton of $U_3O_8$ with grades ranging from about 500 to 1000 ppm, but some pods show contents more than 3 wt% $U_3O_8$.

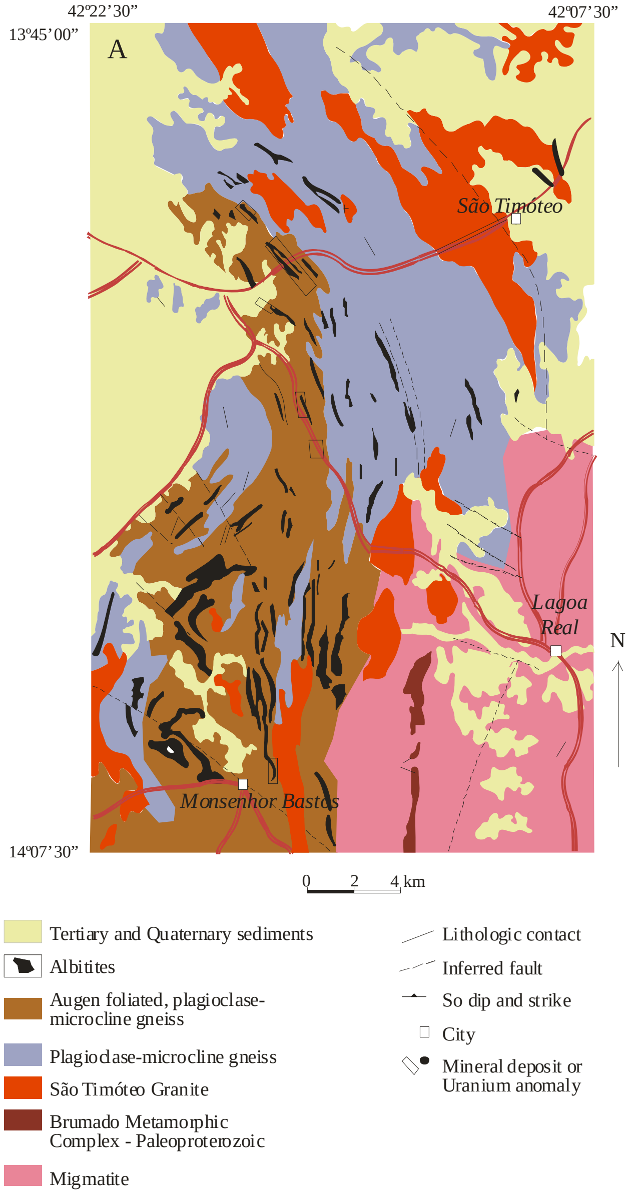


Fig. 31. A: Rabicha mine in the Lagoa Real episyenites (Lobato & Fyfe, 1990). Geological map showing U mineralized bodies.

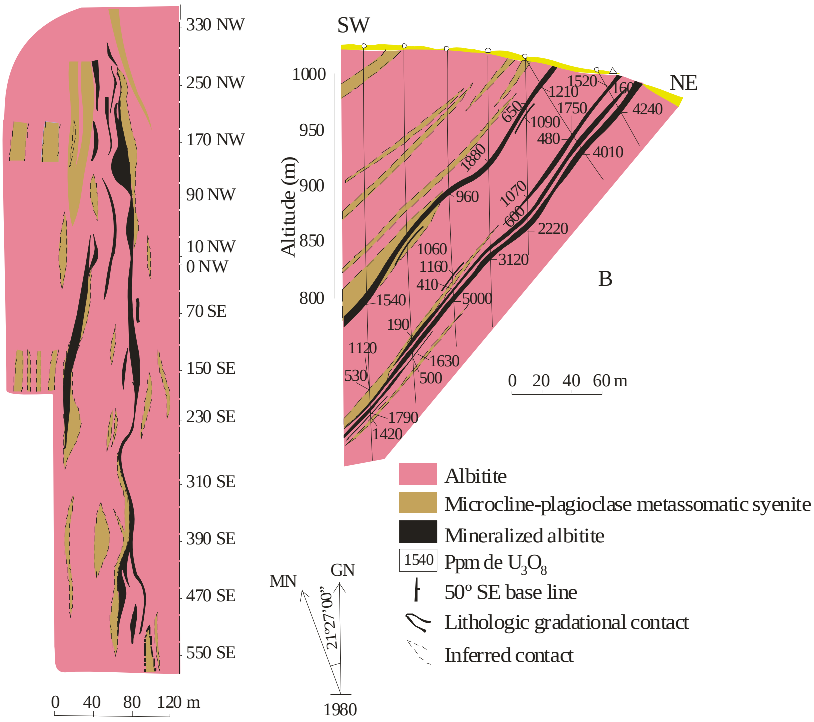


Fig. 31. B: Rabicha mine in the Lagoa Real episyenites (Lobato & Fyfe, 1990). Geological section of the mineralized area.

Itataia episyenite uranium deposit

Itataia (Table 1, n. 34) is the largest uranium episyenite deposit known in Brazil. Different ores occur in paragneisses and associated marble lenses: 1) marble associated bodies with massive collophanites, tens meters thick; 2) "stockworks", where the collophanites fill fractures in the marbles; 3) disseminated collophane and/or apatite in episyenites and, subordinately, in Ca-silicates rocks, marbles and gneisses; 4) powdered carbonaceous and zirconiferous materials cementing shear breccias. The main ore is collophanite, made of more than 80 wt% uraniferous collophane; other minerals present are zirconite, titanite, calcite, pyrite, ankerite, rutile and quartz. The episyenites are pink rocks, coarse to pegmatoid in texture, and contain feldspars, collophane and/or apatite impregnations. The main mineral is albite with subordinate biotite, apatite, epidote, titanite and pyrite. The altered episyenites have sericite, montmorillonite, kaolinite and leucoxene.

Fluid inclusions demonstrated that apatite from the collophanites have been originated at temperatures lower than 50ºC vs. 500-550°C of the episyenites (Lobato & Fyfe, 1990). Positive correlations between $Na_2O$ and of $U_3O_8$ contents and the non-correlated $U_3O_8$ and the phosphate proportions are indicative of relationships between uranium mineralization and episyenitization, and of remobilization by metamorphism and/or by late magmatism of the "sedimentary" uranium from the Proterozoic phosphorites. In this way, the collophanites were formed by supergenic concentration from apatite-rich marbles, previously enriched in uranium through the episyenitization (Mendonça *et al.*, 1985).

The apatite-rich marbles have an age of 2000 to 2500 Ma (Transamazonic cycle), the episyenitization took place at 550 to 600 Ma (Brasiliano cycle) and the formation of the collophanites could have occurred in the Paleozoic times.

In Itataia, 142,500 $U_3O_8$ tons (average grade 0.19 wt% $U_3O_8$) and 18.0 phosphate Mt (26.35 wt% $P_2O_5$) reserves were estimated by Mendonça *et al.* (1985).

Table 5. Genetic classification of the main Brazilian mineral deposits related to alkaline rocks.

| Geological system | Geological subsystem | Geological environment | Model | Brazilian deposits |
|---|---|---|---|---|
| Endomagmatic | Endogenous | Plutonic | Carbonatites with Nb, P and REE in oxide and phosphate minerals<br>Mafic and ultramafic alkaline rocks, nepheline syenites and carbonatites with P<br>Carbonatites with P<br>Carbonatites with Ti<br>Carbonatites with REE in carbonate minerals and with P<br>Sodalite differentiated into nepheline syenites (?) | 1. Primary ore: Barreiro (Araxá)<br>2. Primary ore: Anitápolis<br>3. Primary ore: Jacupiranga<br>4. Primary ore: Angico dos Dias<br>5. Tapira (?)<br>6. Barra do Itapirapuã<br>7. Mato Preto<br>8. Fazenda Hiassu |
| | | Volcanic | Kimberlites (and lamproites?) with diamonds | 1. Coromandel<br>2. Paranatinga<br>3. Três Ranchos-4<br>4. Província Juína-Aripuanã |
| Magmatic hydrothermal | Hydrothermal volcanic or plutonic | Continental volcanic or shallow depth plutonic | U-Mo-Zr disseminated (“porphyry type”) in phonolitic breccia and syenites<br>Mo-U-Zr in brecciated dykes (“fluidization breccia dykes and pipes”)<br>Sideritc carbonatite dykes with REE in carbonate minerals<br>Sideritic carbonatites and beforsites with disseminated and venular fluorspar<br>Magnetite veins with Th and REE<br>Fluorspar veins related to syenite pluton | Usamu Utsumi (Poços de Caldas)<br>1. Agostinho (Poços de Caldas)<br>2. Usamu Utsumi (Poços de Caldas)<br>Barra do Itapirapuã<br>Mato Preto<br>Morro do Ferro (Poços de Caldas)<br>Tanguá-Rio Bonito |
| Metamorphic | Metamorphic thermodynamic | Shear zones | Metasomatic syenites with U (“uranium in episyenites”) | 1. Lagoa Real - U<br>2. Espinharas - U<br>3. Itataia (U ore metasomatic, P ore supergenic) |
| Lateritic (residual and supergenic) | Surface residual and supergenic enrichment | Surficial intemperism. | P, Ti (anatase), Nb, REE, vermiculite (U, Th, Fe) enriched over carbonatites and alkaline rocks | 1. Barreiro (Araxá) - Nb+P+(REE)<br>2. Salitre - P+Ti+Nb<br>3. Tapira - Ti+P+Nb (+REE)<br>4. Catalão I - P+Nb+Ti+vermiculite+(REE)<br>5. Morro dos Seis Lagos - Th+Nb+Ti+Fe+ (REE+Mn)<br>6. Angico dos Dias - P<br>7. Anitápolis - P<br>8. Ipanema - P and vermiculite<br>9. Morro do Serrote - P<br>10. Mutum - (P?)<br>11. Serra Negra - (Ti, Zr?) |
| | | | Al in bauxites over syenites and phonolites.<br>Ni in garnierite over ultrabasic-alkaline rocks | 1. Alcoa, Curimbaba (Poços de Caldas)<br>2. Morro Redondo (Rezende-Itatiaia)<br>1. Ribeirão do Joelho (Jacupiranga)<br>2. Serra de Água Branca<br>3. Santa Fé<br>4. Morro do Engenho<br>5. Salobinha<br>6. Fazenda Furnas<br>7. Rio dos Bois |

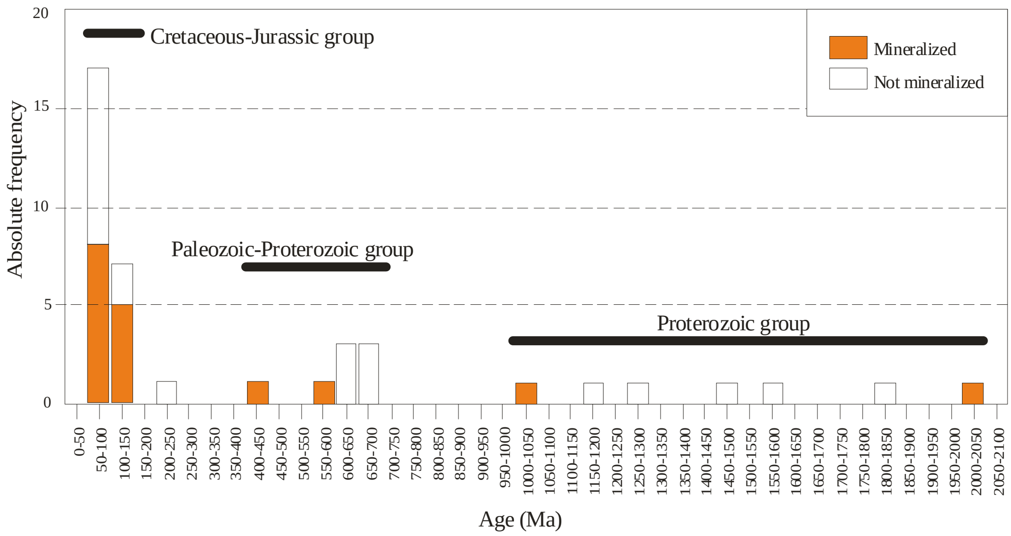


Fig. 32. Histogram of known ages of the main Brazilian alkaline complexes.

Ornamental stones, alkali feldspar, nepheline and sodalite

All the alkaline complexes from Brazil are potential sources for ornamental stones. Evolved rock-types may have economic interest for the ceramic industries because of the high alkali feldspar and foid contents.

Cassedane & Cassedane (1976) studied the mineralogy of a sodalite lens approximately 80x5 m in nepheline syenites (766 to 411 Ma; Cordani *et al*., 1974) from the Itajú da Colônia complex (Table 1, n. 35). Sodalite is a S-rich type (hackmanite) associated with cancrinite, zeolites, aegirine-augite, microcline and calcite. Cassedane (1991) also described sodalitic lens at the nearby Fazenda Hiassu, but further information about the geology of the deposit were not available.

Ages of mineralized Brazilian alkaline complexes

Table 6 shows maximum and minimum known ages of mineralized Brazilian alkaline complexes and various ages of complexes in which mineral concentrations of economic interest are not known.

Figure 32 is a histogram made with these ages. Ages of alkaline complexes having known mineral deposits were stressed, evidencing that the majority are Juro-Cretacic. This can not be understood as a consequence of a greater fertility of the complexes of this period, but simply demonstrates the existence of a large quantity of alkaline complexes formed in Brazil in this period. Mineral deposits associated with alkaline rocks exist since the Proterozoic. It is greatly probable that a detailed prospecting of the Mesoproterozoic complexes of the Amazonian region will reveal many other mineral deposits.

Lateritic deposits (bauxites, garnierites and other deposits formed by residual and supergenic concentrations) were obviously formed in epochs subsequent to that of the intrusions. They are deposits whose genesis is dependent only of the existence of proto-ores and of the permanency of favorable climatic conditions. These are the largest and most important mineral deposits related to alkaline rocks. In Brazil, the great majority of them have Tertiary ages and many are presently still in process of formation and/or growing.

## CONCLUDING REMARKS

Alkaline rocks are particularly enriched in some incompatible elements such as Nb, REE, Zr, P, U and F and may be found as primary sources for these elements (Moller *et al*., 1980; Veksler *et al*., 1998) as well as for industrial commodities (alkali feldspar, nepheline and lime).

It is difficult to classify the wide variety of mineral deposits associated with alkaline rocks because the ores are formed by multiple processes. A classification based on physic-chemical criteria is given in Table 6.

Carbonatite-associated deposits are usually subdivided into magmatic, metasomatic and residual types, but an overlap of the three environments is a very common situation. In general: 1) igneous deposits are related to the crystallization of carbonatites; 2) metasomatic or fenitic deposits are formed by reactions between the fluids released during crystallization and the alkaline intrusions or country-rocks; 3) deposits may be generated through the massive alteration and replacements within the country-rocks and 4) residual deposits are the result of the weathering and erosion of alkaline rocks, being produced either by mechanical accumulation of "inert" minerals, such as apatite, or, secondarily, by chemically enriched concentrations of relatively immobile elements. The latter deposits occur in lateritic or karstic weathered horizons, or in regoliths overlying the complexes.

Table 6. Known ages of the main Brazilian alkaline-carbonatite complexes.

| Alkaline complex | Minimun (Ma) | Observation | Maximum (Ma) | Ore |
|---|---|---|---|---|
| Jacupiranga | 131.5 | K/Ar | 147.1 | |
| Anitápolis | 130.6±3.0 | K/Ar | 136.4±1.6 | $P_2O_5$, "limestone" |
| Morro do Serrote | 131.7±1.6 | K/Ar | 148.2 | $P_2O_5$ |
| Ipanema | 124.9±9.5 | K/Ar | 141.6±5.4 | $P_2O_5$ |
| Barra do Itapirapuã | 96.9±1.9 | K/Ar | 114.7±9.7 | $P_2O_5$, vermiculite |
| Serra Negra | 83.0±3.0 | K/Ar | 83.7 | REE, $P_2O_5$ |
| Poços de Caldas | 62.8 | K/Ar | 80.3 | (Zr, Ti ?) |
| Tanguá | 68 | K/Ar | 70.5 | U, Mo, Zr, Th, REE |
| Mato Preto | 63.2±1.3 | K/Ar | 71.7±4.7 | $CaF_2$ |
| Araxá | 77.4±1.0 | K/Ar | 97.6±6.1 | $CaF_2$, REE |
| Catalão I | 84±4 | K/Ar | 85±6.9 | Nb, $P_2O_5$, REE, (U) |
| Salitre | 79±1.2 | K/Ar | 94.5±1.6 | $P_2O_5$, Nb, REE, Ti, vermiculite |
| Tapira | 71.2±5.1 | K/Ar | 87.2±1.2 | P, Ti, Nb, REE |
| Coromandel | 53 | K/Ar | 87 | Diamond |
| Morro Redondo | 64.6 | K/Ar | 90.5 | Bauxite |
| Itajú da Colônia | 411 | K/Ar | 766 | Sodalite |
| Santo Antonio da Barra | 40.1±1.2 | K/Ar | 61.4±16.9 | |
| Cabo Frio | 50 | K/Ar | 72.4±2.9 | |
| Itatiaia | 64.6±1.0 | K/Ar | 90.5±2.2 | |
| Banhadão | 94.8±1.2 | K/Ar | 111.9±3.1 | |
| Cananéia | 82.7 | K/Ar | 86.6 | |
| Pão de Açúcar | 209.6 | K/Ar | 241.1 | |
| Rio Bonito | 75.9±2.7 | K/Ar | 83.9±2.9 | |
| Cerro Alto | 63.5±1.7 | K/Ar | 107.0±7.8 | |
| Mapari | 1535 | K/Ar | 1680 | |
| Lages | 63 | K/Ar=70 Ma (=avg of 17 determinations) Rb/Sr=82±6 Ma | 78 | |
| | | KNOW AGE (Ma) | | |
| Espinharas | | 395-450(?) | | U (episyenites) |
| Itatiaia | | 550(?) | | U (episyenites) |
| Lagoa Real | | 820(?) | | U (episyenites) |
| Mutum | | 1026±28 | | $P_2O_5$ |
| Angico dos Dias | | 2011±6.0 | | $P_2O_5$ |
| Paratininga | | 121.1 | | Diamond |
| Canami | | 1175 | | |
| Sucunduri | | 1260 | | |
| Cachorra | | 1490 | | |
| Erepecuru | | 1806 | | |
| Itacaré | | 660 | | |
| Potiraguá | | 650 | | |
| Gurupá Mirim | | 610 | | |
| Itarantim | | 570 | | |
| Itabuna | | 560 | | |
| Catrimani | | 100 | | |
| Piedade | | 124.7±3.5 | | |

Dominant rock-associations include: 1) ultramafic rocks, such as dunites, peridotites, pyroxenites etc.; 2) carbonatites associated with ultramafic-dominated complexes; 3) carbonatite-dominated complexes; 4) carbonatites associated with syenite-dominated complexes; 5) nepheline syenites and syenite complexes; 6) peralkaline nepheline syenite complexes; 7) deposits, apparently not associated with alkaline rocks, but interpreted as genetically related (buried source?).

Fig. 33 represents an ideal section for all the rock-types usually found in alkaline-carbonatitic complexes, with some of the mineralized Brazilian occurrences (cf. Table 1) displayed at their present erosional levels. The best preserved intrusions may contain hydrothermal economic concentrations.

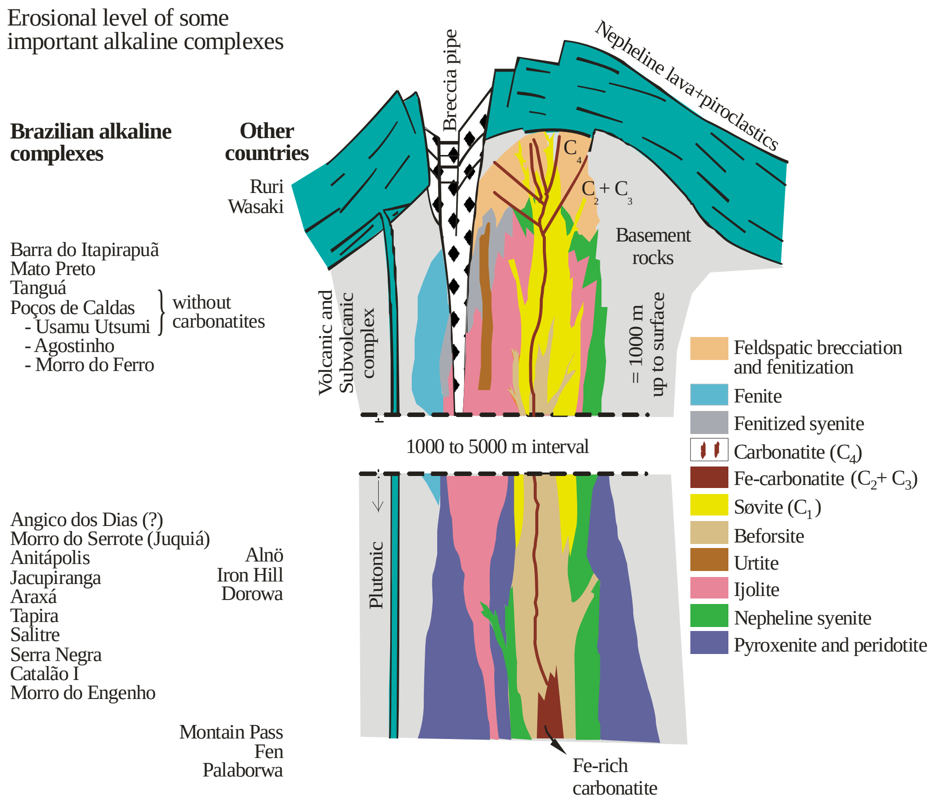


Fig. 33. Idealized sketch of an alkaline-carbonatitic complex. The names of the mineralized Brazilian complexes and of the complexes from other countries are reported in the stratigraphic position corresponding to the supposed erosion level (Le Bas, 1977; modified by Biondi, 1986).

The ore deposits are commonly originated where the fluid pressure ranges from lithostatic to hydrostatic with condensation of the steam phases released by the magma. Under these conditions, for instance, the Poços de Caldas (Usamu Utsumi, Agostinho and Morro do Ferro) U-Mo-Zr ores, the Mato Preto and Tanguá fluorspar deposits and the Barra do Itapirapuã carbonate REE-rich veins have been formed.

The formation of the mineral deposit depends on the composition of the rocks and on the economical interest of the raw material. The alkaline rocks, enriched in one or more industrial elements, show endogenous deposits with primary ore, e.g. at the Barreiro mine in the Araxá complex (carbonatites with 1.6 wt% $Nb_2O_5$), in the Anitápolis complex (ultramafic rocks and nepheline syenites having average grades of 7.41 wt% and 6.27 wt% $P_2O_5$, respectively) and in the Jacupiranga complex (carbonatites with 5.3 wt% $P_2O_5$). Primary and endogenous ore correspond also to the diamond deposits in kimberlites and lamproites.

Although the majority of the mineralized complexes is Juro-Cretacic, this fact is simply a consequence of the great quantity of alkaline complexes formed in Brazil in this period. Mineral deposits associated with alkaline rocks exist since the Proterozoic.

The most important Brazilian deposits associated with the alkaline intrusions are the lateritic, supergenic and/or residual. The great majority of them are from the Tertiary and many are presently still growing. They are formed by the residual and/or supergenic enrichment of minerals (apatite, pyrochlore, anatase etc.) or phases as $Al_2O_3$ and Ni-silicates from alkaline (and ultramafic) rocks playing the role of proto-ores. Some factors may influence somehow the transformation of the proto-ore into a lateritic deposit:

1) The proto-ore contains high amounts of elements or minerals that may form the ore minerals of the associated lateritic deposit.

2) Proto-ores most affected by weather conditions generate major deposits in a short time. For instance, in carbonatites, the water solubility is responsible for proto-ores more efficient than silicate rocks, such as the syenitic rocks, in the genesis of phosphate deposits.

3) The environmental conditions are very important: hot climate and seasons alternating rainy and dry periods tend to favor the development of lateritic profiles and the formation of large deposits of garnierite, bauxite and niobium-laterite and also of deposits containing residual concentrations of resistant minerals such as apatite, pyrochlore, anatase, ilmenite etc.

4) The tectonic stability is also important: tectonically stable regions contribute to the development of erosion surfaces and peneplains that allow the accumulation of lateritic soils. On the other hand, unstable regions modify the drainage level, reactivate the erosion system and displaces the phreatic surfaces. Usually, the latter modifications leads to the destruction of the lateritic deposits.

Finally, the deposits in episyenites are formed in shearing zones where the release of fluids during medium to high degree of metamorphism produces metasomatism and mineralizing processes.

## ACKNOWLEDGEMENTS

I would like to thank the editors, C.B. Gomes and P. Comin-Chiaramonti, for giving me the opportunity for writing this chapter, and for the helpful suggestions to improve the manuscript.

## REFERENCES

Almeida, F.F.M. (1966). Origem e evolução da plataforma brasileira. *Boletim da Divisão de Geologia e Mineralogia do DNPM* **8**, 56p.

Almeida, F.F.M. (1986). Distribuição regional e relações tectônicas do magmatismo pós-paleozóico no Brasil. *Revista Brasileira de Geociências* **16**, 325-349.

Andrade Ramos, J.R. & Fraenkel. M.O. (1974). Principais ocorrências de urânio no Brasil. *Boletim da Comissão Nacional de Energia Nuclear* **12**, 24p.

Araújo, D.P., Gaspar, J.C. & Bizzi, L.A. (2002). Morphology and surface features of diamonds from the Juína kimberlite province, Brazil. *Revista Brasileira de Geociências* **31**, 605-614.

Antonini, P., Comin-Chiaramonti, P., Gomes, C.B., Censi, P., Riffel, B.F. & Yamamoto, E. (2003). The Early Proterozoic carbonatite complex of Angico dos Dias, Bahia State, Brazil: geochemical and Sr-Nd isotopic evidence for an enriched mantle origin. *Mineralogical Magazine* 6**7**, 1039-1057.

Bardet, M.G. (1973). *Géologie du diamant. Part 1: généralités. Mémoires du Bureau de Récherches Géologiques et Minières* **83**, 235p.

Bardet, M.G. (1974). *Géologie du diamant*. Part 2: *gisements de diamants d'Afrique. Mémoires du Bureau de Récherches Géologiques et Minières* **83**, 229p.

Bardet, M.G. (1977). *Géologie du diamant*. Part 3: *gisements de diamants d'Asie, d'Amérique, d'Europe et d'Australasie. Mémoires du Bureau de Récherches Géologiques et Minières* **83**, 169p.

Becker, F.E., Valle. R.R. & Coelho, C.E.S. (1997). Depósitos de fluorita de Tanguá e Itaboraí, Rio de Janeiro. In: Schobbenhaus, C., Queiroz, E.T. & Coelho, C.E.S. (eds.) *Principais depósitos minerais do Brasil - Rochas e minerais industriais*. DNPM-CPRM, vol. VI, parte B, pp. 591-611.

Beccaluva, L., Barbieri, M., Born, H., Brotzu, P., Coltorti, M., Conte, A., Garbarino, C., Gomes, C.B., Macciotta, G., Morbidelli, L., Ruberti, E., Siena, F. & Traversa, G. (1992). Fractional crystallization and liquid immiscibility processes in the alkaline-carbonatite complex of Juquiá

(São Paulo, Brazil). *Journal of Petrology* **33**, 1371-1404.

Berbert, C.O. (1986). O depósito de níquel laterítico de Morro do Engenho, Goiás. In: Schobbenhaus, C., Queiroz, E.T. & Coelho, C.E.S. (eds.) *Principais depósitos minerais brasileiros - Ferro e metais da indústria do aço.* DNPM, vol. 2, pp. 335-340.

Biondi, J.C. (1974). *Contribution à la connaissance des cheminées bréchiques d'origine volcanique.* Docteur Ingénieur Thesis, University of Paris XI, Orsay, 332p.

Biondi, J.C. (1976). Cubagem e avaliação do depósito de urânio do Cercado (C-09). Nuclebrás, Relatório Interno, 26p.

Biondi, J.C. (1986). *Depósitos de minerais metálicos de filiação magmática.* São Paulo: CBMM-T.A. Queiroz, 602p.

Biondi, J.C. (1987). Informações básicas sobre os principais carbonatitos dos Estados de São Paulo, Paraná e Santa Catarina. Companhia Brasileira de Metalurgia e Mineração, Relatório Interno, 73p.

Bonow, C.W. & Issler, R.S. (1980). Reavaliação e aspectos econômicos do jazimento de terras raras e ferro-ligas do Lago Esperança, complexo carbonatítico de Seis Lagos, Amazonas. Brasil. *XXXI Congresso Brasileiro de Geologia, Camboriú, Anais* **3**, 1431.

Born, H. (1971). O complexo alcalino de Juquiá. *XXV Congresso Brasileiro de Geologia, São Paulo, Anais*, pp. 223-225.

Brindley, G.W. (1978). The structure and chemistry of hydrous nickel-containing silicate and aluminate minerals. *Bulletin du Bureau de Récherches Géologiques et Minières*, ser. 2., sec. 2, pp. 233-245.

Brotzu, P., Beccaluva, L., Conte, A., Fonseca, M., Garbarino, C., Gomes, C.B., Leong, R., Macciotta, G., Mansur, R.L., Melluso, L., Morbidelli, L., Ruberti, E., Sigolo, J.B., Traversa, G. & Valença, J.G. (1989). Petrological and geochemical studies of alkaline rocks from continental Brazil. 8. The syenitic intrusion of Morro Redondo, RJ. *Geochimica Brasiliensis* **3**, 63-80.

Burnham, C.W. (1985) Energy release in sub-volcanic environments: implications for breccia formation. *Economic Geology* **80**, 1515-1522.

Carvalho, W.T. (1974). Recursos minerais do complexo ultramáfico-alcalino de Catalão I, Goiás. *XXVIII Congresso Brasileiro de Geologia, Porto Alegre, Anais* **1**, 165-184.

Carvalho, W.T. & Bressan, S.R. (1997). Depósitos de fosfato, nióbio, titânio, terras raras e vermiculita de Catalão I - Goiás. In: Schobbenhaus, C., Queiroz, E.T. & Coelho, C.E.S. (eds.) *Principais depósitos minerais do Brasil - Rochas e minerais industriais.* DNPM-CPRM, vol. VI, parte C, pp. 69-93.

Cassedane, J.P. (1991). Tipologia das jazidas brasileiras de gemas. In: Schobbenhaus, C., Queiroz, E.T. & Coelho, C.E.S. (eds.) *Principais depósitos minerais do Brasil - Gemas e rochas ornamentais.* DNPM-CPRM, vol. VI, parte A, pp. 17-52.

Cassedane, J.P. & Cassedane, J.O. (1976). Étude diffractométrique et physique des minéraux de la lentille de sodalite de la Fazenda Hiassu (BA). *Anais Academia Brasileira de Ciências* **48,** 497-515.

Castro Filho, L.W. & Mattos, S.C. (1986). Depósito de níquel laterítico de Jacaré e Jacarezinho, Município de São Felix do Xingu, Pará. In: Schobbenhaus, C., Queiroz, E.T. & Coelho, C.E.S. (eds.) *Principais depósitos minerais brasileiros - Ferro e metais da indústria do aço.* DNPM, vol. 2, pp. 369-384.

Chaban, N. (1973). Relatório de pesquisa de níquel na região de Morro do Engenho. CPRM, Relatório Interno, 96p.

Coelho, C.E.S., Jost, H., Valle, R.R. & Dardenne, M.A. (1986). O controle estrutural dos depósitos de fluorita do Distrito de Tanguá - Rio de Janeiro. *XXXIV Congresso Brasileiro de Geologia, Goiânia, Anais* **5**, 2089-2104.

Comin-Chiaramonti, P., Gomes, C.B., Castorina, F., Censi, P., Antonini, P., Furtado, S., Ruberti, E. & Scheibe, L.F. (2002). Anitápolis and Lages alkaline-carbonatite complexes, Santa Catarina State, Brazil: geochemistry and geodynamic implications. *Revista Brasileira de Geociências* **32**, 639-653.

Comin-Chiaramonti, P., Gomes, C.B., Ruberti, E., Antonini, P. & Censi, P. (2001). Mato Preto alkaline-carbonatite complex: geochemistry and isotope (O-C, Sr-Nd) constraints. *Geochimica Brasiliensis* **15**, 23-24.

Cordani, U.G., Basei, M.A.S., Sobreiro Neto, A.F. & Mendonça, P.M.M. (1974). Idades potassio-argônio da região leste brasileira. *XXVI Congresso Brasileiro de Geologia, Porto Alegre, Anais,* pp. 71-75.

Fraenkel, M.O., Santos, R.C., Loureiro, F.E.V.P. & Muniz, W.S. (1985). Jazida de urânio no Planalto de Poços de Caldas. Minas Gerais. In: Schobbenhaus, C., Queiroz, E.T. & Coelho, C.E.S. (eds.) *Principais depósitos minerais brasileiros - Recursos minerais energéticos.* DNPM, vol. 1, pp. 89-103.

Frantsesson, E.V. (1970). *The petrology of the kimberlites.* Translation of A. Brown. Department of Geology, Australian National University, Camberra, 195p.

Gaspar, J.C. & Wyllie, P.J. (1983). Magnetite in the carbonatites from the Jacupiranga complex. Brazil. *American Mineralogist* **68**, 195-213.

Germann, A., Marker, A. & Friedrich, G. (1987). The alkaline complex of Jacupiranga. São Paulo. Brazil - Petrology and genetic considerations. *Zentralblatt für Geologie und Paläontologie* **1**, 807-818.

Gierth, E. & Baecker, M.L. (1986). A mineralização de nióbio e as rochas alcalinas associadas no complexo de Catalão I. Goiás. In: Schobbenhaus, C., Queiroz, E.T. & Coelho, C.E.S. (eds.) *Principais depósitos minerais brasileiros - Ferro e metais da indústria do aço.* DNPM, vol. 2, pp. 455-462.

Gomes, C.B., Ruberti, E. & Morbidelli, L. (1990). Carbonatite complexes from Brazil: A review. *Journal of South American Earth Sciences* **3**, 51-63.

Gonzaga, G.M. & Tompkins, L.A. (1991). Geologia do diamante. In: Schobbenhaus, C., Queiroz, E.T. & Coelho, C.E.S. (eds.) *Principais depósitos minerais do Brasil - Gemas e rochas ornamentais*, DNPM-CPRM, vol. VI, parte A, pp. 53-116.

Haggerty, S.E. (1986). Diamond genesis in a multiply-constrained model. *Nature* **320**, 34-38.

Haraly, N.L.E. (1991). Os diamantes de Juína, Mato Grosso. In: Schobbenhaus, C., Queiroz, E.T. & Coelho, C.E.S. (eds.) *Principais depósitos minerais brasileiros - Gemas e rochas ornamentais.* DNPM, vol. 4, pp. 155-160.

Hartmann, L.A., Silva, L.C., Daitx, E. & Girardi, V.A. (1980). O complexo granulítico de Santa Catarina: a Bacia de Campo Alegre e o complexo básico-ultrabásico de Pien. *XXXI Congresso Brasileiro de Geologia, Boletim nº* **3**, *Excursões,* pp. 60-68.

Hasui, Y. & Cordani, U.G. (1962). Idade K-Ar de rochas eruptivas mesozóicas do oeste mineiro e sul de Goiás. *XXII Congresso Brasileiro de Geologia, Rio de Janeiro, Anais* **1**, 139-143.

Issa Filho, A., Lima, P.R.A.S. & Souza, O.M. (1984). Aspectos da geologia do complexo carbonatítico do Barreiro, Araxá, Minas Gerais, Brasil. In: Rodrigues, C.S. & Lima, P.R.A.S. (eds.) *Complexos carbonatíticos do Brasil Geologia*. Companhia Brasileira de Metalurgia e Mineralização, pp. 20-44.

Issa Filho, A., Riffel, B.F. & Souza, C.A.F. (2001). Some aspects of the mineralogy of CBMM niobium deposit and mining and pyrochlore ore processing - Araxá, MG, Brazil. *Proceedings of the International Symposium on Niobium,* Orlando, 14p.

Issler, R.S. & Silva, G.G. (1980). The Seis Lagos Carbonatites complex. *XXXI Congresso Brasileiro de Geologia, Camboriú, Anais* **3**, 1564-1573.

Janse, A.J.A. (1984). Kimberlites - Where and When. In: Glover, J.E. & Harris, P.G. (eds.) *Kimberlites occurrence and origin: a basis for conceptual models in exploration*. The Geology Department and University Extension Courses. The University of Western Australia **8**, 19-61.

Jenkins II, R.E. (1987). Geology of the Clugger fluorspar deposit, Mato Preto, Paraná, Brazil. *Revista Brasileira de Geociências* **17**, 288-294.

Jenkins II, R.E. (1997). Depósitos de fluorita de Mato Preto. Cerro Azul. Paraná. In: Schobbenhaus, C., Queiroz, E.T. & Coelho, C.E.S. (eds.) *Principais depósitos minerais do Brasil - Rochas e minerais industriais*. DNPM-CPRM, vol. VI, parte B, pp.569-573.

Justo, L.J.E.C. & Souza, M.M. (1986). Jazida de nióbio do Morro dos Seis Lagos. Amazonas. In: Schobbenhaus, C., Queiroz, E.T. & Coelho, C.E.S. (eds.) *Principais depósitos minerais brasileiros - Ferro e metais da indústria do aço,* DNPM, vol. 2, pp. 463-468.

Kaminsky, F.V., Zakharchenko, O. D., Khachatryan, G.K. & Shiryaev, A.A. (2002). Diamonds from the Coromandel area, Minas Gerais, Brazil. *Revista Brasileira de Geociências* **31**, 583-596.

King, L.C. (1956). A geomorfologia do Brasil oriental. *Revista Brasileira de Geografia,* Abril-Junho, pp.3-118.

Lapido Loureiro, F.E.V. (1994). *Terras raras no Brasil: Depósitos. Recursos identificados. Reservas. Estudos e Documentos nº 21,* MCT-CNPq-CETEM, 189p.

Le Bas, M.J. (1977). *Carbonatite-nephelinite volcanism - An African case history*. Bristol: John Wiley & Sons, 347 p.

Leinz, V. (1940). Petrologia das jazidas de apatita de Ipanema, SP. *Ministério da Agricultura, Serviço de Publicidade Agrícola, Boletim nº* **40**, 52 p.

Leonardos, O.H. & Ulbrich, M.N.C. (1987). Lamproítos de Presidente Olegário, Minas Gerais. *39º Reunião da Sociedade Brasileira para o Progresso da Ciência, Brasília*.

Lobato, L.M. & Fyfe, W.S. (1990). Metamorphism. metasomatism and mineralization at Lagoa Real, Bahia, Brazil. *Economic Geology* **85**, 968-989.

Lorenz, V. (1985) Maars and diatremes of phreato-magmatic origin: a review. *Transactions of Geological Society of South Africa* **88**, 459-470.

Lorenz, V., McBirney, A.R., & Willians, H. (1970). An investigation of volcanic depressions: maars, tuffrings, tuffcones and diatremes. *NASA Research Grant Report. NGR 38- 003-012*, 198p.

Lumbers, S.B. (1978). Geological setting of alkalic rock-carbonatite complexes in eastern Canada. *I International Symposium on Carbonatites,* Poços de Caldas, Brazil, *Departamento Nacional da Produção Mineral, Anais* **19**, pp. 81-89.

Mariano, A.N. (1987). Analytical report on rocks from Angico dos Dias, Bahia. CBMM, Internal Report, 11p.

McCallum, M.E. (1985) Experimental evidence for fluidization processes in breccia pipe formation. *Economic Geology* **80**, 1523-1543.

Melcher, G.C. (1966). The carbonatites of Jacupiranga. São Paulo. Brazil. In: Tuttle, O.F. & Gittins, G. (eds.) *Carbonatites*. London: Interscience Publishers, pp. 169-181.

Melo, M.T.V. (1997). Depósitos de fosfato, titânio e nióbio de Tapira. Minas Gerais. In: Schobbenhaus, C., Queiroz, E.T. & Coelho, C.E.S. (eds.) *Principais depósitos minerais do Brasil - Rochas e minerais industriais*. DNPM-CPRM, vol. IV, parte C, pp. 41-56.

Melo, M.T.V., Chaban, N., Sad, J.H.G. & Torres, N. (1997). Depósito de fosfato. titânio e nióbio de Salitre. Minas Gerais. In: Schobbenhaus, C., Queiroz, E.T. & Coelho, C.E.S. (eds.) *Principais depósitos minerais do Brasil - Rochas e minerais industriais*. DNPM-CPRM, vol. IV, parte C, pp. 57-68.

Mendonça, J.C.G.S., Campos, M., Braga, A.P.G., Souza, E.M., Favali, J.C. & Leal, J.R.L. (1985). Jazida de urânio de Itataia. Ceará. In: Schobbenhaus, C., Queiroz, E.T. & Coelho, C.E.S. (eds.) *Principais depósitos minerais brasileiros - Recursos minerais energéticos.* DNPM, vol. 1, pp. 121-131.

Milashev, V.A. (1965). *Pétrochimie des kimberlites de Yakoutie et les facteurs de leur minéralisation diamantifère*. Translation by M. Morosoff. *Bureau de Récherches Géologiques et Minières* **5256**, 188p.

Moller, P., Morteani, G. & Schley, F. (1980). Discussion of REE distribution patterns on carbonatites and alkalic rocks. *Lithos* **13**, 171-179.

Morbidelli, L., Beccaluva, L., Brotzu, P., Conte, A., Garbarino, C., Gomes, C.B., Macciotta, G., Ruberti, E., Scheibe, L.F. & Traversa, G. (1986). Petrological and geochemical studies of alkaline rocks from continental Brazil. 3. Fenitization of jacupirangite by carbonatite magmas in the Jacupiranga complex, SP. *Periodico di Mineralogia* **55**, 261-295.

Morbidelli, L., Gomes, C.B., Beccaluva, L., Brotzu, P., Conte, A., G., Ruberti, E. & Traversa, G. (1995). Mineralogical, petrological and geochemical aspects of alkaline and alkaline-carbonatite associations from Brazil. *Earth-Science Review* **39**, 135-168.

Oliveira, A.G., Fuzikawa, K., Moura, L.A.M. & Raposo, C. (1985). Província uranífera de Lagoa Real. Bahia. In: Schobbenhaus, C., Queiroz, E.T. & Coelho, C.E.S. (eds.) *Principais depósitos minerais brasileiros - Recursos minerais energéticos.* DNPM, vol. 1, pp.105-120.

Parisi, C.A. (1988a). Jazidas de bauxita da região de Poços de Caldas, Minas Gerais-São Paulo. In: Schobbenhaus, C. & Coelho, C.E.S. (eds.) *Principais depósitos minerais brasileiros - Metais básicos não ferrosos. Ouro e alumínio.* DNPM, vol. 3, pp. 661-666.

Parisi, C.A. (1988b). Jazidas de bauxita de Morro Redondo. Resende, Rio de Janeiro. In: Schobbenhaus, C. & Coelho, C.E.S. (eds.) *Principais depósitos minerais brasileiros - Metais básicos não ferrosos. Ouro e alumínio.* DNPM, vol. 3, pp. 667-670.

Perkins, D., Essene, E.J., Westrum, E.F. & Wall, V.J. (1979). New thermodynamic data for diaspore and their application to the system $Al_2O_3$-$SiO_2$-$H_2O$. *American Mineralogist* **64**, 1080-1090.

Reis, J.R. (1997). Depósito de fosfato de Jacupiranga, São Paulo. In: Schobbenhaus, C., Queiroz, E.T. & Coelho, C.E.S. (eds.) *Principais depósitos minerais do Brasil - Rochas e minerais industriais*. DNPM-CPRM, vol. IV, parte C, pp. 31-39.

Reynolds, D.L. (1954) Fluidization as a geological process and its bearing on the problem of intrusive granites: *American Journal of Sciences* **1252,** 577-614.

Rodrigues, C.S. & Lima, P.R.A.S. (1984). *Complexos carbonatíticos do Brasil: Geologia*. Companhia Brasileira de Metalurgia e Mineração, Araxá, 44p.

Ruberti, E., Castorina, F., Censi, P., Comin-Chiaramonti, P., Gomes, C.B., Antonini, P. & Andrade, F.R.D. (2002). The geochemistry of the Barra do Itapirapuã carbonatite (Ponta Grossa Arch, Brazil): a multiple stockwork. *Journal of South America Earth Sciences* **15**, 215-228.

Ruberti, E., Castorina, F., Censi, P., Gomes, C.B., Speziale, S. & Comin-Chiaramonti, P. (1997). REE-O-C-Sr-Nd systematics in carbonatites from Barra do Itapirapuã and Mato Preto (southern Brazil). *1st South American Symposium on Isotope Geology, Campos do Jordão, Abstracts*, pp. 271-274.

Ruberti, E., Marguti, R.L. & Gomes, C.B. (1991). O complexo carbonatítico de Jacupiranga, SP: informações gerais. *3º Congresso Brasileiro de Geoquímica, Excursion Guide,* pp.1-20.

Santos, L.C.S. & Anacleto, R. (1985). Jazida de urânio de Espinharas. Paraíba. In: Schobbenhaus, C., Queiroz, E.T. & Coelho, C.E.S. (eds.) *Principais depósitos minerais brasileiros - Recursos minerais energéticos.* DNPM, vol. 1, pp.143-155.

Schobbenhaus, C. (1986). Geologia do níquel. In: Schobbenhaus, C., Queiroz, E.T. & Coelho, C.E.S. (eds.) *Principais depósitos minerais brasileiros - Ferro e metais da indústria do aço.* DNPM, vol. 2, pp. 251-255.

Schobbenhaus, C. & Campos, D.A. (1984). A evolução da Plataforma Sul-Americana no Brasil e suas principais concentrações minerais. In: Schobbenhaus, C., Campos, D.A., Derze, G.R. & Asmus, H.E. (coord.). *Geologia do Brasil - Texto explicativo do mapa geológico do Brasil 1:2.500.000*. DNPM-MME. 501p.

Silva, A.B. (1986). Jazida de nióbio de Araxá, Minas Gerais. In: Schobbenhaus, C., Queiroz, E.T. & Coelho, C.E.S. (eds.) *Principais depósitos minerais brasileiros - Ferro e metais da indústria do aço.* DNPM, vol. 2, pp. 435-453.

Silva, A.B., Liberal, G.S., Issa Filho, A., Rodrigues, C.S. & Riffel, B.F. (1987). Depósito de fosfato em carbonatito do Pré-Cambriano - Angico dos Dias, BA. Companhia Brasileira de Metalurgia e Mineração, Relatório Interno, 8p.

Silva, A.B., Liberal, G.S., Riffel, B.F. & Issa Filho, A. (1997). Depósito de fosfato de Angico dos Dias, Campo Alegre de Lourdes, Bahia. In: Schobbenhaus, C., Queiroz, E.T. & Coelho, C.E.S. (eds.) *Principais depósitos minerais do Brasil - Rochas e minerais industriais*. DNPM-CPRM, vol. VI, parte C, pp.123-130.

Souza, N.B. (1991). Depósitos diamantíferos de Poxoréu, Mato Grosso. In: Schobbenhaus, C., Queiroz, E.T. & Coelho, C.E.S. (eds.) *Principais depósitos minerais brasileiros - Gemas e rochas ornamentais.* DNPM, vol. 4, pp. 149-154.

Ulbrich, H.G.J. & Ulbrich, M.N.C. (2000). The lujavrite and khibinite bodies in the Poços de Caldas alkaline massif, southeastern Brazil: a structural and petrographic study. *Revista Brasileira de Geociências* **30**, 615-622.

Ulbrich, H.G.J., Vlach, S.R.F., Ulbrich, M.N.C. & Kawashita, K. (2002). Penecontemporaneous syenitic-phonolitic and basic-ultrabasic carbonatitic rocks at the Poços de Caldas alkaline massif, SE Brazil: Geologic and geochronologic evidence. *Revista Brasileira de Geociências* **32**, 15-26.

Veksler, I.B., Petibon, C., Jenner, G.A., Dorfman, A.M. & Dingwell, D.B. (1998). Trace element partitioning in immiscible silicate-carbonate liquid system: an initial experimental study using a centrifuge autoclave. *Journal of Petrology* **39**, 2095-2104.

Vergara, V.D. (1997). Depósito de fosfato de Anitápolis. Santa Catarina. In: Schobbenhaus, C., Queiroz, E.T. & Coelho, C.E.S. (eds.) *Principais depósitos minerais do Brasil - Rochas e minerais industriais*. DNPM-CPRM, vol. VI, parte C, pp. 17-30.

Wedow, H. (1967). The Morro do Ferro thorium and rare-earth ore deposit, Poços de Caldas district. *Brazilian Geological Survey Bulletin* nº **1185-D**, 34p.

Weska, R.K & Svisero, D.P. (2002). Aspectos geológicos de algumas intrusões kimberlíticas da região de Paranatinga, Mato Grosso. *Revista Brasileira de Geociências* **31**, 555-562.

Woolsey, T.S. (1975). Modelling of diatreme emplacement by fluidization. *Physics Chemistry of Earth* **9**, 29-42.

*Mesozoic to Cenozoic Alkaline Magmatism in the Brazilian Platform*
*Comin-Chiaramonti, P. & Gomes, C.B. (eds.)*
*Edusp/Fapesp, São Paulo, pp. 707-750, 2005*